

# Some effects of formaldehyde crosslinking on the kinetics of water vapour sorption in cellulose

A. C. Newns

Department of Pure and Applied Physics, University of Salford, Salford M5 4WT, UK  
(Received 28 November 1973; revised 30 May 1974)

New data are presented on the variation in the fraction sorbed with activity in the initial stage of the two stage sorption process for a crosslinked cellulose and compared to those for the original material and analysed in terms of the water-cellulose interaction. For both original and crosslinked material the fractions sorbed in the initial stage depend on the amount sorbed in the first sorption from dryness. The amounts sorbed in the initial stage starting at a given activity and varying the activity increment bear a similar relation to the activity increment as the amounts sorbed at equilibrium bear to activity.

## INTRODUCTION

It has been shown<sup>1-3</sup> that the sorption and desorption kinetics of the cellulose/water system may be explained in terms of a diffusion-relaxation mechanism and under certain circumstances the kinetics separate into two distinct stages. The initial stage is mainly governed by simple diffusion of the water through the polymer matrix, the swelling of the matrix being relatively rapid compared to the diffusion process, whereas the second stage is mainly governed by slow relaxation of the polymer matrix under the swelling stress, for relatively small activity increments, diffusion being the controlling rate when the activity increment is relatively large.

The results in this paper amplify previous work. New facts are presented concerning the fractions sorbed in the initial stage, the variation in the amount sorbed in the initial stage with activity increment and the effect of a crosslinking treatment.

## EXPERIMENTAL

The materials and procedure were the same as those described in previous communications<sup>1,2</sup>. The cellulose was prepared by hydrolysing cellulose acetate films; some specimens were soaked in a solution of formaldehyde + ammonium chloride to induce crosslinks, and the kinetics were determined by weighing on a sensitive quartz spring in water vapour under controlled conditions of temperature and pressure. The experiments reported in this paper were all performed at 15°C and started from equilibrium on the lowest sorption limb of the hysteresis loop.

## RESULTS

The kinetics of water sorption by the cellulose show features similar to those observed for the sorption of small solvent molecules by other polymers at temperatures below the glass transition region<sup>4</sup>. For example, for relatively large concentration changes the curves for the fractional amount sorbed plotted against the square root of the time show a pronounced inflection, and the initial rates of

desorption are far more rapid than the corresponding rates of sorption. If, however, one observes the kinetics for successive small increments of activity then, under certain circumstances, a high initial sorption rate is followed by a low rate of sorption, and the desorption kinetics also exhibit a two-stage behaviour<sup>1</sup>.

### Successive sorptions from dryness

Estimates of the fractions  $F_i$  sorbed in the initial stage as a function of the activity operative during an experiment are shown in Figures 1 and 2 for the original cellulose and the crosslinked material respectively. The total amounts sorbed during the initial and final stages for successive small sorption increments, together with the overall totals, are shown in Figure 3.

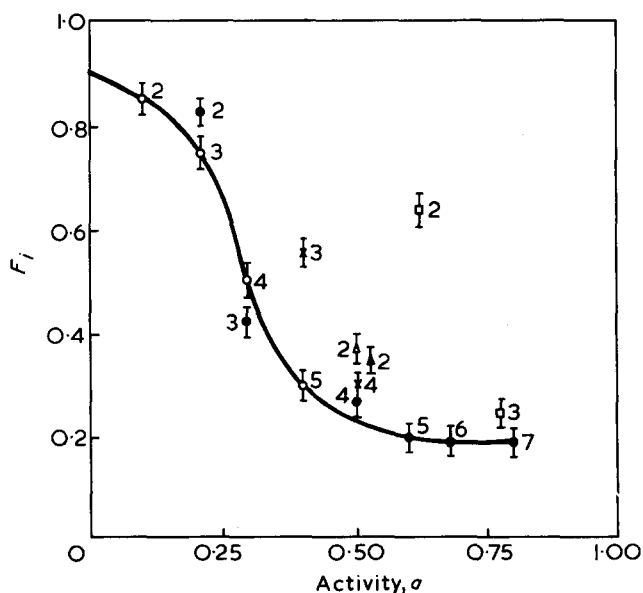


Figure 1 Fraction  $F_i$  sorbed in initial stage as a function of the activity,  $a$  of water vapour for original cellulose. Specimen 2: thickness, 26.2  $\mu\text{m}$ ; X, First cycle; ●, third cycle; ▲, fourth cycle. Specimen 5: thickness, 12.4  $\mu\text{m}$ ; □, fourth cycle; ○, fifth cycle; △, eighth cycle. The number against a point is the number of the interval in a given sequence of measurements

DISCUSSION

Successive sorptions from dryness

The curve in Figure 1 is for small successive increments in activity starting from zero activity of the water. They show that at an activity of about 0.2 the fraction  $F_i$  sorbed in the initial stage decreases rapidly as the activity increases up to an activity of about 0.4, thereafter remaining roughly constant as the activity increases.

This curve may be explained in terms of the water-cellulose interaction. At low activities the water is sorbed onto 'active' sites of the cellulose with the formation of hydrogen bonds. At first the swelling of the cellulose is smaller than the volume of water sorbed, the latter occupying a certain amount of 'free space' in the system available owing to the steric hindrance of the cellulose, and improves the 'packing' of the system. As the activity of the water increases the cellulose swells under the osmotic stress which

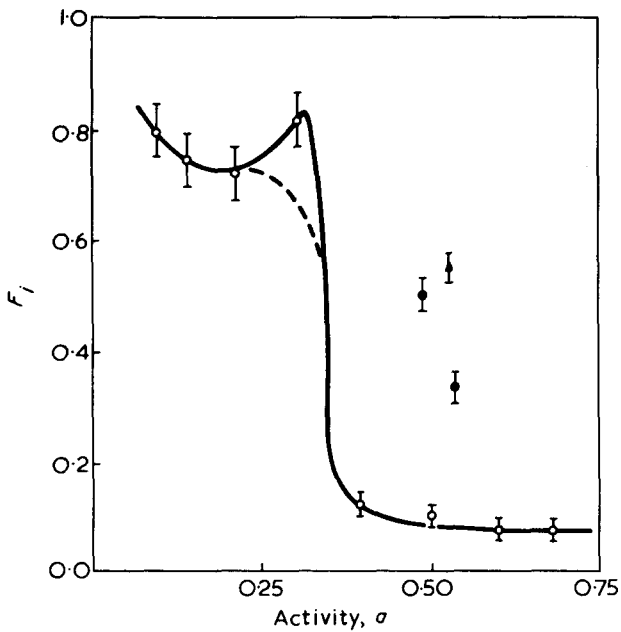


Figure 2 Fraction  $F_i$  sorbed in initial stage as a function of the activity,  $a$  of water vapour for crosslinked cellulose. Film thickness,  $12.4 \mu\text{m}$ ;  $\circ$ , first cycle;  $\bullet$ , third cycle;  $\blacktriangle$ , fifth cycle

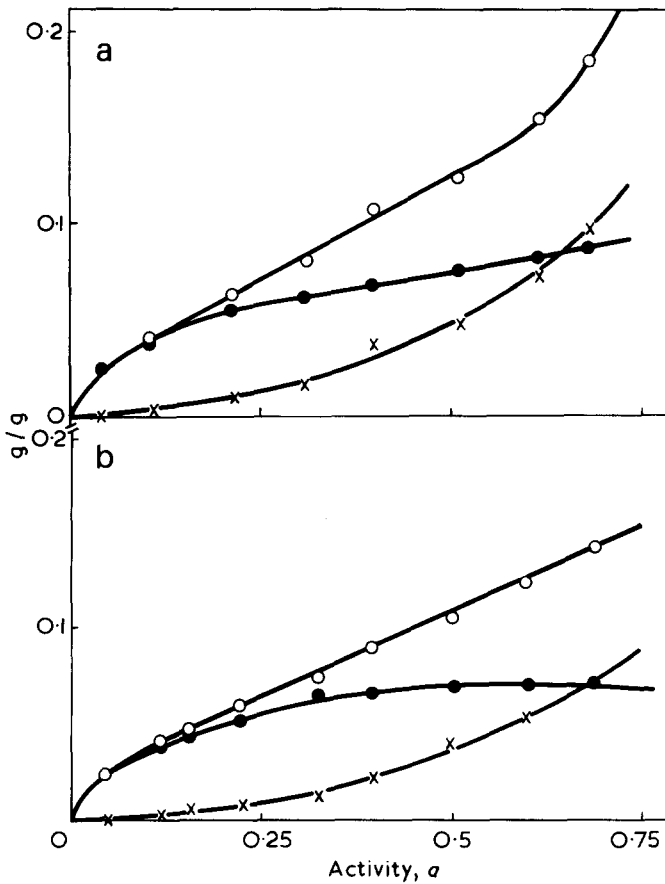


Figure 3 Summation of the amounts sorbed in the initial and final stages. (a) Original cellulose,  $\bullet$ ; (b) treated cellulose.  $\circ$ , Total amount sorbed at a given activity;  $\bullet$ , amount sorbed in the initial stage;  $\times$ , amount sorbed in the final stage

Amounts sorbed in the initial stage with varying activity increment

The amounts sorbed in the initial stage with a given initial activity and varying final activity are plotted against the final activity in Figure 4. The sorption isotherms for the original and crosslinked cellulose are shown in Figure 5.

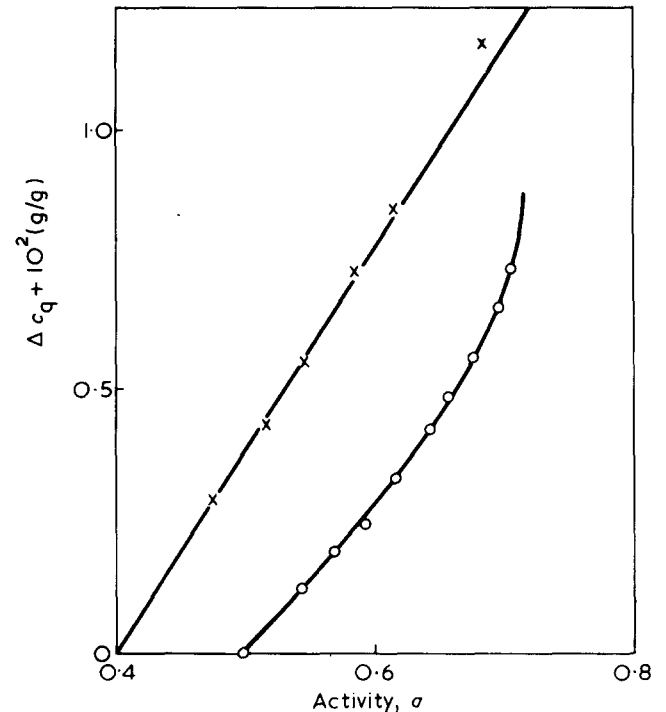


Figure 4 Sorptions in the initial stage from equilibrium at a given activity.  $\circ$ , Original cellulose (initial activity, 0.5);  $\times$ , crosslinked cellulose (initial activity, 0.4). Thickness of the films,  $12.4 \mu\text{m}$

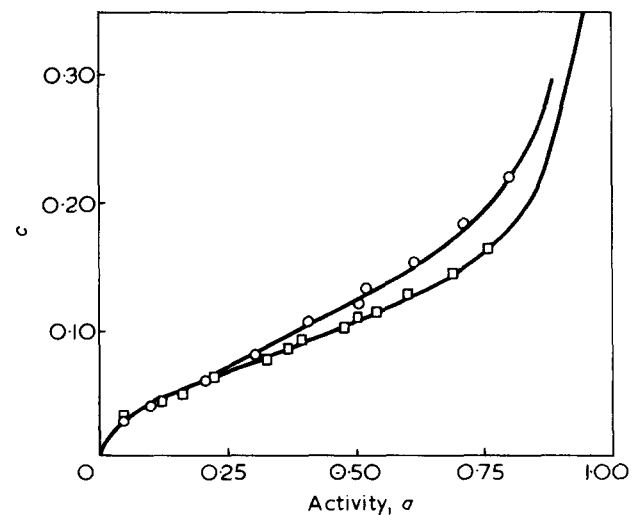


Figure 5 Sorption isotherms.  $\circ$ , Original cellulose;  $\square$ , crosslinked cellulose

overcomes the forces (e.g. hydrogen bonds) holding the chains together. It has been suggested that the kinetics may be interpreted in terms of a coupled diffusion relaxation mechanism in which the increase in free energy during sorption may be separated into the sum of an increase in free energy caused by swelling against unrelaxed internal forces. The kinetics are primarily controlled by diffusion of the water through the system, and an increase in free energy due to mixing as these forces relax, and by the rate of relaxation of the system under the osmotic stress<sup>1</sup>.

Thus an explanation of the curves shown in *Figure 1* is that the water is first sorbed onto active sites. As the 'free space' available to the water is filled, stress is placed on the internal 'bonds' and relaxation occurs producing more free space. Thus, up to an activity of about 0.2, corresponding to the part of the sorption isotherm which is concave to the activity axis (*Figure 5*) the water goes largely onto active sites and gradually fills some 'free space' in the system. Between activities of ~0.2 and 0.4 the water diffuses into 'free space' in the system during the initial stage but an increasing proportion of the 'free space' filled is that due to thermal motion. The activity of the water in solution reaches the activity of the water in the vapour phase as a result of the restricted swelling of the solution owing to internal cohesive forces, e.g. interchain hydrogen bonds. In this way stress is placed on the internal cohesive links which then 'break' and the polymer solution relaxes at a slow rate governed by the relaxation times of these 'links'.

It is to be expected that the relaxation times relevant to the two processes are comparable with those involved in the initial rapid rate of strain followed by the slow rate of strain, or creep, accompanying an external stress applied to the polymer alone. However, as the solution relaxes new 'thermal space' is formed, the activity of the water tends to drop, and the water diffuses in to maintain, as closely as possible, thermodynamic equilibrium throughout the system. This process proceeds until there is sufficient water in the solution for its activity to be constant throughout the system. At this stage the activity of the solution will be governed by the thermodynamics of mixing of the molecular species. At low concentrations the sorption process is diffusion controlled<sup>3</sup> and it would seem that, although there is some relaxation of the polymer matrix, the rate of relaxation is lower than or comparable with the rate of diffusion. Also it would seem that a large proportion of the water is sorbed in the initial diffusion-controlled stage, in which there is sorption with little, if any, breaking of inter- or intra-chain bonds. However, the values of  $F_i$  are uncertain at these low concentrations, and further measurements may clarify the picture. Above a water activity of about 0.4 the fraction sorbed in the final stage bears a roughly constant ratio to the fraction sorbed in the initial stage of 5:1. In this region the sorption isotherm is convex towards the activity axis, as for the rubber/benzene system.

There is a similar variation of  $F_i$  with activity for the crosslinked material (*Figure 2*). However, there are some differences between the results for the two materials. At the higher activities the fraction sorbed in the final stage bears an approximate ratio of 8:1 to the fraction sorbed in the initial stage for the crosslinked material. There are also some differences at lower activities but more data are needed to clarify the picture in this region. The amount of water sorbed at a given activity is less for the crosslinked material than for the original cellulose, as shown in

*Figure 5*. Thus the lower initial stage fraction at high activities means less sorbed in the initial stage by the crosslinked material at these higher activities. The amount sorbed by the crosslinked material in the final stages is also less than that sorbed by the original material as will be seen from *Figure 3*. The crosslinking holds the chains together in the amorphous regions. For this material a smaller amount sorbed will produce the same internal stress resisting swelling as for a larger amount sorbed by the uncrosslinked material. Also the amount of rearrangement of the polymer will also be more restricted for the crosslinked material than for the original material, reducing the amount sorbed in the second stage by the former compared with the latter.

A significant feature of *Figures 1* and *2* is that, although the values of  $F_i$  obtained for successive small increments of activity appear to lie on the lines drawn, if the first sorption is a large one, then the data for  $F_i$  against activity lie to the right of the data for successive small increments. This phenomenon seems to depend on the size of the initial sorption. The greater the value of this, the farther to the right do the points lie for successive small sorptions. If the initial stage corresponds to multilayer sorption, then there must be proportionally more sorbed in the initial stage after a large initial sorption than after a small one. Perhaps this may be due to a relatively smaller proportion sorbed in multilayers in the large initial sorption, the large swelling stress tending to open up the structure more so that a higher fraction is sorbed in the initial stage during the following successive sorptions.

#### Amounts sorbed in the initial stage with varying activity increments

The results plotted in *Figure 4* are for two series of measurements starting at equilibrium on the lowest sorption limb of the hysteresis loop, one for the original cellulose and the other for the crosslinked material. For each of the measurements the activity of the water was increased and the subsequent sorption was allowed to continue until the end of the initial stage. The activity was then decreased to its original state. For the crosslinked material the initial activity was 0.4, and it will be seen that the amount sorbed in the initial stage varies in a linear manner with the activity increment. For the original cellulose the initial activity was ~0.5, and the plot of the amount sorbed in the initial stage against the activity increments is somewhat convex towards the activity axis. Over the activity range covered for the crosslinked material the sorption isotherm (*Figure 5*) is roughly linear whereas over the activity range covered for the original cellulose the isotherm is convex to the activity axis. Thus, for the data presented here the amounts sorbed in the initial stage starting at a given activity and varying the activity increment bear a similar relation to the activity increment as the amounts sorbed at equilibrium bear to the activity. This does not appear to hold for some other systems which exhibit two-stage behaviour (Kishimoto, A. and Fujita, H. personal communication).

#### REFERENCES

- 1 Newns, A. C. *Trans. Faraday Soc.* 1956, 52, 1533
- 2 Newns, A. C. *Trans. Faraday Soc.* 1968, 64, 3147
- 3 Newns, A. C. *JCS Faraday Trans. I* 1973, 69, 444
- 4 Crank, J. and Park, G. S. 'Diffusion in Polymers', Academic Press, London, 1968

# Persistent polarization in a carotenoid polymer, $\beta$ -carotene

P. K. C. Pillai and Malti Goel

Department of Physics, Indian Institute of Technology, New Delhi 29, India  
(Received 18 February 1974; revised 3 June 1974)

Charge retention properties of a carotenoid polymer,  $\beta$ -carotene, have been investigated under photo- and thermal-polarization conditions. Total stored charge has been evaluated. Analysis of thermal current spectra of a polarized sample has been made by obtaining activation energies and relaxation times. The process of ionic and electronic charge trapping is mainly responsible for high charge densities retained for longer times in this polymer. The dipolar contribution is comparatively small.

## INTRODUCTION

It has been suggested<sup>1</sup> that photoconductivity should occur in carotenoid compounds since they have a highly conjugated structure.  $\beta$ -Carotene is a member of the  $C_{40}$  carotenoid group and it has a hydrocarbon composition. It is believed to take part in photosynthesis and phototropic processes. It has also been considered as a precursor of retinene pigment which is involved in all visual receptor systems.

Rosenberg<sup>2-4</sup> has experimentally investigated electronic conduction properties of  $\beta$ -carotene and has determined activation energies. Photoconduction studies in  $\beta$ -carotene single crystals, have been carried out by Chapman *et al.*<sup>5</sup> who reported interesting spectral results. Transient effects in photoconduction of  $\beta$ -carotene glass have also been investigated<sup>6</sup> recently. Thus although photoconduction is an established property of  $\beta$ -carotene, almost nothing has been reported about its charge retention properties observed under suitable experimental conditions. An attempt has thus been made to investigate the persistence of space charge polarization in this polymer.

## EXPERIMENTAL

To study the polarization phenomena in  $\beta$ -carotene, an apparatus in which studies can be made under controlled atmospheric conditions has been designed. The arrangement is shown in *Figure 1*. A sample is placed between two electrodes A and B. The lower electrode is of Nesa-coated glass which enables the sample to be illuminated, while an electric field is applied. The upper electrode is movable and is connected to an insulated micrometer head. The sample is surrounded by an electrostatically shielded heating arrangement<sup>7</sup> which provides a uniform or a variable temperature, changing at a linear rate, as required. A thermocouple (C, D) is placed near the sample for reading the temperature.

For the sample preparation, a thin layer of  $\beta$ -carotene glass was coated on the lower transparent electrode and the upper electrode was pressed over it in such a way that glass film adhered to both electrodes. The photopolarization process has been studied by applying an electrostatic field across the sample and illuminating it in a perpendicular direction. The phenomenon of photodepolarization has been studied in the absence of an external field by observing

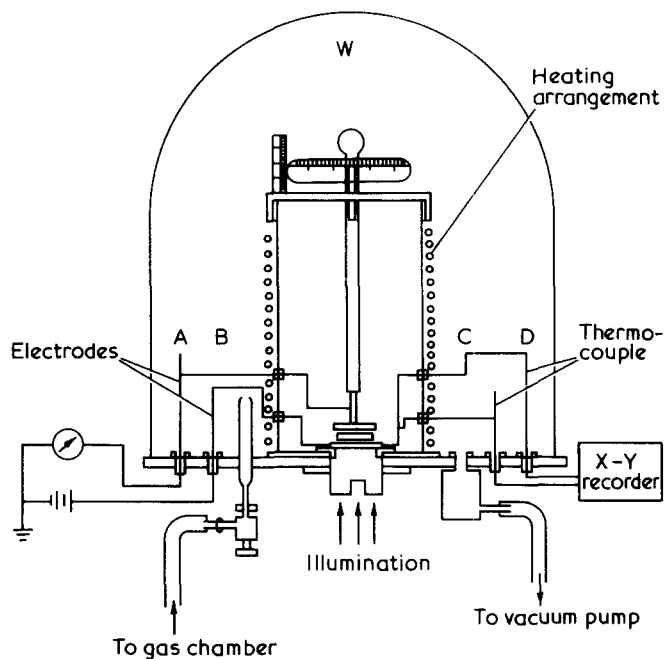


Figure 1 Apparatus for polarization and depolarization studies

the decay of current when the photoelectret (polarized sample) was re-illuminated. For each measurement separate samples were used and all these measurements were carried out at room temperature.

For the study of thermal polarization, a sample was heated to a uniform higher temperature and an electrostatic field was applied to it. This process of polarization was continued for a certain period of time and polarization current as a function of time was measured on a sensitive electrometer. The samples were then cooled to room temperature in the presence of an external field. Thermal depolarization currents of the thermoelectrets, so formed, were observed on reheating the samples at a uniform rate, in the absence of the field.

The essential feature of the present system is that the study of photopolarization and depolarization as well as thermal polarization and depolarization can be carried out without disturbing the sample.

Aplab stabilized power supply Type HV1 was used for

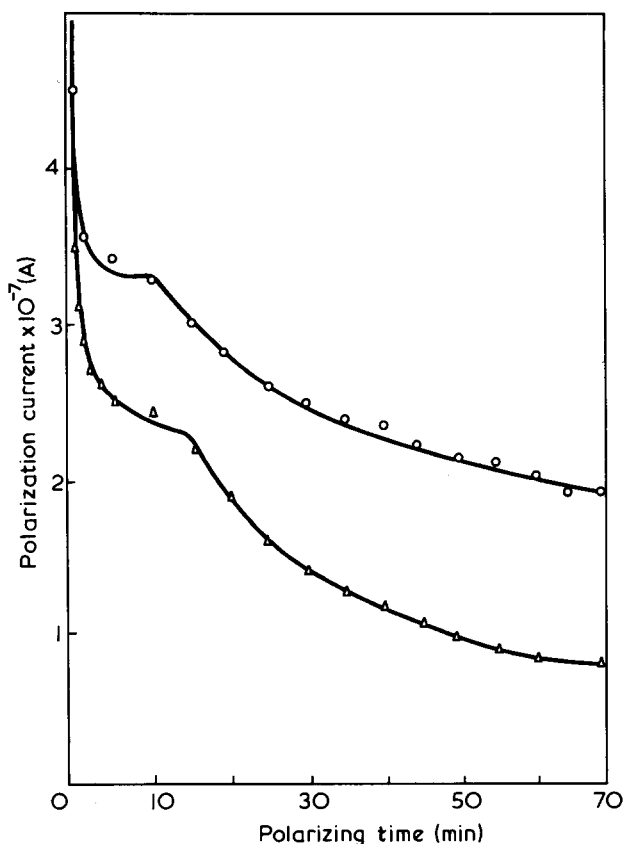


Figure 2 Thermal polarization currents in  $\beta$ -carotene at 343 K ( $\Delta$ ) and 363 K ( $\circ$ ) for constant field strength of 2 kV/cm

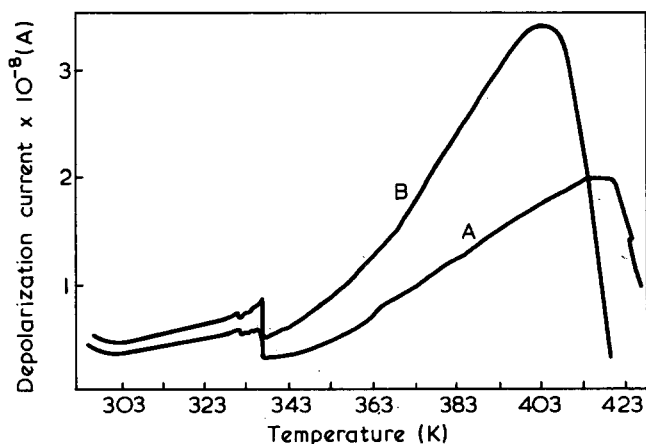


Figure 3 Thermal depolarization current spectra of  $\beta$ -carotene thermoelectrets fabricated at (A) 343 K and (B) 363 K

applying high electrostatic fields across the sample. Current measurements were carried out on a 610C solid state electrometer (Keithley Instruments) and a Hewlett-Packard 7035 B, X-Y recorder was used for studying thermal currents as a function of temperature.

## RESULTS AND DISCUSSIONS

### Thermal polarization in $\beta$ -carotene

A study of  $\beta$ -carotene was made when thermal and electrostatic energies were supplied to it simultaneously. The thermal polarization currents were observed at constant temperature as a function of time. The results are shown in Figure 2 at a forming field strength of 2 kV/cm for two samples polarized at 343 and 363 K respectively. A dis-

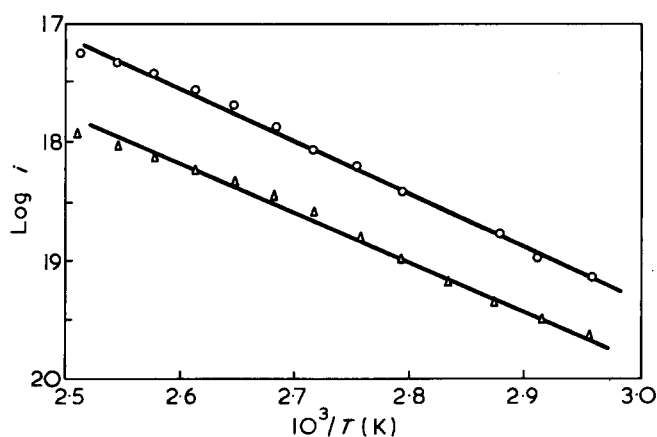


Figure 4 Arrhenius plot obtained for initial half of the current peak observed at 400 K in Figure 3.  $\Delta$ , 343 K;  $\circ$ , 363 K

continuity was observed at about 10–15 min for both samples.

Polarization current attained a constant value in about 75 min. The samples were then slowly cooled to room temperature under the influence of the electrostatic field. The process of polarization was thus continued for a total of 150 min and then the field was switched off. Thermal depolarization studies of these thermoelectrets were carried out by reheating at a uniform rate of 6°C/min. A thermal depolarization current so observed has been plotted as a function of temperature for samples prepared at different temperatures.

In these curves (Figure 3) two peaks, one at 335 K and another at 400 K have been observed. Analysis of the second peak at 400 K has been made by calculating thermal activation energies and relaxation times. According to the initial rise method of Garlick and Gibson<sup>8</sup> the slope of the straight line plot of  $\log i$  vs.  $1/T$  (Figure 4) for the first lower half of the peak gives activation energy, since:

$$\log i(T) = \text{const} - \frac{E}{KT}$$

where  $E$  is activation energy,  $T$  is absolute temperature, and  $K$  is Boltzmann's constant.

Relaxation time of polarization<sup>9</sup> created by ionic motion or by orientation of dipoles is given by the Arrhenius equation:

$$\tau = \tau_0 \exp\left(-\frac{E}{KT}\right)$$

where  $\tau_0$  is a constant corresponding to total charge stored and can be written as,

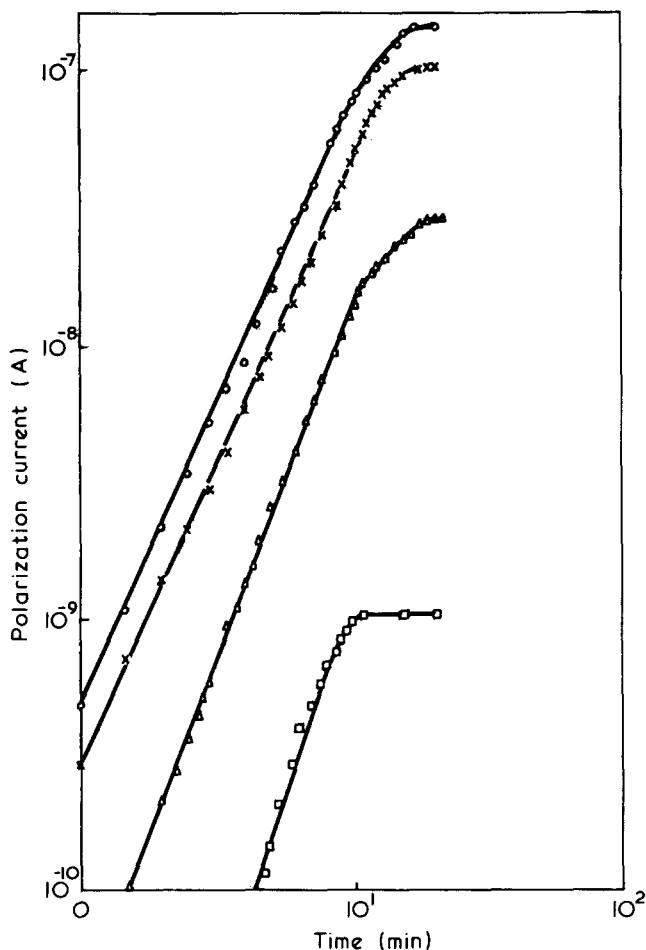
$$\tau_0 = \frac{KT_m^2}{T_1 E \exp(E/KT_m)}$$

where  $T_1$  is the heating rate and  $T_m$  is the peak temperature.

The activation energies and relaxation times obtained from thermal current spectra of Figure 3 are shown in Table 1<sup>10</sup>. The result of activation energy level is in agreement with the result obtained by photoconduction methods. An energy level at 0.356 eV has been postulated<sup>3</sup> as trapping level below triplet state.

Table 1 Results for thermally polarized  $\beta$ -carotene

	Sample 1	Sample 2
Polarizing field (kV/cm)	2	2
Polarizing temperature (K)	343	363
Polarizing time (min)	150	150
Activation energy, $E$ (eV)	0.348	0.355
$\tau_0 \times 10^4$ (min)	1.30	1.377
$\tau$ at room temperature (min)	145	194.9
$\tau$ at $T_m$ (min)	6.386	6.277


 Figure 5 Photopolarization current in  $\beta$ -carotene at various forming field strengths:  $\square$ , 1;  $\triangle$ , 1.8;  $\times$ , 2.5;  $\circ$ , 3.3 kV/cm

#### Photopolarization in $\beta$ -carotene

The photopolarization currents observed in  $\beta$ -carotene in an apparatus described previously are shown in Figure 5 for different field strengths. Non-monochromatic mercury light without any filter has been used for illumination.

Currents have been found to increase and then show a saturation with polarizing time. The polarization time required for attaining saturation depends upon the applied field and irradiation intensity. The positive electrode was illuminated in all the measurements.

The polarization process was carried out for 30 min and then the samples were stored in short circuited condition in the dark<sup>11</sup>. Photodepolarization currents observed on re-illuminating the photoelectret are shown in Figure 6. Currents have been observed as a function of time for various forming fields. Discontinuities in the current-time curves suggested the presence of various decay modes in the substance. While two decay modes are observed at low field, an additional discontinuity is present at higher fields.

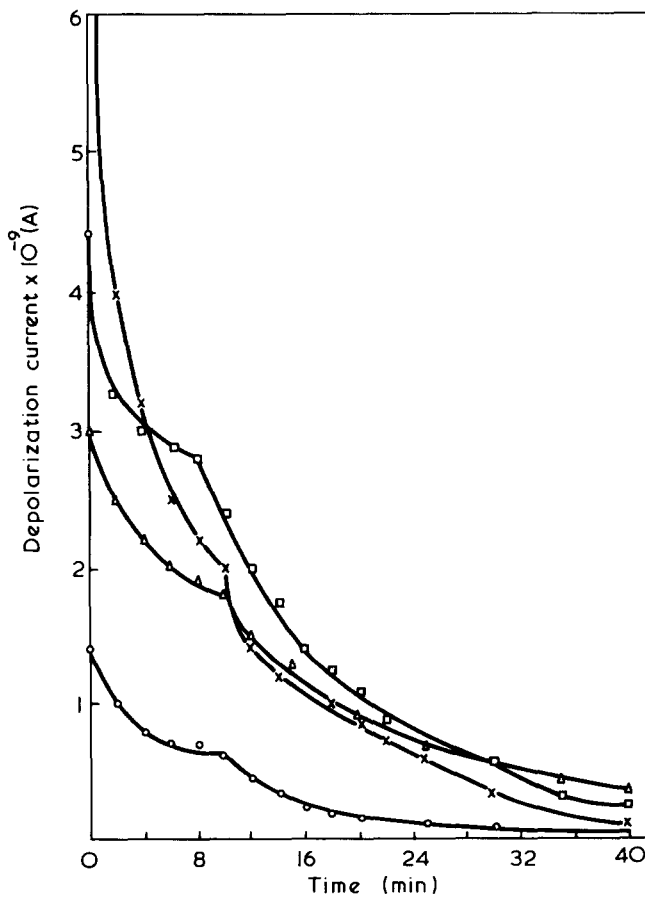
Although the initial value of the photodepolarization

current has been found to increase with increasing forming field the total charge stored in a sample calculated by extrapolating decay curves, does not show a similar dependence<sup>12</sup>. The initial current and total charge of various photoelectrets polarized at different fields is shown in Table 2.

Irradiation with non-monochromatic light generates electric carriers at the surface as well as in the bulk of the sample. Under the influence of the external field carriers migrate in the bulk and subsequently get trapped. If the trapping levels are sufficiently deep, the substance gets polarized and polarization pertains even after the external field is removed and the radiation is switched off. The process of charge decay is dependent on mutual interaction and annihilation of carriers, but it can be accelerated by again irradiating the sample. The discontinuous decay of the kind shown in Figure 6, suggests the presence of various trapping levels in the material. The persistence of thermal polarization also suggests trapping of charge by ionic and

 Table 2 Results for photopolarized  $\beta$ -carotene

Sample No.	Polarizing field (kV/cm)	Polarizing time (min)	Initial depolarization current $\times 10^{-9}$ (A)	Total stored charge $\times 10^{-6}$ (C/cm <sup>2</sup> )
1	1 (dark)	30	0.8	0.384
2	1	30	1.1	5.10
3	1.8	30	3.0	18
4	2.5	30	5.2	8.4
5	3.3	30	7.3	4.2


 Figure 6 Photodepolarization decay curves of  $\beta$ -carotene photoelectrets fabricated as in Figure 5.  $\circ$ , 1;  $\triangle$ , 1.8;  $\square$ , 2.5;  $\times$ , 3.3 V

electronic movements and the trap level activated by the thermal process has been computed as 0.352 eV.

However,  $\beta$ -carotene exists in various isomeric forms. Its *trans* configuration has a minimum dipole moment while the 15-15' configuration has a maximum dipole moment along the perpendicular axis.  $\beta$ -Carotene glass is a combination structure and hence the dipoles will be scattered in all directions in the neutral sample. During polarization processes the external field will exert a force on the dipoles and the orientation will result in dipolar alignment along the external field axis. This dipolar alignment will contribute to persistent polarization, the relaxation of which will depend upon re-orientation of dipoles. The lower peak, observed at 335 K in thermal current spectra (Figure 3) is attributed to dipolar polarization. The contribution of dipoles seems to be comparatively smaller than ionic and electronic polarizations which show a larger relaxation peak at 400 K (Figure 3).

### CONCLUSIONS

The photopolarizing technique produces charge densities in excess of  $10^{-6}$  C/cm<sup>2</sup> in  $\beta$ -carotene, which are retained for reasonably longer times, compared to inorganic substances. This property of retaining high density of charge for longer time, of  $\beta$ -carotene, is possibly correlated with high light sensitivity and memory effects of retinal systems in vertebrates. Thermal polarization technique has also resulted in excessive charge trapping. Analysis of thermal-

ly stimulated currents has helped to determine activation energies and relaxation times.

### ACKNOWLEDGEMENTS

The authors wish to express their appreciation to Professors C. L. Mehta, K. L. Chopra and M. S. Sodha for their continuing encouragement. They also thank Dr K. Jain and Dr P. K. Nair for the helpful discussions in the course of this work.

### REFERENCES

- 1 Chynoweth, A. G. and Schneider, W. G. *J. Chem. Phys.* 1954, **22**, 1021
- 2 Rosenberg, B. *J. Opt. Soc. Am.* 1958, **48**, 581
- 3 Rosenberg, B. 'Electrical Conductivity of Organic Solids', (Eds H. Kallman and M. Silver), 1961, Interscience, New York, p 291
- 4 Rosenberg, B. *J. Chem. Phys.* 1961, **37**, 61
- 5 Chapman, D., Cherry, R. J. and Morrison, A. *Proc. R. Soc. (A)* 1967, **301**, 173
- 6 Kim, E. H. *J. Korean Phys. Soc.* 1971, **4**, 17, 73
- 7 Nair, P. K. unpublished results
- 8 Garlick, G. F. J. and Gibson, A. F. *Proc. Phys. Soc.* 1948, **60**, 574
- 9 Pillai, P. K. C., Jain, K. and Jain, V. K. *Phys. Lett.* 1972, **39A**, 216.
- 10 Perlman, M. M. *J. Appl. Phys.* 1971, **42**, 2645
- 11 Pillai, P. K. C. and Goel, M. *Physica Status Solidi* 1971, **6**, 9
- 12 Pillai, P. K. C. and Goel, M. *Indian J. Pure Appl. Phys.* 1973, **11**, 459

# Conformational study of the sequential (Tyr-Glu)<sub>n</sub> copolymer in aqueous solution

Yves Trudelle

Centre de Biophysique Moléculaire, CNRS, 45045 Orleans-Cedex, France

(Received 23 April 1974)

Conformational properties of the sequential poly(Tyr-Glu) copolymer in aqueous solution were investigated as a function of pH. No transition could be detected over the range pH 13–10.5. Below pH 10.5 an aggregation process takes place, causing a drastic change in all optical properties of the polymer (optical rotation, c.d. and u.v. spectra). By means of i.r. spectroscopy in D<sub>2</sub>O, aggregates were found to be in antiparallel  $\beta$  conformation. The c.d. spectrum of  $\beta$ -aggregates is very similar to that of  $\alpha$ -helical poly(L-tyrosine) in organic solvents, except in the 280 nm region. In addition the aggregation process is accompanied by a strong hyperchromic effect in the 277 nm absorption band. Using space-filling models, different arrangements of the chains in the  $\beta$ -aggregates were shown to be realizable. All result in a close stacking of tyrosyl phenyl groups, which can explain the drastic changes in all optical properties.

## INTRODUCTION

In the present paper we report conformational studies in aqueous solution of the sequential copolymer (Tyr-Glu)<sub>n</sub>, whose synthesis was described elsewhere<sup>1</sup>. This copolymer was expected to form aggregates; thus, tyrosyl and glutamic acid side chains could be brought into close contact and held in a well-defined position, which could induce some enzyme-like activity. Actually, the active site of carboxypeptidase A involves cooperativity of both 248-tyrosine and 270-glutamic acid side chains as well as a Zn<sup>2+</sup> cation.

It is relevant to the present work to give a brief survey of the present state of investigations on poly(L-tyrosine) and poly(L-glutamic acid) and on their copolymers. Since the investigations of Fasman *et al.*<sup>2,3</sup>, poly(L-tyrosine) was considered for a long time to undergo a helix-coil pH-induced transition at about pH 11.5. Fasman<sup>2</sup> pointed out that this transition occurred only when pH was lowered very slowly. If not, the random coiled conformation is retained by entanglement of tyrosyl rings. However, recent results contradict those of Fasman. Patrone *et al.*<sup>4,5</sup> demonstrated convincingly by means of infra-red spectroscopy in D<sub>2</sub>O that poly(L-tyrosine) undergoes a random coil-antiparallel  $\beta$  pH-induced transition. They suspect also that the  $\alpha$ -helical form would exist only in ethanol-water mixtures. Senior *et al.*<sup>6</sup> are in agreement with Patrone and state that the antiparallel  $\beta$ -structure of poly(L-tyrosine) is in the form of  $\beta$ -hairpins. Comparing the c.d. spectra of poly(L-tyrosine) in water and in organic solvents such as trimethylphosphate or methanol, Friedman and Ts'o<sup>7</sup> were led to decide in favour of an  $\alpha$ -helix rather than in favour of a  $\beta$ -structure in water as solvent. They emphasized that theoretical calculations of Chen and Woody<sup>8</sup> predicted a c.d. spectrum for  $\alpha$ -helical poly(L-tyrosine) very similar to that obtained in aqueous solution. It must be pointed out, however, that the c.d. spectrum reported by Friedman and Ts'o is different from that of Fasman. In addition, the u.v. spectra reported by both investigators reveal some discrepancy between degrees of ionization of tyrosyl side chains at pH 11.2.

Hence conformational transition of poly(L-tyrosine) in aqueous solution is not yet unambiguously explained. Although the existence of  $\beta$ -structures has been clearly established by Patrone *et al.*<sup>4,5</sup>, it cannot yet be ruled out that poly(L-tyrosine) in water could exist also under certain circumstances in the  $\alpha$ -helical form.

The pH-induced  $\alpha$ -helix-coil transition of poly(L-glutamic acid) is now well established. In addition, when pH is lowered below 4.6, poly(L-glutamic acid) begins to aggregate<sup>9</sup>.

Few investigations have been devoted to L-glutamic acid/L-tyrosine copolymers. In this connection, it is relevant to mention the fluorescence studies of Fasman<sup>10</sup> concerning glutamic acid-rich copolymers (95%). These exist in  $\alpha$ -helical form at acidic pH. Doty and Gratzer<sup>11</sup> prepared the same random copolypeptide and found that the helix-coil transition causes a blue-shift of the u.v. absorption band at 277 nm of tyrosyl side chains. This effect was identified with the transfer of tyrosyl residues from a helical environment to that of the random coil, which is predominantly that of the solvent. Ramachandran *et al.*<sup>12</sup>, and Schechter *et al.*<sup>13</sup> reported conformational studies on poly(Tyr-Ala-Glu) which would be  $\alpha$ -helical at neutral pH. Tyrosyl and glutamyl side chains would be kept in well defined positions by hydrogen bonding between carboxylate and phenolic groups.

## EXPERIMENTAL

### Materials

The sequential polymer (Tyr-Glu)<sub>n</sub> was obtained by polymerizing *O*-benzyl-L-tyrosyl- $\gamma$ -benzyl-L-glutamyl-*O*-benzyl-L-tyrosyl- $\gamma$ -benzyl-L-glutamyl hydroxyphenyl ester hydrochloride, and subsequent removal of protecting groups by hydrobromic acid in 6.5 N acetic acid, as described previously<sup>1</sup>. This method has been proved to be racemization-free. Molecular weight of the sample was estimated from osmotic pressure measurements at pH 10



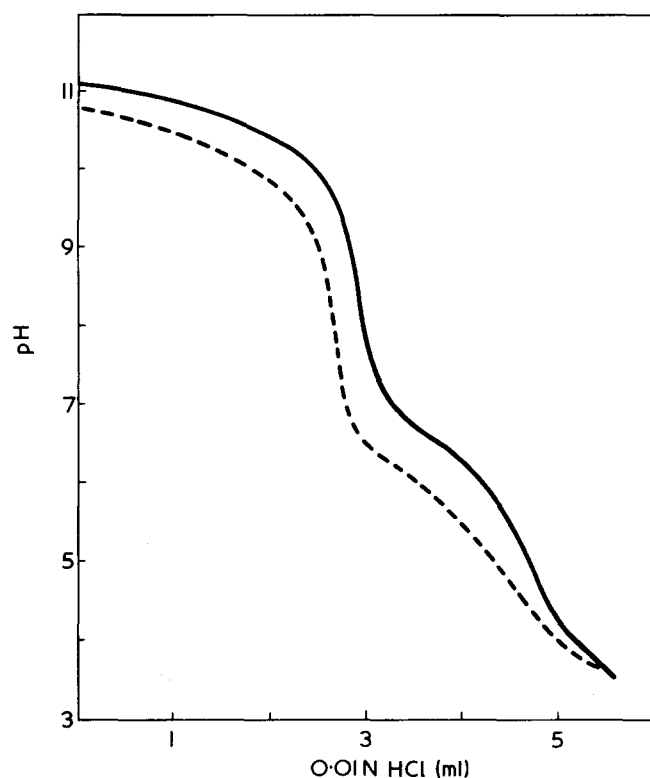


Figure 1 Potentiometric titration of poly(Tyr-Glu): 5.7 mg in 20 ml 0.0025 N NaOH (—); 6.5 mg in 20 ml 0.0025 N NaOH, 0.1 N KCl (---)

to be 15 700. This value may be somewhat overestimated owing to the presence of some aggregated molecules. Intrinsic viscosity was 35.5 ml/g in 0.2 M NaCl, pH 12.

Solutions were prepared by dissolving the polymer in the stoichiometric amount of 0.1 N NaOH evaporating to dryness and adding the adequate dilute buffer in 0.1 M KCl. Buffers were 0.01 M carbonate-bicarbonate (pH 10.5 to 9.5), 0.01 M glycine-NaOH (pH 10 to 8.6), 0.01 M Tris-HCl (pH 8.6 to 7.5) and 1/150 M phosphate (below pH 7.5). The solution was then titrated with 0.1 N NaOH or 0.1 N HCl to the required pH value. For measurements in D<sub>2</sub>O, DCl and NaOD were used instead of HCl and NaOH. No experiments could be performed below pH 6.5 because the polymer begins to precipitate. Concentrations of polymer solutions were determined from the optical density at 294 nm in 0.2 N NaOH as solvent assuming an extinction coefficient of 2200 l mol<sup>-1</sup> cm<sup>-1</sup> per tyrosyl residue.

Methods

Potentiometric titrations were carried out under nitrogen and at room temperature using a Radiometer 26 pH-meter and a GK 2321 electrode. For measurements in D<sub>2</sub>O, pD was considered to be equal to pH<sub>app</sub> + 0.4.

Optical rotations were measured at 546 nm using a 141 M Perkin-Elmer Polarimeter, in a 1 dm microcell.

Circular dichroism (c.d.) spectra were recorded on a Roussel-Jouan 185 model II dichrograph using 1, 0.2, 0.1 and 0.01 mm cells according to the wavelength range. Concentrations of the solutions were in the range 0.05 to 0.2%.

U.v. spectra were recorded on a Beckman Acta III spectrophotometer.

For i.r. spectroscopy, deuteration of the polymer was carried out as described by Patrone *et al.*<sup>4</sup>. Concentrations were in the range 0.1 to 0.8%. Cells were equipped with CaF<sub>2</sub> windows, having an optical path length of 0.05 mm,

and thermostated at 22°C. I.r. spectra were measured on a Beckman IR 11 spectrophotometer, using the transmittance expanded scale.

Analytical gel chromatography was performed on Sephadex G 200, 40-120 μm, at room temperature and using a 2.5 × 45 cm column. Eluants were the same dilute buffers in 0.1 M KCl as used for solutions. The column was monitored by recording the absorbance at 275 nm using a 1 cm flow-cell and a Beckman Acta III spectrophotometer.

RESULTS

Potentiometric and spectrophotometric titration studies in water and in D<sub>2</sub>O

Potentiometric titration curves of poly(Tyr-Glu) are reported in Figure 1. It can be seen that carboxylic species began to be titrated below pH 8. Below pH 6.5 the polymer began to precipitate; nevertheless titrations were achieved on turbid solutions. As expected, ionic strength increased markedly the degree of ionization. Figure 2 shows ionization curves of tyrosyl side chains obtained from u.v. spectroscopic measurements. The degree of ionization was estimated from optical density at 294 nm. Tyrosyl side chains are completely ionized above pH 12.4 (pD 14), while they are fully protonated below pH 8 (pD 8.5). Direct and back titration curves were not exactly superimposed. This resulted probably from a slight difference in ionic strength between both experiments.

Optical rotation

When a polymer solution was titrated over the range pH 12.4-10.5 no significant variation of optical rotation could be detected. At lower pH values, the optical rotation under-

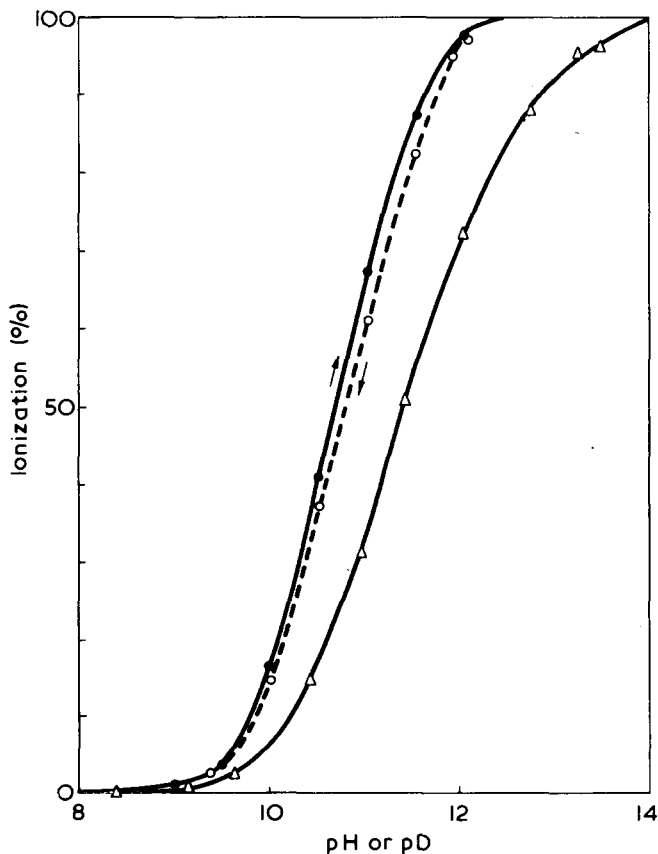


Figure 2 Spectrophotometric titration of 0.2% poly(Tyr-Glu) in 0.1 M KCl in water (●, ○) and in D<sub>2</sub>O (△)

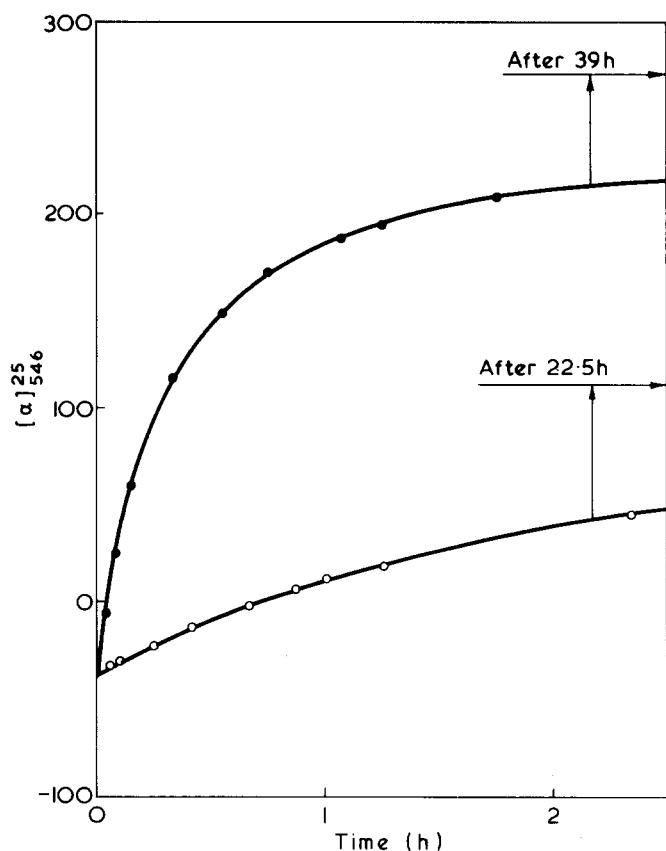


Figure 3 Variation of specific rotation of poly(Tyr-Glu) in 0.1 M KCl, 1/150 M phosphate buffer as a function of time; ●, 0.194%, pH 7.27; ○, 0.056%, pH 7.1

went a slow change with time (Figure 3). At each pH value, two days at least were necessary to reach equilibrium. However the rate of change in optical rotation at a given pH was not reproducible from one run to another and depended also on polymer concentration. Dilute polymer solutions (0.05%) only underwent a small and very slow change. In a few cases, no change at all could be detected. Plotting the optical rotation of a set of equilibrated 0.2% solutions as a function of pH shows (Figure 4) a strong sharp change from pH 10.2 to about 9.5 followed by a less steep change. This pH range corresponds to the protonation of the remaining unprotonated tyrosyl side chains (i.e. 25% of the whole). When titrating an equilibrated solution (solution 1, pH 7 in Figure 4) towards alkaline pH, the optical rotation describes a curve (Figure 4) which is similar to the former, but depends on whether titration was performed slowly or rapidly.

#### Gel chromatography

Two different sets of runs were carried out. In the first one, samples were applied immediately after pH adjustment (Figure 5b). In the second, solutions were titrated to the desired pH value and kept for 4 days at room temperature before being applied to the column (Figure 5c). Chromatograms show that the material was eluted into two fractions. One of them appeared with the hold-up volume which indicates the presence of high molecular weight species. Another fraction was eluted afterwards as a broad peak and corresponds to low molecular weights. As shown in Figure 5b, the peak of high molecular weight increases as the pH becomes more acidic. The same effect can be observed in Figure 5c, but the ratio of high molecular weights to low ones is much larger. This denotes the occur-

rence of a slow aggregation process, occurring below pH 10.5, which must be related to the change in optical rotation described above and in Figure 3. Figure 5a shows pH 6.82, whose optical rotation remained unchanged after pH adjustment, even a few days later. No aggregates could be detected in this solution.

#### I.r. measurements in $D_2O$

Figure 6 shows i.r. spectra of a 0.8% solution of polymer. At pD 13.37, amide I' band is located at  $1648\text{ cm}^{-1}$  amide II' around  $1459\text{ cm}^{-1}$  with a shoulder at about  $1440\text{--}1450\text{ cm}^{-1}$ . When the pH was lowered to 11.16, no shift could be detected either in amide I' or in amide II' bands. However, another amide I' sharp band lying at  $1620\text{ cm}^{-1}$ , as well as a shoulder around  $1685\text{ cm}^{-1}$  developed with time. These are typical of antiparallel  $\beta$ -structures. Figure 7 shows spectra of a dilute (0.18%) solution of polymer at various pD values. In spite of large noise and of parasitic bands of atmosphere, owing to high expansion factor, the typical bands of antiparallel  $\beta$ -structures are still quite visible. We observed that these bands formed slowly and they were found to appear below pD 11 in 0.2% solutions. In addition, the higher the concentration, the faster they formed.

#### Circular dichroism studies

Figure 8 shows the c.d. spectra of a 0.2% solution of poly(Tyr-Glu) at various pH. In alkaline medium (pH 12.05), tyrosinate chromophores give rise to two positive bands located at 285 and 243 nm. The strong negative band at 197.5 nm is probably due to the  $\pi \rightarrow \pi^*$  transition of peptide chromophore in unordered conformation. At

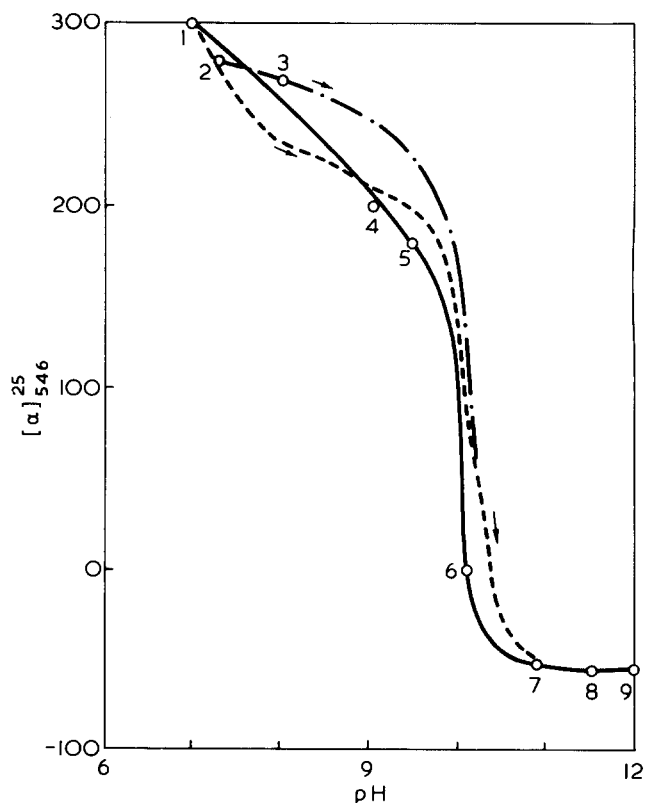


Figure 4 Variation of specific rotation of poly(Tyr-Glu) in 0.1 M KCl as a function of pH; 0.2% solutions (1 to 9) equilibrated for 4 days at room temperature at various pH values in adequate buffer (see text) (○); rapid titration of the equilibrated solution 1 with 1 N NaOH (—); very slow titration of the equilibrated solution 2 with 1 N NaOH (---)

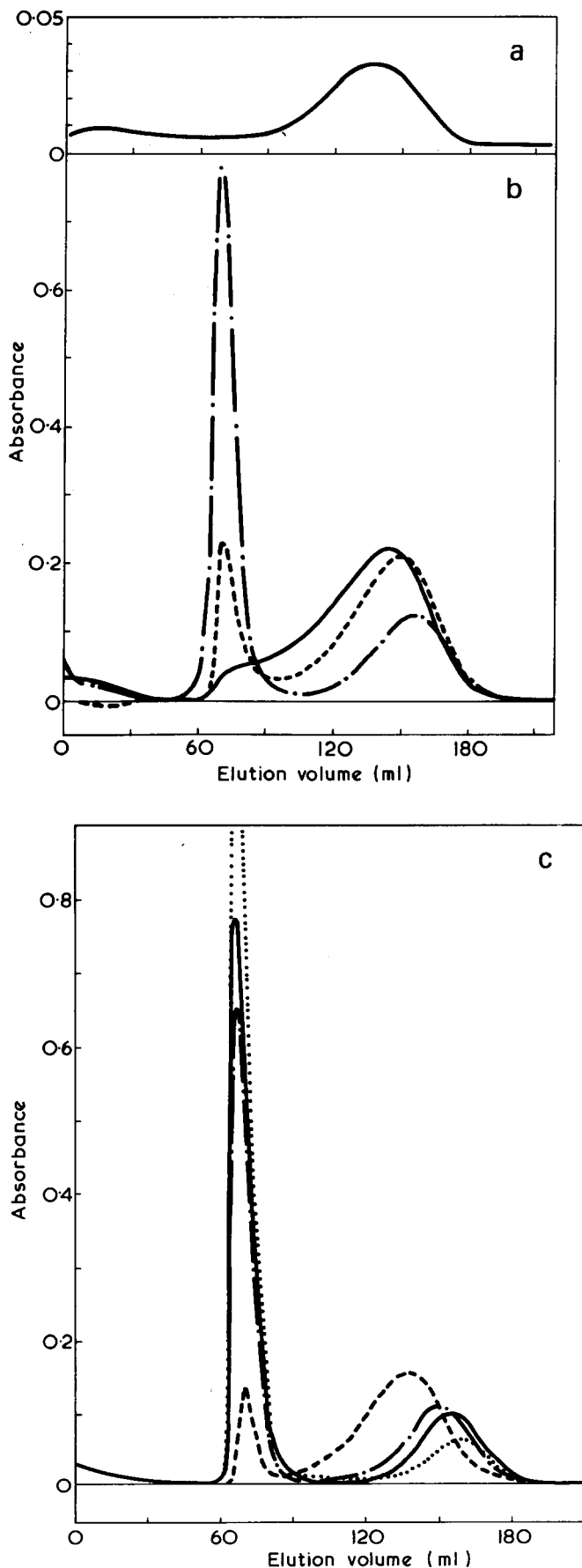


Figure 5 Gel chromatograms of poly(Tyr-Glu) on Sephadex G 200. (a) 0.05% solution (2 ml sample) applied a few days after pH adjustment; (b) 0.2% solutions (1 ml sample) applied immediately after pH adjustment: ---, pH 7.08; - - - -, pH 8.20; —, pH 9.95; (c) 0.2% solutions (1 ml sample) applied 4 days after pH adjustment: · · ·, pH 8.12; —, pH 9.04; - · - ·, pH 9.56; - - - -, pH 10.10

pH 10.56 where the tyrosyl side chains are about 60% protonated, contributions of both tyrosine and tyrosinate are quite visible at 230 and 245 nm respectively. In the 255–300 nm range both contributions seem to overlap and cannot be resolved. The strong negative band is only slightly blue shifted to 196 nm, while its ellipticity decreases slightly. At pH 9.47, tyrosyl side chains are nearly fully protonated and the c.d. spectrum began to undergo a slow and drastic change as a function of time. However, a few minutes after pH adjustment the essential features of the c.d. spectrum remained practically the same as at pH 10.56, except that the 245 nm tyrosinate band vanished completely. A few hours later, the 230 and 273 nm bands were considerably enhanced, while the negative 195 nm one was replaced by a strong positive peak located at 200 nm. Limit spectra (i.e. spectra of solutions equilibrated a few days at a given pH value) as shown in Figure 9 depend on pH. However, the pH affects only the magnitude of c.d. bands but not the shape of the spectrum, which is predominantly that of aggregates. In D<sub>2</sub>O, all phenomena were just the same as in water.

#### U.v. spectroscopy

U.v. studies were carried out on the 277 nm tyrosyl band which is not overlapped by contributions of the peptide chromophores. When titrating rapidly an alkaline solution to neutral pH, in the same way as in c.d. measurements a slow enhancement of the 277 nm band took place (Figure 10). However, this hyperchromic effect occurred without simultaneous shift in wavelength, and the shape of the band remained practically unchanged (Figure 11). The molar absorptivity per tyrosyl residue was increased from about 1320 to more than 1600 in the case of 0.2% solutions. For 0.05% solutions the enhancement was much less pronounced; sometimes no change at all could be detected.

#### DISCUSSION

In alkaline media, at above pH 12, c.d. spectra of poly(Tyr-Glu) exhibit a strong negative band ( $\theta \sim -20\ 000$ ) located at 197.5 nm. This band is probably due to unordered structures. However, its ellipticity seems rather low as

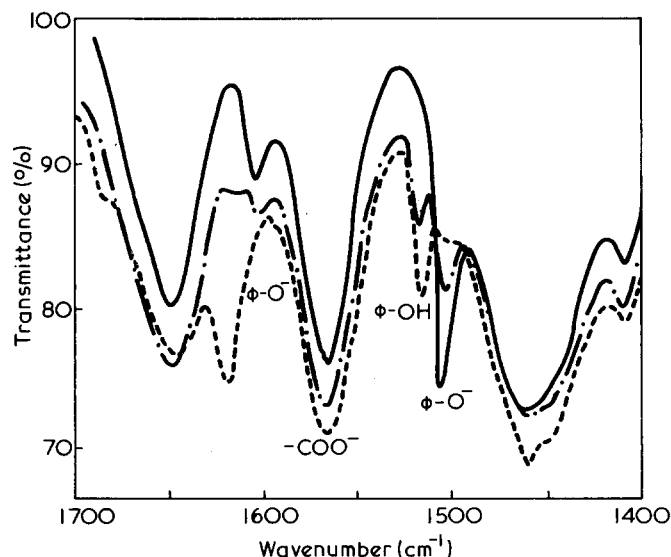


Figure 6 Infra-red spectra of a 0.8% solution of poly(Tyr-Glu) in 0.1 M KCl in D<sub>2</sub>O at various pH. Expansion X3. 0.05 mm path cell. —, pH 13.37; - - - -, pH 11.67; - · - ·, pH 11.16

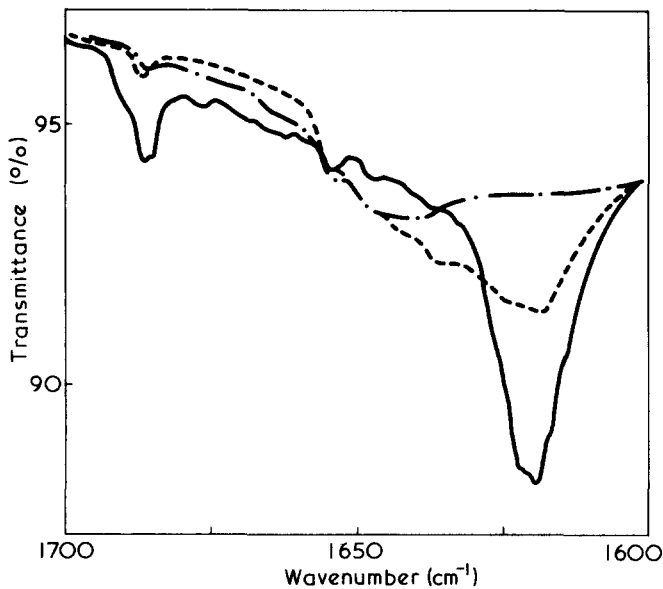


Figure 7 Infra-red spectra of a 0.18% solution of poly(Tyr-Glu) in 0.1 M KCl in D<sub>2</sub>O, 0.01 M Tris buffer. Expansion X 7, 0.05 mm path cell. ---, pD 12.10; - · -, pD 9.67, 60 min after pD adjustment; —, pD 9.65, 2 days after pD adjustment

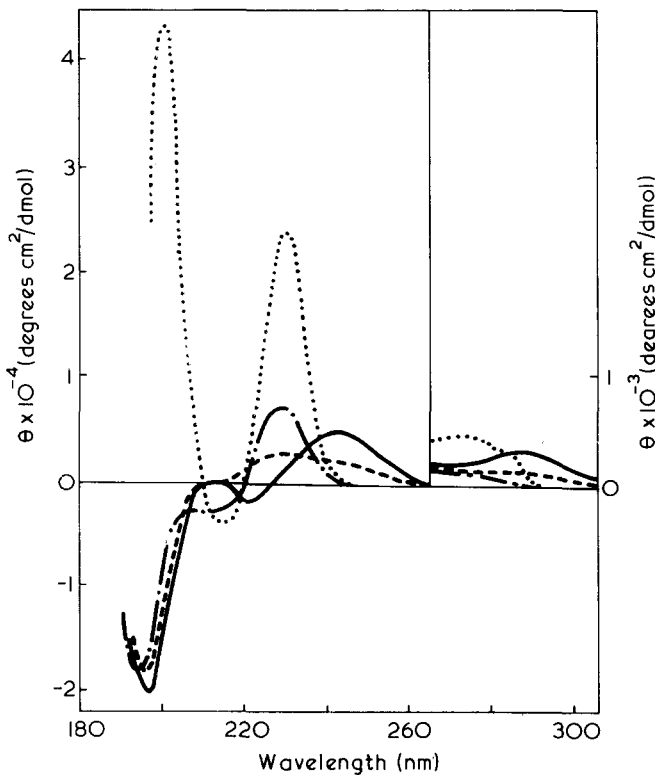


Figure 8 C.d. spectra of a 0.19% solution of poly(Tyr-Glu) in 0.1 M KCl at various pH: —, pH 12.05; ---, pH 10.56; - · -, pH 9.47, 15–30 min after pH adjustment; · · ·, pH 9.47, 20 h after pH adjustment

compared to usual values of unordered structures (–30 000 to –40 000). This difference could result from some positive contribution of tyrosyl side chains. The location of the amide I' (1648.5 cm<sup>-1</sup>) and amide II' (1459 cm<sup>-1</sup>) bands are also in agreement with such a conformation. In the range pH 12 to about 10.5, which corresponds to ~0–60% protonated tyrosyl side chains, no conformational change can be detected. First, the optical rotation undergoes no variation. Second, no significant shift can be observed either on amide I' or amide II' band. Third, the

c.d. spectrum still exhibits a negative 196–197.5 nm band, the only change in c.d. spectrum arising from the protonation of chromophoric tyrosyl side chains. We are thus led to conclude that this polymer undergoes no conformational change over this pH range. Hence, poly(Tyr-Glu) appears to behave quite differently from poly(L-tyrosine), in which lowering of pH induces a sharp transition at pH 11.2.

Below pH 10.5 a slow aggregation process takes place. This process is clearly evidenced by gel chromatography. Molecular weights of aggregates were not estimated. However, since aggregates are eluted with the hold-up volume, these are of the order of 10<sup>5</sup>–10<sup>6</sup> at least. The aggregation process causes drastic changes in all optical properties of the polymer. Optical rotation (Figure 4) undergoes a sharp change around pH 10–10.2, which corresponds to 15–25%

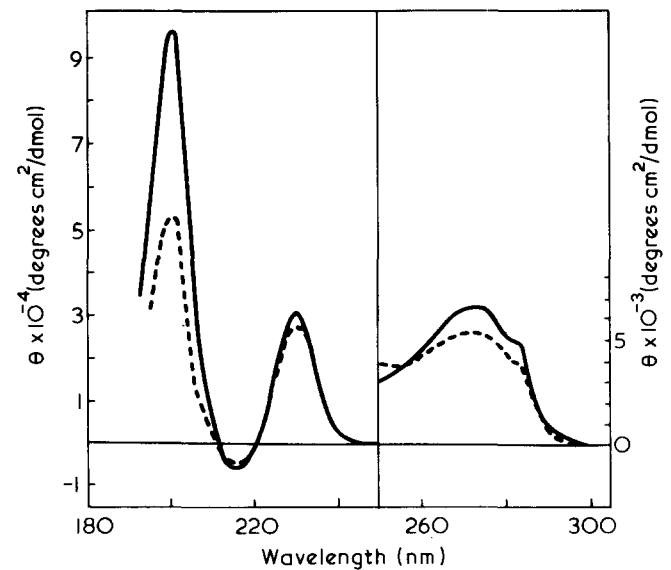


Figure 9 C.d. spectra of two 0.2% solutions of poly(Tyr-Glu) in 0.1 M KCl, equilibrated for two days at room temperature: ---, pH 9.55; —, pH 7.29

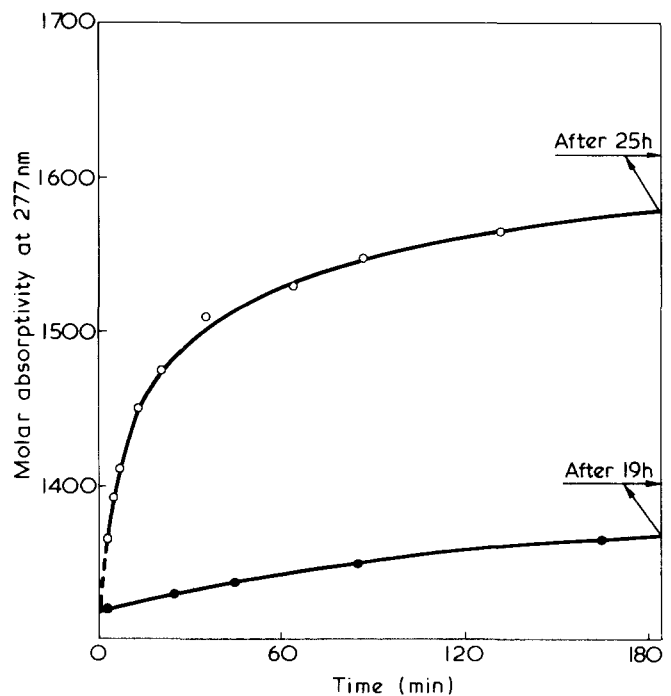


Figure 10 Variation of molar absorptivity at 277 nm of poly(Tyr-Glu) in 0.1 M KCl, 1/150 M phosphate buffer as a function of time. ○, 0.21% solution, pH 7.47; ●, 0.051% solution, pH 7.06

of ionized tyrosyl side chains. When tyrosyl side chains are fully protonated (below pH 8), further lowering of pH gives still rise to a change in optical rotation, probably owing to protonation of some carboxylate groups. It must be pointed out that fast and slow titration curves of Figure 4 are not exactly superimposed. This discrepancy can be easily explained. Actually, addition of 1 N NaOH causes a local but deep pH increase so that a few aggregates are disrupted, which can form again slowly. As expected for such an intermolecular process the concentration has a great effect upon both the rate and the extent of aggregation. This is evidenced in Figures 3 and 9. In a few cases, as already mentioned, no aggregation could be observed on dilute solutions (0.05%). We found that this happened when alkaline solutions were very quickly titrated to the desired pH value. As stated above, Fasman *et al.*<sup>2</sup> found a similar behaviour in the case of poly(L-tyrosine).

From the c.d. spectra, the aggregation process seems to proceed directly from unordered structures, without involvement of any intermediate form. Actually, when an alkaline solution is titrated to pH 9.47, its c.d. spectrum recorded a few minutes later shows that the polymer remains essentially unordered. As the aggregation spreads out, the spectrum changes gradually into that of aggregated species. In addition, unaggregated dilute solutions (0.05%) at neutral pH, present the same c.d. spectra as the unordered form. These lead us to conclude that an intermediate form, if any, is quite unstable. On the contrary, poly(L-tyrosine) would undergo a two-step transition: random coil  $\leftrightarrow$  antiparallel  $\beta$ -monomolecular structures  $\leftrightarrow$   $\beta$ -aggregates<sup>4,6</sup>. However, in a recent paper Patrone *et al.*<sup>5</sup> seem to suspect that the transition could be intermolecular only.

I.r. spectroscopy has clearly evidenced that aggregates were in antiparallel  $\beta$  conformation. It is very interesting to compare the c.d. spectrum of such antiparallel  $\beta$  structures to c.d. spectra of poly(L-tyrosine). It can be seen in Figures 8 and 9 that c.d. spectra of poly(Tyr-Glu) in antiparallel  $\beta$  conformation are very similar to spectra of  $\alpha$ -helical poly(L-tyrosine) in trimethylphosphate<sup>14,15</sup> or in methanol<sup>16</sup>. All spectra exhibit actually strong positive bands located at 195–200 nm and at 230 nm, as well as a trough at about 216 nm. The only qualitative difference lies in the 280 nm region, in which antiparallel  $\beta$ -structures give rise to a weak positive band at 272.5 nm, while for poly(L-tyrosine) Damle<sup>13</sup> found a splitting into a negative and a positive band located at 260 nm and 282 nm respectively. Hence, we should emphasize that much care must be taken in the interpretation of c.d. spectra when rotational strength induced by chromophoric side chains is of utmost importance.

Using space-filling models, two essentially different structures of antiparallel  $\beta$  pleated sheets of poly(Tyr-Glu) could be built up. In the first one (I), aromatic rings are equally distributed on both sides of the pleated sheet. Aromatic rings of a chain will be directed towards one side, those of another chain towards the other. In this structure, aromatic rings are stacked along the chain, and are separated by about 6.9 Å. In the second structure (II), all aromatic rings point to the same side of the pleated sheet, and carboxylates to the other. In this case, one side of the pleated sheet is covered with a compact stacked layer of aromatic rings, which are as distant as  $\sim 6.9$  Å along the chain and 4.7 Å along the perpendicular direction. This aromatic region is likely highly hydrophobic, and it can be suggested that hydrophobic sides of two pleated sheets would come close together, leading to a bi-layer micelle. We cannot, at present, choose between the two structures.

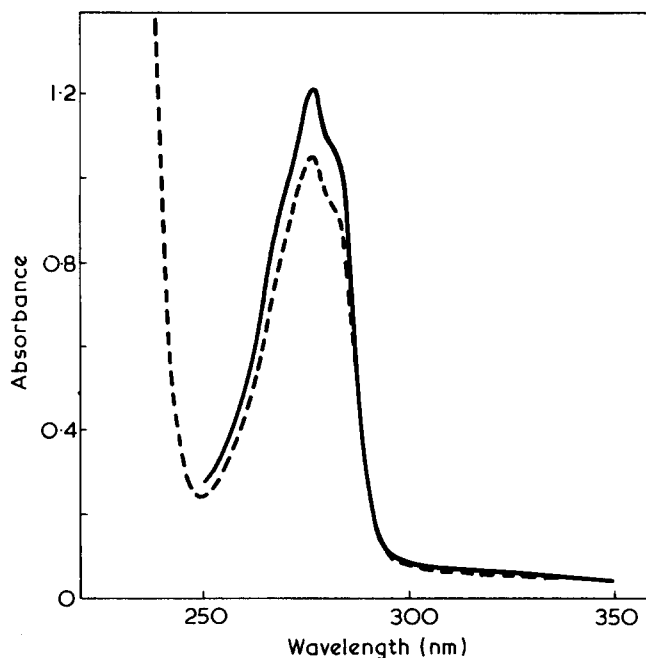


Figure 11 Evolution of the u.v. spectrum of a 0.21% solution of poly(Tyr-Glu) in 0.1 M KCl, 1/150 M phosphate buffer, as a function of time. — —, Immediately after pH adjustment; —, 20 h after pH adjustment

However, in both cases, tyrosyl side chains are arranged in a regular and compact stacking so that they can interact strongly, and give rise to the strong bands observed in the c.d. spectrum. The hyperchromic effect (Figure 11) is rather difficult to explain. As a rule, denaturation of proteins or of polypeptides, as copoly(Tyr, Glu) (5 mol % tyrosine)<sup>2</sup>, induces a blue shift in the 277 nm absorption band of tyrosyl side chains<sup>17</sup>. In addition, Bailey *et al.*<sup>18</sup>, observed that a change of solvent from ethanol to water can lead to a large intensity change in the 277 nm band of tyrosine as well as to a blue-shift, and explained this effect by a decrease of the strength of hydrogen bonds between phenolic groups and the solvent. As pointed out before, as the aggregation of poly(Tyr-Glu) takes place (Figure 11) no shift could be observed, but only a strong hyperchromic effect. This could result from the occurrence of two opposite effects. As aggregation proceeds, interaction between tyrosyl aromatic rings are enhanced, thus leading to a blue shift, as well to a hypochromic effect. At the same time, the hydrogen bonding system of the phenolic groups may change leading to a red shift and to a hyperchromic effect.

## CONCLUSION

Poly(Tyr-Glu) has been found to undergo a random coil- $\beta$ -aggregates transition by lowering the pH. No intermediate form could be detected. Optical properties of  $\beta$ -aggregates indicate that tyrosyl chromophoric side chains interact strongly. Two models of aggregates could be built up using space-filling models, each one resulting in a close stacking of tyrosyl aromatic rings. In one of these models (II), the  $\beta$ -framework is sandwiched between a hydrophobic layer (tyrosyl side chains) and a hydrophilic one (carboxyl groups). Such a structure could lead to the formation of a micelle. However, as yet no experimental evidence can permit the choice of either of these two models.

## ACKNOWLEDGEMENTS

The authors is indebted to Dr Gérard Spach for his helpful advice and to Mrs Anita Caille for her technical assistance.

## REFERENCES

- 1 Trudelle, Y. *JCS Perkin Trans. I* 1973, p 1001
- 2 Fasman, G. D., Bodenheimer, E. and Lindblow, C. *Biochemistry* 1964, 3, 1665
- 3 Beychok, S. and Fasman, G. D. *Biochemistry* 1964, 3, 1675
- 4 Patrone, E., Conio, G. and Brighetti, S. *Biopolymers* 1970, 9, 897
- 5 Conio, G., Patrone, E. and Salaris, F. *Macromolecules* 1971, 4, 283
- 6 Senior, M. B., Gorrell, S. L. H. and Hamori, E. *Biopolymers* 1971, 10, 2387
- 7 Friedman, S. and Ts'o, P. O. P. *Biochem. Biophys. Res. Commun.* 1971, 42, 510
- 8 Chen, A. K. and Woody, R. W. *J. Am. Chem. Soc.* 1971, 93, 29
- 9 Jennings, B. R., Spach, G. and Schuster, T. M. *Biopolymers* 1968, 6, 635; Spach, G. and Constantin, D. *ibid.* 1968, 6, 653; Schuster, T. M., Jennings, B. R. and Spach, G. Nobel Symp. 11, 'Symmetry and Function of Biological Systems at the Macromolecular Level', (Eds A. Engström and B. Strandberg) Almquist & Wiksell, Stockholm, 1969
- 10 Fasman, G., Norland, K. and Pesce, A. *Biopolymers* 1964, 1, 325
- 11 Doty, P. and Gratzer, W. B. 'Polyaminoacids, polypeptides and proteins', (Ed. M. A. Stahmann), Univ. of Wisconsin Press, Madison, 1962
- 12 Ramachandran, J., Berger, A. and Katchalski, E. *Biopolymers* 1971, 10, 1829
- 13 Schechter, B. *et al. Eur. J. Biochem.* 1971, 20, 301
- 14 Damle, V. N. *Biopolymers* 1970, 9, 937
- 15 Engel, J., Liehl, E. and Sorg, C. *Eur. J. Biochem.* 1971, 21, 22
- 16 Shiraki, M. and Imahori, K. *Sci. Pap. Coll. Gen. Educ. Univ. Tokyo* 1966, 16, 215
- 17 Ramachandran, G. N. 'Aspects of Protein Structure', Academic Press, New York, 1963
- 18 Bailey, J. E., Beaven, G. H., Chignell, D. A. and Gratzer, W. B. *Eur. J. Biochem.* 1968, 7, 5

# Circular dichroism study of poly(L-tyrosine), poly(L-glutamic acid) and of random and sequential copolymers of L-glutamic acid and L-tyrosine in trimethylphosphate

Yves Trudelle and Gérard Spach

Centre de Biophysique Moléculaire, CNRS, 45045 Orléans-Cedex, France

(Received 23 April 1974)

Random and sequential copolypeptides containing L-glutamic acid and L-tyrosine, as well as poly(L-tyrosine) and poly(L-glutamic acid) were investigated by means of c.d. spectroscopy in trimethylphosphate as solvent. In random copolymers, variation of ellipticities at 202.5 and 230 nm *versus* tyrosyl content follows a smooth curve, without any sharp change. This led to the conclusion that poly(L-tyrosine)  $\alpha$ -helix is right-handed. From c.d. studies on sequential copolymers we were able to recognize that the 230 nm contribution of tyrosyl side chains is closely related to the array in which tyrosyl residues are arranged in the chain. For instance, it was found that  $(n, n + 2)$  and  $(n, n + 3)$  pairings of tyrosyl side-chains in  $(\text{Tyr-Glu})_n$  and  $(\text{Glu-Tyr-Glu})_n$  respectively, were poorly effective, while the  $(n, n + 4)$  pairing in  $(\text{Glu-Glu-Tyr-Glu})_n$  is more. However, the strongest contribution at 230 nm was observed on the alternating-pairs copolymer  $(\text{Glu-Tyr-Tyr-Glu})_n$ . This result suggests a new conformational arrangement of tyrosyl side chains in sequential copolymers, as well as in poly(L-tyrosine) and other aromatic polypeptides, based on a regular pairing of the aromatic groups, arranged in two contiguous superhelices.

## INTRODUCTION

Several investigators<sup>1-4</sup> have demonstrated the  $\alpha$ -helical structure of poly(L-tyrosine) in trimethylphosphate solution. Among these studies, measurements reported by Damle<sup>1</sup> afford the most convincing proof. Actually, Damle could calculate from viscometric and light scattering determinations the geometrical parameters of the equivalent rod, which are in good agreement with the parameters of an  $\alpha$ -helix.

Theoretical studies of Chen and Woody<sup>5</sup> on circular dichroism (c.d.) supported an  $\alpha$ -helical structure for poly(L-tyrosine). In addition, their calculations give precise details about the sense of the  $\alpha$ -helix which appears to be right-handed. However, such calculations do not take into account the influence of the solvent which can be of importance. For instance, as stated recently by Bradbury *et al.*<sup>4</sup>, poly(L-tyrosine) is likely to be in a random coil conformation in dimethylsulphoxide, contrary to previous assumptions<sup>6</sup>. Moreover, in our opinion, such theoretical predictions must be considered with caution. For example, it was recently shown by infra-red spectroscopy that poly(L-tyrosyl-L-glutamyl) gives  $\beta$ -structures in aqueous solutions below pH 10, whereas its c.d. spectrum (strong positive band at 230 nm, very strong positive band around 200 nm, trough at 216 nm) looks like the one of the poly(L-tyrosine)  $\alpha$ -helix in trimethylphosphate<sup>7</sup>.

The peculiar optical properties of poly(L-tyrosine) are considered to arise from strong excitonic interactions between neighbouring tyrosyl chromophoric side chains. It was of interest to find out what arrays of tyrosyl residues are able to lead to strong rotational strength. In the present paper we have tried to elucidate this problem by studying sequential copolypeptides.

Another question refers to the sense of the  $\alpha$ -helix. Some controversy still stands about this. Damle<sup>1</sup> reported that the amide I band for poly(L-tyrosine) films cast from trimethylphosphate solution lies at  $1662 \text{ cm}^{-1}$ , which seems a somewhat high frequency for a right-handed  $\alpha$ -helix and would rather correspond to a left-handed one. Other results, obtained by Bradbury *et al.*<sup>4</sup> and by Quadrioglio *et al.*<sup>2</sup> contradict those of Damle. These authors found that the amide I band for films or solutions in trimethylphosphate is located at  $1657 \text{ cm}^{-1}$ . Such discrepancies do not seem to be ascribable to differences between wavenumber calibrations and still remain unexplained.

Theoretical predictions are not fully consistent either. Applequist and Mahr<sup>8</sup> predicted a left-handed  $\alpha$ -helix. By another method, Ooi *et al.*<sup>9</sup>, Yan *et al.*<sup>10</sup> and Chen and Woody<sup>5</sup> found the opposite sense.

## MATERIALS AND METHODS

Poly(L-tyrosine) was prepared by polymerization of *O*-benzyloxycarbonyl-L-tyrosine-*N*-carboxyanhydride (NCA)<sup>11</sup> and subsequent removal of the protecting groups by hydrobromic acid in acetic acid.

Samples of random copolymers of L-glutamic acid and L-tyrosine were prepared by copolymerizing *O*-benzyloxycarbonyl-L-tyrosyl NCA and  $\gamma$ -benzyl-L-glutamate NCA<sup>11</sup>. Side chain protections were removed as above.

Synthesis of sequential copolymers, i.e. poly(L-tyrosyl-L-glutamyl), poly(L-glutamyl-L-tyrosyl-L-glutamyl) and poly(L-glutamyl-L-glutamyl-L-tyrosyl-L-glutamyl) is reported elsewhere<sup>12</sup>. Poly(L-glutamyl-L-tyrosyl-L-glutamyl) was obtained following the same experimental procedure.

Table 1 Viscosity and infra-red data for polymer samples

	Tyrosyl content	$\eta$ (ml/g) <sup>b</sup>	Amide I <sup>c</sup> frequency (cm <sup>-1</sup> )
Poly(L-glutamic acid)	0	16.5	1654
—	0	95.5	1654
Poly(L-tyrosine)	1.0	58.5	1661
(Tyr, Glu) random	0.78 <sup>a</sup>	47.6	1658
(Tyr, Glu) random	0.57 <sup>a</sup>	33.8	1656
(Tyr, Glu) random	0.36 <sup>a</sup>	34.1	1655
(Tyr-Glu)	0.50	35.5	1658
(Glu-Tyr-Glu)	0.33	19.0	1655
(Glu-Glu-Tyr-Glu) <sub>n</sub>	0.25	16.2	1655
(Glu-Tyr-Tyr-Glu) <sub>n</sub>	0.50	22.1	1657

<sup>a</sup> Estimated from acid titration of carboxylic groupings in TMP-water as solvent and from spectrophotometric measurements assuming an extinction coefficient of 2200 l mol<sup>-1</sup> cm<sup>-1</sup> at 294 nm, in 0.1 M NaCl, 0.2 N NaOH  
<sup>b</sup> In 0.2 M NaCl, pH 12, at 25°C  
<sup>c</sup> Determined on 1% trimethylphosphate solutions with a Beckman IR 11 spectrometer, carefully calibrated on water vapour

Data for all samples are collected in Table 1.

Most of the samples being not directly soluble in trimethylphosphate, they were first dissolved in dimethylsulphoxide. After exhaustive vaporation of dimethylsulphoxide, the polymer readily dissolved in trimethylphosphate.

C.d. spectra were recorded on a Roussel-Jouan 185 model II dichrograph at 22–24°C.

RESULTS AND DISCUSSION

Figure 1 shows the c.d. spectrum of our sample of poly(L-tyrosine), which is in complete agreement with those reported by others.

The c.d. spectra of random copolymers are also collected in Figure 1. In the 205–240 nm range a gradual overlap of the  $\alpha$ -helix spectrum with the poly(L-tyrosine) one is quite clear. When plotting ellipticities at 230 nm and at 202.5 nm against tyrosyl content no sharp change (Figure 2) can be observed. Such a smooth variation allows us to conclude in favour of a right-handed poly(L-tyrosine). It must be also pointed out that the curves of Figure 2 are not straight lines. This indicates the likely presence of interactions among tyrosyl side chains. However, when plotting ellipticity at 230 nm as a function of the square of tyrosyl content (Figure 3) a straight line was obtained. Extrapolation of the straight line towards zero tyrosyl content gave an ellipticity of -20 000, which is in agreement with the expected value for a right-handed  $\alpha$ -helix.

Assuming that the contribution at 230 nm of a non-interacting tyrosyl side chain, considered as isolated, is negligible, we can suppose that the rotational strength arises solely from pairing between tyrosyl aromatic rings. It is quite clear in this case that the only effective interactions will occur between neighbouring side chains included in a short *n*-mer segment. Thus, the rotational strength induced by a *i*th tyrosyl residue will be:

$$R_i = \sum_{-n/2}^{n/2} k_j(nx) = nx \sum_{-n/2}^{n/2} k_j = Knx$$

where *k<sub>j</sub>* represents the contribution of the (*i, i + j*) pair and (*nx*) the probability to find a tyrosyl residue at any

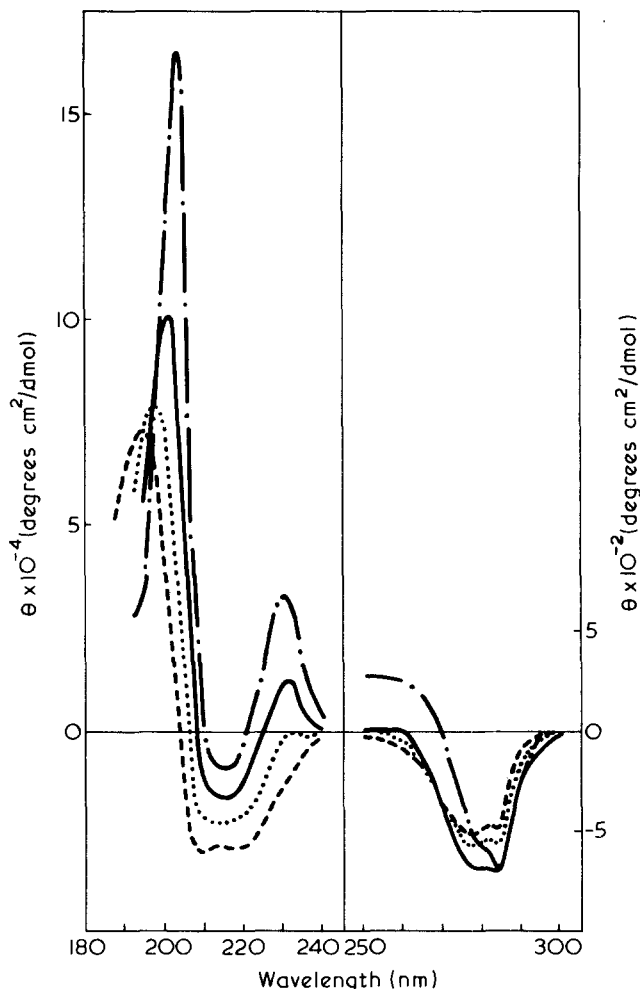


Figure 1 C.d. spectra in TMP of poly(L-tyrosine) (—) and of random copolyptides (Tyr, Glu)<sub>n</sub> of various tyrosyl contents: 0.78 (---); 0.57 (....); 0.36 (-.-.-). Concentrations, ~1 mg/ml

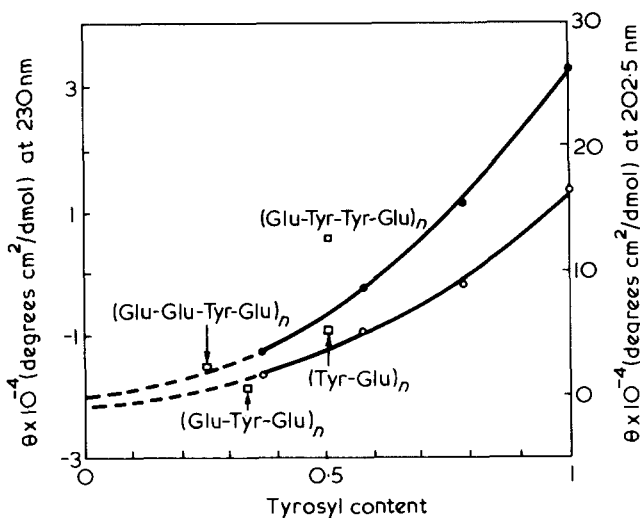


Figure 2 Ellipticities at 230 (●) and 202.5 (○) nm of random copolyptides (Tyr, Glu)<sub>n</sub> as a function of tyrosyl content. □, ellipticities at 230 nm of sequential copolyptides. Concentrations, ~1 mg/ml in TMP

given position in the *n*-mer. Summing over the whole chain (*N* residues) gives:

$$R = Nx \times Knx = NKnx^2$$

Hence, the observed linear relationship is consistent with the hypothesis made above, that the contribution of a



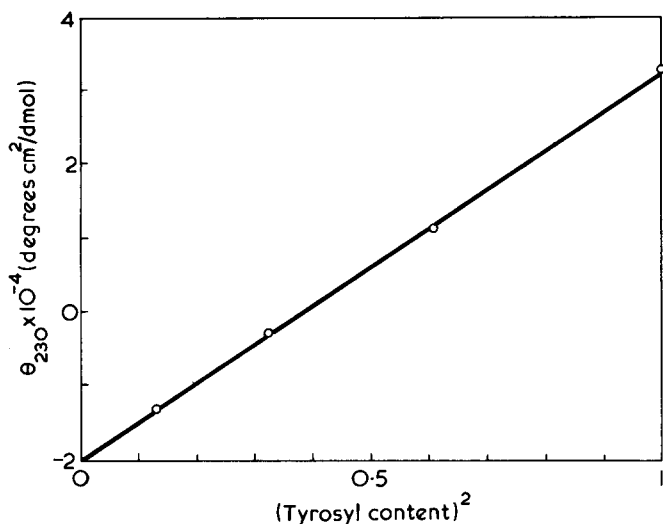


Figure 3 Variation of the ellipticity at 230 nm of random copoly-peptides (Tyr-Glu)<sub>n</sub> against the square of tyrosyl content. Concentrations, ~1 mg/ml in TMP

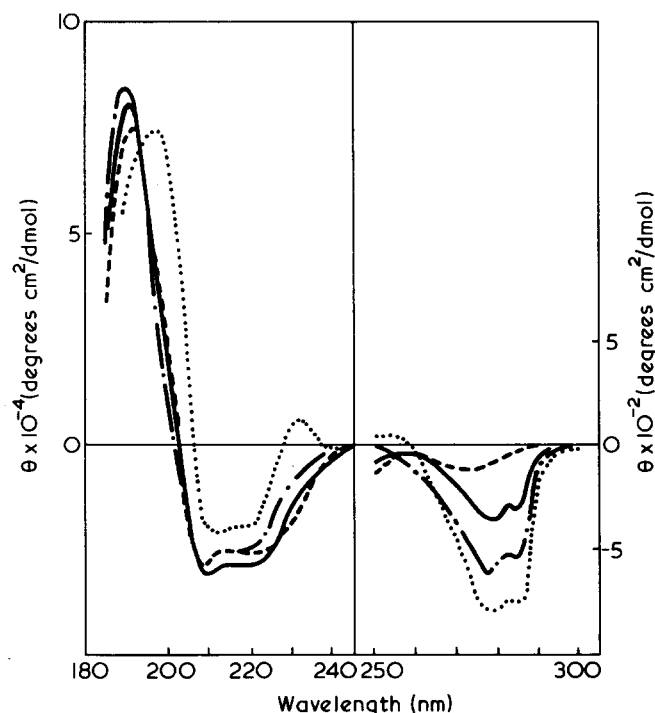


Figure 4 C.d. spectra of sequential copolypeptides in TMP: ····, (Tyr-Glu)<sub>n</sub>; - - -, (Glu-Tyr-Glu)<sub>n</sub>; —, (Glu-Glu-Tyr-Glu)<sub>n</sub>; · · · ·, (Glu-Tyr-Tyr-Glu)<sub>n</sub>. Concentrations, ~1 mg/ml

non-interacting tyrosyl residue is negligible and that interaction between two residues is the only effective mechanism. However, further accurate experiments are required before concluding definitely to the validity of this hypothesis.

In the region below 205 nm, the maximum of the positive band is red shifted from 190 to 202.5 nm as the tyrosyl content increases, whereas the ellipticity first decreases then increases (compare Figures 1 and 5a). This effect results probably from the existence of a strong negative band of poly(L-tyrosine) below 190 nm, which has been already pointed out by others<sup>3</sup>. The 280–285 nm negative band cannot clearly be related to tyrosyl content. There may be two reasons for this. First, it seems that this negative band is overlapped by a positive contribution below 270 nm, which is detectable on the spectrum of poly(L-tyrosine). Secondly, theoretical calculations of Chen and Woody<sup>5</sup> have shown that the 280–285 nm negative band is

very sensitive to the orientation of the aromatic tyrosyl rings.

The c.d. spectra of sequential copolymers are reported in Figure 4. The shapes of poly(Glu-Glu-Tyr-Glu), poly(Glu-Tyr-Glu) and poly(Tyr-Glu) spectra are very similar to the typical spectrum of a right-handed  $\alpha$ -helix. However, ellipticities seem somewhat low compared to the usual values of an  $\alpha$ -helix. This is probably due to the low molecular weights of our samples. Indeed the effect of molecular weight on the c.d. spectrum of poly(L-glutamic acid) is actually quite clearly shown in Figure 5a. More noteworthy seems to be the alternating-pairs copolymer poly(Glu-Tyr-Tyr-Glu) in which the tyrosyl contribution at 230 nm is much enhanced as compared to that of the poly(Tyr-Glu) isomeric copolymer.

Ellipticities of the sequential copolymers are represented in Figure 2. None of the points fit the random copolymer curve, indicating that the rotational strength at 230 nm depends on the tyrosyl residues array.

In Table 2 are listed all the possible pairings between

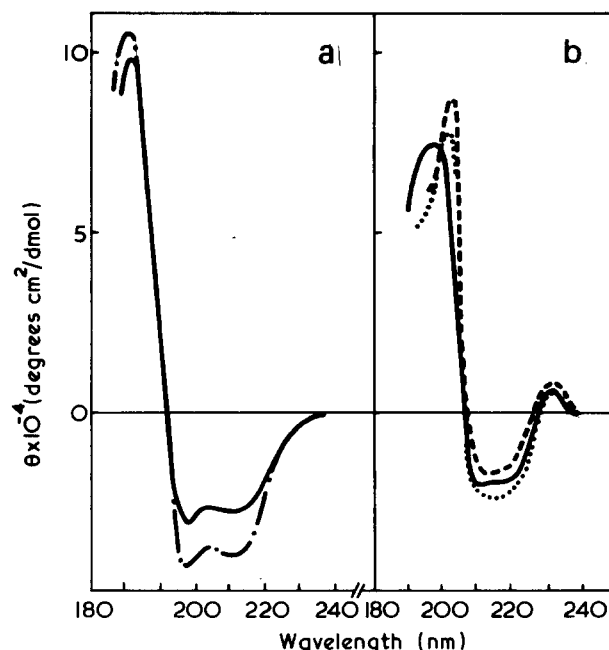


Figure 5a C.d. spectra of poly(L-glutamic acid) in TMP. —,  $[\eta] = 16.5$ ; - - -,  $[\eta] = 95.5$ . Concentrations, ~1 mg/ml  
Figure 5b Difference spectra calculated as outlined in the text, with  $\theta_H$  corresponding to the ellipticity of poly(L-glutamic acid) of  $[\eta] = 95.5$  (· · ·), 16.5 (- - -), as compared to the c.d. spectrum of (Glu-Tyr-Tyr-Glu)<sub>n</sub> (—)

Table 2 Pairing possibilities and c.d. data for poly(L-tyrosine) and sequential copolymers

		$\theta_{230}$	Ellipticity contribution per tyrosyl at 230 nm
poly(L-tyrosine) (Tyr-Glu) <sub>n</sub>	all pairing possibilities	32 000	52 000
(Tyr-Glu) <sub>n</sub>	(n, n + 2) (n, n + 4) (n, n + 6)	-9 500	21 000
(Glu-Tyr-Tyr-Glu) <sub>n</sub>	(n, n + 1), (n, n + 3) (n, n + 4), (n, n + 5)	5 500	51 000
(Glu-Tyr-Glu) <sub>n</sub>	(n, n + 3) (n, n + 6)	-19 000	3 000
(Glu-Glu-Tyr-Glu) <sub>n</sub>	(n, n + 4)	-15 500	18 000

tyrosyl side chains for each sequential copolymer. For this purpose interactions which could occur between side chains separated by more than five residues were neglected. Table 2 also shows the ellipticity contribution per tyrosyl residue calculated assuming a right-handed  $\alpha$ -helix ellipticity of  $-20\ 000$  at 230 nm.

As observed in Table 2 and in Figure 2, the contribution of tyrosyl side chains at 230 nm in poly(Glu-Tyr-Glu) is small. That means that both interactions ( $n, n+3$ ) and ( $n, n+6$ ) as well as the contribution of isolated tyrosyl residues are weak. Comparison of poly(Tyr-Glu) and poly(Glu-Glu-Tyr-Glu) tends to indicate that the ( $n, n+4$ ) interaction is rather effective whereas the ( $n, n+2$ ) is not. But the strongest contribution at 230 nm is obtained with the alternating-pairs copolymer, and is nearly the same as in poly(L-tyrosine). In this connection, Figure 5b shows that, in the range 205–240 nm, at least, the spectrum of this copolymer is similar to a 'reconstituted' spectrum obtained by adding the  $\alpha$ -helix contribution ( $\theta_H$ ) to the half of tyrosyl side chains contribution of poly(L-tyrosine):

$$\theta = \frac{\theta_{\text{polytyr.}} - \theta_H}{2} + \theta_H = \frac{\theta_{\text{polytyr.}} + \theta_H}{2}$$

However, the same agreement is not observed below 205 nm (Figure 5b) where the tyrosyl contribution in the 'reconstituted' spectrum is higher than for the alternating-pairs copolymer. Nevertheless, it seems reasonable to assert that the 230 nm c.d. band in poly(L-tyrosine) arises mainly from the array ( $n, n+1; n+4, n+5$ ). The ( $n, n+1$ ) interaction is likely very effective, but it cannot yet be decided whether interaction between tyrosyl pairs ( $n, n+1$ ), ( $n+4, n+5$ ) etc. is of importance or not.

Using CPK space-filling models as well as Dreiding models, we tried to find out whether some special geometrical arrangement of tyrosyl side chain could be built to account for the c.d. spectrum of the alternating-pairs copolymer as compared to the spectrum of poly(L-tyrosine). It was then found that if the tyrosyl side chains are alternately orientated according to the two sets of  $\chi_1, \chi_2$  angles reported in Table 3, this will result in the formation of two contiguous side chain superhelices ( $n, n+4, n+8 \dots; n+1, n+5, n+9 \dots$  respectively) in which the aromatic rings are nearly parallel to the  $\alpha$ -helix axis and overlap to some extent.

The values of angles  $\chi$  are located near the minimum in the energy map calculated by Ooi *et al.*<sup>9</sup> for poly(L-tyrosine).

In this conformation, consecutive aromatic rings in the same superhelix (i.e. corresponding to  $n, n+4$  residues) are distant by about 6.5–7 Å, while contiguous rings of two different superhelices are nearer (5.5–6 Å). In addition, these contiguous rings are nearly parallel (Figure 6). Each of the superhelices wraps right-handed around a Pauling-Corey  $\alpha$ -helix (18 residues in 5 turns) with a pitch of 54 Å and 9 side chains per turn. We suggest that such a

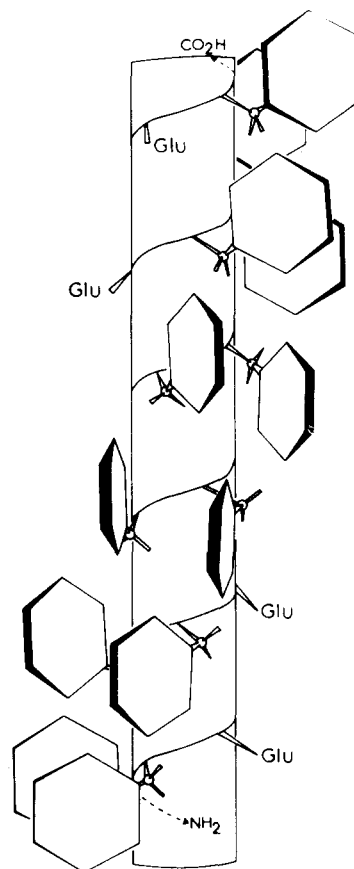


Figure 6 Scheme of the proposed arrangement of the side chains in  $(\text{Glu-Tyr-Tyr-Glu})_n$

model also holds for poly(L-tyrosine). In this case, a tyrosyl side chain held for instance in the conformation ( $\chi_1 \sim 170^\circ, \chi_2 \sim 35^\circ$ ) will pair with one of its two next neighbours held in the other conformation ( $\chi_1 \sim -60^\circ, \chi_2 \sim 120^\circ$ ). The four superhelices thus make two ribbons each wrapping one side of the  $\alpha$ -helical framework. In the free space between the ribbons the  $\alpha$ -helical framework appears to be quite open to the solvent while the other part is hindered.

This can help us to understand why the c.d. contribution at 230 nm in poly(L-tyrosine) is twice that of the alternating-pairs  $(\text{Glu-Tyr-Tyr-Glu})_n$  copolymer. Superhelical ribbons in poly(L-tyrosine) actually are too distant to interact strongly. This newly proposed conformation of tyrosyl side chains can also be valid for other polypeptides bearing aromatic groups. In the same manner, contiguous aromatic side chains included in  $\alpha$ -helical segments of proteins may adopt the same pairing conformation.

## CONCLUSION

Assuming that poly(L-tyrosine) in trimethylphosphate is in  $\alpha$ -helical form which is now largely evidenced, comparison on the basis of c.d. spectra in trimethylphosphate of poly(L-tyrosine) with random copolypeptides of various tyrosyl contents leads to the conclusion of a right-handed helix sense for poly(L-tyrosine).

C.d. studies on sequential copolypeptides  $(\text{Tyr}_x\text{-Glu}_y)$  showed that some tyrosyl residues arrays are able to promote strong rotational strength at 230 nm. We found that ( $n, n+2$ ) and ( $n, n+3$ ) arrays were of poor effectiveness, while the ( $n, n+4$ ) one was much more effective. But the strongest rotational effect arises from the alternating-pairs array ( $n, n+1; n+4, n+5$ ).

Table 3 Proposed conformations of tyrosyl side chains

Order of the residue*	$\chi_1$	$\chi_2^\dagger$
$n, n+4 \dots$	$\sim 165^\circ$	$\sim 35^\circ$
$n+1, n+5 \dots$	$\sim -70^\circ$	$\sim 110^\circ$

\* Numbering the residues from the amino end

†  $\chi_2$  value does not take into account the orientation of the phenolic -OH group

Using atomic models, we have built up the alternating-pairs copolymer ( $x = y = 2$ ) in the form of an  $\alpha$ -helix in which the tyrosyl side chains are arranged as a compact superhelical ribbon wrapping on one side of the  $\alpha$ -helical framework with a pitch of 54 Å. This structure corresponds to two different conformations of the tyrosyl side chains each being defined by a couple of conformational angles  $\chi_1, \chi_2$ . When building up poly(L-tyrosine) in the same way a two-ribboned structure resulted. Such a structure fits well our c.d. results in the range 205–240 nm at least, and may be valid for other aromatic polypeptides.

#### ACKNOWLEDGEMENT

We wish to thank Mrs A. Caille for her technical assistance in obtaining c.d. spectra and measuring intrinsic viscosities.

#### REFERENCES

- 1 Damle, V. N. *Biopolymers* 1970, 9, 937
- 2 Quadrioglio, F., Ius, A. and Crescenzi, V. *Makromol. Chem.* 1970, 136, 241
- 3 Engel, J. *Eur. J. Biochem.* 1971, 21, 22
- 4 Bradbury, E. M., Crane-Robinson, C., Giacotti, V. and Stephens, R. M. *Polymer* 1972, 13, 33
- 5 Chen, A. K. and Woody, R. W. *J. Am. Chem. Soc.* 1971, 93, 29
- 6 Fasman, G. D. *Nature* 1962, 193, 681
- 7 Trudelle, Y. *Polymer* 1975, 16, 9
- 8 Applequist, J. and Mahr, T. G. *J. Am. Chem. Soc.* 1966, 88, 5419
- 9 Ooi, T., Scott, R. A., Vanderkooi, G. and Scheraga, H. A. *J. Chem. Phys.* 1967, 46, 4410
- 10 Yan, J. F., Vanderkooi, G. and Scheraga, H. A. *J. Chem. Phys.* 1968, 49, 2713
- 11 Vollmer, J. P. and Spach, G. *Biopolymers* 1967, 5, 337
- 12 Trudelle, Y. *JCS Perkin Trans. I* 1973, p 1001

# Phosphonitrilic chloride: 23. Substitution reaction of phosphonitrilic chloride trimer with sodium hydroxymethylphenolate and polymerization of substitution products

M. Kajiwara and H. Saito

Department of Applied Chemistry, Faculty of Engineering, Nagoya University, Nagoya, Japan  
(Received 11 January 1974; revised 1 March 1974)

Chlorine substitution reactions of phosphonitrilic chloride trimer  $(\text{PNCl}_2)_3$  with 2-, 3- or 4- $\text{HOH}_2\text{CC}_6\text{H}_4\text{ONa}$  and 2- $\text{NaOH}_2\text{CC}_6\text{H}_4\text{ONa}$  were carried out in dioxane solvent under various experimental conditions. All reactions were completed in 40–200 min in the temperature range  $60^\circ$  to  $100^\circ\text{C}$ . The chemical shifts of P atom were measured by  $^{31}\text{P}$  n.m.r. spectroscopy of  $\text{P}_3\text{N}_3(2\text{-HOH}_2\text{CC}_6\text{H}_4\text{O})_6$  (I),  $\text{P}_3\text{N}_3(3\text{-HOH}_2\text{CC}_6\text{H}_4\text{O})_6$  (II),  $\text{P}_3\text{N}_3(4\text{-HOH}_2\text{CC}_6\text{H}_4\text{O})_6$  (III) and  $\text{P}_3\text{N}_3(2\text{-OH}_2\text{CC}_6\text{H}_4\text{O})_3$  (IV). The  $^{31}\text{P}$  n.m.r. spectra showed the singlet peak. Water vapour and formaldehyde were detected by gas chromatography and polymers were formed when (I), (II) and (III) were heated from  $150^\circ\text{C}$  to  $250^\circ\text{C}$ . The polymers were stable towards water. Further, thermal balance measurements showed that the polymer formed from (I) was the most stable. The resistivity of films formed when (I), (II) and (III) were heated at about  $300^\circ\text{C}$  for 2 min was  $1\text{--}10 \times 10^{13} \Omega\text{-cm}$ . Thermal decomposition occurred rather than ring cleavage reaction when (IV) was heated from  $150^\circ\text{C}$  to  $250^\circ\text{C}$ .

## INTRODUCTION

Various substitution products of cyclophosphazene have been synthesized with cyclophosphazene dichloride trimer  $(\text{PNCl}_2)_3$  and aromatic, aliphatic mono- or di-functional reagents<sup>1</sup>. However, most of the products were not polymerized with ring cleavage on heating as with  $(\text{PNCl}_2)_3$ , cyclophosphazene pseudohalogen compounds or a few substitution products of  $(\text{PNCl}_2)_3$ <sup>2,3</sup>. In recent years, the formation of cyclophosphazene linear or cyclophosphazene matrix polymers has been studied from substitution products of  $(\text{PNCl}_2)_3$ . This paper describes a synthesis of cyclophosphazene derivatives from  $(\text{PNCl}_2)_3$  and sodium hydroxymethylphenolate, and cyclomatrix or cycloliner phosphazene polymers from a condensation reaction with  $-\text{CH}_2\text{OH}$  groups. The physical properties of the polymers are described.

## EXPERIMENTAL

### Preparation of cyclophosphazene dichloride trimer $(\text{PNCl}_2)_3$

Cyclophosphazene dichloride trimer  $(\text{PNCl}_2)_3$  was prepared by the modified method of Saito and Kajiwara<sup>4</sup>. Pure trimer (m.p.  $112^\circ\text{C}$ ) was obtained by repeated fractional crystallization from light petroleum ether.

### Preparation of hydroxybenzyl alcohol and mono- or di-sodium salts of hydroxybenzyl alcohol

2- $\text{HOH}_2\text{CC}_6\text{H}_4\text{ONa}$  was synthesized from phenol and formaldehyde<sup>5</sup>. 3- or 4- $\text{HOH}_2\text{CC}_6\text{H}_4\text{OH}$  were synthesized from *m*- or *p*-hydroxybenzoic acid methyl ester by reduction with  $\text{LiAlH}_4$  or  $\text{NaAlH}_2(\text{OCH}_2\text{CH}_2\text{OCH}_3)_2$ . Hydroxy-

benzyl alcohols were purified by recrystallization from benzene. The melting point of the products were  $86^\circ\text{C}$  (2- $\text{HOH}_2\text{CC}_6\text{H}_4\text{OH}$ ),  $73^\circ\text{C}$  (3- $\text{HOH}_2\text{CC}_6\text{H}_4\text{OH}$ ) and  $125^\circ\text{C}$  (4- $\text{HOH}_2\text{CC}_6\text{H}_4\text{OH}$ ), respectively. The mono- or di-sodium salts of hydroxybenzyl alcohols were prepared by adding Na (2.3 g) into anhydrous ethanol (13% w/w) dropwise to the ethoxide solution. The mixture was refluxed on a water bath for 1 h and then the ethanol was evaporated under reduced pressure. 2- $\text{HOH}_2\text{CC}_6\text{H}_4\text{ONa}$ , 3- $\text{HOH}_2\text{CC}_6\text{H}_4\text{ONa}$ , 4- $\text{HOH}_2\text{CC}_6\text{H}_4\text{ONa}$  and 2- $\text{NaOH}_2\text{CC}_6\text{H}_4\text{ONa}$  were examined using  $^1\text{H}$  n.m.r. The area ratio of  $-\text{CH}_2$  or  $-\text{OH}$  calculated from the spectra, and amounts of sodium determined by chemical analysis were in fair agreement with the theoretical values. It was concluded from the analytical data that the products were formed by this reaction.

### Substitution reaction of cyclophosphazene dichloride trimer with sodium salts of hydroxybenzyl alcohols

The reaction of cyclophosphazene dichloride trimer  $(\text{PNCl}_2)_3$  and the sodium salts of hydroxybenzyl alcohols were carried out in dioxane at various reaction temperatures.  $(\text{PNCl}_2)_3$  (6.86 g) was dissolved in dioxane (200 ml), and was added to a solution of the sodium salt of hydroxybenzyl alcohol in dioxane (19.5 g/100 ml) or the di-sodium salt of hydroxybenzyl alcohol (20.2 g/100 ml). The resulting solutions were warmed on an oil bath at  $60^\circ\text{--}100^\circ\text{C}$  with vigorous stirring. The reaction mixture was separated by filtration, and the filtrate was distilled under vacuum. The product obtained from this reaction was purified from dioxane containing active carbon. No hydrogen chloride gas was evolved. The dioxane insoluble products removed by filtration after the reaction was over, showed the pre-

sence of sodium chloride by X-ray diffraction analysis. The dioxane insoluble products were washed with ethanol several times to remove the unreacted mono- or di-sodium salts of hydroxybenzyl alcohols and the residue was dissolved in distilled water. The degree of conversion was calculated from the quantity of sodium chloride determined with 0.01 N AgNO<sub>3</sub>.

#### Polycondensation of products

The substitution products were heated in an electric furnace at 150°C or 200°C in air for various times and it was found by gas chromatography analysis that water vapour or formaldehyde was formed. After the polycondensation reaction was over, the heat treated materials were separated into the dioxane soluble fraction (a) and the insoluble fraction (b) and their composition was determined by elemental analysis.

#### Molecular weight of products

Molecular weights of the substitution products or polymers obtained with the substitution reactions or polycondensation reaction were measured by the cryoscopic method, or g.p.c. using dioxane.

#### Determination of water and formaldehyde

Water and formaldehyde were determined by gravimetric analysis of an oxidation/reduction titration method using I<sub>2</sub>.

#### Instrumentation

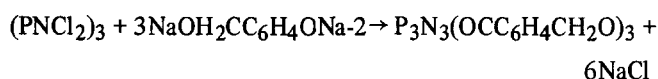
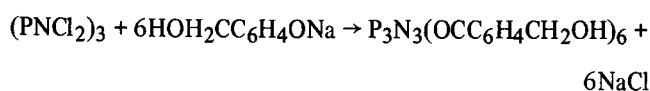
<sup>1</sup>H n.m.r. spectra were measured with a Nihon Denshi JNMC-60 type spectrometer for 60 MHz at 20°C using TMS as internal standard. <sup>31</sup>P n.m.r. spectra were measured with a Nihon Denshi JNMC-60HL type spectrometer using chloroform or DMSO as solvents and H<sub>3</sub>PO<sub>4</sub> as the reference. X-ray diffraction photographs was measured using a Shimadzu Co. VDF-1 type instrument and powder diffraction method. Infra-red absorption spectra were measured with a Shimadzu Co. IRG-2 type spectrometer using the KBr disc technique. The gas chromatograph used was a Shimadzu Co. GC-5A type instrument.

## RESULTS AND DISCUSSION

#### Activation energy of the substitution reaction

Since sodium chloride is formed in the reaction between cyclophosphazene dichloride trimer and the mono- or di-

sodium salts of hydroxybenzyl alcohols and no hydrogen chloride was detected, the following reaction mechanism is proposed:



The extent of the reaction was measured by the amount of sodium chloride formed under various experimental conditions. It was found that the reaction was second order and using equation (1) the value of *k* was determined:

$$k = 1/(n-1)t(1/C^{n-1} - 1/C_0^{n-1}) \quad (1)$$

in which *n* is the reaction order, *t* is the time, *C*<sub>0</sub> is the total sodium chloride when the reaction is complete, *C* is the amount of sodium chloride at reaction time *t*, and *k* is the velocity constant. The values for the activation energies, Δ*E*, determined from Arrhenius plots, are summarized in Table 1.

The solubilities of the mono- or di-sodium salts of hydroxybenzyl alcohols used are also shown in Table 1.

From Table 1 it is apparent that the activation energy of the substitution reaction between cyclophosphazene dichloride trimer and 2-HOH<sub>2</sub>CC<sub>6</sub>H<sub>4</sub>ONa or 3-HOH<sub>2</sub>CC<sub>6</sub>H<sub>4</sub>ONa is the lowest; this is believed to be due to its much higher solubility.

#### Analysis of the substitution reaction products

The products obtained at completion of the reaction are shown in Table 2.

The values for both elemental analysis and molecular weight are in fair agreement with the calculated values. <sup>31</sup>P n.m.r. spectra of the various products are summarized in Table 3.

The <sup>31</sup>P n.m.r. spectra give a singlet peak only for all the products and also, bands characteristic of P=N or P-O-R appeared in the region 1200 cm<sup>-1</sup> or 980–1100 cm<sup>-1</sup>, respectively. The structure of the products are postulated as I–IV respectively. They are soluble in most organic solvents, but insoluble in water.

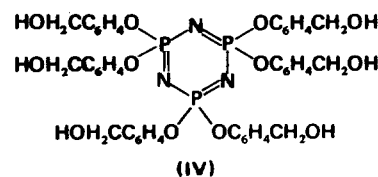
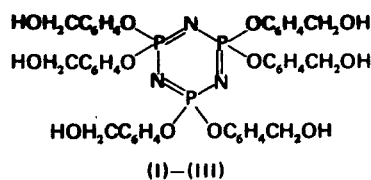


Table 1 Values for the activation energies

Reaction system	Δ <i>E</i> (kcal/mol)	g/100 g dioxane	
		25°C	100°C
(PNCl <sub>2</sub> ) <sub>3</sub> + 2-HOH <sub>2</sub> CC <sub>6</sub> H <sub>4</sub> ONa	8 ± 0.5	1.23	1.28
(PNCl <sub>2</sub> ) <sub>3</sub> + 3-HOH <sub>2</sub> CC <sub>6</sub> H <sub>4</sub> ONa	9	0.59	0.67
(PNCl <sub>2</sub> ) <sub>3</sub> + 4-HOH <sub>2</sub> CC <sub>6</sub> H <sub>4</sub> ONa	16	0	0
(PNCl <sub>2</sub> ) <sub>3</sub> + 2-NaOH <sub>2</sub> CC <sub>6</sub> H <sub>4</sub> ONa	13	0.06	0.43

Table 2 Chemical analysis of the substitution reaction products

Chemical compositions	Calc. (%)			Found (%)			Solidification point (°C)	Appearance
	P	N	Mol. wt	P	N	Mol. wt		
(I) P <sub>3</sub> N <sub>3</sub> (2-HOH <sub>2</sub> CC <sub>6</sub> H <sub>4</sub> O) <sub>6</sub>	10.50	4.76	870	10.61	4.83	850	58–67	solid, paste
(II) P <sub>3</sub> N <sub>3</sub> (3-HOH <sub>2</sub> CC <sub>6</sub> H <sub>4</sub> O) <sub>6</sub>				10.58	4.94	860		liquid
(III) P <sub>3</sub> N <sub>3</sub> (4-HOH <sub>2</sub> CC <sub>6</sub> H <sub>4</sub> O) <sub>6</sub>				10.32	4.51	860		liquid
(IV) P <sub>3</sub> N <sub>3</sub> (2-OH <sub>2</sub> CC <sub>6</sub> H <sub>4</sub> O) <sub>3</sub>	18.07	8.44	498	18.02	8.47	510	54–66	solid, paste

Table 3  $^{31}\text{P}$  n.m.r. spectra of phosphonitrilic derivatives (24.3 MHz, 20°C)

Formula of substitution product	Chemical shift $\delta_p$ (ppm)
(I) $\text{P}_3\text{N}_3(2\text{-HOH}_2\text{CC}_6\text{H}_4\text{O})_6$	-29.9
(II) $\text{P}_3\text{N}_3(3\text{-HOH}_2\text{CC}_6\text{H}_4\text{O})_6$	-17.5
(III) $\text{P}_3\text{N}_3(4\text{-HOH}_2\text{CC}_6\text{H}_4\text{O})_6$	-18.8
(IV) $\text{P}_3\text{N}_3(2\text{-OH}_2\text{CC}_6\text{H}_4\text{O})_3$	+1.58

Table 4 Molecular weight of (a) formed from various substitution products by heating at 200°C for 5 h

Formula of substitution product	Molecular weight of polymer
(I) $\text{P}_3\text{N}_3(\text{HOH}_2\text{CC}_6\text{H}_4\text{O}-2)_6$	3 500
(II) $\text{P}_3\text{N}_3(\text{HOH}_2\text{CC}_6\text{H}_4\text{O}-3)_6$	9 500
(III) $\text{P}_3\text{N}_3(\text{HOH}_2\text{CC}_6\text{H}_4\text{O}-4)_6$	14 500

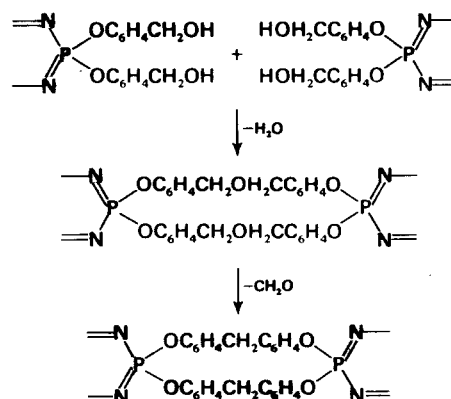
### Polycondensation reaction of the substitution products

I–III were examined by differential thermal analysis (d.t.a.) and thermogravimetry (t.g.). Peaks for exothermic reactions appeared at 170°, 410°, 630°C (I); 160°, 510°C (II); 180°, 360°, 510°C (III), and peaks for endothermic reactions appeared at 460°C (I), 350°C (II), 450°C (III), respectively. It is proposed that the exothermic reaction at 160°–180°C is the polycondensation of  $-\text{CH}_2\text{OH}$  groups present in the substitution products. On heating I–III from room temperature gas chromatographic analysis of the gas formed showed the water vapour or formaldehyde gas was liberated at 160–200°C. The results of d.t.a. and gas chromatography, indicate that polycondensation reaction occurred both intermolecularly or intramolecularly. The results of molecular weight measurement of (a), the soluble fraction obtained by heating at 200°C for 5 h are summarized in Table 4.

Thus, polycondensation of I–III could be brought about most readily. The higher molecular weight of III may be attributed to a symmetrical  $-\text{CH}_2\text{OH}$  group in III. The infra-red absorption spectra of (a) and (b) obtained from I–III showed that the  $\text{P}=\text{N}$  frequencies of (a) and (b) which appeared at  $1200\text{ cm}^{-1}$  shifted to the long wave-number by about  $10\text{ cm}^{-1}$  for the substitution products I–III. On the other hand, the  $\text{P}=\text{N}$  frequency of the rubberlike polymer formed by heating dichlorocyclophosphazene is at  $1365\text{--}1300\text{ cm}^{-1}$  whereas for the trimer the  $\text{P}=\text{N}$  frequency is at  $1218\text{ cm}^{-1}$ . Also, the  $-\text{CH}_2\text{O}-\text{CH}_2-$  bond formed by the polycondensation reaction of  $-\text{CH}_2\text{OH}$  groups appeared at  $1150\text{--}1060\text{ cm}^{-1}$ , but the  $-\text{Ph}-\text{CH}_2-\text{Ph}-$  bond formed by polycondensation of  $-\text{CH}_2\text{O}-\text{CH}_2-$ ,  $-\text{CH}_2\text{OH}$  groups is no longer distinguishable from the other  $-\text{CH}_2-$  groups. The structure of the polymers (a) and (b) could be deduced from the analytical data as follows:

Table 5 Resistivity of films obtained from various substitution products by heating at 300°C for 2 min

Formula of substitution product	Thickness of film (mm)	Resistivity at 20°C $\times 10^{-13}$ ( $\Omega\text{-cm}$ )
(I) $\text{P}_3\text{N}_3(2\text{-HOH}_2\text{CC}_6\text{H}_4\text{O})_6$	0.014	2–10
(II) $\text{P}_3\text{N}_3(3\text{-HOH}_2\text{CC}_6\text{H}_4\text{O})_6$	0.015	1–3
(III) $\text{P}_3\text{N}_3(4\text{-HOH}_2\text{CC}_6\text{H}_4\text{O})_6$	0.029	2–4

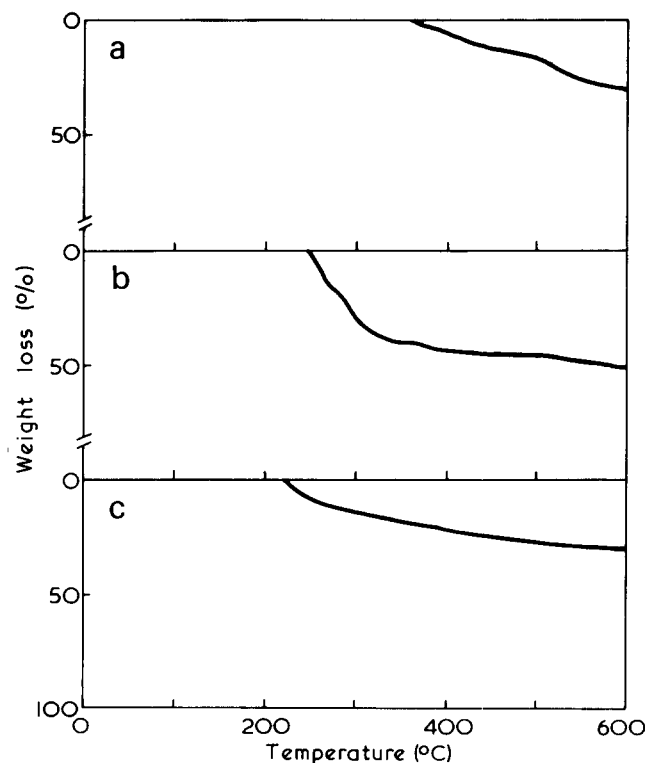


### Ring cleavage polymerization reaction of $\text{P}_3\text{N}_3(2\text{-OH}_2\text{CC}_6\text{H}_4\text{O})_3$ (IV)

The onset of ring cleavage was investigated by d.t.a. and t.g. The exothermic reaction peaks appeared at 160°, 280° and 390°C and the endothermic reaction peaks at 320° and 450°C, respectively. The endothermic reaction at 160°C is due to melting of IV. The nature of the reaction taking place at the other peaks was studied using gas chromatography. It was found that carbon monoxide, carbon dioxide, water vapour, formaldehyde, benzene and methanol were formed when the temperature was raised to 280°C. Thus decomposition occurred without cleavage of the  $\text{P}_3\text{N}_3$  ring, although the mechanism of decomposition cannot be explained.

### Properties of the polymers

The degree of hydrolysis of polymers (a) and (b) formed from I–III was estimated by heating in water at 100°C for 30 min. The extent of hydrolysis was about 0.2–1.6%. By comparison dichlorocyclophosphazene is completely hydrolysed to phosphoric acid, hydrogen chloride and

Figure 1 T.g. curves of polymers obtained by heating at 200°C for 300 min in air at the rate of 5°C/min. (a)  $\text{P}_3\text{N}_3(2\text{-HOH}_2\text{CC}_6\text{H}_4\text{O})_6$ ; (b)  $\text{P}_3\text{N}_3(3\text{-HOH}_2\text{CC}_6\text{H}_4\text{O})_6$ ; (c)  $\text{P}_3\text{N}_3(4\text{-HOH}_2\text{CC}_6\text{H}_4\text{O})_6$

ammonium chloride. The polymers were stable against dilute H<sub>2</sub>SO<sub>4</sub>, HNO<sub>3</sub> or NaOH solution. In air the weight loss by heating was measured on a thermobalance, and the results are shown in *Figure 1*.

Further, it can be seen from the t.g. curves that the most stable polymer is the polymer formed from III, and the stability is related to the degree of condensation. The degradation products formed by heating at 200°C for 300 min are H<sub>2</sub>O, CH<sub>2</sub>O, CH<sub>3</sub>OH (main product), C<sub>6</sub>H<sub>6</sub> (main product), CO and CO<sub>2</sub>.

Although it is found that main products were methanol and benzene, the mechanism of decomposition is uncertain.

The resistivity of films formed from the substitution

products of I–III by heating at 300°C for 2 min are shown in *Table 5*.

#### REFERENCES

- 1 Shaw, R. A., Fitzsimmon, B. W. and Smith, B. C. *Chem. Rev.* 1961, **62**, 247; Allcock, H. R. *Chem. Rev.* 1972, **72**, 315
- 2 Allcock, H. R. 'Phosphorus Nitrogen Compounds', Academic Press, New York and London, 1972, p 303
- 3 Haiduc, I. 'The Chemistry of Inorganic Ring Systems', Wiley-Interscience, New York, 1970, p 662
- 4 Saito, H. and Kajiwara, M. *J. Chem. Soc. Japan (Ind. Chem. Sect.)* 1966, **66**, 618
- 5 Seto, S. and Horiuti, H. *J. Chem. Soc. Japan (Ind. Chem. Sect.)* 1953, **57**, 689

# The role of electrical conduction of macromolecules in certain biomedical problems

Stephen D. Bruck

National Heart and Lung Institute, National Institutes of Health, Bethesda, Maryland 20014, USA  
(Received 26 March 1974)

The electrical properties of selected macromolecules are reviewed in terms of their physico-chemical structures, and these properties are related to interactions with blood. It is suggested that the electrical conduction and semiconduction properties of some natural and synthetic macromolecules may be involved, among other factors, in preventing the initiation of adverse effects on blood components, such as loss of compatibility.

## INTRODUCTION

Electrical conduction and semiconduction can be found in a variety of natural biopolymers and synthetic polymers. In 1946, Szent-Györgyi<sup>1,2</sup> suggested that proteins may have an electronic structure similar to that of semiconductors. Based on his ideas, Evans and Gergely<sup>3</sup> calculated that such conditions may exist in proteins. In 1953, Eley *et al.*<sup>4</sup> reported semiconductivity in albumin, fibrinogen, and edestin, and found that water present in these molecules could decrease the energy gap for the movement of electrons. Later, Cardew and Eley<sup>5</sup> showed that haemoglobin and globin exhibit electrical conductance. Electrical conduction phenomena were also investigated by Rosenberg<sup>6</sup> and Postow and Rosenberg<sup>7</sup>, confirming that electronic conduction and semiconduction exist in a number of proteins. Electrical conduction in collagen has been reported by Eley and Spivey<sup>8</sup> and by Bardelmeyer<sup>9,10</sup>.

Among synthetic polymers, Winslow *et al.*<sup>11,12</sup> showed that the non-volatile pyrolytic degradation products of poly(vinylidene chloride) and pre-oxidized poly(vinyl benzene) exhibit semiconducting properties. Such properties were also reported for the pyrolytic condensation product of polyacrylonitrile by Topchiev<sup>13</sup>, for polymers of phthalocyanine by Marvel and Rassweiler<sup>14</sup>, and for poly(*p*-phenyl) by Mainthia *et al.*<sup>15</sup>. In 1965, Bruck<sup>16</sup> reported a specific electroconduction of 20 ohm<sup>-1</sup> cm<sup>-1</sup> at 25°C for the pyrolytic condensation products of a polypyromellitimide, which is among the highest ever observed in synthetic polymers. With non-polymeric organic substances, Kepler<sup>17</sup> observed very high conductivity of 100 ohm<sup>-1</sup> cm<sup>-1</sup> for salts of tetracyanoquinodimethane (TCNQ).

The role of electrical conduction and semiconduction in various biochemical phenomena has attracted considerable attention since the original suggestion by Szent-Györgyi<sup>1,2</sup> that proteins may have electronic structure resembling semiconductors. For example, it is possible that proteins may be able to conduct electrons in the cytochrome systems of cells<sup>18</sup>, that the transfer of energy may cause chemical reactions to occur in distant protein molecules<sup>5</sup>, and that electronic conduction may be involved in muscle contractions<sup>19</sup>. Bruck<sup>20</sup>, in 1973, suggested that intrinsic semiconduction and electronic conduction may be involved in blood com-

patibility of polymeric systems and described observations *in vitro* in support of such a role with the pyrolytic conversion products of an aromatic polyimide<sup>16,20,21</sup>.

## SOME FUNDAMENTAL CONSIDERATIONS

Electrical conductivity may be either electronic or ionic. Electronic conduction is characteristic of metals in which electrons are the current carriers. On the other hand, ionic conduction is characterized by the presence of charged atoms or groups of atoms, which are the current carriers. Typically, polymers are insulators rather than conductors of electricity. Some polymers, however, can be made 'conductive' by the dispersion of finely powdered metal particles or carbons, or by coating them with metal oxides. Semiconductors are characterized by two energy bands, one that is filled with electrons (valence band), and the other that is empty (conduction band). These two bands are separated by a forbidden energy gap. If an electron acquires sufficient energy, it can jump into the upper conduction band. Electronic conduction may occur that is accompanied by the removal of electrons from the valence bands leaving empty levels and creating the appearance of a flow of positively charged electrons (holes). In a perfect intrinsic semiconductor, the number of electrons in the conduction band is equal to the number of holes. In such a case, electrical conduction will depend on the inherent atomic and crystal structure of the material. On the other hand, in an extrinsic semiconductor, electrical conduction by electrons and holes is caused by impurity atoms present in the crystal lattice. Depending on whether or not the impurity atom (or atoms) donates or accepts an electron (or electrons) from the valence band, the semiconducting material will be *n*-type (because of the negative charge of the carriers) or *p*-type (because of the positive charge of the holes).

Electrical conductivity,  $\sigma$ , which is the reciprocal of resistivity, may be expressed as:

$$\sigma = |e|n(\mu_h + \mu_e) \quad (1)$$

$$= |e|n_h(1 + c) \quad (2)$$



$$= \sigma_0 \exp(E/2kT) \quad (3)$$

where  $|e|$  = electronic charge,  $n$  = concentration of current carriers,  $\mu_{h,e}$  = mobilities of holes and electrons,  $c = \mu_e/\mu_h$ ,  $\sigma_0$  = pre-exponential factor,  $E$  = activation energy to form charge carriers,  $k$  = Boltzmann constant,  $T$  = absolute temperature,  $e$  = base of natural logarithm. The value  $c$  (the ratio of the mobilities of electrons to the mobilities of holes) can be obtained from thermoelectric measurements. These yield the so-called thermoelectric power or Seebeck coefficient,  $Q$ . This represents the thermoelectric force per degree that arises when two different conductors are joined at both ends and the two junctions are kept at slightly different temperatures. By convention, the thermoelectric power is positive when the current flows from the sample to the reference metal at the cold junction. The Seebeck coefficient may be expressed by the following relationship<sup>22</sup>:

$$Q = - \frac{k}{|e|} \left( \frac{c-1}{c+2} \right) - \left( \frac{E}{2kT} \right) + 2 \quad (4)$$

This permits the calculation of the ratio of the mobility of electrons to holes,  $c$ , because  $E$  can be obtained from a study of the temperature dependence of conductivity. If the carrier mobilities are only slightly dependent on temperature, a plot of  $\log \sigma$  vs.  $1/T$  (refer to equation 3) should yield a straight line with a slope of  $-E/2k$ .

Another important effect arises when a current-carrying conductor is placed in a transverse magnetic field, thus producing an electric field,  $E_H$ , that is perpendicular to both the magnetic field and to the flow of current. This is called the Hall effect<sup>23,24</sup>. To understand this phenomenon, consider that when an electric field,  $iE_L$ , is applied, the current carriers moving with a velocity of  $\pm v$  are deflected by the magnetic field,  $kB_z$ , where  $i$  and  $k$  are unit vectors in the directions of  $x$  and  $z$ , respectively. As a result, the excess electrons create an electric field having a force  $eE_H$  which, in a steady state, equals the force on the electrons caused by the magnetic field. Hence,  $eE_H = \pm evB_z$ . Since the velocity of the electrons is  $v = \mu E_L$ , then  $E_H = \mu E_L B_z$ . The current density,  $J$ , can be expressed as:

$$J = nev = ne\mu E_L \quad (5)$$

hence,

$$E_H = \pm(1/ne)BJ \quad (6)$$

where the term  $(\pm 1/ne)$  is called the Hall coefficient,  $R$ . Information can be thus gained on the concentration and sign of the charge carriers. Furthermore, in conjunction with conductivity data, the mobilities of holes and electrons can be calculated.

## ELECTRICAL CONDUCTION IN DEHYDRATED PROTEINS

A number of proteins and synthetic polymers in the dry state exhibit electrical semiconduction. In the case of  $\beta$ -proteins, the energy gap ( $\Delta E$ ) between the top of the filled bands and the bottom of the unfilled bands leads to a value of 3.05 eV according to Evans and Gergely<sup>3</sup>. Such  $\beta$ -proteins are characterized by hydrogen bond structures that presumably enable the movement of electrons and holes through the system. Cardew and Eley<sup>5</sup> have suggested

that  $\alpha$ -proteins would be expected to have similar electrical properties facilitated by the helical structure of the polypeptide chains. Synthetic polyamides also exhibit hydrogen-bonded structures, but the density of such hydrogen bonds is less than in proteins. In such systems, evidence indicates that the observed conduction is caused by protons rather than by electrons<sup>25,26</sup>. Protonic conduction is explained in terms of increased rotational freedom of the polyamide chains caused by the lesser degree of hydrogen bonding in these systems<sup>26</sup>.

The activation energies (energy gaps) for semiconduction of several dry proteins are summarized in *Table 1* as calculated from equation (3) above. The data indicate that the activation energies of these proteins fall within the range of  $\sim 2.3$  to 3.0 eV. The mobility of charge carriers,  $\mu$ , representing the average mobilities of electrons and holes,  $\mu_e + \mu_h$ , as calculated by Eley and Spivey<sup>8</sup> are between  $10^3$  and  $10^5$  cm<sup>2</sup> V<sup>-1</sup> sec<sup>-1</sup> at 400 K. These values are much larger than those of many synthetic aromatic compounds and compare favourably with those of inorganic semiconductors<sup>8</sup>. Although proteins exhibit small electroconductivities in comparison to some synthetic materials, the values are reproducible. *Table 2* shows the calculated specific electroconductivities of selected proteins and polymeric materials. These electroconductivities can be explained in the case of proteins by the movements of the  $\pi$ -electrons in the hydrogen-bonded C=O...H-N systems<sup>8</sup>. In the case of synthetic polymers and their pyrolytic conversion products, the electroconductivities will be also influenced by increased carrier mobilities due to  $\pi$ -orbital overlap in the unsaturated condensed ring structures<sup>12,13,16</sup>. In either case, electroconduction is faci-

*Table 1* Activation energies for semiconduction of selected dry proteins

Protein	$\Delta E$ (eV)	Ref
Haemoglobin (methanol denatured)	2.89	8
Haemoglobin (natural)	2.66	8
Haemoglobin (crystalline)	2.3-2.4	6
Globin (mixture of native and denatured)	2.97	5
Thrombin	2.59	8
Fibrinogen	2.69	8
Elastin	2.91	8
Collagen	2.73	8
Bovine plasma albumin	2.78	8

*Table 2* Specific electroconductivities of some proteins and selected synthetic polymers

Material	Specific electroconductivity (ohm <sup>-1</sup> cm <sup>-1</sup> )	Temp. (°C)	Ref
Thrombin	$3.8 \times 10^{-12}$	27	8
Fibrinogen	$1.6 \times 10^{-12}$	27	8
Bovine plasma albumin	$1.3 \times 10^{-12}$	27	8
Haemoglobin (natural)	$1.8 \times 10^{-12}$	27	8
Collagen	$3.4 \times 10^{-14}$	27	8
Poly [ <i>N,N'</i> -( <i>p,p'</i> -oxydiphenylene) pyromellitimide] (pyrolytic product)	$0.2 \times 10^2$	25	16
Polyphenyleneaminoquinone	$7 \times 10^{-7}$ to $9 \times 10^{-7}$	25	13
Polymeric copper phthalocyanine	$2.5 \times 10^{-2}$	25	14

tated by increased order in the chemical structure of the molecules.

### ELECTRICAL CONDUCTION IN HYDRATED PROTEINS

Several investigators have shown that the electrical conduction of proteins, such as plasma albumin<sup>26</sup> and haemoglobin<sup>6,27</sup>, are influenced by their water content. In particular, it was observed that the main effect of the adsorbed water is manifested in the lowering of the activation energy of conduction. In the case of haemoglobin, Rosenberg<sup>6</sup> proposed that this is due to an increase in the dielectric constant of the protein. This serves to lower the energy needed for charge separation and to stabilize the charge carriers (electrons and holes) so that their numbers will increase. Eley and Leslie<sup>26</sup> considered Rosenberg's hypothesis involving the effect of the dielectric constant as an 'intrinsic mechanism', and they have suggested an alternate 'impurity mechanism' to explain the experimental observations. According to this latter view, the water molecules are adsorbed on polar groups including the C=O---H-N hydrogen bonds to yield a so-called 'charge transfer adsorbed state'<sup>26</sup>. These authors performed experiments to distinguish between the 'intrinsic mechanism' and the 'impurity mechanism' by using various adsorbents such as CH<sub>3</sub>OH (dielectric constant = 33), D<sub>2</sub>O (dielectric constant = 78.7), and H<sub>2</sub>O (dielectric constant = 80.0). There was no significant difference between the activation energy of conductivity between deuterated and non-deuterated proteins, as seen in *Table 3*. Also, only minor changes were observed in the electrical conductivity of these deuterated and non-deuterated proteins. The specific electroconductivities measured as a function of the surface at low adsorbate concentrations were found to increase in the order: H<sub>2</sub>O < D<sub>2</sub>O < CH<sub>3</sub>OH, that is in the direction opposite of their respective dielectric constants. Consequently, Eley and Leslie<sup>26</sup> proposed that this increase in the conductivity may be due to the order of decreasing ionization potentials, rather than to the effect of changes in the dielectric constants as proposed by Rosenberg<sup>6</sup>.

At higher water contents, several authors proposed protonic instead of electronic conduction for proteins<sup>26,27</sup>. This view stems from polarization phenomenon which is manifested by a slow increase of the resistance with time owing to the build-up of a reverse electromotive force. Such a polarization effect has been observed at a water content of 0.9 mol/100 g protein in both native and denatured haemoglobin<sup>26</sup> and in collagen<sup>27</sup>. On the other hand at water contents below 0.9 mol/100 g protein, there are practically no changes in the resistance with time for other proteins, such as bovine plasma albumin and globin<sup>26</sup>. Therefore, it appears that in dry proteins or in proteins at low water contents, the conduction is electronic, whereas at higher water contents, the conduction may be due to protons. Such protons may be transferred between the

adsorbed water molecules, or from the C=O to the H-N groups. This later process would be mediated by the water molecules which may have entered the inside structure of proteins.

In the case of collagen, Bardelmeyer<sup>27</sup> has recently proposed that the current carriers are probably protons rather than electrons when this protein has a water content of about 20 to 45%, and by small inorganic ions beyond a water content of about 65%. He found that at water contents of below 20%, there was good linearity between current and voltage, and the currents were not time-dependent. Above that water content, however, polarization effects predominated. Furthermore, a sharp brake was observed in the plot of the activation energy vs. water content between 45 and 65% water content<sup>27</sup>. This indicates that at the higher water contents, the main charge carriers may not be electrons but protons. Such protonic conduction may occur along the chains of collagen mediated by water molecules adsorbed on polar groups and the C=O---H-N hydrogen bond system<sup>27,28</sup>.

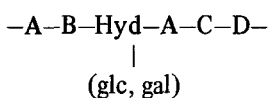
Several authors have used nuclear magnetic resonance (n.m.r.) spectroscopy to study the state of water in collagen<sup>29-31</sup>. Dehl<sup>31</sup> found that about 0.54 g of water/g of collagen does not freeze and retains high mobility to -50°C which represents about 2.6 molecules of unfreezable water per residue of the collagen molecule. Further work by Dehl<sup>32</sup> with MgCl<sub>2</sub> and MgSO<sub>4</sub> in conjunction with n.m.r. spectroscopy and the use of D<sub>2</sub>O suggested that neither the so-called two-state nor the structured-water concept can satisfactorily explain the D<sub>2</sub>O n.m.r. doublet spectrum or the effect of salts on it. The existence of 'structured' water has been invoked previously to explain the n.m.r. spectra of water in anisotropic collagen fibres<sup>28-30</sup>. According to the two-state concept of water in collagen, there would be a rapid exchange between bound and free water in collagen, and furthermore, the n.m.r. doublet splitting,  $\Delta\nu$ , should vary linearly with water content. However, Fung and Siegel<sup>33</sup> have recently shown that this is not the case. In view of these results, it is unlikely that the amount of adsorbed (anisotropic) water in collagen is sufficient to be in equilibrium with an isotropic liquid phase, and that there is a significant quantity of 'structured' water present in collagen<sup>32</sup>.

The existence of 'structured' water to explain the blood compatibility characteristics of some hydrogels has recently been postulated by Bruck<sup>34-36</sup>, and subsequently by Andrade and colleagues<sup>37,38</sup>. It should be pointed out, however, that the structure of collagen fibres is quite different from synthetic hydrogels, so that no generalization is possible. Nevertheless, it is interesting to speculate on the role of water in electroconduction in biopolymers in conjunction with blood compatibility. In the case of collagen, it is well known that when the endothelium of blood vessels is damaged, the underlying collagen attracts platelets which liberate adenosine diphosphate (ADP). The liberated ADP in turn attracts more platelets and the blood vessel might become completely occluded with the formation of a temporary haemostatic plug which is subsequently converted into a mechanically stable thrombus by the activation of the blood coagulation mechanism. The red cells can also release ADP as the result of haemolysis caused by stimuli such as alteration of blood flow patterns, exposure to damaged vascular wall areas or artificial surfaces. Consequently, platelets are apparently not the only formed blood elements which participate in thrombogenesis. Recently, Ganguly<sup>39</sup> presented evidence that while human

*Table 3* Activation energies of conduction of selected deuterated (D) and non-deuterated (N) proteins (compiled from ref 26)

Protein	$\Delta E$ (eV)
Bovine plasma albumin (D)	2.7
Bovine plasma albumin (N)	2.7
Egg albumin (D)	2.95
Egg albumin (N)	2.97
Yeast nucleic acid (D)	2.35
Yeast nucleic acid (N)	2.375

platelets bind thrombin, this by itself is insufficient to cause platelet aggregation and that other reactions seem to be also involved. He also suggested that the receptor of thrombin on platelets may be a protein having a molecular weight in excess of 200 000<sup>39</sup>. The property of collagen to activate and aggregate the platelets appears to be related to its native, triple-helical structure because denatured (random coil) collagen neither promotes the aggregation of the platelets nor initiates the clotting mechanism. It has also been shown that the activation of the Hageman factor may be related to the free carboxyl groups of collagen because esterification of these groups prevents the activation process<sup>40</sup>. Furthermore, the ability of native collagen to aggregate the platelets may be related also to the particular architecture of the collagen molecule. For example, it has been shown that when the positively charged free amino groups are replaced by neutral groups, the aggregation of platelets is drastically diminished<sup>40</sup>. Vertebrate collagens contain small quantities of carbohydrate that constitutes less than 2% by wt of the total weight of the molecule<sup>41</sup>. Butler and Cunningham<sup>42</sup> studied soluble collagen from guinea pig skin and have shown that glucose (glc) and galactose (gal) are linked to the hydroxyl group of hydroxylysine (Hyd) in the peptide chain as follows:



where A = glycine, B = methionine, C = histidine, and D = arginine. Recent studies by Bosmann<sup>43</sup> and by Barber and Jamieson<sup>44</sup> have indicated that platelet-bound glycosyl transferases seem to be needed for the adhesion of platelets to native collagen as the primary step in haemostasis.

The fundamental structural unit of collagen is believed to be the tropocollagen molecule with a diameter of 15 Å, length of 2800 Å, and molecular weight of about 300 000. The tropocollagen molecules are organized into fibrils (~5000 Å long) in such a way that they overlap by about one-quarter of their length<sup>45</sup>. The tropocollagen molecule forms a triple-helix, the structure of which was established by Rich and Crick<sup>46</sup> and Ramachandran<sup>47</sup>. The individual chains are nearly extended with only *intermolecular* hydrogen bonding possible between them. One-third of collagen is glycine, and an additional one-quarter is composed of proline and hydroxyproline. According to Ramachandran and Chandrasekharan<sup>48</sup>, collagen contains one intermolecular hydrogen bond via the N—H— — O=C group plus one intermolecular hydrogen bond via a water molecule per three residues. This is in contrast to other proteins, the architecture of which permits a greater amount of hydrogen bonding to occur. Chang and Chien<sup>49</sup> have recently shown that a variety of electrolytes can affect the stabilization and destabilization of the rod-like superstructure of reconstituted collagen. They showed that ions influence the structural order of reconstituted collagen both at the micron level (association—disassociation of tropocollagen—supermolecular rods of collagen) and at the molecular level (helix—coil transition).

Considering the particular water organization in collagen, Dehl<sup>32</sup> concluded that most of the water in collagen is 'bound' rather than 'free'. In other words, the bound water molecules are oriented by the polar groups of collagen and do not have the freedom of motion characteristic of liquid water. It should be pointed out that 'oriented' or 'bound' water is not equated with 'structured' water<sup>32</sup>.

Collagen, as has been shown above, exhibits electrical conductivity both in the dry and hydrated states. At low water adsorption levels, the conductivity is electronic, but when the water uptake exceeds approximately 10%, the conduction appears to be protonic<sup>27</sup>. Any disturbance to the native structure of this protein (such as increased salt concentration and dehydration) would be expected to affect its triple-helical structure and disrupt at least some of the hydrogen bonds. This in turn should be reflected in increased ion binding propensity and changes in the electrical conduction of the molecule. As a speculative argument, it is proposed that a sufficient alteration in the water structure and hence electrical conductivity may be brought about also as a result of injury to the endothelium of blood vessels by exposing the underlying collagen and the subendothelial components to the inorganic ions and organic polyelectrolytes of blood. The adsorption of these could subsequently affect the platelets which normally carry a net negative charge density and affect the coagulation factors. In other words, fundamental changes may occur in the native collagen molecule when it changes from the milieu that prevails underneath the normal endothelium to the one that becomes operative when collagen is exposed to blood constituents as the result of injuries to the endothelial lining of the blood vessel. These changes are by themselves apparently insufficient to cause denaturation of collagen, but sufficient to initiate the complex biochemical events that lead to platelet adhesion and aggregation. Similar considerations may affect the other subendothelial components in addition to collagen. The question may be raised in what way does electrical conduction influence the nature of the adsorption process of blood constituents and the activation of the blood clotting factors and platelets, leading to thrombosis?

#### ELECTRICAL CONDUCTION IN HYDROPHOBIC SYNTHETIC POLYMERS

It should be pointed out that blood compatibility cannot be related alone to the presence of 'bonded', 'structured', or 'free' water. For example, low-temperature isotropic carbons (so-called *LTI* carbons) have excellent blood compatibility<sup>36</sup>. Also, certain perfluorinated cellulose acetate derivatives have shown very promising *in vivo* non-thrombogenic behaviour<sup>50</sup>. Among synthetic hydrophobic polymers, Bruck<sup>20,36</sup> has recently suggested a possible relationship between intrinsic semiconduction, electronic conduction and blood compatibility.

In general, there are three approaches to the preparation of electroconducting and semiconducting polymers: direct synthesis, modification by complexing and chelation, and pyrolytic conversion of suitable polymers having particular types of chemical structures. In this latter area, Bruck has previously reported the thermal conversion of a specially purified aromatic polyimide, poly [*N,N'*-(*p, p'*-oxydiphenylene)pyromellitimide], into semiconducting and conducting condensation products at temperatures well below the graphitization conditions<sup>16,21</sup>. The thermal conversion process between 500° and 800°C is accompanied by the development of an electron paramagnetic absorption (e.p.r.) spectrum caused by free radicals. The calculated free spin concentration is in excess of 10<sup>19</sup>/g and the relative e.p.r. absorption curves show characteristic maxima as functions of time and temperature of pyrolysis. Initially, there is a decrease in the density owing to the cleavage of the carbonyl bonds and the loss of carbon monoxide and lesser

**Table 4** Physical and *in vitro* biological properties of insulating, semiconducting and electroconducting polypyromellitimides (PPMI) (compiled from refs 16 and 20)

Sample	Specific electro-conductivity at 25°C (ohm <sup>-1</sup> cm <sup>-1</sup> )	No. of spins (g <sup>-1</sup> )	Lee-White coagulation index*	PTT index*	Platelet aggregation and activation
Unmodified PPMI	<10 <sup>-12</sup>	—	0.3	0.5	Heavy and activated
Pyrolytic PPMI	0.1	>10 <sup>19</sup>	2.1	1.3	Very light to none, not activated
Pyrolytic PPMI	11.1	>10 <sup>19</sup>	2.6	1.3	Very light to none, not activated
Pyrolytic PPMI	20.0	>10 <sup>19</sup>	2.5	1.4	Very light to none, not activated

\* Expressed as ratio of clotting times for test specimens and those of siliconized glass (average of three)

quantities of other materials. As the pyrolysis progresses, there is an increase in the density of polymer owing to a polycondensation reaction that gives rise to a condensed polynuclear aromatic and heterocyclic system. This system permits an enhanced  $\pi$ -orbital overlap, and a consequent increase in the mobility of electrons.

It seemed of interest to carry out some *in vitro* biological testing procedures with both control (non-pyrolysed) and pyrolysed samples. These tests consisted of the Lee-White blood coagulation times, partial thromboplastin times (PTT), and platelet activation and aggregation with human platelet-rich plasma<sup>51</sup>. The Lee-White blood coagulation times and PTT were compared with those of siliconized glass<sup>52</sup>. The data summarized in *Table 4* indicate that the semiconducting and conducting pyrolytic polymers have clotting times two to three times longer than those of siliconized glass, whereas the non-conducting (control) sample has a clotting time of approximately one-third that of siliconized glass. Similarly, the electroconducting and semiconducting pyropolymers show very low or no platelet aggregation with no evidence of activation in contrast to the control sample. It seems possible that the electroconducting and semiconducting propensities of these pyropolymers may influence the adsorption and conformation of plasma proteins. This possibility remains to be confirmed experimentally. Although the above observations are preliminary and should not be generalized, they may have importance to the general area of the interactions of blood components with both natural and synthetic surfaces, possibly to the better understanding of the molecular properties of the vascular endothelium, and may also have implications to the pathogenesis of arteriosclerosis.

#### CONCLUDING REMARKS

Electroconduction in natural products such as melanins has recently been suggested by McGinness *et al.*<sup>53</sup> to be related to diseases such as Parkinsonism and schizophrenia. Melanins are polymeric pigments occurring in the skin, hair, retina of the eye, midbrain, and inner ear. They have condensed, unsaturated ring structures, and are formed by the polymerization of oxidation products of tyrosine and dopa (3,4-dihydroxyphenylalanine). McGinness and colleagues have shown that melanins exhibit threshold switching, which until now has been restricted to amorphous inorganic semiconductors. Typically, at the critical threshold voltage, switching occurs that is manifested by 'on' and 'off' states in the current vs. voltage plots. Such electrical switching was also observed with equine cytochrome *c*, but not with bovine serum albumin, myoglobin,

and oxidized cholesterol. The electroconductivity of melanins is in the order of 10<sup>-5</sup> ohm<sup>-1</sup> cm<sup>-1</sup> that increases greatly in the 'on' state<sup>53</sup>. Water absorbed by these pigments is necessary for electrical switching to occur, since dried samples lose this property, apparently due to the alteration in the dielectric constant of the system<sup>53</sup>. However, as it was mentioned in the section on hydrated proteins, ionization potentials could be involved instead in line with the findings of other investigators with deuterated and non-deuterated proteins<sup>26</sup>.

The phenomena of electrical conduction and semiconduction in macromolecules are thus apparently of great significance in a variety of biomedical problems ranging from the pathogenesis of disease to the design of synthetic macromolecules with specific biological effectiveness. The systematic study of selected naturally occurring electroconducting macromolecules offers a rewarding approach towards the better understanding of these problems.

#### ACKNOWLEDGEMENT

The authors thanks his wife, Mrs A. Katherine Bruck, for typing the manuscript.

#### REFERENCES

- 1 Szent-Györgyi, A. *Nature* 1946, **157**, 875
- 2 Szent-Györgyi, A. 'Bioenergetics', Academic Press, New York, 1957
- 3 Evans, M. G. and Gergely, J. *Biochim. Biophys. Acta* 1949, **3**, 188
- 4 Eley, D. D., Parfitt, G. D., Perry, M. J. and Taysum, D. H. *Trans. Faraday Soc.* 1953, **49**, 79
- 5 Cardew, M. H. and Eley, D. D. *Discuss. Faraday Soc.* 1959, **27**, 115
- 6 Rosenberg, B. *J. Chem. Phys.* 1962, **36**, 816
- 7 Postow, E. and Rosenberg, B. *Bioenergetics* 1970, **1**, 467
- 8 Eley, D. D. and Spivey, D. I. *Trans. Faraday Soc.* 1960, **56**, 1432
- 9 Bardelmeyer, G. H. *Biopolymers* 1973, **12**, 2289
- 10 Bardelmeyer, G. H. *Biopolymers* 1973, **12**, 2303
- 11 Winslow, F. H., Baker, W. O. and Yager, W. A. *J. Am. Chem. Soc.* 1955, **77**, 4751
- 12 Winslow, F. H., Baker, W. O., Pape, N. R. and Matreyek, W. *J. Polym. Sci.* 1955, **16**, 101
- 13 Topchiev, A. V. *J. Polym. Sci. (A)* 1963, **1**, 591
- 14 Marvel, C. S. and Rassweiler, J. H. *J. Am. Chem. Soc.* 1958, **80**, 1197
- 15 Mainthia, S. B., Kronick, P. L., Ur, H., Chapman, E. F. and Labes, M. M. *Abstr. ACS 144th Nat. Meet., Los Angeles* 1963, p 11Q
- 16 Bruck, S. D. *Polymer* 1965, **6**, 319
- 17 Keppler, R. G. *Abstr. ACS 144th Nat. Meet., Los Angeles* 1963, p 10Q

- 18 Szent-Györgyi, A. *Nature* 1941, **148**, 157  
19 Gergely, J. in 'Electronic Aspects of Biochemistry', (Ed. B. Pullman), Academic Press, New York, 1964, pp 335-345  
20 Bruck, S. D. *Nature* 1973, **243**, 416  
21 Bruck, S. D. *J. Polym. Sci. (C)* 1967, **17**, 169  
22 Johnson, V. A. and Lark-Horovitz, K. *Phys. Rev.* 1953, **92**, 226  
23 Brophy, J. J. 'Semiconductor Devices', McGraw-Hill, New York, 1964, pp 50-55  
24 Frietsche, H. 'Methods of Experimental Physics', Academic Press, New York, 1959, Vol 6, Part B, Ch 8  
25 Eley, D. D. and Spivey, D. *Trans. Faraday Soc.* 1961, **57**, 2280  
26 Eley, D. D. and Leslie, R. B. in 'Electronic Aspects of Biochemistry', (Ed. B. Pullman), Academic Press, New York, 1964, p 105  
27 Bardelmeyer, G. H. *Biopolymers* 1973, **12**, 2289  
28 Berendsen, H. J. C. *J. Chem. Phys.* 1962, **36**, 3297  
29 Berendsen, H. J. C. and Migchelsen, C. *Fed. Proc. Fed. Am. Soc. Exp. Biol.* 1966, **25**, 998  
30 Dehl, R. E. and Hoeve, C. A. J. *J. Chem. Phys.* 1969, **50**, 3245  
31 Dehl, R. E. *Science* 1970, **170**, 738  
32 Dehl, R. E. *Biopolymers* 1973, **12**, 2329  
33 Fung, B. M. and Siegel, M. M. *Biochim. Biophys. Acta* 1972, **278**, 185  
34 Bruck, S. D. *Trans. Am. Soc. Artif. Int. Organs* 1972, **18**, 1  
35 Bruck, S. D. *J. Biomed. Mat. Res.* 1973, **7**, 387  
36 Bruck, S. D. 'Blood Compatible Synthetic Polymers—An Introduction', C. C. Thomas, Springfield, Ill, 1974  
37 Andrade, J. D., Lee, H. B., Jhon, M. S., Kim, S. W. and Hibbs, Jr J. B. *Trans. Am. Soc. Artif. Int. Organs* 1973, **19**, 1  
38 Jhon, M. S. and Andrade, J. D. *J. Biomed. Mat. Res.* 1973, **7**, 509  
39 Ganguly, P. *Nature* 1974, **247**, 306  
40 Nossel, H. L., Wilner, G. D. and LeRoy, E. C. *Nature* 1969, **221**, 75  
41 Gassman, W. and Schleich, H. *Biochem. Z.* 1935, **277**, 320  
42 Butler, W. T. and Cunningham, L. W. *J. Biol. Chem.* 1966, **241**, 3882  
43 Bosmann, H. B. *Biochem. Biophys. Res. Commun.* 1971, **43**, 1118  
44 Barber, A. J. and Jamieson, G. A. *Biochim. Biophys. Acta* 1971, **252**, 533  
45 Dickerson, R. E. and Geis, I. 'The Structure and Action of Proteins', Harper & Row, New York, 1969  
46 Rich, A. and Crick, F. H. C. *J. Mol. Biol.* 1961, **3**, 483  
47 Ramachandran, G. N. in 'Treatise on Collagen', (Ed. G. N. Ramachandran), Academic Press, New York, 1967, Vol 1, Ch 3  
48 Ramachandran, G. N. and Chandrasekharan, R. *Biopolymers* 1968, **6**, 1649  
49 Chang, E. P. and Chien, J. C. W. *Biopolymers* 1973, **12**, 1063  
50 Rozelle, L. T. and Petersen, R. J. 'Ultrathin Membranes for Blood Oxygenators', North Star Res. and Develop. Inst., Minneapolis, Minn., January 1974 (Public document available from the National Technical Information Service, 5285 Port Royal Road, Springfield, Virginia 22151)  
51 Packham, M. A., Warrior, E. S., Glynn, M. F., Senyi, A. S. and Mustard, J. F. *J. Exp. Med.* 1967, **126**, 171  
52 Frankel, S., Reitman, S. and Sonnenwirth, A. C. (Eds.), 'Gradwohl's Clinical Laboratory Methods and Diagnosis', Mosby, Saint Louis, 1970, Vol 1  
53 McGinness, J., et al. *Science* 1974, **183**, 853

# Absolute reactivity in the cationic polymerization of methyl and other alkyl vinyl ethers

A. Ledwith and E. Lockett

Department of Inorganic, Physical and Industrial Chemistry, University of Liverpool, PO Box 147, Liverpool L69 3BX, UK

and D. C. Sherrington

Department of Pure and Applied Chemistry, University of Strathclyde, Glasgow G1 1XL, UK  
(Received 26 March 1974)

The cationic polymerizations of methyl-, 2-chloroethyl-, ethyl-, cyclohexyl- and t-butyl- vinyl ethers initiated by cycloheptatrienyl hexachloroantimonate in methylene chloride solutions have been studied in detail. Reaction rates were measured by an adiabatic calorimetric technique and rate constants for propagation of each of the monomers,  $k_p$  (obs), were determined by appropriate kinetic analysis of the experimental curves. The results obtained are discussed in terms of current theories regarding ion pair/free ion equilibria in non-aqueous solvents. Although ethyl-, cyclohexyl- and t-butyl- vinyl ethers behave very similarly to isobutyl vinyl ether, and their reactivities are comparable [ $k_p$  (obs)  $\sim 3 \times 10^3 \text{ M}^{-1} \text{ sec}^{-1}$  at  $0^\circ\text{C}$ ] both methyl- and 2-chloroethyl- vinyl ethers show markedly different characteristics to the others, and in particular exhibit a reactivity approximately one order of magnitude less [ $k_p$  (obs)  $\sim 2 \times 10^2 \text{ M}^{-1} \text{ sec}^{-1}$  at  $0^\circ\text{C}$ ]. These variations in reactivity are discussed in terms of preferred monomer conformations, and the resulting differences in activation energy which are likely to arise when such conformers are approached by an electrophile.

## INTRODUCTION

The detailed results from a kinetic study of the cationic polymerization of isobutyl vinyl ether (IBVE), initiated by preformed stable carbonium ion salts, have been reported previously<sup>1</sup>. This present work represents an extension of that study to include a series of alkyl vinyl ether monomers, namely methyl- (MEVE), ethyl- (ETVE), cyclohexyl- (CHVE), t-butyl- (TBVE) and 2-chloroethyl- (CEVE) vinyl ethers. Together with IBVE this group of compounds has aroused considerable interest over the past few years because of the possibility of correlating reactivity with structure. Alkyl vinyl ethers are particularly susceptible to attack from electrophilic reagents, and a number of chemical reactions involving such species have been investigated<sup>2-13</sup> in order to establish some sort of reactivity sequence. In addition various n.m.r. analyses<sup>14-18</sup> have been undertaken to see if such a sequence is compatible with any electronic or structural trends arising within the group.

The aim of the present investigation was to elucidate the absolute reactivity of each of these monomers with respect to polymerization, and in particular to evaluate where possible the rate constants for propagation by free cationic intermediates. It was anticipated that such data might provide an unambiguous comparison of the reactivities of the monomers, since the propagation reaction is a simple bimolecular one, and dissociated free cations should reflect solely on their precursor monomers, and not on any other species in the system (e.g. counter-ions).

Polymerizations were carried out homogeneously in methylene chloride solutions under high vacuum conditions. Initiation was achieved by using preformed cycloheptatrienyl hexachloroantimonate ( $\text{C}_7\text{H}_7^+\text{SbCl}_6^-$ ) as a catalyst, and where possible initiator concentrations were chosen such

that the salt was present predominantly in the form of free ions. Reaction rates were measured by an adiabatic calorimetric method similar to that already reported<sup>1,19</sup>. The technique is most accurate for reactions with half lives  $\sim$  seconds, and in order to effect such rapid polymerization of some of the monomers, notably MEVE, ETVE and CEVE, catalyst concentrations were used such that appreciable proportions of propagating ion pair species may have been present. This possibility and its likely effect on the data is discussed later.

## EXPERIMENTAL

### Materials

Cycloheptatrienyl hexachloroantimonate was prepared and purified as previously reported<sup>1</sup>. Methylene chloride<sup>1</sup>, acetonitrile<sup>19</sup>, ETVE, IBVE, CHVE and TBVE were dried and purified also as already described<sup>5</sup>. CEVE (Koch Light) was washed several times with alkaline water and dried overnight with potassium hydroxide. It was distilled first from fresh potassium hydroxide and then from freshly extruded sodium wire. Finally it was stored *in vacuo* over calcium hydride. MEVE (BDH Ltd) gas was condensed *in vacuo* onto freshly crushed calcium hydride at  $0^\circ\text{C}$ , before a known volume was metered into the reaction calorimeter. A mercury monomer was used to ensure that the vapour pressure of the monomer was constant when volume readings (at  $-62^\circ\text{C}$ ) were taken. The density of MEVE was determined at the same temperature (0.856 at  $-62^\circ\text{C}$ ) and the value agreed with that extrapolated from data reported by Schildknecht<sup>20</sup>.

It was also found necessary to determine the densities of ETVE (0.784 at  $0^\circ\text{C}$ ) and CHVE (0.912 at  $20^\circ\text{C}$ ), since adequate data were not available in the literature.

*Adiabatic calorimeter*

The adiabatic calorimeter differed in three main features from those used earlier<sup>1,19</sup>. A conventional magnetic stirrer and follower replaced the previous mechanical stirring arrangement, a thermistor (Stantel U23US) was used in place of the platinum resistance thermometer, and the two calorimeter sections were united by a large cone and socket joint, rather than ground glass flanges.

The thermistor consisted of an unmounted semi-conducting device, and had a time constant in solution of  $\sim 10^{-3}$  sec. It was held in the calorimeter within a perforated glass envelope. This provided physical protection, yet allowed the reaction mixture to circulate efficiently around the temperature probe. The thermistor formed one arm of a resistance bridge, and a Sefram Gravispot recorder (type GRVAC) measured the small off balance potentials, arising from changes in resistance (i.e. temperature) of the thermistor. Unlike the resistance thermometer used previously, the thermistor was found to have a highly non-linear (exponential) temperature coefficient over the range say  $-20^{\circ}\text{C}$  to  $+20^{\circ}\text{C}$ , though for the temperature rise associated with the polymerization reactions studied ( $\sim 0.5^{\circ}\text{C}$ ), it did approximate to a constant (for a particular reaction temperature). Calibration was achieved by using a Beckmann thermometer at the temperature required. The thermometer and temperature probe were immersed in a stirred methanol bath, and temperature changes were related to resistance changes of the thermistor. Freezing water was used to calibrate the Beckmann thermometer.

The heat capacity,  $H$ , of the reaction vessel and contents was determined by polymerizing IBVE under the same conditions as kinetic runs involving the other monomers. The heat of polymerization of OBVE is known<sup>1</sup>, and hence from the rise in temperature on polymerization,  $H$  was calculated.

*Kinetic technique*

Initiator phials were prepared and placed in the calorimeter as before<sup>1,19</sup>. The catalyst solvent was methylene chloride or a methylene chloride/acetonitrile mixture (96 : 4% v/v). The latter was required for complete dissolution of initiator salt at some of the higher concentrations

Table 1 Calorimeter calibration data

Temperature ( $^{\circ}\text{C}$ )	0.0	11.8
Thermistor resistance, $R_T$ ( $\Omega$ )	5120	3325
Thermistor temperature coefficient, $\theta$ ( $\Omega/\text{deg}$ )	-205.4	-122.5
Heat capacity, $H$ (J/deg)	252.4	269.5

Table 2 Polymerization of ETVE by  $\text{C}_7\text{H}_7^+\text{SbCl}_6^-$  in  $\text{CH}_2\text{Cl}_2$ 

Temperature ( $^{\circ}\text{C}$ )	$[\text{C}_7\text{H}_7^+\text{SbCl}_6^-]_0 \times 10^4$ (M)	$[\text{ETVE}]_0 \times 10^2$ (M)	$k_p(\text{obs}) \times 10^{-3}$ ( $\text{M}^{-1} \text{sec}^{-1}$ )	$-\Delta H$ (polymn) (kJ/mol)	$M_n$
0	0.483	6.52	2.6	70.6	1510
0	3.78	6.47	1.3	81.9	2460
0	5.27	5.97	1.8	78.6	1790
0	6.46	5.33	1.1	74.4	1750
0	6.70	5.88	0.64	84.4	1790
0	average		1.5	78.2	
11.8	5.08	6.20	2.2	89.5	2140
11.8	2.28	6.50	2.6	77.3	1800
11.8	1.33	6.75	3.0	77.3	1550
11.8	0.483	6.52	4.6	74.8	1530
11.8	0.242	13.0	4.6	60.6	1530
	average		3.4	76.1	

of catalyst. Since only  $\sim 1$  ml of this solution was added to 99 ml of methylene chloride in the calorimeter, the effective concentration of acetonitrile in a polymerization reaction never exceeded  $\sim 0.04\%$ . The calorimeter and contents were equilibrated at the required temperature by surrounding the vessel either with a bath of ice/water at  $0^{\circ}\text{C}$ , or freezing dioxane at  $+11.8^{\circ}\text{C}$ . Polymerizations were carried out essentially as before<sup>1,19</sup>, and after quenching the reaction mixture with methanol, the product was transferred quantitatively to a 250 ml flask. Most of the solvent was removed on a water pump, and the concentrated solution was filtered and transferred to a pre-weighed flask. Removal of the last traces of solvent in a vacuum oven overnight allowed the polymer yield to be determined. Molecular weights were calculated from vapour pressure measurements using a Mechrolab osmometer (model 301A).

## RESULTS

*Calibration of the calorimeter*

Kinetic runs were carried out at  $0^{\circ}\text{C}$  and  $+11.8^{\circ}\text{C}$ , and the resistance of the thermistor,  $R_T$ , and its temperature coefficient,  $\theta$ , at each of these temperatures is shown in Table 1. The corresponding mean values of the calorimeter heat capacity,  $H$ , are also shown.

*Kinetic data on ETVE, CHVE and TBVE monomers*

ETVE, CHVE and TBVE produced S-shaped recorder traces similar to those from IBVE polymerizations<sup>1</sup>. Without exception the curves were characterized by a relatively slow build up to a maximum gradient at  $\sim 15\%$  conversion, followed by a steady decay to a horizontal straight line on completion of polymerization. All solutions became coloured after polymerization had ended, with each monomer displaying its own particular succession of colours. The most common sequence observed was a decay from blue, through green, to brown. Similar changes were reported in the case of IBVE, and some speculation concerning the chromophores responsible has been forwarded<sup>1</sup>. Certainly the effect is largely a post-polymerization one and does not constitute a termination reaction. Indeed polymer yields were always  $>80\%$  showing termination to be almost totally absent during kinetic lifetimes. The chart recordings were analysed, therefore, by a mathematical treatment described in detail elsewhere (see Appendix to ref 1), and based on a simple two-stage mechanism involving only initiation and propagation reactions. Such analysis produced the data for rate coefficients for propagation,  $k_p$  (obs), summarized in Tables 2-4.

Table 3 Polymerization of CHVE by  $C_7H_7^+SbCl_6^-$  in  $CH_2Cl_2$ 

Temperature (°C)	$[C_7H_7^+SbCl_6^-]_0 \times 10^5$ (M)	$[CHVE]_0 \times 10^2$ (M)	$k_p(\text{obs}) \times 10^{-3}$ ( $M^{-1} \text{sec}^{-1}$ )	$-\Delta H$ (polymn) (kJ/mol)	$M_n$
0	1.30	4.60	3.1	69.0	1350
0	4.85	4.56	2.5	70.2	760
0	5.02	9.13	3.7	69.8	1150
0	7.22	4.62	2.9	76.5	1110
0	10.0	4.64	4.3	75.2	970
0	average		3.3	72.3	
11.8	1.52	4.62	5.7	61.0	1370
11.8	2.51	4.59	6.4	64.0	850
11.8	5.02	4.59	8.2	76.9	910
11.8	5.02	9.19	6.5	73.6	1290
11.8	10.0	4.51	6.5	73.9	790
11.8	5.02	2.38	6.7	92.0	1210
11.8	average		6.7	73.6	

Table 4 Polymerization of TBVE by  $C_7H_7^+SbCl_6^-$  in  $CH_2Cl_2$ 

Temperature (°C)	$[C_7H_7^+SbCl_6^-]_0 \times 10^5$ (M)	$[TBVE]_0 \times 10^2$ (M)	$k_p(\text{obs}) \times 10^{-3}$ ( $M^{-1} \text{sec}^{-1}$ )	$-\Delta H$ (polymn) (kJ/mol)	$M_n$
0	2.01	5.60	3.4	—	1970
0	5.08	5.46	2.9	86.1	2210
0	10.16	6.43	4.1	88.2	3070
0	average		3.5	87.2	—
11.8	5.08	5.64	3.5	82.3	1570
11.8	10.16	5.79	3.9	101	1460
11.8	2.51	5.64	4.0	88.9	1680
11.8	average		3.8	90.3	—

#### Kinetic data on MEVE monomer

The recorder traces from the kinetic runs using MEVE proved to differ markedly from all the others. First, the overall reaction was more sluggish than those involving the previous three monomers, and some of the higher catalyst concentrations required the use of traces of acetonitrile to maintain solubility, as already described. Secondly, the traces were found to rise sharply as soon as the initiator phial was broken, thus making the rate of polymerization a maximum at zero conversion; similar to the situation found in the polymerization of *N*-vinylcarbazole<sup>19</sup>. Again polymer yields were always >80%, and this apparent absence of termination together with the facile rapid initiation process (compared to subsequent propagation), permitted direct evaluation of the rates of polymerization,  $R_p$ , from the initial slopes of recorder traces. Observed propagation rate coefficients,  $k_p$  (obs), were then obtained from the expression,  $R_p = k_p$  (obs)  $[C_7H_7^+SbCl_6^-]_0 [MEVE]_0$ . The results of these calculations are summarized in Tables 5 and 6.

#### Kinetic data on CEVE monomer

The kinetic traces obtained from the polymerization of this monomer were similar in shape to those of ETVE, CHVE and TBVE. However, polymer yields rarely exceeded ~50% indicating significant termination during kinetic lifetimes. Moreover, unlike any other vinyl ether polymerizations the decaying colour sequences were not visible immediately after polymerization was complete. In order to establish some approximate estimate for the rate constant for propagation it was assumed that initially termination was minimal and the curves were analysed in a manner similar to that used for MEVE. It is recognized, however, that even larger error bars must be associated with these data than for any of the other evaluations. A summary of the figures obtained is shown in Table 7.

Table 5 Polymerization of MEVE by  $C_7H_7^+SbCl_6^-$  in  $CH_2Cl_2$  at 0°C

$[C_7H_7^+SbCl_6^-]_0 \times 10^4$ (M)	$[MEVE]_0 \times 10^2$ (M)	$k_p(\text{obs}) \times 10^{-2}$ ( $M^{-1} \text{sec}^{-1}$ )	$-\Delta H$ (polymn) (kJ/mol)	$M_n$
6.75	13.5	1.3	96.6	1515
6.36	13.8	1.5	79.0	1475
5.38	13.7	1.2	96.6	1530
4.80	13.7	1.3	95.7	1500
4.35	13.6	1.0	75.7	1620
4.24	13.6	1.4	95.7	1590
3.58	13.6	1.7	95.7	1540
2.41	13.8	2.0	76.9	1910
1.74	13.8	2.2	68.1	1690
5.56	7.2	0.87	84.0	1420
5.30	8.8	1.2	95.0	1755
5.38	12.6	1.4	101	1440
5.66	13.3	1.3	95.3	1550
5.10	15.7	1.3	97.4	1500
—	average	1.4	89.5	—

Table 6 Polymerization of MEVE by  $C_7H_7^+SbCl_6^-$  in  $CH_2Cl_2$  at 11.8°C

$[C_7H_7^+SbCl_6^-]_0 \times 10^4$ (M)	$[MEVE]_0 \times 10^2$ (M)	$k_p(\text{obs}) \times 10^{-2}$ ( $M^{-1} \text{sec}^{-1}$ )	$-\Delta H$ (polymn) (kJ/mol)	$M_n$
5.79	13.7	3.8	87.0	1420
5.37	13.7	3.0	73.2	1395
5.35	13.7	4.5	72.3	1480
4.83	13.8	3.7	89.5	1360
1.31	13.8	5.5	69.8	1735
5.21	15.1	5.1	80.7	1245
3.91	14.8	3.3	85.7	1620
2.89	13.5	3.0	64.0	1425
2.62	9.9	4.0	68.5	1455
—	average	4.0	76.9	—



Table 7 Polymerization of CEVE using  $C_7H_7^+SbCl_6^-$  in  $CH_2Cl_2$ 

Temperature (°C)	$[C_7H_7^+SbCl_6^-]_0 \times 10^4$ (M)	$[CEVE]_0 \times 10^2$ (M)	$k_p(\text{obs}) \times 10^{-2}$ ( $M^{-1}\text{sec}^{-1}$ )	$-\Delta H$ (polymn) (kJ/mol)	$M_n$
0	0.755	10.3	2.75	72.7	2120
0	1.37	13.0	3.41	75.2	2120
0	1.44	9.90	2.04	79.8	2240
0	1.46	7.59	1.90	84.4	680
0	2.84	8.85	1.20	85.7	1570
0	5.35	8.58	0.84	85.3	1730
0	—	average	2.0	80.5	—
11.8	0.987	17.5	3.72	71.5	2480
11.8	1.71	17.4	4.82	55.2	1280
11.8	2.82	9.90	1.98	64.8	820
11.8	3.41	17.3	3.14	57.7	2160
11.8	4.55	9.86	2.01	58.5	990
11.8	—	average	3.1	61.5	—

 Table 8 Kinetic and thermodynamic data for the polymerization of alkyl vinyl ethers in  $CH_2Cl_2$ 

Vinyl ether	0°C		+11.8°C		Activation enthalpy (kJ/mol)
	$-\Delta H$ (polymn) (kJ/mol)	$k_p(\text{obs}) \times 10^{-3}$ ( $M^{-1}\text{sec}^{-1}$ )	$-\Delta H$ (polymn) (kJ/mol)	$k_p(\text{obs}) \times 10^{-3}$ ( $M^{-1}\text{sec}^{-1}$ )	
CEVE	80.5	0.20	61.5	0.31	29
MEVE	89.5	0.14	76.9	0.40	59
ETVE	78.2	1.5	76.1	3.4	42
CHVE	72.3	3.3	73.6	6.7	38
TBVE	87.2	3.5	90.3	3.8	~4
IBVE <sup>1</sup>	92.0	6.8	—	—	25

## DISCUSSION

### Polymerization mechanism

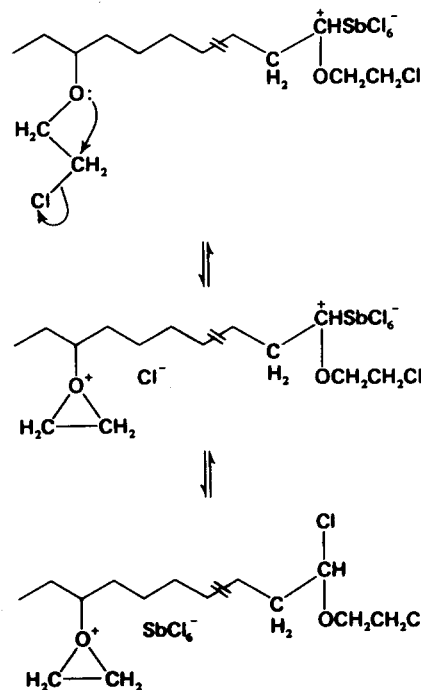
The homogeneous polymerizations of ETVE, CHVE and TBVE initiated by cycloheptatrienyl hexachloroantimonate in methylene chloride parallel exactly those of IBVE<sup>1</sup>. They are characterized by a relatively slow initiation process, followed by a rapid propagation reaction. Termination appears to be insignificant during kinetic lifetimes, as indicated by plots of  $\log_{10}[M]_t$  versus  $t$ , where  $[M]_t$  is the concentration of monomer at time  $t$  (see ref 1). These attain a maximum negative gradient corresponding to the situation where all initiating cations are converted to propagating polymeric species. Since beyond this point, the gradient falls only slowly, the total concentration of active centres in each of the systems,  $[P_n^+]_t$ , thereafter remains constant, to a reasonable approximation, i.e.

$$\frac{-d \ln[M]_t}{dt} = k_p(\text{obs})[P_n^+]_t$$

The molecular weights of polymers are low, a typical average degree of polymerization being ~25, and there seems no reason to indicate that the major chain limiting reaction is anything other than a simple proton transfer to monomer.

In the case of CEVE recorder traces are superficially similar to the others; however, polymer yields are always low and a significant termination reaction must be present. This most likely involves the readily ionizable chlorine atom in the alkoxy substituent. In the polymer the electron lone pairs of the oxygen are no longer conjugated as in the unsaturated monomer, and are therefore much more basic. As a result these may participate in a neighbouring group type reaction to produce chloride ion. The latter

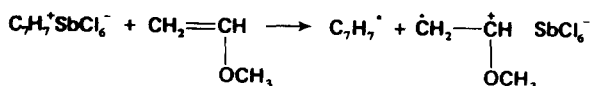
is highly nucleophilic and will readily terminate electrophilic active centres, i.e.



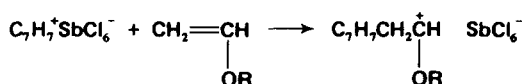
The oxonium ion so formed is likely to be inactive in the kinetic lifetimes of these vinyl polymerizations. Clearly this termination process must compete with transfer mechanisms as the main chain limiting reaction in this case.

The traces from MEVE polymerizations differ most from the remainder, and indicate a fast initiation reaction. In fact as far as the kinetics are concerned initiation can be considered as instantaneous when compared with the subsequent propagation reaction. It would seem that such a

difference could only arise as a result of a different mechanism of initiation, and this argument is reinforced by the data for  $k_p(\text{obs})$  for the various monomers where that for MEVE has the lowest value (see later). In the case of MEVE it might be, for example, that initiation takes place via a fast electron transfer, followed by radical combination processes, i.e.



whereas for the other monomers it seems more likely that a simple addition reaction takes place<sup>1,21,22</sup>:



The higher reactivity of MEVE (over e.g. IBVE) towards the planar initiating cation could be ascribed to the uniquely planar *cis*-conformation (see later discussion) of MEVE, facilitating reaction (whether by primary electron transfer or by direct addition) following ready formation of a charge transfer complex.

#### Significance of kinetic data

A summary of the rate coefficients for propagation and enthalpies of polymerization for the various monomers is shown in Table 8. For completion the corresponding information for IBVE from ref 1 is included, and estimated activation enthalpies are also listed.

The initial concentrations of catalyst used in the polymerization of CHVE and TBVE were such that the salts could be assumed to be fully dissociated to a first approximation. The arguments in support of the assumption that the propagating species will be at least as dissociated as the initiating species at these low concentrations have already been expounded in detail<sup>1</sup>, and since the experimental conditions were almost identical for these two monomers, the discussion will not be repeated here. The observed propagation coefficients can therefore be taken directly as reasonable estimates of the rate constants for the propagation of the free cations derived from these two monomers in methylene chloride solution, i.e.  $k_p^+$ .

In the case of MEVE, and to some extent ETVE, the values of initiator concentrations were of the same order as values of the ion pair dissociation constant,  $K_d$ , for cycloheptatrienyl hexachloroantimonate in methylene chloride<sup>23</sup>. Although the corresponding growing polymeric salts are likely to be more dissociated than the initiator salt at these concentrations, nevertheless, the possibility of some ion pair contribution to propagation cannot be entirely discounted. For these two monomers the observed propagation coefficients,  $k_p(\text{obs})$ , may in fact represent composite data for the rate constant for free ionic propagation ( $k_p^+$ ), and that for propagation by some type (or types) of ion pair species ( $k_p^\ddagger$ ). The simple relationship,  $k_p(\text{obs}) = k_p^+ + \alpha k_p^\ddagger$ , may be assumed to hold, where  $\alpha$  = degree of dissociation of the propagating salt. In anionic systems it has now been clearly demonstrated<sup>24</sup> that polymeric ion pairs propagate several orders of magnitude more slowly than the corresponding free carbanions ( $k_p^-/k_p^\ddagger \sim 10^2-10^3$ ). There seems every reason to suppose that a similar differential exists in cationic systems (i.e.  $k_p^+/k_p^\ddagger \sim 10^2-10^3$ ), though unequivocal experimental evidence confirming this is still lacking. Thus providing free propagating carbonium ions

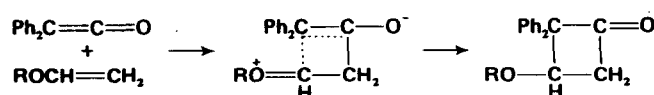
are dominant in these polymerizations (i.e.  $\alpha k_p^\ddagger \gg k_p^+$  or  $\alpha > 10^{-2}-10^{-3}$ ) then the ion pair contribution can be ignored. Under these circumstances the expression for  $k_p(\text{obs})$  collapses to  $k_p(\text{obs}) = \alpha k_p^+$ . As far as MEVE and ETVE are concerned, therefore,  $k_p^+$  may exceed the data for  $k_p(\text{obs})$  by a factor  $1/\alpha$ . A minimum value of  $K_d$  for the propagating species in these two polymerizations would be that for the simple cycloheptatrienyl salt in methylene chloride<sup>23</sup> ( $\sim 3.0 \times 10^{-5}$  M at 0°C). This can be shown to yield a minimum value of  $\alpha$  of  $\sim 0.2$  (i.e. 20% dissociation) for the concentrations of active centres used in these polymerizations. This figure lies well within the limit described above. On these grounds the values of  $k_p^+$  for MEVE and ETVE may be, at a maximum, a factor of  $\sim 5$  larger than the data for  $k_p(\text{obs})$ .

A similar argument can be made in the case of CEVE. However, since a much larger uncertainty already exists in these data owing to the approximate nature of the kinetic analysis used, no quantitative estimation will be included here.

Apart from the possible relative variations considered above, all the data as a whole may be affected in a systematic way by the presence of adventitious impurities. As a result, this set of data should be considered as a valuable guide to orders of magnitude, and no doubt with more refined experimental techniques, more accurate absolute data will eventually emerge. For the time being, however, these values seem to agree well with predictions from the sparse literature which already exists concerning free cationic rate constants in vinyl polymerizations, and indeed represents a very significant addition to the list of numerical data currently available<sup>1,19,25-32</sup>.

#### Relative reactivities of alkyl vinyl ethers

Inspection of the data of Table 8 shows that whilst there may be little significance in the apparent differences between  $k_p(\text{obs})$  (and hence  $k_p^+$ ) for some of the vinyl ethers, there is a significant difference (approximately one order of magnitude) between the data for MEVE and CEVE on the one hand, and the remaining vinyl ethers on the other hand. This result is clear even taking into account the discussion in the previous section. The comparative lack of reactivity of MEVE and CEVE is also reflected in reactions with other electrophiles notably hydronium ion<sup>4,5</sup> and dichlorocarbene<sup>6</sup>, and indeed has been reported before in cationic homopolymerization<sup>9</sup>. Generally reactivity appears to parallel the increased energies required for electronic<sup>11</sup>, charge transfer<sup>11</sup> and photoelectron<sup>35</sup> spectroscopic transitions. More recently the relative rate differences for alkyl vinyl ethers have been highlighted in a detailed study<sup>12</sup> of their 2 + 2 cycloaddition reactions with diphenyl ketene. Although this reaction proceeds with a mechanism exhibiting many features of concerted cycloadditions<sup>34</sup>, the transition state involved has undoubtedly dipolar character<sup>35</sup>, as shown below, and hence the structural and electronic factors affecting reactivity will be similar to those observed for reactions with electrophiles.



In this study a marked increase in reactivity occurs on going from CEVE to TBVE as shown in Table 9.

Considering all the available information it appears that

Table 9 Relative reactivities of alkyl vinyl ethers with diphenylketene in 1,2-dichloroethane at 25°C

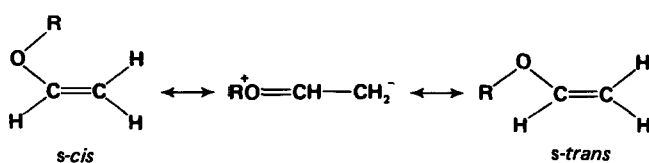
Vinyl ether <sup>a</sup>	Relative reactivity
CEVE	1.0
ETVE	10
IPVE <sup>b</sup>	74
TBVE	250

<sup>a</sup> Experimental conditions precluded the use of MEVE and hence CEVE is used here as its structural model (see subsequent discussion)

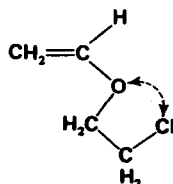
<sup>b</sup> Isopropyl vinyl ether

reactivity towards electrophiles increases in the series: methyl-, 2-chloroethyl- < primary alkyl- < s-alkyl- < t-alkyl- derivatives, with the greatest difference occurring, as in the present study, between methyl and 2-chloroethyl derivatives on the one hand and branched alkyl derivatives on the other.

The greatly enhanced (general) reactivities of alkyl vinyl ethers, compared with simple alkenes, arises from resonance delocalization, viz:



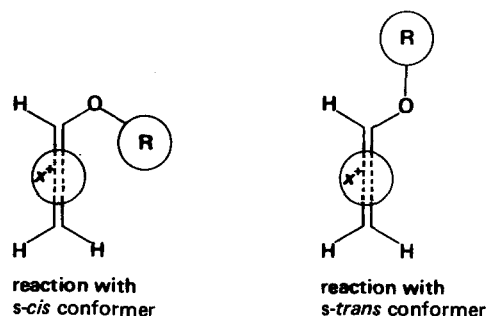
and the contribution of the dipolar canonical structure has the effect of increasing rotational barriers around the R-O-CH= linkage. Resonance in alkyl vinyl ethers contributes to abnormal (for olefins) nuclear magnetic resonance shielding and coupling effects, and since the pioneering study of these monomers by n.m.r. techniques<sup>14</sup>, there have been many subsequent investigations<sup>15-18</sup>. However, possibly the most important study of conformational equilibria in alkyl vinyl ethers is that reported by Owen and Sheppard<sup>36</sup>. These authors established by i.r. techniques that alkyl vinyl ethers exhibit *s-cis/s-trans* conformational equilibria, and that for methyl vinyl ether the planar *s-cis* form is the dominant form at ambient temperatures even in solutions. All the n.m.r. data and more recent i.r. studies<sup>37</sup> are consistent with this view, and the only point at issue is whether alkyl vinyl ethers other than methyl, have stable planar *s-trans* or *gauche* conformations. Certainly, as confirmed by molecular models, branched alkyl vinyl ethers cannot adopt the planar *s-cis* conformation. A major exception is possible in the case of 2-chloroethyl vinyl ether, which like the methyl derivative, may adopt such a planar *s-cis* form because of a significant contribution from a favourable *gauche* interaction between the chlorine and oxygen atoms:



If we now make the generalization that planar *s-cis* conformations are preferred for methyl- and 2-chloroethyl-vinyl ethers, and that progression through other primary and secondary alkyl derivatives to t-butyl vinyl ether involves a gradual change to stable *s-trans* conformations,

it is possible to rationalize the relative reactivities of alkyl vinyl ethers in a rather simple manner.

The transition state for reactions of alkyl vinyl ethers with electrophiles must involve overlap of the  $\pi$ -electrons with a suitable vacant orbital on the electrophile as indicated:



Clearly the planar *s-cis* conformation will offer a greater degree of steric hindrance to the incoming electrophile, than the corresponding *s-trans* (or *gauche*) forms, almost irrespective of the nature of the substituent. It is this steric effect which contributes to ground state strain (i.e. inability to adopt planar *s-cis* conformations) in alkyl vinyl ethers other than methyl- and 2-chloroethyl- derivatives, with a consequent reduction in activation energy for attack by electrophiles, as noted experimentally. In the case of the propagation reaction in polymerization, steric interference in the case of *s-cis* conformers is likely to be exaggerated, since the electrophilic centre is located on the end of an entangled polymer chain. In addition it is tempting to suggest that the apparently zero value for the activation energy in the polymerization of t-butyl vinyl ether arises from a combination of normal Arrhenius behaviour and the ability of the monomer to assume the more hindered *s-cis* conformation at higher temperatures.

#### ACKNOWLEDGEMENTS

We thank the Science Research Council for a scholarship to E.L., and acknowledge the experimental assistance of Mr P. Byrne in the work involving 2-chloroethyl vinyl ether.

#### REFERENCES

- Bawn, C. E. H., Fitzsimmons, C., Ledwith, A., Penfold, J., Sherrington, D. C. and Weightman, J. A. *Polymer* 1971, 12, 119
- Eley, D. D. and Saunders, J. *J. Chem. Soc.*, 1952, p 4167
- Eley, D. D. in 'The Chemistry of Cationic Polymerisation', (Ed. P. H. Plesch), Pergamon, Oxford, 1963, p 375
- Jones, D. M. and Wood, N. F. *J. Chem. Soc.* 1964, p 5400
- Ledwith, A. and Woods, H. *J. Chem. Soc. (B)* 1966, p 753
- Ledwith, A. and Woods, H. *J. Chem. Soc. (B)* 1967, p 973
- Plesch, P. H. *Progr. High Polym.* 1968, 2, 137
- Higashimura, T., Masamoto, J. and Okamura, S. *Kobunshi Kagaku* 1968, 25, 702
- Higashimura, T. in 'Structure and Mechanism in Vinyl Polymerisation', (Ed. T. Tsuruta and K. F. O'Driscoll), Marcel Dekker, New York, 1969, p 313
- Yuki, M., Hatada, K. and Takeshita, M. *J. Polym. Sci. (A-1)* 1969, 7, 667
- Ledwith, A. and Woods, H. *J. Chem. Soc. (B)* 1970, p 310
- Lockett, E. *PhD Thesis* University of Liverpool (1972)
- Tarvin, R. F., Aaki, S. and Stille, J. K. *Macromolecules* 1972, 5, 663
- Feeney, J., Ledwith, A. and Sutcliffe, L. H. *J. Chem. Soc.* 1962, p 2021
- Hatada, K., Takeshita, M. and Yuki, H. *Tetrahedron Lett.* 1968, p 4621

- 16 Higashimura, T., Okamura, S., Morishima, I. and Yonezawa, T. *J. Polym. Sci. (B)* 1969, **7**, 23
- 17 Hatada, K., Nagata, K. and Yuki, H. *Bull. Chem. Soc. Japan* 1970, **43**, 3195
- 18 Masuda, T. *J. Polym. Sci. (Polym. Lett.)* 1973, **11**, 2713
- 19 Bowyer, P. M., Ledwith, A. and Sherrington, D. C. *Polymer* 1971, **12**, 509
- 20 Schildknecht, C. E., Zoss, A. O. and KcKinley, C. *Ind. Eng. Chem.* 1947, **39**, 180
- 21 Kursanov, D. N., Vol'pin, M. E. and Akhrem, I. S. *Dokl. Akad. Nauk. USSR* 1958, **120**, 531
- 22 Vol'pin, M. E., Akhrem, I. S. and Kursanov, D. N. *Zh. Obshchei Khim.* 1960, **30**, 159
- 23 Bowyer, P. M., Ledwith, A. and Sherrington, D. C. *J. Chem. Soc. (B)* 1971, p 1511
- 24 Szwarc, M. 'Carbanions, Living Polymers, and Electron Transfer Processes', Interscience, New York, 1968
- 25 Bonin, M. A., Busler, W. R. and Williams, F. J. *Am. Chem. Soc.* 1965, **87**, 199
- 26 Hubmann, E., *et al.* *Trans. Faraday Soc.* 1966, **62**, 88
- 27 Williams, F., Hayashi, K., Ueno, K., Hayashi, K. and Okamura, S. *Trans. Faraday Soc.* 1967, **63**, 1501
- 28 Ueno, K., Hayashi, K. and Okamura, S. *J. Macromol. Sci. (A)* 1968, **2**, 209
- 29 Taylor, R. B. and Williams, F. *J. Am. Chem. Soc.* 1969, **91**, 3728
- 30 Hayashi, K., Hayashi, K. and Okamura, S. *J. Polym. Sci. (A-1)* 1971, **9**, 2305
- 31 Stannett, V. and Kohler, J. *Polym. Prepr.* 1971, **12**, 98
- 32 Hayashi, K., Hayashi, K. and Okamura, S. *Polym. J.* 1973, **4**, 426
- 33 Cowling, S. unpublished results
- 34 Huisgen, R., Feiler, L. A. and Otto, P. *Chem. Ber.* 1969, **102**, 2405, 3444
- 35 Sustmann, R., Ansmann, A. and Vahrenholt, F. *J. Am. Chem. Soc.* 1972, **94**, 8099
- 36 Owen, N. L. and Sheppard, N. *Trans. Faraday Soc.* 1963, p 634
- 37 Katritzky, A. R., Pinzelli, R. F. and Topsom, R. D. *Tetrahedron* 1972, **28**, 3441

# Preparation and properties of some graft copolymers of the poly(2-chlorocyanurate) ester of bisphenol A

A. G. De Boos\* and G. Allen

Department of Chemistry, University of Manchester, Manchester M13 9PL, UK  
(Received 22 March 1974)

Graft copolymers of poly(2-chlorocyanurate)ester of bisphenol A have been prepared by coupling with polymers containing nucleophilic terminal groups. Polystyrene, poly(ethyl acrylate) and poly(methyl methacrylate) have been prepared. Physical properties of the grafts are characterized by two separate glass transition temperatures characteristic of the two homopolymers involved. The thermostability of the grafts increased with increase in weight fraction of polycyanurate in the copolymers.

## INTRODUCTION

Poly(2-chlorocyanurate)ester of bisphenol A (PCC) is a highly reactive, lightly branched, polydisperse polar macromolecule formed<sup>1</sup> by the polycondensation of cyanuric chloride and 2,2-bis(*p*-hydroxyphenyl) propane. The pendant chlorine group undergoes the normal reactions of organic acid chlorides although the reactivity is somewhat lower. Nucleophilic substitution at the active carbon atom readily occurs in the presence of amine, alcohols, phenols and other hydroxy compounds.

The coupling of PCC to polymers with nucleophilic terminal groups will yield graft copolymers. Whilst the nucleophilic chemistry of the polymer is somewhat complex because substitution at the main chain ether links competes with that at the active chlorine atom<sup>1</sup>, as the molar quantities involved in condensation coupling are small, it is expected that degradative attack on the PCC by the nucleophilic terminal groups of macromolecules will not be a problem in the formation of graft copolymers.

Condensation coupling has not been widely used in the preparation of graft copolymers, nevertheless there are some excellent examples of this technique in the literature. Grahame<sup>2</sup> developed a method in which amine-terminated polystyrene, prepared using a sodium initiator in liquid ammonia, was coupled with polymers containing small amounts of  $\beta$ -isocyanato-ethyl methacrylate as comonomer. Coupling was rapid and efficient, requiring no catalyst. Mutual transesterification between poly(methyl methacrylate) (PMMA) and low molecular weight aliphatic polyesters has also been used<sup>3</sup> to prepare graft copolymers. Similarly by converting the carboxyl end groups of natural and synthetic rubbers to acid chloride groups coupling of these materials to sodium and potassium derivatives of polyamides to form poly(amide-*g*-rubber)copolymers has been effected<sup>4</sup>.

Polymers with amino-terminal groups have been prepared by a number of workers and a series of such polymers have been prepared in this work for coupling with the PCC.

\* Present address: Division of Textile Industry, CSIRO, PO Box 21, Belmont, Victoria 3216, Australia.

## EXPERIMENTAL

### *Purification of reagents*

The solvent, tetrahydrofuran (THF) and the catalyst, triethylamine were refluxed over calcium hydride then distilled as required. Tetrahydrofurfuryl alcohol was vacuum distilled and stored in the dark. Other reagents, all of AR grade, were used as supplied.

### *Preparation of poly(2-chlorocyanurate)ester of bisphenol A*

The polymer was prepared by interfacial polycondensation in the presence of a cationic emulsifying agent by the method described elsewhere<sup>1</sup>.

### *Preparation of amino-terminated polymers*

The polymers were prepared by free radical solution polymerization in the presence of mercaptoethylammonium hydrochloride<sup>5</sup>. Alcohols were used as solvents for the polymerization because of their low radical transfer constants and because they were solvents for both polymer and the radical transfer agent. Tetrahydrofurfuryl alcohol was used as solvent in the polymerization of styrene, butyl and methyl methacrylates and methyl acrylate while propanol was used in the polymerization of ethyl and butyl acrylates. A 3:1 propanol/water mixture was also found to be a suitable solvent for the polymerization of methyl acrylate and methyl methacrylate. Polymers prepared in the different solvents did not differ significantly.

In a typical preparation the initiator, azobisisobutyronitrile (AIBN) (0.1% on weight of monomer) and the transfer agent (1% on the weight of monomer) were dissolved in the appropriate solvent (200% on the weight of monomer) and the required amount of monomer was distilled into the reaction vessel which was then sealed under vacuum and held at 80°C for 24 h. The polymer was precipitated by the slow addition of the polymerizing mixture to an excess of non-solvent (methanol for polystyrene and polymethacrylates and petroleum ether for the polyacrylates), then redissolved in chloroform, reprecipitated and dried under vacuum.

Because of the low molecular weights of the amine-terminated polyacrylates, purification and drying was a considerable problem and consequently characterization was limited to gel permeation chromatography.

#### Preparation of graft copolymers

Because, in the presence of a base catalyst, water caused gelation of PCC<sup>1</sup>, rigorous drying of polymers and solvents was essential before coupling was attempted. In a typical preparation a solution of PCC (10 g) in anhydrous THF (100 ml) was added to a solution of the amine-terminated polymer (20 g) in THF (200 ml). To this mixture was added triethylamine (0.5 ml) and the final mixture was stirred for 24 h. The solution was then added to an excess of acetone [poly(CC-g-DDA) and poly(CC-g-S)] or petroleum ether. The precipitated polymers were redissolved in chloroform, the solutions were filtered to remove triethylammonium chloride and the polymers were reprecipitated in petroleum ether and dried under vacuum.

#### Purification of the graft copolymers

Because of the limited chemical stability of the triazine polymer, selective elution was the only technique used to purify the polymers. The procedure adopted for each graft copolymer was: (a) poly(CC-g-DDA) – none required as dodecylamine was soluble in acetone; (b) poly(CC-g-S) – selective elution with cyclohexane (PS soluble) followed by selective elution with butanone (PCC insoluble); (c) poly(CC-g-MMA) – selective elution with acetonitrile (PMMA soluble) followed by selective elution with butanone, (d) poly(CC-g-EA) – selective elution with diethyl ether (PEA soluble) followed by selective elution with butanone.

No suitable selective solvent could be found for the purification of poly(CC-g-MA).

### CHARACTERIZATION

The polymers were characterized using established techniques. Osmometric measurements were made with a Melabs recording osmometer (Model CSM-2) using THF as solvent. The specific refractive index increments of the polymers in the various solvents were determined using a Brice-Phoenix differential refractometer, which had been previously calibrated with an aqueous sucrose solution. Light scattering studies were performed in a Sofica light scattering photometer, which used monochromatic light ( $\lambda = 546 \text{ nm}$ ) and which was thermostated at  $25^\circ\text{C}$ . Viscosity measurements were made in a Desreux-Bischoff viscometer at  $25^\circ\text{C}$ , the kinetic energy correction of which was negligible for the solvents used. G.p.c. was performed in a Waters Associated Model 200 gel permeation chromatograph, which had been calibrated with low dispersity linear polystyrene and THF was used as solvent. End group analysis was done by labelling the amine terminal groups using fluorodinitrobenzene followed by spectroscopic analysis of the polymer in chloroform solution (at  $350 \text{ nm}$ ), and comparison with a suitable calibration. The end group frequency  $\sigma$  was defined as the number of functional end groups per molecule:

$$\sigma = AM_n$$

where  $A$  = mol end groups/g polymer.

Four techniques were used to determine the composition of the graft copolymers: (1) microanalysis – the polymers

were analysed for chlorine and nitrogen which were specific for the triazine component; (2) ultra-violet spectroscopy – since the polyacrylates, polymethacrylates and dodecylamine do not absorb in the u.v. above  $240 \text{ nm}$  the extinction coefficient of the copolymers at  $254 \text{ nm}$  was used as a measure of composition. This could not be applied to poly(CC-g-S); (3) differential refractometry – as the specific refractive index increments of the components of a graft copolymer are usually additive, the specific refractive index increment was used to determine the composition; (4) infra-red spectroscopy – from the absorbances of the copolymer at wavelengths specific for the components (PCC at  $1540 \text{ cm}^{-1}$ ; PS at  $690 \text{ cm}^{-1}$ ; and PMMA at  $1730 \text{ cm}^{-1}$ ) it was possible to obtain a measure of the composition of the copolymers. The method was calibrated using the spectra of homopolymer mixtures.

The various techniques used to determine the composition of the graft copolymers gave quite consistent results and so the uncertainty in composition was quite small (Table 1)

The problems and errors associated with the solution characterization of the graft copolymers are great, the major ones being due to the products of the side reactions that occurred during the coupling reaction and to the long term degradation of the copolymers during storage. Low molecular weight fragments of PCC are formed when the terminal amino groups attack the main chain ester links of the backbone polymers. These fragments appeared as a low molecular weight tail on the gel permeation chromatograms of poly(CC-g-MMA) and poly(CC-g-EA) but not on that of poly(CC-g-S). These chromatographs are shown in Figure 1. The fragments made impossible any extensive characterization of the copolymers, particularly the determination of number-average molecular weight by osometry.

Light scattering measurements of the graft copolymers, poly(CC-g-MA), poly(CC-g-MMA) and poly(CC-g-EA) were performed in THF. As the specific refractive index increments of these copolymers in this solvent were high, the apparent molecular weight determined<sup>6</sup> was expected to be close to the true weight-average molecular weight of the copolymer. The molecular weight of poly(CC-g-S)-42, determined in benzene, was very close to the true weight-average molecular weight since the specific refractive index increments of the two components were almost identical<sup>6</sup>. The results are shown in Table 2. Although the molecular

Table 1 Composition of graft copolymers

Copolymer*	No.	Weight fraction of PCC (%)				Av.
		Mic†	i.r.	u.v.	SRI‡	
Poly(CC-g-DDA)		88		88	89	88
Poly(CC-g-S)	1	41	43			42
	2	65	64			65
	3	82	84			83
Poly(CC-g-MMA)		37	38	38	38	38
Poly(CC-g-MA)	1	44		42		43
	2	52		54	53	53
Poly(CC-g-EA)	1	30		30		30
	2	55		57		56
	3	68		66		67

\* P(CC-g-DDA) = PCC grafted with dodecylamine  
 P(CC-g-S) = PCC grafted with polystyrene  
 P(CC-g-MMA) = PCC grafted with poly(methyl methacrylate)  
 P(CC-g-MA) = PCC grafted with poly(methyl acrylate)  
 P(CC-g-EA) = PCC grafted with poly(ethyl acrylate)

† From microanalysis

‡ From specific refractive index increments

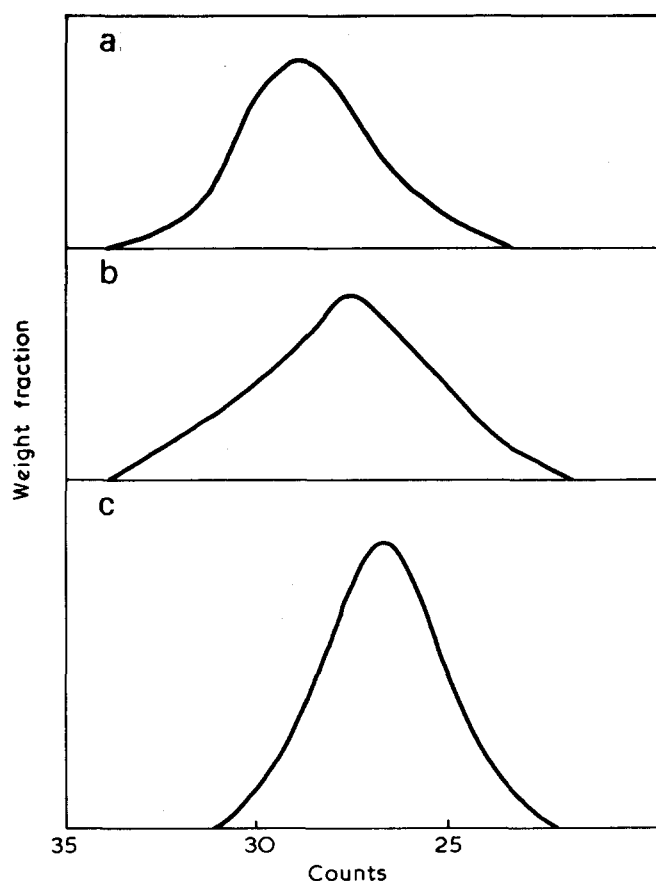


Figure 1 Gel permeation chromatograms of three graft copolymers. (a) Poly(CC-g-MMA); (b) poly(CC-g-EA); (c) poly(CC-g-S)

Table 2 Light scattering studies on PCC graft copolymers

Polymer*	Solvent	$dn/dc$ (ml/g)	$\gamma^\dagger$	$M_g^\ddagger$ $\times 10^{-4}$	$A_2^\S$ $\times 10^4$
Poly(CC-g-DDA)-88	Benzene	0.085	0.44	19	-0.52
Poly(CC-g-S)-42	Benzene	0.096	<0.05	28	1.16
Poly(CC-g-MMA)-38	THF	0.124	0.81	99	<0.2
Poly(CC-g-MA)-53	THF	0.138	0.77	25	1.19

\* Numeral defines the weight fraction of PCC in the graft

† Parameter defined as  $\gamma = \frac{(dn/dc)_{PCC} - (dn/dc)_{graft}}{(dn/dc)_{copolymer}}$

‡ Apparent molecular weight

§ Apparent second virial coefficient

weight of the graft copolymer was greater than that of the reactive prepolymers the difference was not as great as was expected. This was further evidence that scission of the backbone polymer occurred during coupling.

The intrinsic viscosities of the copolymers (Table 3) were determined in three solvents: chloroform, a good common solvent; benzene, a good solvent for the side chains and a very poor solvent for the backbone; butanone, a good solvent for the acrylate side chains, a poor solvent for the polystyrene side chains and a non-solvent for PCC. The solutions of the copolymers in butanone had the characteristic cloudy appearance of micellar solutions. As expected, the order of intrinsic viscosities of the copolymers were:  $[\eta]$  in butanone  $> [\eta]$  in benzene  $> [\eta]$  in chloroform, a consequence of the collapse of the backbone to the 'intramolecular precipitated'<sup>7</sup> state in butanone, which resulted in a contraction of the macromolecules in solution.

In summary, although the graft copolymers have been

partly characterized the instability of the backbone and complications due to side reactions during preparation preclude any application of graft copolymer solution theory.

## PHYSICAL PROPERTIES

In this work, we have concentrated on only three aspects of polymer behaviour, the glass transition temperature, the dynamic mechanical properties and the tensile properties.

The glass transition temperatures of the polymers were determined by differential scanning calorimetry (d.s.c.) using a Dupont 900 Differential Thermal analyser fitted with a DSC cell, at a heating rate of 20°C/min. All polymers were scanned from -100°C to 150°C or higher and duplicate samples were run. The thermal stability of the polymers was determined by thermogravimetric analysis (t.g.a.) in a nitrogen atmosphere at a heating rate of 6°C/min.

Because thermal moulding of PCC and those graft copolymers in which the weight fraction of PCC exceeded 0.5 was not possible even at a temperature of 200°C in a 20 ton (1 ton = 1.016 t) hydraulic press, mechanical testing was performed on films cast on to a clean mercury surface from THF and from butanone. The solvent was allowed to evaporate slowly in air protected from draughts. The films (0.05 cm) were then dried at room temperature under continuous vacuum for 2 months. The residual solvent was determined by heating the films at 150°C to constant weight in an evacuated oven. This caused the films to blow out so that the remnant material was useless for tests. The shear modulus of the cast films and its temperature dependence were determined using a Weissenberg Rheogoniometer. The sample (1.0 × 3.0 × 0.05 cm) was placed between two clamps, one of which was oscillated at 1 Hz and with a maximum amplitude of 1.42°. The movement of the other clamp was measured electronically and output and input signals fed into a computer which calculated the real modulus and the dissipation factor (tan δ). These parameters were measured at 5° intervals until the shear modulus was too low to detect. From a plot of the shear modulus and the dissipation factor against temperature the transition temperature of the film was determined (Figure 2).

The tensile properties of the polymeric films were determined by stretching the samples (1.0 × 0.1 × 4 cm) to break in a tensometer. Duplicate and often triplicate samples were run. As many of the samples were glassy polymers the clamps were modified to prevent any slippage of the sample by placing a strip of emery paper between the sample and the clamp jaws as shown in Figure 3. The samples were stretched at 1 cm/min and a chart to crosshead ratio of 16:1 was used. Samples were conditioned in the testing

Table 3 Intrinsic viscosities of graft copolymers

Polymer	Intrinsic viscosity (dl/g)		
	Chloroform	Benzene	Butanone
Poly(CC-g-DDA)	0.77	0.42	
Poly(CC-g-S)-42	1.05	0.76	0.37
Poly(CC-g-S)-65	0.90	0.60	0.26
Poly(CC-g-S)-83	1.08	0.66	0.28
Poly(CC-g-MMA)-38	1.39	0.81	0.40
Poly(CC-g-MA)-53	0.76	0.42	0.19
Poly(CC-g-EA)-30	0.79	0.50	0.28
Poly(CC-g-EA)-56	0.74	0.40	0.24
Poly(CC-g-EA)-66	0.78	0.42	0.27

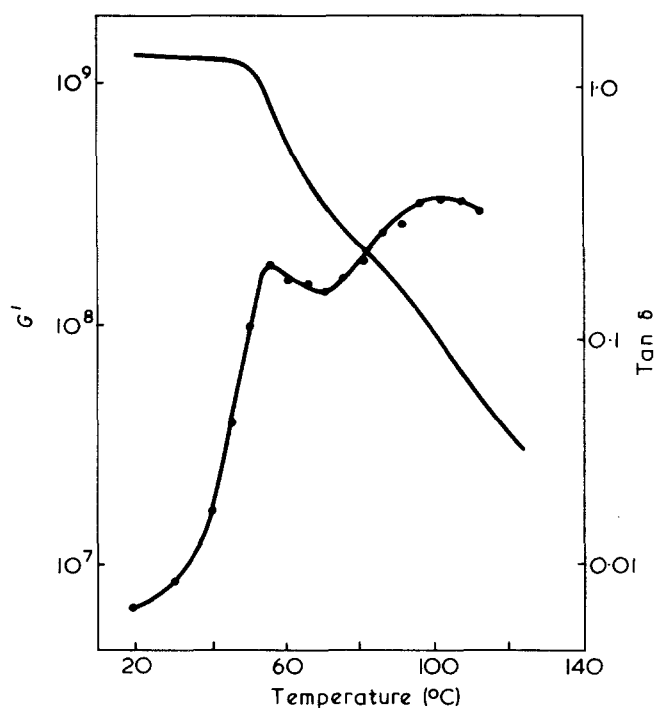


Figure 2 Effect of temperature on the real part of the shear modulus  $G'$  (—) and  $\tan \delta$  (●) for a PCC graft copolymer (solvent cast film)

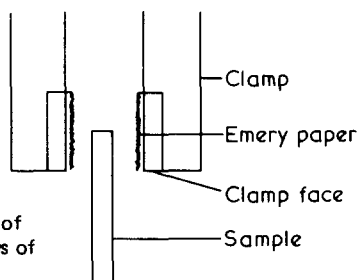


Figure 3 Schematic diagram of modifications made to the jaws of the tensometer clamp

atmosphere (22°C) for more than one hour before they were tested.

## RESULTS AND DISCUSSION

The transition temperature observed by d.s.c. (Table 4) for the triazine homopolymer agreed with that observed by other workers at ~140°C. The graft copolymer, poly(CC-g-DDA) was found to behave like a random copolymer rather than a true graft copolymer, probably because the dodecyl chains were too small to act independently as low molecular weight polyethylene branches. Consequently only one thermal transition was observed at 135°C, the lower thermal transition of the poly(2-chlorocyanurate) ester of bisphenol A, a result of the plasticizing action of the aliphatic side chains. Similar effects have been observed in the poly(acrylic acid) esters, the poly(methacrylic acid) esters and the poly(*p*-alkyl styrenes).

All the true graft copolymers of poly(2-chlorocyanurate) ester of bisphenol A had multiple thermal transitions corresponding to the glass transitions of the component homopolymers. Poly(CC-g-S) copolymers displayed the thermal transitions of the individual components except for poly(CC-g-S)-83 where the weight fraction of the polystyrene component was quite low. Here the transition temperature of the polystyrene component was slightly higher than that

of the polystyrene homopolymer. The polyacrylate and polymethacrylate components of the respective graft copolymers tended to lower the thermal transition of the triazine component. The effect of an increase in grafting frequency on the thermal transition temperature of the backbone can be easily seen from the results obtained from the poly(CC-g-EA) copolymers. Since the molecular weight of the poly(ethyl acrylate) side chains were the same in each case, the grafting frequency was proportional to the weight fraction of the PEA component. The relationship between the thermal transition temperature and the weight fraction of the poly(2-chlorocyanurate) ester of bisphenol A component is shown in Figure 4.

The results derived from the dynamic mechanical testing of the cast films of poly(2-chlorocyanurate) ester of bisphenol A and its graft copolymers shown in Table 5 mirrored the d.s.c. results. The mechanical transitions all represented plasticized glass transitions of the component polymers. The polyacrylate rich phase of the poly(CC-g-MA) film appeared to be almost unplasticized, probably a consequence of the prolonged drying (under vacuum) of the copolymer which allowed most of the solvent to be removed from the rubbery PMA rich phase but not from the glassy phase. The lower mechanical transition of the poly(CC-g-EA)-67 copolymer was below the temperature range investigated.

The d.s.c. and dynamic mechanical result indicated that PCC and polystyrene were incompatible and that microphase separation occurred in the solid state. However, a solvent cast film of the polymer mixture was clear, behaviour not normally observed when polymers are highly incompatible. This apparent anomalous observation was a result of the similar refractive indices of the two materials which prevented any appearance of cloudiness in the blend, even when phase separation had occurred. PCC and the acrylate polymers were much less incompatible and some interaction between the components occurred, probably accompanied by less extensive microphase separation in the bulk state.

Table 4 Thermal transitions of poly(2-chlorocyanurate) graft copolymers

Polymer	Transition temperature (°C)
PCC	140
Poly(CC-g-DDA)-88	135
Poly(CC-g-S)-42	95, 138
Poly(CC-g-S)-83	~99, 138
Poly(CC-g-MMA)-38	103, 131
Poly(CC-g-MA)-53	11, 130
Poly(CC-g-EA)-30	-17, -6, 122
Poly(CC-g-EA)-56	-15, -5, 128
Poly(CC-g-EA)-66	-17, -6, 130
Polystyrene	92
Poly(methyl methacrylate)	119

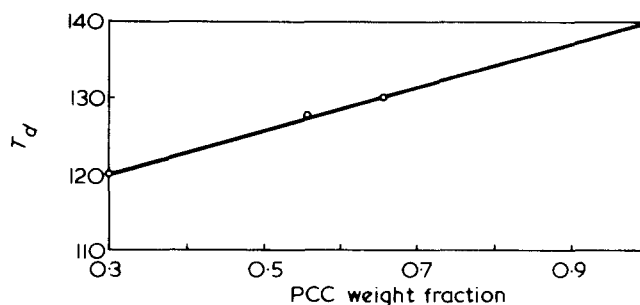


Figure 4 Effect of composition on the upper glass transition temperature of PCC/ethyl acrylate graft copolymers

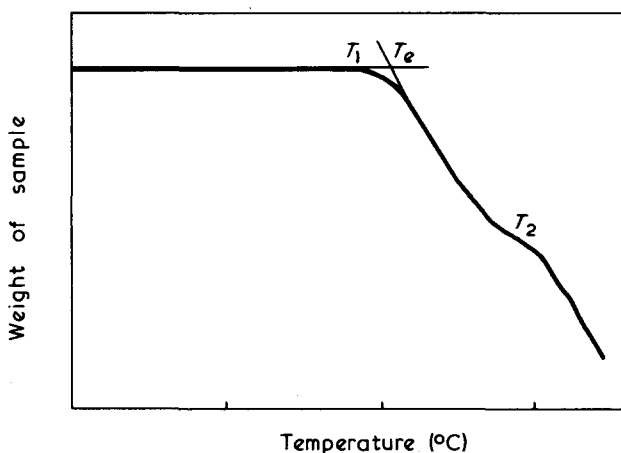


**Table 5** Mechanical properties of solvent cast films of PCC graft copolymers

Polymer	Casting solvent	Residual solvent (%)	Form	Transition temp. (°C)
PCC	THF	7	glass	100
Poly(CC-g-DDA)-88	THF	9	glass	98
Poly(CC-g-S)-42	THF	9	glass	56, 102
Poly(CC-g-S)-83	Butanone	5	glass	66, 108
	THF	8	glass	64, 114
Poly(CC-g-MMA)-38	Butanone	7	glass	65, 116
	THF	11	glass	82, 100
Poly(CC-g-MA)-53	Butanone	8	glass	94, 115
	Butanone	5	ill defined	25, 65
Poly(CC-g-EA)-30	THF		rubber	
	Butanone		rubber	
Poly(CC-g-EA)-66	THF	13	glass	75
	Butanone	7	glass	85

**Table 6** Tensile properties of PCC graft copolymers (solvent cast films)

Polymer	Casting solvent	Initial modulus $\times 10^8$ (N/m <sup>2</sup> )	Strain at break
Poly(CC-g-MA)-53	MEK	8.98	0.03
Poly(CC-g-EA)-66	THF	10.50	0.02
Poly(CC-g-EA)-30	MEK	9.39	0.03
	THF	7.40	0.88
	MEK	2.97	1.00

**Figure 5** T.g.a. curve for a typical PCC graft copolymer

The tensile properties of the solvent cast films of the copolymers in which the grafted side chains were glasses at room temperature could not be determined because the films, including that of the homopolymer were extremely brittle and could not be cut without causing short range fracturing across the line of the cut. While this had little effect on the shear properties of the material it made any meaningful tensile testing impossible. Poly(CC-g-MA)-53 and poly(CC-g-EA)-67 were hard glassy materials of high

**Table 7** Thermal stability of graft copolymers

Polymer	Temperature* (°C)		
	T <sub>1</sub>	T <sub>e</sub>	T <sub>2</sub>
PCC	380	417	
Poly(CC-g-DDA)-88	258		399
Poly(CC-g-S)-42	270	310	422
Poly(CC-g-S)-83	270		426
Poly(CC-g-MMA)-38	265	322	422
Poly(CC-g-MA)-53	270	358	
Poly(CC-g-EA)-30	259	337	
Poly(CC-g-EA)-66	258	330	422

\* Parameters as indicated in *Figure 5*

modulus and low extensibility while poly(CC-g-EA)-30 was a soft rubbery material of lower modulus and higher extensibility. The effect of the casting solvent on the modulus of the polymers can easily be seen from *Table 6*. The films cast from THF had a higher modulus than those cast from butanone, a consequence of the more extended configuration of the poly(2-chlorocyanurate) backbone in the films cast from THF. The difference in moduli of copolymers, in which the weight fraction of the triazine polymer was low, was much greater than that of polymers in which the weight fraction was high and where poly(2-chlorocyanurate) ester of bisphenol A formed the continuous phase irrespective of solvent. The increase in modulus of films of poly(CC-g-EA)-30 occurred without a large decrease in the extensibility of the material.

The high thermal stability of poly(2-chlorocyanurate) ester of bisphenol A and other triazine polymers has been reported by several other workers<sup>8,9</sup>. The stability of the graft copolymers (by t.g.a.) was much lower than that of the poly(2-chlorocyanurate) homopolymer (*Table 7*). A second shoulder, shown in *Figure 5* was observed in the thermograms of those copolymers in which the weight fraction of the triazine polymer was high, corresponding to the degradation of the backbone. We conclude that the lower stability of the graft copolymer is a simple consequence of the low stability of the side chains (the thermal stability of which has been well documented)<sup>10</sup> rather than of any destabilization of the backbone polymer.

## REFERENCES

- Allen, G. and De Boos, A. G. *Polymer* 1974, 15, 56
- Grahame, R. J. *J. Polym. Sci.* 1957, 24, 367
- Kolesnikov, H. and Khan-min, T. K. *IUPAC Macromol. Symp., Moscow* 1960, 3, 236
- Tutorskii, J., Smelyi, Z. and Bistrov, V. *ibid.* p 224
- De Boos, A. *Polymer* 1973, 14, 587
- Grubsic, Z., Benoit, H. and Rempp, P. *J. Polym. Sci. (B)* 1967, 5, 735
- Baltaerd, H. and Tregea, G. 'Graft Copolymers', Interscience, New York, 1967
- Nakamura, Y., Mori, K., Tamura, K. and Saito, Y. *J. Polym. Sci. (A-1)* 1969, 7, 3089
- Sherliker, F. R. *MSc Thesis Manchester University* (1967)
- Grassie, N. and Speakman, J. *J. Polym. Sci. (A-1)* 1971, 9, 919, 931, 949

# Polymerization of acrylonitrile in the presence of vinylsulphone dyes

N. S. Batty and J. T. Guthrie

Department of Colour Chemistry, University of Leeds, Leeds LS2 9JT, UK

(Received 15 March 1974; revised 25 June 1974)

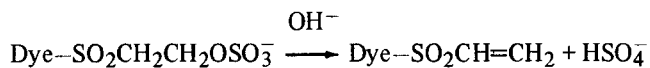
Information regarding the effect of vinylsulphone dyes on the kinetics of polymerization of acrylonitrile is presented in detail. Some of the physical properties of the products, polyacrylonitrile/vinylsulphone dye copolymers, are discussed, although the subject of their thorough characterization is reserved for a later publication. Considerable detail is given concerning the experimental procedures, to ensure ease of understanding of the techniques involved.  $^{60}\text{Co}$   $\gamma$  rays were employed as the polymerization initiator whilst the effect of  $\gamma$  radiation on the chromophore was noted, where relevant.

## INTRODUCTION

The concept of polymeric pigments or colouring matters bound to polymers is an attractive one, since such pigments should be free from many of the problems which bedevil other pigments, for example migration and flocculation. Polymeric pigments could also eliminate the grinding operation which is always necessary in the production of more conventional pigments<sup>1</sup>. Outlets should also exist in moulding, spinning or casting operations, avoiding some of the difficulties involved in the production of intrinsically coloured articles and in mass coloration. These developments would depend largely on the nature of the components of the polymer.

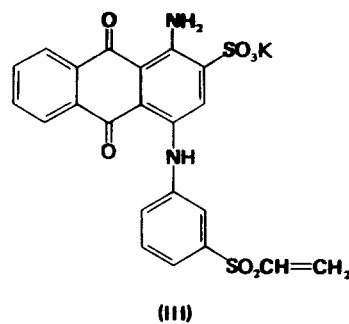
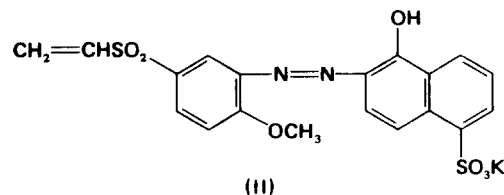
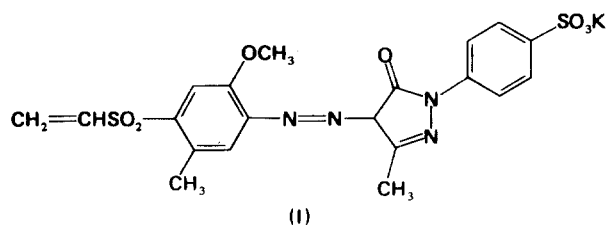
This is an account of some preliminary studies of one possible route to this type of pigment.

Certain commercially available dyes contain vinyl groups, sometimes in the free vinyl form, but often as an addition compound such as the  $\beta$ -sulphatoethylsulphone derivative. For this study three Remazol<sup>®</sup> (Farbwerke Hoechst) dyes were used — a yellow, a red and a blue. The Remazols are reactive dyes intended primarily for dyeing cellulosic fibres. They are sold as  $\beta$ -sulphatoethylsulphones. Under mild alkaline conditions used in dyeing they release the bisulphate anion to yield the free vinylsulphone<sup>2</sup>, thus:



Under alkaline conditions cellulose ionizes and reacts with the vinylsulphone by adding to the  $\beta$  carbon atom of the activated double bond<sup>3</sup>. The reaction is completed by protonation of the  $\alpha$  carbon atom. The sequence of reactions is essentially reversible.

The structures of a number of the Remazol dyes have been elucidated and published<sup>4</sup>. The structures of the free vinyl forms of the three dyes used in this work, Remazol Gold Yellow G (I), Remazol Red B (II) and Remazol Brilliant Blue B (III), are given as:

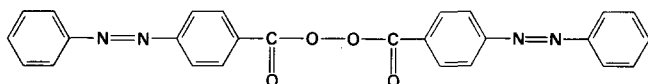


A number of copolymers containing a dye as one of the comonomers have been reported. Lovrien and Waddington<sup>5</sup> copolymerized acrylamide azo dyes with acyclic and methacrylic acids to study the effect of the polymeric environment on the photochromic *cis-trans* isomerism. BASF patented copolymers made from dyes containing polymerizable vinyl groups together with one of a wide range of vinyl monomers<sup>6</sup>. The products are stated to be suitable

for making shaped articles, films, sheets, fibres etc. The concept was extended to include such features as grafting the comonomers to cotton resulting in coloration and modification of the physical properties of the substrate in one operation<sup>7</sup>.

ICI have shown considerable interest in the printing of textiles using dyes containing an acryloylamino group. The dye is polymerized within the interior of the fibre<sup>8</sup>.

There have been a number of papers describing the use of a dye to initiate polymerization. Usually the chromophore becomes attached at one end of the polymer chain. Sometimes it becomes modified during the initiation process and the colour is either changed or destroyed. Kämmerer<sup>9</sup> used a coloured peroxide:



to initiate polymerization. The number of initiator fragments in the polymer were then determined colorimetrically. This was claimed to be a more convenient method of determining the concentration of initiator fragments in the polymer than the more familiar radioactive tracer techniques.

Dyes have also been used as photosensitizers so that polymerization can be initiated by visible light<sup>10</sup>. Much work has been carried out along these lines involving triaryl-methane dyes such as fluorescein<sup>11-14</sup>. The colour of the dye is destroyed during the reaction although it has been shown that the dye molecule becomes bound to the polymer<sup>15</sup>. Simionescu *et al.*<sup>16-18</sup> have used various dyes to photosensitize the polymerization of acrylonitrile. They reported that coloured polymers were produced.

In this study an attempt has been made to copolymerize acrylonitrile with vinylsulphone dyes and to determine the nature of the polymerization process. This has been achieved mainly by considering the effect of the dye on the polymerization reaction.

## EXPERIMENTAL

### Reagents

Acrylonitrile was supplied by BDH Ltd. The inhibitor, 0.005% *p*-methoxyphenol, was removed with potassium hydroxide. An excess of potassium hydroxide pellets was added to the acrylonitrile and it was allowed to stand overnight. The liquid was decanted and distilled from fresh potassium hydroxide, under reduced pressure, at 50°C.

The dyes were all samples from the Remazol range of Farbwerke Hoechst AG and were supplied by Hoechst-Cassella Dyestuffs Ltd, Manchester, UK. The commercial dye was purified and treated to produce the free vinyl form as follows<sup>19</sup>.

Dissolution in a minimum of water at 40°C was followed, on cooling, by titration with 5% sodium hydroxide solution until the pH, measured on a glass electrode, was greater than 10.5. After 10 min (30 min for the blue dye) the pH was checked to ensure that it was still above 10.5. This process liberates the vinylsulphone from the  $\beta$ -sulphatoethylsulphone form of the dye. Caution is needed to maintain the pH of the mixture below 11.5 to 12.0. Above pH 12.0 an essentially irreversible reaction occurs, resulting in the formation of the  $\beta$ -hydroxyethylsulphone from the vinylsulphone form of the dye. Precipitation was completed by the addition of 67% (w/w) potassium acetate solution. The dye

was filtered using Whatman's No.5 filter paper, redissolved in water and precipitated again with potassium acetate. The dye was filtered and this process of dissolving and salting out was repeated. At this stage potassium acetate was the only impurity in the free vinylsulphone dye. The potassium acetate was removed by washing the precipitate repeatedly with ethanol until the washings gave no precipitate with 0.1 M silver nitrate solution. The dye was finally dried in a vacuum desiccator. This purification procedure was used for each of the three vinylsulphone dyes used.

### Pre-irradiation procedure

Polymerizations with each of the dyes were carried out *in vacuo* and in air. The monomer solutions were prepared by dissolving the dye in warm water, cooling and then adding the appropriate amount of acrylonitrile. The mixture was shaken until the acrylonitrile dissolved. Vacuum irradiated samples were sealed off at  $1.33 \times 10^{-3}$  N/m<sup>2</sup>, stored in the dark at 0°C until required and brought to room temperature prior to irradiation.

### Irradiation procedure

Polymerization was initiated by  $\gamma$  radiation from the <sup>60</sup>Co source located in the Department of Physical Chemistry at the University of Leeds. The absorbed dose rate was determined by Frické dosimetry. The dose rates at the four positions used in this work were 5.03, 5.45, 5.27 and 4.75 rad/sec. Owing to difficulties arising from the source design it was not possible to obtain identical dose rates for all the positions used. Hence kinetic data are presented later in terms of rad<sup>-1</sup> as well as sec<sup>-1</sup>.

### Post-irradiation procedure

Post-irradiation polymerization was reduced to a minimum by pouring the contents of each tube, as soon as possible after removal from the irradiation unit (>10 min), into an excess of cold (0°C) methanol containing 50 g/dm<sup>3</sup> of dissolved potassium acetate. The potassium acetate enables the polymer to be separated from the solution. The mixture was centrifuged at approximately 200 m/sec<sup>2</sup> for 20 min. This produced a compact sediment and clear supernatant liquor. The liquor was decanted and passed through a tared sintered crucible (porosity grade 4). The sediment was mixed with 50 cm<sup>3</sup> of methanol and centrifuged again. The clear liquor was passed through the original crucible and further methanol was added to the sediment. This procedure was repeated until no colour was apparent in the solution and until it gave no precipitate with 0.1 M silver nitrate. Thus, removal of all the potassium acetate and dye was ensured.

The resulting sediment was transferred quantitatively to the crucible, washed with methanol and dried to constant weight in a vacuum desiccator. The weight of polymer obtained in each instance was recorded.

## RESULTS AND DISCUSSION

In all the systems irradiated there was an initial period during which no visible change occurred. This was followed by a period of rapid polymerization during which the polymer, being insoluble in the monomer, precipitated as a milky suspension.

Polymer made in the absence of dye was easily filtered from its monomer solution. However, polymers made in

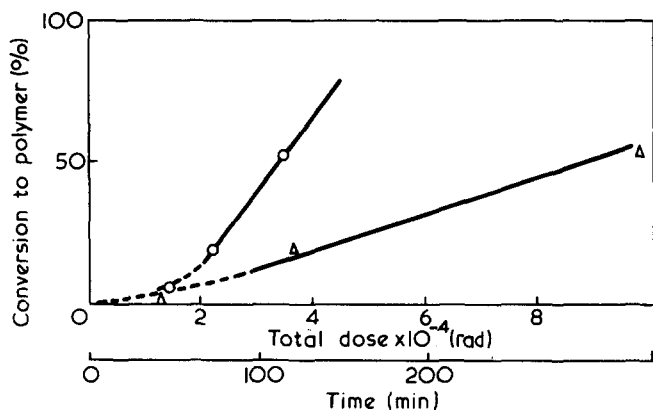


Figure 1 Polymerization of acrylonitrile.  $\circ$ , *in vacuo*;  $\Delta$ , in air

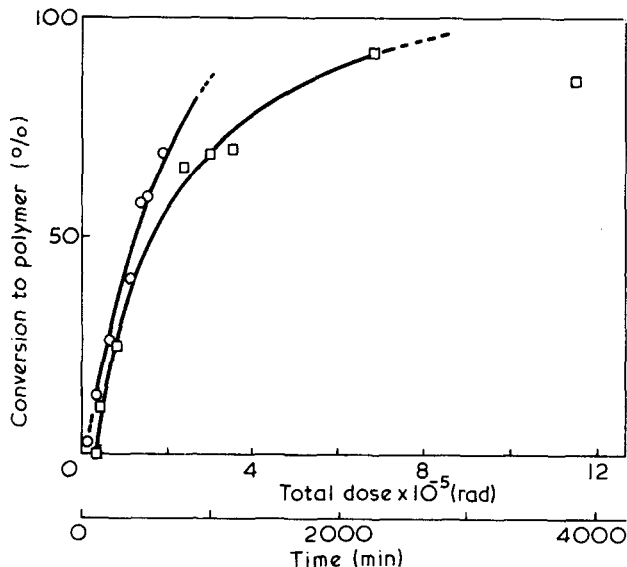


Figure 2 Polymerization of acrylonitrile in the presence of the yellow dye.  $\circ$ , *in vacuo*;  $\square$ , in air

the presence of the dye were extremely difficult to filter. For these, it was necessary to add an electrolyte to coagulate the suspensions before they could be filtered.

The initial period of the polymerization process was not examined at all in this study. In every instance an induction period was observed. This was greatest for irradiations carried out in air and of minor proportions for vacuum irradiated samples. According to Dainton *et al.*<sup>20</sup> and Peebles *et al.*<sup>21</sup> this initial period of polymerization is the time during which the concentration of the propagating species builds up to its steady-state value. When the steady state is reached, the rate of polymerization becomes independent of the monomer concentration up to high conversions. Here, deviations from the steady state will take place.

Some observations were made on the polymerization of acrylonitrile in the absence of dye (Figure 1). The reaction rates in the linear portions of the graphs, corresponding to the steady state period are 27% and 6.9% (w/w) conversion to the polymer per  $10^4$  rad for the reactions *in vacuo* and air. In reality the number of points available in Figure 1 are insufficient to justify a claim that the steady state is reached. Previous workers<sup>20</sup> have found that a steady state is reached after the initial period. This has been assumed in our work and from Figure 1 the conversion rates are seen to be  $3.6 \times 10^{-5}$  and  $9.1 \times 10^{-6}$  mol converted to polymer  $\text{dm}^{-3} \text{rad}^{-1}$  respectively.

Figures 2, 3 and 4 demonstrate the effect of vinylsul-

phone dyes on the polymerization of acrylonitrile *in vacuo* and in air. In every instance there is the same initial behaviour as observed with pure acrylonitrile. From this stage, the rate of polymerization is seen to fall off steadily because of monomer depletion. Here we would expect deviation from steady state conditions. The data are shown in Figures 5, 6 and 7 as plots of  $\log ([M]/[M]_0)$  versus dose, where  $[M]$  denotes the concentration of total monomer (dye + acrylonitrile) in the system at any time and  $[M]_0$  is the original total monomer concentration (dye + acrylonitrile). Reasonably linear plots are shown for the section of the graphs corresponding to the steady state period. This strongly suggests that the steady state process is first order with respect to monomer. If we assume the existence of steady state conditions and that the change in relative monomer concentration is insignificant over the period of investigation then:

$$R_p = k [M]$$

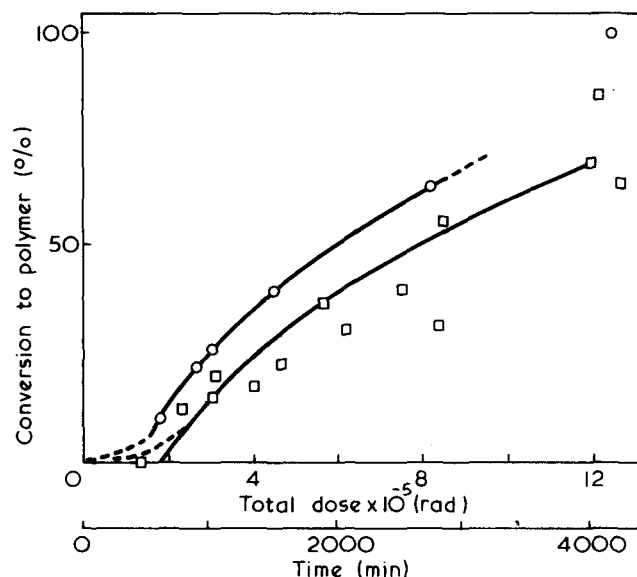


Figure 3 Polymerization of acrylonitrile in the presence of the red dye.  $\circ$ , *in vacuo*;  $\square$ , in air

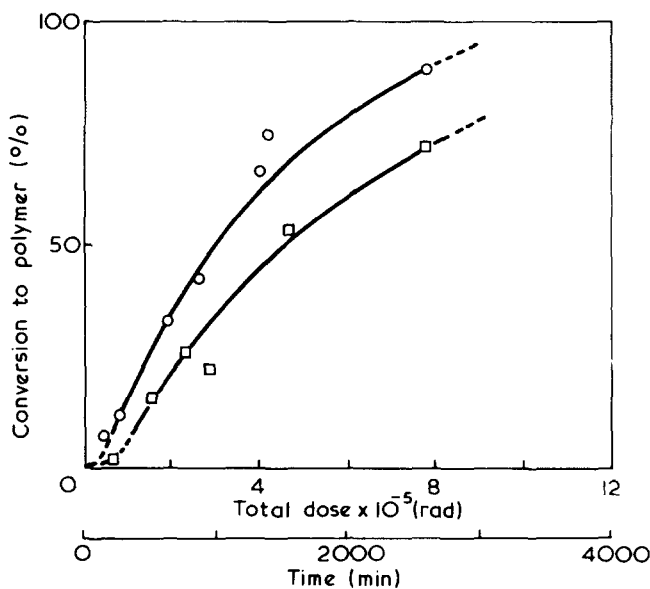


Figure 4 Polymerization of acrylonitrile in the presence of the blue dye.  $\circ$ , *in vacuo*;  $\square$ , in air

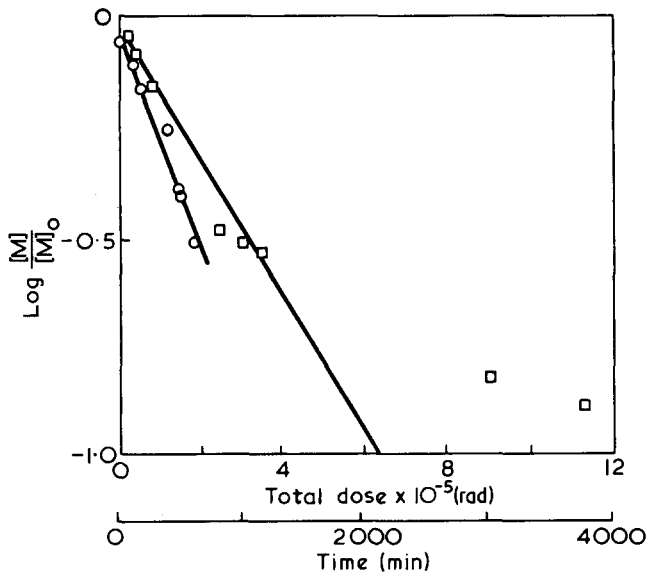


Figure 5 Log (monomer depletion) versus total dose, yellow dye with acrylonitrile.  $\circ$ , *in vacuo*;  $\square$ , in air

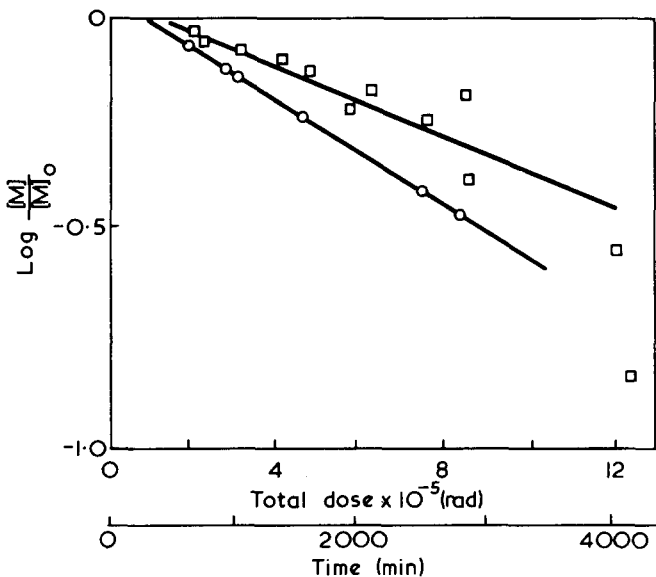


Figure 6 Log (monomer depletion) versus total dose, red dye with acrylonitrile.  $\circ$ , *in vacuo*;  $\square$ , in air

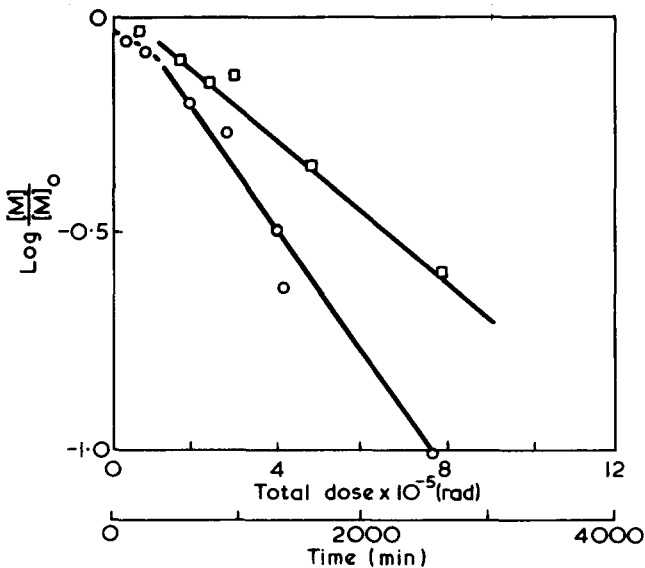


Figure 7 Log (monomer depletion) versus total dose, blue dye with acrylonitrile.  $\circ$ , *in vacuo*;  $\square$ , in air

where  $R_p$  denotes the rate of polymerization and  $k$  is the first order rate constant. For any other dependence of the form  $R_p = k [M]^x$  where  $k$  and  $x$  are constants, a plot of  $\log ([M]/[M]_0)$  against  $\log (\text{dose})$  should give a straight line. Plots given in Figures 8 and 9 can be seen to exhibit continuous curvature. Therefore it is assumed that the reaction is first order in monomer. Here we have a simple method of determining the dependence of the reaction rate on the monomer concentration using data from polymerizations carried out at one monomer concentration. Hence, this affords a much speedier method of acquiring the monomer dependence than is possible using several monomer concentrations in the usual manner. However, the method depends on the validity of the assumptions described.

Polymerizations in air give considerably more scattered points than those carried out *in vacuo*. No attempt was made to control the amount of dissolved oxygen. Oxygen is known to have a marked retarding effect on free radical polymerizations so changes in the concentration of oxygen may account for the observed scatter.

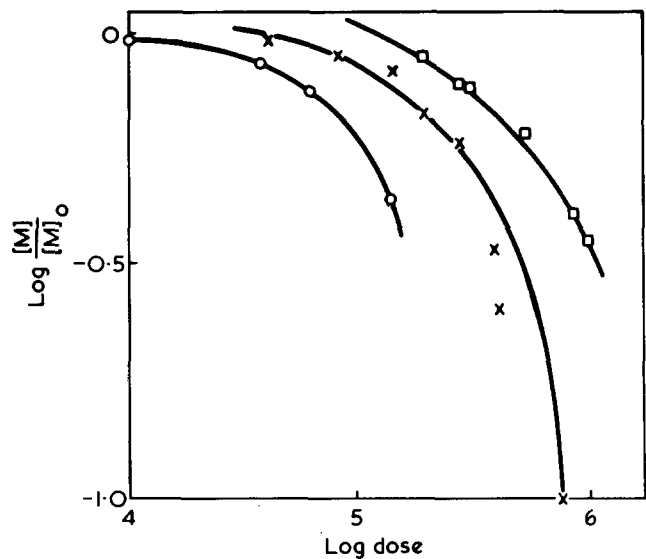


Figure 8 Log-log plot of polymerizations *in vacuo* as log (monomer depletion) versus log (total dose).  $\circ$ , yellow dye;  $\square$ , red dye;  $\times$ , blue dye

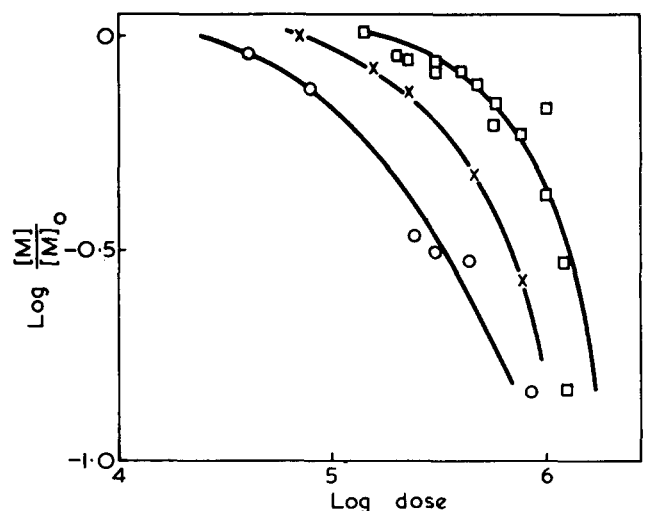


Figure 9 Log-log plot of polymerizations in air as log (monomer depletion) versus log (total dose).  $\circ$ , yellow dye;  $\square$ , red dye;  $\times$ , blue dye

**Table 1** First order rate constants for acrylonitrile (AN) polymerization in the presence of dye, in vacuum and in air

Copolymer	Vacuum		Air	
	$k \times 10^6$ (rad <sup>-1</sup> )	$K' \times 10^6$ (sec <sup>-1</sup> )	$K \times 10^6$ (rad <sup>-1</sup> )	$K' \times 10^5$ (sec <sup>-1</sup> )
AN/yellow dye	2.1	10.0	1.7	8.5
AN/red dye	0.6	3.0	0.35	1.7
AN/blue dye	1.4	7.0	0.8	4.0

The first order rate constants have been calculated for the three dye-acrylonitrile systems, both in air and *in vacuo*, from the slopes of the log  $([M]/[M]_0)$  versus dose plots and are presented in Table 1.

From the nature of the reactions it would seem that the polymerization of acrylonitrile, with or without the dye, follows a similar mechanism. However, there is a considerable difference in the initial reaction rates as shown by the time taken for turbidity to develop. The overall reduction in the polymerization rate, with the dye present is further complicated by the fact that these rates become dependent on the monomer concentration. For concentrated solutions, as used here, the rate of polymerization of acrylonitrile in the absence of dye is independent of the monomer concentration to high conversions. This is explained by assuming that most of the polymerization occurs on the surface of the polymer particles and involves only adsorbed monomer. It is also assumed that the polymer particles become saturated with monomer at concentrations well below the saturation limit of acrylonitrile in water. Provided that the concentration of monomer in the solution is sufficient to ensure saturation of the surface of the polymer particle, the rate should not change significantly with the monomer concentration. Depletion of adsorbed monomer at the surface will result in a corresponding reduction in the polymerization rate. The amount of monomer adsorbed, and hence the polymerization rate, becomes proportional to the concentration of monomer in solution.

If this model is accepted, then the dependence of the polymerization rate on the monomer concentration must mean that the polymer particles are not saturated, even in the more concentrated monomer solutions.

The particles of dye-polymer are stabilized with a smaller size than the particles in the absence of dye, and so would be expected to have a greater total surface area. However, it is difficult to imagine that this could so greatly affect the adsorption. We feel that a more likely explanation involves the increased hydrophilic nature of the polymer resulting from the incorporation of ionic groups. This would promote competition between water and acrylonitrile for the surface sites. Then the greater the acrylonitrile concentration the greater will be its occupation of the surface sites and the faster the polymerization process. Hydrolysis of the cyano groups in the homopolymer results in the formation of acid groups which will be hydrophilic.

Polymerization was carried out without prior degassing of the monomer solutions, to determine the role of air in the process. The results are plotted in Figures 1-7 on the same axes as those of the corresponding degassing reactions, to facilitate comparison. The rates of reaction during the 'steady-state' period are lower in the presence of air. The ratios of the rate constants for vacuum and air are 1:0.8,

1:0.58, 1:0.57 respectively for the yellow, red and blue dye systems, respectively.

Oxygen is well known to have a retarding effect on radical polymerizations. This usually takes the form of almost complete suppression of polymerization until all the oxygen is used up. In the absence of secondary events, polymerization proceeds as normal thereafter.

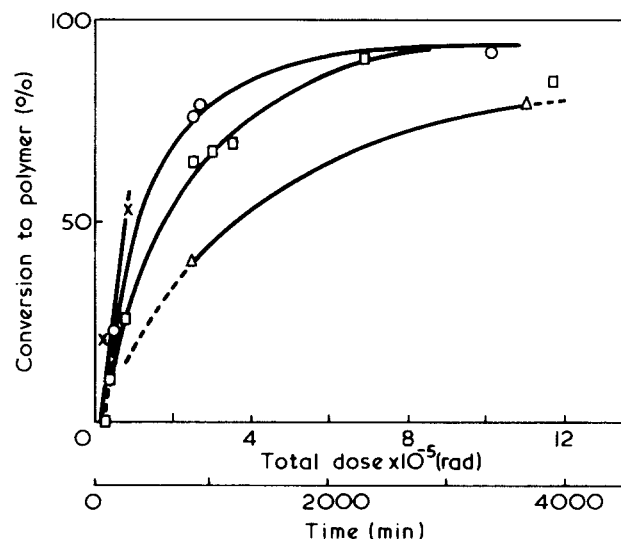
Figure 10 displays the effect of the concentration of the yellow dye on the rate of polymerization. In spite of the paucity of data, the results show clearly that the rate of polymerization decreases with increase in the dye concentration, at a constant concentration of acrylonitrile. One effect of incorporation of dye into the polymer is to reduce the adsorption forces between the monomer and the polymer. Incorporation of more dye into the polymer would further reduce the extent of adsorption.

One possibility is that the growing polymer radical reacts with a dye molecule to produce a less reactive species. This is supported by the fact that all the polymers made in the presence of dye were highly coloured and the colour was not removed by repeated dissolution and precipitation. This lesser reactivity will arise because of the steric protection of the radical on the dye molecule by the bulky chromophore.

Alternatively, the radical could be less reactive because of resonance stabilization. The styryl radical, for example, is markedly deactivated in this way<sup>22</sup>. The sulphur-oxygen bonds in vinylsulphones, however, have very little double bond character<sup>23,24</sup>. Hence the degree of resonance with the aromatic part of the molecule cannot be great. There is no measurable stabilization of phenyl vinylsulphone radicals.

We cannot rule out the possibility of attack by the polymer radical of the dye molecule at positions other than the vinyl group. If the attack were to occur at some part of the conjugated system, the resulting radical would almost certainly be stabilized and unreactive.

Ham has suggested that polymerization of acrylonitrile occurs by a stereospecific helical mechanism<sup>25</sup>. If this is so, a comonomer, such as a vinylsulphone dye, would upset the regularity and reduce the rate of reaction. We feel that the reduced rate of reaction in the presence of dyes is due primarily to reduced adsorption of the monomer onto the polymer particles. However, we appreciate that any one of,


**Figure 10** Effect of the acrylonitrile: dye ratio on polymerization, yellow dye in air. X, acrylonitrile only; O, 40:1 acrylonitrile dye; □, 20:1 acrylonitrile dye; △, 10:1 acrylonitrile dye

or a combination of, the other mechanisms may also take part.

The polyacrylonitrile/dye copolymers were formed as emulsions or suspensions in water. These emulsions were stable. The copolymers could not be removed from the suspension by centrifuging or filtering through a No.4 porosity sinter. This observation is in marked contrast to the precipitates of acrylonitrile produced in the absence of the dyes, which were very easily separated by the sinter.

Every polymer particle produced during the polymerization of acrylonitrile carries a negative charge. The suspension becomes stable when the particles are large enough to carry a charge sufficient to repel other particles and so prevent agglomeration<sup>20</sup>. Molecules of the polymers containing dye have sulphonate groups which are almost completely ionized in water. Hence, the polymer particles have a further inherent negative charge such that repulsion between the particles and stabilization of the suspension can occur at a smaller particle size. This repulsive effect is reduced in the presence of methanol where ionization is inhibited, or in the presence of an electrolyte such as potassium acetate, where it is partly screened by the excess of ions. This facilitates aggregation, allowing the coloured polymer to be separated from its solution. If water is added to the polymer it reforms the emulsion immediately. Once it has been dried, however, the polymer loses its emulsion forming characteristics. On drying, strong intermolecular bonds must form, as in polyacrylonitrile.

The coloured polymers are insoluble in water, alcohols, ethers, hydrocarbons and halogenated hydrocarbons. They are soluble in *N,N*-dimethylformamide and dimethylsulphoxide. If a solution of the polymer in *N,N*-dimethylformamide is poured slowly into water, the polymer is precipitated as a stable suspension. The overall insolubility of the coloured polymers, produced by the methods outlined, should be of value in pigment applications. The stability of their emulsions in aqueous systems is an added advantage. Evidence is available to suggest that copolymerization renders the chromophore more light fast, than the unmodified dyestuff, on normal substrates.

#### ACKNOWLEDGEMENT

We acknowledge the financial support given to one of us (N.S.B.) by the Perkin Bequest.

#### REFERENCES

- 1 Carr, W. J. *Oil Colour Chem. Assoc.* 1971, **54**, 1093
- 2 von der Eltz, H.-U. *Melliand Textilber.* 1959, **40**, 69
- 3 Stamm, O. A. *J. Soc. Dyers Colour.* 1964, **80**, 416
- 4 Panchartek, J., Allen, Z. J. and Poskocil, J. *Coll. Czech. Chem. Commun.* 1962, **27**, 268
- 5 Lovrien, R. and Waddington, J. C. B. *J. Am. Chem. Soc.* 1964, **86**, 2315
- 6 Br. Pat. 877 402, 920 390, 946 472 and 949 404 (BASF)
- 7 Br. Pat. 965 627 (BASF)
- 8 Br. Pat. 1 262 092 (ICI)
- 9 Kämmerer, H. *Chimia* 1965, **19**, 61
- 10 Bamford, C. H. and Dewar, M. J. S. *J. Soc. Dyers Colour.* 1954, **65**, 674
- 11 Oster, G. *Nature* 1954, **173**, 300
- 12 Toppet, S., Delzenne, G. and Smetz, G. *J. Polym. Sci. (A)* 1964, **2**, 1539
- 13 Simionescu, Cr. and Ungureanu, C. *Rev. Roman. Chim.* 1964, **9**, 627
- 14 Sheriff, A. I. M. D. and Santappa, M. *J. Polym. Sci. (A)* 1965, **3**, 3131
- 15 Smetz, G., Winter W. de and Delzenne, G. *J. Polym. Sci.* 1961, **55**, 767
- 16 Simionescu, Cr., Feldman, D. and Noghin, C. *Rev. Roman. Chim.* 1967, **12**, 1481
- 17 Feldman, D., Nuta, V. and Simionescu, Cr. *Rev. Roman. Chim.* 1969, **14**, 1407
- 18 Nuta, V., Feldman, D. and Simionescu, Cr. *Rev. Roman. Chim.* 1972, **17**, 1755
- 19 Robinson, C. and Mills, H. A. T. *Proc. R. Soc. (A)* 1931, **31**, 576
- 20 Dainton, F. S., Seaman, P. H., James, D. G. L. and Eaton, R. S. *J. Polym. Sci.* 1959, **34**, 209
- 21 Peebles, Jr, L. H. in 'Copolymerisation' (Ed. G. E. Ham), Interscience, New York, 1964, Ch IX
- 22 Billmeyer, Jr, F. W. in 'Textbook of Polymer Science', Interscience, New York, 1962, Ch 11c
- 23 Overberger, C. G., Baldwin, D. E. and Gregor, H. P. *J. Am. Chem. Soc.* 1950, **72**, 4865
- 24 Price, C. C. and Morita, H. *J. Am. Chem. Soc.* 1953, **75**, 4747
- 25 Ham, G. E. *J. Polym. Sci.* 1959, **40**, 569

# Melting of thermoplastics in single screw extruders

I. R. Edmondson\* and R. T. Fenner

*Department of Mechanical Engineering, Imperial College of Science and Technology,  
London SW7 2BX, UK*

*(Received 3 May 1974)*

Some experiments on the melting of thermoplastic polymeric materials in single screw extruders are described. Although these were of the now familiar screw extraction type, special care was taken to distinguish between material melted by screw rotation and that melted during the subsequent cooling operation. A barrel which could be split longitudinally was also used, thus avoiding some of the disadvantages of axial extraction. A theoretical model is proposed which, unlike previous models, allows the solid bed of material in the screw channel to accelerate naturally, and also allows for the presence of a film of molten material between the bed and the screw. This model gives satisfactory predictions of melting performance. Comparison with experimental results shows that break-up of the solid bed occurs when the model predicts rapid acceleration of the bed. Bed break-up and the resulting surging may be reduced or prevented by the use of screw cooling which has the effect of inhibiting the formation of a melt film at the screw surface.

## INTRODUCTION

Since most thermoplastic polymeric materials pass at least once through a single screw extruder, there is considerable interest in the design of such machines. Early attempts to understand and analyse the process were concentrated on the flow of the material after melting<sup>1,2</sup>. Attention has also been given to the behaviour of solid feedstocks in the feed sections of screws<sup>3,4</sup>. It is generally agreed, however, that the melting process is often the most important in that it determines the maximum output rate of acceptable quality extrudate. Most experimental work on melting has involved the extraction of the screw from the barrel while still full of polymer, in order to study the melting mechanism<sup>5-8</sup>. Based on the observations, various theoretical models have been proposed<sup>7,9-11</sup>, though all are of a similar type.

The purpose of this paper is to report some improvements to both the experimental techniques for studying melting in extruders and the theoretical analysis of the process<sup>12</sup>. In particular, the latter makes it possible to predict when melting is likely to become unstable, leading to surging of both the output rate and pressure.

## EXPERIMENTAL TECHNIQUE

The essence of the experimental method, both past and present, for studying the melting process in single screw extruders is to first achieve the required steady operating conditions and then to stop the screw and cool the barrel as rapidly as possible. The material in the screw channel is thereby frozen. The screw is then extracted from the barrel and the helical strip of solid polymer removed and sectioned.

Two practical difficulties are usually encountered: first, in achieving a sufficiently rapid rate of cooling to minimize the amount of material melted by thermal conduction after the screw has stopped, and secondly in applying a large enough axial load to the screw to perform the extraction.

It is normally necessary to use water cooling on the barrel, and if possible on the screw as well, to achieve an adequate cooling rate. Powerful screw extraction equipment is also needed, since not only is the screw channel full of polymer, but the extraction must be carried out at as low a temperature as possible. In the present experiments on a 38 mm machine with a screw length-to-diameter ratio of 20, a maximum extraction force of about 10 t was applied by means of an electrically driven screw jack. On larger extruders the required force would be increased in proportion to at least the square of the screw diameter. Even so, it is not always possible to extract the screw at ambient temperature, and the barrel must be partly reheated.

If reheating of the barrel is necessary the softened material near the barrel surface may be disturbed when the screw is extracted. This difficulty was overcome by using a longitudinally split barrel, the two halves being bolted together in use. The barrel heating and cooling jackets could be removed, the barrel split and the screw removed with minimum disturbance of the polymer. In most of the experiments, however, the axial extraction procedure was used, having first established that the barrel splitting method gave the same results.

Owing to the low thermal conductivities of most thermoplastics, a significant amount of melting by conduction after the screw has stopped is unavoidable. While the barrel may be rapidly water cooled, polymer not in contact with the barrel responds much more slowly. During normal extrusion, melting occurs almost exclusively in the regions of intense shear that exist between the solid material and the screw and barrel surfaces. Consequently it is possible to distinguish between extrusion melting and the subsequent conduction melting by whether or not shear deformation is also involved. This is best achieved by adding colouring matter to the solid feedstock. One method is to add a small proportion of granules of the same material and physical form, to which a distinctive colour has been imparted. Another method, and the one that was used in the present experiments, is to mix a very small amount of

\* Present address: Imperial Chemical Industries Limited, Billingham, Teesside.



powdered dry colouring with the feedstock which clings to the surfaces of the granules. When material from the screw channel is sectioned after extraction it is possible to distinguish conduction melting where the outlines of the original granules are still visible, from extrusion melting where the colouring has been distributed by shear.

Pressures at a number of points along the barrel were measured with the aid of Dynisco transducers, Model PT 420, the outputs from which were amplified and recorded by an ultra-violet recorder. The response of this system was sufficiently rapid to follow in detail the variations of pressures as the screw rotated. The back pressure at the delivery end of the extruder was varied with the aid of a range of dies of different diameter.

The materials used in the experiments included a granular and a powdered low density polyethylene (LDPE), granular high density polyethylene, granular polypropylene, crystal polystyrene, plasticized poly(vinyl chloride) (PVC) granules and rigid PVC powder.

**THEORETICAL MODEL**

Figure 1 shows part of the screw and barrel of a typical single screw extruder, where the direction of flow of polymer is from left to right. The coordinate directions  $z$  and  $x$  are respectively parallel and normal to the screw flight, while the third coordinate  $y$  is in the radial direction.

Figure 2 shows the screw channel cross-section normal to the flight, looking in the downstream  $z$  direction. Also shown is the commonly observed form of melting mechanism. The unmelted material is compacted into a solid bed which is approximately rectangular in cross-section (in practice the corners are somewhat rounded). The bed is continuous in the downstream direction and lies just behind the trailing face of the screw flight. Melting occurs mainly at the interface between the upper surface of the solid bed and the narrow melt film between bed and barrel. Much of the melt so formed is swept by the relative motion of screw and barrel into a melt pool formed in front of the leading face of the flight. If the screw is hot enough there may also be melt films formed between the bed and screw surfaces. As melting proceeds the model assumes that the cross-sectional area of the bed decreases until either the bed width or thickness approach zero. In practice the bed may break into discrete pieces as described later.

Figure 2 shows the view from the screw with the barrel moving relative to the observer. A further simplification is to assume that the channel and contents may be unrolled and treated as rectilinear. The solid bed is assumed to move relative to the screw with a velocity  $V_{sz}$  which is independent of  $x$  and  $y$  but may vary with  $z$ . Figure 3 shows the relative velocity diagram for the solid bed, the velocity of

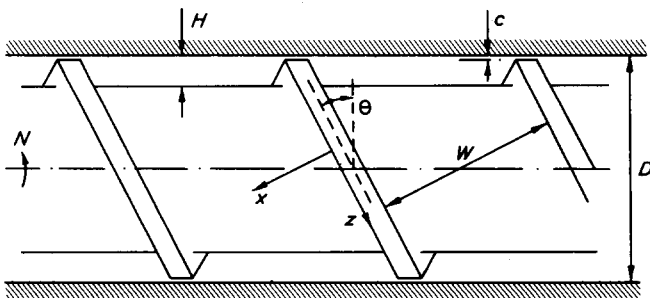


Figure 1 Typical screw extruder geometry

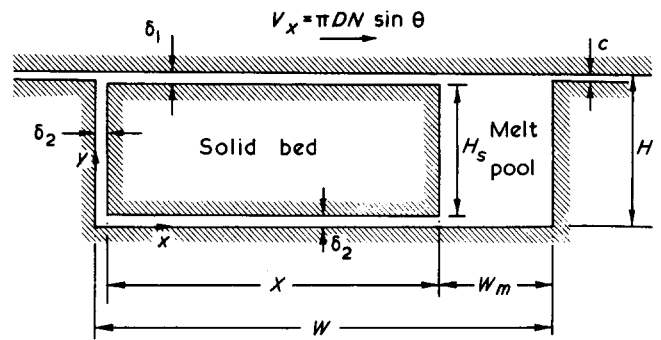


Figure 2 The melting model

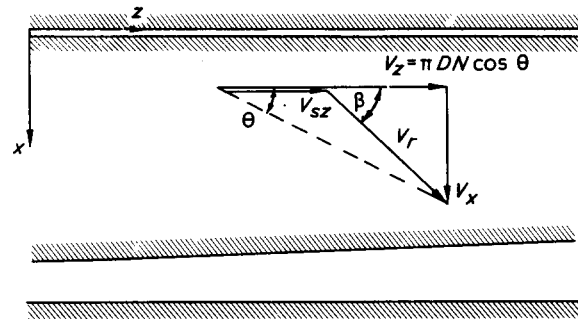


Figure 3 Relative velocity diagram for the solid bed

the barrel relative to the bed using  $V_r$  at an angle  $\beta$  to the downstream direction. In practice the magnitude of  $V_{sz}$  rarely exceeds half that of  $V_z$ .

All the melting models mentioned in the introduction are of the form shown in Figure 2. The earliest ones<sup>7,9</sup> neglected the existence of the lower melt film and assumed the bed velocity,  $V_{sz}$ , to be constant. Apart from small corrections for channel curvature and leakage flow over the screw flights<sup>10</sup>, the main improvement to the basic model has been to allow the bed velocity some freedom to vary. For example, Donovan<sup>11</sup> introduced an empirical 'solid bed acceleration parameter' which allowed  $V_{sz}$  to increase in a prescribed manner along the screw.

In the present model the solid bed velocity is allowed to vary naturally, and the lower melt film is introduced as soon as the screw temperature exceeds the melting point of the polymer. The thicknesses of the melt films at the screw root and flight surfaces are assumed to be the same, in accordance with experimental observations.

**Mass and force balances**

There are four distinct regions in the channel cross-section, namely the upper and lower melt films, the solid bed and the melt pool. Equations for conservation of mass can be stated for each region. For the upper melt film:

$$\left[ \begin{array}{c} \text{Rate of change} \\ \text{of downstream} \\ \text{mass flow rate} \end{array} \right] = \left[ \begin{array}{c} \text{Rate of melting} \\ \text{over interface} \\ \text{with solid bed} \end{array} \right] - \left[ \begin{array}{c} \text{Net trans-} \\ \text{verse flow} \\ \text{rate out of} \\ \text{melt film} \end{array} \right]$$

$$\frac{d}{dz} (m_{1z}X) = \omega_1 X - (m_{1x} - m_{fx}) \quad (1)$$

where the leakage flow rate over the flights may be approximated by assuming a linear velocity profile in the clearance

as:

$$m_{fx} = \frac{1}{2} \rho_m V_x c \quad (2)$$

In the case of the lower film all the melt is retained in the film.

$$\frac{d}{dz} [m_{2z}(X + H_s)] = \omega_2(X + H_s) \quad (3)$$

The downstream mass flow rate in the solid bed decreases owing to the loss of material by melting into the surrounding melt films:

$$\frac{dM_{sz}}{dz} = -\omega_1 X - \omega_2(X + H_s) \quad (4)$$

$$M_{sz} = \rho_s V_{sz} X H_s \quad (5)$$

Since the downstream mass flow rate in the melt pool,  $M_{mz}$ , is required to make up the total mass flow rate which remains constant along the screw, the overall mass balance may be stated as:

$$M_T = m_{1z} X + m_{2z}(X + H_s) + M_{mz} + M_{sz} \quad (6)$$

Neglecting the shear stress at the interface between the melt pool and the solid bed, the downstream force balance for the bed may be used to relate the pressure gradient to the stresses at the interfaces between the bed and the melt films.

$$H_s X (dp/dz) = \tau_{1z} X - \tau_{2z}(X + H_s) \quad (7)$$

Further analyses of the four regions are necessary to obtain the mass flow rates  $m_{1z}$ ,  $m_{1x}$ ,  $m_{2z}$  and  $M_{mz}$ , melting rates  $\omega_1$  and  $\omega_2$ , and shear stresses  $\tau_{1z}$  and  $\tau_{2z}$ .

#### Analysis of the melt films

The flows in both the upper and lower melt films may be treated as being entirely due to the motion of the solid bed relative to the barrel and screw surfaces. While pressure gradients certainly exist in practice, they are not large enough to significantly affect the velocity profiles in the thin films. It is also assumed that the velocity and temperature profiles within the films are locally fully developed. A typical film cross-section is shown in *Figure 4*, where the relative velocity between barrel or screw and solid bed is  $U$  in the direction denoted by  $s$ . The shear stress,  $\tau$ , in the same direction is independent of  $y$  and may be assumed

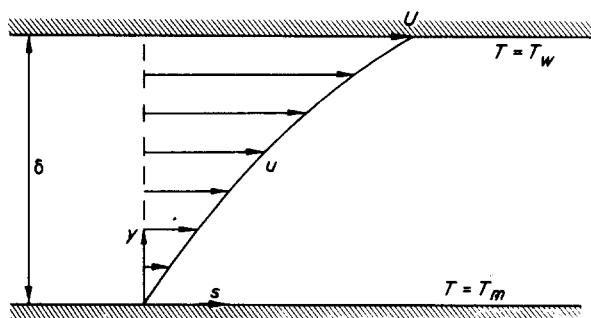


Figure 4 Typical melt film cross-section and velocity profile

to be a power-law function of shear rate and an exponential function of temperature<sup>2</sup>.

$$\tau = \frac{\mu_0}{\gamma_0^{n-1}} \left( \frac{du}{dy} \right)^n \exp[-b(T - T_0)] \quad (8)$$

where  $\mu_0$  is the effective viscosity at a reference shear rate  $\gamma_0$  and temperature  $T_0$ . The temperature profile may be obtained from the energy equation for fully developed flow:

$$k_m \frac{d^2 T}{dy^2} = -\tau \frac{du}{dy} \quad (9)$$

The boundary conditions are

$$\begin{aligned} u = 0, T = T_m \text{ at } y = 0 \\ u = U, T = T_w \text{ at } y = \delta \end{aligned} \quad (10)$$

where  $T_m$  is the melting point of the polymer and  $T_w$  is the metal wall temperature. This is essentially the problem solved by Martin<sup>13</sup> by a largely analytical technique which may be readily adapted to the present situation<sup>12</sup>. For a given film thickness and relative velocity it is possible to derive parameters such as flow rate, shear stress, temperature gradients at the film boundaries and mean melt temperature.

In the case of the lower melt film the relative velocity,  $V_{sz}$ , is in the downstream direction. The main difficulty is in defining the boundary temperature at the screw surface. In the present work axial screw temperature profiles were assumed, based on the observed points at which lower films were formed as the screw temperature exceeded the polymer melting point. The relative velocity in the upper film is  $V_r$  (equivalent to  $U$  in *Figure 4*) at an angle  $\beta$  to the downstream direction as shown in *Figure 3*. Since melted material is entrained in the direction of  $V_r$ , there must be a corresponding increase in film thickness. Consequently  $\delta_1$  is really a function of both  $x$  and  $z$ . In many melting models  $\delta_1$  is assumed to be independent of  $x$ , which is in good agreement with many experimental observations. While  $\delta_1$  must vary across the width of the bed, the variation is often sufficiently small for an average value to be used for analytical purposes. The variation in film thickness in the downstream direction may be substantial, and the present model treats  $\delta_1$  as a function of  $z$ .

From the analysis of the upper film may be obtained the mass flow rate relative to the bed,  $m_1$ , and the shear stress,  $\tau_1$ , both in the direction of  $V_r$ . The required mass flow rate and stress components may therefore be obtained as:

$$m_{1x} = m_1 \sin \beta \quad (11)$$

$$m_{1z} = m_1 \cos \beta + \rho_m \delta_1 V_{sz} \quad (12)$$

$$\tau_{1z} = \tau_1 \cos \beta \quad (13)$$

#### Analysis of the solid bed

Heat transfer in the solid bed is due to a combination of thermal conduction through the thickness of the bed and downstream thermal convection, and is governed by the following energy conservation equation:

$$\rho_s C_{ps} V_{sz} \frac{\partial T}{\partial z} = k_s \frac{\partial^2 T}{\partial y^2} \quad (14)$$

with  $T = T_m$  at the upper and lower faces of the bed. The thickness of the bed slowly diminishes, an effect which amounts to a convection of material into the melting interfaces which can be taken account of in determining the melting rates as described below. Equation (14) is a parabolic partial differential equation for which standard numerical methods of solution are available. The temperature profile at successive bed cross-sections may be found, hence the temperature gradients at the melting interfaces.

*Analysis of the melt pool*

Much of the polymer melted on the upper surface of the solid bed is dragged into the melt pool alongside the bed. The flow patterns in this pool region are very difficult to analyse accurately<sup>14</sup>. So long as the size of the pool is small compared to the channel cross-section, however, a simple but rather inaccurate method may be used without serious effects on the usefulness of the overall model. Assuming the melt to be Newtonian, the total mass flow rate in the pool may be found by superimposing the rates due to the drag flows induced by the motion of the barrel and bed relative to the screw, and the pressure flow due to the downstream pressure gradient.

$$M_{mz} = \rho_m W_m H \left\{ \frac{1}{2} V_z F_D(H/W_m) + \frac{1}{2} V_{sz} F_D(W_m/H) - \frac{H^2(dp/dz)}{12\bar{\mu}} F_P(H/W_m) \right\} \quad (15)$$

where  $F_D(H/W)$  and  $F_P(H/W)$  are respectively the drag and pressure flow shape factors<sup>2</sup> for flow in a rectangular channel of width  $W$  and depth  $H$ . The mean viscosity,  $\bar{\mu}$ , may be evaluated for the mean shear rate in the pool and bulk mean temperature of the melt entering from the upper film.

*Determination of the melting rates*

The melting rates at the interfaces between the solid bed and melt films may be determined from the known temperature gradients:

$$\omega_1 \lambda_1 = k_m \left( \frac{\partial T}{\partial n_1} \right)_m - k_s \left( \frac{\partial T}{\partial n_1} \right)_s \quad (16)$$

$$\omega_2 \lambda_2 = k_m \left( \frac{\partial T}{\partial n_2} \right)_m - k_s \left( \frac{\partial T}{\partial n_2} \right)_s \quad (17)$$

where  $n_1$  and  $n_2$  are the outward normals to the solid bed surface in the two films. Thermal convection in these directions in both the solid and melt may be accounted for by using modified latent heats of fusion.

$$\lambda_1 = \lambda + C_{ps}(T_m - \bar{T}_s) + C_{pm}(\bar{T}_1 - T_m) \quad (18)$$

$$\lambda_2 = \lambda + C_{ps}(T_m - \bar{T}_s) + C_{pm}(\bar{T}_2 - T_m) \quad (19)$$

where  $\bar{T}_s$ ,  $\bar{T}_1$  and  $\bar{T}_2$  are the bulk mean temperatures in solid bed and upper and lower films respectively. The use of these equations assumes that the polymer has a unique

melting point and a definable latent heat of fusion. While this is reasonable for crystalline polymers it is less so for the more amorphous materials. Also it is assumed that the enthalpy is a sufficiently linear function of temperature in the solid and melt regions for mean values of specific heat to be used.

*Solution of the overall problem*

The mathematical problem to be solved is defined by equations (1), (3), (4) and (7), the remaining equations being used to define the various terms appearing in these simultaneous first-order ordinary differential equations. Various combinations of primary variables may be used, for example  $\delta_1$ ,  $\delta_2$ ,  $X$  and  $p$ , or  $m_{1z}$ ,  $m_{2z}$ ,  $M_{sz}$  and  $p$ . In the present work the former set was used. The equations may be integrated numerically with the aid of a digital computer to yield the values of both the primary and secondary variables at intervals along the helical path of the screw channel.

The initial conditions required to start the solution procedure are often difficult to define. At the beginning of the feed section of the screw the temperatures of both screw and barrel are below the melting point of the polymer, owing to the cooling normally applied to the feed pocket. The formation of melt films is therefore delayed until the metal surfaces are hotter than the melting point. This normally occurs first at the barrel surface after two or three turns of the screw. Formation of the melt film on the screw usually occurs several turns later, or may not occur at all if the screw is cooled. Accumulation of molten material in the melt pool does not start until the thickness of the upper film exceeds the radial clearance between the screw flight and barrel. In the present work the starting points for the melt films were based on experimental observations. In the absence of such films it is assumed that Coulomb friction governs the relative motion between the solid bed and metal surfaces.

The downstream solid bed velocity,  $V_{sz}$ , is obtained as a function of  $z$ , and it is assumed that the bed is capable of undergoing the necessary deformation. In practice, excessive acceleration of the bed cannot be sustained and it breaks as described later. Clearly, the present model is inappropriate after break-up of the solid bed has occurred. Also it does not provide a good description of behaviour towards the end of melting when the material is predominantly molten.

**EXPERIMENTAL RESULTS AND COMPARISON WITH THE THEORETICAL MODEL**

Space considerations forbid the presentation of more than a small sample of the experimental results obtained in the present work<sup>12</sup>. Attention is therefore confined to those results which demonstrate particular aspects of the melting process in practice or the theoretical model used to describe it. The main data obtained from the experiments are the pressure variations with time sensed by the pressure transducers, and sections of the frozen helix removed from the screw showing the regions previously solid and molten.

*Pressure profiles*

The variation of mean pressure along the screw is considered in the next section, while this section is concerned with variations detected as the screw rotated. Figure 5 shows typical types of pressure profiles in the absence and

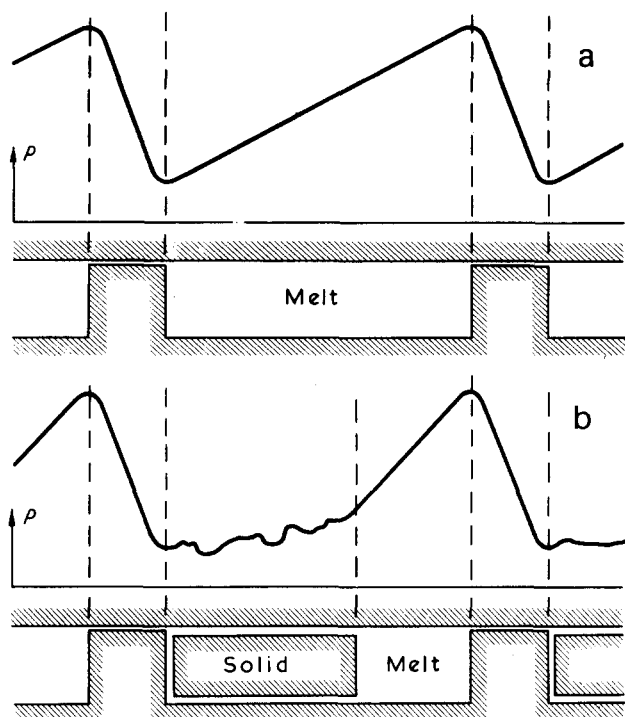


Figure 5 Typical pressure profiles in (a) the absence and (b) the presence of a solid bed

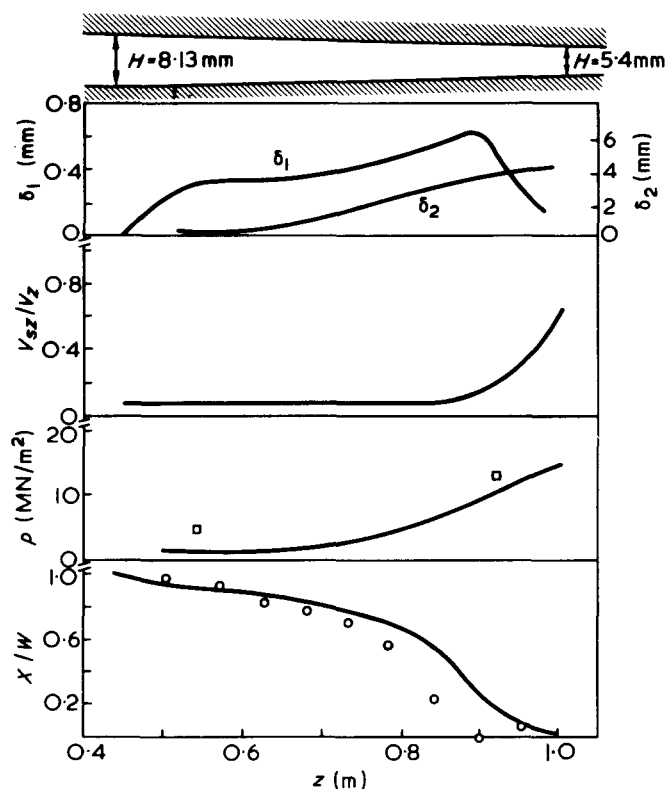


Figure 6 Results and theoretical predictions for an experiment with granular LDPE. —, theoretical predictions. Screw had a compression ratio of 4.0 over an axial length of 10 turns (diameters), and  $c = 0.16$  mm. Barrel temperature =  $150^\circ\text{C}$ ,  $N = 40$  rev/min,  $M_T = 5.0$  kg/h

presence of a solid bed. The finite areas of the sensing diaphragms of the transducers had the effect of rounding any sharp pressure peaks or troughs. In the metering section of a screw where the polymer is completely molten the profile took the form of a relatively smooth saw-tooth shape as shown in Figure 5a. An approximately uniform

pressure gradient was developed in the melt in the channel and a correspondingly steeper gradient was observed in the much narrower flight clearance. In the presence of a solid bed the behaviour was much less regular. Over the bed itself the pressure generally fluctuated more severely and randomly, presumably owing to the passage of individual granules past the diaphragm (powdered feedstocks gave much smoother traces). The mean pressure either remained reasonably uniform as indicated in Figure 5b or rose significantly before the melt pool was reached. Over the melt pool the trace became smoother and the pressure gradient greater.

In principle it is possible to distinguish between melt and solid in the screw channel from the pressure traces alone, based on a combination of change of pressure gradient and smoothness of the profile. This facility is particularly useful on production machines where it is not possible to stop and extract the screw.

#### Solid bed profiles and pressure development

There are at least three ways of comparing measured and theoretical extruder melting performance: in terms of either relative mass flow rates of solid and melt at particular positions along the screw, relative widths or relative cross-sectional areas. The first of these is unsuitable as it requires a knowledge of the solid bed velocity which is not measured. Of the other two, the relative width criterion is easier to apply and is the one used here. Melt film thicknesses are difficult to measure with sufficient accuracy for comparison with the theoretical model.

Figures 6, 7 and 8 show experimental results and the corresponding theoretical predictions for three tests on LDPE granules, LDPE powder and plasticized PVC granules.

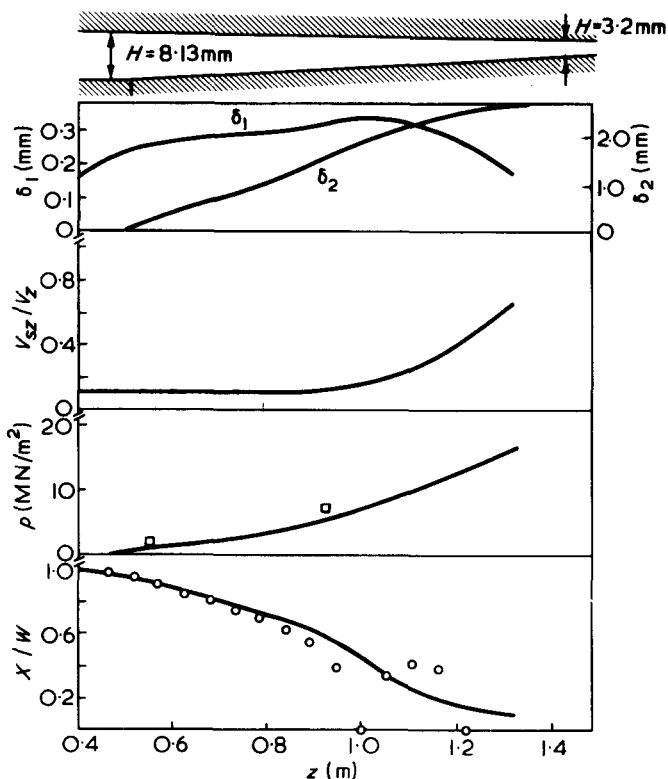


Figure 7 Results and theoretical predictions for an experiment with LDPE powder. —, theoretical predictions. Screw had a compression ratio of 4.0 over an axial length of 10 turns (diameters), and  $c = 0.16$  mm. Barrel temperature =  $150^\circ\text{C}$ ,  $N = 80$  rev/min,  $M_T = 13.3$  kg/h

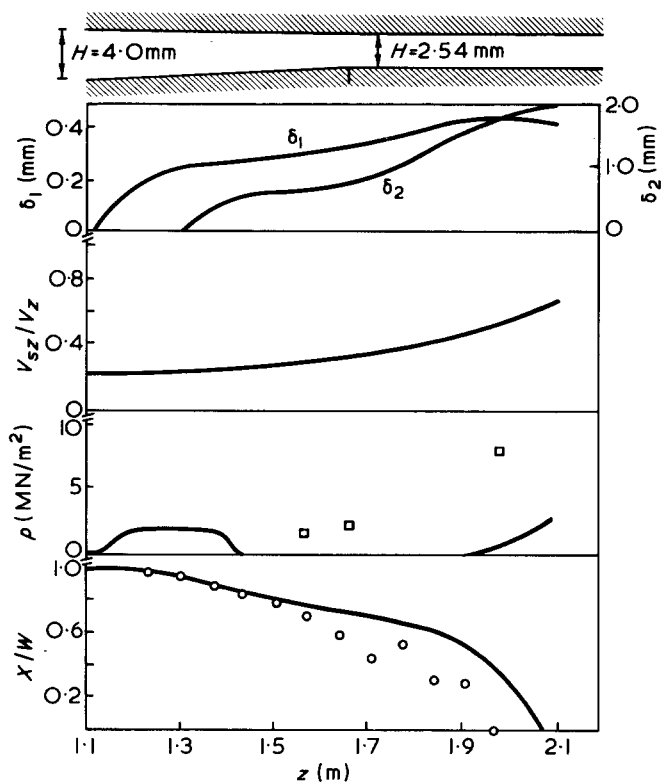


Figure 8 Results and theoretical predictions for an experiment with plasticized PVC granules. —, theoretical predictions. Screw had a compression ratio of 2.25 over an axial length of 10 turns (diameters), and  $c = 0.16$  mm. Barrel temperature =  $160^{\circ}\text{C}$ ,  $N = 80$  rev/min,  $M_T = 22.0$  kg/h

Experimental results are only shown for relative solid bed widths at half-turn intervals along the screw, and mean pressures measured at a limited number of axial locations. The agreement between the measured and predicted solid bed widths is good, particularly during the early stages of melting where the theoretical model is most applicable. The significance of the experimental points showing zero solid bed width in the case of LDPE (Figures 6 and 7) is discussed later. It is worth noting that the end of melting occurs much more rapidly in the case of PVC (Figure 8) than for LDPE, owing to the much lower latent heat of fusion. Once the average temperature of the PVC solid bed is near its melting point very little more heat is required to completely melt it.

The predicted melt film thickness profiles suggest that the upper film grows rapidly at first until the rate of melting is balanced by the rate at which melt is swept into the pool, when the thickness stabilizes (at about twice the radial clearance between the screw flight and barrel). In both the LDPE experiments there is a subsequent rapid reduction in upper film thickness associated with high solid bed acceleration. The mass flow rate in the upper film changes relatively slowly, so an increase in bed velocity must be accompanied by a reduction in film thickness. The lower melt film thickness, on the other hand, shows a more gradual but sustained rate of increase, all the melted material being retained in the film. The predicted lower film thicknesses tend to be rather greater than those observed in practice. This is probably due to the choice of temperature boundary condition at the screw. Estimated screw temperature profiles were employed which took no account of the necessary heat conduction along the screw.

The agreement between the predicted and measured pressure profiles is abnormally good for the LDPE experi-

ments and poor for the PVC. Taking into account other results not reported in detail here, the predicted axial pressure profiles are rather unreliable, although this appears to have very little effect on the quality of the solid bed profile predictions. The computed pressure gradients depend mainly on the melt pool analysis and the force balance on the solid bed. The latter depends on the shear stress in the lower film and hence on the film thickness which, as already mentioned, tends to be overestimated. Also, the melt pool analysis is inaccurate for non-Newtonian melts.

#### Solid bed velocities

Figures 6 to 8 suggest that solid bed velocities do not remain constant along the screw, as has been assumed by previous workers, nor are they generally subject to uniform acceleration. While in the case of PVC the solid bed velocity increased fairly steadily along the screw, with LDPE it tended to remain nearly constant until a region of high acceleration was reached. The differences observed between the two types of materials may be due as much to the difference in screw design as to the materials themselves.

#### Bed break-up and surging

In many of the experiments breaks in the solid bed normal to the screw flights were observed, usually in the compression section of the screw or at the beginning of the metering section. For example, Figures 6 and 7 show bed breaks at 0.9 m and 1.0 m along the channel respectively, whereas in Figure 8 the bed was continuous. Both these and other results show a very high correlation between the onset of bed break-up and high bed acceleration. Breaks generally occurred at regular intervals giving separate pieces of solid bed with lengths between about one and four times, their widths, with regions of melt between. Further evidence for high bed acceleration being the cause of bed break-up is provided by the fact that the lengths of the melt regions between pieces of bed increased as they moved downstream. Since melting was still largely confined to the upper and lower melt films, this suggests acceleration of the pieces.

In the theoretical model no account is taken of the deformation characteristics of the solid bed beyond conserving its mass. This is reasonable so long as the bed remains compacted and continuous, and under these conditions the model appears to be equally applicable to all types of materials in either granular or powder form. If the stresses acting on the solid bed were analysed in detail, a fracture criterion such as the presence of tensile stress might be applicable. In practice, however, high bed acceleration provides an adequate criterion for bed break-up.

Bed break-up in extruders is particularly important because it gives rise to a form of pressure surging. In the present experiments the measured pressures, particularly after bed break, fluctuated at frequencies of the order of 5 to 10 times lower than the variations of the form shown in Figure 5, associated with the screw rotation. This lower frequency could be correlated with the frequency with which bed breaks occurred<sup>12</sup>.

Surging associated with bed break-up has been observed by other workers. For example, Klein<sup>15</sup> reported both this type and another form associated with 'plugging' or wedging of the solid bed in the taper of the screw channel. This latter phenomenon was not observed in the present experiments which used relatively gently tapered screws. In general, surging in extruders appears to be of three main types: (i) variations associated with the rotation of the

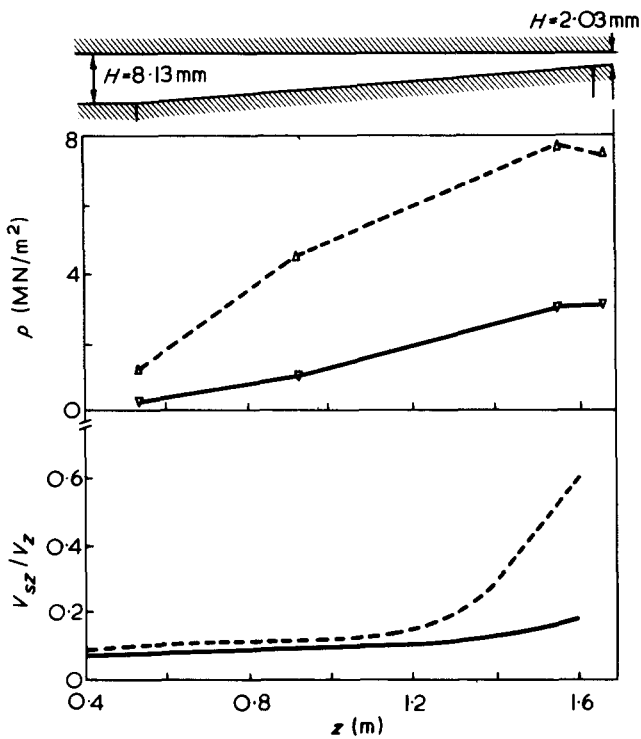


Figure 9 Measured pressure profiles and theoretical solid bed velocities for two experiments with granular polypropylene showing the effects of screw cooling. Screw as in Figures 6 and 7. Barrel temperature = 250°C,  $N = 80$  rev/min,  $M_T = 10.7$  kg/h (---, uncooled) and 8.6 kg/h (—, cooled)

screw and occurring at the same frequency; (ii) fluctuations due to instabilities in the feeding or melting processes and occurring at rather lower frequencies; (iii) very slow variations of temperatures and pressures over periods of minutes or even hours may be caused by instabilities in the temperature control systems.

#### Effects of screw cooling

It can be shown, both experimentally and theoretically, that rapid bed acceleration, and hence break-up, does not normally occur in the absence of a melt film between the bed and screw. One way to prevent the formation of this film is to cool the screw. Figure 9 shows measured pressure profiles and predicted solid bed velocity profiles for two experiments with polypropylene, one with and the other without cold water cooling on the screw. In the case of the cooled screw no lower melt film was formed until melting was nearly complete: the predicted solid bed velocity is nearly constant and the bed was unbroken. With the uncooled screw rapid bed acceleration and break-up occurred. The pressures generated during melting were also much lower, which accounted for the lower output, a lower delivery pressure being available to force melt through the die.

#### CONCLUSIONS

The present theoretical model for the melting of thermoplastics in single screw extruders is an improvement on previous models in that it allows for the formation of a melt film between the unmelted solid bed and the screw, also for the downstream velocity of this bed to vary. It provides adequate predictions of melting behaviour in terms of the reduction in the proportion of solids present at various positions along the screw. It also provides a

simple means of predicting when break-up of the solid bed is likely to occur, namely when the bed is subject to high acceleration. In its present form the model does not provide very accurate predictions of pressure generation although this does not appear to impair its ability to predict melting rates.

Changes in the theoretical model are required to predict melting behaviour after bed break-up, although if this occurs at all it tends to occur towards the end of melting. There is also considerable scope for improvement in the analysis of flow in the melt pool alongside the bed, particularly if the model is to give accurate predictions in the later stages of melting. As has been suggested previously, solid bed break-up gives rise to a form of pressure surging at a frequency lower than that of the screw rotation. One method of controlling the surging is to apply screw cooling which prevents the formation of a melt film on the screw surface, which in turn inhibits bed acceleration. Screw cooling, however, also has the effect of reducing both pressure generating capacity and output from the extruder.

#### NOMENCLATURE

$b$	temperature coefficient of viscosity
$c$	radial clearance between screw flight and barrel
$C_{ps}, C_{pm}$	specific heats of solid and melt
$D$	diameter of the barrel
$F_D, F_P$	drag and pressure flow shape factors
$H$	depth of screw channel
$H_s$	depth of solid bed
$k_s, k_m$	thermal conductivities of solid and melt
$M_{mz}$	downstream mass flow rate in melt pool
$M_{sz}$	downstream mass flow rate in solid bed
$M_T$	total mass flow rate in screw channel
$m_{fx}$	leakage mass flow rate per unit length of flight
$m_1$	mass flow rate per unit width in upper melt film
$m_{1x}$	transverse mass flow rate per unit length of solid bed, in the upper melt film
$m_{1z}, m_{2z}$	downstream mass flow rates per unit bed width in the upper and lower melt films
$N$	screw speed
$n$	power-law index
$n_1, n_2$	directions of outward normals to solid bed in the upper and lower melt films
$p$	pressure
$s$	direction of relative boundary motion in a melt film
$T$	temperature
$T_m$	melting point temperature
$T_w$	boundary wall temperature
$T_0$	reference temperature
$\bar{T}_s$	bulk mean temperature in the solid bed
$\bar{T}_1, \bar{T}_2$	bulk mean temperatures in upper and lower melt films
$U$	relative boundary velocity in a melt film
$u$	melt velocity in a melt film
$V_r$	velocity of barrel relative to the solid bed
$V_{sz}$	downstream velocity of the solid bed relative to the screw
$V_x, V_z$	transverse and downstream velocities of the barrel relative to the screw
$W$	width of the screw channel
$W_m$	width of the melt pool
$X$	width of the solid bed
$x, y, z$	Cartesian screw channel coordinates
$\beta$	angle between $V_r$ and the $z$ axis

$\gamma_0$	reference shear rate
$\delta$	thickness of a melt film
$\delta_1, \delta_2$	thicknesses of upper and lower melt films
$\theta$	helix angle of the screw
$\lambda$	latent heat of fusion
$\lambda_1, \lambda_2$	modified latent heats of fusion for the upper and lower melt films
$\mu_0$	effective viscosity at $\gamma_0$ and $T_0$
$\bar{\mu}$	mean viscosity in the melt pool
$\rho_s, \rho_m$	densities of solid and melt
$\tau$	shear stress in a melt film
$\tau_{1z}, \tau_{2z}$	downstream shear stresses in upper and lower melt films
$\omega_1, \omega_2$	melting rates per unit area in upper and lower melt films

#### ACKNOWLEDGEMENTS

The authors wish to thank Imperial Chemical Industries, Plastics Division for financial support for I. R. E., and the

Science Research Council for funding the research programme on screw extrusion.

#### REFERENCES

- 1 Pearson, J. R. A. 'Mechanical Principles of Polymer Melt Processing', Pergamon Press, Oxford, 1966
- 2 Fenner, R. T. 'Extruder Screw Design', Iliffe, London, 1970
- 3 Darnell, W. H. and Mol, E. A. *J. SPE J.* 1956, 12, 20
- 4 Lovegrove, J. G. A. and Williams, J. G. *J. Mech. Eng. Sci.* 1973, 15, 114, 195
- 5 Maddock, B. H. *SPE J.* 1959, 15, 383
- 6 Street, L. *Int. Plast. Eng.* 1961, 1, 289
- 7 Tadmor, Z., Duvdevani, I. J. and Klein, I. *Polym. Eng. Sci.* 1967, 7, 198
- 8 Martin, G. *Kunststofftechnik* 1969, 8, 238
- 9 Chung, C. I. *Mod. Plast.* 1968, 45, 178
- 10 Hinrichs, D. R. and Lilleht, L. U. *Polym. Eng. Sci.* 1970, 10, 268
- 11 Donovan, R. C. *Polym. Eng. Sci.* 1971, 11, 247
- 12 Edmondson, I. R. *PhD Thesis* University of London (1973)
- 13 Martin, B. *Int. J. Non-linear Mech.* 1967, 2, 285
- 14 Martin, B. *PhD Thesis* University of Cambridge (1969)
- 15 Klein, I. *SPE J.* 1972, 28, 47

# Broadline n.m.r. studies of ultra-high modulus polyethylenes

J. B. Smith, A. J. Manuel and I. M. Ward

*Department of Physics, University of Leeds, Leeds LS2 9JT, UK*

*(Received 8 April 1974; revised 7 June 1974)*

Broadline nuclear magnetic resonance (n.m.r.) measurements have been made for a range of isotropic and drawn high density polyethylene materials with different molecular weight distributions and three well defined thermal treatments during preparation. For the drawn materials the dependence of the n.m.r. spectra on the orientation of the static magnetic field with respect to the draw direction has been studied with respect to both line shape and second moment variation. The spectra in general show three component lines with distinctly different line widths. The broad component shows a high degree of molecular orientation in the drawn samples and can be satisfactorily assigned to the crystalline regions of the polymer. It is proposed that the intermediate component corresponds to high molecular weight molecules which interconnect the crystalline regions and are sufficiently constrained to allow motion about the chain axis only. This component shows an increasing degree of molecular orientation and decreases in intensity with increasing draw ratio. Finally, there is an isotropic narrow component, which is attributed to the mobile fraction. From its intensity in samples of different molecular weight this fraction can be associated with low molecular weight material and the ends of molecules which are rejected from the crystalline regions or the rigid fraction in a drawn sample.

## INTRODUCTION

The composite nature of the broadline nuclear magnetic resonance (n.m.r.) spectrum of crystalline polymers has been discussed in many publications<sup>1-5</sup> since it was first reported in low density polyethylene and polytetrafluoroethylene (PTFE) by Wilson and Pake<sup>6</sup>. In isotropic polymers, two components have sometimes been observed, a broad component corresponding to a rigid lattice signal, and a narrow component corresponding to a mobile fraction. To a first approximation, these broad and narrow components could be attributed to molecules in the crystalline and non-crystalline regions of the polymer respectively, although the exact details of this depended very much on defining the morphology of the polymer and the exact meaning of the term 'crystallinity'.

In some oriented polymers<sup>7</sup>, and in polymer crystals<sup>8</sup>, an additional line of intermediate width has also been observed, to give a signal with three distinguishable components. This remarkable result was first obtained by Hyndman and Origlio for oriented high density polyethylene<sup>7</sup>, and it was suggested that the intermediate line was due to oriented amorphous material and imperfect crystalline structures resulting from the drawing process. In polyethylene crystals, Fischer and Peterlin<sup>8</sup> also observed a third component of similar line width, which they attributed to molecules undergoing coherent rotational motions about the chain axis. Bergmann and Nawotki<sup>5</sup> analysed the n.m.r. spectra of a number of isotropic polyethylene samples and found that the spectra could most satisfactorily be decomposed by assuming that they represented the superposition of three lines arising from three phases of different mobility in the samples.

There is also much to be gained from studying the aniso-

tropy of the n.m.r. spectra of oriented polymers. This anisotropy relates to the distribution of molecular orientations<sup>9,10</sup>, and where there is motion, can also give considerable insight into the molecular nature of these motions<sup>11,12</sup>, and hence structural information concerning the oriented polymer.

In this paper we describe a detailed study of the anisotropy of the composite signals from a series of linear polyethylenes of different structure. The preparation and mechanical properties of four of these materials which have been studied in detail has been discussed in a previous publication<sup>13</sup>, where it was shown that oriented polymers of very high stiffnesses can be produced. In addition some measurements have been made on two samples of materials of high molecular weights. There is very considerable interest in gaining an understanding of the structure of such materials. It will be shown that broadline n.m.r. in conjunction with X-ray diffraction can throw light not only on the final structures, but also on the nature of the processes which produce these structures.

## EXPERIMENTAL

### *Preparation of samples*

Since the full details and methods used to prepare the samples have been discussed in a previous publication<sup>13</sup>, only a summary will be given here. Following the previous work, four commercial grades of Rigidex linear polyethylene homopolymer (BP Chemicals Int. UK Ltd) listed in *Table 1* as samples 1 to 4 were selected for examination. We are indebted to Mr J. M. Squire (BP Research and Development Dept., Grangemouth Division, Grangemouth, UK) for the molecular weight characterization shown in the



Table 1 Molecular weights of polyethylene samples examined

Sample No.		$\overline{M}_n$	$\overline{M}_w$
1	Rigidex Grade 9	6 060	126 000
2	Rigidex Grade 50	6 180	101 450
3	Rigidex Grade 25	12 950	98 800
4	Rigidex Grade 140-60	13 350	67 800
5	Hostalen GUR		3.5 to 4 x 10 <sup>6</sup>
6	R.N.H.		6 to 8 x 10 <sup>6</sup> (est.)

Table. The two high molecular weight samples used were Hostalen GUR (Hoechst AG, Frankfurt (Main), W. Germany) and a sample kindly provided by Professor R. N. Haward (Department of Chemistry, University of Birmingham). These samples are numbered 5 and 6 in Table 2. Sample 6 is referred to by the initials R.N.H. Sheets of the polymers of thickness about 0.5 mm were made by compression moulding at 160°C. The sheets were either allowed to cool slowly to 110°C before being quenched in water (notation 160/110/W), directly quenched in water at room temperature (notation 160/W) or allowed to cool slowly to room temperature (notation 160/RT).

Some of each sheet so prepared was kept aside for the n.m.r. investigation of the isotropic sheet. The remainder was used to prepare oriented material in the following manner.

Dumbbell shaped samples with gauge dimensions 2.0 x 0.5 cm were cut from the sheets and drawn on an Instron tensile testing machine at a cross-head speed (CS) of 10 cm/min where possible, otherwise at 1 cm/min. The draw ratio,  $\lambda$ , was measured from the separation of small ink dots marked at intervals of 1 mm on the undrawn specimen. Since  $\lambda$  varied slightly with drawing time, its value could be controlled to  $\pm 5\%$ . For Rigidex 9 samples of draw ratio 9 only were obtained, for other Rigidex materials draw ratios of 11, 19 and 30 were obtained. The high molecular weight samples (5 and 6 of Table 1) showed a markedly different drawing behaviour from the Rigidex materials. The former draw with little or no sign of a neck and the drawn material deforms elastically if the Instron cross-head is allowed to continue its motion. The Rigidex materials develop the usual neck and any attempt at further extension invariably results in the sample breaking.

Table 2 summarizes the preparation procedures for all the samples.

#### *n.m.r. experimental procedure*

The n.m.r. investigation of these samples was carried out using a Varian DP 60 spectrometer operated at 56.4 MHz. A time-averaging computer was used to add together the signals from several successive sweeps through a spectrum to improve the signal to noise ratio.

Each drawn sample consisted of a thin strip 10 cm long and 1.0 to 1.5 mm wide, depending upon the draw ratio. Strips of the polymer to be investigated were examined and sections with a uniform draw ratio were cut and packed into a slot machined in 6 mm diameter PTFE rod, so that the draw directions of all the pieces were parallel to each other and perpendicular to the PTFE rod. The orientation of the specimen could be varied by rotating the PTFE rod in the n.m.r. spectrometer coil, the angle between the sample draw direction and the static magnetic field being measured by a goniometer head attached to the rod. The angle measured

by the goniometer head was called  $\gamma'$  and spectra were recorded for the values of  $\gamma'$  in steps of 10° between -30° and +120°. Since the measured angle  $\gamma'$  usually differed by a small systematic error from the true angle  $\gamma$  between the static magnetic field and the sample draw direction, a correction was applied so that the variation of the second moments of the spectra with  $\gamma$  showed symmetry about 0° and 90°. The values of second moments were corrected for the modulation amplitude of 0.62 G, using the Andrew correction<sup>14</sup>.

For the isotropic specimens only one spectrum was recorded. A lower modulation amplitude of 0.25 G was used to try to resolve a narrow component.

#### *Wide angle X-ray diffraction measurements*

Wide angle X-ray diffraction measurements (WAXS) were used to obtain a direct measure of the orientation of the crystalline regions of the Rigidex samples. As these samples possess fibre symmetry, this can be done most conveniently by observations on the 002 reflection (for previous work of this nature see, for example, ref 15). In this investigation the measurements were carried out with a Siemens Type F wide angle X-ray diffractometer. A sample of length 1 cm was mounted horizontally using Plasticene, and its position adjusted until it was positioned centrally on the goniometer and exactly perpendicular to the X-ray beam. The value of the Bragg angle for the 002 reflection was found by scanning through the diffraction peak at a rate of 0.1°/min. The detector was then fixed at this Bragg angle and the sample rotated in  $\frac{1}{8}^\circ$  steps. At the end of each step the detector switched on and counted for 200 sec, printing out the count rate at the end. Each step brought different 002 planes into a position to satisfy the diffraction conditions, and the count was therefore directly proportional to the number of 002 planes involved. The appropriate orientation functions were then evaluated from the count rate as a function of angle. Errors were evaluated on the basis that the standard deviation of an X-ray count is simply the square root of that count; they were minimized by counting for a long time (200 sec) at the end of each step.

Table 2 Preparation of samples  
CS: Instron cross-head speed (cm/min);  $t_D$ : drawing time (min)

Sample	160/W	160/RT	160/110/W
Rigidex Grade 9	CS = 10 $t_D$ = 1.5 $\lambda$ = 9	—	—
Rigidex Grade 50	CS = 10 $t_D$ = 1.0 $\lambda$ = 11	CS = 1 $t_D$ = 10 $\lambda$ = 19	CS = 1 $t_D$ = 10 $\lambda$ = 30
Rigidex Grade 25	CS = 10 $t_D$ = 1.5 $\lambda$ = 11	—	CS = 10 $t_D$ = 1.5 $\lambda$ = 19
Rigidex Grade 140-60	CS = 10 $t_D$ = 1.0 $\lambda$ = 11	CS = 10 $t_D$ = 1.5 $\lambda$ = 19	CS = 10 $t_D$ = 1.5 $\lambda$ = 30
Hostalen GUR	CS = 10 $t_D$ = 1.0 $\lambda$ = 3½	—	—
R.N.H.	—	CS = 10 $t_D$ = 1.0 $\lambda$ = 4	—

## RESULTS

## General nature of the n.m.r. results

Figures 1a–1d show the room temperature n.m.r. derivative spectra for the isotropic specimens of the four Rigidex materials following three types of thermal treatment after compression moulding. The two Rigidex 50 specimens which were allowed to cool slowly for part of the time after moulding (160/110/W and 160/RT) show a very narrow line in addition to the broad and intermediate components usually seen in isotropic polyethylene. We believe that this line is present in the spectra of the three other Rigidex materials

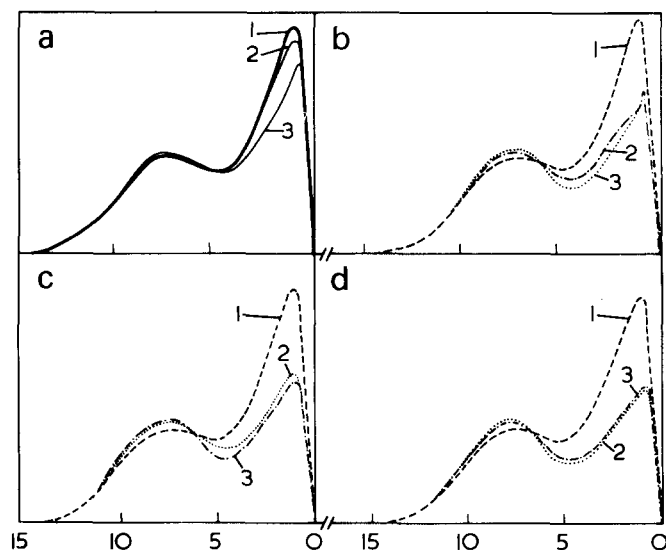


Figure 1 Derivative wide-line n.m.r. spectra for the series of isotropic Rigidex high density polyethylene specimens subjected to different thermal treatments. (a) Rigidex 9; (b) Rigidex 50; (c) Rigidex 25; (d) Rigidex 140-60. The numbers of the curves refer to the thermal treatments described in the text: (1) 160/W; (2) 160/110/W; (3) 160/RT. The abscissae are in G and the ordinates represent absorption derivative normalized to unit (integrated) intensity. Only the low field (left hand) halves of the spectra are shown

to a lesser extent, but that it is swamped by the intermediate component. The spectra for the static magnetic field at  $\gamma = 0, 45$  and  $90$  degrees for the drawn materials are shown in Figures 2a–2d. The spectra of the isotropic and drawn materials may be compared directly since they have been normalized to give unit (integrated) intensity. The three components are noticeably better resolved in the  $\gamma = 0$  spectra of the drawn materials and the narrow component becomes clearly visible in the spectra of Rigidex 50, 25 and 140-60. The spectra of these three materials also show a decrease in the intensity of the intermediate line and an increase in the intensity of the narrow line with increasing draw ratio. However, it should be noted that even at its maximum value the narrow line represents the contribution of only a small fraction of the material.

The existence of three components of differing widths points to the presence of material of three different degrees of molecular motion, both in the isotropic and drawn samples.

The broad component is readily identified as being associated with the crystalline regions and we will show that the observed second moments of the spectra are consistent with this interpretation. The very narrow line is also clearly associated with non-crystalline material. It is the intermediate component which is less easy to be completely certain about. It shows some angular dependence, and has a second moment in a range consistent with hindered rotation of the chain molecules as discussed in detail later.

The spectra were therefore analysed along the following lines. First, the three components can be most readily separated for  $\gamma = 0$ , and this gives a good value for the mass fraction of the three components. Secondly, the total second moment in each case was divided into contributions from the crystalline and intermediate regions. (The very narrow line makes a negligible contribution to the second moment.) Decomposition of the spectra at various angles,  $\gamma$ , enabled orientation functions for the intermediate component to be obtained, on the basis that this arose from molecules undergoing motion about the chain axis, either as chain rotations or torsional vibrations, which can be

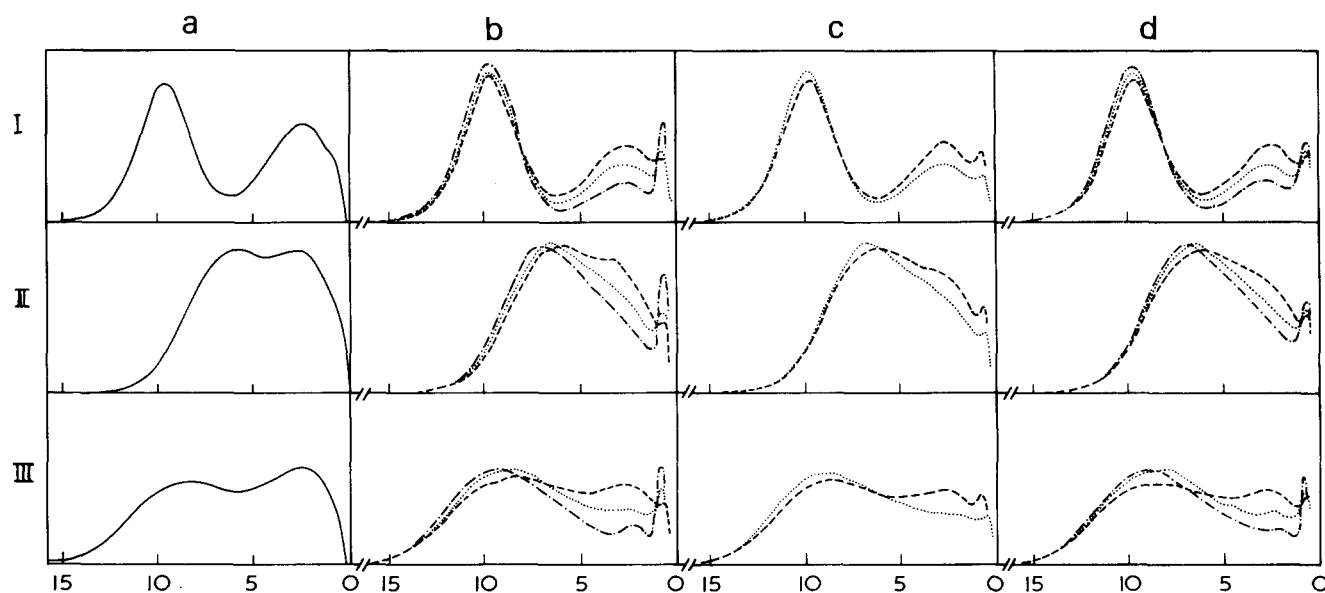


Figure 2 Derivative wide-line n.m.r. spectra for the drawn Rigidex materials for the 3 orientations with respect to the static magnetic field  $\gamma = 0, 45$  and  $90^\circ$ . (a) Rigidex 9, draw ratio  $\lambda = 9$ ; (b) Rigidex 50; (c) Rigidex 25; (d) Rigidex 140-60. — draw ratio  $\lambda = 11$ ; ----, draw ratio  $\lambda = 19$ ; ····, draw ratio  $\lambda = 30$ . I,  $\gamma = 0$ ; II,  $\gamma = 45$ ; III,  $\gamma = 90$ . The abscissae are in G and the ordinates represent absorption derivative normalized to unit (integrated) intensity. Only the low field (left-hand) halves of the spectra are shown.

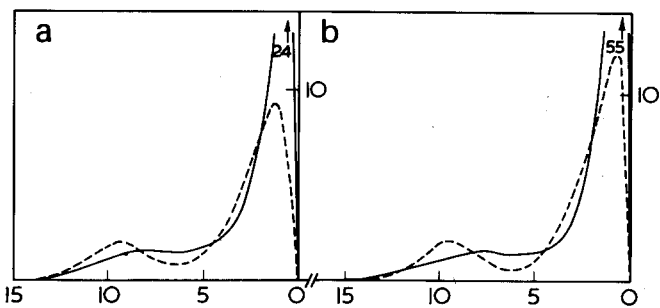


Figure 3 Derivative wide-line n.m.r. spectra for (a) Hostalen GUR, (—, isotropic material; --- drawn to draw ratio  $\lambda = 3.5$ ) and (b) R.N.H. (— isotropic material; --- drawn to draw ratio  $\lambda = 4$ ). The abscissae are in G and the ordinates in arbitrary units normalized to the same integrated intensity. The scale shown is purely to indicate the height of the maxima in the undrawn materials

shown to be a reasonable assumption. The procedures outlined above will be described in detail in the following paragraphs.

The spectra for the materials of high molecular weight (samples 5 and 6 of Table 1) are shown in Figure 3. The derivative spectra of these materials before drawing show a much smaller broad component than the materials discussed earlier, and a narrower component of considerably greater intensity which overlaps the regions in which the narrow and intermediate components of the Rigidex materials occur. The main effect of drawing is to reduce the height and broaden the narrower line giving it a form closer to that of the intermediate line of the Rigidex materials.

*Determination of the crystalline, intermediate and mobile mass fractions of the specimens*

The proportions of crystalline, intermediate and mobile material in each sample were determined from their spectra. The crystalline mass fraction  $f^c$  is given by the ratio of the integrated intensity of the crystalline component to the total integrated intensity. The mass fractions of the intermediate ( $f^i$ ) and mobile ( $f^m$ ) material were determined in a similar manner. The spectra of the materials were each decomposed into their three components as accurately as possible, those for  $\gamma = 0$  being used for the drawn materials because they show the best resolution of the components.

Separation of the narrow components in the drawn material is straightforward. In the isotropic samples it is somewhat more difficult, but the narrowness of the line still ensures that the errors involved will be small. Separation of the broad component from the remainder of the spectrum was, however, rather more difficult. In the isotropic case the room temperature spectrum of an isotropic sample of Rigidex 075-60 grade (Figure 4) prepared by cooling from the melting point ( $251^\circ\text{C}$ ) at a pressure of 5.2 kbar was used as a guide. In this material of high crystallinity the broad component is dominant and can easily be separated to give the room temperature spectrum of an isotropic aggregate of crystalline material. The line shape obtained in this way agreed well with that given by Bergmann and Nawotki<sup>5</sup> and used by them in their work on the decomposition of the spectra of a number of isotropic polyethylene specimens. This shape was used in the decomposition of the spectra of the isotropic Rigidex specimens by matching it to the outer part of the experimental spectrum where the other line components were expected to make no contribution, using a least squares computation. In the drawn case use was made of the results of the X-ray measurements which showed that the crystalline regions of the materials were virtually

fully oriented for the range of draw ratios under consideration. It was therefore possible to use an approximate theoretical calculation<sup>16</sup> (see Appendix and Figure 4) of the rigid lattice line shape for the crystalline material as a guide to decomposing the spectral lines. The theoretically calculated shape was modified to take account of the modulation amplitude and allowance was then made for the effect of some motional narrowing in matching the outer parts of the broad component to the experimental spectrum by the least squares procedure. It was assumed that motion present in the crystalline regions at room temperature would not change the line shape qualitatively. This assumption is most likely to be true for  $\gamma = 0$ . The line shape which gave the best fit in decomposition of the  $\gamma = 0$  spectrum for the 140-60 grade at  $\lambda = 30$ , for which the best resolution occurred, is also shown in Figure 4, and this shape was used in the decomposition of the remaining  $\gamma = 0$  spectra. The doublet structure is partly resolved for the  $\gamma = 0$  direction because for all the  $\text{CH}_2$  groups the internuclear vector joining a pair of protons is closely perpendicular to the direction of the static magnetic field.

*Evaluation of the angular dependence of the second moment of the crystalline component*

The variation with  $\gamma$  of the second moments of the crystalline components of the spectral lines was evaluated from the decomposition of a series of spectra of the Rigidex 140-60 grade for draw ratio 30. This specimen showed the most highly resolved broad component, and it was assumed that because the X-ray results showed the crystalline regions of all the drawn materials to be virtually fully oriented, the second moment variation of the broad component obtained from the spectra of this specimen would be typical of all the other drawn samples. The decompositions were of necessity rather arbitrary, especially for values of  $\gamma$  around  $45^\circ$ . However, the shape of the broad component for an assembly of fully oriented crystals was calculated for each required value of  $\gamma$  (see Appendix) and used as a guide in the decom-

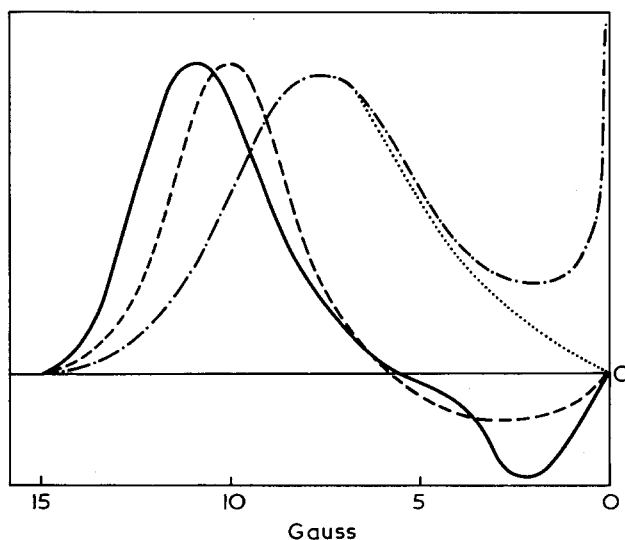


Figure 4 Derivative wide-line n.m.r. line shapes for crystalline polyethylene: —, Rigidex 075-60 prepared by cooling from the melting point of  $251^\circ\text{C}$  at a pressure of 5.2 kbar; ----, modification assumed for isotropic crystalline material in the decomposition of the spectra of Figure 1; ..... rigid lattice line shape for the static magnetic field along the  $c$  axis as calculated in the Appendix; —, line shape giving the best fit to Rigidex 140-60,  $\lambda = 30$  for  $\gamma = 0$  in Figure 2, after allowing for modulation broadening and smoothing and some motional narrowing

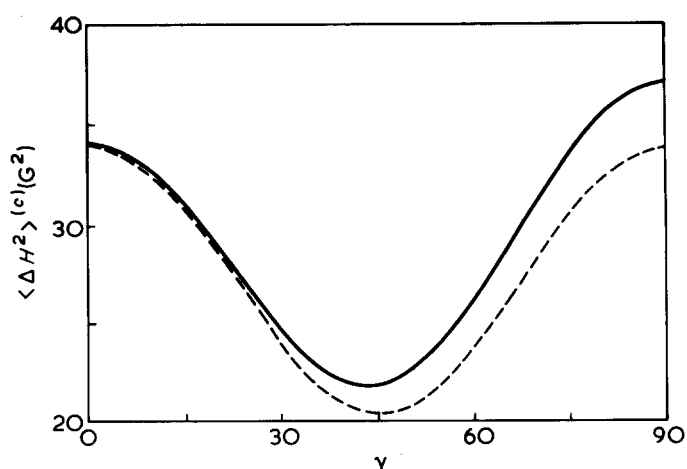


Figure 5 Variation of the second moment  $\langle \Delta H^2 \rangle^c$  for crystalline high density polyethylene with full  $c$  axis orientation along the draw direction and transverse isotropy: —, determined from decomposition of spectra of Rigidex 140-60 at draw ratio  $\lambda = 30$ ; —, calculated by McBrierty and Ward<sup>9</sup> for a rigid polyethylene lattice at  $-196^\circ\text{C}$

positions. Again it was assumed that motion present in the crystalline regions at room temperature would not change these line shapes qualitatively. Each decomposition was checked by verifying that the ratio of the integrated intensity of the broad component to the total integrated intensity remained constant and equal to the crystalline mass fraction of the specimen.

The variation of second moment of the fully oriented crystalline material obtained in this manner is shown in Figure 5.

#### Determination of orientation distribution functions for the intermediate material

The distribution of orientations of the molecular axes of the material giving rise to the intermediate line may be characterized by the values of  $\langle \cos^2 \Delta^i \rangle$  and  $\langle \cos^4 \Delta^i \rangle$  where  $\Delta$  is the angle between the molecular axis and the draw direction of the sample. These two quantities were determined from the variation of the second moment of the intermediate component of the spectra with  $\gamma$ . Since the narrow component arising from the highly mobile fraction gives negligible contribution to the second moment, the second moment of the intermediate component  $\langle \Delta H^2 \rangle^i$  can be obtained from the total second moment  $\langle \Delta H^2 \rangle^c$  and the second moment of the broad component  $\langle \Delta H^2 \rangle^b$ :

$$f^i \langle \Delta H^2 \rangle^i = \langle \Delta H^2 \rangle^c - f^b \langle \Delta H^2 \rangle^b \quad (1)$$

The variation with  $\gamma$  of the second moments for the four Rigidex samples is shown in Figure 6 and the corresponding  $\langle \Delta H^2 \rangle^i$  deduced from them using the data of Figure 5 and equation (1) are shown in Figures 7a-7d.

The shapes of the curves of Figure 7 show qualitative similarity with the theoretical calculations of Folkes and Ward<sup>12</sup> for the second moment variation of an assembly of oriented chains undergoing a rotational motion about their axis. The expression obtained by Folkes and Ward<sup>12</sup> may be written:

$$\begin{aligned} \langle \Delta H^2 \rangle^i = & (G/32) S \{ (11 - 30 \cos^2 \gamma + 27 \cos^4 \gamma) + \\ & \langle \cos^2 \Delta \rangle (252 \cos^2 \gamma - 270 \cos^4 \gamma - 30) + \\ & \langle \cos^4 \Delta \rangle (315 \cos^4 \gamma - 270 \cos^2 \gamma + 27) \} \quad (2) \end{aligned}$$

where  $S$  is a lattice sum given by:

$$S = \frac{1}{N} \sum_{j>k} r_{jk}^{-6} (3 \cos^2 \theta_{jk} - 1)^2 \quad (3)$$

in which  $N$  is the number of protons over which the sum is taken,  $r_{jk}$  the distance between protons  $j$  and  $k$ ,  $\theta_{jk}$  the angle between the vector  $r_{jk}$  and the  $c$  axis of the crystalline material and  $G = 3/2 [I(I+1)g^2\mu_n^2]$ .  $I$  is the nuclear spin number,  $g$  the nuclear  $g$  factor and  $\mu_n$  the nuclear magneton. The present treatment follows closely that adopted by McBrierty and Ward<sup>9</sup>, and Folkes and Ward<sup>12</sup>. The expression (3) for  $S$  is identical to that quoted in these papers, although the factor  $1/N$  was erroneously omitted previously.

The intramolecular contribution to the lattice sum  $S$  for

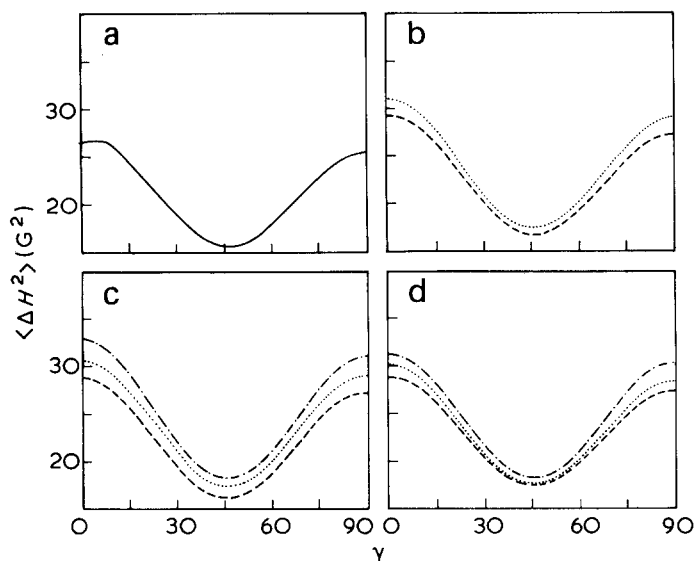


Figure 6 Total second moment  $\langle \Delta H^2 \rangle^c$  as a function of orientation angle  $\gamma$  for the drawn samples of Rigidex high density polyethylene. (a) Rigidex 9,  $\lambda = 9$ ; (b) Rigidex 25; (c) Rigidex 140-60; (d) Rigidex 50. —, Draw ratio  $\lambda = 11$ ; ..., draw ratio  $\lambda = 19$ ; —, draw ratio  $\lambda = 30$

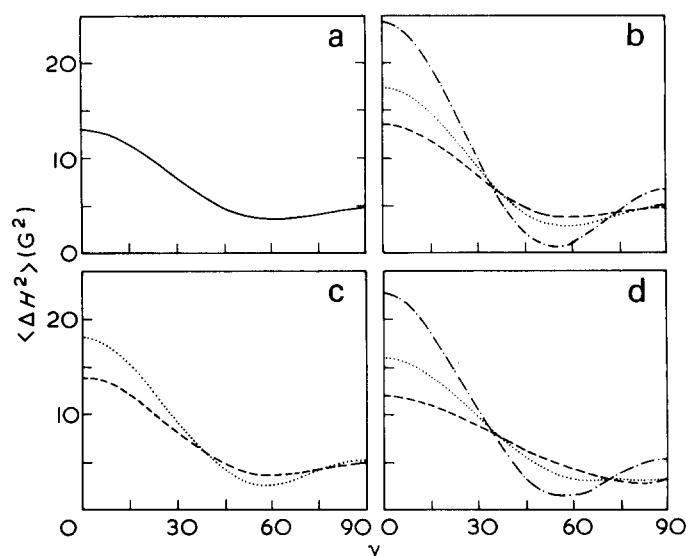


Figure 7 Second moments  $\langle \Delta H^2 \rangle^i$  of the intermediate components of the drawn samples of Rigidex high density polyethylene as function of orientation angle  $\gamma$ , deduced as described in the text. (a) Rigidex 9,  $\lambda = 9$ ; (b) Rigidex 140-60; (c) Rigidex 25; (d) Rigidex 50. —, draw ratio  $\lambda = 11$ ; ..., draw ratio  $\lambda = 19$ ; —, draw ratio  $\lambda = 30$

a system of rotating chains in a polyethylene crystal has been evaluated using (3) as 0.0321. This value has been reduced to 0.030 in our calculations to allow for other motions such as vibrations excited at room temperature. This is consistent with the previous work, but the actual value is approximately one-half that quoted in ref 12. This is because in the earlier papers<sup>9,12</sup> the lattice sums calculated for the two non-equivalent protons of polyethylene have been added together instead of averaged.

In the actual computation, the lattice sum is calculated for  $N$  protons on a crystalline lattice with  $n$  non-equivalent positions, i.e.  $N/n$  of each type. The term in the Van Vleck second moment formula:

$$\frac{1}{N} \sum_{k>j} r_{jk}^{-6} (3 \cos^2 \theta_{jk} - 1)^2$$

may thus be written as:

$$\begin{aligned} & \frac{1}{2} \frac{N}{n} \frac{1}{N} \sum_{m=1}^n \sum_{k \neq m} r_{mk}^{-6} (3 \cos^2 \theta_{mk} - 1)^2 \\ & = \frac{1}{2} \frac{1}{n} \sum_{m=1}^n \sum_{k \neq m} r_{mk}^{-6} (3 \cos^2 \theta_{mk} - 1)^2 \end{aligned}$$

where the index  $m$  runs over the  $n$  non-equivalent protons. This means that for each non-equivalent proton  $m$  the sum

$$\sum_{k \neq m} r_{mk}^{-6} (3 \cos^2 \theta_{mk} - 1)^2$$

is found and one-half of the average of these sums gives the required lattice sum. We have elaborated on this point because the exact connection between the Van Vleck second moment formula and its computation has led to some confusion in previous papers. In one of these<sup>12</sup> it is even incorrectly stated that  $N$  in the second moment formula refers to the number of non-equivalent protons.

Equation (2) was fitted to the experimental results of Figure 7 by a least squares procedure, to give values of  $\langle \cos^2 \Delta \rangle^i$  and  $\langle \cos^4 \Delta \rangle^i$  for the intermediate fraction of the material. The values of these parameters are shown in Table 4.

## DISCUSSION

Figures 6a–6d show the variation of the total second moments with  $\gamma$  for the drawn Rigidex materials at different draw ratios. There is a very clear increase in the total second moment at all orientations as the draw ratio is increased. For any given  $\gamma$ , the second moment of the broad component in the drawn materials will be independent of draw ratio, because the X-ray data show that the crystalline regions are very close indeed to full orientation, even at the lowest draw ratios examined. Moreover, the second moment of the very narrow component is negligible. The increase in total second moment with increasing draw ratio must therefore be due to a change in the fraction of the intermediate component.

We will now attempt to give a more detailed analysis by considering the orientation and proportion of each component separately.

### Broad component

As previously described, the starting point for analysing the broad component was to fit theoretically calculated line shapes for a fully oriented lattice to the room temperature spectra of the Rigidex 140-60 for  $\gamma = 30$ . The second moment variation evaluated from these decompositions is shown in Figure 5 together with the theoretical variation for a fully oriented rigid lattice using the results of McBrierty and Ward<sup>9</sup> for high density polyethylene. The two curves are quite similar, and the observed reduction in second moment with increasing  $\gamma$  is characteristic of the onset of motion about the chain axis. This rotation is, however, clearly very restricted, which is consistent with the view that 'gear wheel' hindrances<sup>12</sup> prevent full rotation below 60°C. The broad component can therefore be confidently attributed to the crystalline regions of the polymer.

The values of  $\langle \cos^2 \Delta \rangle^c$  and  $\langle \cos^4 \Delta \rangle^c$  characterizing the orientation of the crystalline regions obtained from WAXS measurements are given in Table 3. There is clearly a high degree of orientation in all the drawn specimens so that the line shapes of the components of the spectra due to the crystalline fractions are effectively the same. The mass fractions,  $f^c$ , of the crystalline material obtained from the n.m.r. spectra are also given in Table 3. In the drawn materials there is a steady increase in crystalline mass fraction with increasing draw ratio. Although we believe that this is a genuine increase in crystallinity, it is possible that some

Table 3 Crystalline mass fractions for isotropic and drawn materials (n.m.r. measurements) and crystalline orientation functions for drawn materials (WAXS measurements)

Rigidex Grade	Thermal treatment	$f^c$		Draw ratio $\lambda$	$\langle \cos^2 \Delta \rangle^c$	$\langle \cos^4 \Delta \rangle^c$
		Isotropic	Drawn			
9	160/W	0.69	0.70	9	0.996	0.991
	160/RT	0.75	—	—	—	—
	160/110/W	0.75	—	—	—	—
50	160/W	0.68	0.77	11	0.996	0.993
	160/RT	0.79	0.83	19	0.997	0.994
	160/110/W	0.76	0.88	30	0.997	0.995
25	160/W	0.67	0.77	11	0.997	0.994
	160/RT	0.79	—	—	—	—
	160/110/W	0.77	0.84	19	0.998	0.996
140-60	160/W	0.69	0.77	11	0.997	0.995
	160/RT	0.80	0.84	19	0.998	0.996
	160/110/W	0.77	0.90	30	0.998	0.996

**Table 4** Intermediate material mass fractions for isotropic and drawn materials (n.m.r. measurements) and intermediate material orientation functions for drawn materials (n.m.r. measurements)

Rigidex Grade	Thermal treatment	$f_i$		Draw ratio $\lambda$	$\langle \cos^2 \Delta \rangle_i$	$\langle \cos^4 \Delta \rangle_i$
		Isotropic	Drawn			
9	160/W	0.31	0.29	9	0.67	0.55
	160/RT	0.25	—	—	—	—
	160/110/W	0.25	—	—	—	—
50	160/W	0.32	0.22	11	0.7	0.58
	160/RT	0.21	0.16	19	0.83	0.73
	160/110/W	0.24	0.11	30	0.92	0.90
25	160/W	0.33	0.22	9	0.72	0.60
	160/RT	0.21	—	—	—	—
	160/110/W	0.23	0.15	19	0.84	0.75
140-60	160/W	0.31	0.22	11	0.80	0.60
	160/RT	0.20	0.15	19	0.94	0.78
	160/110/W	0.23	0.09	30	0.98	0.92

chains are rigid and fully extended without being incorporated into the crystalline lattice.

It can be seen from *Table 3* that the crystalline mass fraction of the drawn samples correlates with the draw ratio, and not with the crystalline mass fraction of the isotropic starting material. For example, the highest level of crystalline mass fraction amongst the isotropic sheets is to be found in these materials allowed to cool slowly from 160°C to room temperature, whereas amongst the drawn samples it is to be found at the highest draw ratios for the 140-60 and 50 grades. This would seem to imply that, as far as crystallinity is concerned, the drawn materials do not retain any direct memory of the initial isotropic material from which they were drawn. This would be consistent with the morphological evidence that a complete breakdown of the initial morphology takes place when material is drawn to very high draw ratios.

#### Intermediate component

In discussing the results for the intermediate component it is necessary to consider whether our knowledge of the crystallization behaviour of polyethylene can throw any light on the nature of the intermediate component in the isotropic material. Crystallization studies on fractionated samples of linear polyethylene<sup>17</sup> indicate that the half life for crystallization as a function of molecular weight shows a minimum value at a molecular weight of about 20 000. This minimum is most pronounced for crystallization temperatures of ~110–120°C. If we accept that in an unfractionated sample such considerations also apply<sup>13</sup>, then particularly in the case of samples 160/110/W, the broad crystalline component will consist primarily of molecules of intermediate molecular weight. It is plausible to associate the narrow line with those molecules of low molecular weight, which do not crystallize. These molecules would be expected to be highly mobile; consequently this component is narrow and isotropic even in the drawn materials.

The intermediate component can then be associated with the high molecular weight molecules. It is quite possible that parts of these molecules are included in the crystalline regions, so that the intermediate component arises from interlamellar material. Such material would consist of molecular chains whose ends were constrained, their degree of mobility being greater than that of the crystalline regions but much less than that of the mobile fraction. The n.m.r. component from such molecules would be isotropic and of

intermediate linewidth. On drawing, these molecules would become oriented towards the draw direction to an extent depending on the draw ratio. If we accept that the intermediate component corresponds to high molecular weight molecules which are sufficiently constrained by the crystalline material present to allow motion about the chain axis only, the following tentative explanation of effect of draw ratio can be put forward.

The drawing process decreases the proportion of intermediate component (*Table 4*) and correspondingly increases that of the broad (*Table 3*) and narrow components (*Figure 2*). This suggests that a proportion of the high molecular weight chains now become rigid. This probably occurs by their becoming incorporated in the crystalline regions although it is possible that some chains are fully extended and held under stress in a crystalline structure with some imperfections.

The drawing process also increases the orientation of the high molecular weight molecules, i.e. the intermediate component (*Table 4*), this increase being greater for the narrower molecular weight distribution. This result is to be anticipated on purely geometrical grounds, since a given degree of stretching would be expected to produce greater overall orientation in the case where the structure is more homogeneous. The orientation of the intermediate material appears to approach a limiting value at high draw ratios, and it is possible to speculate that this is the limiting degree of orientation possible in these structures by drawing processes alone. Any further orientation could only take place by a recrystallization process, since attempts to produce further alignment and pulling out of molecules will only initiate fracture of the material.

#### Narrow component

Inspection of *Figures 2a–2d* shows that the isotropic narrow component, which is attributed to the mobile fraction, increases markedly with increasing draw ratio in the range from draw ratio 9 to 30. The magnitude of the narrow component is also greater in the samples with lower number-average molecular weight. These results are consistent with the assignment of the mobile fraction to the low molecular weight material which does not crystallize during the cooling or quenching processes, when the isotropic sheets are produced. The increase in the narrow component with increasing draw ratio is also consistent with the breakdown of the initial morphology on drawing. It suggests that both

low molecular weight material and the ends of molecules can be rejected from the crystalline regions or the rigid fraction in a drawn structure.

In the isotropic samples the narrow and intermediate components are only separated in the case of sample 2. Now the intensity of the narrow component relates to  $\overline{M}_n$ , and increases as  $\overline{M}_n$  decreases. The intensity of the intermediate component, on the other hand, relates to  $\overline{M}_w$  and increases as  $\overline{M}_w$  increases. We therefore require a broad distribution as well as a low value of  $\overline{M}_n$  to separate the two components, and this situation is best achieved in our samples by sample 2.

### High molecular weight materials

Figures 3a and 3b show the derivative wide-line n.m.r. spectra for the two high molecular weight samples (5 and 6 of Table 1) before and after drawing. The spectra of the drawn materials are for  $\gamma = 0$ . As before, selective crystallization of a small molecular weight range produces a broad component. Of the molecules left, those with a molecular weight too large to crystallize will produce an intermediate component. These molecules are probably undergoing rotation about their chain axes when there is sufficient crystalline material present to otherwise constrain their motion. This will not be true for high molecular weight samples such as these; there is simply not sufficient crystalline material present to constrain all of the free ends of the long chains. In this case, motion in the intermediate region will be of a more general type, and the corresponding component becomes comparatively narrow. The remainder have a molecular weight too small to crystallize and will give rise to a narrow component; this is swamped by the intermediate component in these spectra and is therefore not resolved. A comparison of the  $\gamma = 0$  spectrum with that of the undrawn material shows that, as before, the broad component increases in intensity and the intermediate component broadens when the material is drawn. This is interpreted as an increase in the crystalline mass fraction and orientation of the intermediate region on drawing. Since there is a relatively small proportion of crystalline material present in the isotropic material, the deformation of these samples will be as a network of entangled long chains. The orientation of the molecules in the intermediate region will be limited since there are so few 'anchor' points available for the ends of the chains.

### ACKNOWLEDGEMENTS

We are especially indebted to Dr G. Capaccio for his advice and assistance in the preparation of the highly oriented sheets. We also wish to thank him for valuable discussions, particularly concerning the interpretation of the n.m.r. spectra of the isotropic compression moulded sheets.

We are also indebted to Dr R. Jakeways for supervising the X-ray diffraction measurements, and to Mr A. G. Gibson for the preparation of the pressure-crystallized chain extended polyethylene.

Finally, we wish to acknowledge the extensive use of the Leeds University Computing facilities and the tenure of a Science Research Council research studentship by J.B.S.

### REFERENCES

- 1 Slichter, W. P. and McCall, D. W. *J. Polym. Sci.* 1957, **25**, 230
- 2 Ward, I. M. *Trans. Faraday Soc.* 1960, **56**, 648

- 3 Fuschillo, N., Rhian, E. and Sauer, J. R. *J. Polym. Sci.* 1959, **25**, 38
- 4 Olf, H. G. and Peterlin, A. *J. Appl. Phys.* 1964, **35**, 3108
- 5 Bergmann, K. and Nawotki, K. *Kolloid-Z.* 1967, **219**, 132
- 6 Wilson, C. W. and Pake, G. E. *J. Chem. Phys.* 1957, **27**, 115
- 7 Hyndman, D. and Origlio, G. F. *J. Polym. Sci.* 1969, **36**, 556
- 8 Fischer, E. W. and Peterlin, A. *Makromol. Chem.* 1964, **74**, 1
- 9 McBrierty, V. J. and Ward, I. M. *J. Phys. (D: Appl. Phys.)* 1968, **1**, 1529
- 10 Kashiwagi, M., Cunningham, A., Manuel, A. J. and Ward, I. M. *Polymer* 1973, **14**, 111
- 11 Olf, H. G. and Peterlin, A. *J. Polym. Sci. (A-2)* 1970, **8**, 753
- 12 Folkes, M. J. and Ward, I. M. *J. Mat. Sci.* 1971, **6**, 582
- 13 Capaccio, G. and Ward, I. M. *Polymer* 1974, **15**, 233
- 14 Andrew, E. R. *Phys. Rev.* 1953, **91**, 425
- 15 Gupta, V. B. and Ward, I. M. *J. Macromol. Sci. (B)* 1970, **4**, 453
- 16 Evans, W. A. B. and Powles, J. G. *Phys. Lett.* 1967, **24A**, 218
- 17 Fatou, J. M. G. and Barrales-Rienda, J. M. *J. Polym. Sci., (A-2)* 1969, **7**, 1755
- 18 Kubo, R. and Tomita, K. *J. Phys. Soc. Japan* 1954, **9**, 888
- 19 Abragam, A. 'The principles of nuclear magnetism', Clarendon Press, Oxford, 1961
- 20 Bunn, C. W. *Trans. Faraday Soc.* 1939, **35**, 482
- 21 Betsuyaku, H. *Phys. Rev. Lett.* 1970, **24**, 934

### APPENDIX

#### Calculation of the n.m.r. line shape for polyethylene crystal assemblies

In a solid such as polyethylene the n.m.r. absorption line shape,  $g(\omega)$ , is mainly determined by the magnetic dipolar interactions between the precessing nuclear spins. These dipolar interactions are also responsible for the decay of the transverse magnetization (the Bloch decay or free induction decay) observed in a pulsed n.m.r. experiment. It can be shown<sup>18</sup> that the n.m.r. absorption line shape,  $\hat{g}(\omega)$ , is the Fourier transform of the amplitude of the Bloch decay,  $G(t)$ . The relationship is discussed fully by Abragam<sup>19</sup> where expansion formulae for  $G(t)$  based on the theory of Kubo and Tomita<sup>18</sup> are considered in some detail. For polyethylene we have used the results of a perturbation expansion calculation by Evans and Powles<sup>16</sup> for the first two terms of an expansion for  $G(t)$ :

$$G(t) = G_0(t) + G_1(t) + \dots \quad (A1)$$

where

$$G_0(t) = \sum_{j=1,2} \prod_{r \neq j} \cos B_{jr} t \quad (A2)$$

$$G_1(t) = \frac{1}{3} \sum_{j=1,2} \prod_{k \neq j} B_{jk} \sin(B_{jk} t) \times$$

$$\left[ t \prod_{r \neq j,k} \cos(B_{jr} t) - \int_0^t dt_1 \prod_{r \neq j,k} \cos\{B_{jr} t + (B_{kr} - B_{jr}) t_1\} \right] \quad (A3)$$

with

$$B_{jk} = \frac{3}{4} \gamma^2 \hbar (1 - 3 \cos^2 \theta_{jk}) r_{jk}^{-3} \quad (A4)$$

$r_{jk}$  is the internuclear vector between protons  $j$  and  $k$  and

$\theta_{jk}$  is the angle between  $r_{jk}$  and the direction of the static magnetic field.

In calculating  $G_0(t)$  and  $G_1(t)$  for the polyethylene lattice, the crystal structure data of Bunn<sup>20</sup> have been used. The summations over  $j = 1, 2$  correspond to terms contributed by the two non-equivalent protons in the polyethylene unit cell and the indices  $r$  and  $k$  have been taken over all neighbours within a sphere of radius 7 Å corresponding to 101 and 103 neighbours respectively for the two non-equivalent protons. The values of  $G_0(t) + G_1(t)$  were calculated for intervals of 1 μsec in  $t$ . The resulting function has an oscillating decay and the calculations were continued to a value for  $t = t_f$  at which the amplitude of  $G_0(t) + G_1(t)$  fell to 0.001 of its initial value. These computations were carried out on an ICL 1906A computer. The Fourier transforms:

$$g(\omega) = \int_0^{t_f} [G_0(t') + G_1(t')] \cos \omega t' dt' \quad (\text{A5})$$

where evaluated numerically on a PDP 8 computer.

The whole calculation was carried out for a sufficient number of orientations of the static magnetic field with respect to the polyethylene crystal axes to form averages appropriate to assemblies of highly oriented crystals with their  $c$  axes along the draw direction and a random distribution of the  $a$  and  $b$  axes in the transverse plane, as in the specimens measured in the present work.

The absorption line shape functions  $g(\omega)$  were transformed to magnetic field units. The result obtained for the static magnetic field along the  $c$  axis is shown in *Figure 4* and discussed in the section on determination of mass fractions.

Since Evans and Powles' work<sup>16</sup>, Betsuyaku<sup>21</sup> has extended the calculation of the series expansion of  $G(t)$  to give an expression for  $G_2(t)$ . The calculations for polyethylene are being extended to determine  $G_2(t)$  and a more detailed account of this work will be published separately.



# Note to the Editor

## Chlorination of 1,4-polybutadiene

J. C. Bevington and L. Ratti\*

Department of Chemistry, The University of Lancaster, Lancaster LA1 4YA, UK  
(Received 2 June 1974; revised 5 August 1974)

### INTRODUCTION

A re-examination of the structures of the products from the photo-chlorination of polystyrene has already been reported<sup>1</sup>. A similar study has been performed on the products of the dark chlorination of 1,4-polybutadiene in solution; if addition of chlorine to the double bonds were the sole reaction, the final product would be 'head-to-head' poly(vinyl chloride) (with repeating unit  $-\text{CH}_2\text{.CHCl.CHCl.CH}_2-$ ) and the number average molecular weight ( $\bar{M}_n$ ) would rise to 2.3 times the value for the original polymer.

### EXPERIMENTAL

Samples of *cis*- and *trans*-1,4-polybutadiene containing respectively 96% *cis* and 93% *trans* units, were obtained from the Phillips Petroleum Company. Chloroform was treated with silica gel to remove ethanol. In most experiments, polymer (0.5 g) was dissolved in chloroform (100 ml); a solution of chlorine (1.5 g) in chloroform (60 ml) was added with stirring over a period of 20 min. The mixture was kept at 20°C in the dark and then purged with nitrogen. The polymer was recovered by precipitation in methanol, purified by solution in tetrahydrofuran followed by precipitation in methanol and finally dried at room temperature in vacuum.

Analyses for chlorine were performed by Strauss of Oxford. For determinations of  $\bar{M}_n$ , a Mechrolab membrane osmometer (type 501) was used at 37°C with solutions in toluene. Infra-red spectra were recorded for polymer samples in KBr discs using a Perkin-Elmer spectrometer 225. Raman spectra were obtained for polymers as powders using a Cary 81L instrument with a CRL krypton laser (model 52) using the green line at 5208  $\text{cm}^{-1}$ . A Varian HR 220 instrument (ICI Corporate Laboratory, Runcorn) was used for n.m.r. studies of polymers dissolved in *o*-dichlorobenzene (at 120°C) or deuterated chloroform (at 55°C).  $\delta$  values (in ppm) are quoted with respect to tetramethylsilane as internal standard. Areas under peaks were compared by the procedure involving cutting and weighing.

### RESULTS

The compositions of polybutadienes chlorinated under the specified conditions reached those corresponding to PVC after about 4 h treatment; reaction, to give higher chlorine contents, continued but at a much lower rate. Results are summarized in Table 1. The calculated values of  $\bar{M}_n$  were deduced from the values of  $\bar{M}_n$  for the original polymers

\* Present address: Montecatini-Edison Research Centre, Bollate, Milan, Italy.

Table 1 Chlorine contents and molecular weights of polymers

Sample	Cl (% w/w)	$\bar{M}_n$	
		Found	Calculated
C-0	0	114 500	—
C-1	34.0	275 500	173 000
C-2	40.0	252 500	190 500
C-5	56.5	—	258 000
T-0	0	45 000	—
T-1	53.2	102 500	96 000
M-1	43.2	242 000	201 000
M-2	37.8	263 000	184 000

C series: *cis*-1,4-polybutadiene

T series: *trans*-1,4-polybutadiene

M series: chlorination of *cis*-polymer in the presence of methanol (3 ml added to standard system for M-1 and 16 ml for M-2)

and the chlorine contents, assuming that the only reaction affecting the polymer was addition of chlorine to the carbon-carbon double bonds.

Murayama and Amagi<sup>2</sup> reported the changes in infra-red spectra brought about by addition of chlorine to 1,4-polybutadiene; their results were fully confirmed. Products M-1 and M-2 showed a prominent band at 1095  $\text{cm}^{-1}$ , absent from the spectra of products from chlorinations performed in the absence of methanol.

The Raman spectrum of *cis*-1,4-polybutadiene included a strong band at 1643  $\text{cm}^{-1}$  with weak bands at 1625 and 1666  $\text{cm}^{-1}$ ; for the *trans*-polymer, the band at 1666  $\text{cm}^{-1}$  was strong and those at 1625 and 1643 were weak. As chlorination proceeded, the intensities of these bands fell but the band at 1666  $\text{cm}^{-1}$  persisted even in a C-product containing 68.8% Cl. Product M-2 showed no appreciable absorption between 1700 and 1600  $\text{cm}^{-1}$ .

Information on n.m.r. spectra is summarized in Table 2.

### DISCUSSION

Both crosslinking and degradation have been found during the chlorination of hydrocarbon polymers. The data on  $\bar{M}_n$  (Table 1) indicate that both processes occur during the chlorination of 1,4-polybutadiene. The values of  $\bar{M}_n$  found for products C-1, C-2 and T-1 exceed the calculated values showing that there is linking together of polymer molecules although not to an extent sufficient to cause insolubility. That degradation also occurs during chlorination is shown by the fact that  $\bar{M}_n$  found for product C-2 is less than that for C-1 although C-2 has the higher chlorine content.

The Raman bands at 1625, 1643 and 1666  $\text{cm}^{-1}$  are associated with pendant  $-\text{CH}=\text{CH}_2$ , *cis* C=C and *trans* C=C respectively. It is significant that the band at 1666  $\text{cm}^{-1}$  persists even in a product containing nearly 70% chlorine

Table 2 N.m.r. spectra of 1,4-polybutadienes and their derivatives

Polymer	Comments
C-0 and T-0	Peaks at $\delta = 5.5$ and $2.1$ ; areas in ratio 1:2
C-5	No peak at $\delta = 5.5$ . Peaks at $\delta = 4.0, 2.13, 2.00$ and $1.85$ ; areas in ratios 1.0:0.5:1.0:0.5
T-1	No peak at $\delta = 5.5$ . Peaks at $\delta = 3.9, 2.33, 2.06$ and $1.80$ ; areas in ratios 1.0:0.5:1.0:0.5
M-1 and M-2	No peak at $\delta = 5.5$ . Peaks at $\delta = 4.05, 3.5$ and $3.4$ . Various peaks between $\delta = 2.5$ and $1.5$ ; further information in text

and formed from the *cis*-polymer; *trans* C=C may be involved in the 'over-chlorination', i.e. the introduction of chlorine beyond that required to give 56.8% w/w. It is possible that *trans* double bonds are continuously generated in the system by elimination of hydrogen chloride and that they are subsequently saturated with chlorine to convert some of the repeating units first to  $-\text{CHCl.CHCl.CHCl.CH}_2-$  and subsequently to more highly chlorinated units. It should be noted that evidence<sup>2</sup> from infra-red spectra pointed to some conversion of *cis* C=C to *trans* C=C during chlorination.

Chlorination of 1,4-polybutadiene in the presence of methanol is expected to introduce methoxy groups into the polymer and there is compelling evidence to this effect. The prominent infra-red band at  $1095\text{ cm}^{-1}$  can be attributed to these groups in the M-products. These products, although containing appreciably less than 56.8% chlorine, have no Raman absorption between  $1700$  and  $1600\text{ cm}^{-1}$  so evidently all C=C bonds have been saturated. The n.m.r. spectra also provide clear evidence for the methoxy groups (see later).

The n.m.r. peaks at  $\delta = 5.5$  and  $2.1$  have areas in the ratio 1:2 for the starting polymers and are associated with the groups  $-\text{CH}=\text{}$  and  $-\text{CH}_2-$  respectively; the peak at  $\delta = 5.5$  disappears during chlorination. Protons in  $-\text{CHCl}-$  give rise to peaks at  $\delta = 4.0$  (C-5),  $3.9$  (T-1) and  $4.05$  (M-1 and M-2). The various peaks between  $\delta = 2.5$  and  $1.5$  are

associated with methylene groups; the total area for these peaks in C-5 or T-1 is twice the area for the peak at  $\delta = 4.0$  for (C-5) or that for the peak at  $\delta = 3.9$  (for T-1) confirming that the products can be regarded as having the repeating unit  $-\text{CH}_2.\text{CHCl.CHCl.CH}_2-$ . Peaks at  $\delta = 3.5$  and  $3.4$  (areas in the ratio 3:1) are present in the spectra for M-1 and M-2 but not in those for C-5 and T-1; they are assigned to protons in  $-\text{CH}(\text{OCH}_3)$  groups. For M-1 and M-2, the sum of the areas for the peaks at  $\delta = 4.05$  and  $3.4$  (associated with protons in  $-\text{CHX}-$  where X is Cl or  $\text{OCH}_3$  respectively) is close to 50% of that corresponding to the peaks between  $\delta = 2.5$  and  $1.5$  indicating that the original  $\text{C}_4\text{H}_6$  unit in the polymer is on average converted to  $\text{C}_4\text{H}_6\text{Cl}_n(\text{OCH}_3)_{2-n}$ . The ratios of the areas associated with the peaks at  $\delta = 4.05$  and  $3.4$  are 4.5:1 and 2:1 for M-1 and M-2 respectively; the corresponding values of  $n/(2-n)$  are therefore 4.5 and 2.0 and those of  $n$  are 1.64 and 1.33. From these results, the calculated chlorine contents of M-1 and M-2 are 47.2 and 38.6% respectively in fair agreement with the values of 43.2 and 37.8% found by direct analysis. Taking the average repeating units in M-1 and M-2 as  $\text{C}_4\text{H}_6\text{Cl}_{1.64}(\text{OCH}_3)_{0.36}$  and  $\text{C}_4\text{H}_6\text{Cl}_{1.33}(\text{OCH}_3)_{0.67}$  respectively, the calculated values of  $\bar{M}_n$  for these products are 261 000 and 259 000. The discrepancies between the calculated and observed values of  $\bar{M}_n$  are much less for these products than for those produced by chlorination in the absence of methanol.

#### ACKNOWLEDGEMENTS

We thank Montecatini-Edison SpA for granting study leave to L. R. We acknowledge advice and assistance from colleagues in the laboratories at Lancaster. The work reported here formed part of a project supported by the Science Research Council.

#### REFERENCES

- 1 Bevington, J. C. and Ratti, L. *Eur. Polym. J.* 1972, 8, 1105
- 2 Murayama, N. and Amagi, Y. *J. Polym. Sci. (B)* 1966, 4, 119

# Letters

## Solution properties of low molecular weight atactic poly(acrylic acid) and its sodium salt

Below a molecular weight of about  $10^4$  most acrylic and vinyl polymers<sup>1</sup> show an extended region where the Mark-Houwink exponent assumes the theta point value of 0.50 ( $[\eta] = K_0 M^{0.50}$ ) even though thermodynamic conditions are far from those of a theta solvent. The constant  $K_0$  is very near to  $K_\theta$  (the characteristic value in a theta solvent) provided specific solvent effects are not large. The only exception to this rule discovered so far is polyethylene<sup>1</sup>. This letter reports another exception — poly(acrylic acid) (PAA) and its sodium salt (NaPA). Viscosity measurements have been performed on characterized samples ranging from the trimer (2,4,6-tricarboxyheptane)<sup>2</sup> to the high polymer ( $M_w = 360\,000$ ).

Low molecular weight PAA was prepared by free radical polymerization in solvents which were chain transfer agents<sup>3</sup>, i.e. ethyl benzene and 2-butanol. The latter solvent gave partly esterified polymers ( $M_w \sim 3000$ ) which were hydrolysed to the pure acid with boiling aqueous alkali. Fractions of PAA were prepared by elution chromatography and fractional precipitation. A Sofica instrument was used to measure  $M_w$  for PAA samples with 2-propanol as solvent. Experimentally it was found that PAA samples of  $M_w < 50\,000$  had zero angular dissymmetry. For each sample the refractive index increment ( $dn/dc$ ) was measured with a Waters differential refractometer (R403).

Values of  $M_n$ , obtained with a Perkin-Elmer 115 vapour pressure osmometer, were used to correct the intrinsic viscosities of the unfractionated samples for the effect of heterogeneity according to the procedure of Kurata and Stockmayer<sup>4</sup>. This correction was small ( $\leq 8\%$ ) for the unfractionated samples. It was not applied to the fractions for lack of complete data but in their case it would have been even less important. Intrinsic viscosities were measured for PAA samples in 2-propanol (30°C) and

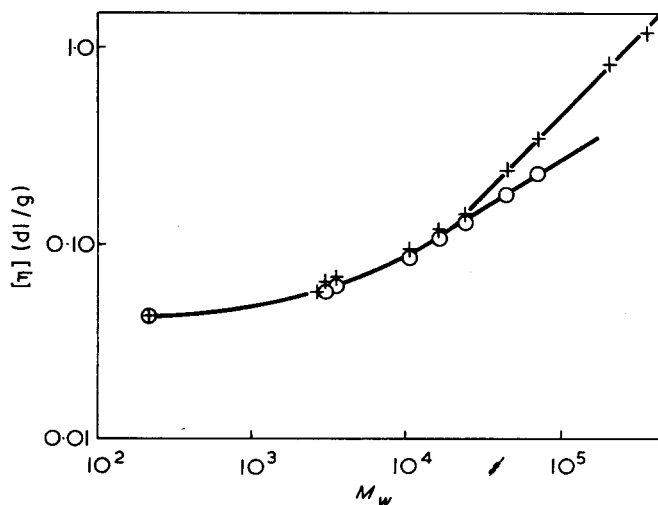


Figure 1 Intrinsic viscosity/molecular weight plots for poly(acrylic acid) in 1,4-dioxane (30°C) (O) and 2-propanol (30°C) (+)

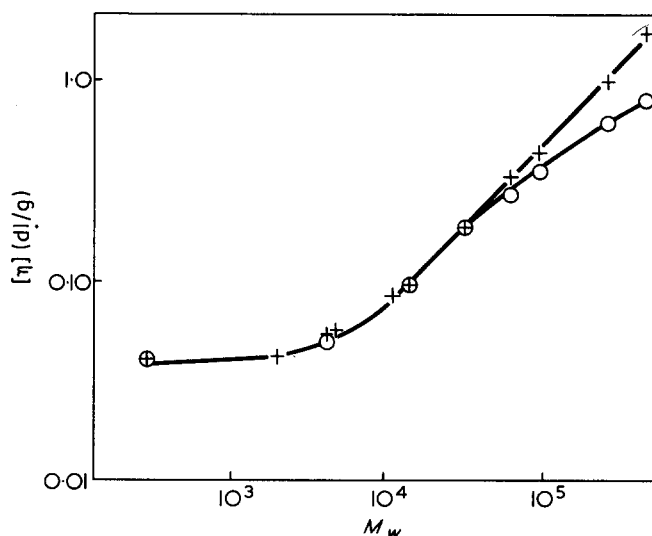


Figure 2 Corrected intrinsic viscosity/molecular weight plots for the sodium-salt of poly(acrylic acid) in 1.5 M NaBr (20°C) (O) and 1.0 M NaCl (30°C) (+)

1,4-dioxane (30°C) and for sodium polyacrylate (NaPA) samples in 1.0 M NaCl (30°C) and 1.50 M NaBr (20°C). Ubbelohde suspended level viscometers with water flow times of 20 min were used with all solvents except 2-propanol for which a shorter flow time viscometer was necessary. The corresponding double logarithmic plots are shown in Figures 1 and 2. The viscosity-molecular weight data in Figure 1 are for the acid form (PAA) but those in Figure 2 have been calculated for the sodium salt taking into account the contribution of the end group to the molecular weight.

The  $[\eta]-M_w$  plots are linear above  $M_w \approx 30\,000$ . The data in this linear region for 1,4-dioxane and 1.5 M NaBr (both theta solvents) correspond very closely to what would be predicted from the corresponding  $[\eta]-M_w$  relationships obtained by other workers<sup>5,6</sup> for higher molecular weight fractions of PAA and NaPA. However,  $[\eta]-M_w$  relationships have not been calculated for the linear portions of the other curves because they are defined by only a small number of points. The viscosity data below  $M_w \approx 10\,000$  are characterized by a strong upward curvature so that below  $M_w \approx 1000$   $[\eta]$  is almost independent of molecular weight. The data for NaPA in 1.5 M NaBr appear to show an additional downward curvature in the range  $M_w \approx 30\,000$  to  $10\,000$ .

These conclusions depend strongly on the accuracy of the data points for 2,4,6-tricarboxyheptane so these have been checked by repeated careful measurement. There is no evidence to suggest that it is invalid to use 2,4,6-tricarboxyheptane as a model for poly(acrylic acid) but it would be useful to have more data for the region below  $M_w \approx 1000$ . What is clear is that although the viscosity of PAA and NaPA becomes independent of solvent power below  $M_w \approx 10\,000$  there is no prolonged region at low molecular weight where the theta point relationship is obeyed. In this respect PAA and NaPAA differ from most vinyl and acrylic polymers so far studied<sup>1</sup> and resemble most closely cellulose and amylose derivatives<sup>1</sup>.

## ACKNOWLEDGEMENTS

The author wishes to thank Dr B. Rossall for a sample of 2,4,6-tricarboxyheptane, Mr R. Sallis and Mr T. J. Lunt for some experimental assistance and Dr C. Price (Manchester University) for helpful discussion.

G. J. Welch

Unilever Research Laboratory,  
Port Sunlight, Wirral,  
Cheshire L62 4XN, UK  
(Received 11 October 1974)

## REFERENCES

- 1 Bianchi, U. and Peterlin, A. *J. Polym. Sci. (A-2)* 1968, 6, 1759
- 2 Clark, H. G. *Makromol. Chem.* 1965, 86, 107
- 3 Sen, I. N., Nadi, U. and Palit, S. R. *J. Indian Chem. Soc.* 1963, 40, 729
- 4 Kurata, M. and Stockmayer, W. H. *Fortschr. Hochpolym. Forsch.* 1963, 3, 196
- 5 Newman, S., Krigbaum, W. R., Laughier, C. and Flory, P. J. *J. Polym. Sci.* 1954, 14, 451
- 6 Takahashi, A. and Nagasawa, M. *J. Am. Chem. Soc.* 1964, 86, 543

## Growth of lamellar crystals of poly( $\gamma$ -benzyl-L-glutamate)

### Introduction

It was shown by Padden and Keith<sup>1</sup> that under suitably chosen conditions polyglycine, poly(L-tyrosine), and probably poly(L-alanine) as well, could crystallize from solution to form single crystals with folded molecular chains. The lamellar crystals were found to exhibit many of the morphological features normally associated with single crystals of more conventional synthetic polymers<sup>2</sup>. With poly(L-tyrosine) and poly(L-alanine) it appeared, however, that solvent was complexed with the polymer even in the crystalline state; evaporation of the solvent resulted in the loss of crystalline order. Later studies carried out by the same school included the growth of single crystals of alkaline earth salts of poly(L-glutamic acid)<sup>3</sup> from aqueous solution and crystals of poly(L-lysine)<sup>4</sup> stabilized by divalent anions.

In this communication we report a method for growing lamellar crystals of poly( $\gamma$ -benzyl-L-glutamate) (PBLG). Because of its solubility in a wide variety of solvents, PBLG has been used by many workers as a useful model compound for investigating the behaviour of fibrous proteins<sup>5</sup>. Numerous dilute solution studies<sup>6-8</sup> have been carried out on the polymer. Crystallization studies have shown that PBLG is able to crystallize from solution in the form of fibrillar aggregates; these may be single strands, ropes, rods or toroids depending on the solvent and precipitation conditions<sup>9</sup>. Also the crystalline structure of the polymer has been analysed by X-ray and electron diffraction studies carried out on stretched solution cast films<sup>10,11</sup>. No direct method of growing lamellar single crystals of PBLG has been reported previously although they have been grown epitaxially on alkali halides from mesitylene solution. In the latter work carried out by Carr *et al.*<sup>12</sup> electron diffraction and microscopy studies indicated that the lamellae contained chain-folded  $\alpha$ -helical main-chain backbones, but that the bulky side groups remained disordered.

## Experimental and Results

### Material

The PBLG was synthesized by polymerizing  $\gamma$ -benzyl-*N*-carboxy-L-glutamate anhydride in benzene for 24 h at 20°C with *n*-hexylamine added as initiator<sup>13</sup>; the concentration of the initial solution was 0.015 g/cm<sup>3</sup> and the molar ratio of anhydride to initiator was 76. An 85% yield of polymer was recovered from the reaction mixture. Solutions of the polymer in *N,N*-dimethylacetamide (0.2–0.5% by wt polymer) were analysed by gel permeation chromatography (g.p.c.) at 50°C; four columns of pore size 7(10)<sup>4</sup>–5(10)<sup>5</sup> nm, 5(10)<sup>3</sup>–1.5(10)<sup>4</sup> nm, 5(10)<sup>2</sup>–1.5(10)<sup>3</sup> nm and 7(10)–2(10)<sup>2</sup> nm were employed. For the unfractionated sample the ratio of the weight-average to number-average molecular weight,  $M_w/M_n$ , = 5.8. The presence of a low molecular weight tail accounted for much of this spread, however, and if its contribution was neglected  $M_w/M_n$  = 2.0. The weight-average molecular weight of the sample determined by light scattering studies on dimethyl formamide solutions was 97 000.

### Fractionation

The polymer was fractionated using methylene chloride/methanol as a solvent/non-solvent system; this system under different experimental conditions has been employed previously for PBLG in fractional precipitation experiments<sup>14,15</sup> and in precipitation chromatography<sup>16,17</sup>. In our procedure, methanol was added slowly with stirring to a solution ( $c = 0.0025$  g/cm<sup>3</sup>) of the polymer in methylene chloride thermostated at 20°C until a persistent turbidity was obtained. Next, the system was heated slowly until the solution became clear (~24°C) and then it was allowed to cool back to 20°C. After a period of 24 h, the crystalline fraction which had precipitated was isolated by syphoning off the supernatant solution through a glass wool plug into another flask. The fraction was collected by dissolution in methylene chloride followed by reprecipitation and filtration, and then it was dried by pumping under vacuum. Fourteen fractions were isolated successively in this manner. G.p.c. analysis showed that all the fractions possessed a narrow molecular weight distribution; the g.p.c. traces of fractions 1, 4, 7, 10 and 12 are shown in *Figure 1*. After making an approximate correction for diffusion broadening<sup>18,19</sup>,  $M_w/M_n$  of each of the fractions is estimated to lie within the range 1.06–1.09. The results show that the solid-liquid fractionation process was very efficient and suggests an almost guillotine-like selection of chain molecules.

### Crystallization from dilute solution

The crystallization results to be reported in the present communication were obtained on fraction 1 for which  $M_w = 129\,000$  and  $M_w/M_n = 1.08$ ; however, similar results have also been obtained for other fractions. Preliminary results showed that well defined lamellar crystals could be grown from dilute solutions of the polymer in hexafluoroisopropanol simply by allowing the system to cool slowly from 65°C to room temperature. Crystallization studies were then carried out under more controlled conditions using a self-seeding technique of the type developed by Blundell *et al.* for polyethylene<sup>20,21</sup>. Because of the low boiling point (58.5°C) of the solvent, all experiments were carried out in sealed glass tubes (3 mm diam.  $\times$  100 mm length); prior to sealing the solutions were degassed on the

## ACKNOWLEDGEMENTS

The author wishes to thank Dr B. Rossall for a sample of 2,4,6-tricarboxyheptane, Mr R. Sallis and Mr T. J. Lunt for some experimental assistance and Dr C. Price (Manchester University) for helpful discussion.

G. J. Welch

Unilever Research Laboratory,  
Port Sunlight, Wirral,  
Cheshire L62 4XN, UK  
(Received 11 October 1974)

## REFERENCES

- 1 Bianchi, U. and Peterlin, A. *J. Polym. Sci. (A-2)* 1968, 6, 1759
- 2 Clark, H. G. *Makromol. Chem.* 1965, 86, 107
- 3 Sen, I. N., Nadi, U. and Palit, S. R. *J. Indian Chem. Soc.* 1963, 40, 729
- 4 Kurata, M. and Stockmayer, W. H. *Fortschr. Hochpolym. Forsch.* 1963, 3, 196
- 5 Newman, S., Krigbaum, W. R., Laughier, C. and Flory, P. J. *J. Polym. Sci.* 1954, 14, 451
- 6 Takahashi, A. and Nagasawa, M. *J. Am. Chem. Soc.* 1964, 86, 543

### Growth of lamellar crystals of poly( $\gamma$ -benzyl-L-glutamate)

#### Introduction

It was shown by Padden and Keith<sup>1</sup> that under suitably chosen conditions polyglycine, poly(L-tyrosine), and probably poly(L-alanine) as well, could crystallize from solution to form single crystals with folded molecular chains. The lamellar crystals were found to exhibit many of the morphological features normally associated with single crystals of more conventional synthetic polymers<sup>2</sup>. With poly(L-tyrosine) and poly(L-alanine) it appeared, however, that solvent was complexed with the polymer even in the crystalline state; evaporation of the solvent resulted in the loss of crystalline order. Later studies carried out by the same school included the growth of single crystals of alkaline earth salts of poly(L-glutamic acid)<sup>3</sup> from aqueous solution and crystals of poly(L-lysine)<sup>4</sup> stabilized by divalent anions.

In this communication we report a method for growing lamellar crystals of poly( $\gamma$ -benzyl-L-glutamate) (PBLG). Because of its solubility in a wide variety of solvents, PBLG has been used by many workers as a useful model compound for investigating the behaviour of fibrous proteins<sup>5</sup>. Numerous dilute solution studies<sup>6-8</sup> have been carried out on the polymer. Crystallization studies have shown that PBLG is able to crystallize from solution in the form of fibrillar aggregates; these may be single strands, ropes, rods or toroids depending on the solvent and precipitation conditions<sup>9</sup>. Also the crystalline structure of the polymer has been analysed by X-ray and electron diffraction studies carried out on stretched solution cast films<sup>10,11</sup>. No direct method of growing lamellar single crystals of PBLG has been reported previously although they have been grown epitaxially on alkali halides from mesitylene solution. In the latter work carried out by Carr *et al.*<sup>12</sup> electron diffraction and microscopy studies indicated that the lamellae contained chain-folded  $\alpha$ -helical main-chain backbones, but that the bulky side groups remained disordered.

### Experimental and Results

#### Material

The PBLG was synthesized by polymerizing  $\gamma$ -benzyl-*N*-carboxy-L-glutamate anhydride in benzene for 24 h at 20°C with *n*-hexylamine added as initiator<sup>13</sup>; the concentration of the initial solution was 0.015 g/cm<sup>3</sup> and the molar ratio of anhydride to initiator was 76. An 85% yield of polymer was recovered from the reaction mixture. Solutions of the polymer in *N,N*-dimethylacetamide (0.2–0.5% by wt polymer) were analysed by gel permeation chromatography (g.p.c.) at 50°C; four columns of pore size 7(10)<sup>4</sup>–5(10)<sup>5</sup> nm, 5(10)<sup>3</sup>–1.5(10)<sup>4</sup> nm, 5(10)<sup>2</sup>–1.5(10)<sup>3</sup> nm and 7(10)–2(10)<sup>2</sup> nm were employed. For the unfractionated sample the ratio of the weight-average to number-average molecular weight,  $M_w/M_n$ , = 5.8. The presence of a low molecular weight tail accounted for much of this spread, however, and if its contribution was neglected  $M_w/M_n$  = 2.0. The weight-average molecular weight of the sample determined by light scattering studies on dimethyl formamide solutions was 97 000.

#### Fractionation

The polymer was fractionated using methylene chloride/methanol as a solvent/non-solvent system; this system under different experimental conditions has been employed previously for PBLG in fractional precipitation experiments<sup>14,15</sup> and in precipitation chromatography<sup>16,17</sup>. In our procedure, methanol was added slowly with stirring to a solution ( $c = 0.0025$  g/cm<sup>3</sup>) of the polymer in methylene chloride thermostated at 20°C until a persistent turbidity was obtained. Next, the system was heated slowly until the solution became clear (~24°C) and then it was allowed to cool back to 20°C. After a period of 24 h, the crystalline fraction which had precipitated was isolated by syphoning off the supernatant solution through a glass wool plug into another flask. The fraction was collected by dissolution in methylene chloride followed by reprecipitation and filtration, and then it was dried by pumping under vacuum. Fourteen fractions were isolated successively in this manner. G.p.c. analysis showed that all the fractions possessed a narrow molecular weight distribution; the g.p.c. traces of fractions 1, 4, 7, 10 and 12 are shown in *Figure 1*. After making an approximate correction for diffusion broadening<sup>18,19</sup>,  $M_w/M_n$  of each of the fractions is estimated to lie within the range 1.06–1.09. The results show that the solid-liquid fractionation process was very efficient and suggests an almost guillotine-like selection of chain molecules.

#### Crystallization from dilute solution

The crystallization results to be reported in the present communication were obtained on fraction 1 for which  $M_w = 129\ 000$  and  $M_w/M_n = 1.08$ ; however, similar results have also been obtained for other fractions. Preliminary results showed that well defined lamellar crystals could be grown from dilute solutions of the polymer in hexafluoroisopropanol simply by allowing the system to cool slowly from 65°C to room temperature. Crystallization studies were then carried out under more controlled conditions using a self-seeding technique of the type developed by Blundell *et al.* for polyethylene<sup>20,21</sup>. Because of the low boiling point (58.5°C) of the solvent, all experiments were carried out in sealed glass tubes (3 mm diam.  $\times$  100 mm length); prior to sealing the solutions were degassed on the

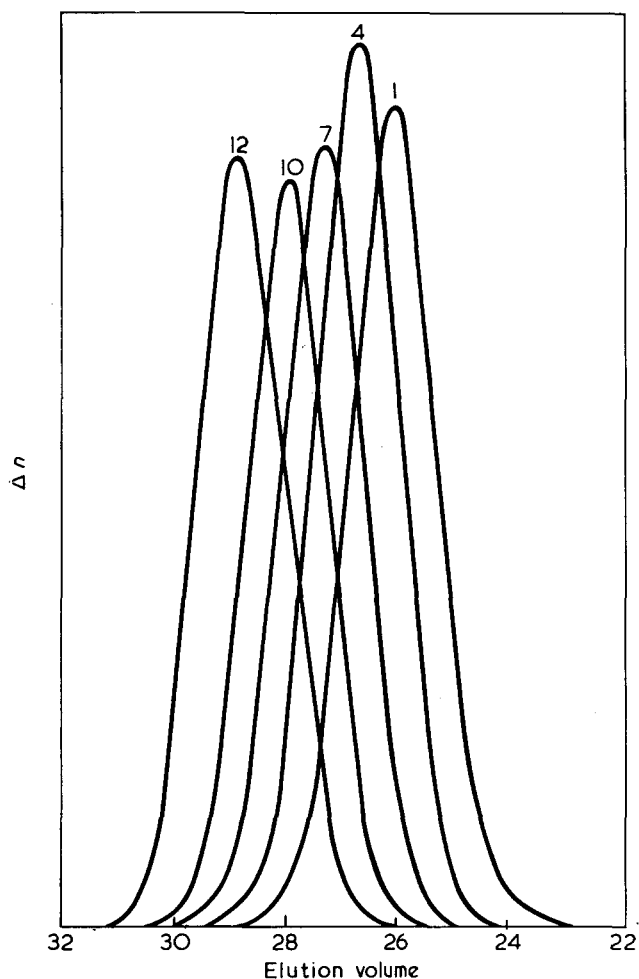


Figure 1 Gel permeation chromatograms (uncorrected) for fractions 1, 4, 7, 10 and 12

vacuum line. The polymer/solvent system ( $w/v = 0.003 \text{ g/cm}^3$ ) was first warmed up slowly ( $\sim 1^\circ\text{C}/\text{min}$ ) and held at  $65^\circ\text{C}$  until the solution became clear. It was then allowed to cool back to room temperature. The system was then plunged into a thermostat bath at  $70 \pm 0.01^\circ\text{C}$  and left for 10 min. Finally, it was plunged into a thermostat bath held at the chosen crystallization temperature; crystallization studies were carried out at 20, 25 and  $30^\circ\text{C}$ . The relatively large temperature increments which separated the dissolution temperature ( $T_d$ ) from the crystallization temperature ( $T_c$ ) made it difficult to achieve completely isothermal growth. So as to facilitate quenching thin walled, narrow bore glass tubes were used in the experiments. Trial runs involving further reductions in bore diameter did not have any noticeable effect on the growth of the crystals.

Lamellar crystals having a basic hexagonal habit were the typical product of growth at each of the crystallization temperatures studied. Figure 2 shows a lamella as viewed with an AEI 6G electron microscope operating in direct transmission; it is mounted on a carbon substrate and shadowed with Pt/C. The lamella is sub-divided into distinct sectors, there being as many sectors as there are prism faces. Many of the lamellae showed evidence of sectorization in this way. Other lamellae revealed no such features. An array of lamellae is shown in Figure 3. This micrograph was selected because the lamellae are heavily fractured. As revealed by many of these lamellae, when fracture occurs it tends to be in a radial direction.

No electron diffraction spots or rings could be observed even when utilizing very low beam intensities, only an amorphous halo was observed. This suggests that the crystals were only stable in the presence of bound solvent. Presumably under the vacuum conditions required for shadowing and electron microscopy the solvent is removed and hence the crystalline order is lost due to local crumpling of chains. A similar argument was invoked by Padden and Keith<sup>1</sup> to explain some of their observations.

The thickness of the lamellae was determined from measurements of shadow lengths. For  $T_c = 20, 25$  and  $30^\circ\text{C}$  the average lamellar thicknesses were found to be 23, 23 and 25 nm respectively. Thus the thicknesses are roughly a third of the value expected for an unfolded PBLG chain. (If we assume the chains adopt an  $\alpha$ -helical conformation<sup>8</sup> along their whole length then the fully extended length of molecules in fraction 1 would be  $\sim 82 \text{ nm}$ .) At this stage, however, we cannot rule out the possibility that evaporation of solvent may be accompanied

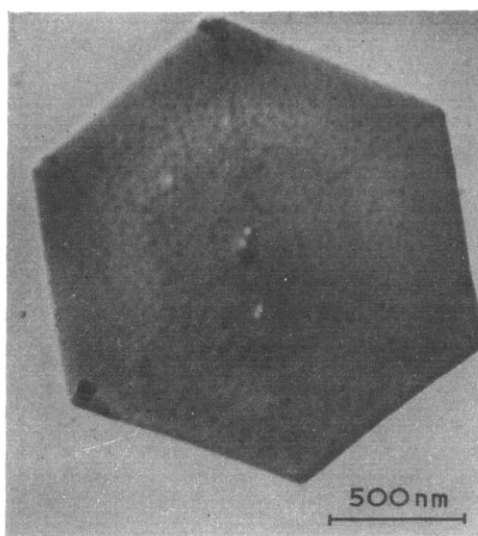


Figure 2 Electron micrograph of a lamella obtained by crystallizing PBLG from hexafluoroisopropanol

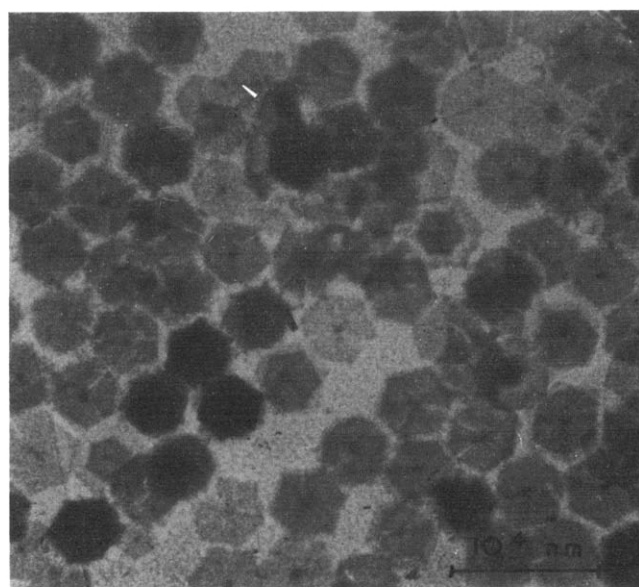


Figure 3 Electron micrograph of an array of lamellae exhibiting extensive fracturing in the radial direction

by significant distortion of the lamellae such as partial collapse and thinning. Certainly many of the lamellae had somewhat rounded edges and this introduced a considerable degree of uncertainty into the measurements of shadow lengths. In future studies it is hoped to obtain unequivocal evidence concerning crystal thicknesses from low-angle X-ray studies made on moist mats. In the meantime, however, supporting evidence that folding occurs is provided by the observations that many crystals are subdivided into distinct sectors. As pointed out by Keller<sup>22</sup> for polyethylene crystals, sectorization must be considered as convincing evidence for the folded-chain model.

#### Acknowledgements

Funding for these studies is being provided by the Science Research Council. We thank Dr C. Booth and Mr D. Roy for assistance with the g.p.c. studies.

C. Price, P. A. Harris, T. J. Holton  
and R. B. Stubbersfield

Department of Chemistry,  
University of Manchester,  
Manchester M13 9PL, UK  
(Received 27 September 1974)

#### References

- 1 Padden, F. J. and Keith, H. D. *J. Appl. Phys.* 1965, 36, 2987
- 2 Keller, A. *Rep. Progr. Phys.* 1968, 31, 623
- 3 Keith, H. D., Giannoni, G. and Padden, F. J. *Biopolymers* 1969, 7, 775
- 4 Padden, F. J., Keith, H. D. and Giannoni, G. *Biopolymers* 1969, 7, 793
- 5 Bamford, C. H., Elliot, A. and Hanby, W. E. 'Synthetic Polypeptides', Academic Press, New York, 1956
- 6 Doty, P., Bradbury, J. H. and Holtzer, A. M. *J. Am. Chem. Soc.* 1956, 78, 947
- 7 Yang, J. T. and Doty, P. *J. Am. Chem. Soc.* 1957, 79, 761
- 8 'Light Scattering from Polymer Solutions' (Ed. M. B. Huglin), Academic Press, London and New York, 1972, Ch 9 and 17
- 9 Rybnikar, F. and Geil, P. H. *Biopolymers* 1972, 11, 271
- 10 Bamford, C. H., Hanby, W. E. and Happey, F. *Proc. R. Soc.* 1951, A205, 30
- 11 Parsons, D. F. and Martius, U. *J. Mol. Biol.* 1964, 10, 530
- 12 Carr, S. H., Walton, A. G. and Baer, E. *Biopolymers* 1968, 6, 469
- 13 Katchalski, E. 'Advances in Protein Chemistry', Academic Press, New York, 1951, Vol 6, pp 123-185
- 14 Scoffone, E., Peggion, E., Cosani, A. and Terbojevich, M. *Biopolymers* 1965, 3, 535
- 15 Spach, G., Freund, L., Daune, M. and Benoit, H. *J. Mol. Biol.* 1963, 7, 468
- 16 Bradbury, E. M., Crane-Robinson, C. and Hartman, P. G. *Polymer* 1973, 14, 543
- 17 Goebel, K. D. and Miller, W. G. *Macromolecules* 1970, 3, 64
- 18 Aldhouse, S. T. E. and Stanford, D. M. *5th Int. GPC Semin. London* 1968
- 19 Tung, L. H. and Runyon, J. R. *J. Appl. Polym. Sci.* 1969, 13, 2397
- 20 Blundell, D. J., Keller, A. and Kovacs, A. J. *J. Polym. Sci., (B)* 1966, 4, 481
- 21 Blundell, D. J. and Keller, A. *J. Macromol. Sci. (B)* 1968, 2, 337
- 22 Keller, A. *Int. Rev. Sci. (Phys. Chem. Ser.)* 1972, 8, 105

# RESOURCES POLICY

the economics, planning and use  
of mineral resources

A NEW QUARTERLY JOURNAL

Second issue · December 1974

#### Main articles

Material resources for the iron  
and steel industry

R.S. Barnes

Potential mineral reserves

V.E. McKelvey

The conservation of building  
materials and the future of the  
built environment

J.K. Page

The current status of the US

mining industry

J.D. Morgan Jr

Policy elements of US resource

supply problems

H.H. Landsberg

#### Other sections

- Current topics
- Conference reports
- Forthcoming meetings
- Book reviews and announcements
- Publications received

**RESOURCES POLICY** will present multi-disciplinary discussions at an upper management/academic level. The aim is to identify policy options for the future supply and demand of mineral resources. It will encompass the many disciplines and examine options as they affect industrial, commercial and social institutions at world and regional levels

Published quarterly in  
March, June, September, December,  
commencing September 1974

One-year subscription (four issues) £20.00 (\$50.00).

For full details apply to: IPC Science and Technology Press Limited (Dept. AD.RP)  
IPC House, 32 High Street, Guildford, Surrey, England GU1 3EW  
Telephone: Guildford (0483) 71661 Telex: Scitechpress Gd. 85556

# Book Reviews

## Reactivity, mechanism and structure in polymer chemistry

Edited by A. D. Jenkins and A. Ledwith

John Wiley, London, 1974, 613 pp. £13.00

Jenkins and Ledwith have performed a notable service by collecting articles which will be of real value to many physical-organic chemists. They support the very reasonable view that polymer chemistry should not be regarded as quite separate from the rest of chemistry; indeed, they have included sections dealing with general aspects of radicals, carbonium ions and carbanions with hardly a specific reference to polymerizing systems. These particular sections could just as well have been included in a corresponding book about general organic chemistry but the material in them is of course necessary for proper appreciation of the various types of polymerization process.

The editors have recruited some famous men to write for them but it is refreshing to see contributions from authors who up to now have not been featured in publications of this type. It is often only too apparent that there is a lack of coherence in books written by large teams of authors; there may also be considerable variations from one contribution to another in style of writing and in depth of treatment. These defects seem not to be significant in this case.

It should be noted that the editors have restricted themselves to various aspects of the process of polymerization in spite of the more general nature of the title; only in a sub-section headed 'Photochemistry processes in high polymers' and occupying less than 10 pages is there any appreciable discussion of the behaviour of polymers themselves. If fault is to be found, it should be with the chosen title.

There can be no doubt that this book will be a valuable and stimulating aid to those involved in advanced teaching, and in research. It deserves wide circulation and not just among those who describe themselves as polymer chemists. It would be niggling to comment on obscurities, errors, unnecessary repetition between sections and presentation of material already available in other accessible publications; there are examples of these faults but they are few. The reviewer must however, demonstrate that he really has looked beyond the list of contents and so report that the index contains a very unusual symbol for the velocity constant for termination in the case of the polymerization of *N*-vinylcarbazole.

J. C. Bevington

## Blood compatible synthetic polymers: an introduction

C. C. Thomas, Springfield, 1974, 131 pp. \$9.75

The field of biomedical polymers is receiving increasing attention from workers in medical engineering and Dr Bruck has set out to provide a short introductory guide for people of all disciplines, be they physicians, engineers, life or materials scientists involved in the development and use of devices which come into direct contact with blood. What it is that makes some synthetic materials more tolerated by the living environment than others is still the subject of much speculation and consequently this monograph deals only briefly with its principal subject matter, giving a summary of the more promising materials found to date which demonstrate a degree of biocompatibility with blood while discussing the attributes mainly associated with a material's surface which might be responsible for the effect.

Understandably the bulk of the text is taken up with a review of polymeric materials and their many chemical, physical and mechanical properties. The emphasis here is on a direct comparison between synthetic and naturally-occurring macromolecules and on those properties which render the former suitable for use in biomedical applications and which might have a bearing on the various theories of blood compatibility.

Additionally, the author has contributed a useful presentation on the composition of blood and its working environment. This serves to highlight the many vital factors which can either influence or be influenced by the presence of a foreign material. For example,

the influence of chemical, physical and mechanical action on the blood's defensive mechanisms are exemplified in relation to the blood coagulation pathways.

The current rate of advance in biomaterials science is such that one can anticipate the appearance of a more comprehensive treatise in the near future. This relatively inexpensive book provides a useful insight into the present state of the art and as the performance requirements expected of synthetic biomaterials increase it will serve to encourage the move from intuitive selection towards the synthesis of macromolecules designed to exist at the interface between a device and both the cellular and non-cellular components of blood.

It must be remembered, however, that while efforts have been made to relate blood compatibility of a material to the composition of that material, the final analysis must take account of the application and the physical form.

T. Gilchrist

## Progress in polymer science Japan, Vol 5

Edited by K. Imahori and S. Murahashi

John Wiley, New York, 1973, 308 pp. £8.75

The volume is a continuation of the series in which Japanese scientists review specific aspects of polymer science, usually concentrating on their own contributions to the subject. The articles provide useful coherent accounts of the authors' work in and philosophy of their particular subject and also provide access to information in original Japanese publications and conference proceedings, which are not readily available to the scientific community at large.

Of the five reviews in this volume three deal with chemical and two with physical aspects of the subject. Four articles originate from university laboratories, one from Kyoto and three from the less well-known but major polymer centre in Hokkaido. The remaining article stems from one of the major government laboratories devoted to polymer science.

In the third article in this series devoted to alternating copolymerizations, Furukawa discusses the mechanisms of reactions which involve donor-acceptor complexes of monomers with Lewis acids and those initiated by Ziegler-type catalysts. After a brief summary of other workers' contributions he develops the subject mainly in terms of the contributions of his own group. The characterization and physical properties of some copolymers are described. Noguchi's article on poly( $\alpha$ -amino acids) is mainly concerned with catalytic hydrolyses by the polymers and the nature of reaction sites. The article also describes polymers and copolymers prepared using *N*-carbothiophenyl derivatives of amino acids and attempts to prepare fibres of poly( $\alpha$ -amino acids) which simulate natural peptide fibres. Hasegawa *et al.* describe four-centre photopolymerizations of diolefinic monomers in the crystalline state. The major monomer used in the work was 2,5-distyrylpyrazine but results obtained with related monomers are also discussed. In a very attractive study of those reactions the authors have investigated they describe various factors which influence the reaction, including the wavelength of the incident illumination, crystallographic effects and, briefly, the properties of some of the novel polymers prepared. In the polymer physics section of the volume Kaneko reviews the viscoelasticity of dilute solutions of flexible and rigid polymers and compares the experimental data with theoretical models. Some data on viscoelasticity of polyelectrolytes are included. Finally, Kobatake and Kamo review transport processes in charged membranes and discuss theoretical mechanisms for transport of ions in terms of experimentally determined parameters existing within the membranes.

The volume is well presented and individual articles will be of value to those working in the specialized areas covered. Unfortunately, but predictably, the price is even higher than that of the preceding volume (see *Polymer* 1974, 15, 255) and is extremely high for most workers who, in view of the spectrum of topics covered, will be specifically interested in only one or two articles.

G. C. Eastmond



# A far infra-red study of conformational disorder in PTFE

H. A. Willis and M. E. A. Cudby

ICI Plastics Division, Welwyn Garden City, Hertfordshire AL7 1HD, UK

and G. W. Chantry, Elisabeth A. Nicol and J. W. Fleming

National Physical Laboratory, Teddington, Middlesex TW11 0LW, UK

(Received 15 May 1974)

The examination of the 250–350  $\text{cm}^{-1}$  region of the infra-red spectrum of polytetrafluoroethylene (PTFE) has been extended by studies of thermally degraded and sintered material. We conclude that a band at 277  $\text{cm}^{-1}$  does not arise from a true mode of the crystal but has its origin in regions where the chain has a bent conformation. Our previous speculation that bands at 292  $\text{cm}^{-1}$  and 312\*  $\text{cm}^{-1}$  (Raman active only, for the isolated chain) acquire their weak activity in the infra-red through conformational disorder is confirmed. It is likely that the conformational disorder in question arises from chain folding in the polymer crystal.

## INTRODUCTION

In our first paper on the far infra-red absorption spectrum of unsintered polytetrafluoroethylene<sup>1</sup>, we reported previously unrecognized lattice modes of the polymer crystal. We subsequently observed<sup>2</sup> further lattice modes and also two relatively weak bands at 292  $\text{cm}^{-1}$  and 312  $\text{cm}^{-1}$  which had not previously been reported. These bands are evidently the counterparts of those observed by Koenig and Boerio<sup>3</sup> in the low temperature Raman spectrum and the two bands can be assigned, according to the calculations of Hannon *et al.*<sup>4</sup>, to the  $\text{CF}_2$  twisting modes in classes  $A_1$  and  $E_2$  respectively. In a line group model both should be inactive in the infra-red. We suggested that these bands are present in the spectrum of a sample measured at liquid nitrogen temperature because the low temperature crystal-line form has more than one molecular chain passing through each unit cell. Above the 19°C transition, however, the crystal unit cell is thought to contain one chain only and we offered a tentative explanation that the persistence of the bands at 292 and 312  $\text{cm}^{-1}$  above this transition might be due to their activation by conformational disorder in the molecule.

Our further experiments on PTFE, which we now report, strongly support the validity of this latter explanation and suggest that the presence of weak bands in the infra-red spectrum, arising from modes which on symmetry grounds should be active only in the Raman effect, is a necessary consequence of the folded chain structure of the polymer crystal<sup>5</sup>.

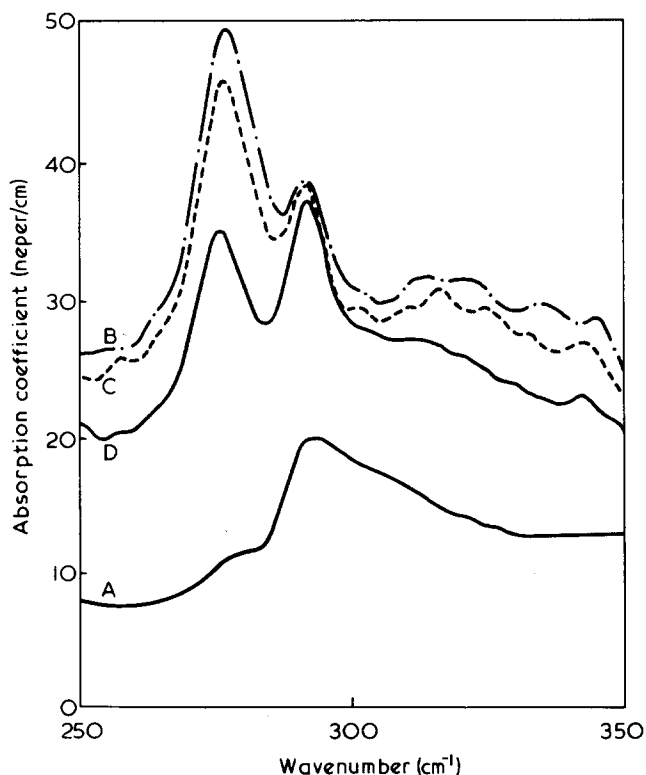
## EXPERIMENTAL

Infra-red spectra were measured with a NPL–Grubb Parsons modular cube interferometer<sup>6</sup> coupled to a Golay cell detector. The highly crystalline unsintered powder was cold pressed into discs of suitable thickness and these were heat treated in air to produce the sintered and thermally degraded samples described in the text.

\* This band is often quoted as 308  $\text{cm}^{-1}$  in the literature but accurate measurement shows it to lie at 312  $\text{cm}^{-1}$ .

## RESULTS

The spectra of a series of samples of PTFE observed in the 250–350  $\text{cm}^{-1}$  region for room temperature are presented in *Figure 1*. The samples were measured in their original unsintered state and after a period of heat treatment at 380°C as indicated. The spectra of the same samples but measured at liquid nitrogen temperature are shown in *Figure 2*.



*Figure 1* Room temperature spectra of a specimen of initially unsintered PTFE after various periods of heat treatment. A, before heat treatment; B, after 1 h at 380°C; C, after 8 h at 380°C; D, after 32 h at 380°C

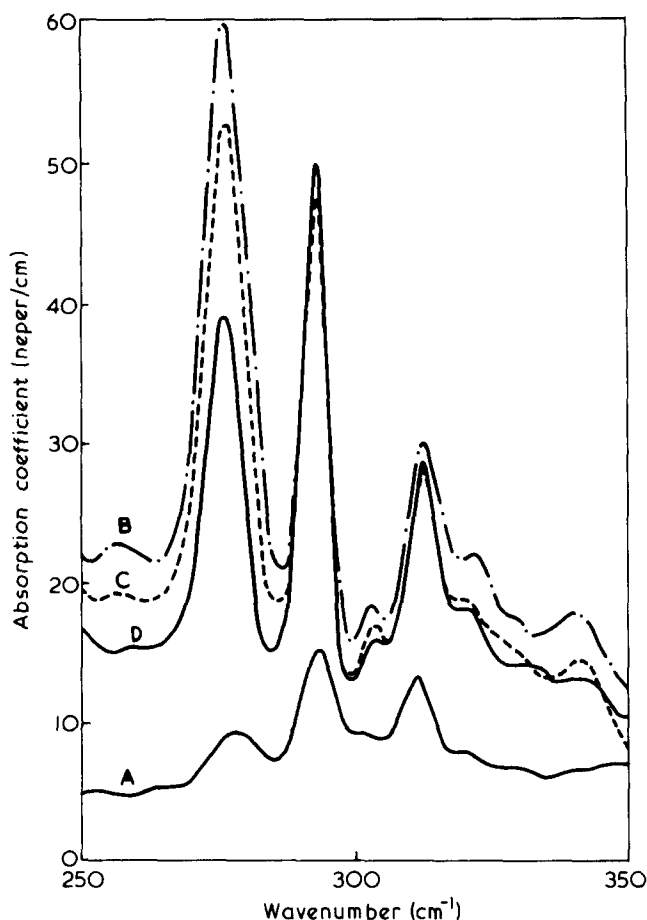


Figure 2 Low temperature (160 K) spectra of a specimen of initially unsintered PTFE after various periods of heat treatment. The distinguishing codes used for the profiles have the same significance as in Figure 1

## DISCUSSION

PTFE is remarkable in that it is very highly crystalline (~95%) as made<sup>7</sup>. However, this form of PTFE, i.e. unsintered, has such poor mechanical properties that it is usual to sinter pre-formed objects, by heating to about 380°C, to make commercial products. If specimens of PTFE are cooled slowly from the sintering temperature, the ultimate crystallinity increases the more slowly the specimen is cooled, although it never reaches that of the original unsintered powder. This is quite different from the behaviour of most partly crystalline polymers where heat treatment generally increases the final crystallinity. The origin of this unusual behaviour lies in the occurrence of mostly chain extended conformers in the unsintered powder<sup>8</sup>. These extended chains pack smoothly side by side to give a high physical density and the predominance of well-aligned regular chains leads to high X-ray estimates of the crystallinity and to low infra-red estimates of amorphous content. This latter estimate is low because the infra-red method is based on measuring the intensity of an absorption band at 770 cm<sup>-1</sup> which arises from a conformational imperfection in the regular progression of the helix<sup>9</sup>.

There is good evidence<sup>10</sup> that in the melt crystallization which takes place on sintering the crystalline habit is changed. The original fully extended helical molecules now pack into chain folded crystals in which, after a succession of monomer units (up to a few hundred) in a regular helical conformation, the conformational order is changed so that

the molecule can bend back and re-enter the crystal in the opposite direction, and once more pack regularly. The 'folds', where the molecule is bending back, lie on a regular surface and a sintered specimen consists of an assembly of these folded chain lamellae, together with interlamellar material which is presumably conformationally irregular. Since the chain folded molecules contain substantial portions which are not packed regularly parallel to other portions the proportion of conformationally irregular units is increased, and consequently both X-ray and infra-red measurements show the sintered material to have a lower crystallinity than the unsintered (i.e. substantially fully extended) original material. It is not surprising that, despite their presumed different crystal habits, the sintered and unsintered materials show similar lattice spectra at low temperatures. For polyethylene, both the extended chain and the folded chain crystals have been shown to have identical lattice spectra<sup>11</sup>. This arises because the segments between folds (100 or so repeat units) are long enough to behave as infinite chains so far as inter-segment motion is concerned. For PTFE one would imagine very similar considerations to apply.

With this background, we may examine Figures 1 and 2. In these three major absorption bands at 277, 292 and 312 cm<sup>-1</sup> will be noticed. The definition of these bands improves as the temperature falls<sup>2</sup> and in the spectrum recorded at liquid nitrogen temperature the bands are very well separated. However, this effect clearly arises only from reduction in the band half-widths as the temperature falls and there are no significant frequency shifts. Hence it may be confidently assumed that all three bands arise from internal molecular motions.

The lowest frequency band of the three, namely that at 277 cm<sup>-1</sup>, has been well known<sup>12</sup> for some years in infra-red absorption and has been universally assigned to a vibrational fundamental of the macromolecular helix, in fact to the E<sub>1</sub> CF<sub>2</sub> scissors mode. The new data shown in Figures 1 and 2 introduce, however, some difficulties which call for a re-examination of this common assumption. The band at 277 cm<sup>-1</sup> increases markedly in intensity in going from the unsintered to the sintered material and from this one can conclude at once that not all of the intensity in the 277 cm<sup>-1</sup> region, observed for sintered samples, arises from the crystalline regions. Of course the simplest assumption is that none of it does and the weak absorption at 277 cm<sup>-1</sup> observed for unsintered samples therefore arises entirely from the remaining 5% of conformationally irregular material. At least the bulk therefore of the absorption at 277 cm<sup>-1</sup> must be connected with molecular motion either in the amorphous (i.e. non-helical) molecules or else in the chain folds, since both these species are more abundant in the sintered material. A similar conclusion can be drawn from close examination of previously published Raman spectra<sup>3,13</sup> and also from our observations<sup>14</sup> of the Raman spectrum of PTFE where a very weak band at 277 cm<sup>-1</sup> for unsintered material becomes very much stronger after sintering. E<sub>1</sub> fundamentals of the regular helix are allowed, of course, in both the infra-red and Raman spectra but the intensification of the 277 cm<sup>-1</sup> band on going to a more conformationally irregular material suggests strongly that this band does not arise from a fundamental of the regular helix.

It is established therefore that, apart from the fortuitous coincidence that the absorption profile near 277 cm<sup>-1</sup> is made up of several components, the band is associated entirely with molecular motion in the conformationally

irregular regions of the crystal. However, it is worth enquiring if it is possible to decide from the spectrum whether the motion in question occurs in the interlamellar amorphous material, in the chain folds or in both. Some light is shed on this question by studies of the effect on the spectrum of prolonged heating of the specimen at 380°C. As the heating time is extended from zero to very long times, the intensity of the 277 cm<sup>-1</sup> band first increases and then slowly decreases. The increase we have already assumed to be due to chain folding and the subsequent decrease can be readily attributed to the effects of chain scission<sup>15</sup>. This has the effect of increasing the rate at which the polymer crystallizes when it is cooled from the melt so that the specimen will become increasingly crystalline as heating is prolonged and therefore the amount of amorphous material will fall. This interpretation of the behaviour of the 277 cm<sup>-1</sup> band strongly points to its origin in the amorphous material; however, the possibility that it arises from a conformer present in both chain folds and amorphous material cannot be eliminated. If the band arose from a bent conformation present in both amorphous regions and chain folds it would show somewhat similar behaviour since the small increase in the number of chain folds with increasing crystallinity would be more than offset by the decrease in amorphous material. We conclude therefore that the 277 cm<sup>-1</sup> band arises from the bent molecular conformation, certainly in the amorphous material but possibly also in the chain folds. This leaves open the question of the identity of the E<sub>1</sub> intersection of B<sub>6</sub> this matter will be discussed in a later publication.

The bands at 292 and 312 cm<sup>-1</sup>, like that at 277 cm<sup>-1</sup>, are considerably stronger in the spectrum of the specimen heated for 1 h at 380°C than they are in the spectrum of the original unsintered material. In other respects however these two bands may be sharply distinguished from that at 277 cm<sup>-1</sup>. First, these bands have obvious counterparts in the Raman spectra of both sintered and unsintered materials and they may be assigned with very little doubt to the A<sub>1</sub> and E<sub>2</sub> fundamentals of the helix. They therefore arise in the crystalline regions. Secondly, prolonged specimen-heating produces only slight changes in the intensities of these two bands rather than the dramatic reduction observed for the 277 cm<sup>-1</sup> band.

If we return to the suggestion which we made in our previous paper<sup>2</sup>, that these Raman active modes acquire infra-red activity through conformational disorder in the molecules, we see that this fits very well with the notions developed above. The original polymer is highly crystalline, but it is also conformationally very regular because the macromolecules occur mostly in the chain-extended form. The presence of a conformational irregularity can make all the modes of the chain active and the observed strength of a 'forbidden' feature will depend on the number of such discontinuities. For the chain-extended macromolecules the number of irregularities is small and the bands at 292 and 312 cm<sup>-1</sup> are weak. After sintering the molecules chain fold, and the ensuing conformational disorder leads to a considerable increase in the intensity of these two bands. Subsequent heating leads to a small increase in the amount

of chain-folded crystalline material and the bands gain in strength. For these two bands, and also for that at 277 cm<sup>-1</sup> it does not appear necessary to draw a major distinction between the observations at liquid nitrogen temperature and those at room temperature. This is in marked contradistinction to the behaviour of the bands lying below 100 cm<sup>-1</sup> where the spectra at room and at liquid nitrogen temperatures are completely different. There can be no doubt that the bands at 277, 292 and 312 cm<sup>-1</sup> are present at both temperatures; all that happens as the temperature falls is that the bands sharpen, become better resolved from one another and therefore more immediately obvious in the spectrum. It therefore seems appropriate to abandon our previous suggestion<sup>2</sup> that the bands are activated by two different processes and instead to conclude that the bands owe their activity solely to conformational disorder and not at all to intermolecular effects. Indeed were the latter significant it would be very difficult to understand why at liquid nitrogen temperature a decrease in crystallinity (subsequent upon sintering) should be accompanied by increasing strength of these bands.

We therefore conclude that the band at 277 cm<sup>-1</sup> is not a fundamental of a conformationally regular PTFE molecule and that the bands at 292 and 312 cm<sup>-1</sup> which are fundamentals, but which should be forbidden in the infra-red, owe their activity to the presence of chain folds in the crystalline regions of the polymer. Similar conclusions have been reached by Professor G. Zerbi and his colleagues and we would like to thank them for sending us preprints of their work<sup>16</sup>.

## REFERENCES

- 1 Chantry, G. W., Fleming, J. W., Nicol, E. A., Willis, H. A. and Cudby, M. E. A. *Chem. Phys. Lett.* 1972, 16, 141
- 2 Chantry, G. W., Fleming, J. W., Nicol, E. A., Willis, H. A., Cudby, M. E. A. and Boerio, F. J. *Polymer* 1974, 15, 69
- 3 Koenig, J. L. and Boerio, F. J. *Chem. Phys.* 1969, 50, 2823
- 4 Hannon, M. J., Boerio, F. J. and Koenig, J. L. *Chem. Phys.* 1969, 50, 2829
- 5 Bunn, C. W., Cobbold, A. J. and Palmer, R. P. *J. Polym. Sci.* 1958, 28, 365; Kirk-Othner, 'Encyclopaedia of Chemical Technology', Vol 9, 2nd Edn, Interscience, New York, 1966, p 821
- 6 Chantry, G. W. 'Submillimetre Physics', Academic Press, London and New York, 1971, Ch 4
- 7 Kirk-Othner. 'Encyclopaedia of Chemical Technology', Vol 9, 2nd Edn, Interscience, New York, 1966, p 819
- 8 Rahl, F. J., Evanco, M. A., Fredericks, R. J. and Reimschuessel, A. C. *J. Polym. Sci. (A-2)* 1972, 10, 1337
- 9 Miller, R. G. J. and Willis, H. A. *J. Polym. Sci.* 1956, 19, 485
- 10 Melillo, L. and Wunderlich, B. *Kolloid Z. Z. Polym.* 1972, 250, 417
- 11 Nicol, E. A. unpublished observation; Martin, D. H. personal communication
- 12 Liang, C. Y. and Krimm, S. *J. Chem. Phys.* 1956, 25, 563
- 13 Peacock, C. J., Hendra, P. J., Willis, H. A. and Cudby, M. E. A. *J. Chem. Soc. (A)* 1970, p 2943
- 14 Willis, H. A. and Cudby, M. E. A. unpublished work
- 15 Sperati, C. A. and Starkweather, H. W. *Adv. Polym. Sci.* 1961, 2, 488
- 16 Zerbi, G. and Sacchi, M. *Macromolecules* 1973, 6, 692; Masetti, G., Cabassi, F., Morelli, G. and Zerbi, G. *Macromolecules* 1973, 6, 700

# Mechanical response of elastomers not too far from equilibrium\*

R. F. Fedors and R. F. Landel

Jet Propulsion Laboratory, California Institute of Technology, Pasadena, California 91103, USA

(Received 23 April 1974; revised 30 July 1974)

For any polymer, the mechanical response can be conveniently represented in terms of the three variables stress,  $\sigma$ , strain,  $\epsilon$ , and time,  $t$ . It is shown that under fairly general conditions, crosslinked elastomers which display weak or moderate viscoelastic character, i.e., are not too far from equilibrium conditions, will yield mechanical response curves including the rupture response that can be superposed onto master curves provided the plotting variables are properly chosen. It is shown that these variables should be: (1) the reduced stress,  $\sigma T_0/\nu_e T$ , where  $T_0$  and  $T$  are an arbitrarily chosen reference temperature and the test temperature respectively, and  $\nu_e$  is the network chain concentration or some other quantity proportional to it; (2) the strain; and (3) the reduced time,  $t/a_T a_x$ , where  $a_T$  is the time-temperature shift factor and  $a_x$  is a shift factor which accounts for the effect of  $\nu_e$  on the time scale.

## INTRODUCTION

Previous studies have indicated that the mechanical response of amorphous gum elastomers can be conveniently described in terms of a family of physical property surfaces, each member of which can be characterized by both its shape and its location in stress, strain, and time space. The surfaces are generated by allowing one or more parameters to assume different values. For temperatures that are sufficiently above the glass-transition temperature  $T_g$ , only a single parameter  $\nu_e$ , the concentration of effective network chains per unit volume of elastomer, seems to be required to specify the shape of the surface to a good first approximation<sup>1</sup>. Little information, however, is available on the number of parameters that determine location although recent work of Plazek<sup>2</sup> would indicate that two, one of which is  $\nu_e$ , may be required.

Fracture in reference to the physical property surfaces represents some limiting boundary or discontinuity to each surface. In general, a distinct space curve is associated with each surface and hence both the shape and location of a space curve might be expected to depend to a large extent on the same parameters that characterize the surface.

The projection of a family of space curves to the stress-time ( $\sigma, t$ ) or strain-time ( $\epsilon, t$ ) planes represents the time dependence of fracture, while the projection to the  $\sigma, \epsilon$  plane is independent of the time scale. The latter projection, known as the failure envelope, has been shown to be independent of  $\nu_e$  over wide ranges of temperature provided the reduced variable  $\sigma_b T_0/\nu_e T$  is used instead of  $\sigma_b$  itself, i.e. a plot of  $\log \sigma_b T_0/\nu_e T$  versus  $\log \epsilon_b$  produces a superposition of the high-temperature portions of individual failure envelopes to yield a master curve for rupture that is essentially independent of variables such as rate, test temperature, chemical nature of the elastomer,  $\nu_e$ , and the presence of small amounts of diluent<sup>1</sup>. Here  $T_0$  and  $T$  are an arbitrarily chosen reference temperature and the test temperature, respectively.

It is easy to demonstrate that these plotting variables will yield a master curve for that segment of the failure envelope in which the elastomer does not exhibit appreciable viscoelastic character, i.e. for test conditions where the system is close to mechanical equilibrium. However, it is a well-established empirical result that segments of the failure envelope where the elastomer is exhibiting weak to moderate viscoelastic response will also fall on the master curve. No explanation for superposition in this region has, as yet, been advanced.

The purpose of this paper is to show that under fairly general conditions, elastomers which display weak to moderate viscoelastic character will yield failure envelopes that will superpose to the master curve. In addition, the effect of weak to moderate viscoelastic character on the physical property surface as well as on the  $\sigma_b, t_b$  and  $\epsilon_b, t_b$  response will also be discussed.

## THE PHYSICAL PROPERTY SERVICE

### General characteristics

In general, for a given test mode, the mechanical response of an elastomer can be conveniently described in terms of at least the four variables  $\sigma T_0/T, \epsilon, t$ , and  $\nu_e$  (the ratio  $T_0/T$  is a temperature correction factor for the stress). If  $\sigma T_0/T, \epsilon$ , and  $t$  are selected as the three plotting variables, then the response can be represented in terms of a family of three-dimensional surfaces, called physical property surfaces; the shape of the high-temperature portion of the surface is determined primarily by the value of  $\nu_e$ .

Rupture can then be defined in terms of a family of space curves that represent some limiting value, boundary, or discontinuity to each surface. Thus, each surface will have associated with it a space curve defining the occurrence of rupture.

The projection of these space curves to the  $\log \sigma T_0/T, \log \epsilon$  plane produces a family of time-independent failure envelopes as shown schematically in *Figure 1a*, where the arrow denotes the direction of increasing  $\nu_e$ . For a given value of  $\sigma_b T_0/T$ , the strain-at-break increases as the network chain concentration decreases. Furthermore, as the test

\* This paper presents the results of one phase of research carried out at the Jet Propulsion Laboratory, California Institute of Technology, under Contract number NAS7-100 sponsored by the National Aeronautics and Space Administration.

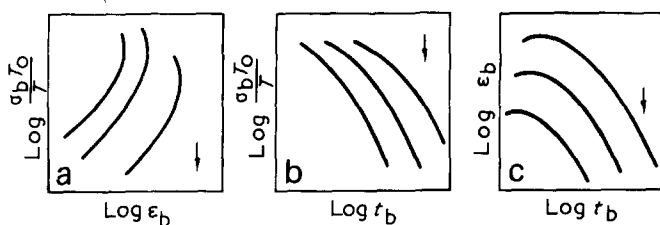


Figure 1 Projections of physical property space curves to: (a)  $\sigma, \epsilon$  plane; (b)  $\sigma, t$  plane; and (c)  $\epsilon, t$  plane

temperature or the time scale of the experiment is decreased, i.e. as the system is moved away from mechanical equilibrium with a concomitant increase in the viscoelastic character, the rupture points move along the failure envelope in an anticlockwise direction. At a sufficiently low temperature,  $\epsilon_b$  passes through a maximum and finally decreases to small values as  $T_g$  is approached.

This failure envelope is of great importance because of this time independence and also because it is approximately independent of the test type so that nearly the same envelope is generated in stress-relaxation, creep, or constant strain rate, provided the test temperatures are well above  $T_g$ .

The projection of the space curve to the  $\log \sigma_b T_0/T$ ,  $\log t_b$  plane provides the time-to-break dependence of  $\sigma_b$  as shown schematically in Figure 1b, while the projection to the  $\log \epsilon_b$ ,  $\log t_b$  plane provides the time-to-break dependence of  $\epsilon_b$  as shown in Figure 1c. It is apparent that  $\sigma_b T_0/T$  increases monotonically while  $\epsilon_b$  passes through a maximum as  $t_b$  decreases. As the system moves away from mechanical equilibrium, the failure points move from right to left in both Figures 1b and 1c. Thus, by increasing the viscoelastic character (by decreasing  $t_b$ ), both  $\sigma_b$  and  $\epsilon_b$  increase. The maximum in  $\epsilon_b$  that is directly related to the network chain concentration  $\nu_e$  is commonly observed to occur at roughly the same time scale at which the stress-relaxation modulus is entering the transition zone. Note that only two of these projections are independent since the third can be generated from the other two by eliminating the common variable.

#### Mathematical description

For elastomers which display weak to moderate viscoelastic character, it has been shown that time and strain are factorable<sup>3-5</sup>. Hence, one can express the stress as a product of two factors, one of which depends on time alone and one which depends on strain:

$$\frac{\sigma}{G_e} = \frac{G(t)}{G_e} f(\epsilon, a_1, a_2, \dots) \quad (1)$$

where  $G_e$  is the shear modulus when the system is at mechanical equilibrium (which may be taken equal to  $\nu_e RT$ , where  $R$  is the gas constant),  $G(t)$  is the time-dependent modulus, and  $f$  is a function that contains the strain dependence as well as possible dependence on additional parameters  $a_1, a_2, \dots$ , as may be required. It is clear from previously cited work that the parameters  $a_i$  can be at most only very weakly dependent on time or temperature except for temperatures near  $T_g$ .

It is more convenient to express equation (1) in the form:

$$\frac{\sigma T_0}{\nu_e T} = g(t) f(\epsilon, a_1, a_2, \dots) \quad (2)$$

where

$$g(t) \equiv \frac{G(t)T_0}{\nu_e T} \equiv \frac{G_p(t)}{\nu_e}$$

and  $G_e$  has been taken equal to  $\nu_e RT$ . As  $t \rightarrow \infty$  or as mechanical equilibrium is approached,  $g(t)$  approaches a limiting value of  $RT_0$ . To the extent that both  $g$  and  $f$  can be taken as universal functions, then equation (2) implies that a single superposed physical property surface will be obtained, provided the plotting variables are chosen to be  $\sigma T_0/\nu_e T$ ,  $\epsilon$ , and  $t$  rather than  $\sigma$ ,  $\epsilon$ , and  $t$ .

The conditions under which both  $g$  and  $f$  can be taken to be universal functions, as a first approximation at least, will now be considered. The time-dependent function  $g$  is considered first.

**Dependence on  $\nu_e$ .** In addition to the usual time-temperature superposition governed by the WLF relationship<sup>6</sup>, Plazek has demonstrated that superposition of the long time or terminal region of the creep compliance curves for both natural rubber (NR) and styrene-butadiene rubber (SBR) gum vulcanizates, having different degrees of cross-linking, can be effected by using  $\nu_e$  as a reduction variable<sup>2</sup>. This fact implies that  $\nu_e$  is the dominant variable that controls the viscoelastic response at small strains in the long-time domain.

The superposed or universal creep compliance response is defined by Plazek in the following manner:

$$J_x \left( \frac{t}{a_x} \right) = J_p \left( \frac{t}{a_x} \right) \frac{J_e(R^*)}{J_e} \quad (3)$$

where  $J_x$  is the universal creep compliance function,  $J_p$  is the response for an elastomer with a given  $\nu_e$  value,  $J_e(R^*)$  is the compliance at mechanical equilibrium for an arbitrarily chosen reference system,  $J_e$  is the compliance at equilibrium at any other  $\nu_e$ , and  $a_x$  is the shift factor along the time scale. For both NR and SBR, the relationship between  $a_x$  and  $\nu_e$  was found to be:

$$\log a_x = 15.4 \log \frac{C}{\nu_e} \quad (4)$$

where  $C$  is a constant. However, NR and SBR had different  $C$  values and this was tentatively ascribed to differences in the monomeric friction coefficients, i.e. to differences in chemical structure for these two materials. Equation (4) indicates the enormous influence of changes in  $\nu_e$  on the time scale and it implies that for a given time scale, the higher the  $\nu_e$  value, the closer the system is to equilibrium.

Various methods exist for converting from one experimentally observable viscoelastic function, such as creep compliance to any other function such as stress relaxation, to any degree of approximation desired<sup>6</sup>. Thus, for example,  $G_p(t)$  can be estimated if  $J_p(t)$  is known by use of the approximate relation:

$$G_p(t) = \frac{\sin m\pi}{m\pi J_p(t)} \quad (5)$$

where  $m$  is the slope of the doubly logarithmic plot of  $J_p(t)$  versus  $t$ . Using this equation, Plazek converted stress-relaxation data, on both NR and SBR as a function of  $\nu_e$ ,

obtained by Chasset and Thirion to a reduced creep compliance function and this was found to be essentially identical to the one that can be obtained by direct experiment. Hence, a universal creep compliance function implies the existence not only of a universal stress-relaxation function but also of other universal viscoelastic functions that can be derived from creep compliance.

Thus, a universal stress-relaxation modulus may be defined in a similar manner to that of the creep function:

$$G_x \left( \frac{t}{a_x} \right) = G_p \left( \frac{t}{a_x} \right) \frac{G_e(R^*)}{G_e} \quad (6)$$

Since  $G_e(R^*)$  is chosen arbitrarily, we can for convenience set it equal to a constant value for all systems and, hence, write

$$\frac{G_p(t/a_x)}{\nu_e} = g(t) = \frac{G_x(t/a_x)}{\nu_e(R^*)} \quad (7)$$

Since  $G_x$  is a universal function, then  $g(t)$  will also be a universal function. This is contingent on the temperature being sufficiently high so that the response is restricted to the terminal region.

*Effect of diluent on g.* Another factor, which greatly affects the nature of the viscoelastic response and hence the approach to mechanical equilibrium, is the presence of a diluent. Fujita and Kishimoto<sup>7</sup> have found, for several polymers containing varying amounts of diluent, that master stress-relaxation curves could be obtained by shifting individual curves horizontally along the time axis. The diluent concentration-time shift factor  $a_c$  for crosslinked systems can be expressed as<sup>8</sup>:

$$\log a_c = \frac{(1/2.303 f_2)(1 - \nu_2)}{(f_2/\beta') + (1 - \nu_2)} \quad (8)$$

where  $f_2$  is the fractional free volume of the polymer,  $\nu_2$  is the volume fraction of the polymer, and  $\beta'$  is a constant for a given system that may be taken as approximately equal to the fractional free volume of the diluent. Values of  $f_2$  and  $\beta'$  can be estimated from the thermal expansion coefficients above and below the glass-transition temperature. It is expected that equation (8) will only be valid for large  $\nu_2$ , i.e. small diluent concentration. It is of interest to note that as  $\nu_2$  decreases, the value of  $-\log a_c$  increases and hence the effective time scale of the experiment increases; thus the system more closely approaches mechanical equilibrium.

*Strain dependent factor, f.* Several explicit forms for the function  $f$  have been reported in the literature. The simplest is provided by the kinetic theory of elasticity and is given by:

$$f = \left( \lambda - \frac{1}{\lambda^2} \right) \quad (9)$$

where  $\lambda = 1 + \epsilon$ . This form, however is known to be useful only when  $\nu_e$  is large and  $\lambda$  is small.

Better fit to experimental data especially at moderate strains is provided by the Mooney-Rivlin expression<sup>9</sup>:

$$f = \left( \lambda - \frac{1}{\lambda^2} \right) \left( 1 + \frac{C_2}{C_1 \lambda} \right) \quad (10)$$

The parameter  $C_1$  is commonly taken equal to  $\nu_e RT$  and the parameter  $C_2$ , of unknown origin, turns out to be an implicit but weak function of both  $\nu_e$  and  $T$  with  $C_2 \rightarrow 0$  as  $\nu_e$  and/or  $T$  increase.

A theoretical equation, which takes into account the finite extensibility of a polymer chain, and provides a good fit to high  $\lambda$  values is given by:

$$f = \frac{n^{1/2}}{3} \left[ \mathcal{L}^{-1} \left( \frac{\lambda}{n^{1/2}} \right) - \frac{1}{\lambda^{3/2}} \mathcal{L}^{-1} \left( \frac{1}{n^{1/2} \lambda^{1/2}} \right) \right] \quad (11)$$

where

$$\mathcal{L}^{-1}(x) = \coth(x) - \frac{1}{x}$$

and  $n$  represents the number of statistical segments per network chain. As  $\lambda/n^{1/2} \rightarrow 1$ ,  $f \rightarrow \infty$  and, hence, the magnitude of  $n$  furnishes an upper limit to the value that  $\lambda$  can attain.

For an ideal network, i.e., one containing no soluble polymer fraction or dangling chain ends, equation (11) leads to the result:

$$(\lambda_b)_{\max} = n^{1/2} = \left( \frac{1}{\nu_e N} \right)^{1/2} \quad (12)$$

where  $(\lambda_b)_{\max}$  is the maximum extensibility at break, and  $N$  is the molar volume of a statistical unit, a quantity that is determined solely by the chemical nature of the chain.

When  $\lambda \ll n^{1/2}$ , equation (11) reduces to the simple kinetic form (equation 9). Hence, equation (11) furnishes a good fit at both small and large strains but a poor fit at intermediate strains; the fit in the latter region improves, however, as  $\nu_e$  is increased.

Thus it may be concluded that no simple equation for  $f$  exists that can provide a fit over the entire strain region. However, since this range can be fitted piecewise by use of these several functional forms, useful deductions can be obtained in the strain region where they are applicable.

For example, for small strains where equation (9) can be employed, the stress-strain response is independent of the chemical structure of the elastomer since  $f$  is a function of  $\lambda$  alone. In the intermediate  $\lambda$  range,  $f$  as given by equation (10) is again apparently independent of chemical structure since at most the strain function includes a contribution from the parameter  $C_2$ , which has been reported to be independent of chemical structure<sup>9</sup>. At high strains, where equation (11) can be employed, the response of an elastomer is now no longer independent of chemical structure since it contains the parameter  $n$  which, as equation (12) shows, is directly related to structure.

Although  $g(t)$  has been shown to be a universal function in the terminal region, no simple universal form for  $f$  apparently exists. However, since the strain region can be fitted at least piecewise by assuming several forms for  $f$ , these several forms taken together can be considered to constitute a universal  $f$ . As a first approximation then, the use of the reduced variables  $\sigma T_0/\nu_e T$ ,  $\epsilon$ , and  $t$  will superpose at least the high-temperature portions of the family of physical property surfaces to a single surface. The superposed surface for elastomers which differ in chemical struc-

ture will at most differ on the time scale by a factor that depends on differences in the value of the monomeric friction coefficient. If this factor is taken into account by suitable shifts along the time scale, then a single universal property surface, independent of chemical structure, will result.

*Effect of test type.* Superposition of segments of the physical property surface as described above was limited to a single test type, e.g. creep, stress-relaxation, or constant strain rate tests. In general, it is expected that a different family of surfaces will be generated for each test type. However, if attention is restricted to the high-temperature portion of the surface, then it turns out that the surfaces are approximately independent of test mode.

For example, in stress-relaxation *versus* creep experiments, factorability of time and strain as expressed by equation (1) is still expected to be valid and, hence, we can write for the stress-relaxation experiment:

$$\frac{\sigma T_0}{\nu_e T} = g(t) f(\epsilon, a_1, a_2, \dots) \quad (13)$$

while for experiments in creep:

$$\frac{\sigma T_0}{\nu_e T} = \frac{1}{j(t)} f(\epsilon, a_1, a_2, \dots) \quad (14)$$

where  $j(t) \equiv J_p(t)/\nu_e$  and  $f$  is taken to be independent of test type. Considering equation (5), which provides a relationship between  $g(t)$  and  $j(t)$ , it may be seen that the response obtained in these two test modes will differ only when the factor  $\sin m\pi/m\pi$  is appreciably less than unity. For example,  $g(t)$  and  $j(t)$  differ by 10% when  $m$  is less than 0.25. For much of the terminal region,  $m$  will most likely be less than 0.25. Hence, in this region, the surfaces and space curves as well are expected to be essentially independent of whether the data are obtained in stress-relaxation or creep experiments.

Considering constant strain rate experiments, Smith<sup>10</sup> has proposed a relationship between the stress-relaxation modulus and the constant strain modulus  $h(t)$  in the form:

$$g(t) = h(t) \left[ 1 + \frac{\partial \log h(t)}{\partial \log t} \right] \quad (15)$$

where the partial derivative can assume values in the interval 0 to -0.67. Here again, if attention is restricted to the terminal zone, the values assumed by this factor should be close to zero and hence  $g(t)$  and  $h(t)$  will not differ appreciably in value.

Thus, the surfaces generated in these three types of experiments may be considered to be essentially the same; this statement applies to the associated space curves and to their projections in the various planes as well. In support of this, it has already been mentioned that experimental data show the failure envelope to be independent of test type.

#### FAILURE BEHAVIOUR

Having shown that superposed physical property surface exists at least for a small region in  $\sigma T_0/\nu_e T$ ,  $\epsilon$ , and  $t$  space, it follows that a universal failure space curve also exists over the same region. Thus, it is expected that a universal or master failure envelope will be produced when the uni-

versal failure space curve is projected to the  $\sigma$ ,  $\epsilon$  plane. Likewise, universal curves will also occur in the  $\sigma$ ,  $t$  as well as the  $\epsilon$ ,  $t$  planes.

The first of these predictions (the existence of a master failure envelope) has been adequately demonstrated by a mass of experimental data<sup>1</sup>. The failure envelopes diverge from the master curve, however, for those conditions where the physical property surfaces do not superpose. The existence of universal  $\sigma_b T_0/\nu_e$  *versus*  $t_b$  and  $\epsilon_b$  curves has been established in that studies have indicated that shifts along the time axis (Plazek shift factor  $a_x$ ) do lead to superposition of segments obtained at high temperatures<sup>11</sup>. This work will be the subject of a future report.

#### IMPLICATIONS AND PRACTICAL APPLICATIONS

##### Physical property surface

To the extent that the Plazek shift factor is universally applicable,  $\nu_e$  can be used as a convenient variable to expand the experimental time scale, i.e. to obtain data for times or temperatures that may not be accessible experimentally. For example, if significant degradation occurs at an elevated temperature for an elastomer having a given  $\nu_e$  value, then equivalent information in the absence of degradation can be obtained by studying the behaviour at lower temperatures for specimens having higher  $\nu_e$  values; these data can then be shifted along the time axis to yield the desired information. The same type of information is produced by a study of swollen specimens; these data can also be shifted along the time axis according to equation (8).

##### Failure behaviour

It is known that both  $\sigma_b$  and  $\epsilon_b$  decrease monotonically with  $t_b$  as mechanical equilibrium is approached. Equations (4) and (8) indicate that increasing  $\nu_e$  or increasing the quantity of diluent also brings the system closer to mechanical equilibrium. Hence, this implies that increasing  $\nu_e$  and adding diluent to a system should produce a reduction in both  $\sigma_b$  and  $\epsilon_b$ ; this is in agreement with experimental data.

Equations (4) and (8) can be employed to obtain semi-quantitative estimates of the effect of both  $\nu_e$  and swelling on failure behaviour. Assuming that the  $\sigma_b$ ,  $t_b$  and  $\epsilon_b$ ,  $t_b$  responses are known at one value of  $\nu_e$ , then the effect of varying both  $\nu_e$  and swelling on the effective time scale can be calculated. Knowing the effective time scale, one can then read off from the  $\sigma_b$ ,  $t_b$  and  $\epsilon_b$ ,  $t_b$  plots in the  $\sigma_b$  and  $\epsilon_b$  values that correspond to the change in  $\nu_e$  or swelling.

#### REFERENCES

- 1 Landel, R. F. and Fedors, R. F. *Rubber Chem. Technol.* 1967, 40, 1049
- 2 Plazek, D. J. *J. Polym. Sci. (A-2)* 1966, 4, 745
- 3 Landel, R. F. and Stedry, P. J. *J. Appl. Phys.* 1960, 31, 1885
- 4 Chasset, R. and Thirion, P. 'Physics of Non-Crystalline Solids', in *Proc. Int. Conf., Delft, 1964*, Interscience, New York, 1965, p 345
- 5 Smith, T. L. *Tech. Docum. Rep. No. ASD-TDR 63-430* Wright-Patterson AFB, Ohio, 1963
- 6 Ferry, J. D. 'Viscoelastic Properties of Polymers', John Wiley, New York, 1961
- 7 Fujita, H. and Kishimoto, A. *J. Polym. Sci.* 1958, 28, 547
- 8 Ferry, J. D. and Stratton, R. A. *Kolloid-Z.* 1961, 171, 107
- 9 Treloar, L. R. G. 'The Physics of Rubber Elasticity', Oxford University Press, New York, 1958
- 10 Smith, T. L. *Tech. Docum. Rep. No. ASD-TDR-62-572* Wright-Patterson AFB, Ohio, 1962
- 11 Fedors, R. F. and Landel, R. F. *J. Polym. Sci. (A-2)* submitted

# Thermal decomposition of polystyrene

Shadi L. Malhotra, Jean Hesse\* and Louis-P. Blanchard

Département de Génie Chimique, Faculté des Sciences et de Génie, Université Laval, Québec, Canada G1K 7P4

(Received 1 May 1974)

Kinetic studies on the decomposition of polystyrene samples with molecular weights ranging from 900 to  $1.8 \times 10^6$  have been carried out making use of the differential thermogravimetric and differential scanning calorimetric techniques. Changes in molecular weight distributions with decomposition, at different temperatures or times, have been studied by gel permeation chromatography. This technique was likewise used to carry out component splitting of the undecomposed polymer samples. These components have been shown to break down statistically primarily by a process of random scissions yielding lower molecular weight products. The major portion of the observed weight loss, by the volatilization of small chain segments, is attributed to a rapid and complete depolymerization of chains. These interpretations are based on changes in polydispersity occurring during the decompositions. Similar components, decomposing in a different manner but under identical operating conditions, are suspected of being different stereoregular forms of the polymer. The order of reaction as computed from the method of Freeman and Carroll has been found to be zero for random scissions and one for the process of depolymerization. The activation energy computed by the method of Coats and Redfern was found to increase with molecular weight reaching a maximum value in the  $10^5$  molecular weight range.

## INTRODUCTION

The thermal decomposition of polystyrene has been the subject of many studies<sup>1-4</sup> in the past and still remains the subject of much discussion. It is generally believed that decompositions such as this proceed in two steps. In the first, it is assumed that random thermal scissions break the polymer chains at weak points<sup>5-7</sup> resulting from factors such as head-to-head linkages, chain branches and unsaturated bonds. In the second step, the shorter chain segments depolymerize into volatile products consisting mainly of monomer and low molecular weight oligomers (e.g. dimers, trimers and tetramers). It is during this second step that the major portion of weight loss occurs in the decomposition process. These conclusions have been reached primarily from kinetic data where the two-step decomposition of polystyrene, attributed to different reaction mechanisms, is said to have zero order kinetics for the first step and first order kinetics for the second<sup>8-13</sup>. Different activation energies for the two processes are also reported in the literature<sup>9-13</sup>.

In thermal decompositions where random scissions and cleavages of chain-ends take place, chain lengths and their distribution in the polymer must of necessity be important factors in determining the course that the reaction process follows with time or temperature. Indeed, studies have been reported in this area<sup>14-16</sup>, but these are based on either theoretical considerations or data obtained with light scattering, osmometry or viscometry which yield limited information. Recently, gel permeation chromatography (g.p.c.) has been used to study the decomposition of polystyrene and detailed information has been reported<sup>17</sup>. In this laboratory, g.p.c. distributions have also been obtained as the decomposition proceeds and they have been

analysed<sup>18</sup> though in a different manner. This has led to speculations regarding the mechanism of decomposition. Kinetics of the reactions have also been studied in order to gain support for the speculated mechanism: the order of reaction and energy of activation being both computed by the method of Freeman and Carroll<sup>19</sup> and by that of Coats and Redfern<sup>20</sup>. The results obtained are discussed in the light of existing theories.

## EXPERIMENTAL

### Materials

Anionically prepared polystyrene standards with molecular weights ranging from 900 to  $1.8 \times 10^6$  were obtained from the Pressure Chemical Company in the USA. A thermally prepared polystyrene sample with a weight-average molecular weight of  $4.3 \times 10^5$ , provided by Farbwerke Hoechst AG was likewise included in the study. The samples were used as such without further purification when preliminary tests with purified (by precipitation) and non-purified samples yielded the same results.

### Apparatus

A Perkin-Elmer model TGS-1 thermobalance, operating under inert nitrogen atmosphere and at heating rates of 1.25°, 5.0° and 20°C/min, was used to study the 1 mg polymer samples selected. A Perkin-Elmer model DSC-1B differential scanning calorimeter likewise operating under inert nitrogen atmosphere and at a heating rate of 20°C/min was also used in this work but with samples each weighing from 2 to 3 mg. The samples were placed between two layers of 100 mesh stainless-steel screening as suggested by Ellerstein<sup>21</sup>.

Analyses of the polystyrene samples both before and after the decompositions were carried out with a Waters Associates model 200 gel permeation chromatograph

\* Present address: Villa Société Nationale des Pétroles Aquitaines No: 6, 64370 Arthez-de-Béarn, France.



operated in a constant temperature ( $25 \pm 0.5^\circ\text{C}$ ) room. The separating system consisted of four 4 ft (1.22 m) columns connected in series, each packed with crosslinked polystyrene gel having (by the Waters method) pore sizes of  $1 \times 10^6$ ,  $1.5 \times 10^5$ ,  $3 \times 10^3$  and  $250 \text{ \AA}$  respectively. The flow of solvent, tetrahydrofuran degassed with nitrogen, was maintained at 1 ml/min while the concentration of polymer in the samples was limited to 0.125 wt % in order to render negligible 'concentration effects' on the peak positions in the chromatograms. The anionic polystyrene standards were used to plot a g.p.c. calibration curve (log molecular weight,  $M$  versus elution volume  $V_e$ ) shown in Figure 1. Molecular weights were then computed by following Smith's method<sup>22</sup>.

*Component splitting of the g.p.c. curves*

Splitting of the raw g.p.c. curves into several components was carried out as described below for the particular case of the  $1.8 \times 10^6$  molecular weight anionic polystyrene standard.

As can be seen from Table 1, at the lower elution volumes which correspond to the higher molecular weight species there is a continuous decrease in the relative weights of the polymer species with reaction temperature, whereas at the higher elution volumes (or lower molecular weights), the weights of the lower molecular weight species increase regularly. If one subtracts from the initial distribution curve of the undecomposed polymer the distribution curve of any subsequently decomposed polymer, one can readily visualize the changes that take place resulting from the decomposition of the higher molecular weight species.

To illustrate the above, the g.p.c. distribution of the undecomposed ( $1.8 \times 10^6$ ) polystyrene standard was compared successively with that of two other samples obtained with the same polymer after it had been decomposed during 50 min periods at 230 and  $330^\circ\text{C}$  respectively. In this manner, it was possible to split the undecomposed polymer sample into three components:  $\alpha$ ,  $\beta$  and  $\gamma$ .

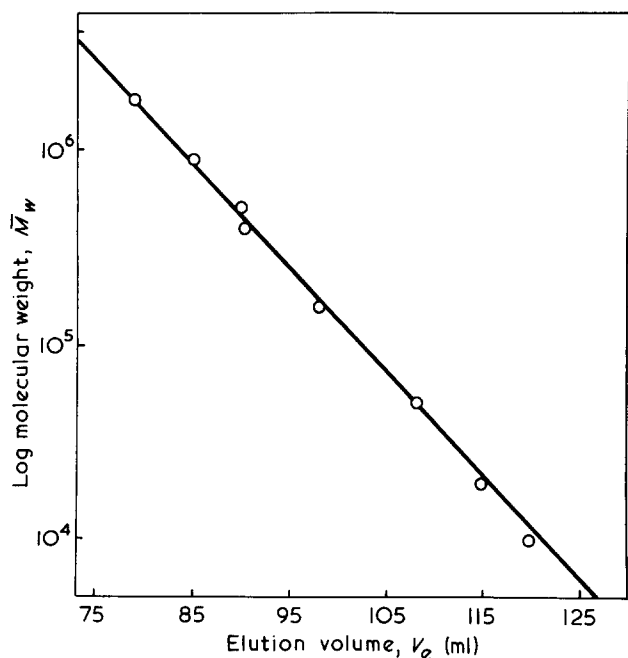


Figure 1 G.p.c. calibration curve prepared with polystyrene standard samples in THF at room temperature at a flow rate of 1 ml/min on the following Waters Associates Styrogel columns linked in the following way:  $7 \times 10^5$  to  $5 \times 10^6 \text{ \AA}$ ,  $1.5 \times 10^5$  to  $7 \times 10^5 \text{ \AA}$ ,  $3.0 \times 10^3 \text{ \AA}$ , and  $250 \text{ \AA}$

Table 1 Relative weights of decomposed and undecomposed fractions of polystyrene standard ( $M_w = 1.8 \times 10^6$ ), at different elution volumes

Elution volume (ml)	Temperature of decomposition ( $^\circ\text{C}$ )					
	20	180	230	280	330	335
	True weight loss (%)					
	0.0	0.4	0.6	0.8	3.0	8.0
70	0.12	0.14	0.14	0.00	0.00	0.00
75	6.75	5.60	2.06	1.35	0.18	0.00
80	6.45	5.80	3.83	2.95	0.75	0.00
85	3.43	4.20	4.61	4.10	1.80	0.00
90	1.81	2.30	4.15	4.40	3.30	0.19
95	0.86	1.10	2.85	3.50	4.30	1.38
100	0.40	0.40	1.45	2.05	4.00	3.79
105	0.15	0.20	0.55	0.95	2.60	5.02
110	0.10	0.20	0.22	0.45	1.60	4.03
115	0.00	0.00	0.04	0.20	0.65	2.46
120	0.00	0.00	0.00	0.00	0.20	1.13
125	0.00	0.00	0.00	0.00	0.02	0.39
Summation of relative weights:	20.07	19.94	19.90	19.95	19.40	18.37

An examination of Figure 2a, where the distribution curves of the undecomposed and decomposed (at  $230^\circ\text{C}$ ) polymer sample are shown, reveals that a part of the high molecular weight species marked  $\alpha$  in the undecomposed sample has been changed, upon heating at  $230^\circ\text{C}$ , into the lower molecular weight species  $\alpha'$ . Figure 2b shows the components of the undecomposed polymer with those of the sample decomposed at  $230^\circ\text{C}$  and this in terms of distributions,  $\alpha$  and  $(\beta + \gamma)$  for the former and  $(\beta + \gamma)$  plus  $\alpha'$  for the latter. These distributions, when derived rigorously from the proportions of their areas, appear as shown by the solid lines. In reality, however, some overlapping of the two distributions undoubtedly takes place as is shown by the broken lines. The tracing of these broken lines is based essentially on the overall shape of the curves be they broad, Gaussian or other in distribution; but they are at best only a first approximation of the true situation.

Figure 2c shows further changes that take place in the  $20^\circ\text{C}$  distribution of the  $1.8 \times 10^6$  polystyrene standard, when it is heated during a 50 min period at  $330^\circ\text{C}$ . It is clear that a greater part of the original distribution,  $(\alpha + \beta)$ , has been changed into species  $(\alpha + \beta)'$  of lower molecular weight. Figure 2d illustrates, in the form of distributions, the areas of  $(\alpha + \beta)$  and  $(\alpha + \beta)'$  again with some overlapping of the two. Tracing of the broken lines was carried out by making extrapolations on both the right-hand and left-hand sides of the  $(\alpha + \beta)$  and  $(\alpha + \beta)'$  distributions respectively, keeping in mind that their areas are essentially the same and that the residual distribution  $\gamma$ , which remains unchanged by the decomposition, is common to the two curves. More explicitly, the areas of  $(\alpha + \beta)$  plus  $\gamma$  and  $\gamma$  plus  $(\alpha + \beta)'$  should be equal. When the distribution of  $\gamma$  has been traced, that of  $\beta$  poses no problem. It can be obtained by subtracting the distribution of  $\alpha$  from that of  $(\alpha + \beta)$  or by tracing those of  $\gamma$  and  $\alpha$  under the distribution curve of the original undecomposed sample, the remaining area should be that of  $\beta$ . This is shown in Figure 2e.

The significance of these components, at this stage, lies in the fact that one can now say that the distribution of a polymer sample made up of components  $\alpha$ ,  $\beta$  and  $\gamma$  at  $20^\circ\text{C}$ , when heated at  $230^\circ\text{C}$  for 50 min, changes to a new distribution involving components  $\beta$ ,  $\gamma$  and  $\alpha'$ . If the sample is

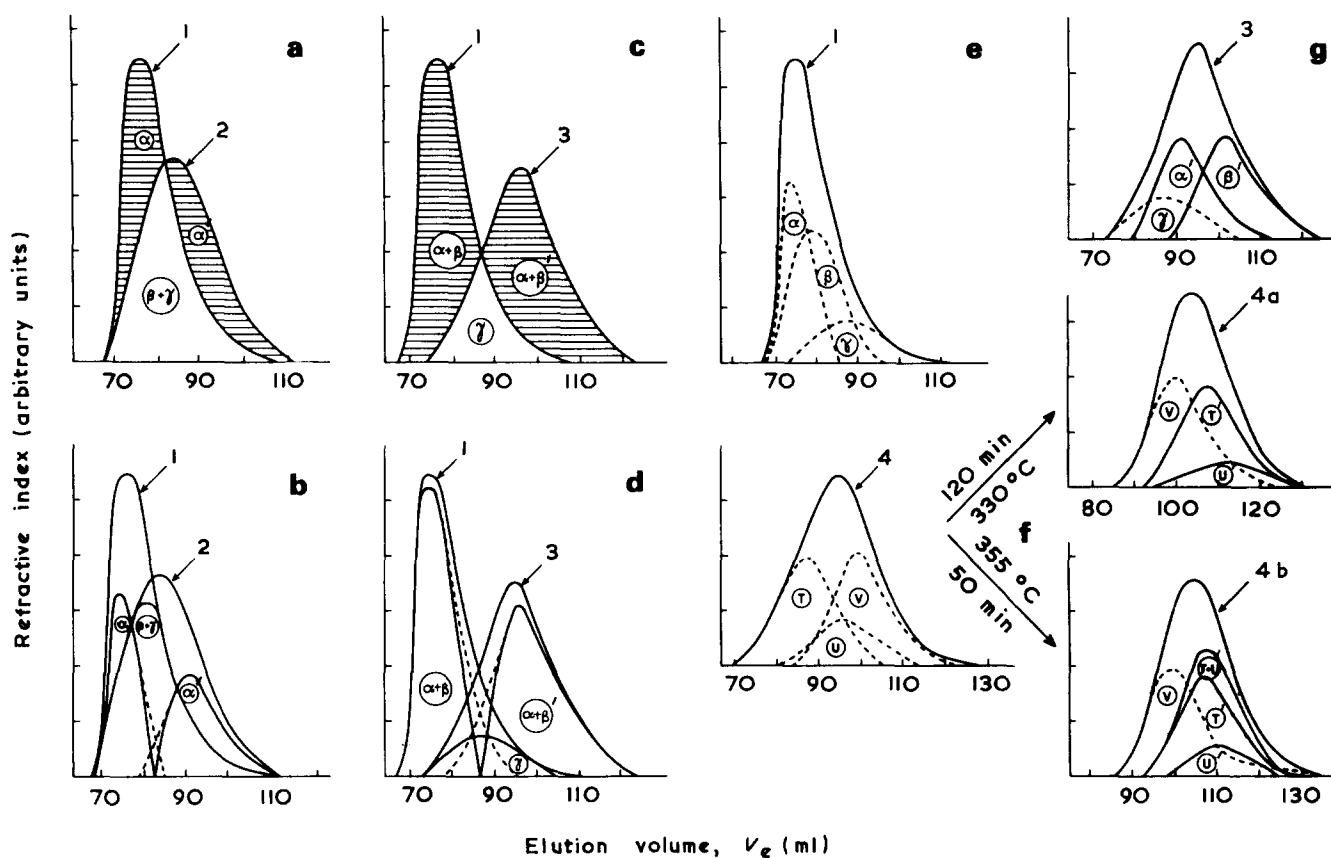


Figure 2 Graphical method of analysis by which g.p.c. distribution curves are broken down into their components: the case of a polystyrene sample PS ( $M_w = 1.8 \times 10^6$ ) subjected to isothermal treatments at several temperatures and for different periods. 1, Undecomposed; 2, 50 min at 230°C; 3, 50 min at 330°C; 4, Hoechst PS ( $M_w = 4.3 \times 10^5$ ) undecomposed; 4a, 120 min at 330°C; 4b, 50 min at 355°C

maintained at 330°C instead of 230°C, for a similar 50 min period, yet another distribution is obtained which is the sum of components  $\gamma$  and  $(\alpha + \beta)'$ . The components  $\beta$  and  $\gamma$  become more meaningful if one finds means to compute their resulting distributions,  $\beta'$  and  $\gamma'$  in a manner similar to that used to evaluate  $\alpha'$ .

This would require that the decomposition studies be made in several steps, starting with the undecomposed polystyrene standard at 20°C and decomposing it for a 50 min period at some given temperature. In a second step, one would use a part of the already decomposed sample and subject it to a further decomposition at a higher temperature for a similar period of 50 min. In this way, one would better understand the decomposition process that is taking place.

In practice, one would find this technique long and cumbersome because of the many difficulties involved in handling large quantities of material in the first decomposition that enough material might be left to carry out six or seven successive stages of decomposition. Furthermore, the kinetic parameters (e.g. activation energy) are not necessarily the same when different initial masses are used for the decompositions. This leads one to use a different approach involving: (1) the division of the original undecomposed sample at 20°C into several 1 mg parts; (2) the study of their decomposition at different temperatures for a period of 50 min; and (3) the analysis of the residues by g.p.c.

The disadvantage of this approach is that one must improvise with the results obtained in order to reach meaningful conclusions as far as the changes in distributions are concerned. To illustrate, one may once again consider the case of the decomposition of the  $1.8 \times 10^6$  polystyrene

standard. As mentioned earlier, on heating this polymer at 230°C for 50 min, the component  $\alpha$  changes to  $\alpha'$  and when the original sample is heated at 330°C for a similar period of 50 min  $(\alpha + \beta)$  changes to  $(\alpha + \beta)'$ . In order to find the value of  $\beta'$ , the products of the second decomposition, one is required to show that the distribution  $(\alpha + \beta)'$  is equivalent to  $\alpha' + \beta'$ . This means that one must assume that the g.p.c. distribution curve of the  $\alpha'$  products, obtained by heating the undecomposed sample at 230°C, will remain the same when the original sample is heated at 330°C.

This assumption originated from experimental results obtained in this laboratory while working on the decomposition of the thermally prepared polystyrene sample mentioned earlier. Figure 2f illustrates the overall distribution of the polystyrene sample and its components T, U and V, their splitting being carried out on a time basis. The use of time as a variable during the decomposition study at a fixed temperature gives meaningful results because these are obtained without having to make assumptions. To illustrate, when considering the changes that occur in distributions on heating a given sample during two different periods (viz. 50 min and 120 min), not only does one obtain results for the two independent times but also information as to what additional decomposition takes place during the latter 70 min. This enables one to trace the distribution of the components in the undecomposed sample; and furthermore it yields the distribution of their decomposed counterparts as shown in Figure 2f. It can be seen that when the sample is heated at 330°C for 120 min, the components T and U are changed into T' and U'. Detailed information about components T, U, and V and their decomposition is given later (Figure 5). Indeed, it was observed that com-

ponent T changed to T' during the first 50 min and component U decomposed into U' during the next 70 min. When the same undecomposed sample was heated at 355°C but for only 50 min, an identical distribution was obtained which is the sum of the distributions V and (T + U)', the decomposed counterpart of the component (T + U). This distribution has also been shown to be made of distributions V, T' and U' with the only difference that the molecular weight of the decomposed component U' is slightly lower, suggesting that (T + U) is equivalent to T' plus U'. Based on these results, one can say that the assumption of  $(\alpha + \beta)$  being equivalent to  $\alpha'$  plus  $\beta'$  is not far-fetched. It can be concluded from this observation that time and temperature play similar roles in the decomposition: higher temperatures require shorter times while lower temperatures require longer times. For comparable weight losses the g.p.c. traces may be expected to be very much the same.

Finally, Figure 2g illustrates the distribution of the  $1.8 \times 10^6$  polystyrene standard, decomposed at 330°C during a 50 min period, which is made up of the undecomposed component  $\gamma$  and two decomposed components  $\alpha'$  and  $\beta'$ . If one were to carry out further decompositions at higher temperatures, the distribution of the decomposed component  $\gamma'$  could then also be traced.

*Nuclear magnetic resonance spectra*

N.m.r. analyses of the polystyrene samples were carried out at the Canadian 220 MHz NMR centre, in Sheridan Park, Ontario. N.m.r. spectra of the polymers were obtained with 15% by wt solutions of the polymers in tetrachloroethylene at 100°C; tetramethylsilane was the internal standard used.

RESULTS AND DISCUSSION

A comparison of g.p.c. distributions of the undecomposed ( $1.8 \times 10^6$ ) polystyrene standard with five of its decomposed counterparts, obtained at different temperatures for 50 min periods, is shown in Figure 3a. Areas under the curves A' to E' are due to the lower molecular weight decomposition products of components A to E which disappear from the original sample when it is heated at successively higher temperatures. The g.p.c. distributions of the undecomposed sample and its five components A to E are shown in Figure 3b. Figures 3c to 3g show successively the g.p.c. distributions of the step-by-step decompositions of this polystyrene standard at temperatures ranging from 180° to 355°C where the weight loss reaches an upper value of 8%. Changes in molecular weights and in polydispersities between the decomposed and the undecomposed components are shown in Table 2. It can be seen that each decomposition reaction is accompanied by an important drop in the molecular weight of the decomposed species when considered on an individual basis; the bulk molecular weight, however, does not seem to change in such a pronounced way. A similar situation is encountered with the polydispersities. The bulk polydispersity does increase as the decomposition progresses, but it does not reveal the fact that, at each decomposition, the polydispersity of the newly formed products is very close to 2.0. One can safely assume from these results that, for a high molecular weight polystyrene sample of low polydispersity, the mechanism of decomposition resulting in a weight loss of less than 10% should be such as to yield a polydispersity of 2.0, the most probable distribution.

Figure 4a illustrates a comparison of g.p.c. distributions obtained with a thermally prepared polystyrene sample of broad initial distribution and molecular weight,  $\bar{M}_w$ , of  $4.3 \times 10^5$  with its decomposed counterparts, where the decompositions were carried out, during 50 min periods, at temperatures of 280°, 330° and 355°C. A fourth distribution of decomposition products was obtained at 370°C but was not included when splitting component parts because of the excessively high polymer weight loss

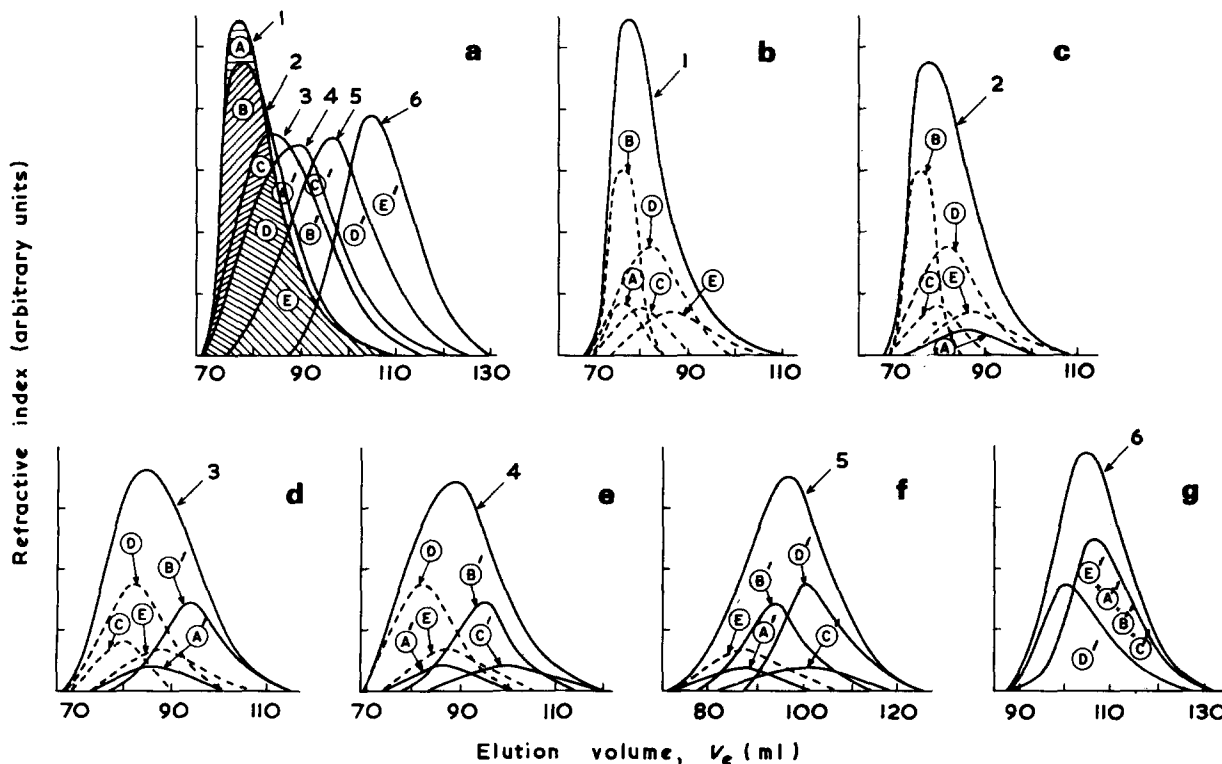


Figure 3 (a) G.p.c. distributions of PS ( $\bar{M}_w = 1.8 \times 10^6$ ) subjected to 50 min isothermal treatments at various temperatures; (b) to (g) components of each of the g.p.c. curves shown in (a). 1, Undecomposed; 2, 180°; 3, 230°; 4, 280°; 5, 330°; 6, 355°C

observed (56.5%). In this study, were considered only those decompositions which involved less than 10% weight loss. *Figure 4b* shows the components L to O of the undecomposed distribution while *Figures 4c to 4f* show successively again by g.p.c. distributions the step-by-step decompositions of this polystyrene sample at the four temperatures mentioned above. The polydispersities of the decomposed components L' to O' are compared in *Table 3* with those of their undecomposed counterparts L to O. The polydispersities of approximately 2.0 remain unchanged after the decompositions.

*Figure 5a* illustrates g.p.c. distributions obtained with the above mentioned undecomposed polystyrene ( $\bar{M}_w = 4.3 \times 10^5$ ) and with the products of its decomposition at 330°C during different periods. Only three curves were considered for component splitting of the undecomposed polymer since the fourth experiment, lasting 4 h involved an excessive 33% weight loss. *Figure 5b* shows three components T, U, and V while *Figures 5c to 5e* show the progression of the decompositions. Molecular weight and polydispersity values of the above components, T, U and V,

**Table 2** Polystyrene standard ( $\bar{M}_w = 1.8 \times 10^6$ ) components and their decomposed counterparts at different temperatures

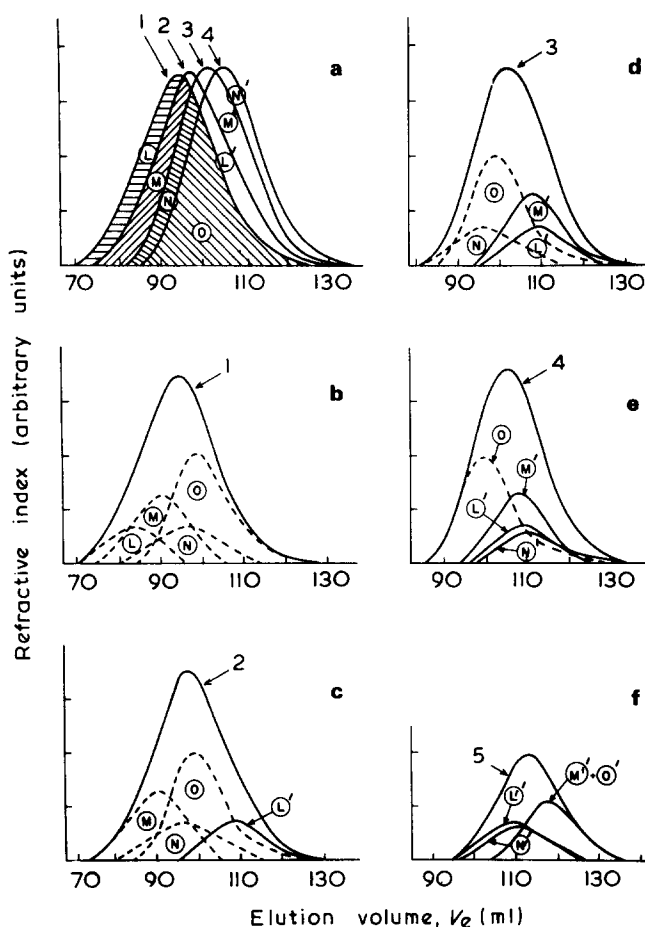
	Undecomposed components at 20°C				
	A	B	C	D	E
$\bar{M}_w \times 10^{-6}$	2.82	2.72	2.05	1.49	0.80
$\bar{M}_n \times 10^{-6}$	2.52	2.48	1.47	0.80	0.40
Polydispersity	1.10	1.10	1.40	1.86	2.0
Temperature of decomposition (°C)	180	230	280	330	355
Time of decomposition (min)	50	50	50	50	50
True weight loss (%)	0.4	0.6	0.8	2.9	8.3
	Decomposed counterparts				
	A'	B'	C'	D'	A'' + B'' + C'' + D'' + E'
$\bar{M}_w \times 10^{-5}$	8.78	3.10	1.80	1.13	0.61
$\bar{M}_n \times 10^{-5}$	4.70	1.57	0.84	0.57	0.31
Polydispersity	1.90	2.00	2.10	2.00	2.00

**Table 3** Components of the thermally prepared polystyrene ( $\bar{M}_w = 4.3 \times 10^5$ ) and their decomposed counterparts at different temperatures and times

	Undecomposed components at 20°C				Undecomposed components at 20°C		
	L	M	N	O	T	U	V
$\bar{M}_w \times 10^{-5}$	12.60	5.78	2.42	1.41	8.25	2.39	1.38
$\bar{M}_n \times 10^{-5}$	7.09	2.89	1.32	0.67	4.18	1.31	0.66
Polydispersity	1.78	2.00	1.85	2.10	1.97	1.86	2.10
Temp. of decomposition (°C)	280	330	355	380	330	330	330
Time of decomposition (min)	50	50	50	50	50	120	240
True weight loss (%)	1.3	5.9	9.6	56.5	5.9	10.0	33.0
	Decomposed counterparts				Decomposed counterparts		
	L'	M'	N'	L'' + M'' + N'' + O'	T'	U'	V'
$\bar{M}_w \times 10^{-4}$	5.07	6.80	2.80	3.60	6.12	3.34	4.60
$\bar{M}_n \times 10^{-4}$	2.95	4.00	1.56	1.80	3.34	1.67	2.39
Polydispersity	1.71	1.70	1.80	2.00	1.83	2.00	1.93

are shown in *Table 3*. The results show clearly that the decomposition products T', U' and V', have the same polydispersity (2.00) as the parent components.

The process whereby the decomposition of a high molecular weight polymer with a polydispersity of 2.0 or less leads to products of lower molecular weight with a most probable distribution, has been attributed to random scissions by Berlin and Yenikolopyan<sup>15</sup>. The polydispersity results obtained in this laboratory agree well with the theoretical values expected for random scissions.



**Figure 4** (a) G.p.c. distributions of Hoechst PS ( $\bar{M}_w = 4.3 \times 10^5$ ) subjected to 50 min isothermal treatments at various temperatures; (b) to (f) components of each of the g.p.c. curves shown in (a). 1, Undecomposed; 2, 280°; 3, 330°; 4, 355°; 5, 390°C

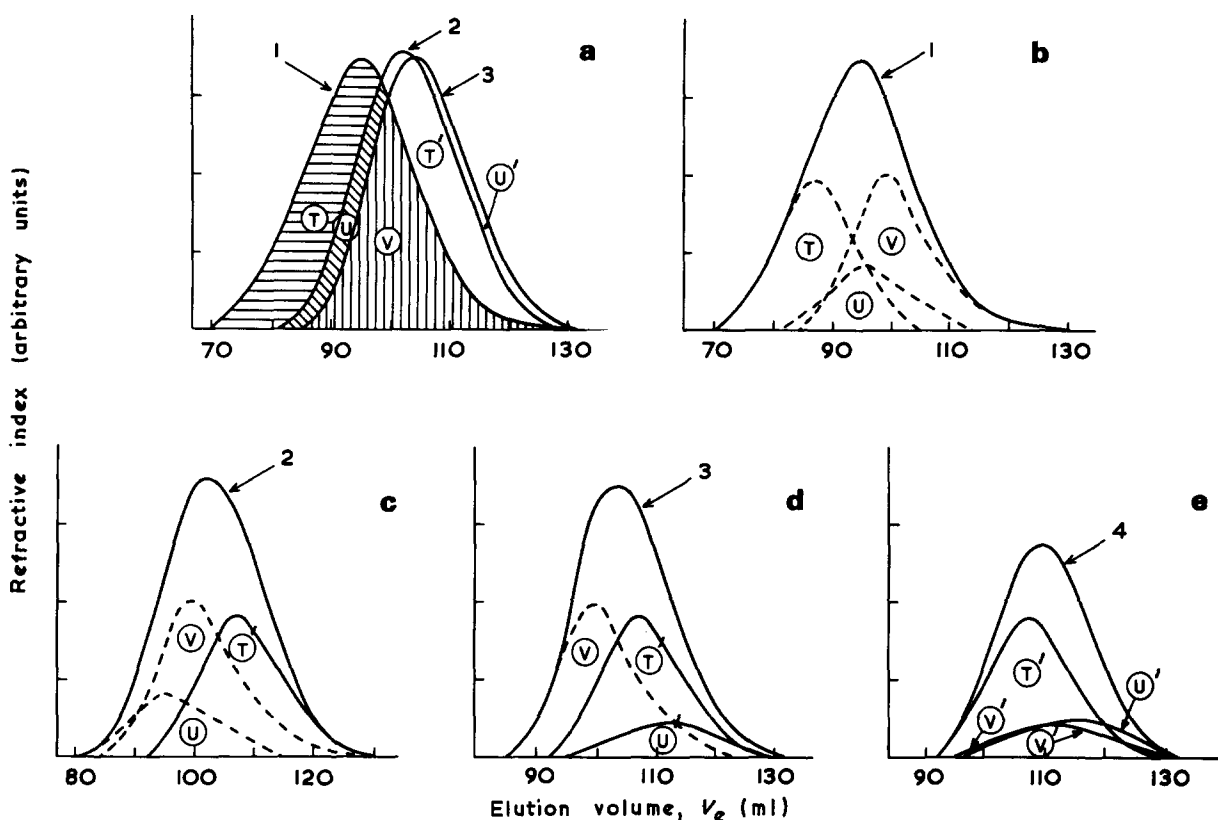
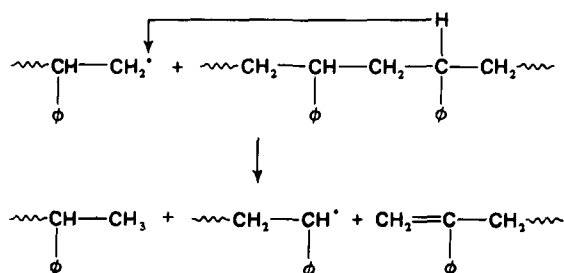


Figure 5 (a) G.p.c. distributions of Hoechst PS ( $\bar{M}_w = 4.3 \times 10^5$ ) subjected at 330°C to thermal treatments during various periods; (b) to (e) components of each of the g.p.c. curves shown in (a). 1, 0 min; 2, 50 min; 3, 120 min; 4, 240 min

Figure 6a shows g.p.c. distributions obtained with an undecomposed polystyrene standard ( $\bar{M}_w = 1.6 \times 10^5$ ) and with its decomposed products at 330°C after 50 and 120 min. A third sample treated at 330°C for 4 h was not used for component splitting because of unusually high weight loss (21%). Figure 6b shows the components X to Z of the undecomposed distribution while Figures 6c to 6e show successively by g.p.c. distributions the step-by-step decompositions of this sample at the three periods mentioned above. The changes in molecular weight distribution and polydispersity on heating are given in Table 4. In this case, the polydispersity values of the decomposed species X' and Y' were all about the same (1.5).

Figure 7a shows a comparison of g.p.c. distributions obtained with the same polystyrene standard ( $\bar{M}_w = 1.6 \times 10^5$ ) but where the decomposition was studied at different temperatures over a fixed time. In Figures 7b to 7e are shown the changes observed in the distributions while the polydispersity values as well as the molecular weights, as computed on the bases of Figures 7c to 7e, are represented in Table 4. Here as before, the components P, Q and R are found to change to P', Q' and R' having polydispersities of 1.5. As suggested by Wall and coworkers, this finding requires, in addition to intermolecular transfer, a radical-radical recombination process which probably takes place by some sort of cage recombination<sup>23</sup> as shown below:



The newly formed radicals,  $\sim\text{CH}_2-\text{C}(\phi)\text{H}$ , must then combine with other radicals.

Figure 8 shows the results of decompositions carried out at different temperatures, as seen through g.p.c. analyses, of a low polydispersity polystyrene standard ( $\bar{M}_w = 1.03 \times 10^4$ ). It is apparent from the g.p.c. traces that there are little or no changes in the molecular weight distributions in the decomposed samples, only weight changes. These are found to decrease. Berlin and Yenikolopyan<sup>15</sup> explain this behaviour by the rapid and complete depolymerization of radical bearing chains. Contrary to chain scissions, depolymerizations invariably occur at polymer chain ends; hence the rate of disappearance of polymer molecules is independent of their length. Thus in depolymerizations, a random proportion of the polymer leaves the reaction medium and this independently of its molecular weight. The number-average and weight-average molecular weights are therefore independent of the extent of the decomposition.

Table 5 summarizes the changes observed in the overall molecular weight and polydispersity values for decompositions carried out at different temperatures and times with the various polystyrene samples discussed individually, in this text, in terms of components. Making use of the values reported, plots of molecular weight with temperature and with fraction decomposed, *a* have been made in Figures 9 and 10, respectively. Figure 9 clearly indicates that the polystyrene standards ( $\bar{M}_w = 1.03 \times 10^4$  and  $1.6 \times 10^5$ ) are very little affected when the temperature is raised up to 330°C; whereas the other two ( $\bar{M}_w = 1.8 \times 10^6$  and  $4.3 \times 10^5$ ) show nearly 5 to 6 fold decreases in their molecular weights. Combining this observation with the results given in Table 5 and Figure 10, the weight loss owing to the decomposition for these two polymers is limited to 9% at 330°C even if there is a substantial drop in molecular weight. As indicated earlier, decompositions involving high

Table 4 Polystyrene standard ( $\bar{M}_W = 1.6 \times 10^5$ ) component and their decomposed counterparts at different temperatures and times

	Undecomposed component at 20°C			Undecomposed component at 20°C		
	P	Q	R	X	Y	Z
$\bar{M}_W \times 10^{-5}$	1.76	1.71	1.21	1.87	1.81	0.83
$\bar{M}_n \times 10^{-5}$	1.63	1.36	0.91	1.55	1.55	0.68
Polydispersity	1.10	1.26	1.33	1.17	1.17	1.22
Temp. of decomposition (°C)	330	355	380	330	330	330
Time of decomposition (min)	50	50	50	50	120	240
True weight loss (%)	2.7	16.0	63.0	2.7	12.0	21.0

	Decomposed counterparts			Decomposed counterparts		
	P'	Q'	R'	X'	Y'	X'' + Y'' + Z'
$\bar{M}_W \times 10^{-4}$	8.73	3.30	3.56	8.30	3.63	3.00
$\bar{M}_n \times 10^{-4}$	5.90	2.24	2.35	5.56	2.30	1.90
Polydispersity	1.48	1.47	1.51	1.52	1.58	1.57

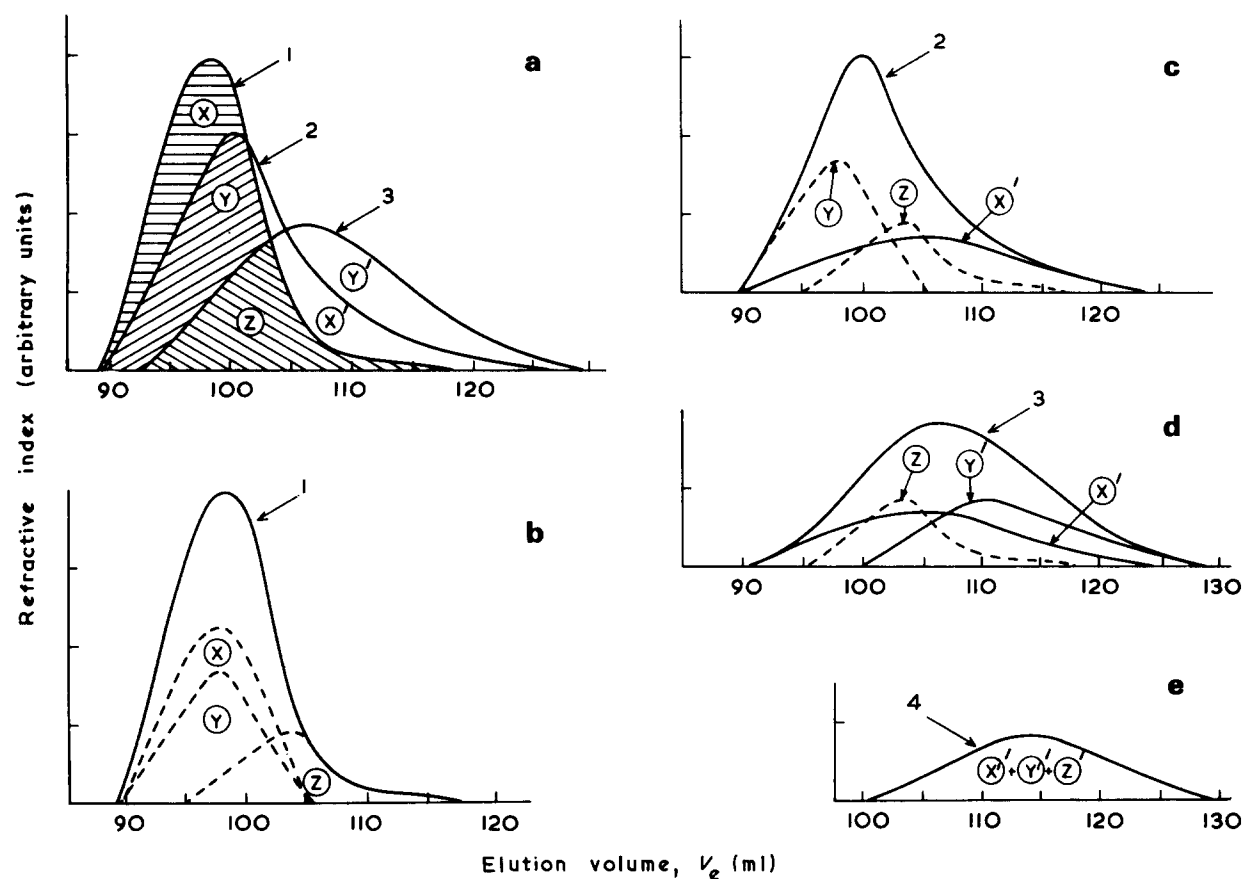


Figure 6 (a) G.p.c. distributions of PS ( $\bar{M}_W = 1.6 \times 10^5$ ) subjected at 330°C to thermal treatments during various periods; (b) to (e) components of each of the g.p.c. curves shown in (a). 1, 0 min; 2, 50 min; 3, 120 min; 4, 240 min

molecular weight samples are termed random scissions when the weight losses are limited to less than 10% and when molecular weights drop by factors of five to six.

When the molecular weights of the fragments drop to a value of around  $10^5$  or less, the process of depolymerization becomes much more important than that of random scissions. This accounts for the major portion of weight loss observed. It is very difficult, however, to point out the exact moment at which the scission step ends and the depolymerization step begins, because the random scissions which break the polymer statistically alter a nearly monodisperse distribution into a modified most-probable one while depolymerization keeps it as such until all of the polymer has disappeared.

When one follows polydispersity changes solely from overall results, one can erroneously be lead to believe that random chain scissions are the only reactions involved while the overall polydispersity of the products varies but progressively with temperature towards the most probable value of 2.0. This is particularly true in certain cases where most probable values of 2.0 are reached only after intensive periods of reaction during which depolymerization has contributed significantly to the weight loss of the samples. This might explain why one obtains an overall polydispersity of only 1.5 for the decomposition of the component parts of the  $1.6 \times 10^5$  polystyrene standard though both random scissions and depolymerization are known to proceed simultaneously.

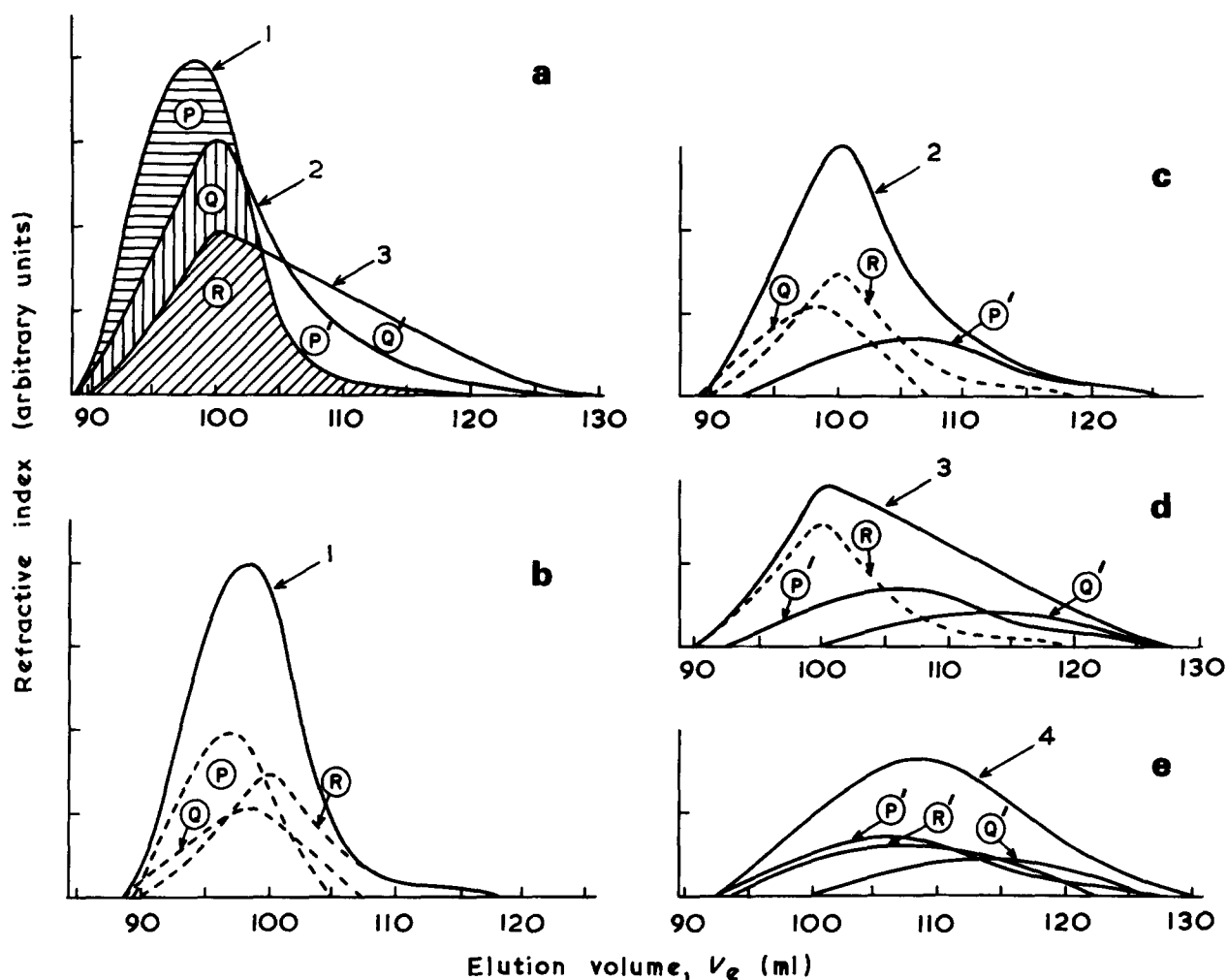


Figure 7 (a) G.p.c. distributions of PS ( $\bar{M}_w = 1.6 \times 10^5$ ) subjected to 50 min isothermal treatments at various temperatures: (b) to (e) components of each of the g.p.c. curves shown in (a). 1, Undecomposed; 2, 330°; 3, 355°; 4, 380°C

*Effect of polymer stereoregularity on the decomposition*

It has been reported<sup>24</sup> that stereoregularity of polystyrene has little or no influence on its decomposition and indeed investigations<sup>10,12,24</sup> have shown that atactic and isotactic samples have similar activation energy values for their decomposition. Boon and Challa<sup>25</sup> found some differences, though slight, when they computed activation energies from melt viscosity data obtained with non-degraded and degraded samples. They attribute the differences, however, to the temperature dependence of activation energy. Their studies were carried out in the 265–320°C temperature range while most others have worked in the lower 200 to 260°C range<sup>26–28</sup>.

In spite of the evidence put forth, it is difficult to visualize that stereoregularity which exerts considerable influence on the mechanical properties of polymers has little or no effect on its thermal properties. Isa and Dole<sup>29</sup> have shown that the heat of fusion of a crystalline polymer is different from that of an amorphous one. One would be led to conclude that, in a mixture made up of isotactic crystalline and atactic amorphous macromolecules of equal molecular weights, one of the two should require less energy to decompose than the other.

With this idea in mind, the decomposition data obtained in this laboratory by g.p.c. were analysed to establish the percentage proportion of isotactic, heterotactic and syndiotactic fractions. The results were compared with those obtained by n.m.r.

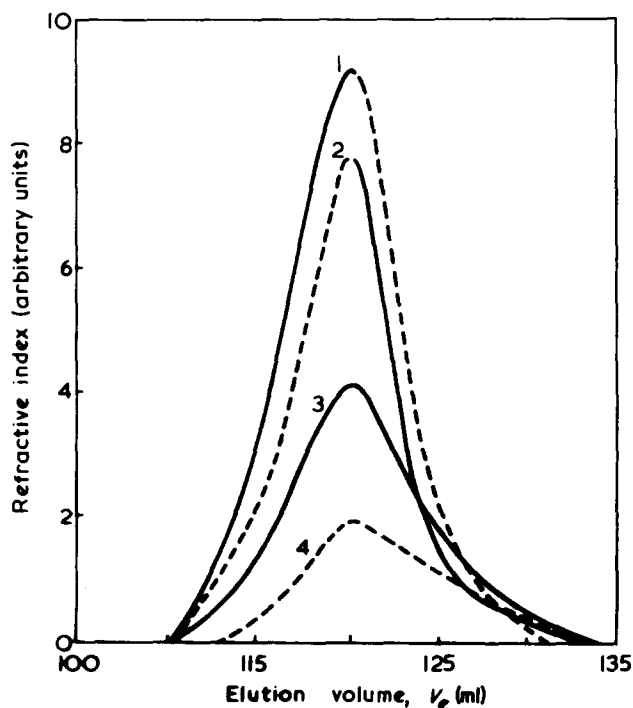


Figure 8 G.p.c. distributions of PS ( $\bar{M}_w = 1.03 \times 10^4$ ) subjected to 50 min isothermal treatments at various temperatures. 1, Undecomposed; 2, 330°; 3, 355°; 4, 380°C

Table 5 Experimental results obtained by gel permeation chromatography

Polystyrene samples	Time of decomposition = 50 min								Temperature of decomposition = 330°C	
	Temperature of decomposition (°C)								Time of decomposition (min)	
	20	180	230	280	330	355	380	120	240	
$1.8 \times 10^6$	$\bar{M}_w \times 10^{-3}$	1870	1560	1020	825	313	81	23	—	—
	Polydispersity	1.66	1.96	2.23	2.57	2.64	2.00	1.64	—	—
	$a$ (%)	0.0	0.4	0.6	0.8	2.9	8.3	84.1	—	—
$4.3 \times 10^5$	$\bar{M}_w \times 10^{-3}$	431	408	363	257	123	86	36	94	53
	Polydispersity	3.18	3.18	3.09	2.91	2.49	2.34	2.00	2.20	2.00
	$a$ (%)	0.0	0.7	0.6	1.3	5.9	9.6	56.5	10.0	33.0
$1.6 \times 10^5$	$\bar{M}_w \times 10^{-3}$	166	—	156	152	120	65	29	87	59
	Polydispersity	1.20	—	1.20	1.23	1.53	1.91	1.96	2.00	2.00
	$a$ (%)	0.0	—	0.3	1.0	2.7	15.9	63.4	12.0	21.0
$1.0 \times 10^4$	$\bar{M}_w \times 10^{-3}$	13.4	—	13.0	13.0	13.0	12.0	10.8	—	—
	Polydispersity	1.20	—	1.20	1.20	1.31	1.30	1.30	—	—
	$a$ (%)	0.0	—	0.3	0.8	9.0	46.8	72.9	—	—

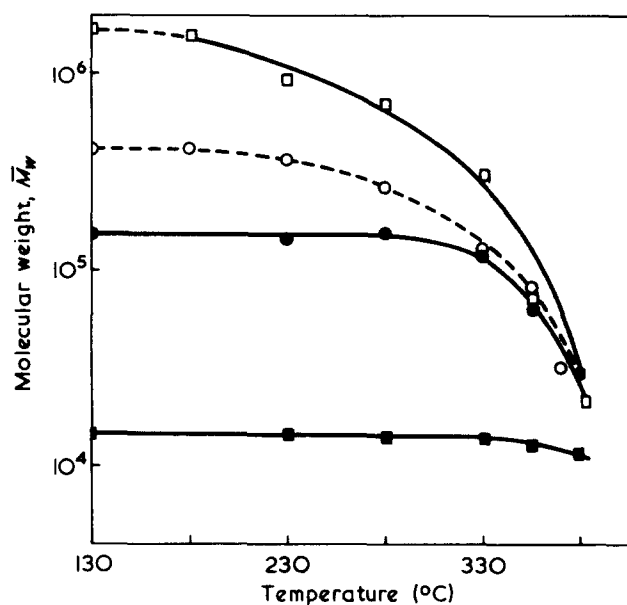


Figure 9 Variation of molecular weight with temperature for several PS samples:  $\square$ ,  $\bar{M}_w = 1.8 \times 10^6$ ;  $\circ$ ,  $\bar{M}_w = 4.3 \times 10^5$  (thermally prepared Hoechst sample);  $\bullet$ ,  $\bar{M}_w = 1.6 \times 10^5$ ;  $\blacksquare$ ,  $\bar{M}_w = 1.03 \times 10^4$

Although the data obtained by the decomposition reactions at different temperatures in the present study have been used to split the g.p.c. curves into many components, there are, in reality, most likely only two or three major components in each case. For example, the components  $\alpha$  and  $\beta$  in Figure 2b correspond, respectively, to the sum of components (A + B) and (C + D) in Figure 3b. This statement is based on the assumption that species of similar molecular weights and identical distributions may actually come from the same parent distribution and thus be combined together. As pointed out earlier, the decomposition reaction itself is random in nature though at any given time, only one component decomposes to lower molecular weight products.

If this is correct, this would mean that the three components  $\alpha$ ,  $\beta$  and  $\gamma$  in Figure 2b, having molecular weights of similar magnitude, decompose at different temperatures and must therefore be different in their formation. Similar

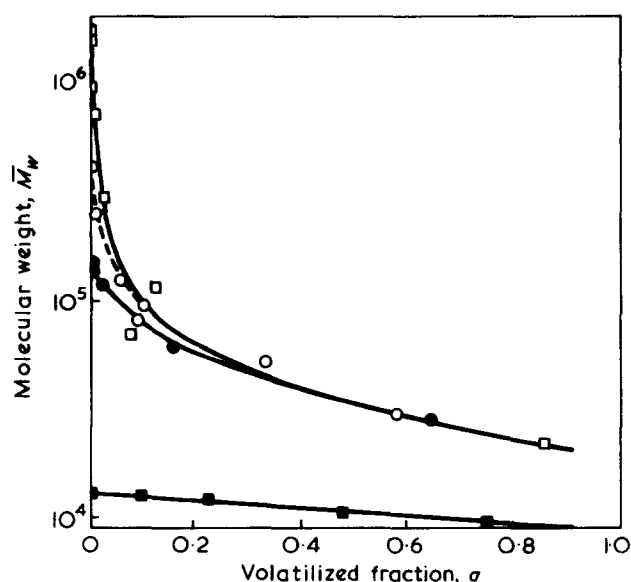


Figure 10 Variation of molecular weight with decomposed fraction,  $\sigma$ , for several PS samples:  $\square$ ,  $\bar{M}_w = 1.8 \times 10^6$ ;  $\circ$ ,  $\bar{M}_w = 4.3 \times 10^5$  (thermally prepared Hoechst sample);  $\bullet$ ,  $\bar{M}_w = 1.6 \times 10^5$ ;  $\blacksquare$ ,  $\bar{M}_w = 1.03 \times 10^4$

observations have also been made in the case of the  $1.6 \times 10^5$  polystyrene standard shown in Figure 6b where the components X and Y have approximately the same molecular weights though component X is the first to decompose. The three polystyrene structures (viz. isotactic, heterotactic and syndiotactic) could be the different formations mentioned earlier.

The validity of this statement can only be checked by the use of n.m.r. spectroscopy; however, the n.m.r. spectra taken even with a 220 MHz instrument at 100°C did not reveal the presence of these stereoregular forms in the four polystyrene samples studied. The n.m.r. spectra in all cases appeared to be identical, indicating that the samples have the same stereoregularity or that the aromatic rings of polystyrene are not sufficiently sensitive to proton spectra. The latter observation is reported in the literature<sup>30</sup> and the possibility that the samples have similar stereoregularities cannot be ruled out. The weight fraction of the least resistant components towards heat, viz.  $\alpha$ , X and T,



is very nearly the same in the three cases (~41%), while the corresponding weight fractions of the other more resistant components do not tally quite so well. The use of an ideal polymer, such as poly( $\alpha$ -methyl styrene), because of its ease of detection in n.m.r., should prove most interesting in further studies to confirm the effects of stereoregularity on their decomposition. The polystyrene proton resonances obtained in this work were, nevertheless found to be different from those already reported in the literature. These are listed in Table 6, and the experimental spectra, in Figure 11. There is a substantial difference in the  $\tau$  values reported<sup>30</sup> for methine and methylene protons and those observed in the present study. Furthermore, a new resonance peak was found at  $\tau = 3.61$ . This peak may form part of the proton resonances for H<sub>(2)</sub> or H<sub>(6)</sub> for which the values of  $\tau = 3.43$  (I) and 3.50 (H) have already been assigned. On the other hand, it may be that H<sub>(2)</sub> and H<sub>(6)</sub> are not identical in value as reported earlier<sup>30</sup>; however, the values for the other proton resonances, H<sub>(3)</sub>, H<sub>(4)</sub> and H<sub>(5)</sub>, show little differences.

Decomposition kinetics

In dynamic thermogravimetry, the rate law for the decomposition of polystyrene can be written in the following general form:

$$\frac{da}{dT} = \frac{k}{q} f(a) \tag{1}$$

where  $a$  is the volatile polymer fraction, defined as the ratio of polymer mass, decomposed at a temperature  $T$ , to its initial mass;  $f(a)$ , a function of  $a$ ;  $q$ , the heating rate (in °C/sec); and  $k$ , the rate constant said to obey the Arrhenius law written in the form:  $k = Z \cdot \exp(-E/RT)$ . Here  $Z$  is the pre-exponential factor (in sec<sup>-1</sup>) and  $E$ , the energy of activation (in kcal/mol).

For decompositions where weight loss is primarily due to depolymerization reactions, Audebert and Aubineau<sup>31</sup> have shown that  $f(a)$  has the following form:

$$f(a) = (1 - a)^n \tag{2}$$

$n$  being the order of reaction. Substituting in equation (1),

Table 6 N.m.r. parameters\* for polystyrene

Benzene protons ( $\tau$ )	Methine protons ( $\tau$ )	Methylene protons ( $\tau$ )
H <sub>(3)</sub> or H <sub>(5)</sub> 3.04, 3.08† (H) 3.06† (I)	H <sub>(A)</sub> : 8.1, b, 7.6†	H <sub>(B)</sub> $\approx$ H <sub>(C)</sub> 8.53, b, 8.34†
H <sub>(5)</sub> or H <sub>(3)</sub> 3.09, 3.08† (H) 3.06† (I)		
H <sub>(4)</sub> 3.15, 3.09† (I and H)		
H <sub>(6)</sub> or H <sub>(2)</sub> 3.44, 3.43† (I)		
H <sub>(2)</sub> or H <sub>(6)</sub> 3.53, 3.61, 3.50† (H)		

\* Based on their comparison with reported literature values  
 † Literature values  
 I = Isotactic polymer; H = heterotactic polymer

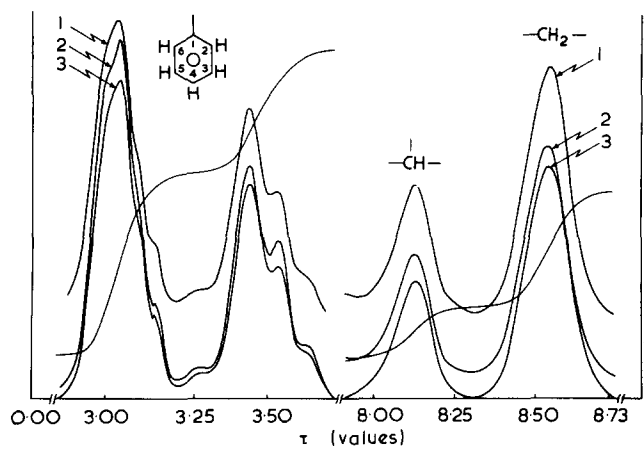


Figure 11 N.m.r. spectra for PS samples. 1,  $\bar{M}_w = 1.6 \times 10^5$ ; 2,  $\bar{M}_w = 4.3 \times 10^5$ ; 3,  $\bar{M}_w = 1.8 \times 10^6$

one obtains:

$$\frac{da}{dT} = \frac{Z}{q} \exp(-E/RT) (1 - a)^n \tag{3}$$

To compute activation energies, Flynn and Wall<sup>32</sup> have suggested the integration of equation (3) between the limits 0 and  $a$ .

Therefore:

$$\int_0^a \frac{da}{(1 - a)^n} = \frac{Z}{q} \int_0^T \exp(-E/RT) dT \tag{4}$$

If one now makes use of the Doyle<sup>33</sup> approximation for the energy of activation  $E$ , one gets:

$$E = -4351 \cdot \frac{d(\log q)}{d(1/T)} \text{ (in Mcal/mol)} \tag{5}$$

Freeman and Carroll<sup>19</sup> have suggested another way of using equation (4). Writing it in logarithmic form and in differential terms one obtains:

$$\frac{\Delta \ln(da/dT)}{\Delta \ln(1 - a)} = \frac{E}{R} \frac{\Delta(1/T)}{\Delta \ln(1 - a)} + n \tag{6}$$

Coats and Redfern<sup>20</sup>, on the other hand, have shown that the integral

$$\int_0^T \exp(-E/RT) dT$$

is equal to  $(RT^2/E) \exp(-E/RT)$ . Thus equation (4) can be written as:

$$\int_0^a \frac{da}{(1 - a)^n} = \frac{Z}{q} \cdot \frac{RT^2}{E} \cdot \exp(-E/RT) \tag{7}$$

The expression on the left-hand side of equation (7) may be referred to as  $f(a)$  and thus:

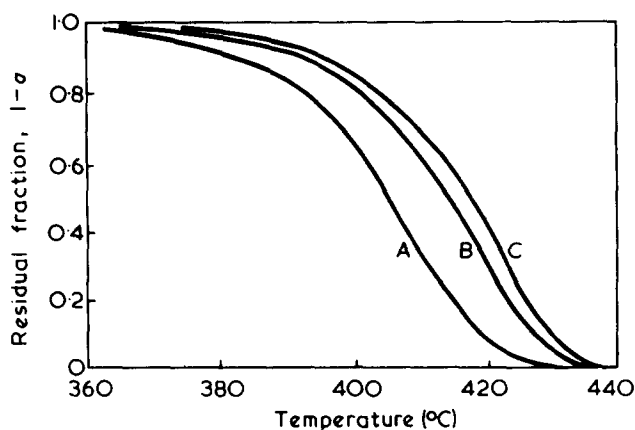


Figure 12 Influence of initial mass on thermograms obtained by dynamic thermogravimetric decomposition of PS ( $\bar{M}_w = 1.03 \times 10^4$ ) at  $50^\circ\text{C}/\text{min}$ . A, 0.996; B, 3.983; C, 6.066 mg

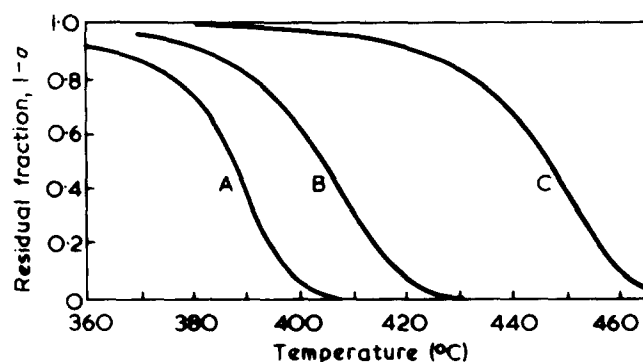


Figure 13 Influence of heating rate on the dynamic thermogravimetric decomposition of a polystyrene standard ( $\bar{M}_w = 1.03 \times 10^4$ ). A, 1.25; B, 5.0; C,  $20^\circ\text{C}/\text{min}$

$$f(a) = \frac{1 - (1 - a)^{(1-n)}}{(1 - n)} \quad \text{for } n \neq 1$$

$$\text{and } = -\ln(1 - a) \quad \text{for } n = 1$$

If  $[f(a)/T^2]$  is plotted as a function of  $1/T$  for different values of  $n$ , the one yielding a straight line is used to compute the value of the activation energy. Based on these expressions, the factors which are most likely to affect the values of the activation energy seem to be the mass of the polymer being decomposed and the heating rate at which the decomposition takes place.

Figure 12 shows dynamic thermogravimetric curves obtained at a heating rate of  $5.0^\circ\text{C}/\text{min}$  with three different initial masses of the  $1.03 \times 10^4$  polystyrene standard. It can be seen that, as the initial mass of the sample is increased, the percentage decomposition at a given temperature decreases. The activation energy values derived from the curves in Figure 12 increase with sample mass. For initial masses of 1, 4 and 6 mg of polymer, the activation energies were 79, 86 and 89 kcal/mol, respectively.

Figure 13 shows differential thermogravimetric (d.t.g.) curves obtained with the  $1.03 \times 10^4$  polystyrene standard using initial samples of 1 mg. These were decomposed at three different heating rates (1.25, 5.0 and  $20.0^\circ\text{C}/\text{min}$ ). It is clear from the Figure that the percentage decomposition at any given temperature decreases with increasing heating rate. This, however, creates no particular problem here, since all the activation energy values have been computed for the three heating rates. Figure 14 shows the d.t.g.

curves of polystyrene standards, with molecular weights ranging from 900 to  $1.8 \times 10^6$ , decomposed at a heating rate of  $1.25^\circ\text{C}/\text{min}$ , the initial mass of the samples being, in all cases, 1 mg. The curves indicate that, for the polystyrene standards situated between 900 and  $1.6 \times 10^5$ , the decomposition begins between 200 and  $350^\circ\text{C}$  depending upon the molecular weight — the higher the value, the higher the starting temperature — but 100% decomposition is achieved at slightly lower temperatures with the two upper molecular weight samples (viz.  $1.03 \times 10^4$  and  $1.6 \times 10^5$ ).

With polystyrene samples having molecular weights of  $1.6 \times 10^5$  and higher, the decomposition reaction begins around  $350^\circ\text{C}$ ; but, as in the previous case, the higher the molecular weight, the lower the ultimate temperature for 100% decomposition. This is reflected in the activation energy values which are found to be lower for polymers of molecular weight greater than  $1.6 \times 10^5$ . This point will be discussed in more detail further on.

The volatile polymer fraction,  $a$ , for thermogravimetric analyses, was defined earlier in the text. The definition, however, changes when it is used in differential scanning calorimetry (d.s.c.), and must be expressed in terms of enthalpic changes that occur during the process. Keeping this in mind, the order of reaction  $n$  can be evaluated with equation (6) proposed by Freeman and Carroll<sup>19</sup> when written in the following form:

$$\frac{\Delta \ln(dH/dT)}{\Delta \ln H_r} = \frac{E}{R} \frac{\Delta(1/T)}{\Delta \ln H_r} + n \quad (8)$$

As with d.t.g., the values of the activation energy are influenced somewhat by the heating rate in the d.s.c. technique. The values, computed with the Borchardt and Daniels<sup>34</sup> expression for different heating rates from d.s.c. thermograms similar to the one shown in Figure 15 for the  $1.03 \times 10^4$  polystyrene standard, are given in Table 7 for first order kinetics as determined with equation (8) in Figure 16. As the values obtained change relatively little, a heating rate of  $20^\circ\text{C}/\text{min}$  was used to study the influence of molecular weight on the activation energy. The values given in Table 8, reveal that the activation energies are somewhat higher for the higher molecular weight standards than those for the lower molecular weights. Similar results were obtained with d.t.g. and are reported below.

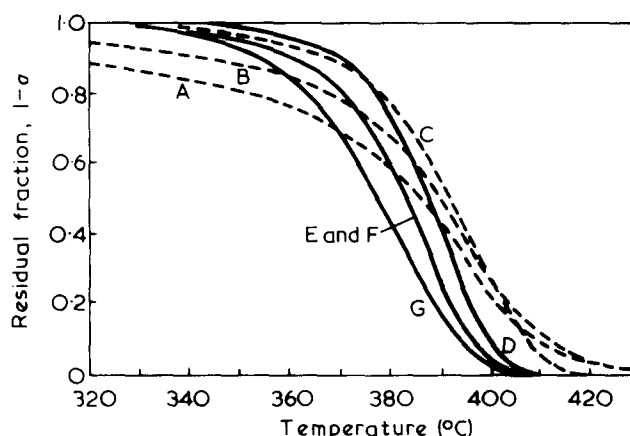


Figure 14 Influence of molecular weight on the dynamic thermogravimetric decomposition of polystyrene standards at  $1.25^\circ\text{C}/\text{min}$  (E, thermally prepared sample). A,  $\bar{M}_w = 900$ ; B,  $\bar{M}_w = 2030$ ; C,  $\bar{M}_w = 10\,300$ ; D,  $\bar{M}_w = 160\,000$ ; E,  $\bar{M}_w = 430\,000$ ; F,  $\bar{M}_w = 498\,000$ ; G,  $\bar{M}_w = 1\,800\,000$

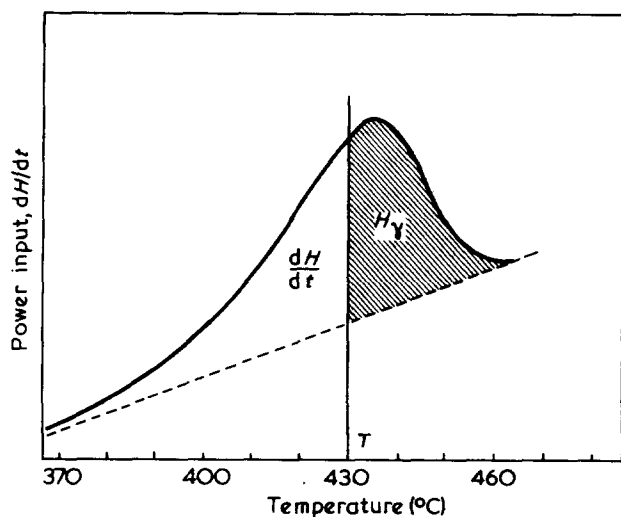


Figure 15 Dynamic differential enthalpic decomposition of polystyrene standard ( $\bar{M}_w = 1.03 \times 10^4$ ) at  $20^\circ\text{C}/\text{min}$  using Ellerstein's modification

Table 7 Activation energy for the decomposition of polystyrene by d.s.c.<sup>34</sup> for first order kinetics: (A) as a function of heating rate (mol wt  $1.03 \times 10^4$ ); (B) as a function of molecular weight (heating rate  $20^\circ\text{C}/\text{min}$ )

A.

Heating rate ( $^\circ\text{C}/\text{min}$ )	2.5	5	10	20	40
Activation energy (kcal/mol)	45	50	48	50	49

B.

Molecular weight, $\bar{M}_w \times 10^{-3}$	0.6	0.9	2.03	12.0	160.0
Activation energy (kcal/mol)	45	45	41	50	60

A close examination of Figure 16 shows that not all of the points fall on the line for a first order reaction. In the initial stages of the process, when the temperature is such that the values of  $a$  are less than 0.15, the order of the reaction is indeed zero. This would mean that even if the process were considered exclusively as one of depolymerization, there must of necessity be random scissions taking place for which the order of reaction is zero. It must be pointed out, however, that the zero order process associated with random scissions is more prominent when dealing with higher molecular weight polystyrenes since depolymerization is not a significant factor. All of the plots are not shown because diagrammatically they all resemble the one shown in Figure 16.

Activation energy values have nevertheless been computed using the method of Coats and Redfern<sup>20</sup> for the two steps involved (chain scissions and depolymerization) in the decomposition of polystyrene standards with molecular weights ranging from 900 to  $1.8 \times 10^6$  and heated at rates of 1.25, 5.0 and  $20.0^\circ\text{C}/\text{min}$ . The results obtained are presented in Table 8. For molecular weights up to  $1.6 \times 10^5$ , there is a steady increase in the activation energy values whereas beyond this point they tend to become constant. Increasing activation energy values with increasing molecular weight appear normal if one considers that longer chain lengths can be expected to require more energy for decomposition than shorter ones.

Constant activation energy values with polystyrenes of still higher molecular weights ( $>1.6 \times 10^5$ ) may be explained on the basis that, for these polymers, very low activation energies are required for their scission into lower molecular weight fragments ( $M_w \approx 1.0 \times 10^5$ ). The values of  $E$ , therefore, lie in the same range as those of a sample whose initial molecular weight is  $1.6 \times 10^5$ .

Under certain conditions the activation energy values for very high molecular weights are sometimes much lower than those of other samples having 10 fold lesser molecular weights, but before attempting any explanation of this effect, one must recall that the activation energy varies with many factors among which are: (a) the rate of heating, (b) the order of reaction, (c) the volatile fraction, (d) the nature of the linkages in the polymer, and (e) branching.

Keeping in mind the numerous factors which influence

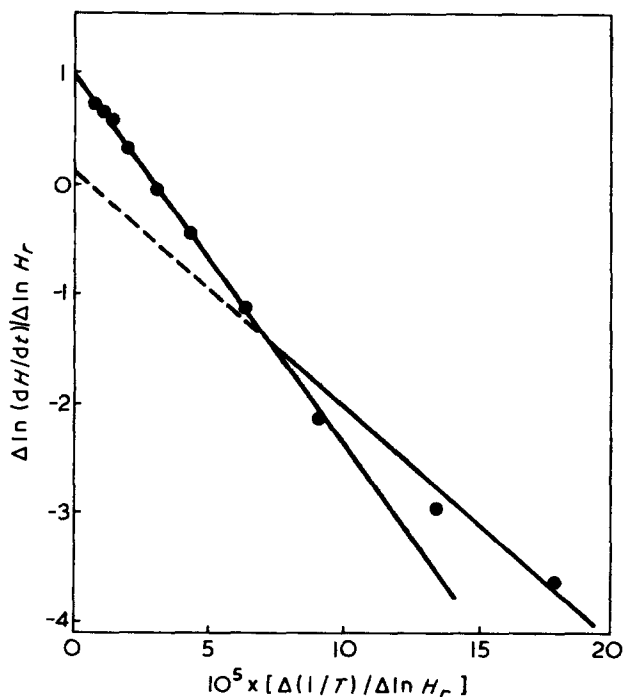


Figure 16 Variation of  $\Delta \ln(dH/dt)/\Delta \ln H_T$  with  $[\Delta(1/T)/\Delta \ln H_T]$  based on d.s.c. data obeying first order kinetics

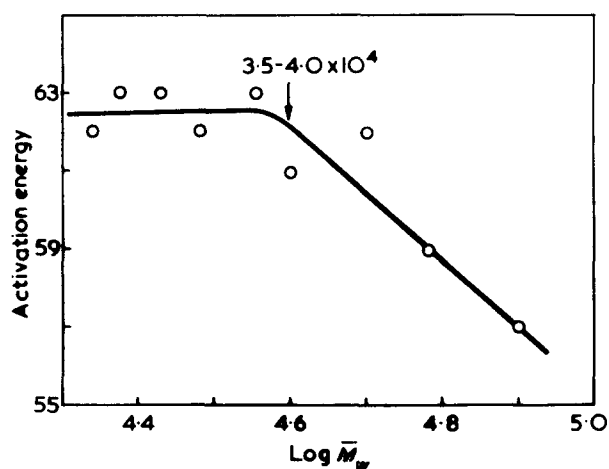
Table 8 Activation energy as a function of molecular weight at three different heating rates<sup>20</sup>

Molecular weight, $\bar{M}_w \times 10^{-3}$	Heating rate ( $^\circ\text{C}/\text{min}$ )		
	1.25	5	20
Zero order kinetics for $a < 0.15$			
0.9	10	9	10
2.0	14	20	21
12.0	38	63	73
160	69	92	91
430	40*	47*	40*
498	41	82	82
1800	42	79	70
First order kinetics for $a > 0.15$			
0.9	34	40	43
2.0	42	50	68
12.0	64	79	82
160	95	108	111
430	83*	87*	90*
498	75	105	115
1800	68	108	117

\* These values have been obtained with a thermally prepared polystyrene sample of polydispersity = 3.17

Table 9 Activation energy as a function of the volatile fraction<sup>19</sup>

Volatile fraction, $a$	Activation energy (kcal/mol)	
	PS ( $1.6 \times 10^5$ )	PS ( $1.8 \times 10^6$ )
0.1	57	37
0.2	59	41
0.3	62	44
0.4	61	45
0.5	63	47
0.6	62	49
0.7	63	50
0.8	63	51
0.9	62	54

Figure 17 Decomposition of a polystyrene standard ( $\bar{M}_w = 1.6 \times 10^5$ ): variation of activation energy with molecular weight

the values of  $E$ , one can ignore minor discrepancies in the experimental data obtained; however, large differences, such as those observed in the case of the  $4.3 \times 10^5$  thermally prepared polystyrene sample, may be attributed to the presence of weak links in the polymer chains owing to its method of preparation. The exact nature of these weak links is difficult to specify; however, the presence of branching in this polymer can be ruled out on the basis of its n.m.r. spectra where the ratio of benzene protons to that of methine as well as methylene protons compares well with that obtained in the case of anionically prepared standard polystyrene samples.

Computed activation energy values at different stages of the decomposition with the expression formulated by Flynn and Wall<sup>32</sup> are presented in Table 9. The results suggest that with the highest molecular weight polymer ( $M_w = 1.8 \times 10^6$ ), the activation energy increases with increasing volatile fraction whereas, with the other ( $M_w = 1.6 \times 10^5$ ), the activation energy remains more or less constant during the whole process. This would tend to confirm that with the higher molecular weight ( $>1.6 \times 10^5$ ) polymer, two processes of decomposition are involved. The one termed as random scissions has undoubtedly a lower activation energy and is therefore the dominant step. With lower molecular weight samples ( $<1.6 \times 10^5$ ), there are still two steps involved in the decomposition process but the dominant one, in this case, is the step termed depolymerization, which appears to have a higher energy of activation.

As mentioned earlier, the point at which the process of depolymerization takes over from that of random scissions is difficult to locate. An attempt has, however, been made in this direction in the case of the  $1.6 \times 10^5$  polystyrene standard by combining the data in Table 9 where activation

energies are shown to vary with the volatile fraction,  $a$ , with that of Figure 10 where the effect of  $a$  on the molecular weights is plotted. These results are shown in Figure 17 and they clearly indicate that the activation energy values increase until the molecular weight has dropped to around  $4.0 \times 10^4$  below which  $E$  remains constant. This may be the limit at which the random scissions step leaves the way entirely to depolymerization. This value though is at best a rough approximation. Further work in this direction is being carried out and will be reported later.

#### ACKNOWLEDGEMENTS

The authors gratefully acknowledge the financial assistance of the Defence Research Board of Canada and the National Research Council of Canada. One of them (J.H.) is grateful to the Canada Council for an assistantship during the period of his MSc studies.

The work described in this paper forms part of the research program of the 'Groupe de Recherche en Sciences Macromoléculaires' at Laval University.

#### REFERENCES

- Wall, L. A. in 'Analytical Chemistry of polymers', (Ed. G. M. Kline), Part II, Interscience, New York, 1962, p 220
- Madorsky, S. L. 'Thermal degradation of organic polymers', Interscience, New York, 1964, pp 26-92
- Cameron, G. G. and Kerr, G. P. *Eur. Polym. J.* 1968, 4, 709; 1970, 6, 423
- Jellinek, H. H. G. 'Encyclopedia of Polymer Science and Technology', Wiley, New York, 1970, Vol 4, p 740
- Jellinek, H. H. G. *J. Polym. Sci.* 1948, 3, 850; 1949, 4, 13
- Grassie, N. and Kerr, W. W. *Trans. Faraday Soc.* 1959, 55, 1050
- Cameron, G. G. and Grassie, N. *Makromol. Chem.* 1962, 51, 130; 1963, 53, 72
- Cascaval, C. N., Vasile, C. and Schneider, I. A. *Makromol. Chem.* 1970, 131, 55
- Wegner, J. and Patat, F. *J. Polym. Sci. (C)* 1970, 31, 120
- Madorsky, S. L. *J. Polym. Sci.* 1952, 9, 133
- Atherton, A. *J. Polym. Sci.* 1950, 5, 378
- Anderson, D. A. and Freeman, E. S. *J. Polym. Sci.* 1961, 54, 253
- Kokta, B. V., Valade, J. L. and Martin, W. N. *J. Appl. Polym. Sci.* 1973, 17, 1
- Simha, R., Wall, L. A. and Blatz, P. J. *J. Polym. Sci.* 1950, 5, 615
- Berlin, A. A. and Yenikolopyan, N. S. *Vysokomol. Soedin. (A)* 1968, 10, 1475
- Boyd, R. H. *J. Polym. Sci.* 1967, 5, 1573
- Hendrickson, J. G. *J. Appl. Polym. Sci.* 1967, 11, 1419
- Hesse, J. *Thèse de maîtrise* Université Laval (1971)
- Freeman, E. S. and Carroll, B. *J. Phys. Chem.* 1958, 62, 394
- Coats, A. W. and Redfern, J. P. *Nature* 1964, 201, 68; *J. Polym. Sci. (B)* 1965, 3, 917
- Ellerstein, S. M. *J. Phys. Chem.* 1965, 69, 2471
- Smith, W. N. *J. Appl. Polym. Sci.* 1967, 11, 639
- Wall, L. A., Strauss, S. and Fetters, L. *J. Polym. Prepr.* 1969, 10, 1472
- Delava, H. *Ind. Chem. Belg.* 1961, 26, 53
- Boon, J. and Challa, G. *Makromol. Chem.* 1965, 84, 25
- Fox, T. G. and Flory, P. J. *J. Am. Chem. Soc.* 1948, 70, 2384
- Rudd, J. F. *J. Polym. Sci.* 1960, 44, 459
- Spencer, R. S. *J. Polym. Sci.* 1950, 5, 591
- Isa, I. A. and Dole, M. *J. Phys. Chem.* 1969, 73, 3384
- Bovey, F. A., Hood, F. P., Anderson, E. W. and Snyder, L. C. *J. Chem. Phys.* 1965, 42, 3900
- Audebert, R. and Aubineau, C. *J. Chem. Phys.* 1969, 66, 414
- Flynn, J. H. and Wall, L. A. *J. Polym. Sci. (B)* 1966, 4, 323
- Doyle, C. D. *J. Appl. Polym. Sci.* 1962, 6, 639
- Borchardt, H. J. and Daniels, F. *J. Am. Chem. Soc.* 1957, 79, 41

# Grafted polymers from poly(4-vinylpyridinium) salts

Denis Ghesquiere, Claude Caze and Claude Loucheux

Laboratoire de Chimie Macromoléculaire, Université des Sciences et Techniques de Lille, BP 36, 59650 Villeneuve d'Ascq, France

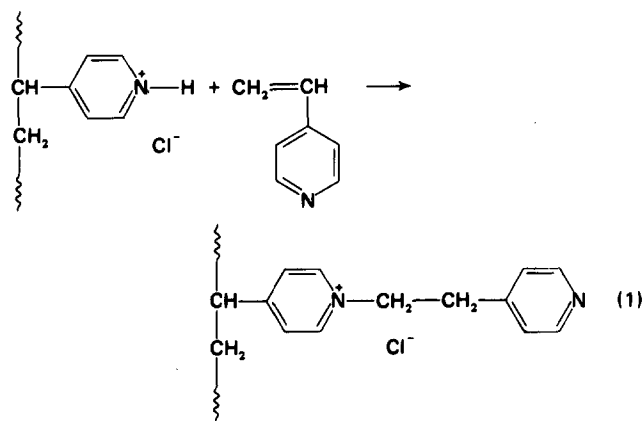
(Received 29 March 1974; revised 22 May 1974)

4-Vinyl pyridine can be added via its vinylic double bond to the quaternary nitrogen atom of poly(4-vinylpyridinium chloride). When this reaction is carried out successively, model grafted polymers with grafts of a constant length with a known number of electric charges, have been obtained. Potentiometric measurements, infra-red and  $^1\text{H}$  n.m.r. spectroscopic studies confirm the structure of the polymers.

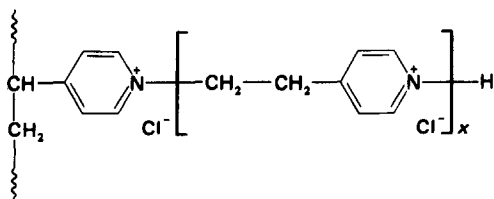
## INTRODUCTION

Quaternized poly(vinyl pyridines) have been extensively studied<sup>1,2</sup>. These polymers are usually obtained either through the reaction of an acid or a halide with the suitable poly(vinyl pyridine), or through the polymerization of the monomeric vinyl pyridine in the presence of a quaternizing reagent<sup>3-5</sup>. Recently a new way of obtaining quaternized pyridines through the action of an electrophilic vinyl type reagent in the presence of various acids, has been published<sup>6</sup>. The aim of the present work was to apply this type of reaction to the poly(4-vinyl pyridine)/4-vinyl pyridine system, in order to prepare poly(4-vinyl pyridines) bearing ionic grafts of controlled length.

The starting poly(4-vinyl pyridine) (P4VP) was quaternized by hydrochloric acid and the addition of 4-vinyl pyridine (4VP) can be written:



The process can be repeated after quaternization by hydrochloric acid of the newly introduced pyridine ring, leading to the following series:



Grafted P4VP polymers with  $x = 1$  and 2 have been synthesized.

## EXPERIMENTAL

### Starting materials

4VP was a Merck commercial product. After washing with a 0.1 N NaOH solution to remove the inhibitor, and drying over calcium chloride, the monomeric 4VP was distilled under reduced pressure just before use.

P4VP was prepared by polymerization in methanol at 60°C, using azobisisobutyronitrile as initiator. Its intrinsic viscosity, measured in ethanol at 25°C, corresponded to a molecular weight  $M_w = 75\,000$ , following the viscosity/molecular weight relationship given by Berkowitz *et al.*<sup>7</sup>.

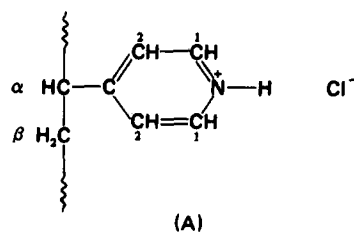
### Grafting

The experimental details are described for reaction (1), but they were quite similar for the successive additions of 4VP. The grafting operations were carried out in two steps: (i) quaternization of the polymer. A methanolic solution of P4VP was reacted at 50°C with a methanolic solution of hydrochloric acid. The quantity of HCl was always in excess. The poly(4-vinylpyridinium chloride) was recovered by precipitation in dry ethyl ether. This precipitation was necessary in order to avoid the polymerization of 4VP in the presence of HCl in the following step<sup>8</sup>; (ii) reaction of 4VP with the quaternized P4VP, in methanolic solution, at 50°C, during several hours. Then the grafted polymer was recovered by precipitation in dry ethyl ether. Both quaternized P4VP and grafted quaternized P4VP were white and strongly hygroscopic products.

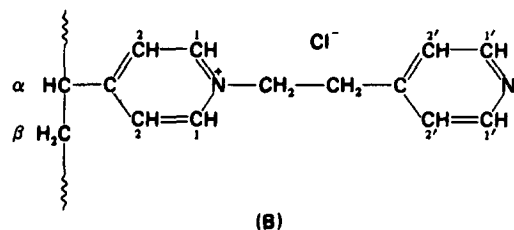
### Characterization of polymers

The potentiometric titrations of  $\text{Cl}^-$  ions were performed in aqueous solutions, using 0.05 N  $\text{AgNO}_3$  as reagent. Radiometer equipment consisted of pH meter 28, Titrator 11, Autoburette ABU 1c and Titrigraph SBR2c. The reference electrode was a glass electrode G202c, and the measurement electrode was a silver electrode P4011. The polymer concentration of titrated solutions was 0.5 g/100 cm<sup>3</sup>. The

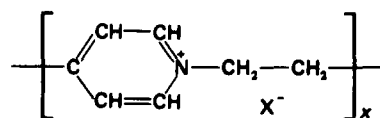




The resonance peaks at 7.55 and 8.55 ppm are assigned respectively to the protons 2 and 1 of the pyridinium ring. The spectrum of B is more complex:



The resonance of  $\gamma$  protons appears as a shoulder at 5 ppm on the flank of the very intense HDO peak. The resonance of the  $\delta$  protons is a peak centred at 3.7 ppm. These two peaks appear more clearly in the spectrum of polymer C which is obtained by hydrochloric quaternization of B. The assignment of these  $\gamma$  and  $\delta$  protons is confirmed by the n.m.r. study of the following polymer<sup>12,13</sup>:



The case of the pyridinic protons is more complex. Owing to the presence of the second pyridine ring one would expect two new resonance peaks from 2' and 1' protons. Actually six peaks (or more) are observed. The comparison with the spectrum of polymer C is interesting and suggests that a stacking effect takes place between two neutral

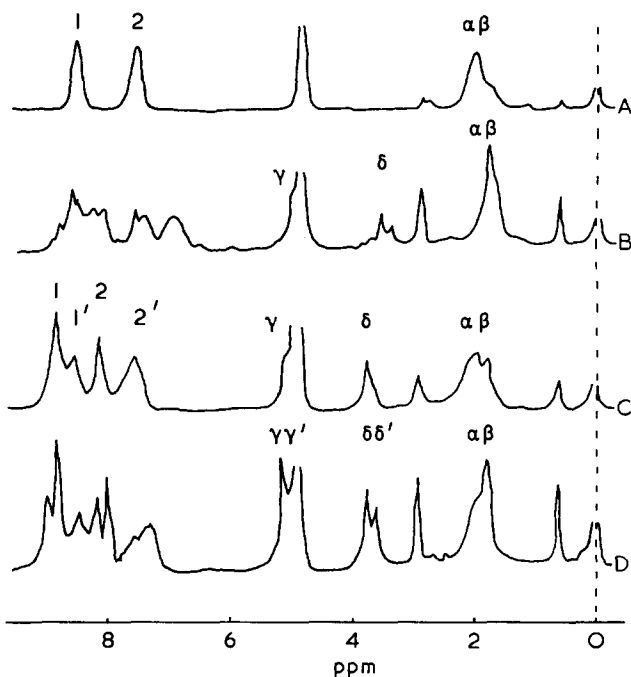


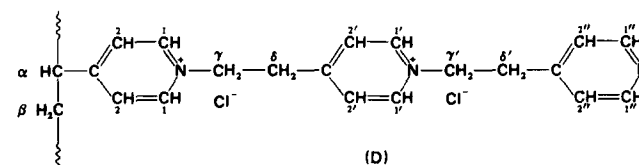
Figure 3 <sup>1</sup>H n.m.r. spectra of polymers A, B, C and D

pyridine rings by an intra- or inter-molecular interaction process. This effect disappears in the spectrum of polymer C, when all the pyridine rings are quaternized, excluding such an hydrophobic effect.

For the spectrum of polymer C the resonances can be assigned as follows:

- $\gamma$  and  $\delta$  protons at 5.05 and 3.65 ppm respectively,
- 1' and 2' protons at 8.5 and 7.55 ppm, respectively,
- 1 and 2 protons at 8.80 and 8 ppm respectively.

The spectrum of polymer D shows that the three pyridine rings are not equivalent.



The  $\delta$  and  $\delta'$  protons appear as unequivalent and give two peaks at about 3.7 ppm, when the  $\gamma$  and  $\gamma'$  protons exhibit one single peak at 5.10 ppm.

## CONCLUSION

The data of potentiometric titrations, infra-red and <sup>1</sup>H n.m.r. spectroscopies confirm that the polymers obtained are those expected. Longer sequences of 4-vinyl pyridine units can be bound to the skeleton, the limit being probably imposed by the solubility of the grafted polymers. These grafted polymers are good models for physical chemistry studies. The B polymer seems to have a special structure which will be the subject of future work.

This type of addition reaction may be largely used in order to modify the chemical and physical properties of polymers and copolymers including amine functions.

## ACKNOWLEDGEMENT

The authors wish to thank Dr C. Chachaty from Centre d'Etudes Nucléaires de Saclay for use of the n.m.r. spectrometer and for helpful discussions.

## REFERENCES

- 1 Hoover, M. F. *J. Macromol. Sci. (A)* 1970, 4, 1327
- 2 Longley, K. 'Cationic surfactants'. Surfactant Science Series. (Ed. E. Jungermann), Marcel Dekker, New York, 1970, Vol 4
- 3 Kabanov, V. A., Kargina, D. V. and Petrovskaya, V. A. *Vysokomol. Soedin. (A)* 1971, 13, 548
- 4 Salamone, J. C., Snider, B. and Fitch, W. L. *J. Polym. Sci. (A-1)* 1971, 9, 1493
- 5 Ringsdorf, H. and Walter, G. *Makromol. Chem.* 1971, 149, 295
- 6 Le Berre, A. and Delecroix, A. *Bull. Soc. Chim. Fr. (II)* 1973, p 640
- 7 Berkowitz, J. B., Yamin, M. and Fuoss, R. M. *J. Polym. Sci.* 1958, 28, 69
- 8 Salamone, J. C., Ellis, E. J., Wilson, C. R. and Bardoliwalla, B. F. *Macromolecules* 1973, 6, 475
- 9 Colthup, N. B., Daly, L. H. and Wiberley, S. E. 'Introduction to infrared and raman spectroscopy', Academic Press, London and New York, 1964
- 10 Bellamy, L. J. 'The infrared spectra of complex molecules', Methuen, London, 1966
- 11 Noel, C., Platzer, N., Monnerie, L. and Basselier, J. J. *J. Chim. Phys.* 1970, 67, 558
- 12 Iwatsuki, S., Kokubo, T., Motomatsu, K., Tsuji, M. and Yamashita, Y. *Makromol. Chem.* 1968, 120, 154
- 13 Salamone, J. C., Snider, B. and Fitch, W. L. *Macromolecules* 1970, 3, 707

# Solvent effect on cationic polymerization of styrene with $\alpha$ - or $\beta$ -methylstyrenes

Kenji Yamamoto and Toshinobu Higashimura

Department of Polymer Chemistry, Kyoto University, Kyoto 606, Japan  
(Received 26 March 1974)

To investigate the steric hindrance in the cationic copolymerization of styrene derivatives, styrene was copolymerized with anethole or with  $\alpha$ -methylstyrene in polar and non-polar solvents by using  $\text{BF}_3\text{O}(\text{C}_2\text{H}_5)_2$  or  $\text{SnCl}_4$ -trichloroacetic acid as catalyst. As the polarity of the solvent increased, the relative reactivity of  $\alpha$ -methylstyrene towards a styryl cation decreased and that of anethole increased. The mode of attack of the propagating carbocation to styrene derivatives in a non-polar solvent is discussed on the basis of these contrasting phenomena.

## INTRODUCTION

It is well known that  $\alpha,\beta$ -disubstituted ethylenes are polymerizable by a cationic mechanism in contrast to no polymerizability in radical polymerizations. Thus one can examine the effect of the  $\beta$ -substituent on the reactivity of vinyl compounds in cationic polymerization.

As to vinyl ethers, the introduction of a  $\beta$ -methyl group increased the reactivity of the monomers. In the cationic copolymerization of vinyl ethers with the corresponding propenyl ethers in non-polar solvents, the reactivity of the monomers decreased in the following order<sup>1,2</sup>:

*cis*-propenyl ether > *trans*-propenyl ether  $\geq$  vinyl ether

However, the relative reactivity of these monomers depends greatly upon the polarity of the solvent, and the reactivity difference becomes smaller in more polar solvents<sup>3,4</sup>. These facts were explained in terms that the location of the attack of a propagating carbocation to a monomer in non-polar solvents differed from that in polar solvents<sup>3,4</sup>.

When a  $\beta$ -methyl group is introduced into styrene derivatives, their reactivity in cationic polymerization decreases considerably because of the steric hindrance of the  $\beta$ -methyl group<sup>5-8</sup>. This result is in contrast to that of propenyl ethers, in which the steric effect of the  $\beta$ -methyl group is not important. Therefore, in the cationic copolymerization of styrene with  $\beta$ -substituted styrenes, one can investigate the dependence of the monomer reactivity ratios on the solvent polarity which might give information concerning the steric hindrance of the  $\beta$ -substituent in the propagation reaction.

Several studies concerning the copolymerization of styrene with  $\beta$ -methylstyrene derivatives have been reported but there has been no report concerning how these reactivities are influenced by the solvent polarity. In this study, styrene was copolymerized with anethole (*p*-methoxy- $\beta$ -methylstyrene) at 30°C in several solvents to investigate the effect of the solvent polarity on the monomer reactivity. In addition, styrene was copolymerized with  $\alpha$ -methylstyrene for comparison. On the basis of these investigations, the mechanism of the propagation reaction of styrene derivatives is discussed.

## EXPERIMENTAL

### Materials

Commercial styrene, *trans*-anethole, and  $\alpha$ -methylstyrene were purified by washing and distillation over calcium hydride under reduced pressure before use. The steric purity of *trans*-anethole was found to be more than 99% by gas chromatography. *cis*-Anethole was synthesized by the decarboxylation of *p*-methoxy- $\beta$ -methylcinnamic acid which was prepared from *p*-anisaldehyde by a Perkin reaction<sup>7,9</sup>. The geometric isomers were separated by fractional distillation through a spinning band column of over 70 theoretical plates (b.p. 99.0–99.5°C at 14 mmHg; lit.<sup>10</sup> 79.0–79.5°C at 2.3 mmHg). After the distillation the monomer contained 98% *cis*-isomer and 2% *trans*-isomer.

Benzene, methylcyclohexane, methylene chloride, and nitroethane as solvents were purified by washing and distillation over calcium hydride before use.  $\text{BF}_3\text{O}(\text{C}_2\text{H}_5)_2$  and  $\text{SnCl}_4$  as catalysts and bromobenzene and chlorobenzene as internal standards for gas chromatography were purified by distillation. Trichloroacetic acid (TCA) (Guaranteed Reagent) was used without further purification.

### Procedure

Copolymerizations were conducted under dry nitrogen in the same manner as reported previously<sup>11</sup>. The concentration of residual water in the reaction system was determined to be 0.2–0.3 mmol/l by Karl-Fischer titration. 5 vol % of chlorobenzene was used as an internal standard for gas chromatography with styrene/ $\alpha$ -methylstyrene copolymerization and 5 vol % of bromobenzene with styrene-anethole copolymerization. Polymer compositions were determined from the amount of residual monomers measured by gas chromatography. Monomer reactivity ratios were calculated according to the improved Fineman-Ross method<sup>12</sup>.

## RESULTS

### Copolymerization of styrene( $M_1$ ) with *cis*-anethole( $M_2$ )

Styrene was copolymerized with *cis*-anethole by  $\text{BF}_3\text{OEt}_2$  as a catalyst in various solvents at 30°C. *Figure 1*



shows the copolymer composition curves and the monomer reactivity ratios are summarized in Table 1. *cis*-Anethole was more reactive than styrene irrespective of the kind of solvent. As the polarity of the solvent increased,  $r_1$  decreased, while  $r_2$  increased. This means that on increasing the solvent polarity *cis*-anethole becomes more reactive than styrene towards either styryl cation or *cis*-anethole cation. However, the influence of the solvent polarity on the monomer reactivity ratio was not so large as in the styrene/*trans*-anethole copolymerization, which will be described below.

#### Copolymerization of styrene( $M_1$ ) with *trans*-anethole( $M_2$ )

Figure 2 shows the copolymer composition curves and the monomer reactivity ratios are summarized in Table 1. *trans*-Anethole was more reactive than styrene irrespective of the kind of solvent. In this copolymerization, in contrast to styrene/*cis*-anethole copolymerization, both  $r_1$  and  $r_2$  decreased as the polarity of the solvent increased, and the product  $r_1 \cdot r_2$  was much smaller than unity in polar solvents. This implies that *trans*-anethole becomes more reactive than styrene towards a styryl cation, while the former becomes less reactive than the latter towards a *trans*-anethole cation with increasing the solvent polarity, i.e. the alternating tendency appears in polar solvents.

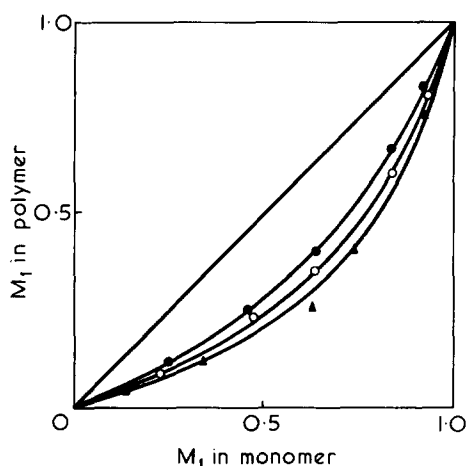


Figure 1 Effect of solvent on copolymer composition (mole fraction) curves in the copolymerization of styrene ( $M_1$ ) with *cis*-anethole ( $M_2$ ): ●, benzene; ○, methylene chloride; ▲, nitroethane.  $[M]_0 = 10$  vol %;  $\text{BF}_3\text{OEt}_2$ ;  $30^\circ\text{C}$

When  $\text{SnCl}_4$ -TCA was used as a catalyst instead of  $\text{BF}_3\text{OEt}_2$  in benzene, the monomer reactivity ratios were nearly the same as in methylene chloride (see Table 1).

#### Copolymerization of *cis*-anethole( $M_1$ ) with *trans*-anethole ( $M_2$ )

The effect of the solvent polarity on the copolymerization of *cis*- and *trans*-anethole was investigated with  $\text{BF}_3\text{OEt}_2$  as a catalyst at  $30^\circ\text{C}$ . Figure 3 shows the copolymer composition curves and the monomer reactivity ratios are summarized in Table 1. *cis*-Anethole was more reactive than *trans*-anethole irrespective of the kind of solvent. As the polarity of the solvent increased,  $r_2$  decreased but  $r_1$  was almost unchanged. This implies that the reaction of *trans*-anethole with a *trans*-anethole cation is difficult in polar solvents.

#### Copolymerization of styrene( $M_1$ ) with $\alpha$ -methylstyrene( $M_2$ )

Styrene was copolymerized with  $\alpha$ -methylstyrene at  $-78^\circ\text{C}$  by use of  $\text{SnCl}_4$  as a catalyst and TCA as a cocatalyst in methylcyclohexane as a non-polar solvent and in methylene chloride or nitroethane as a polar solvent. It is known that the polymerization of  $\alpha$ -methylstyrene accompanies depropagation reactions at high temperatures. However, it is confirmed that in the cationic copolymerization of  $\alpha$ -methylstyrene with styrene at a low temperature such as  $-78^\circ\text{C}$ , the contribution of the depropagation reaction

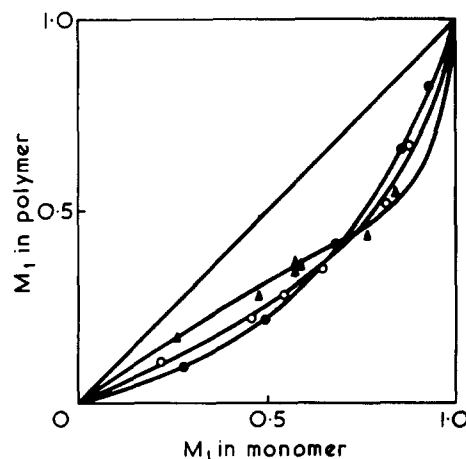


Figure 2 Effect of solvent on copolymer composition (mole fraction) curves in the copolymerization of styrene ( $M_1$ ) with *trans*-anethole ( $M_2$ ): ●, benzene; ○, methylene chloride; ▲, nitroethane.  $[M]_0 = 10$  vol %;  $\text{BF}_3\text{OEt}_2$ ;  $30^\circ\text{C}$

Table 1 Monomer reactivity ratios in the copolymerizations of styrene-anethole and *cis/trans*-anethole (catalyst,  $\text{BF}_3\text{OEt}_2$ ;  $[M]_0 = 10$  vol %;  $30^\circ\text{C}$ )

Monomers <sup>a</sup>		Solvent	$r_1$	$r_2$	$r_1 \cdot r_2$
$M_1$	$M_2$				
St	<i>cis</i> -An	$\text{C}_6\text{H}_6$	$0.40 \pm 0.02$	$2.70 \pm 0.11$	1.08
St	<i>cis</i> -An	$\text{CH}_2\text{Cl}_2$	$0.28 \pm 0.02$	$3.15 \pm 0.12$	0.88
St	<i>cis</i> -An	$\text{C}_2\text{H}_5\text{NO}_2$	$0.22 \pm 0.05$	$3.81 \pm 0.26$	0.83
St	<i>trans</i> -An	$\text{C}_6\text{H}_6$	$0.36 \pm 0.02$	$3.72 \pm 0.16$	1.33
St	<i>trans</i> -An	$\text{C}_6\text{H}_6^b$	$0.15 \pm 0.01$	$2.45 \pm 0.09$	0.37
St	<i>trans</i> -An	$\text{CH}_2\text{Cl}_2$	$0.18 \pm 0.03$	$2.48 \pm 0.16$	0.44
St	<i>trans</i> -An	$\text{C}_2\text{H}_5\text{NO}_2$	$0.08 \pm 0.02$	$1.42 \pm 0.07$	0.11
<i>cis</i> -An	<i>trans</i> -An	$\text{C}_6\text{H}_6$	$1.79 \pm 0.22$	$0.45 \pm 0.06$	0.81
<i>cis</i> -An	<i>trans</i> -An	$\text{CH}_2\text{Cl}_2$	$1.67 \pm 0.11$	$0.34 \pm 0.03$	0.56
<i>cis</i> -An	<i>trans</i> -An	$\text{C}_2\text{H}_5\text{NO}_2$	$1.31 \pm 0.14$	$0.25 \pm 0.06$	0.33

<sup>a</sup> St = styrene; An = anethole

<sup>b</sup> Catalyst,  $\text{SnCl}_4$ -TCA ( $[\text{SnCl}_4]/[\text{TCA}] = 2:1$ )

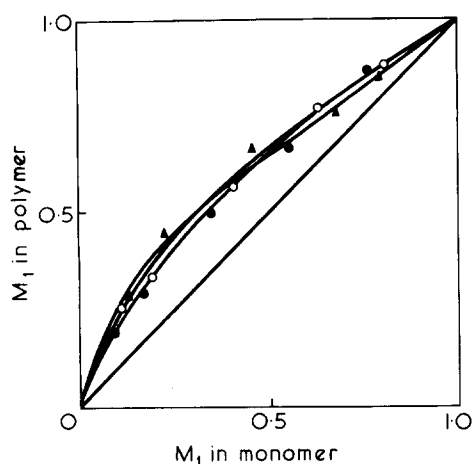


Figure 3 Effect of solvent on copolymer composition (mole fraction) curves in the copolymerization of *cis*-anethole ( $M_1$ ) with *trans*-anethole ( $M_2$ ): ●, benzene; ○, methylene chloride; ▲, nitroethane.  $[M]_0 = 10 \text{ vol } \%$ ;  $\text{BF}_3\text{OEt}_2$ ;  $30^\circ\text{C}$

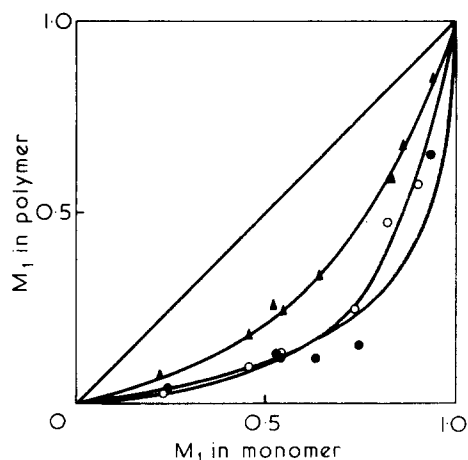


Figure 4 Effect of solvent on copolymer composition (mole fraction) curves in the copolymerization of styrene ( $M_1$ ) with  $\alpha$ -methylstyrene ( $M_2$ ): ●, methylcyclohexane; ○, methylene chloride; ▲, nitroethane.  $[M]_0 = 10 \text{ vol } \%$ ;  $\text{SnCl}_4\text{-TCA}$  ( $[\text{SnCl}_4]/[\text{TCA}] = 2:1$ );  $-78^\circ\text{C}$

Table 2 Monomer reactivity ratios in the copolymerization of styrene ( $M_1$ ) with  $\alpha$ -methylstyrene ( $M_2$ ) (catalyst,  $\text{SnCl}_4\text{-TCA}$ ;  $[\text{SnCl}_4]/[\text{TCA}] = 2:1$ ;  $[M]_0 = 10 \text{ vol } \%$ ;  $-78^\circ\text{C}$ )

Solvent	$r_1$	$r_2$
methylcyclohexane	$0.03 \pm 0.03$	$7.22 \pm 0.99$
$\text{CH}_2\text{Cl}_2$	$0.26 \pm 0.07$	$10.2 \pm 0.99$
$\text{C}_2\text{H}_5\text{NO}_2$	$0.36 \pm 0.02$	$4.17 \pm 0.19$

could be negligible<sup>13</sup>. Therefore, styrene was copolymerized with  $\alpha$ -methylstyrene at  $-78^\circ\text{C}$ . Figure 4 shows the copolymer composition curves and the monomer reactivity ratios are summarized in Table 2.  $\alpha$ -Methylstyrene was much more reactive than styrene irrespective of the kind of solvent. The reactivity difference between the two monomers became small as the polarity of the solvent increased.

## DISCUSSION

In the cationic copolymerization of  $\beta$ -methylstyrenes with styrene, the dependence on the solvent polarity of the relative reactivity of  $\beta$ -methylstyrenes was different from that

found in the copolymerization of  $\alpha$ -methylstyrene with styrene. Both  $\alpha$ -methylstyrene and anethole were more reactive than styrene. But the relative reactivity of  $\alpha$ -methylstyrene towards a styryl cation decreased and that of anethole increased, as the polarity of the solvent increased.

In the copolymerization of styrene with  $\alpha$ -methylstyrene, the relative reactivity of less reactive styrene towards either styryl cation of  $\alpha$ -methylstyryl cation increased with increasing solvent polarity. It is generally accepted that the propagating carbocation becomes more reactive and less selective to attack to monomers when the polarity of the solvent increases<sup>14</sup>. Thus, styrene is much less reactive than  $\alpha$ -methylstyrene in non-polar solvents, but competes well with  $\alpha$ -methylstyrene in polar solvents. This behaviour may be observed with the transition state for the propagation reaction being free from steric hindrance.

Table 3 summarizes the relative reactivity of styrene and anetholes towards various propagating species in polar and non-polar solvents. A and C in Table 3 clearly show that the reactivity of anethole towards a styryl cation is higher than styrene, and that the reactivity difference becomes larger with increasing solvent polarity. This is true for either *cis*- or *trans*-isomer, and is in contrast to the results of the copolymerization of styrene with  $\alpha$ -methylstyrene. If there is no steric hindrance between a propagating styryl cation and the  $\beta$ -substituent of a monomer, the reactivities of the two monomers might be similar in polar solvents, because the reactivity of the propagating carbocation is high in polar solvents. However, the styrene-anethole copolymerization was not the case. Hence, the solvent effect on the styrene-anethole copolymerization seems to be explained in terms of the steric interaction between the propagating carbocation and the  $\beta$ -substituent of the monomer.

In non-polar solvents, we can expect that the propagation reaction of styrene derivatives takes place through a bridged carbocation. However, the propagating carbocation may be very weakly bridged as deduced from the intermediate of the electrophilic halogenation of anethole<sup>15</sup>. This idea is consistent with the mechanism previously proposed by us<sup>4,16</sup> to explain the reactivity of styrene derivatives in terms of open carbocations. The formation of a strongly bridged carbocation from anethole and styryl cation may have been prevented because of the steric repulsion between the substituents. In this respect the reactivity of anethole may have been underestimated in non-polar solvents. As the solvent polarity increases, the propagating styryl cation attacks the monomer from the  $\beta$ -carbon side, so that the steric hindrance between a propagating styryl cation and an anethole monomer diminishes as compared with that in non-polar solvents. Consequently, the reactivity of

Table 3 Summary of relative reactivity of styrene and anetholes towards various propagating species in polar and non-polar solvents (calculated from Table 1)

No.	Propagating chain end <sup>a</sup>	Relative reactivity	Solvent		
			$\text{C}_6\text{H}_6$	$\text{CH}_2\text{Cl}_2$	$\text{C}_2\text{H}_5\text{NO}_2$
A	$\text{St}^+$	<i>cis</i> -An/St	2.50	3.58	4.55
B	<i>cis</i> -An <sup>+</sup>	<i>cis</i> -An/St	2.70	3.15	3.81
C	$\text{St}^+$	<i>trans</i> -An/St	2.78	5.55	12.5
D	<i>trans</i> -An <sup>+</sup>	<i>trans</i> -An/St	3.72	2.48	1.42
E	<i>cis</i> -An <sup>+</sup>	<i>trans</i> -An/ <i>cis</i> -An	0.56	0.60	0.76
F	<i>trans</i> -An <sup>+</sup>	<i>trans</i> -An/ <i>cis</i> -An	0.45	0.34	0.25

<sup>a</sup> St = styrene; An = anethole

anethole relative to styrene towards a styryl cation increases in polar solvents.

Table 3 also shows that the reactivity towards a styryl cation of *trans*-anethole relative to styrene increases much more sharply than that of *cis*-anethole relative to styrene with increasing solvent polarity. This fact is explained by assuming that the ease of the formation of a bridged carbocation is dependent on the geometric structure of anethole, i.e. in non-polar solvents, the steric hindrance with a propagating styryl cation is larger in the reaction of *trans*-anethole than in the reaction of *cis*-isomer. On the other hand, in the point of view of electronic theory the former is more reactive than the latter<sup>8</sup>. These effects cancel each other so that the reactivities of *cis*- and *trans*-anethole are nearly the same in non-polar solvents. In polar solvents, the propagation reaction proceeds through an open carbocation. In this condition, the steric effect of the  $\beta$ -methyl group of a monomer is not affected by the geometric structure of the monomer<sup>4</sup>. So the reactivities of the two monomers are determined by electronic effect, hence *trans*-anethole becomes more reactive towards a styryl cation.

D and F in Table 3 show that the reactivity of *trans*-anethole towards a propagating *trans*-anethole cation as compared with the reactivity of styrene or *cis*-anethole does not increase as the solvent polarity increases. When an open carbocation is involved as an intermediate in the propagation reaction, the geometry of the transition state is similar to that in radical polymerizations. When a propagating *trans*-anethole cation approaches a *trans*-anethole monomer, a large steric interference emerges between the  $\beta$ -methyl group of the monomer and the propagating species to reduce the reactivity of *trans*-anethole. On the other hand, the interference is not important in the addition of an anethole monomer to a propagating *cis*-anethole carbocation, which is substantiated in B and E of Table 3. These results suggest the different conformations of *cis*- and *trans*-anethole carbocations. Further investigations are necessary for this conclusion to be firm.

In the copolymerization of styrene with *trans*-anethole in benzene with SnCl<sub>4</sub>-TCA instead of BF<sub>3</sub>OEt<sub>2</sub> as a catalyst, the monomer reactivity ratios were nearly the same as those obtained with BF<sub>3</sub>OEt<sub>2</sub> in methylene chloride. It has been reported that the catalytic activity of SnCl<sub>4</sub>-TCA is larger than BF<sub>3</sub>OEt<sub>2</sub> in the polymerization of styrene<sup>17</sup> and a propagating carbocation of a loose ion-pair type is formed with SnCl<sub>4</sub><sup>18</sup>. The present result is consistent with this view.

As mentioned in the introduction, propenyl ethers are more reactive than the corresponding vinyl ethers and the reactivity difference is more significant in non-polar sol-

vents than in polar solvents. This has been explained in terms of the formation of a bridged carbocation as an intermediate of the propagation reaction in non-polar solvents<sup>3</sup>. On the other hand, it was observed in this study that the reactivity difference between anethole and styrene was somewhat less significant in non-polar solvents than in polar solvents. For this the following explanations were proposed. The  $\beta$ -methylstyrene derivatives form a weakly bridged carbocation as an intermediate of the propagation reaction even in non-polar solvents because of large steric interactions between the substituents. This sort of intermediate makes the reactivity of anethole close to that of styrene in non-polar solvents. Thus, the different effects of solvent on the copolymerizations of vinyl ether derivatives and styrene derivatives could be related to the different modes of attack of a propagating species to a monomer in non-polar solvents.

## REFERENCES

- Higashimura, T., Kusudo, S., Ohsumi, Y. and Okamura, S. *J. Polym. Sci. (A-1)* 1968, 6, 2523 and the subsequent papers
- Okuyama, T., Fueno, T. and Furukawa, J. *J. Polym. Sci. (A-1)* 1968, 6, 993 and the subsequent papers
- Higashimura, T., Kawamura, K. and Masuda, T. *J. Polym. Sci. (Polym. Chem. Edn)* 1973, 11, 713
- Higashimura, T. and Yamamoto, K. *Makromol. Chem.* 1974, 175, 1139
- Overberger, C. G., Tanner, D. and Pearce, E. M. *J. Am. Chem. Soc.* 1958, 80, 4566
- Mizote, A., Tanaka, T., Higashimura, T. and Okamura, S. *J. Polym. Sci. (A)* 1965, 3, 2567
- Mizote, A., Higashimura, T. and Okamura, S. *J. Polym. Sci. (A-1)* 1968, 6, 1825
- Higashimura, T., Kawamura, K. and Masuda, T. *J. Polym. Sci. (A-1)* 1972, 10, 85
- Johnson, J. R. in 'Organic Reactions' (Ed. R. Adams) Vol 1, Wiley, New York, 1942, p 251
- Naves, Y-R., Ardizio, P. and Favre, C. *Bull. Soc. Chim. France*, 1958, p 566
- Yamamoto, K. and Higashimura, T. *J. Polym. Sci. (Polym. Chem. Edn)* 1974, 12, 613
- Ezriev, A. I., Brokhina, E. L. and Roskin, E. S. *Vysokomol. Soedin.* 1969, 11, 1670
- Inaki, Y., Nozakura, S. and Murahashi, S. *J. Macromol. Sci. (A)* 1972, 6, 313
- Tobolsky, A. V. and Boudreau, R. J. *J. Polym. Sci.* 1961, 51, S53
- Fahey, R. C. and Schneider, H-J. *J. Am. Chem. Soc.* 1968, 90, 4429
- Higashimura, T., Masuda, T., Okamura, S. and Yonezawa, T. *J. Polym. Sci. (A-1)* 1969, 7, 3129
- Okamura, S., Higashimura, T. and Sakurada, Y. *Kobunshi Kagaku* 1959, 16, 49; 1960, 17, 57
- Matsuguma, Y. and Kunitake, T. *Polym. J.* 1971, 2, 353

# Dielectric properties of oligomers:

## 4. Dielectric properties of vinyl acetate and methyl methacrylate oligomers

E. Ikada, T. Sugimura, T. Aoyama and T. Watanabe  
*Faculty of Engineering, Kobe University, Nada, Kobe 657, Japan*  
 (Received 13 May 1974)

Dielectric properties of vinyl acetate and methyl methacrylate oligomers were studied in order to compare the dielectric properties of an oligomer with those of the corresponding high polymers. The two oligomers showed asymmetric dielectric relaxations at room temperatures. The complex dielectric constants vs. angular frequencies for these oligomers were well represented by the Havriliak–Negami equation:

$$\epsilon^* - \epsilon_\infty = \frac{\epsilon_0 - \epsilon_\infty}{[1 + (j\omega\tau_0)^{1-\alpha}]^\beta}$$

The distribution parameters  $(1 - \alpha)$  and  $\beta$  of vinyl acetate and methyl methacrylate oligomer are almost equal to those of poly(vinyl acetate) and poly(methyl methacrylate), respectively. It was concluded that the distribution of relaxation times was independent of the molecular weight of the polymers.

### INTRODUCTION

In the principal dielectric relaxations (so-called ‘ $\alpha$ -relaxation’) of the polymer having polar repeating units the dielectric relaxation times show a broad and asymmetric distribution. In this case the shapes of the Cole–Cole plots of these  $\alpha$ -relaxations on the complex plane are asymmetric<sup>1</sup>. For example, it is well known that the shapes of the Cole–Cole arcs of the principal relaxations of poly(vinyl acetate) (PVAC)<sup>2</sup> apparently resemble the calculated arc of the well-known Davidson–Cole empirical equation<sup>3</sup>:

$$\epsilon^* - \epsilon_\infty = \frac{\epsilon_0 - \epsilon_\infty}{(1 + j\omega\tau_0)^\beta} \quad (1)$$

where  $\epsilon^*$  is the complex dielectric constant,  $\epsilon_0$  and  $\epsilon_\infty$  are the limiting low- and high-frequency dielectric constant, respectively.  $j$  is the imaginary unit,  $\omega$  is the angular frequency,  $\tau_0$  is the mean relaxation time, and  $\beta$  is distribution parameter of relaxation times. This type of relaxation has in most cases been observed in the hydrogen-bonded liquid diol and triol such as glycol and 1,2,6-hexanetriol<sup>3</sup>. However, it was found that the calculated Cole–Cole arc of equation (1) deviates from the experimental arc of  $\alpha$ -relaxations of PVAC<sup>2</sup>. On the other hand, a number of low-frequency  $\alpha$ -relaxations of high polymers have been measured at constant temperature. It was reported that these experimental asymmetric flat loss curves of the polymers are well represented by the equation suggested by Havriliak and Negami<sup>4</sup>

$$\epsilon^* - \epsilon_\infty = \frac{\epsilon_0 - \epsilon_\infty}{[1 + (j\omega\tau_0)^{1-\alpha}]^\beta} \quad (2)$$

where  $(1 - \alpha)$  is another distribution parameter of relaxation times. The applicability of this equation for  $\alpha$ -relaxations of polymers was tested by Havriliak and Negami<sup>4</sup> and Ikada and Watanabe<sup>1</sup>. Further, Williams *et al.*<sup>5</sup> suggested an equation which also fits the  $\alpha$ -relaxations as follows:

$$\frac{\epsilon^* - \epsilon_\infty}{\epsilon_0 - \epsilon_\infty} = \mathcal{L} \left[ - \frac{d\gamma(t)}{dt} \right], \quad \gamma(t) = \exp(-t/\tau) \quad (3)$$

$\mathcal{L}$  indicates the Laplace transform.  $\gamma(t)$  is the normalized decay function.

The low-frequency dielectric relaxations of polar low molecules at the liquid state are attributable to the molecular rotation as a whole<sup>6</sup>. The molecular rotation as a whole in the alternative electric field, however, must become difficult and gradually impossible as the chain length becomes longer beyond the limiting length. This limit cannot be determined definitely. At any rate, the principal dielectric relaxations of long chains differ from those of the low molecules because the relaxing segment of long chains is bound to the neighbouring segment by chemical bonds.

It is interesting to investigate the difference between the molecular rotational relaxation and the segmental relaxation of long chains. As the origins of distribution of relaxation times, several explanations are considered from the characteristic properties of high polymers as follows: (1) the distribution of degree of polymerization in the polymer species yields a distribution of relaxation times; (2) the coexistence of the different relaxation modes in the main chain motions; (3) the relaxation mechanism of segmental motion of main chains consists of the cooperative phenomena; (4) on the relaxation of a long chain the motion is

carried out in the complicated atmosphere.

In order to discuss the above possible deductions, we measured the dielectric relaxations of trifluoromonochloroethylene oligomers  $\text{Cl}-(\text{CF}_2\text{CFCl})_n-\text{Cl}$  ( $n = 2, 3$  and  $4$ ) which have no distribution of degree of polymerization<sup>7</sup>. It was found that the distribution of relaxation times of this fluoro oligomer was also broad and asymmetric as often seen in the distribution of  $\alpha$ -relaxation of high polymers. The distribution parameters  $(1 - \alpha)$  and  $\beta$  of the tetramer of these fluoro oligomers are comparatively small and are equal to the small values of high polymers. The experimental Cole-Cole arc of this tetramer is coincident with the calculated arc of equation (2)<sup>7</sup>. This result leads to the conclusion that the distribution of relaxation times is not attributable to the distribution of degree of polymerization. Further, the dielectric relaxations of 1,2,6-hexanetriacetate and glyceryltriacetate were also investigated at the liquid state<sup>8</sup>. These two acetates have three acetate side groups in a chain. This work was carried out to compare the dielectric properties of the low acetate molecules with those of the high acetate molecule such as PVAC. Consequently, the shapes of the Cole-Cole arcs of both the low- and high-molecular acetates resemble closely each other. That is, the distribution parameters  $(1 - \alpha)$  and  $\beta$  of equation (2) are almost equal for both the samples although their molecular dimensions are quite different. This result leads to the conclusion that the distribution of relaxation times is independent of the chain length. This unexpected result seems to be very suggestive in the study of the dielectric relaxation mechanism of polymers.

On the other hand, the various properties of poly(methyl methacrylate) (PMMA) have been investigated by many workers<sup>9</sup>. Especially, the dielectric properties of this polymer are of interest because  $\beta$ -relaxation plays an important role in PMMA. For example, first, the relaxation intensity of  $\beta$ -relaxation is larger than that of  $\alpha$ -relaxation. Secondly, the temperatures of  $\alpha$ - and  $\beta$ -transition are not so isolated rather than submerged. In this work, comparatively low molecular PVAC and PMMA were prepared and the dielectric properties of the two oligomers were studied in order to compare these results with those of the high molecular weight PVAC and PMMA.

## EXPERIMENTAL

### Preparation of VAC and MMA oligomers

The purified VAC monomer was polymerized in purified acetaldehyde in an ampoule. VAC monomer was added to acetaldehyde in a weight ratio of 1:4. 1 g of benzoyl peroxide was added to 44 g of VAC monomer. Polymerization was carried out in a water bath maintained at  $45 \pm 0.05^\circ\text{C}$  for 110 h. It was reported that in the VAC polymerization in the presence of acetaldehyde a ketone-type aldehyde or an aldehyde-type carboxyl group should be introduced into a polymer chain-end and that in the telomerization of VAC the ketone-type end groups were more preferential than the aldehyde-type carbonyl end group<sup>10</sup>.

MMA oligomer was prepared as follows<sup>11</sup>: purified MMA monomer (0.7 ml) was added to isopropyl alcohol in a volume ratio of 1 to 30 in an ampoule. 0.201 g of di-*t*-butylperoxide was added as initiator. Oligomerization was carried out for 5 h in an oil bath at  $130 \pm 0.5^\circ\text{C}$ . For removal of the unreacted monomer, solvent and initiator, these volatile portions were evaporated in a hot bath at  $42^\circ\text{C}$  under nitrogen gas at the reduced pressure of 60 mmHg.

The residual oligomer, which is an appreciably viscous liquid, was dried in a vacuum drier for a month. The yield of this MMA oligomerization was 72.2%.

### Determination of physical constants

**Molecular weight.** The molecular weight of the oligomers was measured by a vapour pressure osmometer (Mechrolab Inc., model 302). Benzene was used as solvent. *N*-Butylstearate (molecular weight = 340.6) and diphenyl disulphide ( $M_w = 218.3$ ) were used to determine the calibration factor. The experimental molecular weight of MMA oligomer was 375. As each oligo-MMA molecule has a  $(\text{CH}_3)_3\text{CO}$  end group, the average degree of polymerization was calculated as 3.01 subtracting the corresponding molecular weight of this end group from the whole molecular weight. The number-average molecular weight of oligo-VAC was 446.3. This value is equivalent to the average degree of polymerization of  $\sim 5$ . The density and the refractive index of the oligomers were measured by the Lypkin-type pycnometer and Pulfrich refractometer, respectively. The physical constants of the oligomers are collected in Table 1.

**Dielectric measurement.** The dielectric constants and losses were measured by a ratio arm transformer bridge (Ando Electric Co., type TR-1BK) over the temperature range  $-70^\circ$  to  $+60^\circ\text{C}$  and the frequency range 30 Hz to 3 MHz. The dielectric cell was a concentric platinum glass cell whose vacuum capacity was 13.0 pF. The cell temperature was measured by a Pt-Co vs. Cu thermocouple and a standard thermometer. The glass cell was immersed in a well-stirred alcohol bath at the lower temperatures.

## RESULTS AND DISCUSSION

### Static dielectric constant

The experimental static dielectric constants are shown in Figure 1. The values of static dielectric constants of oligo-VAC and oligo-MMA were larger than those of the corresponding high molecular compounds. The dipole moments were calculated from the static dielectric con-

Table 1 Physical properties of the oligomers

	oligo-VAC	oligo-MMA
Molecular weight	446.3	375
Degree of polymerization	5	3.01
Density, $\rho$ (g/ml)	...	1.038 ( $17^\circ$ )
$n_D$	1.46997 ( $20.5^\circ$ )	1.4741 ( $20.1^\circ$ )

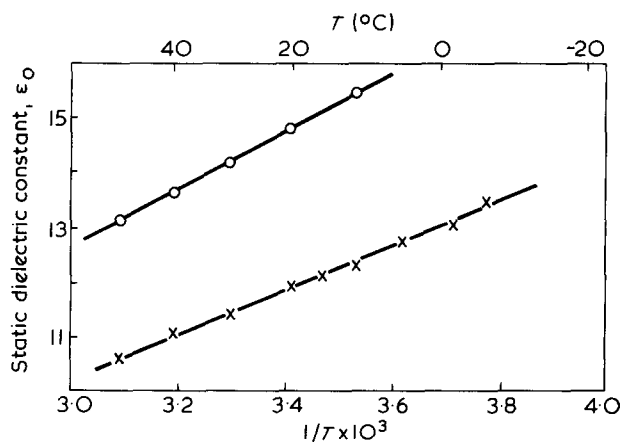


Figure 1 Static dielectric constants of the two oligomers vs. the reciprocal of absolute temperature.  $\circ$ , oligo-MMA;  $\times$ , oligo-VAC

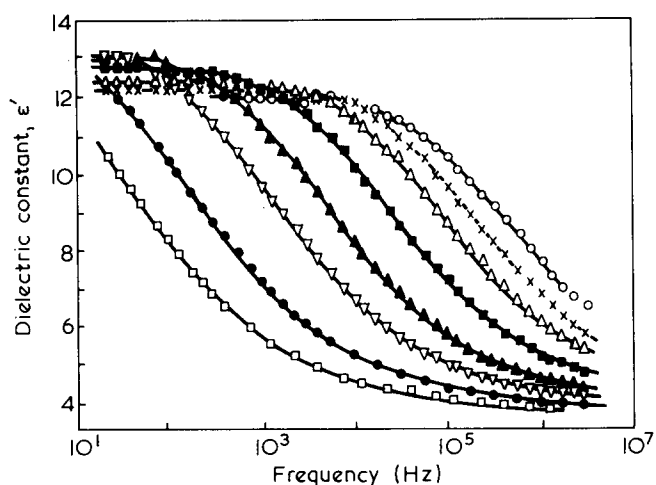


Figure 2 Frequency dependences of the dielectric constants of oligo-VAC at various temperatures:  $\circ$ , 20°;  $\times$ , 15°;  $\triangle$ , 10.0°;  $\blacksquare$ , 2.8°;  $\blacktriangle$ , -4.0°;  $\nabla$ , -9.3°;  $\bullet$ , -16.0°;  $\square$ , -20.0° C

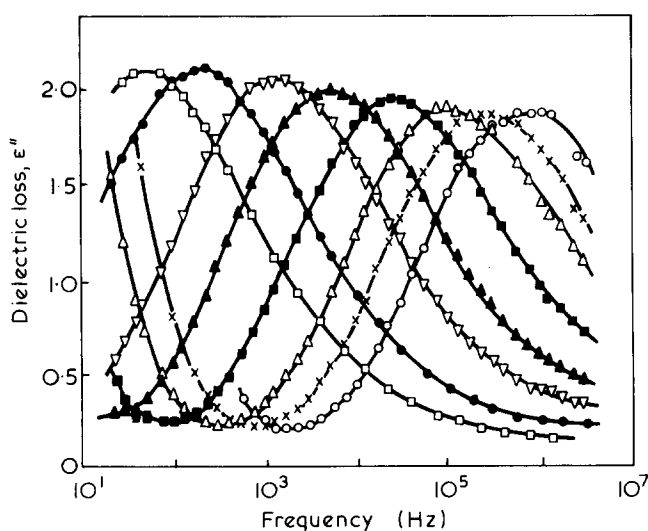


Figure 3 Frequency dependences of the dielectric losses of oligo-VAC at various temperatures. The symbols refer to the same temperatures as in Figure 2

starts by means of the Onsager equation<sup>12</sup>:

$$\epsilon_0 = \epsilon_\infty + \frac{\epsilon_0}{2\epsilon_0 + \epsilon_\infty} \left( \frac{\epsilon_\infty + 2}{3} \right)^2 \frac{4\pi N_0 \mu_0^2}{3kT} \quad (4)$$

where  $\epsilon_0$  and  $\epsilon_\infty$  are the limiting low- and high-frequency dielectric constant, respectively,  $N_0$  is the number of molecules/cm<sup>3</sup>,  $\mu_0$  is the dipole moment *in vacuo* and  $kT$  is the thermal energy. The calculated dipole moments of oligo-VAC and oligo-MMA were 4.8 D and 4.9 D, respectively. These large dipole moments are associated with the dominant quantity of the stretched conformations of the two oligomers. The polar end group (CH<sub>3</sub>CO) contributes to the large dipole moment of oligo-VAC.

#### Dielectric relaxation

The oligomers showed the dielectric dispersion and absorption in the experimental temperature ranges. Frequency dependences of the dielectric constants and losses are shown in Figure 2 and 3, respectively. The loss curves of oligo-VAC are seen to be asymmetric. A number of attempts have been carried out to express the experimental asymmetric arcs of  $\alpha$ -relaxations by a mathematical

equation. It is still especially difficult to explain the relaxation mechanism of a polymer chain explicitly. Thus at the present stage, it seems to be important to determine an equation to express asymmetric  $\alpha$ -relaxation exactly. Applicability of Havriliak–Negami equation was tried for many  $\alpha$ -relaxations of polymers. It seems that this equation is the best-fitting equation to represent the dielectric relaxations of polymers. It was reported that the  $\alpha$ -relaxation of PMMA<sup>4</sup> and PVAC<sup>8</sup> were represented by this equation. Cole–Cole plots of oligo-VAC and oligo-MMA are shown in Figures 4 and 5, respectively. In these Figures, it can be seen that the arcs of both oligomers are as flat as those of the high polymers. The Havriliak–Negami equation was tested for these oligomers. The comparison was shown in Figures 4 and 5. The Havriliak–Negami equation, however, is only an empirical equation to express the experimental dielectric relaxation. The mechanism of  $\alpha$ -relaxation could not be completely explained by this equation.

#### Distribution of relaxation times

The relaxation times of the two oligomers are much shorter than those of the corresponding high polymers. The relationship between the two distribution parameters ( $1 - \alpha$ ) and  $\beta$  in equation (2) and the structure of a polymer is not

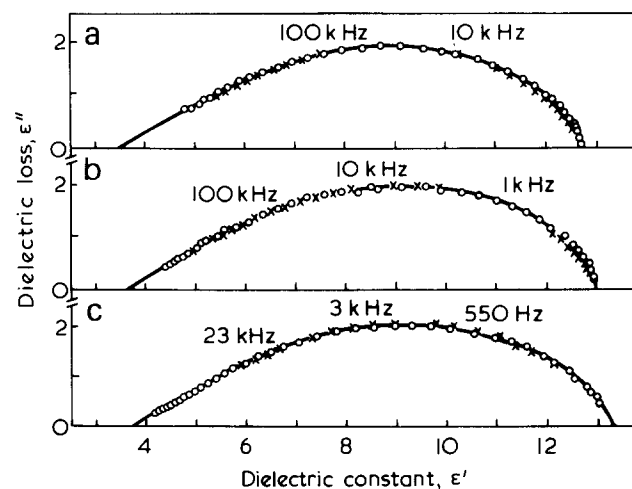


Figure 4 Cole–Cole plots of oligo-VAC at (a) 2.8°, (b) -3.95° and (c) -9.3° C.  $\circ$ , observed points;  $\times$ , calculated points

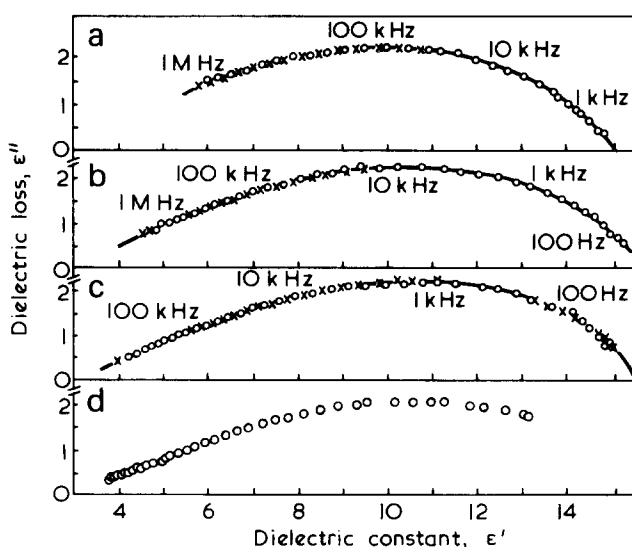


Figure 5 Cole–Cole plots of oligo-MMA at (a) 20.1°, (b) 10.0°, (c) 0.1° and (d) -10.5° C.  $\circ$ , observed points;  $\times$ , calculated points

Table 2 Distribution parameters of PMMA and oligo-MMA

T (°C)	1 - $\alpha$	$\beta$
isotactic PMMA <sup>4</sup> :		
90.1	0.645	0.385
72.0	0.572	0.372
63.0	0.530	0.320
oligo-MMA:		
20.1	0.586	0.451
10.0	0.552	0.469
0.1	0.590	0.437

Table 3 Distribution parameters of PVAC and oligo-VAC

T (°C)	1 - $\alpha$	$\beta$
PVAC:		
70	0.902	0.556
PVAC <sup>4</sup> :		
66	0.910	0.45
oligo-VAC:		
2.8	0.668	0.499
-4.0	0.674	0.495
-9.3	0.632	0.550

clear. To investigate the asymmetric and wide distribution of relaxation times characteristic of the polymers which is more widely distributed at the shorter time side than at the longer time side is an interesting problem to a polymer chemist. The asymmetry of the distribution of relaxation times may lead to an imaginary existence of cooperative relaxation mechanisms. The values of the two distribution parameters and the relaxation times of MMA and VAC polymers and oligomers are collected in Tables 2 and 3, respectively. The oligomers studied are much smaller molecules compared to the high molecular PMMA and PVAC. Nevertheless, the values of the two distribution parameters of PMMA and oligo-MMA do not differ markedly. As described above, the distribution parameters of 1,2,6-hexanetriacetate and glyceryltriacetate were compared with those of PVAC. It was found that the distribution of the dielectric relaxation times of the low molecular triacetates are almost equal to that of high molecular PVAC<sup>8</sup>. These coincidences of the distribution is certainly an interesting result, but this fact does not suggest the significant explanation about the mechanism of the dielectric relaxation of polymers much. As is seen in Table 3, (1 -  $\alpha$ ) of oligo-VAC is smaller than that of PVAC. It was found that this small (1 -  $\alpha$ ) is due to the polar end groups (COCH<sub>3</sub>) of oligo-VAC<sup>13</sup>. The distribution of relaxation times may be more closely related to the molecular structures rather than to the degree of polymerization of the polar polymers. The temperature dependences of relaxation times are shown in Figure 6. The activation energies for the dielectric relaxation were calculated by regarding these two curves as straight lines. The calculated values for oligo-VAC and oligo-MMA were 14.35 and 13.1 kcal, respectively. The literature value for PVAC was 60 kcal<sup>14</sup>.

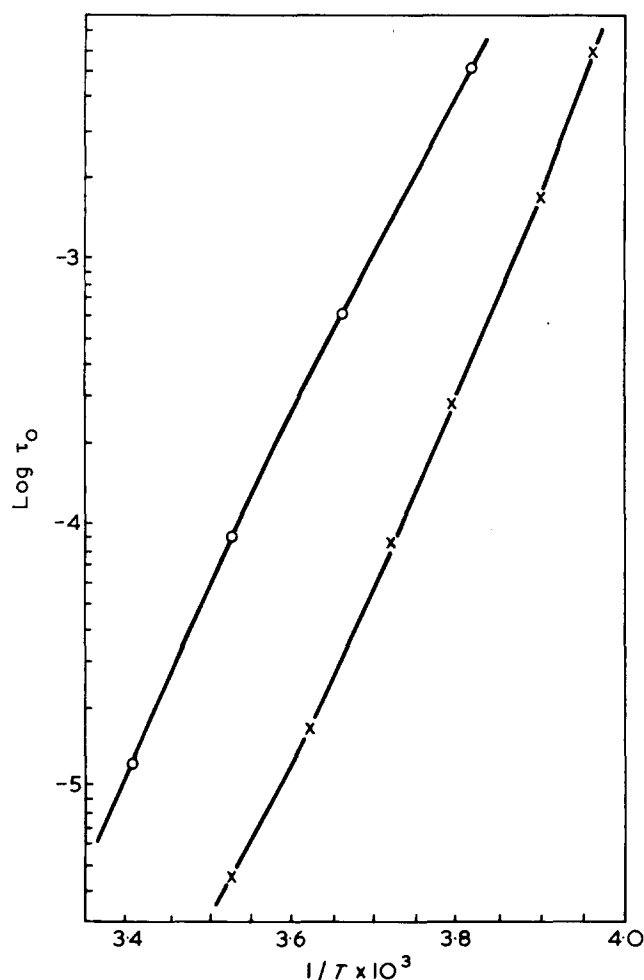


Figure 6 Relaxation times of the two oligomers vs. the reciprocal of absolute temperatures. O, Oligo-MMA; X, oligo-VAC

## REFERENCES

- Ikada, E. and Watanabe, T. *J. Polym. Sci. (A-1)* 1972, **10**, 3457
- Yamafuji, K., Ichikawa, H., Irie, F. and Ishida, Y. *Kolloid-Z. Z. Polym.* 1962, **181**, 160
- Davidson, D. W. and Cole, R. H. *J. Chem. Phys.* 1951, **19**, 1484
- Havriliak, S. and Negami, S. *Polymer* 1967, **8**, 161; *J. Polym. Sci. (C)* 1966, **14**, 99
- Williams, G. et al. *Trans. Faraday Soc.* 1970, **66**, 80
- See e.g. Smyth, C. P. 'Dielectric Behaviour and Structure', McGraw-Hill, New York, 1955
- Ikada, E., Aoyama, T. and Watanabe, T. *Mem. Fac. Eng. Kobe Univ.* 1974, **20**, 271
- Ikada, E. and Watanabe, T. *J. Phys. Chem.* 1974, **78**, 1078
- See e.g. Sasabe, H. and Saito, S. *J. Polym. Sci. (A-2)* 1968, **6**, 1401
- Miyake, Y. and Matsumoto, S. *Kogyo Kagaku Zasshi* 1959, **62**, 1101
- Shimomura, T., Tsuchida, E. and Shinohara, I. *Mem. Sch. Sci. Eng., Waseda Univ.* 1965, **29**, 1
- Onsager, L. *J. Am. Chem. Soc.* 1936, **58**, 1486
- Ikada, E. et al. *J. Polym. Sci.* to be published
- Ishida, Y., Matsuo, M. and Yamafuji, K. *Kolloid-Z. Z. Polym.* 1962, **180**, 108

# Solution properties of poly(propylene sulphide)

D. W. Nash and D. C. Pepper

Chemistry Department, Trinity College, University of Dublin, Dublin 2, Eire

(Received 25 April 1974; revised 7 June 1974)

Poly(propylene sulphide) (PPS) initiated by cadmium bis(phenyl allyl thiolate) was fractionated from benzene-methanol, and the fractions were examined by viscosity, osmotic pressure and light scattering determinations. Gel permeation chromatography with Styragel columns was found unsatisfactory in tetrahydrofuran (THF) and toluene at room temperature. Polymer stored in the dark at room temperature underwent a very slow degradation which broadened the distribution in the fractions. The following quantitative relationships were found at 25°C:

$$\begin{aligned}[\eta] &= 1.40 \times 10^{-2} \bar{M}_w^{0.68} \quad \text{in toluene} \\ (\text{ml/g}) &= 2.58 \times 10^{-2} \bar{M}_w^{0.66} \quad \text{in THF} \\ &= 2.74 \times 10^{-2} \bar{M}_w^{0.63} \quad \text{in benzene} \\ &= 9.42 \times 10^{-2} \bar{M}_w^{0.50} \quad \text{in 31\% n-heptane/toluene}(\theta\text{-mixture})\end{aligned}$$

Extrapolations to derive the unperturbed coil dimensions indicate a possible, but doubtful, solvent effect. The value derived from the  $\theta$ -mixture gives  $A = 696 \times 10^{-11} \text{ cm mol}^{1/2} \text{ g}^{-1/2}$  and a steric factor  $\sigma = 1.49$ , consistent with a high 'chain flexibility' expected from the relatively long C-S-C linkages.

## INTRODUCTION

Examination of their solution properties has shown that polymer chains containing C-O-C linkages have smaller coil-dimensions and lower values of the 'steric factor'<sup>1,2</sup> than the corresponding hydrocarbons. This increased 'flexibility' is even more marked in poly(phenylene oxide) chains containing the long 'virtual' bonds  $\phi\text{-O-}\phi^3$ . The present work was designed to examine the effect of C-S-C links, and also to investigate the discrepancy between different values reported for the Mark-Houwink exponents for poly(propylene sulphide) (PPS) in benzene reported by Eskin<sup>4</sup> and Cooper<sup>5</sup>. The Eskin value of 0.86 is unusually high for a non-cellulosic chain.

## EXPERIMENTAL

### Monomer purification

Propylene episulphide, prepared conventionally from propylene carbonate and potassium thiocyanate<sup>6,7</sup> was purified from thiols by several successive shakings with an alkaline suspension of litharge (2% PbO in 12% aq. NaOH). After washing to neutrality, it was dried first over MgSO<sub>4</sub> and then for several days over CaH<sub>2</sub> and fractionated under nitrogen through a 12 in column of glass helices (b.p. 74°C at 1 atm).

### Polymerization

The catalyst, cadmium bis(phenyl allyl thiolate) was dissolved in bulk monomer; the solutions were twice degassed and sealed into dilatometer-type Pyrex phials. At the catalyst concentration ( $10^{-5}$  to  $10^{-6}$  M) and reaction tem-

peratures (0°–50°C) used the time for apparently complete reaction was between 2 and 20 days. The polymer was broken out of the phials, dissolved in benzene and isolated by freeze drying under high vacuum.

### Fractionation

Turbidimetric studies using a Hilger Spekner Absorptiometer showed that convenient solvent/non-solvent pairs were benzene-methanol (precipitating over the range 23–30% v/v methanol) and carbon tetrachloride/n-hexane (33–43%). Preparative fractionations were carried out with both these pairs, using 10–15 g polymer samples at ~1% initial concentration, yielding 10–11 fractions and virtually quantitative recovery. N.m.r. spectra, at 100 MHz, indicated that all fractions examined had the same tacticity (55% isotactic) as the unfractionated polymer, providing reassurance that the separation was determined by molecular weight, not tacticity.

## RESULTS

### Polymer solubility

In a search for  $\theta$ -solvents, 29 solvents were examined but none were found suitable in the range 0–100°C. At room temperature PPS dissolves easily in aromatic or in chlorinated solvents, and is insoluble in aliphatic hydrocarbons and in very polar solvents. The 'solubility parameter' (cohesive energy density)<sup>1/2</sup>,  $\delta$ , is only partly helpful for prediction. Thus the value calculated for PPS (via 'molar association constants'<sup>2</sup>) is  $9.6 \text{ (cal/cm}^3)^{1/2}$ . As expected, the 'good' solvents listed in Table 1 have  $\delta$ -values fairly close to this



**Table 1** Solvents for PPS and solubility parameters ( $\delta$ ).  $\delta$  (PPS, calc.) =  $9.6 \text{ (cal/cm}^3)^{1/2}$ 

Non-solvents	$\delta$	Solvents	$\delta$
methanol	14.5		
nitromethane	12.7		
ethanol	12.7		
dimethylformamide	12.0		
isopropanol	11.5		
acetic acid	10.1		
acetone	9.9	<i>o</i> -dichlorobenzene	10.0
		cyclohexanone	9.9
		ethylene dichloride	9.8
		methylene chloride	9.7
tetralin	9.5	chlorobenzene	9.5
		furan	9.4
methyl ethyl ketone	9.3	benzene	9.2
		tetrahydrofuran	9.1
		toluene	8.9
decalin	8.8	ethyl benzene	8.8
		xylene	8.8
		n-propyl benzene	8.6
		carbon tetrachloride	8.6
cyclohexane	8.2		
iso-octane	7.6		
diethyl ether	7.4		
n-heptane	7.4		
n-hexane	7.3		

value, and the non-solvents mostly have values much higher or lower. But ketone and cycloalkane solvents having  $\delta$ -values close to that of PPS are nevertheless non-solvents.

By the cloud-point method of Elias<sup>8</sup>, a mixture containing 31.5% v/v of n-heptane in toluene, was found to be a  $\theta$ -mixture for PPS at 25°C.

#### Polymer stability and intrinsic viscosities

PPS samples prepared by cadmium thiolate initiators are said to be somewhat unstable under exposure to light and oxygen<sup>9</sup>. Wragg<sup>10</sup> found rapid degradation above 200°C but believed the polymer to be stable at room temperature in solution. All polymer samples used in the present work were stored in the dark in vacuum desiccators.

The intrinsic viscosities of a number of samples were measured at intervals over a period of one month, and no change was detected. Solutions in THF stored in glass or in stainless-steel containers similarly showed no change in viscosity. However, much longer intervals (up to 12 months) often elapsed between the preparation of a fraction and its ultimate molecular weight measurements. Intrinsic viscosities  $[\eta]$  measured then were found to have fallen by varying amounts (3–20%) below the values for 'fresh' fractions. All  $[\eta]$  values quoted are those of the partly degraded samples, measured shortly after the molecular weight determinations.

Viscosities were measured at 25°C in an Ubbelohde-type suspended level viscometer with negligible kinetic energy correction, and  $[\eta]$  values were derived from this common intercept of Huggins and Kraemer plots. Results in toluene, benzene, THF and the  $\theta$ -mixture are listed in *Table 2*.

#### Molecular weights and chain dimensions

Attempts to derive molecular weights and distributions by g.p.c. from THF or toluene at room temperature proved unsuccessful (see Appendix).

Number average molecular weights,  $\bar{M}_n$ , were obtained from measurements of osmotic pressure ( $\pi$ ) in toluene at 25°C, using a Mechrolab High Speed Membrane Osmometer with gel cellophane membranes. No evidence for polymer

diffusion was observed and linear  $\pi/C$  vs.  $-C$  plots were obtained.

Weight average molecular weights,  $\bar{M}_w$ , were determined (via Zimm<sup>11</sup> plots) from light-scattering in toluene at room temperature, using the Hg green line at 546 nm, in a Brice-Phoenix photometer, series 100. The refractive index increment in toluene for this wavelength was determined to be  $9.6 \times 10^{-2} \text{ cm}^3/\text{g}$  at 25°C.

The results for three series of fractions are shown in *Table 3*. It can be seen that the ratio  $\bar{M}_w/\bar{M}_n$  is often larger than expected for precipitation fractions, and varies erratically; presumably as a result of varying degrees of degradation in different fractions. To make some allowance for this the weight average root mean square end-to-end chain dimensions  $\langle L_w^2 \rangle^{1/2}$  were calculated from the experimentally obtained radii of gyration  $\langle S_z^2 \rangle^{1/2}$ , via the Schultz-Zimm heterogeneity parameter,  $h$ , where

$$\bar{M}_w/\bar{M}_n = (h + 1)/h \quad (1)$$

$$\langle L_w^2 \rangle^{1/2} = [6\langle S_z^2 \rangle^{1/2}(h + 1)/(h + 2)]^{1/2} \quad (2)$$

*Table 3* shows values for these quantities and for the second virial coefficients, determined from both light-scattering and osmotic pressure.

#### DERIVED RELATIONSHIPS

*Mark-Houwink equations*,  $[\eta] = KM^a$

Plots of  $\log [\eta]$  against  $\log \bar{M}_w$  (*Figure 1*) show good consistency between results from sample 6 (fractionated from carbon tetrachloride-hexane) and sample 21 (from benzene-methanol). Values from sample 17 (from benzene-methanol) scatter more widely and appear to indicate lines of higher slope. The best values of the constant, calculated by linear regression analysis, are listed in *Table 4*.

#### Chain dimensions in toluene

The heterogeneity-corrected values for the root mean square end-to-end dimensions in toluene (*Table 3*) depend on  $\bar{M}_w$  with a scatter similar to that of the  $[\eta]$  values. The

**Table 2** Intrinsic viscosities at 25°C

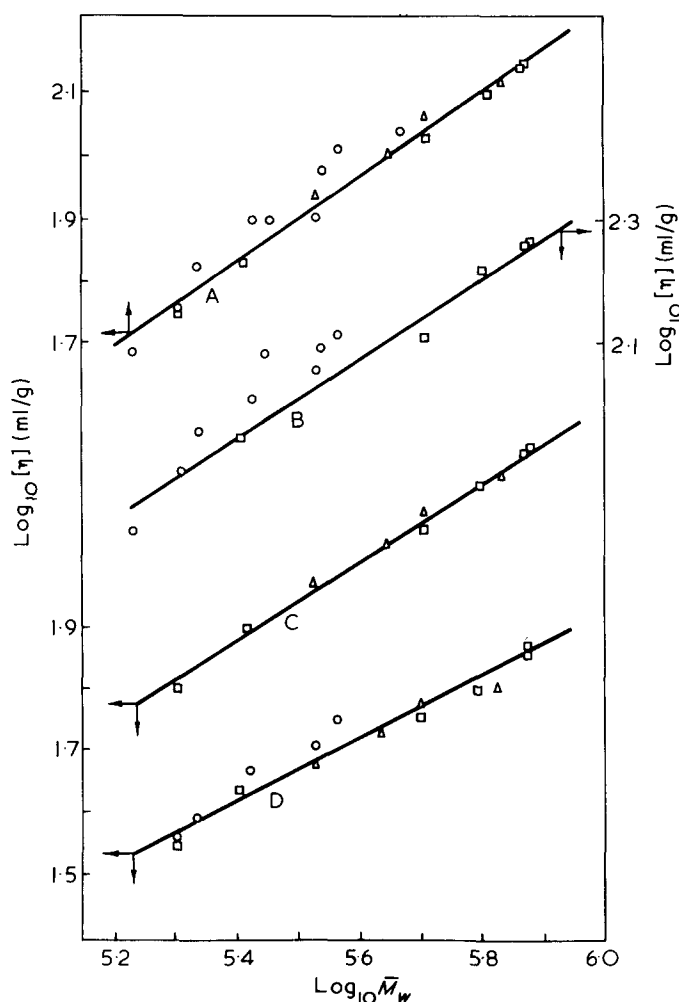
Fraction	$[\eta]$ (cm <sup>3</sup> /g) in			
	Toluene	Benzene	THF	$\theta$ -mixture
6.2	140.5	154	183	72.5
6.3	139.5	149.5	184.5	74.5
6.4	124.5	134	167.5	64
6.5	106.5	115.5	131	57
6.7	67	79	90	43.5
6.8	57	63	79	35
17.2	79.5		115	
17.3	102		130	55
17.4	93.5		124	51
17.5	79		121	—
17.6	78.5		103	47
17.7	66.3		92	39.5
17.8	57		79	36
17.9	49		63	—
21.2	130	138	—	64
21.3	116	123.5		60.5
21.5	100	109		53.5
21.8	86	94		47.5

Table 3 Molecular weights, dimensions and virial coefficients

Fraction	$\bar{M}_w \times 10^5$	$\bar{M}_n \times 10^5$	$\bar{M}_w/\bar{M}_n$	$\langle S_z^2 \rangle^{1/2}$ (Å)	$\langle L_w^2 \rangle^{1/2}$ (Å)	$A_2^\dagger \times 10^4$ (mol cm <sup>3</sup> /g <sup>2</sup> )	$A_2^\ddagger \times 10^4$ (mol cm <sup>3</sup> /g <sup>2</sup> )
6.2	7.39	4.35	1.70	394	813	2.81	5.76
6.3	7.31	3.63	2.01	327	653	3.58	5.28
6.4	6.20	2.61	2.38	257	500	3.74	5.05
6.5	4.95	2.28	2.17	289	570	2.74	4.22
6.7	2.53	2.00	1.26	155	349	3.41	4.85
6.8	2.00	1.09	1.83	132	269	3.84	6.33
17.1	4.69	—	—	290	641	3.07	—
17.2	3.36	2.60	1.30	—	—	—	5.39
17.3	3.64	2.81	1.30	304	673	3.54	4.51
17.4	3.40	2.60	1.31	258	568	4.22	4.39
17.5	2.81	2.42	1.16	212	487	3.82	4.27
17.6	2.64	1.73	1.53	251	530	4.07	3.86
17.7	2.17	1.97	1.10	183	429	4.29	4.95
17.8	2.02	1.10	1.84	155	315	4.75	3.40
17.9	1.70	0.91	1.87	149	301	5.71	3.51
21.2	6.67	3.59	1.85	342	693	3.92	6.01
21.3	5.00	2.47	2.03	313	625	3.77	5.72
21.5	4.35	2.00	2.17	247	490	3.53	5.87
21.8	3.34	2.03	1.64	167	248	3.50	5.97

\* From light scattering

† From osmotic pressure


 Figure 1 Mark-Houwink relationships for PPS. A, toluene; B, THF; C, benzene; D,  $\theta$ -mixture.  $\square$ , points from fractionation no.6;  $\circ$ , points from fractionation no.17;  $\triangle$ , points from fractionation no.21

relationship calculated by linear regression analysis of the points is:

$$\langle L_w^2 \rangle^{1/2} = 3.07 \times 10^{-1} \bar{M}_w^{0.575} \quad (3)$$

 Table 4 Constants in the Mark-Houwink equation ( $[\eta]$  (ml/g) =  $KM^a$ )

Solvent	$K \times 10^2$	$a$
31.5% n-heptane/toluene	9.42	0.49 <sub>5</sub>
Benzene	2.74	0.63 <sub>8</sub>
THF	2.58	0.65 <sub>6</sub>
Toluene	1.40	0.68 <sub>3</sub>

According to Ptitsyn's theory<sup>12</sup>, the exponent in equation (3) should be related to that of the Mark-Houwink equation, having the value  $(a + 1)/3$ . The value thus calculated from  $a = 0.68$  is 0.56, i.e. in reasonable concordance.

#### Unperturbed dimensions and steric factor

The intrinsic viscosities in the different solvents were analysed by the usual extrapolation procedures, capable in principle of yielding the polymer-solvent interaction parameter,  $B$ , and the 'unperturbed' value of the M-H constant ( $K_\theta$ ) and hence the 'unperturbed dimensions' of a PPS chain.

Figure 2 shows a plot according to the Stockmayer-Fixman equation:

$$[\eta]/\bar{M}_w^{1/2} = K_\theta + 0.51\Phi_0 B \bar{M}_w^{-1/2} \quad (4)$$

Within a considerable experimental error the results in a given solvent can be described by a straight line, but the lines for different solvents do not meet in the theoretical common intercept. Plots of the other extrapolation functions (listed in Table 5) showed the same general pattern. Values of  $K_\theta$  calculated from their intercepts are collected in the Table and show good general agreement between the different procedures, and an apparent effect of solvent on  $K_\theta$ .

The values of the 'unperturbed dimension'  $A = (L_0^2/M)^{1/2}$  shown also in Table 5 are derived from  $K_\theta$  via Flory's equation:

$$K_\theta = \Phi_0 \langle L_0^2 \rangle / M^{3/2} \quad (5)$$

using his now recommended value<sup>13</sup> for  $\Phi_0 = 2.6 \times 10^{23}$ . A

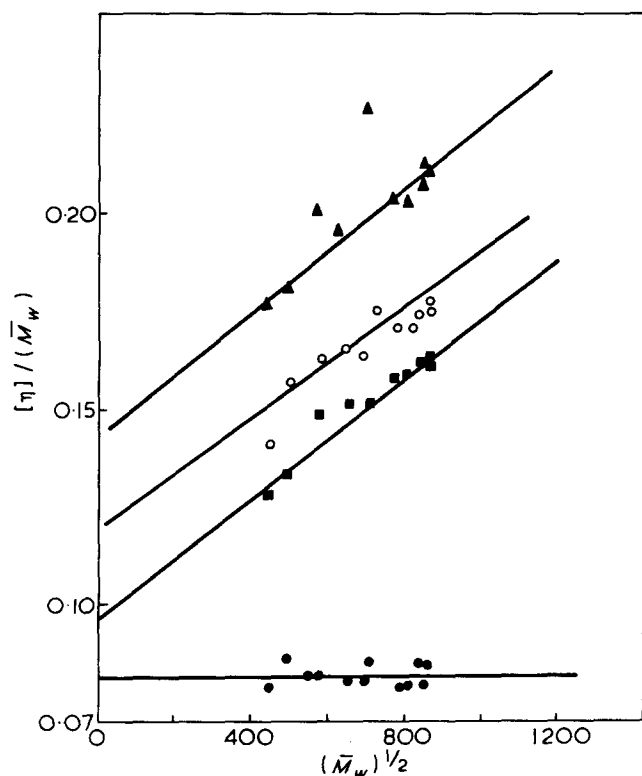


Figure 2 Stockmayer-Fixman plots for PPS.  $\blacktriangle$ , THF;  $\circ$ , benzene;  $\blacksquare$ , toluene;  $\bullet$ ,  $\theta$ -mixture (31.5% n-heptane in toluene)

theoretical value for this dimension of a 'freely rotating' chain,  $A_f = 468 \times 10^{-11} \text{ cm mol}^{1/2} \text{ g}^{-1/2}$  has been calculated from Huglin and Stepto's<sup>14</sup> value for poly(ethylene sulphide), allowing for the higher molecular weight of PPS. The derived values of the steric factor,  $\sigma = A/A_f$ , range from 1.49 to 1.76.

#### Second virial coefficient, $A_2$

Table 3 lists values derived from both osmotic pressure and light-scattering measurements. Those from osmotic pressure are appreciably higher, and in one series (from fractionation 17) show an anomalous apparent increase with molecular weight. Those from light-scattering show the normal decrease with  $\bar{M}_w$ . Log-log plot yields:

$$A_2 = 8.0 \times 10^{-2} \bar{M}_w^{-0.24} \quad (6)$$

the exponent lying within the usual range  $-0.2$  to  $-0.3$ .

#### Coil-expansion factor and excluded volume

Values of the expansion factors  $\alpha$  and  $\alpha_\eta$ , derived from intrinsic viscosities by:

$$\alpha_\eta^3 = \alpha^{2.43} = [\eta] / [\eta]_\theta = [\eta] / K_\theta \bar{M}_w^{1/2}$$

are all lower than often found in good solvents; i.e. all lie in the range 1.07 to 1.27 and trend only slightly with molecular weight (compared with  $\alpha_\eta$  ranging from 1.35 to 1.65 for polystyrene in toluene over a similar  $\bar{M}_w$  range). The values cover too narrow a range of  $\bar{M}_w$  to provide a useful test of the form of the excluded volume function.

The relationship of the  $\alpha_\eta$  values to the virial coefficient is not well defined. They are only slightly less than calculated from the equation of Krigbaum<sup>16</sup>:

$$A_2 \bar{M}_w / [\eta] = 217(1 - \alpha_\eta^{-3}) \quad (7)$$

but considerably less than values calculated by the modified expression of Flory, Krigbaum and Orofino<sup>17</sup>. A plot of  $A_2 \bar{M}_w / [\eta]$  against  $(\alpha_\eta^2 - 1)$ , often useful<sup>18</sup> to distinguish between these and other functions, proves uninformative because of the narrow range of  $\alpha$  values.

#### DISCUSSION

In view of the partial degradation of the fractions during storage, some discussion is needed of the significance of the measurements for quantitative deductions. As judged by the fall in  $[\eta]$  between original fractionation and eventual molecular weight determination, the extent of degradation was variable (3–20%) and unrelated to the original  $[\eta]$  value. The breadth of their molecular weight distributions (as indicated by  $\bar{M}_w / \bar{M}_n$  ratio) was similarly variable, but also unrelated to  $\bar{M}_w$ . The corresponding deviations may therefore be expected to be random rather than systematic, and the uncertainties in the derived Mark-Houwink equations and other relationships to depend more on the relatively limited range of molecular weights examined (only ~5-fold) than on the imperfections of particular samples.

The constants of the Mark-Houwink equations listed in Table 4 are self-consistent, in that for different solvents the  $K$  and  $a$  values show the expected inter-relationship,  $K$  rising smoothly as  $a$  falls. The relatively low values of  $a$  found in all solvents examined are consistent also with the small coil expansion factors calculated by comparison with their unperturbed dimensions. However, the results found in benzene are appreciably different from those quoted by previous authors, e.g. by Stokes<sup>19</sup>:  $[\eta]$  (ml/g) =  $5.0 \times 10^{-3} M^{0.78}$  at 20°C for unfractionated PPS prepared by cadmium thiolates (as here) and by Eskin<sup>4</sup>:  $[\eta]$  (ml/g) =  $3.3 \times 10^{-3} M^{0.86}$  at 31°C for fractions of sodium naphthalene initiated polymer.

When all the relationships in benzene are plotted together in the same graph (Figure 3) it can be seen that Stokes's results and our own are in reasonable concordance up to moderate molecular weights, but appear to diverge above ~300 000. Stokes's samples were unfractionated, but this would account for the divergence only if his samples had progressively narrower distributions the higher the molecular weight, which seems unlikely. Further examination of high molecular weight fractions are needed to resolve this discrepancy.

Figure 3 suggests that Eskin's results for anionically initiated PPS cannot be accommodated by the relationship found here. His results are very self-consistent but extend only up to molecular weights ~ $10^5$ , and it seems possible that over a wider range, an exponent lower than his (un-

Table 5  $K_\theta$  and unperturbed dimensions

Method	$K_\theta \times 10^2$ from viscosities in			
	Toluene	Benzene	THF	$\theta$ -mixture
F-F-S	8.28	11.4	15.0	8.3
K-S	9.50	12.0	14.4	8.2
S-F-B	9.6	12.3	14.3	8.0
Berry	8.7	11.6	14.2	8.3
Bohdanecky	9.4	12.5	14.9	10.1
M-H	—	—	—	9.4
Mean	9.1	12.0	14.5	8.7
$A \times 10^{11}$ i.e. $(K_\theta / 2.6 \times 10^{23})^{1/3}$	704	772	825	696

F-F-S = Flory-Fox-Schaeffgen; K-S = Kurata-Stockmayer; S-F-B = Stockmayer-Fixman-Burchard; M-H = Mark-Houwink

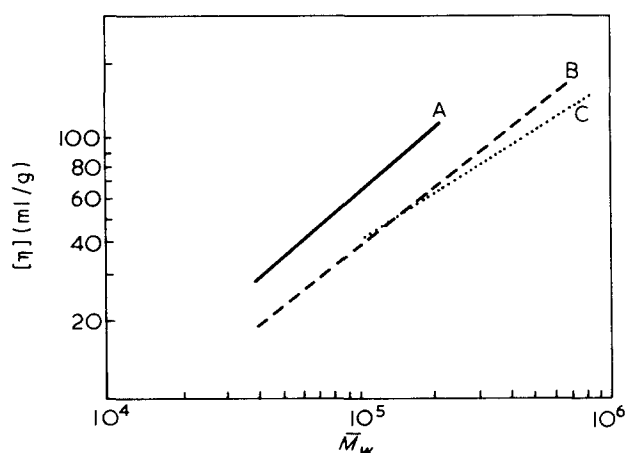


Figure 3 Comparison of M—H relationships for PPS in benzene. A, Eskin (at 31°C); B, Stokes (at 20°C); C, this work (at 25°C)

Table 6 Unperturbed dimensions and steric factors

Polymer	$10^{11} \langle L_0^2 \rangle / M)^{1/2} =$ $10^{11} A$ (cm mol <sup>1/2</sup> g <sup>-1/2</sup> )	$\sigma$	Reference
Poly(ethylene oxide)	930	1.63	24
Poly(ethylene oxide)	840	1.55	22
Poly(propylene oxide)	790	1.62	24
Poly(1-butene oxide)	730	1.71	22
Poly(styrene oxide)	640	1.85	24
Poly(cyclohexene oxide)	592	1.65	25
Poly(propylene sulphide)	600	1.31	4
Poly(propylene sulphide)	696	1.49	this work

usually high) value of 0.86 might apply. But his curve as a whole 'lies high', i.e. corresponds to a value of  $K$  considerably lower than found here, so it seems likely that his anionically initiated polymer may be showing genuinely different relationships corresponding to a different chain structure. The only obvious differences are the presence of a central Cd atom in the present (and Stokes's) samples, and difference in chain tacticity. The former would hardly be expected to have much influence on the overall coil dimensions and hence  $[\eta]$ . Differences in chain tacticity have sometimes been found to influence the M—H equations, especially in the poorer solvents, e.g. with PMMA.

Deductions about chain dimensions in the pure solvents are made more than usually uncertain by the limited range of molecular weights and the scatter of points in the Stockmayer—Fixman (Figure 2) and similar plots. This raises the question whether the present results in good solvents can give accurate derivations of  $K_\theta$ , i.e. whether the variation in values derived is a real indication of a true solvent effect. Such effects have been observed<sup>20,21</sup>, especially when polymer and solvents differ appreciably in polarity. For PPS, this question must at present be left in doubt, especially in the light of Booth's findings<sup>22,23</sup> that with polyoxides, the extrapolation functions often show considerable curvature towards lower molecular weights.

The results for solutions in the  $\theta$ -mixture, however, present no problems of interpretation and lead to a well defined value of  $K_\theta = 8.6 \times 10^{-2}$  and an 'unperturbed dimension'  $A = 696 \times 10^{11}$  cm mol<sup>1/2</sup> g<sup>-1/2</sup>. The derived value for the steric factor ( $=A/A_p$ ) = 1.49 is to be compared with 1.31 derived from Eskin's value of  $A = 600 \times 10^{11}$  for anionically prepared PPS, and with the range of published values for polyoxides listed in Table 6.

It is clear that whichever value is to be taken as more realistic for PPS, it is appreciably lower than shown by any of the polyoxides, consistent with orthodox expectations

that steric interactions of adjacent and nearby chain units should be reduced by the longer C—S—C linkage.

#### ACKNOWLEDGEMENTS

The authors thanks are due to Dr W. Cooper of the Dunlop Research Centre for background information and the gift of a sample of initiator, and to Dr E. Lillie of Queen's University, Belfast, for observation and interpretation of 100 MHz n.m.r. spectra.

#### REFERENCES

- Orofino, T. A. and Mickey, J. W. *J. Chem. Phys.* 1963, **38**, 2512
- Brandrup, J. and Immergut, E. H. 'Polymer Handbook', Interscience, New York, 1966
- Barrales-Rienda, J. M. and Pepper, D. C. *Eur. Polym. J.* 1967, **3**, 535
- Eskin, V. Y. and Nesterov, A. Y. *Polym. Sci. USSR* 1966, **8**, 152
- Cooper, W., Morgan, D. and Wragg, R. T. *Eur. Polym. J.* 1969, **5**, 71
- Sigwalt, P. personal communication
- Searles, G., Hayes, H. A. and Lutz, E. F. *J. Org. Chem.* 1962, **27**, 2828, 2832
- Elias, A. G. *Makromol. Chem.* 1959, **33**, 140
- Morgan, D. personal communication
- Wragg, R. T. *J. Chem. Soc. (B)* 1970, p 404
- Zimm, B. J. *J. Chem. Phys.* 1948, **16**, 1093, 1099
- Ptitsyn, O. B. *Uspekhi Fiz. Nauk* 1959, **49**, 371
- Flory, P. 'Statistical Mechanics of Polymer Chains', Interscience, New York, 1969, p 37
- Huglin, M. B. and Stepto, R. F. T. *Makromol. Chem.* 1970, **132**, 225
- Flory, P. *J. Chem. Phys.* 1959, **17**, 303
- Krigbaum, W. J. *Polym. Sci.* 1955, **18**, 315
- Stockmayer, W. H. *Makromol. Chem.* 1959, **35**, 54
- Banks, W. and Greenwood, C. T. *Eur. Polym. J.* 1968, **4**, 457
- Stokes, A. *Eur. Polym. J.* 1970, **6**, 719
- Cowie, J. M. G. *Polymer* 1966, **7**, 487
- Berry, G. C. J. *Polym. Sci. (B)* 1966, **4**, 161
- Beech, D. R. and Booth, C. J. *Polym. Sci. (A-1)* 1969, **7**, 575
- Booth, C. and Orme, R. *Polymer* 1970, **11**, 626
- Allen, G. *et al. Polymer* 1967, **8**, 391
- Mele, A., Rufo, R. and Santonato, L. *Polymer* 1969, **10**, 233

#### APPENDIX

##### Anomalous behaviour of PPS in gel permeation chromatography

Conventional g.p.c. (Waters Model 200; 5 Styragel columns) proved useless for the present PPS samples in THF or in toluene at room temperature. All chromatograms showed very broad peaks and long 'tails' and indicated apparent molecular weights very much lower than the values derived from light scattering or osmotic pressure. Chromatograms from toluene were less anomalous than those from THF, but still unusable.

In view of the evidence quoted earlier for the slow degradation of PPS it was at first surmised that a faster degradation was occurring in the g.p.c. instrument. Extensive tests of this possibility were made by comparisons of viscosity measurements of solutions stored in presence of the Styragel or in stainless-steel containers. No evidence of degradation could be observed.

It seems likely therefore that the anomalies arise from general adsorption of the polymer on the column material, delaying elution and reducing the resolving power. The fact that Stokes<sup>19</sup> mentions no difficulties in g.p.c. operation in THF at 54°C may be consistent with this conclusion since appreciably less adsorption would be expected at the higher temperature.

# Viscoelastic properties of poly(propylene glycols)

A. John Barlow and Aynur Erginsav

Department of Electronics and Electrical Engineering, University of Glasgow, Glasgow G12 8QQ, UK  
(Received 3 July 1974)

The relaxational and retardational properties of poly(propylene glycol) liquids, of nominal molecular weights 400 and 4000, are described. The viscoelastic behaviour of each liquid has been determined over a wide temperature range, using high frequency shear wave techniques operating at 30 and 454 MHz. It is found that the complex compliance  $J^*(j\omega)$  is described in terms of the viscosity  $\eta$ , the limiting high frequency compliance  $J_\infty$ , the retardational compliance  $J_r$  and a characteristic retardation time  $\tau_r$  by:

$$J^*(j\omega) = J_\infty + 1/j\omega\eta + J_r/(1 + j\omega\tau_r)^\beta$$

where  $\beta$  is a parameter of the retardation time distribution.

For the lower molecular weight liquid,  $J_r/J_\infty = 17.4$ ,  $\beta = 0.45$  and  $\tau_r/\tau_m$  increases with decreasing temperature, reaching a limit of 170 near 0°C. This liquid shows no evidence of polymeric behaviour.

For the other,  $J_r/J_\infty = 85$ ,  $\beta = 0.76$ ,  $\tau_r/\tau_m = 15.4$  and is constant over the temperature range investigated. The main difference between the two liquids appears as an additional retardational or relaxational process for the higher molecular weight material which occurs in the initial or low frequency part of the relaxation region. This process is characterized by a single time, but with relaxation time 1/7 and a stiffness 7 times the values calculated for the first Rouse mode of polymer chain motion.

## INTRODUCTION

In previous publications<sup>1-3</sup> the retardational behaviour of several non-polymeric organic liquids and mixtures has been described. The retardational compliance  $J_r^*(j\omega) = J_1(\omega) - jJ_2(\omega)$  is related to the complex compliance  $J^*(j\omega)$  of a liquid by:

$$J^*(j\omega) = J_\infty + 1/j\omega\eta + J_r^*(j\omega) \quad (1)$$

where  $J_\infty$  is the limiting or high frequency shear compliance ( $=1/G_\infty$ ),  $\eta$  is the steady flow viscosity and  $\omega$  is the angular frequency of the shear stress<sup>4</sup>. In turn,  $J^*(j\omega)$  is related to the shear mechanical impedance,  $Z_L = R_L + jX_L$ , by  $J^*(j\omega) = \rho/Z_L^2$ , where  $\rho$  is the density of liquid.  $J_r^*(j\omega)$  reaches a limiting value of  $J_r$  at low frequency.

For comparatively simple organic liquids, it was found that the retardational compliance could be described by an equation analogous to that used by Davidson and Cole<sup>5</sup> in studies of the dielectric properties of viscous liquids:

$$J_r^*(j\omega) = J_r/(1 + j\omega\tau_r)^\beta \quad (2)$$

Typically, for pure liquids in the supercooled or highly viscous region, the retardational compliance  $J_r$  is 3 to 30 times  $J_\infty$ ,  $\beta$  is 0.5,  $\tau_r$  is greater than the Maxwell relaxation time  $\tau_m (= \eta J_\infty)$  at low temperatures but the ratio  $\tau_r/\tau_m$  decreases rapidly with increasing temperature where the viscosity falls to 1 Pa s or less. These measurements were made possible only by the development of a very accurate experimental system for the determination of both  $R_L$  and  $X_L$ , since  $J^*(j\omega)$  is dominated by the term  $1/j\omega\eta$  at low

frequencies ( $\omega \ll 1/\eta J_\infty$ ) and tends to  $J_\infty$  at high frequencies ( $\omega \gg 1/\eta J_\infty$ ).

This paper describes an extension of the previous work. Two poly(propylene glycol) liquids, of nominal molecular weights 400 and 4000, have been investigated. It was considered that whilst the shorter chain polymer might show behaviour similar to that for the non-polymeric liquids, the longer chain was expected to have distinct polymeric characteristics.

## EXPERIMENTAL

The two samples were kindly supplied by Dr R. F. Boyer and Mr P. C. Dean of The Dow Chemical Co. Inc., Midland, Michigan, and were designated P400 and P4000. Before use they were dried and degassed under vacuum for 12 h at 40°C and subsequently kept in a desiccator with silica gel. The molecular weights were determined by means of a Hitachi-Perkin-Elmer osmometer, and the values obtained are  $M_n = 377$  for P400 and  $M_n = 3034$  for P4000. These results agree with values determined by gel permeation chromatography, although the accuracy of this latter technique is considered to be inferior. For both liquids  $M_w/M_n$  is less than 1.16. It follows that  $n$  in the formula  $\text{HO}(\text{C}_3\text{H}_6\text{O})_n\text{C}_3\text{H}_6\text{OH}$  is approximately 5 for P400 and 50 for P4000.

The viscosity of each liquid was determined using suspended-level viscometers; the results are estimated to be accurate to within  $\pm 0.5\%$ . Measurements were made of P400 in the range 74.8°C to -29.3°C and of P4000 in the range 79.5°C to -20.1°C; the results are shown in Figure 1.

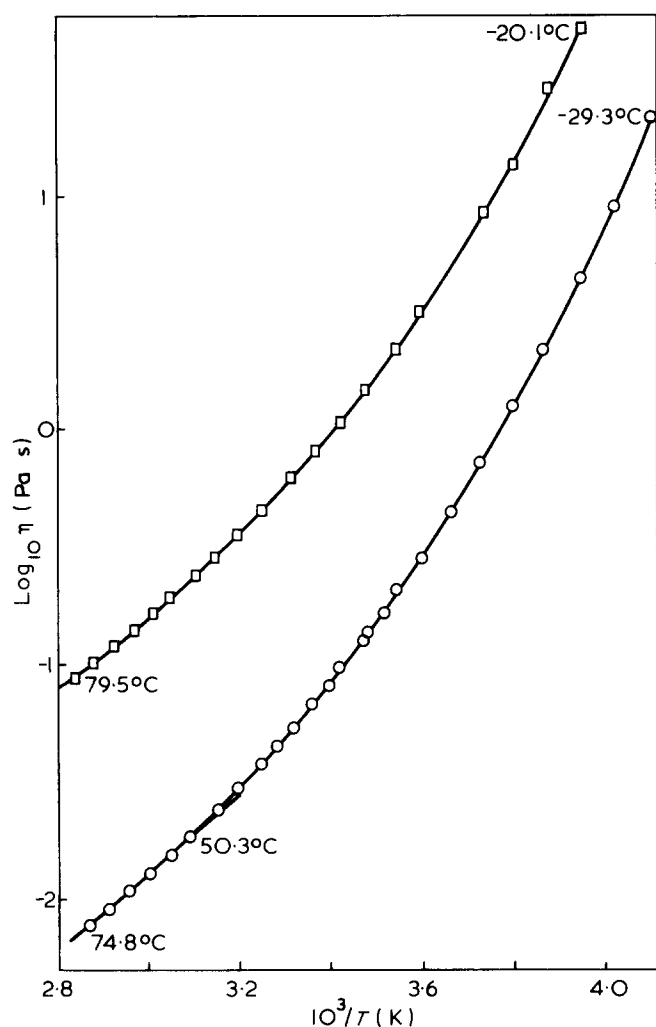


Figure 1 Temperature dependence of the viscosity of poly(propylene glycols): □, P4000; ○, P400

Above 50°C the viscosity of P400 follows an Arrhenius temperature dependence; below 50°C the data are fitted by the empirical equation<sup>6,7</sup>,  $\log_e \eta = A + B/(T - T_0)$ , with the constants given by:

$$\log_e \eta = -10.7744 + 1047.3/(T - 168.4) \quad (3)$$

For P4000, the data are fitted over the full range investigated by:

$$\log_e \eta = -7.172 + 817.2/(T - 180.1) \quad (4)$$

In these equations,  $\eta$  is the viscosity in Pa s and  $T$  is the temperature in Kelvins.

The density,  $\rho$  (kg/m<sup>3</sup>), of each liquid was also determined, and found to vary linearly with temperature, the results obtained being fitted by the equations:

$$\text{P400: } \rho = 1116(1 - 0.000727(T - 168.4)) \quad (5)$$

$$\text{P4000: } \rho = 1063(1 - 0.000696(T - 180.1)) \quad (6)$$

The components  $R_L$  and  $X_L$  of the mechanical shear impedance were determined using plane shear waves at a frequency of 29.426 MHz, and the values obtained are estimated to be accurate to within  $\pm 0.5\% \pm 500 \text{ N s m}^{-3}$ . For P400, measurements were made at eight temperatures from 4.4 to 31.8°C, and for P4000, at five temperatures

from 40.1 to 79.5°C. Measurements of  $R_L$  alone were made at 454 MHz; for P400 results were obtained from 31.8°C to -70.7°C and for P4000 the range was 40.9 to -65.7°C. Some additional measurements were also made at 30 MHz at low temperatures to determine the extent of the region in which  $R_L$  is independent of frequency<sup>8</sup>. The experimental techniques employed have been described in previous publications<sup>9-11</sup>.

## RESULTS AND ANALYSIS

For each liquid the variation with temperature of  $\rho/R_L^2$ , in the region where it defines the compliance  $J_\infty$ , is shown in Figure 2. As has been found for many other liquids<sup>8,12</sup>,  $J_\infty$  increases linearly with temperature. The data are fitted by the equations:

$$\text{P400: } J_\infty = 1.3 \times 10^{-10} + 1.15 \times 10^{-11}(T - 168.4) \quad (7)$$

$$\text{P4000: } J_\infty = 1.0 \times 10^{-10} + 1.85 \times 10^{-11}(T - 180.1) \quad (8)$$

where  $J_\infty$  is the compliance in m<sup>2</sup>/N. These equations have been used to obtain extrapolated values within the relaxation region.

For the definitions given in the previous section, it follows that:

$$J_1(\omega) = \rho(R_L^2 - X_L^2)/(R_L^2 + X_L^2)^2 - J_\infty \quad (9)$$

$$J_2(\omega) = 2\rho R_L X_L/(R_L^2 + X_L^2)^2 - 1/\omega\eta \quad (10)$$

For each temperature at which both  $R_L$  and  $X_L$  are known,  $J_1(\omega)$  and  $J_2(\omega)$  may be determined, using equations (3), (5) and (7) or (4), (6) and (8) as appropriate. Because of experimental limitations which restrict measurement of  $R_L$  and  $X_L$  to a single frequency ( $\omega = 2\pi \times 29.426 \times 10^6 \text{ s}^{-1}$ ) it is not possible to determine the temperature dependence of the retardational modulus  $J_r$ . Following the procedure adopted in previous work<sup>1-3</sup>, the temperature dependencies of  $J_r$  and  $J_\infty$  are assumed to be the same. Accordingly, the values of  $J_1(\omega)/J_\infty$  and  $J_2(\omega)/J_\infty$  have been calculated for each liquid and the results are given in Figures 3 and 4. In each case the relative variation of these normalized com-

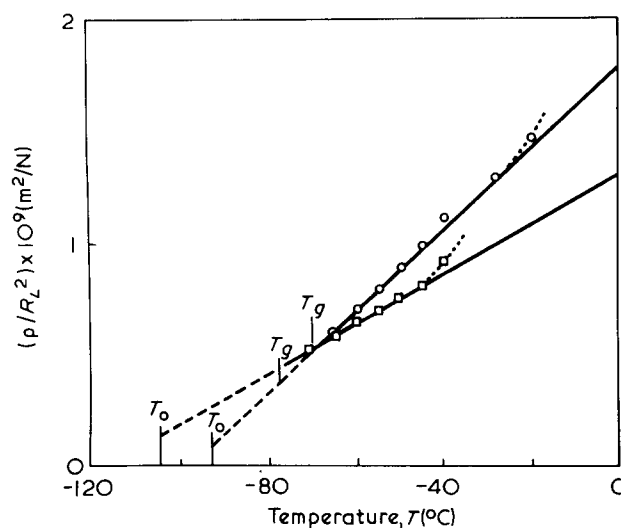


Figure 2 Temperature dependence of  $\rho/R_L^2$  for two poly(propylene glycols): □, P400; ○, P4000. For each liquid the temperature  $T_g$  is the value at which  $\eta = 10^{12} \text{ Pa s}$

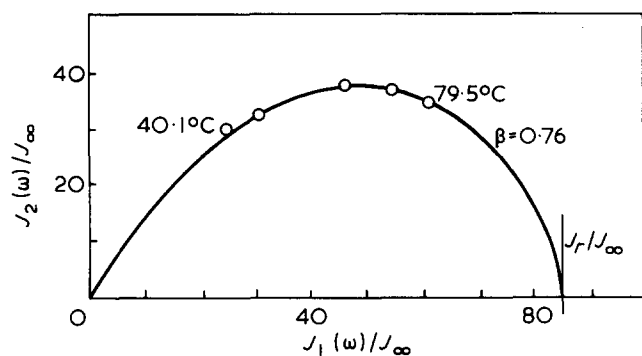


Figure 3 Relative variation of the components of the retardational compliance at 30 MHz for P4000

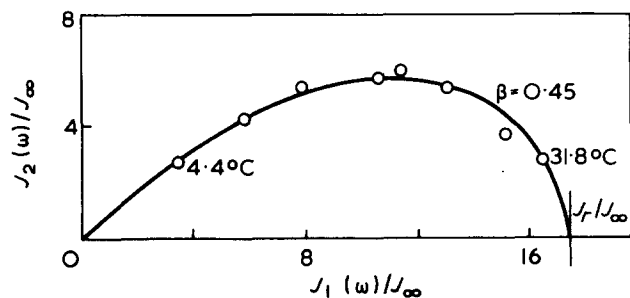


Figure 4 Relative variation of the components of the retardational compliance at 30 MHz for P400

ponents of the retardational compliance is given by a normalized version of equation (2):

$$J_1(\omega)/J_\infty - jJ_2(\omega)/J_\infty = (J_r/J_\infty)/(1 + j\omega\tau_r)^\beta \quad (11)$$

The position of the experimental points on the locus defined by particular values of  $J_r/J_\infty$  and  $\beta$  is determined by  $\omega\tau_r$ ; therefore for each point (i.e. at each temperature of measurement)  $\tau_r$  can be determined.

For P4000,  $J_r/J_\infty = 85$ ,  $\beta = 0.76$ , the ratio  $\tau_r/\tau_m (= \tau_r/\eta J_\infty)$  is 15.4, and is constant over the range 40–80°C. Because of the experimentally limited temperature range of the results these values may be regarded as tentative at this stage of the analysis. However, their use enables a prediction to be made of the properties at other temperatures and frequencies. In particular,  $R_L$  and  $X_L$  may be calculated by means of equations (4), (6) and (8)–(11). In Figure 5 the calculated variations of  $R_L$  and  $X_L$  in normalized form are shown as a function of  $\omega\eta J_\infty$ . Whilst the agreement between the curves and the data at 30 MHz is simply a consequence of the arithmetical accuracy of the analysis, the good agreement between the  $R_L(J_\infty/\rho)^{1/2}$  curve and the 454 MHz data at temperatures from 40.9 to –28.6°C provides substantial confirmation of the predictions, and shows that  $\tau_r/\tau_m = 15.4$  over the full range 80 to –28.6°C. Appreciable discrepancies occur between these results and the predicted curve if any one of the above values of  $J_r/J_\infty$ ,  $\beta$  and  $\tau_r/\tau_m$  is varied by more than  $\pm 10\%$ . The errors in these values are therefore probably less than  $\pm 10\%$ .

For P400, the curve of Figure 4 is obtained using equation (11) with  $J_r/J_\infty = 17.4$  and  $\beta = 0.45$ . However,  $\tau_r/\tau_m$  is not constant but increases from 30 at 31.8°C to 155 at 4.4°C. It is therefore not possible to draw a single curve which describes the frequency dependence of  $R_L$  over this temperature range, a separate curve is required at each temperature. Figure 6 shows the normalized  $R_L$  results plotted as a function of  $\omega\eta J_\infty$ . The lower curve is

predicted using equations (3), (5), (7) and (9)–(11) for a temperature of 31.8°C at which  $\tau_r/\tau_m = 30$ . It can be seen that the curve is in good agreement with the measured value at 31.8°C and 454 MHz. The upper curve is plotted for  $\tau_r/\tau_m = 170$ , and gives a good fit to all the 454 MHz results in the region below 0°C. As in the previous analysis for P4000, the curves are derived using only the data obtained at 30 MHz. The value of  $\tau_r/\tau_m = 170$  is a limiting value which is reached at low temperatures. Curves calculated for intermediate values of  $\tau_r/\tau_m$  at temperatures between 31.8°C and 0°C agree satisfactorily with the 454 MHz data at corresponding temperatures; to avoid confusion these are not shown in Figure 6.

Figure 7 shows the variation of  $\tau_r/\tau_m$  as a function of temperature.

## DISCUSSION

It has been established that the retardational behaviour of each liquid is adequately described by the Davidson–Cole equation (2), and the relaxational behaviour by equations (2) and (1). The properties of the lower molecular weight material P400, as defined by the values of  $\beta$ ,  $\tau_r/\tau_m$  and  $J_r/J_\infty (= 17.4)$ , are similar to those of other non-polymeric liquids of comparable molecular weight and chain length. As examples of liquids with similar values of  $J_r/J_\infty$ , squalane (21.8), tri- $\beta$ -chloroethyl phosphate (26.0) and benzyl benzoate (27.0) may be cited<sup>1,3</sup>. A decrease in  $\tau_r/\tau_m$  with

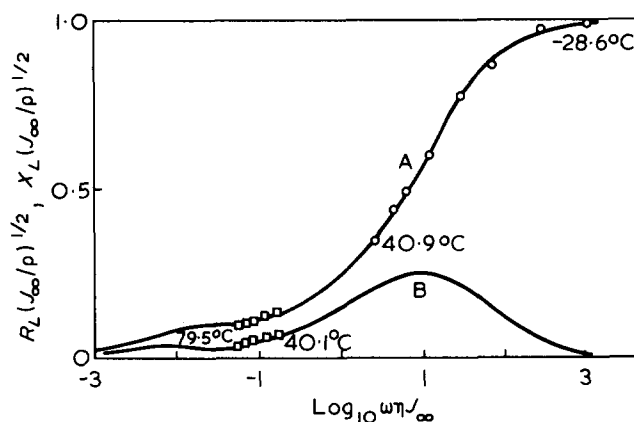


Figure 5 Values of (A)  $R_L(J_\infty/\rho)^{1/2}$  and (B)  $X_L(J_\infty/\rho)^{1/2}$  for P4000 plotted against  $\log_{10} \omega\eta J_\infty$ . The curves are calculated using the values  $J_r/J_\infty = 85$ ,  $\beta = 0.76$  and  $\tau_r/\tau_m = 15.4$ .  $\square$ , 30;  $\circ$ , 454 MHz

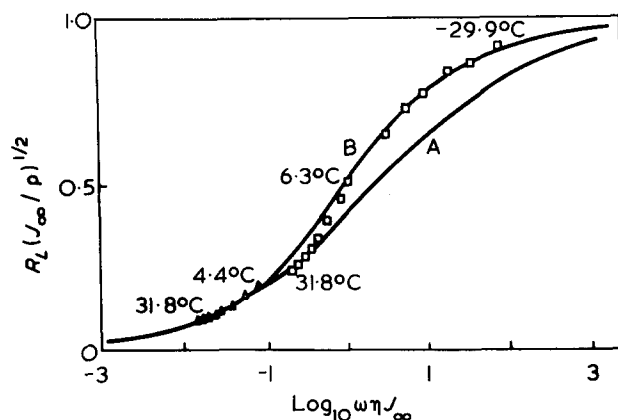


Figure 6 Values of  $R_L(J_\infty/\rho)^{1/2}$  for P400 plotted against  $\log_{10} \omega\eta J_\infty$ . The curves are calculated using the values  $J_r/J_\infty = 17.4$ ,  $\beta = 0.45$  and for  $\tau_r/\tau_m =$  (A) 30 (31.8°C) and (B) 170 ( $T < 0^\circ\text{C}$ ).  $\Delta$ , 30;  $\square$ , 454 MHz

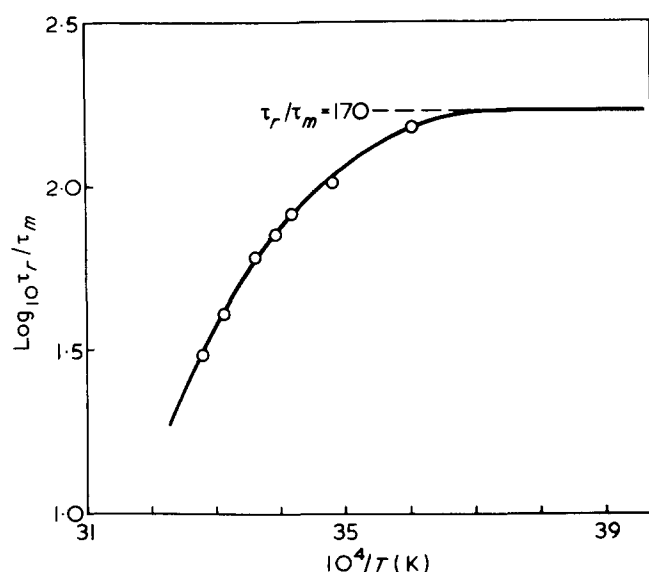

 Figure 7 Temperature dependence of  $\tau_r/\tau_m$  for P400

Table 1 Properties of two poly(propylene glycol) liquids at 0°C

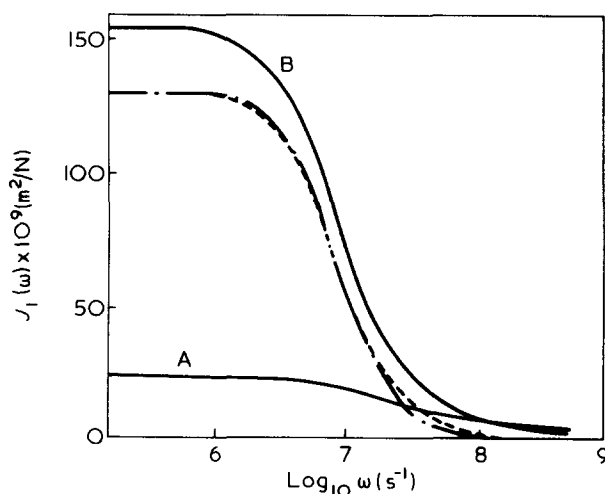
	P400	P4000
$\eta$ (Pa s)	0.46	5.0
$G_\infty$ (N/m <sup>2</sup> )	$7.5 \times 10^8$	$5.5 \times 10^8$
$\tau_m$ (ps)	616	9100
$\tau_r$ ( $\mu$ s)	0.105	0.140
$\tau_r/\tau_m$	170	15.4
$J_\infty$ (m <sup>2</sup> /N)	$1.34 \times 10^{-9}$	$1.82 \times 10^{-9}$
$J_r/J_\infty$	17.4	85
$J_r$ (m <sup>2</sup> /N)	$23.4 \times 10^{-9}$	$155 \times 10^{-9}$
$\beta$	0.45	0.76

increasing temperature is also commonly found for non-polymeric liquids; and it may be noted that the variation of  $\tau_r/\tau_m$  above 0°C for P400 shows that the time-temperature superposition principle does not hold in this region. The evidence therefore shows that P400 has no specifically polymeric characteristics.

In contrast, the higher molecular weight material P4000 has a much greater value of  $J_r/J_\infty$  (=85), a lower ratio  $\tau_r/\tau_m$  and the spectrum parameter  $\beta$  is higher, indicating a narrower retardation spectrum. For comparison, the properties of the two liquids are summarized in Table 1: the values are given at 0°C, thus avoiding the region in which  $\tau_r/\tau_m$  for P400 is temperature dependent. Figure 8 shows  $J_1(\omega)$  for both liquids, calculated using Table 1 and equation (2), plotted as a function of  $\omega$  at 0°C. The difference,  $J_1(\omega)$  (P4000) -  $J_1(\omega)$  (P400), is also shown, and corresponds very closely to the variation pertaining to a single retardation time. The main effect of the increase in molecular weight from P400 to P4000 can therefore be represented by the addition of a single retardation time process to the distributed spectrum for the short chain material. The retardation time,  $\tau_x$ , of this additional component is 0.11  $\mu$ s and its compliance,  $J_{rx}$ , is  $132 \times 10^{-9}$  m<sup>2</sup>/N. The apparently anomalous feature of a narrower retardation spectrum for the higher molecular weight liquid can be regarded as due to the introduction of this dominant, high compliance process with a retardation time close to the longest retardation time ( $\tau_r = 0.105$   $\mu$ s) of the distributed spectrum which describes the short-chain retardation processes. A secondary feature is also noticeable in Figure 8; in the region  $\log_{10} \omega > 8.4$ , the compliance  $J_1(\omega)$  for

P4000 is slightly less than for P400, indicating a smaller amplitude of the retardation spectrum in this range. In effect, some of the highest frequency components present in the spectrum of the shorter chain liquid are diminished in the higher molecular weight polymer. This occurs only where  $J_1(\omega)$  is less than  $4 \times 10^{-9}$  m<sup>2</sup>/N. Since the ratio of the retardation times for the two liquids does not change rapidly with temperature below 0°C, these deductions are not dependent upon the choice of a particular temperature for the comparison, and are valid from 0°C to at least -30°C.

Previously, because of the lack of accurate data of the retardational properties, analyses of the behaviour of short chain polymers have usually been based upon a relaxational model<sup>13,14</sup>. In this model the shear modulus  $G^*(j\omega)$  [ $=G'(\omega) + jG''(\omega) = 1/J^*(j\omega)$ ] is assumed to consist of the sum of components arising from a 'simple-liquid' type of behaviour and contributions from relaxational modes pertaining to changes in the configurations of long polymer chains, the latter being formulated in terms of the theories of Rouse<sup>15</sup> and Zimm<sup>16</sup>. In principle, it is possible to calculate directly the relaxation spectrum from the retardational behaviour<sup>4</sup>. In practice, even for the simply defined retardational behaviour found for P4000, the analysis is almost intractable unless approximation techniques are used. However, the positions and strengths of the relaxation components are very sensitive to the difference between  $\tau_x$  and  $\tau_r$ , and in the present case, where  $\tau_x \approx \tau_r$ , such approximation techniques are not necessarily reliable. It is preferable to calculate the shear modulus components  $G'$  and  $G''$  and to analyse one or both of these. Figure 9 shows the normalized component  $G'/G_\infty$  for P400 and P4000, again calculated at 0°C. The major difference between the two liquids is seen to be the emergence of a 'plateau region' for P4000. Detailed analysis shows that this feature is almost completely accounted for by a single relaxation time process with  $\tau_a = 1/\omega_a = 0.93$   $\mu$ s and  $G_a = 5.2 \times 10^6$  N/m<sup>2</sup>. Analysis of  $G''/G_\infty$  gives a similar result, and these values are also consistent with approximate values calculated from the retardational results. Above  $\log_{10} \omega \approx 8$ , the more rapid approach of  $G'/G_\infty$  for P4000 to the maximum value of unity is again attributable to a smaller contribution from high frequency relaxations in this region; this effect is naturally more apparent in plots of the shear modulus than of its inverse.


 Figure 8 Frequency dependence of  $J_1(\omega)$  for P400 (A) and P4000 (B) at 0°C. --- shows the difference  $J_1(\omega)$  (P4000) -  $J_1(\omega)$  (P400); - - - is for a single retardation time



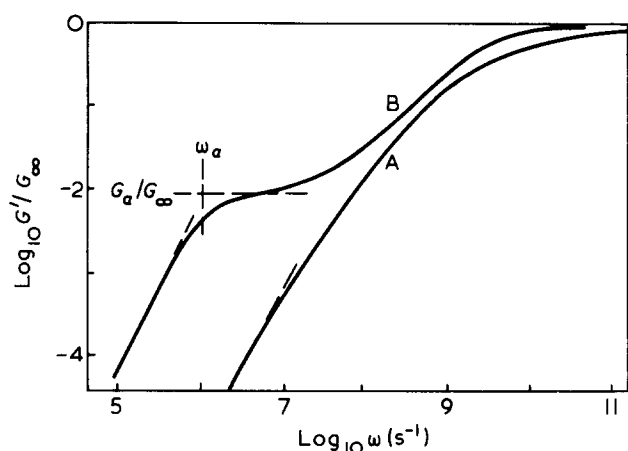


Figure 9 Frequency dependence of the normalized shear modulus component,  $G'/G_\infty$ , for P400 (A) and P4000 (B) at 0°C

The additional single relaxation mode in P4000 is evidence of a 'long chain' mode of relaxation and may tentatively be regarded as the first of the series of 'configurational' modes of the type postulated in the Rouse theory. This theory defines each mode strength as  $\rho RT/M$ , which for P4000 at 0°C amounts to  $7.5 \times 10^5 \text{ N/m}^2$ . The observed mode strength  $G_a$ , is therefore about 7 times the value for the first Rouse mode, and the observed relaxation time  $\tau_a$  is approximately 1/7 of the theoretical time  $\tau_1$  (taken as  $\eta M/\rho RT$ ) for this first mode. The Rouse<sup>15</sup> theory postulates modes of motion associated with polymer chain segments, each segment comprising  $q$  monomer units with the minimum segmental length defined such that the ends of the segment are spatially related according to a Gaussian distribution. For polydimethylsiloxanes a value of  $q \approx 10$  is consistent with the observed viscoelastic behaviour<sup>17,18</sup>, and for unbranched polymers with a  $-C-C-$  backbone, a  $q$  of 25 has been suggested<sup>19,20</sup>. Since the stiffness  $G_a$  for P4000 is greater than the value predicted by the Rouse theory, it may be inferred that the chain length is insufficient for a Gaussian distribution of end-to-end distances, and the value of  $q$  is therefore greater than 50. The comparatively high stiffness of the poly(propylene glycol) molecule is surprising in view of the flexibility of the  $-C-C-O-$  backbone and the small size of the  $\text{CH}_3$  side group, and some restriction of possible orientations by intra- or intermolecular forces may be inferred.

Because of this somewhat unexpected result, an alternative to the preceding direct analysis of the experimental results for P4000 has been attempted, in which the Rouse theory is assumed to apply and the number and strength of the modes is chosen to be consistent with the data. Such an approach could not be dismissed without detailed consideration, since it may be argued that because of experimental limitations  $J_r$  is obtained only by extrapolation, and the true value of  $J_r/J_\infty$  may therefore be quite different

from the value of 85 determined from Figure 3. An equivalent statement is that despite the good agreement between the high frequency results (450 MHz) and the predictions obtained by fitting the Davidson-Cole equation to the 30 MHz data there is no confirmation of the predictions at lower frequencies. This alternative analysis shows that if the mode strength is taken as  $\rho RT/M$ , then the Rouse theory, with any number of modes, is not consistent with the experimental results. If both the mode strength and the number of modes are allowed to be variable, then the best fit to the difference between P4000 and P400 is obtained with one mode, the modulus and relaxation time of this mode agreeing with the values found in the direct analysis of the results.

#### ACKNOWLEDGEMENTS

We thank Professor J. Lamb and Dr G. Harrison for their encouragement and assistance in this work. The determinations of molecular weights were kindly made by Dr R. Petrick of the University of Strathclyde. Support for the research has been provided by the Science Research Council.

#### REFERENCES

- 1 Barlow, A. J. and Erginsav, A. *Proc. R. Soc. (A)* 1972, 327, 175
- 2 Barlow, A. J. and Erginsav, A. *JCS Faraday Trans. II* 1973, 69, 1200
- 3 Barlow, A. J. and Erginsav, A. *JCS Faraday Trans. II* 1974, 70, 885
- 4 Gross, B. 'Mathematical structure of the theories of viscoelasticity', Hermann, Paris, 1953
- 5 Davidson, D. W. and Cole, R. H. *J. Chem. Phys.* 1951, 19, 1484
- 6 Vogel, H. *Phys. Z.* 1921, 22, 645
- 7 Barlow, A. J., Lamb, J. and Matheson, A. J. *Proc. R. Soc. (A)* 1966, 292, 322
- 8 Barlow, A. J., Lamb, J., Matheson, A. J., Padmini, P. R. K. L. and Richter, J. *Proc. R. Soc. (A)* 1967, 298, 467
- 9 Barlow, A. J. and Lamb, J. *Proc. R. Soc. (A)* 1959, 253, 52
- 10 Barlow, A. J., Harrison, G., Richter, J., Seguin, H. and Lamb, J. *Lab. Pract.* 1961, 10, 786
- 11 Barlow, A. J. and Subramanian, S. *Br. J. Appl. Phys.* 1966, 17, 1201
- 12 Barlow, A. J., Erginsav, A. and Lamb, J. *Proc. R. Soc. (A)* 1967, 298, 481
- 13 Barlow, A. J., Day, M., Harrison, G., Lamb, J. and Subramanian, S. *Proc. R. Soc. (A)* 1967, 309, 497
- 14 Barlow, A. J., Dickie, R. A. and Lamb, J. *Proc. R. Soc. (A)* 1967, 300, 356
- 15 Rouse, P. E. *J. Chem. Phys.* 1953, 21, 1272
- 16 Zimm, B. H. *J. Chem. Phys.* 1956, 24, 269
- 17 Barlow, A. J., Harrison, G. and Lamb, J. *Proc. R. Soc. (A)* 1964, 282, 228
- 18 Barlow, A. J. and Erginsav, A. *J. Acoust. Soc. Am.* 1974, 56, 83
- 19 Flory, P. J. 'Principles of Polymer Chemistry', Cornell University Press, Ithaca, 1953, Ch X
- 20 Cerf, R. *Adv. Polym. Sci.* 1959, 1, 382

# Monomeric unit distribution and optical activity of copolymers: random copolymers of acrylic acid and *N*-(*s*-butyl)-*N*-methyl acrylamide antipodes

Christian Braud and Michel Vert

Laboratoire de Chimie Macromoléculaire, Université de Rouen, 76130 Mont-Saint-Aignan, France  
(Received 18 March 1974; revised 23 May 1974)

For copolymers of acrylic acid and *N*-(*s*-butyl)-*N*-methyl acrylamide antipodes as for most copolymers, the dependence of the optical rotatory power was found to be non-linear with regard to their composition. This non-linearity has been discussed generally in terms of conformation or secondary structure. It is proposed that this effect is due to the presence of more than two independent optically active species. The different species were found in terms of triads as the effect of neighbours on the partial specific contribution of a monomeric unit to the total optical activity. A relation was developed for a random copolymer with ideal distribution using eight triads. This relation was applied to acrylic acid/(+) and (–) *N*-(*s*-butyl)-*N*-methyl acrylamide copolymers which can be considered as ideally random; good independent agreement of the optical purity was obtained. The results are discussed in terms of induced optical activity at the level of the electronic transitions of achiral acid unit chromophores.

## INTRODUCTION

The complex optical rotatory dispersion (o.r.d.) of the phenol–formaldehyde type polycondensates of *N*-tosyl *L*-tyrosine prepared in an acidic medium has been explained by a secondary reaction giving rise to a copolymer of two different optically active monomeric units. The dependence of the specific rotatory power  $[\alpha]_{589}^{23}$  on the composition were considered to be anomalous compared to the linear variation shown by mixtures of models of the two types of units<sup>1</sup>.

Similar deviations from linearity for the optical rotation of copolymers with regard to comparable mixtures of homopolymers or to optically active species contents have been reported for partly ionized chiral polyelectrolytes<sup>2–6</sup> as well as for copolymers of chiral and achiral monomers<sup>7–9</sup> and for stereocopolymers with chiral centres in the main chains<sup>10,11</sup> or in the side chains<sup>12</sup>.

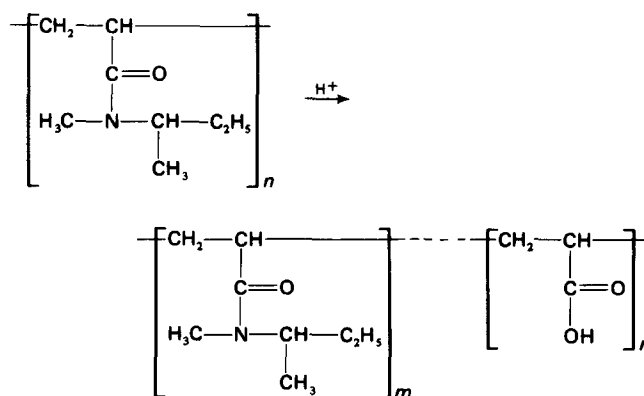
On the other hand, a linear relationship was obtained between the optical rotation at 589 nm and the composition for copolymers of (+) and (–)  $\alpha$ -methylbenzyl methacrylates<sup>13</sup>, (+) and (–) menthylvinyl ethers<sup>14</sup> and (–) menthyl acrylate and styrene<sup>15</sup>.

In most of the cases where linearity was not observed, main chain and/or side chain conformational effects have been invoked<sup>2,3,11</sup>. For copolymers of (–) menthylvinyl ether and arylvinyl ethers<sup>9</sup>, the optical anomalies were attributed to some asymmetric conformations of the initially achiral units induced by the adjacent chiral units giving rise to new Cotton effects at the absorption band of the aromatic chromophores. For copolymers of *S*-4-methyl-1-hexene and 4-methyl-1-pentene<sup>7</sup>, preferential screw sense of helical conformations in 4-methylpentane units were invoked to render them optically active. Theoretical calculations based on conformational parameters of small

sequences extended to long macromolecules were found to fit experimental data with good agreement when moderately blocked or random distribution of monomeric units was considered<sup>16</sup>.

Nevertheless, the above phenol–formaldehyde type polycondensates not being stereoregular, the deviation was assumed to result only from mutual influences of monomeric units attached together since asymmetric preferential conformations are very improbable in this case.

Recently, we have mentioned that o.r.d. of copolymers between acrylic acid and antipodes of *N*-(*s*-butyl)-*N*-methyl acrylamide are not proportional to the content of chiral units<sup>17</sup>. These copolymers were obtained by partial acidic hydrolysis of the corresponding radical polymerized homopolyacrylamide. Then, as for phenol–formaldehyde type polycondensates, stereoregularity and ordered secondary structure could not be invoked. We have assumed the anomalies should depend only on the monomeric unit distribution:



In this paper, we wish to report the results of our attempt

to correlate specific rotatory power of these copolymers to the content of their two units characterized by the molar fraction of the acidic units  $\beta$ . In order to take into account the neighbouring effects in the calculation of the optical rotatory power of a copolymer, we suggest considering the partial contribution of the different units to the total optical activity at least in terms of triads.

RELATION BETWEEN OPTICAL ROTATORY POWER OF AN IDEALLY RANDOM COPOLYMER AND ITS COMPOSITION

The optical rotation of a mixture of independent species is given by the addition of their partial contributions according to:

$$[\Phi] = \sum_i [\Phi]_i C_i / C$$

where

$$C = \sum_i C_i$$

(as molar concentration).

When only two species are involved as usually considered for copolymers, a linear relationship between  $[m]^*$  and the composition should be observed. A non-linear dependence compels us to consider more than two independent species. This is the case for a copolymer if we assume that neighbouring units modify the partial contribution of a unit to the total optical activity.

Thus, in a copolymer with  $a$  and  $b$  units of high optical purity and assuming the long range effects are negligible, changes of the two adjacent units lead to eight different triads:  $aaa, aab, baa, bab, aba, bba,$  and  $bbb$ , that is to say four to each central unit.

To these eight triads  $iii$ , we can associate probabilities  $P_{iii}$  (equal to the molar fractions of  $iii$ ) and specific rotatory power  $[\Phi]_{iii}$ .

Then, the total residue specific rotatory power will result from the sum of the central unit partial contributions of these eight triads according to the relation:

$$[m] = \sum_i P_{iii} [\Phi]_{iii} \tag{1}$$

(It must be noted that relation (1) expressed for specific rotatory power is also suitable for absorption coefficient or ellipticities.)

The problem is actually to determine the molar fractions which depend on the parameters orienting the distribution of the two units.

An interesting situation is found if it is assumed that the different monomeric units are randomly distributed in an ideal manner along the main chain. This is the case of the copolymerization when the reactivity ratios  $r_1$  and  $r_2$  obey the relation  $r_1 r_2 = 1$  for instance<sup>18</sup>, but a similar result can be reached when a chemical reaction on a polymer is performed without orienting effects of the different functional groups.

Let us consider such a copolymer with  $N$  the total number of monomeric units and  $n$  the number of monomeric units of type  $b$ , the degree of copolymerization is then  $\beta = n/N$ . If  $N$  is large and  $1/N$  negligible compared to 1 and  $\beta$ , the probabilities of finding the different triads can be

calculated and reduced as shown in Table 1.

According to the probabilities of the different triads in Table 1, equation (1) can be rewritten and reduced to:

$$\langle [m] \rangle = (1 - \beta)^3 [\Phi]_{aaa} + \beta^3 [\Phi]_{bbb} + \beta(1 - \beta) (\beta\delta + \delta') \tag{2}$$

with

$$\delta = [\Phi]_{bba} + [\Phi]_{abb} - [\Phi]_{baa} - [\Phi]_{aab} + [\Phi]_{bab} - [\Phi]_{aba} \tag{3}$$

and

$$\delta' = [\Phi]_{baa} + [\Phi]_{aab} + [\Phi]_{aba} \tag{4}$$

Without additional interdependent relations between the  $[\Phi]_{iii}$ 's, it is impossible to calculate their respective values; nevertheless,  $\delta$  and  $\delta'$  can be obtained easily from the slopes for  $\beta = 1$  and  $\beta = 0$  respectively.

Differentiating equation (2) with respect to  $\beta$ , one obtains:

$$\frac{d\langle [m] \rangle}{d\beta} = 3\beta^2([\Phi]_{bbb} - [\Phi]_{aaa} - \delta) + 2\beta(3[\Phi]_{aaa} + \delta - \delta') + \delta' - 3[\Phi]_{aaa} \tag{5}$$

For extreme values of  $\beta$ , relation (5) becomes:

$$\left( \frac{d\langle [m] \rangle}{d\beta} \right)_{\beta=0} = \delta' - 3[\Phi]_{aaa} \tag{6}$$

and

$$\left( \frac{d\langle [m] \rangle}{d\beta} \right)_{\beta=1} = 3[\Phi]_{bbb} - (\delta + \delta') \tag{7}$$

Then, relation (2) is completely defined and permits one to correlate experimental data  $[\Phi]_{aaa}, [\Phi]_{bbb}, \delta, \delta', \beta$  and  $\langle [m] \rangle$  when monomeric units are randomly distributed in an ideal manner.

If there are no adjacent unit effects, all the  $[\Phi]_{iai}$ 's on the one hand and all the  $[\Phi]_{ibi}$ 's on the other are identical and relation (2) is reduced to the classical linear law used

Table 1 Probabilities of the different triads found in an ideally random copolymer\*

Triads	Probabilities
$aaa$	$P_{aaa} = \frac{(N-n)(N-n-1)(N-n-2)}{N(N-1)(N-2)} = (1-\beta)^3$
$aab$	$P_{aab} = \frac{(N-n)(N-n-1)n}{N(N-1)(N-2)} = \beta(1-\beta)^2$
$baa$	$P_{baa} = \frac{n(N-n)(N-n-1)}{N(N-1)(N-2)} = \beta(1-\beta)^2$
$bab$	$P_{bab} = \frac{n(N-n-1)(n-1)}{N(N-1)(N-2)} = \beta^2(1-\beta)$
$aba$	$P_{aba} = \frac{(N-n)n(N-n-1)}{N(N-1)(N-2)} = \beta(1-\beta)^2$
$abb$	$P_{abb} = \frac{(N-n)n(n-1)}{N(N-1)(N-2)} = \beta^2(1-\beta)$
$bba$	$P_{bba} = \frac{n(n-1)(N-n)}{N(N-1)(N-2)} = \beta^2(1-\beta)$
$bbb$	$P_{bbb} = \frac{n(n-1)(n-2)}{N(N-1)(N-2)} = \beta^3$

\* The probabilities  $P_{iji}$  calculated in this manner can also be calculated by using the general statistical calculation of the copolymerization reaction in the case of  $r_1 r_2 = 1$ <sup>19</sup>

\* For a copolymer, specific rotatory power is expressed as  $[m] = [\alpha] \bar{M}_r / 100, \bar{M}_r$  being the mean residue weight.

for binary mixture of independent optically active species:

$$\langle [m] \rangle = (1 - \beta)[m]_a + \beta[m]_b$$

where  $[m]_a = [\Phi]_{iai}$  and  $[m]_b = [\Phi]_{ibi}$ .

A similar case is obtained if only two types of triads are present as in block copolymers or in mixtures of homopolymers thus explaining the linear dependence of optical rotations on composition in these two cases.

In a more general manner, relation (2) is available only for ideally random copolymers, probabilities of the different triads being different in the other cases when there are preferential enchainments.

It must be noted that for random vinyl copolymers having a chiral centre in the side chain, the triad *abb* is identical to the triad *bba* (and *aab*  $\equiv$  *baa*) taking into account the different configurations of the pseudo-asymmetric carbons of the main chain. Then, relations (3) and (4) are reduced to:

$$\delta = 2[\Phi]_{bba} - 2[\Phi]_{baa} + [\Phi]_{bab} - [\Phi]_{aba} \quad (3')$$

$$\delta' = 2[\Phi]_{baa} + [\Phi]_{aba} \quad (4')$$

#### APPLICATION TO ACRYLIC ACID/*N*-(*S*-BUTYL)-*N*-METHYL ACRYLAMIDE COPOLYMERS

##### Starting homopolyacrylamides

Stereocopolymers of (+) and (–) *N*-(*s*-butyl)-*N*-methyl acrylamides have been synthesized as optically active homopolyacrylamides, the starting materials for our study on copolymers. Results of radical polymerization of mixtures of the two enantiomers are given in Table 2.

Different enantiomer mixtures give roughly the same yield in crude polymer. After purification by coacervation in methanol–water system, samples having viscosities of the same order have been obtained.

Figure 1 represents the variation of the specific rotatory power of these stereocopolymers as a function of the molar fraction of the antipode (+) in the monomer mixture. The linear variation shows that optical rotations are proportional to the optical purity of the monomer as has been mentioned for other stereocopolymers with chiral centres in the side chain far from the main chain<sup>12,14</sup>.

Table 2 Polymerization of mixtures of (+) and (–) *N*-(*s*-butyl)-*N*-methyl acrylamides with AIBN in toluene and optical rotations of the obtained stereocopolymers

Sample	Monomer		Polymerization <sup>b</sup>			Recovered monomer <sup>a</sup> [ $\alpha$ ] <sub>325</sub> <sup>25</sup>
	[ $\alpha$ ] <sub>325</sub> <sup>25</sup> <sup>a</sup>	(+) (–) + (+)	Yield (%)	$[\eta] \times 10^2$ (cm <sup>3</sup> /g) <sup>c</sup>	[ $\alpha$ ] <sub>270</sub> <sup>25</sup> <sup>d</sup>	
A <sub>1</sub>	+106.0	0.967	93	0.55	–111.7	+105.5
A <sub>2</sub>	+81.8	0.862	87	0.68	–87.5	–
A <sub>3</sub>	+59.0	0.761	72	0.64	–58.0	–
A <sub>4</sub>	+32.0	0.632	80	0.59	–33	–
A <sub>5</sub>	+10.4	0.546	83	–	–11	–
A <sub>6</sub>	–14.8	0.435	88	0.53	+14	–
A <sub>7</sub>	–37.8	0.335	90	0.51	+39.1	–37.6

<sup>a</sup> Neat

<sup>b</sup> Monomer (3 g) in toluene (10 cm<sup>3</sup>) with AIBN (3.4 mg) for 12 h at 60°C

<sup>c</sup> In methanol at 15°C

<sup>d</sup> In methanol:  $c \approx 1$  g/10 cm<sup>3</sup>;  $l = 0.2$  dm

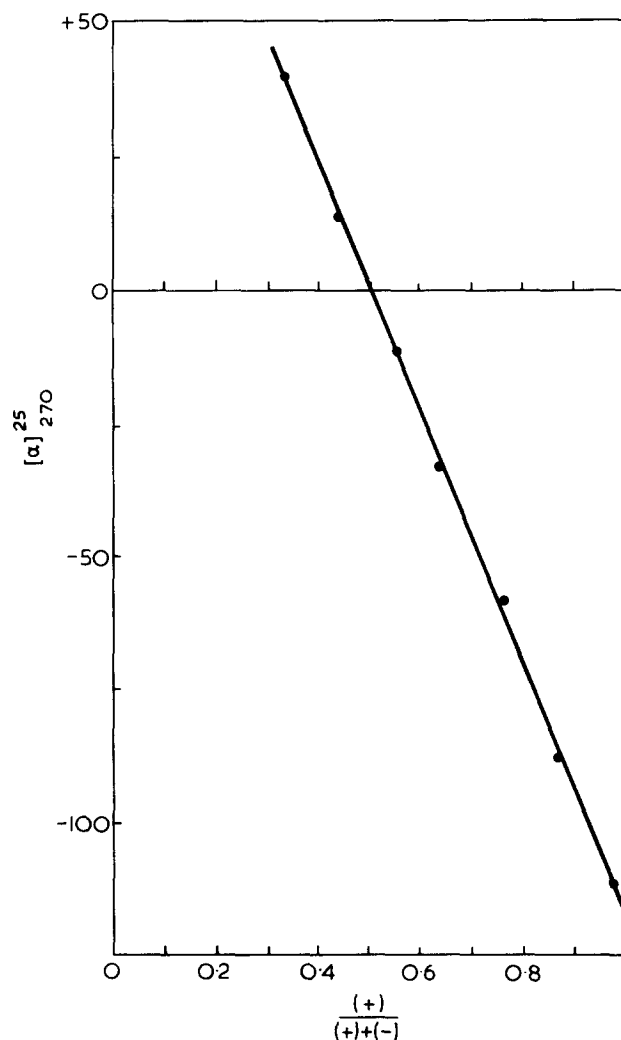


Figure 1 Variation of the specific rotatory power  $[\alpha]_{270}^{25}$  of stereocopolymers of (+) and (–) *N*-(*s*-butyl)-*N*-methyl acrylamides synthesized by radical polymerization as a function of the molar fraction of (+) antipode in the monomeric mixtures (solvent: methanol)

##### Hydrolysis

The reaction of hydrolysis of poly [*N*-(*s*-butyl)-*N*-methyl acrylamide] in acidic medium which is independent of the optical purity of the starting homopolyacrylamide has been described in a previous paper<sup>17</sup>.

In order to determine the nature of this reaction, we have plotted  $\ln 1/(1 - \beta)$  versus time,  $\beta$  being the molar fraction of acrylic acid units in the copolymers thus obtained (Figure 2).

The straight line obtained for the overall hydrolysis shows that in the chosen condition, the reaction is unimolecular and of the first order with regard to the amide groups according to the kinetic equation:

$$-\left(\frac{d \text{ AAm}}{dt}\right) = k (\text{AAm}) \quad (\text{AAm} = \text{acrylamide units})$$

with a rate constant  $k = 3.15 \times 10^{-2} \text{ h}^{-1}$  and  $\theta_{1/2} = 22 \text{ h}$ .

Then, the reaction of hydrolysis in acidic medium does not depend on the degree of hydrolysis and we can assume that acrylic acid units are randomly distributed in an ideal manner along the copolymer chain.

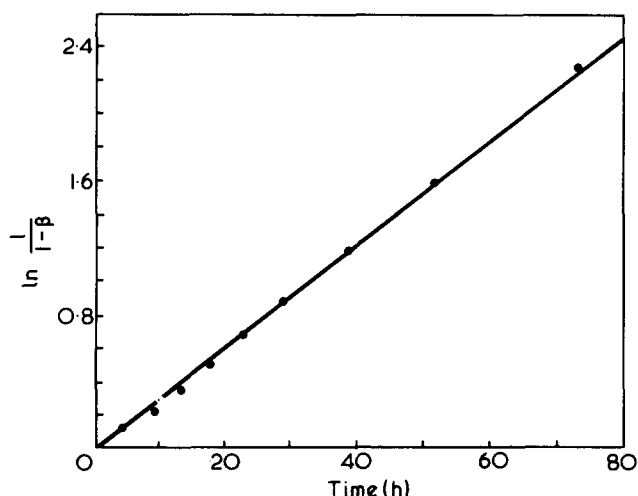


Figure 2 First order kinetic of acidic hydrolysis of poly[N-(s-butyl)-N-methyl acrylamide] ( $\beta$  = molar fraction of acidic unit formed)<sup>17</sup>

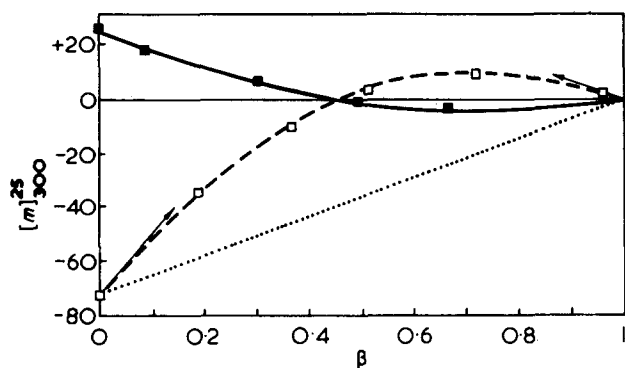


Figure 3 Experimental rotatory powers of two sets of copolymers of acrylic acid and *N*-(s-butyl)-*N*-methyl acrylamide having different optical purities: □, ~93%; ■, ~34% and corresponding variation curves calculated using respectively relation (8) (---) and relation (8) multiplied by the optical purity correction factor  $-25.1/73.5$  (—) (solvent: methanol)

#### Optical activity of copolymers

Figure 3 represents the variation of the specific rotatory power ( $\lambda = 300$  nm) as a function of the proportion of acrylic acid units  $\beta$  for the copolymers derived from homopolyacrylamides A<sub>1</sub> and A<sub>7</sub> (Table 2).

Normally, with independent monomeric units, the curve should be a straight line between the specific rotatory power of the homopolyacrylamide ( $\beta = 0$ ) and 0 ( $\beta = 1$ ) since poly(acrylic acid) is optically inactive. In fact, we observe in Figure 3 a large deviation depending on the degree of hydrolysis  $\beta$  for the two sets of copolymers.

Since proportionality between optical activity of the stereocopolyacrylamides and the molar fraction of one antipode as well as ideally random distribution of the two units have been shown respectively in Figures 1 and 2, we can apply the treatment based on the influence of only eight triads as stated above to the curves in Figure 3.

For the set of copolymers derived from homopolyacrylamide A<sub>1</sub> ( $d[m]_{300}^{25}/d\beta)_{\beta=0}$  and ( $d[m]_{300}^{25}/d\beta)_{\beta=1}$  are respectively 242 and  $-72$ .

Then, using relations (6) and (7), with  $[\Phi]_{aaa} = -73.5$  and  $[\Phi]_{bbb} = 0$ ,  $\delta$  and  $\delta'$  are found to be  $+50$  and  $+22$ .

Relation (2) becomes:

$$[m]_{300}^{25} = -73.5(1 - \beta)^3 + \beta(1 - \beta)(50\beta + 22) \quad (8)$$

The broken line in Figure 3 represents the calculated values of  $[m]_{300}^{25}$  for copolymers of different composition. There is a fairly good agreement with all the corresponding experimental data.

Furthermore, the specific rotation of copolymers depends only on their composition and not on the optical purity of the chiral acrylamide units since relation (8) multiplied by the ratio  $-25.1/73.5$  (corresponding to the difference of optical purity between A<sub>1</sub> and A<sub>7</sub>) also fits the experimental data obtained for the second set of copolymers very well.

These results confirm that optical activity of random copolymers depends mainly on their composition and not on their conformations because the conformations depend certainly on the proportion and the distribution of R and S antipodes.

For the set of copolymers issued from homopolyacrylamide A<sub>1</sub>, relations (3') and (4') give:

$$2[\Phi]_{bba} - 2[\Phi]_{baa} + [\Phi]_{bab} - [\Phi]_{aba} = +50$$

and

$$2[\Phi]_{baa} + [\Phi]_{aba} = +22$$

To a first approximation, it could be assumed that  $[\Phi]_{bba} = [\Phi]_{aba} = 0$  since acrylic acid units are not chiral. So,  $[\Phi]_{baa}$  and  $[\Phi]_{bab}$  would be respectively  $+11$  and  $+72$ . However, the assumption  $[\Phi]_{bba} = [\Phi]_{aba} = 0$  is probably erroneous although  $[\Phi]_{bbb} = 0$  in homopoly(acrylic acid). Optical activity can be induced at the level of the electronic transitions of the carboxyl chromophores or of those corresponding to the aliphatic backbone.

Such inductions have been previously shown for styrene/*R*-dimethyl-3,7-octene-1 copolymers<sup>20,21</sup> and model molecules<sup>22</sup>. It has also been observed for copolymers between (–) menthylvinyl ether and aryl vinyl ethers<sup>9</sup>.

Unfortunately, electronic transitions of C=O chromophores in amide and carboxyl groups near 200 nm overlap and it is difficult to distinguish their respective contribution to circular dichroism (c.d.) in order to prove the optical activity induction in the C=O of COOH.

The use of a copolymer of acrylic acid and a chiral monomer with no absorption bands above 190 nm should permit one to observe a c.d. band at the  $n - \pi^*$  transition of the C=O chromophore of the  $-\text{COOH}$  groups close to 210 nm. Such a copolymer is not yet available.

Using a maleic acid/S(+) methyl-2 butyl vinyl ether copolymer\*, we have effectively observed an optically active c.d. band at 212 nm<sup>23</sup>. However, in this type of copolymer, new chiral centres seem to be induced in the succinic moiety by asymmetric reaction during polymerization<sup>24</sup>. This inconvenience should cancel for copolymers of acrylic acid (or ester) and alkyl vinyl ether if no asymmetric induction occurs in this case. Studies of this type are under investigation.

#### CONCLUSIONS

The non-linear variation of the optical rotation of the hydrolysed poly [*N*-(s-butyl)-*N*-methyl acrylamide] is well

\* Kindly prepared by Dr E. Chiellini, Istituto di Chimica Industriale dell' Università di Pisa, Pisa, Italy.

represented by:

$$\langle [m] \rangle = (1 - \beta)^3 [\Phi]_{aaa} + \beta^3 [\Phi]_{bbb} + \beta(1 - \beta)(\beta\delta + \delta')$$

This relation takes into account only the distribution of the two monomeric units in terms of triads and the short range interactions between them. Of course, in the  $[\Phi]_{iii}$  parameters, local conformational changes of monomeric units are included but no asymmetric structures of macromolecular chains are taken into account.

It now seems that such an interpretation is suitable for most of the copolymers except, perhaps, those with a highly stereoregular main chain where ordered conformations can predominate as for biopolymers.

Under these conditions, the linear dependence observed for some copolymers appears as a limiting case where no neighbouring effects occur. This is the case for block copolymers where the number of triads is practically reduced to the homopolymer triads. A second example is given by optically active copolyamides from (+)-camphoric acid and adipic acid with hexamethylene diamine where asymmetrically perturbed amide groups are separated from each other by achiral long chains<sup>25</sup>. A third case is found in vinylic copolymers when chiral centres are well inside the side chain<sup>12-15</sup>.

As shown recently<sup>26</sup>, the optical activity of stereoirregular polyelectrolytes during neutralization depends mainly on the monomeric unit behaviour and not on macromolecular conformation changes. The non-linear dependence of  $[m]$  observed for all the synthetic optically active polyelectrolytes during neutralization can then be attributed to neighbouring effects. Partial ionization gives rise to a copolymer of the two optically active units in variable amounts with the degree of neutralization. This seems corroborated by the similarities between the curves observed for polyelectrolytes<sup>2-4</sup> and Figure 3 in this paper corresponding to acrylic acid/*N*-(*s*-butyl)-*N*-methyl acrylamide copolymers. However, it must be noted that this comparison is only qualitative. By electrostatic repulsions, an ionized group reduces the probability of the ionization of the neighbouring un-ionized groups so the  $P_{iii}$ 's cannot be determined by an ideally random distribution and relation (2) should be unsatisfied.

Nevertheless, the knowledge of the triad distributions (by <sup>13</sup>C n.m.r. for instance) should permit one to obtain relations between optical activity of copolymers and monomeric unit distribution and confirm our interpretation in the case of polyelectrolytes also.

## ACKNOWLEDGEMENTS

The authors are indebted to Dr C. Ripoll of this Laboratory for suggestions and valuable discussions.

## REFERENCES

- 1 Vert, M. *DSc Thesis*, Rouen (1969); *Eur. Polym. J.* 1972, **8**, 513
- 2 Kulkarni, R. K. and Morawetz, H. *J. Polym. Sci.* 1961, **54**, 491
- 3 Bruschtein, F. B. *PhD Thesis*, Polytechnic Institute of Brooklyn (1965); *Dissert. Abstr.* 1965, **26**, 1931
- 4 Sélégnny, E., Thoai, N. and Vert, M. *C. R. Acad. Sci. Paris* 1966, **262C**, 189
- 5 Vert, M. and Sélégnny, E. *Eur. Polym. J.* 1971, **7**, 1321
- 6 Fenyó, J. C. *DSc Thesis*, Rouen (1974)
- 7 Carlini, C., Ciardelli, F. and Pino, P. *Makromol. Chem.* 1968, **119**, 244
- 8 Yamaguchi, H. and Minoura, Y. *J. Polym. Sci. (A-1)* 1970, **8**, 1467
- 9 Yuki, H., Ohta, K. and Yajima, N. *Polym. J.* 1970, **1**, 164
- 10 Tsuruta, T., Inoue, S., Yoshida, N. and Yokoda, Y. *Makromol. Chem.* 1965, **81**, 191
- 11 Tsuboyama, S. and Yanagita, M. *J. Polym. Sci. (C)* 1968, **23**, 775
- 12 Pino, P., Ciardelli, F. and Zandomenighi, M. *A. Rev. Phys. Chem.* 1970, **21**, 561
- 13 Yuki, H., Ohta, K., Ono, K. and Murahashi, S. *J. Polym. Sci. (A-1)* 1968, **6**, 829
- 14 Matsuzaki, K. and Watanabe, T. *Makromol. Chem.* 1971, **146**, 109
- 15 Schulz, R. C. and Kaiser, E. *Makromol. Chem.* 1965, **86**, 80
- 16 Abe, A. *J. Am. Chem. Soc.* 1970, **92**, 1136
- 17 Braud, C., Vert, M. and Sélégnny, E. *Makromol. Chem.* 1974, **175**, 775
- 18 Champetier, G. and Monnerie, L. 'Introduction à la Chimie Macromoléculaire', Masson & Cie, Paris, 1969, Ch 2, pp 59-74
- 19 'Copolymerization', (Ed. G. E. Ham), Interscience, New York, 1964, Ch 1, pp 1-67
- 20 Pino, P., Carlini, C., Chiellini, E., Ciardelli, F. and Salvadori, P. *J. Am. Chem. Soc.* 1968, **90**, 5025
- 21 Ciardelli, F., Salvadori, P., Carlini, C. and Chiellini, E. *J. Am. Chem. Soc.* 1972, **94**, 6536
- 22 Salvadori, P., Lardicci, L., Menicagli, R. and Bertucci, C. *J. Am. Chem. Soc.* 1972, **94**, 8598
- 23 Braud, C., Vert, M. and Chiellini, E. unpublished results
- 24 Matsuzaki, K. and Sugimoto, T. *Makromol. Chem.* 1973, **164**, 127
- 25 Yamaguchi, H., Ueno, H. and Minoura, Y. *J. Polym. Sci. (A-1)* 1971, **9**, 887; *J. Polym. Sci. (A-1)*, 1971, **9**, 897
- 26 Vert, M. 'Polyelectrolytes', (Ed. E. Sélégnny), D. Reidel, Dordrecht, Holland, 1974, pp 347-370

# Determination of the conformation of polymers in the amorphous solid state and in concentrated solution by neutron diffraction

R. G. Kirste and W. A. Kruse

*Institut für physikalische Chemie der Universität Mainz, 65 Mainz, West Germany*

and K. Ibel

*Institut Max von Laue - Paul Langevin, Grenoble, France*

*(Received 29 March 1974; revised 19 June 1974)*

From the coherent neutron scattering on dilute solid solutions of the ordinary polymer within the deuterated polymer, conformation parameters of polymer chains in amorphous solid states can be determined. In this way vitreous poly(methyl methacrylate) (PMMA) has been investigated. The chains form unperturbed coils and the radius of gyration is very near to the corresponding value in dilute solutions of the same polymer in the low molecular  $\theta$ -solvent butyl chloride. The same principle of measurement has been applied to concentrated solutions of PMMA in D-acetone. The solutions contained 50% polymer, the main part of which (98% and more) was deuterated so that the system was optically dilute for neutron scattering on H-PMMA. A monotonic dependence of the radius of gyration and of thermodynamic parameters on the concentration has been found. A first result is presented for a mixture of two polymers. A dilute solid dispersion of poly( $\alpha$ -methylstyrene) (PMS) within D-PMMA has been investigated at  $M_w = 250\,000$ . The samples are limpid. The PMS forms micelles of 16 molecules (weight average). The radius of gyration of the micelles,  $r_z$  is 170 Å.

## INTRODUCTION

For the determination of conformation parameters of macromolecules in isotropic phases by diffraction experiments we need a dispersion of the macromolecules in which (i) their coherent scattering length density (= scattering power) differs from that of the environments (contrasting condition) and (ii) no correlations exist between their position and orientation. This can be achieved easily in dilute solutions of macromolecules in low molecular weight solvents; if the refractive index or the electron density of the solute and the solvent differ sufficiently, light scattering or small angle X-ray scattering yield the necessary information. For the elimination of the intermolecular interferences it must be extrapolated to zero concentration. There are many experimental data which have been obtained in this way<sup>1-7</sup>.

It is much more difficult to obtain the same information in amorphous solid polymers, in molten polymers or in concentrated polymer solutions. For this purpose a new procedure has been established<sup>8-14</sup>; only a small fraction of the polymer molecules (about 1% or less) contains the normal hydrogen containing compound. All other molecules are perfectly deuterated. Neutron small angle scattering on such a sample yields the required information. A large difference in the coherent scattering length for neutron diffraction between H and D in this way provides the contrast which is needed. The reverse process with a small amount of deuterated polymer molecules dispersed in a large amount of normal hydrogen containing polymer exhibits the same coherent scattering. However, the large

incoherent scattering of hydrogen leads to a large background scattering and less accurate results.

From theoretical considerations as well as from experimental data several conceptions have been derived of the conformation of polymer chains in the amorphous solid state and in concentrated solutions<sup>15-19</sup>. Some of these conceptions, however, are highly speculative. Hence new experimental results have become most desirable.

## SCATTERING THEORY

If a solved particle is hit by electromagnetic or neutron radiation of intensity,  $I_0$ , the coherent scattering intensity,  $I$  is given by the equation:

$$(I/I_0)r^2 \equiv R(\kappa) = \left( \sum_i b_{2i} - \frac{v_2}{v_1} \sum_i b_{1i} \right)^2 P(\kappa) \equiv \Delta b^2 P(\kappa) \quad (1)$$

where  $R(\kappa)$  is the Rayleigh ratio,  $r$  is the distance between scatterer and detector,  $b_{2i}$  and  $b_{1i}$  are the coherent scattering lengths of the nuclei in the solute and the solvent molecule respectively,  $v_2$  and  $v_1$  are the corresponding partial molar volumes,  $P(\kappa)$  is the single particle scattering function and  $\kappa = (4\pi/\lambda) \sin \theta$  is the scattering vector;  $\lambda$  is the wavelength and  $\theta$  is half the scattering angle. The wavelength of neutrons is given by  $\lambda = h/mv$ , where  $m$  and  $v$  are mass and velocity of the neutrons respectively and  $h$  is Planck's constant. In neutron small angle scattering usually neutrons are taken with  $\lambda$  between 5 and 20 Å<sup>20,21</sup>.

If the concentration in g/ml is  $c$  then the number of polymer molecules/ml is  $cN_0/M$ , where  $N_0$  is Avogadro's number and  $M$  is the molar mass of the polymer. Equation (1) has to be multiplied by this value if  $R(\kappa)$  is related to the unit of the scattering volume:

$$R(\kappa) = \Delta b^2 P(\kappa) \cdot c \cdot N_0/M \quad (1')$$

If any non-ideal interaction occurs, one has to take into account the virial coefficients of osmotic pressure. The influence of the thermodynamic solution parameters on the scattering behaviour is well known and has been given by Zimm<sup>22,23</sup>:

$$Kc/R(\kappa) = 1/MP(\kappa) + 2A_2c + \dots \quad (2)$$

$K$  is a constant which depends on the type of scattering and  $A_2$  is the second osmotic virial coefficient. If the solution is ideal,  $A_2$  is zero. By comparison of equation (1') and (2)  $K$  can be evaluated for the case of neutron scattering:

$$K = \Delta b^2 \cdot N_0/M^2 \quad (3)$$

with  $\Delta b$  given by equation (1). From equation (3)  $K$  can be specialized easily for our dispersion of the normal hydrogen containing polymer (= solute) within the deuterated polymer. Only the scattering lengths of D and H enter into  $\Delta b$ :

$$\Delta b = \Sigma b_H - \Sigma b_D = N(b_H - b_D) \quad (4)$$

where  $N$  is the number of hydrogen or deuterium atoms in 1 polymer molecule.

To obtain  $R(\kappa)$  of the solute one has to subtract the scattering of a polymer sample which contains the same amount of D and H but randomly distributed over all molecules. This sample gives the total incoherent scattering and the small fraction of coherent scattering which is due to the supermolecular structure. It is prepared by suitable copolymerization of the normal monomer with the deuterated monomer.

For the evaluation of the conformation of the polymer molecules  $P(\kappa)$  is of greatest interest. It is correlated with the radius of gyration,  $r$ , by  $P(\kappa) = 1 - r^2\kappa^2/3 + \dots$ . For a more detailed knowledge of the conformation one can perform model calculations and compare them with the experimental results.

## EXPERIMENTAL

### Preparation of samples

Neutron scattering experiments were made on samples with weight-average molecular weights,  $M_w = 6100, 34\,500, 78\,000, 250\,000, 505\,000$  and  $1\,034\,000$ . Normal poly(methyl methacrylate) (PMMA) fractions of these molecular weights have been prepared in the usual way by radical polymerization<sup>24</sup> with azoisobutyronitrile (AIBN) and sol-gel fractionation. The molecular weight of these samples has been determined by viscometry<sup>25</sup>.  $M_w/M_n$  of these samples is about 1.35 (determined by gel permeation chromatography). They contain about 80% syndiotactic diads. The calculated amount (0.3–1.2%) of these PMMA fractions has been solved in monomer deuterio methyl methacrylate and the deuterated monomer has been polymerized. This polymerization was initiated by benzoyl peroxide and dodecylmercaptan served as a transfer agent.

The amount of the initiator and of the transfer agent has been apportioned so that (i)  $M_w$  of the resulting deuterated polymer coincided with the same quantity of the solved H-PMMA fraction, and (ii) the total amount of initiator + transfer agent was a minimum<sup>24</sup>. The alteration of the kinetic constants by the H/D isotope effect has been determined experimentally and taken into account.

After degassing, the solution was heated for 7 days at 50°C and afterwards for 3 days at 70°C. The reaction was completed by heating for 6 h at 120°C. Tensions occurring in the material were removed by annealing for a short time at 140°C. The temperature was later lowered at a rate of 0.5°C/h. The obtained deuterated polymer has a Schulz distribution<sup>26</sup> with  $M_w/M_n \approx 2$ .

The samples were rectangular pieces with the dimensions 1.2 cm x 3 cm x 1 cm. The thickness (1 cm) is well known as the optimum thickness of deuterated material (e.g. D<sub>2</sub>O) for neutron diffraction. This rough estimation was justified by the experimentally determined attenuation factor of 2.6 for these samples.

### Neutron scattering experiments

The experimental data which are reported in this paper have been obtained with the neutron small angle scattering device of the Institute Max von Laue - Paul Langevin in Grenoble which is described elsewhere<sup>21</sup>. A part of the data is essentially the same as had been determined already earlier<sup>10,11</sup>. The measurements were carried out with different wavelengths,  $\lambda$ , of the neutrons and at different distances,  $L$ , between sample and detector. The monochromatizing of the neutron beam was performed by speed selectors. Two different types were used. The half-width of the wavelength distribution was  $\pm 17\%$  and  $\pm 4\%$  respectively. The neutron scattering data in Figures 1 and 3 were obtained with both selectors and no perceptible difference was exhibited. The other results were obtained with the broader wavelength distribution. The  $\lambda$  values given in the Tables and Figures are averages.

Instead of the Raleigh ratio the measurement yields a relative scattering intensity  $i(\kappa) = k'R(\kappa)$  where  $k'$  is a constant of the device. From the scattering intensity of a solution of a polymer with known molecular weight according to equation (2) the Rayleigh ratio has been determined, so that also  $k'$  is a known quantity.

## RESULTS

### Vitreous PMMA

Figure 1 shows difference scattering intensities (sample minus background) for  $M_w = 250\,000$  as a function of  $\kappa$  with the concentration  $c$  of H-PMMA as a parameter. The background scattering is  $\approx 0.1 \times 10^3$  counts in the scale of Figure 1 almost independently of  $\kappa$ . It does not vary perceptibly if the H/D ratio varies between 0.003 and 0.012. This means that the measured background scattering is mainly due to supermolecular structure and not to incoherent scattering. The drawn lines in Figure 1 are least error square fits of the theoretical coil scattering function to the experimental values. Debye's expression<sup>27</sup> for monodisperse Gaussian coils has been modified for polydispersity with  $U \equiv M_w/M_n - 1 = 0.36$ <sup>22,28</sup>:

$$P(\kappa) = \frac{2}{(U+1)\xi^2} [(1+U\xi)^{-1/U} - 1 + \xi] \quad (5)$$



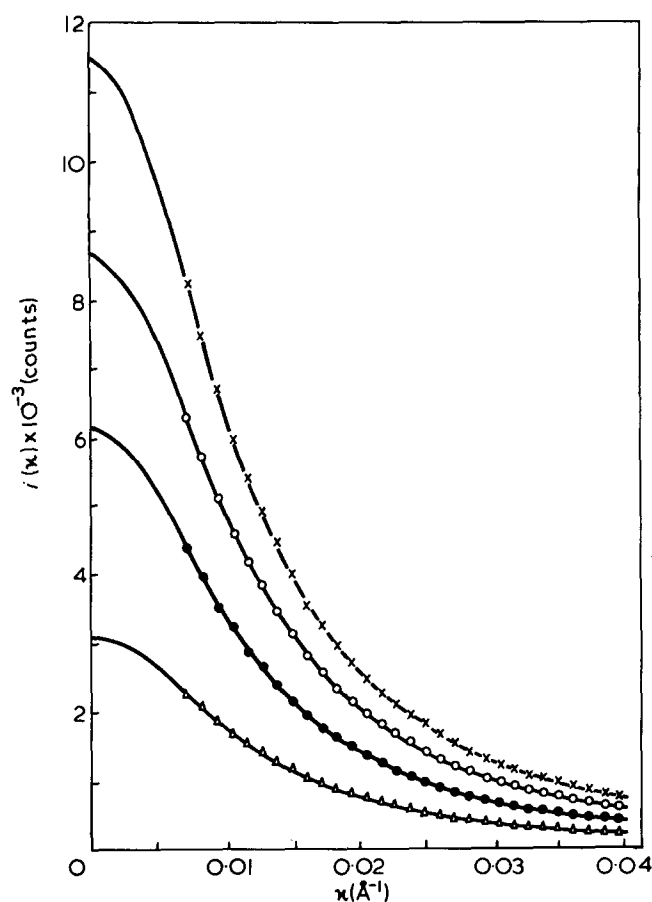


Figure 1 Neutron scattering of PMMA dispersed in D-PMMA ( $\lambda = 6.51 \text{ \AA}$ ,  $L = 8.665 \text{ m}$ ). —, Least error square fits of equation (5) to experimental data. X, 1.19%; O, 0.93%; ●, 0.63%; Δ, 0.31%

with

$$\xi = \frac{\langle r^2 \rangle_z k^2}{1 + 2U}$$

This equation is valid for a Schulz distribution<sup>22,26</sup> of the molecular weight:

$$H(M) = \frac{1}{\Gamma(k+1)} \left( \frac{k+1}{M_w} \right)^{k+1} \cdot M^k \cdot e^{-(k+1)M/M_w} \quad (6)$$

with  $k = 1/U$ . Adjustable parameters for the fits in Figure 1 have been the intersection on the ordinate and  $\langle r^2 \rangle_z$ .

The radii of gyration are converted to the weight average by means of the relation<sup>29</sup>:

$$\langle r^2 \rangle_w = \langle r^2 \rangle_z \cdot \frac{1+U}{1+2U} \quad (7)$$

which is valid for Schulz distributions.

The evaluation has been done in the same way for all experimental data. The result is shown in Table 1. It seems noteworthy that the apparent radius of gyration does not vary with the concentration outside the limits of error at  $c < 1.2\%$ .

The data from Figure 1 have been drawn into a Zimm plot which is very similar to that which had been published earlier<sup>11</sup>.

The second virial coefficient of osmotic pressure  $A_2$  has

been evaluated according to equation (2) from the Zimm plot and the result is that  $A_2$  is zero within the limits of error ( $\pm 2 \times 10^{-5} \text{ cm}^3 \text{ g}^{-2}$ ).

The obtained radii of gyration in the glassy state are compared in Figure 2 with those in dilute solutions in low molecular compounds. The latter have been determined by light scattering and by small angle X-ray scattering<sup>1-7</sup>. According to a least error square fit the data for the vitreous polymer obey the relation:

$$\langle r^2 \rangle_w = 0.096 M_w^{0.98} \quad (8)$$

Thus for the conformation of polymers in the vitreous state all features of unperturbed coils are present, just as it had been predicted by Flory<sup>15,19</sup>. Compared with the results on the  $\theta$ -solvent butyl chloride the coils in the vitreous state in Figure 2 are larger by 10–15%. But there is some evidence that this difference is not real. Neutron measurements on PMMA in D-acetone exhibit radii of gyration which are larger by the same factor than the corresponding values from X-ray measurements on PMMA in normal acetone. So the difference is probably due to systematical errors of the used experimental devices. The results on vitreous PMMA are independent of the temperature within the range  $20^\circ\text{C} < T < 130^\circ\text{C}$ .

In Figures 3 and 4 the difference in neutron scattering of one of the samples is shown within a larger range of scattering vectors. The curve shown is the continuation of the curve  $c = 1.19\%$  in Figure 1. It has been drawn by over-

Table 1 Root mean square radii of gyration ( $\langle r^2 \rangle_w^{0.5} \equiv r_w$ ) from least error square fits of equation (5)

$M_w$	$c \times 10^2$ (g/cm <sup>3</sup> )	$r_w(\text{\AA})$			average	
		$\lambda = 3.41 \text{ \AA}$ $L = 8.665 \text{ m}$	$\lambda = 6.51 \text{ \AA}$ $L = 8.665 \text{ m}$	$\lambda = 8.58 \text{ \AA}$ $L = 8.665 \text{ m}$		
250 000	0.31	130	132	117	126	
	0.63	125	136	130	130	
	0.93	124	132	132	129	
	1.19	121	135	131	129	
1 034 000	0.60	289	291	274	285	
	505 000	0.90	187	196	194	192
	78 000	1.20	68.8	71.2	70.4	70.1
$r_w$ with $\lambda = 9.1 \text{ \AA}$ and $L = 1.33 \text{ m}$ :						
34 500	1.49		50.0			
6 100	1.96		23.3			

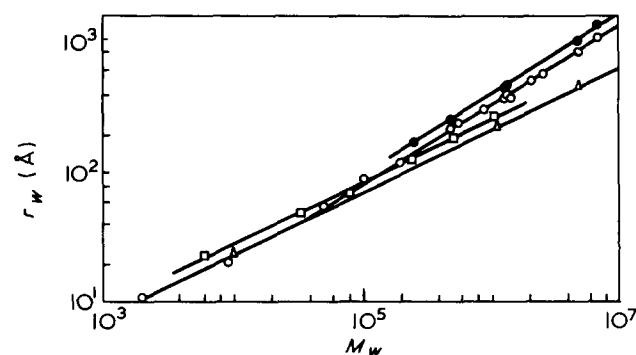


Figure 2 Comparison between the radius of gyration of PMMA in the vitreous state and in dilute solutions in low molecular weight compounds. □, Vitreous PMMA (neutron scattering); ●, dioxane (light scattering); ○, acetone (light- and X-ray scattering); △, butyl chloride =  $\theta$ -solvent (light- and X-ray scattering)

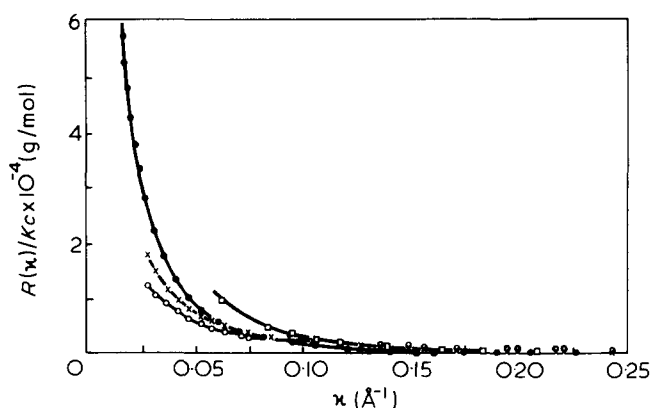


Figure 3 Neutron scattering of PMMA dispersed in D-PMMA with in a larger range of  $\kappa$  (●).  $M_w = 250\,000$ ,  $c = 1.19\%$ . For comparison: small angle X-ray data on dilute solutions of PMMA ( $c = 2\%$ ); x, syndiotactic PMMA,  $M_w = 270\,000$  in benzene; ○, isotactic PMMA,  $M_w = 275\,000$  in benzene; □, syndiotactic PMMA in methylisobutyrate

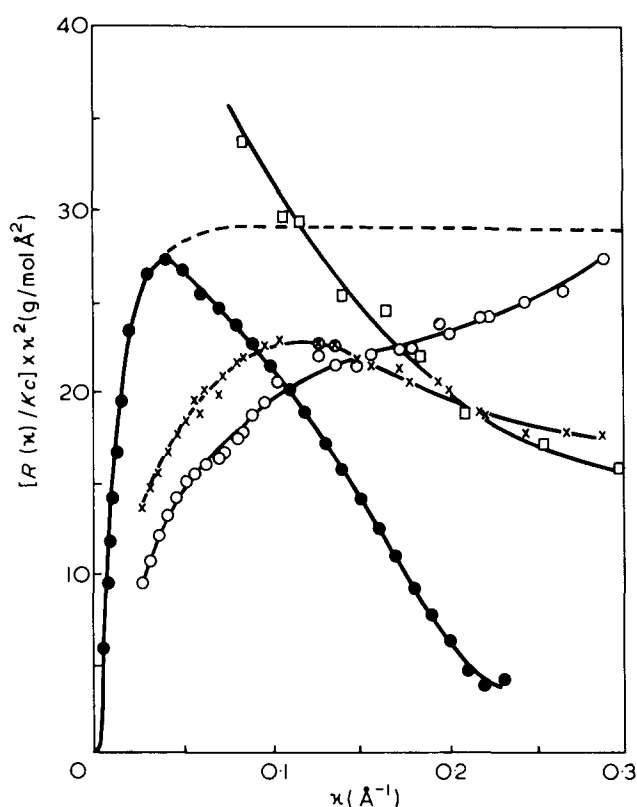


Figure 4 The data of Figure 3 in the plot  $R\kappa^2$  versus  $\kappa$ . ----, equation (5) with  $R/\kappa c = M_w P(\kappa)$

lapping of three measurements: the first is that of Figure 1. The second has been taken at  $L = 2.36$  m with  $\lambda = 3.81$  Å and the third at  $L = 1.33$  m with  $\lambda = 9.10$  Å. A great number of counts per experimental point (up to  $4 \times 10^5$ ) has been recorded. The error due to pulse statistics is less than 1 unit in the ordinate scale of Figure 4.

The result is compared with small angle X-ray scattering on syndiotactic and isotactic PMMA in two solvents<sup>32</sup>. In Figure 4 the data of Figure 3 are plotted as  $R\kappa^2$  versus  $\kappa$ . In Figure 5 a further plot of this kind is shown. From equation (5) one should expect an asymptotic  $\kappa^{-2}$  course of  $R$  for Gaussian coils at large  $\kappa$ . As had been pointed out earlier<sup>6,30-32</sup> this behaviour is not found in the case of PMMA. Also Monte Carlo calculations on some special coil models yielded a different result<sup>6,30</sup>. Isotactic PMMA follows

the scattering function of the persistent coil of Kratky and Porod whereas the scattering of syndiotactic and atactic PMMA can be interpreted by the assumption that the coiling of the thread is superimposed by a certain tendency of helix formation.

#### Concentrated solution of PMMA in acetone and comparison with the dilute solution

The contrast between H and D for coherent neutron scattering can be used also for the determination of the conformation of polymers in concentrated solutions. A preliminary result is shown in Figure 6. The 'concentrated solution' consists of 50% polymer and 50% D-acetone. The polymer consists mainly of D-PMMA. The content of H-PMMA is given as the concentration parameter in the Zimm plot. After conversion of  $r_z$  to  $r_w$  according to equation (7) the result from this Zimm plot is  $A_2 = 0.3 \times 10^{-4} \text{ cm}^3/\text{g}^2$  and  $r_w = 143$  Å.

In the same way a dilute solution of PMMA in D-acetone has been investigated. The result is  $A_2 = 2.1 \times 10^{-4} \text{ cm}^3/\text{g}^2$  and  $r_w = 158$  Å. If one compares these data with the glassy polymer ( $A_2 = 0$ ,  $r_w = 129$  Å) a monotonic change with the

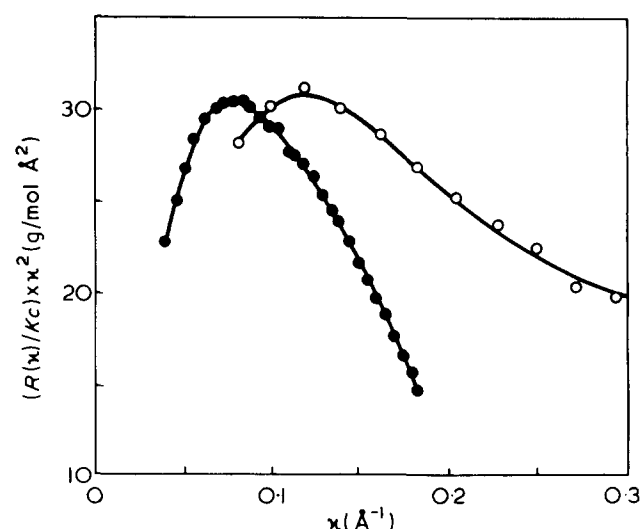


Figure 5 Neutron scattering on a dilute solution of PMMA in D-acetone (●) ( $M_w = 34\,500$ ); X-ray scattering on a dilute solution of syndiotactic PMMA in acetone (○) (independent of  $M_w$  for  $M_w > 10\,000$ )

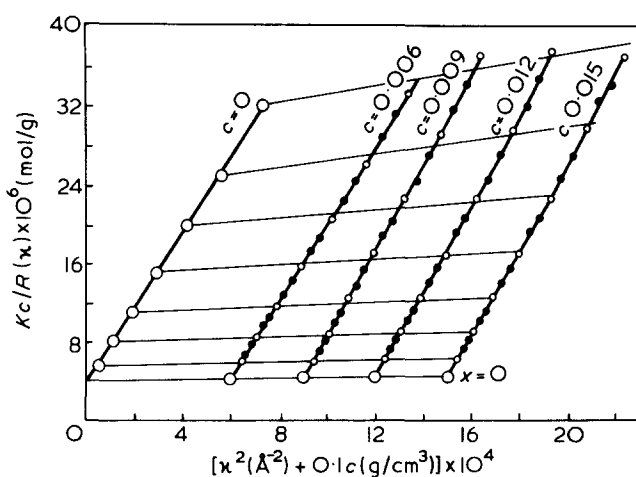


Figure 6 Zimm plot of small angle neutron scattering on solutions of 50% PMMA in D-acetone. The concentration parameter indicates the amount of H-PMMA.  $M_w = 250\,000$

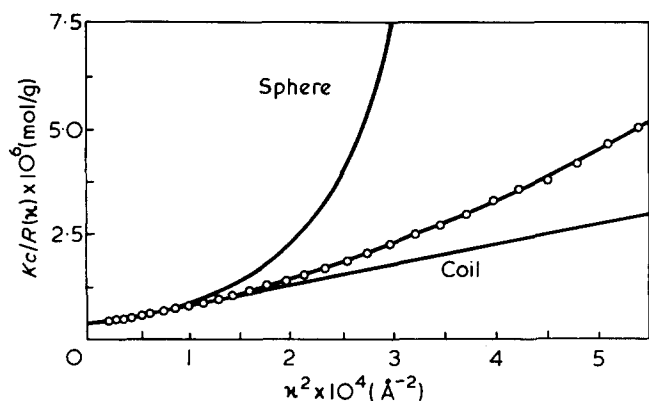


Figure 7 Small angle neutron scattering on a dispersion of 1% PMS in D-PMMA

concentration can be observed.  $A_2$  in the concentrated solution refers to the chemical potential of D-PMMA + D-acetone as a binary solvent.

#### Mixture of two polymers

In Figure 7 a preliminary result of the neutron scattering on a mixture of two polymers is shown. As before the sample consists mainly of D-PMMA. Instead of H-PMMA poly( $\alpha$ -methylstyrene) (PMS) is dispersed within the D-PMMA. The concentration of PMS is 1%, its molecular weight 250 000. It has been prepared by anionic polymerization<sup>33</sup> and therefore its molecular weight distribution is narrow ( $M_w/M_n < 1.01$ ). The sample for neutron scattering has been prepared in the same way as is described for the PMMA samples of Figure 1, the resulting  $M_w$  of the D-PMMA being 250 000.

The experimental scattering function in Figure 7 is not that of a coil. The curve lies between the scattering functions of coil and sphere. The particle weight  $M_w$  is  $\sim 4\,000\,000$ , the radius of gyration  $r_z$  is 170 Å.

This result can be interpreted by spherical particles which have a wide size distribution and are aggregates of about 16 PMS molecules. It shows that the two polymers are not really compatible though they form a clear limpid mixture.

#### ACKNOWLEDGEMENTS

We thank Dr K. C. Berger and Dr G. Löhr for providing us with the fractions of normal PMMA. We thank J. Haas for support in the performance of the measurements. We are further indebted to Mr Hrabak who provided us with a cal-

ulation procedure for the reduction of the huge number of intensity data.

#### REFERENCES

- 1 Cantow, H. J. and Schulz, G. V. *Z. Phys. Chem. (Frankfurt)* 1954, 2, 117
- 2 Cantow, H. J. and Bodmann, O. *Z. Phys. Chem. (Frankfurt)* 1955, 3, 65
- 3 Schulz, G. V. and Craubner, H. *Z. Elektrochem.* 1959, 63, 301
- 4 Schulz, G. V. and Kirste, R. G. *Z. Phys. Chem. (Frankfurt)* 1961, 30, 171
- 5 Cohn-Ginsberg, E., Fox, T. G. and Mason, H. F. *Polymer* 1962, 3, 97
- 6 Kirste, R. G. *Makromol. Chem.* 1967, 101, 91
- 7 Kirste, R. G. and Wunderlich, W. *Z. Phys. Chem. (Frankfurt)*, 1968, 58, 133
- 8 Kirste, R. G. *Jber. 1969, 1970 and 1971 des Sonderforschungsbereichs 41 Mainz* 1970, p47; 1971, p 127; 1972, p 86
- 9 Wignall, G. D. ICI Int. Rep. PQR G 19/70 (1970)
- 10 Kirste, R. G., Kruse W. A. and Schelten, J. *Makromol. Chem.* 1972, 162, 299
- 11 Schelten, J., Kruse, W. A. and Kirste, R. G. *Kolloid-Z. Z. Polym.* 1973, 251, 919
- 12 Cotton, J. P., Farnoux, B., Jannink, G., Mons, J. and Picot, C. *C. R. Hebd Seanc. Acad. Sci. (C)* 1972, 275, 175
- 13 Benoit, H. et al. *Nature (Phys. Sci.)* 1973, 245, 13
- 14 Ballard, D. G. H., Schelten, J. and Wignall, G. D. *Eur. Polym. J.* 1973, 9, 965
- 15 Flory, P. J. *J. Chem. Phys.* 1949, 17, 303
- 16 Kargin, V. A. *J. Polym. Sci.* 1958, 30, 247
- 17 Pechold, W. *Kolloid-Z. Z. Polym.* 1968, 228, 1; 1969, 231, 418
- 18 Vollmert, B. and Stutz, H. *Angew. Makromol. Chem.* 1968, 3, 182
- 19 Flory, P. J. 'IUPAC Macromolecular Chemistry', Butterworths, London, 1973, Vol 8, p 1
- 20 Bacon, G. E. 'Neutron Diffraction', Clarendon Press, Oxford, 1967
- 21 Springer, T., Schmatz, W., Schelten, J. and Ibel, K. *J. Appl. Crystallog.* 1974, 7, 96
- 22 Zimm, B. H. *J. Chem. Phys.* 1948, 16, 1093, 1099
- 23 Flory, P. J. and Bueche, A. M. *J. Polym. Sci.* 1958, 27, 219
- 24 Küchler, L. 'Polymerisationskinetik', Springer, Heidelberg, 1951
- 25 Schulz, G. V. and Meyerhoff, G. *Z. Elektrochem.* 1952, 56, 904
- 26 Schulz, G. V. *Z. Phys. Chem.* 1935, B30, 379; 1939, B43, 25
- 27 Debye, P. *J. Phys. Colloid Chem.* 1947, 51, 18
- 28 Greschner, G. S. *Makromol. Chem.* 1973, 170, 203
- 29 Altgelt, K. and Schulz, G. V. *Makromol. Chem.* 1960, 36, 209
- 30 Kirste, R. G. in 'Small-Angle X-Ray Scattering', Gordon and Breach, New York and London, 1967, p 33
- 31 Kirste, R. G. and Kratky, O. *Z. Phys. Chem. (Frankfurt)* 1962, 31, 363
- 32 Wunderlich, W. and Kirste, R. G. *Z. Elektrochem.* 1964, 68, 646
- 33 Szwarc, M. 'Carbanions, Living Polymers and Electron Transfer Processes', Interscience, New York, 1968

# Nuclear magnetic relaxation in linear and branched polyethylene

Vincent J. McBrierty

*Physical Laboratory, Trinity College, University of Dublin, Dublin 2, Eire*

and Ian R. McDonald

*Department of Chemistry, Royal Holloway College, Englefield Green, Surrey, UK*

*(Received 19 April 1974; revised 9 July 1974)*

An assessment is made of the information provided by n.m.r. second moment, fourth moment and  $T_2$  measurements on oriented samples of branched and linear polyethylene. Detailed theoretical comparisons are made with the previously reported experimental results of a number of workers in order to derive information about the molecular motions which underlie the  $\alpha$ ,  $\beta$  and  $\gamma$  relaxations in the two forms of the polymer. Plausible motional models are presented in each case. Particular attention has been given to the  $\beta$  relaxation which is explained in terms of lamellar fold motion. The relative sensitivity of the various n.m.r. measurements to molecular anisotropy and motion in the polymer is discussed.

## INTRODUCTION

For many years now the nuclear magnetic resonance (n.m.r.) method has featured prominently among those available for the study of polymers by providing an abundance of information on the molecular motions which underlie the various relaxation processes. The technique is capable of probing a motional spectrum over some eight decades, being limited on the low frequency side by the applicability or otherwise of the Slichter–Ailion conditions<sup>1</sup> (rotating frame  $T_{1\rho}$  measurements) and on the high frequency side by the resonant frequency of the spectrometer (spin-lattice  $T_1$  measurements). Second,  $M_2$ , and fourth,  $M_4$ , moments of the resonance absorption envelope and spin–spin,  $T_2$ , relaxation times are sensitive to intermediate correlation frequencies of the order of  $10^{4.5}$  Hz. While the theory underlying all these measurements is well established, the precise interpretation of the experimental data is easiest for  $M_2$ ,  $M_4$  and  $T_2$ . The analysis of data on  $T_1$  and  $T_{1\rho}$  tends to be complicated by factors such as spin diffusion effects<sup>2,3</sup> and the presence of distributions of correlation frequencies<sup>4</sup>.

Fibre materials have been particularly useful in the study of molecular motion as a consequence of the anisotropy which is often observed in n.m.r. measurements when recorded as a function of the orientation,  $\gamma$ , of the fibre axis to the applied laboratory field<sup>5–14</sup>. On the other hand, anisotropic effects may be quite pronounced in some materials<sup>14</sup> and virtually absent in others<sup>15</sup>. In fact the observation or otherwise of anisotropy is dependent on details of the molecular structure of the polymer<sup>16</sup>. Furthermore,  $M_2$  and  $M_4$  may be highly anisotropic when, for the same system,  $T_2$ ,  $T_1$  and  $T_{1\rho}$  exhibit little or no detectable dependence on the angle of orientation<sup>10,16</sup>.

It is our intention in this paper to examine, in a general way, the type of information provided by those measurements which tend to be anisotropic. Polyethylene (PE), both linear and branched, has been chosen as particularly suitable for our purposes. The factors which influence this choice are several. First, there is an abundance of relevant

published n.m.r. data<sup>3,5–13,16–47</sup>. Second, the crystallographic information required for the various lattice sum computations has been determined for PE over a wide range of temperature<sup>48–51</sup>. Third, even with the extensive relaxation data recorded for PE of widely diverse morphologies, the precise molecular mechanisms which underlie these processes are not yet fully understood. Of particular interest is the observed plateau in the amorphous  $T_2$  component for branched PE<sup>42,46</sup>. Fourth, the orientation statistics of partly drawn PE films have been analysed in detail<sup>41,44</sup>. Finally, the fact that there is no detectable anisotropy (<10%) in the  $T_2$  data from the highly drawn material even though  $M_2$  and  $M_4$  are highly anisotropic is a commonly observed feature of n.m.r. data which requires an explanation.

A recently derived theory of motionally averaged fourth moments will be used<sup>16</sup>, in conjunction with the more established theories for  $M_2$  and  $T_2$ <sup>2,52,54</sup>, to compare plausible molecular motional models with the experimental data on linear and branched PE.

## EXPERIMENTAL

An analysis of the broadline spectra for linear PE published by Olf and Peterlin<sup>7</sup> was carried out principally to determine their fourth moments. The material used in their study was Fortiflex A-60-500 (Celanese Corporation of America) for which  $M_n \approx 5-6 \times 10^3$  and  $M_w \approx 8 \times 10^4$ . A sheet of thickness 0.5 mm was compression moulded at +150°C and quenched in ice water. Strips 5 mm wide were drawn at +60°C at a rate of 1 cm/min to a draw ratio of 9. The crystallinity of the material was  $\approx 75\%$ . Five sets of spectra at orientation angles  $\gamma = 0^\circ, 45^\circ$  and  $90^\circ$  within the temperature range  $-196^\circ\text{C}$  to  $+125^\circ\text{C}$  are available.

The published spectra of Foulkes and Ward<sup>43</sup> for low density branched PE were also analysed. The material was again in the form of sheets 5 mm thick which had been compression moulded from Alkathene WNF-15 (ICI Ltd) at +150°C. The melt flow index of the sample was 7 and its density was  $0.917 \text{ g/cm}^3$ . Sections of the sheet  $10 \times 10$

cm were cold drawn at a rate of 1.25 cm/min to a draw ratio of 3.7. Five sets of spectra at orientation angles  $\gamma = 0^\circ, 45^\circ$  and  $90^\circ$  within the temperature range  $-196^\circ\text{C}$  to  $+60^\circ\text{C}$  were analysed. The crystallinity was 60%.

In each case photographic enlargements of the spectra were made from which the second and fourth moments were computed. In those cases where the crystalline and amorphous components were clearly resolvable,  $M_2$  and  $M_4$  were determined for each. It is estimated that these experimental moment values have an uncertainty not greater than 10%. As a partial check on our procedures the  $M_2$  values were compared with those quoted in the respective papers and were found to agree satisfactorily. In addition, the results from the two sides of a spectrum agreed to within 5%.

The  $T_2$  data for branched PE reported by McCall and Falcone<sup>42</sup> and by Fujimoto *et al.*<sup>46</sup> are also of interest. Their materials closely resemble the sample studied by Foulkes and Ward specifically with regard to density and branch content.

The  $T_2$  data for a branched PE sample in highly oriented fibre form were recorded in this laboratory as a function of fibre orientation in the magnetic field but no anisotropy was detected; if anisotropy was present in the  $T_2$  measurements it was certainly less than 10%.

#### BASIC FORMULAE REQUIRED IN THE ANALYSIS

The moment expressions for a semi-crystalline polymer may be written:

$$\langle M_n \rangle = x \langle M_n \rangle_{\text{cryst}} + (1 - x) \langle M_n \rangle_{\text{amorph}} \quad (1)$$

where  $x$  is the crystallinity and  $n = 2$  or  $4$ .

The crystalline second and fourth moments for an oriented polymer may be concisely expressed as<sup>16</sup>:

$$\langle M_2(\gamma) \rangle_{\text{cryst}} = \sum_{n=0}^4 C'(\gamma, n) \overline{P_n(\cos \Delta)} \quad (2)$$

$$M_4(\gamma)_{\text{cryst}} = \sum_{n=0}^8 C(\gamma, n) \overline{P_n(\cos \Delta)} + \langle M_4(\gamma) \rangle_{\text{III}} \quad (3)$$

$\overline{P_n(\cos \Delta)}$  are distribution functions in the form of Legendre polynomials which describe the orientation statistics in the polymer<sup>16</sup>;  $\langle M_4(\gamma) \rangle_{\text{III}}$  is a small correction term due to lattice sums of the type

$$\sum_{i,j,k \neq} B_{ij}^2 B_{ik} B_{jk}$$

(usually designated type III terms) in the fourth moment calculation<sup>52</sup>.  $C(\gamma, n)$  and  $C'(\gamma, n)$  are coefficients which may be determined from a knowledge of the positions of the resonant nuclei in the polymer along with fundamental constants. The summations are taken over even values of  $n$ .

The second moment  $M_{2\text{uo}}$  of an unoriented sample may be determined from calculations on the drawn material according to the relation<sup>8</sup>:

$$M_{2\text{uo}} = 1/15 \{ M_2(0^\circ) + 8M_2(45^\circ) + 6M_2(90^\circ) \} \quad (4)$$

Finally, we shall also make use of the approximate relation-

ship between  $T_2$  and  $M_2$  for solids<sup>42</sup>:

$$T_2 \approx 1/\gamma M_2^{1/2} \quad (5)$$

where  $\gamma$  here is the gyromagnetic ratio (not to be confused with the orientation angle in the applied field).

#### REVIEW OF CURRENT INTERPRETATIONS OF DATA ON PE

Linear and branched PE have both been the subject of extensive study by n.m.r.<sup>3,5-13,16-47</sup>. The overall features of the relaxation behaviour are reasonably well established and have been discussed by various authors<sup>8,38</sup>. There would appear to be two crystalline,  $\alpha_c$  and  $\gamma_c$ , and two amorphous,  $\beta$  and  $\gamma_a$ , relaxation processes.

The  $\alpha$  and  $\gamma$  processes show up clearly in the n.m.r. of linear PE although the presence of  $\gamma_a$  and  $\gamma_c$  contributions to the relaxation can only be inferred. Olf and Peterlin<sup>8,9</sup> have carried out detailed quantitative analyses of the  $\alpha$  and  $\gamma$  processes. They observe a linear correlation between the amorphous content and the strength of the  $\gamma$  relaxation as manifested by the fall in  $M_2$  over the temperature range from  $-196^\circ\text{C}$  to  $+20^\circ\text{C}$  for a wide range of linear PE materials<sup>8</sup>. The dependence of the observed depth on amorphous content of the  $T_1$  minimum at  $-20^\circ\text{C}$ , which is also attributed to the  $\gamma$  process, supports this conclusion<sup>10</sup>. A number of molecular models have been proposed to account for the  $\gamma$  relaxation: the crankshaft model<sup>55</sup>, the kink model<sup>56,57</sup>, vacancies associated with chain ends<sup>58</sup> and the 'sandwich model'<sup>59,63</sup>. The results of Olf and Peterlin tend to rule out the first two mechanisms<sup>8</sup>.

The  $\alpha$  process, which occurs within the temperature range from  $\sim +50^\circ\text{C}$  to the melting point, is clearly a crystalline one for which a number of models have been proposed<sup>8,38,53</sup>: a flip-flop model which entails rotational jumps through  $180^\circ$  between two equilibrium sites coupled with a translation of one  $\text{CH}_2$  unit<sup>8,58,64</sup>; a model which involves rotational oscillations of chains about their long axes plus possible torsion<sup>58,67</sup>; and a defect model<sup>56,58</sup>. Quantitative  $M_2$  considerations, again by Olf and Peterlin<sup>8</sup>, favour the flip-flop model coupled with a small oscillation ( $8^\circ$ ) about the two equilibrium sites. Their results pertain to single crystal mats. McCall and Douglass<sup>3</sup> have observed little change in the crystalline  $T_2$  from the rigid lattice value until temperatures in excess of  $+100^\circ\text{C}$  are reached although there is a substantial fall in  $M_2$  for the crystalline component over the same temperature range. This apparent anomaly will be resolved in the appropriate section to follow. The  $\alpha$  relaxation is very pronounced in the rotating frame results for linear PE in the form of a well defined minimum at  $+95^\circ\text{C}$ <sup>37</sup>.

The pulsed n.m.r.  $T_1$ ,  $T_{1\rho}$  and  $T_2$  data for branched PE<sup>42,46</sup> manifest methyl branch rotations, the  $\gamma$  relaxation, the principal amorphous transition,  $\beta$ , and the  $\alpha$  relaxation. The use of multiple pulse techniques<sup>65,66</sup> by Fujimoto *et al.*<sup>46</sup> has enabled them to separate out three  $T_2$  and  $T_{1\rho}$  components above  $\sim +20^\circ\text{C}$  as compared with two components observed by McCall and Falcone<sup>42</sup>. The longer, amorphous,  $T_2$  in the data of McCall and Falcone appears to be a weighted average of the intermediate and long components recorded by Fujimoto *et al.* Schmedding and Zachmann<sup>47</sup> have examined theoretically the crankshaft motion for a single PE chain as a function of the fixed end-to-end distance of the chain. Their results indicate that this mechanism may well be responsible for the intermediate

component observed by Fujimoto *et al.* In both sets of experimental data<sup>42,46</sup> the  $\beta$  relaxation appears as a two stage process as evidenced by an increase in the amorphous  $T_2$  to an intermediate plateau followed by a further increase to a value appropriate to motions of liquid-like proportions.

The  $\alpha$  relaxation sets in at much lower temperatures in branched PE as compared with the linear form of the polymer. Typically, the  $T_{1\rho}$  minimum for this relaxation occurs at +50°C<sup>42</sup> in branched PE and +95°C in linear PE<sup>37</sup>. McCall and Falcone suggest crystalline chain rotation as the mechanism responsible for the  $\alpha$  process and state further that the high temperature crystalline phase may not be a true rotor phase in which all the molecules are rotating<sup>42</sup>. This conclusion parallels an earlier discussion by Hoffman<sup>68</sup>.

Foulkes and Ward<sup>43</sup>, in their analysis of  $M_2$  data for oriented branched PE, have focused attention on the  $\gamma$  relaxation and propose a chain sliding model for its description.

Bergmann and coworkers<sup>39,45</sup> have performed a detailed line-shape analysis of linear and branched PE spectra, recorded as a function of temperature, in terms of three components attributed, respectively, to rigid, microbrownian and hindered mobile behaviour. This approach has the advantage, in principle, of utilizing all the molecular information contained in the absorption envelope in contrast to linewidth,  $M_2$  or  $M_4$  measurements which only monitor part of the information available. This advantage is offset somewhat by the inherent difficulty associated with all curve fitting procedures of assigning values simultaneously to a number of unknown parameters. However, the accurate prediction of the degree of crystallinity of their materials lends general support to their procedures.

The  $\beta$  relaxation in both forms of the polymer is probably the least well understood and will be a central feature of this paper. The absence of a well defined  $\beta$  relaxation in linear PE in experimental measurements tended to support a branch point mechanism. However, Moore and Matsuoka<sup>69</sup> were able to induce a  $\beta$  peak in a linear PE which had been subjected to suitable heat treatment and observed, in addition, that the peak disappeared when the sample was subsequently annealed.

The results of n.m.r. indicate a shift in the  $\beta$  process to higher temperatures in linear PE<sup>3,38</sup> compared with branched PE and consequently becomes so close to the strong  $\alpha$  relaxation as to be unresolved. Sinnott's high temperature relaxation peak, which is probably a superposition of the  $\alpha$  and  $\beta$  relaxations, was observed to decrease in magnitude when the sample was either annealed or subjected to electron irradiation<sup>40</sup>. A further important conclusion of his work is the observed dependence of the peak upon the motion of the lamellar folds in his single crystal material. The models which are presented later to explain the  $\beta$  relaxation will attempt to reconcile these experimental observations.

The transition maps for linear and branched PE are not superimposable<sup>38</sup> and hence the same molecular mechanisms need not necessarily be responsible for the corresponding relaxations in the two cases.

## MODEL CALCULATIONS

The molecular motions which will be considered in our interpretation of the experimental data are: (1) oscillations about the chain axis, leading ultimately to classical rotation; and (2) a flip-flop motion which involves jumps bet-

ween two equilibrium sites plus a translation of one CH<sub>2</sub> unit.

In the oscillation calculation the chains are displaced as rigid rods through  $\pm\phi$  from their equilibrium position; all displacements in the range  $+\phi$  to  $-\phi$  are equally probable. Indeed the choice of specific probability distributions for the displacements has little effect on the results<sup>8</sup>. Classical rotation corresponds to the case where the angle  $\phi = 360^\circ$ . Chain torsion is neglected.

For the flip-flop calculation the chains are assumed to spend equal time between the two equilibrium sites and, furthermore, all chains are assumed to move coherently. We have not included the refinement of oscillation about the equilibrium sites<sup>8</sup>.

The values of the moments were computed for those specific temperatures for which precise crystallographic data are available within the temperature range  $-196^\circ\text{C}$  to  $+100^\circ\text{C}$ <sup>48-51</sup>. The  $M_2$  and  $M_4$  results are presented in Figures 1-4 for the crystalline component in the cases of a rigid lattice, flip-flop motion and classical rotation for the two extreme temperatures,  $-196^\circ\text{C}$  and  $+100^\circ\text{C}$ . The oscillation data are presented in Figures 5 and 6 for  $-196^\circ\text{C}$  only, to preserve clarity of presentation. The higher temperature behaviour may be easily inferred from the rigid lattice results,  $\phi = 0$ , and the classical rotation results at the other extreme,  $\phi = 360^\circ$ . As already noted by Olf and Peterlin<sup>8</sup>, oscillations at angles greater than  $\phi = 120^\circ$  are essentially indistinguishable from classical rotation.

## RESULTS AND DISCUSSION

### Branched polyethylene

*Rigid lattice.* The rigid lattice n.m.r. of branched PE, draw ratio 3.7, has been the subject of detailed examina-

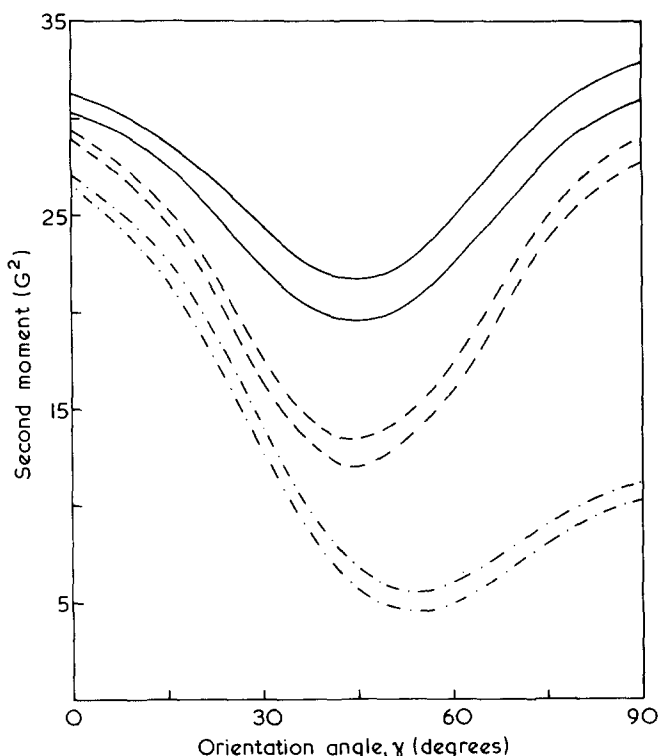


Figure 1 Theoretical dependence of  $M_2$  for branched PE as a function of orientation in the magnetic field for rigid lattice (—), flip-flop motion (---) and classical rotation (- · - · -). The upper curve is for a temperature of  $-196^\circ\text{C}$  and the lower,  $+100^\circ\text{C}$  in each case

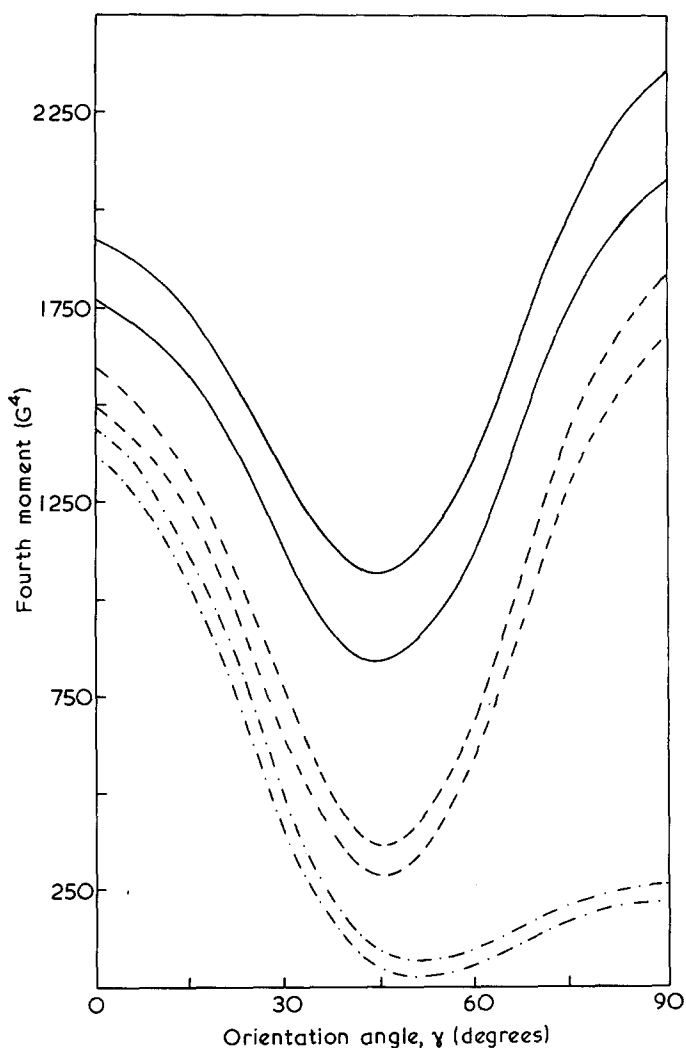


Figure 2 Theoretical dependence of  $M_4$  for branched PE as a function of orientation in the magnetic field for rigid lattice (—), flip-flop motion (---) and classical rotation (- · - · -). The upper curve is for a temperature of  $-196^\circ\text{C}$  and the lower,  $+100^\circ\text{C}$  in each case

tion in two earlier papers<sup>41,44</sup>. The chain distribution statistics for this partly drawn polymer have been fully characterized in terms of the following distribution functions:

$$\overline{P_2(\cos \Delta)} = 0.80$$

$$\overline{P_4(\cos \Delta)} = 0.84$$

$$\overline{P_6(\cos \Delta)} = 0.70$$

$$\overline{P_8(\cos \Delta)} = 0.00$$

The angle  $\Delta$  is the angle between the symmetry axis of a typical structural unit and the draw direction in the polymer. The rigid amorphous contributions, assumed isotropic were assigned the values  $M_{2a} = 24.3 \text{ G}^2$  and  $M_{4a} = 1650 \text{ G}^4$ , respectively. The theoretical predictions based upon these data (referred to as model BI) are compared with the experimental results in Table 1.

**$\gamma$ -Relaxation process.** The clearest manifestation of the  $\gamma$  process by n.m.r. is contained in the isotropic data of McCall and Falcone<sup>42</sup> in the form of a small anomaly in  $T_2$  at  $-100^\circ\text{C}$  (a rise from  $\sim 9 \mu\text{s}$  to  $\sim 10 \mu\text{s}$ ), a  $T_{1\rho}$  minimum at  $-85^\circ\text{C}$  and a  $T_1$  minimum at  $-25^\circ\text{C}$ . The broad-

line  $M_2$  data in the low temperature region display a fairly uniform decrease in magnitude for all orientations without the appearance of a discrete plateau<sup>43</sup>.

McCall and Falcone tend to favour the explanation of Hoffman, Williams and Passaglia (HWP)<sup>58</sup> for the  $\gamma$  process in which it is supposed that there is chain rotation in the amorphous regions,  $\gamma_a$ , and crystalline chain rotations near row vacancies,  $\gamma_c$ . Foulkes and Ward<sup>43</sup> propose chain sliding in the crystalline regions as being the responsible mechanism. Bergmann's results indicate a rigid crystalline component in the region of the  $\gamma$  relaxation process<sup>45</sup>.

Our analysis relates to the  $M_2$  and  $M_4$  data at  $-100^\circ\text{C}$ , that is, the temperature indicated by  $T_2$  measurements<sup>42</sup> and dielectric<sup>45</sup> data for the activation of the  $\gamma$  relaxation. Prompted by the results of Hoffman *et al.*<sup>58</sup> and Bergmann<sup>45</sup>, we have considered two theoretical models. In the first, 20% of the crystalline chains are undergoing flip-flop motion while 75% of the amorphous chains are rotating about their long axes. The model, designated BII, assumes that all the crystalline chains neighbouring row vacancies can undergo flip-flop motion. The second model, BIII, assumes a rigid crystalline component and all the amorphous chains in rotation. The theoretical predictions are compared with the experimental data in Table 1 from which it is evident that there is little to choose between the two models. In the calculation, the reasonable assumption is made that chain rotation in the amorphous regions reduces the rigid lattice moments by half to the respective values  $M_{2a} = 12.1 \text{ G}^2$  and  $M_{4a} = 825 \text{ G}^4$ . The result is not overly sensitive to the percentage of amorphous chains in rotation because of the biasing coefficient 0.4, i.e. the amorphous content. The model of Foulkes and Ward is less attractive in that the description of subsequent relaxation at higher temperatures proves difficult on the basis of predominantly *intra* contributions alone, as

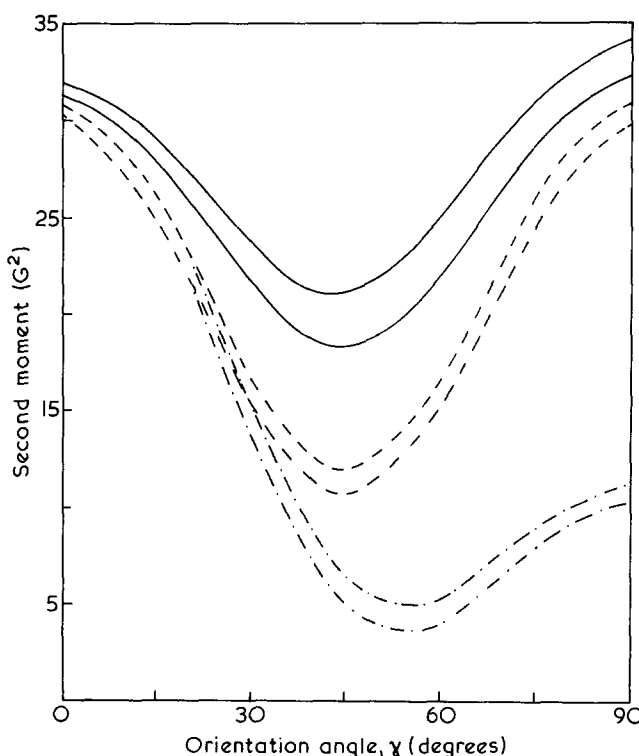


Figure 3 Theoretical dependence of  $M_2$  for linear PE as a function of orientation in the magnetic field for rigid lattice (—), flip-flop motion (---) and classical rotation (- · - · -). The upper curve is for a temperature of  $-196^\circ\text{C}$  and the lower,  $+100^\circ\text{C}$  in each case

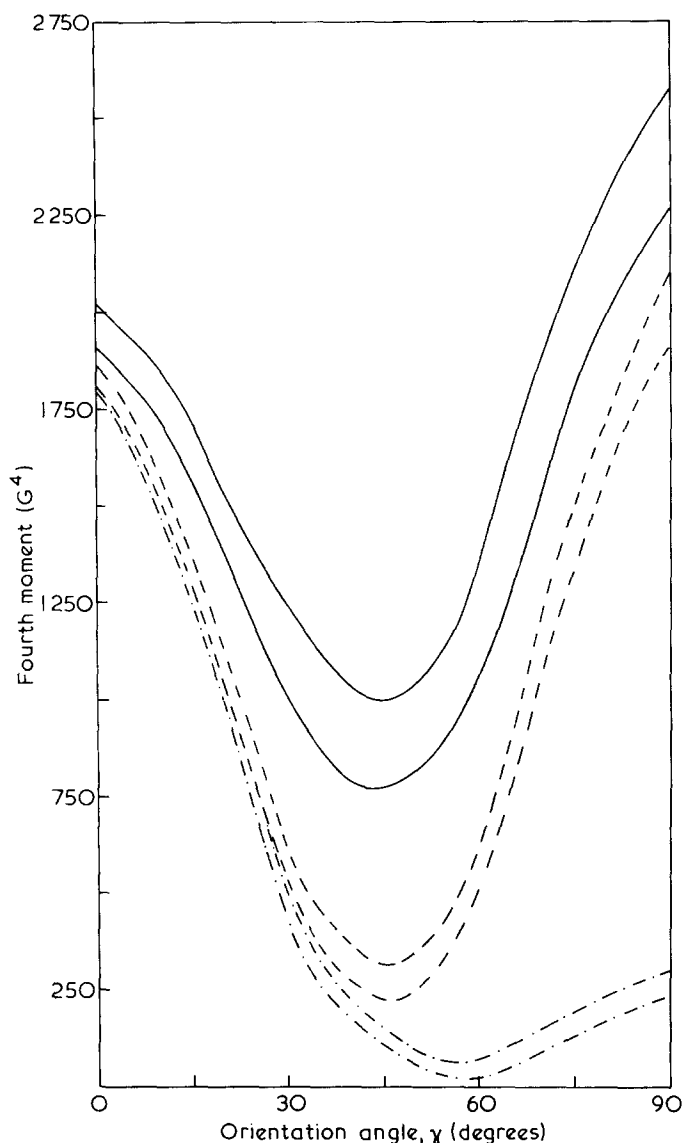


Figure 4 Theoretical dependence of  $M_4$  for linear PE as a function of orientation in the magnetic field for rigid lattice (—), flip-flop motion (---) and classical rotation (- · - · -). The upper curve is for a temperature of  $-196^\circ\text{C}$  and the lower,  $+100^\circ\text{C}$ , in each case

required in their analysis. The models considered here predict an increase in  $T_2$  of  $\sim 1 \mu\text{s}$  with the onset of the  $\gamma$  relaxation process, in agreement with the experimental observations<sup>42</sup>.

**$\beta$ -Relaxation process.** The  $\beta$  relaxation in branched PE corresponds to the conventional glass transition which ultimately indicates liquid-like motions in the amorphous regions. The observation of three components by Bergmann<sup>45</sup> and by Fujimoto *et al.*<sup>46</sup> indicates that there are two discrete types of molecular activity in the amorphous regions. The intermediate  $T_2$  component in the data of Fujimoto *et al.* exhibits a plateau of  $\sim 50 \mu\text{s}$  in the region of  $+60^\circ\text{C}$  while the long component rises sharply to a value of  $\sim 200 \mu\text{s}$  at the same temperatures which indicates extensive motions of a general character. The relative intensities are  $\sim 28\%$  and  $\sim 40\%$  for the long and intermediate components, respectively. A single amorphous component is observed by McCall and Falcone which exhibits a plateau of  $\sim 65 \mu\text{s}$  at about  $+50^\circ\text{C}$ . The magnitude of the plateau in each case falls between the expected values for chain rotation,  $\sim 20\text{--}30 \mu\text{s}$ , at lower temperatures to values of the order of milliseconds appropriate to motions

of liquid-like proportions at higher temperatures<sup>29</sup>. The problem is to find a discrete motional model which will account for the magnitude of the observed plateau in addition to satisfying the other experimental criteria referred to earlier.

It is most probable that this type of hindered motion is associated with the chain folded regions in the polymer. This view is consistent with current ideas of lamellar morphology which embody the results of a host of experimental observations on PE<sup>59-63</sup>. The morphological feature which is of immediate interest is the presence of loose folds which can spread out in a disordered fashion onto the surrounding environment, in addition to the presence of loose chain ends (Figure 7)<sup>63</sup>. These loose folds constitute a sizeable fraction of the amorphous material in branched PE<sup>38</sup>.  $T_2$  data indicate that folds account for about 60%<sup>46</sup>. As the temperature is increased the tendency towards vigorous motion correspondingly increases. However, in the case of folds, the chain ends are anchored at the entry points to

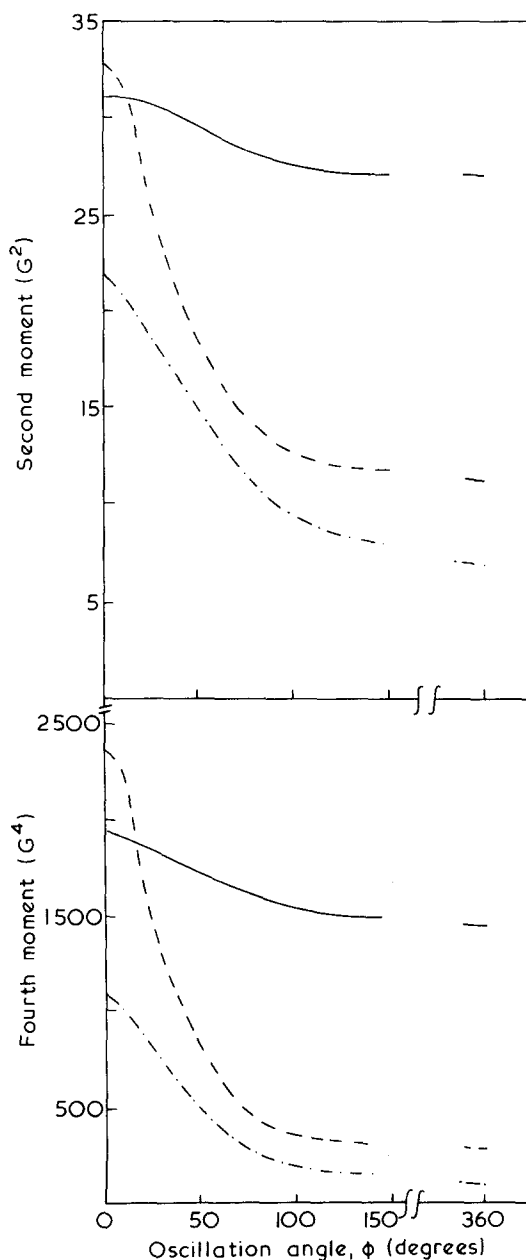


Figure 5 Theoretical dependence of  $M_2$  and  $M_4$  for branched PE as a function of oscillation angle  $\phi$  for  $\gamma = 0^\circ$  (—),  $45^\circ$  (- · - · -) and  $90^\circ$  (---)



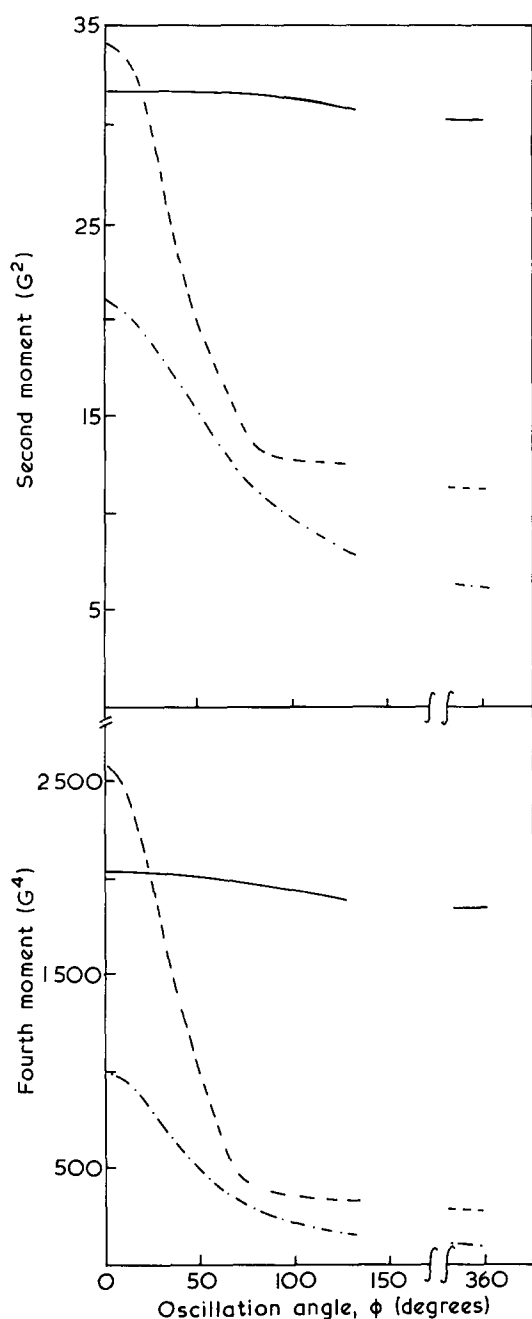


Figure 6 Theoretical dependence of  $M_2$  and  $M_4$  for linear PE as a function of oscillation angle  $\phi$  for  $\gamma = 0^\circ$  (—),  $45^\circ$  (- · - · -) and  $90^\circ$  (---)

the crystalline interior of the lamellae with the result that the degree of vigour which the motion can achieve is limited.

The calculations of Schmedding and Zachmann<sup>47</sup> demonstrate that their crankshaft model is an obvious candidate for the description of fold behaviour. Typical of their results is a decrease in  $M_2$  from  $19 \text{ G}^2$  to  $0.5 \text{ G}^2$  when the end-to-end distance decreases to a value of one half of the stretched chain length. This corresponds to a rise in  $T_2$  from  $8.6 \mu\text{s}$  to  $53 \mu\text{s}$ , in agreement with the experimental observations.

A second more idealized mechanism may be envisaged where the chains as a whole are moving in the highly idealized manner shown in Figure 8. The chains are already considered to be rotating about their own axes at these temperatures ( $\gamma$  process)<sup>42</sup>. This model has been used to predict successfully the observed anisotropy in the amorphous  $T_2$  data of oriented polychlorotrifluoroethylene

fibres<sup>70</sup>. The fold is divided into straight sections and  $T_2$  is computed for each. The vertical part of the fold will be characterized by a  $T_2$  close to the crystalline value; we assume that those parts of the fold at the angle  $\chi$  alone contribute to the amorphous  $T_2$ . Only *intra* contributions are considered. The  $T_2$  expression for this motion may be written<sup>70</sup>:

$$1/T_2^2 = 1.07 \times 10^{10} P_2^2(\cos \xi) \sum_{l=0,2,4} a_l P_l(\cos \gamma) P_l(\cos \chi) \quad (6)$$

where the numerical coefficient has been adjusted to a value appropriate to polyethylene;  $a_0 = 1/5$ ,  $a_2 = 2/7$  and  $a_4 = 18/35$ , respectively. The angles are defined in Figure 8. The expression for an isotropic sample has the much simpler form:

$$1/T_2^2 = 0.214 \times 10^{10} P_2^2(\cos \xi) \quad (7)$$

$T_2$  is graphed as a function of the angle  $\xi$  in Figure 9. Notwithstanding the highly idealized nature of the motion, the results again demonstrate that discrete  $T_2$  values of the correct order of magnitude are predicted for reasonable values of the angle,  $\xi$ .

The two models discussed involve loose folds on the surface of crystal lamellae and as such describe an amorphous phenomenon. It is not surprising, however, that the crystalline regions may exert some influence on the process, as hitherto observed<sup>71</sup>. Upon annealing, the loose folds are drawn into the crystalline interior in the lamellar thickening process<sup>72</sup> which would result in the disappearance of the  $\beta$

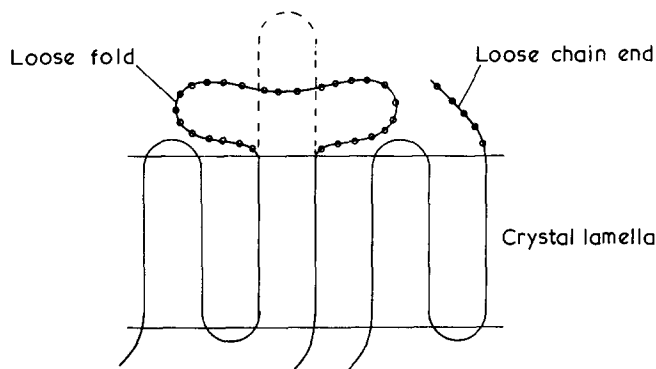


Figure 7 Diagram which illustrates loose chain folds and chain ends on the surface of a crystal lamella

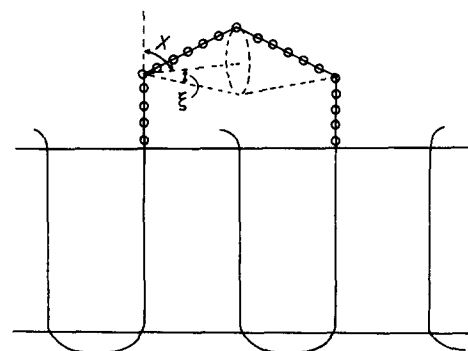
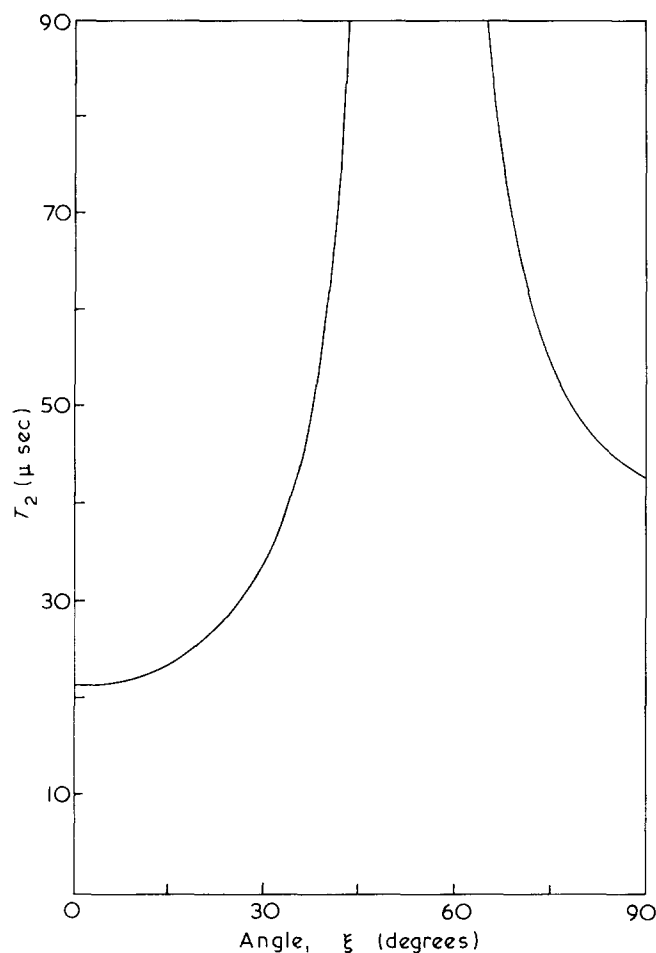


Figure 8 Diagram which illustrates the proposed idealized motion underlying the  $\beta$  relaxation process

**Table 1** Summary of relaxation data for linear and branched PE (the various models are specified in the text)

	$M_2$ ( $G^2$ )			$M_4$ ( $G^4$ )			RMS deviation		Bulk $T_2$ ( $\mu s$ )	Temp. ( $^{\circ}C$ )	Process	Model
	$0^{\circ}$	$45^{\circ}$	$90^{\circ}$	$0^{\circ}$	$45^{\circ}$	$90^{\circ}$	$\Delta M_2$	$\Delta M_4$				
Linear polyethylene:												
Exp.	33.0	21.9	34.0	2240	1120	2580			7.0			
Theor.	31.2	23.2	33.1	1980	1225	2410	1.38	189	7.1	-196	Rigid lattice	LI
Exp.	27.1	16.2	25.0	1650	670	1570			8.0			
Theor.	27.2	16.0	25.8	1650	668	1800	0.48	135	8.2	+25	$\gamma$ process	LII
Theor.	27.2	16.4	25.3	1630	715	1665	0.16	62	8.2			LIII
Exp.	22.5	8.0	18.0	1175	260	940			9.0	+120	$\alpha + \beta$ process	LIV
Theor.	23.0	8.3	15.0	1380	280	860	1.76	127	10.8			
Branched polyethylene:												
Exp.	29.5	23.9	31.0	1870	1300	2100			9.0			
Theor.	29.8	23.7	30.9	1870	1290	2085	0.22	10	7.0	-196	Rigid lattice	BI
Exp.	24.5	19.3	25.2	1420	920	1560			10.0			
Theor.	24.5	18.1	25.2	1520	960	1760	0.70	130	8.0	-100	$\gamma$ process	BII
Theor.	23.5	17.9	24.5	1480	970	1730	1.07	100	8.0			BIII
Exp.	11.3	4.0	5.0	480	60	120			13.5	+60	$\alpha$ process	BIV
Theor.	13.0	3.0	5.3	700	40	120	1.15	128	17.0			



**Figure 9**  $T_2$  as a function of the angle  $\xi$  for the motion illustrated in Figure 8

relaxation. The crosslinking produced by electron irradiation of the folds<sup>40</sup> would certainly curtail motion severely, if not prevent it altogether, with a consequent elimination of the  $\beta$  process.

**$\alpha$ -Relaxation process.** The  $\alpha$  relaxation shows up as a minimum in the crystalline  $T_{1\rho}$  component at  $+50^{\circ}C$ <sup>42</sup>.  $M_2$  and  $M_4$  are decreasing continuously at these higher temperatures although  $M_2, M_4$  ( $\gamma = 90^{\circ}$ ) become less than

$M_2, M_4$  ( $\gamma = 0^{\circ}$ ) above room temperature in contrast to the lower temperature region where the reverse is true<sup>43</sup>. This accelerated fall in the values of the moments for  $\gamma = 90^{\circ}$  is reminiscent of the onset of classical rotation (see Figures 1 and 2).

In our analysis of the data at  $+60^{\circ}C$  it is noted, initially, that an amorphous  $T_2$  value of  $65 \mu s$  corresponds to  $M_{2a} \approx 0.4 G^2$ ; the weighted contribution to the total moment is therefore  $0.16 G^2$ , which may be neglected.  $M_{4a}$  is also deemed to be negligible. Attempts to fit any of the proposed motional mechanisms to the crystalline regions lead on the whole to poor agreement with experiment. A reasonable fit may be achieved, however, (see Table 1) if 10% of the crystalline regions are assumed to have melted and the remaining 90% of the crystalline component (50% mass fraction in all) to be in classical rotation (model BIV). A further improvement is obvious with the assumption of a less perfect orientation which may well be the case above the glass transition temperature: the vigorous motions in the amorphous regions may have a disordering influence upon the oriented crystalline part. The model is compatible with the rapid decrease in density which is observed with increase in temperature above room temperature<sup>73</sup>. Bunn and Alcock<sup>74</sup> have observed premelting in their X-ray measurements in excess of  $+80^{\circ}C$ . This higher temperature may be due to the different preparative histories of the materials or to the relative sensitivities of the X-ray and n.m.r. methods to premelting.

*Linear polyethylene*

**Rigid lattice.** Table 1 shows the optimum agreement which could be achieved between theory and experiment. The polymer was assumed to be fully drawn, in agreement with earlier findings on a comparable sample<sup>41</sup>. The amorphous second and fourth moments were assigned the respective values  $M_{2a} = 29.5 G^2$  and  $M_{4a} = 1900 G^4$ . The model is designated LI. The rather low predicted value at orientation  $\gamma = 0^{\circ}$  and the high value at  $\gamma = 45^{\circ}$  would tend to indicate an oriented amorphous component as suggested by Olf and Peterlin on the basis of the sandwich model<sup>8</sup>. However, the lack of precise morphological information on the amorphous regions precludes a rigorous treatment of amorphous anisotropy for the rigid lattice case. The pre-

dicted rigid lattice  $T_2$  for unoriented material of 7.1  $\mu\text{s}$ , from equations (4) and (5), is in good agreement with the experimental results of  $\sim 7 \mu\text{s}$  obtained at  $-196^\circ\text{C}$  by McCall and Falcone<sup>42</sup>.

**$\gamma$ -Relaxation process.** It has been argued that the fall in  $M_2$  from  $-196^\circ\text{C}$  to  $+25^\circ\text{C}$  is a manifestation of the  $\gamma$  relaxation process in linear PE<sup>8,9</sup>. Any proposed model to explain the  $\gamma$  relaxation must necessarily be compatible with a number of observations. In the first place,  $T_2$  data would appear to preclude any crystalline motion at  $+25^\circ\text{C}$ <sup>3,45</sup>. Secondly, the anisotropy in the amorphous regions, implied in the rigid lattice data, would have a more pronounced effect on the measurements if the chains were rotating about their own axes; the anisotropy in  $M_2$  and  $M_4$  as a function of orientation is much greater for rotating chains than for rigid ones<sup>14</sup>. Thirdly, the predicted amorphous moments for the  $\gamma = 0^\circ$  orientation at  $+25^\circ\text{C}$  must agree with the measured values; at this temperature the n.m.r. trace may easily be decomposed into its two components at orientation  $\gamma = 0^\circ$ . The experimental values are  $M_{2a} = 15.4 \text{ G}^2$  and  $M_{4a} = 770 \text{ G}^4$ , respectively, which are consistent with rotation about the chain axis.

The theory presented above to explain the relaxation in branched PE may be used here to quantify the anisotropic effects of an oriented amorphous component in which the chains are rotating. The angle  $\xi$  is set equal to zero to confine the motion to rotation about the chain axis alone. The experimental amorphous value of  $15.4 \text{ G}^2$  for  $\gamma = 0^\circ$  is predicted by the model when the angle  $\chi$  assumes the value  $25^\circ$ . The corresponding values of  $M_{2a}$  for the  $\gamma = 45^\circ$  and  $\gamma = 90^\circ$  orientations are, respectively,  $5.6 \text{ G}^2$  and  $4.1 \text{ G}^2$ . A rough estimate of the corresponding  $M_{4a}$  values may be made if the line shape parameter<sup>11</sup>  $p = M_{4a}/M_{2a}^2$  is assumed to be the same for the three orientations. At  $\gamma = 0^\circ$ ,  $p$  is experimentally equal to 3.25 which results in  $M_{4a}(45^\circ) = 100 \text{ G}^4$  and  $M_{4a}(90^\circ) = 55 \text{ G}^4$ . The theoretical predictions presented in *Table 1* derive from these amorphous values used in conjunction with rigid lattice moments for the crystalline regions. This model is referred to as LII.

We now examine a second model, designated LIII, to demonstrate that a particular model assignment is by no means unambiguous. The second calculation is based upon the impressive arguments of Hoffman *et al.*<sup>58</sup> in which a vacancy defect model is invoked to explain their dielectric data. This model is similar to the one proposed to explain the  $\gamma$  relaxation in branched PE. Crystalline chains near row vacancies are considered to be undergoing classical rotation in addition to chain rotation in the amorphous regions. To illustrate the flexibility of the approach, we have assumed for simplicity that the amorphous regions are isotropic with  $M_{2a} = 15.4 \text{ G}^2$  and  $M_{4a} = 770 \text{ G}^4$ , i.e. the measured values for orientation  $\gamma = 0^\circ$ . The excellent fit achieved with the experimental data, also shown in *Table 1*, is on the basis of 20% of the crystalline chains rotating near defects. Substitution of flip-flop motion for classical rotation coupled with a small adjustment of the number of crystalline chains in motion also leads to an acceptable fit with the experimental data. The predicted bulk  $T_2$  value of  $8.2 \mu\text{s}$  is only  $1.1 \mu\text{s}$  up on the rigid lattice value, i.e., a marginal increase *vis-à-vis* the observations of McCall and Douglass<sup>3</sup>.

Thus, while a given model may be in excellent agreement with the experimental data it is nevertheless important to keep an open mind on the possibility of alternative mechanisms.

**High temperature relaxation process.** This process is usually designated the  $\alpha$ -relaxation but we should bear in mind that there exists also the overlapping  $\beta$  process which cannot be resolved by n.m.r. in linear PE. We recall that the predictions of Olf and Peterlin for single crystal mats of linear PE support a model in which all the crystalline chains are undergoing flip-flop motion<sup>8</sup>. McCall suggests rotation of crystalline chains where there exists the possibility that the crystalline regions may not be a true rotor phase<sup>38</sup>.

We have analysed the n.m.r. moment data at  $+120^\circ\text{C}$  and note in the first instance, from those traces which may readily be decomposed into two components, that the amorphous moment values are sufficiently small as to be neglected in our calculations. Attempts to ascribe a particular motion to all of the crystalline regions results in poor agreement between theory and experiment. However, the assumption of 45% of the crystalline component remaining essentially rigid and 55% undergoing classical rotation yields the agreement shown in *Table 1* (model LIV). While it is not our intention to inject detailed morphological conclusions into any particular model we are nevertheless tempted to suggest that there may be appreciable amounts of different types of crystalline material present which exhibit characteristic molecular behaviour (for example, chain folded or extended chain forms)<sup>75</sup>.

The predicted  $T_2$  value for the model is  $10.8 \mu\text{s}$  which again is in reasonable agreement with the data of McCall and Douglass<sup>3</sup>.

The absence of a well defined  $\beta$  relaxation in mechanical measurements or in n.m.r. data may be due to the presence only of sharp folds which are unable to rotate as in branched PE or, alternatively, to the steric hindrance to fold motion caused by intercrystalline chain units linking neighbouring lamellae<sup>75,76</sup>.

## CONCLUSIONS

The principal quantitative conclusions of the paper are contained in *Table 1* which summarizes the experimental and theoretical data for the various relaxation mechanisms in linear and branched PE. An interesting and important aspect of these results is the relatively low sensitivity of  $T_2$  to molecular behaviour as compared with  $M_2$  (and  $M_4$ ). This derives from the square root dependence between  $M_2$  and  $T_2$  as shown in equation (5). In particular, preferred orientation in drawn materials can effect large changes in  $M_2$  as a function of orientation angle  $\gamma$  in the applied field and yet  $T_2$  is essentially isotropic for similarly drawn samples. Typically, the low temperature  $M_2$  data for drawn branched PE are 29.5, 23.9 and  $31.0 \text{ G}^2$  for  $\gamma = 0^\circ, 45^\circ$  and  $90^\circ$ , respectively. The equivalent  $T_2$  values, from equation (5), are 6.9, 7.7 and  $6.7 \mu\text{s}$ , respectively. These differences are barely detectible by pulsed n.m.r. as we have experience in this laboratory. Furthermore, the onset of specific motions in the polymer have a much greater effect upon  $M_2$  than on  $T_2$ . For example, the fall in  $M_2$  with the onset of the  $\gamma$  relaxation in linear PE is of the order of  $7 \text{ G}^2$  while the corresponding rise in  $T_2$  is only of the order of  $1 \mu\text{s}$ . As a result  $M_2$  and  $M_4$  are much more sensitive monitors of the onset of molecular motion than  $T_2$ . It is commonly observed that specific motions such as methyl group rotations can remain undetected in  $T_2$  measurements although clearly manifested in  $M_2, T_1$  and  $T_{1\rho}$ <sup>76</sup>.

On the other hand, major experimental difficulties impair the accuracy of  $M_2$  data for magnitudes of the order of a fraction of a (Gauss)<sup>2</sup> as is typical above the glass transition temperature. In such cases,  $T_2$  measurements are to be preferred.

In general, it is important to note that while certain intuitive models are in excellent agreement with the experimental observations they need not necessarily be unique in this respect; there may be other models which are in comparable agreement within the accuracy of the experimental n.m.r. data. In practice one tends to choose the model on the basis of available morphological information rather than adopt the reverse procedure of drawing detailed morphological conclusions from a chosen model.

#### ACKNOWLEDGEMENTS

It is a pleasure to acknowledge helpful discussions with Drs K. Bergmann, D. C. Douglass, D. W. McCall and S. Matsuoka. We are grateful to G. E. Wardell who checked for anisotropy in  $T_2$  for oriented PE fibres.

This work was supported in part by a grant from the National Science Council of Ireland.

#### REFERENCES

- Slichter, C. P. and Ailion, D. *Phys. Rev. (A)* 1964, **135**, 1099
- Abragam, A. 'The Principles of Nuclear Magnetism', Clarendon Press, Oxford, 1961
- McCall, D. W. and Douglass, D. C. *Polymer* 1963, **4**, 433
- Connor, T. M. *Trans. Faraday Soc.* 1963, **60**, 1574
- Meyer, L. H. Thesis Univ. of Illinois (1953)
- McCall, D. W. and Slichter, W. P. *J. Polym. Sci.* 1957, **26**, 171
- Olf, H. G. and Peterlin, A. *J. Appl. Phys.* 1964, **35**, 3108
- Olf, H. G. and Peterlin, A. *J. Polym. Sci. (A-2)* 1970, **8**, 753, 771, 791
- Olf, H. G. and Peterlin, A. *Kolloid-Z.* 1967, **215**, 97
- Crist, B. and Peterlin, A. *J. Polym. Sci. (A-2)* 1969, **7**, 1165
- Powles, J. G. *Polymer* 1960, **1**, 219
- Yamagata, K. and Hirota, S. *Rep. Progr. Polym. Phys. Japan* 1962, **5**, 236
- Hyndman, D. and Origlio, G. F. *J. Polym. Sci.* 1959, **39**, 556
- McBrierty, V. J., McCall, D. W., Douglass, D. C. and Falcone, D. R. *J. Chem. Phys.* 1970, **52**, 512
- McBrierty, V. J., Douglass, D. C. and Falcone, D. R. *JCS Faraday Trans. II* 1972, **68**, 1051
- McBrierty, V. J. and McDonald, I. R. *J. Phys. (D: Appl. Phys.)* 1973, **6**, 131
- Slichter, W. P. and McCall, D. W. *J. Polym. Sci.* 1957, **25**, 230
- Nishioka, A. *J. Phys. Soc. Japan* 1957, **12**, 283
- Sauer, J. A. and Woodward, A. E. *Rev. Mod. Phys.* 1960, **32**, 88
- Herring, M. J. and Smith, J. A. S. *J. Chem. Soc.* 1960, **53**, 273
- Slichter, W. P. *J. Appl. Phys.* 1960, **31**, 1965
- Peterlin, A., Krasovec, F. and Pirkmajer, E. *Makromol. Chem.* 1960, **37**, 231
- Peterlin, A. and Pirkmajer, E. *J. Polym. Sci.* 1960, **46**, 185
- Slichter, W. P. *J. Appl. Phys.* 1961, **32**, 2339
- Thurn, H. *Kolloid-Z.* 1961, **179**, 11
- Odajima, A., Sauer, J. A. and Woodward, A. E. *J. Phys. Chem.* 1962, **66**, 718
- Peterlin, A. and Roeckl, E. *J. Appl. Phys.* 1963, **34**, 102
- Haeberlen, U., Hausser, R. and Noack, F. *Z. Naturforsch.* 1963, **18a**, 689, 1026
- McCall, D. W. and Anderson, E. W. *J. Polym. Sci. (A)* 1963, **1**, 1175
- Hunt, B. I., Powles, J. G. and Woodward, A. E. *Polymer* 1964, **5**, 323
- Trappeniers, N. J., Gerritsma, C. J. and Oosting, P. H. *Physica* 1964, **30**, 997
- Anderson, J. E. and Slichter, W. P. *J. Phys. Chem.* 1965, **69**, 3099
- Koltsov, A. I. and Vokenstein, M. W. *Vysokomol. Soedin.* 1965, **7**, 250
- Peterlin, A., Meinel, G. and Olf, H. G. *J. Polym. Sci. (B)* 1966, **4**, 399
- Peterlin, A. and Olf, H. G. *J. Polym. Sci. (A-2)* 1966, **4**, 587
- Haeberlen, U. *Kolloid-Z.* 1967, **225**, 15
- McCall, D. W. and Douglass, D. C. *Appl. Phys. Lett.* 1965, **7**, 12
- McCall, D. W. 'Proc. 2nd Symp. Molecular Dynamics', (NBS Serial Publ. 301), (ed. R. S. Cater and J. J. Rush), Nat. Bur. Stand., Washington, D.C., 1969, p 475
- Bergmann, K. and Nawotki, K. *Kolloid-Z.* 1967, **219**, 132
- Sinnott, K. M. *J. Appl. Phys.* 1966, **37**, 3385
- McBrierty, V. J. and Ward, I. M. *J. Phys. (D: Appl. Phys.)* 1968, **1**, 1529
- McCall, D. W. and Falcone, D. R. *Trans. Faraday Soc.* 1970, **66**, 262
- Foulkes, M. and Ward, I. M. *J. Mat. Sci.* 1971, **6**, 582
- McBrierty, V. J., McDonald, I. R. and Ward, I. M. *J. Phys. (D: Appl. Phys.)* 1971, **4**, 88
- Bergmann, von K. *Kolloid-Z. Z. Polym.* 1973, **251**, 962
- Fujimoto, K., Nishi, T. and Kado, R. *Polym. J.* 1972, **3**, 448
- Schmedding, von P. and Zachmann, H. G. *Kolloid-Z. Z. Polym.* 1972, **250**, 1105
- Bunn, C. W. *Trans. Faraday Soc.* 1939, **35**, 428
- Cole, E. A. and Holmes, D. R. *J. Polym. Sci.* 1960, **46**, 245
- Swan, P. R. *J. Polym. Sci.* 1962, **56**, 403
- Kobayashi, Y. and Keller, A. *Polymer* 1970, **11**, 114
- Van Vleck, J. H. *Phys. Rev.* 1948, **74**, 1168
- McBrierty, V. J. and Douglass, D. C. *J. Magnet. Res.* 1970, **2**, 352
- Kashiwagi, M., Cunningham, A., Manuel, A. J. and Ward, I. M. *Polymer* 1973, **14**, 111
- Schatzki, T. J. *Polym. Sci.* 1962, **57**, 496; *Polym. Prepr.* 1965, **6**, 646
- Pechhold, W. and Blasenbrey, S. *Kolloid-Z.* 1967, **216/217**, 235
- Pechhold, W. *Kolloid-Z.* 1968, **228**, 1
- Hoffman, J. D., Williams, G. and Passaglia, E. *J. Polym. Sci. (C)* 1966, **14**, 173
- Fischer, E. W. and Lorenz, R. *Kolloid-Z.* 1963, **189**, 97
- Fischer, E. W. and Schmidt, G. *Angew. Chem.* 1962, **74**, 551
- Flory, P. J. *J. Am. Chem. Soc.* 1962, **84**, 2857
- Peterlin, A. and Meinel, G. *J. Polym. Sci. (B)* 1965, **3**, 1059
- Keller, A., Martuscelli, E., Priest, D. and Yudagawa, Y. *J. Polym. Sci. (A-2)* 1971, **9**, 1807
- Frohlich, H. *Proc. Phys. Soc.* 1942, **54**, 422
- Powles, J. G. and Strange, J. H. *Proc. Phys. Soc.* 1963, **82**, 6
- Waugh, J. S. and Wang, C. H. *Phys. Rev.* 1967, **162**, 209
- Okano, K. *Rep. Inst. Phys. Chem. Res. (Tokyo)* 1965, **40**, 273
- Hoffman, J. D. *J. Chem. Phys.* 1952, **20**, 541
- Moore, R. S. and Matsuoka, S. *J. Polym. Sci. (C)* 1964, **5**, 163
- McBrierty, V. J. and Douglass, D. C. to be published
- Nielsen, L. E. *J. Polym. Sci.* 1960, **43**, 357
- Balta Calleja, F. J., Bassett, D. C. and Keller, A. *Polymer* 1963, **4**, 269
- Billmeyer, F. W. 'Textbook of Polymer Science', Wiley-Interscience, New York, 1971, p 383
- Bunn, W. C. and Alcock, T. C. *Trans. Faraday Soc.* 1945, **41**, 317
- Mandelkern, L. *J. Polym. Sci. (C)* 1966, **15**, 129
- Keith, H. D., Padden, F. J., and Vadimsky, R. G. *Science* 1965, **150**, 1026
- Larsen, D. W. and Strange, J. H. *J. Polym. Sci. (A-2)* 1973, **11**, 65, 449

# Developments in radiation-induced graft polymerization to cellulose

J. T. Guthrie

Department of Colour Chemistry and Dyeing, University of Leeds, Leeds LS2 9JT, UK

(Received 19 April 1974; revised 14 May 1974)

## INTRODUCTION

Such is the effort afforded studies of grafting to cellulose that several reviews have already been written on this topic. In many ways one can visualize a situation requiring a review of the reviews! As yet, however, industrial interest has been minimal. Whether or not this debility arises from within industry or the research centres is debatable. It is reasonably clear that, despite having many advantages to offer relative to alternative industrial processes, graft polymerization reactions have not been examined to decide their viability. In view of the simplicity of operation, radiation-induced grafting processes appear worthy of much greater attention. Whilst one may attempt to review completely the developments made in radiation grafting in recent times, the advances made are such that the task is beyond the scope of a single publication. Here we are primarily concerned with modern progress in radiation-induced grafting to cellulose and its more common derivatives. Where necessary, however, reference to other substrates may be made for comparison. The theme throughout is publication of the industrial potential of the technique, those applications already in existence and advantages to be gained through their use.

There are in existence reviews which deal with the subject of grafting to cellulose in varying degrees of detail. In some of these radiation dependent methods are considered along with other methods of initiation. The number of reviews devoted to radiation induced processes is very small. Krassig and Stannett<sup>1</sup> set the standard in general reviews of grafting to cellulose which has yet to be matched for comprehensiveness and lucidity. Battaerd and Tregear<sup>2</sup> covered the general and patent literature though their treatment was less comprehensive. More recent reviews have been published by Hebeish<sup>3</sup>, Nakamura<sup>4</sup>, Matsuzaki and Nakamura<sup>5</sup>, Stannett and Hopfenberg<sup>6</sup>, Rogovin<sup>7</sup> and Le Gall<sup>8</sup>.

Apart from reviews by Moore<sup>9,10</sup> only three other publications are available dealing specifically with the radiation-induced graft polymerization of vinyl monomers to cellulose — by Hoffman<sup>11</sup> and by Arthur<sup>12,13</sup>. The review by Hoffman deals with industrial possibilities whilst Arthur's publications describe advances in the general knowledge of the subject. In the latter instance considerable emphasis is placed on the effects of radiation on the substrate.

As an indication of the interest in grafting processes involving cellulose as the substrate, the proceedings of a symposium held on this topic have recently been published<sup>14</sup>. The field of reference was broad and the treatments given were comprehensive.

In this review a logical progression is followed. Initially,

the techniques available in radiation grafting are outlined. Although the coverage is not absolute, much of the recent literature is cited and should be referred to for further details. Thus literature, relevant to radiation-induced grafting to cellulose, is covered in tabulated fashion. This approach enables easy reference to be achieved. Aspects of the subject which have advanced considerably since the review by Krassig and Stannett<sup>1</sup> and those of Moore<sup>9,10</sup> are dealt with in depth in later sections. Emphasis on applications, characterization, grafting to timber and the patent literature is necessary since these areas have been somewhat neglected in the past.

Those interested in cellulose modification through radiation grafting techniques are advised to consult consistently the work of Arthur *et al.*, Dilli and Garnett, Huang and his group, Stannett *et al.* and Usmanov *et al.* Whereas some of the research concerned with grafting to cellulose is of a repetitive nature, that of the above mentioned is invariably of high quality and original.

It is interesting to note that the bulk of the scientific literature relating to grafting arises from research carried out in academic surroundings and that this work is now reaching the patent application stage. Industry has seemed to be hitherto reluctant to investigate the potential of the process. This observation runs contrary to most areas of research. Possible explanations include an unwillingness to change in industries involved in cellulosic products, problems associated with radiation sources, and the relative novelty of the technique. The present time is ideal for the commercial exploitation, on a wide scale, of radiation-induced grafting in a variety of situations.

## TECHNIQUES OF RADIATION-INDUCED GRAFTING

All modes of graft copolymerization of vinyl monomers to cellulose require that the substrate be accessible to the monomer. For vapour phase processes this is not a particularly restrictive limitation. However, for both pre-irradiation and simultaneous processes in which the grafting system is heterogeneous, the problem of swelling the substrate arises. For cellulose derivatives this does not present any difficulty provided the derivative is soluble in the monomer or alternatively that both the monomer and derivative are soluble in the solvent selected. This need of access of the monomer into the cellulose substrate is not peculiar to cellulose alone but exists irrespective of the nature of the substrate. In the absence of swelling, grafting is limited to the surface regions of the parent matrix whereas with increased swelling volumetric grafts are obtained.

In general, two fundamental processes are available for radiation-induced grafting.

*Pre-irradiation method*

Here the substrate is irradiated, either in the presence of air or its absence, before being brought into contact with the monomer whether in liquid, gaseous or solution form. In the absence of oxygen little or no homopolymer is formed whereas in the presence of oxygen, peroxy-radicals are formed within the substrate. These can be made to decompose on heating in the presence of a monomer, giving grafting and some homopolymerization. This homopolymerization occurs through chain transfer to the monomer.

Difficulties often put forward against the use of pre-irradiation as a technique usually centre around the sensitivity of the substrate to radiation damage and factors related to the swelling of the substrate. Features concerning the substrate sensitivity are dealt with in later sections and the second aspect is now considered.

The effect of any cellulose pre-treatment, monomer type and concentration, presence of additives, the dose rate and total radiation dose and the substrate structure all play some part in the ultimate grafting efficiency. However, the major factor is the allowance, in the grafting procedure, for swelling of the cellulose before exposure to the monomer and subsequent grafting. Vapour phase grafting requires that the monomer be applied in a vapour medium which is able to enhance the swelling and reactivity of the cellulose matrix. This is also true of pre-irradiation grafting in heterogeneous systems using either monomer solutions incorporating a swelling agent or a hydrophilic monomer. Walsh<sup>15</sup> has studied, in detail, the effects of swelling on the pre-irradiation grafting of acrylonitrile onto cellulose during which the extent of grafting was noted to increase markedly provided an aqueous medium was employed. This indicates increased access of the monomer into the interior of the cellulose.

Another feature of importance is the nature of the cellulose substrate as seen through the extent of accessibility of the radical sites to the monomer or monomer solution. Grafting is thought to occur initially in the more accessible regions and then, as the substrate becomes modified in these areas, grafting proceeds in the otherwise less accessible regions. Since areas available to the monomer are also amenable to other reagents, for example oxygen, solvents etc., complications may arise. This is seen in the retardation of grafting by atmospheric oxygen. Hence strict interpretations or logic cannot always be applied. An example of this is the lower rate of grafting usually obtained with highly amorphous regenerated celluloses than occurs with substrates of greater crystallinity. This observation is contrary to expectations if accessibility to the monomer is taken as the sole factor of relevance.

The effect of the dose rate and total dose on the ultimate extent of polymerization is less important with pre-irradiation than with mutual techniques. This does not apply to the substrate which may degrade irrespective of the method of grafting employed if excessive doses are used. Within the context of industrialization the pre-irradiation technique is attractive. One may visualize long-term storage of large batches of substrate paper, textile or timber at low dose rates or short term exposure at high dose rates. Either method may be modified to meet particular needs. In this way particular batches can be called upon as required. Advantages to be gained over simultaneous techniques include ease of storage, personnel protection, plant cost and insulation, chemical efficiency, cost effectiveness, etc. Provided certain precautions are taken, as outlined below, there is little excuse for this type

of process not being utilized more readily in the future than it is at the present time.

Recent data concerning pre-irradiation grafting to cellulose and some of its more common derivatives are given in *Table 1*. Being reasonably comprehensive, the outline indicates that the technique is attracting considerable attention. Also of interest is the gradually increasing drift away from the use of the more conventional monomers into areas dealing with improvements to the substrate. This trend is to be encouraged since, to be commercially viable, the products obtained by graft copolymerization must be designed to meet specific needs such as low cost, high efficiency or superior physical characteristics.

*Simultaneous irradiation technique*

Irradiation of a cellulosic substrate in the presence of the monomer whether in the vapour or liquid phase, bulk or solution system, heterogeneous or homogeneous in nature, is termed the mutual or simultaneous method. Factors of importance to the pre-irradiation technique also apply to simultaneous grafting. These include the nature of the cellulose, its pre-treatments, contributions made to grafting efficiency by swelling agents, transfer agents and additives. Other factors to be considered are the ratio of monomer to solvent in the grafting solution, the ratio of monomer to substrate, diffusion aspects, the possibility of viscosity effects taking place, accurate temperature control, the presence of inhibitors and retarders etc.

Much of the earlier work in grafting has been concerned with mutual techniques, although only recently have the kinetics of the polymerization processes been dealt with in any detail whether qualitatively or quantitatively. Difficulties arose through the inability to determine with accuracy the concentration of monomer in the interior of the substrate during the grafting process. This is of critical significance to monomer/solvent systems since differences may exist between the concentration of monomer within the substrate and the bulk monomer concentration. Use of ultra-violet spectroscopy has resolved these difficulties to a certain extent and has enabled a more reasoned approach to the kinetics to be made.

Extensive volumetric grafting using the mutual process is dependent on swelling of the substrate. Here water has a particular part to play through its ability to break down the hydrogen bonded network in the cellulose. Low concentrations (2%) of water in a monomer/solvent system (assuming that either or both the monomer and solvent are miscible with water) greatly enhances the accessibility of the cellulose to the monomer solution. In the absence of a swelling agent grafting is minimal and is restricted to the substrate surface. From the point of view of general serviceability voluminal grafts are essential.

The swelling behaviour in a given system is dependent on the structure of the substrate cellulose whether cotton, rayon, fibre or film. Equally important is the monomer: solvent ratio which may override all other contributing factors in the grafting process. Areas of general interest include characterization of products, reaction kinetics in terms of chain transfer possibilities and relationships between experimental results and the composition of the monomer solution.

Data relating to the mutual irradiation technique are presented in *Table 2*. The list of observations made is reasonably comprehensive though a fuller treatment may be found in the text.

Table 1 Recent developments in pre-irradiation grafting to cellulose\*

Substrate	M	MP	SA	T (°C)	Remarks	Ref.
Cellulose or derivative	S and AN	solution	Aqueous	RT	i.r. spectroscopy used as means of determining the extent of grafting; samples prepared by KBr pressed disc method; absorption bands at 700 cm <sup>-1</sup> (styrene) and 2249 cm <sup>-1</sup> (acrylonitrile) monitored	16,17
Cotton cellulose	EA	solution	CH <sub>3</sub> OH/H <sub>2</sub> O	25	radical accessibility assessed by e.s.r.; acceleration in rate observed, thought to be due to presence of water; maximum grafting at phase boundary conditions	18
			(CH <sub>3</sub> ) <sub>2</sub> C=O/H <sub>2</sub> O	25	radical scavenging observed by e.s.r.; grafting less than with methanol/water; no Trommsdorff effect observed	19
			CH <sub>3</sub> OH/H <sub>2</sub> O	25	effect of oxygen on grafting observed by e.s.r.; effect of temperature increase on the extent of grafting followed; e.s.r. spectra interpreted	20
Cotton cellulose	MA	solution	Aqueous	25	e.s.r. spectra obtained and interpreted; evidence of existence of poly(methacrylic acid) radicals given	21
	S	solution	Both dry and aqueous	50–117	effect of oxygen on degree of grafting; effect of water decreased the amount of grafting when adsorbed; grafting decreases as T increases; e.s.r. measurements analysed; effect of oxygen on the radical yield determined	22
Cotton cellulose	AN + other monomers	solution	H <sub>2</sub> O CH <sub>3</sub> OH DMSO MEK	25	copolymerization of acrylonitrile and one other monomer from a series of binary mixtures; comprehensive discussion	23
Cellulose fibres	EA	solution	Aqueous	25–35	high grafting yields; grafting yields examined above T <sub>g</sub> ; levels for elasticity outlined; effect of the comonomer dependent on the functionality of the comonomer; grafting rate increases as temperature increases in the range 25–35°C but not above 60°C; electron microscopic study carried out.	24
Cellulose	MVK	solution	H <sub>2</sub> O CH <sub>3</sub> OH DMF	25	effect of DMF on grafting assessed and compared with CH <sub>3</sub> OH; i.r. band at 5.85 μm used to detect C=O group; mechanical properties determined; tensile characteristics reduced on grafting; other desirable properties imparted to the substrate	25
Cellulose	A	vapour	Aqueous	—	evidence of crosslinking of cellulose by acrolein obtained; strength and flexibility deteriorated on grafting; no homopolymerization observed	26
Cellulose	MMA	vapour	RT → 65°C	—	presence of air enhanced grafting; grafting increased with temperature to a maximum at 65°C; beyond this point the rate falls off; E <sub>a</sub> = 640 kJ/mol; radical mechanism indicated	27
Cellulose	S VA 2-VP 4-VP	solution	CH <sub>3</sub> OH	60	various low dose rates used; small amounts of additives employed and their effect assessed; acridine suppressed, anthracene inhibited and halobenzenes sensitized t.a. reaction	28
Cotton rayon	S MMA α-methyl-S	—	—	—	single fibre strength remained unchanged but tenacity in g/denier decreased as grafting increased; apparent degree of grafting > true extent observed	29
Cellulose and cellulose triacetate	S and BA	solution	CH <sub>3</sub> OH	0	irradiation in air; monomer mixtures used; reactivity ratios different than with AIBN initiation; trapped radicals in cellulose and peroxide radicals in cellulose triacetate found to be the active initiation species; kinetics studied	30
Cellulose	BMA	solution	Aqueous CH <sub>3</sub> OH	25	cellulose copolymerized with butyl methacrylate; distribution of monomer within the fibre investigated; grafted fibre shows better resistance and flexural properties	31
Cotton cellulose rayon, cellulose triacetate	MMA MAA	solution	CH <sub>3</sub> OH DMSO	60	polymer structure studies after thorough removal of occluded homopolymers; n.m.r. used to characterize the grafted species	32
Cotton cellulose	VFF	vapour	Aqueous vapour CH <sub>3</sub> OH vapour	—	grafting studied in presence and absence of H <sub>2</sub> O and CH <sub>3</sub> OH; vapours enhanced grafting; excellent laundering and crease resistance characteristics observed; stability to u.v. irradiation increased	33

-cont.

Table 1 Recent developments in pre-irradiation grafting to cellulose\*—cont.

Substrate	M	MP	SA	T (°C)	Remarks	Ref
Ethyl cellulose	MA	vapour	None	25	air retarded the grafting reaction; i.r. used to follow the grafting reaction; identification of the grafted branches attempted; short branches obtained; substrate exposed to vapour of monomer	34
Rayon	EA MMA	solution	H <sub>2</sub> O	50	aqueous emulsion medium used; pre-irradiation and chemical initiation compared; effect of temperature on radiation induced methods covered; the morphology of the copolymer investigated; studies show that elastomeric properties require volumetric grafting which expands and disrupts the rayon fibre	35
Cotton cellulose	VF	vapour	—	—	vinyl fluoride grafted onto cotton cellulose	36
Cellulose acetate (DS 1.84–2.25)	S	solution	pyridine	25	e.s.r. used to investigate the grafting process; radical decay rate at 25°C slow; the e.s.r. spectrum does not change on addition of monomer suggesting that chains grow and terminate rapidly compared with the cellulose radical decay rate; high yields and molecular weights of branches anticipated	37
Cotton cellulose	AN	solution	H <sub>2</sub> O/ZnCl <sub>2</sub>	25	an e.s.r. study; effects of various factors including copolymerization on radical yields and the nature of spectra interpreted; suggested radical sites given	38
Cotton cellulose	AN	solution	H <sub>2</sub> O/ZnCl <sub>2</sub>	25	method of separation of grafts from the backbone quoted; grafts analysed for molecular weight characteristics	39
Cotton cellulose	BMA and AN singly and mixtures	solution	—	23	emphasis on structural determinations by electron microscopy; dye uptake used as monitor of uniformity of grafting	40
Cellulose	AN S	solution	benzene DMF	—	radiochemical yields of graft polymerization reactions of cellulose; mutual and pre-irradiation considered	41
Cotton cellulose	AN S MMA VA	solution	various	various	electron microscopic study of various cellulose—comonomer grafts prepared under both pre-irradiation and simultaneous techniques; location of graft partly dependent on monomer grafted	42
Cellulose acetate	S	solution	CH <sub>3</sub> OH	50 (in N <sub>2</sub> )	radical sites labelled with bromine atoms; methanol remarkably increased the lifetimes of the individual graft radicals but decreased the growth rates	43

\* The symbolism used is given in the Appendix

Table 2 Recent developments in the simultaneous (mutual) irradiation technique\*

Substrate	M	MP	SA	T (°C)	Remarks	Ref.
Cellulose acetate and others	S AN MA VA	solution	—	—	reactivity ratios in various radiation and redox initiated systems compared and discussed; homogeneous and heterogeneous conditions used; abnormal behaviour at low degrees of grafting which normalized with increased grafting	44
Cellulose (regenerated)	MMA	solution	acetone	RT	samples soaked in monomer then irradiated; acetone as solvent for MMA gave enhanced grafting; effect of AQ (none), hydroquinone (marginal) and oxygen (marginal) on grafting monitored	45
Cellulose	S	solution	H <sub>2</sub> O/dioxane	30	quantitative method of determining the concentration of monomer at the grafting sites described in detail using u.v. spectroscopy	46
Cellulose (regenerated)	S	solution	H <sub>2</sub> O/dioxane	30	kinetics of grafting investigated; effect of water on the grafting and swelling characteristics of the substrate studied; cellulose degradation studied viscometrically	47
Cellulose (regenerated)	S	solution	H <sub>2</sub> O/dioxane	30	ratio $k_p^2/k_t$ was 10 <sup>5</sup> greater for grafting than homopolymerization; e.s.r. used to identify radical types and radical decay; values for $G(\text{scission})$ in both air and vacuum obtained	48
Cellulose (regenerated)	S	solution	H <sub>2</sub> O/dioxane	30	technique of isolation of grafted branches from the substrate given; other methods discussed	49
Hydroxyethyl cellulose (DS 0.4)	S	solution	H <sub>2</sub> O/dioxane	RT	kinetics of grafting discussed; comparisons made with cellulose substrates; effect of physical form on grafting ascertained	50

—cont.



Table 2 Recent developments in the simultaneous (mutual) irradiation technique\*—cont.

Substrate	M	MP	SA	T (°C)	Remarks	Ref
Carbanilated celluloses (DS 0 → 0.52)	S	solution	H <sub>2</sub> O/dioxane	30	effect of radiation protection of cellulose on radical yields and grafting behaviour investigated; kinetic appraisal of results made	51
Cellulose	S	solution	CH <sub>3</sub> OH	20–25	effect of additives on grafting investigated; non-aromatic additives reduced grafting, radical scavengers suppressed grafting; non-aromatics showed little change apart from anthracene and acridine; reaction mechanisms discussed	52
Cellulose rayon	various	solution	—	—	general observation of decrease in the substrate strength with increase in dose	53
Cellulosic textiles	AN	solution	acids alcohols and hydrocarbons	25–50	sensitizers used to enhance grafting; grafting observed to increase with increase number of atoms in the additive both in the presence and absence of air	54
Cellulosic fibres	S MMA	—	none and H <sub>2</sub> O comparison	various	simultaneous and pre-irradiation methods considered; various factors examined relating to grafting; problems encountered in grafting critically assessed; semi-review	55
Rayon	S	solution	methanol and water	—	comparison between cellulose and poly(vinyl alcohol) as substrates in terms of characterization of grafted chains; methods of isolation of grafts outlined; mutual and pre-irradiation techniques compared	56
Cellulose and others	S 4-VP 5-methyl-2-VP	solution	various polar solvents	—	effect of substrate type on grafting investigated; for S in CH <sub>3</sub> OH; cellulose exhibited Trommsdorff effect; results interpreted in terms of charge transfer theories	57
Cellulose	S and substituted S MMA VA VP	solution	wetting and non-wetting solvents	—	variety of solvents assessed for effect on grafting; S + <i>o</i> -, <i>m</i> - and <i>p</i> -derivatives investigated; Trommsdorff observed at low doses and dose rates; effect of O <sub>2</sub> , N <sub>2</sub> and vacuum assessed; rate of energy transfer discussed	58
Cellulose	S MMA VA	solution	dioxane DMF acetone	RT	effect of air and vacuum on polymerization investigated; grafting in various cellulose wetting solvents studied; mechanistic interpretation discussed	59
Cellulose	S	solution	CH <sub>3</sub> OH	RT	grafting at low dose rates studied; effect of oxygen ascertained; evidence of Trommsdorff behaviour noticed	60
Cellulose	S and substituted styrenes and others	solution	CH <sub>3</sub> OH	various –196 to +40	effect of temperature on the grafting reaction observed as indication of contribution of ionic mechanisms to the process; various monomers used to correlate grafting results with Hammett constants	61
Cellulose	S MMA VA 2-VP 4-VP	solution	non-wetting solvents	RT	poor grafting yields observed; results interpreted in terms of charge transfer theories; methanol enhanced grafting in all cases	62
Cellulose	S MMA VA 2-VP 4-VP	solution	CH <sub>3</sub> OH	RT	appreciable grafting at room temperature in air and vacuum; dose and dose rate dependence found; evidence of Trommsdorff effect observed; mechanism proposed for the grafting process	63
Cellulose	S	solution	CH <sub>3</sub> OH	RT	kinetics of grafting studied in a non-quantitative manner; dose dependence observed and effect of air and vacuum on grafting investigated; radical scavenging by methanol proposed for poor grafting yields	64
Cotton cellulose	HEMA HPMA	solution	H <sub>2</sub> O CH <sub>3</sub> OH DMF DMSO and combinations	24	kinetic analysis attempted; organic solvents decreased amount of grafting; reactions diffusion controlled and exhibited second order kinetics; various factors investigated, e.g. monomer concentration, dose rate, swelling agents	65
Cotton cellulose	MAA MAN 6-FIPA NVC	solution	1,2-DCE and CH <sub>3</sub> OH/H <sub>2</sub> O	25	textile properties of various cellulose graft copolymers and terpolymers investigated and related to the chemical structures of the monomers and the glass transition temperatures of the homopolymers	66
Cotton cellulose	S AN singly and mixtures	swollen substrate	Primary alcohols	—	industrial potential of grafting process assessed; grafts examined for various physical and structural properties	67

\* The symbolism used is given in the Appendix

## KINETICS OF THE GRAFTING REACTION

Until comparatively recently the mechanism of the grafting process was far from well understood. Considerable difficulties arose from the inability to quantify the concentration of monomer at the grafting sites during the grafting reaction. This position has now been improved through u.v. spectroscopic analysis of ungrafted monomer extracted from the substrate prior to and during grafting<sup>46</sup>. Further problems have been overcome by the use of e.s.r. spectroscopy in ascertaining the locations of the radicals within the cellulose substrate (see later).

Attempts have been made to measure the contribution of various solvents for the monomer, to the grafting reaction. This may take the form of swelling the substrate<sup>33</sup>, solvency for any homopolymeric species, participation in chain transfer processes and so on. The roles of various additives on grafting have been investigated<sup>28,45,52</sup> as have the effects of temperature<sup>61</sup>, viscosity of the grafting medium<sup>47,48</sup>, the nature of the substrate and the value of radiation protection<sup>51</sup>.

A generalized reaction scheme for the radiation-induced grafting of vinyl monomers (M) to cellulose (P) may be written in a manner which is analogous to that of homogeneous homopolymerization, with equations to represent the various stages.

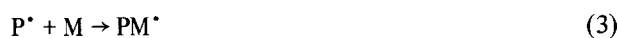
Initiation (radical formation):



and



Initiation (grafting):



and



Propagation:



Termination:



Certain features of this scheme apply to grafting to cellulose. Steps (1), (3), (5), (7) and (8) are important reactions during pre-irradiation induced polymerization whereas all steps are possible using the simultaneous method. Where the  $G$  (radical) value of the monomer is higher than that of the substrate, reaction (2) produces problems through homopolymerization. The converse favours grafting and will be accompanied by correspondingly less homopolymer formation. In the propagation stages, diffusion plays a fundamental part, especially in bulk polymerizations

or polymerizations taken to high conversion. Not allowed for, but equally important, is the part played by the solvent in initiation and termination through transfer. At high extents of grafting, termination reactions become more difficult generally. However, reactions (7) and (8) are likely to be more seriously affected because of restrictions within the matrix.

Before we can proceed further in a kinetic analysis certain assumptions relating to the grafting medium are required. These have been outlined by Guthrie *et al.*<sup>47,48</sup>. Of importance are the nature of the grafting sites in terms of the substrate, the monomer and any swelling agent. One must also consider the effects of radiation on each of the species present in the system. Information required includes the concentration of each of the reactants in terms of the other reagents per unit volume of grafting medium. Thus it is more realistic to express rates of grafting as the number of moles of monomer grafted to the cellulose per unit volume of swollen substrate rather than as amount of add-on per unit mass of original substrate per unit time.

For the grafting process, the following rate equations apply.

Initiation (primary copolymer radicals):

$$R_i = k_i [P^*] [M] \quad (10)$$

Propagation:

$$R_p = k_p [PM_n^*] [M] \quad (11)$$

Termination:

$$R_t = 2k_t [PM_n^*]^2 \quad (12)$$

where  $P^*$  represents cellulose radicals,  $M^*$  the monomer and  $PM_n^*$  the growing polymer radicals respectively.  $k_p$  and  $k_t$  are the rate constants for propagation and bimolecular termination. Equation (11) gives the rate of polymerization. From this we obtain an equation to represent the rate of change of the graft copolymer radical concentration,  $[PM_n^*]$  thus:

$$d[PM_n^*]/dt = k_i [P^*] [M] - 2k_t [PM_n^*]^2 \quad (13)$$

At the steady state the rate of change of  $[PM_n^*]$  is small compared to its rate of formation and disappearance so we may state that:

$$[PM_n^*] = (R_i/2k_t)^{1/2} \quad (14)$$

Combination of equations (11) and (14) yields:

$$R_p = k_p (R_i/2k_t)^{1/2} [M]$$

or alternatively:

$$k_p^2/k_t = 2R_p^2/[M]^2 R_i \quad (15)$$

We must now consider the rate of initiation in the grafting process,  $R_i$ . Odian<sup>68</sup> has shown that in grafting styrene to polyethylene this rate of initiation is adequately expressed as:

$$R_i = GI\rho/100N_A \quad (16)$$

Equation (16) may be applied to cellulose grafting where

the terms have the following significance:  $G$  = the number of radicals formed in the cellulose for each 100 eV of absorbed energy,  $I$  = the radiation intensity ( $\text{eV g}^{-1} \text{s}^{-1}$ );  $\rho$  = the concentration of accessible cellulose ( $\text{g/dm}^3$  of substrate).  $[M]$  is the concentration of monomer at the grafting site expressed as mol of monomer/ $\text{dm}^3$  of swollen substrate. Factors relating to the determination of  $\rho$  and  $[M]$  have been outlined by Guthrie *et al.*<sup>48</sup>

Comparison of values of  $k_p^2/k_t$ , calculated for grafting and attendant homopolymerization systems, can be used to quantify the autoacceleration known to occur in grafting<sup>68</sup>. This approach has been used in the grafting of styrene to cellulose where the value for grafting was  $6.0 \times 10^5$  greater than observed in the corresponding homopolymerization<sup>47,48</sup>. Although this is the first quantitative evidence of the Trommsdorff effect in cellulose grafting several qualitative indications have been reported<sup>64,69,70</sup>. Such evidence centres around the fact that in cellulose grafting, grafts have been obtained with very high molecular weights relative to the homopolymer. Data collected indicate that grafts with molecular weights 30 times those of the homopolymer, are not uncommon.

Validity of the procedures adopted to calculate  $k_p^2/k_t$  is seen in the close agreement between values obtained by Guthrie<sup>47,48</sup>, for radiation-induced styrene homopolymerization ( $2.0\text{--}3.0 \times 10^{-4} \text{ l mol}^{-1} \text{ s}^{-1}$ ) and those published by George<sup>72</sup> in bulk styrene homopolymerization ( $1.0 \times 10^{-4}$  to  $1.8 \times 10^{-4} \text{ l mol}^{-1} \text{ s}^{-1}$ ).

Differences in  $k_p^2/k_t$  for grafting relative to homopolymerization are usually accounted for by viscosity or Trommsdorff effects. However, when solvents are used, the possibility of chain transfer to the solvent cannot be ignored. This transfer would be greater in the bulk solution than in the polymer matrix if the concentration of solvent were less in the substrate. Hence termination is easier in the bulk solution, which results in lower  $k_p^2/k_t$  values being obtained.

In the styrene–cellulose–dioxane–water system extensive transfer to the solvent was demonstrated in homopolymerization<sup>71</sup>. The constant for chain transfer to the solvent (dioxane/water) was  $C_s = 1.24 \times 10^{-4}$ . Ham<sup>73</sup> has shown that the value of  $C_s$  for the styrene–dioxane system is essentially zero. It would seem, therefore, that chain transfer, resulting in lower values of  $k_p^2/k_t$ , arises from the presence of water in the mixed solvent. Any water in the cellulose interior is not so readily available for transfer through being tightly bound to the matrix in preferential adsorption. Hence chain transfer within the growing grafted chains is less likely. However, the preponderance of the Trommsdorff effect arises from physical restrictions within the interior of the graft copolymer.

Unless suitable precautions are taken, simultaneous grafting methods may result in excessive involuntary homopolymerization, a potential nuisance factor to commercialization. This can be avoided by considering only those systems in which  $G$  (radical) substrate  $>$   $G$  (radical) monomer. Other variables such as solvent effects, affinity of the monomer for the substrate and the presence of inhibitors require some attention. Often the proportion of grafting over homopolymerization is improved using comonomers in the grafting process. Examples include butadiene–styrene, styrene–methacrylic esters, styrene–acrylic acid and acrylonitrile–butadiene.

Most kinetic and mechanistic studies of radiation-induced grafting have been carried out at very high dose rates and

total doses. There is a lack of data relating to investigations at low dose rates. Available information<sup>46,47,49,60</sup> contains some interesting observations. These include such features as extremely high average molecular weights in branches and homopolymer at low conversion which decrease with increasing total dose, complex molecular weight distribution patterns as shown by gel permeation chromatography (g.p.c.) and ideality in behaviour with regard to the monomer (to the first power) and the radiation intensity (square root of the dose rate) dependence.

The occurrence of post-irradiation grafting and homopolymerization (by transfer from the substrate), involving trapped radicals within the cellulose interior, has been demonstrated. However, most post-irradiation grafting is minimal compared with pre-irradiation and simultaneous grafting.

Free radical grafting reactions undergo classic inhibition and retardation. Air is seen to retard grafting whilst the addition of low concentrations of an inhibitor, for example *p*-benzoquinone, prevents polymerization by rapid termination of radicals. The interference by oxygen is not well defined though it involves the formation of peroxy-radicals either in the monomer, the cellulose, solvent or any other additive. Subsequent grafting will be dependent on the decomposition of these peroxy-radicals which is a more complex and usually slower process than primary radical formation. Some reports indicate that oxygen plays little part in the grafting process<sup>58,59</sup>, findings which are disputed by others<sup>47</sup>. This contention indicates that further controlled work is needed to clarify the position.

Other factors of importance include adequate temperature control, swelling, and the presence of additives. Studies of grafting to cellulose are not always carried out at carefully controlled temperatures. This is surprising since the temperature can markedly affect the grafting medium via diffusion, increased reactivity and accessibility. Grafting at elevated temperatures favours the more amorphous substrates such as cellophane or rayon whereas lower temperatures are more suitable for cotton. A suitable general temperature range for enhanced grafting is  $60\text{--}70^\circ\text{C}$ . Recent accounts of the effect of swelling agents on grafting<sup>58,59,74–77</sup> indicate that the greater the substrate swelling the more efficient will be the grafting reaction, provided the swelling agent does not chemically interfere. This point has been investigated by Reine *et al.*<sup>74</sup> using aprotic solvents to study the stability of free radicals in  $\gamma$ -irradiated cellulose. Although the substrate becomes highly swollen in solvents such as dimethylformamide or dimethylsulphoxide, the radical concentration is seriously reduced. This suggests that these solvents are unsuitable for cellulose grafting. At elevated temperatures the extent of termination is even more marked owing to greater accessibility of the solvent.

Various additives have been used in cellulose grafting to ascertain their effect on the system. Much of this work has been completed by Dilli and Garnett<sup>52,62–64</sup>. The scope of their investigations incorporated a range of acetone, aniline, benzaldehyde, hydroquinone, thiourea, thiophene, pyridine, benzene, naphthalene, pyrene, phenanthrene, durene, hexamethylbenzene, stilbene, acridine and the halobenzenes. Inhibition was observed when low concentrations ( $10^{-2} \text{ mol}$ ) of non-aromatics were used whereas high concentrations sensitized the reaction. Hydroquinone and thiourea suppressed grafting when present in high concentrations. Anthracene, pyrene and acridine gave reduced yields but other aromatics had only marginal effects. Aro-

matic compounds are known to operate by means of energy transfer and radical scavenging. Inhibition by essentially non-aromatic compounds is thought to arise from competitive radical-additive reactions owing to the high  $G$  (radical) values of the additive. With high concentrations of non-aromatic, polar additives the grafting yields increase presumably owing either to the effect of the additive on the swelling of the substrate or to indirect activation of the cellulose.

Although work has been devoted to the kinetics of grafting much remains to be done in other areas. Prime among these is the need for methods of producing low molecular weight grafts randomly distributed throughout the substrate in reasonable concentrations. Commercial exploitation is more likely to concern multitudinous grafts of relatively low molecular weights since these will have a greater effect on the properties of the substrate.

### EFFECTS OF HIGH ENERGY RADIATION ON CELLULOSE

It is meaningless to speculate on the viability of radiation grafting to cellulose without first considering the effect of radiation on the cellulose. Irrespective of the technique used in grafting, one consequence of exposure to high energy radiation is damage to the substrate. Opinions vary as to the sensitivity of cellulose to high energy radiation. However, it is known that some forms are more prone to degradation than are others. Here we view the problem through changes in physical properties and subsequently show the value of e.s.r. spectroscopy to studies of radical location, cellulose sensitivity and structural interpretation.

#### Cellulose degradation

Several factors contribute to the overall deterioration including the presence of moisture, oxygen, additives, sensitizers, protecting groups, the dose rate and the total dose. The threshold level for radiation damage is relatively low. Fortunately it is recognized that dose levels needed to encourage grafting are significantly below those likely to cause extensive damage to the cellulose.

The effects of radiation on cellulose can be seen in many ways. These include e.s.r. spectroscopy, changes in thermal and mechanical properties, molecular weight determinations, chemical methods such as end-group analysis and spectroscopic methods.

Factors of importance to any study of radiation damage to cellulose are the reaction conditions, substrate composition and morphology, previous chemical and physical modifications and the presence of trapped radicals. Although the main consequence of irradiating cellulose is degradation, there is growing evidence that some crosslinking takes place when cellulose is irradiated in aqueous media<sup>80-82</sup>. This suggests that the events secondary to initial irradiation are highly complex. However, there is little doubt that the major consequence is chain scission. The formation of carboxyl groups, increase in solubility in alkaline solution on progressive irradiation and the development of characteristic e.s.r. spectra indicate the nature of the scission process. The occurrence of chain cleavage during grafting reactions would result in the product containing varying amounts of block copolymer. This might create difficulties in interpreting the nature of the graft copolymer. Normally chain scission is less using simultaneous irradiation than occurs with pre-irradiation grafting unless both reactions are carried out in the absence of air, when equal cleavage occurs.

Guthrie *et al.* have investigated the degradation of regenerated cellulose, viscometrically, using Cadoxen as a solvent for cellulose.  $G$  (scission) values were 24.6 and 13.5 respectively for samples irradiated in air or vacuum. The corresponding threshold values for radiation damage were 10 and 200 J/kg. These threshold values are below previously accepted degradation levels. Exposure of samples irradiated in vacuum or air to the atmosphere at 65% relative humidity gave greatly enhanced degradation even on removal from the radiation source. Examination of samples 21 days after irradiation produced values of  $G$  (scission) of 143.0 and 186.5 for vacuum and air irradiated samples respectively. Similar observations have been made by Leuthy in his derivation of the relationship between the total radiation dose and the intrinsic viscosity of the resulting celluloses<sup>83</sup>.

Arthur *et al.*<sup>84</sup> have studied the oxidative reactions of cellulose initiated by free radicals. The formation of free radicals increases the reactivity of cellulose mainly through dehydrogenation and oxidative depolymerization reactions. Panchenkov *et al.*<sup>85</sup>, in their work on the mechanical properties of filaments of cellulose and its esters, observed reductions in breaking strength and elongation at rupture on irradiation. Decomposition was rapid at high dose rates in either air or vacuum.

In a comprehensive series of papers<sup>86-89</sup> Imamura and Ueno have studied the effects of radiation on a series of dissolving cellulose pulps. The nature of this high energy radiation, whether  $\gamma$ - or X-ray, produced the same chemical and physical effects. The rate of chain cleavage was directly proportional to the dose. Nitration of the irradiated celluloses and their subsequent characterization by g.p.c. gave a decrease in molecular weight and an increase in molecular weight distribution with increase in the total dose. This indicates that the radiation damage is non-random but occurs predominantly in the lower molecular weight regions. Such degradation is enhanced by elevation of the temperature.

Potential industrial processes are suggested from this work especially in aspects of cellulose regeneration. Further investigation has shown that xanthation of these irradiated celluloses, producing useful viscoses, is possible without preliminary ageing. This process is thought to have great practicability provided the total dose is limited to 2 Mrad.

The effect of  $\gamma$ -radiation on the low temperature, dilute acid hydrolysis of cellulose has been investigated by Kunz *et al.*<sup>90</sup> who obtained greater yields of glucose (27%) with irradiated samples than the un-irradiated ones. Such work suggests that low molecular weight products of crude cellulosic materials are obtainable in reasonable yields through preliminary extensive irradiation.

#### Electron spin resonance spectroscopy

Irradiated celluloses have attracted considerable attention for study by e.s.r. spectroscopy. Many of the parameters thought to influence e.s.r. spectra have been investigated. However, the spectra and their interpretations vary considerably depending on the nature of the substrate, the conditions of irradiation and spectra measurement, decay phenomena, the effects of temperature and so on. Ahmed and Rapson<sup>91</sup> interpreted such spectra in terms of the different crystalline structures used. Khamidov *et al.*<sup>92</sup> obtained  $G$ (radical) values for cellulose and some of its derivatives at various temperatures and also studied the kinetics of radical formation. The data indicate that the more crystal-

line celluloses produce a reduction in  $G(\text{radical})$  with increases in temperature which is not observed with the more amorphous samples. A possible cause of this difference is the reduction in mobility of excited species, owing to the greater crystallinity giving less substrate interaction.

One feature of this work is that, in the absence of air, no evidence of degradation was observed as a result of irradiation. This finding is substantiated by Guthrie *et al.*<sup>48</sup>, who in studies with regenerated cellulose, observed a doublet in the e.s.r. spectra of samples irradiated under vacuum which is indicative of radicals at C<sub>1</sub> of the anhydroglucose unit. Air irradiated samples produced a quartet, one cause of which could be main chain cleavage. Exposure of samples, irradiated under vacuum, to the atmosphere and monitoring by e.s.r. spectroscopy showed a gradual change from a doublet to a quartet which indicates the role of oxygen and moisture in the degradation process.

Arthur *et al.*<sup>93</sup> have obtained the e.s.r. spectra of various crystalline modifications of celluloses irradiated in air. Celluloses I, II, III, and IV, partly decrystallized cotton cellulose, ball-milled cotton cellulose, Ramie cellulose and hydrocelluloses of cellulose III and IV were analysed. Radical formation was thought to involve both hydrogenation and chain cleavage. Accessible free radicals were rapidly terminated by water whilst radicals in the inaccessible regions remained unaltered even after long exposure to chemical agents. The e.s.r. spectra were explained in terms of inter- and intra-molecular bonding forces, particularly hydrogen bonding.

The existence of long-lived radicals is supported by Dilli *et al.*<sup>94</sup> who observed that significant concentrations of radicals remained in the cellulose four years after irradiation and storage at ambient temperature. Elevation of the temperature, in the range 25–70°C, caused a rapid reduction in the radical concentration to take place. Beyond 70°C, little effect on the radical decay pattern was noticed. Radical decay was more rapid in vacuum than in air at these elevated temperatures, which again demonstrates the interference by oxygen in decay processes.

Baugh *et al.*<sup>38,95</sup> chose to interpret the e.s.r. spectra of various types of irradiated cellulose in terms of the possible location of the radicals within the anhydroglucose unit. Radicals in cellulose I (containing regain moisture) dehydrogenation at the C<sub>5</sub> atom; radicals in cellulose II, dehydrogenation at the C<sub>5</sub> atom and also dehydrogenation of the OH group or dehydroxylation at C<sub>6</sub>. Since these studies were carried out in air, interference from degradation effects cannot be ruled out. A commonly accepted value for  $G(\text{radical})$  of cellulose irradiated in air is 2.88<sup>79</sup> which comprises both the inaccessible and accessible radicals. A value of  $G(\text{accessible radicals only})$  of 1.6 has been suggested<sup>51</sup>, the residue being inaccessible to chemical attack. Thermal decay of radicals has been shown to be a second order process and the presence of several types of radical of different lifetimes is indicated.

#### INTRAMOLECULAR ENERGY TRANSFER IN CELLULOSES

Energy transfer processes in the solid state are generally considered to be dependent on the mechanism of energy loss by the incident radiation to the molecules, the initial random deposition and dissipation of the energy within the molecule and the rapid localization of the energy resulting in chemical and physical changes. The time required for this localization process is reported to be not less than 10<sup>-13</sup> s.

Grafting reactions and chemical substitution have provided considerable information concerning the processes of intramolecular energy transfer of high energy in carbohydrates<sup>97,98</sup>. Such information is important since this concept offers a means of protecting cellulose against otherwise inevitable damage when irradiated. As such, radiation protection may be an important factor in any commercial exploitation. Considerable work has been carried out in this area in recent years.

Arthur *et al.*<sup>99–102</sup> have investigated the radiation protection given to cellulose through substitution by a wide variety of aromatic groups. These include phenylcarbamoyl, benzoyl, naphthoyl, cinnamoyl, benzyl, benzydryl and trityl groups. All gave protection apart from the benzyl group. The level of substitution required to impart protection was found to depend on the particular group, the nature of its linkage to the cellulose chain and the stability of that linkage. In all cases, in which protection was observed, the substitution affected the localization of energy, reduced both the extent of degradation and also the radical concentration of the substrate. If localization of energy occurs and cleaves the aromatic group from the cellulose chain then the radiation protection of the cellulose chain by the aromatic group is ineffective. Modification of the aromatic group to bring about a reduction in the number of available  $\pi$  electrons results in a corresponding decrease in the level of protection.

Similar studies by Chidambareswaran *et al.*<sup>103</sup>, Guthrie *et al.*<sup>51</sup> and Singh *et al.*<sup>104</sup> have confirmed the protective nature of aromatic groups. Chidambareswaran compared benzylation with allylation and found that, while allylation influenced both the nature and yield of free radicals as seen through e.s.r., benzylation affected only the yield.

Substitution of cellulose using phenyl isocyanate to give products of low degrees of substitution ( $DS$ ) have been achieved by Guthrie *et al.* The carbanilated groups are very effective in protecting cellulose from radiation damage as seen through e.s.r. spectroscopy<sup>51</sup>. Irradiation of the carbanilated celluloses under vacuum produces the cyclohexadienyl radical whose spectrum is shown in Figure 1,

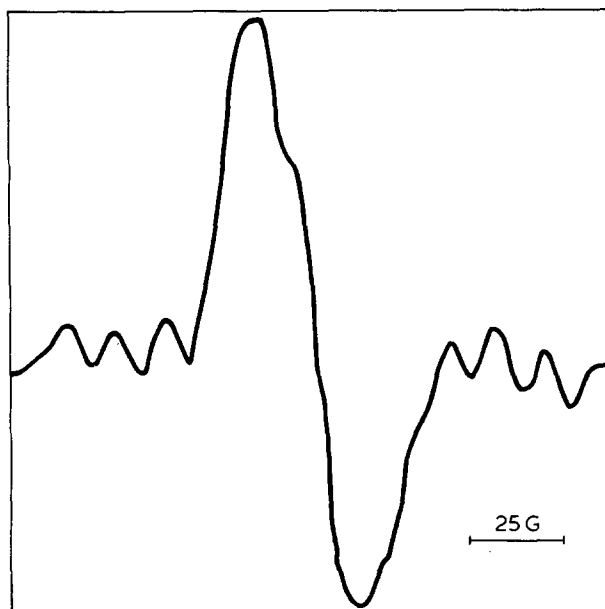


Figure 1 E.s.r. spectrum of a typical cellulose carbanilate sample ( $DS = 2.0$ ), irradiated under vacuum.  $DS$  determined by analysis for nitrogen

whilst that of the unsubstituted irradiated cellulose is given in Figure 2. No cyclohexadienyl radicals were observed in air irradiated samples owing to quenching with atmospheric oxygen and moisture. The lifetime of the cyclohexadienyl radical was approximately five hours after which time spectra similar to those of cellulose irradiated in air were obtained, although of much reduced intensity. Typical  $G(\text{radical})$  values were: cellulose ( $DS = 0.0$ ), 2.86; carbanilated cellulose ( $DS = 0.3$ ), 2.20; carbanilated cellulose ( $DS = 1.00$ ), 1.33; carbanilated cellulose ( $DS = 2.00$ ), 1.19.

In spectra of carbanilated celluloses, irradiated under vacuum, three radical species are indicated, those in inaccessible regions, in accessible regions and the cyclohexadienyl radicals. Quenching of radicals in the inaccessible areas can only be explained in terms of energy transfer to the aromatic group from the cellulose backbone, since the substitution takes place only in the accessible regions. Here we have definite evidence of the contribution made by low degrees of substitution of suitable groups, to the protection of the substrate. Damage to the substrate during further modification can be minimized without altering the nature of the cellulose too drastically. Thus grafting to reasonable extents is easy. Justification for this observation is shown in Figure 3 which relates changes observed in grafting behaviour to the level of substitution of the cellulose. The decrease in grafting is only marginal when compared with the protection offered the substrate.

Kinetic studies on substituted celluloses indicate that values of  $k_p^2/k_t$  decrease with increasing substitution. This suggests that viscosity or Trommsdorff effects are minimized, showing that lower molecular weight grafts are obtained. Such a feature is an asset in radiation-induced

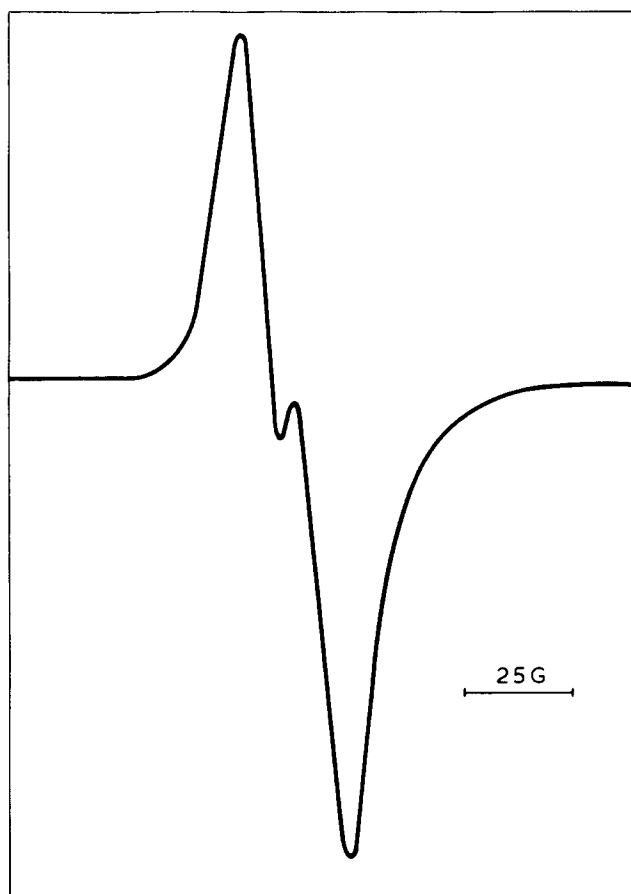


Figure 2 E.s.r. spectrum of a regenerated cellulose sample, irradiated under vacuum

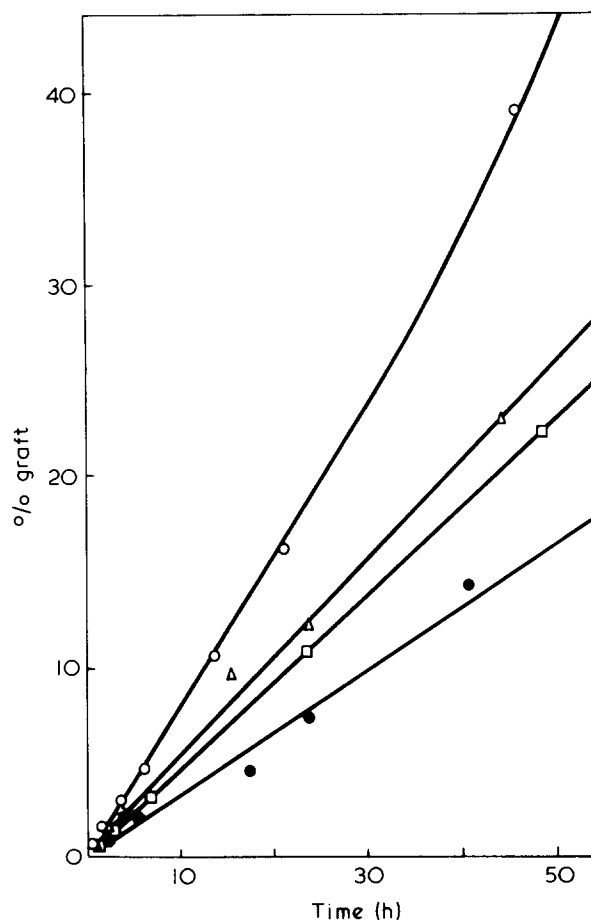


Figure 3 Extent of grafting versus irradiation time for various degrees of substitution ( $DS$ ). Styrene monomer used.  $\circ$ ,  $DS = 0$ ;  $\triangle$ ,  $DS = 0.02$ ;  $\square$ ,  $DS = 0.27$ ;  $\bullet$ ,  $DS = 0.50$ . Temperature =  $30^\circ\text{C}$ . Dose rate =  $0.37 \times 10^{-2}$  W/kg. Monomer concentration ( $S$ ) = 20% (v/v) in dioxane (78% v/v) and water (2% v/v)

modifications requiring many low molecular weight grafts rather than a few of very high molecular weight. Owing to the enhanced swelling imparted to the substrate by substitution, mobility of the grafted chains is facilitated, resulting in easier termination.

Singh *et al.*<sup>104</sup> have studied the protection by the furoate group as seen by substitution of cellulose with 2-furoyl, 5-methyl-2-furoyl, or 5-bromo-2-furoyl groups on fibrous cotton cellulose. Radiation sensitivity was reduced as was the energy localized on carbon atoms  $C_1$  and  $C_4$  of the anhydroglucose unit. This work has been patented<sup>105</sup> though the radiation protective effects are similar to those imparted by benzenoid groups.

Graft polymerization reactions may be used to impart stability to radiation damage in certain instances. In an e.s.r. study of cellulose acetate-styrene grafting, Campbell *et al.*<sup>37</sup> observed a slow decay in the trapped radical concentration after addition of the monomer. Such a reduction in radical concentration can only arise through energy transfer to the grafted areas of the substrate. Since grafting only occurs in the accessible regions, energy transfer from the inaccessible to accessible areas is indicated.

More tangible evidence of the effectiveness of aromatic groups in radiation protection of cellulose is seen in the retention of mechanical properties and the corresponding reduction in chain cleavage. Radiation doses required to start deterioration of celluloses substituted to a low degree are usually at least ten times those required for sterilization and thirty times those needed for grafting reactions.

Hence it appears that the presence of bonded aromatic groups in the cellulose substrate leads to selective absorption of the incident radiation by these groups and dissipation of the energy as heat. This minimizes the localization of the energy which would otherwise cause depolymerization and consequent loss of strength. Where non-grafted protective groups are used, care is needed to ensure that this protection does not result in a reduction in grafting efficiency.

### COPOLYMER CHARACTERIZATION

Since radiation-induced graft copolymerization is a random process with regard to the mode of initiation, the location of the grafts and their molecular weights, it is reasonable to assume that cellulose graft copolymers prepared in this way will have appreciable heterogeneity of composition and molecular weight. This has led to interest in the solution properties and morphological character of cellulose copolymers and their components.

#### Solution properties

Prior to any investigation of the copolymer, the backbone or the grafted branches it is essential that each be obtained in a pure state. Hence, techniques have been developed for separation of the branches from the backbone and also for removal of the ungrafted cellulose from the copolymer. Several methods are available for isolation of the grafts. These usually involve acid hydrolysis of the backbone to water-soluble residues. Huang and Chandramouli<sup>70</sup> adopted a simultaneous acetolysis-hydrolysis procedure which was reported to give useful results. Viscometric analysis of polystyrene branches isolated in this way have been shown to exhibit polyelectrolyte behaviour<sup>49</sup>. Sulphur analyses indicated the presence of one sulphonic acid grouping for every thirty polystyrene repeat units. Thus the hydrolysis procedure, which involves the use of 72% sulphuric acid, results in sulphonation of the aromatic nucleus. This problem does not arise when non-aromatic vinyl monomers are used. The alternative method of hydrolysis devised by Morris *et al.*<sup>39</sup> is satisfactory. This is based on the acid hydrolysis (6 M HCl) of the copolymer, previously swollen in 75% aqueous zinc chloride. The products do not exhibit polyelectrolyte behaviour.

Having isolated the grafts one can evaluate their characteristics. Isolation of the trunk polymer free from grafts is not possible for cellulose substrates, though the position regarding cellulose derivatives is not clear. With unmodified substrates the most satisfactory alternative involves isolation of the ungrafted cellulose and its elucidation. In order to analyse the copolymer, removal of the ungrafted cellulose is essential. This is achieved to some degree by repeated extraction with known solvents for cellulose. Examples include cuprammonium hydroxide, Cadoxen, Cuene etc. The extracted fractions may then be analysed as required. Copolymers of unsubstituted cellulose and vinyl monomers have unusual solubility characteristics. Solvents are unavailable. For this reason it is essential that the cellulose component of the copolymer is converted to some derivative which is soluble in as wide a variety of solvents as possible. Examples include the formation of cellulose acetate or the carbanilate. Unfortunately the substitution of cellulose is accompanied by degradation. Substitution by carbanilate groups is known to give minimum degradation and has been the subject of several investigations<sup>114-117</sup>.

It has been conclusively shown by light scattering, osmometry and viscometry that cellulose graft copolymers, prepared by radiation-induced methods, exhibit extreme heterogeneity in composition and molecular weight<sup>71</sup>. Observations from light scattering phenomena were obtained using solutions of the copolymer, the extracted substrate and the branches in a comprehensive series of single solvents and selected mixed solvents. Although the copolymers studied are, without doubt heterogeneous, it is felt that composition deviations arise from the presence within the copolymers of ungrafted cellulose, which is not removed by conventional extraction.

Certain factors ought to be considered regarding the true extent of grafting relative to the apparent value. Much of the substrate remains free of grafting. Figure 4 shows the apparent and real grafting figures for cellulose-styrene copolymers prepared at low dose rates and total doses. The true extent of grafting is approximately ten times the apparent value at all times. In comparison, Figure 5 gives the variation in the percentage of extractable cellulose (using Cadoxen) with increase in the percentage of grafting. This latter figure indicates that beyond a certain level of grafting, ungrafted cellulose becomes occluded in the copolymer which cannot be removed by repeated extraction. These observations substantiate the composition heterogeneity found in light scattering measurements. The experimental techniques and definition of the terms real and apparent grafting have been fully dealt with previously<sup>48</sup>.

Wellons *et al.*<sup>118,119</sup> have investigated some of the solution properties of cellulose acetate-styrene graft copolymers. Various types of graft copolymer were analysed. The solubility characteristics of the copolymers were considerably different from those of the copolymer components. These

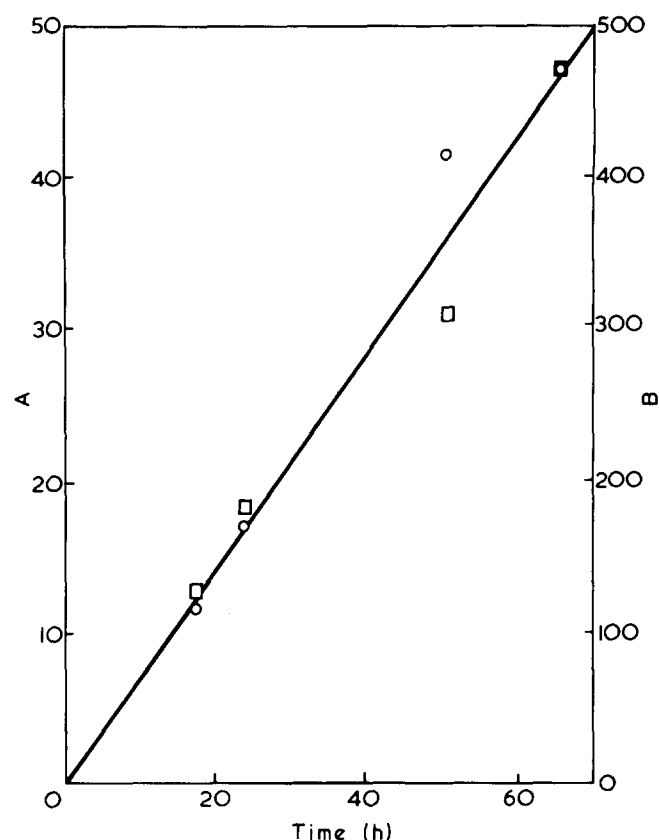


Figure 4 Variation of the extent of grafting with increasing irradiation time; A (○) = apparent; B (□) = real. Styrene monomer used. Dose rate =  $0.37 \times 10^{-2}$  W/kg. Monomer concentration = 20% v/v in dioxane (78% v/v) and water (2% v/v)

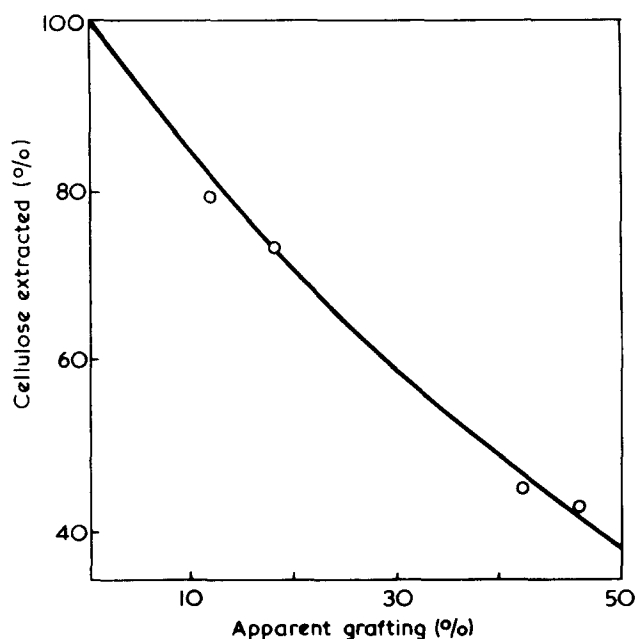


Figure 5 Variation in the extent of cellulose extraction (O) with increasing apparent degree of grafting. Styrene monomer used. Dose rate =  $0.37 \times 10^{-2}$  W/kg. Ungrafted cellulose isolated using Cadoxen<sup>48,71</sup>

differences include their permeability, diffusion and gas absorption properties. The diffusion and solubility behaviour was closer to that of cellulose acetate, whilst the other physical properties generally lay between those of the two homopolymers.

Regardless of limitations of the available extraction procedures, there is little doubt that with the majority of vinyl monomers, the grafted side chains are of higher molecular weight than the corresponding homopolymer chains. This is further evidence of the Trommsdorff effect. Certain abnormalities in molecular weight distributions have been observed. Conventional, non-radiation induced methods produce branches with broad, but otherwise standard monomodal molecular weight distributions. Pre-irradiation methods have been known to produce binodal molecular weight distributions. Such systems continue to attract interest<sup>71</sup>. Even stranger are observations made during simultaneous radiation-induced grafting at very low dose rates, total doses and monomer concentrations. These conditions give rise to trinodal distributions of the molecular weights of the attendant homopolymer. With increasing total dose the distribution became binodal and ultimately monomodal. Such observations are confirmation of the complexity of the grafting process and spotlight the difficulties of interpretation.

In an unusual approach to isolating the components of cellulose-styrene copolymers Ikada *et al.*<sup>120</sup> obtained samples of grafted fibres which were then acetylated. The substituted cellulose fraction was removed by solution in methylene chloride. Munari *et al.*<sup>121</sup> isolated grafts from cellulose diacetate and the measured molecular weights were correlated with the kinetics of the grafting process. It was observed that the molecular weights of the grafted chains were controlled by the physical limitations imposed by the matrix. Copolymers of cellulose with methyl acrylate, methyl methacrylate, styrene and vinyl toluene were prepared by Azizov and Afaki<sup>122</sup>. These were acetylated and comparisons made using the ungrafted cellulose as a standard. Acetylation was more rapid with all the

grafted samples than with cellulose alone. Deformation of the copolymers was measured as a function of temperature. The increased rate of acetylation arises from the enhanced accessibility of the substrate, made possible through grafting and the breakdown of the closely knit structure.

Attempts have been made to study the thermal behaviour of cellulose graft copolymers<sup>123</sup> and of <sup>60</sup>Co-irradiated cellulose<sup>124</sup>. Thermal analysis techniques indicate that extensive degradation occurs at doses beyond 19 Mrad and that a sensitivity threshold exists at 1 Mrad. Such observations are in close agreement with data presented in earlier sections. Byrne and Arthur<sup>124</sup> have shown that cotton cellulose is marginally more radiation resistant than the more accessible forms of cellulose such as rayon or cellophane. This suggests that post-irradiation damage involves secondary chemical attack by air and moisture.

#### Morphological properties

Radiation-induced copolymerization of vinyl monomers and cellulose produces copolymers with heterogeneity in composition and molecular weights. Morphological studies should throw some light on the nature of this heterogeneity. Investigations of pure graft copolymers are not usually possible because of difficulties associated with the complete removal of the ungrafted cellulose. Interest has been restricted mainly to the morphology of the grafted fibre, textile, paper, film or powder in its entirety. This approach is justified by the fact that most end uses require only a low degree of grafting to achieve the desired physical properties.

Electron microscopy is particularly useful for locating polymeric grafts within the substrate and many of the factors known to influence the macrostructure have been elucidated. These include the grafting technique (whether simultaneous or pre-irradiation), prior chemical modification of the cellulose, solvent effects, the total dose and dose rate and degradation processes.

The initial irradiation is known to affect markedly the morphology of cellulose graft copolymers irrespective of the original structural form of the cellulose. Such changes correspond to main chain cleavage and overall fragmentation. Arthur *et al.*<sup>42,102</sup> have correlated these structural changes with modifications in other physical properties such as tensile and elongation characteristics, swelling behaviour and grafting patterns. This group<sup>125</sup> have shown that pre-irradiation grafting of cellulose with acrylonitrile dissolved in zinc chloride shows little change in the natural shape of cotton whereas simultaneous grafting from a solution of the monomer in dimethylformamide causes collapse of the natural fibre shape<sup>111</sup>. Mutual irradiation of cellulose, in the presence of styrene or alkyl methacrylates in methanol solution, produces fibrous structures which are rounded, but not collapsed, existing in a layered network. Here, the extent of layering appears to be dependent on the molecular weight of the original monomer<sup>125</sup>. Copolymerization of cellulose with vinyl acetate from a solution of the monomer in aqueous zinc chloride results in a rounded copolymer structure, though in this instance the poly(vinyl acetate) is evenly distributed throughout the matrix.

Goynes and Harris<sup>40</sup> have used light and electron microscopy to investigate the structure of cotton fibres grafted with butyl methacrylate and acrylonitrile. Uniformity of reaction was indicated by the degree of uptake of dye from solutions of Celliton Fast Red (1% in ethanol) and a Dupont Identification Dye (1% in aqueous solution). Grafting occurred throughout the fibre and increased in uniformity with increase in grafting. Views of highly grafted fibres



showed that coatings of the graft had gradually built up on the surface of the fibre. Similar instrumental techniques were used by Razikov *et al.*<sup>127</sup> on samples of cellulose acetate/poly(methyl methacrylate) copolymers. The overall results suggest globular structures with layering, producing increased flexural strength and lower glass transition temperatures. Using a modified staining technique, dependent on the particular reactivity of osmium tetroxide, Broughton *et al.*<sup>128</sup>, studied the location and distribution of *N*-methylolacrylamide brought about during radiation-induced curing processes. This method is useful for locating unsaturated monomers within cellulosic substrates by photomicrography.

Matsuzaki *et al.*<sup>32</sup> applied n.m.r. spectroscopy to their appraisal of the stereoregularity of poly(methacrylic acid) and poly(methyl methacrylate) grafted viscose rayon and cotton fibres. Copolymers prepared by radiation-induced methods were observed to be markedly different from those prepared in chemically initiated processes. Very similar observations were made by Ogiwara and Hitoshi<sup>109</sup> in their n.m.r. study of the water absorption phenomena of poly(methyl methacrylate)/cellulose graft copolymers.

Much of the knowledge of the morphology of cellulose and its copolymers has come from Arthur and coworkers. Details of earlier surveys are to be found in the many publications of this group. Through data of this type, composite pictures of the physical condition of graft copolymers can be built up, especially when correlated with other factors relevant to improving the characteristics of cellulose or its more common derivatives.

#### APPLICATIONS OF RADIATION-INDUCED CELLULOSE GRAFTING

Considering the attention devoted to applied aspects of radiation-induced grafting to cellulose and the negligible industrialization of such effort, a review of the progress made along these lines is opportune. Much is known of the synthesis, structure, chemical and physical properties, technology, design and fabrication of cellulose copolymers, but few of the original hopes have been realized. Recent international events, the shortage of certain basic raw materials, and the expansion of the textile industries should result in renewed interest in graft copolymerization.

Logic suggests that such interest will be channelled into certain areas. In this section we are concerned with those systems which have particular industrial potential. Technological aspects of grafting were originally discussed by Metz<sup>129</sup>, though more recent additions have been made along similar lines<sup>67,130</sup>. Treatments related to wood cellulose are reserved for the next section.

Modification of cellulose, aimed at improving its rot resistance, abrasion resistance, solvent resistance and mechanical stability, has been achieved by grafting with acrylonitrile<sup>131</sup>. Reductions in moisture uptake by grafting with styrene, methylacrylate and other hydrophobic monomers are particularly satisfactory since only low levels of grafting are required to produce the desired change in physical properties.

Dilli *et al.*<sup>134</sup> have investigated the ion exchange properties of radiation copolymerized celluloses. Cellulose-poly-styrene systems have been shown to be effective in column and paper chromatography. Examples of their applicability include the separation of dyestuffs, metal cations such as  $Zn^{2+}$ ,  $Ni^{2+}$  and  $Cd^{2+}$ , and fatty acids including stearic, myristic and lauric acids. Poly(methyl methacrylate)/cellulose systems separate mixtures of oil-soluble dyes more

readily than does untreated cellulose. Also of interest are the ion exchange properties of grafted celluloses containing  $-NH_2$ ,  $-SO_3H$  functional groups or those involving heterocyclic nitrogen. Among the many advantages claimed for these membranes over other adsorbing media are ease of preparation, greater efficiency and resistance to chemical attack, applicability to reverse phase chromatography, greater radiation stability and ease of separation of complex mixtures.

Mares and Arthur<sup>66,135</sup> have considered the textile applications of graft copolymers and terpolymers. A range of monomers was screened and the products were assessed in terms of improvements to the physical properties and serviceability of the substrate. The copolymers retain some of the properties of cellulose and adopt others of the comonomer. Selective application of monomers can produce products which may be thermoplastic, elastomeric, hydrophobic, soil releasing, rot resistant, mechanically and visually superior, radiation resistant, more easily dyed and washed or with better thermal characteristics. Among the monomers grafted to cellulose to achieve specific modifications are acrylic monomers<sup>136</sup>, *N*-methacryloylpiperidine<sup>137</sup>, acrolein<sup>138</sup> and *N*-methylolacrylamide<sup>139</sup> to induce cross-linking of cellulose; allyl methacrylate *p*-divinylbenzene and ethyleneglycol monomethacrylate<sup>140</sup> to improve the fungus resistance of fabrics; and various monomers designed to improve crease resistance and general usability<sup>141-143</sup>. In most cases the improvement sought in the particular physical property has been achieved.

The use of radiation grafting to provide membranes for studies and applications of osmosis phenomena, particularly reverse osmosis, is gaining in popularity. Hopfenberg *et al.*<sup>144,145</sup> have applied cellulose acetate-styrene graft copolymers to a wide variety of conditions and environments. Similar fundamental studies have been carried out by Dilli and Garnett<sup>134</sup> and Bentvelzen *et al.*<sup>146</sup>. Although still in the experimental stages, this approach seems to hold great prospects for the future.

Ahmed *et al.*<sup>147</sup> have reviewed the potential of radiation grafting with particular reference to its suitability in the developing countries. Substrates considered include wood cellulose, jute, agricultural and stone wastes. The main advantage of the technique lies in the use of materials which are readily available.

Stannett and Stahel<sup>148</sup> have considered the full scale and pilot size plant machinery and isotope sources which would be required for the realistic commercialization of radiation grafting. Among the processes considered are modifications to textiles, curing of coatings and the preparation of wood-polymer composites. Machida<sup>149</sup> has published the results of work concerning the flocculation properties of polyacrylamide-cellulose graft copolymers. A correlation is shown to exist between the length of the grafted chains and the flocculation stability. This work has implications which should be of interest to paint manufacturers in view of the stability of the systems obtained.

The application of radiation-induced graft polymerization to cellulosic textiles has been recently reviewed by Okada<sup>150</sup>. Aspects covered include hydrophilization of the fibres, improvements in the thermal stability, permanent press characteristics and the provision of flame retardant finishes.

Although this survey of recent developments has been brief, the industrial potential of many of the processes outlined is clearly indicated. Further information, relating to earlier predictions of the potential of radiation grafting,

can be obtained from the reviews by Das Gupta<sup>67,130</sup> and Metz<sup>129</sup>.

### RADIATION-INDUCED GRAFTING TO WOOD

Such has been the recent interest in wood-plastic composites and timber preservation that these materials deserve particular attention. One process, using radiation grafting, has been described by Mott and Stannett<sup>151</sup>. This consists essentially of degassing under vacuum to remove air, nitrogen purging, degassing, exposure to the monomer, impregnation of the timber by the monomer under pressure and subsequent irradiation. Low dose rates and total doses are favoured and a variety of monomers has been investigated. The results of grafting, depending on the monomer applied can be related to those observed during textile modifications. Thus improvements are observed in the moisture uptake, rot resistance, tensile strength, compressive strength, dimensional stability, elastic modulus and overall wood hardness<sup>152-154</sup>.

Attempts to fabricate 'wood-plastics' have been successful in certain instances with a wide range of monomers<sup>155</sup>. Much of the research along these lines arises from utilization of natural resources as fully as possible. The outcome is of great interest to the developing nations. In a thorough treatment of the radiation-induced grafting of styrene- and methyl methacrylate-impregnated birch and aspen Shirayeva *et al.*<sup>156</sup> noted improved compression strength, static bonding strength, shear strength and static hardness. Grafting rates were accelerated by the presence of tributylphosphate resulting in lesser doses being required. Alkyl phosphates were observed to impart both fire and bio-organic decay resistance.

Another treatment involving impregnation followed by irradiation was used by Basson<sup>157</sup> in a study of grafting to pine and eucalyptus timbers. The degree of monomer uptake by the eucalyptus was less than that of pine. The investigation included microscopic examination, dose rate effects and mechanical and weathering tests. Both types of treated timber were superior to their untreated counterparts in many respects.

Stannett and his group<sup>158-161</sup> have shown a general interest in grafting to wood and wood pulps. Here, however, the aim has been towards a greater understanding of the nature of the grafting process rather than in improving the physical properties of the timber alone. This theme is adopted by Sakata<sup>162</sup> *et al.* using styrene in grafting to woody fibres. In this instance, the study involved the distribution of grafted polystyrene branches between the lignin and carbohydrate fractions of the parent substrate (1.2 : 4 for lignin : carbohydrate respectively). The branches were removed from lignin sections by treatment with acetic acid and from cellulose by hydrolysis with 72% sulphuric acid (see observations made earlier regarding the use of concentrated sulphuric acid in the acid hydrolysis of cellulose-polystyrene graft copolymers).

Birchwood has attracted attention recently because of the considerable improvements which can be achieved in physical properties by low extents of grafting. Irradiation of unitary and binary monomer impregnated samples has been successfully carried out. Steiners *et al.*<sup>163</sup> have noted the absence of stress and deformation when birchwood is treated with styrene in carbon tetrachloride and then irradiated. Copolymerized samples have greater dynamic compliance and mechanical properties. Glukhov *et al.*<sup>164</sup> used styrene-acrylonitrile mixtures and observed that graft-

ing was much easier than polymerization with either monomer alone. Similar observations were made by Oraby *et al.*<sup>165</sup> in their study of the grafting of these same monomers to wood pulp cellulose.

Modification of timber or wood pulps by radiation-induced grafting offers a simple method of protection against a wide variety of decay-initiating systems. Improvements to physical properties, structural properties and appearance are also achieved. Once grafted, the timber or wood pulp composites are amenable to a much wider range of use than exists for ungrafted materials.

### RECENT PATENT LITERATURE

Perhaps the best guide to the progress and success of a novel technique is the patent literature, for it is here that protection of innovations is sought before their commercial baptism. Whether or not radiation-induced grafting techniques achieve success will depend on their viability when compared with existing methods of cellulose modification. On a numerical basis, comparatively few patents applications have been taken out in recent years, especially when the amount of research effort given to the topic is considered.

As in all aspects of grafting studies. Arthur and his coworkers are frequently found in the patent literature. Typical examples include the selective grafting of vinyl monomers to cellulosic materials by radiation-induced grafting with a view to improving the crease resistance. A recommendation that the total dose be restricted to 1 Mrad is made<sup>166</sup>. A second patent<sup>167</sup> involves the copolymerization of binary monomer mixtures with cellulose in order to produce industrial textiles and cellulosic articles having a rigid construction. In outline, the cellulose is dried to a 2% water content, irradiated and then treated with one of several binary monomer mixtures before final washing and drying.

A patent application granted to BASF<sup>168</sup> concerns grafting 1,4-butyleneglycol methacrylate and acrylamide to cellulose. This produces materials whose properties render them useful as leather substitutes. DasGupta and Slobodian were granted patent rights to the grafting of methyl methacrylate or styrene impregnated cotton or paper in roll form in which diffusion of the monomer into the interior of the substrate is assisted by acetone (for methyl methacrylate) or methanol (for styrene).

The flame-proofing of textiles is one aspect of grafting which shows real promise. Miles and Delasanta<sup>170</sup> have claimed a patent governing the grafting of *N*-methylolacrylamide, acrylamide, acrylonitrile and acrylic acid in binary mixtures with either triallyl phosphate or dimethyl hydrogen phosphite. The addition of the vinyl monomer enhances the flame-proofing action of the phosphate and phosphite.

Improvements to the dyeing properties of rayon (to cationic and acid dyes) as a result of prior modification of the rayon through grafting, is claimed by Igarashi *et al.*<sup>171</sup> Rayon, among other fibres, was grafted with methyl methacrylate before dyeing. Better light fastness properties were observed than with samples treated with cationic dyes alone. Garnett and Martin<sup>172</sup> claimed general patent rights for the process of the simultaneous, radiation-induced liquid phase grafting of 2-vinylpyridine to cellulose in solvent systems containing alkylolamines. Such a process would broaden the range of dyeability of the substrate by use of acid dyes.

In a Russian patent application Makhkamov *et al.*<sup>173</sup> describe the bacteriostatic properties of cellulose-acrylonitrile copolymers on treatment with copper acetate and

sodium sulphide. Since similar properties can be acquired by grafting with various vinyl monomers this modification appears to have little to offer over existing selected copolymers. Recent patent applications are more sophisticated than earlier disclosures. Dotson *et al.*<sup>174</sup> hold a patent concerned with the solvent casting of cellulosic films using previously radiation grafted products. Increased processing rates are reported. This is especially so when cellulose ester dopes used in solvent-cast processes in the production of photographic film base, are modified by addition of a vinyl monomer and the whole irradiated. This polymerizes the compatible monomer portion before the cast layer is stripped from the casting web. Another patent relating to cellulose graft copolymer solutions was awarded to Nakao *et al.*<sup>175</sup>. In this application are described processes for the efficient dissolution of a series of cellulose-vinyl monomer graft copolymers.

Dilli and Garnett<sup>176,177</sup> have taken out patents covering the production of cellulose graft copolymers, containing styrene, using low radiation doses, methanol as a swelling agent and a mineral acid (1.1 M sulphuric acid). High levels of grafting are claimed.

## CONCLUSION

Several factors need to be taken into account in adopting radiation-induced grafting procedures. Prime among these will be the usability of existing equipment as an alternative to wholesale re-equipping with plant. Adaptation should be possible with little inconvenience and cost when compared with the advantages offered. Major decisions will concern the type of radiation source to be employed, the radiation polymerization technique and personnel protection. High grafting yields, though not essential, offer the greatest scope for versatility. Efforts made to achieve extensive grafting should be carefully considered. Simultaneous irradiation of the substrate in the monomer solution produces greater grafting yields at lower doses than would the pre-irradiation method. However, the pre-irradiation technique may be preferred on expansion to full scale production because of simplicity of plant design, continuity of operation, cost effectiveness, ease of personnel protection and the absence of homopolymeric species which would cause serious problems associated with their removal. Economic viability depends on the total cost of operation. Savings made through the absence of homopolymerization will be considerable. Processes which can operate under aqueous conditions have particular advantages. Storage of batches in radioactive isotope source rooms (<sup>60</sup>Co or <sup>137</sup>Cs) may appear simpler though passage of the conventional substrate under an electron beam lends itself to greater flexibility. The latter technique has disadvantages in terms of stray radiation, maintenance and the initial cost.

The reluctance to change from conventional technology, apparent in the textile and paper industries, must be overcome before the techniques outlined will be accepted. Application to timber preservation seems more hopeful. The greatest potential, in the short term lies in the production of materials for specialist uses. Examples include semi-permeable membranes, sterilization without degradation, food preservation and fire-retardant textiles.

Changing world situations could see renewed interest from areas otherwise reluctant to change.

## ACKNOWLEDGEMENTS

The author wishes to thank the Director and staff of The British Library, Lending Division, Thorpe Arch Trading Estate, Wetherby, for making available the facilities of the library; Dr N. Okui, The Department of Colour Chemistry, University of Leeds, for Japanese translations; and Miss Lynne Skelton, for patience and perseverance during the typing of this review.

## REFERENCES

- 1 Krassig, H. A. and Stannett, V. T. *Adv. Polym. Sci.* 1965, 4, 111
- 2 Battaerd, H. A. J. and Tregear, G. W. 'Graft Copolymers', Interscience, New York, 1967
- 3 Habeish, A. *Kolor. Ert.* 1971, 13, 12
- 4 Nakamura, Y. *Sen i To Kogyo* 1972, 5, 359
- 5 Matsuzaki, K. and Nakamura, S. *Kami Pa Gikoyoshi* 1973, 27, 15
- 6 Stannett, V. T. and Hopfenberg, H. B. in 'High Polymers', (Eds. N. M. Bikales and L. Segal), Interscience, New York, 1971, Vol 5, Part 5, p 907
- 7 Ragovin, Z. A. *Cellulose Chem. Technol.* 1972, 6, 17
- 8 Le Gall, M. *Bull. Sci. Inst. Text. France* 1973, 2, 77
- 9 Moore, P. W. AAEC/TM540 (1970)
- 10 Moore, P. W. *Rev. Pure Appl. Chem.* 1970, 20, 139
- 11 Hoffman, A. S. *Isotope Radiat. Technol.* 1970, 8, 84
- 12 Arthur, J. C. Jr as ref 6, p 937
- 13 Arthur, J. C. Jr *Adv. Chem. Ser.* 1969, 91, 574
- 14 see *J. Polym. Sci. (C)* 1972, 37
- 15 Walsh, W. K. *PhD Thesis* North Carolina State University (1967)
- 16 Imrišova, D. and Maryška, S. *J. Appl. Polym. Sci.* 1968, 12, 2007
- 17 Imrišova, D. and Maryška, S. *J. Appl. Polym. Sci.* 1967, 11, 901
- 18 Nakamura, Y., Hinojosa, O. and Arthur, J. C. Jr *J. Appl. Polym. Sci.* 1969, 13, 2633
- 19 Nakamura, Y., Hinojosa, O. and Arthur, J. C. Jr *J. Appl. Polym. Sci.* 1970, 14, 789
- 20 Nakamura, Y., Hinojosa, O. and Arthur, J. C. Jr *J. Appl. Polym. Sci.* 1971, 15, 391
- 21 Hinojosa, O. and Arthur, J. C. Jr *J. Polym. Sci. (B)* 1972, 10, 161
- 22 Okada, T., Kohdera, K. and Sakurada, I. *Jap. Atom. Energy Res. Inst. Osaka Rep. JAERI-5022* p 59
- 23 Harris, J. A. and Arthur, J. C. Jr *J. Appl. Polym. Sci.* 1970, 14, 3113
- 24 Williams, J. L. *PhD Thesis* North Carolina State University (1971)
- 25 Reine, A. H., Arthur, J. C. Jr and George, M. *J. Appl. Polym. Sci.* 1972, 16, 1893
- 26 Ishanov, M. M., Nikonovich, G. V. and Usmanov Kh. U. *Vysokomol. Soedin. (B)* 1969, 11, 763
- 27 Yunusov, M. Yu. and Azizov, U. A. *Uzb. Khim Zh.* 1971, 5, 64
- 28 Dilli, S. and Garnett, J. L. *Aust. J. Chem.* 1971, 24, 981
- 29 Sakurada, I. *Chem. Technol.* 1972, 2, 376
- 30 Matsuzaki, K., Nakamura, S. and Shindo, S. *J. Appl. Polym. Sci.* 1972, 16, 1339
- 31 Harris, J. A., Carra, J. H., DeGruy, I. V. and Arthur J. C. Jr *Text. Res. J.* 1972, 42, 14
- 32 Matsuzaki, K., Kanai, T. and Morita, N. *J. Appl. Polym. Sci.* 1972, 16, 15
- 33 Yul'chibaeva, S. G., Yusupalaev, R. M. and Usmanov, Kh. U. *Uzb. Khim. Zh.* 1973, 7, 60
- 34 Hayakawa, K., Yamakita, H. and Kawase, K. *J. Polym. Sci. (A-1)* 1970, 8, 1227
- 35 Williams, J. L. *et al. Text. Res. J.* 1973, 43, 205
- 36 Yusupaliev, R. M. *Nauch. Trudy Tashkent Univ.* 1971, 403, 75
- 37 Campbell, D., Williams, J. L. and Stannett, V. T. *J. Polym. Sci. (A-1)* 1969, 7, 429
- 38 Baugh, P., Hinojosa, O. and Arthur J. C. Jr *J. Appl. Polym. Sci.* 1967, 11, 1139
- 39 Morris, N. J., Blouin, F. A. and Arthur, J. C. Jr *J. Appl. Polym. Sci.* 1968, 12, 373

- 40 Goynes, W. R. and Harris, J. A. *J. Polym. Sci. (C)* 1972, **37**, 277
- 41 Arthur, J. C. Jr and Blouin, F. A. *J. Appl. Polym. Sci.* 1964, **8**, 2813
- 42 Rollins, M. L., Cannizzaro, A. M., Blouin, F. A. and Arthur, J. C. Jr *J. Appl. Polym. Sci.* 1968, **12**, 71
- 43 Yasukawa, T., Sasaki, Y. and Murakami, K. *J. Polym. Sci. (A-1)* 1973, **11**, 2547
- 44 Odian, G., Kruse, R. L. and Kho, J. H. T. *J. Polym. Sci. (A-1)* 1971, **9**, 91
- 45 Detrick, C. A. and Kelly, J. L. *Nucl. Appl. Technol.* 1969, **7**, 472
- 46 Guthrie, J. T., Huglin, M. B. and Phillips, G. O. *Angew. Makromol. Chem.* 1972, **13**, 199
- 47 Guthrie, J. T., Huglin, M. B. and Phillips, G. O. *J. Appl. Polym. Sci.* 1972, **16**, 1017
- 48 Guthrie, J. T., Huglin, M. B. and Phillips, G. O. *J. Polym. Sci. (C)* 1972, **37**, 205
- 49 Guthrie, J. T., Huglin, M. B. and Phillips, G. O. *J. Appl. Polym. Sci.* 1971, **15**, 1033
- 50 Guthrie, J. T. and Haq, Z. *Polymer* 1974, **15**, 133
- 51 Guthrie, J. T., Huglin, M. B. and Phillips, G. O. *Eur. Polym. J.* 1972, **8**, 747
- 52 Dilli, S. and Garnett, J. L. *Aust. J. Chem.* 1970, **23**, 1767
- 53 Sakurada, I. *Cellulose Chem. Technol.* 1972, **6**, 35
- 54 Vlagiu, I., Petrus, I. and Niculescu, E. *Rev. Roum. Chim.* 1970, **15**, 1077
- 55 Sakurada, I., Okada, T. and Kaji, K. *J. Polym. Sci. (C)* 1972, **37**, 1
- 56 Sakurada, I., Ikada, Y. and Nishizaki, Y. *J. Polym. Sci. (C)* 1972, **37**, 265
- 57 Dilli, S. et al. *J. Macromol. Sci. (A)* 1972, **6**, 719
- 58 Dilli, S., Garnett, J. L., Martin, E. C. and Phuoc, D. H. *J. Polym. Sci. (C)* 1972, **37**, 57
- 59 Dilli, S. and Garnett, J. L. *Aust. J. Chem.* 1968, **21**, 1827
- 60 Garnett, J. L. and Martin, E. C. *J. Macromol. Sci. (A)* 1970, **4**, 1193
- 61 Dilli, S. and Garnett, J. L. *Aust. J. Chem.* 1970, **23**, 1163
- 62 Dilli, S. and Garnett, J. L. *Aust. J. Chem.* 1968, **21**, 397
- 63 Dilli, S. and Garnett, J. L. *J. Appl. Polym. Sci.* 1967, **11**, 839
- 64 Dilli, S. and Garnett, J. L. *J. Appl. Polym. Sci.* 1967, **11**, 859
- 65 Byrne, G. A. and Arthur, J. C. Jr *J. Appl. Polym. Sci.* 1970, **14**, 3093
- 66 Mares, T. and Arthur, J. C. Jr *J. Polym. Sci. (C)* 1972, **37**, 349
- 67 DasGupta, S. *J. Polym. Sci. (C)* 1972, **37**, 333
- 68 Odian, G., Sobel, M., Rossi, A. and Klein, R. *J. Polym. Sci.* 1961, **55**, 663
- 69 Huang, R. Y-M. and Chandramouli, P. *J. Polym. Sci. (A-1)* 1969, **7**, 1393
- 70 Huang, R. Y-M. and Chandramouli, P. *J. Appl. Polym. Sci.* 1968, **12**, 2549
- 71 Guthrie, J. T. *PhD Thesis* University of Salford (1971)
- 72 George, M. H. in 'Kinetics and Mechanisms of Polymerisation', (Ed. G. E. Ham), Edward Arnold, London, 1967, Vol 1
- 73 Ham, G. E. as in ref 72
- 74 Reine, A. H., Hinojosa, O. and Arthur, J. C. Jr *J. Polym. Sci. (B)* 1971, **9**, 503
- 75 Harris, J. A. and Arthur, J. C. Jr *J. Polym. Sci. (B)* 1971, **9**, 915
- 76 Mares, T., Hinojosa, O., Nakamura, Y. and Arthur, J. C. Jr *J. Appl. Polym. Sci.* 1971, **15**, 2349
- 77 Razikov, K. Kh., Tyagai, E. D., Tashpulatov, Yu. T., Saidaliev, T. and Usmanov, Kh. U. *Vysokomol. Soedin. (B)* 1972, **14**, 226
- 78 Vigneron, M. and Deschreider, A. R. *Lebe-Weiss Technol.* 1972, **5**, 198
- 79 Florin, R. E. and Wall, L. A. *J. Polym. Sci. (A)* 1963, **1**, 1163
- 80 Leavitt, F. C. *J. Polym. Sci.* 1950, **45**, 146
- 81 Mares, T. and Arthur, J. C. Jr *J. Polym. Sci. (B)* 1969, **7**, 419
- 82 Johanson, F. and Back, E. L. *Svensk. Pappstid.* 1966, **69**, 199
- 83 Leuthy, H. *Atomkernenergie* 1971, **18**, 93
- 84 Arthur, J. C. Jr and Hinojosa, O. *J. Polym. Sci. (C)* 1971, **36**, 53
- 85 Panchenkov, G. M., Kaushanski, D. A. and Gel'tser, G. A. *Dokl. Akad. Nauk. SSSR* 1972, **16**, 42
- 86 Ueno, T., Yamauchi, T. and Imamura, R. *Kami Pa. Gikoyoshi* 1971, **25**, 242
- 87 Imamura, R., Ueno, T. and Murakami, K. *Bull. Inst. Chem. Res. Kyoto Univ.* 1972, **50**, 51
- 88 Imamura, R. and Ueno, T. *Kami Pa. Gikoyoshi.* 1971, **25**, 121
- 89 Ueno, T., Murakami, M. and Imamura, R. *Kami Pa. Gikoyoshi* 1972, **26**, 164
- 90 Kunz, N. D., Gainer, J. L. and Kelly, J. L. *Nucl. Technol.* 1972, **16**, 556
- 91 Ahmed, A. U. and Rapson, W. H. *J. Polym. Sci. (A-1)* 1972, **10**, 1945
- 92 Khamidov, D. S., Azizov, U. A., Millinchuk, V. K. and Usmanov, Kh. U. *Vysokomol. Soedin. (A)* 1972, **14**, 838
- 93 Arthur, J. C. Jr., Hinojosa, O. and Tripp, V. W. *J. Appl. Polym. Sci.* 1969, **13**, 1497
- 94 Dilli, S., Ernst, I. T. and Garnett, J. L. *Aust. J. Chem.* 1966, **20**, 911
- 95 Baugh, P. J. and Worthington, K. *Cellulose Chem. Technol.* 1971, **5**, 23
- 96 Burton, M. *Discuss. Faraday Soc.* 1963, **36**, 7
- 97 Phillips, G. O., Blouin, F. A. and Arthur, J. C. Jr *Nature* 1964, **202**, 1328
- 98 Phillips, G. O., Blouin, F. A. and Arthur, J. C. Jr *Radiat. Res.* 1964, **23**, 527
- 99 Arthur, J. C. Jr and Mares, T. *J. Appl. Polym. Sci.* 1965, **9**, 2581
- 100 Arthur, J. C. Jr, Mares, T. and George, M. *Text. Res. J.* 1965, **35**, 1116
- 101 Sarkar, I. M., Arthur, J. C. Jr and George, M. *Text. Res. J.* 1968, **38**, 1145
- 102 Arthur, J. C. Jr in 'Energy Transfer in Radiation Processes', (Ed. G. O. Phillips), Elsevier, Amsterdam, 1966
- 103 Chidambareswaran, P. K., Sundaram, V., Prakash, J., Verma, N. C. and Singh, B. B. *CTRL Publ. No.25* 1971; *J. Polym. Sci. (A-1)* 1971, **9**, 2651
- 104 Singh, S., Hinojosa, O. and Arthur, J. C. Jr *J. Appl. Polym. Sci.* 1970, **14**, 1591
- 105 Arthur, J. C. Jr, Singh, S. and Hinojosa, O. US Pat. 3 677 692 (1972)
- 106 Arthur, J. C. Jr, Stannonis, D. J., Mares, T. and Hinojosa, O. *J. Appl. Polym. Sci.* 1967, **11**, 1129
- 107 Westberry, C. J. and Hyden, W. L. *Am. Dyest. Rep.* 1967, **56**, 13
- 108 Betty, R. W. *PhD Thesis* University of Toronto (1968)
- 109 Ogiwara, Y. and Hitoshi, K. *J. Appl. Polym. Sci.* 1971, **15**, 3137
- 110 Stannett, V. T., Wellons, J. D. and Yasuda, H. *J. Polym. Sci. (C)* 1963, **4**, 551
- 111 Blouin, F. A., Morris, N. J. and Arthur, J. C. Jr *Text. Res. J.* 1966, **36**, 309
- 112 Gugliemelli, L. A., Weaver, M. O. and Russell, C. R. *J. Polym. Sci. (B)* 1968, **6**, 509
- 113 Kobayashi, Y. *J. Polym. Sci.* 1961, **51**, 359
- 114 Ohman, J. *Arkiv Kemi* 1970, **31**, 125
- 115 Shanbhag, V. P. *Arkiv Kemi* 1968, **29**, 139
- 116 Burchard, W. *Z. Phys. Chem.* 1964, **42**, 293
- 117 Janeschitz-Kriegl, H. and Burchard, W. *J. Polym. Sci. (A-2)* 1968, **6**, 1953
- 118 Wellons, J. D., Williams, J. L. and Stannett, V. T. *J. Polym. Sci. (A-1)* 1967, **5**, 1341
- 119 Wellons, J. D. and Stannett, V. T. *J. Polym. Sci. (A)* 1965, **3**, 847
- 120 Ikada, Y., Nishizaki, Y. and Sakurada, I. *Bull. Inst. Chem. Res. Kyoto Univ.* 1972, **50**, 20
- 121 Munari, S., Tealdo, G. C., Canepa, G. and Rose, C. *J. Appl. Polym. Sci.* 1970, **14**, 807
- 122 Azizov, U. and Afaki, N. I. *Uzb. Khim. Zh.* 1971, **3**, 51
- 123 Kokta, B. V., Lepoutre, P. and Valade, J. L. *Tappi* 1972, **55**, 370, 375
- 124 Byrne, G. A. and Arthur, J. C. Jr *Text. Res. J.* 1970, **40**, 577
- 125 Blouin, F. A., Cannizzaro, A. M., Arthur, J. C. Jr and Rollins, M. L. *Text. Res. J.* 1968, **38**, 811
- 126 Arthur, J. C. Jr and Blouin, F. A. *J. Appl. Polym. Sci.* 1964, **8**, 2313
- 127 Razikov, K. Kh., Peremkulova, Kh. T., Afaki, N. I. and Usmanov, Kh. U. *Vysokomol. Soedin. (B)* 1972, **14**, 192
- 128 Broughton, R. M., Rollins, M. L. and Walsh, W. K. *Text. Res. J.* 1972, **40**, 672
- 129 Metz, D. J. *Nucleonics* 1958, **16**, 73
- 130 DasGupta, S. *Am. Dyest. Rep.* 1966, **55**, 6, 59
- 131 Saunders, F. L. and Sovish, R. C. *J. Appl. Polym. Sci.* 1963, **7**, 357
- 132 Kesting, R. E. and Stannett, V. T. *Makromol. Chem.* 1963, **63**, 248
- 133 Yoshitake, I., Obuchi, S., Tsuneda, T. and Maeda, H. *J. Soc.*

- 134 Dilli, S., Garnett, J. L. and Martin, E. C. *J. Polym. Sci. (C)* 1972, 37, 291
- 135 Arthur, J. C. Jr *Adv. Chem. Ser.* 1971, 99, 321
- 136 Frick, J. G. Jr and Gautreaux, G. A. *Am. Dyest. Rep.* 1971, 59, 40
- 137 Usmanov, Kh. U., Musaev, U. N., Khaidarov, K., Saidaliev, T. and Azizova, N. *Nauch. Trudy Tashkent Univ.* 1972, 419, 240
- 138 Ishanov, M. M., Azizov, U. A., Nigmankhodzhaeva, M. S. and Usmanov, Kh. U. *J. Polym. Sci. (A-1)* 1971, 9, 1013
- 139 Broughton, R. M. Jr *PhD Thesis* North Carolina State University (1970)
- 140 Ishanov, M. M. *et al. Uzb. Biol. Zh.* 1972, 16, 17
- 141 Dziedziela, W., Kroh, J., Mader, K. and Spondenkiewicz, T. *Przegl. Wlok* 1971, 25, 517
- 142 Agnihotri, V. G. and Sharma, V. N. *Fibres Polym.* 1972, 2, 55
- 143 DasGupta, S. *AECL Rep. 4062* 1971, p 2
- 144 Hopfenberg, H. B., Kimura, F., Rigney, P. T. and Stannett, V. T. *J. Polym. Sci. (C)* 1969, 28, 243
- 145 Hopfenberg, H. B., Stannett, V. T., Kimura, F. and Rigney, P. T. *Appl. Polym. Symp.* 1970, 13, 139
- 146 Bentvelzen, J. M., Kimura, F., Hopfenberg, H. B. and Stannett, V. T. *J. Appl. Polym. Sci.* 1973, 17, 809
- 147 Ahmed, A., Hussain, A. and Rashid, A. *Conf. 710901-364 Dep. NTIS '4th Conference on the Peaceful Uses of Atomic Energy', Geneva, 1971*
- 148 Stannett, V. T. and Stahel, E. P. *A. Rev. Nucl. Sci.* 1971, 21, 397
- 149 Machida, S. *Kyoto Univ. Text. Ind. Text. Dept. Rep.* 1973, 7, 122
- 150 Okada, T. *Senshoku Kogyo* 1969, 17, 575
- 151 Mott, W. E. and Stannett, V. T. *Isotope Radiat. Tech.* 1969, 6, 323
- 152 Czikovsky, T. *Atom. Energy Rev.* 1968, 6, 3
- 153 Stamm, A. J. 'Wood and Cellulose Science', Ronald Press, New York, 1964
- 154 Kenaga, D. L., Fennessey, J. P. and Stannett, V. T. *Forest Product J.* 1962, p 161
- 155 Kandeel, S. A. E. and Etman, M. H. *Alexandria J. Agric. Res.* 1973, 19, 365
- 156 Shirayeva, G. V., Prishchepa, N. D., Gluhov, V. I., Lebedev, V. T. and Karpov, V. L. 'Proc. 3rd Tihany Symp. Radiat. Chem. 1971', (Ed. J. Dobo and P. Hedvig), Akadémiai Kiado, Budapest, 1972, Vol 1, p 783
- 157 Basson, R. A. *Atom. Energy Board, Pretoria Rep. A/Conf. 49/P-668* 1971
- 158 Radi, F. S., Hopfenberg, H. B. and Stannett, V. T. *J. Appl. Polym. Sci.* 1972, 16, 2685
- 159 Phillips, R. B., Brown, W. and Stannett, V. T. *J. Appl. Polym. Sci.* 1971, 15, 2929
- 160 Phillips, R. B., Brown, W. and Stannett, V. T. *J. Appl. Polym. Sci.* 1972, 16, 1
- 161 Phillips, R. B., Brown, W. and Stannett, V. T. *J. Appl. Polym. Sci.* 1973, 17, 443
- 162 Sakata, I., Miyata, N. and Senjui, R. *Mokuzai Gakkaishi* 1972, 18, 593
- 163 Steiners, K., Goldsteins, A., Rocens, K., Dolacis, J. and Rajavaa, E. *Latv. PSR Zinat Akad. Vestis* 1972, 11, 35
- 164 Gluhov, V. I., Shirayeva, G. V. and Karpov, V. L. *Plass. Massy* 1972, 11, 28
- 165 Oraby, W., Hopfenberg, H. B. and Stannett, V. T. *J. Appl. Polym. Sci.* 1971, 15, 2987
- 166 Arthur, J. C. Jr and Harris, J. A. US Pat. 3 634 018 (1972)
- 167 Arthur, J. C. Jr and Harris, J. A. US Pat 3 733 257 (1973)
- 168 Badische Anilin und Soda-Fabrik DDR Pat. 81 475 (1972)
- 169 DasGupta, S. and Slobodian, J. T. FDR Pat. 1 594 881 (1971)
- 170 Miles, T. D. and Delasanta, A. C. US Pat. 3 592 683 (1971)
- 171 Igarashi, Y., Eguchi, T. and Okatani, T. Jap. Pat. 7 129 467 (1971)
- 172 Garnett, J. L. and Martin, E. C. Aust. Pat. 432 730 (1973)
- 173 Makhkamov, K., Kolontarov, I. Ya. and Repina, E. N. USSR Pat. 259 819 (1973)
- 174 Dotson, B. R., Morrison, E. D. and Williams, R. F. Jr US Pat. 3 738 924 (1973)
- 175 Nakao, O. *et al.* US Pat. 3 658 735 (1972)
- 176 Garnett, J. L. and Dilli, S. US Pat. 3 748 241 (1973)
- 177 Garnett, J. L. and Dilli, S. FDR Pat. 2 213 052 (1973)

## APPENDIX

A key to the abbreviations used in *Tables 1* and *2* is outlined below.

M	monomer used in grafting
MP	grafting conditions of monomer (solution or vapour)
SA	swelling agent used to enhance grafting
T	temperature of the grafting process
S	styrene
EA	ethyl acrylate
AN	acrylonitrile
MA	methyl acrylate
MVK	methyl vinyl ketone
A	acrolein
MMA	methyl methacrylate
VA	vinyl acetate
2- and 4-VP	2- and 4-vinylpyridine
$\alpha$ -Methyl-S	$\alpha$ -methylstyrene
BA	butyl acrylate
BMA	butyl methacrylate
MAA	methacrylic acid
VFF	vinylidene fluoride
VF	vinyl fluoride
5-methyl-2-VP	5-methyl-2-vinylpyridine
HEMA	2-hydroxyethyl methacrylate
HPMA	hydroxypropyl methacrylate
MAN	methacrylonitrile
NVC	N-vinylcarbazole
6-FIPA	hexafluoroisopropyl acrylate
DMSO	dimethylsulphoxide
MEK	methyl ethyl ketone
DMF	dimethylformamide
1,2-DCE	1,2-dichloroethylene
AQ	anthraquinone

## Note to the Editor

### Synthesis and characterization of a *cis*-1,4-polyisoprene-*b*-poly(methyl methacrylate) copolymer

D. C. Evans, J. A. Barrie and M. H. George

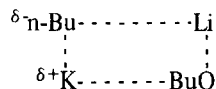
Department of Chemistry, Imperial College of Science and Technology, London SW7 2AY, UK

(Received 22 July 1974)

#### INTRODUCTION

It was recognized several years ago<sup>1</sup> that anionic polymerization provides a convenient route for the synthesis of block copolymers. Since that time, a considerable amount of work on this subject has been reported. However, recent reviews<sup>2-4</sup> contain no reference to the synthesis of a block copolymer of *cis*-1,4-polyisoprene and poly(methyl methacrylate) using anionic techniques, although a block copolymer has been prepared by mastication of natural rubber swollen with methyl methacrylate<sup>5</sup>. A major difficulty in the preparation of this block copolymer is that anionic polymerization of isoprene produces *cis*-1,4-polymer, only if lithium is used as counter-ion in a hydrocarbon solvent. However, anionic polymerization of methyl methacrylate with a lithium counter-ion does not produce living polymer in the normal sense<sup>6</sup>, whereas with a sodium<sup>7</sup> or potassium<sup>8</sup> counter-ion, polymerization proceeds smoothly.

When *n*-butyl lithium (*n*-BuLi) was used as a metalating agent in the presence of *t*-butoxide potassium (*t*-BuOK), it was proposed<sup>9</sup> that complex formation occurred:



Further, the presence of *t*-BuOK during polymerization of dienes, initiated by *n*-BuLi in hydrocarbon solvents, caused suppression of 1,4-addition<sup>10</sup>, suggesting that counter-ion exchange occurred. An attempt has been made to utilize this phenomenon in order to prepare a *cis*-1,4-polyisoprene-*b*-poly(methyl methacrylate) copolymer, as described below.

#### METHOD

Polymerization of isoprene was initiated by *n*-BuLi in *n*-hexane. Since the activation energy for initiation is less than that for propagation in this system<sup>11</sup>, the efficiency of initiation was increased by carrying out the polymerization of isoprene at 0°C for 4 h and then overnight at room temperature.

After polymerization of isoprene was complete, *t*-BuOK was added to the solution of living polyisoprene in order to effect an exchange of counter-ions, as suggested above. This was followed by addition of 1,1'-diphenylethylene (DPE) in tetrahydrofuran (THF) and then sufficient THF to make the final solvent composition approximately 66% (v/v) THF. DPE was added to the living polyisoprene to prevent attack of the ester group by the living polymer upon addition of methyl methacrylate<sup>8</sup>. DPE does not homopolymerize<sup>12</sup> and so only one molecule is added to each of the living polymer molecules.

Polymerization of methyl methacrylate was then carried

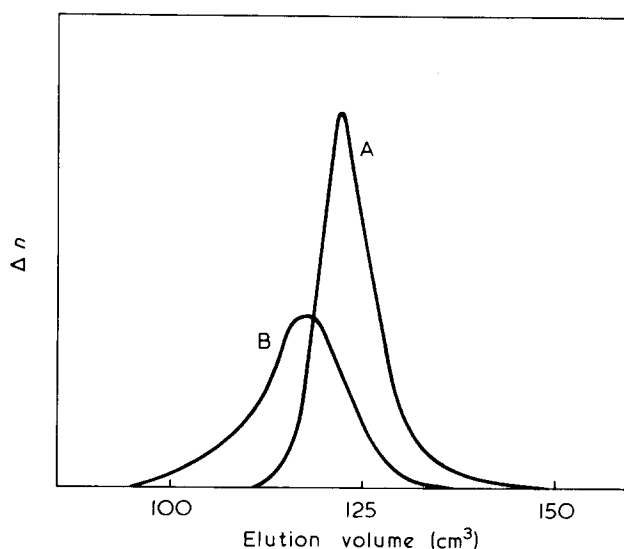
out by dropwise addition of the monomer to the reaction mixture at -78°C. The whole reaction was carried out under vacuum in a sealed, all-glass apparatus. The highly purified materials were stored in breakseal ampoules which were attached to the apparatus.

The block copolymer and a sample of homopolyisoprene removed from the reaction mixture on completion of the first stage of the reaction, were fully characterized with respect to molecular weight, composition and microstructure. Full experimental details have been given elsewhere<sup>13</sup>.

#### RESULTS

Molecular weights and composition of the polymers were close to the predicted values. The molecular weight distribution (*MWD*) of the sample of homopolyisoprene, determined by gel permeation chromatography (g.p.c.), is narrow, as shown in *Figure 1*. The *MWD* of the copolymer is relatively broad (*Figure 1*) but the fact that it consists of a single sharp peak suggests that potassium acted as counter-ion during polymerization of methyl methacrylate, since when lithium does so, very broad or bimodal distributions are obtained<sup>6</sup>. Also, the g.p.c. trace of the copolymer suggests that little or no homopoly(methyl methacrylate), possibly initiated by *t*-BuOK<sup>14</sup>, is present.

The microstructure of the homopolyisoprene was determined by proton n.m.r. spectroscopy. Spectra were interpreted according to published data<sup>15</sup>. The polyisoprene microstructure was, approximately: *cis*-1,4-, 78%; *trans*-



*Figure 1* Gel permeation chromatograms of (A) homopolyisoprene and (B) *cis*-1,4-polyisoprene-*b*-poly(methyl methacrylate), prepared as described in the text

## Note to the Editor/Book Review

1,4-, 20%; 3,4-, 2%; and 1,2-, 0%. These values are close to those reported elsewhere<sup>16</sup> for polyisoprene prepared under similar conditions and analysed by proton n.m.r. spectroscopy.

The chain configuration of the poly(methyl methacrylate) block was also determined by proton n.m.r. spectroscopy. Spectra were interpreted according to literature data<sup>17</sup> and the results are summarized in Table 1. The triad distribution in the poly(methyl methacrylate) block of the isoprene-methyl methacrylate block copolymer (IMMA) is compared to that in a polystyrene-*b*-poly(methyl methacrylate) copolymer (SMMA), in which polymerization of the methyl methacrylate block was initiated by polystyryl potassium in THF. The triad distribution in each copolymer is similar and is also similar to that in homopoly(methyl methacrylate), prepared by anionic polymerization with a potassium counter-ion in polar solvents, as reported elsewhere<sup>18</sup>. When lithium is the counter-ion the results are quite different<sup>18</sup>.

Thus, a *cis*-1,4-polyisoprene-*b*-poly(methyl methacrylate) copolymer of approximately predetermined composition has been prepared. The evidence presented above suggests that counter-ion exchange between polyisoprenyl lithium and *t*-BuOK does occur under the conditions employed.

## ACKNOWLEDGEMENTS

Thanks are due to the Science Research Council for a maintenance award (to D.C.E.). Proton n.m.r. spectra were recorded by Mr S. J. Roberts at Imperial College and g.p.c. measurements were made by Dr J. M. Evans of the Rubber and Plastics Research Association (RAPRA).

## REFERENCES

- 1 Szwarc, M., Levy, M. and Milkovich, R. *J. Am. Chem. Soc.* 1956, 78, 2656

Table 1 Proton n.m.r. spectra of *cis*-1,4-polyisoprene-*b*-poly(methyl methacrylate) (IMMA) and polystyrene-*b*-poly(methyl methacrylate) (SMMA)

Band (ppm) <sup>a</sup>	Assignment <sup>b</sup>	Polymer configuration (%)	
		SMMA	IMMA
1.2	Isotactic	15	14
1.05	Heterotactic	57	56
0.9	Syndiotactic	28	30

<sup>a</sup> Shift from TMS

<sup>b</sup> Assignment of triads from ref 17

- 2 Morton, M. and Fetters, L. J. *J. Polym. Sci. (D)* 1967, 2, 71
- 3 Fetters, L. J. *J. Polym. Sci. (C)* 1969, 26, 1
- 4 Allport, D. C. in 'Block Copolymers' (Eds D. C. Allport and W. H. Janes) 1973, Applied Science, Barking, Ch 3
- 5 Allport, D. C. *ibid.* Ch 2
- 6 Bywater, S. *Adv. Polym. Sci.* 1965, 4, 66
- 7 Roig, A. and Figuerello, J. E. *J. Polym. Sci. (B)* 1965, 3, 171
- 8 Freyss, D., Rempp, P. and Benoit, H. *J. Polym. Sci. (B)* 1964, 2, 217
- 9 Amass, A. J., Duck, E. W., Hawkins, J. R. and Locke, J. M. *Eur. Polym. J.* 1972, 8, 781
- 10 Hsieh, H. L. and Wofford, C. F. *J. Polym. Sci. (A-1)* 1969, 7, 449
- 11 Morton, M., Bostick, E. E., Livigni, R. A. and Fetters, L. J. *J. Polym. Sci. (A)* 1963, 1, 1735
- 12 Szwarc, M. 'Carbanions, Living Polymers and Electron Transfer Processes', Interscience, New York, 1968, p 145
- 13 Evans, D. C. *Thesis* University of London (1974)
- 14 Baca, J., Lochmann, L., Juzl, K., Coupek, J. and Lim, D. *J. Polym. Sci. (C)* 1968, 16, 3865
- 15 Simak, R. and Fahrback, G. *Angew. Makromol. Chem.* 1970, 12, 73
- 16 Worsfold, D. J. and Bywater, S. *Can. J. Chem.* 1964, 42, 2884
- 17 Bovey, F. A. and Tiers, G. V. D. *J. Polym. Sci.* 1960, 44, 173
- 18 Braun, D., Herner, M., Johnsen, U. and Kerner, W. *Makromol. Chem.* 1962, 51, 15

# Book Review

## Polymer molecular weight methods (Advances in Chemistry Series 125)

Edited by Myer Ezrin

ACS, Washington D.C., 1973, 350 pp. \$17.50

Papers from the symposium entitled 'Recent Trends in the Determination of Molecular Weight' cosponsored by the Analytical and Polymer Chemistry Divisions of the American Chemical Society (ACS) form the contents of this volume. The symposium was held during the 162nd ACS national meeting at Washington D.C. in September 1971.

Methods suitable for the measurement of molecular weights (*MW*) from simple molecules to high polymers are covered. Ebulliometry and mass chromatography have been modified to provide useful methods for measuring lower *MW*. More reliable qualitative determinations are achieved with the twin columns and gas density detectors used in the mass chromatograph. Its adoption to pyrolysis gas chromatography should extend the versatility of this technique also.

Twelve of the twenty six published papers concern the technique of gel permeation chromatography (g.p.c.) in some aspect. Some of these represent small but significant improvements to the technique that enjoyed wider coverage at a previous ACS symposium at Houston, Texas, in February 1970. A welcome emphasis has been placed on the reproducibility of derived parameters, both inter- and intra-laboratory. Polymer standards, useful in this connection, are described. Other topics include computerized data acquisition

and processing, calibration and application to the analysis of polypeptides, cellulose, cellulose nitrate, resole phenol-formaldehyde resins and styrene-butadiene block copolymers.

Another advance, electrospray mass spectrometry (e.m.s.) has enabled particles up to a *MW* of  $1.6 \times 10^5$  to be examined by mass spectrometry. The electrospray process consists of feeding a liquid through a metal capillary which is maintained at a high electrical potential with respect to some nearby surface. As liquid reaches the capillary tip, the liquid is dispersed into fine electrified droplets. If the liquid contains macromolecules then, after the solvent has evaporated completely, the macromolecules are left as gaseous macro-ions. Here *MW* is expressed in atomic mass units. This unit is equivalent to the less familiar Dalton ( $1.66 \times 10^{-24}$  g) used in a previous paper.

Diffusion and sedimentation equilibrium are given a good coverage. Diffusion coefficients are reported to be more readily obtained with the newer technique of self-beat spectroscopy. Two papers explore the mathematics for deriving molecular weight distributions from sedimentation equilibrium experiments.

Other techniques covered include light scattering, X-ray scattering, nuclear magnetic resonance spectroscopy, viscosity and thin film dialysis for isolating substances in the intermediate *MW* range.

This is an excellently produced volume in keeping with the standard of the ACS series of publications. The symposium was successful in conveying the importance of a multidisciplinary approach to *MW* measurement. Generally the papers are highly informative and make a useful and very concise reference book.

J. M. Evans

## Note to the Editor/Book Review

1,4-, 20%; 3,4-, 2%; and 1,2-, 0%. These values are close to those reported elsewhere<sup>16</sup> for polyisoprene prepared under similar conditions and analysed by proton n.m.r. spectroscopy.

The chain configuration of the poly(methyl methacrylate) block was also determined by proton n.m.r. spectroscopy. Spectra were interpreted according to literature data<sup>17</sup> and the results are summarized in Table 1. The triad distribution in the poly(methyl methacrylate) block of the isoprene-methyl methacrylate block copolymer (IMMA) is compared to that in a polystyrene-*b*-poly(methyl methacrylate) copolymer (SMMA), in which polymerization of the methyl methacrylate block was initiated by polystyryl potassium in THF. The triad distribution in each copolymer is similar and is also similar to that in homopoly(methyl methacrylate), prepared by anionic polymerization with a potassium counter-ion in polar solvents, as reported elsewhere<sup>18</sup>. When lithium is the counter-ion the results are quite different<sup>18</sup>.

Thus, a *cis*-1,4-polyisoprene-*b*-poly(methyl methacrylate) copolymer of approximately predetermined composition has been prepared. The evidence presented above suggests that counter-ion exchange between polyisoprenyl lithium and *t*-BuOK does occur under the conditions employed.

## ACKNOWLEDGEMENTS

Thanks are due to the Science Research Council for a maintenance award (to D.C.E.). Proton n.m.r. spectra were recorded by Mr S. J. Roberts at Imperial College and g.p.c. measurements were made by Dr J. M. Evans of the Rubber and Plastics Research Association (RAPRA).

## REFERENCES

- 1 Szwarc, M., Levy, M. and Milkovich, R. *J. Am. Chem. Soc.* 1956, 78, 2656

Table 1 Proton n.m.r. spectra of *cis*-1,4-polyisoprene-*b*-poly(methyl methacrylate) (IMMA) and polystyrene-*b*-poly(methyl methacrylate) (SMMA)

Band (ppm) <sup>a</sup>	Assignment <sup>b</sup>	Polymer configuration (%)	
		SMMA	IMMA
1.2	Isotactic	15	14
1.05	Heterotactic	57	56
0.9	Syndiotactic	28	30

<sup>a</sup> Shift from TMS

<sup>b</sup> Assignment of triads from ref 17

- 2 Morton, M. and Fetters, L. J. *J. Polym. Sci. (D)* 1967, 2, 71
- 3 Fetters, L. J. *J. Polym. Sci. (C)* 1969, 26, 1
- 4 Allport, D. C. in 'Block Copolymers' (Eds D. C. Allport and W. H. Janes) 1973, Applied Science, Barking, Ch 3
- 5 Allport, D. C. *ibid.* Ch 2
- 6 Bywater, S. *Adv. Polym. Sci.* 1965, 4, 66
- 7 Roig, A. and Figuerello, J. E. *J. Polym. Sci. (B)* 1965, 3, 171
- 8 Freyss, D., Rempp, P. and Benoit, H. *J. Polym. Sci. (B)* 1964, 2, 217
- 9 Amass, A. J., Duck, E. W., Hawkins, J. R. and Locke, J. M. *Eur. Polym. J.* 1972, 8, 781
- 10 Hsieh, H. L. and Wofford, C. F. *J. Polym. Sci. (A-1)* 1969, 7, 449
- 11 Morton, M., Bostick, E. E., Livigni, R. A. and Fetters, L. J. *J. Polym. Sci. (A)* 1963, 1, 1735
- 12 Szwarc, M. 'Carbanions, Living Polymers and Electron Transfer Processes', Interscience, New York, 1968, p 145
- 13 Evans, D. C. *Thesis* University of London (1974)
- 14 Baca, J., Lochmann, L., Juzl, K., Coupek, J. and Lim, D. *J. Polym. Sci. (C)* 1968, 16, 3865
- 15 Simak, R. and Fahrback, G. *Angew. Makromol. Chem.* 1970, 12, 73
- 16 Worsfold, D. J. and Bywater, S. *Can. J. Chem.* 1964, 42, 2884
- 17 Bovey, F. A. and Tiers, G. V. D. *J. Polym. Sci.* 1960, 44, 173
- 18 Braun, D., Herner, M., Johnsen, U. and Kerner, W. *Makromol. Chem.* 1962, 51, 15

# Book Review

## Polymer molecular weight methods (Advances in Chemistry Series 125)

Edited by Myer Ezrin

ACS, Washington D.C., 1973, 350 pp. \$17.50

Papers from the symposium entitled 'Recent Trends in the Determination of Molecular Weight' cosponsored by the Analytical and Polymer Chemistry Divisions of the American Chemical Society (ACS) form the contents of this volume. The symposium was held during the 162nd ACS national meeting at Washington D.C. in September 1971.

Methods suitable for the measurement of molecular weights (*MW*) from simple molecules to high polymers are covered. Ebulliometry and mass chromatography have been modified to provide useful methods for measuring lower *MW*. More reliable qualitative determinations are achieved with the twin columns and gas density detectors used in the mass chromatograph. Its adoption to pyrolysis gas chromatography should extend the versatility of this technique also.

Twelve of the twenty six published papers concern the technique of gel permeation chromatography (g.p.c.) in some aspect. Some of these represent small but significant improvements to the technique that enjoyed wider coverage at a previous ACS symposium at Houston, Texas, in February 1970. A welcome emphasis has been placed on the reproducibility of derived parameters, both inter- and intra-laboratory. Polymer standards, useful in this connection, are described. Other topics include computerized data acquisition

and processing, calibration and application to the analysis of polypeptides, cellulose, cellulose nitrate, resole phenol-formaldehyde resins and styrene-butadiene block copolymers.

Another advance, electrospray mass spectrometry (e.m.s.) has enabled particles up to a *MW* of  $1.6 \times 10^5$  to be examined by mass spectrometry. The electrospray process consists of feeding a liquid through a metal capillary which is maintained at a high electrical potential with respect to some nearby surface. As liquid reaches the capillary tip, the liquid is dispersed into fine electrified droplets. If the liquid contains macromolecules then, after the solvent has evaporated completely, the macromolecules are left as gaseous macro-ions. Here *MW* is expressed in atomic mass units. This unit is equivalent to the less familiar Dalton ( $1.66 \times 10^{-24}$  g) used in a previous paper.

Diffusion and sedimentation equilibrium are given a good coverage. Diffusion coefficients are reported to be more readily obtained with the newer technique of self-beat spectroscopy. Two papers explore the mathematics for deriving molecular weight distributions from sedimentation equilibrium experiments.

Other techniques covered include light scattering, X-ray scattering, nuclear magnetic resonance spectroscopy, viscosity and thin film dialysis for isolating substances in the intermediate *MW* range.

This is an excellently produced volume in keeping with the standard of the ACS series of publications. The symposium was successful in conveying the importance of a multidisciplinary approach to *MW* measurement. Generally the papers are highly informative and make a useful and very concise reference book.

J. M. Evans



# On the structure of polybutadiene: 4. $^{13}\text{C}$ n.m.r. spectrum of polybutadienes with *cis*-1,4-, *trans*-1,4- and 1,2-units

Karl-Friedrich Elgert, Gunther Quack and Bernhard Stützel

Institut für Makromolekulare Chemie der Universität Freiburg, D-78 Freiburg, West Germany

(Received 18 June 1974)

$^{13}\text{C}$  n.m.r. spectra of polybutadienes with different contents of *cis*-1,4-, *trans*-1,4- and 1,2-units are assigned in the resonance region of the *cis* and *trans* carbon double bond. The observed signals are assigned to configurational triads.

## INTRODUCTION

Investigations of the sequence analysis of polybutadienes by  $^1\text{H}$  n.m.r. spectroscopy indicated triads generated by *cis*-1,4- and *trans*-1,4-units in 1,4-polybutadienes<sup>1,2</sup>. The backbone chain of real polybutadienes, however, consists of sequences of *cis*, *trans* and 1,2-units.  $^{13}\text{C}$  n.m.r. spectroscopy offers more detailed information on this structure problem. In previous papers we reported the sequence analysis of 1,4-polybutadiene<sup>3</sup>, 1,2-polybutadiene<sup>4</sup> and equibinary (*cis*-1,4-/1,2-)polybutadiene<sup>5</sup> by  $^{13}\text{C}$  n.m.r. spectroscopy. In this communication the first results on the determination of the sequence distribution of polybutadienes with different contents of *trans*-1,4-, *cis*-1,4- and 1,2-units are reported.

## EXPERIMENTAL

The polybutadienes were polymerized anionically by *n*-butyl lithium in various *n*-heptane/tetrahydrofuran mixtures. The polymerization temperatures varied between  $-10^\circ\text{C}$  and  $+60^\circ\text{C}$ .

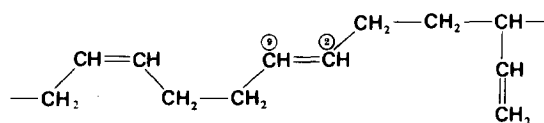
The microstructure of the polybutadienes was determined by i.r. spectroscopy on a Perkin-Elmer spectrometer 125 in  $\text{CS}_2$  solution.

The proton decoupled  $^{13}\text{C}$  n.m.r. spectra were obtained in  $\text{CDCl}_3$  at  $35^\circ\text{C}$  with a HX 270 (Spectrospin AG, CH-8117, Zürich-Fällanden, Switzerland) at 67.88 MHz. The spectrometer conditions were: sweep width, 12 kHz; acquisition time, 0.67 sec; pulse width, 35  $\mu\text{sec}$ ; transients, 8 k; data points, FT interferogram, 16 k. Internal standard was octamethyltetrasiloxane (OMTS) = 0 ppm.

## RESULTS AND DISCUSSION

Six polybutadiene samples have been selected. The polymerization conditions of these samples polymerized anionically by *n*-butyl lithium in suitable *n*-heptane/tetrahydrofuran mixtures are listed in Table 1. The polymerization process is assumed to generate a random sequence distribution of *cis*-1,4-, *trans*-1,4- and 1,2-units. The resonance region of the *cis* and *trans* carbon double bond of the  $^{13}\text{C}$  n.m.r. spectra of these polybutadienes is shown in Figure 1. The spectra are arranged in succession of increasing content of 1,2-units in the polymer. The observed resonance signals result from influences of neighbouring

1,2-, *cis*-1,4- and *trans*-1,4-units on the signal of a central *cis*-1,4 or *trans*-1,4-unit in a sequence of three structure units, e.g. *cis*-1,4(*c*)/*trans*-1,4(*t*)/1,2(*v*) (*c/t/v*):



or 1,2(*v*)/*trans*-1,4(*t*)/1,2(*v*) (*-v/t/-v*):

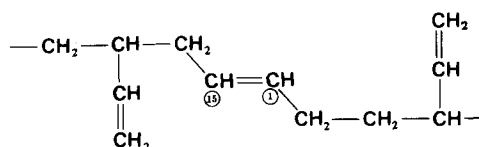


Figure 1 demonstrates the multiplicity of the  $^{13}\text{C}$  n.m.r. spectra caused by the sequence distribution of the structure units. Spectrum (1) represents the polymer sample 1 whose

Table 1 Polymerization of butadiene by *n*-butyl lithium in *n*-heptane/tetrahydrofuran mixtures

Sample	Microstructure (%)			Polymerization temperature ( $^\circ\text{C}$ )	Tetrahydrofuran (%)
	<i>trans</i>	<i>cis</i>	1,2		
1	54	37	9	30	0
2	45	28	27	60	0.2
3	41	27	32	60	0.3
4	31	16	53	30	0.4
5	9	11	80	$-10$	1.0
6	5	7	88	$-10$	100

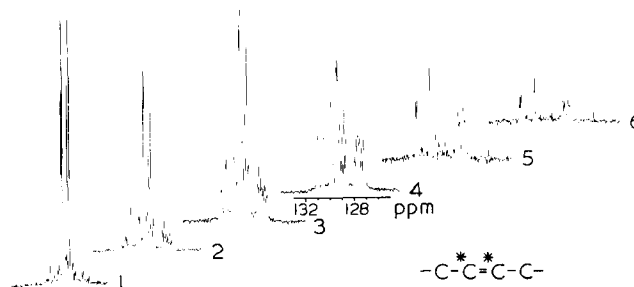


Figure 1  $^{13}\text{C}$  n.m.r. spectra of the *cis*-1,4 and *trans*-1,4 double bond in polybutadienes with different contents of 1,2-units

1,2-units are mainly isolated. With increasing content of 1,2-units as in samples 2, 3 and 4 the relative intensities of the 1,4-block signals are decreasing whereas the signals of sequences containing 1,2-units are increasing. In spectra (5) and (6), 1,4-units are expected to be mainly isolated.

Figure 2 shows the expanded spectrum of a polymer

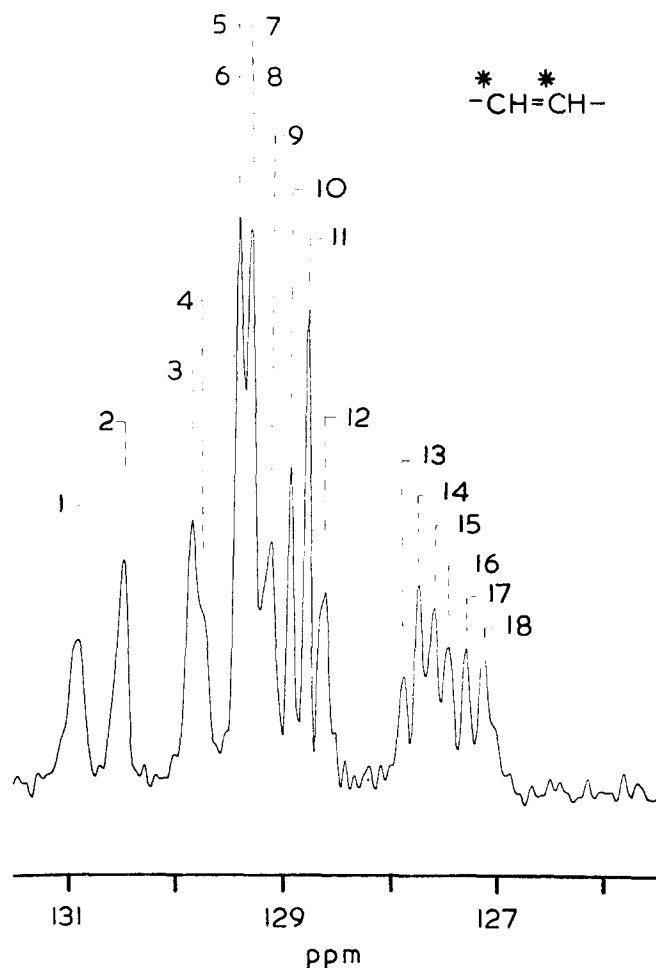


Figure 2 Expanded  $^{13}\text{C}$  n.m.r. spectrum of a polybutadiene with 34% *trans*-1,4-, 24% *cis*-1,4- and 42% 1,2-units

sample containing 34% *trans*-, 24% *cis*- and 42% 1,2-units. Within resolution and sensitivity of the spectrometer 16 signals are completely resolved in the resonance region of the *cis*-1,4- and *trans*-1,4-carbon double bond. The assignment of the resonance signals has been performed stepwise using our previous assignment of the  $^{13}\text{C}$  n.m.r. spectra of 1,4-polybutadienes<sup>3</sup>. Signals (8) and (10) are assigned to *trans-trans* and *cis-cis* sequences. Signals (6) and (11) represent *trans-cis* and *cis-trans* transitions. According to our interpretation of the  $^{13}\text{C}$  n.m.r. spectrum of equibinary (*cis*-1,4-/1,2-)polybutadiene<sup>5</sup> the signals (3), (5), (7), (12), (16), (17) and (18) are assigned to sequences of three units containing a central *cis*-1,4-unit. The residual signals are assigned to sequences of three units containing a central *trans*-unit.

If surrounded by 1,2-units the two carbon atoms of the *cis*-1,4- and *trans*-1,4-carbon double bond have different chemical shifts owing to their different distances from the vinyl side group. Head-to-tail addition is highly probable because no signals for other linkages could be verified.

The assignment of the resonance signals of the *cis*-1,4- and *trans*-1,4-carbon double bond is listed in Table 2. The assignment of the resonance signals including units with a central *trans*-1,4-unit has been verified by comparison of experimental peak intensities with those calculated by Bernoullian statistics. The intensities in all resonance regions have been calculated from peak areas given by the integration procedure of the spectrometer computer rather than from peak heights. The overall composition of the polybutadienes was determined by i.r. spectroscopy. Within experimental error no difference exists between predicted polymer composition and experimental values from  $^{13}\text{C}$  n.m.r. spectra. By quantitative interpretation of  $^{13}\text{C}$  n.m.r. spectra from poly( $\alpha$ -methylstyrene)<sup>6</sup> it was feasible to calculate the relative abundance of  $^{13}\text{C}$  nuclei incorporated in configurational sequences. The quantitative results from  $^{13}\text{C}$  n.m.r. spectra are in excellent agreement with those from corresponding  $^1\text{H}$  n.m.r. spectra. Preliminary evidence suggests this procedure may be applicable on polybutadienes as well, if nuclear Overhauser enhancement and relaxation times do not vary in a strong way.

Table 2  $^{13}\text{C}$  chemical shift data and relative intensities in polybutadienes

Signal	Carbon atom	Sequence	Chemical shift (ppm)	Sample											
				1		2		3		4		5		6	
				Exp.	Calc.	Exp.	Calc.	Exp.	Calc.	Exp.	Calc.	Exp.	Calc.	Exp.	Calc.
1	-C=C*-	-v/t/-v	131.01	0.00	0.00	0.02	0.02	0.04	0.03	0.08	0.09	0.15	0.14	0.23	0.16
2		c/t/-v	130.55	0.02	0.02	0.06	0.06	0.07	0.07	0.07	0.08	0.04	0.04	0.00	0.02
3		-v/c/-v	129.87	0.05	0.03	0.09	0.07	0.13	0.09	0.14	0.13	0.20	0.21	0.23	0.25
4		-v/t/c	129.87	0.05	0.03	0.09	0.07	0.13	0.09	0.14	0.13	0.20	0.21	0.23	0.25
5		c/c/-v	129.41	0.21	0.22	0.19	0.16	0.14	0.15	0.12	0.09	0.04	0.05	0.00	0.03
6		t/t/c	129.41	0.21	0.22	0.19	0.16	0.14	0.15	0.12	0.09	0.04	0.05	0.00	0.03
7		c/t/c	129.30	0.29	0.31	0.19	0.24	0.18	0.21	0.10	0.14	0.04	0.05	0.00	0.03
8		t/t/c	129.30	0.29	0.31	0.19	0.24	0.18	0.21	0.10	0.14	0.04	0.05	0.00	0.03
9	-C*==C-	c/t/-v	129.11	0.00	0.02	0.07	0.06	0.06	0.07	0.07	0.08	0.03	0.04	0.00	0.02
10		c/c/c	128.91	0.17	0.14	0.10	0.08	0.08	0.07	0.05	0.03	0.00	0.01	0.00	0.00
11		c/c/t	128.73	0.21	0.20	0.15	0.13	0.11	0.11	0.06	0.05	0.01	0.01	0.00	0.00
12		c/c/-v	128.56	0.03	0.02	0.04	0.04	0.05	0.04	0.06	0.04	0.06	0.04	0.00	0.03
13		-v/t/c	127.77	0.02	0.02	0.05	0.06	0.06	0.07	0.07	0.08	0.00	0.04	0.00	0.02
14		-v/t/t	127.64	0.02	0.02	0.05	0.06	0.06	0.07	0.07	0.08	0.00	0.04	0.00	0.02
15		-v/t/-v	127.48	0.00	0.00	0.01	0.02	0.03	0.03	0.05	0.09	0.16	0.14	0.17	0.16
16		-v/c/c	127.33	0.00	0.02	0.03	0.04	0.05	0.04	0.08	0.04	0.07	0.04	0.11	0.03
17		-v/c/t	127.15	0.00	0.02	0.03	0.04	0.05	0.04	0.08	0.04	0.07	0.04	0.11	0.03
18		-v/c/-v	126.98	0.00	0.00	0.01	0.01	0.02	0.02	0.07	0.05	0.21	0.18	0.25	0.23

In  $^{13}\text{C}$  n.m.r. spectroscopy of low molecular weight compounds the position of a peak in the spectrum is determined by the local environment of the carbon nucleus. The chemical shift of alkanes<sup>7</sup> and alkenes<sup>8</sup> can be calculated from the sum of empirical shift parameters which take into account the environment of a carbon atom. If additivity holds for polymers, too, it should be possible to find an empirical set of shift parameters which take into account quantitatively the influence of a neighbouring 1,2-unit on a given *cis*-1,4- or *trans*-1,4-unit.

As listed in Table 3 eight parameters are necessary to describe the influence of a neighbouring 1,2-unit on the chemical shift of the resonance signals of the *cis*-1,4- and *trans*-1,4-double bond relative to their block signals at 128.91 ppm and 129.30 ppm, respectively. These parameters hold whether the double bond of the 1,2-unit is three ( $\gamma$ ) or four ( $\delta$ ) carbon bonds away from that 1,4-double bond under consideration. The parameters ( $\gamma'$ ) and ( $\delta'$ ) refer to the influence of the vinyl double bond on the opposite side of that double bond atom.

For example, the chemical shift,  $\Delta$ , of the carbon atoms of the above mentioned examples are calculated as follows:

$$\Delta(\text{C}_1)\text{calc.} = \textit{trans} \text{ block} + \gamma' + \delta = 129.30 + 0.46 + 1.25 = 131.01 \text{ ppm}$$

$$\Delta(\text{C}_1)\text{exp.} = 131.01 \text{ ppm}$$

$$\Delta(\text{C}_{15})\text{calc.} = \textit{trans} \text{ block} + \gamma + \delta' = 129.30 - 1.66 - 0.19 = 127.45 \text{ ppm}$$

$$\Delta(\text{C}_{15})\text{exp.} = 127.48 \text{ ppm}$$

$$\Delta(\text{C}_2)\text{calc.} = \textit{trans} \text{ block} + \delta = 129.30 + 1.25 = 130.55 \text{ ppm}$$

$$\Delta(\text{C}_2)\text{exp.} = 130.55 \text{ ppm}$$

$$\Delta(\text{C}_9)\text{calc.} = \textit{trans} \text{ block} + \delta' = 129.30 - 0.19 = 129.11 \text{ ppm}$$

$$\Delta(\text{C}_9)\text{exp.} = 129.11 \text{ ppm}$$

Carbon atoms 13 and 14 of a central *trans*-1,4-unit and carbon atoms 16 and 17 of a central *cis*-1,4-unit differ only in the neighbouring 1,4-unit. The splitting in these cases is of the same magnitude as the splitting of the signals of isomerized 1,4-polybutadienes<sup>5</sup>. The signal of an atom in the *trans* carbon double bond is shifted downfield by 0.11 ppm, if the *trans* unit is next to a *cis* unit on the opposite side of the double bond, whereas the *cis* signal

Table 3 Shift parameters in polybutadienes

Para- meters	<i>cis</i>	<i>trans</i>
$\gamma$ ,	-1.60	-1.66
$\gamma'$	+0.48	+0.46
$\delta$ ,	+0.48	+1.25
$\delta'$	-0.31	-0.19

is shifted upfield by 0.18 ppm if next to a *trans* unit. Owing to limited resolution and overlapping of signals, however, this splitting is not observable for signals (2) and (5).

As shown in spectra (5) and (6) of Figure 1 the  $^{13}\text{C}$  n.m.r. spectra of polybutadienes containing mainly 1,2-blocks and isolated *cis*-1,4- and *trans*-1,4-units are complicated by an additional fine structure. Signals (1), (15) and (18) split up into two resonance signals. This splitting may be caused by the asymmetric carbon atom of the 1,2-unit or by the influence of the next neighbouring *cis*-1,4 or *trans*-1,4 unit<sup>5</sup>. The shift parameters listed in Table 3 refer only to the upfield signal. The correct interpretation of these signals is subject to current investigation. An important feature of these parameters is that  $^{13}\text{C}$  n.m.r. spectra of polybutadienes can be predicted in the resonance region of the *cis* and *trans* double bond if the sequence distribution generated by the polymerization process is known.

#### ACKNOWLEDGEMENT

The financial support of the Arbeitsgemeinschaft Industrieller Forschungsvereinigungen and the Deutsche Forschungsgemeinschaft is gratefully acknowledged.

#### REFERENCES

- 1 Santee, E. R., Mochel, V. D. and Morton, M. J. *Polym. Sci. (Polym. Lett. Edn)* 1973, **11**, 453
- 2 Hatada, K., Tanaka, Y., Terawaki, Y. and Okuda, H. *Polym. J.* 1973, **5**, 327
- 3 Elgert, K.-F., Stützel, B., Frenzel, P., Cantow, H.-J. and Streck, R. *Makromol. Chem.* 1973, **170**, 257
- 4 Elgert, K.-F., Quack, G. and Stützel, B. *Makromol. Chem.* 1974, **175**, 1955
- 5 Elgert, K.-F., Quack, G. and Stützel, B. *Polymer* 1974, **15**, 612
- 6 Elgert, K.-F., Stützel, B., Cantow, H.-J., Seiler, E. and Frenzel, P. *IV Symp. Polymere 73, Varna* 1973, p 11
- 7 Lindeman, L. P. and Adams, J. Q. *Analyt. Chem.* 1971, **43**, 1245
- 8 Dorman, D. E., Jautelat, M. and Roberts, J. D. *J. Org. Chem.* 1971, **36**, 2757

# Optimum conditions for electron microscopy of radiation-sensitive polymer crystals

J. R. White

*Department of Materials, Queen Mary College, Mile End Road, London E1 4NS, UK*

*(Received 1 April 1974; revised 2 September 1974)*

The use of low electron-image magnifications reduces the electron dose suffered by a specimen during the recording of the image, and can result in a valuable extension of the life-time of a radiation sensitive polymer crystal. At magnifications of approximately 1000x the resolution is determined by the characteristics of the photographic recording plate, and is of the order of 300 Å. It is shown, however, that this is adequate for many of the studies of current interest, and that the benefits resulting from increased lifetime will usually outweigh the detrimental effect on resolution. Particular attention is given to Moiré patterns and dislocation images, and to the problem of focusing when operating at sub-visual levels.

## INTRODUCTION

In a recent paper Thomas and Ast<sup>1</sup> conclude that the use of image intensification in the electron microscopy of radiation sensitive polymer crystals brings a modest improvement, namely that damage during focusing can be minimized. They further estimate that the optimum recording magnification for polyethylene crystals is approximately  $14\,000\ n^{-1/2}$  in bright field and  $4000\ n^{-1/2}$  in dark field, where  $n$  is the number of exposures required from the area under observation. Thomas and Ast concentrate on the case where  $n = 1$ , but it is argued below that very little sacrifice in useful magnification is made when recording images at approximately 1000x, (giving  $n \sim 16$ ). In reaching this conclusion an examination of some of the more important structural features is made, with particular reference to the resolution requirements for adequate observation.

## FOCUSING

### *Focusing procedure*

The advantages of image intensification during focusing have been discussed by Thomas and Ast<sup>1</sup>. The majority of electron microscope users do not have access to this facility, however, and are faced with the choice between subjecting a radiation sensitive specimen to considerable damage during focusing, or focusing on an area remote from that subsequently chosen for photography. The latter has been preferred in this laboratory<sup>2</sup> and in others<sup>3-5</sup> and is employed in the current series of experiments. Focusing is performed with an objective aperture displacement corresponding to a polyethylene orthorhombic (110) reflection. (The instrument used in the investigation described here, a JEOL JEM 7, has no high resolution dark field beam-tilting facility.) A small condenser 2 aperture, (100 μm), and the Wehnelt cylinder bias yielding minimum beam current are used throughout, and after focusing the illumination is further reduced by setting both condenser lenses to maximum over-focus. After focusing the specimen is moved at least three

grid squares, and thence until finding an area which yields above average brightness — still only a glimmer — indicating crystalline diffraction into the objective aperture. Photographic recording of the selected area on fast plates (Ilford XM) is then performed, making adjustments such as goniometry and selection of the dark field beam rapidly and with the beam intensity switched off as much as possible.

Under the conditions of illumination described, exposures of approximately 30 sec are required even with fast plates and a vibration-free, stable microscope is essential.

### *Precision of focusing*

The focusing precision of the above procedure is limited by the following factors: (a) differences in height between the area focused and that chosen for photography; (b) differences in the intermediate and projector lens excitations caused by hysteretical effects which occur when conditions are altered between diffraction and imaging; (c) imprecision of focusing at low primary magnifications; (d) the spherical aberration term, which will differ from one reflection to another when these are at different inclinations.

The first of these is likely to be the most serious, and the one which offers least chance of correction. At present it is impossible to know the quality of the area or of the focusing until completing the series of exposures and processing the plates. If an image intensifier were available it would be used at this stage to perform a check on the suitability of the area for photography — ideally based on the evidence of a single scan recorded on an image storer (e.g. videotape), with still playback facility. Fine focus adjustment assessed by a small number of single scans might be justified.

Hysteretical effects can be minimized by cycling the lenses through a fixed routine, though they are probably unimportant at the resolution levels accepted here. Similarly low magnification focusing is probably adequate.

In dealing with the spherical aberration term it should first be noted that focusing is performed in dark field. This is important when using simple dark field operation since

beams diffracted away from the optic axis have a different focus from the transmitted beam travelling parallel to the optic axis. If the objective lens is free from astigmatism, however, the same focal length will be shared by all beams of the same deflection independent of their azimuth. Hence all  $\{110\}$  reflections will be in focus together, while the  $\{200\}$  reflections occur at a different angle, and so should require a different objective lens setting. By inspection of the phase term in the scattered amplitude<sup>6,7</sup> it can be seen that the contribution of spherical aberration of electrons inclined to the optic axis can be expressed in terms of an equivalent defocus. The difference in this equivalent defocus for beams respectively diffracted by (110) planes and (200) planes is approximately 300 Å for an objective lens with spherical aberration coefficient of 3 mm ( $\sim$ focal length), and using 100 keV electrons<sup>8</sup>, and is insignificant at the levels of resolution involved here. The effect when using a beam-tilt high resolution dark field attachment should be negligible.

## RESOLUTION

Under the conditions of image recording described above, stage drift during the long exposure may limit the resolution. If, on the other hand, this can be neglected, and focusing is likewise good, then resolution will depend on the photographic plate characteristics, and will be approximately 200 Å for images recorded at 1000x magnification<sup>1</sup>. Moiré fringes down to 290 Å spacing have been found in the current series of observations thus confirming that this value is a reasonable estimate. It is now pertinent to examine whether this level of resolution is adequate to yield information of the kind usually sought. It should also be noted that the micrographs of Thomas and Ast contain no detail corresponding to a resolution level approaching their theoretical estimate, such that no benefit has been gained from high magnification recording.

### *Moiré fringes*

The information yielded by Moiré fringes is of two basic types. First, the spacing and orientation of the fringe patterns relate to the relative orientation and relative strains in the superposed lattices which produce them. Secondly defects, in particular dislocations, can often be detected by means of Moiré magnification<sup>9</sup>. In the latter case, the view has been expressed that the detailed shape of the patterns should not be taken as indicative of the strain field associated with the dislocation<sup>9</sup>, and our criteria for resolution appropriate to this application will reduce to those for mere observation of the fringes, which result from misorientation or strain differences in the two crystals, and are dealt with below. In examining the resolution requirements of Moiré pattern observation the three types<sup>9-11</sup> will be dealt with separately.

### *Rotation Moiré patterns*<sup>9</sup>

These should show a continuous range of spacings if the angle of misorientation between the two crystals is random. Spacings as small as 40 Å, corresponding to a misorientation of approximately 6°, have been observed in polyethylene<sup>12</sup>. Larger misorientations produce smaller spacings and are hence unlikely to be detected owing to the resolution limitation. This will not be a serious drawback, however, since such patterns would only be useful insofar as their potential for Moiré magnification is realized. At the opposite end

of the scale, i.e. small misorientation/large spacing, the fringe pattern takes on a modified appearance and has attracted the interest of several workers<sup>3,4,12,13</sup>. When the angular misorientation is very small the fringes become kinked and of irregular thickness instead of being straight or continuously and gently curving, and of constant thickness. This has been interpreted to correspond to the formation of an interfacial dislocation network<sup>3-5,13-15</sup>, which must have the same (vernier) periodicity as would the rotation Moiré pattern formed at the same misorientation in the absence of any interaction<sup>4,12</sup>. The transition from the regular to the irregular type of pattern has been found to depend on the molecular weight of the sample<sup>13,16</sup> and the time of storage of the crystals (in suspension in the preparation solvent), and to be in the range 0.1°–0.3°<sup>4</sup>. The exact nature of the interface has not been established, though it seems unlikely that the folds are completely destroyed to yield a true dislocation network. Intermeshing of the crystals has been suggested to occur<sup>13</sup>, while an alternative hypothesis is that interaction across tight folds is strong enough to cause mutual alignment of the crystals over large areas, relieved by regions in which corresponding planes in the respective crystals are strongly inclined to maintain the same net misorientation<sup>17</sup>. The strains would hence be qualitatively similar to those envisaged by Niinomi and coworkers for true dislocations, and the image appearance consequently similar. What is relevant here is that the Moiré spacing corresponding to this transition is easily within the resolution capability of the technique under scrutiny.

### *Parallel Moiré patterns*<sup>9</sup>

The dark field parallel Moiré pattern which would be produced by a (110) reflection and a (200) reflection falling within the aperture and produced by polyethylene crystals oriented such that these reflections lie on a common radius would have a spacing of approximately 36 Å. Even if such a pattern could be resolved, it would contain no information which could not be obtained from the diffraction pattern, since the contributing beams would be sufficiently separated to be easily distinguished. Consequently the only parallel Moirés to be considered will be those formed between like planes in crystals maintaining different strains. A parallel Moiré pattern spacing of 300 Å in a dark field image would correspond to a relative elastic strain between the two crystals of  $\sim$ 1.4%. Even if the external restraints could be so arranged to share this between the two, with one in tension and the other in compression, such a strain seems too high to make its occurrence likely. Smaller strains would produce larger spacings which would hence be resolvable by the low magnification recording technique.

### *Tilt Moiré patterns*<sup>10,11</sup>

The range of relative tilt between two crystals which produces a tilt Moiré pattern with observable contrast is restricted, and depends on crystal thickness. For most systems encountered in practice, in particular polyethylene crystals of 100–200 Å thickness, the relative tilt must be small, and the lower limit to the corresponding fringe pattern spacing large, and easily resolved by low magnification recording.

### *Dislocations*

Dislocation detection by Moiré magnification will, in general, be possible whenever the Moiré pattern is resolved,

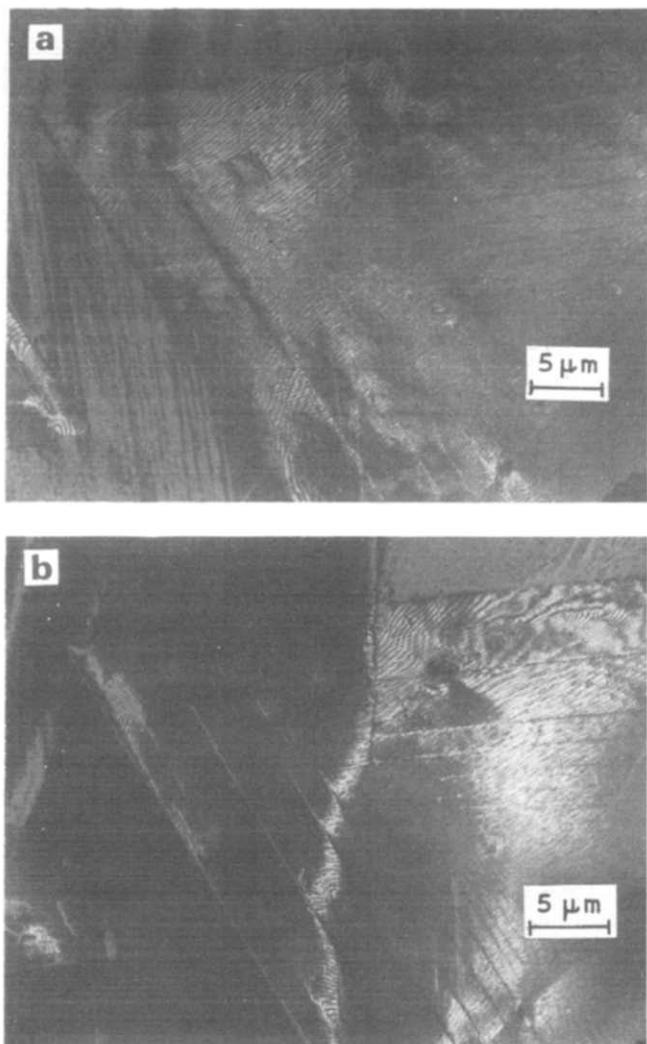


Figure 1 Dark field images taken in the  $(\bar{1}\bar{1}0)$  reflection of polyethylene crystals on a carbon support film. (a) First exposure; (b) thirteenth exposure. (Goniometer adjustments were made between (a) and (b).)

and the remarks in the sections dealing with Moiré patterns are hence again appropriate. A dislocation will also be rendered visible by the diffraction contrast produced by the associated strain field as long as the burgers vector and the diffraction vector are not mutually perpendicular. Dislocation networks have often been reported, even when recorded at low magnifications<sup>3</sup>. These are generally assumed to lie in the interfacial boundary between two overlying crystals, and to be screw dislocations. Some remarks relating to these networks were made in the section on rotation Moiré patterns above. It will further be recalled that dislocation images are only obtained when the separation exceeds a certain value corresponding to a 'critical angle' of misorientation between the crystals<sup>4</sup>. This separation is fairly large and is easily resolved as has been noted above.

The dissociation of the interfacial dislocations is energetically favourable in many instances<sup>15</sup>, and the separation of the partials is often large enough to be easily resolved. In some cases the expected dissociation has not been observed, however, possibly because it is weak and the separation is too small<sup>15</sup>. Better resolution might improve matters, though distinction between an undissociated dislocation image and that of two partials placed close together would not be particularly clear. Care must be taken not to confuse dislocation double images, produced

when  $gb = n = 2$ , with separated partials. Calculated values for the separation of partials and of dislocation double images are in conflict with observations, possibly owing to inadequate data on the elastic constants of the polyethylene crystal<sup>15</sup>, and need improvement before higher resolution can be justified on this account. On the other hand, the reader is reminded of the remarks made earlier regarding the nature of the interfacial dislocations. If the assimilation of the folds into a true twist boundary is incomplete as suggested, the dislocation-like strains might still be expected to dissociate in a manner analogous to that of true dislocations. The difference in strength of the interaction which would occur in a twist boundary at the centre of a crystal of thickness twice the fold period of a monolayer crystal and that present when two monolayer crystals with tight folds are in contact may provide an alternative explanation for the discrepancy between calculated images based on the former model and experimental observations<sup>15</sup>.

## EXPERIMENTAL RESULTS

The observations presented here are extracted from a broader study reported more fully in another paper<sup>18</sup>. Dark field micrographs of single areas using several beams and at different specimen tilts were required. The number of micrographs with good diffraction contrast obtainable from a single area was found consistent with that claimed by Thomas and Ast, as projected to a magnification of 1000x. Figures 1a and 1b show the same area of a polyethylene crystal preparation grown in xylene and deposited onto a thin evaporated carbon support film. They are respectively the first and thirteenth exposures in a series in which dark field recording at 980x magnification was used throughout, with the exception of one selected area diffraction pattern taken as the seventh exposure (Figure 2). The quality of the Moiré patterns in the last of the series is seen still to be very good as long as the large underlying crystal is reflecting, as indicated by projecting the bright bands of the single layered regions into the multi-layered parts. This is a pre-requisite applicable to all of the images, of course, and is dependent on the local crystallographic orientation, which is in turn partly governed by the specimen tilt produced by the goniometer stage. The changing location of Moiré images is hence dependent on the diffracted beam used to form the image and on any goniometer adjustments. Loss of Moiré contrast cannot



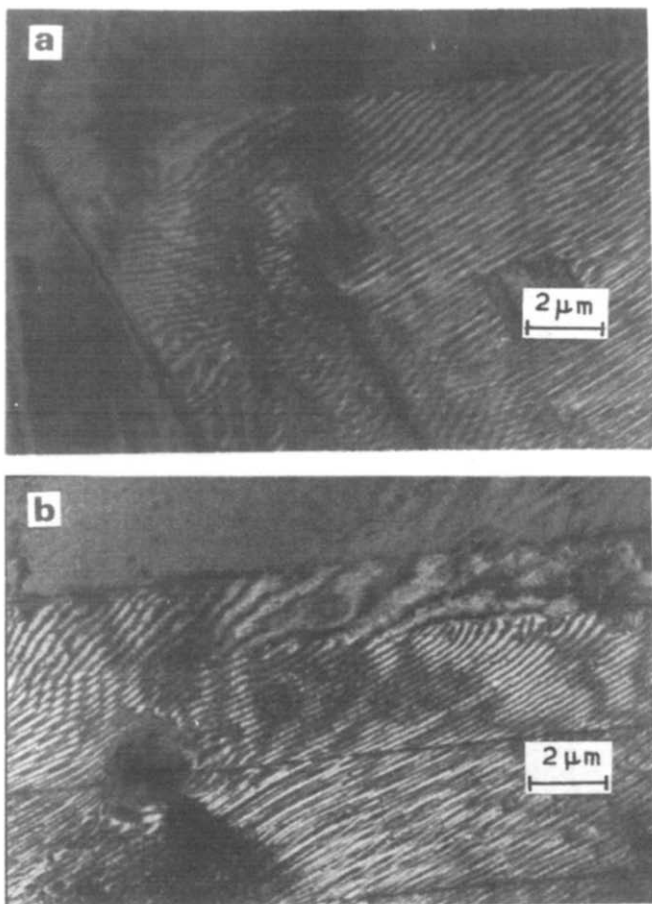
Figure 2 Selected area diffraction pattern from part of the area shown in Figure 1

alone be taken as indication that crystal structure has been destroyed in that area. Parts of this area are shown at higher magnification in *Figures 3a* and *3b*. *Figure 4* shows another area recorded at a primary magnification of 980x at still greater photographic enlargement in which fringe resolution of 290 Å is clearly visible.

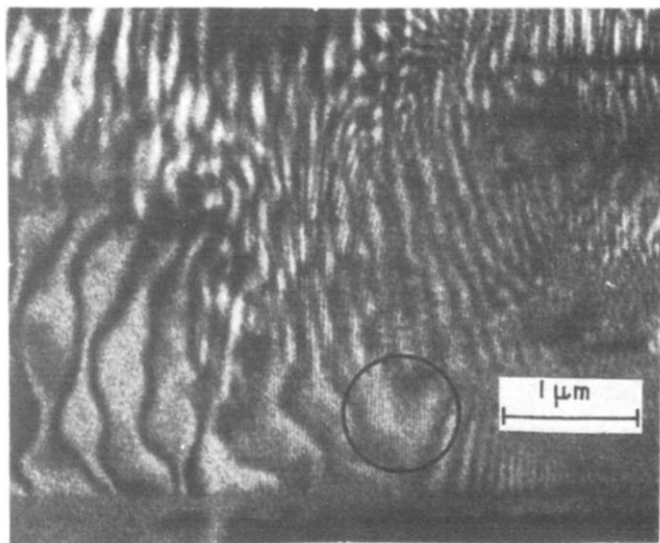
The number of exposures possible at higher beam currents (achieved by concentrating the beam somewhat with condenser lens 2) seems to be smaller than with the minimum current available, though no quantitative assessment has been made. This may mean that the heating effect of the beam contributes to the destruction of the crystals, even when working at sub-visual levels. If this is indeed the case, the balancing of low beam currents against the problem of drift and instability during long exposures would again favour low magnification recording, which minimizes the time of exposure.

## CONCLUSIONS

In the examination of the resolution requirements of polymer crystal observation in the electron image it has been found that important information is unlikely to be lost when low magnification (~1000x) is used for recording, with or without the aid of an image intensifier during focusing. The main consequent benefit is improved crystal lifetime, upwards of ten dark field photographs



*Figures 3a and 3b* Parts of the images shown as *Figures 1a and 1b* at higher magnification



*Figure 4* High enlargement of an image recorded at 980x primary magnification, showing fringe resolution of 290 Å within the circle

being possible from a single area. Additionally, a small magnification means a large field of view, and this is a tremendous advantage when area selection must be made at sub-visual levels.

## ACKNOWLEDGEMENTS

The assistance of Mr R. Whitenstall, who produced photographic enlargements in which every detail resolved on the plate was faithfully preserved, is gratefully appreciated. Financial support was provided by the Science Research Council.

## REFERENCES

- 1 Thomas, E. L. and Ast, D. G. *Polymer* 1974, 15, 37
- 2 Andrews, E. H. and Voigt-Martin, I. G. *Proc. R. Soc. (A)* 1972, 327, 251
- 3 Holland, V. F. and Lindenmeyer, P. H. *J. Appl. Phys.* 1965, 36, 3049
- 4 Niinomi, M., Abe, K. and Takayanagi, M. *J. Macromol. Sci. (B)* 1968, 2, 649
- 5 Bassett, D. C. *Phil. Mag.* 1964, 10, 595
- 6 Heidenreich, R. D. *J. Electron Microsc.* 1967, 16, 23
- 7 Heidenreich, R. D., Hess, W. M. and Ban, L. L. *J. Appl. Crystallog.* 1968, 1, 1
- 8 White, J. R. unpublished calculations
- 9 Hirsch, P. B., Howie, A., Nicholson, R. B., Pashley, D. W. and Whelan, M. J. 'Electron Microscopy of Thin Crystals', Butterworths, London, 1965
- 10 White, J. R. *J. Appl. Phys.* 1974, 45, 588
- 11 White, J. R. *J. Polym. Sci. (Polym. Phys. Edn)* 1973, 11, 2173
- 12 Agar, A. W., Frank, F. C. and Keller, A. *Phil. Mag.* 1959, 4, 32
- 13 Sadler, D. M. and Keller, A. *Kolloid-Z.Z. Polym.* 1970, 239, 641
- 14 Holland, V. F. and Lindenmeyer, P. H. *Science* 1965, 147, 1296
- 15 Holland, V. F., Lindenmeyer, P. H., Trivedi, R. and Amelinckx, S. *Phys. St. Solid.* 1965, 10, 543
- 16 Kloos, F., Go, S. and Mandelkern, L. *J. Polym. Sci. (Polym. Phys. Edn)* 1974, 12, 1145
- 17 Bassett, D. C. *Phil. Mag.* 1968, 17, 37
- 18 White, J. R. *J. Polym. Sci. (Polym. Phys. Edn)* 1974, 12, 2375

# <sup>19</sup>F chemical shift anisotropy in aligned PTFE fibres

A. N. Garroway\*, D. C. Stalker and P. Mansfield

Department of Physics, University of Nottingham, Nottingham NG7 2RD, UK

(Received 28 May 1974)

By applying a nuclear magnetic resonance (n.m.r.) multiple pulse sequence to a powder of randomly aligned crystallites, the principal values of the chemical shift tensor may be measured. However information about alignment of the chemical shift tensor with respect to the crystal axes is lost. To obtain orientation information in polytetrafluoroethylene (PTFE), we have prepared a bundle of drawn PTFE fibres and observed the <sup>19</sup>F line-narrowed n.m.r. spectra for various fibre orientations relative to the direction of the static magnetic field. The data at 77 K indicate that the most screened component of the chemical shift tensor lies along the C–F bond and that the least screened component is aligned at approximately 20° to the molecular chain axis. At 298K the spectrum of a PTFE powder indicates an axially symmetrical tensor whose principal values are consistent with a 20° inclination of the least screened component relative to the chain axis.

## ROTATION SPECTRA OF THE CHEMICAL SHIFT TENSOR

In nuclear magnetic resonance (n.m.r.) the chemical shift tensor  $\underline{\sigma}$  is observed in the laboratory frame along the  $z$  direction, specified by the direction of the static field,  $H_0$ . The observed shift is:

$$\sigma_{zz} = (\mathbf{R}^\dagger \underline{\sigma} \mathbf{R})_{zz} \quad (1)$$

where  $\mathbf{R}$  is the transformation matrix from the coordinate system in which  $\underline{\sigma}$  is known into the laboratory frame. In the principal axis system  $\underline{\sigma}$  is diagonal and equation (1) becomes:

$$\sigma_{zz} = \sigma_{11} \sin^2 \alpha \sin^2 \beta + \sigma_{22} \cos^2 \alpha \sin^2 \beta + \sigma_{33} \cos^2 \beta \quad (2)$$

where  $\alpha$  and  $\beta$  are the Euler angles linking the principal axes system and the laboratory frame. For a polycrystalline sample the Euler angles are spatially averaged and equation (2) leads to the familiar powder lineshape<sup>1</sup>:

$$f_3(\sigma, \theta) = \pi^{-1} (\sigma - \sigma_{11})^{-1/2} (\sigma_{33} - \sigma_{22})^{-1/2} K(k)$$

with

$$k^2 = \frac{(\sigma_{33} - \sigma)(\sigma_{22} - \sigma_{11})}{(\sigma - \sigma_{11})(\sigma_{33} - \sigma_{22})} \quad \text{for } \sigma_{33} \geq \sigma > \sigma_{22} \quad (3a)$$

$$f_3(\sigma, \theta) = \pi^{-1} (\sigma_{33} - \sigma)^{-1/2} (\sigma_{22} - \sigma_{11})^{-1/2} K(k)$$

with

$$k^2 = \frac{(\sigma - \sigma_{11})(\sigma_{33} - \sigma_{22})}{(\sigma_{33} - \sigma)(\sigma_{22} - \sigma_{11})} \quad \text{for } \sigma_{22} > \sigma \geq \sigma_{11} \quad (3b)$$

$$f_3(\sigma, \theta) = 0 \quad \text{for } \sigma > \sigma_{33} \text{ or } \sigma_{11} > \sigma \quad (3c)$$

\* Present address: Chemistry Division, Naval Research Laboratories, Washington D.C. 20375, USA.

Here  $K(k)$  is a complete elliptic integral of the first kind and we have assumed that  $\sigma_{33} > \sigma_{22} > \sigma_{11}$ . The subscript 3 indicates that equation (2) has been averaged over three dimensions and we shall refer to equation (3) as a three-dimensional powder lineshape.

At the other extreme to a powder is a single crystal. The observed chemical shift is found by first transforming from the chemical shift principal axes system to the crystal frame and then to the laboratory frame:

$$\sigma_{zz} = (\mathbf{R}^\dagger \underline{\sigma}^c \mathbf{R})_{zz} \quad (4a)$$

with

$$\underline{\sigma}^c = \mathbf{T}^\dagger \underline{\sigma} \mathbf{T} \quad (4b)$$

From the 'rotation spectra', obtained by rotation about various axes in the laboratory frame, the components of  $\underline{\sigma}^c$  may be determined and then, by diagonalizing  $\underline{\sigma}^c$  may be revealed.

Aligned fibres provide an intermediate to these extremes. Here the fibre axis is the only preferred direction and there is rotation isotropy about this axis. A two-dimensional powder pattern is observed, corresponding to a spatial average about the fibre axis. Under favourable conditions, partial knowledge of the orientation of the chemical shift tensor may be extracted from rotation spectra.

## ROTATION SPECTRA FOR ALIGNED PTFE

Polytetrafluoroethylene (PTFE) is a long chain polymer. As PTFE is extruded, these chains tend to align. We shall assume that there is a high degree of alignment and further that the molecular chain axis coincides with the macroscopic fibre axis. The formalism of the first section is now specialized to the PTFE fibre case.

In *Figure 1* the principal axes system of the chemical shift tensor is denoted by 1, 2, 3. We assume the 3 axis coincides with the C–F bond. The superscript c indicates



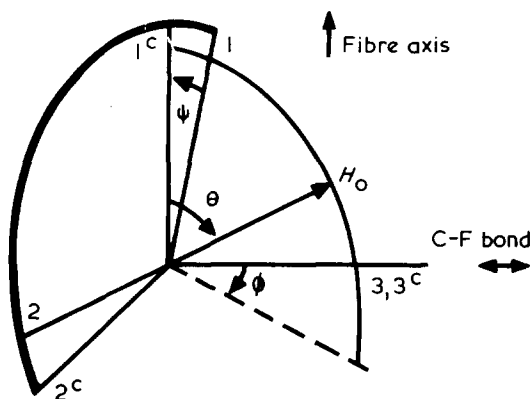


Figure 1 Co-ordinate systems for <sup>19</sup>F chemical shifts. The directions 1,2,3 correspond to the chemical shift principal axis system and the directions 1<sup>c</sup>, 2<sup>c</sup>, 3<sup>c</sup> to the crystal axes

the crystal axes system and the fibre direction defines the 1<sup>c</sup> axis. We shall further assume that the C–F bond is perpendicular to the fibre axis and therefore take the 3<sup>c</sup> axis coincident to the 3 axis. The chemical shift in the crystal frame is obtained via equation (4) by a rotation  $\psi$  about the 3 axis:

$$\underline{\sigma}^c = \begin{pmatrix} \sigma_{11}^c & \sigma_{12}^c & 0 \\ \sigma_{21}^c & \sigma_{22}^c & 0 \\ 0 & 0 & \sigma_{33}^c \end{pmatrix}$$

$$= \begin{pmatrix} \sigma_{11} \cos^2 \psi + \sigma_{22} \sin^2 \psi & (\sigma_{11} - \sigma_{22}) \sin \psi \cos \psi & 0 \\ (\sigma_{11} - \sigma_{22}) \sin \psi \cos \psi & \sigma_{11} \sin^2 \psi + \sigma_{22} \cos^2 \psi & 0 \\ 0 & 0 & \sigma_{33} \end{pmatrix} \quad (5)$$

In Figure 1 the Euler angles  $\phi, \theta$  represent respectively the azimuthal angle about the fibre axis and the inclination of the fibre axis to  $H_0$ . By equations (4) and (5) the chemical shift in the laboratory frame is:

$$\sigma_{zz} = \sigma_{11}^c \cos^2 \theta + (\sigma_{22}^c \sin^2 \phi + \sigma_{33}^c \cos^2 \phi) \sin^2 \theta + 2\sigma_{12} \sin \phi \sin \theta \cos \theta \quad (6)$$

The lineshape is then:

$$f_2(\sigma, \theta) \propto [-\sigma + \sigma_{33}^c \sin^2 \theta + \sigma_{11}^c \cos^2 \theta + \epsilon^c \cos^2 \theta]^{-1/2} \times \left\{ [\sigma - \sigma_{22}^c \sin^2 \theta - \sigma_{11}^c \cos^2 \theta - 2\epsilon^c \cos^2 \theta + 2(\epsilon^c)^{1/2} \cos \theta [-\sigma + \sigma_{33}^c \sin^2 \theta + \sigma_{11}^c \cos^2 \theta + \epsilon^c \cos^2 \theta]^{1/2}]^{-1/2} + [\sigma - \sigma_{22}^c \sin^2 \theta - \sigma_{11}^c \cos^2 \theta - 2\epsilon^c \cos^2 \theta] - 2(\epsilon^c)^{1/2} \cos \theta [-\sigma + \sigma_{33}^c \sin^2 \theta + \sigma_{11}^c \cos^2 \theta + \epsilon^c \cos^2 \theta]^{1/2} \right\}^{-1/2} \quad (7a)$$

$$\text{and } f_2(\sigma, \theta) = 0 \quad (7b)$$

for  $\sigma$  outside the range for which the radicals are real. Here

$\epsilon^c = (\sigma_{12}^c)^2 / (\sigma_{33}^c - \sigma_{22}^c)$  and the subscript 2 indicates a two-dimensional powder average. This lineshape must then be convoluted by a broadening function to account for relaxation broadening or the residual dipolar interactions not fully reduced by the multiple pulse sequence. These effects, in principle quite complicated<sup>2</sup>, are approximated by a simple Gaussian so that the observed lineshape  $g_2(\sigma, \theta)$  is:

$$g_2(\sigma, \theta) = \int_{-\infty}^{\infty} d\sigma' f_2(\sigma', \theta) \exp -[(\sigma - \sigma')^2 / W^2] \quad (8)$$

The characteristic broadening width,  $W$ , is to be determined experimentally.

In this paper, based in part on our preliminary report<sup>3</sup>, we first obtain the chemical shift principal values from a fit to the three-dimensional powder lineshape at 77K and then determine the chemical shift orientation from a rotation study of the aligned fibres. Finally the three-dimensional powder lineshape is measured at 298K to demonstrate the effects of molecular re-orientation about the chain axis.

## EXPERIMENTAL

The sample for rotational studies consisted of extruded 0.01 mm diameter PTFE fibres (kindly provided by D. W. McCall and V. J. McBrierty; Du Pont; batch no. 400-60-0) aligned to within  $\pm 3^\circ$ . A specimen of randomly oriented fibres and also a powder of 5  $\mu\text{m}$  particles (BDH; batch no. 0943980) were used for the three-dimensional powder lineshapes; within experimental error, no difference in the powder lineshape at 77 or at 298K was observed for these two samples. The PTFE polymer is composed of amorphous and crystalline regions. By measuring the density and also by fitting  $T_2$  relaxation data to a two-phase model, we infer a crystallinity of 60–70% for our fibre sample.

In rigid solids the chemical shift lineshape is generally obscured by the nuclear dipolar interaction which can, however, be reduced by employing multiple pulse sequences. All data were taken on a computer controlled line-narrowing spectrometer operating at 9.0 MHz. The  $[[132; 132]]$  sequence<sup>4</sup> was used with  $\tau = 6.4 \mu\text{sec}$  for the low temperature studies. For comparison the <sup>19</sup>F resonance linewidth in single crystal CaF<sub>2</sub> aligned along the  $[111]$  direction with respect to  $H_0$  was 70–95 Hz at a resonance offset of 2 kHz for this sequence. For the powder lineshape at 298K a new sequence<sup>2</sup>,  $[[132; 1\bar{3}2]] [[123; 1\bar{2}3]]$ , was used, again with  $\tau = 6.4 \mu\text{sec}$ . This sequence has a slightly greater line-narrowing efficiency and produced <sup>19</sup>F linewidths of 60–70 Hz in CaF<sub>2</sub> at an offset of 2 kHz.

## RESULTS AND DISCUSSION

### Powder lineshape and rotation pattern at 77K

Figure 2 shows the observed three-dimensional powder lineshape taken at 77K, as well as a computer fit using equations (3) and (8). We find an isotropic chemical shift of –30 ppm measured from a liquid C<sub>6</sub>F<sub>6</sub> reference and traceless components of –80, +10 and +70 ppm. These are consistent with previously reported values<sup>4,5</sup>. To achieve a fit, a broadening width of  $W = 55 \text{ ppm}$  (500 Hz) was used.

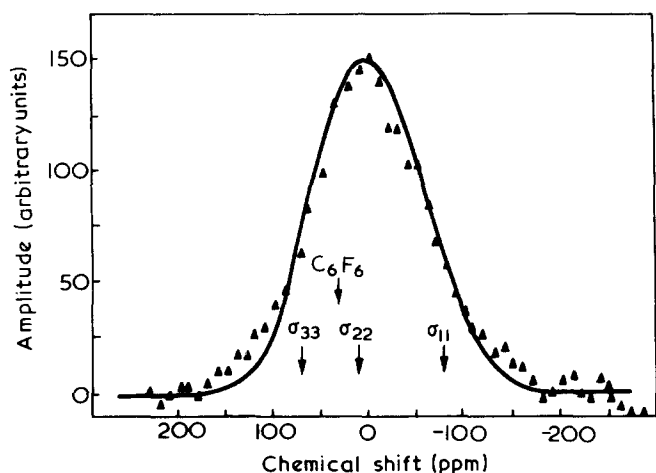


Figure 2 The line narrowed <sup>19</sup>F spectrum of PTFE powder at 77K. The solid line represents the theoretical lineshape, equation (3), convoluted with a Gaussian broadening function, for the principal values indicated.  $\blacktriangle$ , Experimental points

At 77K we obtain the following rotation pattern (Figure 3) for the aligned PTFE. Although equation (7) predicts a rather complex spectrum at each  $\theta$ , owing to residual broadening we see only a single resonance line. The chemical shift plotted represents the first moment of the resonance, with the measured isotropic shift subtracted.

The amorphous region of the PTFE fibre is a complication. If there is indeed no alignment within this region, it follows that the observed spectrum is a superposition of a three-dimensional powder lineshape from the amorphous region and two-dimensional lineshape from the crystalline region; the composite lineshape is:

$$\mathcal{F}(\sigma, \theta) = (1 - a)f_2^c(\sigma, \theta) + af_3^a(\sigma) \quad (9)$$

where  $a$  represents the fraction of nuclei in the amorphous region, and where  $f_2^c(\sigma, \theta)$  and  $f_3^a(\sigma)$  are the lineshapes of the crystalline and amorphous regions respectively. The first moment  $M^c$  of the crystalline region is related to the observed first moment  $M$  and the first moment  $M^a$  of the amorphous region by:

$$M^c(\theta) = \frac{M(\theta) - aM^a}{(1 - a)} \quad (10)$$

and the first moments are defined by:

$$M^a = \int_{-\infty}^{\infty} d\sigma \sigma f_3^a(\sigma) \quad (11a)$$

$$M^c(\theta) = \int_{-\infty}^{\infty} d\sigma \sigma f_2^c(\sigma, \theta) \quad (11b)$$

It should be recalled that the first moment is independent of broadening provided the broadening is represented by an even function, as it is here for the dipolar case.

We take  $a = 0.30$  and by equation (9) calculate from the data of Figure 3 the first moment for the crystalline region only; these results are shown in Figure 4. We may immediately draw conclusions about the alignment of the

shift tensor. For  $\theta = 0$ , equation (6) predicts a line centred at  $\sigma_{11}^c$ . Since, by equation (5),  $\sigma_{11}^c$  is a linear combination of  $\sigma_{11}$  and  $\sigma_{22}$  only, then at least one of these components is negative. For  $\theta = \pi/2$  the predicted shift is just the average of  $\sigma_{22}^c$  and  $\sigma_{33}^c$ . The observed positive shift indicates that  $\sigma_{33}$  is positive and we assign  $\sigma_{33} = +70$  ppm. So the most screened component lies along the C-F bond, as expected. We may arbitrarily assign the  $-80$  ppm value to  $\sigma_{11}$  and now consider the orientation of  $\sigma_{11}$  and  $\sigma_{22}$ .

With the experimental values of  $\sigma_{11} = -80$ ,  $\sigma_{22} = 10$  and  $\sigma_{33} = 70$  ppm, theoretical rotation patterns generated by equation (7) for various choices of  $\psi$  are also shown in Figure 4. A reasonable fit to the data is achieved for  $\psi \approx 20^\circ$  and so we infer that the least screened component ( $\sigma_{11} = -80$  ppm) is at an angle of  $20^\circ$  to the PTFE chain axis. (In our preliminary report<sup>3</sup> the contribution of the amorphous region was not explicitly considered and we found  $\psi = 30$  to  $45^\circ$  but when the data are corrected for this contribution, a reduced value of  $\psi = 20^\circ$  is obtained.)

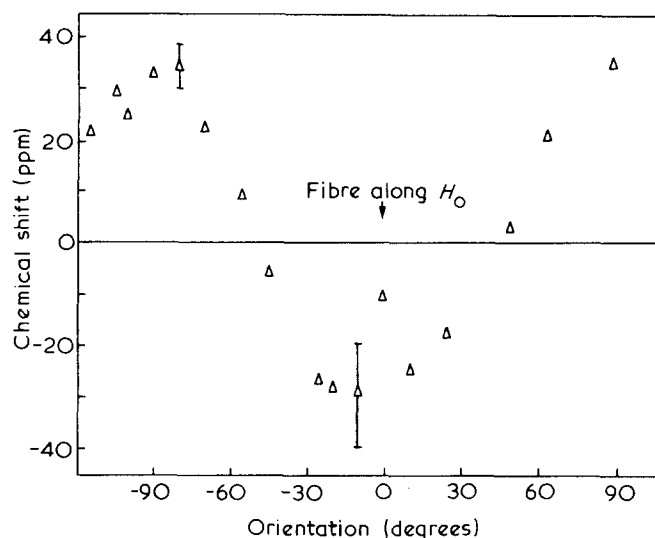


Figure 3 <sup>19</sup>F chemical shift rotation pattern for aligned PTFE fibres at 77K. The first moment is plotted and the measured isotropic shift has been subtracted

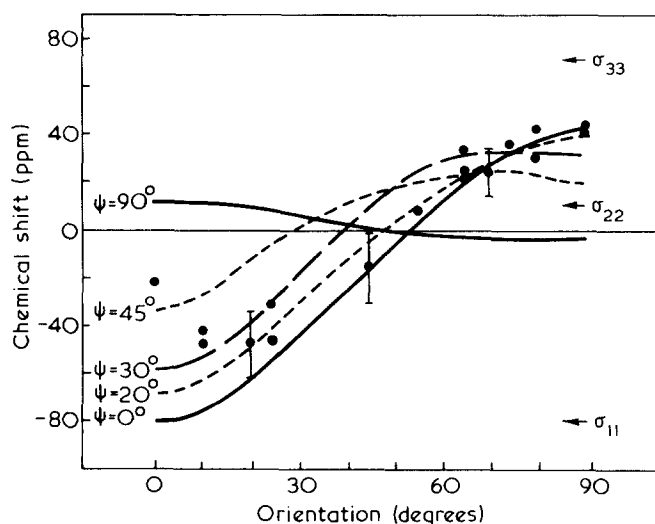


Figure 4 Experimental and theoretical <sup>19</sup>F chemical shift rotation pattern for the crystalline region of PTFE fibres at 77K. The theoretical curves are obtained from equation (7) for various values of  $\psi$ , using the measured chemical shift principal values. The data of Figure 3 are replotted here, after the contribution of the amorphous region of PTFE has been subtracted

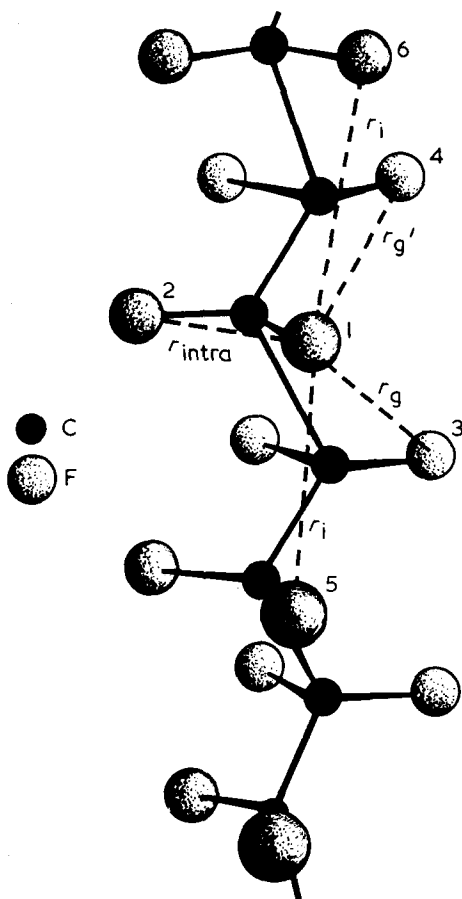


Figure 5 A schematic diagram of a short length along the PTFE helix, showing the *gauche* (3 and 4) and isotactic (5 and 6) fluorine positions

To explain properly the orientation of the chemical shift tensor about the C–F bond requires a calculation of the <sup>19</sup>F chemical shift tensor in PTFE, a calculation we have not attempted. However, this orientation may be understood qualitatively by examining the location of the near fluorine neighbours since it is their electronic interaction which tends to depopulate the filled *p*-orbitals of the fluorine, giving rise to the chemical shift anisotropy. A short segment of the PTFE helix is shown schematically in Figure 5. From X-ray studies<sup>6</sup>, the radii of the carbon and fluorine helices are 0.42 and 1.64 Å respectively. Below the 19°C transition adjacent CF<sub>2</sub> groups are related by a rotation of 12π/13 about the axis of the helix and a translation of 1.30 Å along the axis. Between the 19 and 30°C transitions, the helix uncoils slightly so that the pitch angle is 14π/15 but the CF<sub>2</sub> groups are still separated by 1.30 Å. Iwasaki<sup>7</sup> suggests by comparison to the C–F bond characteristics in CF<sub>2</sub>H<sub>2</sub> that in PTFE the FCF bond angle is 108.5° and the C–F bond length is 1.36 Å. We shall use these values to estimate the distance to near fluorine neighbours.

The nearest neighbour to the fluorine labelled 1 (Figure 5) is the intramolecular fluorine (2) at a distance of 2.21 Å; this distance is of course independent of pitch angle. Since the carbon atoms are arranged on a helix, rather than in a linear zig-zag, the normal to the plane of fluorines 1 and 2 and their associated carbon atom does not coincide with the helix axis but rather makes an angle of 4.5° with this axis. Fluorines 3 and 4 (the *gauche* positions) are at a distance 2.63 and 3.03 Å. Fluorines 5 and 6 are at the isotactic positions at a distance of 2.71 Å.

Other neighbours are further removed. These values are all calculated for the crystal phase below 19°C and will alter slightly when the helix uncoils above 19°C.

The non-bonding *p*-orbitals tend to depopulate preferentially in the direction of the projection of the interacting fluorine onto the plane perpendicular to the C–F bond. Letting χ measure the angle made by this direction with respect to the axis of the helix, we find for the intramolecular fluorine, χ<sub>intra</sub> = –97.5° and for the nearest *gauche* fluorine, χ<sub>g</sub> = 125°. If the dominant perturbation to the *p*-orbitals were due to only the two nearest neighbours, we should expect that the chemical shift tensor would roughly align along a direction intermediate between 82.5° (180° – 97.5°) and 125° to the fibre axis. The competition of the other *gauche* and two isotactic fluorines will alter this angle. We speculate that the dominant effect does indeed come from the two nearest neighbour fluorines by the following argument.

In the Karplus–Das semi-empirical theory<sup>8</sup> for *p*-orbital chemical shifts, the deviation from filled shells, *p*<sub>ii</sub> = 2, etc., is represented by:

$$p_{ii} = 2 - \rho_i \quad (12a)$$

$$p_{ij} = 2 - \rho_j \quad (12b)$$

$$p_{kk} = 2 - \epsilon \quad (12c)$$

with

$$\epsilon = 1 - (I + S - IS) \quad (13)$$

and where ρ<sub>i</sub>, ρ<sub>j</sub> are the double bond characters, *kk* is defined by the bond direction, and *I* and *S* are the ionic character and degree of *sp* hybridization, respectively. The paramagnetic contributions to the chemical shifts are then

$$\sigma_{ii}^p = (3/2) \sigma_0 [\epsilon + \rho_j (1 - \epsilon)] \quad (14a)$$

$$\sigma_{jj}^p = (3/2) \sigma_0 [\epsilon + \rho_i (1 - \epsilon)] \quad (14b)$$

$$\sigma_{kk}^p = (3/2) \sigma_0 [\rho_i + \rho_j - \rho_i \rho_j] \quad (14c)$$

where σ<sub>0</sub> (–863 ppm<sup>8</sup>) is a semi-empirical parameter. Now we have found that the least screened component (–80 ppm) lies at about 20° to the fibre axis. If we identify *ii* with the 20° direction, equations (14a) and (14b) imply then that the deviation from a closed shell is greatest along the 110° direction. This corresponds to an angle approximately intermediate to the intramolecular angle (82.5°) and the nearest *gauche* angle (125°) and so we suggest that the chemical shift orientation about the C–F bond is dominated by the intramolecular and nearest *gauche* interactions. This angle is dependent on the pitch and should change slightly above the 19°C transition. Molecular rotation about the helix axis sets in somewhat below this temperature and produces an axially symmetrical chemical shift tensor. Even with this complication, a rotation spectrum similar to Figure 4 should in principle reflect the slight change in pitch angle. Our resolution at present is not adequate to determine such a change and we have not produced a high temperature rotation spectrum. However, as the next subsection shows, the experimental three-dimensional powder lineshape above the 19°C transition does provide information about the orientation of the chemical shift tensor.

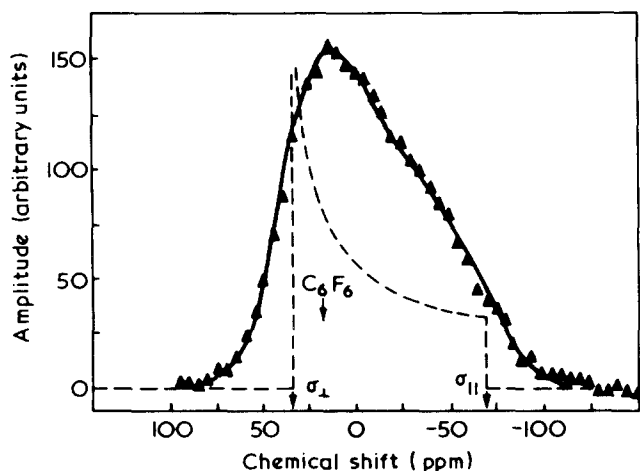


Figure 6 Line-narrowed <sup>19</sup>F spectrum of PTFE powder at 298K. Molecular re-orientation about the chain axis produces an axially symmetrical chemical shift tensor. The theoretical unbroadered lineshape with principal values as indicated is shown as a broken line; the solid line is obtained by convolution with a Gaussian broadening function. ▲, Experimental points

### High temperature

Relaxation studies<sup>9,10</sup> in PTFE have suggested that above the 19°C transition, the molecules in the crystalline region begin to rotate rapidly (10<sup>7</sup> Hz) about the chain axis. (In the amorphous region, this rotation may occur at lower temperature<sup>11</sup>.) We should then expect that the chemical shift tensor will be in effect temporally, rather than spatially, averaged about the axis of rotation. If the axis of rotation does indeed coincide with the chain axis, then the observed component of the chemical shift tensor is from equation (6):

$$\langle \sigma_{zz} \rangle_{\phi} = \sigma_{11}^c \cos^2 \theta + (1/2)(\sigma_{22}^c + \sigma_{33}^c) \sin^2 \theta \quad (15)$$

where  $\langle \rangle_{\phi}$  indicates that an azimuthal average has been performed. This is just the expression for an axially symmetrical chemical shift tensor with parallel component  $\sigma_{\parallel} = \sigma_{11}^c$  and perpendicular component  $\sigma_{\perp} = (1/2)(\sigma_{22}^c + \sigma_{33}^c)$ . Figure 6 shows the observed <sup>19</sup>F spectrum from a PTFE powder at 298K, a temperature selected between the 19 and 30°C transition temperatures. Assuming that the principal values of the chemical shift tensor are essentially independent of temperature from 77 to 298K, we may then use the low temperature results to predict the lineshape at this high temperature. Although the uncoiling of the helix above 19°C alters slightly the angle of the intramolecular and nearest *gauche* fluorines with respect to the fibre axis, we shall still compute the averaged chemical shift components using the experimental value of  $\psi = 20^\circ$ . From equations (15) and (5) we have  $\sigma_{\parallel} = -69.5$  and  $\sigma_{\perp} = 34.7$  ppm. The powder spectrum for an axially symmetrical tensor is generated by a special case of equation (3). The broken line in Figure 6 represents the theoretical powder spectrum for these principal values, in the absence of broadening. A reasonable fit to the experimental spectrum is achieved for

a broadening width of 27 ppm (240 Hz) and is shown as the solid line in the Figure. The rather asymmetrical lineshape in Figure 6, indicative of axial symmetry, should be compared with the more symmetrical lineshape at 77K (Figure 2).

### CONCLUSIONS

N.m.r. rotation studies of aligned PTFE fibres have shown that the most screened component of the <sup>19</sup>F chemical shift tensor lies along the C–F bond and that the least screened component is aligned at approximately 20° to the chain axis. At 298K molecular rotation about the chain axis yields an axially symmetrical chemical shift tensor and the observed powder lineshape is consistent with a 20° orientation of the least screened component with respect to the chain axis. We suggest that the determination of this orientation is dominated by interactions with the fluorine neighbours at the intramolecular and nearest *gauche* positions.

Although we have implicitly assumed a unique fibre direction in the crystalline region, certainly not all the chains are so well aligned. A distribution of alignments will tend to smooth out the observed angular dependence and may well account for the deviation of the experimental results near  $\theta = 0$  from the theoretical curve in Figure 5. The rotation data are unfortunately too imprecise to warrant invoking an alignment distribution model. With improved line-narrowing resolution, further chemical shift studies of polymer fibres should provide a more sensitive measure of polymer alignment.

### ACKNOWLEDGEMENTS

We wish to thank the Science Research Council for an equipment grant, for a research studentship (D.C.S.) and a post-doctoral research assistantship (A.N.G.). We also thank R. Sjöblom and W. Derbyshire for helpful discussions.

### REFERENCES

- Bloembergen, N. and Rowland, T. J. *Phys. Rev.* 1955, **97**, 1679
- Garroway, A. N., Mansfield, P. and Stalker, D. C. *Phys. Rev.* (in press)
- Garroway, A. N., Stalker, D. C. and Mansfield, P. 'Proceedings of the First Specialized "Colloque Ampere"'. (Ed. J. W. Hennel), Institute of Nuclear Physics, Krakow, 1973, pp 135–139
- Mansfield, P., Orchard, M. J., Stalker, D. C. and Richards, K. H. B. *Phys. Rev. (B)* 1973, **7**, 90
- Mehring, M., Griffin, R. G. and Waugh, J. S. *J. Chem. Phys.* 1971, **55**, 746
- Bunn, C. W. and Howells, E. R. *Nature* 1954, **174**, 549
- Iwasaki, M. *J. Polym. Sci. (A)* 1963, **1**, 1099
- Karplus, M. and Das, T. P. *J. Chem. Phys.* 1961, **34**, 1683
- McCall, D. W., Douglass, D. C. and Falcone, D. R. *J. Phys. Chem.* 1967, **72**, 998
- McCall, D. W., Douglass, D. C., McBrierty, V. J. and Hoch, M. R. *Discuss. Faraday Soc.* 1969, **48**, 205
- Hyndman, D. and Origlio, G. F. *J. Appl. Phys.* 1960, **32**, 1849

# Electrical conductivity of PMMA at linearly increasing temperatures

V. Adamec and E. Mateová

Cables and Insulating Materials Research Institute, Bratislava, Czechoslovakia  
(Received 16 April 1974; revised 28 August 1974)

The temperature dependence of electrical conductivity in poly(methyl methacrylate), representing polar polymers, has been measured at linearly increasing temperatures in the range from  $-100$  to  $+100^\circ\text{C}$ . The interpretation by superposition of inherent conductivity and polarization processes is discussed.

## INTRODUCTION

The temperature dependence of electrical conductivity of polymer insulating materials used to be determined in two ways. Either the time dependence of current was measured at several fixed temperatures after the d.c. voltage application to the specimen until the steady-state current was achieved and a plot of temperature dependence of steady-state conductivity values was drawn or, after the voltage application, the temperature was steadily increased and simultaneously the current was measured and recorded. In the former case, some of the authors have not found any inflection on the curve in the region of the second order transition temperature<sup>1</sup>; others have found an inflection<sup>2-4</sup>. With the latter method there is always an inflection on the temperature curve<sup>1-5</sup>, and the measurement being comparatively simple, this method has been applied several times for the determination of the glass transition temperature,  $T_g$ <sup>6</sup>.

The interpretation of the temperature dependence of conductivity in insulating polymers is far from consistent. Some hypotheses have postulated that conductivity above and below the inflection is ionic and electronic in nature, respectively, and yet others are based on the analogy with some other materials, according to which intrinsic conductivity exists above  $T_g$  and impurity conductivity below  $T_g$ . Shishkin and Verzhinina<sup>5</sup> and Warfield and Petree<sup>6</sup> explain the inflection at  $T_g$  by change in environmental conditions for ion mobility at the transition from the glassy state into a highly elastic one. Herwig and Jenckel<sup>1</sup> and Reddish<sup>2</sup> suppose that the inflection appears as a result of the superposition of polarization effects on the conductivity process at temperatures below  $T_g$ , at which the relaxation times become long.

## THEORY

The current,  $I$ , flowing through the circuit with the specimen connected in after the d.c. voltage,  $V$ , application may be expressed as:

$$I(t) = \left( G + \frac{dC}{dt} \right) V \quad (1)$$

where the first term represents the contribution of the

inherent conductance,  $G$  and the second one that of the capacitance,  $C$  change. From equation (1), the effective conductivity may be deduced:

$$\sigma(t) = \sigma_s + \frac{L}{A} \frac{dC}{dt} \quad (2)$$

where  $\sigma_s$  is the steady-state (inherent) conductivity,  $L$  is the thickness of the specimen, and  $A$  is the area of the electrodes. At a linear increase in temperature ( $dT/dt = b$ ) we obtain:

$$\sigma(T) = \sigma_s(T) + \frac{bL}{A} \frac{dC}{dT} \quad (3)$$

Since  $C = \epsilon \epsilon_0 A/L$  and the relative permittivity  $\epsilon = \epsilon_\infty + \sum \epsilon_{ai}$ , where  $\epsilon_\infty$  stands for fast polarization processes and  $\sum \epsilon_{ai}$  for slow processes, and since one may also use the Clausius–Mossotti relation for  $\epsilon_\infty$ , one obtains:

$$\sigma(T) = \sigma_{s0} \exp\left(-\frac{W_c}{kT}\right) + b\beta_L \epsilon_0 [\epsilon - (\epsilon_\infty - 1)(\epsilon_\infty + 2)] + b\epsilon_0 \sum \frac{d\epsilon_{ai}}{dT} \quad (4)$$

where  $\sigma_{s0}$  is the pre-exponential factor,  $W_c$  is the activation energy of the inherent conduction process and  $\beta_L$  is the linear expansion coefficient. The second term on the right hand side represents both the temperature dilatation of the specimen and the temperature dependence of  $\epsilon_\infty$ . Its magnitude is of the order  $10^{-19}$  or  $10^{-18}$  mho/cm and therefore it may be neglected in the present consideration.

Using the known differential equation for permittivity  $d\epsilon_a/dt = (\epsilon_{as} - \epsilon_a)/\tau$  in the case of a process with a single relaxation time  $\tau = \tau_0 \exp(W_a/kT)$ , where  $\tau_0$  is the pre-exponential factor and  $W_a$  is the activation energy of the polarization process, we obtain:

$$\frac{d\epsilon_a}{dT} = \frac{\epsilon_{as} - \epsilon_a}{b\tau_0} \exp\left(-\frac{W_a}{kT}\right) \quad (5)$$

where  $\epsilon_{as}$  is the static value of the permittivity increment corresponding to the polarization process. Assuming  $\epsilon_{as}$  to be roughly temperature independent, we have:

$$\epsilon_a(T) = \epsilon_{as} \left\{ 1 - \exp \left[ -\frac{1}{b\tau_0} \int_{T_0}^T \exp \left( -\frac{W_a}{kT} \right) dT \right] \right\} \quad (6)$$

An anomalous conductivity  $\sigma_a(T)$  corresponds to the change of permittivity in the course of the linear temperature rise:

$$\sigma_a(T) = \frac{\epsilon_{as}\epsilon_0}{\tau_0} \exp \left[ -\frac{W_a}{kT} - \frac{1}{b\tau_0} \int_{T_0}^T \exp \left( -\frac{W_a}{kT} \right) dT \right] \quad (7)$$

The measured effective conductivity at linearly increasing temperatures ought to be determined by both the inherent conductivity and the sum of anomalous conductivities from all relaxation polarization processes in the dielectric.

$$\sigma(T) = \sigma_s(T) + \sum \sigma_{ai}(T) \quad (8)$$

## EXPERIMENTAL AND RESULTS

A sample of a commercial atactic poly(methyl methacrylate) (PMMA) was chosen for the measurement as a representative polar polymer. A disc shape specimen of 0.5 mm thickness was provided with evaporated gold electrodes of 30 mm diameter and guard rings on both surfaces. The specimen was placed in a shielded oven which was provided with liquid nitrogen cooling and resistance heating controlled by a temperature programmer. A highly stable voltage source of 100 V was used and the current was measured and recorded with a vibrating reed electrometer.

After the specimen had been placed in the oven, it was heated for 3 h at 100°C with short-circuited electrodes. Before the proper measurement started, the background current was checked. It was no larger than  $2 \times 10^{-15}$  A. Also with short-circuited electrodes, the specimen was cooled down to -100°C. Then the voltage was applied and after 10 min, when the effective conductivity was lower than  $10^{-18}$  mho/cm, the temperature began to rise at a rate of 2.3°C/min. At +100°C the temperature rise was stopped and the electrodes were short circuited. A repeated measurement showed very good reproducibility. Further measurements were carried out at the rates of 4.3 and 9.1°C/min. The results are shown in Figure 1.

Lastly, the charge,  $Q$  accumulated on electrodes during the heating cycle was measured with a capacitor instead of a resistor connected to the input of the electrometer. These results are given in Figure 2. At the first measurement, the input of the electrometer was opened and then the voltage was applied ( $Q = Q_\infty + \sum Q_{ai} + Q_c$ ), while at the second measurement the reverse procedure was used ( $Q = \sum Q_{ai} + Q_c$ ).

## DISCUSSION

Three polarization processes have been found previously with a similar sample of PMMA at the measurements of frequency dependences of the permittivity and the loss factor, and of the time dependence of the anomalous conductivity at various temperatures in the range from -30 to +120°C<sup>7</sup>. Processes  $\beta$  and  $\alpha$  are due to the motion of the parts of molecules carrying a dipole moment. These processes are detectable also with dynamic mechanical methods. The third process,  $\alpha'$ , which does not have a mechanical analogue, is probably caused by the charge pile-up at the electrodes. The characteristic parameters  $\epsilon_{asi}$ ,  $\tau_{oi}$ ,  $W_{ai}$  for

these processes as well as  $\sigma_{os}$  and  $W_c$  for conduction have been determined from the measurements mentioned. With these data and with the temperature rates used, the  $\sigma_s(T)$  and  $\sigma_{ai}(T)$  dependences were obtained by applying equation (7) and by approximate solving of the integral with the aid of a programmable calculator (broken lines in Figure 1).

The steeply rising part of the function  $\sigma(T)$  is evidently determined by the inherent conductivity and therefore the  $\alpha'$  and partly also the  $\alpha$  process are masked. The calculated  $\sigma_{ai}(T)$  functions are much narrower than the measured ones. This effect may be explained by the existence of a broad distribution of relaxation times instead of a single one. Of course, the equality  $\int \sigma_{ai} dt = \epsilon_{asi}\epsilon_0$  must still hold.

A distribution function, which enables one to deduce simple expressions for the time dependence of the anomalous conductivity, and the frequency dependence of the permittivity and the loss factor is based on a uniform distribution of activation energies according to Fröhlich<sup>8</sup>. If the activation energies of the motion of the molecular segments are uniformly distributed in the interval  $\Delta W$  from  $W_A$  to  $W_B$ , the relation for  $\sigma_a(T)$  would be:

$$\sigma_a(T) = \frac{\epsilon_{as}\epsilon_0}{\tau_0\Delta W} \int_{W_A}^{W_B} \exp \left[ -\frac{W}{kT} - \frac{1}{b\tau_0} \int_{T_0}^T \exp \left( -\frac{W}{kT} \right) dT \right] dW \quad (9)$$

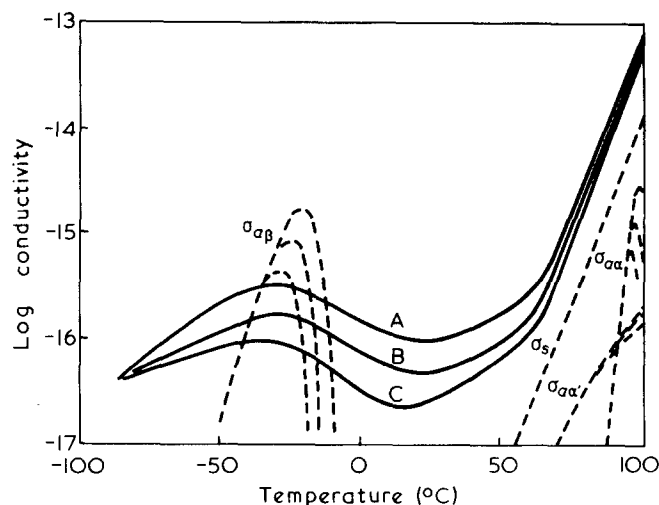


Figure 1 Temperature dependence of effective conductivity of PMMA at various temperature rates: (A, 9.1; B, 4.3; C, 2.3°C/min); —, measured; ----, calculated

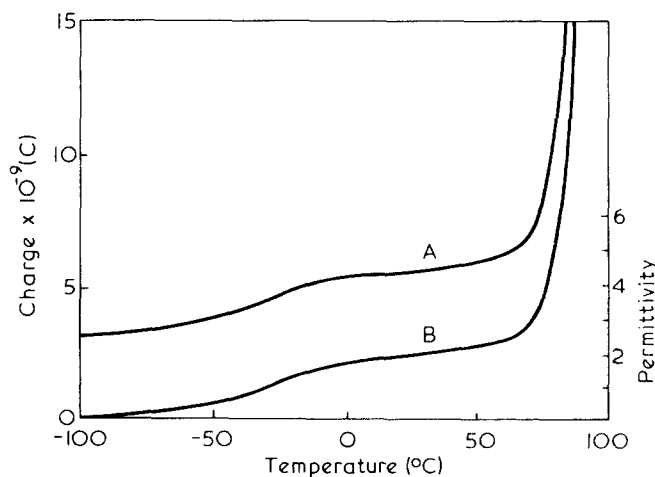


Figure 2 Accumulated charge and respective permittivity during linear temperature rise. A,  $Q_\infty + \sum Q_a + Q_c$ ; B,  $\sum Q_a + Q_c$

The low temperature tail of the peak in case of a single relaxation time is:

$$\sigma_a(T)_{\text{LTT}} = \frac{\epsilon_{as}\epsilon_0}{\tau_0} \exp\left(-\frac{W_a}{kT}\right) \quad (7a)$$

and in case of distributed relaxation times is:

$$\sigma_a(T)_{\text{LTT}} = \frac{\epsilon_{as}\epsilon_0}{\tau_0} \frac{kT}{\Delta W} \left[ \exp\left(-\frac{W_A}{kT}\right) - \exp\left(-\frac{W_B}{kT}\right) \right] \quad (9a)$$

It follows that the broader the distribution, the less steep is the initial rise of  $\sigma_a(T)$ , because  $W_A = W_a - \Delta W/2$ .

From the measurement of absorbed charge (*Figure 2*), one can determine in a simple way the permittivity increment corresponding to the  $\beta$  process:  $\epsilon_{\beta s} = 2.0$ . This is the same value as has been obtained previously from the measurements of frequency dependence of permittivity<sup>7</sup>.

## CONCLUSION

The effective conductivity of PMMA determined at linearly increasing temperatures can be interpreted by superposition of the conduction and polarization processes. It follows

that the inflection on the  $\sigma(T)$  curve does not necessarily correspond to the glass transition temperature  $T_g$ , even though the inherent conductivity becomes a predominating component in the vicinity of  $T_g$ .

Based on further, unpublished results, it is believed that the concept described in this paper applies not only to PMMA and other polar polymers but also to weak polar polymers, e.g. polyethylene, polystyrene, etc. But, in the latter case, the second term in equation (4) may play an important role.

## REFERENCES

- 1 Herwig, H. U. and Jenckel, E. *Z. Elektrochem.* 1959, 63, 360
- 2 Reddish, W. 'The Physical Properties of Polymers', *SCI Monogr. 5* Society of Chemical Industry, London, 1959, p 138
- 3 Oster, A. *Z. Angew. Phys.* 1966, 20, 375
- 4 Ieda, M., Kosaki, M., Ohshina, H. and Shinohara, U. *J. Phys. Soc. Japan* 1968, 25, 1742
- 5 Shishkin, N. I. and Vershinina, M. P. *Fiz. Tverd. Tela* 1959, 1, 798
- 6 Warfield, R. W. and Petree, M. C. *Makromol. Chem.* 1962, 58, 139
- 7 Adamec, V. *Kolloid-Z. Z. Polym.* 1971, 249, 1085
- 8 Fröhlich, H. 'Theory of Dielectrics', Clarendon Press, Oxford, 1958, p 92

# Light scattering Rayleigh linewidth measurements on some solutions of cellulose trinitrate

D. B. Sellen

Astbury Department of Biophysics, University of Leeds, Leeds LS2 9JT, UK  
(Received 31 May 1974)

Light scattering Rayleigh linewidth measurements have been made upon three cellulose trinitrate samples in ethyl acetate by obtaining the autocorrelation function of fluctuations in scattered intensity. The weight average degrees of polymerization ( $DP_w$ ) were in the range 2400 to 3300 and  $DP_w/DP_n \sim 1.3$ . Measurements were made at concentrations below  $2 \times 10^{-3}$  g/ml and no concentration dependence was detected within experimental error ( $\pm 7\%$ ). No effects due to internal motion of the polymer chains were observed even though current theories predict that these effects should be quite large. Reasons for this are discussed and it is suggested that the effects of internal motion are diminished when the second virial coefficient is large and positive. Absolute values of translational diffusion constant calculated from the results lie well within the range of those obtained by other authors using conventional techniques. Over the limited range of degrees of polymerization investigated the equivalent hydrodynamic diameter per monomer unit was found to be  $0.45 \pm 0.03 \text{ \AA}$ . The effects of polydispersity on the results are discussed.

## INTRODUCTION

The diffusion of cellulose trinitrate in solution has been investigated by several authors using conventional techniques<sup>1-6</sup>. During the past decade, however, it has become possible to determine diffusion constants by investigating the spectra of scattered light<sup>7-12</sup>, a technique which is particularly advantageous for very large macromolecules where previously a single determination could take more than a week. The relevant theory is set out in a series of publications by Pecora<sup>13</sup>. For high molecular weight polymers spectral broadening due to fluctuations in the particle scattering factor,  $P(\theta)$ , resulting from configurational changes is predicted, in addition to that resulting from translational diffusion. It is of additional interest therefore to see whether the effects of internal motion can be detected. This paper describes some experiments upon three samples of cellulose trinitrate dissolved in ethyl acetate, each having a low degree of polydispersity.

## EXPERIMENTAL

### Preparation of cellulose trinitrate samples

Cellulose trinitrate is obtained by nitrating cellulose from a natural source. In most investigations the cellulose has been deliberately degraded so as to render it highly polydisperse. Samples of differing degree of polymerization ( $DP$ ) with  $DP_w/DP_n \sim 2$  can then be obtained by fractional precipitation<sup>14</sup>. A considerable amount of work has recently been done on cellulose nitrate in this Department with a view to investigating the degree of polymerization and polydispersity of native cotton cellulose<sup>15</sup>. During this investigation it was found that direct nitration of cotton by the method of Alexander and Mitchell<sup>16</sup> for periods increasing from 2 to 25 hours at 20°C yielded samples of decreasing molecular weight with  $DP_w/DP_n \sim 1.3$  (Table 1). Unfortunately the range of degree of polymerization obtainable by

Table 1 Cellulose trinitrate samples

Nitration time* at 20°C (h)	$DP_w$ (light scattering)	$DP_n$ (osmometry)	$D_{20} \times 10^{8\dagger}$ (cm <sup>2</sup> /sec)
2	3300	2600	5.9
6	2800	2100	7.7
25	2400	1600	9.7

\* Nitrogen content was 13.9% in all cases

† In ethyl acetate

this method is somewhat limited. Samples obtained by nitration for periods shorter than 2 h were found to contain microgel and the higher molecular weights rendered osmotic pressure measurements impossible, whilst very long periods of nitration yielded highly polydisperse material. It was thought, however, that in the first instance it would be advantageous to investigate samples with a low polydispersity, so that this method of preparation was used.

### Investigation of the spectra of scattered light

The apparatus used and its operation have already been described<sup>11,12</sup>. The autocorrelation function of the photoelectric signal due to the scattered light is obtained. This is given by  $\phi(\tau)$  where:

$$\phi(\tau) = \frac{c^2 \gamma^2}{2} [F(\tau)]^2 \quad (1)$$

$\tau$  is the autocorrelation delay time and  $c$  the overall photosensitivity of the detecting system.  $\gamma$  is a coherence factor associated with the geometry of the detecting system.  $F(\tau)$  is the phase correlation function of the scattered light which for a monodisperse system where spectral broadening is due to translational diffusion alone is given by:



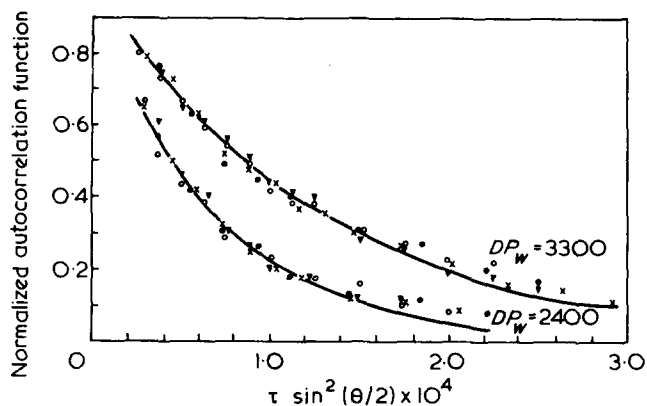


Figure 1 Normalized autocorrelation functions of intensity fluctuations of light scattered from two samples of cellulose trinitrate in ethyl acetate. Concentrations are  $\sim 10^{-3}$  g/ml. X, 45°; O, 60°; ●, 75°; ▽, 90°

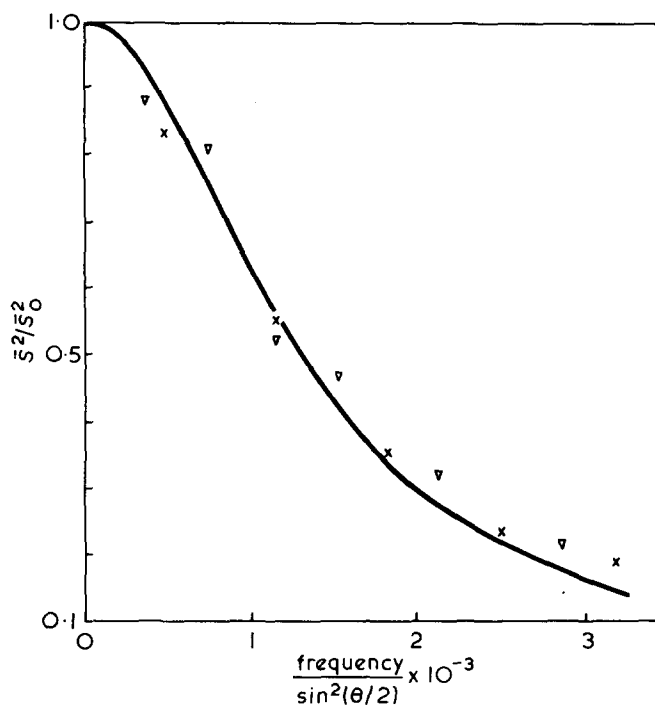


Figure 2 Homodyne beat spectrum for a solution of cellulose trinitrate ( $DP_w = 3300$ ) in ethyl acetate at a concentration of  $\sim 10^{-3}$  g/ml. The solid line is a Lorentzian and corresponds to the exponential shown in Figure 1. X, 45°; ▽, 90°

$$F(\tau) = I \exp(-K^2 D \tau) \quad (2)$$

where  $I$  is the scattered intensity,  $D$  the translational diffusion constant and:

$$K = \frac{4\pi}{\lambda} \sin \theta/2 \quad (3)$$

where  $\lambda$  is the wavelength in the solution and  $\theta$  the angle of scatter.

In the present experiments  $\gamma$  was increased to 0.3 by using smaller stops than previously<sup>12</sup> and removing all lenses from the light receiver system. The bandwidth of the electronic system was 30 Hz to 14 kHz (3db points). The criteria for selection of bandwidth have already been discussed. Corrections were made for any resulting distortion of the autocorrelation function in the manner previously described<sup>12</sup>. The effect of dust in the solutions on measurements of this kind has also already been discussed<sup>12</sup>. Solu-

tions were clarified by centrifuging at 30 000Xg for 2 h and in each case using the top 10 ml of 40 ml in the centrifuge bucket for light scattering measurements<sup>17</sup>. Measurements were made in the angular range 45° to 90°.

At the lower concentrations used in the present work the scattered intensity due to the cellulose trinitrate was approximately equal to that due to ethyl acetate. The Rayleigh linewidth of light scattered from the solvent is, however, very broad compared with that of light scattered from the solute. This was verified experimentally. The autocorrelation function of the photoelectric signal due to light scattered from ethyl acetate, was found to be indistinguishable from that due to light direct from the laser attenuated to the same intensity as the scattered light in the manner previously described<sup>11</sup>.

In view of the low scattered intensities involved, a few experiments were carried out in which the power spectrum of the photoelectric signal was obtained directly by scanning with a wave analyser<sup>11</sup>. This was done in order to confirm the validity of the results obtained from the autocorrelation function computer.

## RESULTS AND DISCUSSION

Figure 1 shows normalized autocorrelation functions plotted against  $\tau \sin^2 \theta/2$  for various angles of scatter for two of the samples. The solid lines are exponentials. The lower molecular weight sample shows a systematic deviation from the exponential curve at longer times independent of angle of scatter. This is the expected effect of polydispersity if the variation in  $P(\theta)$  over the angular range is approximately the same for each molecular species, a condition which will hold if the polydispersity is not too high. Figure 2 shows the results of an experiment on the higher molecular weight sample in which the power spectrum was scanned with a wave analyser. The solid line is a Lorentzian and corresponds to the exponential curve in Figure 1.

The variation of diffusion constant with concentration was investigated in detail for two of the samples and the results are shown in Figure 3. No variation with concentration was detected. This is surprising in view of the high second virial coefficients associated with the ethyl acetate-

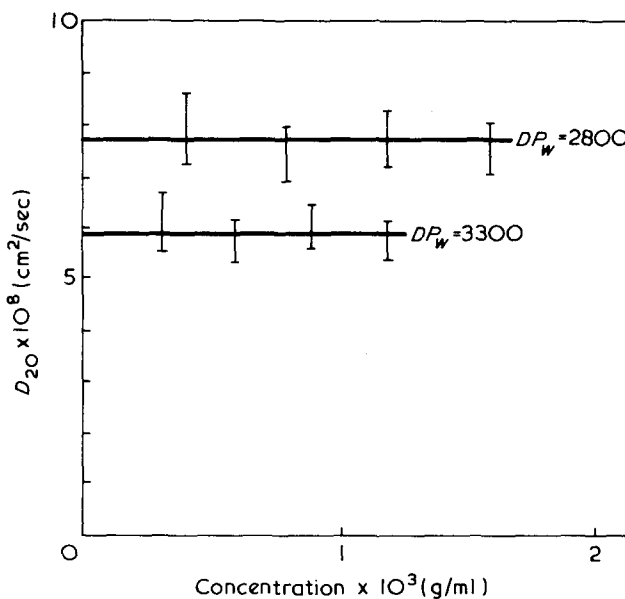


Figure 3 Diffusion constant as a function of concentration for two samples of cellulose trinitrate dissolved in ethyl acetate

cellulose trinitrate system. The author has no explanation to offer at present other than that the effects of thermodynamic and hydrodynamic interaction just cancel out.

In the above discussion the effects of internal motion of the polymer chain have been ignored and the results are in fact those expected for translational diffusion alone. However, the theory due to Pecora<sup>18</sup> suggests that for the samples studied here the effects of internal motion should be quite large. This will therefore be discussed further. The results of Pecora's theoretical investigation into the case of a monodisperse freely draining coil are complicated. The phase correlation function can be expressed in the form:

$$F(\tau) = \frac{I}{P(x)} \left[ P_0(x) \exp(-K^2 D \tau) + \sum P_A(x) \exp - \left( K^2 D + \sum \frac{a}{\tau_n} \right) \tau \right] \quad (4)$$

where  $P(x)$  is the particle scattering factor for a Gaussian coil and:

$$x = \frac{K^2 \bar{r}^2}{6} \quad (5)$$

where  $\bar{r}^2$  is the mean square end to end distance. The contribution due to translation diffusion alone,  $P_0(x)$  is given by:

$$P_0(x) = \frac{\pi}{x} \exp(-x/6) \left[ \operatorname{erf} \left( \frac{\sqrt{x}}{2} \right) \right]^2 \quad (6)$$

$\tau_n$  denotes a relaxation time of the polymer chain and is given by:

$$\tau_n = \frac{\bar{r}^2}{3\pi^2 n^2 D} \quad (7)$$

where  $n$  is an integer.  $\sum(a/\tau_n)$ , where  $a$  is an integer, represents permitted combinations of relaxation times which occur, and for each combination there is a function  $P_A(x)$  the analytical form of which is in general highly complex. Pecora gives numerical values of these functions for  $x < 7$ . For  $x < 1$  the contribution of internal motion is negligible and  $P_0(x) \approx P(x)$ . For  $x < 3$  the summation is dominated by a single term for which  $\sum(a/\tau_n) = 2/\tau_1$  and Pecora denotes the corresponding value of  $P_A(x)$  by  $P_2(x)$ . This term also represents approximately half of the contribution of internal modes at  $x = 7$ , the rest comprising terms for which

$$\sum \frac{a}{\tau_n} = \frac{4}{\tau_1} + \frac{2}{\tau_2} \quad \text{and} \quad \frac{1}{\tau_2} + \frac{2}{\tau_1}$$

A qualitatively similar result to that of Pecora has been obtained by Saitō and Itō<sup>19</sup>. They give an expression which after some rearrangement becomes:

$$F(\tau) = \frac{I}{P(x)} \left[ \left( P(x) - \frac{x^2}{45} \right) \exp(-K^2 D \tau) + \frac{2x^2}{\pi^4} \sum_n \frac{1}{n^4} \exp - (K^2 D + 2/\tau_n) \tau \right] \quad (8)$$

The various functions of  $x$  have here been expressed as power series and limited to the  $x^2$  term. The expression is not quantitatively valid for  $x > 1$ .

Experimentally  $\phi(\tau)$  is obtained and the contribution of internal motion will appear principally as terms of the form  $P_0(x)P_A(x) \exp - [2K^2 D + \sum(a/\tau_n)] \tau$ . All of these have decay times which are shorter than that of the term due to translational diffusion alone and will never give rise to a 'tail' on the exponential decay as was obtained for one of the samples in the present work (Figure 1). This must be attributed to polydispersity as already indicated. If  $P_2(x)$  is assumed to represent the dominant contribution of internal motion then  $\phi(\tau)$  is given to a first approximation by:

$$\phi(\tau) = \frac{c^2 \gamma^2}{2} I^2 \frac{P_0(x)}{[P(x)]^2} \left[ P_0(x) \exp(-2K^2 D \tau) + 2P_2(x) \exp - \left( 2K^2 D + \frac{2}{\tau_1} \right) \tau \right] \quad (9)$$

The ratio of the contribution of the two terms and the ratio of the decay times calculated according to Pecora's theory is shown for the highest molecular weight sample ( $DP_w = 3300$ ) in Table 2. The values of  $x$  are those obtained from conventional light scattering experiments<sup>15</sup>. At first sight the fourth and fifth columns would appear to indicate that the contributions of internal motion are large. However, if plots are made of the sum of the two terms as a function of  $\ln \tau$ , it can be shown that within 1%  $\phi(\tau)$  is indistinguishable from a single exponential over the experimental range. The factor,  $R$ , by which the decay time is reduced from that expected for translational diffusion alone is shown in the last column. Although the effect is less than might be expected a variation of some 25% should have been detectable in the present work. A possible explanation why this was not so is that measurements were made at finite concentrations. A Zimm plot consisting of parallel straight lines may be described by the relation:

$$\frac{KC}{R\theta} = \frac{1}{MP(\theta)} + 2BC \quad (10)$$

where the symbols have their usual meaning. Hence:

$$\frac{d(R\theta)}{R\theta} = \frac{dP(\theta)}{P(\theta)} \frac{1}{1 + 2BCMP(\theta)} \quad (11)$$

so that fluctuations in scattered intensity are less than fluctuations in particle scattering factor for positive values of the second virial coefficient,  $B$ . For the highest molecular weight sample at a concentration of  $10^{-3}$  g/ml the factors by which intensity fluctuations would be reduced on the

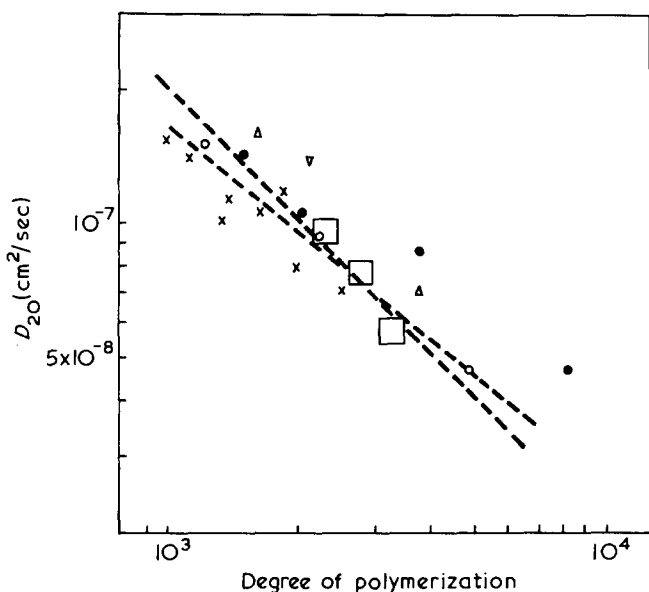
Table 2 Calculated effect of internal motion for the highest molecular weight sample ( $DP_w = 3300$ )

$\theta$ (degrees)	$x$	$P(x)$	$\frac{2P_2(x)}{P_0(x)}$	$\frac{\tau_1 K^2 D}{1 + \tau_1 K^2 D}$ *	$R^\dagger$
45	1.75	0.60	0.10	0.26	0.96
60	3.0	0.46	0.28	0.37	0.85
75	4.5	0.35	0.56	0.47	0.81
90	6.2	0.27	0.84	0.58	0.78 (0.73‡)

\*  $\tau_1 K^2 D = 2x/\pi^2$

† Effective reduction in decay time

‡ Taking account of higher order relaxation times



**Figure 4** Diffusion constant as a function of degree of polymerization for cellulose trinitrate in ethyl acetate. The author's results are represented by the open squares which indicate the limits of error and have been obtained from light scattering Rayleigh linewidth measurements and conventional light scattering measurements. The results of other authors are as follows:  $\nabla$ , Muisimann<sup>1</sup>;  $\times$ , Gralen<sup>2</sup>;  $\Delta$ , Jullande<sup>3</sup>;  $\circ$ , Newman *et al.*<sup>4</sup>;  $\bullet$ , Meyerhoff<sup>5,6</sup>. Where measurements were not made in ethyl acetate the points shown are those expected assuming the validity of the Stokes-Einstein equation

basis of equation (11) are 0.51, 0.57, 0.64, 0.69 at  $45^\circ$ ,  $60^\circ$ ,  $75^\circ$ ,  $90^\circ$  respectively. The values of  $R$  then become 0.97, 0.93, 0.89, 0.88 so that the variation with angle is reduced by about a half and is approximately the same as the experimental error. At concentrations lower than  $10^{-3}$  g/ml measurements were possible only at  $45^\circ$  and  $60^\circ$  due to the low scattered intensity. It is possible that the translational diffusion constants shown in *Table 1* are systematically high due to the neglect of internal motion but it is believed on the basis of the above discussion that the error involved is of the same order as the random error.

The samples investigated in the present work do not have a wide enough range of degree of polymerization to establish a relationship between diffusion constant and molecular weight. The absolute values can, however, be compared with those obtained by other authors using conventional techniques. Such a comparison is illustrated in *Figure 4* which shows diffusion constants for degrees of polymerization above 1000. The author's results lie well within the range of previous results. The dotted lines have slopes of minus unity and  $-0.8$ , the former representing a freely draining coil and the latter representing the minimum value of  $\alpha$  in the expression:

$$D = AM^{-\alpha} \quad (12)$$

consistent with the author's results. The true value of  $\alpha$  must therefore lie between these limits for the range of degree of polymerization investigated.

The results of other authors shown in *Figure 4* were obtained by a combination of diffusion and sedimentation velocity measurements. Polydispersity considerations are

therefore complicated and direct comparison of the results is difficult. It has been shown that light scattering Rayleigh linewidth measurements yield a  $Z$  average diffusion constant if the autocorrelation function is indistinguishable from a single exponential<sup>12</sup>. The molecular weight to which this diffusion constant corresponds is given by  $M_D$  where:

$$M_D = \left[ \frac{\sum_i N_i M_i^2}{\sum_i N_i M_i^{2-\alpha}} \right]^{1/\alpha} \quad (13)$$

$N_i$  is the number of molecules with molecular weight  $M_i$ . Thus  $M_D = M_w$  when  $\alpha = 1$ , i.e. in the case of a freely draining coil. Thus within experimental error the author's values of diffusion constant and degree of polymerization correspond directly. Assuming  $\alpha = 1$  the equivalent hydrodynamic diameter per monomer unit is  $0.45 \pm 0.03$  Å. This, of course, is merely a parameter determining the diffusion constant at high degree of polymerization and has no physical significance.

## CONCLUSIONS

Light scattering Rayleigh linewidth measurements made upon solutions of high molecular weight cellulose trinitrate in ethyl acetate by obtaining the autocorrelation function of fluctuations in scattered intensity, yield diffusion constants which are in good agreement with those obtained by conventional techniques. There is no concentration dependence within experimental error ( $\pm 7\%$ ) and no effects due to internal motion are observed. The latter may in part be due to the high second virial coefficient.

## REFERENCES

- 1 Muisimann, H. *Helv. Chim. Acta* 1943, **26**, 61
- 2 Gralen, N. *Dissert. Univ. of Uppsala* (1944)
- 3 Jullander, I. *Arkiv. Kemi* 1945, **21A**, 8
- 4 Newman, S., Loeb, L. and Conrad, C. M. *J. Polym. Sci* 1953, **10**, 463
- 5 Meyerhoff, G. *Naturwissenschaften* 1954, **41**, 13
- 6 Meyerhoff, G. *J. Polym. Sci.* 1958, **29**, 399
- 7 Cummins, H. Z., Knable, N. and Yeh, Y. *Phys. Rev. Lett.* 1964, **12**, 150
- 8 Dubin, S. B., Lunacek, J. H. and Benedek, G. B. *Proc. Nat. Acad. Sci. US* 1967, **67**, 1164
- 9 Foord, R., Jakeman, E. and Oliver, C. J. *et al. Nature* 1970, **227**, 242
- 10 Ford, N. C., Karasz, F. E. and Owen, J. E. M. *Discuss. Faraday Soc.* 1970, **49**, 228
- 11 Sellen, D. B. *Polymer* 1970, **11**, 374
- 12 Sellen, D. B. *Polymer* 1973, **14**, 359
- 13 Pecora, R. *Discuss. Faraday Soc.* 1970, **49**, 222 and references cited therein
- 14 Holtzer, A. M., Benoit, B. and Doty, P. *J. Phys. Chem.* 1954, **58**, 624
- 15 Holt, C., Mackie, W. and Sellen, D. B. *J. Polym. Sci. (C)* 1973, **42**, 1505
- 16 Alexander, W. J. and Mitchell, R. L. *Analyt. Chem.* 1949, **21**, 1467
- 17 Sellen, D. B. and Levi, M. P. *Polymer* 1967, **8**, 633
- 18 Pecora, R. *J. Chem. Phys.* 1968, **49**, 1032
- 19 Saito, N. and Ito, S. *J. Phys. Soc. Japan* 1968, **25**, 1446

# Relationships between $T_g$ and cohesive energy: 1. Dependence of $T_g$ on the composition of copolymers

K. Marcinčin and A. Romanov

*Polymer Institute of the Slovak Academy of Sciences, Dúbravská cesta, 809 34 Bratislava, Czechoslovakia*

*(Received 10 January 1974; revised 3 September 1974)*

The possibility of expressing the glass transition temperature of copolymers and homopolymers with an n-alkyl side chain as a function of two parameters (cohesive energy and steric factor) is discussed. An empirical equation representing these two factors is proposed. Calculated values are in good agreement with literature data for the investigated systems.

## INTRODUCTION

There are several more-or-less empirical equations available in the literature<sup>1-6</sup> which enable the glass transition temperature of copolymers to be expressed as a function of their composition. Wood<sup>2</sup> proposed an equation of the form:

$$T_g = \frac{k(T_{g2} - T_g)w_2}{1 - w_2} + T_{g1} \quad (1)$$

where  $T_g$  is the glass transition temperature of copolymer,  $w_2$  is the weight fraction of component 2,  $k$  is a non-specified constant and  $T_{g1,2}$  are the glass transition temperatures of the corresponding homopolymers.

The equations put forward by other authors are in most cases identical with equation (1) provided the constant  $k$  is expressed in a convenient form.

For some copolymers the relationship between the glass transition temperature and composition shows a minimum or maximum. It is not possible to describe such a relationship by equation (1). For this reason, Dyvik<sup>7</sup> proposed the equation:

$$T_g = w_1 T_{g1} + w_2 T_{g2} - \phi w_1 w_2 \quad (2)$$

where  $\phi$  is an interaction parameter and its value is a quadruple of the deviation from the linear dependence of  $T_g$  on weight composition at  $w_1 = w_2 = 0.5$ . However, it may be determined only from the relationship between  $T_g$  and composition which has been found experimentally.

$T_g$  of polymers is affected by a number of factors among which intermolecular forces and steric hindrance are the most significant. In order to express the relationship between these factors, Wyman<sup>8</sup> put forward the equation:

$$\log T_g = b \sum n_i E_i + \sum n_i E_{S_i} + C \quad (3)$$

where the symbols  $b$ ,  $n_i$ ,  $C$ ,  $E_i$  and  $E_{S_i}$  denote the constant ( $b = 10^{-5}$ ), molar fraction of component  $i$ , constant ( $\log T_g$  of reference polymer — polyethylene), intermolecular interaction parameter of component  $i$  which is a quantitative measure of cohesive energy, and intramolecular interaction parameter (steric factor) of component  $i$ , respectively.

The values of  $E_{S_i}$  calculated from the known values of  $T_g$  and cohesive energy have been correlated by Wyman with the solution properties of polymers.

Wyman assumes in his equation that the cohesive energy as well as the steric factor is an additive quantity. It follows from the application of the Wyman equation to copolymers that  $\log T_g$  is a linear function of molar composition. Only negative deviation from linear dependence of  $T_g$  as a function of composition is possible should the dependence of  $\log T_g$  on composition be linear. In fact, this dependence of  $T_g$  on composition is observed for many copolymers<sup>2,9</sup>. The Wyman equation, however, fails to describe properly the situation when dependence of  $T_g$  on composition shows a minimum (i.e.  $T_g$  of copolymers in certain composition range fall below  $T_g$  of both homopolymers).

## DEPENDENCE OF COHESIVE ENERGY ON THE COMPOSITION OF POLYMERS

The cohesive energy of polymers cannot be determined immediately from heat of evaporation. It is found indirectly by several methods but the individual methods do not quite give identical results<sup>10,11</sup>.

The cohesive energy may also be obtained by calculation. In general, the Small method of calculation<sup>12</sup> provides quite good results. The calculations are performed according to the formula:

$$E = \rho \frac{(\sum n_i F_i)^2}{M} = \frac{F^2}{V} = F\delta \quad (4)$$

$\rho$ ,  $M$ ,  $F$  and  $\delta$  being density of polymer, molecular weight of repeating unit (monomer), attraction constant, and solubility parameter, respectively. Small<sup>12</sup> published the mean values of attraction constants  $F_i$  for individual structural units.

It follows from equation (4) that the cohesive energy  $E$  changes linearly with the composition of copolymer only in some specific cases (i.e. provided the solubility parameter is equal over the whole range of composition).

Another factor which occurs in equation (4) is the density of polymer, which is a complicated function of inter-

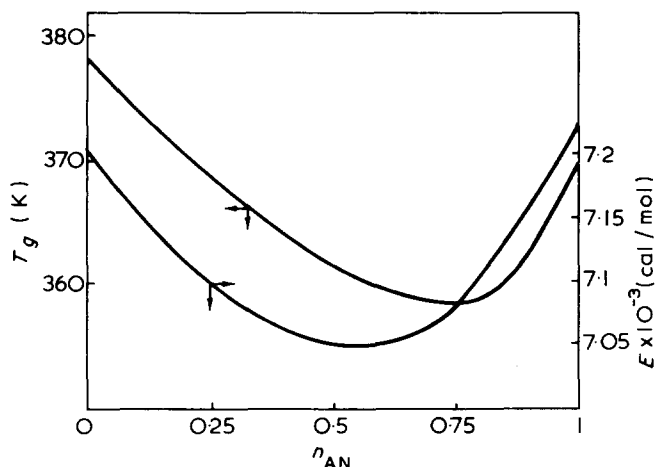


Figure 1 Relationship between  $T_g$  (according to Dyvik<sup>7</sup>) and cohesive energy (calculated according to Small<sup>12</sup> assuming the additivity of volume) on the molar fraction of acrylonitrile (AN) for copolymer methyl methacrylate-acrylonitrile

and intra-molecular interactions. Van Krevelen and Hoftyzer<sup>13</sup>, however, showed the possibility of evaluating the density of polymers on condition that the volume increments of individual structural units are additive:

$$\rho = \frac{M}{\sum V_i} \quad (5)$$

They calculated the average values of volume increments and demonstrated that the agreement of the values calculated from average increments with the real ones was rather good.

Other authors<sup>14</sup> calculated the proper volume of the molecules of polymers on the basis of the volume of individual atoms and the lengths of bonds. They showed that the coefficient of packing:

$$K = \frac{\text{proper volume of molecule}}{\text{real volume}} \quad (6)$$

was approximately a constant quantity, the mean value of which was 0.68. They also calculated the average values of the increments of proper volume for individual atoms considering the kind of atoms to which these atoms were bonded in the molecule.

It follows from the above that the molar volume is approximately an additive quantity consisting of volume increments. The linear dependence of molar volume may be assumed to be still more for copolymers in which the structure of monomer units remains preserved. Provided the volume can be expressed in additive terms corresponding to individual homopolymers, the cohesive energy may be calculated easily for copolymers of different composition on the basis of equation (4).

#### CORRELATION BETWEEN COHESIVE ENERGY AND $T_g$ FOR COPOLYMERS

According to equation (4) the cohesive energy as a function of the composition of copolymer may even show a minimum. In this respect the copolymer methyl methacrylate-acrylonitrile can serve as an illustration. Both the polymers have nearly equal cohesive energies (7206 and 7245 cal/mol respectively) and glass transition temperatures (105° and

96°C respectively). Figure 1 shows the dependence of cohesive energy and glass transition temperature on the composition of this copolymer. The course of both these quantities is analogous (they pass through a minimum).

To express  $T_g$  dependence on copolymer composition we suggest the equation:

$$T_g = S_F 10^{kES_F} \quad (7)$$

where

$$S_F = \frac{1}{\rho \cdot S_L}$$

and  $k$  is a constant ( $10^{-6}$ ),  $S_F$  and  $\rho$  denote the steric factor and density of polymer and  $S_L$  is the parameter which is a linear function of molar composition.

The values of  $T_g$  calculated according to equation (7) are in good agreement with the values measured for the following examples.

#### Methyl methacrylate-acrylonitrile

For this copolymer a decrease of  $T_g$  below the values of corresponding homopolymers<sup>7,16,19</sup> has been found by several authors. Both the homopolymers show approximately equal and relatively high glass transition temperatures. According to the molecular structure the high glass transition temperature of methyl methacrylate is ascribed to the effect of steric hindrance caused especially by the  $-\text{CH}_3$  group in the  $\alpha$ -position. The high glass transition temperature of acrylonitrile is attributed chiefly to the polarity of polymer. The decrease in the glass transition temperature of copolymer may then be interpreted as a decrease in the steric hindrance occurring in methyl methacrylate by the effect of acrylonitrile units and as a disturbance of polar interactions in acrylonitrile by the effect of methyl methacrylate units. In Figure 2 the dependence of glass transition temperature calculated for this copolymer according to equation (7) is compared with the course measured by Dyvik<sup>7</sup> ( $\phi = 60\text{K}$ ). As is clear from this

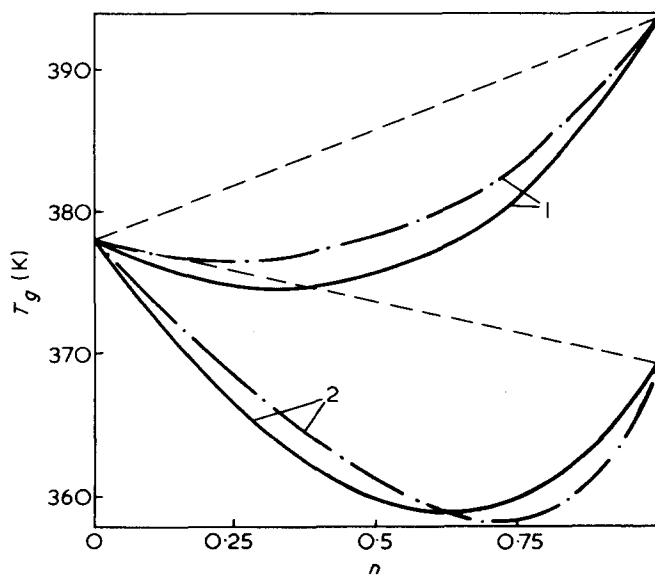


Figure 2  $T_g$  as a function of molar composition for copolymers methyl methacrylate-methacrylonitrile (1) and methyl methacrylate-acrylonitrile (2). —, Calculated on the assumption of a linear relation between  $S_L$  and molar composition; - - -, according to Dyvik<sup>7</sup> for  $\phi = 24\text{K}$  and  $\phi = 60\text{K}$

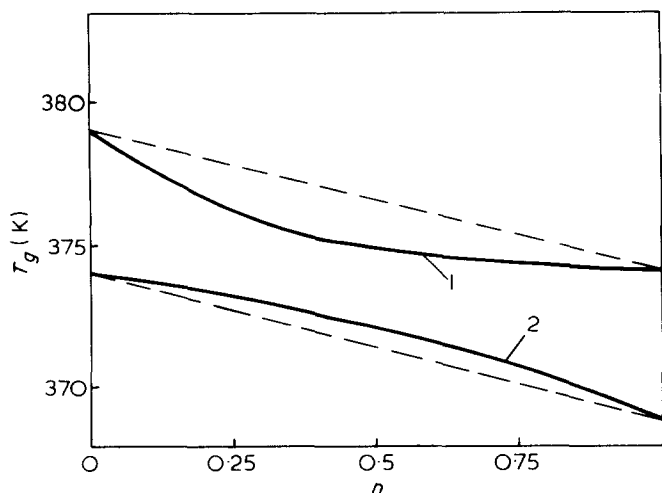


Figure 3  $T_g$  as a function of molar composition for copolymers methyl methacrylate-styrene (1) and styrene-acrylonitrile (2) calculated on the assumption of a linear relation between  $S_L$  and molar composition

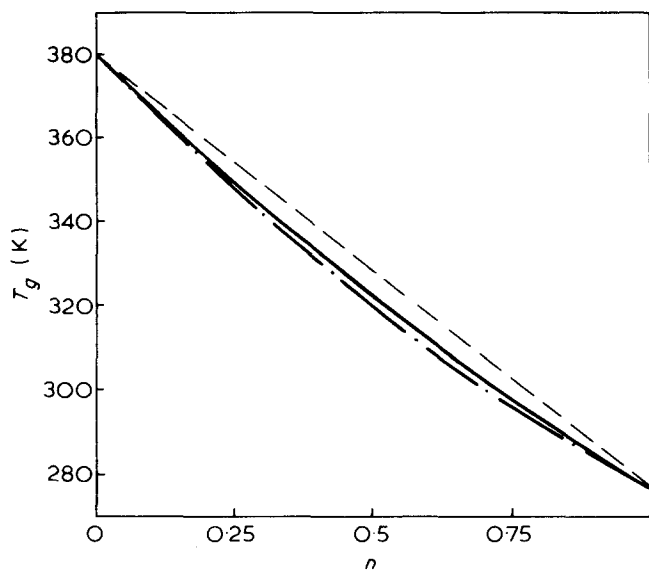


Figure 4  $T_g$  as a function of molar composition for copolymer methyl methacrylate-methylacrylate. ---, according to Dyvik<sup>7</sup> ( $\phi = 40\text{K}$ )

Figure, the decrease in the glass transition temperature may be due to the change in cohesive forces at a practically equal steric factor.

#### Methyl methacrylate-methacrylonitrile

With the copolymer consisting of this pair of monomers the situation is similar to that one which occurs with the pair methyl methacrylate-acrylonitrile. The dependence of glass transition temperature on composition is well described qualitatively by equation (7) (Figure 2). The calculated values are within the whole range of composition smaller than that stated by Dyvik<sup>7</sup> ( $\phi = 24\text{K}$ ) but the difference does not exceed 2K.

#### Methyl methacrylate-styrene

The properties of the copolymer consisting of this pair of monomers to a certain degree depend on the polymerization conditions. In general, a small negative deviation has been found in the dependence between glass temperature and composition and according to Dyvik<sup>7</sup> at the equimolar composition its value is about 3-4K. The curves

calculated according to equation (7) and presented in Figure 3 show a negative deviation also.

#### Styrene-acrylonitrile

The relationship between the glass transition temperature and the composition of this copolymer has been studied previously<sup>15</sup>. They have found that the glass transition temperatures of copolymers are a few degrees higher than those of the corresponding homopolymers. The calculated relation presented in Figure 3 describes this fact although it shows a positive deviation.

#### Methyl methacrylate-methyl acrylate

For this copolymer, either a positive (in one case<sup>16</sup>) or negative (in several cases<sup>2,7,17</sup>) deviation has been published for the relation between glass transition temperature and composition. The relationship calculated according to equation (7) shows a negative deviation but it complies fairly well with the values found experimentally for  $\phi = 40\text{K}$  (Figure 4).

#### Methyl methacrylate-ethyl acrylate

The interaction parameter  $\phi$  of this pair of monomers varies in the range  $\phi = 60-80\text{K}$ <sup>7,18</sup>. A similar relation has been also found for mutually crosslinked mixtures of both homopolymers<sup>8</sup>. The relationship calculated according to equation (7) agrees fairly well with the values for  $\phi = 60\text{K}$  (Figure 5).

#### Change in glass transition temperature due to the prolongation of the side methylene chain

Equation (7) also expresses the change of  $T_g$  due to the prolongation of the side methylene chain. Figure 6 shows the variation of the parameter  $S_L$  with the number of methylene groups in the side chain for 6 homologous polymer series. The dependence is linear in all cases presented. By comparing the course of  $T_g$  or parameter  $S_L$  of the copolymer methyl methacrylate/n-butyl methacrylate<sup>7</sup> and the homologous series of alkyl methacrylates it may be concluded that the effect of a  $-\text{CH}_2-$  group in the side chain is equal and independent whether a greater number of small-

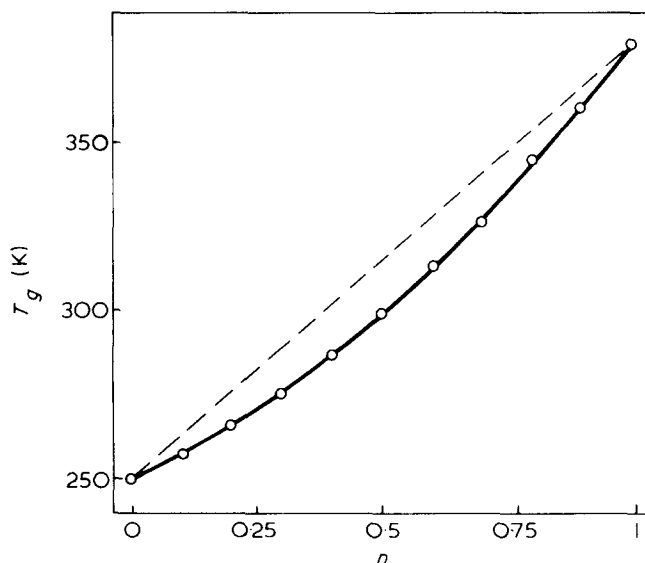


Figure 5  $T_g$  as a function of molar composition for copolymer ethyl acrylate-methyl methacrylate.  $\circ$ , Calculated according to Dyvik<sup>7</sup> for  $\phi = 60\text{K}$ ; ---, calculated on the assumption of linear relation between  $S_L$  and molar composition

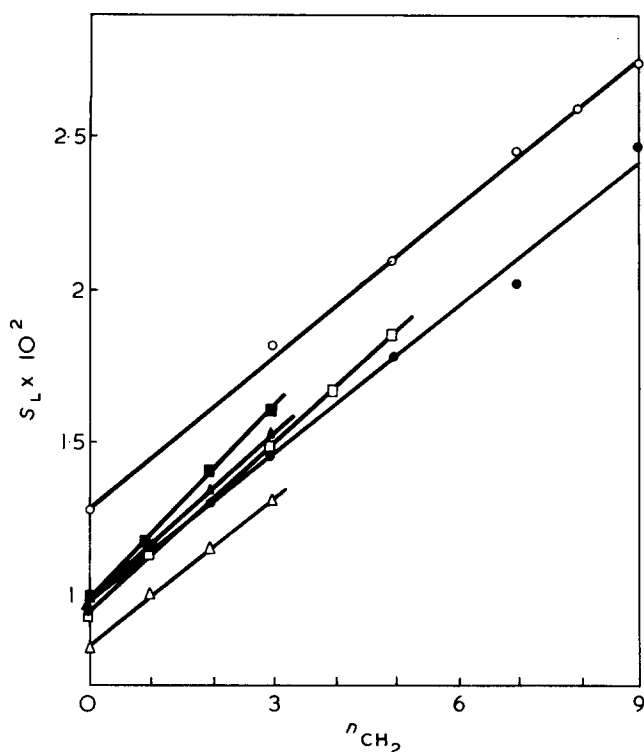


Figure 6 Parameter  $S_L$  as a function of the number of methylene groups in side chain for: ■, poly(alkyl acrylate); ●, poly(alkyl methacrylate); ○, poly(4-alkylstyrenes); △, poly(alkyl chloroacrylates); ▲, polyalkenes; □, poly(vinyl alkyl ethers)

Table 1  $T_g$  and cohesive energy of some polymer isomers (data according to Wyman<sup>8</sup>)

Polymer	$T_g$ (K)	$E$ (cal/mol)
Poly(vinyl acetate)	302	6428
Poly(methyl acrylate)	276	6900
Poly( <i>o</i> -methylstyrene)	393	9043
Poly( <i>p</i> -methylstyrene)	374	9360

ler alkyl groups or proportionally lesser number of longer groups is present.

## DISCUSSION

In equation (7), the product of cohesive energy and the steric factor ( $E, S_F$ ) is taken as the measure of intermolecular forces. The presumption is being introduced that in the case of lower steric hindrances, intermolecular forces of smaller chain section have to be overcome to release molecular motion. The influence of flexible side chain on  $T_g$  may be given as an example. In the polymer of this type

side chains of molecules may perform certain kinds of motions even below the glass temperature. Intermolecular forces (potential barriers) which have necessarily to be overcome at the motion of a certain link (section) of the chain will, in this case, be lower when compared with the one, where the motion (rotation) of the side chain due to steric hindrances is not made possible. The mutual dependence of cohesive energy and steric factor is also referred to by Wyman<sup>8</sup>.

The glass transition temperatures of polymers of similar composition are different in many cases. This can be shown best with polymer isomers (Table 1).

It is interesting that the isomer with lower  $T_g$  shows a higher cohesive energy. According to equation (4) the isomer with higher cohesive energy manifests a higher density. By including the density of polymer into the expression for steric factor (equation 7) we obtain an equal value of the parameter  $S_L$  for isomers. The value of the constant  $k$  in equation (7) was so chosen that this equation might express most accurately the relationship between  $T_g$  and composition for the copolymer methyl methacrylate-acrylonitrile. The calculated  $T_g$  dependences on composition show quite good agreement even for the other copolymers referred to with experimental results.

## REFERENCES

- Gordon, M. and Taylor, J. S. *J. Appl. Chem.* 1952, 2, 493
- Wood, L. A. *J. Polym. Sci.* 1958, 28, 319
- Fox, G. T. *Bull. Am. Phys. Soc.* 1956, 1, 123
- Mandelkern, L., Martin, G. M. and Quin, F. A. *J. Res. Nat. Bur. Stand.* 1957, 58, 137
- Kelley, F. N. and Buecke, F. *J. Polym. Sci.* 1961, 50, 549
- DiMarzio, E. A. and Gibbs, J. H. *J. Polym. Sci.* 1959, 40, 121
- Dyvik, G. K., Bartoe, W. F. and Steck, N. S. *SPE Trans.* 1964, 4, 98
- Wyman, D. P. *J. Appl. Polym. Sci.* 1967, 11, 1439
- Reding, F. P., Faucker, J. A. and Whitman, R. D. *J. Polym. Sci.* 1962, 57, 483
- Lee, W. A. and Lewell, J. H. *J. Appl. Polym. Sci.* 1968, 12, 1397
- Gardon, J. L. 'Encyclopedia of Polymer Science and Technology', Wiley, New York, 1965, Vol 3, p 833
- Small, P. A. *J. Appl. Chem.* 1953, 3, 71
- van Krevelen, D. W. and Hoflyzer, P. J. *J. Appl. Polym. Sci.* 1969, 13, 871
- Slonimskij, G. L., Askadskij, A. A. and Kitajgorodskij, A. I. *Vysokomol. Soedin. (A)* 1970, 12, 494
- Beevers, R. B. and White, E. F. T. *J. Polym. Sci. (B)* 1963, 1, 171
- Illers, K. H. *Kolloid Z.* 1963, 190, 16
- Schen, M. C. and Eisenberg, A. *Progr. Solid State Chem.* 1966, 3, 407; *Rubber Chem. Technol.* 1970, 43, 1
- Sperling, L. H., Taylor, D. V., Kirkpatrick, M. L., George, H. F. and Bardman, D. R. *J. Appl. Polym. Sci.* 1970, 14, 73
- Beevers, R. B. and White, E. F. T. *Trans. Faraday Soc.* 1960, 56, 1529

# Relationships between $T_g$ and cohesive energy: 2. Prediction of $T_g$ of homopolymers

K. Marcinčin and A. Romanov

Polymer Institute of the Slovak Academy of Sciences, Dúbravská cesta, 809 34 Bratislava, Czechoslovakia

(Received 10 January 1974; revised 3 September 1974)

An empirical equation expressing  $T_g$  of polymers as a function of cohesive energy and steric factor is suggested so that the parameter  $V_S$  in this equation may be considered to be an additive quantity. From the data on 44 polymers including 6 homologous series the increments of  $V_S$  were calculated for individual structural units. The agreement of the calculated with the measured values of  $T_g$  found for homopolymers and copolymers is discussed.

## INTRODUCTION

The prediction of the glass transition temperature of polymers from chemical structure is of remarkable theoretical and practical importance. There are several methods<sup>1-3</sup> which have been proposed for the calculation of the glass transition temperature of polymers from the chemical structure of monomer unit. Some authors<sup>1,2</sup> started from the equations describing the dependence of  $T_g$  of copolymers on composition and calculated the additive temperature parameters for individual structural units (groups of atoms). Lee<sup>2</sup> also took into consideration in his calculations how the groups in a molecule of monomer were bonded. Askandskij<sup>3</sup> put forward an empirical equation for the calculation of  $T_g$  of polymers in which he assumed the addi-

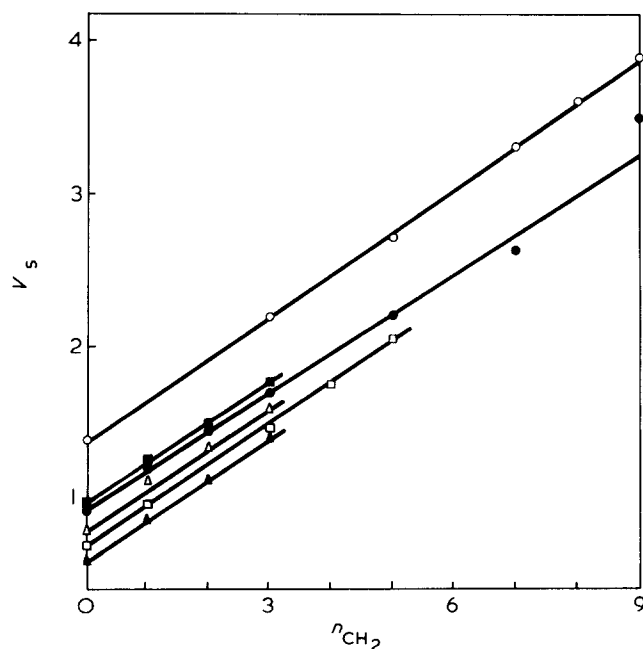


Figure 1 Parameter  $V_S$  as a function of the number of methylene groups in side chain for: ■, poly(alkyl acrylates); ●, poly(alkyl methacrylates); ○, poly(4-alkylstyrenes); △, poly(alkyl chloroacrylates); ▲, polyalkenes; □, poly(vinyl alkyl ethers)

Table 1 Increments  $V_S$  of  $-\text{CH}_2-$  group for individual homologous series

Homologous series	Increment $V_S$ ( $-\text{CH}_2-$ )	Average
Poly(n-alkyl methacrylates)	0.254	0.258
Poly( <i>p</i> -n-alkyl styrenes)	0.272	
Poly(n-alkyl acrylates)	0.270	
Poly(n-alkenes-1)	0.264	
Poly(n-alkyl vinyl ethers)	0.261	
Poly(n-alkyl chloroacrylates)	0.235	

vity of another parameter occurring in this equation (different from temperature). In the equations expressing the relationships between  $T_g$  and cohesive energy some additive parameters are also present<sup>4,5</sup>

## METHOD OF CALCULATION

In Part 1<sup>7</sup> it has been shown that the parameter  $S_L$  in the equation

$$T_g = \frac{1}{\rho S_L} 10^k (F^2 / MS_L) \quad (1)$$

increases linearly if the alkyl side is prolonged and assuming the linear dependence of this parameter on molar composition is valid the equation expresses fairly well the glass transition temperature of copolymers. But the parameter  $S_L$  does not fulfil the postulate of additivity.

It is known that flexible n-alkyl side chain decreases  $T_g$  of polymers more than a non-linear alkyl side chain with the same number of carbon atoms. The polymer with a flexible side chain may be considered as a copolymer consisting of several monomer units. In this case the calculation of steric factor demands that the molar cohesive energy corresponding to such monomer unit be taken into consideration. If we assume for simplification that the number of monomer units is proportional (equal) to molecular weight, equation (1) may be written in the form:



$$T_g = \frac{V}{V_S} 10^k (F^2/MV_S) \quad (2)$$

where  $V$  is molar volume of monomer unit,  $V_S$  is additive parameter ( $V_S = MS_L$ ) and the constant  $k = 10^{-4}$ . The

Table 2 Values of the increments  $V_{S_i}$  for individual structural units

Structural unit	$V_{S_i}$
—CH <sub>2</sub> — 	0.2710
—CH— 	0.6382
—C— 	0.9558
—CH <sub>3</sub>	-0.2824
—CO—O— (ester)	0.3169
—O— (ether)	0.0710
—Cl	-0.4089
—CN	-0.1188
phenyl	0.2602
<i>p/o</i> -phenylene	0.7650

Table 3 Parameters  $V_S$  and  $T_g$  for polymers\*

No.	Polymer	$V_S$	$\sum n_i V_{S_i}$	$V_S - \sum n_i V_{S_i}$	$T_g$ (K) <sup>†</sup>	$T_g$ (calc.) (K)	$\Delta T_g$
1	Polypropylene	0.6175	0.6267	-0.0092	258	265.9	-7.9
2	Poly(vinyl chloride)	0.4975	0.5002	-0.0027	360	355.5	+4.5
3	Polyacrylonitrile	0.7670	0.7903	-0.0233	369	341.8	+27.2
4	Polymethacrylonitrile	0.8670	0.8255	+0.0415	393	450.9	-57.9
5	Poly(vinyl acetate)	0.9311	0.9437	-0.0126	302	292.9	+9.1
6	Poly(vinyl <i>t</i> -butyl ether)	1.1082	1.0886	+0.0196	361	375.9	+14.9
7	Poly(2-methylstyrene)	1.3709	1.3917	-0.0208	393	378.5	+14.5
8	Poly( $\alpha$ -methylstyrene)	1.1808	1.2046	-0.0238	458	437.2	+20.8
9	Polystyrene	1.1829	1.1694	+0.0135	374	380.3	-6.3
10	Poly(4-methylstyrene)	1.3789	1.3917	-0.0128	374	378.2	-4.2
11	Poly(4-butylstyrene)	2.1998	2.2045	-0.0047	289	287.8	-8.8
12	Poly(4-hexylstyrene)	2.6811	2.7463	-0.0652	246	261.6	-15.6
13	Poly(4-octylstyrene)	3.3347	3.2882	+0.0465	228	245.2	-17.2
14	Poly(4-nonylstyrene)	3.6142	3.5591	+0.0551	220	239.1	-19.1
15	Poly(4-decylstyrene)	3.9193	3.8300	+0.0893	208	233.9	-25.9
16	Poly(methyl methacrylate)	0.9553	0.9788	-0.0235	378	362.1	+15.9
17	Poly(ethyl methacrylate)	1.2157	1.2498	-0.0341	338	310.5	+27.5
18	Poly(propyl methacrylate)	1.4491	1.5207	-0.0716	308	280.7	+27.3
19	Poly(butyl methacrylate)	1.6931	1.7916	-0.0985	293	261.5	+31.5
20	Poly(hexyl methacrylate)	2.2249	2.3334	-0.1085	268	241.0	+27.0
21	Poly(octyl methacrylate)	2.6578	2.8753	-0.2175	253	212.5	+40.5
22	Poly(decyl methacrylate)	3.5080	3.4171	+0.0909	208	216.4	-8.4
23	Poly(methyl acrylate)	0.9527	0.9437	+0.0090	279	285.5	-6.4
24	Poly(ethyl acrylate)	1.2820	1.2146	+0.0674	249	255.4	-6.4
25	Poly(propyl acrylate)	1.4912	1.4855	+0.0057	236	238.0	-2.0
26	Poly(butyl acrylate)	1.7877	1.7564	+0.0313	218	226.7	-8.7
27	Poly(1-butene)	0.8751	0.8976	-0.0225	249	235.6	+13.4
28	Poly(1-pentene)	1.1382	1.1685	-0.0303	233	220.3	+12.7
29	Poly(1-hexene)	1.4033	1.4395	-0.0362	223	211.0	+12.0
30	Poly(methyl chloroacrylate)	0.8998	0.8523	+0.0475	398	456.3	-58.3
31	Poly(ethyl chloroacrylate)	1.1382	1.1232	+0.0150	351	362.5	-11.5
32	Poly(propyl chloroacrylate)	1.3497	1.3941	-0.0444	339	314.2	+24.8
33	Poly(butyl chloroacrylate)	1.5949	1.6651	-0.0702	315	285.0	+30.0
34	Poly(vinyl methyl ether)	0.7000	0.6976	+0.0024	242	259.1	-17.1
35	Poly(vinyl ethyl ether)	0.9735	0.9686	+0.0049	230	232.4	-2.4
36	Poly(vinyl butyl ether)	1.4736	1.5104	-0.0368	221	209.8	+11.2
37	Poly(vinyl pentyl ether)	1.7676	1.7813	-0.0137	207	203.9	+3.1
38	Poly(vinyl hexyl ether)	2.0714	2.0522	+0.0192	196	199.8	-3.8
39	Poly(2,3-dimethyl butene-1)	1.0933	1.0177	+0.0756	332	379.9	-47.9
40	Poly( <i>t</i> -butyl acrylate)	1.4237	1.3346	+0.0891	316	368.2	-52.2
41	Poly(4- <i>t</i> -butylstyrene)	1.8495	1.7827	+0.0668	391	428.8	-37.8
42	Poly(3-methyl pentene-1)	1.1832	1.2534	-0.0702	309	271.4	+37.6
43	Poly(2-butyl acrylate)	1.6447	1.5703	+0.0744	251	278.8	-27.8
44	Poly(2-butyl methacrylate)	1.6063	1.6055	+0.0088	326	326.6	-0.6

\* Data of cohesive energy for calculation after Wyman<sup>5</sup> for polymers 1–24 and calculated after Small<sup>10</sup> using additive volume increments<sup>6</sup> for polymers 25–44

† Data after Brandrup and Immergut<sup>11</sup>

value of constant  $k = 10^{-4}$  was chosen so that, for the polymer of molecular weight of monomer unit  $M = 100$ , equation (2) was numerically equal to equation (1) or equation (7) in Part 1<sup>7</sup>.

The values of  $V$ ,  $M$ ,  $F$  were assigned, experimental  $T_g$  being available for 44 polymers including 6 homologous series. The resulting transcendental equations were solved graphically for  $V_S$  of these 44 polymers.

The dependence of the parameter  $V_S$  on the number of —CH<sub>2</sub>— groups in the side chain may be expressed fairly well by a straight line (Figure 1). The slope of lines is almost equal (Table 1) for individual homologous series and represents the increment of the parameter  $V_S$  for methylene groups. The arithmetic mean for six homologous series is  $V_S(-CH_2-) = 0.258$ . The glass transition temperature of polyethylene calculated from this value is 196K and complies well with the value obtained by extrapolating the glass transition temperature of a copolymer of ethylene with different monomers<sup>8,9</sup>. Assuming the additivity of parameter  $V_S$  is valid, the values of the increments  $V_{S_i}$  have been calculated for individual structural units (groups of atoms) using least squares procedures. The calculated values of increments  $V_{S_i}$  are given in Table 2. Table 3 also contains the

differences  $V_S - \sum n_i V_{S_i}$  and the deviations of the transition temperatures calculated by means of the increments  $V_{S_i}$  from the real ones.

## DISCUSSION

The assumption that the molecular weight is proportional to the number of monomer units in equation (2) is only approximate. In the case of vinyl polymers the molecular weight of monomer unit is approximately proportional to the number of atomic groups able to rotate freely around simple bonds except polymers containing structural skeletons (rings) or heavier atoms. Owing to this the increment  $V_S(-CH_2-)$  (Table 1) is the smallest for the homologous series of poly(n-alkyl chloroacrylates) and differs most from the average value. This is also seen in the deviation of the glass transition temperatures obtained from average increments of the parameters  $V_S$  from the real values of  $T_g$  (Table 3, polymers 30–33). For poly( $\alpha$ -methylstyrene) (polymer 8) and homologous series of poly(n-alkyl methacrylates) (polymers 16–22) a positive deviation appears. On the other hand, it is negative in the case of homologous series of poly(n-alkyl acrylates) (polymers 23–26) and poly(p-n-alkyl styrene). It is to a great extent due to the fact that polyacrylonitrile (polymer 3) and polymethacrylonitrile (polymer 4) has also been involved in the calculation of the average values of increments  $V_{S_i}$ . For these polymers the difference in the values of  $V_S$  is rather higher than that contributed by a  $-CH_3$  group of poly( $\alpha$ -methylstyrene) and poly(n-alkyl methacrylate). The deviations occurring with polymers 3 and 4 are also relatively high and of opposite character. High negative deviations also appear in the case of polymers with t-alkyl groups in the side chain (polymers 39–41). It indicates the need of a different evaluation of the  $-CH_3$  group according to the kind of bonding in the molecule. For this reason it would be necessary to introduce another rule.

The values of molar cohesive energy are referred to room temperature. For the correlation of  $T_g$  with cohesive energy it would be more correct to use values of cohesive energy at  $T_g$  of individual polymers. A disagreement may also be due to other factors affecting  $T_g$  of polymers (tacticity, crystallinity, symmetry of molecule etc.) the total of which is difficult to express by a single parameter.

The assumption of additivity of the parameter  $V_S$  (equation 2) provides fairly good results for  $T_g$  of copoly-

Table 4 Glass transition temperatures of copolymers with equimolar composition

Copolymer	$T_g$ (K)			
	Literature data	Calculated		Refs
		Eqn. (1)	Eqn. (2)	
acrylonitrile—methyl methacrylate	361	361	366	9, 12
methacrylonitrile—methyl methacrylate	378	375.5	379	12
styrene—acrylonitrile	374	372	371	13
styrene—methyl methacrylate	373	375	375	12
methyl acrylate—methyl methacrylate	321	323	325	12
methyl methacrylate—butyl methacrylate	329	330	322	12
methyl methacrylate—ethyl acrylate	300	300	300	12, 14

mers. The glass transition temperatures of copolymers with equimolar composition calculated from the values of corresponding homopolymers by means of equations (1) and (2) are compared with real values in Table 4.

## REFERENCES

- 1 Weyland, H. G., Hoftyzer, P. J. and van Krevelen, D. W. *Polymer* 1970, **11**, 79
- 2 Lee, W. A. *J. Polym. Sci. (A-2)* 1970, **8**, 555
- 3 Askadskij, A. A. *Vysokomol. Soedin. (A)* 1967, **9**, 418
- 4 Hayes, R. A. *J. Appl. Polym. Sci.* 1961, **5**, 318
- 5 Wyman, D. P. *J. Appl. Polym. Sci.* 1967, **11**, 1439
- 6 van Krevelen, D. W. and Hoftyzer, P. J. *J. Appl. Polym. Sci.* 1969, **13**, 871
- 7 Marcinčin, K. and Romanov, A. *Polymer* 1975, **16**, 173
- 8 Tobolsky, A. V. 'Properties and Structure of Polymers', Wiley, New York, 1960
- 9 Illers, K. H. *Kolloid Z.* 1963, **190**, 16
- 10 Small, P. A. *J. Appl. Chem.* 1953, **3**, 71
- 11 Brandrup, I. and Immergut, E. H. 'Polymer Handbook', Wiley, New York, 1966
- 12 Dyvik, G. K., Bartoe, W. F. and Steck, N. S. *SPE Trans.* 1964, **4**, 98
- 13 Beevers, R. B. and White, E. F. T. *J. Polym. Sci. (B)* 1963, **1**, 171
- 14 Sperling, L. H., Taylor, D. V., Kirkpatrick, M. L., George, H. F. and Bardman, D. R. *J. Appl. Polym. Sci.* 1970, **14**, 73

# Star polymers from styrene and divinylbenzene

Helmut Eschwey and Walther Burchard

*Institut für Makromolekulare Chemie der Universität Freiburg, D 78 Freiburg i. Br., West Germany*

(Received 28 May 1974)

The principle of anionic block copolymerization of styrene and divinylbenzene, first employed by Rempp and his coworkers, is further developed. Rempp's method (1) of divinylbenzene polymerization with long 'living' polystyrene chains, and our method (2) of the polymerization of styrene with polydivinylbenzene, bearing a number of 'living' carbanionic groups, are shown to be the two limiting cases of the styrene-divinylbenzene block copolymerization. By preparing 'living' polystyrene of shorter chain lengths than was used by Rempp *et al.* all stages of polymerization within the two limits are realized. In particular, star molecules with a large number of short side chains, according to Rempp's method, are prepared in a first step, and these stars with 'living' nuclei are used to prepare stars (3) according to our method. The number of branches of the original star is doubled by this technique. Also mixed stars with both polystyrene and polyisoprene branches are prepared. The latter are characterized by light scattering in benzophenone, which is isorefractive with the polystyrene moiety. The  $g'$  factors of the stars are compared with existing theories, but in no case is satisfactory agreement obtained.

## INTRODUCTION

Common block copolymers of the A-B and B-A-B type are usually prepared by anionic copolymerization with either lithium alkyls or sodium naphthalene as catalysts<sup>1</sup>. In these examples lithium alkyls should be regarded as monofunctional initiators while the sodium naphthalene catalyst leads to a bifunctional initiation.

A new type of block copolymer has been obtained by the anionic copolymerization of divinylbenzene (DVB) with styrene or other suitable monomers. By this technique star-shaped block copolymers are obtained consisting of a nucleus of polydivinylbenzene and rays of linear chains, e.g. polystyrene or polyisoprene etc. The structure of this type of block copolymer is represented in *Figure 1*.

Two different methods of preparation of such star molecules have been described in the literature. In the first case<sup>2-5</sup> living polystyrene bearing one carbanionic end group is copolymerized with a small amount of divinylbenzene resulting in small densely crosslinked nuclei of polydivinylbenzene with several pendant polystyrene chains. By this method Rempp and his coworkers pre-

pared star molecules with four to twenty polystyrene branches.

In the second method<sup>6</sup>, recently developed in our laboratory, divinylbenzene is anionically polymerized in dilute solution by *n*-butyl lithium, where densely cross-linked polydivinylbenzene particles are obtained. These particles bear quite a number of living carbanionic groups capable of polymerizing styrene or other monomers yielding star molecules. The size and functionality of the polydivinylbenzene nuclei are increased by increasing the ratio  $R = [\text{DVB}] / [\text{butyl lithium}]$  and the overall concentration of divinylbenzene.

Both methods have different advantages. According to Rempp's method the star molecules are characterized by a relatively narrow molecular weight distribution but the number of branches is highly controlled by a pronounced diffusion control of the reaction. In contrast to Rempp's method any desired functionality of the nuclei ( $p = 4 - 4 \times 10^5$ ) and any length of the side chains can be prepared by the second method but the products are rather polydisperse.

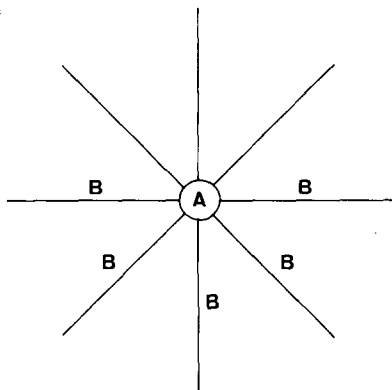
In spite of the differences in principle, these two methods can be considered as two limiting cases of divinylbenzene polymerization. In the first case the initiator is a long 'living polymer' chain ( $\text{PSt-Li}^+$ ,  $DP > 100$ ), while in the second case it is of low molecular weight ( $\text{Bu}^-\text{Li}^+$  = butyl lithium).

From this point of view all stages in between should be capable of synthesis.

## EXPERIMENTAL

### Materials

Toluene and tetrahydrofuran (both Merck) were dried over sodium. Styrene and isoprene (both BASF) were purified in the usual manner and stored over calcium hydride. Butyl lithium supplied by Merck-Schuchardt as a 20% solution in hexane was used without further treatment. The concentration was determined by titration following the description of Gilman and Haubein<sup>7</sup>. *p*-Di-



*Figure 1* Sketch of a star block copolymer

vinylbenzene was separated from the Merck-Schuchardt commercial mixture by means of its tetrabromide as described by Naumann<sup>8</sup>. Purity was checked by n.m.r. and found to be about 98%. Before use, all solvents and monomers were distilled under high vacuum into flamed breakseal ampoules and sealed off.

#### Polymerization procedure

Linear living polystyrene was polymerized under high vacuum at room temperature using a mixture of 98% toluene and 2% THF at a monomer concentration of 5%.

In order to prepare star-shaped molecules according to method (1), the solution mixture of living polystyrene was cooled down to  $-78^{\circ}\text{C}$  and *p*-divinylbenzene was added. At this temperature the rate of polymerization can be neglected and the reactants are allowed to mix completely. The reaction vessel was then warmed up to room temperature and was left about 8 h for complete polymerization. An aliquot of this polymer solution was withdrawn under an inert gas atmosphere and terminated with methanol. For the preparation of star molecules according to method (3), styrene or isoprene was added to the remaining part and polymerized to complete conversion. All samples were precipitated in methanol and dried *in vacuo* at  $35^{\circ}\text{C}$ .

#### Physical measurements

**Viscosity.** All measurements were performed in toluene at  $20^{\circ}\text{C}$  with an Ostwald viscometer which was dimensioned such that the kinetic energy corrections were negligible. For the determination of the  $g'$  factors the intrinsic viscosity/molecular weight relationship of Meyerhoff<sup>9</sup> was used for linear polystyrene.

**Light scattering.** A Sofica photogoniometer (PDG 43 000) instrument was used. All measurements were performed with light of wavelength 436 and 546 nm using benzene at  $20^{\circ}\text{C}$  as solvent for the polystyrene stars and benzophenone at  $60^{\circ}\text{C}$  for the mixed polystyrene-polyisoprene stars. The molecular weights were calculated as usual from Zimm plots. The refractive index increments of polystyrene in benzene were taken from the literature<sup>10</sup>. The same values have been assumed for polydivinylbenzene. The refractive index increments of polystyrene and polyisoprene in benzophenone were found by extrapolation of a plot of  $dn/dc$  in various solvents against the refractive indices of the solvents  $n_D$  using data from the literature<sup>10</sup>. The following values were obtained:

$$\left. \begin{array}{l} \lambda_1 = 436 \text{ nm: } dn/dc = -0.0865 \\ \lambda_2 = 546 \text{ nm: } dn/dc = -0.0915 \end{array} \right\} \text{ polyisoprene}$$

$$\left. \begin{array}{l} \lambda_1 = 436 \text{ nm: } dn/dc = 0.0090 \\ \lambda_2 = 546 \text{ nm: } dn/dc = 0.0055 \end{array} \right\} \text{ polystyrene}$$

## RESULTS AND DISCUSSION

### Divinylbenzene polymerization initiated by short 'living polystyrene' chains

To prove the statement at the end of the introduction, living short chain polystyrene of 4 to 160 monomer units in length were prepared and subsequently copolymerized with DVB at almost constant overall concentration (5%). The stars were characterized by light scattering and viscosity measurements and the number of branches,  $p$ , and the molecular weight of the nuclei were calculated according to:

$$p = \frac{M_w(\text{star})}{M_w(\text{branch})} \times m(\text{styrene}) \quad (1)$$

$$M_w(\text{nucleus}) = M_w(\text{star}) \times m(\text{divinylbenzene}) \quad (2)$$

where  $M_w(\text{star})$ ,  $M_w(\text{branch})$  and  $M_w(\text{nucleus})$  are the weight average molecular weights of respectively the stars, the polystyrene branches and the polydivinylbenzene nuclei, and  $m(\text{styrene})$  and  $m(\text{divinylbenzene})$  are the mass fraction of styrene and divinylbenzene used.

Equations (1) and (2) follow from the three relationships:

$$p = \frac{\Sigma M_w(\text{branch})}{M_w(\text{branch})} \quad (1')$$

$$M_w(\text{star}) = \Sigma M_w(\text{branch}) + M_w(\text{nucleus}) \quad (2')$$

$$\frac{\Sigma M_w(\text{branch})}{M_w(\text{nucleus})} = \frac{m(\text{styrene})}{m(\text{divinylbenzene})} \quad (3')$$

where  $\Sigma M_w(\text{branch})$  is the sum of molecular weights of the  $p$  branches of one star molecule. It should be noticed that equations (1')–(3') are strictly valid only for the number averages, but for branches of homodisperse chain length these equations may be considered as useful approximations.

The molecular parameters of these stars are collected in Table 1. Curve A in Figure 2 shows the dependence of the number of branches,  $p$ , on the degree of polymerization of the initiator. For a better comparison the data obtained by Rempp *et al.*<sup>3</sup> are replotted in Figure 3. Figure 4 demonstrates the interdependence of the size of the nuclei and the number of branches. Line A in Figure 2 reveals two

Table 1 Experimental values for  $M_w(\text{star})$ ,  $M_w(\text{nucleus})$ ,  $DP(\text{nucleus})$  and  $p$  obtained by copolymerization of *p*-divinylbenzene with living polystyrene chains of different length,  $DP(\text{initiator})$ ;  $R = [\text{divinylbenzene}]/[\text{butyl lithium}]$

Sample	$DP(\text{initiator})$	$R$	$M_w(\text{star})$	$p$	$M_w(\text{nucleus})$	$DP(\text{nucleus})$
80	165	5	125 000	7	4 700	36
79	140	5	77 000	5	3 500	27
74	109	3	47 000	4	1 700	13
78	99	5	91 000	8	5 400	41
82	68	5	122 000	16	10 200	78
73	55	3	303 000	50	20 700	159
76	34	5	280 000	67	44 500	342
71	22	3	521 000	192	85 000	654
70	16	3	571 000	279	112 600	866
69	13	3	5 650 000	3 090	1 350 000	10 400
68	11	3	25 800 000	16 600	6 940 000	53 400
77	9	3	Gel	—	—	—
66	5	3	Gel	—	—	—

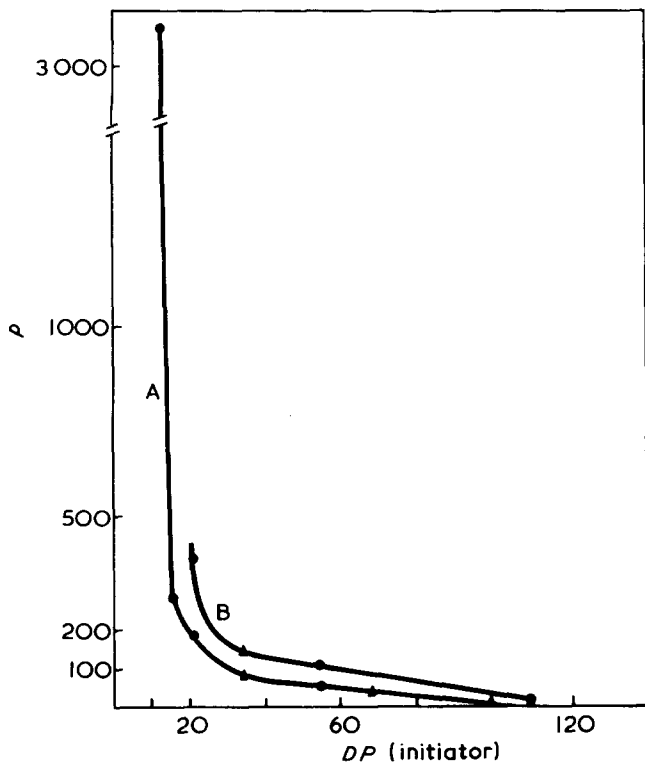


Figure 2 The number of side chains  $p$  as function of the chain length of initiator  $DP(\text{initiator})$ . ●, samples prepared at  $R = 3$ ; ▲, samples prepared at  $R = 5$ . A, stars prepared according to Rempp's method (1); B, stars prepared according to method (3) (see text)

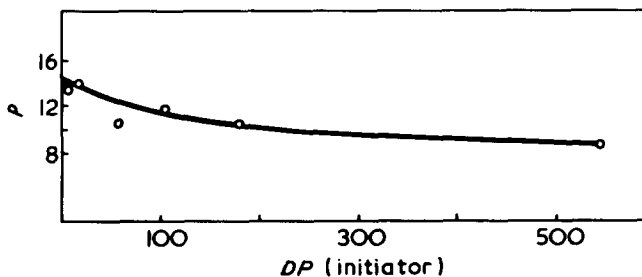


Figure 3 Plot as in Figure 2, but A obtained with data from Worsfold, Zilliox and Rempp<sup>3</sup>

striking features: (i) the two series of experiments with  $R_1 = 3$  and  $R_2 = 5$  yield within experimental error the same curve; (ii) the curve of Rempp *et al.* (Figure 3) was not correctly extrapolated to short chains, actually the number of branches increases sharply with decreasing chain length of the initiator, arriving at  $p \approx 16000$  for  $DP(\text{initiator}) = 10.8$ . The limit of divinylbenzene polymerization with butyl lithium was not accessible in this series of experiments, since under the applied conditions the critical branching is exceeded and gelation occurs. To verify this limit, one has to perform the same series of experiments at much lower concentration<sup>6,11-14</sup>.

These experiments demonstrate that, in the range of short chain initiation, the critical point of gelation depends on both, the concentration of divinylbenzene and on the chain length of the initiator. In the present case the critical chain length is found  $DP_{\text{initiator}}^{\text{crit.}} = 10$  from the plot of Figure 5.

The sharp decrease of the branch numbers per nucleus with increasing chain length resembles the familiar dependence of the grafting efficiency<sup>15</sup> for star and comb molecules, which in the case of four star molecules has been conclusively interpreted by Roovers and Bywater<sup>16</sup> to be due to a diffusion controlled polymer-polymer reaction.

Applying similar considerations, the correlation between polystyrene chain length and number of branches,  $p$ , can be interpreted as follows. The reaction may be conveniently separated into three steps. First, each living polystyrene initiates the polymerization of linear poly(*p*-divinylbenzene) chains with the degree of polymerization of the polydivinylbenzene block  $DP = R$  (see Figure 6). This is in agreement with studies of Black and Worsfold<sup>17</sup>. In the second step, the pendant double bonds will be crosslinked, where each crosslinking necessarily implies one polystyrene branch. However, with increasing polystyrene chains, crosslinking becomes more and more hindered because now the primary chains have to move through a shield of polystyrene branches before crosslinking can take place. Thus in the third step intramolecular ring formation is favoured resulting in particles with a limited number of branches. It is evident that crosslinking becomes also more hindered with increasing chain length in agreement with our experimental results\*.

Figure 4 demonstrates the reasonable finding that for a given  $R$  the branch number increases with the size of the nucleus. The shift of the  $M_w(\text{nucleus})$  versus  $p$  line to

\* These difficulties do not occur in method (2)<sup>6</sup>, where polydivinylbenzene particles are used as anionic initiators, because in this case neither the branch number nor the chain length hinder the propagation step.

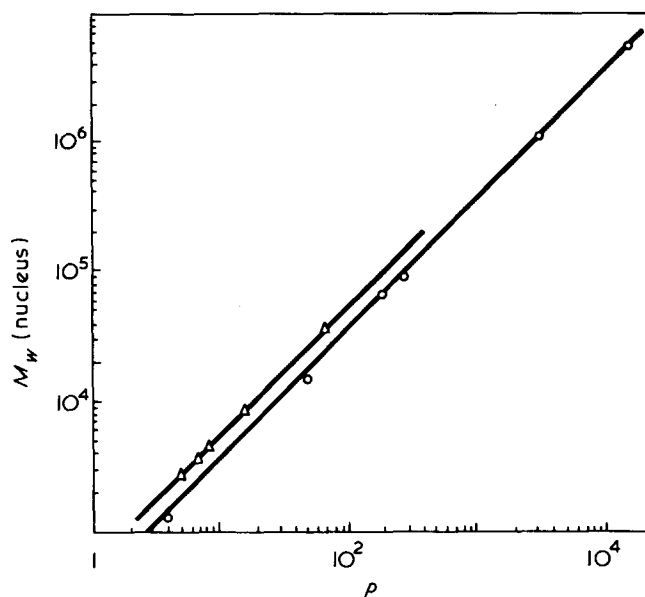


Figure 4 The size of nucleus  $M_w(\text{nucleus})$  as a function of the branch number  $p$ . △,  $R = 5$ ; ●,  $R = 3$

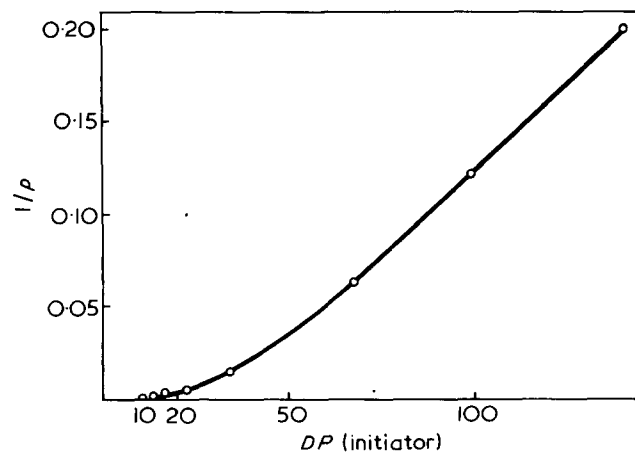
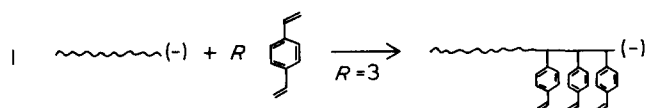
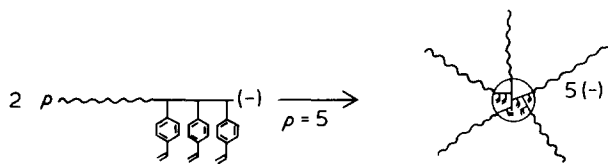


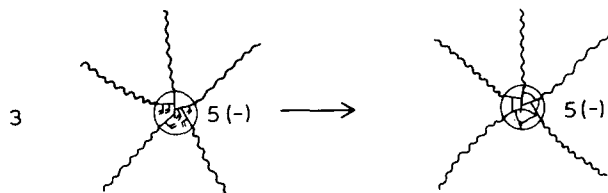
Figure 5 Plot of  $1/p$  versus  $DP(\text{initiator})$  for the determination of the critical chain length  $DP_{\text{initiator}}^{\text{crit.}}$



Formation of linear block copolymers



Crosslinking



Ring formation

**Figure 6** Scheme of the anionic block copolymerization of styrene and *p*-divinylbenzene

higher values of  $M_w$  (nucleus) reflects the simple relationship that with increasing  $R$  the polydivinylbenzene block in the primary chain (see *Figure 6*) is increased by the same factor  $R_2/R_1 = 5/3$ . Thus, *Figure 2* demonstrates that the number of branches is determined by the polystyrene chain length, while *Figure 4* shows that the size of the nuclei for a given  $p$  is controlled by the ratio  $R$ . This is of practical importance for the synthesis of star molecules of different nucleus size but the same number of branches. The control of the crosslinking reaction by the chain length can also be recognized from *Table 1*, because the size of the nuclei and the number of branches increase as the polystyrene chains become shorter. Therefore short polystyrene branches correspond to larger molecular weights of the nucleus and large number of branches,  $p$ .

#### Styrene polymerization initiated by star molecules with 'living' nuclei (method 3)

A star molecule with  $p$  branches, prepared by Rempp's method, bears  $p$  carbanionic groups inside the nucleus, if termination by impurities is excluded. Therefore, it should be possible to use these living nuclei of the star polymers as polyfunctional initiators for the anionic polymerization of styrene or other monomers, in the same manner as we have shown recently for pure polydivinylbenzene particles<sup>6</sup>. This would result in living star molecules and, in the ideal case, the number of branches should be doubled.

The conditions of polymerization were chosen such that the length of the newly polymerized polystyrene branches equal those of the already existing ones. Line B in *Figure 2* shows the results. The increase of the molecular weights agrees well with the values calculated theoretically, with the exception of the stars with very large nuclei, where higher molecular weights and eventually gelation are found. The satisfactory agreement does not necessarily mean that the number of branches is exactly doubled. It is conceivable that the number is smaller, and this would result in longer chains.

To test this, a further quantity defining the number of branches  $p$  is needed. According to theories on star mole-

cules<sup>18,19</sup> such a relationship is given by the  $g'$  factor:

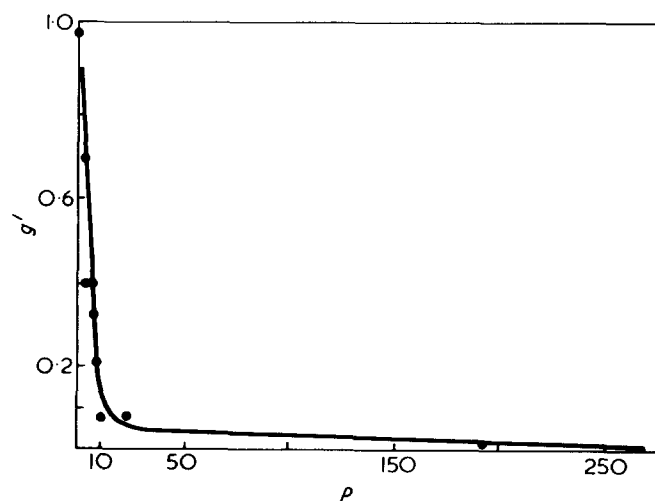
$$g' = [\eta]_{\text{branched}} / [\eta]_{\text{linear}}$$

where the viscosities of the linear and branched materials have to be taken for the same molecular weight. Strictly speaking, the linear and branched samples should also have the same molecular weight distributions. However, these conditions cannot be realized experimentally. Therefore we determined the  $g'$  factors experimentally for stars prepared according to methods (1) and (2)<sup>6</sup> (see *Figure 7*). With the aid of this relationship the number of branches of the stars prepared by method (3) can be estimated independently from their viscosities.

If  $p_1$  is the number of branches of the star prepared due to method (1), and  $p_2$  is the number of branches of the corresponding star prepared by method (3), then (i)  $p_2 = 2p_1$  indicates, that all living carbanionic groups of a star 1 have initiated propagation of chains, while if (ii)  $p_2 < 2p_1$  some of the living ends were wasted, and finally (iii) if  $p_2 > 2p_1$  several stars must have been tied together presumably by free double bonds. *Table 2* shows that  $p_2$  is very close to  $2p_1$ . The possibilities of preparation as described in this and the preceding section are schematically summarized in *Figure 8*.

We are aware that the experimentally determined  $g'$  versus  $p$  relationship cannot be directly compared with existing theories<sup>18,19</sup> mainly for two reasons. First, our samples have a certain molecular weight distribution and secondly, the stars have a more or less extended nucleus and consequently the  $g'$ (star) factor is determined by the number of rays of the star and the  $g'$ (nucleus) factor of the branched nucleus.

Nevertheless, it is instructive to compare the experimental relationship with the theoretical ones for homodisperse point centred stars. This is done in *Figure 9*.


**Figure 7** Plot of  $g'$  versus  $p$  for star molecules prepared according to methods (1) and (2)

**Table 2** Increase of the number of branches  $p$ .  $p_1$  = number of branches of the original star,  $p_2$  = number of branches of the final star

Sample	Star 1			Star 2	
	$g'$	$p_1$	$2p_1$	$g'$	$p_2$
74	0.69	4	8	0.33	$8 \pm 2$
73	0.09	50	100	0.05	$100 \pm 25$

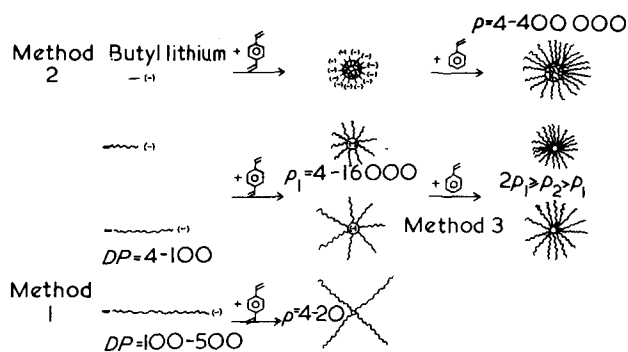


Figure 8 Principles of the anionic star polymerization demonstrated with the example of *p*-divinylbenzene/styrene

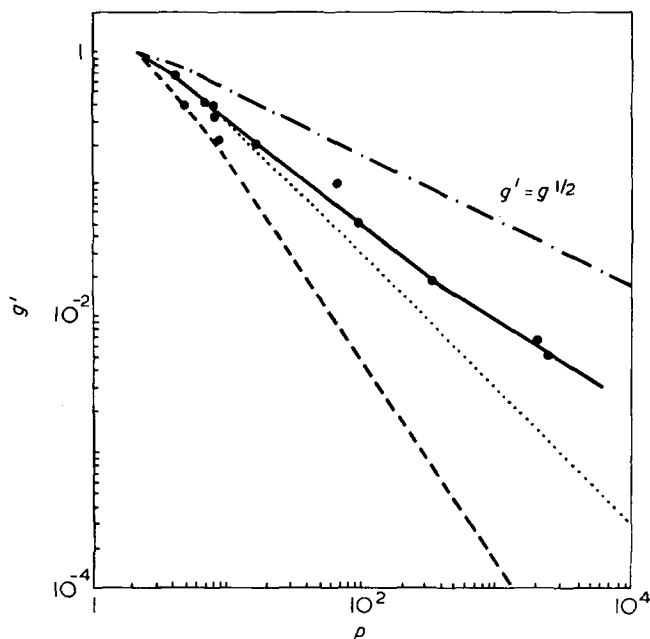


Figure 9 Double-logarithmic plots of  $g'$  versus  $p$ ; ●—, Experimental; - - - - - according to Zimm and Kilb<sup>18</sup>,  $g' = g^{1/2}$ ; ····,  $g = g$  (free draining case of ref 18); - · - · - according to Zimm and Stockmayer<sup>19</sup>,  $g' = g^{3/2}$ .  $g = \langle S^2 \rangle_Z(\text{star}) / \langle S^2 \rangle_Z(\text{linear}) = (3p - 2) / p^2$

Measurements of  $g'$  performed by Zilliox<sup>20</sup> in the range of  $4 \leq p \leq 20$  using method (1) are not shown in this plot. A similar dependence of  $g'$  on  $p$  was found but the values are about 20% larger than found by us. The deviations are probably caused by differences in size of the nuclei. Owing to the present state of knowledge on the viscosity of branched materials it appears to be unjustified to draw any conclusions from this comparison<sup>21</sup>.

#### Isoprene polymerization initiated by 'living' polystyrene star molecules

Instead of polymerizing styrene with 'living' polystyrene star molecules as was shown in the previous section, the living polystyrene stars can be used to initiate isoprene branches. This would result in a 'mixed' star bearing the same number of polystyrene and polyisoprene branches. Such stars are of interest not only because of some remarkable mechanical properties to be expected, but also for a check of light scattering theories on block copolymers<sup>22</sup>.

Polystyrene has a refractive index of  $n_D = 1.59-1.60$ <sup>23</sup> while polyisoprene has a lower one of  $n_D = 1.519$ <sup>24</sup>. Using benzophenone as solvent with  $n_D = 1.5975$  the polystyrene moieties will show no refractive index increment and will therefore scatter no light. Light scattering is caused in such

Table 3 Comparison of the experimental and calculated branch numbers after addition of isoprene to polystyrene stars with living nuclei

	Polystyrene star 76	Polystyrene-polyisoprene star 76
$M_w(\text{star})$	280 000	439 000
$M_w(\text{nucleus})$	44 500	44 500
$p_1$	67	67
$M_w$ of the isoprene branches:		
calc.	—	160 000
exp.	—	159 000
$p_2$	—	$67 + 67 = 134$

a case exclusively by the polyisoprene branches, and the molecular weight obtained is that of the sum of polyisoprene branches if the refractive index increments of polyisoprene are used. Table 3 shows for one example the satisfactory agreement between experimental molecular weight and the predicted one.

#### ACKNOWLEDGEMENTS

One of us (W.B.) is much indebted to Dr S. Bywater (Ottawa) for a very fruitful discussion during his visit at our laboratory in 1972. H.E. thanks the Studienstiftung des Deutschen Volkes for a grant, and we both acknowledge gratefully the technical assistance of Mr K.-H. Glorer.

#### REFERENCES

- 1 Szwarc, M., Levy, M. and Milkovich, R. *J. Am. Chem. Soc.* 1956, **78**, 2656
- 2 Zilliox, J. G., Decker, D. and Rempp, P. *Compt. Rend.* 1966, **262**, 726
- 3 Worsfold, D. J., Zilliox, J. G. and Rempp, P. *Can. J. Chem.* 1969, **47**, 3379
- 4 Rempp, P. *Polym. Prepr.* 1966, **7**, 141
- 5 Rempp, P. and Franta, E. *Pure Appl. Chem.* 1972, **30**, 229
- 6 Eschwey, H., Hallensleben, M. L. and Burchard, W. *Makromol. Chem.* 1973, **173**, 235
- 7 Gilman, H. and Haubein, A. H. *J. Am. Chem. Soc.* 1944, **66**, 1515
- 8 Naumann, G. *J. Prakt. Chem.* 1955, **1**, 277
- 9 Meyerhoff, G. and Cantow, M. *J. Polym. Sci.* 1959, **36**, 503
- 10 Brandrup, I. and Immergut, E. H. 'Polymer Handbook', Interscience, New York, 1966
- 11 Stockmayer, W. H. and Weil, L. L. 'Advancing Fronts in Chemistry', (Ed. S. B. Twiss), Reinhold, New York, 1945, Ch 6
- 12 Jacobson, H. and Stockmayer, W. H. *J. Chem. Phys.* 1950, **18**, 1600
- 13 Frisch, H. L. *Prepr. 128th Meet. ACS Polym. Div., Minneapolis* 1955
- 14 Kilb, R. W. *J. Phys. Chem.* 1958, **62**, 969
- 15 Minoura, Y., Hironaka, H., Kasabo, T. and Ueno, Y. *J. Polym. Sci. (A-1)* 1968, **6**, 2773
- 16 Roovers, J. E. L. and Bywater, S. *Macromolecules* 1972, **5**, 384
- 17 Black, P. E. and Worsfold, D. J. *J. Appl. Polym. Sci.* 1970, **14**, 1671
- 18 Zimm, B. H. and Kilb, R. W. *J. Polym. Sci.* 1959, **37**, 19
- 19 Zimm, B. H. and Stockmayer, W. H. *J. Chem. Phys.* 1949, **17**, 1301
- 20 Zilliox, J.-G. *Makromol. Chem.* 1972, **156**, 121
- 21 see Hoffmann, M. and Kuhn, R. *Makromol. Chem.* 1973, **174**, 149
- 22 Bushuk, W. and Benoit, H. *Can. J. Chem.* 1958, **36**, 1616
- 23 'Styrene, its Polymers, Copolymers and Derivatives' (Eds R. H. Boundy and R. F. Boyer), Reinhold, New York, 1952
- 24 Wood, L. A. and Tilton, L. W. *Proc. 2nd Rubber Technol. Conf. London* 1948, p 142; *J. Res. Nat. Bur. Stand.* 1949, **43**, 57, RP 2004

# Studies on the formation of poly(ethylene terephthalate): 3. Catalytic activity of metal compounds in transesterification of dimethyl terephthalate with ethylene glycol

Kosuke Tomita and Hiroaki Ida

Research and Development Center, Unitika Ltd, 23 Kozakura, Uji, Kyoto 611, Japan

(Received 4 July 1974)

The rate constant of transesterification of dimethyl terephthalate (DMT) with ethylene glycol (EG) in the presence of various metal compounds as catalysts at 197°C, calculated from the quantity of formed methanol, was used to evaluate each metal compound in its catalytic activity. First, in the case of highly basic metal salts the rate constants were found to be extremely large in the initial stage of the reaction. These values depended on the basicity of the metal salts, but decreased rapidly with the progress of the reaction, and reached values which were not appreciably dependent on the basicity. Secondly, in the case of metal salts of lower basicity such a phenomenon was not observed, and single rate constants were recognized throughout the reaction period. These rate constants were logarithmically correlated by a straight line (mountain-shaped) in a plot vs. stability constants ( $\log \beta_1$ ) of dibenzoyl methane (DBM) complexes of the corresponding metal species. Also in the case of highly basic metal salts, the rate constants in the latter stage followed the same straight line. Consequently, the stability constant of DBM complex of each metal species was found very useful as a forecast of catalytic activity of the metal compound. The compound of metal species with values of  $\log \beta_1$  ranging from 9 to 11 was most active as the catalyst.

## INTRODUCTION

Poly(ethylene terephthalate) (PET) is produced by polycondensation of bis(2-hydroxyethyl) terephthalate (BHET) or its oligomers, usually formed by transesterification of dimethyl terephthalate (DMT) with ethylene glycol (EG). This transesterification occurs with removal of formed methanol at a temperature of nearly 200°C under atmospheric pressure, and the presence of a catalyst is essential for the effective formation of BHET or its oligomers.

A knowledge of the catalyst in the transesterification of DMT with EG is important for the polyester-fibre industry, but at the present time little is known about the mode of catalytic activity.

In the present study transesterification of DMT with EG was carried out in the presence of various metal compounds as catalysts, and some rules governing the catalytic activity were found.

## EXPERIMENTAL

### Reagents

DMT was a commercial 'fibre grade' product, and was used without further purification. EG was also a commercial 'fibre grade' product, and was purified by distillation prior to use.

Most of the catalysts were metal acetates. Commercial products (guaranteed reagent grade) were used without further purification. Antimony(III) acetate was synthesized according to the method of Nerdel and Kleinwächter<sup>1</sup>, and aluminium acetate by the method of Pande and Mehrotra<sup>2</sup>.

### Transesterification

Transesterification was carried out at 197°C (DMT/EG = 0.5 mol/1.0 mol) as described in a previous paper<sup>3</sup>, and the progress of the reaction was followed by measuring the quantity of formed methanol.

## EVALUATION OF CATALYTIC ACTIVITY

Previously, Griehl<sup>4</sup> and Sumoto<sup>5</sup> investigated transesterification of DMT with EG, and compared the activities of some catalysts from a plot of quantities of formed methanol vs. reaction time. These are, however, too simple as a means of evaluation, and are insufficient to correlate catalytic activity with reaction mechanism.

Catalytic activity must be evaluated from the rate constant but the only study made from such a standpoint is that by Yoda *et al.*<sup>6</sup>. However, this paper is also insufficient in that the rate equation was too simplified, a treatment of highly basic metal salts was left out of consideration, and the study of low active catalysts was insufficient (their rate constants were regarded as zero).

The authors calculated the rate constants according to the kinetic treatment proposed in a previous paper<sup>3</sup>, and in the case of low active catalysts the reaction could be followed by using the apparatus described in ref 3, and in the case of extremely low active catalysts rate constants could be calculated according to the relationships given earlier<sup>3</sup>.



RESULTS AND DISCUSSION

Figure 1 shows the variation of the reaction with various metal acetates as catalysts ( $1 \times 10^{-4}$  mol/mol DMT).

It is noteworthy that highly basic acetates, e.g., alkali metal acetate, give a different curve from others. This problem is discussed first, and a comprehensive view including other acetates is given later.

Catalytic activity of highly basic metal salt

According to ref 3 the rate equation is:

$$k_a t = \frac{V_{100}}{V_0} \left\{ \frac{V_{100} y}{100 - y} + (V_0 - V_{100}) \log \frac{100}{100 - y} \right\} \quad (1)$$

where  $k_a$  is an apparent rate constant which depends on the catalyst concentration,  $y$  is the degree of conversion (%),  $V$  is a volume of the reaction mixture and the subscripts 0 and 100 are used to denote  $y$ , 0% and 100%, respectively. By application of equation (1) to sodium or calcium acetate catalyst (Figure 1), and plotting the  $Y$  values (the right hand term of equation 1) thus obtained against time, Figure 2 results. The slopes of these rate plots correspond to  $k_a$ . In ref 3, the rate plots for zinc acetate and manganese acetate gave straight lines over a wide conversion range, i.e., single rate constants were recognized throughout the reaction. In Figure 2, however, the rate constants are found to be extremely large in the initial stage, and then rapidly decrease with the progress of the reaction.

The catalytic activity of highly basic metal salt was further investigated by replacing the anionic species of sodium salt ( $1 \times 10^{-3}$  mol/mol DMT). Figures 3 and 4 show the results.

Figure 4 indicates that as the basicity of anionic species decreases the shape of a curve approaches a single straight

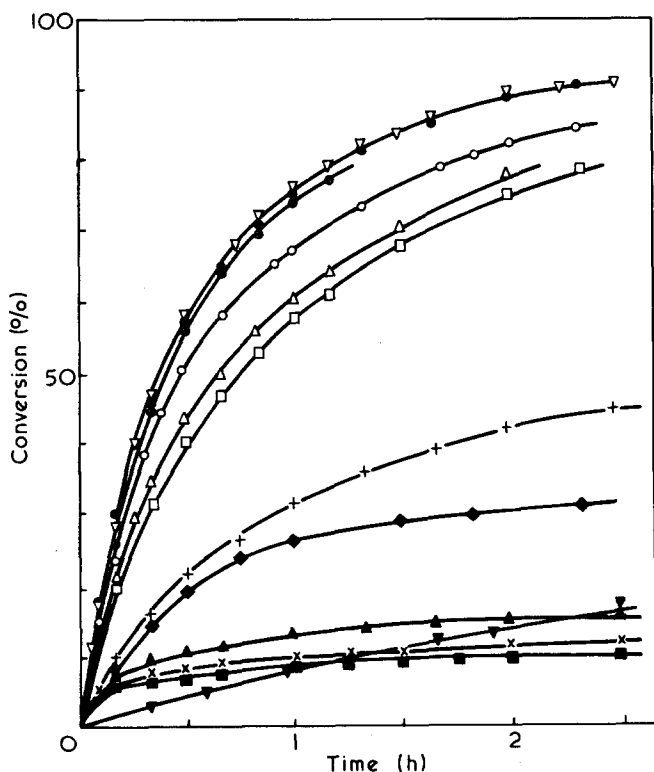


Figure 1 Time-conversion curves of the transesterification of DMT by EG with various metal acetates as catalysts: ●, Zn; ▽, Pb; ⊕, Ce; ○, Mn; △, Co; □, Cd; +, Mg; ◆, Ca; ▲, Li; X, Na; ■, K; ▼, Sn

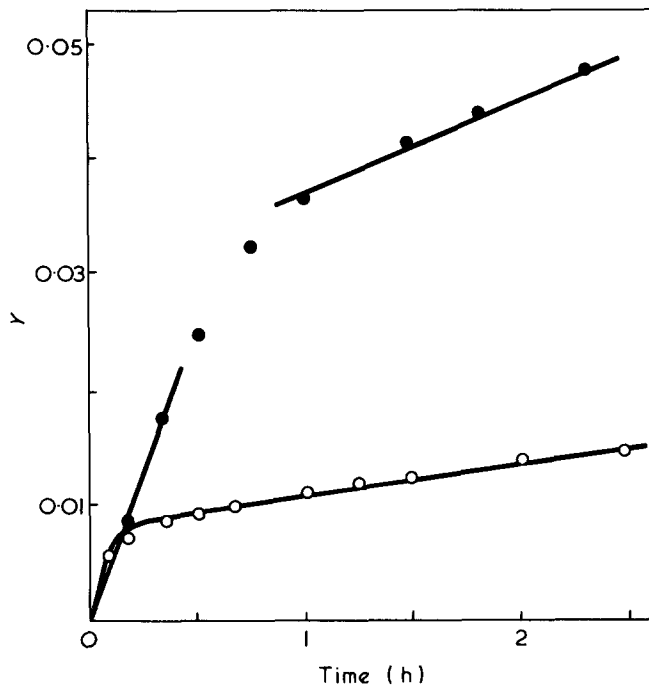


Figure 2 Application of equation (1) to data for sodium acetate and calcium acetate in Figure 1: ○, Na; ●, Ca

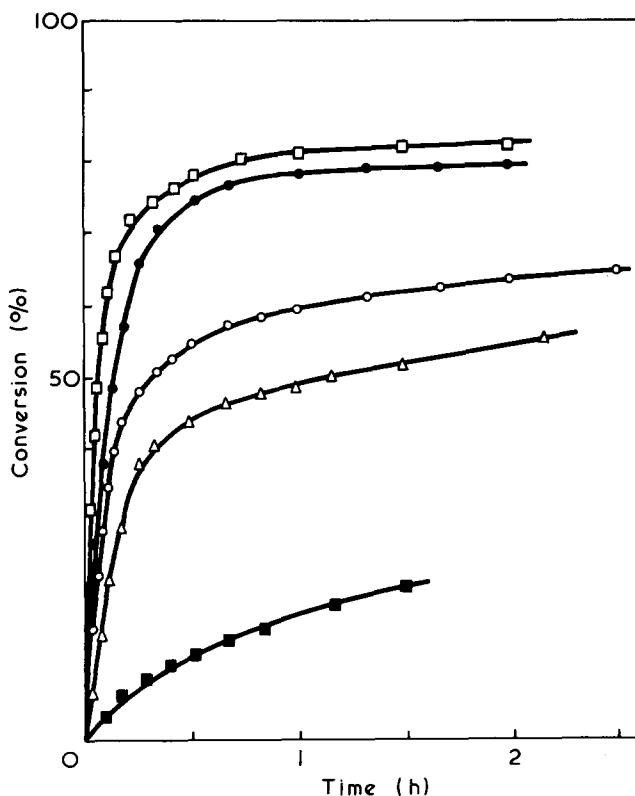


Figure 3 Time-conversion curves of the transesterification of DMT by EG with some sodium compounds as catalysts: □, ethylene glycolate; ●, phenoxide; ○, acetate; △, benzoate; ■, chloride

line, and that after the initial stage the slopes of these rate plots are not appreciably dependent on the anionic species, i.e. the anionic species has an effect mainly on the slopes in the initial stage.

The rate constant in the initial stage and its relationship to the basicity of anionic species are shown in Figure 5. In this figure  $k_{basic}$  is the rate constant in the initial stage and does not depend on the catalyst concentration:  $k_{basic}$  was calculated from  $k_a$  in the initial stage. As shown in Table 1,

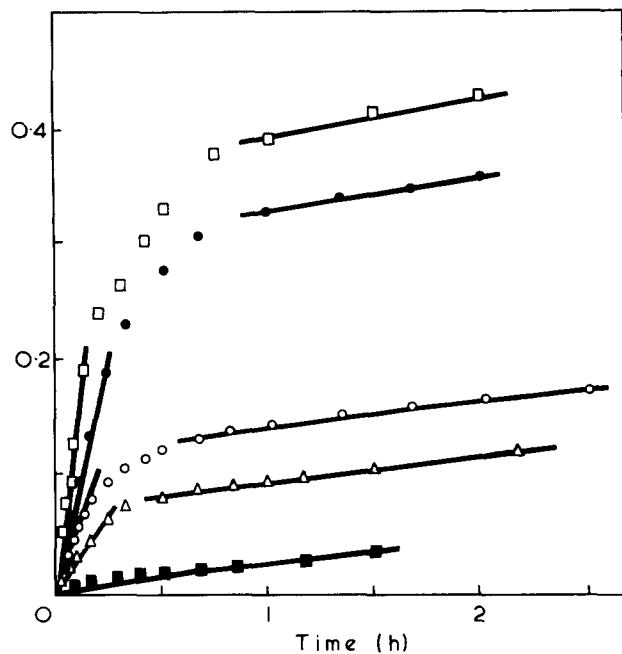


Figure 4 Application of equation (1) to data in Figure 3

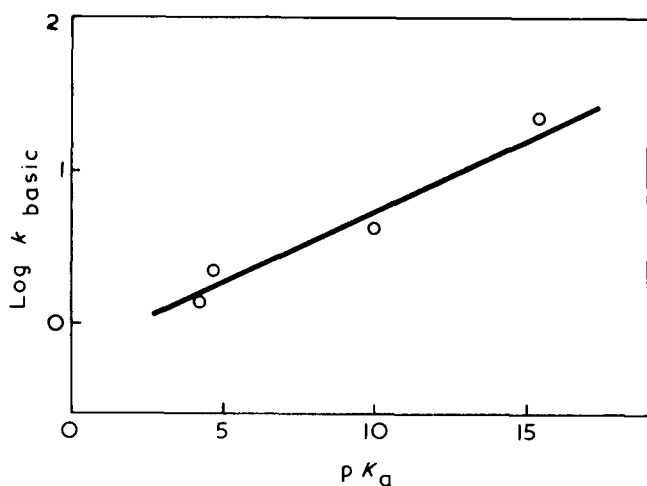


Figure 5 Rate constants in the transesterification of DMT by EG with some sodium compounds against the basicity of the corresponding anionic species

the  $pK_a$  value for the conjugate acid of anionic species is used as the value of basicity of anionic species.

Figure 5 shows that according to an increase in basicity of anionic species the rate constant increases, and that a linear relationship exists between  $\log k_{\text{basic}}$  and  $pK_a$ . This result suggests that the catalytic species of the sodium salt in the initial stage of the reaction is the base.

The degree of breaking of the linear relationship in the rate plot (Figure 4) becomes progressively greater according to the increase in the basicity of anionic species, and becomes negligible with the decrease in the basicity.

This phenomenon may be attributed to the decrease in basicity of highly basic salt with the progress of transesterification. In transesterification of DMT with EG, carboxyl groups will be formed as a result of a side reaction, which may cause the above decrease in the basicity.

On the other hand, after the initial stage of the reaction, the slopes of rate plots are not appreciably dependent on the kind of sodium compounds. Consequently these slopes are considered to show the inherent catalytic activity of sodium compounds. Thus, there are two catalytic species

in a sodium compound: anionic species and another species persisting after the disappearance of basicity.

With regard to the latter, sodium acetate was compared with calcium acetate. Basicity of sodium acetate is evidently higher than that of calcium acetate. This fact corresponds to the relationship between two slopes of their rate plots in the initial stage (see Figure 2). After the initial stage, however, it is seen in Figure 2 that the slope of the rate plot is greater in the later stages contrary to expectation based on basicity. This result suggests that catalytic activity after the initial stage does not depend on basicity but on something of the reverse characteristic, i.e. acidity.

#### Catalytic activity of other metal salts

Figure 1 suggests that each of the metal salts except for the highly basic metal salts do not show the above tendency. In order to clarify this suggestion, equation (1) was applied to these data as shown in Figure 6. Each catalyst gives a linear plot over a wide conversion range, i.e. the rate constant remains constant throughout the reaction period.

Table 1 Basicity of some sodium compounds

Sodium compounds	$pK_a$ values for conjugate acids of anionic species	Ref
ethylene glycoxide	15.4	7
phenoxide	10.0	8
acetate	4.76	8
benzoate	4.20	8

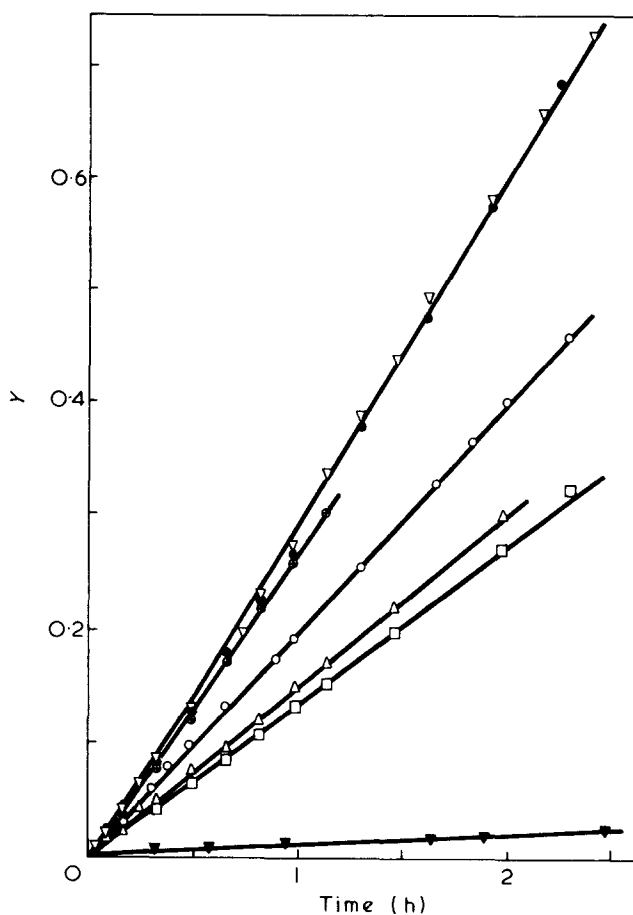


Figure 6 Application of equation (1) to data in Figure 1, except for highly basic metal acetates

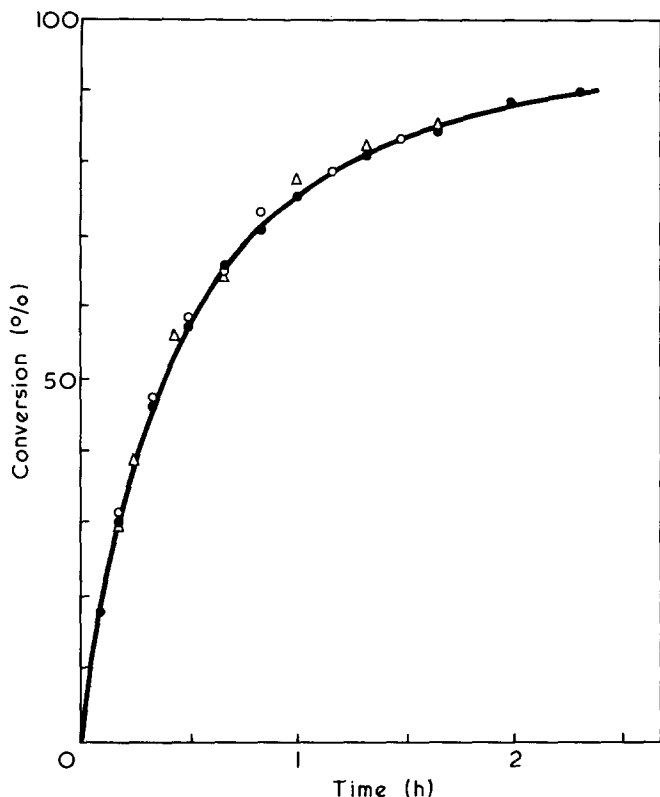


Figure 7 Time-conversion curves of the transesterification of DMT by EG with some zinc compounds as catalysts: ○, phenoxide; ●, acetate; △, benzoate

These metal salts are nearly neutral and therefore, the inactivation of anionic species, as described in the preceding section, may be almost negligible.

In the case of the sodium salt, catalytic activity varies extensively with the kind of anionic species. On the other hand, in the case of the zinc salt ( $1 \times 10^{-4}$  mol/mol DMT) Figure 7 shows that the variation of the anionic species from acetate to phenoxide or benzoate did not influence catalytic activity. The application of equation (1) to these data (Figure 8) shows that a linear relationship exists over a wide conversion range with a slope almost independent of the anionic species.

Consequently, the catalytic activity of low basic metal salt seems to be slightly dependent on the anionic species\*. Furthermore, these metal salts give single rate constants throughout the reaction period and these values are often higher than those for highly basic metal salts.

From the above point of view, the catalytic species is clearly not basic such as the anionic species, but must be acidic such as the cationic species, i.e., the metal species.

#### Ordering of catalytic activity

As described above, catalytic activity of a highly basic metal salt is determined by its basicity at least in the initial stage of the reaction, but that of a metal salt discussed in the preceding section is not determined by its basicity. We now discuss the ordering of catalytic activity in the latter.

The only previous related investigation in transesterification of DMT with EG, is ref 6, where electronegativity of each metal species was proposed as the ordering factor of catalytic activity of the metal compound. This proposal is

\* There are some exceptional cases, e.g., phosphate, etc., which will be discussed in a later paper.

reasonable to a certain degree, but is not entirely satisfactory for the following reasons.

First, catalytic activity changes variously with a reactant, but electronegativity presents only a uniform value regardless of the reactant. Secondly, electronegativity does not accurately follow the change of valency of metal species.

As for the latter, some electronegativities corrected for valency have been proposed<sup>9</sup>, but they are also insufficient.

Table 2 shows the rate constants (which do not depend on the catalyst concentration, calculated from  $k_a$ ) in transesterification of DMT with EG in the presence of various metal acetates as catalysts. These rate constants were logarithmically plotted against electronegativities proposed by Gordy *et al.*<sup>9</sup>, as shown in Figure 9 (the authors consider that the rate constant must be plotted logarithmically, while such a consideration was also overlooked in ref 6). Figure 9 shows wide scatter and this result suggests that it is not cor-

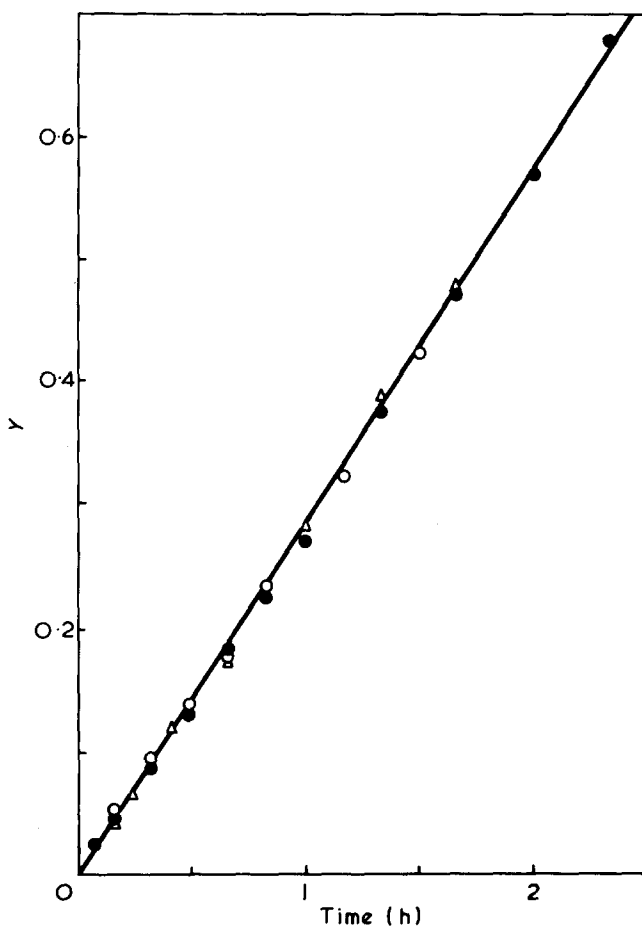


Figure 8 Application of equation (1) to data in Figure 7

Table 2 Rate constants ( $k$ ) in the transesterification of DMT by EG with various metal acetates as catalysts

Metal species	$k$ ( $l^2 \text{ mol}^{-2} \text{ min}^{-1}$ )	Metal species	$k$ ( $l^2 \text{ mol}^{-2} \text{ min}^{-1}$ )
Zn <sup>2+</sup>	$1.45 \times 10$	Sn <sup>2+</sup>	$5.14 \times 10^{-1}$
Pb <sup>2+</sup>	$1.45 \times 10$	Ba <sup>2+</sup>	$3.02 \times 10^{-1}$
Ce <sup>3+</sup>	$1.35 \times 10$	Li <sup>+</sup>	$1.95 \times 10^{-1}$
Mn <sup>2+</sup>	$1.15 \times 10$	Na <sup>+</sup>	$1.34 \times 10^{-1}$
Co <sup>2+</sup>	6.78	Sb <sup>3+</sup>	$8.14 \times 10^{-2}$
Cd <sup>2+</sup>	6.32	Al <sup>3+</sup>	$5.02 \times 10^{-2}$
Mg <sup>2+</sup>	4.18	K <sup>+</sup>	$4.92 \times 10^{-2}$
Ca <sup>2+</sup>	$7.96 \times 10^{-1}$		

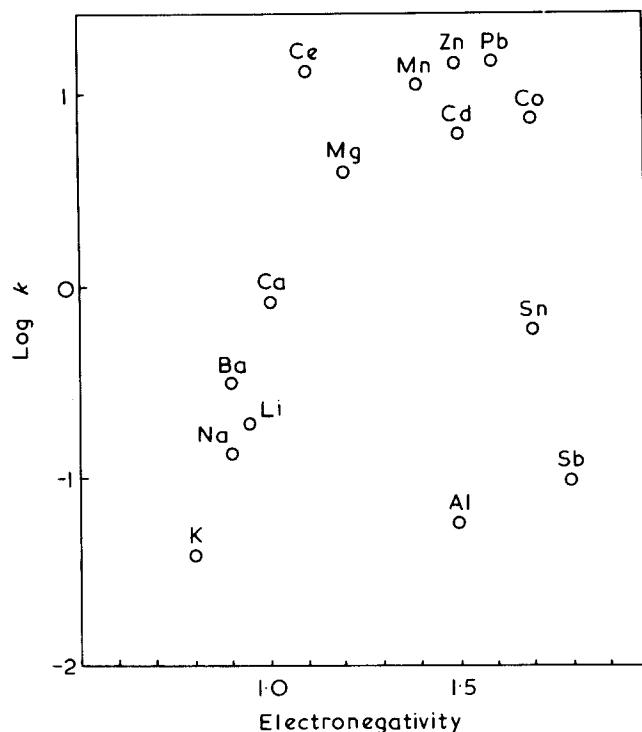


Figure 9 Rate constants in the transesterification of DMT by EG with various metal acetates as catalysts against electronegativities of the corresponding metal species

rect to apply such a common value as electronegativity to this particular catalytic reaction.

As mentioned above, catalytic activity of these metal salts is considered to depend on its acidity, except for highly basic metal salt in the initial stage of the reaction. Transesterification may proceed by the nucleophilic attack of hydroxyl groups in EG upon ester carbonyl groups in DMT. Consequently, it may be natural to present the following hypothesis. The reaction intermediate is regarded as a complex formed by coordination of the ester carbonyl group to the metal species. This coordination lowers the electron density of carbonyl carbon atom and facilitates the nucleophilic attack of the hydroxyl group upon this positively polarized carbon atom.

Thus, the authors considered adopting the degree of facility of coordination of ester carbonyl groups in DMT to metal species as the ordering factor of catalytic activity of metal salt, e.g., concerning the mixture of DMT and each metal salt, the extent of the frequency shift in the infra-red absorption spectra due to coordination of the carbonyl groups to the metal species. However, it is difficult to estimate exactly the extent of such shifts, since many of the metal salts used in this study are relatively weak Lewis acids. Hence the authors paid attention to a compound that has similar structure to DMT and that can be quantitatively estimated in its facility of coordination to metal species, i.e., dibenzoyl methane (DBM).

DBM has carbonyl groups directly connected to benzene rings although it has no ester groups, and these carbonyl groups form a coordination compound with a metal species.

As to the complexing ability of DBM it is convenient to use a stability constant, and those of DBM complexes ( $\log \beta_1$ ) are shown in Table 3 with respect to the metal species used in this study. These values were determined by Van Uiter *et al.*<sup>10</sup> except for  $\text{Sn}^{2+}$  and  $\text{Sb}^{3+}$ . The values for  $\text{Sn}^{2+}$  and  $\text{Sb}^{3+}$  were calculated from the values of the extent of the shift in the frequency of the carbonyl stretch-

ing vibration in the infra-red absorption spectra of xanthone complexes of both metal species ( $\Delta\nu_{\text{C=O}}$ ), since an approximately linear relationship exists between  $\log \beta_1$  of DBM complexes and  $\Delta\nu_{\text{C=O}}$  of xanthone complexes<sup>11</sup>.

The rate constants in Table 2 are plotted as  $\log k$  against  $\log \beta_1$  in Figure 10 and it is easily concluded that the linear relationship is clearly superior to that in Figure 9. Even the rate constants which were regarded as exceptions or wide scatter in Figure 9 fit the linear relationship in Figure 10.

Consequently, it is concluded that the stability constant of the DBM complex is an excellent ordering factor and is very useful as a forecast of the catalytic activity of the metal salt in the transesterification of DMT with EG; further this result is consistent with the hypothesis proposed above in connection with the mechanism of catalytic action.

In addition, this ordering factor has a mechanistic significance because of being the stability constant of the DBM

Table 3 Stability constants ( $\log \beta_1$ ) of DBM complexes of various metal species

Metal species	$\log \beta_1$
$\text{K}^+$	3.67
$\text{Na}^+$	5.14
$\text{Li}^+$	5.95
$\text{Ba}^{2+}$	6.10
$\text{Ca}^{2+}$	7.17
$\text{Mg}^{2+}$	8.54
$\text{Cd}^{2+}$	8.67
$\text{Mn}^{2+}$	9.32
$\text{Pb}^{2+}$	9.75
$\text{Zn}^{2+}$	10.23
$\text{Co}^{2+}$	10.35
$\text{Ce}^{3+}$	10.99
$\text{Sn}^{2+}$	13.1
$\text{Sb}^{3+}$	13.6
$\text{Al}^{3+}$	15.0

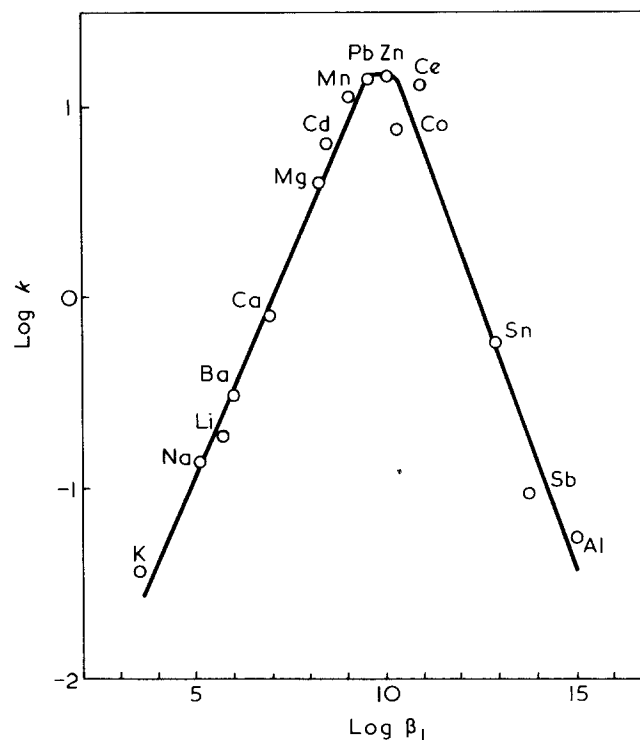


Figure 10 Rate constants in the transesterification of DMT by EG with various metal acetates as catalysts against stability constants ( $\log \beta_1$ ) of DBM complexes of the corresponding metal species

complex. The above clear result is not obtained with a stability constant of a common complex not related to the above hypothesis, e.g. a stability constant of metal acetylacetonate.

The straight line in *Figure 10* is mountain-shaped, and its peak appears in the  $\log \beta_1$  9 to 11 region. Thus the compound made of metal ion species ranging in  $\log \beta_1$  from 9 to 11 is most active as the catalyst in transesterification of DMT with EG. This relationship suggests catalytic effect of so-called 'volcano-shaped activity order'<sup>12</sup>.

#### ACKNOWLEDGEMENT

The authors wish to thank Professor Seizo Okamura (Kyoto University) for his interest in this work and his helpful criticism of the manuscript.

#### REFERENCES

- 1 Nerdel, F. and Kleinwächter, J. *Chem. Ber.* 1957, **90**, 600
- 2 Pande, K. C. and Mehrotra, R. C. *Z. Anorg. Allg. Chem.* 1956, **286**, 291
- 3 Tomita, K. and Ida, H. *Polymer* 1973, **14**, 55
- 4 Griebel, W. and Schnock, G. *Faserforsch. Textiltech.* 1957, **8**, 408; *J. Polym. Sci.* 1958, **30**, 413
- 5 Sumoto, M. and Kifuji, A. *Rep. Osaka Ind. Res. Inst.* 1961, **12**, 214
- 6 Yoda, K., Kimoto, K. and Toda, T. *Kogyo Kagaku Zasshi (J. Chem. Soc. Japan, Ind. Chem. Sect.)* 1964, **67**, 909
- 7 Ballinger, P. and Long, F. A. *J. Am. Chem. Soc.* 1960, **82**, 795
- 8 Kotake, M. 'Constants of Organic Compounds', Asakura, Tokyo, 1963, pp 614, 637
- 9 Gordy, W. and Thomas, W. J. D. *J. Chem. Phys.* 1956, **24**, 436
- 10 Van Uitert, L. G. *et al. J. Am. Chem. Soc.* 1953, **75**, 2736, 2739, 3862; Atomic Energy Commission Document, NYO-3372 (March 5, 1952)
- 11 Tomita, K. in preparation
- 12 Balandin, A. A. *Adv. Catalysis*, 1958, **10**, 120; 1969, **19**, 1

# Effect of molecular weight on spherulite growth rates of high molecular weight poly(ethylene oxide) fractions

J. Q. G. Maclaine and C. Booth

Department of Chemistry, University of Manchester, Manchester M13 9PL, UK

(Received 8 July 1974)

Spherulite growth rates have been determined for a set of poly(ethylene oxide) fractions ranging in molecular weight from  $10^4$  to  $10^6$ . At a given crystallization temperature the spherulite growth rate as a function of molecular weight passes through a maximum. At a given undercooling (as assessed by the method of Mandelkern) the spherulite growth rate is a monotonically decreasing function of molecular weight, and in the range  $6000 < \bar{M}_v < 50\,000$  varies roughly as  $(\bar{M}_v)^{-3}$ . The free energy of formation of the end interface (as assessed by nucleation theory) also decreases as molecular weight increases.

## INTRODUCTION

Many features of the crystallization of polymer fractions are affected by their molecular weight, as are many properties of the crystallized polymers. In this paper we report measurements of the spherulite growth rates of poly(ethylene oxide) fractions of moderate and high molecular weight. We are not directly concerned with low molecular weight fractions which crystallize predominantly in extended-chain form<sup>1-3</sup>. Adequate investigations of low molecular weight poly(ethylene oxide) fractions already exist<sup>3-6</sup>.

## EXPERIMENTAL

We have studied spherulite growth by optical microscopy for a set of well characterized fractions of poly(ethylene oxide) covering the molecular weight range  $10^4$  to  $10^6$  (g/mol).

### Preparation of fractions

Poly(ethylene oxide) samples with narrow molecular weight distributions were obtained from Hoechst Chemicals Limited (prefix H in Table 1) or were prepared, via KOH catalysis with HOCH<sub>2</sub>CH<sub>2</sub>OH initiator, in a stirred pressure reactor (prefix R in Table 1). These samples were purified by dissolving in benzene, filtering, and then precipitating by adding iso-octane. High molecular weight fractions were obtained from samples supplied by Union Carbide Limited, either Polyox WSR-35 (prefix W in Table 1) or Polyox N-750 (prefix N in Table 1), which were fractionated by the addition of iso-octane to a dilute solution in benzene<sup>7</sup>. Polyox samples contain insoluble alkaline earth salts (catalyst residues) which were removed with the first fraction and discarded. Generally the fractions used in the crystallization measurements were obtained by refractionation of original successive fractions.

### Characterization of fractions

The fractions were characterized by dilute solution viscometry and gel permeation chromatography (g.p.c.). Intrinsic viscosities were determined for benzene solutions at

Table 1 Characteristics of poly(ethylene oxide) fractions

Fraction	$[\eta]$ (benzene at 25°C) (cm <sup>3</sup> /g)	$\bar{M}_v$	$\bar{M}_w/\bar{M}_n$ (g.p.c.)	$\bar{x}_n$
H11000	23	11 000	1.20	210
H23000	37	23 000	1.20	440
R42000	59	42 000	1.30	730
W72000	85	72 000	1.21	1300
W84000	95	84 000	1.24	1500
W95000	103	95 000	1.19	1800
N130000	125	126 000	1.35	2200
W190000	168	193 000	1.32	3300
W240000	194	244 000	1.22	4500
W540000	339	538 000	1.53	8000
W740000	421	738 000	2.00	8400
W950000	497	945 000	1.85	12 000

25°C. Modified Desreux-Bischoff<sup>8</sup> or modified Ubbelohde (Fica Model 52 000) viscometers were used. A Kinetic energy correction (+4% of determined intrinsic viscosity) was applied to the results obtained with the Ubbelohde viscometer. Shear corrections were negligible. Viscosity-average molecular weights were calculated using the relation<sup>9</sup>:

$$[\eta] = 0.0397\bar{M}_v^{0.686}$$

Conditions for g.p.c. were: Waters Associates Model 200 GPC; 4 x 4 ft (1.22 m) Styragel columns with nominal pore sizes in the range 10 to 5 x 10<sup>5</sup> nm; *N,N*-dimethylacetamide at 80°C and a flow rate of 1 cm<sup>3</sup>/min; 2 cm<sup>3</sup> solution of concentration near 5 g/dm<sup>3</sup> injected. Correction for peak broadening was by the method of Aldhouse and Stanford<sup>10</sup>: the standard deviation,  $\sigma$ , resulting from adventitious dispersions was estimated by the method of Tung and Runyon<sup>11</sup> to be:

$$\sigma = 6.72 - 0.026v$$

where  $v$  is the elution volume in cm<sup>3</sup>. Calibration was by fractions of poly(ethylene oxide) over the molecular weight range  $10^3$  to  $2 \times 10^6$ . The characterization data are given

in Table 1. Fractions are denoted by a prefix (source) and a number (viscosity-average molecular weight). Approximate number-average chain lengths ( $\bar{x}_n$ , chain units), calculated from the molecular weights and molecular weight ratios, are also listed in Table 1.

Spherulite growth rate

Spherulite growth rates were measured on the hot stage<sup>12</sup> of a polarizing microscope. The hot stage could be held at a steady temperature, to  $\pm 0.02\text{K}$ , by a proportional controller. Calibration was by 9 melting point standards (checked against standardized thermometers) in the range 35–69°C. Polymer films (0.3–0.5 mm thick) were heated to 100°C for 5 min and then transferred to the stage held at the crystallization temperature. Spherulite sizes were measured by reference to an eyepiece scale, either directly or via photographs. The eyepiece was calibrated against a stage micrometer. As a precaution against oxidative degradation a new polymer sample was used for each crystallization. Characterization of certain fractions (W72000, W95000) by g.p.c. after crystallization indicated no degradation, nor did spherulite growth rates of twice-used samples differ from normal.

RESULTS

We made the following observations with the polarizing microscope: (i) spherulites were initiated sporadically with time over the initial part of the crystallization (as noted by Hay *et al.*<sup>13</sup>). Impinged spherulites eventually filled the field of view; (ii) the spherulite number density,  $\nu$ , varied from fraction to fraction. Generally  $\nu$  increased as  $\bar{M}_v$  increased. For a given fraction  $\nu$  was reduced by prolonged heating at high temperatures<sup>13</sup>; (iii) the spherulites had a close-textured appearance which did not differ from fraction to fraction; (iv) spherulite radii increased linearly with time up to the point of impingement. Variation of melting temperature (between 80 and 120°C) and melting time (between 2 and 60 min) did not change the spherulite growth rate.

Spherulite radial growth rates ( $G_s$ ) are listed in Table 2. Values are reproducible to about  $\pm 10\%$ . In Figure 1 we present a double logarithmic plot of  $G_s$  against  $\bar{M}_v$  for selected temperatures. For one crystallization temperature ( $T_c = 53.4^\circ\text{C}$ ) the curve is extended to  $\bar{M}_v = 6000$  by use of data published previously<sup>5</sup>. Plotted in this way the results show broad maxima in spherulite growth rate versus molecular weight at constant crystallization temperature. The maxima

are more pronounced at the higher values of  $T_c$ . The molecular weights at the maxima are  $10^5$  or greater, being higher at the higher values of  $T_c$ . This variation with  $\bar{M}_v$  of  $G_s$  is very similar to the variation with  $\bar{M}_v$  of the bulk (dilatometric) crystallization rates of polyethylene fractions of moderate and high molecular weight<sup>14</sup>.

DISCUSSION

Spherulite growth rate/molecular weight isotherms

The interesting feature of our results is the maximum in the spherulite growth rate,  $G_s$ , measured at constant crystallization temperature,  $T_c$ , when plotted against molecular weight,  $\bar{M}_v$ ; and particularly the increase in  $G_s$  with  $\bar{M}_v$  in the low molecular weight range ( $\bar{M}_v < 10^5$ ). This behaviour at low molecular weights is well established for poly(ethylene oxide) fractions crystallized at temperatures near to the melting point<sup>3–6</sup>. Spherulite growth rates measured<sup>15</sup> for polyethylene fractions ( $\bar{M}_v$  from 3900 to 87 000) also increase with increasing molecular weight when compared at constant  $T_c$ .

By contrast spherulite growth rates measured at con-

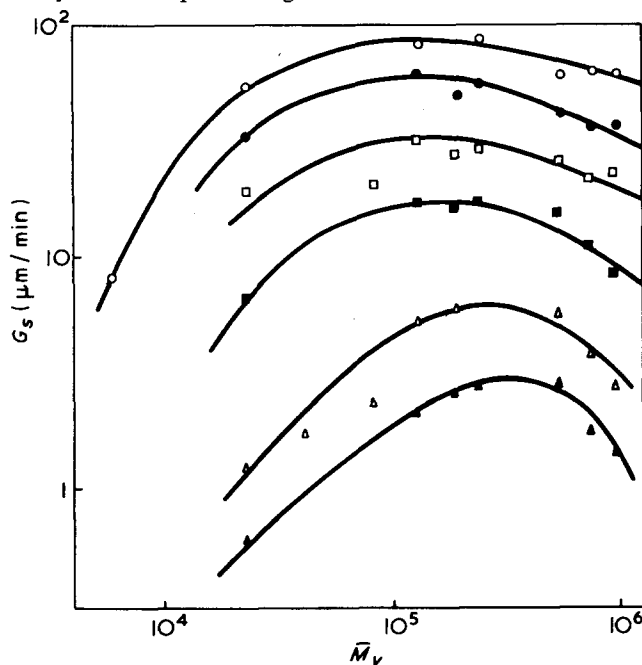


Figure 1 Double logarithmic plot of spherulite growth rate,  $G_s$ , against viscosity-average molecular weight,  $\bar{M}_v$  for poly(ethylene oxide) fractions. Crystallization temperatures ( $^\circ\text{C}$ ):  $\circ$ , 53.4;  $\bullet$ , 54.5;  $\square$ , 55.7;  $\blacksquare$ , 56.9;  $\triangle$ , 58.2;  $\blacktriangle$ , 59.1

Table 2 Spherulite growth rates ( $G_s$ ,  $\mu\text{m}/\text{min}$ ) at crystallization temperature ( $T_c$ ) for poly(ethylene oxide) fractions

Fraction	$T_c$ ( $^\circ\text{C}$ )													
	53.1	53.4	54.0	54.5	55.1	55.7	56.3	56.9	57.6	58.2	58.5	59.1	59.5	
H11000	45	—	21	—	5.2	—	2.0	—	0.39	—	—	—	—	
H23000	82	55	40	33	25	19	11	6.5	3.0	1.2	0.82	0.59	0.34	
R42000	84	—	45	—	25	—	11	—	4.6	1.7	1.6	—	0.41	
W72000	81	—	52	—	33	—	11	—	5.0	—	1.4	—	0.47	
W84000	—	—	—	—	—	20	—	—	—	2.3	—	—	—	
W95000	83	—	66	—	40	—	20	—	6.3	—	2.3	—	0.47	
N130000	—	81	—	62	—	32	—	17	—	5.2	—	2.1	—	
W190000	91	—	60	49	42	28	23	16	9.5	5.9	3.1	2.6	0.69	
W240000	—	86	—	56	—	29	—	17	—	—	—	2.7	—	
W540000	—	60	—	41	—	26	—	15	—	5.7	—	2.8	—	
W740000	—	63	—	36	—	22	—	11	—	3.8	—	1.7	—	
W950000	—	62	—	37	—	23	—	8.1	—	2.7	—	1.4	—	

stant  $T_c$  for many other polymers<sup>16-23</sup> [e.g. poly(tetra-methyl-*p*-silphenylene)-siloxane<sup>20</sup>, poly(ethylene succinate)<sup>21</sup>, *trans*-1,4-polyisoprene<sup>22</sup> and poly(ethylene terephthalate)<sup>23</sup>] decrease with increasing molecular weight within the range of interest. The polymers in this second group all crystallize very slowly compared with poly(ethylene oxide) or polyethylene; at equivalent undercoolings their spherulite growth rates are some 100 times slower than those of poly(ethylene oxide) or polyethylene.

Assuming that crystallization is by a single mechanism, polymer crystal growth rates,  $G$ , can be described in terms of a classical rate equation<sup>24-26</sup> which is written (with sufficient accuracy):

$$G = [G_0 \exp(-\Delta F^a/RT_c)] \exp(-\Delta F^*/RT_c) \quad (1)$$

The term  $[G_0 \exp(-\Delta F^a/RT_c)]$  can be thought of as the elementary rate of transport of chain units across the liquid/crystal interface,  $\Delta F^a$  being the activation free energy for that process. This elementary rate is modified by the term  $\exp(-\Delta F^*/RT_c)$  which incorporates the free energy of formation from the melt of a crystal growth nucleus of critical size,  $\Delta F^*$ . For a given polymer sample and over a limited temperature range well removed from the glass transition temperature,  $G_0$  and  $\Delta F^a/RT_c$  can be treated as constant relative to the term  $\Delta F^*/RT_c$ . For growth of lamella crystals via monolayer nuclei,  $\Delta F^*$  can be written

$$\Delta F^* = \frac{4\sigma_u \sigma_e T_m^e}{\Delta h(T_m^e - T_c)} = \frac{4\sigma_u \sigma_e T_m^e}{\Delta h \Delta T} \quad (2)$$

where  $\sigma_u$  and  $\sigma_e$  are the free energies of formation from the melt of the lateral ( $\sigma_u$ , J/mol chain units) and end ( $\sigma_e$ , J/mol chains emerging) interfaces of the lamella crystal,  $\Delta h$  is the enthalpy of fusion (J/mol chain units) of bulk polymer crystal,  $T_m^e$  is the equilibrium melting point of the sample (i.e. the melting point of the thickest lamella crystal which can be formed from the polymer sample), and  $\Delta T$  is the undercooling ( $T_m^e - T_c$ ). Parameters  $\Delta h$  and  $\sigma_u$  are properties of the polymer and independent of molecular weight. For practical purposes, over a limited temperature range, they (together with  $\sigma_e$ ) may be treated as temperature independent parameters (the temperature range of our experiments is from 324 to 332K).

Provided chain ends are not co-crystallized the equilibrium melting point of a polymer sample is lowered as the molecular weight is lowered. Theory<sup>27</sup> predicts a rapid decrease in  $T_m^e$  at molecular weights less than  $10^5$ : by an amount roughly proportional to the inverse molecular weight. Consequently, at a given  $T_c$  near to  $T_m^e$ ,  $\Delta T$  is reduced as the molecular weight is lowered (particularly at low  $M$ ) and so, given  $G_0$  and  $\Delta F^a$  constant, the prediction is that  $G$  is reduced as  $M$  is lowered. However, it has been argued<sup>20</sup> that the transport term,  $G_0 \exp(\Delta F^a/RT)$ , is also dependent on the inverse molecular weight; thus, at constant  $\Delta T$ , the prediction is that  $G$  is increased as  $M$  is lowered.

Spherulite growth rates of poly(ethylene oxide) fractions bear a one to one correspondence to crystal growth rates over the molecular weight and temperature ranges where the two have been measured<sup>6</sup>. Accordingly we substitute the spherulite growth rate,  $G_s$  for the crystal growth rate,  $G$  in subsequent discussion. Moreover Kovacs and Gonthier<sup>6</sup> have shown that a single mode of (chain-folded) crystallization probably holds for the molecular weight

and temperature ranges we have examined here, so that the theoretical treatment summarized above can be applied to our data. At high values of the undercooling variation of  $T_m^e$  with  $M$  is unimportant in determining the value of the nucleation term and consequently  $G_s$  at constant  $T_c$  will decrease as the molecular weight increases, following the variation of the transport term. The results of Kovacs and Gonthier<sup>6</sup> for poly(ethylene oxide) fractions show that  $G_s$  may consistently decrease as molecular weight increases when the undercooling from  $T_m^e$  exceeds about 20K. Spherulite growth rates of the slowly crystallizing polymers are rarely measured at undercoolings less than 20K<sup>16-23</sup>. At low values of the undercooling both effects will be important and  $G_s$  plotted against  $M$  will show a maximum. The position of the maximum ( $M_{max}$ ) will depend upon the relative importance of the two terms in the rate expression: the greater  $\Delta T$  the lower  $M_{max}$ . Our results (Figure 1) are in accord with this prediction.

#### Temperature dependence of spherulite growth rate

For fractions of the highest molecular weight  $T_m^e$  is equal to the thermodynamic melting point  $T_m^0$ , i.e. the melting point of a crystal of infinite size formed from polymer of infinite molecular weight. For poly(ethylene oxide) extrapolation methods lead<sup>28,29</sup> to a value of  $T_m^0 = 76^\circ\text{C}$ .

According to equations (1) and (2), and taking the transport term to be relatively insensitive to temperature within our temperature range<sup>†</sup>, a plot of  $\log_e G_s$  against  $1/T_c \Delta T$  should be a straight line of slope  $4\sigma_u \sigma_e T_m^e / R \Delta h$ . Such a plot, for the fraction of highest molecular weight, is shown in Figure 2. The straight line drawn through the points has a slope of  $9.2 \times 10^4 \text{K}^2$ .

Within the experimental error of determination of  $G_s$  ( $\pm 10\%$ ) a straight line is as adequate a representation of the data of Figure 2 as any. However, similar plots for fractions of lower molecular weight (but  $\bar{M}_v > 5 \times 10^4$  so that  $T_m^e \approx T_m^0$ ) are curved. This is illustrated in Figure 3. We shall show later that appropriate plots for low molecular

† Plots of  $\log_e G_s + \Delta F^a/RT_c$ , with  $\Delta F^a$  evaluated by an Arrhenius expression<sup>6</sup> or by a WLF expression<sup>24</sup> [ $T_g = -67^\circ\text{C}$  for poly(ethylene oxide)<sup>30</sup>] have identical slopes, within the error of our data, to a plot of  $\log_e G_s$  alone.

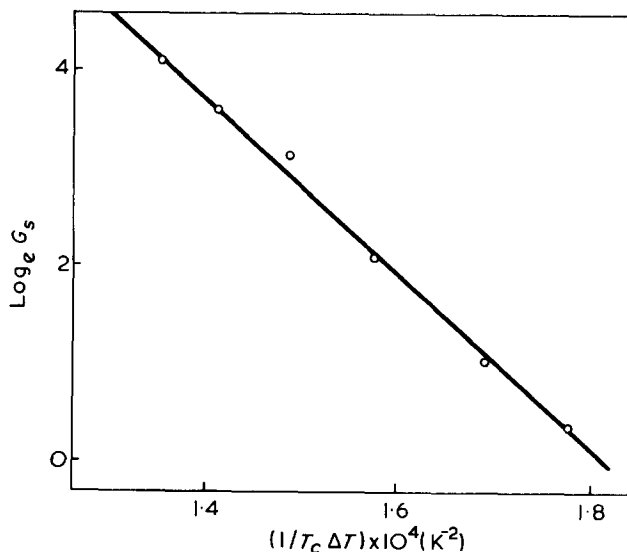


Figure 2 Logarithm of spherulite growth rate,  $G_s$ , against  $1/T_c \Delta T$  ( $\Delta T = T_m^0 - T_c$ ) for poly(ethylene oxide) fraction W950000



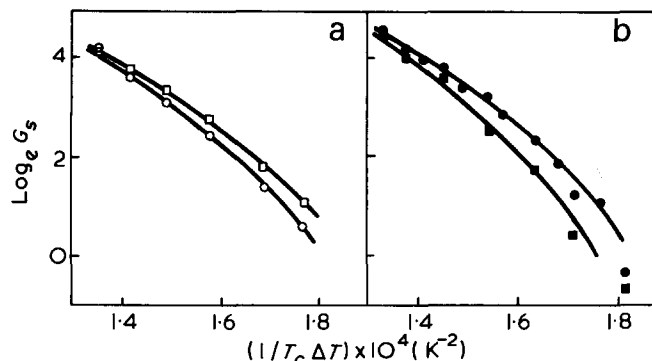


Figure 3 Logarithm of spherulite growth rate,  $G_s$ , against  $1/T_c \Delta T$  ( $\Delta T = T_m^0 - T_c$ ) for (a) poly(ethylene oxide) fractions W740000 (○) and W540000 (□) and (b) poly(ethylene oxide) fractions W190000 (●) and W72000 (■)

Table 3 End interfacial free energies ( $\sigma_e$ ) from temperature dependence of spherulite growth rate

Fraction	$T_c$ (°C)	$\sigma_e$ (kJ/mol)	
		$t = 1$	$t = 4$
6000	49–55	9.0	7.0
H11000	53–58	8.0	6.5
H23000	53–60	7.0	6.0
R42000	53–60	6.0	5.5
W950000	53–60	5.5	5.5

weight fractions ( $\bar{M}_v < 5 \times 10^4$ ) are linear. Ergoz *et al.*<sup>14</sup> have reported similar deviations from linearity in plots of the logarithm of the bulk crystallization rate against  $1/T_c \Delta T$  for polyethylene fractions of similar molecular weight ( $\bar{M}_v$  from about  $5 \times 10^4$  to  $7 \times 10^5$ ). This departure from the theoretical prediction for fractions of intermediate molecular weight casts doubt upon a simple model for the crystallization process. However, the deviation from linearity is slight and in subsequent discussion, mainly concerned with the highest and lowest molecular weight fractions, the problem is ignored.

Fractions of molecular weight lower than  $10^5$  cannot be treated in this way because  $T_m^e$  for low molecular weight polymers is lower than  $T_m^0$ . The value of  $T_m^e$  for a given sample is not generally measurable, nor can  $T_m^e$  be calculated independently of  $\sigma_e$  for polymers of narrow molecular weight distribution<sup>27</sup>. Rather than calculate values of  $T_m^e$  by assuming values of  $\sigma_e$ , we prefer the method of analysis proposed by Mandelkern<sup>31</sup>.

An alternative expression for  $\Delta F^*$  for monolayer growth is:

$$\Delta F^* = 2\sigma_u \zeta^* \quad (3)$$

where  $\zeta^*$  is the thickness of the growth nucleus of critical size given by:

$$\zeta^* = \frac{2\sigma_e - RT_c \log_e I}{\Delta h(T_m^0 - T_c)/T_m^0 - RT_c/\bar{x}_n} \quad (4)$$

where  $\bar{x}_n$  is the number-average chain length of the polymer and  $I$  is the probability that a sequence of length  $\zeta^*$  chain units does not contain a chain end. The number of sequences in a growth nucleus of critical size is given by:

$$\rho^* = \frac{2\sigma_u}{\Delta h(T_m^0 - T_c)/T_m^0 - RT_c/\bar{x}_n - RT_c I' / I} \quad (5)$$

where  $I' = (dI/d\zeta)$  evaluated at  $\zeta^*$ . We here assume that chain folding is via adjacent re-entry and write<sup>5,32</sup>:

$$I = \sum_{s=1}^t \int_{s\zeta^*}^{(s+1)\zeta^*} w(x) \frac{(x - s\zeta^* + 1)}{x} dx + \int_{(t+1)\zeta^*}^{\infty} w(x) \frac{(x - t\zeta^* + 1)}{x} dx \quad (6)$$

where  $w(x)$  is the weight fraction of molecules of chain length  $x$  units, and where it is assumed that the chains fold to their maximum extent (consistent with  $x > s\zeta^*$ ) up to a maximum of number of sequences  $t$ . (If  $t = 1$ , then the nucleus is composed of unrelated sequences.) Our calculations show that the allowance for the molecular weight distribution is important only when the average chain length is low (comparable with  $t\zeta^*$ ).

We assume that the chain length distributions of our fractions are described by the Schulz-Zimm expression<sup>33</sup>, with parameters defined by  $\bar{x}_n$  and  $\bar{M}_w/\bar{M}_n$  (Table 1). For poly(ethylene oxide) at temperatures near 60°C we take  $\Delta h$  to be 8.4 kJ/mol<sup>34</sup>. Use of the relationship<sup>24</sup>  $\sigma_u \approx 0.1\Delta h$  gives a value of  $\sigma_u$  of 840 J/mol (equivalent to 8 erg/cm<sup>2</sup>). Equation (1) predicts that a plot of  $\log_e G_s$  against  $\Delta F^*/RT_c$  has unit slope. Accordingly we calculate  $\Delta F^*$  for several values of  $\sigma_e$  and determine that value (of  $\sigma_e$ ) which leads to unit slope. The procedure is illustrated in Figure 4:  $\sigma_e$  is defined to the nearest 0.5 kJ/mol by this method<sup>†</sup>.

In Table 3 we list values of  $\sigma_e$  so determined for two cases:  $t = 1$  corresponding to unrelated sequences in the

† Previously<sup>5</sup>, in analysing the temperature dependence of spherulite growth rate data for poly(ethylene oxide) fractions we accepted twin restrictions of unit slope for the plot of  $\log_e G_s$  against  $\Delta F^*/RT_c$  and a constant value of the transport term,  $G_0 \exp(-\Delta F^*/RT_c)$ . Within the limits of accuracy of the data, and including data covering the molecular weight range 1500 to 600 000, this double restriction was possible. In view of the data reported by Kovacs and Gonthier<sup>6</sup> we would not now include data for fractions of molecular weight less than 6000 in such an analysis. Comparison of the present representation (Figure 4) with that used earlier (Figure 1 of ref 5), for the higher ( $\bar{M}_v \geq 6000$ ) fractions only, convinces us that restriction to constant  $[G_0 \exp(-\Delta F^*/RT_c)]$  is inconsistent with the bulk of our results.

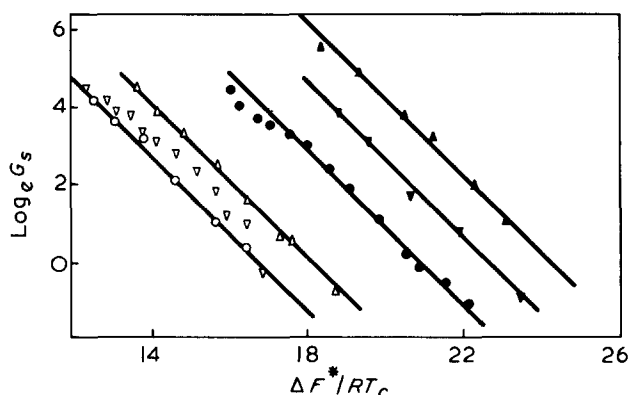


Figure 4 Logarithm of spherulite growth rate,  $G_s$ , against  $\Delta F^*/RT_c$  for poly(ethylene oxide) fractions W950000 (○), W190000 (▽), R42000 (△), H23000 (●), H11000 (▼) and 6000 (▲). Values of  $\sigma_e$  used in calculating  $\Delta F^*$ , with  $t = 1$  in equation (6), are given in Table 3

nucleus;  $t = 4$  corresponding to regularly folded sequences in the nucleus [ $t = 4$  is consistent with the values of  $\rho^*$  calculated from equation (3)]. The results for fraction 6000 (Figure 4 and Table 3) are obtained using data published earlier<sup>5</sup>. The values we quote have relative significance only, being based upon an assumed value for  $\sigma_u$ : that obtained for the high fraction can be compared with the value of 5.5 kJ/mol obtained from Figure 2 by use of the same value of  $\sigma_u$ . We note that fractions with molecular weights in the range  $5 \times 10^4 < \bar{M}_v < 9 \times 10^5$  cannot be analysed by our method because of the curvature of the  $\log_e G_s$  versus  $\Delta F^*/RT_c$  plots, but are best fitted (average slope) with  $\sigma_e$  near 5.5 kJ/mol. The data for fraction W190000 are included in Figure 4 in order to illustrate this point.

We find that  $\sigma_e$  decreases as the molecular weight increases. [We have remarked elsewhere<sup>5</sup> on the difference between our results with poly(ethylene oxide) and those discussed by Devoy and Mandelkern<sup>35</sup>.] The values of  $\sigma_e$  obtained for low molecular weight fractions vary with the model used (reflecting the lower entropy of the regularly folded chain nucleus). Kovacs and Gonthier<sup>6</sup> suggest that the crystallization of all our fractions (in the temperature range used) proceeds via a folded-chain nucleus. Accordingly we lean towards the values obtained for  $t = 4$ .

#### Spherulite growth rate at constant $\Delta F^*/RT_c$

If  $\Delta F^*/RT_c$  is constant then variation in  $G_s$  can be attributed to variation in the transport term,  $G_0 \exp(-\Delta F^a/RT_c)$ , of equation (1). In Table 4 we list values of  $G_s$  estimated (e.g. from Figure 4) at  $\Delta F^*/RT_c = 18$ . The corresponding values of  $T_c$  indicate that the undercooling ( $\Delta T = T_m^e - T_c$ ) is about 15K. The precision of an estimate of  $G_s$  is no better than  $\pm 50\%$  (reflecting the difficulty of defining  $\sigma_e$  to better than 0.5 kJ/mol). The molecular weight dependence of  $G_s$  at constant  $\Delta F^*/RT_c$  is similar to that found for polyethylene. For example, for polyethylene fractions at constant  $1/T\Delta T$  of  $1.7 \times 10^{-4}$  ( $\Delta T$  near 15K),  $G_s$  ( $\mu\text{m}/\text{min}$ ) is 400 for  $\bar{M}_v = 3900$  and 5 for  $\bar{M}_v = 87\,000$ . (These values are taken from Figure 3 of ref 15.)

The values of  $G_s$  at constant undercooling given in Table 4 vary roughly as  $1/\bar{M}_v^3$  provided that  $\bar{M}_v < 5 \times 10^4$ . This is in keeping with a transport process controlled directly in rate by the viscosity of the melt<sup>36</sup>. At molecular weights higher than  $5 \times 10^4$ , so far as we can judge,  $G_s$  at constant undercooling varies very little with

Table 4 Spherulite growth rates of poly(ethylene oxide) fractions estimated for constant  $\Delta F^*/RT_c = 18$

Fraction	$G_s$ ( $\mu\text{m}/\text{min}$ )	
	$t = 1$	$t = 4$
6000	500	130
H11000	100	20
H23000	20	2
R42000	1	0.4
W950000	0.3	0.3

$\bar{M}_v$ . These results are not in keeping with the predicted<sup>20</sup> variation of  $G_s$  (at constant undercooling).

#### ACKNOWLEDGEMENTS

We thank Mr D. J. Roy for assistance with the characterization of the polymers. J. Q. G. M. acknowledges receipt of a Science Research Council Studentship.

#### REFERENCES

- 1 Spegt, P. *Makromol. Chem.* 1970, **140**, 167
- 2 Beech, D. R., Booth, C., Dodgson, D. V., Sharpe, R. R. and Waring, J. R. S. *Polymer* 1972, **13**, 73
- 3 Godovsky, Yu. K., Slonimsky, G. L. and Garbar, N. M. *J. Polym. Sci. (C)* 1972, **38**, 1
- 4 Barnes, W. J., Luetzel, W. G. and Price, F. P. *J. Phys. Chem.* 1961, **65**, 1742
- 5 Beech, D. R., Booth, C., Hillier, I. H. and Pickles, C. J. *Eur. Polym. J.* 1972, **8**, 799
- 6 Kovacs, A. J. and Gonthier, A. *Kolloid-Z.* 1972, **250**, 530
- 7 Booth, C. and Price, C. *Polymer* 1966, **7**, 85
- 8 Desreux, V. and Bischoff, J. *Bull. Chem. Soc. Belg.* 1950, **59**, 93
- 9 Allen, G., Booth, C., Hurst, S. J., Jones, M. N. and Price, C. *Polymer* 1967, **8**, 391
- 10 Aldhouse, S. T. E. and Stanford, D. M. *5th Int. GPC Semin., London* 1968
- 11 Tung, L. H. and Runyon, J. R. *J. Appl. Polym. Sci.* 1969, **13**, 2397
- 12 Hay, J. N. *J. Scient. Instrum.* 1964, **41**, 456
- 13 Hay, J. N., Sabir, M. and Steven, R. L. T. *Polymer* 1969, **10**, 187
- 14 Ergoz, E., Fatou, J. G. and Mandelkern, L. *Macromolecules* 1972, **5**, 147
- 15 Lindenmeyer, P. H. and Holland, V. F. *J. Appl. Phys.* 1964, **35**, 55
- 16 Price, F. P. *J. Am. Chem. Soc.* 1952, **74**, 311
- 17 Burnett, B. B. and McDevitt, W. F. *J. Appl. Phys.* 1957, **28**, 1101
- 18 Lindgren, C. R. *J. Polym. Sci.* 1961, **50**, 181
- 19 McLaren, J. V. *Polymer* 1963, **4**, 175
- 20 Magill, J. H. *J. Appl. Phys.* 1964, **35**, 3249; *J. Polym. Sci. (A-2)* 1967, **5**, 89
- 21 Steiner, K., Lucas, K. J. and Ueberreiter, K. *Kolloid-Z.* 1966, **214**, 23
- 22 Lovering, E. G. *J. Polym. Sci. (C)* 1970, **30**, 329; *J. Polym. Sci. (A-2)* 1970, **8**, 747
- 23 van Antwerpen, F. and van Krevelen, D. W. *J. Polym. Sci. (Polym. Phys. Edn)* 1972, **10**, 2423
- 24 Hoffman, J. D. *SPE Trans.* 1964, p 315
- 25 Mandelkern, L. 'Crystallisation of Polymers', McGraw-Hill, New York, 1964
- 26 Sharples, A. 'Introduction to Polymer Crystallisation'. Arnold, London, 1966
- 27 Flory, P. J. *J. Chem. Phys.* 1949, **17**, 223
- 28 Beech, D. R. and Booth, C. *J. Polym. Sci. (B)* 1970, **8**, 731
- 29 Afifi-Effat, A. M. and Hay, J. N. *JCS Faraday Trans. II* 1972, **68**, 656
- 30 Wetton, R. E. and Allen, G. *Polymer* 1966, **7**, 331
- 31 Mandelkern, L., Fatou, J. G. and Howard, C. *J. Phys. Chem.* 1964, **68**, 3386; 1965, **69**, 956
- 32 Ashman, P. C. and Booth, C. *Polymer* 1972, **13**, 459
- 33 Peebles, L. H. 'Molecular Weight Distributions in Polymers', Interscience, New York, 1971
- 34 Devoy, C. J. *PhD Thesis* Manchester University (1966)
- 35 Devoy, C. J. and Mandelkern, L. *J. Polym. Sci. (A-2)* 1969, **7**, 1883
- 36 Yin, T. P., Lovel, S. E. and Ferry, J. D. *J. Phys. Chem.* 1961, **65**, 534; Porter, R. S. and Johnson, J. F. *Trans. Soc. Rheol.* 1962, **6**, 107

# Crystallization of poly(ethylene oxide) fractions: simultaneous dilatometry and calorimetry

C. Price, K. A. Evans\* and C. Booth

Department of Chemistry, University of Manchester, Manchester M13 9PL, UK

(Received 2 July 1974)

The crystallization of two fractions of poly(ethylene oxide), with molecular weights of 6000 and 360 000, has been studied by simultaneous dilatometry and calorimetry. The crystallization isotherms obtained by the two techniques are identical for the low molecular weight fraction, but differ for the high molecular weight fraction.

## INTRODUCTION

The study of the transformation of a polymer from the liquid to the crystalline state requires the measurement of some property of the system which reflects the extent of the transformation<sup>1,2</sup>. Two such properties are the volume and the enthalpy.

Measurements on a partly crystallized polymer are most simply interpreted in terms of a two-phase model consisting of perfect liquid and perfect crystal. Thus the weight fraction of polymer which is crystalline is defined by:

$$X = \frac{P - P_l^0}{P_c^0 - P_l^0} \quad (1)$$

where  $P$  represents some property of the system ( $V$ ,  $H$ ) and  $P_l^0$  and  $P_c^0$  are the corresponding properties of the system when the polymer is perfectly liquid and perfectly crystalline respectively. Defined in this way  $P_l^0$  and  $P_c^0$  (or their difference,  $P_c^0 - P_l^0$ ) are easily determined<sup>1,2</sup>.

It is found that  $X$  is always less than unity. This is because polymers crystallize in stacked lamellae and the interfacial regions contain partly ordered liquid and/or partly disordered crystal. Since different properties of the system may be affected in different ways by partial ordering or disordering, it is possible that  $X$  will vary according to the property used in its evaluation<sup>1-3</sup>.

An alternative representation for the partly crystallized system is a two-phase model comprising liquid and crystalline phases, the crystalline phase being considered as a whole. This model is suited to a single crystalline process occurring at the liquid-crystal (spherulite) boundary. For this model we define a weight fraction of polymer which has been crystallized as:

$$\chi = \frac{P - P_l^0}{P_c - P_l^0} \quad (2)$$

where  $P_c$  is the property of the crystallized polymer as it exists in the crystalline phase. When crystallization is com-

plete, all the polymer is within the crystalline phase. Accordingly we can write:

$$\chi = \frac{P(t) - P(0)}{P(\infty) - P(0)} \quad (3)$$

where the property is measured at time zero ( $P(0) = P_l^0$ ),  $t$ , and infinity ( $P(\infty) = P_c$ ).

Equations (2) and (3) define the weight fraction of polymer crystallized,  $\chi$ , entirely in terms of the properties of the system as it actually exists. For a single crystallization process,  $\chi$  is independent of the property used in its determination. If secondary processes occur, i.e. processes of whatever nature which occur behind the primary liquid-crystal boundary, or if fractionation (by molecular weight, chain purity, etc.) results in a proportion of polymer which is not incorporated into the spherulites, then  $\chi$  may be dependent on the property used in its determination.

In this work we have studied the crystallization of fractions of poly(ethylene oxide) by simultaneously measuring volume and enthalpy changes. The technique of simultaneous measurement by two techniques precludes inconsistencies due to variation in crystallization conditions. A recent study<sup>4</sup> of the crystallization of poly(ethylene oxide) of molecular weight 20 000 by dilatometry and calorimetry has shown that there are differences in the crystallization isotherms obtained by the two techniques. Here we present results for poly(ethylene oxide) fractions of molecular weight 6000 and 360 000. We have good reason to believe, as a result of dilatometric measurements<sup>5,6</sup>, that the crystallization of poly(ethylene oxide) of molecular weight 6000 is free from secondary processes whereas that of molecular weight 360 000 is more complex.

## EXPERIMENTAL

### Preparation and characterization

Samples of poly(ethylene oxide) were Carbowax Methoxy-5000 and Polyox WSR-35, both supplied by Union Carbide Ltd. These samples were fractionated by precipitation from dilute solution in benzene by addition of iso-octane<sup>7</sup>. Characterization was by methods described

\* Present address: The British Aluminium Company Ltd, Chalfont Technological Centre, Gerrards Cross, Bucks, UK.

Table 1 Molecular characteristics of poly(ethylene oxide) fractions

Fractions	$\bar{M}_n^a$	$\bar{M}_w/\bar{M}_n^b$	$[\eta]^c$ (cm <sup>3</sup> /g)	$\bar{M}_v^d$
6000M	6100	1.1	18.6	—
360 000	—	~1.3 <sup>6</sup>	256	360 000

<sup>a</sup> Vapour pressure osmometry (Mechrolab Inc.); benzene at 25°C

<sup>b</sup> Gel permeation chromatography (Waters Associates); tetrahydrofuran at 40°C

<sup>c</sup> Dilute solution viscometry; benzene at 25°C

<sup>d</sup>  $[\eta] = 0.0397\bar{M}_v^{0.686}$  (ref 9)

fully elsewhere<sup>8</sup>. Characterization data are given in Table 1; the fractions are denoted by their approximate molecular weights.

### Dilatometry and calorimetry

Simultaneous observation of the crystallization process by dilatometry and calorimetry was by use of a Calvet microcalorimeter.

Dilatometers were constructed of glass. The capillary entered the bulb by an internal seal (after the design of Kovacs and Manson<sup>10</sup>). The bulb volume was about 1 cm<sup>3</sup>. The capillary was 0.5 mm internal diameter Veridia tubing, and was of sufficient length (>1 m) to protrude from the top when the dilatometer was inserted into the calorimeter.

The Calvet microcalorimeter (Setram, Lyon) was a standard model (25–200°C). A detailed description of the theory, construction, calibration and operation of the instrument may be found elsewhere<sup>11</sup>. Briefly, the instrument consisted of an aluminium heat sink containing two cavities into which fitted twin cylindrical cells (referred to as 'laboratory' and 'reference' cells). The temperature of the aluminium block was controlled to  $\pm 0.001$ K. In each cavity a thermopile was interposed between cell and block. These thermopiles were connected in opposition and the net output from them was fed to a recorder assembly (Sefram Verispot galvanometer, projection lantern and photodyne spot-follower).

The thermal power,  $W$ , developed in the laboratory cell (relative to the reference cell) at time  $t$  was estimated by use of the Tian equation. It is assumed that the internal boundary which contacts the pile is at uniform temperature, and that this differs from the temperature of the external boundary by  $\theta$ :

$$W = p\theta + \mu(d\theta/dt) \quad (4)$$

where  $p$  is a constant and  $\mu$  is the effective thermal capacity of the cell contents. The voltage generated by the heat flux produces a recorder deflection:

$$\Delta = g\theta \quad (5)$$

where  $g$  is a constant. Hence we can write:

$$W = (p/g)\Delta + (\mu/g)(d\Delta/dt) \quad (6)$$

$$W = (p/g)[\Delta + \tau(d\Delta/dt)] \quad (7)$$

where  $\tau = \mu/p$  is the time constant of the instrument. During the course of an experiment  $\Delta$  is recorded as a function of time. Equation (7) shows that the actual thermokinetic curve (i.e.  $W$  vs.  $t$ ) can be obtained from the observed curve (i.e.  $\Delta$  vs.  $t$ ) by adding at each point an amount  $\tau d\Delta/dt$ . In

the case of the slow thermal processes (such as the crystallization processes studied here) the correction term is small relative to  $\Delta$ . Electrical calibration, carried out in the recommended manner using<sup>11</sup> Joule heating, gave values of  $p/g$  near  $0.966 \times 10^{-4}$  W/cm and  $\tau$  near 6.0 s for the sensitivity range (lowest) used here.

The twin cells (1.7 cm diameter, 8.5 cm long) were constructed of stainless steel and were held on Teflon tubes. The assembly within a cell is shown schematically in Figure 1. The dilatometer bulb (A) was inserted into the cell (B) via the Teflon tube (C). The roof of the cell was formed by a Teflon plug (D) and socket (E). To facilitate heat conduction the dilatometer bulb was immersed in silicone oil (F). The capillary tube of the dilatometer (G) protruded from the top of the instrument through a rubber bung (H).

In practice a known weight of poly(ethylene oxide) (~100 mg) was moulded in high vacuum, sealed into the dilatometer, outgassed and confined with mercury. A similar dilatometer was filled with mercury only, for insertion into the reference cell. In a crystallization experiment the laboratory dilatometer was immersed in boiling water for about 30 min, quickly dried, rinsed in silicone oil held at a temperature a little above the calorimeter temperature, and then inserted into the laboratory cell. At the same time the reference dilatometer was treated similarly and placed in the reference cell. Thermal equilibrium within the calorimeter required about 20 min. This was judged by the movement of the mercury level in the protruding capillary, and also by the establishment of the baseline on the recorder. It was possible to use some of the thermocouples in the pile surrounding the laboratory cell for Peltier cooling and this facility ensured that the temperature of the polymer sample approached the required crystallization temperature fairly quickly. In practice, how-

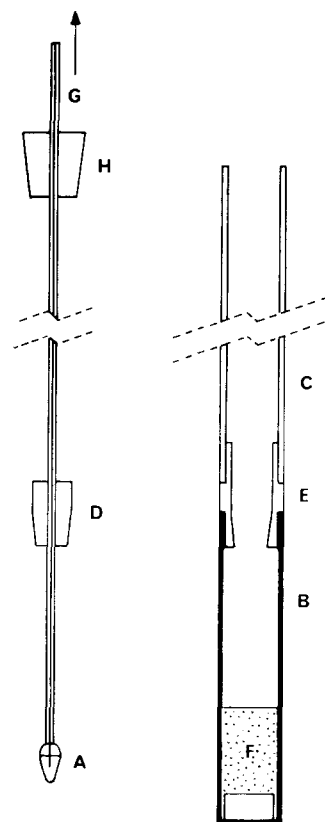


Figure 1 Experimental assembly of the microcalorimeter cell

ever, our experiments were restricted to very slow crystallizations. The time of transfer was taken as the starting time for the crystallization. The height of mercury in the capillary when steady was taken as the starting height for dilatometry.

The volume contraction was followed by measuring the height of the mercury in the capillary by means of a dilatometer (to  $\pm 0.005$  cm). Typically the total contraction was about 4 cm, so that we could record changes in degree of crystallinity of about 0.1% by dilatometry. The sensitivity of the microcalorimeter ( $p/g$ ) was about  $10^{-4}$  J s $^{-1}$  cm $^{-1}$ . Typically the overall heat output was about 20 J, so that the sensitivity in terms of degree of crystallinity was about  $5 \times 10^{-4}\%$  s $^{-1}$  cm $^{-1}$  i.e. about 0.2% per hour produced a deflection of 1 mm from the baseline.

## RESULTS

In the dilatometric experiment we determine the specific volume change on crystallization ( $V - V_l^0$ , cm $^3/g$ ). The specific volume change for perfect crystallization ( $V_c^0 - V_l^0$ , cm $^3/g$ ) can be calculated from the following data.

$$\text{Liquid: } V_l^0(25^\circ\text{C}) = 0.891 \text{ cm}^3/\text{g}^{12}, \\ \alpha_l^0 = 0.00069 \text{ cm}^3/\text{g K}^{12,13}$$

$$\text{Crystal: } V_c^0(25^\circ\text{C}) = 0.813 \text{ cm}^3/\text{g}^{14}, \\ \alpha_c^0 = 0.00015 \text{ cm}^3/\text{g K}^{12}$$

from which:

$$V_c^0 - V_l^0 = -0.078 - 0.00054(T_c - 298)$$

In the calorimetric experiment we determine the specific enthalpy change on crystallization ( $H - H_l^0$ , J/g). This is given by:

$$H - H_l^0 = \int_0^t W dt$$

The specific enthalpy change for perfect crystallization ( $H_c^0 - H_l^0$ , J/g) can be calculated from the following data:  $H_c^0 - H_l^0(67.9^\circ\text{C}) = -210^{15}$  and  $\Delta C_p(\text{J K}^{-1} \text{g}^{-1}) = 1.23 - 0.0016T^{16}$ .

The value of  $-210$  J/g, for the heat of crystallization of a poly(ethylene oxide) crystal of infinite size formed from polymers of infinite molecular weight, is from measurements on mixtures of benzene with a high molecular weight fraction ( $M_v = 800\,000$ ) of poly(ethylene oxide). The technique is discussed elsewhere<sup>17</sup>. A second estimate is available<sup>18</sup> from extrapolation of the heats of crystallization of extended chain crystals formed from low molecular weight crystals to infinite crystal thickness: i.e. 216 J/g at 75°C.

In Figure 2 we show crystallization isotherms,  $X$  vs.  $\log t$ , obtained by dilatometry for fraction 360 000 for a selection of crystallization temperatures. The lowest crystallization temperature illustrated in Figure 2 is 58.8°C. Crystallization isotherms determined at temperatures lower than this (e.g. 57.8°C) overlie that for  $T_c = 58.8^\circ\text{C}$ ; presumably heat cannot be dissipated sufficiently quickly from the dilatometer-cell assembly when the tenth-life of the crystallization is much lower than 100 min. In what follows we con-

fine our attention to slow crystallizations: fraction 6000M at  $T_c \geq 55^\circ\text{C}$  and fraction 360 000 at  $T_c \geq 59.5^\circ\text{C}$ . The results quoted are typical of many obtained under similar conditions.

Examples of calorimetric records (corrected,  $W$  vs.  $t$ ) are shown in Figure 3. The curve for 6000M (Figure 3a) shows pronounced bumps. This is due to the low number density of spherulites in the sample; isotherms recorded for 6000M melted at 75°C (rather than 100°C) showed no peculiarities. Similar effects have been noted by Hay *et al.*<sup>19</sup>; presumably the low number density allows the development of large spherulites with consequent changes in crystallization rate when they impinge with one another or with the sample boundary. These adventitious variations in crystallization rate are less apparent when the data are presented as cumulative crystallization curves (see Figure 4).

Figure 4 shows the crystallization isotherms ( $X$  or  $\chi$  vs.  $t$ ) of fraction 6000M determined both by dilatometry and calorimetry. The isotherms are practically identical: the difference between the  $X$  isotherms is within the error of their determination (i.e. in the assessment of the numerator of equation 1). The  $\chi$ -isotherms cannot be separated. The isotherms terminate abruptly, at or about  $X = 0.80$ , with no indication of a slow secondary process: this is in keeping with other results<sup>5,6</sup>.

Figure 5 shows the corresponding crystallization isotherms for fraction 360 000. For this sample the isotherms

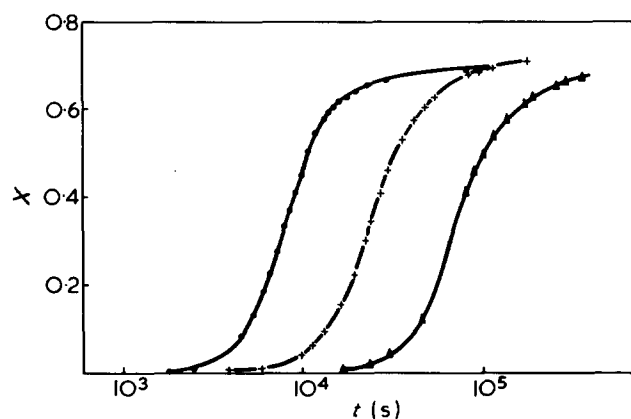


Figure 2 Dilatometric crystallization isotherms for fraction 360 000 at crystallization temperatures of: ●, 58.8°; +, 60.0°; ▲, 60.9°C

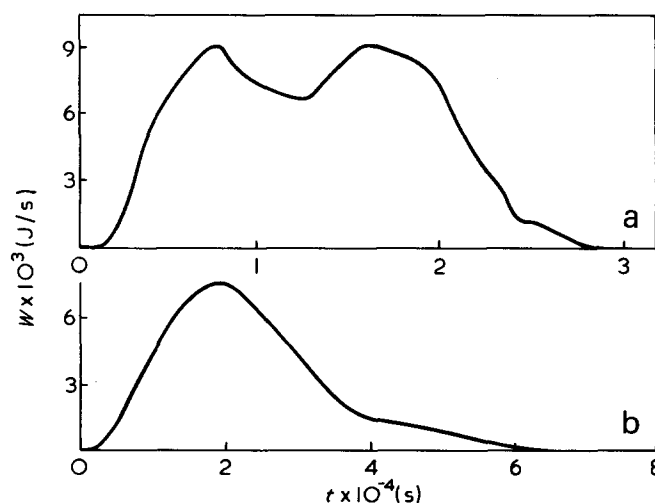


Figure 3 Calorimetric records for (a) fraction 6000M at 56°C and (b) fraction 360 000 at 60°C

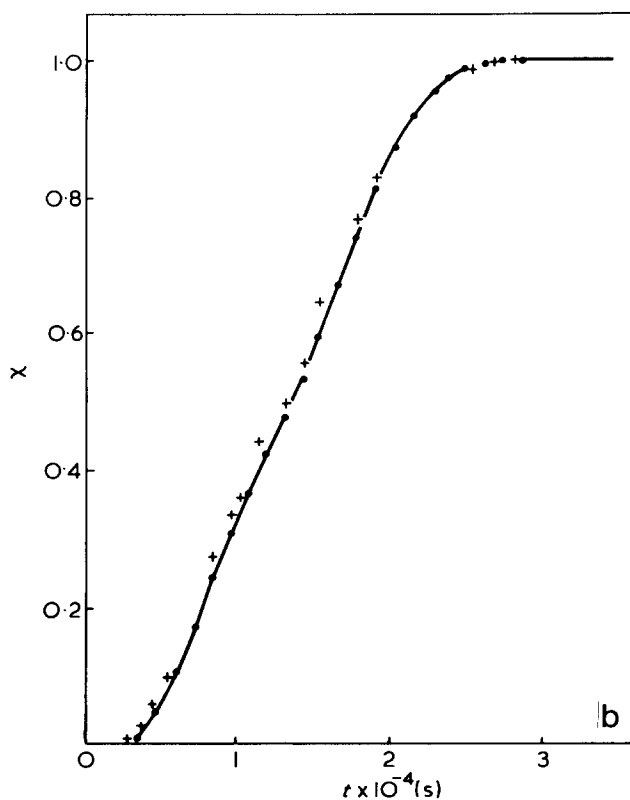
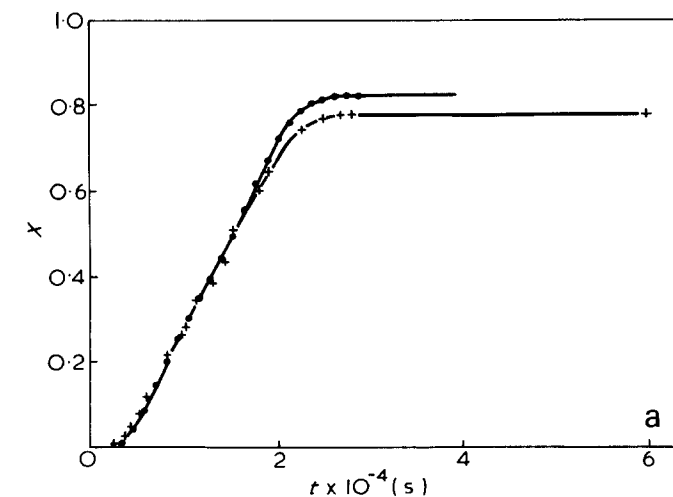


Figure 4 Crystallization isotherms for fraction 6000M at 56°C, obtained by dilatometry (+) and calorimetry (●). (a)  $X$  vs.  $t$ ; (b)  $\chi$  vs.  $t$

determined by the two techniques differ. Two results are noteworthy. First, the dilatometric isotherm lags behind the calorimetric isotherm at all stages of the crystallization. Secondly, the volume of the system continues to contract long after the production of heat at a detectable rate has ceased. From a practical point of view we note that the volume contraction at the time when the heat flow becomes undetectable ( $8.5 \times 10^4$  s) corresponds to a crystallization rate of about  $0.5\% \text{ h}^{-1}$ , i.e. about 2 mm deflection of the recorder\*.

\* Whilst this should be readily detectable, it is just possible that a systematic baseline drift could affect the measurements and to this extent the second result is tentative. By increasing the amount of polymer in the dilatometer and setting up the experiment so that only the later stages of the crystallization process are investigated, an increase in the sensitivity of the experiment by about a factor of 20 is feasible. In this way we hope at a future time to investigate the thermodynamics of the process in a more detailed manner.

Measurements of volume contraction were stopped after two days. Crystallization isotherms (determined by dilatometry) of comparable fractions of Polyox WSR-35 have been presented elsewhere<sup>6</sup>; provided the molecular weight ( $\bar{M}_v$ ) exceeds  $10^5$ , a slow decrease in volume is found, continuing long after the primary crystallization has ceased. We would surmise that the volume of our fraction would have contracted further had it been held at 60°C for a few more days. The calculation of the isotherm  $\chi(t)$  is therefore somewhat arbitrary; the curve illustrated in Figure 5 is calculated assuming  $V(\infty) = V(8.5 \times 10^4 \text{ s})$ .

The data of Godovskii *et al.*<sup>4</sup> for poly(ethylene oxide) of molecular weight 20 000 ( $\chi$  isotherms only are given) are somewhat intermediate between those of 6000M than 360 000: the dilatometric and calorimetric isotherms are identical up to  $\chi \approx 0.9$ ; thereafter the dilatometric isotherm lags behind the calorimetric isotherm.

## DISCUSSION

For both fractions we find final degrees of crystallinity ( $X \approx 0.80$  for 6000M,  $X \approx 0.7$  for 360 000) which are similar whether estimated by dilatometry or calorimetry. This

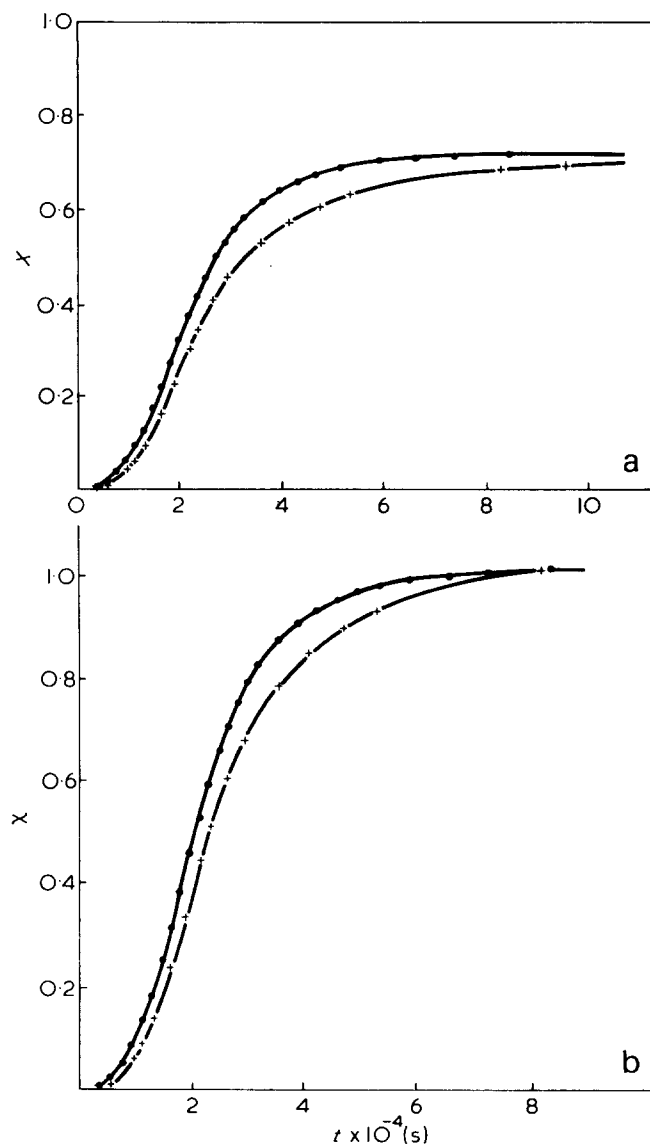


Figure 5 Crystallization isotherms for fraction 360 000 at 60°C, obtained by dilatometry (+) and calorimetry (●). (a)  $X$  vs.  $t$ ; (b)  $\chi$  vs.  $t$

does not necessarily mean that  $X$  has been correctly assessed. It does mean that the volume and enthalpy are similarly affected by partial ordering or disordering in the system.

The observed slow athermal volume contraction at the end of the crystallization of fraction 360 000 (which is absent in fraction 6000M) allows one provisionally to assign the secondary process in high molecular weight poly(ethylene oxide) to a volume relaxation process. The fact that the dilatometric isotherm lags behind the calorimetric isotherm over the whole of the crystallization process implies that the volume relaxation occurs within the spherulites.

It is possible that the volume relaxation process is correctly described by the free volume mechanism assigned to the relaxation of glasses<sup>20</sup> and applied to the crystallization of poly(ethylene) by Banks *et al.*<sup>21</sup>. However, it could only be coincidental that such a process was athermal: changes in the conformational energies of the chain molecules would need to compensate for the energy decrease due to closer packing. We prefer to assign the effect to the formation of macroscopic voids during crystallization<sup>3,22</sup>; the relaxation of a system containing voids will cause a small decrease in enthalpy but a large decrease in volume.

#### ACKNOWLEDGEMENTS

The authors wish to thank Esso Chemicals Research Limited, Abingdon, for the award of a research studentship to K.A.E.

#### REFERENCES

- 1 Miller, R. L. 'Encyclopedia of Polymer Science and Technology', Interscience, New York, 1966, Vol 4, p 449
- 2 Kavesh, S. and Schultz, J. M. *Polym. Eng. Sci.* 1969, 9, 452
- 3 Hoffman, J. D. *SPE Trans.* 1964, 4, 315
- 4 Godovsky, Yu. K., Garbar, N. M. and Slonimsky, G. L. *Vysokomol. Soedin. (A)* 1972, 14, 1833; *Polym. Sci. USSR* 1972, 14, 2053
- 5 Beech, D. R., Booth, C., Dodgson, D. V. and Hillier, I. H. *J. Polym. Sci. (A-2)* 1972, 10, 1555
- 6 Maclaine, J. Q. G. *PhD Thesis* University of Manchester (1975)
- 7 Booth, C. and Price, C. *Polymer* 1966, 7, 85
- 8 Beech, D. R., Booth, C., Dodgson, D. V., Sharpe, R. R. and Waring, J. R. S. *Polymer* 1972, 13, 73
- 9 Allen, G., Booth, C., Hurst, S. J., Jones, M. N. and Price, C. *Polymer* 1967, 8, 391
- 10 Kovacs, A. J. and Manson, J. A. *Kolloid-Z.* 1966, 214, 1
- 11 Calvet, E. and Prat, H. 'Recent Progress in Microcalorimetry', (Ed. H. A. Skinner), Pergamon Press, Oxford, 1963
- 12 Arlie, J. P., Spegel, P. and Skoulios, A. *Makromol. Chem.* 1966, 104, 212
- 13 Simon, F. T. and Rutherford, J. H. *J. Appl. Phys.* 1964, 35, 82
- 14 Price, F. P. and Kilb, R. W. *J. Polym. Sci.* 1962, 57, 395
- 15 Devoy, C. J. *PhD Thesis* University of Manchester (1966)
- 16 Roberts, R. C. *PhD Thesis* University of Manchester (1966); Beaumont, R. H., Clegg, B., Gee, G., Herbert, J. B. M., Marks, D. J., Roberts, R. C. and Sims, D. *Polymer* 1966, 7, 401
- 17 Booth, C., Devoy, C. J. and Gee, G. *Polymer* 1971, 12, 327
- 18 Afifi-Effat, A. M. and Hay, J. N. *JCS Faraday Trans. II* 1972, 68, 656
- 19 Hay, J. N., Sabir, M. and Steven, R. L. T. *Polymer* 1969, 10, 187
- 20 Hirai, N. and Eyring, H. *J. Polym. Sci.* 1959, 37, 51
- 21 Banks, W., Gordon, M., Roe, R.-J. and Sharples, A. *Polymer* 1963, 4, 61
- 22 Matsuoka, S. *J. Appl. Phys.* 1961, 32, 2334

# Influence of tacticity of poly(methyl methacrylate) on the compatibility with poly(vinyl chloride)

J. W. Schurer, A. de Boer and G. Challa

Department of Polymer Chemistry, State University of Groningen, Groningen, The Netherlands

(Received 13 June 1974)

Blends of conventional poly(vinyl chloride) (PVC) and poly(methyl methacrylate) (PMMA) with different tacticities were obtained both from the bulk and from solution. The glass transition temperatures ( $T_g$ ) of the blends were determined with a differential scanning calorimeter and by dynamic mechanical measurements. Some turbidity measurements on films and viscosity measurements on mixed solutions supplied additional information about the state of mixing. From the results it appeared that isotactic (i-)PMMA and PVC form an incompatible system over the entire composition range (two  $T_g$ 's), whereas blends of syndiotactic (s-)PMMA and PVC form a compatible system up to a composition corresponding with a monomer unit ratio of about 1:1. For higher s-PMMA contents phase separation is observed; one phase corresponding with the 1:1 s-PMMA-PVC associate and the other phase representing the excess of pure s-PMMA. This effect of tacticity is discussed in terms of the differences in chain conformation of i- and s-PMMA.

## INTRODUCTION

In the last few decades many polymer blends have been investigated. These studies have been reviewed by Bohn<sup>1</sup>, Rosen<sup>2</sup>, and Krause<sup>3</sup>. In order to say something more definitely about mixing of polymers the concept of compatible polymer pairs has been introduced. Two polymers were considered to be compatible, when a mixture of these polymers gives a transparent film. However, if two polymers have the same refractive index but do not mix, it is to be expected that such blend also gives transparent films.

Another method to find out compatibility comprises determination of the glass transition temperature,  $T_g$ , as a function of the composition of the polymer-polymer system. However, when a polymer-polymer system demonstrates a single  $T_g$ , it does not yet definitely mean that mixing occurred on a molecular scale. Thus, Matsuo<sup>4</sup> has shown by electron microscopy that the poly(vinyl chloride)-copoly(butadiene-acrylonitrile 40:60) system contains heterogeneous domains with diameters up to 100 Å, although dynamic mechanical measurements produced only a single  $T_g$ .

A next example of the controversy around compatibility of polymer pairs is demonstrated by the poly(2,6-dimethyl phenylene oxide)(PPO)-polystyrene(PS) system. Stoelting<sup>5</sup> has shown by differential scanning calorimetry (d.s.c.) measurements that the PPO-PS system has one  $T_g$ . This indication of compatibility was confirmed by Shultz<sup>6</sup> using thermal optical analysis and by Prest and Porter<sup>7</sup> from rheological experiments. However, dynamic mechanical and dielectric relaxation measurements<sup>8</sup> have shown, that PPO and PS form an incompatible system with a PPO rich phase and a PS rich phase.

Another approach to polymer-polymer compatibility starts from well known thermodynamic considerations in terms of solubility parameters  $\delta$ . If there exists a more favourable interaction between mutual structural units

(smaller difference in  $\delta$ ) the chance of compatibility of the polymer-polymer system will become larger. Some examples of compatible systems are poly(methyl methacrylate)-poly(vinylidene fluoride)<sup>9</sup>, polystyrene-poly(vinyl methylether)<sup>10</sup>, and poly(vinyl chloride)-poly( $\epsilon$ -caprolactone)<sup>11</sup>.

Applying this idea to our studies on association phenomena of tactic poly(methyl methacrylates)(PMMA) we selected poly(vinyl chloride)(PVC) as second polymer because  $\delta$  has about the same value for both polymers, viz. 9.5 and 9.6, respectively<sup>12</sup>. In view of the large difference of 80°C in  $T_g$  between isotactic (i-)PMMA and syndiotactic (s-)PMMA we were interested to know whether the tacticity of PMMA would also have a large effect on the compatibility of PMMA with PVC. To this end we investigated the glass transitions of different blends of i- and s-PMMA with PVC. In some preliminary experiments a commercial sample of atactic (a-)PMMA was used.

## EXPERIMENTAL

The polymers i- and s-PMMA were prepared according to known procedures<sup>13,14</sup>, a-PMMA was a commodity of ICI (Diakon MO/900), and PVC a commodity of P echiney et St Gobain (Lucovyl RB 8010). The data of the used polymers are compiled in Table 1. The tacticities of PMMA

Table 1 Data of used polymers

	triads i-h-s	$[\eta]$ (dl/g)	$\bar{M}_v \times 10^{-3}$
i-PMMA	92-3-5	2.03	630
s-PMMA	2-4-94	1.37	370
a-PMMA	5-32-63	0.40	80
PVC		0.71	55



were measured on 5% solution in *o*-dichlorobenzene<sup>15</sup> at 160°C by 60 MHz n.m.r. spectroscopy with a Varian A60 instrument.  $[\eta]$  of the PMMA samples were determined in chloroform at 25°C. For the calculation of  $\bar{M}_v$  we used the relationship<sup>16</sup>:  $[\eta] = 4.8 \times 10^{-5} \bar{M}_v^{0.8}$ .  $[\eta]$  of PVC was determined in cyclohexanone at 25°C and  $\bar{M}_v$  was calculated<sup>17</sup> from  $[\eta] = 173 \times 10^{-5} \bar{M}_v^{0.55}$ .

Blends of PMMA and PVC were prepared in three ways: (a) by evaporation of 3 wt% mixed PMMA-PVC solutions in dimethyl formamide (DMF); (b) by precipitation from 3 wt% mixed PMMA-PVC solutions in DMF in an excess of 10:1 water-methanol mixture. The samples were dried in vacuum at 120°C for 1 h. To remove the last traces of DMF, the samples were finally heated at 170°C for 10 min in vacuum; (c) a-PMMA-PVC blends were also prepared by mixing the molten bulk polymers on a two roll mill (Schwabenthan) rotating with 10 and 12 rev/min at 180°C. PVC was first supplied on the mill and after 2 min a-PMMA was added. After 6 min the sheet was removed from the roll. To oppose degradation of PVC, 1 wt% stabilizer, di-*n*-octyltin-*S,S'*-bisiso-octyl-mercaptoacetate, (Ciba-Geigy) was added. The mixed samples were pressed to bars or d.s.c. tablets at 180°C for 3 min at 50 kgf/cm<sup>2</sup>. The bars or tablets were slowly cooled under pressure.

The glass transition temperatures,  $T_g$ , were measured with a Perkin-Elmer differential scanning calorimeter (DSC 1B) at a heating rate of 8°C/min. All samples were first scanned up to 180°C for relaxation of possible stresses. In the second scan reproducible results were obtained. The beginning of the  $c_p$  jump was taken as  $T_g$ . It appeared from these measurements that the processing conditions had no influence on the course of  $T_g$  with composition of the blends. Dynamic mechanical measurements have been carried out on bars of 7 × 0.7 × 0.3 cm with a torsion pendulum of Nonius/TNO at a frequency of ~1 Hz. The measurements have been performed in the temperature range 20–170°C. From the damped oscillations loss tangents  $\tan \delta$  were calculated. The turbidities of some a-PMMA-PVC blends were quantitatively measured at a wavelength of 550 nm with a Jouan spectrophotometer.

## RESULTS

### Preliminary experiments

In order to test the expected compatibility of a-, i-, and s-PMMA and PVC we first looked for common solvents yielding homogeneous mixed solutions. It appeared that for total polymer concentrations of about 1 g/dl no phase separation occurred at 25°C in solvents such as DMF, cyclohexanone, butanone-2, dioxane-1,4, THF, and *p*-chlorotoluene. Moreover, the reduced viscosities  $\eta_{sp}/c$  of the mixed solutions were practically additive with respect to the values of the separate components.

A further indication of compatibility was obtained from turbidity measurements on 0.6 ± 0.05 mm films of various a-PMMA-PVC mixtures. The results in Figure 1 show that clear films are obtained for blends up to about 60 wt% a-PMMA. Only at higher a-PMMA contents turbidity arises, passing a maximum value and then falling off to the value of pure a-PMMA. From these solubility and turbidity studies we thought it worthwhile to investigate the compatibility with PVC more thoroughly for both stereoregular PMMA's.

### *i*-PMMA-PVC blends

Some characteristic d.s.c. thermograms are shown in Figure 2.  $T_g$  values derived from such thermograms are plotted against the composition of the system *i*-PMMA-PVC in Figure 3. Two  $T_g$ 's are found over a wide composition range, which means that two different phases are present. Moreover, whatever composition is taken the  $T_g$ 's vary less than should be expected in case of partial mixing of *i*-PMMA and PVC. So, it is likely that still two phases are present in the extreme composition ranges, but the sensitivity of

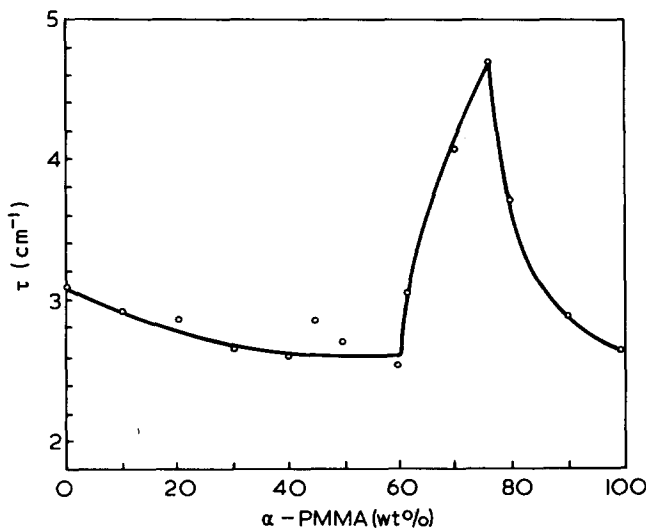


Figure 1 Turbidity ( $\tau$ ) at 550 nm versus wt% a-PMMA for the a-PMMA-PVC system (film thickness 0.6 ± 0.05 mm)

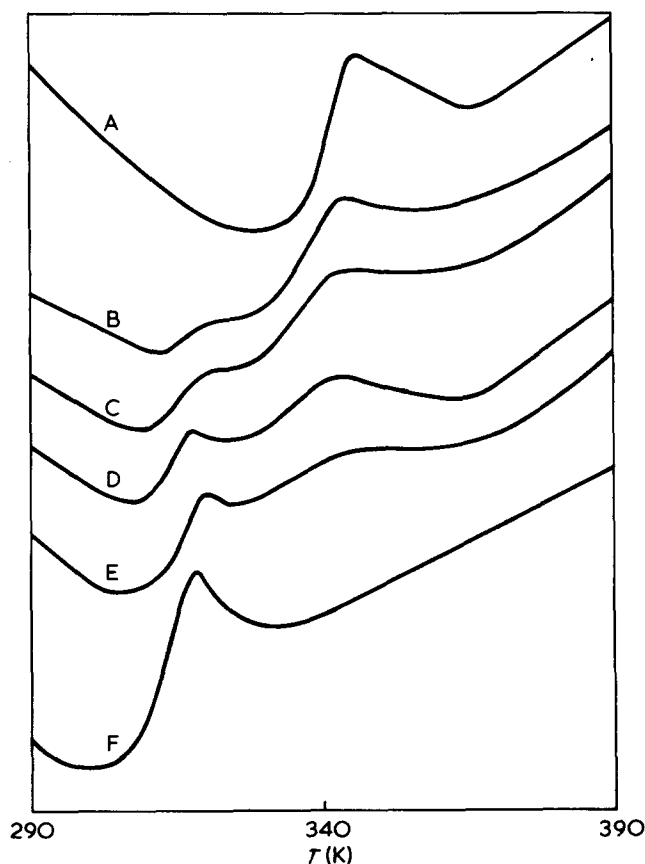


Figure 2 Some characteristic thermograms (heat flow versus temperature) for the *i*-PMMA-PVC system recorded by d.s.c. with a heating rate of 8°C/min. *i*-PMMA-PVC: A, 0:100; B, 40:60; C, 50:50; D, 60:40; E, 70:30; F, 100:0

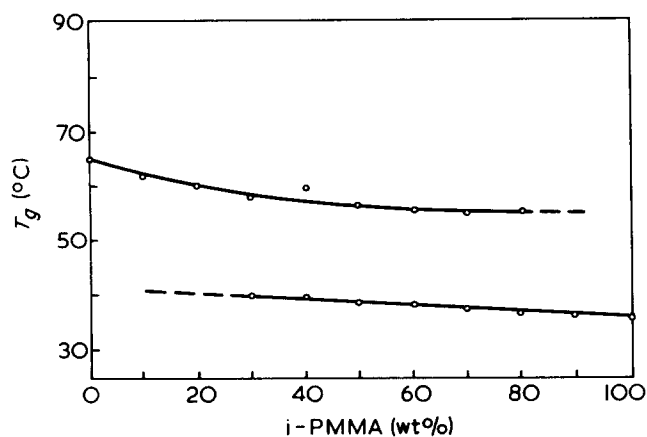


Figure 3 Glass transition temperatures  $T_g$  (determined by d.s.c.) versus wt% i-PMMA for the i-PMMA-PVC system

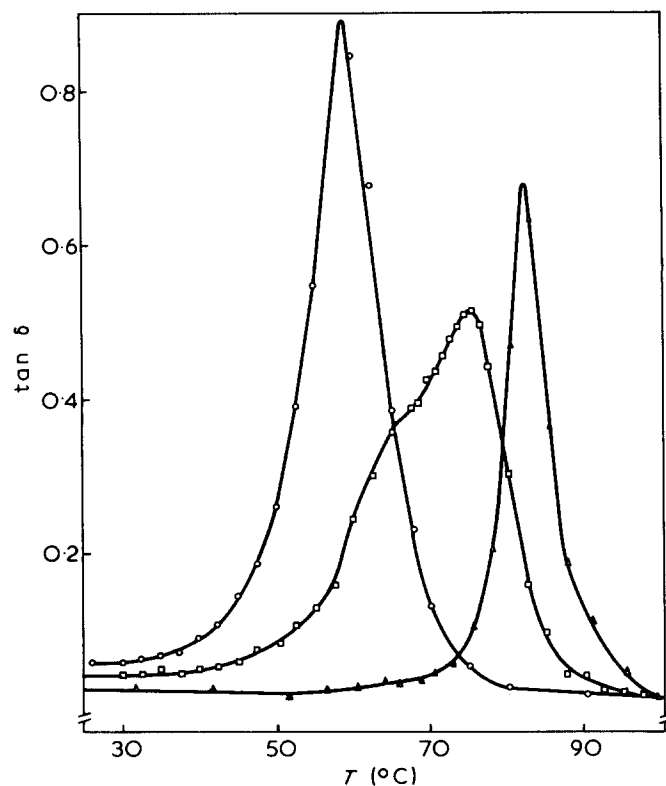


Figure 4 Loss tangent  $\tan \delta$  at about 1 Hz versus temperature for the i-PMMA-PVC system. ○, 100:0; □, 50:50; △, 0:100 i-PMMA-PVC

the d.s.c. is too low to detect the  $T_g$  of the respective small phases.

In order to check the d.s.c. results dynamic mechanical measurements were performed. In Figure 4  $\tan \delta$  is plotted against temperature for three different compositions. From the wide asymmetrical damping curve of the 50:50 sample it seems clear that i-PMMA and PVC form an incompatible system. Asymmetrical curves were also found for 25:75 and 75:25 compositions. Moreover, all the bars of the blends had an opaque appearance pointing to separated phases.

#### s-PMMA-PVC blends

In Figure 5  $T_g$  values found by d.s.c. measurements are plotted against composition for the system s-PMMA-PVC. From these data it appears that  $T_g$  increases regularly with composition up to 60 wt% s-PMMA. At higher s-PMMA

contents this  $T_g$  does not alter anymore, but is accompanied by a second  $T_g$ , of about 120°C, i.e. the value of pure s-PMMA. All this does indicate that a compatible system is formed up to 60 wt% s-PMMA, whereas PVC and s-PMMA form an incompatible system at higher s-PMMA contents. One phase of the incompatible system represents the blend 60:40 s-PMMA-PVC, the other one consists of pure s-PMMA.

Figure 6 shows  $\tan \delta$  of some s-PMMA-PVC systems as a function of temperature. It appears that the weight compositions 30:70 and 60:40 s-PMMA-PVC still give symmetrical damping curves, whereas the broad damping curve of the 80:20 s-PMMA-PVC blend seems to be composed of two curves which partly overlap. These results agree with those of the d.s.c. studies. Up to 60 wt% s-PMMA the polymers PVC and s-PMMA form a compatible system, whereas higher s-PMMA contents produce phase separation between a 60:40 s-PMMA-PVC phase and pure s-PMMA. This is also demonstrated by the turbidity of bars with overall compositions between 60 and 100 wt% s-PMMA.

Since the microstructure of a-PMMA is much more syndiotactic than isotactic it is understandable that blends of a-PMMA with PVC give nearly the same d.s.c. and dynamic mechanical results as presented in Figures 5 and 6. However, Razinskaya *et al.*<sup>18</sup> found a much smaller compatibility range for a-PMMA-PVC blends. This might be explained by the three times higher  $\bar{M}_v$  value of their PVC.

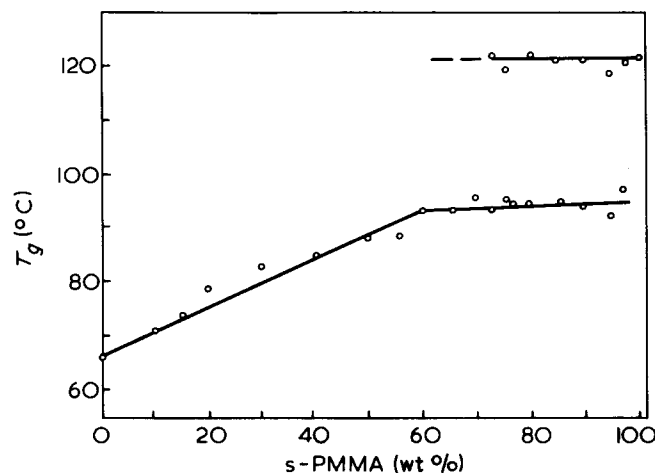


Figure 5 Glass transition temperatures  $T_g$  (determined by d.s.c.) versus wt% s-PMMA for the s-PMMA-PVC system

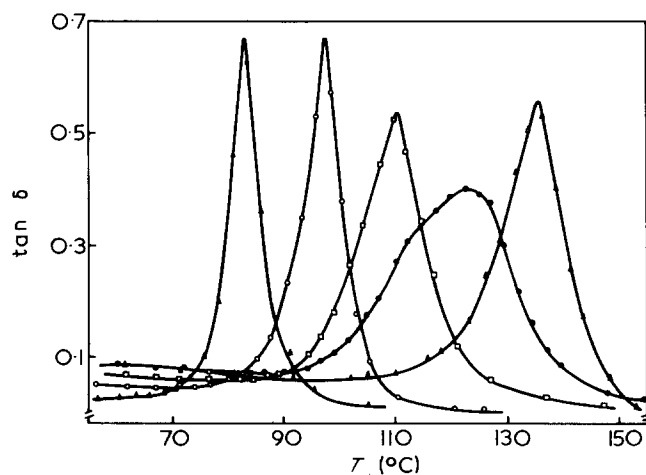


Figure 6 Loss tangent  $\tan \delta$  at about 1 Hz versus temperature for the s-PMMA-PVC system: ▲, 0:100; ○, 30:70; □, 60:40; ●, 80:20; △, 100:0 s-PMMA-PVC

## DISCUSSION

From our studies it can be concluded that i-PMMA and PVC form an incompatible system over the whole composition range, with phase separation between two phases. One phase is very rich in PVC and the other one in i-PMMA. On the contrary, s-PMMA and PVC form a compatible system up to 60 wt% s-PMMA. At higher s-PMMA contents separation occurs between a 60:40 s-PMMA-PVC phase and pure s-PMMA.

Taking into account the different weights of monomer units it appears that the 60:40 s-PMMA-PVC composition corresponds to a monomer unit ratio of nearly 1:1. So, the results show that the interaction between PVC and s-PMMA is so strong that a compatible system is formed up to a monomer unit ratio of 1:1. Possibly, some 1:1 associate is formed from s-PMMA and PVC, which dissolves in excess PVC producing a single  $T_g$  but which is not soluble in excess s-PMMA.

As mentioned in the introduction the solubility parameters are about the same for PVC ( $\delta = 9.6$ ) and a-PMMA ( $\delta = 9.5$ )<sup>12</sup>. Unfortunately, very little is known about the solubility parameters of stereoregular polymers. Only Cowie<sup>19</sup> has reported  $\delta$  values for i- and s-PMMA, viz. 9.28 and 9.55, respectively. These values are in good agreement with the difference in mixing behaviour of i- and s-PMMA with PVC as found by us. This difference might be attributed to the different chain conformations of i- and s-PMMA. i-PMMA prefers a  $S_1$  helix conformation<sup>20</sup>, while s-PMMA chains have predominantly a planar structure<sup>21</sup>. In the  $S_1$  helix the ester groups are rotated somewhat inwards and become less accessible to intermolecular interaction than the ester groups of s-PMMA in the planar conformation. Furthermore the ester group of PMMA is considered to be a proton accepting group, whereas PVC behaves like a weakly proton donating polymer by its  $\alpha$ -H atoms<sup>22</sup>. So, PMMA and PVC are complementary polymers,

for which dipole-dipole or hydrogen bondlike interactions can manifest themselves more strongly when PMMA has a syndiotactic microstructure.

## REFERENCES

- 1 Bohn, L. *Kolloid-Z. Z. Polym.* 1966, 213, 55
- 2 Rosen, S. L. *Polym. Eng. Sci.* 1967, 7, 115
- 3 Krause, S. J. *Macromol. Sci. (C)* 1972, 7, 251
- 4 Matsu, M., Nozaki, C. and Jyo, Y. *Polym. Eng. Sci.* 1969, 9, 197
- 5 Stoelting, J., Karasz, F. E. and MacKnight, W. J. *Polym. Eng. Sci.* 1970, 10, 133
- 6 Shultz, A. R. and Gendron, B. M. *J. Appl. Polym. Sci.* 1972, 16, 461
- 7 Prest, Jr. W. M. and Porter, R. S. *J. Polym. Sci. (A-2)* 1972, 10, 1639
- 8 MacKnight, W. J., Stoelting, J. and Karasz, F. E. *Adv. Chem. Ser.* 1971, 99, 29
- 9 Noland, J. S., Hsu, N. N.-C., Saxon, R. and Schmitt, J. W. *Adv. Chem. Ser.* 1971, 99, 15
- 10 Bank, M., Leffingwell, J. and Thies, C. *J. Polym. Sci. (A-2)* 1972, 10, 1097
- 11 Koleske, J. V. and Lundberg, R. D. *J. Polym. Sci. (A-2)* 1969, 7, 795
- 12 Brandrup, J. and Immergut, E. H. 'Polymer Handbook', Interscience, New York, 1966, Ch IV, p 366
- 13 Goode, W. E., Owens, F. H., Fellmann, R. P., Snyder, W. H. and Moore, J. H. *J. Polym. Sci.* 1960, 46, 317
- 14 Abe, H., Imai, K. and Matsumoto, M. *J. Polym. Sci. (C)* 1968, 23, 469
- 15 Ramey, K. C. *J. Polym. Sci. (B)* 1967, 5, 859
- 16 Bischof, J. and Desreux, V. *Bull. Soc. Chim. Belg.* 1952, 61, 10
- 17 Moore, W. R. and Hutakinson, R. J. *Nature* 1963, 200, 1097
- 18 Razinskaya, J. N., Vidyakina, L. I., Radbil', T. I. and Shtarkman, B. P. *Vysokomol. Soedin. (A)* 1972, 14, 968
- 19 Cowie, J. M. G. *Polymer* 1969, 10, 708
- 20 Tadokoro, H., Chatani, Y., Kusanagi, H. and Yokoyama, M. *Macromolecules* 1970, 3, 441
- 21 Grigo'eva, F. P., Birshtein, T. M. and Gotlib, Yu. Ya. *Vysokomol. Soedin. (A)* 1967, 9, 580
- 22 Adelman, R. L. and Klein, I. M. *J. Polym. Sci.* 1958, 31, 77

# Influence of cure system concentration on crosslink structure in SBR sulphur vulcanizates

C. M. Blow and C. T. Loo\*

*Institute of Polymer Technology, Loughborough University of Technology, Loughborough, Leics LE11 3TU, UK*

*(Received 3 June 1974; revised 8 August 1974)*

A series of pure gum styrene–butadiene copolymer mixes, compounded with a sulphur/*N*-cyclohexyl-2-benzothiazyl sulphenamide (CBS) curing system and vulcanized for various times at 150°C has been subjected to extraction and chemical probe treatments to cleave polysulphidic and disulphidic crosslinks. The changes in the value of  $C_1$  of the Mooney–Rivlin equation, obtained from stress–strain data, and the degree of swelling in *n*-heptane are reported. The weight losses occurring during these treatments have also been determined. If the proportion of vulcanizing ingredients is varied with the ratio of sulphur to CBS held constant, the ratio of monosulphidic to disulphidic crosslinks varies considerably at cure times from 45 to 120 min; no polysulphidic crosslinks were present in the vulcanizates examined. The paper contains values of  $C_2$  (Mooney–Rivlin equation) and of  $\chi$ , the polymer–liquid interaction constant; the latter varies with the cure system and is altered by the chemical probe treatments.

## INTRODUCTION

In much of the published work on the study of the properties of rubber vulcanizates in relation to crosslink density, peroxide-cured materials have been employed in which the crosslink is of one type: carbon–carbon.

If the interest, however, is in accelerated sulphur vulcanizates, the problem of selecting a series of mixes to study the effect of crosslink density is complicated by the fact that sulphur forms mono-, di- and poly-sulphidic crosslinks as well as sulphidic ring structures with the polymer chain and pendant accelerator groups<sup>1</sup>.

An accelerated sulphur mix vulcanized for a range of times and/or at a range of temperatures will produce a series of vulcanizates with varying crosslink densities but, as is well known, the ratio of monosulphide to disulphide to polysulphide crosslinks varies greatly. An alternative approach is to keep the time and temperature of vulcanization constant and vary the curing system, (a) maintaining a constant proportion of sulphur and varying the accelerator proportion, (b) maintaining a constant proportion of accelerator and varying the sulphur proportion, or (c) maintaining the sulphur to accelerator ratio constant and varying the proportion of total ingredients.

There are statements in the literature<sup>2</sup> to the effect that if the last procedure (c) is adopted the crosslink density will be varied but the proportion of each of the several crosslink types will remain constant. Little evidence has, however, come to light in the present authors' searches, and that is conflicting. Farlie<sup>3</sup> gave data on the mono-, di- and poly-sulphidic proportions in two series of pure gum natural rubber (NR) vulcanizates with a constant sulphur to accelerator ratio, vulcanized at 140°C for the same time. In the

first series, a conventional sulphur to *N*-cyclohexyl-2-benzothiazyl sulphenamide (CBS) ratio of 5:1 was used and cure times of 35 min and 120 min representing approximately optimum and overcure respectively. At each cure time the proportions of disulphide and polysulphide crosslinks present in the vulcanizates were substantially constant for a range of sulphur contents from 2 to 4 parts per hundred of rubber (by wt) (phr), there being no monosulphide crosslinks; at the overcure, the monosulphide/disulphide/polysulphide proportions were equal. In the second series, an efficient cure system, sulphur/tetramethyl thiuram disulphide (TMTD)/2-(4-morpholinylmercapto)benzothiazole (MOR) in the ratio 1:1.89:4, was used and a cure time of 50 min. In this case the percentage of monosulphide crosslinks varied from 100 to 85 for a range of sulphur contents from 0.35 to 1.0 phr, the remainder being disulphide links with no polysulphide links.

Studebaker<sup>4</sup> investigated black loaded [50 phr high abrasion furnace (HAF)] NR mixes with the ratio of sulphur to accelerator held constant over a range of sulphur contents from 1 to 6 phr; the accelerators were diphenylguanidine (DPG), MOR, and 2-mercaptobenzothiazole (MBT). Analyses were carried out for polysulphide and monosulphide crosslinks using the lithium aluminium hydride reagent in conjunction with crosslink density estimates from swelling determinations corrected for the carbon black content using the procedure described by Kraus<sup>5</sup>. A decrease in the ratio of polysulphide to monosulphide crosslinks was found to occur with the increasing quantity of curing agents.

In this paper a study is reported of the effect of the proportion of sulphur and CBS (at a constant ratio) on the crosslink types in pure gum styrene–butadiene copolymer (SBR) vulcanizates. SBR mixes were selected because, if the relative proportion of the three crosslink types is con-

\* Present address: Rubber Research Institute of Malaysia, PO Box 150, Kuala Lumpur, Malaysia.

stant, they would be of interest as a series for a failure property study.

## EXPERIMENTAL

### Vulcanizate preparation

The mix formulations are given in *Table 1*, from which it is seen that the sulphur/CBS ratio in the four mixes has been kept constant at 1.81:1. The mixes were prepared on a laboratory mill in a conventional manner and had the same plasticity (Wallace Rapid Plasticity value  $29 \pm 2$ ); vulcanization was carried out in a steam-heated press at  $150^\circ\text{C}$  for a range of times to produce test sheets  $150 \times 150 \times 1$  mm, from which the testpieces were cut.

### Determination of crosslink density and crosslink type

Dumbbell shaped testpieces were punched from the test sheets and treated with propane-2-thiol (0.4 M) and piperidine (0.4 M) in n-heptane solution to cleave the polysulphidic crosslinks and with a solution of (1 M) n-hexane-thiol in piperidine to cleave the di- and poly-sulphidic crosslinks<sup>6</sup>. Additional testpieces were subjected to extraction in the

Table 1 Mix formulations

	A	B	C	D
SBR 1500	100	100	100	100
Zinc oxide	3.5	3.5	3.5	3.5
Stearic acid	2.5	2.5	2.5	2.5
Antioxidant*	1	1	1	1
Sulphur	0.8	1.32	2.0	3.34
CBS	0.44	0.73	1.1	1.84

\* Nonox OD (ICI Ltd.) octylated diphenylamine

Table 2 Stress-strain results

Test-piece no.	Mix no.	Cure time*	$C_1$ values at $25^\circ\text{C} \times 10^6$ (dynes/cm <sup>2</sup> )				
			Original	Extracted <sup>a</sup>	$S_1 + S_2^b$	$S_1^c$	$S_2^d$
1	A	75	0.17	0.19	0.27	soft gel	†
2	A	120	0.29	0.29	0.43	gel	†
3	B	45	0.50	0.53	0.67	gel	†
4	B	75	0.74	0.73	0.86	0.41	0.45
5	B	120	0.76	0.80	0.89	0.48	0.41
6	C	45	1.17	1.22	1.30	0.51	0.79
7	C	75	1.27	1.29	1.31	0.70	0.61
8	C	120	1.31	1.33	1.39	1.02	0.37
9	D	45	2.13	2.18	2.15	1.45	0.70
10	D	75	2.18	2.23	2.21	1.47	0.74
11	D	120	2.08	2.00	2.10	1.64	0.46

\* Minutes at  $150^\circ\text{C}$

<sup>a</sup> After extraction with n-heptane

<sup>b</sup> After propane-2-thiol/piperidine chemical probe treatment

<sup>c</sup> After n-hexane-thiol chemical probe treatment

<sup>d</sup> By difference (b - c)

† Testpieces 1, 2 and 3, after n-hexane-thiol treatment were very soft so that  $C_1$  values could not be obtained; the number of monosulphide crosslinks is, therefore, low in these vulcanizates

Table 3 Values of  $C_2$  (Mooney-Rivlin equation)  $\times 10^6$  (dynes/cm<sup>2</sup>)

	1	2	3	4	5	6	7	8	9	10	11
Original	1.06	1.12	1.24	1.36	1.40	1.53	1.54	1.59	1.90	1.95	1.81
After extraction	1.36	1.43	1.57	1.58	1.64	1.85	1.73	1.82	2.06	2.07	2.14
After propane-thiol probe	1.13	1.26	1.33	1.43	1.45	1.69	1.60	1.56	1.89	1.95	1.89
After hexane-thiol probe	—	—	—	1.36	1.46	1.93	1.41	1.51	1.78	1.62	1.44

cold by n-heptane for times and under conditions similar to those given to the testpieces for chemical destruction of crosslinks.

Stress-strain measurements of the original untreated, n-heptane extracted and chemically treated vulcanizates were carried out, using the technique and apparatus described previously<sup>7</sup>. Good straight line plots were obtained of  $f/2A_0(\lambda - \lambda^{-2})$  against  $\lambda^{-1}$  enabling the  $C_1$  and  $C_2$  values of the Mooney-Rivlin equation to be calculated,  $f$  being the force required to strain a testpiece of cross-sectional area  $A_0$  to an extension ratio,  $\lambda$ .

### Weight losses on extraction and chemical treatment

The losses in weight of testpieces during extraction with n-heptane and during treatment with propane-2-thiol and n-hexane-thiol were determined.

### Determination of swelling in n-heptane

Portions of some of the dumbbells used for the above-mentioned determination of crosslink density and type were swollen in n-heptane at  $20^\circ\text{C}$  for 96 h. From weights in air and liquid, the weight and volume changes were calculated. The weights and volumes of testpieces after removal of the solvent were also obtained so that the volume fraction of rubber in the swollen jelly,  $v_r$ , could be calculated, excluding soluble non-rubber ingredients. No correction was made for the small volume ( $\sim 1\%$ ) of zinc oxide and other non-extractable ingredients and residues.

## RESULTS

The values of  $C_1$  and  $C_2$  obtained on the vulcanizates in the untreated, extracted and chemically treated state are given in *Tables 2* and *3*. The values of  $C_2$ , differing somewhat from some other published values<sup>8</sup>, are only included for completeness; they are not relevant to the subject of this paper. The weight losses occurring during the various treatments are plotted in *Figure 1* against the corresponding  $C_1$  values.

The results of swelling tests (*Table 4*) on vulcanizates of mixes B, C and D, cured for 75 min at  $150^\circ\text{C}$ , (testpieces 4, 7 and 10), include the untreated vulcanizates, those extracted with n-heptane and dried, and those treated with the chemical probes. *Figure 2* is a plot of  $v_r$  against  $C_1$ , showing a correlation; the three n-hexane-thiol treated samples appear to lie on a line separate from the other results. Included in *Table 4* are the values of the polymer-liquid interaction constant,  $\chi$ , calculated according to the Flory-Rehner equation, using the  $C_1$  values as determined above:

$$-RT[\ln(1 - v_r) + v_r + \chi v_r^2] = 2V_1 C_1 (v_r^{1/3} - 1/2v_r)$$

$R$  and  $T$  are the gas constant and the absolute temperature respectively, and  $V_1$  is the molar volume of the liquid. It is to be noted that these  $\chi$  values are all higher than those reported by Bristow and Watson<sup>9</sup> and vary systematically

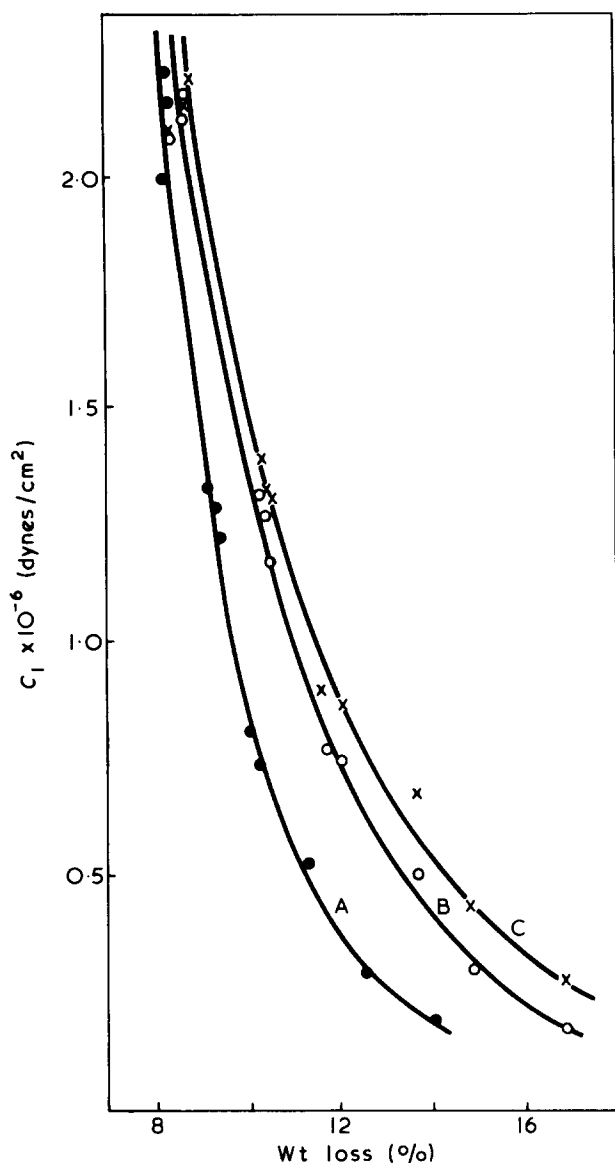


Figure 1 (A) Weight loss on extraction with n-heptane vs. the  $C_1$  value of the extracted testpiece; (B) weight loss on treatment with propane-2-thiol vs. the  $C_1$  value of the untreated testpiece; (C) weight loss on treatment with propane-2-thiol vs. the  $C_1$  value of the test-piece after treatment

Table 4  $v_r$  and  $\chi$  values for swelling in n-heptane at 20°C

Test-piece no.	Original untreated		Extracted n-heptane		Treated propane-thiol		Treated hexane-thiol	
	$v_r$	$\chi$	$v_r$	$\chi$	$v_r$	$\chi$	$v_r$	$\chi$
4	0.355	0.631	0.378	0.650	0.370	0.637	0.314	0.615
7	0.422	0.667	0.423	0.668	0.418	0.664	0.393	0.659
10	0.489	0.707	0.503	0.720	0.493	0.715	0.464	0.702

with the cure system and treatment. The change of  $\chi$  with curing system, cure time and after probe treatment is well documented<sup>10</sup>. Figure 3, a plot of  $v_r$  against  $\chi$ , is included for interest as it shows the linear relation ( $\chi = 0.436 + 0.56v_r$ ) previously pointed out by Kraus<sup>10</sup>.

## DISCUSSION

It should be pointed out that the probe treatment conditions were those developed for natural rubber vulcanizates. These may not be entirely appropriate for a SBR vulcanizate with

its different backbone structure, and some error may be involved in interpreting the data. Furthermore, no attempt has been made to calculate values for the density of chemical crosslinks because of the absence of data, in the case of SBR, to correct for chain ends and entanglements. Consideration is, therefore, confined to  $C_1$  values. Extraction with n-heptane increases the  $C_1$  value slightly and the chemical treatment with propane-2-thiol increases it somewhat more, the amounts of the increase correlating well with the weight losses (Figure 1) which are much in excess of

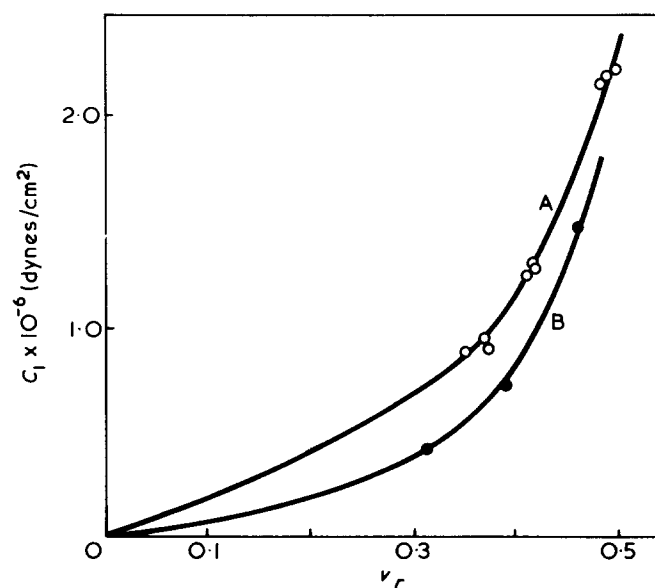


Figure 2 The  $C_1$  value vs.  $v_r$  (the volume fraction of polymer in the rubber swollen in n-heptane at 20°C) of testpieces 4, 7 and 10. A, Untreated, extracted and treated with propane-2-thiol; B, treated with n-hexane-thiol

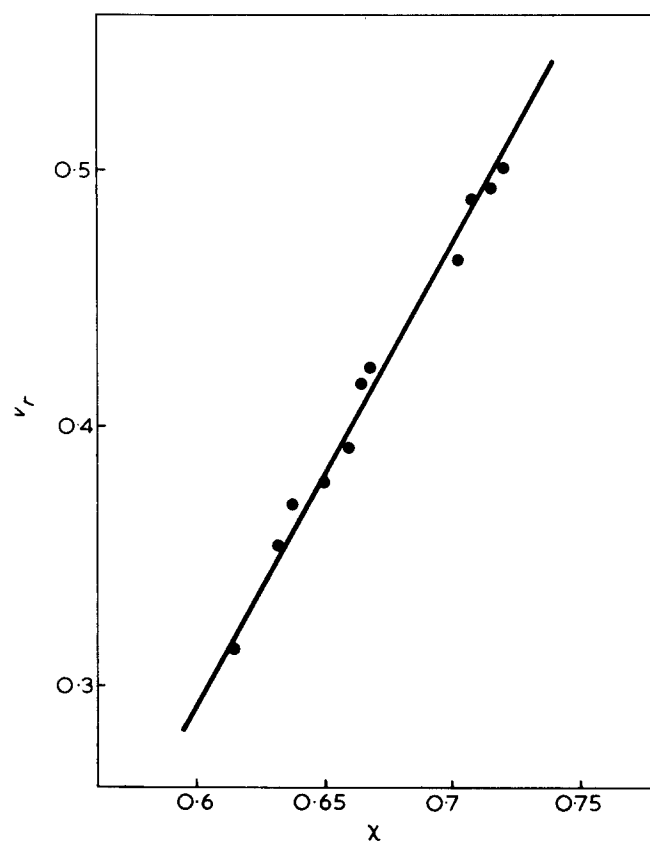


Figure 3  $\chi$  (the polymer-liquid interaction constant) vs.  $v_r$

those normally found in the case of pure gum NR vulcanizates.

Since neither extraction nor chemical probe treatment is carried out at an elevated temperature it can be assumed that no further sulphur crosslinks are added and the possibility of oxidative crosslinking seems remote. The explanation of the increase in  $C_1$  on extraction and probe treatment must lie in the removal of some unbound polymer, which the weight loss data suggest, and in the production of supercoiling and chain entanglements<sup>11</sup>. The lower the state of the cure the more unbound polymer there is likely to be and the greater freedom for the polymer chains to coil and rearrange on its removal.

The  $\nu_r$  values of the pre-extracted samples are somewhat higher than those of the original vulcanizate, although the latter values have been based on the extracted rubber. This fact that an extracted and dried sample swells less than an unextracted one lends weight to the suggestion that increased coiling and entanglement of polymer molecules are present in the extracted vulcanizates.

The conclusion from the data for the samples treated with the propane-2-thiol probe is that there is not a significant number of polysulphidic crosslinks in any of the vulcanizates which is in line with the known lower stability of polysulphides in SBR and their subsequent rapid conversion to monosulphide crosslinks in the case of the semi-efficient curing system employed in this series of mixes<sup>12</sup>. The  $C_1$  values in column 6 of Table 2 can, therefore, be considered to represent the contribution of the mono- and di-sulphide crosslinks. Correspondingly, the values in column 7, obtained on samples treated with hexane-thiol, represent the contribution of the monosulphide crosslinks.

## CONCLUSIONS

It appears justifiable to conclude that the contribution of the disulphide links will be given by the difference between the values in columns 6 and 7. Calculation of the ratio of monosulphide crosslinks to disulphide crosslinks (Table 5) shows that keeping the ratio of sulphur to CBS constant in the mix formulation has not maintained this ratio constant at any of the cure times selected in this series.

Table 5 Ratios of  $C_1$  value due to monosulphide crosslinks to that due to disulphide crosslinks

Cure system (phr)		Cure time at 150°C (min)		
Sulphur	CBS	45	75	120
1.32	0.73	—	0.91	1.17
2.00	1.10	0.65	1.15	2.76
3.34	1.84	2.07	1.99	3.57

## ACKNOWLEDGEMENTS

The authors gratefully acknowledge the interest and encouragement received from Professors R. J. W. Reynolds and A. W. Birley. One of us (C.T.L.) is in receipt of a Malaysian Rubber Research and Development Board post-graduate studentship.

## REFERENCES

- 1 Saville, B. and Watson, W. F. *Rubber Chem. Technol.* 1967, **40**, 100
- 2 Brennan, J. J. and Lambert, D. H. *Rubber Chem. Technol.* 1972, **45**, 94
- 3 Farlie, E. D. *J. Appl. Polym. Sci.* 1970, **14**, 1127
- 4 Studebaker, M. L. *Rubber Chem. Technol.* 1966, **39**, 1359
- 5 Kraus, G. J. *J. Appl. Polym. Sci.* 1963, **7**, 861; *Rubber Chem. Technol.* 1964, **37**, 6
- 6 Campbell, D. S. and Saville, B. *Proc. Int. Rubber Conf., Brighton, 1967* pp 1-14
- 7 Loo, C. T. *Polymer* 1974, **15**, 357
- 8 Gumbrell, S. M., Mullins, L. and Rivlin, R. S. *Trans. Faraday Soc.* 1953, **49**, 1495
- 9 Bristow, G. M. and Watson, W. F. *Trans. Faraday Soc.* 1958, **54**, 1731
- 10 Moore, C. G. and Trego, B. R. *J. Appl. Polym. Sci.* 1964, **8**, 1957; Westlinning, H. and Wolff, S. *Rubber Chem. Technol.* 1968, **41**, 659; Kraus, G. *Rubber World*, 1956, **135**, 67, 254; *J. Appl. Polym. Sci.* 1963, **7**, 1257
- 11 Bristow, G. M. and Porter, M. *J. Appl. Polym. Sci.* 1967, **11**, 2215
- 12 Studebaker, M. L. and Beatty, J. R. *ACS Rubber Div. Meet. Boston 1972* (April)

# The energetic contribution to rubber elasticity in the range of small uniaxial compression and moderate elongation

F. P. Wolf\* and Geoffrey Allen

Department of Chemistry, University of Manchester, Manchester M13 9PL, UK

(Received 9 July 1974)

The relative energetic contribution to the retractive force of a deformed rubber sample,  $f_e/f$ , has been evaluated from thermoelastic measurements at constant pressure. Extension ratios  $\lambda$  have been studied in the range  $0.88 \leq \lambda \leq 1.70$  at 20° and 40°C. The results are given for a reference temperature, 30°C. Since data in the transition region from uniaxial elongation to compression were to be evaluated, a new set of equations was derived on the basis of the Gaussian force law, because the usual equation for measurements at constant pressure tends towards infinity when approaching the undeformed state  $\lambda = 1$ .

Considerable difference between the results obtained by different, though apparently equivalent, equations have their origins in the deviation of the experimental data from ideal Gaussian behaviour. The influence of this inaccuracy on the terms of the equations is discussed and the most reliable functions for small deformations  $0.88 \leq \lambda \leq 1.15$  and for moderate elongation  $\lambda > 1.10$  have been identified. With these precautions the Gaussian force law is a satisfactory approximation for the determination of reliable values of  $f_e/f$ .

The evaluation of data at small deformations is extremely sensitive to experimental error. Even smoothed polynomials  $L(f)$  were not sufficient to eliminate an apparent maximum in the  $f_e/f$  vs.  $\lambda$  curve. Therefore the linear thermal expansion coefficient  $\beta_{lin}(\lambda)$ , which is a major term in all the  $f_e/f$  equations at small deformations, had to be scrutinized critically. Although experimental data in this range showed that  $\beta_{lin}(\lambda)$  is a slightly S-shaped function, a linear approximation is adequate at moderate elongations.

Using one of the new equations together with the linear approximation for  $\beta_{lin}(\lambda)$  in the region of small deformations, and two equivalent equations at moderate elongation, the energetic contribution to the total stress was found to be  $f_e/f = 0.18 \pm 0.02$  for lightly crosslinked natural rubber. Little variation in  $f_e/f$  was observed over the full range of measurements:  $0.88 \leq \lambda \leq 1.70$ .

## INTRODUCTION

The retractive force,  $f$ , of a deformed rubber sample does not originate entirely from entropy changes due to orientation of the macromolecules in the network. An energetic contribution,  $f_e$ , to the total force comes from changes of the conformational free energy of the macromolecules. The relative energetic contribution,  $f_e/f$ , can be related to the temperature coefficient of the unperturbed dimensions of the macromolecular chains<sup>1</sup> and thus provides a means of studying molecular processes.

The quantity  $f_e/f$  has been reported to be a function of extension ratio<sup>2,3</sup>. Furthermore in elongation the most serious deviations have been detected for small strains, where the experiment ought to be in best agreement with the statistical theory. The deviations at high strains in natural rubber can be ascribed, of course, to the onset of crystallization which can be detected by X-ray analysis<sup>4</sup>.

Since the variation of  $f_e/f$  in the range of small elongation may be due to experimental methods and their mathematical evaluation, methods currently in use will be discussed against the background of exact thermodynamical relations and the use of Gaussian theory. Then a new

set of equations will be developed for the evaluation of  $f_e/f$  from thermoelastic measurements. These equations will be applied to experimental data obtained from a rubber sample under small uniaxial deformation in compression as well as in elongation. The results will be compared with data obtained by one of the conventional methods up to moderate extensions.

## THEORY AND REVIEW OF $f_e/f$ DETERMINATIONS

The free energy of a macromolecular network is assumed to consist of two additive terms, the first one accounting for liquid-like intermolecular interactions, the second for intramolecular elastic free energy changes. Thus changes of the conformational free energy can be separated from intermolecular interactions. They are governed by the thermodynamical relationship:

$$dF_{el}(T, V, \lambda) = dU - TdS \quad (1)$$

$U$  being the internal energy,  $S$  the entropy,  $V$  the volume of the sample and  $\lambda = L/L_0$  the uniaxial deformation ratio (actual length divided by undeformed length).

The retractive force  $f$  of the deformed sample is obtain-

\* Permanent address: Fritz-Haber-Institut der Max-Planck-Gesellschaft, D1 Berlin 33 (Dahlem), Germany.



ed by differentiation of the free energy with respect to the actual length  $L$  at constant temperature  $T$  and volume  $V$ :

$$f = \left(\frac{\partial U}{\partial L}\right)_{T,V} - T \left(\frac{\partial S}{\partial L}\right)_{T,V} = f_e + T \left(\frac{\partial f}{\partial T}\right)_{V,L} \quad (2)$$

The first term represents the energetic contribution  $f_e$  to the total retractive force, and

$$f_e/f = 1 - \frac{T}{f} \left(\frac{\partial f}{\partial T}\right)_{V,L} \quad (3)$$

Instead of measuring the temperature coefficient of the force at constant volume and length, the following relationship uses the corresponding coefficient at constant pressure,  $p$  and length,  $L$ :

$$\begin{aligned} \left(\frac{\partial f}{\partial T}\right)_{V,L} &= \left(\frac{\partial f}{\partial T}\right)_{p,L} - \left(\frac{\partial f}{\partial V}\right)_{T,L} \left(\frac{\partial V}{\partial T}\right)_{p,L} \\ &= \left(\frac{\partial f}{\partial T}\right)_{p,L} - \left(\frac{\partial f}{\partial p}\right)_{T,L} \left(\frac{\partial p}{\partial V}\right)_{T,L} \left(\frac{\partial V}{\partial T}\right)_{p,L} \end{aligned} \quad (3a)$$

Introduction of the bulk thermal expansion coefficient  $\beta_L$  and the isothermal compressibility  $\kappa_L$  at constant length  $L$  of the sample, as given in a previous paper<sup>5</sup>, leads to:

$$f_e/f = 1 - \frac{T}{f} \left(\frac{\partial f}{\partial T}\right)_{p,L} - \frac{T}{f} \left(\frac{\partial f}{\partial p}\right)_{T,L} \cdot \frac{\beta_L}{\kappa_L} \quad (4)$$

Equations (3) and (4) have been derived using exact thermodynamical relationships.

Measurements based upon equation (3) are difficult because they require the thermal expansion of the sample to be offset by means of hydrostatic pressure. They have so far been carried out only by Allen *et al.*<sup>6,8</sup> for a few rubbers. Since the apparatus also allowed force vs. pressure measurements to be made, the use of equations (3) and (4) could be compared. The results were in good agreement with one another and although the data showed considerable scatter owing to experimental difficulties, no obvious trend of the  $f_e/f$  values in the region of small elongation ratios could be detected. Apart from these direct measurements, all other evaluations require the knowledge of a force vs. elongation relationship.

Application of Gaussian statistics to macromolecular networks leads to a force law which may be expressed as<sup>5</sup>:

$$\begin{aligned} f &= c \left( L - \frac{qV}{L^2} \right) \\ &= cL_0(\lambda - \lambda^{-2}V/V_0) \end{aligned} \quad (5)$$

where the factor  $V/V_0$  corrects for the difference between elongation ratio  $\lambda$  and anisotropic strain<sup>9</sup>  $\alpha$ , which because of the very small volume changes on deformation is extremely small and can be disregarded normally. The variable  $c$  depends on temperature only and  $q$  is a constant determined by the shape of the sample:

$$q = \frac{L_0^3}{V_0} = \frac{L_0^2}{A_0} \quad (5a)$$

(Subscript 0 refers to the undeformed state of the sample,  $A_0$  being the cross-sectional area.)

The slope  $cL_0$  at  $\lambda = 1$  for the usual Gaussian plot of force  $f$  vs.  $(\lambda - \lambda^{-2})$  is related<sup>5</sup> to the shear modulus,  $G$ :

$$cL_0 \approx A_0 G \quad (5b)$$

The following derivatives of the force  $f$  obtained from equation (5) will be needed later in the paper:

$$\left(\frac{\partial f}{\partial p}\right)_{T,L} = + \frac{cq}{L^2} V \kappa_L \quad (5c)*$$

$$\left(\frac{\partial f}{\partial L}\right)_{T,V} = \frac{c}{L^3} (L^3 + 2qV) \quad (5d)$$

$$\left(\frac{\partial f}{\partial V}\right)_{T,L} = - \frac{cq}{L^2} \quad (5e)$$

$$\left(\frac{\partial f}{\partial T}\right)_{V,L} = \frac{dc}{dT} \left( L - \frac{qV}{L^2} \right) = f \frac{d \ln c}{dT} \quad (5f)$$

Returning now to equation (4), all pressure dependent quantities in the last term can be replaced in order to yield a formula for the evaluation of thermoelastic experiments at constant  $p$  and  $L$ . Using equations (5) and (5c) the following expression is obtained for the relative energetic contribution:

$$f_e/f = 1 - \frac{T}{f} \left(\frac{\partial f}{\partial T}\right)_{p,L} - \frac{\beta_L T}{(\lambda^3 V_0/V - 1)} \quad (6)$$

This equation has been derived by Flory<sup>10</sup> who points out that the last term depends strongly on  $\lambda$ , being infinite for  $\lambda = 1$ . This equation has frequently been used for the evaluation of experimental data, because the conditions of constant  $p$  and  $L$  are easily realized. Owing to the behaviour of the last term, upturns or downturns of  $f_e/f$  when approaching  $\lambda = 1$  have been reported in the literature (for a review see refs 2 and 3), and some authors have tried to find molecular interpretations of this phenomenon<sup>11-13</sup>.

Another formula, originally given by Flory<sup>10</sup> in terms of the anisotropic strain  $\alpha$  has been used with<sup>9</sup>  $\lambda \approx \alpha$  for the evaluation of measurements at constant pressure:

$$f_e/f = 1 - \frac{T}{f} \left(\frac{\partial f}{\partial T}\right)_{p,\lambda} + \frac{\beta_L T}{3} \quad (7)$$

It may be verified using the Gaussian force law (5).

Evaluating the same set of data for silicone rubber in the range  $\lambda > 1.25$ , Ciferri<sup>14</sup> obtained equivalent results within the limits of experimental error by means of equations (6) and (7). Barrie and Standen<sup>15</sup> applied equation (7) to data obtained at constant  $p$  and  $f$ , conditions which are even more suitable from an experimental point of view than those of constant  $p$  and  $L$ . Both the above mentioned references, like the majority of the more recent publications, make use of least square method computer programs (LSMCP) to fit experimental data and to find a reliable value of the unstrained length  $L_0$ . Even with

\*  $(\partial f/\partial p)_{T,L} = (\partial f/\partial V)_{T,L} (\partial V/\partial p)_{T,L} = (\partial V/\partial L)_{T,p}$

LSMCP small inconsistencies<sup>15</sup> such as force  $f \neq 0$  for  $\lambda = 1$  often obtain. This problem has been dealt with in a previous paper<sup>5</sup>.

Another type of experiment has been carried out by Treloar<sup>3,16</sup>, who employed cylindrical samples subjected to combined torsion and axial extension. This method avoids the sensitivity to an accurate determination of  $L_0$  and the deviations which are introduced by equation (6) in the region of small strains. Effects of the volume changes on deformation are much less apparent. On the other hand, combined torsion and extension involve an inhomogeneous state of strain and thus can be compared with uniaxial deformation only in the limit of zero strain. From the experimental point of view, Treloar's measurements are more complicated than stress-strain investigations in simple elongation.

The relative energetic contribution to the total stress can be calculated from the temperature dependence of the shear modulus,  $G$ . Equations (5f) and (5b) yield:

$$f_e/f = 1 - T \frac{d \ln c}{dT} = 1 - T \frac{d \ln G}{dT} - \frac{\beta_0 T}{3} \quad (8)$$

The thermal expansion coefficient  $\beta_0$  (of the isotropic state) has to be taken into account because  $c$  is different from the modulus by the dimension 'length'.

Equation (8) has been used by Shen and Blatz<sup>2</sup> in a new attempt to remove the inadequacy of equation (6). They determined  $G$  from the initial slopes of Gaussian plots in a way similar to equation (5b). The curves of  $f/A_0$  vs. elongation  $(\lambda - \lambda^{-2})$  were calculated by a LSMCP 'forced' through the origin. Since only the 'linear parts' of the Gaussian plots ( $\lambda < 1.3$ ) were used and one single value of  $G$  was obtained for each plot, it was claimed that  $f_e/f$  was strain independent in this region.

#### CHOICE OF EXPERIMENTAL CONDITIONS

Because of the well known difficulties of the constant volume experiment the condition of constant pressure is normally preferred for thermoelastic investigations. Then there remain three variables, one of which must be kept constant: (a) temperature,  $T$ ; (b) force,  $f$  or stress,  $f/A_0$ ; (c) length,  $L$  or elongation,  $\lambda$  (or anisotropic strain  $\alpha$ ). Alternative (c) presents experimental difficulties. Experiments at constant  $T$  were chosen because the apparatus used in the present investigation was designed to allow measurements of length vs. force in the regions of small uniaxial extensions and compressions. Thus the undeformed length  $L_0(T)$ , the determination of which has proved troublesome in other investigations, is obtained with high accuracy by a LSMCP for  $f = 0$ . We have not made  $L$  vs.  $T$  measurements at constant force.

The apparatus and experimental technique have been described previously<sup>5</sup>. The measurements have been evaluated on the basis of various theoretical relationships which render the resulting  $f_e/f$  as a function of either the force  $f$  or elongation ratio,  $\lambda$  and also yield a finite value for  $f_e/f$  at zero force. For comparison the experimental results have been converted into relations between  $f$  and  $T$  at constant  $p$  and  $L$  and an evaluation according to equation (6) has been carried out.

#### EVALUATION OF $f_e/f$ FROM EXPERIMENTAL DATA

In the analysis of our experimental data we have explored a number of formally equivalent procedures for the evaluation of  $f_e/f$ . Without making any assumptions the following equations can be derived from equation (3) using the normal methods of manipulating partial differentials. These manipulations are set out in more detail in the Appendix.

In this section we simply list the equations which have actually been used to interpret the experimental data. Apart from equation (6) these are:

$$f_e/f = 1 + T \left[ \beta_{\text{lin}} + \frac{cL_0}{\lambda^2 V_0/V} \frac{3\beta_{\text{lin}} - \beta_f}{f} \right] \quad (9)$$

$$f_e/f = 1 + T \left[ \beta_{\text{lin}} + \frac{3\beta_{\text{lin}} - \beta_f}{\lambda^3 - 1} \right] \quad (9a)$$

$$f_e/f = 1 + \frac{T}{f} \frac{cL_0}{\lambda^2} \left[ (\lambda^3 + 2)\beta_{\text{lin}} - \beta_f \right] \quad (9b)$$

$$f_e/f = 1 + \frac{T}{f} \left[ \left( \frac{\partial f}{\partial L} \right)_{T,p} \frac{L\beta_{\text{lin}}}{f} - \frac{cL_0}{\lambda^2} \beta_L \right] \quad (9c)$$

$$f_e/f = 1 + T \left[ \left( \frac{\partial f}{\partial L} \right)_{T,p} \frac{L\beta_{\text{lin}}}{f} - \frac{\beta_L}{\lambda^3 - 1} \right] \quad (9d)$$

#### SAMPLE SPECIFICATION AND ASSESSMENT OF THE APPROXIMATIONS

The lightly crosslinked sample of natural rubber had a cylindrical shape of 4.2 cm length and 1.27 cm diameter as described in a previous paper<sup>5</sup>. Length vs. force measurements were taken at 20° and 40°C in the range of  $0.88 \leq \lambda \leq 1.18$ , and an individual set of results at  $\lambda = 1.70$ . Thus thermoelastic quantities could be calculated for a reference temperature of 30°C which is convenient for comparison with the literature.

At 30°C the cross-section area of the sample was  $A_0 = 1.266 \text{ cm}^2$ . For the isothermal compressibility a value of  $\kappa_L = 51.4 \times 10^{-6} \text{ atm}^{-1} \equiv 5.07 \times 10^{-10} \text{ m}^2/\text{N}$  can be extrapolated from ref 18. This quantity is independent of strains<sup>6,19</sup> within an experimental error of 3%.

Two sets of reference marks were attached to the sample, the unstrained distances being about 3.4 cm ('outer marks') and 2.6 cm ('inner marks') respectively. The shear modulus,  $G$  was evaluated according to equation (5b) for 30°C:

$$G = 0.462(0.458) \times 10^6 \text{ N/m}^2$$

for the outer (inner) marks. With the mean value of  $G$  the factor  $G\kappa_L/\lambda$  was obtained:  $G\kappa_L = 2.34 \times 10^{-4}$ . This factor appears in several correction terms which have to be assessed.

(a) Uniaxial deformation of a sample is accompanied by volume changes. The quotient:

$$V_0/V \approx 1 - \frac{\Delta V}{V_0} = 1 - \phi \quad (10)$$

or its inverse value appears together with some power of  $\lambda$  in the force law (5) and in the  $f_e/f$  expressions. The correction  $\phi$  is obtained on the basis of the Gaussian force law as<sup>5</sup>:

$$\phi \approx \frac{\kappa_L}{A_0} \frac{f}{\lambda + 1 + \lambda^{-1}} \approx \frac{G\kappa_L}{\lambda} (\lambda - 1) \quad (11)$$

(b) The bulk thermal expansion coefficient under conditions of constant force (A1e) has been assumed to remain constant for moderate elongation. This assumption has been proved for the corresponding coefficient at constant length<sup>6</sup>. The difference between  $\beta_L$  and  $\beta_f$  may be assessed from equations (5c) and (A1d):

$$\beta_L = \frac{1}{V} \left( \frac{\partial V}{\partial T} \right)_{p,L} = \frac{1}{V} \left( \frac{\partial V}{\partial T} \right)_{p,f} - \frac{1}{V} \left( \frac{\partial V}{\partial L} \right)_{p,T} \left( \frac{\partial L}{\partial T} \right)_{p,f} \quad (12)$$

$$\beta_L = \beta_f \left( 1 - \frac{cq}{L} \frac{\kappa_L \beta_{\text{lin}}}{\beta_f} \right) = \beta_f (1 - \chi) \quad (12a)$$

$$\chi \approx \frac{G\kappa_L}{\lambda} \frac{\beta_{\text{lin}}}{\beta_f} \quad (13)$$

(c) Comparing equations (A2) and (A2a) in the Appendix the bulk thermal expansion coefficients  $\beta_f$  and  $\beta_L$  have been interchanged, and  $(\partial f/\partial L)_{T,V}$  has been replaced by  $(\partial f/\partial L)_{T,p}$ :

$$\left( \frac{\partial f}{\partial L} \right)_{T,p} = \left( \frac{\partial f}{\partial L} \right)_{T,V} + \left( \frac{\partial f}{\partial V} \right)_{T,L} \left( \frac{\partial V}{\partial L} \right)_{T,p} \quad (14)$$

The derivatives in the last term are replaced through equations (5c), (5d), (5e) thus:

$$\begin{aligned} \left( \frac{\partial f}{\partial L} \right)_{T,p} &= \left( \frac{\partial f}{\partial L} \right)_{T,V} \left[ 1 - \frac{cq}{L^2} \frac{cq}{L^2} V\kappa_L \frac{L^3}{c(L^3 + 2qV)} \right] \\ &= \left( \frac{\partial f}{\partial L} \right)_{T,V} (1 - \psi) \end{aligned} \quad (14a)$$

where

$$\psi \approx \frac{G\kappa_L}{\lambda} \frac{1}{\lambda^3 + 2} \quad (15)$$

(d) The Gaussian force law (5) itself is an approximation. To estimate its validity, the experimental data of force and elongation can be inserted so that the experimental correction  $\omega$  is obtained:

$$\omega = 1 - \frac{cL_0(\lambda - \lambda^{-2})}{f} \quad (16)$$

For values of  $\lambda$  in the range studied here, the corrections  $\phi$ ,  $\chi$ ,  $\psi$  and  $\omega$  have been calculated using the experimental results reported previously<sup>5</sup>, and are given in Table 1.

Although experiments have proved that volume changes exceed the values calculated according to Gaussian behaviour<sup>20</sup> the correction  $\phi$  remains negligible compared with  $\omega$ . The same applies to  $\chi$ , and since the experimental accuracy of  $\beta_L$  is about 1%,  $\beta_L$ ,  $\beta_f$  and  $\beta_0$  cannot be discriminated. The correction  $\psi$  too can be disregarded, which means that it is satisfactory to carry out force vs. elongation measurements at constant pressure even if the coefficient at constant volume is needed.

Table 1 Values of  $\lambda$  and the corrections  $\phi$ ,  $\chi$ ,  $\psi$  and  $\omega$  for the studied range

$\lambda$	$\phi$ (%)	$\chi$ (%)	$\psi$ (%)	$\omega$ (%)
0.88	-0.003	0.023	0.010	2.15
1.00	0.0	0.008	0.008	0.0
1.18	0.004	-0.010	0.005	-3.83
1.70	0.010	-0.034	0.002	-13.06

The aforementioned corrections have been calculated on the basis of the force law (5), which may only be exact enough when  $\lambda$  is close to 1. The orders of magnitude of  $\phi$ ,  $\chi$ ,  $\psi$  will remain much the same even for a non-Gaussian equation of state. More troublesome is the influence of  $\omega$  when the force law is applied to transform the exact equation (A2) for the determination of  $f_e/f$ . Even if both derivatives are evaluated by means of the force law (5), there is no guarantee that the deviations cancel out. If, on the other hand, equations with the experimentally determined quantities  $(\partial f/\partial L)_{T,p}$  or  $(\partial f/\partial T)_{p,L}$  are used there remains the uncertainty of the second term in the force law. If the force law is applied to both terms of equation (A2), for  $f = 0$  the difference in  $f_e/f$  is zero because  $\omega = 0$ . Expressions (6) and (9c) and (9d) which contain the force law in one of their terms only can give infinite values of  $f = 0$  resulting from even the most minute experimental scatter. Furthermore equation (7) involves the same uncertainties originating from the force law.

Use of the Mooney-Rivlin equation instead of the Gaussian force law would be of little help in the experimental range of the present work because this equation is not applicable in the vicinity of  $\lambda = 1$  or in uniaxial compression<sup>5</sup>.

## RESULTS

The measurements of lengths vs. force at 20° and 40°C have been described previously<sup>5</sup>. Experimental data in the range of small deformation  $0.88 < \lambda < 1.18$  were represented by fourth power polynomials  $L(f)$  using a LSMCP. From these polynomials mean values for 30°C were calculated giving the constant  $cL_0$  and  $\beta_f$ , and the functions  $\lambda$ ,  $\beta_{\text{lin}}$  and  $(\partial f/\partial L)_{T,p}$  as functions of  $f$ . Then equations (9), (9a), (9b), (9c) and (9d) could be applied to the determination of  $f_e/f$ . For comparison, another LSMCP was used to fit the experimental data by third power polynomials  $f(L)$ . Thus the expansion coefficient  $\beta_L$  and the functions  $f$ ,  $\lambda$  and  $(\partial f/\partial T)_{p,L}$  were obtained at constant increments in length. This evaluation allowed the application of equation (6) to determine  $f_e/f$ .

### Influence of experimental errors in $\beta_{\text{lin}}$

The linear thermal expansion coefficient  $\beta_{\text{lin}}$  is a substantial part of all equations for  $f_e/f$  except equation (6). The results turn out to be strongly dependent on any variation in  $\beta_{\text{lin}}$  which itself is sensitive to experimental errors. To assess the experimental scatter of  $\beta_{\text{lin}}$  this function has been drawn, for the outer and the inner pairs of marks, in Figure 1, rendering the computer-calculated curves for small deformations ( $\lambda = 0.9$  to 1.15) as continuous lines and an averaged curve for the experimental data at moderate elongation up to  $\lambda \approx 1.70$  as a broken line. The continuous curves are slightly S-shaped, the curve for the inner marks showing a downward curvature above  $\lambda \approx 1.12$  which probably is due to experimental inaccuracies. Therefore

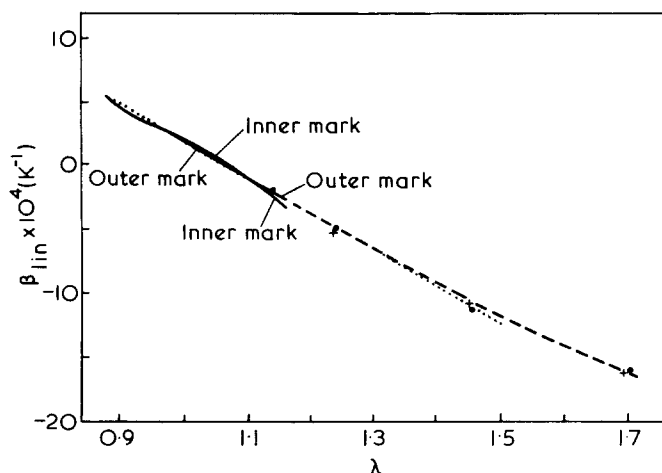


Figure 1 Linear thermal expansion coefficient  $\beta_{lin}$  vs.  $\lambda$ . ●, Outer marks; +, inner marks. —, Computer calculated curves for small deformations; ···, approximated straight line for small deformations; ---, averaged curve for moderate elongations

of the continuous curves only that for the outer marks which connects satisfactorily with the broken line, was used to calculate  $f_e/f$ .

Taking the whole range of measurements and the experimental scatter between inner and outer marks into consideration another method of smoothing out the experimental findings seems reasonable too. In the range of small deformation from  $\lambda \approx 0.90$  to  $\lambda \approx 1.15$ ,  $\beta_{lin}$  might be approximated by a straight line which joins the broken line and the straight line might even be extended through the experimental points measured at moderate elongation up to  $\lambda \approx 1.50$  (dotted line). Only the last two points, for  $\lambda \approx 1.70$ , are not included.

In the isotropic state  $\lambda = 1$  the continuous curves yield for the outer (inner) marks  $\beta_{lin}(0) = 2.134(2.230) \times 10^{-4} \text{ deg}^{-1}$  whereas from the straight approximation  $\beta_{lin}(0) = 2.14 \times 10^{-4} \text{ deg}^{-1}$ . According to equation (9f) the bulk expansion coefficient  $\beta_f$  is to be calculated from  $\beta_{lin}(0)$ . A comparison with  $\beta_L$  as obtained from the second LSCMP (the constant length evaluation) shows good agreement:

$$\beta_f [\times 10^{-4} \text{ deg}^{-1}] = 6.40_1 (6.68_9)$$

$$\beta_L [\times 10^{-4} \text{ deg}^{-1}] = 6.40_9 (6.69_8)$$

The accuracy of these coefficients has previously been estimated at 3%<sup>5</sup>.

Thermoelastic inversion occurs at  $\lambda_{inv} = 1.076$  (1.079) on the continuous curves or at 1.074 in the case of the linear approximation of  $\beta_{lin}(\lambda)$ . Because the curve passes through zero the relative accuracy of  $\beta_{lin}$  depends strongly on its absolute value.

From the continuous curve of  $\beta_{lin}$  from the outer marks,  $f_e/f$  has been calculated by means of equations (9), (9a), (9b), (9c) and (9d) in the region of small deformation and from the experimental data of either pair of marks in moderate elongation (broken lines). Figure 2 shows these results together with values obtained according to equation (6) from the constant length evaluation. All continuous functions (9), (9a) and (9b) yield a distinct value  $(f_e/f)_0 = 0.265$  for  $\lambda = 1$  whereas (9c) and (9d) have sharp poles which only become apparent in the interval  $0.98 < \lambda < 1.02$ . The functions show maxima of different heights for  $\lambda \approx 0.95$  and a rather sharp decrease for smaller  $\lambda$  (more

compression). In elongation there is a negative slope which gradually lessens towards higher  $\lambda$ , being different for each formula and even leading to almost zero slope for (9c) and (9d) in the range of moderate elongation. Equation (6) yields a curve similar to (9c), (9d) but tends towards  $+\infty$  on either side of  $\lambda = 1$  and shows a small decrease in compression.

Even apart from the differences between functions yielding infinite values for  $\lambda = 1$  and the continuous functions in the immediate vicinity of zero deformation, there is a broad scatter of the  $f_e/f$  results obtained by different equations. In compression down to  $\lambda \approx 0.92$  the extreme values of  $f_e/f$  differ by  $\Delta(f_e/f) \leq 0.05$ . In the range of small elongations  $\Delta(f_e/f) < 0.03$  up to  $\lambda \approx 1.12$  but  $\Delta(f_e/f) \geq 0.20$  at moderate elongations for  $\lambda > 1.50$ .

In addition to the variation originating from the use of different functions there is an experimental scatter between values for the outer and inner pair of marks, obtained by the same function. This is shown in Figure 3, in which  $f_e/f$  is represented according to equation (9a) in the range of small deformation as continuous curves and the experimental points for moderate elongation approximated by a broken line. The discrete value  $(f_e/f)_0 = 0.298$  is found from all continuous functions for the inner marks compared with 0.265 for the outer ones.

If, however, the  $f_e/f$  calculation is carried out based upon a smoothed function  $\beta_{lin}$ , the resulting curve in the range of small deformation has a completely different shape. Figure 4 shows  $f_e/f$  in the range of small deformation  $0.90 \leq \lambda \leq 1.15$  as a continuous curve obtained from the straight line approximation of  $\beta_{lin}$  using equation (9a).

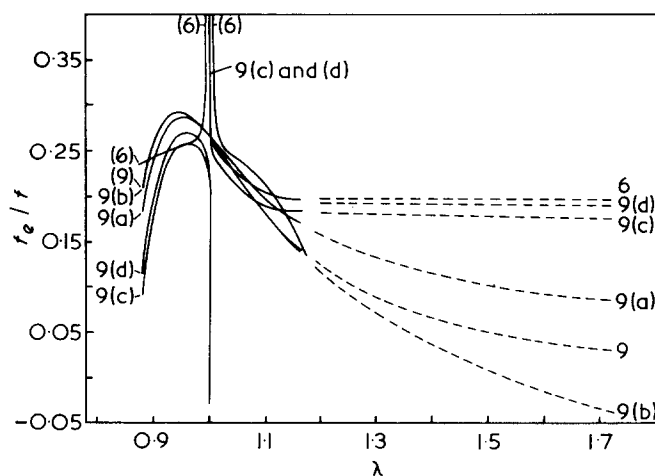


Figure 2  $f_e/f$  vs.  $\lambda$  calculated from various equations

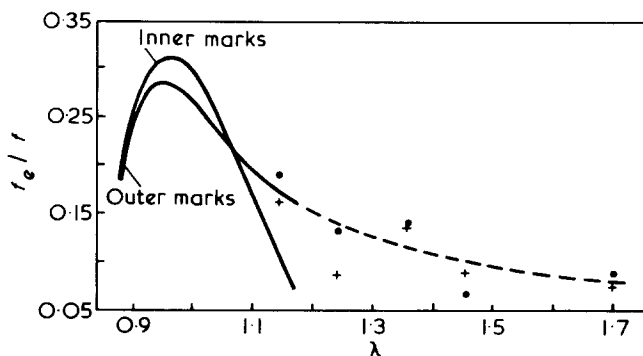


Figure 3  $f_e/f$  vs.  $\lambda$  for outer (●) and inner (+) marks from equation (9a)

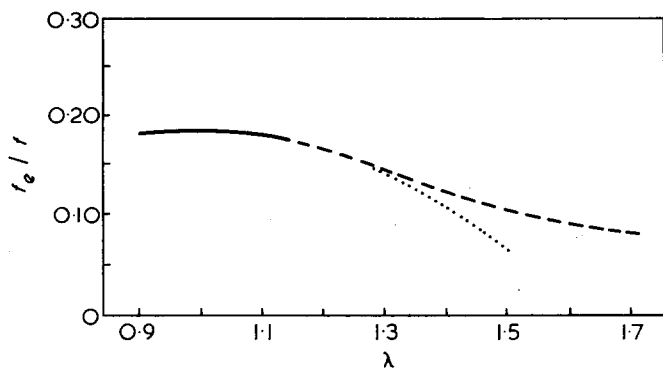


Figure 4  $f_e/f$  vs.  $\lambda$  from equation (9a) with linear approximation of  $\beta_{lin}(\lambda)$

Thus  $f_e/f$  is almost constant in this range with an average value of 0.18.

Continuation of the straight approximation up to  $\lambda \approx 1.50$  leads to  $f_e/f$  values which, by analogy to Figure 1, are given by a dotted line. From the broken line in Figure 1 the broken line in Figure 4 is obtained. Comparing the broken and dotted lines in Figure 4 again it is seen that small changes of  $\beta_{lin}$  (see Figure 1) cause drastic changes of  $f_e/f$ .

We conclude that the influence of experimental errors in  $\beta_{lin}$  on the evaluation of  $f_e/f$  at small deformations is most conveniently dealt with by use of a smoothed function for  $\beta_{lin}$  which is linear in  $\lambda$ .

Restrictions on the use of the force law

The poles displayed by equations (6), (9c) and (9d) show that the application of the Gaussian force law to the evaluation of  $f_e/f$  must be considered critically. Inspection of these three equations reveal that whereas  $-(1/f) \cdot (\partial f / \partial T)_{p,L}$  and  $(\partial f / \partial L)_{T,p} \cdot L \beta_{lin} / f$  can be calculated directly from experimental measurements, the second term in each equation can only be estimated by invoking the force law. At higher elongations they become increasingly important compared with the second terms which can only be determined from the force law. Figure 5 shows that the magnitude of the second term, underlying the inaccurate force law is roughly equal to the first term for  $\lambda \approx 1.15$  but only  $\sim 6\%$  of the first term for  $\lambda \approx 1.70$ . Thus increasing inaccuracy of the force law at higher elongations (see correction  $\omega$ ) is offset by the reduced importance of the term. Preference should be given to equation (9d) rather than (9c) for two reasons: first,  $\beta_L / (\lambda^3 - 1) < (cL_0 / f \lambda^2) \cdot \beta_L$  and therefore has less influence on  $f_e/f$ , and secondly the determination of the slope  $cL_0$ , which may cause additional inaccuracy, is redundant in equation (9d).

Inspection of Figure 5 shows that both the terms of equations (6) and (9d) tend towards infinity in opposite directions as  $\lambda = 1$  is approached. Whereas the increasing influence of the second term is not serious because the force law becomes more and more accurate in this region, it is clear that even minute experimental error causes substantial changes in the sum of both terms. This is the reason why many investigators have found strong upturns or downturns of  $f_e/f$  in this region<sup>11-13</sup> and why even a LSMCP does not avoid the appearance of an infinite value for  $(f_e/f)_0$  as demonstrated in Figure 2 for equations (6), (9c) and (9d). Therefore application of equations (6) and (9d) should be restricted to the range of  $\lambda > 1.10$  for which range the 'functions' in Figure 5 have been given as dotted lines, thus allowing the direct estimation of  $f_e/f$ .

In equations (9) and (9a) the sum of  $\beta_{lin}$  and the second term are given as dotted lines in Figure 6. It must be remembered that both terms of these equations have been derived on the basis of the force law. Therefore the validity of these equations is limited to small deformations up to  $\lambda < 1.15$ . In compression, the range may be larger because the Gaussian force law is more closely obeyed than in elongation<sup>5</sup>. The second term  $(3\beta_{lin} - \beta_f) / (\lambda^3 - 1)$  of equation (9a) should be preferred to the corresponding term in equation (9). Inaccuracy in the determination of  $cL_0$  may be responsible for the non-constancy of  $f_e/f$  at small deformations. Therefore the resulting  $f_e/f$  can be read more reliably from  $F(9a)$  in Figure 6, or directly in Figure 4.

The rule of de l'Hospital (equation A4) yields a discrete value  $(f_e/f)_0$  for zero deformation which may be compared with results obtained by means of measuring the shear modulus  $G$  according to equation (8). Owing to the extreme sensitivity of the calculation in the range of small deformations, even a LSMCP rendering smoother  $L(f)$  polynomials may cause a fairly large scatter in the

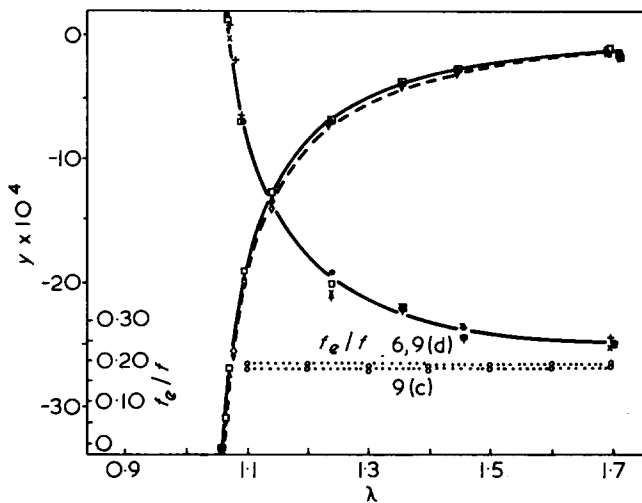


Figure 5 Evaluation of terms in equations (6), (9c) and (9d) vs.  $\lambda$ .  $\gamma = -(\beta_L / \lambda^3 - 1)$ :  $\square$ , inner marks;  $\diamond$ , outer marks.  $\gamma = -(cL_0 / f \lambda^2) \cdot \beta_L$ :  $\nabla$ , inner marks;  $\triangle$ , outer marks.  $\gamma = (\partial f / \partial L)_{T,p} (L \beta_{lin} / f)$ :  $\times$ , inner marks;  $\blacksquare$ , outer marks.  $\gamma = -(1/f) (\partial f / \partial T)_{p,L}$ :  $+$ , inner marks;  $\bullet$ , outer marks

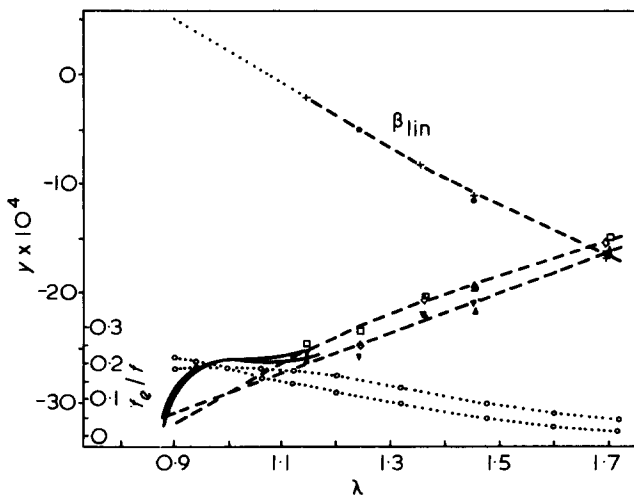


Figure 6 Evaluation of terms in equations (9) and (9a) vs.  $\lambda$ .  $\bullet$ , Outer marks;  $+$ , inner marks.  $\gamma = (3\beta_{lin} - \beta_f) (cL_0 / f)$ :  $\triangle$ , outer marks;  $\nabla$ , inner marks.  $\gamma = (3\beta_{lin} - \beta_f) / (\lambda^3 - 1)$ :  $\square$ , outer marks;  $\diamond$ , inner marks

$f_e/f$  results unless an additional smoothing of the coefficient  $\beta_{\text{lin}}(\lambda)$  is carried out.

From this analysis of results we conclude that of the equations we have used (9a) is most suitable for evaluating  $f_e/f$  at small deformations whereas equations (6) and (9d) are best applied at moderate elongations.

## DISCUSSION

The selective use of equation (9a) for the range of small deformation and (6) and (9d) for moderate elongation results in a consistent pattern of behaviour of  $f_e/f$  in the whole range of the present investigation. Figure 7 demonstrates that a constant relative contribution  $f_e/f \approx 0.18$  has been measured from compression at  $\lambda \approx 0.90$  up to moderate elongation at  $\lambda \approx 1.70$  for  $T = 30^\circ\text{C}$ . Taking into account the experimental scatter between different sets of marks and different evaluations according to equations (6) or (9d) the accuracy is estimated as:  $f_e/f = 0.18 \pm 0.02$ .

It is, of course, satisfactory to find that the relative energetic contribution  $f_e/f$  is not sensitive to the degree of deformation over a fairly wide range of deformation. Since this holds in the transition region between uniaxial elongation and compression too, any speculation of special 'phenomena' accompanying initial deformation can be discarded.

Volume effects too are not serious in the range of small deformations since disregarding the correction  $\phi$  causes no detectable changes of  $f_e/f$ . In the range of small deformation a computer calculation of equation (9) gave differences of  $\Delta(f_e/f) < 0.0001$  when  $\phi$  calculated on the basis of Gaussian behaviour was taken into account.

Since in equations (6) and (9d) the influence of the second term which has to be derived from a force law decreases quickly with increasing elongation as shown in Figure 5, the Gaussian force law can be used without restriction for  $\lambda > 1.10$  to determine  $f_e/f$ . Though the Mooney-Rivlin equation is a better representation of the force vs. length relationship in moderate and higher elongation by means of two constants  $C_1$  and  $C_2$ , the resulting value  $f_e/f$  is not particularly sensitive<sup>8,21</sup> to changes of  $C_2$ .

The result that  $f_e/f = 0.18$  and is independent of the elongation ratio compares well with data from literature obtained for the most part at larger deformations. The same value 0.18 for lightly crosslinked rubber has been found by Smith *et al.*<sup>4</sup> for  $\lambda > 1.30$ . Allen *et al.*<sup>8</sup> obtained this value in the range  $1.2 \leq \lambda \leq 2.1$  by use of the Gaussian equation compared with  $f_e/f = 0.12$  from the direct experimental determination. Measurements of  $L(T)$  at constant  $f$  by Barrie and Standen<sup>15</sup> lead to  $f_e/f = 0.17$ . Treloar's experiments<sup>3</sup> of combined torsion and elongation gave  $f_e/f \approx 0.13$  in the range of axial elongation  $1.13 \leq \lambda \leq 1.25$ .

Shen and Blatz<sup>2</sup> found  $f_e/f = 0.15$  from  $f(T)$  measurements at constant  $L$ , and Shen<sup>17</sup> obtained  $f_e/f = 0.18$  independent of the degree of swelling by a diluent from measuring  $L(T)$  at constant  $f$ . These investigations used equation (8), with the shear modulus  $G$  determined from the slope of the Gaussian plot  $f/A_0$  vs.  $(\lambda - \lambda^{-2})$ .

Comparing these data from the literature with the result of the present investigation the suggestion of Shen and Blatz<sup>2</sup> that  $f_e/f$  depends on the sample geometry, is at least partly refuted. First, the sample used here is much shorter and thicker than usual samples, and secondly, no uniform trend of  $f_e/f$  values measured between the outer

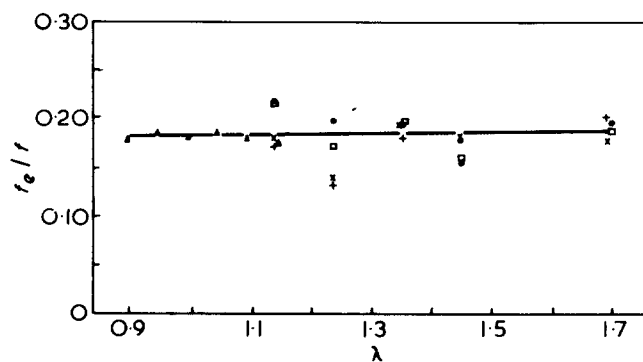


Figure 7  $f_e/f$  vs.  $\lambda$ .  $\Delta$ , Equation (9a). Equation (6):  $\bullet$ , outer marks;  $\times$ , inner marks. Equation (9d):  $\square$ , outer marks;  $\times$ , inner marks

('longer sample') or the inner marks ('shorter sample') can be detected.

The amount of deformation (in either direction) read between the marks is relatively larger than that read between the rigidly fixed ends of a sample. A more homogeneous state of deformation is achieved by using the marks. But under the influence of varying temperature, relative changes of the length, and thus  $f_e/f$  itself, are not changed apparently.

The geometrical dimensions of samples which are appropriate to uniaxial compression do not favour experiments at high elongation. For this reason the slight decrease of  $f_e/f$  which has been reported<sup>13,15</sup> could not be investigated.

## ACKNOWLEDGEMENTS

The authors wish to thank the Science Research Council for financial support and Professor G. Gee for helpful comments.

## REFERENCES

- 1 Flory, P. J., Hoeve, C. A. J. and Ciferri, A. *J. Polym. Sci.* 1959, **34**, 337
- 2 Shen, M. and Blatz, P. J. *J. Appl. Phys.* 1968, **39**, 4937
- 3 Boyce, P. H. and Treloar, L. R. G. *Polymer* 1970, **11**, 21
- 4 Smith, K. J., Greene, A. and Ciferri, A. *Kolloid-Z.* 1964, **194**, 49
- 5 Wolf, F. P. *Polymer* 1972, **13**, 347
- 6 Allen, G., Bianchi, U. and Price, C. *Trans. Faraday Soc.* 1963, **59**, 2493
- 7 Price, C., Padget, J. C., Kirkham, M. C. and Allen, G. *Polymer* 1969, **10**, 573
- 8 Allen, G., Kirkham, M. C., Padget, J. and Price, C. *Trans. Faraday Soc.* 1971, **67**, 1278
- 9 Roe, R. J. *Trans. Faraday Soc.* 1966, **62**, 312
- 10 Flory, P. J. *Trans. Faraday Soc.* 1961, **57**, 829
- 11 Shen, M., McQuarrie, D. A. and Jackson, J. L. *J. Appl. Phys.* 1967, **38**, 791
- 12 Puett, D. *Rubber Chem. Technol.* 1968, **41**, 569
- 13 Tanaka, T., Yokoyama, T. and Yamaguchi, Y. *Rubber Chem. Technol.* 1971, **44**, 127
- 14 Ciferri, A. *Trans. Faraday Soc.* 1961, **57**, 846
- 15 Barrie, J. A. and Standen, J. *Polymer* 1967, **8**, 97
- 16 Treloar, L. R. G. *Polymer* 1969, **10**, 291
- 17 Shen, M. *Rubber Chem. Technol.* 1970, **43**, 270
- 18 Wood, L. A. and Martin, G. M. *Rubber Chem. Technol.* 1964, **37**, 850
- 19 Price, C., Padget, J., Kirkham, M. C. and Allen, G. *Polymer* 1969, **10**, 495
- 20 Christensen, R. G. and Hoeve, C. A. J. *J. Polym. Sci. (A-1)* 1970, **8**, 1503
- 21 Ciferri, A. *J. Polym. Sci. (A)* 1964, **2**, 3089

APPENDIX

Theoretical calculations

The relative energetic contribution can be transformed from the exact equation (3) into:

$$f_e/f = 1 + \frac{T}{f} \left[ \left( \frac{\partial f}{\partial L} \right)_{T,V} \left( \frac{\partial L}{\partial T} \right)_{p,f} + \left( \frac{\partial f}{\partial V} \right)_{T,L} \left( \frac{\partial V}{\partial T} \right)_{p,f} \right] \quad (\text{A1})$$

with the aid of the following relationships:

$$\left( \frac{\partial f}{\partial T} \right)_{V,f} \equiv 0 = \left( \frac{\partial f}{\partial T} \right)_{V,L} + \left( \frac{\partial f}{\partial L} \right)_{V,T} \left( \frac{\partial L}{\partial T} \right)_{V,f} \quad (\text{A1a})$$

$$\left( \frac{\partial L}{\partial T} \right)_{V,f} = \left( \frac{\partial L}{\partial T} \right)_{p,f} - \left( \frac{\partial L}{\partial V} \right)_{T,f} \left( \frac{\partial V}{\partial T} \right)_{p,f} \quad (\text{A1b})$$

$$\left( \frac{\partial f}{\partial V} \right)_{T,f} \equiv 0 = \left( \frac{\partial f}{\partial V} \right)_{T,L} + \left( \frac{\partial f}{\partial L} \right)_{T,V} \left( \frac{\partial L}{\partial V} \right)_{T,f} \quad (\text{A1c})$$

The thermal coefficients at constant pressure  $p$  and force  $f$  may be represented by the usual symbol  $\beta$  with different subscripts, i.e. the linear thermal expansion coefficient:

$$\beta_{\text{lin}} = \frac{1}{L} \left( \frac{\partial L}{\partial T} \right)_{p,f} \quad (\text{A1d})$$

and the bulk thermal expansion coefficient:

$$\beta_f = \frac{1}{V} \left( \frac{\partial V}{\partial T} \right)_{p,f} \quad (\text{A1e})$$

In the isotropic state of the sample ( $f = 0$ ) there is by definition:

$$3\beta_{\text{lin}}(f = 0) = \beta_{f=0} \quad (\text{A1f})$$

Whereas  $\beta_{\text{lin}}$  strongly depends on  $f$  or  $\lambda$  and even changes its sign at a certain elongation  $\lambda_{\text{inv}}$  (thermoelastic inversion), the bulk coefficient  $\beta_f$  remains virtually constant because  $\beta_f$  deviates only slightly from the bulk thermal expansion coefficient  $\beta_L$  taken at constant length. Experimental evidence demonstrates that  $\beta_L$  remains constant<sup>6</sup> within the experimental limits of 1% in the range of moderate elongation up to  $\lambda = 2.2$ . Later the relative difference between  $\beta_f$  and  $\beta_L$  will be shown to be of the order of  $10^{-4} \text{ deg}^{-1}$ . Therefore either of them can be replaced by the coefficient  $\beta_{f=0}$  of the isotropic material<sup>9</sup>.

Inserting the thermal coefficients, equation (A1) transforms into:

$$f_e/f = 1 + \frac{T}{f} \left[ \left( \frac{\partial f}{\partial L} \right)_{T,V} L\beta_{\text{lin}} + \left( \frac{\partial f}{\partial V} \right)_{T,L} V\beta_f \right] \quad (\text{A2})$$

A force vs. length relationship is required now to express the remaining derivatives in equation (A2) in terms of quantities which can be measured under the experimental limitations imposed by the design of the apparatus. A similar equation:

$$f_e/f = 1 + \frac{T}{f} \left[ \left( \frac{\partial f}{\partial L} \right)_{T,p} L\beta_{\text{lin}} + \left( \frac{\partial f}{\partial V} \right)_{T,L} V\beta_L \right] \quad (\text{A2a})$$

is obtained directly from equations (3) and (3a) since:

$$\left( \frac{\partial f}{\partial T} \right)_{p,L} = - \left( \frac{\partial f}{\partial L} \right)_{p,T} \left( \frac{\partial L}{\partial T} \right)_{p,f} = - \left( \frac{\partial f}{\partial L} \right)_{p,T} L\beta_{\text{lin}} \quad (\text{A1g})$$

The first derivative in equation (A2) can be replaced by means of equation (5d) and split into two terms, thus using equations (5) and (5e):

$$f_e/f = 1 + \frac{T}{f} \left[ \left( f + \frac{c}{L^2} 3qV \right) \beta_{\text{lin}} - \frac{cqV}{L^2} \beta_f \right] \quad (\text{A2b})$$

This can be re-written in terms of  $\lambda$  using equation (5a) and  $\lambda = L/L_0$ :

$$f_e/f = 1 + T \left[ \beta_{\text{lin}} + \frac{cL_0}{\lambda^2 V_0/V} \frac{3\beta_{\text{lin}} - \beta_f}{f} \right] \quad (9)$$

where  $cL_0$  may be replaced by the shear modulus according to equation (5b).

Equation (11) becomes indefinite for  $f = 0$ , because according to equation (A1f) the numerator  $3\beta_{\text{lin}} - \beta_f$  tends towards zero as  $f \rightarrow 0$ . The influence of the volume quotient  $V_0/V$  is negligible.

To evaluate measurements by means of (9) the actual length  $L$  has to be known as a function of  $f$  and  $T$ . The temperature coefficient of the length at various constant forces leads to  $\beta_{\text{lin}}$ . An exact determination of length and  $\beta_{\text{lin}}$  at zero force is sufficient to calculate  $\lambda$  and  $\beta_f$  and the slope of the Gaussian plot at this point yields  $cL_0$ .

Equation (9) is not the only one which can be obtained from equation (A2) by means of the force law (5). There are other similar expressions in which, for simplicity, the volume quotient  $V_0/V$  has been omitted:

$$f_e/f = 1 + T \left[ \beta_{\text{lin}} + \frac{3\beta_{\text{lin}} - \beta_f}{\lambda^3 - 1} \right] \quad (9a)$$

$$f_e/f = 1 + \frac{T}{f} \frac{cL_0}{\lambda^2} \left[ (\lambda^3 + 2)\beta_{\text{lin}} - \beta_f \right] \quad (9b)$$

If experimental data are evaluated by means of a LSMCP and the force is known as a polynomial of the length,  $(\partial f/\partial L)_{T,p}$  can be calculated explicitly. Then equation (A2a) may be employed together with the derivative (5e) of the force law to obtain:

$$f_e/f = 1 + \frac{T}{f} \left[ \left( \frac{\partial f}{\partial L} \right)_{T,p} L\beta_{\text{lin}} - \frac{cL_0}{\lambda^2} \beta_L \right] \quad (9c)$$

$$f_e/f = 1 + T \left[ \left( \frac{\partial f}{\partial L} \right)_{T,p} \frac{L\beta_{\text{lin}}}{f} - \frac{\beta_L}{\lambda^3 - 1} \right] \quad (9d)$$

Returning to equation (9) the undeformed state of the sample may be analysed. In the limit of zero force,  $\lambda = 1$  and  $V_0/V = 1$ . Then the indefinite expression is accessible by means of the rule of de l'Hospital if  $\beta_f$  is assumed to be constant:

$$\lim_{f \rightarrow 0} \frac{3\beta_{\text{lin}} - \beta_f}{f} = 3 \left( \frac{\partial \beta_{\text{lin}}}{\partial f} \right)_{p,T,f \rightarrow 0} \quad (9e)$$

Replacing  $\beta_{\text{lin}}(f=0)$  by  $\beta_f/3$  the relative energetic contribution to zero force is obtained as:

$$(f_e/f)_0 = 1 + T \left[ \beta_f/3 + 3cL_0 \left( \frac{\partial \beta_{\text{lin}}}{\partial f} \right)_{p,T,f=0} \right] \quad (\text{A3})$$

where equation (5b) may be taken to express  $cL_0 = A_0G$ .

Another single value of  $f_e/f$  can be calculated using the thermoelastic inversion point. For a particular length  $L_{\text{inv}}$  the temperature derivative  $(\partial f/\partial T)_{p,L_{\text{inv}}}$  is zero<sup>17</sup> which is equivalent to the condition that the temperature coefficient of the sample length is zero for the corresponding force  $f_{\text{inv}}$ :

$$\frac{1}{L_{\text{inv}}} \left( \frac{\partial L}{\partial T} \right)_{p,f_{\text{inv}}} = \beta_{\text{lin}}(f_{\text{inv}}) = 0 \quad (\text{A3a})$$

Inserting this into equation (9a) the quantity  $f_e/f$  is obtained at the thermoelastic inversion point:

$$(f_e/f)_{\text{inv}} = 1 - \frac{\beta_f T}{\lambda_{\text{inv}}^3 - 1} \quad (\text{A4})$$

which is equivalent to Shen's equation<sup>17</sup>.



# Depolymerization behaviour of poly-(*p*-phenylene diacrylic acid diethyl ester)

Fusae Nakanishi and Masaki Hasegawa

Research Institute for Polymers and Textiles, 4 Sawatari, Kanagawa-ku, Yokohama, Japan

and Takeshi Tasai

Somar Kogyo Co. Ltd, Ginza, Tokyo, Japan

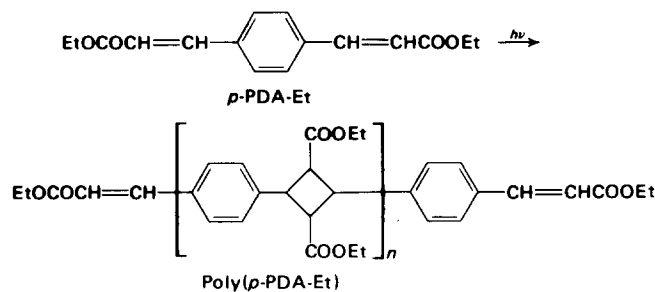
(Received 31 May 1974; revised 2 July 1974)

The photochemical and thermal behaviour of poly(*p*-phenylene diacrylic acid diethyl ester) [poly(*p*-PDA-Et)] has been investigated. It was observed that both photo and thermal depolymerization occurs with cleavage of the cyclobutane ring. Photochemically poly(*p*-PDA-Et) in solution depolymerizes selectively into oligomer, which undergoes *cis-trans* isomerization without further depolymerization to monomer. On the other hand, it depolymerizes thermally at random into low molecular weight polymer and monomer.

## INTRODUCTION

Various types of novel polymers with a cyclobutane ring in the main chain have been prepared by means of four-centre type photopolymerization of diolefinic compounds in the crystalline state<sup>1-3</sup>. It is expected that the presence of a cyclobutane ring in the polymer chain introduces interesting properties to the polymer. Of several cyclobutane derivatives in the solution, it is well known that photocleavage and formation of a cyclobutane ring proceeds reversibly depending on the wavelength of the irradiation. In a polymer system with a cyclobutane ring in the main chain, such a photoreversibility corresponds to the solution photopolymerization and photodepolymerization and such a case was found in poly(2,5-distyryl pyrazine) (PDSP)<sup>4-6</sup>.

The present work was undertaken to investigate the photo and thermal behaviour of poly(*p*-phenylene diacrylic acid diethyl ester) [poly(*p*-PDA-Et)] which is one typical polymer obtained by a crystalline state photopolymerization:



## EXPERIMENTAL

### Preparation of poly(*p*-PDA-Et)

Poly(*p*-PDA-Et) was prepared according to the method described in an earlier paper<sup>2</sup>. Because of poor solubility of as-polymerized polymer crystal, amorphous polymer which is soluble in organic solvents was used for the study on photochemical behaviour in solution. Amorphous polymer was obtained by reprecipitation of trifluoroacetic acid solution of polymer by adding water. The reduced vis-

cosity of the polymer thus obtained was in the range of between 0.4 and 1.2 ( $C = 0.36$  in trifluoroacetic acid).

### Preparation of oligo(*p*-PDA-Et)

Oligo(*p*-PDA-Et) was obtained by extracting high molecular weight crystalline poly(*p*-PDA-Et) with chloroform or benzene. Its molecular weight was about 1000 (tetramer), which was measured by vapour pressure osmometry with a Mechro Lab. Model 301 A.

### Formation of anhydride from oligo(*p*-PDA-Et)

Oligo(*p*-PDA-Et) (100 mg) was hydrolysed by refluxing with 1 N NaOH ethanol solution (10 ml) for 10 h. After removal of ethanol, the residue was dissolved in water and neutralized with dilute hydrochloric acid. The white precipitate obtained was found by i.r. spectroscopy to be hydrolysed oligomer. This acid was refluxed in acetic anhydride for 4 h. After removal of acetic anhydride the residue was washed with ethanol and dried. The obtained product showed the presence of a six-membered ring anhydride by i.r. absorption peaks at 1820 and 1770  $\text{cm}^{-1}$ .

### Preparation of model compounds

*p*-PDA-Et crystals (1 g), dispersed in water (100 ml) at 60–65°C, were irradiated with a 100 W high pressure mercury lamp. The crystal gradually became cohesive. After 6 h the product was collected and dried. The dimer content in this product was found to be about 30% by n.m.r. spectroscopy. The dimer was isolated from unreacted *p*-PDA-Et by washing with *n*-hexane where the dimer is much less soluble than *p*-PDA-Et. The residue was recrystallized from ethanol: m.p. 138°C;  $\lambda_{\text{max}}$  287 nm ( $\epsilon = 58\,000$  in ethanol). Calculated for  $\text{C}_{16}\text{H}_{18}\text{O}_4$ : C, 70.05%; H, 6.61%. Found: C, 70.08%; H, 6.68%. The anhydride derivative from hydrolysed dimer showed i.r. absorption at 1820 and 1770  $\text{cm}^{-1}$ .

### Preparation of diethyl $\alpha$ -truxillate

Diethyl  $\alpha$ -truxillate was prepared by esterification of  $\alpha$ -truxillic acid: m.p. 149°C.

### Preparation of poly(*p*-PDA-Et) film

Relatively low molecular weight polymer ( $\eta_{\text{red}} = 0.8$ ), the terminal double bonds of which are detectable from the i.r. spectrum was used. The film was obtained by casting a chloroform solution of poly(*p*-PDA-Et). In order to check the change of film with the u.v. spectrum, the films were deposited on a quartz plate by evaporation of a solution of the polymer in chloroform.

### Determination of quantum yield

A solution of diethyl  $\alpha$ -truxillate in ethanol ( $2.49 \times 10^{-5}$  mol/l) was irradiated with monochromatic light of 224 nm wavelength. The number of photons absorbed was determined by use of a calibrated thermopile. The amount of ethyl cinnamate formed was determined by measurement of absorption intensity at 278 nm. The quantum yield thus obtained was 0.2 for the formation of ethyl cinnamate by irradiation with light of 224 nm wavelength in ethanol.

### N.m.r. spectroscopy

All spectra were determined in deuteriochloroform solution (5%) using a JOEL-C-60HL instrument. These solutions were subjected to photo-irradiation.

### D.s.c. and t.g.a. measurements

Differential scanning calorimetry (d.s.c.) and thermogravimetric analysis (t.g.a.) were carried out with Rigaku standard d.s.c. and t.g.a. instruments at a heating rate of  $10^\circ\text{C}/\text{min}$  under nitrogen. In order to study the thermal behaviour of poly(*p*-PDA-Et) a few milligrammes of poly(*p*-PDA-Et) was heated in a cell of the d.s.c. apparatus under an atmosphere of nitrogen for 1 h at various temperatures.

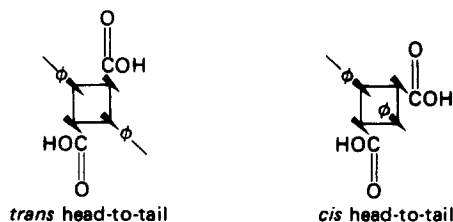
### Light source

The monochromatic light was furnished by a spectroscopic irradiator (JASCO CRM FA) composed of 2000 W xenon lamp as the light source and grating monochromator. Other irradiation lights, 100 W high pressure mercury lamp or 17 W low pressure mercury lamp were used as necessary according to the experiment.

## RESULTS AND DISCUSSION

### Structure of poly(*p*-PDA-Et), its oligomer and *p*-PDA-Et dimer

It is difficult to determine the structure of high molecular weight poly(*p*-PDA-Et) because of poor solubility needed to study the chemical behaviour in solution and the n.m.r. spectrum. However, its oligomer is soluble in common organic solvents and it is easier to study this structure. Therefore, elucidation of the structure was carried out on oligo(*p*-PDA-Et). The oligomer should have the same steric configuration as that of poly(*p*-PDA-Et) concerning the cyclobutane ring as any isomerization is not presumed to occur either by crystalline state photopolymerization or during extraction procedure with chloroform. I.r. spectra of anhydride derivatives of hydrolysed oligo(*p*-PDA-Et) and *p*-PDA-Et dimer shows formation of a six-membered ring anhydride ( $1820$  and  $1770\text{ cm}^{-1}$ ). Formation of the six-membered ring anhydride suggests that the configuration of these compounds is one of the following two types:



In the case of the former, epimerization is assumed during formation of anhydride. However, the structure of *p*-PDA-Et dimer and oligo(*p*-PDA-Et) is most likely to be *trans* head-to-tail from the n.m.r. spectra. The n.m.r. spectra of oligo(*p*-PDA-Et), *p*-PDA-Et dimer and diethyl  $\alpha$ -truxillate are shown in Figure 1 together with that of ethyl cinnamate for comparison. The spectrum of oligo(*p*-PDA-Et) is very similar to *p*-PDA-Et dimer in each chemical shift. Furthermore, the chemical shifts of ethyl, methyl protons which are in ester residue as substituents on the cyclobutane ring, are in agreement with those of ethyl, methyl protons in diethyl  $\alpha$ -truxillate, in which the configuration of its parent acid was established as *trans* head-to-tail type<sup>7</sup>. From these agreements in chemical shifts, the configuration of oligo(*p*-PDA-Et) and *p*-PDA-Et dimer is concluded to be *trans* head-to-tail as described in Figure 1. In addition the fact that a shear rate dependence of the solution viscosity has been observed for a chloroform solution of poly(*p*-PDA-Et) supports the view that the structure of poly(*p*-PDA-Et) is the same as that of oligo(*p*-PDA-Et)<sup>8</sup>.

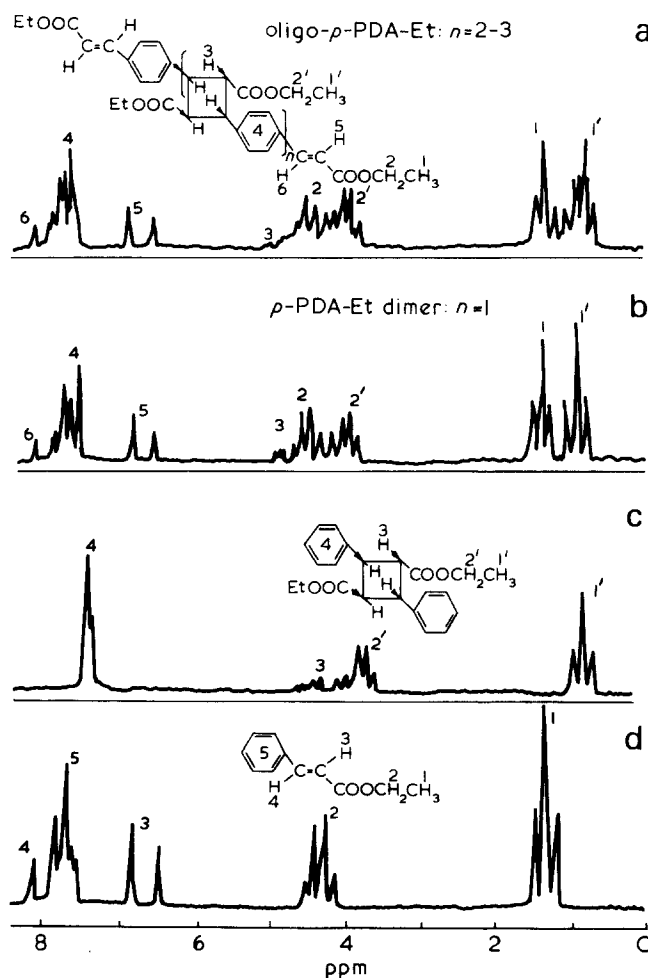


Figure 1 N.m.r. spectra of (a) oligo(*p*-PDA-Et), (b) *p*-PDA-Et dimer, (c) diethyl  $\alpha$ -truxillate and (d) ethyl cinnamate and their structures

Table 1 Change in solution viscosity<sup>a</sup> on irradiation<sup>b</sup>

Vessel	Time (min)				
	0	15	30	75	135
glass tube	1.28	1.24	—	1.18	1.06
quartz tube	1.16	0.61	0.45	0.19	0.11

<sup>a</sup> Reduced viscosity;  $C = 0.36$  in chloroform

<sup>b</sup> Light source: 100 W high pressure mercury lamp; solvent: chloroform

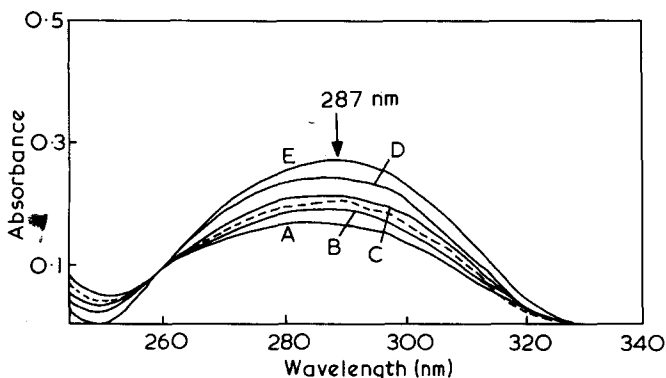


Figure 2 Change in u.v. spectrum of poly(*p*-PDA-Et) on irradiation. — — —, Before irradiation; —, after irradiation. A, 60; B, 150; C, 360; D, 900; E, 1800 sec

#### Photobehaviour of poly(*p*-PDA-Et) and oligo(*p*-PDA-Et)

The effect of photoirradiation on polymer solution has been studied by means of measurement of the change in solution viscosity and u.v. spectrum. The change in solution viscosity on irradiation with 100 W high pressure mercury lamp is shown in Table 1. When the solution of poly(*p*-PDA-Et) in chloroform was irradiated in a glass tube which is transparent above 300 nm wavelength light, a slight decrease in viscosity was observed (1.28 → 1.06). Thus irradiated polymer did not show any change in n.m.r. spectrum and thin-layer chromatogram compared to those of the original polymer. When a quartz tube was used in place of the glass tube the solution viscosity dropped drastically (1.16 → 0.11). At the same time, the n.m.r. spectrum of thus irradiated polymer showed the appearance of the ethyl cinnamyl group (methyl protons, 1.3 ppm; methylene protons, 4.4 ppm; olefinic protons, 6–7 ppm), which is due to the cleavage of the cyclobutane ring in the main chain. In addition, its thin layer chromatogram gave several spots which are considered to be the fragments with different degree of polymerization. However, no monomer was detected in the u.v. spectrum in this photoirradiated product, i.e. irradiation with light of wavelength shorter than 300 nm, makes poly(*p*-PDA-Et) depolymerize into low molecular weight polymer by cleavage of the cyclobutane ring. This photochemical depolymerization was confirmed by following the change of the u.v. spectrum on irradiation. Poly(*p*-PDA-Et) in chloroform was prepared at a concentration high enough to observe the change in absorption at around 280 nm. The change on irradiation with monochromatic light is shown in Figure 2. On irradiation at 287 nm, the absorption intensity decreased slightly and then gradually increased with irradiation time. The first decrease of absorption intensity is due to the isomerization from *trans*- to *cis*-isomer of the terminal ethyl cinnamyl group of the polymer and the subsequent increase is due to a gradual increase in the ethyl cinnamyl group formed by cleavage of the cyclobutane ring in the main chain of the polymer.

Irradiation with the light of wavelength shorter than 287 nm showed the same spectral change; on irradiation at 304 nm, the absorption peak decreased and finally gave a photo-stationary spectrum. So in this case, only isomerization of the terminal ethyl cinnamyl group occurred.

From these data it may be said that photodepolymerization of poly(*p*-PDA-Et) into low molecular weight polymer is favourable with light that excites the benzene ring, while with light that excites the terminal ethyl cinnamyl group ( $\pi-\pi^*$ ) isomerization of *trans* to *cis* occurs efficiently.

As the next step the photochemical behaviour of oligo(*p*-PDA-Et) solution has been investigated. When oligo(*p*-PDA-Et) in deuteriochloroform was exposed to 287 nm light, its n.m.r. spectrum changed as shown in Figure 3. New peaks with a coupling constant of 13 counts/sec were observed at 6–7.5 ppm. With regard to methyl, methylene proton new peaks were found in a slightly higher field. These peaks are assigned to be *cis* protons of the ethyl cinnamyl group.

Almost no change in molecular weight of oligo(*p*-PDA-Et) before (988) and after (995) irradiation supports the occurrence of *cis*-*trans* isomerization of oligo(*p*-PDA-Et) in solution. The change of u.v. spectrum on irradiation of oligo(*p*-PDA-Et) in ethanol solution is shown in Figure 4.

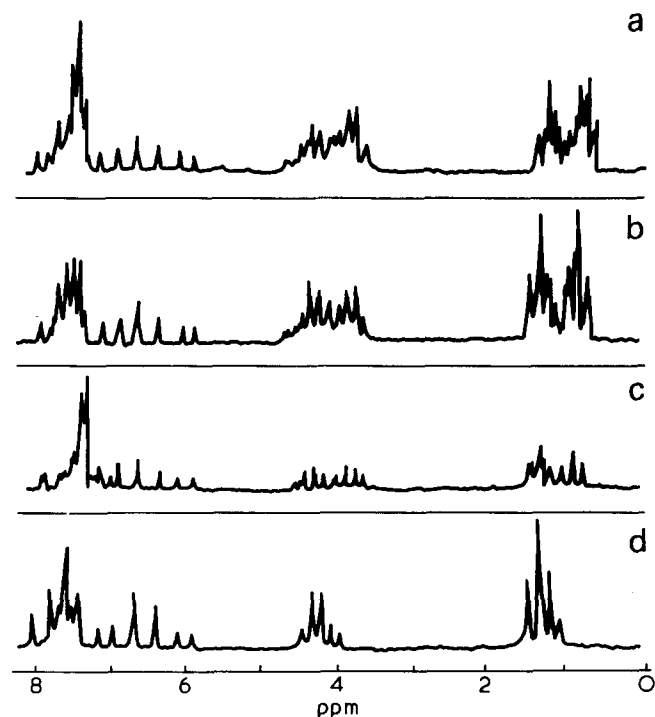


Figure 3 N.m.r. spectra of irradiated (a) oligo(*p*-PDA-Et), (b) *p*-PDA-Et dimer, (c) diethyl  $\alpha$ -truxillate and (d) ethyl cinnamate

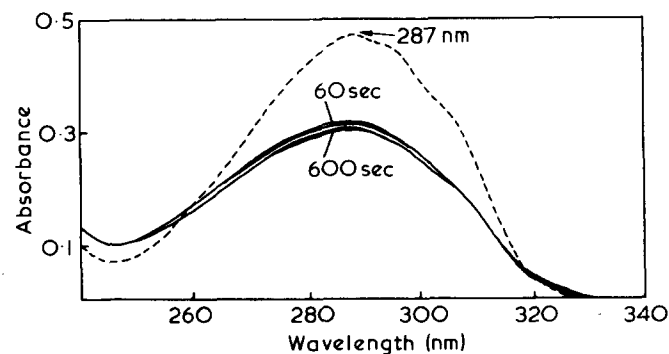


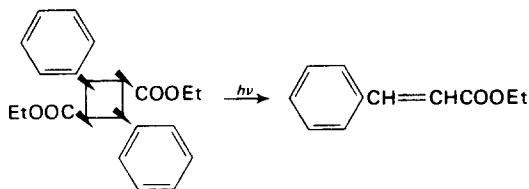
Figure 4 Change in u.v. spectrum of oligo(*p*-PDA-Et) on irradiation. — — —, Before irradiation; —, after irradiation

With irradiation of the absorption peak at 287 nm, a decrease of absorption intensity was observed indicating isomerization of the terminal ethyl cinnamyl group. Thus in the case of oligomer, the absorption of light by the ethyl cinnamyl group is predominant, resulting in *cis*→*trans* isomerization.

It should be noted that PDSP photodepolymerized into the monomer very easily but photodepolymerization of poly(*p*-PDA-Et) into the monomer is rather difficult even on prolonged irradiation.

#### Photoreaction of model compounds

Two model compounds were prepared in the hope that their photoreaction would provide further information to clarify the photodepolymerization of poly(*p*-PDA-Et). One of the model compounds is *p*-PDA-Et dimer for the terminal unit group of the polymer. The other is diethyl  $\alpha$ -truxillate for the repeating unit of the main chain of the polymer. When diethyl  $\alpha$ -truxillate in ethanol solution was irradiated at 224 nm, the absorption peak at 278 nm increased gradually (Figure 5). This band is due to the appearance of ethyl cinnamate and the reaction is considered to proceed as follows:



The quantum yield was 0.2 for the formation of ethyl cinnamate by 224 nm light in ethanol. Irradiation at 260 nm also caused the same reaction. The n.m.r. spectrum of diethyl  $\alpha$ -truxillate in deuteriochloroform after irradiation showed the appearance of both the *cis* and *trans* form of ethyl cinnamate (Figure 3). Figure 6 shows the variation of the u.v. spectrum of *p*-PDA-Et dimer in ethanol with irradiation at 224 nm. The decrease of absorption intensity seems to be due to the slow isomerization of dimer as observed in the case of oligo(*p*-PDA-Et). No detectable amount of *p*-PDA-Et was formed by cleavage of the cyclobutane ring and the quantum yield for the formation of *p*-PDA-Et was negligible under the same irradiation conditions as diethyl  $\alpha$ -truxillate.

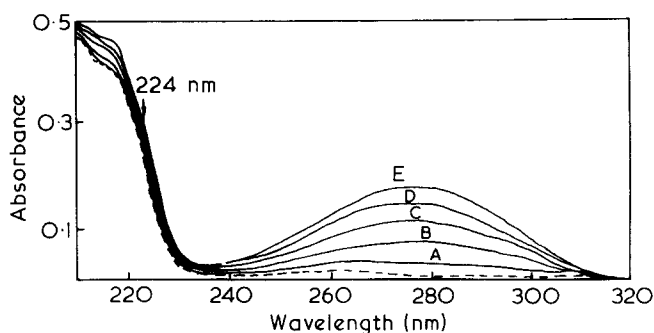
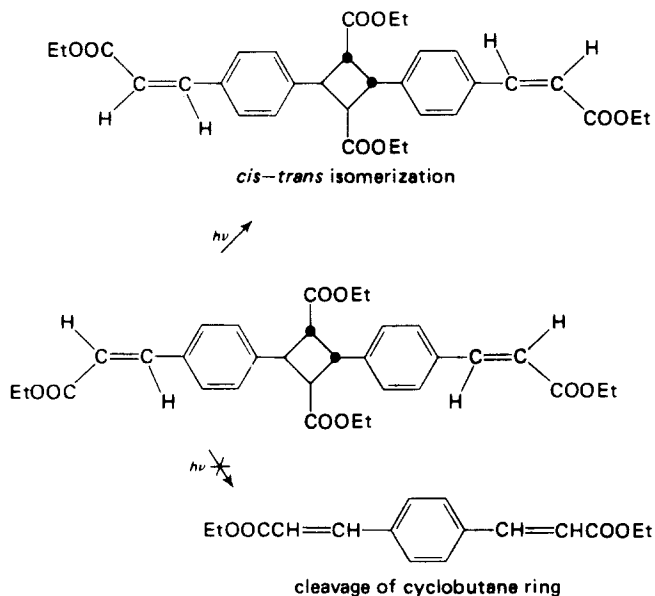
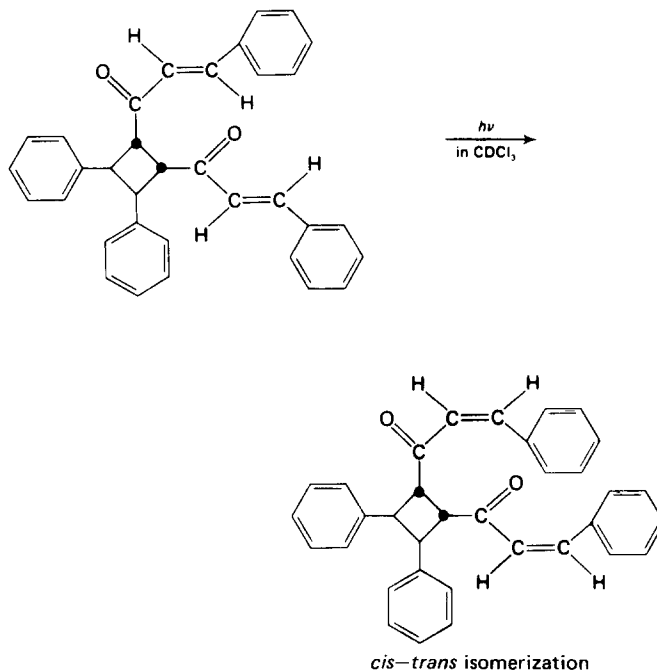


Figure 5 Change in u.v. spectrum of diethyl  $\alpha$ -truxillate on irradiation. — — —, Before irradiation; —, after irradiation. A, 100; B, 300; C, 550; D, 750; E, 950 sec

*Cis*→*trans* isomerization was also confirmed by following the change of the n.m.r. spectrum of *p*-PDA-Et dimer in deuteriochloroform. After irradiation with 100 W high pressure mercury lamp, no peaks corresponding to *p*-PDA-Et were detected, but peaks corresponding to the *cis* form of ethyl cinnamate were found (Figure 3). From the photoreaction of these model compounds it is considered that the absorption of light by a benzene substituent on the cyclobutane ring stimulates photocleavage of the cyclobutane ring, but by substitution of ethyl cinnamyl group on the cyclobutane ring, absorption of light by ethyl cinnamyl group became superior to that of benzene and results in *cis*→*trans* isomerization of ethyl cinnamyl group. A similar case was found in the photoreaction of 1,2-dicinnamoyl-3,4-diphenylcyclobutane in which *cis*→*trans* isomerization takes place without cleavage of the cyclobutane ring:



In summary, the following explanation is reasonable for photodepolymerization of poly(*p*-PDA-Et). There are many benzene rings in the main chain of the polymer and in the first stage they absorb the light resulting in cyclobutane ring cleavage. As a result, the molecular weight of the polymer decreases with an increase in terminal ethyl cinnamyl group. So absorption of light by ethyl cinnamyl group becomes superior to that of benzene and *cis*→*trans* isomerization takes place efficiently without further depolymerization of poly(*p*-PDA-Et).

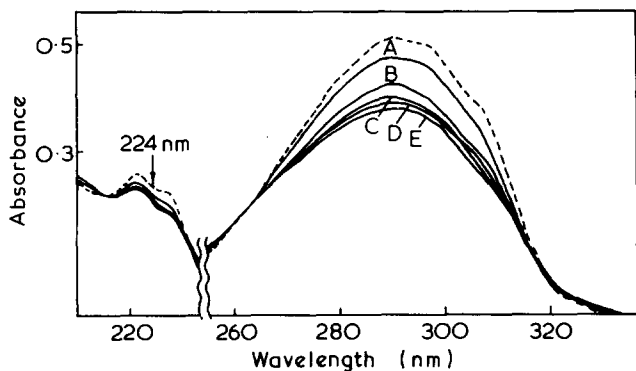


Figure 6 Change in u.v. spectrum of *p*-PDA-Et dimer on irradiation. ---, Before irradiation; —, after irradiation. A, 90; B, 330; C, 520; D, 720; E, 1000 sec

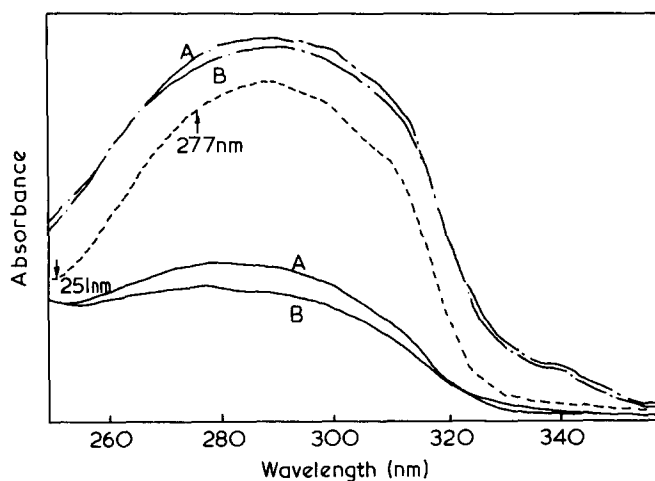


Figure 7 Change in u.v. spectrum of poly(*p*-PDA-Et) film on irradiation. ---, Before irradiation; —, after irradiation at 277 nm; - - - -, after irradiation at 251 nm. A, 1000; B, 2000 sec

#### Photochemical behaviour of poly(*p*-PDA-Et) film

It is noteworthy that the film can be produced from poly(*p*-PDA-Et) with a molecular weight of only 2200 as determined by vapour pressure osmometry. The spectral changes in irradiation of poly(*p*-PDA-Et) film are shown in Figure 7. With irradiation at 277 nm, the absorption peak disappeared, while with irradiation at 251 nm, the intensity of the peak increased. The former may be due to the decrease of terminal cinnamyl group by cyclo-addition, the latter due to the increase of cinnamyl group by cyclobutane ring cleavage. Actually when the film was irradiated with the light of wavelength longer than 280 nm, the decrease of C=C double bonds ( $1640\text{ cm}^{-1}$ ) in the i.r. spectrum was observed with an increase in molecular weight of the film (mol. wt 3000).

It should be pointed out that the photochemical behaviour of poly(*p*-PDA-Et) film is quite different from that of PDSP which becomes brittle following oxidative degradation on irradiation.

#### Thermal behaviour of poly(*p*-PDA-Et)

D.s.c. analysis of poly(*p*-PDA-Et) showed an exothermic peak at  $340^{\circ}\text{C}$  which is the melting point of the polymer. The t.g.a. curve showed slight weight loss near the melting point. Thermal stability of the polymer was examined by heating under a nitrogen atmosphere for 1 h at various temperatures ( $320$ ,  $330$  and  $360^{\circ}\text{C}$ ). From the heat-treatment at  $320^{\circ}\text{C}$ , the polymer did not show any change in spectroscopic analysis and at  $360^{\circ}\text{C}$  it became insoluble material. This may be due to the occurrence of thermal vinyl-type polymerization which leads to formation of gel<sup>9</sup>. At  $330^{\circ}\text{C}$  the polymer became brown material but the result of elemental analysis showed almost no change in composition. Calculated for  $\text{C}_{16}\text{H}_{18}\text{O}_4$ : C, 70.05%; H, 6.61%. Found: C, 70.74%; H, 6.08%.

Further characterization was carried out on this heat-treated polymer. Several spots which are fragments of different degrees of polymerization were found by thin-layer chromatography. The n.m.r. spectrum showed the appearance of a terminal ethyl cinnamyl group (methylene protons, 4.4 ppm; methyl protons, 1.3 ppm; olefinic protons, 6–7 ppm) and the u.v. spectrum had an absorption peak at 290 nm with tailing absorption corresponding to that of the monomer. In the i.r. spectrum the double bond absorption appeared at  $1640\text{ cm}^{-1}$ . From these facts, it is concluded that by heating near its melting point poly(*p*-PDA-Et) thermally depolymerizes into low molecular weight polymer with a small amount of monomer. It should be noted that thermal depolymerization due to cyclobutane ring cleavage seems to occur at any cyclobutane ring in the polymer, while photodepolymerization occurs rather selectively at the cyclobutane ring in the main chain to yield the oligomer without formation of the monomer.

#### REFERENCES

- 1 Hasegawa, M., Suzuki, Y., Suzuki, F. and Nakanishi, H. *J. Polym. Sci. (A-1)* 1969, 7, 743
- 2 Suzuki, F., Suzuki, Y., Nakanishi, H. and Hasegawa, M. *ibid.*, 1969, 7, 2319
- 3 Nakanishi, F. and Hasegawa, M. *ibid.* 1970, 8, 2151
- 4 Hasegawa, M., Suzuki, Y. and Tamaki, T. *Bull. Chem. Soc. Japan* 1970, 43, 3020
- 5 Tamaki, T., Suzuki, Y. and Hasegawa, M. *ibid.* 1972, 45, 1988
- 6 Suzuki, Y., Tamaki, T. and Hasegawa, M. *ibid.* 1974, 47, 210
- 7 Cohen, M. D., Schmidt, G. M. J. and Sonntag, F. I. *J. Chem. Soc.* 1964, p 2000
- 8 Hasegawa, M., Fujishige, S., Koderu, A., Joko, E. and Saito, T. *20th A. Meet. Soc. Polym. Sci. Japan* 1971, to be published
- 9 Nakanishi, H., Nakanishi, F., Suzuki, Y. and Hasegawa, M. *J. Polym. Sci. (A-1)* 1973, 11, 2501

# Dynamic viscoelasticity of entangled polymers

G. Marin

SNPA, Centre de Recherche de Lacq, 64170 Lacq, France

J. J. Labaig

Centre de Recherche sur les Macromolécules, CNRS, 67000 Strasbourg, France

and Ph. Monge

Laboratoire de Thermodynamique, Université de Pau, 64016 Pau, France

(Received 3 May 1974; revised 24 July 1974)

The study of dynamic viscoelastic properties of polystyrene samples shows the influence of molecular parameters on characteristic parameters of linear viscoelastic behaviour. An analysis of complex viscosity in a complex plane shows the influence of polydispersity on the broadness of the relaxation spectrum and on the shape of steady-flow curve  $\eta_a(\dot{\gamma})$ .

## INTRODUCTION

In a previous paper<sup>1</sup>, a method for analysing the dynamic viscoelasticity of molten entangled polymers was described. The study of dynamic viscoelasticity of various molten entangled polymers (polyethylene, polystyrene, poly(methyl methacrylate), polyamide) in the low frequency range (20 to  $10^{-3}$  Hz) showed the convenience of representing the variations of real and imaginary parts of the complex viscosity by:

$$\eta^*(\nu) = \eta'(\nu) - j\eta''(\nu)$$

where  $\eta''(\nu)$  presents a maximum for a value  $\nu_c$  of the frequency and  $\eta'(\nu)$  goes through an inflection point.

In the complex plane ( $\eta'$ ,  $\eta''$ ), experimental points are located for each product on a circular arc.

There are three parameters, namely:  $\eta_0$ , limiting extrapolated viscosity (intersection of the circular arc with the real axis);  $\tau_0$ , characteristic relaxation time such as  $\tau_0 = 1/2\pi\nu_c$ ; and  $h$ , coefficient such that  $(h\pi)/2 = \theta$ , angle between diameter going through the origin and the real axis.

Dynamic measurements have been achieved with a Contraves-Kepes Balance-Rheometer. Complex viscosity was measured in the temperature range 150–200°C.

The accuracy of  $\eta'$  and  $\eta''$  was about 4%.  $\eta_0$  is known to an accuracy of  $\pm 5\%$ ,  $\tau_0$  to an accuracy of  $\pm 10\%$ .

In order to understand the significance of these parameters better, further experiments were carried out on polystyrene samples with a wide range of polydispersity and weight average molecular weight, and are reported in this paper. The results are compared with those obtained in steady-flow experiments.

## EXPERIMENTAL

We used polystyrene samples of various types: 3 anionic polystyrene fractions (PSS62, PS50, PSW39); 3 commercial-type polystyrenes (PS550, PS500, PS506); 7 radical polystyrenes with practically the same polydispersity (PS 1,

PS 3, PS 4, PS 5, PS 6, PS 8, PS 9); a polystyrene of polydispersity 4.2, with a very asymmetrical distribution.

The structural parameters of the samples are shown in Table 1, in which  $P$  represents the polydispersity and  $M_w$  the weight average molecular weight.

## RESULTS

As an example Figures 1 and 2 show the results obtained for samples PSW39 (narrow) and PS550 (commercial type). We have reported in Table 2 the values of the  $h$  parameter obtained on all the samples.

Table 1 Structural parameters of polystyrene samples

Sample	$M_w$	$P$	Sample	$M_w$	$P$
PSS62	125 000	1.25	PS1	257 000	3.38
PS50	160 000	1.10	PS3	311 000	3.52
PSW39	390 000	1.10	PS4	353 000	3.77
PS550	310 000	2.45	PS5	458 000	3.74
PS506	274 000	4.62	PS6	364 000	3.63
PS500	275 000	2.00	PS8	418 000	3.45
PS SAM 327 A	168 000	4.20	PS9	414 000	3.58

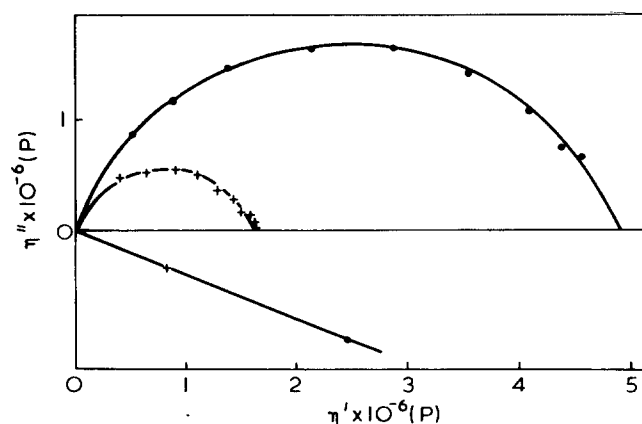


Figure 1 Complex representation of viscosities: PS fraction W39. ●, 179°C; +, 192°C

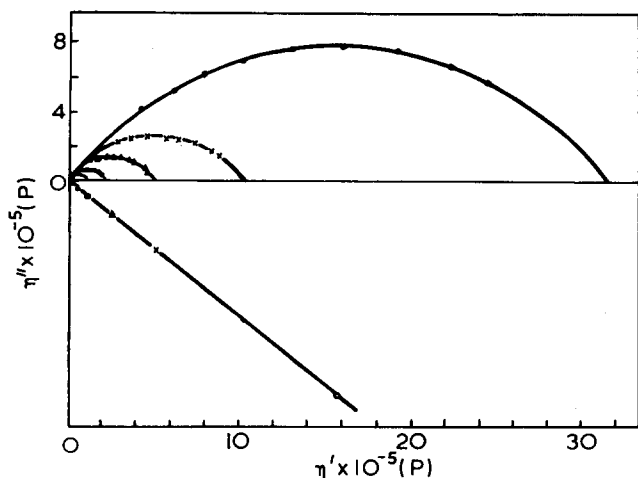


Figure 2 Complex representation of viscosities: commercial PS550. ●, 160°; ×, 170°; ▲, 180° C; ○, 190°; △, 200° C

Table 2 *h* parameters of polystyrene samples

Sample	<i>h</i>	Sample	<i>h</i>
PSS62	0.34	PS1	0.41
PS50	0.14	PS3	0.47
PSW39	0.23	PS4	0.44
PS550	0.40	PS5	0.44
PS506	0.39	PS6	0.45
PS500	0.38	PS8	0.48
PSSAM327A	0.48	PS9	0.48

Variation of *h* parameter

We confirm that the *h* parameter is independent of temperature, whatever the polydispersity value is; it depends greatly on polydispersity, varying from 0.14 for PS50 of polydispersity 1.1, to a value of 0.48 for the SAM 327 A of polydispersity 4.2.

On the contrary it depends weakly on molecular weight at constant polydispersity (PS1 to PS9) and without any correlation.

Figure 3 shows the variation of the *h* parameter with polydispersity for all the samples.

It can be seen that the *h* parameter decreases with polydispersity, the variation being small at large values of polydispersity, and large when *P* tends to 1.

Variation of  $\eta_0$

We show in Figure 4 the variation of  $\eta_0$  (limiting viscosity extrapolated from our dynamic measurements) with weight average molecular weight,  $M_w$ , on a logarithmic scale. The full line is the curve proposed by Suzuki<sup>3</sup> for narrow fractions of polystyrene at 192°C (zero shear rate viscosity measured in steady flow experiments: cone and plate rheometry). The plots for narrow fractions, are located on the line, and we will identify  $\eta_0$  as zero shear rate viscosity.

Variation of  $\tau_0$

We previously defined<sup>1</sup> a characteristic relaxation time  $\tau_0 = 1/\omega_c$  where  $\omega_c$  is the frequency corresponding to the maximum of  $\eta''$ . For narrow fractions,  $\log \tau_0$  varies linearly with  $\log M_w$ , following the line:  $\log \tau_0 = 3.77 \log M_w - 2.55$ . For large samples, at constant polydispersity (PS1 to PS9), the variation is found to be:  $\log \tau_0 = 6.22 \log M_w - 33.69$ .

DISCUSSION

The results obtained on polystyrene, polyethylene, polyamide and poly(methyl methacrylate) samples in the molten state, led us to represent complex viscosity by an analytical expression such as the Cole–Cole complex permittivity for dielectrics:

$$\eta^* = \frac{\eta_0}{1 + (j\omega\tau_0)^{1-h}} \quad (1)$$

This expression accounts quite well for our experimental results; it is valid for entangled polymers in the molten state, at low and moderate frequencies (20 to  $10^{-3}$  Hz).

Many steady-flow experiments have been carried out on polystyrene (cone, plate and capillary rheometers) and

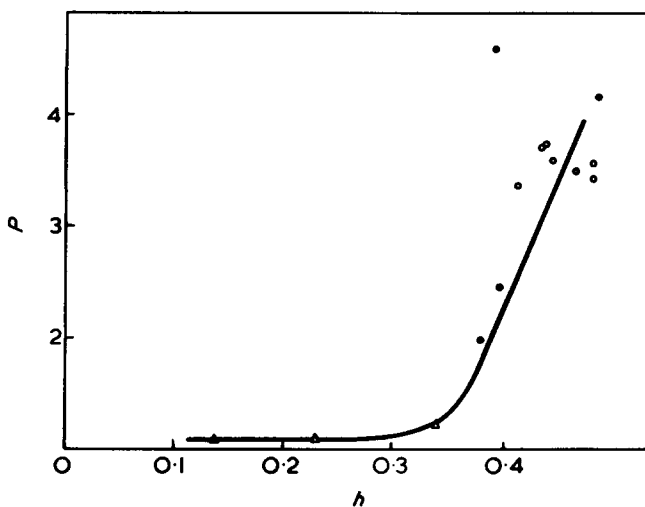


Figure 3 Variation of the *h* parameter with polydispersity. ●, Commercial PS; △, PS fractions; ○, constant polydispersity

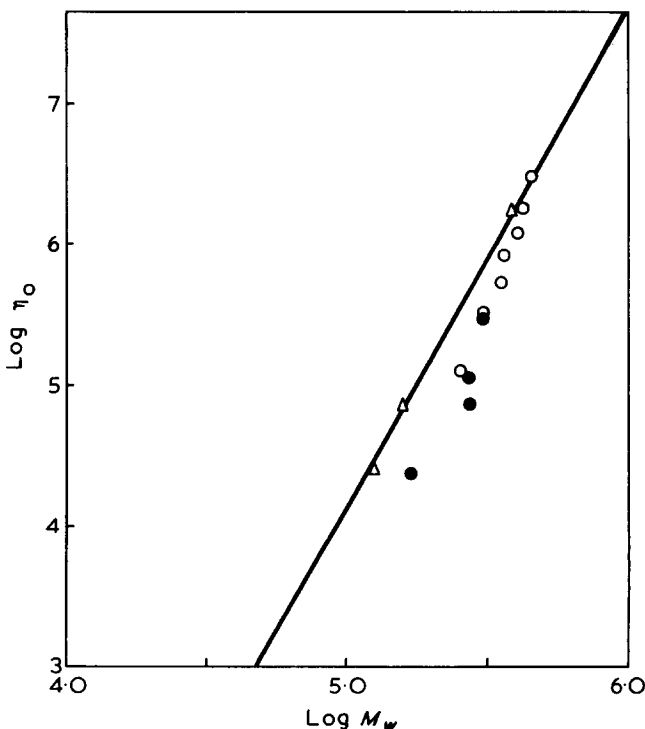


Figure 4 Zero shear viscosities versus weight average molecular weight.  $T = 192^\circ\text{C}$ , ●, Commercial PS; △, PS fractions; ○, constant polydispersity

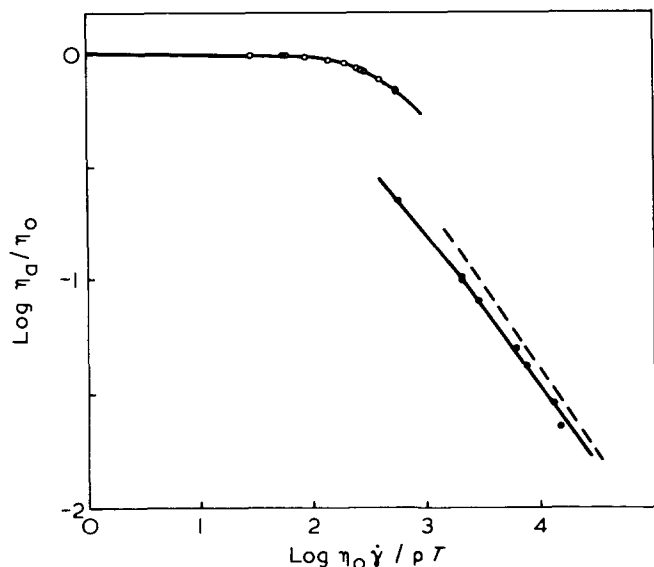


Figure 5 Log (apparent viscosity) versus log (shear rate), in reduced coordinates. Data of Suzuki, superposed on Graessley's theoretical curve. ○, Linear PS fraction  $M_w = 1.2 \times 10^6$ ; ●, star PS

it is interesting to compare them with our dynamical results.

Apparent viscosity  $\eta_a$  is compared either with the modulus of complex viscosity, or with the real part of the complex viscosity<sup>5-7</sup>.

In Figure 5 we show the results obtained by Suzuki<sup>3</sup> for a PS fraction ( $M_w = 1.2 \times 10^6$ ) and star PS approaching the limiting slope. The reduced apparent viscosity is plotted against  $\dot{\gamma}\eta_0/\rho T$ .

On these experimental results, is superposed the theoretical curve of Graessley<sup>8</sup> calculated for a Schultz-Zimm molecular weight distribution:

$$P(n)dn = \frac{(Z+2)^{Z+1}}{Z!} \left(\frac{n}{n\omega}\right)^Z \times \exp\left[-\frac{n}{n\omega}(Z+2)\right] \frac{dn}{n\omega} \quad (2)$$

the polydispersity  $P$  being  $=(Z+2)/(Z+1)$ .  $Z = 10$  is chosen, corresponding to a polydispersity index of 1.09, a reasonable value for anionic polystyrene.

The polystyrene of similar polydispersity (PS50) results in a dynamic parameter  $h$  of 0.14.

We can calculate from equation (1) the analytical form of  $\eta'/\eta_0$  and  $|\eta^*|/\eta_0$  as functions of  $\omega\tau_0$ .

The theoretical curve of  $\log |\eta^*|/\eta_0$  versus  $\log \omega\tau_0$  according to the Cole-Cole expression (equation 1), with  $h = 0.14$  is plotted in Figure 6 (curve B). The curve covers a frequency range much larger than the experimental curve.

It appears that the reduced steady-flow curve ( $\eta_a/\eta_0, \dot{\gamma}\tau_0$ ) calculated from Graessley's theory (and the experimental data of Suzuki) (Figure 5) superimpose quite well with  $|\eta^*|/\eta_0$  calculated (and experimental data for PS50) over a large frequency range (with a shift on the frequency scale corresponding to different reducing parameters).

For large frequencies, the curve ( $|\eta^*|/\eta_0, \omega\tau_0$ ) calculated with the Cole-Cole expression tends to a straight line with slope equal to  $(h-1)$ . For our narrow fractions of polystyrene, this limiting slope varies from  $-0.77$  to  $-0.86$ , according to the experimental values of  $h$ .

For large samples, the limiting slope depends rather weakly on polydispersity index, since the  $h$  parameter depends weakly on  $P$  ( $h \sim 0.5$ ).

We have calculated from equation (1) theoretical curves ( $\log |\eta^*|/\eta_0$  vs.  $\log \omega\tau_0$ ) (Figure 6) for various values of  $h$  ( $h = 0; 0.14; 0.5$ ).

We may conclude that the greater the polydispersity index, the sooner the deviation from Newtonian behaviour appears, which is consistent with experiments.

The choice of an analytical expression for  $\eta^*(\omega)$  imposes the form of the relaxation time distribution function  $H(\tau)$ <sup>9</sup>. It is convenient to note that the analytical expression of  $\eta^*(\omega)$  is a formal expression without physical analogy in dielectric experiments. This analysis fails at high frequencies, where molecular motions are quite different, but can provide the relaxation spectrum at medium and long times in a very simple way<sup>1,10</sup>.

The broadness of the distribution function of the logarithm of the relaxation times depends on  $h$  in the experimental frequency range. This distribution, in reduced coordinates ( $\tau H(\tau)/\eta_0$  vs.  $\log \tau/\tau_0$ ) becomes narrower as the polydispersity index tends to 1 (Figure 7). According to a more classical scheme, we outlined  $\log H(\tau)$  versus  $\log \tau$  for a commercial PS (PS506,  $P = 4.62$ ) (Figure 8). This distribution has been calculated using the analytical expression proposed here above (full line) and is compared with distribution calculated using the Ferry-Williams approximations (circles)<sup>9</sup>.

It is interesting to note that the analytical expression

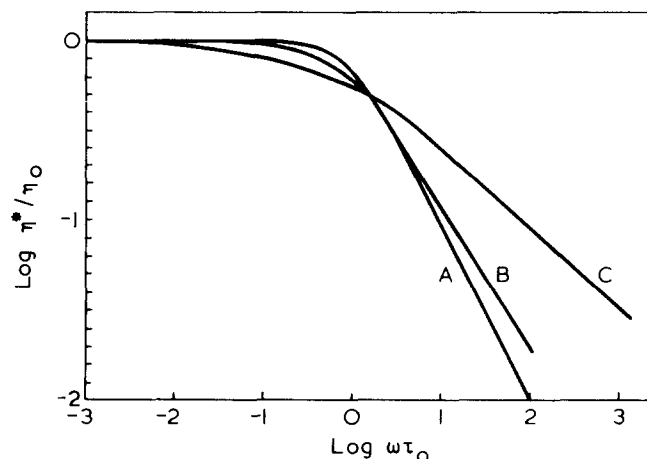


Figure 6 Calculated curves of  $\log |\eta^*|/\eta_0$  versus  $\log \omega\tau_0$ , for different values of  $h$ : A,  $h = 0$ ; B,  $h = 0.14$ ; C,  $h = 0.5$

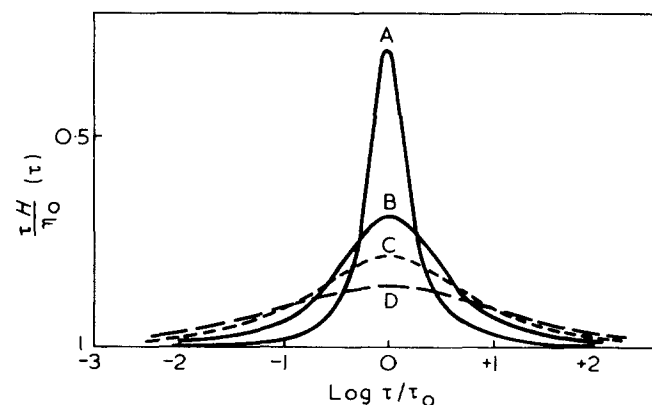


Figure 7 Relaxation spectrum in reduced coordinates. A, PS50 ( $P = 1.11$ ); B, PSS62 ( $P = 1.25$ ); C, PS550 ( $P = 2.45$ ); D, PSSAM327A ( $P = 4.20$ )



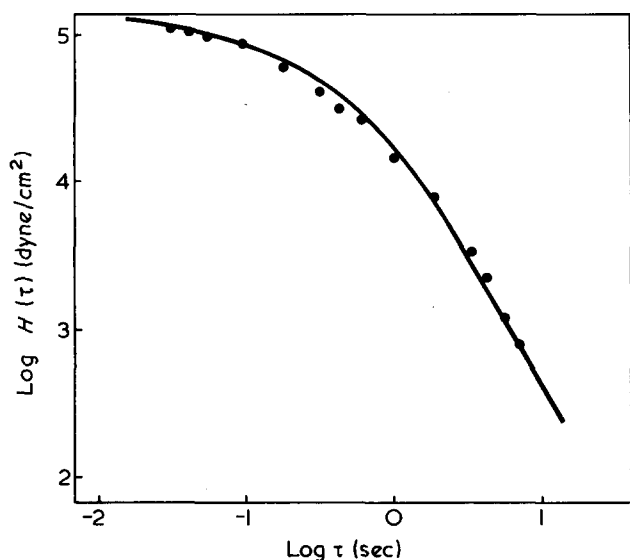


Figure 8 Relaxation times distribution function, in logarithmic scales, for PS506

reproduces the shape of distributions quite well, both for narrow fractions and for samples with broad distributions, in the plateau and terminal zones. It accounts also for the variation of the distribution form with polydispersity<sup>4</sup>.

This analysis fails at short times, where molecular motions do not involve entanglement couplings.

#### CONCLUSION

This study on polystyrene provides the following conclusions: (1) in a complex representation of viscosities, the

experimental plots are located on curves corresponding, within experimental error, to circular arcs whose centres are below the real axis, in the frequency range 20 to  $10^{-3}$  Hz; (2) three parameters  $\eta_0$ ,  $\tau_0$  and  $h$ , characterize the behaviour in dynamical experiments; (3) the  $h$  parameter is independent of temperature, but essentially depends on polydispersity; (4)  $\eta_0$  and  $\tau_0$  depend on temperature, following a WLF type law and also on molecular weight and polydispersity.

#### ACKNOWLEDGEMENTS

The authors wish to express their gratitude to Professor A. J. Kovacs of the Centre de Recherches sur les Macromolécules, Strasbourg, for helpful discussions.

Financial support for the present work was provided by the Société Nationale des Pétroles d'Aquitaine. The support is gratefully acknowledged.

#### REFERENCES

- 1 Labaig, J. J., Monge, Ph. and Bednarick, J. *Polymer* 1973, 14, 384; Labaig, J. J. *Thèse Université de Pau* (1973)
- 2 Pierson, J. *Thèse Université de Strasbourg* (1968)
- 3 Suzuki, R. *Thèse Université de Strasbourg* (1970)
- 4 Onogi, S., Masuda, T. and Kitagawa, K. *Macromolecules* 1970, 3, 309; Onogi, S. and Masuda, T. *Kogyo Kagaku Zashi* 1970, 23, 1255
- 5 Berry, G. C. and Fox, T. G. *Adv. Polym. Sci.* 1968, 5, 261
- 6 Cox, W. P. and Merz, E. H. *J. Polym. Sci.* 1958, 18, 118, 619
- 7 Casale, A., Porter, R. S. and Johnson, J. F. *J. Macromol. Sci. (C)* 1971, 5 (2), 387
- 8 Graessley, W. W. and Prentice, J. S. *J. Polym. Sci. (A-2)* 1968, 6, 1887; Graessley, W. W. *J. Chem. Phys.* 1967, 47, 1942
- 9 Ferry, J. D. 'Viscoelastic properties of polymers', John Wiley, New York, 1961
- 10 Kim, Min Gon *Polymer* 1974, 15, 123

## Note to the Editor

### Effect of a non-uniform distribution of crosslinks on the analysis of Raman polarization data in stretched networks

J. Maxfield\* and I. W. Shepherd

Department of Physics, University of Manchester, Manchester M13 9PL, UK

(Received 20 August 1974; revised 6 November 1974)

In previous work<sup>1</sup> it has been shown that the isomeric populations in a rubber network can be measured as a function of strain using polarized Raman techniques. From these experiments on polydimethylsiloxane (PDMS) it was possible to estimate the value of the constant of proportionality,  $D_2$ , in a rotational isomeric theory of elasticity<sup>2</sup>. This value was found to be  $-8$  for *trans* isomers which was nearly an order of magnitude larger than the theoretical prediction of  $-1.2$ . For the purposes of the experimental determination a uniform network was assumed, and this assumption is not strictly valid. The purpose of this note is to show that the experimental value of  $D_2$  is strongly dependent on deviations from uniformity in the form of extra short chains in the network and that the Raman data provide evidence for the presence of such short chains.

There is independent evidence of inhomogeneities in the form of highly crosslinked regions within networks. Prins *et al.*<sup>3</sup> have observed resonances in the spectra of light scattered from networks which they attribute to oscillation modes of such inhomogeneities and Baer (personal communication) has seen evidence of such regions in crosslinked polystyrene under deformation. In qualitative terms the presence of such defects has the effect of increasing the number of chains or decreasing the average distance between crosslinks. (Entanglements, in as much as they act as crosslinks, will have a similar effect.)  $D_2$  is connected with the change in population of isomer  $\eta$  through the equation:

$$(\Delta n)_{\eta, \alpha} = \nu D_2 \left[ \frac{1}{3} \left( \frac{V}{V_0} \right)^{2/3} \left( \alpha^2 + \frac{2}{\alpha} \right) - 1 \right] \quad (1)$$

where  $\nu$  is the number of chains in the network,  $\alpha$  the extension and  $V$ ,  $V_0$  respectively the unstrained and strained volumes. It is clearly important in evaluating  $D_2$  to have the correct value of  $\nu$  or, equivalently, the average chain length. These quantities, and hence  $D_2$ , will be sensitive to the presence of highly crosslinked, short chain regions.

\* Present address: Polymer Research Center, University of Massachusetts, Amherst, Mass. 01002, USA.

This can be illustrated by using a simple model in which a fraction of short chains  $L$ , is introduced into an otherwise uniform network of chains length  $L_2 = 10L_1$ . The experimental data of ref 1 can now be used to calculate  $D_2$  as a function of the weight fraction of short chains  $F$ . The value of  $D_2$  falls sharply with increasing  $F$  and at  $F = 0.1$  yields a value of  $D_2 = -3.9$  in agreement with recent measurements of PDMS in solution<sup>4</sup>. Agreement with the theoretical value occurs at  $F \sim 0.5$ . Thus it seems that the presence of short chains can explain the large difference between theory and experiment. Unfortunately, because the Raman technique is only sensitive to the average chain length it cannot be used to study the network inhomogeneities themselves.

In summary, it is clear that an experimental determination of  $D_2$  in networks by Raman scattering depends critically on the network morphology and an accurate value will only be obtained if this morphology is known from an independent measurement. However, the fact that the value of  $D_2$  obtained in solution is much lower than the value obtained assuming a uniform network provides strong evidence that imperfections incorporating short chains exist and confirms the work of Prins *et al.*<sup>3</sup> and Baer.

#### ACKNOWLEDGEMENTS

The authors wish to acknowledge helpful discussions with Professor S. F. Edwards and Dr D. H. Reneker. Professor E. Baer is thanked for sending details of his work on polystyrene.

#### REFERENCES

- 1 Maxfield, J. and Shepherd, I. W. *Chem. Phys. Lett.* 1973, **19**, 541; *Chem. Phys.* 1973, **2**, 433
- 2 Abe, Y. and Flory, P. J. *J. Chem. Phys.* 1970, **52**, 2814
- 3 Prins, W., Rimai, L. and Chomppf, A. J. *Macromolecules* 1972, **5**, 104
- 4 Speak, R. and Shepherd, I. W. *J. Polym. Sci. (A-2)* submitted

## Letters

**Comments on Letter: 'Dilatometric study of monovalent counter-ion association with poly-methacrylate'** (J. Komiyama, Y. Takeda, M. Ando and T. Iijima, *Polymer* 1974, 15, 468-470)

In a recent communication, Komiyama *et al.*<sup>1</sup> reported volume changes ( $\Delta V$ ) upon protonation of alkali metal (AM) and tetraalkylammonium (TAA) salts of poly(methacrylic acid) (PMA). The results given indicate: (i) that the  $\Delta V$  upon protonation of AM salts of PMA does not depend on the nature of the alkali metal ( $\Delta V = 19.8 \text{ cm}^3/\text{mol}$ ), except for  $\text{Li}^+$ , and that therefore the binding of AM by polyions cannot be specific; (ii) in contrast, the larger the TAA ion, the larger the volume change upon protonation of TAA-PMA salts ( $\Delta V = 26.2, 27.3$  and  $28.8 \text{ cm}^3/\text{mol}$  for the protonation of T(Methyl)A, T(Propyl)A and T(Butyl)A-PMA salts, respectively).

From these results as well as results from other studies<sup>2,3</sup> the authors 'suggest that in aqueous solutions, AM salts of PMA do not associate to an extent that the primary hydrations of respective ions are perturbed and in contrast, TAA salts are under an interaction leading to the volume contraction'. Since some of our results<sup>3</sup> were used to reach this conclusion we feel entitled to report several facts which show that the experimental procedure used by Komiyama *et al.*<sup>1</sup> is not very well fitted to the problem investigated and which lead to conclusions opposite to those of these workers.

It must be first remembered that for polyelectrolytes considerable precautions must be taken in both density measurements (to obtain partial molal volumes) and dilatometry (to obtain volume changes) in order to obtain accurate results. These precautions, which have been described at length elsewhere<sup>3</sup>, concern more the preparation of the polysalt solutions (thorough purification of the polyacids and hydroxides used to prepare the polysalts, determination of their concentration to within 0.1 to 0.2%, etc.)<sup>3</sup> than the density or volume change measurements which are usually of sufficient accuracy. In particular, an incomplete purification may lead to large errors (several  $\text{cm}^3/\text{mol}$  on partial molal volumes). The absence of any detail about the experimental procedure by Komiyama *et al.*<sup>1</sup> does not permit us to discuss this point further. It must be pointed out however that the data of Ise and Okubo<sup>2</sup> used by Komiyama *et al.*<sup>1</sup> to further substantiate their conclusion have been shown<sup>3</sup> to be systematically too large by several  $\text{cm}^3/\text{mol}$ . In this respect they certainly do not offer a good experimental basis for a discussion on whether the  $\Delta V$  upon protonation of PMA salts depends on the nature of the counter-ion.

It must also be remembered that the dilatometric study of Strauss and Leung<sup>4</sup> which has provided us with the first evidence of a dependence of the volume change upon counter-ion binding on the nature of the AM counter-ion, consists in the measurement of the  $\Delta V$  upon addition of an AM-chloride to a TMA polysalt solution at constant ionic strength. If  $\Delta V_{\text{AM}}$  and  $\Delta V_{\text{TMA}}$  are the volume changes upon binding of AM and TMA, respectively, by the polyion, these volume changes would be those measured in an idealized experiment where counter-ions alone are

added to a counter-ion-free solution of polyion. The experimental volume change is then given by:

$$\Delta V_{\text{exp}} = \Delta V_{\text{AM}} - \Delta V_{\text{TMA}} \quad (1)$$

$\Delta V_{\text{TMA}}$  has been found to be very close to zero<sup>4</sup> (this point is further substantiated below). Therefore  $\Delta V_{\text{exp}}$  is very close to  $\Delta V_{\text{AM}}$ . The variation of  $\Delta V_{\text{exp}}$  for different counter-ions may reach 1 to 2  $\text{cm}^3/\text{mol}$  for  $\Delta V_{\text{exp}} \approx 5$  to 6  $\text{cm}^3/\text{mol}$ <sup>3</sup>. As the accuracy on  $\Delta V_{\text{exp}}$  is usually of about 5%, the variations of  $\Delta V_{\text{exp}}$  for different counter-ions are well above the experimental error. They can therefore be measured and have in fact been measured for several polyions<sup>4-6</sup>.

Such is not the case when the Komiyama *et al.*<sup>1</sup> procedure is used. Indeed these authors measured the  $\Delta V$  upon protonation of AM-PMA. With the same assumption as above, the measured volume change can be now written:

$$\Delta V_{\text{exp}} = \Delta V_{\text{H}} - \Delta V_{\text{AM}} \quad (2)$$

Note that  $\Delta V_{\text{H}}$  and  $\Delta V_{\text{AM}}$  are positive because they are associated with a release of hydration water. The main drawback of this procedure lies in the fact that  $\Delta V_{\text{H}}$  has been consistently found to be much larger than  $\Delta V_{\text{AM}}$ <sup>3-7</sup> (20  $\text{cm}^3/\text{mol}$  compared to 2 to 6  $\text{cm}^3/\text{mol}$ ). As a result, the ion specific contribution to  $\Delta V_{\text{exp}}$ , which shows up only through  $\Delta V_{\text{AM}}$ , represents a much smaller part of  $\Delta V_{\text{exp}}$  than in the Strauss *et al.* procedure. This part is, in many instances, smaller than the experimental error on  $\Delta V_{\text{exp}}$  and can thus go undetected. Also, the purification of the solutions as well as the determination of their concentration become more critical.

Another minor drawback in the Komiyama *et al.* procedure is that the ionic strength,  $\mu$ , is not held constant during the experiment. Indeed additions of HCl to AM-PMA increase the AM-Cl content of the solution. This variation of  $\mu$  depends on the degree of neutralization,  $\alpha$ . The increase of  $\mu$  appears to be sizeable since the initial concentration of AM-Cl is 0.01 M and that of AM-PMA 0.046 M. Thus at  $\alpha = 0$  the final concentration of AM-Cl is 0.056 M. Volume changes upon binding have been found to decrease with increasing  $\mu$ <sup>4,8</sup> and the magnitude of this decrease appears to depend on the counter-ion<sup>8</sup>. This may have been of importance in the work of Komiyama *et al.*

In addition to the dilatometric work of Strauss *et al.*<sup>4-6</sup>, there is other evidence of the dependence of the volume change upon binding on the nature of the bound AM ion. This evidence has been obtained through the measurement of the excess ultrasonic absorption of solutions of polysalts, with TMA polysalts used as reference<sup>9</sup>. It must be first recalled that in aqueous solutions, an excess ultrasonic absorption arises from a chemical process such as counter-ion binding, only if a volume change is associated with this process because the enthalpy term is usually very small with respect to the volume change term, owing to the very low value of the thermal expansion coefficient of water<sup>10</sup>. Thus, in water where studies of polyelectrolytes are usually performed, the existence of an excess absorption implies that of a volume change. Upon neutralization of polyacids by TMA hydroxide we have observed very *small* changes

of absorption for weak polyacid solutions and *no* change of absorption for solutions of strong polyacids<sup>9</sup>. The ultrasonic absorption titration curves obtained upon neutralization with AM hydroxides are always above those relative to a neutralization by TMA hydroxide. Finally, additions of AM-Cl to TMA-polysalts (including TMA-PMA) consistently result in an increase of absorption whose magnitude is extremely sensitive to the nature of the counter-ion. All of these results are consistent with the existence of a positive volume change upon binding of AM ions by polyions, and a negligible  $\Delta V$  upon binding of TMA. The same conclusion was reached by other workers in an ultrasonic study of solutions of chelates of AM and TMA ions<sup>11</sup>. Therefore, in the Komiyama *et al.*<sup>1</sup> report the difference between the  $\Delta V$  upon protonation of AM and TMA polymethacrylates must not be attributed to a volume contraction due to the interaction between TMA and PMA but to the volume increase upon binding of AM ions by PMA. The negligible volume change upon binding of TMA or formation of chelates including TMA appears to be the result of a compensation between the various contributions to the hydration of TMA ions. As a result, this ion has practically no influence on the volume of the surrounding water molecules<sup>12</sup>. We agree, however, that a small contraction (1 to 2 cm<sup>3</sup>/mol) may occur from the interaction of TPA and TBA ions with PMA. We have ourselves observed that the partial molal volumes of the poly(ethylene sulphonic) ion calculated from those of its TEA, TPA and TBA salts are smaller than that obtained from the partial molal volume of the TMA poly(ethylene sulphonate)<sup>13</sup>. Note, however, that this difference cannot be the result of a simple hydrophobic interaction between TAA ions and polyions because a volume increase would be then expected.

Finally, mention must be made about whether the primary hydration layer of AM ions is affected upon binding by PMA and other polyions. We have reported<sup>14</sup> n.m.r. evidence that several polyions, including polyacrylate which is chemically very similar to PMA, appear capable of causing a release of some primary hydration of Co<sup>2+</sup> upon binding of this ion (4 to 5 water molecules from the Co<sup>2+</sup> inner hydration shell appear to be released upon binding by polyacrylate<sup>14</sup>). Since the interaction of Co<sup>2+</sup> with the water molecules constituting its primary hydration is much stronger than in the case of AM ions it seems likely that the primary hydration of AM ions will be affected upon binding. This conclusion is also in contrast with that of Komiyama *et al.*<sup>1</sup>.

Christian Tondre and Raoul Zana

Centre de Recherches sur les Macromolécules, CNRS,  
Strasbourg 67083, France

(Received 18 September 1974; revised 9 December 1974)

#### References

- 1 Komiyama, J., Takeda, Y., Ando, M. and Iijima, T. *Polymer* 1974, **15**, 468
- 2 Ise, N. and Okubo, T. *J. Am. Chem. Soc.* 1968, **90**, 4527
- 3 Tondre, C. and Zana, R. *J. Phys. Chem.* 1972, **76**, 3451
- 4 Strauss, U. and Leung, P. *J. Am. Chem. Soc.* 1965, **87**, 1476
- 5 Begala, J. and Strauss, U. *J. Phys. Chem.* 1972, **76**, 254
- 6 Hen, J. and Strauss, U. *J. Phys. Chem.* 1974, **78**, 1013
- 7 Ikegami, A. *J. Polym. Sci. (A)* 1964, **2**, 907; *Biopolymers* 1968, **6**, 431
- 8 Rinaudo, M. and Pierre, C. *C. R. Acad. Sci.* 1969, **269**, 1280
- 9 Tondre, C. and Zana, R. *IUPAC Symp. Macromolécules, Leiden* 1970, **1**, 387; *J. Phys. Chem.* 1971, **75**, 3367; *J. Chim. Phys.* 1971, **68**, 1258; *Biophys. Chem.* 1974, **1**, 367

- 10 Tamm, K. in 'Dispersion and Absorption of Sound by Molecular Processes', (Ed. D. Sette), Academic Press, New York, 1963, p 189
- 11 Eigen, M. *Pure Appl. Chem.* 1963, **6**, 97; 1969, **20**, 93
- 12 Conway, B., Desnoyers, J. and Verrall, R. *J. Phys. Chem.* 1971, **75**, 3031 and references therein
- 13 Tondre, C. and Zana, R. unpublished results
- 14 Spegt, P., Tondre, C., Weill, G. and Zana, R. *Biophys. Chem.* 1973, **1**, 55

#### Study of structural change in linear polyethylene by elongation in view of behaviour of free radicals induced by $\gamma$ -irradiation

The behaviour of free radicals formed in solid polymers by  $\gamma$ -irradiation has been closely correlated to molecular motions by many investigators. We have reported in a study of  $\gamma$ -irradiation effects on polymers that radicals preferentially form in the non-crystalline phase including defects and the amorphous phase<sup>1,2</sup>. Therefore, the observation of radical behaviour in irradiated polymers may become an invaluable tool for studying the defect of polymer crystals. Actually, we have used this method to elucidate the structural change in the crystalline phase of polyethylene subjected to a cyclic tensile stress<sup>3</sup>.

This communication deals with the application of the method for studying the structural change in polyethylene by elongation. Pellets of high density polyethylene (Hizex 1200J, Mitsui Petrochemical Co.) were melted and pressed to form sheets, and then quenched in ice water. The quenched sheets were drawn with different elongations at 60 and 90°C. Additionally, a suspension of solution grown crystals was obtained by maintaining a 0.08% xylene solution of the polyethylene in a Dewar vessel overnight, and then filtering to form single crystal mats. The mats were dried under reduced pressure for more than 3 days. The specimens (0.26 × 3 × 10 mm) were cut out of the original sheets, and sealed in glass tubes under a pressure of less than 10<sup>-4</sup> mmHg. They were irradiated by <sup>60</sup>Co  $\gamma$ -rays to a total dose of about 10<sup>7</sup> rad at liquid nitrogen temperature. The electron spin resonance studies were made with a Nihon Denshi JES-3BSX spectrometer using the x-band and 100 kHz field modulation.

As shown previously<sup>1,2</sup>, the amount of radicals formed in the crystalline polymers at liquid nitrogen temperature depends on the polymer morphology. Therefore, we called the radical concentration after  $\gamma$ -irradiation at liquid nitrogen temperature 'radical trapping capacity', which is a measure of polymer morphology. *Figure 1* shows the plots of alkyl radical concentration *versus* elongation. The radical trapping capacity is found to linearly decrease until the elongation reaches 160 and 180% for the samples drawn at 60 and 90°C, respectively. Above these elongations the radical trapping capacity, in turn, linearly increases slightly up to 400%. The capacity of the single crystals was found to be 80% of the bulk sample. The decrease in the capacity with increasing elongation suggests a decrease of non-crystalline phase. Further since little change of density crystallinity by elongation was found, this decrease of radicals may be due to the decrease of crystal defects. It is interesting to compare this fact with the result that the radical trapping capacity increased owing to the increase of crystal defects when linear polyethylene sheets were subjected to the cyclic stress to cause fatigue<sup>3</sup>. In *Figure 1* the radical trapping capacity of the 60°C drawn sample is

of absorption for weak polyacid solutions and *no* change of absorption for solutions of strong polyacids<sup>9</sup>. The ultrasonic absorption titration curves obtained upon neutralization with AM hydroxides are always above those relative to a neutralization by TMA hydroxide. Finally, additions of AM-Cl to TMA-polysalts (including TMA-PMA) consistently result in an increase of absorption whose magnitude is extremely sensitive to the nature of the counter-ion. All of these results are consistent with the existence of a positive volume change upon binding of AM ions by polyions, and a negligible  $\Delta V$  upon binding of TMA. The same conclusion was reached by other workers in an ultrasonic study of solutions of chelates of AM and TMA ions<sup>11</sup>. Therefore, in the Komiyama *et al.*<sup>1</sup> report the difference between the  $\Delta V$  upon protonation of AM and TMA polymethacrylates must not be attributed to a volume contraction due to the interaction between TMA and PMA but to the volume increase upon binding of AM ions by PMA. The negligible volume change upon binding of TMA or formation of chelates including TMA appears to be the result of a compensation between the various contributions to the hydration of TMA ions. As a result, this ion has practically no influence on the volume of the surrounding water molecules<sup>12</sup>. We agree, however, that a small contraction (1 to 2 cm<sup>3</sup>/mol) may occur from the interaction of TPA and TBA ions with PMA. We have ourselves observed that the partial molal volumes of the poly(ethylene sulphonic) ion calculated from those of its TEA, TPA and TBA salts are smaller than that obtained from the partial molal volume of the TMA poly(ethylene sulphonate)<sup>13</sup>. Note, however, that this difference cannot be the result of a simple hydrophobic interaction between TAA ions and polyions because a volume increase would be then expected.

Finally, mention must be made about whether the primary hydration layer of AM ions is affected upon binding by PMA and other polyions. We have reported<sup>14</sup> n.m.r. evidence that several polyions, including polyacrylate which is chemically very similar to PMA, appear capable of causing a release of some primary hydration of Co<sup>2+</sup> upon binding of this ion (4 to 5 water molecules from the Co<sup>2+</sup> inner hydration shell appear to be released upon binding by polyacrylate<sup>14</sup>). Since the interaction of Co<sup>2+</sup> with the water molecules constituting its primary hydration is much stronger than in the case of AM ions it seems likely that the primary hydration of AM ions will be affected upon binding. This conclusion is also in contrast with that of Komiyama *et al.*<sup>1</sup>.

Christian Tondre and Raoul Zana

Centre de Recherches sur les Macromolécules, CNRS,  
Strasbourg 67083, France

(Received 18 September 1974; revised 9 December 1974)

#### References

- 1 Komiyama, J., Takeda, Y., Ando, M. and Iijima, T. *Polymer* 1974, **15**, 468
- 2 Ise, N. and Okubo, T. *J. Am. Chem. Soc.* 1968, **90**, 4527
- 3 Tondre, C. and Zana, R. *J. Phys. Chem.* 1972, **76**, 3451
- 4 Strauss, U. and Leung, P. *J. Am. Chem. Soc.* 1965, **87**, 1476
- 5 Begala, J. and Strauss, U. *J. Phys. Chem.* 1972, **76**, 254
- 6 Hen, J. and Strauss, U. *J. Phys. Chem.* 1974, **78**, 1013
- 7 Ikegami, A. *J. Polym. Sci. (A)* 1964, **2**, 907; *Biopolymers* 1968, **6**, 431
- 8 Rinaudo, M. and Pierre, C. *C. R. Acad. Sci.* 1969, **269**, 1280
- 9 Tondre, C. and Zana, R. *IUPAC Symp. Macromolécules, Leiden* 1970, **1**, 387; *J. Phys. Chem.* 1971, **75**, 3367; *J. Chim. Phys.* 1971, **68**, 1258; *Biophys. Chem.* 1974, **1**, 367

- 10 Tamm, K. in 'Dispersion and Absorption of Sound by Molecular Processes', (Ed. D. Sette), Academic Press, New York, 1963, p 189
- 11 Eigen, M. *Pure Appl. Chem.* 1963, **6**, 97; 1969, **20**, 93
- 12 Conway, B., Desnoyers, J. and Verrall, R. *J. Phys. Chem.* 1971, **75**, 3031 and references therein
- 13 Tondre, C. and Zana, R. unpublished results
- 14 Spegt, P., Tondre, C., Weill, G. and Zana, R. *Biophys. Chem.* 1973, **1**, 55

#### Study of structural change in linear polyethylene by elongation in view of behaviour of free radicals induced by $\gamma$ -irradiation

The behaviour of free radicals formed in solid polymers by  $\gamma$ -irradiation has been closely correlated to molecular motions by many investigators. We have reported in a study of  $\gamma$ -irradiation effects on polymers that radicals preferentially form in the non-crystalline phase including defects and the amorphous phase<sup>1,2</sup>. Therefore, the observation of radical behaviour in irradiated polymers may become an invaluable tool for studying the defect of polymer crystals. Actually, we have used this method to elucidate the structural change in the crystalline phase of polyethylene subjected to a cyclic tensile stress<sup>3</sup>.

This communication deals with the application of the method for studying the structural change in polyethylene by elongation. Pellets of high density polyethylene (Hizex 1200J, Mitsui Petrochemical Co.) were melted and pressed to form sheets, and then quenched in ice water. The quenched sheets were drawn with different elongations at 60 and 90°C. Additionally, a suspension of solution grown crystals was obtained by maintaining a 0.08% xylene solution of the polyethylene in a Dewar vessel overnight, and then filtering to form single crystal mats. The mats were dried under reduced pressure for more than 3 days. The specimens (0.26 × 3 × 10 mm) were cut out of the original sheets, and sealed in glass tubes under a pressure of less than 10<sup>-4</sup> mmHg. They were irradiated by <sup>60</sup>Co  $\gamma$ -rays to a total dose of about 10<sup>7</sup> rad at liquid nitrogen temperature. The electron spin resonance studies were made with a Nihon Denshi JES-3BSX spectrometer using the x-band and 100 kHz field modulation.

As shown previously<sup>1,2</sup>, the amount of radicals formed in the crystalline polymers at liquid nitrogen temperature depends on the polymer morphology. Therefore, we called the radical concentration after  $\gamma$ -irradiation at liquid nitrogen temperature 'radical trapping capacity', which is a measure of polymer morphology. *Figure 1* shows the plots of alkyl radical concentration *versus* elongation. The radical trapping capacity is found to linearly decrease until the elongation reaches 160 and 180% for the samples drawn at 60 and 90°C, respectively. Above these elongations the radical trapping capacity, in turn, linearly increases slightly up to 400%. The capacity of the single crystals was found to be 80% of the bulk sample. The decrease in the capacity with increasing elongation suggests a decrease of non-crystalline phase. Further since little change of density crystallinity by elongation was found, this decrease of radicals may be due to the decrease of crystal defects. It is interesting to compare this fact with the result that the radical trapping capacity increased owing to the increase of crystal defects when linear polyethylene sheets were subjected to the cyclic stress to cause fatigue<sup>3</sup>. In *Figure 1* the radical trapping capacity of the 60°C drawn sample is

Letters

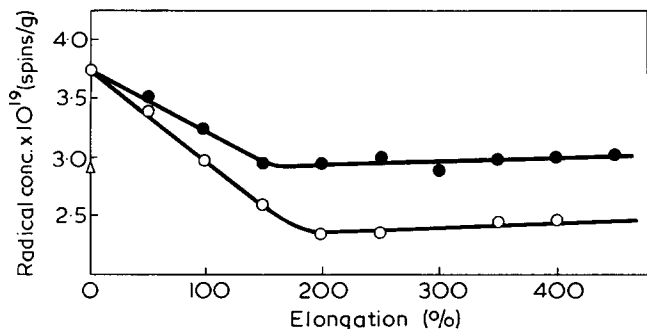


Figure 1 Plots of radical concentration versus elongation.  $\circ$ , Drawn at  $90^{\circ}\text{C}$ ;  $\bullet$ , drawn at  $60^{\circ}\text{C}$

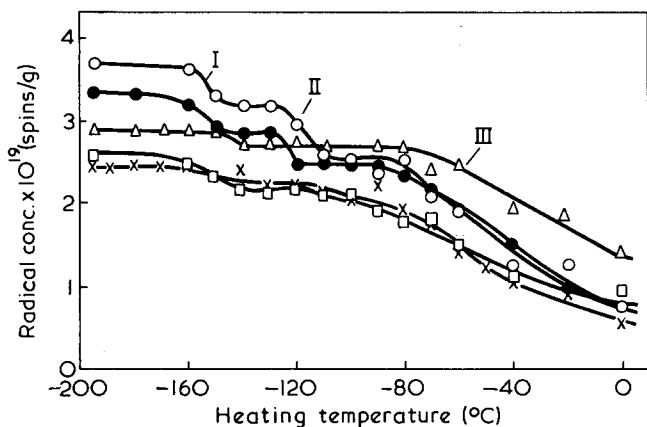


Figure 2 Plots of radical concentration versus heating temperature.  $\circ$ , Bulk;  $\bullet$ , 50% elongation;  $\square$ , 150% elongation;  $\times$ , 350% elongation;  $\Delta$ , solution grown crystal

always larger than that of the  $90^{\circ}\text{C}$  drawn sample. This fact can be interpreted by the mechanism that the  $60^{\circ}\text{C}$  drawn sample originally has much larger amount of non-crystalline phase than the  $90^{\circ}\text{C}$  drawn sample because of its low elongation temperature. The fact that the radical trapping capacity becomes almost constant at 160–180% elongation implies that the crystalline texture has settled to form fibre structure above this elongation range.

Further, experiments on radical decay by elevating sample temperature give us valuable information about the cause of change in the radical trapping capacity. Figure 2 shows the plots of the radical concentration versus heating temperature for the bulk, the solution grown and the  $90^{\circ}\text{C}$  drawn samples. These curves were obtained by measuring the radical concentration at liquid nitrogen temperature after heating the samples for 3 min at a regulated temperature increased stepwise from liquid nitrogen temperature. For the bulk sample three stepwise decays are clearly seen. The first step begins at about  $-160^{\circ}\text{C}$  (region I), the second one at about  $-130^{\circ}\text{C}$  (region II) and the final one at about  $-80^{\circ}\text{C}$  (region III). This result is very similar to those obtained by Nagamura<sup>3</sup>, Tamura<sup>4</sup>, and Nara<sup>5</sup>. The activation energy of the radical decay was estimated to be 0.5, 5 and 15 kcal/mol for regions I, II and III, respectively, by the method described previously<sup>3</sup>. These values are similar to those obtained by Nara<sup>5</sup>. The cause of radical decay in region I has been ascribed to a very small scale motion of the amorphous chains and in region II to the local relaxation mode at the lamellar surface, because the activation energies and the temperature locations of these radical decays are similar to those of molecular motions detected by mechanical relaxation<sup>5</sup>. However, we are inclined to ascribe

region II to the localized motion of molecules within the lamellar crystal throughout our recent work<sup>1,3</sup>. This discrepancy originally comes from the interpretation of the  $\gamma$ -process in the mechanical relaxation. The decay datum for the single crystals in the same figure may afford the proof of the above supposition in the present work. Region II almost cannot be seen in the single crystal which is believed to have few defects within it from the Moiré pattern technique<sup>6–8</sup> and n.m.r. data<sup>1</sup>. Similar results were obtained for the  $60^{\circ}\text{C}$  drawn sample.

Figure 3 shows the plots of the step height in the decay curve versus elongation for the  $90^{\circ}\text{C}$  drawn sample. It is noteworthy that the amount of decay considerably decreases and the temperature locations are shifted to higher temperatures in region II with increasing elongation, while the amount of decay in region I only slightly decreases.

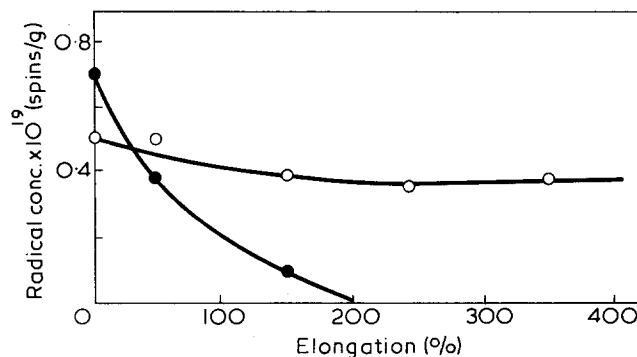


Figure 3 Plots of decay amount of radicals versus elongation.  $\circ$ , Region I;  $\bullet$ , region II

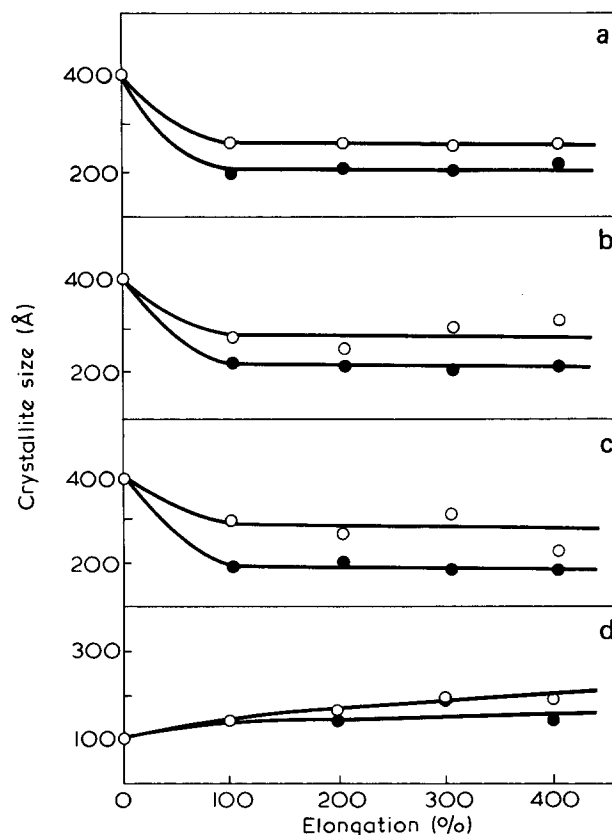


Figure 4 Plots of crystallite size versus elongation. (a) (110); (b) (200); (c) (020); (d) (002).  $\circ$ , Drawn at  $90^{\circ}\text{C}$ ;  $\bullet$ , drawn at  $60^{\circ}\text{C}$

From these results it follows that the defects within the crystals which cause region II decreased by elongation. This mechanism agrees well with the result obtained in the study on the radical trapping capacity of the crystalline phase of the drawn polypropylene treated by fuming nitric acid<sup>2</sup>. In this work it was found that the crystal core of drawn sample stripped by etching has little crystal defects. As to the cause of the decrease of defects, one possible mechanism is that the crystal decomposes into smaller ones cleaving from the defects within the crystal. At the cleaved planes of lamellar crystals molecular chains will have larger mobilities, and hence the radical trapping capacity decreases. On the other hand, it has been deduced that elongation causes the remelt-recrystallizing process of crystallites<sup>9,10</sup>. It was found that the long period after elongation was independent on that before elongation, but determined by elongation temperature. This fact seems to be contradictory to the above interpretation, but our experimental range is confined only in the initial stage of elongation where the other data did not cover.

Figure 4 shows the plots of crystallite size versus elongation, estimated from the width of wide angle X-ray line profiles using Scherrer's equation. As far as the present data are concerned, both temperature and elongation were found to determine the crystallite size. The progressive increase in crystallite size along the *c*-axis from the original size with increasing elongation is seen, and the abrupt decrease in the size seen earlier<sup>9,10</sup> was not observed. The increase of the size along the *c*-axis may possibly be caused by annealing at elongation temperature and additional heat generation by viscous flow of the microstructure to cause thickening of the lamellar crystals.

From the above considerations we propose here a possible model of the structural change in the early stage of elongation as shown in Figure 5. In this model it is emphasized that the lamellar crystal cleaves from the defects within the lamella, shown by the broken lines, to form smaller crystal blocks which have little defects. The model shows the case where complete cleavage occurs, although the actual aspect of the cleavage depends on the draw direction to the lamella. It is comprehensible that the lamellar crystals cleave from the defects within the crystals because the van der Waals force between the crystals plays a predominant role in transmitting the external stress to the element of supramolecular structure in the initial stage of elongation. At this time amorphous tie chains afford to some extent and the external stress acts on the whole unit through van der Waals forces and hence the crystals cleave from the defects. The cleavage from the defects could also

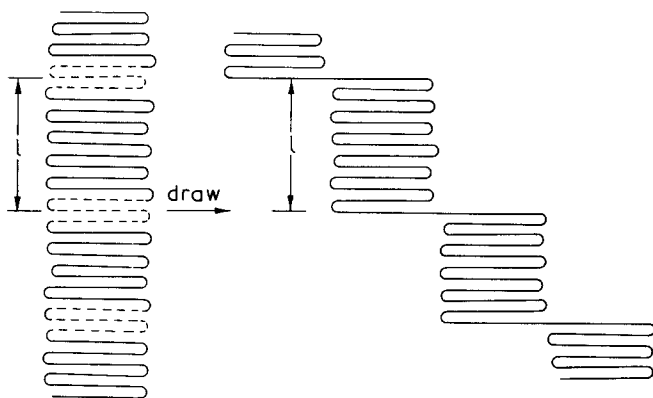


Figure 5 Schematic representation of cleavage of crystallite by elongation

be caused by the thickening process if it proceeds similar to the case of single crystal according to the theory of crystal block formation<sup>1</sup>.

Present address:  
Department of Macromolecular Science,  
Case Western Reserve University,  
Cleveland, Ohio 44106, USA

N. Kusumoto

and Y. Haga and Y. Motozato

Department of Synthetic Chemistry,  
Faculty of Engineering, Kumamoto University,  
Kumamoto 860, Japan  
(Received 16 December 1974)

#### References

- 1 Kusumoto, N., Yamamoto, T. and Takayanagi, M. *J. Polym. Sci. (A-2)* 1971, 9, 1173
- 2 Kusumoto, N., Matsumoto, K. and Takayanagi, M. *J. Polym. Sci. (A-1)* 1969, 7, 1773
- 3 Nagamura, T., Kusumoto, N. and Takayanagi, M. *J. Polym. Sci. (Polym. Phys. Edn)* 1973, 11, 2357
- 4 Tamura, N. *Rep. Progr. Polym. Phys. Japan* 1964, 7, 347
- 5 Nara, S., Shimada, S., Kashiwabara, H. and Sohma, J. *J. Polym. Sci. (A-2)* 1968, 6, 1435
- 6 Holland, V. H. *J. Appl. Phys.* 1964, 35, 3255
- 7 Bassett, D. C. *Phil. Mag.* 1968, 17, 37
- 8 Abe, K., Niinomi, M. and Takayanagi, M. *J. Macromol. Sci. (B)* 1970, 4, 87
- 9 Corneliussen, R. and Peterlin, A. *Makromol. Chem.* 1967, 105, 193
- 10 Peterlin, A. and Corneliussen, R. *J. Polym. Sci. (A-2)* 1968, 6, 1273

#### Conference Announcement

##### Rheometry: methods of measurement and analysis of results

Shrivenham, 8–11 April 1975

The British Society of Rheology and the Italian Society of Rheology are organizing the above conference at the Royal Military College of Science, Shrivenham, Wiltshire from April 8 to 11, 1975. The conference will provide a forum for discussion and debate about measuring techniques and the interpretation of rheological data. Further details may be obtained from Dr F. N. Cogswell, 67 Daniells, Welwyn Garden City, Herts. AL7 1QT, UK.

The Proprietors of British Patent No. 1163502, for "Method for activating cycloaliphatic polyamines as curing agents for reaction with epoxide compounds", desire to enter into negotiations for the sale of the patent, or for the grant of licences thereunder. Further particulars may be obtained from Marks & Clerk, 57-60 Lincoln's Inn Fields, London WC2A 3LS.

## Book Reviews

### The physics of glassy polymers

*Edited by R. N. Haward*

Applied Science, Barking, 1973, 620 pp. £15

This is a large and ambitious work containing an introduction and ten chapters on various aspects of the structure and physical properties of amorphous polymers at temperatures below their glass-rubber transition. Some sixteen authors are involved and the subject matter is mainly, but not entirely, devoted to mechanical behaviour. Topics covered include thermodynamics of the glassy state, X-ray diffraction studies of amorphous structures, relaxation processes, creep, yield, post yield behaviour, cracking and crazing, and the diffusion and sorptions of gases and vapours. There are also chapters on the behaviour of rubber-modified thermoplastics and regular block copolymers.

Inevitably in a compendium of this sort the style and standards vary from chapter to chapter and there is no progressive, logical development of the subject as one progresses through the book. Indeed each contribution stands on its own as a separate review of a particular subject area.

The nature of the reviews varies considerably; a few are critical, authoritative presentations in which the necessary concepts are presented in a fairly detailed manner which will help the reader achieve some real understanding. Others, less usefully, lack authority and critical appraisal and are little more than an introduction to the literature.

It is perhaps in this latter role, as an up to date introduction to and survey of the literature that the book will be most useful. Each chapter has an extensive bibliography and contains a large amount of experimental data and information on behaviour in the form of numerous diagrams and tables drawn from the literature. There is also an excellent subject index but no author index.

Overall the book will be disappointing to those coming new to the subject and seeking detailed development, basic understanding and critical appraisal. It is likely to have most appeal to those having a good general background in polymer physics who seek mainly a series of 'state of the art' reviews.

The book is well produced and commendably free from editorial and printing errors.

*D. W. Saunders*

### Advances in polymer science

*Volume 12*

Springer-Verlag, Berlin, 1973, 190 pp. \$32.00

This slim volume fully maintains the high standard reached by some of the earlier volumes in this series.

The first chapter by K. Osaki (Kyoto University, Japan) is on the 'Viscoelastic properties of dilute polymer solutions', and is a comprehensive account both of theoretical and experimental studies of dilute polymer solutions. The author sets out to describe systematically the experimental results which have been obtained and to evaluate the success of present molecular-based theoretical explanations. It is of interest to note that in the field of viscoelastic properties of flexible polymers at infinite dilution that several molecular theories were constructed prior to the determination of successful experimental measurements. Considerable attention is paid to the Zimm theory in its different forms as well as to those of Rouse and Ogasa and Imai. Perhaps the most valuable section is that dealing with an evaluation of the experimental validity of the various theories. The final section in this review surveys more recent work on viscoelastic studies at higher frequencies, again considering both theoretical and experimental studies. The author somewhat confidently concludes that sufficient data now exist to allow the theoretical elucidation of the dynamics of polymer solutions on a molecular basis. Certainly an optimistic note on which to end!

The second review is by W. L. Carrick, on the 'Mechanism of olefin polymerization' by Ziegler-Natta catalysts, and attention is naturally paid to the contribution to this field which has come from the Union Carbide Research and Development Department at Bound Creek, New Jersey. The author states that his report is

intended to serve as an illustrative, but not exhaustive review of some of the work carried out on olefin polymerization with Ziegler-Natta catalysts. He thus sets out to provide answers to such questions as: what are the co-catalyst interactions?; what is the structure of the active site?; what activates the olefin?; how is stereoregularity achieved? In an area of enormous complexity this is an excellent approach. The answers given are sometimes oversimplified but the author is to be congratulated on the clarity of his account and the considerable insight which he shows into this complex area of polymerization. He rightly stresses the contribution to our present understanding which has come from copolymerization studies and also the role of complex formation reactions between monomer and catalyst so that the necessary degree of stereoregular orientation can be achieved. This brief review should serve as a good introduction to this field of study.

The third review on the 'Applications of infra-red spectroscopy to ethylene-propylene copolymers' is by C. Tosi and F. Ciampelli of the Montecatini Edison Central Research Group in Milan, Italy. It is indeed fitting that this group should be responsible for this review owing to the considerable contribution which they have made to this field. Also, as the authors remark, this is probably the right moment to present a review due to the likely impact of  $^{13}\text{C}$  n.m.r. spectroscopy. This is one of the best reviews of its kind and is most readable covering critically the applications of i.r. spectroscopy to  $\text{C}_2$ - $\text{C}_3$  copolymers up to mid-1972. In dealing with methods for the analysis of composition the authors rightly stress the importance of useful standards and the selection of bands of clear assignment.

The final review on the 'ESR study of photodegradation of polymers' by K. Tsuji of the Sumitomo Chemical Co. Ltd, Osaka, Japan, is timely in view of recent developments in degradable plastics. This is a fairly exhaustive review. The author begins with a consideration of the fundamental steps involved in the photodegradation of polymers. This consideration is followed by a long section on the structure and behaviour of types of free radicals produced after u.v. irradiation of polymers. An exhaustive variety of polymers are examined including polyolefins, poly(vinyl chloride), polystyrene, poly(methyl methacrylate), polyethers, polyamides, polysiloxanes, etc. There is no doubt that this review will be a most useful source of reference to workers in this field.

*P. J. T. Tait*

### The solid state of polymers

*Edited by P. H. Geil, E. Baer and Y. Wada*

Marcel Dekker, New York, 1974, 708 pp. \$47.50

This book contains thirty-three of the forty-one papers delivered at the October 1972 joint seminar in Cleveland, and includes then-current research reports from several leading groups in the USA and Japan. The subject matter divides, somewhat unevenly, into the following sections: deformation of crystalline polymers (3 papers); structure-property relationships in oriented polymers (4 papers); morphology-crystalline polymers (5 papers); morphology-amorphous polymers (3 papers); relaxation behaviour (9 papers); fracture, yield and crazing (8 papers).

The papers individually are of a high standard, but several of the researches are described in outline only; some merely supplement previous publications by their authors whilst others have been superseded by later or amplified papers in journals (this state of affairs is not helped by the appearance of the proceedings nearly two years after the event).

The main value of the work probably lies in the access it provides to some recent Japanese work which might otherwise not have been published in the West. Some of the papers (e.g. Lindenmeyer on Molecular configurations in molten and glassy polymers) will, no doubt, take a significant place in the literature, but the book viewed as a *collection* of papers has no greater coherence than is to be expected from such an exercise. In no way does it constitute a text on, or provide a full coverage of, the solid state of polymers and in that respect its title is somewhat misleading, but research workers in the field will find it a useful reference book.

*E. H. Andrews*



# Sequence peptide polymers: 3. Synthesis and conformational study in solution of poly (L-leucyl-L-leucyl- $\epsilon$ -N-carbobenzyloxy-L-lysine)\*

L. Bravin and M. D'Alagni<sup>†</sup>

Istituto di Chimica delle Macromolecole, Nucleo di Roma, c/o Laboratorio di Chimica Fisica, Università di Roma, 00185 Roma, Italy

(Received 16 April 1974; revised 5 August 1974)

The synthesis and characterization of poly[Leu-Leu-( $\epsilon$ -Z)-Lys] and its conformational study in organic solvents are reported. The sequential polypeptide has been obtained with a satisfactory optical purity by the self-condensation method of the *p*-nitrophenyl ester of the corresponding tripeptide derivative according to the general procedure of De Tar *et al.* Poly[Leu-Leu-( $\epsilon$ -Z)-Lys] showed a right-handed  $\alpha$ -helical conformation in solution of helicogenic solvents, as displayed by circular dichroism measurements and ultra-violet absorption spectra. The presence of the  $\alpha$ -helix has been also detected in the solid state by infra-red spectroscopy. The helix stability of the polypeptide in chloroform-dichloroacetic acid solution is considerably high. This property may be related to the ordered sequence of the bulky leucyl residues which give rise to a screening effect, protecting the chain backbone from the acid solvent molecules.

## INTRODUCTION

In order to examine the role of the specific contribution of some factors determining the secondary and tertiary structure of polypeptides and proteins, we have undertaken the synthesis and the conformational study in water and organic solvents of some sequential polypeptides. In previous papers<sup>1,2</sup> we have reported the syntheses and the conformational aspects of sequential poly(leucyl-leucyl-aspartic acid- $\beta$ -benzyl-ester) (PLLAB), and its acid derivative, poly(leucyl-leucyl-aspartic acid) (PLLAA). This paper describes the synthesis and some conformational features of poly(leucyl-leucyl- $\epsilon$ -N-carbobenzyloxy-lysine) (PLLLZ) in organic solvents. This particular sequence of amino acid residues was chosen in order to obtain a sequential polypeptide which could serve as a model in the study of side chain interactions involving polar as well as non-polar groups. In fact, the investigation in water<sup>3</sup> of the polypeptide with the lysine residue in the unblocked form, poly(leucyl-leucyl-lysine) (PLLL), allowed us to extend the previous work<sup>2</sup>, i.e. to examine in aqueous solution and at different pH values the conformation, the charge and the thermal stability of PLLL having the same leucyl-leucyl hydrophobic sequence and, in addition, a residue with an ionizable side chain group further from the backbone than the carboxyl of the aspartic acid of PLLAA.

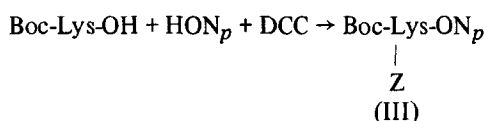
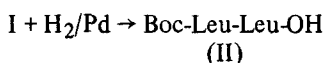
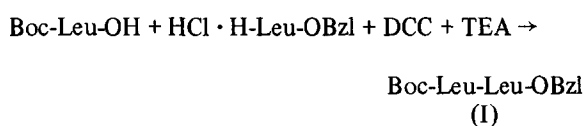
The polytripeptide PLLLZ was obtained by the poly-

condensation of leucyl-leucyl- $\epsilon$ -Z-lysine-*p*-nitrophenyl ester in dimethylsulphoxide. The conformational study of the polypeptide in organic solvents at different polarity was performed by optical methods and the presence of a right-handed  $\alpha$ -helical structure was established by ultra-violet (u.v.) and circular dichroism (c.d.) measurements in TFE and HFI. The surrounding medium affected the conformational state of PLLLZ, an increase of the  $[\theta]$  values was obtained in going from HFI to TFE, showing a marked dependence on the  $\alpha$ -helical content.

A random coil conformation was exhibited in MSA and a transition from the  $\alpha$ -helical conformation to a random coil was displayed in a solution of chloroform-dichloroacetic acid (25:75 v/v).

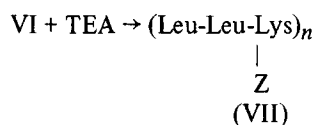
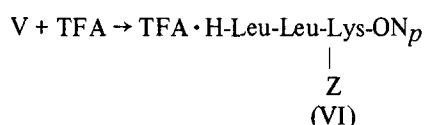
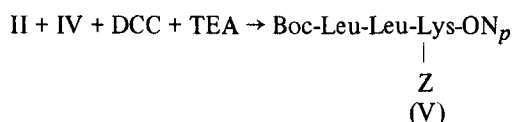
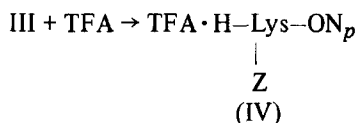
## EXPERIMENTAL

The synthesis of poly[Leu-Leu-( $\epsilon$ -Z)-Lys] was carried out in a similar way to the preparation of poly[Leu-Leu-Asp(OBzl)]<sup>1</sup> by polymerization of the *p*-nitrophenyl ester of the tripeptide and is summarized in the following scheme:



\* The following abbreviations are used in this paper: Boc = *t*-butyloxycarbonyl; Z = carbobenzyloxy; OBzl = benzyl ester; TEA = triethylamine; DCC = dicyclohexylcarbodiimide; DCU = dicyclohexylurea; HON<sub>*p*</sub> = *p*-nitrophenol; TFA = trifluoroacetic acid; DCA = dichloroacetic acid; H-Leu-OH = L-leucine; H-Lys-OH = L-lysine; MSA = methanesulphonic acid; TFE = trifluoroethanol; HFI = hexafluoroisopropanol.

<sup>†</sup> To whom enquiries should be addressed.



### Synthesis of peptides<sup>‡</sup>

Boc-Leu-Leu-OBzl and Boc-Leu-Leu-OH were obtained as described<sup>1</sup> previously.

*Boc-(εZ)-Lys-ON<sub>p</sub>*. DCC (2.713 g; 13.15 mmol) was added to a cooled (0–5°C) solution of Boc-(εZ)-Lys-OH (5.0 g; 13.15 mmol) and of HON<sub>p</sub> (1.829 g; 13.15 mmol) in anhydrous and purified ethyl acetate (120 ml) and allowed to react with stirring for 2 h at –5°C and then at 4°C overnight. After a thin-layer chromatography control on silica gel, the reaction mixture was filtered to remove the DCU. The filtrate was evaporated *in vacuo* and the residue obtained was crystallized by ethyl acetate/hexane mixture (1:2.5 by vol) (yield 82%). Recrystallization by the same solvent mixture gave a chromatographically pure (chloroform–methanol 95:5 by vol as eluant) crystalline product: m.p. 74–74.5°C;  $[\alpha]_{\text{D}}^{25} = -13.80$  ( $c = 0.96\%$  in CHCl<sub>3</sub>). Calculated for C<sub>25</sub>H<sub>31</sub>N<sub>3</sub>O<sub>8</sub>; C = 59.86%; H = 6.23%; N = 8.38%. Found: C = 59.73%; H = 6.31%; N = 8.41%.

*TFA.H-(εZ)-Lys-ON<sub>p</sub>*. Boc-(εZ)-Lys-ON<sub>p</sub> (3.6 g) was dissolved in 10 ml of TFA, allowed to stand at room temperature for 15 min and then evaporated *in vacuo* at 25–30°C. The viscous product was treated twice with CH<sub>2</sub>Cl<sub>2</sub>, removed *in vacuo*; the residue obtained was triturated with ether and the resulting solid was purified by crystallization from acetonitrile–ether (1:2 by vol). After two recrystallizations from acetonitrile a colourless chromatographically pure product (n-butanol/acetic acid/water 60:15:25 by vol and chloroform–methanol 95:5 by vol as eluants) was obtained. Yield 80%; m.p. 124.5–125°C;  $[\alpha]_{\text{D}}^{25} = +9.69$ ;  $[\alpha]_{546}^{25} = +12.08$  ( $c = 0.720\%$  in CH<sub>3</sub>CN). Calculated for C<sub>22</sub>H<sub>24</sub>N<sub>3</sub>O<sub>8</sub>F<sub>3</sub>; C = 51.26%; H = 4.69%; N = 8.15%. Found: C = 51.34%; H = 4.67%; N = 7.95% and H = 4.72%; N = 8.02%.

*Boc-Leu-Leu-(εZ)-Lys-ON<sub>p</sub>*. TFA.H-(εZ)-Lys-ON<sub>p</sub> (1.599 g; 3.1 mmol) was added to a cooled (–5°C) stirred solution of DCC (0.640 g; 3.1 mmol) in acetonitrile (30 ml). A solution of Boc-Leu-Leu-OH (1.074 g; 3.12 mmol) and of TEA (0.432 ml) in 50 ml of acetonitrile was added in portions over a period of 30 min to the suspension previously obtained.

The reaction mixture was kept under stirring for 2 h at –5°C and overnight at 0–4°C. The DCU formed was fil-

tered and the filtrate was evaporated to yield an oily residue which was crystallized from ethyl acetate/ether. Further recrystallizations from ethyl acetate/hexane mixtures gave a chromatographically pure product (chloroform–methanol 95:5 by vol. as eluant) in 58% yield: m.p. 156–157°C;  $[\alpha]_{\text{D}}^{25} = -54.35$ ;  $[\alpha]_{546}^{25} = -65.64$  ( $c = 0.780\%$  in chloroform). I.r. spectrum in KBr pellet showed bands at: 1760 cm<sup>-1</sup> (COON<sub>p</sub>); 1690 cm<sup>-1</sup> (Z); 1650 cm<sup>-1</sup>; 1545 cm<sup>-1</sup> (CONH); 1530 cm<sup>-1</sup> (NO<sub>2</sub>); 1390 cm<sup>-1</sup> and 1370 cm<sup>-1</sup> (t-Bu). Calculated for C<sub>37</sub>H<sub>53</sub>N<sub>5</sub>O<sub>10</sub>; C = 61.43%; H = 7.38%; N = 9.68%. Found: C = 61.25%; H = 7.41%; N = 9.78%; and C = 61.31%; N = 9.75%.

*TFA.H-Leu-Leu-(εZ)-Lys-ON<sub>p</sub>*. Chromatographically pure Boc-Leu-Leu-(εZ)Lys-ON<sub>p</sub> (0.8 g) was treated with 5 ml of TFA, allowed to stand at room temperature for 10 min, and then evaporated under vacuum at 25–30°C. The residue was dissolved in anhydrous chloroform and concentrated under vacuum to a small volume. This operation was repeated. The solid obtained was crystallized from ethyl acetate/ether.

Further recrystallization from acetonitrile gave a pure compound. Yield 72%; m.p. 142.5–143.5°C;  $[\alpha]_{\text{D}}^{25} = -22.50$ ;  $[\alpha]_{546}^{25} = -26.87$  ( $c = 0.781\%$  in CH<sub>3</sub>CN–DMF, 90:10 by vol). Calculated for C<sub>34</sub>H<sub>46</sub>N<sub>5</sub>O<sub>10</sub>F<sub>3</sub>; C = 55.05%; H = 6.25%; N = 9.44%. Found: C = 54.92%; H = 6.24%; N = 9.25%.

*Poly[Leu-Leu-(εZ)-Lys]*. TFA.Leu-Leu-(εZ)Lys-ON<sub>p</sub> (0.775 g) was dissolved in dimethylsulphoxide (0.85 ml).

Anhydrous TEA (0.144 ml) was added while stirring for 3 min. The reaction mixture was kept in the dark for five days at room temperature.

The product obtained was solubilized in 500 ml of chloroform, washed several times with trishydroxymethyl aminomethane buffer (pH = 7.2), water, and dried over anhydrous sodium sulphate. The solvent was removed in vacuum and the residue was extracted with dry ether. The polymer was redissolved in chloroform and precipitated with ether, dried to constant weight under high vacuum at 110°C and over P<sub>2</sub>O<sub>5</sub>. Yield 85%; m.p. 225–232°C. Calculated for C<sub>26</sub>H<sub>40</sub>N<sub>4</sub>O<sub>5</sub>; C = 63.91%; H = 8.25%; N = 11.46%. Found: C = 63.90%; H = 8.28%; N = 11.41%.

### Determination of optical purity of the polymer

The optical purity of the polypeptide was established by the hydrolysis procedure on the decarbobenzoylated polymer, that is the PLLL·HCl. A treatment with 6 N hydrochloric acid at 106°C for 48 h in degassed sealed tubes gave complete hydrolysis of the polymer. A duplicate comparison was made on the specific rotation of the amino acids solution obtained by the hydrolysed polymer with the specific rotation of the amino acid components exposed to the same treatment. Because of the initial low concentration in PLLL·HCl a wavelength of 297 nm was used. The specific rotations were the following:  $[\alpha]_{297}^{25} = +175.31$  for the totally hydrolysed solution obtained from the PLLL·HCl, in 6 N hydrochloric acid;  $[\alpha]_{297}^{25} = +179.69$  and +172.33 for the leucine and lysine solution respectively. The optical purity, calculated from the reported values, was 99.2 ± 2%. This result led to the conclusion that no significant racemization occurred during the synthesis of PLLLZ.

### Physical measurements

U.v. absorption spectra were measured on a Beckman DK-2A recording spectrophotometer.

<sup>‡</sup> The elemental analyses were performed by Dr A. Bernhardt of the Microanalytical Laboratory. The melting points were taken on a Kofler apparatus.

Circular dichroism (c.d.) measurements were obtained on a Cary 61 CD spectropolarimeter. All measurements of u.v. and c.d. spectra below 210 nm were made in 0.01 or 0.50 cm path length quartz cells, so that the total cell absorbances were kept below 1.2. The slit width was maintained sufficiently small to ensure a wavelength accuracy of better than 0.5 nm. Prepurified nitrogen was flushed to remove oxygen from the light path. In calculating  $\epsilon$  and  $[\theta]$  values one-third of the repetitive unit (leu-leu- $\epsilon$ Z-lys) was used as residue molecular weight of the polypeptide.

Infra-red absorption spectra were recorded by a Perkin-Elmer 257 instrument during the synthesis of peptides, and on a Beckman IR 9 apparatus for the study of the conformational aspects.

Optical rotation measurements were performed using a Perkin-Elmer 141 M spectropolarimeter at 25°C ( $c = 0.1-0.15\%$ ) and a 1 dm path length cell.

## RESULTS AND DISCUSSION

The reactions leading to the sequential polypeptide PLLLZ are shown in the scheme previously reported.

Information about the molecular weight distribution have been deduced studying the polymer PLLL·HCl. The main fractions obtained on gel filtration, as described elsewhere<sup>3</sup>, had an average molecular weight of over 94 000, corresponding to over seven hundred amino acid residues per polypeptide chain. The presence of fractions at such a degree of polymerization and the optical purity of PLLLZ provide further evidence<sup>1</sup> on the usefulness of the polycondensation method of tripeptide *p*-nitrophenyl esters for obtaining sequential polypeptides<sup>4-7</sup>.

The conformational study of PLLLZ was carried out by u.v. absorption spectra and c.d. measurements in solution and by i.r. spectra in solid state.

Figure 1 shows the u.v. spectra of PLLLZ obtained in

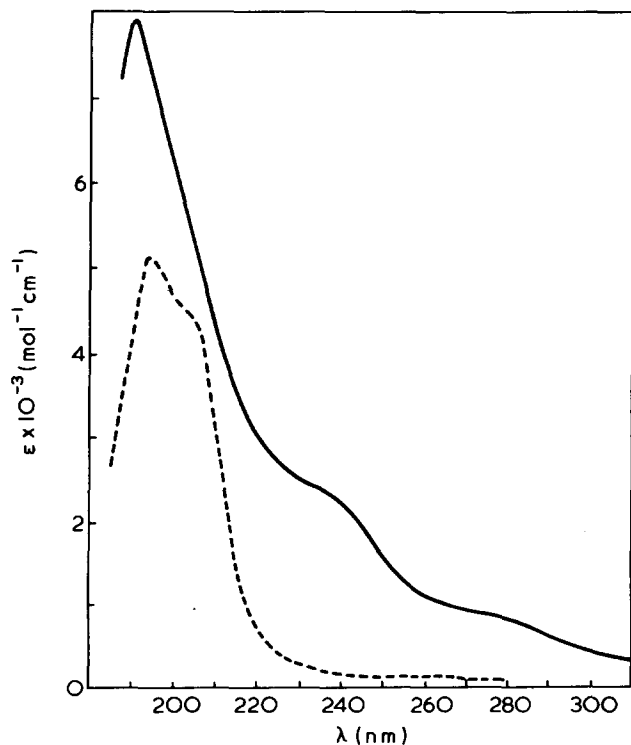


Figure 1 Ultra-violet absorption spectra of PLLLZ in MSA (—) and in TFE (---)

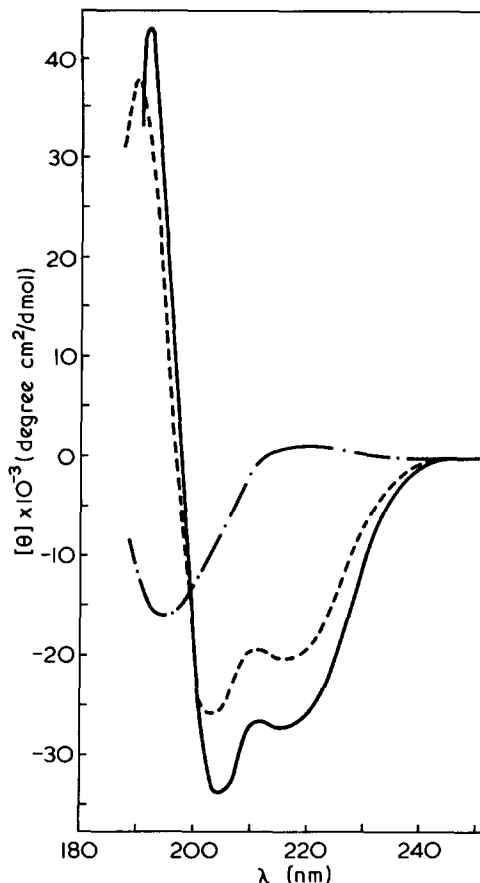


Figure 2 Circular dichroism spectra of PLLLZ in MSA (- · - ·), in HFI (- - -) and in TFE (—)

two different solvents, in MSA and in TFE. As is evident, the molar residue absorptivity value results are highly dependent on the solvent medium in which the polypeptide is examined. A large decrease in the molar absorptivity and a different spectral resolution ensued in going from MSA to TFE. A different conformational state in the two solvents considered, namely random coil in the former and  $\alpha$ -helical in the latter may be assumed to be present. It can be seen that the molar residue absorptivity values are in both cases higher than those reported<sup>8</sup> for these conformational states, being the molar absorptivities of the peptide band at the maximum  $7000 \pm 100$  and  $4300 \pm 100 \text{ mol}^{-1} \text{ cm}^{-1}$  respectively for a random and  $\alpha$ -helical chain. The difference in the values of  $\epsilon_{\text{max}}$  obtained can be ascribed to the side chain  $\epsilon$ -carbobenzyloxy absorption contribution. In fact considering the molar residue absorption maximum in both curves,  $\Delta\epsilon_{\text{max}} = 2910 \pm 100 \text{ mol}^{-1} \text{ cm}^{-1}$  is obtained. This value is equal or very near to that reported<sup>9</sup> in the conformational transition from random coil to  $\alpha$ -helix. Moreover, a prominent shoulder between 205 and 210 nm, due to the splitting of the  $\pi-\pi^*$  peptide transition in the  $\alpha$ -helical conformation<sup>9-11</sup>, is displayed for TFE. This evidence together with the characteristic hypochromism at 190 nm, may be used as convincing proof for the presence of the  $\alpha$ -helical conformation in TFE and of the random coil in MSA.

The results obtained by circular dichroism, where there is no interference from extraneous sources of optical activity contribution, are presented in Figure 2. PLLLZ easily dissolves in pure MSA. The dichroic spectrum in this solvent, registered soon after dissolution of the polypeptide,

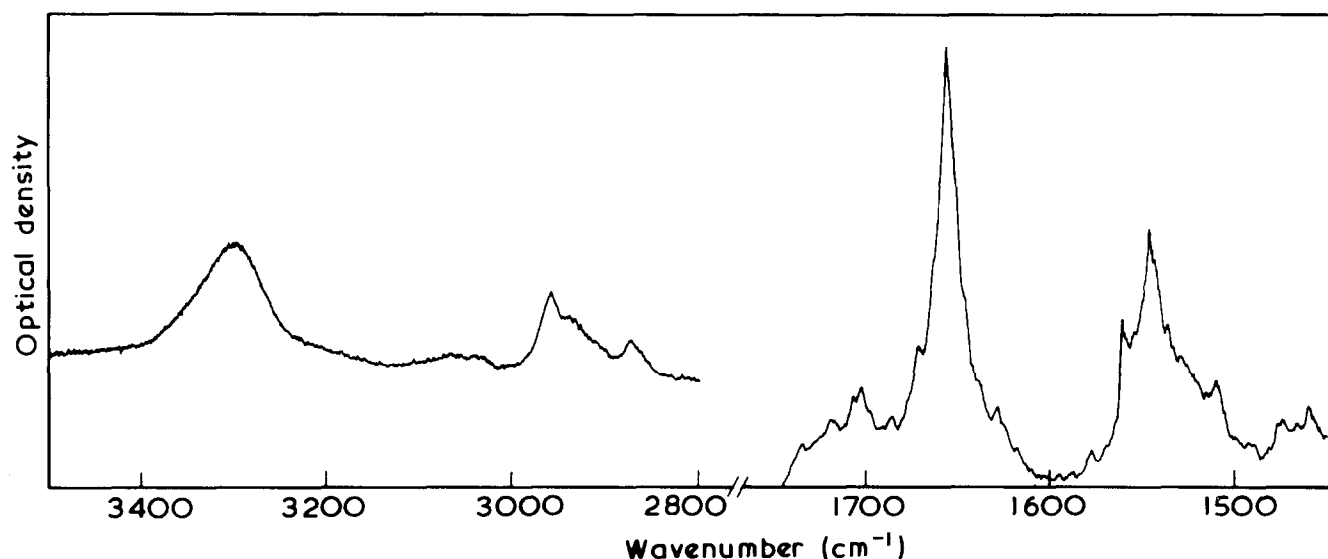


Figure 3 Infra-red spectrum of PLLLZ: unoriented film cast from chloroform solution

is characterized by a negative dichroic band located at about 196 nm ( $[\theta]_{196} = -15\,260 \pm 1300$  degree  $\text{cm}^2/\text{dmol}$ ) and a weak positive dichroic band located at 218 nm. The profile of the dichroic curve is typical<sup>12-14</sup> of polypeptides in the random coil conformation, but exhibits absolute molar ellipticity values lower than those normally obtained for polypeptides in such conformational state. This behaviour, which has been already observed in the case of poly( $\gamma$ -ethylglutamate)<sup>15</sup> and of polycyclohexylalanine<sup>16</sup> studied in MSA, is similar to that reported<sup>17</sup> in 0.2 M  $\text{NaClO}_4$  for the polyelectrolyte poly(L-glutamate) sodium salt (NaPG) and the non-ionizable poly[ $N^5$ -(2-hydroxyethyl)-L-glutamide] (PHEG). Heating a solution at pH 7.7 in 0.2 M  $\text{NaClO}_4$  of NaPG and PHEG, which are in random conformation in this condition, the absolute molar ellipticity gradually decreased and reached at 198 nm the same limiting value of  $-16\,000$  at  $90^\circ\text{C}$  for both polymers. Since the heating at such a temperature of these polypeptides solutions should increase the randomness of the polymer, the lower ellipticity values obtained in MSA for poly( $\gamma$ -ethyl-L-glutamate), poly(L-cyclohexylalanine) and PLLLZ may be ascribed as due to a higher degree of randomness rather than to solvent effects on the  $\pi$ - $\pi^*$  peptide transition<sup>16</sup>.

Three ellipticity peaks are displayed by the c.d. spectra of PLLLZ in HFI and TFE: a positive peak at  $190$ – $192 \pm 2$  nm, and two negative peaks located at  $204$ – $205 \pm 1$  nm and at  $217 \pm 1$  nm. The c.d. crossover points are obtained at  $197$ – $197.5 \pm 1$  nm. The ellipticities values, and the c.d. crossover points, are consistent with the presence of the  $\alpha$ -helicoidal state in HFI and TFE, in agreement, for the latter solvent, with the u.v. absorption analysis. However, the substantial differences in the ellipticities values of the two spectra indicate an  $\alpha$ -helical content greater in TFE than in HFI. Furthermore it should be noted that the c.d. profiles examined are characterized by a blue shift of the two negative dichroic bands and by a marked difference in their absolute magnitudes, i.e., the peak at 217 nm, due<sup>12</sup> to the  $n$ - $\pi^*$  transition is lower than that at 205 nm, owing to the parallel-polarized component of the  $\pi$ - $\pi^*$  transition. Similar results have been found for  $\alpha$ -helical polypeptides such as polyalanine<sup>18</sup> in TFE-TFA (98.5:1.5 by vol) and poly( $\gamma$ -methylglutamate) in TFE<sup>12</sup> and in HFI<sup>19</sup>. These features found in the c.d. spectra of PLLLZ may be ascribed,

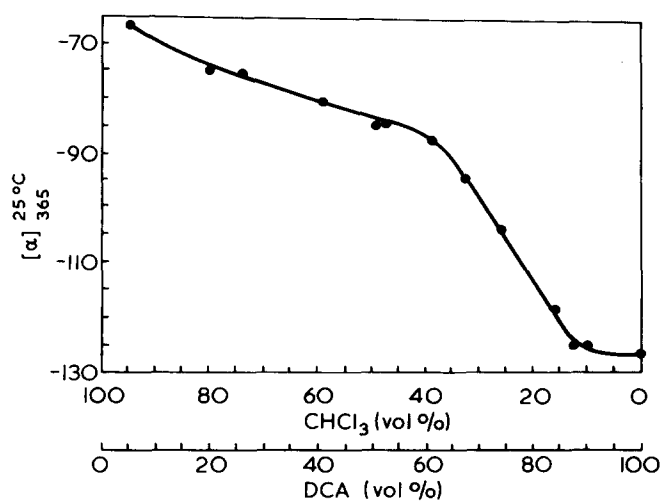


Figure 4  $[\alpha]_{365}^{25^\circ}$  of PLLLZ versus solvent composition (chloroform/dichloroacetic acid mixtures)

ed, besides the residues forming the main chain, to solvent effects which may induce changes in the positions and intensities of the transitions and may cause conformational variations in the polypeptide chain as is observed in the comparison between the solutions in TFE and HFI.

The i.r. spectrum of PLLLZ obtained on a film cast from chloroform is reported in Figure 3. Sharp and strong absorption bands at  $1655 \pm 2$   $\text{cm}^{-1}$  and at  $1547 \pm 2$   $\text{cm}^{-1}$  are shown respectively for the amide I and II bands. The correlation<sup>20</sup> between the amide I and II band frequencies and the conformations, establishes the prevalence of the  $\alpha$ -helical conformation in the PLLLZ also in the solid state.

The PLLLZ  $\alpha$ -helical stability in solution has been investigated by observing the dependence on the  $\alpha$ -helix random coil transition from the solvent mixture. The variation of the specific rotation at 365 nm with solvent composition is shown in Figure 4 for mixtures of chloroform, a helix favouring solvent and DCA, a random coil favouring solvent. The  $[\alpha]_{365}$  of PLLLZ showed a marked decrease on addition of small amounts of DCA and an abrupt change is obtained as the proportion of DCA is increased above 75% (by vol) in the chloroform solution, thus indicating the helix  $\rightarrow$  random coil transition had

occurred. This last result proves that the stability of the helical structure of PLLZ in solution is comparable to that of the PLLAB previously studied<sup>1</sup> and, moreover, that the aliphatic hydrocarbon side chains of the leucyl residues provide a more efficient shield for the hydrogen bonded  $\alpha$ -helical backbone than those of the poly( $\epsilon$ -carbobenzyl-oxy-lysine), for which the helix  $\rightarrow$  random coil transition occurs at about 36% dichloroacetic acid in chloroform solution<sup>21</sup>.

In PLLZ it is possible to consider that the bulky isobutyl groups forming a compact hydrocarbon surface decrease the accessibility of the hydrogen bonds of the backbone to the polar hydrogen bond breaker dichloroacetic acid.

#### REFERENCES

- 1 D'Alagni, M., Bemporad, P. and Garofolo, A. *Polymer* 1972, **13**, 419
- 2 Carità Morelli, M. and D'Alagni, M. *Polymer* 1972, **13**, 515
- 3 Corsi, E. and D'Alagni, M. *J. Phys. Chem.* in press
- 4 De Tar, D. F. *et al. J. Am. Chem. Soc.* 1963, **85**, 2873
- 5 De Los, F. *et al. J. Am. Chem. Soc.* 1967, **89**, 3039
- 6 Fraser, R. D. B., MacRae, T. P., Stewart, F. H. C. and Suzuki, E. *J. Mol. Biol.* 1965, **11**, 706
- 7 Stewart, F. H. C. *Aust. J. Chem.* 1966, **19**, 489
- 8 Gratzer, B. W. in 'Poly- $\alpha$ -amino acids', (Ed. G. D. Fasman), Marcel Dekker, New York, 1967, Vol I, p 178
- 9 Rosenheck, K. and Doty, P. *Proc. Nat. Acad. Sci. US* 1961, **47**, 1775
- 10 Tinoco, I., Halpern, A. and Simpson, W. T. in 'Polyamino Acids, Polypeptides and Proteins', (Ed. M. A. Stahman), Univ. Wisconsin Press, Madison, 1962, p 147
- 11 Goodman, M., Listowsky, I., Masuda, Y. and Boardman, F. *Biopolymers* 1963, **1**, 33
- 12 Holzwart, G. and Doty, P. *J. Am. Chem. Soc.* 1965, **87**, 218
- 13 Timasheff, S. N. *et al.* in 'Conformation of Biopolymers', (Ed. G. N. Ramachandran), Academic Press, New York, 1967, Vol I, p 173
- 14 Myer, Y. P. *Macromolecules* 1969, **2**, 624
- 15 Steigman, J., Peggion, E. and Cosani, A. *J. Am. Chem. Soc.* 1969, **91**, 1822
- 16 Peggion, E., Strasorier, L. and Cosani, A. *J. Am. Chem. Soc.* 1970, **92**, 381
- 17 Adler, A. J., Hoving, R., Potter, J., Wells, M. and Fasman, G. D. *J. Am. Chem. Soc.* 1968, **90**, 4736
- 18 Quadrifoglio, F. and Urry, D. W. *J. Am. Chem. Soc.* 1968, **90**, 2755
- 19 Parrish, J. R. and Blout, E. R. *Biopolymers* 1971, **10**, 1491
- 20 Miyazawa, T. and Blout, E. R. *J. Am. Chem. Soc.* 1961, **83**, 712
- 21 Fasman, G. D., Idelson, M. and Blout, E. R. *J. Am. Chem. Soc.*, 1961, **83**, 709

# Effect of molecular weight on the morphology and drawing behaviour of melt crystallized linear polyethylene

G. Capaccio and I. M. Ward

Department of Physics, University of Leeds, Leeds LS2 9JT, UK  
(Received 16 May 1974; revised 16 October 1974)

The effect of molecular weight on the cold drawing behaviour of melt crystallized linear polyethylene has been studied. It is shown that the draw ratio achieved under comparable conditions rises with decreasing  $\bar{M}_w$ , very high draw ratios ( $\sim 36$ ) being possible for optimum morphology of the undrawn polymer. The yield behaviour was also examined, and it is shown that the yield stress is affected in a complex fashion by both crystallization conditions and molecular weight. These results are discussed in terms of the crystallization and morphology of the melt crystallized polymer.

## INTRODUCTION

In recent papers, the drawing behaviour of melt-crystallized linear polyethylene (LPE) was discussed<sup>1,2</sup>. The draw ratios obtainable were shown to depend on the molecular weight characteristics of the polymer and on the crystallization procedure, the extent of the effects being markedly dependent on the latter, and hence on the morphology of the undrawn polymer.

The present paper is one of a series in which particular aspects of these discoveries are covered in some detail. Here we consider the molecular weight effects by examining a much wider range of samples than was previously available. On the basis of the previous work two very contrasting crystallization conditions have been chosen, one in which the polymer is rapidly cooled from the melt by directly quenching in water, and one in which the polymer is first slow cooled to 110°C and subsequently quenched. The latter process, when combined with suitable drawing procedures produces oriented material which is substantially different from those previously obtained for comparable draw ratios<sup>3,4</sup>, with Young's moduli reaching  $\sim 7 \times 10^{10}$  N/m<sup>2</sup>. This value is close to theoretical values for fully aligned LPE<sup>5,6</sup> and gives a material of considerable technological potential<sup>7</sup>, quite apart from its interest for studies of structure and physical properties.

## EXPERIMENTAL

The molecular weight characteristics of the linear polyethylene homopolymers studied are shown in *Table 1*. Both  $\bar{M}_w$  and  $\bar{M}_n$  were obtained from gel permeation chromatography, unless otherwise stated.

Compression moulded sheets were prepared according to the procedure described previously<sup>2</sup>. As discussed in the introduction, only two thermal treatments were selected; one in which crystallization occurs during rapid quenching in water from 160°C, and a second in which before quenching in water, the sample is allowed to cool from 160°C to 110°C at a rate of 7–9°C/min.

The density of the compression moulded sheets was

measured at 23°C in a diethyleneglycol/isopropyl alcohol density gradient column.

Dumbbell samples of dimensions 2 cm x 0.2 cm were cut and drawn in air on an Instron Tensile machine at 75°C at a speed of 10 cm/min for drawing times of either 60 sec or 90 sec

Optical micrographs of the morphology of the isotropic sheets were obtained with crossed polarizers using sections 20  $\mu$ m thick for sample 4 and 5  $\mu$ m thick for sample 9.

## RESULTS AND DISCUSSION

### Density and crystallization

The results of the density measurements (*Figure 1*) will be discussed first as they provide information regarding the crystallization behaviour. All the samples of the present investigation have been crystallized under non-isothermal conditions; they have been cooled very rapidly to room temperature either from the melt or after slow cooling to 110°C. In the latter case, the cooling curves were measured in the previous investigation and from the exotherm at 120–123°C we could conclude that an appreciable amount of crystallization occurred in this temperature range. Looked at superficially this crystallization route gives rise

*Table 1* Molecular weight characteristics of linear polyethylenes studied

Sample	Polymer grade	$\bar{M}_w$	$\bar{M}_n$
1	Rigidex 140–60 <sup>a</sup>	67 800	13 350
2	b	93 800	16 800
3	Rigidex 25 <sup>a</sup>	98 800	12 950
4	Rigidex 50 <sup>a</sup>	101 450	6 180
5	Rigidex 9 <sup>a</sup>	126 600	6 060
6	b	213 000	16 600
7	b	265 000	26 300
8	H020–54P <sup>a</sup>	300 000–400 000 <sup>†</sup>	20 000–30 000 <sup>†</sup>
9	Hostalen GUR <sup>c</sup>	3 500 000–4 000 000*	–

<sup>a</sup> BP Chemicals Ltd production grade

<sup>b</sup> Experimental grade polymer

<sup>c</sup> Farbwerke Hoechst AG production grade

<sup>†</sup> Estimate from melt viscosity data

\* Light scattering

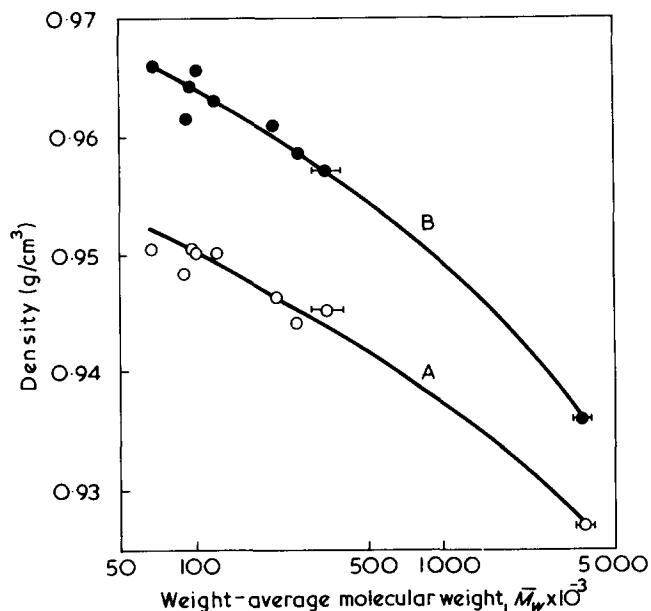


Figure 1 Density,  $\rho$ , of the isotropic samples as a function of  $\bar{M}_w$ . A, samples quenched in water from 160°C; B, samples quenched from 110°C

to an increase in density from  $\sim 0.950$  to  $\sim 0.966$  g/cm<sup>3</sup> at low molecular weights and from  $\sim 0.927$  to  $\sim 0.936$  g/cm<sup>3</sup> at high molecular weights. More significantly at this stage the substrate is produced on which further crystallization will take place during the subsequent rapid cooling. It would appear as if this particular phenomenon might be associated with important morphological modifications which are observed in the final product as a function of its thermal history and which will be discussed later in this section. Consideration of the measured crystallization rates of LPE fractions crystallized isothermally<sup>8-10</sup> show that for the rapidly quenched samples negligible crystallization can occur above 120°C, i.e. rapid cooling will not only reduce the extent of crystallization, but cause the initial growth of the lamellae to occur at lower temperatures. We believe that this has important consequences for the proportions of different molecular weight species which take part in the crystallization and hence for the morphology, and this part will be elaborated later.

First, let us consider the effect of molecular weight on density for the different heat treatments. Figure 1 shows that in both cases there is a clear correlation between the density  $\rho$  and  $\bar{M}_w$ ,  $\rho$  decreasing monotonically with  $\bar{M}_w$ , with the samples quenched from the higher temperature showing a systematically lower density, as expected.

The trend is very similar to that found for LPE fractions crystallized isothermally<sup>11</sup>. This would support the view that it is justifiable, at any rate for qualitative considerations, to extrapolate from results on fractionated polymers to polydisperse systems. This conclusion has important consequences, because it implies that the isothermal crystallization data for fractionated polymers can be combined with a knowledge of the imposed thermal history to provide an understanding of the crystallization of an unfractionated polymer for a wide range of arbitrarily selected crystallization conditions.

It is interesting to note that the differences in density between samples of different thermal treatment are somewhat reduced at high values of  $\bar{M}_w$ . This observation is consistent with the view that the longest molecules are responsible for the decrease of  $\rho$  with  $\bar{M}_w$ . The long molecules are characterized by low mobility which is responsible for two

interrelated effects, a decrease in crystallization rates and increased disorder on the lamellar fold surfaces, both effects reducing the overall level of crystallinity. Molecular weight effects on the interfacial morphology have been observed for isothermally crystallized LPE fractions<sup>12</sup> and could be even more pronounced in unfractionated polymers crystallized non-isothermally.

It is known from other studies that the crystallization of medium and high molecular weight species in LPE is closely related to the transport factor in the kinetic equation<sup>8</sup> and hence to the internal viscosity. It is therefore reasonable that the molecular weight dependence of the crystallization can be so well expressed in terms of  $\bar{M}_w$ . This is analogous to the strong dependence of the melt viscosity on  $\bar{M}_w$ .

The importance of the transport factor suggests that the effect of molecular weight and thermal treatment on the rate of crystallization of polymers must be also linked to the development of other important features which are also diffusion-controlled, i.e. the degree of order of the fold surface of the crystals and the morphology of the crystalline aggregates. Thus not only will the slow cooled polymers be more crystalline than the rapidly cooled polymers and the low  $\bar{M}_w$  slow cooled polymers more crystalline than the high  $\bar{M}_w$  slow cooled polymers, but the concentration of chains folding regularly back into the same crystalline lamellar will also increase.

The optical micrographs in Figures 2a and 2b show how much the morphology of the samples can be affected by the thermal treatment. The rapid cooling clearly produces a conventional spherulitic structure with banded spherulites, whereas slow cooling yields much coarser and often hardly recognizable spherulites.

It is known<sup>13</sup> that in conditions of relatively high viscosity the spherulitic geometry develops in a complex process of radial lamellar growth and/or branching at different angles with the radial direction. At low viscosities, however, the secondary nucleation which gives rise to the branching mechanism becomes less likely and the spherulitic radiation cannot occur in the same fashion.

This is exactly what the optical micrographs confirm. Sample 4 exhibits a spherulitic texture when quenched from 160°C, i.e. crystallized at very high degree of supercooling, hence high melt viscosity (Figure 2a). The opposite happens when it is slow cooled, i.e. crystallized at a low degree of supercooling hence low viscosity (Figure 2b). At much higher molecular weight (sample 9) where the viscosity of the melt always remains high, differences in crystallization temperature produce a less obvious morphological distinction (Figures 3a and 3b).

#### Drawing behaviour

In a previous paper it was observed that there was a very considerable increase in the yield stress as the quenching temperature following slow cooling was decreased below 120°C, showing the effect of crystallization on the yield stress. This is confirmed by the present investigation over a much wider range of molecular weights (Figure 4). It is, however, at first sight remarkable that the yield stress appears to be independent of molecular weight because we know that there is an appreciable reduction in crystallinity at higher molecular weights. We can therefore conclude that not only does the yield stress increase with crystallinity at constant molecular weight but also that at constant thermal treatment it increases with molecular weight. The

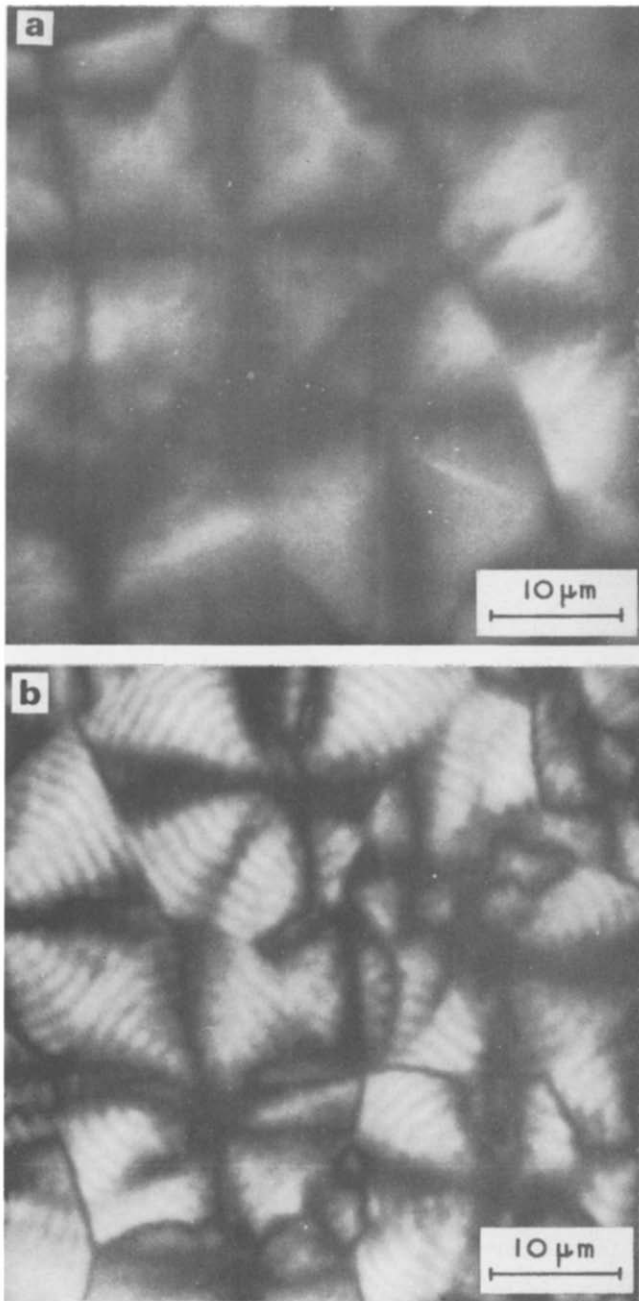


Figure 2 Photomicrographs of sample 4, photographed between crossed polarizers. (a) quenched from 160°C; (b) quenched from 110°C

larger molecules introduce more interlamellar tie molecules and physical entanglements, probably changing the nature of the yield process so that it involves higher stresses in the non-crystalline regions. Although this gives rough equivalence to increasing crystallinity from the phenomenological measure provided by the yield stress, these processes may not be capable of allowing such high degrees of molecular alignment as are produced by the pulling out of chain folds. Hence there is a dramatic effect of molecular weight and crystallization procedure on the draw ratio as we will now discuss.

The results are summarized in Figures 5 and 6. The most striking feature is shown by samples quenched from 110°C and drawn for 90 sec. There is a clear correlation between the draw ratio achieved and  $\bar{M}_w$ . As found previously, but with much less certainty<sup>2</sup>,  $\bar{M}_n$  does not produce any comparable effect, although there may be points of detail

which are obscured in this very wide span of  $\bar{M}_w$ . Detailed arguments have been presented previously as to how molecular weight distribution can be considered to affect the results<sup>2</sup>.

The effect of  $\bar{M}_w$  on draw ratio is also shown in the case of the quenched polymers, although the magnitude of the change is considerably reduced and here some effect of  $\bar{M}_n$  may also be seen (Table 2). It is to be noted in particular that samples 2, 3 and 4 now reverse their order in terms of draw ratio. Without ruling out the possibility that the effect is due to small fluctuations in the crystallinity of the initial materials, a plausible explanation of this fact can also be given along the following lines. When the crystallization occurs under less discriminating conditions from the viewpoint of molecular weight, shorter molecules can become incorporated in more than one lamella. In the case of polymers with a larger low molecular weight fraction this pos-

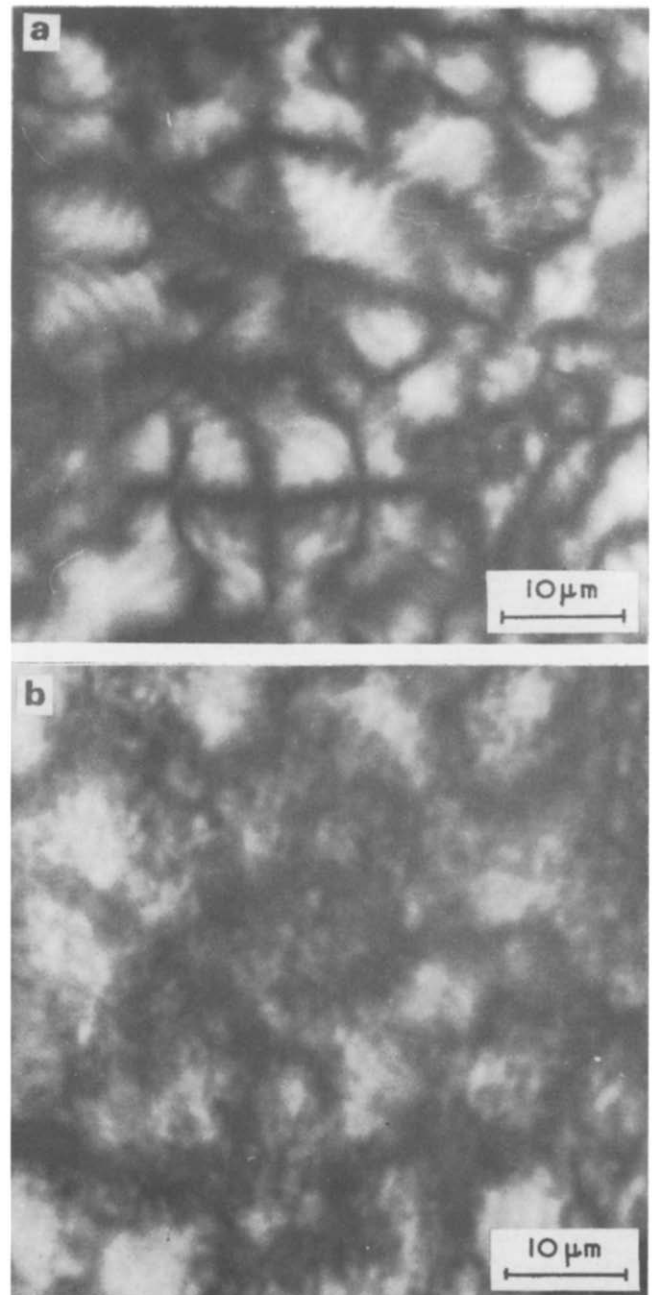


Figure 3 Photomicrographs of sample 9, photographed between crossed polarizers. (a) quenched from 160°C; (b) quenched from 110°C



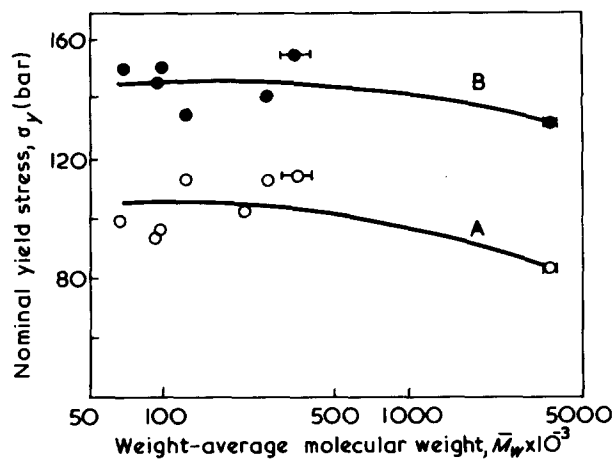


Figure 4 Yield stress,  $\sigma_y$ , as a function of  $\bar{M}_w$  for samples quenched in water from a temperature of 160°C (A) and from a temperature of 110°C (B)

Table 2 Samples quenched from 160°C and drawn for 60 sec

Sample	Draw ratio, $\lambda$
1	10.7
2	8.6
3	9.0
4	9.2
5	7.7
6	6.7
7	6.4
8	5.6
9	3.4

sibility will be reduced and the draw ratio would be expected to increase with decreasing  $\bar{M}_n$  as is observed.

Figures 5 and 6 also show that the draw ratio achieved is dependent on the time of drawing, and this is particularly so at low values of  $\bar{M}_w$ . At low values of  $\bar{M}_w$ , and especially for the polymer which was slow cooled to 110°C before quenching, the deformation is very time dependent and the polymer behaves as a viscoelastic material. With increasing values of  $\bar{M}_w$ , on the other hand, the effect of drawing time becomes less and less pronounced and the deformation proceeds by the movement of a stable neck along the specimen in a manner which approximates to the behaviour of an elastic-plastic material. It is interesting to relate this observation to two possible deformation mechanisms. The first deformation mechanism, yielding lower and less time-dependent draw-ratios, is dominated by the plastic characteristics of a network superstructure originated by the non-crystalline material<sup>14</sup>. It involves limited breakdown and subsequent orientation of crystalline lamellae. In the second mechanism, operative at high draw ratios, we believe that the predominant process is the simultaneous pulling out of chain folds and alignment of much longer lengths of molecular chain. This second process must therefore involve both the breakdown of the lamellar structure and the straightening out of interlamellar material. It is much more time-dependent and dependent on the topology of long lengths of molecular chain. This gives rise to the dependence of the draw ratio achieved on  $\bar{M}_w$ .

The present results show clearly that, for given drawing conditions, the initial morphology affects the local deformation rate in the necked region, so that for a given drawing time drawn samples can be obtained from slow cooled polymers, which exhibit a draw ratio higher than that for

drawn quenched polymers. It is also evident that the magnitude of this effect decreases with increasing molecular weight. It is, however, not possible at this stage to formulate any definite conclusions regarding the effect of initial morphology on the ultimate draw ratio attainable from a sample of given molecular weight. However, studies which are now in progress do suggest that for intermediate values of  $\bar{M}_w$ , much higher draw ratios can be obtained than those shown in Figure 6 simply by extending the drawing time. The isochronal draw ratio/ $\bar{M}_w$  curves of Figure 6 therefore do not represent an absolute upper limit for the plastic deformation. Rather, they indicate different deformation patterns as a function of initial morphology and molecular weight. It seems likely that with increasing drawing times the draw ratios will converge to an envelope curve which defines the limiting or ultimate extensibility of the initial polymer as a function of  $\bar{M}_w$ . The research required to substantiate or deny this hypothesis is at present being undertaken and will be reported in due course.

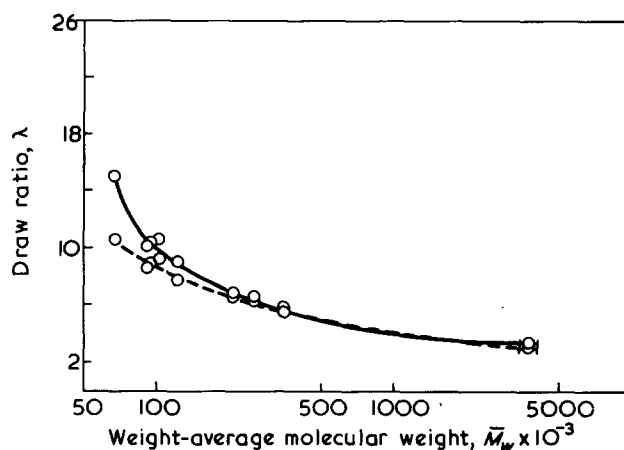


Figure 5 Draw ratio,  $\lambda$ , as a function of  $\bar{M}_w$  and drawing time for samples quenched from 160°C. ---, 60 sec drawing; —, 90 sec drawing

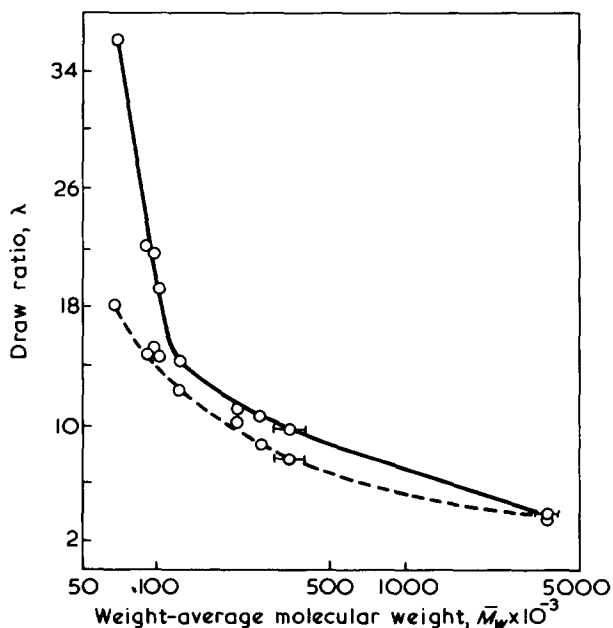


Figure 6 Draw ratio,  $\lambda$ , as a function of  $\bar{M}_w$  and drawing time for samples quenched from 110°C. ---, 60 sec drawing; —, 90 sec drawing

## CONCLUSIONS

Studies of the influence of molecular weight and thermal treatment on the plastic deformation of LPE polymers suggest that these two factors affect both the morphology of the isotropic polymer and the draw ratio in a similar manner. The differences in molecular weight between different samples manifest themselves as a monotonic increase in draw ratio with decreasing  $\bar{M}_w$ . This relates to the part played in the morphology by the longer molecules in the molecular weight distribution. These molecules, in comparatively small concentration, can form a network superstructure in which physical crosslinking is supplied by molecular entanglements in the non-crystalline regions and by crystalline domains sharing segments of the same molecule. High values of  $\bar{M}_w$ , and crystallization under conditions where there are many tie molecules linking the crystalline domains, both affect the morphology in a similar manner and reduce the draw ratio achieved under standard conditions of draw.

## ACKNOWLEDGEMENTS

We wish to thank Mr N. Hazelwood for his assistance in the experimental work, and Mr M. A. Wilding for taking the optical micrographs. With regard to the latter, we are

indebted to Dr F. P. Chappel, ICI Fibres Ltd for helpful discussion. We also wish to acknowledge that one of us (G.C.) was supported by the Science Research Council.

## REFERENCES

- 1 Capaccio, G. and Ward, I. M. *Nature (Phys. Sci.)* 1973, **243**, 143
- 2 Capaccio, G. and Ward, I. M. *Polymer* 1974, **15**, 233
- 3 Peterlin, A. and Meinel, G. *J. Appl. Phys.* 1965, **36**, 10, 3028
- 4 Meinel, G., Peterlin, A. and Sakaoku, K. 'Analytical Calorimetry', (Ed. R. S. Porter and J. F. Johnson), Plenum Press, New York, 1968, Vol 1, p 135
- 5 Frank, F. C. *Proc. R. Soc. (A)* 1970, **319**, 127
- 6 Sakurada, I., Ito, T. and Nakamae, K. *J. Polym. Sci. (C)* 1966, **15**, 75
- 7 Capaccio, G. and Ward, I. M. Br. Pat. Appl. 10746/73 (filed 6.3.73)
- 8 Mandelkern, L., Fatou, J. M. G. and Ohno, K. *J. Polym. Sci. (B)* 1968, **6**, 615
- 9 Fatou, J. M. G. and Barrales-Rienda, J. M. *J. Polym. Sci. (A-2)* 1969, **7**, 1755
- 10 Barrales-Rienda, J. M. and Fatou, J. M. G. *Polymer* 1972, **13**, 407
- 11 Mandelkern, L. *J. Polym. Sci. (C)* 1966, **15**, 129
- 12 Mandelkern, L. *J. Polym. Sci. (C)* 1973, **43**, 1
- 13 Wunderlich, B. 'Macromolecular Physics', Academic Press, New York, 1973, Vol 1, pp 313-324
- 14 Steidl, J. and Pelzbauer, Z. *J. Polym. Sci. (C)* 1972, **38**, 345

# Phase equilibria in quasi-binary poly( $\alpha$ -methylstyrene) solutions

J. M. G. Cowie and I. J. McEwen

Department of Chemistry, University of Stirling, Stirling, FK9 4LA, UK  
(Received 20 June 1974; revised 7 August 1974)

Upper (*UCST*) and lower (*LCST*) critical solution temperatures have been measured for poly( $\alpha$ -methylstyrene) in four solvents. The extent of solvent-polymer interaction was found to be reflected in the miscibility range exhibited by these systems. The data could be described by theoretical curves derived using the Patterson-Delmas theory, if an arbitrary selection of the reference temperature was made for each quasi-binary system. Curves showing the relative contributions of the cohesive energy and free volume contribution to the polymer-solvent interaction parameter were also derived from this theory; these illustrated that while the free volume factors predominated at the *LCST*, the cohesive energy contribution could still play a significant role.

## INTRODUCTION

Phase separation in polymer-solvent systems, owing to the difference in thermal expansion between solvent and solute, occurs as the liquid-vapour critical point of the solvent is approached. By examining this high temperature region one can locate lower critical solution temperatures (*LCST*) which, in conjunction with the well-known upper critical solution temperatures (*UCST*), define the phase-temperature relations for polymer solutions<sup>1-3</sup>. In this paper we report the threshold temperatures for poly( $\alpha$ -methylstyrene) (*P $\alpha$ MS*) in four relatively poor solvents in which both upper and lower critical phase separation is observable. The solvents are cyclohexane, methylcyclohexane, *n*-butyl chloride and propylene oxide.

The results are analysed by the Patterson-Delmas theory<sup>4,5</sup> based on the principle of corresponding states as applied to polymer solutions by Prigogine and his associates<sup>6</sup>.

## EXPERIMENTAL

Four *P $\alpha$ MS* samples were prepared by anionic polymerization and have been characterized previously<sup>7</sup>; they have a very narrow molecular weight distribution. A sample of *P $\alpha$ MS* was obtained by polymerization in methylene chloride at 203 K with  $\text{BF}_3$  initiator. Two fractions were selected from a seven-fold fractionation of this material and their viscosity-average molecular weights were calculated from the relation<sup>8</sup>:  $[\eta] = 7.81 \times 10^{-5} M_v^{0.73}$ . Fraction molecular weights are collected in *Table 1*.

The solvents were dried by standard techniques and fractionated before use.

Cloud point curves were established as described elsewhere<sup>1,3</sup> by measuring the temperature of phase separation of polymer solutions in the concentration range 0-20%. Since *P $\alpha$ MS* degrades at elevated temperatures<sup>9</sup>, the validity of the *LCST* obtained was always checked by recooling solutions to the previously determined *UCST* and noting the new temperature of phase separation. In no instance did this differ by more than a degree from the original value. It has been assumed, therefore, that thermal degradation

does not affect the *LCST* values reported when these occur below 530 K.

In the case of the *UCST* in *n*-butyl chloride and propylene oxide the cloud point curves had to be established by first cooling the solutions to 195 K and noting the temperature at which the polymer redissolved when the solutions were warmed, with constant shaking. This technique gave reproducible cloud points whereas those obtained by noting the temperature of phase separation on cooling were unreproducible and at much lower temperatures than the former. This behaviour has been encountered previously<sup>1</sup> but remains unexplained.

Light-scattering measurements on *P $\alpha$ MS*/propylene oxide solutions were made in a Sofica P.G.D. 42000 instrument using unpolarized blue light ( $\lambda = 436 \text{ nm}$ ). Solutions were clarified by passage through Millipore filters, grade 0.45  $\mu\text{m}$ , into Pyrex cells designed to fit standard Sofica cell holders. These were subsequently flame-sealed under vacuum. Readings were made in the temperature range 285-360 K at an angle of  $\theta = 90^\circ$ .

The specific volume of propylene oxide was measured, as a function of temperature, by standard dilatometric techniques. The propylene oxide used was fractionated, dried over calcium hydride under vacuum for three days, distilled three times on a vacuum line, discarding generous head and tail fractions, and finally flame-sealed, under vacuum, in a calibrated dilatometer with a precision bore (0.05 cm) capillary tube. Measurements were made over the temperature range 288-345 K at approximately 2 K intervals.

The thermometers used in the study were Arno Amarell works certificated thermometers with a quoted accuracy of

*Table 1* Molecular weights of *P $\alpha$ MS* samples used

<i>P<math>\alpha</math>MS</i>	$M_w$ or $M_v$	$M_w/M_n$
2	$1.40 \times 10^6$	<1.10
8	$8.45 \times 10^5$	<1.10
2, 5*	$3.20 \times 10^5$	—
1, 3*	$1.02 \times 10^5$	—
LMB	$1.0 \times 10^4$	~1.5
LMD	$5.7 \times 10^3$	~1.2

\* Polymerized by  $\text{BF}_3$  initiation

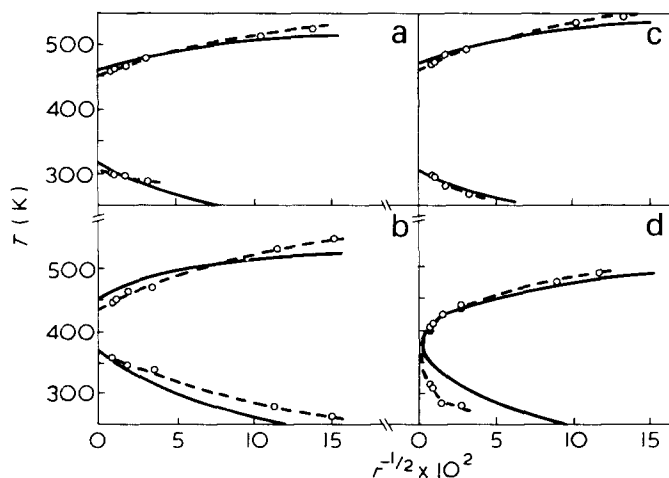


Figure 1 Experimental threshold temperatures (○) and theoretical CST curves (—) for P $\alpha$ MS-solvent systems: (a) cyclohexane; (b) methylcyclohexane; (c) butyl chloride; (d) propylene oxide. P $\alpha$ MS/propylene oxide system  $A_2 =$  zero conditions indicated (●)

$\pm 0.05$  K in the range 273–323 K falling to  $\pm 0.3$  K in the range 473–523 K.

## RESULTS AND DISCUSSION

Threshold temperatures for P $\alpha$ MS in the four solvents are shown, plotted as a function of  $r$ , in Figure 1 where  $r$  is taken as the ratio of molar volumes of the polymer and solvent at 298 K. The results, as depicted in Figure 1, show a considerable variation in type. In cyclohexane, which is an established  $\theta$  solvent for P $\alpha$ MS<sup>10</sup> the upper and lower  $\theta$ -temperatures ( $\theta_U$  and  $\theta_L$ ) are well separated. Extrapolation to infinite molecular weight gives  $\theta_U = 308$  K, in good agreement with results reported by Cowie and Bywater<sup>10</sup> and a value of 307.5 K obtained by Kato *et al.*<sup>11</sup>. The value of  $\theta_L$  for this system is found to be 456 K. The miscibility range, defined by ( $\theta_L - \theta_U$ ) is 148 K which can be compared with ( $\theta_L - \theta_U$ ) = 179 K for the polystyrene-cyclohexane system reported by Kuwahara *et al.*<sup>12</sup>.

In contrast to P $\alpha$ MS-cyclohexane, the P $\alpha$ MS/propylene oxide system shows considerable curvature and cannot be unambiguously extrapolated to intercept the  $T$  axis. In order to clarify this point the second virial coefficient,  $A_2$ , was measured by light scattering for two fractions of P $\alpha$ MS in propylene oxide.

If separate  $\theta_U$  and  $\theta_L$  exist for this system they should correspond to the two temperatures at which  $A_2$  becomes zero<sup>13</sup> and these temperatures should be identical for fractions of differing chain length. Measurements from light-scattering  $C/I_{90}$  vs.  $C$  plots in the quasi-ternary system polystyrene-methylcyclohexane-diethyl ether have shown<sup>14</sup> that zero slope correlates well with  $\theta$ -conditions extrapolated from CST measurements. The results of similar measurements in the P $\alpha$ MS/propylene oxide system, for two fractions of considerably different molecular weights, are shown in Figure 2. The upper limit of temperature was 360 K due to distillation within the light-scattering cell but the slopes of the  $C/I_{90}$  vs.  $C$  plots for the two fractions cannot be sensibly extrapolated to zero slope at the same temperature. For a molecular weight of  $1.40 \times 10^6$  this temperature is 348 K while for a molecular weight of  $1.02 \times 10^5$  it is estimated to be about 384 K. Both are shown in Figure 1 and tend to mirror the threshold temperature curve. Since there is no unique, molecular weight independent temperature where  $A_2$  is zero in the P $\alpha$ MS/propylene

oxide system the  $T$  vs.  $r^{-1/2}$  curve cannot be extrapolated to intersect the  $T$  axis at separate temperatures corresponding to  $\theta_U$  and  $\theta_L$ .

The P $\alpha$ MS/propylene oxide system is thus of the same type as the polystyrene-acetone and polystyrene-ether system<sup>2,3</sup>. In this instance, however, the solvent is relatively 'good' in the sense that it can dissolve quite high molecular weight polymer compared with, for example, polystyrene in acetone where the solubility limit is reached at a molecular weight of about  $2 \times 10^4$ <sup>2,3</sup>. For the P $\alpha$ MS/propylene oxide system the solubility limit is estimated to be  $M \approx 10^7$ .

The data for P $\alpha$ MS/methylcyclohexane extrapolate to  $\theta_U = 366$  K and  $\theta_L = 431$  K, indicating a small miscibility range of only 65 K compared with polystyrene in the same solvent<sup>12</sup> where ( $\theta_L - \theta_U$ ) = 140 K. This reflects the poorer nature of the solvent for P $\alpha$ MS but is not accompanied by the predicted high curvature<sup>15</sup> in the  $T$  vs.  $r^{-1/2}$  plots.

The P $\alpha$ MS/butyl chloride system presents a much higher degree of curvature but ( $\theta_L - \theta_U$ ) has the considerable value of 149 K. It appears that high curvature in these plots is not necessarily indicative of small miscibility gaps contrary to the prediction of the Patterson-Delmas theory<sup>15</sup>.

An alternative treatment of CST data is given by the Schultz-Flory expression which is based on the original Flory-Huggins theory<sup>16</sup>:

$$\frac{1}{T_c} = \frac{1}{\theta} \left\{ 1 + \frac{1}{\psi_1} \left( \frac{1}{r^{1/2}} + \frac{1}{2r} \right) \right\} \quad (1)$$

This predicts a linear dependence of  $T_c^{-1}$  on ( $r^{-1/2} + 1/2r^{-1}$ ). For the P $\alpha$ MS-solvent systems described here, equation (1) is only valid over the whole molecular weight range in the upper critical regions of the P $\alpha$ MS-cyclohexane and P $\alpha$ MS-methylcyclohexane systems. By drawing tangents to the remaining data, which is curved,  $\theta$ -temperatures and entropy parameters,  $\psi_1$ , for all the systems can be obtained and these are shown in Table 2. The thermodynamic condition that the excess entropy of solution should

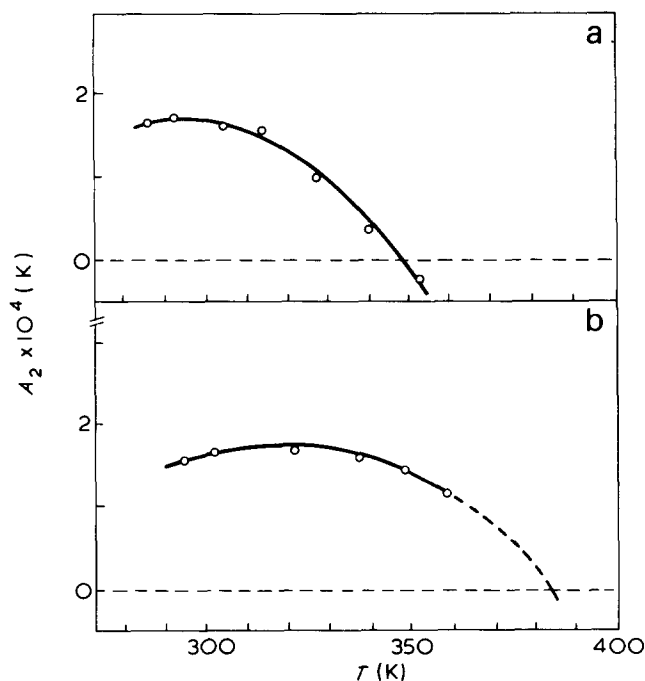


Figure 2 (a) Slopes ( $A_2$ ) of  $C/I_{90}$  vs.  $C$  plots for P $\alpha$ MS fraction 2 ( $1.40 \times 10^6$ ). (b) Slopes ( $A_2$ ) of  $C/I_{90}$  vs.  $C$  plots for P $\alpha$ MS fraction 1, 3 ( $1.02 \times 10^5$ )

Table 2 Schultz-Flory parameters for P&amp;MS-solvent systems studied

Solvent	$\theta_U$ (K)	$\theta_L$ (K)	$\psi_{1U}$	$-\psi_{1L}$	$\theta_L/T_{crit}$	$\alpha \times 10^3$ at $\theta_L$
cyclohexane	308	456	0.51	0.70	0.83	2.21
methylcyclohexane	366	431	0.41	0.26	0.75	1.30
butyl chloride	263	412	0.12	0.35	0.79	1.70

$$\alpha(\text{polymer}) = 5.72 \times 10^{-4} \text{K}^{-1}$$

be negative for a LCST is exemplified by the negative values of  $\psi_{1L}$  shown in Table 2. Also tabulated is the ratio  $\theta_L/T_{crit}$  for each system, where  $T_{crit}$  is the solvent-vapour critical temperature.

The original polymer solution theory proposed by Flory<sup>16</sup> and Huggins<sup>17</sup> does not predict the existence of the LCST. Patterson and Delmas<sup>4,5</sup> have extended the statistical thermodynamic theory based on the corresponding state principle developed by Prigogine and his coworkers<sup>6</sup> to account for this phenomenon. This theory is essentially similar to that recently proposed by Flory *et al.*<sup>18</sup>, and expresses the  $\chi_1$  interaction parameter as:

$$\frac{\chi_1(P, T)}{c_1} = \frac{-\tilde{U}(\tilde{P}, \tilde{T})\nu^2}{T} + \frac{\tilde{C}_p(\tilde{P}, \tilde{T})\tau^2}{2} \quad (2)$$

where  $\tilde{U}$  is the reduced configurational energy of the solvent,  $\nu^2$  is a parameter describing differences in force fields and segment sizes between polymer and solvent and  $c_1$  is the number of external degree of freedom of the solvent molecule.  $\nu^2$  is normally treated as an adjustable parameter although it can be defined by the theory.  $c_1$  and  $\tau$  are measured directly from experimental expansion coefficients,  $\alpha_i$ , and thermal pressure coefficients,  $\gamma_i$ , for the solvent (1) and polymer (2) via the following expressions:

$$c_i = \frac{P_i^* V_i^*}{T_i^* R} \quad (3)$$

$$\tau = 1 - \frac{T_1^*}{T_2^*} \quad (4)$$

$$\tilde{V}_i^{1/3} = \frac{\alpha_i T}{3(1 + \alpha_i T)} + 1 \quad (5)$$

$$T_i^* = \frac{T \tilde{V}_i^{4/3}}{(\tilde{V}_i^{1/3} - 1)} \quad (6)$$

$$P_i^* = \gamma_i T \tilde{V}_i^2 \quad (7)$$

Characteristic reduction parameters (asterisked) are related to reduced quantities (tilde) by:

$$\tilde{X}_i = \frac{X_i}{X_i^*} \quad (8)$$

In equation (2) the function  $\tilde{C}_p$  has the property of increasing with temperature to an infinite limit at the gas-liquid critical point. By assuming a smoothed cell model and a van der Waals dependence of the configurational energy on liquid volume, the following expressions for  $\tilde{U}$  and  $\tilde{C}_p$  have been derived<sup>5,18</sup>:

$$\tilde{U} = -\tilde{V}^{-1} \quad (7)$$

$$C_p^{-1}(P, T) = \left(1 - \frac{2}{3} \tilde{V}^{-1/3}\right) - \frac{2(1 - \tilde{V}^{-1/3})}{(P\tilde{V}^2 + 1)} \quad (8)$$

Combination of equations (2), (6), (7) and (8) leads to

$$\chi_1 = \frac{T_1^* c_1 \nu^2}{T \tilde{V}_1} + \frac{c_1 \tau^2}{2 \left( \frac{4}{3} \tilde{V}_1^{-1/3} - 1 \right)} \quad (9)$$

at zero pressure. The first term on the right hand side of equation (9) may be regarded as an alternative expression of the Flory-Huggins dependence of  $\chi_1$  on temperature. If solvent quality were solely described by such an expression it is predicted to be an ever increasing function of temperature. The second term on the right-hand side of equation (9) expresses the effect of free-volume differences between the components. It is this latter expression which predominates at high temperatures when the solvent is relatively highly expanded compared with the polymeric solute and causes the overall value of  $\chi_1$  to increase rapidly near the gas-liquid critical point. The relative contribution of each term to  $\chi_1$  is clearly seen in Figure 3, as a function of the temperature in each system. Using the Flory-Huggins expression we have

$$\chi(\text{crit}) = \frac{1}{2} (1 + r^{-1/2})^2 \quad (10)$$

Equations (9) and (10) can be solved to provide the theoretical dependence of CST on chain length,  $r$ , when  $c_1$ ,  $T_1^*$ ,  $T_2^*$  and  $\nu^2$  are known. Following procedures described elsewhere<sup>1,3,14</sup> theoretical curves for the four systems described here have been calculated and are shown in Figure 1. The equation of state and reduction parameters required have been collated in Table 3. Expansion and compressibility coefficients were obtained from the literature for cyclohexane, methylcyclohexane and butyl chloride. Thermal expansion data for propylene oxide was established from the following least squares expression from the results of our own dilatometric study:

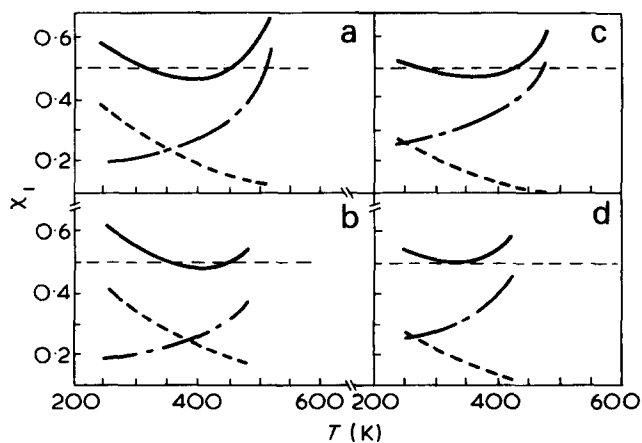


Figure 3 Theoretical  $\chi_1$  (—),  $\chi_1^{CE}$  (---) and  $\chi_1^{FV}$  (-·-·-) curves calculated as described in text for P&MS-solvent systems: (a) cyclohexane; (b) methylcyclohexane; (c) butyl chloride; (d) propylene oxide

Table 3 Characteristic reduction and equation of state parameters for systems

	$T$ (K)	$V$ (cm <sup>3</sup> /g)	$\alpha \times 10^3$ (K <sup>-1</sup> )	$\tilde{V}$	$V^*$ (cm <sup>3</sup> /g)	$T^*$ (K)	$\gamma$ (J cm <sup>-3</sup> K <sup>-1</sup> )	$P^*$ (J/cm <sup>3</sup> )	$c_1$	Refs
Cyclohexane	298	1.2923	1.217	1.2906	1.0012	4720	1.067	530	1.13 <sub>8</sub>	20, 21
	433*	1.571	1.69	1.485	1.058	5208	—	—	—	
Methylcyclohexane	298	1.3079	1.105	1.2688	1.0308	4960	1.23	589	1.44 <sub>8</sub>	14, 22
	363	1.4106	1.216	1.3387	1.0534	5248	0.74	483	1.14 <sub>4</sub>	
Butyl chloride	303	1.1440	1.292	1.3087	0.8742	4626	1.158	601	1.27 <sub>0</sub>	23, 24
	423*	1.365	1.760	1.490	0.916	5065	—	—	—	
Propylene oxide	298	1.2161	1.545	1.3498	0.9010	4232	—	—	0.82 <sub>4</sub> <sup>†</sup>	25
	383*	1.417	2.01	1.501	0.944	4545	—	—	—	
P $\alpha$ MS	298*	0.888	0.572	1.153	0.770	7420	—	—	—	19

\* Data extrapolated

† Estimate from comparison with other hydrocarbons

$$V(\text{cm}^3) = 1.1725 + 1.5970 \times 10^{-3}T + 5.653 \times 10^{-6}T^2 \quad (11)$$

where here  $T$  is in degrees Celsius.

Theoretically  $T_1^*$  should be a constant but when measured experimentally is found to vary with temperature<sup>14</sup>. This temperature variation has been used to select a  $T_1^*$  value, for each of the four solvents, which provides a close absolute prediction of the experimental  $CST$  values. In this and other systems studied<sup>1-3,12</sup> use of  $T_1^*$  values calculated from expansion data pertaining to room temperatures has led to theoretical  $CST$  vs.  $r^{-1/2}$  curves which are displaced by varying amounts from the experimental ones. By selecting  $T_1^*$  values at a new, higher reference temperature a fit is obtained which is absolute and no worse than that obtained by displacing the curves calculated from room temperature data. Unfortunately the actual choice of a new reference temperature is completely arbitrary and is governed only by the 'best fit' criterion used previously<sup>14</sup>. It is found that the reference temperatures required are normally in the region bounded by the  $UCST$  and  $LCST$  and in this sense are reasonable. It should be noted we are using extrapolated expansion data which will introduce small unavoidable errors in the selection of the reference temperature.

An indication of the temperature variation of  $T_1^*$  values in the four systems can be obtained from Table 3 where both room temperature and higher reference temperature values are tabulated. In each of the systems it is the second value of  $T_1^*$  which is used in constructing the theoretical curves shown in Figure 1.

The temperature variation of  $\chi_1$ , for the four systems, is shown in Figure 3. This function has been calculated from equation (9) using the parameters listed in Table 4. Since  $T_1^*$  is not a constant it has been necessary to generate an artificial dependence of  $\tilde{V}_1$ , on temperature by solving equation (6) using the chosen value of  $T_1^*$  for each of the systems. This artificial  $\tilde{V}_1(T)$  function coincides with the experimental  $\tilde{V}_1(T)$  function calculated from equation (5) only at the chosen reference temperature. It is, however, the function implicitly used in the calculation of the theoretical  $CST$  vs.  $r^{-1/2}$  curves shown in Figure 1.

In Figure 3 there are several noteworthy features;  $\chi_1$  attains its limiting value of 1/2 at both the theoretically predicted  $LCST$  and  $UCST$  in the three systems P $\alpha$ MS-cyclohexane, P $\alpha$ MS-methylcyclohexane and P $\alpha$ MS/butyl chloride, whereas in the P $\alpha$ MS/propylene oxide system  $\chi_1$  is always greater than 1/2 implying that no distinct  $\theta_U$  and

Table 4 Parameters used in the construction of  $\chi_1$  curves for the four systems

Solvent	$T_{\text{ref}}$ (K)	$T_1^*$	$c_1 r^2$	$c_1 \nu^2$ $\times 10^3$
Cyclohexane	433	5208	0.101	21.89
Methylcyclohexane	363	5248	0.098	25.06
Butyl chloride	423	5065	0.128	15.08
Propylene oxide	383	4545	0.124	19.19

$\theta_L$  temperatures exist in the system. The two separate components of  $\chi_1$ , corresponding to the two terms on the right-hand side of equation (9), have been identified here with a free volume contribution and a cohesive energy contribution and correspondingly labelled  $\chi_1^{\text{FV}}$  and  $\chi_1^{\text{CE}}$  in the Figure. In each case  $\chi_1^{\text{FV}}$  is shown to be rapidly increasing at high temperatures. The effect of this, in the P $\alpha$ MS-cyclohexane, P $\alpha$ MS-methylcyclohexane and P $\alpha$ MS/butyl chloride systems, is that there is a more rapid increase in total  $\chi_1$  through the  $LCST$  region than the corresponding decrease through the  $UCST$  region.

The ratio  $\theta_L/T_c$  gives an indication of how close one must approach the critical temperature of the solvent before phase separation occurs. It is instructive to compare this with the expansion coefficient of the solvent at the  $\theta_L$  and one finds that they are in the same relative order. While the simple picture of the  $LCST$  is one in which the free volume control of the phenomenon is emphasized, this shows that the cohesive energy contribution is still an important consideration. Thus the difference in free volume between solvent and polymer, as reflected in the difference in expansion coefficients, might be expected to be of the same order of magnitude for a polymer in different solvents at  $\theta_L$  if this was the only contributing factor. This is clearly not the case. In cyclohexane solutions the solvent is much more expanded at the temperature of phase separation than is methylcyclohexane, but the cohesive energy contribution is considerably less favourable in methylcyclohexane. This means that phase separation will take place in methylcyclohexane solutions when the difference in free volume is smaller than that required for phase separation to occur in cyclohexane. This is reflected in the lower value of  $\theta_L/T_c$ . The ratio  $\theta_L/T_c$  for butyl chloride solutions has an intermediate value.

Consequently, while the predominant factor governing phase separation is entropic in origin, its effect is tempered by the enthalpic contribution. This is clearly illustrated in the curves shown in Figure 3.

Three main points of interest emerge from this study.

The first is confirmation of our previous observations that the Patterson-Flory theory is capable of describing the phase equilibria in a qualitative sense, but that quantitative agreement requires an arbitrary choice of reference temperature. We have not yet been able to rationalize this selection. The second highlights the importance of examining the broader aspects of phase equilibria in polymer solutions. This is exemplified in the propylene oxide solutions where polymer insolubility is manifest only at very high molecular weights. This type of behaviour immediately indicates that the liquid will not act as a theta solvent. This system is unusual, however, in that insolubility as a function of chain length has normally been reported for systems where the polymer solubility limit is much lower<sup>2,3</sup>. The final point is that the miscibility range appears to provide a good indication of polymer-solvent interaction, and this is being investigated further, for other binary systems.

#### ACKNOWLEDGEMENTS

The authors wish to thank the SRC for financial support of this work, in particular for the fellowship to I. J. McE.

#### REFERENCES

- 1 Cowie, J. M. G., Maconnachie, A. and Ranson, R. J. *Macromolecules* 1971, **4**, 57
- 2 Siow, K. S., Delmas, G. and Patterson, D. *Macromolecules* 1972, **5**, 29
- 3 Cowie, J. M. G. and McEwen, I. J. *JCS Faraday Trans. 1* 1974, **70**, 171
- 4 Patterson, D. and Delmas, G. *Trans. Faraday Soc.* 1969, **65**, 708
- 5 Patterson, D. *J. Polym. Sci. (C)* 1968, **16**, 3379
- 6 Prigogine, I. (in collaboration with Bellmans, A. and Mathot, V.), 'The Molecular Theory of Solutions', North-Holland, Amsterdam, and Interscience, New York, 1957
- 7 Cowie, J. M. G., Bywater, S. and Worsfold, D. J. *Polymer* 1967, **8**, 105
- 8 McCormick, H. W. *J. Polym. Sci.* 1959, **41**, 327
- 9 Bywater, S. and Black, P. E. *J. Phys. Chem.* 1965, **69**, 2967
- 10 Cowie, J. M. G. and Bywater, S. *J. Polym. Sci. (A-2)* 1968, **6**, 499
- 11 Noda, I., Mizutani, K., Kato, T., Fujimoto, T. and Nagasawa, M. *Macromolecules* 1970, **3**, 787
- 12 Saeki, S., Kuwahara, N., Konno, S. and Kaneko, M. *Macromolecules* 1973, **6**, 246
- 13 Delmas, G. and Patterson, D. *Polymer* 1966, **7**, 513
- 14 Cowie, J. M. G. and McEwen, I. J. *Macromolecules* 1974, **7**, 291
- 15 Delmas, G. and Patterson, D. *J. Polym. Sci. (C)* 1970, **30**, 1
- 16 Flory, P. J. 'Principles of Polymer Chemistry', Cornell University Press, Ithaca, 1953
- 17 Huggins, M. L. *Ann. N.Y. Acad. Sci.* 1942, **43**, 1
- 18 Flory, P. J. *et al. J. Am. Chem. Soc.* 1964, **86**, 3507; 1965, **87**, 1833, 1838
- 19 Cowie, J. M. G. and Toporowski, P. M. *J. Macromol. Sci. (B)* 1969, **3**, 81
- 20 Wood, S. A. and Gray, J. A. *J. Am. Chem. Soc.* 1952, **74**, 3729
- 21 Holder, G. A. and Whalley, E. *Trans. Faraday Soc.* 1962, **58**, 2095
- 22 Abas-Zade, A. K., Kerimov, A. M., Agaev, N. A. and Apaev, T. A. *Teplofiz. Svaistva Zhidk., 3rd Mater. Vses. Teplofiz. Korf. Svoistvam Veshchestv Vys. Temp.* 1968, p 34
- 23 Timmermans, J. 'Physico-Chemical Constants of Pure Organic Compounds', Elsevier, New York, 1950
- 24 Skinner, J. F., Cussler, E. L. and Fouss, R. M. *J. Phys. Chem.* 1968, **72**, 1057
- 25 Patterson, D. and Delmas, G. *IUPAC Int. Symp. Macromol. Chem., Toronto* 1968

# Domain structure and crystalline morphology of AB and ABA type block copolymers of ethylene oxide and isoprene cast from solutions\*

Eiji Hirata<sup>†</sup>, Toshikazu Ijitsu, Toshiichi Soen<sup>‡</sup>, Takeji Hashimoto and Hiromichi Kawai  
*Department of Polymer Chemistry, Faculty of Engineering, Kyoto University, Kyoto, Japan*  
(Received 17 June 1974)

The domain structure and crystalline morphology of AB and ABA type block copolymers of ethylene oxide (EO) and isoprene (Ip) were investigated by using two kinds of casting solvents, non-selective (benzene) and selective (ethyl benzene) solvents. The domain structures of both types of block copolymers are identical, as in the case of amorphous block copolymers, depending mostly on the fractional compositions of each block segment but hardly on the sequence arrangements.

When benzene is used as a cast solvent, the change of domain structure with increase of Ip fraction follows, in general, a role established for amorphous block copolymers, except for the fact that the EO segment is crystallizable so that the above role is considerably modified, especially when the EO fraction is dominant, to form spherulitic crystalline texture. The domain structure of mixed system of block copolymer with homo-PEO, cast from benzene solution, also follows the above role, simply depending on fractional composition as a whole, of each component, unless the molecular weight of the homopolymer is much larger than that of corresponding block segment.

On the other hand, when ethyl benzene is used as a cast solvent, the domain structure is quite different from that cast from benzene solution, giving single crystal-like texture of EO segments on which Ip segments are segregated to form Ip layer even for a copolymer having an EO fraction as small as 20%. The above contrast of domain formation mechanism between the two kinds of casting solvents is interpreted in terms of an interrelation of two binodal surfaces, critical concentration of crystallization of EO segments and critical concentration of micelle formation of EO and Ip segments, in the phase diagram of the system at a given temperature.

## INTRODUCTION

Thermodynamic incompatibility of A and B block segments of amorphous block copolymers has been shown to involve the microphase separation at a critical micelle concentration<sup>1,2</sup>. The micelles formed at the concentration are believed to be essentially maintained through the solvent evaporation process to result in the domain structures observed in the solid state<sup>2-4</sup>. The shape and size of the micelles, and consequently of the domains, depend upon the incompatibility, molecular weight, and fractional composition of the block copolymers, and solvent used for casting, and temperature of casting<sup>3-8</sup>.

When one component of the amorphous block copolymers is replaced by a crystalline polymer, the domains (or crystalline textures) formed by the solvent cast should depend upon, at least, the following two factors: (i) crystalline blocks; and (ii) the microphase separation resulting from the incompatibility of the A and B blocks. The cry-

stalline textures observed in solid state are considered to depend upon a relative contribution of the two factors. It is the purpose of this paper to investigate the role of the casting solvent and fractional composition on the domain structure and domain formation mechanism of AB and ABA type block copolymers of ethylene oxide and isoprene.

## EXPERIMENTAL AND RESULTS

### *Preparation of AB and ABA type block copolymers of ethylene oxide and isoprene*

The block copolymers were synthesized by an anionic polymerization technique primarily after the method of Szwarc<sup>9</sup>, using cumyl potassium and sodium naphthalene as initiators for ethylene oxide/isoprene (EO/Ip) diblock copolymer and ethylene oxide/isoprene/ethylene oxide (EO/Ip/EO) triblock copolymer, respectively, and varying the fractions of the ethylene oxide and isoprene segments from zero to unity.

Isoprene and ethylene oxide monomers, as well as tetrahydrofuran (THF), the polymerization solvent, were carefully purified by conventional methods and collected under a vacuum ( $10^{-6}$  mmHg) in separate ampoules equipped with breakable seals. Polymerization of the isoprene monomer, and then of the ethylene oxide monomer, was performed in a block copolymerization apparatus connected to

\* Presented partly at the 22nd Annual Meeting of the Society of Polymer Science, Japan, Kyoto, May 1972, and partly at the 23rd Annual Meeting of the Society of Polymer Science, Japan, Tokyo, May 1973.

<sup>†</sup> Present address: Toyama Mill, Mitsubishi Rayon Co. Ltd, Toyama, Japan.

<sup>‡</sup> Present address: Department of Textile Engineering, Faculty of Fiber Technology, Kyoto University of Industrial Arts and Fiber Technology, Kyoto, Japan.



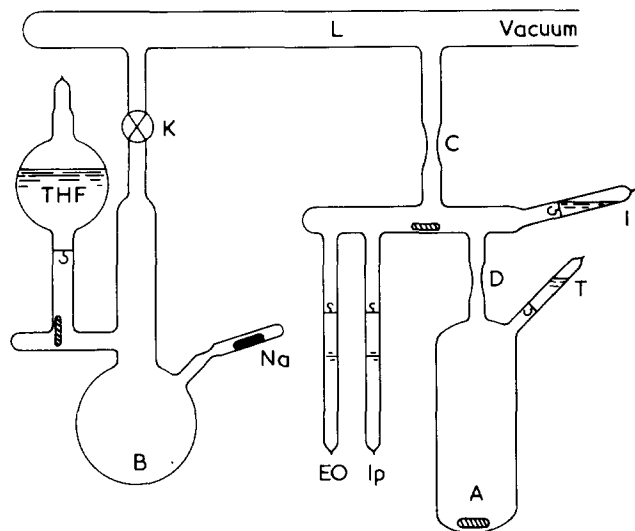


Figure 1 Schematic diagram of block copolymerization apparatus: B, purification flask for solvent (THF); Na, sodium lumps; EO, ethylene oxide monomer; Ip, isoprene monomer; A, copolymerization flask; I, polymerization initiator for isoprene (cumyl potassium or sodium naphthalene in THF); T, polymerization terminator (glacial acetic acid in THF)

a vacuum line, as illustrated schematically in the right hand side of Figure 1. The THF solvent was further purified by means of the Na mirror technique in flask B, flash-distilled to flask A through stopcock K and main vacuum line L, and stored in the block copolymerization apparatus by fusing off the apparatus at the portion C from the main vacuum line.

The polymerization of isoprene was then initiated by mixing the initiator solution (cumyl potassium or sodium naphthalene in THF), I, and the isoprene monomer, Ip, at dry ice-methanol temperature around  $-75^{\circ}\text{C}$ . The reaction, which gave a pale yellow colour of living isoprenyl potassium or naphthalene anion, was allowed to continue for 6 to 24 h, depending on the molecular weight of the isoprene block, until the monomer was completely consumed. Then, block copolymerization of ethylene oxide to the polyisoprene sequence was carried out by adding the ethylene oxide monomer, EO, to the solution containing poly(isoprenyl potassium) or naphthalene anion as the initiator. The reaction rate was usually very low, as reported by O'Malley *et al.*<sup>10</sup> as well as by Richards and Szwarc<sup>9</sup>, but the reaction was performed, at first, at relatively low temperature near room temperature for about 24 h and then at gradually elevated temperatures up to  $60^{\circ}\text{C}$  for a period as long as 10 days, to avoid blowing up the ethylene monomer within the copolymerization apparatus. The reaction was terminated by adding a solution of glacial acetic acid in THF, T.

The copolymers thus synthesized were precipitated from the solutions in THF by adding n-hexane for EO rich copolymers, methanol for Ip rich copolymers, or their mixtures for intermediate copolymers. These precipitates were dried under a vacuum ( $10^{-3}$  mmHg) at room temperature, followed by freeze drying in benzene to remove traces of the solvents.

#### Characterization of block copolymers

The block copolymers thus obtained were characterized by velocity ultra-centrifugation, osmotic pressure, and ordinary element analysis in order to investigate the degrees of monodispersity of the copolymers as well as of contamination with corresponding homopolymers, the number-average

molecular weight, and the fractional compositions of the block sequences, respectively.

**Sedimentation pattern.** The sedimentation pattern of the copolymers was observed at  $20^{\circ}\text{C}$  in a Spinco Model E ultracentrifuge of a benzene solution (0.3–0.5 g/l in concentration) at 56 000 rev/min. The pattern exhibited a relatively sharp single peak, as demonstrated in Figure 2b in terms of the Schlieren picture, for most of the copolymers, suggesting that the copolymers synthesized must be genuine AB or ABA type block copolymers having considerably sharp distribution of molecular weights. But some of the copolymers gave twin peaks, as demonstrated by the lower pattern in Figure 2a, suggesting that the copolymers may be contaminated with homopolyisoprene. The fractionation to remove the homopolymer was repeated by using n-hexane or methanol as a precipitant for relatively dilute solutions (less than 5% in concentration) of EO rich or Ip rich copolymers both in benzene, respectively, until their sedimentation patterns gave a single peak.

**Molecular weight.** The number-average molecular weights, as determined in a toluene solution at  $37.0^{\circ}\text{C}$  with a high-

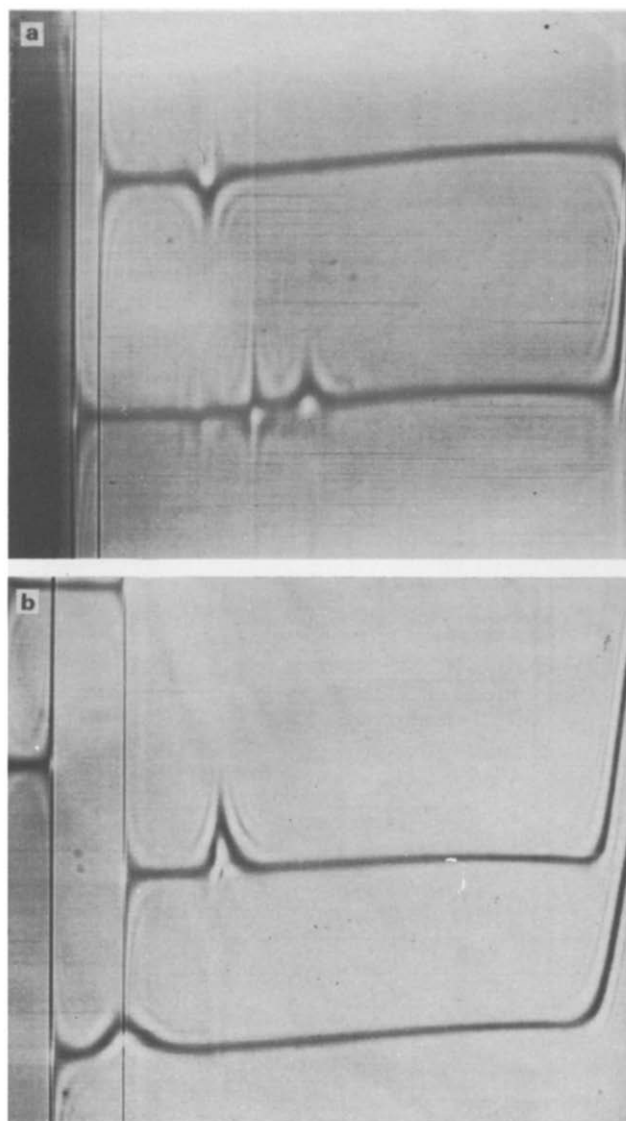


Figure 2 Sedimentation patterns from Spinco Model E ultracentrifuge: (a) (lower curve) 0.5 g/l benzene solution of a block copolymer contaminated by homopolyisoprene at 56 100 rev/min; (b) 0.5 g/l benzene solutions of a genuine block copolymer and a well fractionated block copolymer both at 56 000 rev/min

speed membrane osmometer, are listed in Table 1, together with specimen codes of the respective copolymers.

**Fractional compositions of AB and ABA block sequences.** The weight fraction of each block sequence was determined from ordinary element analysis, and was double-checked by using an infra-red absorption of 0.5 g/l solution in CCl<sub>4</sub> in terms of a characteristic band for polyisoprene at 1638 cm<sup>-1</sup>. The fraction by the infra-red method agreed with that by the element analysis within experimental error, so that their arithmetic mean was listed in terms of wt % fraction of EO sequence in Table 1.

**Degree of crystallinity and melting point of EO crystal.** The degree of crystallinity and melting point of the EO crystal in the film specimens cast from benzene solutions of the block copolymers, were investigated by means of d.s.c. analysis using a Perkin-Elmer Model DSC-1B differential scanning calorimeter, under a given elevating temperature rate ~10°C/min. The results were also listed in Table 1, where the degree of crystallinity and melting point were evaluated from the endothermic peak area over a temperature range from about 40 to 70°C, as illustrated in Figure 3 for some of the test specimens, by taking a literature value of heat of fusion of homo-PEO crystal, 45 cal/g<sup>12</sup> as a reference and from the endothermic peak position along the temperature scale, respectively.

As can be recognized from the Table, the degree of crystallinity in EO phase decreases linearly, in general, but more rapidly for the ABA series than the AB series, with decrease of the EO fraction. On the other hand, the melting point of the EO crystals, which are considerably lower than a literature value for homo-PEO crystal, 68.5°C<sup>12</sup>, remains almost constant, a little higher than 60°C, unless the EO fraction and the molecular weight of the EO block sequence become extremely small.

Figure 4 shows X-ray diffraction pictures for the series of AB type block copolymers including homopolyisoprene and homo-PEO as extremes. The Figure demonstrates that the crystal system of the block copolymers is identical with that of homo-PEO even for a block copolymer of less crystallinity and lower melting point as EO/Ip 5, and that somewhat diffused characteristics in the X-ray diffraction picture from the EO/Ip 5 must arise mostly from smaller size of less grown crystallites than the others.

#### Electron and polarized light microscopy

Ultrathin film specimens (~700 to 1000 Å in thickness) were prepared for electron microscopic observations by pouring a drop of 0.1% benzene or ethyl benzene solutions on to the microscope mesh coated by collodion and carbon, and by evaporating the solvents as gradually as possible at 30°C. Ethyl benzene was used as a selective solvent good for the Ip but poor for EO block segments, while benzene

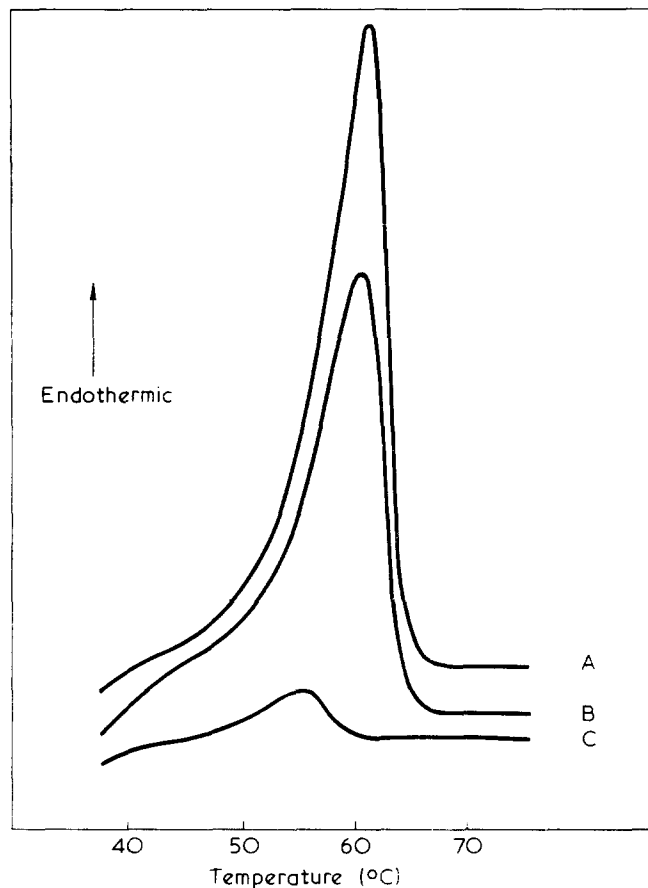


Figure 3 D.s.c. thermogram with an elevating temperature rate ~10°C/min, demonstrating endotherm due to EO crystal melting for a series of EO/Ip/EO specimens cast from benzene solutions. A, EO/Ip/EO 2; B, EO/Ip/EO 3; C, EO/Ip/EO 6

Table 1 Characterization of AB and ABA type block copolymers of ethylene oxide and isoprene synthesized

Specimen code	Fraction of ethylene oxide* (wt %)	Number-average molecule weight x 10 <sup>4</sup>			Degree of crystallinity† (%)	Melting point‡ (0°C)
		Total**	Ip-block	EO-block		
EO/Ip 1	87.0	135.8	17.7	118.1	79.5	62.2
EO/Ip 2	76.0	98.8	23.7	75.1	81.0	64.0
EO/Ip 3	72.0	65.2	18.3	46.9	72.7	63.3
EO/Ip 4	60.0	53.0	21.2	31.8	61.5	60.0
EO/Ip 5	23.0	24.9	19.2	5.7	10.1	50.8
EO/Ip/EO 1	78.4	31.5	7.1	12.2	88.0	62.5
EO/Ip/EO 2	74.6	21.9	5.6	8.2	86.4	61.5
EO/Ip/EO 3	67.4	29.9	9.7	10.1	83.6	61.0
EO/Ip/EO 4	52.4	31.5	14.9	8.3	60.0	60.5
EO/Ip/EO 5	14.0	34.3	30.0	2.4	—	—
EO/Ip/EO 6	11.8	68.9	61.1	3.9	35.0	55.5
EO/Ip/EO 7	8.8	48.5	44.2	2.1	—	—
PEO 1	100	21.0	0.0	21.0	—	—
PEO 2	100	3.8	0.0	3.8	—	—
Pip 1	0.0	7.8	7.8	0.0	—	—

\* Determined from ordinary element analysis as well as from infra-red absorption at 1638 cm<sup>-1</sup>, a characteristic band for polyisoprene

\*\* Measured by a high-speed membrane osmometer in toluene at 37°C

† Relative value determined from the d.s.c. thermogram taking a literature value of heat of fusion for homo-PEO crystal as reference

‡ Measured from peak position of endotherm in the d.s.c. thermogram

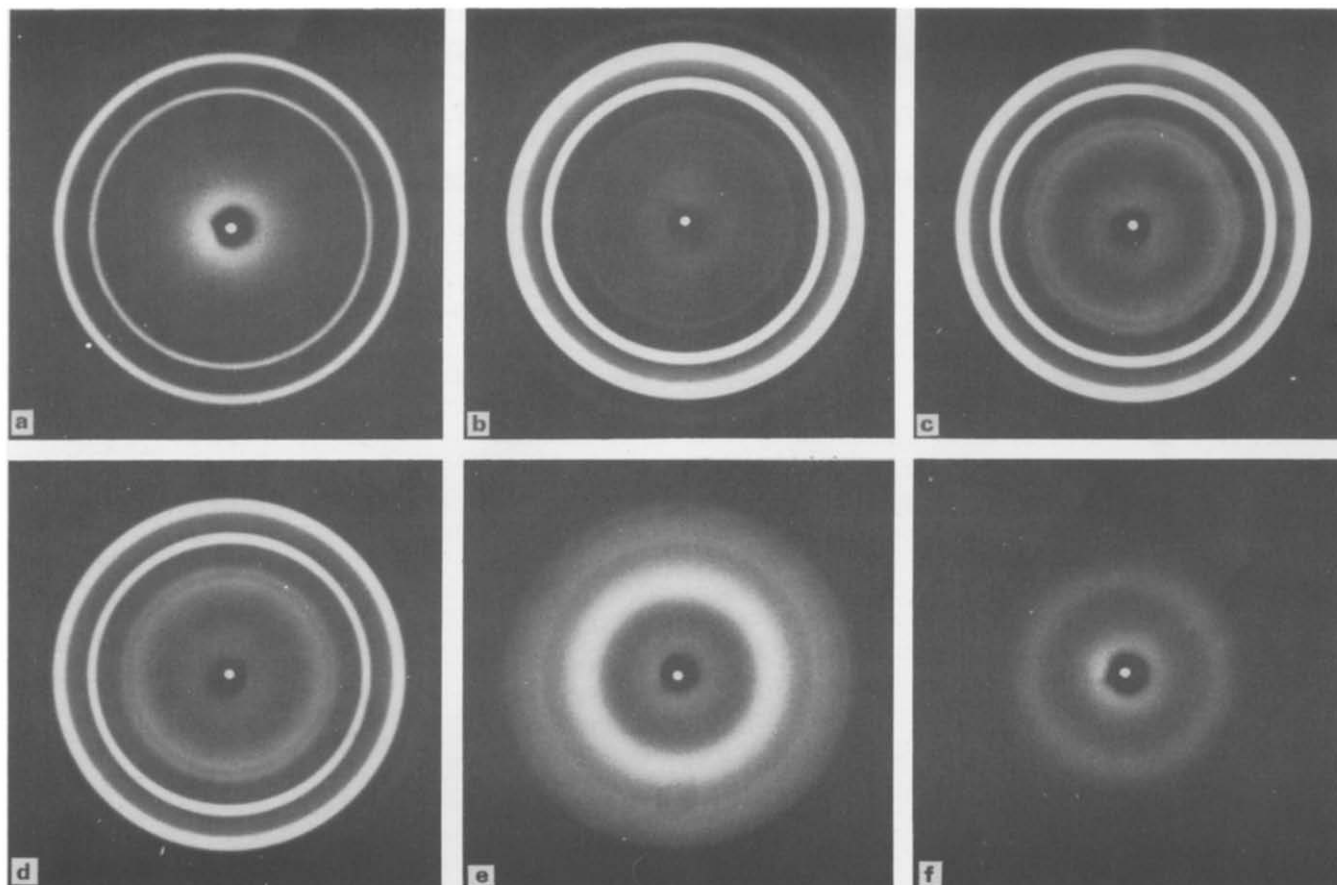


Figure 4 X-ray diffraction diagrams for a series of EO/Ip block copolymers including homo-PEO and homopolyisoprene, as extremes, all cast from benzene solutions. (a) Homo-PEO; (b) EO/Ip 1; (c) EO/Ip 3; (d) EO/Ip 4; (e) EO/Ip 5; (f) homopolyisoprene

was used as a non-selective solvent good for both block segments. The results for the selective solvent may be compared with those recently studied by Kovacs *et al.*<sup>13,14</sup> and by Kawai *et al.*<sup>15</sup>

The electron microscopic observations were made in the following two ways: (i) the specimens were stained by OsO<sub>4</sub> vapour which selectively stains Ip phase in order to observe the domain structure (the microphase separation) with deep contrast; or (ii) they were shadowed by Pt-Pd in order to observe morphology of crystalline EO phase. It was not possible to prepare ultrathin sections by ultramicrotome even after the OsO<sub>4</sub> fixation treatment proposed by Kato<sup>16</sup>, partly because the EO segment is hydrophilic and makes the specimen too ductile to perform the ultrathin sectioning, and partly because there are no adequate liquids of common poor solvent for both segments on which the ultrathin sections are floated in order to mount the sections on the microscope mesh.

*Domain structure and crystalline morphology of EO/Ip/EO tri-block copolymers cast from benzene solutions.* In Figure 5 are shown cross-polarized photomicrographs of the PEO 1; EO/Ip/EO 2, EO/Ip/EO 3, and EO/Ip/EO 4 specimens all cast from 1% benzene solutions at 30°C. It is seen from the Figure that spherulitic texture with negative birefringence becomes less perfect, leading to less clear Maltese-cross, with increasing fraction of the amorphous Ip segments. The texture of the other specimens having EO fractions less than 50% was not clearly observed by the light microscope. Most of the block segments must be considered to locate within the spherulites for the EO/Ip/EO 1 to EO/Ip/EO 4 specimens, since the spherulites are impinged on another. Fine structure of the spherulites, especially location of the

Ip phase within the spherulites was examined as a function of EO fraction by transmission electron microscopy.

The fine structure of the EO/Ip/EO tri-block copolymers cast from 0.1% benzene solution at 30°C are shown in Figure 6. These Figures show typical structures of the copolymers having weight fraction of EO segments: (i) greater than 75% (Figures 6a and 6b for EO/Ip/EO 2 stained and shadowed, respectively); (ii) less than 75% but greater than ~40% (Figures 6c and 6d for EO/Ip/EO 3 and EO/Ip/EO 4, respectively); and (iii) less than ~40% (Figures 6e and 6f for EO/Ip/EO 5 and EO/Ip/EO 7, respectively).

The micrograph on the stained specimen of EO/Ip/EO 2 (Figure 6a) indicates that the dark spherical domains of ~1000 Å in diameter are dispersed in the bright matrix. The dark and bright phases should correspond to the Ip and EO phases which are stained and unstained by OsO<sub>4</sub>, respectively. Texture of the EO matrix is seen clearly to be spherulitic from the micrograph on the shadowed specimen (Figure 6b). The spherical Ip domains are not regularly arranged in the spherulitic EO matrix as in the case of amorphous block copolymers.

Upon increasing the Ip fraction, the spherical Ip domains are interconnected to result in the texture of rod-like Ip domains dispersed in spherulitic EO matrix as seen in Figure 6c. With further increase of the Ip fraction, the rod-like Ip domains are interconnected to result in both Ip and EO being continuous phases as seen in Figure 6e. The EO phase, however, is still seen to be spherulitic, although disordered, from the electron micrographs on the shadowed specimens or in the cross-polarized photograph (Figure 5d). Finally a phase inversion occurs in which, as shown, for example in Figure 6e, spherical EO domains having average

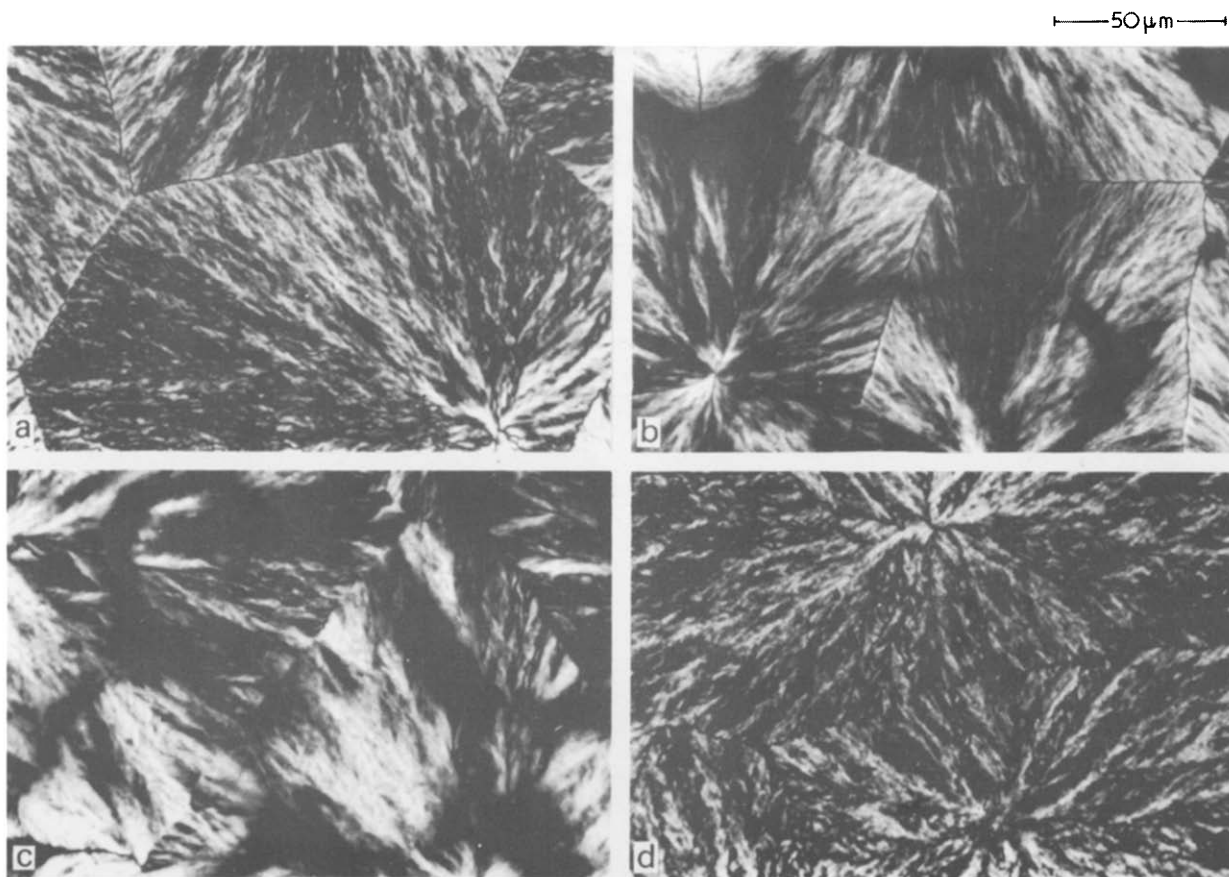


Figure 5 Cross-polarized photomicrographs of film specimens, a series of EO/lp/EO block copolymers having relatively large fractions of EO segments, all cast from 1% benzene solutions at 30°C, demonstrating less perfect development of spherulitic crystalline texture with increase of lp fraction. (a) Homo-PEO; (b) EO/lp/EO 2; (c) EO/lp/EO 3; (d) EO/lp/EO 4

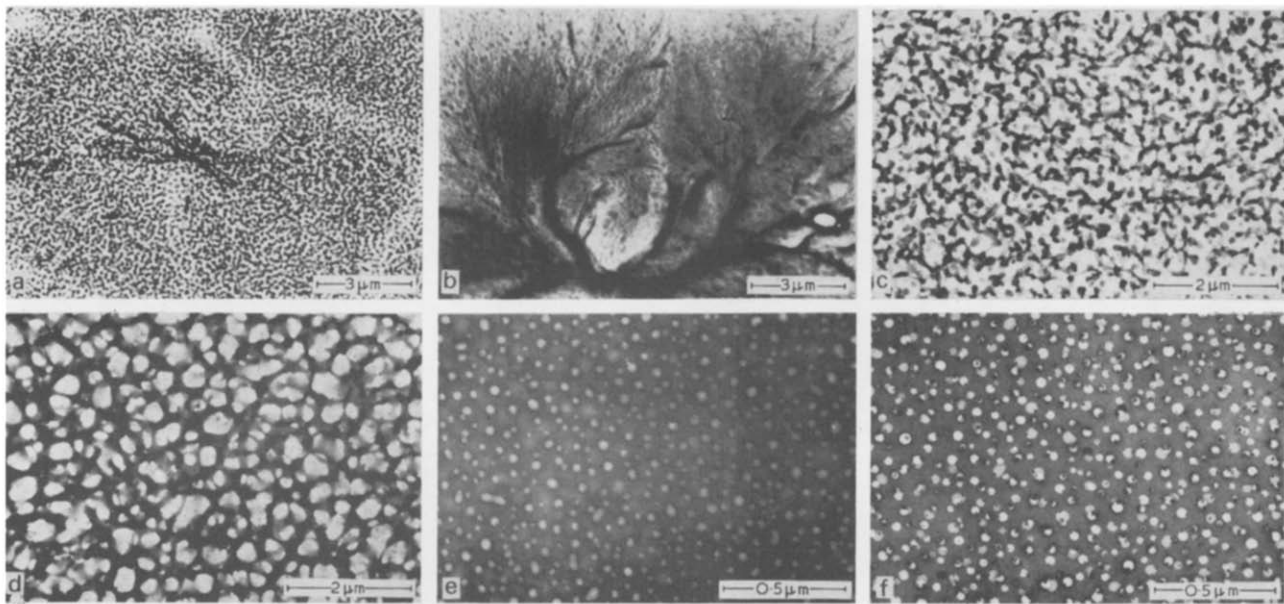


Figure 6 Electron micrographs of ultrathin films cast from 0.1% benzene solutions of a series of EO/lp/EO block copolymers at 30°C: (a) EO/lp/EO 2 stained by OsO<sub>4</sub>; (b) EO/lp/EO 2 shadowed by Pt-Pd; (c) EO/lp/EO 3 stained by OsO<sub>4</sub>; (d) EO/lp/EO 4 stained by OsO<sub>4</sub>; (e) EO/lp/EO 5 stained by OsO<sub>4</sub>; and (f) EO/lp/EO 7 stained by OsO<sub>4</sub>

diameter of  $\sim 400$  Å are dispersed in an lp matrix. The spherical EO domains are known to be crystallized, as mentioned before, by wide-angle X-ray diffraction and d.s.c. thermogram investigations on the thin films. The size of the dispersed EO domains,  $\sim 400$  Å in diameter for EO/lp/EO 5,  $\sim 750$  Å for EO/lp/EO 6, 400 Å for EO/lp/EO 7, is not necessarily in agreement with that theoretically expected

for amorphous AB and ABA type block copolymers<sup>3-6</sup>. This may be due to an effect of crystallization of one component.

*Domain structure and crystalline morphology of AB type block copolymers cast from benzene solutions.* Figure 7 shows cross-polarized photographs of EO/lp 1 to EO/lp 4 specimens all cast from 1% benzene solutions at 30°C. It is

seen again that spherulitic texture, which becomes less perfect with increasing fraction of the amorphous Ip segments, grows unless the fraction of crystalline EO segments is relatively small, being less than around 50%.

The fine structure of the EO/Ip di-block copolymers cast from 0.1% benzene solutions at 30°C are shown in Figure 8. The electron micrograph on the stained specimen of EO/Ip 2 (Figure 8a) indicates that the Ip spherical domains of ~1300 Å in diameter are dispersed in the EO matrix. Texture of the EO matrix is seen clearly to be spherulitic from the micrograph on the shadowed specimen (Figure 8b). With increasing the Ip fraction, the spherical Ip domains are interconnected to form a texture of irregular rod-like domains dispersed in spherulitic EO matrix as seen in Figure 8c. With further increase of the Ip fraction up to an extent comparable with EO fraction, the irregular rod-like domains of Ip component become more regular and orient parallel to each other in the radial direction of the spherulitic texture of EO component as seen in Figure 8d for EO/Ip 4. When the Ip fraction becomes more dominant, the phase inversion occurs, as seen in Figure 8e for EO/Ip 5, in which the spherical EO domains are dispersed in a matrix of the amorphous Ip component.

Comparing the results for the EO/Ip di-block series with those for the EO/Ip/EO tri-block series, it may be suggested that the morphological behaviour of the di-block series is quite similar to that of the tri-block series, depending mostly on the fractional compositions of the block segments but hardly on the sequence arrangements, as in the case of amorphous AB and ABA type block copolymers<sup>17</sup>.

*Domain structure and crystalline morphology of ABA and AB type block copolymers cast from ethyl benzene solutions.* Figures 9a and 9c show cross-polarized micrographs of the EO/Ip/EO 2 and EO/Ip/EO 4 specimens, respectively, both

cast from 1% solutions in ethyl benzene, a good solvent for the Ip segments but a poor solvent for the EO segments, at 30°C. Figure 9b also shows a cross-polarized micrograph of a thin film specimen, which was obtained by melting and annealing the EO/Ip/EO 2 specimen cast from the solution on a microscope deck. As can be seen in the Figures, the crystalline texture is generally much less developed than that obtained from benzene solutions.

When the specimens were cast from 0.1% ethyl benzene solution at 30°C, the texture seen in the electron micrographs for both the stained and shadowed specimens turned out to be those characteristic of single crystal-like lamellae (hedrites) having a square shape of a few micrometres in size, irrespective of the fractions of EO segments if it is approximately greater than 20%. Typical electron micrographs are shown in Figure 10 for EO/Ip/EO 2 (Figure 10a) and EO/Ip 5 (Figure 10c). Close observation of the micrographs suggests that disc-like domains of Ip segments appear on the free surface of the EO single crystals. The Ip phase is considered to exist in interlamellar region, as proposed by Kovacs et al.<sup>13,14</sup> and by Kawai et al.<sup>15</sup>, when the copolymers are cast from more concentrated solutions so as to result in a stack of lamellae.

There is, however, an exception for the copolymers having nearly equal fractions of the Ip and EO segments, for which the development of crystalline texture is quite unstable, forming either sheaf-like texture, an undeveloped texture of spherulite as shown in Figure 10b, or hedrite having a square shape of a few micrometres in size. Despite the exceptions, it must be emphasized that the crystalline texture of the EO component and, in turn, the domain structure of the amorphous Ip component obtained by casting with ethyl benzene are very different from those obtained by casting with benzene. In the case of casting with ethyl

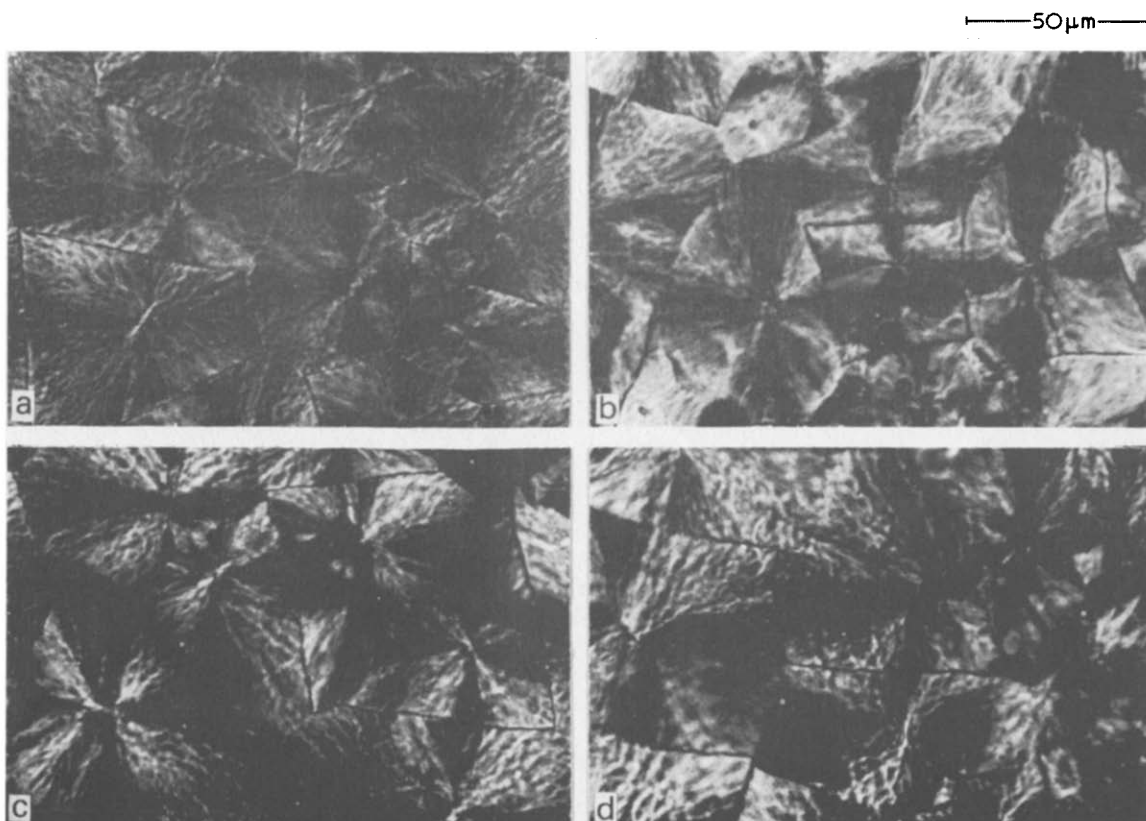
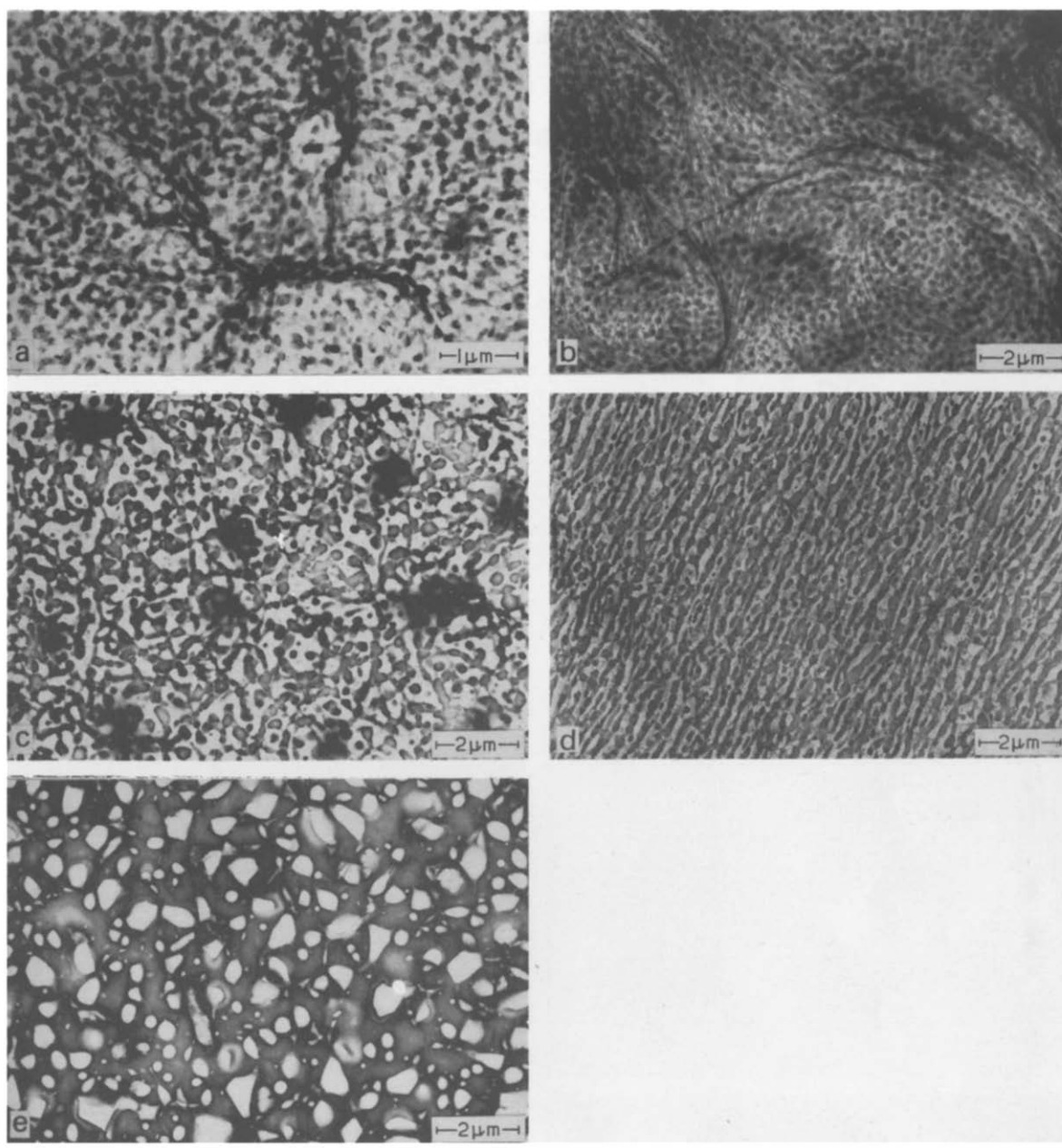


Figure 7 Cross-polarized photomicrographs of film specimens, a series of EO/Ip block copolymers having relatively large fractions of EO segments, all cast from 1% benzene solutions at 30°C, demonstrating less perfect development of spherulitic crystalline texture with increase of Ip fraction. (a) EO/Ip 1; (b) EO/Ip 2; (c) EO/Ip 3; (d) EO/Ip 4



**Figure 8** Electron micrographs of ultrathin films cast from 0.1% benzene solutions of a series of EO/Ip block copolymers at 30°C: (a) EP/Ip 2 stained by OsO<sub>4</sub>; (b) EO/Ip 2 shadowed by Pt-Pd; (c) EO/Ip 3 stained by OsO<sub>4</sub>; (d) EO/Ip 4 stained by OsO<sub>4</sub>; (e) EO/Ip 5 stained by OsO<sub>4</sub>

benzene, the crystallization of the EO segments must occur in advance of the micelle formation owing to microphase separation of the block segments and/or in association with relatively less entanglements between the EO segments due to contraction of individual EO segments in the poor solvent. These must make the crystallization less dislocated to result in the hedrite with a square shape as large as a few micrometres in size and on which surfaces the Ip segments may be segregated to form the Ip layers. In the case of casting with benzene, on the other hand, the situation may be just the opposite and makes the crystallization much dislocated resulting in the dendritic or spherulitic textures or the spherical domain structure of the EO component dispersed in a matrix of the Ip component for the EO rich or Ip rich copolymers, respectively.

Figure 11 shows wide-angle X-ray diffraction and small-angle X-ray scattering patterns obtained from through radiation (Figure 11a) and edge radiation (Figure 11b) for a film specimen of EO/Ip/EO 2 copolymer, which was cast from

3% solution in ethyl benzene, at first at a relatively elevated temperature around 60°C and then at gradually lowered temperatures down to 30°C. The patterns indicate preferential orientation of paratropic crystal planes, such as (120) plane, perpendicular to the film surface as well as planar orientation of crystal lamellae parallel to the film surface. The first and second order scattering peaks, which are observed from meridional intensity scanning as shoulders at 33.6 and 67.2 min, arise from a single interlamellar spacing of 157 Å (from the Bragg equation). By assuming the densities of crystalline and amorphous phases of EO component and of amorphous phase of Ip component as 1.234 and 1.130 and 0.913 g/cm<sup>3</sup>, respectively, and by using the fractional composition of the EO and Ip segments of the copolymer, the layer thickness of the crystalline and amorphous EO phases and of amorphous Ip phase are calculated to be 96 and 10 and 51 Å, respectively. The thickness of the crystalline EO phase agrees fairly well with that reported for homo-PEO<sup>12</sup>.

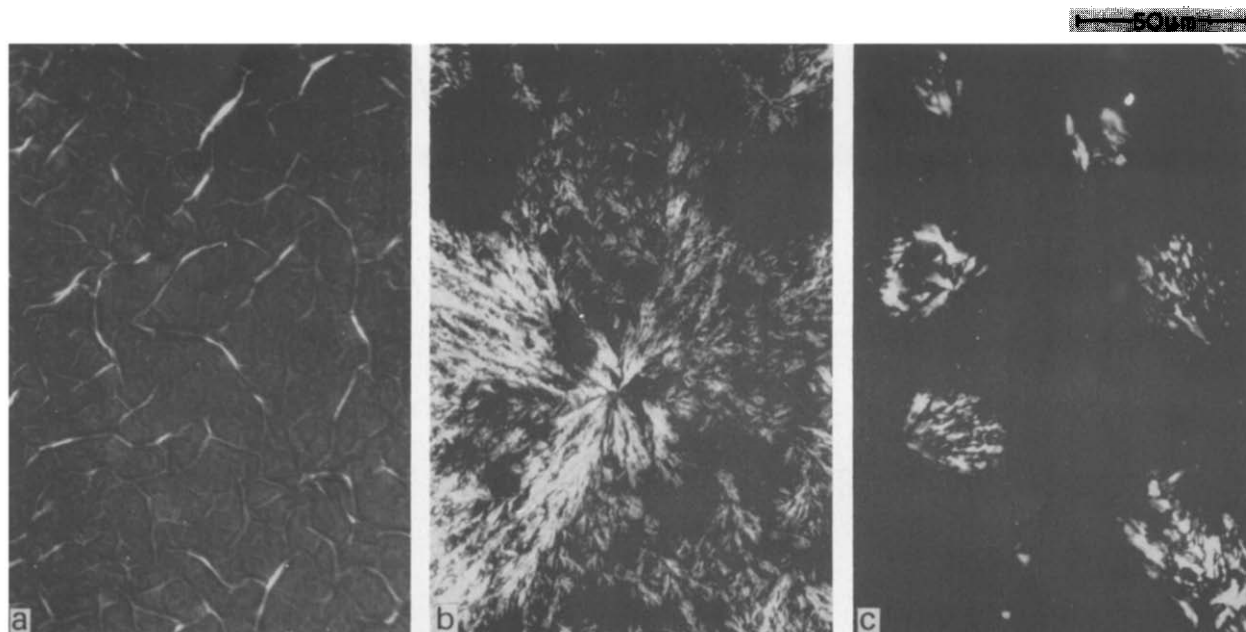


Figure 9 Cross-polarized photomicrographs of film specimens, EO/Ip/EO block copolymers having relatively large fractions of EO segments, all cast from 1% ethyl benzene solutions at 30°C: (a) EO/Ip/EO 2 (as cast); (b) EO/Ip/EO 2 (molten and annealed); (c) EO/Ip/EO 4 (as cast)

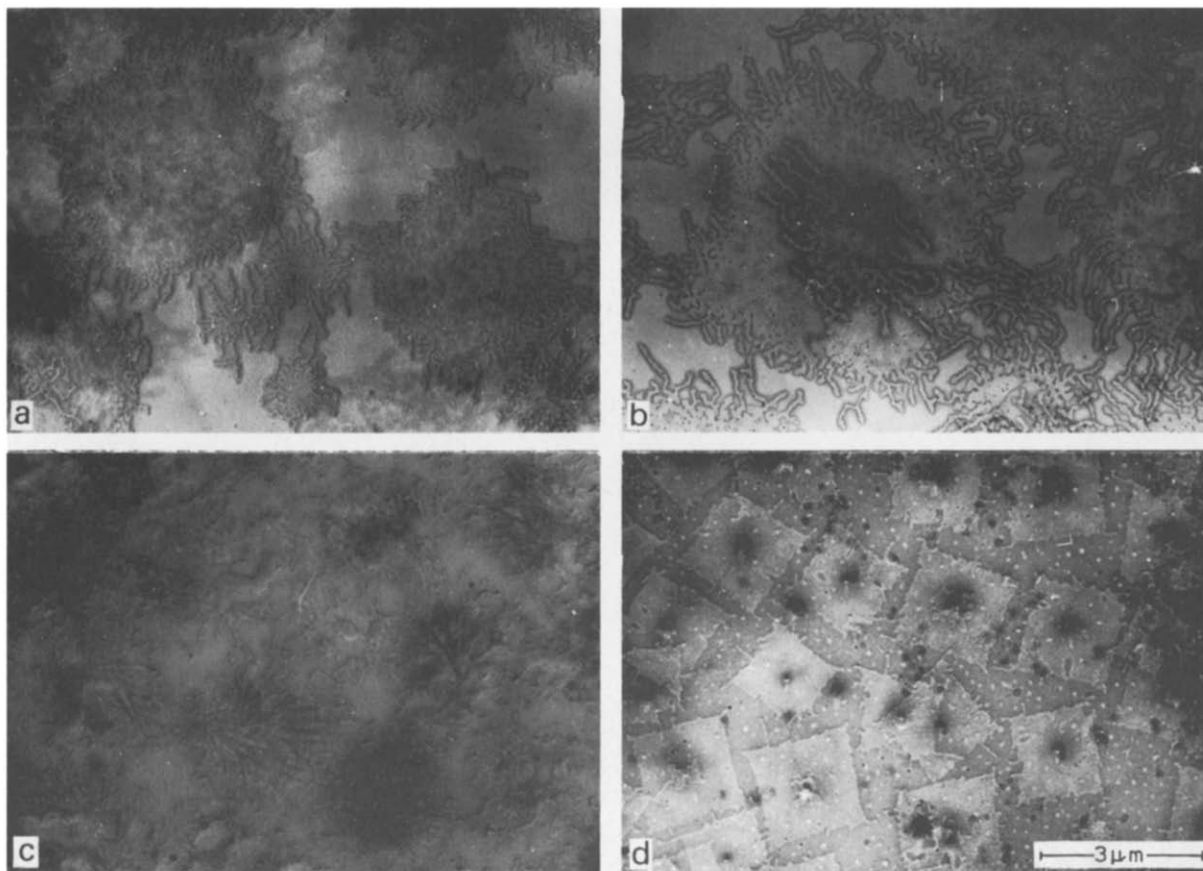


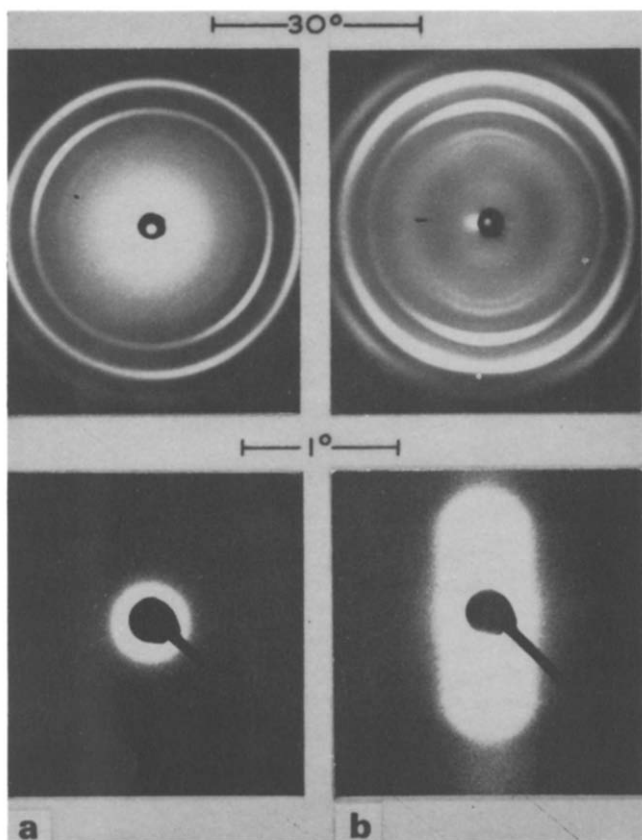
Figure 10 Electron micrographs of ultrathin films cast from 0.1% ethyl benzene solutions at 30°C: (a) EO/Ip/EO 2 shadowed by Pt-Pd; (b) EO/Ip/EO 2 stained by OsO<sub>4</sub>; (c) EO/Ip/EO 4 shadowed by Pt-Pd; and (d) EO/Ip 5 shadowed by Pt-Pd

Similar investigations of the wide-angle X-ray diffraction and small-angle X-ray scattering were performed for a film specimen of EO/Ip/EO 4 copolymer cast from 3% solution in benzene. Although much less preferential orientation of (120) crystal plane and planar orientation of crystal lamellae than the above were observed, the meridional intensity distribution was too monotonous to detect the long period.

*Domain structure and crystalline morphology of mixed system of block copolymer with homo-polymer.* In order to investigate the solubilization of homo-polymer into the corresponding domains of block copolymer, EO/Ip/EO 6 was mixed with homo-PEA 2 in various fractions and was cast into ultrathin films from 0.1% solutions in benzene at 30°C. The homo-PEO was chosen so that its molecular weight was

comparable to that of the EO segment of the block copolymer<sup>18</sup>, and the mixed specimens were designated as Co 90 to Co 30 in accordance with the mixed fractions of the copolymer in wt % from 90 to 30.

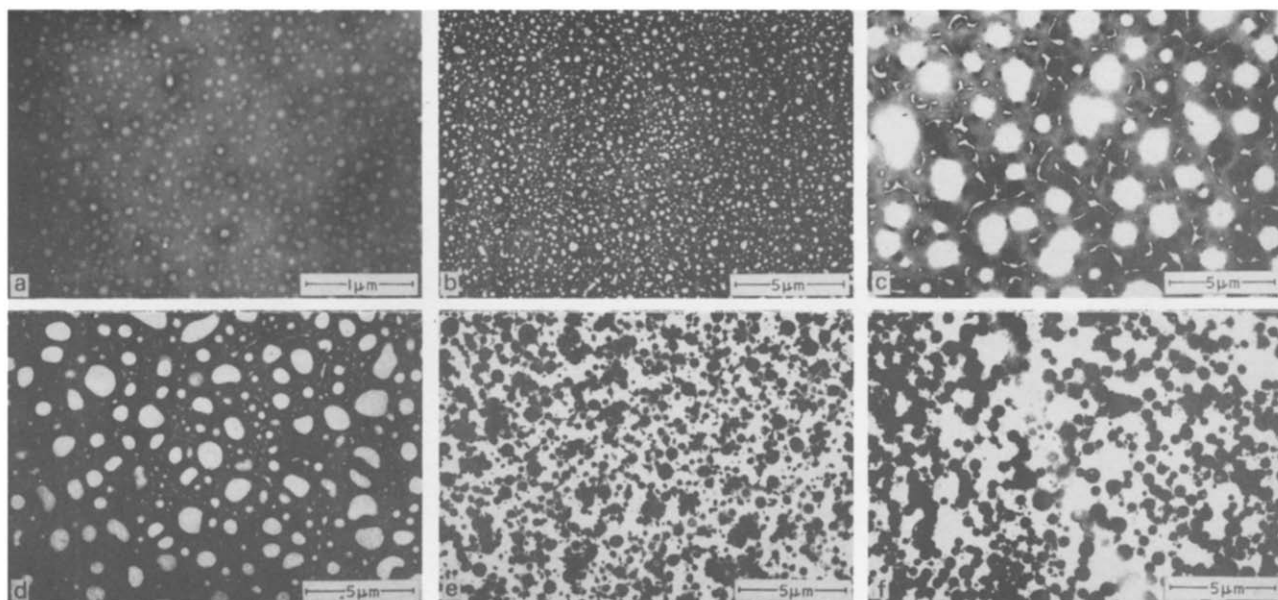
Electron micrographs of the stained specimens including EO/Ip/EO 6 itself are shown in *Figure 12*. As can be seen, the morphological behaviour of the mixed system with



**Figure 11** Wide-angle X-ray diffraction ( $30^\circ$ ) and small-angle X-ray scattering ( $1^\circ$ ) patterns of film specimen cast from 3% ethyl benzene solution of EO/Ip/EO 2, at first, at around  $60^\circ\text{C}$  and then at gradually lowered temperatures down to  $30^\circ\text{C}$ : (a) through radiation; and (b) edge radiation (film normal is in horizontal and vertical directions for the wide- and small-angle X-ray patterns respectively)

increasing fractions of homo-PEO is very similar to that of the series of EO/Ip/EO tri-block copolymers with increasing fractions of EO segment, as demonstrated in *Figure 6*. When the fraction of the Ip component remain: still dominant, the Ip component occupies the matrix phase in which spherical domains of EO component disperse with their diameters increasing with increase of homo-PEO fraction, as seen in *Figures 12a* and *12b*; when the fraction of the Ip component becomes comparable to that of the total fraction of the EO component, the spherical EO domains are interconnected resulting in both Ip and EO phases being continuous and interpenetrating each other, as seen in *Figures 12c* and *12d*; and when the total fraction of the EO component becomes dominant, the EO component occupies the matrix phase in which spherical or rod-like domains of the Ip component are dispersed, as seen in *Figures 12e* and *12f*. Sheaf-like or spherulitic crystalline textures, which are not shown here, can be also observed under cross-polarized microscope for the mixed systems of Co 75 to Co 30. These suggest that the morphological behaviour of the mixed system is mostly affected by the fractional composition of each component, as a whole, in association with a complete solubilization of the homo-PEO into the corresponding domains, unless the molecular weight of homo-PEO is considerably larger than that of EO segment of copolymer, as concluded for the amorphous block copolymer systems<sup>18</sup>.

*Effect of heat treatment upon the domain structure and crystalline morphology of as-cast copolymers.* The effect of heat treatment upon the domain structure and crystalline texture of as-cast films of the block copolymers from benzene solutions was investigated. The ultrathin films were, at first, cast on the electron microscope mesh from 0.1% solutions in benzene, and then heat-treated under vacuum ( $10^{-3}$  mmHg) at  $70^\circ\text{C}$  for 2 h followed by gradual cooling down to room temperature. *Figure 13* shows the stained and shadowed micrographs demonstrating the effect of the treatment for EO/Ip/EO 4, EO/Ip 4 and EO/Ip 5. By comparing the results with those for the as-cast specimens in *Figures 6d*, *8d* and *8e*, respectively, the domains of Ip component are seen to be considerably distorted as the EO crystalline texture is being developed.



**Figure 12** Electron micrographs of ultrathin films cast from 0.1% benzene solutions of mixtures of EO/Ip/EO 6 with PEO 2 in various fractions at  $30^\circ\text{C}$  and stained by  $\text{OsO}_4$ . The numbering designation is weight fraction of EO/Ip/EO 6; (a) EO/Ip/EO 6; (b) Co 90; (c) Co 75; (d) Co 65; (e) Co 50; (f) Co 30





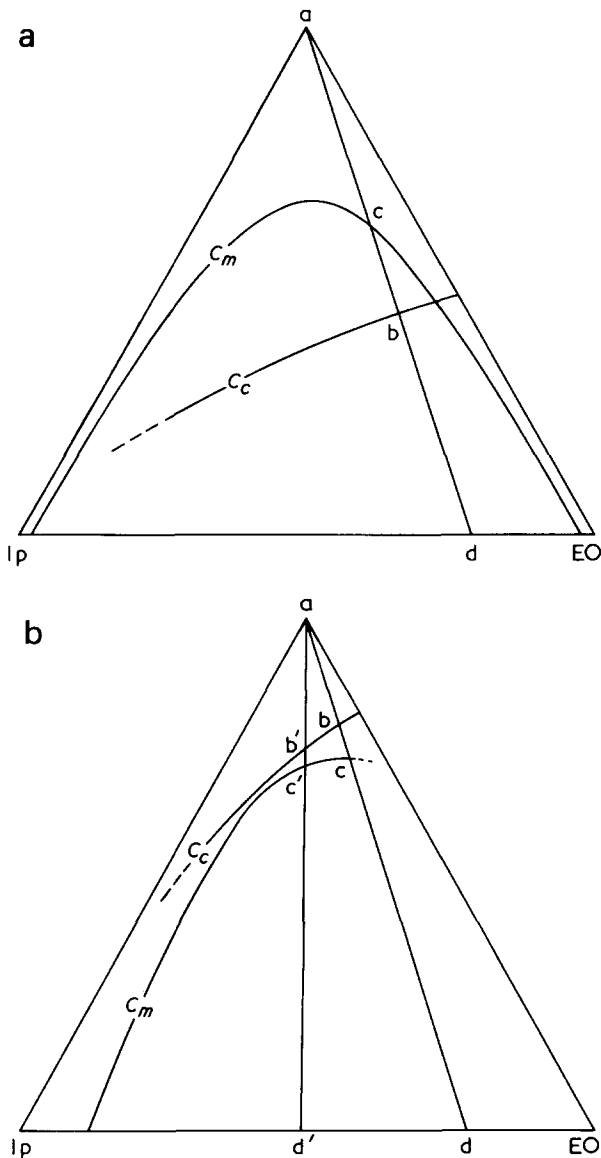


Figure 15 Schematic representations of the triangular phase diagram at a given temperature, room temperature  $\sim 30^\circ\text{C}$ ; (a) benzene, and (b) ethyl benzene as cast solvent

phase is dispersed in a matrix of lp component, so that the crystallization is limited in the dispersed EO domain. This gives a spherical crystalline texture embedded in the amorphous lp matrix, as shown in Figures 6e, 6f and 8e. The lp domains or matrix interrupt crystal growth and may cause disorders in the EO crystal as schematically shown in Figure 16b.

In the case of amorphous AB or ABA type block copolymers, the domain structure is regularly arranged in space and varies with increasing A component: (i) A sphere, (ii) A rod in B matrix, (iii) alternating lamellae of A and B, (iv) B rod and (v) B sphere in A matrix. In the case when one component B is replaced by a crystalline component, the domain structure and mutual arrangement of the domain are disordered as seen in Figures 6 and 8. The domain structure (iii) is modified to result in Figures 6d and 8d, and structure (iv) is not observed but is modified to result in structure (v). The effect of crystallization on the domain structure occurs because the decrease of free energy level of the system due to the crystallization must be larger than that due to the micelle formation, when a given common stage of high free energy level, if any, is taken as a reference state. In other

words, the crystallization must occur, in general, more easily than the micelle formation, resulting in the above modifications for the domain structures of (iii) and (iv) having rather higher level of free energy in the micelles than the others, as pointed out by Inoue *et al.*<sup>3</sup>. The effect of heat treatment of the as-cast specimens, shown in Figure 13, can be interpreted in terms of the same principle.

On the other hand, if ethyl benzene is used as a cast solvent,  $C_c$  is expected to be lower than  $C_m$  at room temperature, as illustrated in Figure 15b, since the solvent is good for the lp segments but poor for the EO segments. Therefore, crystallization is a predominant factor which governs the solid texture, and there is little effect of the phase separation on the solid texture. For the EO/lp/EO 2 copolymer, the EO component is crystallized into single crystal-like texture at point 'b' (Figure 15b) and lp component is segregated into interlamellar region, as schematically shown in Figure 10d, even for a copolymer having EO fraction as small as  $\sim 20\%$ , such as for EO/lp 5. It should be, however, noted that the texture is exceptionally ill defined and not single crystal-like but rather a less perfect spherulite for copolymers having nearly equal fraction of the EO and lp

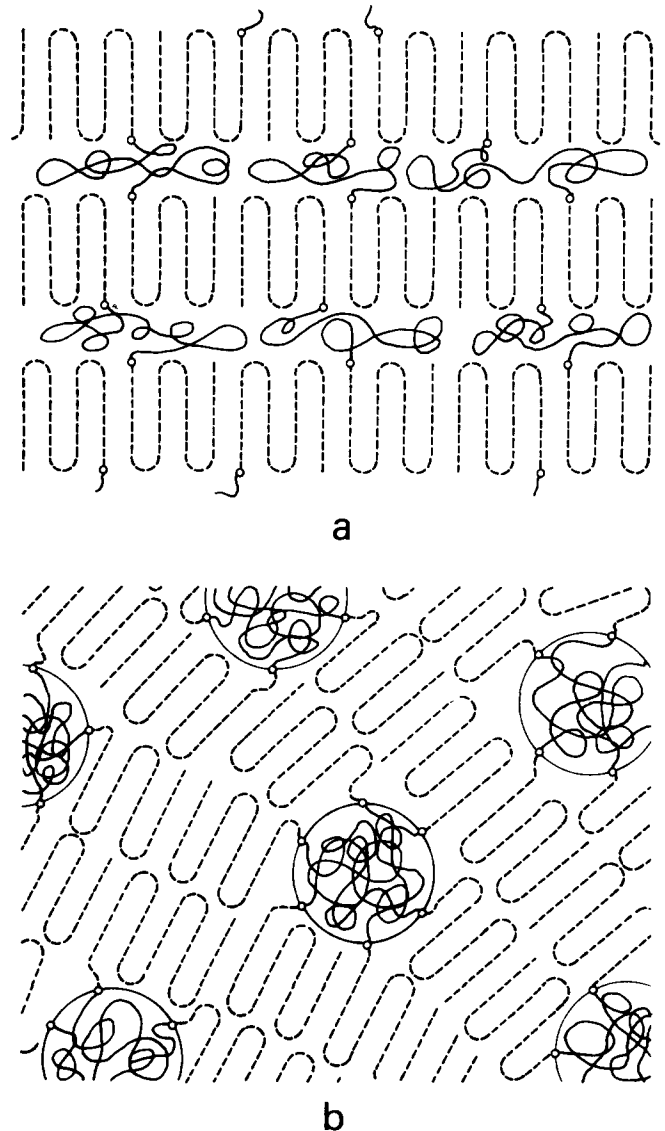


Figure 16 Schematic representation of the textures of EO/lp/EO block copolymers cast from (a) ethyl benzene and (b) benzene solutions

segments, as illustrated in Figure 10c for EO/Ip/EO 4. This may be interpreted as arising from an effect of the micro-phase separation on the crystallization, which, in turn, may occur because  $C_c$  is close to  $C_m$ , as shown in Figure 15b in terms of another straight line 'ab'c'd' for the copolymers.

Solution behaviour of similar block copolymers (styrene/ethylene oxide, and styrene/propylene oxide) in selective solvent of both block chains has been intensively studied by Skoulios and coworkers<sup>20-23</sup>. They give, at high concentrations, highly organized, mesomorphic structures which could be detected by analyses of small angle X-ray scattering. This organization, in the range 100-500 Å, is shown to be of the lamellar, rod-like, or spherical type.

The domain structure of the EO/Ip and EO/Ip/EO copolymers as expected when the selective solvent good for the homo-PEO is used should be similar to that as expected when the non-selective solvent is used, in that the micro-phase separation occurs prior to the crystallization of the crystallizable EO segment. The domain structure formed by the phase separation would correspond to the mesomorphic organization found in concentrated solutions by Skoulios and coworkers. On the other hand, when the selective solvent good for the non-crystallizable block chain is used, crystallization of the EO block chain is shown to occur at very low concentration, i.e. lower than the critical micelle concentration, and to result in single crystal-like texture. In this case the mesomorphic organization observed by Skoulios et al. will be, therefore, expected to correspond to the dispersed single crystal-like texture in solutions.

Our findings on the domain structure and domain formation mechanism are also in rough accord with those by Crystal et al.<sup>24,25</sup>, although the detailed submicroscopic domain structures were not necessarily fully investigated by them because the osmium tetroxide staining method could not be satisfactorily used on their copolymers of styrene/ethylene oxide.

#### ACKNOWLEDGEMENTS

This work was supported in part by a grant from the Scientific Research Funds (Kagaku Kenkyu-hi, 743020-1973) of

the Ministry of Education, Japan, and in part by a grant from the Bridgestone Tire Co. Ltd, Tokyo, Japan and Japan Synthetic Rubber Co. Ltd, Tokyo, Japan.

#### REFERENCES

- 1 Sadron, C. *Angew. Chem.* 1963, **75**, 472
- 2 Vanzo, E. *J. Polym. Sci. (A-1)* 1965, **4**, 1727
- 3 Inoue, T., Soen, T., Hashimoto, T. and Kawai, H. *J. Polym. Sci. (A-2)* 1969, **7**, 1283
- 4 Soen, T., Inoue, T., Miyoshi, K. and Kawai, H. *J. Polym. Sci. (A-2)* 1972, **10**, 757
- 5 Meier, D. J. *J. Polym. Sci. (C)* 1969, **26**, 81
- 6 Meier, D. J. *Polym. Prepr.* 1970, **11**, 400
- 7 Matsuo, M., Sagae, S. and Asai, H. *Polymer* 1969, **10**, 79
- 8 Leary, D. F. and Williams, M. C. *J. Polym. Sci. (Polym. Phys. Edn)* 1973, **11**, 345
- 9 Richards, D. H. and Szwarc, M. *Trans. Faraday Soc.* 1959, **56**, 1944
- 10 O'Malley, J., Crystal, R. G. and Erhardt, P. F. 'Block Copolymers', (Ed. S. L. Aggarwal), Plenum Press, New York, 1970, p 163
- 11 Zbinden, R. 'Infrared Spectroscopy of High Polymers', Academic Press, New York, 1964, p 240
- 12 Mandelkern, L. 'Crystallization of Polymers', McGraw-Hill, New York, 1964, p 78
- 13 Kovacs, A. J. and Lotz, B. *Kolloid-Z. Z. Polym.* 1966, **209**, 97
- 14 Lotz, B., Kovacs, A. J., Bassett, G. A. and Keller, A. *Kolloid-Z. Z. Polym.* 1966, **209**, 115
- 15 Kawai, T. et al. *Makromol. Chem.* 1969, **128**, 252
- 16 Kato, K. *Polym. Eng. Sci.* 1967, **7**, 38
- 17 Uchida, T., Soen, T., Inoue, T. and Kawai, H. *J. Polym. Sci. (A-2)* 1972, **10**, 101
- 18 Inoue, T., Soen, T., Hashimoto, T. and Kawai, H. *Macromolecules* 1970, **3**, 87
- 19 Sadron, C. and Gallot, B. *Makromol. Chem.* 1973, **164**, 301
- 20 Skoulios, A., Fianz, G. and Parrod, J. C. *R. Acad. Sci.* 1960, **251**, 739
- 21 Skoulios, A. and Fianz, G. *C. R. Acad. Sci.* 1961, **253**, 265
- 22 Skoulios, A. and Fianz, G. *J. Chim. Phys.* 1962, **59**, 473
- 23 Skoulios, A., Tsoulade, G. and Franta, E. *J. Polym. Sci. (C)* 1963, **4**, 507
- 24 Crystal, R. G., Erhardt, P. F. and O'Malley, J. J. 'Block Copolymers', (Ed. S. L. Aggarwal), Plenum Press, New York, 1970, p 179
- 25 Crystal, R. G. 'Colloidal and Morphological Behavior of Block and Graft Copolymers', (Ed. G. E. Molau), Plenum Press, New York, 1971, p 279

# Thermomechanical heat of deformation studies on *cis*-polybutadiene

C. Price, G. Allen and N. Yoshimura

Department of Chemistry, University of Manchester, Manchester M13 9PL, UK

(Received 16 August 1974)

Thermomechanical heat of torsional deformation measurements have been made on crosslinked *cis*-polybutadiene by means of a Calvet microcalorimeter operated at 30°C. When corrected for volume changes utilizing the Gaussian statistical theory of elasticity, the data gave a value for the relative energy contribution to the torsional couple,  $M_e/M$ , of  $0.14 \pm 0.02$ . Measurements were also made on a sample subjected to simple tensile deformations. The relative energy contribution to the tensile force ( $f_e/f$ ) was found to agree within experimental error with the value obtained for  $M_e/M$ , and the two results gave an average value for  $d \ln \langle r_0^2 \rangle / dT$  of  $4.1 \times 10^{-4} \text{ K}^{-1}$ .

## INTRODUCTION

The Gaussian statistical theory of rubber elasticity predicts that the equilibrium couple required to maintain a rubber cylinder of length,  $L$  in torsion at an angular rotation,  $\theta$ , is given by<sup>1</sup>:

$$M = (\pi/2)(\nu kT/V_u)(\langle r_i^2 \rangle / \langle r_0^2 \rangle)(\theta/L)a_0^4 \quad (1)$$

where  $\nu$  is the number of active network chains,  $k$  is Boltzmann's constant,  $V_u$  is the volume in the stress free state,  $\langle r_i^2 \rangle$  is the mean-square end-to-end distance of the chains in the network and  $\langle r_0^2 \rangle$  the corresponding value for free chains in the bulk state, and  $a_0$  is the unstrained radius of the cylindrical sample. From a thermodynamic stand-point the equilibrium couple may be considered to consist of an entropic and an energetic (or enthalpic) contribution:

$$\begin{aligned} M &= (\partial U / \partial \theta)_{T,V,L} - T(\partial S / \partial \theta)_{T,V,L} \\ &= (\partial U / \partial \theta)_{T,V,L} + T(\partial M / \partial T)_{\theta,V,L} \end{aligned} \quad (2)$$

and

$$\begin{aligned} M &= (\partial H / \partial \theta)_{T,P,L} - T(\partial S / \partial \theta)_{T,P,L} \\ &= (\partial H / \partial \theta)_{T,P,L} + T(\partial M / \partial T)_{\theta,P,L} \end{aligned} \quad (3)$$

where, to a very good approximation<sup>2</sup>,

$$(\partial H / \partial \theta)_{T,P,L} = (\partial U / \partial \theta)_{T,P,L} \quad (4)$$

In terms of the classical theory of elasticity, torsion is a constant volume deformation, and hence  $(\partial U / \partial \theta)_{T,P,L}$  and  $(\partial U / \partial \theta)_{T,V,L}$  are equivalent<sup>3</sup>. For finite deformations of rubber-like materials, Flory *et al.*<sup>4</sup> indicated this would not hold. Considering the combined case of torsion about a cylindrical axis and extension in the axial direction, Treloar<sup>1</sup> showed from equation (1) that:

$$(\partial U / \partial \theta)_{T,V,L} = (\partial U / \partial \theta)_{T,P,L} + M\beta T \quad (5)$$

where  $\beta$  is the coefficient of cubical expansion.

The correction term  $M\beta T$  arises because a torsional deformation at constant pressure is accompanied by a small, but significant, reduction in volume ( $\Delta V$ ) i.e. according to the Gaussian theory:

$$(\partial V / \partial \theta)_{T,P,L} = -M\kappa \quad (6a)$$

and

$$\Delta V = -M\theta\kappa/2 \quad (6b)$$

where  $\kappa$  is the bulk compressibility.

To-date very few studies have been made of the energetics of torsional deformations of rubber-like materials. From torsional couple vs. temperature measurements carried out at constant  $P$ ,  $L$  and  $\theta$ , Boyce and Treloar<sup>5</sup> determined  $M_e/M$  for natural rubber by means of equations (3), (4) and (5). Again from thermoelastic measurements, but using a somewhat refined apparatus, Gent and Kuan<sup>6</sup> determined  $M_e/M$  for natural rubber, *cis*-polybutadiene, *trans*-polyisoprene and polyethylene at a series of uniaxial extensions. Recently, the present authors<sup>7</sup> reported a thermomechanical, heat of torsional deformation study of natural rubber from which values of  $M_e/M$  could be obtained. In the present contribution we report the results of a similar thermomechanical study for *cis*-polybutadiene. Measurements have also been made of the energetics of simple extension in order to obtain a direct comparison of the analogous quantities  $M_e/M$  and  $f_e/f \equiv (\partial U / \partial L)_{T,V} / f$ . All the measurements were made at 30°C at atmospheric pressure.

## EXPERIMENTAL

The *cis*-1,4-polybutadiene (BR-01) was obtained from the Japanese Synthetic Rubber Co. (JSR). The polymer was crosslinked in the form of cylindrical rods by the Rubber and Plastics Research Association, Great Britain; the recipe involved heating at 153°C for 60 min with 2 parts by weight of dicumyl peroxide (per 100 parts of rubber). The

cylinders were approximately 21 mm in length and 13 mm in diameter for torsion experiments (and designated BR.A) and 21 mm in length and 3 mm in diameter for simple extension experiments (and designated BR.B). Mild steel end-pieces were bonded on to the samples. Uncrosslinked material and excess curing reactant were not extracted.

Before any experiments were made, each sample was relaxed by annealing at 48–55°C for about 65 h at a higher deformation than the maximum deformation to be developed in the experiments.

#### Thermomechanical studies

On deformation of a rubber sample at constant pressure, the change in enthalpy,  $\Delta H$ , is given by  $q + w$ , where  $q$  is the heat absorbed by the system and  $w$  is the work done on the system other than that arising from volume changes. In torsion,

$$w = \int_{\theta_1}^{\theta_2} M d\theta$$

where  $\theta_1$  and  $\theta_2$  are the initial and final angles of torsion, and for simple extension,

$$w = \int_{L_1}^{L_2} f dL$$

where  $L_1$  and  $L_2$  are the initial and final lengths in the extension direction. For both torsion and simple extensions  $q$  was measured in a Calvet microcalorimeter thermostated at 30°C. Values of  $w$  were determined in the first case from torsional couple *versus* angle of twist measurements and in the second from tensile force *versus* extension measurements. Ideally, for any given deformation  $q$  and  $w$  should have been determined simultaneously. Since this proved difficult to achieve experimentally, values of  $w$  were determined in separate deformation experiments carried out under similar conditions to those used in the calorimeter.

A detailed description of the theory, construction and calibration of the Calvet microcalorimeter<sup>8</sup> and the experimental arrangement used in the determination of heats of deformation<sup>7</sup> are fully described elsewhere. Details of the procedures and apparatus used in the force–deformation experiments have also been described<sup>7</sup>.

The thermomechanical, heat of torsional deformation, measurements were carried out in an axially unstretched state. A torsional twist was first applied to the sample (BR.A) and the system left for 1 hour to reach equilibrium. The angle of torsion was then reduced and the calorimetric response was monitored until the recorder showed a steady base line. Measurements were made for a number of increments over the range  $\theta = \pi \rightarrow 0$  (radians). The heat changes observed were additive, i.e.  $q(\theta_A \rightarrow \theta_C) = q(\theta_A \rightarrow \theta_B) + q(\theta_B \rightarrow \theta_C)$ .

In the heat of extension measurements the sample (BR.B) was first deformed to a chosen extension ratio and kept at this value for 1 hour. The sample was then allowed to retract to a lower extension ratio. This process was repeated until the sample had completely retracted. A wide range of experiments were carried out starting and finishing at different extensions. As in torsion it was found that the

observed heat changes were additive. A number of exploratory runs showed that the calorimetric results were insensitive to moderate variations in the retraction rate.

As in previous experiments, the arrangement within the 'reference' cell of the microcalorimeter was similar to that employed in the 'laboratory' cell except for the omission of the sample<sup>7</sup>. The microcalorimeter was calibrated in the recommended manner using Joule heating<sup>8</sup>.

## RESULTS AND DISCUSSION

### Torsion

As shown in *Figure 1*, there was found to be a linear dependence of heat of untwisting on  $\psi^2$  over the range studied (i.e.  $\psi = 1.57 \rightarrow 0$  rad/cm). The value of  $\gamma (=q/a_0^2 V_u \psi^2)$  was calculated to be 0.137 J/cm<sup>3</sup> using the method of least squares.

In agreement with the results of earlier force–deformation experiments on rubber-like materials<sup>9</sup>, the plot of torsional couple  $M$  *versus*  $\psi$  was linear: from the gradient, the shear modulus [ $G = (2/\pi a_0^4) ML/\theta$ ] was calculated to be 0.516 J/cm<sup>3</sup>. A simple analytical expression for the mechanical work,  $w$ , may be obtained by integrating the torque over the angle of twist  $\theta$ :

$$w = \int_0^{\theta} M d\theta = a_0^2 V_u G \psi^2 / 4 \quad (7)$$

Combining expressions for  $q$  and  $w$  we obtain:

$$\frac{\Delta H}{a_0^2 V_u} = \left( \frac{G}{4} - \gamma \right) \psi^2 \quad (8)$$

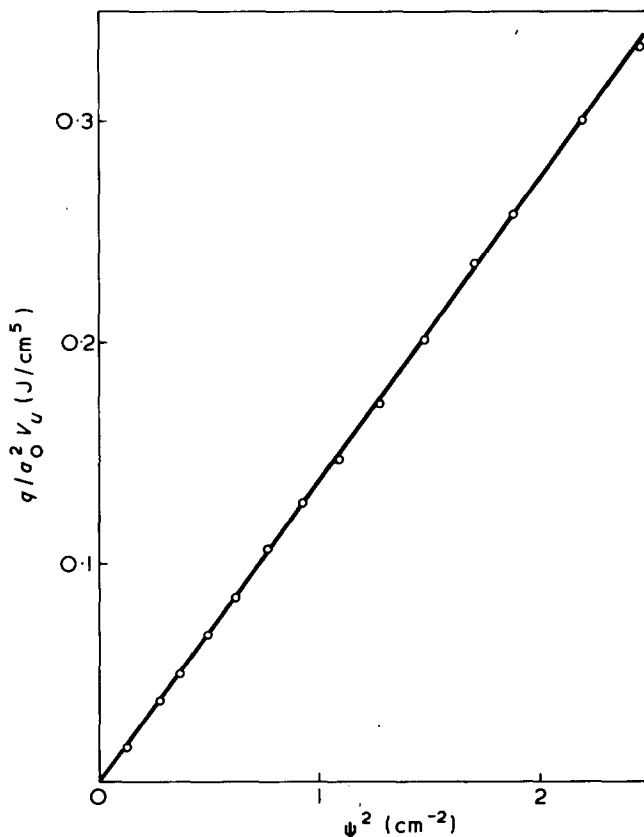


Figure 1 Heat absorbed on untwisting a sample of crosslinked cis-polybutadiene from torsion  $\psi (= \theta/L)$  to the unstrained state

By partial differentiation,

$$\left(\frac{\partial H}{\partial \theta}\right)_{T,P,L} = \left(1 - \frac{4\gamma}{G}\right)M \quad (9)$$

Finally, from equations (3)–(5) and (9):

$$\frac{M_e}{M} = \left(1 - \frac{4\gamma}{G}\right) + \beta T \quad (10)$$

Substitution of the experimental data into this expression yields  $M_e/M = 0.14 \pm 0.02$ . This result is in satisfactory agreement with the values of  $M_e/M$  obtained recently by Gent and Kuan from thermoelastic studies on *cis*-polybutadiene; they obtained  $M_e/M = 0.10 \pm 0.04$  at  $\alpha \approx 1.0$ , and  $M_e/M = 0.07$  on averaging seven determinations made within the range  $\alpha = 1.0 \rightarrow 3.0$ . Whilst thermomechanical experiments offer a more direct method of determining  $M_e/M$  than thermoelastic experiments, it should be emphasized that both approaches are dependent on a volume correction term derived from the Gaussian statistical theory of rubber elasticity.

#### Simple extension

Thermomechanical studies were made within the range  $\alpha = 1.7 \rightarrow 1.0$ . The results are plotted together in Figure 2. The mechanical work was obtained by graphical integration of the force–extension curve established under similar conditions to those employed in the calorimetric experiments.

The relative energy contribution to the tensile force at constant volume ( $f_e/f$ ) may be calculated from the data using one of the following expressions derived from the Gaussian statistical theory:

$$f_e/f = (\partial H/\partial L)_{P,T}/f - \beta T/(\alpha^3 - 1) \quad (11)^{10,11}$$

$$f_e/f = [\Delta H - VT\beta f'(1 - \alpha^{-1})/(\alpha - \alpha^{-2})]/w \quad (12)^7$$

where  $f'$  is the force per unit cross-sectional area of the unstrained rubber, and  $\Delta H$  and  $w$  are the enthalpy changes and the work done on the bulk sample. Estimation of the slope of  $\Delta H$  versus  $\alpha$  in Figure 2 at  $\alpha = 1.65, 1.55, 1.45, 1.35$  and  $1.25$  to obtain  $(\partial H/\partial L)_{T,P}$  and correction of these values to constant volume conditions by means of equation (11) gave the following results for  $f_e/f$ : 0.12, 0.13, 0.13, 0.13 and 0.11 respectively.

Application of equation (12) provides a more satisfactory method of analysis, however, since any inaccuracies which might be introduced in estimating slopes are avoided. It also circumvents the problem associated with the determination of  $f_e/f$  at low extension ratios, since the equation yields an average value for the range covered. Over the range  $\alpha = 1.0 \rightarrow 1.65$  we find  $f_e/f = 0.11 \pm 0.02$  which is in fair agreement with the results reported from thermoelastic studies. From five thermoelastic studies<sup>12–16</sup> on conventionally crosslinked *cis*-polybutadiene (cited in a recent review article by Mark<sup>17</sup>) an average value for  $f_e/f = 0.13$  is obtained.

For natural rubber it has been established that the Gaussian statistical theory underestimates the magnitude of the volume correction term for the case of simple extension<sup>18</sup>. Whilst the effect on  $f_e/f$  is small and barely outside experimental error, it does lead to systematically high values for this parameter. Unfortunately, dilation measurements have only been made on one sample<sup>18</sup> of *cis*-poly-

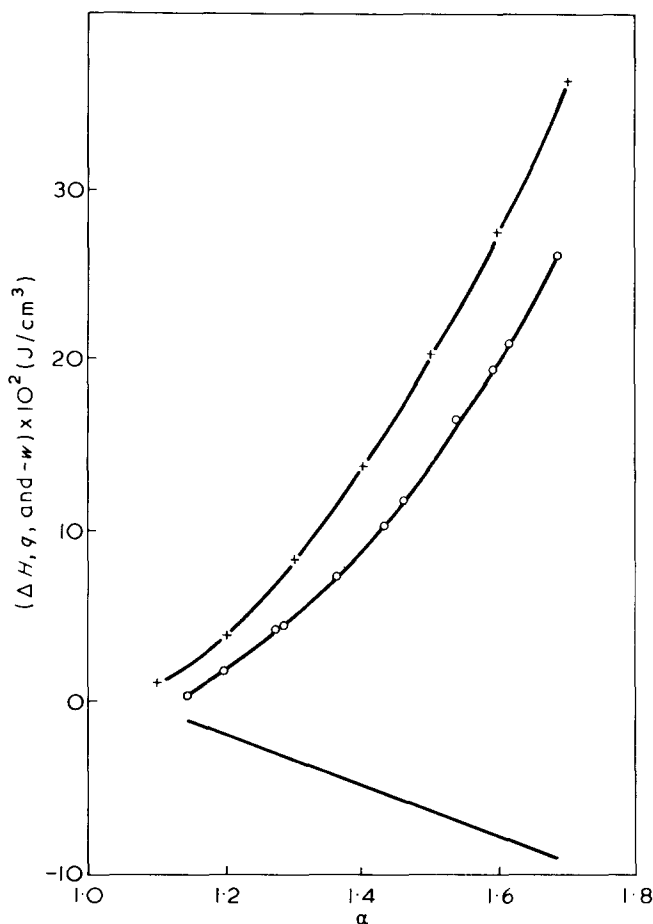


Figure 2 Enthalpy change,  $\Delta H$ , heat absorbed,  $q$ , and work done by ( $-w$ ) a sample of crosslinked *cis*-polybutadiene on retraction from extension ratio  $\alpha$  to the unstrained state;  $\circ$ , values of  $q$ ;  $+$ , values of  $w$ , and  $\Delta H = q + w$

butadiene; furthermore this sample had a considerably lower shear modulus than those used in the present study. The limited dilation results available, however, suggest that as with natural rubber the Gaussian statistical theory may very slightly underestimate the volume correction term.

On the basis of the Gaussian statistical theory, values of  $M_e/M$  and  $f_e/f$  should be directly comparable since both quantities are equivalent to  $Td \ln \langle r_0^2 \rangle / dT$ . In keeping with this prediction, the values obtained in the present study ( $0.14 \pm 0.02$  and  $0.11 \pm 0.02$  respectively) agree within experimental error, and give an average value for  $d \ln \langle r_0^2 \rangle / dT$  of  $4.1 \times 10^{-4} \text{ K}^{-1}$ . There do not appear to be any solution data suitable for the calculation of  $d \ln \langle r_0^2 \rangle / dT$ . Using the rotational isomeric state theory, however, Mark<sup>19</sup> has shown that a positive value for *cis*-polybutadiene arises because the lowest energy conformations about  $\text{CH}_2\text{-CH=CH-CH}_2$  rotatable bonds are  $\pm 60^\circ$ ,  $\pm 60^\circ$  and  $\mp 60^\circ$ ,  $\pm 60^\circ$  states, which are relatively compact.

#### ACKNOWLEDGEMENTS

The authors wish to thank the Bridgestone Tire Co. (Japan) who financed N.Y. during the course of this work. We are also grateful to Dr S. Morrell (RAPRA) for crosslinking the *cis*-polybutadiene samples.

#### REFERENCES

- 1 Treloar, L. R. G. *Polymer* 1969, **10**, 291
- 2 Flory, P. J. 'Principles of Polymer Chemistry', Cornell University Press, Ithaca, 1953, Ch 11

*Heat of deformation studies on cis-polybutadiene: C. Price et al.*

- 3 Meyer, K. H. and van der Wyk, A. J. A. *Helv. Chim. Acta* 1946, 28, 1842
- 4 Flory, P. J. *et al. J. Polym. Sci.*, 1960, 45, 235
- 5 Boyce, P. H. and Treloar, L. R. G. *Polymer* 1970, 11, 21
- 6 Gent, A. N. and Kuan, T. H. *J. Polym. Sci.* 1973, 11, 1723
- 7 Allen, G., Price, C. and Yoshimura, N. *JCS Faraday Trans. I* to be published
- 8 Calvet, E. and Prat, H. 'Recent Progress in Microcalorimetry', (Ed. H. A. Skinner), Pergamon Press, Oxford and New York, 1963
- 9 Rivlin, R. S. and Saunders, D. W. *Phil. Trans. R. Soc. (A)* 1951, 243, 251
- 10 Flory, P. J., Hoeve, C. A. J. and Ciferri, A. *J. Polym. Sci.* 1959, 34, 337
- 11 Flory, P. J. *Trans. Faraday Soc.* 1961, 57, 829
- 12 Crespi, G. and Flisi, U. *Makromol. Chem.* 1963, 60, 191
- 13 Becker, R. H. *MSc Thesis* Polytechnic Institute of Brooklyn (1972)
- 14 Ishikawa, T. and Nagai, K. *J. Polym. Sci. (A-2)* 1969, 7, 1123
- 15 Shen, M. C., Gebhard, H. M. and Strong, G. D. *Polym. Prepr.* 1969, 10, 80; Shen, M. C., Chen, T. Y., Cirilin, E. H. and Gebhard, H. M. in 'Polymer Networks, Structure and Mechanical Properties', (Ed. A. J. Chompff and S. Newman), Plenum Press, New York, 1971
- 16 van der Hoff, B. M. E. *J. Macromol. Sci. (A)* 1971, 5, 661
- 17 Mark, J. E. *Rubber Chem. Technol.* 1973, 46, 593
- 18 Price, C. and Allen, G. *Polymer* 1973, 14, 577
- 19 Mark, J. E. *J. Am. Chem. Soc.* 1966, 88, 4354

# Effect of thermal decomposition on dielectric relaxation process of poly(vinyl chloride)

Yasuharu Kihira

Department of Industrial Chemistry, Faculty of Engineering,  
Kinki University, Kure, Japan

Kikuo Matsusaka

Research Institute, Toyo-Kohan Co. Ltd, Kudamatsu, Japan

and Ichiro Murakami

Department of Chemistry, Faculty of Science, Hiroshima  
University, Hiroshima 730, Japan

(Received 4 March 1974; revised 29 July 1974)

Dielectric absorption caused by the molecular relaxation of thermally decomposed poly(vinyl chloride) in air was studied on samples in the form of thin films. It was found that, with the progress of thermal decomposition, the magnitude of  $\alpha$  dielectric absorption changes in three stages: (1) initial decrease in magnitude corresponding to the process of the formation of polyene sequences caused by dehydrochlorination; (2) ensuing increase corresponding to the deformation of polyene sequences attributed to oxidation; (3) final decrease corresponding to the formation of crosslinks.

## INTRODUCTION

Studies<sup>1-11</sup> on the thermal decomposition of poly(vinyl chloride) (PVC) in air, by means of determining hydrogen chloride evolved, viscosity measurement, infra-red spectroscopy, thermal gravimetric analysis, and Brabender Plastograph, have so far revealed that both dehydrochlorination and polyene formation take place in the initial stage of the thermal decomposition, then in the second stage, oxidation, and finally in the third stage, crosslinking and chain scission take place.

Kisbényi and Hedvig<sup>12,13</sup> have reported that, by continuously recording the a.c. conductivity and the dielectric spectra, the degradation of sheet PVC samples interposed between electrodes can be kinetically measured and that information on changes in the physical structure of the samples can be obtained.

For the purpose of observing the dielectric absorption due to the molecular relaxation, the usual dielectric method for measuring the decomposition process, however, is unsatisfactory as the absorption is masked from observation by electrical conduction caused by ionic matters resulting from decomposition.

In the present study, thin films of PVC degraded in an air oven were employed, so that most ionic compounds such as hydrogen chloride derived from the decomposition could be released from the film into the air and electric conduction caused by ionic compounds remaining in the film would be minimal, thus eliminating the difficulty mentioned above. From the results obtained, the relation between the dielectric absorption caused by molecular relaxation and structural changes in the thermal decomposition process of PVC is clarified.

## EXPERIMENTAL

### Sample

PVC films used in the present study were prepared thus; Geon 103 EP (product of Nippon Geon Co.) was dissolved in tetrahydrofuran (THF), and the solution was poured onto a glass plate and left for 2 days until a sheet of film was formed. To remove the remaining THF, the film was steeped in methanol for two days and dried *in vacuo* at 50–60°C. The films thus obtained were decomposed thermally in a thermal ageing tester (a gear oven produced by Tabai Co., model GS-11) at 150°C and 190°C ( $\pm 2^\circ\text{C}$ ) for a given time. After an appropriate time lag, one of the films was taken out from the oven and then quenched in liquid nitrogen. The thickness of these sample films was 0.04–0.1 mm.

### Method

Each sample film was set in an electrode arrangement. The complex dielectric constant ( $\epsilon^* = \epsilon' - j\epsilon''$ , where real term,  $\epsilon'$ , is the dielectric constant and imaginary term,  $\epsilon''$ , the dielectric loss) of the sample was calculated from the values of capacitance ( $C$ ) and conductance ( $G$ ) measured by the inductive ratio arm bridge (manufactured by Ando Electric Co., model TR-10C) in the frequency range of 30 to  $10^6$  Hz at varied temperature. The thickness of the sample was not changed during the dielectric measurement. To compare the degradation in the air oven, a thick PVC plate interposed between measuring electrodes (in a closed system) was decomposed in a state in which the decomposition products remained in the sample.

In order to see the physical nature of the degraded films, the dynamic modulus, the d.c. conductivity, the glass transi-



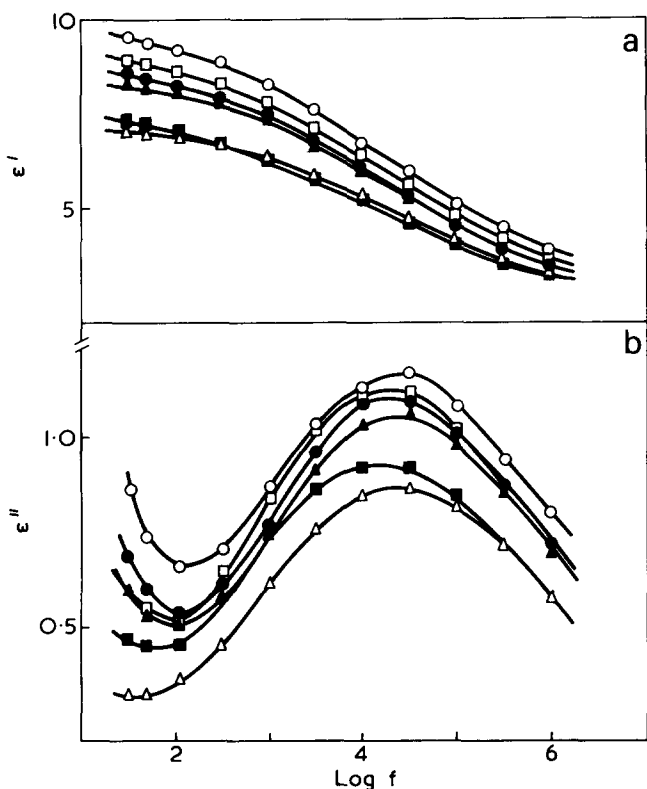


Figure 1 Frequency dependences of  $\epsilon'$  and  $\epsilon''$  at  $110^\circ\text{C}$  for PVC films decomposed at  $150^\circ\text{C}$  in the air oven. Time of decomposition:  $\circ$ , 0;  $\bullet$ , 0.5;  $\Delta$ , 2;  $\blacktriangle$ , 3;  $\square$ , 4;  $\blacksquare$ , 8 h

tion temperature, X-ray diffraction and infra-red absorption spectra were measured.

### RESULTS AND DISCUSSION

As for the thin films of the original and those decomposed at  $150^\circ\text{C}$  in the air oven, the frequency dependence of  $\epsilon'$  and  $\epsilon''$  calculated directly from the value measured by the inductive ratio arm bridge (hereafter, a.c. bridge) at  $110^\circ\text{C}$  are shown in Figure 1. It is clear that the dielectric absorption observable in Figure 1 is ascribable not to the electric conduction attributed to the ionic matters derived from the decomposition, but to the molecular relaxation. On the other hand, for the films decomposed in the closed system, the d.c. conduction ( $G_0$ ) increased with progress of decomposition; for example, the d.c. conductivity,  $\sigma(\Omega^{-1}\text{cm}^{-1})$  ( $\sigma = G_0 \cdot d/S$  where  $d$  is the thickness of the film and  $S$  is the area of electrode) increases as expressed by:

$$\log \sigma = 2.2t - 10.9$$

where  $t$  is the time of decomposition (h), and the value of  $\sigma$  for the decomposed film for 3 h was found to be about  $10^4$  times that of the thin film decomposed in the air oven for the same period and at the same temperature. As for the case of the closed system, the dielectric loss ( $\epsilon''_T$ ) calculated directly from a.c. conductance ( $G_a$ ) measured by the a.c. bridge, and the loss ( $\epsilon''_D$ ) calculated from the value subtracting  $G_0$  from  $G_a$ , are plotted against the frequency in Figure 2. Although  $\epsilon''_T$  which increases with the progress of decomposition shows no peak of dielectric absorption,  $\epsilon''_D$  shows a peak of dielectric absorption which coincides with that observed in Figure 1. It is inferred from these results that when the thick plate of PVC sample is being decomposed

thermally, most of the ionic compounds such as hydrogen chloride derived from the decomposition remain in the sample, hence the dielectric loss calculated directly from  $G_a$  of the sample plate increases with the decomposition.

In the case of the present study using thin films decomposed in the air oven, it is considered that because of the diffusion of split ionic compounds from the film into the air, the ionic conduction becomes very small. Thus the dielectric loss ascribed to the orientation of dipoles can be determined directly from  $G_a$  without measuring d.c. conduction of the sample, although a small increase of  $\epsilon''$  is observed at the low frequency side as shown in Figure 1, which is attributed to the electric conduction caused by the ionic compounds remaining in the film.

The analysis of X-ray diffraction patterns measured for the original and decomposed PVC films revealed that the sample films are not crystallized during treatment in the present experiments.

The glass transition temperature,  $T_g$ , was found to be  $77^\circ\text{C}$  for the original film, and ranged between  $77^\circ$  and  $83^\circ\text{C}$  for the decomposed films. The value of  $T_g$  changes to a lesser extent with decomposition.

The frequency dependence of  $\epsilon''$  of the films decomposed at  $190^\circ\text{C}$  is shown in Figure 3. The dielectric absorptions shown in Figure 1 and 3, observed at temperatures above the glass transition region, are the so-called  $\alpha$  absorptions ascribed to the micro-Brownian motion of segments in amorphous region<sup>14-17</sup>. The  $\beta$  absorptions which have been considered as deriving from the local motion of frozen main chain below  $T_g$ <sup>14-17</sup> were observed at temperatures lower than  $70^\circ\text{C}$ . The discussion with respect to the  $\beta$  absorptions is omitted from this paper, since little influence is caused by the thermal decomposition.

As for the sample films decomposed at  $150^\circ\text{C}$  and  $190^\circ\text{C}$ , the apparent activation energy,  $H^*$  of the  $\alpha$  relaxation process for each film was determined from the slopes of  $\log f_m$  vs.  $1/T$  curves ( $f_m$  is the relaxation frequency,  $T$  is the absolute temperature at which the dielectric constants were measured), and the time dependence of  $H^*$  in the thermal decomposition is shown in Figure 4a. It is observed in this Figure that  $H^*$  changes in three stages.

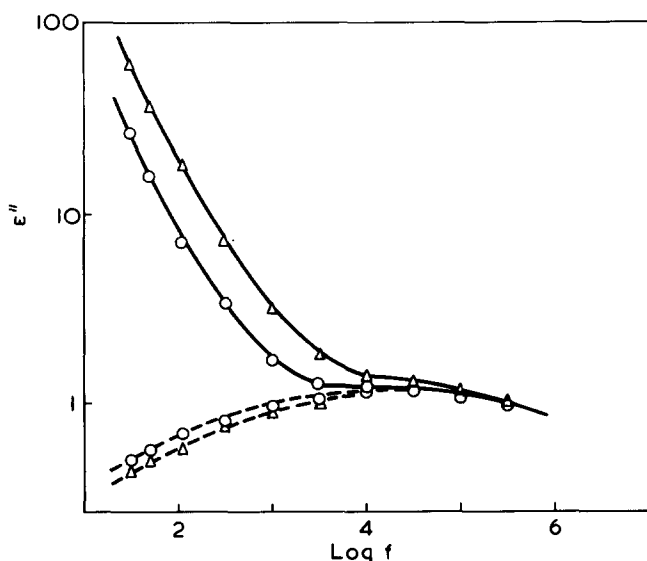


Figure 2 Frequency dependences of  $\epsilon''_T$  at  $110^\circ\text{C}$  for PVC plate decomposed at  $150^\circ\text{C}$  by interposing between electrodes (closed system) (—). ---, loss,  $\epsilon''_D$ . Time of decomposition:  $\circ$ , 40;  $\Delta$ , 60 min

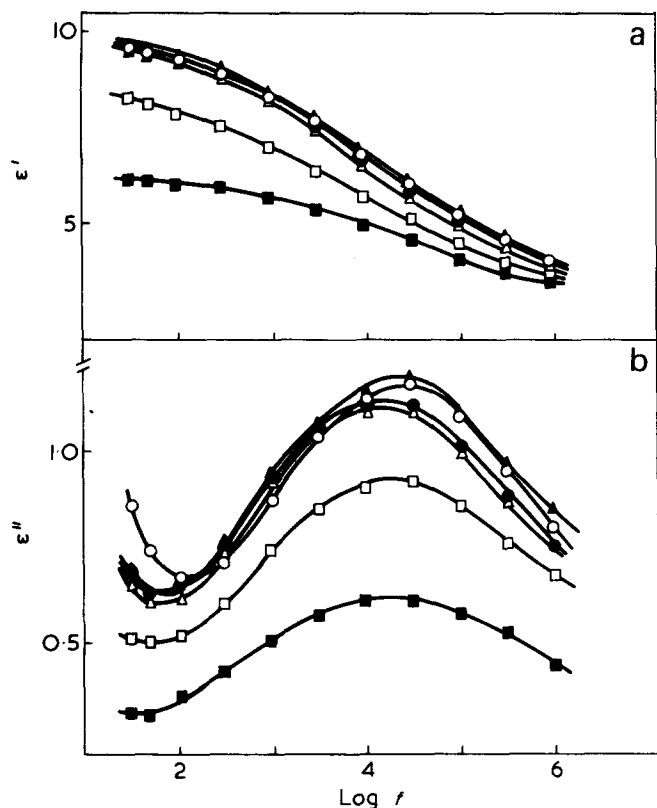


Figure 3 Frequency dependences of  $\epsilon'$  and  $\epsilon''$  at 110°C for PVC films decomposed at 190°C in the air oven. Time of decomposition:  $\circ$ , 0;  $\bullet$ , 10;  $\triangle$ , 30;  $\blacktriangle$ , 40;  $\square$ , 60;  $\blacksquare$ , 180 min

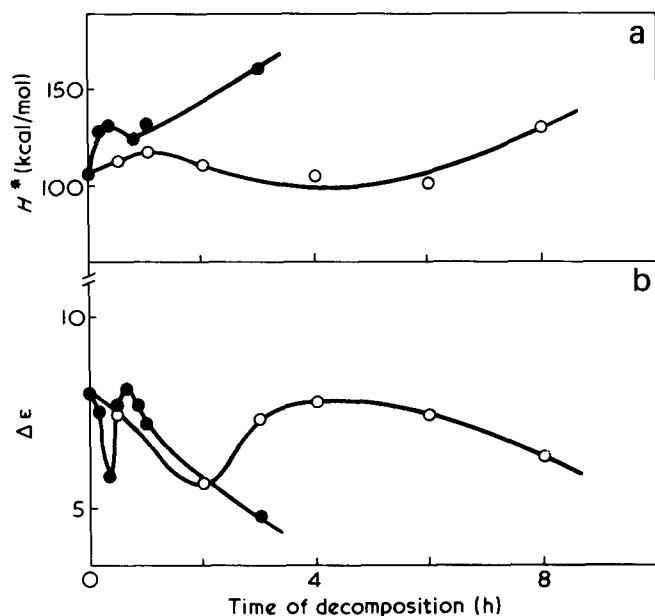


Figure 4 (a) Change of apparent activation energy,  $H^*$  ( $\alpha$ relaxation process) with the progress of thermal decomposition.  $\circ$ , Decomposed at 150°C;  $\bullet$ , decomposed at 190°C. (b) Change of  $\Delta\epsilon$  at 110°C with the progress of thermal decomposition.  $\circ$ , Decomposed at 150°C;  $\bullet$ , decomposed at 190°C

In order to clarify the behaviour of the polar groups in PVC, the value of  $\Delta\epsilon = \epsilon_0 - \epsilon_\infty$  as a magnitude of the dielectric absorption ( $\epsilon_0$  and  $\epsilon_\infty$  are low and high frequency limiting values of  $\epsilon'$ ) was determined from the Cole circular arc plots<sup>18</sup>. The value of  $\Delta\epsilon$ , here, is independent of the frequency and proportional to  $N\mu^2/kT$ , as shown in Fröhlich's formula<sup>19</sup> ( $\mu$  is the mean dipole moment;  $N$ , the concentration of dipoles;  $k$ , Boltzmann's constant;  $T$ , the absolute

temperature). The time dependence of  $\Delta\epsilon$  in the thermal decomposition process is shown in Figure 4b, which shows the  $\alpha$  absorptions for the films decomposed at 150°C and 190°C. The value of  $\Delta\epsilon$  in both cases decreases in the initial stage of the decomposition, then increases and again decreases after reaching a maximum. The rate of change in  $\Delta\epsilon$  with the decomposition at 190°C is greater than that for those decomposed at 150°C.

At the initial stage of the thermal decomposition of PVC, the predominant reaction is known to be the dehydrochlorination which is accompanied by the formation of a series of conjugated double bonds<sup>4-9</sup>. For the purpose of finding the change in number of conjugated double bonds and the carbonyl groups of PVC during the thermal decomposition, the absorbance at 1600 and 1725  $\text{cm}^{-1}$  arising from the conjugated double bonds and the carbonyl groups was measured by i.r. spectroscopy, and these results are shown in Figures 5a and 5b. Figure 5a shows that the conjugated double bonds increase at the initial stage of the decomposition. From this fact and that  $H^*$  increases at the initial stage, it can be considered that the decrease of  $\Delta\epsilon$  in the initial stage corresponds to the decrease of the molecular mobility caused by the formation of polyene sequences.

At the second stage, the decrease of the absorbance due to the conjugated double bonds and the increase of the absorbance due to the carbonyl groups take place at the same time as shown in Figures 5a and 5b. It has been

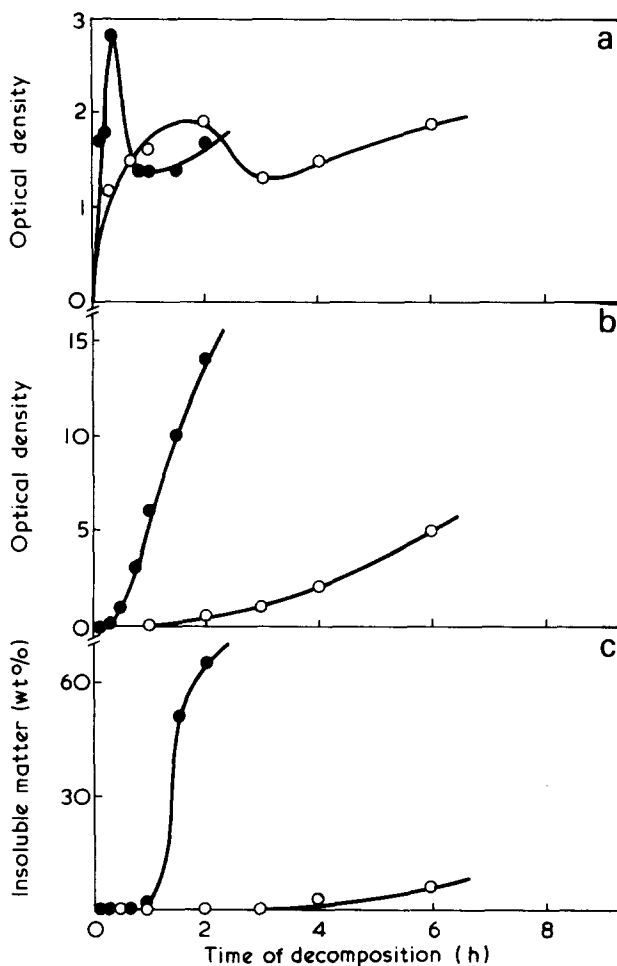


Figure 5 (a) Change of polyene absorption intensity (1600  $\text{cm}^{-1}$ ) with the progress of thermal decomposition. (b) Change of carbonyl absorption intensity (1725  $\text{cm}^{-1}$ ) with the progress of thermal decomposition. (c) Formation of insoluble compounds in the thermal decomposition of PVC films.  $\circ$ , Decomposed at 150°C;  $\bullet$ , decomposed at 190°C

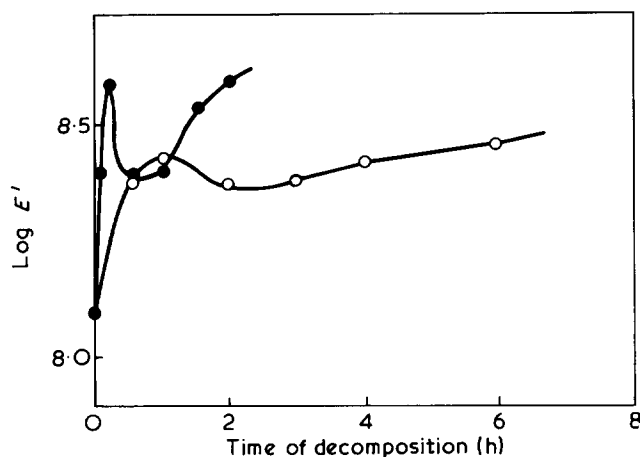


Figure 6 Change of elastic modulus,  $E'$ , (at 110°C and at 110 Hz) by thermal decomposition. ○, Decomposed at 150°C; ●, decomposed at 190°C

reported that polyene sequences derived from the decomposition are shorter in the presence of oxygen than in its absence<sup>4,6,9</sup>. Therefore, it is suggested that the deformation of polyene sequences caused by oxidation takes place at the second stage. Further,  $H^*$  decreases at this stage in the decomposition as shown in Figure 4a. From these facts, it is considered that the segmental motion restricted in the initial stage is restored temporarily by the deformation of polyene sequences caused by oxidation. The increase of  $\Delta\epsilon$  at the second stage, therefore, is considered to correspond to the increase of chain mobility attributed to the deformation of polyene sequences caused by oxidation.

In order to examine the decomposition process of the final stage, a portion of the decomposed sample was taken and again dissolved in THF; the solution was then filtered and the residue was dried and weighed. The time dependence of the insoluble matter, as shown in Figure 5c, indicates that at 190°C crosslinking commences about 50 min after the onset of decomposition and that at 150°C, it commences about 3 h after the onset, as observed by Collins and Krier<sup>3</sup>. Furthermore, it was found that the  $T_g$  of the samples in the final stage above 81°C is greater than that of the original sample (77°C), and that  $H^*$  increases at the final stage as shown in Figure 4a. These findings support the above observation of the formation of crosslinks in the final stage. Since the segmental motion is restricted by the crosslinks, the decrease of  $\Delta\epsilon$  in the final stage can be considered to correspond to the increase of crosslinks.

It is also possible to obtain information on the molecular mobilities from the viscoelastic properties<sup>20-22</sup>. In order to examine the rigidity of the sample, the dynamic modulus,  $E'$ , was measured by a viscoelastic spectrometer at 110°C and at 110 Hz, for the decomposed PVC samples, and is shown in Figure 6 as a function of the time of decomposition. Log  $E'$  changes in three stages as observed for the case of  $H^*$  in Figure 5a. This result is evidence in support of the consideration related to the dielectric properties.

#### ACKNOWLEDGEMENT

The authors wish to thank Professor H. Yamamura, Hiroshima University, for his valuable guidance and discussion in this research.

#### REFERENCES

- 1 Minematsu, Y. Kanbara, N. and Kobayashi, T. *Kobunshi Kagaku* 1959, 16, 724
- 2 Ouchi, I. *J. Polym. Sci. (A)* 1965, 3, 2685
- 3 Collins, E. A. and Krier, C. A. *J. Appl. Polym. Sci.* 1966, 10, 1573
- 4 Onozuka, M. and Ashahina, M. *J. Macromol. Sci. (C)* 1969, 3, 235
- 5 Kelen, T., Balint, G., Galambos, G. and Tüdös, F. *Eur. Polym. J.* 1969, 5, 597
- 6 Braun, D. and Bender, R. F. *Eur. Polym. J. Suppl.* 1969, p 269
- 7 Guyot, A. and Bert, M. *Polym. Prepr.* 1971, 12, 303
- 8 Anderson, K. B. and Sorvik, E. M. *J. Polym. Sci. (C)* 1971, 33, 247
- 9 Morikawa, T. *Bull. Osaka Munic. Tech. Res. Inst.* 1971, 48, 1
- 10 Henson, J. H. L. and Hybart, F. J. *J. Appl. Polym. Sci.* 1972, 16, 1653
- 11 Bataille, P. and Van, B. T. *J. Polym. Sci. (A-1)* 1972, 10, 1097
- 12 Kisbényi, M. and Hedvig, P. *Prepr. IUPAC Int. Symp. Macromol. Chem.* 1969, 5, 163
- 13 Hedvig, P. *J. Polym. Sci. (C)* 1971, 33, 315
- 14 Reddish, W. *Soc. Chem. Ind. Monogr.* 5 1959, p 138
- 15 Yamafuji, K. *J. Phys. Soc. Japan* 1960, 15, 2295
- 16 Tanaka, K. *Rep. Progr. Polym. Phys. Japan* 1962, 6, 138
- 17 Ishida, Y. *J. Polym. Sci. (A-2)* 1969, 7, 1835
- 18 Cole, R. H. and Cole, K. S. *J. Chem. Phys.* 1941, 9, 341
- 19 Fröhlich, H. 'Theory Dielectrics', 2nd Edn, Oxford Univ. Press, Oxford, 1958
- 20 Sommer, W. *Kolloid Z.* 1959, 167, 97
- 21 Takayanagi, M. et al. *Rep. Progr. Polym. Phys. Japan* 1963, 6, 121
- 22 Kinjo, N. and Nakagawa, T. *Polym. J.* 1973, 4, 143

# Thermal decomposition of a vinyl chloride/vinyl acetate copolymer

Shadi L. Malhotra, Jean Hesse\* and Louis-P. Blanchard

Département de Génie Chimique, Faculté des Sciences, Université Laval, Québec, G1K 7P4, Canada  
(Received 1 May 1974)

The thermal decomposition of an 85% vinyl chloride/15% vinyl acetate copolymer and its different fractions obtained by precipitation was studied by the thermogravimetric scanning (t.g.s.) technique. Analyses of the t.g.s. thermograms revealed the existence of two major steps in the decomposition reaction. The first occurs between 180 and 380°C during which hydrogen chloride and hydrogen acetate are given off. In the second, which occurs between 420 and 480°C, degradation of the carbon chain takes place. Both the order of reaction and the activation energy were found to be dependent on the molecular weight of the copolymer and on the heating rate at which the experiments were carried out. Analyses of the samples carried out by gel permeation chromatography (g.p.c.) after each decomposition revealed that, besides the two steps mentioned above, yet another step, viz. crosslinking, may be taking place at 180°C or below where the weight loss of copolymer is too small to be detected by t.g.s. The process of crosslinking, however, may take place at other temperatures as well. A higher degree of crosslinking has been associated with a higher acetate content in the copolymer. A comparison of g.p.c. results with those obtained by nuclear magnetic resonance spectra showed that, out of the three steric configurations of the copolymer, syndiotactic sequences are least resistant to thermal treatment followed in order by heterotactic and isotactic sequences.

## INTRODUCTION

Studies of the thermal decomposition of poly(vinyl chloride) (PVC)<sup>1</sup> and of poly(vinyl acetate) (PVAC)<sup>2</sup> have yielded very interesting results. The respective decompositions are known to begin around 180°C with the elimination of hydrogen chloride (HCl) from PVC by a free radical mechanism and of hydrogen acetate (HAC) from PVAC by a molecular mechanism. The remaining products in both cases are conjugated residues which can undergo at much higher temperatures (>400°C) further decomposition by carbon chain scissions.

As for the thermal decomposition of vinyl chloride/vinyl acetate copolymers P(VC/VAC), the first investigations reported in the literature are those of Lehrle and Robb<sup>3</sup> who showed that the volatile decomposition products (viz. HCl and HAC) are given off in proportions corresponding to the amounts of each monomer in the copolymers. Vymazal<sup>4</sup> who studied the elimination of HCl from an 87% VC copolymer between 143 and 164°C reports an overall activation energy of 27 kcal/mol in air and 31 kcal/mol in nitrogen.

In a recent study, Grassie *et al.*<sup>5</sup> have shown that once the reaction has been initiated neither HCl nor HAC is given off preferentially. Their studies on the thermal decomposition of these copolymers by pyrotechnique analysis over the full range of compositions showed that copolymers having vinyl acetate contents of 40 to 50% were indeed the least stable. While examining the development of conjugation along the polymer chain, they also found that for a given rate of decomposition, the conjugation sequences were longest for copolymers having vinyl acetate contents of 20 to 30%.

Little is reported in the literature on the thermal decomposition of P(VC/VAC) copolymers by the thermogravi-

metric scanning (t.g.s.) technique. Furthermore little interest seems to have been shown in the second step of this reaction, namely, the thermal decomposition of poly-conjugated chains formed by the acid eliminating step. This is why a t.g.s. investigation<sup>6</sup> was undertaken in this laboratory to elucidate kinetic aspects of the two-step process responsible for the thermal decomposition of an 85:15 wt % VC/VAC copolymer and some of its fractions with differing molecular weights. Changes in distribution resulting from thermal effects were also studied by gel permeation chromatography (g.p.c.). The results of these studies form the subject of this communication.

## EXPERIMENTAL

### Materials

The vinyl chloride/vinyl acetate copolymer (VS-814) used in this work was kindly provided by the Shawinigan Chemicals Division of the Gulf Oil Company in Canada. The product had been synthesized by suspension polymerization and contained 15% by wt of vinyl acetate. This material was purified by total precipitation from a tetrahydrofuran (THF) solution using distilled water as the precipitating agent. It was then dried at 60°C under vacuum prior to its use in the decomposition study. Fractions with differing molecular weights were also obtained by partial precipitation from a 1% by wt solution of the copolymer in THF. The precipitations were carried out in a large pear-shaped separatory funnel by adding progressively small quantities of distilled water to the well agitated solution. Before withdrawing a precipitated phase, the total solution was allowed to settle for at least 24 h in order to favour equilibrium exchanges between the upper solution and the lower precipitated phase. After drying, each fraction was examined by g.p.c.<sup>7</sup>

\* Present address: Villa Société Nationale de Pétroles Aquitaines (6), 64370 Arthez-de-Béarn, France.

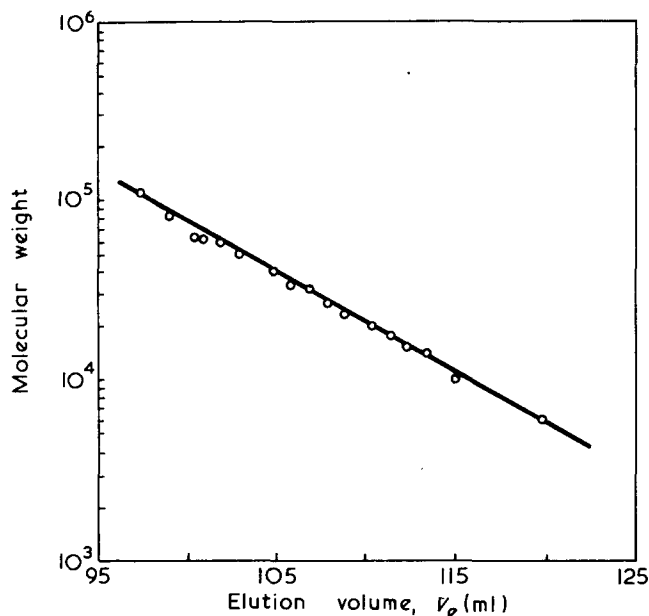


Figure 1 G.p.c. calibration curve prepared under normal operating conditions with several P(VC/VAC) copolymer fractions

#### Apparatus

The decompositions were carried out with a Perkin-Elmer (model TGS-1) thermobalance. It was operated at three different heating rates (1.25, 5.0 and 20.0°C/min), under a dynamic (27 ml/min) nitrogen atmosphere. The samples used weighed approximately 1.0 mg.

Molecular weight distribution analyses of the P(VC/VAC) copolymers, both before and after the decompositions, were carried out with a Waters Associates (model 200) gel permeation chromatograph, operated at a constant temperature of  $25 \pm 0.5^\circ\text{C}$ .

The separating system, consisting of four 4 ft (1.22 m) long columns connected in series and packed with cross-linked polystyrene gels having nominal permeabilities (by the Waters method) of  $1.0 \times 10^6$ ,  $1.5 \times 10^5$ ,  $3.0 \times 10^3$  and  $250 \text{ \AA}$  respectively, was fed with solvent, THF degassed with nitrogen, at a controlled flow rate of 1 ml/min. The concentration of all g.p.c. sample solutions was adjusted to 0.125% by wt in order to render negligible 'concentration effects' on the peak position in the chromatograms. The P(VC/VAC) copolymer fractions, characterized by membrane and vapour pressure osmometry as well as light scattering, were used to plot a g.p.c. calibration curve ( $\log M$  versus elution volume,  $V_e$ ) shown in Figure 1. Molecular weight calculations were computed following Smith's method.

#### Component splitting of the g.p.c. curves

The raw g.p.c. curves were broken down into three distinct components (L, M and N shown in Figure 2a) by the method described below for the particular case of the P(VC/VAC) ( $M_n = 2.8 \times 10^4$ ) copolymer. The relative weights of the above mentioned copolymer as a function of the elution volume for decompositions carried out during 50 min periods at different temperatures are summarized in Table 1. The results show that between 20 and 180°C the weight loss due to decomposition is negligible. Furthermore there is little or no change in the relative weights of the samples treated in this temperature range when compared to those of the initial copolymer. On heating them at 230°C for a similar period of 50 min, over and above the 7% weight

loss, a significant change in the relative weights was observed. At the lower elution volumes (95 to 110 ml), these show a decrease whereas at higher elution volumes (115 to 130 ml), there is a corresponding increase in the relative weights. If one subtracts from the initial distribution curve of the undecomposed polymer, the distribution of any subsequently decomposed polymer, one can readily visualize the changes brought about by the decomposition of the higher molecular weight species. This is shown in Figure 2b where the area marked L in the initial undecomposed copolymer is found to disappear at 230°C, while a corresponding area marked L' appears at a lower elution volume. Figure 2c shows these areas (L and L') in the form of distributions where both meet at a common elution volume of 111 ml. In reality, however, some overlapping is believed to

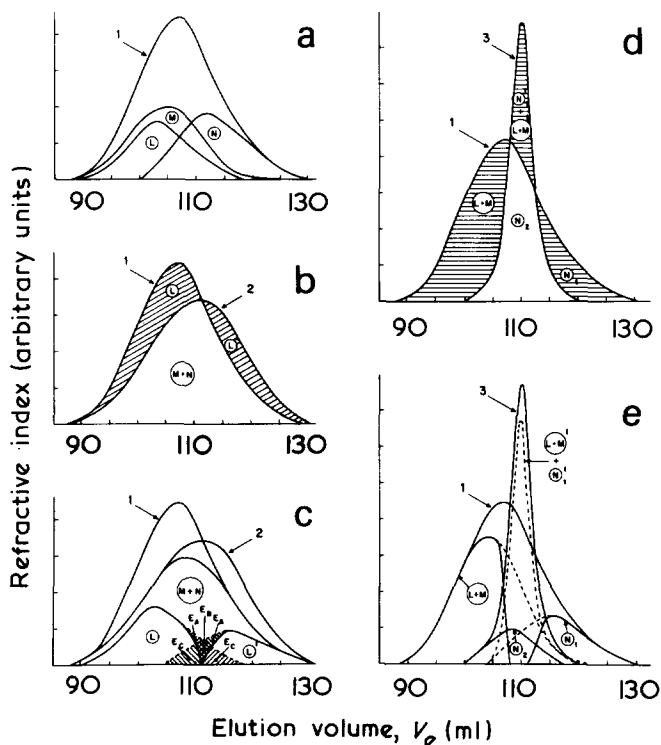


Figure 2 (a) G.p.c. distribution of a P(VC/VAC) copolymer ( $M_n = 2.80 \times 10^4$ ) and distribution tracings of its three components. (b) to (e) G.p.c. distributions of the same copolymer before and after isothermal treatment (50 min periods at various temperatures) plus distribution tracings of components (undecomposed, decomposed and crosslinked counterparts). 1, 20°C; 2, 230°C; 3, 330°C

Table 1 Relative weights (arbitrary units) of decomposed and undecomposed copolymer P(VC/VAC) molecular weight  $M_n = 2.80 \times 10^4$  at different elution volumes (decomposition time = 50 min)

Elution volume (ml)	True weight loss (%)				
	0.0 at 20°C	0.44 at 130°C	0.73 at 180°C	7.0 at 230°C	44.0 at 280°C
90	0.18	0.25	0.18	0.19	—
95	1.28	1.31	1.21	0.80	—
100	3.62	3.72	3.53	2.00	—
105	5.33	5.36	5.32	3.60	1.0
110	4.97	4.82	4.95	4.80	9.8
115	2.84	2.90	2.95	4.00	1.0
120	1.28	1.26	1.28	2.20	—
125	0.43	0.33	0.40	0.80	—
130	0.07	0.05	0.09	0.10	—
Summation of relative weights	20.00	20.00	19.91	18.49	11.8

take place between the two distributions as shown in the Figure by the broken lines. The tracing of these lines is based essentially on the overall shape of the curves, be they broad, Gaussian or other in distribution; and they are at best only a first approximation of the true situation. This correction, when applied to component L of the undecomposed polymer results in the addition of areas  $E_A$ ,  $E_B$  and  $E_C$  to its distribution. A corresponding compensation in the  $L'$  distribution is then necessary and is made by using the same areas. Figure 2d illustrates two g.p.c. distributions, one obtained with an undecomposed sample, the other after the sample has been heated at 280°C for 50 min. The areas marked (L + M) and  $N_1$  in the original distribution show up in the second as the alternate areas  $(L + M)'$  and  $N_1'$ . This would mean that the higher molecular weight portions (L + M) of the original distribution are decomposed into lower molecular weight species  $(L + M)'$ , while a lower molecular weight portion  $N_1$  is altered to form a higher molecular weight one  $N_1'$  by a process believed to involve crosslinking. Species  $N_1$  could possibly follow an alternative route and decompose completely into volatile products: however, as additional experimental data will show, this is not believed to be the case. Rather, the possibility of crosslinking appears to be the more logical choice.

Figure 2e shows these areas in the form of distributions. As can be seen, the (L + M) and  $N_1$  distributions show abrupt endings at elution volumes of 108 and 111 ml, respectively. Unlike the situation shown in Figure 2e, there are no clear guide-lines to indicate how these two distributions might be overlapping; therefore, the broken line extensions based on the Gaussian nature of the overall curves were made by simply tracing the mirror images of the (L + M) and  $N_1$  distributions. The summation of these two distributions when subtracted from the area under the undecomposed copolymer curve yields a fourth distribution  $N_2$ , which has remained unchanged until now. Distributions  $N_1$  and  $N_2$  have been considered here as forming a part of a single distribution N rather than introducing a fourth distribution O. This has enabled the number of components to be kept to three, L, M and N, in order that they might be compared with the three possible steric forms of the copolymer. Subtracting the distribution assigned to component L from that of (L + M) yields M, while subtracting that of the (L + M) component from the distribution of the undecomposed copolymer yields an area assignable to N which is also the

sum of the  $N_1$  and  $N_2$  components. If one then subtracts the distribution of  $N_2$  from the distribution of a sample decomposed at 280°C, that of  $(L + M)' + N_1'$  poses no problem to trace.

#### Nuclear magnetic resonance (n.m.r.) spectra

N.m.r. analyses were carried out on several P(VC/VAC) copolymer samples at the Canadian 220 MHz NMR Centre in Sheridan Park, Ontario. Spectra were obtained using solutions of the copolymers (15% by wt) in dichlorobenzene at 100°C, with hexamethyldisiloxane as internal standard.

#### RESULTS AND DISCUSSION

The changes observed in components L, M and N when samples of the initial copolymer were heated for 50 min periods at different temperatures are summarized in Table 2. It is interesting to note that the molecular weights,  $M_n$  and  $M_w$ , of component L undergo a five-fold drop in value, while its weight loss due to decomposition attains but 26%. Moreover, the polydispersity of the decomposed component does not change significantly. These observations suggest that one of the initial processes responsible for lowering of the molecular weight must be that of random chain scissions. Once these have made their contribution some other mechanism of decomposition invariably takes over. The process whereby the initial polydispersity of the polymeric species is unaffected by decomposition and where changes occur only in the weight of the sample has been explained in detail by Berlin and Yenikolopyan<sup>9</sup> on the basis of complete and rapid depolymerization of the chains. There is yet another condition attached to this depolymerization process: this demands that no abrupt changes take place in the molecular weight of the decomposing species. In the present case, however, the molecular weight of the copolymer did in fact change from  $6.05 \times 10^4$  to  $1.32 \times 10^4$ . It is therefore difficult to say if this observation should be attributed entirely to the process of random scissions or in part to a chain depolymerization process.

On heating the copolymer at 280°C, component M disappears and is replaced by a new distribution  $M'$  having a lower molecular weight and a lower polydispersity. Lowering of both the molecular weight and the polydispersity of component M, coupled with its weight loss attaining between 43 and 90%, suggests that chain depolymerization

Table 2 Components of the initial P(VC/VAC) copolymer, molecular weight  $\bar{M}_n = 2.8 \times 10^4$  and their decomposed counterparts at different temperatures and times

	Undecomposed components							S	T
	L	(L + M)	M	[ $N_1$ + $N_2$ = N]					
$\bar{M}_w \times 10^{-4}$ (g.p.c.)	6.05	6.11	6.10	1.18	2.67	1.64	3.94	0.89	
$\bar{M}_n \times 10^{-4}$ (g.p.c.)	3.66	3.40	3.24	0.78	2.15	0.98	2.80	0.53	
Polydispersity	1.65	1.80	1.88	1.51	1.24	1.67	1.41	1.68	
Decomposition time (min)	50	50	50	50	50	50	120	240	
Temperature (°C)	230	280	280	280	280	280	180	180	
True weight loss, $\alpha$ (%)	7.0	44.0	44.0	44.0	44.0	44.0	1.29	1.41	
	Decomposed counterparts							S'	T'
	L'	(L + M)'	M'	[ $N_1'$ + $N_2'$ = N']					
$\bar{M}_w \times 10^{-4}$ (g.p.c.)	1.23	2.01	2.01	2.01	—	—	34.6	15.2	
$\bar{M}_n \times 10^{-4}$ (g.p.c.)	0.78	1.88	1.88	1.88	—	—	26.9	12.6	
Polydispersity	1.60	1.07	1.07	1.07	—	—	1.29	1.20	

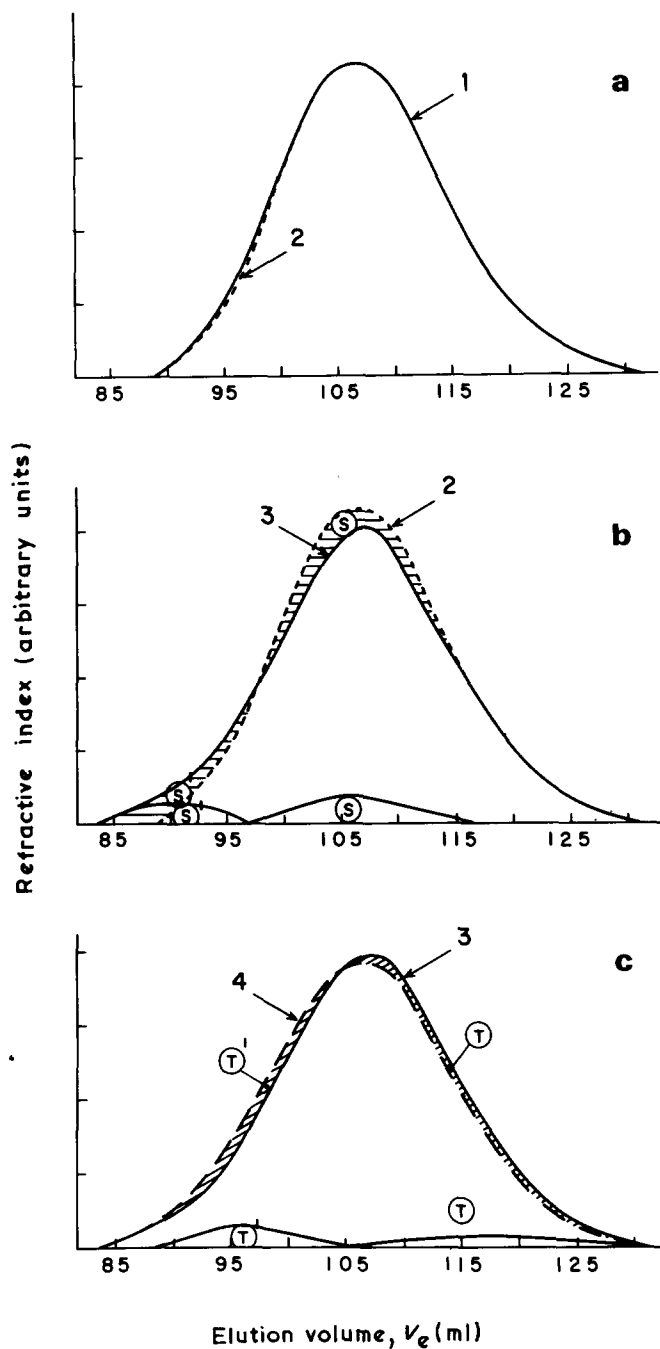


Figure 3 (a) to (c) G.p.c. distributions of a P(VC/VAC) copolymer ( $\bar{M}_n = 2.80 \times 10^4$ ) before and after isothermal treatment (various periods at 180°C) plus distribution tracings of the components (decomposed and crosslinked counterparts). 1, 0; 2, 50; 3, 120; 4, 240 min

is very much the predominant process in this reaction. Estimation of the weight loss range for M is based on results given in Table 2 which show that at 280°C the 44% overall weight loss observed in the copolymer comes primarily from components (L + M). The lower weight loss limit (43%) in M is based on the assumption that component L has been completely volatilized, whereas the upper limit (90%) corresponds to the 26% weight loss of L alone recorded on heating the copolymer at 230°C. A part, N<sub>1</sub>, of component N may also undergo changes without weight loss when the copolymer is heated at 280°C for 50 min. As suggested earlier in the text, crosslinking may be responsible for the resulting changes observed. If this assumption is valid, the number of chains should decrease and their lengths should

increase thereby affecting the polydispersity of the resulting crosslinked component.

In all probability, one should expect the polydispersity to decrease. The change observed (from 1.5 in L to 1.07 in L') supports the concept of crosslinking which is put forth here.

Figures 3a to 3c illustrate the changes observed in the g.p.c. curves of the initial P(VC/VAC) copolymer when it is heated at 180°C for periods of 50, 120 and 240 min. In Figure 3a, it is evident that the thermal treatment of the sample at 180°C during a 50 min period does not affect its g.p.c. distribution; however, on heating it for 120 min, a part of the lower molecular weight species S disappears while higher molecular weight ones S' are found to appear. After 240 min at the same temperature another part T likewise disappears and is replaced by the higher molecular weight species denoted by T'. In both cases the thermal treatment was accompanied by a weight loss on only 1.3 and 1.4%, respectively. It seems evident that intermolecular crosslinking of the conjugated polymeric species yield higher molecular weight products. The decrease in polydispersity observed when components S and T undergo crosslinking again adds support to the existence of such a process.

One should note that the copolymer species which are most susceptible to crosslinking are those that are situated in the relatively lower molecular weight range ( $0.9 \times 10^4$ , the approximate molecular weight of components N<sub>1</sub> and T, and  $4 \times 10^4$ , that of component S). In order to verify this observation a study was made on the decomposition of two fractions, C and J, of this copolymer<sup>7</sup> having molecular weights ( $\bar{M}_n$ ) of  $6.05 \times 10^4$  and  $3.18 \times 10^4$  respectively.

Figures 4a to 4d and Table 3 summarize the results obtained for the decomposition of fraction C which was heated at 180°C for different periods of time. In Figure 4a are shown the g.p.c. curves of the initial undecomposed sample and of samples treated at 180°C for 50, 120 and

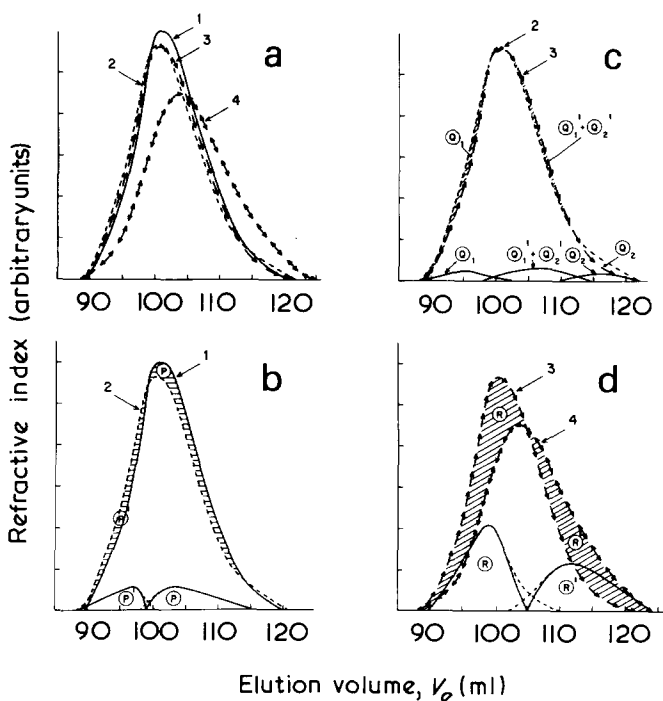


Figure 4 (a) G.p.c. distributions of P(VC/VAC) copolymer fraction C ( $\bar{M}_n = 6.05 \times 10^4$ ) before and after isothermal treatment (various periods at 180°C); (b) to (d) distribution tracings of components (undecomposed, decomposed and crosslinked counterparts). 1, 0; 2, 50; 3, 120; 4, 240 min

**Table 3** Components of fraction C, ( $\bar{M}_n = 6.05 \times 10^4$ ) of the initial copolymer P(VC/VAC) and their decomposed counterparts at different times

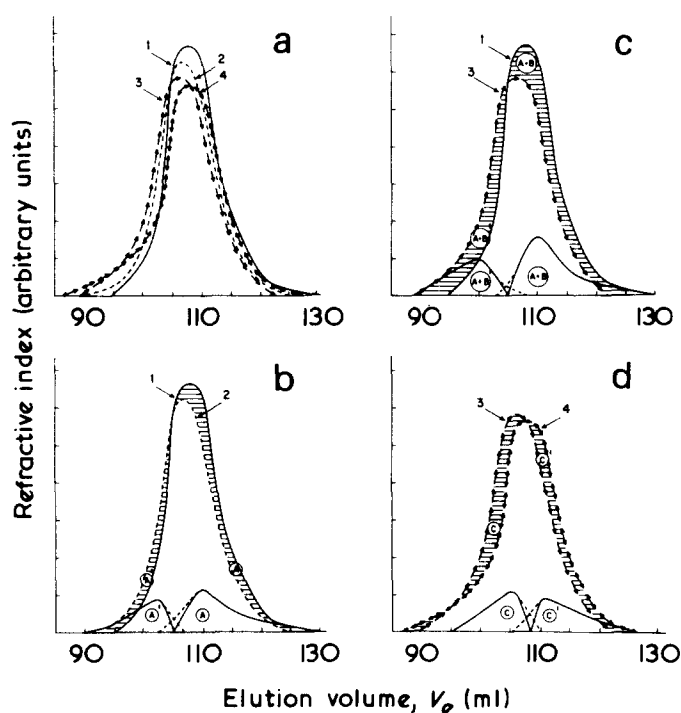
	Undecomposed components			
	P	Q <sub>1</sub>	Q <sub>2</sub>	R
$\bar{M}_w \times 10^{-4}$ (g.p.c.)	4.76	15.80	0.87	9.86
$\bar{M}_n \times 10^{-4}$ (g.p.c.)	3.77	13.80	0.82	8.00
Polydispersity	1.26	1.14	1.06	1.23
Decomposition times (min)	50	120	120	240
Temperatures (°C)	180	180	180	180
True weight loss, $\alpha$ (%)	5.0	5.0	5.0	8.0
	Decomposed counterparts			
	P'	Q' <sub>1</sub> + Q' <sub>2</sub>	R'	
$\bar{M}_w \times 10^{-4}$ (g.p.c.)	17.0	4.04	1.89	
$\bar{M}_n \times 10^{-4}$ (g.p.c.)	14.7	3.21	1.30	
Polydispersity	1.16	1.26	1.46	

240 min, respectively. It is difficult to draw definite conclusions from this Figure because, from all appearances, the first three g.p.c. curves shown (viz. that of the initial sample and those of the samples treated for 50 and 120 min respectively) appear to be very much the same. If one attempts to study the changes that occur at each step, however, one observes that during the first 50 min, a component P having a molecular weight of  $4.76 \times 10^4$  has been converted to a new component P' of higher molecular weight ( $\bar{M}_w = 17.0 \times 10^4$ ). On heating the sample for an additional 70 min, a component Q<sub>1</sub> ( $\bar{M}_w = 15.8 \times 10^4$ ) decomposes and a lower molecular weight component Q'<sub>1</sub> ( $\bar{M}_w = 2.01 \times 10^4$ ) appears. At the same time, a component Q<sub>2</sub> ( $\bar{M}_w = 0.87 \times 10^4$ ) undergoes crosslinking to yield Q'<sub>2</sub> ( $\bar{M}_w = 2.01 \times 10^4$ ). This shows the complexities involved in attempting to study the kinetics of this reaction, where processes take place involving random scissions, chain depolymerizations, crosslinking as well as the decomposition of conjugated residues at higher temperatures ( $>400^\circ\text{C}$ ). Figure 4d shows the changes that occur when sample C is treated at  $180^\circ\text{C}$ , first for 120 and then for 240 min. Though no additional weight loss is observed, a component R with a molecular weight of  $9.86 \times 10^4$  is replaced in the 240 min treatment by a lower molecular weight component R' ( $\bar{M}_w = 1.89 \times 10^4$ ) arising most probably from a random scission process.

Figures 5a to 5d summarize the results obtained with fraction J. Here as in the case of fraction C, one can see that the distributions, when compared as a group, appear as a cluster (Figure 5a); however, when these are considered on an individual basis, they show trends similar to those observed with the higher molecular weight fraction C. The principal difference appears to be in the greater extent of crosslinking that takes place in the lower molecular weight fraction J. As shown in Figures 5b and 5c, on heating fraction J at  $180^\circ\text{C}$  for 50 min, component A is replaced by a new component A' of higher molecular weight whereas on heating it at the same temperature but for 120 min, components (A + B) give rise to a new still higher molecular weight component (A + B)' as a result of intermolecular crosslinking. The changes that occur during the latter 70 min, involving the formation of B' from B are not shown in Figure 5 but the analytical results are listed in Table 4.

The changes that occur to fraction J in the time interval of 120 to 240 min, involve a decrease in molecular weight for species C due, in all probabilities, to random scissions because the polydispersity of the species is found to increase while no additional weight loss is observed during the period.

Figures 6a to 6c show the changes that take place in g.p.c. distributions based on studies of the decomposition of fraction J at 180 and  $230^\circ\text{C}$  for periods of 50 min. Here, as before, the lower molecular weight components X and (X + Y) are replaced by the higher molecular weight components X' and (X + Y)' as a result of intermolecular crosslinking.


**Figure 5** (a) G.p.c. distributions of P(VC/VAC) copolymer fraction J ( $\bar{M}_n = 3.18 \times 10^4$ ) before and after isothermal treatment (various periods at  $180^\circ\text{C}$ ); (b) to (d) distribution tracings of components (undecomposed, decomposed and crosslinked counterparts). 1, 0; 2, 50; 3, 120; 4, 240 min

**Table 4** Components of fraction J, ( $\bar{M}_n = 3.18 \times 10^4$ ) of the initial copolymer P(VC/VAC) and their decomposed counterparts at different times and temperatures

	Undecomposed components				
	X	(X + Y)	A	B	C
$\bar{M}_w \times 10^{-4}$ (g.p.c.)	1.62	2.26	1.81	2.00	5.49
$\bar{M}_n \times 10^{-4}$ (g.p.c.)	1.09	1.49	1.13	1.75	4.91
Polydispersity	1.49	1.52	1.60	1.15	1.12
Decomposition times (min)	50	50	50	120	240
Temperatures (°C)	180	230	180	180	180
True weight loss, $\alpha$ (%)	6.0	9.0	6.0	7.0	7.0
	Decomposed counterparts				
	X'	(X + Y)'	A'	B'	C'
$\bar{M}_w \times 10^{-4}$ (g.p.c.)	8.00	15.2	8.36	15.7	1.37
$\bar{M}_n \times 10^{-4}$ (g.p.c.)	6.55	9.15	6.76	12.8	0.97
Polydispersity	1.22	1.66	1.24	1.23	1.40



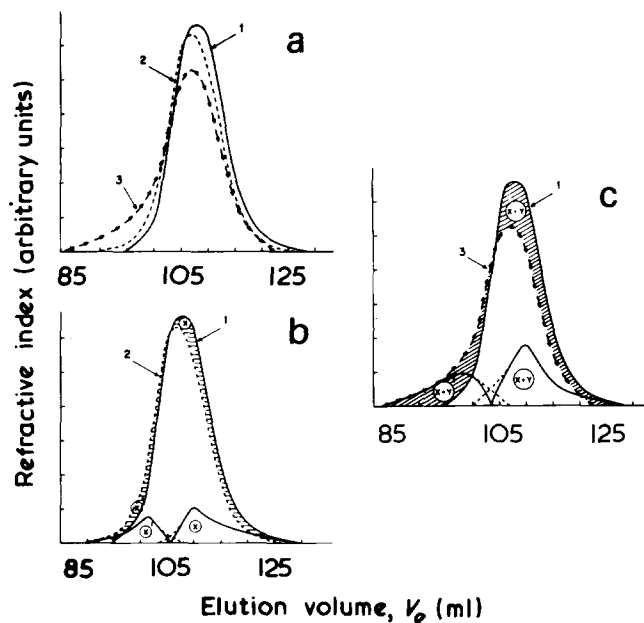


Figure 6 (a) G.p.c. distributions of P(VCl/VAc) copolymer fraction J ( $M_n = 3.18 \times 10^4$ ) before and after isothermal treatment (50 min periods at various temperatures); (b) and (c) distribution tracings of components (undecomposed and crosslinked counterparts). 1, 20°; 2, 180°; 3, 230°C

The maximum extent of crosslinking observed for these fractions varies between 20 and 24%, the former value being for component (A + B) of fraction J when it is heated for 120 min at 180°C and the latter for component (X + Y) (also of fraction J) when it is heated at 230°C for only 50 min. As mentioned earlier, these values obtained under identical conditions are lower in the case of fraction C, the maximum value not exceeding 8%.

#### Stereoregularity and crosslinking

It has been shown earlier that the lower molecular weight fraction J shows a greater tendency to crosslink than does the higher molecular weight fraction C. Before attempting to study the effect of molecular weight of the copolymer on its tendency to crosslink, it is necessary to establish initially that all of the samples have the same structure because branching as well as the different steric arrangements in the copolymer may influence its mode of decomposition. In order to elucidate these characteristics, the initial copolymer and its two fractions C and J were subjected to n.m.r. spectroscopy.

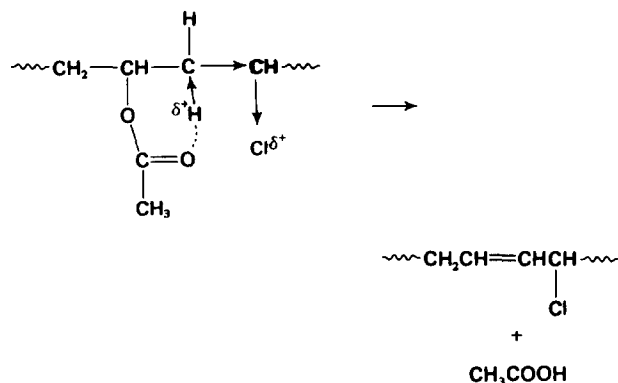
The criterion generally used for the determination of stereoregularity through n.m.r. spectroscopy for a P(VCl/VAc) copolymer is the triplet yielded by the methyl protons of the acetate  $-\text{OCOCH}_3$  group. If one obtains a well resolved triplet, then the areas under the three peaks can easily be computed. These correspond, in ascending order of magnetic field, to the proportions of isotactic, heterotactic and syndiotactic sequences in the sample. In the event that the resolution of the triplet is poor, one can alternatively use the methine protons of the vinyl chloride  $-\text{CHCl}$  units. These yield three pentuplets assigned, in ascending order of magnetic field respectively, to syndiotactic, heterotactic and isotactic sequences. The spectra of the initial copolymer was obtained in order to relate its steric structure with the pattern of its decomposition at different temperatures. Figure 7 shows n.m.r. spectra of the three copolymers. The assignment of the chemical shifts for the protons of the vinyl chloride part of the copolymer

was based on results reported by Heatley and Bovey<sup>10</sup>, that for the protons of the vinyl acetate part, on the work of Bovey and coworkers<sup>11</sup> and that of Ramey and Field<sup>12</sup>. The chemical shifts observed in this work for the VC part agree well with the literature<sup>10</sup>; however, those for the VAc part are at some variance<sup>11,12</sup>. It is not unlikely that the chemical shifts recorded in the lower magnetic field ( $\tau = 4.70$ ) for the methine protons ( $-\text{CH}$ ) of the VAc part of the copolymer and those in the higher magnetic field ( $\tau = 8.40$  and  $8.69$ ) for the methylene protons ( $-\text{CH}_2$ ) are caused by the presence of VC units in the vicinity instead of the VAc units usually present in vinyl acetate homopolymer.

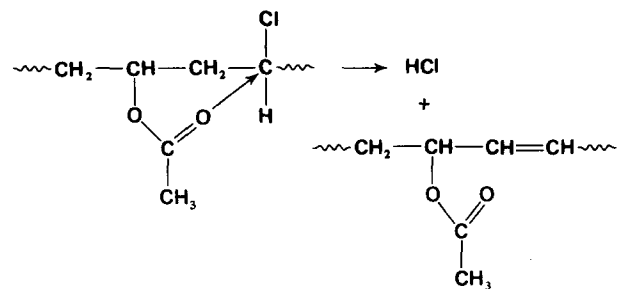
A comparison of the n.m.r. spectra obtained with the C and J copolymer fractions reveals that the percentages of syndiotactic (25%), heterotactic (40%) and isotactic (35%) sequences are essentially the same in both. The acetate content of the lower molecular weight fraction J would seem to be higher than that of the lower molecular weight fraction C. Moreover, there appears to be differences in the proportions and nature of methylene protons ( $\tau = 8.40$  and  $8.69$ ) in the vinyl acetate part of the copolymer. How these differences bring about an increase in the process of crosslinking is not as yet fully understood.

Grassie and coworkers<sup>11</sup> have made suggestions concerning the role played by the chloride and acetate groups in the elimination of acids. These may be represented as follows.

For the elimination of HAC:



For the elimination of HCl:



The inductive effect of the chlorine atoms weakens the C-H bonds of the methylene group and thus facilitates the elimination of acetic acid. Elimination of HCl on the other hand has been attributed to the participation of acetate groups which finds its support from the role of acetic acid as a catalyst in a study reported on by Capon<sup>13</sup> who showed instances where the elimination of small molecules is assisted by the acetate groups. Grassie and coworkers<sup>11</sup> have shown further that vinyl acetate content in the copolymer controls the chain lengths of the conjugated sequences. It was found that in copolymers with a vinyl acetate content of 20 to 30%, the proportion of long conjugated sequences was at a maximum. This might explain the higher degree of

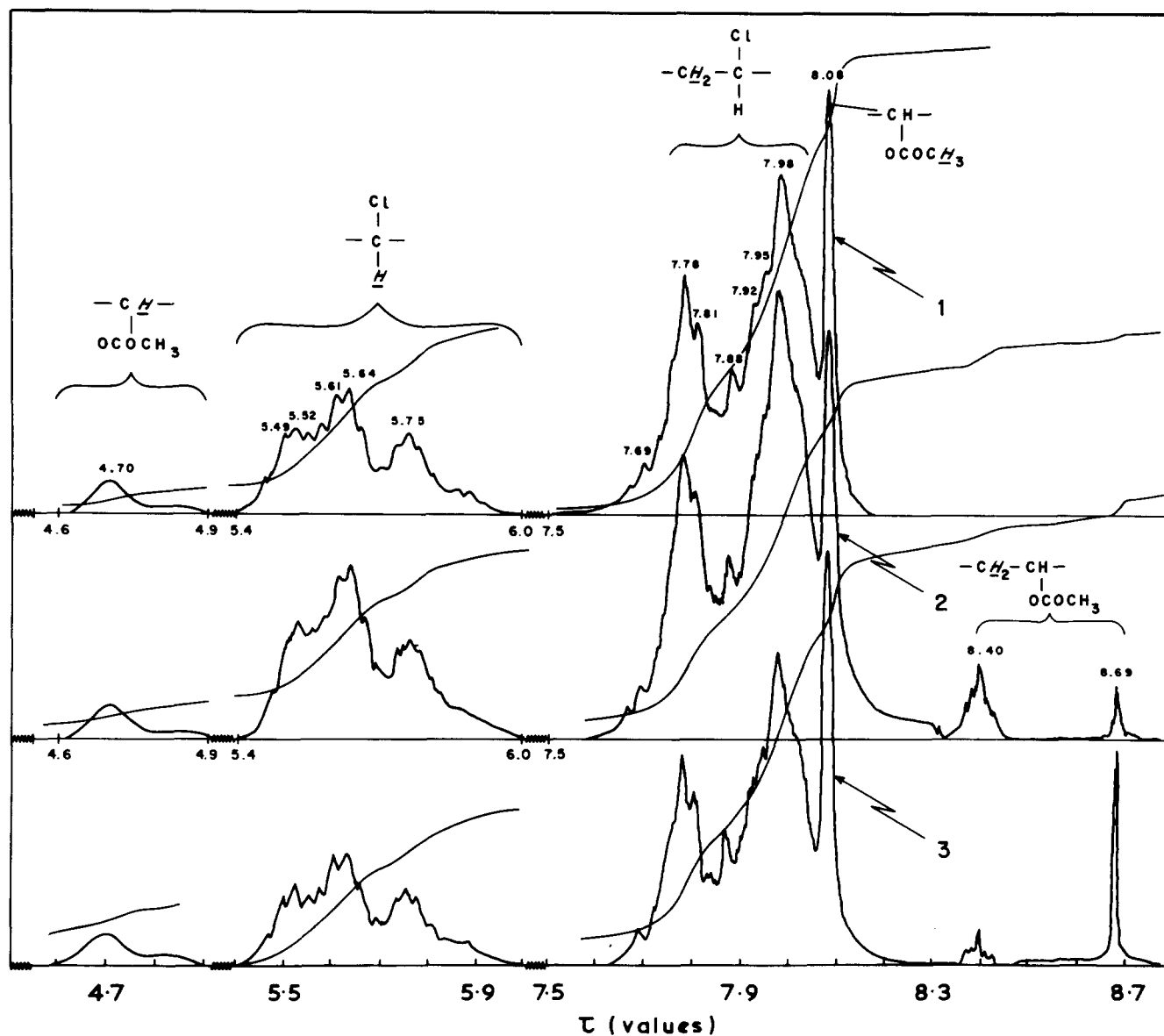


Figure 7 N.m.r. spectra for three P(VCl/VAc) samples. 1, Initial copolymer ( $\bar{M}_n = 2.80 \times 10^4$ ); 2, fraction C ( $\bar{M}_n = 6.05 \times 10^4$ ); 3, fraction J ( $\bar{M}_n = 3.18 \times 10^4$ )

crosslinking observed in the lower molecular weight copolymer J, which carries a higher acetate content.

The n.m.r. spectrum of the unfractionated copolymer is also shown in Figure 7 with the exception of that part situated between  $\tau$  values of 8.10 and 10.00. Based on the integral of the curve produced by the methine protons ( $\tau = 5.40$  and 6.00) of the vinyl chloride units and the specific areas under the three peaks  $\tau = 5.52$ , 5.62 and 5.75, the syndiotactic, heterotactic and isotactic sequence contents of the copolymer are found to be 25, 40 and 35%, respectively. If one compares these values with the corresponding values obtained for the areas of each of the components L (27%), M (40%) and N (33%) in the initial copolymer, one is led to speculate that the syndiotactic sequences are the first to decompose followed by the heterotactic and finally the isotactic sequences. It remains very difficult to say whether this is indeed the order followed in the decomposition of the three steric structures present in the copolymer.

#### Kinetics of the decomposition

In dynamic thermogravimetry, the rate law for the decomposition of a polymer may be written, in a general form,

as follows:

$$\frac{d\alpha}{dT} = \frac{k}{q} \cdot F(\alpha) \quad (1)$$

where  $\alpha$  is the fraction of initial polymer volatilized at a temperature  $T$ ;  $F(\alpha)$  is a function of  $\alpha$ ;  $q$  (in  $^{\circ}\text{C}/\text{sec}$ ) is the heating rate; and  $k$  is a rate constant presumed to follow the Arrhenius law in the form  $k = Z \exp(-E/RT)$ . Here  $Z$  (in  $\text{sec}^{-1}$ ) is the pre-exponential factor and  $E$  (in kcal/mol) is the energy of activation.

It is evident from this expression that the heating rate has a definite influence on the rate of decomposition. Figure 8 shows, for three specific heating rates, typical thermograms obtained during the decomposition of copolymer samples at temperatures ranging from 220 to 520 $^{\circ}\text{C}$ . At first glance, though the shapes of the curves are similar in all three cases, the influence of the heating rate is reflected in variations of the initial and final temperatures of decomposition. The curves are made up of two parts located in successive regions of the temperature scale. This observation agrees well with that of Grassie and coworkers<sup>5</sup> who showed that the first

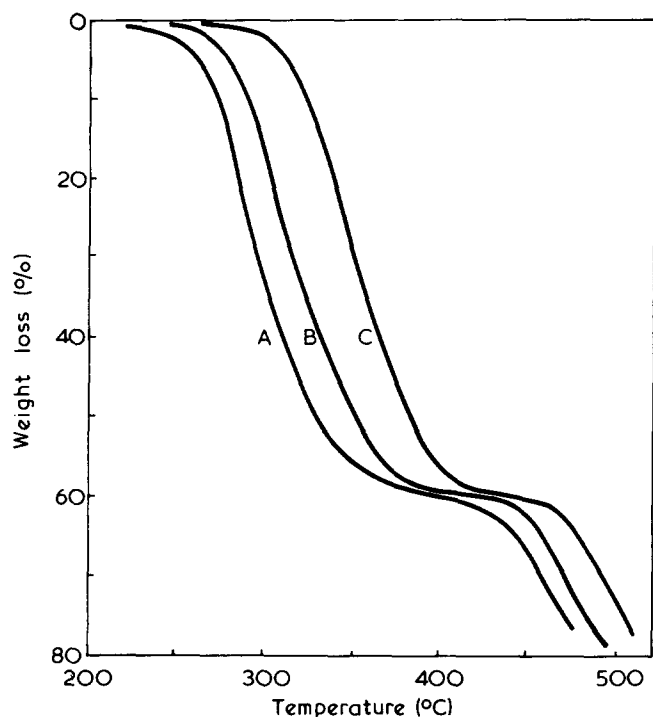


Figure 8 Influence of heating rate on the dynamic thermogravimetric decomposition of P(VC/VAC) copolymer ( $\bar{M}_n = 2.80 \times 10^4$ ). A, 5.0°C/min; B, 10.0°C/min; C, 20.0°C/min

region is characterized by the elimination of acid (HCl and HAC) and the second by the degradation of polyconjugated chains. They did not, however, establish the kinetic parameters of these reactions. Keeping this in mind, an analysis of the curves shown in Figure 8 has been carried out in order to determine, for each part, the order of reaction and the energy of activation, using the expression derived by Coats and Redfern<sup>14</sup>. This method, based on equation (1), consists of plotting  $\ln [F(\alpha)/T^2]$  as a function of  $1/T$ , where

$$F(\alpha) = \left[ \frac{1 - (1 - \alpha)^{1-n}}{1-n} \right]$$

for  $n \neq 1$  and

$$F(\alpha) = [-\ln(1 - \alpha)]$$

for  $n = 1$ .  $\alpha$  is the volatilized fraction of the polymer and  $T$  (K) is the absolute temperature.

Different values of  $n$  are tested and that which yields the most linear correlation is retained as the order of reaction. The slope of the line obtained with the accepted value of  $n$  is  $(-E/R)$  from which the activation energy is readily obtained.

Figure 9 shows, for several values of  $n$ , plots of  $\ln [F(\alpha)/T^2]$  versus  $1/T$  for each of the two parts involved in the decomposition at three specific heating rates of initial

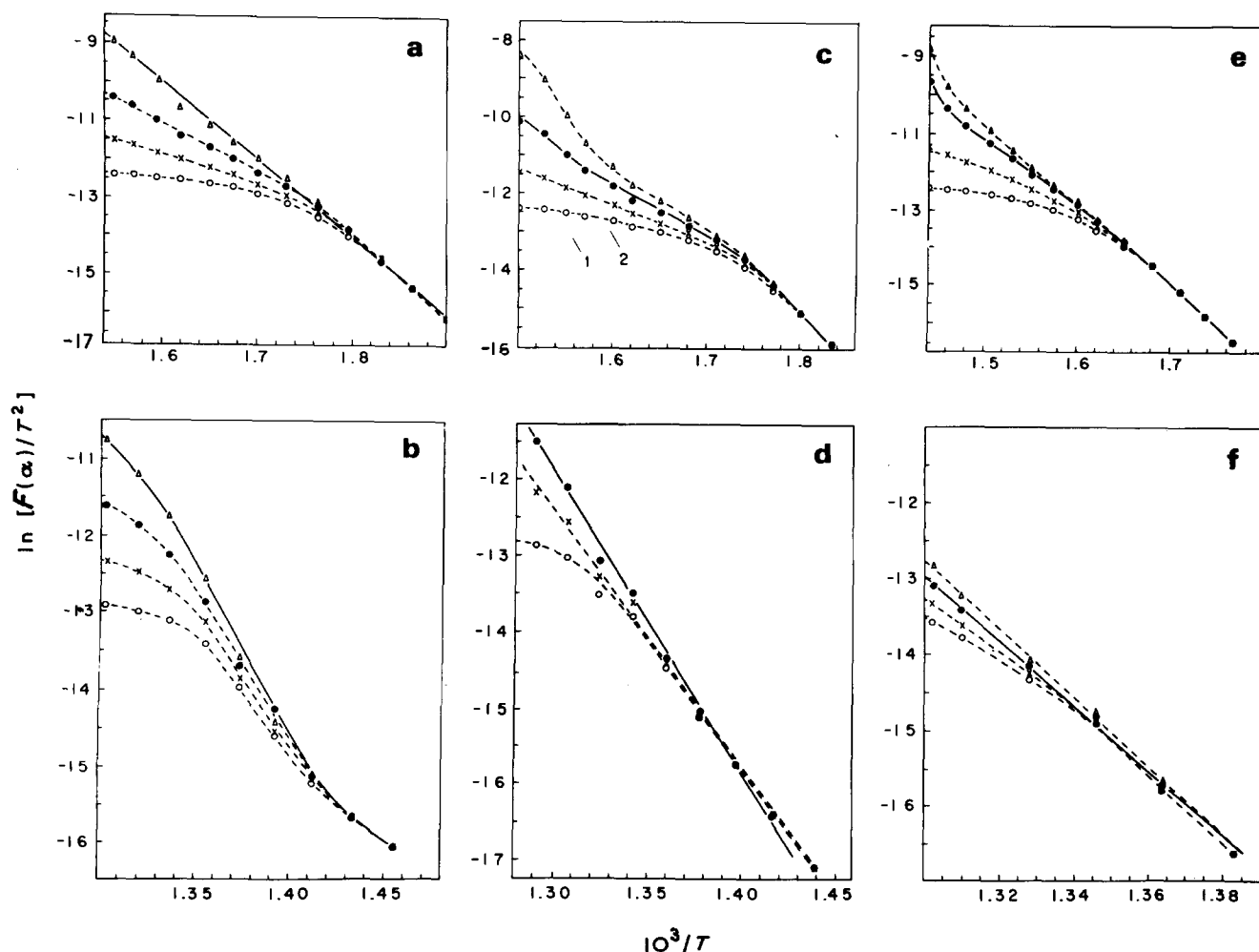


Figure 9 Variation of  $\ln [F(\alpha)/T^2]$  with  $1/T$  for the two-step decomposition of P(VC/VAC) copolymer ( $\bar{M}_n = 2.80 \times 10^4$ ) at three different heating rates and several values of  $n$ , the order of reaction: 1, 5.0°C/min (first-step in a, second-step in b); 2, 10.0°C/min (first-step in c, second-step in d); 3, 20.0°C/min (first-step in e, second-step in f); O,  $n = 0.5$ ; x,  $n = 1.0$ ; ●,  $n = 1.5$ ; ▲,  $n = 1.7$ ; △,  $n = 2.0$

copolymer samples. Similar plots have been made (though not shown here) for the two fractions C and J. The order of reaction and the energies of activation have been computed and are presented in Tables 5 and 6. It is evident from the data given in these Tables, that the order of reaction for the same phenomenon is different for each of the heating rates. Moreover, the results show a dependency on the molecular weight. In all probability, the principal factor responsible for this dependency lies in the interpretation given to the value of  $n$  since in many cases, one can trace near-linear relationships for  $\ln [F(\alpha)/T^2]$  versus  $1/T$  with several values of  $n$  and it becomes a difficult problem to select the true value. This also has an effect on the activation energy values which are based directly on the accepted order of reaction  $n$ . Based on the data obtained, one can only say that the value of the activation energy for the first part of the decomposition, involving the elimination of acids, lies between 30 and 40 kcal/mol while that for the second (viz. decomposition of polyconjugated chains) lies between 50 and 90 kcal/mol, depending upon the molecular weight of the sample: the lower the molecular weight, the lower the energy of activation.

In conclusion, one can say that crosslinking begins to take place at 180°C even though the weight loss is negligible. This may take place as well at higher temperatures in other stages of the reaction. A higher degree of crosslinking in the lower molecular weight copolymer has been attributed to its higher acetate content. Furthermore during the course of the process leading to the elimination of acids (viz. HCl and HAC) from chain ends, as suggested by Grassie and co-workers<sup>11</sup>, random scissions also participate in breaking down the polymeric chains. The activation energy values (Table 6) computed for the second step lie in the range of 50–90 kcal/mol assigned to the dissociation of C–C bonds<sup>15</sup>, which may be responsible for the decomposition of polyconjugated chains in the copolymer. N.m.r. spectroscopy has led to speculations that syndiotactic sequences are the least resistant to thermal treatment, followed by heterotactic and finally isotactic sequences.

The experimental limitations and the corresponding interpretations limit the number of conclusions that can be

Table 5 Activation energy of the acid elimination process calculated by the method of coats and redfern<sup>14</sup>

Copolymer samples <sup>7</sup>	$M_n \times 10^{-4}$	Heating rate (°C/min)					
		1.25		5.0		20.0	
		$n$	$E$	$n$	$E$	$n$	$E$
Initial	2.80	2.0	40.0	1.6	34.3	1.5	39.1
Fractions:							
C	6.05	2.0	38.0	2.0	43.1	1.6	41.0
F	4.24	—	—	1.2	26.3	1.2	28.6
H	3.55	—	—	1.5	33.2	1.4	35.0
J	3.18	2.0	41.5	1.7	39.1	1.8	41.2
M	2.00	—	—	1.6	36.4	1.3	33.5
O	1.54	—	—	1.5	34.5	1.3	29.4
Q	0.85	1.6	33.2	1.5	33.7	1.3	34.3

$n$  = order of reaction;  $E$  = activation energy (kcal/mol)

Table 6 Activation energy of the decomposition of polyconjugated chains, calculated by the method of Coats and Redfern<sup>14</sup>

Copolymer samples <sup>7</sup>	$M_n \times 10^{-4}$	Heating rate (°C/min)					
		1.25		5.0		20.0	
		$n$	$E$	$n$	$E$	$n$	$E$
Initial	3.80	1.3	59.0	1.1	69.1	2.0	92.5
Fractions:							
C	6.05	1.6	71.5	0.8	68.3	0.5	75.8
F	4.24	—	—	1.1	63.8	0.8	66.2
H	3.55	—	—	0.5	68.9	1.6	84.7
J	3.18	1.5	78.5	1.4	84.6	2.0	79.6
M	2.00	—	—	1.0	78.4	0.5	63.5
O	1.54	—	—	1.1	66.6	0.5	68.7
Q	0.85	0.5	43.7	0.5	48.9	1.0	62.4

$n$  = order of reaction;  $E$  = activation energy (kcal/mol)

drawn from this work. Nevertheless, it should prove interesting to establish eventually the role played by the molecular weight and likewise by the heating rate. To do this, other techniques would be required such as differential scanning calorimetry. These would prove more helpful in the lower temperature range (180 to 220°C) where the t.g.s. technique is less effective because of negligible weight losses though other activities, e.g. crosslinking which consumes energy, are operative.

#### ACKNOWLEDGEMENTS

The authors are grateful to Mrs Hsiao-Rong Chen for supplying the purified and fractionated copolymer samples and to the National Research Council of Canada for financial assistance in support of this work. One of the authors (J.H.) acknowledges receipt of a postgraduate bursary from the Canada Council.

The work described in this paper forms part of the general research program of the 'Groupe de Recherches en Sciences Macromoléculaires' at Laval University.

#### REFERENCES

- McNeill, I. C. and Neil, D. *Eur. Polym. J.* 1970, 6, 569
- Grassie, N. *Trans. Faraday Soc.* 1952, 48, 379; 1953, 49, 835
- Lehrle, R. S. and Robb, J. C. *Nature* 1959, 183, 1671
- Vymazal, Z. *Gummi Asbest. Kunststoffe* 1967, 5, 514
- Grassie, N., McLaren, I. F. and McNeill, I. C. *Eur. Polym. J.* 1970, 6, 679, 865
- Hesse, J. *Master's Thesis* Laval University (1971)
- Chen, H. R. and Blanchard, L. P. *J. Appl. Polym. Sci.* 1972, 16, 603
- Smith, W. N. *J. Appl. Polym. Sci.* 1967, 11, 639
- Berlin, A. A. and Yenikolopyan, N. S. *Vysokomol. Soedin. (A)* 1968, 10, 1475
- Heatley, F. and Bovey, F. A. *Macromolecules* 1969, 2, 241
- Bovey, F. A., Anderson, E. W., Douglass, D. C. and Manson, J. A. *J. Chem. Phys.* 1963, 39, 1199
- Ramey, K. C. and Field, N. D. *J. Polym. Sci. (B)* 1964, 2, 69
- Capon, B. *Q. Rev. Chem. Soc.* 1964, 18, 45
- Coats, A. W. and Redfern, J. P. *J. Polym. Sci. (B)* 1965, 3, 917
- Tsang, W. J. *J. Chem. Phys.* 1966, 44, 4283

# Reactivity ratios for the copolymerization systems styrene/*p*-ethoxystyrene and methyl methacrylate/*p*-ethoxystyrene

D. Margerison, D. R. Bain, K. Lindley, N. R. Morgan and Lindsay Taylor

Department of Inorganic, Physical and Industrial Chemistry, University of Liverpool, PO Box 147, Liverpool L69 3BX, UK

(Received 26 July 1974)

Reactivity ratios for the systems styrene/*p*-ethoxystyrene and methyl methacrylate/*p*-ethoxystyrene have been determined at 50°C. The values found by the computational method of Tidwell and Mortimer were 1.08 and 0.74 for the first system, and 0.37 and 0.24 for the second; the 90% joint confidence limit envelopes were also calculated.

## INTRODUCTION

The theory of free-radical copolymerization leads to the conclusion that the composition of the copolymer is determined by the reactivity ratios,  $r_1$  and  $r_2$ , and the ratio of the concentrations of the two monomers. Since the composition of the polymerization mixture normally changes with time, the theory predicts the composition of the copolymer formed in an infinitesimal period of time in which the two monomer concentrations may be regarded as constant. The result is:

$$y_2 = \frac{x_1 x_2 + r_2 x_2^2}{r_1 x_1^2 + 2x_1 x_2 + r_2 x_2^2}$$

where  $y_2$  is the mole fraction of monomer 2 in the infinitesimal amount of copolymer formed in the time interval in which the mole fractions of monomer 1 ( $M_1$ ) and monomer 2 ( $M_2$ ) in the feed are  $x_1$  and  $x_2$ . Several authors<sup>1-5</sup> have recently discussed the procedures by which the reactivity ratios can be evaluated from determinations of copolymer compositions at known feeds. Here, we report the application of the Tidwell-Mortimer<sup>1</sup> method to the determination of the reactivity ratios of two systems: styrene ( $M_1$ )/*p*-ethoxystyrene ( $M_2$ ), and methyl methacrylate ( $M_1$ )/*p*-ethoxystyrene ( $M_2$ ).

## EXPERIMENTAL

Inhibitor was removed from the three monomers by washing with 10% aqueous sodium hydroxide. After washing with de-ionized water and drying over anhydrous sodium sulphate, the monomers were distilled under vacuum. All polymerizations were carried out at 50°C under vacuum ( $<10^{-3}$  mmHg permanent gas pressure) using AZBN as initiator. Toluene was added as a diluent in the methyl methacrylate systems. The polymerizations were followed dilatometrically and stopped at about 5% conversion. The polymers were recovered by precipitation from methanol. Their number-average molecular weights were in the range  $5 \times 10^4$  to  $2.5 \times 10^5$ .

In the case of the styrene systems, the initial composition of the comonomer mixture was fixed by pipetting accurate-

ly known volumes of the two monomers into the reaction vessel; with the methyl methacrylate systems, a weighing technique was used instead.

The composition of each of the copolymers was found by elemental analysis (Alfred Bernhardt, West Germany), or by u.v. spectrophotometry using a peak located at about 279 nm in the absorption spectrum of both the homopolymer of *p*-ethoxystyrene and the two copolymers studied here. Neither polystyrene nor poly(methyl methacrylate) absorb appreciably at this wavelength so that a determination of the absorbance of the copolymer at this point gives directly its composition, once the extinction coefficient for *p*-ethoxystyrene segments is known.

## RESULTS AND TREATMENT OF DATA

### *Extinction coefficient of p-ethoxystyrene at 279 nm*

The absorbances of 4 solutions of poly(*p*-ethoxystyrene) in  $\text{CHCl}_3$  were measured in a 1 cm cell over the concentration range 20–50 mg/l. A simple least squares line constrained to pass through the origin was put through the points and the extinction coefficient calculated to be  $1.131 \times 10^4$   $\text{cm}^2/\text{g}$  with negligible error.

### *Compositions of the monomer feed and the copolymer for the system styrene ( $M_1$ )/p-ethoxystyrene ( $M_2$ )*

Two groups of four copolymers were prepared. Each copolymer was analysed for carbon, hydrogen, and oxygen by elemental analysis and for *p*-ethoxystyrene by u.v. spectrophotometry. The mole fractions,  $y_2$ , of *p*-ethoxystyrene in the products is shown in Table 1.

The figures indicate the precision obtainable; *p*-ethoxystyrene contents determined from H analysis do not appear because the precision of the method is inadequate. It will be noted that there is good agreement between the three methods used.

### *Compositions of the monomer feed and the copolymer for the system methyl methacrylate ( $M_1$ )/p-ethoxystyrene ( $M_2$ )*

A similar procedure to that above was employed to determine the copolymer compositions at different feeds

Table 1 Compositions of styrene/*p*-ethoxystyrene copolymers

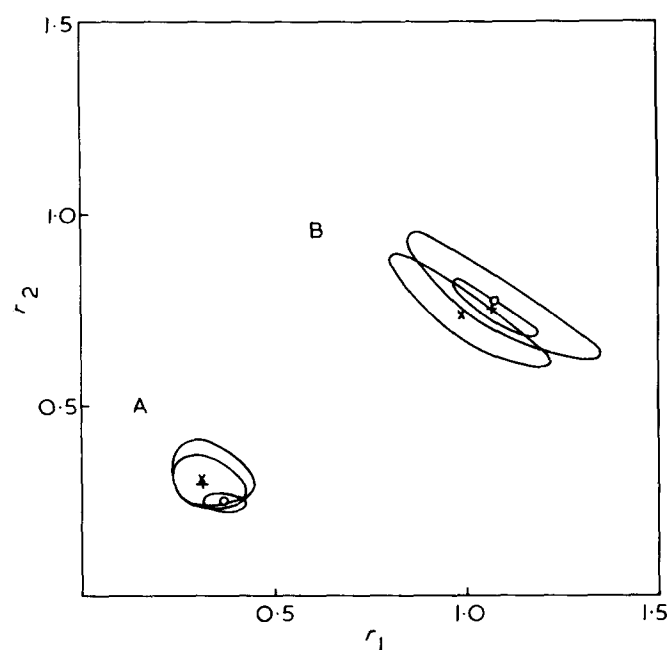
$x_1$	$y_2$ from		
	C analysis	O analysis	U.v. analysis
0.363	0.594	0.596	0.603
	0.590	0.589	0.602
	0.593	0.582	0.582
	0.586	0.582	0.569
0.571	0.406	0.390	0.388
	0.378	0.386	0.388
	0.399	0.392	0.394
	0.411	0.394	0.393

 Table 2 Compositions of methyl methacrylate/*p*-ethoxystyrene copolymers

$x_1$	$y_2$ from		
	C analysis	O analysis	U.v. analysis
0.873	0.223	0.235	0.224
0.876	0.264	0.255	0.222
0.878	0.216	0.220	0.219
0.877	0.253	0.249	0.221
0.230	0.605	0.597	0.600
0.256	0.641	0.633	0.593
0.255	0.651	0.644	0.611
0.249	0.646	0.642	0.619

 Table 3 Least squares estimates of  $r_1$  and  $r_2$ 

Analytical method	S/ <i>p</i> -EtOS		MMA/ <i>p</i> -EtOS	
	$\hat{r}_1$	$\hat{r}_2$	$\hat{r}_1$	$\hat{r}_2$
C analysis	1.00	0.72	0.33	0.31
O analysis	1.08	0.74	0.33	0.29
U.v. analysis	1.09	0.75	0.37	0.24


 Figure 1 Least squares estimates  $r_1$  and  $r_2$  for (A) methyl methacrylate/*p*-ethoxystyrene and (B) styrene/*p*-ethoxystyrene. X, carbon analysis; +, oxygen analysis; o, u.v. analysis; the corresponding 90% joint confidence limit envelopes are approximately centred on these points

in this system. The results are shown in Table 2. Again reasonable agreement between the three analytical methods is observed.

#### Estimation of $r_1$ and $r_2$ and the error envelopes for both systems

The procedure for calculating the least squares estimates of  $r_1$  and  $r_2$  which was described by Tidwell and Mortimer was found to work very satisfactorily. Usually, only three or four iterations were required to reach more or less stationary values of these quantities. The results are shown in Table 3.

The differences in the estimates from one analytical method to another are not significant. This can be seen from Figure 1 where the 90% joint confidence limit envelopes are plotted. (To construct these envelopes, an extension of Tidwell and Mortimer's approximate procedure was devised to facilitate computation; the method is described in the Appendix.) The numerical values listed in Table 3 illustrate a well-known difficulty in the estimation of reactivity ratios, namely that  $r_1$  and  $r_2$  cannot be independently estimated from the same set of data; when one estimate is shifted by a change of analytical procedure or the use of an alternative computational method, then so is the other. This fact is the basic reason why joint confidence limits provide the best representation of the experimental error.

It only remains to select final values of the estimates of  $r_1$  and  $r_2$  for the two systems studied. We choose the values associated with the confidence limit envelope with the smallest area. These are:

Styrene/*p*-ethoxystyrene:  $\hat{r}_1 = 1.08$   
(oxygen analysis)  $\hat{r}_2 = 0.74$

Methyl methacrylate/*p*-ethoxystyrene:  $\hat{r}_1 = 0.37$   
(u.v. analysis)  $\hat{r}_2 = 0.24$

These two sets of values are self-consistent in the sense that each gives essentially the same  $e$  value<sup>6</sup> for *p*-ethoxystyrene; we obtain  $-1.3$  from the styrene system and  $-1.2$  from the methyl methacrylate system. Furthermore, the first pair of reactivity ratios is very similar to the pair found by Ceccorulli *et al.*<sup>7</sup> for the analogous system styrene/*p*-methoxystyrene. These workers found  $\hat{r}_1 = 1.16$  and  $\hat{r}_2 = 0.82$  using u.v. rather than oxygen content to characterize the copolymers.

#### REFERENCES

- Tidwell, P. W. and Mortimer, G. A. *J. Polym. Sci. (A)* 1965, 3, 369
- Behnken, D. W. *J. Polym. Sci. (A)* 1964, 2, 645
- Tidwell, P. W. and Mortimer, G. A. *J. Macromol. Sci. (Rev. Macromol. Chem.)* 1970, 4, 281
- Braun, D., Brendlein, W. and Mott, G. *Eur. Polym. J.* 1973, 9, 1007
- Tosi, C. *Eur. Polym. J.* 1973, 9, 357
- Price, C. C. *J. Polym. Sci.* 1948, 3, 772
- Ceccorulli, G., Pizzoli, M., Stea, G. and Gechele, G. B. *Ann. Chim.* 1968, 58, 314

#### APPENDIX

##### Computation of the joint confidence limit envelope

Using the notation,  $\ln \hat{r}_1 = \hat{t}_1$  and  $\ln \hat{r}_2 = \hat{t}_2$ , Tidwell and Mortimer derived the following approximate equation for the coordinates ( $t'_1$ ,  $t'_2$ ) of the joint confidence limit envelope at the 100(1 -  $p$ ) per cent level, where  $0 < p < 1$

$$\begin{aligned} (t'_1 - \hat{t}_1)^2 a_{11} + 2(t'_1 - \hat{t}_1)(t'_2 - \hat{t}_2) a_{12} + \\ (t'_2 - \hat{t}_2)^2 a_{22} = 2s^2 F_p(2, n - 2) \end{aligned} \quad (1)$$

Here,  $a_{11}$ ,  $a_{12}$ ,  $a_{22}$ , and  $s^2$  are quantities evaluated in the estimation of  $r_1$  and  $r_2$ , and  $F_p(2, n - 2)$  is the value of the statistic  $F$  at the significance level  $p$  with  $(2, n - 2)$  degrees of freedom,  $n$  being the number of copolymers used. Equation (1) represents an ellipse in  $(t_1, t_2)$  space with its centre at  $(\hat{t}_1, \hat{t}_2)$ .

By shifting the origin of the coordinate system to the point  $(\hat{t}_1, \hat{t}_2)$  and then rotating the coordinate axes through an angle  $\theta$  given by:

$$\tan 2\theta = \frac{2a_{12}}{a_{22} - a_{11}}$$

we can reduce equation (1) to the simple form:

$$\frac{x^2}{A^2} + \frac{y^2}{B^2} = 1$$

where

$$\left. \begin{aligned} t'_1 - \hat{t}_1 &= x \cos \theta - y \sin \theta \\ t'_2 - \hat{t}_2 &= x \sin \theta + y \cos \theta \end{aligned} \right\} \quad (2)$$

and

$$\left. \begin{aligned} A^2 &= \frac{2}{\alpha + \gamma - \delta} \\ B^2 &= \frac{2}{\alpha + \gamma + \delta} \end{aligned} \right\} \quad (3)$$

Here,  $\alpha = a_{11}/2s^2F$ ,  $\beta = a_{12}/s^2F$ ,  $\gamma = a_{22}/2s^2F$ , and  $\delta^2 = \beta^2 + (\gamma - \alpha)^2$ ;  $F$  in these expressions stands for  $F_p(2, n - 2)$ . The virtue of this transformation is that the coordinates of the confidence limit envelope in the new coordinate system can be computed through the expressions:

$$\left. \begin{aligned} x &= A \cos \phi \\ y &= B \sin \phi \end{aligned} \right\} \quad (4)$$

where  $\phi$  is a dummy variable to be incremented in the range 0 to  $2\pi$ .

The computation of the confidence limit envelope on  $\hat{r}_1, \hat{r}_2$  in  $(r_1, r_2)$  space thus proceeds as follows: (1) having chosen  $p$ , the significance level, compute  $A$  and  $B$  from equation (3) and the associated definitions of  $\alpha, \beta, \gamma$ , and  $\delta$ ; (2) compute the locus of the elliptical envelope in  $(x, y)$  space using equation (4); (3) calculate the quantities  $(t'_1 - \hat{t}_1)$  and  $(t'_2 - \hat{t}_2)$  using equation (2); (4) calculate  $t'_1$  and  $t'_2$ , the coordinates of the elliptical envelope in  $(t_1, t_2)$  space; (5) transform to  $r'_1 = \exp(t'_1)$  and  $r'_2 = \exp(t'_2)$  to obtain the joint confidence limit envelope in  $(r_1, r_2)$  space.

# Vinyl polymerization initiated with alkali metal adducts of triphenylamine and triphenylphosphine

Koichi Yamaguchi, Takero Yoshida and Yuji Minoura

Research Institute for Atomic Energy, Osaka City University, Osaka, Japan

(Received 25 April 1973; revised 3 October 1974)

The polymerizations of styrene, methyl methacrylate, isoprene, butadiene and acrylonitrile initiated with alkali metal adducts of triphenylamine or triphenylphosphine at 0°C in tetrahydrofuran take place by an anionic mechanism. Biphenyl alkali metal anion radical and alkali metal adducts of benzene, aniline and diphenylamine are formed in the reaction of triphenylamine with the alkali metal and it was shown that styrene was polymerized with both the anion radical and alkali metal adducts of benzene, whereas methyl methacrylate and acrylonitrile were polymerized by all anion species.

## INTRODUCTION

It is well known that alkali metal amides initiate an anionic polymerization of styrene (S), methyl methacrylate (MMA) and acrylonitrile (AN) in liquid ammonia<sup>1</sup>, and that alkali metal salts of aniline and diphenylamine initiate the polymerization of AN and MMA in diethyl ether or liquid ammonia<sup>2</sup>. Primary and secondary amines<sup>3,4</sup> or tertiary amines and phosphines<sup>5</sup> [e.g. triphenylamine (TPA) and triphenylphosphine (TPP)] readily react with alkali metals and in this paper, the polymerizations of S, MMA, AN, isoprene, and butadiene with the potassium adducts of TPA or TPP were investigated in tetrahydrofuran (THF) at 0°C. The difference between the reactivity of TPA and TPP with various alkali metals was examined.

## EXPERIMENTAL

### Materials

Triphenylamine (TPA) prepared by the reaction<sup>6</sup> of diphenylamine with phenyl iodide was recrystallized from ethyl acetate (m.p. 127°C). Diphenylamine and triphenylphosphine were purified by recrystallization from benzene and all solvents used were purified by distillation before use.

All vinyl monomers used were dried over calcium hydride, and distilled under nitrogen.

### Reaction of triphenylamine with potassium metal

A mixture of potassium (0.0346 mol) and TPA (0.0204 mol) was stirred in 50 ml of dried THF under nitrogen atmosphere at room temperature until the potassium dissolved (about 100 h). The green solution resulting was filtered through the glass filter under a stream of nitrogen gas, and the filtrate was used immediately.

### Reaction of triphenylphosphine with potassium metal

A mixture of potassium (0.00785 mol) and TPP (0.00308 mol) was stirred in 50 ml of dried THF under nitrogen atmosphere at -15°C until the potassium dissolved (about 40 h). The red solution was used after filtering as described above.

### Alkali salts of aniline and diphenylamine

The reaction of aniline (0.052 mol) with potassium (0.0511 mol) in 20 ml of THF to give mono-potassium aniline, and that of diphenylamine (0.041 mol) with potassium (0.043 mol) in 20 ml of THF to form mono-potassium diphenylamine were carried out at 70°C for 6 h.

Di-potassium aniline was obtained by the reaction of aniline (0.056 mol) with potassium (0.113 mol) in 20 ml of THF at room temperature for 4 h.

The identification of those products was carried out by elemental analysis and by reaction with benzyl chloride. The products of the latter reaction were benzyl aniline (m.p. 35.0°C), benzyl diphenylamine (m.p. 88.0°C) and dibenzyl phenylamine (m.p. 69.5°C), respectively.

### Polymerization

The alkali metal adduct in THF solution was added to the degassed monomer-solvent mixture by means of a syringe. The polymerization was carried out in a sealed tube at 0°C. The reaction mixture was poured into a large excess of methanol containing dilute hydrochloric acid and the precipitated polymer was filtered off, washed with methanol and dried in vacuum to constant weight.

### Measurements

The intrinsic viscosity of polymer was measured in benzene by means of a Ubbelohde viscometer and the degree of polymerization was calculated from:

$$\bar{P}_n = 1770 \times [\eta]^{1.40} \text{ (for polystyrene)}^7$$

$$\bar{P}_n = 2200 \times [\eta]^{1.13} \text{ (for PMMA)}^7$$

Molecular weights of the reaction products and of the oligomers were determined with a Knauer vapour pressure osmometer, using benzene as solvent.

E.s.r. measurements were carried out on a JES ME 3X Type spectrometer (x-band, 100 kHz irregularity) with 100 kilocycles modulation.

The visible absorption spectrum was measured by means of a Hitachi-EPS-2 Type ultra-violet spectrometer and the



infra-red spectra of polymer, oligomer, and reaction products as film or pellets using a Jasco IR-E infra-red spectrometer.

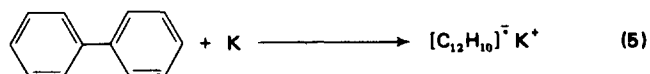
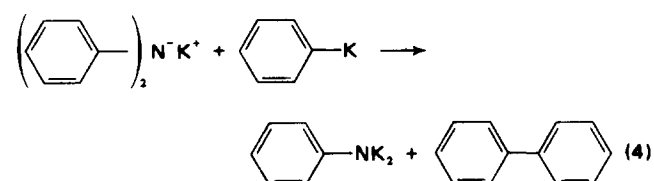
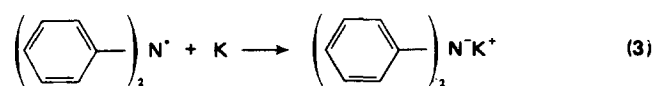
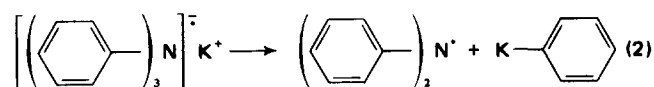
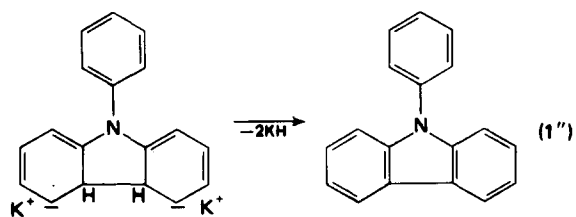
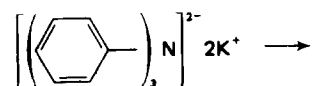
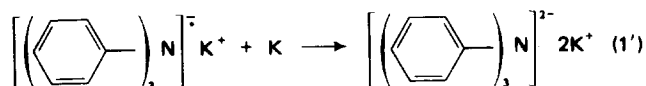
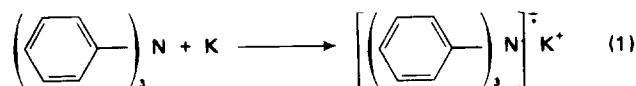
## RESULTS AND DISCUSSION

### Reaction of triphenylamine with potassium metal

**Anion radical.** The reaction of TPA with potassium, sodium, lithium was investigated at room temperature, and only the more highly electron donating potassium reacted. The e.s.r. signal of a THF solution of TPA with potassium metal showed a nine line spectrum centred at 3300 G, and each signal split into five fractions at 0.41 G. This signal was the same as that of biphenyl anion radical<sup>8</sup>, but e.s.r. signals from triphenylamine anion radical or any radical on nitrogen were not observed. The formation of the reaction product was confirmed by the absorption band at 600 nm from biphenyl anion radical.

**Reaction products.** By treating the solution obtained by reacting TPA with potassium described above with a few drops of water, followed by hydrogen chloride, aniline hydrochloride (0.41 g, m.p. 192.2°C) was isolated by the filtration. Biphenyl (0.51 g), *N*-phenylcarbazole (0.11 g), benzene (0.4 ml), and unreacted TPA (2.22 g) were isolated from the filtrate by column chromatography on silica gel (developing solvent; mixed solvent of diethyl ether and petroleum ether). The formation of aniline, was confirmed by reaction of the product with *p*-toluenesulphonyl chloride to give phenyl *p*-toluenesulphonamide (m.p. 103.0°C).

From these results, the following reactions are assumed:



As the electronegativity of nitrogen atom (3.0) is larger than that of carbon atom (2.5), alkali metal was thought to react directly at the nitrogen atom. It was found by thin-layer chromatography (silica gel, developing solvent; mixed solvent of diethyl ether and petroleum ether,  $R_f = 0.16$  for aniline and 0.41 for diphenylamine), that a little  $\text{C}_6\text{H}_5\text{NH}_2$  was formed by the reaction of  $(\text{C}_6\text{H}_5)_2\text{NK}$  with *n*-butyl lithium, which has smaller  $pK_a$  than  $\text{C}_6\text{H}_5\text{K}$  (>40). Therefore, aniline was assumed to be produced by the reaction of  $(\text{C}_6\text{H}_5)_2\text{NK}$  with  $\text{C}_6\text{H}_5\text{K}$ , (reaction 4) and that benzene was formed from reaction (2) and *N*-phenylcarbazole by reaction (1), and that the main reaction products were obtained by the reactions (2)–(5) rather than reaction (1).

### Polymerization with potassium adducts of triphenylamine

The results are shown in Table 1.  $J$  values<sup>9</sup> of PMMA were 95~100. The microstructure of the polyisoprene and polybutadiene was calculated from the intensity of i.r. spectrum as follows:

	<i>cis</i> -1,4 (%)	<i>trans</i> -1,4 (%)	1,2 (%)	3,4 (%)
polyisoprene	0	0	24.0	76.0
polybutadiene	30.2	28.5	41.3	—

Further, copolymerizations of S–MMA, S–AN, and AN–MMA carried out under the same conditions gave the results shown in Table 2.

The results show that the polymerization took place by an anionic mechanism.

In order to confirm the initiation reaction, an oligomer of MMA was prepared by use of high concentration of potassium adducts of TPA (MMA: 0.048 mol; TPA: 0.041 mol; potassium: 0.053 mol). The i.r. spectrum of the oligomer (which had been purified by reprecipitation from petroleum ether) showed an absorption band at 1600  $\text{cm}^{-1}$  due to phenyl group, a molecular weight of 1700, and nitrogen content 0.09 wt %. Similarly, an oligomer of S prepared under the same conditions had a molecular weight of 1800, and nitrogen content zero. From these results, it was assumed that the polymerization of MMA was induced

by  $\text{C}_6\text{H}_5\text{NK}_2$ ,  $(\text{C}_6\text{H}_5)_2\text{NK}$ ,  $\text{C}_6\text{H}_5\text{K}$ , and  $\left[\text{C}_6\text{H}_5\text{---C}_6\text{H}_5\right]^- \text{K}^+$

and that of S by  $\text{C}_6\text{H}_5\text{K}$  and  $\left[\text{C}_6\text{H}_5\text{---C}_6\text{H}_5\right]^- \text{K}^+$

as previously shown by Morton *et al.*<sup>10</sup>

Table 1 Polymerization of vinyl monomers with triphenylamine–potassium adducts in tetrahydrofuran at 0°C for 6 h

Monomer	[M] (mol/l)	Adducts (mol/l)	Yield (%)	$\bar{P}_n$
S	4.56	$8.7 \times 10^{-3}$	100	900
S	4.56	$1.7 \times 10^{-2}$	100	620
MMA	4.71	$8.7 \times 10^{-3}$	70	360
MMA	4.71	$1.7 \times 10^{-2}$	87	250
AN	3.56	$8.7 \times 10^{-3}$	34	—
AN	3.56	$1.7 \times 10^{-2}$	68	—

**Table 2** Copolymerization of vinyl monomers with triphenylamine–potassium adducts in tetrahydrofuran at 0°C for 6 h

	Monomer		
	S	S	MMA
[M <sub>1</sub> ] (mol/l)	2.28	2.28	3.36
Comonomer	MMA	AN	AN
[M <sub>2</sub> ] (mol/l)	2.36	1.78	1.78
[Adducts] (mol/l)	2.0 × 10 <sup>-2</sup>	2.0 × 10 <sup>-2</sup>	2.0 × 10 <sup>-2</sup>
Yield (%)	54	21	33
Composition of polymer*	S:MMA 10:90	S:AN 10:90	MMA:AN 10:90

\* Calculated from elemental analysis

**Table 3** Polymerization and copolymerization of vinyl monomers with potassium salts of aniline and diphenylamine in tetrahydrofuran at 0°C for 6 h

Salts	[Salts] (mol/l)	Monomer	[M] (mol/l)	Polymer yield (%)	Composition of copolymer (mol %)*
(C <sub>6</sub> H <sub>5</sub> ) <sub>2</sub> NK	2.6 × 10 <sup>-1</sup>	S	4.55	0	
C <sub>6</sub> H <sub>5</sub> NK <sub>2</sub>	1.0 × 10 <sup>-1</sup>	S	4.55	0	
C <sub>6</sub> H <sub>5</sub> NHK	1.5 × 10 <sup>-1</sup>	S	4.55	0	
(C <sub>6</sub> H <sub>5</sub> ) <sub>2</sub> NK	1.6 × 10 <sup>-2</sup>	MMA	4.71	79 <sup>†</sup>	
(C <sub>6</sub> H <sub>5</sub> ) <sub>2</sub> NK	3.3 × 10 <sup>-2</sup>	MMA	4.71	99 <sup>†</sup>	
C <sub>6</sub> H <sub>5</sub> NHK	1.5 × 10 <sup>-2</sup>	MMA	4.71	35 <sup>†</sup>	
C <sub>6</sub> H <sub>5</sub> NK <sub>2</sub>	5.0 × 10 <sup>-2</sup>	MMA	4.71	36 <sup>†</sup>	
C <sub>6</sub> H <sub>5</sub> NK <sub>2</sub>	1.0 × 10 <sup>-1</sup>	MMA	4.71	27 <sup>†</sup>	
(C <sub>6</sub> H <sub>5</sub> ) <sub>2</sub> NK	1.6 × 10 <sup>-2</sup>	AN	3.56	35	
(C <sub>6</sub> H <sub>5</sub> ) <sub>2</sub> NK	3.3 × 10 <sup>-2</sup>	AN	3.56	67	
C <sub>6</sub> H <sub>5</sub> NK <sub>2</sub>	5.0 × 10 <sup>-2</sup>	AN	3.56	75	
C <sub>6</sub> H <sub>5</sub> NK <sub>2</sub>	1.0 × 10 <sup>-1</sup>	AN	3.56	82	
C <sub>6</sub> H <sub>5</sub> NHK	1.5 × 10 <sup>-1</sup>	AN	3.56	39	
(C <sub>6</sub> H <sub>5</sub> ) <sub>2</sub> NK	3.3 × 10 <sup>-2</sup>	MMA	2.36	23	10
		AN	1.79		90
C <sub>6</sub> H <sub>5</sub> NHK	1.5 × 10 <sup>-2</sup>	MMA	2.36	23	20
		AN	1.78		80

\* Calculated from elemental analysis

† The degree of polymerization was 300 to 760, and *J* value was 92 to 95

#### Polymerization with potassium salts of aniline and diphenylamine

In order to elucidate the polymerization with *N*-metal compounds derived from the reaction of TPA with potassium, the polymerizations of vinyl monomer with aniline mono-potassium salt, aniline di-potassium salt and diphenylamine mono-potassium salt were carried out, and the results shown in *Table 3*, include also the copolymerization of AN and MMA with these salts.

AN and MMA were found to undergo polymerization with these potassium salts but S did not polymerize. The PMMA was found to be syndiotactic. The copolymer was found to contain more AN than MMA. The results show that the alkali salts initiate an anionic polymerization of MMA and AN.

In order to confirm the initiation mechanism, the reaction of MMA (0.0472 mol) with aniline (0.0104 mol) and potassium (0.0225 mol) and of MMA (0.0283 mol) with diphenylamine (0.0075 mol) and potassium (0.0071 mol) in 10 ml of THF were carried out at room temperature. The oligomers formed were found to contain phenyl group and nitrogen by i.r. spectrum and elemental analysis and it was concluded that the fragment of C<sub>6</sub>H<sub>5</sub>NK<sub>2</sub> and (C<sub>6</sub>H<sub>5</sub>)<sub>2</sub>NK was linked at the chain end of PMMA.

#### Reaction of triphenylphosphine with alkali metal

In order to compare the reactivity of TPA and TPP the polymerization of vinyl monomers with TPP–alkali metal adducts were studied. The reaction of TPP with alkali metal in THF or liquid ammonia has been shown<sup>11–15</sup> to lead to the formation of anion radical products.

A study of the reaction of potassium, sodium and lithium with TPP and TPA in THF at room temperature showed that TPP reacted readily with these alkali metals, whereas TPA reacted only with potassium.

It was considered that the difference of reactivity arises from the smaller energy differences in the 4s–3d orbitals of phosphorus relative to that of the 3s–4d orbitals of nitrogen. The former situation would promote electron delocalization into the *pπ* system in TPP<sup>-</sup> thus stabilizing the molecule.

#### Polymerization with alkali metal adducts of triphenylphosphine

The results are shown in *Table 4*. The *J* values of PMMA were 92–95, and the PMMA had a syndiotactic structure. The micro-structure of polyisoprene and polybutadiene obtained was calculated from the intensity of the infra-red spectrum as follows:

	<i>cis</i> -1,4 (%)	<i>trans</i> -1,4 (%)	1,2 (%)	3,4 (%)
Polyisoprene	0	0	35–32	65–68
Polybutadiene	25.4	29.6	45.0	—

The results agreed with those of the classical anionic polymerization in polar solvents.

The results of the copolymerizations of S–AN, MMA–S, and MMA–AN were carried out under the same conditions and are shown in *Table 5*.

In order to confirm the polymerization mechanism, PMMA and polystyrene of low degree of polymerization were prepared by use of high concentration of initiator, viz.: ([monomer] = 1.0 mol/l, [I] = 0.162 mol/l) in THF at room temperature. The oligomer of MMA and that of S formed had molecular weights of 1300 and 1800, respectively. The qualitative analysis for phosphorus<sup>16</sup> was positive for oligomeric MMA, and was negative for oligomeric S. PMMA had an absorption band at 1600 cm<sup>-1</sup> due to phenyl group. Therefore, the oligomer of MMA had a

**Table 4** Polymerization of vinyl monomers with triphenylphosphine–alkali metal adducts in tetrahydrofuran at 0°C for 6 h

Alkali metal	[Adducts] (mol/l)	Monomer	[M] (mol/l)	Polymer yield (%)
K	7.73 × 10 <sup>-3</sup>	S	4.55	98
K	1.55 × 10 <sup>-2</sup>	S	4.55	100
Na	6.05 × 10 <sup>-3</sup>	S	4.55	92
Na	1.21 × 10 <sup>-2</sup>	S	4.55	100
K	7.73 × 10 <sup>-3</sup>	MMA	4.71	45
K	1.55 × 10 <sup>-2</sup>	MMA	4.71	67
Na	6.05 × 10 <sup>-3</sup>	MMA	4.71	42
Na	1.21 × 10 <sup>-2</sup>	MMA	4.71	45
K	7.80 × 10 <sup>-3</sup>	AN	3.56	16
K	1.56 × 10 <sup>-2</sup>	AN	3.56	36
Na	6.10 × 10 <sup>-3</sup>	AN	3.56	30
Na	1.22 × 10 <sup>-2</sup>	AN	3.56	41
K	1.08 × 10 <sup>-2</sup>	Butadiene	4.80	83
K	5.40 × 10 <sup>-3</sup>	Isoprene	4.50	83
K	1.01 × 10 <sup>-2</sup>	Isoprene	4.50	94
Na	1.47 × 10 <sup>-2</sup>	Isoprene	4.50	100
Na	2.97 × 10 <sup>-2</sup>	Isoprene	4.50	100

Table 5 Copolymerization of vinyl monomers with triphenylphosphine-alkali metal adducts in tetrahydrofuran at 0°C for 6 h

Monomer	[M <sub>1</sub> ] (mol/l)	Comonomer	[M <sub>2</sub> ] (mol/l)	Alkali metal	[Adducts] (mol/l)	Yield (%)	Composition of copolymer M <sub>1</sub> :M <sub>2</sub> (mol/l)
S	2.28	AN	1.78	K	1.53 × 10 <sup>-2</sup>	12	10:90
S	2.28	AN	1.78	Na	1.43 × 10 <sup>-2</sup>	15	10:90
MMA	2.36	AN	1.78	K	1.54 × 10 <sup>-2</sup>	14	10:90
MMA	2.36	AN	1.78	Na	1.43 × 10 <sup>-2</sup>	13	15:85
S	2.28	MMA	2.36	K	1.27 × 10 <sup>-2</sup>	54	10:90
S	2.28	MMA	2.36	Na	1.18 × 10 <sup>-2</sup>	67	10:90

fragment of complex as initiator in the polymer end, but the oligomer of S did not.

The results show that the main difference between nitrogen (TPA) with phosphorus (TPP) was the reactivity with alkali metal.

#### REFERENCES

- Sanderson, H. *J. Am. Chem. Soc.* 1949, **71**, 1595
- Higginson, W. C. and Wooding, N. S. *J. Chem. Soc.* 1952, p 774
- Greenlee, K. W. and Henne, A. L. 'Inorganic Syntheses', McGraw-Hill, New York, 1967, Vol II, p 19
- Stephens, J. R. US Pat. 3 084 191 (1963)
- Wittenberg, D. and Gilman, H. *J. Org. Chem.* 1958, **23**, 1663
- Weith, M. *Org. Chem.* 1952, **B6**, 1514
- Tobolski, A. V. *J. Polym. Sci.* 1952, **9**, 171
- Nishiguchi, H. *et al. J. Chem. Phys.* 1962, **40**, 241
- Goode, W. E. *et al. J. Polym. Sci.* 1960, **46**, 371
- Morton, A. A. and Grovenstein, Jr. E. *J. Am. Chem. Soc.* 1952, **74**, 5434
- Young, S. 'Inorganic Synthesis', McGraw-Hill, New York, 1946, Vol I, p 128
- Britt, A. D. and Kaiser, E. T. *J. Phys. Chem.* 1965, **69**, 2775
- Wittenberg, D. and Gilman, H. *J. Org. Chem.* 1968, **23**, 1063
- Aguiar, A. M., Beisler, J. and Mills, A. *J. Org. Chem.* 1962, **27**, 1001
- Santhaman, K. S. V. and Bard, A. J. *J. Am. Chem. Soc.* 1968, **78**, 1118
- Masoero, M. and Perini, N. *Chim. Ind. (Milan)* 1955, **37**, 945

# Cloud point curves for poly(vinyl methyl ether) and monodisperse polystyrene mixtures

T. Nishi\* and T. K. Kwei

Bell Laboratories, Murray Hill, New Jersey 07974, USA

(Received 14 May 1974; revised 24 July 1974)

The compatibility behaviour of poly(vinyl methyl ether) (PVME) and monodisperse polystyrene (PS) is studied for solution cast films. The molecular weight of monodisperse PS ranges from 2100 to 2 000 000 whereas the PVME used is polydisperse and has weight-average molecular weight of 51 500. When cast from toluene solution, the mixtures undergo phase separation at elevated temperatures. The cloud point curves move to markedly lower temperatures with increasing molecular weight which is similar to the lower critical solution temperature (*LCST*) behaviour for polymer solutions. They move to lower temperatures until the molecular weight of PS reaches about 51 500.

The effect of molecular weight distribution on the cloud point of equal amounts of PS and PVME mixtures simulated by mixing two monodisperse polystyrenes of different molecular weight for PS part is accurately predicted by using weight-average molecular weight for PS in this range. However, if the molecular weight of PS exceeds about 110 000 the molecular weight dependence of cloud point temperature is reversed and the prediction for polydisperse polymer by using weight-average molecular weight fails. This phenomenon is discussed from several viewpoints including the possibility of the effect of chain entanglement.

Mixtures of PVME and PS of  $M_w = 20\,400$  were also cast from an 'incompatible' solvent, trichloroethylene. Compatibility is found to be dependent on composition and even phase-separated samples show at least one cloud point, indicating at least partial mixing of the two polymers. Finally, it is demonstrated that crosslinking of compatible films can be achieved by electron irradiation to form true interpenetrating networks. The cloud point temperatures are increased drastically after crosslinking.

## INTRODUCTION

Only a few pairs of polymers that show mutual compatibility are known<sup>1,2</sup> because of the small entropy of mixing for long polymer chains and the positive energy of mixing usually observed between polymers. However, recent results for the mixtures of polystyrene (PS) and poly(vinyl methyl ether) (PVME)<sup>3,4</sup> show their compatibility for a wide range of composition<sup>3</sup> and temperature, although compatibility is reported to depend on the nature of the solvent used. The compatible films show reversible phase separation at high temperatures<sup>4</sup>, and this cloud point temperature is associated with the lower critical solution temperature (*LCST*)<sup>5</sup>.

Detailed studies of the nature of compatibility of this system have been conducted including density, vapour sorption, diffusion and pulsed n.m.r. measurements<sup>6</sup>. The two different polymer chains in the compatible system are found to mix extensively, although pulsed n.m.r. measurements suggest that the mixture is not completely free of microheterogeneity. Negative interaction parameters were obtained for certain compositions, and it was also suggested that both *LCST* and upper critical solution temperature (*UCST*) appeared to exist for this system.

According to the thermodynamics of mixtures, the most influential factors which determine *LCST* or *UCST* behaviour in a polymer-polymer mixture<sup>5</sup> are the interaction parameter, thermal expansion or thermal pressure coefficient,

and molecular weight and molecular weight distribution. Although the contribution of each parameter was calculated for model monodisperse polymer pairs<sup>5</sup>, experimental results were too scarce to permit meaningful comparison. This is to be contrasted with the case of polymer-solvent mixtures where the effect of molecular weight and the nature of the solvent on *UCST* or *LCST*<sup>7,8</sup> have been studied in detail and compared with theory<sup>9,10</sup>.

In order to elucidate cloud point behaviour of polymer-polymer mixtures, the PS and PVME system is thought to be ideal since monodisperse PS with widely different molecular weights is available. In this paper, monodisperse PS with molecular weights ranging from 2100 to 2 000 000 are mixed at various compositions with polydisperse PVME of  $\bar{M}_w = 51\,500$  and cast from toluene solution to obtain compatible films. The effects of molecular weight and molecular weight distribution on the cloud point curves are studied. The influence of molecular weight distribution is studied by blending monodisperse PS simultaneously with PVME. We have also examined films cast from trichloroethylene solution since the latter was reported to give always incompatible films<sup>3</sup> for high molecular weight PS and PVME. In our case, a low molecular weight monodisperse PS ( $M_w = 20\,400$ ) was mixed with PVME and examined.

PS and PVME can be crosslinked by radiation<sup>11</sup>. This provides a unique opportunity to prepare a truly interpenetrating network from a compatible mixture. To examine the effect of irradiation on cloud point curves, samples were irradiated by 1 MeV electron beam at doses from 5 to 200 Mrad.

\* Resident Visitor: Tokyo Research Laboratory, Bridgestone Tire Co. Ltd, Tokyo, Japan.

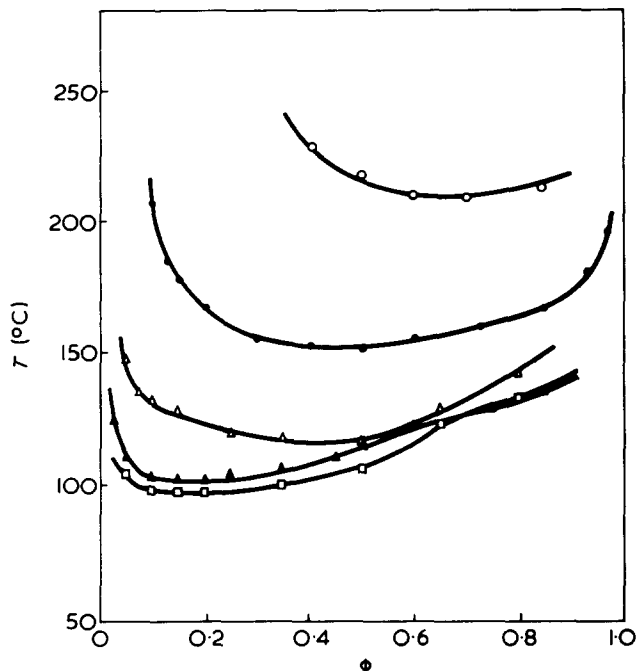


Figure 1 Cloud point curves for PVME and monodisperse PS mixture where molecular weight ( $\bar{M}_w$ ) of PS is changed:  $\circ$ , 10 000;  $\bullet$ , 20 400;  $\triangle$ , 51 000;  $\blacktriangle$ , 110 000;  $\square$ , 200 000.  $\phi$  is the weight fraction of PS

## EXPERIMENTAL

### Materials

The monodisperse PS polymers were obtained from the Pressure Chemical Co. and Table 1 lists their nominal molecular weights and the ratios of weight-average molecular weight,  $\bar{M}_w$ , to number-average molecular weight,  $\bar{M}_n$ . PVME was obtained from Cellomer Associates, Inc. and the intrinsic viscosity was 0.51 (100 cm<sup>3</sup>/g) in benzene at 20°C. The  $\bar{M}_w$  was computed to be 51 500. Both polymers were used without further purification.

Films containing PS and PVME mixtures were cast from toluene or trichloroethylene solution on glass surfaces. Initial polymer concentration was about 3 g/100 ml. The solvent evaporation process has been described elsewhere<sup>6</sup>. Film thicknesses ranged from 0.01 to 0.03 cm.

### Electron irradiation

Five samples of films, cut into about 5 mm square, were placed in a chamber with a thin polyethylene window (about 0.005 cm) and irradiated simultaneously at each dosage. A van de Graaff accelerator was used. The electron energy was 1 MeV and the dose rate was 0.5 Mrad/sec. Irradiation was carried out at room temperature under circulating nitrogen gas.

### Cloud point measurements

The film was cut into 2–3 mm square and mounted on a glass microscope slide. To ensure good heat transfer during measurements, thin spacers with 0.01 cm thickness were placed around the specimen and a cover glass was applied to protect the sample. The assembly was carefully pressed above the glass transition temperature of the film to get uniform thickness and air bubble free geometry between the glasses and the film. It was slowly cooled down to room temperature to relax residual stress due to the above operation. The assembly was then placed on a microscope hot

stage (manufactured by Reichert Co., Austria). A thermometer attached to the hot stage served as a temperature indicator. Temperature was increased at about 10°C/min and the sample was monitored through a stereomicroscope (manufactured by Bausch & Lomb Co.). The temperature at which blue coloration was first detected was recorded as the cloud point. The heating rate dependence of the bluish coloration temperature of the film was slight<sup>4</sup> and was less than 3°C from 1°C/min to 10°C/min heating rate probably because of good heat transfer for our thin samples. The temperature was increased further until slightly white opalescence appeared. Subsequently, temperature was gradually lowered. Compatible films became transparent again after this treatment. All the measurements were carried out within one week after sample preparation to avoid any effect which may arise as a result of slow phase separation<sup>6</sup>.

## RESULTS AND DISCUSSION

### Effect of molecular weight

Figures 1 and 2 show the cloud point curves of films cast from toluene. The effect of molecular weight and weight fraction,  $\phi$ , of PS on the cloud point curves are typical of the LCST phenomena commonly observed for polymer–solvent mixtures. Owing to thermal degradation of PVME above ~240°C the cloud point curves are shown only for PS with molecular weight above 10 000. These are probably the first experimental data to show the molecular weight dependence of cloud point curves for polymer–polymer mixtures of sufficiently high molecular weight.

When the molecular weight of PS is below 51 500 the cloud point curves depend greatly on the molecular weight of PS and the composition of the mixture especially at very low PS or PVME concentrations. It should be noted, however, that the molecular weight dependence of the cloud point curves levels off or even reverses with PS having molecular weight above 110 000. The significance of this unusual observation will be discussed in a later section.

In the case of polydisperse polymer–solvent systems the

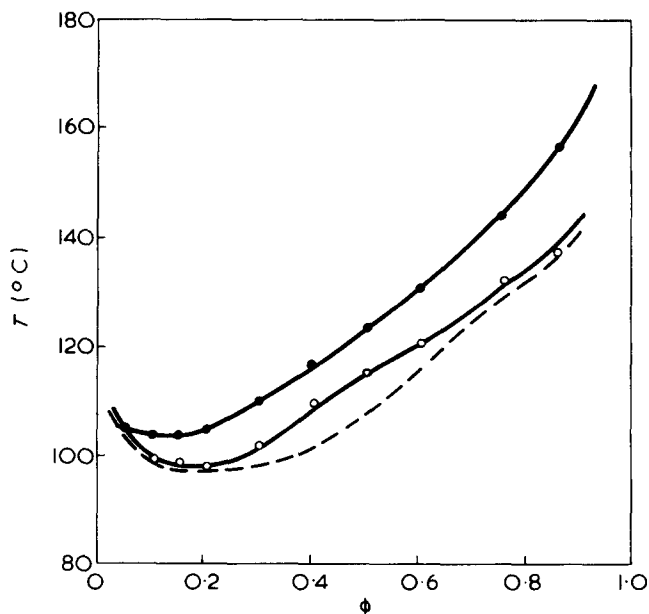


Figure 2 Cloud point curves for PVME and monodisperse PS mixture where molecular weight ( $\bar{M}_w$ ) of PS is 498 000 ( $\circ$ ) and 2 000 000 ( $\bullet$ ).  $\phi$  is the weight fraction of PS and broken line shows the result for PS with  $\bar{M}_w = 200 000$  in Figure 1

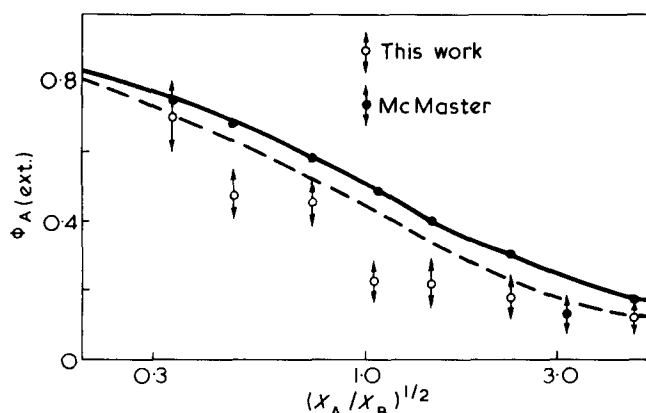


Figure 3 Composition of the extremum point  $\phi_{A(\text{ext.})}$  and reduced variables  $X_A$  and  $X_B$ , where  $X_A$  and  $X_B$  mean degree of polymerization of PS and PVME, respectively. —, equation (1); - - -, equation (2)

extremum of cloud point curve and critical point does not coincide with each other<sup>21,22</sup>. The critical point tends towards the right-hand branch of the cloud point curve as the polydispersity of the polymer increases. However, it may be worthwhile to discuss the extremum of the cloud point curve and the critical point of this system since it is systematically changing with molecular weight of PS.

Figures 3 and 4 show the composition of the extremum point,  $\phi_{A(\text{ext.})}$  and the extremum temperature,  $T_{\text{ext.}}$ , plotted against the parameter  $(X_A/X_B)^{1/2}$ , where  $X_A$  and  $X_B$  are the degree of polymerization for PS and PVME, respectively. The weight-average molecular weight is used since it is found to be a proper parameter for cloud point curves for polydisperse polymers as will be shown in the next section.

In Figure 3, McMaster's data<sup>5</sup> of extremum composition are shown as the solid circle and the agreement with our data is within experimental error. In his experiment,  $\bar{M}_w$  of PS and PVME were 236 600 and 13 320, respectively, and both were polydisperse. According to the theory of polymer solution the critical composition  $\phi_{A(\text{crit.})}$ , can be estimated for monodisperse polymer mixtures from equation (1)<sup>12</sup> based on the Flory-Huggins approximation<sup>13,14</sup>. The calculated values are indicated as a solid line in Figure 3.

$$\phi_{A(\text{crit.})} = \frac{1}{1 + (X_A/X_B)^{1/2}} \quad (1)$$

Our experimental data seem to parallel the trend predicted by equation (1), but this always predicts a higher value of  $\phi_{A(\text{crit.})}$ . One reason for the discrepancy may be due to polydispersity of PVME. For polydisperse polymer mixtures Stockmayer's equation<sup>19</sup> is more appropriate:

$$\phi_{A(\text{crit.})} = \frac{1}{1 + (X_{Aw}/X_{Bw})(X_{Bz}/X_{Az})^{1/2}} \quad (2)$$

where subscripts w and z mean weight- and z-average, respectively.

As a first approximation, we assume  $X_{Az} \approx X_{Aw}$  for PS and  $X_{Bz} \approx 3/2 X_{Bw}$  for PVME, using Schulz-Flory's most probable distribution<sup>20</sup>. Then the denominator in equation (2) becomes  $1 + 1.225 (X_{Aw}/X_{Bw})^{1/2}$  and the calculated values of  $\phi_{A(\text{crit.})}$  are represented by the broken line. Although the agreement between equation (2) and experimental results is still far from perfect, the correction for polydispersity is certainly in the right direction.

In Figure 4, the data by McMaster and by Bank *et al.*<sup>4</sup> on extremum temperatures are shown and they differ from our data. Bank *et al.* gave only number-average molecular weight  $\bar{M}_n$  for PS and PVME.  $\bar{M}_n$  for PS was given as 104 000 or 150 000 and  $\bar{M}_n$  for PVME as 524 000. They did not specify which PS was used. Therefore their results have less importance in this report. The rather high extremum temperature found by McMaster may be ascribed to the low molecular weight PVME used in his study.

In order to explain the results in Figures 1–4, it may be necessary to take into account not only the molecular weight and molecular weight distribution of each polymer but also the difference between the thermal expansion and the thermal pressure coefficients of the two polymers as suggested by McMaster<sup>5</sup>. According to his model calculation, a difference of several per cent in thermal expansion coefficients or thermal pressure coefficients is enough to change  $T_{\text{crit.}}$  drastically. Whether McMaster's contention is sufficient to account for our observation cannot be assessed at present because of lack of experimental data.

Another possibility which we like to entertain is the influence of molecular entanglement. For PS, the critical chain length for the formation of entanglement is about 300 to 500 ( $M_w \approx 30\,000$  to  $50\,000$ )<sup>15–17</sup>. For PVME, the entanglement chain length is not known but it is probably about 300 ( $M_w \approx 17\,000$ ) or less because the chain is more flexible. The two polymers are supposed to be mixed well in toluene and there should be many molecular entanglements between PS and PVME molecules in concentrated solutions, i.e. as solvent evaporates. After evaporation of the solvent, the entanglement between different chains can be preserved and can act to hinder the phase separation at high temperatures although separation is favoured on thermodynamic grounds. This can explain qualitatively the decrease of molecular weight dependence of cloud point curves where  $\bar{M}_w$  of PS exceeds 51 000 or 110 000. Based on this reasoning, we have attempted to introduce permanent entanglement (i.e. crosslinks) into the system by electron irradiation. As will be seen later, crosslinking increases the cloud point temperature quite drastically.

The other possibility to explain the reversal in extremum temperatures of the cloud point curves at higher molecular weight range for PS is the polydispersity of the monodisperse PS in the polymer-polymer mixtures. From Table 1,

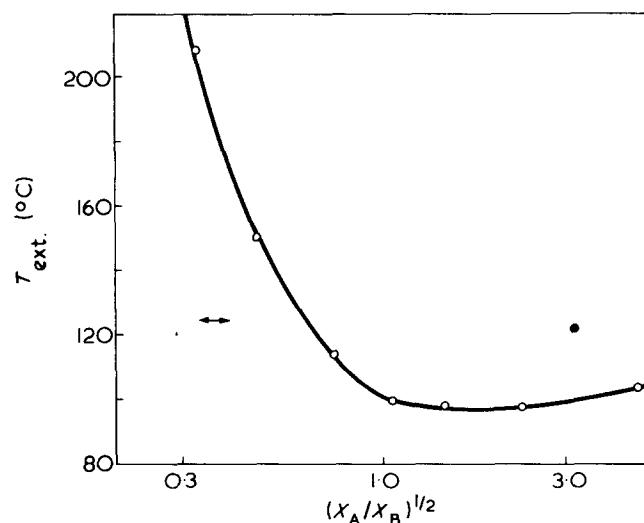
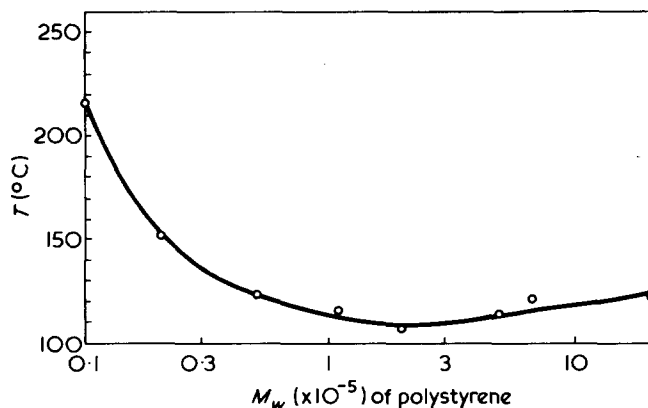


Figure 4 Temperature of the extremum point  $T_{\text{ext.}}$  and reduced variables  $X_A$  and  $X_B$ , where  $X_A$  and  $X_B$  mean degree of polymerization of PS and PVME, respectively.  $\circ$ , This work;  $\bullet$ , McMaster;  $\leftrightarrow$ , Bank *et al.*

Table 1 Monodisperse polystyrene samples

Nominal molecular weight	$\bar{M}_w/\bar{M}_n (\leq)$
2 100	1.10
4 000	1.10
10 000	1.06
20 400	1.06
51 000	1.06
110 000	1.06
200 000	1.06
498 000	1.20
670 000	1.10
2 000 000	1.20


 Figure 5 Molecular weight  $\bar{M}_w$  dependence of cloud point temperature for PS/PVME = 50:50 mixtures

the polydispersity of the monodisperse PS increases slightly as the molecular weight of PS exceeds 498 000. However, this will cause the sharpening of the cloud point curves and the extremum temperature would decrease with increase in molecular weight distribution of monodisperse PS if we take into account the model calculation for polydisperse polymer-polymer<sup>5</sup> and polymer-solvent<sup>21</sup> systems by McMaster and Koningsveld *et al.*\* Their calculations are contrary to our experimental results. Moreover, the results in Figure 6 for the effect of molecular weight distribution indicate that it may not be the increased polydispersity of the higher molecular weight monodisperse PS that causes this effect.

The last possibility is the influence of the microheterogeneous structure in the mixture, as described in our earlier paper<sup>6</sup>, which was detected by pulsed n.m.r. as two spin-spin relaxation times. This concept is now under investigation and will be reported in the near future.

#### Effect of molecular weight distribution

Figure 5 shows molecular weight dependence of PS of the cloud point temperature for PS/PVME = 50:50. The effect of molecular weight distribution is simulated by mixing different amounts of two PS polymers of different molecular weights. The composition was always kept at PS/PVME = 50:50. Blends of PS with  $\bar{M}_w = 110\ 000$  and 10 000 or with  $\bar{M}_w = 670\ 000$  and 10 000 were chosen since the trend in cloud temperature changes when  $\bar{M}_w$  of PS is above 110 000.

\* Koningsveld *et al.* calculated the effect of polydispersity for polymer-solvent system with UCST and they showed that extremum temperature would increase with the polydispersity of the polymer. On the other hand, our system has lower critical solution temperature behaviour and the extremum temperature would decrease with the polydispersity of the polymer.

Figure 6 shows the results for PS blends with  $\bar{M}_w = 110\ 000$  and 10 000. As the concentration of PS with  $\bar{M}_w = 10\ 000$  increases, the cloud point increases as expected from Figure 5. Also in Figure 6, cloud point temperatures predicted from  $\bar{M}_n$ ,  $\bar{M}_w$ , and  $\bar{M}_z$  for the PS blends are indicated by using equations (3) to (5) and Figure 5:

$$\bar{M}_n = \frac{M_1 M_2}{\phi M_2 + (1 - \phi) M_1} \quad (3)$$

$$\bar{M}_w = \phi M_1 + (1 - \phi) M_2 \quad (4)$$

$$\bar{M}_z = \frac{\phi M_1^2 + (1 - \phi) M_2^2}{\phi M_1 + (1 - \phi) M_2} \quad (5)$$

where  $M_1$  and  $M_2$  are the molecular weights for each monodisperse PS respectively and  $\phi$  is the weight fraction of PS with  $M_1$ . It is apparent that  $\bar{M}_w$  is a good measure for predicting the cloud point curves of polydisperse polymers. It is also consistent with theoretical prediction<sup>5</sup>.

Figure 7 shows similar results for mixed PS with  $\bar{M}_w = 670\ 000$  and 10 000. In this case, however, minima in cloud temperatures appear at  $\phi = 0.025, 0.64$  and 0.992 for curves predicted from  $\bar{M}_n$ ,  $\bar{M}_w$  and  $\bar{M}_z$ , respectively, because of the minimum cloud point temperature around  $\bar{M}_w = 250\ 000$  in Figure 5. The agreement between the data and those calculated from  $\bar{M}_z$  below  $\phi = 0.7$  is fortuitous. The reason for the discrepancy is not clear, and it might be due to the effect of molecular entanglement or other causes discussed in the previous section.

#### Effect of solvent

Figure 8 shows the cloud point curve for PS-PVME mixtures cast from trichloroethylene solution. The molecular

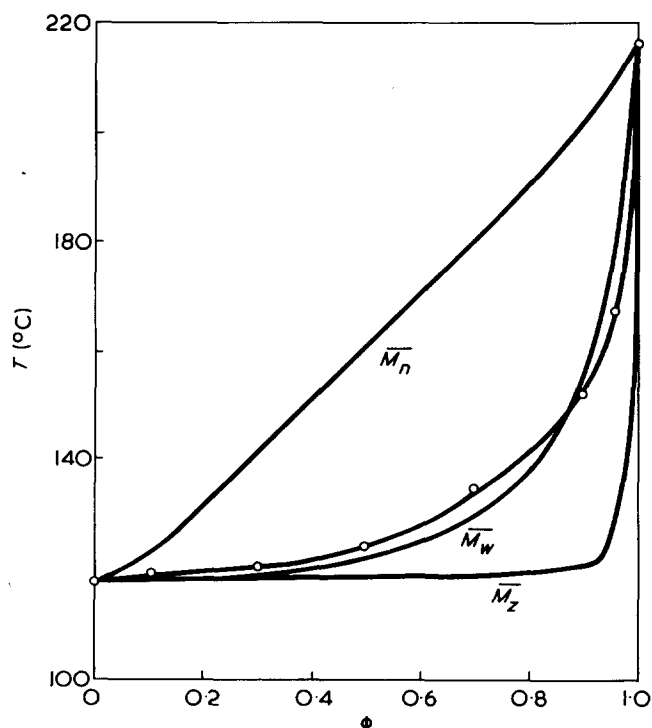


Figure 6 Cloud point temperatures for PS/PVME = 50:50 mixture where PS is a mixture of two monodisperse PS (1) and PS (2). The weight fraction of PS (1) is  $\phi$  and the molecular weights of PS (1) and PS (2) are 10 000 and 110 000, respectively.  $\bar{M}_n$ ,  $\bar{M}_w$  and  $\bar{M}_z$  curves are predicted based on equations (3)–(4) and Figure 5 for the PS (1) and PS (2) mixture

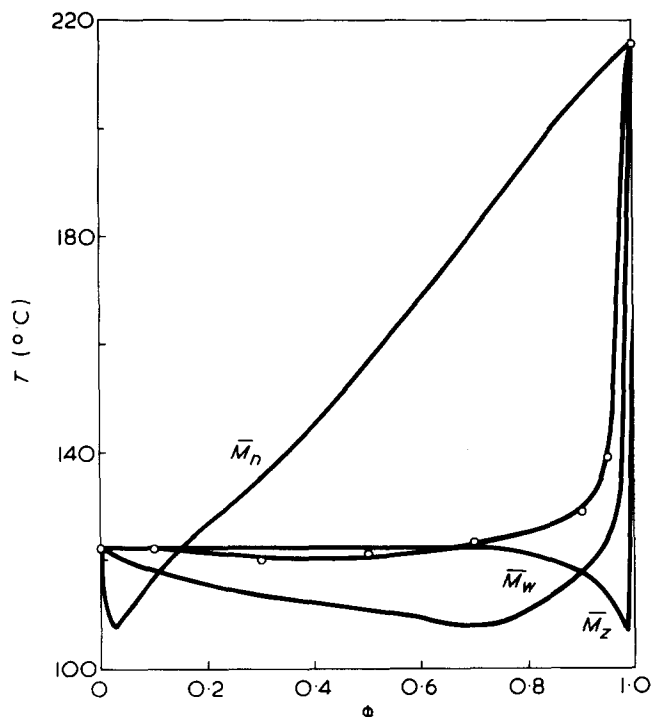


Figure 7 Cloud point temperatures for PS/PVME = 50:50 mixture where PS is a mixture of two monodisperse PS (1) and PS (2). The weight fraction of PS (1) is  $\phi$  and the molecular weights of PS (1) and PS (2) are 10 000 and 670 000, respectively.  $\bar{M}_n$ ,  $\bar{M}_w$  and  $\bar{M}_z$  curves are predicted based on equations (3)–(5)

weight of the monodisperse PS was 20 400. Homogeneous, clear films were obtained at room temperature when the PS weight fraction  $\phi$  was lower than 0.25. Films were almost clear yet had slight heterogeneity when  $\phi$  was between 0.25 and 0.30 or when  $\phi$  was higher than 0.97. For PS fractions between 0.40 and 0.93 films were usually heterogeneous.

Upon heating, the clear films gave the same cloud point temperature as that cast from toluene solution. The solid line in Figure 8 represents the cloud point curve for films cast from toluene solution. For the heterogeneous films two cloud points appeared to exist. If we describe heterogeneities in these films as islands in the sea, then either the sea or the islands became cloudy first and then the rest of the film also turned cloudy at a higher temperature. For films with  $\phi$  between 0.4 and 0.7 the sea part became cloudy first and between 0.8 and 0.93 the island part first. The first cloud point temperature was almost constant ( $\sim 157^\circ\text{C}$ ) regardless of the composition of the film. It was difficult to detect accurately the second cloud point temperature except for the film with  $\phi = 0.97$  since at higher temperature the sea or the island part which showed first cloud point became too whitish. Upon cooling, all films returned to their original appearances if the temperature was not brought up much higher than the first cloud point temperature.

It is clear from Figure 8 that the heterogeneous films are not completely phase separated into pure PS and PVME domains. Rather, PVME rich and PS rich phases result upon evaporation of trichloroethylene. In order to explain our observation it seems logical to assume the existence of upper critical solution temperature (UCST) for this system. If the UCST curve crosses room temperature at  $\phi \approx 0.30$  and  $\approx 0.97$ , samples with  $\phi$  between 0.30 and 0.97 should always separate into PVME rich phase ( $\phi \approx 0.30$ ) and PS rich phase ( $\phi \approx 0.97$ ). Upon heating, the PVME rich phase which happens to have lower cloud point temperature

would show an almost constant first cloud point temperature.

The experiments reported by Bank *et al.*<sup>3</sup> used PS and PVME of much higher molecular weight than ours and the crossing points between the UCST curve and room temperature must have occurred at very low and very high  $\phi$ . Therefore, they obtained all incompatible films and they concluded, quite properly, that phase separation resulted in almost pure PS and PVME as evidenced by their  $T_g$  results.

In the next series of experiments, the solvent trichloroethylene was rapidly evaporated and the resulting films ( $0.97 > \phi > 0.30$ ) became heterogeneous on a very fine scale and looked white. They were found to turn transparent again after annealing at  $60\text{--}90^\circ\text{C}$  for a period of 10 to 100 min and they showed the same cloud point temperatures as the films cast from toluene solution when heated above  $150^\circ\text{C}$ . Apparently, there seems to be a critical size of heterogeneity below which annealing can bring the system to the thermodynamically favoured state. However, it was very difficult to obtain UCST curves accurately.

It is known that a small difference in polymer–solvent interaction has a marked effect on polymer incompatibility in the polymer–polymer–solvent ternary system<sup>18</sup>. Therefore, the observed effect of solvent on the properties of solid films can be regarded as an extrapolation of the effect of asymmetry in the polymer–solvent interactions in the ternary system.

#### Effect of electron irradiation

Figure 9 shows effect of electron irradiation on a cloud point temperatures for PS/PVME = 50:50 mixture where the molecular weight of monodisperse PS has been changed from 51 000 to 2 000 000. The cloud point temperature increases drastically at around 50 to 100 Mrad. In this range it was noticed that the temperature gap between the onset of blue coloration and white opalescence also increased greatly. For samples which show cloud point temperatures higher than  $195^\circ\text{C}$  in Figure 9, the whitish coloration is limited only to the periphery of the film. The phase separation behaviour observed in this limited area was probably accompanied by oxidative degradation and it was not reversible after cooling.

Both PS and PVME are classified as radiation crosslink-

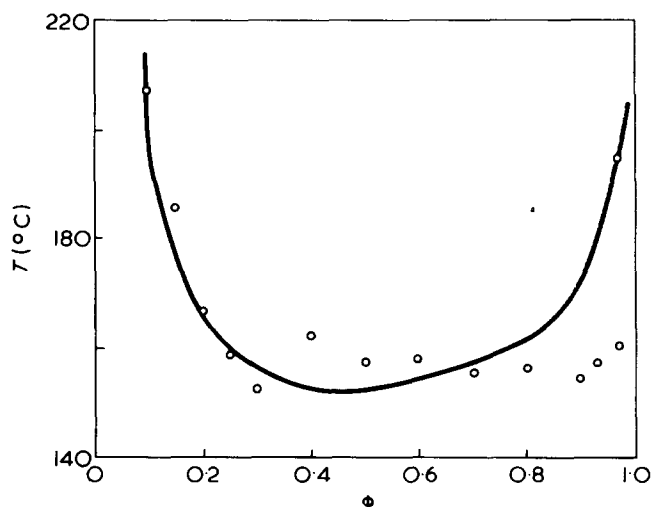


Figure 8 Cloud point curve for PVME and monodisperse PS with molecular weight 20 400 cast from trichloroethylene solution ( $\circ$ ).  $\phi$  is the weight fraction of PS and solid line represents the cloud point curve for the same composition cast from toluene solution



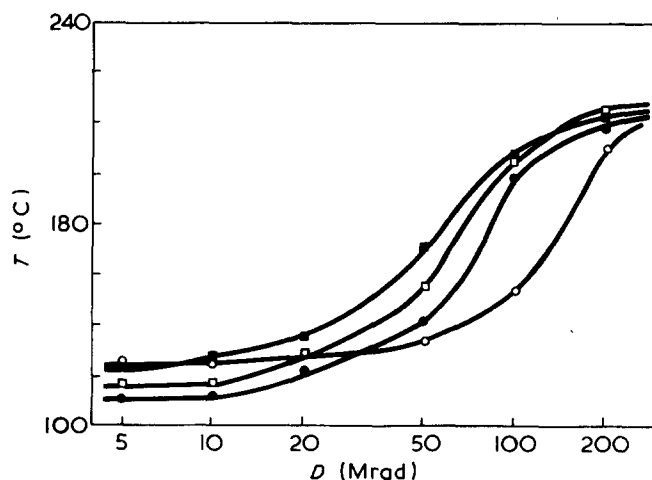


Figure 9 Electron irradiation dose  $D$  dependence of cloud point temperature for PS/PVME = 50:50 where the molecular weight of PS has been changed:  $\circ$ , 51 000;  $\bullet$ , 110,000;  $\square$ , 498 000;  $\blacksquare$ , 2 000 000

able polymers<sup>11</sup> and the irradiated mixtures swell but do not dissolve in toluene. The doses for incipient gel formation are dependent on the molecular weights of monodisperse PS in the mixture and they are about 10, 20, 50 and 100 Mrad for the mixtures with PS molecular weight 2 000 000, 498 000, 110 000 and 51 000, respectively. It is most probable that the crosslinking between PS and PVME has taken place to form an interpenetrating network and the cloud point temperature increases as a result of the restricted mobility of the chains.

## CONCLUSIONS

Many aspects of polymer-polymer compatibility behaviour are clarified experimentally by using polydisperse PVME and monodisperse PS samples with molecular weight varying from  $1 \times 10^4$  to  $2 \times 10^6$ .

The molecular weight dependence of cloud point curves for polymer-polymer mixtures is obtained for the first time for polymer pairs having sufficiently high molecular weight. For PS-PVME mixtures cast from toluene, LCST behaviour is observed and the cloud points decrease rapidly with increase in PS molecular weight until about 51 000. However, the molecular weight dependence of cloud point curves levels off or even reverses for mixtures with PS having molecular weight higher than about 110 000. Several possibilities for the phenomena are suggested based on thermodynamic effect, effect of molecular entanglement and effect of microheterogeneous structure in the mixture.

The effect of molecular weight distribution on cloud point curves is simulated by mixing PVME with a blend of two PS fractions of different molecular weight. When the

molecular weight of both PS are lower than 110 000, the cloud point temperature is accurately predicted by using weight average molecular weight. However, if the molecular weight of either PS is higher than 110 000, the above prediction is found to be ineffective and again the possibility of the effect of molecular entanglement is suggested.

The effect of the nature of solvent is studied using trichloroethylene. The compatibility behaviour is dependent on the composition of the mixture and even in heterogeneous films phase separation is incomplete. This is explained adequately by the existence of UCST near room temperature. These solvent effects can be rationalized as the consequence of the effect of asymmetry in the polymer-solvent interactions in the ternary system.

Finally, it is demonstrated that the electron irradiation can crosslink compatible films to form an interpenetrating network and drastically increase the cloud point temperature.

## ACKNOWLEDGEMENT

We are grateful to H. N. Vazirani for irradiating our films with electron beams.

## REFERENCES

- 1 Bohn, L. *Kolloid Z.* 1966, 213, 55
- 2 Krause, S. J. *Macromol. Sci. (C)* 1972, 7, 251
- 3 Bank, M., Leffingwell, J. and Thies, C. *Macromolecules* 1971, 4, 44
- 4 Bank, M., Leffingwell, J. and Thies, C. *J. Polym. Sci. (A-2)* 1972, 10, 1097
- 5 McMaster, L. P. *Macromolecules* 1973, 6, 760
- 6 Kwei, T. K., Nishi, T. and Roberts, R. F. *Macromolecules* 1974, 7, 667
- 7 Freeman, P. I. and Rowlinson, J. S. *Polymer* 1960, 1, 20
- 8 Siow, K. S., Delmas, G. and Patterson, D. *Macromolecules* 1972, 5, 29
- 9 Orofino, T. A. and Flory, P. J. *J. Chem. Phys.* 1957, 26, 1067
- 10 Eichinger, B. E. and Flory, P. J. *Trans. Faraday Soc.* 1968, 64, 2035
- 11 Chapiro, A. 'Radiation Chemistry of Polymeric Systems', Interscience, New York, 1962
- 12 Scott, R. L. *J. Chem. Phys.* 1949, 17, 279
- 13 Huggins, M. L. *J. Chem. Phys.* 1941, 9, 440
- 14 Flory, P. J. *J. Chem. Phys.* 1941, 9, 660
- 15 Fox, T. G. and Flory, P. J. *J. Polym. Sci.* 1954, 14, 314
- 16 Beng, G. C. and Fox, T. G. *Adv. Polym. Sci.* 1968, 5, 261
- 17 Porter, R. S. and Johnson, J. F. *Rheol. Acta* 1968, 7, 332
- 18 Zeman, L. and Patterson, D. *Macromolecules* 1972, 5, 513
- 19 Stockmayer, W. H. *J. Chem. Phys.* 1949, 17, 588
- 20 Flory, P. J. 'Principles of Polymer Chemistry', Cornell Univ. Press, Ithaca, 1953
- 21 Koningsveld, R. and Staverman, A. J. *J. Polym. Sci. (A-2)* 1968, 6, 349
- 22 Šolc, R. *Macromolecules* 1970, 3, 665

# Effects of molecular weight and chain ends on glass transition of polystyrene

Alfred Rudin and Dennis Burgin

Department of Chemistry, University of Waterloo, Waterloo, Ontario N2L 3G1, Canada

(Received 28 May 1974; revised 2 August 1974)

The main glass transition temperatures,  $T_g$  of narrow distribution anionic polystyrene samples have been measured by differential thermal analysis (d.t.a.). The d.t.a. data were verified by differential scanning calorimetry. Effects of heating rates were eliminated by extrapolating observed  $T_g$  values to a standard heating mode of  $1^\circ\text{C}/\text{min}$  in a  $T_g$  vs.  $\log$  (heating rate) relation. The variations of  $T_g$  peak height and temperature with heating rate and polymer molecular weight ( $M$ ) agree with conclusions from other reports of d.t.a. work. The  $T_g$  values corrected for heating rate effects agree well with figures reported in studies with d.t.a. and other techniques for locating vitrification temperatures.

The volumes attributable to end groups differ significantly between anionic and thermally initiated polystyrenes at temperatures above  $T_g$ . A comparison of  $T_g$  values of both polystyrene types provides a direct test of the iso-free volume model of the vitrification process. A common  $T_g$  vs.  $M$  relation was found for anionic and thermally initiated polystyrenes, regardless of chain end nature. This comparison is not consistent with the concept that vitrification is governed by free volume defined as the difference between specific volume of the polymer and a reference volume. Our results are compatible with several other mechanisms which have been suggested for the glass transition.

## INTRODUCTION

The glass transition of a polymer sample is observed when the short time limit of viscous response at the particular temperature and pressure is comparable to the time scale of the experiment. The fundamental mechanistic problem involves the means whereby temperature, pressure and molecular weight changes influence the polymer relaxation time. A large number of explanations have been offered<sup>1-3</sup>. This paper focuses on the assumption that the glass transition is an iso-free volume state. Our concern here is not primarily with questions as to whether the glass transition can be related to thermodynamic state variables<sup>4</sup>, existence of multiple transitions<sup>2</sup>, or even with the choice of a particular reference specific volume in the definition of free volume<sup>5</sup>.

Fox and Flory<sup>6</sup> first proposed that the glass transition represents an iso-free volume state. This conclusion has been variously supported and challenged, depending on the particular experimental results<sup>1-5</sup>. Some of the difficulties in this connection are evidently related to experimental inaccuracies and to uncertainties in the meanings of viscosity and free volume at the glass transition.

Particular evidence may tend to favour one view<sup>5</sup> or the other<sup>7</sup>, but clear-cut answers evidently require further information. Much of the available evidence can be interpreted in terms of alternate models and a case may even be made<sup>1</sup> that there is no inherent controversy between the various views.

The present report contributes some additional evidence regarding the nature of the transition phenomenon. It is a direct test of current iso-free volume concepts and concerns results on polystyrenes, which formed the initial basis of this model. The influence of molecular weight on the glass transition,  $T_g$ , of this polymer is examined in experiments which parallel the important pioneering work of Fox and Flory<sup>6,8</sup>.

Free volume derives from three principal sources: motion of chain ends, motion of side chains and motion of the main chain<sup>5</sup>. This study examines the glass transitions of polystyrenes which differ only in the specific volumes assignable to chain ends. The conclusions are independent of the particular model used to estimate free volume from chain end volumes if it is accepted that differences in the latter volumes must lead to free volume variations.

Fox and Flory<sup>6,8</sup> studied the effects of molecular weight on  $T_g$  and specific volumes of thermally initiated polystyrenes. A recent study from this laboratory<sup>9</sup> has shown that volumes attributable to end groups differ significantly between anionic and thermally initiated polymers. Specific volumes of end groups in anionic polystyrene liquids are larger and increase more rapidly with temperature in the temperature range (170–237°C) studied. Data of Bender and Gaines<sup>10</sup> which were developed in a different context and extend to lower temperatures, are also consistent with this conclusion. One would expect from the iso-free volume model that  $T_g$  values of anionic and thermally initiated polystyrenes would coincide at reasonably high molecular weights and differ significantly at low molecular weights where chain end concentrations are relatively more important. This assumption is tested in this report and it is shown that the two polymer types do not differ significantly in  $T_g$  at given molecular weight.

Glass transition temperatures were measured in this work by differential thermal analysis (d.t.a.). Application of this technique for  $T_g$  measurements of polymers was first reported by Keavney and Eberlin<sup>11</sup>. Its use in the study of molecular weight effects on polystyrene  $T_g$  has been reported once, for whole polymers<sup>12</sup>. A method is described in this report for eliminating d.t.a. instrument effects on  $T_g$  and the validity of the present data is established by comparison with results of other workers.

The d.t.a. data obtained here were verified by differential

scanning calorimetry (d.s.c.) measurements. A relation between molecular weight of narrow distribution polymers and  $T_g$  is presented here which seems to be universally applicable and which permits estimation of  $T_g$  of infinitely high molecular weight samples ( $T_g^\infty$ ) from data on lower molecular weight polymers.

## EXPERIMENTAL

### Materials

The anionic polystyrenes studied are commercial samples available from Pressure Chemical Co. Molecular weights of these materials are listed in Table 1. These values were determined as reported elsewhere<sup>9</sup>. A Dow anionic sample (S102)<sup>13</sup> was also included in this study. The influence of uncertainties in molecular weight ( $M$ ) values on conclusions which can be reached in studies such as this has been noted before<sup>9</sup>.

All the usual molecular weight averages coincide within experimental error for samples with molecular weight distributions as narrow as those used in this work. It is not necessary, then, to distinguish between  $\bar{M}_w$ ,  $\bar{M}_n$  and so on, although  $\bar{M}_n$  is clearly the average which determines specific volume and presumably free volume<sup>6,8,9,14</sup>.

### Methods

A Du Pont model 900 differential thermal analyser was used. Nitrogen atmosphere was provided by flushing the

gas through the sample holder at a controlled rate. Thermocouple contacts were surrounded with glass wool for shielding from drafts caused by the nitrogen flow. Dynamic gas flow has been reported to increase peak heights, without changing peak temperatures<sup>15</sup>.

Before each experiment the chromel-alumel sample thermocouple tip was cleaned by burning off contamination in a gas flame. Care was taken to prevent heating of the thermocouple past a dull red colour. Thermocouples and samples tubes were handled with rubber gloves to prevent transfer of moisture from the operator's fingers.

Glass beads were used as the reference substance. The sample cell contained undiluted polymer. The polymer samples were obtained as powders and were used as received. In all cases 3 mm of sample (or reference) was packed as uniformly and reproducibly as possible into 2 mm diameter glass 'micro' tubes supplied with the d.t.a. apparatus. The thermocouples were centred in the tubes and positioned to touch the bottoms of the glass cells.

$T_g$  of polystyrenes was obtained by Martin and Kase<sup>12</sup> from d.t.a. thermograms as the temperature corresponding to intersection of extrapolated base line and peak curves. This procedure, which relates  $T_g$  to the temperature of onset of the endotherm in the heating mode, was not applicable in the present experiments because non-linear base lines made extrapolation uncertain. Instead,  $T_g$  was defined as the intersection temperature from extrapolation of the longest straight line portions of the peak sides. This is the

Table 1  $T_g$  data for polystyrene

Sample* Code	Molecular weight	Heating rate (°C/min)	$T_g$ (obs.) (°C)	$T_g$ (corr.) (°C)	$\Delta T$ (°C) at $T_g$	Degree of polymerization
12b	2 100	1.8	—	—	0.0	20.2
	2 100	4.5	68.0	63.0	0.14	20.2
	2 100	9.0	70.3	63.0	0.26	20.2
	2 100	9.0	70.0	62.7	0.27	20.2
	2 100	17.9	31.8	62.2	0.30	20.2
	2 100	26.4	73.8	62.9	0.60	20.2
	2 100	34.7	74.5	62.7	0.39	20.2
	2 100	34.7	75.0	63.2	0.92	20.2
	2 100	34.7	74.8	63.0	0.62	20.2
	2 100	43.7	75.4	62.9	0.65	20.2
	11a, 11b	4 000	17.9	80.5	70.9	0.03
4 000		26.4	82.0	71.1	0.26	39.2
4 000		26.4	82.0	71.1	0.10	39.2
4 000		34.7	88.0	76.2	—	39.2
4 000		34.7	88.0	76.2	0.41	39.2
4 000		34.7	88.0	76.2	0.43	39.2
4 000		43.7	89.0	76.5	0.40	39.2
4 000		43.7	89.0	76.5	0.42	39.2
8b	10 000	34.7	100.0	88.2	0.07	96.2
	10 000	34.7	99.5	87.7	0.11	96.2
	10 000	43.7	100.8	88.3	0.08	96.2
2b	20 400	34.7	105.5	93.7	0.06	196
	20 400	34.7	105.3	93.5	0.03	196
	20 400	43.7	106.5	94.0	0.06	196
7a	51 000	9.0	107.5	100.2	0.02	490
	51 000	17.9	109.3	99.7	0.02	490
	51 000	26.4	109.8	98.9	0.02	490
	51 000	34.7	111.8	100.0	0.03	490
	51 000	34.7	112.0	100.2	0.06	490
	51 000	43.7	112.8	100.3	0.07	490
Dow S102	82 000	34.7	109.3	97.5	0.06	788
	97 200	34.7	112.5	100.7	0.03	934
4a	97 200	34.7	112.5	100.7	0.03	934
	97 200	43.7	114.3	101.8	0.06	934
1c	200 000	34.7	112.5	100.7	0.03	1920
	200 000	43.7	114.3	101.8	0.05	1920
5a	498 000	34.7	112.5	100.7	~0.005	4780
14a	1 800 000	34.7	—	—	0.00	17320

\* Pressure Chemical Co.

method used to locate phase transitions by Vassallo and Harden<sup>16</sup> and others. Martin and Kase<sup>12</sup> reported  $T_g = 100^\circ\text{C}$  for an anionic polystyrene with  $\bar{M}_w$  187 000. Our data, given below, indicate a  $T_g$  of about  $101^\circ\text{C}$  for a narrow molecular weight distribution polymer with the given molecular weight. The agreement between the two studies is thus good, considering the differences in interpretation of the differential thermograms.

It has been reported that annealing was necessary to obtain good thermograms of commercial polystyrenes. This was attributed to the presence of stresses frozen into the polymer during extrusion and subsequent granule cutting<sup>12</sup>. A differential scanning calorimeter study of a commercial polystyrene has also indicated that prolonged annealing at  $200^\circ\text{C}$  was required to erase the influence of thermal history on the specific heat of the polymer<sup>17</sup>. The effects on  $T_g$  were minimal, however, in the latter report.

In this study annealing was found to be unnecessary and, in fact, undesirable. Duplicate specimens which were not annealed showed excellent reproducibility at fixed experimental conditions. Samples which were annealed by heating to  $130^\circ\text{C}$  in an initial experiment and were tested again after cooling had much smaller or no endothermic peaks. When a peak was obtained in second or subsequent heating experiments its location was found to coincide with the endothermic peak in the first experiment, to within the normal experimental error.

The present results appear to be consistent with both cited reports. Our anionic polystyrene samples have very different shear and thermal histories from the commercial polymers studied by Martin and Kase<sup>12</sup>. The anionic polymers have presumably never been heated into the melt temperature range and are free of extrusion and freezing stresses. Thus, annealing does not shift the observed  $T_g$ . Inadvertent annealing during the experimental heating cycle does apparently change the relative heat capacities of the material above and below  $T_g$  sufficiently to diminish the observed endotherm in the glass transition range. This is qualitatively consistent with the report of Currie and Dole<sup>17</sup>. The apparent elimination of  $T_g$  effects with some of our samples is an artifact of the particular sample, the time-temperature conditions during the heating cycle and the sample size and instrument sensitivity.

The effect of sample size on  $T_g$  was not investigated. The largest sample size consistent with the use of 'micro' sample tubes in the Du Pont d.t.a. apparatus was used to maximize the endothermic peak observed during heating. This corresponded to a sample depth of 3 mm in the particular cell.

No exothermic peak could be detected during cooling of the polystyrene samples. Two factors seem to be responsible for this observation. In the first place, annealing of the specimens during the heating mode would reduce the magnitude of the cooling mode  $T_g$  exotherm for reasons mentioned above. Secondly, the apparatus used limited cooling rates to a maximum of about  $20^\circ\text{C}/\text{min}$ . These relatively low cooling rates produce smaller d.t.a. peaks. Linear cooling rates were not attainable over the whole temperature range in any event.  $T_g$  is most easily detected by this method with lower molecular weight polystyrenes. In these cases the glass temperatures are at lower absolute temperatures where the non-linear cooling rates which could be achieved were even slower. Thus the sizes of the most easily detectable peaks were depressed the most. All  $T_g$  values reported here were measured during heating experiments.

The absolute value of the d.t.a. temperature scale was confirmed by measuring melting points of *trans*-azobenzene,

benzil and acetanilide. The respective temperatures cited in the literature are  $68.5^\circ$ ,  $95.0^\circ$  and  $114.3^\circ\text{C}$ . This range coincides with the limits of the polystyrene  $T_g$  values reported here. The melting points were identified as the intersection of the peak sides, in accord with the procedure used to locate polystyrene glass transition temperatures. The measured melting points coincided with the values cited to within  $0.5^\circ\text{C}$  at heating rates  $\leq$  about  $10^\circ\text{C}$ . We conclude that the  $T_g$  temperatures reported for anionic polystyrenes are free of systematic error.

## RESULTS

### Peak magnitudes

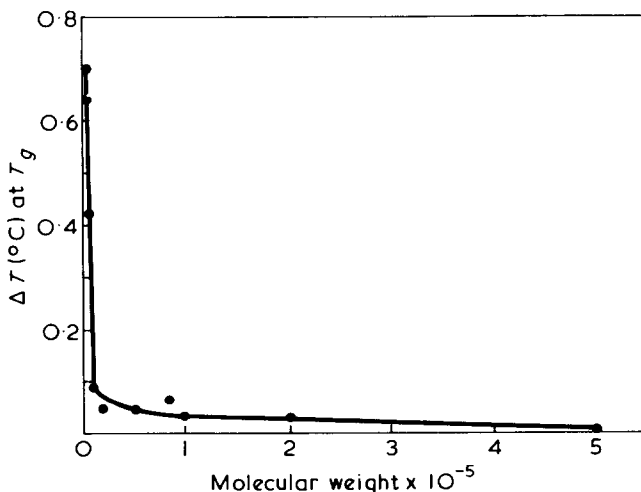
Subject to certain simplifying assumptions, the temperature difference,  $\Delta T$ , between a sample of fixed dimensions and the reference in the d.t.a. experiment is expected to be proportional to the heating rate and inversely related to the thermal diffusivity of the sample material<sup>18</sup>. Since thermal diffusivity will be related directly to polymer viscosity and hence inversely to molecular weight,  $\Delta T$  may be predicted to be less for high than for low molecular weight polymers.

This is indeed the observed effect. *Figure 1* records  $\Delta T$  ( $^\circ\text{C}$ ) figures for  $34.7^\circ\text{C}/\text{min}$  heating rate abstracted from the complete set of results in *Table 1*. The shape of the experimental curve is as expected. A sample with molecular weight  $1.8 \times 10^6$  produced no detectable  $T_g$  (i.e.  $\Delta T = 0$ ) under the particular experimental conditions with a heating rate of  $34.7^\circ\text{C}/\text{min}$ . This datum point, which is consistent with the others, is not shown in *Figure 1*.

The expected increase of  $\Delta T$  of a given sample at higher heating rates was observed. The data, which are somewhat scattered, are recorded in *Table 1*. A linear relation, however, was not found between  $\Delta T$  and heating rate. Some of the variations in replicate values of  $\Delta T$  may be attributed to differences in sample packing and thermocouple placements.

### Heating rate effects

As expected, the  $T_g$  values measured during the heating mode increased at faster heating rates. *Figure 2* summarizes the experimental data. The data are linear in a temperature/log (heating rate) representation. This relation is as reported by Wunderlich and Bodily<sup>19</sup> for d.t.a. of an annealed polystyrene with  $\bar{M}_w \sim 350\,000$ . Our data points for anionic poly-



*Figure 1* Endotherm peak height ( $\Delta T$ ) as a function of sample molecular weight at heating rate of  $34.7^\circ\text{C}/\text{min}$

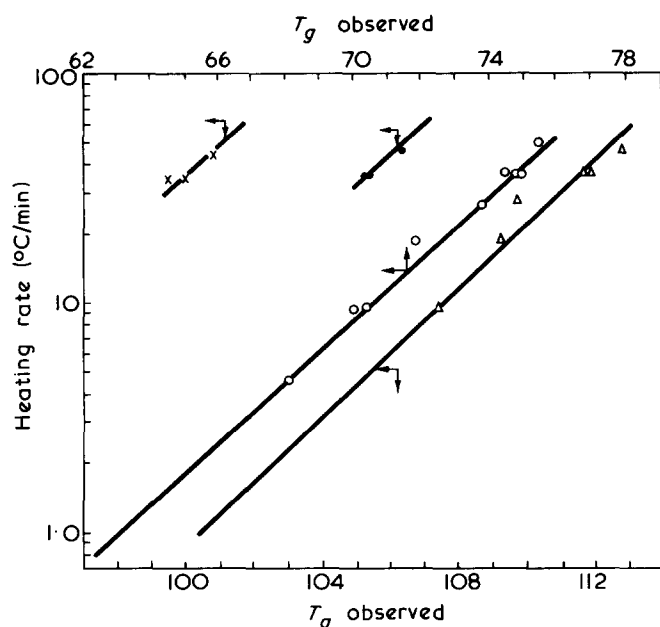


Figure 2 Observed  $T_g$  values as functions of d.t.a. heating rates. x,  $M = 10\,000$ ; •,  $M = 20\,400$ ; o,  $M = 2100$ ;  $\Delta$ ,  $M = 51\,000$

styrenes with molecular weights  $\geq 200\,000$  fit the heating rate relation given in this reference.

Plots such as those in Figure 2 allow extrapolation of measured  $T_g$  values to standard conditions of  $1^\circ\text{C}/\text{min}$  heating rates [ $\log(\text{heating rate}) = 0$ ]. The estimated  $T_g$  at this heating rate is presumably a 'true' value independent of experimental artifacts. Comparison with results of other measurements below indicates that this expectation is realized.

Experimentally,  $T_g$  could not be detected at a heating rate of  $1.8^\circ\text{C}/\text{min}$  even with the molecular weight 2100 polystyrene which yielded the largest endotherms. Thus the only way to determine a true  $T_g$  was by extrapolation from faster, experimentally accessible heating rate results. Fortunately, the change in  $T_g$  with a given change in heating rate is essentially the same for all the polystyrenes. The extrapolated  $1^\circ\text{C}/\text{min}$   $T_g$  was  $11.6^\circ\text{C}$  less than the  $T_g$  measured at  $34.7^\circ\text{C}/\text{min}$  heating rate with the 2100 molecular weight sample, for example, and the corresponding difference was  $11.9^\circ\text{C}$  with the 51 000 molecular weight polystyrene. It was thus assumed that the correction factor depended only on the heating rate and not at all on the polymer molecular weight. The heating rate  $T_g$  correction factor curve is shown in Figure 3.

Table 1 lists the observed and corrected  $T_g$  values. All corrected (to  $1^\circ\text{C}/\text{min}$  heating rate)  $T_g$  figures agreed to within  $1.4^\circ\text{C}$  except for the 4000 molecular weight sample. Higher  $T_g$  temperatures were observed in replicate experiments which produced larger, sharp peaks than when broader endotherms with lower  $\Delta T$  values were obtained. This may reflect packing variations in the sample cell. The higher  $T_g$  values were used below for 4000 molecular weight polystyrene. These results coincide with d.s.c. figures mentioned below. The corrected  $T_g$  value for infinite molecular weight obtained in this study was  $101^\circ\text{C}$ . This agrees with the figure reported from other measurement techniques<sup>6,8,14</sup> and is further evidence for the reliability of the present results. Our data on low molecular weight samples seem to be in reasonable agreement with the d.s.c. values given by Bender and Gaines<sup>10</sup> for three Pressure Chemical Co. polystyrenes.

#### Differential scanning calorimetry

The anionic polystyrene samples mentioned above were also examined with a Perkin Elmer DSC-1B differential scanning calorimeter (d.s.c.). This instrument is superior to d.t.a. for measurement of heat energy interchanges at transitions but was less satisfactory for the primary aim of this research, which was the location of transition temperatures. Some details of the d.s.c. results are nevertheless recorded here as they will be of value to other workers in this area.

A series of standard crystalline materials was examined to calibrate the temperature scale on the d.s.c. instrument. The absolute errors in measured melting temperatures were found to vary with the temperature level, and the effect of heating rate was not strictly linear in a melting point vs. log (heating rate) plot. These effects are shown in Figure 4.

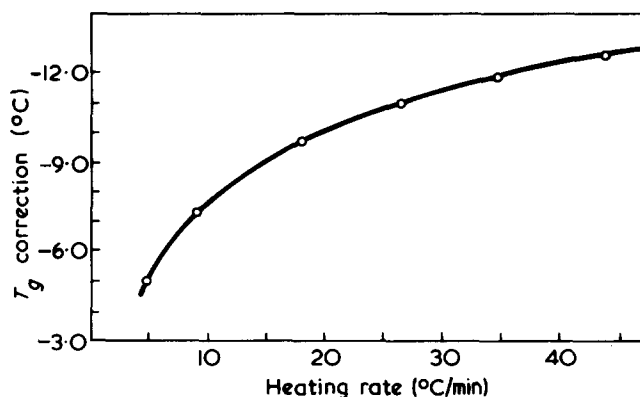


Figure 3  $T_g$  corrections for various experimental heat rates

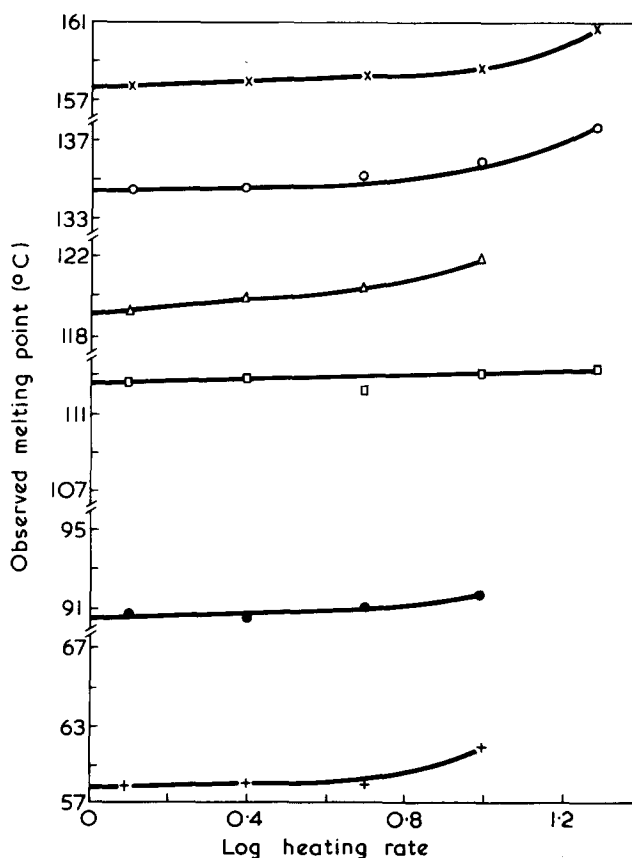


Figure 4 D.s.c. melting point vs. log (heating rate) plot. x, Indium (m.p.  $156.6^\circ\text{C}$ ); o, phenacetin (m.p.  $134.5^\circ\text{C}$ );  $\Delta$ , benzoic acid (m.p.  $122^\circ\text{C}$ );  $\square$ , acetanilide (m.p.  $114.3^\circ\text{C}$ ); •, benzil (m.p.  $95.0^\circ\text{C}$ ); +, *trans*-azobenzene (m.p.  $68.5^\circ\text{C}$ )

Table 2 D.s.c. and d.t.a. results

Sample code*	Molecular weight	D.s.c. heating rate (°C/min)	No. d.s.c. experiments	D.s.c. $T_g$ (°C)		Mean d.s.c. $T_g$ (°C)	D.t.a. $T_g$ (°C)
				Observed	Corrected		
12b	2 100	1.25	2	55.5	64	64	63
		2.5	2	57.3	63		
		5.0	2	60.1	64		
		10.0	2	62.9	63		
		20.0	2	67.6	64		
		40.0	2	73.4	64		
11b	4 000	1.25	1	~72	68	77	76
		2.5	1	73.1	77		
		5.0	1	74.6	76		
		10.0	1	77.7	76		
		20.0	1	81.8	76		
		40.0	2	88.5	78		
8b	10 000	5.0	3	~92	86	85	88
		10.0	1	94.9	85		
		20.0	1	98.8	85		
		40.0	1	103.2	84		
2b	20 400	5.0	2	~92.6	92	90	94
		10.0	1	94.4	91		
		20.0	1	97.6	90		
		40.0	1	99.4	87		
7a	51 000	10.0	1	103.8	99	98	100
		20.0	1	106.6	98		
		40.0	1	111.8	98		
Dow S102	82 000	10.0	1	~99.2	95	95	97.5
		20.0	2	102.5	95		
		40.0	1	107.9	95		
4a	97 200	10.0	1	104.0	100	99	101
		20.0	1	107.8	99		
		40.0	1	111.8	98		
1c	200 000	10.0	1	104.4	100	100	101
		20.0	1	108.4	100		
		40.0	1	114.7	101		
5a	498 000	40.0	1	112.0	100	100	101
14a	1 800 000	40.0	1	106.5	98	98	101

All d.s.c. measurements were made in the heating mode to correspond to the d.t.a. procedure. D.s.c. transitions were located at the intersection of the base line and extrapolated peak side. The discrepancy between this temperature and the peak temperature varied with the breadth of the transition, and hence with polystyrene molecular weight.

An average heating rate correction for all polystyrene samples was obtained by a procedure similar to that described above in d.t.a. studies. Apparent polystyrene  $T_g$  values were obtained at a standard heating rate of 1°C/min by reference to a heating rate correction vs. log (heating rate) curve similar to the d.t.a. plot in Figure 3. A plot of temperature correction versus apparent temperature was made from the data shown in Figure 4 and used to adjust the absolute values of the 1°C/min heating-rate  $T_g$  figures.

Table 2 lists the d.s.c. results and corresponding d.t.a. figures. The d.t.a.  $T_g$  values are slightly higher, in general, since these are taken from peak side intersections while the d.s.c. temperatures are those at which the peak side intersected the base line. D.s.c.  $T_g$  temperatures taken at the peak maxima averaged 3–4°C higher than the figures recorded in Table 2.

The coincidence shown in Table 2 is good, and we conclude that the d.s.c. and d.t.a. measurements are in essential agreement. The d.t.a. figures are taken as reference values since the non-uniform absolute temperature corrections noted above in connection with the d.s.c. values make the latter somewhat more uncertain.

Table 3  $T_g$  vs.  $M$  relations for polystyrene

Present results			Fox and Flory <sup>8</sup>		
$M$	$10^5/M$	$T_g$ (K)	$M$	$10^5/M$	$T_g$ (K)
2 000	47.6	336	1 220*	82.0	313
4 000	25.0	349	1 670*	59.9	326
10 000	10.0	361	2 180*	45.9	335
20 400	4.9	367	2 630*	38.0	338
51 000	2.0	373	3 200*	31.2	348
97 200	1.0	374	4 750*	21.1	351
200 000	0.5	374	6 720*	14.9	350
498 000	0.02	374	13 300	7.5	359
			19 300	5.2	362
			85 000	1.2	373

\*  $M$  from intrinsic viscosity data of Fox and Flory<sup>8</sup> and Mark-Houwink equation of Altares and coworkers<sup>22</sup> for low molecular weight polystyrenes

#### Effect of molecular weight on $T_g$

The influence of molecular weight on  $T_g$  has been studied by several groups and an inverse<sup>6,8,14,20</sup> relation to molecular weight of fractionated samples has been clearly established.

Our data are summarized in the appropriate form in Table 3. A plot of  $T_g$  against  $1/M$  is not strictly linear. This is shown in Figure 5, which also includes data points from the work of Fox and Flory.

Comparison of the present data with those of Fox and

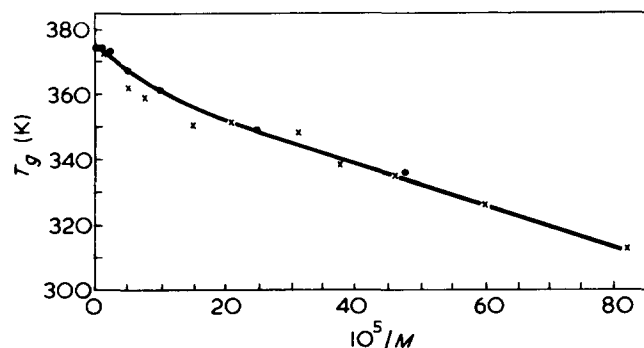


Figure 5  $T_g$  as a function of  $1/M$  for polystyrene. •, Present data; x, Fox and Flory<sup>8</sup> as given in Table 3

Flory is instructive, since the former are measured with anionic polystyrenes and the latter with fractions of thermally initiated polymers. Fox and Flory determined polystyrene molecular weights from dilute solutions viscosities using a relation given by Pepper<sup>21</sup>. However, the Mark-Houwink constants reported more recently by Altares and coworkers<sup>22</sup> for low molecular weight polystyrenes account for the data of Pepper as well as those of other workers. These latter constants were used for molecular weights of the Pressure Chemical Co. anionic polystyrenes. A consistent comparison of our data with those of Fox and Flory requires use of the same Mark-Houwink relations and this is fortunately possible because the constants appropriate for low molecular weight species do not depend on solvent or end groups<sup>22</sup>. We have therefore recalculated the molecular weights given by Fox and Flory<sup>8</sup> using the Mark-Houwink values reported by Altares and coworkers<sup>22</sup> for molecular weights up to 10 000. These molecular weights and the corresponding  $T_g$  values are given in Table 2.

A plot of the recalculated data of Fox and Flory coincides within experimental uncertainty with the present data, as shown in Figure 5. It is clear that the same  $T_g/M$  dependence applies to both the anionic and thermally initiated polymers.

The data of Ueberreiter and Kanig<sup>14</sup>, which are also for thermally initiated polystyrene fractions, differ systematically from those shown in Figure 5 in that  $T_g$  at low molecular weights tend to be lower than the values reported here and by Fox and Flory. This discrepancy has been noted by others<sup>2</sup> but its cause is not clear.

The slight inflection in the  $T_g$  vs.  $M^{-1}$  plot at degrees of polymerization between 100 and 200 is not confined to the present data. The results of Beevers and White<sup>20</sup> for poly-(methyl methacrylate) samples and the polystyrene data of Fox and Flory also reveal a similar tendency. The effects noted are minor but they seem to be general<sup>23</sup>.

The observed inverse relation between  $T_g$  and  $M$  and the occurrence of a limiting value,  $T_g^\infty$ , of  $T_g$  at sufficiently high  $M$  suggest the following general relation:

$$T_g x = T_g^\infty (x - \text{constant}) \quad (1a)$$

where  $x$  is the degree of polymerization of the particular vinyl polymer. The form of this equation is similar to those derived from different premises by Fox and Flory<sup>6</sup> and Somcynsky and Patterson<sup>24</sup> and others. The constant in equation (1a) is a small number which depends on the particular polymer type. We have found it useful for some applications to assume the form given in equation (1b):

$$T_g x = T_g^\infty (x - 1) \quad (1b)$$

Although this relation is not strictly correct, a plot of  $T_g x$  against  $(x - 1)$  is always rectilinear through the origin because deviations of the constant from unity are negligible compared to the experimental uncertainties and the range of  $x$ . This linear representation facilitates comparison of  $T_g$  data from different sources, as shown below. The slope of the relation equals  $T_g^\infty$  whether or not a zero intercept is theoretically acceptable. This technique provides a reliable method for estimating  $T_g^\infty$  values without measurements of the behaviour of very high molecular weight polymers, which respond sluggishly to changes in experimental conditions.

Polystyrene data are plotted in Figure 6, according to equation (1b). The slope yields a value of  $100^\circ\text{C}$  for  $T_g^\infty$ . Data of Fox and Flory<sup>8</sup> and of Ueberreiter and Kanig<sup>14</sup> are included in this plot along with the results of this study. Since the ordinate is rather compressed in Figure 6, low molecular weight data from the three sources are replotted with an expanded ordinate in Figure 7. The degree of polymerization in the latter plot is such that  $2 \leq x \leq 44$ . The slope in Figure 7 is lower than the corresponding value in Figure 6, which was equal to  $T_g^\infty$ . This difference in slopes reflects the non-linearity noted in Figure 5.

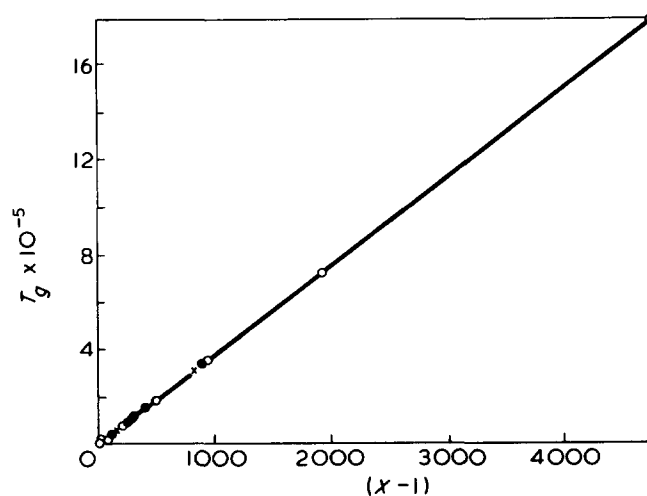


Figure 6 Plot of equation (1b) for polystyrene fractions. ○, Present data; x, Fox and Flory<sup>8</sup>; ●, Ueberreiter and Kanig<sup>14</sup>

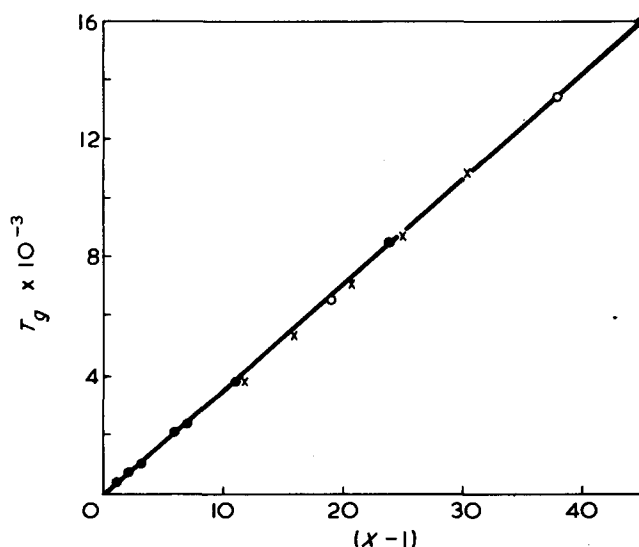


Figure 7 Plot of equation (1b) for low molecular weight polystyrenes. ○, Present data; x, Fox and Flory<sup>8</sup> as given in Table 2; ●, Ueberreiter and Kanig<sup>14</sup>

Anionic and thermally initiated polystyrenes fall on the same lines in Figures 6 and 7, showing that the two polystyrene types have the same dependence of  $T_g$  on molecular weight at all molecular weights which have been studied.

The 82 000 molecular weight polystyrene listed in Table I is the Dow S-102 sample. This polymer has slightly lower  $T_g$  than the value expected from the Pressure Chemical Co. samples. Its molecular weight determination is, however, stated to be uncertain<sup>25</sup> from consideration of Newtonian viscosity data. This may be the reason for the minor difference in  $T_g$  behaviour noted here with this material.

## DISCUSSION

The comparisons with other reports given above establish the validity of the present d.t.a. method for locating  $T_g$ . Also, the fact that the  $T_g/M$  relation found here for anionic polystyrenes agrees at all  $M$  values with figures developed by others for thermally initiated fractions is indirect but nevertheless very strong evidence that the present  $T_g$  values are comparable to those obtained by other experimental methods.

This appears to be the first direct study of effect of  $M$  on  $T_g$  with polymer fractions which differed only in end-groups. The specific volumes attributable to end groups in anionic and thermally initiated polystyrene melts differ significantly<sup>9,10</sup> and it seems unlikely that these discrepancies would disappear under glass transition conditions. Since free volume is defined operationally as the difference between specific volume and a reference volume the two species may reasonably be expected to differ in free volume regardless of the definition of the reference state.

As shown in Figures 5–7, the various polystyrene fractions with different end group volumes have the same  $T_g$  at equivalent molecular weight. It seems clear, then, that free volume and main glass transition are not cause and effect. This conclusion does not preclude the possibility that the glass transition and an operationally defined estimate of free volume may vary in parallel with changing experimental conditions or polymer structure.

The present results are not consistent with the idea that free volume is a constant at the glass transition. Our comparison of polystyrene fractions with different end group volumes is compatible with a number of other explanations which have been offered for the main glass transition. A recent article by Morley<sup>26</sup>, for example, concludes that the nature of end groups should have no strong influence on  $T_g$ .

Our data are also consistent with the concept<sup>3,7</sup> of  $T_g$  as an isoviscosity state characteristic of segmental rather than molecular movement. This idea is pursued briefly below because it leads to certain interesting conclusions regarding the influence of free volume on melt viscosity.

The iso-segmental viscosity mechanism is compatible with the observation noted above that the  $T_g$  vs.  $M^{-1}$  relation deviates from linearity at molecular weights at which studies of Newtonian viscosity indicate that segmental flow becomes more important than molecular translation of polymer molecules<sup>25</sup>.

In the low molecular weight region the Newtonian viscosities of polystyrene melts are directly proportional to molecular weights of fractions, indicating that molecular rather than segmental flow mechanisms dominate. It might be expected in this region that  $T_g$  of anionic and thermally initiated polymers would still differ even if the determining

role in the vitrification process is not the achievement of a constant free volume. This assumes that free volume is related to molecular mobility at given  $M$  and  $T$ . At sufficiently low molecular weights (which are in the range of the samples examined in this and the cited work<sup>6,8,14</sup> of others) the different end group volumes in the two polystyrene types would be expected to result in different free volumes and hence in different Newtonian viscosities and vitrification temperatures. With these particular oligometric samples in which segmental flow is absent, this model predicts that  $T_g$  and end group volume should be related if only indirectly through the influence of free volume on molecular mobility.

In fact, there is no detectable difference in  $T_g$  of low molecular weight polystyrenes, as is shown most clearly in Figure 7. If the glass transition is an iso-viscosity state then this observation brings into question the role of free volume in viscosity and suggests that Newtonian viscosities of anionic and thermally initiated polystyrenes will not differ at given  $M$  and  $T$  despite the differences in end group volumes. The two different polymer types have indeed been reported to give equivalent viscosities under these conditions<sup>27</sup>, in agreement with the results of the present  $T_g$  experiments.

## ACKNOWLEDGEMENT

Financial support of this research was provided in part by the National Research Council of Canada.

## REFERENCES

- 1 Shen, M. and Eisenberg, A. *Rubber Chem. Technol.* 1970, **43**, 95
- 2 Boyer, R. F. *Rubber Chem. Technol.* 1963, **36**, 1303
- 3 Haward, R. N. *J. Macromol. Sci. (C)* 1970, **4**, 191
- 4 Adam, G. and Gibbs, J. H. *J. Chem. Phys.* 1965, **43**, 139
- 5 Kaelble, D. H. in 'Rheology', (Ed. F. R. Eirich), Academic Press, New York, 1969, Vol 5
- 6 Fox, T. G. and Flory, P. J. *J. Appl. Phys.* 1950, **21**, 581
- 7 Gee, G. *Polymer*, 1966, **7**, 177
- 8 Fox, T. G. and Flory, P. J. *J. Polym. Sci.* 1954, **14**, 315
- 9 Chee, K. K. and Rudin, A. *J. Macromol. Sci. (B)* 1973, **7**, 503
- 10 Bender, G. W. and Gaines, Jr G. L. *Macromolecules* 1970, **3**, 128
- 11 Keavney, J. J. and Eberlin, E. C. *J. Appl. Polym. Sci.* 1960, **3**, 47
- 12 Martin, A. F. and Kase, H. F. *Ind. Eng. Chem. (Prod. Res. Dev.)* 1967, **6**, 104
- 13 Rudd, J. F. *J. Polym. Sci.* 1962, **60**, 57
- 14 Ubbereiter, K. and Kanig, G. *J. Colloid Sci.* 1952, **7**, 569
- 15 Schwenker, R. K. and Luecarello, R. L. *J. Polym. Sci. (C)* 1964, **6**, 1
- 16 Vassallo, D. A. and Harden, J. C. *Analyt. Chem.* 1962, **34**, 132
- 17 Currie, J. A. and Dole, M. *Polym. Prepr.* 1968, **9**, 814
- 18 Strella, S. *J. Appl. Polym. Sci.* 1963, **7**, 509
- 19 Wunderlich, B. and Bodily, D. M. *J. Polym. Sci. (C)*, 1964, **6**, 137
- 20 Beevers, R. B. and White, E. F. T. *Trans. Faraday Soc.* 1960, **56**, 744
- 21 Pepper, D. C. *Sci. Proc. R. Dublin Soc.* 1951, **25**, 239
- 22 Altares, Jr, T., Wyman, D. P. and Allen, V. R. *J. Polym. Sci. (A)* 1964, **2**, 4533
- 23 Boyer, R. F. *Macromolecules* 1973, **7**, 142
- 24 Somcynsky, T. and Patterson, D. *J. Polym. Sci.* 1962, **62**, S151
- 25 Casale, A., Porter, R. S. and Johnson, J. F. *J. Macromol. Sci. (C)* 1971, **5**, 387
- 26 Morley, D. C. W. *J. Mat. Sci.* 1974, **9**, 619
- 27 Allen, V. R. and Fox, T. G. *J. Chem. Phys.* 1964, **41**, 337



# The design of large hot melt extruders\*

R. T. Fenner

*Department of Mechanical Engineering, Imperial College of Science and Technology,  
London SW7 2BX, UK*

*(Received 14 August 1974)*

A method is proposed for the rational design of large single screw extruders for processing hot molten thermoplastics, which is based on a theoretical analysis of polymer flow. A typical design study for an homogenizer for low density polyethylene is examined in detail, with particular attention being paid to the effects of screw diameter, length and channel depths on melt temperatures, degree of mixing, residence time, machine cost and power consumption. Owing to the physical properties of polymer melts, heat transfer by conduction is very inefficient. Barrel cooling serves to draw power from the motor rather than heat from the polymer, and in order to achieve a given level of mixing there is a largely unavoidable increase in melt temperature.

## INTRODUCTION

Large single screw extruders for processing thermoplastic polymeric materials are particularly difficult to design and operate because of heat transfer limitations. The amount of heat that can be conducted into or out of the bulk of the flowing polymer is very limited. In the present context 'large' extruders are those with diameters of 200 mm or more. The main application for such machines is in homogenization during polymer manufacture. Although attention is confined here to the design of extruders for homogenizing molten low density polyethylene (LDPE), the method is applicable to other materials. Many of the topics discussed are also relevant to the design of both smaller and plasticating extruders.

The main function of a LDPE homogenizer is to thoroughly mix the melt produced by the polymerization process, prior to granulation. During hot mixing, the melt undergoes shear and thermal degradation which result in a breakdown not only of agglomerates, but also of individual molecules with molecular weights higher than the average, resulting in a change in material properties<sup>1</sup>. The current trend in a number of European countries is to use a single extruder to homogenize up to 10 000 kg/h or more of melt. The diameter of such an extruder would be at least 400 mm, and in some cases machines with length-to-diameter ratios of as much as 40 are in use.

## ANALYSIS OF PERFORMANCE

The approach described here for designing large hot melt extruders is based on a mathematical analysis of the melt flow. The complexity of this analysis makes it unsuitable for presentation in the form of algebraic design formulae. Numerical solutions to specific problems may be obtained, however, with the aid of a digital computer. The purpose of the present paper is not to dwell on the mathematical details of the analysis but to concentrate on its application to design problems.

\* Presented at a conference on Engineering Design of Plastics Processing Machinery held at the University of Bradford, April 1974.

## *Mathematical model*

The details of the mathematical model, which was first proposed and solved by Yates<sup>2</sup>, are outlined in the Appendix. This model is sufficiently simple to be used in routine design studies, while retaining all the important features of the melt flow, particularly the developing thermal effects. It has been used successfully to aid in the design of large extruders.

## *Performance parameters*

The flow analysis should ideally provide estimates of the following extruder performance parameters. (1) Output. (2) Mean melt temperature (see equation (A11) in the Appendix). The most useful single temperature parameter is the mean delivery temperature,  $\bar{T}_{out}$ . (3) Delivery pressure. As indicated later, delivery pressure is closely linked with filled length, the effect of which is examined below. (4) Mechanical power consumption. The power required to drive the screw may be calculated as the rate of working at the interface between the melt and barrel<sup>3</sup>. (5) Heat transfer at the barrel surface. The amount of barrel heating or cooling required to maintain a particular barrel temperature can be estimated from the computed temperature profiles. (6) Mean degree of (distributive) mixing. The degree of mixing imparted by an extruder is one of its most important performance parameters. Mixing is of two main types, namely dispersive and distributive. The former is obtained by applying high stresses to the material to break up inhomogeneous lumps, whereas the latter is obtained by applying large deformations which spread such lumps into thin layers over large areas. In a polymer extruder, distributive mixing is the more important, and the overall degree of mixing imparted may be thought of as:  $M = (\text{mean shear rate}) \times (\text{mean residence time})$ . Thus  $M$  is the mean shear strain applied to the material. The formal definition of the mixing parameter is given by equation (A12) in the Appendix. (7) Mean shear rate (see equation (A13) in the Appendix). It appears that mixing is best carried out at a reasonable shear rate, generally of the order of  $100 \text{ s}^{-1}$ . At this level there may be a significant amount of dispersive mixing, but the rate is not so high as

to lead to excessive degradation. (8) Residence time is also important for a readily degradable material.

The mean degree of mixing is just one aspect of extrudate quality. The variation of the degree of mixing about this mean is also significant, as is the variation of thermal history of different particles of material passing through the extruder.

#### Mixing aids

The screws of some large hot melt extruders are fitted with mixing aids such as dams or rows of cylindrical pins. The main functions of these appear to be to provide some dispersive mixing and to disturb the established flow patterns in the melt. Extrudate quality is thus improved by narrowing the distributions of shear and thermal history.

#### Typical example

Suppose it is required to homogenize a 0.2 MFI LDPE supplied at a rate of 5000 kg/h and a uniform temperature of 250°C. In a typical LDPE plant the material range is generally 0.1 to 30 MFI, although extruder performance for a 0.2 MFI grade is usually the one specified. The physical properties of such a material are:

$$\mu_0 = 16.0 \text{ kNs/m}^2 \text{ at } \dot{\gamma}_0 = 1 \text{ s}^{-1} \text{ and } T_0 = 250^\circ\text{C},$$

$$n = 0.30, b = 0.01^\circ\text{C}^{-1},$$

$$\rho = 750 \text{ kg/m}^3, C_p = 0.80, k = 0.30 \text{ W/m}^\circ\text{C}$$

For the remainder of this paper, certain assumptions are made concerning extruder screw geometry. The lengths of the feed and compression sections ( $L_f$  and  $L_c$  in Figure 9a) are chosen as  $2D$ , where  $D$  is the barrel diameter. For melt extruders such lengths are adequate. The flight width,  $e$ , is taken to be  $0.1D$ , and flight lead as  $D$  (helix angle  $\theta = 17.65^\circ$ ).

The compression ratio,  $H_f/H_m$ , is chosen to be 4, based on the following reasoning. The output of a hot melt extruder is normally determined by the feed section, and practical experience shows that the value of the dimensionless flow rate there,  $Q/BV_2H_f$ , is usually very close to 0.10. As indicated later, however, the dimensionless flow rate in the metering section (equation A10) should be about 0.4. A compression ratio of 4 therefore ensures a reasonable balance between the feed and metering sections of the screw.

Initially one set of machine geometry is considered, variations in the main dimensions being examined in the next section. The barrel diameter is chosen as  $D = 300$  mm, overall length  $L = 25D = 7.5$  m, and  $H_m = 12$  mm. A value of  $\pi_Q = 0.4$  is assumed, from which the screw speed may be determined as  $N = 97$  rev/min. The other operating conditions include barrel temperature,  $T_b = 250^\circ\text{C}$ , and filled length,  $L_{fill} = L_m$ .

The performance predicted by the analysis is as follows:

Bulk mean delivery temperature, $\bar{T}_{out}$	= 326°C
Mechanical power consumption (excluding motor and gearbox losses)	= 690 kW = 0.138 kWh/kg
Barrel cooling rate	= 200 kW
Mean degree of mixing, $M$	= 4400
Mean shear rate, $\bar{\gamma}$	= 121 s <sup>-1</sup>

Figure 1a shows the predicted temperature profile over the channel depth at the delivery end of the screw. The two temperature peaks correspond to the regions of greatest shear rate. Despite the steepness of the profile near the barrel the amount of heat conducted out is comparatively small, owing to the low thermal conductivity of the melt. Figure 1b shows the predicted increase in bulk mean temperature along the extruder. Clearly the flow is far from being 'fully developed' (velocities and temperatures independent of distance along the screw channel) even at the delivery end of the machine. Indeed, a machine with a  $L/D$  ratio very much larger than 25 would be required to achieve this condition, which is fortunate because excessively high temperatures would be generated.

Melt temperatures actually measured in large extruders generally do not show the considerable increases implied by the predicted profiles. In the author's experience this is largely due to inaccurate measurements. A temperature recorded at the barrel surface is unrepresentative of the bulk of the material, as is the temperature of a small sample leaked through the barrel wall. Most temperature measurements tend to be strongly influenced by the temperature of the metal component on which the thermocouple is mounted, which may be 50°C or more below that of the bulk of the flowing polymer.

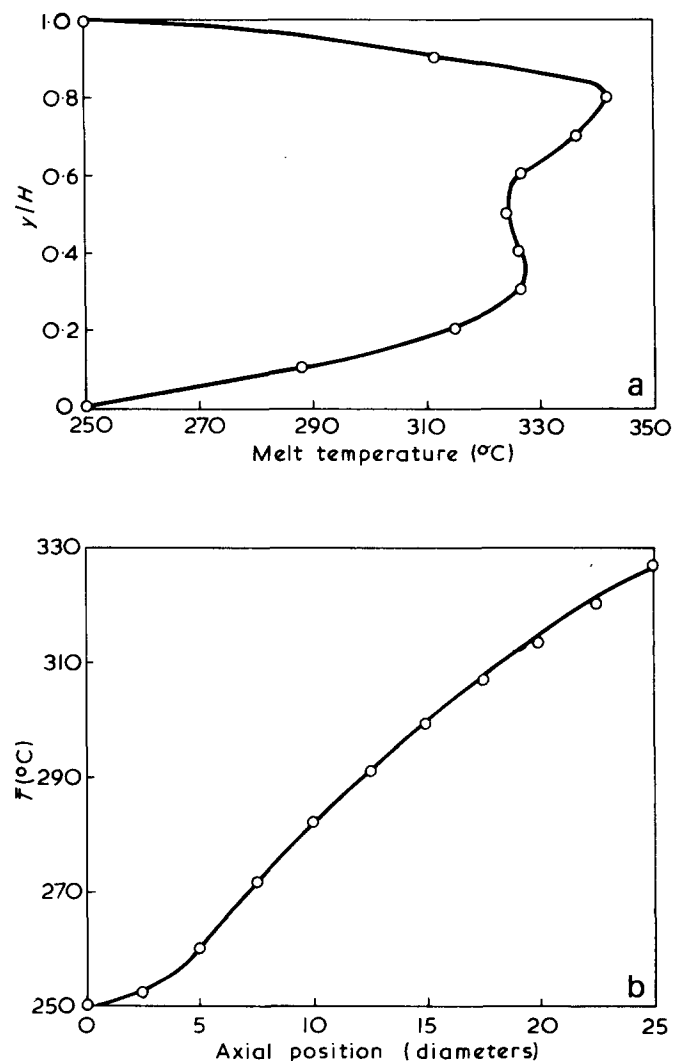


Figure 1 (a) Melt temperature profile at delivery. (b) Increase in bulk mean temperature

## APPLICATION TO DESIGN

In the above example the method of melt flow analysis is applied to an extruder whose geometry is prescribed. An even more important application for such an analysis is to the design of new machines for particular duties. In order to do this it is necessary to establish the appropriate design criteria.

## Design criteria

The constraints to be satisfied in the design of a large extruder for homogenizing a given flow rate of melt include the following: (1) adequate mixing; (2) minimum bulk mean delivery temperature; (3) minimum machine size and cost; (4) minimum power consumption; (5) reasonable screw  $L/D$  ratio; (6) reasonable speed and shear rate. These requirements are of course highly interdependent. For example, delivery temperature and power consumption increase with the degree of mixing. It is difficult to predict what constitutes 'adequate' mixing, although trials on laboratory scale equipment can in principle establish the appropriate level. The mean degree of mixing imparted by melt homogenizers is generally between 2000 and 6000, although at the lower end of this range the machines serve as no more than melt pumps.

The last two of the above design criteria are concerned with the mechanical aspects of extruder design. Previous work<sup>4</sup> has shown that large extruders with high  $L/D$  ratios tend to be mechanically unstable, owing to a combination of buckling and whirling. High  $L/D$  machines are also more difficult and therefore more expensive to manufacture, and occupy large areas of plant. For all these reasons it is desirable to restrict  $L/D$  ratios to about 25. Similarly, as speeds are increased, screws tend to whirl and the rates of wear increase. For large extruders, 100 rev/min is a reasonable upper limit. The choice of mean shear rate was discussed earlier, where a figure of about  $100 \text{ s}^{-1}$  was suggested.

The main geometric variables available to the designer are the diameter,  $L/D$  ratio, metering section channel depth and helix angle. For present purposes, secondary variables such as feed and compression section lengths, flight width and compression ratio are fixed as indicated above. Operating variables which affect the design include the screw speed, barrel temperature profile and delivery pressure.

## Typical design problem

Suppose it is required to select a suitable screw design for the application described earlier, namely the homogenization of 5000 kg/h of a 0.2 MFI LDPE supplied at  $250^\circ\text{C}$ . The effects of the various operating variables and helix angle are examined before considering the main screw dimensions.

Figure 2 shows bulk mean delivery temperature plotted against mean degree of mixing, two of the principal performance parameters. The geometric and operating variables are as defined before, except that helix angle, dimensionless flow rate (speed) and filled length are varied in turn over the ranges indicated. For all of these variations there is a direct proportionality between temperature rise and degree of mixing. This result may be interpreted as meaning that the helix angle, dimensionless flow rate, and filled length do not significantly affect machine performance, because they do not affect the ratio of temperature rise to degree of mixing. The required level of mixing can be

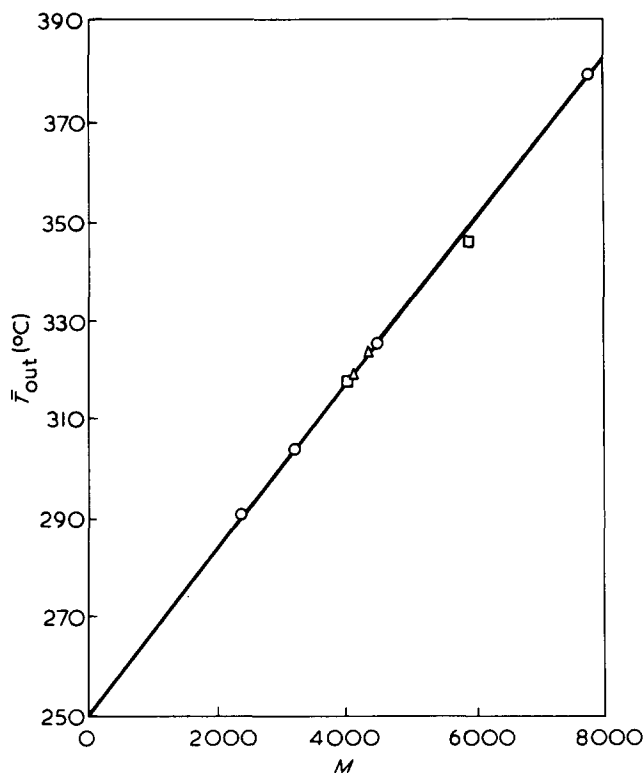


Figure 2 Effect of varying helix angle,  $\pi_Q$  and filled length.  $\circ$ ,  $10^\circ < \theta < 35^\circ$ ;  $\square$ ,  $0.3 < \pi_Q < 0.45$ ;  $\triangle$ ,  $9D < L_{fill} < 21D$ . 0.2 MFI LDPE; 5000 kg/h at  $250^\circ\text{C}$ .  $D = 300 \text{ mm}$ ;  $L/D = 25$ .  $L_f = L_c = 2D$ .  $H_f = 48 \text{ mm}$ ;  $H_m = 12 \text{ mm}$ .  $N = 97 \text{ rev/min}$  (when  $\pi_Q = 0.4$ );  $T_b = 250^\circ\text{C}$

equally well achieved by a suitable choice of channel depths, as shown below. It should be noted that the effect of relatively large variations in the filled length, and hence the delivery pressure, have very little effect on performance in terms of melt temperatures and mixing. For the remainder of this paper the values  $\theta = 17.65^\circ$ ,  $\pi_Q = 0.4$  and  $L_{fill} = L_m$  are used.

The effects of varying barrel temperature are shown in Figure 3, in which the predicted bulk mean delivery temperature, mechanical power input and barrel cooling are plotted. The degree of mixing is not significantly affected by barrel temperature. In practice, the temperature of the barrel is controlled by the amount of cooling applied to it. According to Figure 3, the delivery temperature actually decreases as the barrel temperature is increased (eventually reaching a minimum), although the rate of decrease is relatively small. Practical evidence for this phenomenon can be obtained by removing the cooling from one or more barrel zones of a large hot melt extruder, and noting the very small effect on melt temperatures measured beyond the end of the screw. In large extruders the heat generated by the dissipation of mechanical work tends to be convected downstream, causing a continual rise in the bulk mean temperature, rather than be conducted out through the barrel. This can be attributed to the low thermal conductivity, and makes it very difficult to conduct heat into or out of the bulk of the flowing polymer.

Figure 3 also shows the large variations in power input and barrel cooling associated with the changing barrel temperature. In view of the much smaller effects on the main performance parameters, mixing and temperature rise, a number of conclusions may be drawn as follows. The main effect of barrel cooling is to draw power from the motor rather than heat from the polymer. It would appear to be

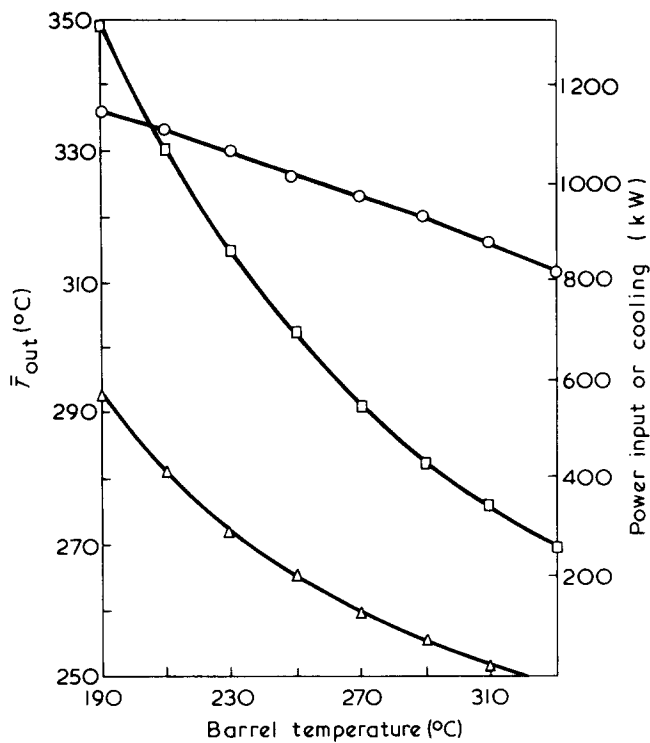


Figure 3 Effects of varying barrel temperature.  $\circ$ ,  $\bar{T}_{out}$ ;  $\square$ , power input;  $\triangle$ , cooling. Same conditions as in Figure 2.  $\theta = 17.65^\circ$ .  $\pi Q = 0.4$  ( $N = 97$  rev/min).  $L_{fill} = 21 D$

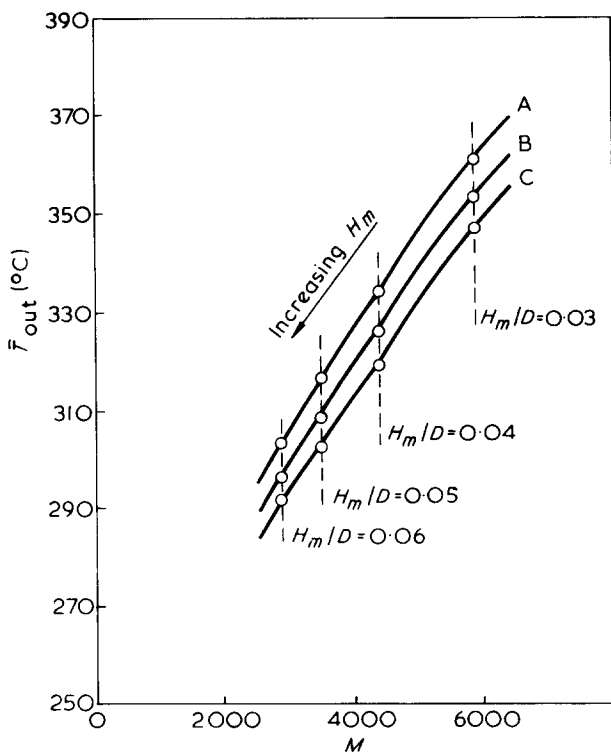


Figure 4 Effect of varying screw diameter. A,  $D = 250$  mm; B,  $D = 300$  mm; C,  $D = 350$  mm.  $L/D = 25$ ;  $T_b = 250^\circ\text{C}$

possible to run large melt homogenizers with no barrel cooling and a considerable saving in power consumption. The common practice of quoting specific power consumption as a measure of the degree of mixing imparted can be misleading.

It now remains to examine the effects of the main geometric variables of diameter, length and channel depths.

Figure 4 shows the effect of varying screw diameter for a fixed  $L/D$  ratio of 25. For each of the diameters there is nearly a direct proportionality between mean temperature rise and degree of mixing, with metering section channel depth as the variable. For a given value of the ratio  $H_m/D$ , the degree of mixing is virtually constant. The main point to note is that machine performance is improved by increasing the screw diameter, since a cooler melt can be achieved for a given level of mixing. Considering the relatively massive increases in extruder dimensions however, the temperature reductions are modest. Owing to the difficulty of transferring heat by conduction, increases in barrel surface area have relatively little effect.

According to the design criteria, screw speed and mean shear rate should also be considered. These are shown in Table 1 for the range of machine dimensions employed in Figure 4. Clearly, the use of a 250 mm extruder for the present application would lead to excessive speeds and shear rates, whereas those for 300 or 350 mm machines are reasonable.

Figure 5 shows the effect of varying the length of a 300 mm extruder. For each of the five lengths there is nearly a direct proportionality between mean temperature rise and degree of mixing, with metering section channel depth as the variable. The downward displacement of the

Table 1 Screw speed and mean shear rates

$H_m/D$	Screw speeds (rev/min)			Shear rates, $\bar{\gamma}$ ( $\text{s}^{-1}$ )		
	Diameter (mm)			Diameter (mm)		
	250	300	350	250	300	350
0.03	225	131	81	375	217	134
0.04	168	97	60	208	121	75
0.05	133	77	48	132	76	47
0.06	110	63	39	91	52	33

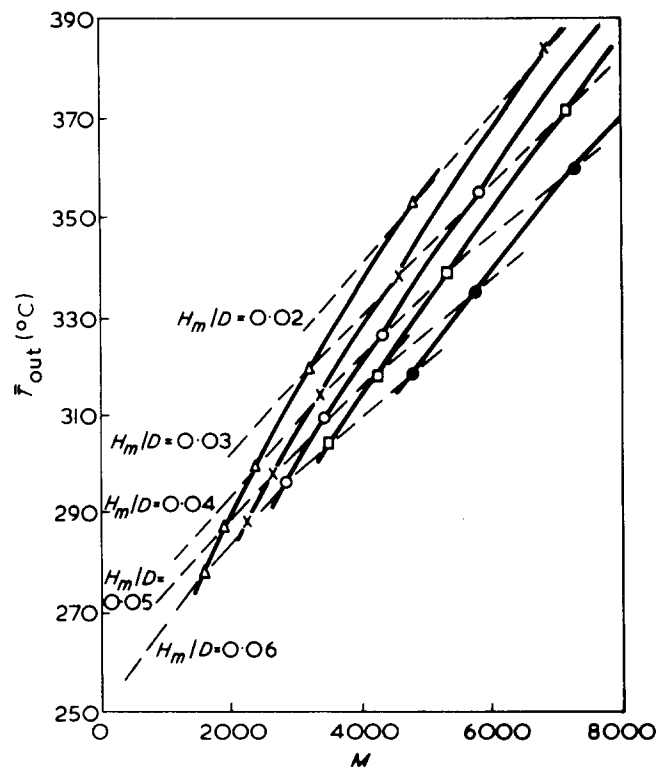


Figure 5 Effect of varying  $L/D$  ratio:  $\triangle$ , 15;  $\times$ , 20;  $\circ$ , 25;  $\square$ , 30;  $\bullet$ , 40.  $D = 300$  mm;  $T_b = 250^\circ\text{C}$

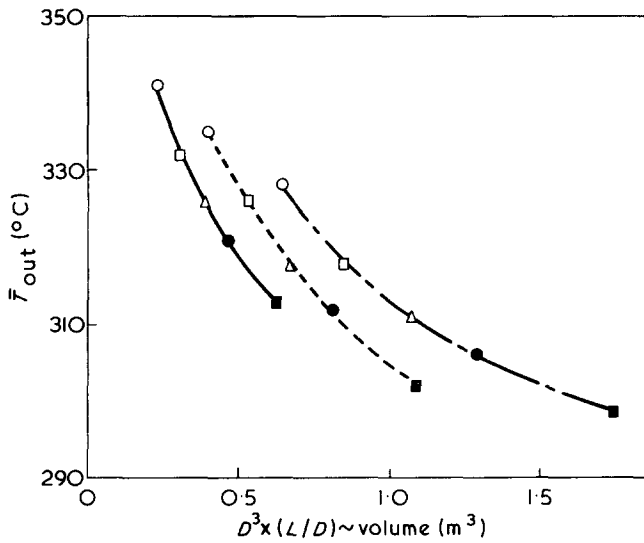


Figure 6 Effect of machine volume (cost) on bulk mean temperature rise.  $L/D$ :  $\circ$ , 15;  $\square$ , 20;  $\triangle$ , 25;  $\bullet$ , 30;  $\blacksquare$ , 40. —,  $D = 250$  mm; ---,  $D = 300$  mm; - · - ·,  $D = 350$  mm.  $M = 4000$ ;  $T_b = 250^\circ\text{C}$

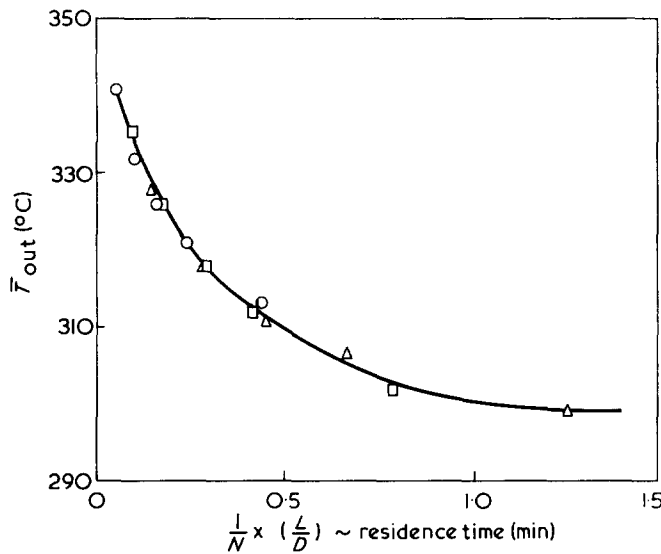


Figure 7 Effect of residence time on bulk mean temperature rise.  $\circ$ ,  $D = 250$  mm;  $\square$ ,  $D = 300$  mm;  $\triangle$ ,  $D = 350$  mm.  $M = 4000$ ;  $T_b = 250^\circ\text{C}$

curves with increasing  $L/D$  implies that machine performance is improved by increasing its length, but not by very large amounts. As indicated in the previous section, however, considerations of screw stability and ease and cost of manufacture suggest that  $L/D$  ratios should be limited to about 25.

From the point of view of performance, the extruder should be as large as possible. In practice, the costs of building, housing and running such a machine are also important considerations. As a rough approximation, the cost of manufacture is proportional to the volume of the machine, which in turn is proportional to  $D^3 \times (L/D)$ . Figure 6 shows the effect of this parameter on the bulk mean delivery temperature for a particular level of mixing,  $M = 4000$ . There are two main conclusions to be drawn. First, that a long thin extruder is better than a short fat one having the same volume (cost), from the point of view of minimizing melt temperature rise. Secondly, that the delivery temperature tends to become independent of the size of the machine as the latter is increased. In the present example, it is not possible to reduce the delivery tempera-

ture to significantly less than  $300^\circ\text{C}$  for the particular level of mixing imposed. A 300 mm, or at most a 350 mm, extruder represents a reasonable compromise between delivery temperature and cost.

With some materials, the residence time in an extruder is important from the point of view of thermal degradation, particularly if elevated temperatures are unavoidable. For a given dimensionless flow rate, the residence time is proportional to  $(1/N) \times (L/D)$ . Figure 7 shows the effect of this parameter on the bulk mean delivery temperature, for  $M = 4000$ . The computed results all lie close to a single curve. A limiting minimum delivery temperature is again reached as the residence time (machine size) is increased. For some materials a thermal damage criterion, possibly based on a product of temperature and residence time, might be appropriate for helping to choose a screw design.

The final choice of screw design is based on  $L/D = 25$  for the reasons already given, and  $D = 300$  mm for reasons of cost. Figure 8 shows bulk mean delivery temperature plotted against the degree of mixing for metering section channel depths between 9 and 18 mm. The upper limit of the useful range on this curve is determined by the maximum acceptable screw speed, and the lower limit by inadequate mixing and low shear rate. A channel depth of  $H_m = 12$  mm is a reasonable choice, unless a very high degree of mixing is required, and is the case considered earlier.

#### Range of machines

Attention has so far been confined to extruders for processing 5000 kg/h of LDPE melt. Even larger machines are being designed and built. Following the procedure outlined in the above design study, the range of machine designs show in Table 2 may be proposed.

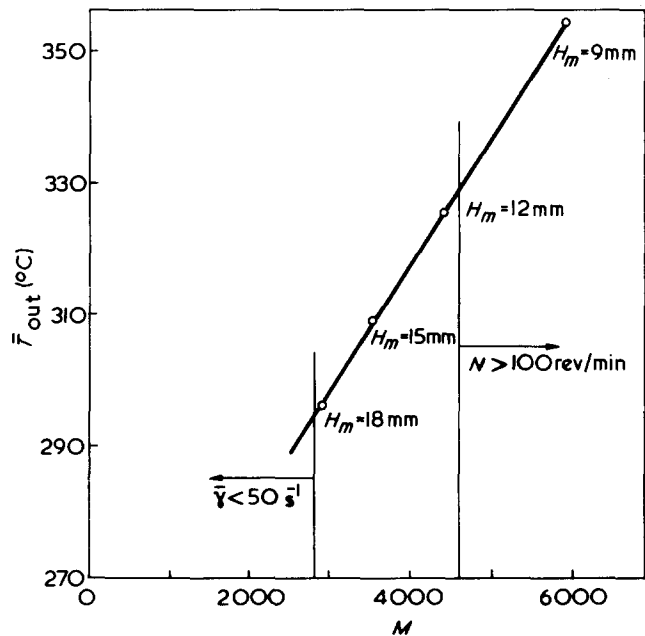


Figure 8 Final choice of screw.  $D = 300$  mm;  $L/D = 25$ ;  $\pi Q = 0.4$ ;  $T_b = 250^\circ\text{C}$

Table 2 A range of LDPE homogenizers

Output (kg/h)	$D$ (mm)	$L/D$	$H_m$ (mm)
5 000	300	25	12
10 000	400	25	16
15 000	450	25	18

All three machines are very similar in terms of mixing performance, bulk mean temperature rise and specific power consumption, for the same barrel temperatures. The screw speeds for the 400 and 450 mm machines are in the range of 80–90 rev/min.

## NOMENCLATURE

$a$	axial component of velocity,
$B$	screw channel width,
$b$	temperature coefficient of viscosity,
$C_p$	specific heat,
$D$	internal diameter of extruder barrel,
$e$	screw flight width,
$H$	screw channel depth,
$H_f$	screw channel depth in feed section,
$H_m$	screw channel depth in metering section,
$I_2$	second invariant of rate of deformation tensor,
$k$	thermal conductivity,
$L$	axial length of screw,
$L_c$	axial length of compression section,
$L_f$	axial length of feed section,
$L_{fill}$	axial filled length,
$L_m$	axial length of metering section,
$M$	mean degree of (distributive) mixing,
$N$	screw speed,
$n$	power-law index,
$p$	pressure,
$Q$	volumetric flow rate,
$T$	temperature,
$\bar{T}$	bulk mean temperature,
$\bar{T}_{out}$	bulk mean delivery temperature,
$T_b$	barrel temperature,
$T_0$	reference temperature for viscosity data,
$u, v, w$	velocity components in $(x, y, z)$ directions,
$V_x, V_z$	transverse and downstream components of velocity of barrel relative to screw,
$x, y, z$	Cartesian coordinates,
$\bar{\gamma}$	mean shear rate in metering section,
$\gamma_0$	reference shear rate for viscosity data.
$\theta$	helix angle,
$\mu$	viscosity,
$\mu_0$	effective viscosity at reference shear rate and temperature.
$\pi Q$	dimensionless flow rate in metering section,
$\rho$	density,
$\tau_{xy}, \tau_{yz}$	viscous stress components.

## REFERENCES

- 1 Konoval, I. V., Evdokimov, E. I., Gilim'yanov, F. G., Muzykantova, A. I., and Vysotskaya, M. I. *Sov. Plast.* 1972, (7), pp 6–8
- 2 Yates, B. *PhD Dissertation*, University of Cambridge (1968)
- 3 Fenner, R. T. 'Extruder Screw Design', Iliffe, London, 1970
- 4 Fenner, R. T. and Williams, J. G. *Polym. Eng. Sci.* 1971, 11, 474

## APPENDIX

### Mathematical model

Figure 9a shows, in very diagrammatic form, the basic geometry of a single screw extruder. From the analytical point of view the difference between single and multi-start screws is very slight, although the latter may offer advantages in terms of mechanical symmetry and improved feeding. Note the choice of  $x$  and  $z$  for the transverse and down-

stream channel directions respectively. If it is assumed that the channel may be treated as though it were unrolled, then the views from the screw in the  $z$  and  $x$  directions are as shown in Figures 9b and 9c.

### Flow theory

The channel depth,  $H$ , changes slowly with  $z$  and is small compared with the width,  $B$ . Consequently, the local velocity profiles can be obtained from the following simplified momentum equations for slow viscous flow<sup>3</sup>:

$$\frac{\partial p}{\partial z} = \frac{d\tau_{yz}}{dy}, \quad \frac{\partial p}{\partial x} = \frac{d\tau_{xy}}{dy} \quad (A1)$$

where  $p$  is pressure and  $\tau_{yz}$  and  $\tau_{xy}$  are viscous stresses, given by:

$$\tau_{zy} = \mu \frac{dw}{dy}, \quad \tau_{xy} = \mu \frac{du}{dy} \quad (A2)$$

where  $\mu$  is viscosity. The velocity components ( $u, v, w$ ) are in the  $(x, y, z)$  directions, and the assumptions imply that  $u = u(y), v = 0, w = w(y)$ .

The same level of approximation cannot, however, be applied to the melt temperatures because of the dominant effect of thermal convection. Assuming that the only significant thermal conduction is in the  $y$  direction, the energy equation becomes:

$$\rho C_p \left( w \frac{\partial T}{\partial z} + u \frac{\partial T}{\partial x} \right) = k \frac{\partial^2 T}{\partial y^2} + \tau_{yz} \frac{dw}{dy} + \tau_{xy} \frac{du}{dy} \quad (A3)$$

convection                  conduction                  dissipation

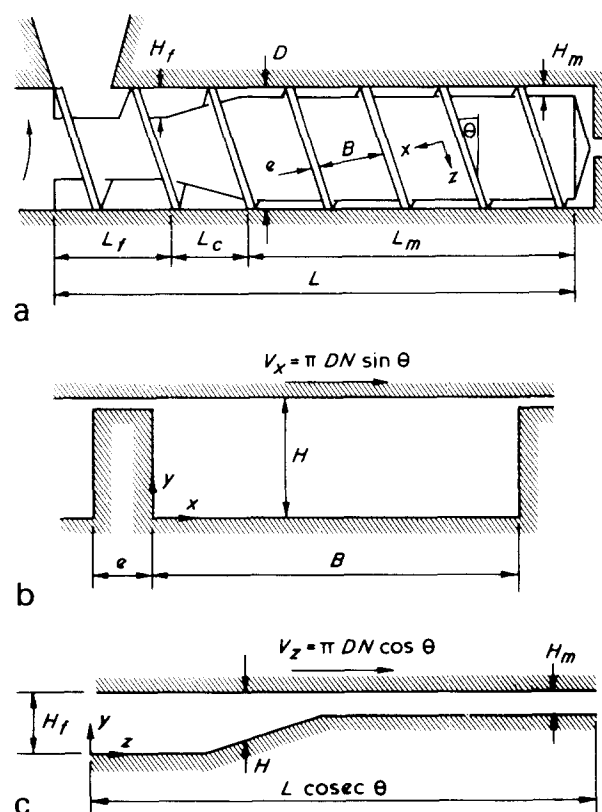


Figure 9 (a) Extruder geometry; (b) view in the  $z$  direction; (c) view in the  $x$  direction

where  $\rho$ ,  $C_p$ ,  $k$  and  $T$  are respectively the density, specific heat, thermal conductivity and temperature of the melt. As the thermal conductivity is low, heat derived from the dissipation of mechanical work tends to be convected along the screw channel rather than conducted out through the barrel. Unfortunately, it is not possible in the present model to include the effects of transverse convection because of the simplification already applied to the velocity profiles. Thus it is necessary to assume that:

$$u \frac{\partial T}{\partial x} \ll w \frac{\partial T}{\partial z} \quad (A4)$$

so that the second term on the left hand side of equation (A3) may be omitted. The disadvantages of making this assumption can be largely offset by a suitable choice of boundary conditions.

#### Constitutive equation

The non-Newtonian viscosity of polymer melts can generally be represented empirically as a power-law function of the local rate of deformation and an exponential function of temperature<sup>3</sup>:

$$\mu = \mu_0 \left( \frac{\sqrt{4I_2}}{\gamma_0} \right)^{n-1} \exp[-b(T - T_0)] \quad (A5)$$

where  $\mu_0$  is the effective viscosity at a reference shear rate  $\gamma_0$  and temperature  $T_0$ .  $n$  is the power-law index and  $b$  the temperature coefficient of viscosity. In the present model, the second invariant of the local rate of deformation tensor is:

$$I_2 = \frac{1}{4} \left[ \left( \frac{dw}{dy} \right)^2 + \left( \frac{du}{dy} \right)^2 \right] \quad (A6)$$

#### Boundary conditions and flow rate

The boundary conditions are assumed to be:

$$u = 0, w = 0, T = T_b \text{ at } y = 0 \quad (A7)$$

$$u = V_x, w = V_z, T = T_b \text{ at } y = H$$

where  $T_b$  is the barrel temperature. The temperature boundary condition at the screw ( $y = 0$ ) is chosen to allow for the omission from equation (A3) of transverse convection, the effect of which is to keep the temperature of the screw close to that of the barrel.

Neglecting leakage over the flights, the transverse flow rate in the channel is zero:

$$\int_0^H u dy = 0 \quad (A8)$$

while the downstream volumetric flow rate, which is the output from the machine, is given by:

$$Q = B \int_0^H w dy \quad (A9)$$

It is convenient to define a dimensionless flow rate:

$$\pi_Q = \frac{Q}{BV_z H_m} \quad (A10)$$

which can be thought of as the ratio between the actual flow rate and the rate that would be achieved if the melt in the metering section all moved downstream with the same velocity as the barrel relative to the screw. A value for  $\pi_Q$  between about 0.4 and 0.5 corresponds to the drag flow condition, where no pressure gradient is generated. As this represents the maximum output for melt-fed machines,  $\pi_Q = 0.4$  is a reasonable value to assume for design purposes.

#### Filled length

So far it has been implicitly assumed that the channel is always full of melt. In the early part of the screw, before pressure generation starts, the channel is in practice only partly full. This situation can be analysed with only minor modifications to the mathematical model. The axial filled length,  $L_{fill}$ , is determined by the pressure required at the delivery end of the screw. As indicated, however, variations of the filled length have relatively small effects on machine performance.

#### Method of solution

The mathematical equations can in general only be solved numerically, with the aid of a digital computer. Equation (A3) is used to step downstream to compute the developing temperature profiles. At each step equations (A1) are used to find the velocity profiles with the aid of equations (A2), (A5)–(A9). Note that the temperature and velocity profiles are linked by the temperature dependence of viscosity in equation (A5).

#### Performance parameters

From the computed temperature and velocity profiles may be obtained performance parameters which are of more direct practical use. For example, the temperature profile can be described in terms of a bulk mean temperature at any position along the extruder

$$\bar{T} = \frac{\int_0^H aT dy}{\int_0^H a dy} \quad (A11)$$

where

$$a = w \sin \theta - u \cos \theta$$

is the melt velocity component in the axial direction.

Distributive mixing is discussed in the paper. The mean degree of mixing may be formally defined as<sup>3</sup>:

$$M = \frac{B}{Q} \int_0^{L \csc \theta} \int_0^H \sqrt{4I_2} dy dz \quad (A12)$$

Finally, the mean shear rate in the metering section may be defined as

$$\bar{\gamma} = V_z / H_m \quad (A13)$$

# Notes to the Editor

## Viscosity of Newtonian suspensions\*

R. F. Fedors

*Jet Propulsion Laboratory, California Institute of Technology, Pasadena, California 91103, USA*  
(Received 23 December 1974)

In a recent paper, Nicodemo and Nicolais<sup>1</sup> reported the effect of asymmetric glass fibres (of average length 0.053 cm, average diameter 0.0014 cm and hence of aspect ratio 37.8) on the viscosity of aqueous solutions of poly(ethylene oxide). They showed that the dependence of the relative viscosity,  $\eta_r$ , at zero shear rate on volume fraction of glass fibre,  $\phi$  could be described by an equation of the form:

$$\eta_r = \exp(8.52\phi) \quad (1)$$

A comparison of the experimentally measured  $\eta_r$  and that calculated using equation (1) is shown in *Table 1* where as may be seen, the agreement is quite satisfactory.

It is our purpose to show that the  $\eta_r, \phi$  response can also be adequately described by an equation proposed previously for the Newtonian viscosity of suspensions of aggregates<sup>2</sup>. It is given by:

$$\eta_r = \left(1 + \frac{1.25\phi}{\phi_m - \phi}\right)^2 \quad (2)$$

where  $\phi_m$  is the maximum volume fraction to which the suspended particles can be randomly packed. In principle, the value of  $\phi_m$  can be estimated independently from measurements such as sedimentation volume or packing fraction. We have used equation (2) to fit the  $\eta_r, \phi$  data and the results are also shown in *Table 1*. For this fit,  $\phi_m$  was taken to have the value 0.31 which is reasonable for the random packing of high aspect ratio rods. This value means that a randomly packed bed of rods contains 69% void volume.

If we expand equation (1) to the second power in  $\phi$  (which is adequate to fit the experimental data), we have:

$$\eta_r \approx 1 + 8.52\phi + \frac{(8.52)^2}{2} \phi^2 \quad (3)$$

while expansion of equation (2) provides:

\* This paper represents the results of one phase of research carried out at the Jet Propulsion Laboratory, California Institute of Technology, under Contract No. NAS7-100, sponsored by the National Aeronautics and Space Administration.

*Table 1* Dependence of  $\eta_r$  on  $\phi$  for glass fibres in aqueous poly(ethylene oxide)

	$\phi$				
	0	0.01	0.03	0.05	0.07
$\eta_r$ (exp.)	1.0	1.12	1.3	1.5	1.85
$\eta_r$ (calc. eqn.1)	1.0	1.09	1.29	1.53	1.82
$\eta_r$ (calc. eqn.2 $\phi_m = 0.31$ )	1.0	1.09	1.29	1.54	1.86
$\eta_r$ (calc. eqn.2 $\phi_m = 0.29$ )		1.09	1.31	1.59	1.95

$$\eta_r \approx 1 + \frac{5\phi}{2\phi_m} + \frac{65}{16} \frac{\phi^2}{\phi_m^2} \quad (4)$$

Equating like coefficients of powers of  $\phi$ , we have  $\phi_m = 0.293$  from the  $\phi$  term and  $\phi_m = 0.334$  from the  $\phi^2$  term. Taking the average of these two values, we get  $\phi_m = 0.314$  which is in satisfactory agreement with the value of this parameter obtained directly from application of equation (2) to the experimental data.

In a further effort to show that  $\phi_m = 0.31$  is a reasonable value, packing experiments were carried out using approximately 2500 pieces of steel wire 0.12 cm in diameter and 4.0 cm in length (i.e., wire with an aspect ratio of 34). This size was chosen for convenience in handling as described below. Also it is well-known that  $\phi_m$  does not depend on particle size except in that region where the high surface area to volume ratio causes particle to particle sticking. For example,  $\phi_m$  for large sphere of glass, steel, Plexiglass, nylon<sup>3</sup> 0.32 cm in diameter is 0.63 while  $\phi_m$  for glass spheres 0.003 cm in diameter is also 0.63<sup>4</sup>. Hence, we can reasonably expect that  $\phi_m$  for the 0.12 cm diameter wire should be comparable to  $\phi_m$  for the glass fibre used by Nicodemo and Nicolais.

The  $\phi_m$  value for the wire was estimated as follows. The wire was placed in small, very flexible plastic bags and then immersed in water; the volume of water displaced was assumed to be equal to the total volume,  $V_T$ , occupied by the wire.  $\phi_m$  was then taken equal to  $v/V_T$  where  $v$  is the volume of the wire which is equal to the weight of the wire, 899 g, divided by its density, 7.70 g/cm<sup>3</sup>.

The plastic bags were sufficiently flexible so that they for the most part conformed to the outline of the bed of wire. However, in practice, the wire ends usually produced small punctures in the bag. Hence two bags were used one over the other. The inner bag opening was simply twisted closed but otherwise left unsealed while the outer bag was sealed with a rubber band. It soon became apparent that an appreciable air space existed between the two bags. To eliminate the air, small holes were made in the outer bag and the bags and wire were gently kneaded by hand to expel air. The total occupied volume was then taken to be the minimum volume of water displaced. To monitor the quantity of water getting into the bags to the wire, the bags containing the wire were removed periodically and weighed. When the volume of displaced water had decreased and stabilized at 405 cm<sup>3</sup>, the difference between the weight after kneading under water and the initial dry weight amounted to less than 4%. This weight increase is equal to the weight of water which had flowed in the plastic bags. From the numerical data obtained,  $\phi_m$  for the wire is estimated to be 0.29, a value in excellent agreement with the value of 0.31 required for fit of equation (2) to the experimental data.

If one takes the  $\phi_m$  value for the glass fibres to have



the same value as estimated for the wire, the  $\eta_r$ ,  $\phi$  response calculated using equation (2) and  $\phi_m = 0.29$  is within 6% of the experimentally determined response. Thus, we have been able to estimate  $\eta_r$  as a function of  $\phi$  to within 6% using equation (2) and independently estimating the parameter  $\phi_m$  by means of an auxiliary experiment.

## Evidence for aggregation in solutions of poly(ethylene oxide)

Carla Cuniberti

Istituto di Chimica Industriale dell'Università di Genova, Via Pastore 3, 16132 Genova, Italy  
(Received 23 October 1974; revised 18 November 1974)

It was shown in previous papers<sup>1,2</sup> that dilute solutions of high molecular weight poly(ethylene oxide) (PEO) in dimethylformamide (DMF) above room temperature contain supermolecular particles arising from molecular associations. In order to investigate the ability of these particles to act as crystallization centres on cooling, the isothermal crystallization of PEO-DMF solutions with different thermal histories was studied.

Three procedures were used to prepare the solutions: (a) direct dissolution of the sample at a temperature above its solution point; (b) dissolution of the sample at 80°C, followed by full crystallization at 0°C and heating of the suspension up to a temperature above the clearing point (the solution was maintained 30 min at this temperature); (c) dissolution of the sample at 110°C, followed by slow cooling (10°C/h) to lower temperatures.

The time at the dissolution temperature was 1 h and 0.1% diphenylamine was added to avoid polymer degradation.

Quenching from the final temperature reached by the solution,  $T_d$ , to the crystallization temperature,  $T_c$ , was carried out in each case.

The sample was a well annealed film obtained by evaporation at 50°C of a benzene solution of a PEO fraction with molecular weight  $3.5 \times 10^5$ . Solutions of concentration 0.155% were employed. The dissolution temperature of the appropriate amount of polymer in DMF was 38°C and the clearing point of the crystalline suspension 21.6°C. The crystallization temperature 12.8°C was chosen because it was possible to achieve the complete phase separation within acceptable times in all the cases here studied. The crystallization process was followed by measuring the increase of the turbidity, a method particularly suited to the investigation of the initial part of the phase separation in dilute solutions<sup>3</sup>.

In Figure 1 the measured induction time,  $t_i$ , for the crystallization of PEO is plotted against the temperature  $T_d$ . The increase of  $t_i$  with  $T_d$  reveals the presence of destroyable heterogeneities in all the solutions but, while induction times falling approximately on the same curve are obtained by means of procedures (b) and (c), the crystallization is much faster in case (a) at  $T_d < 80^\circ\text{C}$ . Furthermore, in Figure 1a curve bc (circles) shows a sensible increase of  $t_i$  in two separate intervals of the explored temperature range. The low temperature variation covers about 25 degrees above the clearing point of the suspension and must be connected with crystallization seeds that decrease in number with increasing temperature, as

## REFERENCES

- 1 Nicodemo, L. and Nicolais, L. *Polymer* 1974, 15, 589
- 2 Fedors, R. F. *J. Colloid Interfacial Sci.* 1974, 46, 545
- 3 Scott, G. D. and Kilgour, D. M. *Br. J. Appl. Phys. (D)* 1969, 2, 863
- 4 Fedors, R. F. unpublished results

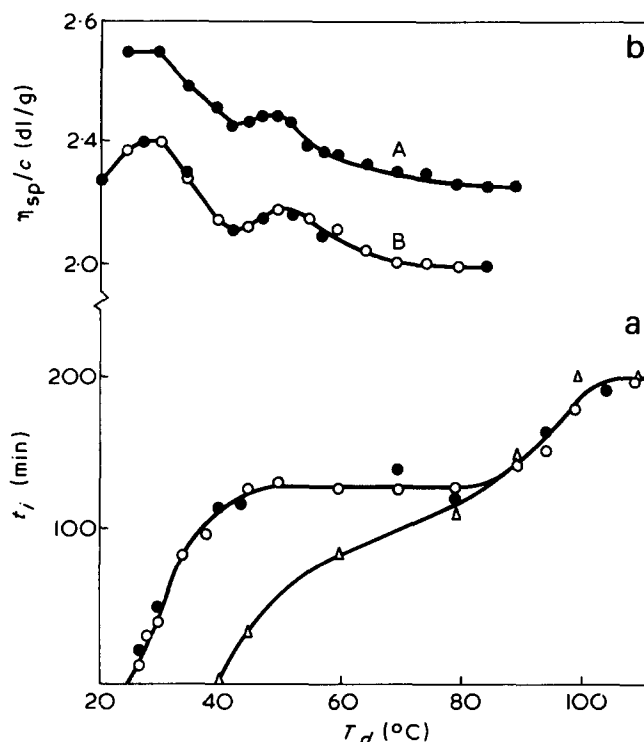


Figure 1 (a) Dependence of induction time,  $t_i$ , on the final temperature of the solution ( $T_d$ ) reached by procedures (a) ( $\Delta$ ), (b) ( $\circ$ ) and (c) ( $\bullet$ ). (b) Dependence of the reduced viscosity on temperature for solutions 0.155% (A) and 0.082% (B);  $\bullet$ , points obtained by decreasing the temperature;  $\circ$ , points obtained by increasing the temperature

was shown for polyethylene in xylene<sup>4</sup>. These seeds are completely destroyed above 45–50°C. On the same line, the increase of  $t_i$  between 80° and 110°C gives evidence of a second kind of crystallization seeds that disappear only above 110°C. The stability of these particles above the melting point of the polymer<sup>5</sup> and their reduced ability to grow crystals show that, besides numerical or dimensional differences, a different morphology must be involved. The identical crystallization rates obtained with procedures (b) and (c) show moreover that both kinds of seeds are in equilibrium with dissolved polymer molecules. That non-equilibrium residues give rise to much shorter induction times is shown by curve a (triangles) in Figure 1a, obtained when the sample is directly dissolved at  $T_d$ . At  $T_d$  lower than about 80°C residual seeds from the crystalline film require heating times longer than 1 h to reach equilibrium

the same value as estimated for the wire, the  $\eta_r$ ,  $\phi$  response calculated using equation (2) and  $\phi_m = 0.29$  is within 6% of the experimentally determined response. Thus, we have been able to estimate  $\eta_r$  as a function of  $\phi$  to within 6% using equation (2) and independently estimating the parameter  $\phi_m$  by means of an auxiliary experiment.

## Evidence for aggregation in solutions of poly(ethylene oxide)

Carla Cuniberti

Istituto di Chimica Industriale dell'Università di Genova, Via Pastore 3, 16132 Genova, Italy  
(Received 23 October 1974; revised 18 November 1974)

It was shown in previous papers<sup>1,2</sup> that dilute solutions of high molecular weight poly(ethylene oxide) (PEO) in dimethylformamide (DMF) above room temperature contain supermolecular particles arising from molecular associations. In order to investigate the ability of these particles to act as crystallization centres on cooling, the isothermal crystallization of PEO-DMF solutions with different thermal histories was studied.

Three procedures were used to prepare the solutions: (a) direct dissolution of the sample at a temperature above its solution point; (b) dissolution of the sample at 80°C, followed by full crystallization at 0°C and heating of the suspension up to a temperature above the clearing point (the solution was maintained 30 min at this temperature); (c) dissolution of the sample at 110°C, followed by slow cooling (10°C/h) to lower temperatures.

The time at the dissolution temperature was 1 h and 0.1% diphenylamine was added to avoid polymer degradation.

Quenching from the final temperature reached by the solution,  $T_d$ , to the crystallization temperature,  $T_c$ , was carried out in each case.

The sample was a well annealed film obtained by evaporation at 50°C of a benzene solution of a PEO fraction with molecular weight  $3.5 \times 10^5$ . Solutions of concentration 0.155% were employed. The dissolution temperature of the appropriate amount of polymer in DMF was 38°C and the clearing point of the crystalline suspension 21.6°C. The crystallization temperature 12.8°C was chosen because it was possible to achieve the complete phase separation within acceptable times in all the cases here studied. The crystallization process was followed by measuring the increase of the turbidity, a method particularly suited to the investigation of the initial part of the phase separation in dilute solutions<sup>3</sup>.

In Figure 1 the measured induction time,  $t_i$ , for the crystallization of PEO is plotted against the temperature  $T_d$ . The increase of  $t_i$  with  $T_d$  reveals the presence of destroyable heterogeneities in all the solutions but, while induction times falling approximately on the same curve are obtained by means of procedures (b) and (c), the crystallization is much faster in case (a) at  $T_d < 80^\circ\text{C}$ . Furthermore, in Figure 1a curve bc (circles) shows a sensible increase of  $t_i$  in two separate intervals of the explored temperature range. The low temperature variation covers about 25 degrees above the clearing point of the suspension and must be connected with crystallization seeds that decrease in number with increasing temperature, as

## REFERENCES

- 1 Nicodemo, L. and Nicolais, L. *Polymer* 1974, 15, 589
- 2 Fedors, R. F. *J. Colloid Interfacial Sci.* 1974, 46, 545
- 3 Scott, G. D. and Kilgour, D. M. *Br. J. Appl. Phys. (D)* 1969, 2, 863
- 4 Fedors, R. F. unpublished results

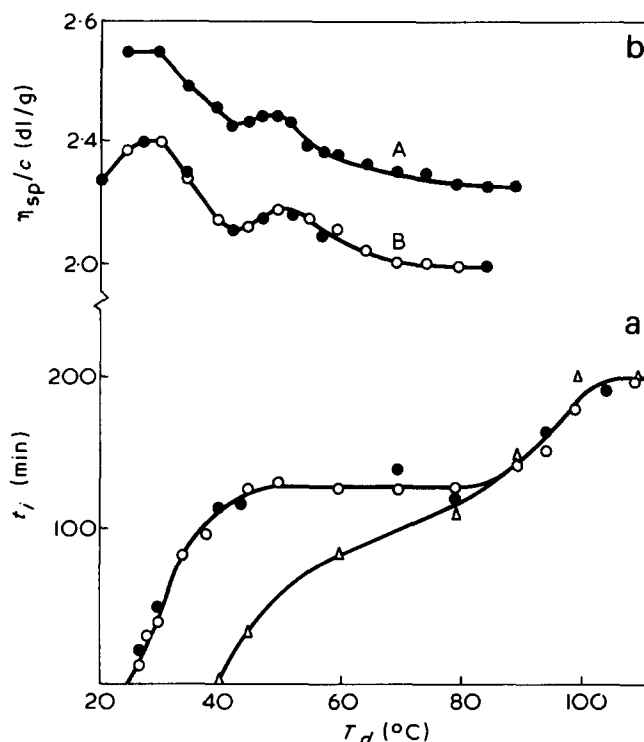


Figure 1 (a) Dependence of induction time,  $t_i$ , on the final temperature of the solution ( $T_d$ ) reached by procedures (a) ( $\Delta$ ), (b) ( $\circ$ ) and (c) ( $\bullet$ ). (b) Dependence of the reduced viscosity on temperature for solutions 0.155% (A) and 0.082% (B);  $\bullet$ , points obtained by decreasing the temperature;  $\circ$ , points obtained by increasing the temperature

was shown for polyethylene in xylene<sup>4</sup>. These seeds are completely destroyed above 45–50°C. On the same line, the increase of  $t_i$  between 80° and 110°C gives evidence of a second kind of crystallization seeds that disappear only above 110°C. The stability of these particles above the melting point of the polymer<sup>5</sup> and their reduced ability to grow crystals show that, besides numerical or dimensional differences, a different morphology must be involved. The identical crystallization rates obtained with procedures (b) and (c) show moreover that both kinds of seeds are in equilibrium with dissolved polymer molecules. That non-equilibrium residues give rise to much shorter induction times is shown by curve a (triangles) in Figure 1a, obtained when the sample is directly dissolved at  $T_d$ . At  $T_d$  lower than about 80°C residual seeds from the crystalline film require heating times longer than 1 h to reach equilibrium

with their environment. This behaviour shows that the polymer film is characterized by a more extensive order than the crystals grown in solution, since it is presumably the more ordered parts of the crystallites that resist dissolution. Only above 80°C is  $t_i$  completely independent of the thermal history of the solution, this suggesting that the aggregation mechanism<sup>3</sup> involved has no connection with crystallization.

The equilibrium between crystal seeds and polymer molecules found for PEO solutions just above the clearing point is different from the behaviour reported for polyethylene solutions, where the destruction of crystals has been described as an irreversible process<sup>6</sup>. One must therefore conclude that in PEO solutions the mechanism for recreating seeds is connected with the high temperature aggregation.

Viscosity measurements on solutions prepared after procedure (c) give further support to this result. *Figure 1b* shows the change of the reduced viscosity for the  $c = 0.155$  per cent solution (curve A), together with results previously

obtained<sup>2</sup> at higher dilution (curve B). The two maxima at different temperatures indicate that two different aggregation mechanisms are involved<sup>7</sup>; the increased prominence of the maxima with dilution shows that the average size of the two species is different. The larger weight of the peak on the left suggests further that the high temperature aggregates must act as nuclei for the growth of the low temperature species.

#### REFERENCES

- 1 Cuniberti, C. and Ferrando, R. *Polymer* 1972, 13, 379
- 2 Cuniberti, C. *Eur. Polym. J.* 1974, 10, 1175
- 3 Raciti, R. and Cuniberti, C. *Nuova Chim.* 1973, 49, (11), 35
- 4 Blundell, D. J., Keller, A. and Kovacs, A. J. *J. Polym. Sci. (B)* 1966, 4, 481
- 5 Beech, D. R. and Booth, C. *J. Polym. Sci. (B)* 1970, 8, 731
- 6 Keller, A. and Sadler, D. M. *J. Polym. Sci. (A-2)* 1970, 8, 1457
- 7 Nakajima, A. and Hamada, F. *IUPAC VIII Macromol. Microsymp. Prague* 1971, p 1

# RESOURCES POLICY

the economics, planning and use  
of mineral resources

A NEW QUARTERLY JOURNAL  
Third issue • March 1975

Copper resource appraisal  
**S.P. Wimpfen and H.J. Bennett**

Resource implications of materials waste  
in engineering manufacture  
**P.E. Becker and H.J. Pick**

The economic and environmental  
benefits of increased use of pfa and  
ground granulated slag  
**M.A. Smith**

Materials recovery and recycling in the  
USA — a report  
**M.E. Henstock**

#### Other sections

- Current topics
- Conference reports
- Forthcoming meetings
- Book reviews and announcements
- Publications received

**RESOURCES POLICY** will present multi-disciplinary discussions at an upper management/academic level. The aim is to identify policy options for the future supply and demand of mineral resources. It will encompass the many disciplines and examine options as they affect industrial, commercial and social institutions at world and regional levels

Published quarterly in  
March, June, September, December,  
commencing September 1974

One-year subscription (four issues) £20.00 (\$52.00)

For details apply to: IPC Business Press (Sales and Distribution Ltd.)  
Oakfield House, Perry Mount Road, Haywards Heath, Sussex, England RH6 3DH  
Telephone Haywards Heath (0444) 53281 Telex: Bisnespress Ldn 25137

## Dielectric behaviour of ethylene-vinyl acetate copolymers

Previous studies<sup>1-3</sup> of electrical properties of ethylene-vinyl acetate copolymers have demonstrated their use for determining the composition of the copolymers. Eidel'nant *et al.*<sup>3</sup> designated three relaxations  $\alpha$ ,  $\beta$  and  $\gamma$  in descending order of temperature at a fixed frequency. The  $\alpha$  process was observed only for copolymers with vinyl acetate contents up to 20% by wt and was assigned to crystalline regions and the  $\beta$  relaxation to segmental motion in amorphous regions. The  $\gamma$  relaxation process occurred in the glassy state at about  $-100^\circ\text{C}$  for frequencies in the audio-region and presumably was associated with local motion on a small scale. The  $\alpha$  and  $\gamma$  loss peaks were very small compared with the  $\beta$  one. McNight and Tretault<sup>4,5</sup> in dynamic mechanical and dielectric measurements on ethylene/vinyl acetate/vinyl alcohol terpolymers observed only two relaxations in the relevant copolymers (their samples A<sub>1</sub> and B<sub>1</sub>) corresponding to the  $\beta$  and  $\gamma$  relaxations above.

To assist clarification of these mechanisms we have made further studies of these copolymers and describe in some detail, not previously published, the parameters associated with segmental motion in amorphous regions. This includes information about the shape and width of loss curves and activation energies as a function of vinyl acetate content.

The copolymers studied were supplied by ICI Ltd as Evatane 18-02, 28-05, 33-25 and 40-50 (all random with the first number designating the wt/wt concentration of vinyl acetate) with crystallinities of 37, 22, 15 and 4% respectively as deduced from an empirical relationship<sup>6</sup>. The glass transitions  $T_g$  of the samples were evaluated from d.s.c. data and fell in the range  $-20^\circ\text{C}$  to  $-30^\circ\text{C}$ . The average molecular weights of the samples were at least 20 000. The samples were examined *in vacuo* as discs 5.08 cm in diameter by about 1 mm thick in the form of a three-terminal guarded electrode system, after cleaning and careful drying to constant weight over P<sub>2</sub>O<sub>5</sub>. They were placed in a shielded electrode assembly in a cryostat controlling temperature to  $\pm 0.3^\circ\text{C}$ . Dielectric measurements were made over the frequency range  $10^2$  to  $10^5$  Hz using a GR 1615A capacitance bridge.

Careful measurements on the 18-02 sample over the temperature range  $-25^\circ\text{C}$  to  $+40^\circ\text{C}$  (and frequency range above) revealed only one ( $\alpha$ ) relaxation contrary to the results of Eidel'nant *et al.*<sup>3</sup> and over the temperature range  $-90^\circ\text{C}$  to  $+40^\circ\text{C}$  all the copolymers exhibited only 2 relaxations ( $\alpha$  and  $\beta$ ) corresponding to the  $\beta$  and  $\gamma$  of Eidel'nant *et al.*<sup>3</sup>. The magnitude of the  $\alpha$  relaxation was much greater than that of the  $\beta$ .

The  $\alpha$  relaxation occurred in the temperature region  $-10^\circ\text{C}$  to  $-25^\circ\text{C}$  and is clearly due to the large scale segmental motion (manifestation of  $T_g$ ) in amorphous regions. The shape of the relatively broad  $\alpha$  relaxation is shown in detail by the normalized plots of ratio of loss factor  $\epsilon''$  to maximum loss factor  $\epsilon''_m$  against log ratio of frequency  $f$  to frequency of maximum loss  $f_m$  in Figure 1. As the vinyl acetate content is increased, the plots narrow consistent with a lower crystallinity<sup>7</sup> from a half width of about 5.6

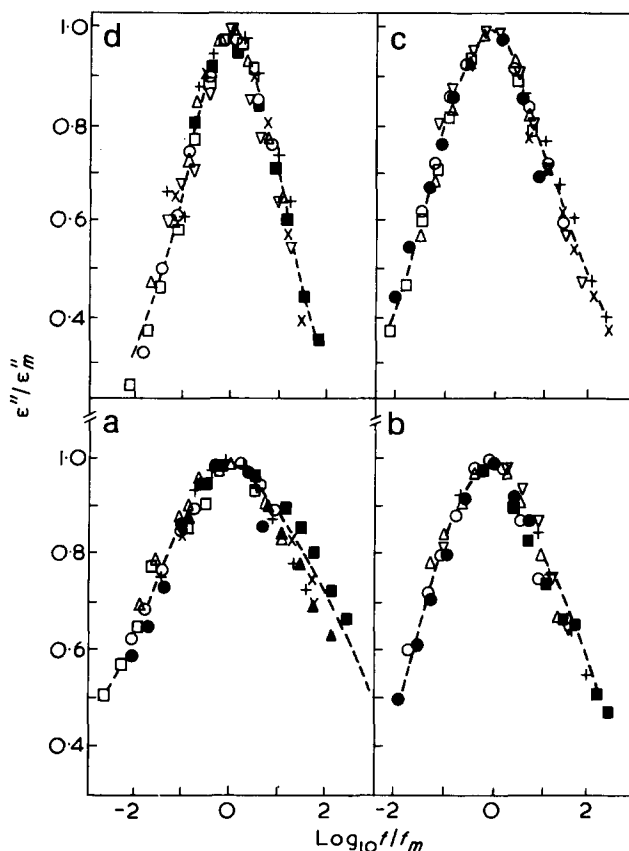


Figure 1 Normalized plots of  $\epsilon''/\epsilon''_m$  against  $\log f/f_m$  for the  $\alpha$  relaxation in samples with varying concentrations of vinyl acetate. (a) 18-02:  $\square$ ,  $-9.5^\circ\text{C}$ ;  $\bullet$ ,  $-11.5^\circ\text{C}$ ;  $\circ$ ,  $-13.5^\circ\text{C}$ ;  $\Delta$ ,  $-16.0^\circ\text{C}$ ;  $+$ ,  $-19.5^\circ\text{C}$ ;  $\times$ ,  $-21.4^\circ\text{C}$ ;  $\blacktriangle$ ,  $-23.5^\circ\text{C}$ ;  $\blacksquare$ ,  $-25.0^\circ\text{C}$ . (b) 28-05:  $\bullet$ ,  $-11.0^\circ\text{C}$ ;  $\circ$ ,  $-13.5^\circ\text{C}$ ;  $\Delta$ ,  $-16.0^\circ\text{C}$ ;  $\nabla$ ,  $-18.0^\circ\text{C}$ ;  $+$ ,  $-20.0^\circ\text{C}$ ;  $\blacksquare$ ,  $-25.5^\circ\text{C}$ . (c) 33-25:  $\square$ ,  $-9.0^\circ\text{C}$ ;  $\circ$ ,  $-14.0^\circ\text{C}$ ;  $\Delta$ ,  $-15.5^\circ\text{C}$ ;  $\nabla$ ,  $-19.0^\circ\text{C}$ ;  $+$ ,  $-21.0^\circ\text{C}$ ;  $\times$ ,  $-22.5^\circ\text{C}$ . (d) 40-50:  $\square$ ,  $-9.5^\circ\text{C}$ ;  $\circ$ ,  $-13.5^\circ\text{C}$ ;  $\Delta$ ,  $-16.5^\circ\text{C}$ ;  $\nabla$ ,  $-18.5^\circ\text{C}$ ;  $+$ ,  $-20.0^\circ\text{C}$ ;  $\times$ ,  $-22.5^\circ\text{C}$ ;  $\blacksquare$ ,  $-25.5^\circ\text{C}$ .

decades for the 18-02 sample to 2.8 decades for the 40-50 sample; but an interesting point is that the broader loss curves for samples of lower vinyl acetate content are broader on the high frequency side instead of the low frequency side<sup>7</sup>. The relatively small scatter in the data for each normalized plot is due to the fact that the width of the loss curves varies somewhat with temperature and this scatter is much reduced in the nearly amorphous 40-50 specimen, which has a half width somewhat greater than that for poly(vinyl acetate)<sup>14</sup> (2.0 decades). The position of the loss peak is little affected by the vinyl acetate content and this is illustrated in Figure 2 in the plots of log frequency of maximum loss against  $1/T$  on a fairly sensitive scale. Over the frequency and temperature range used the points for the three samples 18-02, 28-05 and 33-25 fall on a roughly common plot corresponding to an activation energy of about 160 kJ/mol as determined from the slopes of lines fitted by the method of least squares to the points for each sample separately. However, the data for the 40-50 sample are slightly shifted to the lower temperature side (at fixed frequency) corresponding to a reproducibly lower activation energy of about 90 kJ/mol as determined from the slope of the line (again) fitted to the corresponding

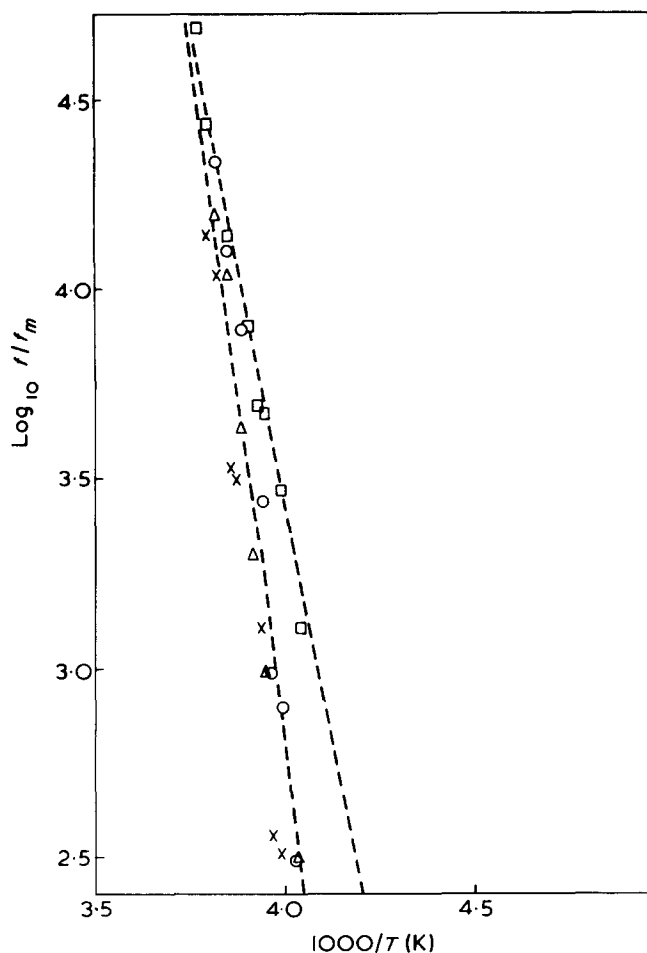


Figure 2 Loci plots of  $\log f_m$  against  $1/T$  (K) for the  $\alpha$  relaxation in samples with varying concentrations of vinyl acetate.  $\circ$ , 18-02;  $\triangle$ , 28-05;  $\times$ , 33-25;  $\square$ , 40-50

points by the method of least squares. This can be explained by the relatively low crystallinity (4%) of this sample, whereas the lack of variation of activation energy of the other three samples can be explained by the effect of varying crystallinity, (higher crystallinity shifting the loss peaks to higher temperatures at a fixed frequency<sup>8,9</sup>) being counteracted by the increased polarity of the chain molecules as the vinyl acetate content is increased. All the copolymers have a lower activation energy than that quoted for poly(vinyl acetate)<sup>14</sup> (250 kJ/mol).

The magnitude of the relaxation was calculated assuming the relationship<sup>10,11</sup>:

$$\epsilon_s - \epsilon_\infty = 1.75\epsilon_m'' \Delta \log f \quad (1)$$

where  $\Delta \log f$  is the half width (for  $\epsilon'' = \epsilon_m''/2$ ) and assuming that the plots of  $\epsilon''$  vs.  $\log f$  can be represented by a Fuoss-Kirkwood relationship. The error involved in this assumption is likely to be small<sup>11</sup>. The calculations were made using average values of  $\epsilon_m''$ , the  $\Delta \log f$  values being taken from the normalized plots, so that the values of  $\epsilon_s - \epsilon_\infty$  are averages over the range of temperature used ( $-10^\circ\text{C}$  to  $-25^\circ\text{C}$ ). Values of  $\epsilon_\infty$  were obtained by short extrapolations from arc plots. The plots of  $\epsilon_s - \epsilon_\infty$  against vinyl acetate content were approximately linear, suggesting that the effective dipole moment for the average repeat unit



is approximately independent of dipolar vinyl acetate con-

centration and the linear variation arises because of the increasing number of dipoles per unit volume. The dipole moment,  $\mu$  for an average repeat unit was calculated from the Onsager<sup>12</sup> formula (MKS system):

$$\mu^2 = \frac{9\epsilon_0 k T (2\epsilon_s + \epsilon_\infty)(\epsilon_s - \epsilon_\infty)}{N\epsilon_s(\epsilon_\infty + 2)^2} \quad (2)$$

where  $k$  is Boltzmann's constant,  $T$  the temperature (K) and  $N$  is the number of dipolar repeat units per unit volume, equal to  $N_A \rho / M$  where  $N_A$  is Avogadro's number,  $\rho$  is the density and  $M$  is the molecular weight of the average repeat unit. In view of the usual inherent errors involved in applying this formula to polymers the values of dipole moment are only estimates. However, the results shown in Table 1 support the previous suggestion since the dipole moment values are approximately equal for the four samples used. Eidel'nant *et al.*<sup>3</sup> quoted slightly higher values (about 1.7 Debye) probably because they were evaluated for room temperature, suggesting a dependence of dipole moment on temperature. These dipole moment values probably characterize the effective dipole moment of the vinyl acetate unit when surrounded by mainly ethylene units as the values of  $\bar{m}$  (in the repeat unit) varied from 14 for the 18-02 sample to about 5 for the 40-50 sample.

The  $\beta$  loss peaks are quite small and the data have been found to be somewhat variable. Generally with 33-25 and 40-50 samples the half width of the loss peaks is 4-5 decades and the size of  $\epsilon_m''$  is of the order of 0.01. This is about 20 to 30 times smaller than the corresponding peak heights for the  $\alpha$  relaxation and an estimate for the magnitude  $(\epsilon_s - \epsilon_\infty)_\beta$  for the relaxation using equation (1) is of the order of 0.10. The loss peaks appear in the region of 10 kHz for temperatures in the range  $-70^\circ\text{C}$  to  $-85^\circ\text{C}$ , i.e. roughly in the same place as for poly(vinyl acetate)<sup>13,14</sup> with a relaxation magnitude (0.10) of just over half that found in poly(vinyl acetate) (0.14). Thus the  $\beta$  relaxation in these copolymers probably arises from a similar side group motion (in the glassy state) to that in poly(vinyl acetate).

The absence of a higher temperature relaxation equivalent to the  $\alpha$  of Eidel'nant *et al.*<sup>3</sup> on the 18-02 sample is not surprising as these authors assigned their  $\alpha$  relaxation to crystalline regions. These will contain only ethylene groups and the relaxation magnitude will normally be negligible even when allowing for residual dipole moments, unless accidental impurities or oxidation cause the presence of extraneous carbonyl groups<sup>8,9</sup>. Thus, whilst these may have been present in the samples of lower vinyl acetate content examined by Eidel'nant *et al.*<sup>3</sup> giving his small  $\alpha$  relaxation, this relaxation should normally be negligible

Table 1 Parameters of the  $\alpha$  relaxation (approximate average values over the range  $-10^\circ\text{C}$  to  $-25^\circ\text{C}$ )

Copolymer	Crystallinity (%)	Half-width from normalized plots	Peak height, $\epsilon_m''$	Relaxation magnitude, $\epsilon_s - \epsilon_\infty$	Dipole moment estimate (D) *
18-02	37	5.6	0.06	0.6	1.4
28-05	22	4.0	0.13	0.9	1.3
33-25	15	3.8	0.19	1.2	1.3
40-50	4	2.8	0.34	1.7	1.4

\* 1 Debye  $\equiv 3.33 \times 10^{-30}$  C m

and not usually observable in ethylene–vinyl acetate copolymers over a wide range of concentration of vinyl acetate.

For our  $\alpha$  relaxation the lack of variation of dipole moment with vinyl acetate concentration (and a corresponding change in the degree of crystallinity) is attributed to the fact that the vinyl acetate units occur only in amorphous regions<sup>15,16</sup> and not in crystalline regions which contain only ethylene groups. Generally the changes in width of the normalized plots in *Figure 1* are consistent with the corresponding changes in crystallinity except that there seems to be no obvious explanation for the curves for the 18–02 sample being broader on the high frequency side than on the low frequency side. In view of the curved  $\log f_m$  against  $1/T$  plot found by Eidel'nant *et al.*<sup>3</sup> for a sample with a vinyl acetate content of 11% (as might be expected from the WLF relationship<sup>17</sup>), it is interesting that the data for all our copolymers definitely fit a linear relationship better than a curved one over the frequency and temperature range used. Also, we can separate the locus and lower activation energy for the 40–50 sample from those for the other three samples. Extension of our frequency range by d.c. step response measurements (down to  $10^{-4}$  Hz) might well then show the curved plots typical of WLF behaviour. The much larger relaxation magnitude for the  $\alpha$  relaxation  $(\epsilon_s - \epsilon_\infty)_\alpha$  as compared with that for the  $\beta$  relaxation  $(\epsilon_s - \epsilon_\infty)_\beta$  is explained by the much freer movement of the vinyl acetate group in large scale segmental motion as compared with its small scale side group motion in the glassy state.

Further work (including measurements on samples of higher vinyl acetate content) is required to determine the exact shape of the loci for the  $\alpha$  relaxation at lower frequencies in the region of  $T_g$  and to determine the causes of variability in the  $\beta$  relaxation and hence evaluate its parameters more accurately.

#### Acknowledgements

The authors wish to thank Mr L. J. Maisey (Rubber and Plastics Research Association) for the d.s.c. measurements.

Martin E. Baird and Eve Houston

Department of Applied Physics and Electronics,  
UWIST, Cathays Park, Cardiff, CF1 3NU, UK  
(Received 20 December 1974)

#### References

- 1 Würstlin, F. *Kolloid-Z. Z. Polym.* 1966, **213**, 79
- 2 Terteryan, R. A., Barash, Yu. I. and Shapkina, L. N. *Vysokomol. Soedin. (A)* 1968, **10**, 673; *Polym. Sci. USSR* 1968, **10**, 1940
- 3 Eidel'nant, M. P., Duntov, F. I., Krundel, V. Kh. and Sazhin, B. I. *Vysokomol. Soedin. (A)* 1973, **15**, 533; *Polym. Sci. USSR* 1973, **A15**, 601
- 4 McNight, W. J. and Tetrault, R. J. *J. Polym. Sci. (C)* 1971, **35**, 117
- 5 McNight, W. J. and Tetrault, R. J. *Polym. Prepr.* 1971
- 6 Kawath, P. A. and Wakefield, R. W. *J. Appl. Polym. Sci.* 1965, **9**, 3153
- 7 Ishida, Y., Yamafuji, K., Ito, H. and Takayanagi, M. *Kolloid-Z. Z. Polym.* 1962, **184**, 97
- 8 McCrum, N. G., Read, B. E. and Williams, G. 'Anelastic and Dielectric Effects in Polymeric Solids', John Wiley, London, 1967
- 9 Baird, M. E. 'Electrical Properties of Polymeric Materials', Plastics Institute, London, 1973
- 10 Fuoss, F. M. and Kirkwood, J. G. *J. Am. Chem. Soc.* 1941, **63**, 385
- 11 Williams, G., Watts, D. C., Dev, S. B. and North, A. M. *Trans. Faraday Soc.* 1971, **67**, 1323
- 12 Bottcher, C. J. F. 'Theory of Electric Polarisation', Elsevier, Amsterdam, 1952
- 13 Veselovskii, P. F. and Slusker, A. I. *Zh. Tekh. Fiz.* 1955, **25**, 939; *Sov. Phys. Tech. Phys.* 1955, **25**, 1204
- 14 Ishida, Y., Matsuo, M. and Yamafuji, K. *Kolloid-Z.* 1962, **180**, 108
- 15 Kargin, V. A., Terteryan, R. A. Konstantipol'skaya, M. B. and Berestneva, Z. Ya. *Vysokomol. Soedin. (A)* 1969, **11**, 2585; *Polym. Sci. USSR* 1969, **11**, 2940
- 16 Personal communication from ICI Ltd, Plastics Group
- 17 Williams, M. L., Landel, R. F. and Ferry, J. D. *J. Am. Chem. Soc.* 1955, **77**, 3701

### An improved model for studying the concentration dependence of the configurational behaviour of chain molecules

Theoretical studies of the configurational behaviour of polymer molecules in high concentration solutions have been impeded by the lack of appropriate models. A model considered in the past for Monte Carlo calculations assumes that the chain molecule is confined to an impenetrable 'cell' which simulates the free volume available to the molecule<sup>1</sup>. The concentration varies with the 'cell' size. This model implies an unjustifiable constraint that the maximum length which the molecule can assume will not exceed the dimensions of the 'cell'. Further, the model does not take into account interchain interactions in a valid manner. The purpose of this letter is to put forward an improvement in the model in an attempt to avoid the above shortcomings.

An important consideration in the computer simulation studies is the computational feasibility of the model. Even the most efficient computational machines available at present permit calculations on only single chains of moderate length without incurring unrealistic expenditure. Therefore, an acceptable improvement in the model should incorporate the interchain interactions in such a way that the behaviour of a single chain as the basis of the model is retained, if calculations are not to be limited to short chains. This can be accomplished by postulating that although the positions of chain segments are no longer restricted to the confines of the cell, the system conforms to the periodic boundary conditions such that the number of segments in the 'cell' remains constant. Previously, we have mentioned the use of these conditions in the development of a model for studying the configurational behaviour of adsorbed chains as function of surface coverage<sup>2</sup>. Some other workers also have alluded to such conditions in the context of chain molecular models<sup>3,4</sup>.

A two-dimensional pictorial representation of the model with the proposed periodic boundary conditions is given in *Figure 1*. The square ABCD represents the basic 'cell' surrounded by replicas with chain molecular configurations identical to those in the 'cell' itself. In the particular configuration shown the chain molecule leaves the basic 'cell' at b. The parts bc, cd and de exist in the replicas 1, 2 and 3, which are represented in the basic 'cell' by 'b'c, 'c'd and 'd'e respectively. Then, in addition to the intramolecular interactions, the interchain interactions between ab, 'b'c, 'c'd and 'd'e have to be considered. In three dimensions the number of replicas in the immediate vicinity of the basic 'cell' will be 26.

Assuming the above model we have carried out some preliminary Monte Carlo calculations on 10-, 20-, 30- and 40-bond chains confined to a tetrahedral lattice. The basic 'cell' contained 64 lattice sites. Sufficiently large samples

and not usually observable in ethylene–vinyl acetate copolymers over a wide range of concentration of vinyl acetate.

For our  $\alpha$  relaxation the lack of variation of dipole moment with vinyl acetate concentration (and a corresponding change in the degree of crystallinity) is attributed to the fact that the vinyl acetate units occur only in amorphous regions<sup>15,16</sup> and not in crystalline regions which contain only ethylene groups. Generally the changes in width of the normalized plots in *Figure 1* are consistent with the corresponding changes in crystallinity except that there seems to be no obvious explanation for the curves for the 18–02 sample being broader on the high frequency side than on the low frequency side. In view of the curved  $\log f_m$  against  $1/T$  plot found by Eidel'nant *et al.*<sup>3</sup> for a sample with a vinyl acetate content of 11% (as might be expected from the WLF relationship<sup>17</sup>), it is interesting that the data for all our copolymers definitely fit a linear relationship better than a curved one over the frequency and temperature range used. Also, we can separate the locus and lower activation energy for the 40–50 sample from those for the other three samples. Extension of our frequency range by d.c. step response measurements (down to  $10^{-4}$  Hz) might well then show the curved plots typical of WLF behaviour. The much larger relaxation magnitude for the  $\alpha$  relaxation  $(\epsilon_s - \epsilon_\infty)_\alpha$  as compared with that for the  $\beta$  relaxation  $(\epsilon_s - \epsilon_\infty)_\beta$  is explained by the much freer movement of the vinyl acetate group in large scale segmental motion as compared with its small scale side group motion in the glassy state.

Further work (including measurements on samples of higher vinyl acetate content) is required to determine the exact shape of the loci for the  $\alpha$  relaxation at lower frequencies in the region of  $T_g$  and to determine the causes of variability in the  $\beta$  relaxation and hence evaluate its parameters more accurately.

#### Acknowledgements

The authors wish to thank Mr L. J. Maisey (Rubber and Plastics Research Association) for the d.s.c. measurements.

Martin E. Baird and Eve Houston

Department of Applied Physics and Electronics,  
UWIST, Cathays Park, Cardiff, CF1 3NU, UK  
(Received 20 December 1974)

#### References

- 1 Würstlin, F. *Kolloid-Z. Z. Polym.* 1966, **213**, 79
- 2 Terteryan, R. A., Barash, Yu. I. and Shapkina, L. N. *Vysokomol. Soedin. (A)* 1968, **10**, 673; *Polym. Sci. USSR* 1968, **10**, 1940
- 3 Eidel'nant, M. P., Duntov, F. I., Krundel, V. Kh. and Sazhin, B. I. *Vysokomol. Soedin. (A)* 1973, **15**, 533; *Polym. Sci. USSR* 1973, **A15**, 601
- 4 McNight, W. J. and Tetrault, R. J. *J. Polym. Sci. (C)* 1971, **35**, 117
- 5 McNight, W. J. and Tetrault, R. J. *Polym. Prepr.* 1971
- 6 Kawath, P. A. and Wakefield, R. W. *J. Appl. Polym. Sci.* 1965, **9**, 3153
- 7 Ishida, Y., Yamafuji, K., Ito, H. and Takayanagi, M. *Kolloid-Z. Z. Polym.* 1962, **184**, 97
- 8 McCrum, N. G., Read, B. E. and Williams, G. 'Anelastic and Dielectric Effects in Polymeric Solids', John Wiley, London, 1967
- 9 Baird, M. E. 'Electrical Properties of Polymeric Materials', Plastics Institute, London, 1973
- 10 Fuoss, F. M. and Kirkwood, J. G. *J. Am. Chem. Soc.* 1941, **63**, 385
- 11 Williams, G., Watts, D. C., Dev, S. B. and North, A. M. *Trans. Faraday Soc.* 1971, **67**, 1323
- 12 Bottcher, C. J. F. 'Theory of Electric Polarisation', Elsevier, Amsterdam, 1952
- 13 Veselovskii, P. F. and Slusker, A. I. *Zh. Tekh. Fiz.* 1955, **25**, 939; *Sov. Phys. Tech. Phys.* 1955, **25**, 1204
- 14 Ishida, Y., Matsuo, M. and Yamafuji, K. *Kolloid-Z.* 1962, **180**, 108
- 15 Kargin, V. A., Terteryan, R. A. Konstantipol'skaya, M. B. and Berestneva, Z. Ya. *Vysokomol. Soedin. (A)* 1969, **11**, 2585; *Polym. Sci. USSR* 1969, **11**, 2940
- 16 Personal communication from ICI Ltd, Plastics Group
- 17 Williams, M. L., Landel, R. F. and Ferry, J. D. *J. Am. Chem. Soc.* 1955, **77**, 3701

### An improved model for studying the concentration dependence of the configurational behaviour of chain molecules

Theoretical studies of the configurational behaviour of polymer molecules in high concentration solutions have been impeded by the lack of appropriate models. A model considered in the past for Monte Carlo calculations assumes that the chain molecule is confined to an impenetrable 'cell' which simulates the free volume available to the molecule<sup>1</sup>. The concentration varies with the 'cell' size. This model implies an unjustifiable constraint that the maximum length which the molecule can assume will not exceed the dimensions of the 'cell'. Further, the model does not take into account interchain interactions in a valid manner. The purpose of this letter is to put forward an improvement in the model in an attempt to avoid the above shortcomings.

An important consideration in the computer simulation studies is the computational feasibility of the model. Even the most efficient computational machines available at present permit calculations on only single chains of moderate length without incurring unrealistic expenditure. Therefore, an acceptable improvement in the model should incorporate the interchain interactions in such a way that the behaviour of a single chain as the basis of the model is retained, if calculations are not to be limited to short chains. This can be accomplished by postulating that although the positions of chain segments are no longer restricted to the confines of the cell, the system conforms to the periodic boundary conditions such that the number of segments in the 'cell' remains constant. Previously, we have mentioned the use of these conditions in the development of a model for studying the configurational behaviour of adsorbed chains as function of surface coverage<sup>2</sup>. Some other workers also have alluded to such conditions in the context of chain molecular models<sup>3,4</sup>.

A two-dimensional pictorial representation of the model with the proposed periodic boundary conditions is given in *Figure 1*. The square ABCD represents the basic 'cell' surrounded by replicas with chain molecular configurations identical to those in the 'cell' itself. In the particular configuration shown the chain molecule leaves the basic 'cell' at b. The parts bc, cd and de exist in the replicas 1, 2 and 3, which are represented in the basic 'cell' by 'b'c, 'c'd and 'd'e respectively. Then, in addition to the intramolecular interactions, the interchain interactions between ab, 'b'c, 'c'd and 'd'e have to be considered. In three dimensions the number of replicas in the immediate vicinity of the basic 'cell' will be 26.

Assuming the above model we have carried out some preliminary Monte Carlo calculations on 10-, 20-, 30- and 40-bond chains confined to a tetrahedral lattice. The basic 'cell' contained 64 lattice sites. Sufficiently large samples

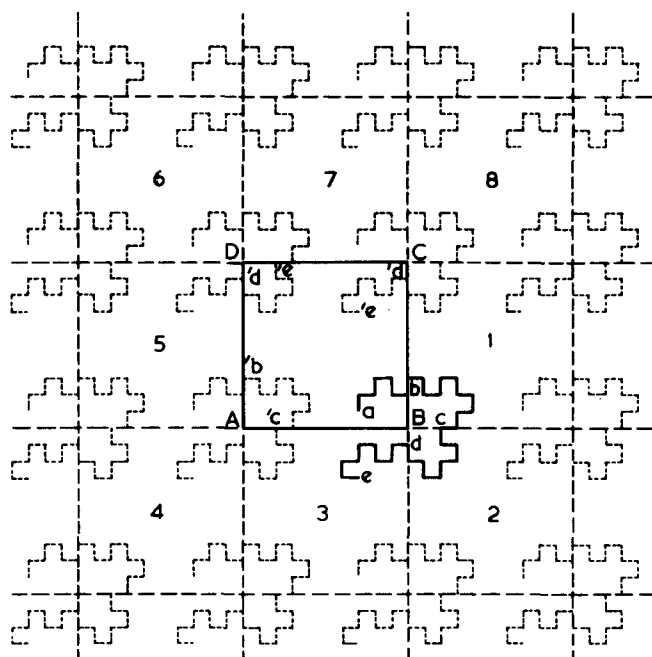


Figure 1 A pictorial representation of the periodic boundary conditions

of configurations (40 000–200 000 configurations) were generated on a computer following a procedure analogous to the Metropolis sampling technique<sup>5</sup>. Only those configurations were accepted which maintained intramolecular as well as intermolecular excluded volume condition. Mean values of the configurational quantities over the samples thus generated converge to the canonical ensemble averages. The description of the procedure as applied to an isolated chain appeared in a previous publication<sup>6</sup>; details of its extension to the present model will be provided later. Computed values of the mean square of the end-to-end distance,  $\langle(R_N^2)\rangle_\phi$ , for the chains of various lengths ( $N$ ) are given in Table 1. Volume fractions, quoted in the second column, are simply the ratio between the number of segments in the chain ( $N + 1$ ) and the number of lattice sites in the basic 'cell'. For the sake of comparison we have included in Table 1 the mean values of  $R_N^2$  for systems in the limit of zero concentration (excluded volume isolated chains),  $\langle(R_N^2)\rangle_{\phi \rightarrow 0}$ , and under the theta condition (chains without excluded volume),  $\langle(R_N^2)\rangle_\theta$ . It is interesting to note that for 10-, 20- and 30-bond chains the values of  $\langle(R_N^2)\rangle_\phi$  lie

Table 1 Values of the mean square of the end-to-end distance for the chains of various lengths

No. of bonds ( $N$ )	$\phi$	$\langle(R_N^2)\rangle_\phi$	$\langle(R_N^2)\rangle_{\phi \rightarrow 0}$	$\langle(R_N^2)\rangle_\theta$
10	0.172	$59.2 \pm 0.3$ (sample size: 40 000 conf.)	$60.4^{7,8}$	55.5
20	0.328	$128.8 \pm 0.6$ (sample size: 100 000 conf.)	$140^{7,9}$	115.5
30	0.484	$204 \pm 3$ (sample size: 100 000 conf.)	$228^{9,10}$	175.5
40	0.640	$212 \pm 9$ (sample size: 200 000 conf.)	$321^{10}$	235.5

between  $\langle(R_N^2)\rangle_{\phi \rightarrow 0}$  and  $\langle(R_N^2)\rangle_\theta$ , but as the chain length increases to 40 bonds  $\langle(R_N^2)\rangle_\phi$  assumes a value lower than  $\langle(R_N^2)\rangle_\theta$ .

In forthcoming publications we shall consider the effect of concentration on such configurational features as chain molecular shape, chain flexibility and chain/chain entanglements. Also, we shall attempt to evaluate pressure/volume relationships.

The present model, in which there are no interactions other than the excluded volume effect, may be considered to represent athermal solutions. Models representing non-athermal solutions would contain non-zero segment/segment interactions. In future studies we hope to extend the present approach to such models.

A. T. Clark and M. Lal

Unilever Research Laboratory,  
Port Sunlight, Wirral,  
Cheshire L62 4XN, UK  
(Received 27 November 1974)

#### References

- 1 Bluestone, S. and Vold, M. J. *J. Chem. Phys.* 1965, **42**, 4175
- 2 Lal, M. and Spencer, D. *167th A.C.S. Nat. Meet. Los Angeles 1974*, Abstract COLL 145
- 3 Belleman, A. and De Vos, E. J. *Polym. Sci. (C)* 1973, **42**, 1195
- 4 Nakata, Y. and Suzuki, K. *Rep. Progr. Polym. Phys. Japan* 1973, **16**, 1
- 5 Metropolis, N. *et al. J. Chem. Phys.* 1953, **21**, 1087
- 6 Lal, M. *Mol. Phys.* 1969, **17**, 57
- 7 Wall, F. T. and Hioe, F. T. *J. Phys. Chem.* 1970, **74**, 4416
- 8 Kumbar, M. and Windwer, S. *J. Chem. Phys.* 1969, **50**, 5257
- 9 Jurs, P. C. and Reisner, J. *J. Chem. Phys.* 1971, **55**, 4948
- 10 Wall, F. T. and Whittington, S. G. *J. Phys. Chem.* 1969, **73**, 3953

#### ERRATA

'Conformational study of the sequential (Tyr-Glu)<sub>n</sub> copolymer in aqueous solution' by Yves Trudelle, *Polymer* 1975, **16**, 9–15.

Page 11, right hand column, lines 3–4 should read:

Figure 5a shows the chromatogram of a dilute sample, 0.05%, pH 6.82, etc.

'Circular dichroism study of poly(L-tyrosine), poly(L-glutamic acid) and of random and sequential copolymers of L-glutamic acid and L-tyrosine in trimethylphosphate' by Yves Trudelle and Gérard Spach, *Polymer* 1975, **16**, 16–20.

Page 16, right hand column, 2 lines from bottom:

for Poly(L-glutamyl-L-tyrosyl-L-glutamyl)  
read Poly(L-glutamyl-L-tyrosyl-L-tyrosyl-L-glutamyl) etc. We apologize for these errors.



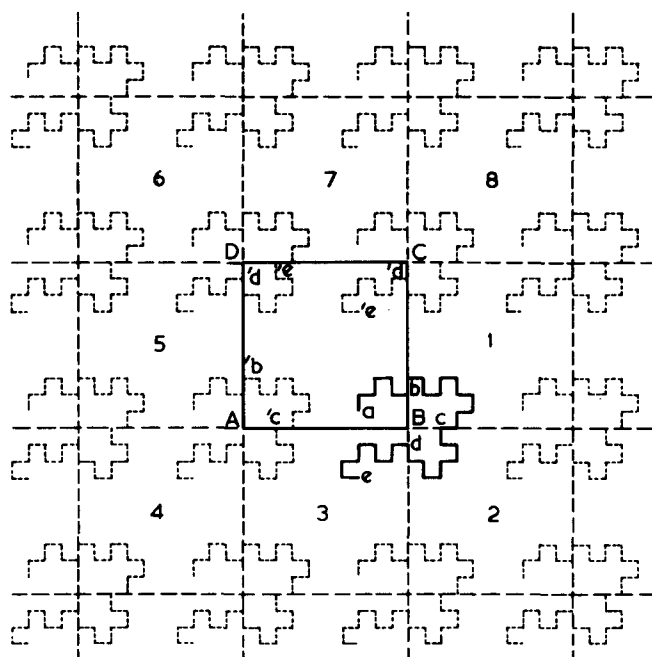


Figure 1 A pictorial representation of the periodic boundary conditions

of configurations (40 000–200 000 configurations) were generated on a computer following a procedure analogous to the Metropolis sampling technique<sup>5</sup>. Only those configurations were accepted which maintained intramolecular as well as intermolecular excluded volume condition. Mean values of the configurational quantities over the samples thus generated converge to the canonical ensemble averages. The description of the procedure as applied to an isolated chain appeared in a previous publication<sup>6</sup>; details of its extension to the present model will be provided later. Computed values of the mean square of the end-to-end distance,  $\langle(R_N^2)\rangle_\phi$ , for the chains of various lengths ( $N$ ) are given in Table 1. Volume fractions, quoted in the second column, are simply the ratio between the number of segments in the chain ( $N + 1$ ) and the number of lattice sites in the basic 'cell'. For the sake of comparison we have included in Table 1 the mean values of  $R_N^2$  for systems in the limit of zero concentration (excluded volume isolated chains),  $\langle(R_N^2)\rangle_{\phi \rightarrow 0}$ , and under the theta condition (chains without excluded volume),  $\langle(R_N^2)\rangle_\theta$ . It is interesting to note that for 10-, 20- and 30-bond chains the values of  $\langle(R_N^2)\rangle_\phi$  lie

Table 1 Values of the mean square of the end-to-end distance for the chains of various lengths

No. of bonds ( $N$ )	$\phi$	$\langle(R_N^2)\rangle_\phi$	$\langle(R_N^2)\rangle_{\phi \rightarrow 0}$	$\langle(R_N^2)\rangle_\theta$
10	0.172	$59.2 \pm 0.3$ (sample size: 40 000 conf.)	$60.4^{7,8}$	55.5
20	0.328	$128.8 \pm 0.6$ (sample size: 100 000 conf.)	$140^{7,9}$	115.5
30	0.484	$204 \pm 3$ (sample size: 100 000 conf.)	$228^{9,10}$	175.5
40	0.640	$212 \pm 9$ (sample size: 200 000 conf.)	$321^{10}$	235.5

between  $\langle(R_N^2)\rangle_{\phi \rightarrow 0}$  and  $\langle(R_N^2)\rangle_\theta$ , but as the chain length increases to 40 bonds  $\langle(R_N^2)\rangle_\phi$  assumes a value lower than  $\langle(R_N^2)\rangle_\theta$ .

In forthcoming publications we shall consider the effect of concentration on such configurational features as chain molecular shape, chain flexibility and chain/chain entanglements. Also, we shall attempt to evaluate pressure/volume relationships.

The present model, in which there are no interactions other than the excluded volume effect, may be considered to represent athermal solutions. Models representing non-athermal solutions would contain non-zero segment/segment interactions. In future studies we hope to extend the present approach to such models.

A. T. Clark and M. Lal

Unilever Research Laboratory,  
Port Sunlight, Wirral,  
Cheshire L62 4XN, UK  
(Received 27 November 1974)

#### References

- 1 Bluestone, S. and Vold, M. J. *J. Chem. Phys.* 1965, **42**, 4175
- 2 Lal, M. and Spencer, D. *167th A.C.S. Nat. Meet. Los Angeles 1974*, Abstract COLL 145
- 3 Belleman, A. and De Vos, E. J. *Polym. Sci. (C)* 1973, **42**, 1195
- 4 Nakata, Y. and Suzuki, K. *Rep. Progr. Polym. Phys. Japan* 1973, **16**, 1
- 5 Metropolis, N. *et al. J. Chem. Phys.* 1953, **21**, 1087
- 6 Lal, M. *Mol. Phys.* 1969, **17**, 57
- 7 Wall, F. T. and Hioe, F. T. *J. Phys. Chem.* 1970, **74**, 4416
- 8 Kumbar, M. and Windwer, S. *J. Chem. Phys.* 1969, **50**, 5257
- 9 Jurs, P. C. and Reisner, J. *J. Chem. Phys.* 1971, **55**, 4948
- 10 Wall, F. T. and Whittington, S. G. *J. Phys. Chem.* 1969, **73**, 3953

#### ERRATA

'Conformational study of the sequential (Tyr-Glu)<sub>n</sub> copolymer in aqueous solution' by Yves Trudelle, *Polymer* 1975, **16**, 9–15.

Page 11, right hand column, lines 3–4 should read:

Figure 5a shows the chromatogram of a dilute sample, 0.05%, pH 6.82, etc.

'Circular dichroism study of poly(L-tyrosine), poly(L-glutamic acid) and of random and sequential copolymers of L-glutamic acid and L-tyrosine in trimethylphosphate' by Yves Trudelle and Gérard Spach, *Polymer* 1975, **16**, 16–20.

Page 16, right hand column, 2 lines from bottom:

for Poly(L-glutamyl-L-tyrosyl-L-glutamyl)  
read Poly(L-glutamyl-L-tyrosyl-L-tyrosyl-L-glutamyl) etc. We apologize for these errors.

# Book Reviews

## Metals, ceramics and polymers

Oliver H. Wyatt and David Dew-Hughes

Cambridge Univ. Press, London, 1974, 625 pp. £12

This book can be recommended as a reference book to any serious student of materials science. In one volume the authors have combined the atomistic, microscopic and macroscopic approaches to materials and covered metals, ceramics, glasses and high polymers. The properties considered are mechanical, electrical and magnetic. Most of the standard proofs are given, often with an historical basis, which makes for interesting reading. There are many tables containing a great deal of useful, factual information and the diagrams and illustrations are excellent. The authors have chosen a physical, engineering approach to their subject which will be welcomed by physicists and applied scientists, but may be less useful to the polymer chemist who might, with some justification, feel that he has not received his 'fair bite of the cherry'. Although polymers are discussed throughout the book, only 55 pages out of 625 are devoted exclusively to them.

Inevitably there must be omissions in a book which attempts to cover as broad a field as this one. The authors realize this and argue that sensible selection of material is preferable to a wider coverage and superficiality. This is probably true, but it is arguable whether the complete omission of fabrication techniques in the section on polymers can be justified in view of the importance that these techniques have in the choice of polymers in competition with other materials. Also the importance of correct design for plastics is not discussed, and there is nothing on environmental stress cracking. Spherulites are described briefly but there is no mention of the role of impurities in causing constitutional undercooling, although this is a feature which is common to the growth of spherulites in polymers and to cellular growth in impure metals. In the discussions on metals it is surprising that temper brittleness and blue brittleness are dismissed in one sentence.

This is an ambitious book which largely achieves its objectives. It is written with style and humour, and each chapter ends with a selection of novel, often searching, questions.

The price of the hard-back version, £12, is not excessive in these inflationary times; the paper-back version, at just under £5, is excellent value for money.

J. R. Atkinson

## Polymer materials science

J. M. Schultz

Prentice-Hall, Englewood Cliffs, NJ, 1974, 511 pp.

Not since Geil's 1963 *Polymer Single Crystals* has there been an attempt to embrace the entire field of polymeric physical structure and dependent properties in a single volume. That book, written in the heyday of morphological inquiry, was able to give a comprehensive account of all textural studies then made plus the first rudimentary efforts to relate these to properties. To cover the same, now vastly more extensive, area today is a formidable task, but one which Professor Schultz has set himself in *Polymer Materials Science*. This is a postgraduate text comprising eleven chapters: Introduction dealing with chain conformations; Single crystals; Melt-crystallized polymers; Degree of crystallinity; Polymerization; Methods of measuring molecular weight averages and stereo-regularity; Mechanics of amorphous polymers; Time-dependent mechanical behaviour; Crystallization kinetics and mechanism; Electrical and electro-optical behaviour; and Mechanical behaviour of semi-crystalline polymers. The student is helped by needing little background knowledge, by detailed explanations of several investigative techniques and by the separation into appendixes of aspects of diffraction theory. There are also problems, some rather esoteric, attached to the earlier chapters.

The very long second chapter is partly, the author explains, to convince us that 'in many ways the science of polymeric materials is an extension of the science of copper or lithium fluoride or steel.' There is no doubt that Professor Schultz's enthusiasm, which is always evident, knows few bounds whenever he is dealing with such familiar metallurgical topics as dislocations, on which there are 14 pages plus 3 in an appendix. Nowadays one would think that the pendulum of opinion has swung back and that it is appreciated

that with polymers the meaning of 'crystal' has to be extended beyond the usage in simpler solids. It may be partly for this reason that the book seems a little old-fashioned; it is also because the subject matter is strangely out of date. Excepting a slight sprinkling of the author's own papers, there are only nine references to work published after 1970, one on morphology, the rest on mechanical properties. Had work appearing even a few months later been included such erroneous information as e.g. that nitric acid attacks polyethylene in two separate stages (p 72) or that pressure-crystallized polyethylene contains fully-extended molecules (p 182) could have been corrected. Early work on inter- and intra-lamellar deformation was then also available.

The chronological line has, nevertheless, to be drawn somewhere. It is the author's decisions on what to omit from established work which are the more disconcerting. Figure 2.21 is of an energetically vibrating dendrite to illustrate an early idea for the genesis of screw dislocations along re-entrant sector boundaries, but one which can hardly be of general application. Of the more extensive research which established that in non-planar lamellae a deviating sector boundary must lead to the observed overlaps, there is no mention. Nor is there the slightest indication of how morphologically complicated systems other than polyethylene typically are. Most surprising of all, however, is the treatment of spherulites – surely a major point of contact in the relation of properties to structure. Yet the main plank in our understanding of their microstructure, the theory of impurity segregation advanced by Keith and Padden, is referred to only *a propos* dendritic crystallization from solution, a context where mass transport is the dominant diffusion process. In the chapter on melt crystallization the theory is not mentioned. Instead there is a dangerous intermingling of 'dendritic' and 'spherulitic' and Keith and Padden's related work would only have been referred to in passing, as having made measurements on growth rates, had not a whole batch of references on this topic been mistakenly left out of the text.

All things considered, it is undoubtedly useful to have all these topics brought together in a single volume, notwithstanding a certain awkwardness in the sequence of chapters. Indeed any book attempting to fill students' needs in polymer materials science at the present time has to be welcomed. For Professor Schultz's text, however, which in many ways is a disappointment, that welcome must, regrettably, be muted.

D. C. Bassett

## European Plastics Buyer's Guide 1975

to be published in APRIL

The re-titled *europlastics yearbook* is the ONLY complete guide to the European plastics industry and will be the most extensive yet produced.

The buyer's guide has comprehensive sections on:

- materials and semi-finished products
- plant, ancillary equipment and engineering services
- processing services
- manufactured products and components

There is also an index to products (in English, French, German, Italian and Spanish) and trade names as well as information about more than 12 500 companies.

Price £12 (or £8 to subscribers to *European Plastics News*)

Orders to: IPC Industrial Press Ltd,  
33–40 Bowling Green Lane,  
London EC1R 0NE, England

Typeset by Mid-County Press, London SW19  
Printed by Kingprint Ltd, Richmond, Surrey

# Crosslinked poly [acryloyl *N,N*-bis-(2,2-dimethoxyethyl) amine] and crosslinked poly [acryloylmorpholine/ acryloyl *N,N*-bis(2,2-dimethoxyethyl) amine] gel networks and their application to the immobilization of $\beta$ -D-glucosidase

R. Epton, Barbara L. Hibbert and G. Marr

Department of Physical Sciences, Wolverhampton Polytechnic, Wolverhampton WV1 1LY, UK  
(Received 10 October 1974)

The synthesis and homopolymerization of acryloyl *N,N*-bis(2,2-dimethoxyethyl)amine is described. Gel networks were obtained by copolymerization of acryloyl *N,N*-bis(2,2-dimethoxyethyl)amine and *N,N'*-methylene diacrylamide (molar ratio 8:1) and by copolymerization of acryloyl morpholine, acryloyl *N,N*-bis(2,2-dimethoxyethyl)amine and *N,N'*-methylene diacrylamide (molar ratio 8:2:1). Following treatment of the gel networks with tartaric dihydrazide in dilute hydrochloric acid and subsequent activation with nitrous acid, conjugates of  $\beta$ -D-glucosidase were prepared. In both cases the immobilized enzyme was more resistant to heat denaturation than the native enzyme in solution. The nature of the polymer-enzyme linkage is discussed with reference to studies on the model compound phenylacetyl *N,N*-bis(2,2-dimethoxyethyl)amine.

## INTRODUCTION

The range of non-ionic, hydrophilic matrices in common use for the immobilization of enzymes is limited to derivatives of polysaccharides, crosslinked polyacrylamide and porous glass<sup>1-3</sup>. There is a need for alternative types of support to provide for enzyme immobilization within micro-environments of differing chemical functionality.

Recently, we have described the synthesis and properties of a new type of support matrix for enzyme immobilization, namely, crosslinked poly(acryloyl aminoacetaldehyde dimethylacetal) (Enzacryl<sup>®</sup> polyacetal)<sup>3</sup>. Controlled acid hydrolysis of this material leads to reactive aldehydrol groups effective in enzyme binding. Immobilization takes place within a novel and intensely hydrophilic micro-environment and in a number of cases the immobilized enzyme exhibits enhanced stability to heat denaturation<sup>4,5</sup>.

In view of the efficacy of Enzacryl polyacetal as an enzyme carrier, we have investigated other gel networks of the polyacetal and polyether type. This paper deals with the synthesis of two such materials. The first, crosslinked poly[acryloyl *N,N*-bis(2,2-dimethoxyethyl)amine] is structurally related to Enzacryl polyacetal. The second, a cross-linked copolymer of acryloyl morpholine and acryloyl *N,N*-bis(2,2-dimethoxyethyl)amine, molar ratio 4:1, may be regarded as a functional derivative of crosslinked poly(acryloyl morpholine) (Enzacryl<sup>®</sup> gel), a hydrophilic matrix introduced recently by us as a packing for gel permeation chromatography. The new gel networks have been evaluated

as matrices for the immobilization of the enzyme  $\beta$ -D-glucosidase.

## EXPERIMENTAL

### Synthesis of *N,N*-bis(2,2-dimethoxyethyl)amine

Aminoacetaldehyde dimethylacetal (315 g, 3 mol) (Koch-Light Ltd, UK) was added with vigorous mechanical stirring to a slurry of sodium carbonate (212 g, 2 mol) and water (500 cm<sup>3</sup>) at 100°C. Bromoacetaldehyde dimethylacetal (355 g, 2 mol) (prepared by the method of Bedoukian<sup>6</sup>) was added slowly over a period of 20 min and the mixture was boiled under reflux for 48 h.

After cooling to 0°C, the organic layer was siphoned off after which the aqueous layer was saturated with sodium chloride and extracted exhaustively with ether. The original organic layer and ether extracts were combined. Evaporation of the ether followed by fractional distillation under reduced pressure gave *N,N*-bis(2,2-dimethoxyethyl)amine (194 g, 39%), b.p. 100–114°C at 5 mmHg,  $\eta_D^{25}$  1.42687,  $\nu_{\max}$  (liquid film) 3325 (amine N–H str.), 1130 and 1080 cm<sup>-1</sup> (acetal C–O str.),  $\delta$  (CDCl<sub>3</sub>; 60 MHz) 1.42 (H, bs, CH<sub>2</sub>NHCH<sub>2</sub>), 2.75 (4H, d,  $J \sim 2$  Hz, NHCH<sub>2</sub>CH), 3.30 [12H, s, CH(OCH<sub>3</sub>)<sub>2</sub>] and 4.42 ppm [2H, t,  $J \sim 6$  Hz, CH<sub>2</sub>CH(OCH<sub>3</sub>)<sub>2</sub>]. (Found: C, 49.32; H, 10.71; N, 6.92; O, 33.60%. C<sub>8</sub>H<sub>19</sub>NO<sub>4</sub> requires C, 49.73; H, 9.91; N, 7.25; O, 33.12%.) A higher boiling fraction proved to be *N,N,N*-tris(2,2-dimethoxyethyl)amine (88.1 g, 19%), b.p. 130–

132°C at 5 mmHg,  $\eta_D^{25}$  1.42886. (Found: C, 50.99; H, 9.73; O, 34.25; N, 5.16%.  $C_{12}H_{27}NO_6$  requires C, 51.23; H, 9.68; O, 34.24; N, 4.98%.)

#### Synthesis of acryloyl *N,N*-bis(2,2-dimethoxyethyl)amine

Peroxide-free, dry ether was used throughout this experiment. Acryloyl chloride (4.52 g, 0.05 mol) (Koch-Light Ltd, UK) in ether (100 cm<sup>3</sup>) was maintained at 0°C and a mixture of *N,N*-bis(2,2-dimethoxyethyl)amine (19.3 g, 0.10 mol) and ether (100 cm<sup>3</sup>) was added dropwise, with mechanical stirring, over 0.5 h. The reaction mixture was stirred for a further 0.5 h after which the precipitate of *N,N*-bis(2,2-dimethoxyethyl)amine hydrochloride was removed by filtration and washed with ether (10 cm<sup>3</sup>). Evaporation of the combined ether solutions gave acryloyl *N,N*-bis(2,2-dimethoxyethyl)amine (11.9 g, 97%) b.p. 120–123°C at 1 mmHg,  $\eta_D^{25}$  1.46061,  $\nu_{\max}$  (liquid film) 1650 (amide C=O str.), 1130 and 1080 cm<sup>-1</sup> (acetal C–O str.),  $\delta$  (CDCl<sub>3</sub>; 60 MHz) 3.45 [16H, CH(OCH<sub>3</sub>)<sub>2</sub> and NCH<sub>2</sub>CH] 4.48 [2H, m,  $J \sim 12$  Hz, CH<sub>2</sub>CH(OCH<sub>3</sub>)<sub>2</sub>], 5.65 (H, dd,  $J \sim 8$  and 5 Hz, CH<sub>2</sub>=CHCO) and 6.45 ppm (2H, m, CH<sub>2</sub>=CHCO). (Found: C, 53.25; H, 8.66; N, 5.60; O, 32.47%.  $C_{11}H_{21}NO_5$  requires C, 53.49; H, 8.57; N, 5.67; O, 32.39%.)

#### Preparation of polymers

*Poly[acryloyl N,N-bis(2,2-dimethoxyethyl)amine]*. The monomer (4.94, 0.02 mol) was mixed with deoxygenated 80% ethanol/water (9 cm<sup>3</sup>). An aliquot (1 cm<sup>3</sup>) of a solution of 0.5% w/v ammonium persulphate in the same solvent was added and the mixture was maintained at 40°C for 3 days. The resulting viscous solution was diluted with ethanol, poured into an excess of distilled water and the precipitate was collected by filtration. Removal of excess solvent by lyophilization gave pure *poly[acryloyl N,N-bis(2,2-dimethoxyethyl)amine]* (3.75 g, 75%). (Found: C, 53.47; H, 8.77; O, 32.32; N, 5.53%.  $C_{11}H_{21}NO_5$  requires C, 53.49; H, 8.57; O, 32.39; N, 5.67%.) Intrinsic viscosity = 0.57 dl/g at 25°C (CHCl<sub>3</sub>),  $\nu_{\max}$  (film) 1645 (amide C=O str.), 1090 and 1130 cm<sup>-1</sup> (acetal C–O str.). The homopolymer is soluble in acetone, benzene, carbon tetrachloride, chloroform, ethanol and ether but is insoluble in methanol, light petroleum and water.

Polymerization of acryloyl *N,N*-bis(2,2-dimethoxyethyl)amine in aqueous solution led to direct precipitation of the homopolymer.

*Crosslinked poly[acryloyl-N,N-bis(2,2-dimethoxyethyl)amine]* was prepared in gel form in 80% ethanol/water. The technique was similar to that described for the homopolymer, acryloyl-*N,N*-bis(2,2-dimethoxyethyl)amine (4.9 g, 0.020 mol) and the crosslinker, *N,N'*-methylene diacrylamide, (0.38 g, 0.0025 mol) being dissolved in a mixture of deoxygenated 80% ethanol/water (13 cm<sup>3</sup>) and 0.5% w/v ammonium persulphate solution (2 cm<sup>3</sup>). The block of gel obtained was broken up in a mortar, pressed several times through a wire sieve (75  $\mu$ m) and stored in suspension in ethanol/water. The weight of the crosslinked poly[acryloyl *N,N*-bis(2,2-dimethoxyethyl)amine], (*copolymer A*) was 2.5 g (40%) (estimated by drying out a sample of the hydrated gel).

*Crosslinked poly[acryloyl morpholine/acryloyl N,N-bis(2,2-dimethoxyethyl)amine]* molar ratio 4:1, was obtained as gel beads by aqueous suspension polymerization in liquid paraffin. Liquid paraffin (100 cm<sup>3</sup>) ( $\rho^{20}$  0.85 g/

cm<sup>3</sup>),  $\eta^{20}$  3.5–4.0 N sec m<sup>-2</sup>) and a surfactant mixture, HLB<sup>7</sup> 3.0, consisting of sorbitan trioleate (7 cm<sup>3</sup>) and polyoxyethylene(20)sorbitan trioleate (1 cm<sup>3</sup>) were placed in a 500 cm<sup>3</sup> glass polymerization vessel fitted with a semi-circular paddle stirrer. Nitrogen was bubbled through the mixture for 1 h after which a nitrogen atmosphere was maintained in the flask. A saturated solution of potassium persulphate in water (1 cm<sup>3</sup>) was added rapidly, with stirring to an oxygen-free solution of acryloyl morpholine (2.27 g, 0.016 mol), acryloyl *N,N*-bis(2,2-dimethoxyethyl)amine (0.99 g, 0.004 mol) and *N,N'*-methylene diacrylamide (0.030 g, 0.0002 mol) in distilled water (32 cm<sup>3</sup>). The solution of monomers was added immediately to the paraffin in the polymerization vessel and the stirring rate was adjusted to give droplets of approximately 10–40  $\mu$ m. Polymerization was evident within 1 h and was assumed to be complete in 5 h.

After allowing the gel beads to settle overnight, most of the paraffin was decanted and the beads were washed three times with light petroleum ether (b.p. 40–60°C) (500 cm<sup>3</sup>), three times with acetone (500 cm<sup>3</sup>) and three times with distilled water (500 cm<sup>3</sup>). The beads were stored in suspension in distilled water. The weight of the crosslinked copolymer matrix, (*copolymer B*) within the gel was 3.1 g, (97%) (estimated by drying out a sample of the hydrated gel).

#### Synthesis of phenylacetyl *N,N*-bis(2,2-dimethoxyethyl)amine

*N,N*-bis(2,2-dimethoxyethyl)amine (9.70 g, 0.05 mol) was mixed with dry ether (75 cm<sup>3</sup>) and maintained at 0°C with magnetic stirring while a solution of phenylacetyl chloride (4.0 g, 0.026 mol) in dry ether (25 cm<sup>3</sup>) was added. Stirring was continued for 0.5 h after which the reaction mixture was filtered and the precipitate of *N,N*-bis(2,2-dimethoxyethyl)amine hydrochloride was discarded. On evaporation of the ether solution a yellow oil was obtained which was repeatedly triturated with 2 M aqueous sodium hydroxide solution, washed with distilled water and taken up in light petroleum ether (b.p. 40–60°C). After drying over anhydrous magnesium sulphate the solution was chilled to –78°C to precipitate phenylacetyl *N,N*-bis(2,2-dimethoxyethyl)amine (8.02 g, 62%)  $\nu_{\max}$  (liquid film) 1650 (amide C=O str.), 1130 and 1080 cm<sup>-1</sup> (acetal C–O str.),  $\delta$  (CCl<sub>4</sub>; 60 MHz) 3.30–3.48 [16H, CH(OCH<sub>3</sub>)<sub>2</sub> and NCH<sub>2</sub>CH], 3.65 (2H, s, C<sub>6</sub>H<sub>5</sub>CH<sub>2</sub>CO), 4.08–4.40 [2H, m, CH<sub>2</sub>CH(OCH<sub>3</sub>)<sub>2</sub>] and 7.15 ppm (5H, s, C<sub>6</sub>H<sub>5</sub>). (Found: C, 61.68; H, 8.34; N, 5.07%.  $C_{16}H_{25}NO_5$  requires C, 61.17; H, 8.42; N, 4.50%.)

#### Studies on phenylacetyl *N,N*-bis(2,2-dimethoxyethyl)amine

*Acid hydrolysis.* This reaction was investigated by dissolving the amine (0.5 cm<sup>3</sup>) in an aliquot (4.5 cm<sup>3</sup>) of a solution of 2 M DCl in D<sub>2</sub>O/CH<sub>3</sub>OD (1:1, v/v) and following the change in the p.m.r. spectrum over 24 h (*Figure 3*). The hydrolysis was repeated using H<sub>2</sub>O/CH<sub>3</sub>OH over the same period, after which the reaction mixture was neutralized with the minimum amount of Na<sub>2</sub>CO<sub>3</sub> and the solvent was removed under high vacuum at 25°C over 24 h to give a clear viscous oil  $\delta$  (CHCl<sub>3</sub>; 60 MHz) 2.65 (4H, d,  $J \sim 5$  Hz, NCH<sub>2</sub>CH), 3.55 (2H, s, C<sub>6</sub>H<sub>5</sub>CH<sub>2</sub>CO), 4.30 [2H, t,  $J \sim 5$  Hz, CH<sub>2</sub>CH(OH)O], 7.15 (5H, s, C<sub>6</sub>H<sub>5</sub>CH<sub>2</sub>) and 7.95–8.35 (D<sub>2</sub>O labile) ppm (2H, b s, CH(OH)O).

**Acid mediated reaction with acetyl hydrazide.** A solution of amine (0.1 cm<sup>3</sup>) and acetyl hydrazide (0.1 g) in D<sub>2</sub>O/CD<sub>3</sub>OD (1:1, v/v) (1 cm<sup>3</sup>) was prepared and a control p.m.r. spectrum recorded  $\delta$  (60 MHz) 1.82 (s, CH<sub>3</sub>CONHNH<sub>2</sub>), 3.29 [12H, s, CH(OCH<sub>3</sub>)<sub>2</sub>], 3.48 (4H, d,  $J \sim 5$ Hz, NCH<sub>2</sub>CH), 3.70 (2H, s, C<sub>6</sub>H<sub>5</sub>CH<sub>2</sub>CO), 4.35 [2H, m, CH<sub>2</sub>CH(OCH<sub>3</sub>)<sub>2</sub>] and 7.16 ppm (5H, s, C<sub>6</sub>H<sub>5</sub>). A reaction solution consisting of amine (0.1 cm<sup>3</sup>) and acetyl hydrazide (0.1 g) in 5 M DCl in D<sub>2</sub>O/CD<sub>3</sub>OD (1 cm<sup>3</sup>) was prepared and the p.m.r. spectrum recorded after 1 h at 25°C,  $\delta$  (60 MHz) 1.82 (s, CH<sub>3</sub>CONHNH<sub>2</sub>), 3.25 [2H, s, possibly CD<sub>2</sub>CH(N)O] and 7.15 ppm (5H, s, C<sub>6</sub>H<sub>5</sub>).

#### Activation of copolymer gels and coupling with $\beta$ -D-glucosidase

Samples of the solvated (gel) copolymers A and B were suspended in separate aliquots of a 5% w/v solution of tartaric acid dihydrazide<sup>8</sup> in 1 M HCl. After 18 h at ambient temperature each gel was washed with distilled water until tartaric acid dihydrazide could no longer be detected in the washings on testing with trinitrobenzene sulphonic acid reagent<sup>9</sup>.

For enzyme coupling samples of both treated gels (each equivalent to 100 mg of dry copolymer) were equilibrated with 2 M HCl. After centrifuging and discarding the supernatant, each gel was resuspended in an aliquot (5 cm<sup>3</sup>) of 2 M HCl, cooled to 0°C with magnetic stirring, and an aliquot (4 cm<sup>3</sup>) of ice-cold 2% sodium nitrite solution was added. Reaction was allowed to proceed for 15 min. The gels were washed four times with aliquots (10 cm<sup>3</sup>) of 50 mM acetate buffer (pH 5.5). Each washing was of 3 min duration and was carried out with magnetic stirring at 0°C. After discarding the final washings an aliquot (0.5 cm<sup>3</sup>) of a 1% w/v solution of  $\beta$ -D-glucosidase (ex. sweet almonds, Koch-Light Ltd UK) in 50 mM acetate buffer was added to each gel and coupling allowed to proceed for 18 h at 0–4°C with magnetic stirring. The resulting conjugates were subjected to five washing cycles each consisting of a wash with an aliquot (15 cm<sup>3</sup>) of 50 mM acetate buffer (pH 5.5) and a wash with an aliquot (15 cm<sup>3</sup>) of 1 M sucrose in 1 M NaCl solution. The  $\beta$ -D-glucosidase conjugates derived from copolymers A and B, designated conjugate AG and conjugate BG respectively, were each suspended in acetate buffer (10 cm<sup>3</sup>), and stored at 0–4°C.

#### Determination of immobilized protein

The amino acids produced on hydrolysis of samples of each conjugate by treatment with 6 M HCl at 110°C for 18 h were separated into groups<sup>10</sup> by paper chromatography and estimated by quantitative ninhydrin determination<sup>11</sup>. A standard graph, obtained on chromatographic assay of a hydrolysate of  $\beta$ -D-glucosidase was used to calculate the amount of bound protein originally present in the conjugates.

#### Determination of $\beta$ -D-glucosidase activity

The method due to Agrawal and Bahl<sup>12</sup> was adapted. A solution of the substrate *p*-nitrophenyl  $\beta$ -D-glucopyranoside (75 mg) in 50 mM sodium acetate buffer (pH 5.5, 10 cm<sup>3</sup>) was prepared immediately prior to each determination. This solution was stirred magnetically and maintained at 30°C. An aliquot (0.25 cm<sup>3</sup>) of conjugate suspension was added. At intervals, samples (0.25 cm<sup>3</sup>) of the reaction mixture were withdrawn, diluted with 200 mM aqueous sodium carbonate solution (0.7 cm<sup>3</sup>) and centrifuged briefly. The

change in extinction (420 nm) recorded was related to *p*-nitrophenol concentration with the aid of a standard graph. One unit of  $\beta$ -D-glucosidase activity was taken to be that which released one  $\mu$ mol of *p*-nitrophenol in 1 min.

#### Stability of immobilized $\beta$ -D-glucosidase

**Heat stability** was determined on incubation of samples of the conjugates in suspension in 25 mM acetate buffer (pH 5.5 at 50°C). Enzyme activity was determined at intervals. A control experiment was performed using a solution of the native enzyme in the same buffer.

**Storage stability** was evaluated by re-determining the activity of each conjugate after 8 weeks in suspension at 0–2°C in 25 mM acetate buffer (pH 5.5).

## RESULTS AND DISCUSSION

For an enzyme to retain significant bio-catalytic activity following immobilization it must remain accessible to its substrate in solution. One of the best ways of ensuring this is to effect immobilization by anchorage of the dissolved enzyme molecule to the solvated, three dimensional, space network of polymer chains of a typical xerogel matrix. Coincidentally, high enzyme binding capacities result from this technique. The potential to form an aqueous xerogel is a desirable property in any organic matrix intended for use as an enzyme support.

Crosslinked poly(acryloylaminoacetaldehyde dimethylacetal) (*Figure 1a*) undergoes gelation readily in water and synthesis of the copolymer in this solvent results inevitably in xerogel formation. Since the hydrophilic nature of the copolymer arises as a result of its pendant dimethylacetal groups, it seemed reasonable to expect that crosslinked poly[acryloyl *N,N*-bis-(2,2-dimethoxyethyl)amine (*Figure 1b*) would also be obtained in gel form if synthesized in water. However, this approach resulted merely in precipitation of the crosslinked polymer from solution.

It was observed that poly[acryloyl *N,N*-bis(2,2-dimethoxyethyl)amine] could be prepared by solution polymerization in 80% ethanol/water. This homopolymer proved to be insoluble in pure water but could be brought into solution on hydrolysis of some of the dimethylacetal groups with dilute acid. Subsequently, successful experiments were conducted in which a xerogel network incorporating crosslinked poly[acryloyl *N,N*-bis-(2,2-dimethoxyethyl)amine (copolymer A) was prepared by direct copolymerization in 80% ethanol/water and activated for enzyme coupling in an aqueous acid reaction medium. This ensured that the copolymer remained in solution both during the activation process and the concurrent substitution of water as the solvent component of the xerogel.

Acryloyl *N,N*-bis(2,2-dimethoxyethyl)amine is related structurally to acryloyl morpholine and the two monomers copolymerize readily. Crosslinked poly(acryloyl morpholine) is a relatively cheap copolymer which is known to form xerogel networks readily<sup>13,14</sup>. Recently these have been characterized quite rigorously<sup>15</sup>. Furthermore these networks may be prepared in bead form by aqueous suspension polymerization in liquid paraffin. It was evident that the crosslinked poly(acryloyl morpholine) matrix had considerable potential as an enzyme support provided that a way of introducing the necessary groups functionally active binding could be devised. It was with this in mind that an aqueous xerogel network incorporating the crosslinked poly-

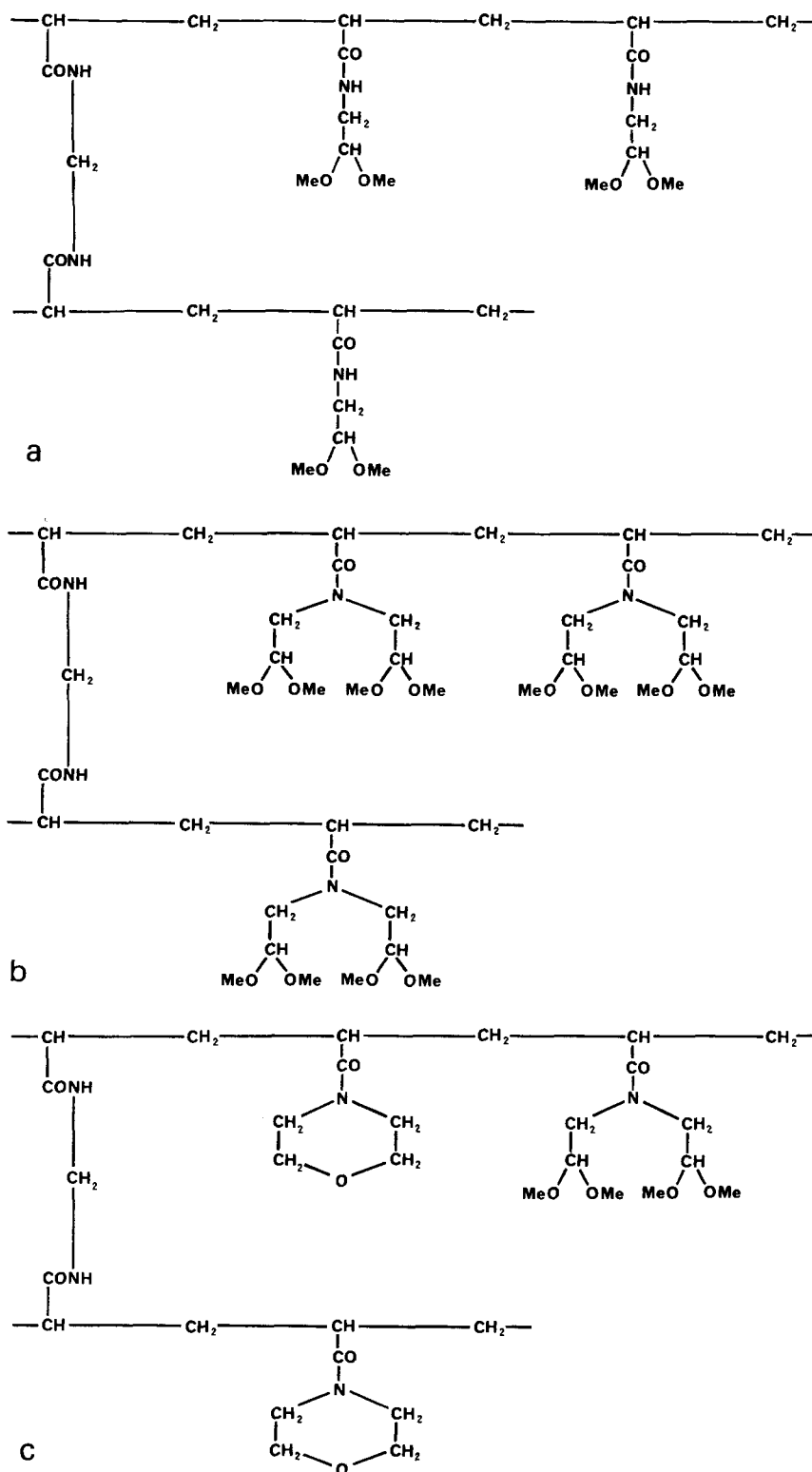


Figure 1 (a) Crosslinked poly(acryloylaminoacetaldehyde dimethylacetal); (b) crosslinked poly[acryloyl *N,N*-bis(2,2-dimethoxyethyl)amine]; (c) crosslinked poly[acryloyl morpholine/acryloyl *N,N*-bis(2,2-dimethoxyethyl)amine]

[acryloyl morpholine/acryloyl *N,N*-bis(2,2-dimethoxyethyl)amine] matrix (copolymer B) (Figure 1c) was synthesized. Copolymer B may be regarded essentially as a substituted poly(acryloyl morpholine) since acryloyl morpholine is used in four fold excess for its preparation.

Controlled acid hydrolysis of homopolymeric poly[acryloyl *N,N*-bis(2,2-dimethoxyethyl)amine] or its cross-linked analogue, copolymer A, does not lead to the extensive generation of aldehydrol groups, as in the related hydro-

lysis of poly(acryloylaminoacetaldehyde dimethylacetal). Consequently, the aldehydrol enzyme binding reaction was impractical in this work and it was necessary to adopt the reaction scheme outlined in Figure 2.

It is probable that acid hydrolysis of the *N,N*-bis(2,2-dimethoxyethyl)amine residues lead to pyranose rings of the bis-hemiacetal type which, in the absence of other reactive species, condense spontaneously with their near neighbours to give acetal linkages. Such behaviour has been

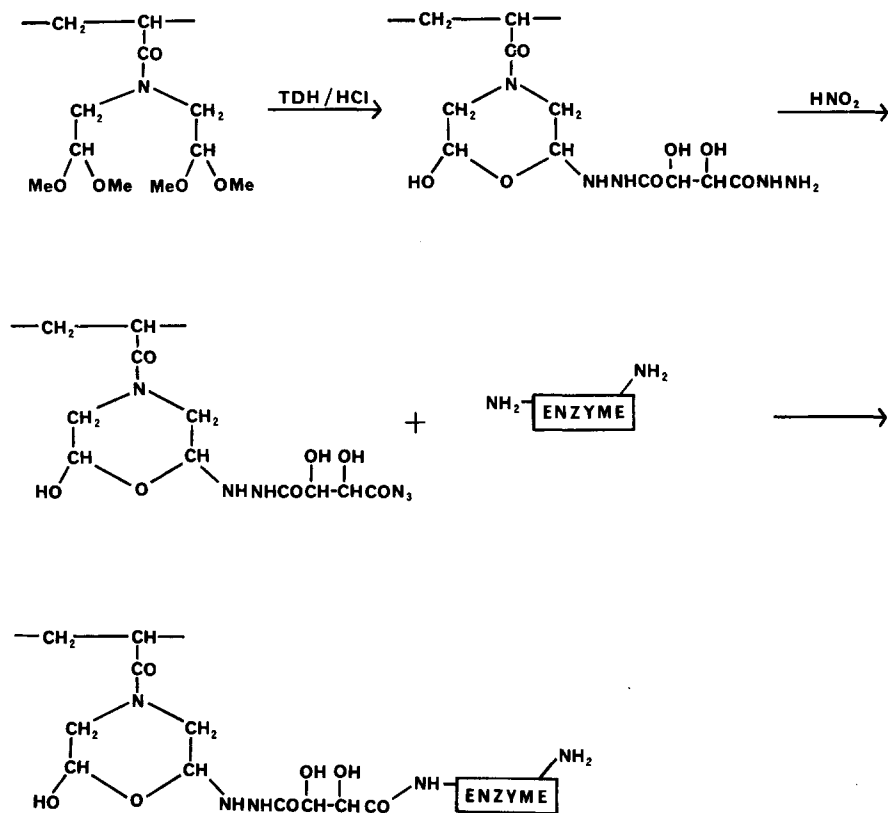


Figure 2 Reaction scheme for the immobilization of  $\beta$ -D-glucosidase

observed in the case of polyacetaldehyde. With this polymer aldehyde or aldehydrol groups condense spontaneously to give an extended system of fused pyran rings<sup>16</sup>.

Evidence for a pyranose bis-hemiacetal structure has been obtained from p.m.r. studies on the DCl catalysed hydrolysis of the model compound phenylacetyl *N,N*-bis-(2,2-dimethoxyethyl)amine in D<sub>2</sub>O/CD<sub>3</sub>OD as solvent. It is evident from Figure 3 that the broad symmetrical signal at  $\delta$  4.75 ppm arising from the methine protons of the two CH<sub>2</sub>CH(OCH<sub>3</sub>)<sub>2</sub> groups is replaced, on hydrolysis, by simple triplets,  $\delta$  4.73 and 4.94 ppm integrating for 0.6 and 1.4 protons respectively. Non-equivalent integration and chemical shifts might arise if two types of molecule, with methine protons in different chemical environments, are formed. This could be consistent with a mixture of structural units of the type:



Attempts to isolate the products of acid hydrolysis of phenylacetyl *N,N*-bis(2,2-dimethoxyethyl)amine from larger scale experiments in water resulted in degeneration of the methine proton signal. This suggests possible reversion to a more stable structural unit. It is significant that the p.m.r. spectrum of the aqueous hydrolysis product exhibited a signal,  $\delta$  7.95–8.35 ppm, corresponding to two deuterium labile protons. Almost certainly, these are the two hydroxyl groups of the pyranose bis-hemiacetal.

In the activation of copolymers A and B for enzyme coupling, acid hydrolysis was carried out in the presence of tartaric dihydrazide, a water-soluble, bifunctional, reagent. By this device it was possible to exploit the activity of the hemiacetal and any aldehydrol groups before extensive homocondensation could take place. The exact course of

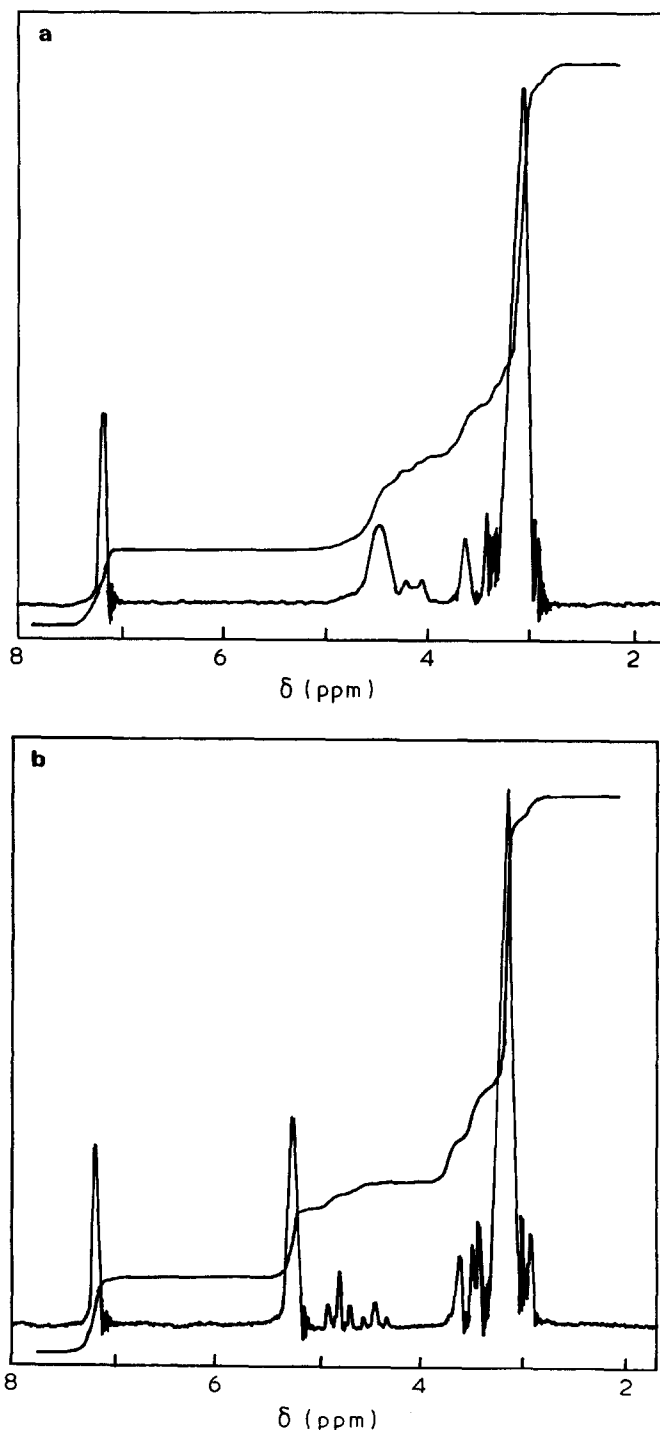
reaction with tartaric dihydrazide is difficult to study. However, it would seem likely that, as in the reaction of a simple hexose with a single molecule of a substituted hydrazide, the pyranose ring may be preserved<sup>17</sup>.

An attempt to obtain direct evidence for the pyranose intermediate by means of a p.m.r. study of the DCl mediated condensation between the model compounds acetyl hydrazide and phenylacetyl *N,N*-bis(2,2-dimethoxyethyl)amine was made. This was complicated by the relatively high reagent concentrations necessary in order to obtain an acceptable signal to noise ratio. Owing to the high DCl concentration a number of the more active protons in the reacting amine were replaced by deuterium. However, it is significant that no peak between  $\delta$  7.8 and 8.0 ppm, characteristic of the non-labile azomethine proton, was recorded.

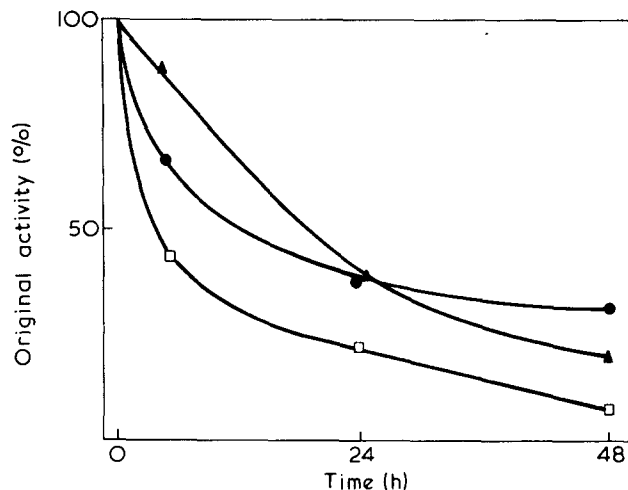
Enzyme coupling to the two copolymers was effected following conversion of the pendant acyl hydrazide residues to acyl azide groups. Acid azide coupling is well established as an immobilization procedure<sup>18</sup>. The protein bound in the  $\beta$ -D-glucosidase conjugate AG, 12 mg/g and the  $\beta$ -D-glucosidase conjugate BG, 42 mg/g reflects the relative gelation and swelling properties of the respective copolymers, A and B, from which they are derived. The xerogel network derived from crosslinked poly(acryloyl morpholine) (copolymer B) was much the easier to prepare.

In common with most enzymes, the activity of  $\beta$ -D-glucosidase diminished on immobilization. The  $\beta$ -D-glucosidase activities per mg of bound protein in conjugates AG and BG were 2.58 and 0.66 enzyme units respectively while the activity of the native enzyme was 20.50 units per mg. The respective activity retentions of conjugates AG and BG were thus 12.8 and 3.2%. No change in pH-activity profile occurred on immobilization. Rigorous tests for re-solubilized  $\beta$ -D-glucosidase activity in the supernatant solutions derived from centrifuged incubation mixtures involving the two conjugates proved negative.

Previous workers have immobilized  $\beta$ -D-glucosidase by covalent coupling to the semi-synthetic carrier, cellulose *trans*-2,3-carbonate<sup>19</sup> and to the totally synthetic carrier, poly(allyl carbonate)<sup>20</sup>. In the case of cellulose *trans*-2,3-carbonate the amount of enzyme bound was too low (<0.2 mg/g of carrier) to estimate accurately. Poly(allyl carbonate) was effective in binding up to 6 mg of  $\beta$ -D-gluco-



**Figure 3** Proton magnetic resonance study of the acid catalysed reaction of phenylacetyl *N,N*-bis(2,2-dimethoxyethyl)amine with D<sub>2</sub>O. (a) Spectrum before addition of DCl:  $\delta$  3.30–3.48 [16H, NCH<sub>2</sub>CH and CH(OCH<sub>3</sub>)<sub>2</sub>], 3.65 (2H, s, C<sub>6</sub>H<sub>5</sub>CH<sub>2</sub>CO), 4.08–4.40 [2H, m, CH<sub>2</sub>CH(OCH<sub>3</sub>)<sub>2</sub>], 4.49 (HOD) and 7.15 ppm (5H, s, C<sub>6</sub>H<sub>5</sub>). (b) Spectrum after DCl catalysed hydrolysis:  $\delta$  3.15–3.45 (NCH<sub>2</sub>CH and CH<sub>3</sub>OD), 3.60 (2H, s, C<sub>6</sub>H<sub>5</sub>CH<sub>2</sub>CO), 4.73 [0.6H, t, *J* ~ 6 Hz, possibly CH<sub>2</sub>CH(OH)OCH or CH<sub>2</sub>CH(OH)<sub>2</sub>], 4.94 [1.4H, t, *J* ~ 6 Hz, possibly CH<sub>2</sub>CH(OH)OCH or CH<sub>2</sub>CH(OH)<sub>2</sub>], 5.27 (HOD) and 7.15 ppm (5H, s, C<sub>6</sub>H<sub>5</sub>)



**Figure 4** Heat denaturation of soluble and immobilized forms of  $\beta$ -D-glucosidase on incubation in acetate buffer at 50°C. ●,  $\beta$ -D-glucosidase conjugate AG; ▲,  $\beta$ -D-glucosidase conjugate BG; □, soluble  $\beta$ -D-glucosidase

sidase per g of carrier although, under reaction conditions most effective for retention of enzyme activity, the binding capacity was lower (2 mg/g of carrier). Probably the much higher binding capacities obtained in the present studies is a result of effecting immobilization by means of a xerogel network rather than a classical solid support.

The retention of enzyme activity per mg of protein immobilized in conjugates AG and BG was inferior to that of the most active  $\beta$ -D-glucosidase–poly(allyl carbonate) derivative (30%). However, it is apparent that the overall activity of conjugate BG was similar to that of the poly(allyl carbonate) derivative and that of conjugate AG was much better. High overall activity is important for any conjugate in practical applications.

A pleasing feature of the conjugates of this report was the enhanced stability to heat denaturation of the immobilized enzyme as compared to the native enzyme in solution. This property is exhibited by relatively few enzyme–polymer conjugates<sup>1</sup>. It is apparent from *Figure 4* that, whereas the  $\beta$ -D-glucosidase–copoly(acryloyl morpholine) conjugate BG is the more stable initially to heat denaturation, it is less stable, over a longer period, than the conjugate AG derived from poly[acryloyl *N,N*-bis(2,2-dimethoxyethyl)amine]. This result reflects the activity retentions of conjugate AG (79%) and conjugate BG (28%) on storage in acetate buffer suspension for 2 months at 0–2°C.

These studies demonstrate that xerogel networks derived from crosslinked poly[acryloyl *N,N*-bis(2,2-dimethoxyethyl)amine] and poly[acryloyl morpholine/acryloyl *N,N*-bis(2,2-dimethoxyethyl)amine] are viable supports for the immobilization of  $\beta$ -D-glucosidase. As totally synthetic materials they are non susceptible to microbial attack. It is probable that they would be effective for the immobilization of other enzymes. This is of some importance since both provide for enzyme immobilization within a new and distinctive chemical micro-environment.

#### ACKNOWLEDGEMENT

We thank Mr G. A. Sniezko-Blocki for his technical assistance and advice on p.m.r. studies.



REFERENCES

- 1 Melrose, G. J. H. *Rev. Pure Appl. Chem.* 1971, **21**, 83
- 2 Gryszkiewicz, J. *Folia Biologica* 1971, **19**, 119
- 3 Epton, R., McLaren, J. V. and Thomas, T. H. *Polymer* 1974, **15**, 564
- 4 Epton, R., McLaren, J. V. and Thomas, T. H. *Biochem. J.* 1971, **123**, 21P
- 5 Epton, R., McLaren, J. V. and Thomas, T. H. *Carbohydr. Res.* 1972, **22**, 301
- 6 Bedoukian, P. Z. *J. Am. Chem. Soc.* 1944, **66**, 651
- 7 Sherman, P. 'Emulsion Science', Academic Press, London and New York, 1968, p 140
- 8 Curtius, T. *J. Prakt. Chem.* 1917, **95**, 214
- 9 Inman, J. K. and Dintzis, H. M. *Biochemistry* 1969, **8**, 4074
- 10 Epton, R. and Thomas, T. H. 'An Introduction to Water-Insoluble Enzymes', Broglia Press, London, 1970, p 26
- 11 Entenman, C., Harris, D. C. and Kay, R. E. *Arch. Biochem. Biophys.* 1956, **63**, 14
- 12 Agrawal, K. M. L. and Bahl, O. P. *J. Biol. Chem.* 1968, **243**, 98
- 13 Epton, R., Holloway, C. and McLaren, J. V. *J. Appl. Polym. Sci.* 1974, **18**, 179
- 14 Epton, R., Holloway, C. and McLaren, J. V. *J. Chromatog.* 1974, **90**, 249
- 15 Epton, R., Holding, S. and McLaren, J. V. *Polymer* 1974, **15**, 466
- 16 Maher, G. G., Douglas, J. A. Russell, C. R. and Rist, C. E. *J. Polym. Sci. (A-1)* 1970, **8**, 1537
- 17 Mester, L. *Adv. Carbohydr. Chem.* 1958, **13**, 105
- 18 Mitz, M. A. and Summaria, L. *J. Nature* 1961, **189**, 576
- 19 Barker, S. A., Doss, S. H., Gray, C. J., Kennedy, J. F., Stacey, M. and Yeo, T. H. *Carbohydr. Res.* 1971, **20**, 1
- 20 Kennedy, J. F., Barker, S. A. and Rosevear, A. J. *J. Chem. Soc. (C)* 1972, p 2568

# Study of relationship between network structure of g.p.c. gels and molecular size of permeable substance

Y. Motozato, N. Kusumoto\*, C. Hirayama, R. Murakami† and H. Isozaki

Department of Synthetic Chemistry, Faculty of Engineering, Kumamoto University, Kumamoto 860, Japan

(Received 17 April 1974; revised 6 January 1975)

Attempts were made to correlate the average size of the network of crosslinked vinyl acetate–glycidyl methacrylate (GMA) copolymer to the maximum size of permeable molecules when the copolymers were used as g.p.c. packing materials. The root-mean-square of the end-to-end distance  $(\bar{r}^2)^{1/2}$  and of the hydrodynamic radius  $(\bar{s}^2)^{1/2}$ , which characterizes the maximum extent of the molecules, were calculated. Meanwhile, the average size of the copolymer network,  $r_c$ , was estimated from the average molar weight between crosslinkages, this being calculated from the equilibrium rubber elastic modulus,  $E_r$ , obtained by dynamic viscoelastic measurements. It was found that the maximum size which can permeate the copolymer decreases as the content of GMA in the copolymer increases. From viscoelastic measurements,  $E_r$  was found to increase as the content of GMA in the copolymer increases. Further, linear relationships were obtained among  $r_c$ ,  $(\bar{r}^2)^{1/2}$ , and  $(\bar{s}^2)^{1/2}$  covering the wide range of the copolymer composition.

## INTRODUCTION

Recently, many studies on synthesis of packing materials for gel permeation chromatography (g.p.c.) and its application have been made. G.p.c. seems to now be accepted as a useful tool for separating high polymers according to molecular size.

For separation of hydrophobic polymers polystyrene gel<sup>1</sup> and poly(vinyl acetate) gel<sup>2,3</sup> and for hydrophilic polymers dextran gel<sup>4</sup>, agar gel<sup>5</sup> and polyacrylamide gel<sup>6</sup> have been described. The authors have studied the synthesis of vinyl acetate–glycidyl methacrylate (VAC–GMA) copolymer<sup>7,8</sup>. These gels can be classified into two prototypes: one is a homogeneous gel which separates substances by its network swelled in a solvent; and the other is a heterogeneous gel which separates substances by its so called macroreticular structure.

The size of the network of homogeneous gels is represented by the crosslinking density, which is usually represented by the charge amount of the crosslinking agent. However, the relation between the network size and the size of permeable substances has not yet been described. Therefore, the present work aims to correlate the network size of homogeneous gel of VAC–GMA copolymer to the molecular size of the permeable substance.

## EXPERIMENTAL

### Preparation of gel plates and beads

Commercial VAC monomer was purified by distillation under atmospheric pressure at its boiling point of 72.5–73.0°C. GMA was distilled at 75–80°C under 4–5 mmHg. The purified VAC and GMA were mixed at the ratios listed

\* Present address: Department of Macromolecular Science, Case Western Reserve University, Cleveland, Ohio 44106, USA.

† Present address: Department of Industrial Chemistry, Kumamoto Technical University, Kumamoto 860, Japan.

in Table 1, and then 1 wt % of benzoyl peroxide (BPO) was added as initiator. A polyethylene gasket of 0.4 mm thickness was placed between glass plates (8 × 4 × 0.3 cm), and the gap between the plates was filled with the monomer mixture. The polymerization was carried out at 55°C for 24 h.

To obtain the g.p.c. packing material, suspension polymerization was conducted as follows. A water system was prepared by dissolving 5 g of gelatin in 400 ml of distilled water. A monomer mixture the same as that mentioned above was suspended in the water system and reacted at 60–65°C for 7 h under continuous agitation to form beads of the copolymer; calcium carbonate was used as a stabilizer. Then, the beads were washed with 1 N hydrochloric acid and hot water to remove the calcium carbonate and gelatin.

### G.p.c. operation

Substances with different molecular sizes are separated on the basis of the difference in permeability of the substances in the gels. The large molecules which cannot permeate the gel are first eluted at a volume equal to the interstitial volume of the gel beads. Smaller molecules can

Table 1 Charging ratio of monomers

Film No.	Gel No.	Feed (vol %)	
		VAC	GMA
F-1		100	0
	G-1	80	20
F-2	G-2	70	30
F-3	G-3	60	40
F-4	G-4	50	50
F-5	G-5	40	60
F-6	G-6	30	70
F-7	G-7	0	100

Table 2 Sample characteristics

No.	Material	$M_n$	Conc. (wt %)
E1	EG	62	2
E2	OEG	200	2
E3	OEG	633	2
E4	OEG	2 250	2
E5	OEG	3 400	2
E6	OEG	9 700	2
E7	PEG	18 700	2
E8	PEG	28 300	2

permeate the gel and are delayed. The gel was packed into a glass column with a diameter of 0.75 cm, 120 cm long, and then 0.3 ml of 2% sample was eluted at room temperature with dimethylformamide as eluant at 0.85 ml/min. Ethylene glycol (EG), oligo(ethylene glycol) (OEG) and poly(ethylene glycol) (PEG) with different molecular weights were used, as listed in Table 2. Quantitative analysis of the effluent was made using a differential refractometer (Waters Associates, Model 403).

The calibration curves were obtained by plotting the average molecular weights against the peak elution volumes. Further, the straight line at the centre of the calibration curve was extrapolated to the outer volume and the excluded molecular weight,  $M_{lim}$ , was obtained.

#### Viscosity measurements

The viscosity of DMF solution was measured for PEG samples differing in molecular weight using a Ubbelohde viscometer at 30°C, and an experimental viscosity equation was obtained.

#### Ebrioscropy

The molecular weight of the sample,  $M_n$ , was estimated by ebrioscropy using an ebriometer (Takara Kogyo, Model L4). Benzene was used as solvent.

#### Density measurement

The density of the copolymer at room temperature was measured by the flotation method using a water-CaCl<sub>2</sub> system. Further, dilatometry was carried out to obtain the density at higher temperatures by raising the temperature at the rate of 0.5°C/min.

#### Viscoelastic measurements

Dynamic viscoelastic measurements were carried out for the sheets of the copolymer by using the direct reading dynamic viscoelastometer (Toyo-Bouldwin, Vibron Model DDV-1).

## RESULTS AND DISCUSSION

#### Temperature dependency of viscoelastic properties

Figure 1 shows the variation of the dynamic storage modulus,  $E'$  with temperature for the copolymer. In this Figure for GMA copolymer a rapid decrease of  $E'$  can be seen around 60°C, after which it becomes constant again at around 140°C. This region, where  $E'$  rapidly decreases, corresponds to the glass transition at which micro-Brownian motion of chain segments takes place. The rubbery plateau is at higher temperatures. The lowest curve in the Figure is for the VAC homopolymer, and the curves between those for GMA and PVAC were obtained for the copolymers differing in content of VAC and GMA. The copolymers show

similar viscoelastic behaviour to that of PGMA, but the temperature region where the glass transition occurs shifts to lower temperatures as the content of VAC increases. PVAC shows a somewhat different curve; a more rapid decrease of  $E'$  is seen compared with the copolymers.

#### Change of density with composition of gel

Figure 2 shows plots of the density of the copolymers measured at 20°C and 160°C against composition of the copolymer. The curves at 20°C are similar to those at 160°C, with a rapid change occurring near 50% VAC content.

#### Average molar weight between crosslinkages

According to the theory of rubber elasticity the rubber elastic modulus  $E_r$  is related to the average molecular weight between the crosslinks by the following equation<sup>9</sup>:

$$M_c = 3\rho RT/E_r \quad (1)$$

where  $\rho$  is the density of the copolymer,  $R$  is the gas constant, and  $T$  is absolute temperature.

In the present study, the dynamic storage modulus  $E'$  in the rubbery plateau in Figure 1 can be taken as  $E_r$ .  $E_r$  and  $\rho$  at 160°C were taken although  $E_r$  shows some tendency to continue to decrease, since this temperature is the maximum achieved in this experiment. For samples F-4 and F-5,  $E_r$  at 160°C was obtained by extrapolating the curves to 160°C.  $E_r$  of the samples whose VAC content is more than 70% was hard to estimate.

Figure 3 shows plots of  $M_c$  calculated from equation (1) against copolymer composition.  $M_c$  is found to decrease as the content of GMA increases. This fact indicates that GMA acts as crosslinking agent, and the larger the content of GMA, the larger the crosslinking density becomes. The relation between composition of the copolymer and net-

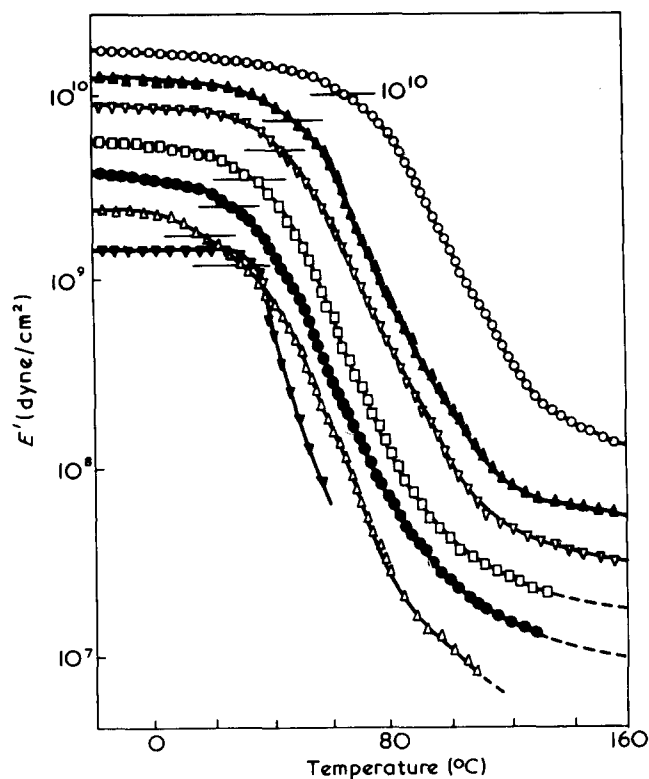


Figure 1 Plots of  $E'$  versus temperature.  $\circ$ , F-1;  $\blacktriangle$ , F-2;  $\nabla$ , F-3;  $\square$ , F-4;  $\bullet$ , F-5;  $\triangle$ , F-6;  $\blacktriangledown$ , F-7

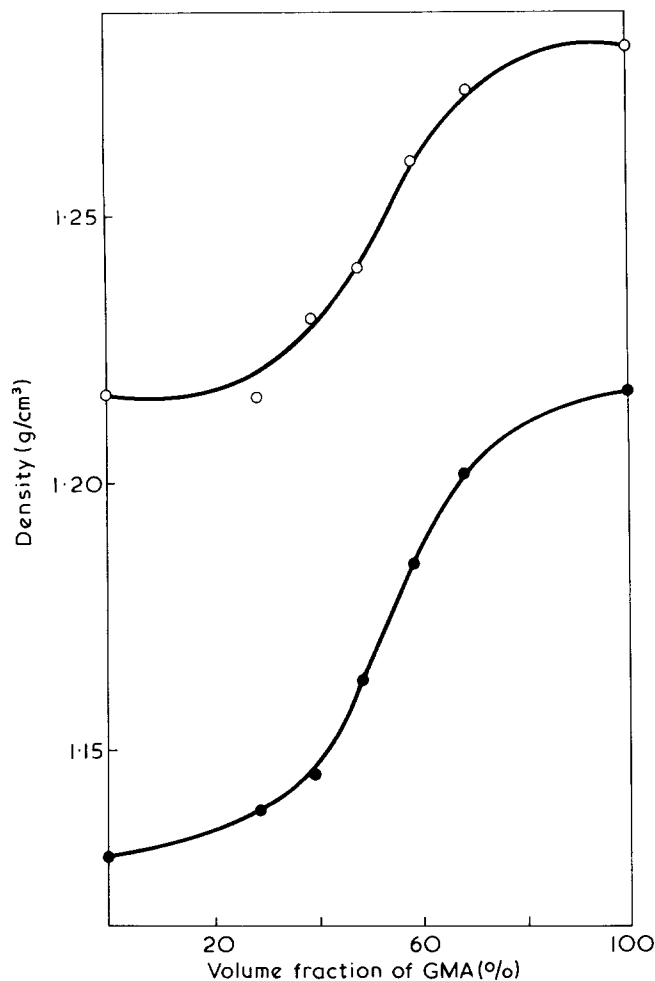


Figure 2 Plots of density versus composition of copolymer. ○, 20°C; ●, 160°C

work radius,  $r_c$ , is also shown in Figure 3. The value of  $r_c$  was derived from  $M_c$  and the average molar weight of the repeating unit of the copolymer, assuming that the molecules in the network structure are completely extended and the network is a circle. Similar to  $M_c$ ,  $r_c$  decreases as the GMA content increases. The gel swells and the chains between the crosslinks are extended in an eluant. However,  $r_c$  calculated assuming that the chains take the completely extended structure may be larger than the actual size in the equilibrium swelling state.

#### Change of degree of swelling with composition of gel

Figure 4 shows plots of the degree of swelling of the gels in DMF, THF, benzene, and methanol against composition of the gel. The swelling is largest for DMF and becomes smaller in the order of THF, benzene and methanol. In the case of methanol and benzene a maximum is seen for the composition VAC-GMA = 70:30, but is not seen for DMF and THF. In this study, DMF was selected as an eluant, since it shows the maximum swelling, the data obtained will be suitable for discussions related to the network size estimated from the viscoelastic data.

#### G.p.c.

Figure 5 shows the g.p.c. calibration curves for EG and PEG with different molecular weights using DMF as eluant. It is found that these gel systems have similar line shape, but are different in the elution point where the vertical line crosses the inclined one except for the G-2 gel, indicating

that  $M_{lim}$  is shifted to higher molecular weights. This is in accordance with the results obtained for the poly(vinyl alcohol) gel in the previous work<sup>7</sup>. A similar result has also been shown by Heitz for PVAC gel<sup>2</sup>.

Figure 6 shows the relation between  $M_{lim}$  and the molecular composition of the gels. The value of  $M_{lim}$  is found to be dependent on the composition of the gels. The larger the content of GMA, which may partially act as a cross-linking agent, the smaller the value of  $M_{lim}$ , i.e. it becomes more difficult for molecules with large molecular weight to permeate as the content of GMA increases.

#### Extent of permeable molecules with maximum size

$M_{lim}$  gives a measure of molecular size in relation to the network of the gels, but the actual extent of the molecules in a solution depends on the eluant used for g.p.c. Therefore, it is desirable to estimate the actual molecular size in

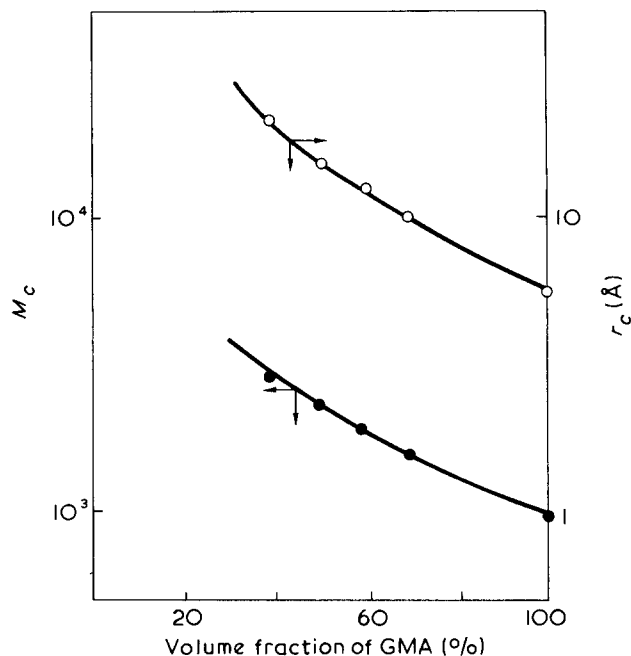


Figure 3 Plots of  $M_c$  and  $r_c$  versus composition of copolymer. ●,  $M_c$ ; ○,  $r_c$

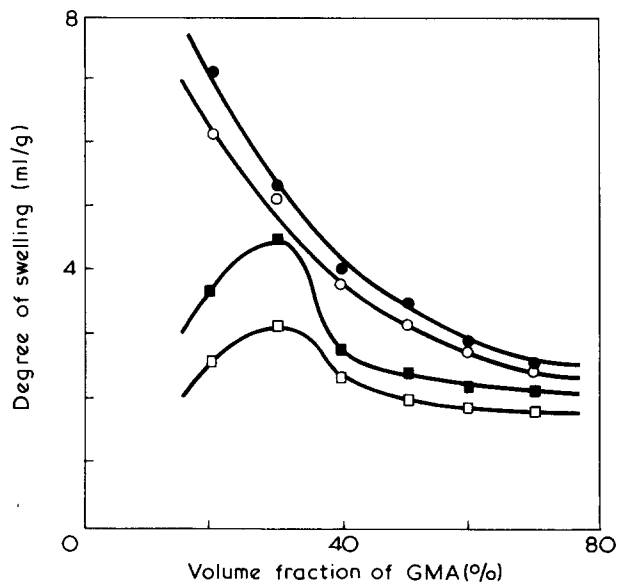


Figure 4 Plots of degree of swelling versus composition of copolymer: ●, DMF; ○, THF; ■, benzene; □, methanol

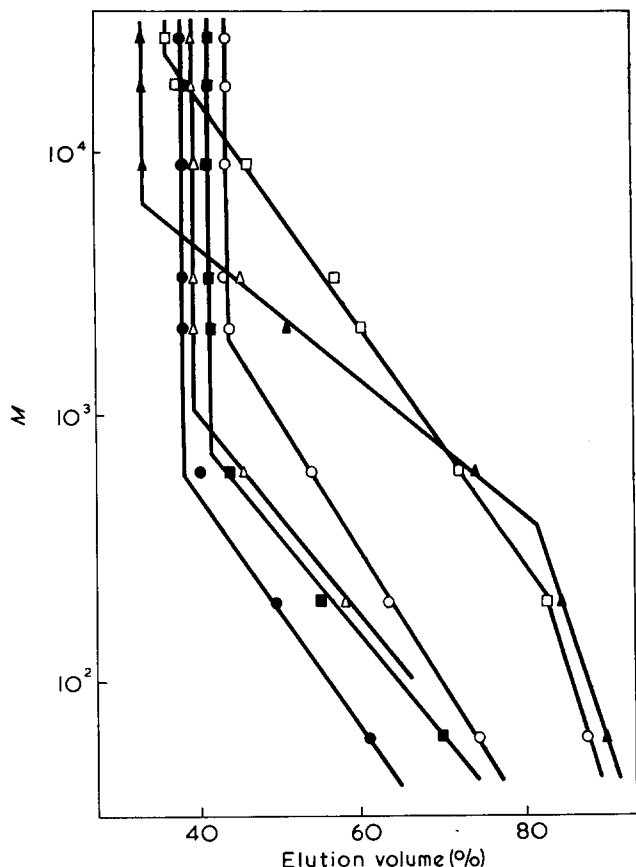


Figure 5 Calibration curve for copoly(VAC-GMA) gels. □, G-1; ▲, G-2; ○, G-3; △, G-4; ■, G-5; ●, G-6

an eluant to discuss the relation between  $r_c$  and the molecular size. For this purpose, the root-mean-square end-to-end distance  $(\bar{r}^2)^{1/2}$  and the root-mean-square hydrodynamic radius  $(\bar{s}^2)^{1/2}$  were first estimated by the method of Ptitsyn and Eizner<sup>11</sup>:

$$[\eta] = \Phi(\epsilon)(\bar{r}^2)^{1/2}/M = \Phi(\epsilon)(\bar{s}^2)^{1/2}/\sqrt{6} M \quad (2)$$

$$\Phi(\epsilon) = 2.86 \times 10^{23}(1 - 2.63\epsilon + 2.86\epsilon^2) \quad (3)$$

where  $[\eta]$  is the intrinsic viscosity and  $M$  is the molecular weight.  $\epsilon$  is determined by the exponent of the viscosity equation (5) as follows.

$$\alpha = (1 + 3\epsilon)/2 \quad (4)$$

in the range of molecular weight of the all samples except for EG. The viscosity equation obtained is:

$$[\eta] = KM^\alpha \quad (5)$$

$$K = 6.14 \times 10^{-4}, \quad \alpha = 0.63$$

As to the determination of the value of  $\Phi$ , it has been pointed out that  $\Phi$  depends on molecular weight<sup>11</sup>. However, the values of  $(\bar{r}^2)^{1/2}$  and  $(\bar{s}^2)^{1/2}$  estimated using the method of Kirkwood and Riseman were not found to differ significantly from those of Ptitsyn and Eizner<sup>10</sup>. According to their theory, the exponent of the viscosity relation varies with molecular weight, but in our case variation of the exponent can be ignored so that the results obtained are reliable in the range of the present work.

Figure 7 shows the logarithmic plot of  $(\bar{r}^2)^{1/2}$  and

$(\bar{s}^2)^{1/2}$  against composition of the gel. It should be noticed that parallel relations are seen among  $r_c$ ,  $(\bar{r}^2)^{1/2}$  and  $(\bar{s}^2)^{1/2}$ , covering the wide range of gel composition. The value of  $r_c$  lies between those of  $(\bar{r}^2)^{1/2}$  and  $(\bar{s}^2)^{1/2}$ . It thus seems satisfactory that  $r_c$  obtained by viscoelastic measurement is comparable with  $(\bar{r}^2)^{1/2}$  and  $(\bar{s}^2)^{1/2}$  obtained by the viscosity equation. From these parallel relations it follows that  $r_c$  is proportional to  $(\bar{r}^2)^{1/2}$  and  $(\bar{s}^2)^{1/2}$  as follows:

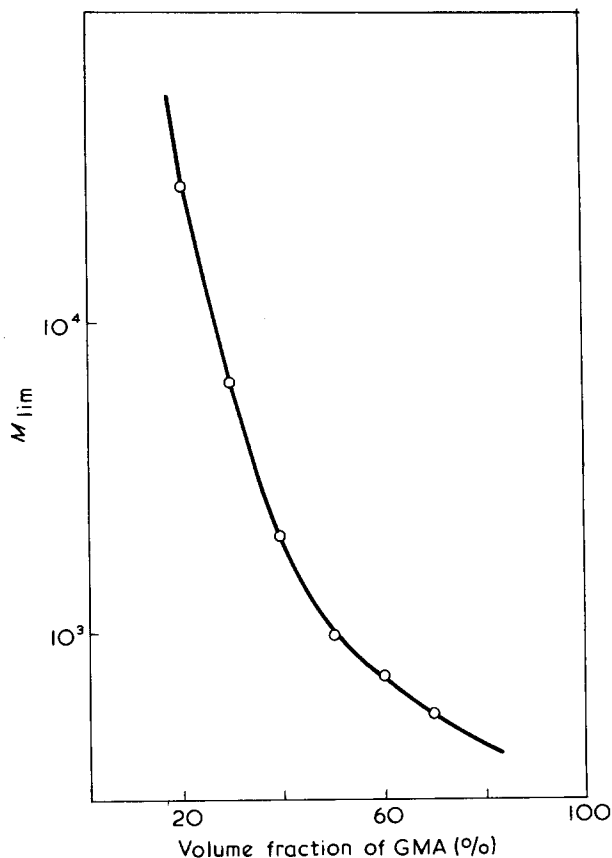


Figure 6 Plot of  $M_{lim}$  versus composition of copolymer.

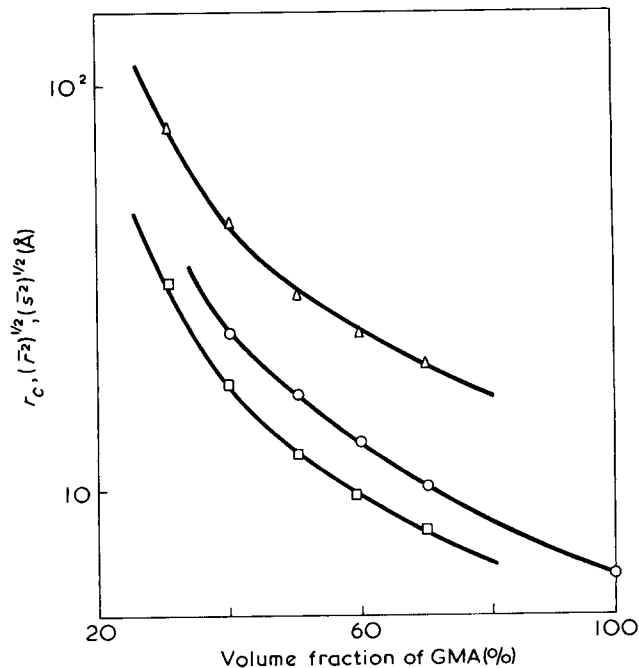


Figure 7 Plots of  $r_c$ ,  $(\bar{r}^2)^{1/2}$  and  $(\bar{s}^2)^{1/2}$  versus composition of copolymer. ○,  $r_c$ ; △,  $(\bar{r}^2)^{1/2}$ ; □,  $(\bar{s}^2)^{1/2}$

$$r_c = 0.55 (\bar{r}^2)^{1/2} = 1.33 (\bar{s}^2)^{1/2} \quad (6)$$

The discrepancy between  $r_c$  and the molecular size  $(\bar{r}^2)^{1/2}$  may come from the fact that  $(\bar{r}^2)^{1/2}$  is related to the maximum network size, while  $r_c$  is the average size. This discrepancy may be decreased as the homogeneity of the network structure increases.

The value of the exponent of equation (5), 0.63, suggests that the molecular shape in the eluant is almost spherical. As a result, the above relations give us a clear microscopic view that in g.p.c. operations the molecular spheres are passing through the swollen networks whose size is proportional to, or larger than, the sphere.

#### CONCLUSION

Linear relations were found among the size of the network of the VAC-GMA copolymer gel and the root-mean-square end-to-end distance and the root-mean-square hydrodynamic radius of molecules in DMF eluant when the gels were used as g.p.c. packing materials covering a wide range of copolymer composition.

#### ACKNOWLEDGEMENT

The authors thank Professor Arichi for useful discussions and encouragement during this work.

#### REFERENCES

- 1 Moore, J. C. *J. Polym. Sci. (A-2)* 1964, **10**, 835
- 2 Heitz, W., Ullner, H. and Haker, H. *Makromol. Chem.* 1966, **98**, 42
- 3 Heitz, W. *Angew. Makromol. Chem.* 1970, **10**, 115
- 4 Porath, J. and Flodin, P. *Nature* 1959, **183**, 1657
- 5 Polson, A. *Biochim. Biophys. Acta* 1961, **50**, 565
- 6 Hjerten, S. and Mosbach, R. *Analyt. Biochem.* 1962, **3**, 109
- 7 Motozato, Y., Hirayama, C. and Matsumoto, K. *Kogyo Kagaku Zasshi* 1971, **74**, 1904
- 8 Motozato, Y. and Hirayama, C. *Nihon Kagaku Zasshi* 1972, p 1087
- 9 Nielsen, L. E. 'Mechanical Properties of Polymers', Reinhold, New York, 1962
- 10 Ptitsyn, O. B. and Eizner, Yu. E. *Sov. Phys. Tech. Phys. (Eng. Transl.)* 1960, **4**, 1020
- 11 Kirkwood, J. G. and Riseman, J. *J. Chem. Phys.* 1948, **16**, 565

# Stress – strain isotherms and thermoelastic properties of crosslinked amorphous polyoxyethylene in compression

C. U. Yu and J. E. Mark

Department of Chemistry and the Macromolecular Research Center, University of Michigan, Ann Arbor, Michigan 48104, USA

(Received 22 July 1974)

Stress–strain isotherms at a number of temperatures in the range 45–85°C have been determined for a compressed, amorphous polyoxyethylene network swollen with a constant amount of non-volatile diluent. The observed isotherms showed much smaller departures from the form indicated by the molecular theories of rubberlike elasticity than is generally the case for polymer networks in elongation. The thermoelastic behaviour of the network was characterized by the dependence of the stress on temperature at constant deformation. The value of the temperature coefficient of the unperturbed dimensions of polyoxyethylene calculated from these data is in good agreement with values obtained both from thermoelastic measurements on polyoxyethylene networks in elongation, and from viscosity–temperature studies on isolated polyoxyethylene chains in a thermodynamically good solvent.

## INTRODUCTION

It has recently been demonstrated that it is quite feasible to use compression measurements to study both stress–strain relationships and stress–temperature coefficients of amorphous polymer networks<sup>1</sup>. In such studies, it is frequently most convenient to determine stress–strain isotherms, at a number of temperatures. One thereby immediately obtains information on the degree to which the observed isotherms differ from the form indicated by the statistical or molecular theories of rubberlike elasticity<sup>2</sup>. In addition, such a series of isotherms directly provides values of the stress as a function of temperature at fixed deformation. As has now been well established, such ‘thermoelastic’ data may be used to calculate both the fraction  $f_e/f$  of the stress which is due to energetic effects, and the temperature coefficient  $d \ln \langle r^2 \rangle_0 / dT$  of the unperturbed dimensions of the network chains<sup>3</sup>.

In the present study, compression measurements were carried out on polyoxyethylene (POE)  $[\text{CH}_2\text{--CH}_2\text{--O}]_x$ , a particularly important polymer to be studied in this way because some serious disagreements<sup>4–6</sup> regarding the value of  $d \ln \langle r^2 \rangle_0 / dT$  for this chain molecule have only recently been resolved<sup>7</sup>, and this temperature coefficient plays a crucial role in the understanding of the configuration-dependent properties of polyoxide chains in general<sup>7,8</sup>.

## EXPERIMENTAL

### Preparation of networks

The sample of POE (Polyox WSR-205, Union Carbide) employed had a molecular weight of approximately 600 000 and a melting point of approximately 65°C (in the undiluted, uncrosslinked state). A portion of this material was moulded, under pressure and at approximately 68°C, into a cylindrical pellet having a diameter of 1.76 cm and a length of 3.50 cm. This sample was then crosslinked

under vacuum at room temperature, using approximately 16.4 Mrad of  $\gamma$ -radiation. After the small amount of soluble material present in the sample was extracted, approximately 8% of the antioxidant *N*-phenyl-2-naphthylamine was incorporated into the network by means of a swelling–deswelling technique<sup>4</sup>. Sufficient *m*-cresol, a non-volatile diluent, was then incorporated into the network to decrease the volume fraction  $v_2$  of polymer to 0.75, thus further decreasing the melting point of the POE network. The thermal expansion coefficient  $\beta = (\partial \ln V / \partial T)_p$  of the swollen network in the vicinity of 65°C was obtained from dilatometric measurements; it was found to be  $0.509 \times 10^{-3} \text{ K}^{-1}$ .

### Stress–compression measurements

Stress–strain isotherms were obtained for this swollen POE network in compression, at 45, 55, 65, 75, and 85°C, in the manner described in detail elsewhere<sup>1,9</sup>. A slurry of graphite in low molecular weight dimethylsiloxane fluid applied to the Teflon compression plates aided in preventing non-uniform deformation of the network. Values of the relative length or compression  $\alpha = L/L_i$  of the sample were in the range 1.00–0.80. The isotherms were found to be reversible and there was no evidence of crystallization under the conditions employed in these measurements.

## RESULTS AND DISCUSSION

The experimental data were used to calculate values of the ‘reduced force’  $[f^*]$  defined by:

$$[f^*] = f v_2^{1/3} / A^* (\alpha - \alpha^{-2}) \quad (1)$$

where  $f$  is the elastic force or stress, and  $A^*$  is the cross-sectional area of the unswollen, undistorted sample at 45°C. Values of the deformation or compression,  $\alpha$ , were

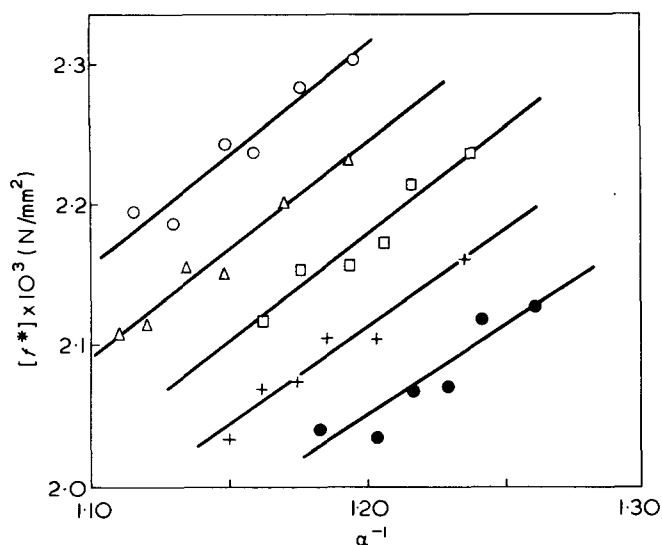


Figure 1 Stress-strain isotherms for polyoxyethylene in compression. The deformation  $\alpha$  is defined by  $L(T)/L_i(T)$ , i.e., the length of the sample at the specified temperature relative to the undeformed length at the same temperature. ●, 45°; +, 55°; □, 65°; △, 75°; ○, 85° C

calculated relative to the initial length,  $L_i$ , at the particular temperature of measurement, and values of the reduced force were expressed in  $\text{N/mm}^2$ . (In order to facilitate comparison of these results with others already in the literature, it may be helpful to point out that  $1 \text{ N/mm}^2 = 1 \text{ MN/m}^2 = 10.20 \text{ kg/cm}^2$ .) The values of  $[f^*]$  thus calculated were plotted against the reciprocal of the compression,  $\alpha$ , as suggested by the semi-empirical Mooney-Rivlin equation<sup>10</sup>:

$$[f^*] = 2C_1 + 2C_2\alpha^{-1} \quad (2)$$

The results are shown in Figure 1; each line, representing a stress-strain isotherm, was located by the method of least squares. The slopes of these lines represent values of the constant  $2C_2$ , which is a measure of the departure of the observed stress-strain relationship from the theoretical prediction that  $[f^*]$  be independent of  $\alpha$ <sup>11</sup>. From these results,  $2C_2 = 0.0014(\pm 0.0002) \text{ N/mm}^2$ , a result very much smaller than the values of this correction generally obtained for networks in elongation<sup>11</sup>. Similarly small values of  $2C_2$  have been reported for several other polymers which have been studied in compression<sup>1</sup>.

Values of the reduced force at selected values of  $\alpha$  in the range 0.95–0.80 were obtained from each stress-strain isotherm by means of interpolation and limited extrapolation. The values of  $[f^*]$  thus obtained were found to vary linearly with temperature. Typical results are presented in Figure 2, where the lines shown were again located by least-squares analysis. The slopes of these lines were used to calculate<sup>1</sup> values of the coefficient  $[\partial \ln([f^*]/T)/\partial T]_{p,\alpha}$  at the average temperature, 65°C, employed in this study; these results are given in the second column of Table 1. The quantities  $f_e/f$  and  $d \ln \langle r^2 \rangle_0/dT$  were then calculated from the equations<sup>1,12</sup>:

$$\begin{aligned} f_e/f &= T d \ln \langle r^2 \rangle_0/dT \\ &= -T[\partial \ln([f^*]/T)/\partial T]_{p,\alpha} + \beta T/3 \end{aligned} \quad (3)$$

Values of these quantities are given in the last two columns

of the Table. They are seen to vary only slightly with  $\alpha$ , and give the average results  $f_e/f = 0.06(\pm 0.01)$  and  $d \ln \langle r^2 \rangle_0/dT = 0.19(\pm 0.03) \times 10^{-3} \text{ K}^{-1}$ .

The value of  $d \ln \langle r^2 \rangle_0/dT$  for POE which is obtained in the present study is in very good agreement with the value  $0.23(\pm 0.02) \times 10^{-3} \text{ K}^{-1}$  resulting from a thermoelastic study of a POE network in elongation<sup>4</sup>, and with the value  $0.2(\pm 0.2) \times 10^{-3} \text{ K}^{-1}$  obtained from viscosity-temperature measurements on isolated POE chains in a thermodynamically good solvent<sup>7</sup>. (Other thermoelastic results<sup>5,13</sup> of lower reliability<sup>6,13</sup> are in fair agreement with the results cited above. Values calculated from viscosity-temperature studies on POE chains of low molecular weight<sup>5</sup> have been shown to be unreliable<sup>7</sup>, and are therefore not presented here.)

The fact that there is good agreement between values of  $d \ln \langle r^2 \rangle_0/dT$  obtained in compression and elongation has some bearing on the alleged existence of intermolecularly ordered domains<sup>14,15</sup> or 'supermolecular structures'<sup>5</sup> in polymers in the amorphous state. Since any such ordering would reasonably be expected to respond differently to (uniaxial) elongation and compression (mechanically equivalent to biaxial elongation<sup>11</sup>), the absence of any difference between the values of  $d \ln \langle r^2 \rangle_0/dT$  obtained using these two different types of deformation would seem to represent yet another piece of evidence<sup>16</sup> against the existence of ordered regions in amorphous polymers.

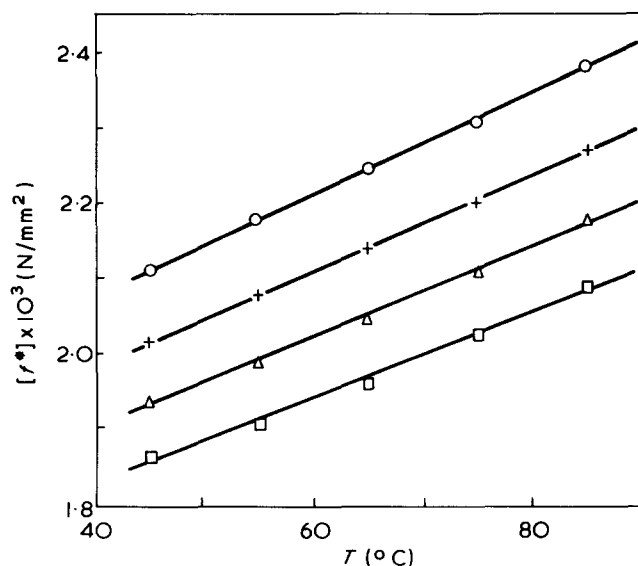


Figure 2 Reduced force shown as a function of temperature for selected values of the deformation,  $\alpha$ . These results were obtained from Figure 1, in which  $\alpha = L(T)/L_i(T)$ , and thus pertain to constant deformation rather than constant length. ○,  $\alpha = 0.80$ ; +,  $\alpha = 0.85$ ; △,  $\alpha = 0.90$ ; □,  $\alpha = 0.95$

Table 1 Thermoelastic results on polyoxyethylene in compression

$\alpha$	$[\partial \ln([f^*]/T)/\partial T]_{p,\alpha} \times 10^3$	$f_e/f$	$d \ln \langle r^2 \rangle_0/dT \times 10^3$
0.950	-0.0658	0.08	0.24
0.925	-0.0501	0.07	0.22
0.900	-0.0335	0.07	0.20
0.875	-0.0169	0.06	0.19
0.850	-0.0008	0.06	0.17
0.825	0.0167	0.05	0.15
0.800	0.0346	0.05	0.14



ACKNOWLEDGEMENTS

Acknowledgement is made to the donors of the Petroleum Research Fund, administered by the American Chemical Society, for partial support of this research. In addition, C. U. Y. wishes to acknowledge the predoctoral fellowship provided by the Macromolecular Research Center of the University of Michigan.

REFERENCES

- 1 Chen, R. Y. S., Yu, C. U. and Mark, J. E. *Macromolecules* 1973, 6, 746
- 2 see Mark, J. E. *J. Am. Chem. Soc.* 1970, 92, 7252
- 3 see Mark, J. E. *Rubber Chem. Technol.* 1973, 46, 593
- 4 Mark, J. E. and Flory, P. J. *J. Am. Chem. Soc.* 1965, 87, 1415
- 5 De Candia, F., Vittoria, V., Bianchi, U. and Patrone, E. *Macromolecules* 1972, 5, 493
- 6 Mark, J. E. and Flory, P. J. *Macromolecules* 1973, 6, 300
- 7 Bluestone, S., Mark, J. E. and Flory, P. J. *Macromolecules* 1974, 7, 325
- 8 Flory, P. J. 'Statistical Mechanics of Chain Molecules', Interscience, New York, 1969
- 9 Yu, C. U. *PhD Thesis*, University of Michigan (1974)
- 10 Mooney, M. J. *Appl. Phys.* 1940, 11, 582; Rivlin, R. S. *Phil. Trans. R. Soc. (A)* 1948, 240, 459, 491, 509
- 11 Treloar, L. R. G. 'The Physics of Rubber Elasticity', 2nd Edn, Clarendon Press, Oxford, 1958
- 12 Flory, P. J., Ciferri, A. and Hoeve, C. A. J. *J. Polym. Sci.* 1960, 45, 235
- 13 De Candia, F. *Makromol. Chem.* 1971, 141, 177
- 14 Yeh, G. S. Y. *Crit. Rev. Macromol. Sci.* 1972, 1, 173
- 15 Yeh, G. S. Y. *Polym. Prepr.* 1973, 14, 718
- 16 Flory, P. J. *Pure Appl. Chem. (Macromol. Chem. Suppl. 8)* 1973, 33, 1

# Light scattering in an electric field: variations of the $H_H(\theta)$ component around $\theta = 90^\circ$

J. C. Ravey and P. Mazon

Laboratoire de Biophysique, Université de Nancy I, 54037 Nancy Cedex, France  
(Received 26 June 1974; revised 13 August 1974)

The studies of the changes  $\Delta H_H$  of the  $H_H$  component of the light scattered by dilute suspensions of particles oriented by an electric field  $E_0$  are shown to be convenient and reliable methods for obtaining simultaneous information on the electrical ( $\mu$ ), geometrical ( $\omega$ ) and optical ( $\delta$ ) anisotropies of the particles. Indeed, when  $E_0$  is applied in three particular directions, which are related to the exterior and interior bisectrices of the observation angle  $\theta$ ,  $\Delta H_H(\theta = 90^\circ)$  generally has the same sign as  $(-\mu\omega)$ ,  $(+\mu\omega)$  or  $(-\mu)$ , according to the direction of  $E_0$ . Moreover, under the same conditions, the slopes of  $\Delta H_H(\theta)$  versus  $\theta$  are shown to be much more informative than those of  $\Delta H_H(\theta)/H_H(\theta)$ , having the sign of  $(-\mu\delta)$ ,  $(+\mu\delta)$  or  $(-\mu\delta\omega)$ . Experiments on TMV particles illustrate in a very satisfactory manner these theoretical conclusions.

## INTRODUCTION

When the Rayleigh–Gans–Debye approximation is used, the light scattering method is a simple and powerful tool for studying the size of diluted particles. Moreover, the measurements of the depolarized components  $H_V$  and  $H_H$  of the scattered light allow the determination of optical and geometrical parameters which are unattainable by usual light scattering experiments. For example, the algebraic value of the optical anisotropy,  $\delta$ , can be found by measuring the angular position of the minimum of  $H_H$  if the shape of the scatterer is known<sup>1</sup>. Likewise it has been shown<sup>2</sup> that the value of  $[(H_H - H_V)/H_V]_{\theta=90}$  determines whether the particles are elongated or flattened.

Furthermore if the particles are oriented by means of an electric field  $E_0$ , information concerning optical, geometrical and electrical anisotropies, namely the induced and/or permanent moments of the particles can be obtained<sup>6–9</sup>.

Let  $\omega$  be the anisometry of the scatterer ( $\omega = p^2 - 1$ , where  $p$  is its ellipticity), and  $\mu = c + b^2/2$ , where  $b$  and  $c$  are proportional respectively to its electrical-permanent moment and anisotropy (see below).

In the presence of the electric field, the resulting variation  $\Delta V_V$  of the  $V_V(\theta)$  component:

$$\Delta V_V(\theta) = V_V(\theta, E_0) - V_V(\theta, 0)$$

has the same sign as  $(\mu\omega)^{3,4,10}$  for a particular (vertical) direction of  $E_0$ , at least for weaker orientation rates. When  $b = 0$ ,  $(\mu\omega)$  is always positive, whatever the shape of the spheroidal scatterer. In that case and with such a measurement, the signs of  $\omega$  and  $\mu$  cannot be found separately.

Until now, electric light scattering experiments have been only used for obtaining values of the electrical parameters ( $b$  and  $c$ ) of scatterers, the shape and size of which were already known. Moreover, the optical anisotropy  $\delta$  was generally disregarded. If we wish the algebraic values of  $\delta$ ,  $\omega$ ,  $\mu$  to be determined with the help of very few measurements, other light scattered components must be studied, as done in the present paper.

On the other hand, studies of  $H_V$  and  $H_H$  and of their changes are believed to be more fruitful, for they do permit the determination of the sign of each quantity of interest,  $\mu$ ,  $\delta$ ,  $\omega$ ; the present work deals with the  $H_H$  component which seems most suitable.

## DEFINITIONS AND SYMBOLS

Throughout the text, the following functions and symbols are used.

$\beta_1, \beta_2, \beta_3$  are the direction cosines of the  $\vec{\xi}$  axis of the scattering spheroid, in the reference frame  $(\vec{s}, \vec{s}', \vec{z})$  built on the exterior  $\vec{s}$  and interior  $\vec{s}'$  bisector of the observation angle,  $\theta$ .

$R(\Phi)$  is the normalized interference factor of the scatterer for which  $\vec{\xi} \cdot \vec{s} = \beta_1 = \cos \Phi$ .

$H_H(\theta)$  and its changes due to an electric orientating field may be expressed in terms of the following integrals introduced by Ravey<sup>3</sup>:

$$I_{pqr} = \frac{1}{4\pi} \int R(\Phi) \beta_1^{2p} \beta_2^{2q} \beta_3^{2r} d\Omega$$

the properties of which have been indicated in a previous paper<sup>3</sup>. The full expressions of  $\Delta H_H$  are rather complicated, and can be found elsewhere<sup>4</sup>.

When the particles are oriented by an electric field, their orientation is described by the distribution function  $p(\nu)$ :

$$p(\nu) = \frac{1}{4\pi U} \exp(b \cos \nu + c \cos^2 \nu) \quad (1)$$

where  $\cos \nu = \vec{\xi} \cdot \vec{E}_0 / |\vec{E}_0|$ ,  $U$  being a normalization constant.  $b$  describes the orientation due to a permanent dipole (along  $\vec{\xi}$ ), and  $c$  the one due to induced moment<sup>6–9</sup>.

For lower degrees of orientation:

$$4\pi U p(\nu) \simeq 1 + \mu \cos^2 \nu$$

where

$$\mu = c + b^2/2 \text{ and } U = 1 + \mu/3 + \dots$$

For time-dependent electric fields,  $\mu$  must include the rotational diffusion constant of the particles<sup>6-9</sup>.

GENERAL THEORETICAL RELATIONS

Any scattered component,  $I$ , of the scattered intensity can be expressed by the following integral<sup>3</sup>:

$$I = \frac{1}{4\pi U} \int p(\nu) R(\Phi) f(\theta, \beta, \delta) d\Omega \tag{2}$$

where  $f$  is a function of the scattering angle,  $\theta$ , the two principal optical polarizabilities per unit volume of the spheroid (or cylinder)  $g_1$  and  $g_2$ , and of the direction cosines  $\beta_1, \beta_2, \beta_3$ . The various expressions of  $f$  corresponding to the components  $H_H, H_v, V_H, V_v$  can be found in previous papers<sup>3,11</sup>. In order to avoid complicated expressions, only the cases where  $\vec{E}_0$  is directed along the  $\vec{s}, \vec{s}', \vec{z}$  direction will be considered here, the resulting changes of  $H_H$  being noted respectively by  $(\Delta H_H)_s, (\Delta H_H)_{s'}$ , and  $(\Delta H_H)_z$ . More general expressions (arbitrary direction of  $\vec{E}_0$ , any direction of scattering, form- and polarizability ellipsoids not coinciding) may be also deduced<sup>3</sup>.

General expressions of  $H_H(\theta)$  (within RGD approximation)

Scattered intensity without orientating field. By setting  $\theta = \pi/2 + 2\alpha$  in the general expressions giving  $H_H^0$ <sup>3</sup>, the following expression is obtained:

$$H_H^0(\theta) = \frac{9\delta^2}{4} (I_{200} + I_{002} - 2I_{101}) + 6\delta(1 - \delta)\alpha(I_{001} - I_{100}) + 9\delta^2\alpha(I_{002} - I_{200}) + \alpha(\alpha^2) \tag{3}$$

whatever the shape and the size of the spheroid (or cylinder) are, and for any value of the optical anisotropy,  $\delta$ , where

$$\delta = (g_1 - g_2)/(g_1 + 2g_2)$$

The  $\theta$ -derivatives of the  $I_{pqr}$  integrals are always finite, and these functions vary not much around  $\theta = 90^\circ$ . Moreover,  $\delta^2$  is generally negligible compared with  $\delta$  for most of the anisotropic scatterers. Since the  $\theta$ -derivative of the first term of equation (3), where  $\alpha$  does not explicitly appear, contains the  $\delta^2$  factor, the  $\theta$ -derivative of  $H_H^0(\theta)$  will be given to a good approximation by the following term:

$$\left[ \frac{d}{d\theta} H_H^0(\theta) \right]_{\theta=90^\circ} \approx 3\delta(I_{001} - I_{100})$$

Case of weaker orientation rates. The use of the  $I_{pqr}$  formalism allows an immediate obtainment of the results as shown below. From equation (1):

$$4\pi p(\nu) \approx 1 + \mu \left( \beta_1^2 - \frac{1}{3} \right)$$

when  $\vec{E}_0$  is directed along  $\vec{s}$  ( $\cos \nu \equiv \beta_1$ ).

Thus the absolute change  $\Delta H_H$  is simply:

$$\Delta H_H = \mu \left( \Delta' H_H - \frac{1}{3} H_0^0 \right) \tag{4}$$

where  $\Delta' H_H$  is derived from  $H_H^0$  in equation (3) by changing the index  $p$  in  $p + 1$  in the  $I_{pqr}$  functions. Thus we get:

$$\left( \frac{\Delta H_H}{\mu} \right)_s = \frac{9\delta^2}{4} (I_{300} + I_{102} - 2I_{201}) + 6\delta(1 - \delta)\alpha(I_{101} - I_{200}) + 9\delta^2\alpha(I_{102} - I_{300}) - \frac{1}{3} H_H^0 + \sigma(\alpha^2) \tag{5}$$

for any value of  $\delta$ , and for any shape of the revolution scatterers. As before, the  $\theta$ -derivative of  $\Delta H_H$  is approximately given by the factor  $(2\alpha)$  which is proportional to  $\delta$ .

It is clear that  $(\Delta H_H)_s'$  and  $(\Delta H_H)_z$  will be obtained in the same manner from equation (4);  $(\Delta' H_H)_s$  and  $(\Delta' H_H)_z$  are deduced from  $H_H^0$  by replacing the  $I_{pqr}$  functions respectively by  $I_{p,q+1,r}$  and  $I_{p,q,r+1}$ .

Case of higher orientation extent. The various changes of the  $H_H$  component have been directly evaluated by numerical integration of equation (2), on a computer. The results will be presented later.

However, for the zero scattering angle, or for very small particles  $R(\Phi) \approx 1$ , and the problem has been solved<sup>3,10</sup> by introduction of the so-called generalized Langevin functions<sup>5</sup>.

Expression of the  $I_{pqr}$  integrals

Calculations have been performed on cylinders, rods, discs and spheroids. Let us recall here some results.

The normalized interference factor of a spheroid, the semi-axes of which are  $a, a, pa$ , is:

$$R(x) = \frac{9\pi}{2} \left[ \frac{\mathcal{F}_{3/2}(x)}{x^{3/2}} \right]^2$$

where  $\mathcal{F}_{3/2}(x)$  is a Bessel function of  $x$ , and

$$x = \frac{4\pi a}{\lambda} \sin \frac{\theta}{2} (1 + \omega\beta_1^2)^{1/2} \tag{6}$$

$\lambda$  is the wavelength in the medium,  $\omega = p^2 - 1$ .

The orientation of the spheroid is such that  $\vec{\xi} \cdot \vec{s} = \beta_1$ .

For quasi-spherical spheroids ( $\omega \rightarrow 0$ ),  $R(\beta_1)$  may be expanded in a MacLaurin series of  $\omega$ , from which it follows:

$$I_{pqr} \approx G_q^r [J_{q+r}^p P_0 - \omega J_{q+r}^{p+1} P_0' + \sigma(\omega^2)] \tag{7}$$

where these various functions are given in the Appendix.

The expansion (7) is quite similar to the following one:

$$I_{pqr} = G_q^r [J_{q+r}^p P - \omega J_{q+r}^{p+1} P' + \sigma(\rho^4/\lambda^4)] \tag{8}$$

$$\left( h = \frac{4\pi}{\lambda} \sin \frac{\theta}{2} \right)$$

which is valid for small particles, the square radius of gyration of which is  $\rho^2 \ll \lambda^2$ , where  $P = 1 - h^2\rho^2/(\omega + 3)$  and

$P' = h^2 \rho^2 / (\omega + 3)$ ; small and quasi-spherical particles behave then in the same manner.

For large discs ( $\omega \rightarrow -1$ ) and rods ( $\omega \rightarrow \infty$ ), the asymptotic behaviour of  $\Delta H_H$  is deduced from the following properties of the  $I_{pqr}$  functions<sup>3</sup>.

For large rods, all of the  $I_{pqr}$  becomes negligible compared with the  $I_{oqr}$ :

$$I_{oqr} \rightarrow \frac{2}{H} G_q^r \text{Si}(2H)$$

where  $H = (2\pi L/\lambda) \sin \theta/2$ ;  $L$  is the length of the rod, and  $\text{Si}(x)$  is the function integral sine.

For large discs, all of the  $I_{pqr}$  becomes negligible compared with the  $I_{poo}$ :

$$I_{poo} \rightarrow \frac{2}{H^2} \text{ for any } p$$

where  $H = (4\pi R/\lambda) \sin \theta/2$ ,  $2R$  being the diameter of the disc.

## THEORETICAL RESULTS AND DISCUSSION

### $H_H$ component scattered by small or very large particles

From the above considerations, the following results may be derived (smaller orientation rates).

*Case of small ( $h^2 \rho^2 < 1/5$ ) and quasi-spherical particles*

If  $P$  and  $P'$  are the quantities previously defined, we get:

$$H_H^0 = \frac{3}{5} \delta^2 \left( P - \frac{3\omega}{7} P' \right) + \alpha \frac{4}{5} \delta \left( 1 + \frac{2\delta}{7} \right) \omega P' \quad (9)$$

$$\left( \frac{\Delta H_H}{\mu} \right)_s = \frac{2\delta^2}{35} (P - 2\omega P') - \frac{4}{5} \delta \alpha \left[ P \left( 1 + \frac{2\delta}{7} \right) - \frac{\omega P'}{21} (11 + 4\delta) \right] \quad (10)$$

$$\left( \frac{\Delta H_H}{\mu} \right)_{s'} = \frac{2\delta^2}{35} (P + \omega P') + \frac{4}{5} \alpha \delta \left( 1 + \frac{2\delta}{7} \right) \left( P - \frac{\omega}{3} P' \right) \quad (11)$$

$$\left( \frac{\Delta H_H}{\mu} \right)_z = -\frac{4\delta^2}{35} \left( P - \frac{\omega}{2} P' \right) - \frac{16}{105} \alpha \delta \left( 1 + \frac{\delta}{2} \right) \omega P' \quad (12)$$

The behaviour of quasi-spherical spheroids ( $\omega \rightarrow 0$ , any size) is obtained by replacing  $P$  and  $P'$  by  $P_0$  and  $P'_0$  in these relations respectively (see Appendix).

For smaller particles, all the expressions between parentheses or brackets containing both  $P$  and  $P'$  [e.g.:  $(P - (3\omega/7)P')$ ] are positive.

For quasi-spherical spheroids (of any size) the sign of this quantity depends on the size in a very oscillatory way, due to the presence of the Bessel functions  $\mathcal{J}_{3/2}$  and  $\mathcal{J}_{5/2}$  in  $P_0$  and  $P'_0$ . For this reason, we shall exclude from our

study the values of ellipticity between  $p = 2/3$  and  $p = 3/2$ , for which no general conclusion can be easily drawn if the particle sizes are relatively large ( $\rho/\lambda \geq 1/3$ ).

*Asymptotic behaviour.* The following expressions can be easily obtained for large discs (the  $2/H^2$  term has been omitted), from the properties of the  $I_{pqr}$  integrals:

$$H_H^0 \rightarrow \frac{9\delta^2}{4} - 6\alpha\delta \left( 1 + \frac{\delta}{2} \right) \quad (13)$$

$$\left( \frac{\Delta H_H}{\mu} \right)_s \rightarrow \frac{3}{2} \delta^2 - 4\alpha\delta \left( 1 + \frac{\delta}{2} \right) \quad (14)$$

$$\left( \frac{\Delta H_H}{\mu} \right)_{s'} = \left( \frac{\Delta H_H}{\mu} \right)_z = -\frac{1}{2} \left( \frac{\Delta H_H}{\mu} \right)_s \quad (15)$$

For large rods the factor  $2/H \text{Si}(2H)$  is omitted also:

$$H_H^0 \rightarrow \frac{9\delta^2}{4} \cdot \frac{3}{16} + \frac{3}{2} \alpha \delta \left( 1 + \frac{\delta}{8} \right) \quad (16)$$

$$\left( \frac{\Delta H_H}{\mu} \right)_s \rightarrow -\frac{1}{3} H_H^0 \quad (17)$$

$$\left( \frac{\Delta H_H}{\mu} \right)_{s'} \rightarrow \frac{9\delta^2}{4} \cdot \frac{3}{32} + \frac{5}{8} \alpha \delta \left( 1 + \frac{7\delta}{20} \right) \quad (18)$$

$$\left( \frac{\Delta H_H}{\mu} \right)_z \rightarrow -\frac{9\delta^2}{4} \cdot \frac{1}{32} - \frac{\alpha\delta}{8} \left( 1 + \frac{5}{4} \delta \right) \quad (19)$$

### Study of $[\Delta H_H/H_H^0]_{\theta=90}$

We shall now study how the expressions change when  $p$  increases from zero (discs) to infinity (rods), for various values of the radius of gyration,  $\rho$ .

*Case of weaker orientation rates.* The results derived from the above equations are summarized in Table 1.

It can be seen that the sum of the variations corresponding to  $\vec{E}_0$  directed along  $\vec{s}$ ,  $\vec{s}'$ ,  $\vec{z}$  is zero as it must be<sup>4,11</sup>.

Numerical computations of  $(\Delta H_H/H_H^0)_{\theta=90}$  for other values of  $\omega$  have allowed the curves of Figure 1 to be drawn in a logarithmic scale for  $p$ . These computations have been made by using two particle shapes: the spheroid and the cylinder. The results are generally very close to each others for these two models. For simplicity, only the spheroid-like particles will be considered in the present paper. The curves illustrate the following conclusions: let  $w = 4\pi\rho/\lambda$ .

If  $w < 1$  (smaller particles), the relative change  $[\Delta H_H/H_H^0]_{\theta=90}$  is about  $(2/21)\mu$  for  $\vec{E}_0$  directed along  $\vec{s}$  or  $\vec{s}'$ .

Table 1 Theoretical values of  $(1/\mu)[(\Delta H_H)/H_H^0]_{\theta=90}$  for the three particular directions of  $\vec{E}_0$ , obtained for smaller or quasi-spherical particles, large discs and large rods

$\vec{E}_0$ directed along	$\omega \rightarrow 0$ (spheres of any size)	$\omega \rightarrow -1$ (large discs)	$\omega \rightarrow \infty$ (large rods)
	small particles		
$\vec{s}$	2/21	2/3	-1/3
$\vec{s}'$	2/21	-1/3	1/2
$\vec{z}$	-4/21	-1/3	-1/6

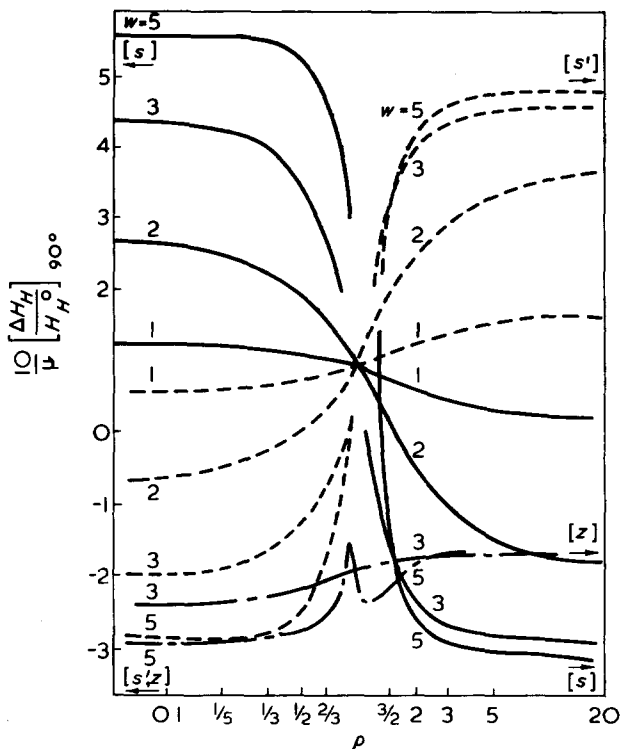


Figure 1 The ratio  $(1/\mu)[(\Delta H_H/H_H^0)]_{90^\circ}$  for smaller orientation rates as a function of the ellipticity  $\rho$  of the particles for various values of the size ( $w$ ) and for  $\vec{E}_0$  oriented along  $\vec{s}$ , ( $\text{---}$ ),  $\vec{s}'$  ( $\text{---}$ ) or  $\vec{z}$  ( $\text{---}$ ). A decimal logarithmic scale is used for  $\rho$ . The common value of the curves for spheres is  $2/21$  ( $s$  and  $s'$ ) and  $-4/21$  ( $z$ ). The horizontal arrows represent the asymptotical values given in Table 1

and about  $(-4/21 \mu)$  for  $\vec{E}_0$  along  $\vec{z}$ , for any values of  $\delta$  and  $\omega$ .

For  $1.5 < w < 6$  (values of  $w$  greater than 6 are generally out of the scope of the Rayleigh-Gans-Debye approximation), we recall that we exclude here the values of  $\rho$  between  $2/3$  and  $3/2$ . Whatever  $\delta$  and  $\omega$  are:

$(\Delta H_H/H_H^0)_{90}$  has the sign of  $(-\mu\omega)$ ,  
for  $\vec{E}_0$  directed along  $\vec{s}$

$(\Delta H_H/H_H^0)_{90}$  has the sign of  $(+\mu\omega)$ ,  
for  $\vec{E}_0$  directed along  $\vec{s}'$

$(\Delta H_H/H_H^0)_{90}$  has the sign of  $(-\mu)$ ,  
for  $\vec{E}_0$  directed along  $\vec{z}$

$(\Delta H_H)_{90,z}$  has thus always the sign of  $(-\mu)$  for any  $\delta$ ,  $\omega$  and  $w$ . Such a measurement supplies then the sign of the electric parameter  $\mu$ , independently of the values of  $\omega$  and  $\delta$ .

**Higher orientating field strength: the effect of the saturation.** How are the previous results modified with increasing orientating field strength,  $E_0$ ? The effect depends on the direction of  $\vec{E}_0$ , the size of the particle and on its ellipticity. The curves of related figures are drawn for an orientation due to the induced moment only ( $b = 0$ ), so that  $\mu \equiv c$ .

$\vec{E}_0$  directed along  $\vec{z}$ . In this case,  $(1/\mu)[(\Delta H_H)/(H_H^0)]_{90,z}$  slightly increases, but remains negative when  $E_0$  increases, whatever the shape and the size of the scatterers are, a very useful result.

$\vec{E}_0$  directed along  $\vec{s}'$ . Let us consider elongated particles ( $\rho > 1$ ). It can be seen from Figure 2 ( $w = 2$ ) that for increasing values of  $c$  the effect is becoming first larger and

then less important, but the sign of the ratio  $(1/\mu)[(\Delta H_H)/(H_H^0)]_{90,s'}$  does not change. This conclusion is still true for other values of  $w$ : increasing values of  $w$  only shifts the curves towards higher values (Figure 3). For flattened particles, the ratio  $(1/\mu)[(\Delta H_H)/(H_H^0)]_{90,s'}$  is generally negative, and becomes more and more negative with increasing values of  $w$ . But for quasi-spherical or smaller particles, its sign may be reversed (Figure 2).

$\vec{E}_0$  directed along  $\vec{s}$ . As shown in Figure 4, the value of  $(1/\mu)[(\Delta H_H)/(H_H^0)]_{90,s}$  generally decreases with  $\mu$ . Its sign does not change, except for smaller particles (Figures 3 and 4) or for small values of  $\omega$  (Figure 4). When  $w$  increases, the curves are shifted 'downward' for elongated particles, and 'upward' for flattened ones.

As a conclusion, the previous theoretical results concerning the sign of  $(\Delta H)_{90}$  are generally not changed under electrical saturation effects: a change of sign may occur only in the case of smaller or quasi-spherical particles.

**Study of the slope of  $[\Delta H_H(\theta)]_{\theta=90}$**

The absolute slope of  $[\Delta H_H(\theta)]_{\theta=90}$  have been divided by  $H_H^0(90)$ , and denoted by  $m_a$ :

$$m_a = \left[ \frac{d}{d\theta} \Delta H_H(\theta) \right]_{\theta=90} / H_H^0(90)$$

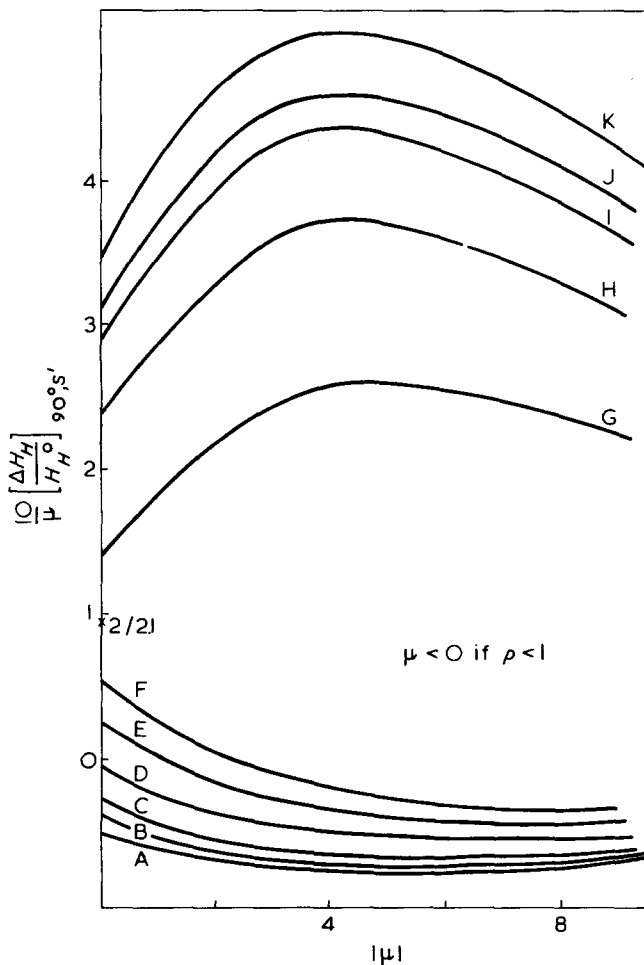


Figure 2  $(1/\mu)[(\Delta H_H/H_H^0)]_{90,s'}$  as a function of the electrical parameter  $\mu$  for various values of the ellipticity of the particles for which  $w = 2$ . The orientation is assumed to be due to the induced electric moment only, so that  $\mu$  has the same sign as  $(\rho - 1)$ . The upper and lower curves do not correspond to ellipsoids but to cylinders of length  $L$  and diameter  $2R$  ( $L/2R = 10$  or  $0.1$ ).  $\rho$ : A, 0.1; B, 0.25; C, 0.33; D, 0.5; E, 0.66; F, 0.8; G, 1.25; H, 2.0; I, 3.0; J, 4.0; K,  $L/2R = 10$

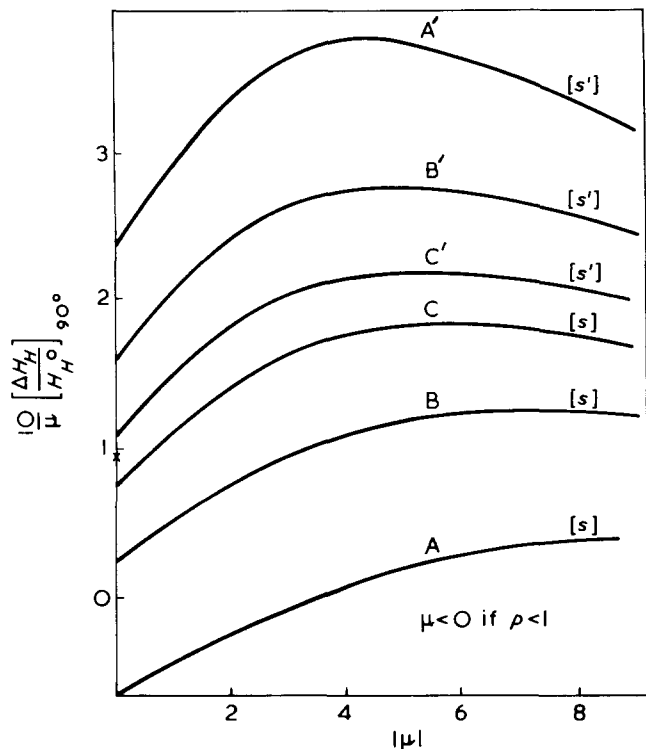


Figure 3  $(1/\mu)[(\Delta H_H/H_H^0)]_{90^\circ}$  as a function of  $\mu$  for various small anisotropic elongated ( $\rho = 10$ ) particles.  $w$ : A, A', 1.5; B, B', 1.0; C, C', 0.5. It should be noted that for the lower curve (A) the sign of the above ratio is changed

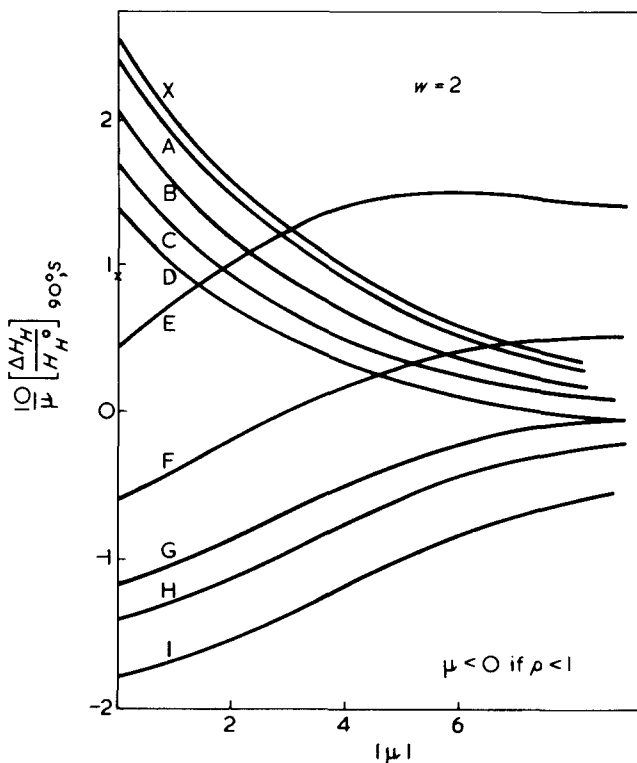


Figure 4  $(1/\mu)[(\Delta H_H/H_H^0)]_{90^\circ,s}$  as a function of  $\mu$  for anisotropic ellipsoids or cylinders of various ellipticities  $\rho$  ( $\rho = L/2R$  for cylinders). X,  $L/2R = 0.1$ .  $\rho$ : A, 0.25; B, 0.5; C, 0.66; D, 0.8; E, 1.25; F, 2.0; G, 3.0; H, 4.0; I, 10.0

Case of lower orientation rates. As stated above the various absolute slopes (or  $\theta$ -derivatives) are approximately given in expressions (9)–(19), as half of the factor of  $\alpha$ : it is seen that they are nearly proportional to the optical anisotropy,  $\delta$ ; they depend on  $\omega$  chiefly when  $\vec{E}_0$  is directed along  $\vec{z}$ . Let us give the following approximate asymptotic

expressions, where the slopes are expressed as variations per unit radian (they are approximate in the sense that only the term proportional to  $\delta$  is kept).

$$\text{smaller particles} \left\{ \begin{aligned} (m_a)_s &= -\frac{2\mu}{3\delta} \left( 1 + \frac{2\delta}{7} \right) \\ (m_a)_{s'} &= -(m_a)_s \\ (m_a)_z &= 0 \end{aligned} \right.$$

$$\text{large discs} \left\{ \begin{aligned} (m_a)_s &\approx -\frac{8\mu}{9\delta} \\ (m_a)_{s'} &= -\frac{1}{2}(m_a)_s = (m_a)_z \end{aligned} \right.$$

$$\text{large rods} \left\{ \begin{aligned} (m_a)_s &\approx -\frac{16\mu}{27\delta} \\ (m_a)_{s'} &\approx +\frac{20\mu}{27\delta} \\ (m_a)_z &= -(m_a)_s - (m_a)_{s'} \end{aligned} \right.$$

These values should be multiplied by  $\pi/180$  before being marked on Figure 5, where  $\theta$  is expressed in degrees rather than in radians.

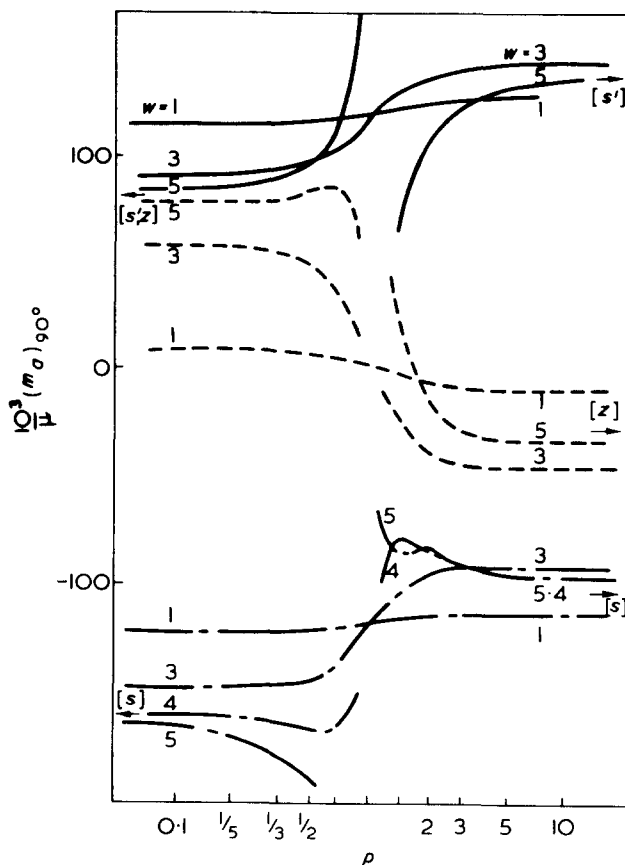


Figure 5 Absolute slope  $(m_a)_{90^\circ}$  for smaller orientation rates as a function of the ellipticity  $\rho$  (decimal logarithmic scale) of anisotropic ( $\delta = 0.1$ ) spheroids and for various values of the size. —,  $\vec{E}_0$  along  $\vec{s}'$ ; ---,  $\vec{E}_0$  along  $\vec{z}$ ; - · - · -,  $\vec{E}_0$  along  $\vec{s}$ . Arrows represent the asymptotic values for larger particles, discs and rods. Identical curves can be obtained for cylinders (except for  $2/3 < \rho < 3/2$ ) For  $\delta = -0.1$ , one has roughly the general shape of the corresponding curves by multiplying the above ones by  $-1$

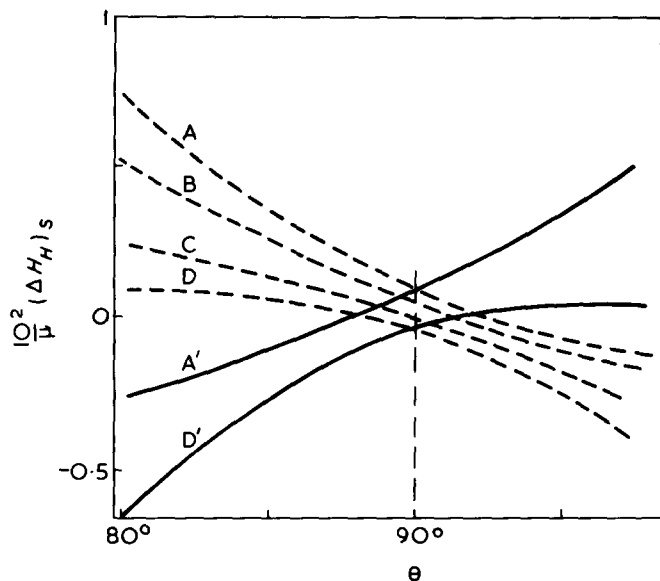


Figure 6 Absolute change  $(1/\mu)(\Delta H_H)_s$  versus  $\theta$  for a spheroid ( $w = 2, \delta = 0.1$ ) and for lower orientation rates. When  $p$  increases from 0.1 to 10, the curvature of the curve changes but the slope at  $\theta = 90^\circ$  has always the same sign. For  $\delta < 0$ , this sign is changed. —,  $\delta = -0.1$ ; ---,  $\delta = +0.1$ .  $p$ : A, A', 0.1; B, 0.8; C, 2.0; D, D', 10.0

For the general case, the slopes have been numerically calculated on a computer, by using the Richardson and Romberg extrapolation method<sup>12</sup>. These exact theoretical results are represented on the curves of Figure 5 (where the slopes are expressed as variations per degree); the following conclusions, valid for  $w < 6$  except for  $\omega \approx 1$ , can be drawn:

$(m_a)_s$  has the sign of  $(-\mu\delta)$ , for any  $\omega$

$(m_a)_s'$  has the sign of  $(+\mu\delta)$ , for any  $\omega$

$(m_a)_z$  has the sign of  $(-\mu\delta\omega)$

As it must be, the absolute slope for small particles is nearly independent of  $p$ .

By measuring the experimental variations of  $H_H$  due to  $E_0$  in the vicinity of  $\theta = 90$ , it is thus easy to determine the sign of  $\mu, \delta$  and  $\omega$ .

All of these conclusions [both for the absolute slope and for the values of  $(\Delta H_H/H_H^0)_{90}$ ] may be ascertained by considering the curves in Figures 6–8.

**Effects of the saturation.** The numerical computations show that the above results remain unchanged for higher electrical field strength,  $E_0$  (until  $\mu = 12$ ). Figure 8 indicates how the various curves are modified when  $|\mu|$  increases from 1 to 10.

#### Study of the relative change $\Delta H_H(\theta)/H_H^0(\theta)$

*A priori* it would have seemed more natural to study the relative changes of  $H_H(\theta)$  as far as experiments are concerned. The present question is to know whether such a study supplies more information and is more fruitful or not than the previous one.

**Slope,  $m_r$ , of the relative change.** Let  $m_r = \{(d/d\theta)[\Delta H_H(\theta)/H_H^0(\theta)]\}_{\theta=90}$  be the relative slope.

For smallest particles ( $w < 1$ )  $m_r$  and  $m_a$  are of the same order of magnitude. The conclusions deduced from  $m_a$  are also valid for  $m_r$ .

For increasing  $w, m_r$  rapidly decreases, and tends to zero for disc-like particles.

For rod-like scatterers, we get:

$$(m_r)_s' \rightarrow -\frac{4}{27} \frac{\mu}{\delta} = -(m_r)_z$$

$$(m_r)_s \rightarrow 0$$

It is then clear that the study of  $m_r$  is much less fruitful than the study of  $m_a$ , as shown by comparison of Figure 5 and Figure 9.

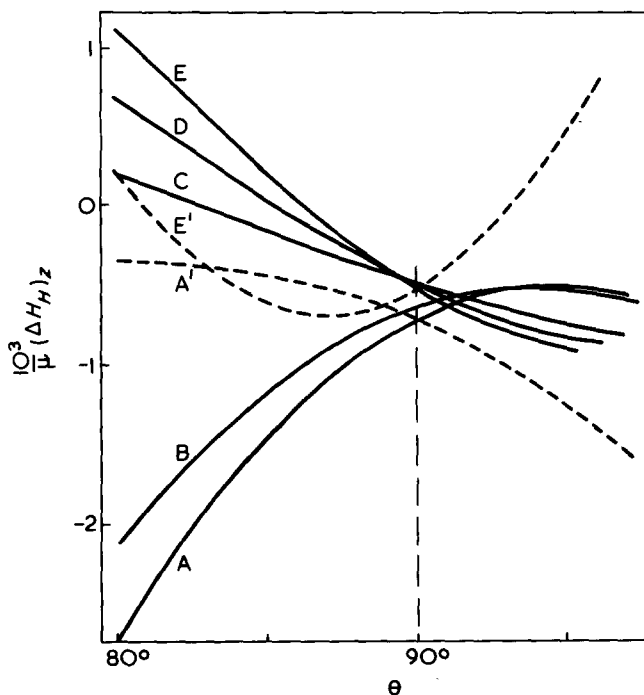


Figure 7 Absolute change  $(1/\mu)(\Delta H_H)_z$  versus  $\theta$  for spheroids ( $w = 2$ ) and for lower orientation rates. —,  $\delta = +0.1$ ; ---,  $\delta = -0.1$ . When  $p$  increases, both the curvature and the slope at  $\theta = \pi/2$  change their sign. This conclusion is still valid for  $\delta$  negative.  $p$ : A, A', 0.1; B, 0.5; C, 2.0; D, 3; E, E', 7

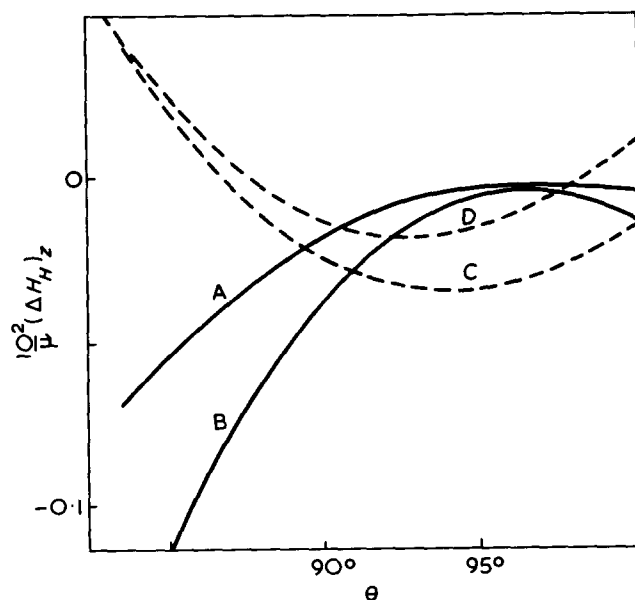


Figure 8 Influence of the electrical saturation on  $(1/\mu)(\Delta H_H)_z$  for spheroids [ $p = 4$  (---) and 0.1 (—),  $w = 4, \delta = 0.1$ ]. The absolute slope keeps always the same sign as  $\mu$  increases: A, -10; B, -0.1; C, 0.1; D, 10

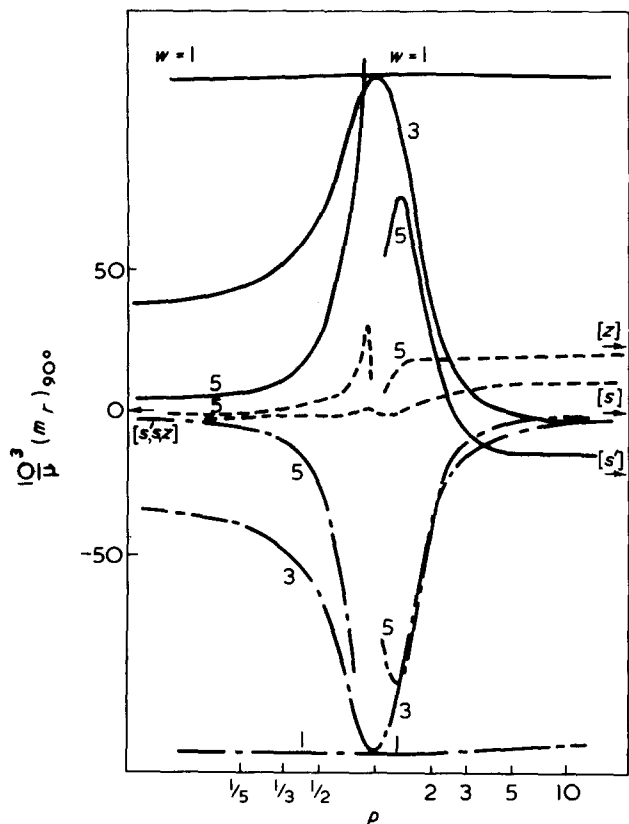


Figure 9 Relative slope  $(m_r)_{90^\circ}$  for smaller orientation rates as a function of the ellipticity  $\rho$  (decimal logarithmic scale) of anisotropic ( $\delta = 0.1$ ) spheroids and for various values of their size. —,  $\vec{E}_0$  along  $\vec{s}$ ; - - -,  $\vec{E}_0$  along  $\vec{s}$ ; - · - ·,  $\vec{E}_0$  along  $\vec{z}$ . Horizontal arrows represent the asymptotic values for larger particles, discs and rods.  $(m_r)_{90^\circ}$  rapidly decreases with  $\rho$  or increasing values of  $w$

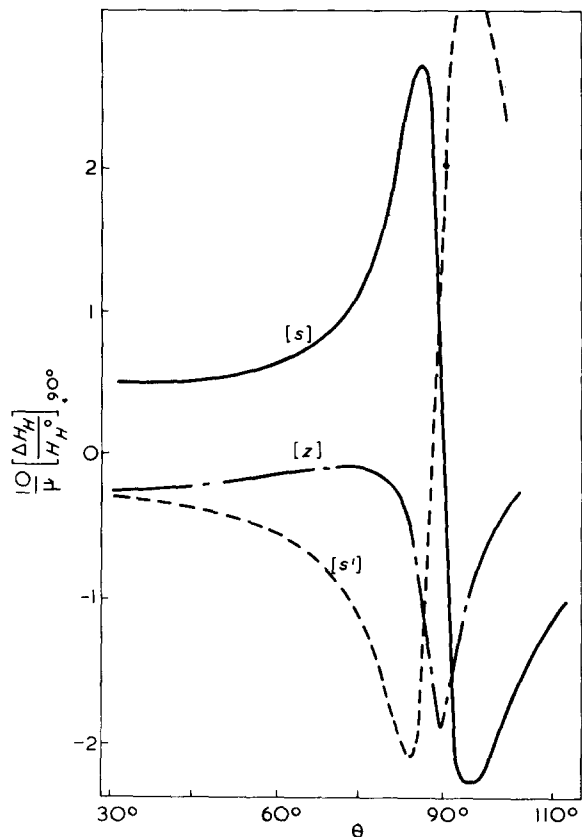


Figure 10 General shape of the relative change  $(1/\mu)(\Delta H_H/H_H^0)$  versus  $\theta$  for small orientation rates. These curves correspond to anisotropic ( $\delta = 0.1$ ) small rods of length  $L$  such that  $2\pi(L/\lambda) = 2$ , and to the three principal directions of the electric field,  $\vec{E}_0: \vec{s}, \vec{s}', \vec{z}$

General shape of the relative curves. In order to avoid tedious descriptions of curves, only some typical results will be presented.

The relative curves  $\Delta H_H(\theta)/H_H^0(\theta)$  generally present very pronounced effects around  $\theta = 90$ : a maximum ( $M$ ) and/or a minimum ( $m$ ) occur near  $\theta = 90$  as shown on the curves of Figure 10. It should be noted that for small disc-like particles without permanent moment ( $\mu \equiv c < 0$ ), the related shapes of relative curves  $(1/\mu)(\Delta H_H/H_H^0)$  are quite similar to those shown in Figure 10.

Let  $\theta_M$  and  $\theta_m$  be the respective angular positions of the maximum  $M$  and the minimum  $m$  which occur near  $\theta = 90$ .

$\vec{E}_0$  directed along  $\vec{s}$ . Whatever  $\omega$  and  $w$ , we have  $\theta_M < \theta_m$  if  $(\mu\delta)$  is positive, and vice versa as shown in Figures 11 and 12, corresponding to various values of the particle sizes. Moreover, the electrical saturation has little effect on the general shape of these curves.

$\vec{E}_0$  directed along  $\vec{s}'$ . We get a similar conclusion, but for  $\mu\delta > 0$ ,  $\theta_m < \theta_M$ .

$\vec{E}_0$  directed along  $\vec{z}$ . The quantity  $(m_r)_z$  very rapidly vanishes (Figure 9) so that in most cases an extremum should be observed for  $(\Delta H_H/H_H^0)_z$  very close to  $\theta = 90$ . For any value of  $\delta$ , this extremum is a maximum if  $\mu < 0$ , and vice versa; in other words, the curves  $(1/\mu)[(\Delta H_H/H_H^0)]_z$  always present a minimum near  $\theta = 90$ . For increasing particle size these last curves are modified as follows:

a maximum rises for  $\theta_M < 90$ , if  $(\delta\omega)$  is positive

it rises for  $\theta_M > 90$ , if  $(\delta\omega)$  is negative (Figure 13)

Electrical saturation has little effect on the general shape of these curves.

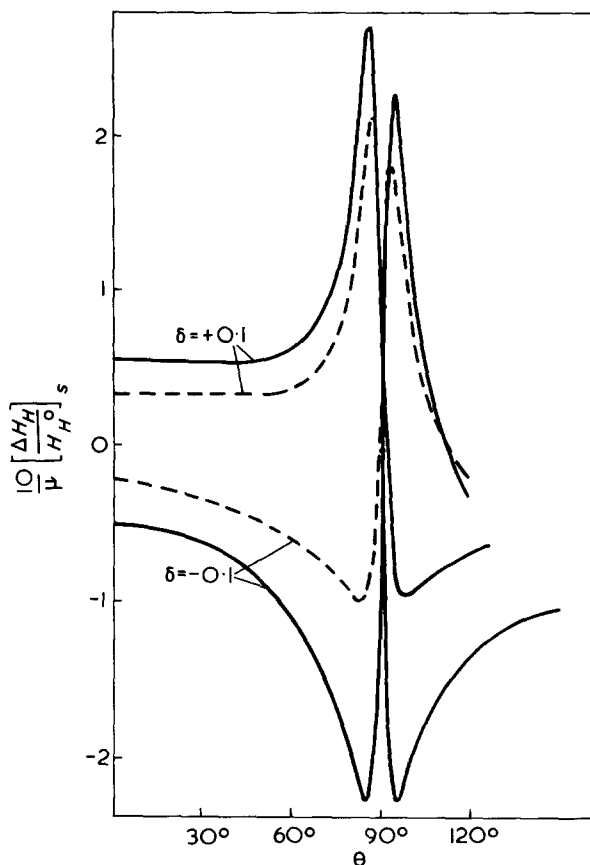


Figure 11 Relative change  $(1/\mu)[(\Delta H_H/H_H^0)]_s$  versus  $\theta$  for a rod of length  $L$  such that  $2\pi(L/\lambda) = 2$ , for two values of  $\delta$  and two values of  $\mu$ : —, 0.1; - - -, 10



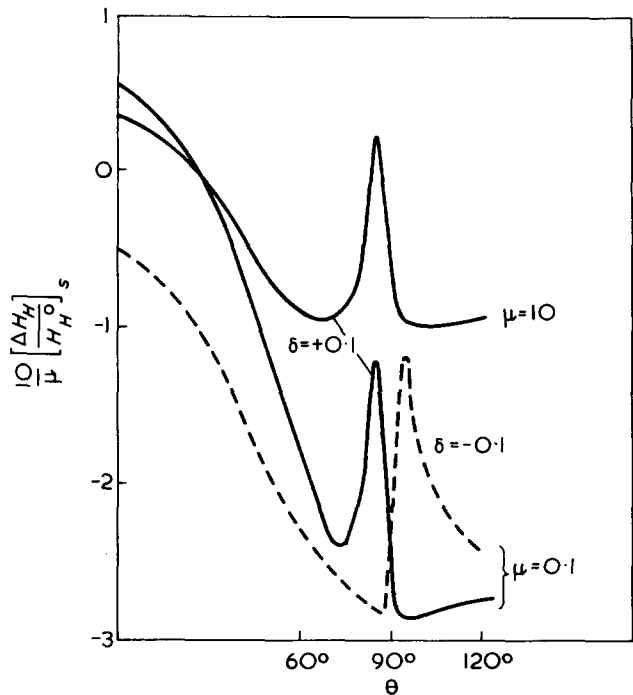


Figure 12 Relative change  $(1/\mu)[(\Delta H_H/H_H^0)]_s$  versus  $\theta$  for a rod such that  $2\pi(L/\lambda) = 6$ , as a function of  $\mu$  and  $\delta$ . (Compare with Figure 11 for the influence of the size.)

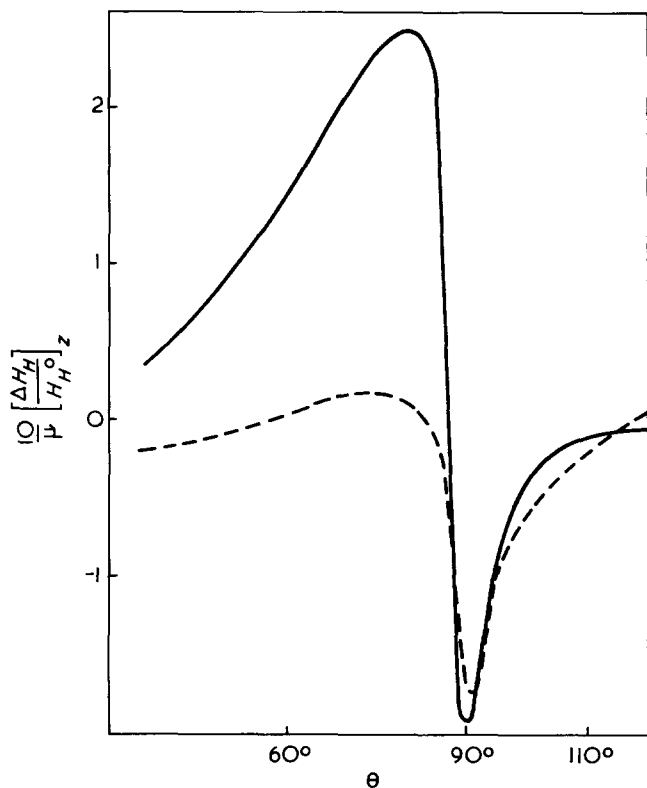


Figure 13 Relative change  $(1/\mu)[(\Delta H_H/H_H^0)]_z$  versus  $\theta$  for two spheroids of different size  $w = 2$  (—) and  $5$  (---). (Small orientation rates).  $\rho = 2$ ;  $\delta = 0.1$

EXPERIMENTAL AND CONCLUSION

As previously stated, the study of the depolarized components of the light scattered by particles, although experimentally difficult because of the weakness of the intensities to be measured, seems to be very suitable for obtaining reliable information concerning geometrical, optical and electrical parameters of the scatterers.

In the present work, it is shown that the study of the

changes of  $H_H(\theta)$  under an electric field is a fruitful method: of particular interest is the study of  $(\Delta H_H)_{z,90}$ , the sign of which is the same as  $(-\mu)$ , for any  $\delta, \omega, w$ , and is not modified by electrical saturation. Likewise studying the absolute slope  $m_a$  is a very sure way to ascertain the sign of  $\delta, \omega$  and  $\mu$ .

An application of this method is given in Figure 14, which represents the absolute change  $\Delta H_H(\theta)$  occurring when tobacco mosaic virus (TMV) (rod-like particle) solutions are subjected to an electric field directed along  $\vec{s}$  or  $\vec{s}'$ . The slopes of the  $s$  and  $s'$  graphs are consistent, as they should be, with positive values of  $\mu\delta$ ; the values of  $[\Delta H(90)]_s$  and  $s'$  are consistent with positive values of  $(\mu\omega)$ , i.e. positive values of  $\mu$ , since  $\omega > 0$  (as expected, and previously shown<sup>1</sup>); as a result,  $\delta$  has a positive value<sup>2</sup>.

As far as relative values of  $\Delta H_H/H_H^0$  are concerned, the following comments can be made (TMV suspensions) (Figures 15 and 16).

$\vec{E}_0$  directed along  $\vec{s}$ . Figures 12, 15 and 17 have the same appearance:  $\Delta H_H$  is negative between  $\theta = 60^\circ$  and  $\theta = 120^\circ$ ; and the angular position of the maximum  $\theta_M$  is about  $86^\circ$ , the minimum occurring for  $\theta_m > 90^\circ$ .

$\vec{E}_0$  directed along  $\vec{s}'$ . Figures 10, 16 and 17 are to be compared (although Figure 10 is related to small particles). Here we have  $\theta_M \approx 100^\circ > \theta_m \approx 86^\circ$  which is also consistent with  $\mu\delta > 0$ .

$\vec{E}_0$  directed along  $\vec{z}$ .  $\Delta H_H$  is probably negative, (i.e.  $\mu > 0$ ) at its minimum. A flat maximum occurs at  $\theta_M \approx 80^\circ < 90^\circ$ , which proves that  $\mu\delta\omega$  is positive.

Such results are then compatible with positive values of

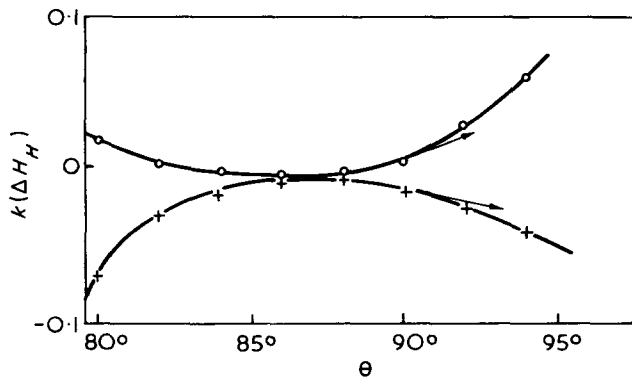


Figure 14 Experimental variation of  $(\Delta H_H)_s$  (+) and  $(\Delta H_H)_{s'}$  (o) as a function of  $\theta$  for tobacco mosaic virus solutions. Electric field strength = 300 V/cm. Frequency = 1000 Hz.  $k$  = arbitrary scale factor

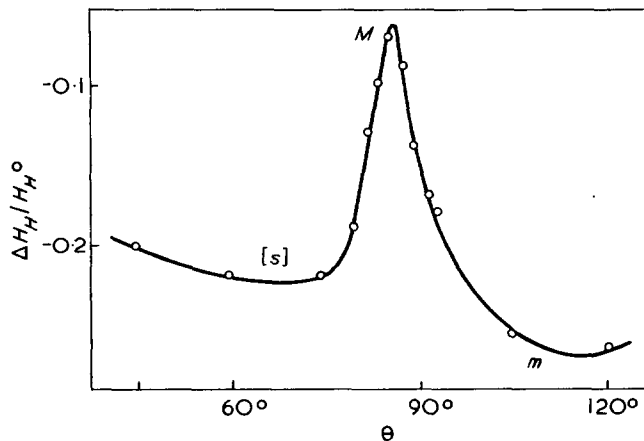


Figure 15 Experimental relative variation of  $H_H$  obtained for TMV when the electric field direction is along  $s$ , versus  $\theta$ ; electric field strength = 300 V/cm; frequency = 1000 Hz

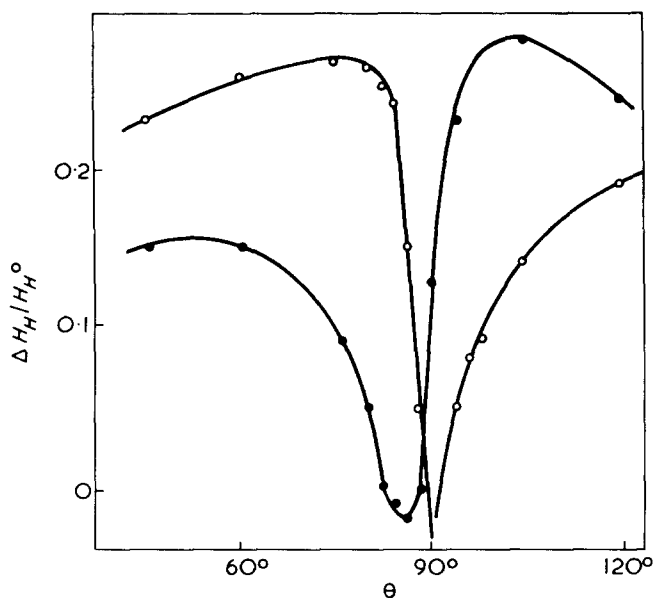


Figure 16 Experimental variation of  $(\Delta H_H/H_H^0)_{s'}$  (●), and  $(\Delta H_H/H_H^0)_z$  (○) as a function of  $\theta$  for TMV. Electric field strength = 300 V/cm; frequency = 1000 Hz

$\mu$ ,  $\delta$ ,  $\omega$  and illustrate in a very satisfactory manner the theoretical relations of the present paper.

Other experiments have been carried out on carbon black suspensions; the results are also consistent with the theory and will be presented elsewhere.

## REFERENCES

- 1 Ravey, J. C. and Mazon, P. *Polym. J.* 1974, **6**, 279
- 2 Ravey, J. C., Mazon, P. and Sere, Y. *Polymer* 1974, **15**, 77
- 3 Ravey, J. C. *Eur. Polym. J.* 1972, **8**, 937; 1973, **9**, 47
- 4 Ravey, J. C. and Mazon, P. *J. Macromol. Sci. (B)* 1974, **10**, 271
- 5 Kielich, S. *Acta Phys. Polym.* 1969, **36**, 495
- 6 Benoit, H. *Ann. Phys. (Paris)* 1951, **6**, 561; *J. Chem. Phys.* 1952, **49**, 517
- 7 Stoylov, S. P. *Adv. Colloid Interface Sci.* 1971, **3**, 51
- 8 Plummer, H. and Jennings, B. R. *J. Chem. Phys.* 1969, **50**, 1033
- 9 Tinocco, I. and Yamaoka, K. *J. Phys. Chem.* 1959, **63**, 423
- 10 Ravey, J. C. *Thèse Université Nancy* (1973)
- 11 Ravey, J. C. *J. Chim. Phys.* 1970, **67**, 1787
- 12 Filippi, S. and Engels *Elektron. Datenverarb.* 1966, (2), 57

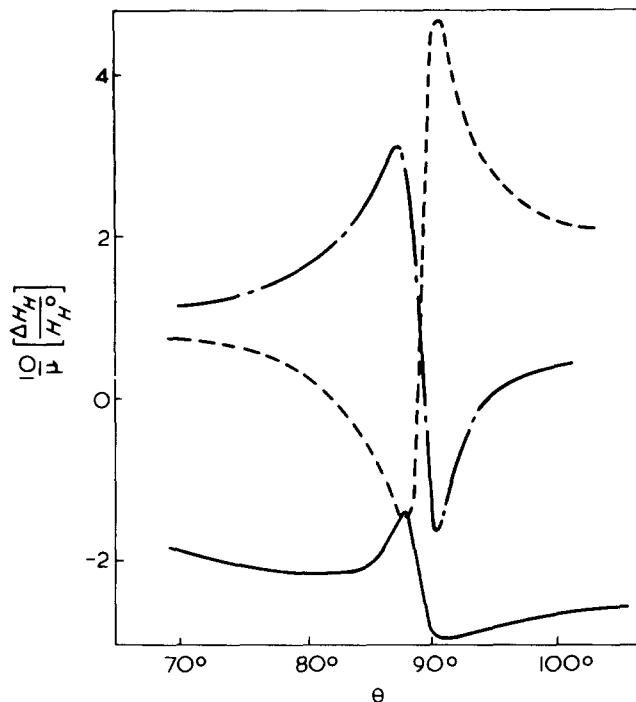


Figure 17 Theoretical relative variations of  $\Delta H_H/H_H^0$  on  $\vec{s}^-$  (—),  $\vec{s}'$  (---) and  $\vec{z}$  (-·-·-) versus  $\theta$  for rod-like particles;  $\delta = 0.03$ ;  $4\pi\rho/\lambda = 3$

## APPENDIX

The following functions are used in relation (7):

$$J_k^p = \frac{(2p)!k!(k+p)!2^{2k+1}}{p!(2p+2k+1)!}$$

$$G_k^p = \frac{(2p)!(2k)!}{2^{2p+2k+1}p!k!(p+k)!}$$

$P_0$  is the interference factor of a sphere of radius,  $a$ :

$$P_0 = \frac{9\pi}{2} \left[ \frac{\mathcal{F}_{3/2}(ha)}{(ha)^{3/2}} \right]^2$$

$$P_0' = \frac{9\pi}{2} \frac{\mathcal{F}_{3/2}(ha)\mathcal{F}_{5/2}(ha)}{(ha)^2}$$

where  $\mathcal{F}_{3/2}$  and  $\mathcal{F}_{5/2}$  are Bessel functions and  $h = (4\pi/\lambda) \sin \theta/2$ .

# N.m.r. studies of butadiene – styrene copolymers

A. L. Segre, M. Delfini and F. Conti

*Istituto Chimico dell'Università di Roma, 00185 Roma, Italy*

and A. Boicelli

*Laboratorio CNR, Ozzano Emilia, Bologna, Italy*

(Received 29 April 1974)

An analysis of the  $^{13}\text{C}$  nuclear magnetic resonance spectra of copolymers of butadiene–styrene, both block or random type, shows the possibility of observing the microstructure of the copolymers themselves. The microstructure of the copolymers was analysed in terms of triads of monomeric sequences. The units present in the copolymers are of the type: *trans*-1,4-butadiene, *cis*-1,4-butadiene, 1,2-butadiene and styrene. An assignment for all the experimental bands observed is proposed on the basis of correlation with homopolymers as well as on the basis of the frequencies for the single triads, calculated by additivity rules.

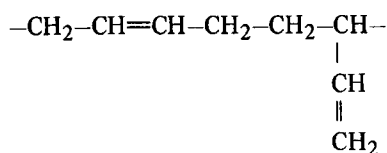
## INTRODUCTION

In the sphere of characterization of butadiene–styrene copolymers, until now no exhaustive analysis of the microstructure of the polymeric chains in terms of the distribution of monomeric sequences has been carried out. In the case of SB or SBS copolymers, a differentiation was made on the basis of different ways of preparation<sup>1</sup>. Only scant knowledge of the microstructure of the block or random copolymers has been obtained, even with the help of proton nuclear magnetic resonance (n.m.r.) spectroscopy<sup>2</sup>, for other types of comonomer,  $^1\text{H}$  n.m.r. gave definite information regarding the polymeric chain microstructure<sup>3</sup>. We have studied certain types of butadiene–styrene copolymers using  $^{13}\text{C}$  n.m.r. and the results obtained are given here.

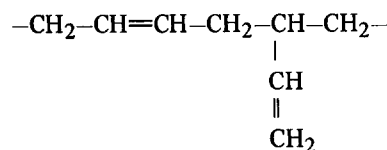
### Mechanism of copolymerization

The addition of a butadiene monomeric unit to a polymeric chain in growth can occur in the 1,4-position or across the double bond (1,2-).

In the case of the 1,4- addition the butadiene unit can be in a *cis* or *trans* configuration. In the case where the polymeric chain in growth ends with a 1,4- unit the addition of a 1,2-unit can result in two ways:



or

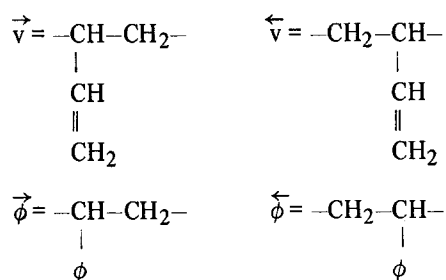


while if the chain in growth ends with a 1,2-unit the addition of another 1,2-unit takes place regularly.

With regard to the butadiene units which can be *cis*-1,4-, *trans*-1,4 or 1,2-, the styrene residues can attach themselves either by the head ( $-\text{CH}_2-\text{C}(\phi)\text{H}-$ ) or by the tail ( $\phi-\text{CH}-\text{CH}_2-$ ), resulting in different sequences; i.e. with respect to the last growing unit the entering styrene monomeric unit can present itself either with its head or its tail.

The great sequential multiplicity which can result from the different possible combinations is therefore evident.

To simplify the notation and to keep in mind all the combinations we mark differently the units which can present themselves by the head and by the tail, i.e.:



and with *c* and *t* respectively the 1,4-units in a *cis* or *trans* configuration.

The number of possible triads is  $6^3 = 216$ , each of which will give rise to two resonances, which might or might not be different as far as the backbone carbon atoms are concerned.

As a matter of fact, considering that due to the steric hindrance,  $\overleftarrow{\phi}\vec{v}$  additions do not seem very likely and, as will be seen, have not been observed, and considering that the  $\vec{v}\vec{v}$  and  $\overleftarrow{\phi}\overleftarrow{\phi}$  additions are not present in the homopolymers<sup>4,5</sup> the number of possible triads is reduced to 152, each of which must be considered twice, owing to the fact that in the backbone, whichever monomeric unit is considered, this has two saturated carbon atoms.

Calculation of the backbone  $^{13}\text{C}$  chemical shifts

All the central units of possible triads give rise to two n.m.r. signals, corresponding to the saturated carbon atoms of the backbone. However, the two signals in certain cases can be coincidental by symmetry.

The assignment of different resonance signals to the possible sequences has been done either by direct comparison with corresponding homopolymers expressly prepared, or by calculating the chemical shifts relative to various groups according to additivity rules<sup>6</sup>, i.e. adding the contributions relative to  $\alpha$ ,  $\beta$  and  $\gamma$  positions. Contributions relative to the  $\delta$  position and those that follow have been neglected. Obviously no steric effect can be kept in consideration with this type of approach.

By using the data relative to homopolymers, considered as model compounds, it has been possible to evaluate the contributions relative to  $\alpha$ ,  $\beta$  and  $\gamma$  positions of various groups.

In fact, if model compounds, such as octene, heptene etc. for the vinyl contribution, and ethyl benzene, butyl benzene etc., for the phenyl contribution, are used, the calculated values for the spectra relative to homopolymers show a very poor fit.

On the contrary, values for  $\alpha$ ,  $\beta$  and  $\gamma$  contribution for *cis* and *trans* double bond in the backbone, are consistent with the values obtained by Roberts *et al.*<sup>7</sup>.

In order to obtain the vinyl group contribution we carefully studied various polymers of butadiene (with different content of 1,2-, *cis*-1,4- and *trans*-1,4-units, so that the vinyl contributions on the polymeric chain were obtained\*.

A study of the same type has been done on polystyrene, in order to ascertain the phenyl contribution on the backbone carbon atoms. Finally, branching corrections as indicated by Grant and Paul<sup>8</sup> were added.

The polyethylene chemical shift, 29.9 ppm from tetramethylsilane (TMS), was chosen as starting point, in which all  $\text{CH}_2$  contributions must be considered nil.

The values for the contributions are:

Starting chemical shift	29.9 ppm
Corrections for $\text{CH}_2$ ( $\alpha = \beta = \gamma$ etc. = 0)	
Corrections for CH tertiary saturated	$\alpha = -2.5$ $\beta = 0$ $\gamma = 0$
Contribution for a <i>cis</i> double bond	$\alpha = -2.5$ $\beta = 0$ $\gamma = -0.5$
Contribution for a <i>trans</i> double bond	$\alpha = +3.0$ $\beta = 0$ $\gamma = -0.5$
Contribution for a vinyl group	$\alpha = 13.5$ $\beta = 8.4$ $\gamma = -2.4$
Contribution for a phenyl group	$\alpha = 18.9$ $\beta = 7.9$ $\gamma = -2.2$

Thus it is possible to calculate the values of chemical shifts relative to different C atoms in the different triads, and these values can be compared with the observed peaks experimentally.

## Calculation of the intensities (random copolymers)

Let us consider now the case of a random copolymer. If  $p_i$  = probability of the  $i$ th monomer and  $n_i$  = percentage of the  $i$ th monomer,  $\delta_{ij} = 1$  or 0, where  $\delta_{ij}$  is zero only if  $\overleftarrow{i} \overrightarrow{j}$ ,  $\overleftarrow{i} \overleftarrow{i}$  or  $\overrightarrow{i} \overrightarrow{i}$ , otherwise it is 1. Then with this notation, the probability  $\Phi_{ij}$  of a diad  $ij$  is:

$$\Phi_{ij} = \frac{p_i p_j \delta_{ij}}{\sum p_i p_j \delta_{ij}}$$

Thus, in the case of random copolymers, knowing the different percentages  $n_i$ , it is possible to compare the experimental and calculated intensities.

The latter are coincidental with the triad probabilities themselves:

$$\Phi_{\text{triad } ijk} = \frac{n_i n_j n_k \delta_{ij} \delta_{jk}}{\sum_{i,j,k} n_i n_j n_k \delta_{ij} \delta_{jk}} \quad (1)$$

and clearly:  $n_{\overrightarrow{\phi}} = n_{\overleftarrow{\phi}} = 1/2 n_{\phi}$  and  $n_{\overrightarrow{v}} = n_{\overleftarrow{v}} = 1/2 n_v$ . The quantitative determination of  $n_{\phi}$ ,  $n_v$ ,  $n_c$  and  $n_t$  is possible by running both the  $^1\text{H}$  and  $^{13}\text{C}$  n.m.r. spectra. In the proton spectrum three groups of resonances are present, with chemical shift values of  $\sim 7$ ,  $\sim 5.5$  and  $\sim 1.5$  ppm from TMS, respectively, from aromatic groups, vinyl and vinylic groups, and aliphatic groups. If A = percentage of styrene units, B = percentage of 1,4-polybutadiene units ( $c + t$ ), C = percentage of 1,2-polybutadiene units, then peak at 7 ppm = 5A, peak at 5.5 ppm = 2B + 3C, and peak at 1.5 ppm = 4B + 3C + 3A from which it is easy to obtain A, B and C<sup>9</sup>. In order to obtain  $n_c$  and  $n_t$ , these can easily be obtained from the  $^{13}\text{C}$  spectrum, by considering the peaks at 130.75 and 130.25 ppm from TMS, respectively due to *trans* and *cis* double bonds<sup>10</sup>. The use of the peaks at 27.4 and 32.7 ppm, relative to ethylene groups adjacent to a *cis* or *trans* double bond (see ref 10 and references quoted therein), is not a good choice, because, in that range of the spectrum, in the copolymers, there is a very large number of peaks, which partially overlap.

Finally, by considering that  $\overrightarrow{v}$  and  $\overleftarrow{v}$  are equally populated, as well as  $\overrightarrow{\phi}$  and  $\overleftarrow{\phi}$ , it is possible to obtain the following resolution:

$$\left. \begin{array}{l} n_{\overrightarrow{\phi}} = n_{\overleftarrow{\phi}} = A/2 \\ n_{\overrightarrow{v}} = n_{\overleftarrow{v}} = C/2 \\ n_{\text{cis}} + n_{\text{trans}} = B \\ n_{\text{cis}}/n_{\text{trans}} = \frac{\text{peak at } 130.25}{\text{peak at } 130.75} \end{array} \right\} \begin{array}{l} ^1\text{H spectrum} \\ ^{13}\text{C spectrum} \end{array}$$

from which it is possible to get the values of equation (1) giving  $\Phi_{ijk}$ .

Thus it is possible to compare experimental and calculated intensities for a random copolymer.

## EXPERIMENTAL

We studied four copolymers whose preparation was as follows.

Sample A: block copolymer SB type. Catalyst, n-butyl-Li. Adiabatic reaction between 50°C and 115°C.

Sample B: random copolymer. Catalyst, n-butyl-Li/

\* Note added in proof – Conti, F., Delfini, M., Segre, A. L., Pini, D. and Porri, L. *Polymer* 1974, 15, 816

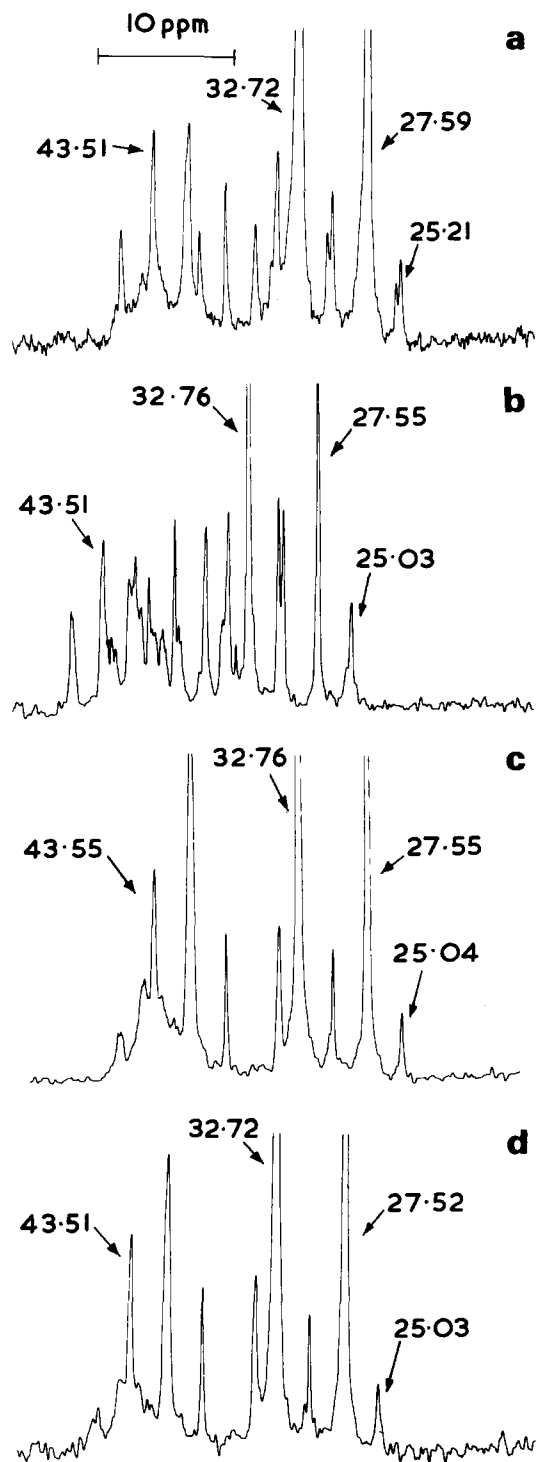


Figure 1 Spectra of samples (a) A, (b) B, (c) C and (d) D in the upper field range. Shift values are given in Table 1

tetrahydrofuran. Adiabatic reaction between 50°C and 110°C.

Sample C: block copolymer SB type. Catalyst, n-butyl-Li/tetrahydrofuran. Adiabatic reaction between 50°C and 95°C.

Sample D: same as C but different composition.

The analysis in terms of percentages of composition of units in the copolymer (by <sup>1</sup>H and <sup>13</sup>C n.m.r. spectra) is given below. A: styrene, 16.0; 1,2-butadiene, 11.2; *cis*-1,4-butadiene, 30.5; *trans*-1,4-butadiene, 42.3. B: styrene, 16.0; 1,2-butadiene, 26.0; *cis*-1,4-butadiene, 19.0; *trans*-1,4-butadiene, 39.0. C: styrene, 28.2; butadiene, 9.0; *cis*-1,4-butadiene, 24.9; *trans*-1,4-butadiene, 37.9. D: sty-

rene, 20.9; 1,2-butadiene, 8.0; *cis*-1,4-butadiene, 28.8; *trans*-1,4-butadiene, 42.3.

The butadiene-styrene ratio has been verified by elemental analysis.

<sup>13</sup>C n.m.r. spectra have been run on 10% (by wt) solution in CDCl<sub>3</sub>, with TMS as an internal reference and under the following conditions: pulse width, 9 μsec; repetition, 1.1 sec; data points, 8 K; frequency range, 4 K. The spectrometer was a Jeol PFT 100.

## RESULTS AND DISCUSSION

Spectra relative to different samples of styrene-butadiene copolymers are reported in Figures 1 and 2.

The chemical shift values, relative to the observed resonances in different samples of copolymers as well as homopolymers, are reported in Tables 1 and 2 together with the relative normalized intensities. Finally in Table 3 the calculated values are reported together with different assign-

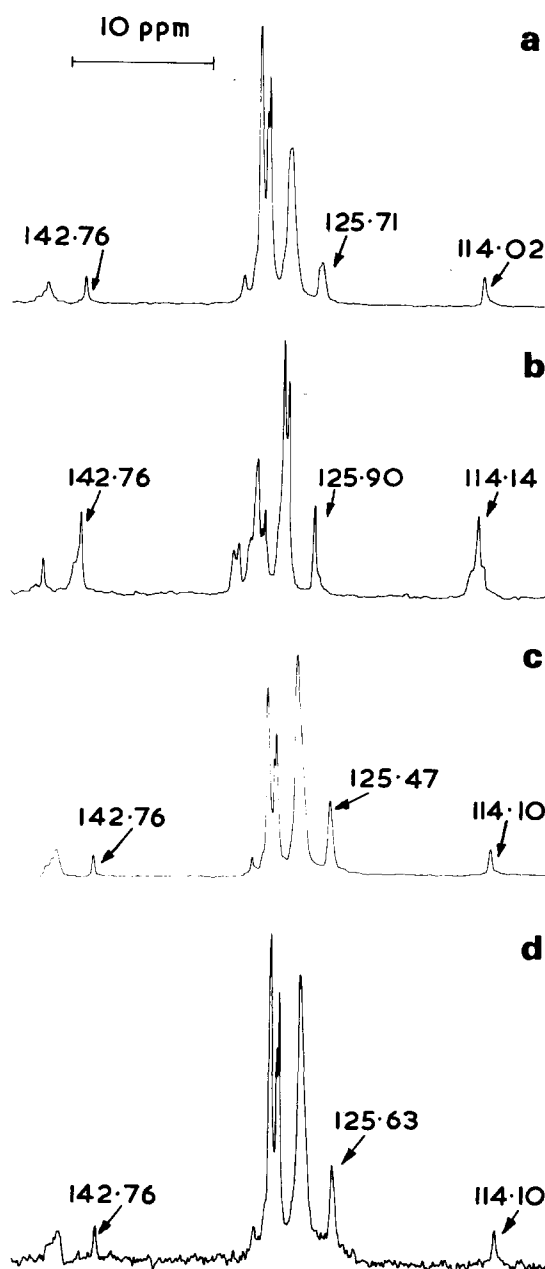


Figure 2 Spectra of samples (a) A, (b) B, (c) C and (d) in the lower field range. Shift values are given in Table 2

Table 1

Peak No.	A		B		C		D		Atactic polystyrene exp. frequency (ppm)
	Exp. frequency (ppm)	Intensity	Exp. frequency (ppm)	Intensity	Exp. frequency (ppm)	Intensity	Exp. frequency (ppm)	Intensity	
1	25.21	0.87	25.03	2.37	25.04	0.85	25.03	0.62	
2	25.42	0.47	25.38	0.47	—	—	—	—	
3	27.59	33.45	27.55	11.66	27.55	29.12	27.52	32.85	
4	30.15	2.05	30.15	5.04	30.19	2.27	30.16	2.04	
5	30.50	1.33	30.51	5.40	—	—	—	—	
6	—	—	32.33	1.87	—	—	—	—	
7	32.72	45.91	32.76	23.27	32.76	44.05	32.72	47.04	
8	—	—	33.65	1.15	—	—	—	—	
9	34.31	2.72	34.23	4.99	34.23	2.80	34.23	2.81	
10	—	—	34.56	1.86	—	—	—	—	
11	35.90	1.47	35.86	4.57	—	—	—	—	
12	—	—	37.72	1.21	—	—	—	—	
13	—	—	37.88	1.69	—	—	—	—	
14	38.15	2.20	38.19	4.76	38.19	2.65	38.15	2.57	
15	—	—	38.89	0.92	—	—	—	—	
16	—	—	39.05	1.58	—	—	—	—	
17	—	—	39.60	1.62	—	—	—	—	
18	—	—	39.83	1.62	—	—	—	—	
19	40.09	1.34	40.09	3.09	—	—	—	—	
20	40.67	3.18	40.68	2.21	40.80	7.89	40.76	5.24	40.76
21	—	—	41.14	3.69	—	—	—	—	
22	—	—	41.51	3.03	—	—	—	—	41.49
23	—	—	—	—	42.15	1.05	—	—	42.15
24	—	—	42.62	1.05	—	—	—	—	
25	—	—	42.93	1.35	43.00	1.41	42.91	0.89	43.01
26	43.51	3.04	43.51	4.17	43.55	4.06	43.51	3.63	44.25
27	44.36	0.59	—	—	44.33	1.59	44.23	0.96	44.44
28	—	—	45.82	1.91	—	—	—	—	45.11
29	45.96	1.35	45.92	2.09	46.00	0.77	45.91	0.51	45.96
30	—	—	—	—	46.35	0.77	46.10	0.44	46.28

Table 2 Low field spectra

	D		C		B		A		
	ppm	Intensity	ppm	Intensity	ppm	Intensity	ppm	Intensity	
A	146.18	0.69	146.18	1.12	146.20	0.55	—	—	C. quat. arom. seq. $\phi\phi\phi$
B	145.75	1.39	145.79	1.95	145.70	1.26	—	—	C. quat. arom. seq. $\phi\phi\phi$
C	145.40	2.02	145.45	2.95	145.51	1.70	145.51	2.34	C. quat. arom. seq. $\phi\phi\phi$ + $\phi$ interspersed between 1,4-units
D	—	—	—	—	—	—	143.30	2.03	$C_{\beta}$ between 1,2- and $\phi$ -units
E	142.76	2.45	142.76	2.24	142.76	2.34	142.76	6.10	$C_{\beta}$ between 1,4- units
F	—	—	—	—	—	—	131.77	3.09	C=C
G	131.30	2.34	131.34	2.17	131.34	2.64	131.38	3.64	C=C
H	—	—	—	—	—	—	130.53	4.10	C=C
I	130.06	26.00	130.10	22.26	130.10	26.72	130.10	10.33	$ttt + 1/2ttt + 1/2 - ctt + ctc$
L	129.67	16.99	129.67	13.75	129.67	18.43	129.67	4.85	$ccc + 1/2cct + 1/2tcc$
M	129.48	20.74	129.48	16.48	129.52	21.60	129.51	6.28	$tct + 1/2cct + 1/2tcc$
N	—	—	—	—	—	—	128.55	5.03	
O	—	—	—	—	—	—	128.20	19.63	ortho
P	127.96	18.88	128.00	26.04	128.00	14.81	127.84	16.44	meta and ortho
Q	—	—	—	—	125.85	3.59	—	—	
R	125.63	5.91	125.47	8.44	125.71	3.74	125.89	6.65	para
S	—	—	—	—	—	—	114.61	1.64	$C_{\alpha}$
T	114.10	2.59	114.10	2.60	114.02	2.54	114.14	5.93	$C_{\alpha}$
U	—	—	—	—	—	—	113.71	1.97	$C_{\alpha}$

ments in term of triads relative to all observed resonance peaks.

Interesting considerations of the different spectral assignments, follow from an analytical inspection of all resonance lines.

1. Peak at 25.07 ppm. Present in all copolymer samples. Present also in homopolymers of butadiene containing 1,2-units and *cis*-1,4-units. It is due to the  $\gamma$  effect of a vinyl group on a *cis*-1,4-unit.

2. Peak at 25.40 ppm. Present in samples A and B. By analogy with the attribution of peak 1, this peak is attribut-

ed to the  $\gamma$  effect of a phenyl group on *cis*-1,4-units. This attribution is supported by the lack of this peak in block samples C and D, where these sequences ought to be extremely low.

3. Peak at 27.55 ppm. Present in all copolymer samples, it has also been observed by Grant<sup>11</sup> in homopolymers of butadiene in a *cis*-1,4-configuration. All sequences, having a central *cis*-1,4-unit and to which the neighbouring contribution has no effect, should give rise to this signal.

4. Peak at 30.16 ppm. Present in all copolymer samples. Present also in homopolymers of butadiene containing



polymer and tentatively assigned to sequences with a central vinyl surrounded by a vinyl and a neighbouring styrene.

13. *Peak at 37.88 ppm.* Present only in the random copolymer. Attributed to the  $\beta$  effect of a phenyl group on *trans*-1,4-units. The assignment of peaks 12 and 13 can be switched.

14. *Peak at 38.17 ppm.* Present in all copolymer samples, as well as in a homopolymer of 1,2-polybutadiene containing *trans*-1,4-units. It is attributed to ethylenes of *trans*-1,4-units with a vinyl group in  $\beta$  position.

15. *Peak at 38.89 ppm.* Tentatively assigned to methines of vinyl units interspersed between neighbouring styrene units. It has been observed only in the random copolymer.

16. *Peak at 39.05 ppm.* Present only in the random copolymer; tentatively assigned to methines in  $\vec{v} \vec{v} \vec{\phi}$  sequences.

17. *Peak at 39.60 ppm.* Present only in the random copolymer; the assignment again is only a tentative one, owing to the fact that this peak is very near and has the same intensity of peak 18. Assignments of peaks 17 and 18 can be interchanged. It is tentatively attributed to the CH<sub>2</sub> group between two neighbouring styrenes adjacent to 1,4-units. May also be due to the CH of two 1,2-units adjacent to 1,4-units.

18. *Peak at 39.83 ppm.* Present only in the random copolymer. Tentatively assigned to a CH<sub>2</sub> group between two neighbouring styrenes adjacent to a 1,2-unit. Plus probably the CH groups of sequences of the type (1,4-)/(1,2-)/(styrene) (see Table 3).

19. *Peak at 40.09 ppm.* Present only in the random copolymer. It might be due to sequences of the type (1,4-)/(1,2-)/(styrene). The assignment is mainly due to the calculated and experimental intensities of this peak.

20. *Peak at 40.73 ppm.* Present in all the copolymers and due to the CH<sub>2</sub> groups of styrene blocks. It is also present in polystyrene (see Table 1 and Figure 3).

21. *Peak at 41.14 ppm.* Present in the random copolymer (at high vinyl content) and also in a 1,2-polybutadiene sample containing 1,4-type units (*cis* and *trans*). From off

resonance experiments this peak is mainly due to CH<sub>2</sub> groups. It is attributed to two 1,2-units, neighbouring 1,4-units. It might also be due to mixed sequences of CH groups of 1,2-units having in the  $\gamma$  position either a vinyl group or a phenyl group (see Table 3). Assignment among bands 21 and 22 which might be and probably are, mixed together.

22. *Peak at 41.51 ppm.* Present only in the random copolymer. It must be observed that many calculated sequences lie between 41.2 and 41.7 ppm (see Tables 1 and 3). All these sequences should give rise to peaks 21 and 22. The attribution of these two bands is quite reliable as a whole, but we do not know which sequences contribute to peak 21 and which ones to peak 22. The total assignment of the sum of peaks 21 and 22 as shown in Table 3 is in satisfactory agreement with the experimental data.

23. *Peak at 42.15 ppm.* Present only in sample C (block copolymer with high styrene content). It is present in the spectrum of atactic polystyrene as one of the peaks in which the CH signal is split due to configurational effect. It is attributed to polystyrene blocks (see Figure 3).

24. *Peak at 42.62 ppm.* Present only in the random copolymer. Its intensity is very weak. Tentatively it is assigned to 1,2-units interspersed between styrene units. As another tentative assignment it might be due to the methines of  $\vec{\phi} \vec{v}$  sequences. This last assignment must be considered solely a tentative one.

25. *Peak at 42.98 ppm.* Present in copolymers B, C and D and in the spectrum of atactic polystyrene. It is attributed to polystyrene blocks. It might also be due (low probability) to styrene adjacent to 1,2-units.

26. *Peak at 43.52 ppm.* Present in all copolymer samples. Present in 1,4-polybutadiene containing low percentages of 1,2-units, in which off resonance experiments demonstrate that it is due to the superimposition of CH and CH<sub>2</sub> resonances. It is attributed to the CH of 1,2-units interspersed between 1,4-units and also to the CH<sub>2</sub> groups of units of the type 1,4-, 1,2-.

27. *Peak at 44.26 ppm.* Present in copolymers B, C and D and in atactic polystyrene. Attributed to CH of polystyrene blocks (see Figure 3).

28. *Peak at 45.82 ppm.* Present only in the random copolymer. By comparison of the intensities it might be due to a set of mixed sequences as shown in Table 3. This assignment is only a tentative one.

29. *Peak at 45.95 ppm.* Present in all copolymer samples. Present also in the atactic polystyrene. It is due to polystyrene blocks. Moreover, it might be due to other sequences (see Table 3), which present a calculated chemical shift in reasonable agreement.

30. *Peak at 46.22 ppm.* Present only in samples C and D. Present in atactic polystyrene. Attributed to polystyrene blocks (see Figure 3).

No peak has been assigned to the CH groups relative to sequences of the type  $\vec{c\phi v}^*$ ,  $\vec{t\phi v}^*$ ,  $\vec{v\phi t}^*$ ,  $\vec{v\phi c}^*$  (calculated at 48.8) because any assignment would have been absolutely hypothetical. Sequences  $\vec{v v v}$  and  $\vec{v v v}$ , of which the chemical shift values, both for CH and CH<sub>2</sub>, were known, were not found.

It must be remarked that sequences  $\vec{\phi \phi}$  or  $\vec{\phi v}$  not considered in this analysis, have calculated values higher than 60 ppm; no peak higher than 46 ppm has been observed. The use of additivity rules has no meaning in the spectral range between 110 and 150 ppm. In this range, assignments have been made only on direct comparison with homopolymers. Assignments as well as experimental values are reported in Table 2.

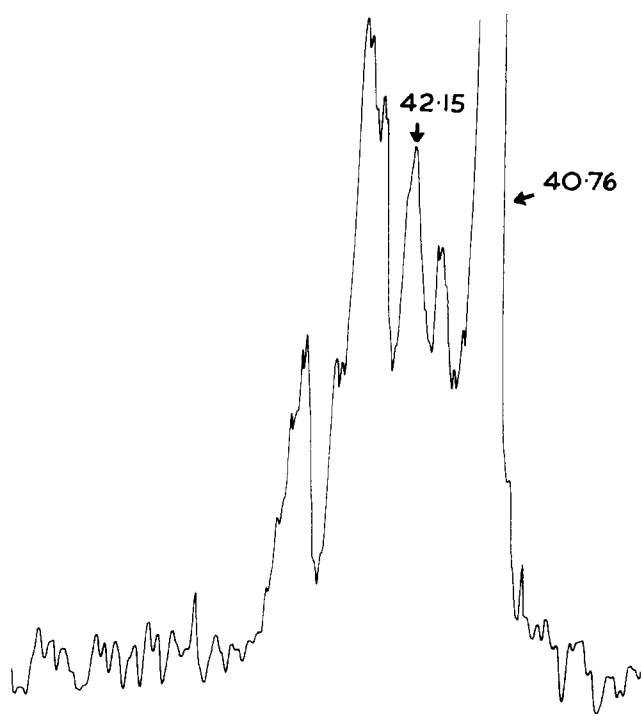


Figure 3 Spectrum of an atactic high molecular weight polystyrene sample, upper field range; shift values are given in Table 1



Bands A, B, C, P and R have been assigned on the basis of the results obtained on polystyrene: A, B, C, aromatic quaternary carbon atom; P, *meta* and *ortho*; R, *para*.

It must be observed that the P peak is a very broad one, as observed in samples B, C and D and in high molecular weight atactic polystyrene; while it is split in sample A. In this sample the O peak is assigned to C atoms in an *ortho* position, while the P peak is assigned to the *meta* positions; the N peak is probably due to styrene, but is probably dependent on the sequences.

Peaks I, L and M belong to sequences due to 1,4-butadiene.

Peaks D, E, S, T and V are also present in the spectrum of 1,2-polybutadiene and in samples of 1,4-polybutadiene containing small percentages of 1,2-units; these peaks can be assigned to vinyl groups. In the random sample these peaks are partly split probably due to the presence of different sequences. Peak G, present in all copolymers, is due to vinylic groups of 1,4-units adjacent to 1,2-units.

Peaks F and H might be due (tentative) to vinylic carbon atoms of 1,4-units adjacent to styrene units.

## CONCLUSION

From the reported results the possibility of obtaining information on the distribution of comonomers in chains of copolymers of the SB type is evident. These data, even if not strictly quantitative, give us a knowledge of the microstructure of polymer chains, that can be considered a base for a more rational correlation with technological

properties of this important class of copolymers.

With regards to this, we are studying polymers of the SBS type, polymers at very different content of comonomers and polymers prepared with different catalysts.

## ACKNOWLEDGEMENT

The authors thank Professor L. Porri for the preparation of polybutadiene samples.

## REFERENCES

- 1 Bishop, E. T. and Davison, S. *J. Polym. Sci. (C)* 1969, **26**, 59
- 2 Mochel, V. D. and Claxton, W. E. *J. Polym. Sci. (A-1)* 1971, **9**, 345
- 3 Bovey, F. A. 'High Resolution NMR of Macromolecules', Academic Press, New York, 1972
- 4 Natta, G. *Makromol. Chem.* 1960, **35**, 94
- 5 Natta, G. *Rubb. Plast.* 1957, **38**, 495; Natta, G., Corradini, P. and Porri, L. *Atti Accad. Naz. Lincei* 1956, **20**, 728; Natta, G., Porri, L., Corradini, P. and Morero, D. *Atti Accad. Naz. Lincei* 1956, **20**, 560
- 6 Levy, G. C. and Nelson, G. L. 'Carbon-13 Nuclear Magnetic Resonance for Organic Chemists', Wiley-Interscience, New York, 1972, Ch 3
- 7 Dorman, D. E., Jautelat, M. and Roberts, J. D. *J. Org. Chem.* 1971, **36**, (19), 2757
- 8 Grant, D. M. and Paul, E. G. *J. Am. Chem. Soc.* 1964, **86**, 2984
- 9 Morton, M., McGrath, J. and Juliano, P. C. *J. Polym. Sci. (C)* 1969, **26**, 99
- 10 Conti, F., Segre, A., Pini, D. and Porri, L. *Polymer* 1974, **15**, 5
- 11 Duch, M. W. and Grant, D. M. *Macromolecules* 1970, **3**, 165

# Conformational studies of *N*-acetyl-*N*-methyl-L-alanine dimethylamide-*d*<sub>6</sub> by n.m.r. spectroscopy\*

Yukio Imanishi, Kazuya Kugimiya and Toshinobu Higashimura

Department of Polymer Chemistry, Kyoto University, Kyoto, Japan

(Received 14 June 1974)

Nuclear magnetic resonance of *N*-acetyl-*N*-methyl-L-alanine dimethylamide-*d*<sub>6</sub> in methylene chloride-*d*<sub>2</sub>/dichloroacetic acid was investigated. In methylene chloride-*d*<sub>2</sub> the amide assumed nearly all-*trans* conformation. Small signals corresponding to trace amounts of *cis* conformation were observed. Dichloroacetic acid induced the shift of the resonance signals immediately after the addition. On leaving the solution containing dichloroacetic acid, the amide nitrogen was protonated and the isomerization around the amide bond took place. After a sufficient time lapse a complex spectrum resulted, which corresponded to at least five different conformations. On heating the solution several signals disappeared without coalescence and the resonance signals corresponding to three different conformations remained at 120°C. These conformations should include non-planar conformations as well as planar *cis* and *trans* conformations.

## INTRODUCTION

Simple amides have been useful models for polypeptides in respect to their conformational properties. In fact the conformational changes of simple amides under suitable conditions have been a basis for considering the conformational behaviour of polypeptides. A particular interest has been paid to the presence of a *cis* amide bond in poly(imino acids). The *cis*-*trans* isomerism of simple substituted amides has long been known<sup>1</sup>. With poly(L-proline)<sup>2</sup> and polysarcosine<sup>3,4</sup> the presence of a *cis* amide bond was observed mainly by nuclear magnetic resonance (n.m.r.) spectroscopy, and the conformational behaviour of these poly(imino acids) was discussed in comparison with the corresponding monomeric amides. With poly(*N*-methyl-L-alanine)<sup>5,6</sup>, the open chain analogue of poly(L-proline), the presence of a *cis* amide bond was suggested by the calculation of potential energies and was observed by n.m.r. spectroscopy, and the conformational transition was discussed in terms of the *cis*-*trans* isomerism of the amide bonds. However, no such investigation has been carried out with the monomeric amide. Recently Goodman *et al.*<sup>7</sup> reported the n.m.r. investigation of *N*-acetyl-*N*-methyl-L-alanine methyl ester. They investigated the *cis*-*trans* isomerism (thermodynamics and kinetics) of the ester only in the so-called helix-supporting solvents.

In our study of enzyme-model reactions<sup>8</sup> using various polypeptides, we became interested in the conformational behaviour of poly(*N*-methyl-L-alanine). So we investigated at first *N*-acetyl-*N*-methyl-L-alanine dimethylamide in methylene chloride-*d*<sub>2</sub> (CD<sub>2</sub>Cl<sub>2</sub>)/dichloroacetic acid (DCA) mixed solvent. We believe that the amide is a better model for poly(*N*-methyl-L-alanine) than the ester. Furthermore, the conformational studies in strongly solvating DCA are directly related to the conformational transition of poly(*N*-methyl-L-alanine) in so-called helix-breaking solvents. In the present paper we will describe the n.m.r. studies of *N*-acetyl-*N*-methyl-L-alanine dimethylamide. The observations with poly(*N*-methyl-L-alanine) will be described in the following paper<sup>9</sup>.

\* Presented at the 21st Society of Polymer Science, Japan Symposium on Macromolecules, Osaka, November 1972.

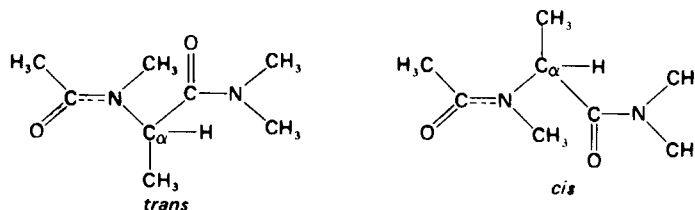
## EXPERIMENTAL

*N*-Methyl-L-alanine *N*-carboxyanhydride (NCA) was synthesized from commercial L-alanine as reported previously<sup>10,11</sup>. The NCA was added in portions to a large excess of dimethylamine cooled by Dry Ice and allowed to react for 15 min. After the excess dimethylamine was evaporated, the residual oil, *N*-methyl-L-alanine dimethylamide was acetylated with acetic anhydride/pyridine. *N*-Acetyl-*N*-methyl-L-alanine dimethylamide was purified by distillation. When *N*-acetyl-*N*-methyl-L-alanine dimethylamide-*d*<sub>6</sub> was synthesized, dimethylamine-*d*<sub>6</sub> was used (b.p. 89–92°C at 4 mmHg).

100 and 220 MHz n.m.r. spectra were recorded with Varian HA-100 and HA-220 spectrometers, respectively. Tetramethylsilane was used as an internal standard. CD<sub>2</sub>Cl<sub>2</sub> (Merck, 99%) was used without further purification. DCA was purified by vacuum distillation.

## RESULTS

*N*-Acetyl-*N*-methyl-L-alanine dimethylamide can be represented in either *cis* or *trans* form:



The 100 MHz n.m.r. spectrum of *N*-acetyl-*N*-methyl-L-alanine dimethylamide dissolved in CD<sub>2</sub>Cl<sub>2</sub> is shown in Figure 1. For the peak assignment the n.m.r. spectra of *N*-acetyl-*N*-methyl-L-alanine methyl ester<sup>7</sup> and *N*-acetyl sarcosine dimethylamide<sup>4</sup> were referred to: C<sub>α</sub>-H resonance appeared as a quartet (4.52τ, *J* = 6.67 cycles/sec), C<sub>α</sub>-CH<sub>3</sub> resonance appeared as a doublet (8.82τ, *J* = 6.67 cycles/sec), and acetyl-CH<sub>3</sub> (7.95τ) and *N*-CH<sub>3</sub> (7.15τ) resonances appeared as a singlet. There are two signals for the terminal amide-CH<sub>3</sub> (7.06τ, 7.11τ), which correspond to *cis* and *trans* CH<sub>3</sub>.

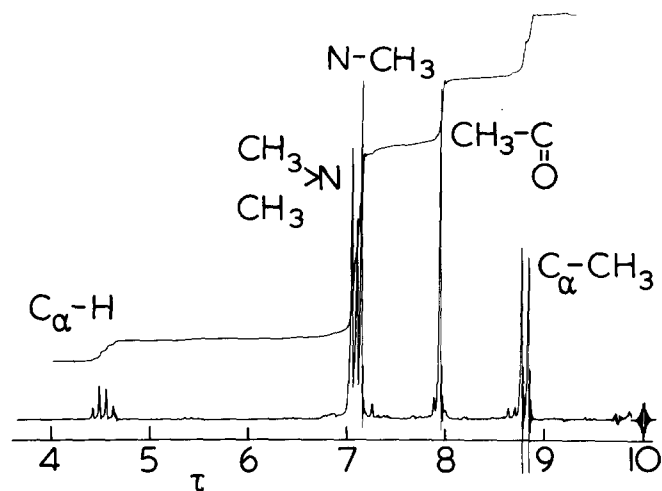


Figure 1 100 MHz n.m.r. spectrum of *N*-acetyl-*N*-methyl-L-alanine dimethylamide in  $\text{CD}_2\text{Cl}_2$  at  $31.5^\circ\text{C}$ ; concentration 5% w/v

However, in  $\text{CD}_2\text{Cl}_2$  a small doublet for  $\text{C}_\alpha\text{-CH}_3$  and a small singlet for  $\text{N-CH}_3$  appeared in addition to the main signals. Goodman *et al.*<sup>7</sup> assigned these resonances to the presence of *cis* form. The experimental results which appear subsequently confirmed Goodman's proposal. These small resonance signals were not observed in  $\text{CCl}_4$ . These results indicate that *N*-acetyl-*N*-methyl-L-alanine dimethylamide exists in  $\text{CCl}_4$  as completely *trans* form and in  $\text{CD}_2\text{Cl}_2$  as nearly all *trans* form.

DCA promotes the transition of an ordered structure of polypeptide to a randomly coiled structure owing to its strongly solvating ability. DCA would induce more drastic isomerization of amide bond of *N*-acetyl-*N*-methyl-L-alanine dimethylamide than  $\text{CD}_2\text{Cl}_2$ . So, we examined the effect on the n.m.r. spectrum of increasing amount of DCA added to the  $\text{CD}_2\text{Cl}_2$  solution of *N*-acetyl-*N*-methyl-L-alanine dimethylamide- $d_6$ . Hereafter the deuterated amide was used to eliminate the complication due to the terminal methyl signals. Figure 2 shows the effect of DCA. The spectra were recorded immediately after the addition of DCA. The addition of small amount of DCA (2–13% v/v) caused a peak shift towards lower magnetic field. The effect was most marked with  $\text{N-CH}_3$  and  $\text{C}_\alpha\text{-CH}_3$  resonances, and least marked with  $\text{C}_\alpha\text{-H}$  resonance. It should be noted here that on adding DCA only the peak shift was observed, and that neither the peak-splitting nor the appearance of new signals was observed. This peak shift induced by DCA is a fast process.

It was found that the n.m.r. spectrum of *N*-acetyl-*N*-methyl-L-alanine dimethylamide- $d_6$  in  $\text{CD}_2\text{Cl}_2$ /DCA mixed solvent was time-dependent. In Figure 3 the change with time of the n.m.r. spectrum of the amide- $d_6$  dissolved in DCA/ $\text{CD}_2\text{Cl}_2$  (9:1 v/v) mixed solvent is shown. Immediately after DCA was added to the  $\text{CD}_2\text{Cl}_2$  solution (Figure 3a), the signals are seen to have shifted to a lower magnetic field as compared with Figure 2a. At this stage new signals appeared only to a minor extent. When the solution was kept for several days at room temperature, the peak shift was no longer observed, but the peak intensity changed drastically and consequently a number of new signals were observable. After 27 days the n.m.r. spectrum became very complicated (Figure 3d), and  $\text{C}_\alpha\text{-H}$  resonance which originally centred at  $4.53\tau$  became very obscured because of the peak broadening and the spin side band of DCA. The assignment of other resonance signals was made on the basis of the chemical shift and the peak area. Roughly five resonance signals are observed for each of  $\text{C}_\alpha\text{-CH}_3$ ,  $\text{N-CH}_3$  and

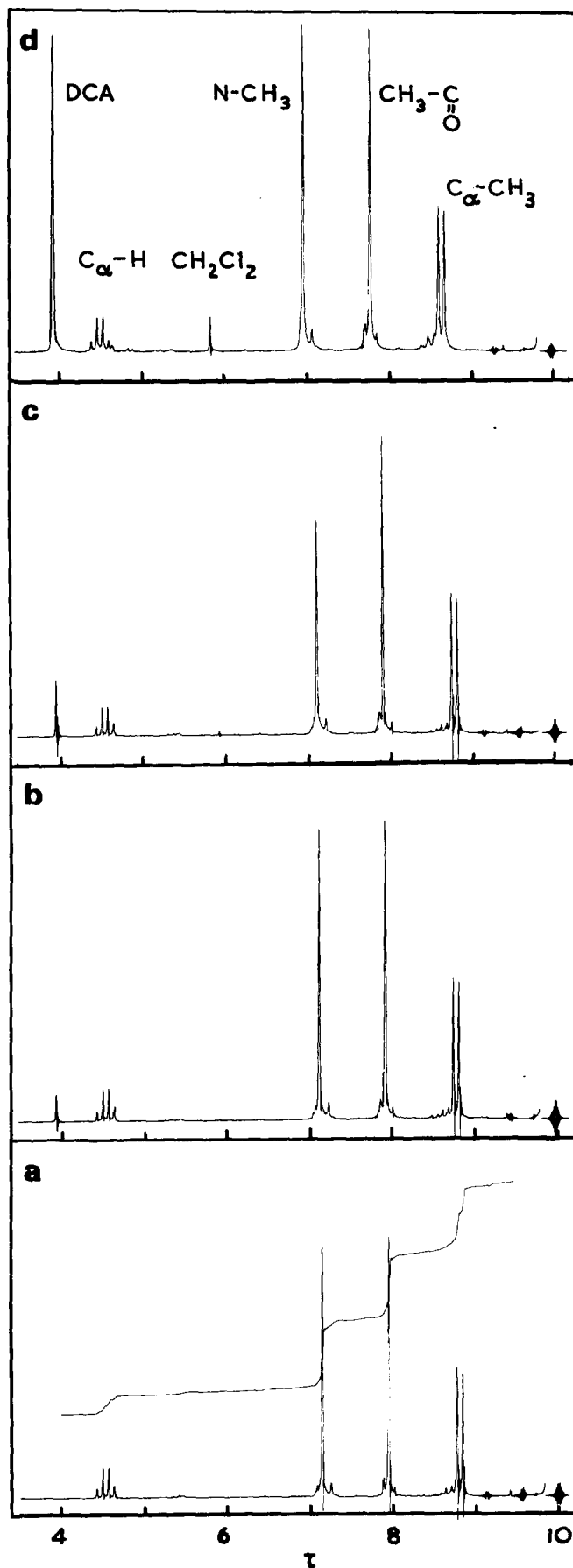


Figure 2 100 MHz n.m.r. spectra of *N*-acetyl-*N*-methyl-L-alanine dimethylamide- $d_6$  in  $\text{CD}_2\text{Cl}_2$  at  $31.5^\circ\text{C}$ ; concentration 25.76% w/v; (a) 0; (b) 1.96; (c) 3.85; (d) 13% v/v DCA

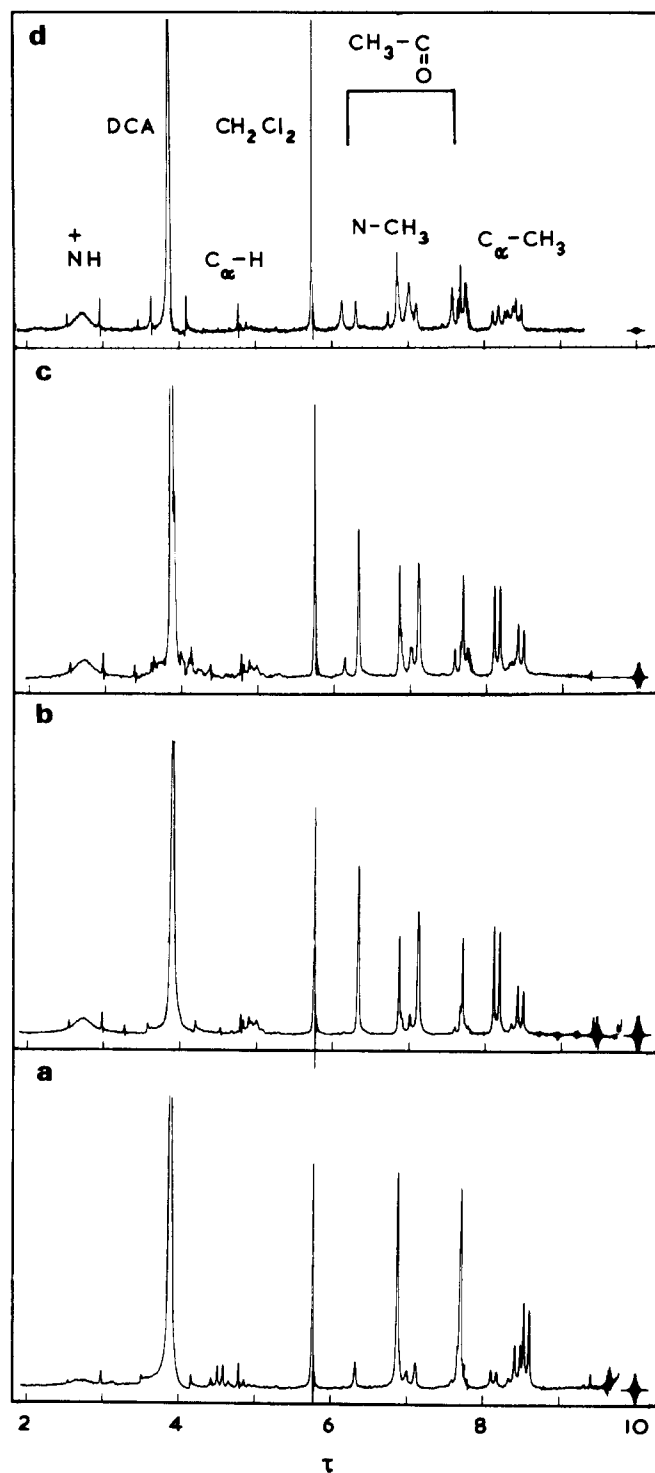


Figure 3 100 MHz n.m.r. spectra of *N*-acetyl-*N*-methyl-L-alanine dimethylamide- $d_6$  in  $CD_2Cl_2$ /DCA (1:9 v/v) mixed solvent at  $31.5^\circ C$ ; concentration 13% w/v. Measured after the preparation of solution: (a) immediately; (b) 24 h; (c) 6 days; (d) 27 days

acetyl- $CH_3$ ,  $N-CH_3$  so that the amide should exist as a mixture of at least five different conformers (see also Figure 4a). It was interesting to note that the peak splittings were accompanied by the appearance of a new broad singlet centred at  $2.7\tau$ . The latter could be assigned to  $N-H$  resonance signal which was formed by the protonation of amide nitrogen (see later discussion). Both the splittings of signals and the protonation of amide nitrogen are a slow process.

To investigate further the peak splittings, the n.m.r. spectrum of *N*-acetyl-*N*-methyl-L-alanine dimethylamide- $d_6$

dissolved in DCA/ $CD_2Cl_2$  (9:1 v/v) mixed solvent and stored at room temperature for 27 days was measured at varying temperatures. Figure 4 represents the effect of temperature on the methyl resonance region of the n.m.r. spectrum. At  $36^\circ C$  at least five signals are observable for each of  $C_\alpha-CH_3$ ,  $CH_3-CO$ , and  $N-CH_3$  protons (Figure 4a). At  $120^\circ C$  three of the five remain (Figure 4e). On cooling the solution, the original spectrum appeared again so that this change is reversible. It should be noted that the disappearance of the peaks with increasing temperature did not take place through coalescence but through the decrease of the intensity. It should also be noted that three different conformations still existed at  $120^\circ C$ .

## DISCUSSION

*N*-Acetyl-*N*-methyl-L-alanine dimethylamide was found to assume all-*trans* conformation in  $CCl_4$  at room temperature. A small amount of *cis* conformation was observed in  $CD_2Cl_2$ .

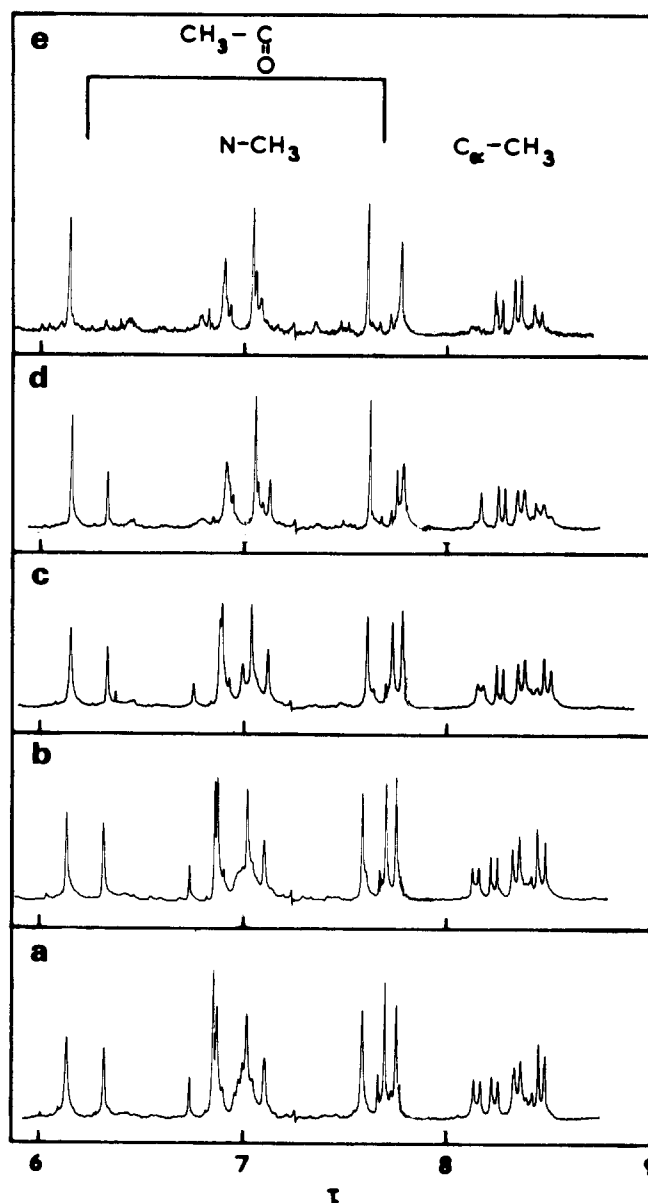
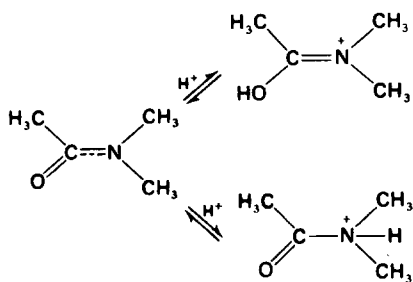


Figure 4 220 MHz n.m.r. spectra of *N*-acetyl-*N*-methyl-L-alanine dimethylamide- $d_6$  in  $CD_2Cl_2$ /DCA (1:9 v/v) mixed solvent 27 days after the preparation; concentration 13% w/v. Measured at: (a)  $36^\circ$ ; (b)  $60^\circ$ ; (c)  $70^\circ$ ; (d)  $100^\circ$ ; (e)  $120^\circ C$

Weakly hydrogen bonding  $CD_2Cl_2$  may have caused the difference.

Addition of DCA to the  $CD_2Cl_2$  solution caused a fast change and a slow change of the n.m.r. spectrum. The fast change is a shift of signals towards a lower magnetic field. The same effect has been reported in many papers<sup>12,13</sup> in which the effects of a strong acid on the chemical shift of simple amides are investigated. A stronger hydrogen bonding by DCA than  $CD_2Cl_2$  would have caused the shift. On the other hand, the slow change is peak-splitting accompanied by *N*-protonation. This change is of similar type as that observed with the change of solvent from  $CCl_4$  to  $CD_2Cl_2$ . Hence the spectral change is associated with the conformational change. We shall explain this in terms of an isomerization around the amide bond induced by the protonation of amide nitrogen.

Relatively strong acids, such as DCA and trifluoroacetic acid, induce a helix-coil transition of polypeptides. It has been a subject of controversy whether polypeptides are protonated or hydrogen bonded by acids at the transition. For some instances, simple amides are protonated more easily than polypeptides<sup>12,14</sup>. With regard to the mechanism of amide protonation, *O*-protonation and *N*-protonation have been considered. Although the fact that amides protonate predominantly on oxygen in strongly acidic media has been established for some time<sup>15</sup>, predominant protonation is on nitrogen in dilute acid<sup>14,16-18</sup>. The present authors took *N*-protonation because a new peak appeared at  $2.72\tau$  on adding DCA. Allowing for the chemical shift and the shape this signal is reasonably assigned to  $\equiv\overset{+}{N}-H$  resonance<sup>19</sup>.  $>C=O-H$  resonance signal has been reported to appear at about  $0\tau$  only at low temperatures<sup>20</sup>. Intermediately fast exchanging  $\equiv\overset{+}{N}-H$  would appear as a broad singlet and its coupling with *vicinal* protons would be negligible. Amide nitrogen having electron-releasing substituents seems to be easily protonated. As is seen in *Figure 3*, the appearance of a signal at  $2.72\tau$  was accompanied by the conformational change. This gives further support to *N*-protonation. The *N*-protonation decreases the double bond character of the amide bond, making the isomerization easier, whereas *O*-protonation increases the double bond character, according to the mechanism shown for the protonation of *N,N*-dimethylacetamide below:



In *Figure 3d* five signals ascribable to different conformations are observed for each methyl proton. This complicated spectrum cannot be explained in terms of *cis-trans* diad of the amide bond, because *N*-acetyl-*N*-methyl-*L*-alanine dimethylamide possesses only one isomerizable amide bond. A restricted rotation around  $C_\alpha$  bonds<sup>5</sup> could result in different stable conformations. However, the spectral change shown in *Figure 3* does not seem to be explained on this basis. One day after the addition of DCA (*Figure 3b*), *trans*- $C_\alpha-CH_3$  resonance (doublet  $8.58\tau$ ,  $J = 6.67$  cycles/sec) disappeared and a new doublet at  $8.14\tau$  became predominant. At the same time a new  $CH_3-CO$  resonance at  $6.34\tau$ , and a

new  $N-CH_3$  resonance at  $7.13\tau$  increased their intensities. These changes and in particular the large shift observed with  $CH_3-CO$  resonance can hardly be explained by the isomerization around  $C_\alpha$  bonds. Although on a quite different ground, Goodman *et al.*<sup>7</sup> also considered that the isomerization of *N*-acetyl-*N*-methyl-*L*-alanine methyl ester is associated with the amide bond (not with the  $C_\alpha$  bonds).

The new signal at  $6.34\tau$  was assigned to  $CH_3-CO$  resonance on the basis of peak area and the fact that this signal was not observed with poly(*N*-methyl-*L*-alanine)<sup>9</sup>. The chemical shift difference of  $CH_3-CO$  resonance between the original peak at  $7.94\tau$  and the new one at  $6.34\tau$  is very large. Such a large shift must have arisen from a twisted acetyl group adjacent to nitrogen carrying a positive charge. To explain such a complex spectrum as *Figure 3d* in terms of the isomerization around a single amide bond, non-planar amide conformations should be taken into account in addition to planar *cis* and *trans* conformations. Non-planar amide conformations have been considered to be unfavourable, because the conjugation  $\overset{-}{N}-C=O$  is lost. However, in the present case nitrogen is protonated to use up its lone-pair electrons. Thus the amide bond became a pure single bond, the rotation around which became less hindered. In this connection it should be remembered that the large splitting of  $CH_3-CO$  resonance as well as the moderate splitting of other methyl protons commenced when the amide nitrogen was protonated. Furthermore, the peak splittings progressed with increasing peak intensity at  $2.72\tau$ .

A strong support for the isomerization around the peptide bond is obtained from the temperature effect. Three different conformations still remains at as high a temperature as  $120^\circ C$  (*Figure 4e*). Restricted rotations around  $C_\alpha$  bonds at  $120^\circ C$  are hardly acceptable<sup>21</sup>. On cooling the solution the spectrum *Figure 4a* was restored. It is most plausible that there are planar and non-planar conformations of the amide bond, and that some of them are relatively unstable at higher temperatures. The long-lived (on n.m.r. time scale) non-planar amide conformers are unique, but they are acceptable if one takes into account the steric interactions among methyl groups in the acetylated imino acid amide. Recently, the n.m.r. chemical shift of oligopeptides containing proline residue was explained by the proline stereoisomerism due to a slow nitrogen inversion<sup>22</sup>. This idea would involve steric interactions among substituents and non-planar amide links.

It is not known whether the deprotonation of the protonated amide took place during the temperature rise, because at higher temperatures only the regions of  $N-CH_3$  and  $C_\alpha-CH_3$  resonance signals were examined.

## REFERENCES

- 1 Stewart, W. E. and Siddall, III, T. H. *Chem. Rev.* 1970, **70**, 517
- 2 Deber, C. M., Bovey, F. A., Craver, J. P. and Blout, E. R. *J. Am. Chem. Soc.* 1970, **92**, 6191
- 3 Bovey, F. A., Ryan, J. J. and Hood, F. P. *Macromolecules* 1971, **4**, 246
- 4 Sisido, M., Imanishi, Y. and Higashimura, T. *Biopolymers* 1972, **11**, 399
- 5 Conti, F. and DeSantis, P. *Biopolymers* 1971, **10**, 2581
- 6 Goodman, M., Chen, F. and Prince, F. R. *Biopolymers* 1973, **12**, 2549
- 7 Goodman, M., Chen, F. and Lee, C.-Y. *J. Am. Chem. Soc.* 1974, **96**, 1479
- 8 Imanishi, Y. 'Enzymes and Polymer Catalysts', Kagaku-Dojin, Kyoto, 1972

- 9 Imanishi, Y., Kugimiya, K. and Higashimura, T. *Polymer* 1975, **16**, 350
- 10 Quitt, P., Hellerbach, J. and Voller, K. *Helv. Chim. Acta* 1963, **46**, 327
- 11 Imanishi, Y., Kugimiya, K. and Higashimura, T. *Biopolymers* 1973, **12**, 2643
- 12 Stewart, W. E., Mandelkern, L. and Glick, R. E. *Biochemistry* 1967, **6**, 150
- 13 Nawrot, C. F. and Veis, A. *J. Am. Chem. Soc.* 1970, **92**, 3903
- 14 Stewart, W. E., Mandelkern, L. and Glick, R. E. *Biochemistry* 1967, **6**, 143
- 15 O'Connor, C. J. *Q. Rev. Chem. Soc.* 1970, **24**, 553
- 16 Berger, A., Loewenstein, A. and Meiboom, S. *J. Am. Chem. Soc.* 1959, **81**, 62
- 17 Liler, M. *Chem. Commun.* 1971, p 115
- 18 Liler, M. *Chem. Commun.* 1972, p 527
- 19 Silverstein, R. M. and Bassler, G. C. 'Spectrometric Identification of Organic Compounds', 2nd Edn, John Wiley, New York, 1967
- 20 Gillespie, R. J. and Birchall, T. *Can. J. Chem.* 1963, **41**, 148
- 21 Love, A., Alger, T. and Olsen, K. *J. Phys. Chem.* 1972, **76**, 853
- 22 Sugiyama, H., Shiraishi, H. and Seto, S. *Chem. Lett.* 1973, p 621

# Conformational studies of poly(*N*-methyl-L-alanine) by n.m.r. spectroscopy\*

Yukio Imanishi, Kazuya Kugimiya and Toshinobu Higashimura

Department of Polymer Chemistry, Kyoto University, Kyoto, Japan

(Received 14 June 1974)

Nuclear magnetic resonance (n.m.r.) and circular dichroism of poly(*N*-methyl-L-alanine) in methylene chloride-*d*<sub>2</sub>/dichloroacetic acid were investigated. In methylene chloride-*d*<sub>2</sub> poly(*N*-methyl-L-alanine) was found to consist of nearly all-*trans* amide bonds and assume a stable secondary structure. Trace amounts of *cis* amide bonds were also present. The addition of dichloroacetic acid destroyed the secondary structure and induced a drastic change of the n.m.r. spectrum, which was similar to that observed with the monomeric amide, *N*-acetyl-*N*-methyl-L-alanine dimethylamide. In comparison of the polymer with the monomeric amide, it was concluded that the transition of poly(*N*-methyl-L-alanine) was caused by the isomerization of amide bonds. The complex n.m.r. spectrum was interpreted in terms of the distribution along the polymer chain of various non-planar amide links as well as planar *cis* and *trans* amide links. The difference of the mechanism of conformational transition between poly(amino acid) and poly(imino acid) is also discussed.

## INTRODUCTION

Synthetic polypeptides have been used as simplified model systems to investigate enzymic reactions<sup>1</sup>. In our laboratories poly(*N*-methyl-L-alanine) was used as a catalyst to initiate the polymerization of  $\alpha$ -amino acid *N*-carboxyanhydride<sup>2,3</sup>. Poly(*N*-methyl-L-alanine) showed an interesting stereoselectivity in the polymerization, and the selectivity seemed to be related to a unique conformation of poly(*N*-methyl-L-alanine) in solution.

There have been a few papers published on the conformation of poly(*N*-methyl-L-alanine). Pioneering work by Goodman *et al.*<sup>4</sup> showed that this polymer consisted of all-*trans* amide bonds and assumed an ordered structure in methylene chloride. Later, the calculations made by Goodman *et al.*<sup>5</sup> and Liquori *et al.*<sup>6</sup> suggested the possibilities for stable secondary structures of poly(*N*-methyl-L-alanine).

The present authors were interested in the conformation of poly(*N*-methyl-L-alanine) in strongly acidic media as well as in non-polar media. Soon after the present authors started the investigation on the effect of dichloroacetic acid, Conti *et al.*<sup>7</sup> published a paper concerning the effect of trifluoroacetic acid. They observed a complex multiplet for each proton resonance in nuclear magnetic resonance (n.m.r.) spectrum in trifluoroacetic acid and explained the spectrum in terms of multiple energy minima in the rotation around C $\alpha$  bond in combination with *cis* and *trans* amide bonds. However, their conclusion came mainly from calculation and little experimental work was made with n.m.r. spectroscopy. More recently Goodman *et al.*<sup>8</sup> made a more detailed study on the same problem and suggested that the addition of trifluoroacetic acid to the methylene chloride solution of poly(*N*-methyl-L-alanine) induced the *trans*  $\rightarrow$  *cis* isomerization of amide bonds. Thus, *cis* and *trans* amide bonds

became randomly distributed along the polymer chain, and the secondary structure was destroyed in trifluoroacetic acid. However, their n.m.r. work was not detailed enough to give a complete explanation to the nature of the isomerization around amide bond. They investigated only the effect of trifluoroacetic acid concentration on the n.m.r. spectrum.

The present authors investigated the effect of dichloroacetic acid on the n.m.r. spectrum of poly(*N*-methyl-L-alanine) in more detail and found a number of interesting features which were observed neither by Conti *et al.* nor by Goodman *et al.* These aspects are described and discussed here in comparison with the effect of dichloroacetic acid on *N*-acetyl-*N*-methyl-L-alanine dimethylamide, the monomeric analogue of poly(*N*-methyl-L-alanine)<sup>9</sup>. Part of the experimental results have been reported in a previous paper<sup>2</sup>, together with the properties of poly(*N*-methyl-L-alanine) as an initiator for the polymerization of phenylalanine *N*-carboxyanhydride.

## EXPERIMENTAL

Poly(*N*-methyl-L-alanine) was synthesized by the polymerization of *N*-methyl-L-alanine *N*-carboxyanhydride with *N*-methyl-L-alanine diethylamide as an initiator in methylene chloride. Details of the synthesis and the control of the degree of polymerization have been described in a previous paper<sup>2</sup>. The degree of polymerization of poly(*N*-methyl-L-alanine) used for the present investigation was 15 or 30. Poly(*N*-methyl-DL-alanine) having a degree of polymerization of 30 was synthesized for comparison as reported previously<sup>10</sup>.

N.m.r. spectra of the polypeptides were measured as described in the preceding paper<sup>9</sup>. Methylene chloride-*d*<sub>2</sub> (CD<sub>2</sub>Cl<sub>2</sub>) (Merck, 99%) was used without further purification and dichloroacetic acid (DCA) was purified by distillation.

\* Presented at the 21st Society of Polymer Science, Japan Symposium on Macromolecules, Osaka, November 1972

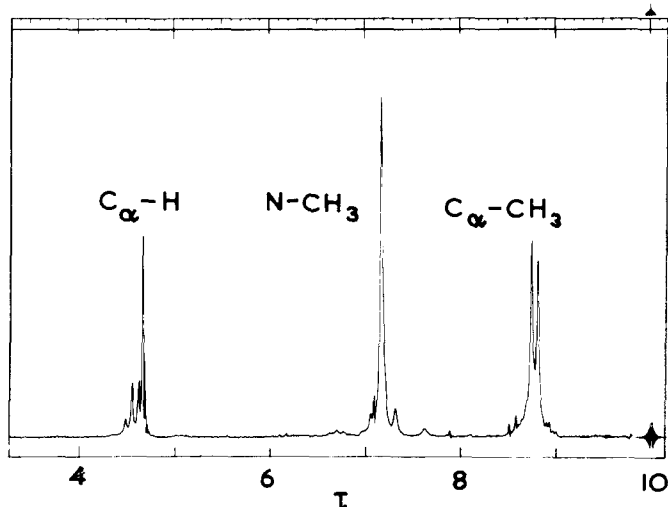
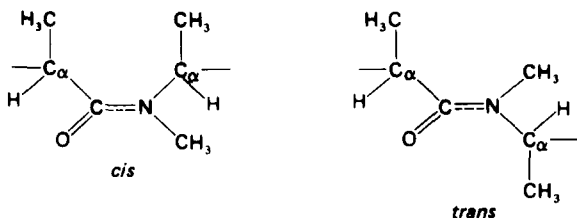


Figure 1 100 MHz n.m.r. spectrum of poly(*N*-methyl-L-alanine) ( $DP = 30$ ) in  $CD_2Cl_2$  at  $31.5^\circ C$ ; concentration 5% w/v

## RESULTS

Poly(*N*-methyl-L-alanine) can be represented in either *cis* or *trans* form as:



100 MHz n.m.r. spectrum of poly(*N*-methyl-L-alanine) having a degree of polymerization of 30 in  $CD_2Cl_2$  is shown in Figure 1. The spectrum is identical with that reported by Goodman *et al.*<sup>4,8</sup>  $N-CH_3$  resonance signal appeared as a singlet at  $7.2 \tau$  and  $C_\alpha-CH_3$  resonance signal appeared as a doublet at  $8.75 \tau$  ( $J = 6.7$  cycles/sec).  $C_\alpha-H$  resonance signal appeared as a quartet at  $4.58 \tau$  ( $J = 6.3$  cycles/sec), which was obscured by the resonance signal of methylene chloride. According to the peak assignment proposed by Goodman *et al.*<sup>4,8</sup> poly(*N*-methyl-L-alanine) in  $CD_2Cl_2$  possesses nearly all-*trans* amide bonds. A small doublet at a lower magnetic field than the main  $C_\alpha-CH_3$  doublet, and a small singlet at a higher magnetic field than the main  $N-CH_3$  singlet are ascribed to the presence of a small amount of *cis* amide bond. Under this condition poly(*N*-methyl-L-alanine) assumes an ordered structure which is evident from the circular dichroism spectra reported in a previous paper<sup>2</sup>.

100 MHz n.m.r. spectra of poly(*N*-methyl-L-alanine) were recorded soon after the addition of a small amount of DCA to the  $CD_2Cl_2$  solution (Figure 2). The  $C_\alpha-CH_3$  and the  $N-CH_3$  signals shifted slightly towards a lower magnetic field and the  $C_\alpha-H$  signal shifted a little towards a higher magnetic field. New signals for  $C_\alpha-CH_3$  and  $N-CH_3$  resonances began to appear only to a minor extent. This change is similar to that observed with *N*-acetyl-*N*-methyl-L-alanine dimethylamide<sup>9</sup>. It is interesting to note that a broad singlet appeared at  $4.35 \tau$  (DCA 0.60% v/v) or at  $3.40 \tau$  (DCA 1.18% v/v). The chemical shift of the signal was dependent on the concentration of DCA. Thus the signal appeared at  $2.07 \tau$ , when the solution contained 90% v/v DCA.

When the solution of poly(*N*-methyl-L-alanine) containing DCA was left for standing, the chemical shifts of the proton

resonances no longer changed, but the intensities of the original signals decreased and new signals appeared. Figure 3 shows the effect of standing for 24 h on the methyl resonance region of the 100 MHz n.m.r. spectra. The time-dependent n.m.r. spectra and the mode of peak splittings are very similar to those observed with *N*-acetyl-*N*-methyl-L-alanine dimethylamide<sup>9</sup>. However, the n.m.r. spectra of the polymer in DCA-containing solvent after standing for 24 h were more complex than those of the simple amide. Under this condition poly(*N*-methyl-L-alanine) is in a random-coil form, which has been evidenced by optical rotatory dispersion as reported in a previous paper<sup>2</sup>. This change was found to be reversible; i.e. after the recovery of the polymer from the solution, it was redissolved in  $CD_2Cl_2$  to give a n.m.r. spectrum very similar to Figure 1.

Figure 4 shows the n.m.r. spectra of poly(*N*-methyl-DL-alanine) in  $CD_2Cl_2$  and in DCA/ $CD_2Cl_2$  (9:1 v/v) mixed solvent. 100 MHz n.m.r. spectrum of poly(*N*-methyl-DL-alanine) in  $CD_2Cl_2$  is very similar to that of poly(*N*-methyl-L-alanine). The  $N-CH_3$  signal split into two sharp peaks. The peak splitting was maintained at higher temperatures, so it may be related with the configurational (L or D) diad. However, it is not known why the configuration of  $C_\alpha$  affects only the  $N-CH_3$  resonance signal. The addition of DCA gave a complex spectrum, which is very similar to the spectrum of poly(*N*-methyl-L-alanine) in a solvent containing DCA.

Poly(*N*-methyl-L-alanine) was dissolved in DCA/ $CD_2Cl_2$  (9:1 v/v) mixed solvent and left at room temperature for 14 days. The solution was then heated up to  $130^\circ C$  and the change of n.m.r. spectra ( $C_\alpha-CH_3$  and  $N-CH_3$  regions only) was followed (Figure 5). At  $31.5^\circ C$  the signals were overlapped and broad, but at least six singlets for  $N-CH_3$

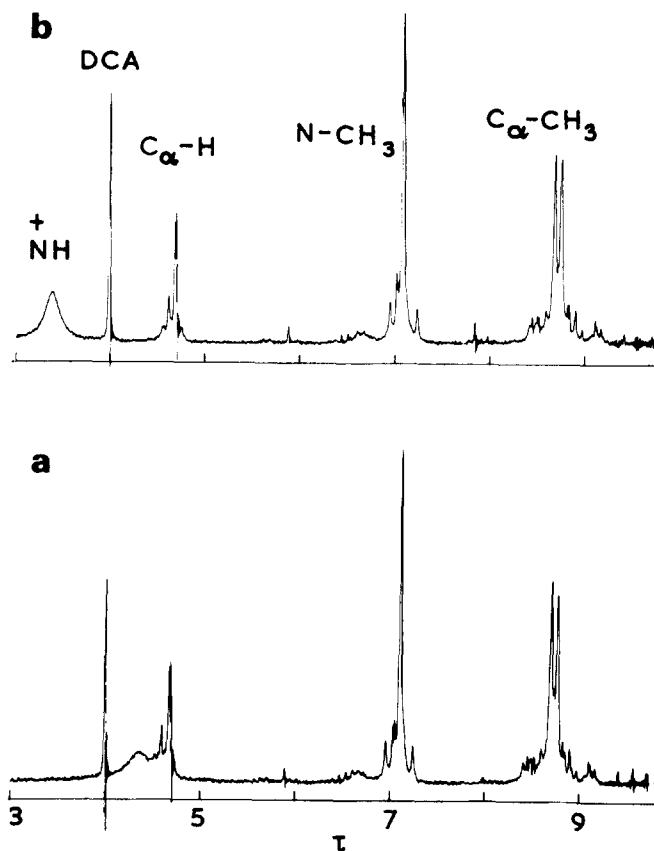


Figure 2 100 MHz n.m.r. spectra of poly(*N*-methyl-L-alanine) ( $DP = 15$ ) in  $CD_2Cl_2$  at  $31.5^\circ C$ . (a) 0.60%; (b) 1.18% v/v DCA



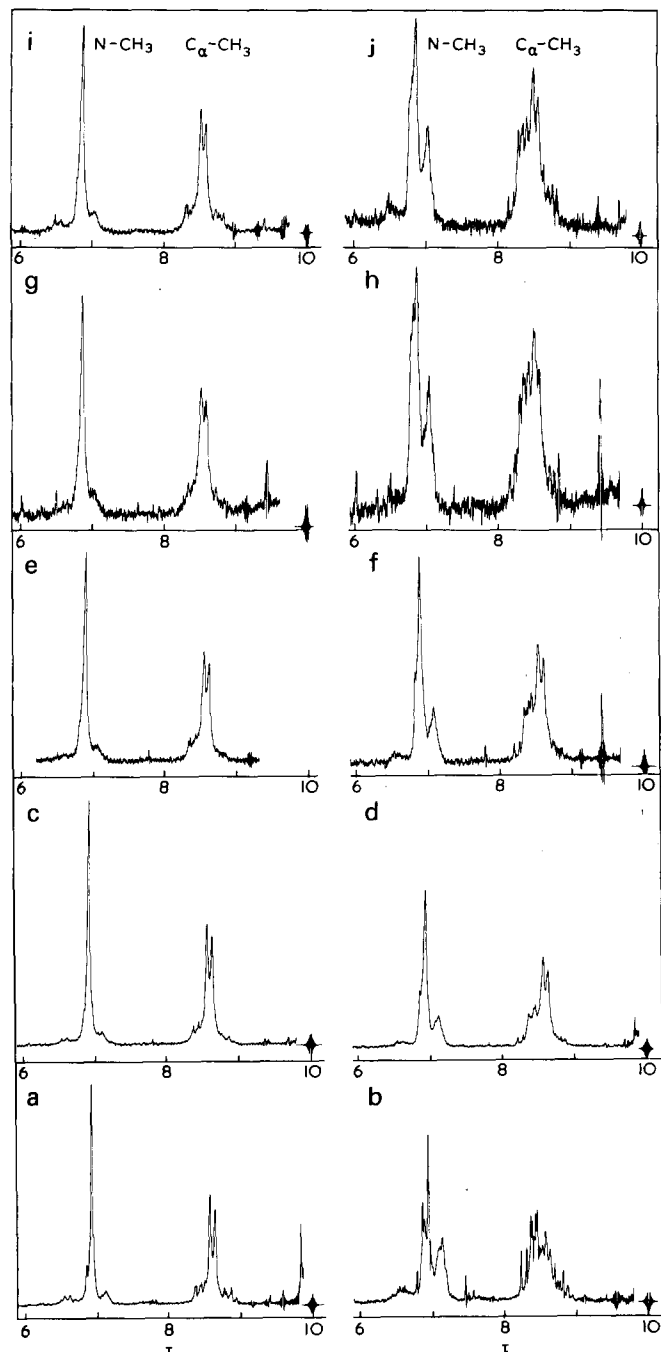


Figure 3 100 MHz n.m.r. spectra of poly(*N*-methyl-L-alanine) ( $DP = 15$ ) at  $31.5^\circ\text{C}$ . (a)  $\text{CD}_2\text{Cl}_2/\text{DCA}$  9:1 v/v soon after preparation; (b)  $\text{CD}_2\text{Cl}_2/\text{DCA}$  9:1 v/v 4 days after preparation; (c)  $\text{CD}_2\text{Cl}_2/\text{DCA}$  7:3 v/v soon after preparation; (d)  $\text{CD}_2\text{Cl}_2/\text{DCA}$  7:3 v/v 24 h after preparation; (e)  $\text{CD}_2\text{Cl}_2/\text{DCA}$  5:5 v/v soon after preparation; (f)  $\text{CD}_2\text{Cl}_2/\text{DCA}$  5:5 v/v 24 h after preparation; (g)  $\text{CD}_2\text{Cl}_2/\text{DCA}$  3:7 v/v soon after preparation; (h)  $\text{CD}_2\text{Cl}_2/\text{DCA}$  3:7 v/v 24 h after preparation; (i)  $\text{CD}_2\text{Cl}_2/1:9$  v/v soon after preparation; (j)  $\text{CD}_2\text{Cl}_2/\text{DCA}$  1:9 v/v 24 h after preparation

resonance signals and six doublets for  $\text{C}_\alpha\text{-CH}_3$  resonance signal were observed. On heating, the signals shifted slightly towards a higher magnetic field and were sharpened. A sudden change of the relative peak intensities occurred at a temperature rise from  $70^\circ\text{C}$  to  $90^\circ\text{C}$ . At  $130^\circ\text{C}$ , two main resonance signals and one minor resonance signal were observed for either  $\text{N-CH}_3$  or  $\text{C}_\alpha\text{-CH}_3$  proton. During this procedure, the chemical shift difference for the  $\text{N-CH}_3$  signals decreased a little, but that for the  $\text{C}_\alpha\text{-CH}_3$  signals did not change significantly. The coupling constant of the  $\text{C}_\alpha\text{-CH}_3$  doublet was little affected by the temperature.

## DISCUSSION

Poly(*N*-methyl-L-alanine) was found to consist of all-*trans* amide bonds and assume an ordered conformation in  $\text{CD}_2\text{Cl}_2$ . The preponderance of *trans* amide bonds in  $\text{CDCl}_3$  have also been observed with the monomeric amide, *N*-acetyl-*N*-methyl-L-alanine dimethylamide. The same observations have been made by Goodman *et al.*<sup>4,8</sup>.

The addition of DCA induced a shift of the resonance peaks. This change took place immediately after the addition of DCA, so that it may have been caused by the solvation, hydrogen bonding with added DCA being involved. The same phenomenon has been observed with the monomeric amide<sup>9</sup>.

On adding 0.60% v/v DCA a broad singlet appeared at  $4.35\tau$ . The chemical shift of this resonance peak was dependent on the concentration of DCA, and finally moved to  $2.07\tau$  at the DCA concentration of 90% v/v. The protonated amide nitrogen was considered to be the origin of this new signal. This consideration came from the comparison with the n.m.r. spectrum of the monomeric amide in DCA-containing solvent<sup>9</sup>. The chemical shift value ( $2.07\tau$ ) is reasonable for  $\equiv\text{N}^+\text{-H}$  resonance<sup>11</sup>. The signal was broad because of quadrupole moment of nitrogen, but less broad than that of monomeric amide because of a slower molecular motion of the polypeptide<sup>12,13</sup>.

It has been the subject of controversy whether polypeptides are protonated or not at the conformational transition in strong acids. Some papers<sup>14,15</sup> have been published in favour of protonation, and others<sup>16,17</sup> against it.  $\equiv\text{N}^+\text{-H}$  resonance signal observed in the present investigation unam-

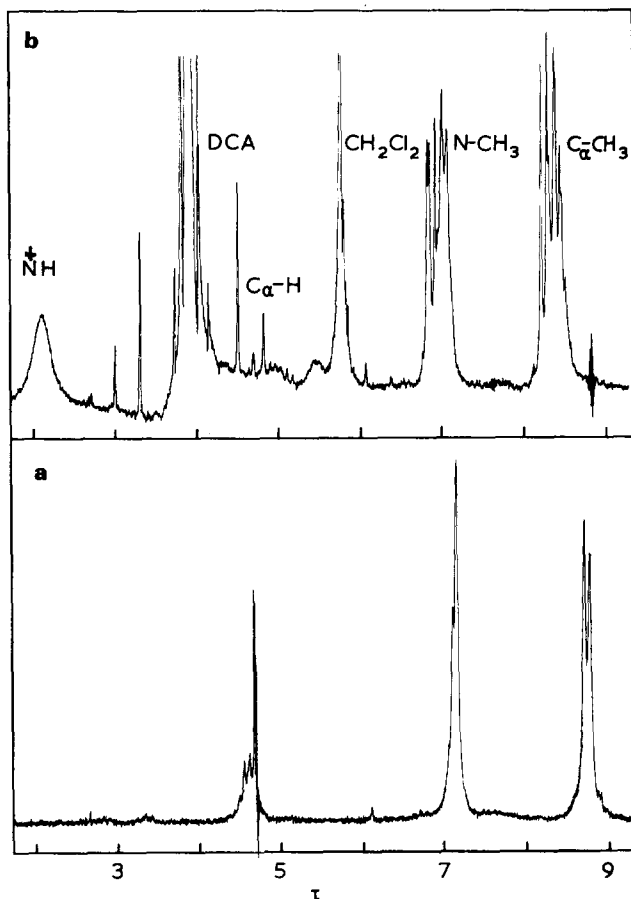


Figure 4 100 MHz n.m.r. spectra of poly(*N*-methyl-DL-alanine) ( $DP = 30$ ) at room temperature; concentration 5% w/v; (a) in  $\text{CD}_2\text{Cl}_2$ ; (b) in  $\text{CD}_2\text{Cl}_2/\text{DCA}$  1:9 v/v mixed solvent 8 days after preparation

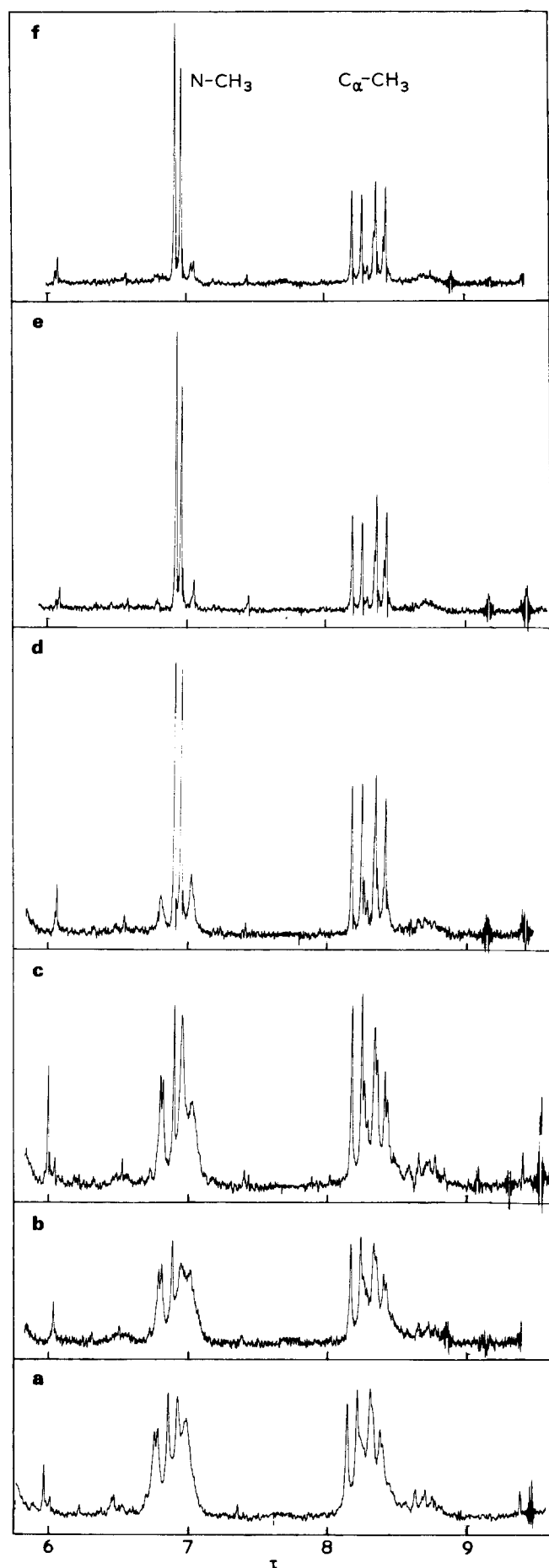


Figure 5 100 MHz n.m.r. spectra of poly(*N*-methyl-L-alanine) ( $DP = 15$ ) in  $CD_2Cl_2/DCA$  (1:9 v/v) mixed solvent measured 14 days after preparation; (a)  $31.5^\circ$ ; (b)  $50^\circ$ ; (c)  $70^\circ$ ; (d)  $90^\circ$ ; (e)  $110^\circ$ ; (f)  $130^\circ C$

biguously indicates the occurrence of protonation at least in case of poly(*N*-methyl-L-alanine).

The resonance peak at 2.07  $\tau$  increased the intensity without changing the chemical shift on standing at room temperature. Together with this, the resonance peaks for  $C_\alpha-CH_3$  and  $N-CH_3$  protons began to change. This mode of change is very similar to that observed with the monomeric amide. So we considered that the amide nitrogen of the polypeptide was slowly protonated by DCA and the increased single bond character made the amide bonds take various rotational states. The restricted rotation around the single bond could have resulted from the strict steric interaction among substituents, which is characteristic of poly(imino acids).

Comparison can be made between poly(*N*-methyl-L-alanine) and poly(*N*-methyl-DL-alanine) for the n.m.r. spectra in  $CD_2Cl_2$  (Figure 1 and Figure 4a) and in  $DCA/CD_2Cl_2$  (9:1 v/v) mixed solvent (Figure 3j and Figure 4b). In either solvent, two polymers gave similar spectra; that is, the configuration of  $C_\alpha$  affects little the pattern of n.m.r. spectrum. A complex spectrum observed in DCA-containing solvent is no doubt a result of the isomerization around amide bond.

Goodman *et al.*<sup>8</sup> observed the similar effect of trifluoroacetic acid on the n.m.r. spectrum of poly(*N*-methyl-L-alanine), and proposed that the multiplets stem from the sensitivity of the n.m.r. spectrum to triads of adjacent *N*-methyl-L-alanine residues along the polymer chain. Their conclusion was drawn mainly from the fact that two sets of *N*-methyl multiplets were observed. However, their idea was not tested further. A similarity shown up between poly(*N*-methyl-L-alanine) and the monomeric amide, in the latter the *cis-trans* triad being impossible, strongly suggests that the multiplets reflect the multiple energy minima involved in the restricted rotation around the protonated amide bond.

A further support for the above conclusion is obtained from the n.m.r. spectra at higher temperatures. A complex spectrum in DCA-containing solvent became simple at higher temperatures. In that event, the coalescence was never observed, but the relative intensities of the resonance signals changed. This excludes the possibility for the *cis-trans* triad and supports the multiple energy minima around amide bond. It is not clear whether amide nitrogens still protonate at higher temperatures. Deprotonation might have bearing on a sudden change of the n.m.r. spectrum observed at the temperature rise from  $70^\circ C$  to  $90^\circ C$ . Two main signals survived at  $130^\circ C$  could be assigned to planar *cis* and *trans* amide conformers. One small resonance observed at  $130^\circ C$  should be ascribed to a minor non-planar conformation of amide bond.

With poly(*N*-methyl-L-alanine) and its monomeric amide the effects of DCA and temperature on the n.m.r. spectrum were very similar but not completely the same. Some difference of the steric interactions among substituents and hence the different behaviour of n.m.r. spectra have been noted between poly(*N*-alkylglycines) and their monomeric amides, too<sup>18</sup>.

It is conceivable that the nature of the denaturation of poly(imino acid) is different from poly(amino acid). Poly(amino acids) consist of *trans* amide bonds and a uniform conformation around  $C_\alpha$  is essential to assume a secondary structure. Intra- or inter-molecular hydrogen bond stabilizes the uniform conformation. Strong acids destroy these hydrogen bonds and thereby the secondary structure. With poly(imino acids) severe steric interactions among substitu-

ents confine the conformation of C $\alpha$  into a unique one without the help of hydrogen bonding. A uniform (*cis* or *trans*) conformation of amide bond is necessary for the polypeptide to assume a secondary structure. Strong acids enhance the isomerization of amide bonds and hence destroy the secondary structure.

#### REFERENCES

- 1 Noguchi, J. *Progr. Polym. Sci. Japan* 1973, 5, 65
- 2 Imanishi, Y., Kugimiya, K. and Higashimura, T. *Biopolymers* 1973, 12, 2643
- 3 Imanishi, Y., Kugimiya, K. and Higashimura, T. *Biopolymers*, 1974, 13, 1205
- 4 Goodman, M. and Fried, M. *J. Am. Chem. Soc.* 1967, 89, 1264
- 5 Mark, J. E. and Goodman, M. *Biopolymers* 1967, 5, 809
- 6 Liquori, A. M. and DeSantis, P. *Biopolymers* 1967, 5, 815
- 7 Conti, F. and DeSantis, P. *Biopolymers* 1971, 10, 2581
- 8 Goodman, M., Chen, F. and Prince, F. R. *Biopolymers* 1973, 12, 2549
- 9 Imanishi, Y., Kugimiya, K. and Higashimura, T. *Polymer* 1975, 16, 345
- 10 Sisido, M., Imanishi, Y. and Okamura, S. *Biopolymers* 1970, 9, 791
- 11 Silverstein, R. M. and Bassler, G. C. 'Spectrometric Identification of Organic Compounds', 2nd Edn, John Wiley, New York, 1967
- 12 Roberts, J. D. *J. Am. Chem. Soc.* 1956, 78, 4495
- 13 Bovey, F. A. and Tiers, G. V. D. *J. Polym. Sci. (A)* 1963, 1, 849
- 14 Hanlon, S., Russo, S. F. and Klotz, I. M. *J. Am. Chem. Soc.* 1963, 85, 2024
- 15 Bradbury, J. H., Fenn, M. D. and Moritz, A. G. *Aust. J. Chem.* 1969, 22, 2443
- 16 Stewart, W. E., Mandelkern, L. and Glick, R. E. *Biochemistry* 1967, 6, 143
- 17 Steigman, J., Verdini, A. S., Montagner, C. and Strasorier, L. *J. Am. Chem. Soc.* 1969, 91, 1829
- 18 Sisido, M., Imanishi, Y. and Higashimura, T. *Biopolymers* 1973, 12, 2375

# On the theory of the Ising model of the macromolecular solution

L. Georgescu

Faculty of Physics, University of Bucharest, Măgurele, Bucharest, Romania

(Received 25 June 1974; revised 13 September 1974)

The partition function of a macromolecular binary solution is transposed in the partition function in Ising's model. On the basis of this model the macrocanonical function is explained by the presence of the interaction forces, in the one-dimensional as well as in the two-dimensional cases. The chemical potential of the macromolecular solution is calculated in both cases and compared with the results obtained by Flory and Huggins.

## INTRODUCTION

The chemical potential of the athermal macromolecular solution has been calculated by Flory<sup>1</sup> and Huggins<sup>2</sup>, the flexible macromolecular chain being introduced in a pseudorecticular lattice (model lattice proposed by Bethe<sup>3</sup>). The entropy of mixing was calculated by a combination method.

Later, the calculations were improved by Miller<sup>4</sup> and Guggenheim<sup>5</sup>. Interaction forces between the macromolecules and solvent molecules were taken into account by Orr<sup>6</sup> and Guggenheim<sup>7</sup> who studied the irregular solution, starting from the above described quasichemical approximation.

The historical evolution with regard to the calculation of the chemical potential of the macromolecular solutions as well as other papers in this field may be found in Tompa's and Petrea's<sup>8</sup> monographs.

In this paper the same problem is discussed again, i.e. the calculation of the chemical potential of a macromolecular solution on the Ising model base is adopted for a binary solution<sup>9</sup>. The lattice model is maintained and in each cell of the lattice it is possible to introduce either a solvent molecule or a monomer unit of the macromolecule. In the language of Ising's model we may say that a state  $j$  of the lattice can be represented by a quantity  $\sigma_j$  that can take two values only,  $\pm 1$ . In the event when  $\sigma_j = 1$ , the lattice  $j$  is occupied by a particle of type 1 (a solvent molecule) and when  $\sigma_j = -1$  the lattice  $j$  is occupied by a particle of type 2 (a monomer unit of the macromolecule).

The quantity  $(1 + \sigma_j)/2$  that also takes the value 1, may be defined if the lattice cell  $j$  is occupied by the particle of type 1, and the quantity  $(1 - \sigma_j)/2$  that also takes the value 1 if the particle of type 2 is present in the  $j$  cell. In this manner the number of particles of type 1 and 2 is:

$$N_1 = \frac{1}{2} \sum_{j=1}^N (1 + \sigma_j) \quad (1)$$

$$N_2 = \frac{1}{2} \sum_{j=1}^N (1 - \sigma_j) \quad (2)$$

with  $N_1 + N_2 = N$ .

Macrocanonical partition function of the binary solution is transformed into the equivalent form of Ising's model. On this basis, the chemical potential is calculated in Ising's one-dimensional model, either when the interaction forces are neglected or in the presence of the interaction forces between the neighbouring particles to the lattice of 1-1, 2-2 and 1-2 types.

Later the chemical potential in Ising's two-dimensional model is calculated again in the presence of the interaction forces. In fact, one can calculate the free energy of mixing where by derivation, the chemical potential of the solvent or macromolecule may be obtained.

## GENERAL FORMULATION OF THE THEORY

We consider a binary solution which consists of solvent molecules (1) and of macromolecules (2), each particle being introduced in a lattice cell only. The flexible macromolecular chain is supposed to be homogeneous with the degree of polymerization  $\sigma$ . We choose the macrocanonical partition function of the binary solution in the following form:

$$Z = \sum_N \sum_m \exp \left( N_1 \ln \phi_1 + N_2 \ln \phi_2 - \frac{E_m}{kT} \right) \quad (3)$$

where

$$\phi_1 = \frac{n_1}{n_1 + \sigma n_2} \quad \text{and} \quad \phi_2 = \frac{\sigma n_2}{n_1 + \sigma n_2}$$

are the respective concentrations, with  $N_i = n_i N_A$  ( $N_A$  is the Avogadro number), and  $E_m$  the system energy in the state  $m$ . This energy may be expressed in the form:

$$E_m = \sum_{i,j=1}^N \frac{1}{2} a_{ij} A(\sigma_i, \sigma_j) \quad (4)$$

where

$$A(\sigma_i, \sigma_j) = \frac{1}{4} E_{11} (1 + \sigma_j) (1 + \sigma_j) +$$

$$\frac{1}{4} E_{22}(1 - \sigma_i)(1 - \sigma_j) + \frac{1}{2} E_{12}(1 - \sigma_i \sigma_j) \quad (5)$$

represents the energy between the pairs  $j$  and  $i$  and  $a_{ij}$  can take only the values 1 and 0.1 if  $j$  is a near neighbour of  $i$  and zero in the any other case. When we have mentioned relation (5), relations (1) and (2) were taken into account, as well as the fact that two neighbouring cells of the lattice can be occupied only by 1-1, 2-2, 1-2 pairs type with the corresponding energies  $E_{11}$ ,  $E_{22}$  and  $E_{12}$ .

Considering equations (4) and (5), relation (3) can also be expressed as:

$$Z = \sum_{\sigma_1 = \pm 1} \dots \sum_{\sigma_N = \pm 1} \exp \left\{ \frac{N}{2} \left[ \ln \phi_1 + \ln \phi_2 - \frac{z}{4kT} (E_{11} + E_{22} + 2E_{12}) \right] + \frac{1}{4} \left[ 2 \ln \phi_1 - 2 \ln \phi_2 - \frac{z}{kT} (E_{11} - E_{22}) \right] \sum_j \sigma_j - \frac{1}{8kT} (E_{11} + E_{22} - 2E_{12}) \sum_{i,j} a_{ij} \sigma_i \sigma_j \right\} \quad (6)$$

where

$$z = \sum_{j=1}^N a_{ij}$$

is the number of the nearest neighbours.

If we introduce the relations:

$$\alpha = \frac{1}{2} \left[ \ln \phi_1 + \ln \phi_2 - \frac{z}{4kT} (E_{11} + E_{22} + 2E_{12}) \right] \quad (7)$$

$$J = -\frac{1}{8kT} (E_{11} + E_{22} - 2E_{12}) \quad (8)$$

$$B = \frac{1}{4} \left[ 2 \ln \phi_1 - 2 \ln \phi_2 - \frac{z}{kT} (E_{11} - E_{22}) \right] \quad (9)$$

relation (6) can be condensed as:

$$Z = e^{N\alpha} \sum_{\sigma_1 = \pm 1} \dots \sum_{\sigma_N = \pm 1} \exp \left[ J \sum_{i,j} a_{ij} \sigma_i \sigma_j + B \sum_j \sigma_j \right] \quad (10)$$

or

$$Z = e^{N\alpha} Z_1 \quad (11)$$

where  $Z_1$  is the partition function in Ising's model. This

partition function can be expressed either in the one-dimensional model, or in the two-dimensional one in the form:

$$Z_1 = \lambda^N \quad (12)$$

where  $\lambda$  is the maximum eigenvalue of matrix  $P$ , that is connected to the partition function through the relation  $Z_1 = SpP^N$ <sup>10</sup>. The maximum eigenvalue  $\lambda$  can be explained as a function of the adopted model, which may be one- or two-dimensional.

### CHEMICAL POTENTIAL OF A MACROMOLECULAR SOLUTION IN ISING'S ONE-DIMENSIONAL MODEL

In the case of Ising's one-dimensional model, the maximum eigenvalue has the form:

$$\lambda = e^J [chB + (ch^2B - 2e^{-2Jsh^2J})^{1/2}] \quad (13)$$

and the macromolecular partition function, according to equation (12), will be:

$$Z = e^{N\alpha} e^{JN} [chB + (ch^2B - 2e^{-2Jsh^2J})^{1/2}]^N \quad (14)$$

the quantities  $\alpha$ ,  $J$  and  $B$  being given by relations (7)–(9). If the interaction forces are not considered ( $E_{11} = E_{22} = E_{12} = 0$ ), then relations (7)–(9) can be written in the form:

$$\alpha = \frac{1}{2} [\ln \phi_1 + \ln \phi_2]$$

$$J = 0 \quad (15)$$

$$B = \frac{1}{2} [\ln \phi_1 - \ln \phi_2]$$

In this case, relation (14) takes the simplified form:

$$Z = e^{N\alpha} [e^B + e^{-B}]^N \quad (16)$$

For the very diluted solutions  $[2chB]^N \approx e^{B(2N_1 - N)}$  because of the relation

$$\sum_j \sigma_j = 2N_1 - N$$

Then relation (16) becomes:

$$Z = \exp(N_1 \ln \phi_1 + N_2 \ln \phi_2) \quad (17)$$

which is analogous to that obtained by Flory<sup>1</sup> and Huggins<sup>2</sup>, because, if we pass to the chemical potential of the solvent, the well known relation:

$$\Delta\mu_1 = RT \left[ \ln(1 - \phi_2) + \phi_2 \left( 1 - \frac{1}{\sigma} \right) \right]$$

is obtained. If  $N \gg N_1$  with  $N \rightarrow \infty$ ,  $e^{-B}$  may be always neglected with respect to  $e^B$ . Here the macrocanonical partition function (16) takes the form:

$$Z = e^{(N_1 + N_2) \ln \phi_1} \quad (18)$$

and the solvent chemical potential:

$$\Delta\mu_1 = \frac{\partial\Delta F_m}{\partial n_1} = RT \left[ \ln(1 - \phi_2) + \phi_2 \left( 1 + \frac{\phi_2}{\sigma\phi_1} \right) \right] \quad (19)$$

for the reason of the case of the macrocanonical distribution  $\Delta F_m = kT \ln Z$ .

When the chemical potential of the solvent is calculated from relation (16), without any approximation, we obtain the following relation:

$$\Delta\mu_1 = RT \left\{ \frac{1}{2} (\ln \phi_1 + \ln \phi_2) + \ln \left[ \exp \frac{1}{2} (\ln \phi_1 - \ln \phi_2) + \exp \left( -\frac{1}{2} (\ln \phi_1 - \ln \phi_2) \right) \right] + \phi_2 \left( 1 + \frac{\phi_2}{\sigma\phi_1} \right) \right\} \quad (20)$$

When in relation (20)  $e^{-B}$  is neglected again with respect to  $e^B$  we find a new relation (19).

If the interaction forces are taken into account and we introduce the notations:

$$\frac{E_{11}}{kT} = \epsilon_{11}, \quad \frac{E_{22}}{kT} = \epsilon_{22}, \quad \frac{E_{12}}{kT} = \epsilon \quad (21)$$

the relations (7)–(9) become:

$$\alpha = \frac{1}{2} \left[ \ln \phi_1 + \ln \phi_2 - \frac{z}{4} (\epsilon_{11} + \epsilon_{22} + 2\epsilon) \right] \quad (22)$$

$$J = -\frac{1}{8} (\epsilon_{11} + \epsilon_{22} - 2\epsilon) \quad (23)$$

$$B = \frac{1}{2} [2 \ln \phi_1 - 2 \ln \phi_2 - z(\epsilon_{11} - \epsilon_{22})] \quad (24)$$

and the maximum eigenvalue can be also expressed as:

$$\lambda = e^J chB + (e^{2Jsh^2B} + e^{-2J})^{1/2} \quad (25)$$

If we consider  $e^{-2J}$  negligible with respect to  $e^{2Jsh^2B}$ , then relation (25) becomes:

$$\lambda = e^{J+B} \quad (26)$$

and the macrocanonical partition function will be:

$$Z = e^{N\alpha} \lambda^N = \exp \frac{N}{2} \left[ \ln \phi_1 + \ln \phi_2 - \frac{z}{4} (\epsilon_{11} + \epsilon_{22} + 2\epsilon) \right] \times \left\{ \exp \left[ -\frac{1}{8} (\epsilon_{11} + \epsilon_{22} - 2\epsilon) \right] \times \exp \frac{1}{4} [2 \ln \phi_1 - 2 \ln \phi_2 - z(\epsilon_{11} - \epsilon_{22})] \right\}^N \quad (27)$$

Now the chemical potential of the solvent may be calculated for the binary solution when we consider also the interaction between the neighbouring pairs without any

approximation as follows:

$$\Delta\mu_1 = RT \left[ \ln(1 - \phi_2) + \phi_2 \left( 1 - \frac{1}{\sigma} \right) - \phi_2^2 \left\{ \frac{1}{8} \epsilon_{11}(1 + 3z) + (z - 1) \frac{\epsilon_{22}}{8} - \frac{\epsilon}{4} (z - 1) \right\} \right] \quad (28)$$

#### CHEMICAL POTENTIAL OF A MACROMOLECULAR SOLUTION IN ISING'S TWO-DIMENSIONAL MODEL

In the framework of the two-dimensional model in the absence of external fields, the eigenvalue  $\lambda$  has the form<sup>10</sup>:

$$\lambda = \frac{1}{2} \ln [2sh(2J)] + \frac{1}{2} \ln \frac{2ch^2J}{sh^2J} + \mathcal{J} \quad (29)$$

where

$$\mathcal{J} = \frac{1}{2\pi} \int_0^\pi d\varphi \ln \frac{1}{2} [1 + (1 - \kappa^2 \sin^2 \varphi)^{1/2}] \quad (30)$$

with

$$\kappa = \frac{1}{ch2Jcth2J}$$

The free energy per particle may be expressed as:

$$\beta F = \alpha - \ln(ch2J) - \mathcal{J} \quad (31)$$

or as

$$\beta F = \alpha + \frac{1}{2} \ln(2sh2J) + \frac{1}{2} \ln \frac{2ch^2J}{sh^2J} + \mathcal{J} \quad (32)$$

with  $\beta = 1/kT$ .

If neither interaction forces nor the external field are taken into consideration, then  $J \rightarrow 0$ . In this case, taking into account the compound of the field of the matrix

$$V_3 = \exp \left( B \sum_j \sigma_j \right)$$

we have:

$$\beta F = N\alpha + B \sum_j \sigma_j = N_1 \ln \phi_1 + N_2 \ln \phi_2$$

and we have found again at the limit, Flory's results.

In the event when the interaction forces are considered, such as:

$$\beta F = N(\alpha + \ln \lambda) + B \sum_j \sigma_j \quad (33)$$

the free energy of mixing can be expressed in the form:

$$\begin{aligned} \Delta F_m = RT[n_1 \ln \phi_1 + n_2 \ln \phi_2 - \\ \frac{nz}{8} (\epsilon_{11} + \epsilon_{22} + 2\epsilon) - n \ln (2ch2J) - \\ n\mathcal{J} - \frac{2n_1 - n}{4} z(\epsilon_{11} - \epsilon_{22})] \end{aligned} \quad (34)$$

On the basis of relation (34) the chemical potential of the solution may be calculated:

$$\begin{aligned} \Delta\mu_1 = RT \left[ \ln \phi_1 + \phi_2 \left( 1 - \frac{1}{\sigma} \right) - \right. \\ \left. \phi_2^2 \left\{ \frac{z}{8} (3\epsilon_{11} - \epsilon_{22} + 2\epsilon) - \ln (2ch2J) - \mathcal{J} \right\} \right] \end{aligned} \quad (35)$$

the elliptical integral  $\mathcal{J}$  might be evaluated from tables<sup>11</sup>.

If  $\exp(-2J)$  is neglected with respect to  $\exp(2J)$ , relation (35) takes the final simplified form:

$$\begin{aligned} \Delta\mu_1 = RT \left[ \ln \phi_1 + \phi_2 \left( 1 - \frac{1}{\sigma} \right) - \left\{ \frac{\epsilon_{11}}{8} (3z - 1) + \right. \right. \\ \left. \left. \frac{\epsilon_{22}}{4} \left( 1 + \frac{z}{2} \right) - \frac{\epsilon}{2} \left( 1 + \frac{z}{2} \right) - \mathcal{J} \right\} \phi_2^2 \right] \end{aligned} \quad (36)$$

Analogously, the chemical potential of the solute may be calculated by deriving the free energy of mixing, relation (34), with respect to the variable  $n_2$ .

The expression of the solvent chemical potential for a binary macromolecular solution, expression (34), at the limit, coincides with the expression given by Flory for the athermal solutions which is in accordance with Ising's

two-dimensional lattice. Different results appear in the presence of the interaction forces, and the chemical potential is different depending on the forces of types  $\epsilon_{11}$ ,  $\epsilon_{22}$  and  $\epsilon$  as well as on the nearest neighbour number  $z$ .

In the one-dimensional model, the chemical potential expression is given by Flory, but it must not be forgotten that Ising's one-dimensional model no longer corresponds to a two-dimensional lattice from Flory's model.

At the limit only, in the case of very dilute solutions and in the absence of interaction forces, the results are analogous. The chemical potential also differs depending upon the interaction forces in the two models, see relations (28) and (34). The dependency on  $z$  is different too, stressing still more the essential differences between the one-dimensional model and the two-dimensional one, the latter being nearer to a flexible macromolecular chain.

#### ACKNOWLEDGEMENT

The author wishes to thank Professor I. Petrea for several useful discussions.

#### REFERENCES

- 1 Flory, P. J. *J. Chem. Phys.* 1942, 10, 51
- 2 Huggins, M. L. *J. Phys. Chem.* 1942, 46, 151
- 3 Bethe, H. A. *Proc. Roy. Soc. (A)* 1935, 150, 552
- 4 Miller, A. R. *Proc. Cambridge Phil. Soc.* 1943, 39, 54, 151
- 5 Guggenheim, F. A. *Proc. Roy. Soc. (A)* 1944, 183, 203
- 6 Orr, W. J. C. *Trans. Faraday Soc.* 1944, 40, 320
- 7 Guggenheim, E. A. *Proc. Roy. Soc. (A)* 1944, 183, 213
- 8 Tompa, H. 'Polymer Solutions', Butterworths, London, 1956;
- 9 Petrea, I. 'Termodinamica statistică a macromoleculilor', E.D.P., Bucharest, 1968
- 10 Gordon, F. N. and Montroll, E. W. *Rev. Mod. Phys.* 1953, 25, 353
- 11 Kerson Huang, 'Statistical Mechanics', John Wiley, New York, 1963
- 12 Hancock, H. 'Elliptic Integrals', Dover, New York, 1958

# Flow birefringence studies of polymer conformation: cellulose tricarbanilate in two characteristic solvents\*

J. W. M. Noordermeer, R. Daryanani and H. Janeschitz-Kriegl

Laboratory of Physical Chemistry, Delft University of Technology, Delft 8, The Netherlands

(Received 12 July 1974)

Flow birefringence measurements are reported on ten samples of cellulose tricarbanilate ( $14.1 \times 10^3 < M < 2180 \times 10^3$ ). Phenyl benzoate, dioxane and mixtures of both were used as solvents. The ratio of Maxwell constant to intrinsic viscosity  $[n]/[\eta]$  strongly depends on temperature and kind of solvent. In ether solvents this polymer has a stiffer conformation than in an ester or a ketone. With the aid of the theory of Gotlib and Svetlov quantitative conclusions about chain stiffness can be drawn from the observed molecular weight dependence of  $[n]/[\eta]$ . A number of 50 monomer units per random link were obtained in dioxane at 25°C. This agrees quite well with light scattering and intrinsic viscosity data. According to Burchard an interpretation of the great chain stiffness of this polymer in ether solvents can be given in terms of the formation of intramolecular hydrogen bonds. The tremendous influence of a change in stiffness on  $[n]/[\eta]$  must be ascribed to the varying sterical hindrance of rotation of the phenyl rings in the side groups of the chain. Unfortunately, no valuable information with respect to chain stiffening can be deduced from extinction angle data. Relatively small effects, as expected from theory, are almost completely masked by the influence of the polydispersity of the samples.

## INTRODUCTION

It is well known that, under certain conditions, biopolymers and their synthetic analogues can retain well ordered conformations after dissolution. These ordered conformations are usually stabilized by intramolecular hydrogen bonds and are extremely stable in the sense, that breaking of a single hydrogen bond is not advantageous. Only with the simultaneous breakage of a large number of adjacent hydrogen bonds does the ordered conformation collapse<sup>1</sup>.

At the present time conformational transitions in biological as well as synthetical macromolecules, are the subject of very intensive experimental and theoretical studies. Surprisingly, the technique of flow birefringence has been applied to the study of conformational transitions only in a few cases. As an example, Tsvetkov *et al.*<sup>2,3</sup> carried out experiments on the helix-coil transition of poly( $\gamma$ -benzyl-L-glutamate) in mixtures of dichloroethane and dichloroacetic acid. In the rather apolar solvent dichloroethane this macromolecule occurs as an  $\alpha$ -helix. In the strongly polar solvent dichloroacetic acid, however, the molecule assumes a randomly coiled conformation. At this transition the reduced viscosity  $\eta_{sp}/c$  of the polymer solution changes by a moderate factor of 2.5. In contrast, the intrinsic optical anisotropy of the molecules, which can be determined with the aid of flow birefringence, appears to decrease by a factor of about 50. This example clearly indicates the importance of flow birefringence as a technique for the study of conformational transitions in polymers.

In a recent paper<sup>4</sup> we have shown for a polyelectrolyte that valuable information concerning coil expansion can be

derived from flow birefringence data. In the present work we extend our flow birefringence studies to cellulose tricarbanilate in a series of solvents. Previously, flow birefringence of cellulose tricarbanilate has been measured by Janeschitz-Kriegl and Burchard<sup>5</sup> only in a single solvent but for a number of sharp fractions of various molecular weights. As a solvent benzophenone was used. Meanwhile new information has been gathered concerning this polymer. This information gives rise to the supposition that the formation of intramolecular hydrogen bonds between CO- and NH- groups of neighbouring carbamate groups, as already proposed by one of the mentioned authors<sup>6</sup>, would be more pronounced in ethers rather than in esters or ketones<sup>7</sup>. In fact, when the mentioned hydrogen bonds are formed, cellulose tricarbanilate assumes a kind of ladder conformation which has a greater chain stiffness than the conformation occurring in the absence of these hydrogen bonds.

The aim of the present investigation was to produce an independent check of the reported sensitivity of flow birefringence to changes of chain stiffness, as caused by changes in solvent composition.

Because of the considerable chain stiffness which is a property of all cellulose derivatives, and owing to the additional effect of the phenyl rings in the carbamate side-groups, cellulose tricarbanilate has an extraordinarily high intrinsic optical anisotropy. As under these circumstances form birefringence will hardly influence the measurements, the choice of solvent is greatly simplified; one can admit rather high refractive index increments without taking the risk of a disturbing influence of form birefringence. As is well known, this birefringence becomes considerable if a large difference exists between the refractive indices of polymer and solvent. In such a case the macromolecule as a whole contrasts with the solvent.

In the following measurements are reported on several samples of cellulose tricarbanilate covering a molecular

\* This communication comprises part of the work done by J. W. M. N. for his doctoral thesis. Another part has already been published<sup>4</sup>. A third part on the non-linear behaviour of the investigated polymer solutions will be published in due course.



weight range from  $14 \times 10^3$  to  $2180 \times 10^3$ . As an ester solvent we have chosen phenyl benzoate. Its refractive index is very close to that of the polymer. As an ether solvent we have chosen dioxane. Admittedly, the refractive index of the latter solvent differs quite considerably from that of the polymer. However, as will be shown below, the influence of form birefringence lies within the accuracy of the measurements. A considerable temperature range, viz. from  $25^\circ\text{C}$  to  $100^\circ\text{C}$ , has been covered by the reported experiments.

## THEORY

Flow birefringence is characterized by two quantities which can be measured separately, viz. the extinction angle and the birefringence, both as functions of shear rate. In addition the viscosities of the solution and of the solvent are needed for a proper interpretation of the results. For the theoretical background of flow birefringence reference can be made to the literature<sup>8</sup>. However, for the present purpose some additional remarks must be made.

A description of the hydrodynamic behaviour of a macromolecule in dilute solution was worked out in its most general form by Kramers<sup>9</sup>, Kirkwood and Fuoss<sup>10-12</sup>. These authors derived a general diffusion equation, which was the starting point for nearly all theoretical work on specialized model chains, as for example on the well known bead-spring model of Rouse<sup>13</sup>, Bueche<sup>14</sup> and Zimm<sup>15</sup>. It should be emphasized, however, that from such a diffusion equation only a linear elasticoviscous behaviour can be derived, in principle. A diffusion equation in the above sense is not consistent with non-linear constitutive equations which have often been used to describe non-Newtonian viscosity and non-linear flow birefringence behaviour of polymer fluids. In this connection we should refer to an early discussion between Saito and Prigogine<sup>16</sup> and to a recent report published by Merk<sup>17</sup>. According to Kirkwood<sup>11</sup> the generalized diffusion equation only holds for 'systems departing from equilibrium'. As a matter of fact, without rather arbitrary modifications introduced into this diffusion equation only linear results can be obtained. In particular, only Newtonian viscosities can be derived for polymer solutions.

As a consequence of the limitation of the linear theory to only small disturbances of the equilibrium situation we have to carry out proper extrapolations of our experimental results to zero shear rate in order to enable a correct interpretation. Notwithstanding the fact that cellulose tricarbanilate solutions show considerably non-linear behaviour, an unambiguous extrapolation into the range of linear behaviour appeared to be possible in all cases which are of interest for the present investigation. An attempt to describe the non-linear behaviour of cellulose tricarbanilate solutions is postponed to a later paper.

As is well-known, cellulose derivatives usually have a too low degree of polymerization for the formation of a Gaussian distribution of the end-to-end distances of the molecular coils. It has become customary to describe the flow birefringence of such non-Gaussian polymers with the aid of a molecular weight dependent coefficient  $[n]/[\eta]$  defined by:

$$\Lambda = [n]/[\eta] = (\Delta n \sin 2\chi - \Delta n_s)/q(\eta - \eta_s) \quad (1)$$

where  $\Delta n$  is the flow birefringence,  $\chi$  the extinction angle,  $\eta$  the viscosity of the solution and  $\Delta n_s$  the flow birefrin-

gence of the pure solvent, all these quantities being measured at the same shear rate,  $q$ . The solvent viscosity,  $\eta_s$ , usually does not depend on the shear rate. Notwithstanding the fact that the Maxwell constant  $[n]$  and the intrinsic viscosity  $[\eta]$  are separately defined only for the limiting cases of zero shear rate,  $q$  and concentration,  $c$ , i.e.:

$$[n] = \lim_{\substack{c=0 \\ q=0}} (\Delta n - \Delta n_s)/cq\eta_s; \quad [\eta] = \lim_{\substack{c=0 \\ q=0}} (\eta - \eta_s)/c\eta_s \quad (2)$$

the right hand side of equation (1) is independent of concentration, if the form birefringence effect is absent<sup>18,19</sup>, and also independent of shear rate, if the molecular weight of the polymer is sufficiently high. For such a solution of Gaussian chain molecules  $\Lambda$  has reached an upper limiting value  $\Lambda_\infty$ , no longer dependent on the molecular weight (the suffix stands for 'infinite' molecular weight). This means that a restriction of the definition of  $\Lambda_\infty$  to the limiting cases of zero shear rate and zero concentration becomes irrelevant. However, for non-Gaussian polymers, an extrapolation to zero shear rate has to be carried out anyway.

The quantity  $\Lambda_\infty$  is related to the structure of the macromolecular chain in the following way:

$$\Lambda_\infty = (4\pi/45) [(n^2 + 2)^2/n] (\alpha_1 - \alpha_2)/kT \quad (3)$$

where  $n$  is the refractive index of the solution,  $kT$  has its usual meaning and  $(\alpha_1 - \alpha_2)$  is the anisotropy of polarizability of the statistical random link with respect to directions parallel and perpendicular to its extension. Equation (3), which does not contain molecular weight, concentration and shear rate as parameters, can be obtained from all variants of the linear theory for Gaussian chains. In particular,  $\Lambda_\infty$  is also independent of the degree of hydrodynamic interaction ('free draining' or 'non-draining'). However, this is strictly valid only if the refractive index of the solvent is equal to that of the polymer ('matching solvent'). Otherwise the form birefringence gives a complicated contribution. The  $\Lambda_\infty$  value, undisturbed by form birefringence, as given by equation (3), depends roughly on two quantities: the temperature and the anisotropy  $(\alpha_1 - \alpha_2)$ , where the latter quantity should again be considered as a function of temperature. As to the temperature dependence of  $\Lambda_\infty$  very little is known. For the very flexible polymers polystyrene and polyethylene, for instance, nearly no influence of temperature on  $\Lambda_\infty$  could be observed in the accessible temperature range<sup>8</sup>. On the contrary, a strong temperature dependence of  $\Lambda_\infty$  was found for cellulose tricarbanilate in benzophenone<sup>5</sup> and for undiluted polydimethylsiloxanes<sup>20</sup>. The temperature dependence of  $\Lambda_\infty$  for cellulose tricarbanilate in some other solvents will be discussed in the experimental part of this work.

The anisotropy  $(\alpha_1 - \alpha_2)$  has formally been related separately to the length of the random link, the chemical structure of the chain<sup>18,21</sup> and to the degree and kind of solvation of the chain<sup>22</sup>. A change of one of these properties will lead to a change of the anisotropy which, on its part, can be observed as a change of the value of  $\Lambda_\infty$ . The conformation of the macromolecule is strongly related to the first two properties. Consequently, it must be expected that valuable information concerning conformational transitions of polymers can be deduced from the experimental values of  $\Lambda_\infty$ . However, if a change of solvent or solvent composition is involved in such a conformational transition, solvation effects may have a disturbing influence. Investi-

gations with atactic polystyrene, for instance, have shown that the solvent influence on the value of  $\Lambda_\infty$  can amount to 30% of its value for the polymer melt<sup>8</sup>. Unfortunately, correction methods or ways to exclude this influence are not known, so that solvation influences will cause some uncertainty in the interpretation of the experimental results. One can only hope that the extraordinarily high intrinsic optical anisotropy of the chain of cellulose tricarbaniolate will be predominant under all circumstances.

Whereas  $\Lambda_\infty$  is independent of molecular weight in the range of sufficiently high molecular weights, it appears that  $\Lambda$  decreases with decreasing molecular weight for non-Gaussian polymers. Gotlib and Svetlov<sup>23</sup> have made a successful approach to a calculation of the molecular weight dependence of  $\Lambda$ . For their calculations they used the model of a wormlike chain as described by Kratky and Porod<sup>24</sup>. For the calculation of the Maxwell constant, in principle, a detailed distribution function of chain coordinates is required, while for the calculation of the intrinsic viscosity only average chain dimensions are needed<sup>8</sup>. Gotlib and Svetlov calculated these quantities separately for the free draining case. They considered an assembly of 'frozen' random conformations of the wormlike chain. Brownian motion was taken into account only as far as rotary diffusion of the random conformations was concerned. In such a case only the average orientations of 'frozen' macromolecules determine their contributions to the flow birefringence of the streaming solution. In this way a first order distribution function with respect to shear rate is obtained, which holds for the limit of zero shear rate. Since  $\Lambda_\infty$  is independent of the degree of hydrodynamic interaction, the same is assumed for  $\Lambda$ . This justifies the use of the free draining approximation. Gotlib and Svetlov have derived the following relation for the dependence of  $\Lambda$  on chain length  $L$  and  $\Lambda_\infty$ :

$$\Lambda = (3/10)[x\phi_1(x)/\phi_2(x)]\Lambda_\infty \quad (4)$$

where  $x = L/a$  and  $a$  is the persistence length<sup>24</sup> of the wormlike chain. As is well known, this length is half the length of the statistical random link as introduced by Kuhn. The functions  $\phi_1(x)$  and  $\phi_2(x)$  depend in a complicated manner on  $x$ . They are explicitly given by Gotlib and Svetlov. This theory predicts  $\Lambda$  values which increase continuously with molecular weight and level off at  $\Lambda_\infty$ .

Equation (4) has been shown to give a good description of the molecular weight dependence of  $\Lambda$  for many polymer systems<sup>8</sup>. In particular, Janeschitz-Kriegl and Burchard<sup>5</sup> have shown its validity for cellulose tricarbaniolate fractions in benzophenone. Some further examples will be given in the experimental part of this paper.

Another point of interest is the behaviour of the extinction angle. It has become quite customary to interpret the optically measured extinction angles in terms of the hydrodynamic theory of the bead-spring model of Rouse<sup>13</sup> and Zimm<sup>15</sup>. For a solution of Gaussian chain molecules this is a permitted procedure, since in this case the contributions of the polymer molecules to the deviatoric components of the stress tensor and the refractive index tensor of the streaming solution are proportional. This means that the tensor ellipsoids are coaxial<sup>19</sup>. With this coaxiality taken for granted, the Rouse-Zimm theory yields the following result for Gaussian coils:

$$\cot 2\chi_c = \cot 2\chi' = J_{eR}\beta_N \quad (5)$$

where  $\chi_c$  is the extinction angle, as corrected for the solvent contribution to the flow birefringence of the solution, and  $\chi'$  is the orientation angle of the stress ellipsoid\*. The appropriate correction formula for the extinction angle  $\chi_c$  reads:

$$\cot 2\chi_c = \cos 2\chi / (\sin 2\chi - \Delta n_s / \Delta n) \quad (6)$$

For the symbols used see equation (1).

In equation (5)  $J_{eR}$  is the reduced steady-state shear compliance<sup>25</sup> and  $\beta_N$  is the reduced shear rate<sup>26</sup> defined by:

$$\beta_N = \frac{Mq(\eta_N - \eta_s)}{cRT} \quad (7)$$

where  $M$  is the molecular weight of the polymer and  $R$  the gas constant. The suffix  $N$  is used to indicate that the zero shear viscosity of the solution  $\eta_N$  is inserted. The use of the parameter  $\beta_N$  should result in a reduction of experimental data with respect to temperature, molecular weight and concentration. Owing to the linear character of the Rouse-Zimm theory the value of  $J_{eR}$  should be independent of shear rate. The numerical range quoted for Gaussian coils reads<sup>15</sup>:

$$\text{Gaussian coils} \left\{ \begin{array}{l} \text{'free draining'} \quad J_{eR} = 0.4 \\ \text{'non draining'} \quad J_{eR} = 0.205 \end{array} \right. \quad (8)$$

As the validity of this theory is restricted to very small shear rates, it can be expected that equation (5) is valid only for sufficiently small values of  $\beta_N$ .

In dealing with stiff, non-Gaussian chain molecules several difficulties arise. Primarily, the coaxiality condition, equation (5), does not hold for these cases. Secondly, recent work<sup>27-29</sup> on the bead-spring model has shown that the introduction of a certain kind of chain stiffness into this model causes a rise of the numerical value of  $J_{eR}$ .

For a demonstration of these facts we can look at the model of a rigid rodlike pearl necklace, which can be considered as the best approximation for a really rigid rodlike macromolecule. If the influence of hydrodynamic interaction is disregarded, the relations between the respective angles  $\chi'$  and  $\chi_c$  and the reduced shear rate  $\beta_N$  read<sup>30,31</sup>

$$\text{Rigid rodlike pearl necklace} \left\{ \begin{array}{l} J_{eR} = \cot 2\chi' / \beta_N = 0.6 \\ \cot 2\chi_c / \beta_N = 1.0 \end{array} \right. \quad (9)$$

For this model clearly no coaxiality exists. However, one can also conclude that the effects of varying chain stiffness on the value of  $J_{eR}$  and even on the value of the ratio  $\cot 2\chi_c / \beta_N$  are moderate. In this connection one has to keep in mind that a broad molecular weight distribution can produce changes of at least the same order of magnitude. In fact, it can be deduced that for a polydisperse system of Gaussian chain molecules equation (5) must read:

$$\cot 2\chi_c = pJ_{eR} \langle \beta_N \rangle_n \quad (10)$$

\* The reader may observe that the direction of each ellipsoid can be described by a single angle. Because of symmetry, one axis of the ellipsoid is perpendicular to the flow direction and lies in the shearing plane. The other two axes lie in a plane perpendicular to the shearing plane. The smallest angle between the shearing plane and one of the latter axes is chosen for convenience.

where  $p$  is a polydispersity factor and the angular brackets  $\langle \rangle_n$  mean that the number average molecular weight  $\langle M \rangle_n$  of the polymer is inserted in equation (7). For a description of the calculation of  $p$ , which can become rather large and dependent on solvent power, reference is made to the literature<sup>32-34</sup>.

Finally, the result should be quoted of a theory which describes the molecular weight dependence of the intrinsic viscosity of stiff polymers. Eizner and Ptitsyn<sup>35</sup> derived the following equation for the intrinsic viscosity of wormlike chains:

$$[\eta] = \frac{2^{3/2}(b/M_0)\Phi_0 N \chi(N/\lambda)}{[45(2\pi/3)^{1/2}/32(3 - 2^{1/2})](b/\lambda r_0) + (1/\lambda^{3/2})\phi(\lambda, N)N^{1/2}} \quad (11)$$

where  $\Phi_0$  is the Flory-Fox constant<sup>36</sup> equal to  $2.86 \times 10^{23} \text{ mol}^{-1}$ ;  $N$  is the degree of polymerization;  $r_0$  is the hydrodynamic radius of the monomer unit;  $M_0$  is the molecular weight of this unit; and  $\lambda$  is the ratio of the persistence length  $a$  to the length  $b$  of the monomer unit, i.e.  $\lambda = a/b$ . The ratio  $N/\lambda$  equals the parameter  $x = L/a$ , used in equation (4). The function  $\chi(N/\lambda)$  describes the ratio of the real mean square radius of gyration of the considered wormlike chain to the quantity  $aL/3$ . It is separately calculated by Eizner and Ptitsyn. The function  $\phi(\lambda, N)$  describes the intramolecular hydrodynamic interaction as a function of  $\lambda$  and  $N$ . It was tabulated by Kurath *et al.*<sup>37</sup>.

It should be emphasized that, from a physical point of view, equation (11) is valid only for an infinitively thin (persistent) thread. The hydrodynamic radius  $r_0$  is only a kind of friction factor for relative translational movements between chain units and solvent. In a double logarithmic plot equation (11) yields a continuously curved line which has a slope two at low molecular weights and a slope of one half at high molecular weights (non-draining limit).

The theories reviewed here are all valid only for theta solvents in which the excluded volume of the polymer chain is taken to be zero. For short or stiff chains in reasonably good solvents this may be a much less serious restriction than for long and intensively coiled molecules.

## EXPERIMENTAL

The investigations were done on ten samples of cellulose tricarbaniolate. Data on these samples are gathered in Table 1. The low molecular weight samples of the series CCI and CC II were prepared by partial precipitation from solutions in acetone with the aid of water. CC III was prepared from saponified cellulose 2½-acetate (Lonza). CC IV originates from bleached Linters cotton. The chemical origin of the sample CC V was not traced back\*.

Weight average molecular weights  $\langle M \rangle_w$  were determined by light scattering from solutions in dioxane<sup>7</sup>. No details about the heterogeneity of the low molecular weight fractions are known. Table 1 also contains the intrinsic viscosities of the samples, as determined in dioxane at 20°C.

The solvents were prepared in the following ways: 1, 4-dioxane (UCB) was dried over  $\text{MgSO}_4$  and distilled after-

wards. Phenyl benzoate (Fluka AG) was recrystallized from ethanol and thoroughly dried in vacuum.

Solutions were prepared by weighing dried polymer samples and freshly prepared solvent. In dioxane the samples dissolved within 1 or 2 days at room temperature. The phenyl benzoate solutions were prepared by shaking at 75°C for a few hours in a nitrogen atmosphere. Solutions in mixtures of both solvents were prepared by dissolving a certain amount of the sample in the calculated quantity of dioxane at room temperature and adding afterwards the required amount of phenyl benzoate. The compositions of the mixed solvents will be expressed in weight percentages.

Data of the pure solvents are given in Table 2 for the temperatures at which measurements were carried out. Pure phenyl benzoate shows a measurable flow birefringence. This means that all measurements carried out in this solvent and in mixtures with dioxane, have to be corrected for the solvent contribution to the flow birefringence of the solutions [cf. equations (1) and (6)]. Since, for low molecular weight fluids, a plot of flow birefringence against shear rate is always linear, Table 2 only contains the slopes of these plots. Data for the mixed solvents had to be determined separately, but are not quoted. Phenyl benzoate can be considered as a matching solvent, i.e. the refractive index increment  $dn/dc$  of cellulose tricarbaniolate is almost zero in this solvent. In dioxane, however, this quantity amounts to a measurable value of  $dn/dc = 0.156 \text{ cm}^3/\text{g}$  at 20°C<sup>6</sup>. Normally such a high value results in a relatively large contribution of form birefringence to the measured value of  $\Lambda$ . This contribution  $\Lambda_f$  can be calculated for Gaussian coils [equation (5.3) of Janeschitz-Kriegl<sup>8</sup>]. Using the above given value of  $dn/dc$  one obtains for the high molecular weight sample CC IV in dioxane:

$$(\Lambda_f/\Lambda_\infty) = 2.3 \times 10^{-2} \quad (12)$$

where the value of  $\Lambda_\infty$  is taken from the measurements at 25°C to be described below. In this comparison the

Table 1 Data of samples investigated

Code	$\langle M \rangle_w \times 10^{-3}$	$[\eta]$ at 20°C in dioxane (cm <sup>3</sup> /g)	$\frac{\langle M \rangle_w}{\langle M \rangle_n}$
CC 13	14.1	13.7	unknown
CC 14	14.0	13.4	unknown
CC 15	15.1	13.0	unknown
CC 17	15.1	13.3	unknown
CC 19	12.8	10.8	unknown
CC 112	8.2	9.1	unknown
CC II	3.1	5.35	unknown
CC III	185	168	1.59
CC IV	620	555	1.5
CC V	2180	—	1.2

Table 2 Data of pure solvents

Solvent	Temp. (°C)	Density (g/cm <sup>3</sup> )	Viscosity $\times 10^2$ (P)	$\Delta n_s/q \times 10^{11}$ (s)
Dioxane	25	1.0283	1.193	—
	35	1.0171	1.017	—
	50	0.9998	0.816	—
	60	0.9893	0.718	—
	75	0.9735	0.611	—
	90	0.9543	0.514	—
Phenyl benzoate	75	1.0893	2.699	1.137
	90	1.0766	1.982	0.843
	100	1.0682	1.693	0.733

\* Several of these samples (CC IV, CC V) were kindly supplied by Professor W. Burchard, Freiburg; others (CCI and CC II) were fractionated by one of our former cooperators (Mr A. Ghijsels) during his stay at the Institute of Macromolecular Chemistry of the University of Freiburg under kind supervision of Dr B. Pfannemüller.

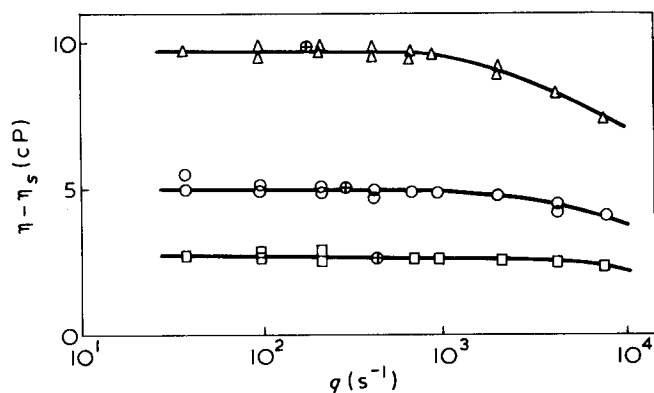


Figure 1 Shear dependence of solute contribution to the viscosity of solutions of CC IV in phenyl benzoate at 75°C. Concentrations are given in g/100 ml. □, 0.3%; ○, 0.5%; △, 0.8%. Experimental points obtained with the aid of Ubbelohde viscometers are indicated by ⊕

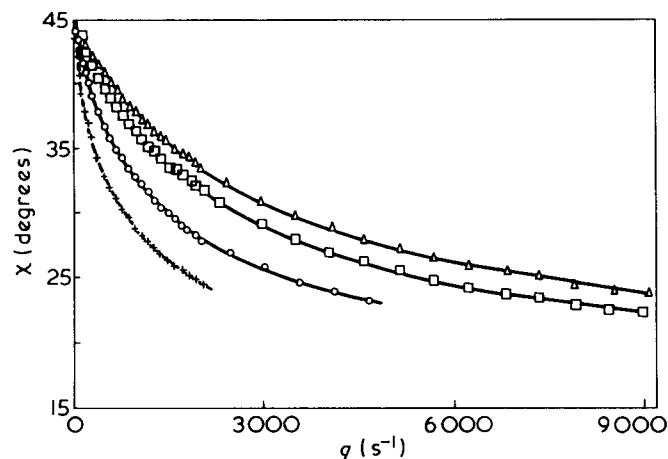


Figure 2 Extinction angles against shear rate for a series of solutions of CC IV in dioxane at 25°C. Concentrations are given in g/100 ml: △, 0.2; □, 0.3; ○, 0.5; +, 0.8

influence of a difference of 5°C between the temperatures of measurements of  $dn/dc$  and  $\Lambda_\infty$  is disregarded. It appears that the relative contributions of  $\Lambda_f$  for this high molecular weight sample is small enough to lie completely within the accuracy limits of the flow birefringence technique. If one keeps in mind that, from a theoretical point of view<sup>18</sup>, the form birefringence of the molecular coils should decrease with decreasing molecular weight, one arrives at the conclusion that this effect can be disregarded throughout the present investigation.

Flow birefringence measurements were carried out in the equipment previously described<sup>8,38</sup>. Viscosity measurements were done with the aid of ordinary Ubbelohde viscometers. A check with a special viscometer for non-Newtonian viscosities<sup>39</sup> showed that, except for the sample CC V, Ubbelohde measurements were always in fair agreement with the Newtonian viscosities at small shear rates. A few examples are given in Figure 1 for a series of solutions of CC IV in phenyl benzoate at 75°C. To remove dust all solutions were filtered through glass filters.

## RESULTS

Figure 2 gives extinction angle curves for a series of solutions of various concentrations of sample CC IV in dioxane at 25°C. The corresponding measurements of the birefringence  $\Delta n$  are given in Figure 3. For the lowest concentra-

tion the dependence of flow birefringence on shear rate appears to be linear. For higher concentrations some downward deviation can be noticed with increasing shear rate. With decreasing molecular weight the deviation of the extinction angle from 45° decreases rapidly, as can be seen in Figure 4. In this Figure extinction angles are given for a 1.32% (w/v) solution of sample CC III in pure phenyl benzoate at 75° and 90°C. In this connection it is important that the viscosities of dioxane and of phenyl benzoate are of the same order of magnitude at the respective temperatures of the measurements. This means that solvent viscosities cannot account for the differences between Figures 2 and 4. For the lowest molecular weight samples the deviations from 45° angle were so small that no reliable measurements could be done.

With the aid of equation (1) the experimental values of  $\Lambda$  can be calculated from these measurements. In Figure 5  $\Lambda$  values, as extrapolated to zero shear rate, are plotted for the sample CC IV in pure dioxane, respectively in pure phenyl benzoate, against concentration and with temperature as a parameter. In both solvents no significant influence of concentration on the results is observed. A relative scatter of about 10% is quite normal for these types of results, as they are calculated from three separate measurements of limited accuracy. The independence of  $\Lambda$  of concentration was found for all CC samples in all kinds of solvents. The importance of this fact for the interpretation will be discussed in the next paragraph.

On the other hand,  $\Lambda$  strongly depends on temperature in both solvents. This is quite a striking result, because

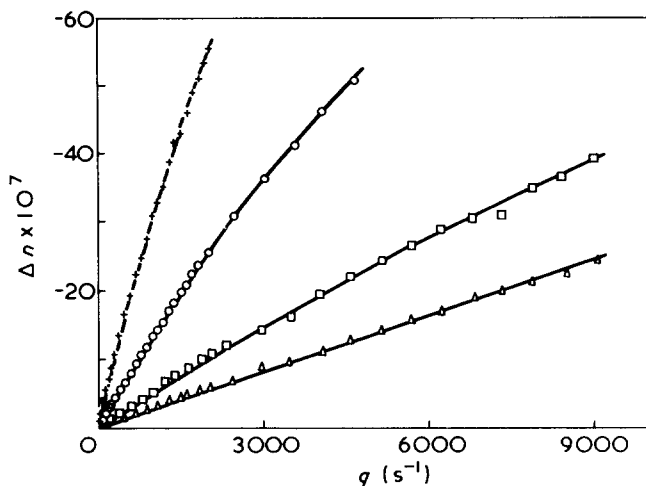


Figure 3 Flow birefringences against shear rate for solutions specified in the caption to Figure 2

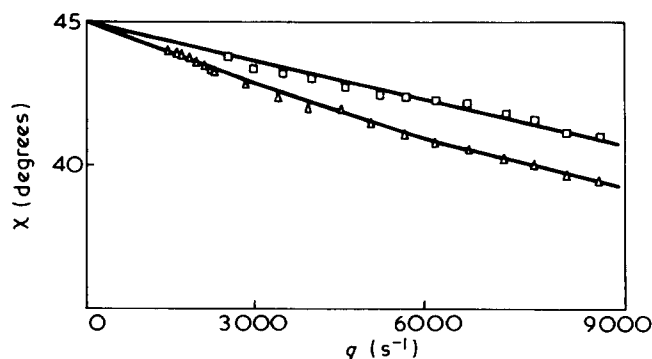


Figure 4 Extinction angle curves for a solution of CC III in phenyl benzoate at two temperatures: △, 75°; □, 90°C. Concentration = 1.32 g/100 ml

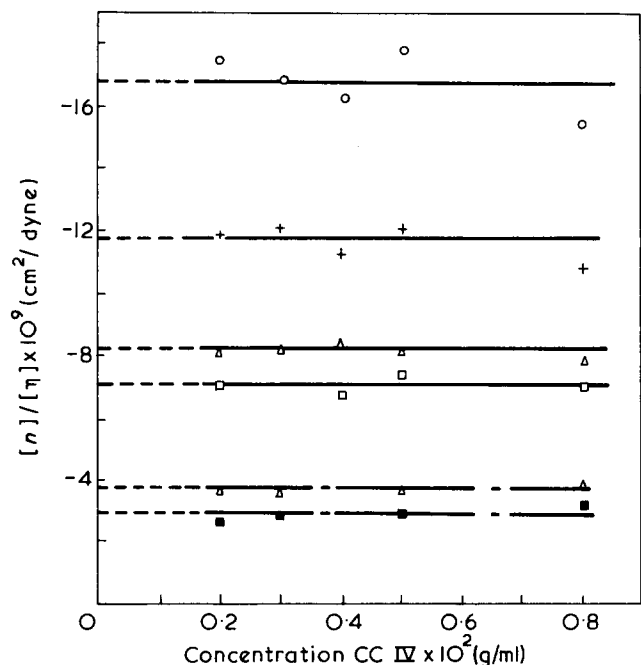


Figure 5 Ratios  $[n]/[\eta]$  against concentration for solutions of CC IV in dioxane (—) and phenyl benzoate (---) at several temperatures:  $\circ$ , 25°C; +, 50°C;  $\Delta$ , 75°C;  $\square$ , 90°C;  $\blacksquare$ , 100°C

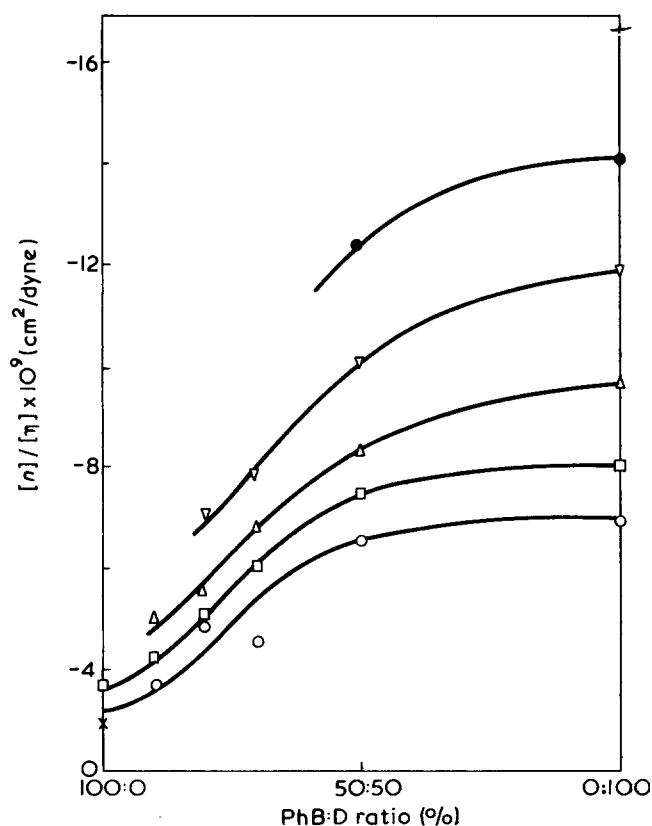


Figure 6 Ratios  $[n]/[\eta]$  after extrapolation to zero concentration for CC IV as functions of solvent composition (phenyl benzoate-dioxane).  $\bullet$ , 35°C;  $\nabla$ , 50°C;  $\Delta$ , 60°C;  $\square$ , 75°C;  $\circ$ , 90°C;  $\times$ , 100°C

until now no other polymer is known to have a  $\Lambda$ , which is so strongly temperature dependent. Moreover,  $\Lambda$  appears to be considerably larger for CC IV in dioxane than in phenyl benzoate at corresponding temperatures. To investigate this difference in more detail we have measured the value of  $\Lambda$  for CC IV in a series of mixtures of both solvents. The results, given in Figure 6, are averages of the values obtained on at least two concentrations. Phenyl benzoate melts at

about 70°C. Consequently, on the ester side no measurements could be carried out at low temperatures. In Figure 6 a clear transition can be observed, which almost entirely takes place in the range of high phenyl benzoate contents of the solvent.

A similar transition can also be observed in the intrinsic viscosity of CC IV as measured with changing composition of the solvent mixture at the same temperatures at which also flow birefringence measurements were carried out. This is shown in Figure 7. A comparison with Figure 6 shows that both transitions occur at about the same solvent composition. However, the total effect, as observed on the intrinsic viscosity, appears to be much smaller than that observed on the value of  $\Lambda$ , although the transition in the intrinsic viscosity is much sharper.

To understand the observed transitions more quantitatively, the dependence of  $\Lambda$  on molecular weight has been determined. For these measurements also the other CC samples, mentioned in Table I, were used. In Figure 8  $\Lambda$  values, as obtained in pure phenyl benzoate and in pure

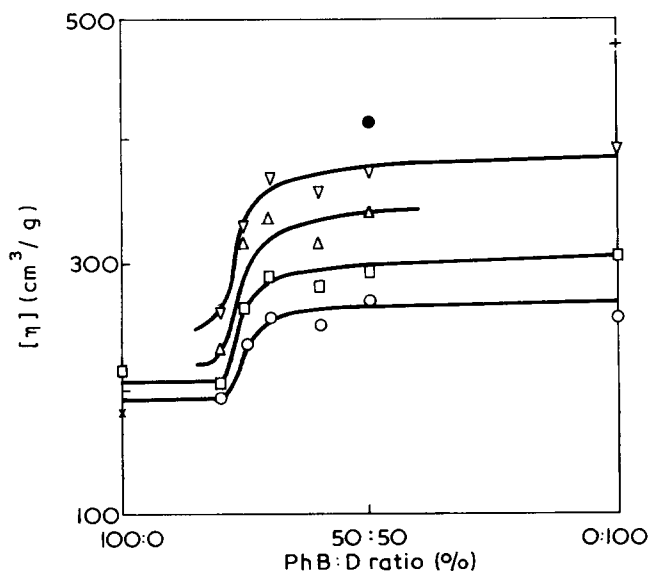


Figure 7 Intrinsic viscosities of CC IV at several temperatures as function of solvent compositions. For symbols see caption to Figure 6. +, 25°C

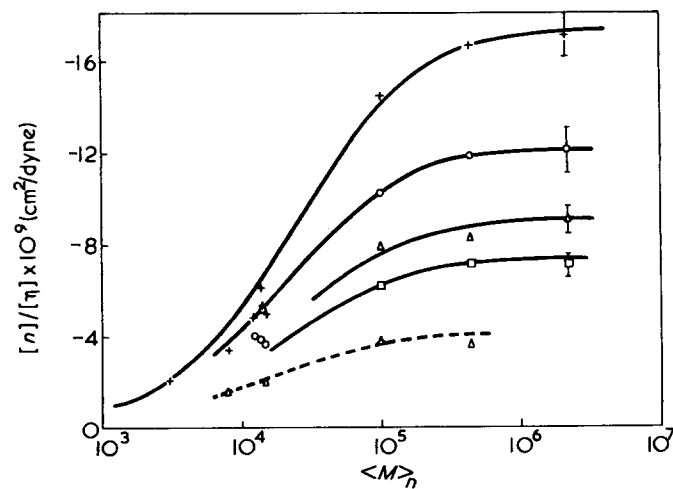


Figure 8 Plot of the values of ratio  $[n]/[\eta]$  against the logarithm of molecular weight for a series of samples of CC in dioxane (—) and phenyl benzoate (---) at several temperatures: +, 25°C;  $\circ$ , 50°C;  $\Delta$ , 75°C;  $\square$ , 90°C. The lines are theoretical curves according to the Theory of Gotlib and Svetlov. The pertinent parameters are enlisted in the first paragraph of the discussion

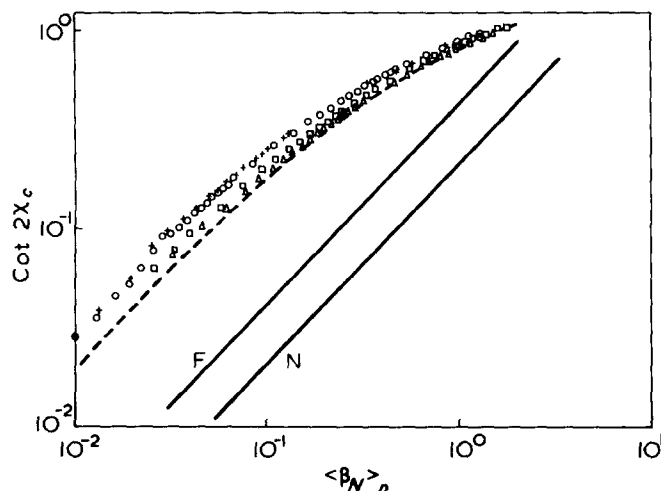


Figure 9 An example for the poor reducibility of extinction angle curves with respect to concentration. The indicated points are obtained with CC IV in dioxane at 25°C. For symbols see caption to Figure 2. - - -, Extrapolated curve for zero concentration; —, from Zimm's theory for the free draining case (F) and the non-draining case (N)

dioxane, are given as functions of the estimated number average molecular weights of the samples for the temperatures indicated. For the samples with weight average molecular weights between 3000 and 15 000 no number average molecular weights could be estimated. As a consequence, for these samples the  $\Lambda$  values are plotted against the weight average molecular weights. Most  $\Lambda$  values are averages of measurements on at least two concentrations. Of the high molecular weight sample CC V only a small amount was available, so that measurements could be carried out at only one concentration. The non-Newtonian behaviour of the viscosity of this solution, which was expected to be more pronounced than for the other samples, could not be measured either. As for CC V Ubbelohde measurements will lie in the non-Newtonian region of shear rates, no exact values of  $\Lambda$  can be determined. Shear rates at the capillary wall in the Ubbelohde viscometers were estimated on the approximate assumption of a parabolic flow profile. Values of  $\Lambda$ , however, as calculated according to equation (1) for those finite shear rates, can only be lower than the 'true'  $\Lambda$  for zero shear rate. This is a general experience for non-Gaussian polymers. For cellulose tricarbaniolate it is supported by Figure 10 of ref 5. On the other hand, flow birefringence data, which are first extrapolated to zero shear rate and then combined with the mentioned Ubbelohde viscosities, must give too high values of  $\Lambda$ . Both limits are given in Figure 8 by the endpoints of the vertical lines. As the best approximations for the true zero shear values of  $\Lambda$  the averages of both limits have been taken, as indicated by the symbols.

In Figure 9 an example is given for a plot of extinction angle curves against reduced shear rate  $\langle\beta_N\rangle_n$ . The points correspond to the measurements reproduced in Figure 2. The curves show an upwards shift with increasing concentration. This means that the reduction of the extinction curves with respect to concentration is not successful, as was found also for anionic polystyrenes by Daum<sup>40</sup> and Janeschitz-Kriegl<sup>8</sup>. Furthermore, a clear curvature can be observed for all concentrations at sufficiently high values of  $\langle\beta_N\rangle_n$ . Only for the lowest  $\langle\beta_N\rangle_n$  values a linear relationship between  $\cot 2\chi_c$  and  $\beta_N$ , as predicted by the linear theory, seems approximately valid. For CC IV in phenyl benzoate no measurements could be done at shear rates, low enough

to reach the linear region. In this connection it should be admitted that, with decreasing shear rate, the inaccuracy in the measurement of extinction angles becomes considerable. From Figure 9 it can be concluded that the results on the high molecular weight sample CC IV are not very useful for a determination of the zero shear values of the ratio of  $\cot 2\chi_c$  and  $\langle\beta_N\rangle_n$ .

In fact, the determination of this ratio is equivalent with a direct determination of the initial slope of the extinction angle curve. The accuracy of this determination mainly depends on the number of reliable extinction angle measurements carried out in the vicinity of the 45° angle. In this respect the measurements on sample CC III, which has a much lower molecular weight, look more promising as is seen from Figure 4. For this sample the initial slopes can be determined directly and with great accuracy.

The values of the ratio of  $\cot 2\chi_c$  and  $\langle\beta_N\rangle_n$ , as obtained for sample CC III according to this more direct method, are given in Figure 10. In the upper part of this Figure one finds the results for dioxane, in the lower part those for phenyl benzoate. The temperatures are indicated near the respective experimental curves. For solutions in dioxane at 90°C the extinction angles deviate so little from 45° that a reasonable estimate of  $\cot 2\chi_c/\langle\beta_N\rangle_n$  becomes impossible. From Figure 10 it may be concluded that the ratios of  $\cot 2\chi_c$  and  $\langle\beta_N\rangle_n$ , as extrapolated to zero shear rate do not only depend on concentration but also on temperature, at least for the solutions in dioxane. However, the temperature influence diminishes when the concentration is lowered. In other words, the reduction with respect to temperature may hold for infinite dilution. For finite concentrations it does not hold for CC III in dioxane. In the phenyl benzoate part of this Figure, however, the temperature difference between both series of measurements seems too small to show up in the results. A comparison of the results in both solvents shows that the values of  $\cot 2\chi_c/\langle\beta_N\rangle_n$  for the solutions in phenyl benzoate seem to lie below those for the dioxane solutions. The same trend was also observed for the solutions of CC IV. An extrapolation of the results in Figure 10 to zero concentration can be made with reasonable accuracy. Strictly speaking, however, the differences between the obtained results are so small that they nearly lie within the accuracy limits of the extrapolations. So it must be concluded that, if the transitions in  $\Lambda$  and in intrinsic viscosity

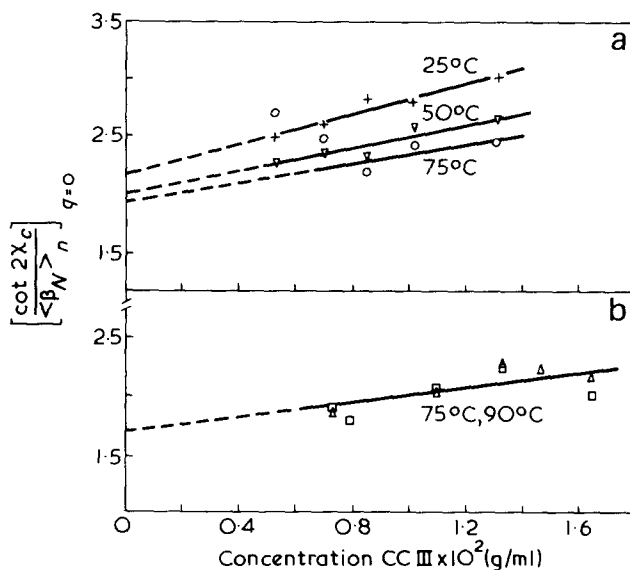


Figure 10 Values of  $[\cot 2\chi_c/\langle\beta_N\rangle_n]$  against concentration for CC III in (a) dioxane and (b) phenyl benzoate at several temperatures

Table 3 Properties of two samples of cellulose tricarbanilate in a series of solvents

Sample	Mol. wt. $\times 10^{-5}$	Solvent	Temp. (°C)	$[\eta]$ (cm <sup>3</sup> /g)	$[\eta]/[\eta] \times 10^9$ (cm <sup>2</sup> /dyne)	$(\alpha_1 - \alpha_2) \times 10^{25}$ (cm <sup>3</sup> )	S	$d(\ln[\eta])$	$d(\ln \alpha_1 - \alpha_2 )$
								$\frac{dT}{T} \times 10^2$	$\frac{dT}{T} \times 10^2$
CC IV	4.4	Dioxane	25	472	-16.60	-2270	50.0		
			50	390	-11.80	-1730	42.5	-0.98	-1.02
			75	305	-8.10	-1370			
			90	255	-7.00	-1167	38.6		
CC IX <sub>4</sub>	5.0	Phenyl benzoate	75	215	-3.72	-510	30.0	-0.71	-0.72
			100	180	-2.90	-426	-		
		Benzophenone	55	206	-3.96	-519	36.6	-0.68	-0.74
			80	174	-3.08	-430	34.7		

of cellulose tricarbanilate are accompanied by a change of the value of  $\cot 2\chi_c / \langle \beta_N \rangle_n$ , this change must be a very small one.

## DISCUSSION

The experimental results clearly demonstrate that cellulose tricarbanilate undergoes a kind of conformational transition when the solvent composition is changed from ester to ether. The simultaneous growths of  $\Lambda$  and of the intrinsic viscosity (Figures 6 and 7) probably point to a stiffening of the chain. The most direct proof for the character of the transition can be derived from Figure 8. The measurements represented in this Figure can be interpreted straightforwardly by the theory of Gotlib and Svetlov<sup>23</sup>. In fact, the full lines connecting these points are theoretical curves with the following parameters.

Dioxane: 25°C  $\Lambda_\infty = -17.52 \times 10^{-9}$  cm<sup>2</sup>/dyne,  $S = 50.0$   
 50°C  $\Lambda_\infty = -12.34 \times 10^{-9}$  cm<sup>2</sup>/dyne,  $S = 42.5$   
 75°C  $\Lambda_\infty = -9.10 \times 10^{-9}$  cm<sup>2</sup>/dyne,  $S = 42.5$   
 90°C  $\Lambda_\infty = -7.40 \times 10^{-9}$  cm<sup>2</sup>/dyne,  $S = 38.6$

Phenyl benzoate: 75°C  $\Lambda_\infty = -4.12 \times 10^{-9}$  cm<sup>2</sup>/dyne,  $S = 30.0$

where  $S$  is the number of monomer units per statistical random link (i.e. twice the number of units per length of persistence).

The lowest molecular weight samples usually give too low values when compared with theory. In the first place, this may be caused by the fact that for these samples the experimental values of  $\Lambda$  are plotted against the weight average instead of the number average molecular weight. This means that the points are probably shifted to the right. In the second place, for these low molecular weights, the chain can no longer be considered as an 'infinitely thin' persistent thread. Consequently, the theory of Gotlib and Svetlov cannot hold exactly for these samples. In the third place, Tsvetkov<sup>41</sup> has shown that, at sufficiently low degrees of polymerization, the anisotropy of the side-groups can take over the function of the anisotropy of the main chain which, for cellulose tricarbanilate, can result in an extraordinary descent of the absolute value of  $\Lambda$  with decreasing molecular weight and, in the worst case, even in a change of sign of the birefringence. Finally, it should be noticed that a logarithmic molecular weight scale is used in Figure 8. This overemphasizes the importance of the experimental points at low molecular weights.

Special attention should be paid to the high value of  $S = 50.0$  for cellulose tricarbanilate in dioxane at 25°C. From light-scattering measurements in a mixture of dioxane and

methanol of 56.5:43.5 (vol %), which is a  $\theta$ -solvent at 20°C, Burchard<sup>6,42</sup> calculated a length of the statistical random link of 282 Å. He assumed a symmetric rotational potential around  $\beta$ -glycosidic bonds with respect to a straight zig-zag conformation of the chain. The best fit of experimental results was obtained when an average monomer length of 5.50 Å was assumed. Using these values one obtains  $S = 51.3$ , which is close to the value given above for the dioxane solutions at 25°C.

From the above given values of  $S$  it can be concluded that the stiffness of cellulose tricarbanilate increases with a decrease of temperature. Moreover, it appears that also the transition, as observed with a change of solvent composition, must be ascribed to a changing stiffness of the chain; in the ester phenyl benzoate the chain is less stiff than in the ether dioxane at comparable temperatures.

In Table 3 a survey is given of the results obtained on sample CC IV in both pure solvents. In addition, results are mentioned which were obtained on the sharp fraction CC IX<sub>4</sub> of comparable molecular weight in benzophenone<sup>5</sup>. Before drawing conclusions from the values of  $\Lambda$  or  $\Lambda_\infty$ , one should realize that  $\Lambda_\infty$  is influenced by the refractive index of the solution and also explicitly by temperature. This means that it will be more adequate to use the values of the anisotropy ( $\alpha_1 - \alpha_2$ ) as calculated from  $\Lambda_\infty$  with the aid of equation (3). In the case of phenyl benzoate at 100°C the value of  $\Lambda_\infty$  is not known, as only one sample, i.e. CC IV, was investigated at that temperature. However, a look at Figure 8, where results for phenyl benzoate are given for 75°C, leads us to the conclusion that the molecular weight of CC IV is sufficiently high to yield a value of  $\Lambda$  which is practically equal to  $\Lambda_\infty$ . The calculated values of ( $\alpha_1 - \alpha_2$ ) are given in Table 3. The influences of temperature on the intrinsic viscosity and on the anisotropy of these polymer samples in the different solvents can be compared if the temperature coefficients of both quantities are calculated from the data in Table 3 (the results are given in columns 9 and 10).

Two groups of solvents can easily be discerned: on the one hand, the ether dioxane, in which cellulose tricarbanilate has a relatively high stiffness, on the other the ester phenyl benzoate and the ketone benzophenone, in which this polymer is more flexible. Also the high temperature coefficients of the intrinsic viscosity and of the anisotropy in dioxane must be noticed, compared with those for both other solvents. It further strikes that both coefficients are nearly equal in the same solvent. The temperature coefficients of the viscosity in phenyl benzoate and in benzophenone are of the same order of magnitude as those found for other cellulose derivatives<sup>43</sup>. The value found in dioxane is higher than the just mentioned ones. An interpretation of these facts in terms of the formation of a certain number

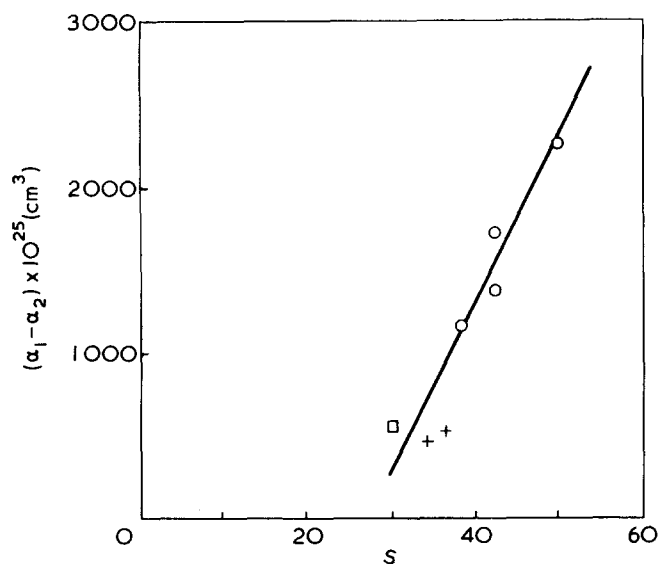


Figure 11 Anisotropy ( $\alpha_1 - \alpha_2$ ) of the statistical random link against the number  $S$  of monomer units per random link for CC in three solvents and at several temperatures.  $\circ$ , Dioxane;  $+$ , benzophenone;  $\square$ , phenyl benzoate

of intramolecular hydrogen bonds for cellulose tricarbaniolate in ethers<sup>7</sup> seems quite obvious.

In Figure 11 the results given in Table 3 are plotted graphically to illustrate the tremendous influence of  $S$  on the anisotropy ( $\alpha_1 - \alpha_2$ ); the latter quantity increases much more than proportional to the length of the statistical random link. Consequently, besides chain stiffening, which would lead to a linear relation between ( $\alpha_1 - \alpha_2$ ) and  $S$ , also other effects must play a role in the change of the anisotropy ( $\alpha_1 - \alpha_2$ ). Changes of the following effects can be responsible: (1) form birefringence; (2) polymer-solvent interaction resulting in variations of solvation as well as excluded volume; (3) stereochemical structure and conformation of the molecular chain. This classification is certainly quite arbitrary, as the different effects are usually inter-related. There are reasons, however, to expect a simpler situation with cellulose tricarbaniolate.

As to the effect of form birefringence, it has already been argued that this effect should be negligible even in dioxane. In fact, if form birefringence is of importance,  $\Lambda$  shows a systematic concentration dependence<sup>44</sup>. With a negative intrinsic anisotropy, as in the case of cellulose tricarbaniolate, an increase of the absolute value of  $\Lambda$  should be expected with increasing concentration. This was never found, which confirms that this effect can be neglected.

With a value of  $S = 50.0$  in dioxane at 25°C one molecule of the sample CC IV comprises only 17 random links. With such a small number of random links the molecule will only approximately form a Gaussian coil. In such a case, however, excluded volume cannot play a role of importance. On the other hand, in the transition of the anisotropy ( $\alpha_1 - \alpha_2$ ), as observed with a change of solvent composition, a change of solvation is certainly involved to some extent.

Undoubtedly, however, the strong change of the anisotropy with temperature and also with solvent composition, is mainly due to a change of the stereochemical structure of the chain. The fact that the anisotropy of the cellulose tricarbaniolate is negative, is caused by the presence of the phenyl rings in the side-groups. The polarizability of the phenyl groups, probably enhanced by the -CONH- links with the main chain, is certainly greater in the plane of the ring than in a direction perpendicular to the ring. The

extent to which these groups influence the anisotropy of the chain can be expected to depend on the average orientation of the rings with respect to the direction of the chain. A similar hypothesis has been put forward and evaluated quantitatively for the comparison of atactic and isotactic polystyrene<sup>21,45</sup>. When cellulose tricarbaniolate gets a stiffer structure by the formation of intramolecular hydrogen bonds, the phenyl groups become more closely packed. This can be seen with the help of a molecular model. The angle of rotation of the phenyl rings becomes nearly zero. A greater flexibility of the chain is accompanied by a greater freedom for rotation of the phenyl rings, which certainly explains a decrease of the negative anisotropy ( $\alpha_1 - \alpha_2$ ).

Another point of discussion is the interpretation of the transition found with the measurements of intrinsic viscosity (Figure 7). Before starting this discussion, however, the molecular weight dependence of the intrinsic viscosity in pure solvents should be interpreted.

In this context it is of importance that Burchard *et al.*<sup>46</sup> had already measured the molecular weight dependence of the intrinsic viscosity of cellulose tricarbaniolate in dioxane at 20°C. For these measurements a great number of samples with narrow molecular weight distribution ( $M_w/M_n < 1.1$ ) was used. The respective results are given in Figure 12. This Figure also contains measurements on a series of sharp fractions in benzophenone at 55°C<sup>5</sup> and on the samples CC I<sub>5</sub>, CC I<sub>12</sub>, CC III and CC IV in phenyl benzoate at 75°C.

With the aid of the Eizner-Ptitsyn theory<sup>35</sup> we have calculated the molecular weight dependence of the intrinsic viscosity of cellulose tricarbaniolate in dioxane at 20°C. The molecular weight of the monomer unit  $M_0$  is 519. For the length  $b$  of the monomer unit a value of 5.15 Å was taken, as obtained from X-ray diffraction data on cellulose<sup>47</sup>. For the number of monomer units per random link  $S = 2\lambda$  we used the value of 50.0, in accordance with our flow birefringence data, as obtained on solutions in dioxane at 25°C. The difference of 5°C between the temperatures of the flow birefringence and viscosity measurements seem to us of minor importance. For the hydrodynamic radius  $r_0$  of the monomer unit a value of 9.2 Å was chosen, which agrees

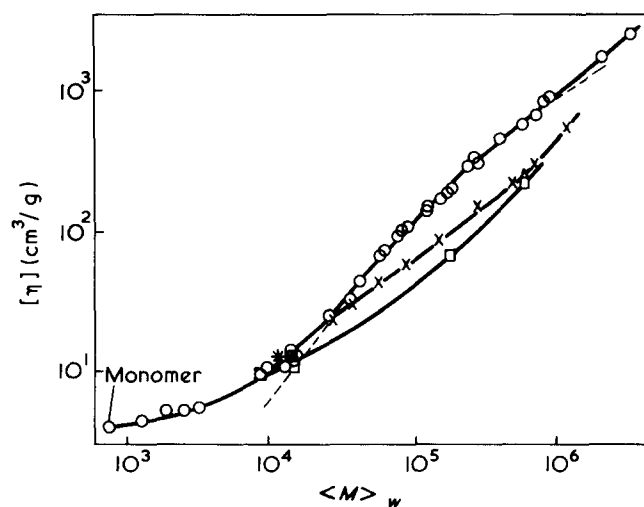


Figure 12 Intrinsic viscosity of cellulose tricarbaniolate fractions against molecular weight in various solvents:  $\circ$ , dioxane at 20°C according to ref 46;  $\times$ , benzophenone at 55°C according to ref 5;  $\square$ , phenyl benzoate. - - -, theory of Eizner and Ptitsyn for the parameters indicated; \*, theoretical point for a rigid prolate ellipsoid of one persistence length and appropriate thickness.  $b = 5.15$  Å;  $r_0 = 9.2$  Å;  $S = 50$



with the one used by Janeschitz-Kriegl and Burchard<sup>5</sup>. The results of this calculation are given by the broken line in *Figure 12*. Except for the lowest and highest molecular weights the experimental and theoretical lines completely coincide, which means that the flow birefringence and viscosity measurements on cellulose tricarbanilate in dioxane at 20° and 25°C respectively are in excellent agreement.

For the low molecular weight samples the model of an infinitely thin wormlike chain, as used by Eizner and Ptitsyn, cannot be realistic. For these samples the finite thickness of the chain will have a pronounced influence on the intrinsic viscosity. As has been pointed out by Janeschitz-Kriegl and Burchard<sup>5</sup>, short wormlike chains of finite thickness can better be approximated by prolate ellipsoids. For these ellipsoids the well known theory of Simha<sup>48</sup> can be used to calculate the intrinsic viscosity. Following this idea we calculated the intrinsic viscosity for a particle of a length equal to one persistence length  $a (= bS/2)$ . As such a particle contains about 25 monomer units in dioxane at 20°C, its molecular weight is  $13 \times 10^3$ . In fact, some mistake was made in ref 5 in the calculation of the volumes of the equivalent ellipsoids. This mistake resulted in too low values of the intrinsic viscosity for these ellipsoids, when no effective increase of thickness was assumed as a consequence of solvation. The value obtained by the present authors on assuming a value of 5.15 Å for the monomer length and a value of 9.2 Å for the mean radius of the cross-section of the chain, is indicated in *Figure 12* by an asterisk. This value agrees quite well with the experimental results for dioxane.

The character of the curves drawn through the experimental points for benzophenone and phenyl benzoate, however, is quite different from the theoretically predicted curve. In fact, contrary to the theoretical prediction these curves show an upwards curvature in the whole range of molecular weights. The minor differences between the experimental curves in benzophenone and phenyl benzoate are probably due to the fact that the samples measured in the latter solvent are polydisperse. The curves obtained for benzophenone and phenyl benzoate are below the one for dioxane. According to the Eizner–Ptitsyn theory this would correspond to a lower value of  $S$ , in accordance with flow birefringence data. As already suggested<sup>5</sup> the opposite curvature of these experimental curves must be ascribed to the influence of the excluded volume effect which can be expected to show up at a lower molecular weight for a more flexible chain. As a matter of fact, for the stiff chains in dioxane one can see a slight deviation from the theoretical line due to excluded volume only at the highest molecular weights. Finally, it can be observed in *Figure 12* that all experimental curves seem to converge at small molecular weights, where the influences of chain stiffness as well as excluded volume vanish.

At this point it is no longer difficult to interpret the transition of intrinsic viscosity, as observed in *Figure 7* for sample CC IV, when dissolved in various mixtures of dioxane and phenyl benzoate. From an inspection of *Figure 12* one can learn that, for a molecular weight of about 500 000, the transition occurs from a  $[\eta]$  value in pure dioxane, which is practically uninfluenced by excluded volume, to a lower  $[\eta]$  value in phenyl benzoate, which is due to an increased flexibility. This  $[\eta]$  value would be even lower, if there would be no influence of excluded volume. In connection with this last statement it is convenient to know that the concave experimental curve for phenyl benzoate and a convex theoretical curve according to equation (11) with  $S = 2\lambda = 30$  just touch each other at a molecular weight some-

what higher than  $10^5$ . The same has been shown for benzophenone<sup>5</sup>.

As a final point of discussion we now choose the behaviour of the extinction angle. For this purpose *Figures 9* and *10* are considered. For a comparison of these measurements with the results of Zimm's<sup>15</sup> treatment of the bead-spring model, two theoretical lines are also drawn in *Figure 9*. The upper line, denoted by  $F$ , stands for the free-draining approximation of a Gaussian coil molecule, the lower one, designated by  $N$ , for the non-draining case (see equation 8). Apart from a considerable upwards shift with respect to the theoretical lines, which is due to the polydispersity of the sample CC IV, this *Figure* clearly shows the non-linear behaviour of the extinction angle curves of this sample. The low molecular weight CC III, does not show a non-linear behaviour. By this fact an extrapolation to zero shear rate becomes possible. But even then it is rather difficult to draw conclusions from the observed changes of  $\cot 2\chi_c / \langle \beta_N \rangle_n$ , as shown in *Figure 10*. However, a general trend can be deduced from this *Figure*: the value of  $\cot 2\chi_c / \langle \beta_N \rangle_n$  shows a tendency to grow with increasing stiffness of the chain. The temperature and the solvent influence on the chain stiffness can be recognized in a change of  $\cot 2\chi_c / \langle \beta_N \rangle_n$ . If one assumes that the behaviour of  $\cot 2\chi_c / \langle \beta_N \rangle_n$  reflects that of the quantity  $pJ_{eR}$ , one can conclude that the prediction put forward in the theoretical part of this paper, viz. that  $J_{eR}$  increases with growing stiffness is confirmed by these experiments. However, in view of the limited accuracy of the extrapolation procedures the question remains in how far the observed changes can be considered as significant. Moreover, also a possible influence of chain stiffness on the value of the polydispersity factor  $p$  can be responsible for the observed effects.

To get an idea of the values of  $J_{eR}$  for a monodisperse sample, certain assumptions can be made. If we assume that the molecular weight distribution of sample CC III is of the Schulz–Zimm type, we can calculate a value of  $p$  according to Peterlin<sup>32,34</sup> and Daum<sup>33</sup>. For this purpose we need the polydispersity index of this sample, as given in *Table 1*, and the exponent  $\alpha$  in the Mark–Houwink equation. As is well known, this equation reads  $[\eta] = KM^\alpha$ . However, the value of  $\alpha$  is not a constant for cellulose tricarbanilate in all solvents and at all temperatures used (see the curved lines in *Figure 12*). But from *Figure 12* a smoothed exponent  $\alpha$  of about 1.0 can be deduced for CC III in dioxane at 20°C. On using this value we obtain a polydispersity factor:

$$p = 3.80 \quad (13)$$

If we further assume that this value will approximately hold in dioxane at the slightly different temperature of 25°C, it can be used for a correction of  $\cot 2\chi_c / \langle \beta_N \rangle_n$ , as extrapolated in *Figure 10* to infinite dilution. One obtains in this way:  $J_{eR} \sim 0.57$ . This value lies only slightly above the range quoted for Gaussian coils (see equation 8). As a matter of fact, this is surprising, as sample CC III comprises in dioxane at 25°C only about 4 random links.

The conclusion can be drawn that the influence of chain stiffness on the behaviour of the extinction angle is very small; it nearly lies within the limits of experimental error. Moreover, the influence of polydispersity masks the effects to such an extent that no quantitative conclusion can be drawn. It appears that the behaviour of the extinction angle hardly gives any valuable information concerning the observed stiffening of cellulose tricarbanilate.

## ACKNOWLEDGEMENTS

The authors are indebted to Professor W. Burchard and Dr B. Pfannemüller, University of Freiburg, for supplying samples and still unpublished results as well as for suggestions and discussions. They also thank Mr U. Daum for providing the opportunity to measure non-Newtonian viscosities at the Central Laboratory TNO.

## REFERENCES

- 1 Birshtein, T. M. and Ptitsyn, O. B. 'Conformations of Macromolecules', (High Polymers: Vol XXII) Interscience, New York, 1966
- 2 Tsvetkov, V. N., Shtennikova, I. N., Ryumtsev, Ye. I. and Pirogova, G. F. *Vysokomol. Soedin. (A)* 1967, **9**, 1583
- 3 Tsvetkov, N. V., Shtennikova, I. N., Skazka, V. S. and Ryumtsev, Ye. I. *J. Polym. Sci. (C)* 1968, **16**, 3205
- 4 Noordermeer, J. W. M., Janeschitz-Kriegl, H. and Horvath, A., *Polymer* 1973, **14**, 178
- 5 Janeschitz-Kriegl, H. and Burchard, W. *J. Polym. Sci. (A-2)* 1968, **6**, 1953
- 6 Burchard, W. *Makromol. Chem.* 1965, **88**, 11
- 7 Burchard, W. personal communication
- 8 Janeschitz-Kriegl, H. *Adv. Polym. Sci.* 1969, **6**, 170
- 9 Kramers, H. A. *J. Chem. Phys.* 1946, **14**, 415; 1948, **16**, 565
- 10 Kirkwood, J. G. and Fuoss, R. M. *J. Chem. Phys.* 1941, **9**, 328
- 11 Kirkwood, J. G. *Rec. Trav. Chim. Pays-Bas* 1949, **68**, 649; *J. Polym. Sci.* 1954, **12**, 1
- 12 Kirkwood, J. G. 'Macromolecules', (Ed. P. L. Auer), Gordon and Breach, New York, 1967
- 13 Rouse, P. E. *J. Chem. Phys.* 1953, **21**, 1272
- 14 Bueche, F. J. *J. Chem. Phys.* 1954, **22**, 603
- 15 Zimm, B. H. *J. Chem. Phys.* 1956, **24**, 269
- 16 Saito, N. and Prigogine, I., discussion remarks in ref 12, p 31
- 17 Merk, H. J. *Rep. WTHD 46*, Delft University of Technology (May 1973)
- 18 Tsvetkov, V. N. in 'Newer Methods of Polymer Characterisation', (Ed. B. Ke), Interscience, New York, 1964
- 19 Janeschitz-Kriegl, H. *Makromol. Chem.* 1960, **40**, 140
- 20 Wales, J. L. S. personal communication
- 21 Birshtein, T. M., Volkenshtein, M. V., Gotlib, Yu. Ya. and Ptitsyn, O. B., *Vysokomol. Soedin.* 1962, **4**, 670
- 22 Frisman, E. V., Dadivanyan, A. K. and Dyuzhev, G. A. *Dokl. Akad. Nauk SSSR* 1963, **153**, 1062
- 23 Gotlib, Yu. Ya. and Svetlov, Yu. E. *Dokl. Akad. Nauk SSSR* 1966, **168**, 621; *Ukr. Fiz. Zh.* 1967, **12**, 331
- 24 Kratky, O. and Porod, G. *Rec. Trav. Chim. Pays-Bas* 1949, **68**, 1106
- 25 Tschoegl, N. W. *J. Chem. Phys.* 1966, **44**, 4615
- 26 Peterlin, A. *J. Chem. Phys.* 1963, **39**, 224
- 27 Thurston, G. B. and Morrison, J. D. *Polymer* 1969, **10**, 421
- 28 Lodge, A. S. and Yeen-jing Wu, Paper presented at Soc. Rheol. Winter Meet., Salt Lake City (February 1971)
- 29 Noda, I. and Hearst, J. E. *J. Chem. Phys.* 1971, **54**, 2342
- 30 Kotaka, T. *J. Chem. Phys.* 1959, **30**, 1566
- 31 Kuhn, W., Kuhn, H. and Buchner, P. *Ergeb. Exakt. Naturw.* 1951, **25**, 1
- 32 Peterlin, A. *J. Chem. Phys.* 1963, **39**, 224
- 33 Daum, U. *J. Polym. Sci. (A-2)* 1968, **6**, 141
- 34 Peterlin, A. and Munk, P. in 'Physical Methods of Chemistry', Vol I, Part III c (Eds A. Weissberger and B. Rossiter), John Wiley, New York, 1972, p 271
- 35 Eizner, Yu. E. and Ptitsyn, O. B. *Vysokomol. Soedin.* 1962, **4**, 1725
- 36 Fox, T. G. and Flory, P. J. *J. Am. Chem. Soc.* 1951, **73**, 1909
- 37 Kurath, S. F., Schmitt, Ch. A. and Bachhuber, J. J. *J. Polym. Sci. (A)* 1965, **3**, 1825
- 38 Janeschitz-Kriegl, H. and Nauta, R. J. *J. Sci. Instrum.* 1965, **42**, 880
- 39 Daum, U. and Janeschitz-Kriegl, H. *Rheol. Acta* 1968, **7**, 349
- 40 Daum, U. unpublished results
- 41 Tsvetkov, V. N. *Dokl. Akad. Nauk SSSR* 1970, **192**, 380
- 42 Burchard, W. *Br. Polym. J.* 1971, **3**, 214
- 43 Flory, P., Spurr, O. K. and Carpenter, D. K. *J. Polym. Sci.* 1958, **27**, 231
- 44 Janeschitz-Kriegl, H. *Makromol. Chem.* 1959, **33**, 55
- 45 Tsvetkov, V. N. and Magarik, S. Ya. *Dokl. Akad. Nauk SSSR* 1959, **127**, 840
- 46 Burchard, W., et al. unpublished results
- 47 Meyer, K. H. and Misch, L. *Ber.* 1937, **70B**, 226; *Helv. Chim. Acta* 1937, **20**, 232
- 48 Simha, R. *J. Phys. Chem.* 1940, **44**, 25

# Polymers from acrylonitrile polymerized in the presence of vinylsulphone dyes

N. S. Batty and J. T. Guthrie

Department of Colour Chemistry and Dyeing, University of Leeds, Leeds LS2 9JT, UK

(Received 24 July 1974)

The properties of a series of 'copolymers' of acrylonitrile and various vinylsulphone dyes are discussed. Information relating to molecular size, the nature of the linkage between the chromophore and the backbone and the reactivity ratios of the two 'monomers' is given. These reactivity ratios are calculated from extinction coefficients on the assumption that there is no appreciable breakdown of the chromophore during polymerization. Factors governing the role of the dye in the polymerization process are considered in some detail. Thermal analysis techniques have been used to investigate the thermal stability of the products of polymerization. The thermograms have been used to assess the potential of these materials as pigments and to study the nature of their decomposition.

## INTRODUCTION

In a previous paper<sup>1</sup> we outlined a method for making coloured polymers by copolymerizing a dye with vinyl monomers. The kinetics of the reaction of acrylonitrile with three vinylsulphone dyes were investigated. This paper deals with the properties of the polymers so produced, attempts at their characterization and some of their uses. Work of this type falls within the concept of intrinsically coloured polymers, a topic which has been neglected somewhat in the past, especially outside industrial circles. However, there are notable exceptions<sup>2</sup>. We are mainly interested in the potential of such materials as pigments, though other avenues are not forgotten.

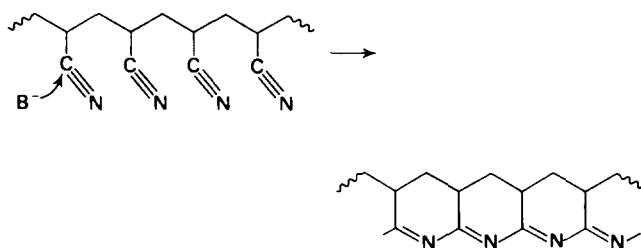
The properties desirable in a pigment depend on its end use. Fastness to migration and to light are generally required but may not be essential in particular applications. Good thermal stability is often necessary, especially in the pigmentation of moulded plastics. The cost of the pigment is important and may be an overriding factor. Problems of migration which are commonplace in many pigment applications should be overcome by using polymeric pigments, as the higher molecular weight will inhibit any tendency to migration.

It is well known that the light fastness of many dyes on polyacrylonitrile fibres is increased out of all proportion to the values obtained on wool or other fibres<sup>3</sup>. We hoped to take advantage of this fact by placing the chromophore in a compact environment of polyacrylonitrile through copolymerization. In this way we hoped to make polymeric pigments having improved light fastness over the unmodified chromophore.

A grinding operation is required to produce the full tinctorial value from all conventional pigments. In some cases the intensity of colour changes quite sharply with particle size<sup>4</sup>. Grinding is a long and expensive process, usually accounting for a large proportion of the cost of manufacturing the pigment. Using polymeric pigments this operation could become redundant.

The thermal stability of polyacrylonitrile and its copolymers has been extensively studied by Grassie and his co-workers<sup>5</sup>. On heating the polymer above 200°C, it becomes coloured, yellow then red and ultimately black. The same

sequence of coloration can be produced by the action of a basic catalyst on a solution of polyacrylonitrile<sup>6</sup>. There are some differences but the coloration in each case has been attributed to the formation of a conjugated  $-C=N-$  system; for example, by cyclization of the nitrile groups, thus:



The mechanism of this conjugation has been considered in detail by Gachkovskii<sup>7</sup>. The colour intensifies as the number of rings in sequence increases and the reaction is exothermic in character<sup>8</sup>.

## EXPERIMENTAL

In view of some of the problems encountered, the experimental procedure is given in considerable detail. The preparation of the copolymers of acrylonitrile and vinylsulphone dyes has already been described<sup>1</sup>.

### Osmometry

A Hewlett-Packard Series 500 high-speed osmometer was used for number-average molecular weight determinations. Each sample of polymer was dissolved in freshly distilled *N,N*-dimethylformamide (DMF) to give solutions of known concentration. The osmotic pressure between each polymer solution and the pure solvent at 37°C was measured. Initially the 'solvent-resistant' membranes (type 0-8) recommended by the manufacturer of the instrument were used. At best these membranes lasted only two days in the solvent before they began to disintegrate. Small pieces of debris from the membrane then obstructed the smooth flow of solvent through the capillary and its connecting tubes. The results became erratic and irreproducible.

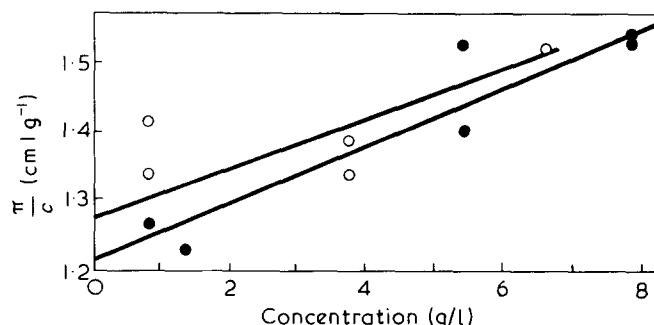


Figure 1 Plot of  $\pi/c$  ( $\text{cm l g}^{-1}$ ) against  $c$  (g/l) for sample of yellow 'copolymer' in DMF. Total dose: ○,  $6.3 \times 10^4$ ; ●,  $1.4 \times 10^5$  rad

This problem was overcome using modified hydroxyethyl cellulose membranes, whose preparation we have already disclosed<sup>9</sup>. Results obtained with these membranes were more reproducible and the useful lifetime of the membrane was far greater than that of the type 0-8 membrane. Indeed, membranes are still in service after six months in contact with DMF.

#### Spectroscopy

Infra-red spectra were recorded on a Perkin-Elmer recording spectrophotometer, model 157G, using the pressed disc technique and a constant polymeric pigment: potassium bromide ratio. Visible and ultra-violet spectra, recorded on a Unicam SP800 recording spectrophotometer, were obtained for samples in solution in DMF.

#### Thermal analysis

Samples were examined by differential thermal analysis (d.t.a.). Approximately 5 mg of sample were sealed in an aluminium pan and heated at  $10^\circ\text{C}/\text{min}$  from  $30^\circ$  to  $350^\circ\text{C}$  using a DuPont Model 900 Thermal Analyzer. An empty pan was used as the reference and the chamber purged with nitrogen during heating. One sample of each of the polymers made with yellow, red or blue dye was examined and compared with both the pure vinylsulphone dyes and polyacrylonitrile homopolymer.

#### Light fastness

Simple paints were made using the coloured polymers as pigments, drawn into even films on paper and dried at  $40^\circ\text{C}$ . The pigment was used both in full strength and reduced with titanium dioxide. Strips of the printed paper, 2.5 cm x 1.0 cm, were cut out and stapled across a 2.5 cm x 8.0 cm card. A similar card was prepared with dyed wool light fastness standards, supplied by the British Standards Institution. The cards were mounted in frames so that half of each sample was masked, then placed in a Xenotest (Quarzlampen GmbH, Hanau, Germany) 150 xenon arc fading lamp at  $33^\circ \pm 2^\circ\text{C}$  and  $63\% \pm 2\%$  relative humidity. Samples and standards were examined periodically until the contrast between the protected and exposed parts was judged to be equivalent to grade 3 of the Grey Scale for assessing change in colour<sup>10</sup>. The light fastness was then the number of the standard which had faded to the same extent.

#### Fibre-forming characteristics

Fibres were spun using 25% of the yellow 'copolymer' with 75% of commercial polyacrylonitrile. The respective amounts of polymer were dissolved in DMF to give a 30%

w/v solution. This solution, under a nitrogen atmosphere, was forced at  $110^\circ\text{C}$  through a spinneret and dried in a stream of air at  $190^\circ\text{C}$ . The fibres were collected as 8 filaments each of approximately 10 dtex. Their light fastness was assessed in the same way as the paint films.

#### Sulphur analysis

As a further check of the composition of the 'copolymers', quantitative sulphur analyses of a number of samples were carried out by the Microanalytical Section of the School of Chemistry, University of Leeds. The results were then compared with those obtained from spectroscopic analysis. From these results, values of the reactivity ratio,  $r_{\text{AN}}$  were derived, where  $r_{\text{AN}}$  denotes the reactivity ratio of the acrylonitrile monomer.

## RESULTS

#### Osmometry

DMF was used throughout as a solvent for the polymers. It is not an ideal solvent for osmometry because it rapidly attacks conventional membranes and has a strong affinity for water. Hence, moisture is constantly absorbed from the atmosphere and markedly reduces the efficiency of the solvent for polyacrylonitrile. In addition there is a tendency for small bubbles to form on and around the membrane during measurements.

The results of measurements on the coloured polymers are shown in Figures 1 to 4. Figures 1a and 1b relate to two yellow copolymers, (acrylonitrile with Remazol Golden Yellow G), made by exposing the mixed monomer solutions *in vacuo* to  $6.3 \times 10^4$  (a) and  $1.4 \times 10^5$  (b) rad of  $\gamma$  radiation. Although there is some scatter in the plots of  $\pi/c$  against concentration, values for  $\bar{M}_n$  of  $21\,900 \pm 1000$  and  $23\,000 \pm 1000$  g/mol were obtained for the two polymers respectively.

Plots of some of the other yellow samples, (identical monomers but various total doses of high energy radiation), are given in Figure 2. These indicate a decrease in the molecular weight with increasing total dose (Figure 3). This observation must be treated with reservation owing to the limited number of points available for each sample. In fact in several examples there was only sufficient sample for one concentration to be used. Here we have assumed the nature of polymer-solvent interactions to be identical to those

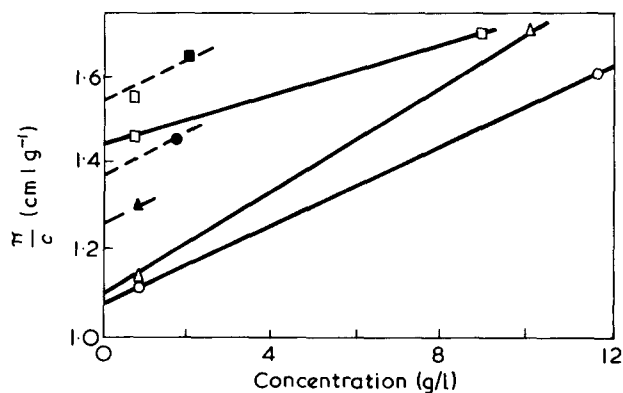


Figure 2 Plot of  $\pi/c$  ( $\text{cm l g}^{-1}$ ) against  $c$  (g/l) for a series of yellow copolymers for various total doses. Solid symbols indicate only one measurement carried out through lack of sample (see text). —, *in vacuo*; - - - -, in air. ○,  $0.36 \times 10^5$ ; ●,  $0.76 \times 10^5$ ; △,  $1.2 \times 10^5$ ; ■,  $1.4 \times 10^5$ ; □,  $1.8 \times 10^5$ ; ▲,  $2.4 \times 10^5$  rad

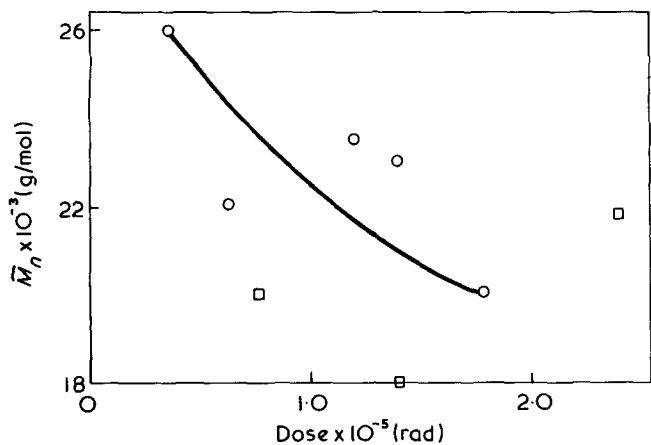


Figure 3 Variation in  $\bar{M}_n$  with increasing dose (rad); yellow 'copolymer'.  $\square$ , In air;  $\circ$ , in *vacuo*

observed with the yellow copolymers in DMF. With caution, certain observations can be made but these will require subsequent confirmation.

The data for 'red' and blue copolymers are shown in Figure 4. They are more erratic than the results from the yellow polymers. The values of  $\pi/c$  at equivalent concentrations are significantly higher.

Membrane osmometry is not normally suitable for measuring molecular weights of unfractionated polymers with number-average molecular weights below about 20 000 g/mol<sup>11</sup>. Significant amounts of smaller molecular species diffuse through the membrane and do not contribute to the osmotic pressure. The derived value of  $\bar{M}_n$  then becomes too high. Values obtained for the coloured 'copolymers' cannot be considered to be accurate, particularly in the case of the blue and 'red' copolymers, but they give a useful indication of the probable range and of relative values.

Visible spectroscopy

Measurements of the absorption peaks were made on the three free Remazol dyes at a series of dilutions in DMF and were found to obey the Beer-Lambert law. The extinction coefficient,  $E$ , was calculated for each dye and was used to calculate the concentration of the chromophore in solutions of the coloured polymers. This approach was suitable for polymers made with the yellow and blue dyes but not the red. The red copolymers presented problems which will be discussed later.

The absorption peaks of the free yellow, red and blue dyes in DMF were at 433, 512 and 584 nm respectively, with corresponding extinction coefficients of 3.18, 3.97 and 2.32 m<sup>2</sup>/g.

The spectra of the solutions of the yellow and blue polymers were identical in shape to those of the parent dyes, with the absorption maxima at the same wavelengths. In these instances it can be assumed that there has been no change in the chromophore on polymerization and, therefore, that the extinction coefficient has not been altered. The extinction coefficient of the polymer in comparison with that of the free dye then gives a direct measure of the chromophore content of the 'copolymer'. It is useful to consider one example in detail. A sample of the yellow copolymer had an extinction coefficient of 8.16 x 10<sup>-2</sup> m<sup>2</sup>/g. The chromophore content of the copolymer is found by dividing the extinction coefficient of the pure dye (3.18 m<sup>2</sup>/g) by that of the copolymer, thus 3.18/8.16 x 10<sup>2</sup> = 39.0. This means that 39 g of coloured copolymer

contains 1 g of dye and therefore 38 g of polyacrylonitrile residues. Thus the composition of the coloured copolymer is 1 mol of dye: 380 mol of acrylonitrile. (The monomer molecular weights are 530 and 53 respectively.)

Such composition data can be used to derive the reactivity ratio,  $r$ , of the two monomer types. The Mayo and Lewis<sup>12</sup> integrated copolymer equation can be simplified if it is assumed that the large bulk of the dye molecules pre-vents two of them adding consecutively to the chain, that is,  $r_{\text{dye}} = 0$ . This is a reasonable assumption when one considers the structures of the three dyes used<sup>1</sup>. The modified equation is then:

$$\log \left( \frac{[\text{dye}]_0}{[\text{dye}]} \right) = \left\{ \frac{1}{(1 - r_{\text{AN}})} \right\} \log \left\{ \frac{(r_{\text{AN}} - 1) \left( \frac{[\text{AN}]}{[\text{dye}]} \right) + 1}{(r_{\text{AN}} - 1) \left( \frac{[\text{AN}]_0}{[\text{dye}]_0} \right) + 1} \right\}$$

The calculated values of  $r_{\text{AN}}$  are shown in Table 1. These were calculated on the assumption that the reactivity ratios are constant for each system. For polymerizations with the yellow dye in *vacuo*, consistent values (2.5 ± 0.3) were

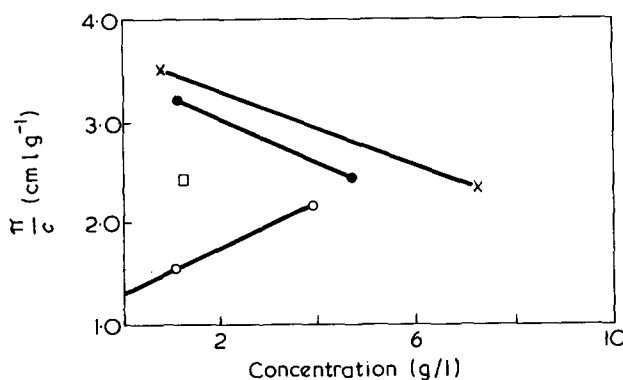


Figure 4 Plot of  $\pi/c$  (cm l g<sup>-1</sup>) against concentration for red ( $\circ$ ,  $\times$ ) and blue ( $\square$ ,  $\bullet$ ) 'copolymers', obtained after irradiation in *vacuo* for the specified dose:  $\square$ , 0.7 x 10<sup>5</sup>;  $\circ$ , 1.9 x 10<sup>5</sup>;  $\times$ , 2.7 x 10<sup>5</sup>;  $\bullet$ , 12.6 x 10<sup>5</sup> rad

Table 1 Spectroscopic and kinetic data

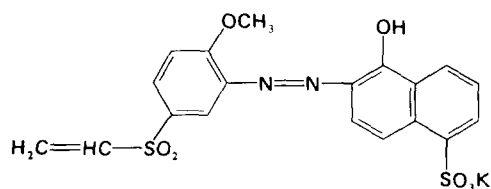
Total dose x10 <sup>-5</sup> (rad)	Environment	[AN] <sub>0</sub> /[dye] <sub>0</sub>	Conversion to polymer (%)	Extinction coefficient, E <sub>i</sub> , at 512 nm x 10 <sup>2</sup> (m <sup>2</sup> /g)	Reactivity ratio, r <sub>AN</sub>
<b>Yellow 'copolymers'</b>					
0.3	vac	20:1	14	7.56	2.2
0.6	vac	20:1	26	6.34	2.7
1.2	vac	20:1	40	8.16	2.3
1.4	vac	20:1	57	7.90	2.5
1.8	vac	20:1	68	8.64	2.4
0.4	air	20:1	11	9.66	1.3
0.8	air	20:1	24	8.90	1.9
1.3	air	20:1	46	8.49	2.1
2.4	air	20:1	66	8.64	2.4
3.0	air	20:1	68	7.45	1.8
11.5	air	20:1	87	5.89	4.5
10.9	air	10:1	82	12.98	3.8
10.1	air	40:1	94	3.07	6.0
<b>Blue 'copolymers'</b>					
0.8	vac	20:1	11	8.43	1.45
1.5	vac	20:1	15	8.34	1.50
4.1	vac	20:1	74	9.02	1.45
2.9	air	20:1	22	8.87	1.50

obtained. Considerably greater deviation in  $r_{AN}$  was observed for reactions carried out in air. For the blue dye systems, the value of  $r_{AN}$  was found to be about 1.5, both in air and *in vacuo*.

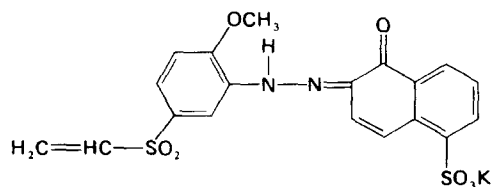
The visible spectra of solutions of samples of 'copolymer' made with the red dye were recorded similarly in DMF. The wavelength of maximum absorption moved from 512 nm in the free red dye to 440 nm in the coloured 'copolymer'. The polymers and their solutions were yellow instead of the expected deep red. During polymerization, the chromophore must have been modified, so the extinction coefficient found for the free dye cannot be applied. There is a large spread in the extinction coefficients of the 'red copolymers' made in air with no clear trend, as shown in Table 2.

One useful aspect of the change in peak absorption is that any free dye remaining in the polymer sample is detected through its absorption at 512 nm. Thus, less than 0.1% by weight of free dye in the copolymer should be apparent. This is important since it enables an efficient purification system to be devised for the 'copolymer'. It can be extended to systems which do not undergo changes in the structure of the chromophore. No peaks at 512 nm were found which indicates that the extraction and washing procedures, given in detail in ref 1, are effective in removing free dye. This removal of free dye will become an essential feature of the envisaged use of this type of polymeric pigment, since the presence of free dye will introduce problems of migration.

The structure of the red dye has previously been quoted as<sup>1</sup>:



However, this type of phenylazo-1-naphthol derivative exists in two tautomeric forms, the hydroxyazo and the hydrazone<sup>13</sup>. In this case the hydrazone form has the structure:



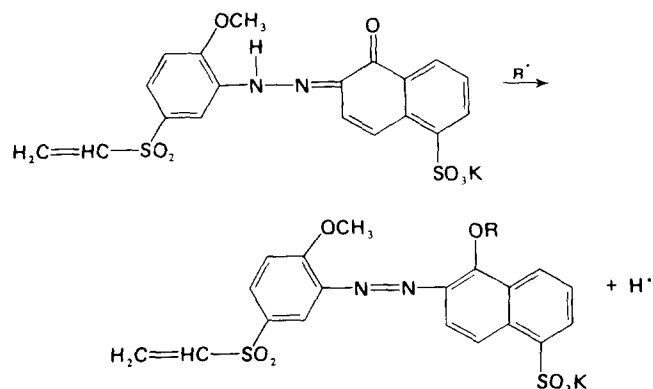
Usually, the forms of a dyestuff are markedly different in colour, the hydroxyazo being yellow and the hydrazone being red. The equilibrium between the two forms may also be affected by the solvent. The red dye in DMF solution must be almost exclusively in the hydrazone form as there is no evidence of the hydroxyazo form in the spectrum (400–500 nm region).

The hypsochromic shift (from a deeper to a lighter colour) on polymerization probably arises through conversion to the hydroxyazo form. One possible cause of this change could be the different environment of the chromophore. In the polymer it will be surrounded by polar nitrile groups. It should be possible to make a metal complex of the dye after it has been incorporated into the polymer. Such complexing would deepen the colour again.

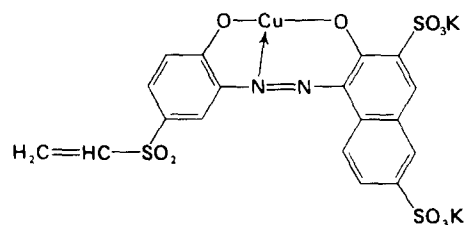
20% of pyridine was added to a solution of the polymer in DMF. A solution of nickel acetate in pyridine was added, the mixture shaken, allowed to stand for several minutes

and then warmed gently to its boiling point. There was no colour change at any stage of this sequence, so no nickel complex was formed. It is possible that the polymer molecules were so tightly coiled in the poor solvent that the nickel ions could not reach the chromophore. This seems unlikely, however, especially as heating had no effect whatever.

A more probable explanation is that the chromophore is altered during polymerization, changing into the hydroxyazo form and so preventing the possibility of complexing with nickel ions. This could occur if the polymerizing radical became attached to the chromophore through the hydroxyl oxygen atom instead of through the vinyl group:



Preliminary work has been undertaken using mixtures of acrylonitrile and Remazol Red 3B, whose structure is given as:



Here, conversion from the hydrazone to hydroxyazo form of the dye cannot take place because of the presence of the metal atom. 'Copolymers' made using this system are red, with the same wavelength of maximum absorption as the parent dye. We may assume that the above mechanism for conversion from the hydrazone to hydroxyazo form is valid.

These observations may have important consequences for polymeric pigments. Inexpensive dyes, able to exist in such tautomeric forms could take part in termination in the manner described, thus providing useful pigments with relative ease.

Table 2 Extinction coefficients of red copolymers with change in total dose

Total dose $\times 10^{-5}$ (rad)	Environment	Extinction coefficient, $E$ , at 440 nm ( $m^2/g$ )
1.9	vac	10.55
2.7	vac	10.71
2.0	air	6.77
2.2	air	9.53
6.2	air	13.02
8.4	air	11.99
12.2	air	6.39

Table 3 Sulphur analysis of the 'copolymers' and the derived reactivity ratios,  $r$ . [AN] : [dye] = 20:1

Dye	Environment	Total dose $\times 10^{-5}$ (rad)	Sulphur content (%)	$r_{AN}$
red	vac	2.7	0.70	1.1
red	air	6.2	0.65	1.1
red	air	12.2	0.45	1.0
yellow	air	11.5	0.55	1.4
blue	vac	4.1	0.55	1.2

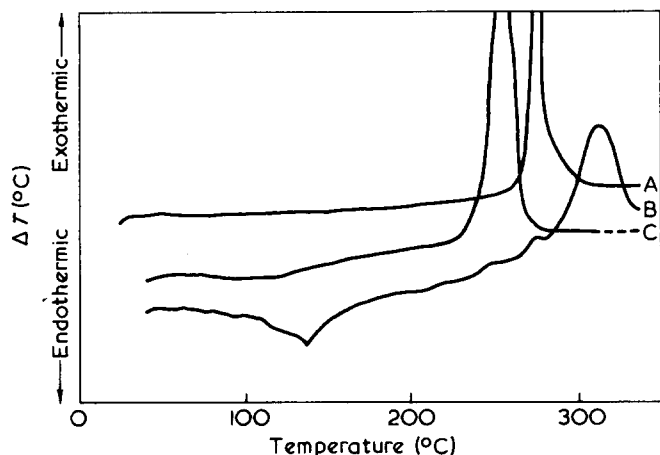


Figure 5 Differential thermal analysis thermogram. Variation in  $\Delta T$  ( $^{\circ}\text{C}$ ) with increasing temperature ( $^{\circ}\text{C}$ ) for polyacrylonitrile (A), pure dye (B) and the yellow 'copolymer' (C)

#### Infra-red spectroscopy

The coloured 'copolymers' were examined by infra-red spectroscopy. This proved that the colour was derived from the chromophores of the dyes and not from degradation of the acrylonitrile. Such degradation is thought to involve the formation of a  $-\text{C}=\text{N}-$  conjugated system and can arise from the action of heat or a base on polyacrylonitrile. During this process the sharp nitrile peak at  $2240\text{ cm}^{-1}$  decreases in intensity while new peaks appear at  $1627\text{ cm}^{-1}$  and  $1772\text{ cm}^{-1}$ .

In the spectrum of pure polyacrylonitrile, prepared in the same manner as the coloured polymers, there were small peaks at  $1627\text{ cm}^{-1}$  and  $1722\text{ cm}^{-1}$ , showing the presence of some  $-\text{C}=\text{N}-$  groups, although no colour was apparent in the sample. The spectra of the coloured 'copolymers' show additional peaks, nearly all of which correspond to absorption peaks in the dye. Composite spectra can be built up almost completely by addition of a suitable proportion of the spectra of the pure dyes to the spectrum of pure polyacrylonitrile. The peaks at  $1627\text{ cm}^{-1}$  and  $1722\text{ cm}^{-1}$  are very weak in all the samples. Clearly, colour is due to incorporation of the chromophore and not to the formation of a conjugated  $-\text{C}=\text{N}-$  system.

A small peak occurred at  $1580\text{ cm}^{-1}$  in several 'copolymer' samples. This peak cannot be attributed to either the dye or polyacrylonitrile. A peak in this position is indicative of the carboxylate anion<sup>15</sup>. This is probably due to a small amount of hydrolysis of the nitrile groups. It seems unlikely that any potassium acetate could remain in the polymer from the original precipitation stage<sup>1</sup>. The washing process was effective in removing all the free dye from the polymer (shown by the absence of a  $512\text{ nm}$  peak in the visible spectra of the copolymers of the red dye) and potassium acetate is far more soluble in methanol. Thorough washing of a finely ground sample with methanol gave no reduction in the peak at  $1580\text{ cm}^{-1}$ .

The infra-red spectra confirm that the chromophore is an integral part of each copolymer. Further, the heights of the absorption peaks change with the dye content in the polymers made from 40:1, 20:1 and 10:1 (w/w), acrylonitrile/dye starting mixtures. The extinction coefficients of solutions of the copolymers increase in regular fashion with each increase in the above dye/acrylonitrile ratio (Table 1).

#### Sulphur analysis

Each dye chromophore contains two atoms of sulphur. Since there is no other sulphur in the system, it should be possible to calculate the proportions of dye and acrylonitrile in the 'copolymers' from the sulphur content. The reactivity ratios calculated from the analysis figures are shown in Table 3, together with the sulphur contents. The agreement of the reactivity ratios with values calculated from spectroscopic data is poor. This implies that degradation of the chromophore is occurring to some extent, presumably during irradiation, which lowers the visible absorption. In this way some sulphur-containing fragments may be incorporated into the polymer, increasing the sulphur content but not the extinction coefficient.

#### Differential thermal analysis

D.t.a. was carried out on one sample of each of the 'copolymers' containing yellow, red and blue dye, the free vinylsulphone dyes and pure polyacrylonitrile. The results are shown in Figures 5 to 7. The thermogram of polyacry-

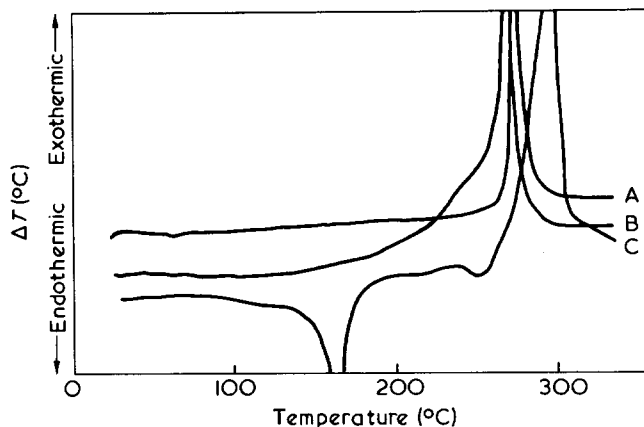


Figure 6 Differential thermal analysis thermogram. Variation in  $\Delta T$  ( $^{\circ}\text{C}$ ) with increasing temperature ( $^{\circ}\text{C}$ ) for polyacrylonitrile (A), the red 'copolymer' (B) and the pure dye (C)

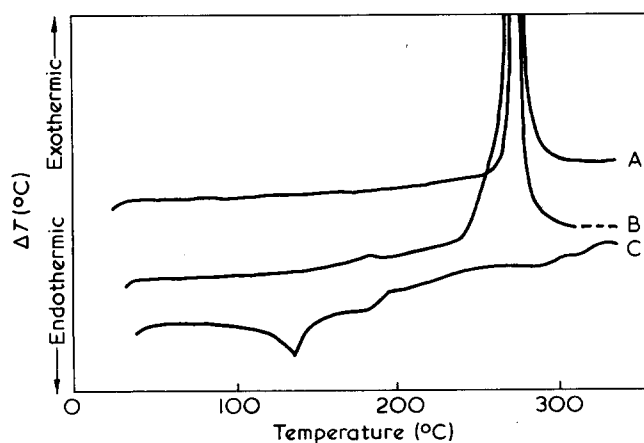


Figure 7 Differential thermal analysis thermogram. Variation in  $\Delta T$  ( $^{\circ}\text{C}$ ) with increasing temperature ( $^{\circ}\text{C}$ ) for polyacrylonitrile (A), the blue 'copolymer' (B) and the pure dye (C)

Table 4 Light fastness properties of the 'copolymeric' pigments in fibre and paint form

Sample	Ratio polymer:TiO <sub>2</sub>	Approx. depth (ISD)	Fastness rating
Yellow fibre	—	1/1	3
Yellow paint	mass tone	1/2	5-6
	1:2.6	1/10	5
	1:32	1/100	4-5
Red paint	mass tone	1/1	5
	1:2.6	1/10	5
	1:32	1/100	4-5
Blue paint	mass tone	1/1	5
	1:2.6	1/20	6-7
	1:32	1/200	6-7

lonitrile is shown, for comparison, in all three Figures. Polyacrylonitrile provides a steady thermogram with no deviations up to  $278 \pm 2^\circ\text{C}$  when a sharp exotherm occurs, corresponding to decomposition. The 'copolymer' containing the yellow dye showed an exotherm, beginning at  $110^\circ\text{C}$  and gradually increasing up to the decomposition temperature of  $259^\circ\text{C}$ , about  $20^\circ\text{C}$  lower than for polyacrylonitrile. The red and blue 'copolymers' both give gradually increasing exotherms from  $140^\circ$  or  $150^\circ\text{C}$  up to  $278 \pm 2^\circ\text{C}$ . With the blue 'copolymer' a slight exotherm at  $180^\circ\text{C}$  is in evidence. The decomposition temperature is only slightly affected by incorporation of the red and blue dyes into polyacrylonitrile, but is lowered significantly by the yellow dye.

The thermograms of the pure yellow and red vinylsulphone dyestuffs show gradual decomposition, roughly parallel to the exotherms of the polymers. The blue dye is much more thermally stable than the other two, showing no strong exotherm below  $350^\circ\text{C}$ . The blue copolymer is also thermally stable. The exotherms seen with all the 'copolymers' may arise from decomposition of the chromophore only, the environment having no significant effect. Alternatively, the exotherms could be due to the occurrence of conjugation already mentioned. In polyacrylonitrile this reaction can start at as low a temperature as  $175^\circ\text{C}$ <sup>16</sup> and increases with increase in temperature. It is accelerated by nucleophilic agents such as acids and phenols. The extended isotherms observed with the yellow and red 'copolymers' could well be due to this reaction, catalysed by the dye residues. The heat stability of this type of product may well be improved by using more suitable vinylsulphone dyes.

#### Light fastness

The light fastnesses of the three types of 'copolymers' red, yellow and blue were assessed in simple paint films. The light fastness of a pigment usually falls as the proportion of white pigment, incorporated in the mix, is increased. The results, shown in Table 4, show that the above observation is substantiated by the yellow and red polymeric pigments but that the fastness of the blue paint actually increases on reduction. Explanations of such differences are beyond the scope of this paper and are the subject of further work.

#### Fibre and film-forming character

Fibres spun from a mixture of 25% of the yellow 'copolymer' and 75% Courtelle (polyacrylonitrile fibre) have physical properties which compare well with a sample of Courtelle spun in the same way. The fibres have a very attractive appearance and are highly coloured. However, the fastness of the yellow polymer is much better in the

paint than in the fibre form. The reason for this is not clear. Possibly it arises from degradation which occurs in the spinning process. It has been shown that some degradation can occur at temperatures as low as  $130^\circ\text{C}$  and this is well below the tower temperature used in drying the fibre.

The 'copolymers' could also be made into films by spreading their solutions in DMF and either immersing them in water or methanol or allowing a combination of moisture adsorption and solvent evaporation to precipitate the polymer. The films, although tough and flexible initially, become very brittle over extended periods as the last traces of solvent evaporate. However, such films facilitate investigation by infra-red spectroscopy provided allowance is made for residual solvents.

#### CONCLUSIONS

The polymers described in this paper represent a potentially useful class of pigment. The high molecular weight should prevent migration. A further advantage lies in the insolubility of polymers with a high acrylonitrile content in virtually all common solvents. This type of pigment is admirably suited to the manufacture of water-based paints. The emulsion form in which they are produced is quite stable and, unless they have been allowed to dry out, the polymers emulsify spontaneously in water without the need of additives. In principle, it should be possible to form a paint by adding a water-soluble film-forming agent to such an emulsion. By selection of the vinyl monomer, polymeric pigments can be visualized which will form stable emulsions and act as their own film former. Such materials would represent a considerable advance in pigment technology.

The system is by no means limited to the three vinylsulphone dyes that have been described. There is a large number of commercially available dyes of the vinylsulphone and related acrylamide types. More convenient initiator systems could also be used. Benzoyl peroxide, potassium persulphate and azobisisobutyronitrile have all been used successfully in preliminary experiments using the three acrylonitrile/dye systems already described. Various vinyl monomers are also being investigated in this context to assess the factors involved in 'copolymer' formation and to evaluate their physical properties.

On the whole the strength of colour in the polymers is rather weak. It must always, of course, be much weaker than that of the parent dye. Some increase should be obtainable by use of higher initiation rates and dye concentrations, but this would be at the expense of the molecular weight. It appears that the polymer-dye system is not 'copolymeric' in the accepted sense. Rather, it would seem that the dye is involved in reaction termination though this position is by no means clear.

The concept of intrinsically coloured polymers could be extended into other areas. These include polymers which are stable to light and oxidative degradation, intrinsically fluorescing polymers and so on.

#### ACKNOWLEDGEMENT

We are grateful to the Perkin Bequest for supplying the necessary finance for one of us (N.S.B.).



REFERENCES

- 1 Batty, N. S. and Guthrie, J. T. *Polymer* 1975, **16**, 43
- 2 Paikachev, Yu, S., Bikou, A. N. and Borodin, V. F. *Khim. Volokna* 1968, **2**, 22
- 3 'Colour Index', 3rd Edn, 1971, Society of Dyers and Colourists, Bradford
- 4 Carr, W. J. *Oil Colour Chem. Assoc.* 1971, **54**, 155
- 5 Grassie, N. and McGuchan, R. *Eur. Polym. J.* 1971, **7**, 1091
- 6 Freireich, S., Gertner, D. and Zilkha, A. *J. Polym. Sci. (A-1)* 1972, **10**, 3109
- 7 Gachkovskii, V. F. *Vysokomol. Soedin. (A)* 1971, **13**, 2207
- 8 Houtz, R. *Textile Res. J.* 1950, **20**, 786
- 9 Batty, N. S. and Guthrie, J. T. *Polymer* 1974, **15**, 127
- 10 I.S.O. Recommendation R.105, Part 2
- 11 Staverman, A. J., Pals, D. T. F. and Kruissink, C. A. *J. Polym. Sci.* 1957, **23**, 57
- 12 Mayo, F. R. and Lewis, F. M. *J. Am. Chem. Soc.* 1944, **66**, 1594
- 13 Griffiths, J. J. *Soc. Dyers Colour.* 1972, **88**, 106
- 14 Moore, W. R. and Saito, K. *SCI Monogr.* 1967, **26**, 236
- 15 Dyer, J. R. in 'Applications of Absorption Spectroscopy of Organic Compounds', Prentice-Hall, Englewood Cliffs, NJ, 1965, p 34
- 16 Grassie, N. and McGuchan, R. *Eur. Polym. J.* 1971, **7**, 1357

# Network properties: 2. A broadline n.m.r. study of molecular motions in some multicomponent crosslinked polymers

C. H. Bamford, G. C. Eastmond and D. Whittle\*

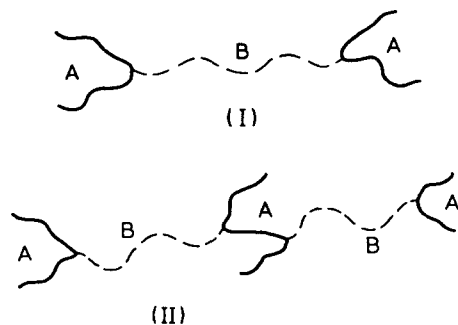
Department of Inorganic, Physical and Industrial Chemistry, University of Liverpool, PO Box 147, Liverpool L69 3BX, UK

(Received 3 October 1974)

A series of multicomponent polymers of known structure and consisting of poly(vinyl trichloroacetate) crosslinked with poly(methyl methacrylate) (PMMA) have been examined by broadline n.m.r. Both enhanced and retarded rotation of the  $\alpha$ -methyl groups on the PMMA chains, compared with those in PMMA homopolymer, have been observed. A previous assessment of the morphologies of the same polymers, based on the results of dilatometric studies, has been extended. The modifications to the rotations of the  $\alpha$ -methyl groups have been correlated with the morphologies of the multicomponent polymers and it is proposed that both effects arise as a result of changes in the distribution of conformations adopted by the PMMA chains in the multicomponent polymers compared with that in the pure homopolymer.

## INTRODUCTION

A previous series of publications described a general method for preparing multicomponent crosslinked polymers of known structure<sup>1-4</sup>. These materials, which we refer to as ABCPs, consist of chains of a polymer A crosslinked with chains of a chemically different polymer B. The ABCPs are prepared by reacting a preformed polymer A, containing reactive chlorine or bromine atoms in side groups, with a suitable metal derivative in the presence of a free-radically polymerizable monomer. The metal derivative specifically removes a halogen atom from a side group of the A polymer to generate a polymeric radical species. This radical then initiates the graft polymerization of the monomer to form propagating B-chains attached to the A-chains. Combination termination of the propagating radicals produces a cross-linked species consisting of two A-chains linked by a B-chain; i.e. an H-shaped species in which the A-chains form the limbs of the H, as represented in structure I. Disproportionation termination of the propagating radicals gives rise to branched structures. As reaction proceeds more multicomponent species are produced and, by using additional side groups on previously reacted A-chains, structures of greater complexity are produced, e.g. structure II.



All propagating radicals we have examined undergo combination termination at least to some extent<sup>4</sup> and ultimately

\* Present address: British Steel Corporation, Strip Mills Division, Product Development Centre, Deeside, Clwyd, CH5 2NH, UK.

the reaction mixture gels with the formation of infinite network structures. Continued reaction beyond the gel point increases the crosslink density and incorporates more A- and B-chains into the infinite networks. The major structural parameters of the ABCPs, including crosslink length and density, are calculable on a statistical basis from the reaction kinetics. The branch/crosslink ratio is determined by the relative rates of the two termination reactions.

In the preceding paper of this series<sup>5</sup> we described the preparation of a series of ABCPs, in which poly(vinyl trichloroacetate) (PVTCA) was used as the A-component and poly(methyl methacrylate) (PMMA) was the B-component, and we discussed the results of a dilatometric study of the solid PVTCA/PMMA ABCPs. The major structural parameters of these polymers are given in Table 1. The dilatometric data showed the existence of multiple glass-transition temperatures, indicating microphase separation of the incompatible component polymers, even at high crosslink densities. From the values of the glass-transition temperatures and coefficients of expansion of the ABCPs it was concluded that microphase separation was incomplete and that mixed phases, containing both A- and B-chains were present in the polymers; the compositions of the mixed phases were estimated.

The present paper describes the results of a broadline n.m.r. study of the materials referred to in Table 1 and a more detailed analysis of the previous dilatometric data. Effects on the rotation of the  $\alpha$ -methyl groups in the PMMA chains are discussed in terms of polymer morphology.

Table 1 Structural parameters of PVTCA/PMMA ABCPs

Sample	PVTCA in network (% w/w)	$\bar{P}_n$ of PMMA crosslinks	Branches: crosslinks	$\gamma_r$
I	21.4	4560-4740	4	3
II	8.0	5060-5440	4	9
III	3.3	6900-8000	4	16-18
IV	23.7	11 820	8	1
V	7.7	11 700	8	3.5
VI	3.0	16 760	8	7

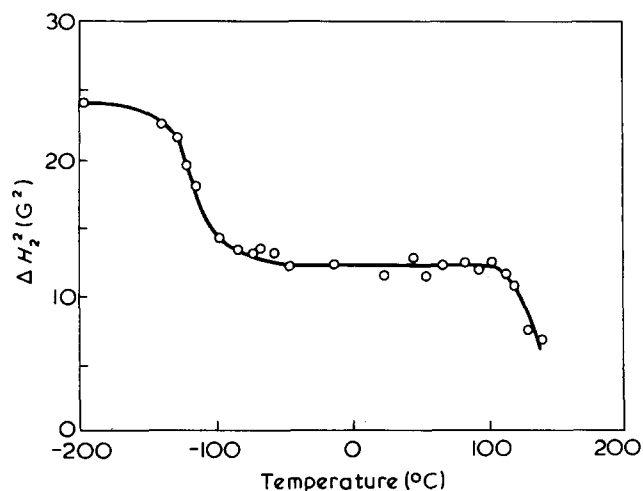


Figure 1 Variation in second moment ( $\Delta H_2^2$ ) of n.m.r. absorption line of poly(methyl methacrylate) with temperature

## EXPERIMENTAL

The reaction conditions used to prepare the ABCPs referred to in Table 1 were presented in a previous paper<sup>5</sup>. The PVTCA was a copolymer of poly(vinyl trichloroacetate) and poly(vinyl alcohol) prepared by trichloroacetylation of poly(vinyl alcohol) to 60.4% conversion; the polymer had a glass-transition temperature of 59°C.  $\bar{P}_w$  of the trichloroacetate residues in the PVTCA was 2600. Crosslink densities of the ABCPs are described by values of the relative crosslinking index  $\gamma_r$  which is the crosslinking index relative to that at the gel point and is equal to the reaction time divided by the gel time; where appropriate, corrections have been applied for initiator consumption and a small amount of transfer to monomer.

Solid polymers were isolated from solutions or gels swollen in methyl methacrylate by evaporation of the solvent and heating under vacuum at 100°C.

N.m.r. spectra were recorded using a Varian DP60 spectrometer. Second moments of the absorption spectra were calculated from the derivative spectra<sup>6</sup> and corrected for modulation broadening<sup>7</sup>.

In samples I and IV over 80% of the protons, and in the other samples investigated in this study over 90% of the protons, are contained in the PMMA chains so that the n.m.r. signals arise predominantly from the PMMA.

## RESULTS AND DISCUSSION

### N.m.r. observations

Figure 1 shows the variation in second moment ( $\Delta H_2^2$ ) of the n.m.r. absorption line with temperature for a sample of PMMA homopolymer prepared under the same conditions as the PMMA chains in the ABCPs, except that the PVTCA component of the initiating system was replaced by ethyl trichloroacetate. The shape of the curve in Figure 1 is virtually identical with that obtained by previous workers<sup>8,9</sup>. Absolute values of  $\Delta H_2^2$  at -196° and 0°C obtained in this study were 24.0 and 12.0 G<sup>2</sup> respectively, compared with corresponding values of 18.6 and 10.5 G<sup>2</sup> reported by Sinnott<sup>8</sup> and 19–20.5 and 11.5–12.5 G<sup>2</sup> found by Odajima et al.<sup>9</sup> for various samples of PMMA. The differences in values of  $\Delta H_2^2$  reported by various workers possibly reflect differences in sample preparation; we therefore compare

the n.m.r. data from the ABCPs with the data in Figure 1. Slichter and Mandell<sup>10</sup> have confirmed that the reduction in  $\Delta H_2^2$  when samples were warmed from -196° to -75°C is due to the establishment of  $\alpha$ -methyl group rotation; the ester methyl groups are rotating at all temperatures above -200°C. The decrease in  $\Delta H_2^2$  at about 100°C is due to the development of segmental motion associated with the glass transition.

A blend of PVTCA and PMMA containing 22% (w/w) PVTCA, a higher PVTCA content than in any of the PVTCA/PMMA ABCPs, gave values of  $\Delta H_2^2$  indistinguishable from those for PMMA. This result is consistent with previous dilatometric data which indicated complete micro-phase separation of the component polymers, and also confirms that the n.m.r. signals from the ABCPs can be effectively attributed to the PMMA component.

Variation of  $\Delta H_2^2$  with temperature for the PVTCA/PMMA ABCPs I–VI are given in Figures 2, 3 and 4. Significant differences exist between the data for the ABCPs and those for PMMA homopolymer (shown as a dotted line without experimental points on each graph for comparative purposes). Absolute values of  $\Delta H_2^2$  at -196°C and in the plateau region between the establishment of  $\alpha$ -methyl group rotation and the onset of segmental motion are generally higher for the ABCPs than for PMMA. Comparing these data with the parameters in Table 1 we see that samples I and IV, which have the highest PVTCA content and lowest crosslinking index, have the highest values of  $\Delta H_2^2$ . As  $\gamma_r$  and the PMMA content increase, values of  $\Delta H_2^2$  approach those for PMMA.

Other major differences between the broadline data for the ABCPs and for PMMA are associated with the transition region corresponding to the development of  $\alpha$ -methyl group rotation. For samples II and III (Figure 2)  $\Delta H_2^2$  decreases, and methyl group rotation develops more slowly than for PMMA, the transition region covering a comparatively large temperature range. For PMMA all  $\alpha$ -methyl groups are rotating at temperatures above -40°C but in samples II and III rotation of the methyl groups is not fully developed until temperatures in excess of 0°C are attained. By contrast, with samples I, IV and V (Figures 3 and 4)  $\alpha$ -methyl group rotation both sets in and is fully established at temperatures lower than for PMMA. There appears to be no direct correlation between these data and the structural parameters and overall compositions in Table 1. These

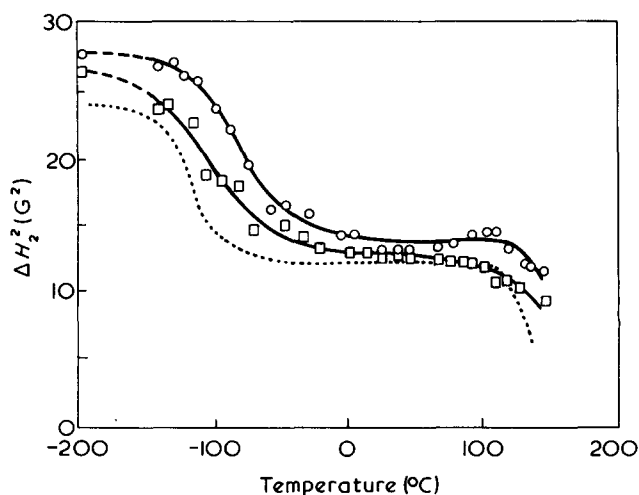


Figure 2 Variation in second moments of n.m.r. absorption lines with temperature for PVTCA/PMMA ABCPs.  $\circ$ , Sample II;  $\square$ , sample III. -----, refers to PMMA

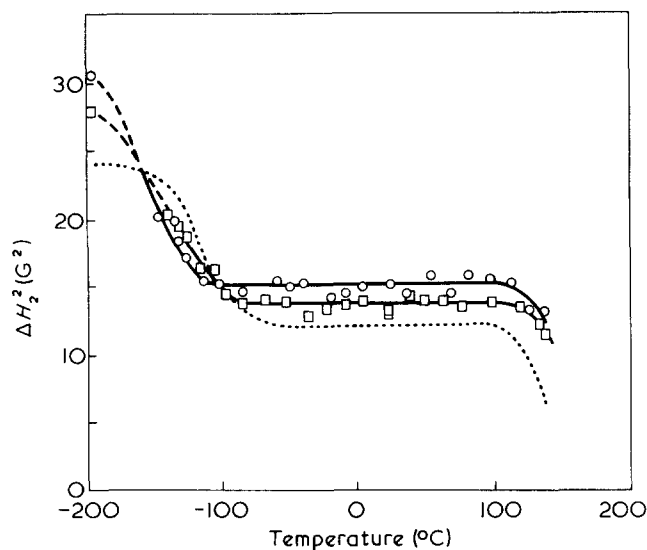


Figure 3 Variation in second moments of n.m.r. absorption lines with temperature for PVTCA/PMMA ABCPs.  $\circ$ , Sample IV;  $\square$ , sample V. -----, refers to PMMA

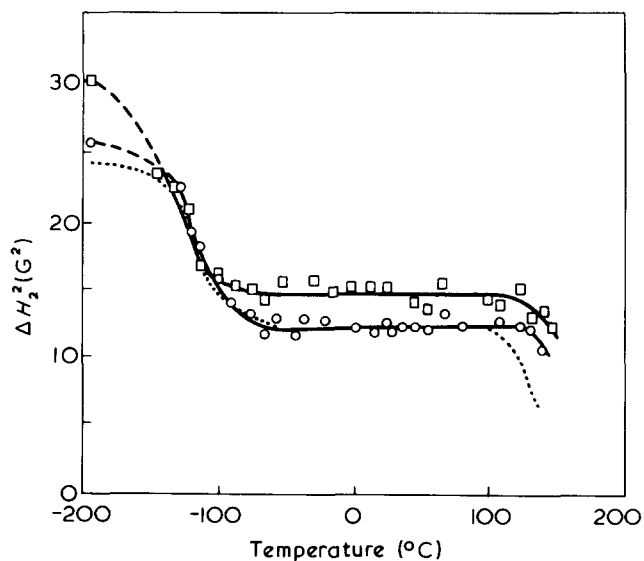


Figure 4 Variation in second moments of n.m.r. absorption lines with temperature for PVTCA/PMMA ABCPs.  $\square$ , Sample I;  $\circ$  sample VI. -----, refers to PMMA

effects will be discussed later in terms of polymer morphology.

Sample VI which contains 97% (w/w) PMMA exhibited only one  $T_g$  at about 100°C and produced n.m.r. data almost identical with those of pure PMMA; data for this sample are not discussed further.

Decreases in  $\Delta H_2^2$  associated with the development of segmental motions appear to be similar for the ABCPs and for PMMA homopolymer, within the limited temperature range investigated. Possibly sample II (Figure 2) shows significantly different behaviour. So far we have been unable to identify any trends in behaviour in this temperature range which can be interpreted in terms of structure and morphologies of the polymers. Pulsed n.m.r. studies of segmental motions appear to be more informative<sup>11</sup> than broadband studies and these will be discussed in a subsequent publication.

#### Re-assessment of dilatometric data

In our previous publication<sup>5</sup> we reported volume–temperature data for PVTCA/PMMA ABCPs I to VI. We

analysed the data quite simply in terms of two glass-transition temperatures, drawing three straight lines through the dilatometer plots. For PVTCA/PMMA blends the two glass-transition temperatures identified correspond to those of the component homopolymers (Table 2). The lower glass-transition temperatures  $T_{g1}$  for the PVTCA/PMMA ABCPs were 10–15°C higher than  $T_g$  for PVTCA, while the higher glass-transition temperatures  $T_{g2}$  appeared to correspond to that of PMMA; values of  $T_{g1}$  and  $T_{g2}$  identified in this way are given in Table 2. Sample VI contained only 3% PVTCA and did not exhibit a lower glass-transition temperature.

While the appearance of two glass-transition temperatures indicates microphase separation of the incompatible constituent polymers, the elevated values of  $T_{g1}$  for the ABCPs were taken to indicate that microphase separation was incomplete. The results were interpreted in terms of formation of a mixed phase containing PVTCA and PMMA and a phase of pure PMMA. On the basis of volume additivity and normal coefficients of expansion for the liquid polymers in the mixed phase above  $T_{g1}$ , the compositions of the mixed phases were calculated from the coefficients of expansion. The compositions of the mixed phases calculated in this way are given in Table 2;  $W$  is the weight of PMMA associated with unit weight of PVTCA in the mixed phase. From the values of  $W$  and the overall compositions of the polymers the distribution of the PMMA between the mixed and pure PMMA phases can be calculated; the percentages of PMMA in each phase is given in Table 2. This simple analysis requires some elaboration.

Glass-transition temperatures for mixtures of amorphous materials, for which simple additivity of free volume applies, can be calculated from the coefficients of expansion of the glassy and liquid materials and their volume fractions and glass-transition temperatures by use of the Kelley–Bueche equation<sup>12</sup>. This equation has been successfully applied to polymer–diluent systems<sup>12</sup>, compatible mixtures of PMMA and poly(ethyl methacrylate)<sup>13</sup> and certain PVTCA/poly(styrene) ABCPs which show a single glass transition<sup>14</sup>. Assuming simple additivity of volumes applies to mixtures of PVTCA and PMMA in the mixed phase we can calculate the  $T_g$  of the mixed phase from the values of  $W$  given in Table 2. Values of  $T_{g1}$  calculated in this way are given in Table 2, and are seen to be consistently higher than the observed values of  $T_{g1}$ . The calculated values of  $T_{g1}$  also vary monotonically with composition of the mixed phase whereas observed values do not. Validity of the Kelley–Bueche equation to mixtures of PVTCA and PMMA can only be checked by producing homogeneous mixtures of the polymers of known composition. This has not yet been achieved.

Table 2 Glass transitions and compositions of phases in PVTCA/PMMA ABCPs

Sample	$T_{g1}$ (obs)	$T_{g2}$	$W$	% (w/w) of PMMA in mixed phase	% (w/w) of PMMA in pure PMMA phase	$T_{g1}$ (calc.)
I	74	97.5	1.2	32.6	67.4	82.6
II	71	102	1.7	14.8	85.2	86.6
III	69	101	2.1	7.1	92.9	88.4
IV	74	99	2.8	87.0	13.0	91.1
V	71	102	4.5	37.2	62.8	95.7
VI		103				
Blend (52% w/w PVTCA)	59	103				

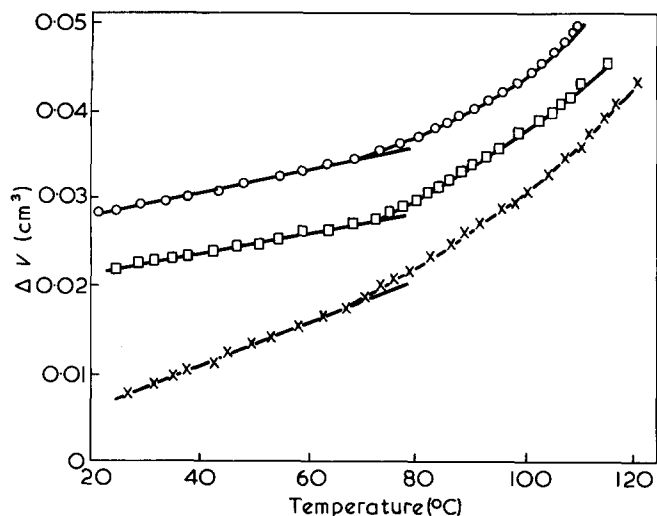


Figure 5 Dilatometric data for PVTCA/PMMA ABCPs.  $\circ$ , Sample I;  $\square$ , sample IV;  $\times$ , sample V

In the absence of information to the contrary we shall continue to assume that the Kelley–Bueche equation is applicable to mixed phases in PVTCA/PMMA ABCPs and look elsewhere for an explanation of the discrepancy between the observed and calculated values of  $T_{g1}$

Further examination of the dilatometer plots reveals that the data are not accurately represented by three straight lines; in general the dilatometer plots above  $T_{g1}$  are curved as is clearly seen in Figure 5 in which the original dilatometric data for samples I, IV and V are redrawn. Figure 6 shows data for samples II and III which also exhibit multiple transitions with a well defined upper glass-transition. The curvature in the dilatometer plots indicates that the PVTCA/PMMA ABCPs do not undergo microphase separation into a mixed phase of well defined composition (with a unique  $T_g$ ) and a pure PMMA phase, rather the mixed phase can have a continuous variation of composition. Thus, if each portion of the mixed phase exhibits a  $T_g$  according to its composition the sample will effectively exhibit a broad glass-transition region. The range of compositions of the mixed phase may reflect domains of different composition through that phase. The values of  $W$  calculated on the basis of the original analysis will represent average compositions of the mixed phase and the lower glass-transition temperatures (which are usually well defined) will arise from those regions of the mixed phases richest in PVTCA.

For samples I, IV and V (Figure 5) the dilatometer plots are smooth curves through  $T_g$  of PMMA. There is no sharp transition corresponding to pure PMMA and it must be concluded that essentially all the PMMA is incorporated in the mixed phase; i.e. the distribution of the PMMA between the phases given in Table 2 and based on the simple analysis for samples I, IV and V, is incorrect. In contrast, samples II and III exhibit well defined transitions at about  $100^\circ\text{C}$  so that, in addition to the mixed phase, these materials contain an essentially pure PMMA phase. From the coefficients of expansion it can be estimated that the fractions of the PMMA existing in the pure PMMA phase in samples II and III are 0.85 and 0.93, respectively.

#### Correlation of broadline n.m.r. data with morphology

Comparison of the n.m.r. and dilatometric data brings to light a definite correlation between polymer morphology and the onset of  $\alpha$ -methyl group rotation in the PMMA

chains. In samples I, IV and V the  $\alpha$ -methyl group rotation starts, and is fully established, at lower temperatures than in pure PMMA, and dilatometry leads to the conclusion that for these samples essentially the whole of the PMMA is in the mixed phase. For samples II and III the  $\alpha$ -methyl group rotation develops more slowly, with increasing temperature than, for pure PMMA and dilatometry suggests that in these samples most of the PMMA is in a pure PMMA phase. Thus, enhancement of the methyl-group rotation arises in the mixed phase and retardation of the rotation in the PMMA phase.

The temperature range over which the  $\alpha$ -methyl group rotation in pure PMMA develops, as observed by n.m.r. must reflect the energy barriers to rotation of the methyl groups and hence the conformations of the PMMA chains which control the local environments of those groups. Thus, the breadth of the transition will be influenced by the variety of local environments which are present in the amorphous polymer. Modifications to the development of  $\alpha$ -methyl group rotations, as observed in the ABCPs, must result from changes in the environment of the methyl groups. Recent neutron scattering studies<sup>15</sup> have demonstrated that torsional vibration frequencies of the  $\alpha$ -methyl groups in isotactic and syndiotactic PMMA are different, the differences arising from changes in chain conformation in consequence of the different chain configurations. Modifications to  $\alpha$ -methyl group rotations in the ABCPs, however, cannot arise from differences in tacticity since all the PMMA chains are predominantly syndiotactic and samples I (enhanced rotation) and II (retarded rotation) were prepared under identical conditions (PMMA polymerization at  $80^\circ\text{C}$ ) and should have the same tacticity.

To explain the modifications to  $\alpha$ -methyl group rotation observed in this work it is necessary to consider the PMMA chain conformations in the mixed phase and in the pure PMMA phase in the ABCPs. It is not known whether the PMMA and PVTCA chains in the mixed phase are intimately mixed on a segmental level or if some very small-scale microphase separation exists. In either case it must be presumed that in order to pack efficiently in the solid state the PMMA chains must adopt a distribution of conformations different from those adopted by PMMA chains in PMMA homopolymer. We believe that in this situation the conformations adopted are such that on average steric restrictions to  $\alpha$ -methyl group rotation are reduced, so that

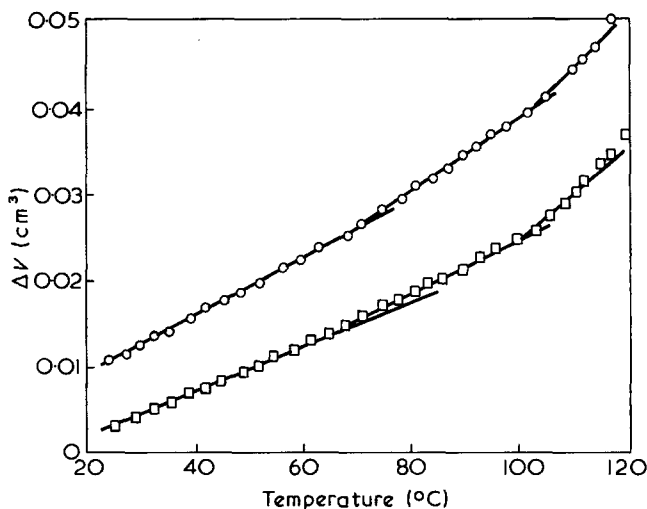


Figure 6 Dilatometric data for PVTCA/PMMA ABCPs.  $\circ$ , Sample II;  $\square$ , sample III

methyl group rotation in samples I, IV and V is observed at a lower temperature than in PMMA homopolymer.

The essential difference between PMMA chains in the homopolymer and in the essentially pure PMMA phase in the ABCPs is the presence of a domain-matrix interface in the latter. In the ABCPs all the PMMA chains are attached to PVTCA chains, consequently the interdomain separation (assuming the PMMA forms the matrix) must be comparable with the PMMA chain dimensions and a large proportion of each PMMA chain must be in close proximity to the interface. A PMMA chain emerging from a PVTCA domain will necessarily adopt conformations which provide good space filling on the surface of the domain. We believe that this can only be achieved if the PMMA chains adopt conformations different from those adopted by a 'free' PMMA chain in the homopolymer, and that the retardation of the methyl group rotation arises as a result of the enhanced barrier to methyl group rotation in the vicinity of the interface. At the present time it is impossible to determine how far the influence of the interface is transmitted into the PMMA phase.

Davis and Slichter<sup>16</sup> have recently observed that when tetraethylene glycol dimethacrylate is polymerized and crosslinked within a poly(vinyl chloride) matrix molecular motions, including rotation of the  $\alpha$ -methyl groups, are impeded.

Absolute values of  $\Delta H_2^2$  are determined by the inter-proton distances and the motions of the protons together with a contribution from the other nuclei with non-zero spin. No satisfactory quantitative interpretation of the absolute values of  $\Delta H_2^2$  observed for the ABCPs in this work

has been obtained so far. However, the relatively high values of  $\Delta H_2^2$  obtained for the ABCPs may arise from the unusual conformations adopted by the PMMA chains which must influence the inter-proton distances and modify both the intra- and inter-molecular contributions to  $\Delta H_2^2$ .

## REFERENCES

- 1 Bamford, C. H., Dyson, R. W. and Eastmond, G. C. *J. Polym. Sci. (C)* 1967, **16**, 2425
- 2 Bamford, C. H., Dyson, R. W., Eastmond, G. C. and Whittle, D. *Polymer* 1969, **10**, 759
- 3 Bamford, C. H., Eastmond, G. C. and Whittle, D. *Polymer* 1969, **10**, 771
- 4 Bamford, C. H., Dyson, R. W. and Eastmond, G. C. *Polymer* 1969, **10**, 885
- 5 Bamford, C. H., Eastmond, G. C., and Whittle, D. *Polymer* 1971, **12**, 247
- 6 Pake, G. E. and Purcell, E. M. *Phys. Rev.* 1948, **74**, 1184
- 7 Andrew, E. R. *Phys. Rev.* 1953, **91**, 425
- 8 Sinnott, K. M. *J. Polym. Sci.* 1960, **42**, 3
- 9 Odajima, A., Woodward, A. E. and Sauer, J. A. *J. Polym. Sci.* 1961, **55**, 181
- 10 Slichter, W. P. and Mandell, E. R. *J. Appl. Phys.* 1959, **30**, 1473
- 11 Smith, E. G. *PhD Thesis* University of Liverpool (1973)
- 12 Kelley, F. N. and Bueche, F. J. *J. Polym. Sci.* 1961, **50**, 549
- 13 Noland, J. S., Hsu, N. N.-C., Saxon, R. and Schmitt, J. M. *Adv. Chem. Ser.* 1971, **99**, 15
- 14 Maguire, D. unpublished results
- 15 Higgins, J. S., Allen, G. and Brier, P. N. *Polymer* 1972, **13**, 157; Allen, G., Wright, C. J. and Higgins, J. S. *Polymer* 1974, **15**, 319
- 16 Davis, D. D. and Slichter, W. P. *Macromolecules* 1973, **6**, 728

# Notes to the Editor

## Solvent effects on the optical behaviour of poly(L-leucyl-L-leucyl-L-aspartic acid) and poly(L-leucyl-L-leucyl-L-lysine)

M. D'Alagni\*

*Istituto di Chimica delle Macromolecole, Nucleo di Roma, c/o Laboratorio di Chimica Fisica, Istituto Chimico, Università di Roma, 00185 Roma, Italy*

and E. Giglio

*Laboratorio di Chimica Fisica, Istituto Chimico, Università di Roma, 00185 Roma, Italy*  
(Received 12 August 1974)

### INTRODUCTION

Two topics of interest in recent years have been the study of the solvent effects on the physico-chemical properties of biopolymers<sup>1-6</sup> and the conformational analysis of sequential polypeptides<sup>7-10</sup>. Research on these subjects may throw light both on the role that the hydrophobic interactions play in proteins, displaying the contribution of the water molecules in such biological systems, and on the influence of different sequences of peptide residues in connection with the macromolecular geometry.

The copolymers poly(L-leucyl-L-leucyl-L-aspartic acid)<sup>11,12</sup> (PLLAA) and poly(L-leucyl-L-leucyl-L-lysine)<sup>13,14</sup> (PLLL) were synthesized and hence investigated in aqueous solution by potentiometric and spectral measurements. The experimental results were in agreement with the presence of  $\alpha$ -helical segments stabilized by hydrophobic interactions both in PLLAA and PLLL. Moreover the  $\Delta H^0$  values seem to point to the existence of a more compact hydrophobic state in PLLAA than in PLLL (6173 and 2784 cal/repetitive unit respectively).

As a development of the research programme concerning PLLAA and PLLL circular dichroism (c.d.) spectra in mixed solvents were recorded in order to obtain some information about the influence of the medium dielectric constant and of the electric dipole moment of the solvent molecules on the PLLAA and PLLL conformation.

### EXPERIMENTAL

Stock solutions of PLLAA<sup>12</sup> and PLLL  $\cdot$  HCl<sup>14</sup> were prepared by dissolving the polymer in double-distilled water (conductivity less than  $2.5 \times 10^{-6}$  ohm<sup>-1</sup> cm<sup>-1</sup> at 20°C) and then adding the appropriate amount of spectroscopic grade solvents (Merck). PLLAA was dissolved in water by adding a small amount of 0.1 N NaOH.

The concentrations of the polymer stock solutions were obtained by a Beckman 120 C amino acid analyser after complete hydrolysis in 6 N HCl at 106–110°C in sealed tubes under vacuum. The concentration range was  $1 \times 10^{-4}$  to  $2 \times 10^{-4}$  M (referred to the mass weight of one third of the repetitive unit).

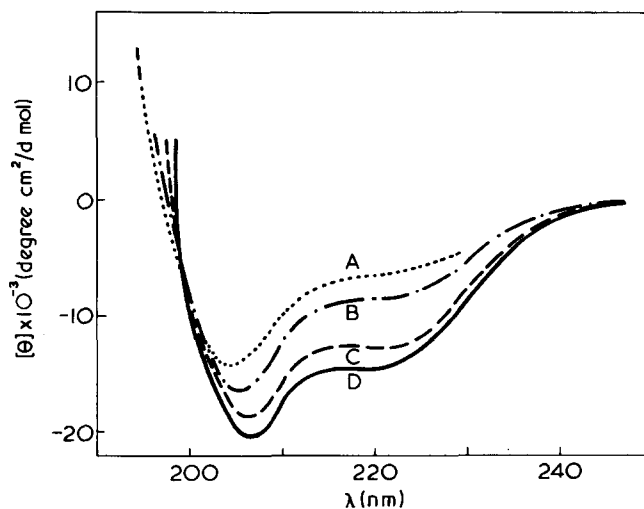
pH was measured on a Radiometer pH meter 26 which was standardized at several pH values with buffers in aqueous media. Thus we report the apparent pH for mixed solvent solutions.

The c.d. spectra were recorded on a Cary 61 and a Cary 60 spectropolarimeter with c.d. attachment. No time effect was detected in the spectral patterns of the polymers in the charged state. The spectra within the pH range corresponding to the region near to the uncharged state were collected by making sure that no precipitation occurred in solution as well as that the pH had reached a constant value. This was done in order to handle data describing equilibrium states.

### RESULTS AND DISCUSSION

Two series of c.d. measurements were accomplished for PLLAA and PLLL in methanol–water solvent mixtures and some spectra are displayed in *Figures 1* and *2* for PLLAA (pH  $\approx$  10.9) and PLLL (pH  $\approx$  5.5) in the charged state. In addition the molar ellipticity  $[\theta]$  of the two polymers at 205 and 220 nm is reported in *Figure 3* as a function of the methanol concentration. From inspection of this Figure it is clear that both the polypeptides show a rather constant  $[\theta]$  value within almost wide range of the methanol percentage. However, the plateau's start at a very different solvent composition and the slope in the first part of the curves is greater for PLLL than for PLLAA.

PLLL exhibits a higher  $\alpha$ -helical content in water than PLLAA. The helicity increases more rapidly by adding less methanol for PLLL than for PLLAA and at 90:10% (v/v) methanol–water PLLL is nearly completely  $\alpha$ -helical. The



*Figure 1* C.d. curves of PLLAA as a function of methanol concentration at 27°C. A, 0; B, 20; C, 50; D, 80% methanol

\*To whom enquiries should be addressed

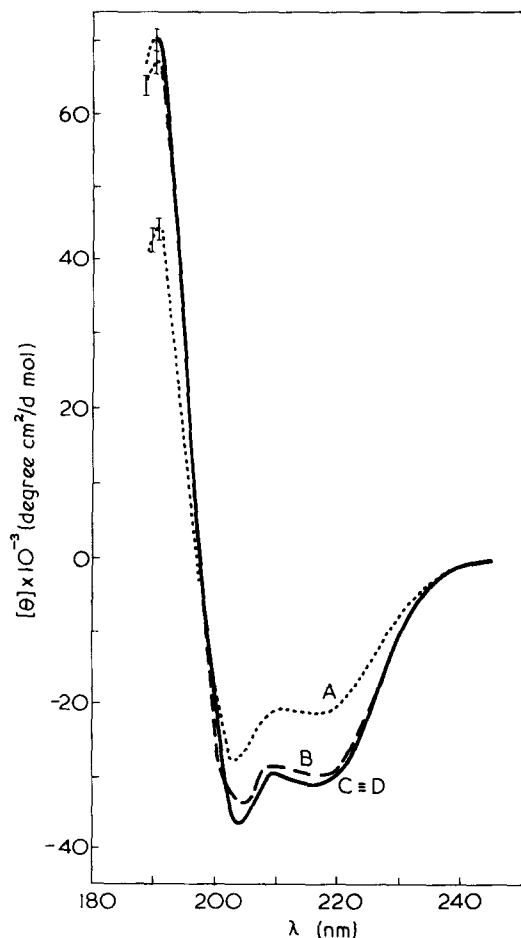


Figure 2 C.d. curves of PLLL as a function of methanol concentration at 27°C. A, 18; B, 36; C, 54; D, 72% methanol. The C and D profiles coincide

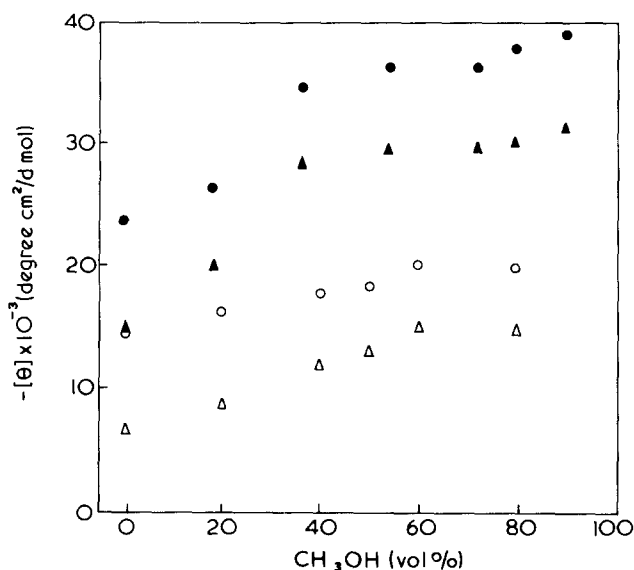


Figure 3 Molar ellipticity vs. methanol concentrations at 27°C. PLLAA:  $\circ$ ,  $\lambda = 205$  nm;  $\triangle$ ,  $\lambda = 220$  nm. PLLL:  $\bullet$ ,  $\lambda = 205$  nm;  $\blacktriangle$ ,  $\lambda = 220$  nm. The  $[\theta]$  values of PLLL at 0 and 90% of methanol are taken from spectra reported in ref 14

curves of PLLL seem to indicate that the increase in helicity occurs in two distinct stages, the second of which causes only a small change in  $[\theta]$ . Thus methanol might give rise to a double-step process characterized by two different types of interaction states. In this connection it may be reasonable to suppose that bulky and hydrophobic side

chains, as those of the leucine and lysine, suitably interact with the apolar parts of the solvent molecules. These molecules produce a short-range ordered structure around the protruding side chains in such a way as to support the  $\alpha$ -helix. For this reason the smaller  $\alpha$ -helical content of PLLAA may be explained as due to the low solvation ability of the aspartyl side chain residue, which is very near to the backbone chain.

It should be mentioned that the  $\alpha$ -helical conformation is just as stable when higher alcohols are used<sup>2,4</sup>, because the hydrophobic part of the solvent molecule is increased. A similar effect is found in water and in methanol-water mixtures for a series of polymers of the *N*<sup>5</sup>-( $\omega$ -hydroxyalkyl)-L-glutamines<sup>1</sup> and for poly(diaminobutyric acid), polyornithine and polylysine<sup>5</sup> as a direct function of the number of methylene groups within the side chain.

C.d. spectra were performed for PLLL in the charged state in order to evaluate the influence of solvents with various dielectric constants on the conformation of the polypeptides. Solvent mixtures containing 80% of methanol, acetonitrile or dioxane and 20% of water were employed. No remarkable change of  $[\theta]$  was detected (see Figure 4) although the dielectric constants of methanol and acetonitrile, which are nearly equal, differ from that of dioxane<sup>15</sup>. On the other hand the electric dipole moments, increasing from dioxane to acetonitrile, seem to be ineffective in stabilizing the  $\alpha$ -helix.

The ellipticity of PLLAA in methanol-water (80:20% v/v) was measured at various pH values. Only three illustrative curves are reported in Figure 5. A similar plot is given in Figure 6, where the charge effect is studied in the aceto-

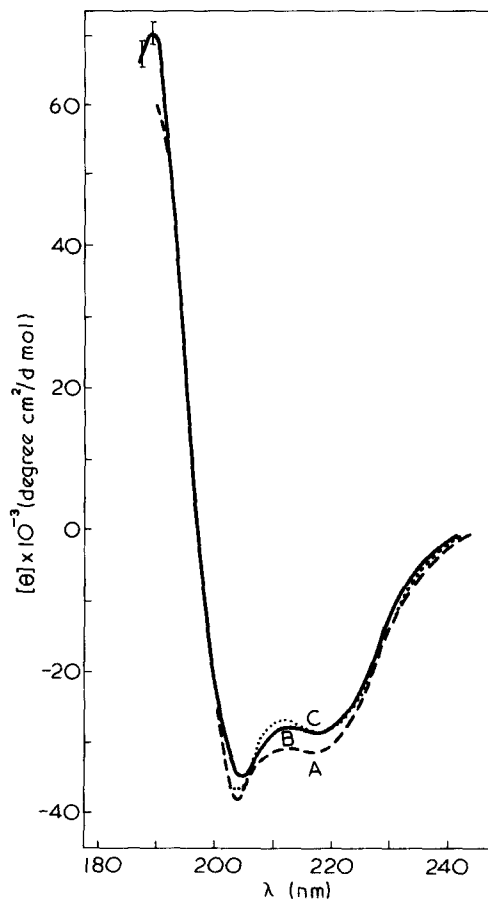


Figure 4 C.d. spectra of PLLL in different solvent mixtures containing 20% (v/v) of water at 27°C. A: methanol, pH = 5.52; B: acetonitrile, pH = 4.96; C: dioxane, pH = 4.60



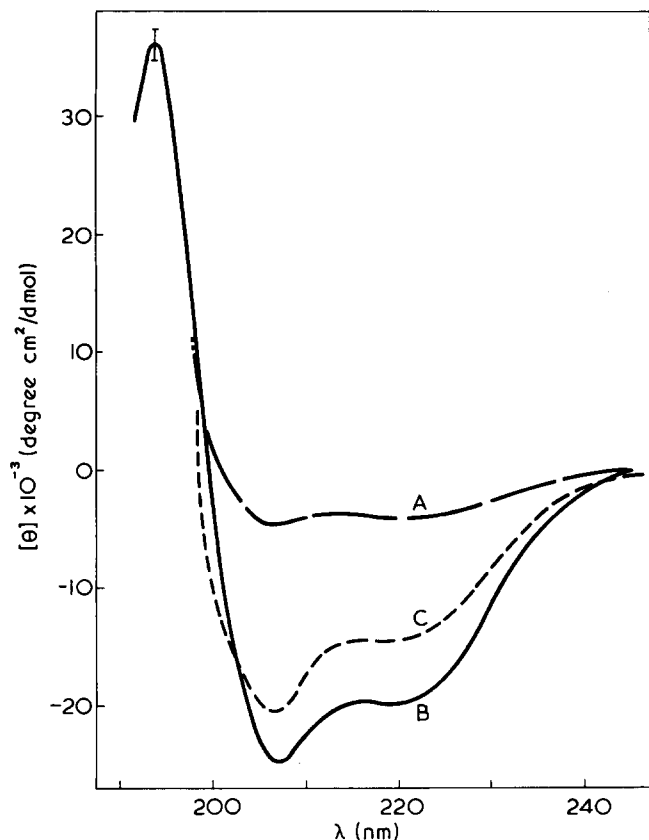


Figure 5 C.d. spectra of PLLAA in methanol-water (80:20% v/v) at 27°C. A, pH = 4.49; B, pH = 6.38; C, pH = 11.22

nitrile-water mixture.  $[\theta]$  decreases slightly more for methanol than for acetonitrile by lowering the pH in the charged state region. However, a fast decrease of the absolute magnitude of  $[\theta]$  appears for the uncharged polymer (curve A of Figures 5 and 6). This peculiar behaviour seems to denote the existence of inter- or intra-molecular aggregation. Clearly the lack of repulsive Coulombic interactions in the uncharged state and the very hydrophobic side chains of PLLAA and PLLL may strongly favour aggregation states.

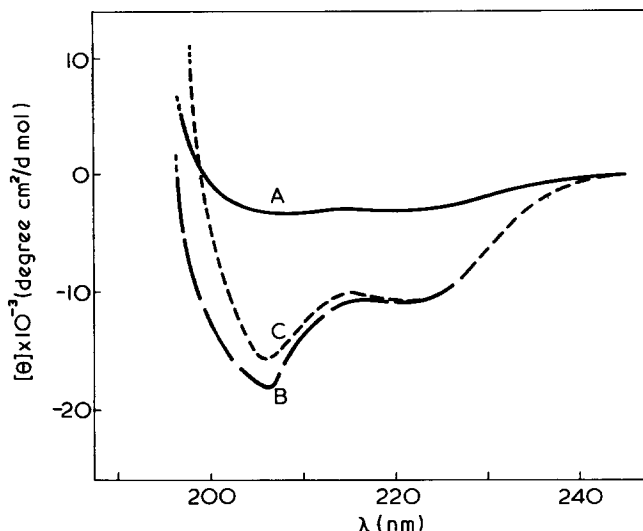


Figure 6 C.d. spectra of PLLAA in acetonitrile-water (80:20% v/v) at 27°C. A, pH = 4.91; B, pH = 8.59; C, pH = 10.30

## REFERENCES

- 1 Lotan, N., Yaron, A. and Berger, A. *Biopolymers* 1966, 4, 365
- 2 Epand, R. F. and Scheraga, H. A. *Biopolymers* 1968, 6, 1383
- 3 Ptitsyn, O. B. *J. Polym. Sci. (C)* 1970, 30, 615
- 4 Pederson, D., Gabriel, D. and Hermans, Jr. *J. Biopolymers* 1971, 10, 2133
- 5 Grouke, M. J. and Gibbs, J. H. *Biopolymers* 1971, 10, 795
- 6 Chou, P. Y., Wells, M. and Fasman, G. D. *Biochemistry* 1972, 11, 3028
- 7 Fraser, R. D. B. *et al. J. Mol. Biol.* 1965, 14, 423
- 8 Brack, A. and Spach, G. *Biopolymers* 1972, 11, 563
- 9 Rippon, W. and Walton, A. G. *J. Am. Chem. Soc.* 1972, 94, 4319
- 10 Brown, F. R., Di Corato, A., Lorenzi, G. P. and Blout, E. R. *J. Mol. Biol.* 1972, 63, 85
- 11 D'Alagni, M., Bemporad, P. and Garofolo, A. *Polymer* 1972, 13, 419
- 12 Carità Morelli, M. and D'Alagni, M. *Polymer* 1972, 13, 515
- 13 Bravin, L. and D'Alagni, M. *Polymer* 1975, 16, 234
- 14 Corsi, E. and D'Alagni, M. *J. Phys. Chem.* in press
- 15 Riddick, J. A. and Bunger, W. B. (*Organic Solvents*, (Ed. A. Weissberger), Wiley-Interscience, New York, 3rd Edn, 1970, Vol 2

## Active centre determination in donor-modified Ziegler-Natta polymerization

D. R. Burfield

Department of Chemistry, University of Malaya, Kuala Lumpur 22-11, Malaysia  
(Received 20 October 1974; revised 30 December 1974)

### INTRODUCTION

Recently a detailed kinetic study of the effect of addition of triethylamine to the catalyst system  $VCl_3/Al(iBu)_3$  for the polymerization of 4-methylpentene-1, has been reported<sup>1</sup>. It was conjectured that differing rates encountered, when using various orders of addition of polymerization components, could be ascribed to variation in the number of active centres. This proposal has been tested by further tritium quench experiments which are now described.

### EXPERIMENTAL

Details of catalysts, solvents and procedure have already been published<sup>1-3</sup>.

### RESULTS AND DISCUSSION

#### Kinetic isotope effect

The correction factor,  $K$ , for the kinetic isotope effect arising from difference in reactivity between the oxygen-hydrogen and oxygen-tritium bonds in the quench methanol, was determined as described previously<sup>3</sup>. A value of  $1.7 \pm 0.2$  was obtained in the donor-modified system, this being the mean of three determinations. This is within the range of values of 1-3.7 obtained by other workers<sup>4-8</sup>, but is significantly lower than that of  $3.20 \pm 0.15$  found previously for the same system in the absence of donor<sup>3</sup>. This observation clearly demonstrates the necessity of determination of the correction factor for meaningful comparison of

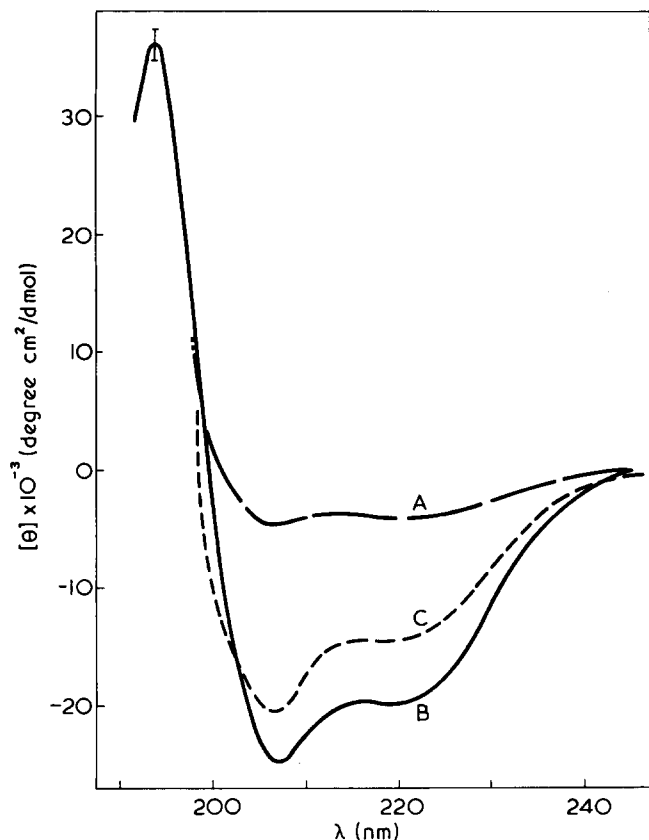


Figure 5 C.d. spectra of PLLAA in methanol-water (80:20% v/v) at 27°C. A, pH = 4.49; B, pH = 6.38; C, pH = 11.22

nitrile-water mixture.  $[\theta]$  decreases slightly more for methanol than for acetonitrile by lowering the pH in the charged state region. However, a fast decrease of the absolute magnitude of  $[\theta]$  appears for the uncharged polymer (curve A of Figures 5 and 6). This peculiar behaviour seems to denote the existence of inter- or intra-molecular aggregation. Clearly the lack of repulsive Coulombic interactions in the uncharged state and the very hydrophobic side chains of PLLAA and PLLL may strongly favour aggregation states.

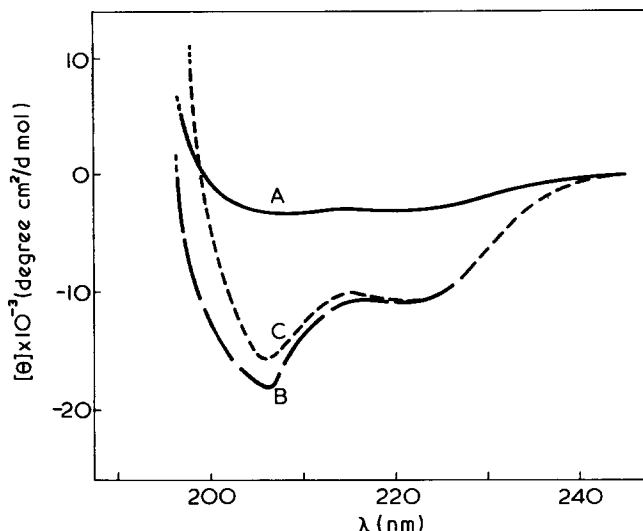


Figure 6 C.d. spectra of PLLAA in acetonitrile-water (80:20% v/v) at 27°C. A, pH = 4.91; B, pH = 8.59; C, pH = 10.30

## REFERENCES

- 1 Lotan, N., Yaron, A. and Berger, A. *Biopolymers* 1966, 4, 365
- 2 Epand, R. F. and Scheraga, H. A. *Biopolymers* 1968, 6, 1383
- 3 Ptitsyn, O. B. *J. Polym. Sci. (C)* 1970, 30, 615
- 4 Pederson, D., Gabriel, D. and Hermans, Jr. *J. Biopolymers* 1971, 10, 2133
- 5 Grouke, M. J. and Gibbs, J. H. *Biopolymers* 1971, 10, 795
- 6 Chou, P. Y., Wells, M. and Fasman, G. D. *Biochemistry* 1972, 11, 3028
- 7 Fraser, R. D. B. *et al. J. Mol. Biol.* 1965, 14, 423
- 8 Brack, A. and Spach, G. *Biopolymers* 1972, 11, 563
- 9 Rippon, W. and Walton, A. G. *J. Am. Chem. Soc.* 1972, 94, 4319
- 10 Brown, F. R., Di Corato, A., Lorenzi, G. P. and Blout, E. R. *J. Mol. Biol.* 1972, 63, 85
- 11 D'Alagni, M., Bemporad, P. and Garofolo, A. *Polymer* 1972, 13, 419
- 12 Carità Morelli, M. and D'Alagni, M. *Polymer* 1972, 13, 515
- 13 Bravin, L. and D'Alagni, M. *Polymer* 1975, 16, 234
- 14 Corsi, E. and D'Alagni, M. *J. Phys. Chem.* in press
- 15 Riddick, J. A. and Bunger, W. B. (*Organic Solvents*, (Ed. A. Weissberger), Wiley-Interscience, New York, 3rd Edn, 1970, Vol 2

## Active centre determination in donor-modified Ziegler-Natta polymerization

D. R. Burfield

Department of Chemistry, University of Malaya, Kuala Lumpur 22-11, Malaysia  
(Received 20 October 1974; revised 30 December 1974)

### INTRODUCTION

Recently a detailed kinetic study of the effect of addition of triethylamine to the catalyst system  $VCl_3/Al(iBu)_3$  for the polymerization of 4-methylpentene-1, has been reported<sup>1</sup>. It was conjectured that differing rates encountered, when using various orders of addition of polymerization components, could be ascribed to variation in the number of active centres. This proposal has been tested by further tritium quench experiments which are now described.

### EXPERIMENTAL

Details of catalysts, solvents and procedure have already been published<sup>1-3</sup>.

### RESULTS AND DISCUSSION

#### Kinetic isotope effect

The correction factor,  $K$ , for the kinetic isotope effect arising from difference in reactivity between the oxygen-hydrogen and oxygen-tritium bonds in the quench methanol, was determined as described previously<sup>3</sup>. A value of  $1.7 \pm 0.2$  was obtained in the donor-modified system, this being the mean of three determinations. This is within the range of values of 1-3.7 obtained by other workers<sup>4-8</sup>, but is significantly lower than that of  $3.20 \pm 0.15$  found previously for the same system in the absence of donor<sup>3</sup>. This observation clearly demonstrates the necessity of determination of the correction factor for meaningful comparison of

results obtained in donor-modified and conventional Ziegler systems. The lower kinetic isotope effect in the presence of triethylamine may possibly reflect the increased reactivity of the donor-complexed polymeric alkyl in the quench reaction.

In addition, it was noticed that at very high conversions (>80%), when the reaction mixture had become extremely viscous, the rate of the quench reaction (as judged by the colour change<sup>3</sup>) became much slower, requiring up to 30 min for complete catalyst penetration compared to about 1–3 min under normal conditions. At the same time, the value of the correction factor for the kinetic isotope effect was found to approach unity, which is to be expected if the quench reaction had become diffusion controlled. This observation introduces a further complication in the tritium quench method of active centre determination since the isotope effect may be dependent on the viscosity of the reaction medium under extreme conditions. However, all values used in this study were obtained outside the viscosity dependent region.

#### Active centre measurements

The number of active centres was determined as previously described<sup>3</sup> by following the variation of the concentration of metal–polymer bonds (MPB) during polymerization. The active centre concentration ( $C_0$ ) is taken as the intercept, at zero conversion, of a plot of [MPB] versus  $\log_{10}(100 - \% \text{ conversion})^3$ .  $C_0$  was determined in the absence of Et<sub>3</sub>N (control experiment) and in the presence of Et<sub>3</sub>N: (i) where the donor is added prior to the monomer (order A); and (ii) where the donor is added subsequent to monomer addition (order B). The  $C_0$  values together with the rates of polymerization and experimental conditions are summarized in Table 1.

The results show that the number of active centres in the donor modified system is dependent on the order of addition of triethylamine to the catalyst (VCl<sub>3</sub>), in particular whether the donor is added before or after the addition of monomer. Prior addition of triethylamine to the catalyst leads to a significant drop in the number of active centres as has been previously suggested<sup>1</sup>. That the rate of polymerization, in this case, remains almost unchanged is probably due to the simultaneous increase in the value of the concentration of adsorbed monomer,  $\theta_M$ , since the rate of polymerization has been shown to be governed by the equation:

$$R_p = k_p \theta_M C_0 \quad (1)$$

The increase in  $\theta_M$  arises through the removal of adsorbed aluminium alkyl species, from the catalyst surface, by complexation with donor.

Where triethylamine is added after monomer addition  $C_0$  is only marginally higher and is in fact within experimental

error of the control value. The large increase in rate of polymerization, in this case, is seen to be mainly due to an increase in  $\theta_M$  rather than in the number of active centres.

These results confirm the importance of the initial monomer/catalyst interaction, and are suggestive of some intermediate species necessary for active centre formation.

#### Chain transfer with metal alkyl

Besides the effect of donor on the number of active centres it is also possible to determine its influence on the rate of transfer with metal alkyl ( $R_{ta}$ ). The rate of transfer with metal alkyl is found<sup>3</sup> directly from the gradient of a plot of [MPB] versus  $t$ . The results for the control and donor-modified polymerization are summarized in Table 1.

It is apparent that the donor may either increase or decrease the rate of transfer with metal alkyl dependent upon the order of addition and concentration. This partly reflects the observed<sup>9</sup> dependence of  $R_{ta}$  upon  $C_0$  of:

$$R_{ta} = k_a \theta_A C_0 \quad (2)$$

Thus the rate of transfer decreases in order A, where  $C_0$  is decreased and increases in order B where  $C_0$  is increased, relative to the control.

The effect of donor on the rate of chain transfer is not, however, totally expected since the polymerization activation has been explained<sup>1</sup> in terms of complexation of metal alkyl, which should also reduce the value of  $\theta_A$ , and hence the ratio  $R_{ta}/C_0$  (Table 1). This apparent discrepancy may well arise if the denominator of  $\theta_A$  contains additional terms, i.e.  $\theta_A$  is given by the modified equation:

$$\theta_A = \frac{K_A [A]}{1 + K_M [M] + K_A [A] + K_{A'} [A']} \quad (3)$$

where the additional term  $K_{A'} [A']$  represents the adsorption of aluminium chloroalkyl species. Such modification is consistent with earlier results<sup>1</sup>. If the aluminium chloroalkyl species are strongly adsorbed, as seems likely, and are preferentially complexed by donor then  $\theta_A$  could remain virtually unchanged or even somewhat increased on addition of triethylamine.

What, however, is more significant is the fact that the ratio of  $R_p/R_{ta}$  increases in the presence of donor by a factor of about 2. As it has been shown<sup>10</sup> that in this system transfer with metal alkyl is a major molecular weight limiting reaction, this would be expected to lead to a significant increase in the molecular weight. Such molecular weight increases have been generally observed on donor modification of conventional catalyst systems<sup>11–19</sup>. Thus it may be speculated that the increase in molecular weight in the presence of electron donors is largely due to the reduction in rate of chain transfer with metal alkyl relative to the rate of polymerization.

Table 1 Comparison of active centre concentration and rate of chain transfer with aluminium alkyl in control and donor modified polymerization

	$R_p$ (mol l <sup>-1</sup> min <sup>-1</sup> VCl <sub>3</sub> <sup>-1</sup> )	$C_0 \times 10^4$ (mol/mol VCl <sub>3</sub> )	$R_{ta} \times 10^6$ (mol l <sup>-1</sup> min <sup>-1</sup> VCl <sub>3</sub> <sup>-1</sup> )	$R_p/R_{ta}$ $\times 10^{-5}$	$R_{ta}/C_0 \times 10^2$ (min <sup>-1</sup> )
Control	0.270	3.8 ± 0.4	3.2	0.83	0.85
Order A <sup>a</sup>	0.292	2.1 ± 0.3	2.6	1.1	1.2
Order B <sup>b</sup>	0.684	4.6 ± 0.5	4.1	1.7	0.88

[4-MP-1] = 2.0 mol/l; [VCl<sub>3</sub>] = 18.5 × 10<sup>-3</sup> mol/l; [Al(iBu)<sub>3</sub>] = 37.0 × 10<sup>-3</sup> mol/l; solvent = benzene; temperature = 30°C

<sup>a</sup> [NEt<sub>3</sub>] = 18.5 × 10<sup>-3</sup> mol/l

<sup>b</sup> [NEt<sub>3</sub>] = 27.8 × 10<sup>-3</sup> mol/l

## REFERENCES

- 1 Burfield, D. R. and Tait, P. J. T. *Polymer* 1974, 15, 87
- 2 McKenzie, I. D., Tait, P. J. T. and Burfield, D. R. *Polymer* 1972, 13, 307
- 3 Burfield, D. R. and Tait, P. J. T. *Polymer* 1972, 13, 315
- 4 Schnecko, H. and Kern, W. *IUPAC Macromol. Symp. Budapest* 1969
- 5 Feldman, C. F. and Perry, E. J. *J. Polym. Sci.* 1960, 46, 217
- 6 Kohn, E., Schuurmans, H. J. L., Cavender, J. V. and Mendelson, E. A. *J. Polym. Sci.* 1962, 58, 681
- 7 Coover, R. W., Guillet, J. E., Combs, R. L. and Joyner, F. S. *J. Polym. Sci. (A-1)* 1966, 4, 2583
- 8 Bier, G., Hoffman, W., Lehmann, G. and Seydel, G. *Makromol. Chem.* 1962, 58, 1
- 9 Burfield, D. R., Tait, P. J. T. and McKenzie, I. D. *Polymer* 1972, 13, 321
- 10 McKenzie, I. D. and Tait, P. J. T. *Polymer* 1972, 13, 510
- 11 Boor, J. Jr. *J. Polym. Sci. (A)* 1965, 3, 995
- 12 Vesely, K., Ambroz, J., Vilim, R. and Hamrik, O. *J. Polym. Sci.* 1961, 55, 25
- 13 Coover, H. W. Jr. and Joyner, F. B. *J. Polym. Sci. (A)* 1965, 3, 2407
- 14 Pirogov, O. N. and Chirokov, N. M. *Vysokomol. Soedin.* 1965, 7, 491
- 15 Milovskaya, Ye. B. and Dolgopolskaya, T. I. *Vysokomol. Soedin.* 1962, 4, 145
- 16 Razuvaev, G. A., Minsker, K. S., Fedoseeva, G. T. and Bykhovskii, U. K. *Vysokomol. Soedin.* 1960, 2, 404
- 17 Boor, J. and Short, G. A. *J. Polym. Sci. (B)* 1971, 9, 235
- 18 Razuvaev, G. A., Minsker, K. S., Fedoseeva, G. T. and Savel'er, L. A. *Vysokomol. Soedin.* 1959, 1, 1961
- 19 Razuvaev, G. A., Minsker, K. S., Chernovskaya, R. P. and Burlakova, G. I. *Vysokomol. Soedin* 1965, 7, 39

## Properties of poly(*p*-biphenyl methacrylate) in dilute solution

J. B. Alexopoulos, N. Hadjichristidis and A. Vassiliadis

Department of Industrial Chemistry, University of Athens, 13A Navarinou Street, Athens 144, Greece

(Received 2 December 1974)

As part of a research programme for the investigation of solution properties of polymethacrylate esters as a function of the chemical structure of the side groups, we present here the results for poly(*p*-biphenyl methacrylate).

The *p*-biphenyl methacrylate<sup>1</sup> was polymerized at 50°C in benzene solution under vacuum with azobisisobutyronitrile as initiator. Fractions of the polymer were obtained by stepwise precipitation from benzene solutions using methanol as precipitant. The fractions were analysed by gel permeation chromatography (g.p.c.). Finally six fractions (B1 to B6) were chosen among those obtained from five polymerizations.

Viscosity, light scattering, osmotic pressure sedimentation and g.p.c. results are given in Table 1. The methods used have been described elsewhere<sup>2-4</sup>.

### RESULTS AND DISCUSSION

The experimental values of the constants for the relations:

$$[\eta] = K_a \bar{M}_w^a \quad (S_0) = K_c \bar{M}_w^c \quad A_2^* = K_d \bar{M}_w^d$$

$$A_2 = K_e \bar{M}_n^e \quad (\bar{r}_z^2)^{1/2} = K_f \bar{M}_w^f$$

are given in Table 2. The values of the constants *c* and *f* calculated

from the Mark-Houwink constant  $a(c = (2 - a)/3, f = (a + 1)/3)$  are 0.475 and 0.57 in excellent agreement with the experimental values.

The value of  $k = k_s/[\eta]$  varies from 1.4 to 1.6 in good agreement with theory<sup>5</sup>. The average value of  $\Phi^{1/3}P^{-1}$  of the Mandelkern-Flory equation<sup>6</sup> is  $2.3 \times 10^6$ .

The value of  $K_\theta$  leading to the unperturbed dimension  $(\bar{r}_0^2)^{1/2}$ :

$$K_\theta = \Phi \left( \frac{\bar{r}_0^2}{M} \right)^{3/2}$$

has been calculated by the well known relations of Stockmayer-Fixman<sup>7</sup> and Kamide-Moore<sup>8</sup>. The values of  $K_\theta$  obtained by these relations are:  $43 \times 10^{-5}$  dl/g (S-F) and  $45 \times 10^{-5}$  dl/g (K-M) (Figures 1 and 2).

Adopting the value of  $44 \times 10^{-5}$  dl/g for  $K_\theta$ , the relation between  $(\bar{r}_0^2)^{1/2}$  and molecular weight is:

$$(\bar{r}_0^2)^{1/2} = 0.60QM^{1/2} (\text{\AA})$$

taking the value of  $2.0 \times 10^{21}$  for  $\Phi$ .

The root-mean-square end-to-end distance, assuming completely free rotation around the bonds or  $(\bar{r}_{0f}^2)^{1/2}$ ,

Table 1 Experimental values of poly(*p*-biphenyl methacrylate) at 25°C

	Solvent	B1	B2	B3	B4	B5	B6	
[η] (dl/g)	CHCl <sub>3</sub>	1.330	0.767	0.425	0.272	0.190	0.112	$K_H$ (av. value)
	THF	1.105	0.682	0.373	0.240	0.168	0.105	
	Dioxane	0.872	0.583	0.330	0.215	0.155	0.100	
	Benzene	0.635	0.445	0.275	0.185	0.140	0.095	
$\bar{M}_w \times 10^{-6}$	CHCl <sub>3</sub>	1.180	0.618	0.282	0.140	0.0847	0.0434	$dn/dc$ (cm <sup>3</sup> /g)
		$A_2^* \times 10^4$ (cm <sup>3</sup> mol g <sup>-2</sup> )	1.03	1.63	2.22	2.45	3.33	
$(\bar{r}_z^2)^{1/2}$ (Å)		1085	727	460	318	245	—	
$\bar{M}_n \times 10^{-6}$	C <sub>6</sub> H <sub>5</sub> Cl*	—	0.487	0.200	0.107	0.0470	0.0236	$\bar{V}$ (cm <sup>3</sup> /g)
		$A_2 \times 10^4$ (cm <sup>3</sup> mol g <sup>-2</sup> )	—	1.21	2.08	2.86	4.10	
$(S_0) \times 10^{15}$	Benzene	49.69	37.75	26.17	18.69	14.23	10.68	$\bar{V}$ (cm <sup>3</sup> /g)
$k_s$		0.91	0.69	0.44	0.30	0.17	0.07	
$\bar{M}_w/\bar{M}_n$ by g.p.c.	THF	1.4	1.4	1.3	1.3	1.6	1.6	

\* Measurements at 37°C

## REFERENCES

- 1 Burfield, D. R. and Tait, P. J. T. *Polymer* 1974, 15, 87
- 2 McKenzie, I. D., Tait, P. J. T. and Burfield, D. R. *Polymer* 1972, 13, 307
- 3 Burfield, D. R. and Tait, P. J. T. *Polymer* 1972, 13, 315
- 4 Schnecko, H. and Kern, W. *IUPAC Macromol. Symp. Budapest* 1969
- 5 Feldman, C. F. and Perry, E. J. *J. Polym. Sci.* 1960, 46, 217
- 6 Kohn, E., Schuurmans, H. J. L., Cavender, J. V. and Mendelson, E. A. *J. Polym. Sci.* 1962, 58, 681
- 7 Coover, R. W., Guillet, J. E., Combs, R. L. and Joyner, F. S. *J. Polym. Sci. (A-1)* 1966, 4, 2583
- 8 Bier, G., Hoffman, W., Lehmann, G. and Seydel, G. *Makromol. Chem.* 1962, 58, 1
- 9 Burfield, D. R., Tait, P. J. T. and McKenzie, I. D. *Polymer* 1972, 13, 321
- 10 McKenzie, I. D. and Tait, P. J. T. *Polymer* 1972, 13, 510
- 11 Boor, J. Jr. *J. Polym. Sci. (A)* 1965, 3, 995
- 12 Vesely, K., Ambroz, J., Vilim, R. and Hamrik, O. *J. Polym. Sci.* 1961, 55, 25
- 13 Coover, H. W. Jr. and Joyner, F. B. *J. Polym. Sci. (A)* 1965, 3, 2407
- 14 Pirogov, O. N. and Chirokov, N. M. *Vysokomol. Soedin.* 1965, 7, 491
- 15 Milovskaya, Ye. B. and Dolgopolskaya, T. I. *Vysokomol. Soedin.* 1962, 4, 145
- 16 Razuvaev, G. A., Minsker, K. S., Fedoseeva, G. T. and Bykhovskii, U. K. *Vysokomol. Soedin.* 1960, 2, 404
- 17 Boor, J. and Short, G. A. *J. Polym. Sci. (B)* 1971, 9, 235
- 18 Razuvaev, G. A., Minsker, K. S., Fedoseeva, G. T. and Savel'er, L. A. *Vysokomol. Soedin.* 1959, 1, 1961
- 19 Razuvaev, G. A., Minsker, K. S., Chernovskaya, R. P. and Burlakova, G. I. *Vysokomol. Soedin* 1965, 7, 39

## Properties of poly(*p*-biphenyl methacrylate) in dilute solution

J. B. Alexopoulos, N. Hadjichristidis and A. Vassiliadis

Department of Industrial Chemistry, University of Athens, 13A Navarinou Street, Athens 144, Greece

(Received 2 December 1974)

As part of a research programme for the investigation of solution properties of polymethacrylate esters as a function of the chemical structure of the side groups, we present here the results for poly(*p*-biphenyl methacrylate).

The *p*-biphenyl methacrylate<sup>1</sup> was polymerized at 50°C in benzene solution under vacuum with azobisisobutyronitrile as initiator. Fractions of the polymer were obtained by stepwise precipitation from benzene solutions using methanol as precipitant. The fractions were analysed by gel permeation chromatography (g.p.c.). Finally six fractions (B1 to B6) were chosen among those obtained from five polymerizations.

Viscosity, light scattering, osmotic pressure sedimentation and g.p.c. results are given in Table 1. The methods used have been described elsewhere<sup>2-4</sup>.

### RESULTS AND DISCUSSION

The experimental values of the constants for the relations:

$$[\eta] = K_a \bar{M}_w^a \quad (S_0) = K_c \bar{M}_w^c \quad A_2^* = K_d \bar{M}_w^d$$

$$A_2 = K_e \bar{M}_n^e \quad (\bar{r}_z^2)^{1/2} = K_f \bar{M}_w^f$$

are given in Table 2. The values of the constants *c* and *f* cal-

culated from the Mark-Houwink constant  $a(c = (2 - a)/3$ ,  $f = (a + 1)/3$ ) are 0.475 and 0.57 in excellent agreement with the experimental values.

The value of  $k = k_s/[\eta]$  varies from 1.4 to 1.6 in good agreement with theory<sup>5</sup>. The average value of  $\Phi^{1/3}P^{-1}$  of the Mandelkern-Flory equation<sup>6</sup> is  $2.3 \times 10^6$ .

The value of  $K_\theta$  leading to the unperturbed dimension  $(\bar{r}_0^2)^{1/2}$ :

$$K_\theta = \Phi \left( \frac{\bar{r}_0^2}{M} \right)^{3/2}$$

has been calculated by the well known relations of Stockmayer-Fixman<sup>7</sup> and Kamide-Moore<sup>8</sup>. The values of  $K_\theta$  obtained by these relations are:  $43 \times 10^{-5}$  dl/g (S-F) and  $45 \times 10^{-5}$  dl/g (K-M) (Figures 1 and 2).

Adopting the value of  $44 \times 10^{-5}$  dl/g for  $K_\theta$ , the relation between  $(\bar{r}_0^2)^{1/2}$  and molecular weight is:

$$(\bar{r}_0^2)^{1/2} = 0.60QM^{1/2} (\text{\AA})$$

taking the value of  $2.0 \times 10^{21}$  for  $\Phi$ .

The root-mean-square end-to-end distance, assuming completely free rotation around the bonds or  $(\bar{r}_{0f}^2)^{1/2}$ ,

Table 1 Experimental values of poly(*p*-biphenyl methacrylate) at 25°C

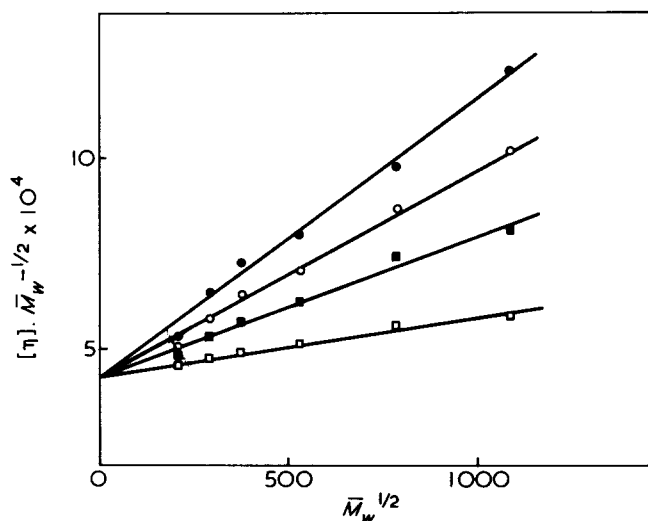
	Solvent	B1	B2	B3	B4	B5	B6	
[η] (dl/g)	CHCl <sub>3</sub>	1.330	0.767	0.425	0.272	0.190	0.112	<i>K<sub>H</sub></i> (av. value)
	THF	1.105	0.682	0.373	0.240	0.168	0.105	
	Dioxane	0.872	0.583	0.330	0.215	0.155	0.100	
	Benzene	0.635	0.445	0.275	0.185	0.140	0.095	
$\bar{M}_w \times 10^{-6}$	CHCl <sub>3</sub>	1.180	0.618	0.282	0.140	0.0847	0.0434	<i>dn/dc</i> (cm <sup>3</sup> /g)
		$A_2^* \times 10^4$ (cm <sup>3</sup> mol g <sup>-2</sup> )	1.03	1.63	2.22	2.45	3.33	
$(\bar{r}_z^2)^{1/2}$ (Å)		1085	727	460	318	245	—	
$\bar{M}_n \times 10^{-6}$	C <sub>6</sub> H <sub>5</sub> Cl*	—	0.487	0.200	0.107	0.0470	0.0236	$\bar{V}$ (cm <sup>3</sup> /g)
		$A_2 \times 10^4$ (cm <sup>3</sup> mol g <sup>-2</sup> )	—	1.21	2.08	2.86	4.10	
$(S_0) \times 10^{15}$	Benzene	49.69	37.75	26.17	18.69	14.23	10.68	$\bar{V}$ (cm <sup>3</sup> /g)
<i>k<sub>s</sub></i>		0.91	0.69	0.44	0.30	0.17	0.07	
$\bar{M}_w/\bar{M}_n$ by g.p.c.	THF	1.4	1.4	1.3	1.3	1.6	1.6	

\* Measurements at 37°C

Table 2 Constants of the different empirical relations at 25°C

	CHCl <sub>3</sub>	THF	Dioxane	Benzene	C <sub>6</sub> H <sub>5</sub> Cl*
$K_d \times 10^5$	5.22	6.37	9.72	20.51	
$a$	0.72	0.695	0.65	0.575	
$K_c \times 10^{17}$				6.64	
$c$				0.475	
$K_d \times 10^2$	3.1				
$d$	(-0.4)				
$K_e \times 10^2$					9.07
$e$					(-0.5)
$K_f$	0.37				
$f$	0.57				

\* Measurements at 37°C

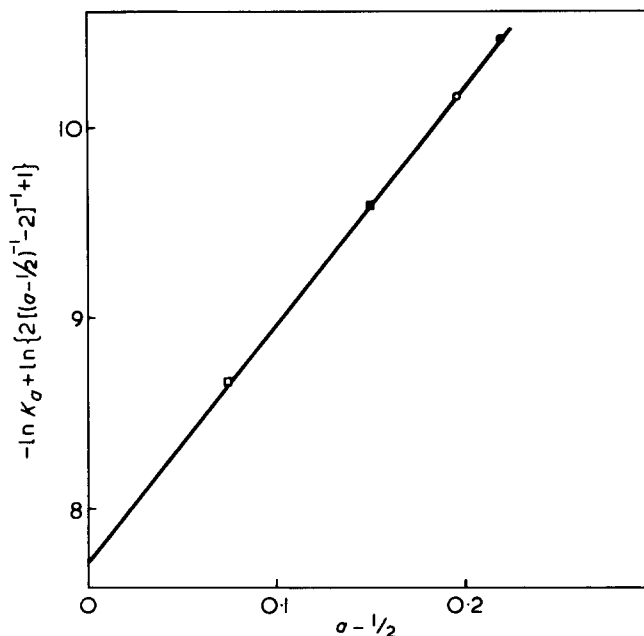
Figure 1 Stockmayer-Fixman plot for poly(*p*-biphenyl methacrylate) in different solvents at 25°C. ●, CHCl<sub>3</sub>; ○, THF; ■, dioxane; □, benzene

is given by the relation:

$$(\bar{r}_{0f}^2)^{1/2} = 0.20M^{1/2} (\text{Å})$$

The value  $(\bar{r}_0^2)^{1/2}/(\bar{r}_{0f}^2)^{1/2}$  or  $\sigma$ , representing the effect of steric hindrance on the flexibility of the chain, is consequently equal to 3.0.

In conclusion, poly(*p*-biphenyl methacrylate), as with other aromatic polymethacrylates<sup>2,3</sup>, has a high rigidity probably because of the specific interactions between the aromatic rings.

Figure 2 Kamide-Moore plot for poly(*p*-biphenyl methacrylate) at 25°C. ●, CHCl<sub>3</sub>; ○, THF; ■, dioxane; □, benzene

#### ACKNOWLEDGEMENT

Part of the experimental work has been carried out by one of us (N.H.) in Professor V. Desreux's laboratories, at Liège University, to whom we are gratefully indebted.

#### REFERENCES

- 1 Patai, S., Bentov, M. and Reichmann, M. E. *J. Am. Chem. Soc.* 1952, **74**, 845
- 2 Hadjichristidis, N., Devaleriola, M. and Desreux, V. *Eur. Polym. J.* 1972, **8**, 1193
- 3 Hadjichristidis, N. and Desreux, V. *J. Macromol. Sci. (C)* 1972, **6**, 1227
- 4 Di Marco, A., Hadjichristidis, N., Niezette, J. and Desreux, V. *Bull. Soc. R. Sci. Liège* 1973, **5-6**, 253
- 5 Gralén, N. *Thesis Uppsala* (1944)
- 6 Mandelkern, L. and Flory, P. J. *J. Chem. Phys.* 1952, **20**, 212
- 7 Stockmayer, W. and Fixman, M. J. *J. Polym. Sci. (C)* 1963, **1**, 137
- 8 Kamide, K. and Moore, W. R. *J. Polym. Sci. (B)* 1964, **2**, 809

## Letters

### Solvent sorption of heat treated vinyl chloride polymers

#### Introduction

The results reported here are part of an investigation into the effect of heat treatment on structural order in vinyl chloride polymers. The solvent sorption technique described is based on that used by Blackadder and Vincent<sup>1</sup> for following small morphological changes in polypropylene and poly(ethylene terephthalate). Changes in the solvent sorption behaviour of heat treated suspension polymerized poly(vinyl chloride) have been reported by Illers<sup>2</sup>, but long annealing times (100 h at 65°C, 94 h at 90°C) were used. In the present work the effect of much shorter heat treatments

on solvent sorption is examined for three vinyl chloride polymers. The shorter heat treatments are used in an attempt to find out whether structural changes are likely to occur during the processing of PVC.

#### Experimental

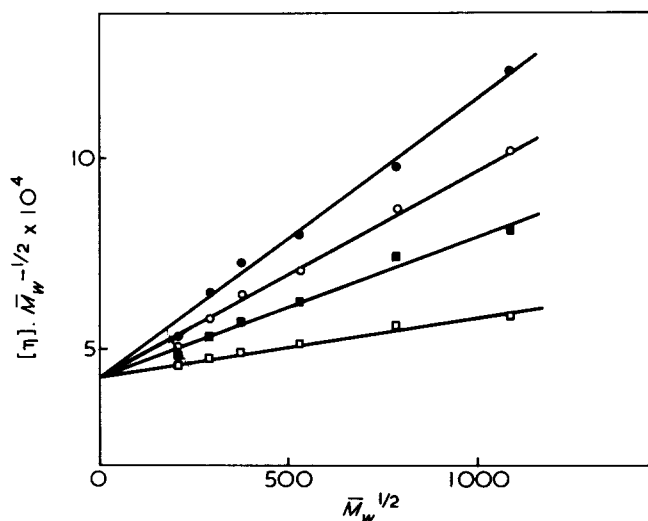
**Materials.** The three polymers were as follows: (1) PVC 2 (a BP suspension homopolymer supplied by RAPRA Polymer Supply and Characterisation Centre); (2) Breon AS 60/41 X15 (a BP suspension polymer containing 15% vinyl acetate); (3) a PVC homopolymer polymerized at -30°C (Montecatini Edison).

Glass transition temperatures of the polymers, measured by a du Pont thermomechanical analyzer, are listed below.

Table 2 Constants of the different empirical relations at 25°C

	CHCl <sub>3</sub>	THF	Dioxane	Benzene	C <sub>6</sub> H <sub>5</sub> Cl*
$K_d \times 10^5$	5.22	6.37	9.72	20.51	
$a$	0.72	0.695	0.65	0.575	
$K_c \times 10^{17}$				6.64	
$c$				0.475	
$K_d \times 10^2$	3.1				
$d$	(-0.4)				
$K_e \times 10^2$					9.07
$e$					(-0.5)
$K_f$	0.37				
$f$	0.57				

\* Measurements at 37°C

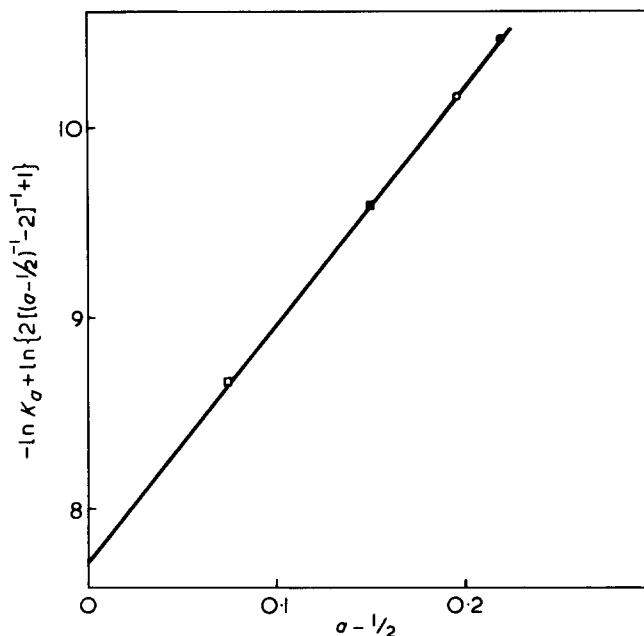
Figure 1 Stockmayer-Fixman plot for poly(*p*-biphenyl methacrylate) in different solvents at 25°C. ●, CHCl<sub>3</sub>; ○, THF; ■, dioxane; □, benzene

is given by the relation:

$$(\bar{r}_{of}^2)^{1/2} = 0.20M^{1/2} (\text{Å})$$

The value  $(\bar{r}_0^2)^{1/2}/(\bar{r}_{of}^2)^{1/2}$  or  $\sigma$ , representing the effect of steric hindrance on the flexibility of the chain, is consequently equal to 3.0.

In conclusion, poly(*p*-biphenyl methacrylate), as with other aromatic polymethacrylates<sup>2,3</sup>, has a high rigidity probably because of the specific interactions between the aromatic rings.

Figure 2 Kamide-Moore plot for poly(*p*-biphenyl methacrylate) at 25°C. ●, CHCl<sub>3</sub>; ○, THF; ■, dioxane; □, benzene

#### ACKNOWLEDGEMENT

Part of the experimental work has been carried out by one of us (N.H.) in Professor V. Desreux's laboratories, at Liège University, to whom we are gratefully indebted.

#### REFERENCES

- 1 Patai, S., Bentov, M. and Reichmann, M. E. *J. Am. Chem. Soc.* 1952, **74**, 845
- 2 Hadjichristidis, N., Devaleriola, M. and Desreux, V. *Eur. Polym. J.* 1972, **8**, 1193
- 3 Hadjichristidis, N. and Desreux, V. *J. Macromol. Sci. (C)* 1972, **6**, 1227
- 4 Di Marco, A., Hadjichristidis, N., Niezette, J. and Desreux, V. *Bull. Soc. R. Sci. Liège* 1973, **5-6**, 253
- 5 Gralén, N. *Thesis Uppsala* (1944)
- 6 Mandelkern, L. and Flory, P. J. *J. Chem. Phys.* 1952, **20**, 212
- 7 Stockmayer, W. and Fixman, M. J. *J. Polym. Sci. (C)* 1963, **1**, 137
- 8 Kamide, K. and Moore, W. R. *J. Polym. Sci. (B)* 1964, **2**, 809

## Letters

### Solvent sorption of heat treated vinyl chloride polymers

#### Introduction

The results reported here are part of an investigation into the effect of heat treatment on structural order in vinyl chloride polymers. The solvent sorption technique described is based on that used by Blackadder and Vincent<sup>1</sup> for following small morphological changes in polypropylene and poly(ethylene terephthalate). Changes in the solvent sorption behaviour of heat treated suspension polymerized poly(vinyl chloride) have been reported by Illers<sup>2</sup>, but long annealing times (100 h at 65°C, 94 h at 90°C) were used. In the present work the effect of much shorter heat treatments

on solvent sorption is examined for three vinyl chloride polymers. The shorter heat treatments are used in an attempt to find out whether structural changes are likely to occur during the processing of PVC.

#### Experimental

**Materials.** The three polymers were as follows: (1) PVC 2 (a BP suspension homopolymer supplied by RAPRA Polymer Supply and Characterisation Centre); (2) Breon AS 60/41 X15 (a BP suspension polymer containing 15% vinyl acetate); (3) a PVC homopolymer polymerized at -30°C (Montecatini Edison).

Glass transition temperatures of the polymers, measured by a du Pont thermomechanical analyzer, are listed below.

	$T_g(^{\circ}\text{C})$
PVC 2	82
Breon AS 60/41 X15	75
Low temperature polymerized PVC	91

The polymers were selected to represent a typical commercial suspension polymer, a copolymer in which structural order would be disrupted by bulky acetate groups, and a low temperature polymerized PVC which is known to have a higher syndiotacticity, hence a higher crystallinity than a typical commercial PVC homopolymer<sup>3</sup>.

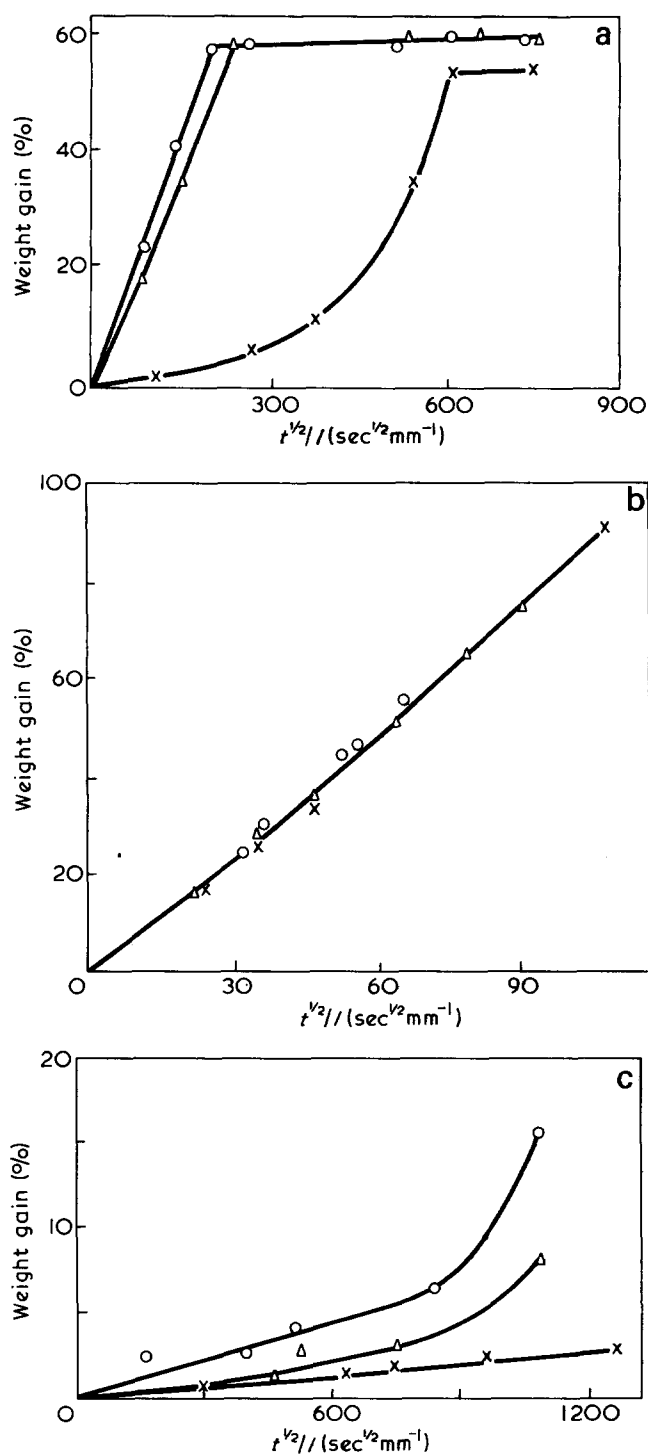


Figure 1 Sorption curves for (a) PVC 2 (b) PVC/PVAC copolymer and (c) low temperature polymerized PVC. ○, pre-treated and quenched; △, pre-treated, quenched and heated 8 h at 70°C; X, pre-treated, quenched and heated 8 h at 110°C

After dry blending with 4 parts per hundred (by weight) of dibasic lead stearate each polymer was milled, then compression moulded to form sheet approximately 0.5 mm thick.

**Heat treatment.** In an attempt to destroy existing order and to ensure a uniform heat history all samples were first heated under nitrogen for 3 min and then quenched in an ice/water mixture. The pre-treatment temperatures used were: PVC 2, 200°C; PVC/PVAC copolymer, 175°C; low temperature polymerized PVC, 220°C.

Selected samples were further heat treated at 70°C and 110°C, i.e. above and below their glass transition temperature.

**Solvent sorption.** The heat treated sheet was cut into strips 13 mm x 40 mm for the solvent sorption measurements. The weight and average thickness of each strip were measured, and the samples were immersed in toluene in stoppered jars which were placed in a water bath thermostated at  $30 \pm 0.1^{\circ}\text{C}$ . Samples were removed after selected intervals of time. Each sample was quickly dabbed with a tissue to remove excess toluene, and a plot of its weight against time was used to find the sample weight at the time of its removal from toluene.

### Results and Discussion

In Figures 1a–1c the % weight gain due to solvent sorption for the three polymers are plotted against  $t^{1/2}/l$  where  $t$  is the immersion time of the strip in toluene, and  $l$  its average thickness in mm. The term  $t^{1/2}/l$  is used to correct for any slight thickness differences of the samples. Results for the three polymers, heat treated for 8 h at 110°C are compared in Figure 2.

The PVC/PVAC copolymer absorbed over 90% of its own weight of toluene in 1 h. During the same time PVC 2 and the low temperature polymerized PVC absorbed less than 1% of toluene. After longer immersion times the two homopolymers exhibited different behaviour. For PVC 2 the rate of solvent sorption increased, then the weight gain reached an equilibrium value of 50–60% after about 24 h. For the low temperature polymerized PVC the rate of solvent sorption increased more slowly and an equilibrium value had not been reached after 4 days. For the copolymer it is clear that the equilibrium weight gain must be higher than for PVC 2.

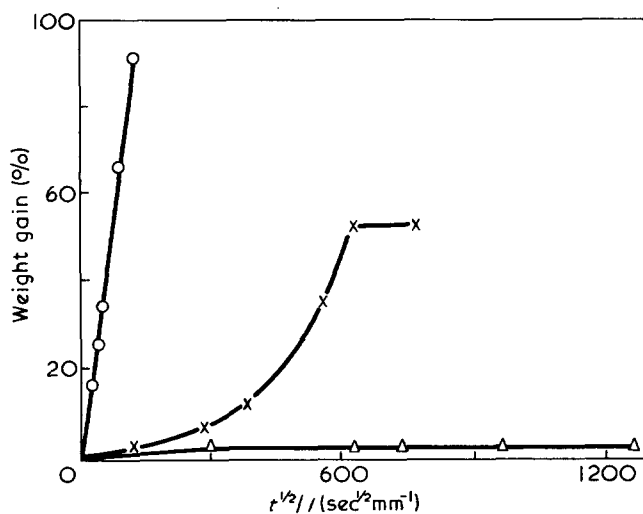


Figure 2 Sorption curves for three vinyl chloride polymers heat treated 8 h at 110°C. X, PVC 2; ○, PVC/PVAC copolymer; △, low temperature polymerized PVC



The different solvent sorption behaviour of the three polymers may be due to several factors. Some X-ray diffraction work currently in progress has shown that, as expected, the PVC/PVAC copolymer appears to be virtually amorphous while the low temperature polymerized PVC has the highest crystallinity. Crystallinity is expected to have a significant effect on solvent sorption since the polymer chains are packed more closely in crystalline regions thus restricting solvent penetration. The results obtained for the two PVC homopolymers may be explained on this basis. In the copolymer chain packing is also reduced by the bulky acetate groups present and the decrease in polar forces between chains caused by the replacement of chlorine atoms by these groups.

Heat treatment changed the solvent sorption behaviour of the two homopolymers (Figures 1a and 1c) but had no significant effect on the solvent sorption of the copolymer (Figure 1b). For PVC 2 (Figure 1a), the quenched sample, in which order would be expected to be lowest, absorbs solvent most rapidly. The sample heat treated at 70°C (i.e. below the glass transition temperature of the polymer) absorbs solvent slightly more slowly, but the weight gain reaches the same equilibrium value. The sample heat treated at 110°C (i.e. above the glass transition temperature) absorbs solvent more slowly and reaches a lower equilibrium value. Also the solvent sorption curve is S-shaped in the latter case, while for the quenched sample and the sample heat treated at 70°C the initial part of the plot of weight gain versus  $t^{1/2}/l$  appears linear before the equilibrium value is reached.

The effect of heat treatment on the solvent sorption behaviour of the low temperature polymerized PVC appears

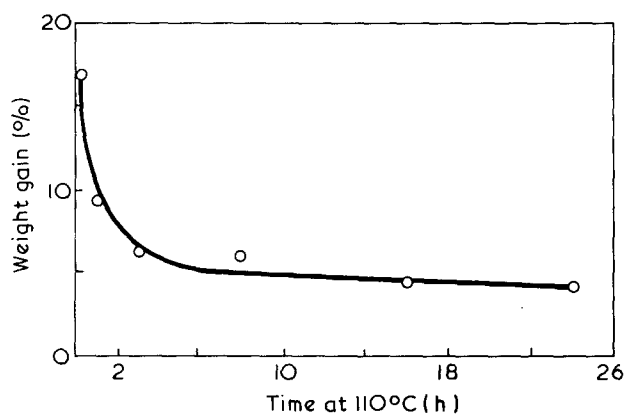


Figure 3 Solvent uptake for PVC 2 immersed 4 h in toluene as a function of heat treatment time at 110°C

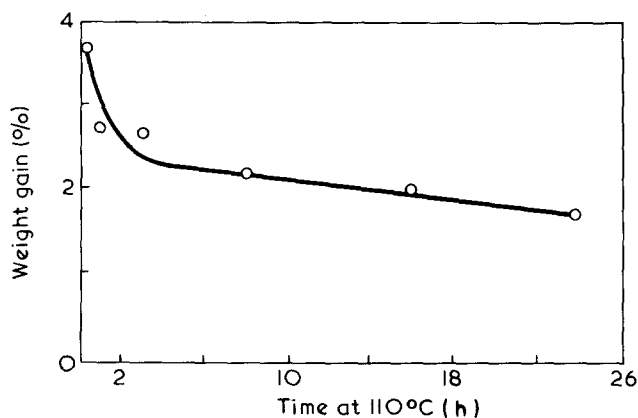


Figure 4 Solvent uptake for low temperature polymerized PVC immersed 72 h in toluene as a function of heat treatment time at 110°C

to be similar to that of PVC 2, but the rates of solvent sorption were much slower and none of the experiments were continued to equilibrium.

The above results can be explained tentatively as follows. Heat treatment is considered to have no effect on solvent sorption behaviour of the copolymer either because the rapid uptake of solvent is governed only by the presence of acetate groups, or because the polymer structure is too irregular for crystallization to occur.

For the two homopolymers results were similar to those reported by Illers<sup>2</sup>. Quenching would be expected to remove order, and actually resulted in more rapid solvent sorption in each case. The different solvent sorption behaviour for samples heat treated above and below  $T_g$  has been attributed to changes in crystallinity and free volume respectively<sup>2</sup>; further evidence (from density measurements, thermal analysis and X-ray diffraction) will be presented later.

Figures 3 and 4 illustrate the effect of time of heat treatment at 110°C on solvent sorption and provide some information about the rate of the crystallization or ordering process occurring. These results suggest that structural changes occur within quite short times. However, it is necessary to examine the effects of short term heat treatment in more detail.

#### Acknowledgement

The authors are grateful to the Science Research Council for the award of a Research Studentship to A.G.

A. Gray

Present address:

BP Chemicals International Ltd,  
Sully, Penarth, Glamorgan, UK

and Marianne Gilbert

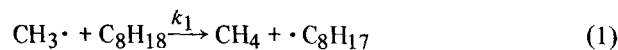
Institute of Polymer Technology,  
Loughborough University of Technology,  
Loughborough, Leics LE11 3TU, UK  
(Received 4 February 1975)

#### References

- 1 Blackadder, D. A. and Vincent, P. I. *Polymer* 1974, 15, 2
- 2 Illers, K. H. *Makromol. Chem.* 1969, 127, 1
- 3 Pezzin, G. *Plastics and Polymers* 1969, 37, 295

#### Evaluation of relative reactivities of vinyl monomers towards t-butoxy radical by means of spin trapping technique

Szwarc<sup>1</sup> developed a concept of 'methyl affinity', i.e. a measure of relative reactivities of various compounds, including vinyl monomers, towards the methyl radical produced by the thermal decomposition of diacetyl peroxide in iso-octane. To determine the relative reactivities, the following competitive reactions were used:



where M represents a vinyl monomer. It has also been

The different solvent sorption behaviour of the three polymers may be due to several factors. Some X-ray diffraction work currently in progress has shown that, as expected, the PVC/PVAC copolymer appears to be virtually amorphous while the low temperature polymerized PVC has the highest crystallinity. Crystallinity is expected to have a significant effect on solvent sorption since the polymer chains are packed more closely in crystalline regions thus restricting solvent penetration. The results obtained for the two PVC homopolymers may be explained on this basis. In the copolymer chain packing is also reduced by the bulky acetate groups present and the decrease in polar forces between chains caused by the replacement of chlorine atoms by these groups.

Heat treatment changed the solvent sorption behaviour of the two homopolymers (Figures 1a and 1c) but had no significant effect on the solvent sorption of the copolymer (Figure 1b). For PVC 2 (Figure 1a), the quenched sample, in which order would be expected to be lowest, absorbs solvent most rapidly. The sample heat treated at 70°C (i.e. below the glass transition temperature of the polymer) absorbs solvent slightly more slowly, but the weight gain reaches the same equilibrium value. The sample heat treated at 110°C (i.e. above the glass transition temperature) absorbs solvent more slowly and reaches a lower equilibrium value. Also the solvent sorption curve is S-shaped in the latter case, while for the quenched sample and the sample heat treated at 70°C the initial part of the plot of weight gain versus  $t^{1/2}/l$  appears linear before the equilibrium value is reached.

The effect of heat treatment on the solvent sorption behaviour of the low temperature polymerized PVC appears

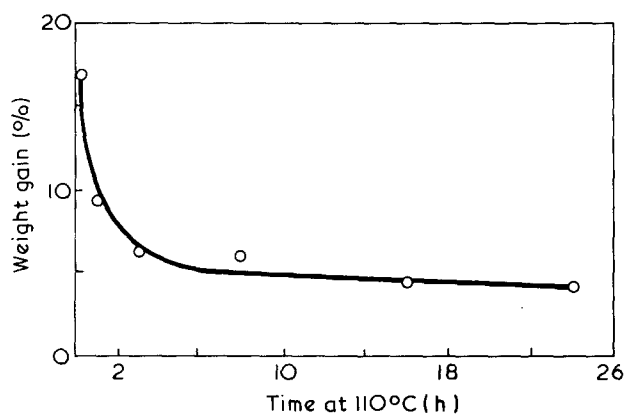


Figure 3 Solvent uptake for PVC 2 immersed 4 h in toluene as a function of heat treatment time at 110°C

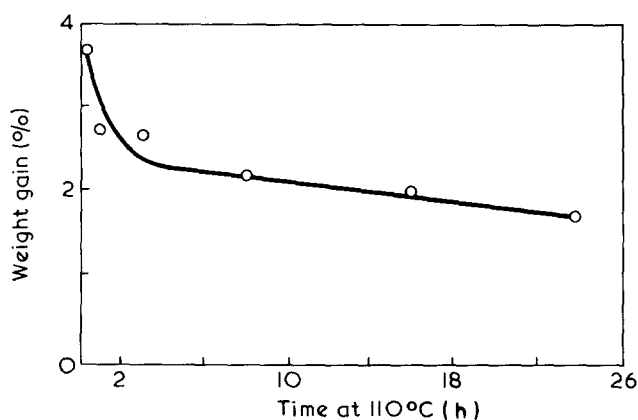


Figure 4 Solvent uptake for low temperature polymerized PVC immersed 72 h in toluene as a function of heat treatment time at 110°C

to be similar to that of PVC 2, but the rates of solvent sorption were much slower and none of the experiments were continued to equilibrium.

The above results can be explained tentatively as follows. Heat treatment is considered to have no effect on solvent sorption behaviour of the copolymer either because the rapid uptake of solvent is governed only by the presence of acetate groups, or because the polymer structure is too irregular for crystallization to occur.

For the two homopolymers results were similar to those reported by Illers<sup>2</sup>. Quenching would be expected to remove order, and actually resulted in more rapid solvent sorption in each case. The different solvent sorption behaviour for samples heat treated above and below  $T_g$  has been attributed to changes in crystallinity and free volume respectively<sup>2</sup>; further evidence (from density measurements, thermal analysis and X-ray diffraction) will be presented later.

Figures 3 and 4 illustrate the effect of time of heat treatment at 110°C on solvent sorption and provide some information about the rate of the crystallization or ordering process occurring. These results suggest that structural changes occur within quite short times. However, it is necessary to examine the effects of short term heat treatment in more detail.

#### Acknowledgement

The authors are grateful to the Science Research Council for the award of a Research Studentship to A.G.

A. Gray

Present address:

BP Chemicals International Ltd,  
Sully, Penarth, Glamorgan, UK

and Marianne Gilbert

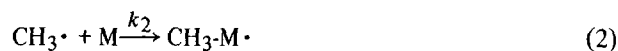
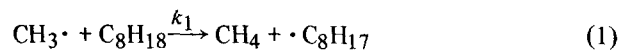
Institute of Polymer Technology,  
Loughborough University of Technology,  
Loughborough, Leics LE11 3TU, UK  
(Received 4 February 1975)

#### References

- 1 Blackadder, D. A. and Vincent, P. I. *Polymer* 1974, 15, 2
- 2 Illers, K. H. *Makromol. Chem.* 1969, 127, 1
- 3 Pezzin, G. *Plastics and Polymers* 1969, 37, 295

#### Evaluation of relative reactivities of vinyl monomers towards t-butoxy radical by means of spin trapping technique

Szwarc<sup>1</sup> developed a concept of 'methyl affinity', i.e. a measure of relative reactivities of various compounds, including vinyl monomers, towards the methyl radical produced by the thermal decomposition of diacetyl peroxide in iso-octane. To determine the relative reactivities, the following competitive reactions were used:

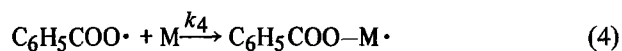
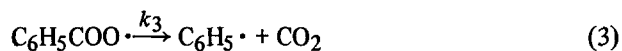


where M represents a vinyl monomer. It has also been

Letters

pointed out that the observed relative reactivities ( $k_2/k_1$ ) of vinyl monomers towards the methyl radical correlated well with those towards a polystyryl radical<sup>2</sup>.

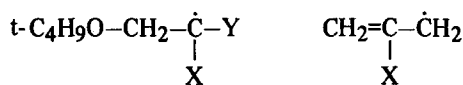
Subsequently Bevington and his coworkers<sup>3,4</sup> attempted to evaluate the reactivity ( $k_3/k_4$ ) of the benzoyloxy radical towards vinyl monomers by using <sup>14</sup>C-labelled benzoyl peroxide. In this case, the reactivities were determined by the <sup>14</sup>C-labelled end group analysis of the polymers obtained as the result of the following competitive reactions:



They also emphasized that polar effects were more important in the reaction of the benzoyloxy radical than that of methyl radical with the monomers<sup>4</sup>.

Although order of reactivity to the methyl radical towards vinyl monomers was confirmed to be similar to that of ethyl<sup>5</sup>, n-propyl<sup>5</sup> and phenyl radicals<sup>6,7</sup>, no data with respect to the reactivity of the oxy radicals except benzoyloxy radical towards vinyl monomers were found.

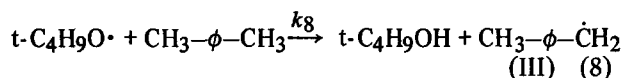
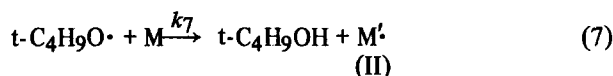
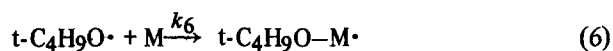
Recently, we have succeeded to trap with 2-methyl-2-nitrosopropane (BNO) as a spin trapping agent, the intermediate radical species (I and II) produced from the reactions of a number of vinyl and  $\alpha$ -methyl-vinyl monomers having X substituents with the t-butoxy radical produced by the thermal decomposition of di-t-butyl peroxalate<sup>8</sup>:



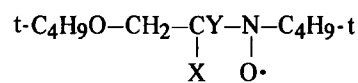
(I; Y=H, CH<sub>3</sub>)

(II)

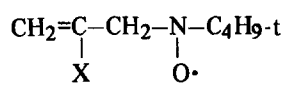
When decomposition is carried out in *p*-xylene in the presence of a monomer, the t-butoxy radical produced participates in competitive reactions:



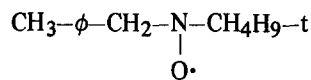
If this reaction is performed in the presence of BNO, the radicals (I, II and III) produced react readily with BNO to give the respective nitroxides:



(IV)



(V)



(VI)

Figures 1 and 2, for example, show the e.s.r. spectra of the reaction mixtures of styrene and methyl methacrylate, respectively, with di-t-butyl peroxalate in the presence of BNO without *p*-xylene at 25°C.

From the e.s.r. spectrum of Figure 1, it is seen that only a nitroxide was produced and assigned as IV ( $A_N = 14.2$  G,  $A_H^\beta = 2.3$  G and  $A_H^\gamma (2H) = 0.6$  G) in which X and Y are C<sub>6</sub>H<sub>5</sub> and H, respectively. However, Figure 2 appears to be the combined spectra of the nitroxides IV (X=COOCH<sub>3</sub>, Y=CH<sub>3</sub>;  $A_N = 14.9$  G) and V (X=COOCH<sub>3</sub>;  $A_N = 14.8$  G,  $A_H^\beta (2H) = 9.8$  G). When reactions are carried out in *p*-xylene, of course, the e.s.r. spectrum due to the nitroxide VI ( $A_N = 15.0$  G,  $A_H^\beta (2H) = 7.5$  G) is superimposed on the respective spectra of Figures 1 and 2.

Therefore, if the relative concentrations of the nitroxides ([IV], [V] and [VI]) produced are determined from the areas of the peaks due to the respective nitroxides in the absorption spectra obtained from integration of the observed first derivative e.s.r. spectra, the relative reactivities ( $k_6/k_8$  and  $k_7/k_8$ ) of the t-butoxy radical towards the monomers can be evaluated by using the following equations

$$\frac{[IV]}{[VI]} = \frac{k_6}{k_8} \frac{[M]}{[CH_3-\phi-CH_3]} \quad (9)$$

$$\frac{[V]}{[VI]} = \frac{k_7}{k_8} \frac{[M]}{[CH_3-\phi-CH_3]} \quad (10)$$

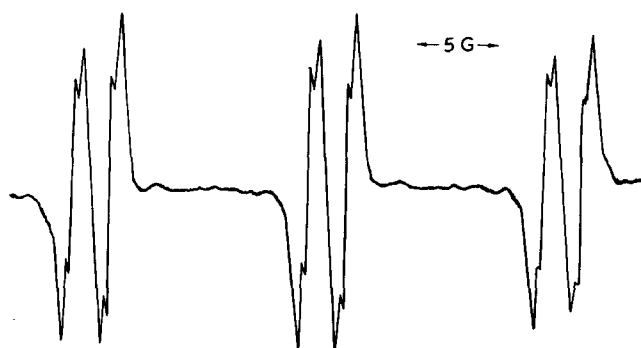


Figure 1 E.s.r. spectrum of the reaction mixture of styrene and di-t-butyl peroxalate in the presence of BNO

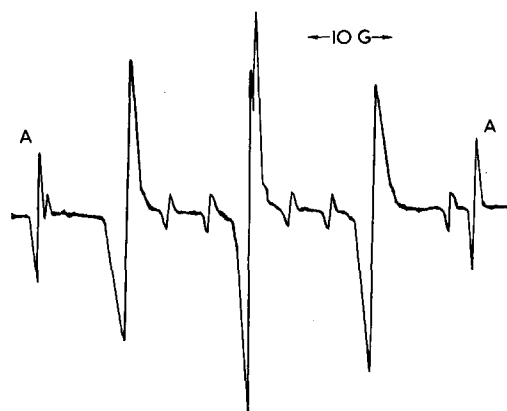


Figure 2 E.s.r. spectrum of the reaction mixture of methyl methacrylate and di-t-butyl peroxalate in the presence of BNO; the peaks A are due to t-butyl-t-butoxynitroxide which is obtained from the reaction of BNO with t-butoxy radical

Table 1 Relative reactivities of vinyl monomers towards t-butoxy radical at 25°C: comparison with those towards benzoyloxy, methyl and phenyl radicals

Monomer	$e$	$Q$	t-C <sub>4</sub> H <sub>9</sub> O•		C <sub>6</sub> H <sub>5</sub> COO• <sup>a</sup>	CH <sub>3</sub> • <sup>b</sup>	C <sub>6</sub> H <sub>5</sub> • <sup>c</sup>
			$k_6/k_8$	$k_7/k_8$	$k_4$ (rel. value)	$k_2/k_1$	$k_5$ (rel. value)
Isobutyl vinyl ether	-1.77	0.023	9.06	—	—	—	—
α-Methylstyrene	-1.27	0.98	6.90	<0.05	—	926	1.24
t-Butyl vinyl sulphide	-1.1	0.32	7.43	—	—	—	—
Styrene	-0.8	1.0	29.8	—	1.0	792	1.0 (1.0)
Vinyl acetate	-0.22	0.026	0.28	—	0.36	31	0.23 (≥0.08)
Methyl methacrylate	0.4	0.74	1.73	1.09	0.12	1440	1.78 (1.7)
Methyl isopropenyl ketone	0.53	1.49	2.47	0.74	—	—	—
Methyl acrylate	0.6	0.52	1.54	—	—	1030	0.78
Methyl vinyl ketone	0.68	0.69	2.68	—	—	1900	—
Methacrylonitrile	0.81	1.12	0.71	1.56	—	2120	2.46
Acrylonitrile	1.2	0.60	0.52	—	≤0.05	1730	— (0.8)

<sup>a</sup>Data of Bevington *et al.*<sup>3,4</sup> at 60°C

<sup>b</sup>Data of Szwarc<sup>1</sup> at 65°C

<sup>c</sup>Data of Pryor *et al.*<sup>7</sup>, who determined these values through tritium abstraction reaction of a phenyl radical, produced by phenyl azotriphenylmethane, with tritiated pentanethiol at 60°C, as the standard. The values in parentheses indicate the data of Bevington *et al.*<sup>6</sup> who used hydrogen abstraction reaction from dimethylformamide by a phenyl radical, produced by decarboxylation of benzoyloxy radical, as the standard

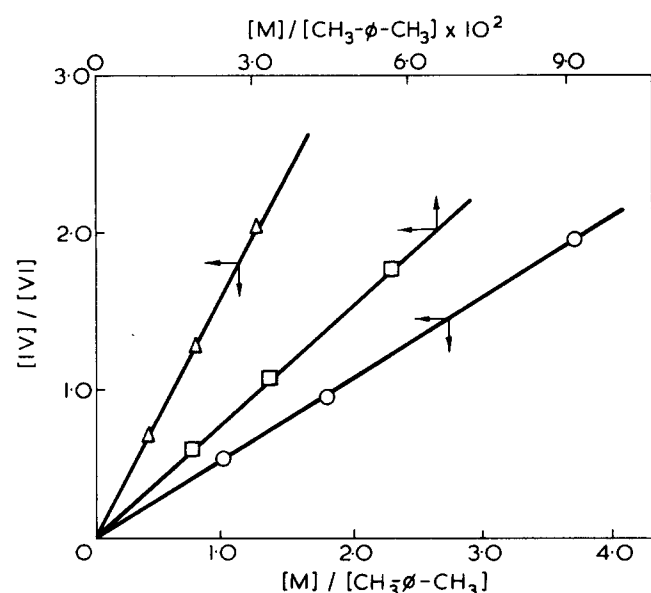


Figure 3 Plots of [IV]/[VI] with  $[M]/[CH_3-\phi-CH_3]$ :  $\Delta$ , Methyl acrylate,  $\square$ , styrene;  $\circ$ , acrylonitrile

where  $[M]$  and  $[CH_3-\phi-CH_3]$  are initial concentrations of monomer and *p*-xylene, respectively.

Figure 3 shows the plots of [IV]/[VI] with  $[M]/[CH_3-\phi-CH_3]$  for the reactions of di-*t*-butyl peroxalate with styrene, methyl acrylate and acrylonitrile in *p*-xylene in the presence of BNO at 25°C. As can be seen from this Figure, linear relationships are obtained, and the relative reactivities of these monomers towards the *t*-butoxy radical are determined from their slopes.

The results are summarized in Table 1, in which the relative reactivities of vinyl monomers towards methyl, phenyl and benzoyloxy radicals are also indicated.

It is of interest that the relative reactivities ( $k_6/k_8$ ) of the monomers towards addition of the *t*-butoxy radical are related more with their  $e$  values than their  $Q$  values, indicating that the polar effect is more important than resonance effect, similar to the case of the benzoyloxy radical<sup>4</sup>. In connection with these results, it is also noted that the *t*-butoxy radical can easily abstract the allylic hydrogen of  $\alpha$ -methyl-vinyl monomers such as methyl methacrylate and

methacrylonitrile. This observation seems to be related to that found for the benzoyloxy radical<sup>4</sup>, and to provide important information on the initiation mechanism of radical polymerization of vinyl monomers with the oxy radical.

Tsuneyuki Sato and Takayuki Otsu

Department of Applied Chemistry, Faculty of Engineering,  
Osaka City University, Osaka 558, Japan  
(Received 22 January 1975; revised 11 February 1975)

#### References

- 1 Szwarc, M. *J. Polym. Sci.* 1955, 16, 367
- 2 e.g., Otsu, T. *Progr. Polym. Sci. Japan* 1971, 1, 1
- 3 Bevington, J. C. and Brooks, C. S. *J. Polym. Sci.* 1956, 22, 257
- 4 Bevington, J. C. 'Radical Polymerization', Academic Press, London, 1961
- 5 Smid, J. and Szwarc, M. *J. Am. Chem. Soc.* 1956, 78, 3322
- 6 Bevington, J. C. and Ito, T. *Trans. Faraday Soc.* 1968, 64, 1329
- 7 Pryor, W. A. and Fiske, T. R. *ibid.* 1969, 65, 1865
- 8 Sato, T. and Otsu, T. *Makromol. Chem.* in press

#### Conference Announcement

### Polymer Physics

Shrivenham, Wilts, 24–26 September 1975

The Polymer Physics Group will be holding its biennial meeting at the Royal Military College of Science, Shrivenham, Wiltshire from 24 to 26 September 1975. Contributed papers (20 minutes) are invited. The subject matter of this meeting is deliberately wide and is meant to include all aspects of the physics of polymers and macromolecules, including the morphology, mechanical, electrical and optical properties of solids, melts and solutions. Intending contributors are asked to send a title and short abstract (250 words) to Mrs H. Higdon, Department of Physics, Brunel University, Uxbridge, Middlesex UB8 3PH, UK by 31 May 1975. Further details and application forms will be available in June from the Institute of Physics, 47 Belgrave Square, London SW1X 8QX, UK.

# Book Reviews

## Particle size analysis

Z. K. Jelinek

John Wiley, New York (for Ellis Horwood) 1974,  
178 pp. £5

This book, which is a translation of a Czechoslovak text is a welcome addition to the few books on this subject already available. The others I have seen relate primarily to powders. This book also includes critical accounts of the determination of the size or molecular weight distributions in colloid systems, mostly of polymers, besides chapters on surface area and pore size measurement.

The depth of the criticism of the interpretation of experimental results and of the theoretical basis of the methods should appeal to the research specialist in disperse system analysis. I agree with the publisher's claim that this book should also interest any chemist or chemical engineer who desires a rapid insight into the practical application of dispersoid analysis. This could best be achieved by reading the excellent practical examples of the applications, extracted from the literature, which accompany the description of each method of size analysis. Polymer chemists will appreciate the fact that twelve out of the seventeen applications described refer to polymer systems.

Well written practical instructions in most of the methods of size analysis are given. I would, however, have preferred a longer more detailed description of representative sampling.

The book includes all the normal methods of size analysis namely by optical, ultra and electron microscopy, X-ray analysis, sieve analysis, ultrafiltration, gel permeation, sedimentation, centrifugation, diffusion, osmometry, viscometry and permeametric methods.

The book is well produced and worth the price of £5.

W. E. Laird

## Fluorine chemistry reviews: Vol 7

Edited by Paul Tarrant

Marcel Dekker, New York, 1974, \$24.50

This series of reviews sets out to provide articles which cover the international literature comprehensively and are aimed mainly at research workers in the field of fluorine chemistry but also provide a means for others outside the field to keep abreast of developments.

This volume contains two articles, the first on Nucleophilic substitution in polyfluoroaromatic compounds by L. S. Kobrina,

and the second on the Preparation and reactions of polyfluorinated aromatic heterocyclic compounds by G. G. Yakobson, T. D. Petrova and L. S. Kobrina. They originally covered the literature to the end of 1970 but, owing to delays in printing, the authors have added, in the first case, a list of pertinent papers up to the end of 1972 and, in the second case, a short commentary and list of papers which take us into early 1973. Both reviews are excellent, they cover their fields very thoroughly indeed and are particularly useful in putting work in Russia in perspective with work in the western world. Since it is eighteen months to two years from the time of their submission before English translations of Russian papers (and then not all papers) are available, and presumably there is a similar delay in reverse, there has tended to be some duplication of effort.

Points worth special mention are that both articles bring out the importance of solvent polarity in controlling the nature of reaction products (an area where there has been considerable Russian work); and they clearly indicate the need for more kinetic measurements to help rationalize reaction mechanisms with complete confidence.

Apart from a few awkward grammatical word formations and some typing errors, the latter particularly in the list of references, the articles are well written and easy to read. The errors are, in the main, easily resolved and one must pay tribute both to the authors' command of English and to the efforts of the editor. Presumably these efforts, together with postal delays, caused the original delay in publication. This delay, while disappointing for the authors when the field is so active, does not detract from the quality and usefulness of the articles as sources of reference to research workers and also to those teaching undergraduate courses in this field.

At \$24.50 (£10-£11) the price is fairly high but the book is well worth the money.

W. K. R. Musgrave

## Polymer synthesis: Vol 1

Stanley R. Sandler and Wolf Karo

Academic Press, New York, 1974, 572 pp. £18.95

The title indicates coverage of an enormous topic. The authors have reduced this to this one volume by selecting only the preparation of uncomplicated 'linear' polymers for review by functional group classes. They deviate, for no adequate reason, from this format in chapters entitled 'Thermally stable polymers' and 'Organophosphorus polymers' and incorporate two chapters comprising sixty-five pages on peroxidic initiators which seem to me to be an unnecessary inclusion. The various chapters discuss a number of classes of addition and condensation polymers and each chapter comprises a general introduction, a set of experimental methods and a list of titles for miscellaneous preparations with copious references. The more complicated polymers such as blocks, grafts, gels or more commercially interesting systems such as alkyds, urea-formaldehyde and melamine-formaldehyde resins are omitted.

A more serious criticism of this book is that it presents an inadequate and often incorrect view of polymer science to the intended audience—industrial research workers, graduate and advanced undergraduate students in polymer, organic or medicinal chemistry. The book uses extracts from older references without updating the terminology and, annoyingly, mixes and confuses crystalline melting temperature and softening point. The introductions to the chapters contain too many errors of fact. For example 'ethylene can be initiated by all except the anionic type' (page 2) and 'cationic polymerizations such as the  $\text{BF}_3 \cdot \text{H}_2\text{O}$  complex-catalysed polymerization of isobutylene is considered a "living" type polymer', this latter statement having been taken from a 1950 literature reference.

My assessment of this book is that it is a useful factual reference work for libraries, more useful for the critical experienced polymer chemist and industrial research chemist than undergraduate or graduate students. The price is high and I would not recommend it for purchase by individuals.

As this is volume 1, further volumes can be anticipated. I hope that they will not contain similar flaws as this could be a quite useful series.

N. B. Graham

### Conference Announcement

## Polymer science: achievements and prospects

in honour of

Paul J. Flory, Nobel Laureate in Chemistry, 1974

Pittsburgh, USA, 17 June 1975

A symposium to honour Paul J. Flory, Nobel Laureate in Chemistry, 1974 will be held at the Carnegie-Mellon University, Pittsburgh, USA on 17 June 1975. The symposium will deal with the current status and future directions of key areas in polymer science. The speakers will include M. Morton, E. F. Casassa, L. Mandelkern, W. H. Stockmayer, J. E. Mark and W. O. Baker. Further information can be obtained by writing to Hershel Markovitz, Department of Chemistry, Carnegie-Mellon University, 4400 Fifth Avenue, Pittsburgh, Pa 15213, USA.

## Polymer engineering

Over the years there has been a suggestion that more research and basic training are essential for satisfactory progress in the polymers industry. Here is a field of industrial enterprise where it is said that scientific and technical innovation in the provision of polymeric materials, their use in many forms and applications, and fabrication by a variety of processing methods have often been made in advance of sound understanding of the basic principles. One may argue that this is far from the true picture since study of polymeric materials has long been a discipline in its own right, especially with regard to synthesis, structure and physical properties. However, this is polymer science and it is clear that polymer engineering, i.e., the operations concerned with design, fabrication, and properties of the final products, has been less well studied. A glance at the contents of most journals devoted to polymer research and development may give support to this; papers on polymer science are far more numerous than those on polymer engineering.

In two decades manufacture and usage of polymers have become a major industry in developed countries and call for much effort in training, research, development and production. Low levels of such effort cause short term concern and can have more serious consequences in the long run. The need to encourage research and advanced training to meet growing requirements in the UK was recognized in 1969 when the Science Research Council formed the Polymer Science Committee, which body selected polymer engineering as one area for preferential support and approached academic institutions for research proposals. Again, in 1972, the Chemicals EDC Plastics Working Party of NEDO stressed that industry should upgrade its technology through improved knowledge of plastics materials and development of processes and machinery.

However, polymer engineering still appeared to be taking second place to polymer science. Although the SRC Polymer Science Committee received requests for research support in all branches of polymers, it was significant that there were far fewer applications for investigations in polymer engineering compared with those for polymer science. Last year the SRC set up a working party under the chairmanship of Professor G. Allen to examine the national needs for effective research and development and for suitably trained manpower. Their findings have recently been issued\* and give new impetus to encouragement of work in this field. The report outlines a number of proposals by which positive progress should be possible, following a study of the current industrial background and requirements.

In personnel, the industry requires graduate engineers and technicians trained specially for production activities while on the research front it stresses that there is much scope for technological improvement in processes and applications, i.e., in processing machinery and knowledge of physical and mechanical properties associated with product design and fabrication methods. These are areas which call for large-scale equipment and the capital costs and provision of facilities for such research have often proved prohibitive to other than a few university departments. The report stresses that there are too few research students in polymer engineering. One might add that also there are probably too few lecturers and experienced research workers in this same subject. The advanced courses in polymers supported by the SRC are more closely related to science than engineering and this may in part be due to the scarcity of expert staff. In the past when efforts have been made to recruit teaching staff specifically for polymer engineering the number of suitably qualified applicants has generally been small.

In setting out a sound course of action, the SRC paper puts forward a number of possibilities but wisely decides against single, narrow, and often fragmented, research proposals or even on relying implicitly on those centres of polymer

---

\* Polymer Engineering: The Report of an SRC Working Party, Science Research Council, London, 1975.

research established through major SRC funding over the last five years. It indicates that while there is no single remedy to promote adequate polymer engineering and training, one needs fully to exploit existing facilities but in a coordinated manner. There is recommended, then, the establishment of a Polymer Engineering Directorate as a primary move in a two-phase activity; this could be followed, as necessary, by formation of an Engineering Institute which would provide (in association with other organizations where convenient) a facility for experimental work and training in areas not now fully catered for by industry or university.

The Directorate, comprising a Director and appropriate supporting staff and working in collaboration with a small task force or management committee appointed by SRC, is thus to establish a group of coordinated centres in university and polytechnic engineering departments so as to form a coherent training and research programme. Such a programme would be drawn up in consultation with representative bodies of the polymer-making and -using industries and, when accepted, be funded by SRC. The cost of the Directorate is estimated at £60 000 per year for a five year period, together with up to £2M to meet the costs of the researches proposed.

These recommendations are full of interest and have the merit of ensuring, when implemented, that live engineering centres for polymer research and training are brought into being and receive both adequate recognition and adequate finance. Science, technology and commerce would profit by such a move and one looks forward to the introduction of research and teaching which is not subject to any fragmentation as was sometimes experienced in past endeavours. The immediate concerns will be to appoint an active Director who is knowledgeable in polymer engineering and appreciates fully the needs in training and research and to formulate practical programmes which will lead to positive action and findings of rapid benefit to the industry. One hopes to see, in due course, papers in POLYMER which arise from research contained in the Directorate programme.

The Science Research Council will welcome comments on and offers of assistance in implementing the proposals.

*R. J. W. Reynolds*

Readers of POLYMER may also be interested to learn that Dr J. G. Williams, one of our UK Editorial Board members since July 1973, has recently had conferred on him the title of Professor of Polymer Engineering in the Department of Mechanical Engineering at Imperial College, London. Hopefully, this should encourage both technical and graduate staff to enter the relatively new discipline of polymer engineering.

# Helix – coil transition of poly-( $\epsilon$ -carbobenzyloxy-L-lysine) in *m*-cresol

Toshio Hayashi, Shingo Emi and Akio Nakajima

Department of Polymer Chemistry, Kyoto University, Sakyo-ku, Kyoto, Japan

(Received 6 August 1974; revised 25 September 1974)

The thermodynamic parameters for the helix–coil transition of poly( $\epsilon$ -carbobenzyloxy-L-lysine) (PCBL) in *m*-cresol have been determined calorimetrically by determining the heat capacity of the solution in the transition region, and spectropolarimetrically by measuring the helix content of the polypeptide as functions of temperature. From the former measurements, the enthalpy of transition,  $\Delta H_0$ , was calculated directly. The values of  $\Delta H_0$  in *m*-cresol determined from the polarimetric measurements, using experimental data of PCBL samples with rather high molecular weights, are found to be larger than the published data but agree fairly well with the calorimetric values presented in this paper. Further, the transition curves are independent of the concentration of the polymer over the concentration range studied. The values of  $\Delta H_0$  in *m*-cresol determined from the calorimetric measurements may be considered to be independent of the molecular weights of PCBL.

## INTRODUCTION

A number of papers have reported in the past few years on the helix–coil transitions of un-ionized polypeptides using solvents that destroy the helix such as dichloroacetic acid (DCA) and trifluoroacetic acid (TFA)<sup>1,2</sup>. It was found that poly( $\epsilon$ -carbobenzyloxy-L-lysine)(PCBL) underwent thermal transition of an inverse type in DCA containing a proper amount of 1,2-dichloroethane (DCE) or chloroform, and efforts were made to determine the thermodynamic parameters of the helix–coil transitions from polarimetric measurements<sup>3,4</sup> or from calorimetric measurements<sup>5,6</sup>. However, the results were divergent with respect to both the transition enthalpy,  $\Delta H_0$ , and the cooperativity parameter,  $\sigma$ . For a number of reasons, the transition always occurred in a finite temperature range, depending on the kinds of solute and solvent and on the molecular weight of the polypeptide. It is therefore useful to define an apparent heat of transition,  $\Delta H$ , which is obtained from the van't Hoff equation. In the formulation of Zimm–Bragg<sup>7</sup> and Applequist<sup>8</sup>,  $\Delta H$  is related to the transition enthalpy,  $\Delta H_0$ , by the equation  $\Delta H = \Delta H_0/\sigma^{1/2}$ . The parameter  $\sigma$  may be related to the statistical length of a helical section of polypeptide at the middle point,  $T_c$ , of the transition. We found *m*-cresol to be an exceptional single solvent in which PCBL exhibits an extremely sharp thermal transition of the inverse type<sup>9</sup>. Recently, Matsuoka *et al.*<sup>4</sup> reported a similar sharp transition of PCBL in *m*-cresol. They investigated helix–coil transitions of PCBL in *m*-cresol by optical rotation measurements. On the other hand, no calorimetric measurements to obtain the transition enthalpy  $\Delta H_0$  have been carried out for PCBL in *m*-cresol. We therefore attempted a detailed study of the thermal transitions in *m*-cresol by calorimetric as well as polarimetric measurements.

## EXPERIMENTAL

### Materials

The monomer, CBL–NCA, was prepared by the method proposed by Blout and Karlson<sup>10</sup>, and purified by repeated

recrystallizations from an ethyl acetate solution with the addition of petroleum ether. Polymerization of the CBL–NCA was carried out at 25°C in a 1:1(v/v) mixture of dioxane and methylene dichloride in the presence of triethylamine (TEA) as an initiator. The solvents and the initiator were purified by the usual means described in the literature and finally distilled by the use of a long column. The fractionation of the PCBL samples was done by fractional precipitation of the polymer from a solution in *N,N'*-dimethylformamide (DMF), using ethanol as the precipitant. The resulting fractions were dissolved in dioxane and filtered through a sintered glass plate, freeze dried, and stored in a refrigerator.

The number-average molecular weights,  $M_n$ , of the fractions were determined by osmotic pressure measurements. An Electronic Membrane Osmometer (Knauer Co.) equipped with a variable temperature controller was employed. Regenerated cellulose membrane SD (Sartorius-Membran-Filter GmbH) for organic solvents was used. The solvent used for the measurements was DMF and the temperature was fixed at 30°C. Table 1 gives the value of  $M_n$  of the seven PCBL fractions used in the optical rotatory dispersion (o.r.d.) and calorimetric experiments.

### Measurements

The calorimeter employed was a Calvet differential twin-type microcalorimeter manufactured by Setaram of Lyon. A general description of this precision apparatus is given elsewhere<sup>11</sup>. The principle for the measurement of the spe-

Table 1 Molecular weights of PCBL fractions used for experiments

Fractions	$M_n$	$N_n$
PCBL-1	400 000	1525
PCBL-2	320 000	1220
PCBL-3	300 000	1145
PCBL-4	238 000	905
PCBL-5	202 000	770
PCBL-6	170 000	650
PCBL-7	140 000	570



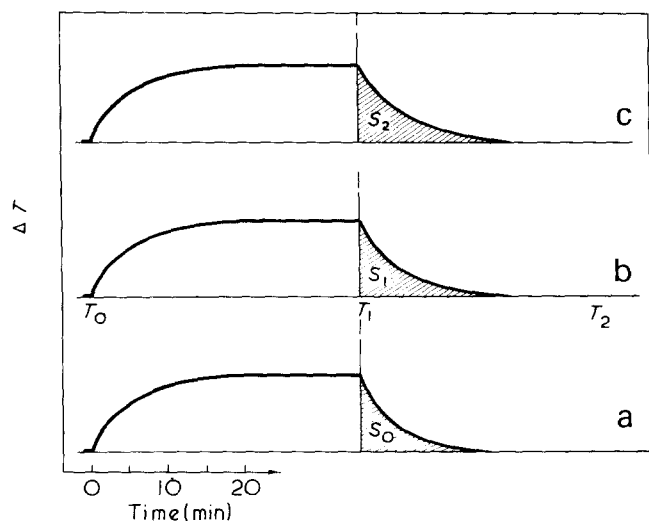


Figure 1 Schematic  $\Delta T$  vs. time curves with (a) an empty cell, (b) a cell containing pure water, and (c) a cell containing the sample at the constant temperature of 22.4°C

cific heat consists of: (1) making the system containing the cell an equilibrium constant temperature; (2) changing the temperature of the cell by a definite increment using the Peltier effect<sup>11</sup>; (3) maintaining the calorimetric unit at a constant temperature; and (4) measuring the energy evolved to return to the original equilibrium temperature (i.e., the temperature of the cell is identical to the temperature of the calorimetric unit). The evolved energy, which can be measured by the flow-meter immediately after cutting off the Peltier current by automatic commutation, is proportional to the total heat capacity of the cell. Three successive operations, with an empty cell, a cell with calibrated medium and a cell with sample, make it possible to measure the specific heat of the sample at each temperature. Figure 1 illustrates a typical scheme of the chart for these three operations. Integration of the recorder trace was obtained by the area of the chart. If  $S_0$ ,  $S_1$ , and  $S_2$  are the areas corresponding to the three successive experiments, i.e., with the empty cell, cell containing a specimen of known heat capacity ( $C_1$ ) (in this case, we use a pure water as standard specimen), and cell containing the sample ( $C_2$ ), the heat capacity,  $C_2$ , is determined by the relation:

$$C_2 = C_1 \cdot \frac{S_2 - S_0}{S_1 - S_0} \cdot \frac{M_2}{M_1} \quad (1)$$

where  $M_1$  and  $M_2$  are the weight of pure water and sample solution in the cells, respectively. A glass vessel stopped with Teflon stoppers and covered with a stainless-steel jacket for measuring the heat capacity was designed by the authors, and had an internal volume of about 15 ml. The polymer concentration was in all cases about 2 wt %. A measurement of the heat capacity of solution over a temperature range of 20°C can be made with a precision of  $\pm 3\%$ . The heat of mixing of benzene and carbon tetrachloride was measured as a test of the accuracy of the calorimeter and of the cell. The average of several replicate experiments led to a value of 22.3 cal/mol for the heat of mixing, which agreed within 1.2% with the published value of 22.0 cal/mol<sup>12</sup>.

O.r.d. in a temperature range from 5° to 50°C was measured with a Yanagimoto OR-100 type spectropolarimeter using a tungsten lamp as light source. The wavelengths used

ranged from 325 to 610 nm. The concentration of polymer solutions was about 1.0 g/dl throughout these measurements. The o.r.d. data were fitted to the Moffitt–Yang equation<sup>13</sup> to obtain values of the helix parameter  $b_0$  for PCBL in *m*-cresol. A value of 212 nm was used for the constant  $\lambda_0$  of the Moffitt–Yang equation. In addition, correction was also made for the change in concentration of the polymer due to the change in volume of the solvent mixture at different temperatures from experimental data by the density measurements for sample solution at each temperature. The average error in the determination of  $b_0$  from the slope of the least-squares Moffitt–Yang plot was estimated to be  $\pm 3$  units in  $b_0$  throughout the range of values of  $b_0$ .

## RESULTS AND DISCUSSION

### Polarimetric measurements

The thermally induced conformational transition of PCBL from the coil conformation at low temperatures to the helix conformation at high temperatures was studied in *m*-cresol by o.r.d., using the fractionated PCBL samples listed in Table 1. The course of the transition was followed by the change in the value of  $b_0$  of the polypeptide solution with temperature (see Figure 2). The transition was found to be completely reversible, as was first observed by Doty and Yang<sup>14</sup>. The transition temperature  $T_c$  of PCBL in *m*-cresol is about 25°C, and the decrease in molecular weight of PCBL broadens and shifts the transition curve towards higher temperature. Furthermore, it is shown that the value of  $b_0$  at the lower temperature side gives a positive value of about +150; this value is larger than that ( $b_{0,c} = 0$ )<sup>15,16</sup> found for coil conformation in DCA–DCE mixture. While at the higher temperature side the value of  $b_0$  is in a range of  $-350$  to  $-400$ ; these values of  $b_0$  are largely remote from the value of  $-550$  for helix conformation obtained in DMF or chloroform<sup>4,16</sup>. Matsuoka *et al.*<sup>4</sup> reported a similar result for the thermal transition of PCBL in *m*-cresol.

Figure 3 shows the relation between two coefficients relating to the helix content in the modified two-term Drude equation<sup>17</sup>:  $[M'] = A_{193}\lambda_{193}^2/(\lambda^2 - \lambda_{193}^2) + A_{225}\lambda_{225}^2/(\lambda^2 - \lambda_{225}^2)$ , where  $A_{225}$  is plotted against  $A_{193}$  for PCBL in *m*-cresol. Since  $A_{193}$  and  $A_{225}$  are directly related to the

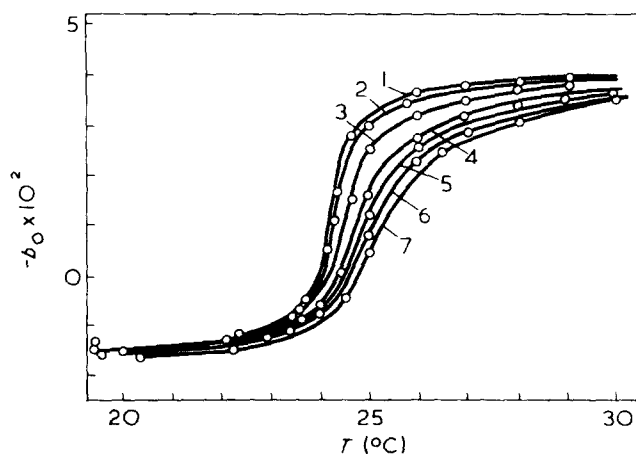


Figure 2 Temperature dependence of Moffitt–Yang parameter  $b_0$  of PCBL in *m*-cresol. 1, PCBL-1,  $N_n = 1525$ ; 2, PCBL-2,  $N_n = 1220$ ; 3, PCBL-3,  $N_n = 1145$ ; 4, PCBL-4,  $N_n = 905$ ; 5, PCBL-5,  $N_n = 770$ ; 6, PCBL-6,  $N_n = 650$ ; 7, PCBL-7,  $N_n = 570$

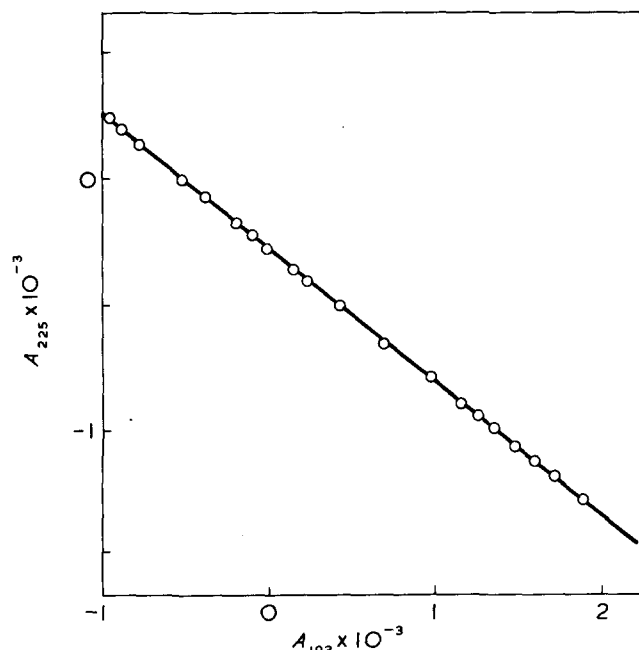


Figure 3 Plot of  $A_{193}$  against  $A_{225}$  for PCBL in *m*-cresol. Solid straight line denotes the relation;  $A_{225} = -0.55 A_{193} - 280$  given by Schechter and Blout<sup>17</sup>

rotational strength of the Cotton effects due to the  $\alpha$ -helix and random coil conformations, respectively, a definite linear relation should be found between  $A_{193}$  and  $A_{225}$  for mixtures of  $\alpha$ -helix and random coil conformations. A failure to fit the relation is taken as an indicator of the presence of another structure such as  $\beta$ -conformation<sup>17</sup>. The straight line in Figure 3 represents the relation  $A_{225} = -0.55 A_{193} - 280$  obtained by Schechter and Blout<sup>17</sup> by assuming that polypeptides exist either in  $\alpha$ -helix or random coil conformation, and not contain other conformations. As is shown in Figure 3, all the points fall on the straight line; therefore, it should be concluded that PCBL does not include structures other than  $\alpha$ -helix and random coil in *m*-cresol.

#### Calorimetric measurements

A linear dependence of the measured heat capacity on temperature is obtained for pure solvent without polymer. The heat capacity of the PCBL in *m*-cresol was measured as a function of temperature over a 20°C range centred about  $T_c$ . The maxima in the heat capacity curves appeared at 24.5°C and 25.2°C with PCBL-1 and PCBL-7, respectively, in excellent agreement with the o.r.d. data. Heat capacity curves, referred to a smoothed baseline, are shown as a function of temperature in Figures 4a and 4b, with PCBL-1 and PCBL-7, respectively. The area surrounded by the curve and the baseline is directly proportional to  $\Delta H_0$ . Our results yield a value of +1200 cal/mol with PCBL-1 and of +1150 cal/mol with PCBL-7. The effect on the molecular weight on the transition behaviour is shown in Figure 4 for two samples of nearly equal PCBL concentration. For the sample of lower molecular weight (PCBL-7), the transition region locates at a higher temperature and the transition temperature  $T_c$  is a higher value, while the area surrounded by the curve and the baseline is approximately equal to that obtained for the sample of higher molecular weight (PCBL-1). Thus, the values of  $\Delta H_0$  in *m*-cresol determined from the calorimetric measurements may be considered to be independent of the molecular weight of PCBL.

#### Thermodynamic parameter for thermally induced coil-to-helix transition

The experimental data of o.r.d. measurements relating to the thermally induced conformational transition have been analysed in terms of the Zimm-Bragg theory<sup>7</sup>. The helix content  $f_H$  was obtained as a function of temperature at a fixed solvent composition; hence the value of  $\Delta H$ , van't Hoff heat of transition, is readily determined experimentally from the slope of the  $b_0$  against temperature plot using the equation<sup>18</sup>:

$$\left(\frac{df_H}{dT}\right)_{T_c} = \frac{1}{b_{0,h} - b_{0,c}} \left(\frac{db_0}{dT}\right)_{T_c} = \frac{\Delta H}{4RT_c^2} \quad (2)$$

The values of  $b_{0,h}$  and  $b_{0,c}$  for the complete helix and complete coil, respectively, required for the computation of the fractional helix content from  $b_0$ , were obtained as follows. The value of  $b_{0,c}$  was assumed to be +150 from measurements, judging that PCBL seems to be completely random coil conformation below 22°C. While  $b_{0,h}$  was assumed to be -480, considering that a relation  $b_{0,c} - b_{0,h} = 630$  obtained for PBLG in DCA-DCE mixture<sup>16</sup> may be expected to hold even for PCBL in *m*-cresol.  $f_H$  was then calculated from  $f_H = -(b_0 - 150)/630$ . The error involved in computing  $f_H$  should include not only the error in  $b_0$  mentioned earlier but also the possible error in the limiting values of  $b_{0,h}$  and  $b_{0,c}$ .

The  $\Delta H$  values calculated for PCBL in *m*-cresol with various molecular weights are illustrated in Figure 5 as a function of the reciprocal of degree of polymerization,  $1/N_n$ . It should be pointed out that the  $\Delta H$  value decreases with decreasing molecular weight. A similar curve was obtained with PCBL in DCA-DCE mixture<sup>16</sup> (see the broken line in Figure 5).

Although the value of  $\Delta H_0$  should directly be measured by the calorimetric method as described above, it also can be estimated from the o.r.d. data. In the present work, experimental data obtained with PCBL in *m*-cresol (see Figure 2) are analysed by the method proposed by Okit et al.<sup>19</sup>. They proposed a new procedure to estimate the parameters  $\Delta H_0$  and  $\sigma$  independently from the o.r.d. measurements by using Nagai's theory<sup>20</sup> for the helix-coil transition in polypeptide. It has been shown that the helix content  $f_H$  of a polypeptide having  $N_n$  degrees of polymerization is represented to a good approximation by<sup>19</sup>:

$$f_H = f_H^0 = \frac{2f_H^0{}^{3/2}(1 - f_H^0)^{1/2}}{N_n \sigma^{1/2}} \quad (3)$$

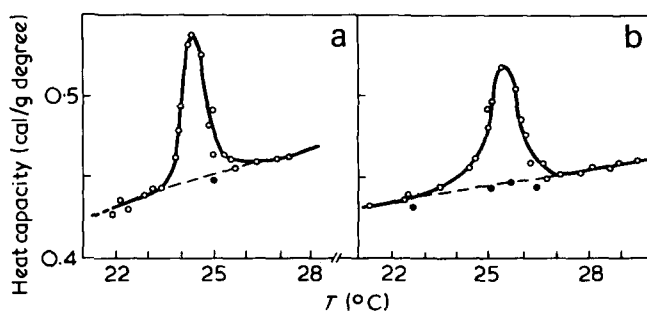


Figure 4 Heat capacity as a function of temperature of PCBL solution: (a) PCBL-1 ( $N_n = 1525$ ) at 0.0179 g PCBL/g of solution; (b) PCBL-7 ( $N_n = 570$ ) at 0.0188 g PCBL/g of solution. ● data for *m*-cresol

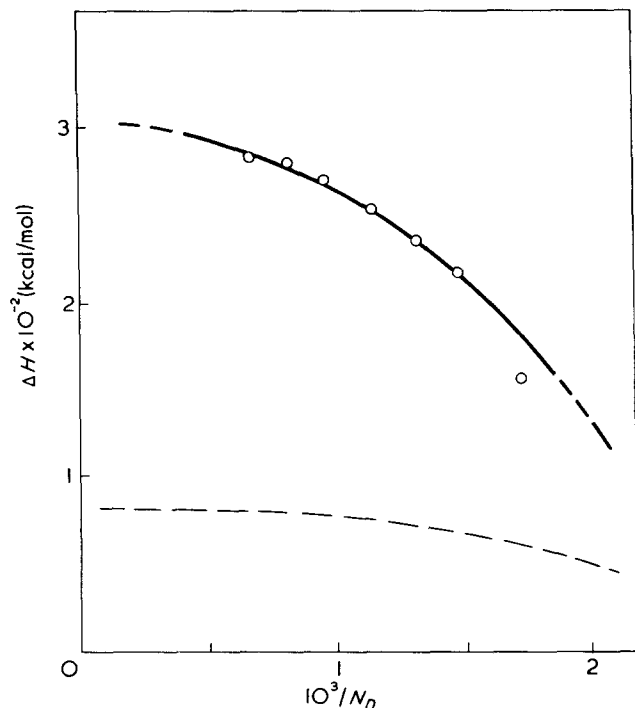


Figure 5 The van't Hoff heat of transition,  $\Delta H$ , for the thermal transition of PCBL in *m*-cresol as a function of  $1/N_n$ . ----, data obtained in DCA-DCE mixture<sup>16</sup>

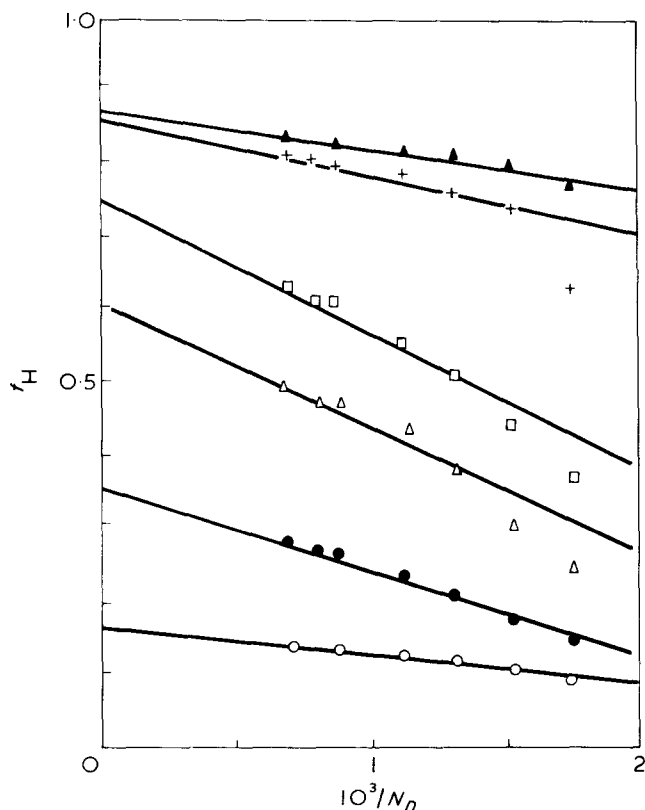


Figure 6 Plots of  $f_H$  vs.  $1/N_n$  for PCBL in *m*-cresol at temperatures: ○, 23.3°C; ●, 24.1°C; △, 24.3°C; □, 24.7°C; +, 26.2°C; ▲, 29.3°C

provided that  $\sigma^{1/2} \ll 1$ ,  $N_n \gg 1$  and  $N_n \sigma^{1/2} \gg 2$ . Here,  $f_H^0$  denotes the value of  $f_H$  for infinitely large  $N_n$  and is related to  $\sigma$ . Figure 6 illustrates plots of the helix content  $f_H$  against the reciprocal  $1/N_n$  of number-average degrees of polymerization from data in Figure 2. In Figure 6, the solid lines represent the theoretical curves calculated by using equation (3) with sets of proper values of  $f_H^0$  and  $\sigma$

to fit the experimental data at each temperature. The sets of values of  $f_H^0$  and  $\sigma^{1/2}$  used are 0.60 and  $0.35 \times 10^{-2}$  at 24.3°C, and 0.74 and  $0.40 \times 10^{-2}$  for at 24.7°C. Thus, the average value  $0.38 \times 10^{-2}$  is given for  $\sigma^{1/2}$  in the transition region for PCBL in *m*-cresol. Similar sets of  $f_H^0$  and  $\sigma^{1/2}$  were applied to the data at other temperatures. The results for  $f_H^0$  and  $\sigma^{1/2}$  as functions of temperature are summarized in Table 2. Table 3 lists the estimated values of thermodynamic parameters from the o.r.d. data as well as values of  $\Delta H_0$  obtained by the calorimetric measurement.

The thermal transition curves of PCBL-1 in *m*-cresol were also obtained by o.r.d. measurements at various PCBL concentrations from 0.5 to 3.0 % w/v (see Figure 7). The values of  $\Delta H$  estimated from these curves agreed with each other within experimental error, while the values of  $T_c$  slightly decreased with increasing concentrations of PCBL. Therefore, it may be concluded that the values of  $\Delta H$  are independent of the polypeptide concentration over the concentration range studied. Ananthanarayanan *et al.*<sup>21,22</sup> investigated the helix-coil transition of PBLG in DCA-DCE mixtures from both polarimetric and calorimetric measurements and concluded that  $\Delta H_0$  is independent of the concentration of the polypeptide from 0.35 to 2.5 % w/v. Therefore, for a comparison of the polarimetric with the calorimetric data, the difference of less than 1% in polymer concentration between them was neglected. The values of  $\Delta H_0$ , estimated from the o.r.d. data using  $\sigma^{1/2} = 0.38 \times 10^{-2}$  derived from the o.r.d. data of PCBL samples having a

Table 2 Sets of  $f_H^0$  and  $\sigma^{1/2}$  for PCBL in *m*-cresol

Temperature (°C)	$f_H^0$	$\sigma^{1/2} \times 10^2$
23.3	0.16	0.30
24.1	0.35	0.30
24.3	0.60	0.35
24.7	0.74	0.40
26.2	0.85	0.80
29.3	0.87	1.0

Table 3 Thermodynamic parameters for PCBL in *m*-cresol

Sample No.	$N_n$	$\Delta H$ (kcal/mol)	$\Delta H_0$ (cal/mol)	$\sigma^{1/2} \times 10^2$
PCBL-1	1525		$1200 \pm 100$	
PCBL-7	570		$1150 \pm 100$	
PCBL-1	1525	$280 \pm 30$	$1065 \pm 100$	0.38
PCBL-2	1220	$275 \pm 30$	$1045 \pm 100$	0.38
PCBL-3	1145	$265 \pm 30$	$1010 \pm 100$	0.38

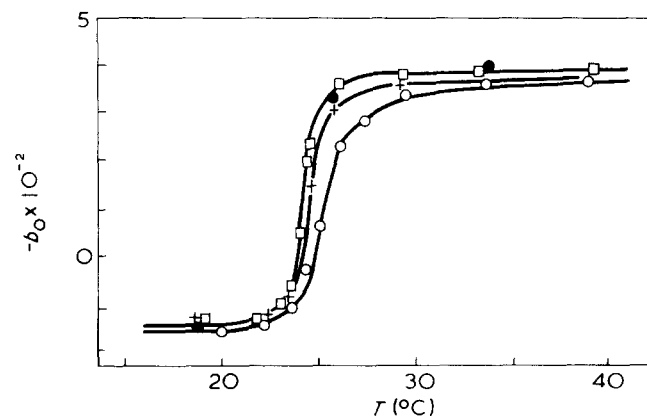


Figure 7 Temperature dependence of Moffitt-Yang parameter  $b_0$  of PCBL-1 ( $N_n = 1525$ ) in *m*-cresol. PCBL concentration: □, 0.50; ●, 1.00; +, 2.05; ○, 3.00 g/dl

degree of polymerization greater than 1000, are in fair agreement with those obtained by calorimetric measurements. If we use the values of  $0.38 \times 10^{-2}$  for  $\sigma^{1/2}$  to estimate the value of  $\Delta H_0$  for PCBL samples having rather low degrees of polymerization, such as PCBL-7, the value of  $\Delta H_0$  calculated by  $\Delta H = \Delta H_0/\sigma^{1/2}$  from the experimental values of  $\Delta H$  (see Figure 5) is +650 cal/mol. This value of  $\Delta H_0$  is much smaller than that obtained by our calorimetric measurement (see Table 3). This fact suggests that the dependence of thermodynamic parameters,  $\sigma$  and  $\Delta H$ , for helix-coil transition, on  $N_n$  is quite remarkable for PCBL in *m*-cresol. Thus, it should be noted that the estimation of these parameters from the o.r.d. data is valuable only for samples with a considerably high degree of polymerization ( $N_n > 1000$ ) for PCBL in *m*-cresol. In conclusion, in any event, the sharp transition of PCBL in *m*-cresol is mainly attributed to an unusually large value of  $\Delta H_0$ , and to a small value of  $\sigma$ .

#### REFERENCES

- 1 Applequist, J. and Doty, P. in 'Polyamino Acids, Polypeptides and Proteins', (Ed. M. A. Stahman), Univ. Wisconsin Press, Madison, 1962, p 161
- 2 Fasman, G. D. in 'Poly- $\alpha$ -Amino Acids', (Ed. G. D. Fasman), Marcel Dekker, New York, 1967
- 3 Cortijo, M., Roig, A. and Blanco, F. G. *Biopolymers* 1969, **7**, 315
- 4 Matsuoka, M., Norisuye, T., Teramoto, A. and Fujita, H. *Biopolymers* 1973, **12**, 1515
- 5 Karasz, F. E., O'Reilly, J. M. and Bair, H. E. *Biopolymers* 1965, **3**, 241
- 6 Giacometti, G., Turolla, A. and Boni, R. *Biopolymers* 1970, **9**, 979
- 7 Zimm, B. H. and Bragg, J. K. *J. Chem. Phys.* 1958, **28**, 1246
- 8 Applequist, J. *J. Chem. Phys.* 1963, **38**, 934
- 9 Nakajima, A., Hayashi, T. and Emi, S. *17th Polym. Symp. Kobe (Japan)* 1971
- 10 Blout, E. R. and Karlson, H. A. *J. Am. Chem. Soc.* 1956, **78**, 941
- 11 Calvet, E. and Prat, H. in 'Recent Progress in Microcalorimetry', (Ed. H. A. Skinner) Pergamon Press, Oxford and New York, 1963
- 12 Murakami, S. and Fujishiro, R. *Kogyo Kagaku Zasshi* 1966, **69**, 1627
- 13 Moffitt, W. and Yang, J. T. *Proc. Nat. Acad. Sci. US* 1956, **42**, 596
- 14 Doty, P. and Yang, J. T. *J. Am. Chem. Soc.* 1956, **78**, 498
- 15 Fasman, G. D., Idelson, M. and Blout, E. R. *J. Am. Chem. Soc.* 1961, **83**, 709
- 16 Hayashi, T. *Thesis* Kyoto University (1973)
- 17 Shechter, E. and Blout, E. R. *Proc. Nat. Acad. Sci. US* 1964, **51**, 695
- 18 Nakajima, A. and Hayashi, T. *Bull. Inst. Chem. Res., Kyoto Univ.* 1968, **46**, 62
- 19 Okita, K., Teramoto, A. and Fujita, H. *Biopolymers* 1970, **9**, 717
- 20 Nagai, K. *J. Chem. Phys.* 1961, **34**, 887
- 21 Ananthanarayanan, V. S., Leroy, E. and Scheraga, H. A. *Macromolecules* 1973, **6**, 553
- 22 Ananthanarayanan, V. S., Davenport, G., Stimson, E. R. and Scheraga, H. A. *Macromolecules* 1973, **6**, 559

# Preferential and absolute adsorption on poly (L-glutamic acid) in water – dioxane mixtures

Michel Morcellet and Claude Loucheux

Laboratoire de Chimie Macromoléculaire, Université des Sciences et Techniques de Lille, BP 36, 59650 Villeneuve d'Ascq, France

(Received 25 July 1974; revised 14 October 1974)

The preferential adsorption exhibited by poly(L-glutamic acid) (PLGA) in water–dioxane mixtures has been determined by measuring the specific refractive index increments at constant concentration and at constant chemical potential. These measurements have been carried out at two values of pH (12 and 4.5) and in the presence or in absence of a strong electrolyte (NaCl). At pH 12, in the absence of dioxane, the conformation of the PLGA macromolecule is an ionized chain. When adding low concentrations of dioxane (whether NaCl is present or not) a preferential adsorption of dioxane takes place. While increasing the dioxane concentration the preferential adsorption of dioxane increases and then after passing through a maximum, it decreases and an inversion of the preferential adsorption is observed at higher concentrations of dioxane, water being now preferentially adsorbed. The conformation of PLGA is  $\alpha$ -helical, showing that a transition takes place from a disordered ionized state to an ordered one by the addition of dioxane. At pH 4.5, in the absence of dioxane, the conformation of PLGA is  $\alpha$ -helical. When adding dioxane in the presence of NaCl, a preferential adsorption of dioxane occurs. While increasing the dioxane concentration no change of the preferential adsorption is observed.

## INTRODUCTION

A conformational transition is usually induced in water-soluble polypeptides from a disordered conformation to an ordered one ( $\alpha$ -helical for instance), by changing the pH of the solution<sup>1–5</sup>. However, at pH 7.0, the transition from the ionized disordered chain to an  $\alpha$ -helical conformation has been obtained by Tiffany and Krimm<sup>5</sup> by adding methanol to poly(L-glutamic acid) (PLGA) solutions. The same transition has been observed by Giancotti *et al.*<sup>6</sup> by adding pyridine and by Iizuka and Yang<sup>7</sup> by adding dioxane to PLGA solutions.

To date the variation of the preferential adsorption on PLGA when adding increasing quantities of an organic solvent at a constant value of the pH has never been determined.

The aim of this work is to study the preferential adsorption on PLGA in water–dioxane mixtures at two values of pH (when the macromolecule is ionized and when it is not) and eventually in the presence of a strong electrolyte. Such studies have been made by Inoue and Timasheff<sup>8</sup> on the  $\beta$ -lactoglobulin/water/2-chloroethanol system. They have pointed out that for low 2-chloroethanol concentrations a preferential adsorption of this alcohol takes place. However, for higher 2-chloroethanol concentrations, an inversion of the preferential adsorption occurs and water is then preferentially adsorbed. The addition of increasing quantities of 2-chloroethanol induces a transition from the native  $\alpha$ -helix poor state of the protein to an  $\alpha$ -helix rich one, as shown by the study of the dichroic spectra. This inversion of the preferential adsorption has been interpreted<sup>9</sup> in terms of water polar group interactions and organic solvent hydrophobic zone interactions. In the case of PLGA the side chains of the macromolecule are always polar ones and it is interesting to see whether such an inversion of preferential adsorp-

tion exists and to seek a correlation with the disordered conformation  $\approx$   $\alpha$ -helix transition.

## THEORY

The notation used here is that of Scatchard<sup>10</sup> and Stockmayer<sup>11</sup> for three component systems, in which the polymer is referred to as component 2, water as component 1 and the organic solvent as component 3. In the case where a strong soluble electrolyte is added the system may be considered as a pseudo-3 component system in which component 1 becomes water + electrolyte.

The measurement of the specific refractive index increment,  $\partial n/\partial C_2$  can be made in two experimental conditions, either at constant concentration  $m_3$  or at constant chemical potential  $\mu_3$  of the organic solvent. These two values  $(\partial n/\partial C_2)_{m_3}$  and  $(\partial n/\partial C_2)_{\mu_3}$  are obtained by measuring the specific refractive index increment respectively before and after a dialysis against the water–organic solvent mixture which has been used to dissolve the polymer. The following relationship can be written<sup>9</sup>:

$$\left(\frac{\partial g_3}{\partial g_2}\right)_{\mu_1, \mu_3} = \frac{1}{(1 - V_3 C_3)} \left[ \frac{\left(\frac{\partial n}{\partial C_2}\right)_{\mu_3}}{\left(\frac{\partial n_0}{\partial C_3}\right)_{m_2}} - \frac{\left(\frac{\partial n}{\partial C_2}\right)_{m_3}}{\left(\frac{\partial n_0}{\partial C_3}\right)_{m_2}} \right] \quad (1)$$

$g$  is the concentration (in g/g of component 1),  $C$  is the concentration (in g/ml of solution),  $V$  is the partial specific volume.  $(\partial n_0/\partial C_3)_{m_2}$  is the refractive index increment of the mixed solvent as a function of the concentration of

Table 1 Preferential adsorption data as a function of the dioxane content (% v/v) at pH 12.5 in the absence (A) and in the presence (B) of NaCl

Dioxane (% v/v)	$\bar{v}_3$ (ml/g)	$\left(\frac{\partial n_0}{\partial C_3}\right)_{m_2}$ (ml/g)	$\left(\frac{\partial g_3}{\partial g_2}\right)_{\mu_1, \mu_3}$ (g/g)	
			A	B
0		0.098		
10	0.911	0.100	0.19	0.21
20	0.917	0.099	0.07	0.08
30	0.925	0.098	-0.17	0.03
33		0.097		-0.25
40	0.931	0.097	-0.32	
45	0.936	0.092		

component 3 (organic solvent), and  $\partial g_3/\partial g_2_{\mu_1, \mu_3}$  is the preferential adsorption coefficient of component 3 on component 2 (the macromolecule). If this coefficient is positive, there is a preferential adsorption of the organic solvent; if it is negative there is a preferential adsorption of water which can be measured by the coefficient  $(\partial g_1/\partial g_2)_{\mu_1, \mu_3}$ . We have the following relation between these two coefficients:

$$\left(\frac{\partial g_1}{\partial g_2}\right)_{\mu_1, \mu_3} = -\frac{g_1}{g_3} \left(\frac{\partial g_3}{\partial g_2}\right)_{\mu_1, \mu_3} \quad (2)$$

## EXPERIMENTAL

### PLGA sample

The PLGA sample has been prepared in the laboratory by debenzoylation of a poly( $\gamma$ -benzyl-L-glutamate) according to the method of Idelson and Blout<sup>12</sup>. Its intrinsic viscosity, measured at 25°C, pH 7.3, in a 0.2 M NaCl solution, is 60.4 ml/g corresponding to a weight-average molecular weight  $M_w = 26\,000$ , if using a calibration given by Wada<sup>13</sup>.

### Preparation of solutions

**Undialysed solutions.** The water-dioxane mixtures used were prepared by adding a given volume of dioxane to an aqueous solution of 0.125 N NaOH (or 0.125 N NaOH + 0.2 M NaCl for experiments in the presence of NaCl). The basic solutions were obtained by dissolving directly a weighed quantity of PLGA to the mixed solvent. The value of the pH was  $12.5 \pm 0.15$ . These solutions were used directly to measure the values of  $(\partial n/\partial C_2)_{m_3}$  at constant concentration at higher pH.

The acidic solutions of PLGA cannot be obtained directly by dissolution of PLGA in a water-dioxane mixture at a convenient pH. A solution was prepared as mentioned above at pH 12.5 and then the pH was adjusted to 4.5. The mixed water-dioxane solvent was adjusted separately at the same pH. In these conditions the values of  $(\partial n/\partial C_2)_{m_3}$  at constant concentration for lower values of pH can be determined.

In both cases the concentration of the starting solution was approximately  $6 \times 10^{-3}$  g/ml. In order to extrapolate the specific refractive index increment measurements at zero the solution of a given composition was diluted with the corresponding water-dioxane mixture. In all cases it has been verified that the variation of pH by dilution was negligible (within  $\pm 0.1$  pH unit).

**Dialysed solutions.** The dialysis was carried out in the same way whether the solutions were acidic or basic. The

solution in the mixed solvent was introduced in a dialysis bag (Union Carbide Co.) which was brought into equilibrium with the solvent. In order to prevent the evaporation of the solvent, the dialysis was performed in a vessel sealed with Parafilm wax (Marathon Division, American Can Co.) and a rubber band until a few moments before filling the refractometer cells. As mentioned by Tuzar and Kratochvil<sup>14</sup> the time needed to reach the equilibrium depends on the experimental conditions. Preliminary measurements have shown that for our experiments the equilibrium is always reached within 12 h of dialysis. Under these conditions the measurements of refractive index increments were made at constant chemical potential.

### Specific refractive index increment measurements

They were performed using a Brice-Phoenix BP 2000 differential refractometer (15) at 20°C. The value of the increment  $(\partial n/\partial C_3)_{m_2}$  was also determined by using the differential refractometer.

### Circular dichroism

Circular dichroism spectra were recorded in order to ascertain the conformation of PLGA under different experimental conditions. A Roussel-Jouan dichrograph model II equipped with a xenon source was used with 0.1 mm cells under a dried oxygen-free nitrogen flow. The concentrations used were  $\sim 5 \times 10^{-4}$  g/cm<sup>3</sup>.

## RESULTS AND DISCUSSION

### Study of PLGA at pH 12.5

The measurements of the specific refractive index increment have been made in the presence and in the absence of NaCl, varying the dioxane from 0 to 45% in the absence of NaCl and from 0 to 33% in the presence of NaCl, the precipitation of PLGA taking place beyond this percentage of dioxane. This precipitation phenomenon has been mentioned by Iizuka and Yang<sup>7</sup>.

Table 1 gives the values of the preferential adsorption coefficient  $(\partial g_3/\partial g_2)_{\mu_1, \mu_3}$  as a function of the percentage of dioxane in the mixed solvent, in the absence or in the presence of NaCl respectively. This coefficient has been calculated from equation (1) using the values of  $\partial n/\partial C_2$  plotted in Figure 1. The values of the partial specific volume  $\bar{v}_3$  of dioxane in the mixed solvent have been found in the literature<sup>16</sup> and are also reported in Table 1.

Figures 1a and 1b show the values of  $(\partial n/\partial C_2)$  before

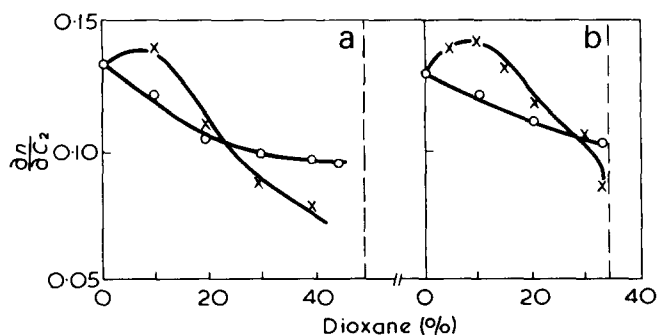


Figure 1 Variation of the specific refractive index increments of PLGA versus the dioxane composition (% v/v) before (O) and after (X) dialysis. (a) In the absence of NaCl; (b) in the presence of 0.2 M NaCl

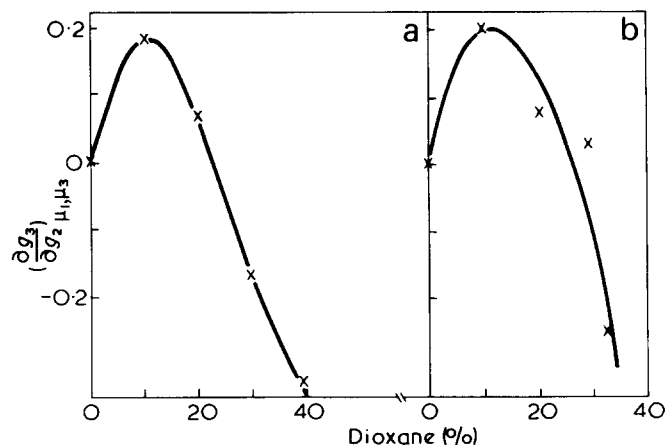


Figure 2 Variation of the preferential adsorption coefficient in basic solutions of PLGA versus the dioxane composition (% v/v). (a) In the absence of NaCl; (b) in the presence of 0.2 M NaCl

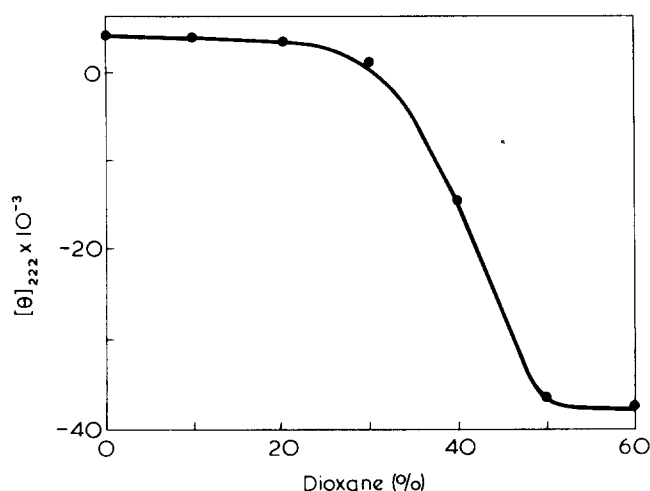


Figure 3 Variation of the ellipticity  $[\theta]_{222}$  at 222 nm as a function of the dioxane composition, in basic solutions of PLGA, in the absence of NaCl

and after dialysis, in the absence and in the presence of NaCl respectively versus the percentage of dioxane. In each case one observes an intersection which corresponds to an inversion of preferential adsorption. This inversion occurs at 22% of dioxane in the absence of NaCl and approximately 30% of dioxane in the presence of NaCl. The vicinity of the precipitation point of the solutions in the last case makes the determination of this inversion point less sure. Figures 2a and 2b give the variation of the preferential adsorption coefficient as a function of the percentage of dioxane, in the absence and in the presence of NaCl respectively. In both cases, while increasing the percentage of dioxane, the preferential adsorption coefficient increases, then passes through a maximum, decreases and becomes zero and even negative in the absence of NaCl. This kind of variation means that dioxane is first preferentially adsorbed, then this preferential adsorption decreases, and is replaced by a preferential adsorption of water when the coefficient becomes negative. The maximum of preferential dioxane adsorption lies in both cases at  $\sim 10\%$  dioxane.

It is important to determine the conformation adopted by the PLGA macromolecule before and after this inversion of preferential adsorption. The measurement of the ellipticity at 222 nm  $[\theta]_{222}$  on the dichroic spectra can be an estimation of the helix content of the polypeptide. This

value is reported in Figure 3 as a function of the percentage of dioxane for PLGA solutions in the absence of NaCl. This curve exhibits a broad transition range between 30 and 50% of dioxane, much broader than the transition obtained when varying the pH. The dichroic spectra for lower (30%) and higher (50%) dioxane concentrations are given in Figure 4. The former corresponds to a disordered conformation and the latter to an  $\alpha$ -helix. It is difficult to find any correlation between the variation of the preferential adsorption coefficient (Figure 2a) and the variation of the ellipticity during the transition, when adding dioxane. It is important to point out that the preferential adsorption coefficient represents a comparison of the solvent compositions in bulk and in the immediate domain of the polymer. In order to determine the absolute adsorption of the organic solvent onto the polymer, Inoue and Timasheff<sup>17,18</sup> suggest splitting the preferential adsorption coefficient into two terms:

$$\left(\frac{\partial g_3}{\partial g_2}\right)_{\mu_1, \mu_3} = A_3 - A_1 g_3 \quad (3)$$

$A_1$  and  $A_3$  are respectively the number of grammes of water and of dioxane bound to one gramme of polymer. In equation (3)  $A_1$  and  $A_3$  are unknown. If one makes an assumption for the number of water molecules bound to a carboxylic group,  $A_3$  can be calculated. Timasheff and Inoue<sup>9</sup> think that a hydrophilic site of a globular protein retains six to eight water molecules. We have considered that the number of water molecules bound to a carboxylic group in PLGA does not change when dioxane is added. This assumption is probably an oversimplification of the problem because this number changes very likely when the transition: disordered conformation  $\rightleftharpoons$   $\alpha$ -helix occurs. However,

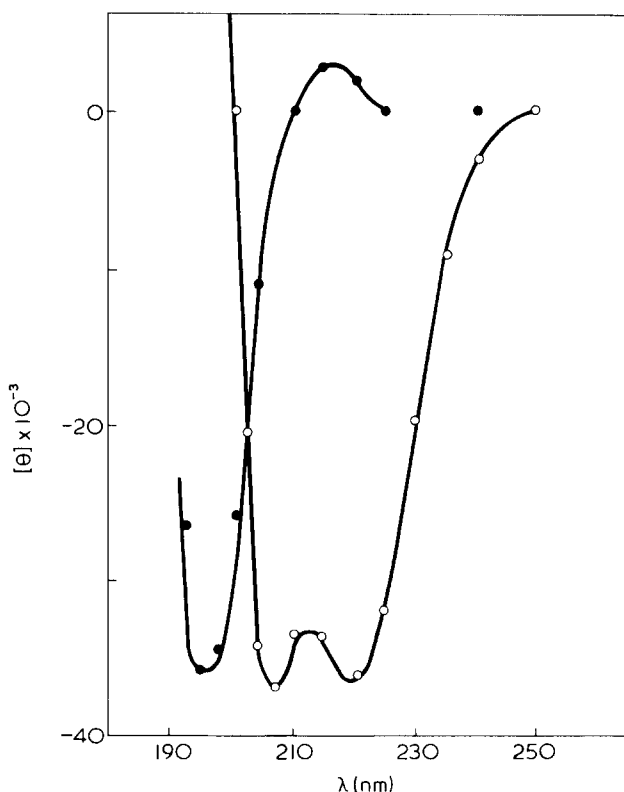


Figure 4 Dichroic spectra of basic solutions of PLGA in the absence of NaCl, for different values of the dioxane content: ●, 30% v/v; ○, 50% v/v

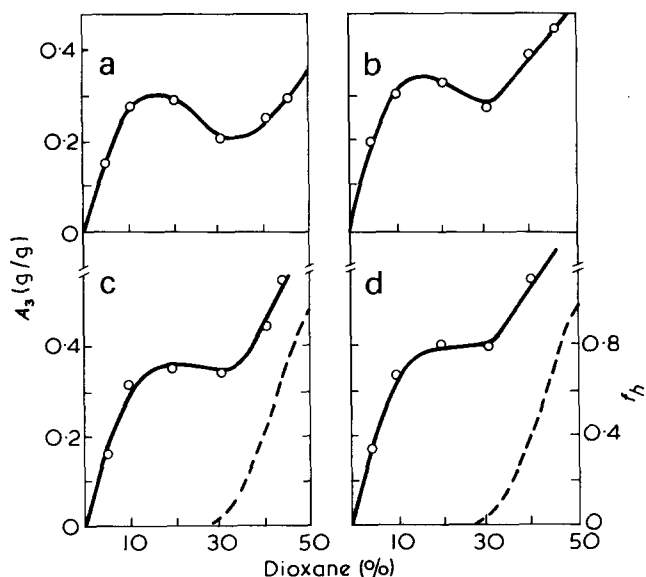


Figure 5 Variation of the absolute adsorption of dioxane as a function of the solvent composition (% v/v of dioxane) assuming (a) 6, (b) 7, (c) 8 and (d) 9 water molecules adsorbed on each residue of PLGA

under these conditions, fixing successively this number,  $n$ , of water molecules adsorbed on a carboxylic group at 6, 7, 8 and 9, we have obtained 4 corresponding variations of the absolute coefficient  $A_3$  which describes the absolute fixation of dioxane onto the PLGA molecule, as a function of the percentage of dioxane added in the solution (Figures 5a, 5b, 5c and 5d). The common feature of these four graphs is that the  $A_3$  coefficient undergoes a change of behaviour at a value of approximately 15% dioxane. Then the value of  $A_3$  levels off in the case of 8 or 9 water molecules bound to a carboxylic group. In all cases the absolute amount of dioxane adsorbed on the macromolecule increases again, when reaching about 30% dioxane in the mixed solvent.

The value of the helix content  $F_H$  has been calculated using the relation:

$$F_H = \frac{4000 - [\theta]_{222}}{41\,000} \quad (4)$$

The variation of  $F_H$  versus the percentage of dioxane is also plotted in Figures 5c and 5d (broken lines). It can be seen that the macromolecule is almost entirely disordered until 30% of dioxane. Then the transition occurs and  $F_H$  increases, paralleling the increase of  $A_3$ . Thus, the plateau observed between 15 and 30% of dioxane refers to the adsorption of dioxane on the disordered conformation. A second plateau in the  $A_3$  variation should be obtained after the end of the transition, but measurements in this domain are not possible because of the limit of solubility. On the contrary, dichroic spectra can be recorded up to 60% dioxane, probably owing to the fact that the concentration needed is smaller — of an order of magnitude in this case. Assuming successively 6, 7, 8 and 9 water molecules bound to a carboxylic group, the absolute number of dioxane molecules adsorbed on a residue has been calculated. For 20% of dioxane these numbers are respectively 0.43, 0.48, 0.53 and 0.58 mol/residue. For 45% dioxane, at the end of the conformational transition, these numbers are respectively 0.43, 0.63, 0.77, 0.86 mol/residue. Assuming 8 or 9 water molecules bound to a residue in the  $\alpha$ -helical conformation should be about 1.0 when the transition is achieved. The curves of

Figures 5c or 5d seem to be more reliable in describing the adsorption phenomenon. Inoue and Timasheff<sup>17</sup> have calculated the mean number of organic solvent molecules bound to a non-polar residue for  $\beta$ -lactoglobulin as between 2 and 3. In the case of PLGA the residue is a polar one and the mean number of organic solvent molecules bound to each residue is much lower,  $\sim 1.0$ , but this type of adsorption does exist and hence the maximum of preferential adsorption is reached more easily.

#### Influence of NaCl

In the presence of NaCl, such calculations are more hazardous owing to the proximity of the precipitation range for the solutions. The presence of NaCl is known to stabilize the disordered structure and the addition of 0.2 M NaCl to a water/dioxane mixture (2:1 v/v) shifts the transition of one pH unit towards the lower pH value. A similar behaviour has been observed in our preferential adsorption experiments: the addition of NaCl shifts the zero value of the  $(\partial g_3/\partial g_2)_{\mu_1, \mu_3}$  coefficient from 22 to 33% of dioxane. Such similar effects may suggest a correlation between the conformational transition and the inversion of the preferential adsorption.

#### Study of PLGA at pH 4.5

The measurements of the specific refractive index increment have been made with mixed solvent in the presence of 0.2 M NaCl, varying the dioxane content from 0 to 33%. (Beyond this value precipitation of PLGA occurs.) The preferential adsorption coefficient  $(\partial g_3/\partial g_2)_{\mu_1, \mu_3}$  has been calculated as above, using equation (1). Between 10 and 30% of dioxane, the values of  $(\partial n/\partial C_2)_{m_3}$  and  $(\partial n/\partial C_2)_{\mu_3}$  are almost constant (about 0.110 and 0.135 ml/g respectively). Thus, the value of the preferential adsorption coefficient is positive and practically constant in this range of solvent composition and dioxane is preferentially adsorbed on PLGA.

Whatever the percentage of dioxane, the conformation of PLGA in the mixed solvent at pH 4.5 is always  $\alpha$ -helical.

The shape of the dichroic spectra and the values of the ellipticities at 222 nm indicate an  $\alpha$ -helical structure without ambiguity (in good agreement with the results of Holzwarth and Doty<sup>3</sup>).

Measurements have been made in a solvent containing 33% of dioxane with the pH varying between 4.5 and 5.15. The results obtained show that pH has little effect on the extent of the preferential adsorption on the  $\alpha$ -helical conformation (Table 2).

#### CONCLUSION

The results obtained show that, in acidic solutions, the preferential adsorption on PLGA is essentially a preferential

Table 2 Preferential adsorption data in a mixture of 0.2 M NaCl/dioxane (67:33% v/v) for different pH values

pH	$\left(\frac{\partial n}{\partial C_2}\right)_{m_3}$ (ml/g)	$\left(\frac{\partial n}{\partial C_2}\right)_{\mu_3}$ (ml/g)	$\left(\frac{\partial g_3}{\partial g_2}\right)_{\mu_1, \mu_3}$ <sup>a</sup> (g/g)
4.5	0.085	0.129	0.664
4.8	0.089	0.140	0.770
5.15	0.089	0.120	0.468

<sup>a</sup> Calculated by using  $\bar{v}_3 = 0.927$  ml/g and  $(\partial n_0/\partial C_3)_{m_2} = 0.097$  ml/g



adsorption of dioxane, in the whole range of composition studied. At the same time, the dichroic spectra indicate no conformational change in the macromolecule. In basic solutions, an inversion in the preferential adsorption is observed and the dichroic spectra show a transition between a disordered and an  $\alpha$ -helical conformation. This transition is closely related to the variation of the absolute adsorption of dioxane. Unfortunately, in the case of the system PLGA/water/dioxane, the experimental conditions make the description of the whole transition by a preferential adsorption study difficult. This system had been chosen because it was the first used to define the disordered conformation  $\rightleftharpoons$   $\alpha$ -helix transition for PLGA, by Doty and coworkers<sup>2</sup>. Other systems with a broader range of solubility for the PLGA would be more convenient for preferential adsorption studies. Moreover, studies in the absence of salt should be more interesting because of the larger range of solubility of the polymer.

#### REFERENCES

- 1 Fasman, G. D. in 'Poly( $\alpha$ -amino acids)', Marcel Dekker, New York, 1967
- 2 Doty, P., Wada, A., Yang, J. T. and Blout, E. R. *J. Polym. Sci.* 1957, **23**, 851
- 3 Holzwarth, G. and Doty, P. *J. Am. Chem. Soc.* 1965, **87**, 218
- 4 Tiffany, M. L. and Krimm, S. *Biopolymers* 1969, **8**, 347
- 5 Tiffany, M. L. and Krimm, S. *Biopolymers* 1968, **6**, 1379
- 6 Giancotti, V., Quadrifoglio, F. and Crescenzi, V. *Makromol. Chem.* 1972, **158**, 53
- 7 Iizuka, E. and Yang, J. T. *Biochemistry* 1965, **4**, 1249
- 8 Inoue, H. and Timasheff, S. N. *J. Am. Chem. Soc.* 1968, **90**, 1890
- 9 Timasheff, S. N. and Inoue, H. *Biochemistry* 1968, **7**, 2501
- 10 Scatchard, G. *J. Am. Chem. Soc.* 1946, **68**, 2315
- 11 Stockmayer, W. H. *J. Chem. Phys.* 1950, **18**, 58
- 12 Idelson, M. and Blout, E. R. *J. Am. Chem. Soc.* 1958, **80**, 4631
- 13 Wada, A. *Mol. Phys.* 1960, **3**, 409
- 14 Tuzar, Z. and Kratochvil, P. *Coll. Czech. Chem. Commun.* 1967, **32**, 3358
- 15 Brice, B. A. and Halwer, M. *J. Opt. Soc. Am.* 1951, **41**, 1033
- 16 Malcolm, G. N. and Rowlinson, J. S. *Trans. Faraday. Soc.* 1957, **53**, 921
- 17 Inoue, H. and Timasheff, S. N. *Biopolymers* 1972, **11**, 737
- 18 Timasheff, S. N. *Acc. Chem. Res.* 1970, **3**, 62

# Effect of oligo-amine (or polyamine) on the vinyl chloride polymerization by alkyl aluminium compounds

Akira Akimoto

Central Research Laboratory, Toyo Soda Manufacturing Co. Ltd., Yamaguchi-ken, Japan

(Received 17 May 1974; revised 21 October 1974)

Polymerization of vinyl chloride was investigated in the presence of  $AlR_3$ , oligo-amine (or polyamine) as a multidentate ligand, and  $CCl_4$ . Among oligo-amines and polyamines, diethylenetriamine gives the best yield. The yield of polymer decreased with increase of  $n$  in compounds of the type  $(n)$ ethylene  $(n + 1)$ amine. The addition of monodentate amine such as ethylamine and *n*-butylamine markedly reduced the rate of polymerization. It is suggested that the formation of the hexa-coordinated complex between  $AlR_3$  with oligo-amine is important in the initiation process.

## INTRODUCTION

In a previous paper<sup>1</sup>, the author showed that the catalyst system  $AlEt_3$ /Lewis base/ $CCl_4$  can initiate vinyl chloride (VC) polymerization, particularly in the presence of diethylenetriamine (DETA). A kinetic study showed that the polymerization occurred by a free radical mechanism, and the formation of the complex between  $AlEt_3$  and DETA greatly contributes to the initiation reaction<sup>2</sup>.

The present paper deals with a detailed study of the catalytic behaviour of oligo-amine as a multidentate ligand.

The polymerization was carried out in the presence of  $AlR_3$ , oligo-amine (or polyamine) and  $CCl_4$ , in order to clarify the relationship between the structural character of the  $AlR_3$ -amine complex and its activity for initiating polymerization.

## EXPERIMENTAL

VC was dried and purified by passing it through columns containing calcium chloride and phosphorus pentoxide. Vinyl monomers, i.e. methyl methacrylate (MMA), styrene (S) and vinyl acetate (VAC) were purified in the usual manner.

Organo-aluminium compounds, i.e.  $AlEt_3$  and  $Al(iBu)_3$ , were distilled in the presence of nitrogen under reduced pressure and preserved under nitrogen atmosphere.

Commercial ethylenediamine (EDA), tetramethylethylenediamine (TMEDA), DETA, triethylenetetramine (TETA), and tetraethylenepentamine (TEPA) were used as the multidentate ligands. Polyethyleneimine (PEI) was obtained by cationic polymerization of ethyleneimine with *p*-toluenesulphonic acid ( $[\eta] = 0.18, 0.08$  and  $0.03$ , respectively, in water at  $30^\circ C$ ). These amines except polyethyleneimine were purified by distillation before use.

$CCl_4$  was washed with concentrated sulphuric acid, then with water, and distilled before use.

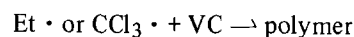
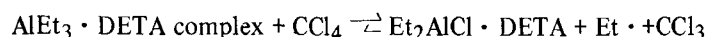
Polymerization was carried out in a sealed tube at  $40^\circ C$ , as reported earlier<sup>1</sup>.

The intrinsic viscosity of the polymers was measured in nitrobenzene solution at  $30^\circ C$ .

The n.m.r. spectra of a mixture of  $AlEt_3$  and amine in benzene were measured at room temperature on a 100 MHz n.m.r. spectrometer with benzene as the internal standard.

## RESULTS AND DISCUSSION

As previously reported,  $AlEt_3/CCl_4$  was found to be an effective initiating catalyst system for the polymerization of VC in the presence of DETA<sup>1</sup>. It was assumed that the reaction between the  $AlEt_3 \cdot DETA$  complex and  $CCl_4$  might be involved in the initiation process:



From these considerations, it seems probable that other oligo-amines and polyamines may also be effective for initiation. Therefore, the polymerization of VC was investigated by the  $AlR_3$ /oligo-amine (or polyamine)/ $CCl_4$  catalyst system.

Table 1 lists the effect of varying the structure of amine complexed with  $Al(iBu)_3$  on the polymerization in the presence of  $CCl_4$ . Good activity was also observed with compounds of the type oligo( $n$ )ethylene( $n + 1$ )amine, which have multidentate ligands, in the case of  $Al(iBu)_3$  as well as  $AlEt_3$ <sup>1</sup>. However, alkylamines having a monodentate ligand showed low catalytic activities and as expected from Breslow's data<sup>3</sup> their basicity did not influence the activity of the catalyst. Although Breslow reports that tertiary amines give fairly active catalysts, the catalysts containing triethyl-

Table 1 Effect of various amines on polymerization of vinyl chloride with  $Al(iBu)_3/CCl_4$  catalyst system<sup>a</sup>

No.	Amine	Yield (%)	$[\eta]$
1	Ethylamine	0.2	—
2	Diethylamine	0.2	—
3	Triethylamine	0.2	—
4	EDA	1.5	—
5	TMEDA	0.0	—
6	DETA	21.3	0.03
7	TEDA	18.6	0.03
8	TEPA	16.8	0.03

<sup>a</sup> VC, 5 ml;  $C_6H_6$ , 5 ml;  $Al(iBu)_3$ , 1 mol % on monomer;  $Al(iBu)_3$ /amine/ $CCl_4 = 1:1:1$ ; polymerization for 20 h

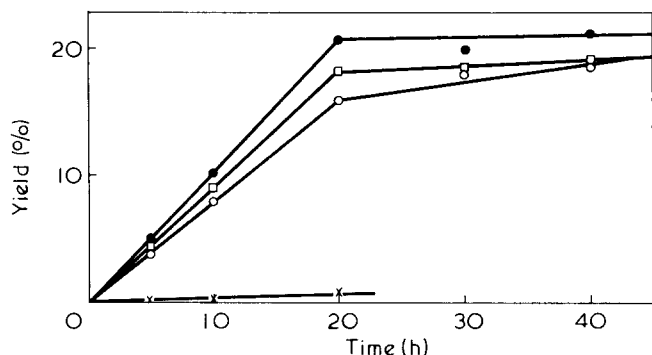


Figure 1 Plot of yield (%) versus time. VC, 5 ml;  $C_6H_6$ , 5 ml;  $Al(iBu)_3$ , 1 mol % on monomer;  $Al(iBu)_3/amine/CCl_4 = 1:1:1$ . X, EDA; ●, DETA; ○, TEPA; □, TETA

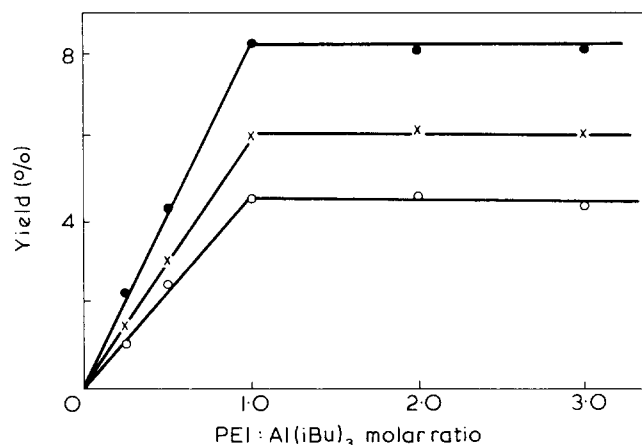


Figure 2 Plot of yield (%) versus PEI:  $Al(iBu)_3$  molar ratio. VC, 5 ml;  $C_6H_6$ , 5 ml;  $Al(iBu)_3$ , 1 mol % on monomer;  $Al(iBu)_3/CCl_4 = 1:1:1$ ; polymerization for 20 h.  $[\eta]$ : ●, 0.03; X, 0.08; ○, 0.18

amine did not show the activity under the experimental conditions used in this work.

Figure 1 shows a typical plot of percentage yield against time for the catalyst system  $Al(iBu)_3/CCl_4$  in the presence of oligo-amine. It can be seen that there is a moderate fall off in rate, which is a characteristic of the VC polymerization. With oligo-amines, the order of the catalytic activity was found to be: DETA > TETA > TEPA  $\gg$  EDA, in the initial period of polymerization.

Figure 2 presents the results obtained in the presence of PEI (concentration expressed in base mol/l of ethyleneimine) for the  $Al(iBu)_3/CCl_4$  catalyst system. The concentrations of monomer,  $CCl_4$  and  $Al(iBu)_3$  remained constant, whilst molar ratio of PEI to  $Al(iBu)_3$  was varied from 0.25:1.0 to 3.0:1.0.

PEI is representative of a polymeric ligand, and 'polymer effect' as a catalyst<sup>4</sup> has been noticed by many authors. Although the polymerization starts immediately in the presence of suspended PEI, it can be seen that with PEI having various values of  $[\eta]$  the rate of polymerization increases as the molar ratio of PEI to  $Al(iBu)_3$  is increased, and then flattens out as the ratio is equal to or greater than one, similar to DETA<sup>2</sup>. However, the yield of polymer was lower in the presence of PEI than of oligo-amine, and decreased with increase of the degree of polymerization. This seems to be due to the insolubility of PEI and the existence of non-coordinated amine in the polymer. The approach of  $Al(iBu)_3$  to the surface of polymer is likely to be hindered and apparently the polymerization occurs from the surface of the PEI.

Although the excessive amounts of free amines do not influence the polymerization in the case of oligo-amine and

polyamine, excessive amounts of monodentate alkylamine such as ethylamine and n-butylamine leads to the retardation of the polymerization. As shown in Table 2, the mixtures of DETA and ethylamine, and of TETA and n-butylamine have the lower catalytic activity.

Table 3 presents the results with  $AlEt_3/DETA/CCl_4$  catalyst system in various diluents. Expected yields of polymer were obtained in n-hexane, while tetrahydrofuran, dioxane and ethyl acetate were poor diluents. In acetone and in hexamethyl phosphoric acid triamide the polymerization was inhibited.

All the experimental results point out the effectiveness of oligo-amines except EDA and this may be ascribed to the chemical activity of the complex between  $AlR_3$  with oligo-amine. The change of the catalytic activity of organo-aluminium compounds, when combined with a Lewis base, has been reported in the MMA polymerization, and it was interpreted on the basis of the change of electronegativity of a central aluminium ion<sup>5</sup>. This is not so in the present work. In Table 4 the internal chemical shifts are presented for free  $AlEt_3$  and for  $AlEt_3$  with some amines (1:1 molar ratio)<sup>6</sup>. The shifts, i.e. the electronegativity, show little relationships with the catalytic activity given in Table 1.

Figure 3 presents the n.m.r. spectrum of the mixture of DETA with  $AlEt_3$  (1:1 molar ratio). The A, B, C and D

Table 2 Vinyl chloride polymerization with  $Al(iBu)_3/CCl_4$  catalyst system in the presence of mixed amines<sup>a</sup>

No.	Oligo-amine	Mol % on monomer	Alkyl-amine	Mol % on monomer	Yield (%)
6	DETA	1.0	—	—	21.3
12	DETA	0.5	—	—	13.0
13	DETA	0.5	$EtNH_2$	0.5	5.8
7	TETA	1.0	—	—	18.6
14	TETA	1.5	—	—	18.3
15	TETA	1.0	n-BuNH <sub>2</sub>	0.5	13.4
16	DETA	1.0	—	—	21.0
	TETA	0.5	—	—	21.0

$EtNH_2 =$  ethylamine; n-BuNH<sub>2</sub> = n-butylamine. <sup>a</sup>VC, 5 ml;  $C_6H_6$ , 5 ml;  $Al(iBu)_3$ , 1 mol % on monomer;  $Al(iBu)_3/CCl_4 = 1:1:1$ ; polymerization for 20 h

Table 3 Polymerization of vinyl chloride in various diluents<sup>a</sup>

No.	Diluent	Yield (%)
17	Benzene	32.5
18	n-Hexane	32.0
19	Acetone	trace
20	Ethyl acetate	4.6
21	Dioxane	10.3
22	Tetrahydrofuran	20.4
23	Hexamethyl phosphoric acid triamide	trace

<sup>a</sup> VC, 5 ml; diluent, 5 ml;  $AlEt_3$ , 1 mol % on monomer;  $AlEt_3/DETA/CCl_4 = 1:1:1$ ; polymerization for 20 h

Table 4 Internal chemical shifts of the methyl and methylene protons in n.m.r. spectrum of  $AlEt_3^+$  amine complexes

Amine	$\Delta(CH_3-CH_2)^a$ (ppm)
Triethylamine	1.26
TMEDA	1.30
DETA	1.28
TETA	1.26
—	0.80

<sup>a</sup> Internal chemical shifts,  $\Delta(CH_3-CH_2)$ , were measured with benzene as internal standard at room temperature

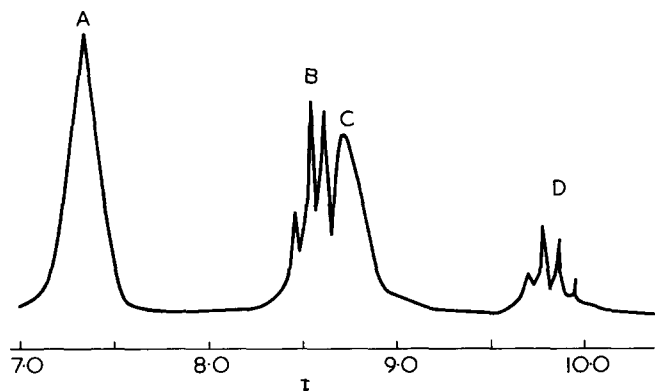
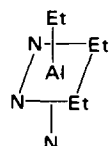


Figure 3 N.m.r. spectrum of a mixture of DETA and  $\text{AlEt}_3$

peaks are assigned to the  $-\text{NH}-\text{CH}_2-\text{CH}_2-$ ,  $\text{C}-\text{CH}_3$ ,  $-\text{NH}_2$  and the  $\text{CH}_2$  hydrogens, respectively.

Extensive work has been carried out on the study of the structure of  $\text{AlR}_3$  and amine having multidentate ligands. According to Fetter<sup>7,8</sup>,  $\text{AlMe}_3$  reacts with  $\text{Me}_2\text{N}(\text{CH}_2)_2\text{NMe}_2$  and  $\text{Me}_2\text{N}(\text{CH}_2)_3\text{NMe}_2$  to give complexes with two molecules of  $\text{AlMe}_3$  per amine, the structures being a penta-coordinated aluminium atom with a linear  $\text{N} \rightarrow \text{Al} \leftarrow \text{N}$  covalent bond. According to Thiele<sup>9,10</sup>, however,  $\text{AlMe}_3$  and  $\text{AlEt}_3$  yield 2:1 complexes with TMEDA and the aluminium atom has in these compounds the coordination number of 4. In the n.m.r. spectrum of Figure 3 there is a single  $\text{NH}_2$  peak, indicating that both of the amine groups are equivalent, as mentioned in a previous paper<sup>2</sup>. If the aluminium was bonded to only one of the nitrogens, the  $\text{NH}_2$  groups would be expected to show two peaks in the spectrum because the environment of the  $\text{NH}_2$  group attached to the quadruple bonded nitrogen should differ from that of the  $\text{NH}_2$  group attached to triple bonded nitrogen. The change of the chemical shifts of the  $-\text{NHCH}_2\text{CH}_2-$  of DETA in the presence of  $\text{AlEt}_3$  means that the  $-\text{NHCH}_2\text{CH}_2-$  group of DETA interacts with  $\text{AlEt}_3$ . One possible complication in the interpretation of the spectrum is that the state of aggregation is not known. However, in benzene solution of DETA/ $\text{AlEt}_3$  molecular weight determination indicates the presence of a monomeric species.

These results indicate that  $\text{AlEt}_3 \cdot \text{DETA}$  may be a species involving a hexa-coordinated aluminium atom:



Such a scheme is a better rationalization of both n.m.r. and molecular weight data, than the penta-coordinated structure proposed earlier<sup>1,2</sup>.

The high catalytic activity with DETA may be ascribed to the presence of this type of complex whereas the low catalytic activity with EDA and TMEDA may be attributed to the impossibility of the formation of this type of complex. Furthermore, the difficulty of formation of the complex with long chain molecules causes the retardation of polymerization with PEI. The fact that the catalytic activity with DETA is highest is important.  $\text{AlR}_3/\text{CCl}_4/\text{TETA}$  and TEPA catalyst systems showed less activity, probably because of the existence of a residual free amino group in the tetradentate and pentadentate ligands. Free amino groups may retard the polymerization as seen with monodentate alkylamine.

As mentioned before, the rate of polymerization was

Table 5 Copolymerization of VC and VAC<sup>a</sup>

No.	VC (mol %)	VAC (mol %)	Yield (%)
24	80	20	1.2
25	90	10	1.4
26	95	5	1.2

<sup>a</sup> Total monomer, 5 ml;  $\text{C}_6\text{H}_6$ , 5 ml;  $\text{AlEt}_3$ , 1 mol % on total monomer;  $\text{AlEt}_3/\text{DETA}/\text{CCl}_4 = 1:1:1$ ; polymerization for 40 h

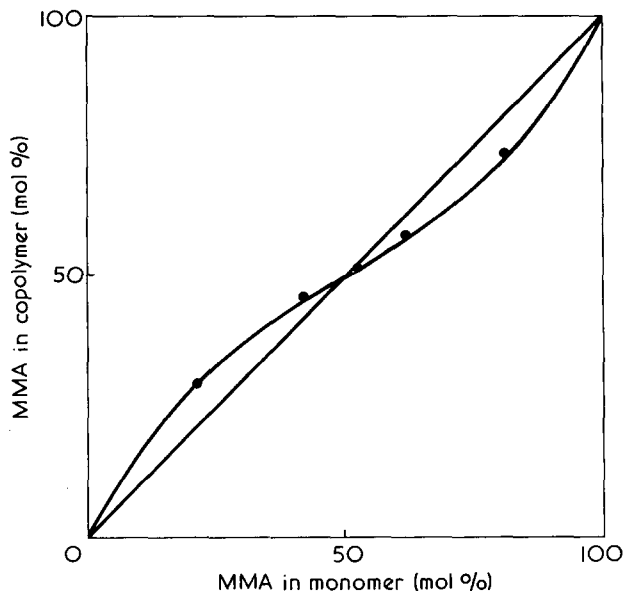


Figure 4 Composition diagram for the copolymerization of MMA with S. Total monomer, 5 ml;  $\text{C}_6\text{H}_6$ , 5 ml;  $\text{AlEt}_3$ , 1 mol % on total monomer;  $\text{AlEt}_3/\text{DETA}/\text{CCl}_4 = 1:1:1$ ; polymerization for 10 h

reduced by addition of the alkylamine on the  $\text{Al}(\text{iBu})_3/\text{amine}$  (having a multidentate ligand)/ $\text{CCl}_4$  catalyst system or by polymerizing in a polar solvent. These results can be interpreted in terms of a competitive solvation or coordination of amine to the catalyst site so as to hinder the formation of this type of complex.

The copolymerization of VC and VAC was retarded even in the presence of small amounts of the latter monomer (Table 5), because VAC coordinates the catalyst active site. However, copolymerization of MMA with S was successful with the  $\text{AlEt}_3/\text{DETA}/\text{CCl}_4$  catalyst system. The monomer-copolymer composition curve is shown in Figure 4. For each experiment monomer mixtures were polymerized in the range 5–10% by weight. The results show the free radical character of the polymerization.

#### ACKNOWLEDGEMENTS

The author is grateful to Dr Y. Kosaka and Mr S. Imura for valuable discussions.

#### REFERENCES

- 1 Akimoto, A. *Polymer* 1974, **15**, 216
- 2 Akimoto, A. *Polymer* 1974, **15**, 717
- 3 Breslow, D. S., Christman, D. L., Espy, H. N. and Lukach, C. A. *J. Appl. Polym. Sci.* 1967, **11**, 73
- 4 Inaki, Y., Kimura, K. and Takemoto, K. *Makromol. Chem.* 1973, **171**, 19
- 5 Ikeda, M., Hirano, T. and Tsuruta, T. *ibid.* 1971, **150**, 127
- 6 Narasimhan, P. T. and Rogers, M. T. *J. Am. Chem. Soc.* 1960, **82**, 5983
- 7 Fetter, N. R., Bartocha, B., Brinckman, F. E. and Moore, D. W. *Can. J. Chem.* 1963, **41**, 1359
- 8 Fetter, N. R. and Moore, D. W. *ibid.* 1964, **42**, 885
- 9 Thiele, K. H., Müller, H. K. and Brüser, W. *Z. Anorg. Allgem. Chem.* 1966, **345**, 194
- 10 Thiele, K. H. and Brüser, W. *ibid.* 1967, **349**, 33

# Biomedical applications of polymeric materials and their interactions with blood components: a critical review of current developments\*

Stephen D. Bruck

National Heart and Lung Institute, National Institutes of Health, Bethesda, Maryland 20014, USA

(Received 8 August 1974)

A critical review is presented of some of the current developments in the biomedical applications of polymeric materials, with emphasis on naturally occurring macromolecules present in blood vessel walls, synthesis and surface modifications, mechanical properties, and interactions between surfaces and blood components.

## INTRODUCTION

Polymeric materials in prosthetic devices have attracted considerable attention, and several aspects of this complex problem have been discussed by Bruck<sup>1-4</sup>, Salzman<sup>5</sup>, Berger and Salzman<sup>6</sup>, Mason<sup>7</sup>, and Leininger<sup>8</sup>. In previous publications some of the biological test methods<sup>9</sup>, problems of sterilization<sup>10,11</sup>, hydrogels<sup>12</sup>, and specially prepared segmented polyether-urethanes<sup>13</sup> have been discussed by the present author.

It is the purpose of this paper to review critically some of the latest developments in blood compatible polymeric materials and in the interactions of blood components with surfaces. In order to present the subject matter in a logical manner, attention is focused on the following areas:

(1) naturally occurring macromolecules present in the cardiovascular wall, (2) some newer synthetic polymers and surface modifications, (3) mechanical properties, and (4) interactions between blood components and surfaces.

As indicated previously<sup>1-4</sup>, materials that are to be useful for prostheses in blood should not cause: (a) thrombosis, (b) destruction of the cellular elements of the blood, (c) alteration of the plasma proteins, (d) destruction of enzymes, (e) depletion of electrolytes, (f) adverse immune responses, (g) damage to adjacent tissue, (h) cancer, and (i) toxic and allergic reactions; furthermore, the biomaterials should not deteriorate in the biological environment (if used for prostheses which must perform appropriate mechanical functions), or during sterilization with resultant changes in their physical, chemical, and surface characteristics. Usually, polymers that are blood compatible are also tissue compatible, but the reverse is not always true. It is most important that all biomaterials be free of leachable impurities or additives of unknown composition which could adversely affect the physiological environment.

Figure 1 illustrates some of the major areas involved in biomaterials research and development. Investigations include both basic and more applied areas, since without an adequate understanding of basic phenomena, applied research and development efforts would remain empirical.

These studies involve work in the areas of: (a) natural macromolecules present in the cardiovascular wall and their chemical modifications, (b) synthetic macromolecules, (c) microfibre tissue culture approaches, (d) technological problems, (e) biological properties, (f) physico-chemical properties, and (g) biological testing according to a carefully devised protocol. It is very important that the biological testing of candidate biomaterials be done in such a way that statistically significant data may be derived from it. This involves a relatively large number of various tests, including *in vitro*, *in vivo* and *ex vivo*, with the same materials, prepared, fabricated, sterilized, and handled in an identical manner. All too often, residual solvents, degradation products due to careless fabrication processes, impurities due to improper handling, and unsuitable sterilization techniques can affect the biological performance of even the best materials. Biomedical materials should be handled in a clean room environment throughout the various operations.

## MACROMOLECULAR COMPONENTS OF THE VASCULAR WALL: THE BIOLOGICAL INTERFACE WITH BLOOD

The eventual development of blood compatible synthetic materials depends on a better understanding of the physico-chemical and biological characteristics of components of the vascular wall and their interactions with blood. The components of the vascular wall are proteins which differ in their complexity from synthetic polymers. Nevertheless, the study of the former are especially important for the development of synthetic blood compatible polymeric materials as nature provides the best guidance in this area. Consequently, brief descriptions are given below of the vascular wall components.

### *Endothelium*

The inside of the vascular wall is lined with endothelial cells and this lining is characteristic of blood vessels as well as lymph capillaries. It is the healthy and intact endothelium on the innermost surface of blood vessels that prevents thrombosis.

\* Based partly on a lecture presented at the International Symposium on Artificial support systems for acute hepatic failure, King's College Hospital Medical School, London, September 1974.

BIOMATERIALS R&D

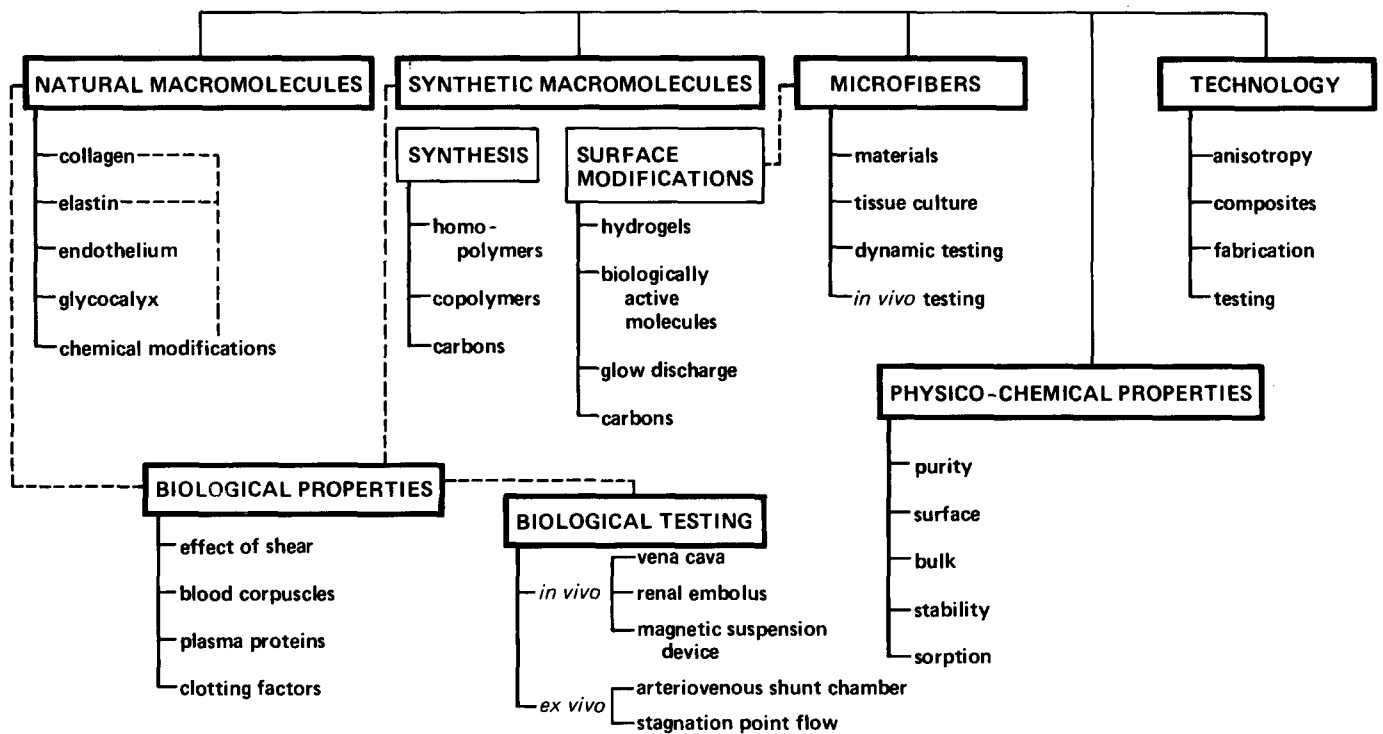


Figure 1 Biomaterials R & D

The thrombotic events may be subdivided into the intrinsic and extrinsic pathways, both of which involve a series of complex reactions of blood factors (including calcium ions), and phospholipids<sup>4,14,15</sup>. The intrinsic pathway can be initiated by a variety of stimuli, including the contact of blood with glass, many artificial materials, native collagen, and may be influenced by disturbances in blood flow<sup>16</sup>, as well as by the abnormal functioning of the clotting factors arising from hereditary disorders<sup>17</sup>. The extrinsic pathway is triggered when blood contacts an injured blood vessel, thus exposing the underlying surface to which platelets and other blood elements can adhere. When platelets do adhere to this surface, they can release their granules and liberate adenosine diphosphate (ADP), serotonin and other substances. Alternately, the red cells also can release ADP as the result of haemolysis<sup>18</sup>, caused by stimuli such as alteration of blood flow patterns and by plaques that may be present as a result of previous injury to the endothelial lining. The release of ADP in turn attracts more platelets with the alteration in the shape of the platelets by the formation of so-called pseudopods<sup>19</sup>. Eventually, the blood vessel might become completely occluded with the formation of a temporary haemostatic plug. This is converted into a mechanically stable thrombus by the activation of the blood coagulation mechanism, mentioned above.

The surface coating (glycocalyx) of the endothelium is approximately 500–1000 Å thick and appears to be a mucopolysaccharide<sup>20</sup>. The endothelial cells and the surface coating can stretch and contract with the dilation and contraction of the blood vessels. The endothelial cells exhibit a low turnover rate<sup>21</sup> but this varies depending on their location in the organism. The endothelial cells of veins and pulmonary arteries are likely involved in fibrinolysis<sup>22,23</sup> (dissolution of fibrin strands) and appear to have an antigenic site<sup>14</sup>. Recently, Jaffe *et al.*<sup>24</sup> have been able to culture endothelial cells *in vitro*, thus enabling their more detailed study.

*Subendothelium and basement membrane*

Immediately below the endothelium is the subendothelium which in larger blood vessels is approximately 1000 Å wide. In capillaries, the subendothelium consists of a well-defined morphological structure called the basement membrane, which seems to have a trilaminar structure<sup>25</sup>. Adjacent to the outermost region of the basement membrane are collagen fibres<sup>25</sup>. These fibres are not in contact with the blood elements, unless the endothelium and the basement membrane are injured. In such an event, collagen will initiate thrombosis by adversely interacting with platelets and the coagulation factors.

The basement membrane has some chemical similarity to collagen fibres, although there is considerable controversy on its exact structure. For example, Lazarow and Speidel<sup>26</sup> have shown that the basement membrane of isolated glomeruli can be digested by collagenase and trypsin, and appeared to be a complex glycoprotein. Dische<sup>27</sup> showed that the lens capsule of the eye seems to be composed largely of a protein similar to collagen.

The subendothelium is associated with the internal elastic lamina<sup>28</sup>, and in the arteries of rabbits consists of elastin, microfibrils of elastin, and vestiges of the basement membrane<sup>28</sup>. In man, the space between the endothelium and the internal elastic lamina is characterized by the presence of cells and connective tissue. Elastin does not come in direct contact with the endothelium unless both the basement membrane and the microfibrils covering the elastin are lost.

*Collagen*

Once the endothelium and the subendothelial lining are damaged, collagen may become exposed than can initiate the thrombotic process by causing platelet adhesion, aggregation, release of the platelet constituents, and by activating some of the coagulation factors<sup>28,29</sup>.

The fundamental structural unit of collagen appears to be the tropocollagen molecule having a diameter of 15 Å, length of 2800 Å, and molecular weight of about 300 000. The tropocollagen molecules are organized into approximately 5000 Å long fibrils in such a way that they overlap by a quarter of their length<sup>30</sup>. The tropocollagen molecule forms a triple helix, the structure of which was established by Rich and Crick<sup>31</sup> and by Ramachandran<sup>32</sup>. The individual chains are nearly extended so that only intermolecular hydrogen bonding is possible between them. One-third of collagen is glycine, and an additional quarter is composed of proline and hydroxyproline. According to Ramachandran and Chandrasekharan<sup>33</sup>, collagen contains one intermolecular hydrogen bond via the N-H...O=C group, plus one intermolecular hydrogen bond via a water molecule per three residues. This is in contrast to other proteins, the architecture of which permits a greater amount of hydrogen bonding to occur. Chang and Chien<sup>34</sup> have shown that a variety of electrolytes can affect the stabilization and destabilization of the rod-like superstructure of reconstituted collagen. Apparently, ions influence the structural order of reconstituted collagen both at the micron level (association–disassociation of tropocollagen–supermolecular rods of collagen) and at the molecular level (helix–coil transition). Concerning the water structure in collagen, Dehl<sup>35</sup> has concluded that most of the water in collagen is 'bound' rather than 'free'. In other words, the bound water molecules are oriented by the polar groups of collagen and do not have the freedom of motion characteristic of liquid water. It should be pointed out that 'oriented' or 'bound' water should not be equated with 'structured' water<sup>35</sup>.

The triple-stranded helical structure of collagen is formed by intracellular processes involving the three  $\alpha$ -polypeptide chains which constitute the collagen sub-units. A precursor, called procollagen, is involved in the biosynthesis of collagen and consists of polypeptide chains with molecular weight in the range of 120 000 to 125 000. Cysteine residues in procollagen give rise to disulphide crosslinks between the  $\alpha$ -polypeptide chains. These crosslinks seem to have a stabilizing effect for the formation of the triple-stranded helix which has a molecular weight of  $\sim 360\,000$ <sup>36</sup>. The stabilizing effect of disulphide crosslinks was also suggested by Grant *et al.*<sup>37</sup>. These investigators found that procollagen secreted by chick embryonic lens cells was in the triple-helical conformation, while the intracellular lens collagen contained no disulphide bonds and was in a random coil conformation. Further evidence for the role of the disulphide crosslinks in the formation of the triple-helical conformation was provided by Schofield *et al.*<sup>38</sup> and by Uitto and Prockop<sup>39</sup>. These latter studies suggested that the  $\alpha$ -polypeptide chains of procollagen must be linked by disulphide crosslinks prior to the formation of the triple helix. In other words, it appears that without such crosslinks, the production of a triple-helical structure would not be possible. The triple-helical conformation of procollagen polypeptides is apparently stabilized by the presence of hydroxyproline in the molecule and contributes to the thermal stability of the collagen molecule<sup>40</sup>.

### Elastin

The components of the subendothelium also contain elastin that accounts for the elastic properties of arteries, lung tissue and skin, and apparently is a gel consisting of randomly coiled, crosslinked peptide chains<sup>41,42</sup>. The crosslinks arise from oxidized lysine groups<sup>43</sup>, and are responsible

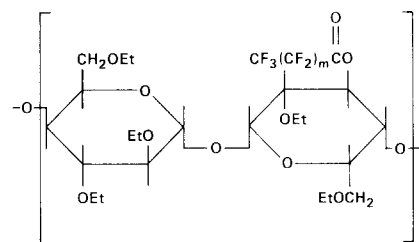
for the insolubility of mature elastin. In the absence of crosslinks, elastin remains soluble and the isolated product has a molecular weight of 70 000<sup>44,45</sup>. Two basic types of regions have been reported in elastin: one which is apparently involved with the formation of the crosslinks and the other which influences extensibility<sup>42</sup> of the molecule. The crosslinking regions could favour an  $\alpha$ -helical conformation<sup>42</sup>. The helical content of hydrated elastin is estimated to vary from 10 to 25%, with the crosslinking areas contributing 15 to 20% of the  $\alpha$ -helical content<sup>42</sup>.

As will be discussed later, elastin apparently does not directly cause platelet aggregation.

## SYNTHETIC POLYMERS

### Perfluorinated ethylcellulose

There is considerable interest in extracorporeal circulatory assistance devices, such as blood oxygenators, for which polymeric membranes are needed having both good blood compatibility and high gas transmission rates towards oxygen and carbon dioxide. Among such polymers are the perfluoroacyl derivatives of ethylcellulose<sup>46</sup>.



These polymers are amorphous materials exhibiting neither glass transition nor melting temperatures, have good tensile properties, and dissolve readily in a number of organic solvents. Based on the vena cava and renal embolus tests, the perfluorobutyryl ethylcellulose shows very promising thromboresistance in dogs. These properties compare favourably to low temperature isotropic (*LTI*) carbons (developed at Gulf Oil Corporation) and are widely used in artificial heart valve prostheses<sup>2,9</sup>. Although the gas-to-gas *permeabilities* towards oxygen and carbon dioxide are low in comparison to polydimethylsiloxane (*Table 2*), ultra-thin membranes in the range of 1–3  $\mu\text{m}$  can be prepared and laminated to porous polyolefin paper (Tyvek 1073) to give the membrane adequate physical support. Such ultra-thin membranes exhibit approximately a four-fold increase in the gas-to-gas *transmission rates* towards oxygen and carbon dioxide in comparison to polydimethylsiloxane (*Table 1*). The gas-to-blood permeabilities and gas-to-blood transfer rates towards oxygen are at least as high as those exhibited by

*Table 1* Gas-to-gas transmission rates of ultra-thin membranes of perfluorobutyryl ethylcellulose<sup>46</sup>

Membrane	Gas transmission rate ( $\text{cm}^3/\text{min m}^2 \text{ atm}$ )	
	O <sub>2</sub>	CO <sub>2</sub>
Perfluorobutyryl ethylcellulose*	880 $\pm$ 160	4680 $\pm$ 580
Polydimethylsiloxane†	195 $\pm$ 25	1090 $\pm$ 150

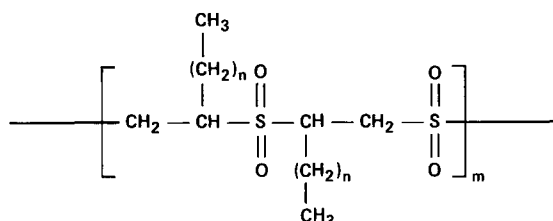
\* 2 to 3  $\mu\text{m}$  membrane coated onto Tyvek 1073 with 1.5 to 2  $\mu\text{m}$  layer of Dow Corning No.282 Silicone adhesive

† 127  $\mu\text{m}$  (5 mil) fabric-reinforced Dow Corning Silastic

polydimethylsiloxane under typical clinical flow conditions<sup>46</sup>. The combination of the promising biological properties and high gas transfer rates towards oxygen and carbon dioxide make the perfluorobutyl ethylcellulose membranes potentially useful candidates for blood oxygenators and for blood compatible surface coatings. This could eliminate the need to use heparinized materials in oxygenator applications, such as heparinized polydimethylsiloxanes, to prevent thrombosis. While specially purified polydimethylsiloxane has many desirable attributes (such as flexibility, relative inertness to body fluids, non-toxicity, and sterilizability by steam autoclaving), its overall blood compatibility is relatively poor<sup>4,9</sup>.

#### Poly(alkyl sulphones)

Other polymers with possible applications for membrane oxygenators and surface coatings are the poly(alkyl sulphones)<sup>47,48</sup>. Polymers and copolymers of poly(alkyl sulphones) can be prepared from the C<sub>16</sub> and C<sub>18</sub> straight chain  $\alpha$ -olefins and sulphur dioxide yielding the general structure illustrated below:



Although gas-to-gas permeabilities towards oxygen and carbon dioxide are about one-tenth of those of polydimethylsiloxane (Table 2), ultra-thin (2.5  $\mu\text{m}$ ) membranes can be made and coated onto a microporous polypropylene (Celgard<sup>®</sup> of Celanese Corporation). This composite membrane exhibits gas-to-gas *transfer rates* towards oxygen which are approximately double of those typical of polydimethylsiloxane<sup>48</sup>. The gas-to-blood transfer rates (measured with a large spiral channel membrane cell) are  $\sim 20\%$  higher with oxygen and approximately three times higher with carbon dioxide in comparison to polydimethylsiloxane<sup>48</sup>.

Poly(alkyl sulphones) have molecular weights over one million and  $M_w/M_n$  ratios between 5 and 7. Thermal decomposition begins at approximately 200°C and the polymer starts to soften between 75° and 90°C. Owing to these properties, steam autoclaving cannot be used. However, ethylene oxide gas gives a satisfactory means for sterilization, provided that a careful outgassing procedure is followed<sup>10,11</sup>. The biological properties of the poly(alkyl sulphones) based on the vena cava test in dogs appear promising and additional evaluations are in progress.

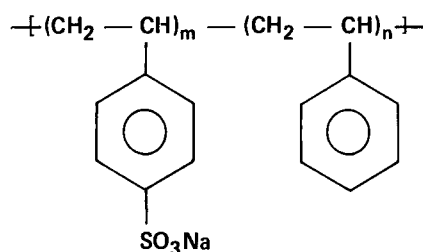
Table 2 Gas-to-gas permeabilities of various membranes<sup>46,48</sup>

Membrane	'Barrier' permeability $\times 10^{10}$ (cm <sup>3</sup> (STP) cm/cm <sup>2</sup> sec cmHg)	
	O <sub>2</sub>	CO <sub>2</sub>
Ethylcellulose	7–15	42–90
Perfluorobutyl ethylcellulose	40–50	200–250
Poly(alkyl sulphone)*	60	260
Poly(dimethylsiloxane-co-carbonate)	140–160	790–970
Polydimethylsiloxane (Dacron-reinforced)	500–640	2530–2800

\* 50:50 wt % copolymer of C<sub>16</sub> and C<sub>18</sub> straight chain  $\alpha$ -olefins

#### Sulphonated polystyrenes

Other polymers which may be useful as blood compatible surface coatings are the sulphonated polystyrenes<sup>49</sup>.



The biological properties of these polymers may be associated with the sulphate groups<sup>50,51</sup> and with the rigid spacing of these anionic groups<sup>52,53</sup>. Optimum blood thromboresistance (based on the vena cava and renal embolus test systems) is exhibited by the styrene-sulphonate copolymers having sulphonate contents in the range of 8.3 to 14.5%. The adhesion of these polymers to specially prepared segmented polyether-urethanes is good.

#### Surface modifications of polymers

One approach to the preparation of blood compatible surfaces involves hydrogels. These are coherent three-dimensional polymeric networks that can imbibe large quantities of water without dissolution of the polymeric network<sup>54</sup>. Wichterle and Lim<sup>55</sup> in 1960 were the first to call attention to the potential biological use of hydrogels based on 2-hydroxymethylmethacrylate (HEMA) in soft contact lenses. Until recently, a major problem with hydrogels was their lack of good mechanical strength. In 1971, a microwave discharge grafting technique was developed by Kronick<sup>56</sup>. Also in 1971, Halpern and colleagues<sup>57</sup>, using chemical means, successfully grafted polyacrylamide hydrogels onto polyurethanes and other polymers. On the author's recommendation, the grafting technique was applied to prosthetic devices which extended the usefulness of hydrogels by combining mechanical strength with blood compatibility. Following these developments, other investigators using high energy irradiation have grafted hydrogels onto polymeric substrates<sup>58</sup>.

Bruck has recently reviewed the physical and biological aspects of hydrogels for biomedical applications<sup>12</sup>. The evidence strongly suggests that the presence of negatively charged ionic groups on certain synthetic hydrogels is not essential for blood compatibility<sup>2,4,12</sup>. The biological performance of hydrogels apparently depends on a critical level of water uptake, chemical composition, purity, crosslinking density, porosity, the possible existence of a quasi-organized water structure, and on the thermodynamic interaction parameters between the components of the biological environment and the gel<sup>2,4,12</sup>. The possible existence of a quasi-organized water structure in certain hydrogels was subsequently also proposed by others<sup>59</sup>. However, solid experimental evidence is lacking in support of this. Small amounts of impurities can influence the blood compatibility of the hydrogel. Hydrogels based on acrylamide have been also grafted onto several substrate polymers<sup>57</sup>. Optimum blood compatibility was achieved only with highly purified monomers and small quantities of crosslinking agent. It should be stressed that not all hydrogels perform well and therefore each of these materials must be identified and treated individually. This is especially important since it is likely that blood components (especially proteins) interact



differently with the various types of hydrogel surfaces.

Recent evidence suggests that there is practically no penetration by plasma proteins into the covalently grafted hydrogels based on polyacrylamide or PHEMA. Smaller molecules, ions, and oxygen and carbon dioxide can penetrate into the network. These properties of covalently grafted hydrogels permit their use in oxygenators where high gas transfer rates and good blood compatibility are essential. Also under development are hydrogels based on poly(vinyl acetate-*co*-crotonic acid) grafted onto polymeric surfaces by high energy irradiation from a  $^{60}\text{Co}$  source<sup>60</sup>. These hydrogels, which carry anionic groups, are being evaluated for their blood compatibility.

Certain hydrogels have been also studied as coatings for copper intrauterine devices in rabbits<sup>61</sup>. Other applications involve the encapsulation of activated charcoal particles with hydrogels for extracorporeal blood perfusion to impart blood compatibility to them<sup>62,63</sup>. Materials other than hydrogels for the microencapsulation of charcoal have been reported earlier by Chang<sup>64-66</sup>. Recently, Castino and colleagues encapsulated charcoal particles with hydrophilic cellulose triacetate for artificial kidney applications<sup>67</sup>.

In addition to the covalent grafting of hydrogels onto polymeric substrates, microwave discharge techniques can also be used to treat polymer surfaces with or without the deposition of polymer coatings<sup>68-70</sup>. The technique permits the preparation of very low as well as very high surface energy polymeric surfaces, and some of these exhibit interesting biological performance in preliminary tests<sup>70</sup>.

Still another approach to the surface modification of polymers involves the ionic and covalent bonding of biologically active molecules. The use of heparin has been adequately described by several authors<sup>71-78</sup>. Ionically bonded heparin surfaces have been used successfully in short-term clinical applications. Although heparin has been covalently bonded to hydrogels and other polymers, the biological activity of these is diminished in comparison to ionically bonded heparin surfaces<sup>58</sup>.

Work is currently underway to attach covalently platelet protective agents to polymeric surfaces, including prostaglandin E<sub>1</sub> and others<sup>79</sup>. The covalent attachment of fibrinolytic enzymes has also been reported<sup>80</sup>.

In order to extend the usefulness of *LTI* carbons with their excellent biological properties, investigations are being conducted to deposit carbons onto appropriate polymeric and non-polymeric substrates by vacuum-vapour and ion-plating techniques<sup>81</sup>, and by ion-beam processes<sup>82</sup>. Studies showed that both the vacuum-vapour and ion-plating techniques yield carbon surfaces on polymeric substrates which are nearly impermeable to gases at a thickness of 0.1  $\mu\text{m}$ . The coatings adhere well to a number of polymers, including polyimides, cellulose acetate, and segmented polyether-urethanes<sup>81</sup>. The biological evaluation of these composite carbon structures are under investigation<sup>81,82</sup>.

## MICROFIBRES

Although woven fabrics, velours, and flocked surfaces have been used in clinical practice (especially in large blood vessel replacements), the blood compatibility of these materials depends on the formation of a fibrin layer and subsequent vascularization<sup>83</sup>. In prosthetic devices that undergo repeated flexing and stretching, such an approach is not entirely satisfactory. Furthermore, in comparison to many animals, the regeneration of a pseudo-intimal lining in man is slow.

An important alternate approach is the use of microfibrils as scaffold structures for the anchoring of viable cells and for the production of a vascular intima<sup>84,85</sup>. Such cellular linings must be able to survive the shearing forces of blood and the pressure differentials between cardiac contraction and relaxation. To date, the best results were obtained with diploid WI-38 cells from embryonic human lung tissue which were uniformly seeded onto non-woven microfibrils<sup>85</sup>, including those made from specially prepared poly(tetramethylene terephthalate) and parylene-C coated polypropylene<sup>85</sup>. In order to use the microfibre-scaffold cellular linings for prosthetic applications in humans, autologously derived cells must be available for the seeding of devices. Work is currently underway to accomplish this objective<sup>85</sup>.

## MECHANICAL PROPERTIES

The components of the cardiovascular system, such as the arteries, veins, and heart valves, are composite materials, the stress-strain properties of which vary in the transverse and longitudinal directions. This stiffness *anisotropy* is important in the performance of physiological functions as it prevents buckling of the blood vessels and provides for the accommodation of the vessels to systolic and diastolic blood pressure changes. This anisotropy also plays an important role in the operation of natural heart valves. Several authors have called attention to the role of the anisotropic property of natural tissues<sup>4,86-88</sup>.

To imitate some of the mechanical properties of the components of the cardiovascular system, investigations are underway with specially prepared segmented polyether-urethanes<sup>89</sup>. It should be stressed that the aim is to provide the required mechanical properties rather than blood compatibility. Although these polyether-urethanes have shown fairly good blood compatibility especially in short range applications<sup>9,13</sup>, their overall biological performance for longer use can be enhanced further by various surface modifications (*Figure 2*). To impart anisotropy specially synthesized segmented polyether-urethanes<sup>13</sup> are used which are cast in 6 mil thick films (plies) with the careful removal of residual solvent (dimethylformamide). These individual plies are then stretch-oriented to produce the desired stiffness anisotropy. After quenching, the individual stretched plies are stacked at 0°, 90°, 90° and 0° and compression moulded at a moderate temperature to form composite

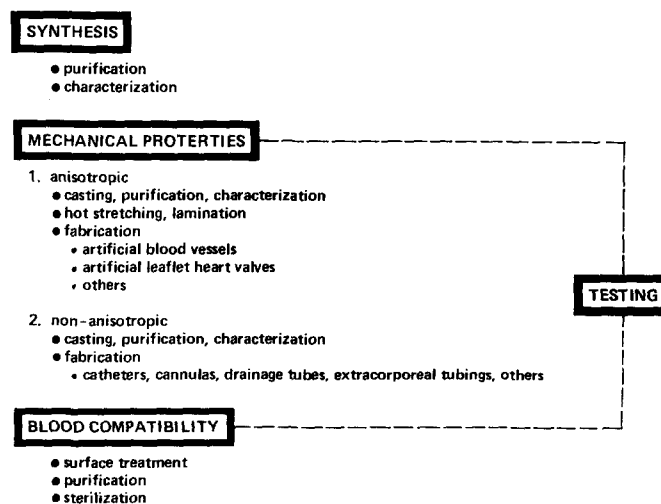


Figure 2 Blood compatible composite materials

laminates with a thickness of 24 mil. Exposure of the plies to whole blood for 32 days showed no significant change in the anisotropy, although some relaxation occurred. Cyclic biaxial straining experiments indicated some irreversible creep for the polymer and investigations are underway to minimize this property<sup>89,90</sup>.

Another approach involves the so-called 'springy' polypropylenes<sup>91</sup>. These are strong, tough, resilient, and dynamic materials and have the ability to recover immediately from extensions of 100 to 1000% in excess of the 'yield point'. The polymers can be steam autoclaved and no changes in the mechanical properties have been noted after prolonged immersion in isotonic saline solution. They are also non-toxic and can be surface-treated to impart blood compatibility to them. Although these polymers are not anisotropic, their mechanical properties (including high resistance to fatigue and abrasion) indicate a potential utility in prosthetic applications.

## INTERACTIONS OF BLOOD COMPONENTS WITH MATERIALS

When synthetic surfaces come in contact with blood, the available evidence indicates that most, if not all of them, become coated with plasma proteins within a very short time. This rapid adsorption process most likely influences the activation of factor XII (Hageman factor) and possibly other coagulation factors as well, and affects the adhesion of platelets. Depending on these initial events, thrombosis may or may not take place. The adsorption phenomenon is influenced by a combination of factors, including surface smoothness, ionic and electronic charge, wettability by blood components, chemical structure, and haemodynamic parameters. However, no single factor alone can explain the relative blood compatibility of some materials in comparison to others<sup>4</sup>.

The situation is even more complex in the case of natural surfaces. It is well known that platelets adhere to the sites of injured blood vessels as the result of exposure of the sub-endothelial tissue and native collagen<sup>92</sup>. As a result of this interaction, the platelets release ADP, which causes platelet aggregation. Also, when platelets aggregate they release phospholipids which are essential for the coagulation process. Several blood coagulation factors may be adsorbed on them, thus accelerating the coagulation.

Recently, Ganguly<sup>93</sup> presented evidence that while human platelets bind thrombin, this by itself is insufficient to cause platelet aggregation and that other reactions seem to be also involved. He suggested that the receptor of thrombin on platelets may be a protein having a molecular weight in excess of 200 000. The property of collagen to activate and aggregate the platelets appears to be related to its native, higher-ordered structure because denatured (random coil) collagen neither promotes the aggregation of platelets nor initiates the clotting process. It has been shown also that the activation of the Hageman factor may be related to the free carboxyl groups of collagen because esterification of these groups prevents the activation process<sup>94</sup>. The aggregation of platelets is drastically reduced when the positively charged free amino groups of collagen are replaced by neutral groups, suggesting that rigidly spaced polar groups in the molecule may be required for platelet aggregation<sup>94</sup>. Furthermore, the ability of native collagen to aggregate the platelets may be related also to the particular architecture of the collagen molecule because

monodisperse *tropocollagen* with its triple helix is apparently insufficient for platelet aggregation<sup>95</sup>. However, this does not necessarily rule out the possibility that the more complex triple helical structure of multimeric tropocollagen or collagen fibrils is not involved in the observed platelet aggregation.

Vertebrate collagens contain small quantities of carbohydrate that constitutes less than 2% by wt of the molecule<sup>96</sup>. Studies with soluble collagen from guinea pig skin have shown that glucose and galactose are linked to the hydroxyl groups of hydroxylysine in the peptide chain<sup>97</sup>. Suggestions were also made that an enzyme (platelet-bound glycosyl transferase) may be needed for the adhesion of platelets to native collagen as the primary step in haemostasis when the blood vessels are injured<sup>98,99</sup>.

Recently, Bruck has called attention to the fact that the known electrical conduction properties of collagen may have a role in blood compatibility<sup>100,101</sup>. At low water adsorption levels, the conductivity is electronic, but when the water uptake exceeds approximately 10%, the conduction appears to become protonic<sup>102</sup>. Any disturbance to the native structure of this protein (such as increased salt concentration and dehydration) would be expected to affect its fibrillar structure and partly disrupt the supermolecular architecture. This in turn should be reflected in increased ion binding and changes in the electrical conduction of the molecule. As a speculative argument, it was proposed<sup>100</sup> that a sufficient alteration in the water structure and hence in the electrical conductivity of the molecule may be brought about also as a result of injury to the endothelium of blood vessels by exposing the underlying subendothelial components and collagen to the inorganic ions and organic polyelectrolytes of blood. The adsorption of these could subsequently affect both the platelets, which normally carry a net negative charge density, and also the coagulation factors. In other words, fundamental changes may occur in the native collagen molecule when it changes from the milieu that prevails underneath the normal endothelium to the one that may become operative when collagen is exposed to blood constituents as the result of injuries to the endothelial lining of the blood vessels. These changes are by themselves apparently insufficient to cause the denaturation of collagen, but sufficient to initiate the complex biochemical events that lead to platelet adhesion, aggregation, and the release of platelet constituents. The question may be raised in what way does electrical conduction influence the nature of the adsorption of plasma proteins and the activation of the blood clotting factors and the platelets, leading to thrombosis<sup>100?</sup>

In the absence of severe vascular injury and hence the exposure of collagen fibres, other subendothelial components, such as basement membranes and microfibrils, may be involved in the thrombogenic process. Work by Sterman and his colleagues<sup>103</sup> suggests that microfibrils exhibit affinity for platelets. The basement membranes of the blood vessels have also been implicated in platelet adhesion<sup>104</sup>. On the other hand, elastin does not seem to cause platelet adhesion and aggregation<sup>105</sup>.

Red cells contain a factor that can cause platelet adhesion and aggregation<sup>106</sup>, which was subsequently identified as ADP<sup>107</sup>. The red cells also contain a clot-promoting factor called erythrocytin, which can be released on haemolysis<sup>108,109</sup>. Based on these and other observations, Stormorken<sup>110</sup> suggested including haemolysis in the theory of thrombogenesis.

Damage to the red cells can result from rheological

stresses and from the interaction with surfaces<sup>111,112</sup>. Shear-induced haemolysis is a common occurrence in various prosthetic devices<sup>113</sup>. A good correlation was demonstrated between critical surface free energy and haemolysis in a rotating shearing device for various polymeric surfaces<sup>113</sup>. Other investigators<sup>114</sup> reported that the adhesion of red cells to glass, siliconized glass, polyethylene and Teflon is governed by shear stresses which must exceed a minimum critical value before the cells will detach and that the minimum critical shear stress for detachment from clean surfaces correlates with the critical surface tension of the materials. This is in agreement with the finding of other investigators<sup>113</sup>. Exposure of blood to foreign surfaces also results in damage to the white cells, causing morphological changes, altered oxygen utilization, and impairment of their phagocytic activity<sup>115</sup>.

As it was mentioned earlier, the exposure of synthetic surfaces to whole blood results, in most cases, in protein adsorption in a very short time, preceding the arrival of the formed elements, such as the platelets, red cells, and white cells. As pointed out elsewhere<sup>4</sup>, several questions remain to be answered. Is there protein adsorption in every case (for example with hydrogels), and if so, what is the nature of the *first* layer of protein that is adsorbed during the initial contact? What conformational changes occur in this initially adsorbed protein? Is this protein denatured as the result of sufficiently large changes in its molecular architecture? What is the nature of the proteins that are adsorbed by this initially adsorbed protein layer? How do these adsorbed proteins trigger the blood clotting process and the adsorption and activation of platelets?

One way to study the adsorption of protein films on surfaces is by ellipsometry. Rothen<sup>116</sup> in 1945 designed the first ellipsometer (and coined its name) that can measure the thickness of thin transparent films up to several thousand Ångstroms adsorbed on solid surfaces. The ellipsometer determines the change in the elliptical polarization of a beam of light which is reflected from a surface coated with a thin film<sup>117</sup>. Vroman and Adams<sup>118</sup> investigated the adsorption of blood plasma proteins on metallic and anodized tantalum, oxidized and non-oxidized silicon, and polymeric substrates using a recording ellipsometer to follow the rate of adsorption. They have found that oxidized silicon surfaces adsorbed fibrinogen from blood plasma within two seconds, that is subsequently converted by a plasma component<sup>118</sup>. Platelets adhere to unconverted fibrinogen films deposited on glass<sup>118</sup>. Others have observed similar effects<sup>119-121</sup>. On the other hand, albumin-coated surfaces did not seem to attract platelets, whereas  $\gamma$ -globulin coatings caused not only platelet adhesion but also aggregation and the release of platelet constituents<sup>119</sup>. Other investigators have also reported on the interaction of fibrinogen, albumin, and prothrombin with various surfaces using ellipsometry and infra-red bound fraction measurements aimed at elucidating the molecular conformational changes that occur during the adsorption process<sup>122,123</sup>. Apparently, no change occurred in the extension of the proteins for a given surface during the time period while the adsorbance increases, suggesting a lack of molecular re-arrangement. Furthermore, the equilibrium extension values increased with decreasing surface energy, while the quantities of protein adsorbed at physiological concentrations remained approximately constant. These findings indicate that molecular conformation is dependent on surface energy. Other workers are investigating the thermodynamics of the interactions between selected blood plasma proteins and synthetic surfaces using

a sensitive microcalorimeter without an air/protein interface<sup>124,125</sup>. For  $\gamma$ -globulin adsorbed on glass powder, the enthalpy values suggest that the greatest interaction energies are evolved by those molecules which are directly exposed to the surface in the first monolayer of protein. Molecules in the second and successive layers of the protein give rise to exponentially decreasing enthalpy values with increasing molar surface concentrations<sup>125</sup>.

Finally, the interaction of platelets with surfaces can be influenced by various agents and drugs. For example, the adherence of platelets to fibrinogen-coated glass surfaces and the release of platelet constituents are inhibited by divalent cations, prostaglandin E<sub>1</sub>, and caffeine, all of which increase the level of cyclic AMP (adenosine monophosphate) in platelets<sup>126</sup>. Non-steroidal anti-inflammatory drugs also inhibit platelet adhesion to collagen-coated surfaces<sup>127</sup>. Prostaglandins are unsaturated fatty acids which are synthesized by many types of cells in very small quantities and released upon stimuli to the cell membranes. Prostaglandin E<sub>1</sub> is an especially powerful inhibitor of platelet aggregation<sup>128</sup>, while prostaglandin E<sub>2</sub> enhances the second wave of platelet aggregation induced by ADP<sup>129</sup>. Certain antihistamines also inhibit platelet aggregation<sup>130</sup>. Other low molecular weight substances, such as derivatives of benzamidine, phenylguanidine and benzylamine, likewise inhibit platelet aggregation induced by ADP, collagen, and thrombin<sup>131</sup>. Among macromolecules, polyphloretinphosphate (a polyester of phloretin and phosphoric acid) has been shown recently to inhibit platelet adhesion on a polypropylene surface<sup>132</sup>.

The above developments substantially widen the horizon for biomaterials research and applications, and emphasize the need for close interactions between the physical, biological, and medical disciplines.

## ACKNOWLEDGEMENT

The author wishes to thank his wife, Mrs A. Katherine Bruck, for typing the manuscript.

## REFERENCES

- 1 Bruck, S. D. *J. Biomed. Mat. Res.* 1972, **6**, 173
- 2 Bruck, S. D. *Trans. Am. Soc. Artif. Int. Organs* 1972, **18**, 1
- 3 Bruck, S. D. *Biomat., Med. Dev., Artif. Organs* 1973, **1**, 79
- 4 Bruck, S. D. 'Blood compatible synthetic polymers - an introduction', Charles C. Thomas, Springfield, Ill., 1974
- 5 Salzman, E. W. *Blood* 1971, **38**, 509
- 6 Berger, S. and Salzman, E. W. in 'Progress in Hemostasis and Thrombosis', (Ed. T. H. Spaet), Grune & Stratton, New York, 1974, Vol 2, p 273
- 7 Mason, R. G. in 'Progress in Hemostasis and Thrombosis', (Ed. T. H. Spaet), Grune & Stratton, New York, 1972, Vol 1, p 141
- 8 Leininger, R. I. *CRC Crit. Rev. Bioeng.* 1972, **1**, 333
- 9 Bruck, S. D., Rabin, S. and Ferguson, R. J. *Biomat., Med. Dev., Artif. Organs* 1973, **1**, 191
- 10 Bruck, S. D. *J. Biomed. Mat. Res.* 1971, **5**, 139
- 11 Bruck, S. D. *Int. J. Radiat. Steril.* 1973, **1**, 177
- 12 Bruck, S. D. *J. Biomed. Mat. Res.* 1973, **7**, 387
- 13 Brash, J. L., Fritzing, B. K. and Bruck, S. D. *J. Biomed. Mat. Res.* 1973, **7**, 313
- 14 Nemerson, Y. and Pitlick, F. A. in 'Progress in Hemostasis and Thrombosis', (Ed. T. H. Spaet), Grune & Stratton, New York, 1972, Vol 1, p 1
- 15 Biggs, R. and Macfarlane, R. G. 'Human Blood Coagulation and its Disorders', 3rd Edn., Blackwell, Oxford, 1962
- 16 Murphy, E. A., Rowsell, H. C., Downie, H. G., Robinson, G. A. and Mustard, J. F. *Can. Med. Assoc. J.* 1962, **87**, 259

- 17 Ratnoff, O. D. and Bennett, B. *Science* 1973, **179**, 1291
- 18 Hellem, A. J., Borchgrevink, C. F. and Ames, S. B. *Br. J. Haematol.* 1961, **7**, 42
- 19 Hovig, T. *Ser. Haemat. (Vol I)* 1968, **2**, 3
- 20 Luft, J. H. *Fed. Proc. Fed. Am. Soc. Exp. Biol.* 1966, **25**, 1773
- 21 Altschul, R. 'Endothelium: its Development, Morphology, Function and Pathology', MacMillan, New York, 1954
- 22 Todd, A. S. *J. Clin. Pathol.* 1964, **17**, 324
- 23 Kwaan, H. C. and Astrup, T. *Circulation Res.* 1965, **17**, 477
- 24 Jaffe, E. A., Nachman, R. L. and Becker, C. G. *Abstr. 3rd Congr., Int. Soc. Thrombosis and Haemostasis* 1972, p 366
- 25 Majno, G. in 'Handbook of Physiology III', (Ed. W. F. Hamilton and H. Dow), American Physiological Society, Washington, D.C., 1965, p 2293
- 26 Lazarow, A. and Speidel, E. in 'Small Blood Vessel Involvement in Diabetes Mellitus', (Ed. M. D. Siperstein, A. R. Colwell and K. Meyer), American Institute of Biological Sciences, Washington, D.C., 1966
- 27 Dische, Z. in 'Small Blood Vessel Involvement in Diabetes Mellitus', (Ed. M. D. Siperstein, A. R. Colwell and K. Meyer), American Institute of Biological Sciences, Washington, D.C., 1966
- 28 Stemerman, M. B. in 'Progress in Hemostasis and Thrombosis', (Ed. T. H. Spaet), Grune & Stratton, New York, 1974, Vol 2, p 1
- 29 Wilner, G. D., Nossel, H. L. and LeRoy, E. C. *J. Clin. Invest.* 1968, **47**, 2608
- 30 Dickerson, R. E. and Geis, I. 'The Structure and Action of Proteins', Harper & Row, New York, 1969
- 31 Rich, A. and Crick, F. H. C. *J. Mol. Biol.* 1961, **3**, 483
- 32 Ramachandran, G. N. in 'Treatise on Collagen', Vol 1, (Ed. G. N. Ramachandran), Academic Press, New York, 1967, Ch 3
- 33 Ramachandran, G. N. and Chandrasekharan, R. *Biopolymers* 1968, **6**, 1649
- 34 Chang, E. P. and Chien, J. C. W. *Biopolymers* 1973, **12**, 1063
- 35 Dehl, R. E. *Biopolymers* 1973, **12**, 2329
- 36 Monson, J. M. and Bornstein, P. *Proc. Nat. Acad. Sci. US* 1973, **70**, 3521
- 37 Grant, M. E., Schofield, J. D., Kefalides, N. A. and Prockop, D. J. *J. Biol. Chem.* 1973, **248**, 7432
- 38 Schofield, J. D., Uitto, J. and Prockop, D. J. *Biochemistry* 1974, **13**, 1801
- 39 Uitto, J. and Prockop, D. J. *Biochem. Biophys. Res. Commun.* 1973, **55**, 904
- 40 Jimenez, S., Harsch, M. and Rosenbloom, J. *Biochem. Biophys. Res. Commun.* 1973, **52**, 106
- 41 Partridge, S. M. *Nature* 1967, **213**, 1123
- 42 Gray, W. R., Sandberg, L. B. and Foster, J. A. *Nature* 1973, **246**, 461
- 43 Thomas, J., Elsdon, D. F. and Partridge, S. M. *Nature* 1963, **200**, 651
- 44 Sandberg, L. B., Weissman, N. and Smith, D. W. *Biochemistry* 1969, **8**, 2940
- 45 Smith, D. W., Brown, D. M. and Carnes, W. H. *J. Biol. Chem.* 1972, **247**, 2427
- 46 Rozelle, L. T. and Petersen, R. J. 'Ultrathin Membranes for Blood Oxygenators', *A. Rep. PB 231324* (January 1974), (available from National Technical Information Service, Springfield, Va 22151, USA)
- 47 Ketteringham, J. M., et al. *Trans. Am. Soc. Artif. Int. Organs* 1973, **19**, 61
- 48 Ketteringham, J. M., Nelsen, L. L., Stevenson, K. K., Birkett, J. D. and Massucco, A. A. 'Polyalkylsulfones: Blood Compatible Polymers for Membrane Lung', *A. Rep. PB 231328* (March 1974) (available from National Technical Information Service, Springfield, Va 22151, USA)
- 49 Brash, J. L., Fritzing, B. K. and Loo, B. H. 'Development of Materials for Heart Assist Devices', *A. Rep. PB 210665* (April 1972) and *A. Rep. PB 223165* (May 1973) (available from National Technical Information Service, Springfield, Va 22151, USA)
- 50 Marshall, D. W., Cross, R. A. and Bixler, H. J. *J. Biomed. Mat. Res.* 1970, **4**, 357
- 51 Lovelock, J. E. and Porterfield, J. S. *Nature* 1951, **167**, 39
- 52 Nossel, H. L., Wilner, G. D. and LeRoy, E. C. *Nature* 1969, **221**, 75
- 53 Leonard, F. *Trans. Am. Soc. Artif. Int. Organs* 1969, **15**, 15
- 54 Jirgensons, B. and Straumanis, M. E. 'A Short Textbook of Colloid Chemistry', 2nd Edn., MacMillan, New York, 1962, p 377
- 55 Wichterle, O. and Lim, D. *Nature* 1960, **185**, 117
- 56 Scott, H., Kronick, P. L. and Hillman, E. E. 'Active-Vapor Grafting of Hydrogels in Medical Prostheses', *A. Rep. PB 206499* (August 1971); also *A. Rep. PB 221846* (February 1973) and *PB 230308* (January 1974) (available from National Technical Information Service, Springfield, Va 22151, USA)
- 57 Halpern, B. D., Akkapeddi, M. K. and Ledis, S. L. 'Polymer Studies Related to Prosthetic Cardiac Materials Which are Non-Clotting at a Blood Interface', *A. Rep. PB 230310* (February 1974); also *A. Rep. PB 200987* (January 1971), *PB 212724* (September 1972) and *PB 215886* (February 1973) available from National Technical Information Service, Springfield, Va 22151, USA)
- 58 Hoffman, A. S., Schmer, G., Harris, C. and Kraft, W. G. *Trans. Am. Soc. Artif. Int. Organs* 1972, **18**, 10
- 59 Andrade, J. D. et al. *Trans. Am. Soc. Artif. Int. Organs* 1973, **19**, 1
- 60 Creasy, W. S., Kwiatkowski, G. T., Byck, J. S., Gaasch, J. F. and Gonsior, L. J. *Abstr. 20th A. Meet. Am. Soc. Artificial Internal Organs, Chicago* 1974, Vol 3, p 14; *A. Rep. PB 211790* (August 1972) and *PB 225636* (August 1973) (available from National Technical Information Service, Springfield, Va 22151, USA)
- 61 Scott, H. et al. *Biomat., Med. Dev., Artif. Organs* 1973, **1**, 681
- 62 Andrade, J. D. et al. *Trans. Am. Soc. Artif. Int. Organs*, 1971, **17**, 222
- 63 Andrade, J. D. et al. *Trans. Am. Soc. Artif. Int. Organs* 1972, **18**, 473
- 64 Chang, T. M. S. *Science* 1964, **146**, 524
- 65 Chang, T. M. S. 'Artificial Cells', Charles C. Thomas, Springfield, Ill, 1972
- 66 Chang, T. M. S. and Migchelson, M. *Trans. Am. Soc. Artif. Int. Organs* 1973, **19**, 314
- 67 Castino, F., Malchesky, P. S., Kiraly, R. J., Denti, E. and Nosé, Y. *Abstr. 20th A. Meet. Am. Soc. Artif. Int. Organs, Chicago* 1974, Vol 3, p 12
- 68 Yasuda, H. and Lamaze, C. E. *J. Appl. Polym. Sci.* 1973, **17**, 1519
- 69 Yasuda, H., Lamaze, C. E. and Sakaoku, K. *J. Appl. Polym. Sci.* 1973, **17**, 137
- 70 Yasuda, H., Bumgarner, M. O. and Morosoff, N. C. 'A Study of Electrodeless Glow Discharge as a Means of Modifying the Surface of Polymers', *A. Rep. PB 229097* (December 1973) (available from National Technical Information Service, Springfield, Va 22151, USA)
- 71 Gott, V. L. et al. *Surgery* 1961, **50**, 382
- 72 Lagergren, H., Johansson, L. and Eriksson, J. C. *Thoraxchir. Vask. Chir.* 1964, **12**, 172
- 73 Leininger, R. I., Cooper, C. W., Falb, R. D. and Grode, G. A. *Science* 1966, **152**, 1625
- 74 Leininger, R. I., Epstein, M. M., Falb, R. D. and Grode, G. A. *Trans. Am. Soc. Artif. Int. Organs* 1966, **12**, 151
- 75 Merker, R. L., Elyash, L., Mayhew, S. H. and Wang, J. Y. C. in 'Proceedings of the Artificial Heart Program Conference', (Ed. R. J. Hegyeli), U.S. Government Printing Office, Washington, D.C., 1969, p 29
- 76 Merrill, E. W. et al. *Trans. Am. Soc. Artif. Int. Organs* 1966, **12**, 139
- 77 Salzman, E. W. et al. *Surgery* 1967, **61**, 1
- 78 Lagergren, H. R. and Eriksson, J. C. *Trans. Am. Soc. Artif. Int. Organs* 1971, **17**, 10
- 79 Grode, G. A., Pitman, J., Crowley, J. P., Leininger, R. E. and Falb, R. D. *Abstr. 20th A. Meet. Am. Soc. Artif. Int. Organs, Chicago* 1974, Vol 3, p 29
- 80 Kusserow, B. K., Larrow, R. and Nichols, J. *Trans. Am. Soc. Artif. Int. Organs* 1971, **17**, 1
- 81 Meyer, C. H. Jr., Kaae, J. L., Perez, J. and Shim, H. 'Development of Carbon-Film Composites for Use in Prosthetic Devices', *A. Rep. PB 228964* (January 1974) (available from National Technical Information Service, Springfield, Va 22151, USA)
- 82 Aisenberg, S. and Chabot, R. W. 'Ion Beam Deposited Carbon Coatings for Bio-Compatible Materials', *A. Rep. PB 229810* (December 1973) (available from National Technical Information Service, Springfield, Va 22151, USA)
- 83 Litwak, R. S. *Bull. NY Acad. Med.* 1972, **48**, 406
- 84 Kahn, R. H. and Burkel, W. E. *In Vitro* 1973, **8**, 451
- 85 Kahn, R. H. and Burkel, W. E. 'Multiple-Layered Intimal Linings by Perfusion Culture', *A. Rep. PB 226863* (November

- 1973) (available from National Technical Information Service, Springfield, Va 22151, USA)
- 86 Yamada, H. 'Strength of Biological Materials', (Ed. F. G. Evans), Williams and Wilkins, Baltimore, 1970
- 87 Clark, R. E. *J. Thorac. Cardiovasc. Surg.* 1973, **66**, 202
- 88 Patel, D. J., Janicki, J. S. and Carew, T. E. *Circulation Res.* 1969, **25**, 765
- 89 Kardos, J. L., Thies, C., Clark, R. E., Mehta, B., Apostolou, S. F. and Wu, E. M. 'Materials Development and Testing', *A. Rep. PB 230309* (January 1974) (available from National Technical Information Service, Springfield, Va 22151, USA)
- 90 Moacanin, J., Fedors, R. F., Ingham, J. D. and Cuddihy, E. F. 'Effects of the Physiological Environment on the Long-Term Physical Performance of Polymeric Materials', *A. Rep. PB 232641* (March 1974) (available from National Technical Information Service, Springfield, Va 22151, USA)
- 91 Statton, W. O., Cannon, S. L. and King, R. N. 'Characterization and Evaluation of Springy Polypropylene as a Prosthetic Device', *A. Rep. PB 229335* (December 1973) (available from National Technical Information Service, Springfield, Va 22151, USA)
- 92 Mustard, J. F. and Packham, M. A. in 'Research on Acute Myocardial Infarction', (Ed. S. Bondurant), American Heart Association, New York, 1969, p IV-20
- 93 Ganguly, P. *Nature* 1974, **247**, 306
- 94 Wilner, G. D., Nossel, H. L. and Procupez, T. L. *Am. J. Physiol.* 1971, **220**, 1074
- 95 Muggli, R. and Baumgartner, H. R. *Thrombosis Res.* 1973, **3**, 715
- 96 Grassman, W. and Schleich, H. *Biochem. Z.* 1935, **277**, 320
- 97 Butler, W. T. and Cunningham, L. W. *J. Biol. Chem.* 1966, **241**, 3882
- 98 Bosmann, H. B. *Biochem. Biophys. Res. Commun.* 1971, **43**, 1118
- 99 Barber, A. J. and Jamieson, G. A. *Biochim. Biophys. Acta* 1971, **252**, 533
- 100 Bruck, S. D. *Polymer* 1975, **16**, 25
- 101 Bruck, S. D. *Nature* 1973, **243**, 416
- 102 Bardelmeyer, G. H. *Biopolymers* 1973, **12**, 2289
- 103 Stemerman, M. B., Baumgartner, H. R. and Spaet, T. H. *Lab. Invest.* 1971, **24**, 179
- 104 Hugues, J. and Mahieu, P. *Thromb. Diath. Haemorrh.* 1970, **24**, 395
- 105 Spaet, T. H. and Erichson, R. B. *Thromb. Diath. Haemorrh. Suppl.* 21 1966, p 67
- 106 Hellem, A. J. *Scand. J. Clin. Lab. Invest.* 1960, **12**, Suppl. 51
- 107 Gaarder, A. *et al. Nature* 1961, **192**, 531
- 108 Lechler, E. *Thromb. Diath. Haemorrh. Suppl.* 22 1967, p 139
- 109 Quick, A. J., Georgatsos, J. G. and Hussey, C. V. *Am. J. Med. Sci.* 1954, **228**, 207
- 110 Stormorken, H. *Fed. Proc. Fed. Am. Soc. Exp. Biol.* 1971, **30**, 1551
- 111 Bernstein, E. F. *ibid.* 1971, **30**, 1510
- 112 Indeglia, R. A. and Bernstein, E. F. *Trans. Am. Soc. Artif. Int. Organs* 1970, **16**, 37
- 113 Lampert, R. H. and Williams, M. C. *J. Biomed. Mat. Res.* 1972, **6**, 499
- 114 Mohandas, N., Hochmuth, R. M. and Spaeth, E. E. *J. Biomed. Mat. Res.* 1974, **8**, 119
- 115 Kusserow, B., Larrow, R. and Nichols, J. *Fed. Proc. Fed. Am. Soc. Exp. Biol.* 1971, **30**, 1516
- 116 Rothen, A. *Rev. Sci. Instrum.* 1945, **16**, 26
- 117 Rothen, A. in 'Progress in Surface and Membrane Science', (Ed. D. A. Cadenhead, J. F. Danielli and M. D. Rosenberg), Academic Press, New York, 1974, Vol 8
- 118 Vroman, L. and Adams, A. L. *J. Biomed. Mat. Res.* 1969, **3**, 43
- 119 Packham, M. A., Evans, G., Glynn, M. F. and Mustard, J. F. *J. Lab. Clin. Med.* 1969, **73**, 686
- 120 Zucker, M. B. and Vroman, L. *Proc. Soc. Exp. Biol. Med.* 1969, **131**, 318
- 121 Vroman, L., Adams, A. L. and Klings, M. *Fed. Proc. Fed. Am. Soc. Exp. Biol.* 1971, **30**, 1494
- 122 Fenstermaker, C. A., Grant, W. H., Morrissey, B. W., Smith, L. E. and Stromberg, R. R. 'Interaction of Plasma Proteins with Surfaces', *A. Rep. PB 232629* (March 1974) (available from National Technical Information Service, Springfield, Va 22151, USA)
- 123 Morrissey, B. W. and Stromberg, R. R. *J. Colloid Interface Sci.* 1974, **46**, 152
- 124 Nyilas, E., Chiu, T. H. and Herzlinger, G. A. *Abstr. 20th Meet. Am. Soc. Artif. Int. Organs, Chicago* 1974, Vol 3, p 52
- 125 Nyilas, E., Chiu, T. H., Herzlinger, G. A. and Federico, A. 'Microcalorimetric Study of the Interaction of Plasma Proteins with Synthetic Surfaces: I. Construction of the Microcalorimeter and Preliminary Studies', *A. Rep. PB 231776* (February 1974) (available from National Technical Information Service, Springfield, Va 22151, USA)
- 126 Jenkins, C. S. P., Packham, M. A., Guccione, M. A. and Mustard, J. F. *J. Lab. Clin. Med.* 1973, **81**, 280
- 127 Cazenave, J. P., Packham, M. A., Guccione, M. A. and Mustard, J. F. *J. Lab. Clin. Med.* 1974, **83**, 797
- 128 Weeks, J. R., Sekhar, N. C. and Ducharme, D. W. *J. Pharm. Pharmacol.* 1969, **21**, 103
- 129 Shio, H. and Ramwell, P. *Nature (New Biol.)* 1972, **236**, 45
- 130 Thomson, C., Forbes, C. D. and Prentice, C. R. M. *Thromb. Diath. Haemorrh.* 1973, **30**, 547
- 131 Glusa, E., Barthel, W. and Markwardt, F. *Thromb. Diath. Haemorrh.* 1974, **31**, 172
- 132 Swedenborg, J., *et al. Thrombosis Res.* 1974, **4**, 687

# A phenomenological description of the non-linear viscoelastic properties of polymer melts and concentrated solutions

M. G. Brereton

Department of Physics, University of Leeds, Leeds LS2 9JT, UK

(Received 12 September 1974; revised 11 November 1974)

The non-linear stress response of molten polymers and concentrated solutions to an applied strain is formulated in terms of a material response function. The response function is considered to depend explicitly on the resulting stress history and it is shown how many of the non-linear features of these systems can be described both qualitatively and quantitatively. The particular equations used involve one non-linear term in addition to the usual linear response terms. Finally the non-linear equation is interpreted in terms of a plausible model process.

## INTRODUCTION

For polymer melts and concentrated solutions highly non-linear effects dominate all aspects of both the transient and steady state behaviour. The data shown in *Figure 1*, from Vinogradov and Belkin<sup>1</sup>, illustrate this point. It is typical for a whole class of concentrated polymer systems and shows the shear stress response to a suddenly imposed, steady state of simple shear flow. Above a certain strain rate the shear stress shows a characteristic overshoot behaviour where the stress actually decreases with increasing strain.

In the steady state the system exhibits a non-Newtonian viscosity, i.e. the shear stress depends non-linearly on the shear rate. In stress relaxation after the cessation of steady flow a very sudden drop in the stress at high shear rates followed by a comparatively slow relaxation is almost universally observed<sup>2-6</sup>. Also in many systems the stress relaxation after the cessation of a large shear rate can fall below that from small rates<sup>7</sup>. Other modes of testing such as stress relaxation from a constant strain<sup>8</sup> and from a repeated stop-start flow experiment<sup>9</sup> also show quite distinctive non-linear features.

Clearly we might hope to find a common explanation for these features which will enable the results from the different modes of testing to be correlated. It is the object of this paper to suggest in fairly general terms a possible mechanism to account for many of the non-linear features seen in concentrated polymer systems. Our description will be phenomenological in that, in this paper, no attempt will be made to set up a three-dimensional constitutive stress-strain relation. Instead we will aim at describing both qualitatively and quantitatively a wide range of non-linear viscoelastic behaviour in terms of the applied shear rate  $\dot{\gamma}$  and resulting shear stress  $\sigma(t)$ . The equations to be described are, therefore, one-dimensional relations between  $\sigma(t)$  and  $\gamma(t')$ . However, the form of this relation can still be usefully compared to the multiple integral representation for non-linear constitutive relations.

## NON-LINEAR STRESS-STRAIN RELATION

There are many approaches used in understanding the rheological properties of polymers, ranging from formal constitutive relations through phenomenological analysis to empirical relations. Useful surveys of these methods have been given by Middleman<sup>10</sup>, Christensen<sup>11</sup> and Spriggs<sup>12</sup>. In the linear regime the viscoelastic properties of polymers can be described by expressions of the form:

$$\frac{\text{stress}}{\text{strain}} = \int_0^t (\text{response function}) \begin{cases} \text{stress}(t') \\ \text{strain}(t') \end{cases} dt' \quad (1)$$

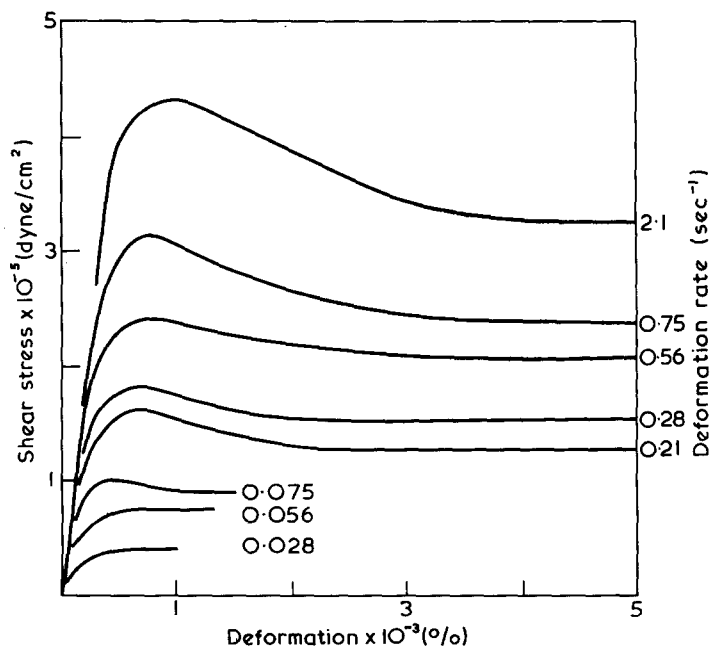


Figure 1 Stress relaxation data re-drawn from Vinogradov and Belkin. [Reproduced from *J. Polym. Sci. (A)* 1965, 3, 917 by permission of John Wiley, New York ©]

For example, the shear stress  $\sigma(t)$  response to an applied shear strain can be written as:

$$\sigma(t) = \int_0^t g(t-t')\gamma(t')dt' \quad (2)$$

where  $\gamma(t')$  is the shear strain acting between the times 0 and  $t$ . (In this paper both  $\sigma$  and  $\gamma$  will be assumed to be zero for negative times.)

The response function  $g(t)$  is related to the stress relaxation modulus,  $G$  by:

$$G(t) = \int_0^t g(t-t')dt' \quad (3)$$

To extend this formulation to non-linear phenomena, we propose that the material response function  $g$  should now be dependent on the resulting stress response history  $\{\sigma\}$ , so that

$$\sigma(t) = \int_0^t g(t-t'; \{\sigma\})\gamma(t')dt' \quad (4)$$

Because the output stress is related to the input strain history  $\{\gamma\}$  it might be argued that we could just as well consider  $g$  to be dependent on  $\{\gamma\}$ . At least in this latter case the stress would be expressed as an explicit function of the strain. However, by adopting the original form (4) we introduce the idea that the state of the material is *directly* affected by the resulting output. The stress is now determined by an implicit equation and the situation becomes very analogous to a feedback process. In fact by introducing the simplest form of feedback we can model all the non-linear behaviour described in the introduction. More specifically we will regard the non-linearity as a modification of the linear response function  $g$  by some as yet unspecified functional  $U(t'; \{\sigma\})$  of the output acting at time  $t'$  intermediate between the times  $t$  and  $t_1$ . The situation is diagrammatically represented in *Figure 2*. As a result of the 'interaction', the linear response function  $g(t' - t_1)$  is changed to another form  $L(t - t_1)$ . Separating out the linear term (2) we can write

$$\sigma(t) = \int_0^t g(t-t')\gamma(t')dt' + \int_0^t dt' \int_0^{t'} dt_1 L(t-t')U(t'; \{\sigma\})g(t'-t_1)\gamma(t_1) \quad (5)$$

For the functional term we will choose the simplest form where  $U$  is proportional to  $\sigma$  and in order that the second term of equation (5) should act so as to reduce the stress, we take

$$U(t'; \{\sigma\}) = -c\sigma(t') \quad (6)$$

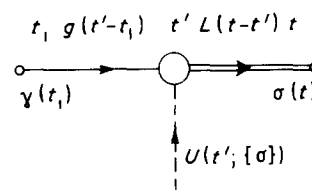


Figure 2 Diagrammatic representation of the proposed non-linearity

By defining the linear response term:

$$\sigma_L(t) = \int_0^t g(t-t')\gamma(t')dt' \quad (7)$$

and absorbing the constant  $c$  into the function  $L(t)$ , we can write equation (5) as:

$$\sigma(t) = \sigma_L(t) - \int_0^t L(t-t')\sigma_L(t')\sigma(t')dt' \quad (8)$$

This equation will form the basis for the rest of the paper. It has the form of an integral equation which if iterated would produce a series expansion similar to a multiple integral representation.

In the next section we will analyse the predictions of this non-linear form for an imposed shear rate.

## SHEAR RATE CONTROLLED EXPERIMENT

### Non-Newtonian viscosity

Under the action of a constant shear rate  $\dot{\gamma}$  the flow reaches, at long times, a steady state stress level and we can define a viscosity  $\eta$  by:

$$\sigma(t \rightarrow \infty) \equiv \sigma_\infty = \eta\dot{\gamma} \quad (9)$$

where  $\eta$  will also depend on  $\dot{\gamma}$ . Using our proposed non-linear relation (8) we can find the long time limit for  $\sigma(t)$  by integrating by parts the integral part of equation (8). The result is that:

$$\sigma(\infty) = \sigma_L(\infty) - l\sigma(\infty)\sigma_L(\infty) \quad (10)$$

where

$$l = \int_0^\infty L(t')dt'$$

The linear stress response is given in terms of the Newtonian viscosity  $\eta_0$  as  $\sigma_L(\infty) = \eta_0\dot{\gamma}$  and equation (10) can be written as:

$$\sigma(\infty) = \left( \frac{\eta_0}{1 + \tau\dot{\gamma}} \right) \dot{\gamma} \quad (11)$$

where  $\tau = l\eta_0$ .

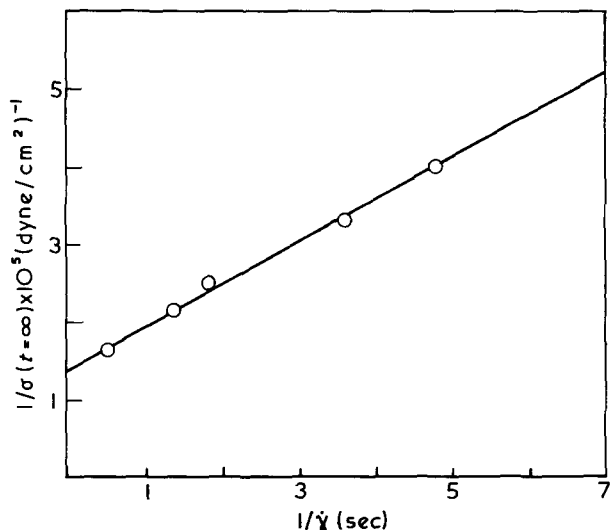


Figure 3 Steady state stress data from Figure 1 plotted according to equation (14). Straight line fit gives  $\eta_0 = 9.10 \times 10^5$  dyne/cm<sup>2</sup> sec.  $\tau = 2.54$  sec

Consequently we can identify the non-Newtonian viscosity,  $\eta$ , as:

$$\eta(\dot{\gamma}) = \frac{\eta_0}{1 + \tau\dot{\gamma}} \quad (12)$$

Cross<sup>17</sup> has correlated an extensive amount of literature data on the shear dependence of the viscosity of concentrated polymer systems on the basis of a four parameter equation:

$$\frac{\eta_0 - \eta_\infty}{\eta - \eta_\infty} = 1 + (\tau\dot{\gamma})^m \quad (13)$$

where  $\eta_0$ ,  $\eta_\infty$ ,  $\tau$  and  $m$  are the parameters. Briefly his results indicate that for monodisperse systems  $m \approx 1$  and  $\eta_\infty$  is small. Consequently our result (12) gives a reasonable description of the experimental data for monodisperse systems. In particular we can apply the data of Vinogradov and Belkin by writing equation (11) as:

$$\frac{1}{\sigma_\infty} = \frac{1}{\eta_0\dot{\gamma}} + \frac{\tau}{\eta_0} \quad (14)$$

which predicts a linear relation between  $1/\sigma(t \rightarrow \infty)$  and  $1/\dot{\gamma}$ . Figure 3 shows the data of Vinogradov plotted in this manner, the result is an excellent straight line from which  $\eta_0$  and  $\tau$  were determined as  $\eta_0 = 9.10 \times 10^5$  dyne cm<sup>-2</sup> sec<sup>-1</sup> and  $\tau = 2.54$  sec.

#### Transient overshoot behaviour

The results of Vinogradov shown in Figure 1 for Alkathene are typical of the dynamic response for a large class of concentrated polymer systems<sup>3,4,7,13-16</sup>. To describe these data using equation (8) we need to know the linear stress response term  $\sigma_L(t)$  and the non-linear function  $L(t)$ . In the rest of this paper we will tentatively take  $L(t)$  to be a simple memory function:

$$L(t) = K\delta(t) + \rho e^{-\mu t} \quad (15)$$

For the linear term  $\sigma_L(t)$  we will first consider the effect of

a Newtonian viscosity i.e.  $\sigma_L(t) = \eta_0\dot{\gamma}$ . Equation (8) can then be solved analytically for  $\sigma(t)$  and the result is:

$$\sigma(t) = \eta_0\dot{\gamma} \left[ \frac{\tau\dot{\gamma} \exp\{-\mu(1 + \tau\dot{\gamma})t\} + 1}{1 + \tau\dot{\gamma}} \right] \quad (16)$$

where  $\tau$  defined by equation (11) and for the simple form (15) for  $H(t)$  is given by:

$$\tau = \frac{\rho\eta_0}{\mu} \quad (17)$$

We have also put  $K = 0$  for further simplicity. This result shows that at  $t = 0$ ,  $\sigma(t) = \eta_0\dot{\gamma}$  which is just the linear response term  $\sigma_L$ , whilst as  $t \rightarrow \infty$  the stress level drops to  $\eta_0\dot{\gamma}/(1 + \tau\dot{\gamma})$  in agreement with the non-Newtonian viscosity result discussed in the previous section. The relaxation of stress is governed by a shear rate dependent relaxation rate  $\mu(1 + \tau\dot{\gamma})$  which can also be written as  $\mu\eta_0/\eta(\dot{\gamma})$ .

We still, as yet, have not got the short time behaviour correct, as our result (16) does not show the experimentally observed overshoot behaviour. This is because of the oversimplified Newtonian form we adopted for  $\sigma_L(t)$ . At short times there will be some elastic effects which we can model by putting

$$\sigma_L(t) = \eta_0\dot{\gamma}(1 - e^{-\lambda t}) \quad (18)$$

Unfortunately with this form for  $\sigma_L$  it is no longer possible to solve equation (8) for  $\sigma(t)$  in terms of known functions. However, we can anticipate that there will be a competition between the build up of stress coming from the elastic term in the linear response and the relaxation of stress caused by the non-linear interaction. As the relaxation rate  $\mu(1 + \tau\dot{\gamma})$  is governed by the applied shear rate  $\dot{\gamma}$ , becoming faster as  $\dot{\gamma}$  is increased, then we can anticipate that an overshoot behaviour will appear as  $\dot{\gamma}$  is increased. In fact in the Appendix we have derived a condition on  $\dot{\gamma}$  for the appearance of the overshoot behaviour. Using equation (18) for  $\sigma_L$  and equation (15) for  $L(t)$ , we find that:

$$\tau\dot{\gamma} > \frac{\mu - \lambda}{\lambda} \quad (19)$$

A numerical iteration of equation (8) was performed using equation (18) for  $\sigma_L$  and taking  $K = 0$ ,  $\rho = 1$ ,  $\mu = 0.2$ ,  $\eta_0 = 10$ ,  $\lambda = 0.1$  as model values for the parameters involved. The results are shown in Figure 4 and confirm our expectations about the origin of the overshoot behaviour. The next step was to see how well actual experimental data could be modelled by using equation (8). The data chosen, largely because they were the most comprehensive available, were those of Vinogradov and Belkin on Alkathene at 114°C. Using the simple parameterizations (15) and (18) for  $L(t)$  and  $\sigma_L(t)$  respectively we found, by trial and error, values for the parameters to fit the whole range of data. The result is shown in Figure 5 together with the actual values of the parameters used. In view of the simple parameterization used the overall fit is quite good.

#### OTHER PROGRAMMED SHEAR INPUTS

In principle equation (8) can be solved numerically for any shear input behaviour. The choice of inputs considered in



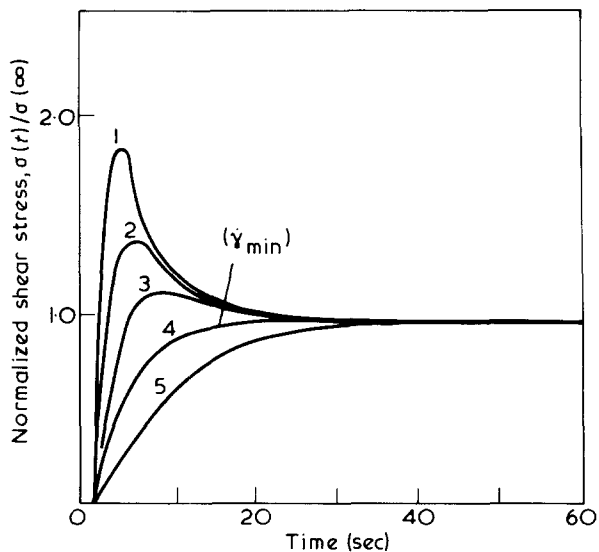


Figure 4 Numerical iteration of equation (8). Parameters used:  $\eta_0 = 10$ ,  $\lambda = 0.1$ ,  $K = 0$ ,  $\rho = 1$ ,  $\mu = 0.2$ . Shear rates: 1, 0.2; 2, 0.1; 3, 0.05; 4, 0.01; 5, 0.001

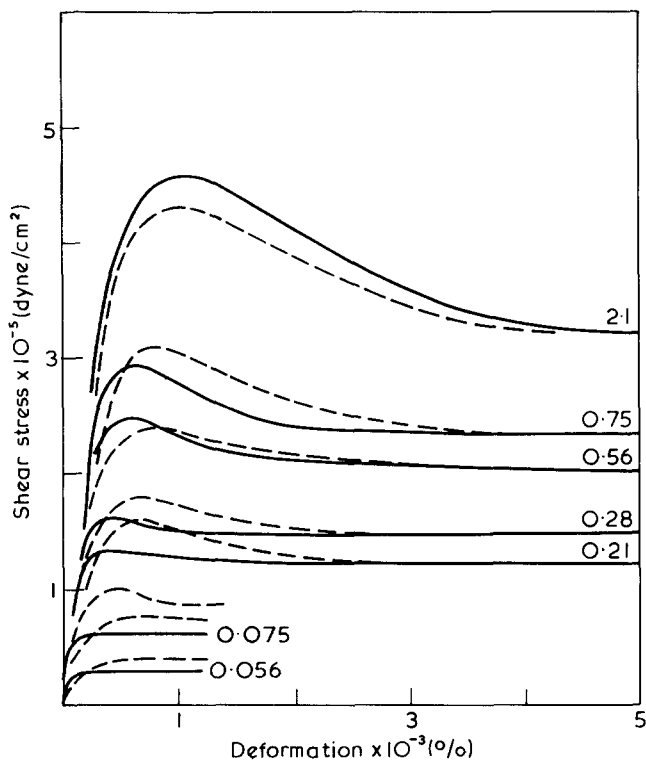


Figure 5 Theoretical predictions based on equations (8), (15) and (18) (—). Experimental data from Figure 1 (-----)

this section has been dictated by the availability of experimental data.

#### Stress relaxation after the cessation of steady flow

The linear stress response  $\sigma_L$  to a steady imposed flow is taken to be modelled by the viscoelastic form (18). If the flow is stopped at some  $t_0$  then the linear stress relaxation is given for  $t > t_0$ :

$$\sigma_L(t) = \eta_0 \dot{\gamma} (1 - e^{-\lambda t_0}) e^{-\lambda(t-t_0)} \quad (20)$$

The full non-linear response  $\sigma(t)$  is found by solving equation (8). Using equations (18) and (20) for  $\sigma_L$  and (15) for  $H(t)$ , we have numerically evaluated this equation using

$K = 0$ ,  $\rho = 1$ ,  $\mu = 0.2$ ,  $\eta_0 = 10$ . The results are shown in Figure 6 and show a very sudden drop in the stress at high shear rates followed by a comparatively slow relaxation. This kind of behaviour is almost universally observed<sup>2-6</sup>.

Another feature frequently observed is the fact that the stress relaxation after the cessation of large shear rates can fall below that from small rates<sup>7</sup>. By decreasing the non-linear relaxation rate  $\mu$  from 0.2 to 0.1 we can also model this kind of behaviour. Figure 7 shows the computed results for  $\mu = 0.1$ .

The reason for the sudden drop in stress can be seen from the structure of equation (8) if we write it as:

$$\sigma(t) = \sigma_L(t) - F(t) \quad (21)$$

where  $F(t)$  is the feedback term  $\int_0^t L(t-t') \sigma_L(t') \sigma(t') dt'$ . Basically  $\sigma(t)$  is determined through a competition between the linear response term  $\sigma_L(t)$  and the feedback term  $F(t)$ . As the linear term  $\sigma_L$  begins to decrease after the cessation of flow,  $F(t)$  still has a 'memory' of the previously high values of  $\sigma$  and  $\sigma_L$  and correspondingly subtracts a greater

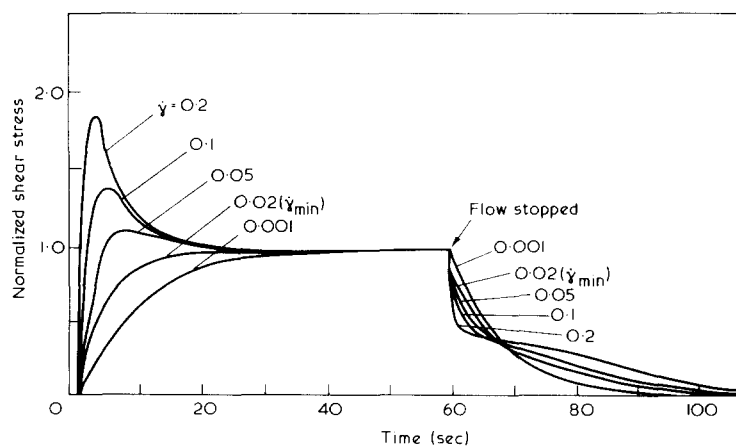


Figure 6 Theoretical curves of stress relaxation based on equation (8). Parameters used:  $\eta_0 = 10$ ,  $\lambda = 0.1$ ,  $\rho = 1$ ,  $\mu = 0.2$

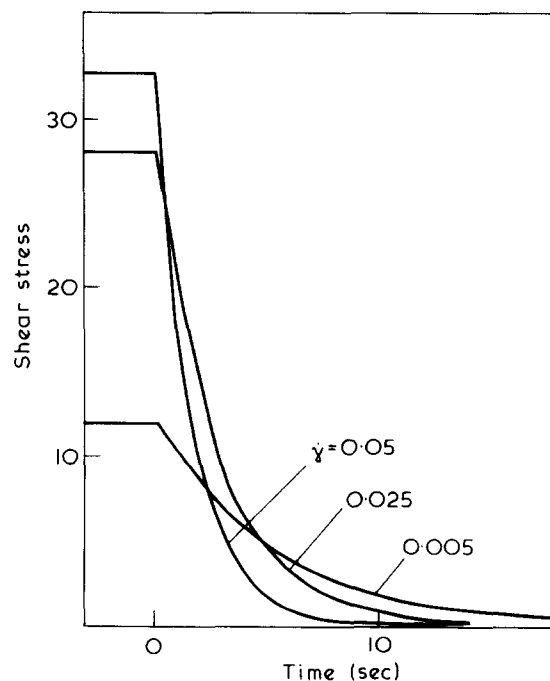


Figure 7 Curves of stress relaxation, after the cessation of steady flow, predicted by equation (8). Parameters used:  $\eta_0 = 10$ ,  $\lambda = 0.1$ ,  $K = 0$ ,  $\rho = 1$ ,  $\mu = 0.1$

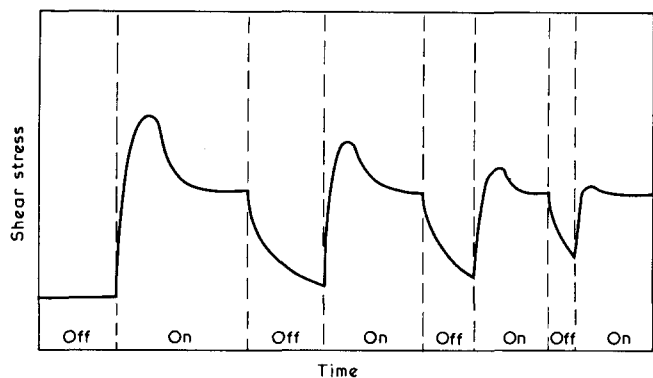


Figure 8 Data of Stratton and Butcher<sup>9</sup> on the stress relaxation obtained from a 'stop-start' experiment

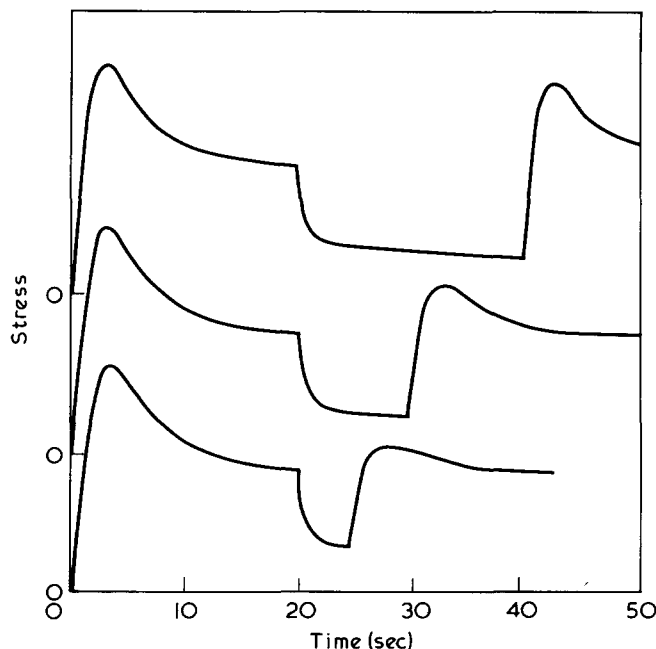


Figure 9 Stress relaxation predicted from equation (8) using a 'start-stop' flow input. Parameters used:  $\eta_0 = 10$ ,  $\lambda = 0.1$ ,  $K = 0$ ,  $\rho = 1$ ,  $\mu = 0.2$  and flow rate  $\dot{\gamma} = 0.2$

contribution from  $\sigma_L$ . By increasing the 'memory' of this term, i.e. by decreasing  $\mu$  we increase further the contribution of  $F(t)$  as shown in Figure 7. For essentially the same argument we get the overshoot behaviour at the start up of a flow experiment. In this case  $F(t)$  has a memory of previously low values of  $\sigma$  and  $\sigma_L$ , correspondingly it is not until the lapse of some time before it can effectively begin to subtract from  $\sigma_L$ .

The existence of this feedback term with a memory of the past stress history can be further demonstrated in a repeated stop-start flow experiment.

#### Stress relaxation in a repeated stop-start flow experiment

In this kind of experiment, a constant flow rate is imposed for one period of time, then switched off for another period and then switched on again etc. Such an experiment has been performed by Stratton and Butcher<sup>9</sup> on a polyisobutylene solution. The kind of results they obtained are reproduced in Figure 8. The main feature is a decreasing maximum with decreasing 'off-time'.

The predictions based on the use of equation (8) are shown in Figure 9 and qualitatively agree with the experimental results. This behaviour can easily be understood

from the feedback structure of the equation. In an 'off' period the stress is given by:

$$\sigma_{\text{off}}(t) = \sigma_{L\text{off}}(t) - F(t) \quad (22)$$

But at the start of an 'on' period the driving term  $\sigma_{L\text{off}}$  changes rapidly to  $\sigma_{L\text{on}}$  which is an increasing function of time. However, the feedback term  $F(t)$  cannot change so quickly and continues to subtract from the linear term. Only if the 'off' period has been sufficiently long to allow this term to decay completely, will a full stress maximum be developed on the start up of the experiment.

#### Stress relaxation from a constant strain

Few measurements have been taken on the stress relaxation of concentrated polymer systems in the non-linear regime. Recently, however, a systematic series of measurements on polystyrene in solution under conditions of large strain were carried out by Einaga *et al.*<sup>8</sup> Their results are reproduced in Figure 10. The relaxation modulus is clearly strain dependent, but the terminal relaxation time remains unaffected. The stress relaxation predicted by equation (8) is shown, for a wide range of strains, in Figure 11. The parameters are the same as those previously used. The selection of curves enclosed in the broken square show good qualitative agreement with the experimental ones. Again at long times the curves come together because in this approach only the linear term survives.

#### A MODEL INTERPRETATION

The approach adopted in this paper has so far avoided any specific molecular or mechanistic models. A non-linear equation has been proposed where the non-linearity comes from a simple feedback scheme. If we adopt very simple

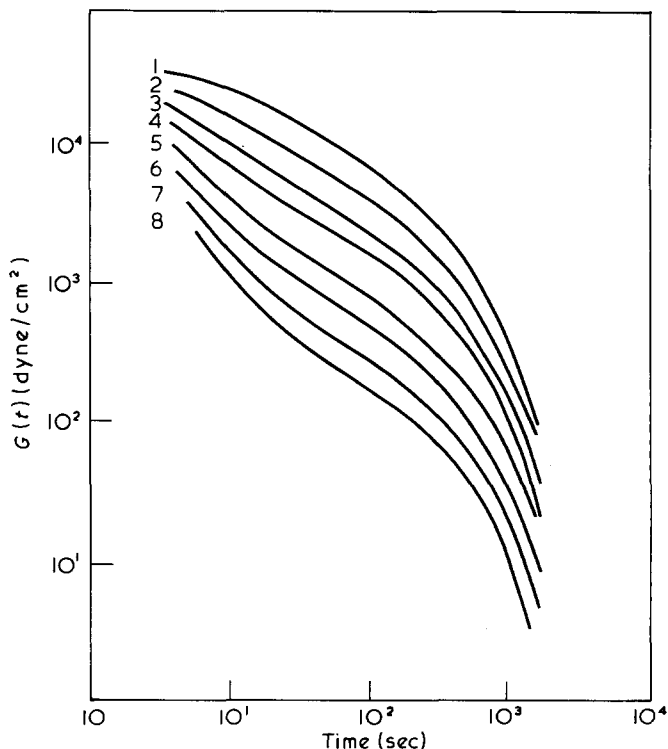


Figure 10 Stress relaxation modulus  $G(t) = \sigma(t)/\dot{\gamma}$  for a 20% solution of narrow distribution polystyrene in chlorinated diphenyl. Data taken from Einaga *et al.*<sup>8</sup>

forms for the terms  $\sigma_L$  and  $L$  occurring in this equation, then in these circumstances (and only in these circumstances) we can re-interpret our approach in terms of a simple mechanistic model. For example in a constant shear rate test, if we take the linear stress  $\sigma_L$  as given by the Newtonian result  $\eta_0\dot{\gamma}$  and  $L(t)$  given by equation (15) with  $K=0$ , then the full stress response is given by equation (16) i.e.

$$\sigma(t) = \eta_0\dot{\gamma} \left[ \frac{\tau\dot{\gamma}e^{-\mu(1+\tau\dot{\gamma})t} + 1}{1 + \tau\dot{\gamma}} \right] \quad (23)$$

If we write this as:

$$\sigma(t) = \eta_0\dot{\gamma}n(t) \quad (24)$$

then this suggests that we interpret  $n(t)$  as the fraction  $N(t)/N_0$  of stress bearing units present at the time  $t$  and that the contribution of each of these units to the total stress is  $\bar{\eta}\dot{\gamma}$  where  $\bar{\eta} = \eta_0/N_0$  and  $N_0$  is the total number of units available in the absence of any external force. If we use a 'switch' to signify whether a unit is contributing to the total stress or not, then this model can be represented by the mechanistic model shown in Figure 12. From the solution (23) we have that the fraction of switches closed is:

$$n(t) = \frac{\tau\dot{\gamma}e^{-\mu(1+\tau\dot{\gamma})t} + 1}{1 + \tau\dot{\gamma}} \quad (25)$$

By differentiating equation (25) we see that  $n(t)$  satisfies the following simple rate equation:

$$\frac{dn}{dt} = -\mu(\tau\dot{\gamma})n + \mu(1 - n) \quad (26)$$

This implies that the activation (opening) of the switches is governed by a shear rate dependent rate constant (first term

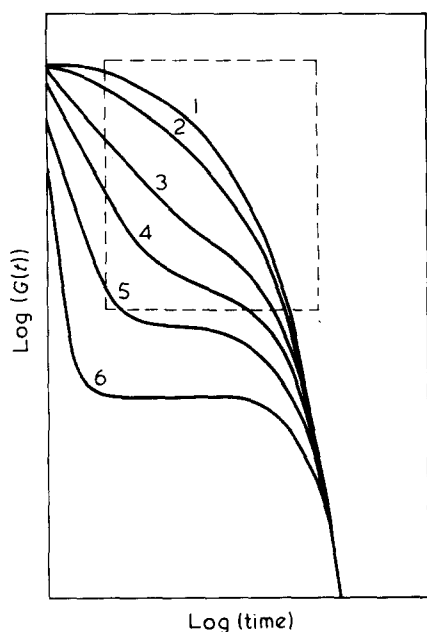


Figure 11 Stress relaxation modulus  $G(t) = \sigma(t)/\dot{\gamma}$  predicted from equation (8) using a constant strain input. Strain values used: 1, 0.01; 2, 0.1; 3, 0.5; 4, 1.0; 5, 2.0; 6, 5.0. Parameters:  $\eta_0 = 10$ ,  $\lambda = 0.1$ ,  $K = 0$ ,  $\rho = 1$ ,  $\mu = 0.2$

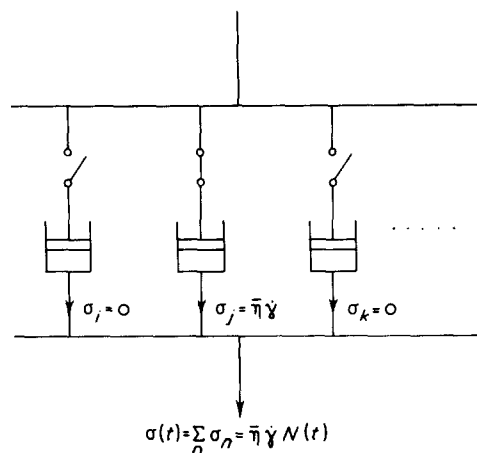


Figure 12 Dashpot model representation of the non-linear relation between stress and strain rate

of equation 26), whereas the restoration of the original closed state of the switches is simply governed by the departure from the equilibrium fraction, i.e. the second term  $\mu(1 - n)$  in equation (26).

Clearly this particular model could be developed in a more realistic way in terms of the formation and destruction of network bonds<sup>18,19</sup>. The main point of introducing it here was to show how a specific model could be encompassed within the more general formalism described earlier.

## CONCLUSION

We have proposed a new approach to the non-linear viscoelastic properties of molten polymers and concentrated solutions. The material response function describing the stress response to an applied strain was considered to depend explicitly on the output stress history  $\{\sigma\}$ . In this paper we expanded the dependence of the response function on  $\{\sigma\}$  to first order in  $\{\sigma\}$  and have shown both qualitatively and quantitatively how many of the non-linear features of these systems can be described. The formulation of the non-linear equation was accomplished by the introduction of a further phenomenological response function  $L(t)$ , in addition to the usual linear response terms. By adopting simple forms for the response functions involved, we could interpret the non-linear equation in terms of a plausible model process.

## REFERENCES

- 1 Vinogradov, G. V. and Belkin, I. M. *J. Polym. Sci. (A)* 1965, 3, 917
- 2 Spriggs, T. W. *et al. Trans. Soc. Rheol.* 1963, 7, 391
- 3 Elliot, J. J. *J. Appl. Polym. Sci.* 1969, 13, 755
- 4 White, J. *et al. J. Appl. Polym. Sci.* 1971, 15, 1181
- 5 Vinogradov, G. V. and Malkin, A. *J. Polym. Sci. (A-2)* 1966, 4, 135
- 6 Alioso, C. J., Matsuoka, S. and Maxwell, B. *J. Polym. Sci. (A-2)* 1966, 4, 113
- 7 Trapeznikov, A. A. *Proc. Fifth Int. Congr. Rheology* 1968, 4, 257
- 8 Einaga, Y., Osaki, K. and Kurata, M. *Polym. J.* 1971, 2, 550
- 9 Stratton, R. and Butcher, A. *J. Polym. Sci. (Phys. Edn)* 1973, 11, 1747
- 10 Middleman, S. 'The Flow of High Polymers', Interscience, New York, 1968
- 11 Christensen, R. M. 'Theory of Viscoelasticity', Academic Press, New York, 1971
- 12 Spriggs, T. W. *et al. Trans. Soc. Rheol.* 1966, 10, 191
- 13 Meissner, J. *J. Appl. Polym. Sci.* 1972, 16, 2877
- 14 Bianchi, U. and Peterlin, A. *Kolloid-Z.* 1969, 232, 749

- 15 Lewis, W. E. and Brodkey, R. *Proc. Fifth Int. Congr. Rheology* 1968, 4, 141  
 16 Kim, H. T. and Brodkey, R. *AIChE J.* 1968, 14, 61  
 17 Cross, M. J. *Appl. Polym. Sci.* 1969, 13, 765  
 18 Graessley, W. W. *J. Chem. Phys.* 1965, 43, 2696  
 19 Storey, B. T. and Merrill, E. W. *J. Polym. Sci.* 1958, 33, 361

APPENDIX

Condition on the shear rate for the appearance of the overshoot behaviour

For  $L(t)$  given by equation (15) with  $K = 0$ , the non-linear equation (8) for  $\sigma(t)$  can be differentiated to give:

$$\frac{d\sigma}{dt}(t) + \{\mu + \rho\sigma_L(t)\} = \frac{d\sigma_L}{dt}(t) + \mu\sigma_L(t) \quad (A1)$$

The condition for a maximum in  $\sigma(t)$  is that:

$$\frac{d\sigma}{dt} = 0 \text{ and } \frac{d^2\sigma}{dt^2} < 0 \quad (A2)$$

If we write the linear stress term  $\sigma_L$  as:

$$\sigma_L(t) = \dot{\gamma}f(t) \quad (A3)$$

then the condition for the overshoot behaviour (maximum is  $\sigma(t)$ ) can be shown, using equations (A1) and (A2), to be:

$$\dot{\gamma} > \frac{\mu}{\rho} \left\{ \frac{\mu\dot{f} + \ddot{f}}{\dot{f}^2 - f\ddot{f}} \right\} \quad (A4)$$

For the simple viscoelastic parameterization (18) we have used for  $\sigma_L$ :

$$f(t) = \eta_0(1 - e^{-\lambda t}) \quad (A5)$$

and consequently the condition on  $\dot{\gamma}$  can be written as:

$$\tau\dot{\gamma} > \frac{\mu - \lambda}{\lambda} \quad (A6)$$

where, as usual,  $\tau = \eta_0\rho/\mu$ .

# Studies on poly (iso-butene oxide):

## 3. Elastic hard fibre of poly (iso-butene oxide)

T. Yamazaki and S. Oya

Department of Textile Chemistry, Kyoto University of Industrial Arts & Textile Fibers, Matsugasaki, Kyoto, Japan

and N. Tsukane, K. Tanaka, H. Toba and K. Yamagishi

Central Research Laboratory, Daicel Co.Ltd, 171 Tsurugaoka, Ohi-machi, Iruma-gun, Saitame-ken, Japan

(Received 30 July 1974)

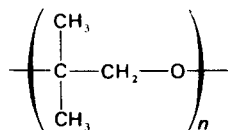
Poly(iso-butene oxide), a highly crystalline polyether, gives an 'elastic hard fibre', having excellent elastic recovery, on melt-spinning under appropriate drafting conditions. The interrelation between fabricating conditions and elastic recovery has been studied and the mechanism of the appearance of the elastic recovery is discussed. The mechanical, thermal and chemical properties of the fibre have been investigated.

### INTRODUCTION

In recent years, it has been found that 'elastic hard fibres', having the property of high elastic recovery, are formed from highly crystalline polymers such as polypropylene<sup>1</sup>, polyacetal<sup>2</sup>, poly(3-methylbutene-1)<sup>3</sup> and polypivalolactone<sup>4</sup>, under special fabricating conditions.

The mechanism of the elastic recovery of these 'elastic hard fibres' has been explained by Quynn and coworkers<sup>5</sup> as due to reversible 'bending' of the stacked crystalline lamellae. Clark<sup>6</sup> who discussed the elastic behaviour in terms of the 'RENKER WEB' model, (similar to network structure) explained the elastic property as arising from the formation of tie molecules in 'row' structure lamellae.

We have found out that poly(iso-butene oxide) (PIBO):



a highly crystalline polyether, becomes an excellent 'elastic hard fibre', and a detailed study is underway. In this paper, we discuss mainly the processing and apparent behaviour of the fibre.

PIBO is easier to restrain in the lower degree of crystallinity on quenching than polyacetal, because it has a lower rate of crystallization as shown in *Figure 1*. Moreover, it is characteristic of this polymer that the polymer molecules readily orientate by rolling in the unmelted state (unpublished results).

We discovered that the filaments of PIBO exhibit very excellent elastic recovery when melt extruded, and stretched at the appropriate draft ratio under cooling conditions leading to crystallization. The characteristic mechanical and thermal properties of PIBO fibre, such as high elastic recovery and excellent low temperature properties, as well as the good chemical property compared to those of Spandex elastic fibre are described.

### EXPERIMENTAL

#### Materials

Poly(iso-butene oxide) (PIBO) was prepared, using diethyl zinc, water and cyclohexylamine catalysts system<sup>7</sup> (molar ratio of ZnEt<sub>2</sub>/H<sub>2</sub>O/C<sub>6</sub>H<sub>11</sub>NH<sub>2</sub> was 3:1:1) in hexane at 75°C in a bench-scale reactor.

The residue of catalysts was extracted after polymerization, and the polymer was pelleted after addition of antioxidants such as 0.9 pph tetra-kis[methylene-3-(3,5-di-*t*-butyl-4-hydroxyl phenyl)propionate] methane and 0.1 pph dibenzildisulphide, and 0.5 pph 2-(2-hydroxy-5-methyl-phenyl)-benzotriazole as ultra-violet absorber.

The PIBO resin thus obtained has excellent mechanical, chemical and thermal properties, and is highly crystalline with m.p. of 172°C.

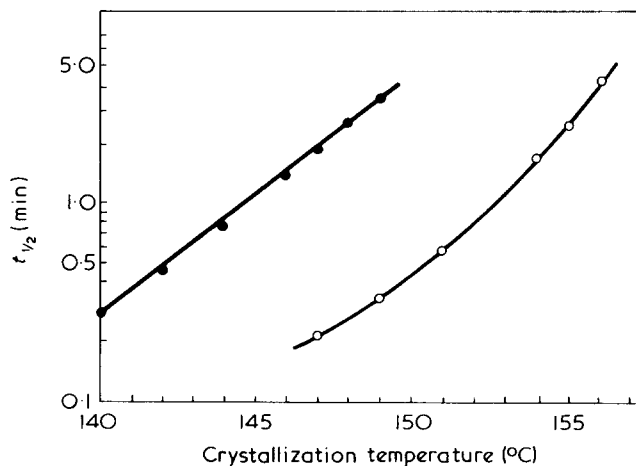


Figure 1 Crystallization rate of PIBO (●) and polyacetal (○). The values of half time of overall crystallization,  $t_{1/2}$ , were calculated from the half area of d.s.c. curves due to polymer crystallization

Table 1 Relationship between fabricating conditions and the elastic recovery of PIBO fibres

Runs	Nozzle (holes)	Temperature of cylinder and die (C <sub>1</sub> -C <sub>2</sub> -D)* (°C)	Speed of winding (m/min)	Crystallization condition	Elastic recovery
1	12	205-225-250	135	cooled in air	excellent
2	12	215-230-260	125	cooled in air	good
3	1	190-215-235	100-130	cooled in air	fair
4	1	190-200-220	55	cooled in air	poor
5	20	185-210-260	30-50	cooled in air	after heat-treated, fair
6	1	230-240-260	120	quenched in chilled ice-water (-10°C)	poor
7	12	210-230-260	90	treated in warmed cylinder (50°C)	poor

\* C = cylinder; D = die

Melt spinning apparatus

The melt spinning die connected to a single hole nozzle having a diameter of 1 mm, or multi-hole nozzle of twelve or twenty holes, was attached to the extruder, the cylinder of which had a diameter of 25 mm, and a length of 420 mm. Single or multi-filaments passed on to a guide-roll and were wound up on a winding-roll placed at a distance of about 2m from the nozzle.

Measurements

Mechanical properties of the PIBO fibre and Spandex fibre were measured with a 'Tensilon UTM-II' (made by Toyo-Bowling Corp., Japan) in elongation-retraction cycles. A uniaxial stretching tool with scale was used to fix the fibre in elongated state for 24 h. Both energy for elongation and energy loss during elongation-retraction cycles were measured with a planimeter on the stress-strain curves.

RESULTS AND DISCUSSION

Relationship between fibre fabricating conditions and elastic recovery

The experimental results summarized in Table 1 show that the elastic recovery of PIBO filaments is good for higher speeds of winding and crystallizing in ambient air, in comparison with crystallizing in water (run 6) or in a warm cylinder (run 7).

In the melt-spinning process, the draft ratio (DR) of filament is defined as:

$$DR = V_1/V_0 \tag{1}$$

where V<sub>1</sub> is winding speed and V<sub>0</sub> is the extruding speed of filament.

Since the extruded volume per unit time, Q, of the twelve and twenty hole nozzles are the same:

$$V_0 = Q/n \cdot \pi \cdot \phi^2 \tag{2}$$

where n is the number of nozzle holes, and φ is the radius of the nozzle hole.

The values of V<sub>0</sub> in both cases are also equal. Thus, the comparison between DR for twelve and twenty hole nozzles, is equivalent to the comparison between the corresponding V<sub>1</sub> values.

According to Table 1, the higher the draft ratio the better the elastic recovery in the cases of multi-hole nozzles, and

this indicates that the most important factors controlling the elastic recovery are shear stress and thermal conditions for the crystallization in good agreement with the mechanism of elastic recovery proposed by Quynn and coworkers.

On the other hand, V<sub>0</sub> in the case of a single hole nozzle is about five times larger than in the case of multi-hole nozzles and therefore, V<sub>1</sub> must be about five times larger for the multi-hole nozzles to get the equivalent draft ratio. Thus, the inferior elastic recovery of the filament of run 3 in comparison with that of run 2 could be ascribed to the lower draft ratio of the former.

The other factor influencing elastic recovery is the ratio of length to diameter of the nozzle hole (L/D). The L/D ratio of a single hole nozzle is larger than that of the multi-hole nozzles and it is likely that the smaller the value, the more excellent the elastic recovery.

Although it cannot be concluded from the results in Table 1 that the temperature of the cylinder and die influence elastic recovery, it is our experience that the elastic recovery of filaments extruded at the slightly higher temperature than the melting point of PIBO is better than that of the filaments extruded at much higher temperatures. These facts may be understood if we consider that the higher 'spinning-stress' results in the superior elastic recovery of the filaments.

Furthermore, as shown in Table 2, the elastic recovery of PIBO filaments is very closely related to the orientation of filaments. This indicates that the adequate draft of PIBO filaments during crystallization is a main factor in determining the elastic recovery.

Measurements show that all samples had similar crystal structures.

We also found that PIBO filaments in the stretched state spontaneously lose the elastic recovery, when sprayed with organic solvents such as toluene, acetone, and regain it with

Table 2 Relationship between birefringence and the elastic recovery of PIBO fibres

Samples*	Birefringence, Δn x 10 <sup>-3</sup>	Elastic recovery
1	32.67	excellent
8†	35.20	excellent
2	32.10	good
4	16.46	poor
7	23.77	poor

\* Numbers of samples are referred to as 'runs' in Table 1.

† Sample 8 is sample 1 extended by 50% and aged at 150°C for 30 min

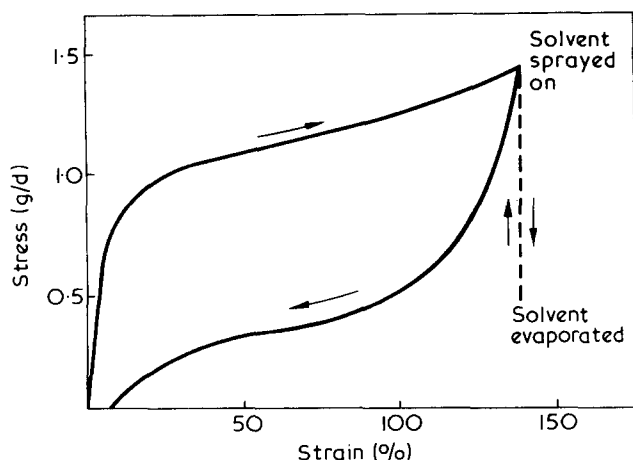


Figure 2 Stress-strain curve of PIBO elastic hard fibre and the effects of organic solvents sprayed on it

Table 3 General and mechanical properties of PIBO elastic hard fibre and Spandex fibre\*

Property	PIBO	Spandex
Denier	20–300	20–2920
Appearance	lustrous, tactual like hemp	opaque
Density (g/cm <sup>3</sup> )	1.02	1.0–1.2
Moisture contents at equilibrium (%)	0.2	0.4–1.3
Strength at break (g/d.)	1.0–1.7	0.6–1.2
Elongation at break (%)	165	450–800
Strength (hooked) (g/d.)	2.24	1.2–1.8
Strength (knotted) (g/d.)	1.33	0.5–0.9
Elasticity at 50% elongation:		
elastic recovery (%) <sup>†</sup> (fixed for 5 min)	96	94–99
elastic recovery (%) (fixed for 24 h)	96	81–91
retractive force (g/d.)	0.6–0.7	0.03–0.04
energy for elongation (erg/d.)	2300–2900	80.2
energy loss (%)	60	20
Elasticity at 100% elongation:		
elastic recovery (%) (fixed for 5 min)	80	98
elastic recovery (%) (fixed for 24 h)	96	—
retractive force (g/d.)	1.0–1.6	0.06–0.07
energy for elongation (erg/d.)	6000–10 000	312
energy loss (%)	60	30

\* At 20°C and 65% r.h.

<sup>†</sup> Elastic recovery was measured after the filament was fixed in the elongated state for a constant time, and then relaxed for 10 min

evaporation of the solvent. This behaviour is shown in Figure 2 and suggests that the elastic recovery force could be intimately correlated to the surface energy and presumably interfacial energy of crystal interfaces.

#### Mechanical properties of PIBO fibre

Physical and mechanical properties of PIBO elastic hard fibre are compared with those of Spandex fibre in Table 3. The PIBO fibre has higher tensile strength, higher retracted force, higher energy required for elongation, lower elongation ratio at break and higher energy loss during elongation and retraction cycles. It may be considered that these characteristic properties are due to the mechanism of the elastic recovery of hard fibre which is different from that of 'entropic' elastic recovery of a crosslinked rubber.

#### Elastic recovery at low temperature

Table 4 shows that PIBO elastic hard fibre has very excellent low temperature properties. On the other hand, Spandex fibre shows an elastic recovery of only about 10% at the temperature of  $-75^{\circ}\text{C}$ . These facts also suggest the former has sufficient elastic recovery at a much lower temperature below its glass transition temperature and the mechanism of the elastic recovery of the elastic hard fibre is different from that of rubber elasticity.

#### Chemical properties of PIBO fibre

In Table 5, some chemical properties of PIBO elastic hard fibre are compared with those of Spandex fibre. PIBO has excellent resistivity against chemical reagents and is more resistant against such reagents as sodium hypochlorite, tetrachloroethylene, carbon tetrachloride and dimethyl formamide than Spandex fibre.

Table 4 Mechanical properties at low temperature of PIBO elastic hard fibre

Temperature (°C)	Elongation at break (%)	Elastic recovery (%) (50% elongated)
R.T.	165	96.0
0	150	98.4
-5	—	96.8
-10	—	96.8
-30	—	89.7
-75	130–150	85.5
-193	130	20–40*

\* Completely retracted immediately after being taken out into room temperature

Table 5 Chemical properties of PIBO and Spandex elastic fibre

Reagents	PIBO degree of swelling (weight loss) (%)	Spandex weight loss (%)
60 min in boiling aq. H <sub>2</sub> SO <sub>4</sub> (0.5 cm <sup>3</sup> /l)	no change	no change
60 min in boiling aq. acetic acid (0.5 cm <sup>3</sup> /l)	no change	3.3
60 min in boiling aq. oxalic acid (1 g/l)	no change	no change
60 min in boiling aq. sodium hydroxide	no change	3.1
60 min in boiling aq. sodium carbonate (10 g/l)	no change	no change
sodium hypochlorite (effective chlorine contents: 2 g/l) at 20°C, 24 h	no change	4.1
tetrachloroethylene (20°C, 24 h)	no change	yellowish, mechanical properties change to worse
carbon tetrachloride (20°C, 24 h)	no change	slightly yellowish, mechanical properties change to worse
Soxhlet extraction (3 h):		
benzene	(3.3)	—
methanol	(3.2)	—
benzene	(3.0)	—
Warmed dimethyl formamide	no change	swollen or soluble
Hot dichlorobenzene, or xylene (100–140°C)	swollen or soluble	—

Table 6 Weathering\* and thermal stability of PIBO and Spandex elastic fibres

Tests	PIBO	Spandex fibre
Weathering stability:		
colour	no change	slightly yellowish
retention percentages of tensile strength	87-100	slightly decreased
retention percentages of elongation	100	—
elastic recovery	no change	—
Thermal stability (120°C, 5 h, in air)	no change	yellowish

\* Weathering meter, 60°C, 40 h

#### Weathering resistivity and thermal stability

As shown in Table 6, the weathering resistivity and thermal stability of PIBO is superior to those of Spandex fibre

and has excellent properties also from the point of view of practical use.

#### ACKNOWLEDGEMENT

The authors are very grateful to Daicel Co. Ltd for permission to publish.

#### REFERENCES

- 1 Boltaiaw, A. U.S. Pat. 3 323 190 (1967)
- 2 Coplan, M. J. et al. U.S. Pat. 3 608 044 (1971); 3 661 853 (1972)
- 3 Quynn, R. G. and Sprague, B. S. *J. Polym. Sci. (A-2)* 1970, **8**, 1971
- 4 Japan Pat. 9810 (1966)
- 5 Quynn, R. G. and Brody, H. *J. Macromol. Sci.(B)* 1971, **5**, 721
- 6 Clark, E. S. *ACS Meet. Div. Org. Coat. Plastics Chem. Prepr.* 1972, **32**, 19
- 7 Furukawa, J. 'Encyclopedia of Polymer Science and Technology', John Wiley, New York, 1967, Vol 6, pp 191-193



# Some kinetic aspects of radical copolymerization: influence of the reaction medium on the reactivity ratios

Giorgio Bontà, Bianca M. Gallo and Saverio Russo

*Istituto di Chimica Industriale, Università Genova, 16132 Genova, Italy*

*(Received 9 May 1974; revised 30 September 1974)*

The reactivity ratios for the free radical copolymerization of styrene and methyl methacrylate at 50°C have been evaluated in dioxane, acetone and dimethylformamide solutions. In all these systems there is a marked solvent effect on both  $r_1$  and  $r_2$ , which can be correlated to the variation in the dielectric constant of the solvent. The role of solvents in enhancing the polarization of growing chains and the alternation tendency is discussed.

## INTRODUCTION

In the past few years we have undertaken a thorough study of the fundamental aspects of the free radical copolymerization reaction. In particular we have proposed<sup>1</sup> a novel approach for interpreting the behaviour of the overall copolymerization rate in place of the older inadequate reaction schemes, and at present we are studying in detail the many still obscure aspects in the kinetics and mechanisms which control the stages of initiation, propagation and termination.

As far as the propagation stage is concerned, we have evaluated<sup>2</sup> the temperature dependence of reactivity ratios for the pair styrene–methyl methacrylate polymerized in bulk at temperatures ranging from 40° to 80°C [initiator  $\alpha, \alpha'$ -azobisisobutyronitrile (AIBN)]. Changes in composition due to temperature variations were found to be not very pronounced, because of the small differences between the activation energies associated with the four rate constants in the propagation stage.

It is well known that, besides temperature and pressure, the reaction medium can affect reactivity ratios. This is clearly evident in systems including ionogenic monomers such as acrylic and methacrylic acids, sodium styrene sulphonate, etc.<sup>3–6</sup> and it has been observed also in the radical copolymerization of non-ionizable monomers, such as acrylamide<sup>7–10</sup>, *N*-monosubstituted acrylamides<sup>11,12</sup>, methacrylamide<sup>13</sup>, acrylonitrile<sup>14</sup>, methacrylonitrile<sup>15</sup>. Moreover, some recent papers<sup>16,17</sup>, conflicting with earlier reports in the literature<sup>18,19</sup>, show an appreciable effect of the reaction medium on the reactivity ratios for the pair styrene–methyl methacrylate.

Several interpretations have been proposed for the variation of the reactivity ratios as functions of the reaction medium. Monomer solvation, complex formation, stabilization of the growing chains, hydrogen bonding ability, polarization, proton donating tendency of the solvent, microphase separation and hot radical theory are among the most common ones.

In the present paper we refer to the solvent dependence of reactivity ratios for the pair styrene–methyl methacrylate polymerized at 50°C. The solvents used are acetone, dioxane, and *N,N'*-dimethylformamide (DMF).

## EXPERIMENTAL

### Materials

Purification of styrene (S) (Carlo Erba RP) and methyl methacrylate (MMA) (B. H. Shilling) monomers was carried out following previously described techniques<sup>1</sup>.

Acetone (Baker) was distilled twice at atmospheric pressure. DMF was purified following the method described by Ritchie *et al.*<sup>20</sup>, i.e., it was dried by molecular sieves and vacuum distilled in a nitrogen stream over phosphorus pentoxide. Dioxane (Baker) was distilled twice at reduced pressure.

AIBN initiator (Merck) was purified as described previously<sup>1</sup>.

### Procedure

All experiments were performed in glass ampoules covered by aluminium foil to prevent photoinitiation. Sampling of monomers and solvents in the ratio 1 : 2 (v/v) was carried out using conventional techniques. The mixtures were flushed with helium, degassed and vacuum distilled into the ampoule containing a known amount of initiator. The ampoules were sealed under a pressure  $\leq 10^{-5}$  mmHg. Initiator, monomer and solvent concentrations, temperature of sampling and reaction, polymerization times and yields were carefully determined. The polymerization temperature was  $50^\circ \pm 0.05^\circ\text{C}$ . The maximum monomer conversions were  $\leq 3\%$ .

The copolymers were precipitated twice using benzene or methyl ethyl ketone as solvents and methanol as precipitant.

### Copolymer analysis

Copolymer composition was determined by elemental analysis, using a Carlo Erba CHNO automatic analyser model 1102. Monomer reactivity ratios were calculated on the basis of the curve-fitting method recently proposed by Braun *et al.*<sup>21</sup>.

### Infra-red spectroscopy

The absorption bands in the region of C=C stretching for styrene and methyl methacrylate were recorded in

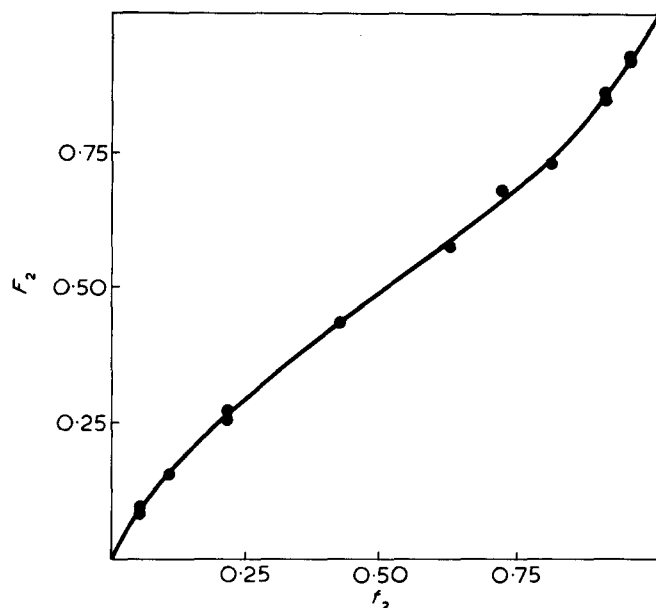


Figure 1 Copolymer composition for the copolymerization of S (1) and MMA (2) in dioxane at 50°C

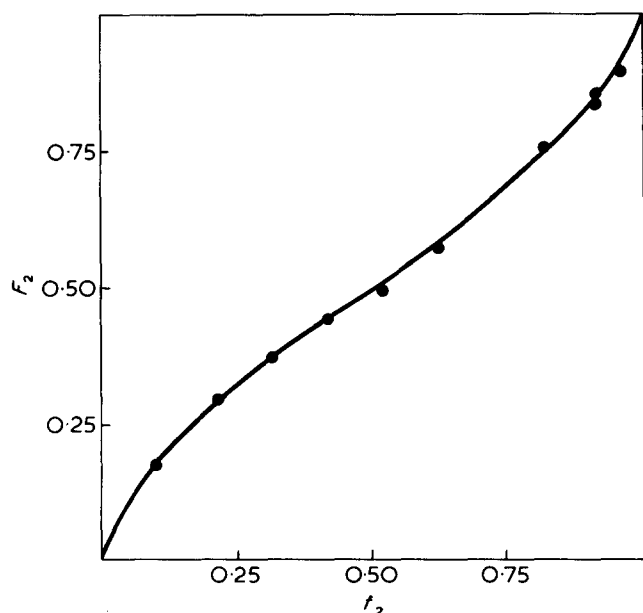


Figure 2 Copolymer composition for the copolymerization of S (1) and MMA (2) in acetone at 50°C

In order to evaluate whether solvent interaction influences the monomer or the growing radicals, we have measured the i.r. absorption of monomer mixtures with the different solvents. The spectroscopic data related to the stretching frequencies of the alkene groups are reported in Table 2. The strong absorption bands of DMF in that wavelength region prevented any measure of DMF–monomer interactions.

The above data do not show any change in the stretching frequencies of vinyl and vinylidene groups for the different monomer–solvent mixtures. Even if the above experimental evidence cannot be considered conclusive owing to the contrasting opinions on the validity of this argument<sup>15,22,23</sup>, we suggest that interactions with solvents, if any, are not so remarkable as to affect monomer reactivities in an appreciable way.

Figure 4 shows  $r_1$  and  $r_2$  as functions of the solvent dielectric constant,  $\epsilon$  at 50°C. For evaluating  $\epsilon_{50^\circ}$  interpolations and extrapolations of literature values have been used<sup>24,25</sup>. A good correlation between monomer reactivity ratios and  $\epsilon$  is evident. An increase of solvent dielectric constant corresponds to a decrease of both reactivity ratios, which is more pronounced for  $r_1$  than for  $r_2$ . The

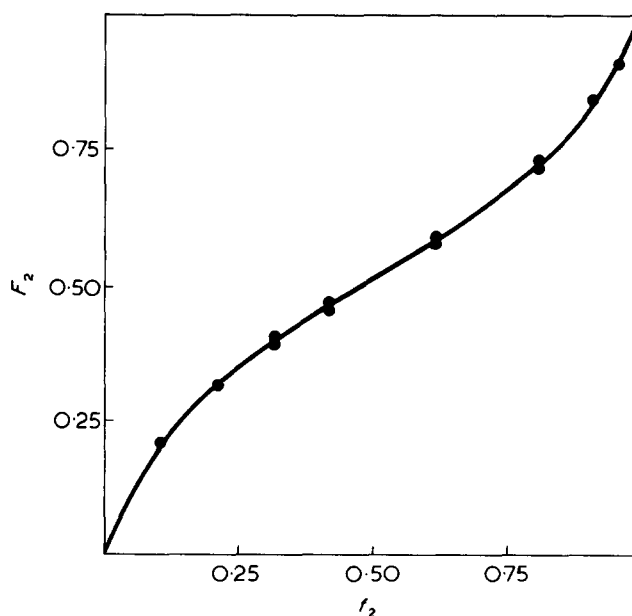


Figure 3 Copolymer composition for the copolymerization of S (1) and MMA (2) in DMF at 50°C

sodium chloride microcells (0.075 mm pathlength), using 15% (v/v) solutions. A Perkin-Elmer grating spectrometer Model 225 was employed.

## RESULTS AND DISCUSSION

Copolymer composition data as functions of monomer feed are reported in Figures 1–3 and refer to acetone, dioxane and DMF solutions, respectively. Monomer reactivity ratios are quoted in Table 1. For comparison, the values referred to bulk copolymerization at 50°C are also given. The slight discrepancy with previous data in bulk<sup>2</sup> is due to the novel method used for the calculation of  $r_1$  and  $r_2$ <sup>21</sup>.

From the data of Table 1 it is evident that all solvents used in the copolymerization experiments affect copolymer composition considerably. Both  $r_1$  and  $r_2$  are significantly changed.

Table 1 Reactivity ratios for the copolymerization of S and MMA at 50°C in various solvents

Solvent	$r_1$	$r_2$	$r_1 \cdot r_2$
dioxane	0.56 <sub>2</sub>	0.53 <sub>1</sub>	0.29 <sub>8</sub>
acetone	0.49 <sub>2</sub>	0.49 <sub>6</sub>	0.24 <sub>4</sub>
DMF	0.38 <sub>0</sub>	0.45 <sub>3</sub>	0.17 <sub>2</sub>
bulk	0.47 <sub>7</sub>	0.45 <sub>8</sub>	0.21 <sub>9</sub>

Table 2 Stretching frequencies (in  $\text{cm}^{-1}$ ) of alkene groups from i.r. spectra of S and MMA in various solvents

Solvent	C=C <sub>S</sub>	C=C <sub>MMA</sub>
dioxane	1631	1637
acetone	1629	1637
DMF	—	—
bulk	1630	1639

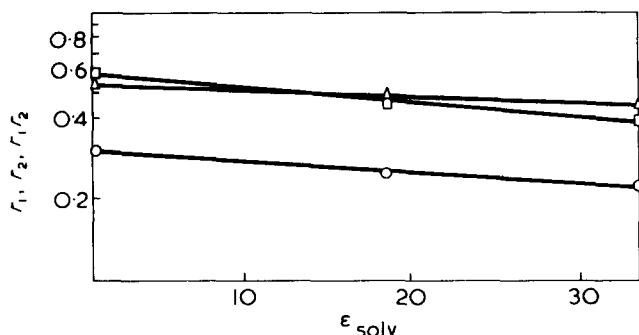


Figure 4 Reactivity ratios and alternation tendency of S-MMA pair as functions of solvent dielectric constant at 50°C. □,  $r_1$ ; △,  $r_2$ ; ○,  $r_1 r_2$

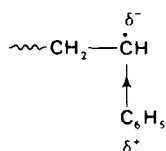
simultaneous decrease of both monomer reactivity ratios determines a marked increase of the alternating tendency, inversely proportional to the product  $r_1 \cdot r_2$ .

As has been recently recalled<sup>15</sup>, Bamford *et al.*<sup>26</sup> already foresaw the variation of reactivity ratios by changing the dielectric constant of the reaction medium; the assumption<sup>19</sup> of growing chains almost insensitive to the environment, because of their radical character, has been mainly based on earlier results<sup>18</sup>, affected by large experimental errors in the determination of monomer reactivity ratios. Quite recently<sup>27</sup>, Joshi has reviewed the various published methods of calculating  $r_1$  and  $r_2$ . All the earlier methods are considered inadequate and obsolete, whereas new computer programs<sup>28-30</sup> for minimizing errors lead to the maximum reliable information about monomer reactivity ratios.

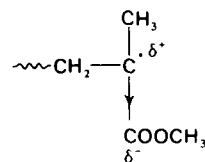
Using a very accurate set of analytical data for copolymer composition and a newer computer method<sup>21</sup> we have obtained the values of  $r_1$  and  $r_2$  given in Table 1. They do show an unequivocal solvent effect, which seems to be mainly due to changes in the dielectric constant. Variations in the propagation rate constants for the homopolymerization of styrene<sup>31,32</sup> and methyl methacrylate<sup>33-35</sup> in several solvents have been recently discovered. Often, the solvent effects show an opposite trend for the two monomers; a decrease of  $k_p$  for styrene polymerization corresponds to an increase of  $k_p$  for methyl methacrylate. Such effects are not confined only to aromatic solvents, but seem to be more general. Bamford *et al.*<sup>33</sup> and later Cameron *et al.*<sup>32</sup> interpret the above results in terms of stability and reactivity of the complex between growing radical and solvent as compared to the reactivity of the growing chain towards the monomer. This interpretation, supported by indirect evidence<sup>36,37</sup> is an extension of the well known radical complex theory by Henrici-Olivé and Olivé<sup>38-41</sup>. In a more general sense, it has been stated<sup>42</sup> that polymer radical 'complexing' can be regarded as an enhanced form of radical solvation by monomer and/or solvent.

The polarity of the medium would be expected to affect activation energies and entropies of propagation, by enhancing polarized forms of the growing radical in the transition state, although no charged species are directly involved in propagation. The polar character of polymer radicals has been recently reviewed by Jenkins<sup>43</sup>.

The growing chains ending with a styrene unit are mainly polarized by the electron-donating phenyl group:



whereas the electron-withdrawing ester group gives methyl methacrylate growing ends which are oppositely polarized:



On these grounds, the alternation tendency in the copolymerization of styrene and methyl methacrylate can be easily derived. Polar solvents will enhance the role of the polarized forms, resulting in a marked increase of the alternation tendency. The stronger effect on  $r_1$  in comparison to  $r_2$  may be ascribed to an opposite behaviour of  $k_{11}$  in solution as compared to  $k_{22}$ . The same patterns already discovered for bromobenzene<sup>32,33</sup>, diethyl malonate<sup>32,35</sup> and benzonitrile<sup>32,33</sup>, which increase  $k_{22}$  but decrease  $k_{11}$ , has been recently found to be valid also for the solvents considered in other studies of the present work<sup>44</sup>.

Also from the results of Ito and Otsu<sup>16</sup>, who were the first to point out a solvent effect in the copolymerization of styrene and methyl methacrylate, it is clearly evident that both  $r_1$  and  $r_2$  decrease as the dielectric constant of the solvent increases, although owing to large experimental errors, the data points do not fit a straight line\*. Nevertheless, here again  $r_1$  seems to be more solvent-dependent than  $r_2$ .

## CONCLUSIONS

The solvent effects on the monomer reactivity ratios for the pair styrene-methyl methacrylate appear to be connected mainly with the polarity of the polymerizing medium. The enhancement of polarized forms of the growing radicals by polar solvents can explain the increase of the alternating tendency.

From our results it may be expected that highly polar solvents would give rise to alternating-type copolymers.

Further work in this area seems to be needed in the future.

## ACKNOWLEDGEMENT

This work has been supported by the Italian CNR (project no.2/72.0057.03 115.0780).

## REFERENCES

- Bontà, G., Gallo, B. M. and Russo, S. *JCS Faraday Trans. I* 1973, **69**, 328
- Russo, S., Gallo, B. M. and Bontà, G. *Chim. Ind. (Milan)* 1972, **54**, 521
- Izumi, Z., Kiuchi, H., Watanabe, M. and Uchiyama, H. *J. Polym. Sci. (A)* 1965, **3**, 2721
- Kerber, R. *Makromol. Chem.* 1966, **96**, 30
- Nikolayev, A. F. and Gal'perin, V. M. *Vysokomol. Soedin. (A)* 1967, **9**, 2469
- Ryabov, A. V., Semchikov, Yu. D. and Slavnikskaya, N. N. *Vysokomol. Soedin. (A)* 1970, **12**, 553
- Saini, G., Leoni, A. and Franco, S. *Makromol. Chem.* 1971, **144**, 235
- Johnston, N. W. and McCarthy, N. J., Jr. *Polym. Prepr.* 1972, **13**, 1278

\* The curve-fitting method proposed by Braun *et al.*<sup>21</sup> clearly shows the poor confidence limits of the experimental points and the implied errors in the derived monomer reactivity ratios.

- 9 Jacob, M., Smets, G. and De Schryver, F. *J. Polym. Sci. (B)* 1972, **10**, 669
- 10 Perek, L. *J. Polym. Sci. (B)* 1973, **11**, 267
- 11 Franco, S. and Leoni, A. *Polymer* 1973, **14**, 2
- 12 Leoni, A., Franco, S. and Saini, G. *Makromol. Chem.* 1973, **165**, 97
- 13 Saini, G., Leoni, A. and Franco, S. *Makromol. Chem.* 1971, **147**, 213
- 14 Guillot, J., Graillat, G. and Guyot, A. *IUPAC Int. Symp. Macromolecules Aberdeen* 1973, Abstract B6
- 15 Cameron, G. G. and Esslemont, G. F. *Polymer* 1972, **13**, 435
- 16 Ito, T. and Otsu, T. *J. Macromol. Sci. (A)* 1969, **3**, 197
- 17 Azikonda, L. and Chapiro, A. *Proc. 3rd Symp. Radiat. Chem., Tihany, Hungary* 1971 1972, p 555
- 18 Price, C. C. and Walsh J. G. *J. Polym. Sci.* 1951, **6**, 239
- 19 Walling, C. in 'Free Radicals in Solution', John Wiley, New York, 1957, p 102
- 20 Ritchie, C. D., Skinner, G. A. and Badding, V. G. *J. Am. Chem. Soc.* 1967, **89**, 1447
- 21 Braun, D., Brendlein, W. and Mott, G. *Eur. Polym. J.* 1973, **9**, 1007
- 22 Zubov, V. P. et al. *J. Polym. Sci. (C)* 1968, **23**, 147
- 23 Bamford, C. H. and Brumby, S. *Makromol. Chem.* 1970, **134**, 159
- 24 'Handbook of Chemistry and Physics', 49th Edn, The Chemical Rubber Co., Cleveland, 1968
- 25 Bass, S. J., Nathan, W. I., Meighan, R. M. and Cole, R. H. *J. Phys. Chem.* 1964, **68**, 509
- 26 Bamford, C. H., Barb, W. G., Jenkins, A. D. and Onyon, P. F. 'The kinetics of Vinyl Polymerization by Radical Mechanisms', Butterworths, London, 1958, p 162
- 27 Joshi, R. M. *J. Macromol. Sci. (A)* 1973, **7**, 1231
- 28 Mortimer, G. A. and Tidwell, P. W. *J. Polym. Sci. (A)* 1965, **3**, 369
- 29 Yezrielev, A. I., Brokhina, E. L. and Roskin, Y. S. *Vysokomol. Soedin. (A)* 1969, **11**, 1970
- 30 Mortimer, G. A. and Tidwell, P. W. *J. Macromol. Sci. (C)* 1970, **4**, 281
- 31 Cameron, G. G. and Cameron, J. *Polymer* 1973, **14**, 107
- 32 Burnett, G. M., Cameron, G. G. and Joiner, S. N. *JCS Faraday Trans. I* 1973, **69**, 322
- 33 Bamford, C. H. and Brumby, S. *Makromol. Chem.* 1967, **105**, 122
- 34 Burnett, G. M., Cameron, G. G. and Zafar, M. M. *Eur. Polym. J.* 1970, **6**, 823
- 35 Zafar, M. M. *Makromol. Chem.* 1972, **157**, 219
- 36 Kalashnikova, L. A., Buchachenko, A. L. and Neiman, M. B. *Russ. J. Phys. Chem.* 1968, **42**, 598
- 37 Burnett, G. M., Cameron, G. G. and Cameron, J. *JCS Faraday Trans. I* 1973, **69**, 864
- 38 Henrici-Olivé, G. and Olivé, S. *Makromol. Chem.* 1963, **68**, 219
- 39 Henrici-Olivé, G. and Olivé, S. *Z. Phys. Chem. (Frankfurt)* 1965, **47**, 286
- 40 Henrici-Olivé, G. and Olivé, S. *Z. Phys. Chem. (Frankfurt)* 1966, **48**, 35, 51
- 41 Henrici-Olivé, G. and Olivé, S. *Makromol. Chem.* 1966, **96**, 221
- 42 Scott, G. E. and Senogles, E. *J. Macromol. Sci. (C)* 1973, **9**, 49
- 43 Jenkins, A. D. 'Chemical Transformations of Polymers', *IUPAC Int. Conf. Bratislava, 1971* Butterworths, London, 1972, p 167
- 44 Bontà, G. et al. *JCS Faraday Trans. I* in press

# Synthesis and characterization of some copolycarbonates of 2,2-bis(4-hydroxyphenyl) propane (bisphenol A) and 1,4-bis-(hydroxymethyl) decafluoro-bicyclo(2.2.1) heptane

G. A. Adam, I. W. Parsons and R. N. Haward

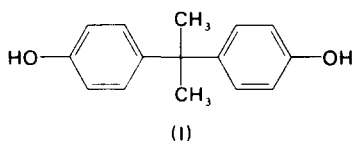
Department of Chemistry, University of Birmingham, PO Box 363, Birmingham B15 2TT, UK

(Received 2 December 1974)

The preparation and properties of the copolycarbonates of bisphenol A (I) and 1,4-bis(hydroxymethyl) decafluoro-bicyclo (2.2.1) heptane (II) are described. Most of the copolymers were prepared by reaction with phosgene in a mixture of pyridine and methylene dichloride. Bisphenol A polycarbonate molecular weights could be controlled by the use of small quantities of *p*-cresol. Increasing quantities of II led to a slight reduction in the glass transition temperature ( $T_g$ ) of the copolymers and to an increased solubility in, for example, acetone. At the same time the heat stability, as measured thermogravimetrically, increased. Even small quantities of II in the copolymer have a substantial effect in reducing the tendency to crystallize and in limiting annealing effects. When heated at 120–140°C polycarbonate (I) shows an increase in yield strength and develops a substantial peak in the d.s.c. curve at  $T_g$ . These changes are much reduced by small amounts of copolymerized II. Dynamic mechanical properties were measured on a Rheovibron dynamic viscoelastometer.

## INTRODUCTION

The polymers prepared by the reaction of 2,2-bis(4-hydroxyphenyl) propane (bisphenol A) (I) with phosgene to give 'polycarbonate' plastics have assumed increasing importance in recent years and a number of analogous polymers and copolymers have been prepared and studied<sup>1–4</sup>.

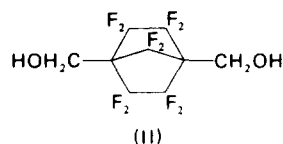


Further, as 'polycarbonate resin' has become commercially available and widely applied, more has been learnt about their valuable properties and also about their limitations. Thus several originally unsuspected characteristics have come to light, many of which are not understood and most of which were not included in early studies of copolymers or analogous polyacrylates.

Among the properties of polycarbonate which have recently become of interest we may include a tendency to slow and partial crystallization and their response to annealing<sup>5–8</sup>. When annealed at elevated temperatures below the glass transition temperature,  $T_g$ , polycarbonate develops a nodular structure visible under the electron microscope<sup>5</sup>; this is accompanied by an increase in yield strength and a characteristic peak observable at  $T_g$  in a differential scanning calorimeter. These annealing effects are accompanied by a decrease in impact strength<sup>8,9</sup>, although there are only very minor changes in low temperature relaxation behaviour<sup>9</sup>. The polymer is also rather sensitive to solvent stress cracking<sup>10,11</sup>.

In view of these features we decided to prepare some

polycarbonate copolymers containing fluorine and to study their physical properties and since a new fluorine containing diol had been prepared in this Department we decided to use it in these studies. The compound was 1,4-bis(hydroxymethyl) decafluoro-bicyclo (2.2.1) heptane (II):



In the present work particular interest was attached to the question of a possible relation between the response to annealing and crystallization properties. Some theories of annealing behaviour propose significant analogies between the two processes<sup>12,13</sup> and if they are correct then both annealing and crystallization should be affected in the same way by the introduction of comonomers.

The preparation and properties of the copolymers are described below.

## EXPERIMENTAL

### Materials

Bisphenol A was a gift from Shell Chemicals UK Ltd. It was recrystallized to m.p. 160°C. Phosgene, nitrogen, dichloromethane, pyridine and tetrahydrofuran (THF) were purified by standard methods before use. *p*-Cresol (BDH Ltd) was used as supplied. 1,4-Bis(hydroxymethyl) decafluoro-bicyclo (2.2.1) heptane was prepared by a modified procedure as follows. To a stirred mixture of 1*H*, 4*H*-decafluoro-bicyclo (2.2.1) heptane<sup>14</sup> (20.0 g), 37–41% (w/v) formalin (300 cm<sup>3</sup>) and dimethylsulphoxide (1 dm<sup>3</sup>) were

added portionwise 50 g of KOH pellets. The mixture was stirred at room temperature for ~2 h and then for 16 h at 75°C. The cooled mixture was then acidified with concentrated HCl, poured into water (0.5 dm<sup>3</sup>) and extracted with ether (3 x 0.5 dm<sup>3</sup>). The ethereal extracts were washed with water and dried (MgSO<sub>4</sub>) before removal of the solvent by fractional distillation. The residue was sublimed to give a crude product (21.5 g) which was recrystallized twice from CCl<sub>4</sub> to give 19.0 g of 1,4-bis(hydroxymethyl)decafluorobicyclo (2.2.1) heptane, m.p. 210°C (lit. 210–210.5°C<sup>15</sup>) with a correct i.r. spectrum<sup>16</sup>.

**Polymerization procedures**

**Homogeneous systems.** Some homogeneous polymerizations were carried out in pure pyridine but most polymers, including all the copolymers, were made on a 70 g scale in a mixed solvent system, using CH<sub>2</sub>Cl<sub>2</sub>/C<sub>5</sub>H<sub>5</sub>N, which gave higher molecular weights. The techniques employed followed closely those described in ref 17.

**Heterogeneous systems.** A series of two phase polymerizations were carried out using the procedure described in ref 18. Several batches of homopolymers were prepared in this system both with and without *p*-cresol as molecular weight modifier. Copolymerizations in this system proved unsuccessful (see text).

**Polymer characterization**

The following procedures were employed

**Viscometry,** using Ubbelohde suspended level viscometers at 25 ± 0.01°C. The solvent used was CH<sub>2</sub>Cl<sub>2</sub> and the values used in the Mark–Houwink equation<sup>19</sup> are:

$$K = 1.11 \times 10^{-2} (\eta \text{ in cm}^3/\text{g})$$

$$\alpha = 0.82$$

The results obtained with commercial materials agreed with the values supplied by the manufacturer<sup>20</sup>.

**Vapour pressure osmometry (v.p.o.),** using a Perkin-Elmer Hitachi model 115 instrument, with CHCl<sub>3</sub> as solvent at 32 ± 0.2°C.

**Gel permeation chromatography (g.p.c.),** using a Waters Association analytical instrument fitted with a differential refractometry detector. Solutions of 2.5 g polymer/dm<sup>3</sup>

THF were employed at 25°C. Calibration was against standard polystyrenes.

**Infra-red (i.r.) spectroscopy,** using a Perkin-Elmer 257 grating instrument.

**<sup>1</sup>H n.m.r. spectroscopy,** using a Perkin-Elmer R12 instrument, operating at 60 MHz; samples were run as CDCl<sub>3</sub> solutions, with an internal TMS standard.

**Tensile tests,** were performed on an Instron floor model TT-BM or a metric table model Tm-M. The tests were carried out in a controlled environment at 23 ± 1°C and 50 ± 5% relative humidity.

**Dynamic mechanical properties** of the materials were determined on a Rheovibron Direct Reading Viscoelastometer, Model DDVII.

**Differential scanning calorimetry (d.s.c.)** was performed on a Perkin-Elmer DSC-2 machine.

**Differential thermal gravimetry** was performed using a Perkin-Elmer Thermobalance, Model TGS-1.

**Preparation of copolymers and homopolymers**

Three systems were tried for these polymerizations, viz. two homogeneous systems (one using pure pyridine as solvent) and one with a mixed pyridine/dichloromethane solvent) and a heterogeneous (two phase) system. Initial trials showed that all three of these systems gave efficient homopolymerizations of bisphenol A, with a heterogeneous system giving generally higher molecular weights, but that only the homogeneous system with mixed solvents gave good copolymerizations. The heterogeneous system gave crude 'copolymers' which certainly contained fluorine, as evidenced by elemental analyses, but partial extraction of these materials with dichloromethane gave fractions which differed greatly in their fluorine contents, showing that these copolymers were not uniform. Further efforts at copolymerizations were therefore concentrated on the homogeneous system.

In the homogeneous systems it was found that use of a pure pyridine solvent gave materials of rather low molecular weight, but that the mixed solvent system gave high molecular weight material. The range of materials prepared and used are described in Table 1.

The early trials showed the necessity of allowing separately for the effects of molecular weight and fluorocarbon (como-

Table 1 Properties of the main polymers referred to in this work

Type of polymer	Mol % by elemental analysis	% by n.m.r.	$\bar{M}_n \times 10^{-3}$ by V.P.O.	G.p.c. results			$[\eta]$ (cm <sup>3</sup> /g)	$\bar{M}_v \times 10^{-3}$	$T_g$ (K) from d.s.c.
				$\bar{M}_n \times 10^{-3}$	$\bar{M}_w \times 10^{-3}$	$\bar{M}_w/\bar{M}_n$			
Mobay Grade M39	—	—	14.3	12.4 12.0*	31.3 27*	2.53 2.25*	45.5	25.5	421
Makrolon 5705	—	—	—	—	82–84*	—	115	78	431
Makrolon 5730	—	—	—	—	74–77*	—	106	71	429
Synthetic polycarbonate	—	—	—	—	—	—	117	80	430
2% Copolymer	1.5	1.3	27	35	80	2.3	113	77	429
5% Copolymer	4.0	3.5	11	17	40	2.3	62	38	422
10% Copolymer	9.8	7.1	21	24	58	2.4	84	54	421
15% Copolymer	15.4	12.0	60 ± 20†	65	130	2.3	130	92	422
20% Copolymer	19.6	15.4	23	25	59	2.3	73	45	415
50% Copolymer	50	43	15	16	36	2.3	40.0	22	390

\* Information supplied by the manufacturer

† This value is outside the accurate range of the instrument used

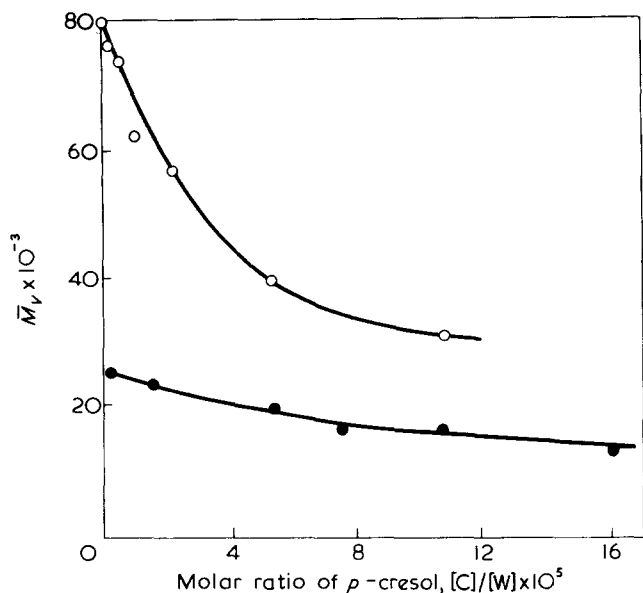
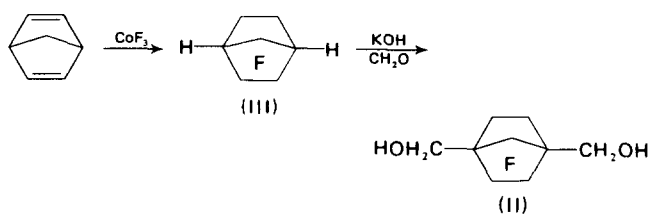


Figure 1 Effect of added *p*-cresol on the molecular weight of polycarbonate prepared by homogeneous (●) and heterogeneous (○) polymerization processes

nomer) content upon some of the physical properties of the polymers. Consequently, efforts were made to prepare a range of bisphenol A polycarbonates of differing molecular weights. Two approaches were made to this problem. First, using both the heterogeneous and homogeneous systems, the rate of phosgenation was varied, particularly towards the end of the reaction. This did vary the molecular weights somewhat, but did not produce a wide enough range; also, the reproducibility of this method was poor. Secondly, *p*-cresol was used as a molecular weight modifier, following the method of Weilgosz *et al.*<sup>21</sup>. This produced an acceptable range of molecular weights, using the heterogeneous system for high molecular weights, and the (pure pyridine) homogeneous system for the lower ones.

#### Synthesis of the fluorocarbon diol

This compound was prepared by the following (schematic) route:



where F in the ring denotes 'all unmarked bonds to fluorine'.

In this sequence the intermediate 1*H*,4*H*-decafluoro-bicyclo (2.2.1) heptane (III) was available to us<sup>15</sup>, but the published method for the second stage proved difficult to scale up. A modified procedure has therefore been developed (see above) which consistently gives large batches of pure product. It should be pointed out that even small deviations from this procedure give much reduced yields.

Simple theory shows that in a closed condensation polymerization system where the molecular weight is determined by adventitious terminating agents, T:

$$\bar{M}_n = \frac{2[W]}{[T]}$$

where [W] is the initial monomer concentration. Thus, when an artificial terminator C is introduced:

$$\bar{M}_n = \frac{2[W]}{[T + C]}$$

Since [T] will be different for the two systems which we have studied, a plot of  $\bar{M}_n$ , or  $\bar{M}_v$  for these polymers against the concentration of *p*-cresol will give two separate curves (Figure 1).

Also, for any system:

$$\frac{1}{\bar{M}_n} - \frac{1}{\bar{M}_{n0}} = \frac{[C]}{2[W]}$$

where  $\bar{M}_{n0}$  is the number average molecular weight obtained with a given system in the absence of added terminator.

Further we have found from g.p.c. measurements (with homopolymers) that  $\bar{M}_v \sim 2.5 \bar{M}_n$  so that in this case:

$$\frac{1}{\bar{M}_v} - \frac{1}{\bar{M}_{v0}} = \frac{[C]}{[W]}$$

A plot of results from both systems in this form is given in Figure 2 where the gradient is found to be 0.23, i.e. it is in good agreement with expectation for simple theory and also suggests that our preparation methods are reasonably satisfactory.

## RESULTS AND DISCUSSION

### Polymer characterizations

The physical methods employed give the results shown in Table 1. Some comments are, however, required. The most

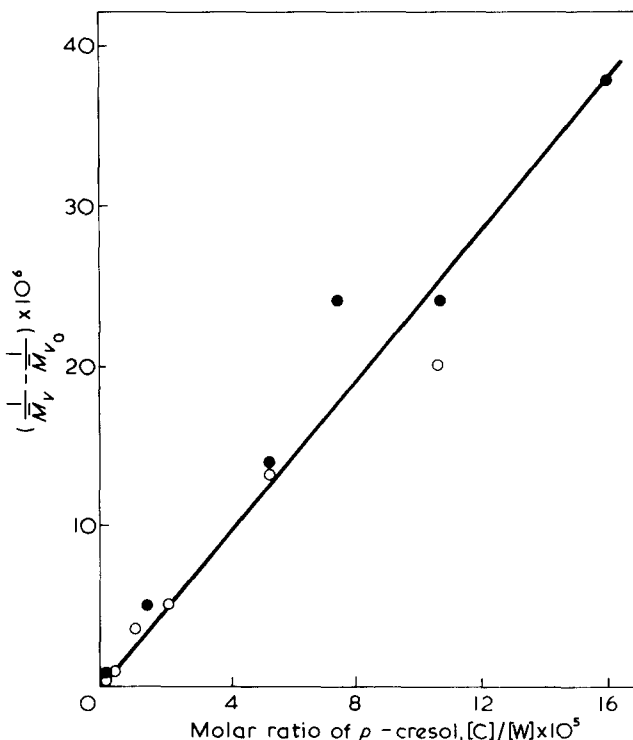
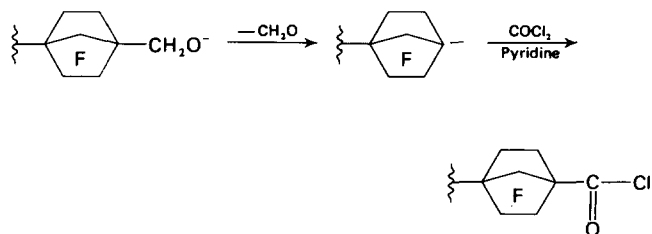


Figure 2 Relation between the reciprocal molecular weight and the concentration of added chain terminator. ● Homogeneous; ○, heterogeneous system

general characterization procedures are of course those of d.s.c. and g.p.c. The g.p.c. results require interpretation, however, since they depend upon the size of the polymer molecules per unit molecular weight, which is a variable from polymer to polymer. In this work the most internally consistent set of all molecular weights is obtained if the molecular weight of the polymer is worked out by calculating the weight per Å of the extended copolymer chain, using the figure for percentage fluorocarbon incorporation calculated from the elemental analysis figures, doing the same for polystyrene, and then assuming that these two (rather different) chains behave similarly with respect to coil volume, degree of extension in the solvent, etc. These results are the ones included in *Table 1*. The intrinsic viscosities of the copolymers are, of course, experimental data, but their conversion into  $\bar{M}_v$  numbers is a difficulty. This has been done using values for  $K$  and  $\alpha$  appropriate to homopolymer. It is realised that inaccuracies will occur here, but this procedure seems to be the best available.

However, since the  $\bar{M}_n$  values were directly measured for the copolymers and were generally more relevant to the comparison of physical properties of different polymers the difficulty over  $\bar{M}_v$  does not play a very significant part in the subsequent discussion.

Two further points need to be made concerning the copolymers. First, i.r. spectroscopy could be used qualitatively to determine the incorporation of fluorocarbon into the copolymer: a band at  $935\text{ cm}^{-1}$  appeared to belong to the fluorocarbon unit, and one at  $890\text{ cm}^{-1}$  to belong to the bisphenol A unit. Secondly, the amount of fluorocarbon incorporated could be estimated from  $^1\text{H}$  n.m.r. spectroscopy, by integrating a band at  $4.8\text{--}4.95$  ( $\text{CH}_2\text{O}$ ) against bands at  $1.5\text{--}1.755$  ( $-\text{CH}_3$ ) and/or the aromatic protons. Calculations based on these results suggest lower comonomer contents than do the elemental analyses. Whilst we can offer no proof, we suggest the following reaction sequence as a possible explanation of this:



In this way, there would be less than two  $\text{CH}_2\text{--O}$  units per fluorocarbon unit incorporated into the chain.

#### Thermal stability of copolymers

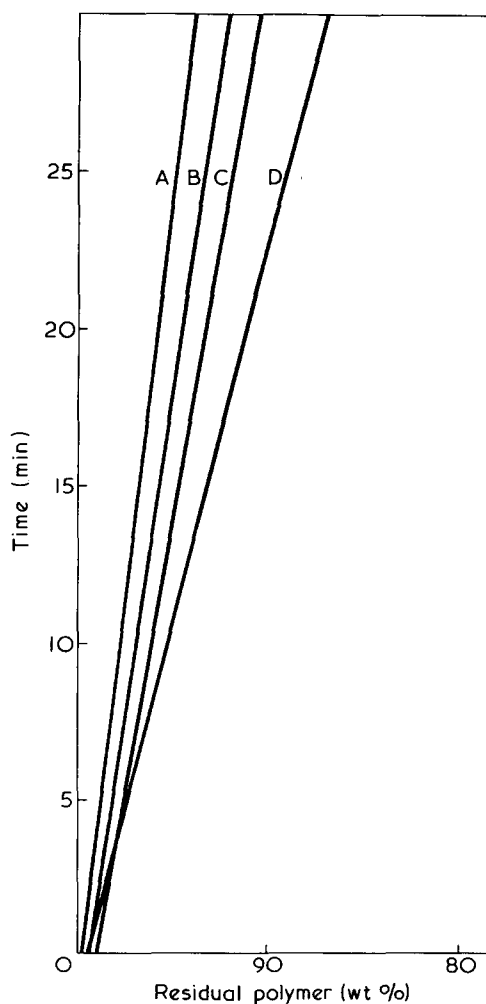
It is important that any copolymer of polycarbonate should have an adequate thermal stability, since processing (e.g. moulding) must inevitably take place above the relatively high glass transition temperatures (around  $160^\circ\text{C}$  — see below). In order to estimate thermal stability at high temperatures it is convenient to employ thermogravimetric analysis, i.e. the specimen is heated to a high temperature and changes of weight are observed. Although the method is quite simple to apply it is necessary to ensure that the copolymers and homopolymers studied are themselves truly comparable. For this purpose we note that the degradation of polycarbonate has been reported to depend on the active hydrogen present either as water or as end groups<sup>22</sup>. The latter will lead to an influence due to molecular weight, which will be described in detail elsewhere<sup>23</sup>, but for the

present purpose it will be enough to ensure that all polymers compared lie within a reasonably narrow band of molecular weight ( $\bar{M}_n$ ).

Four polymers of this type are shown in *Figure 3* where the isothermal weight loss at  $410^\circ\text{C}$  is plotted as a function of time. It will be seen that the two copolymers have a thermal stability superior to the homopolymer prepared in the same way. However, the equivalent commercial polymer is better than the laboratory materials, probably indicating the use of a stabilizer or stabilizing treatment. Nevertheless direct comparison of equivalent homopolymers and copolymers shows that no special difficulty need be expected from this source.

#### Crystallization of polycarbonate copolymers

The polycarbonates studied in the present work were all 100% amorphous (as shown by d.s.c.) unless they were specially treated. However, it is well known that the polycarbonate of I may be crystallized in a number of ways. These include heating for long times at temperatures above  $T_g$ <sup>24</sup> and treatment with solvents<sup>25</sup>. We found it possible to obtain powdery products with relatively high crystallinity by dissolving the polymers in boiling 1,2-dichloroethane ( $78^\circ\text{C}$ ) and precipitating at  $80^\circ\text{C}$  in petroleum ether (b.p.  $80\text{--}100^\circ\text{C}$ ). The fine precipitates were dried under vacuum at  $100^\circ\text{C}$  for 8 h. A second method of treatment consisted



*Figure 3* Thermogravimograms of polymers and copolymers heated at  $410^\circ\text{C}$ . A, Makrolon 5730; B, 10% copolymer; C, 2% copolymer; D, synthetic polycarbonate



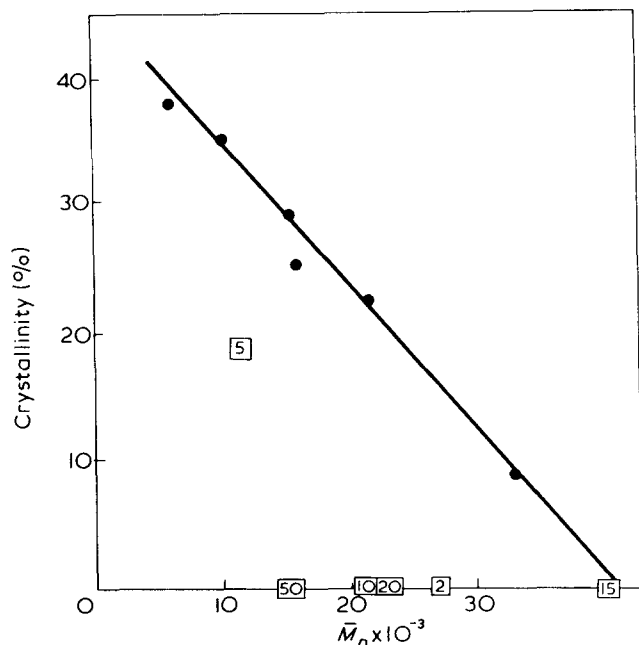


Figure 4 Crystallinity of copolymers and homopolymers precipitated from solution. ●, Homopolymers; □, copolymers with number showing percentage II. The homopolymers were synthesized to give a range of molecular weights

of simply heating the polymer at 195°C under vacuum for 8 and 21 days respectively. In each case the percentage crystallinity ( $T_m$  250–260°C) was determined by d.s.c. measurements assuming a heat of fusion of 30.7 cal/g. This value was obtained by averaging our own estimates and those quoted by Wineman<sup>26</sup>.

As the amount of crystallization achieved with a particular treatment was shown to depend on the molecular weight of the homopolymers, we have presented our results to show the percentage crystallinity measured for a copolymer of a particular molecular weight in such a way that the value can be related to that of a similar homopolymer (Figures 4 and 5). It will be seen that even small quantities of the comonomer (II) have a substantial effect on crystallization and that above 15% comonomer the amount of crystallization is virtually zero.

An unexpected property of the copolymers was their increased solubility in several organic solvents, those having 20% or more of the comonomer II being soluble in acetone and xylene. Probably for this reason the differences in crystallinity between copolymers and homopolymers was not as great when crystallinity was induced by soaking in acetone, though in this case also the copolymer did show a lower crystallization than the homopolymers. It was possible to measure the crystalline melting points of several copolymers and these were shown to fall with increasing comonomer content. At 15% of II the melting point was reduced by about 30°C.

As might be expected from the above, tensile experiments on films of copolymers containing appreciable amounts of II, carried out in organic solvents suggested that they were more solvent-sensitive than the homopolymer.

#### Glass transition temperature of copolymers

The effect of introducing II on the glass transition temperature of the copolycarbonates was not very large. Nevertheless the comonomer did have a significant effect in reducing  $T_g$  whether measured on the d.s.c. or from the high

temperature relaxation peak of the Rheovibron (using a cast film). With low comonomer concentrations the Rheovibron measurements gave higher values of  $T_g$  than those obtained by the d.s.c. (Figure 6) a result which was reasonable since the Rheovibron measurements were made at 11 Hz whereas the d.s.c. experiments were extrapolated to zero heating rate. However, the Rheovibron results also seemed to be more sensitive to the presence of comonomer and gave lower

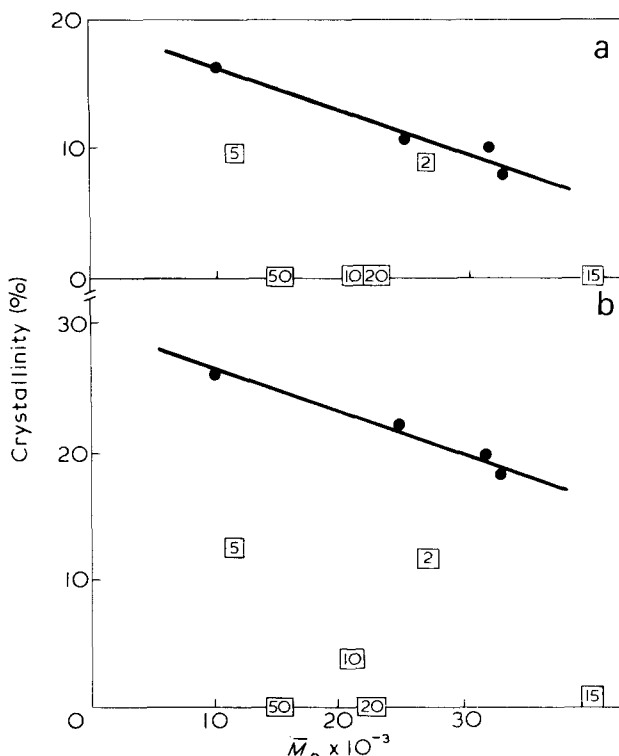


Figure 5 Crystallinity of polymers heated at 195°C for different periods: (a) 8 days; (b) 21 days. ●, Homopolymers; □, copolymers with number showing percentage II. The homopolymers were synthesized to give a range of molecular weights

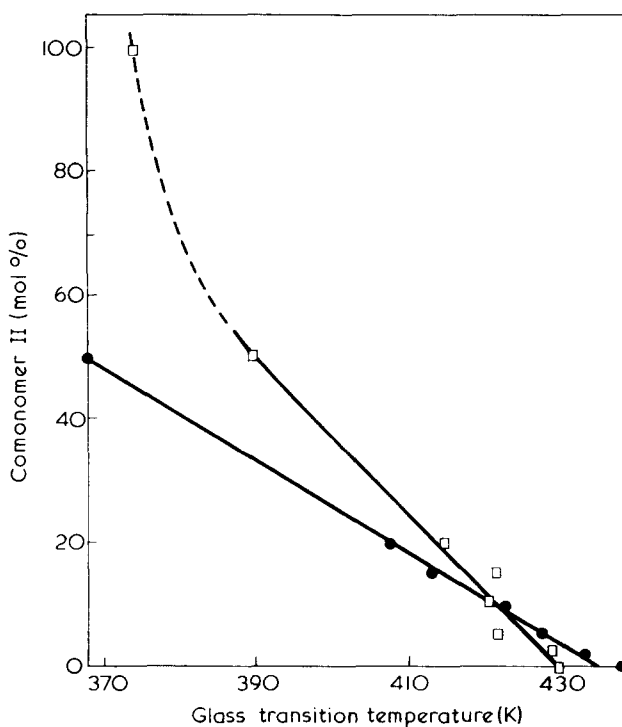


Figure 6 Glass transition temperature of homopolymers and copolymers. □, Measured by d.s.c.; ●, measured by the Rheovibron

Table 2 Mechanical properties of the copolymers

Fluorocarbon in copolymer (%)	Yield stress* (MN/m <sup>2</sup> )	Elongation		$M_n \times 10^{-3}$
		A	B	
0	61	150	156	33
2	60	180	190	27
5	59	208	†	11.2
10	58	215	†	21.2
15	56.5	240	260	40
20	56	217	†	22.5
50	37.5	135	†	15.2

\* Each value is the average of four tests which agree within  $\pm 1$  MN/m<sup>2</sup>

† The neck was not propagated along the whole specimen

A = Residual elongation (%) from bench marks after fracture

B = Elongation at break (%)

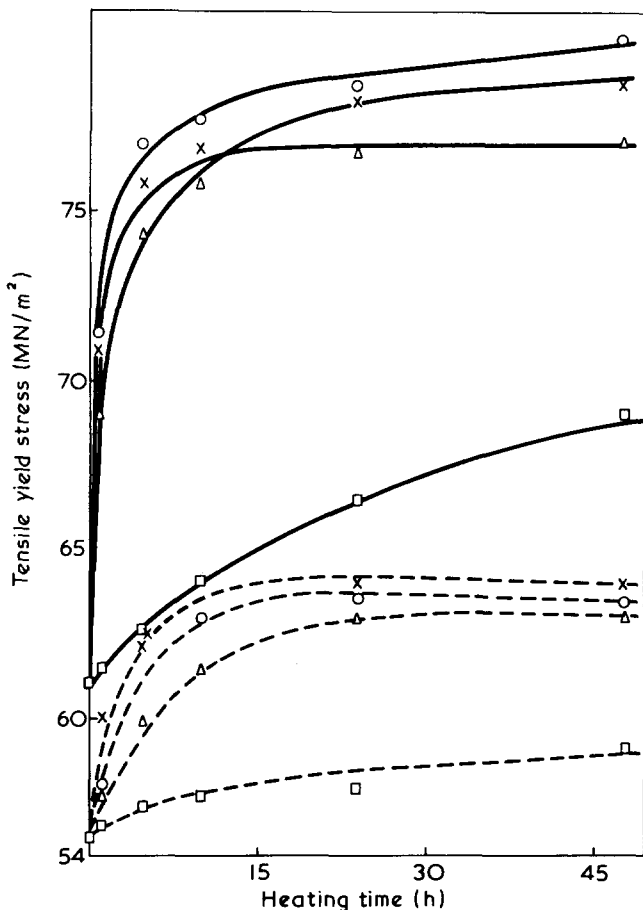


Figure 7 Effect of annealing below  $T_g$  on the tensile yield stress of synthetic polycarbonate and the 15% copolymer (---). □, 110°; △, 120°; ○, 130°; X, 140°C

values of  $T_g$  at higher monomer concentrations. The reason for this is not known. On the other hand, the observed reduction in  $T_g$  with increased amounts of II could be ascribed to the greater frequency of flexible linkages along the chain.

#### Tensile properties

Tensile experiments were carried out on films 0.5–1.5 mm thick. These were cast from 20% methylene chloride solution on glass plates and progressively dried out, first at room temperature for 12 h, then at 35°C for 5 h and finally at 80°C in vacuum. This temperature was chosen because it had been reported that annealing effects as measured mechanically were small below 80°C<sup>8</sup>.

Tensile test-pieces were cut from the films according to BS 2782 (1970) Fig 301.12, Method 301K, and tested on an Instron tester under standard conditions ( $23 \pm 1^\circ\text{C}$ ;  $50 \pm 2\%$  r.h.).

The results which are shown on Table 2 are in line with the observations on  $T_g$ . Increasing the comonomer leads to a small reduction in yield stress and to an increase in elongation at break. Molecular weight has been separately shown to have only a minimum effect on yield stress but it does effect elongation at break. Only polymers having  $\bar{M}_n > 27\,000$  exhibited necking along the whole length of the test-piece before fracture.

More interest attaches to the effect of annealing on tensile properties, since polycarbonates are known to become more brittle when annealed<sup>8,9</sup>. However, in studying annealing effects allowance might be necessary for differences in  $T_g$  since the most sensitive annealing temperatures might be lower for the copolymers than for the homopolymer. However, it will be seen from Figure 7 that synthetic polycarbonate and the 15% copolymer show the same differences in annealing response over a wide range of temperatures. At every temperature the homopolymer shows a much greater increase in yield stress than the copolymer.

The effect of copolymer composition may therefore be conveniently illustrated by annealing a series of materials for a standard time; e.g. 130°C for 48 h. The results can then be represented in terms of the relative increase in yield stress,  $\Delta\sigma/\sigma_0$ , due to the treatment, plotted against composition (Figure 8). It will be seen that even small quantities of the comonomer have a substantial effect on the magnitude of the annealing changes.

#### Study of annealing effects by d.s.c.

The influence of annealing in causing an endothermic peak at  $T_g$  in the differential scanning calorimeter has been known for some time<sup>6,7,27</sup>. These peaks therefore offer an alternative means of studying annealing effects to the measurement of yield stress. Again we studied similar materials to those used in the previous section and in Figures 9a and 9b we show the annealing behaviour of a homo-BPA polycarbonate compared with a 15% copolymer. The results

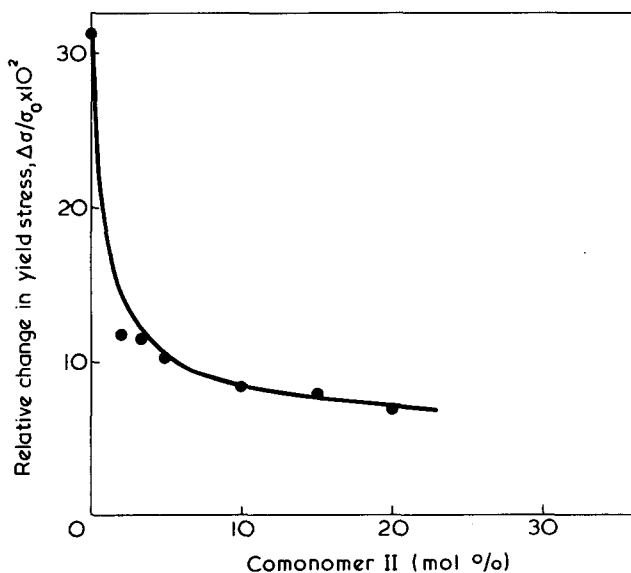


Figure 8 Relationship between copolymer composition and the relative change in yield stress due to annealing (heated at 130°C for 48 h)

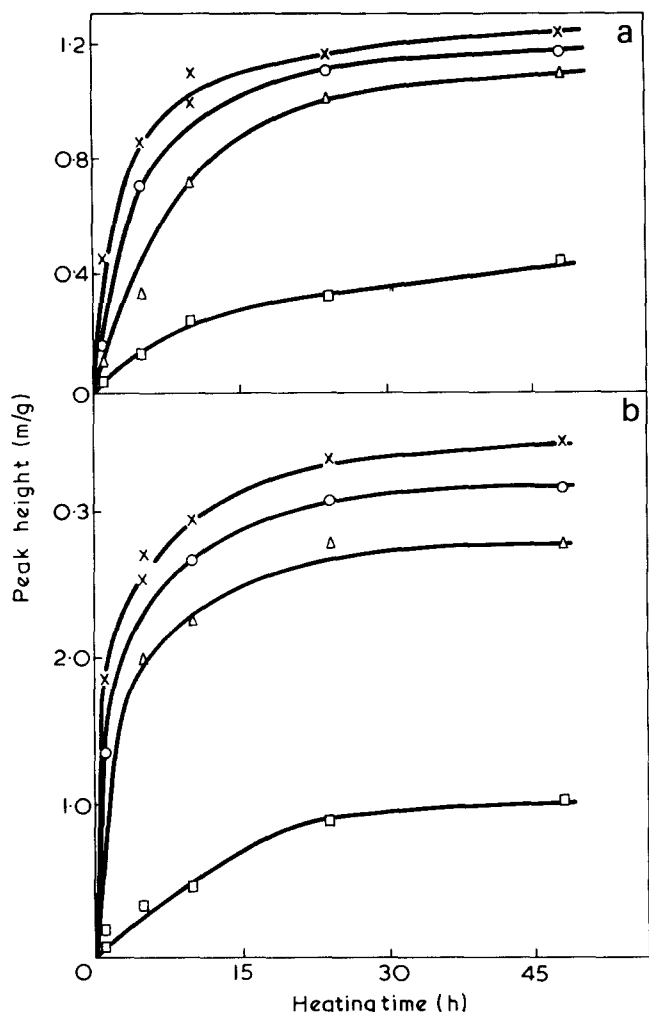


Figure 9 Effect of annealing time on d.s.c. peak height for polycarbonates. (a) 15% copolymer; (b) synthetic polycarbonate. □, 110°; △, 120°; ○, 130°; X, 140°C

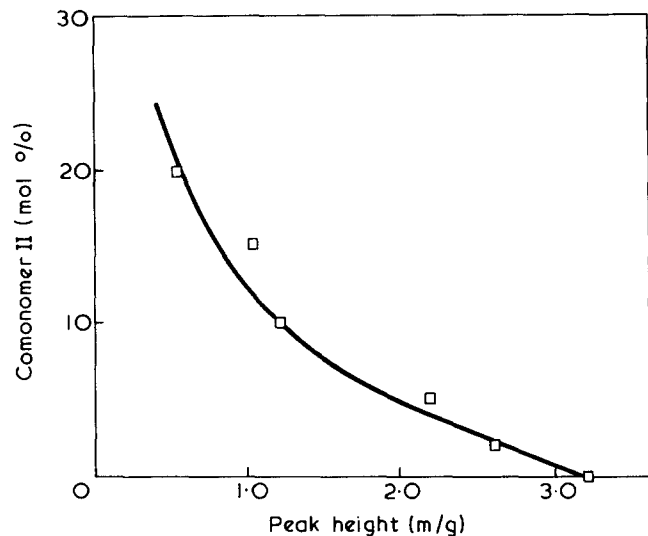


Figure 10 Effect of the fluorinated comonomer on the d.s.c. peak height developed by heating at 130°C. Time of heating, 48 h

obtained are analogous to these observed with yield stress. In every case the copolymer is much less affected by annealing than the homopolymer and the effect of comonomer content under constant annealing conditions may also be readily demonstrated (Figure 10).

Thus the introduction of the comonomer also reduces the effects due to annealing as measured by d.s.c.

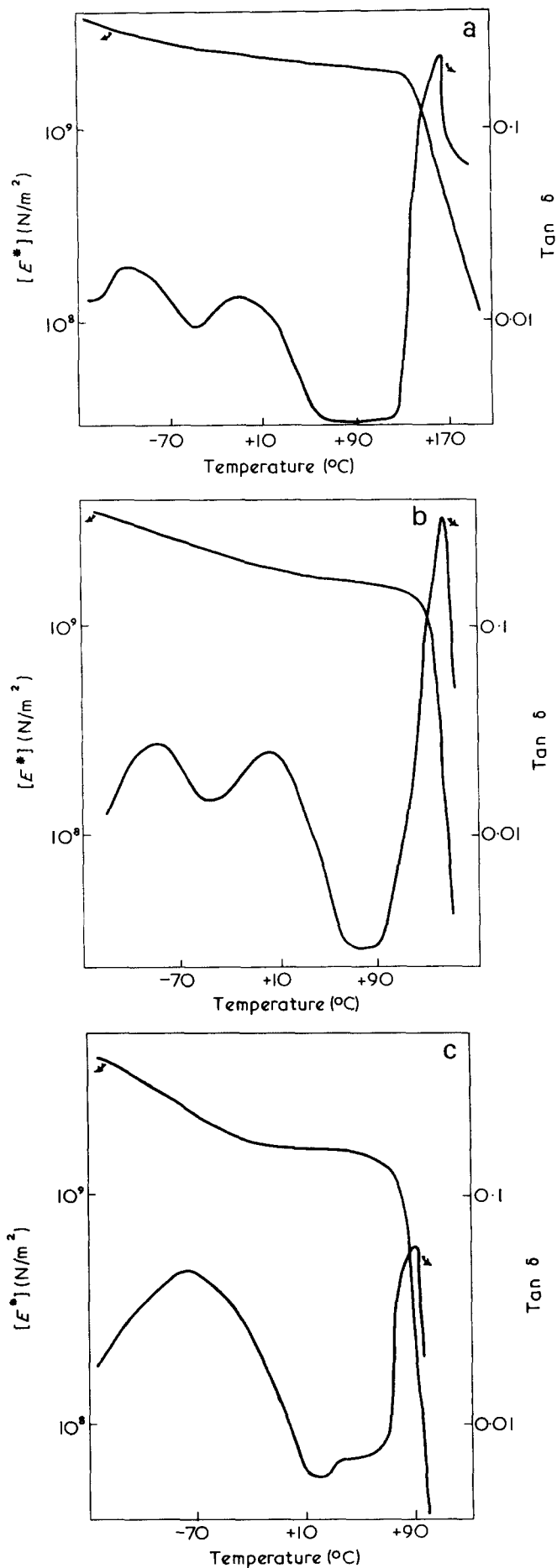


Figure 11 Dynamic mechanical measurements on polycarbonate homopolymer and copolymers. (a) Homopolymer,  $\bar{M}_v$  80 000; (b) 15% copolymer; (c) 50% copolymer

Dynamic mechanical properties

Dynamic measurements were carried out by means of a Rheovibron dynamic viscoelastometer using films cast from a 10% solution in 1,2-dichloroethane and dried out in vacuum for 24 h at 80°C.

Three examples of the curves obtained are shown in Figure 11, where typical results are given for the synthetic homopolymer, and the 15% and 50% copolymers. Briefly the results obtained may be summarized as follows.

(1) The main  $\alpha$  or glass transition peak remains sharp for all the materials used, suggesting a reasonably random copolymer structure. It moves to a lower temperature with increasing comonomer content (as previously stated).

(2) Two low temperature ( $\beta$ ) peaks are observed with the pure polycarbonate and with those copolymers which contain only small quantities of II. With 50% of II, however, only one low temperature peak is observed. Two peaks have not always been observed with polycarbonate<sup>9,28</sup> but Illers and Breuer<sup>29</sup> observed a broad loss peak which they ascribed to these overlapping peaks at -40, -100, and -150°C (1 Hz) while Le Grand and Erhardt<sup>30</sup> found two n.m.r. loss peaks at -150°C and -50°C (at  $2 \times 10^4$  Hz) which might well correspond with our results.

(3) The two peaks respond differently to the introduction of comonomer. The position of the low temperature peak, starting at -110°C for pure polycarbonate, rises steadily to -75°C with the 50% copolymer. On the other hand, the position of the -10°C peak does not vary significantly with comonomer content, but disappears completely when the level of II is raised to 50%.

While we do not propose to comment on the different behaviour of the two peaks we may note that the loss of specificity (broad peak) associated with the 50% copolymer may well correspond with a low degree of structural regularity in the glassy state.

ACKNOWLEDGEMENTS

We are indebted to Dr J. N. Hay for advice on differential scanning calorimetry and to Mr N. J. Mills and to Dr J. Berry of the University of Manchester Institute of Science and Technology for help in the use of the Rheovibron.

One of us (G.A.A.) wishes to thank the Iraqi Ministry of Higher Education for financial support.

REFERENCES

- 1 Schnell, H. 'The Chemistry and Physics of Polycarbonates', Wiley, New York, 1964
- 2 Ikeda, K. and Sekine, Y. *Ind. Eng. Chem. (Prod. Res. Dev.)* 1973, 12, 202, 212
- 3 Taimr, L. and Smith, J. G. *J. Polym. Sci. (A-1)* 1971, 9, 1203
- 4 Bier, G. *Polymer* 1974, 15, 527
- 5 Siegman, A. and Geil, P. H. *J. Macromol. Sci. (B)*, 1970, 4, 239
- 6 Ali, M. S. and Sheldon, R. P. *J. Appl. Polym. Sci.* 1970, 14, 2619
- 7 Ali, M. S. and Sheldon, R. P. *J. Polym. Sci. (C)* 1972, 38, 97
- 8 Golden, J. H., Hammant, B. L. and Hazell, E. A. *J. Appl. Polym. Sci.* 1967, 11, 1571
- 9 Allen, G., Morley, D. C. W. and Williams, T. *J. Mat. Sci.* 1973, 8, 1449
- 10 Millar, G. W., Visser, S. A. D. and Morecroft, A. S. *Polym. Eng. Sci.* 1971, 11, 73
- 11 Kambour, R. P., Grumer, C. L. and Romagosa, E. E. *Macromolecules* 1974, 7, 248
- 12 Yeh, G. S. Y. *Pure Appl. Chem.* 1972, 31, 65
- 13 Hoseman, R. *J. Polym. Sci. (C)* 1967, 20, 1
- 14 Campbell, S. F., Stephens, R. and Tatlow, J. C. *Tetrahedron* 1965, 21, 2997
- 15 Brown, P. J. N., Stephens, R. and Tatlow, J. C. *JCS Perkin Trans. I* 1972, p 937
- 16 Stephens, R. personal communication
- 17 Sorenson, W. R. and Campbell, T. W. 'Preparative Methods of Polymer Chemistry', 2nd Edn, Interscience, New York, 1968, p 140
- 18 *Idem, ibid.* p 141
- 19 Schulz, G. V. and Horbach, A. *Makromol. Chem.* 1959, 29, 93
- 20 Backus, J. K. (Mobay Chem. Co., Pittsburgh, USA) personal communication
- 21 Weilgosz, Z., Dobkowski, Z. and Krajewski, B. *Eur. Polym. J.* 1972, 8, 1113
- 22 Davis, A. and Golden, J. H. *J. Macromol. Sci. (C)* 1969, 3, 49
- 23 Adam, G., Hay, J. N., Parsons, I. W. and Haward, R. N. to be published
- 24 Van Falkai, B. and Rellensmann, W. *Makromol. Chem.* 1964, 75, 112
- 25 McNulty, B. J. *J. Polym. Sci. (A-1)* 1969, 7, 3038; *Polymer* 1968, 9, 41
- 26 Kambour, R. P. *et al. J. Polym. Sci. (A-2)* 1966, 4, 327; O'Reilly, J. P. *et al. J. Polym. Sci. (C)* 1964, 6, 109
- 27 Illers, K. H. *Makromol. Chem.* 1967, 127, 1
- 28 Boyer, R. F. *Polym. Eng. Sci.* 1968, 8, 161
- 29 Illers, K. H. and Breuer, H. *Kolloid Z.* 1961, 176, 110; *J. Colloid Sci.* 1963, 18, 1
- 30 Le Grand, D. G. and Erhardt, P. F. *J. Appl. Polym. Sci.* 1969, 13, 1707

# Sorption of water vapour by atactic and isotactic poly (methyl methacrylate)

Z. Miyagi and K. Tanaka

Department of Chemistry, Faculty of Science, Science University of Tokyo, Tokyo, Japan

(Received 5 August 1974)

For the purpose of studying the relation between the stereoregularity and the sorption properties of atactic (a-PMMA) and isotactic (i-PMMA) poly(methyl methacrylate) samples, the isotherms for the sorption of water vapour by these polymers were determined. The glass transition temperatures,  $T_g$  and the densities of both PMMA samples were also measured under different conditions of moisture content. The amount of water vapour sorbed by i-PMMA was found, in this study, to be greater than that by a-PMMA. This is rather peculiar when we consider that the former has a high crystallinity (76%) and the latter is non-crystalline in nature. It was concluded that water vapour is sorbed by a-PMMA by a mechanism whereby the water molecules sorbed, fill pre-existing sites (polar groups) and spaces occupied by microvoids or free volumes in the polymer without causing any swelling in the latter; and that the extra sorption of water vapour by i-PMMA was due to a mechanism by which the water molecules sorbed cause the polymer to swell, and thus increase its sorption capacity.

## INTRODUCTION

The present work was undertaken to study the effects of stereoregularity on the water vapour sorption properties of poly(methyl methacrylate) (PMMA) samples. It is well known that the sorption properties of polymeric materials for the vapours of various solvents depend not only on the chemical structures of the polymers, but also on their higher-order structures, and there are numerous reports<sup>1,2</sup> on the effects of crystallinity on the water vapour sorption properties of polymers. Formerly, it was assumed that the sorption occurred only in the non-crystalline part of the sorbent and that the crystalline part did not have any effect on this. However, it has been reported recently that water molecules sorbed by poly(vinyl alcohol)<sup>3</sup> and nylon-6<sup>4</sup> cause changes in the lattice constants of the crystals, and also that a meaningful relationship does not necessarily exist between an increase in the degree of crystallinity and a decrease in the amount of organic vapours sorbed by polyethylene<sup>5</sup>, whose degree of crystallinity has been increased by elongation and heat treatment.

Thus, the sorption properties of polymers are influenced in a complicated way, by their chemical structures and physical properties. Moreover, differences in the stereoregularity of polymers cause differences in their physical properties. However, since no specific discussion on the relationship between the stereoregularity and the sorption properties of polymers had so far been reported, we studied this relationship by measuring the amount of water vapour sorbed by atactic (a-) and isotactic (i-) PMMA samples. The changes in the  $T_g$  and in the densities of both samples, with changes in the moisture content of the polymers, were also determined.

## EXPERIMENTAL

### Materials and methods

a-PMMA ( $\bar{M}_v = 1.10 \times 10^5$ ) manufactured by Sumitomo Chemical Co. and i-PMMA ( $\bar{M}_v = 6.01 \times 10^5$ ) synthesized

by the authors were used as samples. The a-PMMA was purified and prepared as follows: it was dissolved in 5 wt % acetone, precipitated in methanol, decanted and collected by filtration, a procedure which was repeated 4 times. It was then dried under reduced pressure, and films were prepared by casting the polymer from a 10 wt % benzene solution onto glass sheets. i-PMMA was synthesized and refined by the method that had been reported previously by Watanabe<sup>6</sup>. The conditions for polymerization were as follows: Grignard reagent with isobutyl bromide as the base was used as the catalyst, the molar ratios of monomer: solvent (toluene) and catalyst: monomer were  $4.70 \times 10^{-1}$  and  $1.88 \times 10^{-2}$ , respectively, and the temperature was 0°C. The films of i-PMMA were prepared in a similar manner as the a-PMMA ones, from a 3–5 wt % benzene solution of the polymer. The film thickness of both a- and i-PMMA samples was 0.08–0.1 mm, and these samples were vacuum-dried for 50 days at  $10^{-5}$  mmHg and stored in sealed glass tubes. The moisture content of the samples for  $T_g$  and density measurements were adjusted by allowing the sample to stand in the vapour of saturated solutions of various salts. The samples for the  $T_g$  study were sealed in aluminium pans to prevent evaporation during measurement.

### Sorption measurement

Measurements of the amount of water vapour sorbed by both a- and i-PMMA samples were carried out on about 300 mg of the samples by the gravimetric method using the usual quartz spiral balance. Standard drying of the samples was carried out for 4 days at  $10^{-6}$  mmHg and 35°C. The sensitivity of the quartz spiral balance was 1.0523 mm/mg at 30°C. Since amount of water vapour sorbed by polymers depends greatly on temperature, the whole sorption apparatus was made of double tubes, and the temperature was kept constant by circulating thermostatically controlled water.

Table 1 Characteristics of both a- and i-PMMA samples

Samples	$M_v \times 10^{-5}$	Densities (g/cm <sup>3</sup> )		Crystallinity (%)	Isotacticity (%)
		20°C	30°C		
a-PMMA	1.10	1.163	1.158	—	—
i-PMMA	6.01	1.224	1.223	76	99

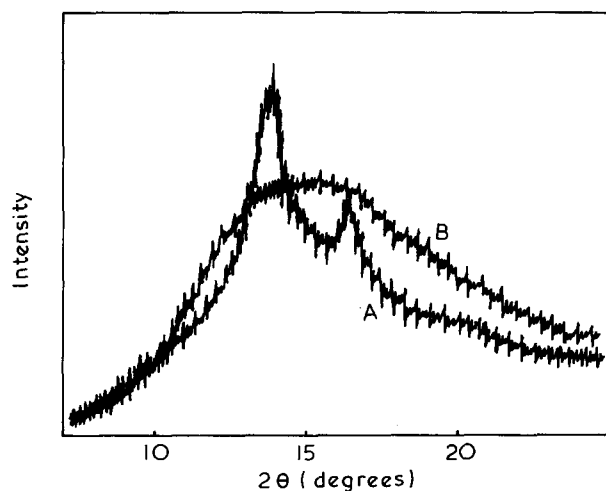


Figure 1 Intensity of X-ray diffraction of PMMA samples: A, i-PMMA; B, a-PMMA

#### $T_g$ and density measurements

The  $T_g$  and densities of a- and i-PMMA samples were measured under different conditions of moisture. The  $T_g$  was measured with a Perkin-Elmer Model DSC-1b differential scanning calorimeter. The rate of temperature rise was 8°C/min. Density measurements were carried out rapidly at 20°C and 30°C, by the density-gradient tube method, using zinc chloride and methanol.

#### Determination of isotacticity

The isotacticity was determined by the i.r. method. As i-PMMA shows an absorption at 757 cm<sup>-1</sup> that was not found in a-PMMA, the absorbancy ratio  $D_{749}/D_{757}$  was calculated from the absorbancies at 749 cm<sup>-1</sup> and 757 cm<sup>-1</sup>, and the isotacticity was determined from the calibration curve previously reported by Watanabe<sup>7</sup>.

## RESULTS AND DISCUSSION

The characteristics of both a- and i-PMMA samples are listed in Table 1. As shown in Table 1, the isotacticity of i-PMMA is 99%. Consequently, it is a suitable substance for studying the effects of stereoregularity on the sorption properties of a polymer. A clear difference in degree of crystallinity between a- and i-PMMA samples can be seen from the densities listed in Table 1 and from the results of X-ray diffraction shown in Figure 1. a-PMMA is composed almost entirely of non-crystalline substance, whereas a considerable portion has crystallized in i-PMMA. The degree of crystallinity of i-PMMA, calculated from the densities<sup>8-10</sup>, is 76%.

#### Sorption isotherms

The isotherms for the sorption of water vapour by a- and i-PMMA samples at 30°C are shown in Figure 2. It can be seen from Figure 2 that the amount of water vapour sorbed

by i-PMMA with a crystallinity of 76% was greater than that sorbed by non-crystalline a-PMMA. This is contrary to previous thinking that 'increase in the degree of crystallinity of polymers causes decrease in the amount of water vapour sorbed by them'. In order to elucidate this singular phenomenon in a- and i-PMMA samples resulting from the difference in their chemical structure, the BET theory<sup>11</sup> was applied to the isotherms shown in Figure 2. This does not mean that the isotherms necessarily satisfy the BET theory, but it is convenient for studying the mechanism of sorption with respect chiefly to the point at which the observed amount of water vapour sorbed deviates from the theoretical value. The results are shown in Figure 3. The BET theory is expressed by the following equation:

$$\frac{x}{a(1-x)} = \frac{1}{a_0c} + \frac{(c-1)x}{a_0c} \quad (1)$$

where  $a$  is the weight of the sorbate in g sorbed/g of polymer,  $a_0$  is the weight of the sorbate sorbed to form a monomolecular layer,  $x$  is the relative vapour pressure and  $c$  is a constant related to the heat of sorption.

As shown in Figure 3, BET plots of the isotherms are linear in a narrow range of lower relative vapour pressures ( $RVP$ ), but deviate from straight lines with increase in  $RVP$ , as in water vapour sorption by other polymeric materials<sup>12,13</sup>. However, BET plots for water vapour sorption of PMMA samples is different from those other polymeric

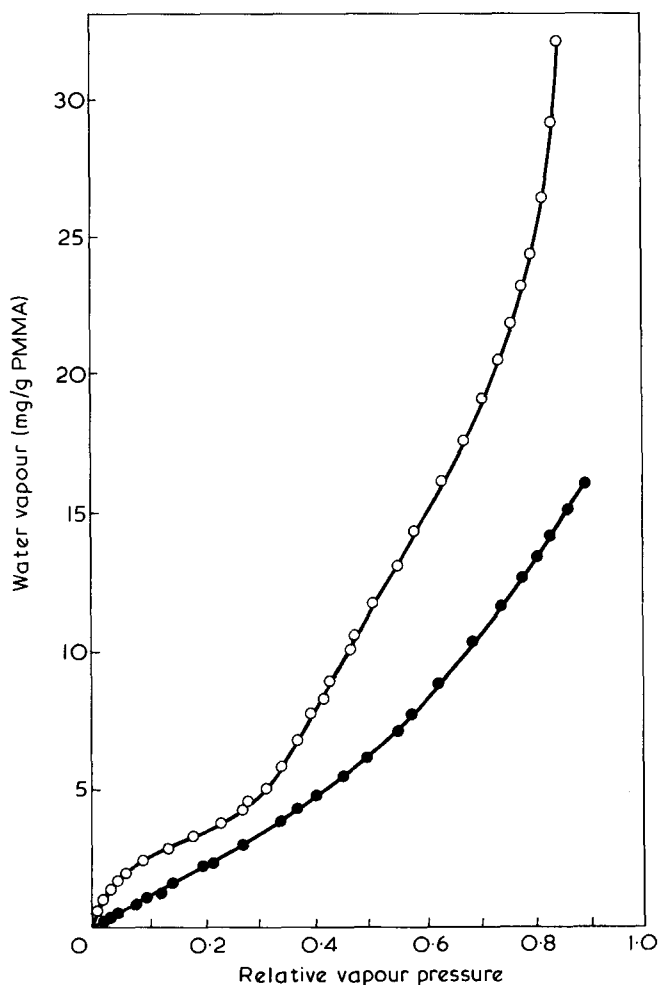


Figure 2 Sorption isotherms of PMMA samples at 30°C: ●, a-PMMA; ○, i-PMMA

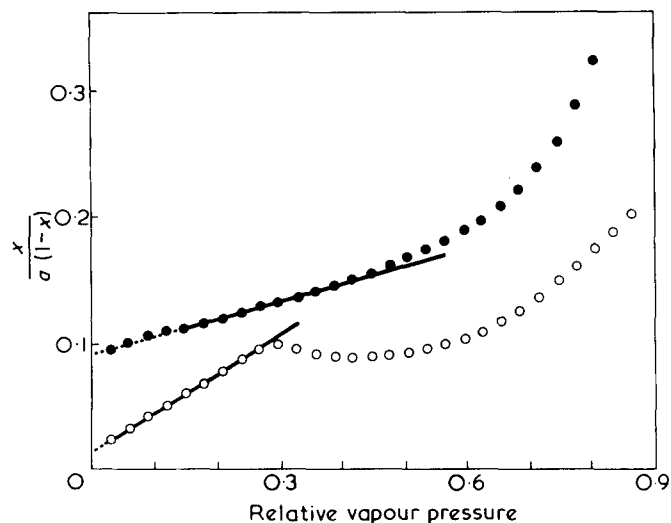


Figure 3 BET plots of the isotherms of Figure 2: ●, a-PMMA; ○, i-PMMA

Table 2 BET constants of both *a*- and *i*-PMMA samples

Samples	$a_0$ (mg/g)	$x_0$ (%)	$n_0$	$n_0^*$	$E$ (kcal/mol)
a-PMMA	4.42	38.8	40.6	40.6	0.520
i-PMMA	3.17	16.9	56.8	13.4	1.850

$a_0$  = weight of sorbate sorbed to form a monomolecular layer  
 $x_0$  = relative vapour pressure corresponding to  $a_0$   
 $n_0$  = number of sorption sites occupied by one molecule of the sorbate in a monomolecular layer  
 $n_0^*$  = value corrected in  $n_0$  for crystallinity  
 $E$  = heat of sorption

materials, because BET plots for water vapour sorption of *a*- and *i*-PMMA samples show that the deviations from straight lines are mutually in the opposite directions to those suggested by the theory. The deviation of BET plot from the theoretical values for sorption in the *a*-PMMA/water vapour system is negative<sup>13</sup> (the observed  $a$  values are much smaller than those predicted by the theory), whereas the *i*-PMMA/water vapour system shows a positive deviation (the observed  $a$  values are much larger than those predicted by the theory). This suggests that there is a clear difference between the mechanisms of water vapour sorption by *a*- and *i*-PMMA samples. That is, the sorption capacity of *a*-PMMA is restricted, while that of *i*-PMMA is increased during the sorption process. This is considered in further detail by assuming that sorption occurs by two mechanisms<sup>12</sup>: adsorption of the Langmuir type and by dissolution. The amount of water vapour sorbed by adsorption of the Langmuir type, is represented by the  $a_0$  value in the BET constants listed in Table 2. It is clear from Table 2 and Figure 2 that the amount of water vapour sorbed by *a*-PMMA by adsorption of the Langmuir type is greater than that sorbed by *i*-PMMA, despite the fact that the amount of water vapour sorbed by *i*-PMMA is greater than that sorbed by *a*-PMMA. This indicates that the dissolution mechanism corresponding to the increase of sorption capacity makes a large contribution in water vapour sorption by *i*-PMMA, and that the adsorption mechanism, in which an increase of sorption capacity is not expected, greatly affects the water vapour sorption of *a*-PMMA.

#### $T_g$ and density

To obtain further information on such difference between the mechanisms of water vapour sorption of *a*- and

*i*-PMMA samples, the changes in  $T_g$  and densities of both samples with changes in moisture content in the polymers were determined. The results are shown in Figure 4 and Figure 5, respectively. The tendency for  $T_g$  to decrease, with increase in moisture content in both *a*- and *i*-PMMA samples, can be seen. The  $T_g$  of *i*-PMMA drops to below 30°C near an  $a$  value of 0.44 wt % ( $RVP = 28\%$ ), where the

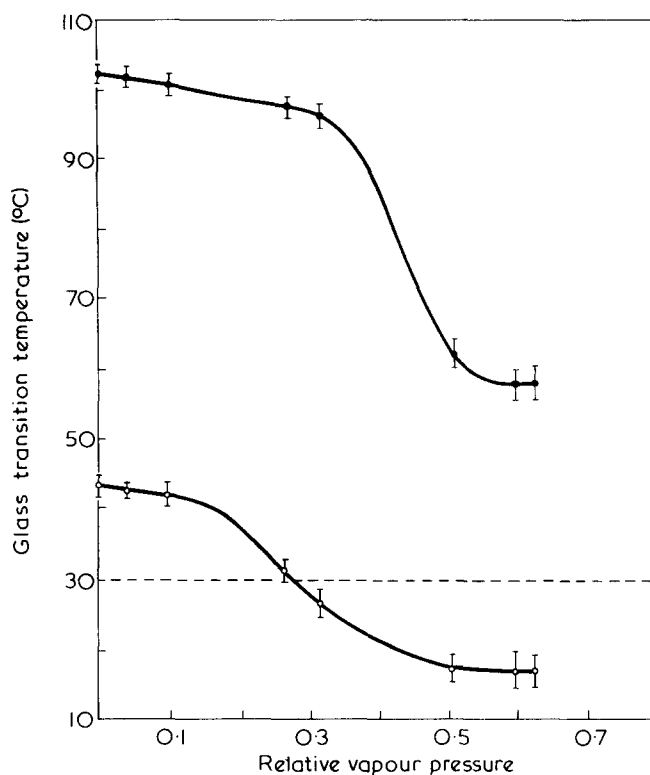


Figure 4 Variations of  $T_g$  of PMMA samples as a function of  $RVP$ : ●, a-PMMA; ○, i-PMMA

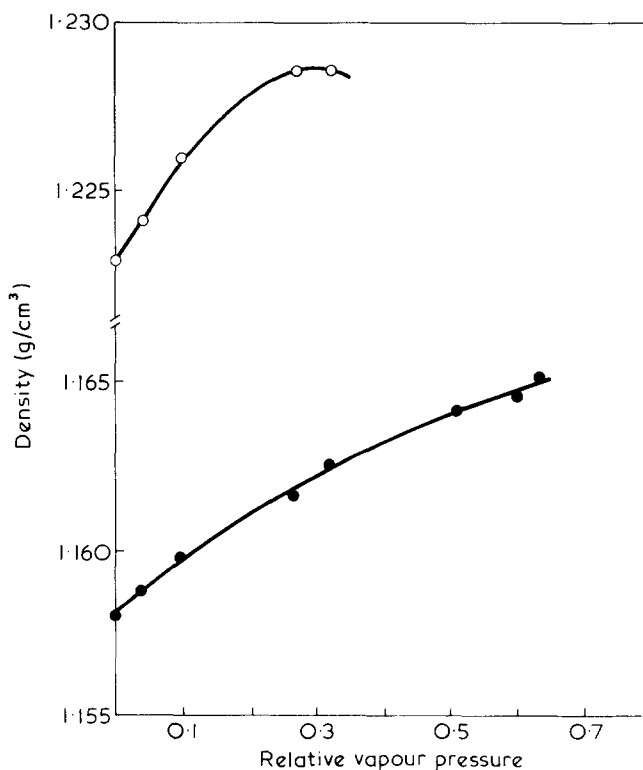


Figure 5 Variation of density of PMMA samples as a function of  $RVP$ : ●, a-PMMA; ○, i-PMMA

BET plot shows a positive deviation from the straight line expected by the theory, i.e. it becomes lower than the temperature of sorption measurement above a *RVP* value of 28%. Therefore the motion of the polymer chain, which had been fixed, rises above 28% *RVP* and the sorption capacity increases in *i*-PMMA. Consequently, the amount of water vapour sorbed in *i*-PMMA is much larger than that predicted by the BET theory, and the BET plot shows a positive deviation from the theoretical value, as shown in *Figure 3*. No decrease in the  $T_g$  of *a*-PMMA below 50°C was observed within the range measured. As the measurement of the amount of water vapour sorbed by *a*-PMMA was consequently carried out in conditions in which the molecular motion of the main chain of the polymer was in a fixed state, the amount of water vapour sorbed by *a*-PMMA was much smaller than that predicted by the BET theory and the BET plot shows a negative deviation from the theoretical value, as shown in *Figure 3*.

When the water molecules sorbed by PMMA samples cause swelling in a polymer, its density should decrease correspondingly with the moisture content, when we consider that the density of water (0.9998 g/cm<sup>3</sup> at 30°C) is smaller than that of *a*- and *i*-PMMA samples, 1.158 and 1.223 g/cm<sup>3</sup> at 30°C, respectively. Moreover, when the water molecules cause no swelling, but merely fill the spaces where there are microvoids or free volumes in the polymer, the density should increase corresponding to the moisture content. As shown in *Figure 5*, the density of *a*-PMMA increased over the entire range measured with increases in the moisture content, i.e., 0.58% over the dry sample density, with a water vapour sorption of 0.80 wt %. This shows that *a*-PMMA had hardly swelled at all over the entire range measured, and since the value of 0.22% is much smaller than the density increase estimate based on the amount of water added (i.e. the moisture content of 0.80 wt %), the difference of 0.22% between density increase and moisture content is explained reasonably, in terms of the sorption mechanism of water vapour by the pre-existing sites (polar groups) exposed on the surface. The density of *i*-PMMA showed a maximum in the vicinity of an *a* value of 0.44 wt % (*RVP* = 28%), and a decrease of 0.02% of the dry sample value with an increase of moisture content of 0.10 wt % from 0.44 wt % (*RVP* = 28%). This suggests that *i*-PMMA swelled above the *RVP* value of 28%.

From the discussion of the isotherms,  $T_g$  and density, it was concluded that water vapour had been sorbed by *a*-PMMA by a mechanism in which the water molecules sorbed fill the pre-existing sites (polar groups) and spaces occupied by microvoids or free volumes in the polymer, causing no swelling in the latter. The extra sorption of water vapour by *i*-PMMA, was concluded to have occurred by a mechanism whereby the water molecules sorbed caused swelling in the polymer, as well as increasing the sorption capacity of the polymer. Consequently, since the  $T_g$  of polymers generally increases with increase in the degree of crystallinity, the sorption properties of polymers may be said to be affected by the degree of crystallinity. However, the  $T_g$  of crystalline *i*-PMMA is lower than that of non-crystalline *a*-PMMA and the sorption capacity of the former is greater than that of the latter. Furthermore, it has been reported previously that the amount of water vapour sorbed by nylon-6<sup>14</sup> is different after heat treatment, even at the same degree of crystallinity. Accordingly, if the sorption properties of such singular polymers as PMMA, nylon-6, etc., are discussed concurrently, it should be taken that they are controlled by their  $T_g$  rather than their degree of crystallinity.

#### REFERENCES

- 1 Lasoski, S. W. Jr. and Cobbs, W. H. Jr. *J. Polym. Sci.* 1959, 36, 21
- 2 Howard, W. and Starkweather, Jr. *J. Appl. Polym. Sci.* 1959, 2, 129
- 3 Ishikawa, K., Miyasaka, K. and Yamamoto, Y. *Kobunshi Kagaku* 1968, 25, 50
- 4 Boukal, I. *J. Appl. Polym. Sci.* 1967, 11, 1483
- 5 Peterlin, A., Williams, J. L. and Stannett, V. *J. Polym. Sci. (A-2)* 1967, 5, 957
- 6 Watanabe, H. *Denki Tsushin Kenkyushoho* 1961, (1607), 31
- 7 Watanabe, H. *Kogyo Kagaku Zasshi* 1961, 61, 1851
- 8 Tadokoro, H., Chatani, Y., Kusanagi, H. and Yokoyama, M. *Macromolecules* 1970, 3, 441
- 9 Stroup, J. D. and Hughes, R. E. *J. Am. Chem. Soc.* 1958, 80, 2341
- 10 Fox, T. G., *et al.* *J. Am. Chem. Soc.* 1958, 80, 1768
- 11 Brunauer, S. 'Adsorption of Gases and Vapors', Princeton Univ. Press, Princeton, 1943, p 154
- 12 Takizawa, A., Negishi, T. and Ishikawa, K. *J. Polym. Sci. (A-1)* 1968, 6, 475
- 13 Miyagi, Z. and Tanaka, K. *Kolloid-Z. Z. Polym.* 1973, 251, 739
- 14 Koshimo, A. and Tagawa, T. *J. Appl. Polym. Sci.* 1965, 9, 45



# Pressure dependence of upper critical solution temperatures in the polystyrene–cyclohexane system

S. Saeki, N. Kuwahara, M. Nakata and M. Kaneko

Department of Polymer Science, Hokkaido University, Sapporo, Japan

(Received 5 August 1974; revised 11 September 1974)

The pressure dependence of the upper critical solution temperature  $(dT/dp)_c$  in the polystyrene–cyclohexane system has been measured over the pressure range of 1 to 50 atm. The value of  $(dT/dp)_c$  determined over the molecular weight ( $M_w$ ) range of  $3.7 \times 10^4$  to  $\sim 145 \times 10^4$  greatly depends on the molecular weight of polystyrene. The value of  $(dT/dp)_c$  for a polystyrene solution of low molecular weight ( $M_w = 3.7 \times 10^4$ ) is positive ( $3.14 \times 10^{-3}$  degree atm $^{-1}$ ), while the values are negative ( $-0.52 \times 10^{-3} \sim -5.64 \times 10^{-3}$  degree atm $^{-1}$ ) for solutions of polystyrene over the high molecular weight range of  $11 \times 10^4$  to  $\sim 145 \times 10^4$ . The Patterson–Delmas theory of the corresponding state and the newer Flory theory have been used to explain this behaviour.

## INTRODUCTION

Thermodynamic phenomena such as phase separation behaviour at the upper critical solution temperature (*UCST*) and the lower critical solution temperature (*LCST*)<sup>1–10</sup>, excess volume of mixing<sup>11–18</sup>, concentration dependence of the  $\chi$  parameter<sup>11–17,19,20</sup>, and both endothermic and exothermic behaviour<sup>5,21,22</sup> have been extensively investigated in non-polar polymer solutions. The temperature dependence of polymer chain dimensions<sup>23,24</sup> in dilute polymer solutions has been correlated with the temperature dependence of  $\chi_1$ ; the polymer chain dimension attains a maximum in the vicinity of the minimum value of  $\chi_1$ . The recent theories of polymer solution thermodynamics by Patterson<sup>2,21,24–29</sup> and Flory<sup>17,30–32</sup> successfully predict these phenomena. In these theories the polymer–solvent interaction parameter,  $\chi_1$ , consists of a decreasing function of temperature from the contact interaction and an increasing function from the free volume or equation of state terms.

Systematic examinations have been carried out by introducing pressure as a thermodynamic variable on the second virial coefficient<sup>33–35</sup>, the mean square end-to-end distance of polymer in dilute solution<sup>33–35</sup> and the upper and lower critical solution temperatures<sup>36–39</sup>. Determinations of the pressure dependence of the *UCST* and *LCST* are of great interest for investigation of the thermodynamic properties of the polymer solution and also for obtaining information about the third derivative of the chemical potential with respect to concentration<sup>40</sup>.

The present work was done to supply the phase diagram in temperature–pressure–concentration space in the vicinity of the *UCST* in the polystyrene–cyclohexane system and to apply recent theories of polymer solution thermodynamics.

## EXPERIMENTAL

Polystyrene samples were obtained from the Pressure Chemical Co. Characterization for samples of  $M_w = 3.7 \times 10^4$  to

$67 \times 10^4$  has been described elsewhere<sup>7–9</sup>. A sample designated by 14b-3 was obtained by the solution fractionation described in detail elsewhere<sup>7</sup>. The 14b-3 fraction  $M_w = 145 \times 10^4$  and  $M_w/M_n < 1.10$  was used in this work. Cyclohexane was reagent grade and was further purified before use. The solvent was treated over silica gel and fractionally distilled by use of a column<sup>7–9</sup>. The middle fraction was dried over phosphorus pentoxide and redistilled through the same column. The apparatus for determination of the cloud-point temperature under pressure consisted of three parts: a pressure reservoir made of stainless steel, a calibrated Bourdon-type pressure gauge of 45 cm diameter (Heise Co., to 50 kg/cm<sup>2</sup>), and a pressure cell consisting of a brass block with a hole to hold the solution cell and two glass windows for passage of the He–Ne laser beam. The solution cell was sealed by the use of mercury. Compressed nitrogen gas was used as the pressure source.

Upper critical solution temperatures were estimated from cloud-point curves. Several solutions in cyclohexane, prepared from each sample in the concentration range 1 to  $\sim 22$  wt %, were stirred for a day and sealed by pure mercury inside the solution cells. The cloud-point temperatures for the *UCST* were determined with an accuracy of  $\pm 0.005^\circ\text{C}$  by the aid of the pattern of He–Ne laser beam, as described elsewhere<sup>7</sup>. The cloud-point temperatures obtained by cooling very slowly ( $0.0005^\circ$  to  $\sim 0.001^\circ\text{C}/\text{min}$ ) in a water bath controlled to  $\pm 0.002^\circ$  agreed within  $\pm 0.005^\circ\text{C}$  by the aid of the pattern of He–Ne laser beam, as very slowly ( $0.03$  to  $\sim 0.05$  atm/min).

## RESULTS

Figures 1 to 4 show the cloud-point curves at different pressures for solutions of polystyrenes of  $M_w = 3.7 \times 10^4$  to  $\sim 145 \times 10^4$  in cyclohexane. Although the maximum point is not the critical point, the difference of the maximum point from the critical point should be quite small because of the small values of  $M_w/M_n$  for the four samples in this work<sup>41,42</sup>.

The pressure dependence of the *UCST*  $(dT/dp)_c$  for the

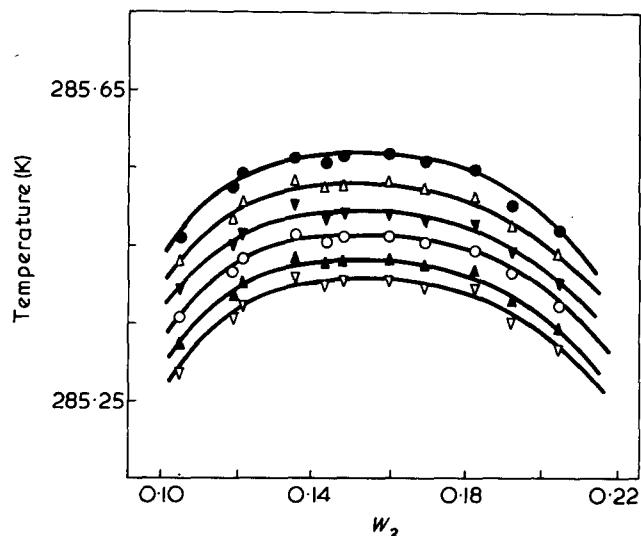


Figure 1 Temperature/weight fraction phase diagram for the polystyrene ( $M_w = 3.7 \times 10^4$ )-cyclohexane system under various pressures:  $\nabla$ , 1 atm;  $\blacktriangle$ , 10 atm;  $\circ$ , 20 atm;  $\blacktriangledown$ , 30 atm;  $\triangle$ , 40 atm;  $\bullet$ , 50 atm

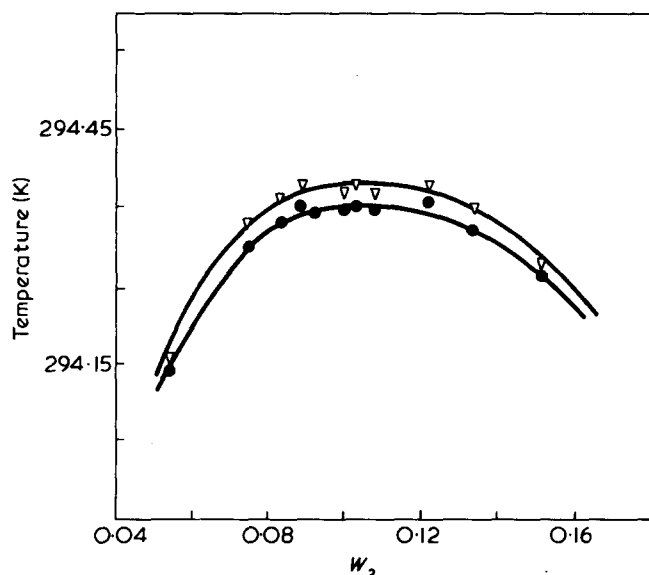


Figure 2 Temperature/weight fraction phase diagram for the polystyrene ( $M_w = 11 \times 10^4$ )-cyclohexane system under various pressures:  $\nabla$ , 1 atm;  $\bullet$ , 50 atm

solutions is shown in Figure 5 and the values of  $(dT/dp)_c$  are collected in Table 1. The values of  $(dT/dp)_c$  are positive for the polymer sample of  $M_w = 3.7 \times 10^4$ , slightly negative for  $M_w = 11 \times 10^4$ , and more negative for  $M_w = 67 \times 10^4$  and  $145 \times 10^4$ . Although the increase or decrease of the precipitation temperature in the pressure range of 50 atm is very small, it is detectable by the use of the optical determination of the cloud-point temperature. Since the meniscus between two coexisting phases appears in the polystyrene-cyclohexane system after lapse of half a day at a temperature  $0.003^\circ\text{C}$  lower than the temperature of a dramatic change of the pattern of a He-Ne laser beam passed through the solution cell, the cloud-point temperatures determined in this work are sufficiently reliable.

## DISCUSSION

Ham *et al.*<sup>37</sup> have determined the precipitation temperatures of polystyrene solutions in cyclohexane as a function of pressure up to 400 atm. The values of  $(dT/dp)_c$  estimated

from their data over the pressure range of 1 to 100 atm are  $2.5 \times 10^{-3}$  degree atm<sup>-1</sup> for  $M_w = 26.7 \times 10^4$  and  $3.1 \times 10^{-3}$  degree atm<sup>-1</sup> for  $M_w = 8.2 \times 10^4$ . Their values are very different in sign and magnitude from our experimental values corresponding to  $M_w = 26.7 \times 10^4$  and  $8.2 \times 10^4$ . The difference should be attributed to the method for determination of cloud-point temperatures under pressure.

The Patterson<sup>25-29</sup> and Flory theories<sup>17,30-32</sup> of polymer solution thermodynamics predict the pressure dependence of the UCST and its variation with molecular weight of polymer. The  $\chi_1$  parameter obtained by Patterson *et al.*

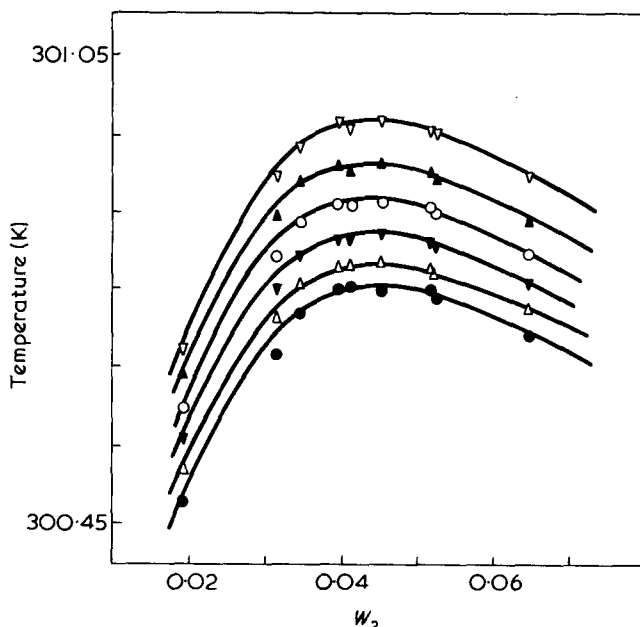


Figure 3 Temperature/weight fraction phase diagram for the polystyrene ( $M_w = 67 \times 10^4$ )-cyclohexane system under various pressures:  $\nabla$ , 1 atm;  $\blacktriangle$ , 10 atm;  $\circ$ , 20 atm;  $\blacktriangledown$ , 30 atm;  $\triangle$ , 40 atm;  $\bullet$ , 50 atm

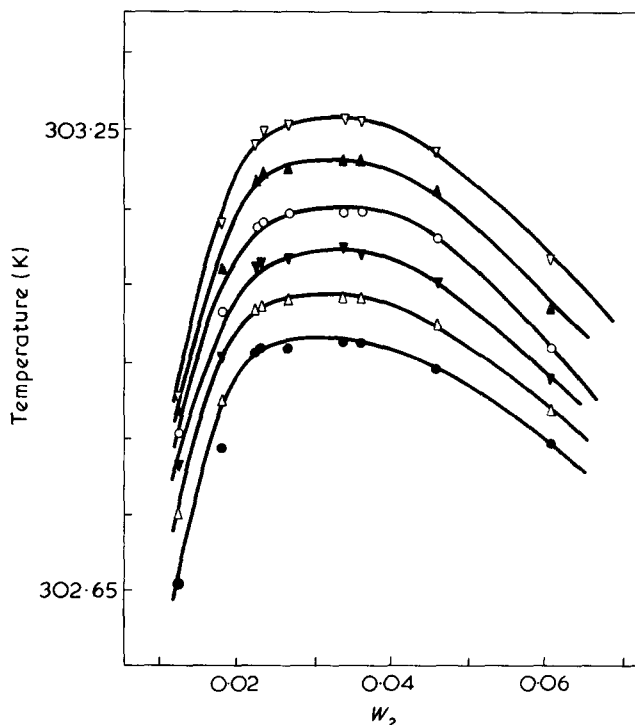


Figure 4 Temperature/weight fraction phase diagram for the polystyrene ( $M_w = 145 \times 10^4$ )-cyclohexane system under various pressures:  $\nabla$ , 1 atm;  $\blacktriangle$ , 10 atm;  $\circ$ , 20 atm;  $\blacktriangledown$ , 30 atm;  $\triangle$ , 40 atm;  $\bullet$ , 50 atm

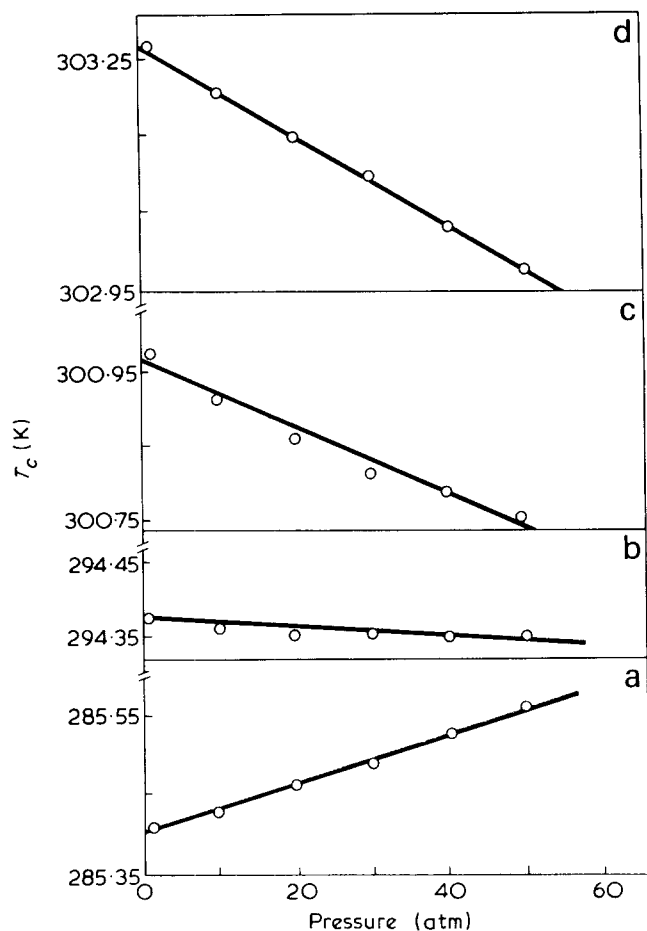


Figure 5 Pressure dependence on upper critical solution temperatures in the polystyrene–cyclohexane system for the samples: (a)  $M_w = 3.7 \times 10^4$ ; (b)  $M_w = 11 \times 10^4$ ; (c)  $M_w = 67 \times 10^4$ ; (d)  $M_w = 145 \times 10^4$

and Flory *et al.* from the viewpoint of the corresponding state law is essentially the same expression except for the definition of the molecular parameters<sup>3,26</sup>, and is expressed as a function of temperature and pressure. The equation of state in reduced form derived by Flory *et al.* is given by<sup>30</sup>:

$$\tilde{P}\tilde{V}/\tilde{T} = (1 - \tilde{V}^{-1/3})^{-1} - (\tilde{V}\tilde{T})^{-1} \quad (1)$$

By use of the van der Waals expression,  $\tilde{U} = -\tilde{V}^{-1}$ , for the dependence of the configurational energy on volume, the Patterson theory<sup>25–28,35</sup> gives:

$$\chi_1(P, T)/c_1 = -(\tilde{U}_1(\tilde{P}_1, \tilde{T}_1)/T_1)\nu^2 + (\tilde{C}_{p,1}(\tilde{P}_1, \tilde{T}_1)/2)(\tau + \pi\tilde{P}_1/\alpha\tilde{T}_1)^2 \quad (2)$$

where

$$\tilde{C}_{p,1}^1(\tilde{P}_1, \tilde{T}_1) = (1 - (2/3)\tilde{V}_1^{-1/3}) - 2(1 - \tilde{V}_1^{-1/3})/(\tilde{P}_1\tilde{V}_1^2 + 1) \quad (3)$$

and

$$\beta\tilde{P}_1/\alpha\tilde{T}_1 = \tilde{P}_1\tilde{V}_1^2/(\tilde{P}_1\tilde{V}_1^2 + 1) \quad (4)$$

The Flory theory<sup>12,15–17,30–32</sup> gives:

$$\chi_1 = (P_1^*V_1^*/\tilde{V}_1RT)(A^2\alpha_1T/2 + Y_{12}) - V_1^*Q_{12}/R(s_1/s_2)^2 \quad (5)$$

where

$$A = (1 - T_1^*/T_2^*)(P_2^*/P_1^*) - (s_2/s_1)(X_{12}/P_1^*) \quad (6)$$

and

$$Y_{12} = (X_{12}/P_1^*)(s_2/s_1)^2 \quad (7)$$

In the Patterson theory,  $-\tilde{U}_1$  is the reduced vaporization energy of the solvent,  $\tilde{C}_{p,1}$  is the reduced configurational heat capacity of the solvent, and  $\alpha$  and  $\beta$  are respectively the reduced thermal expansion coefficient and the isothermal compressibility of the solvent. The  $\nu^2$  parameter is related to the difference of cohesive energy and size between the solvent molecule (1) and polymer segment (2). The  $\tau$  parameter is related to the difference between the thermal expansion coefficient of the solvent (1) and the polymer (2) and is defined by:

$$\tau = 1 - T_1^*/T_2^* \quad (8)$$

where  $T_i^*$  is the characteristic temperature reduction parameter of the components (1) and (2). The  $\pi$  parameter is similarly related to the difference between the pressure reduction parameter of the components and is defined by:

$$\pi = P_1^*/P_2^* - 1 \quad (9)$$

The parameter  $c_1$  is one-third the total number ( $3c_1$ ) of external degrees of freedom of the solvent molecule. In the Flory theory the parameter  $X_{12}$  measures the interchange energy on formation of contacts between unlike molecules,  $Q_{12}$  is analogously defined to represent the entropy arising from interchange of neighbouring molecules, and  $s_1$  and  $s_2$  denote the number of surface sites (or surface area) for segments of respective species, segments being of equal core volumes ( $V^*$ ).

The pressure dependence of the critical solution temperature under the critical condition is expressed<sup>40</sup> by the ratio of second derivative of volume and enthalpy on concentration:

$$(dT/dp)_c = T(\partial^2V/\partial\phi_2^2)_c/(\partial^2H/\partial\phi_2^2)_c \quad (10)$$

where  $\phi_2$  is the segment fraction of polymer<sup>12,17</sup>. By assuming  $\chi$  independent of concentration, equation (10) can be written as:

$$(dT/dp)_c = -(\partial\chi_1/\partial p)_T/(\partial\chi_1/\partial T)_p \quad (11)$$

Values of  $(\partial^2H/\partial\phi_2^2)_c$  are negative for the UCST corresponding to the endothermic condition and positive for the LCST corresponding to the exothermic condition. Rough estimations of  $(dT/dp)_c$  have been carried out by the aid of the Patterson and Flory theories. The pressure coefficients of

Table 1 Pressure dependence of upper critical solution temperatures in the polystyrene–cyclohexane system

Sample	$M_w \times 10^{-4}$ (g mol wt)	$M_w/M_n$	UCST at $p = 1$ atm (K)	$(dT/dp)_c \times 10^3$ (degree atm <sup>-1</sup> )
7b	3.7	<1.06	285.41	3.14
4b	11.0	<1.06	294.38	-0.52
13a	67.0	<1.15	300.97	-4.40
14b-3	145.0	<1.10	303.26	-5.64

Table 2 Calculated value of pressure dependence of upper critical solution temperatures in the polystyrene–cyclohexane system

Sample	$\tilde{T}_{1,UCST} \times 10^2$ at $p = 1$ atm	$(\partial\chi_1/\partial p) \times 10^5$ (atm <sup>-1</sup> )			$(dT/dp)_c \times 10^2$ (degree atm <sup>-1</sup> )	
		Patterson	Flory	$(\partial\chi_1/\partial T) \times 10^3$ (degree <sup>-1</sup> )	Patterson	Flory
7b	6.051	-7.48	-7.15	-2.79	-2.68	-2.56
4b	6.241	-8.60	-8.33	-2.62	-3.28	-3.18
13a	6.381	-8.83	-8.57	-2.51	-3.51	-3.41
14b-3	6.429	-8.99	-8.73	-2.47	-3.64	-3.53

$\chi_1$  (equations 2 and 5) have been determined from the variation of volume with pressure at the critical solution temperature by use of equation (1). The values of  $(\partial\chi_1/\partial T)$  at 1 atm have been estimated from the experimental values of the UCST over the molecular weight range of  $3.7 \times 10^4$  to  $\sim 145 \times 10^4$  and the critical values of  $\chi_1$ :

$$\chi_1(\text{crit}) = (1/2)(1 + r^{-1/2})^2 \quad (12)$$

where  $r$  is defined by the ratio of the molar volume reduction parameters (core volume),  $V^*/V^{\dagger}$ <sup>17</sup>. The values of  $(dT/dp)_c$  calculated by using these values of  $(\partial\chi_1/\partial p)_c$  and  $(\partial\chi_1/\partial T)$  at 1 atm are listed in Table 2, in which the pressure and temperature dependence of  $\chi_1$  are also included. The molecular parameters of the Flory theory obtained by using  $X_{12}$ ,  $s_1/s_2$ , and the equation of state parameters<sup>14</sup> are given by  $Y_{12} = 0.0205$ ,  $A^2 = 0.1129$ , and  $c_1 = 1.14$ , while the parameters of the Patterson theory are  $v^2 = 0.0159$ ,  $\tau^2 = 0.119$ , and  $c_1 = 1.01$ ; all these parameters are determined by comparison of experimental critical solution temperatures for the UCST and LCST with theory and the equation of state parameters<sup>7</sup>. A qualitative prediction of the experimental results is obtained by use of the Patterson and Flory theories, although the positive value for the solution of polystyrene of low molecular weight ( $M_w = 3.7 \times 10^4$ ) is not predicted.

The expression proposed by Flory *et al.*<sup>12-17</sup> for the volume change on mixing in polymer solutions is given by:

$$\tilde{V}E = \tilde{V} - \tilde{V}^0 \quad (13)$$

and

$$\tilde{V}^0 = \phi_1 \tilde{V}_1 + \phi_2 \tilde{V}_2 \quad (14)$$

where  $\phi_i$  is the segment fraction of the component  $i$ . The value of  $\tilde{V}$  for the solution is obtained by equation (1) at zero pressure. The characteristic temperature  $T^*$  of the solution is given by:

$$1/T^* = (\phi_1 P_1^*/T_1^* + \phi_2 P_2^*/T_2^*)/P^* \quad (15)$$

and

$$P^* = \phi_1 P_1^* + \phi_2 P_2^* - \phi_1 \theta_2 X_{12} \quad (16)$$

where  $\theta_2$  is the site fraction of the polymer. The segment fraction and the site fraction for the polymer molecule (2) are defined by

$$\phi_2 = m_2 V_{sp,2}^*/(m_1 V_{sp,1}^* + m_2 V_{sp,2}^*) \quad (17)$$

and

$$\theta_2 = (s_2/s_1)\phi_2/(\phi_1 + (s_2/s_1)\phi_2) \quad (18)$$

where  $m_i$  is the mass of the component  $i$  and  $V_{sp,i}^*$  is the characteristic reduction volume per gramme of the component  $i$ . The value of the excess volume for the polystyrene solution of  $M_w = 3.7 \times 10^4$  at 12.25°C and 16 wt % of polymer calculated by the Flory theory is  $\tilde{V}E/\tilde{V}^0 = -0.13 \times 10^{-2}$ . The negative value is consistent with the prediction of a negative  $(dT/dp)_c$ .

The value of  $(dT/dp)_c$  for  $M_w = 3.7 \times 10^4$  is to be compared with the small value of the negative excess volume of mixing for the solution of polystyrene ( $M_w = 5.1 \times 10^4$ ) in cyclohexane at 25°C obtained by Flory *et al.*<sup>14</sup>. The pressure dependence of the second virial coefficient  $(\partial A_2/\partial p)$  in the polystyrene ( $M_w = 10 \times 10^4$ )–cyclohexane system obtained by Schulz-Lechner<sup>34</sup> is negative at 40°C and positive at 45° and 50°C over the pressure range of 1 to 400 atm. In the polystyrene–*trans*-decalin system<sup>33,34</sup> the values of  $(\partial A_2/\partial p)$  are negative over temperature range of 15° to 35°C and slightly positive at 40°C. This behaviour of  $(\partial A_2/\partial p)$  as a function of temperature can be related to the excess volume of mixing being positive at low temperature and being negative at high temperature<sup>33,35</sup>. Baba *et al.*<sup>22</sup> have recently observed the molecular weight dependence of the excess volume of mixing in the polystyrene–ethyl acetate system at 30°C. The excess volume of mixing is zero for solutions of polystyrene of  $M_w = 0.21 \times 10^4 \sim 1.0 \times 10^4$  and negative, depending on concentration, for  $M_w = 2.04 \times 10^4 \sim 67 \times 10^4$ . In the light of these facts it is suggested that the value of the excess volume of mixing in the polystyrene–cyclohexane system changes sign depending both on the molecular weight of polystyrene and temperature.

#### ACKNOWLEDGEMENT

The authors thank Dr C. Nakayama and Dr K. Kamide of Textile Research Laboratory, Asahi Chemical Industry Co. Ltd, for their helpful support.

#### REFERENCES

- 1 Freeman, P. I. and Rowlinson, J. S. *Polymer* 1960, **1**, 20
- 2 Delmas, G. and Patterson, D. *Int. Symp. Macromol. Chem., Toronto* 1968
- 3 Siow, K. S., Delmas, G. and Patterson, D. *Macromolecules* 1972, **5**, 29
- 4 Cowie, J. M. G., Maconnachie, A. and Ranson, R. J. *Macromolecules* 1971, **4**, 57
- 5 Liddell, A. H. and Swinton, F. L. *Discuss. Faraday Soc.* 1970, **49**, 115
- 6 Nakajima, A., Hamada, F., Yasue, K., Fujisawa, K. and Shiomi, T. *Makromol. Chem.* 1974, **175**, 197
- 7 Saeki, S., Kuwahara, N., Konno, S. and Kaneko, M. *Macromolecules* 1973, **6**, 246
- 8 Saeki, S., Kuwahara, N., Konno, S. and Kaneko, M. *Macromolecules* 1973, **6**, 589

- 9 Saeki, S., Konno, S., Kuwahara, N., Nakata, M. and Kaneko, M. *Macromolecules* in press
- 10 Kuwahara, N., Saeki, S., Chiba, T. and Kaneko, M. *Polymer* 1974, **15**, 777
- 11 Baker, C. H., Brown, W. B., Gee, G., Rowlinson, J. S., Stubbley, D. and Yeadon, R. E. *Polymer*, 1962, **3**, 215
- 12 Flory, P. J. and Hocker, H. *Trans. Faraday Soc.* 1971, **67**, 2258
- 13 Hocker, H. and Flory, P. J. *Trans. Faraday Soc.* 1971, **67**, 2270
- 14 Hocker, H., Shih, H. and Flory, P. J. *Trans. Faraday Soc.* 1971, **67**, 2275
- 15 Flory, P. J. and Shih, H. *Macromolecules* 1971, **5**, 761
- 16 Flory, P. J., Ellenson, J. L. and Eichinger, B. E. *Macromolecules* 1968, **1**, 279
- 17 Eichinger, B. E. and Flory, P. J. *Trans. Faraday Soc.* 1968, **64**, 2035, 2053, 2061, 2066
- 18 Orwoll, R. A. and Small, J. A. *Macromolecules* 1973, **6**, 755
- 19 Okazawa, T. and Kaneko, M. *Polym. J.* 1971, **2**, 747
- 20 Sugamiya, K., Kuwahara, N. and Kaneko, M. *Macromolecules* 1974, **7**, 66
- 21 Delmas, G., Patterson, D. and Somcynsky, T. J. *Polym. Sci.* 1962, **57**, 79
- 22 Baba, Y., Katayama, H. and Kagemoto, A. *Makromol. Chem.* 1974, **175**, 209
- 23 Kuwahara, N., Saeki, S., Konno, S. and Kaneko, M. *Polymer* 1974, **15**, 66
- 24 Delmas, G. and Patterson, D. *Polymer* 1966, **7**, 513
- 25 Bardin, J. M. and Patterson, D. *Polymer* 1969, **10**, 247
- 26 Biros, J., Zeman, L. and Patterson, D. *Macromolecules* 1971, **4**, 30
- 27 Patterson, D. and Delmas, G. *Trans. Faraday Soc.* 1969, **65**, 708
- 28 Patterson, D. *Macromolecules* 1969, **2**, 672
- 29 Patterson, D. and Delmas, G. *Discuss. Faraday Soc.* 1970, **49**, 98
- 30 Flory, P. J., Orwoll, R. A. and Vrij, A. J. *Am. Chem. Soc.* 1964, **86**, 3507
- 31 Flory, P. J., Orwoll, R. A. and Vrij, A. J. *Am. Chem. Soc.* 1964, **86**, 3515
- 32 Flory, P. J. *J. Am. Chem. Soc.* 1965, **87**, 1833
- 33 Schulz, G. V. and Lechner, M. *J. Polym. Sci. (A-2)* 1970, **8**, 1885
- 34 Schulz, G. V. and Lechner, M. in 'Light Scattering from Polymer Solutions', (Ed. M. B. Huglin), Academic Press, New York, 1971
- 35 Gaeckle, D. and Patterson, D. *Macromolecules* 1972, **5**, 136
- 36 Ehrlich, P. and Kurpen, J. J. *J. Polym. Sci. (A)* 1963, **1**, 217
- 37 Ham, J., Bolen, M. C. and Hughes, J. K. *J. Polym. Sci.* 1962, **57**, 25
- 38 Allen, G. and Baker, C. H. *Polymer* 1965, **6**, 181
- 39 Myrat, C. D. and Rowlinson, J. S. *Polymer* 1965, **6**, 645
- 40 Prigogine, I. and Defay, R. 'Chemical Thermodynamics', Longmans, London, 1954
- 41 Koningsveld, R., Kleitjens, L. A. and Shultz, A. R. *J. Polym. Sci. (A-2)* 1970, **8**, 1261
- 42 Kuwahara, N., Nakata, M. and Kaneko, M. *Polymer* 1973, **14**, 415

# Deformation mechanisms in polytetrafluoroethylene

Robert J. Young

Department of Engineering, University of Cambridge, Cambridge CB2 1PZ, UK  
(Received 29 August 1974; revised 11 December 1974)

The deformation of isotropic and oriented polytetrafluoroethylene has been examined by wide-angle X-ray diffraction and electron microscopy. The deformation mechanisms which have been found to operate are  $\{10\bar{1}0\}\langle 0001\rangle$  chain direction slip and  $\{10\bar{1}0\}\langle 12\bar{1}0\rangle$  transverse slip. At 20°C the critical resolved shear stress for chain direction slip has been found to be about 2.5 MN/m<sup>2</sup> and that for transverse slip to be about 15 MN/m<sup>2</sup>.

## INTRODUCTION

Polytetrafluoroethylene (PTFE) normally crystallizes in the form of banded lamellae up to 1 μm thick and containing striations parallel to the chain direction<sup>1</sup>. The size of the banded lamellae has been found by Speerschneider and Li<sup>2,3</sup> to depend upon the crystallization conditions. They also found that when the banded material was deformed above -70°C the striations tended to shear past each other whereas at lower temperatures deformation by kinking of the striations appeared to be more common<sup>3</sup>.

The deformation of PTFE has also been studied by X-ray diffraction. Uniaxially oriented material has been found to have a texture with the chain axes,  $\langle 0001\rangle$  parallel to the draw direction<sup>4</sup>. The texture of rolled PTFE has been investigated by pole-figure analysis<sup>5,6</sup>. Hot-rolled PTFE has a simple texture with  $\{10\bar{1}0\}$  in the plane of the sheet and  $\langle 0001\rangle$  parallel to the extension direction. McCrum and his coworkers<sup>5,6</sup> interpreted this texture in terms of chain direction slip on the closest-packed planes (i.e.  $\{10\bar{1}0\}\langle 0001\rangle$  slip). The crystal structures of PTFE and polyoxymethylene (POM) are similar in that both have molecules in a helical conformation and a hexagonal crystal structure. It is not surprising therefore that the texture of hot-rolled POM is similar to that of hot-rolled PTFE<sup>5</sup>.

The texture of cold-rolled POM is rather complex<sup>5-9</sup>. Preedy and Wheeler<sup>8</sup> suggested that the difference in texture between the hot-rolled and cold-rolled material might be due to POM undergoing a phase transformation to an orthorhombic cell. Miles and Mills<sup>9</sup> found no evidence for a new phase in POM and suggested that the complex low temperature texture was probably due to the simultaneous occurrence of  $\{10\bar{1}0\}\langle 0001\rangle$  slip and  $\{10\bar{1}0\}\langle 12\bar{1}0\rangle$  slip. It is difficult to roll PTFE at room temperature and so little work has been done upon the structure of cold-rolled material. In this present work a technique has been used to obtain biaxially oriented PTFE at various temperatures by the use of a constrained compression die<sup>10</sup>. The texture of the oriented material has been interpreted in terms of deformation mechanisms. The constrained compression technique has been used to prepare oriented material with a well-defined texture which has then been used for further study of the individual deformation mechanisms.

## DEFORMATION OF ISOTROPIC PTFE

The PTFE material used in this work was Fluon coarse dispersion polymer kindly supplied by ICI Ltd in the form of 6 mm thick sintered sheet. During fabrication, the material had been cooled slowly to produce the thick banded lamellae<sup>1</sup>.

### Experimental

Bars of PTFE were compressed at various temperatures between -40°C and 220°C in the die illustrated schematically in Figure 1 which is similar to the one used by Young *et al.*<sup>10</sup>. It had been modified to include electrical heaters which were able to hold the temperature constant to better than ±3°C up to 250°C. When the material is compressed, the die allows the PTFE to extrude from the ends as the height is reduced but at the same time the sample is con-

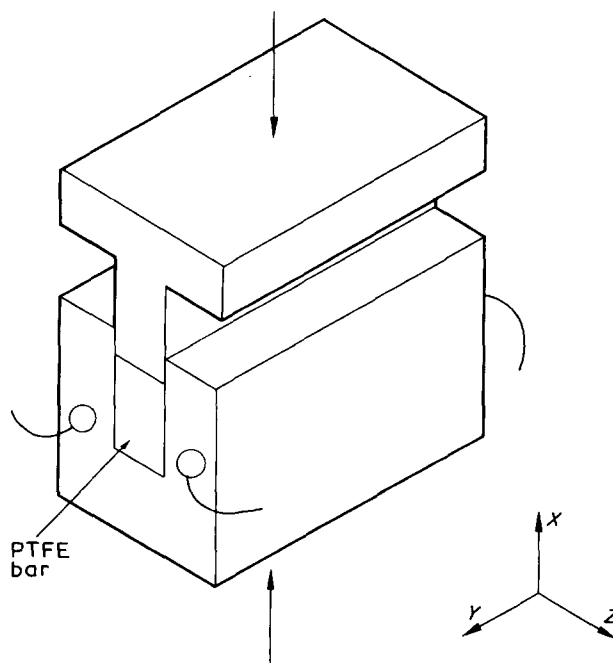


Figure 1 The heated compression die used to prepare the oriented material. X is parallel to the compression direction, Y and Z are in the plane of the sheet with Y parallel to the extension direction

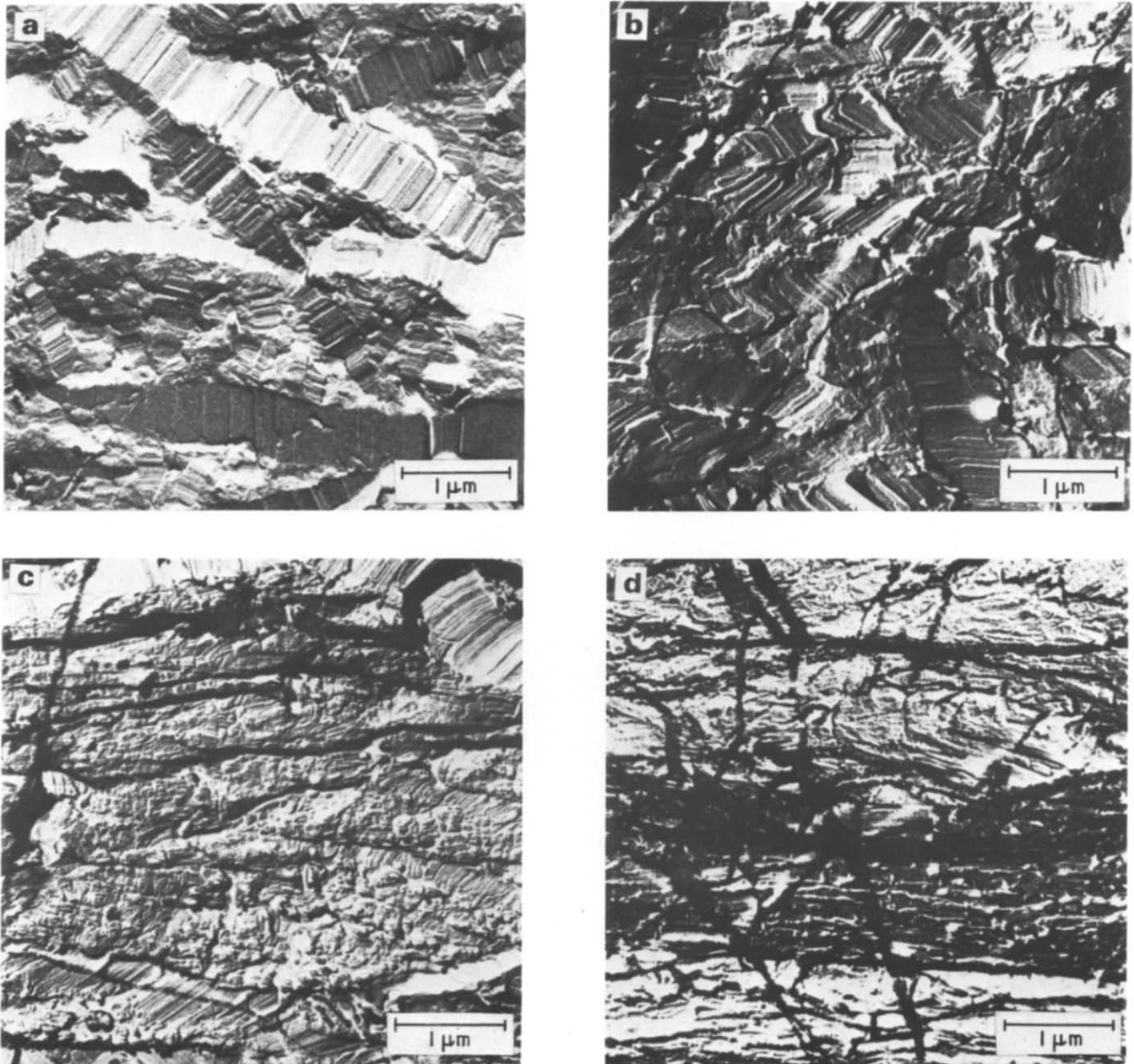


Figure 2 Electron micrographs of PTFE (a) before and (b)–(d) after deformation at different temperatures: (b)  $-40^{\circ}$ ; (c)  $21^{\circ}$ ; (d)  $70^{\circ}\text{C}$

strained to constant width. This produces a plane strain deformation similar to that of rolling but has the added advantage of not allowing any increase in width due to bulging<sup>7</sup>.

In each case the sample was compressed to the maximum strain that could be tolerated before fracture intervened and the hot samples were quenched by water-cooling to room temperature at about  $30^{\circ}\text{C}/\text{min}$ .

#### Electron microscopy

Replicas of fracture surfaces of the PTFE samples were obtained before and after deformation and were examined in an electron microscope. The fracture surfaces were obtained by cleaving specimens in liquid nitrogen. Carbon replicas, shadowed by gold–palladium, were obtained using cellulose acetate as described by Young and Bowden<sup>11</sup> for HDPE.

An electron micrograph of a replica of a fracture surface of an undeformed sample is given in Figure 2a. The surface

consists of lamella crystals up to  $1\ \mu\text{m}$  thick. The striations within the crystals are parallel to the chain axes of the crystals<sup>1</sup> and approximately perpendicular to the surfaces of the lamellae. Figure 2b is a replica from a specimen compressed to a strain of 45% at  $-40^{\circ}\text{C}$ . The section was taken in the plane strain plane with the *X* direction vertical and *Y* horizontal (Figure 1). In some of the crystals the striations appear to have sheared past each other and are no longer perpendicular to the surfaces of the lamellae. Figure 2c shows a similar specimen compressed at  $21^{\circ}\text{C}$  to a strain of 70%. In this case all the striations have tilted over sharply and in some cases crystals have started to break up. In the central area of the micrograph the broken crystals appear to have started to recrystallize and where this has happened the striations in the new crystals are approximately parallel to the extension direction (*Y*). Figure 2d is taken from a specimen compressed at  $70^{\circ}\text{C}$  to a strain of about 80%. In this case the original crystal structure is completely destroyed and a fibre structure produced.

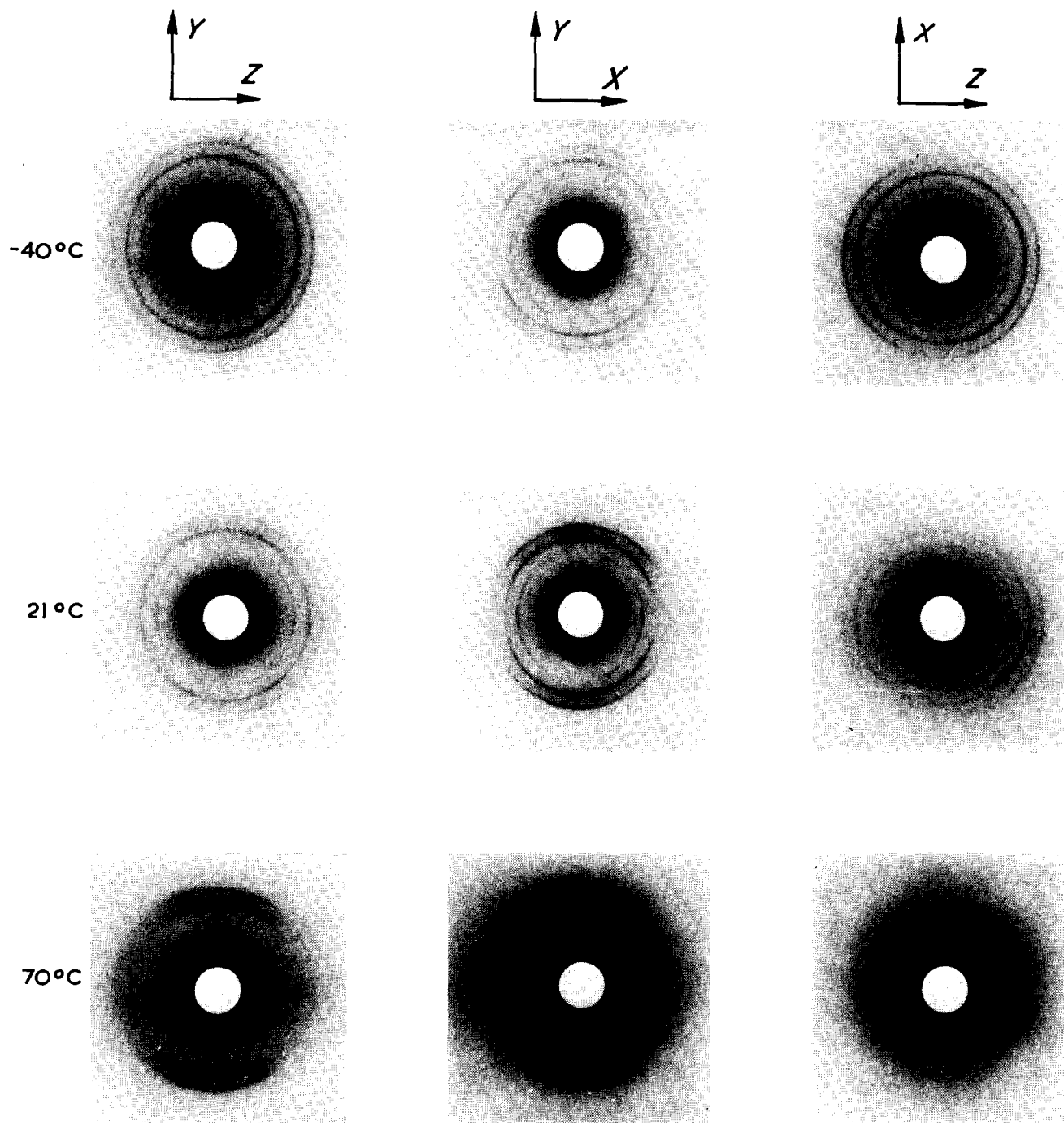


Figure 3 Wide-angle X-ray diffraction patterns of PTFE deformed at three different temperatures. Patterns have been obtained with the beam parallel to X, Z and Y respectively

The behaviour outlined above is consistent with the model for the deformation of polyethylene and polypropylene by rolling or drawing put forward by Peterlin<sup>12</sup>. It is thought that first of all the molecules shear past each other within the crystals until they are aligned close to the extension direction. The crystals are then thought to start to break up and recrystallize such that the new crystals are all approximately transverse to the extension direction and the molecules are parallel to the extension direction. Previously most of the evidence for this model for deformation had been obtained by using indirect methods such as X-ray diffraction. The micrographs in Figure 2 show clearly how this process takes place in PTFE on the molecular level.

#### X-ray diffraction

The X-ray diffraction patterns which were obtained at  $25 \pm 2^\circ\text{C}$  with the X-ray beams parallel to X, Z and Y for specimens deformed at  $-40^\circ$ ,  $21^\circ$  and  $70^\circ\text{C}$  are given in Figure 3.

The patterns obtained with the beam parallel to X and Y for specimens deformed at  $-40^\circ\text{C}$  show almost complete rings and are not very different from the pattern obtained from the undeformed structure. The pattern obtained with the beam parallel to Z is quite different showing a well-defined hexagonal pattern. The reflections in the inner ring are of the  $\{10\bar{1}0\}$  type and the positions of the maxima correspond to 3 sets of  $\{10\bar{1}0\}$  planes parallel to Z as illustrated in Figure 4a. One set is also parallel to X



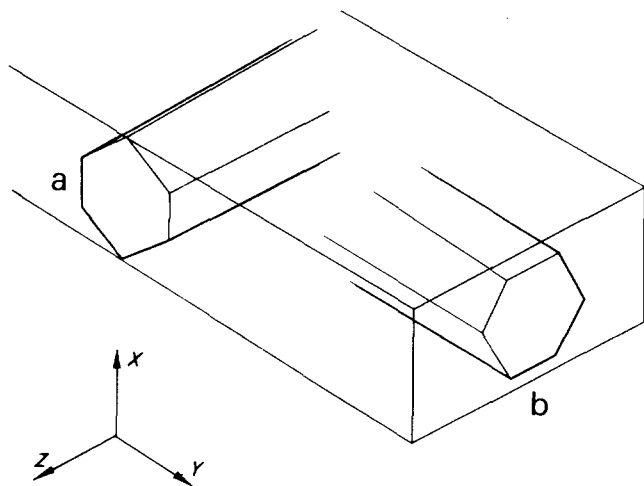


Figure 4 Schematic diagrams of the texture in oriented PTFE. (a) Transverse texture obtained at  $-40^{\circ}\text{C}$ ; (b) normal texture obtained by hot rolling or compression orientation

and the other two are at  $\pm 60^{\circ}$  to  $X$ .

For specimens deformed at higher temperatures the three diffraction patterns are found to change. In the pattern obtained with the beam parallel to  $X$  the inner rings start to intensify at the equator and become quite intense at  $70^{\circ}\text{C}$ . With the beam parallel to  $Z$  intensification on the equator also starts to occur at higher temperatures and the hexagonal symmetry found at  $-40^{\circ}\text{C}$  starts to be destroyed. The intensification of these patterns about the equator is characteristic of molecular orientation when  $(hki0)$  reflections intensify perpendicular to the extension direction ( $Y$ ). However, the pattern obtained with the beam parallel to  $Z$  at  $70^{\circ}\text{C}$  still has a maximum on the meridian of the  $\{10\bar{1}0\}$  ring indicating the presence of  $\{10\bar{1}0\}$  planes perpendicular to  $Y$ .

The patterns obtained with the beam parallel to  $Y$  do not show a great deal of orientation and do not change greatly as the temperature is raised. However, careful examination of the  $\{10\bar{1}0\}$  ring in the specimen deformed at  $70^{\circ}\text{C}$  shows that there is a variation of intensity around the ring. There is intensification on the meridian and at  $\pm 60^{\circ}$  to the meridian. Along with the other patterns obtained from the  $70^{\circ}\text{C}$  material this implies that the texture is made up of  $\{10\bar{1}0\}$  planes in the  $ZY$  plane and also at  $\pm 60^{\circ}$  to the  $ZY$  plane as illustrated schematically in Figure 4b. This is precisely the texture obtained by McCrum and coworkers<sup>5,6</sup> for hot-rolled PTFE.

#### INTERPRETATION OF TEXTURE IN TERMS OF DEFORMATION MECHANISMS

The interpretation of texture in deformed polymers in terms of deformation mechanisms has been discussed in detail by Bowden and Young<sup>13</sup> and essentially their approach will be used again here. The deformation mechanisms that have been suggested for PTFE are  $\{10\bar{1}0\}$   $\langle 0001 \rangle$  chain direction slip<sup>5,13</sup> and  $\{10\bar{1}0\}$   $\langle 12\bar{1}0 \rangle$  transverse slip<sup>13</sup>. For both of these two mechanisms there are three slip systems, two of which are independent. In total, therefore, there are four independent slip systems for the PTFE crystal. It has been shown<sup>14</sup> that five independent slip systems are required to be able to operate before any polycrystalline material may undergo a general shape change. As PTFE can deform plastically without cracking, it must be concluded that shape changes are to some extent taken up by the amorphous material between the crystals<sup>13</sup>.

#### Hot-oriented PTFE

The simplest texture of PTFE to interpret is that of hot rolled or hot compression-oriented material. The texture consists of  $\{10\bar{1}0\}$  planes transverse to the compression direction ( $X$ ) and  $\langle 0001 \rangle$  chain axis parallel to the extension direction ( $Y$ ). McCrum and coworkers<sup>5,6</sup> interpreted such a texture as being due to  $\{10\bar{1}0\}$   $\langle 0001 \rangle$  chain slip. Bowden and Young<sup>13</sup> showed that such a texture could not be produced by chain direction slip alone and went on to show that in order to produce such a texture during plane strain deformation, slip would have to take place on  $\{10\bar{1}0\}$  in both  $\langle 0001 \rangle$  and  $\langle 12\bar{1}0 \rangle$  directions (i.e. transverse slip was needed as well).

#### Orientation at lower temperatures

The texture found by orienting PTFE at lower temperatures is more unusual than that found at higher temperatures. The amount of strain that can be produced before cracking is less at lower temperatures and this may account for some of the differences. Figure 4a gives a schematic illustration of the texture of compression-oriented PTFE deformed at  $-40^{\circ}\text{C}$ . The chain axis  $\langle 0001 \rangle$  is transverse to the extension direction and the  $\{10\bar{1}0\}$  planes perpendicular to the extension direction ( $Y$ ) and at  $\pm 60^{\circ}$  to  $Y$ . In order to interpret this texture it is necessary to consider what the X-ray beam is sampling. For any given orientation of the X-ray beam the reflections on the diffraction pattern are from planes which are oriented at the Bragg angle to that beam. In polymers strong reflections are only normally obtained from low index planes. The spacing of the  $\{10\bar{1}0\}$  planes in PTFE is  $4.9 \text{ \AA}$  which using  $\text{CuK}\alpha$  radiation leads to a Bragg angle of about  $9^{\circ}$ . This is within the limits of the spread of the texture that would be expected and so it may be assumed that for this analysis  $\{10\bar{1}0\}$  planes giving rise to the  $\{10\bar{1}0\}$  reflection are effectively parallel to the beam.

As there is no high degree of overall orientation at  $-40^{\circ}\text{C}$ , it appears that the texture found in the pattern obtained with the beam parallel to  $Z$  may be due to the deformation of crystals which were oriented initially with their chain axes approximately parallel to  $Z$ . This transverse texture is probably due to slip within these crystals only. The chain axes of the crystals are perpendicular to the plane strain ( $XY$ ) and so during deformation  $\{10\bar{1}0\}$   $\langle 12\bar{1}0 \rangle$  transverse slip will be favoured. Because of the hexagonal symmetry of PTFE there are three possible slip systems at  $60^{\circ}$  to each other. Slip will take place on the

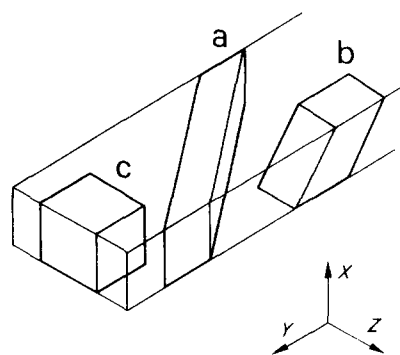


Figure 5 Illustration of the three different ways in which specimens were cut from the oriented sheets. (a) Specimen for shear on  $XY$ ; (b) specimen for shear on  $YZ$ ; (c) specimen for shear perpendicular to the molecular chains ( $Y$ )

$\{10\bar{1}0\}$  plane which experiences the highest resolved shear stress and the crystal rotates until this plane is at  $60^\circ$  to the compression direction ( $X$ ). At this point another plane is also at  $60^\circ$  to  $X$  and slip then takes place on both of these planes simultaneously. This is known as *Duplex slip* and there is no further rotation of the crystal (see later). The texture found in the specimen compressed at  $-40^\circ\text{C}$  is consistent with this type of deformation. At higher tem-

peratures and in specimens deformed to higher strains, crystals of all original orientations will have to deform to accommodate the strain.  $\{10\bar{1}0\}\langle 0001\rangle$  chain slip will then take place as well as transverse slip and the high temperature texture will be produced. However, even at  $70^\circ\text{C}$  there are still  $\{10\bar{1}0\}$  planes perpendicular to  $Y$  due to Duplex slip in crystals which were originally oriented with their chain axes ( $\langle 0001\rangle$ ) parallel to  $Z$ .

Table 1 Measured values of  $\theta_0$ ,  $\theta_1$ ,  $e$  and bulging for specimens of oriented PTFE sheared in two different ways parallel to the chain direction ( $\theta_1$  has also been calculated using equation 1)

Mode	$\theta_0$ (degrees)	$\theta_1$ (degrees)	$e$ (%)	$\theta_1$ (calc.) (degrees)	Bulging (%)
Shear	17	38	26.7	45	21
on	36	47	22.5	51	3
XY	52	62	22.8	61	7
Shear	27	46	20.5	45	7
on	43	56	26.0	57	1
YZ	60	66	22.0	67	~0

#### DEFORMATION OF ORIENTED PTFE

The oriented material used in this section had been compressed as described in the experimental section to a strain of 83% which corresponds to a compression ratio of about 6. This material was similar to that compressed at  $70^\circ\text{C}$  with  $\{10\bar{1}0\}$  planes parallel to and at  $\pm 60^\circ$  to the plane of the sheet ( $YZ$ ). The X-ray diffraction patterns of this material were more well-defined showing that deformation at higher temperatures produced a higher degree of orientation. No extra reflections were observed in the X-ray diffraction patterns after deformation so it was assumed that

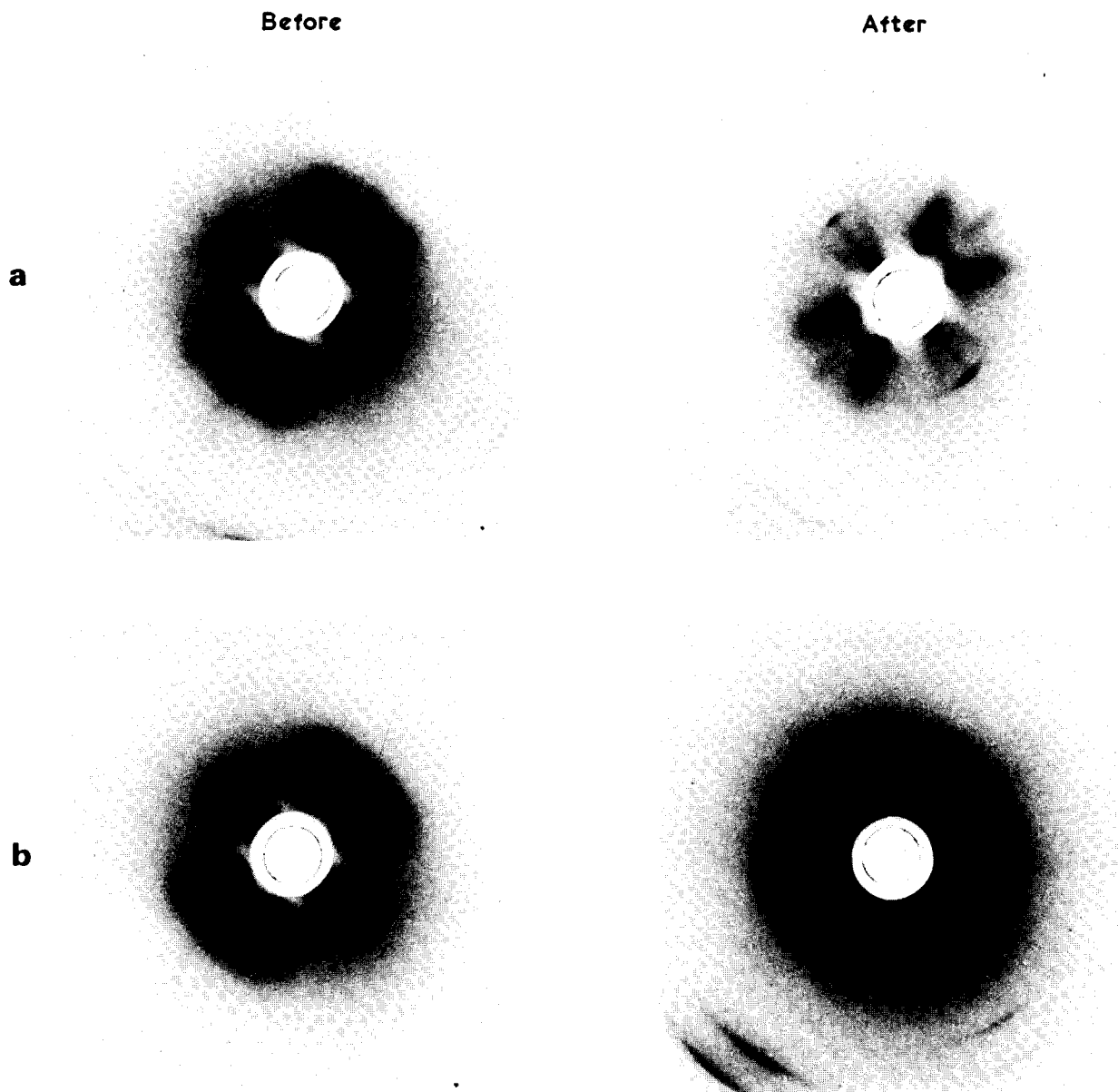


Figure 6 Wide-angle X-ray diffraction patterns obtained before and after deformation for specimens with  $\theta_0 \sim 40^\circ$ . The compression direction is vertical and  $\theta$  was measured using the innermost ( $\{10\bar{1}0\}$ ) arcs. (a) Specimen sheared on XY (X-ray beam parallel to  $X$ ); (b) specimen sheared on YZ (X-ray beam parallel to  $Z$ )

the PTFE crystals had not undergone a stress-induced phase change as in the case of deformed PE<sup>10,15</sup>.

#### Shear parallel to the molecules

Specimens were cut from the oriented sheets at angles to the chain direction in two different ways as shown in *Figures 5a* and *5b*. They were then compressed between steel dies at various angles to the chain direction as described for PE by Young *et al.*<sup>10</sup> and deformation was found to take place principally by slip parallel to the chain direction. The angle between the chain direction and the compression direction has been defined as  $\theta$  and for the two types of specimen samples were cut out at  $\theta$  values of approximately 20°, 40°, and 60°.

Stress-strain curves were obtained for each specimen and  $\theta$  was measured before ( $\theta_0$ ) and after ( $\theta_1$ ) deformation using wide-angle X-ray diffraction and CuK $\alpha$  radiation. The measured values of  $\theta_0$  and  $\theta_1$  are given in *Table 1*. Pairs of X-ray diffraction patterns for the two types of specimens both with  $\theta_0 \sim 40^\circ$  are given in *Figure 6*. In all cases it was found that  $\theta$  had increased after deformation which is consistent with the deformation having taken place by single slip parallel to  $c$ <sup>10</sup>. For this type of deformation the relationship between  $\theta_0$  and  $\theta_1$  is given by<sup>10</sup>:

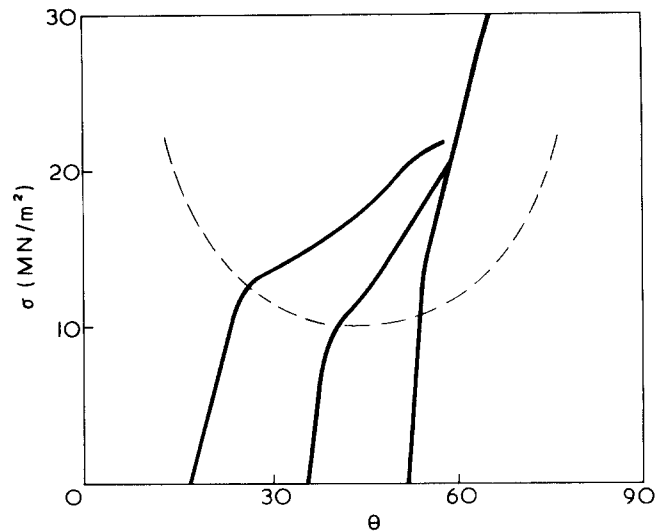
$$\frac{\cos \theta_1}{\cos \theta_0} = 1 - e \quad (1)$$

where  $e$  is the specimen strain. Values of  $\theta_1$ , calculated using this equation with the measured values of  $\theta_0$  and  $e$ , are also given in *Table 1*. For shear on  $YZ$  it can be seen that the measured and calculated values of  $\theta_1$  agree to within one degree which shows that for this case, the deformation took place essentially by single slip parallel to the chain direction. For specimens sheared on  $XY$  this agreement was somewhat worse. The increase in specimen width due to bulging perpendicular to the compression direction was also greater. This shows that there was some deviation from plane strain deformation. Both of these observations show that in this orientation, the specimens deformed by other mechanisms as well as single slip parallel to the chain direction.

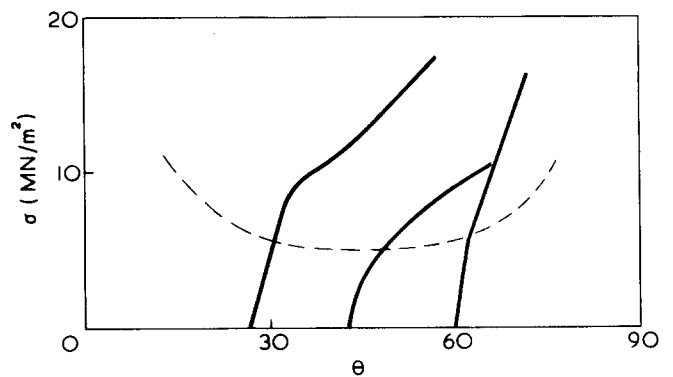
The stress-strain curves were converted into plots of stress against  $\theta$  using equation (1). The curves for shear on  $XY$  are given in *Figure 7* and those for shear on  $YZ$  in *Figure 8*. In a previous paper<sup>10</sup> upon PE an attempt was made to interpret similar data in terms of slip parallel to  $c$  at a constant critical resolved shear stress,  $\tau$ . The yield or flow stress  $\sigma$  is then given by the equation,

$$\sigma = \tau / \sin \theta \cos \theta \quad (2)$$

This equation is plotted as broken lines in *Figures 7* and *8* fitted approximately to the yield stresses of each of the curves by choosing an appropriate value of  $\tau$ . For shear upon  $XY$  (*Figure 7*)  $\tau$  is 5 MN/m<sup>2</sup> and for shear upon  $YZ$  (*Figure 8*)  $\tau$  is 2.5 MN/m<sup>2</sup>. It may be noted that, although the yield points of the curves lie approximately upon the broken lines, after yield the curves rise steeply above them. This may be contrasted with similar investigations into the deformation of compression-oriented and annealed HDPE<sup>10</sup>. In this case, it was found that the oriented HDPE yielded and flowed at a constant critical resolved shear stress. However, compression-oriented HDPE which had not been annealed did show similar strain-hardening during plastic flow.



*Figure 7* Plots of stress as a function of  $\theta$  for specimens sheared on  $XY$



*Figure 8* Plots of stress as a function of  $\theta$  for specimens sheared on  $YZ$

#### Deformation mechanisms induced by shear parallel to the molecules

In the previous section it was shown that slip parallel to the molecules would take place upon both the  $XY$  and  $YZ$  planes. However, it was also shown that slip was easier upon  $YZ$  as there was a lower value of  $\tau$  required, much less bulging (*Table 1*) and good agreement with equation (1). This gives a strong indication of the slip plane for the chain direction ( $\langle 0001 \rangle$ ) slip process. In the oriented PTFE that has been used there is a set of  $\{10\bar{1}0\}$  planes in the plane of the sheet ( $YZ$ ). Since slip is very much easier on the  $YZ$  plane, the slip plane with the lowest critical resolved shear stress must therefore be  $\{10\bar{1}0\}$ . The  $\{10\bar{1}0\}$  planes are at  $\pm 30^\circ$  to the  $XY$  plane and so for slip to take place on  $\{10\bar{1}0\}$  planes in a specimen sheared on  $XY$ , the stress needed for  $\langle 0001 \rangle$  slip is higher by a factor of  $(\cos 30^\circ)^{-1}$  (1.15). Since the measured ratio of the  $\tau$  values is of the order of 2 and in some specimens there was considerable amounts of bulging (*Table 1*) any quantitative interpretations of this form of deformation would appear to be difficult.

#### Shear perpendicular to the molecules

Specimens were cut from the sheets of oriented PTFE as shown in *Figure 5c* so that they could be compressed in directions perpendicular to the molecular chains. They were compressed in uniaxial compression in a similar way

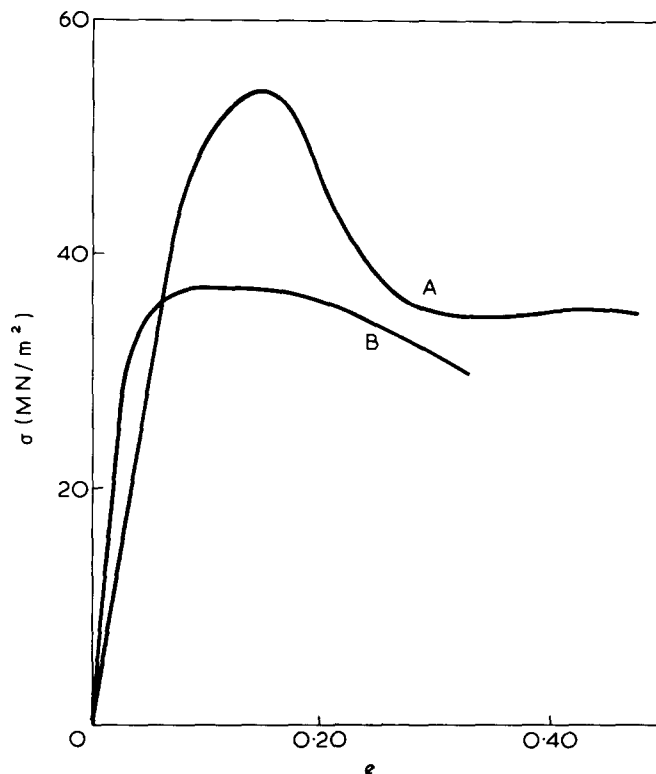


Figure 9 Stress-strain curves for specimens compressed in directions transverse to the chain axis (Y). A, Specimen compressed parallel to X; B, specimen compressed parallel to Z

to the compression of oriented and annealed HDPE described by Young and Bowden<sup>15</sup>. Two particular specimens were used. One was compressed parallel to X and the other parallel to Z. In both cases there was no measurable change in specimen length parallel to Y and so the deformation could be considered to be essentially plane strain. Plots of true stress against nominal strain were obtained for the two specimens and they are both given in Figure 9.

Wide-angle X-ray diffraction patterns were also obtained from each specimen before and after deformation and they are given in Figure 10. In each case the X-ray beam is parallel to Y and the compression direction is vertical. The first pair of diffraction patterns (Figure 10a) were obtained from the specimen compressed parallel to X. Before deformation, the pattern has hexagonal symmetry corresponding to  $\{10\bar{1}0\}$  transverse to and at  $\pm 30^\circ$  to the compression direction. After deformation, the pattern is less well-defined but careful examination of the  $\{10\bar{1}0\}$  ring shows maxima corresponding to planes parallel to and at  $\pm 60^\circ$  to the compression direction. The second pair of patterns (Figure 10b) are for the specimen compressed parallel to Z. The pattern obtained before deformation has hexagonal symmetry again and the  $\{10\bar{1}0\}$  maxima correspond to planes parallel to and at  $\pm 60^\circ$  to the compression direction. After deformation the pattern is less well-defined but the position of the maxima remains unchanged. This means that this time the  $\{10\bar{1}0\}$  planes have not rotated during deformation but have remained stationary at  $\pm 60^\circ$  to the compression direction.

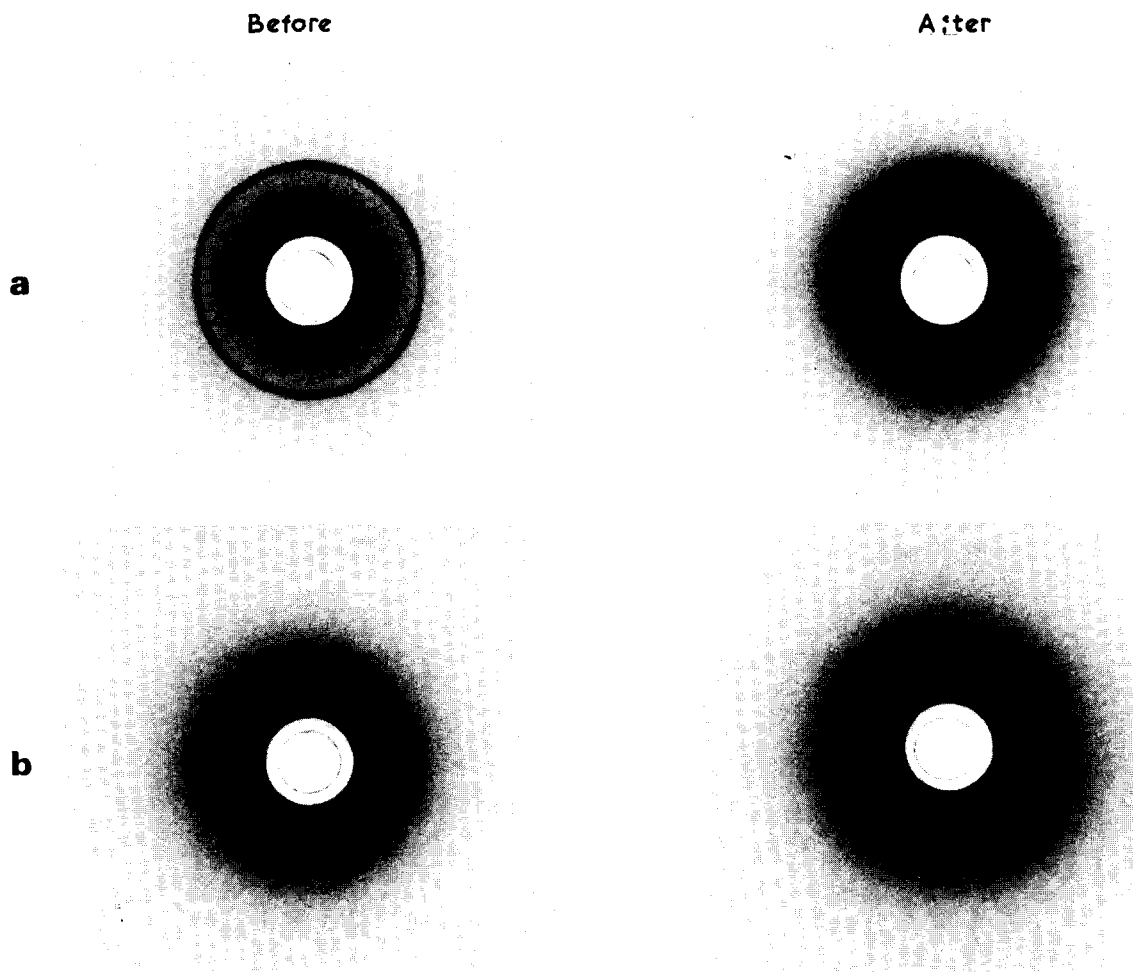


Figure 10 Wide-angle X-ray diffraction patterns for the specimens used in Figure 9 obtained with the beam parallel to Y. (a) Specimen compressed parallel to X; (b) specimen compressed parallel to Z

### Deformation mechanisms induced by shear transverse to the molecules

From the X-ray diffraction patterns obtained in the previous section it is possible to determine the deformation mechanisms which were operating during transverse deformation. For both specimens the X-ray patterns obtained after deformation are identical with  $\{10\bar{1}0\}$  planes parallel to and at  $\pm 60^\circ$  to the compression direction.

The orientation of the unit cell for compression perpendicular to the chain direction and parallel to  $X$  is illustrated schematically in Figure 11. In this orientation  $\{10\bar{1}0\}$   $\langle 12\bar{1}0 \rangle$  transverse slip will take place on the  $\{10\bar{1}0\}$  plane which experiences the highest resolved shear stress, i.e. one of the planes at  $30^\circ$  to the compression direction. The plane is rotated by the slip process and the resolved shear stress is continuously reduced until it reaches a minimum when the plane is at  $45^\circ$  to the compression direction. Any further rotation of the plane increases the resolved shear stress but slip continues until it is at  $60^\circ$  to the compression direction as it is still the plane which experiences the highest resolved shear stress. When the slip plane is at  $60^\circ$  to the compression direction, there is then another plane also at  $60^\circ$  to the compression direction (Figure 11). In this position any further rotation of the original slip plane reduces the angle of the second plane. This is a position of Duplex slip<sup>16</sup> since slip will take place simultaneously on the two  $\{10\bar{1}0\}$  planes without any overall rotation of the crystal.

It is now possible to explain the stress-strain curves in Figure 9 in terms of Duplex slip. For curve B the stress increases as the specimen is loaded until it reaches a constant value. In this specimen the  $\{10\bar{1}0\}$  planes were originally at  $\pm 60^\circ$  to the compression direction. The yield and flow stress in this orientation is  $36 \text{ MN/m}^2$  and since there is no change in orientation during Duplex slip, there is no overall change in stress during flow. It must be noted that there is no apparent strain hardening as was found for chain direction slip. The critical resolved shear stress,  $\tau$ , for  $\{10\bar{1}0\}\langle 12\bar{1}0 \rangle$  slip may be estimated from equation (2). In this case, the  $\{10\bar{1}0\}$  slip planes are always at  $\pm 60^\circ$  to the compression direction which means that  $\theta$  equals  $60^\circ$ . The yield and flow stress for compression parallel to  $Z$  is about  $36 \text{ MN/m}^2$  which gives a value of  $\tau$  of about  $15 \text{ MN/m}^2$  for  $\{10\bar{1}0\}\langle 12\bar{1}0 \rangle$  slip at  $20^\circ\text{C}$ . Curve A in Figure 9 eventually settles at about  $36 \text{ MN/m}^2$  at strains above 30% when the  $\{10\bar{1}0\}$  slip planes have rotated to the position for Duplex slip to take place.

## DISCUSSION AND CONCLUSIONS

The deformation mechanisms which have been found to operate in PTFE are  $\{10\bar{1}0\}\langle 0001 \rangle$  chain slip and  $\{10\bar{1}0\}\langle 12\bar{1}0 \rangle$  transverse slip. Both of these two mechanisms give rise to three slip systems, only two of which are independent. This gives a total of four independent slip systems. For an isotropic polycrystalline material to undergo a general shape change without cracking five independent slip systems must be able to operate<sup>13,14</sup>. However, the amorphous material between the crystals can accommodate the change in shape of the individual crystals and may therefore allow the material to undergo a general shape change without the necessity of five independent slip systems<sup>13</sup>.

The critical resolved shear stress for  $\{10\bar{1}0\}\langle 0001 \rangle$

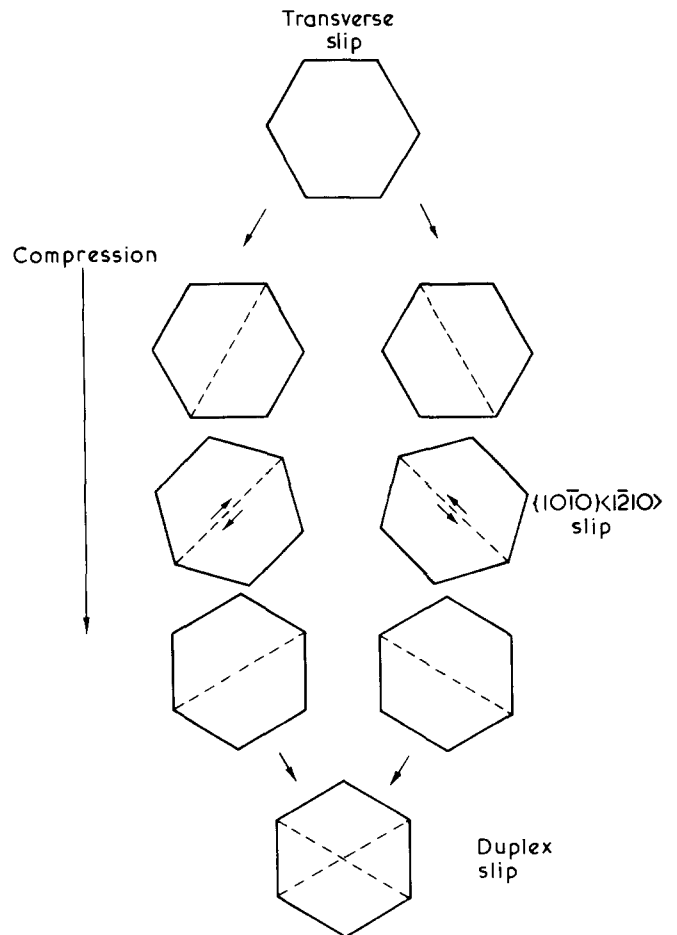


Figure 11 A schematic diagram of the rotation of the hexagonal unit cell of PTFE by compression perpendicular to the chain direction. The slip planes are represented by broken lines

chain direction slip has been found to be about  $2.5 \text{ MN/m}^2$  and that for  $\{10\bar{1}0\}\langle 12\bar{1}0 \rangle$  transverse slip to be about  $15 \text{ MN/m}^2$ . Chain direction slip also appears to show a large amount of strain hardening but transverse slip shows remarkably little.

Recent work<sup>17</sup> has shown that dislocations may be activated thermally during the deformation of HDPE by means of chain direction slip. The energy of a dislocation depends strongly upon the Burgers vector which for chain direction slip in PTFE is extremely large ( $19.5 \text{ \AA}$ ). For this type of deformation to take place with such ease, slip must occur by means of partial dislocations or the rotation of molecules during deformation<sup>18</sup>.

## ACKNOWLEDGEMENTS

Part of this work was carried out in the Department of Metallurgy and Materials Science in the University of Cambridge and the author wishes to acknowledge his indebtedness to the late Dr P. B. Bowden for valuable discussion during the course of the work. He would also like to thank Dr H. Browning of ICI (Plastics Division) for supplying the material and the Master and Fellows of St John's College, Cambridge for support in the form of a Research Fellowship.

REFERENCES

- 1 Sherratt, S. 'Encyclopedia of Chemical Technology', Interscience, New York, 1966, Vol 9, p 803
- 2 Speersneider, C. J. and Li, C. H. *J. Appl. Phys.* 1962, **33**, 1871
- 3 Speersneider, C. J. and Li, C. H. *J. Appl. Phys.* 1963, **34**, 3004
- 4 Wecker, S. M., Davidson, T. and Baker, D. W. *J. Appl. Phys.* 1972, **43**, 4345
- 5 Gray, R. W. and McCrum, N. G. *Nature (Phys. Sci.)* 1971, **234**, 117
- 6 Chang, E. P., Gray, R. W. and McCrum, N. G. *J. Mat. Sci.* 1973, **8**, 397
- 7 Gezovich, D. M. and Geil, P. H. *J. Mat. Sci.* 1971, **6**, 509
- 8 Preedy, J. E. and Wheeler, E. J. *Nature (Phys. Sci.)* 1972, **236**, 60
- 9 Miles, M. J. and Mills, N. J. Paper presented at Inst. of Phys., Polymer Physics Group Conference, Shrivenham, 1973
- 10 Young, R. J., Bowden, P. B., Ritchie, J. M. and Rider, J. G. *J. Mat. Sci.* 1973, **8**, 23
- 11 Young, R. J. and Bowden, P. B. *J. Mat. Sci.* 1973, **8**, 1177
- 12 Peterlin, A. *J. Mat. Sci.* 1971, **6**, 490
- 13 Bowden, P. B. and Young, R. J. *J. Mat. Sci.* 1974, **9**, 2034
- 14 Kelly, A. and Groves, G. W. 'Crystallography of Crystal Defects', Longman, London, 1970
- 15 Young, R. J. and Bowden, P. B. *Phil. Mag.* 1974, **29**, 1061
- 16 Bowen, D. K. and Christian, J. W. *Phil. Mag.* 1965, **12**, 369
- 17 Young, R. J. *Phil. Mag.* 1974, **30**, 85
- 18 Flack, H. D. *J. Polym. Sci. (Polym. Phys. Edn)* 1974, **12**, 81

# Notes to the Editor

## Voiding in glass fibre reinforced thermoplastics mouldings

M. W. Darlington and G. R. Smith

*Department of Materials, Cranfield Institute of Technology, Cranfield, Bedfordshire MK43 0AL, UK  
(Received 16 December 1974)*

### INTRODUCTION

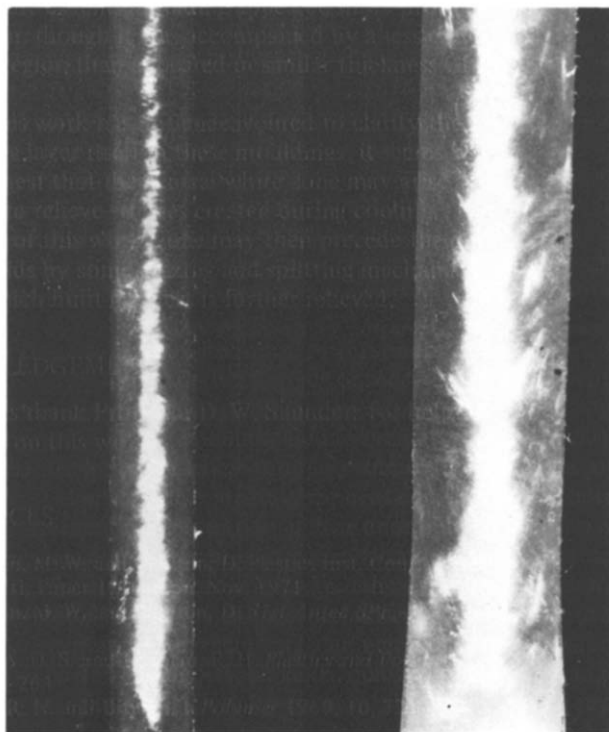
The tensile creep behaviour of short fibre reinforced thermoplastics has been studied in these laboratories using highly accurate equipment in which all three orthogonal strains are measured simultaneously. This has enabled volume changes associated with voiding during uniaxial tensile creep to be calculated and these have been correlated with the incidence of permanent damage (in the form of deterioration in mechanical properties) resulting from the deformation of the fibre-matrix system<sup>1,2</sup>. The detailed development of the voiding has not yet been studied.

The nature of these composites makes the preparation of well oriented (or indeed, perfectly random) and homogeneous samples extremely difficult, and the fibre orientation distribution in typical injection mouldings of these materials is usually complex and inhomogeneous. Nevertheless, a detailed characterization of the fibre orientation distribution and all other relevant features of the composite is essential if the mechanical data are to have any real significance. Some guidance on fibre orientation distributions in the above samples has been obtained by optical examination of surfaces cut in a variety of directions through the samples and polished using standard metallographic polishing techniques.

In preparation for an extension of the above studies to creep in liquid environments, a new batch of short glass fibre reinforced thermoplastics injection mouldings were obtained from a different source (referred to as moulder B) to that of the original batch (from moulder A). During an initial characterization of these mouldings a new feature became apparent. This took the form of a central white zone and was initially observed in the through-thickness cross-section of short glass fibre reinforced polypropylene (GFPP) edge-gated discs of nominal thickness 3 mm and 6 mm. On re-examination, a similar, though less marked and discontinuous, central white zone was noted in the cross-section of the GFPP 3 mm thick edge-gated discs previously supplied by moulder A. The appearance of the cross-section for the samples from moulder B is shown in *Figure 1*. The weight fraction of glass fibres was  $28 \pm 1\%$  in all samples.

Although voids were known to occur in GFPP mouldings with thick sections, enquiries and a search of the literature produced no clear statement on the nature of the white zone, or even on the occurrence of voids, in the thinner sections. In view of the possible effects of voids on mechanical properties in air, and the proposed creep study in liquids, it was considered essential to examine the central white zone, with particular regard to any occurrence of voids.

A detailed determination of fibre content in the mouldings indicated little change through thickness, but the central white zone was found to have a lower density than the



*Figure 1* Photograph of the cross-section of 3 mm and 6 mm thickness edge-gated discs of GFPP supplied by moulder B, showing the central white zone

surrounding regions. Subsequent optical examination of the 6 mm thick GFPP disc moulding indicated the existence of voids in the central white zone, large enough to be resolved by a low power stereo-optical microscope at a magnification of 60. It was considered that the occurrence of the narrow central white zone in the 3 mm thickness moulding should be an effect similar to that observed in the 6 mm mouldings, though occurring on a smaller scale. As stereo-optical microscopy provided no evidence of the existence of voids in the 3 mm thickness mouldings, scanning electron microscopy was employed in an attempt to locate such features in the central white region.

The surface preparation technique was that mentioned above for the determination of fibre orientation distributions. Although this surface preparation technique appears to be reasonably well established for the examination of glass fibre reinforced thermosets<sup>3</sup>, and has been shown to be useful for fibre orientation distribution studies in short fibre reinforced thermoplastics, it does not appear to be readily acceptable for the study of features such as voids in the latter group of composite materials. The purpose of this note is therefore to establish the validity of the preparation technique for the study of voids and to report some of the interesting features observed in the central white

regions of some short glass fibre reinforced thermoplastics injection mouldings.

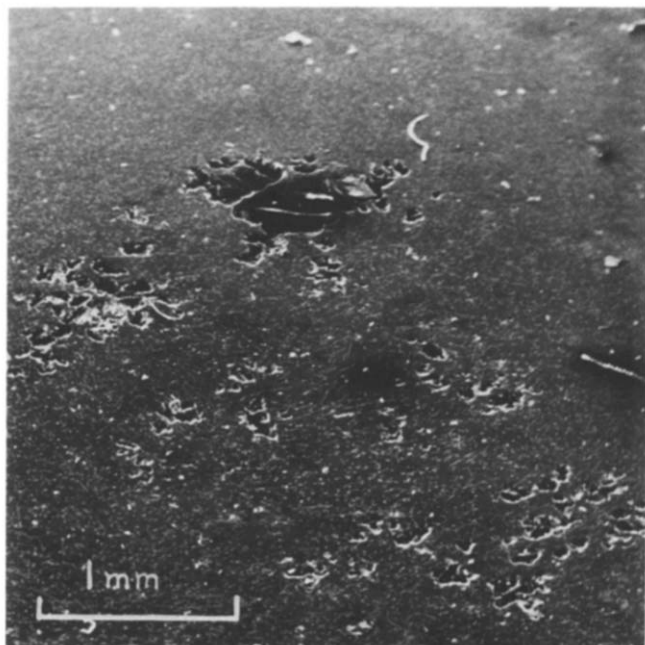
It is concluded that (1) the polishing technique is superior to microtome methods in this context and that (2) voids occur in all the mouldings examined, but that the scale of the effect changes substantially with mould thickness.

## EXPERIMENTAL

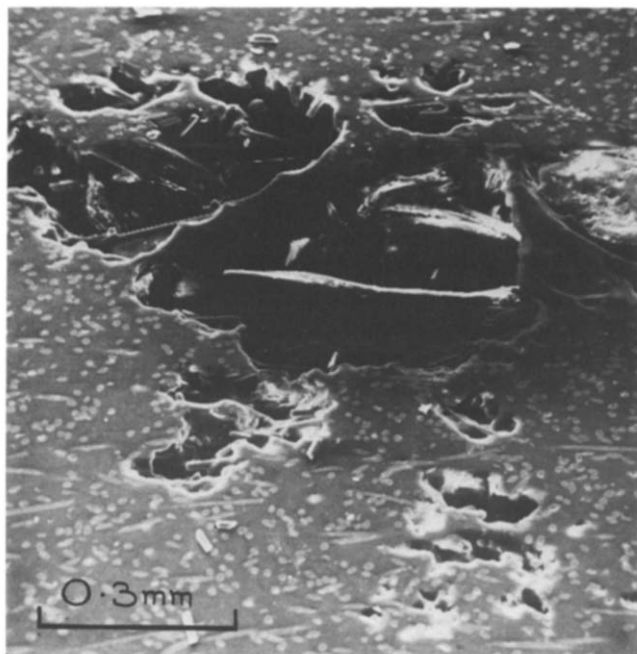
Examination techniques have been refined from standard metallographic sectioning and polishing procedures in order to reduce to a minimum the number of spurious observations of surface features associated with polishing brittle glass fibres embedded in a flexible matrix. Sections were cut along planes parallel and orthogonal to the moulding surfaces from a number of glass fibre reinforced nylon (GF nylon) mouldings, as well as from those GFPP mouldings described above. These sections were then embedded in a cold curing mounting compound prior to progressive polishing on graded emery papers followed by polishing on five graded diamond wheels down to  $0.25\ \mu\text{m}$ . Examination of the polished surfaces for defects by reflection optical microscopy then preceded careful extraction of the sections from the embedding medium and remounting on metal studs. These remounted, polished specimens were then coated under vacuum with a gold/palladium alloy before examination by scanning electron microscopy.

## RESULTS AND DISCUSSION

The most severe instance of voiding observed during this study was noted in a 12 mm square cross-section GF nylon-6,6 impact test bar provided by moulder A. Here holes clearly visible to the naked eye could be observed in the central white region. *Figure 2* presents a low magnification scanning electron micrograph of the central region of a cross-section plane cut and polished from this impact bar. In addition to the large voids visible by eye, a wide range of smaller size voids can also be seen in this micrograph. *Figure 3* then concentrates on the area around the largest void visible in



*Figure 2* Scanning electron micrograph of the central zone of a section cut perpendicular to the longitudinal axis of a 12 mm square cross-section impact bar of GF nylon supplied by moulder A



*Figure 3* Detail of a large void appearing in the micrograph of *Figure 2*

*Figure 2* and here it can be seen that void sizes range over at least two orders of magnitude (from approximately 1 mm across down to a few  $\mu\text{m}$ ).

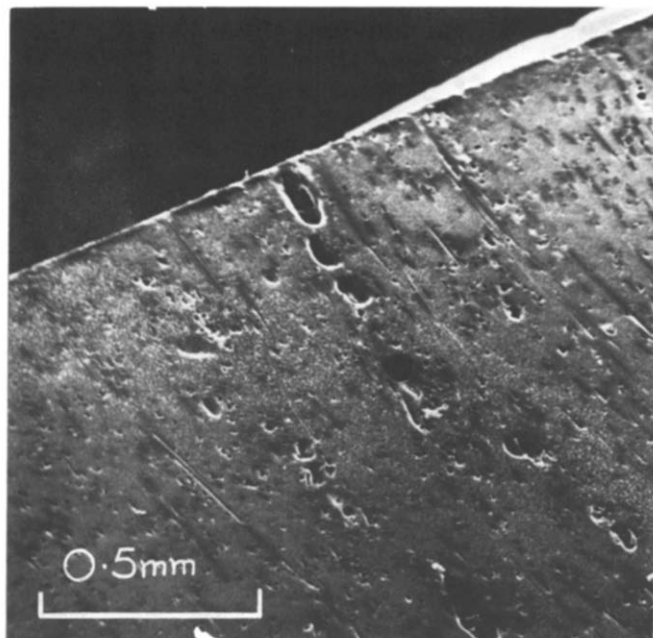
A similar pattern of voids has been observed in the central white region of 6 mm thickness GFPP edge-gated discs. In addition to the large voids described earlier for this material many smaller voids were visible at higher magnifications by scanning electron microscopy. The largest void sizes observed in the 6 mm GFPP disc (about 0.3 mm across) were far smaller than the large void visible in *Figures 2* and *3*. However, a wide range of void sizes was observed and the pattern of voiding in the central white region of the 6 mm thickness GFPP disc was quite similar to that observed in the GF nylon impact bar.

The incidence of a central white layer through the cross-section of 3 mm thickness GFPP edge-gated discs was far less developed than in the 6 mm GFPP disc moulding. However, this central white layer was easily observable in the 3 mm thickness disc supplied by moulder B. A wide void size range was noted in the central white zone of sections cut through the disc cross-section and in sections cut parallel to the moulding surface at half-thickness through the disc. The overall impression obtained was that void sizes in this 3 mm thickness disc (from 0.1 mm down to several  $\mu\text{m}$ ) were smaller than those observed in the 6 mm disc provided by the same moulder.

It is worth noting that sections cut at half-thickness through the disc parallel to the mould surface were found preferable to sections through the disc cross-section for the observation of these smaller holes. As the plane of these 'half-thickness' sections was the plane in which most fibres lay (the fibre distribution in the central zone of these discs being generally aligned in the plane of the disc), damage occurring at polished fibre ends was thus minimized. Examination of sections cut parallel to the surface outside the central white layer of the specimens described above produced no detectable voids (i.e. features greater than 2 or 3  $\mu\text{m}$  across).

Observation of voiding in the discontinuous and narrow central white layer of the 3 mm thickness GFPP disc produced by moulder A presented a greater problem. Sections





**Figure 4** Voiding appearing in the central white layer of a GFPP 3 mm thickness edge-gated disc supplied by moulder A. (See text for detail of sectioning.)

cut parallel to the mould surface at half thickness invariably polished through the narrow white layer during preparation. To overcome this difficulty, a section was cut through this narrow central white layer at an angle to the plane of the disc. The section was cut near to the disc edge where this central white zone had become slightly more apparent in the disc cross-section.

*Figure 4* presents a micrograph of this section from the GFPP 3 mm thickness disc produced by moulder A. It could be seen visually that this section had sliced through the narrow white layer and observations of this section at different magnifications under the scanning electron microscope showed that the site of the white layer coincided with the region in which the voids visible in *Figure 4* occurred. Again, a large size range of voids can be seen (from 0.05 mm across to a few  $\mu\text{m}$ ). It should be noted that the edge visible in this micrograph is not a moulded disc edge, but a cut edge of the section examined.

Once again many sections cut parallel to the surface outside the white region in this edge-gated disc produced no voids of size greater than several  $\mu\text{m}$ . Indeed very few holes even in this size range were observed. This, and the observation of holes only in the white zone, is seen as support for the contention that the holes down to this size range are inherent in the moulding and not artefacts of the preparation process.

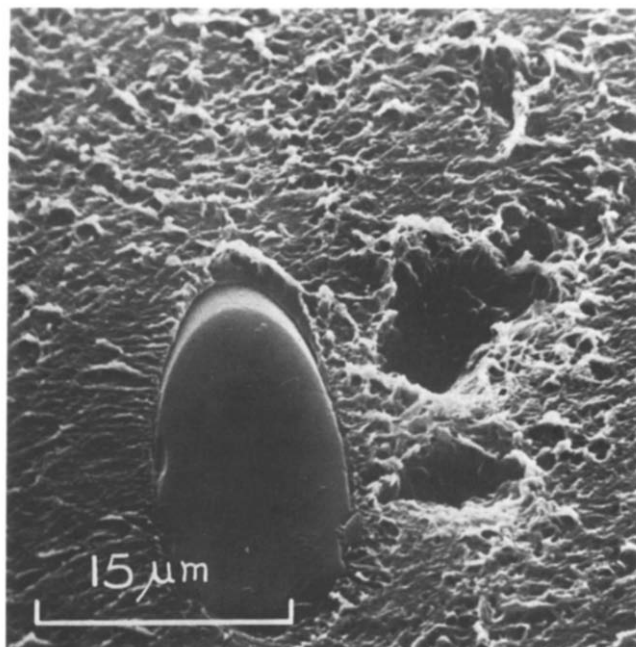
*Figure 5* presents a micrograph of a small void observed in the white zone of the 3 mm GFPP disc from moulder B. This hole is approximately 5  $\mu\text{m}$  across. It is thought that such a void represents the lower bound in size range which can be regarded as an inherent fault in the material when using this metallographic preparation technique. Below this size, problems of interpretation may arise due to surface damage caused by small glass particles.

*Figure 5* may also be used to illustrate the nature of the general polished surface at high magnification. The polished surfaces produced in the manner described above have been found to be far superior to surfaces produced in

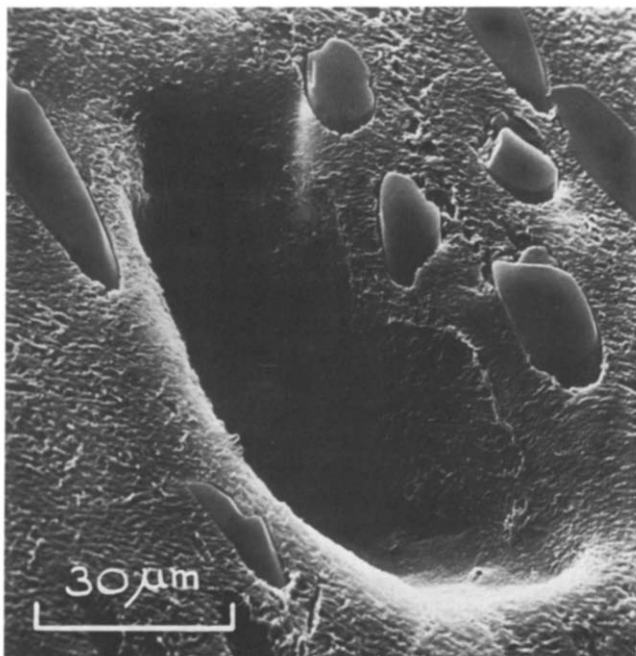
these laboratories by microtome techniques for the observation of voids in these composites. The polishing technique is also considered superior for the simpler problem of observing fibre orientation distributions.

*Figure 6* concentrates on one of the voids visible near the cut edge shown in the micrograph of *Figure 4*. The slight effects of fibre damage and of rounding the edge of the void, both due to the polishing technique, can be observed in this micrograph.

It was possible with the void shown in *Figure 6* to scan down into the void, beyond the effects of polished edge-rounding, to observe the micro-structure of the void wall. This is depicted in *Figure 7*. It is interesting to compare



**Figure 5** Small voids appearing in the central white region of the cross-section of a 3 mm thickness GFPP edge-gated disc supplied by moulder B



**Figure 6** Detail of a large void which can be observed in the scanning electron micrograph of *Figure 4*

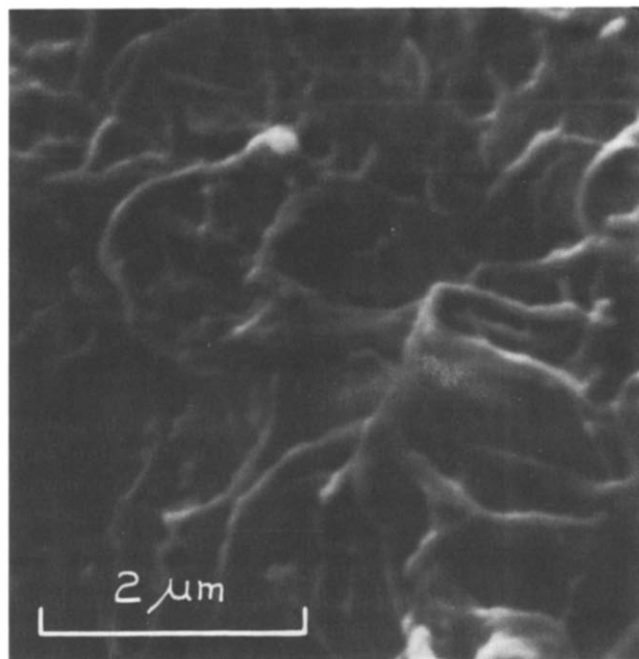


Figure 7 Scanning electron micrograph of the wall of the void shown in Figure 6

the fibrillar structure of this void wall with previously published<sup>4</sup> stereo and transmission electron micrographs of an unoriented polystyrene fracture surface in which the fibrillar structure of the fracture surface is of a similar nature to the structure observed on the void wall. Other small voids have also been observed with fibrillar material across the void suggesting that the void may have occurred as a craze parted and developed into a crack.

From this work it appears that wherever a white central

zone occurs in the cross-section of a glass fibre reinforced thermoplastic injection moulding, it is an example of the same phenomenon and involves voiding. The extent of this whitening phenomenon and the scale of voiding have been seen to be dependent on the thickness of the moulding and perhaps, more particularly, on moulding conditions.

Trends with thickness in different glass fibre reinforced thermoplastics are also worth noting. While a visible white zone and voids existed in 3 mm thickness GFPP mouldings, no whitening was observed in GF nylon mouldings of a similar thickness (though it should be noted, of different fibre length distribution). However, in thicker cross-section specimens the extent of voiding appeared more pronounced in GF nylon, though it was accompanied by a less extensive white region than appeared in similar thickness GFPP mouldings.

While this work has not endeavoured to clarify the origin of the white layer itself in these mouldings, it seems reasonable to suggest that the central white zone may arise as crazing occurs to relieve stresses created during cooling. The occurrence of this white zone may then precede the development of voids by some crazing and splitting mechanism through which built-in stress is further relieved.

#### ACKNOWLEDGEMENT

The authors thank Professor D. W. Saunders for helpful discussions on this work.

#### REFERENCES

- 1 Darlington, M. W. and Clayton, D. *Plastics Inst. Conf., Research Projects III*, Paper 1, London, Nov. 1971
- 2 Darlington, M. W. and Clayton, D. *31st Antec SPE, Montreal 1973*
- 3 Diggwa, A. D. S. and Norman, R. H. *Plastics and Polymers* 1972, 40, 263
- 4 Haward, R. N. and Brough, I. *Polymer* 1969, 10, 724

## Multiple melting in poly(butylene terephthalate)

S. Y. Hobbs and C. F. Pratt

General Electric Company, Corporate Research and Development Center, PO Box 8, Schenectady, NY 12301, USA  
(Received 17 December 1974)

#### INTRODUCTION

Calorimetric investigations have revealed that a number of crystalline polymers including polyethylene<sup>1,2</sup>, polyoxymethylene<sup>3</sup>, nylon<sup>4</sup>, and poly(ethylene terephthalate)<sup>5-8</sup> may exhibit multiple melting peaks. This behaviour is closely tied to the thermal history of the samples and may arise from: (1) the presence of alternate crystal modifications; (2) molecular weight segregation accompanying crystallization; (3) variations in morphology; (4) orientation effects; or (5) melting, recrystallization and annealing processes taking place in the calorimeter. Identification of the specific causes of multiple melting in a particular polymer is an important aspect of its thermal characterization. We wish to report some recent calorimetric studies of multiple melting in poly(butylene terephthalate) (PBT), a polymer currently experiencing rapid growth as an injection mouldable engineering thermoplastic.

#### EXPERIMENTAL

PBT samples were supplied by the GE Plastics Division (Pittsfield, Mass.) and had intrinsic viscosities ranging from 1.21 to 1.53 dl/g. All thermal measurements were carried out in a Perkin-Elmer DSC-2 calorimeter. The samples were first melted in the calorimeter for 2 min at 250°C, recrystallized by slow cooling to room temperature, and then remelted. Wide angle X-ray diffraction measurements were made on a GE XRD-5 machine using CuK $\alpha$  radiation.

#### RESULTS

Since similar d.s.c. traces were obtained on all samples over the available molecular weight range only data for a sample having an intrinsic viscosity in hexafluoroisopropanol (HFIP) at 25°C of 1.31 dl/g are presented in this report. Crystallization exotherms for samples cooled at rates from

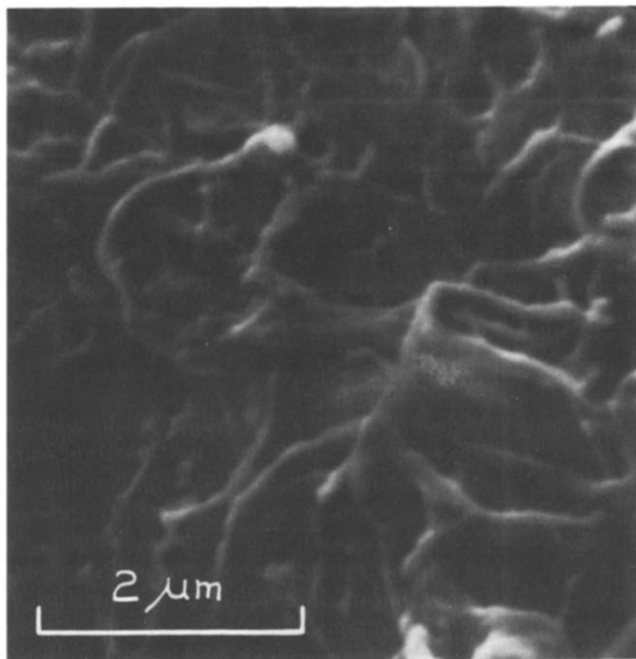


Figure 7 Scanning electron micrograph of the wall of the void shown in Figure 6

the fibrillar structure of this void wall with previously published<sup>4</sup> stereo and transmission electron micrographs of an unoriented polystyrene fracture surface in which the fibrillar structure of the fracture surface is of a similar nature to the structure observed on the void wall. Other small voids have also been observed with fibrillar material across the void suggesting that the void may have occurred as a craze parted and developed into a crack.

From this work it appears that wherever a white central

zone occurs in the cross-section of a glass fibre reinforced thermoplastic injection moulding, it is an example of the same phenomenon and involves voiding. The extent of this whitening phenomenon and the scale of voiding have been seen to be dependent on the thickness of the moulding and perhaps, more particularly, on moulding conditions.

Trends with thickness in different glass fibre reinforced thermoplastics are also worth noting. While a visible white zone and voids existed in 3 mm thickness GFPP mouldings, no whitening was observed in GF nylon mouldings of a similar thickness (though it should be noted, of different fibre length distribution). However, in thicker cross-section specimens the extent of voiding appeared more pronounced in GF nylon, though it was accompanied by a less extensive white region than appeared in similar thickness GFPP mouldings.

While this work has not endeavoured to clarify the origin of the white layer itself in these mouldings, it seems reasonable to suggest that the central white zone may arise as crazing occurs to relieve stresses created during cooling. The occurrence of this white zone may then precede the development of voids by some crazing and splitting mechanism through which built-in stress is further relieved.

#### ACKNOWLEDGEMENT

The authors thank Professor D. W. Saunders for helpful discussions on this work.

#### REFERENCES

- 1 Darlington, M. W. and Clayton, D. *Plastics Inst. Conf., Research Projects III*, Paper 1, London, Nov. 1971
- 2 Darlington, M. W. and Clayton, D. *31st Antec SPE, Montreal* 1973
- 3 Diggwa, A. D. S. and Norman, R. H. *Plastics and Polymers* 1972, 40, 263
- 4 Haward, R. N. and Brough, I. *Polymer* 1969, 10, 724

## Multiple melting in poly(butylene terephthalate)

S. Y. Hobbs and C. F. Pratt

General Electric Company, Corporate Research and Development Center, PO Box 8, Schenectady, NY 12301, USA  
(Received 17 December 1974)

#### INTRODUCTION

Calorimetric investigations have revealed that a number of crystalline polymers including polyethylene<sup>1,2</sup>, polyoxymethylene<sup>3</sup>, nylon<sup>4</sup>, and poly(ethylene terephthalate)<sup>5-8</sup> may exhibit multiple melting peaks. This behaviour is closely tied to the thermal history of the samples and may arise from: (1) the presence of alternate crystal modifications; (2) molecular weight segregation accompanying crystallization; (3) variations in morphology; (4) orientation effects; or (5) melting, recrystallization and annealing processes taking place in the calorimeter. Identification of the specific causes of multiple melting in a particular polymer is an important aspect of its thermal characterization. We wish to report some recent calorimetric studies of multiple melting in poly(butylene terephthalate) (PBT), a polymer currently experiencing rapid growth as an injection mouldable engineering thermoplastic.

#### EXPERIMENTAL

PBT samples were supplied by the GE Plastics Division (Pittsfield, Mass.) and had intrinsic viscosities ranging from 1.21 to 1.53 dl/g. All thermal measurements were carried out in a Perkin-Elmer DSC-2 calorimeter. The samples were first melted in the calorimeter for 2 min at 250°C, recrystallized by slow cooling to room temperature, and then remelted. Wide angle X-ray diffraction measurements were made on a GE XRD-5 machine using CuK $\alpha$  radiation.

#### RESULTS

Since similar d.s.c. traces were obtained on all samples over the available molecular weight range only data for a sample having an intrinsic viscosity in hexafluoroisopropanol (HFIP) at 25°C of 1.31 dl/g are presented in this report. Crystallization exotherms for samples cooled at rates from

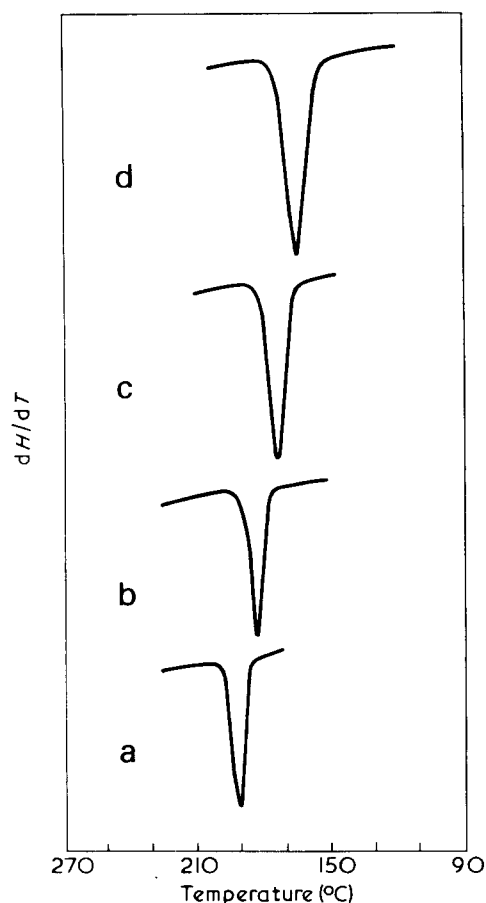


Figure 1 Crystallization exotherms for PBT samples cooled at different rates. The traces are not normalized for differences in sample weight. Cooling rates: (a) 5; (b) 10; (c) 20; (d) 40°C/min

5 to 40°C/min are reproduced in Figure 1. In each case only one peak was observed which was displaced downwards in temperature with increased cooling rate. The size of the crystallization exotherm was constant at 11.5 cal/g. Wide angle X-ray diffraction patterns obtained on these samples showed little variation in relative line intensity and could be indexed to the triclinic unit cell ( $\alpha$  modification) proposed for PBT<sup>9</sup>. No secondary crystal modification was observed.

The corresponding melt endotherms for these samples taken at a scan rate of 20°C/min are presented in Figure 2. The average heat of fusion was approximately 12 cal/g indicating very little additional crystallization occurred during heating. In all cases a double melting peak was observed. With decreasing cooling rate the high temperature peak decreased in size but remained centred at 220–222°C. In contrast, the low temperature endotherm increased in size at the expense of the high melting peak and showed a small upward temperature shift from 205 to 216°C at lower cooling rates. The approximate fractions of the total melt endotherm under each peak are listed in Table 1.

Melt endotherms taken at scan rates from 5 to 80°C/min on samples cooled from the melt at 20°C/min and showing a single crystallization exotherm are shown in Figure 3. Double melting was again observed at all heating rates although at 5°C/min the low temperature peak was barely visible. As the heating rate was increased the low

temperature peak grew in size (see Table 1) and superheated approximately 8°C before disappearing as a shoulder on the high temperature peak at a heating rate of 80°C/min. The high temperature peak showed only a small temperature shift (220 to 223°C) over the range of heating rates. A small, very broad shoulder was seen to develop in the region of 190–200°C at the highest scan speed.

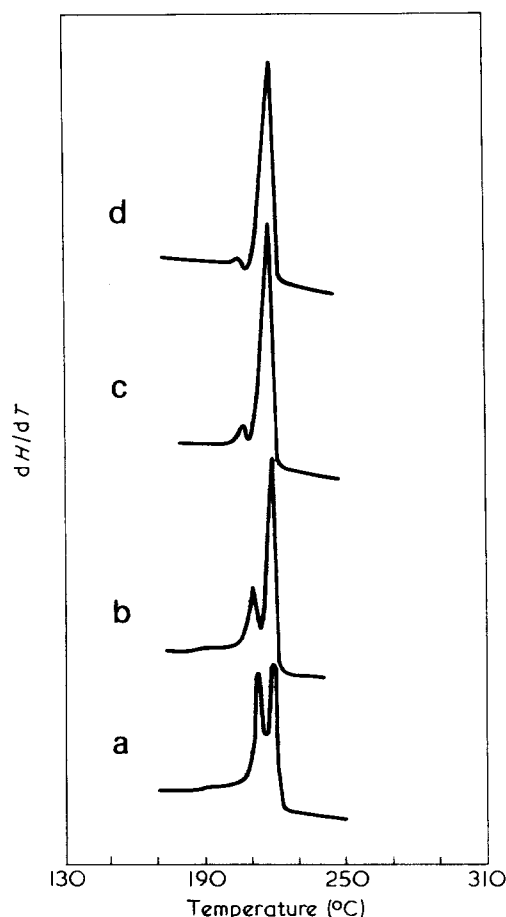


Figure 2 Melting exotherms for PBT samples crystallized at different cooling rates. All scans at 20°C/min. The traces are not normalized for differences in sample weight. Cooling rates: (a) 5; (b) 10; (c) 20; (d) 40°C/min

Table 1 Relative d.s.c. melting peak areas

Heating rate = 20°C/min (constant)		
Cooling rate (°C/min)	Low melting peak (%)	High melting peak (%)
40	2.0	98.0
20	9.4	90.6
10	27.4	72.6
5	51.0	49.0
Cooling rate = 20°C/min (constant)		
Heating rate (°C/min)	Low melting peak (%)	High melting peak (%)
5	—	100
10	3.6	96.4
20	7.7	92.3
40	35.0	65.0
80	40.7	59.3

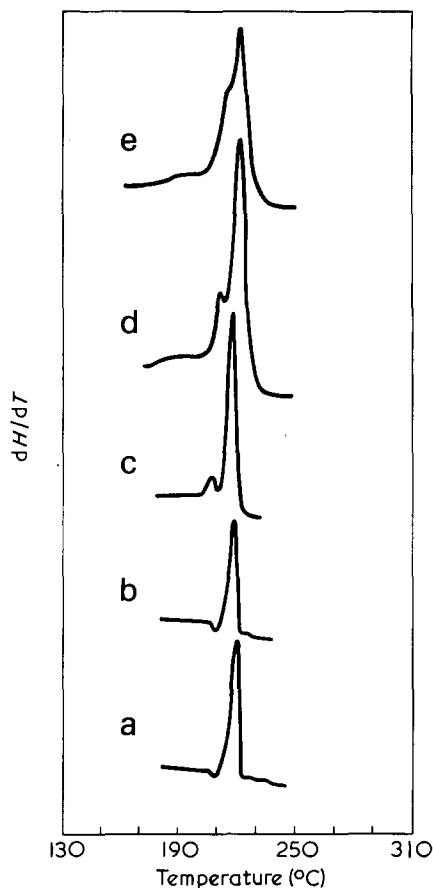


Figure 3 Melting exotherms for PBT samples heated at different rates. All samples crystallized at a cooling rate of 20°C/min. The traces are not normalized for differences in sample height. (a) 5; (b) 10; (c) 20; (d) 40; (e) 80°C/min

## DISCUSSION

Our results suggest that multiple melting in PBT is most convincingly interpreted in terms of reorganization processes occurring during heating in the d.s.c. The variations in both the positions and relative heights of the two melting peaks with different cooling and heating schedules can be explained on this basis as follows.

Crystals which are formed at the highest cooling rate are inherently unstable and anneal on heating at 20°C/min only to melt under a single endotherm centred at 220°C. As the degree of supercooling is reduced and the time of crystallization is increased, crystals of increased perfection are formed. Since the rate of reorganization of these crystals is on the same time scale as the heating rate, melting begins to occur in preference to annealing and a low temperature peak appears in the d.s.c. trace. This peak continues to grow in size at the expense of the high melting peak as the original cooling rates are decreased and greater numbers of crystals which are resistant to reorganization are produced. In addition, the low temperature peak shows the expected upward displacement with increasing crystallization temperature<sup>10</sup> while little or no upward temperature shift of the high temperature is observed.

When the cooling rate is held constant and the heating rate is increased (see Figure 3) the low temperature peak again increases in size as less and less time is available for reorganization of the metastable crystals. The small, broad peak which appears at ~195°C at the highest heating rates is attributed to a limited number of crystals containing predominantly low molecular weight species which reorganize very quickly and are not seen at scan rates less than 40°C/min. A small percentage of such low molecular weight species has been observed in g.p.c. traces on this sample. The observed superheating of the low temperature peak at fast heating rates is sufficiently large to suggest that there is some entropic restriction imposed on the melting process as noted by other authors<sup>11,12</sup>. It is unlikely that such superheating is associated with chain extension since all crystallizations were carried out in the absence of shear at low pressures.

## CONCLUSIONS

The results of our calorimetric studies on poly(butylene terephthalate) are in qualitative agreement with similar studies on poly(ethylene terephthalate)<sup>6-8</sup>. Of the two primary melt endotherms shown by PBT samples crystallized non-isothermally from the melt, only the lower temperature peak can be identified with crystals produced during the original cooling. Extrapolation of our heating rate data on samples crystallized by cooling at 20°C/min indicate that at heating rates above 200°C/min only the low temperature melting peak will be observed. The high temperature peak develops as a result of reorganization processes during heating and is not characteristic of the material in its room temperature state. There is no experimental evidence of a conversion from a high to low melting crystal form or for the presence of a secondary crystal modification.

## REFERENCES

- 1 Wunderlich, B. and Arakawa, T. *J. Polym. Sci. (A)* 1964, 2, 3697
- 2 Prime, R. B., Wunderlich, B. and Melillo, L. *J. Polym. Sci. (A-2)* 1969, 7, 2091
- 3 Jaffe, M. and Wunderlich, B. *Kolloid-Z.* 1967, 216, 203
- 4 Bell, J. P. and Dumbleton, J. H. *J. Polym. Sci. (A-2)* 1969, 7, 1033
- 5 Nealy, D. L., Davis, T. G. and Kibler, C. J. *J. Polym. Sci. (A-2)* 1970, 8, 2141
- 6 Holdsworth, P. J. and Turner-Jones, A. *Polymer* 1971, 12, 149
- 7 Sweet, G. E. and Bell, J. P. *J. Polym. Sci. (A-2)* 1972, 10, 1273
- 8 Roberts, R. C. *J. Polym. Sci. (B)* 1970, 8, 381
- 9 Boye, C. A., Jr. and Overton, J. R. Paper presented at Am. Phys. Soc. Meet., Div. High Polymers, Philadelphia, Pa. (March 1974)
- 10 Hoffman, J. D. and Weeks, J. J. *J. Res. Nat. Bur. Stand.* 1962, 66A, 13
- 11 Miyagi, A. and Wunderlich, B. *J. Polym. Sci. (A-2)* 1972, 10, 1401
- 12 Zachman, H. G. *Kolloid-Z. Z. Polym.* 1965, 206, 25





**Table 4** Tetrad and hexad intensities in the  $^{13}\text{C}$  n.m.r. spectrum of poly( $\alpha$ -methylstyrene). Resonance region of the methylene carbons

Sequence		Chem. shift		Intensity	
Tetrad	Hexad	ppm	Hz	Obs.	Calc.*
rmr	mrmrm	62.64	22	0.01 <sub>4</sub>	0.016
	rrmrm	62.09	16	0.06 <sub>3</sub>	0.066
	rrmrr	61.85		0.08 <sub>0</sub>	0.066
mnr + rmm	mmrrr	61.52	20	0.04 <sub>3</sub>	0.033
	mmrrm	61.23	14	0.01 <sub>3</sub>	0.016
	rmmrr	61.03	6	0.06 <sub>1</sub>	0.065
	rmmrm	60.94		0.02 <sub>6</sub>	0.033
rrr	rrrrm	60.81	22	0.13 <sub>2</sub>	0.132
	rrrrr	60.48	44	0.13 <sub>1</sub>	0.133
	mrrrm	59.83		0.02 <sub>6</sub>	0.033
mmm	—	59.24	<10 <sup>†</sup>	0.04 <sub>0</sub>	0.037
mrm	—	59.10	<10 <sup>†</sup>	0.08 <sub>0</sub>	0.074
mrr + rrm	rmrrm	58.48	19	0.06 <sub>3</sub>	0.066
	rmrrr	58.20	13	0.13 <sub>6</sub>	0.132
	mmrrr	58.01	13	0.06 <sub>3</sub>	0.066
	mmrrm	57.82		0.03 <sub>5</sub>	0.033

\* Calculated for Bernoullian statistics;  $m = 0.332$ ,  $r = 0.668$

† Estimated

**Table 5** Triad and pentad intensities in the  $^{13}\text{C}$  n.m.r. spectrum of poly( $\alpha$ -methylstyrene). Resonance region of the non-protonated carbon

Sequence		Chem. shift		Intensity	
Triad	Pentad	ppm*	Hz	Obs.	Calc.†
rr	mrrm	42.82	5	0.03 <sub>6</sub>	0.026
	mrrr	42.74	7	0.19 <sub>9</sub>	0.205
	rrrr	42.66		0.40 <sub>4</sub>	0.405
mr + rm	rmrr	42.50	4	0.19 <sub>6</sub>	0.205
	mmrm	42.46	4	0.01 <sub>2</sub>	0.013
	rmrm	42.42	3	0.05 <sub>3</sub>	0.052
	mmrr	42.39		0.05 <sub>7</sub>	0.052
mm	—	42.36	<2 <sup>‡</sup>	0.04 <sub>4</sub>	0.041

\*  $^{13}\text{C}$  frequency 90.51 MHz

† Calculated for Bernoullian statistics;  $m = 0.203$ ,  $r = 0.797$

‡ Estimated

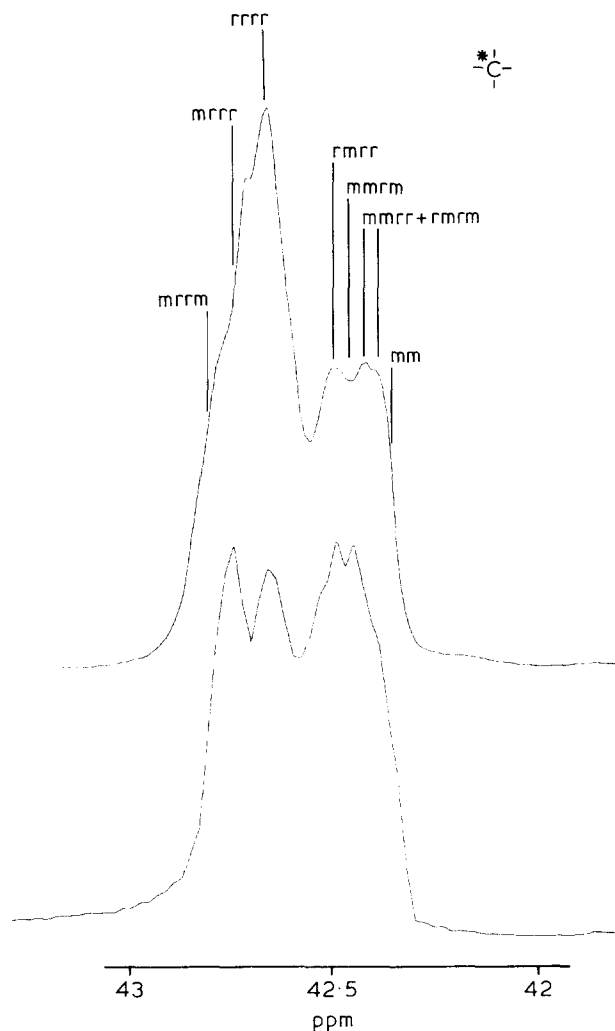
Despite line broadening and severe overlapping the assignment could be performed in analogy to the aromatic  $\text{C}_1$ .

As shown in spectra 2,3,4 and 5  $^{13}\text{C}$  n.m.r. spectroscopy at 67.88 MHz and 90.51 MHz is capable of yielding important and detailed stereochemical information of poly( $\alpha$ -methylstyrene). In principle the enchainment can be determined from six individual  $^{13}\text{C}$  nuclei in four resonance regions. Peak positions as well as sequence fractions can be determined even if the splitting of the resonance region, e.g. of the non-protonated carbon, does not match that of the aromatic  $\text{C}_1$  carbon.

#### Experimental

The poly( $\alpha$ -methylstyrenes) were polymerized by *n*-butyl lithium in tetrahydrofuran at temperatures between +25 and  $-78^\circ\text{C}$ . The stereochemical structure of these samples was determined by  $^1\text{H}$  n.m.r. spectroscopy using a Varian HR 220 at 220 MHz.

The proton decoupled  $^{13}\text{C}$  n.m.r. spectra were obtained in  $\text{CDCl}_3$  at  $35^\circ\text{C}$  using a Bruker-Spectrospin HX 270 and HXS 360 operating at frequencies of 67.88 and 90.51 MHz,



**Figure 5**  $^{13}\text{C}$  n.m.r. spectrum of poly( $\alpha$ -methylstyrene) at 90.51 MHz. Expanded resonance region of the non-protonated carbon;  $^{13}\text{C}$  enrichment 10%; upper trace:  $m = 0.203$ ,  $r = 0.797$ ; lower trace:  $m = 0.312$ ,  $r = 0.688$

respectively. Internal standard was octamethyltetrasiloxane (OMTS) = 0 ppm.

Simulations and quantitative analysis of the observed spectra were performed using a DuPont 310 curve resolver.

#### Acknowledgement

The financial support of the Deutsche Forschungsgemeinschaft is gratefully acknowledged.

K.-F. Elgert, R. Wicke, B. Stützel and W. Ritter

Institut für Makromolekulare Chemie,  
Universität Freiburg,  
D-78 Freiburg i. Br., West Germany  
(Received 17 February 1975)

#### References

- 1 Elgert, K.-F., Quack, G. and Stützel, B. *Polymer* 1975, **16**, 154
- 2 Inoue, Y., Nishioka, A. and Chűjű, R. *Makromol. Chem.* 1972, **156**, 207
- 3 Elgert, K.-F., Seiler, E., Puschendorf, G., Ziemann, W. and Cantow, H.-J. *Makromol. Chem.* 1971, **144**, 73
- 4 Elgert, K.-F. and Seiler, E. *Makromol. Chem.* 1971, **145**, 95
- 5 Brownstein, S., Bywater, S. and Worsfold, D. J. *Makromol. Chem.* 1961, **48**, 127
- 6 Fujii, K., Worsfold, D. J. and Bywater, S. *Makromol. Chem.* 1968, **117**, 275
- 7 Bovey, F. A. 'Polymer Conformation and Configuration', Academic Press, London, 1969, p 49
- 8 Ferguson, R. C. *Macromolecules* 1969, **2**, 237



## Structure and radical reactivities of vinyl monomers: copolymerization reactivities of alkyl vinyl ketones

Recently, vinyl ketones have frequently been used as comonomers for preparing photodegradative polymers<sup>1</sup>. However, systematic investigations on their radical copolymerization behaviour, especially their relationship between structure and reactivity, have been little attempted.

Since 1961, we have studied the radical copolymerization of vinyl monomers having a series of substituents in order to determine the effect of the substituent<sup>2</sup>. In a series of monomers, in which the substituents were conjugated with a reacting vinyl group, such as nuclear-substituted styrenes, the results show that their copolymerization reactivities were correlated by the generalized Hammett equation<sup>2,3</sup>:

$$\log(\text{rel. react.}) = \rho\sigma + \gamma E_R \quad (1)$$

where  $\sigma$  and  $E_R$  are polar and resonance substituent constants, respectively, and  $\rho$  and  $\gamma$  are reaction constants. Equation (1) was found to be also applicable in a number of radical reactions of substituted compounds<sup>2</sup>.

However, in a series of aliphatic monomers in which the reaction sites were not conjugated with the substituents, such as alkyl acrylates and methacrylates, their reactivities were expressed by the Taft equation<sup>2,4</sup>:

$$\log(\text{rel. react.}) = \rho^*\sigma^* + \delta E_s \quad (2)$$

where  $\sigma^*$  and  $E_s$  are, respectively, polar and steric substituent constants, in which the corresponding methyl-substituted compound was taken as the standard, and  $\rho^*$  and  $\delta$  are reaction constants. Equation (2) was also applied to a number of alkyl-substituted monomers<sup>2</sup>.

Since alkyl vinyl ketones (RVK) in which the reacting vinyl group is a cross-conjugated system with the substituents, it is interesting to clarify the correlation between the reactivity and alkyl substituents. The present communication deals with the results of radical copolymerizations of RVK with styrene, and of the effect of alkyl substituents on their reactivities.

Six RVK monomers were prepared, and copolymerized with styrene ( $M_1$ ) in bulk in the presence of  $\alpha, \alpha'$ -azobisisobutyronitrile (AIBN) at 60°C. The composition of the copolymers obtained was determined from their elemental analysis, and the monomer reactivity ratios ( $r_1$  and  $r_2$ ) were obtained by a curve-fitting method. The copolymerization parameters obtained are shown in Table 1.

As can be seen from this Table, the  $r_1$  and  $r_2$  values change somewhat with the alkyl substituents in RVK.

Table 1 Copolymerization parameters for the copolymerizations of RVK ( $M_2$ ) with styrene ( $M_1$ ) at 60°C<sup>a</sup>

RVK	R in RVK	$r_1$	$r_2$	$Q_2^b$	$e_2^b$
MVK	CH <sub>3</sub>	0.27	0.40	1.12	0.69
EVK	C <sub>2</sub> H <sub>5</sub>	0.45	0.31	0.87	0.69
IPVK	CH(CH <sub>3</sub> ) <sub>2</sub>	0.40	0.30	0.78	0.66
t-BVK	C(CH <sub>3</sub> ) <sub>3</sub>	0.40	0.30	0.78	0.66
CMVK	CH <sub>2</sub> Cl	0.13	0.52	2.07	0.84
PVK	C <sub>6</sub> H <sub>5</sub>	0.21	0.48	1.40	0.74

<sup>a</sup> Conditions:  $M_1 + M_2 = 4$  ml; [AIBN] =  $3.5 \times 10^{-3}$  mol/l

<sup>b</sup> Calculated by assuming that  $Q_1$  and  $e_1$  for styrene are 1.0 and -0.8, respectively

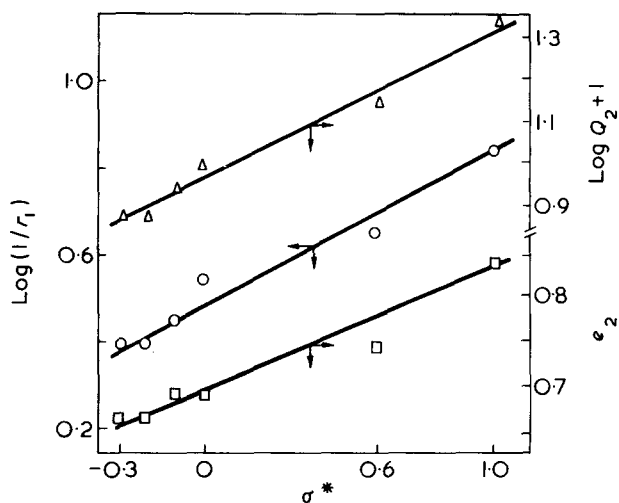


Figure 1 Plots of  $\log(1/r_1)$  (O),  $Q_2$  ( $\Delta$ ) and  $e_2$  ( $\square$ ) with  $\sigma^*$  constants of alkyl substituents of RVK in the copolymerization parameters of styrene ( $M_1$ )—RVK( $M_2$ ) system

Although the relative reactivities towards the polystyryl radical were applied to equation (1), an accurate correlation was not found, because the values of  $\sigma$  and  $E_R$  of the substituents in RVK used here were very close to each other.

Previously Yokota *et al.*<sup>5,6</sup> reported that the copolymerization reactivities of nuclear-substituted phenyl vinyl ketones were correlated by equation (1) in which  $\rho = 0.34$  and  $\gamma = 2.0^5$ , indicating that both polar and resonance effects in this case are influenced by the reactivity.

However, when the reactivities of RVK used here were plotted with the  $\sigma^*$  constants in equation (2), a good linear relationship with  $\rho^* = 0.40 \pm 0.05$  and  $\delta = 0$  was observed as shown in Figure 1. In this case, only the polar effect of the alkyl substituents was seen to have an important influence on the reactivity. Similar results were observed in a number of alkyl-substituted monomers such as alkyl acrylates<sup>7</sup>, alkyl thiolacrylates<sup>8</sup>, alkyl methacrylates<sup>9</sup> and vinyl esters<sup>10</sup>.

From Table 1, it was found that the  $Q$  and  $e$  values of RVK increase with increasing the  $\sigma^*$  constants of their alkyl substituents (Figure 1). This may indicate that both polar and resonance effects are generally affected by the reactivities of RVK. As pointed out in alkyl methacrylate studies<sup>2,9</sup>, these effects are explained on the basis of u.v. and n.m.r.<sup>10</sup> data of RVK from the fact that polarization of the carbonyl group is increased by the electron-donating alkyl groups, and that the resonance of the reacting double bond with the carbonyl group is reduced, resulting in decreased reactivities of the RVK monomer.

From the results of copolymerizations of methyl vinyl ketone (MVK) with styrene in solvents it was also found that relative reactivities of MVK towards the polystyryl radical were found to increase with increasing  $E_T$  values of the solvents, and with decreasing energy differences in  $n - \pi$  interaction determined from u.v. spectroscopy data. These results seem to support the above consideration.

Takayuki Otsu and Hitoshi Tanaka

Department of Applied Chemistry, Faculty of Engineering,  
Osaka City University, Osaka 558, Japan  
(Received 18 February 1975)

### References

- 1 Dan, E. and Guillet, J. E. *Macromolecules* 1973, 6, 230;  
Kato, M. and Yoneshige, Y. *Makromol. Chem.* 1973, 164, 159

- 2 Otsu, T. *Progr. Polym. Sci. Japan* 1971, 1, 1
- 3 Yamamoto, T. and Otsu, T. *Chem. Ind.* 1967, p 787
- 4 Taft, R. W. 'Steric Effects in Organic Chemistry', (Ed. M. S. Newman), Wiley, New York, 1956, p 556
- 5 Suzuki, T., Yokoto, T. and Takada, Y. *Prepr. 16th A. Meet. High Polym. Soc. Japan* 1967, p 134
- 6 Yokota, T., Suzuki, T., Nakazawa, S., Nakamoto, K. and Takada, T. *A. Rep. Fac. Eng., Hokkaido Univ.* 1971, 60, 63
- 7 Otsu, T., Ito, T., Fukumizu, T. and Imoto, M. *Bull. Chem. Soc. Japan* 1966, 39, 2259
- 8 Otsu, T., Tsuda, K. and Fujumizu, T. *Makromol. Chem.* 1968, 119, 140; 1969, 124, 282
- 9 Otsu, T., Ito, T. and Imoto, M. *J. Polym. Sci. (A-1)* 1966, 4, 733
- 10 Hayashi, K. and Otsu, T. *Makromol. Chem.* 1969, 127, 54

### Preparation of ultra-high modulus linear polyethylenes: effect of initial crystallization conditions

In previous publications<sup>1-4</sup> we have reported the cold drawing behaviour of linear polyethylene and the preparation of very stiff oriented samples by means of ultra-high draw ratio. The essence of the previous work was to show that the draw ratios achieved under standard drawing conditions were markedly dependent on the molecular weight and morphology of the initial polymer. It was also shown that under the standard procedures adopted, the room temperature value of the Young's modulus of the oriented polymer was related only to the draw ratio to a good approximation.

In the most recent publication on the drawing behaviour<sup>4</sup>, it was also reported that the draw ratio was very time dependent for polymer of low and intermediate weight-average molecular weight,  $\bar{M}_w$ . It was emphasized that the isochronal draw ratio/ $\bar{M}_w$  curves reported did not represent an absolute upper limit for the plastic deformation, but higher draw ratios could often be obtained by extending the drawing time. It appeared to be of particular interest to prepare a series of oriented samples, varying both initial morphology and drawing time, to determine whether the apparently unique relationship between Young's modulus and draw ratio still held.

We have recently undertaken a detailed comparison of the drawing behaviour and the modulus/draw ratio relationship over a wide range of molecular weights for two very different initial crystallization conditions. Although this extensive study is still being completed, we believe that there is one result which is worthy of immediate publication.

Figure 1 shows the room temperature Young's modulus as a function of draw ratio for Rigidex 50 grade linear polyethylene (BP Chemicals International Ltd).

As in the previous work, the Young's modulus is quoted at 0.1% strain and obtained from isochronal stress-strain curves constructed from the 10 sec creep response. The results are compared for two extreme initial morphologies, produced by the thermal treatments described in the previous papers. In one case the compression moulded sheets were quenched immediately into cold water, in the other case the sheets were slow cooled, at a rate of 7-9°C/min to 110°C and subsequently quenched.

The quenched polymer shows the typical banded spherulitic morphology whereas the slow cooled material shows a coarser structure with hardly recognisable spherulites<sup>4</sup>. In each case a range of draw ratios was produced by drawing at a constant rate (Instron cross-head speed of 10 cm/min on a 2 cm gauge length sample) at 75°C for different times. It can be seen that there is a unique relationship between the modulus and the draw ratio. There are some differences between the moduli achieved for a given draw ratio and those reported earlier but these

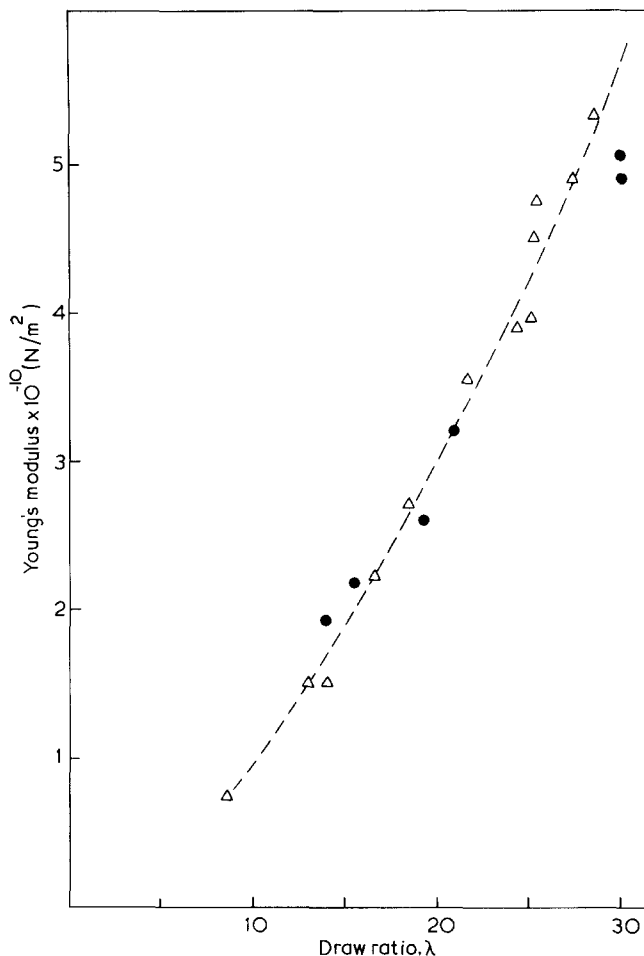


Figure 1 Room temperature Young's modulus as a function of draw ratio.  $\Delta$ , Quenched immediately into water;  $\bullet$ , slow cooled and quenched

are only significant at the highest draw ratios ( $\sim 30$ ) where very small differences in the sample homogeneity and preparation become important.

We therefore conclude that there is a unique relationship between modulus and draw ratio irrespective of the initial morphology. Moreover, it has been found that both high draw and very high modulus can be achieved for samples with conventional spherulitic morphology by extending the draw times under appropriate drawing conditions. The morphology of the initial material, however, is very important in determining the detailed nature of the plastic deformation. This is of interest both in understanding the mechanisms of deformation and in the development of practical procedures for production of these high modulus materials<sup>5</sup>. It is intended to deal with these aspects in a future publication, when our present studies have been completed.

G. Capaccio, T. J. Chapman and I. M. Ward

Department of Physics,  
University of Leeds,  
Leeds LS2 9JT, UK  
(Received 21 March 1975)

#### References

- 1 Capaccio, G. and Ward, I. M. *Nature (Phys. Sci.)* 1973, 243, 143
- 2 Capaccio, G. and Ward, I. M. *Br. Pat. Appln* 10746/73 (filed 6.3.1973)
- 3 Capaccio, G. and Ward, I. M. *Polymer* 1974, 15, 233
- 4 Capaccio, G. and Ward, I. M. *Polymer* 1975, 16, 239
- 5 Capaccio, G. and Ward, I. M. *Br. Pat. Appln* 52644/74 *et seq.* (filed 3.10.73)

- 2 Otsu, T. *Progr. Polym. Sci. Japan* 1971, 1, 1
- 3 Yamamoto, T. and Otsu, T. *Chem. Ind.* 1967, p 787
- 4 Taft, R. W. 'Steric Effects in Organic Chemistry', (Ed. M. S. Newman), Wiley, New York, 1956, p 556
- 5 Suzuki, T., Yokoto, T. and Takada, Y. *Prepr. 16th A. Meet. High Polym. Soc. Japan* 1967, p 134
- 6 Yokota, T., Suzuki, T., Nakazawa, S., Nakamoto, K. and Takada, T. *A. Rep. Fac. Eng., Hokkaido Univ.* 1971, 60, 63
- 7 Otsu, T., Ito, T., Fukumizu, T. and Imoto, M. *Bull. Chem. Soc. Japan* 1966, 39, 2259
- 8 Otsu, T., Tsuda, K. and Fujumizu, T. *Makromol. Chem.* 1968, 119, 140; 1969, 124, 282
- 9 Otsu, T., Ito, T. and Imoto, M. *J. Polym. Sci. (A-1)* 1966, 4, 733
- 10 Hayashi, K. and Otsu, T. *Makromol. Chem.* 1969, 127, 54

### Preparation of ultra-high modulus linear polyethylenes: effect of initial crystallization conditions

In previous publications<sup>1-4</sup> we have reported the cold drawing behaviour of linear polyethylene and the preparation of very stiff oriented samples by means of ultra-high draw ratio. The essence of the previous work was to show that the draw ratios achieved under standard drawing conditions were markedly dependent on the molecular weight and morphology of the initial polymer. It was also shown that under the standard procedures adopted, the room temperature value of the Young's modulus of the oriented polymer was related only to the draw ratio to a good approximation.

In the most recent publication on the drawing behaviour<sup>4</sup>, it was also reported that the draw ratio was very time dependent for polymer of low and intermediate weight-average molecular weight,  $\bar{M}_w$ . It was emphasized that the isochronal draw ratio/ $\bar{M}_w$  curves reported did not represent an absolute upper limit for the plastic deformation, but higher draw ratios could often be obtained by extending the drawing time. It appeared to be of particular interest to prepare a series of oriented samples, varying both initial morphology and drawing time, to determine whether the apparently unique relationship between Young's modulus and draw ratio still held.

We have recently undertaken a detailed comparison of the drawing behaviour and the modulus/draw ratio relationship over a wide range of molecular weights for two very different initial crystallization conditions. Although this extensive study is still being completed, we believe that there is one result which is worthy of immediate publication.

Figure 1 shows the room temperature Young's modulus as a function of draw ratio for Rigidex 50 grade linear polyethylene (BP Chemicals International Ltd).

As in the previous work, the Young's modulus is quoted at 0.1% strain and obtained from isochronal stress-strain curves constructed from the 10 sec creep response. The results are compared for two extreme initial morphologies, produced by the thermal treatments described in the previous papers. In one case the compression moulded sheets were quenched immediately into cold water, in the other case the sheets were slow cooled, at a rate of 7-9°C/min to 110°C and subsequently quenched.

The quenched polymer shows the typical banded spherulitic morphology whereas the slow cooled material shows a coarser structure with hardly recognisable spherulites<sup>4</sup>. In each case a range of draw ratios was produced by drawing at a constant rate (Instron cross-head speed of 10 cm/min on a 2 cm gauge length sample) at 75°C for different times. It can be seen that there is a unique relationship between the modulus and the draw ratio. There are some differences between the moduli achieved for a given draw ratio and those reported earlier but these

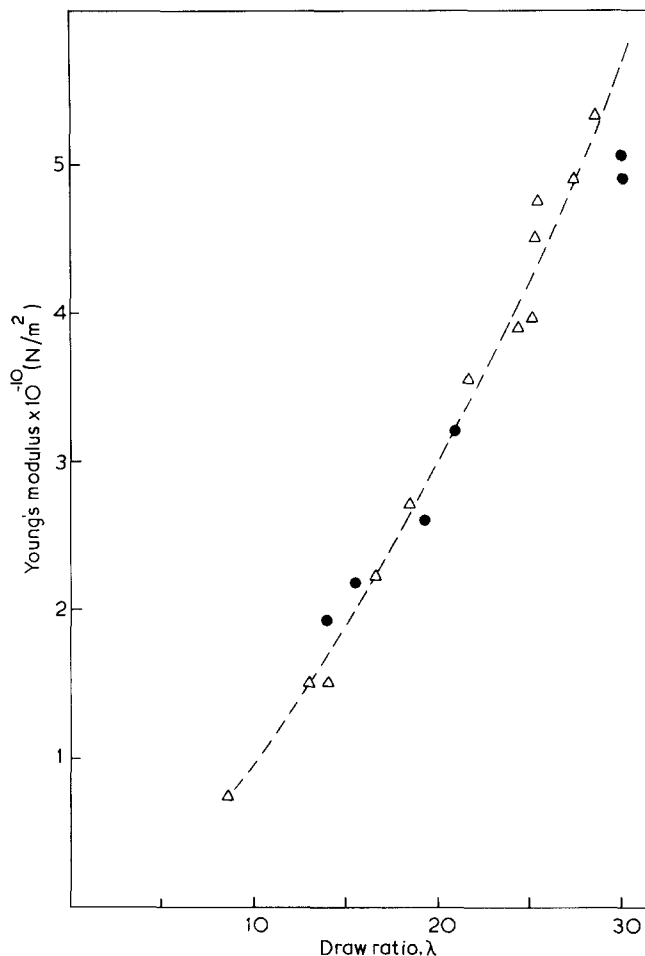


Figure 1 Room temperature Young's modulus as a function of draw ratio.  $\Delta$ , Quenched immediately into water;  $\bullet$ , slow cooled and quenched

are only significant at the highest draw ratios ( $\sim 30$ ) where very small differences in the sample homogeneity and preparation become important.

We therefore conclude that there is a unique relationship between modulus and draw ratio irrespective of the initial morphology. Moreover, it has been found that both high draw and very high modulus can be achieved for samples with conventional spherulitic morphology by extending the draw times under appropriate drawing conditions. The morphology of the initial material, however, is very important in determining the detailed nature of the plastic deformation. This is of interest both in understanding the mechanisms of deformation and in the development of practical procedures for production of these high modulus materials<sup>5</sup>. It is intended to deal with these aspects in a future publication, when our present studies have been completed.

G. Capaccio, T. J. Chapman and I. M. Ward

Department of Physics,  
University of Leeds,  
Leeds LS2 9JT, UK  
(Received 21 March 1975)

#### References

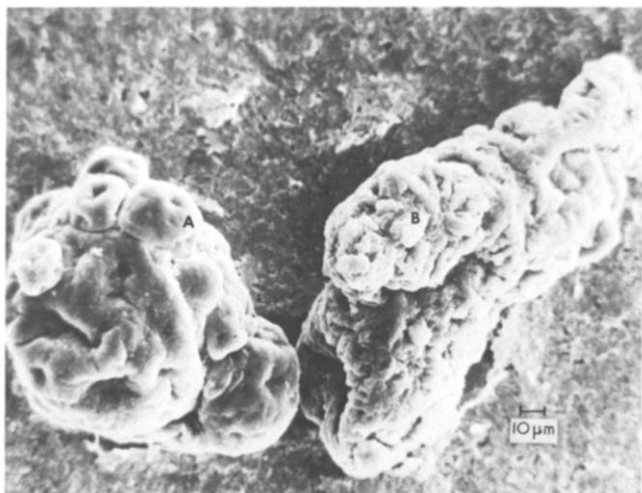
- 1 Capaccio, G. and Ward, I. M. *Nature (Phys. Sci.)* 1973, 243, 143
- 2 Capaccio, G. and Ward, I. M. *Br. Pat. Appln 10746/73* (filed 6.3.1973)
- 3 Capaccio, G. and Ward, I. M. *Polymer* 1974, 15, 233
- 4 Capaccio, G. and Ward, I. M. *Polymer* 1975, 16, 239
- 5 Capaccio, G. and Ward, I. M. *Br. Pat. Appln 52644/74 et seq.* (filed 3.10.73)

## Particle structure and fusion of suspension poly(vinyl chloride)

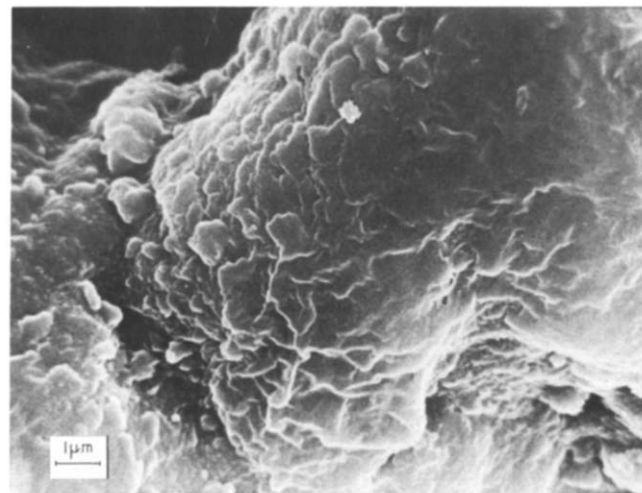
Although it is known that incomplete fusion of resin granules results in anomalous flow effects during the extrusion of suspension PVC<sup>1</sup>, the relation between these anomalies and resin granule morphology is not well understood. This situation exists partly because few details on the structure of suspension PVC granules are published in the literature.

The information which is available<sup>2</sup> does not fully emphasize the heterogeneous nature of the particles in a given PVC formulation. As an example *Figure 1* shows typical granules from a commercial suspension PVC as photographed with a scanning electron microscope. This particular PVC sample was manufactured by Norsk Hydro and had average molecular weights (determined by g.p.c.) of  $\bar{M}_w = 128\,000$  and  $\bar{M}_n = 56\,000$ .

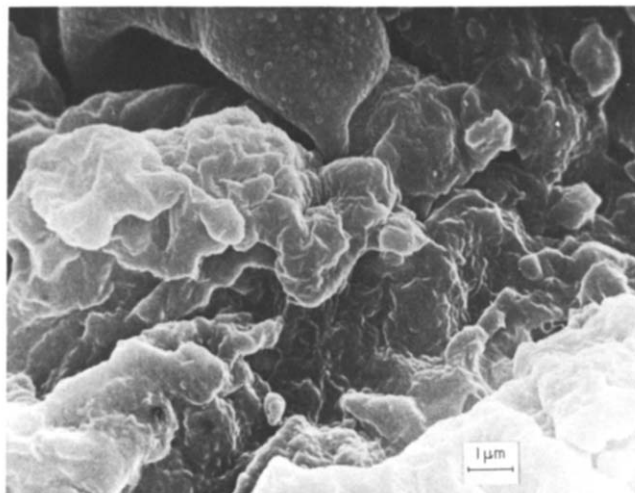
The granules in *Figure 1* are different in size, shape, surface characteristics, and porosity. Other photographs of granules from this sample show many different particle shapes and sizes ranging from 50 to 150  $\mu\text{m}$ . Close-up views of small regions of the same granules (*Figures 2 and 3*) indicate a complex aggregate morphology with a multitude of particles of submicron size. For each granule the surface



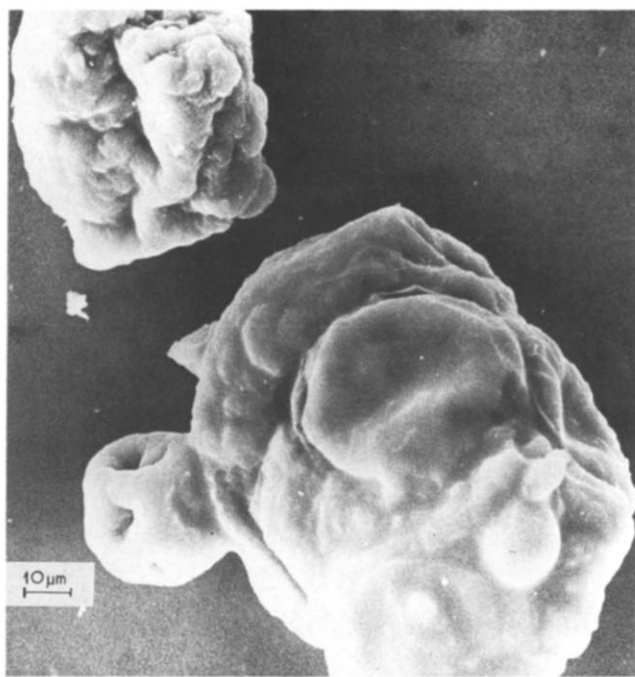
*Figure 1* Two typical suspension PVC granules with varied characteristics (scanning electron photomicrograph)



*Figure 2* Close-up view of PVC granule A showing aggregate structure and complex particulate morphology (scanning electron photomicrograph)



*Figure 3* Close-up view of PVC granule B showing complex particulate structure different from granule A (scanning electron photomicrograph)



*Figure 4* Suspension PVC granules partly fused after heating at 190°C; note that basic particulate structure is still apparent (scanning electron photomicrograph)

texture and state of aggregation are different; it appears also that granule B is more porous than granule A.

Some granules from a portion of the same PVC sample which had been treated with 2.5 pph dibutyltin di-octylthioglycolate stabilizer were heated to 190°C for 4 min. In *Figure 4* we see that some fusion has occurred but the basic particulate structure is still present. *Figure 5* is a close-up of a partly 'melted' portion of a similar PVC granule. It is clear from this that the fusion of these suspension granules at a temperature in the normal processing range is not complete. The surface is heterogeneous with both particulate and smooth regions apparent. The appearance of the granules in *Figure 4* suggests that they are heterogeneous on the inside as well.

While pressure, shear, and increased temperature all will contribute to enhance fusion, preliminary studies on the same PVC extruded at 205°C indicate that a heterogeneous particulate morphology persists. Moreover, granules heated to 220°C in the same manner as those described in *Figure 4*

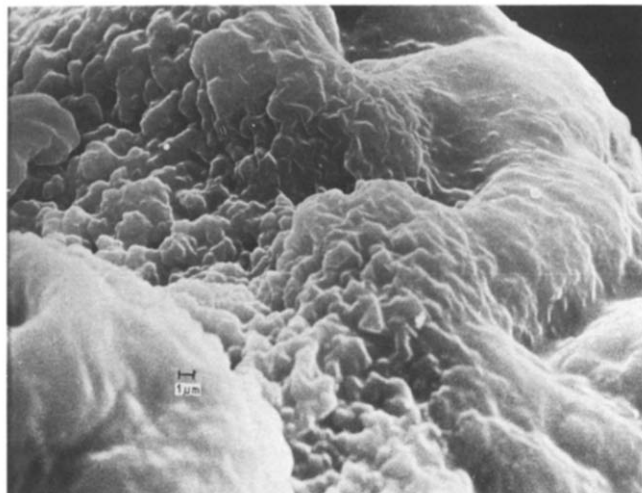


Figure 5 Close-up of a partly fused PVC granule surface; both particulate and smoother regions are apparent (scanning electron photomicrograph)

still retain their basic shapes and some of their original surface texture, although they appear a good deal smoother than those 'melted' at 190°C. 220°C is above normal processing temperatures for PVC.

If the basic granule morphology of a suspension PVC is heterogeneous we expect a considerable influence on fusion and the resulting morphology of the processed polymer.

Some of the PVC samples we have examined are less heterogeneous with uniform particle sizes and shapes. In these materials extrudate homogeneity may improve accordingly. At this point we have not determined whether this is true. However, our studies to obtain additional data on extrudate fusion are continuing.

#### Acknowledgements

Funding for these studies is being provided by The Royal Norwegian Council for Scientific and Industrial Research. The author thanks Dr Normann Bergem for much useful technical advice and Miss Kari Baardseth for assistance with the scanning electron microscope.

The author is on academic leave from University of Cincinnati, Cincinnati, Ohio, USA.

Richard P. Chartoff

Central Institute for Industrial Research,  
Forskningsveien 1,  
Blindern, Oslo 3, Norway  
(Received 10 March 1975)

#### References

- 1 Berens, A. R. and Folt, V. L. *Trans. Soc. Rheol.* 1967, 11, 95; *Polym. Eng. Sci.* 1968, 8, 5
- 2 Eliassaf, J. J. *Macromol. Sci. (A)* 1974, 8, 459 and references cited therein

# SCIENCE & PUBLIC POLICY

the international journal of the Science Policy Foundation

current awareness for busy people in

**government · industry · business ·  
education · research**

#### SCIENCE & PUBLIC POLICY

- provides information on national policies for science and technology and their effects
- examines the roles of science and technology in the operations of government (local, national and international), industry and business
- analyses the social and political environments within which science and technology operate
- assesses appropriate methodologies, information systems and organisational forms
- explores various types of public participation and their influence on national and international policies

The journal contains short, pithy news items, concise reports, comment, commissioned reviews, facts in figures, book reviews and extensive bibliographies.

The information is gathered through a worldwide network of national correspondents who are intimately involved in researching and applying science and public policy in their country.

Subscription £25.00 (\$65.00) per year (12 issues) including postage by fastest route. A special annual rate of £10.00 (\$26.00) is available for the individual who certifies that the copies are for his/her personal use and who is the full-time employee of a current full-price establishment subscriber at the same address.

**IPC Business Press Ltd, Oakfield House, Perrymount Road,  
Haywards Heath, Sussex, England**

Published monthly by IPC Science and Technology Press Ltd:  
publishers of *FUTURES*, *ENERGY POLICY* and *RESOURCES POLICY*.

# Book Reviews

## Functional monomers

Edited by R. H. Yocum and E. B. Nyquist  
Marcel Dekker, New York, 1973, Vol 1, 715 pp.  
\$39.50; 1974, Vol 2, 817 pp. \$46.50

In these two volumes, written and edited by six members of the Dow Chemical Company staff, one obviously benefits from the technical and information resources of a large organization, resulting in a competent and comprehensive review. The title refers to monomers which undergo addition polymerization and, which although generally used only in small amount in relation to other polymerizable compounds, introduce into the final polymers groups capable of further modification or reaction so as to provide specific properties such as ability to crosslink, modified surface behaviour, or enhanced solubility, adhesion or dye receptivity. Thus the subject is one which will have appeal to a wide range of readers, many of whom are concerned with preparation and polymerization or with macromolecular design and behaviour to meet specific end-uses.

The chapters in both volumes show commendable uniformity in treatment and include sections on synthesis, chemical reactions, physical properties and polymerizability, technical applications and some, but probably far from complete, commercial information regarding suppliers and costs. Much of the information on structure, synthesis and properties is summarized and presented in tabular form, thus providing for quick review and reference. At the end of each chapter there are many hundreds of references to the relevant literature which serve to bring the subjects up to early 1970, although as the editors indicate, in an area such as this where scientific and technical advance is rapid, the books cannot be regarded as the last word. However, they will obviate the need for much time-consuming literature searching and for this reason alone could be welcomed.

In the first volume are four chapters dealing with acrylamide and other  $\alpha,\beta$ -unsaturated amides; reactive halogen-containing monomers (but excluding for very obvious reasons vinyl and allyl halides and chloroprene); hydroxy monomers such as hydroxyalkyl acrylate esters, allyl alcohol, *N*-methylolacrylamides; and ethylene-, allyl- and styrene-sulphonic acids and 2-sulphoethyl methacrylate. The second volume comprises three chapters on reactive heterocyclic monomers containing three, five and six-membered rings (thus covering compounds such as glycidyl methacrylate, allyl glycidyl ether, vinyl oxazolones and pyrazoles, vinylene carbonate, and unsaturated dioxolanes – vinyl pyridine and maleic anhydride are more adequately dealt with in later chapters); acidic monomers based on maleic, fumaric, itaconic and crotonic acids; and basic monomers such as the vinyl pyridines and aminoalkyl acrylates and methacrylates.

Apart from some omissions in the compounds covered, e.g., reactive vinyl esters like the chloroacetate, *N*-substituted maleimides and vinyl propiolactone, the several types of functional monomer are well represented and the more important ones considered very fully. Particular aspects of preparation and manufacture, reactions, polymerization behaviour, and properties receive detailed attention, although discussion is generally based on the publications concerned and there may be a lack of critical review of some of the references or expert appraisal of some of the technical information, particularly that based on patent disclosures.

Lay-out of the text, formulae and binding are good but the printed format relies on photoreduced typescript of only moderate contrast which compares unfavourably with conventional type. Again, the numbering systems used for compounds, reactions and references can lead to some confusion. There are some errors in the typescript but these are generally of a minor nature. Author and subject indexes are included although the latter seem to be quite inadequate in view of the comprehensive nature of the work, and fuller itemization would have been an advantage.

The volumes are, perhaps understandably, somewhat expensive (together they amount to \$86, equivalent to some £36) but to those interested in the preparation, reactions and uses of the monomers or in technical applications of derived polymers and copolymers, they are a worthwhile investment, providing a well informed source of information and means of rapid reference. Many academic and industrial workers will find it useful to have access to these books.

R. J. W. Reynolds

## Polymer spectroscopy

Edited by D. O. Hummel  
Verlag Chemie, Weinheim, 1974, 401 pp. DM 125

The book is intended for practising chemists and spectroscopists concerned with polymers in industry and in universities. Apart from diffraction techniques, spectroscopic methods offer the main means of elucidating the structures of polymers: these methods have been brought together here. The chapter entitled Vibrational spectroscopy is sub-divided into the contributions: Vibrational analysis of highly ordered polymers by H. Tadokoro and M. Kobayashi; Applied infrared spectroscopy by D. O. Hummel; Raman spectroscopy by P. J. Hendra; at 180 pages this is the longest chapter. The remaining chapters are High resolution nuclear magnetic resonance spectroscopy by E. Klesper and G. Sietlaff (95 pages); Electron spin resonance by H. Fisher, D. O. Hummel, H. D. Schüddemage and K. Rübenaeker (31 pages). The size of the articles is in direct proportion to the importance and level of treatment given to the various branches of spectroscopy. The book is well printed and bound and it is profusely illustrated: there is a subject but not a name index.

The scientific literature is cluttered with spectroscopic compendia claiming to give special insight into some topic but mainly they represent well-documented basic material. This book, however, rarely deviates from its intended purpose of describing the applications of spectroscopic methods to polymer systems. Thus the reviewer can recommend the book to anyone interested in the structural aspects of polymers

L. H. Sutcliffe

## Structured polymer properties

R. J. Samuels  
John Wiley, New York, 1974, 251 pp. £10.60

This book aims to present a unified approach to the quantitative correlation of crystalline polymer structure with both fabrication and end use property behaviour, in such a way that it will be of interest to polymer physicists, chemists and engineers as well as advanced course students.

Following a short introductory chapter on the nature of crystallinity in polymers with special reference to polypropylene, a second chapter is devoted to details of techniques used in the characterization of polycrystalline polymer structure including those of wide angle X-ray diffraction, sonic modulus, birefringence, infra-red dichroism and small angle light scattering in the context of actual application. The third chapter concerns structural interpretation of the fabrication processes for polypropylene film and fibre formation. The last chapter which precedes some concluding remarks deals with the quantitative correlation of polymer structure with end-use properties, using polypropylene and poly(ethylene terephthalate) as examples.

The overall impression of this book is that it is authoritative reflecting a great deal of the author's personal experience as an industrial and academic scientist. Indeed so much does the impression come through, occasionally as in say, chapter 3 where coded reference to polymer samples used, one almost has the feeling of reading an original paper. On the other hand, experimental details of technique provide an air of conviction from which the most casual reader can only presume an expert acquaintance of the author with his subject. Despite one or two minor irritations such as a suggestion for further reading to a book still in preparation or a different type face for the index compared with the main text, the book appears to be remarkably free from errors and its easy style makes it most readable.

The book is particularly recommended to workers in the general as well as specific field and to more advanced students. Other readers may have some difficulty in appreciating the significance of the account in the broader area of polymeric materials as a whole, although after reading the book they would then be well armed to seek this significance.

R. P. Sheldon

# Specific refractive index increments of certain polysaccharide systems

C. T. Greenwood\* and D. J. Hourston†

Department of Chemistry, University of Edinburgh, Edinburgh, UK

(Received 24 July 1974; revised 22 November 1974)

The specific refractive index increments of amylose, amylose acetate, amylopectin and glycogen in various aqueous and non-aqueous solvents have been determined. These were measured by the direct determination of deviation method.

## INTRODUCTION

Experimentally determined values of specific refractive index increment ( $dn/dc$ ) are presented for the starch polymers amylose and amylopectin and the very similar mammalian polymer, glycogen, in a variety of solvents. Huglin<sup>1</sup> has published a compilation of  $dn/dc$  data for a very wide variety of polymer systems.

## EXPERIMENTAL

The differential refractometer used in this work was that designed by Brice and Hawler<sup>2</sup> and manufactured by the Brice-Phoenix Precision Instrument Corporation, Philadelphia, USA.

Initially calibration was attempted using solutions of anhydrous  $\text{Na}_2\text{SO}_4$ <sup>3</sup>, but the hygroscopic nature of this salt made the preparation of accurate solutions by weighing difficult. For this reason Analar sucrose was used instead and proved very satisfactory. Calibration was performed using a range of concentrations of sucrose solutions (0.1–5.0 g/100 ml) at wavelengths of 546 and 436 nm. The refractive index increment for sucrose in water at 25°C and 546 nm wavelength was taken as 0.1430 ml/g<sup>4</sup> and the corresponding value at 436 nm as 0.1449 ml/g<sup>3</sup>. The calibration constants were checked by measuring the refractive index increments of two systems, polystyrene in toluene and Ludox (a commercially available colloidal silica) in a 0.05 M NaCl solution. The results were in very good agreement with literature values.

All measurements were made at  $25 \pm 0.01^\circ\text{C}$  on solutions which had not been dialysed against the respective solvents. The results reported were generally found to be reproducible to within less than 1%.

Starch was isolated from potatoes (cv. Redskin) as previously described<sup>5</sup>. Fractionation was achieved by aqueous dispersion and the amylose was purified by recomplexing, three times, from hot aqueous n-butanol. The amylose/n-butanol complex was dehydrated by protracted stirring with n-butanol and finally dried in vacuum at 50°C. The

amylopectin was obtained by freeze-drying the residual aqueous dispersion.

Amylose isolated as above was acetylated according to the procedure of Higginbotham and Morrison<sup>6</sup>.

The glycogen was a commercial sample of oyster glycogen (Koch-Light Laboratories Ltd).

## RESULTS AND DISCUSSION

Table 1 presents data for amylose, amylopectin and glycogen in aqueous solvents commonly used in hydrodynamic studies of these natural polymers, but it also includes  $dn/dc$  values for amylose acetate in nitromethane.

The value of the  $dn/dc$  for amylose acetate in nitromethane at 436 nm was found to be 0.0885 ml/g which agreed well with values of 0.0875 ml/g<sup>7</sup> and 0.0857 ml/g<sup>8</sup>. The former literature value was obtained at 30°C. At 546 nm the experimental value was in exact accord with literature data<sup>9,10</sup> which, however, were measured at 20°C.

Glycogen in water was found to have a  $dn/dc$  value of 0.153 ml/g at 436 nm which compared very well with the value reported by Burchard *et al.*<sup>11</sup> of 0.151 ml/g at 20°C.

Data for amylopectin and glycogen in a range of aqueous solvents are presented in Table 2. The solvents investigated were 1% aqueous sodium lauryl sulphate, 1% aqueous cetyltrimethyl ammonium bromide, 15% aqueous  $\text{MgCl}_2$ , 8 M urea and 8 M guanidine hydrochloride.

Tables 3 and 4 present a survey of literature values of  $dn/dc$  for amylose, amylopectin, their various derivatives and for glycogen.

Table 1 Specific refractive index increments of various polysaccharide systems

Polymer	Solvent	$dn/dc$ (ml/g)	
		436 nm	546 nm
Amylose	0.33 M KCl	0.144	0.143
Amylose acetate	Nitromethane	0.0885	0.0835
Amylopectin	Water	0.160	0.157
Amylopectin	0.33 M KCl	0.153	—
Amylopectin	0.1 M NaCl	0.156	—
Glycogen	Water*	0.153	0.151
Glycogen	0.1 M NaCl	0.158	0.156

\* Unbuffered

\* Present address: Flour Milling and Baking Research Association, Chorleywood, Rickmansworth, Hertfordshire, UK.

† Present address: Department of Chemistry, University of Lancaster, Lancaster LA1 4YA, UK.

Table 2 Specific refractive index increments of amylopectin and glycogen in various aqueous solvents

Polymer	Solvent	dn/dc (ml/g)	
		436 nm	546 nm
Amylopectin	1% aqueous sodium lauryl sulphate	0.158	0.153
Amylopectin	1% aqueous cetyl trimethyl ammonium bromide	0.146	0.143
Amylopectin	15% aqueous MgCl <sub>2</sub>	0.112	0.111
Amylopectin	8 M urea	0.106	0.100
Amylopectin	8 M guanidine hydrochloride	0.128	0.125
Glycogen	1% aqueous sodium lauryl sulphate	0.155	0.150
Glycogen	1% aqueous cetyl trimethyl ammonium bromide	0.154	0.150
Glycogen	15% aqueous MgCl <sub>2</sub>	0.102	0.097
Glycogen	8 M urea	0.102	0.095
Glycogen	8 M guanidine hydrochloride	0.131	0.127

Table 3 Literature values of specific refractive index increments of solutions of amylose and its derivatives

Polymer	Solvent	dn/dc (ml/g)		Temp. (°C)	Ref
		436 nm	546 nm		
Amylose	DMSO	0.0676	0.0659		12
	Aq. KCl		0.146		13
	1 M KOH		0.146		13
	4.2 M GHCl*	0.118	0.116	25	14
	Aq. NaIO <sub>3</sub>	0.153	0.152		15
Amylose acetate	Nitro-methane	0.0875		30	7
	Nitro-methane	0.0857			8
	Nitro-methane		0.0835	20	9
	Nitro-methane		0.0835	20	10
Amylose tricarbanilate	Pyridine		0.0973	25	16
	Acetone	0.2279	0.2164	27	17
	Acetone	0.2218	0.2094	7	17
	Dioxane	0.163	0.151	20	18
		0.178†			
Sodium amylose xanthate	0.1 M NaCl		-0.1460	25	19
	0.25 M NaCl		-0.1480	25	19
	0.50 M NaCl		-0.1555	25	19
	1.0 M NaCl		-0.1741	25	19
Sodium carboxymethyl amylose	0.35 M NaCl	0.1325		35	20
	0.0065 M NaCl	0.138		30	21
	0.01 M NaCl	0.138		30	21
	0.03 M NaCl	0.138		30	21
	0.035 M NaCl	0.134		30	21
	1.0 M NaCl	0.124		30	21
	2.5 M NaCl	0.103		30	21

\* Guanidine hydrochloride

† 361 nm

## REFERENCES

- Huglin, M. B. 'Light Scattering from Polymer Solutions', Academic Press, London, 1972
- Brice, B. A. and Hawler, M. *J. Opt. Soc. Am.* 1951, **41**, 1033
- Norberg, P. H. and Sundelöf, L-O. *Makromol. Chem.* 1964, **77**, 77
- Gosting, L. J. and Morris, M. S. *J. Am. Chem. Soc.* 1949, **71**, 1998

- Banks, W., Greenwood, C. T. and Thomson, J. *Makromol. Chem.* 1959, **31**, 197
- Higginbotham, R. S. and Morrison, G. A. *Shirley Inst. Mem.* 1948, **22**, 148
- Cowie, J. M. G. *J. Polym. Sci.* 1961, **49**, 455
- Patel, R. S. and Patel, R. D. *Makromol. Chem.* 1966, **90**, 262
- Banks, W. and Greenwood, C. T. *Staerke* 1967, **19**, 394
- Banks, W., Greenwood, C. T. and Hourston, D. J. *Trans. Faraday Soc.* 1968, **64**, 363
- Burchard, W., Keppler, D. and Decker, K. *Makromol. Chem.* 1968, **115**, 250
- Everett, W. B. and Foster, J. F. *J. Am. Chem. Soc.* 1959, **81**, 3459
- Paschall, E. F. and Foster, J. F. *J. Polym. Sci.* 1952, **9**, 85
- Griffin, H. L., Erlander, S. R. and Senti, F. R. *Staerke* 1967, **19**, 8
- Erlander, S. R. and Griffin, H. L. *Staerke* 1967, **19**, 139
- Banks, W., Greenwood, C. T. and Sloss, J. *Eur. Polym. J.* 1971, **7**, 263
- Burchard, W. and Husemann, E. *Makromol. Chem.* 1961, **44**, 358

Table 4 Literature values of specific refractive index increments of solutions of amylopectin, its derivatives and glycogen

Polymer	Solvent	dn/dc (ml/g)		Temp. (°C)	Ref
		436 nm	546 nm		
Amylopectin	Water	0.156	0.154		22
	Water	0.155	0.151		23
	Water		0.152		24, 25
	Water		0.152		26
	0.2 M NaCl		0.150		27
	Ethylene diamine	0.098	0.098		28
	Ethylene diamine hydrate	0.092	0.092		28
	Formamide	0.069	0.069		28
	4.2 M GHCl*		0.140		24, 25, 26
	1 M KOH	0.142	0.142		28
	0.2 M NaOH	0.142			22
	DMSO/H <sub>2</sub> O (50:50)		0.110	25	25, 26
	DMSO/H <sub>2</sub> O (60:40)		0.101	25	25, 26
	DMSO/H <sub>2</sub> O (75:25)		0.087	25	25, 26
	DMSO/H <sub>2</sub> O (80:20)		0.083	25	25, 26
DMSO/H <sub>2</sub> O (85:15)		0.078	25	25, 26	
DMSO/H <sub>2</sub> O (90:10)		0.074	25	25, 26	
DMSO		0.066	25	25, 26	
Amylopectin acetate	Acetone	0.118			22
	Chloroform	0.051			22
	Acetonitrile	0.128			22
	Nitro-methane	0.088			22
	Dioxane	0.057			22
Sodium amylopectin xanthate	1 M NaOH		0.1550		29
	Water	0.136			30, 31
Glycogen	Water (un-buffered)	0.151		20	11
	15% Aq. MgCl <sub>2</sub>	0.136			32

\* Guanidine hydrochloride



*Specific refractive index increments of polysaccharides: C. T. Greenwood and D. J. Hourston*

- |    |  |    |  |
|----|--|----|--|
| 18 | Burchard, W. <i>Makromol. Chem.</i> 1965, <b>88</b> , 11                                 | 26 | Erlander, S. R. and Tobin, R. <i>Makromol. Chem.</i> 1968, <b>111</b> , 212                    |
| 19 | Pramanik, A. and Choudhury, P. K. <i>J. Polym. Sci. (A-1)</i> 1968, <b>6</b> , 1121      | 27 | Banks, W., Geddes, R., Greenwood, C. T. and Jones, I. G. <i>Stärke</i> 1972, <b>24</b> , 245   |
| 20 | Patel, J. R., Patel, C. K. and Patel, R. D. <i>Stärke</i> 1967, <b>19</b> , 330          | 28 | Stacy, C. J. and Foster, J. F. <i>J. Polym. Sci.</i> 1956, <b>20</b> , 57                      |
| 21 | Patel, J. R. and Patel, R. D. <i>Polymer</i> 1969, <b>10</b> , 167                       | 29 | Manna, P. K. and Choudhury, P. K. <i>J. Polym. Sci. (A-1)</i> 1972, <b>10</b> , 2159           |
| 22 | Witnauer, L. P., Senti, F. R. and Stern, M. D. <i>J. Polym. Sci.</i> 1955, <b>16</b> , 1 | 30 | Putzeys, P. and Verhoeven, L. <i>Rec. Trav. Chim.</i> 1949, <b>68</b> , 817                    |
| 23 | Debye, P. J. <i>Phys. Colloid Chem.</i> 1947, <b>51</b> , 18                             | 31 | Holme, T., Laurent, T. and Palmstierna, H. <i>Acta Chem. Scand.</i> 1957, <b>11</b> , 757      |
| 24 | Erlander, S. R. and Griffin, H. L. <i>Stärke</i> 1967, <b>19</b> , 134                   | 32 | Stetten, M. R., Katzen, H. M. and Stetten, D. Jr. <i>J. Biol. Chem.</i> 1956, <b>222</b> , 587 |
| 25 | Erlander, S. R. and Tobin, R. <i>Makromol. Chem.</i> 1968, <b>111</b> , 194              |    |  |

# Cavity field for axially symmetric dielectrics

K. H. Lau and K. Young

Department of Physics, The Chinese University of Hong Kong, Shatin, Hong Kong

(Received 11 November 1974)

A useful parameter for characterizing drawn polymers is the anisotropy,  $v$ , in the average molecular polarizability,  $\alpha$ . We examine, for an axially symmetric dielectric, the relation of  $v$  to the experimentally measurable anisotropy,  $u$ , in the permittivity,  $\epsilon$ . The relatively simple limit of negligible electronic polarizability is studied explicitly and the resulting mathematical problem of finding the cavity field in an axially symmetric dielectric is solved to second order in the anisotropy,  $u$ . Our result is compared to the *ad hoc* modifications of the isotropic Onsager equation previously used in the literature and it is found that these formulae give anisotropies that may be in error by up to 10%. This amounts to a few degrees in the equivalent angle for the orientation function.

## INTRODUCTION

Dielectric measurements are useful for studying the microscopic structure of polymers possessing permanent dipole moments. Studies of dielectric absorption, in particular the anisotropy in the absorption, are often valuable in identifying the nature of the underlying relaxation processes. In cases where the geometrical relation between the molecular dipoles and the polymer chain is unambiguous, the measured anisotropy can be used to determine the orientation function for the chains.

In all such measurements, the experimental output is the permittivity,  $\epsilon$  (real and imaginary parts as a function of temperature and frequency). This is to be confronted with models of microscopic structure, which predict (or attempt to relate to other quantities) the average molecular polarizability. If short range interactions are neglected, the polar contribution  $\alpha$  to the average molecular polarizability can be obtained from the experimentally measured  $\epsilon$  by Onsager's<sup>1</sup> equation:

$$\epsilon - n^2 = 4\pi N\alpha \left( \frac{3\epsilon}{2\epsilon + n^2} \right) \left( \frac{n^2 + 2}{3} \right)^2 \quad (1)$$

Here  $N$  is the number of dipoles per unit volume and  $n^2$  is the high frequency dielectric constant arising from electronic polarizability. For a dipole  $\mu_0$  completely free to rotate:

$$\alpha = \frac{\mu_0^2}{3kT} \quad (2)$$

Onsager's equation (1) is derived for an isotropic substance whereas one's interest in using dielectric absorption as a tool in polymer science lies often in drawn polymers, which are of course anisotropic. Previous analyses of anisotropic data have either used the *ad hoc* prescription of replacing each quantity in equation (1) by principal

values, e.g.<sup>2</sup>:

$$\epsilon_{xx} - (n^2)_{xx} = 4\pi N\alpha_{xx} \left( \frac{3\epsilon_{xx}}{2\epsilon_{xx} + (n^2)_{xx}} \right) \left[ \frac{(n^2)_{xx} + 2}{3} \right]^2 \quad (3)$$

or assumed<sup>3</sup> that the factor:

$$\left( \frac{3\epsilon}{2\epsilon + n^2} \right) \left( \frac{n^2 + 2}{3} \right)^2$$

is isotropic, so that:

$$\epsilon_{xx} - (n^2)_{xx} = B\alpha_{xx} \quad (4)$$

where  $B$  is a constant taken to be independent of draw ratio.

When the anisotropy itself is the object of interest, such *ad hoc* treatments as equations (3) or (4) make one somewhat uneasy especially in the absence of an estimate on the likely size of the error. Our purpose here is to consider the proper modification to Onsager's equation in the case of an anisotropic medium. Hopefully, this will lead to a theoretically more satisfactory framework for the analysis of anisotropic data. At the very least this will give an estimate of the error involved in previous treatments.

## THE CAVITY FIELD

In order to focus on just one important aspect of the problem, we shall assume that the electronic polarizability can be ignored. Setting  $n^2 = 1$  in equation (1), we get:

$$\epsilon - 1 = 4\pi N\alpha \left( \frac{3\epsilon}{2\epsilon + 1} \right) \quad (5)$$

This is the formula to be generalized to the anisotropic case. The factor  $3\epsilon/(2\epsilon + 1)$  is easily recognized as due to the so-

called cavity field. We do not mean to claim that  $n^2 \approx 1$  is a particularly good approximation for most polymers. The purpose for neglecting  $n^2 - 1$  is two-fold. First, we wish to address a relatively simple problem in order not to obscure the physics. Secondly, by comparing the results of the correct treatment with equations (3) and (4) in this limit, we shall get an idea of the size of the error in equations (3) and (4). A complete treatment including the electronic polarizability will be given elsewhere.

In an anisotropic medium, the average molecular polarizability will be represented by a tensor  $\alpha_{ij}$  and the permittivity by  $\epsilon_{ij}$ . These are defined as follows. The average polarization of an isolated molecule in an electric field  $\vec{G}$  is:

$$\langle \mu_i \rangle = \alpha_{ij} G_j \quad (6)$$

The induced polarization density in the dielectric medium in the presence of a macroscopic field  $\vec{E}$  is:

$$P_i = \frac{1}{4\pi} (\epsilon_{ik} - \delta_{ik}) E_k \quad (7)$$

Now if there are  $N$  dipoles per unit volume, then:

$$P_i = N \langle \mu_i \rangle$$

hence,

$$(\epsilon_{ik} - \delta_{ik}) E_k = 4\pi N \alpha_{ij} G_j \quad (8)$$

The crux of the matter is that the field  $\vec{G}$  available to orient a dipole is not the same as the macroscopic field,  $\vec{E}$ . The field  $\vec{G}$  is the resultant field due to all external sources plus all induced dipole moments *except* that due to the dipole in question. (The argument is the same as the isotropic case, and details may be found in Onsager's paper<sup>1</sup>.) Thus one is to imagine the dipole in question removed from the medium, leaving a hole.  $\vec{G}$  is then the field at the centre of this hole when the field far away is  $\vec{E}$ . For this reason  $\vec{G}$  is referred to as the cavity field. (Equivalently, one may remove a sphere containing many dipoles, but ignore the short range interaction among these dipoles. The mathematics is identical.)

For a linear dielectric, the relation between  $\vec{G}$  and  $\vec{E}$  must be of the form:

$$G_j = X_{jk} E_k \quad (9)$$

so that equation (8) becomes:

$$\epsilon_{ik} - \delta_{ik} = 4\pi N \alpha_{ij} X_{jk} \quad (10)$$

or in matrix notation ( $\hat{\cdot}$  denotes a matrix)

$$\hat{\epsilon} - \hat{1} = 4\pi N \hat{\alpha} \hat{X} \quad (11)$$

### THE MATHEMATICAL PROBLEM

The problem is simply to calculate  $\hat{X}$ . If we treat the medium minus the cavity macroscopically,  $\hat{X}$  will be a function of  $\hat{\epsilon}$  only. Let the cavity be spherical, with radius  $R$  and let the electric field be given by  $-\nabla\psi(x)$  for  $r < R$  and  $-\nabla\phi(x)$  for  $r > R$ . Gauss' law requires:

$$\nabla^2 \psi = 0 \quad (12a)$$

$$\epsilon_{ij} \partial_i \partial_j \phi = 0 \quad (12b)$$

The boundary condition at the origin is:

$$|\psi| < \infty \text{ as } r \rightarrow 0 \quad (13)$$

and at infinity:

$$\phi \rightarrow -\vec{E} \cdot \vec{r} \text{ as } r \rightarrow \infty \quad (14)$$

Across the boundary  $r = R$ , we must have:

$$\psi = \phi \quad (15a)$$

$$\left. \begin{aligned} \frac{\partial \psi}{\partial r} &= n_i (\epsilon_{ij} \partial_j \phi) \end{aligned} \right\} \text{ at } r = R \quad (15b)$$

Here  $\vec{n}$  is the unit outward normal. Equations (12)–(15) completely specify the problem. The cavity field  $\vec{G}$  is then

$$\vec{G} = -\vec{\nabla} \psi |_{r=0} \quad (16)$$

We now specialize to the case of axial symmetry, say about the  $z$  axis. This is the most common situation in polymers. The problem is not in principle more difficult for the general anisotropic case, but will be quite tedious in practice. It will be convenient to use the matrix:

$$\hat{\eta} = \begin{pmatrix} 1 & & \\ & 1 & \\ & & -2 \end{pmatrix}$$

in terms of which we may write:

$$\epsilon_{ij} = \epsilon (\delta_{ij} + u \eta_{ij}) \quad (17)$$

where

$$\epsilon = 1/3 \text{tr} \epsilon_{ij} \quad (18)$$

is the mean value (over the principal directions) of the permittivity and

$$u = \frac{\epsilon_{xx} - \epsilon_{zz}}{2\epsilon_{xx} + \epsilon_{zz}} \quad (19)$$

measures the anisotropy in the tensor  $\epsilon_{ij}$ . The potentials will now be expanded as a power series in  $u$ :

$$\psi = \sum u^n \psi_n$$

$$\phi = \sum u^n \phi_n \quad (20)$$

Then equations (12)–(15) become:

$$\nabla^2 \psi_n = 0 \quad (21a)$$

$$\nabla^2 \phi_n = D \phi_{n-1} \quad D \equiv -(\partial_1^2 - 2\partial_2^2) \quad (21b)$$

$$|\psi_n| < \infty \quad \text{as } r \rightarrow 0 \quad (22)$$

$$\phi_0 \rightarrow -\vec{E} \cdot \vec{r} \quad \text{as } r \rightarrow \infty$$

$$\phi_n \rightarrow 0 \quad \text{as } r \rightarrow \infty \quad n \geq 1 \quad (23)$$

$$\psi_n = \phi_n \quad (24a)$$

$$\left. \frac{1}{\epsilon} \left( \frac{\partial \psi_n}{\partial r} \right) = \frac{\partial \phi_n}{\partial r} + D' \phi_{n-1} \right\} \text{ at } r = R \quad (24b)$$

$$D' \equiv n_1 \partial_1 - 2n_2 \partial_2$$

The zeroth order is nothing but the isotropic case and is trivial<sup>4</sup>. With the zero order solution, we compute  $D\phi_0$  and  $D'\phi_0$ . These are the inhomogeneities 'driving' the next order. Physically  $D\phi_0$  corresponds to an induced volume charge density while  $D'\phi_0$  corresponds to a surface charge density. The next order can then be solved in a straightforward manner by separating variables in spherical coordinates.

We have carried the iteration to second order in  $u$ , with the result:

$$\begin{aligned} X_{ij} = & \left( \frac{3\epsilon}{2\epsilon + 1} \right) \delta_{ij} + u \left\{ \frac{3}{5} \left( \frac{\epsilon(3\epsilon + 2)}{(2\epsilon + 1)^2} \right) \eta_{ij} \right\} + \\ & u^2 \left\{ \frac{6}{25} \left( \frac{\epsilon(9\epsilon^2 - 4\epsilon - 6)}{(2\epsilon + 1)^3} \right) \delta_{ij} + \right. \\ & \left. \frac{3}{175} \left( \frac{\epsilon(-3\epsilon^2 + 26\epsilon + 12)}{(2\epsilon + 1)^3} \right) \eta_{ij} \right\} + \\ & 0(u^3) \end{aligned} \quad (25)$$

The first term is the well-known isotropic result. It is convenient to write:

$$X_{ij} = X(\delta_{ij} + w\eta_{ij}) \quad (26)$$

where from equation (25):

$$\begin{aligned} X = & \frac{3\epsilon}{2\epsilon + 1} + u^2 \left\{ \frac{6}{25} \left( \frac{\epsilon(9\epsilon^2 - 4\epsilon - 6)}{(2\epsilon + 1)^3} \right) \right\} + 0(u^3) \\ w = & u \left\{ \frac{3\epsilon + 2}{5(2\epsilon + 1)} \right\} + u^2 \left\{ \frac{1}{175} \left( \frac{-3\epsilon^2 + 26\epsilon + 12}{(2\epsilon + 1)^2} \right) \right\} + \\ & 0(u^3) \end{aligned} \quad (27)$$

In the following we shall be concerned only with  $w$ . It will be convenient to use:

$$\bar{u} = \left( \frac{\epsilon}{\epsilon - 1} \right) u \quad (28)$$

which is the anisotropy in  $\hat{\epsilon} - \hat{1}$ :

$$\epsilon_{ij} - \delta_{ij} = (\epsilon - 1)(\delta_{ij} + \bar{u}\eta_{ij}) \quad (29)$$

In terms of  $\bar{u}$ , equation (27) is:

$$\begin{aligned} w = & \frac{\bar{u}}{u} \left\{ \frac{(\epsilon - 1)(3\epsilon + 2)}{5\epsilon(2\epsilon + 1)} \right\} + \\ & \bar{u}^2 \left\{ \frac{1}{175} \frac{(\epsilon - 1)^2(-3\epsilon^2 + 26\epsilon + 12)}{\epsilon^2(2\epsilon + 1)^2} \right\} + \\ & 0(\bar{u}^3) \equiv \Sigma A_n(\epsilon) \bar{u}^n \end{aligned} \quad (30)$$

Table 1 Coefficients for relating the anisotropy  $w$  of the cavity field factor  $X_{ij}$  to the anisotropy  $\bar{u}$  in  $\epsilon_{ij} - \delta_{ij}$ :  $w = \Sigma A_n(\epsilon) \bar{u}^n$

$\epsilon$	$A_1$	$A_2 \times 10^3$
1	0	0
2	0.160	2.97
3	0.210	3.26
4	0.233	2.69
6	0.256	1.40
8	0.268	0.42
10	0.274	-0.20
$\infty$	0.300	-4.29

Values of  $A_1(\epsilon)$  and  $A_2(\epsilon)$  are given in Table 1. It is evident that the expansion of  $w$  in terms of  $\bar{u}$  is converging, and in fact the linear term will be sufficient for all practical purposes.

#### RELATION TO $\hat{\alpha}$ AND THE ORIENTATION FUNCTION

If equation (26) is substituted in equation (11),  $\hat{\alpha}$  can be solved in terms of  $\hat{\epsilon}$ . It will be convenient to parameterize  $\hat{\alpha}$  in the same way as  $\hat{\epsilon}$  and  $\hat{X}$ :

$$\alpha_{ij} = \alpha(\delta_{ij} + v\eta_{ij}) \quad (31)$$

In general,  $v$  is the quantity desired. A little arithmetic yields:

$$v = \frac{\bar{u} - w}{1 - w - 2w\bar{u}} \quad (32)$$

and making the linear approximation for  $w$  as discussed in the last section:

$$v = \frac{(1 - A_1)\bar{u}}{1 - A_1\bar{u} - 2A_1\bar{u}^2} \quad (33)$$

It is useful to compare this with equation (3), which for  $n^2 = 1$  reduces to:

$$\epsilon_{xx} - 1 = 4\pi N\alpha_{xx} \left( \frac{3\epsilon_{xx}}{2\epsilon_{xx} + 1} \right) \quad (34)$$

with a similar equation for the  $zz$  component. The resulting equation for  $v$  is:

$$\frac{1 + v}{1 - 2v} = \left( \frac{1 + \bar{u}}{1 - 2\bar{u}} \right) \left\{ \frac{1 - 2 \left( \frac{\epsilon - 1}{\epsilon} \right) \bar{u}}{1 + \left( \frac{\epsilon - 1}{\epsilon} \right) \bar{u}} \right\} \left\{ \frac{1 + 2 \left( \frac{\epsilon - 1}{2\epsilon + 1} \right) \bar{u}}{1 - 4 \left( \frac{\epsilon - 1}{2\epsilon + 1} \right) \bar{u}} \right\} \quad (35)$$

Also, we compare our results with equation (4). For  $n^2 = 1$ , equation (4) reads:

$$\epsilon_{xx} - 1 = B\alpha_{xx} \quad (36)$$

with a similar equation for the  $zz$  component. This clearly leads to:

$$v = \bar{u} \quad (37)$$

For the same measured values of  $\epsilon$  and  $\bar{u}$ , the three methods of analyses: equations (33), (35), (37) which we

shall label as (a), (b), (c) respectively, will lead to different values for  $\nu$ . To display this difference more graphically, it is best to consider the orientation function.

To be definite, we assume the following model<sup>3</sup>. The dipoles are perpendicular to the polymer chain and free to rotate in the plane normal to the chain. The angle between the chain and the  $z$  axis will be called  $\theta$ . It can be shown that for such a model<sup>3</sup>:

$$\alpha_{xx} = K \left( \frac{1 + \langle \cos^2 \theta \rangle}{4} \right) \quad (38)$$

$$\alpha_{zz} = K \left( \frac{1 - \langle \cos^2 \theta \rangle}{2} \right)$$

where  $K$  is a constant. The anisotropy  $\nu$  is then:

$$\nu = \frac{1}{4} [-1 + 3\langle \cos^2 \theta \rangle] \quad (39)$$

Incidentally this demonstrates the simple relation between  $\nu$  and the Hermans<sup>5</sup> orientation function:

$$f = [3\langle \cos^2 \theta \rangle - 1]/2 \quad (40)$$

within this model. Solving for the mean angle:

$$\langle \cos^2 \theta \rangle = (1 + 4\nu)/3 \quad (41)$$

An equivalent angle  $\theta_0$  can be defined by:

$$\cos^2 \theta_0 = \langle \cos^2 \theta \rangle \quad (42)$$

i.e. if the  $\theta$ -distribution is sharp, it peaks at  $\theta_0$ .

With these definitions in hand, we are ready to consider one numerical example. We take  $\bar{u} = 1/3$ . The values for  $\nu$  and  $\theta_0$  are computed according to the three formalisms and displayed as a function of  $\epsilon$  in Table 2.

The discrepancy is a few degrees for  $\theta_0$ , which is at the level of typical experimental errors. This will affect the details of data-fitting but not any qualitative conclusions.

It has been claimed<sup>2</sup> that equation (3) should be good for small anisotropy, since it is obtained from an isotropic formula. We should point out that this is not quite the

Table 2 Values of  $\nu$  and  $\theta_0$  computed by the three different formalism for  $\bar{u} = 1/3$

$\epsilon$	$\nu$			$\theta_0$ (degrees)		
	(a)	(b)	(c)	(a)	(b)	(c)
1	0.333	0.333	0.333	28.1	28.1	28.1
2	0.307	0.314	0.333	30.5	29.9	28.1
3	0.298	0.288	0.333	31.3	32.2	28.1
4	0.294	0.313	0.333	31.6	29.9	28.1
5	0.289	0.317	0.333	32.0	29.6	28.1
8	0.287	0.319	0.333	32.2	29.4	28.1
10	0.286	0.321	0.333	32.3	29.2	28.1
$\infty$	0.280	0.333	0.333	32.8	28.1	28.1

case. Equations (3) and (4) give exactly correct values of  $\nu$  for both zero and maximum anisotropy. This is best seen from equations (33), (35) and (37). All three equations have the property that  $\nu = \bar{u}$  when  $u = 0, 1/2$  or  $-1$ . Maximum discrepancy occurs at intermediate values of the anisotropy  $u$ , though even for such values, the error is not very large.

## CONCLUSION

The implication of the present analysis is simply that the error involved in using equation (3) or (4) is not very large, though for accurate work a correction should perhaps be made. The electronic polarizability, which has been neglected here, is expected to give an error of about the same order.

## ACKNOWLEDGEMENTS

We thank Professor B. Hsu and Dr C. L. Choy for discussions.

## REFERENCES

- 1 Onsager, L. *J. Am. Chem. Soc.* 1936, 58, 1486
- 2 Barés, J. *Kolloid-Z.* 1969, 239, 552
- 3 Phillips, P. J., Kleinheins, G. and Stein, R. S. *J. Polym. Sci. (A-2)* 1972, 10, 1593
- 4 Jackson, J. D. 'Classical Electrodynamics', Wiley, New York, 1962
- 5 Hermans, J. J., Hermans, P. H., Varmaas, D. and Weidinger, A. *Rec. Trav. Chim.* 1946, 65, 427

# Ultrasonic studies of three fluoropolymers \*

S. F. Kwan, F. C. Chen and C. L. Choy

Physics Department, The Chinese University of Hong Kong, Shatin, Hong Kong

(Received 9 September 1974)

The ultrasonic velocities and attenuations of poly(vinylidene fluoride), polytrifluoroethylene and polychlorotrifluoroethylene at 10 MHz from 170 to 300 K have been measured by the pulse echo-overlap and the pulse-height comparison methods, respectively. Discontinuities in the slopes of the velocity-temperature curves and concurrent sharp rises of attenuations were observed, and were identified with previously reported transitions. An analysis of the fractional changes in the corresponding temperature coefficients was made. The velocity data extrapolated to 0 K by Rao's rule were combined with presently available thermal data to yield the effective three-dimensional intermolecular force constants in the Tarasov model, and to confirm the existence of low-frequency vibrational modes contributing to the specific heat of polychlorotrifluoroethylene. The magnitude and temperature dependence of the elastic moduli and the Poisson ratio in relation to those of the velocities are also discussed.

## INTRODUCTION

It has long been recognized<sup>1</sup> that the substitution of fluorine atoms for the hydrogen atoms in polyethylene may lead to a reduction of the intermolecular attraction. However, nearly all the ultrasonic studies<sup>2-5</sup> on fluorinated polyethylene concentrated on the relaxation regions and were not extended to sufficiently low temperatures to allow unambiguous evaluation of the intermolecular interaction. While in principle ultrasonic velocity measurements near 0 K should be used to calculate the intermolecular interaction, this is not really strictly necessary, because if one makes measurements at temperatures below the strong relaxation regions then the data can be extrapolated quite reliably to 0 K. The results so obtained are also useful for studying the acoustic contribution to the specific heat of polymers at low temperatures.

We have measured the ultrasonic velocities and attenuations at 10 MHz of three fluorine-containing polymers, poly(vinylidene fluoride) (PVF<sub>2</sub>), polytrifluoroethylene (PVF<sub>3</sub>) and polychlorotrifluoroethylene (PCTFE) between 170 and 300 K. From results of mechanical relaxation studies<sup>6</sup> down to 6 K, it appears that such linear crystalline polymers should not exhibit any mechanical relaxation at 10 MHz below 220 K. Our results can therefore be extrapolated to low temperatures with some confidence through the application of Rao's empirical formula<sup>7</sup>, especially since the temperature dependence is already very weak at the lower end of our measurement range.

The extrapolated velocities can be understood in both the Debye<sup>8</sup> and the Tarasov model<sup>9</sup> of a solid, thus enabling us to evaluate the Tarasov three-dimensional spring constant of the polymers studied. At low temperatures the Debye model gives the specific heat of a substance as<sup>8</sup>:

$$C/T^3 = \frac{2\pi^2 k^4}{5h^3 \rho} \frac{1}{\bar{v}^3} \quad (1)$$

where  $T$ ,  $h$  and  $k$  have their usual meanings,  $\rho$  is the density, and  $\bar{v}$  is the appropriate average velocity of sound at 0 K:

$$\frac{1}{\bar{v}^3} = \frac{1}{3} \left( \frac{1}{v_L^3} + \frac{2}{v_T^3} \right) \quad (2)$$

Both here and in the following the subscripts L and T refer to longitudinal and transverse elastic waves, respectively. The Debye temperature  $\theta_D$ , which depends on the choice of the vibrating unit, is given by<sup>10</sup>:

$$\theta_D = \frac{h}{k} \left( \frac{2\pi^2 N n}{V} \right)^{1/3} \quad (3)$$

where  $N$  is the Avogadro number,  $V$  is the molar volume,  $n$  is the number of degrees of freedom per vibrating unit. For polymers it is customary to choose the repeating unit of the polymer chain as the vibrating unit<sup>11</sup>. For our samples, there are two backbone carbon atoms per repeating unit and in general six skeletal vibration modes are expected. However, the C-C stretching modes of these atoms are of high frequency<sup>11</sup> (about  $10^3 \text{ cm}^{-1}$ ) and are not excited at low temperature, so that there are actually only four modes per repeating unit,  $n = 4$ . Combining equations (1) and (3) we therefore write the molar heat capacity as:

$$\frac{C}{T^3} = \frac{4\pi^4 N n k}{5} \frac{1}{\theta_D^3} \quad (4)$$

In our case this model is unrealistic in that the polymer consists of many long-chain molecules capable of linear vibrations so it would not behave simply like a Debye solid. Tarasov<sup>9</sup> proposed a more realistic model by assuming its density of states to be a one-dimensional continuum arising from the vibration of individual chains superimposed on a three-dimensional continuum arising from interchain vibrations. Mathematically it is given by:

\* Based on part of a thesis (1974, unpublished) submitted by S. F. Kwan to the Graduate School of The Chinese University of Hong Kong in partial fulfilment of the requirement of the MPhil degree.

$$g(\omega) = \begin{cases} \frac{N'}{3\omega_1\omega_3^2} & (0 < \omega < \omega_3) \\ \frac{N'}{\omega_1} & (\omega_3 < \omega < \omega_1) \end{cases} \quad (5)$$

where  $\omega_1$  and  $\omega_3$  are two characteristic cut-off frequencies and  $N'$  is the total number of states. The heat capacity for a single branch of acoustical vibration can then be shown to be:

$$\begin{aligned} \frac{C_d(T)}{R} &= D(\theta_3, \theta_1, T) \\ &= D_1\left(\frac{\theta_1}{T}\right) - \frac{\theta_3}{\theta_1} \left[ D_1\left(\frac{\theta_3}{T_1}\right) - D_3\left(\frac{\theta_3}{T_1}\right) \right] \end{aligned} \quad (6)$$

where  $R$  is the gas constant,  $\theta_i = \hbar\omega_i/k$ , ( $i = 1, 3$ ) and the  $n$ -dimensional Debye function  $D_n$  is:

$$D_n(x) = \frac{n}{x^n} \int_0^x \frac{x^{n+1} e^x}{(e^x - 1)^2} dx \quad (n = 1, 3) \quad (7)$$

Suppose all acoustical branches have the same characteristic temperatures  $\theta_3$  and  $\theta_1$ . The total acoustical heat capacity contributions is then:

$$C_d(T) = nRD(\theta_3, \theta_1, T) \quad (8)$$

which at low temperatures ( $T \ll \theta_3$ ) reduces to the Debye form:

$$\frac{C_d(T)}{T^3} = \frac{4\pi^4 Nnk}{5} \frac{1}{\theta_1 \theta_3^2} \quad (9)$$

Upon comparison of equations (4) and (9) we arrive at the relation  $\theta_D^3 = \theta_1 \theta_3^2$ .

Through equations (2) and (3) the extrapolated results of our measurements lead to  $\theta_D$ , which, together with the recently available data on  $\theta_1$ <sup>12</sup>, yield  $\theta_3$ . To gauge the strength of the intra- and inter-molecular forces in the polymer, it is also useful to compute the effective one- and three-dimensional spring constants  $k_1$  and  $k_3$  defined as:

$$k_i = \bar{M}(k\theta_i/\hbar)^2 \quad (i = 1, 3) \quad (10)$$

where  $\bar{M}$  is the average mass of the group of atoms associated with each carbon atom of the backbone.

It has been pointed out<sup>13-17</sup> that low-frequency Einstein modes of vibrations may contribute to the specific heats of amorphous materials at low temperature, so as to explain the excess of the calorimetrically determined specific heat over the acoustic contributions given by equation (1). Since thermal values for PCTFE became available recently<sup>18</sup>, our results would also allow us a check on this assertion.

## EXPERIMENTAL

The experimental techniques employed in this experiment are quite conventional, and have already been reported in detail<sup>19</sup>, so only brief descriptions will be given here.

### Sample preparation

The samples of PVF<sub>2</sub> and PCTFE were obtained from Cellomer Associates, Inc. and 3M Co., respectively. The sample of PVF<sub>3</sub> was supplied by Dr R. E. Florin of the National Bureau of Standards of the USA and was mildly crosslinked. They were formed into stocks by slow heating to above the melting point in a mould, pressing for 30 min and then being gradually cooled to room temperature. For PCTFE, sample stocks of four different crystallinities were obtained by quenching in ice water and by annealing for various lengths of time. Crystallinity was determined by the buoyancy method in water to an accuracy of 3–5%. However, the effect of crystallinity on the elastic moduli will be the subject of a separate paper, and the PCTFE data discussed here refer mostly to just one crystallinity (0.53), even though the rest of the PCTFE data do have some bearing on the problem of the excess specific heat discussed below.

After moulding the stocks were cut into thin discs of 1.3 cm diameter and between 2 to 8 mm thickness. The two surfaces of each disc were then ground parallel to within 2  $\mu$ m/cm and polished flat.

### Temperature control and measurement

The copper sample chamber containing the sample and transducers was suspended at the end of a long stainless-steel tube in the middle of a double-wall, separately evacuable cryostat, which in turn was immersed in liquid nitrogen. A copper–constantan thermocouple junction calibrated against a standard platinum resistance thermometer to an accuracy of 0.01 K and mounted next to the sample on the same plate served both as the temperature indicator and the sensor for temperature control. A five-digit differential voltmeter (Hewlett-Packard (HP) 740B) provided digital dialling of temperature settings and also supplied an amplified control signal to the automatic temperature controller (Artronix 5309 and 2202). The overall temperature stability and accuracy was better than 0.05 K.

### Ultrasonic instrumentation

Radiofrequency (r.f.) elastic waves were produced in the sample disc by 10 MHz X- or Y-cut quartz transducers (supplied by the Valpey-Fisher Corporation) bonded to it by silicone oil (Edwards 704). The bond was quite satisfactory between 170 and 300 K (below 250 K for shear wave).

The repetition rate of the r.f. pulses was derived from a sine oscillator (HP 651B) and monitored on a 7-digit frequency counter (HP 5306B). The oscillator output was converted to the actual triggering pulses by a decade divider (Matec 122) which drove the r.f. pulse generator and detector (Matec 6000, with plug-in 950 and 960). A pulse comparator (Matec 666B) triggered by another pulse generator (HP 214A) provided r.f. pulses of calibrated amplitude variable in 0.1 dB steps over a range of 4 decades. The signals were viewed on an oscilloscope (HP 140A with plug-in 1421A and 1402A) with calibrated sweep and delay.

### Measurements and systematic errors

Velocity measurements were made by the pulse echo-overlap technique<sup>20,21</sup>, with a sensitivity of better than 0.1% and an accuracy estimated to be 0.5%. Attenuation measurements were made by pulse-height comparison of the successive echoes<sup>22</sup> with standard pulses. The results

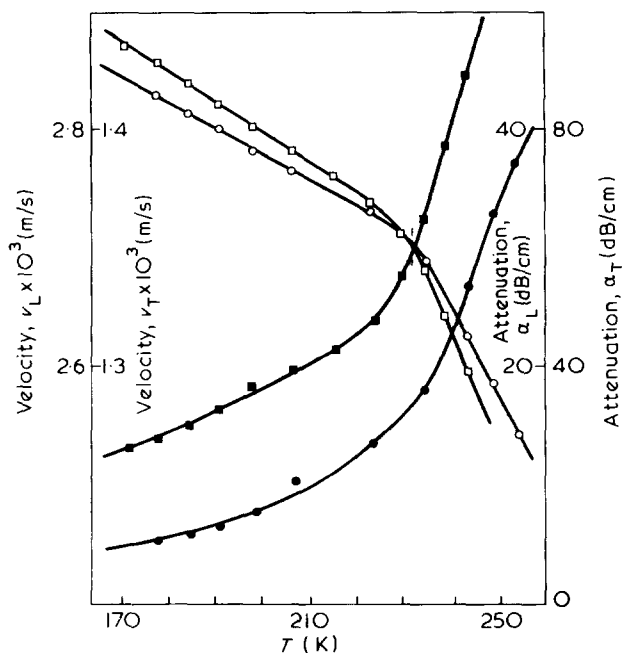


Figure 1 Velocities ( $v_L$ ,  $v_T$ ) and attenuations ( $\alpha_L$ ,  $\alpha_T$ ) in PVF<sub>2</sub> as functions of temperature,  $T$ . ---,  $T_d$ . ○,  $v_L$ ; □,  $v_T$ ; ●,  $\alpha_L$ ; ■,  $\alpha_T$

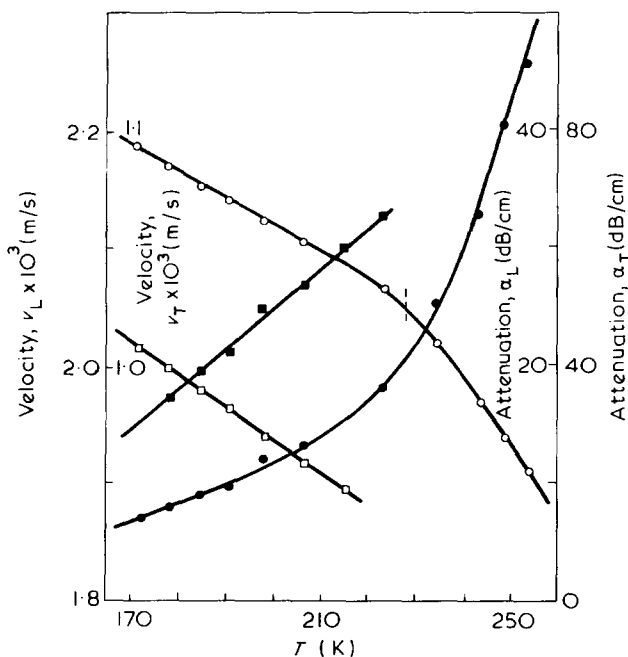


Figure 2 Velocities and attenuations in PVF<sub>3</sub> as functions of temperature. Legend same as for Figure 1

have a much larger uncertainty, say 3–5%. The most important factors giving rise to errors are the bond effect and, in the case of attenuation, the width of the oscilloscope trace.

We have corrected for systematic errors wherever possible. The bond effect was eliminated by making measurements on PCTFE samples of several different thickness  $d$  and then plotting the attenuation coefficient and the echo transit-time in the sample against  $d$ . It turned out that the bond absorption was quite large for longitudinal wave (4.0 dB or 10–30%) but practically zero for transverse wave. The shortening of transit time due to the phase-shift at the sample–bond interface was comparatively small, but still amounted to 60 ns and 36 ns, or 1–3%, for longitudinal

and transverse waves, respectively. These effects were temperature independent to within experimental error. We assumed all bonds to be similar and applied the above corrections to all of our data.

The error arising from the thermal contraction of the sample discs could be readily corrected for by use of the volumetric data on PVF<sub>2</sub> and PCTFE available in literature<sup>23,24</sup>, but this could not be done for PVF<sub>3</sub> owing to the lack of similar data. Diffraction in the sample disc could also be a source of error, but estimates by use of the Papadakis formula<sup>25</sup> showed that such effects were quite negligible.

## RESULTS AND DISCUSSION

The corrected data of the ultrasonic velocities and attenuations of PVF<sub>2</sub>, PVF<sub>3</sub> and PCTFE are summarized in Figures 1, 2 and 3.

### Transition regions

It is apparent from the Figures that each velocity–temperature curve has a break at the point which we called the temperature of discontinuity,  $T_d$ .

In the two velocity curves of PVF<sub>2</sub> (Figure 1) the magnitudes of both slopes increase by a factor of about 3.7 over a 10 K interval around the break, whereas away from this region the slopes practically do not change over intervals as large as 50 K. Near the break there is apparently also a sudden rise in both of the absorption coefficients. It is natural to identify this break, which can be located at 232 K to within  $\pm 5$  K, with the glass-transition temperature,  $T_g$  at 238 K reported in the volumetric measurement of Mandelkern *et al.*<sup>23</sup>. It was suggested by Wada<sup>26</sup> and Work<sup>27</sup> that because of strong dependence of the modulus on the specific volume one can always expect a break at the static glass-transition point irrespective of the characteristic frequency of the modulus. Subsequently many authors confirmed that the temperature where the break appears is independent of frequency, which may range from the

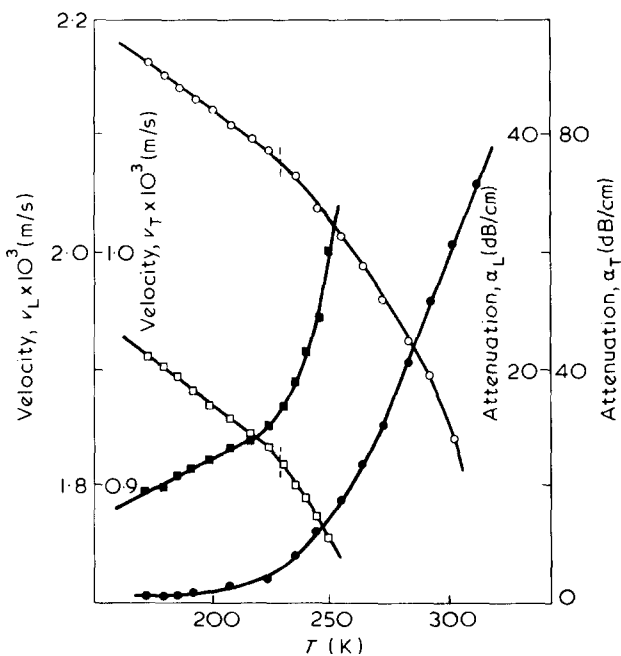


Figure 3 Velocities and attenuations in PCTFE as functions of temperature. Legend same as for Figure 1



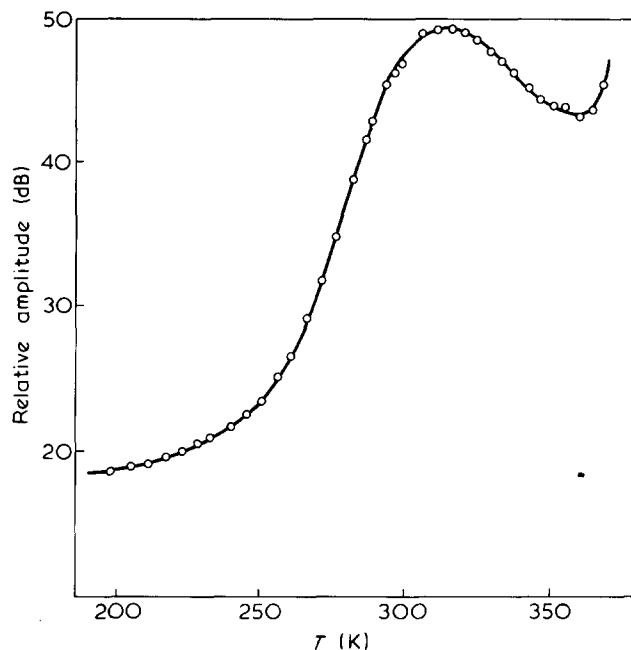


Figure 4 Relative amplitude of the first transmitted pulse of longitudinal wave in PVF<sub>2</sub> as a function of temperature

static region<sup>28</sup> up to the MHz region<sup>29</sup>. In view of their results, our identification seems quite justified.

The dynamic relaxation peak corresponding to the above glass-transition point was observed at approximately 317 K (i.e. 85 K above  $T_d$ ) in the curve of the relative attenuation (Figure 4), which is deduced from the amplitude of the first transmitted longitudinal ultrasonic signal in PVF<sub>2</sub>. Since we were not able to observe the subsequent echoes in this measurement, there is, of course, some uncertainty in the interpretation of this curve, especially regarding the exact location of the peak. Nevertheless it does seem clear that the character of the peak and its approximate position (with an error of perhaps  $\pm 5$  K) are quite beyond doubt. In particular, together with the dielectric data of Kabin *et al.*<sup>30</sup> and Nakagawa and Ishida<sup>31</sup>, this 10 MHz peak at 317 K can be fitted reasonably well by the empirical formula of Williams, Landel and Ferry (WLF)<sup>32</sup> (Figure 5) if the considerable error in its position is taken into account.

The glass-transition point for PCTFE at 325 K<sup>33</sup> is above our measurement range and not observed. However, we did observe a slightly rounder break in the two velocity curves of PCTFE (Figure 3) at  $230 \pm 5$  K, where both slopes change by a factor of 2 within an interval of 10 K. This could possibly be the same break at 223 K observed by Baccaredda and Butta<sup>34</sup> at a lower frequency range (4–16 kHz). Similar breaks below the glass-transition points of a number of polymers and at different frequencies had been previously reported by Wada *et al.*<sup>35</sup>. They discussed this problem in connection with their own observations in the 33 kHz to 1 MHz region, and suggested that the most probable mechanism of such 'secondary discontinuities' was the activation of the end-groups or side-group rotations. Since there are no side-groups in the polymers studied, the observed breaks are probably associated with the motion of a section of the backbone involving a few carbon atoms and correspond to the low-temperature peak at about 230 K observed in dynamical mechanical measurements at 1 Hz<sup>36</sup>. A sudden rise of the absorption curves of PCTFE is also observed around the

same temperature, but any relaxation peak which may correspond to it lies beyond our measurement range.

We also observed a break in the longitudinal velocity curve of PVF<sub>3</sub> (Figure 2) at about 230 K, with an accompanying sharp rise in the attenuation. This corresponds to the onset of motion also observed in nuclear magnetic resonance (n.m.r.) measurements<sup>37</sup> as a decrease in the line-widths of both the proton and fluorine resonance lines, and was attributed to the rotation of a few chain segments of the carbon backbone. Mechanical and dielectric relaxation measurements<sup>38</sup> at low frequencies also show an absorption peak near 230 K, which is presumably due to this limited motion.

Back in 1956 Work<sup>27</sup> attempted to explain the discontinuity in the temperature coefficient of the ultrasonic velocity data of poly(methyl methacrylate) and polystyrene in terms of the discontinuity in the expansion coefficient  $\beta$  through the following thermodynamic relation derived at constant frequency:

$$\left(\frac{\partial v}{\partial T}\right)_P + K\beta\left(\frac{\partial v}{\partial P}\right)_T = \left(\frac{\partial v}{\partial T}\right)_V \quad (11)$$

where  $v$  (i.e.  $v_L$  or  $v_T$ ) and  $K$  (the bulk modulus) are functions of the frequency, temperature  $T$  and pressure  $P$ , but  $\beta$  and  $V$  (volume) depend on  $T$  and  $P$  only. It was argued that  $(\partial v/\partial T)_V \sim 0$  well below the relaxation region, and for these two polymers this was indeed found to be the case. On the assumption that  $K$  and  $(\partial v/\partial P)_T$  were continuous at  $T_d$ , the fractional change of  $(\partial v/\partial T)_P$  should then be equal to that of  $\beta$  by virtue of equation (11). This was well borne out by the experimental data<sup>27</sup>. Following this suggestion, Wada *et al.*<sup>35</sup> verified the same equality for several other polymers at both glass and secondary transitions.

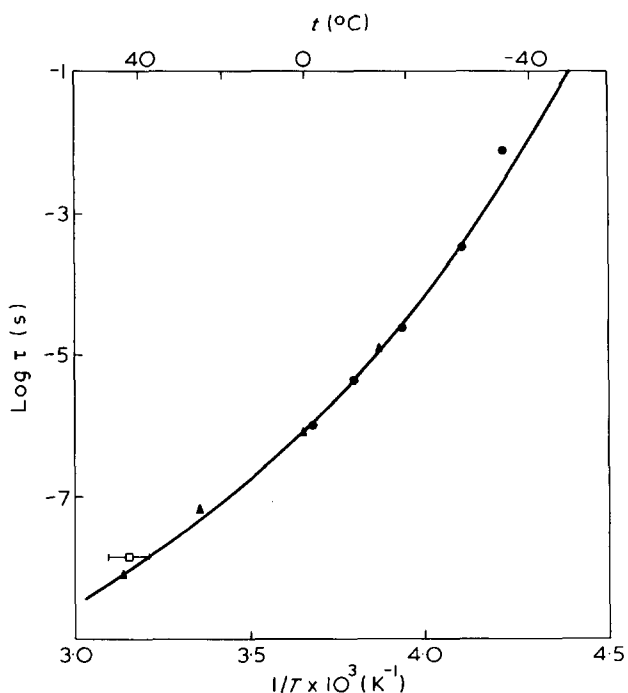


Figure 5 Plot of  $\log \tau$  against  $1/T$  for PVF<sub>2</sub>.  $\tau = 1/2\pi f$ , where  $f$  is the frequency of the measurements. —, Theoretical curve computed from the WLF equation using the parameters given in ref 31. ●, dielectric loss data  $\epsilon''$  taken from ref 31; ▲, dielectric loss tangent data ( $\tan \delta$ ) taken from ref 30; □, our ultrasonic data

However, the above theory is not applicable to the discontinuities observed in this experiment. In Table 1 we have listed  $T_d$ ,  $\beta$  and the temperature coefficient of velocity  $\gamma$  (defined as  $(\partial v/\partial T)_P/v$ ) of the three polymers studied, the primed and unprimed quantities referring to values above and below  $T_d$ , respectively.  $\beta$  is computed from the volume-temperature curves of PVF<sub>2</sub><sup>23</sup> and PCTFE<sup>24</sup> but is omitted for PVF<sub>3</sub>, for which no data exist. It is easily seen that  $\beta'/\beta$  is much smaller than  $\gamma'/\gamma$ , such that the discontinuity in  $\beta$  cannot possibly account for the discontinuity in  $\gamma$  completely. In fact,  $\beta$  and  $\gamma$  are related as follows:

$$\gamma = \frac{-\beta\rho}{v} \left( \frac{\partial v}{\partial \rho} \right)_P \quad (12)$$

While  $\rho$  and  $v$  are continuous, the discontinuities in both  $\beta$  and  $(\partial v/\partial \rho)_P$  are expected to contribute to that of  $\gamma$ . To verify this point we compute  $(\partial v/\partial \rho)_P$  from the velocity-density curve obtained by combining our data and the available volumetric<sup>23,24</sup> data, both of which have been measured at atmospheric pressure. The  $\ln v$  vs.  $\ln \rho$  curves for PCTFE as shown in Figure 6 are straight lines with different slopes above and below  $T_d$ , and therefore can be represented by what is known as Rao's Rule<sup>7</sup>:

$$\ln v = A \ln \rho + B \quad (13)$$

where the constants  $A$  and  $B$  are different above and below  $T_d$ . Similar curves are also obtained for PVF<sub>2</sub>. Combining equations (12) and (13) we arrive at the relation  $\gamma = -\beta A$ . Table 1 shows the good agreement between  $\gamma'/\gamma$  and  $(\beta'/\beta)(A'/A)$ , bringing out the fact that the hitherto neglected factor  $A'/A$  is at least as important as  $\beta'/\beta$  in our

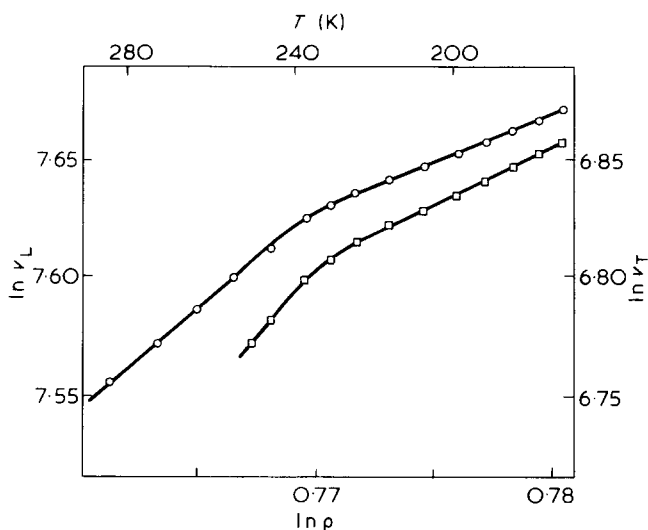


Figure 6 Plot of  $\ln v$  vs.  $\ln \rho$  for PCTFE.  $\circ$ ,  $\nu_L$ ;  $\square$ ,  $\nu_T$

Table 1 Temperature of discontinuity and temperature coefficients of the velocities

Polymer	Velocities	$T_d$ (K)	$-\gamma \times 10^{-3}$ (degrees <sup>-1</sup> )	$-\gamma' \times 10^{-3}$ (degrees <sup>-1</sup> )	$A$	$A'$	$\frac{\gamma'}{\gamma}$	$\frac{\beta'}{\beta}$	$\frac{A'}{A}$	$\left(\frac{\beta'}{\beta}\right)\left(\frac{A'}{A}\right)$
PVF <sub>2</sub>	$\nu_L$	232	0.78	3.0	3.6	9.2	3.8	1.6	2.6	4.2
	$\nu_T$	232	1.1	4.5	4.5	11.1	4.1	1.6	2.5	4.0
PVF <sub>3</sub>	$\nu_L$	230	1.1	2.7			2.5			
PCTFE	$\nu_L$	230	0.68	1.4	3.9	8.3	2.1	1.1	2.1	2.3
	$\nu_T$	230	0.89	1.9	4.9	10.6	2.1	1.1	2.2	2.4

case. At secondary transitions where the change in  $\beta$  is small,  $A'/A$  may even become the dominant factor. The velocity measurement may then be a much more sensitive method for detecting such transitions than the volumetric measurement, PCTFE being a good example. The reason why  $\gamma'/\gamma$  simply equals  $\beta'/\beta$  for the several polymers investigated by Work<sup>27</sup> and Wada *et al.*<sup>35</sup> is not clear, but it may be connected with the fact that all these polymers are amorphous, whereas the ones we studied have considerable crystallinity.

From our data and those of Wada *et al.*<sup>35</sup> it also seems a general feature that the ratio  $\gamma'/\gamma$  is considerably larger at glass transitions than at secondary transitions, with typical values of 4 and 2, respectively. This ratio may therefore serve as a parameter for distinguishing between these two kinds of transitions. Under this criterion and other corroborative evidences<sup>38</sup> it is reasonable to assign the break in the velocity curve of PVF<sub>3</sub> at 230 K ( $\gamma'/\gamma = 2.5$ ) as a secondary transition.

#### Intermolecular interaction

In addition to transitions one can also learn something about the specific heat and the effective intermolecular force constant of the polymers from our data extrapolated to 0 K by the use of equation (13) together with the available volumetric data on PVF<sub>2</sub><sup>23</sup> and PCTFE<sup>24</sup>. Since no such data are available for PVF<sub>3</sub>, and the constant  $A$  does not seem to change much from PVF<sub>2</sub> to PCTFE, we simply use the average values of them for PVF<sub>3</sub>. The values of  $\nu_L$  and  $\nu_T$  so extrapolated to 0 K lead to the values of the average velocity at 0 K,  $v$ , and of  $C/T^3$ ,  $\theta_D$ ,  $\theta_3$  and  $k_3$  through equations (1)–(4), (9) and (10). The results are shown in Table 2, where the corresponding quantities for polyethylene (PE)<sup>11</sup> and polytetrafluoroethylene (PTFE)<sup>17</sup> are also listed for comparison.

Among the three polymers studied the only thermal determination of  $C/T^3$  available in literature is that of PCTFE, which was reported by Reese and Tucker<sup>18</sup> to be 559 erg/K<sup>4</sup> g for a sample of crystallinity 0.34\*. In comparison, the corresponding acoustic value listed in Table 2 is 314 erg/K<sup>4</sup> g, which has been obtained by linearly extrapolating the  $C/T^3$  values of our four PCTFE samples to the same crystallinity. The latter  $C/T^3$  values are based on the measured values of both  $\nu_L$  and  $\nu_T$  for one sample but only on  $\nu_T$  for the other three samples, the fact that  $\nu_L \sim 2\nu_T$  being used in the latter cases. The error involved in this approximation is probably quite small, since the  $1/\nu_L^3$  term contributes only about 7% to  $1/\bar{\nu}^3$  in equation (2). In any case this certainly would not affect our main conclusion, namely that the thermal value of  $C/T^3$  for PCTFE exceeds the acoustic value by a sizable factor (1.7).

\* This crystallinity seems too low for the commercial rod used in ref 18. However, this does not affect the conclusion stated below since the acoustic  $C/T^3$  values range only from 320 to 386 erg/K g when the crystallinity increases from 0.4 to 0.75.

Table 2  $\theta_3$ ,  $k_3$  and  $C/T^3$  values of the polymers studied

Polymer	Repeating unit	$\bar{M}$ (amu)	$\bar{v} \times 10^3$ (m/s)	$\theta_D$ (K)	$\theta_1^C$ (K)	$k_1^C \times 10^5$ (dynes/cm)	$\theta_3$ (K)	$k_3 \times 10^4$ (dynes/cm)	$(C/T^3)$ acoustic (ergs/K <sup>4</sup> g)
PE <sup>a</sup>	CH <sub>2</sub> -CH <sub>2</sub>	14	—	227	540	1.16	147	0.87	—
PVF <sub>2</sub>	CH <sub>2</sub> -CF <sub>2</sub>	32	1.73	148	357	1.16	95	0.82	126
PVF <sub>3</sub>	CHF-CF <sub>2</sub>	41	1.22	99	308	1.11	56	0.37	325
PTFE <sup>b</sup>	CF <sub>2</sub> -CF <sub>2</sub>	50	1.24	97	270	1.05	58	0.48	278
PCTFE	CClF-CF <sub>2</sub>	58	1.18	87	235	0.91	52	0.45	338

<sup>a</sup> Data taken from ref 11

<sup>b</sup> Data taken from ref 17

<sup>c</sup> Data taken from ref 12

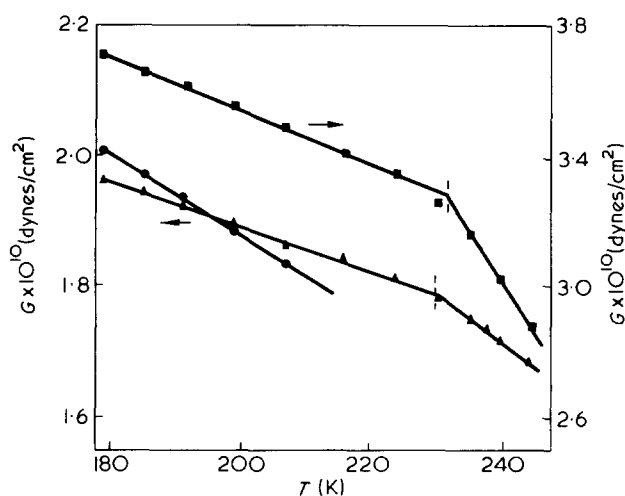


Figure 7 Shear moduli of PVF<sub>2</sub> (■), PVF<sub>3</sub> (●) and PCTFE (▲) as functions of temperature

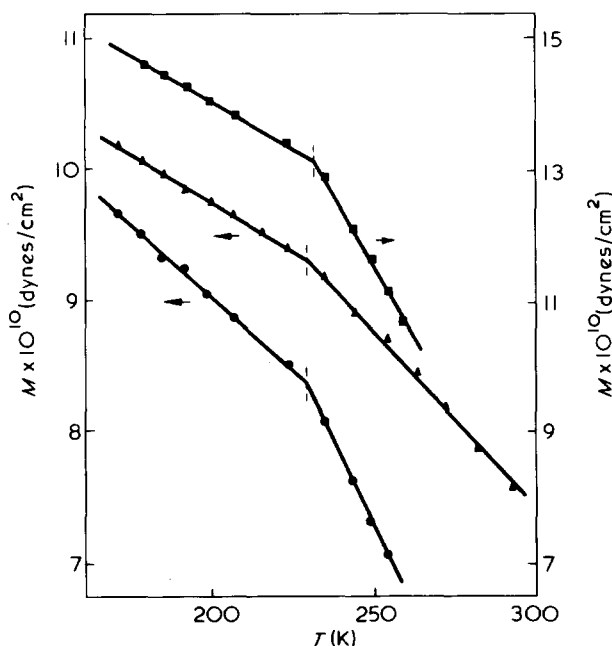


Figure 8 Longitudinal moduli of PVF<sub>2</sub> (■), PVF<sub>3</sub> (●) and PCTFE (▲) as functions of temperature

The existence of excess low-temperature specific heat in amorphous material was first pointed out by Anderson<sup>10</sup> and subsequently observed in various inorganic glasses<sup>13,14</sup> and polymers<sup>15-17</sup>. This implies there may be low-frequency modes in addition to the Debye acoustical vibrations. Rosenstock<sup>39</sup> suggested that the vibrating units contained in or adjacent to cavities present in disordered struc-

tures would only be weakly bound to the rest of the lattice, and might vibrate independently at low frequency.

As already mentioned, the three-dimensional force constant  $k_3$  is a measure of the interchain van der Waals interaction. Table 2 seems to show that the substitution of  $n$  hydrogen atoms by halogen atoms for two carbon atoms of PE does not have any substantial effect on this interaction for  $n = 2$ , since  $k_3$  decreases only marginally when PE changes to PVF<sub>2</sub>; but that a drastic effect is produced for  $n = 3$  or 4, since  $k_3$  decreases by a factor of 2 when PE changes to PVF<sub>3</sub>, PTFE or PCTFE. Qualitatively this is probably due to the larger size of the halogen atoms, so that the substitution causes an increase in the effective intermolecular distance and a consequent weakening in the interaction. As a matter of fact, the polymer chains of PTFE and PCTFE are known to have a helical conformation with an outer halogenated sheath<sup>1</sup>, which may be the cause of the considerable decrease in  $k_3$  when  $n$  increases from 2 to 4. It is somewhat unexpected that the value for PVF<sub>3</sub> is slightly lower than even PCTFE and PTFE, but this probably reflects only the crudeness of the Tarasov model and may not have any real physical significance.

We also note that the one-dimensional force constant  $k_1$  is greater than  $k_3$  by a factor of 10 to 20, which is quite understandable since the covalent bonds responsible for the intrachain interaction should be much stronger than the van der Waals force responsible for the interchain interaction.

#### Elastic moduli and the Poisson ratio

The shear modulus  $G$ , longitudinal modulus  $M$  and bulk modulus  $K$  are related to the velocities  $v_T$  and  $v_L$  of the transverse (T) and longitudinal (L) waves by<sup>40</sup>:

$$G = \rho v_T^2 \quad (15)$$

$$M = \rho v_L^2 \quad (16)$$

$$K = \rho v_T^2 \left( y^2 - \frac{4}{3} \right) \quad (17)$$

where  $y = v_L/v_T$  and we have neglected factors of the form  $(1 - \eta^2)/(1 + \eta^2)^2$  on the right of equations (15) and (16), since in our temperature range, which is below the relaxation regions, the quantity  $\eta = \nu\alpha/\omega$  ( $\alpha$  being the attenuation) is  $\ll 1$  for both waves. The Poisson ratio  $\sigma$  can then be written as<sup>40</sup>:

$$\sigma = \frac{1}{2} \left( 1 - \frac{1}{y^2 - 1} \right) \quad (18)$$

The three moduli and the Poisson ratios are shown in Figures 7 to 10. The moduli for PVF<sub>3</sub> and PCTFE are

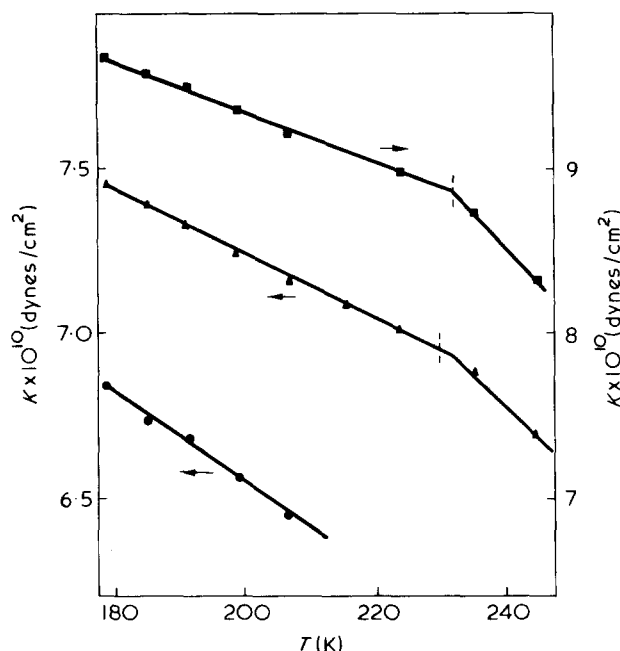


Figure 9 Bulk moduli of PVF<sub>2</sub> (■), PVF<sub>3</sub> (●) and PCTFE (▲) as functions of temperature

approximately equal but are much smaller than those of PVF<sub>2</sub>. This is a reflection of the decrease in  $k_3$  when the number of halogen atoms per repeat unit increases from 2 to either 3 or 4.

The breaks at  $T_d$  are observed in all moduli. This is quite natural, since the temperature coefficients of the latter are, according to equations (15)–(17), simply twice the corresponding values of  $\gamma$ , the contribution of  $\rho$  and  $y$  being rather small. We note that  $y$  has the approximately constant value 2 for all three polymers throughout the temperature covered, including the transition regions. This means that the Poisson ratio  $\sigma$  should always be about  $1/3$ , as is indeed the case. Actually  $\sigma$  does have a small temperature coefficient  $\gamma_\sigma$  which, as can be deduced from equation (18), should be roughly equal to  $4/3(\gamma_L - \gamma_T)$ , where  $\gamma_L$  and  $\gamma_T$  refer to the temperature coefficients of the velocities of longitudinal and transverse waves, respectively. In addition,  $\sigma$  is also observed to have breaks around  $T_d$ , which can be characterized by  $\gamma'_\sigma/\gamma_\sigma$ . This ratio (computed to be 4.7 and 2.4 and observed to be 5.0 and 3.0 for PVF<sub>2</sub> and PCTFE, respectively) is about the same as the  $\gamma'/\gamma$  characterizing the velocity curves, which is a consequence of  $\gamma'_T/\gamma_T$  and  $\gamma'_L/\gamma_L$  being approximately equal. However, these breaks were not observed in similar curves obtained by Wada *et al.*<sup>35</sup> for other polymers and at slightly lower frequencies, possibly owing to the difference in materials.

## CONCLUSION

From the foregoing analysis it can be seen that ultrasonics is a precise and sensitive tool for studying transitions in polymers, especially the secondary transitions, where the effects in other static quantities may be quite small; it is also useful for studying the intermolecular forces, even though this is necessarily model dependent, and cannot be expected to reveal any fine details of the interaction.

In the future it would be interesting to study the  $\gamma'/\gamma$  ratio systematically for several polymers such as PE, PCTFE and poly(ethylene terephthalate), at all transitions and at different crystallinities, to confirm that it does take

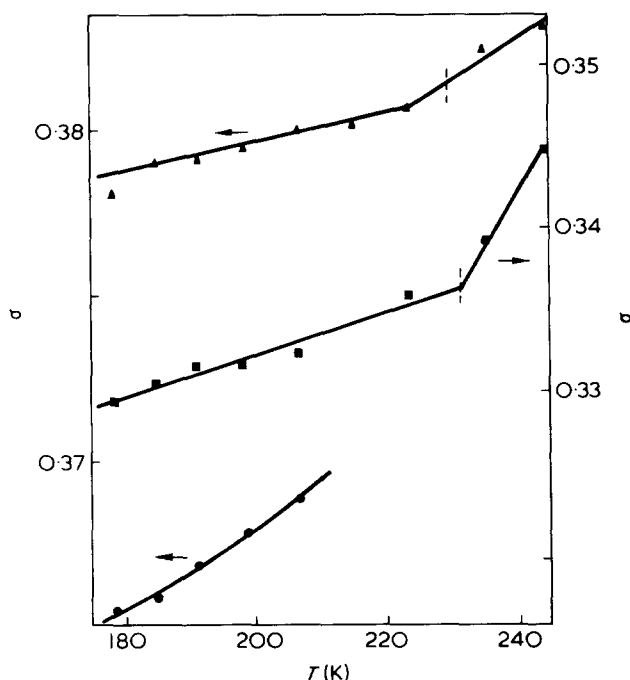


Figure 10 Poisson ratios of PVF<sub>2</sub> (■), PVF<sub>3</sub> (●) and PCTFE (▲) as functions of temperature

on distinctively different values for different kinds of transitions, and to determine whether the contribution of  $\beta'/\beta$  indeed decreases with crystallinity. It may also be worthwhile to repeat the experiment for a different series of polymers, such as those resulting from the chlorination of PE, and see if the variation of the van der Waals force shows the same features as we have observed here.

## ACKNOWLEDGEMENTS

The authors are indebted to Dr R. E. Florin of the National Bureau of Standards, USA for supplying the sample of polytrifluoroethylene and Mr W. B. Isaacson of the 3M Co. for supplying Kel-F pellets. We are also grateful for the financial support of the Institute of Science and Technology of the Chinese University of Hong Kong.

## REFERENCES

- 1 Koo, G. P. 'Fluoropolymers' (Ed. L. A. Wall), Wiley-Interscience, New York, 1972, p 507
- 2 Kabin, S. P. *Soviet Phys. (Tech. Phys.)* 1956, 1, 2542
- 3 Kono, R. *J. Phys. Soc. Japan* 1961, 16, 1580
- 4 Eby, R. K. and Sinnott, K. M. *J. Appl. Phys.* 1961, 32, 1765
- 5 Eby, R. K. and Wilson, F. C. *J. Appl. Phys.* 1962, 33, 2951
- 6 Sauer, J. A. *J. Polym. Sci. (C)* 1971, 32, 69
- 7 Rao, M. R. *Indian J. Phys.* 1940, 14, 109
- 8 Kittel, C. 'Introduction To Solid State Physics', 4th Edn, Wiley, New York, 1971, Ch 6
- 9 Tarasov, V. V. *Zh. Fiz. Khim.* 1950, 24, 111
- 10 Anderson, O. L. *J. Phys. Chem. Solids* 1959, 12, 41
- 11 Wunderlich, B. and Baur, H. *Adv. Polym. Sci.* 1970, 7, 151
- 12 Lee, W. K. and Choy, C. L. to be published
- 13 Flubacher, P., Leadbetter, A. J., Morrison, J. A. and Stoicheff, B. P. *J. Phys. Chem. Solids* 1959, 12, 53
- 14 Antoniou, A. A. and Morrison, J. A. *J. Appl. Phys.* 1965, 36, 1873
- 15 Reese, W. J. *J. Appl. Phys.* 1966, 37, 3959
- 16 Choy, C. L., Hunt, R. G. and Salinger, G. L. *J. Chem. Phys.* 1970, 52, 3269
- 17 Athougies, A. D., Peterson, B. T., Salinger, G. L. and Swartz, C. P. *Cryogenics* 1972, 12, 125
- 18 Reese, W. and Tucker, J. E. *J. Chem. Phys.* 1965, 43, 105

- 19 Kwan, S. F. *MPhil Thesis* Chinese University of Hong Kong (1974)
- 20 Papadakis, E. P. *J. Appl. Phys.* 1964, **35**, 1474
- 21 Papadakis, E. P. *J. Acoust. Soc. Am.* 1967, **42**, 1045
- 22 Roderick, R. L. and Truell, R. *J. Appl. Phys.* 1952, **23**, 267
- 23 Mandelkern, L., Martin, G. M. and Quinn, F. A. *J. Res. Nat. Bur. Stand.* 1957, **58**, 137
- 24 Laquer, H. L. and Head, E. L. *US At. Energy Commiss. Rep. AECU-2161* 1952
- 25 Papdakis, E. P. *J. Acoust. Soc. Am.* 1972, **52**, 847
- 26 Wada, Y. *J. Appl. Phys. Japan* 1955, **24**, 159
- 27 Work, R. N. *J. Appl. Phys.* 1956, **27**, 69
- 28 Hideshima, T. and Okano, K. *J. Appl. Phys. Japan* 1958, **27**, 281
- 29 Wada, Y. and Yamamoto, K. *J. Phys. Soc. Japan* 1956, **11**, 887
- 30 Kabin, S. P. *et al. Vysokomol. Soedin.* 1961, **3**, 618
- 31 Nakagawa, K. and Ishida, Y. *J. Polym. Sci. (A-2)* 1973, **11**, 1503
- 32 Williams, M. L., Landel, R. F. and Ferry, J. D. *J. Am. Chem. Soc.* 1955, **77**, 3701
- 33 Hoffman, J. D. and Weeks, J. J. *J. Res. Nat. Bur. Stand.* 1958, **60**, 465
- 34 Baccaredda, M. and Butta, E. *J. Polym. Sci.* 1960, **44**, 421
- 35 Wada, Y., Hirose, H. and Asano, T. *J. Phys. Sci. Japan* 1959, **14**, 1064
- 36 McCrum, N. G. *J. Polym. Sci.* 1962, **60**, 53
- 37 Slichter, W. P. *J. Polym. Sci.* 1957, **24**, 173
- 38 Choy, C. L., Tse, Y. K., Tsui, S. M. and Hsu, B. S. *Polymer* 1975, **16**, 501
- 39 Rosenstock, H. B. *J. Phys. Chem. Solids* 1962, **23**, 659
- 40 Landau, L. D. and Lifshitz, E. M. 'Theory of Elasticity', Addison-Wesley, Reading, Mass., 1964, Ch 1 and 3

# A study of solvent motion in acetone – PMMA solutions using $^{13}\text{C}$ and $^1\text{H}$ spin-lattice relaxation measurements

Frank Heatley and J. H. Scrivens

Department of Chemistry, University of Manchester, Manchester M13 9PL, UK

(Received 2 September 1974)

The  $^{13}\text{C}$  and  $^1\text{H}$  spin-lattice relaxation times of acetone in solutions containing from 0 to 20% poly(methyl methacrylate) have been measured from  $-55^\circ\text{C}$  to  $120^\circ\text{C}$ . The  $^{13}\text{C}$  measurements show that except at low temperature and the higher polymer concentrations, solvent rotation is little affected by the presence of polymer molecules. By assuming that the  $^{13}\text{C}$  relaxation time is entirely intramolecular in origin, and by progressive deuteration of the acetone, the  $^1\text{H}$  relaxation time has been separated into intramolecular, acetone–acetone intermolecular and acetone–polymer intramolecular contributions. These results show that up to 10% of polymer or so does not affect solvent diffusion, but for 20% polymer, solvent diffusion is perceptibly slowed down, and the activation energy increased by 50%. The data give no indication of polymer conformational transitions in this temperature range, as suggested by others elsewhere, but this may be because of the very short-range sensitivity of n.m.r. measurements.

## INTRODUCTION

For obvious reasons, the majority of investigations into molecular motion in polymer solutions have concentrated on the behaviour of the polymer molecules. A number, however, have been directed towards the motion of the solvent, since this often provides more useful interpretable information on polymer–solvent interactions. Nuclear magnetic relaxation (n.m.r.) measurements have proved an important experimental technique<sup>1–8</sup> in this respect, especially  $^1\text{H}$  relaxation times which are well-known to be sensitive to both intramolecular and intermolecular interactions. Some workers<sup>1,5,6</sup> have investigated preferential polymer solvation by one component of a poor solvent/good solvent mixture while others<sup>2,3,8</sup> have used various methods of separating the three principal contributions to solvent proton relaxation – intramolecular, solvent–solvent intermolecular and solvent–polymer intermolecular – in order to distinguish the effect of the polymer on the solvent rotational and translational diffusion. This paper is of the second type, the system studied being acetone–poly(methyl methacrylate) (PMMA). This system was chosen to complement an earlier study<sup>3</sup> along these lines of the benzene–PMMA system, and also because of a recent paper<sup>9</sup> suggesting a conformational transition of PMMA in acetone at about  $35^\circ\text{C}$ , which may be reflected in the solvent motion. In this work, the intramolecular relaxation contributions were determined using  $^{13}\text{C}$  n.m.r., the  $^1\text{H}$  acetone–acetone contribution was determined by the usual deuterium replacement technique, and the acetone–PMMA contribution to the  $^1\text{H}$  acetone relaxation was then determined by difference.

## EXPERIMENTAL

The polymer used in this work was a mainly syndiotactic sample of  $M_n = 90\,000$ , supplied by the Rubber and Plastics

Research Association, Shrewsbury, England. The proton n.m.r. spectrum showed that the polymer was 70% syndiotactic, with random placement of diads. All samples were degassed and sealed *in vacuo* before use.  $^{13}\text{C}$   $T_1$  measurements were made on a Varian Associates XL-100 Fourier Transform Spectrometer operating at 25.14 MHz, using the 'progressive saturation' technique<sup>10</sup>.  $^1\text{H}$   $T_1$  measurements were made on a Varian Associates HA-100 Spectrometer using the adiabatic rapid passage with sampling method<sup>12</sup>.  $^{13}\text{C}$  Nuclear Overhauser enhancement factors<sup>11</sup> (NOEF) were determined from the ratio of the intensity of the completely  $^1\text{H}$  noise decoupled spectrum to the intensity with the decoupling field offset by 30 kHz on continuous wave operation. This procedure eliminated changes in sample temperature occurring on switching the decoupler on or off.

## RESULTS AND DISCUSSION

Figures 1 and 2 show the variation of the spin-lattice relaxation time and NOEF of the methyl  $^{13}\text{C}$  nucleus in acetone as a function of temperature for pure solvent and solutions containing 0.05, 0.1 and 0.2 weight fraction PMMA. In each case the acetone was actually a 2:1 mixture of  $\text{CH}_3\text{COCH}_3$  and  $\text{CD}_3\text{COCD}_3$ , but since the intermolecular contribution to relaxation of protonated  $^{13}\text{C}$  nuclei is insignificant<sup>13</sup>, the sources of the methyl  $^{13}\text{C}$  relaxation are entirely intramolecular, and are determined by overall molecular plus internal rotation. For all four samples, the  $T_1$  passes through a common maximum (within the experimental scatter) at  $30^\circ\text{C}$ , and follows a common path on the high temperature side of the maximum. The occurrence of this maximum indicates the presence of two  $^{13}\text{C}$  relaxation mechanisms, namely dipolar interaction with attached protons dominant at lower temperatures, and the spin-rotation mechanism dominant at higher temperatures. The

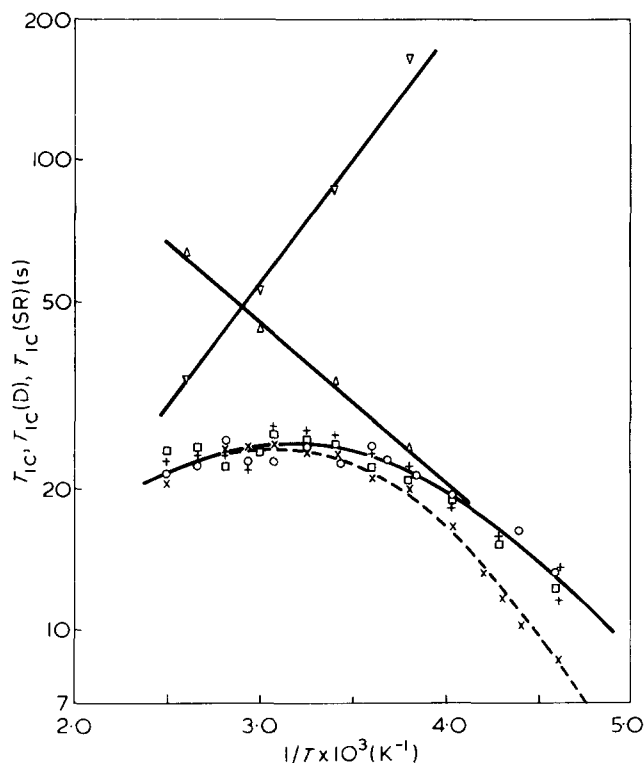


Figure 1 Variation of  $T_{1C}$  with temperature for the methyl carbon in pure acetone ( $\circ$ ) and solutions of PMMA in acetone:  $\square$ , 0.05;  $+$ , 0.1;  $\times$ , 0.2 wt fraction PMMA.  $T_{1C}(D)$  ( $\triangle$ ) and  $T_{1C}(SR)$  ( $\nabla$ ) for pure acetone are also shown. For clarity, only a single curve (---) has been drawn for  $T_{1C}$  of pure acetone and the solutions of weight fraction 0.05 and 0.1

NOEF also shows this, gradually falling from its theoretical maximum of 2 at low temperatures as the temperature increases and the spin-rotation mechanism increases in efficiency<sup>13</sup>. The two contributions will be discussed more quantitatively below, for there are two noteworthy features of these results worth discussing at this point. First, the presence of up to 0.1 weight fraction polymer has very little effect at any temperature on either the magnitude or rate of change with temperature of the solvent relaxation time, but 0.2 weight fraction polymer has a marked effect on the low temperature behaviour, increasing the activation energy from 7.6 kJ/mol for pure solvent to 10.9 kJ/mol for the 0.2 weight fraction sample. Earlier measurements of the benzene-PMMA system<sup>3</sup>, and recent results for the methylene dichloride-polystyrene system<sup>8</sup>, both indicate very little effect on solvent rotational mobility of up to 40% polymer. However, both investigations were made at a constant temperature of 35°C, at which temperature in this study polymer concentration indeed has little effect. In benzene and methylene dichloride, the spin-rotation relaxation mechanism is small compared to that present in acetone, but extrapolation of the Arrhenius low temperature dependence of  $T_{1C}$  back to 35°C for pure solvent and the 0.2 weight fraction solution, reveals that this is approximately the temperature at which the plots cross. Thus the results shown here are consistent with earlier results at a single temperature, but from the temperature dependence it is clear that above a certain concentration, the polymer does influence solvent motion. Both benzene and acetone are good solvents for PMMA, so it is unlikely that the difference in behaviour may be explained by different polymer-solvent interactions.

Secondly, we note that the spin-rotation relaxation must arise from coupling with internal rotation of the methyl group and not overall rotation, otherwise the 0.2 weight fraction solution would differ in its high temperature relaxation times from the pure solvent, since the correlation times for the dipolar and spin-rotation mechanisms are inversely related<sup>14</sup>. Rotation of the methyl group will be determined entirely by intramolecular factors.

The dipolar and spin-rotation contributions may be obtained from the equations<sup>11</sup>:

$$T_{1C}(D) = \frac{2}{\eta} \cdot T_{1C} \quad (1)$$

and

$$\frac{1}{T_{1C}} = \frac{1}{T_{1C}(D)} + \frac{1}{T_{1C}(SR)} \quad (2)$$

where  $T_{1C}$  is the experimental  $^{13}\text{C}$  relaxation time, and the suffixes (D) and (SR) are self-explanatory.  $\eta$  is the nuclear Overhauser enhancement factor<sup>11</sup>. Figure 1 shows the contributions to  $T_{1C}$  for pure acetone. The polymer solutions may be treated similarly but the results do not add anything significant.

The observed acetone proton relaxation time ( $T_{1H}$ ) arises from three sources - intramolecular [ $T_{1H}(\text{intra})$ ], acetone-acetone intermolecular interactions [ $T_{1H}(\text{a-a})$ ] and acetone-polymer intermolecular interactions [ $T_{1H}(\text{a-p})$ ], which are related by:

$$\frac{1}{T_{1H}} = \frac{1}{T_{1H}(\text{intra})} + \frac{1}{T_{1H}(\text{a-a})} + \frac{1}{T_{1H}(\text{a-p})} \quad (3)$$

$T_{1H}(\text{intra})$  may contain dipolar and spin-rotation terms as for  $T_{1C}$ , related by an equation similar to (2).  $T_{1H}(\text{a-a})$  is easily isolated by substitution of  $\text{CH}_3\text{COCH}_3$  by  $\text{CD}_3\text{COCD}_3$  in the usual way<sup>3</sup>. If deuterated polymer were available,  $T_{1H}(\text{a-p})$  could be measured likewise, but we have chosen to calculate  $T_{1H}(\text{intra})$  from  $T_{1C}(D)$  and then obtain  $T_{1H}(\text{a-p})$  from equation (3) by difference. It was found experimentally from the temperature dependence of  $T_{1H}(\text{intra})$  in pure acetone, that both dipolar and spin-rotation mechanisms operated for  $^1\text{H}$  as well as  $^{13}\text{C}$  relaxation at higher temperatures although  $T_{1H}(\text{intra})$  did not

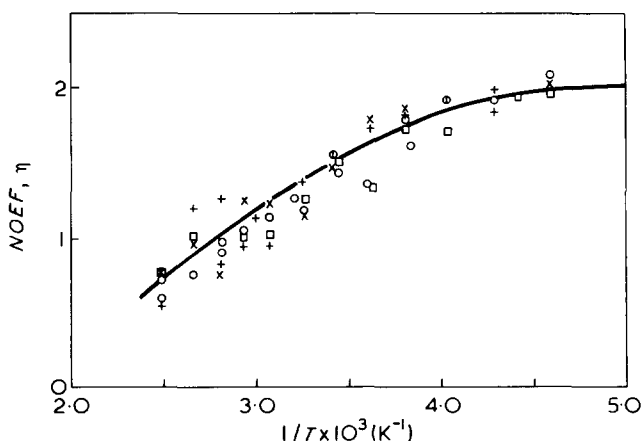


Figure 2 Variation of NOEF with temperature for the methyl carbon in pure acetone and solutions of PMMA in acetone. Symbols as in Figure 1

pass through a maximum so the spin-rotation mechanism is less significant. It is straightforward to calculate  $T_{1H}(D)$  from  $T_{1C}(D)$ , as the relationship between them is strictly geometrical, but  $T_{1H}(SR)$  and  $T_{1C}(SR)$  depend on  $^1H$  and  $^{13}C$  spin-rotation coupling constants which are not simply related.  $T_{1H}(SR)$  was therefore obtained from the difference between the experimental value of  $T_{1H}(intra)$  and the calculated value of  $T_{1H}(D)$  for pure acetone, and was assumed to be the same for all polymer concentrations by analogy with  $T_{1C}(SR)$ . This approximation is not serious, as it proved possible to derive reliable values of  $T_{1H}(a-p)$  only at lower temperatures where  $T_{1H}(SR)$  is insignificant.  $T_{1H}(D)$  was calculated as follows.

In the extreme narrowing limit applicable to small mobile molecules,  $T_{1C}(D)$  for a methyl carbon is given by<sup>13</sup>:

$$\frac{1}{T_{1C}(D)} = \frac{3\gamma_H^2\gamma_C^2\hbar^2}{r_{CH}^6} \cdot \tau_C \quad (4)$$

where  $\gamma_{H,C}$  are the magnetogyric ratios of  $^1H$  and  $^{13}C$  nuclei respectively,  $r_{CH}$  is the internuclear distance and  $\tau_C$  is a dipolar correlation time embracing overall rotation (possibly anisotropic) and internal motions. The corresponding expression for  $^1H$  relaxation is:

$$\frac{1}{T_{1H}(D)} = \frac{3\gamma_H^2\hbar^2}{r_{HH}^6} \cdot \tau_H \quad (5)$$

$\tau_H$  is not necessarily equal to  $\tau_C$  because of anisotropic and/or internal rotation. To make the calculation of  $\tau_H$  tractable, isotropic overall rotation has been assumed, it is suggested quite reasonably, since the moments of inertia of the acetone molecule about three perpendicular axes do not differ greatly. However, the barrier to methyl rotation in acetone is<sup>15</sup> only 3.4 kJ/mol, and methyl rotation is therefore rapid enough to have a significant influence on correlation times. The problem of calculating relaxation times for a system undergoing simultaneous overall and internal rotation has been considered by Woessner *et al.*<sup>16</sup> who give the following expression for the dipolar correlation time:

$$\tau = \frac{1}{4} \left\{ \frac{(1 - 3 \cos^2 \Delta)^2}{6D_1} + \frac{(\sin^2 2\Delta + \sin^4 \Delta)}{6D_1 + D} \right\} \quad (6)$$

where  $D_1$  is the isotropic rotational diffusion constant.  $D$  is defined as<sup>16</sup>: '3/2 x the total rate of jumping of a methyl group from any of its three equivalent orientations', and  $\Delta$  is the angle between the internuclear vector and the axis of internal rotation. To obtain  $D$ , one may use the equation<sup>17</sup>:

$$Z = \frac{1}{2\pi} \left( \frac{f}{m} \right)^{1/2} \exp(-E^*/kT)$$

which gives the rate of passage  $Z$  of particles of mass  $m$  from a harmonic potential well of force constant  $f$  over a potential barrier  $E^*$ . Applying this to the case of a threefold internal rotation potential:

$$u(\phi) = \frac{1}{2} V_0 (1 - \cos 3\phi)$$

and changing  $m$  to the moment of inertia of the methyl top, one obtains:

$$D = \frac{9}{8\pi} \left( \frac{V_0}{I} \right)^{1/2} \exp(-V_0/kT)$$

For  $V_0 = 3.4$  kJ/mol at  $-55^\circ C$ ,  $D = 8.43 \times 10^{11} s^{-1}$ . Knowing the structure of acetone<sup>18</sup> ( $r_{CH} = 0.1084$  nm,  $r_{HH} = 0.1765$  nm,  $\Delta_{CH} = 110.3^\circ$ ,  $\Delta_{HH} = 90^\circ$ ), one may then apply equation (6) obtaining  $\tau_H/\tau_C = 1.34$  and combine equations (4) and (5) to obtain  $T_{1C}(D)/T_{1H}(D) = 1.14$ . (A small correction has been applied to the equation for  $T_{1H}$  to take account of inter-methyl interactions.)

At  $-55^\circ C$ ,  $T_{1C}(D)$  is 13.1 s for pure acetone, whence one calculates  $T_{1H}(D) = 11.5$  s compared with the experimental value of 11.9 s for  $T_{1H}(intra)$ . At this temperature, both  $^{13}C$  and  $^1H$  relaxation are completely dipolar, and the excellent agreement between the calculated  $T_{1H}(D)$  and  $T_{1H}(intra)$  is substantial justification for the method. To gain exact correspondence between  $T_{1H}(D)$  and  $T_{1H}(intra)$  at these low temperatures, the relationship  $T_{1C}(D)/T_{1H}(D) = 1.1$  has actually been used. With the aid of this equation one may then evaluate  $T_{1H}(D)$  and  $T_{1H}(SR)$  for pure acetone and hence  $T_{1H}(a-p)$  for the polymer solutions. Figures 3 and 4 show respectively the quantities  $W_a \times T_{1H}(a-p)$  and  $(W_p/0.05) \times T_{1H}(a-p)$  as a function of temperature for the same solutions as in Figure 1, where  $W_a$  and  $W_p$  are the weight fractions of acetone and polymer respectively. The purpose of multiplying  $T_{1H}(a-p)$  by  $W_a$  and  $T_{1H}(a-p)$  by  $W_p/0.05$  is to eliminate the concentration dependence of intermolecular relaxation contributions, thus showing more clearly relative changes in solvent translational mobility.  $T_{1H}(a-p)$  is thus normalized to give the value one would expect for pure acetone if the translational mobility remained the same as in the polymer solution, and  $T_{1H}(a-p)$  is normalized to the value one would expect for a 5% polymer solution if the same happened.

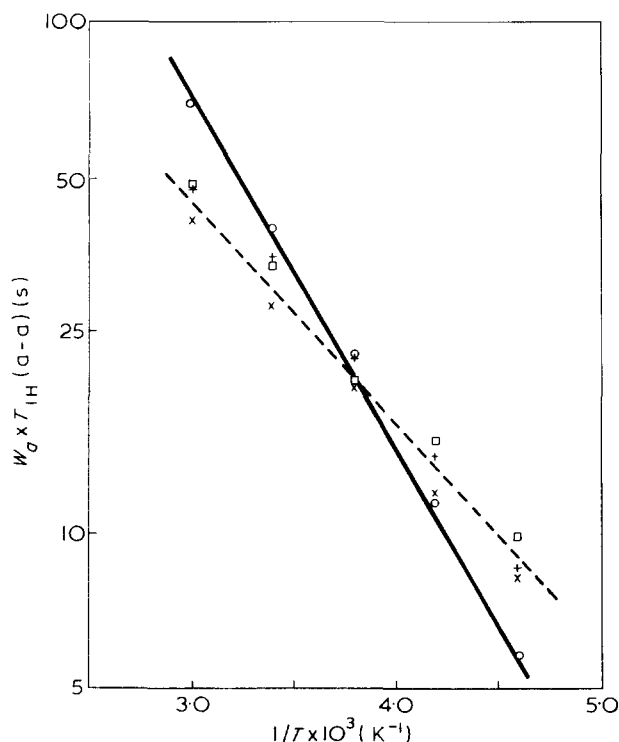


Figure 3 Variation of  $W_a \times T_{1H}(a-p)$  with temperature for pure acetone ( $\square$ ) and solutions of PMMA in acetone:  $+$ , 0.05;  $\times$ , 0.1;  $\circ$ , 0.2 wt fraction PMMA. For clarity only one line has been drawn for pure acetone and the solutions of weight fraction 0.05 and 0.1



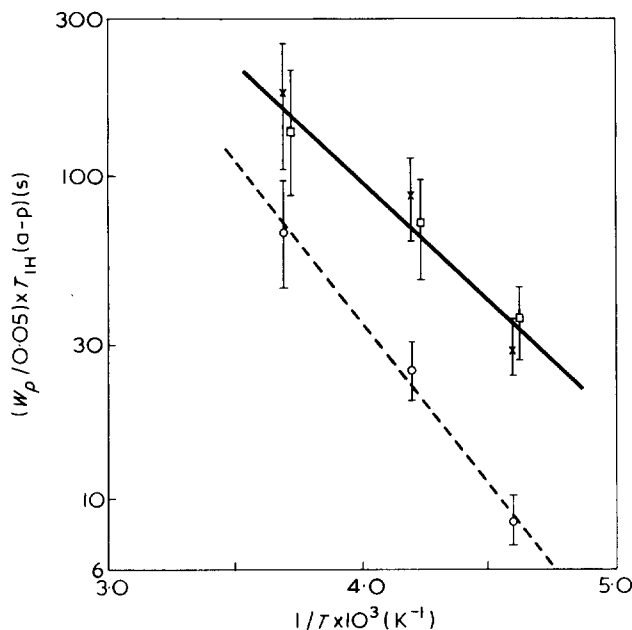


Figure 4 Variation of  $(W_p/0.05) \times T_{1H}(a-p)$  with temperature for the acetone protons in solutions of PMMA:  $\square$ , 0.05;  $\times$ , 0.1;  $\circ$ , 0.2 wt fraction PMMA. For clarity only one line has been drawn for the solutions of weight fraction 0.05 and 0.1

From these results, it is clear once again that the presence of up to 10% polymer has little effect on solvent or polymer translational mobility, but 20% polymer has a marked effect on the activation energy. For the pure solvent and polymer solutions of 0.05 and 0.1 weight fraction, the activation energies for  $T_{1H}(a-a)$  and  $T_{1H}(a-p)$  are 10 and 15.5 kJ/mol respectively, rising to 14.5 and 22 kJ/mol respectively for the 0.2 weight fraction polymer solution. The hindrance to solvent rotation afforded by 20% polymer noted earlier is not unexpectedly also a hindrance to solvent diffusion. In the benzene-PMMA system<sup>3</sup>, it was found that up to 35% polymer had little effect on solvent translation, at 35°C. As with the  $T_{1C}$  measurements described earlier, at this temperature in the present work there is relatively little variation of either  $T_{1H}(a-a)$  or  $T_{1H}(a-p)$  (extrapolated) with solution composition. The effect of the polymer on solvent motion is revealed most clearly by the temperature dependence of the relaxation contributions.

Because of the fairly sharp increase in the hindrance to solvent motion on going from 10% to 20% polymer, it is likely that the explanation lies in the formation of an entangled network rather than in the replacement of relatively weak solvent-solvent contacts by stronger solvent-polymer contacts which would be more gradual in their effect. It is also significant that the change in solvent

mobility occurs at a solvent/monomer molecular ratio of 7:1 (0.2 weight fraction polymer) at which point the immediate environment of a solvent molecule (i.e. the first and second solvation shells) begins to look less like pure solvent. There is evidence<sup>19</sup> that the motion of polymer chains is determined only by the very local viscosity of polymer solution, and this may also be true of solvent motion.

Finally, it is worth noting that there is no indication of any departure from Arrhenius temperature dependence of any relaxation contributions which might occur because of possible conformational transitions in the polymer chain. However, if the molecular motion is sensitive only to nearest and next-nearest neighbours, then a long-range change in polymer dimensions would not be detectable by the n.m.r. method.

#### ACKNOWLEDGEMENTS

Grateful thanks are extended to R. F. Warren for assistance with instrumentation, Professor G. Allen for valuable discussions and to the SRC for the provision of the n.m.r. spectrometer.

#### REFERENCES

- 1 Liu, K. J. *J. Polym. Sci. (A-2)* 1967, **5**, 697
- 2 Liu, K. J. and Ullman, R. J. *J. Chem. Phys.* 1968, **48**, 1158
- 3 Anderson, J. E. and Liu, K. J. *J. Chem. Phys.* 1968, **49**, 2850
- 4 Glasel, J. A. *J. Am. Chem. Soc.* 1970, **92**, 375
- 5 Sato, K. and Nishioka, A. *J. Polym. Sci. (A-2)* 1972, **10**, 489
- 6 Brownstein, S., Bywater, S. and Cowie, J. M. G. *Trans. Faraday Soc.* 1969, **65**, 2480
- 7 Lutje, H. *Makromol. Chem.* 1970, **133**, 295; 1971, **142**, 81
- 8 Rothschild, W. G. *Macromolecules* 1968, **1**, 43; 1972, **5**, 37
- 9 Dondos, A., Rempp, P. and Benoit, H. *Makromol. Chem.* 1973, **171**, 135
- 10 Freeman, R. and Hill, H. D. W. *J. Chem. Phys.* 1971, **54**, 3367
- 11 Kuhlmann, K. F., Grant, D. M. and Harris, R. K. *J. Chem. Phys.* 1970, **52**, 3439
- 12 Anderson, J. E., Steele, J. and Warnick, A. *Rev. Sci. Instrum.* 1967, **38**, 1139
- 13 Kuhlmann, K. F. and Grant, D. M. *J. Chem. Phys.* 1971, **55**, 2998
- 14 Schmidt, C. F. and Chan, S. I. *J. Magn. Res.* 1971, **5**, 151
- 15 Lowe, J. P. *Progr. Phys. Org. Chem.* 1968, **6**, 1
- 16 Woessner, D. E., Snowden, B. S. and Meyer, G. H. *J. Chem. Phys.* 1969, **50**, 719
- 17 Kramers, H. A. *Physica* 1940, **7**, 284
- 18 'Tables of Interatomic Distances', (Ed. L. E. Sutton), Special Publication No. 11, The Chemical Society, London, 1958; Supplement 1962
- 19 Heatley, F. *Polymer* 1975, **16**, 493

# Molecular motion in polyisobutylene and poly(propylene oxide) studied by $^{13}\text{C}$ nuclear magnetic relaxation

Frank Heatley

Department of Chemistry, University of Manchester, Manchester M13 9PL, UK

(Received 2 September 1974)

The  $^{13}\text{C}$  spin-lattice relaxation times of low molecular weight (up to 2500) samples of polyisobutylene and poly(propylene oxide) have been measured as a function of molecular weight, temperature and concentration in chloroform solution. For both polymers there is little dependence on molecular weight indicating a flexible conformation in the liquid state, but the relaxation time increases with increasing dilution in  $\text{CHCl}_3$ . The motion of the polymer backbone therefore depends on the microviscosity of the solution, rather than the bulk viscosity. In polyisobutylene the methyl re-orientation rate increases in parallel with the backbone re-orientation rate, showing that the two motions are interlinked. In poly(propylene oxide) the methyl re-orientation rate is independent of the backbone motion.

## INTRODUCTION

In recent years  $^{13}\text{C}$  n.m.r. relaxation measurements have supplemented the well-established  $^1\text{H}$  n.m.r. technique as a means of investigating molecular motion in polymers.

$^{13}\text{C}$  n.m.r., although much less sensitive than  $^1\text{H}$  n.m.r. has a number of advantages, among which are: (i) when run under  $^1\text{H}$  decoupled conditions,  $^{13}\text{C}$  spectra consist of single lines for each type of carbon present, separated by chemical shifts an order of magnitude greater than  $^1\text{H}$  chemical shifts; (ii) the relaxation times of protonated  $^{13}\text{C}$  nuclei are determined entirely by dipolar interaction with the attached protons, provided the correlation time for the molecular motion is greater than  $10^{-11}$  s, a condition which is fulfilled for polymers, even in dilute solution.

These advantages have been used by a number of workers<sup>1-7</sup>, who have established for polymers in solution that (a) for a fixed monomer unit concentration and high molecular weight,  $^{13}\text{C}$   $T_1$  values are independent of molecular weight for many vinyl polymers, indicating that the relaxation is controlled by internal motions of the polymer chain, which are rapid compared to overall rotation; (b) the correlation time for relaxation of backbone  $^{13}\text{C}$  nuclei is typically  $5 \times 10^{-10}$  s at normal temperature; (c) the correlation time for relaxation of side-group  $^{13}\text{C}$  nuclei may be the same as the backbone, e.g. polystyrene<sup>1</sup>, indicating that internal rotation of the side-group is strongly hindered, or much shorter than the backbone, e.g. polypropylene<sup>4</sup>, indicating rapid internal rotation of the side-group compared to motion of the polymer chain to which it is attached.

In this work, the  $^{13}\text{C}$  relaxation in low molecular weight polyisobutylene (PIB) and poly(propylene oxide) (PPO), both in bulk and in solution in  $\text{CHCl}_3$ , has been investigated as a function of temperature, molecular weight and concentration, with particular attention being paid to the concentration and temperature dependence of the correlation times for backbone motion and internal rotation of the

methyl groups. One objective was to compare the barrier to methyl rotation with that obtained from neutron inelastic scattering<sup>8</sup>.

## EXPERIMENTAL

The PIB samples were provided by W. R. Grace Ltd, Port Talbot, Wales. Two samples were used, one of  $M_n = 900$ , with  $M_w/M_n = 1.8$ , and the other of  $M_n = 2900$ , with  $M_w/M_n = 3.0$ . The PPO samples were obtained from Waters Associates, Framingham, Mass., USA. Two samples were also used with  $M_n = 790$  and 2020, both having  $M_w/M_n < 1.1$ . All samples were viscous liquids.

$^{13}\text{C}$  spin-lattice relaxation times were measured on a Varian Associates XL-100 Fourier Transform spectrometer operating at 25.14 MHz, using the standard  $\pi - \pi/2$  pulse sequence.

## RESULTS AND DISCUSSION

In both polymers, all  $^{13}\text{C}$  resonances appeared as singlets, although there is the possibility of sequences of different tacticities in PPO. The peak positions, essentially unaffected by concentration, molecular weight or temperature are, in ppm downfield from TMS, 22.0, 74.0 and 76.0 for the  $\text{CH}_3$ ,  $\text{CH}_2$  and  $\text{CH}$  carbons in PPO, and 33.3, 40.0 and 61.9 for the  $\text{CH}_3$ , C and  $\text{CH}_2$  carbons in PIB. In the bulk polymers, all peaks were broad, with a linewidth exceeding 20 Hz. The  $\text{CH}_2$  in PIB was particularly broad, with a linewidth of 240 Hz. All peaks decreased markedly in width on dilution with  $\text{CDCl}_3$  and/or raising the temperature, the  $\text{CH}_2$  peak in PIB to the greatest extent.

The variation of the spin-lattice relaxation time of all protonated carbons with solution composition in  $\text{CDCl}_3$  is shown in Figures 1 and 2, in the form of a plot of  $T_1$  against the ratio of solvent molecules to monomer units.

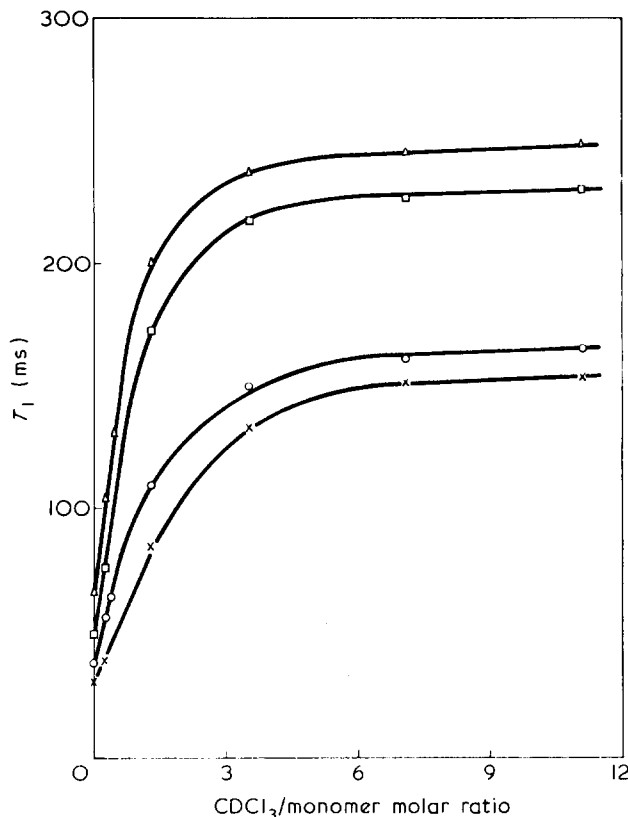


Figure 1 Variation of  $^{13}\text{C}$   $T_1$  values of PIB with concentration in  $\text{CDCl}_3$ .  $\circ$ ,  $M_n = 900$ ,  $\text{CH}_2$ ;  $\triangle$ ,  $M_n = 900$ ,  $\text{CH}_3$ ;  $\times$ ,  $M_n = 2900$ ,  $\text{CH}_3$ ;  $\square$ ,  $M_n = 2900$ ,  $\text{CH}_2$

The sample temperature was  $30^\circ\text{C}$ . The feature common to both polymers is a rapid rise in  $T_1$  with the initial addition of  $\text{CDCl}_3$  to the bulk polymer, and the attainment of a plateau in  $T_1$  at a  $\text{CDCl}_3$ /monomer molecular ratio of about 5, corresponding to a polymer weight fraction of 0.1. At greater dilutions,  $T_1$  is practically independent of polymer concentration and therefore of bulk sample viscosity, which may vary with concentration by an order of magnitude even for quite dilute polymer solutions. There is a slight variation of approximately 10% in  $T_1$  between the samples of different  $M_n$  used here, which are of much lower molecular weight than those used previously. Again, however, this is much less than the factor of 2–3 by which the bulk viscosity changes. These results are in agreement with the independence of  $T_1$  and molecular weight and polymer concentration in dilute solution observed by earlier workers<sup>1,3</sup>. However, the rapid rise in  $T_1$  with initial addition of solvent is a novel feature which shows that the polymer motion is not independent of its environment. This observation suggests that although the polymer motion is not correlated with bulk sample viscosity, it does depend on the frictional forces exerted by the immediate environment of a polymer segment. Since the plateau in  $T_1$  is reached at a  $\text{CDCl}_3$ /monomer molecular ratio of 5, the immediate environment in this case means the first solvation shell, i.e. enough solvent to separate the polymer molecules. Thus it seems that in these two polymers, and presumably others of a like flexibility, the chain segmental motion loses correlation in a short range, of the order of two or three monomer units possibly, otherwise  $T_1$  would be dependent on molecular weight, and forces determining the segment re-orientation rate are not entirely intramolecular, but are controlled in part at least by the very local

viscosity of the segment. It is clear that the Gierer and Wirtz<sup>9</sup> 'microviscosity' theory of n.m.r. relaxation times, which takes the microscopic structure of liquids into account and which has been successfully applied to small molecules<sup>10</sup>, is unable to account for polymer relaxation times, since it contains the inverse proportionality between  $T_1$  and the bulk viscosity. Hill's theory<sup>11</sup> employing an inertial model and the concept of a 'mutual viscosity' may be applicable, but the theory requires a fairly precise knowledge of the solution structure, and there are severe problems in evaluating for a polymer solution some of the moments of inertia needed.

In both polymers the backbone and side-group carbon relaxation times parallel each other, but the side-group  $T_1$  values are considerably longer, indicating the presence of internal methyl rotation which is comparable to the rate of segmental motion. Woessner *et al.*<sup>12</sup> have analysed theoretically the relaxation times of nuclei undergoing simultaneous overall and internal rotation and this formulation has been employed to separate the two motions in these polymers. This theory is based on the single correlation time description of overall motion, and may not be strictly applicable to polymers for which Schaefer<sup>13</sup> has shown that a distribution of correlation times is indicated by experimental fact. However, results obtained from Woessner's theory will not be qualitatively in error. Isotropic segmental motion has been assumed which may also lead to systematic quantitative error.

For isotropic diffusional re-orientation, the relaxation time of the  $^{13}\text{C}$  nucleus in a  $\text{CH}_n$  group which is relaxed by

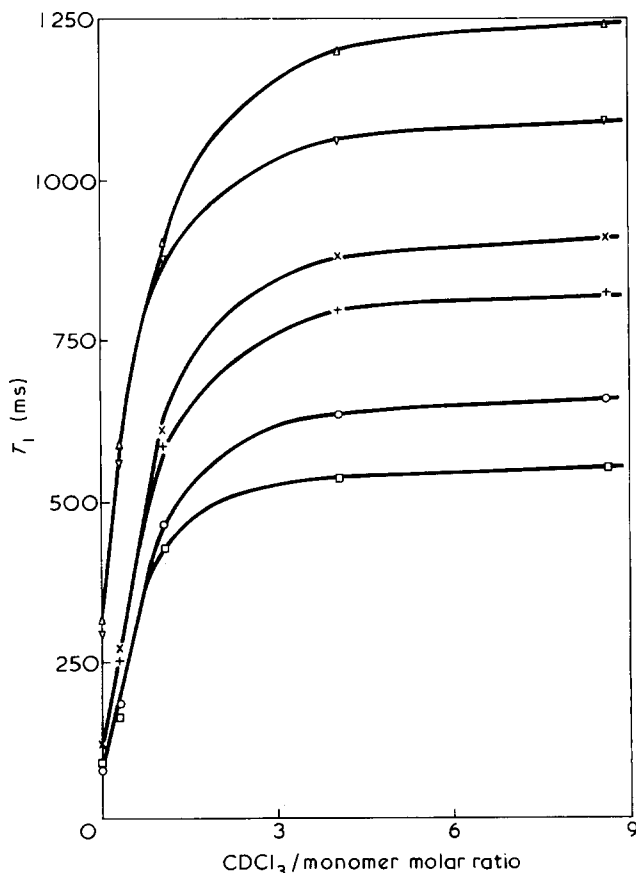


Figure 2 Variation of  $^{13}\text{C}$   $T_1$  values of PPO with concentration in  $\text{CDCl}_3$ .  $\circ$ ,  $M_n = 790$ ,  $\text{CH}_2$ ;  $\times$ ,  $M_n = 790$ ,  $\text{CH}$ ;  $\triangle$ ,  $M_n = 790$ ,  $\text{CH}_3$ ;  $\square$ ,  $M_n = 2020$ ,  $\text{CH}_2$ ;  $+$ ,  $M_n = 2020$ ,  $\text{CH}$ ;  $\nabla$ ,  $M_n = 2020$ ,  $\text{CH}_3$

dipolar interaction with the protons is given by:

$$\frac{1}{T_1} = \frac{n\gamma_C^2\gamma_H^2\hbar^2}{10r_{CH}^6} \left\{ \frac{\tau_1}{1 + (\omega_H - \omega_C)^2\tau_1^2} + \frac{3\tau_1}{1 + \omega_C^2\tau_1^2} + \frac{6\tau_1}{1 + (\omega_H + \omega_C)^2\tau_1^2} \right\} \quad (1)$$

where  $\gamma_C$  and  $\gamma_H$  are the magnetogyric ratios of  $^{13}\text{C}$  and  $^1\text{H}$  nuclei respectively,  $r_{CH}$  is the internuclear distance and  $\omega_C$  and  $\omega_H$  are the  $^{13}\text{C}$  and  $^1\text{H}$  resonance frequencies.  $\tau_1$  is the n.m.r. correlation time and is related to the rotational diffusion constant  $D_1$  by:  $\tau_1 = 1/6D_1$ . In the presence of internal rotation about a three-fold potential barrier this equation becomes<sup>12</sup>:

$$\frac{1}{T_1} = \frac{n\gamma_C^2\gamma_H^2\hbar^2}{40r_{CH}^2} \left\{ (1 - 3\cos^2\Delta)^2 \left[ \frac{\tau_1}{1 + (\omega_H - \omega_C)^2\tau_1^2} + \frac{3\tau_1}{1 + \omega_C^2\tau_1^2} + \frac{6\tau_1}{1 + (\omega_H + \omega_C)^2\tau_1^2} \right] + 3(\sin^2 2\Delta + \sin^4\Delta) \left[ \frac{\tau_2}{1 + (\omega_H - \omega_C)^2\tau_2^2} + \frac{3\tau_2}{1 + \omega_C^2\tau_2^2} + \frac{6\tau_2}{1 + (\omega_H + \omega_C)^2\tau_2^2} \right] \right\} \quad (2)$$

$\Delta$  is the angle between the C-H bond and the axis of internal rotation, and  $\tau_2$  is defined by:  $\tau_2 = 1/(6D_1 + D_{\text{int}})$  where  $D_{\text{int}}$  is  $3/2 \times$  the total rate of jumping of a methyl group from any of its three equivalent orientations<sup>12</sup>. When the extreme narrowing condition applies:  $(\omega_H + \omega_C)^2\tau_2^2 \ll 1$  corresponding to  $nT_1 > 150$  ms, these equations simplify considerably. This condition was fulfilled in all samples except the bulk polymers and more concentrated PIB solutions. To separate  $D_1$  and  $D_{\text{int}}$ ,  $D_1$  was obtained from the relaxation time of the  $\text{CH}_2$  carbon in PIB and the CH carbon in PPO, using equation (1). For a methyl group,  $\Delta = \cos^{-1}(1/3)$ , and this was then substituted, together with  $D_1$ , into equation (2) to obtain  $D_{\text{int}}$ . In both cases  $r_{CH}$  was assumed to be 0.11 nm.

The effect of dilution in  $\text{CDCl}_3$  on  $D_1$  and  $D_{\text{int}}$  is shown in Figure 3 for the higher molecular weight samples.  $D_1$  of course parallels the behaviour of the corresponding  $T_1$  values shown in Figures 1 and 2. The significant feature is that for PIB the plot of  $D_{\text{int}}$  follows closely the plot of  $D_1$ , whereas for PPO,  $D_{\text{int}}$  is essentially independent of  $D_1$ . Also  $D_{\text{int}}$  for PPO is at least an order of magnitude greater than  $D_1$  for PIB. Two conclusions may be drawn: (1) the barrier to methyl rotation in PIB is greater than in PPO; and (2) the barrier in PIB depends on the environment, whereas the barrier in PPO does not. Examination of molecular models shows that PIB is indeed a good deal more sterically crowded than PPO, so much so in fact that steric repulsion of neighbouring methyl groups is so strong that the chain bonds must necessarily be forced out of the usually favoured staggered conformation by  $20^\circ$  or so. Even then, rotation of the methyl groups is still strongly hindered, and can proceed most freely by a co-operative process involving neighbouring methyls and motion about the chain bonds.

Thus the relationship between methyl and segmental rotation diffusion constants in PIB is simply a manifestation of the interdependence of the molecular potential barriers of the two processes. In PPO, on the other hand, the methyl groups are well separated, nor need they necessarily interfere with each other or with rotation about chain bonds. The rate of methyl rotation is thus determined solely by intramolecular factors, intermolecular effects being minimized by the three-fold symmetry.

Activation energies have been obtained for the temperature variation of  $D_1$  and  $D_{\text{int}}$  for the bulk polymers and for solutions in  $\text{CDCl}_3$  of polymer weight fraction 0.3, corresponding approximately to a  $\text{CDCl}_3$ /monomer molecular ratio of unity. The values obtained are listed in Table 1, together with values of the barrier obtained from torsional oscillation data provided by neutron inelastic scattering<sup>8</sup>. We note that in PPO, the activation energy for  $D_{\text{int}}$  is much less than that for  $D_1$ , and is independent of dilution with

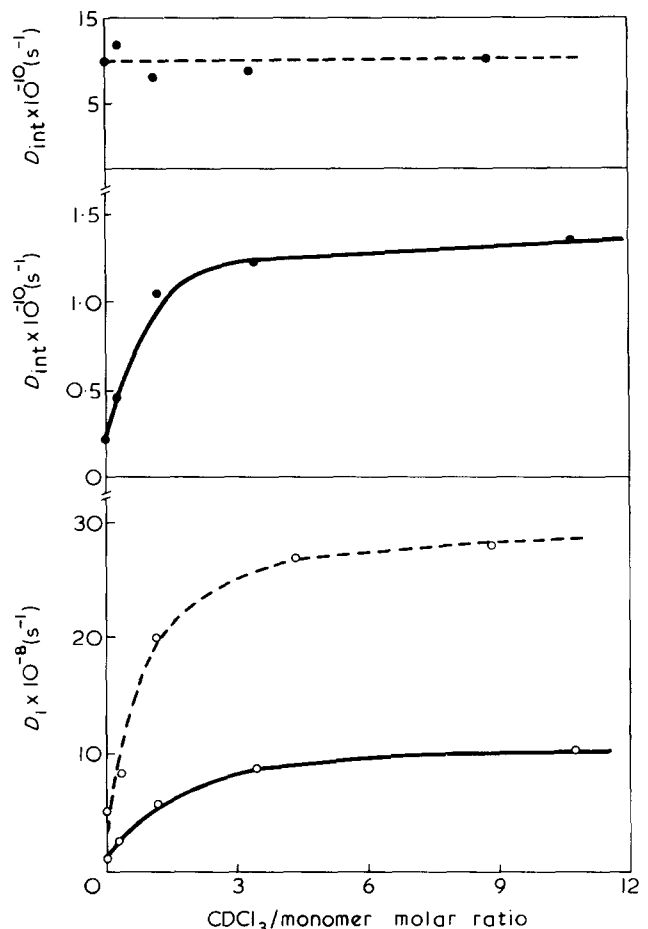


Figure 3 Variation of  $D_1$  (○) and  $D_{\text{int}}$  (●) of PIB (—) and PPO (---) with concentration in  $\text{CDCl}_3$ .  $M_n$ : PIB = 2900; PPO = 2020

Table 1 Activation energies of  $D_1$  and  $D_{\text{int}}$  for PIB and PPO

Sample		Activation energy (kJ/mol)		Barrier from neutron scattering <sup>8</sup> (kJ/mol)
		$D_1$	$D_{\text{int}}$	
PPO	bulk	$27 \pm 2$	$10.5 \pm 2$	13
	0.3 wt fraction in $\text{CDCl}_3$	$21 \pm 2$	$11 \pm 2$	
PIB	bulk	$24 \pm 2$	$25 \pm 2$	24
	0.3 wt fraction in $\text{CDCl}_3$	$18 \pm 2$	$18 \pm 2$	

$\text{CDCl}_3$ , whereas in PIB the two activation energies are equal within experimental error, and both vary with polymer concentration. The activation energies for  $D_1$  for both polymers are similar for the same concentration. There is excellent agreement between the activation energies for  $D_{\text{int}}$  and the methyl barrier from neutron scattering, although the results obtained here for PIB show that the assumption of no coupling between methyl torsion and other vibrational modes made in the neutron scattering experiment may not be even approximately valid.

#### ACKNOWLEDGEMENTS

Grateful thanks are extended to R. F. Warren for assistance with instrumentation, Professor G. Allen for valuable discussions and to the SRC for the provision of the n.m.r. spectrometer.

#### REFERENCES

- 1 Allerhand, A. and Hailstone, R. K. *J. Chem. Phys.* 1972, **56**, 3718
- 2 Schaefer, J. and Natusch, D. F. S. *Macromolecules* 1972, **5**, 416
- 3 Schaefer, J. *Macromolecules* 1972, **5**, 427
- 4 Inoue, Y., Nishioka, A. and Chujo, R. *Makromol. Chem.* 1973, **168**, 163
- 5 Chachaty, C., Forchioni, A. and Ronfard-Haret, J. C. *Makromol. Chem.* 1973, **173**, 213
- 6 Inoue, Y., Nishioka, A. and Chujo, R. *J. Polym. Sci. (Polym. Phys. Edn)* 1973, **11**, 2237
- 7 Levy, G. C. *J. Am. Chem. Soc.* 1973, **95**, 6117
- 8 Higgins, J. S., Allen, G. and Brier, P. N. *Polymer* 1972, **13**, 157
- 9 Gierer, A. and Wirtz, K. *Z. Naturforsch.* 1953, **A8**, 532
- 10 Sato, K. and Nishioka, A. *J. Magn. Res.* 1972, **6**, 231
- 11 Hill, N. E. *Proc. Phys. Soc. (B)* 1954, **67**, 149; 1955, **68**, 209
- 12 Woessner, D. E., Snowden, B. S. and Meyer, G. H. *J. Chem. Phys.* 1969, **50**, 719
- 13 Schaefer, J. *Macromolecules* 1973, **6**, 882

# Synthesis and properties of completely crystalline POM copolymers

M. Dröscher\*, G. Lieser, H. Reimann and G. Wegner\*†

*Institut für Physikalische Chemie, Universität Mainz, D-65 Mainz, West Germany*

*(Received 8 November 1974)*

Extended chain crystals of polyoxymethylene copolymers have been prepared by cationic copolymerization of trioxane and dioxolane. These crystals do not contain amorphous regions and behave like an ideal solid solution of  $-\text{CH}_2\text{CH}_2\text{O}-$  units in the crystal of  $-\text{CH}_2\text{O}-$  units up to a mole fraction of  $x_{\text{CH}_2\text{CH}_2\text{O}} = 0.1$ . Melting points, melting enthalpies, specific heat, density and lattice parameters were measured as a function of mole fraction up to  $x_{\text{CH}_2\text{CH}_2\text{O}} = 0.2$ . Comparison of the dependence of lattice parameters on mole fraction for the extended chain crystals and melt or solution crystallized copolymers indicates, that in the semi-crystalline samples the comonomer units are not distributed at random between amorphous and crystalline phase but the comonomer units are enriched in the amorphous phase.

## INTRODUCTION

In their early work Staudinger and his coworkers showed that polymerization of formaldehyde or cyclic oligomers of formaldehyde give rise to highly crystalline polyoxymethylene (POM) by simultaneous polymerization and crystallization<sup>1,2</sup>. In a recent investigation<sup>3</sup> our group has demonstrated that true single crystals of POM can be obtained by cationic polymerization of trioxane in nitrobenzene. These crystals possess the well known hexagonal structure of POM crystals but differ greatly from the so-called solution grown 'single-crystals' of POM with regard to morphology, melting behaviour and degree of crystallinity. All relevant data on the formation and properties of these crystals<sup>3</sup> indicate that they may be called extended chain crystals according to the definition given by Wunderlich<sup>4</sup>.

We now have studied the crystals of the copolymer which are formed during cationically induced copolymerization of trioxane and 1,3-dioxolane. Again, extended chain crystals of the copolymers are formed in which the comonomer ( $-\text{OCH}_2\text{CH}_2-$ ) units are distributed at random throughout the lattice of the  $-\text{CH}_2\text{O}-$  units. It is interesting to look for the dependence of melting behaviour, density, specific heat and other characteristic data on the mole fraction of comonomer units, because these copolymer crystals do not contain amorphous regions. Thus, all effects are directly related to disturbances created by the comonomer units inside the POM crystal. Therefore, we believe to have found a system in which the thermodynamical properties of a copolymer crystal can be measured directly for the first time. So far only measurements on semi-crystalline copolymers were possible, which are obscured by the fact that the distribution of the comonomer units between the crystalline and amorphous phase is generally not known<sup>5-7</sup>.

\* Present address: Institut für Makromolekulare Chemie, Universität Freiburg, D-78 Freiburg, West Germany

† To whom all correspondence should be addressed.

## EXPERIMENTAL

Trioxane (m.p.  $62^\circ\text{C}$ ) was refluxed over sodium-potassium alloy for 48 h and then distilled under nitrogen prior to polymerization. 1,3-Dioxolane (b.p.  $74.5^\circ\text{C}$ ) was refluxed over  $\text{LiAlH}_4$  for 48 h and then distilled under nitrogen prior to polymerization. Nitrobenzene was refluxed over  $\text{P}_2\text{O}_5$  for 20 h and then fractionated *in vacuo*. Methylene chloride was stored over  $\text{CaH}_2$  for several days, refluxed over  $\text{LiAlH}_4$  for 48 h and then distilled under nitrogen.

For polymerization, a solution of trioxane in nitrobenzene or in dichloromethylene was transferred under an atmosphere of dry nitrogen into a 100 ml polymerization flask which was decontaminated from water by evacuating and heating with a torch. The flask was set in a thermostat at  $30^\circ\text{C}$ . A solution of the catalyst ( $\text{BF}_3 \cdot \text{Et}_2\text{O}$ ) in nitrobenzene or dichloromethylene was added by means of a syringe through a rubber stopper. Dioxolane was added in the same way. Total concentration of the monomers was varied between 1.8 and 4 mol/l and the concentration of the initiator was 1 mmol/l. After a period of several days polymerization was stopped by adding a solution of triethylamine in methanol in five-fold excess with regard to the initiator concentration.

The polymer crystals were carefully filtered without applying suction and were washed repeatedly with acetone. The polymer was dried *in vacuo* at room temperature. Molecular weight was determined by viscometry with hexafluoroacetone sesquihydrate as solvent according to the procedures described by Jaacks *et al.*<sup>8</sup> using the viscosity-molecular weight relationship for the homopolymer as a first approximation. Thermal data were measured with a Perkin-Elmer 1B differential scanning calorimeter (d.s.c.). A heating rate of  $8^\circ\text{C}/\text{min}$  was used in determination of melting points. Melting enthalpy was measured at heating rates of 16, 32 and  $64^\circ\text{C}/\text{min}$ .

The composition of the copolymers was analysed by gas chromatography. 100 mg of the copolymer were reacted

at room temperature with 1 ml acetic anhydride and one drop of a 3.8 M solution of perchloric acid in acetic anhydride. After addition of 1,4-butanediol diacetate as an internal standard the concentration of the reaction products, formaldehyde diacetate and ethylene glycol diacetate, were determined with a Varian Aerograph 1700 gas chromatograph using a Porapak-P column of 1 m length.

Surface replicas for electron micrographs were obtained as described previously<sup>3</sup>.

Lattice constants of the copolymer single crystals were determined by means of a Guinier camera with a precision monochromator using the powder method. Densities were determined in a density gradient consisting of mixtures of CCl<sub>4</sub> and n-hexane.

## RESULTS AND DISCUSSION

The copolymerization of trioxane and 1,3-dioxolane is a reversible polyreaction in which the crystalline copolymer is in equilibrium with the dissolved monomers. Chain growth proceeds by two different reactions, namely 'normal' addition of the cyclic monomers onto cationically active chain ends presumably by an S<sub>N</sub>2 reaction<sup>9</sup> and by insertion of the monomer into the chain folds of the lamellar crystals formed in the very beginning of the polymerization by a transacetalization mechanism<sup>3</sup>. In the closed polymerization system practically all the initiator stays alive over an extended period of time so that the copolymer crystals are allowed to reach their equilibrium composition and comparatively large sizes by the well known mechanism of crystal coarsening (Ostwald ripening)<sup>3,10</sup>. In other words, copolymer crystals grow under thermodynamically controlled conditions and contrary to crystallization of copolymers from solution or melt which is clearly controlled by kinetic factors<sup>5,6</sup>.

Under our reaction conditions crystalline copolymers were obtained up to a mole fraction of -CH<sub>2</sub>CH<sub>2</sub>O- units in the isolated copolymer of  $x_{\text{CH}_2\text{CH}_2\text{O}} \leq 0.2$ . Copolymers richer in -CH<sub>2</sub>CH<sub>2</sub>O- units are soluble in the reaction medium and consequently could not be obtained as extended chain crystals. Figures 1a and 1b show crystals containing 1.8 mol% -CH<sub>2</sub>CH<sub>2</sub>O- units. Size and morphological features such as growth spirals are very similar to the crystals obtained in homopolymerization of trioxane<sup>3</sup>. The micrographs show the fracture surfaces of such copolymer crystals obtained by fracturing a slightly compressed cake of the crystals at liquid nitrogen temperature. The sample consists of lamellae with a rather small distribution in crystal thickness. Average crystal thickness is about 0.14 μm; some crystals are, however, as thick as 0.6 μm. As was shown previously<sup>3</sup>, the polymer chains run perpendicular to the lamella surfaces. An average molecular weight of  $M_n = 23\,000$  was determined from viscosity measurements corresponding to a length of about 0.15 μm, if one assumes an extended 9/5 POM helix. The molecular weights of all the polymers investigated in this work were in the range of  $2 \times 10^4$  to  $6 \times 10^4$ . The comonomer units have to be distributed at random throughout these crystals, since it has been well established that random copolymers are formed in this copolymerization<sup>11,12</sup>. The randomness of comonomer distribution is indeed the key in the stabilization of technical polyacetal resins, prepared in a similar manner by bulk polymerization.

POM crystallizes as a 9/5 helix in a hexagonal unit cell<sup>13,14</sup>. The dependence of the lattice parameters on the

mole fraction of comonomer units is shown in Figure 2. The lattice is expanded in a lateral direction almost linearly with increasing content in comonomer units up to a mole fraction of about 0.1 and then remains nearly constant with further increase of -CH<sub>2</sub>CH<sub>2</sub>O- units. The chain axis (c-axis) is contracted linearly up to  $x_{\text{CH}_2\text{CH}_2\text{O}} = 0.1$  and then increases again. A correspondence between lattice parameters and concentration of comonomer units has already been demonstrated by Holdsworth and Fischer<sup>14</sup> using melt crystallized samples. However, melt or solution crystallized copolymers seem to behave differently as it is seen from Figures 2a and 2b, if one just plots the observed lattice parameters against mole fraction of comonomer units. In reality a segregation occurs in the recrystallized samples leading to a higher concentration of the comonomer units in the amorphous phase as compared to the

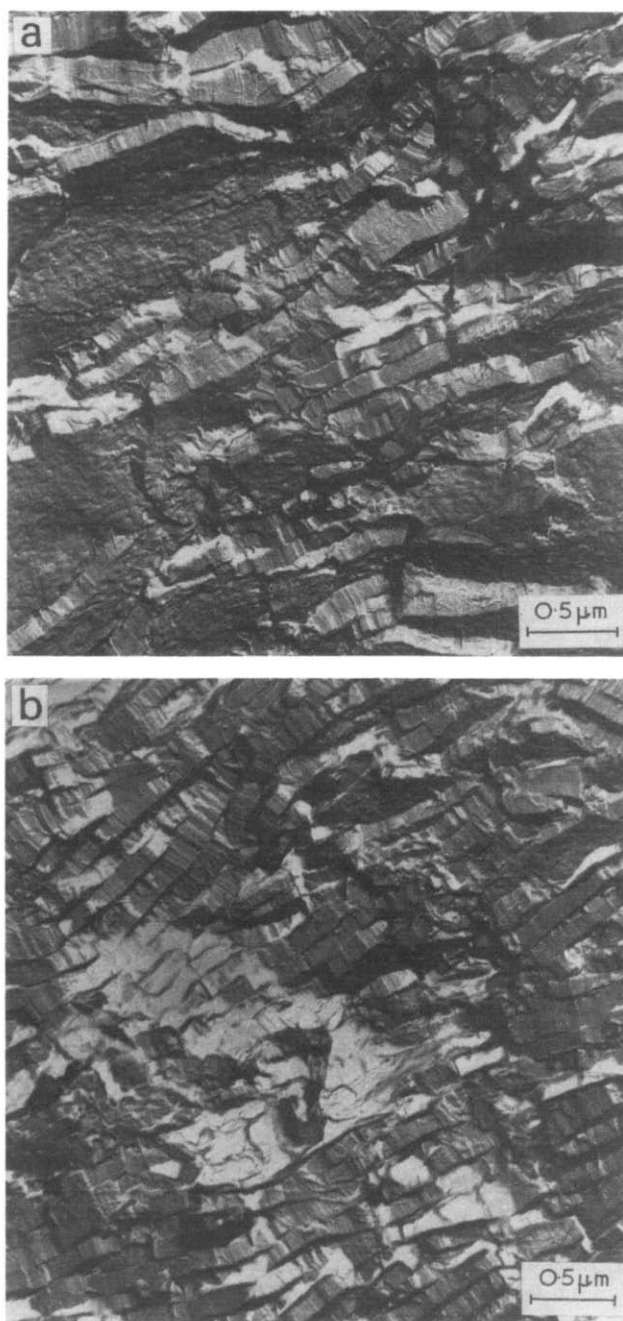


Figure 1 Electron micrographs of fracture surfaces (replica) of a POM copolymer containing 1.8 mol % of CH<sub>2</sub>CH<sub>2</sub>O units

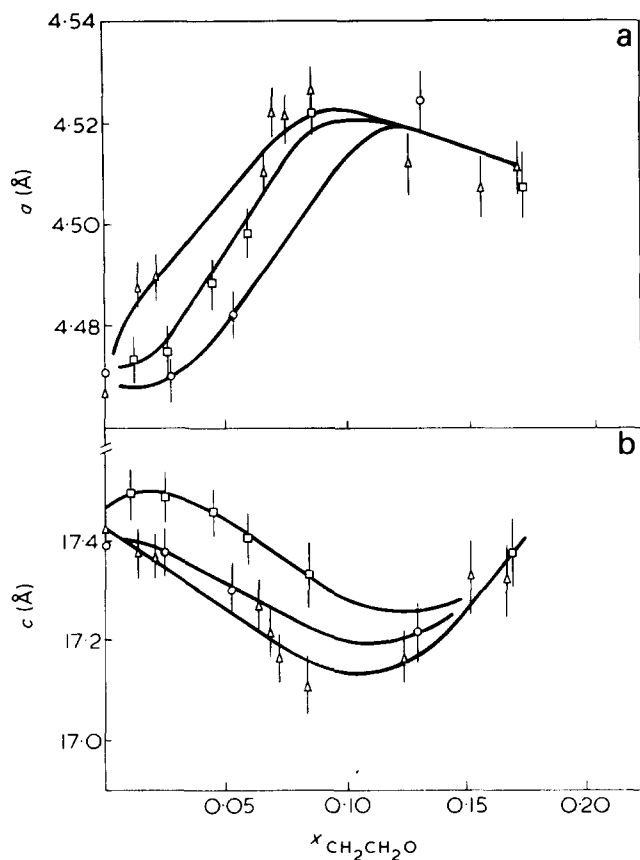


Figure 2 Unit cell spacings as a function of mole fraction of  $-\text{CH}_2\text{CH}_2\text{O}-$  units in crystals as polymerized ( $\Delta$ ), as crystallized from solution ( $\square$ ) and from the melt ( $\circ$ ). Melt data according to Holdsworth and Fischer<sup>14</sup>

crystalline phase. This segregation was verified by a neutron scattering experiment using a copolymer in which the oxyethylene units were fully deuterated. A peak was observed in the low angle diffraction diagram with much higher intensity than the peak observed in the neutron low angle scattering diagram of a non-deuterated standard sample of POM copolymer with the same mole fraction of comonomer units. The diffraction peak is due to density differences in the non-deuterated sample and density differences plus concentration differences of  $\text{CD}_2$  groups in the deuterated sample yielding a much higher scattering length density of the non-crystalline phase. From the diffraction angle the same long spacing was calculated as was observed with X-ray small angle scattering within the limits of error ( $\sim 100 \text{ \AA}$ ). Therefore, the deviation from the lattice parameters of pure POM with increasing content of comonomer units seems to be less for solution or melt crystallized samples because the crystalline phase contains actually considerably less comonomer units than the total polymer.

Figure 3 shows a plot of the experimentally observed density of the copolymers as polymerized against mole fraction of comonomer units. Density decreases linearly with increasing content of  $\text{CH}_2\text{CH}_2\text{O}$  units. A density of  $\rho = 1.4670 \text{ (g/cm}^3\text{)}$  is observed directly for the homopolymer and  $\rho = 1.476$  is extrapolated from the best fit of the line through all points which can be represented by:

$$\rho = 1.476 - 0.665x_{\text{CH}_2\text{CH}_2\text{O}} \quad (1)$$

On the other hand, a value of  $\rho = 1.492 \text{ g/cm}^3$  is reported by Uchida and Tadokoro as based on their determination

of unit cell parameters (X-ray density) and we derive a value of  $\rho = 1.4857$  from our measurements shown in Figures 2a and 2b. At present we cannot explain the difference in densities as measured by the density gradient and derived from X-ray data except by the assumption that the polymer contains voids which would not contribute to the wide angle scattering but would very much show up in density measurements. The discrepancy between the two values is less than 2% in any case. Recently Iguchi and co-workers<sup>15</sup> have reported density values as high as 1.494 to 1.50  $\text{g/cm}^3$  for crystals obtained by polymerization and crystallization of trioxane in cyclohexane. Unfortunately we were not able to obtain similar samples by the techniques described by these authors and we believe that the methods of density measurement used by them (floating and volume exclusion) are much more apt to experimental errors than X-ray determination of unit cell parameters and density gradient.

The melt behaviour of the extended chain copolymer crystals was measured by d.s.c. methods. The half-width of the melting peak is only 3–5°C at a heating rate of 8°C/min. The melting point  $T_m(x)$  as defined by the maximum of melt-peak decreases at first considerably with increasing comonomer content, reaches a plateau between 10 and 20 mol % comonomer units and then decreases again very considerably. The complete melting diagram going from pure POM to pure polydioxolane is shown in Figure 4. The

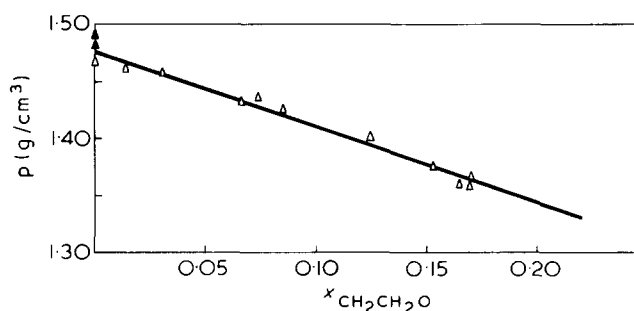


Figure 3 Density as a function of mole fraction of  $-\text{CH}_2\text{CH}_2\text{O}-$  units for as-polymerized crystals

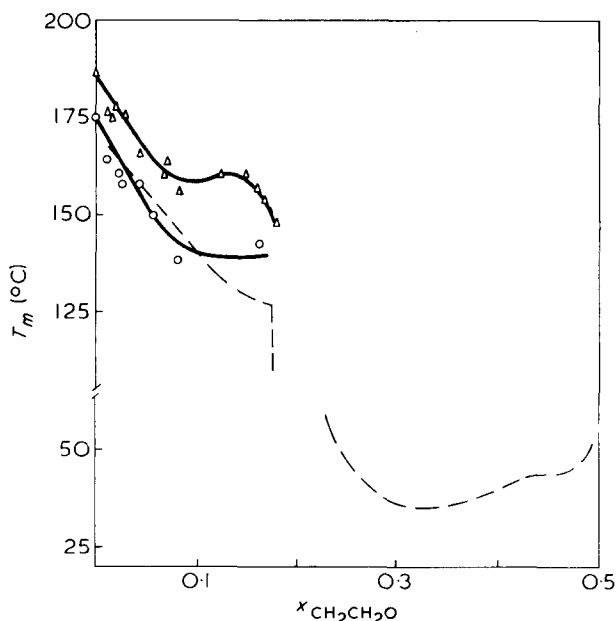


Figure 4 Melting point vs. mole fraction of  $-\text{CH}_2\text{CH}_2\text{O}$  units of crystals as-polymerized ( $\Delta$ ) and recrystallized from solution ( $\circ$ ). — —, according to the data of Wilski<sup>20</sup>



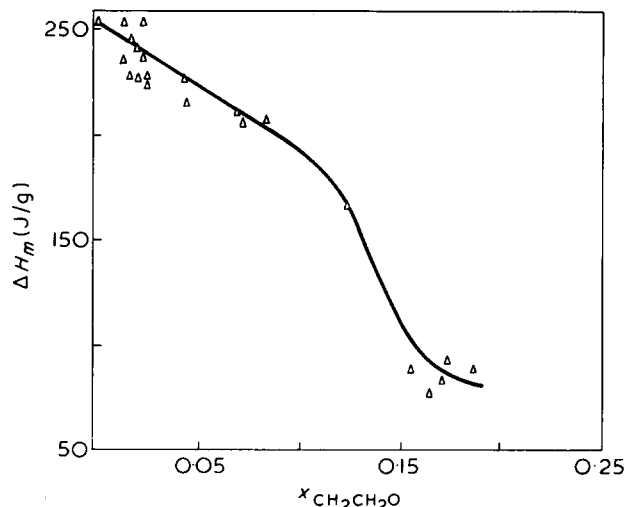


Figure 5 Heat of melting as a function of mole fraction of  $\text{CH}_2\text{CH}_2\text{O}$  units of crystals as-polymerized

region of extended chain crystals extends from pure POM to  $x_{\text{CH}_2\text{CH}_2\text{O}} = 0.2$ . If the polymers are recrystallized from melt or solution the well known folded-chain crystals are formed which show a melting point depression of  $5\text{--}18^\circ\text{C}$  depending on the crystallite thickness and on the degree of segregation of the comonomer units between the crystalline and amorphous phase.

From the slope of the linear part of the melting point curve for extended chain crystals ( $x_{\text{CH}_2\text{CH}_2\text{O}} < 0.1$ ) according to Eby<sup>5</sup> the defect enthalpy  $\Delta H_D$  can be determined by:

$$\begin{aligned} T_m(x) &= (1 - A \cdot x_{\text{CH}_2\text{CH}_2\text{O}})T_m(0) \\ &= \left(1 - \frac{\Delta H_D}{\Delta H_m(0)} \cdot x_{\text{CH}_2\text{CH}_2\text{O}}\right)T_m(0) \end{aligned} \quad (2)$$

$$T_m(x) = (1 - 0.765 \cdot x_{\text{CH}_2\text{CH}_2\text{O}})458 \quad (3)$$

where the terms with (0) refer to the pure POM crystal and  $\Delta H_D$  is the defect enthalpy.

The change in melt enthalpy caused by introduction of comonomer units into the POM lattice is  $\Delta H_D = 5.82 \text{ kJ/mol}$  of  $\text{CH}_2\text{CH}_2\text{O}$  units as derived from the experimentally observed equation (3) with  $\Delta H_m(0) = 7.61 \text{ kJ/mol}$ .

The enthalpy of melting as a function of comonomer units is shown in Figure 5. A similar dependence as already discussed for the melting points is observed. Since

we deal with fully crystalline copolymers, the curve describes the ideal enthalpies of melting as a function of comonomer units, which can be used in determination of the crystallinity of semi-crystalline copolymers by d.s.c. methods. The enthalpy of melting for the pure POM extended chain crystals is found to be  $254 \pm 4 \text{ J/g}$  in excellent agreement with the value of  $250 \text{ J/g}$  reported in the literature<sup>17-19</sup>.

A plot of the melting enthalpies per mole of  $\text{CH}_2\text{O}$  units against the mole fraction of the counts shows a linear function.

$$\Delta H_m(x) = \Delta H_m(0) - \Delta H_D x_{\text{CH}_2\text{CH}_2\text{O}} (x_{\text{CH}_2\text{CH}_2\text{O}} < 0.1) \quad (4)$$

$$\Delta H_m(x) = 7.52 - 7.5x_{\text{CH}_2\text{CH}_2\text{O}} \quad (5)$$

The slope gives the defect enthalpy  $\Delta H_D = 7.5 \text{ kJ/mol}$  of  $\text{CH}_2\text{CH}_2\text{O}$  units. The difference between the two values of  $\Delta H_D$  found by melting point and melting enthalpies studies implies that the excess melting entropy is not zero as was assumed by Eby.

## REFERENCES

- 1 Staudinger, H. *et al. Justus Liebigs Ann. Chem.* 1929, **474**, 145
- 2 Staudinger, H. *et al. Z. Phys. Chem.* 1927, **126**, 425
- 3 Mateva, R., Wegner, G. and Lieser, G. *J. Polym. Sci. (Lett. Edn)* 1973, **11**, 369
- 4 Wunderlich, B. *Angew. Chem.* 1968, **80**, 1009
- 5 Sanchez, J. C. and Eby, R. K. *J. Res. Nat. Bur. Stand.* 1973, **77A**, 353
- 6 Helfand, E. and Lauritzen, J. I. *Macromolecules* 1973, **6**, 631
- 7 Fischer, E. W., Sterzel, H.-J. and Wegner, G. *Kolloid-Z. Z. Polym.* 1973, **251**, 980
- 8 Höhr, L. *et al. Makromol. Chem.* 1967, **103**, 279
- 9 Jaacks, V. *Adv. Chem Ser.* 1969, **91**, 371
- 10 Wagner, C. *Ber. Bunsenges. Phys. Chem.* 1961, **65**, 581
- 11 Burg, K. H., Schlaf, H. and Cherdron, H. *Makromol. Chem.* 1971, **145**, 247
- 12 Fleischer, D. and Schulz, R. C. *Makromol. Chem.* 1972, **152**, 311
- 13 Uchida, I. and Tadokoro, H. *J. Polym. Sci. (A-2)* 1967, **5**, 63
- 14 Holdsworth, P. J. and Fischer, E. W. *Makromol. Chem.* 1974, **175**, 2635
- 15 Iguchi, M., Murase, I. and Watanabe, K. *Br. Polym. J.* 1974, **6**, 61
- 16 Eby, R. K. *J. Appl. Phys.* 1963, **34**, 2442
- 17 Muñoz-Escalona, A. *Dissertation* University of Mainz (1970)
- 18 Inoue, M. *J. Polym. Sci.* 1961, **51**, S18
- 19 Starkweather, H. W. and Boyd, R. H. *J. Phys. Chem.* 1960, **64**, 410
- 20 Wilski, H. *Makromol. Chem.* 1971, **150**, 209

# Mechanical and dielectric relaxations in polytrifluoroethylene

C. L. Choy, Y. K. Tse, S. M. Tsui and B. S. Hsu

Physics Department, The Chinese University of Hong Kong, Shatin, N.T., Hong Kong

(Received 14 October 1974)

Molecular motions in polytrifluoroethylene are studied by dynamic mechanical and dielectric measurements. Two absorption peaks ( $\alpha_a$ ,  $\beta$ ) have been observed in the frequency range from 3 Hz to 300 kHz and in the temperature range from  $-150^\circ$  to  $130^\circ\text{C}$ . The molecular mechanisms for these absorptions are discussed, and the results are compared with ultrasonic, heat capacity and n.m.r. measurements. It is concluded that the  $\alpha_a$  absorption located at  $45^\circ\text{C}$  (10 Hz) is associated with the large-scale motion of the main chains and the  $\beta$  absorption at  $-35^\circ\text{C}$  (10 Hz) is attributed to the limited motion of a few segments of the frozen main chains. In contrast to polychlorotrifluoroethylene the  $\alpha_c$  absorption associated with crystalline regions has not been observed in polytrifluoroethylene. At high temperatures a steep rise in dielectric absorption is observed, which has been ascribed to a d.c. ionic conduction process.

## INTRODUCTION

Numerous work has been carried out on the mechanical and dielectric relaxations in polychlorotrifluoroethylene (PCTFE)<sup>1</sup>. However, not a single study has been reported on the relaxations in polytrifluoroethylene (PVF<sub>3</sub>) which differs from PCTFE only in that the chlorine atoms is substituted by a hydrogen atom. Recently, it has been found<sup>2</sup> that the ultrasonic velocity (10 MHz) in PVF<sub>3</sub> exhibits a change in slope at  $-40^\circ\text{C}$ , which has been attributed to limited motion within the chain backbone. Similar change in slope at  $40^\circ\text{C}$  has also been observed in the heat capacity<sup>3</sup> but it is difficult to associate this change with any motion solely from the heat capacity data.

Dynamic mechanical<sup>4,5</sup> and dielectric<sup>6</sup> investigations of PCTFE reveal three loss peaks  $\alpha_c$ ,  $\alpha_a$  and  $\beta$  which, at 1 Hz, are located at  $140^\circ$ ,  $100^\circ$  and  $-40^\circ\text{C}$  respectively. The small  $\alpha_c$  peak is exhibited only by samples of the highest crystallinity and is connected with the occurrence of chain-folded lamellar spherulites. The  $\alpha_a$  peak decreases in magnitude as the crystallinity increases and is associated with the glass transition at  $52^\circ\text{C}$  found by dilatometric measurements<sup>7</sup>. The relatively low activation energy of the  $\beta$  relaxation suggests that only a small number of segments of the chain backbone are involved in the motion. It would be interesting to make similar mechanical and dielectric relaxation measurements on PVF<sub>3</sub> so as to compare with the relaxations in PCTFE.

## EXPERIMENTAL

The sample of PVF<sub>3</sub> was supplied in the form of coarse powder by Dr R. E. Florin of the National Bureau of Standards, (USA) and was mildly crosslinked. The powder was pressed into sheets at  $160^\circ\text{C}$  and slowly cooled to room temperature at a rate of  $2^\circ\text{C}/\text{min}$ . In an attempt to prepare samples of different crystallinities, some samples were quenched either in air or in ice water. Cracks were found in these samples which were not used in our measurements.

The dynamical tensile modulus was measured with a viscoelastic spectrometer (Iwamoto Seisakusho Co. Ltd.) at 3, 10 and 100 Hz, between  $-150^\circ$  and  $+100^\circ\text{C}$ . The samples had a thickness of 0.3 mm and lateral dimensions of  $5 \times 50$  mm. The dielectric measurements were carried out with an Ando transformer ratio-arm bridge between  $-110^\circ$  and  $+130^\circ\text{C}$  from 30 Hz to 300 kHz. The details of the measurements have been described previously<sup>8</sup>. The samples were discs of diameter 2.7 cm and thickness 0.5 mm. Electrodes were applied by vacuum deposition of silver.

## RESULTS AND DISCUSSION

### Mechanical measurements

The tensile modulus  $E'$  and the mechanical loss tangent  $\tan \delta$  at 10 Hz are shown as functions of temperature in *Figures 1a* and *1b*. A predominant peak is observed at  $45^\circ\text{C}$ . Because this peak is comparatively narrow and is associated with a large drop in  $E'$  within a narrow temperature range it is probably associated with the glass transition and is therefore denoted as the  $\alpha_a$  transition. Unfortunately, we have not been able to prepare samples of different crystallinities to check this assignment and no dilatometric measurements have been carried out for this polymer. The only other corroborative evidence is the change in slope of the heat capacity at  $40^\circ\text{C}$  mentioned above<sup>3</sup>. In fact, there should be a jump in the heat capacity at the glass transition; probably because PVF<sub>3</sub> is a crystalline polymer the jump is so small that it exhibits only as a change in slope.

The low temperature peak at  $-35^\circ\text{C}$ , assigned as the  $\beta$  relaxation, is probably due to the motion of a few segments in the carbon backbone. This motion had been observed as the narrowing of both the proton and fluorine resonance linewidths in nuclear magnetic resonance measurements<sup>9</sup>. Further evidence for the  $\beta$  relaxation is shown in the change in slope of the ultrasonic velocity curve at  $-40^\circ\text{C}$ <sup>2</sup>.

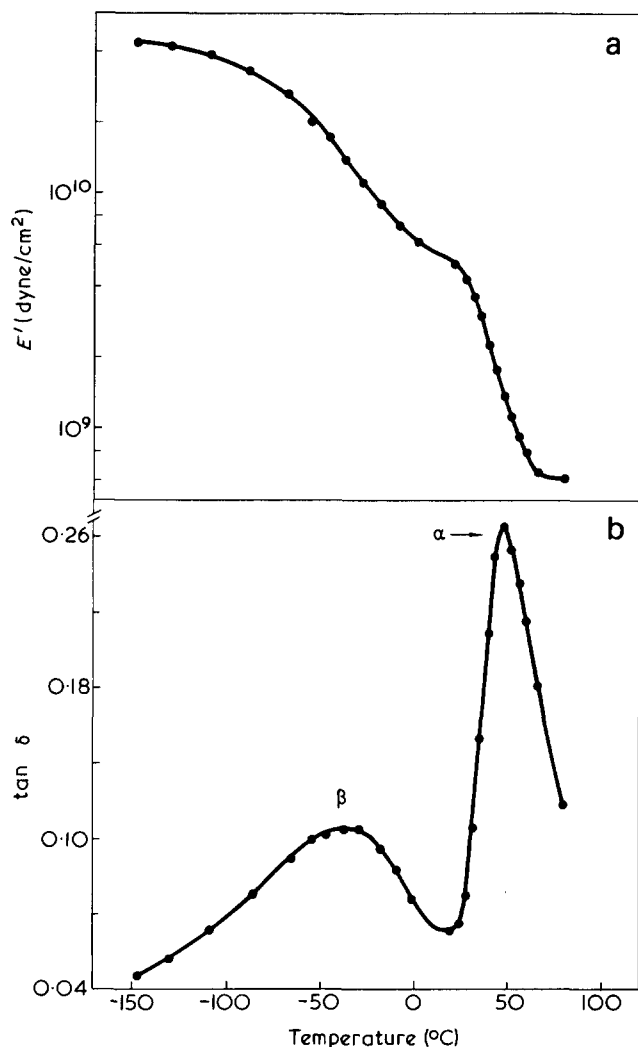


Figure 1 Temperature dependence of (a) tensile modulus,  $E'$  and (b) loss tangent  $\tan \delta$  at 10 Hz for polytrifluoroethylene

Dielectric measurements

The dielectric losses  $\epsilon''$  at 300 Hz, 3 kHz and 100 kHz are plotted as functions of temperature in Figure 2. In contrast to the mechanical measurements the prominent peak in  $\epsilon''$  is the  $\beta$  relaxation which is located at  $-40^\circ\text{C}$  (30 Hz). The frequency dependence of the dielectric constant and loss in the  $\beta$  relaxation region is illustrated in Figures 3 and 4. From the Cole-Cole plots<sup>10</sup> of these data, the dielectric increment  $\Delta\epsilon = \epsilon_R - \epsilon_U$  ( $\epsilon_R$  and  $\epsilon_U$  are the relaxed and unrelaxed dielectric constants) and the Cole-Cole distribution parameters  $\beta$  are obtained and shown in Figure 5. It is easily seen that  $\Delta\epsilon$  for the  $\beta$  relaxation decreases as the temperature decreases. The broadening of the loss peak with decreasing temperature is also represented as a decrease in the Cole-Cole distribution parameter.

Figure 2 also shows that for the lower frequencies (below 1 kHz)  $\epsilon''$  increases very steeply above  $90^\circ\text{C}$  and the  $\alpha_a$  peak is almost covered by this absorption process. The  $\alpha_a$  relaxation shows up as the shoulder in the  $\epsilon''$  curve at 300 Hz and a shallow maximum at 3 kHz. Above 3 kHz, there is considerable overlap between the  $\alpha_a$  and  $\beta$  relaxations and at 100 kHz the  $\alpha_a$  relaxation is completely covered by the tail of the  $\beta$  relaxation. The rise in  $\epsilon''$  at high temperatures is probably due to a d.c. ionic conduction mechanism because of the sharp increase with increasing temperature

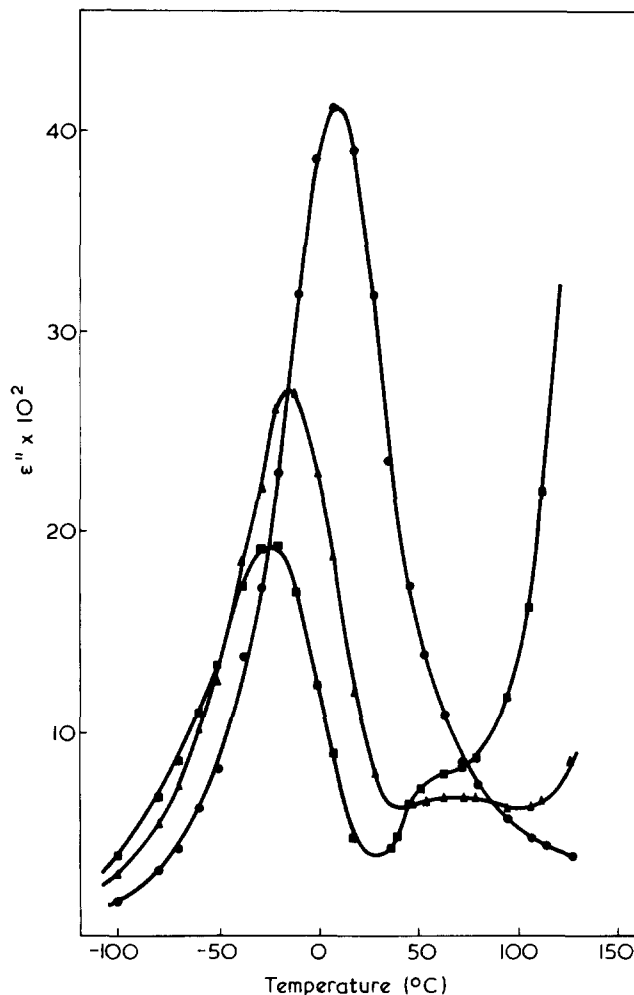


Figure 2 Temperature dependence of the dielectric loss  $\epsilon''$  at 300 Hz ( $\blacksquare$ ), 3 kHz ( $\blacktriangle$ ) and 100 kHz ( $\bullet$ ) for polytrifluoroethylene

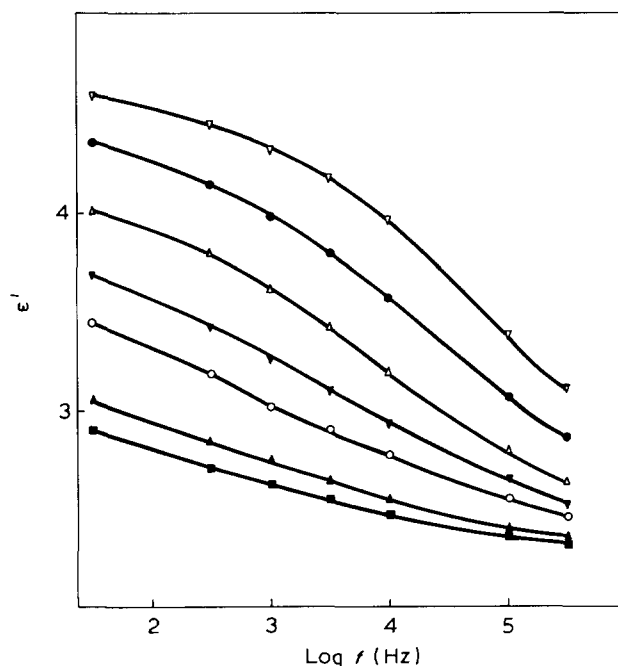


Figure 3 Frequency dependence of the dielectric constant  $\epsilon'$  for polytrifluoroethylene in the  $\beta$  relaxation region.  $\nabla$ ,  $0^\circ$ ;  $\bullet$ ,  $-10^\circ$ ;  $\triangle$ ,  $-20^\circ$ ;  $\nabla$ ,  $-28^\circ$ ;  $\circ$ ,  $-38^\circ$ ;  $\triangle$ ,  $-50^\circ$ ;  $\blacksquare$ ,  $-60^\circ\text{C}$

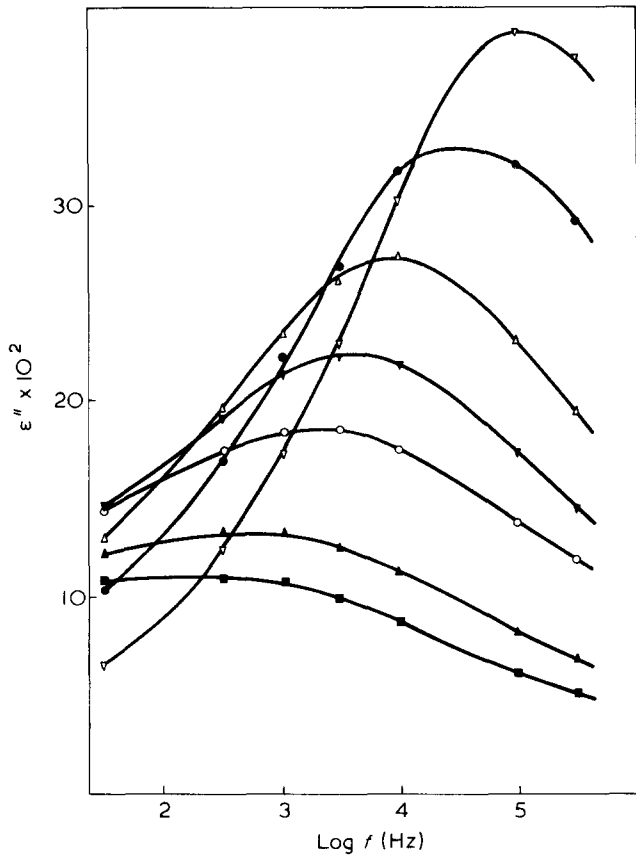


Figure 4 Frequency dependence of the dielectric loss  $\epsilon''$  for polytrifluoroethylene in the  $\beta$  relaxation region. Same symbols as in Figure 3

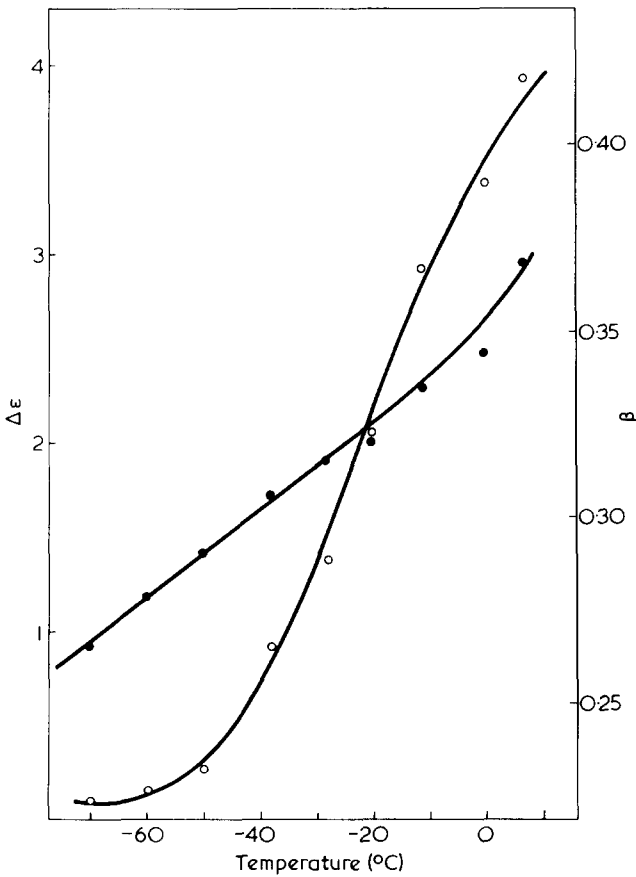


Figure 5 Temperature dependence of the dielectric increment  $\Delta\epsilon$  (●) and the Cole-Cole distribution parameters  $\bar{\beta}$  (○) for polytrifluoroethylene in the  $\beta$  relaxation region

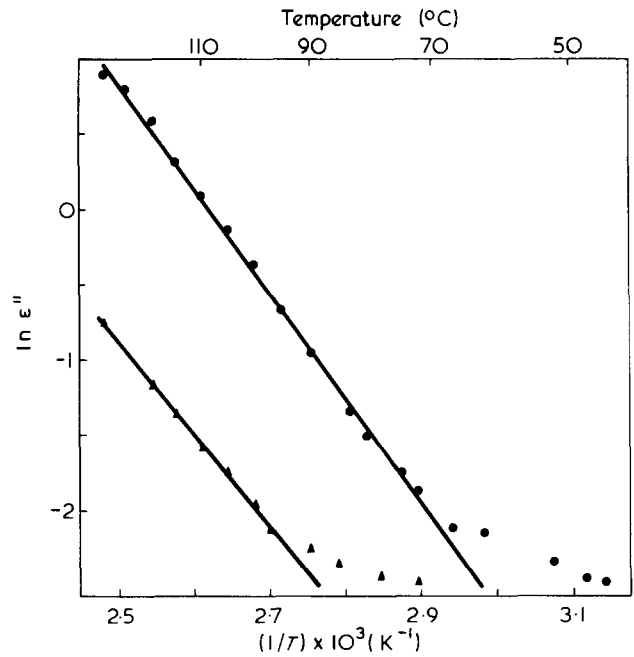


Figure 6 Plots of  $\ln \epsilon''$  at 30 (●) and 300 (▲) Hz against  $1/T$  for polytrifluoroethylene in the high temperature range

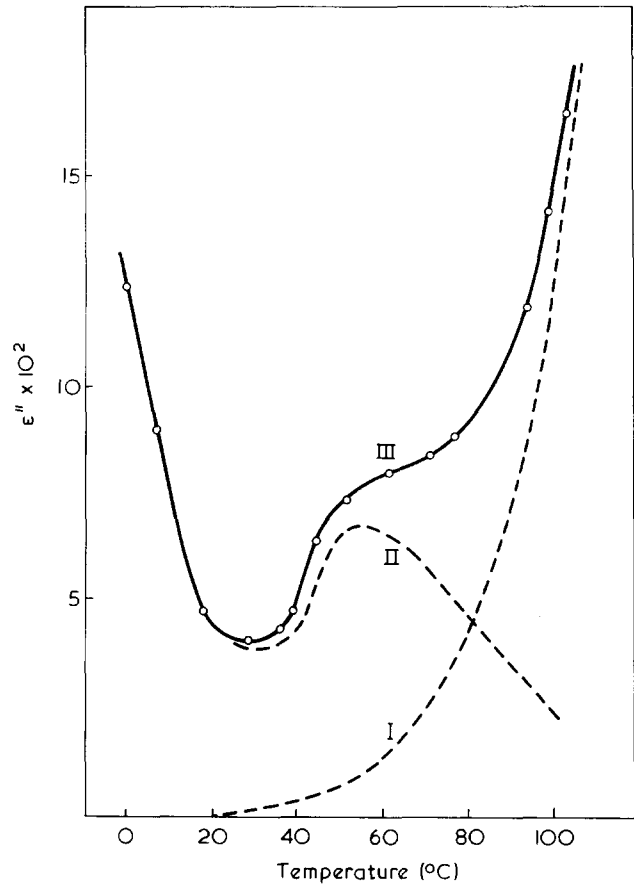


Figure 7 Separation of the dielectric loss  $\epsilon''$  at 300 Hz for polytrifluoroethylene into two components. I: Contribution of d.c. ionic conduction; II: contribution due to dipolar absorption; III: experimental data

and decreasing frequency. Similar contributions to  $\epsilon''$  have been observed in other halogen polymers such as poly(vinyl chloride)<sup>11</sup> and poly(vinyl fluoride)<sup>12,13</sup>. Figure 6 shows the plots of  $\ln \epsilon''$  at 30 and 300 Hz against  $1/T$ , which are straight lines above 90°C, illustrating the fact that  $\epsilon'' =$

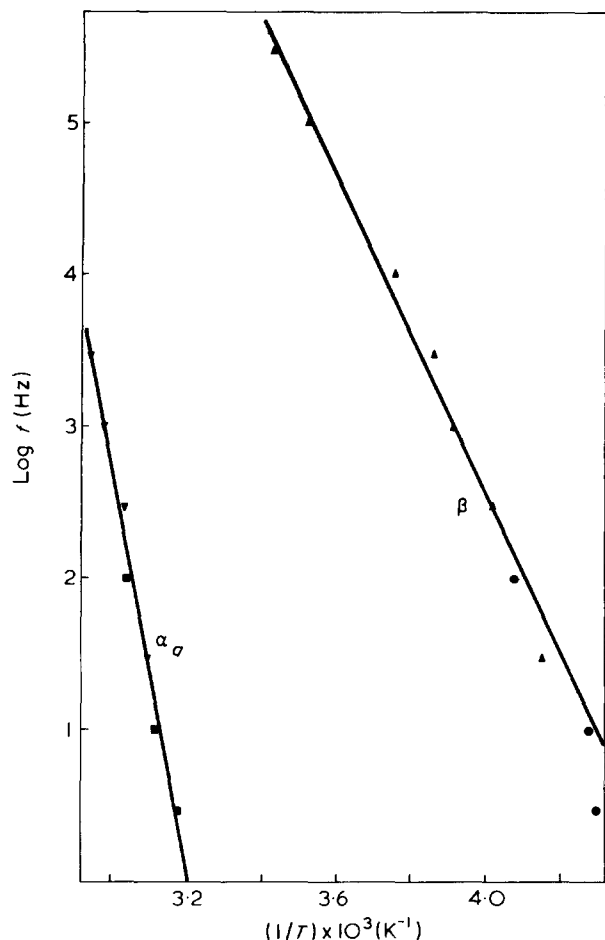


Figure 8 Plots of  $\log f$  against  $1/T$  for polytrifluoroethylene. ■, ●, Mechanical data; ▼, ▲, dielectric data

$A\sigma/f^1$  (where  $A$  is a constant,  $\sigma$  the d.c. conductivity,  $f$  the frequency) increases exponentially with temperature. Below  $90^\circ\text{C}$  the data points lie above the straight lines indicating the existence of the  $\alpha_a$  relaxation. Using straight lines similar to those in Figure 6 the  $\epsilon''$  values due to d.c. ionic conduction are extrapolated to lower temperatures for the data obtained from 30 Hz to 3 kHz. Curve I in Figure 7 is an example of this extrapolation for the  $\epsilon''$  data at 300 Hz. Curve II is obtained by subtracting curve I from the experimental data (curve III) and reveals the  $\alpha_a$  relaxation peak. From curve II the temperature at which  $\epsilon''$  exhibits a maximum is obtained and used in the  $\log f$  against  $1/T$  plot in Figure 8.

#### Activation energies

From Figure 6 the activation energy of the ionic conduction process is found to be 13 kcal/mol. For PCTFE,

the corresponding energies obtained from direct d.c. conductivity measurements are 5 and 32 kcal/mol, respectively, in the glassy and rubbery state<sup>24</sup>. The  $\log f$  against  $1/T$  plots for both the  $\alpha_a$  and  $\beta$  relaxations are shown in Figure 8.

From the slopes of these curves the activation energies of the  $\alpha_a$  and  $\beta$  relaxations are found to be 60 and 24 kcal/mol, respectively. The relatively large activation energy for the  $\alpha_a$  relaxation confirms our assignment that it is associated with the large scale motion of the glass transition.

Although the  $\log f$  versus  $1/T$  plot for this relaxation should obey the WLF equation<sup>15</sup>, it seems to be linear in the limited temperature region ( $40$ – $70^\circ\text{C}$ ) and thus the activation energy is independent of temperature. This is in contrast to the corresponding relaxation in PCTFE where the activation energy decreases from 67 kcal/mol at  $90^\circ\text{C}$  to 34 kcal/mol at  $120^\circ\text{C}$ <sup>6</sup>. The activation energy for the limited motion of the main chain in the  $\beta$  relaxation is slightly higher than the corresponding energies of 13.5 (crystallinity = 1) to 17.4 (crystallinity = 0) kcal/mol for PCTFE<sup>6</sup>.

In conclusion, both the  $\alpha_a$  and  $\beta$  relaxations are observed in PVF<sub>3</sub> and have activation energies similar to those of PCTFE. The  $\beta$  relaxation occurs at nearly the same temperature as that of PCTFE but the  $\alpha_a$  relaxation occurs at  $55^\circ\text{C}$  lower. The  $\alpha_c$  relaxation associated with crystalline regions has not been observed.

#### ACKNOWLEDGEMENTS

The authors are grateful to Dr R. E. Florin of the National Bureau of Standards (USA) for supplying the sample of polytrifluoroethylene and for enlightening discussion.

#### REFERENCES

- 1 see McCrum, N. G., Read, B. E., and Williams, G. 'Anelastic and Dielectric Effects in Polymeric Solids', Wiley, London, 1967, pp 464–477
- 2 Kwan, S. F., Chen, F. C. and Choy, C. L. *Polymer* 1975, **16**, 481
- 3 Lee, W. K. and Choy, C. L. *J. Polym. Sci. (A-2)*, in press
- 4 Crissman, J. M. and Passaglia, E. *J. Polym. Sci. (C)* 1966, **14**, 237
- 5 McCrum, N. G. *J. Polym. Sci.* 1962, **60**, 53
- 6 Scott, A. H. et al. *J. Res. Nat. Bur. Stand. (A)* 1962, **66**, 269
- 7 Hoffman, J. D. and Weeks, J. J. *J. Res. Nat. Bur. Stand.* 1960, **60**, 465
- 8 Hsu, B. S. and Kwan, S. H. *Nature (Phys. Sci.)* 1971, **230**, 46
- 9 Slichter, W. P. *J. Polym. Sci.* 1957, **24**, 173
- 10 Cole, R. H. and Cole, K. S. *J. Chem. Phys.* 1941, **9**, 341
- 11 Isida, Y. *J. Polym. Sci. (A-2)* 1969, **7**, 1835
- 12 Isida, Y. and Yamafuji, K. *Kolloid Z.* 1964, **200**, 50
- 13 Sacher, E. *J. Polym. Sci. (A-2)* 1968, **6**, 1813
- 14 Saito, S., Sasabe, H., Nakajima, T. and Yada, K. *J. Polym. Sci. (A-2)* 1968, **6**, 1297
- 15 Williams, M. L., Landel, R. F. and Ferry, J. D. *J. Am. Chem. Soc.* 1955, **77**, 3701

# Conformation of poly(ethylene oxide) in the solid state, melt and solution measured by Raman scattering

J. Maxfield and I. W. Shepherd

Physics Department, University of Manchester, Manchester M13 9PL, UK

(Received 16 July 1974; revised 8 October 1974)

The Raman spectrum of poly(ethylene oxide) (PEO)  $\overline{M}_w = 3 \times 10^6$  and  $6 \times 10^3$  has been measured in bulk as a function of temperature and in aqueous and chloroform solution as a function of solvent concentration. The spectral features are assigned to particular isomeric configurations and the changes on melting are found to be consistent with a helix-coil transition. In both solvents the ordered nature of the polymer is largely lost at a critical concentration, approximately 50% by weight; residual ordering in dilute aqueous solution is lost and the random coil configuration attained only above the melting temperature. The wavenumber change of the  $862 \text{ cm}^{-1}$  mode as a function of water concentration showed formation of a complex involving three water molecules and was consistent with a simple H-bonding model. The differences between the spectra in the two solvents are explained by this H-bonding. The results are in general agreement with n.m.r. work.

## INTRODUCTION

The conformation of polymer molecules in solution has been a subject of interest over many years and several different experimental techniques have been used in the study<sup>1-4</sup>. Biopolymers in particular have been shown to take up ordered forms in aqueous solution and the stability of the ordering is generally critically dependent on the solution variables. Studies of biological molecules are clearly of great importance but the extremely complex nature of these makes detailed analysis very complicated. In this work we present detailed Raman studies on poly(ethylene oxide) (PEO) which we believe is an ideal molecule for solution studies. It is a synthetic molecule of great industrial importance and has been studied by several different techniques, which we review briefly below. Furthermore it displays some basic features of proteins and can be thought of as a simple model compound. The most important feature is that the monomer contains one hydrophobic region ( $-\text{CH}_2-\text{CH}_2-$ ) and one hydrogen bonding site ( $-\text{O}-$ ).

Raman spectroscopy has great potential in the study of polymer conformations, particularly in aqueous solution because the water spectrum is weak and does not obscure any of the polymer bands. The present paper examines the changes in the Raman spectrum between the crystalline phase and the melt and relates these to the breakdown of ordering. The differences in the spectra of solutions in water and chloroform are presented and discussed in terms of the hydrogen bonding of water to the polymer chain. The solution spectra are also compared with the melt spectrum. At all stages the deductions from the Raman data are compared with previous work, using other techniques, which is briefly reviewed below.

It is well established from X-ray analysis<sup>5</sup> that poly(ethylene oxide) crystallizes in a helical configuration, and spectroscopic studies<sup>6,7</sup> show that the symmetry is isomorphous with the factor group  $D(4\pi/7)$ . The helical form of this

polymer is constructed with a succession of *trans* (CCOC), *gauche* (OCCO), and *trans* (COCC) conformers along the chain, with bond angles of  $192^\circ$ ,  $60^\circ$  and  $192^\circ$  respectively<sup>8</sup>. The normal coordinate analysis for this system has been carried out on the basis of the  $7_2$  helix by Yoshihara *et al.*<sup>6</sup> and the calculated frequencies agree fairly well with the observed infra-red<sup>9</sup> and Raman<sup>10</sup> bands.

In aqueous solution the configuration of the PEO chain will be influenced by the hydrophobic nature of the interaction between the ethylene groups and the polar solvent molecules. Ultrasonic attenuation measurements<sup>11</sup> show that there is a single relaxation time in aqueous solution, which is attributed to a polymer/solvent interaction involving hydrogen bonding of the water molecules to oxygen atoms along the chain, modified by hydrophobic interactions within the polymer and by water clusters near the hydrophobic groups. The data also imply that a minimum molecular size of the solvent-macromolecule structure, of the order of 75 units, is required before cooperativity is displayed<sup>12,13</sup>. The requirement of a minimum molecular size has also been demonstrated in the case of the helix-coil transition in polypeptides<sup>14</sup>.

Liu<sup>15,16</sup> has made an extensive study of PEO solution structures using n.m.r. techniques. The chemical shift of the ethylene protons was found to increase almost linearly with water concentration until a certain composition was reached ( $\sim 50\%$  by vol), after which it remained constant. The hydroxyl protons exhibited an almost analogous behaviour. These results indicate that there is a linear change in the average segmental environment of PEO until 50% concentration is reached, after which there is negligible segmental environment change. This behaviour corresponds to the formation of a hydrogen bonded complex containing approximately three water molecules per monomer unit. The ethylene proton chemical shift in chloroform solution was found to change linearly with solvent content over the entire concentration range. The hydroxyl proton behaviour

was quite different. The chemical shift was constant with increasing chloroform concentration until a particular value was reached ( $\sim 40\%$  by vol) and then fell off sharply. The ethylene proton chemical shifts show that without any specific interaction between the polymer and solvent, the segmental environment changes linearly with solvent content over the entire composition range. The hydroxyl proton behaviour is a measure of the strong molecular association through intermolecular hydrogen bonding. The sharp fall off is associated with the breakdown of this bonding on reaching a specific dilution.

The diffusion constant,  $D$ , of PEO has been measured as a function of concentration in  $D_2O$  solution by neutron scattering<sup>17</sup>. This parameter, which measures the local motions occurring over a number of monomer units, has been measured at several temperatures. At each temperature the behaviour is essentially the same,  $D$  decreases with increasing solvent content until approximately 1 molecule of  $D_2O$  per monomer unit has been added, after this point  $D$  starts to increase. So far measurements have only been made with up to 3 molecules of  $D_2O$  present. In an organic solvent, toluene- $d_8$ , the diffusion constant increases rapidly as the solvent content is increased.

The Raman spectrum of crystalline PEO has been studied by several groups, notably by Yoshihara *et al.* in their analysis of the normal vibrations<sup>6</sup>. Koenig and Angood<sup>18</sup> have published spectra taken in both solution and melt. In the next section we shall present a more intensive study of solutions using Raman scattering methods, with the aim of investigating the structural changes suggested from the n.m.r., ultrasonic, and neutron scattering data of previous workers.

## EXPERIMENTAL AND RESULTS

### Method

The exciting source was an argon ion laser operating with a power of 800 mW in the 5145 Å line. The scattered light was analysed using a Cary 82 spectrometer. Two samples of PEO with molecular weights  $M_w = 3 \times 10^6$  and  $6 \times 10^3$  were used in these experiments. The melting points were determined from differential thermal analysis to be  $61.1 \pm 0.2^\circ\text{C}$  and  $53.8 \pm 0.5^\circ\text{C}$  respectively. The sample cells were square and of spectroscopic quality. Temperatures above ambient were attained by wrapping heating wire and insulation round the cell leaving small areas free for the incident and scattered beams. The temperature was measured using a Comark electronic thermometer and was controlled to  $\pm 0.25^\circ\text{C}$ .

### Raman spectra of PEO in the crystalline and molten states

Raman spectra of pure PEO,  $M_w = 3 \times 10^6$ , are shown in Figure 1 at various temperatures above and below the melting temperature of  $61.1^\circ\text{C}$ . The various well resolved band splittings observed in the crystalline material (lower trace), e.g. at  $846\text{--}860\text{ cm}^{-1}$ , are a result of the ordered helical conformation and disappear at the higher temperatures. The very weak band at  $810\text{ cm}^{-1}$  is of particular interest, and has been assigned to the *trans* conformation of the (OCCO) grouping following the assignment of the IR mode at  $811\text{ cm}^{-1}$ <sup>19,20</sup>. In the crystal state most of the (OCCO) groups are in the *gauche* state and the low intensity of the  $810\text{ cm}^{-1}$  mode is consistent with this assignment. Previous Raman workers<sup>18</sup> have assigned this mode to (OH) end groups or, rather ambiguously, as an 'amorphous'

band. However, our observations discussed below agree with the assignment from IR measurements.

Changes in the spectrum caused by melting occur over a range of several degrees, owing to the distribution of chain lengths within the sample. The molten PEO spectrum is radically different from that of the crystalline material. Such changes are to be expected in going from a highly ordered state exhibiting considerable molecular symmetry to a disordered, essentially random structure. The loss of order is reflected in the disappearance of much of the band splitting observed in the solid state. There are also some frequency shifts of existing bands, and the appearance of new bands, which can be associated with the formation of new conformational structure in the melt. The frequencies of the Raman bands in both the crystalline and molten states are listed in Table 1, together with their probable assignments which are based on previous work<sup>6,9,10</sup>.

In this study, the bands in the region  $800\text{ to }1100\text{ cm}^{-1}$  have been investigated in most detail. These bands arise from combinations of chain backbone modes, in particular the (C—O—C) stretching vibration, and the ethylene rocking modes and are most likely to be susceptible to hydrogen bonding effects. The changes in the remainder of the spectrum were considered to be relatively unimportant, being mainly attributable to the loss of crystalline order. The bands at  $810$ ,  $846$  and  $884\text{ cm}^{-1}$  in the melt spectrum are all attributed to ethylene rocking vibrations. The  $846\text{ cm}^{-1}$  band is at the same frequency as the crystalline band and hence is assigned to the *tgt* conformation. The  $810\text{ cm}^{-1}$  band, as stated above is due to the *trans* conformation of the (OCCO) group. There are several possible structures for the (CCOCCOCC) sequence arising from rotations about the (C—O) and (C—C) bonds. The closeness of the methylene groups for the *gauche* conformation of the (C—O) bonds indicate that this state is highly unfavourable<sup>21</sup>; certainly this conformation will be distorted. The retention of the  $846\text{ cm}^{-1}$  band in the melt also provides confirmation that the *trans* form is largely retained. In view of this, the  $810\text{ cm}^{-1}$  band can be associated with the *ttt* conformational sequence. The band at  $884\text{ cm}^{-1}$  is most probably due to *gauche* structures of the type *tgg* or *ggg*. The small intensity of this band is again consistent with the limitations on the *gauche* form of the (C—O) bond.

The doublet at  $1065\text{--}1075\text{ cm}^{-1}$  in the crystalline state, attributed to  $(\text{COC})_s + r(\text{CH}_2)_a$  and  $(\text{COC})_s + r(\text{CH}_2)_s$  motions respectively, is lost in the melt, and a broad band

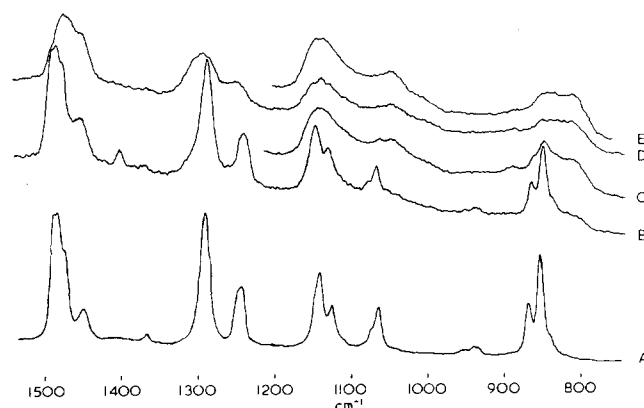


Figure 1 Raman spectra of PEO in the range  $800\text{--}1500\text{ cm}^{-1}$  measured at various temperatures: A,  $25.0^\circ\text{C}$ ; B,  $40.5^\circ\text{C}$ ; C,  $61.0^\circ\text{C}$ ; D,  $62.0^\circ\text{C}$ ; E,  $71.9^\circ\text{C}$ . The sample had molecular weight  $M_w = 3 \times 10^6$  and melting point  $61.1 \pm 0.2^\circ\text{C}$

**Table 1** Observed PEO Raman bands in the frequency range 800–1500  $\text{cm}^{-1}$  for the crystalline structure, the melt and for aqueous and chloroform solutions. The assignments are based on the work of Yoshihara *et al.*<sup>6</sup>. The listed conformations refer to the (CCOC), (OCCO) and (COCC) groups. The conventional notations used are interpreted as follows. Band intensities: w (weak); m (moderate); s (strong). Band resolution: sh (sharp). Mode assignments: r (rocking); t (torsion);  $\nu$  (stretching);  $\omega$  (wagging). The assignment subscripts a and s refer the asymmetric and symmetric motions with respect to the 2-fold axis perpendicular to the helix axis and passing through the O atom or through the centre of the C–C bond

Crystal	Raman frequency ( $\text{cm}^{-1}$ )			Assignment	Conformation
	Melt	Aq. Soln	$\text{CHCl}_3$ Soln		
810 w	810 w	810 ms	810 s	$r(\text{CH}_2)$	ttt
834 sh	834 sh	832 sh	832 sh	End groups	
846 vs	846 s	851 s	845 s	$r(\text{CH}_2)$	tgt
862 m				$r(\text{CH}_2)_s\nu(\text{COC})_s$	tgt
	884 w	884 w	884 w	$r(\text{CH}_2)_a$	tgg, ggg
948 w		943 w		$r(\text{CH}_2)_s\nu(\text{COC})_a$	tgt
936 w				amorphous	
	1043 m	1041 m	1038 m	$r(\text{CH}_2)_s\nu(\text{COC})_a$	tgg
1065 m		1061 m	1055 m	$r(\text{CH}_2)_a\nu(\text{COC})_s$	tgt, ttt
1075 sh				$r(\text{CH}_2)_s\nu(\text{COC})_s$	tgt
1112 vw		1116 vw		$\nu(\text{COC})_s$	tgt
1127 m	1134 s	1123 sh	1128 m	$\nu(\text{COC})_s$	ttt, tgt
1143 m	1141 s	1139 s	1139 m	$\nu(\text{COC})_a$	t, g
1234 m		1230 vw	1236 m	$t(\text{CH}_2)_a$	ttt, ttg, tgt
1239 w	1242 m	1248 m	1246 sh	$t(\text{CH}_2)_s$	tgt, ggg
1286				amorphous	
1283 vs	1283 ms	1285 s	1283 s	$t(\text{CH}_2)_s t(\text{CH}_2)_a$	ttt, tgt
	1295 s	1298 s	1298 s	$t(\text{CH}_2)_s t(\text{CH}_2)_a$	t, g
1364 w				$\omega(\text{CH}_2)_s\nu(\text{CC})$	tgt
		1372 vw	1373 vw	$\omega(\text{CH}_2)_s\nu(\text{CC})$	tgg, ggg
1398 w				$\omega(\text{CH}_2)_s\nu(\text{CC})$	tgt
1448 m	1448 m	1452 m	1446 m	$\delta(\text{CH}_2)_s$	tgg, tgt
1473 sh	1471 s	1474 s	1471 s	$\delta(\text{CH}_2)_a$	tgt
1487 s				$\delta(\text{CH}_2)_s$	tgt

appears at 1043  $\text{cm}^{-1}$ . This band is also due to a combination of *gauche* conformations, the frequency shift being at least partly a result of the breaking of intermolecular hydrogen bonds present in the helical configuration.

These data show that the *trans* to *gauche* ratios change on melting but at present there is no method of making a reliable quantitative experimental estimate to compare with the random coil ratios of 2.8 for (C–C) bonds and 7.3 for (C–O) bonds<sup>22</sup>.

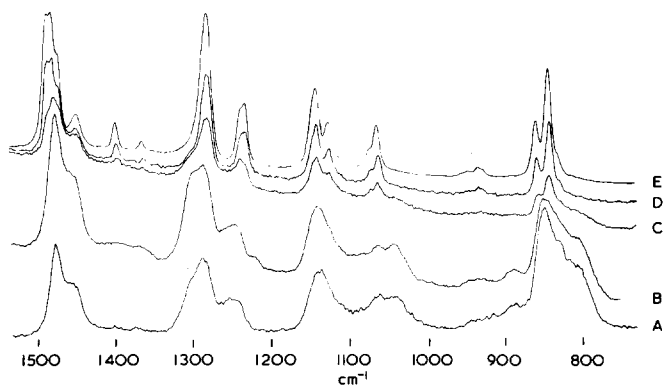
#### Raman spectra of PEO in aqueous solution

The Raman spectra for several concentrations are shown in Figure 2. The frequencies of the dilute solution bands are given in Table 1, where they can be compared with the bands of the molten form. The region 1100 to 1500  $\text{cm}^{-1}$  is very similar to that of the melt, except that the bands are slightly narrower which is to be expected at the lower temperature. The solution spectrum for the region 800 to 1100  $\text{cm}^{-1}$  on the other hand shows considerable differences from the melt. The band at 1043  $\text{cm}^{-1}$  in the melt is split into two bands, at 1041 and 1061  $\text{cm}^{-1}$ , and the ethylene rocking mode at 846  $\text{cm}^{-1}$  occurs at 851  $\text{cm}^{-1}$  with an increased relative intensity.

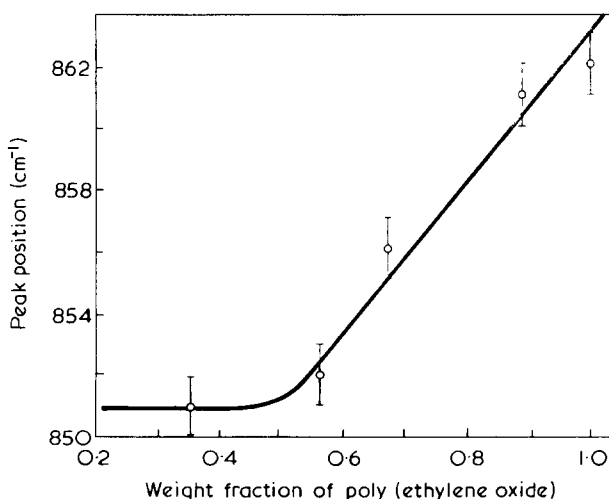
The relatively low intensity of the 810  $\text{cm}^{-1}$  band in dilute solution, compared with the melt spectrum, can be taken as an indication of the greater retention of the *tgt*

conformation of the helix. This fact is emphasized by the retained splitting of bands at 1280  $\text{cm}^{-1}$ . The behaviour of the doublet at 846 and 862  $\text{cm}^{-1}$  on dilution is quite complex. In the work of Koenig<sup>18</sup>, it was reported that the splitting was lost, leaving only the band at 846  $\text{cm}^{-1}$  in solution. Our results show that this is incorrect. It was found that the band at 862  $\text{cm}^{-1}$  decreased in frequency with dilution, while the band at 846  $\text{cm}^{-1}$  remained unchanged, until the composition reached 50% by volume, whereupon the two bands merged to form a hybrid band at 851  $\text{cm}^{-1}$ . The band at 862  $\text{cm}^{-1}$  in the solid state is attributed to a combination of a symmetric rocking motion of the ethylene groups, with a symmetric stretching involving the oxygen atom in the backbone chain. We would therefore expect this vibration to be sensitive to hydrophobic as well as hydrogen bonding interactions.

The major, large scale changes observed in these spectra follow the trends observed by Liu using n.m.r. The spectral changes, loss of ordered modes and appearance of new bands, occur as a smooth function of water concentration until 50% water content is reached. At this point the polymer–solvent structure is completely formed, and no further changes occur in the spectrum on further dilution. This behaviour is characterized by the behaviour of the 862  $\text{cm}^{-1}$  band. In Figure 3 the frequency of this band is plotted as a function of dilution in aqueous solution. There is a sharp fall in frequency with decreasing polymer



**Figure 2** Raman spectra of PEO–water system in the range 800–1500  $\text{cm}^{-1}$ . A, 33.5; B, 56.3; C, 66.7; D, 88.3; E, 100% polymer ( $M_w = 3 \times 10^6$ )



**Figure 3** Frequency of the PEO ethylene rocking mode plotted as a function of water concentration. The mode energy in the pure crystal state is 862  $\text{cm}^{-1}$



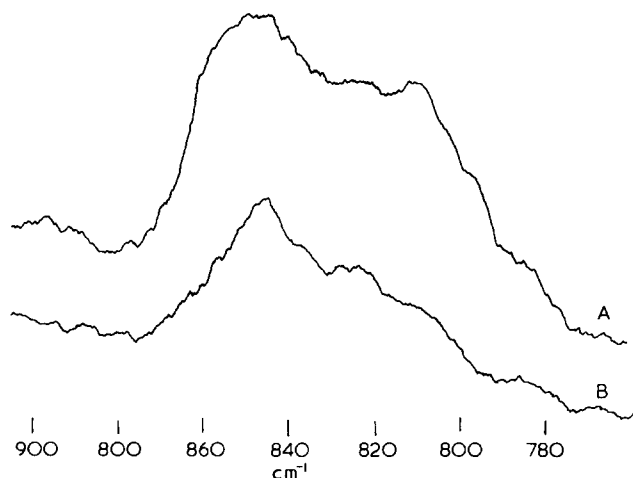


Figure 4 Raman spectra of PEO ( $\bar{M}_w = 3 \times 10^6$ ) in water solution measured above and below the melting temperature of 61.1°C. A, 83.9°C; B, 24.5°C

concentration until the composition reaches 50% water content, and then the frequency curve levels off, giving no further change with dilution. This trend is in direct agreement with the n.m.r. data of Liu, and provides further evidence for the formation of a hydrogen bonded water complex with a composition of three water molecules per repeat unit. The structure of this complex will be discussed later, but it is clear that the helical form is largely lost and the structure tends towards that of the molten state.

In Figure 4, the Raman spectra of a dilute aqueous solution (~30%) is shown for two temperatures above and below the melting point of the polymer. The high temperature spectrum is identical to that of the melt, the band at 810  $\text{cm}^{-1}$  is increased in intensity and the ethylene rocking mode occurs at 846  $\text{cm}^{-1}$ . The cooperative structure of the low temperature solution is therefore destroyed at temperatures above the polymer melting point.

#### Raman spectra of PEO in chloroform solution

The PEO spectra in chloroform solution were studied for two reasons. The first was to observe the breakdown of the molecular association at a particular concentration and thus confirm the n.m.r. results. The second reason was to provide a non-polar solution 'reference' with which to compare the aqueous solution spectra. Spectra showing the variation with concentration in chloroform solution are given in Figure 5. The frequencies of the dilute solution bands are given in Table 1 for comparison with the melt and dilute water solutions. In the region 1100 to 1500  $\text{cm}^{-1}$  the chloroform and aqueous solutions spectra are almost identical. Both spectra show more ordering than in the melt, although much less than the crystalline solid. The major differences from the aqueous solution spectra are for the ethylene stretching modes at ~1050  $\text{cm}^{-1}$  and the rocking modes around 850  $\text{cm}^{-1}$ . The band at 810  $\text{cm}^{-1}$  is also much stronger in the chloroform solution and the relative intensity is comparable to that of the melt. This fact, together with other smaller differences, would point to there being slightly greater order in the aqueous than the chloroform solution.

The spectra of Figure 5 show that the helical structure of the PEO is largely maintained in chloroform solution until the composition reaches 55% by weight solvent concentration. At this point there is a fairly sudden breakdown of the ordered structure and the spectrum takes the form

for the dilute solution structure. This behaviour is analogous to that observed with n.m.r. by Liu. The presence of strong intramolecular hydrogen bonds is sufficient to prevent the breakdown of the helix until a particular dilution is reached.

#### DISCUSSION

We have seen that the spectra of chloroform and aqueous solutions of PEO differ only in the region 800 to 1100  $\text{cm}^{-1}$  and it is on this region that we concentrate. In Figure 3, the frequency dependence of the 862  $\text{cm}^{-1}$  band on water concentration was shown. This band is a complex mode involving two motions: an ethylene rocking mode and a backbone stretching vibration. If the band had been associated solely with the backbone mode we would expect the presence of hydrogen bonded molecules at the oxygen atom to increase the frequency of the vibration, the exact opposite to the observed behaviour. (The apparent anomaly that the addition of a mass should increase the stretching frequency is explained by the fact that the additional mass is not fixed but is held by a comparatively weak force.) The effect of the bonded water on the rocking mode must therefore be critical. This motion will be affected by the hydrophobic interaction of the ethylene groups with the polar solvent. It is difficult to be very precise about this interaction, but we can make a few comments. First, it must act in such a way as to decrease the frequency, outweighing the effect of bonded water on the backbone vibration contribution. This type of behaviour has also been observed in polyamides<sup>23</sup> where again the pendant group motion is predominant. Secondly, such an interaction is likely to cause a perturbation of the electron cloud of the methylene groups. Such an interaction would be a smoothly varying function of water concentration until the stable polymer/solvent structure is formed, whereupon no further water molecules can enter the area of the polymer chain, and so we would expect no further change.

Such an explanation is compatible with the results of Figure 3, where we see a smoothly varying decrease in frequency up to 50% water content, followed by no further change.

The two bands at 1061 and 1041  $\text{cm}^{-1}$  in the aqueous solution are also combinations of ethylene rocking motions and (C-O-C) stretching vibrations for the *tgt* and *tgg* con-

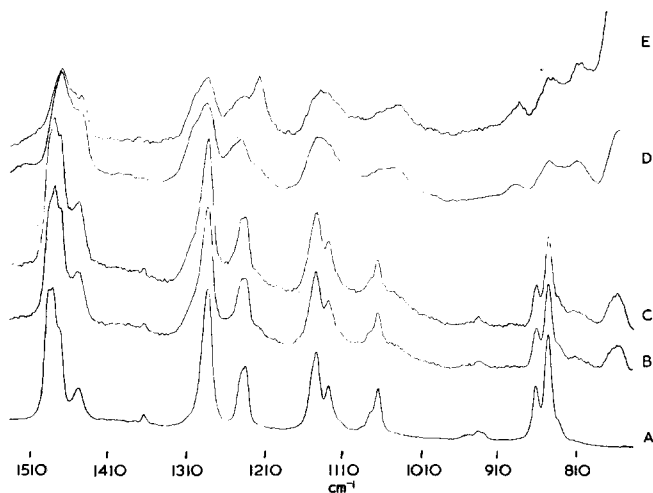


Figure 5 Raman spectra of PEO ( $\bar{M}_w = 3 \times 10^6$ ) in chloroform solution. A, 100; B, 68.7; C, 54.7; D, 49.25; E, 26.9% polymer

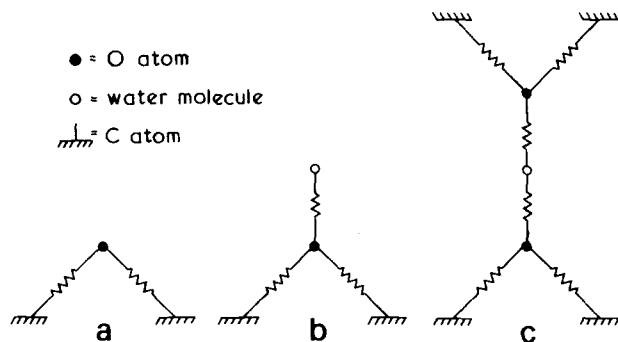


Figure 6 Simple models for the backbone stretching motion in PEO. (a) Unperturbed system; (b) one hydrogen bonded water molecule; (c) a water molecule forming a crosslink

figurations respectively. In the chloroform solution spectrum, these bands occur at  $1055$  and  $1038\text{ cm}^{-1}$ , and we can infer a frequency increase between the non-polar and polar solvents. Such frequency shifts are qualitatively in agreement with the model of water forming hydrogen bonds onto the oxygen atom involved in the backbone stretching vibration. The relative intensities of these bands increase on dilution, until 50% water concentration is reached, exactly the behaviour outlined above. Finally, the potential energy distribution of the  $1065\text{ cm}^{-1}$  band contains a larger percentage of the backbone stretching vibration than does the  $862\text{ cm}^{-1}$  band, and it is reasonable to assume that this mode is dominant in this case. A simple calculation can be done to estimate the effect on the stretching vibration of the bonded water based on the models shown in Figure 6. For water single-bonded onto a backbone oxygen the estimated shift is about  $5\text{ cm}^{-1}$  which is in reasonable agreement with the differences between  $1061\text{ cm}^{-1}$  ( $\text{H}_2\text{O}$ ) and  $1055\text{ cm}^{-1}$  ( $\text{CHCl}_3$ ) and between  $1041\text{ cm}^{-1}$  ( $\text{H}_2\text{O}$ ) and  $1038\text{ cm}^{-1}$  ( $\text{CHCl}_3$ ). It seems probable, then, that the differences observed in these mode energies in the two solvents are due to simple hydrogen bonding of water molecules. The more complicated arrangement in which the water molecules form a crosslink by bonding to oxygens in neighbouring chains gives a frequency shift of the order of  $10\text{ cm}^{-1}$ . This is much larger than the observed shifts and suggests that this form of bonding is unlikely in solution. Indeed this is borne out by simple observation: a predominance of such crosslinks would result in a gel, for which there is no evidence in low molecular weight samples. For high molecular weights, at low concentration, gel behaviour is observed but this is most probably due to entanglements.

## CONCLUSIONS

From the data presented above we can confirm that the PEO molecule forms a hydrogen bonded complex in aqueous solution in which three water molecules are involved with one repeat unit. The helical structure of the crystal is lost in aqueous solution, as in the melt and

chloroform solution. In the melt, the structure would seem to move towards the random coil configuration with an increase in *trans* conformation of the (C-C) bond typified by the increase in the intensity of the  $810\text{ cm}^{-1}$  band. Both of the solution spectra, however, exhibit some retention of ordering. The band at  $\sim 1060\text{ cm}^{-1}$  from the *tgt* conformation, for example, is present in both solutions but not in the melt. The difference between the chloroform and aqueous solution spectra can be explained by the hydrogen bonded water perturbing the ethylene rocking modes and the backbone stretching modes. There is, therefore, very little difference between the conformational structures for the two solutions. Finally, if the aqueous solution is taken above the melting point of the pure polymer, the spectrum becomes that of the melt. This would suggest that the hydrogen bonded structure is destroyed.

## ACKNOWLEDGEMENTS

The authors wish to acknowledge helpful discussions with Dr Liu, Dr A. Maconochie and Professor G. Allen. This work was supported by the SRC Polymer Committee.

## REFERENCES

- 1 Birshtein, T. M. and Ptitsyn, O. B. 'Conformations of Macromolecules', Wiley-Interscience, New York, 1966, Ch 7
- 2 Billmeyer, F. W. 'Textbook of Polymer Science', Wiley-Interscience, New York, 1970, Ch 2
- 3 Flory, P. J. 'Statistical Mechanics of Chain Molecules', Wiley-Interscience, New York, 1969
- 4 Tanford, C. 'Physical Chemistry of Macromolecules', Wiley, New York, 1963
- 5 Tadokoro, H., Chatani, Y., Yoshihara, T., Tahara, S. and Murahashi, S. *Makromol. Chem.* 1964, 73, 109
- 6 Yoshihara, T., Tadokoro, H. and Murahashi, S. *J. Chem. Phys.* 1964, 41, 2902
- 7 Miyazawa, T., Fukushima, K. and Ideguchi, Y. *J. Chem. Phys.* 1963, 37, 2764
- 8 Davison, W. H. T. *J. Chem. Soc.* 1955, p 3270
- 9 Tadokoro, H. *Macromol. Rev.* 1967, 1, 119
- 10 Schaufele, R. F. *J. Opt. Soc. Am.* 1967, 57, 105
- 11 Hammes, G. G. and Roberts, P. B. *J. Am. Chem. Soc.* 1968, 90, 7119
- 12 Hammes, G. G. and Pace, C. N. *J. Phys. Chem.* 1968, 72, 2227
- 13 Grunwald, E. and Ralph, E. K. *J. Am. Chem. Soc.* 1967, 89, 4405
- 14 Goodman, M., Langsam, M. and Rosen, I. F. *Biopolymers* 1966, 4, 305
- 15 Liu, K. J. *Macromolecules* 1968, 1, 213
- 16 Liu, K. J. and Parsons, J. L. *Macromolecules* 1969, 2, 529
- 17 Allen, G. and Maconochie, A. *Polym. Prepr.* 1974, 15, 106
- 18 Koenig, J. L. and Angood, A. C. *J. Polym. Soc. (A-2)* 1970, 8, 1787
- 19 Kuroda, Y. and Kubo, M. *J. Polym. Sci.* 1959, 39, 453
- 20 Matsura, H. and Miyazawa, T. *J. Polym. Sci. (A-2)* 1969, 7, 1735
- 21 Yokoyama, M., Ishihara, H., Iwamoto, R. and Tadokoro, H. *Macromolecules* 1969, 2, 184
- 22 Mark, J. E. and Flory, P. J. *J. Am. Chem. Soc.* 1965, 87, 1415; 1966, 88, 3702
- 23 Peticolas, W. L., Small, E. W. and Fanconi, B. 'Polymer Characterization', Plenum Press, New York, 1971

# E.s.r. study of $\gamma$ -irradiated isotactic and atactic polypropylene

Toshitami Ooi

Research Center, Mitsui Toatsu Chemicals Inc., Totsuka-ku, Yokohama-City, Japan

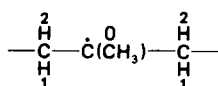
and Masami Shiotsubo, Yoshimasa Hama and Kenichi Shinohara

Science and Engineering Research Laboratory, Waseda University, Tokyo, Japan

An e.s.r. study of  $\gamma$ -irradiated isotactic (i-) and atactic (a-) polypropylene (PP) was carried out. Both the 17 line (or 9 line) spectrum for i-PP and the 6 line spectrum for a-PP are attributed to the tertiary carbon radical,  $-\text{CH}_2-\dot{\text{C}}(\text{CH}_3)-\text{CH}_2-$ . The difference in the hyperfine structure between the spectrum of i-PP and that of a-PP can be explained by different radical conformations owing to the stereoregularity. Hyperfine coupling and the radical conformation for the tertiary carbon radical in i- and a-PP were determined from the  $\cos^2 \theta$  rule. It is shown that the  $\delta$  methylene proton as well as the  $\beta$  methylene proton contribute to the slight anisotropy in the stretched sample. The spectral change from 9 lines to 17 lines with elevation of temperature, observed at low temperature in i-PP, could be explained by the hindered oscillation of the  $\beta$  methylene proton.

## INTRODUCTION

Free radicals produced in irradiated polypropylene (PP) have been studied by many authors<sup>1-7</sup> using electron spin resonance (e.s.r.) spectroscopy. It seems, however, that the ultimate interpretation of the spectrum has not yet been obtained. It is well known that isotactic polypropylene (i-PP),  $\gamma$ -irradiated at room temperature, gives a well-resolved 17 line e.s.r. spectrum at room temperature. Fisher *et al.*<sup>2</sup> reported that this 17 line spectrum is due to  $-\text{CH}(\text{CH}_3)-\dot{\text{C}}(\text{CH}_3)-\text{CH}-\text{CH}(\text{CH}_3)-$  radical, from experiments with oriented samples. Ayscough *et al.*<sup>5</sup>, however, reported that the 17 line spectrum can be assigned to the tertiary carbon radical:



which gives a hyperfine coupling constant of  $a_0 = 21 \pm 1$ ,  $a_1 = 9 \pm 0.6$ ,  $a_2 = 43 \pm 2$ , for the isotropic term in  $\beta$  methylene protons and  $b_1 = \pm 0.6 \pm 0.3$ ,  $b_2 = \mp 1.0 \pm 0.3$  for the anisotropic term in  $\beta$  methylene protons, respectively. An e.s.r. study of  $\gamma$ -irradiated i-PP carried out by Iwasaki *et al.*<sup>6</sup> has shown that the 17 line spectrum appears as a 9 line spectrum by measurement at  $-196^\circ\text{C}$ , and that when the sample is exposed to u.v. light for a short time this 9 line spectrum converts to a 4 line spectrum due to  $-\text{CH}_2-\text{CH}(\dot{\text{C}}\text{H}_2)-\text{CH}_2-$  radical. The fact that this last radical gives a 4 line spectrum was also reported by Loy<sup>3</sup>.

On the other hand, e.s.r. studies of  $\gamma$ -irradiated atactic (a-) PP have seldom been reported. It is expected that the difference of the stereoregularity between i- and a-PP affects the e.s.r. spectrum.

In the present investigation, an e.s.r. study of  $\gamma$ -irradiated i- and a-PP was carried out, and an attempt was made to explain the difference of the steric configuration, and to propose a possible radical structure giving such e.s.r. spectrum, simulating the spectrum with a computer.

## EXPERIMENTAL

i-PP and a-PP (Mitsui Toatsu Chemicals Inc.) were purified by Soxhlet extraction. For experiments using anisotropic samples, sheets of i-PP stretched at  $90^\circ\text{C}$  to the extent of 500% after being extracted by ether were used. These samples were dried sufficiently and then sealed in a vacuum of about  $10^{-4}$  mmHg. The sealed samples were irradiated to a dose of 0.5–1 Mrad by  $\gamma$ -rays from a  $^{60}\text{Co}$  source at room temperature or at  $-196^\circ\text{C}$ .

E.s.r. spectra were measured with an X-band spectrometer with 100 kHz field modulation. The microwave power was attenuated to a level sufficient to remove the effect of power saturation. The anisotropy of the spectrum was investigated by placing the stretched sample either parallel or perpendicular to the applied magnetic field.

Two different procedures were adopted in observing the e.s.r. spectra. In one the measurement was begun at  $-196^\circ\text{C}$  and the temperature was raised in steps to room temperature. In the other, the spectrum was observed at  $-196^\circ\text{C}$  after heat-treating the sample at various temperatures.

The simulation of the spectrum was made with JEC-6 spectrum computer manufactured by Japan Electron Optics Laboratory Co. Ltd.

## RESULTS AND DISCUSSION

### E.s.r. spectrum of i-PP

When the i-PP was irradiated by  $\gamma$ -rays at  $-196^\circ\text{C}$  and measured immediately at  $-196^\circ\text{C}$ , e.s.r. spectra as shown in *Figure 1* were obtained. A sharp singlet observed at the centre of the spectrum in *Figure 1A* can be attributed to trapped electrons because it is subjected easily to power saturation and also it disappears by photobleaching with i.r. light. *Figure 1B* shows the e.s.r. spectrum obtained at  $-196^\circ\text{C}$  after the disappearance of the trapped electrons. This is similar to the spectrum reported by Iwasaki *et al.*<sup>6</sup>



still lower temperature of  $-196^\circ\text{C}$ , a 9 line spectrum was observed instead of the 19 or 20 line spectrum. The overall spread of the spectrum was about 170 and 174 G for  $\theta = 0^\circ$  and  $\theta = 90^\circ$ , respectively.

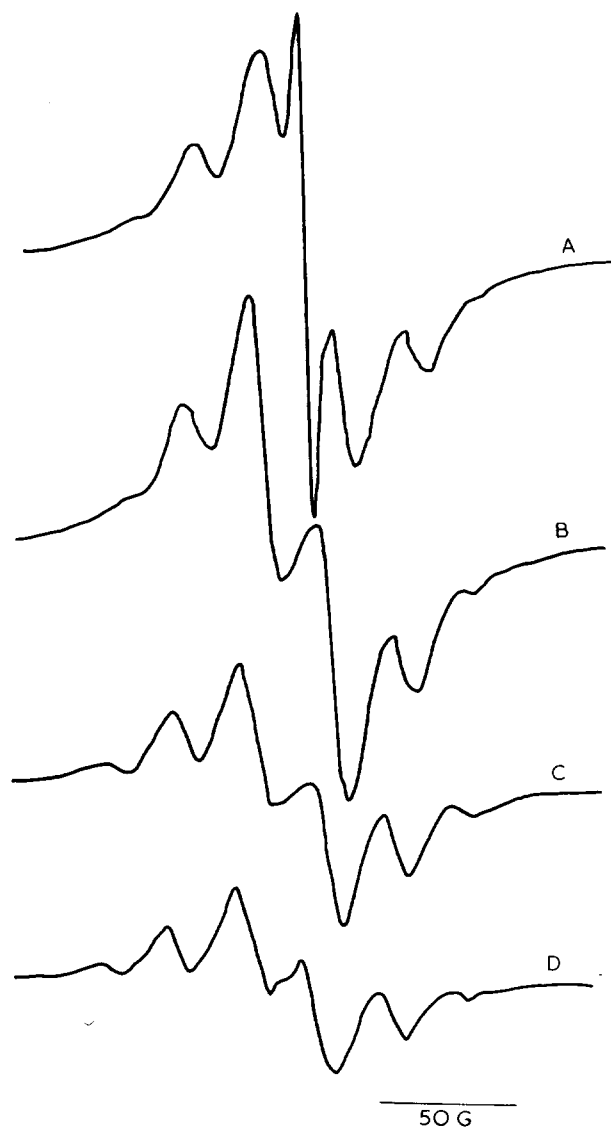


Figure 4 First derivative e.s.r. spectra of a-PP  $\gamma$ -irradiated at  $-196^\circ\text{C}$ : A, observed at  $-196^\circ\text{C}$  immediately after irradiation; B, observed at  $-196^\circ\text{C}$  after photobleaching; C, observed at heat-treating the sample at  $-38^\circ\text{C}$  for 3 min; D, observed at  $-133^\circ\text{C}$  for the sample of C

E.s.r. spectrum of a-PP

E.s.r. spectra of a-PP irradiated by  $\gamma$ -rays at  $-196^\circ\text{C}$ , then kept at various temperatures for 3 min, and measured at  $-196^\circ\text{C}$ , are shown in Figure 4. The spectrum of Figure 4A, obtained at  $-196^\circ\text{C}$  immediately after irradiation, is composed mainly of a broad quartet and a sharp singlet due to trapped electrons in the centre of the spectrum, although a weak peak is observed at both outskirts of the broad quartet. The maximum slope width of the sharp singlet is about 15 G which is not very different from that of polar materials. The broad quartet is similar to one observed at  $-196^\circ\text{C}$  for  $\gamma$ -irradiated i-PP and is due to radical (I)<sup>3,6</sup>.

On heat treatment, even at the low temperature of  $-160^\circ\text{C}$  the sharp singlet due to trapped electrons disappears. The spectral intensity of the quartet decreases with elevation of the temperature of heat-treatment and a broad 6 line spectrum having average hyperfine splitting of 28 G appears. These subsequent heat-treatments not only cause the decrease of the intensity of the broad quartet but also that of the total intensity of the spectrum. Weak peaks observed at both outskirts of the spectrum obtained at  $-196^\circ\text{C}$ , however, increase intensity with elevation of the temperature of heat-treatment. This fact together with the appearance of a 6 line spectrum on heat-treatment at higher temperature, shows that these two peaks belong to the 6 line spectrum.

Change of the 6 line spectrum to another spectrum could not be observed by measurement at or above  $-196^\circ\text{C}$ , unlike the case of i-PP.

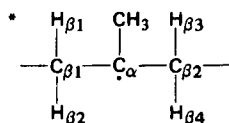
Origin of the 9 line and 17 line spectra, and the 6 line spectrum

As described above, when a sample of i-PP is irradiated by  $\gamma$ -rays at  $-196^\circ\text{C}$  and then measured after being kept at room temperature, a 9 line spectrum is obtained at  $-196^\circ\text{C}$  and a 17 line spectrum at room temperature. On the other hand, a 6 line spectrum is observed for a-PP irrespective of the temperature of measurement. The 9 line spectrum and the 17 line spectrum are attributed to the tertiary carbon radical (II) as shown in some previous reports<sup>3,5,6</sup>.

It may be reasonable to suppose that the 6 line spectrum obtained for a-PP is also due to the tertiary carbon radical (II), because the e.s.r. spectrum obtained at  $-196^\circ\text{C}$  after  $\gamma$ -irradiation at  $-196^\circ\text{C}$  shows a broad quartet which is similar to the spectrum obtained for i-PP under the same condition. The 9 line spectrum observed for i-PP and the

Table 1 Hyperfine coupling constants and radical conformation for i-PP

H.f. coupling constant (G)	Conformational angle (degrees)	Radical conformation*
$\Delta H(\text{CH}_3)$ 21.4		
$\Delta H(\text{C}-\text{H}_{\beta 1})$ 39.6	$\theta_1$ 15.5	
$\Delta H(\text{C}-\text{H}_{\beta 2})$ 15.1	$\theta_2$ 53.5	
$\Delta H(\text{C}-\text{H}_{\beta 3})$ 42.1	$\theta_3$ 6.6	
$\Delta H(\text{C}-\text{H}_{\beta 4})$ 9.1	$\theta_4$ 62.5	



6 line spectrum in a-PP can, therefore, be attributed to the same radical, which appeared through the radical conversion shown by equation (1) due to heat treatment. The difference of the hyperfine structure between the spectrum of i-PP and that of a-PP was supposed to arise from different radical conformations.

*Hyperfine coupling and radical conformation of  $-\text{CH}_2-\text{C}(\text{CH}_3)-\text{CH}_2-$  radical*

It is assumed that the hyperfine splitting of  $\beta$  proton is given by the following  $\cos^2 \theta$  rule<sup>8</sup>:

$$\Delta H(\text{C}-\text{H}_{\beta i}) = B\rho \cos^2 \theta_i \quad (2)$$

Results obtained from analysis of the experimental spectrum and simulation of the spectrum by computer are summarized in Table 1.

In the case of i-PP, the hyperfine coupling constant due to a methyl proton is estimated to be 21.4 G since a methyl group rotates rapidly around the three-fold axis even at  $-196^\circ\text{C}$ . Four protons belonging to two methylene groups give a different hyperfine coupling constant as shown in Table 1 for i-PP. From these values of coupling constant, a value of 42.8 G is obtained for the constant  $B\rho$ . Such hyperfine coupling constants also lead to the computed

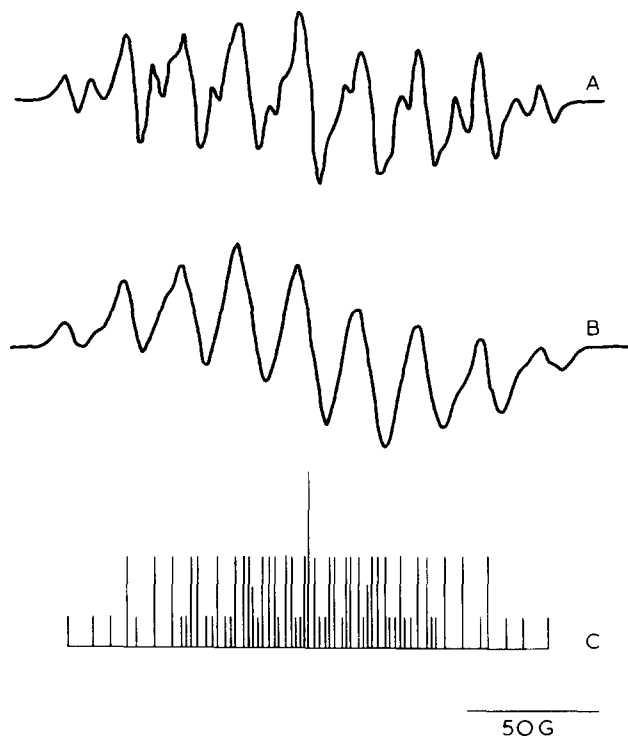


Figure 5 Computed spectrum of tertiary carbon radical for i-PP: A, 17 line spectrum; B, 9 line spectrum; C, line spectrum

spectrum shown in Figure 5, which seems to represent the observed feature of e.s.r. spectra rather well. From the  $\cos^2 \theta$  rule, the conformational angle  $\theta_i$  are determined and they are also given in Table 1. The radical conformation shown in Table 1 is slightly distorted from the original  $3_1$  helical conformation<sup>9</sup>. The different conformational angle obtained for four protons of two  $\beta$  methylenes may be attributed to a  $3_1$  helical structure of the trapping site of radical.

The hyperfine coupling constants for the a-PP are summarized in Table 2. The computed spectrum obtained from these coupling constants is shown by the solid curve in Figure 6B. The computed spectrum is different from the experimental curve in the spectral centre. Addition of a broad singlet shown by the broken line in Figure 6B to the computed spectrum leads to a spectrum which fits the experimental spectrum, shown in Figure 6A quite well. In the case of a-PP also, the conformational angle for two methylene groups is obtained, which is summarized in Table 2 together with the radical conformation expected from these conformational angles.

When the methylene group (Table 1) is projected on the

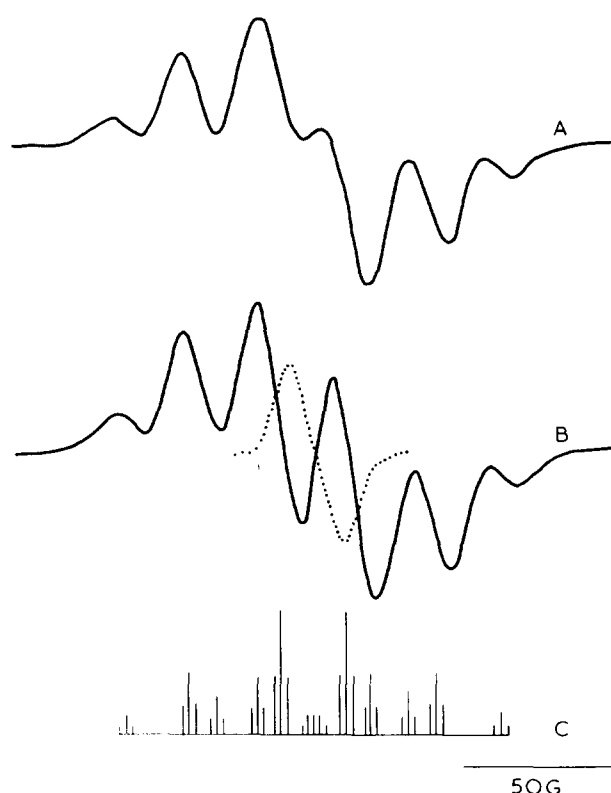


Figure 6 Computed spectrum of tertiary carbon radical for a-PP: A, obtained by superposition of a solid curve and a broken curve in B; B, 6 line spectrum computed by the coupling constant given in Table 2 (—); C, line spectrum

Table 2 Hyperfine coupling constants and radical conformation for a-PP

H.f. coupling constant (G)	Conformational angle (degrees)	Radical conformation
$\Delta H(\text{CH}_3)$ 21.4		
$\Delta H(\text{C}-\text{H}_{\beta 1})$ 1.8	$\theta_1$ 78.2	
$\Delta H(\text{C}-\text{H}_{\beta 2})$ 30.0	$\theta_2$ 33.0	
$\Delta H(\text{C}-\text{H}_{\beta 3})$ 30.0	$\theta_3$ 33.0	
$\Delta H(\text{C}-\text{H}_{\beta 4})$ 1.8	$\theta_4$ 78.2	

plane perpendicular to the direction  $C_{\alpha}-C_{\beta}$ , the angle between two projected C-H bonds is  $111^{\circ}$  for both i-PP and a-PP. This value deviates from that of  $120^{\circ}$  of the original helical structure. Such deviation of the projected bond angle was also reported in a paper by Ohnishi *et al.*<sup>10</sup> on their e.s.r. study of irradiated polyethylene. Similar deviation has also been observed in the e.s.r. study of low molecular weight organic compounds<sup>8,11-15</sup>. The different e.s.r. spectra in i-PP and in a-PP, i.e. a 17 line spectrum and a 9 line spectrum in the former and a 6 line spectrum in the latter, can thus be explained by assuming different conformations for the same kind of radical.

#### Temperature dependence of e.s.r. spectral shape

As described above, the e.s.r. spectrum in i-PP, observed as a 9 line spectrum at  $-196^{\circ}\text{C}$  changes into a 17 line spectrum at  $-150^{\circ}\text{C}$ . The motional narrowing due to the motion of the polymer molecule cannot arise at such low temperatures, since the radical under consideration is produced in a crystalline region and also the temperature of  $-150^{\circ}\text{C}$  is far lower than the glass transition temperature of polypropylene. Ohnishi *et al.*<sup>10</sup> reported in their e.s.r. study of irradiated polyethylene that the spectral change of allylic radicals with temperature can be attributed to the motional narrowing caused by the hindered oscillation of the  $\beta$  methylene proton of the allylic radical. It seems possible to explain the spectral change of the tertial carbon radical  $-\text{CH}_2-\dot{\text{C}}(\text{CH}_3)-\text{CH}_2-$  from a 9 line spectrum to a 17 line spectrum observed in the present investigation, in a similar way. If the  $\beta$  methylene proton can oscillate by a small amplitude of  $\Delta\theta$  around  $\theta_i$  given in Table 1 and if the frequency of oscillation becomes higher than the difference of the hyperfine coupling frequency at both positions,  $\theta_i$  and  $\theta_i + \Delta\theta$ , by elevation of temperature, the hyperfine coupling constant is averaged to give the value determined by  $\theta_i$ .

At a temperature below  $-150^{\circ}\text{C}$ , the frequency of oscillation of  $\beta$  methylene proton becomes lower than the hyperfine coupling frequency. The width of each 17 line spectrum becomes broader and because of the overlap of lines the 17 line spectrum takes an appearance of a 9 line spectrum. Such change of the computed 17 line spectrum to a 9 line spectrum by broadening of the linewidth has also been ascertained by computation. This computed 9 line spectrum is shown in Figure 5B. The computed 9 line spectrum differs slightly from the observed spectrum. The difference is caused probably because the computation was carried out so that  $\Delta\theta$  gives only the breadth to the spectral lines.

In the case of a-PP, change of the 6 line spectrum with elevation of temperature was not observed. This fact may be explained by taking the view that the oscillation of  $\beta$  methylene protons is taking place fairly rapidly even at  $-196^{\circ}\text{C}$  and that the irregular structure due to low tacticity makes the linewidth quite broad.

#### Anisotropic interaction in the stretched polymer

As seen above, the e.s.r. spectrum of the stretched i-PP shows a slight anisotropy. The tertial carbon radical, however, does not have an  $\alpha$  proton. Ayscough *et al.*<sup>5</sup> suggested the possibility that the anisotropy is due to one of two  $\beta$  methylene protons. However, in the  $3_1$  helical structure of i-PP, it can be seen that one of the  $\delta$  methylene protons exists near the  $\alpha$  carbon. The distance between this  $\delta$

methylene proton and the carbon atom, estimated from the  $3_1$  helical structure, is about 1.8 Å. If  $(3 \cos^2 \theta - 1)$  in the term of the anisotropic interaction is nearly equal to unity, the anisotropic hyperfine splitting turns out to be about 4.8 G from the distance of 1.8 Å. Other three  $\delta$  carbon protons are situated far from the  $\alpha$  carbon atom to give only a weak dipole-dipole interaction.

The value of 4.8 G due to the  $\delta$  carbon proton is comparable to that of the dipole-dipole interaction of the  $\beta$  protons. The computation of the e.s.r. spectrum shows that the spectrum for  $\theta = 90^{\circ}$  in the stretched sample can be obtained by adding a splitting of 4-5 G to the spectrum of bulk sample. This fact suggests that the anisotropy of the spectrum observed at  $\theta = 90^{\circ}$  is attributed to the dipole-dipole interaction with the  $\delta$  carbon proton rather than that with four protons of the  $\beta$  methylene which has both anisotropic and isotropic interaction. The slight change of the hyperfine coupling constant from that of the bulk sample, due to slight anisotropy of the  $\beta$  methylene proton, may mainly give rise to a broadening of the linewidth in the spectrum at  $\theta = 90^{\circ}$ .

As for the spectrum observed at  $\theta = 0^{\circ}$ , it can be obtained by a slight change of the hyperfine coupling constant due to  $\beta$  methylene protons; therefore, the anisotropic interaction contributing to this spectrum may be supposed to be caused by the  $\beta$  methylene protons rather than the  $\delta$  methylene proton which is located in the position to make the value of  $(3 \cos^2 \theta - 1)$  fairly small in such a case.

By measurement of the stretched sample at  $-196^{\circ}\text{C}$ , a poorly resolved 17 line spectrum and 9 line spectrum were observed at  $\theta = 0^{\circ}$  and  $\theta = 90^{\circ}$ , respectively. This may be attributed to the following reasons: as the 17 line spectrum observed at  $\theta = 0^{\circ}$  is well-resolved, it may still remain the 17 line spectrum even if the linewidth increases at  $-196^{\circ}\text{C}$ , owing to the decrease of the oscillation frequency of the  $\beta$  methylene proton, though its resolution is made poorer. On the contrary, the poorly resolved spectrum observed at  $\theta = 90^{\circ}$  may convert to the 9 line spectrum by slight increase of the linewidth.

#### REFERENCES

- Ohnishi, S., Ikeda, Y., Kashiwagi, M. and Nitta, I. *Polymer* 1961, **2**, 119
- Fisher, H. and Hellwedge, K. H. *J. Polym. Sci.* 1962, **56**, 33
- Loy, B. R. *J. Polym. Sci. (A)* 1963, **1**, 2251
- Forrestol, L. J. and Hodgson, W. G. *J. Polym. Sci. (A)* 1964, **2**, 1273
- Ayscough, P. B. and Munari, S. *J. Polym. Sci. (B)* 1966, **4**, 503
- Iwasaki, M., Ichikawa, T. and Toriyama, K. *J. Polym. Sci. (B)* 1967, **5**, 427
- Nara, S., Kashiwabara, H. and Sohma, J. *J. Polym. Sci. (A-2)* 1967, **5**, 929
- Heller, C. and McConnell, H. M. *J. Chem. Phys.* 1960, **32**, 1535
- Natta, G. and Corradini, P. *Nuovo Cimento* 1960, **15**, (Suppl. 1) 40
- Ohnishi, S., Sugimoto, S. and Nitta, I. *J. Chem. Phys.* 1962, **37**, 1283
- Pooley, D. and Whiffen, D. H. *Mol. Phys.* 1961, **4**, 81
- Horsfield, A., Morton, J. R. and Whiffen, D. H. *Mol. Phys.* 1961, **4**, 169
- Morton, J. R. and Horsfield, A. *Mol. Phys.* 1961, **4**, 219
- Ogawa, S. *J. Phys. Soc. Japan* 1961, **16**, 1488
- McCarthy, R. L. and MacLachlan, A. *J. Chem. Phys.* 1961, **35**, 1625

# Association of stereoregular poly(methyl methacrylates): 2. Formation of stereocomplex in bulk

E. L. Feitsma, A. de Boer and G. Challa

Department of Polymer Chemistry, State University of Groningen, Groningen, The Netherlands

(Received 17 September 1974; revised 18 December 1974)

Blends of isotactic and syndiotactic poly(methyl methacrylate) (*i*- and *s*-PMMA) are obtained by precipitation from chloroform and acetone solutions. By differential scanning calorimetry and dynamic-mechanical measurements the formation of stereocomplexes from *i*- and *s*-PMMA in bulk is demonstrated. After annealing of the blends at 130–160°C a melting endotherm is detected and it is established by X-ray analysis that this endotherm is caused by formation of crystalline stereocomplex. The rate of complex formation is maximal at 140°C and the extent of complex formation is maximal at an isotactic-rich composition. It appears that the difference in solvent history can be removed by heating to 240°C. The subsequent S-shaped course of glass transition temperature,  $T_g$ , with composition is explained by the occurrence of some complex formation during cooling from 240°C. Asymmetry and shift of the dynamic-mechanical damping curves after annealing are also explained by the formation of complexes. A mechanism is proposed with helical isotactic chains acting as nuclei for a fringed micelle type of complex formation.

## INTRODUCTION

In previous papers it was reported<sup>1–5</sup> that complex formation between isotactic and syndiotactic poly(methyl methacrylate) (*i*- and *s*-PMMA) can occur in suitable solvents, even at concentrations far below that with homogeneous segmental distribution. Spěvácěk *et al.*<sup>6</sup> have shown by high resolution n.m.r. investigations that fixed structures are present in the complexes in solution. The physical properties of isolated stereocomplexes are different from those of the composing components. The complexes are crystalline, as shown by X-ray analysis<sup>2</sup> and their melting points are different from those of *i*- and *s*-PMMA<sup>1</sup>.

As the solvents have different influence on complex formation, we divided them in three types: A, strongly complexing solvents; B, weakly complexing solvents; C, non-complexing solvents. This classification was clearly illustrated in the course of reduced viscosity with composition of mixtures of *i*- and *s*-PMMA in different solvents<sup>1</sup>. The heats of complex formation of *i*- and *s*-PMMA in different solvents, as reported by Byros *et al.*<sup>7</sup> are also in agreement with this classification. Moreover, Buter *et al.*<sup>8</sup> had found that the effect of solvent on replica polymerization of methyl methacrylate (MMA) along stereoregular PMMA is in line with its complexing ability.

Pyrlik *et al.*<sup>9</sup> reported that complex formation occurred even in very concentrated (22.4%) solutions of *i*- and *s*-PMMA in *o*-xylene. At the same time we were interested to know whether *i*- and *s*-PMMA can associate not only in solution but also in bulk. Therefore, blends of *i*- and *s*-PMMA of different origins were subjected to calorimetric and dynamic-mechanical investigations.

## EXPERIMENTAL

The polymers *i*- and *s*-PMMA were prepared according to known procedures<sup>10,11</sup>. The data of the used polymers are

Table 1 Data of used polymers

	Number	triads <i>i</i> - <i>h</i> - <i>s</i>	$[\eta]$ (dl/g)	$\bar{M}_v \times 10^{-3}$
<i>i</i> -PMMA	<i>i</i> MA-103	91 : 6 : 3	1.95	570
	<i>i</i> MA-107	91 : 6 : 3	1.99	600
<i>s</i> -PMMA	<i>s</i> MA-102	5 : 9 : 86	1.33	350
	<i>s</i> MA-106	4 : 8 : 88	1.37	370

compiled in Table 1. The tacticities of PMMA were measured on 5% solutions in *o*-dichlorobenzene<sup>12</sup> at 160°C by 60 MHz n.m.r. spectroscopy with a Varian A-60 instrument.  $[\eta]$  of the PMMA samples were determined in chloroform at 25°C. For the calculation of  $\bar{M}_v$  we used the relationship<sup>13</sup>:  $[\eta] = 4.8 \times 10^{-5} \bar{M}_v^{0.8}$ .

Samples of *i*- and *s*-PMMA blends were prepared by mixing 1 wt% chloroform solutions of *i* MA-103 and *s* MA-102 in various ratios under continuous stirring. After 2 h the mixed solutions were precipitated in excess petroleum ether (b.p. 40–60°C) and the precipitates were dried at 40°C in vacuum for 5 days. In the same way blends were prepared from acetone solutions.

Glass transitions,  $T_g$ , and melting temperatures,  $T_m$ , were measured with a differential scanning calorimeter (Perkin-Elmer, DSC-1B) at a heating rate of 8°C/min. The beginning of the  $c_p$  jump was taken as  $T_g$  and the maximum of the melting endotherm as  $T_m$ .

Dynamic-mechanical measurements were performed on  $7 \times 0.7 \times 0.3$  cm bars with a torsion pendulum of Nonius/TNO at a frequency of ~1 Hz in the temperature range 20–170°C. The samples were obtained by precipitation from *i* MA-107 and *s* MA-106 solutions in acetone and they were heated in a press for 10 min at 240°C. The bars were obtained by pressing the samples at 50 kg/cm<sup>2</sup> for 2 min at the same temperature. After fast cooling to 150°C the bars were cooled slowly down to room temperature



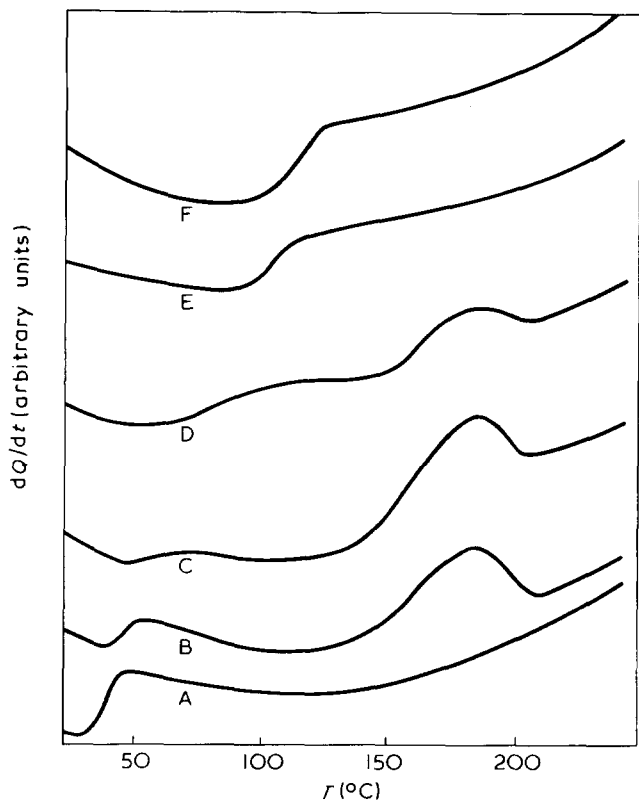


Figure 1 Some characteristic thermograms of samples precipitated from chloroform after annealing for 2 min at 140°C in the d.s.c. A, 100 : 0; B, 80 : 20; C, 60 : 40; D, 40 : 60; E, 20 : 80; F, 0 : 100 i/s-PMMA

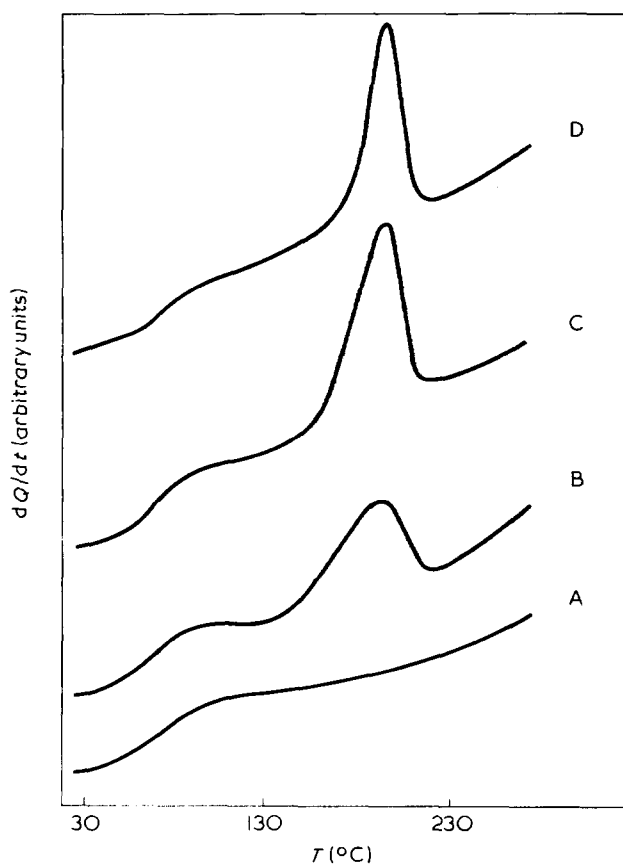


Figure 2 Thermograms of 60 : 40 (w/w) i/s PMMA precipitated from chloroform after annealing for various times at 140°C. A, not annealed; B, 2 min; C, 4 h; D, 40 h annealed

under pressure. From the damped oscillations loss moduli  $G''$ , storage moduli  $G'$  and loss tangents  $\tan \delta$  of the samples were calculated.

## RESULTS

### D.s.c. experiments

In Figure 1 some characteristic thermograms are plotted for samples obtained from the non-complexing solvent chloroform, recorded after annealing at 140°C for 2 min in the d.s.c. An endotherm with a maximum of about 190°C is found for most of the blends. Figure 2 shows the effect of annealing times at 140°C on the area of the endotherm for the 60 : 40 i/s-PMMA composition. The endotherms in Figures 1 and 2 indicate that complex formation of i- and s-PMMA in bulk can occur.

Annealing experiments were carried out for the whole composition range with 21 mg samples from chloroform at different temperatures of complex formation ( $T_c$  130–170°C). In Figure 3 the area of the endotherm at about 190°C as recorded by d.s.c. is plotted against composition after annealing at 140°C and 150°C for 4 and 40 h. The values measured after 2 min at 140°C (Figure 1) give a somewhat lower curve than those after 4 h. The extent of complex formation reaches an end-value after 40 h at 140°C. More than 75 h are needed at 130 and 150°C to reach the same end-value, whereas the rate of complex formation is almost zero at 170°C. Thus, it is clear that the rate of complex formation of i- and s-PMMA in bulk is maximal at about 140°C. Moreover, it appears from Figure 3 that the complex formation curve shifts to lower s-PMMA content for increasing temperature and decreasing time of complex formation. Finally, it is evident that pure i-PMMA and pure s-PMMA do not crystallize at all under these conditions.

For the sake of completeness, Figure 4 shows that there is a great resemblance between the X-ray diffractograms of an annealed sample from chloroform and that of stereo-complex crystallized from dilute solution in acetone. These diffractograms differ strongly from those of pure i- or s-PMMA<sup>8</sup>. So, the crystalline material in bulk consists of stereocomplexes of i- and s-PMMA indeed.

In Figure 5  $T_g$  and  $T_m$  are plotted against composition for mixtures obtained from the strongly complexing solvent acetone. The  $T_m$  of about 205°C originates from complexes, which were already formed in the acetone solutions<sup>1</sup>. Only at the left and right side of the composition range were  $T_g$  values detected.

$T_g$  values measured after premelting for 2 min at 240°C

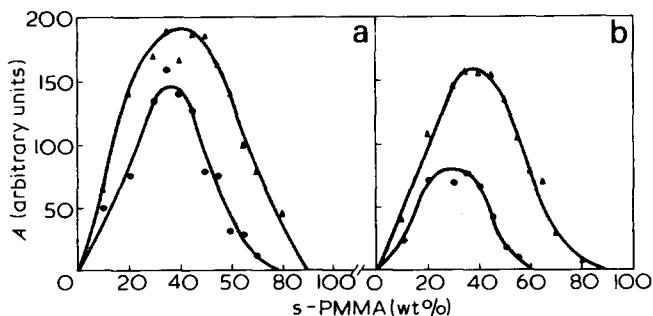


Figure 3 Area (A) of the endotherm recorded by d.s.c. after annealing at (a) 140°C and (b) 150°C versus wt% s-PMMA of samples precipitated from chloroform. Annealing time: ●, 4 h; ▲, 40 h. Experimental error about 10%

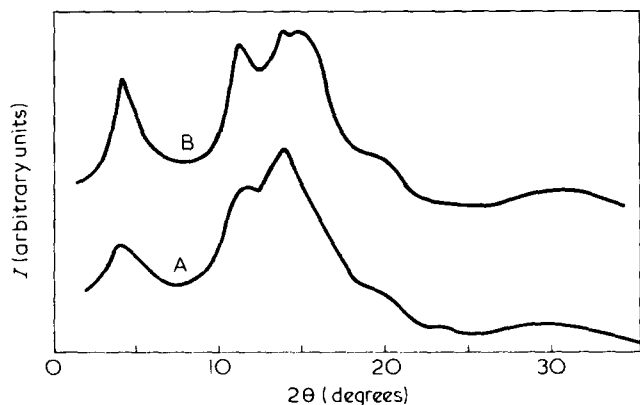


Figure 4 X-ray diffraction intensity,  $I$ , versus diffraction angle  $2\theta$  of: (A) 60:40 (w/w) i/s PMMA precipitated from chloroform after annealing for 3 days at  $140^\circ\text{C}$ ; (B) stereocomplex of 67:33 (w/w) i/s PMMA separated from 0.2 wt% acetone solution

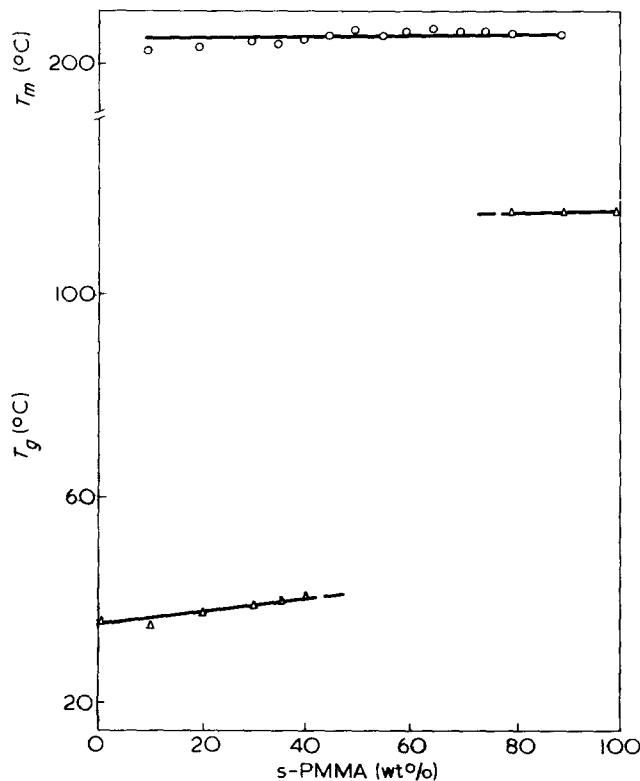


Figure 5 Glass transition temperatures ( $T_g$ ) by d.s.c. of samples precipitated from acetone versus wt% s-PMMA. Melting temperatures ( $T_m$ ) are also presented

in the d.s.c. are plotted against composition in Figures 6 and 7 for blends from acetone and chloroform respectively. To indicate the width of the glass transition the end of the  $c_p$  jump is also presented. No endotherm is measured. It is clear that Figures 6 and 7 are almost identical. Samples from the weakly complexing solvent toluene (type B solvent) demonstrate the same course.

#### Dynamic-mechanical measurements

In order to check the d.s.c. results dynamic-mechanical measurements were performed. In Figure 8  $\tan \delta$  is plotted against temperature for various compositions. After the measurements the bars were annealed at  $140^\circ\text{C}$  for 120 h. The effect of annealing is shown in Figure 9, where  $\tan \delta$  is plotted against temperature for some pairs of not-annealed and annealed bars. When the logarithm of the loss modulus

( $\log G''$ ) is plotted against temperature a similar picture is obtained. It is seen from the curves in Figure 9 that not all material is complexed after annealing for 120 h, not even for i-PMMA rich compositions although d.s.c. would not detect a glass transition anymore.

#### DISCUSSION

Acetone is a strongly complexing solvent and the melting endotherms of samples obtained from acetone originate

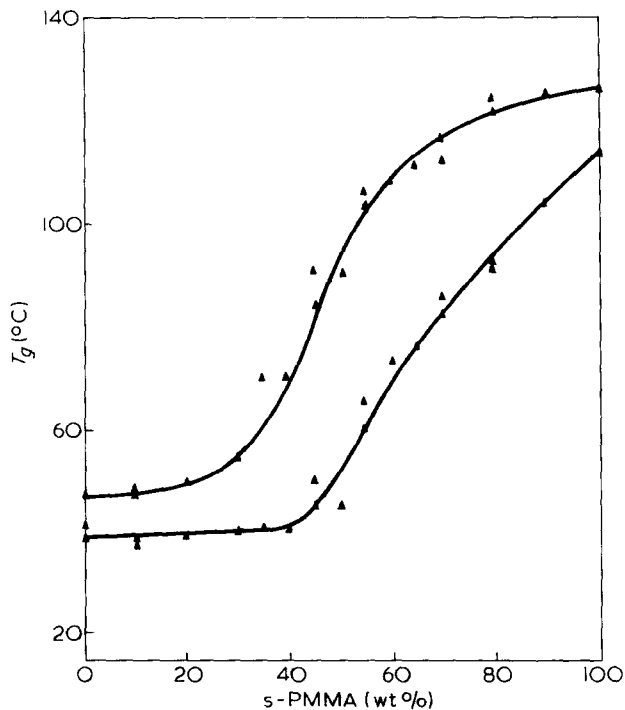


Figure 6 Temperatures of beginning and end of the glass transition of samples precipitated from acetone versus wt% s-PMMA after pre-melting for 2 min at  $240^\circ\text{C}$  in the d.s.c.

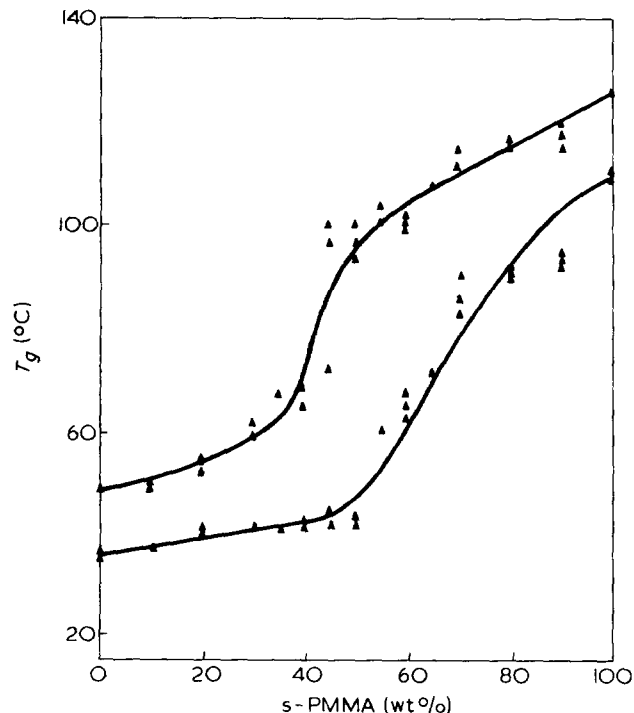


Figure 7 Temperatures of beginning and end of the glass transition of samples precipitated from chloroform versus wt% s-PMMA after pre-melting for 2 min at  $240^\circ\text{C}$  in the d.s.c.

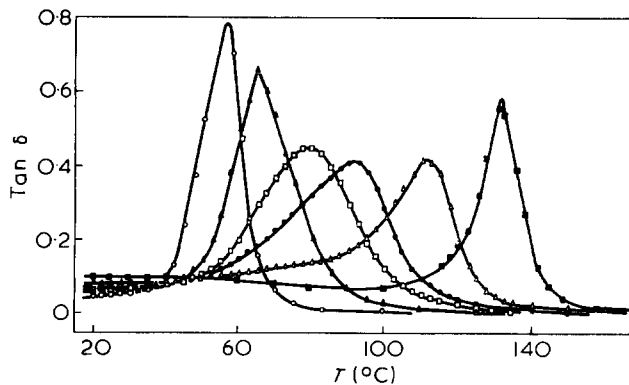


Figure 8 Loss tangent,  $\tan \delta$  at about 1 Hz versus temperature for various i/s PMMA compositions.  $\circ$ , 100:0;  $\blacktriangle$ , 80:20;  $\square$ , 60:40;  $\bullet$ , 40:60;  $\triangle$ , 20:80;  $\blacksquare$ , 0:100 i/s-PMMA

from stereocomplexes already formed in solution (Figure 5). The measured  $T_g$  at the left and right side of the composition range is probably caused by non-complexed excess i-PMMA and s-PMMA, respectively. The course of  $T_g$  with composition for samples from acetone becomes almost identical to that of samples from chloroform after premelting at 240°C (Figures 6 and 7). So, it can be concluded that the solvent history is removed by heating to 240°C. After such elimination of solvent history equal compositions become comparable with respect to complex formation irrespective of their origin.

From Figures 1–4 it is evident that formation of crystalline complex takes place in bulk in the temperature range of 130–160°C with a maximum rate at 140°C.

Previous results<sup>1</sup> indicated that in very dilute solutions of type A solvents maximum complex formation occurs at an i/s ratio of 1:2 with  $T_m = 210^\circ\text{C}$  of the separated complex. At higher concentrations the i/s ratio tended to shift to higher values. In type B solvents (weakly complexing) maximum complex formation appears, even at low concentrations, at an i/s ratio of 1:1 with  $T_m \approx 200^\circ\text{C}$ . In line with this trend maximum complex formation in bulk always occurs at ratios below 1:1 (Figure 3) with  $T_m \approx 190^\circ\text{C}$ . Moreover, it follows from the area of the endotherms that the maximum amount of crystalline complex in the blends is almost two times lower than that of the complexes separated from acetone (see also Figure 4). So, complex formation in bulk is a less selective process than it is in dilute solution and probably yields smaller and less regular regions of complexed material.

Figure 2 suggests that it is quite possible that some complex is formed in the bulk just during cooling from 240°C in the d.s.c. although no distinct endotherm could be measured. Thus at low s-PMMA contents all s-PMMA chains may be locally fixed in complexes and the measured  $T_g$  values in Figures 6 and 7 originate from non-complexed excess i-PMMA. At increasing s-PMMA content no longer can all s-PMMA chains be complexed during cooling. Hence complex formation gives rise to a distribution of local compositions of non-complexed material. This is demonstrated by a broadening of the glass transition in Figures 6–8. Above 50 wt% s-PMMA the rate of complex formation in bulk decreases strongly (Figures 1 and 3), which means that the composition of non-complexed material approaches the overall composition. At high s-PMMA contents no complex formation occurs at all and the glass transition corresponds to that of the overall composition.

Krause *et al.*<sup>14</sup> investigated dilatometrically the course of  $T_g$  with composition of i- and s-PMMA blends obtained

from chloroform. Examining their results it appears that the glass transitions are very broad. So it is quite possible that in those blends complex formation in bulk has taken place too.

Figure 9 shows clearly that annealing at 140°C produces an additional broadening of the glass transition towards higher temperatures. The largest effect is seen in the middle of the composition range, where complex formation is most pronounced (Figure 3). The shift towards higher temperatures may be partly due to stresses created in the amorphous regions as a result of formation of tie molecules between the complex crystallites. Moreover, we know from Figure 2 that the endotherms sharpen during annealing, which points to improvement of complex crystallites. The complexed regions probably approach their optimum composition by further association of material in some stoichiometric ratio, which results in a larger asymmetry of the damping curve during longer annealing times. Since the optimum composition of complexes in bulk seems to be somewhat richer in i-PMMA (Figure 3), the non-complexed material tends to include more s-PMMA than corresponds with the overall composition. As s-PMMA has the highest  $T_g$  this compositional change yields a further shift of the damping curves towards higher temperatures.

Figure 3 showed that the complex formation is most fast at 140°C in i-PMMA rich compositions. Further, we know from Figure 2 that more than half of the transformation takes place within 2 min. Since 140°C is near to the glass transition temperature of s-PMMA it is reasonable to assume that chain segments of i-PMMA form nuclei for complex formation, probably by attaining the favourable helix conformation<sup>2,15</sup>. Then chain segments of s-PMMA partly associate with the helices, initiating crystallization according to the fringed micelle model. This mechanism of molecular nucleation is supported by the observation that samples preheated to 300°C crystallize with the same rate as samples which have been preheated only 20°C above  $T_m$ .

If the number of crystallites was increasing in time, this

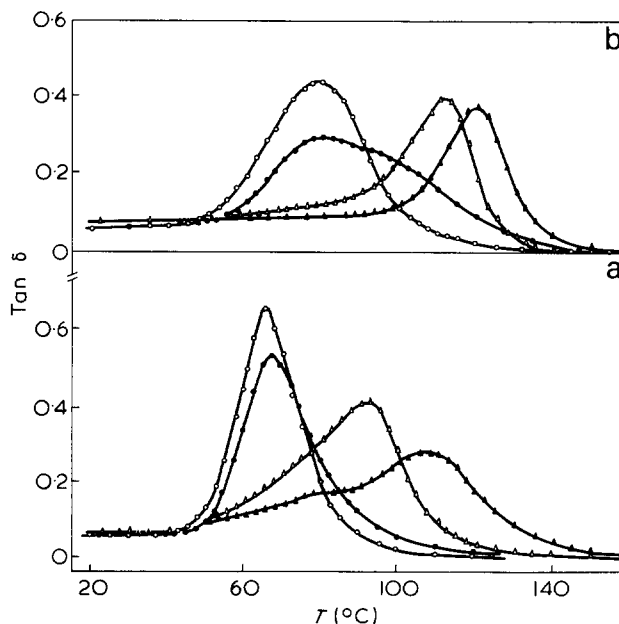


Figure 9 Effect of annealing on loss tangent,  $\tan \delta$  at about 1 Hz versus temperature for four i/s-PMMA compositions. (a):  $\circ$ , 80:20;  $\triangle$ , 40:60; (b):  $\circ$ , 60:40;  $\triangle$ , 20:80;  $\bullet$ ,  $\blacktriangle$ , after annealing for 120 h at 140°C

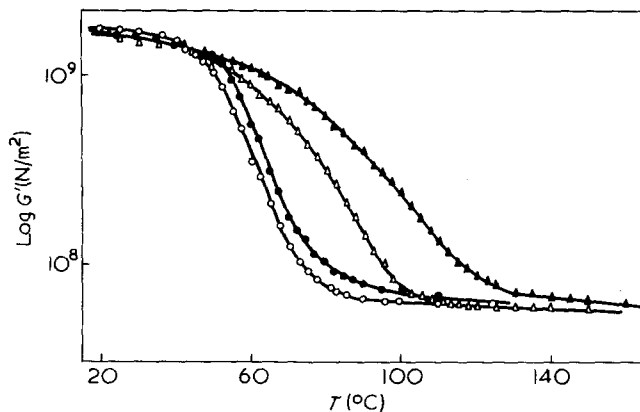


Figure 10 Effect of annealing on storage modulus ( $\log G'$ ,  $\text{N/m}^2$ ) at 0.65 Hz versus temperature for two *i/s*-PMMA compositions.  $\circ$ , 80:20;  $\triangle$ , 40:60;  $\bullet$ ,  $\blacktriangle$ , after annealing for 120 h at 140°C

should result in a tighter network with a higher value of the storage modulus  $G'$  above the glass transition. However, Figure 10 shows that the values of  $\log G'$  interpolated to a fixed frequency of 0.65 Hz are practically the same for annealed and not-annealed bars. In our opinion this suggests that the main process taking place in bulk during annealing comprises growth of complex crystallites as

was first supposed by Pyrlík *et al.*<sup>9</sup> for stereocomplexes of *i*- and *s*-PMMA in concentrated solutions in *o*-xylene.

## REFERENCES

- 1 Challa, G., de Boer, A. and Tan, Y. Y. *Int. J. Polym. Mat.* in press
- 2 Liquori, A. M. *et al. Nature* 1965, **206**, 358
- 3 Chiang, R., Burke, J. J., Threlkeld, J. O. and Orofino, T. A. *J. Phys. Chem.* 1966, **70**, 3591
- 4 Liu, H. Z. and Liu, K. J. *Macromolecules* 1968, **1**, 157
- 5 Borchard, W., Kalawrytinis, G., Mohadjer, B., Pyrlík, M. and Rehage, G. *Angew. Makromol. Chem.* 1973, **29/30**, 471
- 6 Spěvácěk, J. and Schneider, B. *Makromol. Chem.* 1974, **175**, 2939
- 7 Biròs, J., Máša, Z. and Pouchlý, J. *Eur. Polym. J.* 1974, **10**, 629
- 8 Buter, R., Tan, Y. Y. and Challa, G. *J. Polym. Sci. (Polym. Chem. Edn)* 1973, **11**, 2975
- 9 Pyrlík, M., Borchard, W., Rehage, G. and Uerpmann, E. P. *Angew. Makromol. Chem.* 1974, **36**, 133
- 10 Goode, W. E., Owens, F. H., Fellmann, R. P., Snyder, W. H. and Moore, J. H. *J. Polym. Sci.* 1960, **46**, 317
- 11 Abe, H., Imai, K. and Matsumoto, M. *J. Polym. Sci. (C)* 1968, **23**, 469
- 12 Ramey, K. C. *J. Polym. Sci. (B)* 1967, **5**, 859
- 13 Bischof, J. and Desreux, V. *Bull. Soc. Chim. Belg.* 1952, **61**, 10
- 14 Krause, S. and Roman, H. *J. Polym. Sci. (A)* 1965, **3**, 1631
- 15 Tadokoro, H., Chatani, Y., Kusanagi, H. and Yokoyama, M. *Macromolecules* 1970, **3**, 441

# Kinetics of graft polymerization of styrene on *cis*-1,4-polybutadiene

P. Manaresi, V. Passalacqua and F. Pilati

*Istituto Chimico, Facoltà di Ingegneria, Università di Bologna, Bologna, Italy*  
(Received 16 July 1974; revised 31 October 1974)

By measurements of polymerization rate, grafting efficiency and number-average molecular weight of free and grafted polystyrene, the  $\alpha$ -dicumyl peroxide initiated polymerization of styrene on *cis*-1,4-polybutadiene at 100°C and at low extents of reaction was studied. The polymerization rate and the polystyrene molecular weights decreased with the rubber content of the solution. The grafting efficiency was found to be substantially independent of the peroxide concentration, but to increase with rubber content. A rigorous mathematical model of the reaction was developed, from which it has been possible to confirm the proposed mechanism and to establish the value of many kinetic constants.

## INTRODUCTION

In previous papers<sup>1-3</sup> we have studied the dicumyl peroxide initiated graft polymerization of styrene with *cis*-1,4-polybutadiene, mainly by measurement of overall polymerization rates and grafting efficiencies. It has been possible to outline an initial reaction mechanism of direct attack by hydrogen abstraction of initiator radicals onto rubber, to derive a rate equation and to establish the value of a combined kinetic constant. Some approximations were introduced in the mathematical treatment, and chain transfer reactions, thermal initiation and termination between rubber radicals were neglected.

This paper deals with an experimental and theoretical extension of the previous work. A more rigorous mathematical treatment is developed with the aid of a computer, and the calculated values of polymerization rates, number-average degrees of polymerization of free and grafted polystyrene, and grafting efficiencies are compared with the experimental data. This was done to establish the complete initial reaction mechanism and to determine the values of the kinetic constants.

## EXPERIMENTAL

### Materials

*cis*-1,4-Polybutadiene used was Taktene 1202 S (Polysar Italiana SpA) (content: *cis*-1,4 = 96.1%; *trans*-1,4 = 2.1%; vinyl = 1.8% by i.r. analysis). Other characteristics were:  $[\eta]^{30} = 2.2$  dl/g in toluene;  $\bar{M}_n = 90\,000$  (osmometry); gel content < 0.1%. The polybutadiene was freed of antioxidants by repeated acetone extractions, and the disappearance of the u.v. band at 240–280 nm was verified.

Styrene was supplied by Montedison SpA, and had a styrene content > 99.8%. The monomer was twice distilled under reduced pressure prior to use.

$\alpha$ -Dicumyl peroxide was supplied by Noury & Van der Lande, and was purified from two recrystallizations with ethanol.

Di-*t*-butyl hydroperoxide was obtained from Merck-Schuchardt and osmium tetroxide from Carlo Erba SpA.

The solvents benzene, toluene, chlorobenzene, methanol, methyl ethyl ketone, *t*-butyl alcohol and benzaldehyde were Carlo Erba reagent grade products.

### Grafting reaction

Grafting was carried out in dilatometers, starting from styrene solutions of polybutadiene (2–9 wt %) containing  $\alpha$ -dicumyl peroxide (0.1–0.3 wt %) as initiator. Dilatometers were filled under vacuum with repeatedly de-aerated solutions, and the polymerizations were carried out at  $100.0 \pm 0.1^\circ\text{C}$ . Usually monomer conversion did not exceed 10%; only in a few cases have conversions up to 25% been purposely reached. Polymerization rates, after dilatometer calibration, were calculated from the initial slopes of the dilatometric plots. The crude polymerizate was precipitated in an excess of methanol, washed and then vacuum dried at 50°C and weighed. The extent of polymerization  $C$  (%) is given by:

$$C = \frac{100(A - R)}{100 - R}$$

where  $A$  is the amount (wt %) of gross polymer in the solution after the polymerization, and  $R$  is the polybutadiene (wt %) in the initial solution.

### Separation of free polystyrene from grafted polystyrene

As described in previous papers, free polystyrene was separated from the gross polymer by repeated extractions with methyl ethyl ketone and subsequent centrifuging in order to get a better separation of the two phases. Grafting efficiency was calculated from the amount of polystyrene in the grafted fraction, determined by n.m.r. analysis of the CS<sub>2</sub> solution<sup>4</sup>. Grafting efficiency,  $E$  (%) is given by:

$$E = \frac{10^4 \times PR}{C(100 - P)(100 - R)}$$

where  $P$  is the polystyrene (wt %) in the grafted fraction.

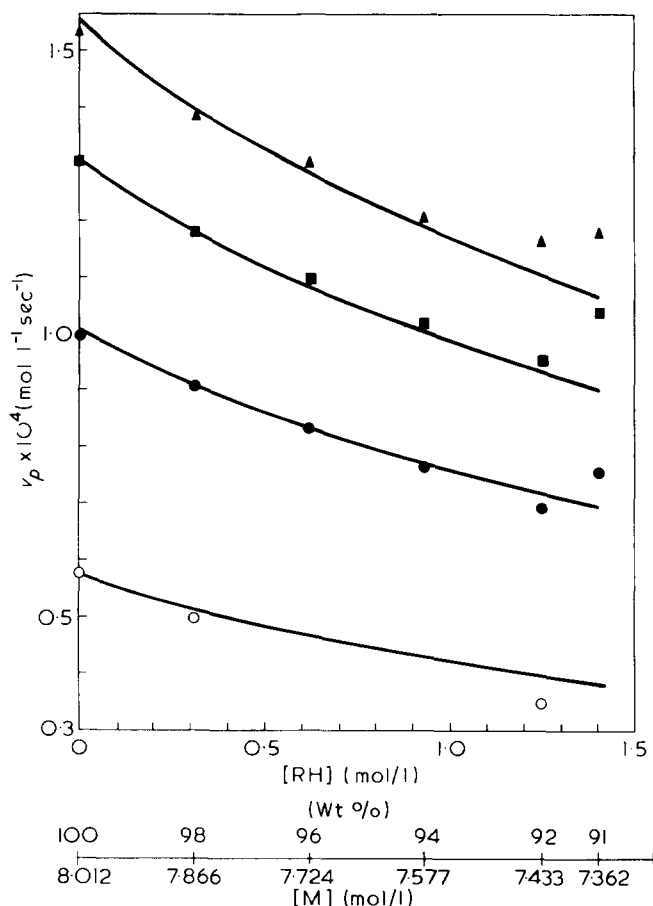


Figure 1 Calculated curves and experimental data for overall polymerization rate.  $\circ$ , thermal;  $\bullet$ , 0.00310;  $\blacksquare$ , 0.00620;  $\blacktriangle$ , 0.00930 mol/l of peroxide

#### Degradation of rubber backbone

In order to obtain reliable molecular weight data for grafted polystyrene, it is necessary to make use of a degradation technique which leaves unaffected polystyrene grafts. The method proposed by Hubin<sup>5</sup> and Locatelli *et al.*<sup>6</sup> based on the polybutadiene degradation with hydroperoxides and  $\text{OsO}_4$  in presence of benzaldehyde was employed.

#### Molecular weight determination

Number-average molecular weights of polystyrenes were determined by osmometry (toluene,  $38^\circ\text{C}$ ) with a Mechrolab Model 502 high-speed membrane osmometer. Non-aqueous Schleicher and Schuell type 0.8 membranes were used. Data were taken at four or five different concentrations and graphical extrapolations were made of  $\pi/c$  versus  $c$  plots to zero concentration.

### RESULTS AND TREATMENT OF DATA

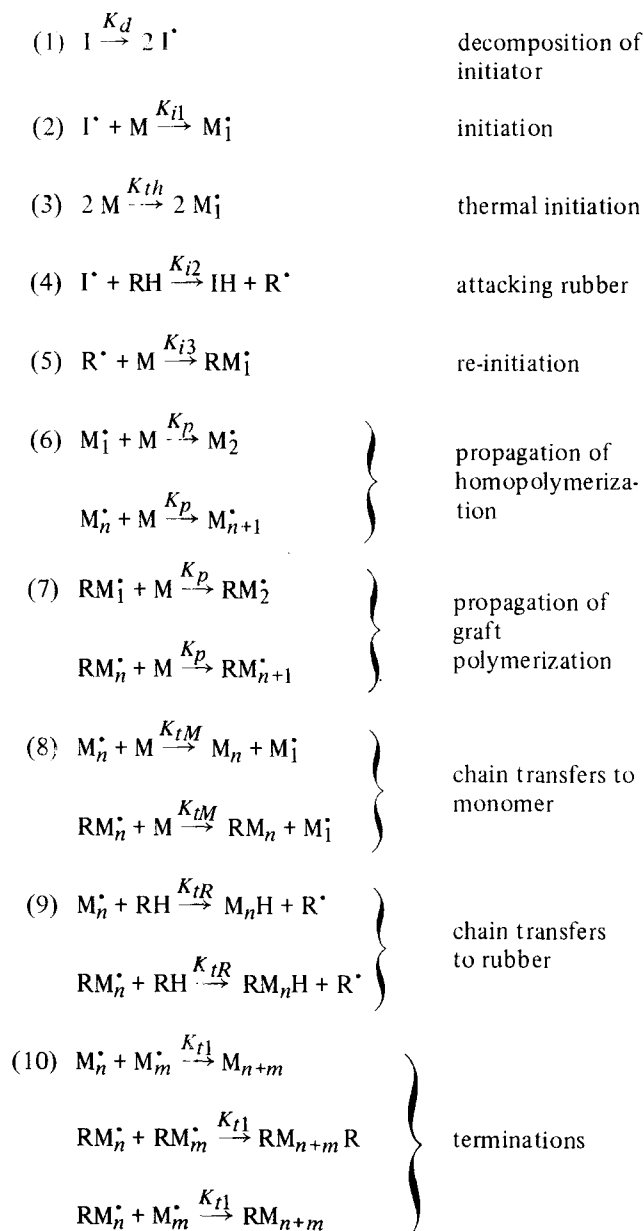
In Figure 1 the results pertaining to the initial rate of polymerization as a function of rubber and initiator concentrations are reported. The data indicate that the presence of *cis*-1,4-polybutadiene lowers the rate of styrene polymerization. This takes place regularly only up to a rubber concentration of about 8%, where the rate has a minimum value.

Table 1 summarizes the results obtained for the grafting efficiency and number-average degree of polymerization of free and grafted polystyrene. As may be seen, the grafting efficiency is slightly lower in the absence than in the presence of initiator, but is almost independent of initiator

concentration. The grafting efficiency increases with the rubber concentration and, at high rubber concentrations decreases strongly with increasing styrene conversion. The number-average degree of polymerization of free polystyrene is noticeably decreased in the presence of polybutadiene, and the magnitude of such effect is increasing with rubber concentration, at the same catalyst concentration. The number-average degree of polymerization of grafted polystyrene is slightly lower than that of free polystyrene at low rubber contents, but greatly increases with increasing rubber concentration. From such molecular weight data it is also evident that in the grafted fraction there exists some unreacted free rubber.

Therefore, it is likely that grafting occurs by initiator radical attack on polybutadiene as previously proposed, but the molecular weight data indicate that chain transfer processes cannot be neglected. The reaction mechanism previously proposed was therefore extended by introducing chain transfer with rubber and with monomer, termination between rubber radicals and, owing to the relatively high polymerization temperature, thermal initiation.

Therefore the mechanism proposed for low extents of reaction and low rubber concentrations is:





$$\frac{d[I^*]}{dt} = 0 = 2K_d[I] - K_{i1}[I^*][M] - K_{i2}[I^*][RH] \quad (1)$$

$$\frac{d[M_{tot}^*]}{dt} = 0 = K_{i1}[I^*][M] + 2K_{th}[M]^2 + K_{i3}[R^*][M] - K_{tR}[RH][M_{tot}^*] - 2K_{t1}[M_{tot}^*]^2 - K_{t2}[R^*][M_{tot}^*] \quad (2)$$

$$\frac{d[R^*]}{dt} = 0 = K_{i2}[I^*][RH] + K_{tR}[RH][M_{tot}^*] -$$

$$K_{i3}[R^*][M] - K_{t2}[R^*][M_{tot}^*] - 2K_{t3}[R^*]^2 \quad (3)$$

From equation (1) it follows:

$$[I^*] = \frac{2K_d[I]}{K_{i1}[M] + K_{i2}[RH]} \quad (4)$$

By introducing equation (4) into equation (2), equation (5) follows:

$$[R^*] = \frac{2[M_{tot}^*]^2 + \frac{K_{tR}}{K_{t1}}[RH][M_{tot}^*] - \frac{2K_{th}}{K_{t1}}[M]^2 - \frac{2K_d[I]}{K_{t1}\left(1 + \frac{K_{i2}[RH]}{K_{i1}[M]}\right)}}{\frac{K_{i3}}{K_{t1}}[M] - \frac{K_{t2}}{K_{t1}}[M_{tot}^*]} \quad (5)$$

By introducing equations (4) and (5) into equation (3), and rationalizing, it is possible to obtain the equation:

$$[M_{tot}^*]^4(1 - 4\theta) + [M_{tot}^*]^3(1 - 4\theta)\gamma[RH] + [M_{tot}^*]^2 \left[ \frac{8\theta\delta[I]}{\left(1 + \alpha \frac{[RH]}{[M]}\right)} + 8\theta J[M]^2 - \theta\gamma^2[RH]^2 - J[M]^2 - \beta^2[M]^2 - \beta\gamma[RH][M] - \delta[I] \frac{\left(1 - \alpha \frac{[RH]}{[M]}\right)}{\left(1 + \alpha \frac{[RH]}{[M]}\right)} \right] + [M_{tot}^*] \left[ \frac{4\theta J\gamma[M]^2[RH] + \frac{4\theta\gamma\delta[RH][I]}{\left(1 + \alpha \frac{[RH]}{[M]}\right)}}{\left(1 + \alpha \frac{[RH]}{[M]}\right)} + \frac{2\beta\alpha\delta[RH][I]}{\left(1 + \alpha \frac{[RH]}{[M]}\right)} \right] + \delta\beta^2[M]^2[I] + J\beta^2[M]^4 - 4\theta J^2[M]^4 - \frac{4\theta\delta^2[I]^2}{\left(1 + \alpha \frac{[RH]}{[M]}\right)^2} - \frac{8\theta\delta J[M]^2[I]}{\left(1 + \alpha \frac{[RH]}{[M]}\right)} = 0 \quad (6)$$

where

$$\theta = \frac{K_{t1}K_{t3}}{K_{t2}^2}; J = \frac{K_{th}}{K_{t1}}; \delta = \frac{K_d}{K_{t1}}; \beta = \frac{K_{i3}}{K_{t2}}; \gamma = \frac{K_{tR}}{K_{t1}}; \alpha = \frac{K_{i2}}{K_{i1}} \quad (7)$$

From equation (6) it is possible to calculate, for fixed values of the kinetic constants, the concentration of  $M_{tot}^*$  and the overall polymerization rate  $v_p = K_p[M][M_{tot}^*]$ .

In order to calculate number-average degrees of polymerization of free and grafted polystyrene and grafting efficiencies, the concentrations of radicals  $M^*$  and  $RM^*$  were separated in the calculus. Equation (2) pertaining to the stationary state for radicals  $M_{tot}^*$  becomes:

$$\frac{d[M^*]}{dt} = 0 = K_{i1}[I^*][M] + 2K_{th}[M]^2 + K_{tM}[M][RM^*] - K_{tR}[RH][M^*] - 2K_{t1}[M^*]^2 - 2K_{t1}[M^*][RM^*] - K_{t2}[R^*][M^*] \quad (8)$$

$$\frac{d[RM^*]}{dt} = 0 = K_{i3}[M][R^*] - K_{tM}[M][RM^*] - K_{tR}[RH][RM^*] - 2K_{t1}[RM^*]^2 - 2K_{t1}[RM^*][M^*] - K_{t2}[R^*][RM^*] \quad (9)$$

By introducing (4) and (5) into equation (8), substituting ( $[M_{tot}^*] - [M^*]$ ) for  $[RM^*]$ , it is possible to obtain an equation (eqn.10) for the concentration of radicals  $M^*$ :

$$[M^*] = \frac{\frac{2\beta\delta[I][M]}{\left(1 + \alpha \frac{[RH]}{[M]}\right)} + 2\beta J[M]^3 + \beta\epsilon[M]^2[M_{tot}^*] - \frac{2\delta[I][M_{tot}^*]}{\left(1 + \alpha \frac{[RH]}{[M]}\right)} - 2J[M]^2[M_{tot}^*] - \epsilon[M][M_{tot}^*]^2}{2\beta[M][M_{tot}^*] - \epsilon[M][M_{tot}^*] - \frac{2\delta[I]}{\left(1 + \alpha \frac{[RH]}{[M]}\right)} - 2J[M]^2 + \beta\epsilon[M]^2 + \beta\gamma[M][RH]} \quad (10)$$



where

$$\epsilon = \frac{K_{tM}}{K_{t1}} = C_M \frac{K_p}{K_{t1}}$$

Now the number-average degree of polymerization of the growing polystyrene radicals (free and grafted), namely the kinetic chain length  $\lambda$  is given by:

$$\lambda = \frac{\text{rate of growth of polystyrene radicals}}{\text{rate of disappearance of polystyrene radicals}};$$

$$\lambda = \frac{K_p [M] [M_{tot}^*]}{2K_{t1} [M_{tot}^*]^2 + K_{t2} [R^*] [M_{tot}^*] + K_{tM} [M] [M_{tot}^*] + K_{tR} [RH] [M_{tot}^*]};$$

$$\lambda = \frac{K_p [M]}{K_{t1} \left( 2[M_{tot}^*] + \frac{K_{t2}}{K_{t1}} [R^*] + \epsilon [M] + \gamma [RH] \right)} \quad (11)$$

where from equation (5):

$$\frac{K_{t2}}{K_{t1}} [R^*] =$$

$$\frac{2[M_{tot}^*]^2 + \gamma [RH] [M_{tot}^*] - 2J[M]^2 - \frac{2\delta [I]}{\left( 1 + \alpha \frac{[RH]}{[M]} \right)}}{\beta [M] - [M_{tot}^*]} \quad (12)$$

The number-average degree of polymerization of free polystyrene  $\bar{x}_{n,f}$  is evidently given by:

$$\bar{x}_{n,f} = \lambda \left( \frac{\text{number of polyradicals disappearing to form free polystyrene}}{\text{number of free polystyrene molecules formed}} \right)$$

and hence:

$$\bar{x}_{n,f} = \lambda \cdot \frac{K_{tM} [M] [M^*] + K_{tR} [RH] [M^*] + 2K_{t1} [M^*]^2}{K_{tM} [M] [M^*] + K_{tR} [RH] [M^*] + K_{t1} [M^*]^2};$$

$$\bar{x}_{n,f} = \lambda \cdot \left[ 1 + \frac{1}{1 + \epsilon \frac{[M]}{[M^*]} + \gamma \frac{[RH]}{[M^*]}} \right] \quad (13)$$

Analogously the number-average degree of polymerization of grafted polystyrene  $\bar{x}_{n,g}$  will given by equation (14):

$$\bar{x}_{n,g} = \lambda \left[ \frac{K_{tM} [M] [RM^*] + K_{tR} [RH] [RM^*] + 2K_{t1} [RM^*]^2 + 4K_{t1} [RM^*] [M^*] + K_{t2} [R^*] [M^*] + K_{t2} [R^*] [RM^*]}{K_{tM} [M] [RM^*] + K_{tR} [RH] [RM^*] + K_{t1} [RM^*]^2 + 2K_{t1} [RM^*] [M^*] + K_{t2} [R^*] [M^*] + K_{t2} [R^*] [RM^*]} \right]$$

$$\bar{x}_{n,g} = \lambda \left[ 1 + \frac{1}{1 + \frac{\epsilon [M]}{[M_{tot}^*] + [M^*]} + \frac{\gamma [RH]}{[M_{tot}^*] + [M^*]} + \frac{K_{t2} [R^*] [M_{tot}^*]}{K_{t1} ([M_{tot}^*]^2 - [M^*]^2)}} \right] \quad (14)$$

The grafting efficiency,  $E$  (%) will evidently be given by:

$$E = 100 \times \frac{\text{moles of styrene grafted}}{\text{total moles of styrene polymerized}};$$

$$E = 100 \times \frac{K_p [M] [RM^*] + 2\lambda K_{t1} [RM^*] [M^*] + \lambda K_{t2} [M^*] [R^*]}{K_p [M] [M_{tot}^*]}$$

Substituting  $([M_{tot}^*] - [M^*])$  for  $[RM^*]$ , it follows:

$$E = 100 \left[ 1 - \frac{[M^*]}{[M_{tot}^*]} + \frac{\lambda [M^*]}{\frac{K_p}{K_{t1}} [M] [M_{tot}^*]} \left( \frac{K_{t2}}{K_{t1}} [R^*] + 2[M_{tot}^*] - 2[M^*] \right) \right] \quad (15)$$

In equations (6) and (10)–(15) there are many kinetic constants, which were evaluated as follows:

$$\delta = \frac{K_d}{K_{t1}} \text{ and } J = \frac{K_{th}}{K_{t1}}$$

The constants have been obtained from the experimental data pertaining to the styrene polymerization ( $[RH] = 0$ ), by plotting the square of the polymerization rate *versus* initiator concentration, from the equation:

$$v_{p,0}^2 = \frac{K_d}{K_{t1}} K_p^2 [M]^2 [I] + \frac{K_{th}}{K_{t1}} K_p^2 [M]^4 \quad (16)$$

A linear relationships was observed. By introducing for the propagation constant a value of  $K_p = 1.67 \times 10^3 \text{ sec}^{-1} \text{ mol}^{-1}$  (at  $100^\circ\text{C}$ ) obtained by a least squares plot of the literature data<sup>9</sup>, the following values were obtained:  $\delta = K_d/K_{t1} = 1.2 \times 10^{-14} \text{ mol/l}$ ;  $J = K_{th}/K_{t1} = 2.8 \times 10^{-19}$ . Analogously the constants  $\epsilon = K_{tM}/K_{t1}$  and  $K_p/K_{t1}$  were evaluated from the data pertaining to the styrene polymerization by plotting  $1/\bar{x}_{n,0}$  against the polymerization rate, following the equation:

$$\frac{1}{\bar{x}_{n,0}} = \frac{K_{t1}}{K_p^2 [M]^2} v_{p,0} + \frac{K_{tM}}{K_p} \quad (17)$$

A linear relationships was observed, from which the following values were obtained:  $K_{tM}/K_p = 2.0 \times 10^{-4}$ ;  $K_{t1}/K_p^2 = 67.3 \text{ sec mol l}^{-1}$  and consequently:  $\epsilon = K_{tM}/K_{t1} = 1.8 \times 10^{-9}$ ;  $K_p/K_{t1} = 8.9 \times 10^{-6}$ . For the constant  $\alpha = K_{i2}/K_{i1}$  a fixed value of 2 was chosen, as approximately found in our previous studies\*. Moreover, since the crosslinking

\* The value in that case was about 1, because we considered in the calculus of  $[RH]$  the presence of two reactive hydrogens in each monomeric unit. In the present work, for reasons of homogeneity, the molecular weight of the unit was taken as equal to that of butadiene.

Table 2 Computer data of values calculated for  $\theta = 0.01$ 

[M] (mol/l)	[RH] (mol/l)	[I] (mol/l)	$[M_{tot}^*]$ $\times 10^9$ (mol/l)	$v_p$ $\times 10^4$ (mol l <sup>-1</sup> s <sup>-1</sup> )	$[M^*]$ $\times 10^9$ (mol/l)	$\frac{K_{t2}}{K_{t1}} [R^*]$ $\times 10^9$ (mol/l)	$\lambda$	$\bar{x}_{n,f}$	$\bar{x}_{n,g}$	E (%)
7.866	0.309	—	3.945	0.517	3.536	0.433	2737	3202	3442	14.8
7.866	0.309	0.00309	6.948	0.908	6.300	0.880	2186	2771	2911	15.5
7.866	0.309	0.00618	8.991	1.178	8.222	1.186	1922	2543	2607	15.4
7.866	0.309	0.00928	10.649	1.397	9.801	1.438	1751	2385	2393	15.2
7.724	0.620	—	3.685	0.475	2.989	0.851	2428	2742	2946	25.3
7.724	0.620	0.00310	6.538	0.842	5.401	1.712	1970	2388	2532	26.8
7.724	0.620	0.00620	8.463	1.089	7.100	2.313	1748	2204	2291	26.8
7.724	0.620	0.00930	10.017	1.289	8.500	2.810	1601	2077	2119	26.7
7.577	0.931	—	3.443	0.436	2.546	1.226	2171	2388	2558	33.2
7.577	0.931	0.00311	6.167	0.778	4.662	2.501	1785	2086	2224	35.4
7.577	0.931	0.00621	7.982	1.008	6.161	3.388	1594	1932	2028	35.6
7.577	0.931	0.00932	9.448	1.194	7.408	4.126	1467	1825	1887	35.6
7.433	1.245	—	3.226	0.400	2.188	1.575	1954	2107	2247	39.5
7.433	1.245	0.00311	5.826	0.722	4.046	3.252	1624	1844	1970	42.2
7.433	1.245	0.00622	7.550	0.936	5.376	4.420	1459	1710	1807	42.6
7.433	1.245	0.00934	8.936	1.108	6.486	5.393	1348	1618	1689	42.6
7.362	1.402	—	3.124	0.383	2.304	1.740	1858	1987	2115	42.1
7.362	1.402	0.00312	5.674	0.697	3.782	3.619	1551	1740	1860	45.0
7.362	1.402	0.00622	7.346	0.903	5.029	4.919	1398	1615	1711	45.5
7.362	1.402	0.00935	8.699	1.067	6.080	6.010	1293	1529	1601	45.6

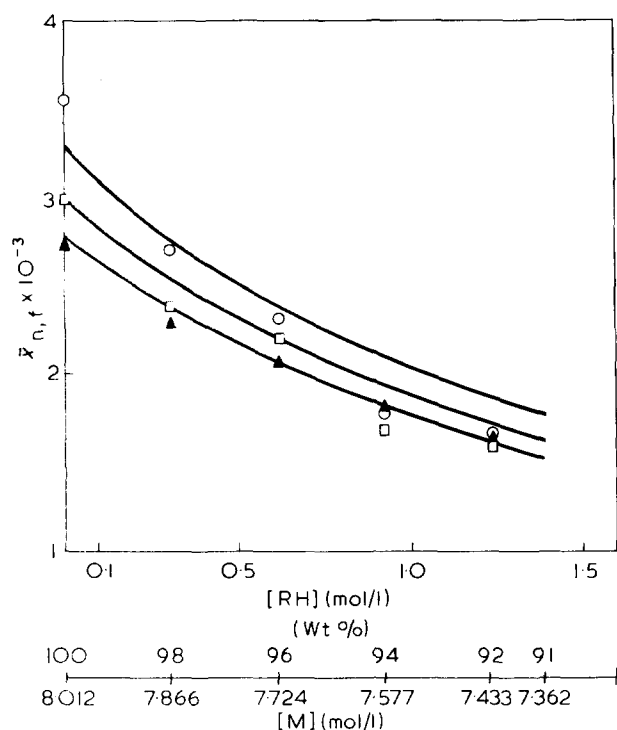


Figure 2 Calculated curves and experimental data for the number-average degree of polymerization of free polystyrene.  $\circ$ , 0.00310;  $\square$ , 0.00620;  $\blacktriangle$ , 0.00930 mol/l of peroxide

reaction, if present, is insignificant at low conversions (the grafted fraction is completely soluble), the constant  $\theta = K_{t1}K_{t3}/K_{t2}^2$  was assumed to be small, from 0 to 0.05. Now, by introducing into equations (6) and (10)–(15) fixed values of these kinetic constants, it was possible to calculate with the aid of a computer (for  $[M_{tot}^*]$  real, positive and  $>[M^*]$ ) values of  $v_p$ ,  $\bar{x}_{n,f}$ ,  $\bar{x}_{n,g}$ ,  $E$ , for different values of  $\beta$ ,  $\gamma$  and  $\theta$ . By comparing calculated values with experimental ones, it was possible to obtain for the constants  $\beta$  and  $\gamma$ :  $\beta = K_{i3}/K_{t2} = 3.0 \times 10^{-9}$ ;  $\gamma = K_{iR}/K_{t1} = 1.0 \times 10^{-8}$ . The value of  $\theta$  between 0.0005 and 0.05 was seen to have only very little influence.

Calculated values of  $[M_{tot}^*]$ ,  $[M^*]$ ,  $v_p$ ,  $(K_{t2}/K_{t1})[R^*]$ ,

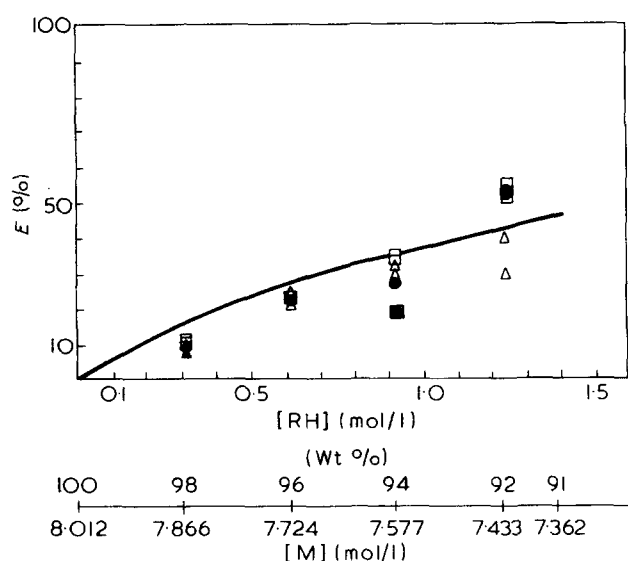


Figure 3 Calculated curve and experimental data for the grafting efficiency.  $\bullet$ , 0.00310;  $\square$ , 0.00620;  $\triangle$ , 0.00930 mol/l of peroxide

$\bar{x}_{n,f}$ ,  $\bar{x}_{n,g}$ ,  $\lambda$  and  $E$  are summarized in Table 2.

In Figure 1 calculated curves of the polymerization rate are reported in comparison with experimental data. It appears that the agreement is good up to a rubber concentration of about 8% ( $[RH] = 1.25$  mol/l).

In Figure 2 calculated curves concerning  $\bar{x}_{n,f}$  are compared with experimental data. The agreement is good enough, particularly at higher peroxide concentration.

The calculated values of  $\bar{x}_{n,g}$  (Table 2) are slightly higher than those of  $\bar{x}_{n,f}$ ; experimental and calculated  $\bar{x}_{n,g}$  values are close together only at low rubber concentrations.

In Figure 3 the calculated curve of  $E$  is reported; the experimental data are generally lower than the calculated ones, owing to the influence of the conversion.

## DISCUSSION

Grafting of styrene on polybutadiene proceeds evidently by two ways: direct attack by hydrogen abstraction of

initiator radicals and chain transfer on the rubber.

While the first process is practically the sole one at low temperatures<sup>10</sup>, the data reported here clearly demonstrate that at 100°C it is necessary to consider also chain transfer with polybutadiene.

Values evaluated for the kinetic constants are suitable or in agreement with literature data. Indeed the value for  $\alpha = K_{i2}/K_{t1} = 2$  can be justified by the better resonance-stabilization of the allyl radicals with respect to the styryl ones, in agreement with the results of Fischer<sup>11</sup>. The low value of  $\theta = K_{t1}K_{i3}/K_{t2}^2$  is also attributed to the stability of the allyl radical and to the steric hindrance for the cross-linking reaction. Analogously the value of the constant  $\beta = K_{i3}/K_{t2} = 3.0 \times 10^{-9}$  is very low if compared with the ratio  $K_p/K_{t1} = 8.9 \times 10^{-6}$ ; this again can be justified by the relative stability of the allyl radical ( $K_{i3} < K_p$ ).

The  $K_p^2/K_{t1} = 1.48 \times 10^{-2} \text{ l mol}^{-1} \text{ sec}^{-1}$  value is in good agreement with that extrapolated at 100°C from the literature data<sup>8</sup>. From the value of  $K_p = 1.67 \times 10^3 \text{ l mol}^{-1} \text{ sec}^{-1}$ , it follows:  $K_{t1} = 1.9 \times 10^8 \text{ l mol}^{-1} \text{ sec}^{-1}$ ; from the  $\delta$  value,  $\delta = K_d/K_{t1} = 1.2 \times 10^{-14} \text{ (mol/l)}$ , one obtains  $K_d = 2.3 \times 10^{-6} \text{ sec}^{-1}$ , in good agreement with values reported by several authors in different solvents<sup>12,13</sup>.

From the constant  $\epsilon = K_{tM}/K_{t1} = 1.8 \times 10^{-9}$ , it follows  $C_M = (K_{t1}/K_p)\epsilon = 2.0 \times 10^{-4}$ . Such a value for the transfer constant to styrene is in excellent agreement with those in the literature<sup>9</sup>. After all, from the  $\gamma$  value:  $\gamma = K_{tR}/K_{t1} = 1.0 \times 10^{-8}$  one obtains for the transfer constant to polybutadiene:  $C_R = (K_{t1}/K_p)\gamma = 1.1 \times 10^{-3}$ , a value of the same order as that reported by Fischer<sup>11</sup> for some polybutadienes at 110°C, by Minoura et al.<sup>14</sup> for the natural rubber at 50°C, and of those reported for unsaturated hydrocarbons<sup>9</sup>. When the polybutadiene concentration is very high (for instance 9%), a disagreement between experimental and calculated values appears, and molecular weights and grafting efficiencies become strongly dependent of the extent of reaction. This effect clearly is due to the phase separation, which arises for these rubber concentrations at very low styrene conversions (<1%). All the concentrations could be different in the two phases and, owing to the different medium viscosities, also the kinetic constants (particularly the termination constants and  $K_d$ ) could be different and strongly conversion-dependent.

## CONCLUSIONS

The development of a rigorous mathematical model has shown that the mechanism proposed for the initial stages of reaction is in complete agreement with experimental data, in the case of styrene solutions with low polybutadiene content. Deviations arising at high polybutadiene concentrations are related exclusively to the phase separation, which makes it impossible to study this reaction in an entirely homogeneous phase. It must be realized that the general reaction mechanism is still valid in each phase, provided one considers their different compositions and physical characteristics.

## ACKNOWLEDGEMENTS

The authors wish to thank Professor P. Chiorboli for encouraging this work, and the Consiglio Nazionale delle Ricerche for financial support.

## REFERENCES

- 1 Manaresi, P., Passalacqua, V. and Simonazzi, T. *Chim. Ind. (Milan)* 1969, **51**, 351
- 2 Manaresi, P. and Passalacqua, V. *Chim. Ind. (Milan)* 1970, **52**, 234
- 3 Manaresi, P., Zappia, G. and Sandrolini, F. *Chim. Ind. (Milan)* 1971, **53**, 915
- 4 Passalacqua, V. and Marchetti, L. personal communication
- 5 Hubin-Eschger, P. *Angew. Makromol. Chem.* 1972, **26**, 107
- 6 Locatelli, J. L. and Riess, G. *Angew. Makromol. Chem.* 1972, **26**, 117
- 7 Locatelli, J. L. and Riess, G. *J. Polym. Sci. (Polym. Chem. Edn)* 1973, **11**, 3309
- 8 Ham, G. E. 'Vinyl Polymerization', Part I, Marcel Dekker, New York, 1967, pp 147-189
- 9 Brandrup, J. and Immergut, E. H. 'Polymer Handbook', Interscience, New York, 1966
- 10 Brydon, A., Burnett, G. M. and Cameron, G. C. *J. Polym. Sci. (Polym. Chem. Edn)* 1973, **11**, 3255
- 11 Fischer, J. P. *Angew. Makromol. Chem.* 1973, **33**, 35
- 12 Bailey, H. C. and Godin, G. W. *Trans. Faraday Soc.* 1956, **52**, 68
- 13 Kharasch, M. S., Fono, A. and Nudenberg, W. *J. Org. Chem.* 1951, **16**, 105
- 14 Minoura, Y., Mori, Y. and Imoto, M. *Makromol. Chem.* 1957, **24**, 205

# Kinetic studies of the free cationic polymerization of ethyl vinyl ether and isobutyl vinyl ether initiated by triphenylmethyl hexachloroantimonate

Y. J. Chung, J. M. Rooney, D. R. Squire and V. Stannett

Department of Chemical Engineering, North Carolina State University, Raleigh, North Carolina 27607, USA

(Received 18 October 1974)

The absolute rate constants for the cationic polymerization of ethyl and isobutyl vinyl ethers have been determined in methylene chloride solution. Under the conditions used, the polymerization proceeded by 'free ions'. Extremely rigorous drying procedures were used and the values obtained were somewhat higher than those reported in the literature. The values were in reasonable agreement with the 'free cation' values obtained by a combination of rate and conductivity measurements of bulk polymerizations, initiated with gamma radiation under 'super dry' conditions. The activation energies were also in good agreement.

## INTRODUCTION

Cationic polymerization lags behind free radical and anionic polymerization in the extent of our understanding of the precise mechanisms involved and our knowledge of the absolute rate constants for the propagation termination and transfer reactions. The present status of the field has been well reviewed recently by Sigwalt<sup>1</sup>. A study of systems which proceed essentially by 'free' cations, not complicated by the presence of gegenions should add considerably to our knowledge. Cationic polymerization initiated by ionizing radiations is such a system and in the capable hands of Williams *et al.*<sup>2</sup> did indeed provide us with orders of magnitude for the propagation rate constants for a number of monomers. However, even when such rate studies are combined with electrical conductivity measurements, only approximate values can be obtained since a number of assumptions are involved concerning both the initiation and termination rates. The development of the stable carbenium ion salts which, in the correct solvent—monomer systems, give essentially instantaneous initiation and non-terminating polymerizations, has made it possible to measure rather accurately the absolute rate constants for a number of vinyl monomers. This work has been mainly carried out by Bawn and Ledwith and their coworkers and has been reviewed in detail recently by Ledwith<sup>3</sup>.

In these laboratories, kinetic studies of radiation-induced cationic polymerization of a series of alkyl vinyl ethers have been carried out systematically under 'super dry' conditions to determine the relative reactivities of the series<sup>4,5</sup>. Under 'super dry' conditions, the radiation-induced polymerization occurs through 'free-cationic' propagation and in theory the polymerization follows a square-root dose-rate dependence. The apparent rate constant of the radiation-induced cationic polymerization of ethyl vinyl ether (EVE) was found to be somewhat smaller than that of isobutyl vinyl ether (IBVE) and there were alarming differences between the chemical and radiation propagation

rate constants<sup>4</sup>. To shed further light on the radiation-induced cationic polymerization of the vinyl ethers, it was decided to study chemically initiated cationic polymerization of EVE under experimental conditions such that propagation might occur through a free ion mechanism. Bawn *et al.*<sup>6</sup> have reported an excellent and detailed kinetic study of the 'free' cationic polymerization of IBVE in methylene chloride initiated by stable carbenium ion salts. Using concentrations low enough to permit virtually complete dissociation of these salts, they have obtained rate constants and the activation energy of propagation by free cations. In this paper some further kinetic studies of the cationic polymerization of isobutyl vinyl ether and ethyl vinyl ether have been conducted according to their well established approach. In particular the results of a study of the kinetics of the free cationic polymerization of ethyl vinyl ether initiated by triphenylmethyl hexachloroantimonate are presented. Isobutyl vinyl ether was studied briefly in order to check the procedures against those of Ledwith *et al.*

## EXPERIMENTAL

At the beginning of the current series of experiments, methylene chloride was purified according to the procedure of Bawn *et al.*<sup>6</sup>. The solvent was washed with sulphuric acid, water and alkaline solution, dried over calcium, refluxed over calcium hydride, fractionated and degassed over calcium hydride. The solvent was then transferred to a 'scavenge' vessel containing triphenylmethyl hexachloroantimonate. It was later found that reproducibility of rate constants and high conversions could also be obtained with simpler purification methods. Approximately 500 cm<sup>3</sup> of methylene chloride was stirred for 2 h over 75 cm<sup>3</sup> sulphuric acid, decanted and washed with water adjusted with KOH pellets to a pH of 8.5 (6 x 200 cm<sup>3</sup>). After drying overnight on anhydrous CaCl<sub>2</sub>, a first fraction of 350 cm<sup>3</sup> was

vacuum-distilled into a receiving flask from which it was poured into a scavenge vessel containing  $\text{Ph}_3\text{CSbCl}_6$ . Approximately 0.1 g of triphenylmethyl hexachloroantimonate was added to 80–140  $\text{cm}^3$  of methylene chloride. The solution was then degassed through several freeze–thaw cycles under liquid nitrogen and sealed off at a pressure of less than  $10^{-4}$  mmHg. The degassing was carried out in a flask equipped with a side-arm containing a break-seal, so the solvent vessel could be connected directly to a vacuum line for transfer to the reactor.

EVE and IBVE were both purified by techniques conventional in 'super dry' radiation polymerization studies<sup>4,5</sup>. About 200  $\text{cm}^3$  of the monomer were washed in water, adjusted with KOH to a pH of 8.5 and stored over KOH pellets for 24 h in a round-bottom flask. The monomer was then refluxed over fresh reagent grade sodium metal (J. T. Baker Chemical Co.) in a spinning band distillation column for 24 h. After refluxing, the middle fraction was collected in a receiving flask equipped with a side arm containing a break-seal. The flask containing pure monomer was attached to a vacuum line and degassed to  $10^{-5}$  mmHg. The degassed monomer was then transferred to a sodium mirror flask *in vacuo* and stored for several days. When the sodium mirror disappeared, the monomer was transferred to a new flask, and the process was repeated until the condition of the monomer permitted the sodium mirror to remain intact. The resulting monomer was transferred in quantities of about 10  $\text{cm}^3$  to an ampoule containing anhydrous barium oxide which had been baked out overnight at 400°C and  $10^{-5}$  mmHg. After several days, ~1  $\text{cm}^3$  of the monomer was transferred to an empty ampoule with a break-seal which had been baked out overnight at 480°C *in vacuo* and sealed off under high vacuum. This ampoule was attached directly to the vacuum line for transfer to the reactor.

Triphenylmethyl hexachloroantimonate was prepared as described by Bawn *et al.*<sup>6</sup>. All phials of initiator solution (triphenylmethyl hexachloroantimonate in methylene chloride) were prepared under a vacuum of less than  $1 \times 10^{-5}$  mmHg.

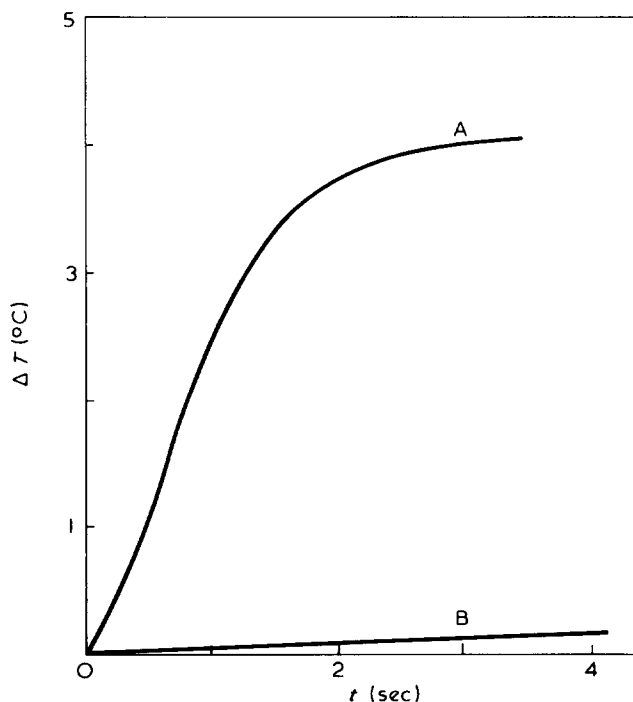
The progress of the polymerization reaction was followed by an adiabatic calorimetric technique using a system similar to that developed by Biddulph and Plesch<sup>7</sup>. A glass jacket enveloped the lower half of the reaction vessel. When evacuated, this jacket provided a region of negligible heat transfer during polymerization. The top of the reactor was equipped with a variable-speed stirrer, a thermocouple (copper–constantan) and a phial-breaking device. The shaft of the stirrer was sealed to the reactor by an O ring and Teflon bearings (Fisher Cat. No. 14-513-100). The copper–constantan thermocouple (250 mm diameter) leads were sheathed in Teflon to within 6.0 mm of the tip. A circular electromagnet was used to activate a phial-breaking rod. Phials of catalyst solution were held in place by fixed glass supports with space provided for two phials. The thermocouple was attached through an automatic reference junction compensator (Con-Ohmic Devices, Carle Place, NY) to a high speed recorder (Leeds & Northrup Speedomax XL-602) which was calibrated in mV with a potentiometer. The thermocouple voltage was virtually linear over the desired temperature range (usually 10°C), permitting direct readout of temperature *versus* time. The chart speed of the recorder during the polymerization reaction was 25.4 mm/sec. The response time of the recorder was 0.3 sec for a full-scale deflection and that of the thermocouple was less than 0.1 sec.

### Procedure

Following the placement of an initiator phial in the phial holder, the two halves of the reaction vessel were sealed together with Apiezon Q compound. The entire vacuum line and the reactor were then subjected to mechanical pumping overnight. When the pressure had been reduced to less than  $1 \times 10^{-5}$  mmHg, the pumping valves were closed, and a measured amount of solvent (70–125  $\text{cm}^3$ ) was distilled into the vessel along with the monomer. When the temperature was stabilized at the desired level, the Dewar jacket was evacuated, the stirring speed increased and the recorder switched to maximum speed (25.4 mm/sec). The electromagnet was then activated and the catalyst phial was crushed. When the recorder indicated that the polymerization was complete, the stirrer was stopped and the entire calorimeter was opened to the atmosphere. A strong jet of methanol was used to quench the mixture. The thermocouple, stirrer and breaker were washed with benzene, the washings were added to the polymer solution and finally the solvent was evaporated slowly. Molecular weights of polymers were measured by using a vapour pressure osmometer (Hewlett-Packard Series 300).

### RESULTS AND DISCUSSION

The upper curve (A) of *Figure 1* shows a typical plot of temperature rise during an experiment, and the lower curve (B) shows the temperature rise due to the heat of both breaking an initiator phial and mixing the initiator solution with solvent in the absence of monomer. The difference between the two curves corresponds to the temperature rise due to the heat of polymerization alone. Since it was found that adiabatic conditions held for the duration of the reaction, the maximum temperature rise could be equated to the polymerization yield which was usually well in excess of 90%. By equating the total temperature rise to the yield of polymerization, the concentration of mono-



*Figure 1* Plot of  $\Delta T$  vs.  $t$ . A, Temperature rise during a typical experiment; B, temperature rise due to both breaking catalyst phial and mixing catalyst solution with solvent in absence of monomer

Table 1 Data from a typical polymerization of ethyl vinyl ether at 15°C. Initiator concentration =  $2.35 \times 10^{-4}$  mol/l

Time (sec)	$\Delta T$ (°C)	Monomer concentration (mol/l)	$-\log[M]$
0.000	0.00	0.1446	0.840
0.125	0.15	0.1385	0.859
0.250	0.33	0.1325	0.878
0.375	0.60	0.1228	0.911
0.500	0.90	0.1118	0.951
0.625	1.35	0.0954	1.020
0.750	1.68	0.0806	1.094
0.875	2.01	0.0712	1.148
1.000	2.50	0.0533	1.273
1.125	2.70	0.0460	1.337
1.250	2.95	0.0368	1.434
1.375	3.15	0.0296	1.529
1.500	3.30	0.0241	1.618
1.625	3.45	0.0186	1.730
1.750	3.57	0.0142	1.848
1.875	3.65	0.0114	1.943
2.000	3.73	0.0084	2.076
2.125	3.77	0.0069	2.161
2.250	3.84	0.0042	2.377
2.375	3.87	0.0032	2.495
2.500	3.90	0.0021	2.678
2.625	3.92	0.0018	2.745
2.750	3.92	0.0015	2.824
2.875	3.93	0.0012	2.921
3.000	3.94	0.0010	3.000
3.125	3.95	0.0007	3.155
3.250	3.96	0.0004	3.398
3.375	3.97	0.0002	4.000
3.500	3.98	—	—

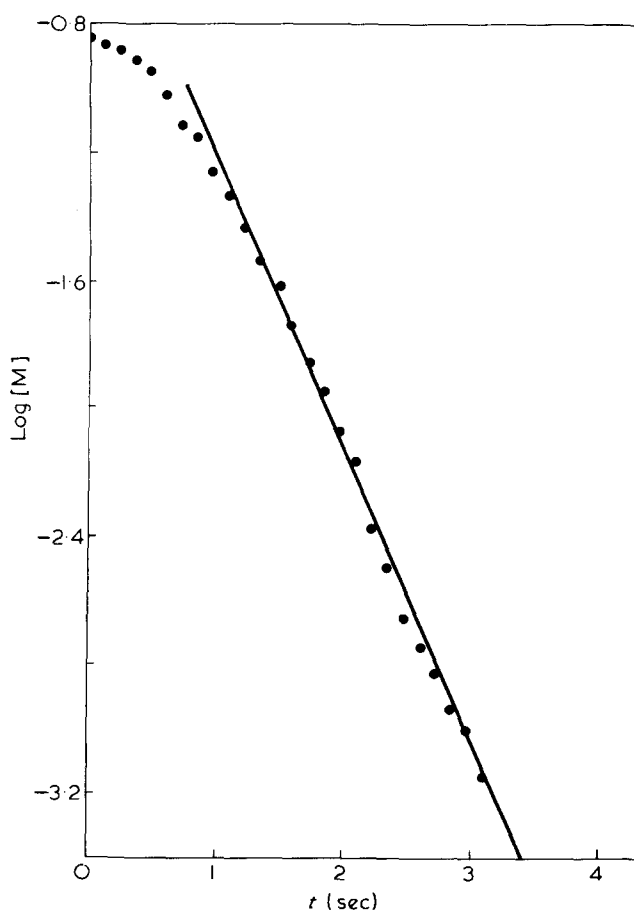


Figure 2 Plot of  $\log [M]$  vs.  $t$  during a typical experiment

mer was obtained as a function of time, and typical data are presented in Table 1. A plot of  $\log [M]$  vs. time yields a straight line after a brief induction period as shown in Figure 2, indicating that the propagation reaction can be considered first order with respect to monomer concentration. Consequently, the concentration of the propagating species can be assumed to be constant under the experimental conditions. This assumption is substantiated by the results obtained from successive polymerization. After  $\sim 90\%$  conversion of the monomer, a second equivalent amount of the same monomer was introduced *in situ* to the polymerization mixture and the observed rate of the second polymerization was similar to that of the first.

From the slope of the  $\log [M]$  vs.  $t$  plot shown in Figure 2, the pseudo-first order rate constant was found to be 2.1. This value is equal to the rate constant of propagation ( $k_p$ ) times the concentration of the propagating species. Assuming that all initiator molecules participated in initiating polymerization\*, the propagation rate constant was calculated to be  $9.2 \times 10^3 \text{ l mol}^{-1} \text{ sec}^{-1}$  at 15°C. All experimental data have been analysed similarly and results are presented in Table 2. The temperature quoted in Table 2 is the initial temperature of the reaction mixture. An Arrhenius plot (Figure 3) of average values of  $\log k_p$  vs.  $1000/T$  gives rise to an activation energy of 9.9 kcal/mol from  $-25^\circ\text{C}$  to  $+15^\circ\text{C}$ .

Molecular weight measurements conducted on polymer samples prepared from more highly concentrated reaction mixtures gave evidence of extensive chain transfer reactions. Polymerization for which the original monomer and initiator concentrations were 0.7 mol/l and  $2 \times 10^{-4}$  mol/l respectively yielded polymers of an approximate molecular weight of 4000 at reaction temperatures of 0–25°C. The molecular weight theoretically possible under the given conditions is about 250 000. This prevalence of chain transfer in similar cationic systems has also been noted by Ledwith<sup>3,6</sup>.

Table 3 presents the average propagation rate constants and activation energies for both isobutyl and ethyl vinyl ethers obtained in this work together with the literature values and the results obtained from radiation-induced polymerization studies. It can be seen that the rate constants for isobutyl vinyl ether are, indeed, consistently higher than for ethyl vinyl ether but not by a large margin. The

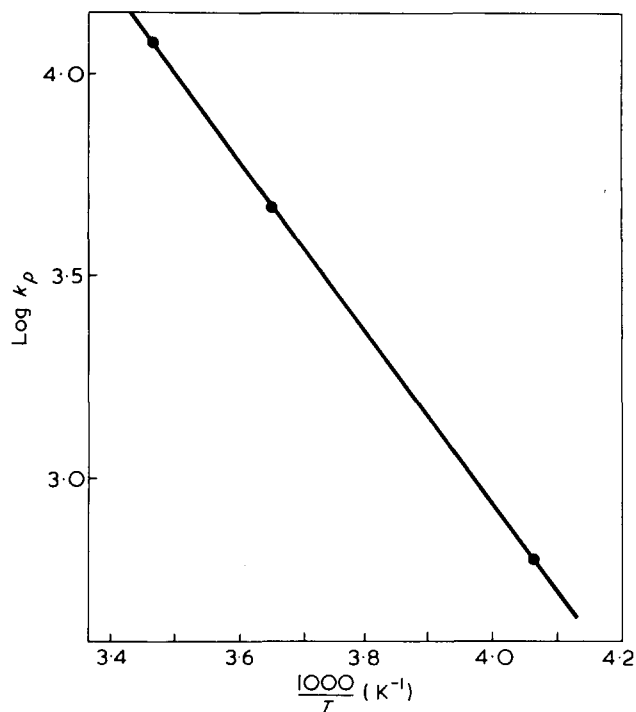
\* This assumption has been challenged recently, however, by Plesch<sup>10</sup>

Table 2 Polymerization of isobutyl and ethyl vinyl ethers initiated by triphenylmethyl hexachloroantimonate in methylene chloride solution

$T$ (°C)	[M]	[I] $\times 10^4$	$k_p \times 10^{-3}$	$\Delta H_p$
IBVE:				
-25	0.065	0.48	3.4	22.5
0	0.101	1.89	9.2	21.0
+15	0.063	0.42	24.2	20.2
EVE:				
-25	0.191	2.26	0.75	15.8
-25	0.114	1.05	0.57	15.0
0	0.172	2.56	4.7	17.4
0	0.206	2.30	7.1	19.3
0	0.195	2.30	5.7	18.2
0	0.090	1.60	2.8	15.2
15	0.141	2.46	7.7	16.5
15	0.145	2.35	9.2	16.9
15	0.106	0.46	18.5	16.0
15	0.075	0.46	17.5	16.8

Table 3 Average values for the propagation rate constant and the activation energies for isobutyl and ethyl vinyl ethers

Monomer	T (°C)	$k_p$			$E_a$		
		This work	Literature <sup>3,6</sup>	Radiation	This work	Literature <sup>3,6</sup>	Radiation
IBVE	-25	$3.4 \times 10^3$	$1.5 \times 10^3$	$6.4 \times 10^3$ <sup>8,9</sup>			
	0	$9.2 \times 10^3$	$4.1 \times 10^3$	$3.8 \times 10^4$	7.1	6.0	$9.6 \pm 2.8$ <sup>9</sup>
	15	$2.44 \times 10^4$	—	$9.5 \times 10^4$			$7.7$ <sup>4,5</sup>
EVE	-25	$6.6 \times 10^2$	—	$\sim 3 \times 10^2$ <sup>4,5</sup>			
	0	$5.1 \times 10^3$	$1.5 \times 10^3$	$3.5 \times 10^3$	9.9	10.0	$10.4$ <sup>4,5</sup>
	15	$1.32 \times 10^4$	—	$7.0 \times 10^3$			

Figure 3 Arrhenius plot of  $\log k_p$  against  $1/T$ 

reasons for this have been discussed by Ledwith<sup>3,6</sup>. With regard to the chemically initiated polymerization the  $k_p$  values from this study are consistently somewhat higher than the literature values. This is almost certainly due to the more rigorous drying conditions used. The activation energies and the  $k_p$  values are, however, in good agreement with the literature considering the experimental difficulties involved.

Considering now the results obtained with radiation initiation, it can be seen that the activation energies are in good agreement. The propagation rate constants are seen to be somewhat higher for the radiation polymerizations compared with chemical in the case of isobutyl vinyl ether and about half as large for the ethyl vinyl ether. Considering the assumptions made, however, with both initiating systems the agreement can be regarded as excellent. This removes one of the more vexing problems of free ion cationic polymerization as pointed out by Sigwalt<sup>1</sup>. Studies of cationic polymerization with free ions whether produced by stable carbenium ion salts or by radiation can be continued therefore with considerable confidence.

#### ACKNOWLEDGEMENT

We would like to thank the US Army Research Office for their generous support of this work.

#### REFERENCES

- 1 Sigwalt, P. *Makromol. Chem.* 1974, 175, 1017
- 2 Williams, F. in 'Fundamental Processes in Radiation Chemistry', (Ed. P. Ausloos), Interscience, New York, 1968, p 515
- 3 Ledwith, A. *Makromol. Chem.* 1974, 175, 1117
- 4 Kohler, J., Suzuki, Y., Goineau, A. and Stannett, V. to be published
- 5 Goineau, A. *Thesis* North Carolina State University (1972)
- 6 Bawn, C. E. H., Fitzsimmons, C., Ledwith, A., Penfold, J., Sherrington, D. C. and Weightman, J. A. *Polymer* 1971, 12, 119
- 7 Biddulph, R. and Plesch, P. H. *Chem. Ind.* 1959, p 1482
- 8 Williams, F., Hayashi, Ka, Ueno, K., Hayashi, K. and Okamura, S. *Trans. Faraday Soc.* 1967, 63, 1501
- 9 Hayashi, Ka, Hayashi, K. and Okamura, S. *J. Polym. Sci. (A-1)* 1971, 9, 2305
- 10 Plesch, P. H. *Makromol. Chem.* 1974, 175, 1065

# Three-block copolymers: morphologies and stress – strain properties of samples prepared under various experimental conditions

Enrico Pedemonte, Giovanni Dondero and Giovanni C. Alfonso

*Istituto di Chimica Industriale dell'Università di Genova, 16132 Genova, Italy*

and Francesco de Candia

*Laboratorio di Ricerche su Tecnologia dei Polimeri e Reologia, CNR, 80072 Arco Felice (Napoli), Italy*

*(Received 1 July 1974; revised 1 November 1974)*

The structural and morphological characterization of a styrene–butadiene–styrene thermoelastic three-block copolymer (Kraton 1101) is reported together with the stress–strain properties of specimens prepared with different techniques (compression moulding, extrusion, solution casting). The influences of the extrusion and of the annealing treatment at high temperature on the morphology (and therefore on the stress–strain properties) are considered in detail because the structure of the specimen becomes particularly simple; it consists of polystyrene cylinders arranged along the extrusion direction and embedded into the rubbery matrix. The rods along the axis lead to a continuous polystyrene phase, so that the plugs exhibit the Mullins and hardening effects already observed for other copolymers. Films cast from toluene are also investigated; the rate of evaporation of the solvent shows a remarkable influence on the morphology of the material and, of course, on its physical properties. An explanation for the hardening effects at high values of deformation is also suggested, supported by optical birefringence measurements on compression moulded specimens after strain.

## INTRODUCTION

The correlation between physical properties and composition of SXS three-block copolymers (S = styrene, X = butadiene or isoprene) has been widely studied. Some years ago<sup>1–6</sup> the influence of the amount of polystyrene was investigated in detail and the conclusion was reached that the glassy or rubber-like behaviour of the material depends on it. Nevertheless at that time no attempt was made to state the principles concerning the relationship between stress–strain behaviour and morphology; only the high values of the Young's modulus and the stress-softening effects which are often shown by the stress–strain curves were explained assuming a polystyrene continuous phase whose weaker ties are progressively broken with increasing load.

It must be stressed that the physical properties of SXS three-block copolymers depend on the morphology which the material, owing to its polystyrene content, is able to assume in consequence of thermal or mechanical treatments carried on in the course of the specimen preparation<sup>7</sup>.

Extrusion and annealing at high temperature have been considered in detail in our experiments. Copolymers with low amount of polystyrene ( $\approx 10\%$ ) do not show any orientation of the domains after the extrusion; the annealing induces a 'polycrystalline type' structure and an arrangement of spherical domains in a body centred cubic lattice<sup>8</sup>. When higher amounts of polystyrene are considered ( $\approx 25\%$ ), the polystyrene domains have a cylindrical shape<sup>9</sup> and are

highly oriented along the axis by extrusion; the annealing treatment leads to a 'single crystal' with parallel and continuous rods, hexagonally packed in the rubbery matrix<sup>10–12</sup>. The stress–strain plot of the former is similar to that of the ordinary vulcanized rubbers while the latter shows a large influence of the annealing treatment on the physical behaviour<sup>7</sup> as well as both stress-softening and hardening effects for low and high values of the deformation respectively.

On the other hand, the statement that the stress-softening was due to the breaking off of the weaker ties of the polystyrene continuous phase was always taken for granted as far as the experimental results could reasonably be assumed. Recently we have experimentally supported this hypothesis<sup>13</sup>.

In this paper we report the molecular characteristics of another SBS copolymer, the influence of compression moulding, extrusion and annealing on its morphology and on the corresponding stress–strain behaviour; finally, when films cast from dilute solution are prepared, the effect of the solvent evaporation rate on the physical properties will be taken into consideration. The aim of the work is to find an explanation for the hardening effect which comes out at the highest values of the load and, beside this, to stress that the total amount of polystyrene in the copolymer is not the conclusive parameter defining the mechanical properties of the material but only the necessary starting point leading to specific morphologies on which the physical properties actually depend.



Table 1 Molecular characteristics of Kraton 1101 copolymer

$\bar{M}_w^{14}$	$1.02 \times 10^5$
$\bar{M}_n^{14}$	$8.4 \times 10^5$
PS (% by wt)	33
Molecular weight of each PS end block	$1.7 \times 10^4$
Molecular weight of the central PB block	$6.8 \times 10^4$
Configurational composition of the rubbery matrix:	
trans-1,4-PB (%)	42
cis-1,4-PB (%)	49
1,2-PB (%)	9

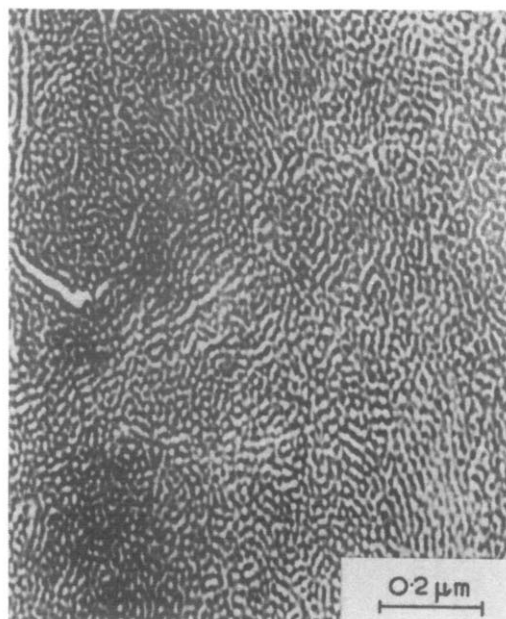


Figure 1 Electron micrograph of the original K 1101 copolymer, as supplied

## EXPERIMENTAL

### Material and molecular characterization

The copolymer employed in our experiments was commercial Kraton 1101 supplied by Shell Co. It is a styrene-butadiene-styrene three-block copolymer whose molecular characterization, performed with techniques already described in detail elsewhere<sup>8</sup>, gives the results summarized in Table 1; these are in good agreement with those previously reported by other authors<sup>14,15</sup>.

The amount of polystyrene and the total molecular weight were higher than the corresponding K 1102 previously studied<sup>7,9-12</sup>; the polystyrene end blocks were longer and therefore the chain mobility was highly hindered.

The toluene used to cast the films was a commercial distilled product.

### Methods

The copolymer was studied as supplied by the manufacturer, after extrusion and/or annealing, and as a film.

The extrusion was carried out at high temperature (220°C and 9.7 kg/cm<sup>2</sup>) and plugs of about 2 mm in diameter were obtained. The annealing was carried out under vacuum ( $\approx 10^{-3}$  mmHg) at 150–170°C. Films were obtained either by die-casting at 110°C under slight pressure or from dilute solutions in toluene at 50°C on a mercury surface at two different evaporation rates (about 20 and 0.5 cm<sup>3</sup>/h). These latter specimens were completely dried under vacuum at the same temperature; their thickness was about 0.2–0.4 mm.

The morphological analysis was performed by electron microscopy on ultra-thin sections cut by low temperature ultramicrotomy<sup>16</sup>. The staining was obtained by exposing the sections to vapour of aqueous OsO<sub>4</sub> solutions at room temperature for several minutes; consequently in the electron micrographs the butadiene phase will appear dark and the styrene bright.

The stress-strain measurements were done by simple extension at room temperature ( $\approx 20^\circ\text{C}$ ) and with a deformation rate of 10 mm/min. The stress  $\sigma$  (kg/cm<sup>2</sup>) is defined by the ratio  $f/s_i$ ,  $f$  being the load applied and  $s_i$  the original cross-section of the specimen; the extension ratio  $\alpha$  is defined by  $(\Delta L + L_i)/L_i$  where  $L_i$  is the original length of the sample and  $\Delta L$  the deformation.

Compression moulded films were observed in polarized light in order to give evidence of anisotropy phenomena.

## RESULTS AND DISCUSSION

### Original copolymer

Figures 1 and 2 show the morphologies of the K 1101 original copolymer, as supplied by Shell and after an annealing treatment of about one month.

The original material does not show any regular morphology. Figure 1 makes evident polystyrene domains of different size and shape (mainly circular and rod-like) together with large aggregates which can be due to small amounts of homopolymer in the copolymer<sup>17</sup>.

Taking into account that the sections viewed in the electron microscope are about 500 Å thick and that the osmium tetroxide stains the whole thickness of the section, the micrograph of Figure 1 does not allow us to draw any conclusion on the morphology of the original copolymer. We looked at the projection on the observation plane of the three-dimensional structure of the sample: therefore circular domains of polystyrene may appear from spheres or from the exact cross-sectional view of cylinders with orientation perpendicular to the cutting section; on the other

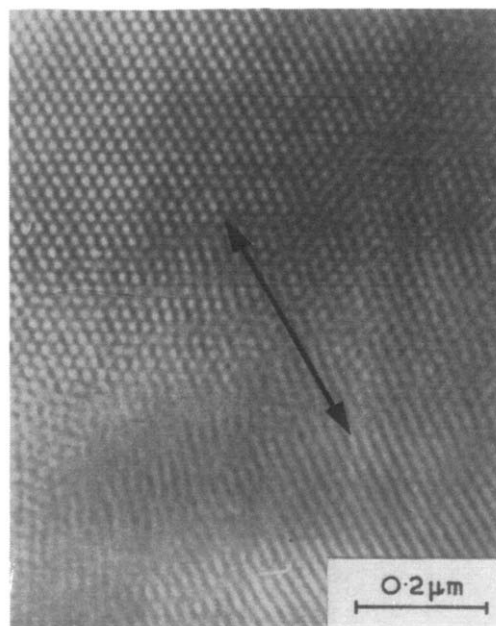


Figure 2 Electron micrograph of the K 1101 annealed under vacuum for one month at 150–170°C. The arrow indicates crystal grains in which rod-like and hexagonally assembled circular polystyrene domains are present

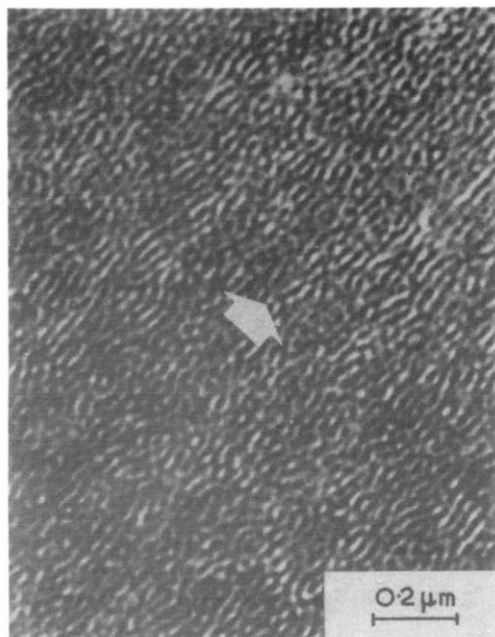


Figure 3 Electron micrograph of a K 1101 extruded plug (diameter, 2 mm) cut along the extrusion axis (indicated by the arrow)

hand, streaks could be due either to a true rod-like structure or to the projection of spherical domains lying down on the same row but at different depths in the section<sup>8</sup>. The copolymer composition would suggest a rod-like polystyrene structure, characterized by very short cylinders randomly embedded in the rubbery matrix<sup>18</sup>.

This hypothesis is supported by Figure 2, showing the equilibrium morphology that appears after one month of annealing at high temperature. Actually we can see crystal grains in which rod-like and hexagonally assembled circular polystyrene domains are present; it can be explained only if one assumes that the polystyrene end blocks supply regularly packed cylinders, variously oriented in adjacent regions of the cross-sectional plane of the specimen. The structure of the whole specimen is that one of a polycrystalline material.

Therefore we reach the conclusion that the original material is also characterized by rod-like polystyrene domains, as with the theoretical prediction of Inoue<sup>19</sup> and Meier<sup>20</sup>.

#### Extruded and extruded-annealed specimens

Figures 3 and 4 show an extruded plug, cut along the extrusion direction, and an extruded-annealed specimen, sectioned both along and perpendicularly to the extrusion axis.

The polystyrene cylinders, which characterize the morphology of the original material, are arranged along the axis of the plug during the extrusion (Figure 3). By annealing it could reach the 'single crystal' structure completely similar to that obtained with the K 1102 copolymer<sup>10-12</sup>, where hexagonally packed continuous rods of polystyrene are regularly embedded in the rubbery matrix<sup>21</sup>; a more regular distribution of the rod-like domains along the extrusion axis is observed (Figure 4) but the single crystal is more difficult to obtain in this case owing to the size of the molecular weight and to the length of the polystyrene end blocks, which highly reduce the macromolecular mobility.

The morphology of extruded and extruded-annealed

specimens is well defined and sufficiently simple, allowing us to give an interpretation of their mechanical properties (Figures 5 and 6) without any unreasonable assumption, on the basis of the older hypothesis<sup>1-6</sup>.

(i) The high values of the Young's modulus (Figures 5a and 6) are justified by the continuous polystyrene phase owing to the arrangement of polystyrene rods along the extrusion axis. It has been shown that the specimens are anisotropic; by stretching the plugs perpendicularly to the extrusion direction a rubber-like behaviour is produced<sup>22</sup>.

(ii) The improvement of the phase separation due to the annealing treatment gives rise to a more regular and continuous distribution of the polystyrene cylinders in the rubbery matrix; therefore the annealed plugs are stiffer than the extruded ones (Figures 5a and 6).

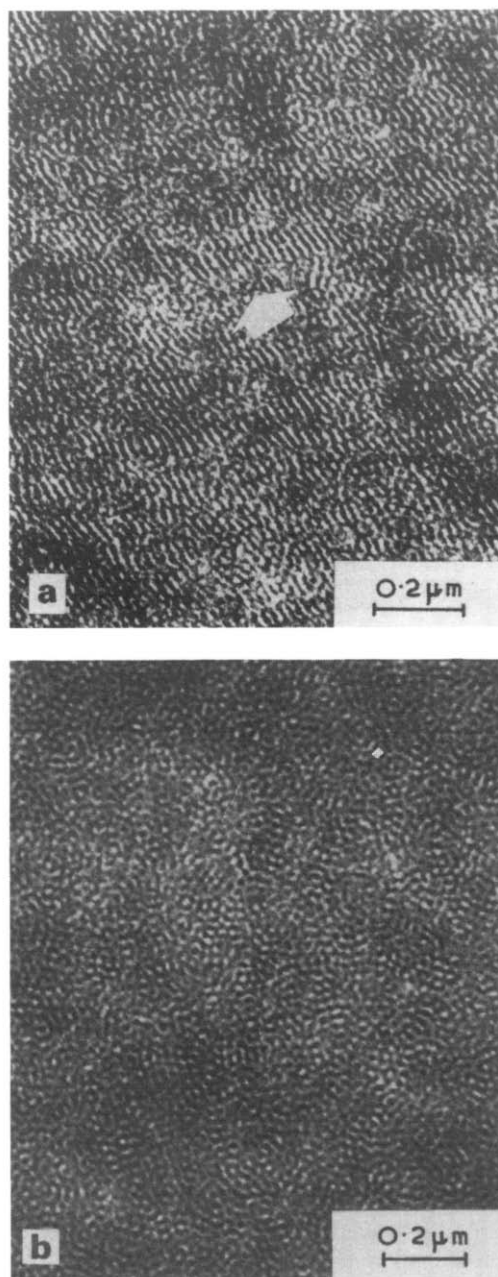


Figure 4 Electron micrographs of a K 1101 extruded and annealed plug (diameter, 2 mm; annealing time, 1 month). (a) Section parallel to the extrusion axis (indicated by the arrow); (b) section perpendicular to the plug axis

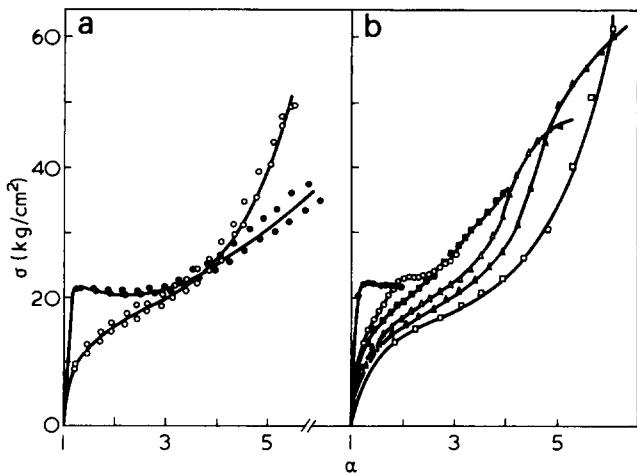


Figure 5 Simple extension stress-strain plots of extruded K 1101 copolymer. (a) First (●) and second (○) deformation run. Between the two successive deformations the specimen has been relaxed, at zero load, for 10 min; (b) consecutive stretching of the sample with the maximum deformation progressively increased

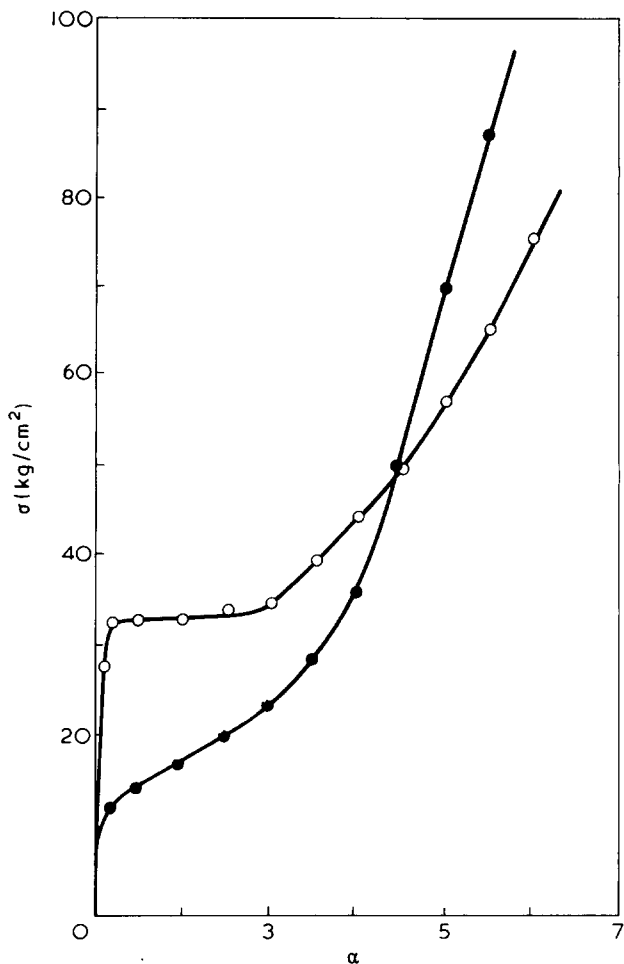


Figure 6 Stress-strain isotherms obtained with an extruded-annealed sample (annealing time, 1 week). ●, First run; ○, second run after 10 min of relaxation

(iii) The yield point (Figures 5a and 6) is easily explained if one takes into account that the rods are not regularly assembled everywhere and do not have constant diameters (Figures 3 and 4a). Many dislocations are present and thin ties often link consecutive cylinders. These defects clearly act as points where the strength of the material is strongly

reduced; when the load becomes sufficiently high, a large number of interconnections between rods in a row can be suddenly broken and therefore a well defined yield point appears.

(iv) The stress-softening (Figure 5b) is another consequence of the tie breaks: by increasing the load the number of ties which are broken off becomes progressively larger and larger. We have recently experimentally supported this hypothesis<sup>13</sup>, which also explains the difference between the first and the second stretching at low values of deformation.

Only the hardening effect, which appears at the higher strain values, is still unexplained.

#### Solution cast films

Figure 7 shows the morphologies of toluene cast films prepared at different solvent evaporation rates. The cor-

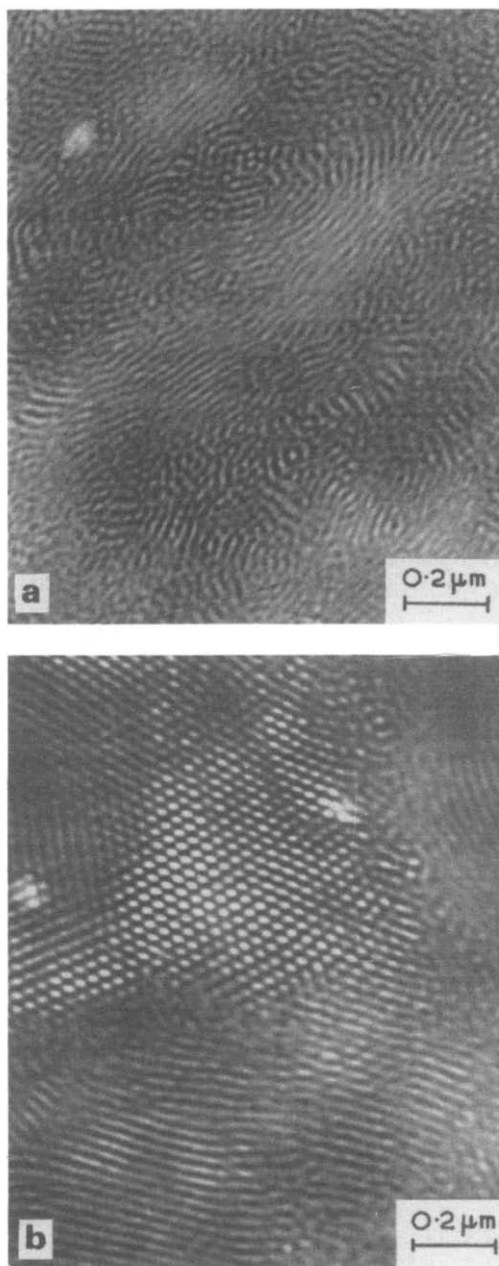


Figure 7 Electron micrographs of K 1101 films cast from toluene. (a) Fast evaporation; (b) slow evaporation. The sections are perpendicular to the film surface. Evaporation temperature = 50°C

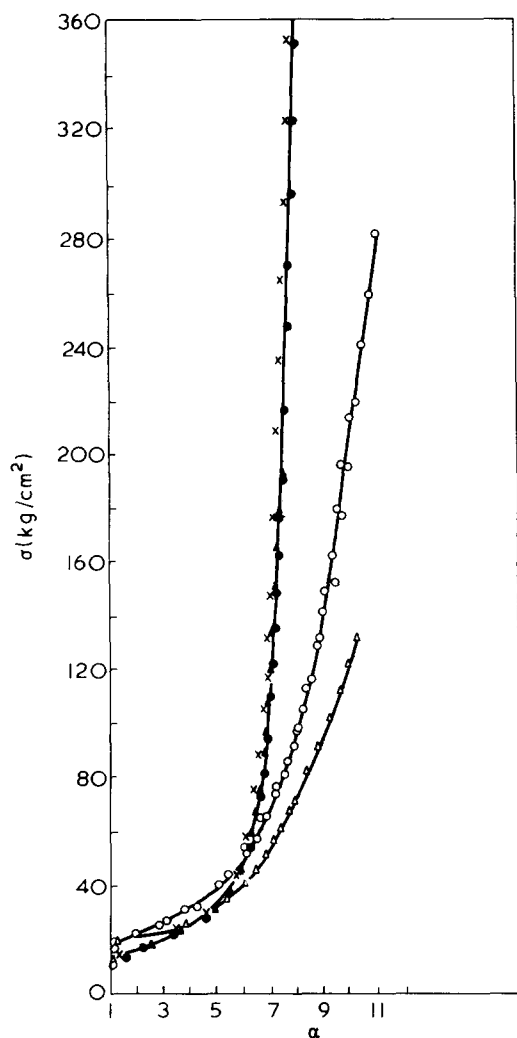


Figure 8 Simple extension stress-strain plots of toluene cast K 1101 films. Fast evaporation: first ( $\Delta$ ) and second ( $\blacktriangle$ ) deformation run; slow evaporation: first ( $\circ$ ) second ( $\bullet$ ) and third ( $\times$ ) deformation run. In both the experiments the storage time of the specimen at zero load is 10 min

responding stress-strain curves are plotted in Figures 8 and 9.

It is well known<sup>14, 19, 23-29</sup> that both the thermodynamic power and the evaporation rate of the solvent influence the morphology of the film. Figure 7 supports this conclusion as far as the evaporation rate is concerned, although the differences between films obtained with fast and slow rate of evaporation are not striking. The morphology of samples prepared at high rate do not show any regular arrangement of the polystyrene domains, which anyway seem to have a rod-like shape; on the contrary, the morphology of samples prepared at low evaporation rate is rather similar to that of the original annealed material (Figure 2) and leads to the same conclusion -- a polycrystalline structure where cylinders are hexagonally packed in the rubbery matrix.

Our results cast some doubts on the conclusions of a previous paper<sup>15</sup>, from which it follows that the morphology of a toluene cast film of K 1101 would be basically a simple cubic geometry of spherical domains. The disagreement between results obtained by electron microscopy and by low angle X-ray diffraction was already pointed out when films of the same copolymer were cast from mixtures

of tetrahydrofuran and methyl ethyl ketone<sup>30, 31</sup>. We do not have any conclusive explanation for this. From the experimental point of view two parameters are able to modify the morphology of films cast from a well known solvent, i.e. the evaporation rate of the solvent itself and the annealing treatment carried on the dry film; in this case: (i) Brown *et al.*<sup>15</sup> do not give any data on the evaporation rate experimentally used in their experiments; nevertheless Figure 7 shows clearly that the morphology of K 1101 toluene cast films is always characterized by polystyrene rods embedded in the rubbery matrix; (ii) Brown *et al.*<sup>15</sup> did not anneal their specimens at high temperatures which underlines the basic feature of the first order diffraction pattern remaining unaltered up to 130°C, leading to the conclusion that the structure does not change at all. Our experiments show that the equilibrium morphology, obtained after a long treatment at high temperature, is still characterized by polystyrene rods (Figure 2).

We therefore feel that perhaps the low angle X-ray diffraction results might be more critically considered. This topic has been recently reviewed by Krigbaum *et al.*<sup>32</sup>.

The small differences between fast and slow evaporated films so far discussed also appear if the corresponding stress-strain curves are taken into consideration. The

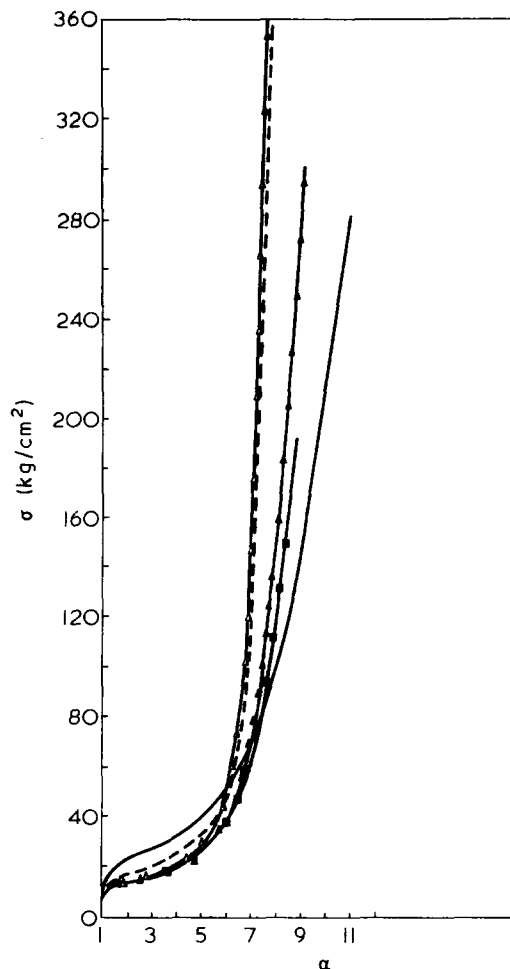


Figure 9 Simple extension stress-strain plots of slowly evaporated toluene cast K 1101 films. —, First deformation; - - -, second deformation after 10 min of relaxation at zero load;  $\blacktriangle$ , second deformation after 1 day of relaxation at zero load;  $\blacksquare$ , second deformation after 1 week of relaxation at zero load;  $\triangle$ , third deformation after 10 min of relaxation of the sample ( $\blacktriangle$ )

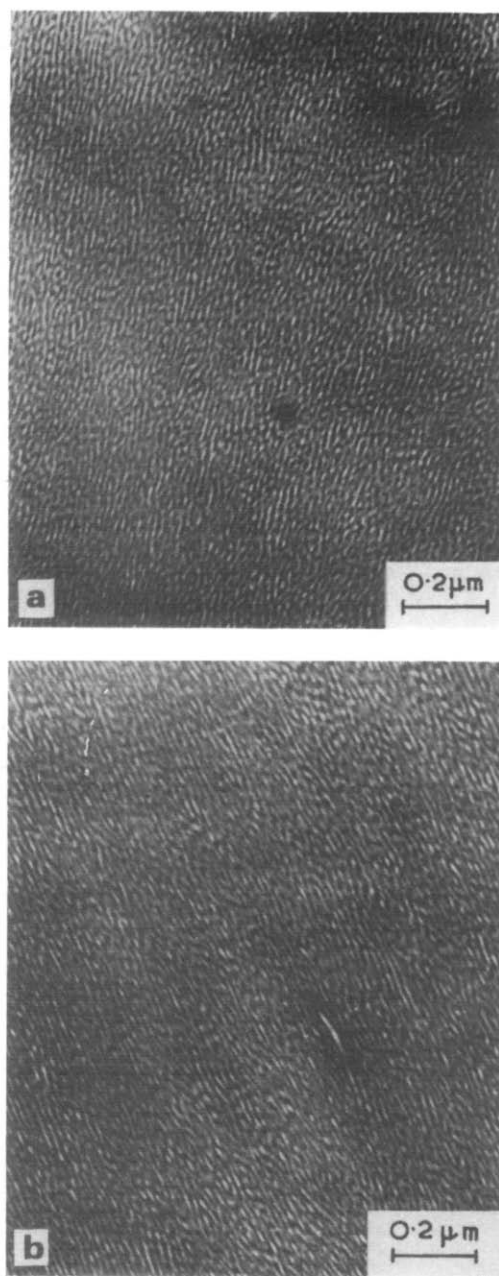


Figure 10 Electron micrographs of a K 1101 compression moulded film. (a) Section parallel to the compression surface; (b) section perpendicular to the compression surface

first deformations are not too different (Figure 8); the slowly evaporated sample does not show any well defined yield point and seems to be slightly more stiff. However, it is noteworthy that the stress-strain curves of the second deformation are exactly coincident; according to the current model this would correspond to the same number of tie breaks.

Figure 9 concerns the influence on the stress-strain curves of the storage time at zero load between following deformations. The complete irreversibility of the first mechanical response of the material appears quite clearly; even after one week of relaxation the softening at low deformation and the hardening at high strain are still present. The main result is nevertheless obtained by stretching a specimen three times after different relaxations; when

the sample, stored for 1 day between the first and second deformation, is strained again after only 10 min we obtain the same plot as obtained without any storage. The suggestion that the hardening effect at high strain values could have a kinetic explanation. We can reasonably assume that, when the load is removed, the recovery of the original structure needs a rather long time owing to the hindered mobility of the copolymer macromolecules; this also occurs when the original dimension of the specimen is apparently restored. Therefore if a deformation is followed immediately by another one, macromolecules that are still strained by the previous deformation run are stretched.

#### Compression moulded films

Figures 10 and 11 show sections of compression moulded films in the original state and after stretching. The corresponding stress-strain plots are reported in Figure 12 and finally in Figure 13 the films are observed in polarized light.

In the moulded film the polystyrene phase is embedded in the rubber as rod-like domains and no particular orientation of the cylinders is present, as is clearly seen from the comparison of the two orthogonal sections of Figure 10. The cylinders are oriented by the stretching and the original morphology is not immediately restored (Figure 11). At  $\alpha = 4$  the polystyrene cylinders are still rather long and oriented in the stretching direction more regularly than in the unstrained material (Figure 10a); when the deformation is larger ( $\alpha = 8$ ) the continuity of the polystyrene phase seems to be broken so that the cylinders are shorter. We believe that the orientation of the polystyrene cylinders needs an irreversible work which can give its contribution

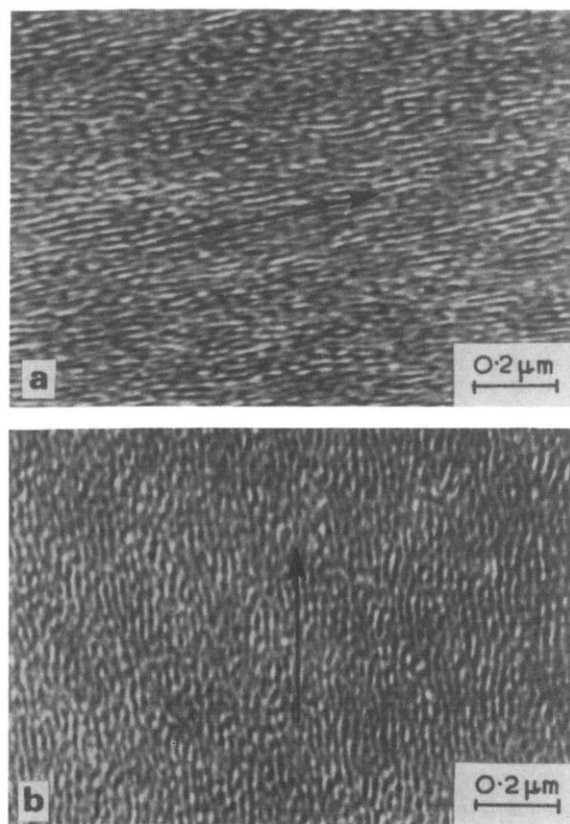


Figure 11 Electron micrographs of die-casting films stretched and relaxed before cutting. Sections parallel to the compression surface. (a)  $\alpha = 4$ ; (b)  $\alpha = 8$

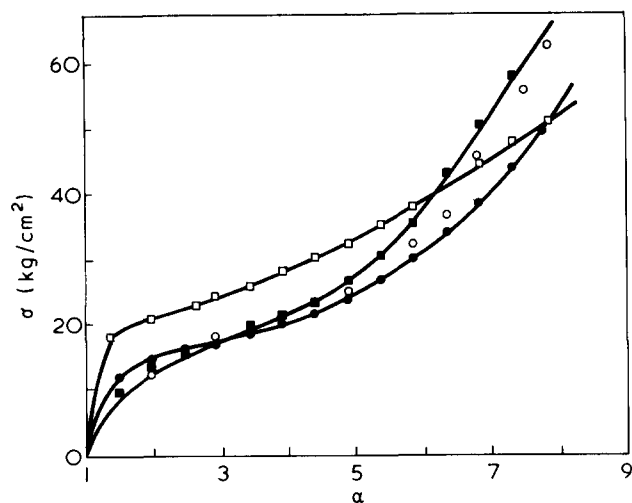


Figure 12 Stress-strain isotherms obtained with a die-casting film. □, First run; ■, second run, after 10 min; ●, third run after one week; ○, fourth run, 10 min after the third

to the softening effect together with the mechanism of breaking.

On the other hand, the hypothesis that the hardening process could be caused by macromolecules in stretched and oriented state at zero load seems to find further support in Figure 13. The distribution of the dark zones is related to the distribution of the force field and therefore to the degree of orientation in the sample. It is evident that, at the same value of the strain, in the second deformation we have a more regular distribution of isotropic zones parallel to the strain direction pointing towards a higher degree of orientation.

## CONCLUSIONS

From the result it would seem that the polystyrene content of the copolymer is certainly an important parameter in order to define the morphology of the material but nevertheless many different morphologies can be obtained from a copolymer as a result of mechanical and/or thermal treatment.

In addition, some experimental evidence indicates that the hardening effect, which appears when two successive deformations are carried out without storage at zero load between them, could have a kinetic explanation. The hindered mobility of the macromolecules of the copolymer does not allow the recovery of the starting conformation; chains which are still strained are stretched again and therefore higher loads are necessary to reach the same values of deformation.

## ACKNOWLEDGEMENT

The assistance of Mr G. Romano and Mr A. Tagliatela with the many measurements involved in this investigation is deeply appreciated.

## REFERENCES

- 1 'Block Copolymers' *J. Polym. Sci. (C)* 1969, 26
- 2 Holden, G., Bishop, E. T. and Legge, N. R. *J. Polym. Sci. (C)* 1969, 26, 37
- 3 Morton, M., McGrath, J. E. and Juliano, P. C. *J. Polym. Sci. (C)* 1969, 26, 99

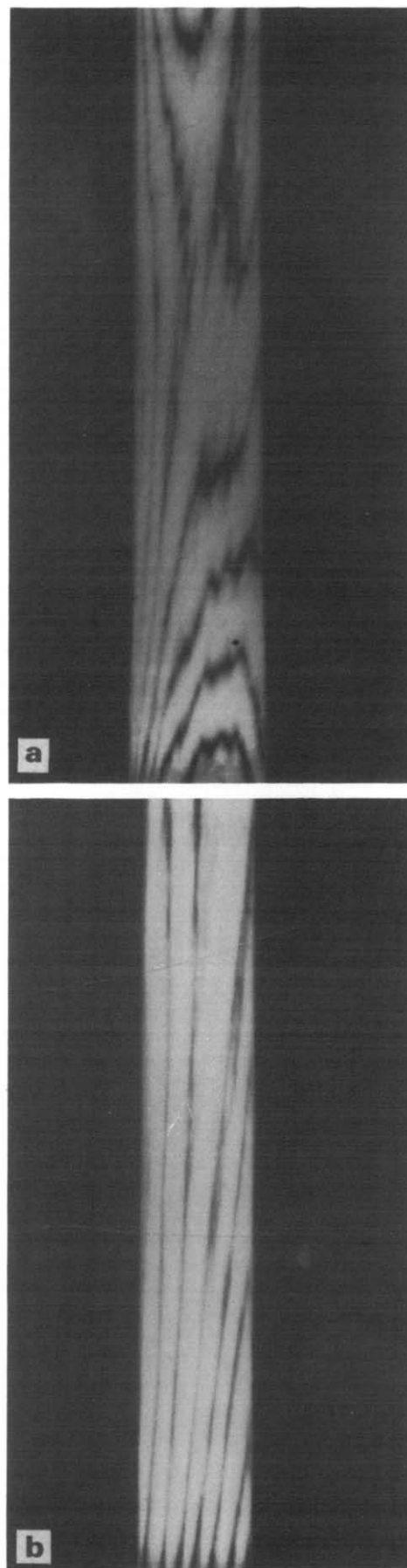


Figure 13 Stretched films observed in polarized light ( $\alpha = 6$ ): (a) first deformation run; (b) second deformation run after 10 min of relaxation

*Morphology and stress-strain properties of three-block copolymers: E. Pedemonte et al.*

- 4 Beecker, J. F., Merker, L., Bradford, R. D. and Aggarwall, S. L. *J. Polym. Sci. (C)* 1969, **26**, 117
- 5 Estes, G. M., Cooper, S. L. and Tobolsky, A. V. *J. Macromol. Sci. (C)* 1970, **4**, 313
- 6 Cunningham, R. E., Auerback, H. and Floyd, W. J. *J. Appl. Polym. Sci.* 1972, **16**, 168
- 7 Turturro, A., Bianchi, U., Pedemonte, E. and Ravetta, P. *Chim. Ind. (Milan)* 1972, **54**, 782
- 8 Pedemonte, E., Turturro, A., Bianchi, U. and Devetta, P. *Polymer* 1973, **14**, 145
- 9 Bianchi, U., Pedemonte, E., Turturro, A. and Tombini, M. *Chim. Ind. (Milan)* 1972, **54**, 603
- 10 Keller, A., Pedemonte, E. and Willmouth, F. M. *Kolloid-Z. Z. Polym.* 1970, **238**, 385
- 11 Dlugosz, J., Keller, A. and Pedemonte, E. *Kolloid-Z. Z. Polym.* 1970, **242**, 1125
- 12 Keller, A., Dlugosz, J., Folkes, M. J., Pedemonte, E., Scalisi, F. P. and Willmouth, F. M. *J. Phys.* 1971, **32**, Ca-295
- 13 Pedemonte, E., Turturro, A. and Dondero, G. *Br. Polym. J.* 1974, **6**, 277
- 14 Lewis, P. R. and Price, C. *Polymer* 1971, **12**, 258
- 15 Brown, D. S., Fulcher, K. U. and Wetton, R. E. *J. Polym. Sci. (B)* 1970, **8**, 659
- 16 Dondero, G., Olivero, L., Devetta, P., Cartasegna, S. and Pedemonte, E. *Nuova Chimica* 1972, **48**, 1
- 17 Fetters, L. J., Meyer, B. H. and McIntyre, D. *J. Appl. Polym. Sci.* 1972, **16**, 2079
- 18 Folkes, M. J. and Keller, A. in 'Physics of Glassy Polymers', (Ed. R. N. Haward), Elsevier, Amsterdam, 1973
- 19 Inoue, T., Soen, T., Hashimoto, T. and Kawai, H. *J. Polym. Sci. (A-2)* 1969, **7**, 1283
- 20 Meier, D. *J. Polym. Prepr.* 1970, **11**, 400
- 21 Pedemonte, E. *et al. Chim. Ind. (Milan)* 1973, **55**, 861
- 22 Folkes, M. J. and Keller, A. *Polymer* 1971, **12**, 222
- 23 Sadron, C. *Angew. Chem. (Int. Edn)* 1963, **2**, 248
- 24 Gallot, B., Mayer, B. and Sadron, C. *C. R. Acad. Sci. Paris* 1966, **263C**, 42
- 25 Vanzo, E. *J. Polym. Sci. (A-1)* 1966, **4**, 1727
- 26 Molau, G. E. 'Block Polymers' (Ed. S. L. Aggarwall), Plenum Press, New York, 1970, p 79
- 27 Uchida, T., Soen, T., Inoue, T. and Kawai, H. *J. Polym. Sci. (A-2)* 1972, **10**, 101
- 28 Price, C. *et al. Br. Polym. J.* 1972, **4**, 413
- 29 Pedemonte, E., Cartasegna, S. and Turturro, A. *Chim. Ind. (Milan)* 1974, **56**, 3
- 30 Campos-Lopez, E., McIntyre, D. and Fetters, L. *J. Macromolecules* 1970, **6**, 415
- 31 Pedemonte, E. and Alfonso, G. *C. Macromolecules* 1975, **8**, 85
- 32 Krigbaum, W. R., Yazgan, S. and Tolbert, W. R. *J. Polym. Sci. (A-2)* 1973, **11**, 511

# Effect of temperature and frequency in fatigue of polymers

J. C. Radon and L. E. Culver

Department of Mechanical Engineering, Imperial College of Science and Technology, London SW7 2BX, UK

(Received 14 June 1974; revised 12 March 1975)

The effects of frequency and temperature on fatigue crack propagation rate in poly(methyl methacrylate) and polycarbonate have been studied using centrally notched plate specimens cycled in tension between constant stress intensity limits. Crack growth was monitored at frequencies between 0.1 Hz and 100 Hz and at temperatures between  $-60^{\circ}\text{C}$  and  $40^{\circ}\text{C}$ . A linear relationship between the cyclic crack growth rate  $d(2a)/dN$  and appropriate levels of toughness,  $K$ , has been proposed:  $d(2a)/dN = A\phi^{\alpha}$ , where  $\phi = (\lambda - \lambda_{\text{th}})/(K_{\text{IC}}^2 - K_{\text{max}}^2)$ ,  $\lambda = K_{\text{max}}^2 - K_{\text{min}}^2$ ,  $\lambda_{\text{th}}$  is the threshold limit and  $A$  and  $\alpha$  are constants. Also, the influence of mean stress intensity was briefly discussed.

## INTRODUCTION

Polymeric materials are now frequently used by engineering designers wherever they can suitably replace more conventional materials. Some possible advantages are the favourable strength to weight ratio, good damping properties and wear resistance and the possibility of economic manufacture of intricately shaped components.

Thus, in recent years, with the continuous development of industrial plastics of improved mechanical properties, considerable interest has been created in their behaviour under monotonic and cyclic loading conditions. While static fracture has received by far the most attention, attempts to analyse specific fatigue failure processes, in particular those connected with the evaluation of crack growth rates, have been relatively scarce.

The study of crack propagation under cyclic loading aims to provide data in a form suitable for use in stress analysis and design. A great deal of fatigue research is now being directed towards a detailed investigation of the influence of environment, temperature, frequency and other factors on subcritical crack growth from the initiation period up to the critical crack size. The development of linear elastic fracture mechanics (*LEFM*) concepts provided a promising approach to investigations of crack growth in statically loaded structures; stress intensity factors,  $K$ , are now known for a wide range of cracked configurations. Subsequent application of *LEFM* methods in cyclically loaded situations offered yet further possibilities for reliable evaluations of engineering materials. Recent work<sup>1,2</sup> provided some evidence that the *LEFM* approach may be conveniently used to describe the propagation of cracks under fatigue conditions in a range of polymers.

In the last ten years a number of fatigue crack growth 'laws' have been proposed and are fully described by Hoepfner and Krupp<sup>3</sup>. While some of the laws suggest that the critical parameter may be a function of stress or of strain, the majority are based on *LEFM* concepts. The basic and probably most widely known crack propagation equation, due to Paris, has been successfully applied to the analysis of cyclic crack growth in many materials for elastic

or, quasi-elastic situations:

$$d(2a)/dN = C_1(\Delta K)^m \quad (1)$$

where  $2a$  is the crack length,  $N$  is the number of cycles,  $\Delta K$  is the range of the stress intensity factor,  $K = K_{\text{max}} - K_{\text{min}}$  and  $C_1$ ,  $m$  are constants dependent on the material tested, the environment and the conditions of cyclic loading.

Recent results of a comprehensive programme of work on fatigue crack propagation at room temperature using a range of polymers<sup>2</sup> provided detailed information on the effects of the mean level,  $K_m$ , and the amplitude,  $\Delta K$ , of the stress intensity factor; they led to a crack propagation model of the form:

$$d(2a)/dN = \beta\lambda^n \quad (2)$$

where  $\lambda = K_{\text{max}}^2 - K_{\text{min}}^2 = 2\Delta K \cdot K_m$ , and  $\beta$  and  $n$  are constants dependent upon the test conditions. Because of the encouraging correlation of the polymer results analysed by equation (2) with other published data, it was decided to apply the method for the evaluation of crack growth in tests similar to those in ref 2 but performed over a range of temperatures and frequencies. Preliminary tests indicated that this particular criterion could probably find a wider application. However, it should be mentioned that the tests<sup>2</sup> had been restricted to a comparatively narrow range of  $\Delta K$  and in particular, cycling at very low values of  $K$ , usually described as region I, was not investigated in detail.

The purpose of the present paper is to report on a study of the effect of temperature between  $-60^{\circ}\text{C}$  and  $+40^{\circ}\text{C}$  and of frequencies between 0.1 Hz and 100 Hz in PMMA and PC under repeated tension fatigue. Some additional tests indicating the significance of mean stress intensity  $K_m$  and the threshold value  $\Delta K_{\text{th}}$  are also discussed.

## EXPERIMENTAL

The two polymers chosen for the present programme were poly(methyl methacrylate) (PMMA) and polycarbonate



(PC). It was shown previously<sup>1</sup> that PMMA (manufactured by ICI, UK) was a suitable material for fracture toughness studies and results on fatigue crack propagation with particular reference to the mean value of stress intensity  $K$  were reported. The fracture properties of polycarbonate of bisphenol A (Makrolon, manufactured by Bayer, Germany), available in the form of extruded sheets, are less well known than those of PMMA<sup>4,5</sup>. However, its increasing use in engineering applications results in the need for full information about its mechanical properties.

Specimens were made in the shape of 6.25 mm thick rectangular plates 180 x 300 mm for PC, and 350 x 400 mm for PMMA. Each was provided with a small central hole 6 mm diameter extended into a sharp crack 25 mm long. Notching procedure and other pertinent details were previously described in detail<sup>1</sup>. Two fatigue testing machines were used: a Dowty electrohydraulic machine suitable for higher frequencies and a hydraulic Denison T42C2 for tests at 0.1 Hz. Repeat tests performed on both machines confirmed that their stiffnesses were comparable and the repeatability of the results was within 5%.

The specimen, in self-aligning shackles, was assembled in an environmental chamber fixed to the machine crosshead. A refrigerator-heater unit (Haake, model KT32) provided temperature regulation ( $\pm 0.5^\circ\text{C}$ ), the regime investigated in this programme being between  $-60^\circ\text{C}$  and  $+40^\circ\text{C}$  and the temperature was automatically recorded using a number of thermocouples attached to each side of the specimen close to the crack path. Each specimen was subjected to cyclic tension under selected maximum and minimum values of stress intensity factor  $K$  at the chosen temperature and frequency and the resulting crack growth was monitored using a cathetometer via narrow observation windows fitted on both sides of the chamber; this arrangement proved to be both simple and adequate.

The limits of the stress intensity range investigated and the maximum testing times were decided by reference to the calculated values of  $K$  for a centrally notched plate, according to the ASTM recommended procedure<sup>6</sup>. The highest level of  $K$  used in the cyclic tests was  $0.8K_{1C}$ . The plastic zone size corresponding to this  $K_{\text{max}}$ , calculated in the usual way, was very small when compared with the plate thickness (for both materials it was below  $10^{-2}$  mm), thus plane strain conditions were assured. In the preliminary tests performed above  $0.8K_{1C}$  a certain amount of cyclic creep was observed, but this was negligible at lower  $K$  levels. As expected, in tests at a low level of  $K_{\text{max}}$ , the crack growth rate  $d(2a)/dN$  decreased considerably and  $0.5K_{1C}$  was the lowest level of  $K_{\text{max}}$  investigated in detail. However, some tests were performed at still lower values of  $K_{\text{max}}$  (or  $\Delta K$ ) to establish whether crack growth would cease when cycling below a certain threshold stress intensity  $\Delta K_{\text{th}}$ <sup>7</sup>.

## RESULTS AND DISCUSSION

### Influence of temperature

Typical linear crack growth records obtained from the constant  $\lambda$  tests on PC at different temperatures but at constant frequency are shown in Figure 1. As the temperature was reduced from  $27^\circ\text{C}$  to  $-60^\circ\text{C}$  the crack growth rates decreased distinctly, the decrease amounting to 60% in the case of PC and 90% for PMMA. A comparable decrease was observed at other frequencies, as mentioned below.

Information on the effect of temperature on crack growth rate is scarce, but some results<sup>8</sup> report an increasing growth

rate  $d(2a)/dN$  with temperature decreasing from  $50^\circ\text{C}$  to  $-10^\circ\text{C}$ . The current tests have so far covered a temperature range between  $-60^\circ$  and  $40^\circ\text{C}$  and the first results obtained at 5 Hz on PMMA are included in Figure 2. It can be seen that the general tendency of all the tests is that of a decreasing crack growth with decreasing temperature. The crack growth rate also decreased with decreasing  $\lambda$ , the factor in

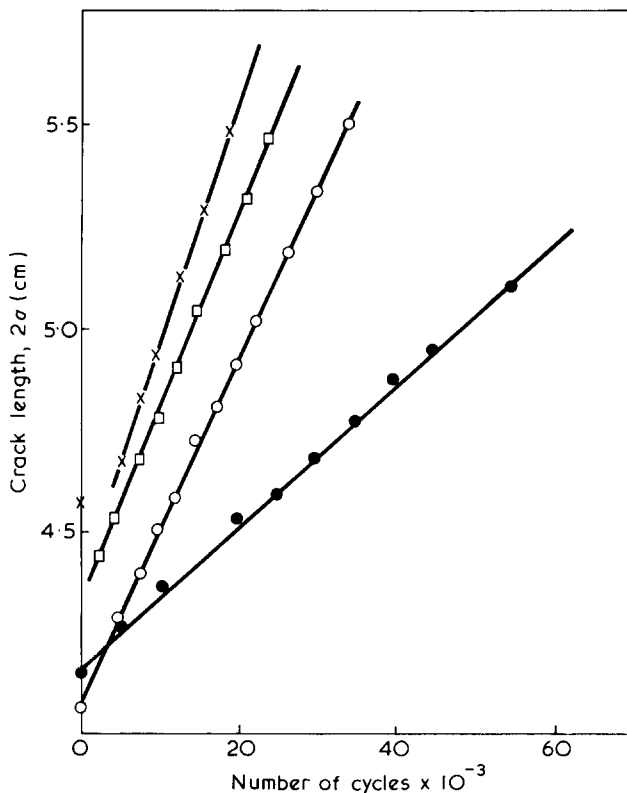


Figure 1 Variation of crack growth at 5 Hz and at different temperatures for PC. ●,  $-60^\circ$ ; ○,  $7^\circ$ ; □,  $21^\circ$ ; X,  $27^\circ\text{C}$ .  $K_{\text{max}} = 0.82 \text{ MN/m}^{3/2}$ ;  $K_{\text{min}} = 0.05 \text{ MN/m}^{3/2}$

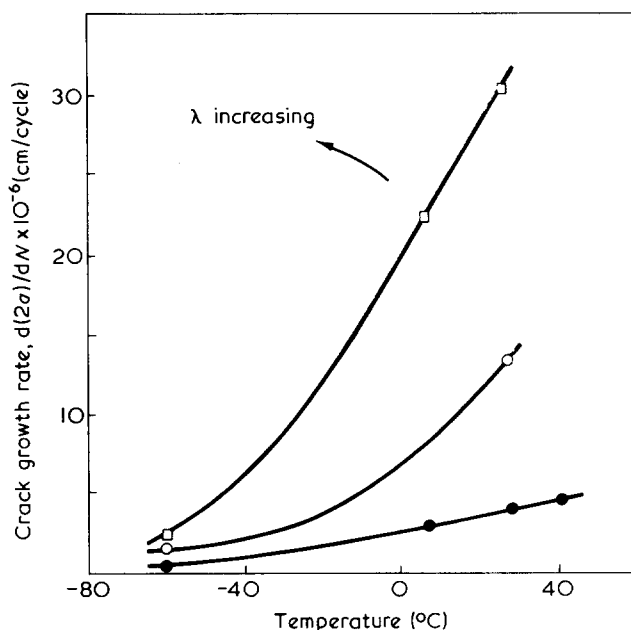


Figure 2 Crack growth rate vs. temperature at 5 Hz for PMMA. ●,  $K_{\text{max}} = 0.66$ ,  $K_{\text{min}} = 0.22 \text{ MN/m}^{3/2}$ ; ○,  $K_{\text{max}} = 0.74$ ,  $K_{\text{min}} = 0.08 \text{ MN/m}^{3/2}$ ; □,  $K_{\text{max}} = 0.82$ ,  $K_{\text{min}} = 0.28 \text{ MN/m}^{3/2}$

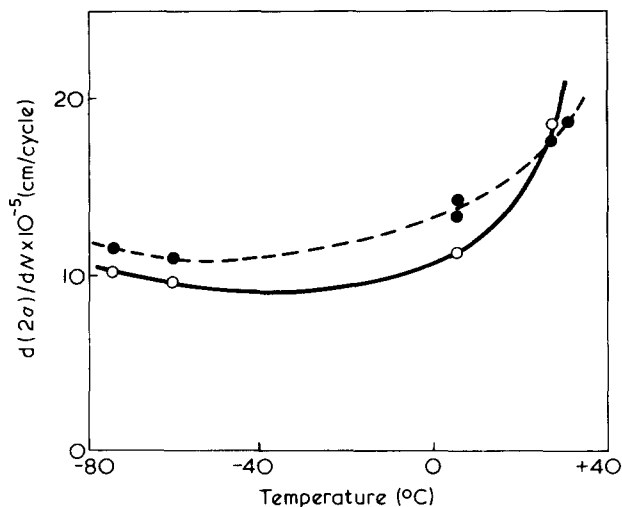


Figure 3 Crack growth rate vs. temperature for PC.  $\circ$ , 5;  $\bullet$ , 20 Hz.  $K_{\max} = 0.93 \text{ MN/m}^{3/2}$ ;  $K_{\min} = 0.05 \text{ MN/m}^{3/2}$

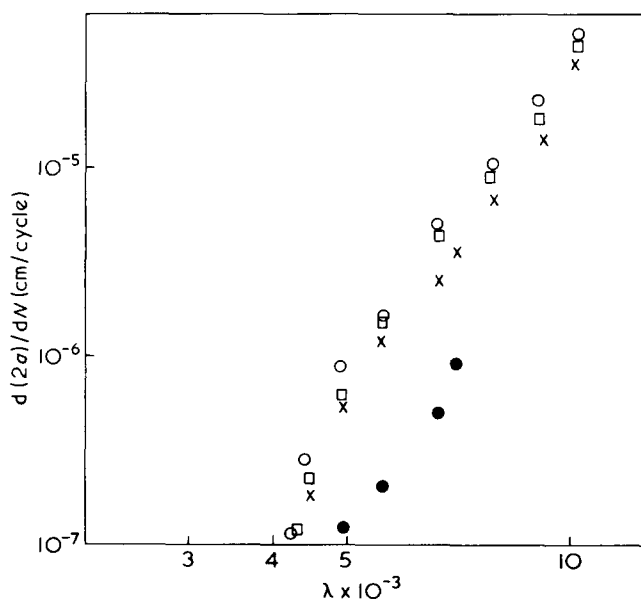


Figure 4 Crack growth rate vs.  $\lambda$  at 20 Hz for PMMA.  $\bullet$ ,  $-60^\circ$ ;  $\times$ ,  $7^\circ$ ;  $\square$ ,  $27^\circ$ ;  $\circ$ ,  $40^\circ \text{C}$

equation (2), and it appears that the influence of  $\lambda$  is dominant at higher temperatures, at least in PMMA. A similar trend, namely that of decreasing crack growth rate with decreasing temperature is shown in Figure 3 on PC, although it should be noted that the observed change was relatively small.

Additional tests on PMMA at different temperatures and at various values of stress intensity factors are shown in Figure 4, where  $d(2a)/dN$  is plotted as a function of  $\lambda$  at 20 Hz. In the investigated region the relationships are essentially linear and have approximately the same slope. Other results obtained from tests on PMMA performed at the same value of  $\Delta K$  but at two different temperatures,  $+27^\circ \text{C}$  and  $-60^\circ \text{C}$  are plotted in Figure 5. It can be seen that for a given frequency within the temperature range investigated the crack growth rates decreased noticeably with decreasing temperature.

The differences in the crack growth rates were larger as frequency decreased, but the slope remained unchanged. Additional tests at still lower temperatures will provide further insight into the changes of crack growth rates with

temperature and it is to be expected that the value of the slope may change also.

#### Influence of frequency

Tests were conducted on sheet specimens as before but at a range of frequencies, namely 5, 20 and 100 Hz. Tests at 0.1 Hz are now in progress, but frequencies below 0.1 Hz were not used because of excessively long testing times, while preliminary tests showed that frequencies above 100 Hz would lead to a considerable heat build-up in the specimen which would influence crack growth and finally result in a thermal failure of the material. Similarly, values of  $K_{\max}$  were limited, as it became clear that fatigue crack growth at levels close to the critical  $K$  would be accompanied by a certain amount of creep damage. In all cyclic tests at constant  $K$  values the crack growth will include a component of cyclic creep, but preliminary tests at  $21^\circ \text{C}$  on PMMA confirmed that the contribution of cyclic creep would not become significant except at  $K_{\max}$  levels greater than  $0.93 \text{ MN/m}^{3/2}$ . A similar limiting value of  $K_{\max}$  was found for PC ( $1.0 \text{ MN/m}^{3/2}$ ) and tests were not performed at higher levels at  $21^\circ \text{C}$ . However, it was possible to increase slightly both limits in testing at lower temperatures and/or higher frequencies.

Data available on the effect of loading frequency on the fatigue crack growth rate even in metals are rather scarce. In general, only small changes in crack growth caused by frequency variation are recorded<sup>9</sup>. In some materials, such as mild steels, the evidence is inconclusive. However, in very strain-rate sensitive materials, such as polymers, changes in frequency may have a definite effect.

In a previous paper<sup>10</sup>, tests performed at  $21^\circ \text{C}$  on PMMA showed an increasing crack growth rate with decreasing

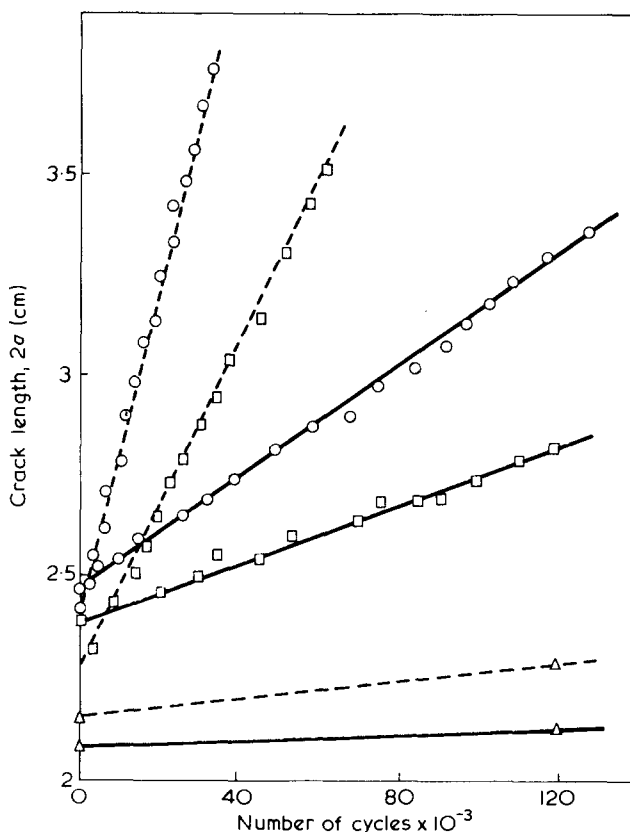


Figure 5. Crack growth at various frequencies and temperatures for PMMA. —,  $-60^\circ$ ; ---,  $+27^\circ \text{C}$ .  $\circ$ , 5;  $\square$ , 20;  $\triangle$ , 100 Hz.  $K_{\max} = 0.66 \text{ MN/m}^{3/2}$ ;  $K_{\min} = 0.22 \text{ MN/m}^{3/2}$

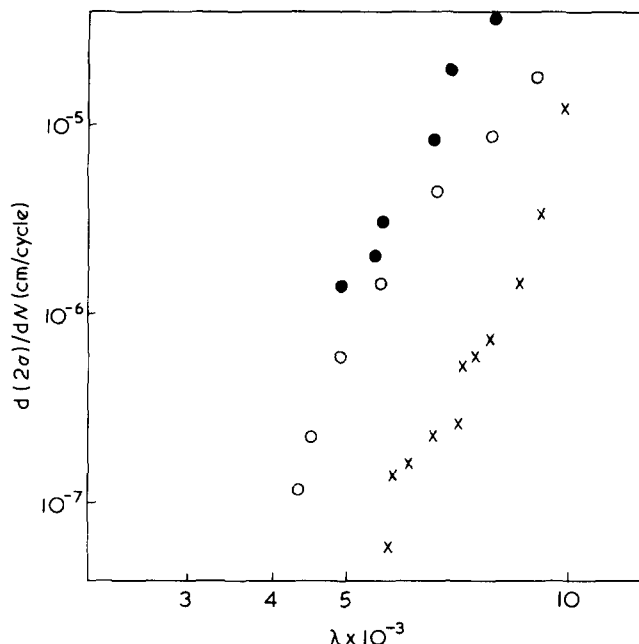


Figure 6 Crack growth rate vs.  $\lambda$  at different frequencies and at 27°C for PMMA. ●, 5; ○, 20; ×, 100 Hz

frequency and current tests at other temperatures confirm this tendency (Figure 5). The relationship between crack length and number of cycles at all frequencies was again linear, as has been similarly reported for metals<sup>11</sup>. Crack growth at high frequencies was extremely slow and decreased by one order of magnitude with frequency increasing from 5 to 100 Hz.

Constant temperature tests may provide an alternative insight into the cyclic process. Crack growth rates in PMMA at a range of frequencies but at constant temperatures are shown in Figure 6. These results indicate a considerable frequency dependence in the growth rates at higher temperatures, although distinctly smaller changes were observed at -60°C. At 27°C the crack growth rate at a frequency of 100 Hz was approximately two orders of magnitude lower than that observed in the tests at 5 Hz, but at -60°C this difference was not more than 50%. Preliminary tests performed on PC at higher than ambient temperatures showed that the crack growth rate may change only marginally with increasing frequency.

However, the results now available on PC (Figure 3) suggest that at temperatures below +25°C the situation reversed. Tests at yet higher temperatures may clarify this point. A slight increase in the crack growth rate appears to occur again below -60°C indicating that the minimum growth rate may occur at approximately -40°C.

In the tests discussed so far the crack growth rate and its dependence on  $\Delta K$  was investigated using tensile cycling, i.e.  $R = (K_{\min}/K_{\max}) = 0$ . It should be recalled that in metals, such as steels and Al alloys, mean stress intensity,  $K_m$ , effects may become important. Also, it is known that the influence of  $K_m$  decreases with increasing toughness<sup>9</sup>. The behaviour of polymers under the conditions  $R \neq 0$  is therefore of interest.

In a further series of tests,  $\Delta K$  was maintained constant whilst  $K_m$  was varied under given temperature and frequency conditions. Again a linear relationship between the crack growth rate and number of load cycles similar to Figure 1 was obtained, but the rate of increase of the crack growth was not proportional to  $K_m$ . These tests indicate

that both  $K_m$  and  $\Delta K$  exert a distinct influence on the crack growth rates. Figure 7 shows results obtained at 5 Hz and 21°C on PMMA in the tests at  $K_m$  equal to 0.27, 0.54 and 0.80 MN/m<sup>3/2</sup>, compared with the basic growth rate curve for  $R = 0$ . It can be seen that the crack growth increases with increasing values of  $K_m$ . A similar behaviour could be expected at other frequencies and tests at 100 Hz; Figure 8 confirms this. Comparable results are recorded for PC at  $K_m = 0.85$  MN/m<sup>3/2</sup> and 5 Hz in Figure 9. As already mentioned, contrary to the behaviour observed on PMMA, the crack growth rate in PC increased with increasing frequency (20 Hz). Basic growth rate curves,  $R = 0$ , showing decreasing growth with increasing frequency in PMMA are shown in Figure 10; in all these graphs experimental points have been omitted for the sake of clarity.

As the results obtained in the present tests show some similarities with the previous data on polymers, obtained under comparable testing conditions (temperature, frequency, etc.), the use of equation (2) may again be appropriate. A logarithmic plot of the results (Figure 11) including those from the tests in which  $R = 0$  show a family of fatigue crack growth curves converging into a single line at higher values of  $\lambda$ .

Fatigue crack growth curves can be divided into three parts. In region I crack initiation and primary crack growth, usually described as stage I (along primary slip planes) becomes more important with decreasing values of  $\lambda$ . At very low crack growth rates the factor  $\lambda$  is strongly dependent on  $K_m$ . The lower limit of region I represents fatigue thresholds. The existence of this critical range of stress intensity, below which crack propagation occurs either

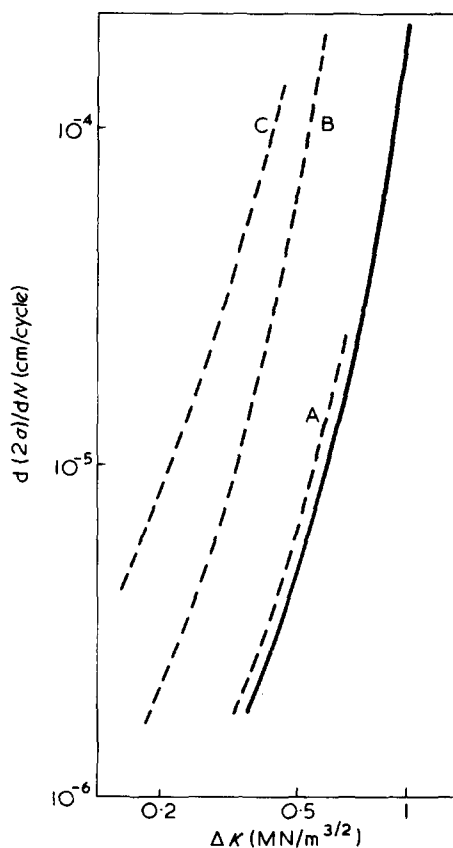


Figure 7 Effect of  $K_m$  on PMMA at 21°C and at 5 Hz. —,  $K_{m,0} = 0$ .  $K_m$ : A, 0.28; B, 0.56; C, 0.84 MN/m<sup>3/2</sup>

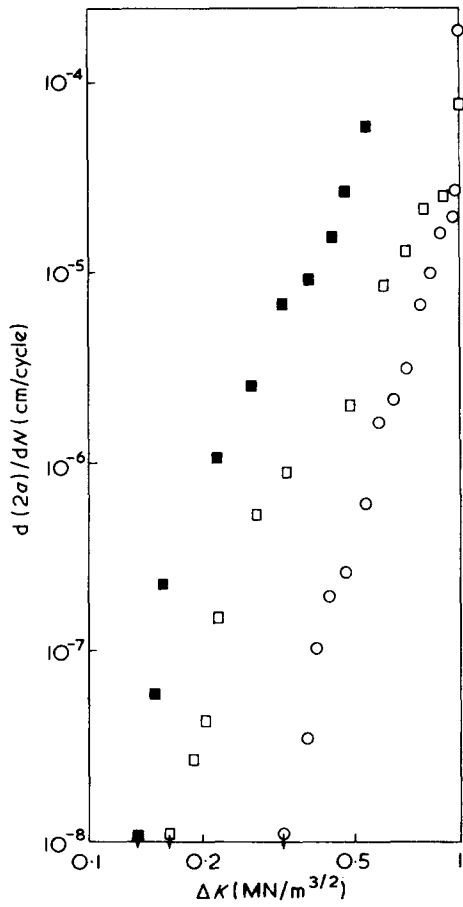


Figure 8 Crack growth vs.  $\Delta K$  at 100 Hz in air at 21°C for PMMA.  $\circ$ ,  $R = 0$ ;  $\square$ ,  $K_m = 0.55$  MN/m<sup>3/2</sup>;  $\blacksquare$ ,  $K_m = 0.825$  MN/m<sup>3/2</sup>

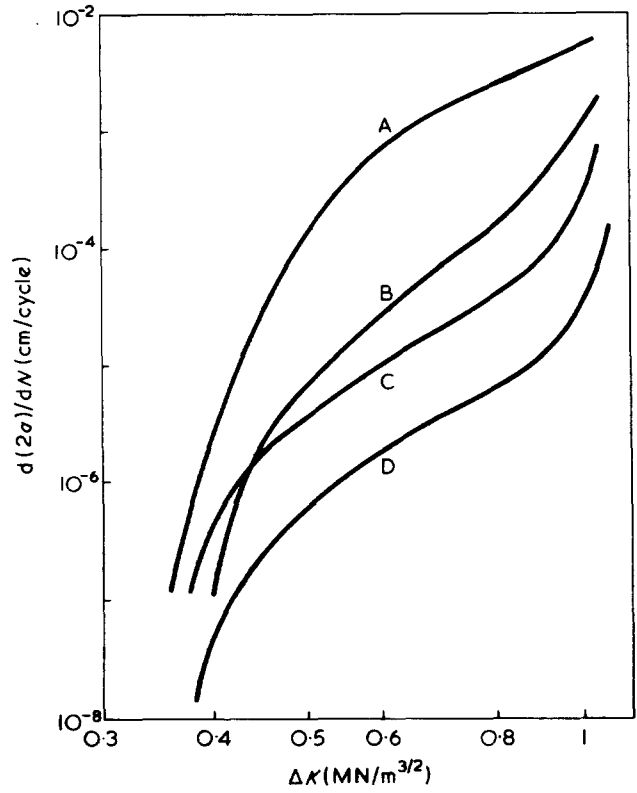


Figure 10 Crack growth rate vs.  $\Delta K$  for PMMA at various frequencies at 21°C in air,  $R = 0$ . A, 0.1; B, 5; C, 20; D, 100 Hz

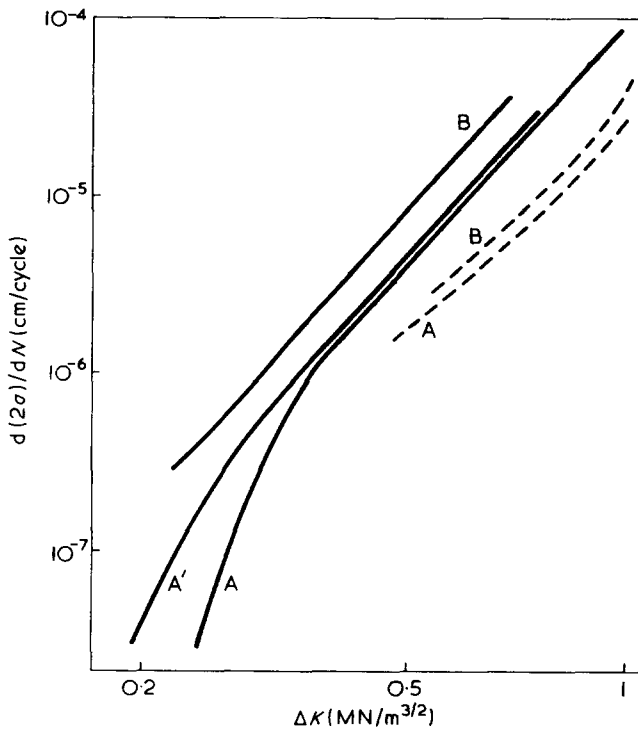


Figure 9 Effect of frequency on PC at +21°C (—) and -60°C (---). A, 5 Hz; A', 5 Hz,  $K_m = 0.88$  MN/m<sup>3/2</sup>; B, 20 Hz

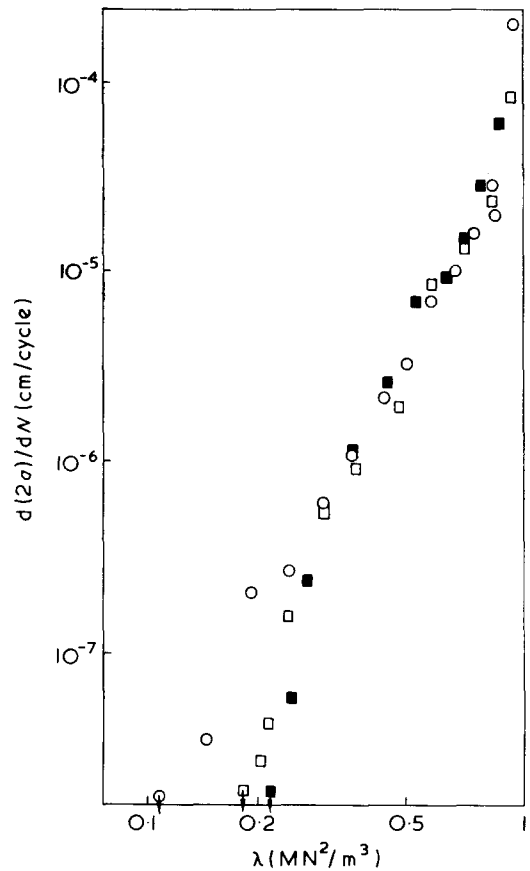


Figure 11 Crack growth vs.  $\lambda$  at 100 Hz in air at 21°C for PMMA.  $\circ$ ,  $R = 0$ ;  $\square$ ,  $K_m = 0.55$ ;  $\blacksquare$ ,  $K_m = 0.825$  MN/m<sup>3/2</sup>

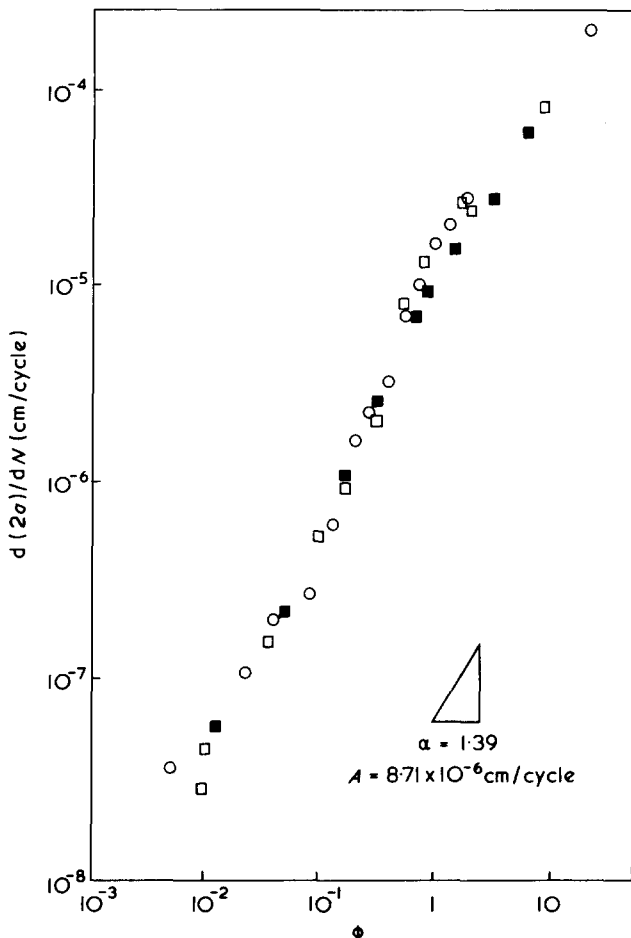


Figure 12 Crack growth vs.  $\phi$  at 100 Hz in air at 21°C for PMMA.  $\circ$ ,  $R = 0$ ;  $\square$ ,  $K_m = 0.55$ ;  $\blacksquare$ ,  $K_m = 0.825 \text{ MN/m}^{3/2}$

extremely slowly or may not occur at all, has been confirmed for some steels and Al alloys<sup>7,9</sup>. The existence of a threshold in the present polymeric materials is also indicated in Figures 7, 8 and 9, where the rapid fall in growth rates at low  $\Delta K$  values would allow the threshold  $\Delta K_{th}$  to be inferred at a rate of about  $10^{-9}$  cm/cycle. The figures also show that  $\Delta K_{th}$  decreases rapidly as  $K_m$  increases. This threshold value  $\Delta K_{th}$  seems to be dependent on the basic material properties, but detailed information is not yet available<sup>7</sup>.

The higher crack growth rate in region II can be described by basic equations such as equation (2). A yet faster growth rate is observed in region III culminating in a half-cycle loading when  $K_{max}$  reaches its critical value. In this region, static modes of fracture become more important with increasing levels of  $K_{max}$ .

The threshold value  $\lambda_{th}$  will influence crack growth in region I (Figure 11) which is highly dependent on  $K_m$ , whereas  $K_{IC}$  is the critical parameter at the instability point, region III. These two values provide the limiting conditions:

$$\left. \begin{aligned} \lim_{\lambda \rightarrow \lambda_{th}} \frac{d(2a)}{dN} &= 0 \\ \lim_{K_{max} \rightarrow K_{IC}} \frac{d(2a)}{dN} &= \infty \end{aligned} \right\} \quad (4)$$

which leads to a generalized equation:

$$\frac{d(2a)}{dN} = A\phi^\alpha \quad (5)$$

where

$$\phi = \frac{\lambda - \lambda_{th}}{K_{IC}^2 - K_{max}^2}$$

as indicated in Figure 12,  $\alpha = 1.39$  and  $A = 8.71 \times 10^{-6}$  cm/cycle.

### CONCLUSIONS

1. In the investigated regime the cyclic crack growth rate decreases with decreasing temperature and increasing frequency.
2. Fatigue crack growth rate was found to be dependent upon the range of stress intensity factor  $\Delta K$  and its mean value  $K_m$ .
3. Fatigue crack growth rate can be described as:

$$\frac{d(2a)}{dN} = A\phi^\alpha$$

where  $\phi = (\lambda - \lambda_{th}) / (K_{IC}^2 - K_{max}^2)$ ,  $\lambda = K_{max}^2 - K_{min}^2$ ,  $\lambda_{th}$  is the threshold value of  $\lambda$  and  $A$  and  $\alpha$  are constants.

4. The threshold stress intensity factor  $\Delta K_{th}$  decreases with increasing  $K_m$ .

### ACKNOWLEDGEMENTS

Some of the data reported here were obtained by Mr P. Chauhan and Mr C. M. Branco, under the authors' supervision.

### REFERENCES

1. Arad, S., Radon, J. C. and Culver, L. E. *J. Mech. Eng. Sci.* 1971, 13, 75
2. Arad, S., Radon, J. C. and Culver, L. E. *Proc. IIIrd Int. Conf. Fracture Munich* 1973, 7, paper VI-323
3. Hoepfner, D. W. and Krupp, W. E. *Eng. Fract. Mech.* 1974, 6, 47
4. Glover, A. P., Johnson, F. A. and Radon, J. C. *Polym. Eng. Sci.* 1974, 14, 420
5. Higuchi, M. and Ishii, H. *Rep. Res. Inst. Appl. Mech., Kyushu Univ.* 1968, 16, 69
6. ASTM-STP 410 (1966)
7. Frost, N. E., Pook, L. P. and Denton, K. *Eng. Fract. Mech.* 1971, 3, 109
8. Kurobe, T. and Wakashima, H. *15th Japan Congr. Mat. Res. (Non-metallic Materials)* 1972, p 137
9. Feeny, J. A., McMillan, J. C. and Wei, R. P. *Metall. Trans.* 1970, 1, 1741
10. Arad, S., Radon, J. C. and Culver, L. E. *J. Mech. Eng. Sci.* 1972, 14, 328
11. Radon, J. C., Arad, S. and Culver, L. E. *Eng. Fract. Mech.* 1974, 6, 195

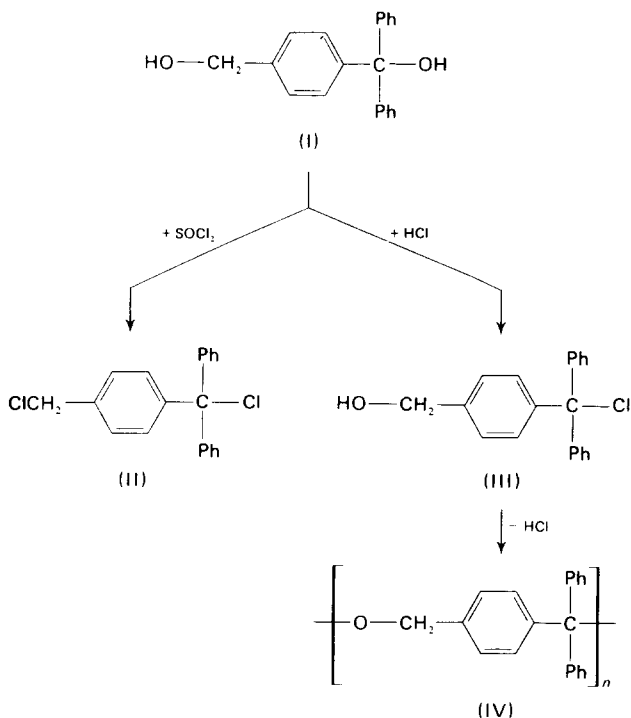
# Notes to the Editor

## Poly(oxybenzhydrylidene-1,4-phenylenemethylene)

D. Braun and U. Platzek

Deutsches Kunststoff-Institut, 61 Darmstadt, Schlossgartenstrasse 6R, West Germany  
(Received 31 December 1974)

It is known that triphenylmethanol and benzyl alcohol react readily with thionyl chloride or hydrogen chloride to yield triphenylmethyl chloride and benzyl chloride respectively<sup>1</sup>. Accordingly, reaction of diphenyl(4-hydroxymethylphenyl)methanol (I), which contains the structure elements of both the above alcohols with thionyl chloride, produces a good yield of diphenyl(4-chloromethylphenyl)methyl chloride (II). However, it is noteworthy that the reaction of diol (I) with hydrogen chloride in benzene, results in the formation of a polyether rather than the expected dichloride. The mode of formation and structure of this polyether (IV) have become of particular interest to us. The equations below illustrate the differences between the two reactions:



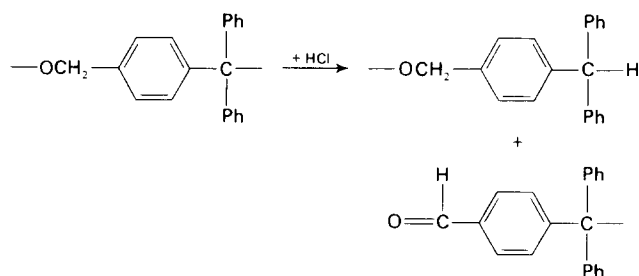
Reaction of (I) with hydrogen chloride may proceed by exchange of the hydroxyl group on the tertiary carbon atom with the halogen. In this manner a phenyl analogue of chlorhydrin (diphenyl(4-hydroxymethylphenyl)methyl chloride) (III) is formed, which easily yields the corresponding ether (IV) by splitting off hydrogen chloride.

In contrast to the above reaction, the conversion of the diol with thionyl chloride may possibly proceed via its ester with chlorosulphinic acid<sup>3</sup>. However, Carré and Libermann could not obtain the chlorosulphite intermediate with either benzyl alcohol or triphenylmethanol and they assumed the formation of the chloride to be a direct reaction<sup>4</sup>. In the conversion of the diol (I) with thionyl chloride, hydrogen chloride is also formed and owing to this a small amount of polyether is obtained as a byproduct.

The structure of the polyether was confirmed by infrared (i.r.) spectrometry and nuclear magnetic resonance (n.m.r.) spectrometry. The i.r. spectrum displayed very strong ether group vibrations at 1070 and 1090 cm<sup>-1</sup> (triphenylmethyl methyl ether 1077 and 1089 cm<sup>-1</sup>)<sup>3</sup>, whereas the n.m.r. spectrum (Figure 1), shows absorptions due to aromatic protons between  $\tau = 2.1$  and 3.1 ppm and due to the oxymethylene group at  $\tau = 5.85$  ppm. As expected, hydroxyl groups could not be detected.

The end groups of the polyethers deserve particular consideration. In the i.r. spectrum there is a carbonyl absorption at 1705 cm<sup>-1</sup> which can be attributed to an aromatic aldehyde. The aldehyde proton can be easily detected in the n.m.r. spectrum at  $\tau = 0.16$  ppm. Moreover, the spectrum contains signals due to methine protons from triphenylmethane end groups at  $\tau = 4.6$  ppm, and due to chloromethylene end groups at  $\tau = 5.6$  ppm.

It is known that triphenylmethyl ethyl ether, in the presence of hydrogen chloride, decomposes to triphenylmethane and acetaldehyde<sup>6</sup>. By analogy, during the formation of the polyether, triphenylmethane and benzaldehyde end groups may be formed by the following reaction:



Such a degradation could be responsible for the osmometric number-average molecular weight of the polyether (IV) being only 890. This molecular weight corresponds to a number-average degree of polymerization of 3.3.

The gel chromatogram of the polyether (IV) on Merckogel 5000 in tetrahydrofuran (Figure 2), provides some indication of the molecular weight distribution. As in our earlier publication on poly(1,4-phenylene-1,1-diarylethylene)<sup>7</sup>, the fraction at  $V_e = 246$  ml corresponds to the monomer fraction; whilst that at  $V_e = 200$  ml corresponds to the dimer fraction etc.

From the chromatogram it is clear that molecules with a degree of polymerization greater than 15 are present in only minute quantities.

### EXPERIMENTAL

Hydrogen chloride gas was passed through a solution of diphenyl(4-hydroxymethylphenyl)methanol in dry benzene (3.36 g in 50 ml), whereupon the solution became red in colour. After 20 to 30 min the solvent was removed under vacuum, leaving a glassy, light brown mass. This substance was dissolved in methanol and precipitated in

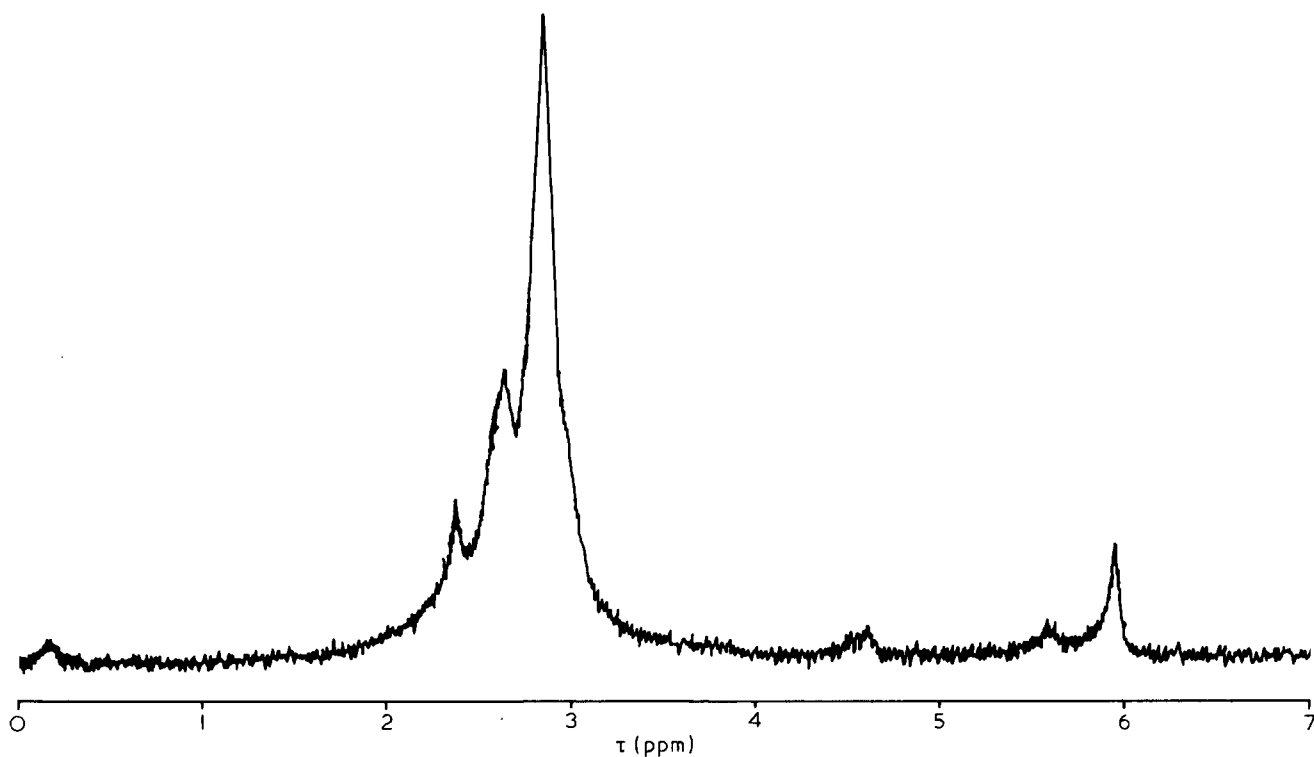


Figure 1 N.m.r. spectrum of polyether (IV) in  $CS_2$

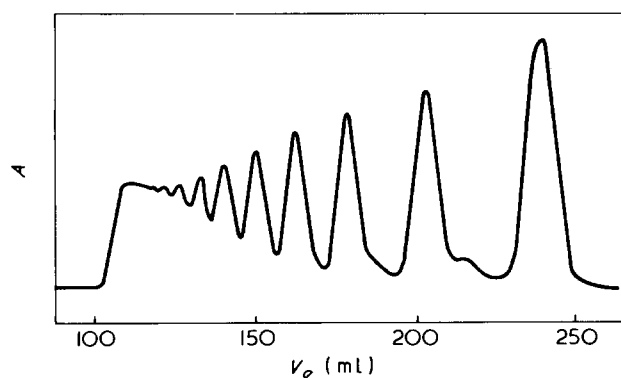


Figure 2 Gel permeation chromatogram of polyether IV (Merckogel 5000/THF)

water. The yield obtained was 82% of the theoretical value, being 2.58 g. Details of the measurement of the n.m.r. spectrum and the gel chromatogram are provided in an earlier publication<sup>7</sup>.

#### REFERENCES

- 1 Clark, R. H. and Streight, H. R. L. *Proc. Trans. R. Soc. Can. Sect. 3* 1929, **23**, 77; Gomberg, M. *Ber. Dtsch. Chem. Ges.* 1902, **35**, 2401
- 2 Braun, D. and Platzek, U. *Makromol. Chem.* 1973, **164**, 55
- 3 Hine, J. 'Reaktivität und Mechanismus in der organischen Chemie', G. Thieme, Stuttgart, 1960, p 113
- 4 Carré, P. and Libermann, D. *Bull. Soc. Chim. Fr.* 1933, **53**, 1050; Carré, P. *C. R. Acad. Sci.* 1933, **196**, 1409, 1806; 1934, **198**, 274
- 5 Moravec, J., Kourim, P. and Horak, M. *Coll. Czech. Chem. Commun.* 1965, **30**, 2298
- 6 Funakubo, E. and Matsui, T. *Ber. Dtsch. Chem. Ges.* 1937, **70**, 2437
- 7 Braun, D. and Platzek, U. *Makromol. Chem.* 1973, **164**, 41

## Measurement of crystallinity of polyamide-6 by d.s.c.

G. Coppola, R. Filippini and B. Pallesi

*Snia Viscosa, Centro Sperimentale F. Marinotti, 20031 Cesano Maderno, Milano, Italy*  
(Received 23 December 1974)

#### INTRODUCTION

The aim of this work was to provide a calibration plot for routine measurements of the degree of crystallinity of commercial polyamide-6 through enthalpies of fusion,  $\Delta H_f$ , derived by differential scanning calorimetry (d.s.c.).

#### EXPERIMENTAL

Some commercial samples of polyamide-6 were moulded at different temperatures to films of 1 mm thickness, thus achieving various degrees of crystallinity (up to 50%). One totally amorphous sample was prepared by quenching in

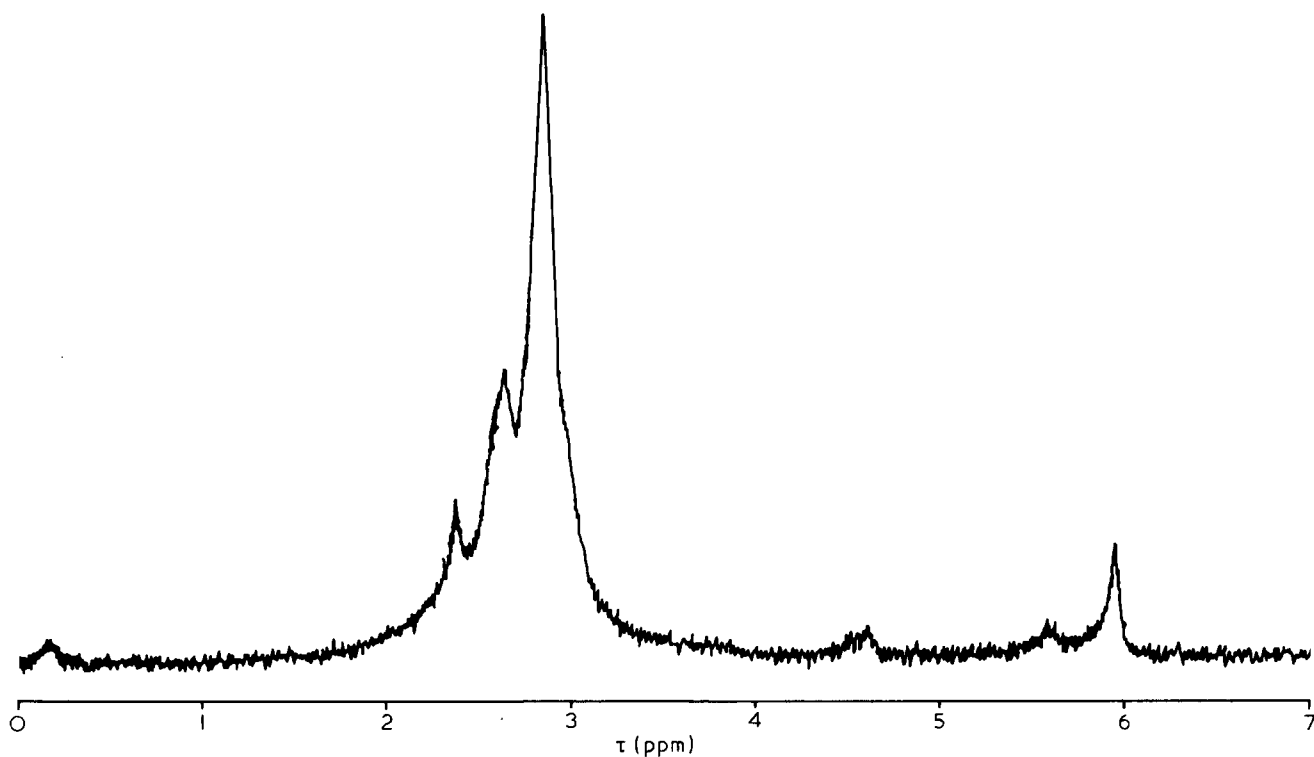


Figure 1 N.m.r. spectrum of polyether (IV) in  $CS_2$

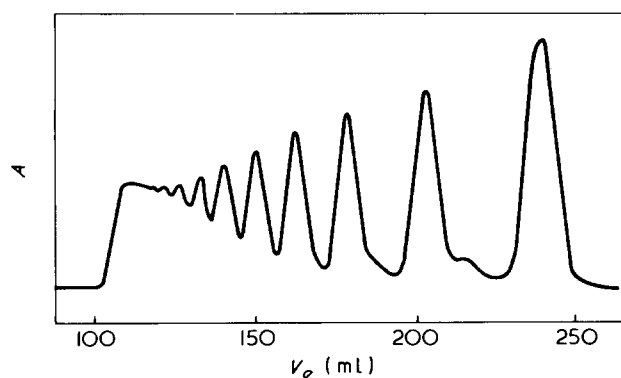


Figure 2 Gel permeation chromatogram of polyether IV (Merckogel 5000/THF)

water. The yield obtained was 82% of the theoretical value, being 2.58 g. Details of the measurement of the n.m.r. spectrum and the gel chromatogram are provided in an earlier publication<sup>7</sup>.

#### REFERENCES

- 1 Clark, R. H. and Streight, H. R. L. *Proc. Trans. R. Soc. Can. Sect. 3* 1929, **23**, 77; Gomberg, M. *Ber. Dtsch. Chem. Ges.* 1902, **35**, 2401
- 2 Braun, D. and Platzek, U. *Makromol. Chem.* 1973, **164**, 55
- 3 Hine, J. 'Reaktivität und Mechanismus in der organischen Chemie', G. Thieme, Stuttgart, 1960, p 113
- 4 Carré, P. and Libermann, D. *Bull. Soc. Chim. Fr.* 1933, **53**, 1050; Carré, P. *C. R. Acad. Sci.* 1933, **196**, 1409, 1806; 1934, **198**, 274
- 5 Moravec, J., Kourim, P. and Horak, M. *Coll. Czech. Chem. Commun.* 1965, **30**, 2298
- 6 Funakubo, E. and Matsui, T. *Ber. Dtsch. Chem. Ges.* 1937, **70**, 2437
- 7 Braun, D. and Platzek, U. *Makromol. Chem.* 1973, **164**, 41

## Measurement of crystallinity of polyamide-6 by d.s.c.

G. Coppola, R. Filippini and B. Pallesi

*Snia Viscosa, Centro Sperimentale F. Marinotti, 20031 Cesano Maderno, Milano, Italy*  
(Received 23 December 1974)

#### INTRODUCTION

The aim of this work was to provide a calibration plot for routine measurements of the degree of crystallinity of commercial polyamide-6 through enthalpies of fusion,  $\Delta H_f$ , derived by differential scanning calorimetry (d.s.c.).

#### EXPERIMENTAL

Some commercial samples of polyamide-6 were moulded at different temperatures to films of 1 mm thickness, thus achieving various degrees of crystallinity (up to 50%). One totally amorphous sample was prepared by quenching in



liquid nitrogen ( $-196^{\circ}\text{C}$ ) after melting at  $250^{\circ}\text{C}$ . This sample did not show any crystallinity by observation under a polarizing microscope.

Degrees of crystallinity were calculated from the density values measured by a gradient column, using the well known equation:

$$C = \frac{d_x - d_a}{d_c - d_a} \cdot \frac{100d_c}{d_x} \quad (1)$$

were  $C$  is the percentage crystallinity,  $d_x$ ,  $d_a$  and  $d_c$  are the densities of the sample, of the totally amorphous and totally crystalline polymer, respectively. The density of the quenched sample was  $1.098 \text{ g/cm}^3$ , in good agreement with published data<sup>1</sup>.

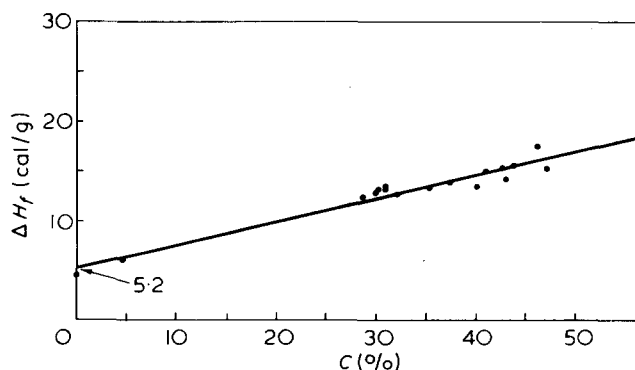
$\Delta H_f$  values were measured, on samples of 20 mg each, by a Du Pont Model 900 thermal analyser equipped with a d.s.c. cell, at a temperature scanning speed of  $30^{\circ}\text{C}/\text{min}$  and under a nitrogen atmosphere. These conditions have been adopted in order to minimize sample crystallization during heating. For samples of low crystallinity, however, crystallization above  $T_g$  (glass temperature) is unavoidable; in these cases, the exothermic peak was always subtracted from the melting area.

## RESULTS AND DISCUSSION

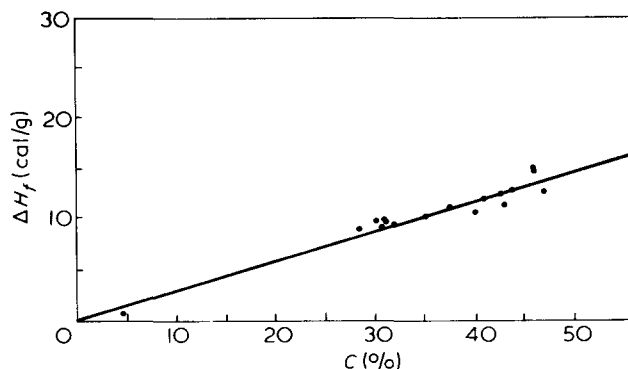
In order to derive  $C$  values from equation (1) we tentatively substitute the value of  $d_c = 1.220 \text{ g/cm}^3$ ; this is an average value of various published data<sup>2-4</sup> which are not in good agreement, however, since they range from 1.243 to 1.133  $\text{g/cm}^3$ . By plotting  $\Delta H_f$  against  $C$ , we obtain, nevertheless, not one but two straight lines; subsequent analysis by X-rays<sup>5</sup> showed that samples rich in  $\alpha$  crystalline form gave one line, distinct from the other on which samples rich in  $\gamma$  form were allocated. This finding is in complete agreement with Illers' conclusions<sup>1</sup>.

Since our object was to produce a simple calibration plot of  $C$  vs.  $\Delta H_f$  to be used for samples (films, monofilaments, etc.) where density measurements are difficult, the existence of two lines complicates the whole matter, requiring X-ray analysis of each sample in order to determine the crystalline form. We have therefore plotted in *Figure 1* only the values concerning those samples in which one of the two forms ( $\alpha$  or  $\gamma$ ) was prevailing; in equation (1) two  $d_c$  values were used: 1.235 for  $\alpha$  crystals and 1.190 for  $\gamma$  crystals, which are averages of published data<sup>4-6</sup>.

By the least squares method we calculated the single



*Figure 1* Calibration curve: values concern samples having only  $\alpha$  or  $\gamma$  forms



*Figure 2* Corrected calibration curve considering the amorphous crystallization after  $T_g$

upper line shown in *Figure 1*. We assumed that  $\Delta H_f$  values for  $\alpha$  and  $\gamma$  forms are practically identical; with this assumption the plot is valid whatever the crystal composition of any sample. *Figure 1* shows that the calibration line does not pass through the origin but cuts the ordinate axis at a value of  $\Delta H_f = 5.20 \text{ cal/g}$ . This same observation was made by Illers<sup>1</sup>, who explained it by assuming the existence of some ordered structures in the amorphous phase. This is probably true for their samples, which were quenched, after melting, in carbon tetrachloride at  $0^{\circ}\text{C}$ . Our samples, quenched at a much lower temperature, suggest a better explanation, i.e. to assume a slow crystallization of the sample during heating in the calorimeter. Polyamides-6 can easily crystallize owing to their low  $T_g$  values. Crystallization is known to occur immediately above  $T_g$  and is put into evidence by an exothermic peak but the phenomenon probably takes place even after this peak, until the polymer melts; this is not easily shown being included in the base line. This effect produces values of  $\Delta H_f$  which are 20–30% higher than those expected from the crystallinity of the original samples. Since, however,  $\Delta H_f$  values have been correlated with degrees of crystallinity measured by density values, the plot of *Figure 1* is still good for the purpose we wanted.

As an indication of the correctness of our hypothesis, we can assume that the amount of crystallinity introduced into the sample on heating is proportional to the original amorphous content; by multiplying this value for 5.2 cal/g and subtracting this quantity from the measured  $\Delta H_f$ , we obtain a new line, shown in *Figure 2*, which passes through the origin.

## ACKNOWLEDGEMENT

We are particularly grateful to Professor U. Bianchi (Istituto di Chimica Industriale dell'Università di Genova) for critical reading of the manuscript.

## REFERENCES

- Illers, K. H. and Haberkorn, H. *Makromol. Chem.* 1971, **142**, 31
- Holmes, D. R., Bunn, C. W. and Smith, D. I. *J. Polym. Sci.* 1955, **17**, 159
- Ruscher, C. and Schröder, H. *J. Faserforsch. Textiltech.* 1960, **11**, 165
- Roldan, L. G. and Kaufman, H. S. *J. Polym. Sci. (B)* 1963, **1**, 603
- D'Alò, B., Coppola, G. and Pallesi, B. *Polymer* 1974, **15**, 130

# A new catalytic system for the polymerization of THF

H. W. Siesler\* and B. Tittle

Department of Chemistry, University of the Witwatersrand, Jan Smuts Avenue, Johannesburg, South Africa

(Received 23 December 1974)

## INTRODUCTION

The polymerization of tetrahydrofuran (THF) with various catalytic systems has been studied by many workers<sup>1-4</sup>. THF polymerizes by a cationic mechanism with the initial formation of an oxonium ion and successive nucleophilic attack of monomer oxygen on the carbon atom in  $\alpha$ -position to the positive oxygen<sup>5</sup>. The influence of various catalysts, solvents and reaction temperatures on the physical and chemical properties of polytetrahydrofuran (PTHF) has been discussed in numerous publications<sup>6-8</sup>.

Here we wish to report the preparation and the results obtained in THF polymerization by a so far unreported catalyst system.

A literature report<sup>9</sup> indicates that phosphorus tricyanide,  $P(CN)_3$ , when isolated from the reaction mixture of phosphorus trichloride,  $P(Cl)_3$ , with silver cyanide,  $AgCN$ , in acetonitrile is initially white and that on standing the product changes from white through yellow to orange. These authors<sup>9</sup> state that the colour change did not affect the reactions of  $P(CN)_3$  which they were studying. We find that  $P(CN)_3$  in this orange-yellow form is an active catalyst for the bulk polymerization of THF to high molecular weight products. Although the exact nature of the catalyst species has not yet been elucidated, we have demonstrated that the change from white to orange form only occurs in the solid state when residual acetonitrile is present.

$P(CN)_3$  has been shown to exist as a dimer in acetonitrile solution<sup>10</sup>. Although acetonitrile is tenaciously retained by  $P(CN)_3$  on isolation, no definite stoichiometry could be detected and sublimation or prolonged evacuation will remove the last traces of solvent.  $P(CN)_3$  purified by vacuum sublimation and shown by mass spectrometry not to contain acetonitrile does not catalyse the polymerization and no change on standing in a sealed vessel to the active form occurs. Similarly complete removal of acetonitrile under high vacuum when isolating  $P(CN)_3$  produces a product which does not revert to the orange active form. On prolonged exposure to the atmosphere a brown product is obtained which, even in the presence of residual acetonitrile, does not act as catalyst in the polymerization reaction and is the result of hydrolysis of the  $P(CN)_3$ .

In view of the uncertainty in the elemental analysis results owing to the hygroscopic nature of the catalyst we do not attempt to propose a mechanism and the nature of the ions involved in the initiation step of the polymerization. Notwithstanding this uncertainty in the exact composition of the catalyst system it can be derived from our observations that residual acetonitrile is a necessary cocatalyst.

## EXPERIMENTAL

### Preparation of catalyst

$P(CN)_3$  was prepared by adding 5 g of  $P(Cl)_3$  in 20 ml acetonitrile (dried over  $P_2O_5$  and distilled) to 15 g of  $AgCN$

vigorously stirred in 200 ml of acetonitrile under dry nitrogen. After 2 h at room temperature the product was filtered under nitrogen and the acetonitrile was removed on a rotary evaporator with a bath temperature of 45°C. When a solid residue was obtained, air was admitted and the flask stoppered. On standing for 24 h the change from white to orange form occurred. This product was used in the polymerization studies.

### Preparation of polymer

Previous to its use in the polymerization reaction THF (predried over KOH) was distilled from sodium and collected over molecular sieve. To 4 ml (~50 mmol) THF approximately 0.1 g of the above-mentioned catalyst was added and the mixture was shaken at room temperature. Within a few minutes the yellow colour of the solution intensified and concomitantly the viscosity increased until the original solution solidified to a transparent yellow-brown solid after about 1 h. After standing for 2 days the reaction mixture was dissolved in 100 ml THF and the polymer was precipitated by adding this solution dropwise to 1 l of ice-cold water in a high speed blender. The polymer precipitated as white rubbery solid which accumulated mainly on the stirrer blades.

The dissolution and precipitation operations were repeated and the yield of white tough product, finally dried in the vacuum oven at 25°C for 48 h varied between 43 and 54% in different experiments.

## CHARACTERIZATION OF THE POLYMER

The intrinsic viscosity  $[\eta]$  determined in chlorobenzene as solvent at 30°C scattered between 0.75 and 1.0 dl/g for products obtained in a series of 6 experiments. In a previous paper Makletsova *et al.* have published their results of viscosity and light scattering studies on PTHF<sup>11</sup>. Applying their relationship between the intrinsic viscosity (measured in methyl ethyl ketone and chlorobenzene solutions respectively) and molecular weight  $\bar{M}_w$  of PTHF:  $[\eta] = 2.1 \times 10^{-3} M^{0.5}$ , we derive molecular weights ranging from 130 000 to 230 000 in our products. The elemental analysis of the polymer (Table 1) is in good agreement with the theoretical values for PTHF. A thermogram of the polymer by differential scanning calorimetry showed an endotherm at the crystalline melting point between 37 and 44°C. For the i.r. spectroscopic investigation 40 mg of polymer were dissolved in 5 ml dry benzene and part of the solution was spread evenly on a KBr disc. The solvent was evaporated in a vacuum oven at 50°C for 48 h. The i.r. spectra of the sample recorded at 50°C and after recrystallization for a week at 20°C were identical to those of amorphous and crystalline PTHF<sup>12</sup>.

Table 1 Elemental analysis of PTHF,  $[(CH_2)_4-O]_n$

	C (%)	H (%)	O (%)
Exp.	66.3	11.2	22.3
Calc.	66.7	11.1	22.2

\* Present address: Bayer AG, Werk Dormagen, Postfach 1140 D 4047 Dormagen, West Germany.

In conclusion we may say that experimental evidence proves that application of the catalyst under investigation yields crystalline high molecular weight products in the bulk polymerization of THF at room temperature.

## REFERENCES

- 1 Meerwein, H., Delfs, D. and Morshel, H. *Angew. Chem.* 1960, 72, 927
- 2 Bawn, C. E. H., Bell, R. M., Fitzsimmons, C. and Ledwith, A. *Polymer* 1965, 6, 661
- 3 Sims, D. *Makromol. Chem.* 1966, 98, 245
- 4 Saegusa, T., Matsumoto, S., Ueshima, T. and Imai, H. *Makromol. Chem.* 1967, 105, 132
- 5 Burrows, R. C. *Polym. Prepr.* 1965, 6, 600
- 6 Hall, H. K. Jr. *Polym. Prepr.* 1965, 6, 535
- 7 Dreyfuss, P. and Dreyfuss, M. P. 'Encyclopedia of Polymer Science and Technology', (Ed. H. F. Mark and N. G. Gaylord), Wiley, New York, 1970, Vol 13, p 670
- 8 Dreyfuss, P. *Polym. Prepr.* 1972, 13, 46
- 9 Jones, C. E. and Coskran, K. J. *Inorg. Chem.* 1971, 10, 1536
- 10 Kirk, P. G. and Smith, T. D. *J. Inorg. Nucl. Chem.* 1968, 30, 892
- 11 Makletsova, N. V., Epelbaum, I. V., Rozenberg, B. A. and Lyudvig, Ye. B. *Polym. Sci. USSR* 1965, 7, 73
- 12 Saegusa, T. *et al. Makromol. Chem.* 1962, 56, 55

## Letter

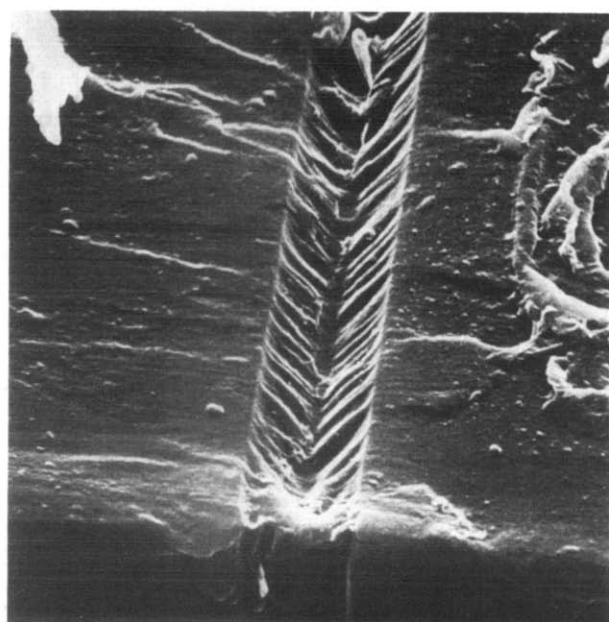
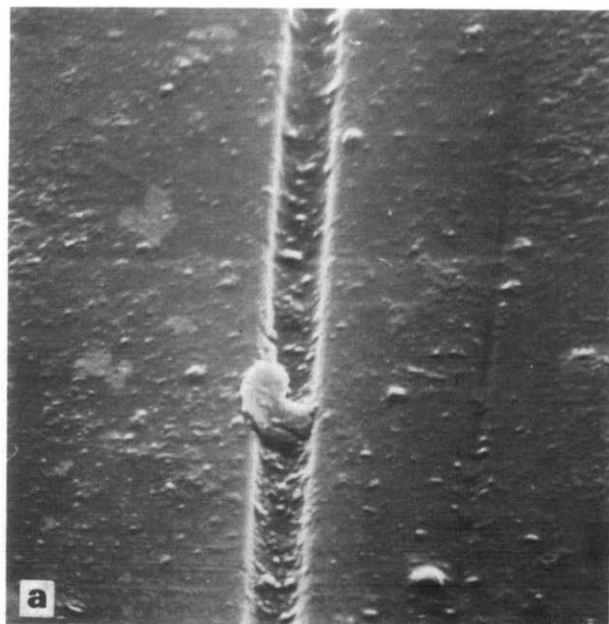


Figure 1 (a) Typical craze in bisphenol A polycarbonate formed by action of *n*-propanol as seen under a scanning electron microscope (2000x). (b) Same as (a) but with a strain of 2.0% (2000x)

### Observations of craze structure in bisphenol A polycarbonate

During the course of work concerned with the effect of crazes on the quality of performance of polycarbonate material, it became desirable to be able to examine the structure of a craze. This letter describes the means by which this has been achieved.

Many techniques have been used to study craze structure in glassy polymers. A popular and useful technique has been transmission electron microscopy of thin films, sections, or replicas from bulk specimens. Good examples of the use of these techniques have been described by Kambour<sup>1</sup>, and Beahan *et al.*<sup>2</sup>. The transmission electron microscope used in their work enables high magnifications to be obtained ( $\sim 250\,000\times$ ), but requires a lot of sample preparation and restricts the type of specimen which can be observed. The scanning electron microscope (stereoscan) enables thick specimens of crazed polymer to be observed without sectioning or replication. The specimen merely needs to be coated with a thin conducting metal layer to prevent it charging in the electron beam. However, although the crazes can be seen, the detailed structure within the craze is often obscured. A typical craze observed by this method is seen in *Figure 1a*. In the work now reported

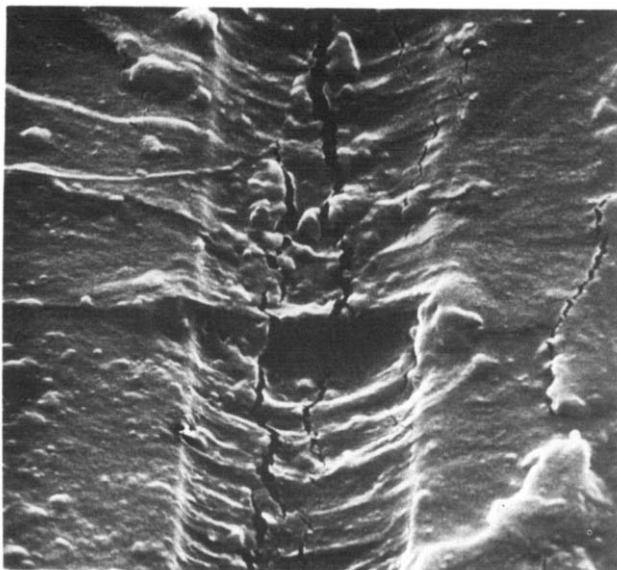


Figure 2 Craze shown in *Figure 1b* but with application of stress to the specimen (4100x)

In conclusion we may say that experimental evidence proves that application of the catalyst under investigation yields crystalline high molecular weight products in the bulk polymerization of THF at room temperature.

## REFERENCES

- 1 Meerwein, H., Delfs, D. and Morshel, H. *Angew. Chem.* 1960, 72, 927
- 2 Bawn, C. E. H., Bell, R. M., Fitzsimmons, C. and Ledwith, A. *Polymer* 1965, 6, 661
- 3 Sims, D. *Makromol. Chem.* 1966, 98, 245
- 4 Saegusa, T., Matsumoto, S., Ueshima, T. and Imai, H. *Makromol. Chem.* 1967, 105, 132
- 5 Burrows, R. C. *Polym. Prepr.* 1965, 6, 600
- 6 Hall, H. K. Jr. *Polym. Prepr.* 1965, 6, 535
- 7 Dreyfuss, P. and Dreyfuss, M. P. 'Encyclopedia of Polymer Science and Technology', (Ed. H. F. Mark and N. G. Gaylord), Wiley, New York, 1970, Vol 13, p 670
- 8 Dreyfuss, P. *Polym. Prepr.* 1972, 13, 46
- 9 Jones, C. E. and Coskran, K. J. *Inorg. Chem.* 1971, 10, 1536
- 10 Kirk, P. G. and Smith, T. D. *J. Inorg. Nucl. Chem.* 1968, 30, 892
- 11 Makletsova, N. V., Epelbaum, I. V., Rozenberg, B. A. and Lyudvig, Ye. B. *Polym. Sci. USSR* 1965, 7, 73
- 12 Saegusa, T. *et al. Makromol. Chem.* 1962, 56, 55

## Letter

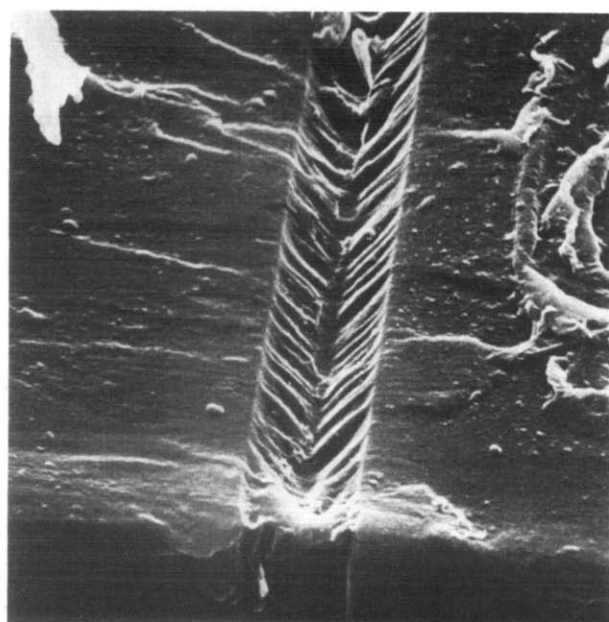
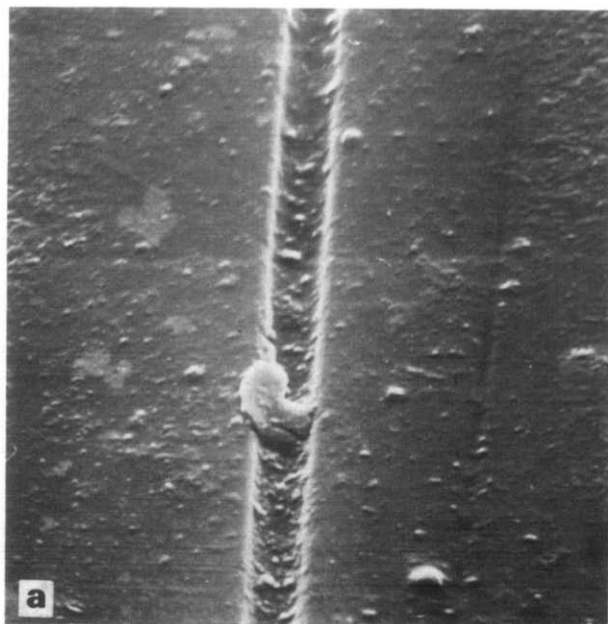


Figure 1 (a) Typical craze in bisphenol A polycarbonate formed by action of *n*-propanol as seen under a scanning electron microscope (2000x). (b) Same as (a) but with a strain of 2.0% (2000x)

### Observations of craze structure in bisphenol A polycarbonate

During the course of work concerned with the effect of crazes on the quality of performance of polycarbonate material, it became desirable to be able to examine the structure of a craze. This letter describes the means by which this has been achieved.

Many techniques have been used to study craze structure in glassy polymers. A popular and useful technique has been transmission electron microscopy of thin films, sections, or replicas from bulk specimens. Good examples of the use of these techniques have been described by Kambour<sup>1</sup>, and Beahan *et al.*<sup>2</sup>. The transmission electron microscope used in their work enables high magnifications to be obtained ( $\sim 250\,000\times$ ), but requires a lot of sample preparation and restricts the type of specimen which can be observed. The scanning electron microscope (stereoscan) enables thick specimens of crazed polymer to be observed without sectioning or replication. The specimen merely needs to be coated with a thin conducting metal layer to prevent it charging in the electron beam. However, although the crazes can be seen, the detailed structure within the craze is often obscured. A typical craze observed by this method is seen in *Figure 1a*. In the work now reported

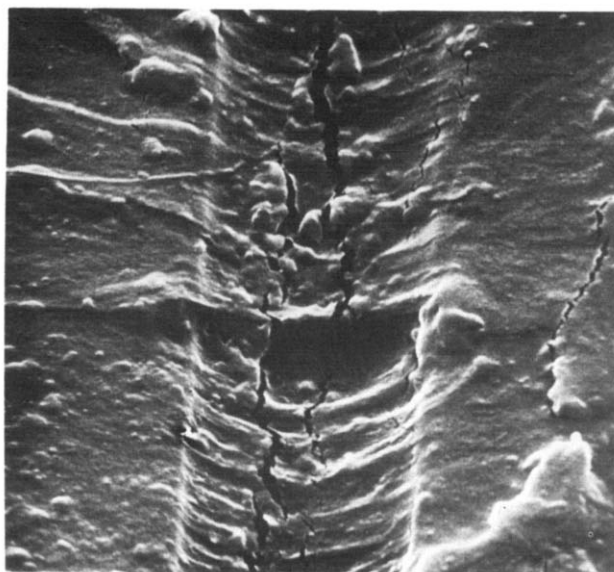


Figure 2 Craze shown in *Figure 1b* but with application of stress to the specimen (4100x)

## Letter

the specimen has been fractured in a brittle manner across the crazing, at right angles to the direction of craze growth. This enables the structure through the depth of the crazes to be examined.

The crazes examined to date by this method have been formed by the action of ethanol and n-propanol on polycarbonate specimens under stress. Large crazes were grown in specimens cut from compression-moulded sheet (thickness 0.8 mm), by the application of tensile stress in a bench-mounted jig, and the chosen environment. The specimens were then notched with a sharp blade, cooled to liquid nitrogen temperatures, and fractured perpendicular to the craze growth direction by rapid flexure. The sample thus obtained was then mounted on a straining device fitted to a stereoscan stub, coated with a thin metal film, and the exposed craze cross-section examined in the stereoscan.

Figure 1b shows a craze formed by the action of n-propanol under a strain of  $\sim 2.0\%$  (part of the original specimen surface is also shown). The craze exhibits V-shaped bridging with a central discontinuity. It is probable that

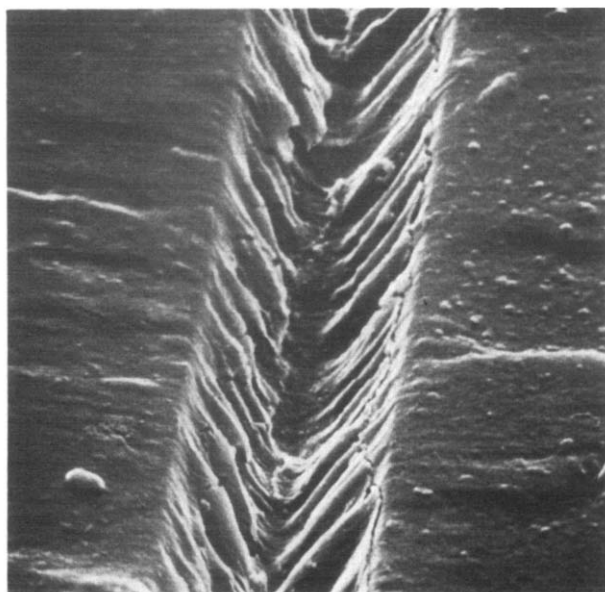


Figure 3 Craze shown in Figures 1b and 2 after strain removal (4100x)

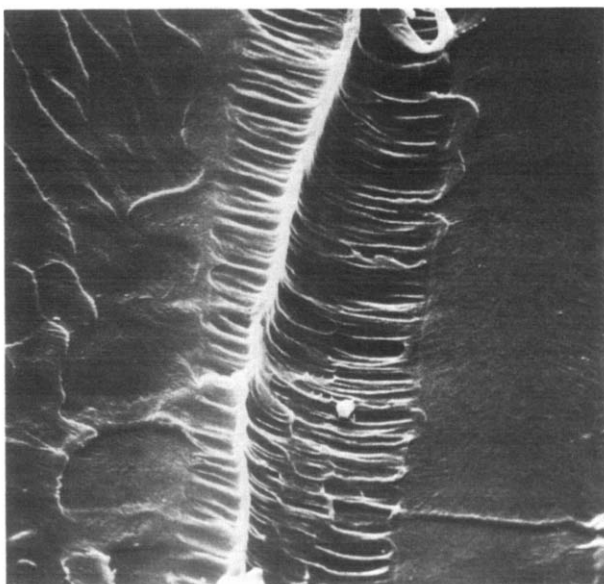


Figure 4 Typical craze in bisphenol A polycarbonate formed by action of ethyl alcohol (1640x)

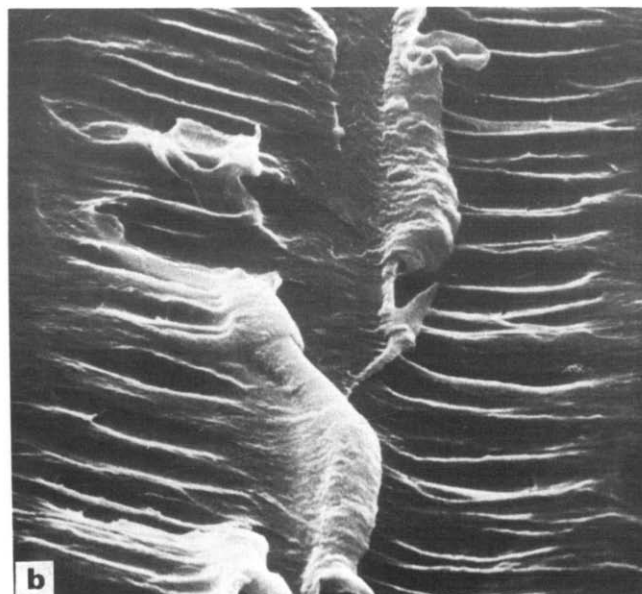
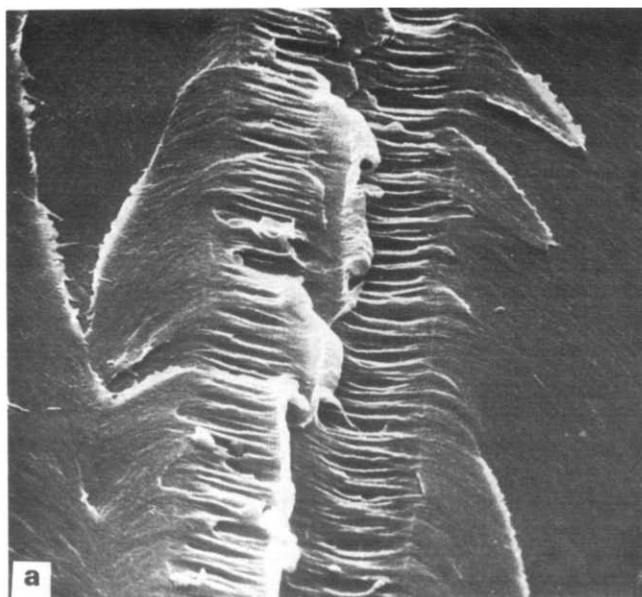


Figure 5 About 4% strain applied to the specimen seen in Figure 4. (a) 1640x; (b) 4100x

some details have been modified by the fracture process, and by relaxation of the craze structure. However, the general appearance of the material would correspond to that found in the craze interior prior to fracture. This craze is about  $8\ \mu\text{m}$  in width and the fibrils are  $0.2\text{--}0.5\ \mu\text{m}$  thick. Figure 2 shows this craze upon the application of stress to the specimen. The overall strain on the specimen was 2–3%, and the craze has increased in width by about 10%, hence the craze material is seen to elongate more than the bulk; this agrees with previous work<sup>3</sup>. The structure gives the appearance of having been pulled taut, and cracks have started to form; these are probably caused by the action of the electron beam. Figure 3 shows the craze in Figures 1b and 2 after strain removal. The structure has clearly been severely affected, and the craze has narrowed somewhat ( $\sim 5\%$ ) compared to the original.

Figure 4 shows a craze formed in ethanol under similar conditions to the previous example. The structure, however, appears to be of a considerably different form, and

the craze is also somewhat wider at  $\sim 17 \mu\text{m}$ . The fibrils appear to be more densely packed, more extended, and there is a prominent ridge of material running down the craze. Additionally, there appear to be smaller fibrils connecting the transverse structure in a similar way to that observed by Beahan *et al.*<sup>2</sup>. Applying strain to this craze, as before, produced little effect at first. Under similar conditions as applied to the craze in *Figure 2*, the only observable change was a very slight widening of the craze. On applying further strain (to the limit of the device used – about 4%) some breakdown of the structure was observed as shown in *Figures 5a* and *5b*. It appears that the material in the ridge has undergone some kind of tearing; the thin fibrils do not seem to be much affected. The bulk material surrounding the craze also seems to have been torn, perhaps illustrating the strength of this type of craze.

Thus it is seen that this technique enables craze structure to be observed with the minimum of sample preparation, and preliminary observations of the effects of strain so far

carried out show that different craze structures can have very different physical properties.

#### Acknowledgement

Thanks are due to Dr R. E. J. Fryer for work on the stereoscan.

[© Controller, HMSO, London, 1975]

Graham Durnal

Materials Quality Assurance Directorate,  
Royal Arsenal East, London SE18 6TD, UK  
(Received 26 February 1975; revised 18 March 1975)

#### References

- 1 Kambour, R. P. and Holik, A. S. *J. Polym. Sci. (A-2)* 1969, 7, 1393
- 2 Beahan, P., Bevis, M. and Hull, D. *Phil. Mag.* 1971, 24, 1267
- 3 Kambour, R. P. *Polym. Eng. Sci.* 1968, 8, 281

## Book Reviews

### Blood compatible synthetic polymers: an introduction

S. D. Bruck

C. C. Thomas, Springfield, 1974, 131 pp. \$9.75

The field of biomedical polymers is receiving increasing attention from workers in medical engineering and Dr Bruck has set out to provide a short introductory guide for people of all disciplines, be they physicians, engineers, life or materials scientists involved in the development and use of devices which come into direct contact with blood. What it is that makes some synthetic materials more tolerated by the living environment than others is still the subject of much speculation and consequently this monograph deals only briefly with its principal subject matter, giving a summary of the more promising materials found to date which demonstrate a degree of biocompatibility with blood while discussing the attributes mainly associated with a material's surface which might be responsible for the effect.

Understandably the bulk of the text is taken up with a review of polymeric materials and their many chemical, physical and mechanical properties. The emphasis here is on a direct comparison between synthetic and naturally-occurring macromolecules and on those properties which render the former suitable for use in biomedical applications and which might have a bearing on the various theories of blood compatibility.

Additionally, the author has contributed a useful presentation on the composition of blood and its working environment. This serves to highlight the many vital factors which can either influence or be influenced by the presence of a foreign material. For example, the influence of chemical, physical and mechanical action on the blood's defensive mechanisms are exemplified in relation to the blood coagulation pathways.

The current rate of advance in biomaterials science is such that one can anticipate the appearance of a more comprehensive treatise in the near future. This relatively inexpensive book provides a useful insight into the present state of the art and as the performance requirements expected of synthetic biomaterials increase it will serve to encourage the move from intuitive selection towards the synthesis of macromolecules designed to exist at the interface between a device and both the cellular and non-cellular components of blood.

It must be remembered, however, that while efforts have been made to relate blood compatibility of material to the composition of that material, the final analysis must take account of the application and the physical form.

T. Gilchrist

### Polymer-plastics technology and engineering

Edited by Louis Naturman

Marcel Dekker, New York, Vol 2, 1974. 262 pp. \$25.50

In order to better reflect the broadening of its subject matter in years to come, particularly in the polymer processing and application fields, the *Journal of Macromolecular Science (D: Reviews in Polymer Technology)* has changed its title to *Polymer – Plastics Technology and Engineering*, it being intended that a series of publications be arranged, on the basis of two issues per volume, providing timely intensive reviews of the state of the art in various branches of polymer technology and engineering.

Volume 2 presents papers on controlled u.v. degradation of plastics, metal plating of polymeric surfaces, fracture of polymers and polyblends, cationic coupling agents for thermoplastics, drilling of multi-layer printed boards, review of properties of polycarbonate resins, pressure sensitive adhesives, and impact behaviour of polymeric foams.

This particular volume in the series, in terms of its value to research and development workers, is difficult to assess there being wide variation in standards between individual authors. For instance the chapter on controlled u.v. degradation contains important open literature and patent material not previously published in a collected form. An example would be the key additives used to promote controlled polymer degradation namely, and unexpectedly, dibutyl dithiocarbonate salts, iron stearate, are listed alongside known polymer pro-oxidants based on copper, manganese, cobalt, and chromium salts. Such and similar data are undoubtedly very useful to newcomers and experienced workers. In like category are the chapters on drilling of multi-layer printed circuit boards, metal plating, pressure sensitive adhesives, and these alone would possibly justify the volume to specialized readers. Against these benefits some of the other chapters, listed above, have in various forms, featured elsewhere in the new voluminous polymer technology literature.

These criticisms may, of course, diminish as the series grows, the reviewer recognizing the considerably editorial problems initially in attracting new technology material written to adequate scientific standards. Change there should be if the present aims of intensive timely reviews are to be realized and, given such improvements, this series would find a place in the libraries and reference rooms of most research and tertiary educational institutions concerned with polymer technology.

Book binding, paper, printing and type-setting are of adequate quality and the price normal by present day standards for what

the craze is also somewhat wider at  $\sim 17 \mu\text{m}$ . The fibrils appear to be more densely packed, more extended, and there is a prominent ridge of material running down the craze. Additionally, there appear to be smaller fibrils connecting the transverse structure in a similar way to that observed by Beahan *et al.*<sup>2</sup>. Applying strain to this craze, as before, produced little effect at first. Under similar conditions as applied to the craze in *Figure 2*, the only observable change was a very slight widening of the craze. On applying further strain (to the limit of the device used – about 4%) some breakdown of the structure was observed as shown in *Figures 5a* and *5b*. It appears that the material in the ridge has undergone some kind of tearing; the thin fibrils do not seem to be much affected. The bulk material surrounding the craze also seems to have been torn, perhaps illustrating the strength of this type of craze.

Thus it is seen that this technique enables craze structure to be observed with the minimum of sample preparation, and preliminary observations of the effects of strain so far

carried out show that different craze structures can have very different physical properties.

#### Acknowledgement

Thanks are due to Dr R. E. J. Fryer for work on the stereoscan.

[© Controller, HMSO, London, 1975]

Graham Durnal

Materials Quality Assurance Directorate,  
Royal Arsenal East, London SE18 6TD, UK  
(Received 26 February 1975; revised 18 March 1975)

#### References

- 1 Kambour, R. P. and Holik, A. S. *J. Polym. Sci. (A-2)* 1969, 7, 1393
- 2 Beahan, P., Bevis, M. and Hull, D. *Phil. Mag.* 1971, 24, 1267
- 3 Kambour, R. P. *Polym. Eng. Sci.* 1968, 8, 281

## Book Reviews

### Blood compatible synthetic polymers: an introduction

S. D. Bruck

C. C. Thomas, Springfield, 1974, 131 pp. \$9.75

The field of biomedical polymers is receiving increasing attention from workers in medical engineering and Dr Bruck has set out to provide a short introductory guide for people of all disciplines, be they physicians, engineers, life or materials scientists involved in the development and use of devices which come into direct contact with blood. What it is that makes some synthetic materials more tolerated by the living environment than others is still the subject of much speculation and consequently this monograph deals only briefly with its principal subject matter, giving a summary of the more promising materials found to date which demonstrate a degree of biocompatibility with blood while discussing the attributes mainly associated with a material's surface which might be responsible for the effect.

Understandably the bulk of the text is taken up with a review of polymeric materials and their many chemical, physical and mechanical properties. The emphasis here is on a direct comparison between synthetic and naturally-occurring macromolecules and on those properties which render the former suitable for use in biomedical applications and which might have a bearing on the various theories of blood compatibility.

Additionally, the author has contributed a useful presentation on the composition of blood and its working environment. This serves to highlight the many vital factors which can either influence or be influenced by the presence of a foreign material. For example, the influence of chemical, physical and mechanical action on the blood's defensive mechanisms are exemplified in relation to the blood coagulation pathways.

The current rate of advance in biomaterials science is such that one can anticipate the appearance of a more comprehensive treatise in the near future. This relatively inexpensive book provides a useful insight into the present state of the art and as the performance requirements expected of synthetic biomaterials increase it will serve to encourage the move from intuitive selection towards the synthesis of macromolecules designed to exist at the interface between a device and both the cellular and non-cellular components of blood.

It must be remembered, however, that while efforts have been made to relate blood compatibility of material to the composition of that material, the final analysis must take account of the application and the physical form.

T. Gilchrist

### Polymer-plastics technology and engineering

Edited by Louis Naturman

Marcel Dekker, New York, Vol 2, 1974. 262 pp. \$25.50

In order to better reflect the broadening of its subject matter in years to come, particularly in the polymer processing and application fields, the *Journal of Macromolecular Science (D: Reviews in Polymer Technology)* has changed its title to *Polymer – Plastics Technology and Engineering*, it being intended that a series of publications be arranged, on the basis of two issues per volume, providing timely intensive reviews of the state of the art in various branches of polymer technology and engineering.

Volume 2 presents papers on controlled u.v. degradation of plastics, metal plating of polymeric surfaces, fracture of polymers and polyblends, cationic coupling agents for thermoplastics, drilling of multi-layer printed boards, review of properties of polycarbonate resins, pressure sensitive adhesives, and impact behaviour of polymeric foams.

This particular volume in the series, in terms of its value to research and development workers, is difficult to assess there being wide variation in standards between individual authors. For instance the chapter on controlled u.v. degradation contains important open literature and patent material not previously published in a collected form. An example would be the key additives used to promote controlled polymer degradation namely, and unexpectedly, dibutyl dithiocarbonate salts, iron stearate, are listed alongside known polymer pro-oxidants based on copper, manganese, cobalt, and chromium salts. Such and similar data are undoubtedly very useful to newcomers and experienced workers. In like category are the chapters on drilling of multi-layer printed circuit boards, metal plating, pressure sensitive adhesives, and these alone would possibly justify the volume to specialized readers. Against these benefits some of the other chapters, listed above, have in various forms, featured elsewhere in the new voluminous polymer technology literature.

These criticisms may, of course, diminish as the series grows, the reviewer recognizing the considerably editorial problems initially in attracting new technology material written to adequate scientific standards. Change there should be if the present aims of intensive timely reviews are to be realized and, given such improvements, this series would find a place in the libraries and reference rooms of most research and tertiary educational institutions concerned with polymer technology.

Book binding, paper, printing and type-setting are of adequate quality and the price normal by present day standards for what

must be a limited and specialized market. Somewhat brief author and subject indexes are provided and regretfully but expectedly as this is a USA publication, imperial units predominate. This volume could usefully be referred by both chemists, physicists and engineers the writing style being suitable for most technically orientated people from diverse backgrounds.

C. Hepburn

**Hot melt adhesives: manufacture and application**

M. J. Satriana

Noyes Data Corporation, Park Ridge, NJ, 1974, \$36.00

This review of the US Patent literature relevant to the field of interest accurately described in the title immediately wins the heart of anyone who has had to try to extract the important information from an official patent document. The author has done an expert job in transposing such documents into a text comprehensible to the adhesives technologist for whom one presumes the book is primarily intended. The reader is left in little doubt that Mr Satriana, like the other Noyes Data Corporation authors, is well versed in this art.

It is believed that anyone in the adhesives industry should have access to this book since it succeeds in achieving one of the objectives in the foreword in describing a very wide area of available hot melt adhesive technology which should stimulate ideas in the reader and lead to technological transfer between the diverse industries which use adhesives.

The patents described cover such a wide field of adhesive use that one hesitates to make too general comments, but extrapolating from familiar fields then the book gives the impression of a vast store of adhesives technology which has not been made use of practically.

The book is well produced and is intended to earn its keep; however, the small print does not suit lengthy periods of reading for any but the most accommodating eyes.

The book is expensive since one would have thought that the production processes claimed to have been chosen to give rapid publication (and no doubt responsible for the print style) might have been expected to have resulted in a lower cost production. However, if one accounts for the time saved in reading lengthy patent documents then the book is well worth its price to the busy technologist.

No claim is made for the degree of coverage achieved by the book and its performance in this respect is difficult to judge but the reviewer is aware of a number of patents in his own field which have not been referred to.

I would recommend any adhesives technologist to read this book whether he is involved directly in hot melts or not, but I do feel that the book would be of increased value if the extensive contents list had been supplemented by an alphabetical subject index.

D. Pettit

*Conference Announcement*

**Canadian High Polymer Forum**

Hamilton, Ont., 20–22 August 1975

The 18th Canadian High Polymer Forum will be held at McMaster University, Hamilton, Ontario from 20 to 22 August 1975 and will cover all aspects of polymer science. It will be sponsored by the Macromolecular Science Division of the Canadian Chemical Society and the Division of Polymer Chemistry of the ACS. Further details may be obtained from Dr J. Prud'homme, Secretary-Treasurer 18th Canadian High Polymer Forum, Department of Chemistry, University of Montreal, PO Box 6210, Montreal, Quebec, Canada.

**Mechanical properties of polymers and composites**

Lawrence E. Nielsen

Marcel Dekker, New York, 1974. Vol 1: 255 pp. \$24.50. Vol 2: 231 pp. \$28.75

This book is one of the few truly comprehensive accounts of mechanical properties of polymers and composites. In addition, it includes elements of current research ideas and activities. It is intended for both the non-specialist scientist who may require a grasp of properties for engineering design and for the polymer scientist embarking on a detailed investigation of some particular aspect. Both these aims are satisfied, although the non-specialist will gain more from the material selection and concise description than the potential specialist who might suffer from an absence of critical account. (The specialist, however, will benefit enormously from the many thousands of well indexed literature references.)

The contents of the book are intended to cover the general mechanical behaviour of polymers to both environmental and structural factors, together with a broad account of composite properties. These aims are achieved, especially as there are chapters on mechanical tests and polymer transitions, elastic moduli, creep and stress relaxation, dynamic mechanical properties, stress-strain behaviour and strength, particulate-filled polymers, fibre-filled composites and other composites and other mechanical properties. In addition each chapter includes a useful summary and a section on problems (without answers).

The writing style is lively and lucid, although the print presentation is poor. The book is in two volumes and can only be recommended as a whole, particularly as several helpful appendixes and the author and subject indexes only appear in the second volume. The cost of the complete book is over £20. This is a formidable cost but on balance the book is good value for money, mainly because the eminent Nielsen has cleverly and creatively compiled the right material.

D. R. Moore

**Injection moulding of rubber**

M. A. Wheelans

Newnes-Butterworths, London, 1974, 241 pp. £6.75

The start of the book is somewhat disappointing since the first chapter is a comprehensive review of the history of injection moulding comprising some 208 references! However, it is not long before the practical knowledge of the author and the resources of MRPA become evident. The effects of various machine parameters are detailed and this is followed by a chapter on rubber compound design: the comment might here be made that a certain bias towards natural rubber can be detected. Examples of injection moulding are given complete with photographs in many cases, and details of machines and machine settings. A short but very practical troubleshooting guide follows and the book concludes with a chapter on the economics of injection moulding, incorporating criticisms of previous authors on this complex subject.

The book is well written and the reviewer's interest was revived once the first chapter was over and the more practical aspects were being described. The typescript can best be denoted as 'imitation typewritten characters' which are not easy to read, and unfortunately the notes beneath some of the tables tend to merge with the text. Examples of this are to be found on pp 83, 101 and 169. Nine items of errata were supplied with the book, and apart from a misprint in the last full paragraph of p 7 and the omission of a reference (41) to Geschwind on p 74, the reviewer did not find any other mistakes. The index appears to be adequate to enable the reader to refer quickly to important passages.

It is a pity, however, that the author has not included some of the recently published work on thermosetting resins and thermoplastics with regard to processing variables and mould design. This work is very relevant to the injection moulding of rubbers and mention of it would have helped the reader to appreciate that in many ways the processing behaviour of rubber is not so different from that of plastics, with which he may be more familiar. With this exception, the book is a very complete guide to the subject and can safely be recommended to students of rubber technology, experienced rubber technologists and engineers, even those of the latter category who have not previously been involved in the production of rubber articles. The binding is attractive and the book is well worth the price for the information it contains.

S. H. Morrell



the craze is also somewhat wider at  $\sim 17 \mu\text{m}$ . The fibrils appear to be more densely packed, more extended, and there is a prominent ridge of material running down the craze. Additionally, there appear to be smaller fibrils connecting the transverse structure in a similar way to that observed by Beahan *et al.*<sup>2</sup>. Applying strain to this craze, as before, produced little effect at first. Under similar conditions as applied to the craze in *Figure 2*, the only observable change was a very slight widening of the craze. On applying further strain (to the limit of the device used – about 4%) some breakdown of the structure was observed as shown in *Figures 5a* and *5b*. It appears that the material in the ridge has undergone some kind of tearing; the thin fibrils do not seem to be much affected. The bulk material surrounding the craze also seems to have been torn, perhaps illustrating the strength of this type of craze.

Thus it is seen that this technique enables craze structure to be observed with the minimum of sample preparation, and preliminary observations of the effects of strain so far

carried out show that different craze structures can have very different physical properties.

#### Acknowledgement

Thanks are due to Dr R. E. J. Fryer for work on the stereoscan.

[© Controller, HMSO, London, 1975]

Graham Durnal

Materials Quality Assurance Directorate,  
Royal Arsenal East, London SE18 6TD, UK  
(Received 26 February 1975; revised 18 March 1975)

#### References

- 1 Kambour, R. P. and Holik, A. S. *J. Polym. Sci. (A-2)* 1969, 7, 1393
- 2 Beahan, P., Bevis, M. and Hull, D. *Phil. Mag.* 1971, 24, 1267
- 3 Kambour, R. P. *Polym. Eng. Sci.* 1968, 8, 281

## Book Reviews

### Blood compatible synthetic polymers: an introduction

S. D. Bruck

C. C. Thomas, Springfield, 1974, 131 pp. \$9.75

The field of biomedical polymers is receiving increasing attention from workers in medical engineering and Dr Bruck has set out to provide a short introductory guide for people of all disciplines, be they physicians, engineers, life or materials scientists involved in the development and use of devices which come into direct contact with blood. What it is that makes some synthetic materials more tolerated by the living environment than others is still the subject of much speculation and consequently this monograph deals only briefly with its principal subject matter, giving a summary of the more promising materials found to date which demonstrate a degree of biocompatibility with blood while discussing the attributes mainly associated with a material's surface which might be responsible for the effect.

Understandably the bulk of the text is taken up with a review of polymeric materials and their many chemical, physical and mechanical properties. The emphasis here is on a direct comparison between synthetic and naturally-occurring macromolecules and on those properties which render the former suitable for use in biomedical applications and which might have a bearing on the various theories of blood compatibility.

Additionally, the author has contributed a useful presentation on the composition of blood and its working environment. This serves to highlight the many vital factors which can either influence or be influenced by the presence of a foreign material. For example, the influence of chemical, physical and mechanical action on the blood's defensive mechanisms are exemplified in relation to the blood coagulation pathways.

The current rate of advance in biomaterials science is such that one can anticipate the appearance of a more comprehensive treatise in the near future. This relatively inexpensive book provides a useful insight into the present state of the art and as the performance requirements expected of synthetic biomaterials increase it will serve to encourage the move from intuitive selection towards the synthesis of macromolecules designed to exist at the interface between a device and both the cellular and non-cellular components of blood.

It must be remembered, however, that while efforts have been made to relate blood compatibility of material to the composition of that material, the final analysis must take account of the application and the physical form.

T. Gilchrist

### Polymer-plastics technology and engineering

Edited by Louis Naturman

Marcel Dekker, New York, Vol 2, 1974. 262 pp. \$25.50

In order to better reflect the broadening of its subject matter in years to come, particularly in the polymer processing and application fields, the *Journal of Macromolecular Science (D: Reviews in Polymer Technology)* has changed its title to *Polymer – Plastics Technology and Engineering*, it being intended that a series of publications be arranged, on the basis of two issues per volume, providing timely intensive reviews of the state of the art in various branches of polymer technology and engineering.

Volume 2 presents papers on controlled u.v. degradation of plastics, metal plating of polymeric surfaces, fracture of polymers and polyblends, cationic coupling agents for thermoplastics, drilling of multi-layer printed boards, review of properties of polycarbonate resins, pressure sensitive adhesives, and impact behaviour of polymeric foams.

This particular volume in the series, in terms of its value to research and development workers, is difficult to assess there being wide variation in standards between individual authors. For instance the chapter on controlled u.v. degradation contains important open literature and patent material not previously published in a collected form. An example would be the key additives used to promote controlled polymer degradation namely, and unexpectedly, dibutyl dithiocarbonate salts, iron stearate, are listed alongside known polymer pro-oxidants based on copper, manganese, cobalt, and chromium salts. Such and similar data are undoubtedly very useful to newcomers and experienced workers. In like category are the chapters on drilling of multi-layer printed circuit boards, metal plating, pressure sensitive adhesives, and these alone would possibly justify the volume to specialized readers. Against these benefits some of the other chapters, listed above, have in various forms, featured elsewhere in the new voluminous polymer technology literature.

These criticisms may, of course, diminish as the series grows, the reviewer recognizing the considerably editorial problems initially in attracting new technology material written to adequate scientific standards. Change there should be if the present aims of intensive timely reviews are to be realized and, given such improvements, this series would find a place in the libraries and reference rooms of most research and tertiary educational institutions concerned with polymer technology.

Book binding, paper, printing and type-setting are of adequate quality and the price normal by present day standards for what

must be a limited and specialized market. Somewhat brief author and subject indexes are provided and regretfully but expectedly as this is a USA publication, imperial units predominate. This volume could usefully be referred by both chemists, physicists and engineers the writing style being suitable for most technically orientated people from diverse backgrounds.

C. Hepburn

**Hot melt adhesives: manufacture and application**

M. J. Satriana

Noyes Data Corporation, Park Ridge, NJ, 1974, \$36.00

This review of the US Patent literature relevant to the field of interest accurately described in the title immediately wins the heart of anyone who has had to try to extract the important information from an official patent document. The author has done an expert job in transposing such documents into a text comprehensible to the adhesives technologist for whom one presumes the book is primarily intended. The reader is left in little doubt that Mr Satriana, like the other Noyes Data Corporation authors, is well versed in this art.

It is believed that anyone in the adhesives industry should have access to this book since it succeeds in achieving one of the objectives in the foreword in describing a very wide area of available hot melt adhesive technology which should stimulate ideas in the reader and lead to technological transfer between the diverse industries which use adhesives.

The patents described cover such a wide field of adhesive use that one hesitates to make too general comments, but extrapolating from familiar fields then the book gives the impression of a vast store of adhesives technology which has not been made use of practically.

The book is well produced and is intended to earn its keep; however, the small print does not suit lengthy periods of reading for any but the most accommodating eyes.

The book is expensive since one would have thought that the production processes claimed to have been chosen to give rapid publication (and no doubt responsible for the print style) might have been expected to have resulted in a lower cost production. However, if one accounts for the time saved in reading lengthy patent documents then the book is well worth its price to the busy technologist.

No claim is made for the degree of coverage achieved by the book and its performance in this respect is difficult to judge but the reviewer is aware of a number of patents in his own field which have not been referred to.

I would recommend any adhesives technologist to read this book whether he is involved directly in hot melts or not, but I do feel that the book would be of increased value if the extensive contents list had been supplemented by an alphabetical subject index.

D. Pettit

*Conference Announcement*

**Canadian High Polymer Forum**

Hamilton, Ont., 20–22 August 1975

The 18th Canadian High Polymer Forum will be held at McMaster University, Hamilton, Ontario from 20 to 22 August 1975 and will cover all aspects of polymer science. It will be sponsored by the Macromolecular Science Division of the Canadian Chemical Society and the Division of Polymer Chemistry of the ACS. Further details may be obtained from Dr J. Prud'homme, Secretary-Treasurer 18th Canadian High Polymer Forum, Department of Chemistry, University of Montreal, PO Box 6210, Montreal, Quebec, Canada.

**Mechanical properties of polymers and composites**

Lawrence E. Nielsen

Marcel Dekker, New York, 1974. Vol 1: 255 pp. \$24.50. Vol 2: 231 pp. \$28.75

This book is one of the few truly comprehensive accounts of mechanical properties of polymers and composites. In addition, it includes elements of current research ideas and activities. It is intended for both the non-specialist scientist who may require a grasp of properties for engineering design and for the polymer scientist embarking on a detailed investigation of some particular aspect. Both these aims are satisfied, although the non-specialist will gain more from the material selection and concise description than the potential specialist who might suffer from an absence of critical account. (The specialist, however, will benefit enormously from the many thousands of well indexed literature references.)

The contents of the book are intended to cover the general mechanical behaviour of polymers to both environmental and structural factors, together with a broad account of composite properties. These aims are achieved, especially as there are chapters on mechanical tests and polymer transitions, elastic moduli, creep and stress relaxation, dynamic mechanical properties, stress-strain behaviour and strength, particulate-filled polymers, fibre-filled composites and other composites and other mechanical properties. In addition each chapter includes a useful summary and a section on problems (without answers).

The writing style is lively and lucid, although the print presentation is poor. The book is in two volumes and can only be recommended as a whole, particularly as several helpful appendixes and the author and subject indexes only appear in the second volume. The cost of the complete book is over £20. This is a formidable cost but on balance the book is good value for money, mainly because the eminent Nielsen has cleverly and creatively compiled the right material.

D. R. Moore

**Injection moulding of rubber**

M. A. Wheelans

Newnes-Butterworths, London, 1974, 241 pp. £6.75

The start of the book is somewhat disappointing since the first chapter is a comprehensive review of the history of injection moulding comprising some 208 references! However, it is not long before the practical knowledge of the author and the resources of MRPA become evident. The effects of various machine parameters are detailed and this is followed by a chapter on rubber compound design: the comment might here be made that a certain bias towards natural rubber can be detected. Examples of injection moulding are given complete with photographs in many cases, and details of machines and machine settings. A short but very practical troubleshooting guide follows and the book concludes with a chapter on the economics of injection moulding, incorporating criticisms of previous authors on this complex subject.

The book is well written and the reviewer's interest was revived once the first chapter was over and the more practical aspects were being described. The typescript can best be denoted as 'imitation typewritten characters' which are not easy to read, and unfortunately the notes beneath some of the tables tend to merge with the text. Examples of this are to be found on pp 83, 101 and 169. Nine items of errata were supplied with the book, and apart from a misprint in the last full paragraph of p 7 and the omission of a reference (41) to Geschwind on p 74, the reviewer did not find any other mistakes. The index appears to be adequate to enable the reader to refer quickly to important passages.

It is a pity, however, that the author has not included some of the recently published work on thermosetting resins and thermoplastics with regard to processing variables and mould design. This work is very relevant to the injection moulding of rubbers and mention of it would have helped the reader to appreciate that in many ways the processing behaviour of rubber is not so different from that of plastics, with which he may be more familiar. With this exception, the book is a very complete guide to the subject and can safely be recommended to students of rubber technology, experienced rubber technologists and engineers, even those of the latter category who have not previously been involved in the production of rubber articles. The binding is attractive and the book is well worth the price for the information it contains.

S. H. Morrell

# Gel permeation chromatography: universal calibration for rigid rod and random coil polymers

J. V. Dawkins\* and Malcolm Hemming†

ICI Corporate Laboratory, The Heath, Runcorn, Cheshire, WA7 4QE, UK

(Received 27 June 1974; revised 11 November 1974)

The g.p.c. behaviour of poly( $\gamma$ -benzyl-L-glutamate) (PBLG) samples, polystyrene standards and poly(2-vinyl pyridine) has been examined in *N,N*-dimethylacetamide (DMA) at 80°C. Solution viscosity measurements show that DMA is a good solvent for the flexible random coil polystyrene and that it promotes a helical rigid-rod shaped PBLG. Comparison of polystyrene and poly(2-vinyl pyridine) confirms that polystyrene separates strictly according to steric exclusion and that polymer/gel interactions are not involved. A PBLG calibration curve predicted from the polystyrene calibration by the  $[\eta]M$  universal calibration procedure was used to calculate average molecular weight and  $M_{\text{peak}}$  data from the PBLG chromatograms. The calculated  $\bar{M}_v$  values are in good agreement with experimental data. Plots of  $\log [\eta]M_{\text{peak}}$  against retention volume for PBLG and polystyrene were coincident. These results suggest that the product  $[\eta]M$  is a valid universal calibration parameter for PBLG and polystyrene which have significantly different shapes. Comparison of theoretical equations relating the diameter of polystyrene hydrodynamic spheres to the half-length of PBLG helices suggests that the parallel-plane model may be a useful mathematical representation of pore geometry.

## INTRODUCTION

Column chromatography separations with porous cross-linked organic gels are now of major importance in characterizing natural and synthetic polymers<sup>1</sup>. The dependence of retention volume  $V_R$  on solute size may be represented by the standard chromatography equation

$$V_R = V_0 + K_D V_i \quad (1)$$

where  $V_0$  is the volume of mobile phase (interstitial volume) and  $V_i$  is the volume of stationary phase (volume of solvent within gel pores). The distribution coefficient  $K_D$  determines the fraction of  $V_i$  accessible to a solute of given size. The dependence of  $K_D$  on solute size and the pore size distribution may be calculated assuming a steric exclusion separation mechanism which is controlled by the loss in conformational entropy when a solute transfers from the mobile phase to a pore. Theoretical expressions for  $K_D$  have been given in terms of the mean external length for rigid biopolymers<sup>2</sup> and in terms of the radius of gyration for random coil polymers<sup>3</sup>. Experimental observations have suggested that the separation is determined by the hydrodynamic volume of the solute. Thus, the separation of globular proteins in aqueous solution can be predicted from the Stokes radii of rigid spheres<sup>4</sup>, whilst the separation of linear and branched homopolymers and copolymers in tetrahydrofuran is predicted by representing these random coils as impermeable hydrodynamic spheres<sup>5</sup>.

In order to rationalize theory and experiment, separa-

tions with polymers having different shapes are required, since hydrodynamic behaviour, as judged by dilute solution viscosity<sup>6</sup>, is markedly influenced by solute geometry. Gel permeation chromatography (g.p.c.) with crosslinked polystyrene gels was developed for separations of synthetic polymers in organic solvents<sup>7</sup>. Very few synthetic high polymers have non-spherical conformations in organic media but poly( $\gamma$ -benzyl-L-glutamate) (PBLG) exists as an  $\alpha$ -helix in the solid state and retains a rigid rod conformation when dissolved in some organic solvents, e.g. *N,N*-dimethylformamide (DMF) and *m*-cresol. However, the choice of solvent is exceedingly critical. Thus, very polar solvents disrupt the helix-stabilizing intramolecular hydrogen bonds, whilst solvents less polar than DMF do not prevent intermolecular PBLG association<sup>6</sup>.

Grubisic *et al.*<sup>8</sup> compared the g.p.c. separation of PBLG samples and polystyrene (PS) standards in DMF with crosslinked polystyrene gels. They suggested that both polymers fell on the same curve of  $\log [\eta]M$  versus  $V_R$ , where  $[\eta]$  is intrinsic viscosity and  $M$  is molecular weight. However, their PBLG samples had relatively broad molecular weight distributions with the ratio of the weight-average to number-average molecular weight  $\bar{M}_w/\bar{M}_n$  lying between 1.3 and 1.6. Therefore, the PBLG values of  $[\eta]M$  will depend on the average molecular weight chosen. Furthermore, subsequent g.p.c. studies<sup>9-11</sup> have suggested that DMF is not entirely satisfactory for PS separations on crosslinked polystyrene gel, because  $V_R$  is higher than expected from a steric exclusion mechanism. This behaviour is due to solute-gel interactions which influence the separation of PS in poor and theta solvents with crosslinked polystyrene gels<sup>12,13</sup>. Then,  $V_R$  is given by

$$V_R = V_0 + K_D K_p V_i \quad (2)$$

\* Present address: Department of Chemistry, Loughborough University of Technology, Loughborough, Leics LE11 3TU, UK.

† Present address: Rank Xerox Limited, Bessemer Road, Welwyn Garden City, Herts, UK.

where  $K_p$  is a distribution coefficient representing the retardation of PS in the stationary phase due to solute-gel interactions ( $K_p > 1.0$ ). PS separates solely by steric exclusion ( $K_p = 1.0$ ) only when the exponent  $\alpha$  in the Mark-Houwink equation:

$$[\eta] = KM^\alpha \quad (3)$$

exceeds 0.65. PS in DMF over the temperature range 20–80°C has  $\alpha$  values in the range 0.60–0.64<sup>9–11,14–17</sup>. Although Grubisic *et al.*<sup>8</sup> did not specify their g.p.c. separation temperature, it is unlikely to be above 80°C.

In this paper the relationship between  $\log[\eta]M$  and  $V_R$  is reported for g.p.c. separations of PBLG samples and PS standards in *N,N*-dimethylacetamide (DMA) with cross-linked polystyrene gels at 80°C. The results are related to the solute size dependence of  $K_D$  in equation (1). Particular attention has been paid to the following points. The molecular weight at the peak of a gel permeation chromatogram ( $M_{\text{peak}}$ ) for PBLG samples was calculated by the procedure developed by Frank *et al.*<sup>18,19</sup>. In order to demonstrate the absence of solute-gel interactions, g.p.c. separations of poly(2-vinyl pyridine) (PVP) and PS were compared (PVP is a random coil polymer having a similar molecular size to PS and a similar polarity to PBLG and DMA). Dilute solution viscosity measurements were performed in order to show that DMA is a good solvent for PS ( $\alpha = 0.68$ ) at 80°C, that high molecular weight PBLG has a rigid rod conformation ( $\alpha = 1.75$ ) in DMA, and that PBLG does not associate in DMA (Huggins constant,  $k' \sim 0.5$ ).

## BACKGROUND TO SOLUTION VISCOSITY

The dilute solution viscosity behaviour of macromolecules may be represented by the Einstein-Simha equation:

$$[\eta] = \gamma \frac{NV_h}{M} \quad (4)$$

where  $V_h$  is the hydrodynamic volume,  $N$  is Avogadro's number whilst  $[\eta]$  (dl/g) and  $M$  are as defined previously. The Simha parameter  $\gamma$  is constant (0.025) for spheres but varies with the molecular weight of non-spherical macromolecules. For a prolate ellipsoid having axial ratio  $p = a/b$ , where  $a$  and  $b$  are respectively the semi-major and semi-minor axes, the increase in the value of  $\gamma$  with augmenting  $p$  has been derived by Simha<sup>20</sup> and expressed graphically by Tanford<sup>21</sup>. For small values of  $p$  the graph is curved but for  $p$  greater than about 50 (corresponding to PBLG molecular weights greater than approximately  $10^5$ ),  $\gamma$  and  $(a/b)$  are linearly related by:

$$\gamma = 0.14 \left( \frac{a}{b} \right)^{1.8} \quad (5)$$

In order to convert equation (4) into a form suitable for cylindrical rigid rods<sup>6</sup>, the volume ( $4\pi ab^2/3$ ) and length ( $2a$ ) of a prolate ellipsoid are equated respectively with the volume ( $\pi d^2L/4$ ) and length ( $L$ ) of a cylinder having diameter  $d$ . Substituting in equation (4) gives:

$$[\eta] = 4.58 \times 10^{22} d^{0.2} L^{2.8} \frac{1}{M} \quad (6)$$

Then replacing  $L$  by  $Mh/m$ , where  $h$  is the length per repeat unit of molecular weight  $m$ , and remembering that  $d$  is constant for a homologous series of cylindrical molecules leads to:

$$[\eta] = K'M^{\alpha'} \quad (7)$$

This equation resembles the Mark-Houwink viscosity relationship (3), but the value of the exponent  $\alpha'$  (1.8) is much larger than for spherical macromolecules ( $\alpha = 0.5$  to 0.8). Also the constant  $K'$  for rigid rods is fundamentally different from and numerically smaller than  $K$  values for spheres. The form of equation (4) for random coil polymers is:

$$[\eta] = 0.025N \frac{4\pi}{3} \left( \frac{D}{2} \right)^3 \frac{1}{M} \quad (8)$$

where  $D$  is the diameter of the rigid equivalent hydrodynamic sphere which increases solution viscosity by the same amount as the flexible random coil.

It has been shown<sup>22–24</sup> that the dilute solution viscosity behaviour of high molecular weight PBLG ( $M > 5 \times 10^4$ ) in solvents of suitable polarity follows equation (7) with  $\alpha' = 1.7$ . This suggests that the rigid cylindrical  $\alpha$ -helix, characteristic of the solid state<sup>25,26</sup> persists in solution. For PBLG molecular weights lower than  $5 \times 10^4$ ,  $\alpha'$  gradually decreases towards 0.8 as predicted by Simha<sup>20</sup> and Tanford<sup>21</sup>.

## EXPERIMENTAL

### Materials

The narrow distribution PS standards were supplied by Pressure Chemical Company, Pittsburgh. The  $M_{\text{peak}}$  values in Table 1 are those recommended by Waters Associates except in the case of PS 10, for which a  $\bar{M}_n$  value obtained by vapour pressure osmometry is preferred<sup>10,27,28</sup>. The  $\bar{M}_w$  and polydispersity  $\bar{M}_w/\bar{M}_n$  data in Table 2 were given by the supplier.

The PBLG samples were used as supplied by Miles-Yeda Ltd, Rehovot, Israel. The viscosity average molecular weights,  $\bar{M}_v$ , in Table 3 were calculated from the supplier's DMF (25°C) intrinsic viscosities. The intrinsic viscosity molecular weight relations given by Fujita *et al.*<sup>23</sup> and Spach *et al.*<sup>24</sup> were used for the calculations in preference to the

Table 1 Peak molecular weight, intrinsic viscosity,  $[\eta]M$  and g.p.c. data for polystyrene in *N,N*-dimethylacetamide at 80°C

Standard	$M_{\text{peak}}$	$[\eta]_{\text{DMA}}^{80}$	$[\eta]M_{\text{peak}}$	$V_R(D)$ (5 ml counts)	$V_R(F)$ (8 ml counts)
PS1	1 900 000	2.50	4 750 000	24.2	16.2
PS2	867 000	—	1 300 000	25.6	17.1
PS3	498 000	1.10	550 000	26.4	17.6
PS4	411 000	—	400 000	26.8	17.9
PS5	160 000	0.51	81 500	28.1	18.8
PS6	98 200	—	35 000	29.0	19.3
PS7	51 000	0.22	11 000	30.4	20.3
PS8	19 800	0.12	2 500	32.7	21.7
PS9	10 300	—	800	34.3	22.8
PS10	3 700	0.04	150	36.4	24.2

Table 2 Average molecular weight and polydispersity data for polystyrene standards

Standard	Experimental		G.p.c., DMA (Set F)		G.p.c., DMA (Set D)	
	$\bar{M}_w$	$\bar{M}_w/\bar{M}_n$	$\bar{M}_w$	$\bar{M}_w/\bar{M}_n$	$\bar{M}_w$	$\bar{M}_w/\bar{M}_n$
PS1	1 900 000	1.20	—	—	2 300 000	1.40
PS2	867 000	1.12	—	—	910 000	1.24
PS3	507 000	1.25	470 000	1.20	530 000	1.30
PS4	394 000	1.05	—	—	380 000	1.33
PS5	173 000	1.06	177 000	1.17	163 000	1.17
PS6	96 200	1.06	115 000	1.13	96 300	1.13
PS7	50 500	1.04	53 000	1.10	52 500	1.12
PS8	19 800	1.04	20 000	1.06	19 900	1.10
PS9	10 000	1.06	—	—	11 000	1.09
PS10	5 000	1.09	—	—	5 200	1.06

Table 3 Molecular weight and viscosity data for PBLG

Sample	$[\eta]_{\text{DMF}}^{25}$ <sup>a</sup>	$\bar{M}_v$	$[\eta]_{\text{DMA}}^{80}$	$(k')_{\text{DMA}}^{80}$
D95	3.20	290 000	4.20	0.56
C100	1.26	160 000	1.60	0.63
C72	0.90	130 000	0.90	0.52
B65	0.25	45 000	0.22	0.48
A89	0.05	9 000	0.05	—

<sup>a</sup> Supplier's values

earlier relationships of Doty *et al.*<sup>22</sup> which would give lower  $\bar{M}_v$  values.

The narrow distribution PVP samples were prepared at the ICI Corporate Laboratory, Runcorn, by Dr D. Brown using an anionic method<sup>29</sup>. Disodium  $\alpha$ -methylstyrene tetramer initiator was formed in tetrahydrofuran at room temperature and the polymerization was performed at  $-80^\circ\text{C}$  in the same solvent. The  $\bar{M}_n$  and  $\bar{M}_w$  values in Table 4 were measured with a Mechrolab membrane osmometer (methyl ethyl ketone,  $37^\circ\text{C}$ ) and a Sofica light-scattering instrument (chloroform,  $30^\circ\text{C}$ ) respectively.

The DMA, 99% pure, was supplied by Honeywell and Stein, and was degassed at  $120^\circ\text{C}$  to remove water and other low boiling point impurities.

#### Gel permeation chromatography

The g.p.c. measurements were obtained with a Waters Associates model 200 gel permeation chromatograph at ICI Organics Division, Blackley, Manchester. The PBLG and PVP data were obtained with different column sets, designated D and F respectively. Both sets comprised five Waters Associates Styragel columns,  $10^5$ ,  $10^5$ ,  $10^4$ ,  $10^3$  and  $10^3$  Å, which were calibrated with the PS standards. The eluent flow rate was 1 ml/min, and the concentrations of PS, PVP and PBLG solutions were 0.25, 0.17 and 0.50% respectively. Peak retention volumes for PBLG chromatograms recorded with 1.00, 0.70, 0.50 and 0.25% solutions of sample D95 agreed to within  $\pm 0.2$  count, indicating the absence of PBLG concentration effects. The toluene plate counts of 450 ppf, obtained by injecting a 1% (w/v) solution for 15 sec, were rather low. However, PS polydispersities (Table 2) calculated<sup>30</sup> from chromatograms indicate a low degree of broadening. This suggests that the plate counts are anomalously low, probably owing to the inclusion of two  $10^3$  Å columns in each set.

Peak retention volume data for PS, PVP and PBLG are shown in Tables 1, 4 and 5 respectively. Average molecular weights and polydispersities were calculated from

chromatograms by the method of Pickett *et al.*<sup>30</sup>. Values of  $M_{\text{peak}}$  for PVP fractions and PBLG samples ( $\bar{M}_w/\bar{M}_n > 1.3$ ) and corresponding values of the constants  $A$  and  $B$  in the calibration equation:

$$\log M = A - BV_R \quad (9)$$

were obtained by the method of Frank *et al.*<sup>18,19</sup>. Details are given in the results section.

#### Solution viscosity

Viscosities were measured with two Ubbelohde suspended level dilution viscometers having 12 cm capillaries of diameter 0.3 and 0.5 mm. The flow times for DMA in the two viscometers were 380 and 114 sec respectively, and kinetic energy corrections are therefore not significant. The wider bore viscometer was used for all of the measurements except for those on standards PS7, PS8 and PS10. The ratio of radius to length was such that shearing stresses were very low, and orientation of PBLG was avoided. The solution concentrations were corrected for solvent expansion from room temperature to  $80^\circ\text{C}$ . Data at four or five concentrations, giving relative viscosities in the range 1.1 to 1.9, were extrapolated linearly to infinite dilution by Huggins and Kraemer plots giving  $[\eta]$  and the Huggins constant  $k'$  and Kraemer constant  $k''$ .

Values for  $k'$  for PS were in the range 0.3 to 0.4 and the sums of  $k'$  and  $k''$  were  $0.50 \pm 0.02$ . The  $[\eta]$  values in Table 1 are shown as a double logarithmic plot against peak molecular weight in Figure 1. This plot is well represented by:

$$[\eta]_{\text{DMA}}^{30} = 1.4 \times 10^{-4} M^{0.68} \quad (10)$$

The exponent in this equation is typical of a flexible random coil polymer in a good solvent.

For PBLG values for  $k'$  shown in Table 3 are in the range 0.5 to 0.6 whilst values for  $k''$  were about 0.01. Such  $k'$  and  $k''$  values are typical of PBLG in a helicogenic solvent and suggest that the macromolecules are not associated<sup>6</sup>. A double logarithmic plot of  $[\eta]_{\text{DMA}}^{80}$  (Table 3) against  $\bar{M}_v$  (DMF,  $25^\circ\text{C}$ ) is shown in Figure 2. For molecular weights greater than  $5 \times 10^4$ , the data obey the typical rigid rod relation:

$$[\eta]_{\text{DMA}}^{80} = 2.2 \times 10^{-9} \bar{M}_v^{1.75} \quad (11)$$

and suggest that samples D95 and C100 have sufficiently large  $p$  values for equation (7) to be valid. For lower mole-

Table 4 Average molecular weight data for poly(2-vinyl pyridine) samples

Fraction	Experimental			G.p.c., DMA (80°C)				
	$\bar{M}_n^a$	$\bar{M}_w^b$	$\bar{M}_w/\bar{M}_n$	$\bar{M}_n$	$\bar{M}_w$	$\bar{M}_w/\bar{M}_n$	$M_{\text{peak}}$	$V_R$
52/1	23 000	25 500	1.11	24 200	27 600	1.14	26 000	21.1
52/2	38 500	46 500	1.20	36 000	42 000	1.16	46 000	20.2

<sup>a</sup> By membrane osmometry

<sup>b</sup> By light scattering

Table 5 G.p.c. data and average molecular weights for PBLG samples

Sample	$V_R$	$\bar{M}_v$	G.p.c., DMA (80°C)							
			$\bar{M}_n^a$	$\bar{M}_w^a$	$\bar{M}_w/\bar{M}_n^a$	$\bar{M}_v^a$	$M_{\text{peak}}^b$	$[\eta]M_{\text{peak}}$	$A$	$B$
D95	25.75	290 000	159 000	247 000	1.56	286 000	227 000	950 000	21.8	0.37
C100	26.90	160 000	106 000	163 000	1.53	186 000	138 000	220 000	21.5	0.54
B65	30.50	45 000	32 000	40 000	1.22	45 000	40 000	8 800	18.7	0.26
A89	34.50	10 000	8 700	12 000	1.23	10 000	11 000	550	18.7	0.26

<sup>a</sup> Calculated as in ref 30

<sup>b</sup> Calculated as in refs 18 and 19

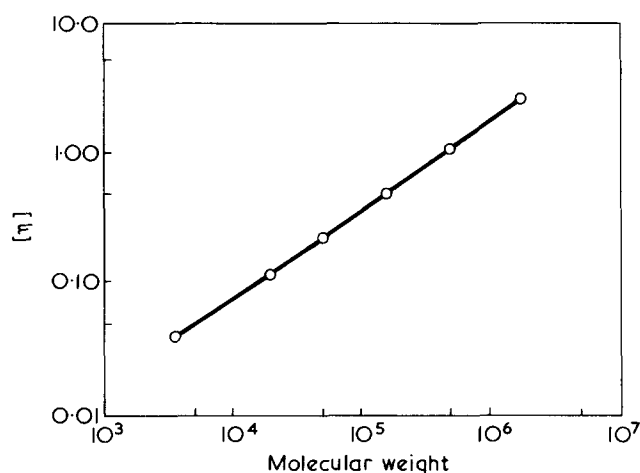


Figure 1 Double logarithmic plot of intrinsic viscosity versus molecular weight for polystyrene standards in *N,N*-dimethylacetamide at 80°C

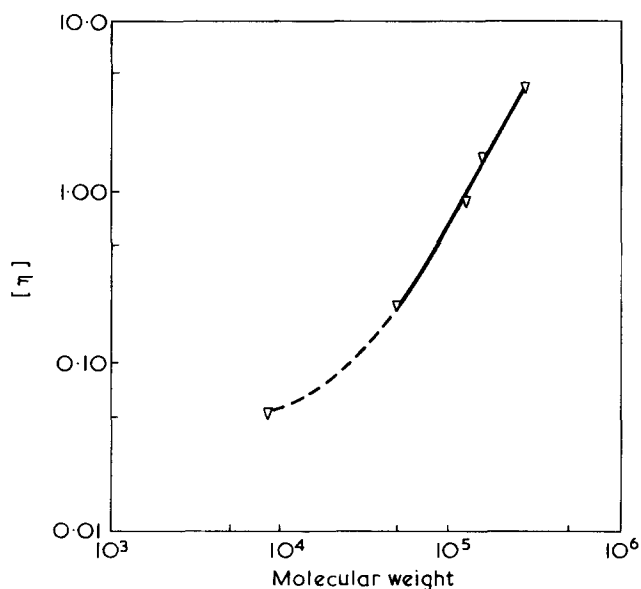


Figure 2 Double logarithmic plot of intrinsic viscosity versus molecular weight for PBLG samples in *N,N*-dimethylacetamide at 80°C

cular weights, the data approximate to:

$$[\eta]_{\text{DMA}}^{80} = 2.2 \times 10^{-5} \bar{M}_v^{0.84} \quad (12)$$

## RESULTS AND DISCUSSION

### Effect of eluent power and polarity

Results discussed elsewhere<sup>12,13</sup> suggest that interactions between PS and crosslinked polystyrene gel can occur when the solubility parameter,  $\delta$  for the eluent is greater than that for PS. In the present case,  $\delta$  (DMA) is 10.8 and  $\delta$  (PS) is 9.1<sup>31</sup> and therefore it is necessary to confirm that, when DMA (80°C) eluent is used, PS is fractionated according to steric exclusion only. Thus, PS has been compared with PVP for which  $\delta$  is approximately 10.5. These two polymers have similar unperturbed dimensions,  $(L_0^2/M)^{1/2}$  (PS) = 0.67 Å<sup>31</sup> whilst  $(L_0^2/M)^{1/2}$  (PVP) = 0.66 Å<sup>31,32</sup>. Solution viscosity determinations show that DMF is a good solvent for PVP ( $\alpha = 0.69$ )<sup>17</sup> and it is assumed that polymer/solvent interactions will be similar in DMA.

The PS calibration curve for column set F, shown in Figure 3, was used to calculate  $\bar{M}_w$  and  $\bar{M}_w/\bar{M}_n$  values for PS and PVP chromatograms. The PS values in Table 2 are in good agreement with the experimental values confirming the absence of the unsymmetrical broadening phenomena which accompany solute/gel interaction effects<sup>12,13</sup>. Also, the PVP results in Table 4 are in good agreement with the experimental values, reflecting the similarities in PS and PVP unperturbed dimensions and suggesting that the separation of PS in DMA (80°C) is controlled by steric exclusion only. The  $M_{\text{peak}}$  values for PVP shown in Table 4 were calculated from the chromatograms using the experimental  $\bar{M}_n$  and  $\bar{M}_w$  values. For both samples the values of calibration constants  $A$  and  $B$  were 25.3 and 0.71 respectively. The PVP  $M_{\text{peak}}$  values are plotted against corresponding peak retention volumes in Figure 3. The two points are coincident with the PS curve.

### Universal calibration for PBLG

If the product  $[\eta]M$  is a valid universal calibration parameter for the rigid-rod molecule PBLG and the random coil

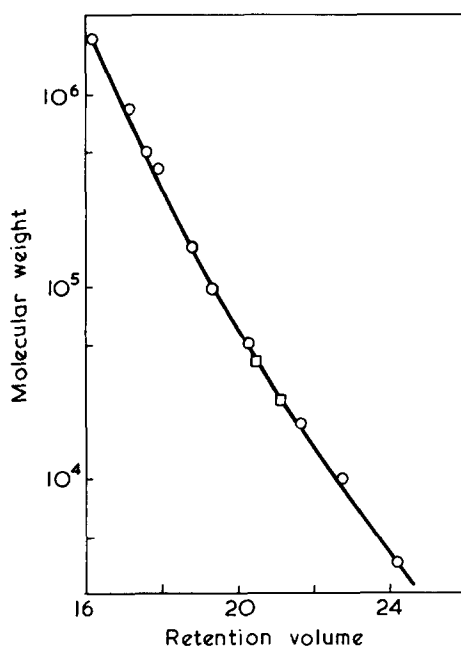


Figure 3 Molecular weight calibration plot for column set F with *N,N*-dimethylacetamide at 80°C; ○,  $M_{\text{peak}}$  polystyrene standards; □,  $M_{\text{peak}}$  poly(2-vinyl pyridine) samples

PS, then at a given retention volume:

$$[\eta]M(\text{PS}) = [\eta]M(\text{PBLG}) \quad (13)$$

Substituting equations (3) and (7) for PS and PBLG respectively gives:

$$K(\text{PS})M^{1+\alpha(\text{PS})} = K'(\text{PBLG})M^{1+\alpha'(\text{PBLG})} \quad (14)$$

Taking logarithms and rearranging leads to:

$$\log M(\text{PBLG}) = \frac{1 + \alpha(\text{PS})}{1 + \alpha'(\text{PBLG})} \log M(\text{PS}) + \frac{1}{1 + \alpha'(\text{PBLG})} \log \frac{K(\text{PS})}{K'(\text{PBLG})} \quad (15)$$

This equation should predict a valid PBLG molecular weight calibration from a PS calibration curve. Alternatively, plots of  $\log [\eta]M_{\text{peak}}$  against appropriate PS and PBLG retention volumes should be coincident.

The PS calibration curve for column set D, shown in Figure 4, was used to calculate average molecular weight and polydispersity data from the PS chromatograms. The results in Table 2 are in good agreement with the accepted values and with the data obtained with column set F, indicating that PS was separated according to equation (1).

A PBLG molecular weight calibration was derived from the PS curve in Figure 4 by substituting into equation (15) the DMA (80°C) intrinsic viscosity relations (10) for PS and (11) for PBLG ( $M > 5 \times 10^4$ ). For lower PBLG molecular weights, equation (15) was modified to accommodate  $K'$  and  $\alpha'$  values for PBLG in relation (12). The complete PBLG calibration curve, shown as a broken line in Figure 4, was used to calculate average molecular weight and polydispersity data from the PBLG chromatograms. The results are shown in Table 5. The viscosity average molecular weights for the three highest molecular weight samples were

calculated with a Mark-Houwink exponent of 1.75, whilst 0.84 was used for sample A89. For all of the samples, the calculated  $\bar{M}_v$  values are in very good agreement with the experimental ones. This suggests that the PBLG calibration predicted from equation (15) is valid, and is also consistent with the very small degree of broadening. The calculated polydispersities for the PBLG samples, particularly D95 and C100, indicate that precise calculation of  $M_{\text{peak}}$  is necessary before assignment to peak retention volumes.  $M_{\text{peak}}$  values were calculated<sup>18,19</sup> from experimental viscosity average molecular weight values and g.p.c. number-average molecular weights. The results are shown in Table 5, which also contains values of constants  $A$  and  $B$  and  $[\eta]M_{\text{peak}}$  data. The PBLG  $M_{\text{peak}}$  values are plotted against peak retention volume in Figure 4 and are in very good agreement with the calibration curve predicted from equation (15). Semi-logarithmic plots of  $[\eta]M_{\text{peak}}$  against peak retention volume for PBLG and PS are also coincident (Figure 5).

The results for PBLG in DMA (80°C) therefore show that the g.p.c. separation of rigid-rod molecules (at 1 ml/min) may be represented by the viscometric size parameter  $[\eta]M$  and that equation (15) is applicable to such systems. This suggests that at normal flow rates, the g.p.c. separation is an equilibrium-controlled distribution of macromolecules of differing size between the mobile phase and stationary phase ( $K_p = 1$ ). Therefore, PBLG in DMA at 80°C is not influenced by solute-gel interaction effects ( $K_p > 1$ ) which affect the separation of some polyamides in phenol-type solvents<sup>33</sup>.

#### Separation mechanism

Retention volumes may be related to the distribution coefficient  $K_D$  by equation (1). Giddings *et al.*<sup>2</sup> applied

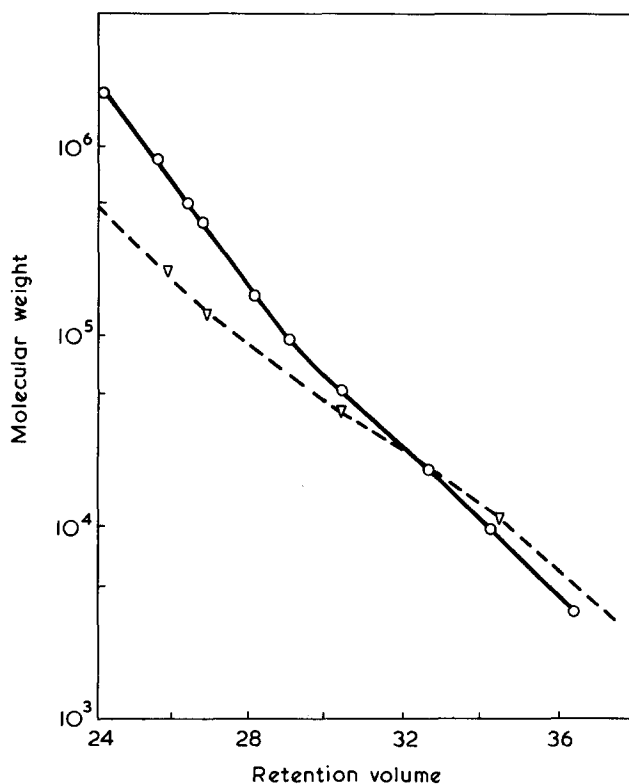


Figure 4 Molecular weight calibration plot for column set D with *N,N*-dimethylacetamide at 80°C. ○,  $M_{\text{peak}}$  polystyrene standards; ▽,  $M_{\text{peak}}$  PBLG samples; ---,  $M(\text{PBLG})$  calibration from equation (15)

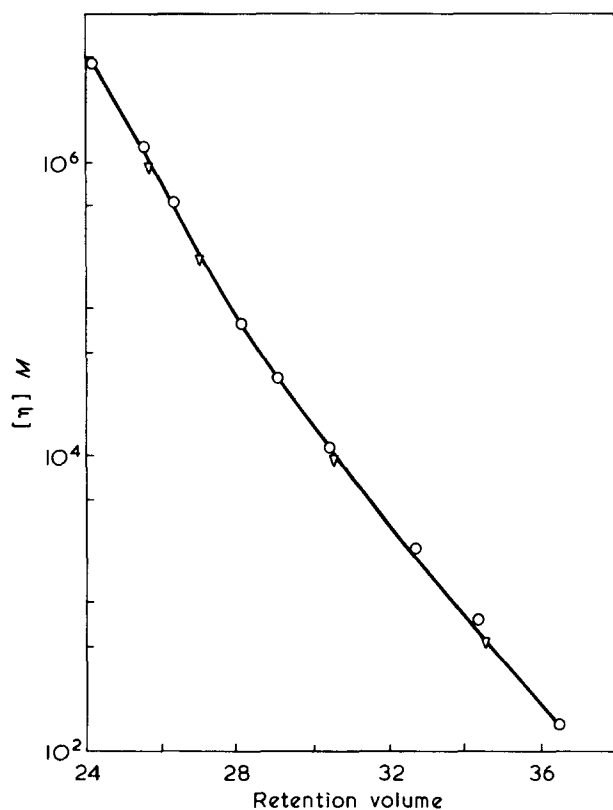


Figure 5 Universal calibration plot of  $\log[\eta]M_{\text{peak}}$  against retention volume; symbols as in Figure 4

statistical mechanics to the distribution of rigid particles, including spheres and rods, in several idealized pore structures. They derived the variation of  $K_D$  with the diameter  $D$  of spheres and with the half-length  $L/2$  of rods for a variety of pore shapes, including random planes, spherical cavities and parallel planes. The relations for random planes predict that at a given value of  $K_D$ , and consequently at a given retention volume,  $D$  and  $L/2$  are equal. For spherical cavities  $D$  is predicted to be greater than  $L/2$  at a given  $K_D$ , whilst for parallel planes  $D$  is expected to be smaller than  $L/2$ .

The PBLG and PS results were used to assess the suitability of these simple pore models for representing g.p.c. behaviour. The half-lengths  $L/2$  at  $M_{\text{peak}}$  for the two high molecular weight PBLG samples were calculated from  $L = Mh/m$  using  $m = 219$  and  $h = 1.3 \text{ \AA}$ <sup>23</sup>. Corresponding values of  $D$  for PS at the same  $V_R$  were calculated from equation (8) assuming a rigid hydrodynamic sphere. The resulting values of  $L/2$  and  $D$  are shown in Table 6.

Of the three pore models under consideration, only the parallel plane shape predicts a relationship between  $L/2$  and  $D$  consistent with that found experimentally. The theoretical variation of  $K_D$  and  $L/2D$  is shown in Figure 6. Values of  $K_D$  from this graph were substituted in equation (1) together with the corresponding retention volumes. Solving the simultaneous equations gives a value of 21.5 counts for  $V_0$  and 19.0 counts for  $V_i$ . The value of  $V_0$  is in reasonable agreement with the upper exclusion limit. The sum of the  $V_0$  and  $V_i$  values, 40.5, is in very good agreement with the experimental retention volume, 41.0, for toluene. It would therefore appear that the parallel plane model is a useful mathematical representation of pore geometry. This is consistent with Casassa's observation<sup>3</sup> that the data of Moore and Arrington<sup>34</sup>, for PS, porous glass and a binary theta-solvent, are in good agreement with the parallel plane or 'slab' model.

Table 6 Molecular dimension and distribution coefficient data for PBLG rods and polystyrene spheres

$V_R$	$L/2$ (Å) (PBLG)	$D$ (Å) (PS)	$\frac{L}{2D}$	$K_D$ (parallel planes)
25.75	678	485	1.49	0.22
26.90	410	318	1.29	0.28

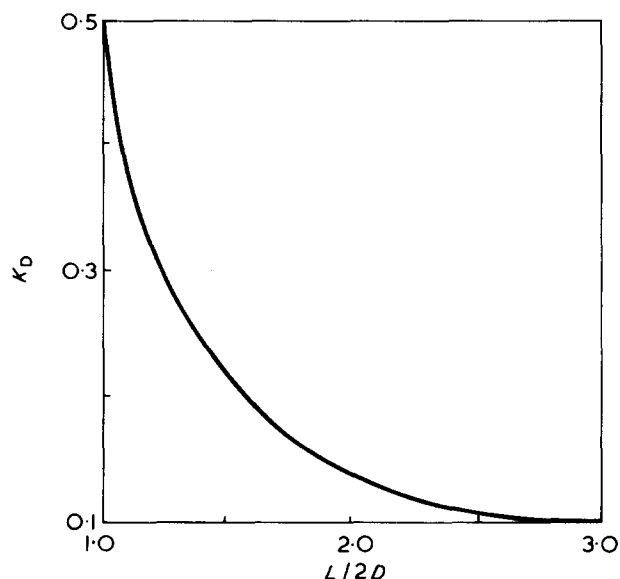


Figure 6 Theoretical variation of distribution coefficient  $K_D$  with the ratio of rod half-length to sphere diameter for parallel plane pore model

#### ACKNOWLEDGEMENTS

This work was undertaken as part of the Research Student Community Scheme at the ICI Corporate Laboratory. The authors acknowledge the interest of Professor J. C. Bevington of Lancaster University. We are indebted to Mr A. E. Ambler of ICI Organics Division for the g.p.c. measurements.

#### REFERENCES

- Determann, H. 'Gel Chromatography', Springer-Verlag, Berlin, 1969
- Giddings, J. C., Kucera, E., Russell, C. P. and Myers, M. N. *J. Phys. Chem.* 1968, **72**, 4397
- Casassa, E. F. and Tagami, Y. *Macromolecules* 1969, **2**, 14
- Siegel, L. M. and Monty, K. J. *Biochim. Biophys. Acta* 1966, **112**, 346
- Grubisic, Z., Rempp, P. and Benoit, H. *J. Polym. Sci. (B)* 1967, **5**, 753
- Bradbury, J. H. in 'Physical Principles and Techniques of Protein Chemistry', Part B, (Ed. S. J. Leach), Academic Press, New York, 1970
- Moore, J. C. *J. Polym. Sci. (A)* 1964, **2**, 835
- Grubisic, Z., Reibel, L. and Spach, G. *C. R. Acad. Sci. (C)* 1967, **264**, 1690
- Kranz, D., Pohl, U. and Baumann, H. *Angew. Makromol. Chem.* 1972, **26**, 67
- Screaton, R. M. and Seemann, R. W. *Appl. Polym. Symp.* 1969, **8**, 81
- Zinbo, M. and Parsons, J. L. *J. Chromatogr.* 1971, **55**, 55
- Hemming, M. in 'Industrial Polymers: Characterisation by Molecular Weight', (Eds J. H. S. Green and R. Dietz) Transcripta Books, London, 1973
- Dawkins, J. V. and Hemming, M. *Makromol. Chem.* submitted



*G.p.c.: universal calibration for rigid rod and random coil polymers: J. V. Dawkins and M. Hemming*

- 14 Tsimpris, C. W., Suryanarayanan, B. and Mayhan, K. G. *J. Polym. Sci. (A-2)* 1972, **10**, 1837
- 15 Coppola, G., Fabbri, P., Pallesi, B. and Bianchi, U. *J. Appl. Polym. Sci.* 1972, **16**, 2829
- 16 Cha, C. Y. *J. Polym. Sci. (B)* 1969, **7**, 343
- 17 Ho-Duc, N., Daoust, H. and Gourdenne, A. *Polym. Prepr.* 1971, **12**, 639
- 18 Frank, F. C., Ward, I. M. and Williams, T. *J. Polym. Sci. (A-2)* 1968, **6**, 1357
- 19 Dawkins, J. V. *Eur. Polym. J.* 1970, **6**, 831
- 20 Simha, R. *J. Phys. Chem.* 1940, **44**, 25
- 21 Tanford, C. 'Physical Chemistry of Macromolecules', Wiley, New York, 1961, p 335
- 22 Doty, P., Bradbury, J. H. and Holtzer, A. M. *J. Am. Chem. Soc.* 1956, **78**, 947
- 23 Fujita, H., Teramoto, A., Yamashita, T., Okita, K. and Ikeda, S. *Biopolymers* 1966, **4**, 781
- 24 Spach, G., Freund, L., Daune, M. and Benoit, H. *J. Mol. Biol.* 1963, **7**, 468
- 25 Parry, D. A. D. and Elliott, A. *Nature* 1965, **206**, 616
- 26 Saludjian, P. and Luzzati, V. *J. Mol. Biol.* 1966, **15**, 681
- 27 Dawkins, J. V., Maddock, J. W. and Coupe, D. *J. Polym. Sci. (A-2)* 1970, **8**, 1803
- 28 Runyon, J. R. *Sep. Sci.* 1971, **6**, 249
- 29 Lee, C. L., Smid, J. and Szwarc, M. *Trans. Faraday Soc.* 1963, **59**, 1192
- 30 Pickett, H. E., Cantow, M. J. R. and Johnson, J. F. *J. Appl. Polym. Sci.* 1966, **10**, 917
- 31 Brandrup, J. and Immergut, E. H. 'Polymer Handbook', Wiley-Interscience, New York, 1966
- 32 Dondos, A. *Makromol. Chem.* 1970, **135**, 181
- 33 Walsh, E. K. *J. Chromatogr.* 1971, **55**, 193
- 34 Moore, J. C. and Arrington, M. C. *Prepr. Third Int. GPC Semin., Geneva* 1966

# Light scattering Rayleigh linewidth measurements on some dextran solutions

D. B. Sellen

Astbury Department of Biophysics, University of Leeds, Leeds LS2 9JT, UK

(Received 20 November 1974)

Light scattering Rayleigh linewidth measurements have been made upon eight fractions of dextran from *Leuconostoc mesenteroides* B512 with molecular weights ranging from 10 to 500 kg/mol and the relationship  $D_{20} = 2.25 \times 10^{-4} M^{-0.45}$  ( $D$  in  $\text{mm}^2/\text{s}$ ,  $M$  in  $\text{kg}/\text{mol}$ ) was established. No concentration dependence of diffusion constant was detected within experimental error ( $\pm 3\%$ ). The measurements were corrected for the polydispersity of the fractions. The results are compared with diffusion constants obtained by conventional techniques and with viscosity data.

## INTRODUCTION

Investigation of the spectra of light scattered from macromolecular solutions is now an established technique for the determination of translational diffusion constants<sup>1-7</sup>. The most convenient method of making these measurements is by means of the optical homodyne technique in which the power spectrum of a photoelectric signal is investigated. In recent years it has been found advantageous to do this by obtaining the autocorrelation function by use of a suitable computer<sup>4,5,7</sup>. The present paper describes some experiments of this type upon eight fractions of dextran with molecular weights ranging from 10 to 500 kg/mol.

## EXPERIMENTAL

Dextran is a branched polymer of D-glucopyranose with  $\alpha(1 \rightarrow 6)$  linkages in the main and side chains and  $\alpha(1 \rightarrow 3)$  linkages at the branch points. The dextrans used in this work were commercial samples (Pharmacia Fine Chemicals, Uppsala, Sweden) consisting of fractions of material synthesized from sucrose by the bacterial species *Leuconostoc mesenteroides* strain B512. Dextran produced in this way has a number of branch points equal approximately to 5% of the degree of polymerization<sup>8,9</sup>.

Both conventional light scattering measurements and light scattering Rayleigh linewidth measurements were made on all the samples. The same solutions were used for both types of measurement, the solvent being glass distilled water. Solutions were clarified by centrifuging for 1 h at  $20\,000 \times g$  and passing through a  $1.2 \mu\text{m}$  Millipore filter directly into the light scattering cell.

Conventional light scattering measurements were made with the Aminco (American Instrument Co. Inc., Silver Spring, Maryland, USA) apparatus. The light scattering Rayleigh linewidth apparatus and its operation have already been described<sup>6,7</sup>. Where spectral broadening is due to translational diffusion alone the autocorrelation function of the photoelectric signal resulting from light scattered from a polydisperse solution of macromolecules is given by:

$$\phi(\tau) = \frac{c^2 \gamma^2}{2} [\sum_n I_n \exp(-K^2 D_n \tau)]^2 \quad (1)$$

$c$  is the overall photosensitivity of the detecting system and  $\gamma$  a coherence factor depending upon the geometry of the optics<sup>6</sup>.  $\tau$  is the autocorrelation delay time,  $I_n$  the scattered intensity from that component having diffusion constant  $D_n$  and:

$$K = \frac{4\pi}{\lambda} \sin \theta / 2 \quad (2)$$

where  $\lambda$  is the wavelength in the solution and  $\theta$  the angle of scatter.

## RESULTS AND DISCUSSION

The results are summarized in *Table 1*. With the exception of the T20 sample (the results for this sample will be discussed later) the weight-average molecular weights agree within experimental error with the gel filtration data supplied with the samples. There was no dissymmetry of scatter except in the case of the T500 sample where the dissymmetry indicated a  $Z$ -average polar radius of gyration of  $26 \pm 5 \text{ nm}$ . The refractive index increment was measured in a Rayleigh differential refractometer and found to be  $0.148 \pm 0.001 \text{ ml/g}$ ; no variation was detected with wavelength within the visible region.

Equation (1) shows that if  $\ln \phi(\tau)$  is plotted against  $\tau$  the slope of the graph at  $\tau = 0$  is  $-2K^2 D_z$  where  $D_z$  is the  $Z$ -average diffusion constant<sup>7</sup>. When the degree of polydispersity is not high enough for the autocorrelation function to differ significantly from a single exponential this graph will be a straight line of slope  $-2K^2 D_z$ . However, in the present work some of the samples had a high enough degree of polydispersity for this not to be the case and *Figure 1* shows the autocorrelation function at various angles of scatter for the T500 sample. As predicted theoretically the data all lie on the same curve<sup>6,7</sup>. The exponential fit at shorter values of  $\tau$  yields  $D_z$ .

*Figure 2* shows diffusion constant as a function of concentration for three of the samples. No concentration dependence was detected.

*Figure 3* shows a double logarithmic plot of diffusion constant as a function of molecular weight. The diffusion

Table 1 Summary of results

Fraction	$M_w$ (kg/mol)		Second virial coefficient $\times 10^4$ (mol m <sup>3</sup> kg <sup>-2</sup> ) by light scattering	$M_w/M_n^*$	$M_D/M_w$	$D_{20} \times 10^5$ (mm <sup>2</sup> /s) by light scattering
	Gel filtration*	Light scattering				
T10	9.3	9.8 ± 0.5	8 ± 1	1.6	1.11	7.3 ± 0.3
T20†	20.4	20†		1.2	1.05	5.8 ± 0.4†
T40	40	43 ± 2	5 ± 1	1.3	1.07	3.9 ± 0.1
T70	70	75 ± 4	4.5 ± 0.5	1.6	1.11	3.1 ± 0.1
T110	106	110 ± 5	4.3 ± 0.5	1.4	1.08	2.8 ± 0.1
T150	154	150 ± 7	3.3 ± 0.3	1.8	1.13	2.3 ± 0.1
T250	231	230 ± 10	2.8 ± 0.2	2.1	1.15	1.90 ± 0.05
T500	460	490 ± 30	1.7 ± 0.2	2.3	1.17	1.25 ± 0.05

\* Gel filtration data supplied by Pharmacia  
 † See text

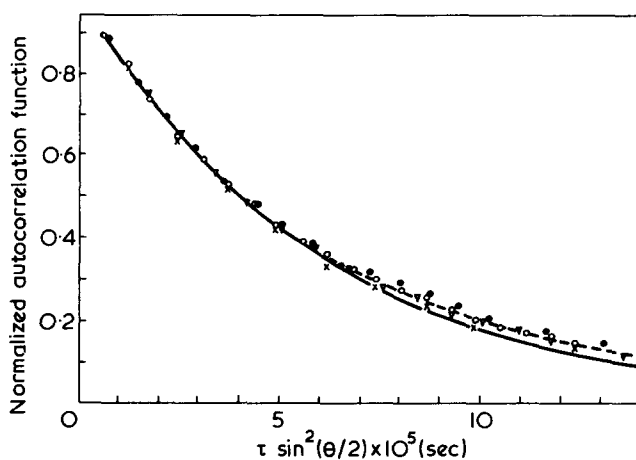


Figure 1 Normalized autocorrelation function of intensity fluctuations of light scattered from a 0.3% solution of dextran fraction T500 (Table 1) in distilled water. ●, 45°; ○, 60°; ×, 90°; ▽, 135° C

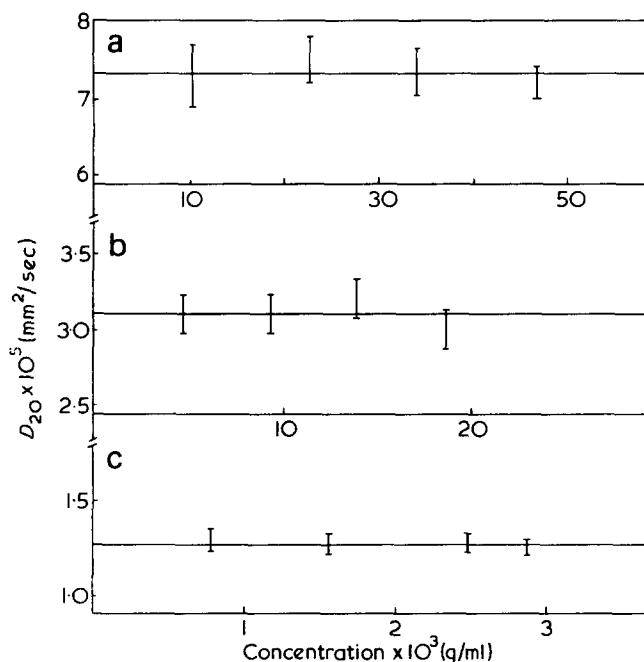


Figure 2 Diffusion constant as a function of concentration for three dextran fractions: (a) T10; (b) T70; (c) T500. Measurements were made in distilled water

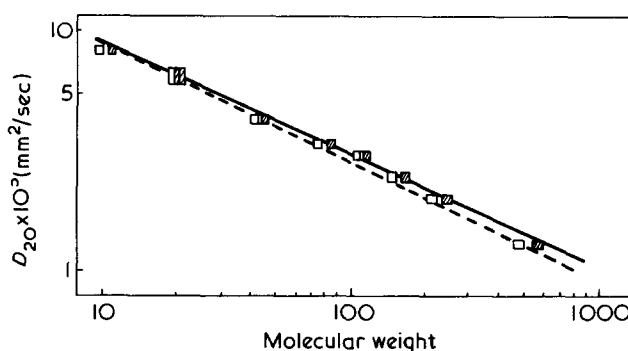


Figure 3 Diffusion constant as a function of molecular weight (kg/mol) for dextran. The open squares indicate the limits of error and the shaded squares represent the data corrected for polydispersity. ---, Variation predicted from viscosity data (see text)

constants were corrected from room temperature to 20°C assuming the validity of the Stokes–Einstein equation. The plot is approximately a straight line, i.e.

$$D = AM^{-\alpha} \tag{3}$$

It is necessary, however, to consider the polydispersity of the samples. The Z-average diffusion constant corresponds to a molecular weight  $M_D$  given by<sup>7</sup>:

$$M_D = \left[ \frac{\sum_i N_i M_i^2}{\sum_i N_i M_i^{2-\alpha}} \right]^{1/\alpha} \tag{4}$$

$N_i$  is the number of molecules having molecular weight  $M_i$ . In the case of a Schulz–Zimm distribution<sup>10</sup>:

$$M_D = \frac{M_w}{1 + \alpha} \left[ \frac{\Gamma(a + 2)}{\Gamma(a + 2 - \alpha)} \right]^{1/\alpha} \tag{5}$$

where

$$a = 1/(r - 1) \tag{6}$$

and

$$r = M_w/M_n \tag{7}$$

The gel filtration data supplied with the samples do in fact indicate distributions approximately equivalent to the

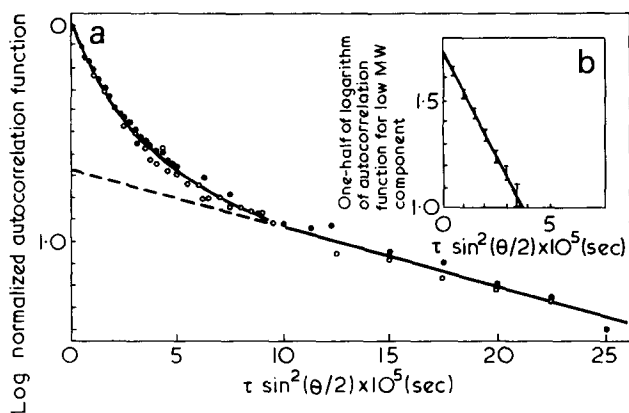


Figure 4 (a) Autocorrelation function for the T20 sample (Table 1) which contains a high molecular weight impurity (see text). ●, 60°; ○, 90° C. (b) Graph to find the diffusion constant for the low molecular weight component (see text)

Shulz-Zimm function. Values of  $M_D$  were accordingly calculated taking values of  $r$  from the gel filtration data and using an approximate value of  $\alpha$  taken from the uncorrected light scattering data. Figure 3 shows that data corrected in this way lie on a straight line within experimental error. In principle the true value of  $\alpha$  should be found by successive approximations, i.e. recorrecting the data using the corrected value of  $\alpha$ . In this case however further corrections do not materially alter the values of  $M_D$ .

Conventional light scattering measurements on the T20 sample yielded, after centrifugation at 40 000  $\times g$  for 2 h, a weight-average molecular weight of 40 kg/mol and a Z-average polar radius of gyration of 30 nm, the result depending upon the time and speed of centrifugation. These two figures are clearly inconsistent with each other for a single dextran fraction and the dissymmetry must arise from a small amount of high molecular weight impurity. Figure 4a shows a logarithmic plot of the autocorrelation function for this sample. At long times this becomes a straight line yielding a Z-average diffusion constant for the high molecular weight component of  $4.3 \times 10^{-6}$  mm<sup>2</sup>/s. The Z-average diffusion constant of the low molecular weight component may be found from the autocorrelation function at shorter times if use is made of the extrapolated straight line. The following procedure, which is justified by equation (1), was adopted. At each value of  $\tau$  the antilogarithm of one-half of the ordinate corresponding to the autocorrelation function and the extrapolated straight line were taken. These two values were then subtracted and the logarithm of the result plotted against  $\tau$  to yield a straight line of slope  $-K^2 D_z / 2.3$  (Figure 4b). This value of  $D_z$  is shown in Table 1 and Figure 3. The intercept of the extrapolated straight line at  $\tau = 0$  indicates that the high molecular weight component accounts for approximately 50% of the scattered intensity, whilst the molecular size as indicated by the diffusion constant of this component suggests that it accounts for only a very small proportion of the total concentration. Thus the true molecular weight of the dextran fraction in this case is one-half of the measured value i.e. 20 kg/mol. This agrees with the gel filtration data. It must be emphasized that in general the results for a two-component system can only be analysed in this way if the two diffusion constants are different by an order of magnitude or more, and the polydispersity of the high molecular weight component is low enough for the  $\log \phi(\tau)$  plot to be a straight line at longer times.

From Figure 3 the values  $\alpha = 0.45$  and  $A = 2.25 \times 10^{-4}$  are obtained. The diffusion constants of dextrans of the type investigated here have also been investigated using conventional techniques by Granath<sup>11</sup> and by Ingelman and Halling<sup>12</sup>. The results presented here agree within experimental error with those of the earlier authors for molecular weights above 70 kg/mol. At lower molecular weights the results using conventional techniques are higher. Granath's value of diffusion constant for a molecular weight of 11.2 kg/mol (determined by the sedimentation velocity method) is  $8.8 \times 10^{-5}$  mm<sup>2</sup>/s and his results lie in a straight line with  $\alpha = 0.50$ . Granath made measurements in phosphate buffer. Measurements were therefore repeated on the T10 sample with 0.05 M phosphate buffer (pH = 7) as solvent. The values of diffusion constant and weight-average molecular weight so obtained were the same within experimental error as those found from measurements in distilled water. (Measurements were also similarly repeated on the T20 sample but a high molecular weight impurity was still observed.) It was not possible to make light scattering measurements on the T10 sample at a concentration below 1%. This does not explain the discrepancy, however, as Granath did not detect any concentration dependence.

There is also the possibility that the T10 sample contained some large aggregates. Whereas these would not materially affect conventional diffusion measurements, it has been shown that, in the case of light scattering measurements, the effect of a small number of large aggregates is to increase the weight-average molecular weight and decrease the Z-average diffusion constant in equal proportions<sup>13</sup>. The aggregates would have to contribute some 25% of the scattered intensity to account for the discrepancy. This is difficult to reconcile with the fact that gel filtration and light scattering measurements yielded the same weight average molecular weight, unless of course the gel filtration calibration for low molecular weights depended upon light scattering measurements on a sample similar to the T10 sample investigated in this work. The presence of a small amount of high molecular weight impurity in the T10 sample still remains a possibility therefore, although in this case the aggregates would have to be small enough in size so as not to produce a dissymmetry of scatter.

It is of interest to compare the results of diffusion constant measurements with those of intrinsic viscosity. The latter are usually analysed in terms of the Mark-Houwink equation:

$$[\eta] = BM^\beta \quad (8)$$

For any theoretical model involving an equivalent hydrodynamic sphere in which the hydrodynamic diameters for translation and shear are assumed to be proportional to each other<sup>14</sup>:

$$3\alpha = \beta + 1 \quad (9)$$

Granath obtained  $\beta = 0.43$  which yields  $\alpha = 0.477$ . If the hydrodynamic diameter for translation and shear are assumed to be identical then:

$$A = \frac{kT}{3\pi\eta} \left( \frac{2.5\pi N_0}{6B} \right)^{1/3} \quad (10)$$

where the symbols have their usual meaning. The variation of diffusion constant with molecular weight predicted in

this way from Granath's viscosity data is shown by the broken line in *Figure 3*. The agreement with the diffusion data is somewhat better than that obtained for unbranched polymers where the measured diffusion constant is usually some 20% lower<sup>14</sup>.

#### CONCLUSION

Diffusion constants of dextran fractions obtained by light scattering Rayleigh linewidth measurements are in good agreement with those obtained by conventional techniques for molecular weights above 70 kg/mol. For lower molecular weights diffusion constants are obtained which are lower than those obtained by conventional techniques. The possible presence of high molecular weight impurities might wholly or partly explain this discrepancy. The diffusion constant/molecular weight relationship obtained from light scattering measurements is:

$$D_{20} = 2.25 \times 10^{-4} M^{-0.45}$$

This is in fair agreement with the variation predicted from viscosity data. There is no concentration dependence of

diffusion constant within experimental error ( $\pm 3\%$ ).

#### REFERENCES

- 1 Pecora, R. *Discuss. Faraday Soc.* 1970, 49, 222 and references cited therein
- 2 Cummins, H. Z., Knable, N. and Yeh, Y. *Phys. Rev. Lett.* 1964, 12, 150
- 3 Dubin, S. B., Lunacek, J. H. and Benedek, G. B. *Proc. Nat. Acad. Sci. US* 1967, 67, 1164
- 4 Foord, R., Jakeman, E., Oliver, C. J., Pike, E. R., Blagrove, R. J., Wood, E. and Peacocke, A. R. *Nature* 1970, 227, 242
- 5 Ford, N. C., Lee, W. and Karasz, J. J. *J. Chem. Phys.* 1969, 50, 3098
- 6 Sellen, D. B. *Polymer* 1970, 11, 374
- 7 Sellen, D. B. *Polymer* 1973, 14, 359
- 8 Van Cleve, J. W., Schaefer, W. C. and Rist, C. E. *J. Am. Chem. Soc.* 1956, 78, 4435
- 9 Lindberg, S. and Svensson, S. *Acta Chem. Scand.* 1968, 22, 1907
- 10 Schulz, G. V. *Z. Phys. Chem.* 1939, B43, 25; Zimm, B. H. *J. Chem. Phys.* 1948, 16, 1099
- 11 Granath, K. A. *J. Colloid Sci.* 1958, 13, 308
- 12 Ingelman, B. and Halling, M. S. *Arkiv Kemi* 1949, 1, 61
- 13 Sellen, D. B. *Polymer* in press
- 14 Flory, P. J. 'Principles of Polymer Chemistry', Cornell University Press, Ithaca, 1953

# Transitions of a series of regularly alternating linear polyesteramides

C. Borri, E. Sorta and L. Zotteri

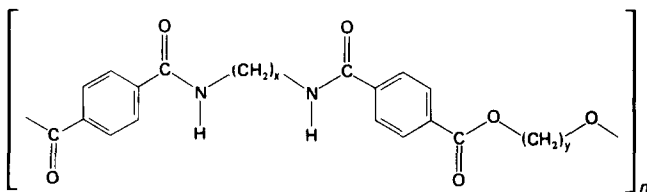
Laboratori Ricerche Polimeri, Snamprogetti, 20097 San Donato Milanese, Milano, Italy

(Received 14 October 1974; revised 1 April 1975)

The systematic detection of the relaxations of a series of regularly alternating linear polyesteramides, based on terephthalic acid, was effected using dynamic-mechanical, thermal and thermomechanical means, thus making it possible to support certain hypotheses as to the attribution of the motions involved in these relaxations. Sufficient data were collected to allow firm prediction of the glass transitions of homologous or similar polymers and copolymers.

## INTRODUCTION

A series of polymers of the following types were synthesized in the Fibre Department of Snamprogetti:



with various  $x$  and  $y$  values conventionally referred to with the symbols  $xNTy$ . The rheological properties of melt 12NT6<sup>2</sup> and the thermodynamics of such melting<sup>3</sup>, determined both experimentally and by means of statistical mechanics calculations, have already been studied.

In carrying out this work, an attempt was made to establish and ascertain the nature of the transition of the polymers under examination, by dynamic-mechanical, thermal and thermomechanical tests. The criteria adopted in order to specify which particular molecular motion or structural defect has brought about the process of relaxation are those typical of other spectroscopic techniques, i.e., based on the comparison of polymer spectra which differ in the monomeric unit, and in the case of one polymer, the comparison of the spectrum of samples with different thermal or thermomechanical history.

## EXPERIMENTAL

### Samples

Circular-section fibres of three polyesteramides (6NT6, 12NT6, 12NT12) were prepared for the forced vibration dynamic-mechanical tests by means of spinning under optimum conditions.

For each type of polymer, three different thermomechanical histories (see Table 1) were taken into consideration: (A) thread as spun (lowest degree of crystallinity compatible to a process on a semi-industrial level); (B) thread as spun and then annealed; and (C) drawn and subsequently annealed thread. The samples marked B were obtained by means of a thermal treatment in a stove for 15 min under a pre-tension of  $5.75 \times 10^5$  N/m<sup>2</sup> at different temperatures (see Table 1). The samples marked C were drawn on pin and plate at

temperatures of 150° and 80°C respectively with a drawing ratio of 1:5.2 and taken up at rate of 50 m/min.

Subsequently, the samples were treated in the stove in the same way as for samples B, with a pre-tension of  $5.75 \times 10^6$  N/m<sup>2</sup>.

The films for the Rheovibron viscoelastometer tests were obtained by means of evaporation of trifluoroacetic acid solutions and were then annealed in a stove (see Table 1).

The samples for the thermal analysis tests were subjected to suitable quenching in order to make their crystallinity so low that a net peak of cold crystallization was observed under thermal analysis.

The wt % crystallinity  $C_x$  was determined for each sample, from the relative density as measured in a gradient tube. The following values of  $\rho_a$  and  $\rho_c$  were used to define  $C_x$  respectively:

	6NT6	12NT6	12NT12
$\rho_a$ (g/cm <sup>3</sup> )	1.1875	1.135	1.100
$\rho_c$ (g/cm <sup>3</sup> )	1.314	1.251	1.210

The relative amorphous density values were obtained from the dilatometric data of Manzini *et al.*<sup>3</sup>

Table 1 Samples used for the dynamic-mechanical tests

Polymer	Sample	Thermal treatment			$C_x$ (%)	$n \times 10^2$
		Temp. (°C)	Time (min)	Density (g/cm <sup>3</sup> )		
6NT6	A	—	—	1.2025	13.0	1.009
	B	185	15	1.2365	41.2	2.224
	C	185	15	1.2405	44.4	19.968
	Film	180	20	1.2500	52.0	—
12NT6	A	—	—	1.1640	26.9	0.839
	B	170	15	1.1740	35.8	2.874
	C	170	15	1.1800	41.1	15.596
	Film	160	20	1.1870	47.2	—
12NT12	A	—	—	1.1302	29.4	1.844
	B	150	15	1.1450	43.2	4.899
	C	150	15	1.1462	44.3	10.793
	Film	140	20	1.1515	49.2	—

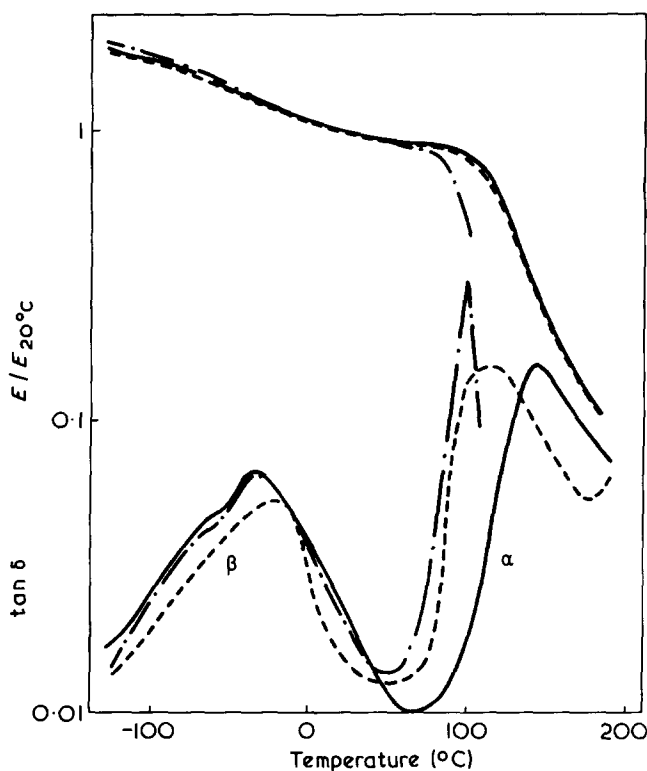


Figure 1 Plot of  $\tan \delta$  and  $E/E_{20}$  versus temperature for 6NT6 ( $100 < \nu < 400$  Hz). ---, Sample A; ---, sample B; —, sample C

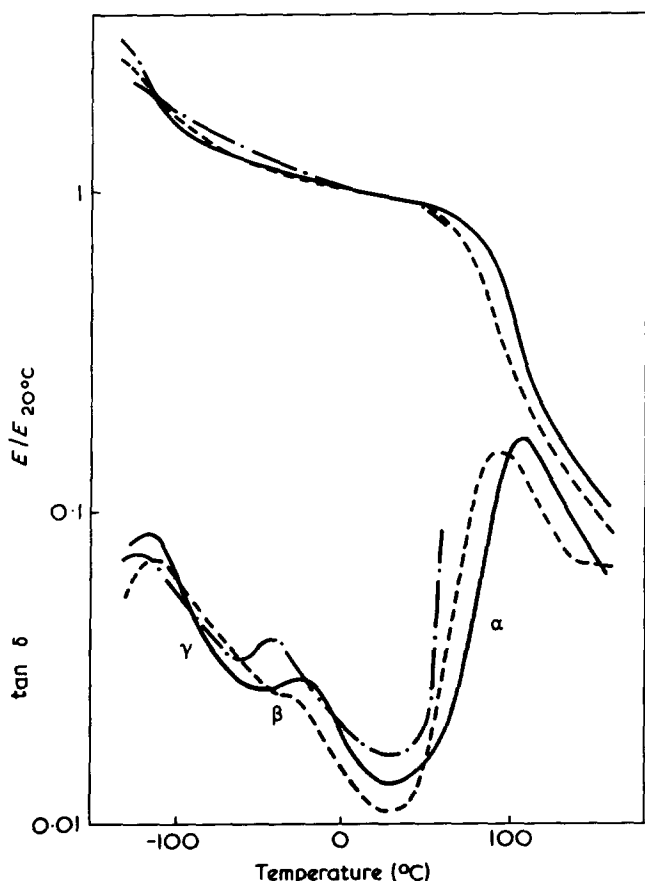


Figure 2 Plot of  $\tan \delta$  and  $E/E_{20}$  versus temperature for 12NT6 ( $100 < \nu < 400$  Hz). ---, Sample A; ---, sample B; —, sample C

The 100% crystallinity density data were obtained through the determination of the elementary cell of RX spectrum of the fibre in a cylindrical chamber<sup>4</sup>. Orientation indexes for the fibres were obtained from the birefringence

expressed as:  $\Delta n = R_0/D$  where  $\Delta n$  is the difference in refractive index parallel and perpendicular to the axis of the fibre,  $R_0$  is the retardation of the light and  $D$  is the thickness of the sample.

*Dynamic-mechanical tests*

The dynamic-mechanical tests were carried out both by means of forced resonance vibration techniques<sup>5</sup>, and by means of a Rheovibron dynamic viscoelastometer (Toyo Instruments Co. Ltd).

The cell for the forced vibrations was slightly modified to allow a range of temperatures from  $-150^\circ$  to  $250^\circ\text{C}$ . With this apparatus, the frequency depends on the modulus and is not therefore constant through the temperature range. Some constant frequency recordings (110 Hz) were taken using a Rheovibron Dynamic Viscoelastometer.

A heating speed of approximately  $1^\circ\text{C}/\text{min}$  was chosen for both dynamic-mechanical measurements.

*Thermal and thermomechanical analyses*

The d.s.c. standard cell and Du Pont 941 Thermo Mechanical Analyzer (t.m.a.) connected to the Du Pont 900 console was used. A heating speed of  $10^\circ\text{C}/\text{min}$  was chosen for the d.s.c. measurements and a heating speed of  $5^\circ\text{C}/\text{min}$  for t.m.a. measurements.

RESULTS

Figures 1 to 4 show the dynamic-mechanical behaviour of the polyesteramides under examination. The dynamic-mechanical data relating to  $\alpha$ ,  $\beta$  and  $\gamma$  relaxations are summarized in Tables 2 and 3.

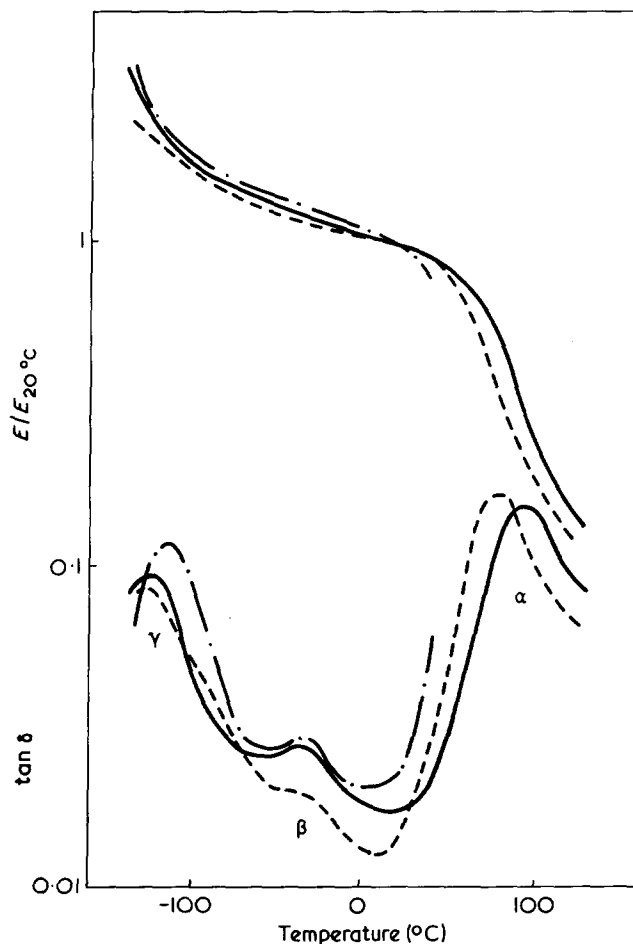


Figure 3 Plot of  $\tan \delta$  and  $E/E_{20}$  versus temperature for 12NT12 ( $100 < \nu < 400$  Hz). ---, Sample A; ---, sample B; — sample C

It was not possible to complete the spectrum on the low crystallinity sample (samples A) since at such temperatures cold crystallization occurs.

Thermal and thermomechanical data of the quenched samples are reported in Table 4 where  $T_f$  (t.m.a.) and  $T_f$  (d.s.c.) are the transition temperatures measured by means of t.m.a. and d.s.c. techniques,  $T_{cc}$  is the temperature at the maximum point of the cold crystallization peak and  $T_m$  is the temperature of the maximum point of the melting peak.

Since the specific heat represents a property which is thermodynamically related to the volume there should be a correspondence between the transition temperatures measured using the d.s.c. and t.m.a. techniques. The dif-

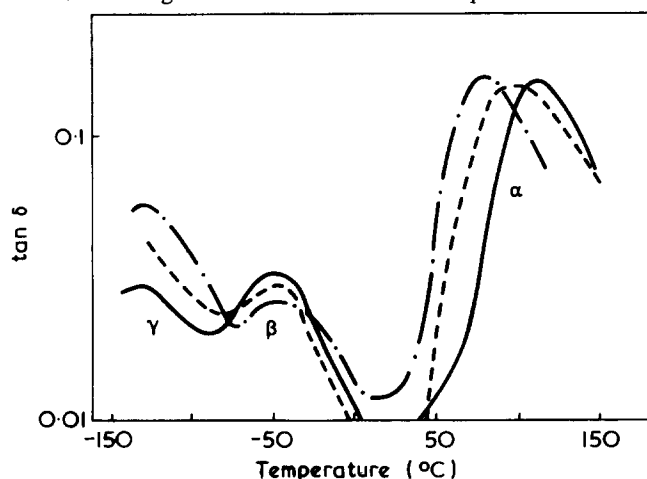


Figure 4 Plot of  $\tan \delta$  versus temperature for 6NT6 (—), 12NT6 (---) and 12NT12 (- - -) at 110 Hz

Table 2 Summary of  $\alpha$  relaxation data

Polymer	Samples	$T_\alpha$ (°C)	( $\tan \delta$ ) <sub>max</sub>	$\nu_{max}$ (Hz)*
6NT6	B	120	0.16	140
	C	140	0.15	150
	Film	110	0.15	110
12NT6	B	95	0.16	145
	C	110	0.17	145
	Film	95	0.15	110
12NT12	B	80	0.17	150
	C	94	0.16	150
	Film	80	0.15	110

\* An error of 2% refers only to samples B and C

$\nu_{max}$  is the resonance frequency at the corresponding relaxation temperature

Table 3 Summary of  $\beta$  and  $\gamma$  relaxation data

Polymer	Initial	$\beta$			$\gamma$		
		$T_\beta$ (°C)	( $\tan \delta$ ) <sub>max</sub>	$\nu_{max}$ (Hz)*	$T_\gamma$ (°C)	( $\tan \delta$ ) <sub>max</sub>	$\nu_{max}$ (Hz)*
6NT6	A	-42	0.064	275	-110	0.068	370
	B	-35	0.044	275	-100	0.052	355
	C	-10	0.049	260	-115	0.062	370
	Film	-50	0.034	110	-130	0.030	110
12NT6	A	-40	0.041	280	-125	0.076	410
	B	-30	0.026	270	-115	0.070	360
	C	-25	0.029	270	-115	0.084	360
	Film	-45	0.030	110	-120	0.040	110
12NT12	A	-35	0.036	290	-120	0.105	430
	B	-35	0.020	275	-125	0.066	380
	C	-35	0.029	295	-125	0.090	380
	Film	-45	0.021	110	-130	0.056	110

\* An error of 2% refers to samples A, B and C

ferences are therefore due to operative variables. Differences of this degree were found by Miller<sup>6</sup> using the same instrument.

## DISCUSSION

### $\alpha$ -Relaxation

There are considerable similarities between the glass transition of the poly(methylene terephthalates)<sup>7</sup> and the  $\alpha$ -relaxation of the polymers under examination. In fact, the transition is dominant in both series of polymers. Moreover,  $T_\alpha$ , temperature corresponding to the maximum point of  $\tan \delta$  (see Table 2) and  $T_f$  (see Table 4) decrease as the number of methylenes increases in a manner roughly parallel to the melting point as observed in the case of the poly(methylene terephthalates). This fact indicates that similar enthalpic and entropic factors act upon the melting point and the  $\alpha$ -relaxation. It is accepted that the same parameters which influence the glass transition ( $T_g$ ) also influence the melting point<sup>8</sup>. Moreover, the  $\alpha$ -relaxations shift to higher temperatures as crystallinity and orientation increase.

In the case of samples having a similar thermomechanical history, the  $\tan \delta$  value at the maximum point of the peak ( $\tan \delta$ )<sub>max</sub> is almost constant in the series of polyesteramides examined. These facts support the hypothesis that the  $\alpha$ -relaxation is due to movements of the entire chain and is not limited to certain groups. Crystallization was not observed at temperatures below  $T_f$ . It would seem to us that there is sufficient evidence to affirm that the  $\alpha$ -relaxation is the glass transition for the polymers under examination.

Some observations may also be made in accordance with the logical scheme of properties and structures by means of comparison with data concerning 'related' polymers. If the amide links of the 6NT6 are replaced with ester links poly(hexamethylene terephthalate) chain is formed; meanwhile if the ester links are replaced with amide links the poly(hexamethylene terephthalamide) chain is formed. From other<sup>7</sup> dynamic-mechanical data relating to a sample of poly(hexamethylene terephthalate), an  $\alpha$ -relaxation at 45°C at a frequency of 165 Hz results. This result should

Table 4 Thermal and thermomechanical data of quenched samples

Polymer	$T_f$ (t.m.a.) (°C)	$T_f$ (d.s.c.) (°C)	$T_{cc}$ (°C)	$T_m$ (°C)
6NT6	49	59	80	251
12NT6	39	43	61	215
12NT12	33	27	53	191



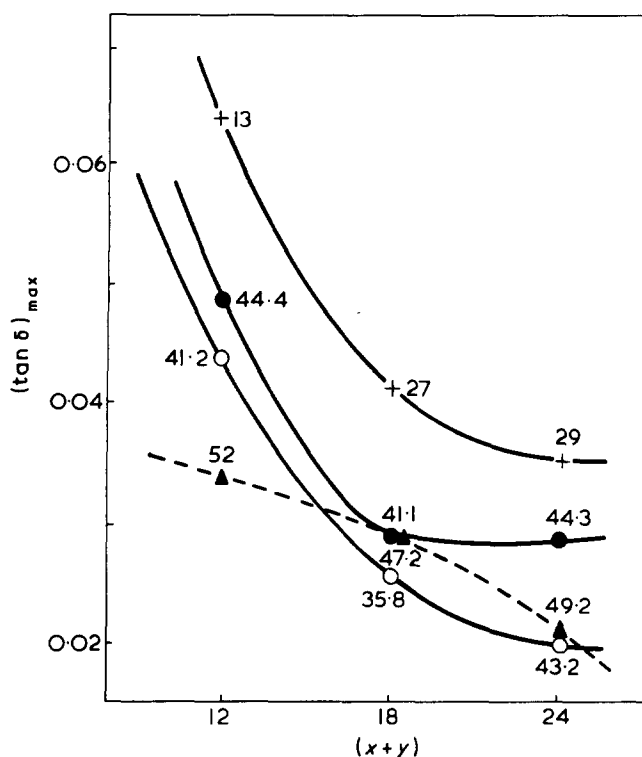


Figure 5 Plot of  $(\tan \delta)_{\max}$  versus total number of  $\text{CH}_2$  ( $x + y$ ) for 6NT6, 12NT6, 12NT12. +, Sample as spun; O, crystallized sample; ●, draw and crystallized sample; ▲, crystallized film. The numbers are the % crystallinity

be comparable to our spectrum of sample B of the 6NT6 ( $T_g$  at  $120^\circ\text{C}$  and at 140 Hz). It may therefore be observed that the introduction of alternating amide links brings about an increase of  $\sim 75^\circ\text{C}$  of the glass transition. The thermal analysis verifies that the glass transition of a sample of poly(hexamethylene terephthalate)<sup>9</sup> ( $T_m = 152^\circ\text{C}$ ) falls to  $\sim 0^\circ\text{C}$  whilst that of 6NT6 measured by means of the same techniques rises to  $59^\circ\text{C}$ .

There are no data available concerning poly(hexamethylene terephthalamide) but the dynamic-mechanical properties of its higher homologue, poly(heptamethylene terephthalamide)<sup>10</sup> are available. The dynamic-mechanical spectrum of the poly(heptamethylene terephthalamide) shows that the total introduction of amide links leads to a further and considerable increase in the temperature of the relaxation to  $\sim 200^\circ\text{C}$  at 1000 Hz. Butta<sup>10</sup> records also a  $T_g$  obtained by means of thermal analysis at  $177^\circ\text{C}$ . In any case, more precise comparison is not possible since the above-mentioned paper does not specify the thermomechanical history of the sample. Unlike the polyesteramides, the poly(heptamethylene terephthalamide) shows, however, a distinct shoulder at  $\sim 100^\circ\text{C}$  connected with the aromatic parts of the chain. In the case of polyesteramides, this relaxation is not recorded as it is preceded by the micro-Brownian motion of the entire chain.

#### $\beta$ -Relaxation

For each polymer the  $\beta$  relaxation peak moves towards higher temperatures in the sequence A, B and C; this fact can be more distinctly observed for the 6NT6 rather than the 12NT6 whilst it tends to disappear in the 12NT12. The intensity of the peaks decrease in relation to the increase of the crystallinity. The irregularity observed for the oriented samples, the intensity of which is slightly higher than that of sample B, is probably due to the difference between the morphological nature of the crystals formed during drawing and annealing and therefore has a different

effect on the movements of the amorphous part. The frequency differences corresponding to the maximum point of the peak are not such as to invalidate the qualitative value of the observations made. All such observations support the hypothesis that the  $\beta$  relaxation occurs in the amorphous part.

The comparison between samples of different polymers is more difficult since the diverse degree of crystallinity and water content must be taken into consideration because the water absorption depends on the crystallinity and polar group content. With the data at our disposal the absorption of water decreases in proportion to an increase in the crystallinity as in the case of aliphatic polyamides and therefore, in the biphasic approximation, it may be affirmed that the water is absorbed by the amorphous region. Our samples were not dried before the tests; in each case and for each type of polymer, the absorption of water was less than 1.6% at 66% r.h. and therefore was less than the absorption of some aliphatic polyamides (e.g. nylon-6 and nylon-6,6). By reason of the low water content, the absorption remains nearly independent of the density of the chain polar groups. The comparison of the intensity of the  $\beta$  relaxations with similar degrees of crystallinity (see Figures 4 and 5) shows that the relaxation mechanism finds its origin in polar groups in the amorphous part.

#### $\gamma$ -Relaxation

The  $\gamma$ -relaxation in the polyesteramides under examination occurs approximately at the same temperature and frequency as the  $\gamma$ -peak of aliphatic polyamides<sup>11</sup>, partly aromatic polyamides<sup>10</sup> and polyethylene<sup>11</sup>. This similarity enables the designation of the  $\gamma$ -relaxation in polyamides to the movements of the  $\text{CH}_2$  units between the amide links. This interpretation is considered valid also in the case of the  $\gamma$ -relaxation of the polyesteramides, emphasis being laid on the fact that the movements of the  $\text{CH}_2$  units is predominant in the relaxation mechanism since the phenomenon is more intense in the 12NT12 as compared to the 12NT6 and to the 6NT6 (see Figure 4).

#### CONCLUSIONS

The results of this research can serve to predict the glass transitions in polymers having a similar structure. There is evidence both on the effect of the variation of the number of  $\text{CH}_2$  units and of the effect of the introduction of a greater number of amide links. Therefore it is possible to approximately predict the glass transition temperature of a polymer of the  $x\text{NT}y$  type with varying  $x$  and  $y$  and of other alternating polyesteramides obtained by means of the polycondensation of a glycol with a diester, which contains more than two preformed amide links.

#### REFERENCES

- 1 Ital. Pat. No. 908 493; 908 844
- 2 Capaccioli, T., Crosta, R. and Sorta, E. *Proc. 2nd Meet. Ital. Soc. Rheol.*, Siena 1973
- 3 Manzini, G. et al. *Eur. Polym. J.* 1973, 9, 941
- 4 Cesari, M. and Perego, G. to be published
- 5 Meredith, R. and Bay-Sung Hsu *J. Polym. Sci.* 1962, 61, 271
- 6 Miller, G. W. 'Analytical Calorimetry', (Ed. R. S. Porter and J. G. Johnson), Plenum Press, New York, 1968, p 71
- 7 Farrow, G. et al. *Makromol. Chem.* 1960, 38, 147
- 8 Boyer, R. F. *Rubber Chem. Technol.* 1963, 36, 1310
- 9 Borri, C. unpublished results
- 10 Butta, E. *Proc. 2nd Meet. Ital. Soc. Rheol. Siena* 1973
- 11 McCrum, N. G., Read, B. E. and Williams, G. 'Anelastic and Dielectric Effects in Polymeric Solids', Wiley, London, 1967

# Conformational properties of poly(alkene sulphone)s in solution:

## 1. Relation between the dielectric properties in solution and the structure of the repeat unit

A. H. Fawcett and K. J. Ivin

Department of Chemistry, The Queen's University of Belfast, Belfast BT9 5AG, UK  
(Received 19 September 1974; revised 13 December 1974)

A survey of the available evidence shows that the central C—C bonds in  $\beta$ -disulphones and polysulphones have a mainly *trans*, and sometimes an exclusively *trans*, conformation.

Calculations of the coulombic interactions in the 27 possible conformational sequences in  $-\text{SO}_2\text{CH}_2\text{CH}_2\text{SO}_2-$  show that certain sequences having *gauche* C—C bonds are unlikely to be significantly populated. Others such as (*t*,  $g^-$ ,  $g^+$ ) and ( $g^-$ ,  $g^-$ ,  $g^+$ ) involve a certain amount of steric interaction but are likely to be comparable in energy with those having a *trans* C—C bond. One alkyl substituent or two at the same carbon atom eliminates some but not all of the accessible sequences having a *gauche* C—C bond. Substituents at both carbon atoms cause such strong steric interactions that only *trans* C—C bonds are allowed. It is shown how such considerations account satisfactorily for the two types of dielectric behaviour of poly(alkene sulphone)s in solution.

Preliminary experiments indicate that poly(norbornene sulphone), unlike polysulphones of other 1,2-disubstituted alkenes, does have a permanent dipole because of the inability of adjacent C—S bonds to take up anti-parallel positions.

A close resemblance is noted between the conformation about the main-chain C—C bond in poly(cyclohexene sulphone) and that about the main-chain C—C bond in poly(but-2-ene sulphone) in its most stable configuration.

### INTRODUCTION

The dielectric behaviour of six poly(alkene sulphone)s in solution has been reported<sup>1-3</sup>. The polymers fall into two distinct groups: group A in which the alkene unit is hex-1-ene or 2-methylpent-1-ene; and group B in which the alkene unit is but-2-ene, hex-2-ene, cyclohexene or cyclopentene. Members of group A show a dispersion in the range  $10^3$ – $10^6$  Hz and the critical frequency is strongly dependent on molecular weight<sup>1,2</sup>, indicating relaxation by overall motion of the molecule. Members of group B show no dispersion in the range  $10^2$ – $10^7$  Hz, indicating zero dipole moment. The essential difference between the two groups of polymers is thought to reside in the proportion of *gauche* conformations taken up by the main-chain C—C bonds. The zero dipole moment for group B implies that all the main-chain C—C bonds are in the *trans* conformation, while the finite dipole moment for group A implies that at least a proportion of the main-chain C—C bonds are in a *gauche* conformation at any one time.

The purpose of the present paper is first, to summarize the available evidence concerning conformations about C—C bonds in  $\beta$ -disulphones and polysulphones, and also about C—S bonds in sulphones; second, to consider the factors which operate to determine the conformational populations in sulphones and polysulphones, and to examine the importance of coulombic interactions between adjacent sulphone groups; and third, to consider the relationships between the structures of polymers in group B.

### CONFORMATIONS IN SULPHONES

Apart from the dielectric evidence on the polysulphones in solution there are five pieces of information concerning the conformation of the central C—C bonds in  $\beta$ -disulphones and polysulphones.

First, the magnitude of one of the vicinal coupling constants ( $\sim 9.5$  Hz) in the  $^1\text{H}$  n.m.r. spectrum of poly(propene sulphone)<sup>4</sup> indicates a preference for the *trans* conformation about the main-chain C—C bond, as in poly(propene sulphide)<sup>5</sup>.

Second, for  $\text{Pr}^n\text{SO}_2\text{CH}_2\text{CH}_2\text{SO}_2\text{Pr}^n$  in the polar solvent dimethyl sulphoxide- $d_6$  the  $^{13}\text{C}$  side band of the  $^1\text{H}$  n.m.r. spectrum of the central protons indicates a preference for the *trans* C—C conformation<sup>6</sup>; the enthalpy difference is estimated to be about 6 kJ/mol in favour of the *trans* conformation<sup>7</sup>.

Third,  $\text{Pr}^n\text{SO}_2\text{CH}_2\text{CH}_2\text{SO}_2\text{Pr}^n$  in the solid state obeys the rule of mutual exclusion for the Raman and infrared bands, showing that it has a centre of symmetry<sup>8</sup>. Intermolecular forces in the crystal thus assist to ensure that all the central C—C bonds adopt a *trans* conformation.

Fourth, the dipole moments of  $\text{Pr}^n\text{SO}_2\text{CH}_2\text{CH}_2\text{SO}_2\text{Pr}^n$  and  $\text{Pr}^n\text{SO}_2\text{CHMeCH}_2\text{SO}_2\text{Pr}^n$  in dioxane solution are both  $3.6 \text{ D}^7$ , which is not equal to any of the values which would be expected (0, 5.8 or 8.2 D) were any one of the 27 possible conformations of the S—C—C—S bonds exclusively adopted. In both of these molecules there must be present in the moderately polar solvent dioxane several conforma-

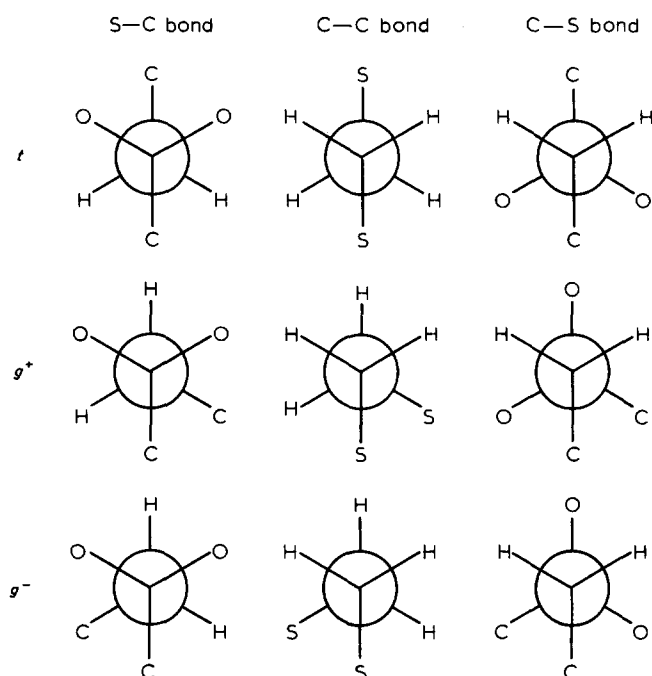


Figure 1 Rotational states about the three bonds in  $-\text{SO}_2-\text{CH}_2-\text{CH}_2-\text{SO}_2-$

tions of comparable enthalpy.

Fifth, in the  $^{13}\text{C}-\{^1\text{H}\}$  n.m.r. spectrum of poly(but-2-ene sulphone), the two chemical shifts observed for the methyl carbon are consistent with an all-*trans* conformation for the main chain C-C bond and two alternative relative configurations about adjacent main-chain carbon atoms<sup>9</sup>; also see final section.

Thus all the evidence indicates a substantial preference for the *trans* conformation of the central C-C bonds in  $\beta$ -disulphones and polysulphones. However, *gauche* conformations are significant in some molecules and their energies must then lie fairly close to those for the *trans* conformation.

We may note in passing that in compounds of the type  $\text{RSO}_2\text{CH}_2-\text{CH}_2\text{CH}_3$  the temperature dependence of the n.m.r. spectra again indicates a preferred *trans* conformation, the *gauche* conformations about the  $\alpha$ - $\beta$  C-C bond having an excess enthalpy of the order of 4 kJ/mol ( $\text{R} = \text{CH}_2\text{CH}_2\text{SO}_2\text{Pr}^n, \text{Me}, \text{Pr}^n, \text{Bu}^t, \text{OH}$ )<sup>7,10</sup>.

Knowledge of the potential energy function for rotation about C-S bonds in sulphone is limited to the determination of the barrier height to internal rotation in dimethyl sulphone. This has been estimated from third law arguments to be 14 kJ/mol, assuming a three-well cosine function<sup>11</sup>. Substituents at the carbon atom may be expected to remove the symmetry of the energy function but without affecting the angular positions of the minima.

#### FACTORS CONTRIBUTING TO THE POTENTIAL FUNCTIONS FOR ROTATION ABOUT THE MAIN-CHAIN BONDS

Since we are dealing with main-chain atoms that are each bonded to four other atoms, we assume that the potential function for rotation about each of the main-chain bonds will show three minima, situated to a first approximation at dihedral angles of 0,  $2\pi/3$  and  $-2\pi/3$  and corresponding to conformational states *t*, *g*<sup>+</sup>, *g*<sup>-</sup>. The rotational states of the three bonds in a repeat unit are depicted in Figure 1. We may expect the energies of the minima and their dihed-

ral angle positions to be affected by steric repulsions, dispersion attractions and dipole-dipole interactions.

Sulphones have relatively large dipole moments<sup>2</sup> so that dipole-dipole interactions between two sulphone groups separated by two carbon atoms may be quite large. Thus, taking each dipole as 4.4 D and representing it as a pair of electronic charges separated by 100 pm, a pair of parallel dipoles separated by 400 pm in a medium of relative permittivity 2 is calculated to have an energy 17 kJ/mol in excess of that for a pair of anti-parallel dipoles at the same distance. This is considerably more than RT so that the orientation of each dipole in the chain will be strongly correlated with those of its neighbours. More detailed calculations of the coulombic interactions are described below and we then go on to consider how the situation is modified by the introduction of substituents.

#### CALCULATIONS OF COULOMBIC INTERACTION ENERGIES BETWEEN ADJACENT SULPHONE GROUPS IN THE STRUCTURE $-\text{SO}_2\text{CH}_2\text{CH}_2\text{SO}_2-$

It is assumed that the rotational states are as shown in Figure 1, the bond lengths being taken as: C-S, 180 pm; C-C, 154 pm; and S-O, 144 pm, in accordance with published data<sup>12</sup>. The dipole moments of *n*-propyl and isopropyl sulphones<sup>2</sup> in benzene have a mean value of 4.42 D. In calculating coulombic interactions between adjacent sulphone groups we have assumed that each dipole may be represented by charges of  $8.87 \times 10^{-20}\text{C}$  and  $17.74 \times 10^{-20}\text{C}$  located on the oxygen and sulphur atoms respectively.

The total coulombic energy  $E_c$  arising from the interaction of adjacent sulphone groups in the 27 possible sequences of conformations has been calculated from:

$$E_c = \sum_i \sum_j (q_i q_j / 4\pi r_{ij} \epsilon_r \epsilon_0) \quad (1)$$

and the results are shown in Table 1.  $q_i$  and  $q_j$  are the charges associated with the interacting atoms  $i$  and  $j$  on different sulphone groups separated by a distance  $r_{ij}$  calculated from the geometry of the system.  $\epsilon_r$  is the relative permittivity of the medium, taken as 2.0 (close to the value of dioxane and benzene) and  $\epsilon_0$  is the permittivity of a vacuum. It is likely that the true value of  $\epsilon_r$  is less than 2.0 when the interacting atoms are very close together. It may also be affected by specific solvent interactions, as will be shown in another paper<sup>17</sup>.

It will be seen from Table 1 that there are in fact only nine distinct values of  $E_c$ ; sequences with the same value of  $E_c$  bear a structural relationship to each other through simple symmetry operations. It may also be seen that when the C-C bond has a *gauche* conformation, there is a larger range of energies than when the C-C bond has the *trans* conformation. This is because the sulphone groups are brought closer together in the former case so that

Table 1 Dipole-dipole interaction energies (kJ/mol) for a pair of sulphone groups in the structure  $-\text{SO}_2-\text{CH}_2-\text{CH}_2-\text{SO}_2-$  (positive values imply repulsion; negative values attraction)

C-C	<i>t</i>			<i>g</i> <sup>+</sup>			<i>g</i> <sup>-</sup>			
	<i>t</i>	<i>g</i> <sup>+</sup>	<i>g</i> <sup>-</sup>	<i>t</i>	<i>g</i> <sup>+</sup>	<i>g</i> <sup>-</sup>	<i>t</i>	<i>g</i> <sup>+</sup>	<i>g</i> <sup>-</sup>	
C-S	<i>t</i>	<i>g</i> <sup>+</sup>	<i>g</i> <sup>-</sup>	<i>t</i>	<i>g</i> <sup>+</sup>	<i>g</i> <sup>-</sup>	<i>t</i>	<i>g</i> <sup>+</sup>	<i>g</i> <sup>-</sup>	
S-C	<i>t</i>	0.8	5.9	5.9	25.8	29.3	-0.4	25.8	-0.4	29.3
	<i>g</i> <sup>+</sup>	5.9	9.8	5.8 <sub>5</sub>	29.3	25.0	8.8	-0.4	25.0	8.8
	<i>g</i> <sup>-</sup>	5.9	5.8 <sub>5</sub>	9.8	-0.4	8.8	25.0	29.3	8.8	25.0

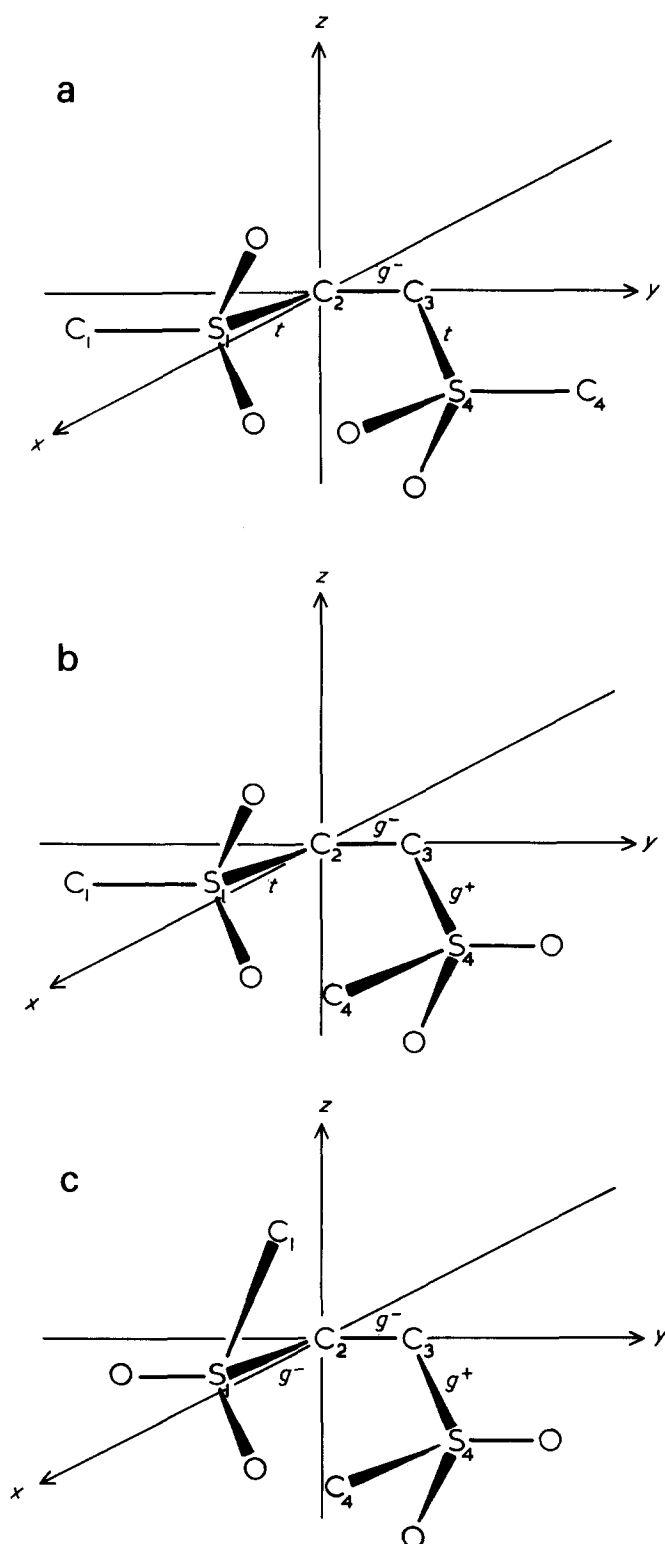


Figure 2 Conformational sequences in  $-\text{SO}_2-\text{CH}_2-\text{CH}_2-\text{SO}_2-$ : (a)  $(t, g^-, t)$ ; (b)  $(t, g^-, g^+)$ ; (c)  $(g^-, g^-, g^+)$

neighbouring dipoles are then more strongly correlated in orientation.

In Figure 2 we show three different sequences in which the C-C bonds have a *gauche* conformation: Figure 2a illustrates one  $(t, g^-, t)$  which is typical of the high energy sequences, while the others are examples of lower energy  $(t, g^-, g^+)$ ,  $(g^-, g^-, g^+)$ . In the first case two oxygen atoms of adjacent sulphone groups are brought very close together, and the repulsive contribution to  $E_c$  from this pair of atoms is probably underestimated by the use of the value

of 2.0 for  $\epsilon_r$ . Even neglecting this factor, sequences of high energy ( $>25$  kJ/mol) in Table 1 are not likely to be appreciably populated, and can be eliminated from further consideration. The sequences of real interest to the present discussion are therefore those with the C-C *gauche* conformation which have energies such as those of the sequences shown in Figures 2b and 2c, together with those with C-C *trans* conformations. The uncertainties in the calculations mean that one cannot be sure of the actual relative energies of these conformational sequences; some light will be thrown on this problem in the next paper<sup>17</sup>

#### STERIC FACTORS AND EFFECT OF SUBSTITUENTS

If we examine the 'low energy' sequences depicted in Figures 2b and 2c in more detail we find that the interatomic distance between  $C_4$  and the nearest oxygen atom to it attached to  $S_1$  is only 171 pm, which is considerably less than the sum of the van der Waals radii of an oxygen atom doubly bonded to a sulphur atom (140 pm) and a methylene group (200 pm)<sup>13</sup>. This would cause a considerable repulsive force, which will, however, be relieved by a relatively small change in the dihedral angles and perhaps by some change in the bond angles<sup>14</sup>. From the different laws of force of coulombic interaction on the one hand and steric repulsion on the other, small changes in the angles may relieve steric strain in the segment under consideration, while not greatly changing coulombic energies. Thus *gauche* states of the C-C bonds in the polymers may be significantly populated. The states of the bond can still be designated  $g^+$  and  $g^-$ , though it is likely that the minima will occur at dihedral angles somewhat different from  $2\pi/3$  and  $-2\pi/3$ ; the C-S bond rotational minima may likewise be displaced from the 'ideal' dihedral angles. Such distortion will be less significant when the C-C bond has the *trans* conformation.

Next we consider the effect of replacing the hydrogen atoms by one or two alkyl groups on the same carbon atom. Poly(2-methylpent-1-ene sulphone) and poly(hex-1-ene sulphone) are known to have a head-to-tail structure<sup>15</sup> so that we may place the alkyl substituent(s) on  $C_1$  and  $C_3$  in Figures 2b and 2c. It can be seen that this will not greatly affect the conformational energy. The sequences  $(t, g^-, g^+)$  and  $(g^-, g^-, g^+)$  are thus accessible in the sense of not having much higher energies than certain other sequences; likewise the symmetry-related sequences  $(t, g^+, g^-)$  and  $(g^+, g^+, g^-)$  are also accessible. If, however, we place the alkyl substituents on  $C_2$  and  $C_4$  in Figures 2b and 2c, an additional and severe steric hindrance arises between the alkyl group(s) on  $C_4$  and the oxygen of the adjacent sulphone group; the sequences  $(t, g^-, g^+)$ ,  $(g^-, g^-, g^+)$ ,  $(t, g^+, g^-)$  and  $(g^+, g^+, g^-)$  are then inaccessible. This is equivalent to demonstrating that with substituents on  $C_1$  and  $C_3$  the symmetry-related sequences  $(g^+, g^-, t)$ ,  $(g^+, g^-, g^-)$ ,  $(g^-, g^+, t)$ , and  $(g^-, g^+, g^+)$  are inaccessible. Thus with one or two substituents on the same carbon atom, the number of accessible sequences having a *gauche* C-C bond is more limited.

Coming now to the case of one substituent on each main-chain carbon atom we may predict from the above considerations that all the sequences with *gauche* C-C (main chain) conformations will be of high energy as a result of steric effects, leaving only the *trans* C-C conformations significantly populated. The zero dipole moment in poly(but-2-ene sulphone) is thus accounted for, as well as the <sup>13</sup>C chemical shifts of the methyl carbons (see next section).



# Conformational properties of poly(alkene sulphone)s in solution:

## 2. A rotational isomeric state study of the poly(cyclohexene sulphone) chain

A. H. Fawcett and K. J. Ivin

Department of Chemistry, The Queen's University of Belfast, Belfast BT9 5AG, UK

(Received 19 September 1974; revised 13 December 1974)

The rotational isomeric states model, coupled with the Flory matrix method, was applied to the calculation of the unperturbed mean-square end-to-end distance in poly(cyclohexene sulphone) as a function of several parameters. The calculations were performed for atactic, isotactic and syndiotactic chains; the tacticity arises from the two possible ways, D and L, in which the rings can be attached to the main chain, assuming that the C—C bonds are all in the *t* conformation, as indicated by dielectric measurements. One of the three conformations about each C—S bond is strongly hindered and was given zero statistical weight whereas the other two were assigned weights determined by second-order effects, operating over three or more consecutive bonds, and dependent on the chirality of the rings and the coulombic interactions between adjacent dipoles.

The calculations for the atactic model, in which a Monte Carlo procedure was used to generate the chain, were found to agree with experiment only if the parameter  $\alpha$  was given a value of 5 or greater. This parameter is determined by the relative orientation of successive sulphone dipoles and was expected to have a value less than unity. It appears that specific solvation effects help to stabilize (*t, g*) and (*g, t*) C—S—C bond pairs relative to *t, t*. Other parameters are not so important.

The calculations for the isotactic and syndiotactic models show interesting features, particularly for certain limiting conditions when cyclic or helical structures are generated. For these models there is a greater sensitivity to the various parameters than in the atactic case.

### INTRODUCTION

It was shown in Part 1<sup>1</sup> that neighbouring sulphone dipoles in poly(olefin sulphones) are likely to be correlated in orientation by dipole—dipole interactions. From the absence of a dielectric dispersion in the range  $10^2$  to  $2 \times 10^8$  Hz in solutions of poly(cyclohexene sulphone) it was deduced that the sulphone groups attached to each cyclohexene ring take up a 1,2-diaxial configuration<sup>2</sup>. There are therefore in effect only two axes of rotation between each pair of neighbouring dipoles, since of the three main-chain bonds between the sulphone groups one (the C—C bond) adopts solely the *trans* conformation with respect to the main chain. The simple matrix scheme of Flory<sup>3</sup>, which allows the expression of second order Markov correlations of bond rotation, may thus be applied to this polymer to include explicitly the dipole—dipole interactions, without further elaboration to express third-order correlations<sup>3</sup>.

There are two distinguishable ways of substituting the chair form of the cyclohexane ring with 1,2-diaxial substituents. For this study we arbitrarily define the D and L forms as those depicted in Figure 1. The existence of these two chiral forms of the repeat unit allows the possibility of tacticity in the chain. Proceeding along such a chain the D and L units may be distributed randomly (atactic polymer), or they may occur alternately (syndiotactic polymer), or each unit may have the same chirality as the previous one (isotactic polymer). The results of the calculations will be independent of our arbitrary labelling of the chiral centres.

In this paper the influence of dipole—dipole correlation and tacticity upon the characteristic dimensions of the polymer is studied. The  $^{13}\text{C}\{^1\text{H}\}$  n.m.r. spectrum of poly(cyclohexene sulphone) made by the radical copolymerization of cyclohexene and sulphur dioxide shows two peaks of equal area for the main chain carbon<sup>4</sup>, which indicates an atactic structure, as was also deduced for poly(propene sulphone) made in the same way<sup>5</sup>. The properties of the rotational isomeric state model of the atactic chain considered in this paper may thus be compared with experimental data on the atactic polymer and an assessment

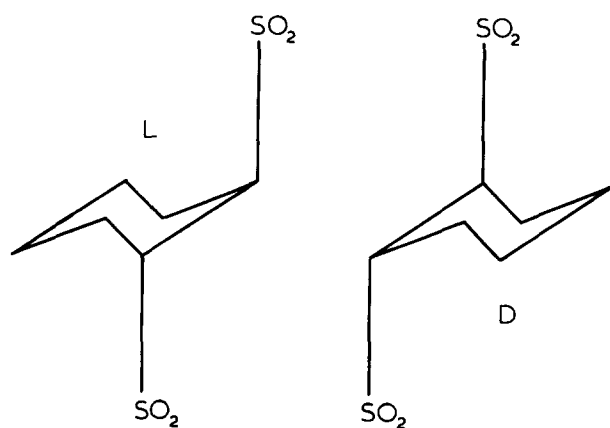


Figure 1 The two chiral forms of 1,2-diaxially substituted cyclohexane rings, L and D, as defined in the text

made of the reliability of the calculations of dipole-dipole correlations, made in Part 1.

### EXPERIMENTAL VALUES OF THE CHARACTERISTIC DIMENSION

The characteristic dimensions of the polymer have been determined at 25°C in two solvent systems<sup>2</sup>, although not under  $\theta$ -conditions.  $K_\theta$  was obtained from viscosity measurements made in the good solvent benzene by the Stockmayer-Fixman<sup>6</sup> and the Inagaki-Suzuki-Kurata methods<sup>7</sup>, and had a mean value of  $(5.4 \pm 0.4) \times 10^{-2} \text{ cm}^3/\text{g}$ . The Stockmayer-Fixman plot of the viscosity measurements obtained with the poor solvent system dioxane-cyclohexane (59:41% v/v) gave  $K_\theta = (5.56 \pm 0.06) \times 10^{-2} \text{ cm}^3/\text{g}$ . Since there is no rotation about the C-C main chain bond,  $\langle R^2 \rangle/z$ , the mean-square end-to-end distance per repeat unit is a more significant quantity than the characteristic ratio  $(\langle R^2 \rangle/n(I^2)_{av})$ . It is obtained from:

$$K_\theta = \frac{[\eta]_\theta}{M_n^{1/2}} = \frac{\Phi \left[ \frac{\langle R^2 \rangle}{z M_0} \right]^{3/2}}{q} \quad (1)$$

where  $\Phi$  is Flory's  $\theta$  constant<sup>8</sup>,  $z$  is the number of repeat units in the chain,  $M_0$  is the weight of a mole of repeat units,  $q$  is a polydispersity factor<sup>9</sup> equal to  $(M_w/M_n)^{1.5}$ .  $\Phi$  was given the value  $2.6 \times 10^{23} \text{ g}^{-1}$ , from theoretical<sup>10</sup> and experimental determinations<sup>11</sup>, and  $(M_w/M_n)$  was assumed the same as that  $(1.13 \pm 0.02)$  estimated for poly(hex-1-ene sulphone)<sup>12</sup> fractions obtained by similar fractionation techniques. The value of  $\langle R^2 \rangle/z$  so obtained from the dioxane/cyclohexane results,  $59 (\pm 2) \times 10^{-20} \text{ m}^2$  (repeat unit)<sup>-1</sup>, was taken to represent the chain dimensions in benzene also.

### ROTATIONAL ISOMERIC STATE CALCULATION

Rotational isomeric state treatments of polymer chains relate a mean-square moment characteristic of a polymeric molecule to: (i) moments associated with individual bonds; (ii) the bond angles and dihedral angles of each rotational state; and (iii) statistical factors which express the relative probabilities of the various possible configurations at each bond. It is well established that these statistical factors should not only express the form of the rotational potential about each bond, but should also include the influence of the rotational states of the neighbouring bonds<sup>3</sup>. A method has been developed for performing such calculations in a convenient manner<sup>13</sup>, which also allows the expression of tactic effects in the proper way. The present calculations were based upon equation (2), which is taken from the paper by Flory and Jernigan<sup>14</sup>,

$$\langle M^2 \rangle/n(m^2)_{av} = 1 + \left( \frac{2}{Zn(m^2)_{av}} \right) | \mathbf{J}^t \mathbf{0} \dots \mathbf{0} | \mathbf{G}_1^{n-1} \begin{vmatrix} 0 \\ \vdots \\ \mathbf{J} \otimes \mathbf{m}_n \\ \mathbf{J} \end{vmatrix} \quad (2)$$

in which  $n$  is the number of bonds in the chain,  $M$  is the molecular moment,  $\mathbf{m}$  is the bond moment vector,  $\mathbf{J}$  is the  $r \times 1$  column matrix with all elements unity, and  $\mathbf{J}^t$  is its transpose.  $r$  is the number of rotational states for the bonds,  $\mathbf{G}_1^{n-1}$  is the product  $\mathbf{G}_1 \mathbf{G}_2 \dots \mathbf{G}_{n-1}$  (the serial pro-

duct),  $\mathbf{G}_i$  is a function<sup>14</sup> of  $\mathbf{U}_i$ ,  $\mathbf{m}_i$  and  $\mathbf{T}_i(\phi_1) \dots \mathbf{T}_i(\phi_r)$ ,  $\otimes$  indicates the direct matrix product,  $\mathbf{U}_i = [u_{pq}]_i$ , the statistical weight matrix for bond  $i$ ,  $u_{pq} = \exp\{-\epsilon_{(i,p)} + \epsilon_{(i,p;i-1,q)}/kT\}$ ,  $\epsilon_{(i,p)}$  is the energy to promote the bond  $i$  to the  $p$ th state,  $\epsilon_{(i,p;i-1,q)}$  is the energy of the interaction which occurs when the bond  $(i-1)$  is then promoted to the  $q$ th state.  $\mathbf{T}_i(\theta, \phi_s)$  is the matrix to transform orthogonally from the coordinate system of bond  $(i+1)$  to that of bond  $i$ , which has the rotational angle  $\phi_s$ .  $\theta$  is the angle between the two bond vectors,  $\mathbf{Z}$  is the partition function  $\mathbf{J}^t \mathbf{U}_1 \mathbf{U}_2 \dots \mathbf{U}_{n-1} \mathbf{J}$ .

The definition of the element  $u_{pq}$  of the statistical weight matrix in terms of simple Boltzmann factors<sup>15</sup> carries the assumption, which may not be strictly valid, that the conformational entropy differences are zero.

### TRANSFORMATION MATRICES

A segment of the main chain is shown in Figure 2. The three bonds S-C, C-C and C-S are labelled as vectors  $\mathbf{a}$ ,  $\mathbf{v}$  and  $\mathbf{w}$ , and are all shown in the *trans* conformation. In our calculations the virtual bond  $\mathbf{b}$ , equal to  $\mathbf{v} + \mathbf{w}$ , replaces the two real bonds  $\mathbf{v}$  and  $\mathbf{w}$ ; this may be done because  $\mathbf{v}$  is fixed in conformation. Bond lengths used were those employed in Part 1, and tetrahedral bond angles were assumed. The four right-handed coordinate systems shown in Figure 2 follow the usual conventions<sup>3</sup>.

$\mathbf{T}_a(\chi, \phi_a)$  is simply given by:

$$\mathbf{T}_a(\chi, \phi_a) = \begin{vmatrix} \cos \chi & \sin \chi & 0 \\ \sin \chi \cos \phi_a & -\cos \chi \cos \phi_a & \sin \phi_a \\ \sin \chi \sin \phi_a & -\cos \chi \sin \phi_a & -\cos \phi_a \end{vmatrix} \quad (3)$$

but because  $\mathbf{w}$ , the second axis of internal rotation in the repeat unit, does not coincide with the second bond vector  $\mathbf{b}$ , the transformation matrix  $\mathbf{T}_b(\theta, \phi_b)$  is formulated as the product of three successive transformations:  $\mathbf{T}_w(\psi, \phi_w)$ , which has the same form as  $\mathbf{T}_a(\chi, \phi_a)$ , and transforms to system  $\mathbf{w}$ ; and two further transformations  $\mathbf{T}(\delta)$  and  $\mathbf{T}(\pi)$ , respectively given by:

$$\mathbf{T}(\delta) = \begin{vmatrix} \cos \delta & -\sin \delta & 0 \\ \sin \delta & \cos \delta & 0 \\ 0 & 0 & 1 \end{vmatrix} \quad (4)$$

and

$$\mathbf{T}(\pi) = \begin{vmatrix} 1 & 0 & 0 \\ 0 & -1 & 0 \\ 0 & 0 & -1 \end{vmatrix} \quad (5)$$

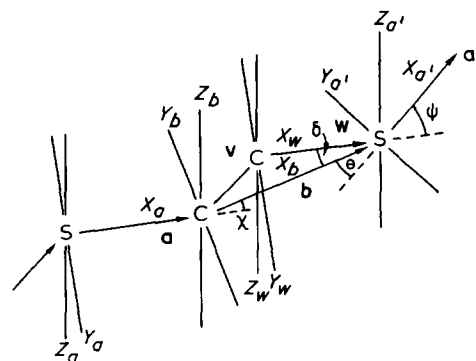


Figure 2 Coordinate systems of the repeat unit of poly(cyclohexene sulphone)

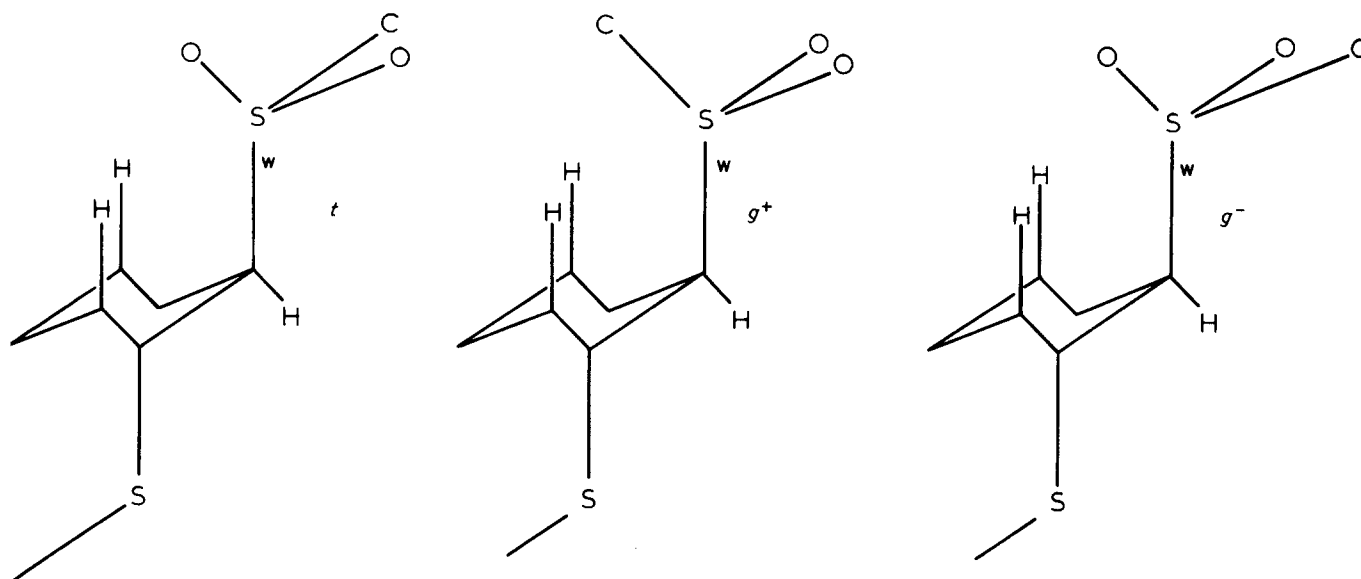


Figure 3 Rotational states  $t$ ,  $g^+$  and  $g^-$  of the C-S bond  $w$  attached to an L-ring

which describe successive rotations to transform from system  $w$  to system  $b$ . Thus:

$$T_b(\theta_\phi, \phi_b) = T_w(\psi, \phi_w)T(\delta)T(\pi) \quad (6)$$

(The subscript in  $\theta_\phi$  is used because the angle between bonds  $b$  and  $a'$  depends upon the conformation adopted by bond  $w$ , and thus upon  $\phi_w$ ).

## STATISTICAL WEIGHT PARAMETERS

### First order effects

In considering first order effects in poly(cyclohexene sulphone) we have to deal with rotation about only one type of bond, namely the C-S bond. Conclusions concerning first order effects for the C-S bond may be applied equally to the neighbouring S-C bond. Figure 3 shows the rotational states of the C-S bond  $w$  attached to an L-ring. The  $t$  state is that in which the main-chain bonds are in the planar zig-zag configuration.

In the  $t$  and  $g^-$  states an oxygen atom is located above the ring, whereas in the  $g^+$  state a carbon atom, to which is attached a hydrogen and two other carbon atoms (part of the next ring, not shown), is in this position. In order to assess the relative importance of these three states we may compare the internuclear distances with the sums of the appropriate van der Waals radii.

For the  $g^+$  state the carbon atom above the ring will be in close proximity to the two axial hydrogen atoms shown, which each form part of a methylene group. The distance between the carbon nucleus above the ring and the carbon nuclei to which these axial hydrogens are attached is 283 pm, which is appreciably less than twice the van der Waals radius of a methylene group (400 pm). In reality the sum of the van der Waals radii for the interacting groups will be substantially greater than this since the carbon atom above the ring is in fact part of a methine group in a substituted cyclohexane ring. Turning now to the  $t$  and  $g^-$  states the distance between the oxygen nucleus above the ring and the carbon nuclei of the ring methylene groups is 273 pm, which is again somewhat less than the sum of the individual van der Waals radii for a methylene group and

an oxygen atom (340 pm). However, in this case there is likely to be an attractive force arising from the dipole induced in the C-H bonds by the neighbouring S-O dipole, thereby decreasing the effective van der Waals radii. Such an effect appears to operate in poly(trimethylene oxide) where there is an attractive interaction<sup>16</sup> between oxygen atoms and methylene groups at a separation of 290 pm.

Thus there are strong reasons for believing that the  $t$  and  $g^-$  states will be greatly preferred over the  $g^+$  state. We therefore assign statistical weights of 1, 0 and 1 to the  $t$ ,  $g^+$  and  $g^-$  states respectively, for an L-ring. The corresponding weights for a D-ring are 1, 1 and 0 respectively. Second order effects, considered in the next section, modify this otherwise very simple situation.

### Second order effects

Here we have two things to consider. First, the effect of the rotational states of bond  $w$  on those of the subsequent bond  $a$  (the direction of the chain is defined in Figure 2); and second, the effect of the rotational states of bond  $a$  on those of the subsequent bond  $w$ . In both cases steric effects arise which depend on the chirality of the rings in the neighbourhood of the bond; but coulombic interaction between adjacent dipoles arises only in the second case, and is independent of the chirality of the rings.

*Correlation parameters for bond a.* The interactions associated with the  $(w, a)$  bond pair depend on the chirality of the two rings adjacent to the bonds and on the conformations about each bond. There are four possibilities so far as the chirality is concerned, namely DD, LD, DL, LL, and three possibilities for the conformations about each of the two bonds, although, as discussed earlier, one of these for each bond may be assumed to have zero weight. In deciding what parameters to introduce at this stage we therefore need to examine  $4 \times 2 \times 2 = 16$  possible structures. Of these, four are depicted in Figure 4a and four in Figure 4b, the other eight being mirror images of these. It should be noted that sulphur atoms are attached to each ring either at  $S_L$  or  $S_D$ , the chirality of the ring then being denoted by the subscript. It will be seen that four structures summarized in Figure 4a have the same steric interactions but arise from four different combinations of configuration and conformation as listed in Table 1; likewise



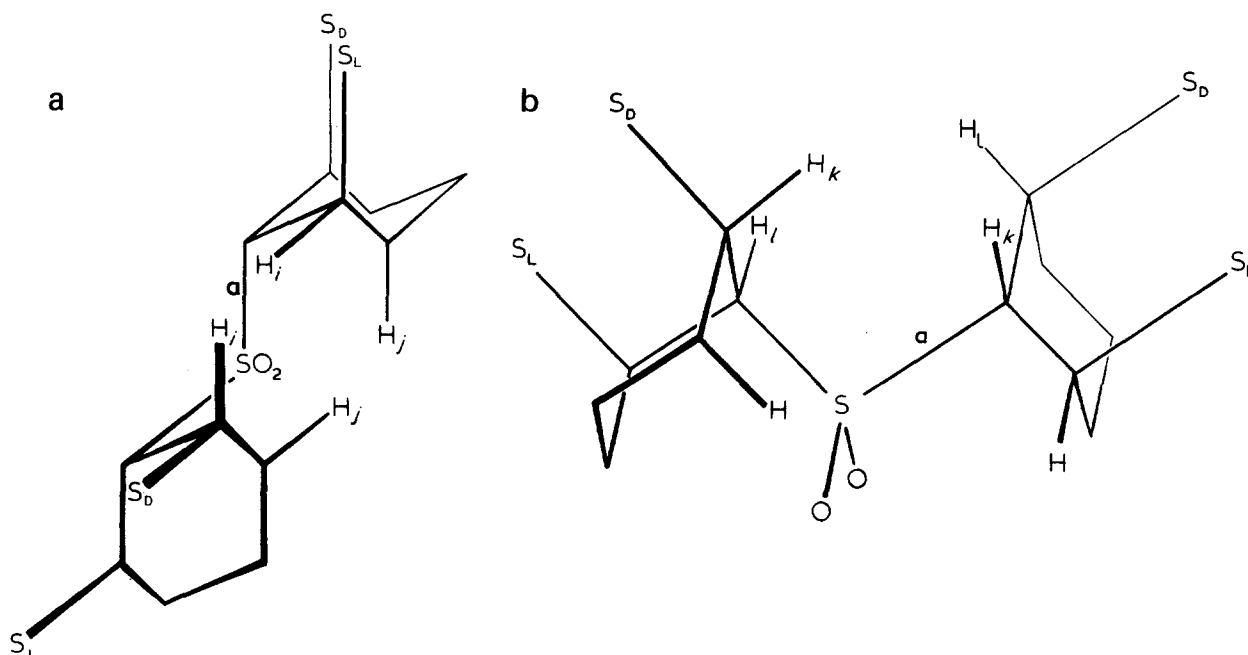


Figure 4 Representation of eight of the sixteen accessible structures in relation to bond a. On each ring only one of the two positions labelled  $S_D$  and  $S_L$  is actually occupied by a sulphur atom; if the sulphur is attached at  $S_D$  the ring has D-chirality, similarly for  $S_L$ . (a) depicts four of the combinations and (b) the other four as listed in Table 1

Table 1 Combinations of configuration and conformation corresponding to Figure 4

	Configura- tion of ring attached to bond w	Conforma- tion of bond w	Conforma- tion of bond a	Configura- tion of ring attached to bond a
Figure 4a	L	t	t	D
	D	$g^+$	t	D
	D	$g^+$	$g^-$	L
Figure 4b	L	t	$g^-$	L
	L	t	$g^+$	D
	D	$g^+$	$g^+$	D
	D	$g^+$	t	L
	L	t	t	L

Table 2 The four pairs of configurations/conformations corresponding to the structures in Figure 4b and their mirror images

Combina- tion	Configura- tion of ring attached to bond w	Confor- mation of bond w	Confor- mation of bond a	Configura- tion of ring attached to bond a	Statisti- cal weight
1	L	t	t	L	1
2	L	$g^-$	$g^-$	L	$\sigma$
3	L	t	$g^+$	D	1
4	L	$g^-$	t	D	1
5	D	$g^+$	t	L	1
6	D	t	$g^-$	L	1
7	D	$g^+$	$g^+$	D	$\sigma$
8	D	t	t	D	1

for the four structures summarized in Figure 4b. The eight mirror-image structures may be derived from those listed in Table 1 by exchanging L and D, and  $g^+$  and  $g^-$ .

For the structures shown in Figure 4a there are two possible interactions to consider, that between the two hydrogens labelled  $H_i$  and that between the pair labelled  $H_j$ . For

a tetrahedral lattice the internuclear distance for each pair of atoms is 132 pm, which will give rise to a severe steric repulsion. From Hendrickson's data<sup>17</sup> we may estimate the repulsion energy at this distance to be in excess of 36 kJ/mol. It is likely that the  $H_j$  interaction will be relieved by a small twist from the tetrahedral lattice, but the  $H_i$  interaction will be less easily accommodated. For the structures shown in Figure 4b, there may be much smaller interactions between pairs of hydrogen atoms  $H_k$  and  $H_l$ , their internuclear distance on a tetrahedral lattice being 214 pm. To take account of this difference between the two groups of structures we introduce the parameter  $f$  as the statistical weight of the structures shown in Figure 4a relative to those shown in Figure 4b.  $f$  is expected to be very much smaller than 1.

Let us now examine the more highly populated structures shown in Figure 4b and their four mirror images in more detail. They form four pairs in which the chirality of the rings is fixed but the two bonds w and a have a different sequence of conformations. Combination 3 is the reverse of combination 5, which is the mirror image of combination 4. Combinations 3 and 4 may therefore be assigned equal weights of unity; likewise for combinations 5 and 6. However, combinations 1 and 2, and also 7 and 8 may have different weights and we introduce the parameter  $\sigma$  as indicated in Table 2 to take account of this possibility. Examination of Figure 4b shows that in combination 7 alternate sulphone groups, labelled  $S_D$  and  $S_D$ , are brought closer together than in combination 1 (which is the mirror image of combination 8) where the alternate sulphone groups are labelled  $S_L$  and  $S_L$ . There is, however, no steric interaction and we may expect  $\sigma$  to be close to unity.

The statistical weight matrices for bond a are summarized in Table 3. If, as the above arguments suggest,  $f$  is zero, and  $\sigma$  is unity it is apparent that (w, a) bond pairs are limited to very few possibilities, namely the eight shown in Table 2 which will be restricted still further if the chain is isotactic or syndiotactic. For example if successive rings have D chirality and bond w has t conformation then bond a

must also have *t* conformation. This absolute determination is an important feature of the model of which use is made in the next section.

**Correlation parameters for bond w.** Here we consider how the rotational state of bond *w* is affected by that of bond *a* which precedes it in the chain, and which lies on the other side of a cyclohexane ring. Three possible sequences are shown in *Figure 5*. We shall not for the moment consider the dispositions of the chain before *C<sub>a</sub>* or beyond *C<sub>w</sub>*, but simply recall that the conformations of the bonds immediately outside this segment are exactly determined as summarized in *Table 2*.

The first point to note is that as the conformations in the (*a*, *w*) bond pair vary, so does the relative orientation of the two sulphone dipoles. *Figure 5a* shows the all-*trans* conformational sequence (on an L-ring), which is taken as the reference state so far as coulombic interactions of the sulphone dipoles are concerned. When either bond *a* or bond *w* is converted to the *g*<sup>-</sup> state, as for example in *Figure 5b*, the sulphone dipoles take up a relative orientation which we will define as an  $\alpha$ -interaction, characterized by a statistical weight of  $\alpha$ . When both bonds *a* and *w* are in the *g*<sup>-</sup> state, as in *Figure 5c*, there is a different relative orientation of the dipoles, and we give this arrangement a statistical weight of  $\gamma$ . As previously concluded when examining first order effects, *g*<sup>+</sup> states of bonds attached

to an L-ring may be assigned a statistical weight of zero. For bonds attached to D-rings, it is the *g*<sup>-</sup> states of the bonds which have zero statistical weight and the  $\alpha$  and  $\gamma$  interactions then correspond to the (*a*, *w*) bond pairs (*t*, *g*<sup>+</sup>) or (*g*<sup>+</sup>, *t*), and (*g*<sup>+</sup>, *g*<sup>+</sup>) respectively. The calculations in Part 1 show that the excess energies associated with  $\alpha$  and  $\gamma$  ( $\epsilon_\alpha = -kT \ln \alpha$ ;  $\epsilon_\gamma = -kT \ln \gamma$ ) might be expected to be of the order of 5 and 9 kJ/mol respectively. This would suggest that  $1 > \alpha > \gamma$ . However, the assumption of a constant relative permittivity of the medium and the neglect of specific solvent effects could well upset this order and we have therefore not restricted the values of  $\epsilon_\alpha$  and  $\epsilon_\gamma$  in the calculations.

One further type of interaction can be taken into account as a result of the severe restriction of available conformational sequences. If one examines sequences of three rings there are 8 possible combinations of chiralities coupled with four possible conformational sequences of the four bonds (two *a* and two *w*). Of these 32 arrangements, models show that in two (D *g*<sup>+</sup> *g*<sup>+</sup> D *g*<sup>+</sup> *g*<sup>+</sup> D and its mirror image) there is severe overlap at the ends of the sequence. Account of this has been taken by introducing an additional parameter  $\omega$  in the statistical weight matrix for the *w* bond.

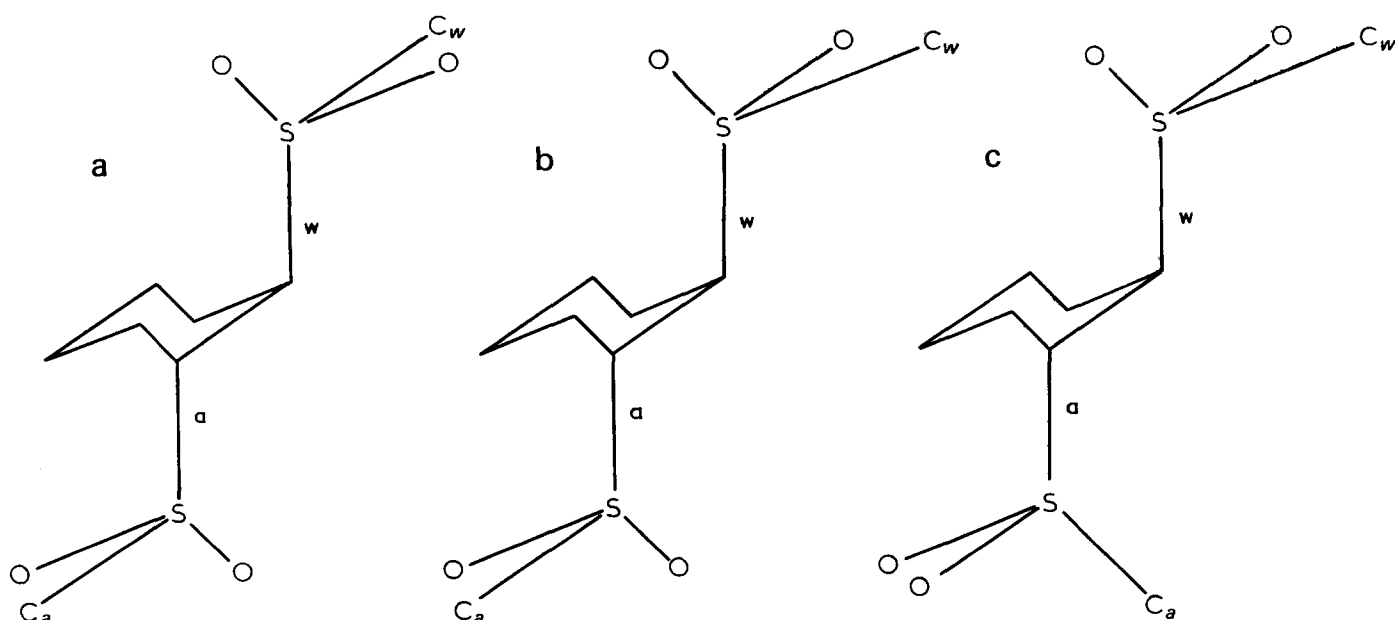
The statistical weight matrices for bond *w* are summarized in *Table 4*.

*Table 3* Statistical weight matrices for bond *a*

Chirality of ring adjacent to bond <i>w</i>	Bond <i>w</i>	Bond <i>a</i>					
		Chirality of ring adjacent to bond <i>a</i>					
		L			D		
		<i>t</i>	<i>g</i> <sup>+</sup>	<i>g</i> <sup>-</sup>	<i>t</i>	<i>g</i> <sup>+</sup>	<i>g</i> <sup>-</sup>
L	<i>t</i>	1	0	<i>f</i>	<i>f</i>	1	0
	<i>g</i> <sup>+</sup>	0	0	0	0	0	0
	<i>g</i> <sup>-</sup>	<i>f</i>	0	$\sigma$	1	<i>f</i>	0
D	<i>t</i>	<i>f</i>	0	1	1	<i>f</i>	0
	<i>g</i> <sup>+</sup>	1	0	<i>f</i>	<i>f</i>	$\sigma$	0
	<i>g</i> <sup>-</sup>	0	0	0	0	0	0

## THE COMPUTER PROGRAM

Equation (2) was computer-programed in Algol 60 to perform the calculations,  $\langle R^2 \rangle / z$  being subsequently obtained using the relationship  $n(l^2)_{av}/z = a^2 + b^2 = 10.7 \times 10^{-20} \text{ m}^2$  (cf *Figure 2*). *Table 5* contains the U matrices deduced for the rotatable bonds of the repeat units of the tactic polymers. The rotational states there shown with zero weights were excluded from the calculations, reducing the problem in effect to a 2-state model, with a consequently smaller requirement of computer time. For the atactic chain the random sequence of ring chiralities was simulated by a Monte Carlo technique<sup>13</sup>, 400 or 800 chemical repeat



*Figure 5* An (*a*, *w*) bond pair on an L-ring showing three conformational sequences having different coulombic interactions between adjacent sulphone groups: (a) all-*trans* structure (the reference state); (b) bond *a*, *g*<sup>-</sup>; bond *w*, *t* (an example of the  $\alpha$ -interaction); (c) bonds *a* and *w* both *g*<sup>-</sup> (the  $\gamma$ -interaction)

Table 4 Statistical weight matrices for bond w

Bond a	Bond w						
	Chirality of central ring						
	L			D			
	t	g <sup>+</sup>	g <sup>-</sup>	t	g <sup>+</sup>	g <sup>-</sup>	
Isotactic triads (LLL, DDD)	t	1	0	α	1	α	0
	g <sup>+</sup>	0	0	0	α	ωγ	0
	g <sup>-</sup>	α	0	ωγ	0	0	0
Other triads (DLL, LLD, DLD, LDD, DDL, LDL)	t	1	0	α	1	α	0
	g <sup>+</sup>	0	0	0	α	γ	0
	g <sup>-</sup>	α	0	γ	0	0	0

Table 5 U matrices for the isotactic and syndiotactic repeat units. The matrices refer to the bonds in heavier type.

Isotactic*	Syndiotactic*					
$\left[ \text{---} \left( \overset{\text{D}}{\text{C}} \right) \text{---} \left( \text{S} \right) \text{---} \right]$	$\left[ \text{---} \left( \overset{\text{L}}{\text{C}} \right) \text{---} \left( \text{C} \right) \text{---} \left( \overset{\text{D}}{\text{C}} \right) \text{---} \left( \text{S} \right) \text{---} \right]$					
$\begin{vmatrix} 1 & f & 0 \\ f & \sigma & 0 \\ 0 & 0 & 0 \end{vmatrix}$	$\begin{vmatrix} 1 & \alpha & 0 \\ \alpha & \gamma & \omega \\ 0 & 0 & 0 \end{vmatrix}$	$\begin{vmatrix} f & 0 & 1 \\ 1 & 0 & f \\ 0 & 0 & 0 \end{vmatrix}$	$\begin{vmatrix} 1 & 0 & \alpha \\ 0 & 0 & 0 \\ \alpha & 0 & \gamma \end{vmatrix}$	$\begin{vmatrix} f & 1 & 0 \\ 0 & 0 & 0 \\ 1 & f & 0 \end{vmatrix}$	$\begin{vmatrix} 1 & \alpha & 0 \\ \alpha & \gamma & 0 \\ 0 & 0 & 0 \end{vmatrix}$	

\* The main chain is shown as a planar zig-zag viewed from above, with the atoms in parenthesis being below the level of the adjacent atoms. The semi-circles represent the remainder of the 6-membered ring, the chirality being indicated as D or L.

units being generated. Matrix squaring was then used to find a limiting value of  $\langle R^2 \rangle / z$ . The standard deviation of the mean characteristic dimensions of several such Monte Carlo chains was taken as an indication of the reliability of the simulation process.

### RESULTS OF CALCULATIONS AND DISCUSSION

We give first the results for the atactic chain since here we can make a direct comparison with experiment. The results for the isotactic and syndiotactic chains show some interesting features which may have a wider bearing than on the particular polymer under consideration.

#### Atactic chain

A preliminary calculation was made using the following values, based on the earlier discussion:  $f = 0$ ,  $\sigma = 1$ ,  $\omega = 0$ ,  $\epsilon_\alpha = 5.1$  kJ/mol ( $\alpha = 0.13$  at 25°C),  $\epsilon_\gamma = 9.0$  kJ/mol ( $\gamma = 0.026$ ). This gave  $\langle R^2 \rangle / z = (211 \pm 33) \times 10^{-20}$  m<sup>2</sup> (repeat unit)<sup>-1</sup> which is nearly four times the experimental value. Since the discrepancy is most likely to stem from an incorrect estimation of  $\alpha$  and  $\gamma$  (the coulombic parameters) these were varied first in order to discover what values were necessary to bring the calculated values into line with experiment.

Figure 6a shows that there is marked dependence of  $\langle R^2 \rangle / z$  on  $\epsilon_\alpha$  for all values of  $\epsilon_\gamma$  used. The important thing to notice is that the calculated values of  $\langle R^2 \rangle / z$  lie in the region of the experimental value only for values of  $\epsilon_\alpha$  more negative than -4.0 kJ/mol ( $\alpha \geq 5.0$ ). The dependence on  $\epsilon_\gamma$  in this region is only slight, as shown in Figure 6b. We have also tested the effect of making  $f$  and  $\omega$  finite, and of allowing  $\sigma$  to depart from unity. The results are shown

in the form of plots of  $\langle R^2 \rangle / z$  against the appropriate  $\epsilon$  value in Figures 7a, 7b and 7c. It will be seen that in the regions close to  $f = 0$  (high  $\epsilon_\omega$ ),  $\omega = 0$  (high  $\epsilon_\omega$ ), and  $\sigma = 1$  ( $\epsilon_\sigma = 0$ ) there is no significant dependence of  $\langle R^2 \rangle / z$  upon any of these parameters taken singly.

Thus the most important parameter, so far as the atactic chain is concerned, is  $\alpha$  and, unexpectedly this has to be assigned a value considerably greater than unity in order to obtain agreement with experiment. We must now consider what this means in physical terms and how it can be explained.  $\alpha$  is the statistical weight of (a, w) bond pairs which have one  $t$  and one  $g$  conformation, relative to those in which both are  $t$ . This means that although in the polymer chain all the C-S bond dipoles cancel for both types of bond pair (since the C-C bonds are always  $t$ ) the adjacent sulphone groups prefer to take up a non-parallel arrangement in benzene or in dioxane/cyclohexane mixtures despite the fact that simple coulombic considerations suggest that such an arrangement should have the higher energy. The difference in coulombic energies is changed in magnitude but not in sign if a different value of the relative permittivity of the medium is used in the calculation. In order to account for a value of  $\alpha$  greater than 1 it is necessary to postulate a differential solvation effect,

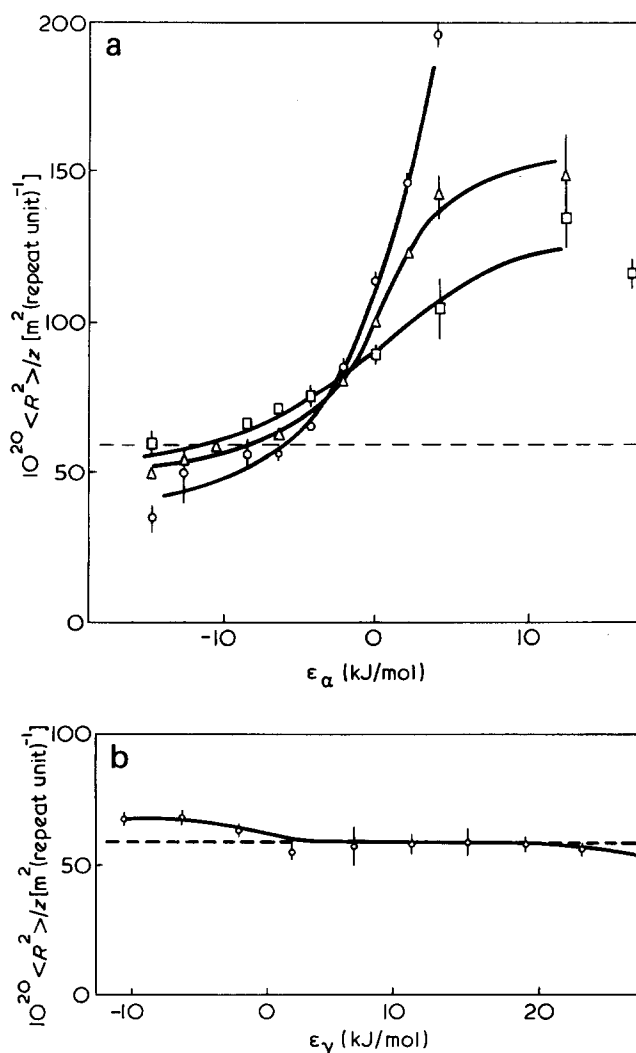


Figure 6 Atactic chain. (a) Dependence of  $\langle R^2 \rangle / z$  on  $\epsilon_\alpha$  for values of  $\epsilon_\gamma$  equal to 10.5 (O), 0 ( $\Delta$ ), and -10.5 ( $\square$ ) kJ/mol, and taking  $f = \omega = 0$ ,  $\sigma = 1$ . (b) Dependence of  $\langle R^2 \rangle / z$  on  $\epsilon_\gamma$  taking  $\epsilon_\alpha = -6.28$  kJ/mol,  $f = \omega = 0$ ,  $\sigma = 1$ . Lengths of vertical lines are equal to two standard deviations. ---, denotes experimental value of  $\langle R^2 \rangle / z$

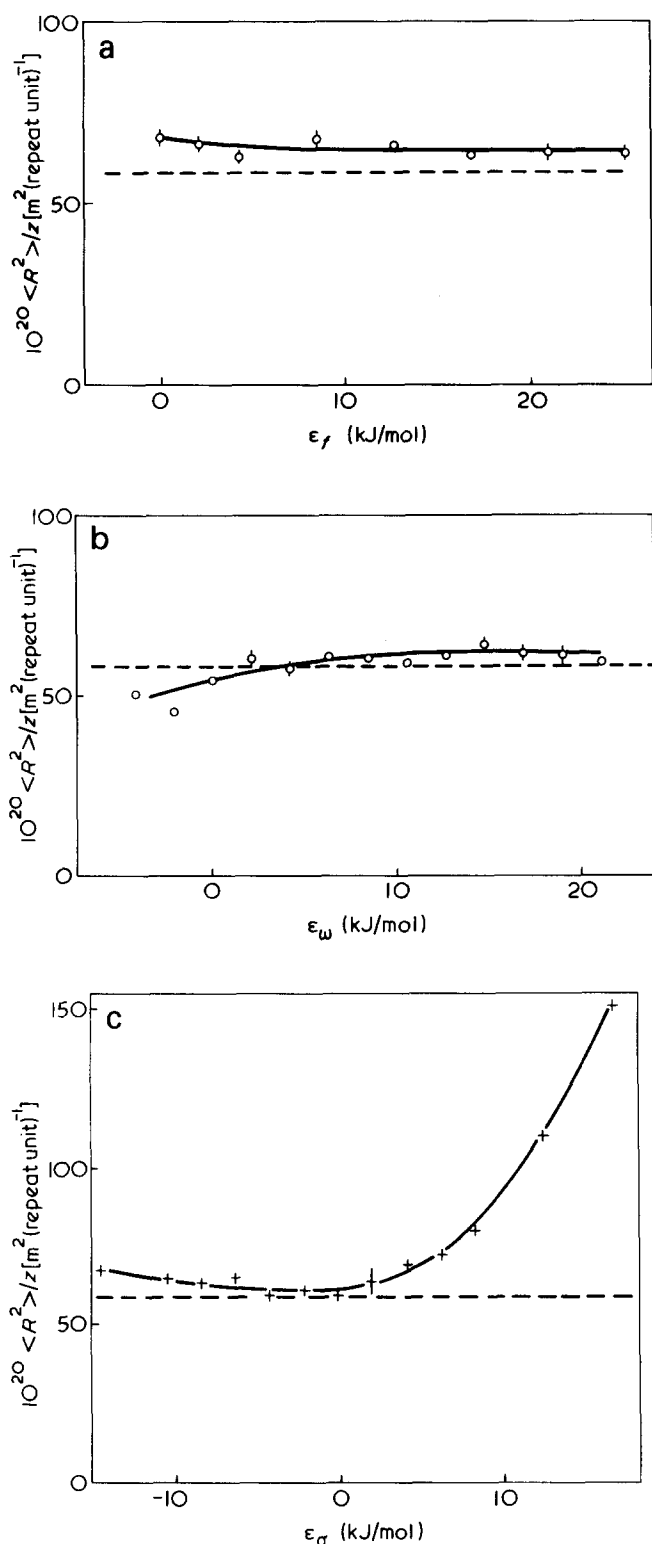


Figure 7 Atactic chain. (a) Dependence of  $\langle R^2 \rangle / z$  on  $\epsilon_f$ , taking  $\epsilon_\alpha = -5.24$  kJ/mol,  $\epsilon_\gamma = -2.1$  kJ/mol,  $\sigma = 1$ ,  $\omega = 0$ . (b) Dependence of  $\langle R^2 \rangle / z$  on  $\epsilon_\omega$ , taking  $\epsilon_\alpha = -6.28$  kJ/mol,  $\epsilon_\gamma = -2.1$  kJ/mol,  $\sigma = 1$ ,  $f = 0$ . (c) Dependence of  $\langle R^2 \rangle / z$  on  $\epsilon_\sigma$  taking  $\epsilon_\alpha = -6.28$  kJ/mol,  $\epsilon_\gamma = -2.1$  kJ/mol,  $f = \omega = 0$ . ---, denotes experimental value of  $\langle R^2 \rangle / z$

in which the solvent tends to stabilize the  $(t, g)$  or  $(g, t)$  bond pair relative to the  $t, t$  bond pair. Such an effect has indeed been observed with small molecules such as 1,2-dichloroethane<sup>18</sup> where both benzene and dioxane have been found to solvate the *gauche* form preferentially; likewise for 1,2-dibromoethane in benzene<sup>19</sup>. In the second case it has

been estimated that the *g* form is stabilized by this effect to the extent of 1.7 kJ/mol. Other things being equal, this effect will be proportional to the square of the moment of the dipole interacting with the solvent (regarding the effect as arising from a dipole-induced dipole attraction). The sulphone dipole is more than twice as big as the C-Cl and C-Br bond dipoles, so that an effect of the order of 8 kJ/mol in the present system is not unreasonable and will reconcile the value of  $\alpha$  deduced from the chain dimensions with that estimated from simple coulombic interactions. The presence of the cyclohexane ring to one side of the chain contour may also be a factor assisting differential solvation of the  $(t, g)$  and  $(t, t)$  states. It may be noted that differential solvation is also believed to be an important factor in the interpretation of solvent effects on n.m.r. chemical shifts<sup>20</sup>, end-to-end distances<sup>21</sup> and mean-square dipole moments per repeat unit in polysulphones<sup>22</sup>.

In an earlier paper<sup>2</sup> we noted that the free rotation parameter,  $(\langle R^2 \rangle / \langle R_f^2 \rangle)^{1/2}$ , had a value of 1.24,  $\langle R_f^2 \rangle$  being derived on the basis of two freely rotating C-S bonds per repeat unit. It was concluded that the energy levels for the three conformations about the C-S bonds were close together. The present, more refined, treatment shows that this is not correct; the number of available conformational sequences is much more restricted and the fact that  $(\langle R^2 \rangle / \langle R_f^2 \rangle)^{1/2}$  is close to unity is fortuitous.

#### Isotactic chain

In the calculations for the isotactic chain the parameters  $\gamma$  and  $\omega$  always occur as a product (see Table 5) so that we may treat  $\gamma\omega$  as a single variable. Plots of  $\langle R^2 \rangle / z$  against  $\epsilon_\alpha$ ,  $\epsilon_\sigma$  and  $(\epsilon_\gamma + \epsilon_\omega)$  are shown in Figures 8a, 8b and 8c respectively.

Comparison with Figures 6 and 7 show that there is a marked difference in the nature of the curves for the atactic and isotactic chains. For the isotactic chains the calculated characteristic ratio is very sensitive not only to the value of  $\alpha$  but also to the values of  $\sigma$  and  $\gamma\omega$ . However, it may be noted that the minima of many of the curves lie close to the experimental value for the atactic chain. The much greater dependence of  $\langle R^2 \rangle / z$  upon any one parameter is a consequence of the much stronger correlations imposed by the tacticity of the chain. This means that on the rising parts of the curves there is a strong tendency towards helix formation and it is necessary to go to very high values of  $z$  before a limiting value of  $\langle R^2 \rangle / z$  is reached. For example in Figure 8b, at the minimum in curve C, the limit was reached within  $0.02 \text{ m}^2 (\text{repeat unit})^{-1}$  at  $z = 2050$ , whereas for the point at  $\epsilon_\sigma = 12.6$  kJ/mol the limit was only reached at  $z = 130\,000$ .

#### Syndiotactic chain

For this model, two parameters,  $\alpha$  and  $\gamma$ , have been varied,  $f$  being taken as zero (see Table 5). The calculated values of  $\langle R^2 \rangle / z$  are plotted in Figures 9a and 9b. When either  $\alpha$  or  $\gamma$  is zero an extreme type of behaviour is exhibited. Let us consider these in turn.

(1).  $\alpha > \gamma = 0$ . This corresponds to the right-hand side of Figure 9b. Under these conditions, the four rotatable bonds in the repeat unit have the sequence  $(g^-, t, g^+, t)$ , in the limit of large  $z$ . The chemical repeat unit then has two bonds in the *trans* conformation, and the third in a *gauche* conformation. *Gauche* conformations along the chain have alternate sign, and the chain describes a ring. This is why the limiting value of  $\langle R^2 \rangle / z$  is zero for all finite values of  $\alpha$ .

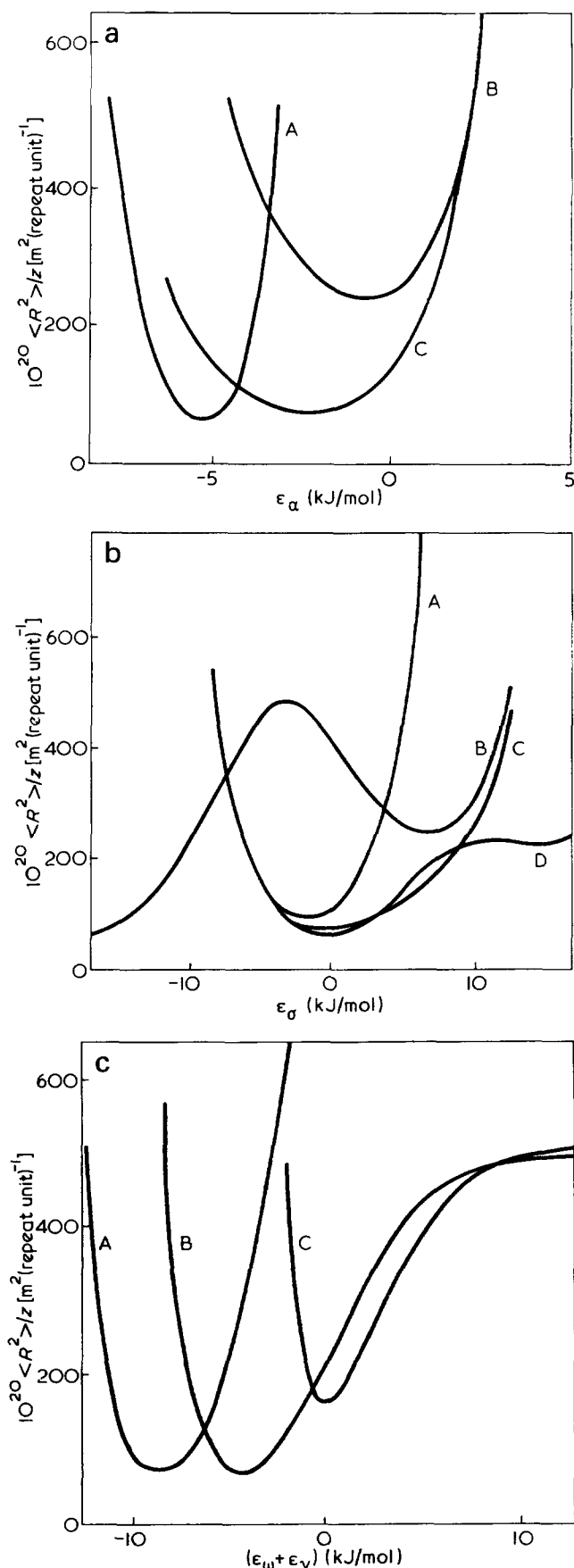


Figure 8 Isotactic chain. (a) Dependence of  $\langle R^2 \rangle / z$  on  $\epsilon_\alpha$  for values of  $(\epsilon_\gamma + \epsilon_\omega)$  of (A)  $-6.3$ , (B)  $-2.1$ , (C)  $8.4$  kJ/mol; with  $\sigma = 1$ ,  $f = 0$ . (b) Dependence of  $\langle R^2 \rangle / z$  on  $\epsilon_\sigma$  for values of (A)  $\epsilon_\gamma + \epsilon_\omega = \epsilon_\alpha = 0$ , (B)  $\epsilon_\gamma + \epsilon_\omega = -\epsilon_\alpha = 4.2$ , (C)  $\epsilon_\gamma + \epsilon_\omega = \epsilon_\alpha = -4.2$ , (D)  $\epsilon_\gamma + \epsilon_\omega = \epsilon_\alpha = -8.4$  kJ/mol; with  $\sigma = 1$ ,  $f = 0$ . (c) Dependence of  $\langle R^2 \rangle / z$  on  $(\epsilon_\gamma + \epsilon_\omega)$  for values of  $\epsilon_\alpha$  of (A)  $-8.4$ , (B)  $-4.2$ , (C)  $2.1$  kJ/mol; with  $\sigma = 1$ ,  $f = 0$

(2).  $\gamma > \alpha = 0$ . This corresponds to the right-hand side of Figure 9a. Two sequences of conformations for the repeat unit are equally probable under these circumstances. These are  $(g^-, g^-, t, t)$  and  $(t, t, g^+, g^+)$ , and their repetition generates respectively right-handed and left-handed helices, for which  $\langle R^2 \rangle / z \propto z$  and has no limit. The two helices cease to be mutually exclusive if the condition  $\alpha = 0$  is relaxed. As  $\alpha$  increases relative to  $\gamma$ , the points along the chain at which transitions between the two helix forms occur come closer and closer together, until eventually the random coil form of the chain is obtained.

The convergence of  $\langle R^2 \rangle / z$  to the limiting value in a variety of polymers has been found to be from below<sup>14,23</sup>. With certain values of  $\alpha$  and  $\gamma$ , when conditions are close to those which lead to the chain describing a ring, it was found that the limiting value of  $\langle R^2 \rangle / z$  was approached from above. This type of convergence arises from the quasi-ring structure of the polymer.

A consequence of the form of the statistical weight matrices is that a set of values of  $\epsilon_\alpha$  and  $\epsilon_\gamma$  exist for each value of  $\langle R^2 \rangle / z$ . It was found that for each set there was relationship between  $\epsilon_\alpha$  and  $\epsilon_\gamma$  of the form  $\epsilon_\gamma = 2\epsilon_\alpha + \text{constant}$ .

### CONCLUSIONS

The main conclusion from this work is that, for the atactic polymer, the parameter  $\alpha$  unexpectedly has a value greater

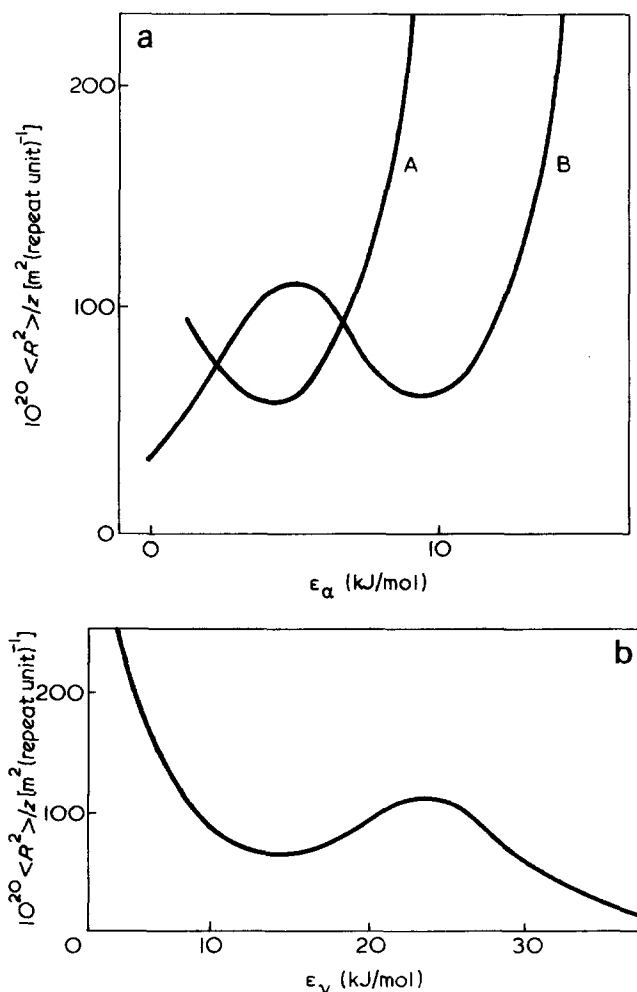


Figure 9 Syndiotactic chain. (a) Dependence of  $\langle R^2 \rangle / z$  on  $\epsilon_\alpha$  for values of  $\epsilon_\gamma$  equal to (A)  $10.5$ , (B)  $21$  kJ/mol, with  $f = 0$ . (b) Dependence of  $\langle R^2 \rangle / z$  on  $\epsilon_\gamma$  for  $\epsilon_\alpha = 6.3$  kJ/mol,  $f = 0$

than unity, perhaps even bigger than 5, whereas a simple treatment in terms of coulombic interactions between adjacent dipoles would have suggested a value less than unity. It thus appears that specific solvation effects help to stabilize (*t, g*) and (*g, t*) states for C—S—C bond pairs in poly(cyclohexene sulphone).

For the isotactic and syndiotactic models the value of  $\langle R^2 \rangle / z$  is much more sensitive to the various parameters than in the atactic case and a marked dependence of the solution properties of such polymers on solvent is to be expected.

#### ACKNOWLEDGEMENT

A. H. F. thanks the Inter-University Council for the award of a Fellowship.

#### REFERENCES

- 1 Fawcett, A. H. and Ivin, K. *J. Polymer* 1975, **16**, 569
- 2 Fawcett, A. H. and Ivin, K. *J. Polymer* 1972, **13**, 439
- 3 Flory, P. J. 'Statistical Mechanics of Chain Molecules', Interscience, John Wiley, London, 1969
- 4 Ivin, K. J. and Stewart, C. D. unpublished results
- 5 Ivin, K. J. and Navrátil, M. *J. Polym. Sci. (A-1)* 1970, **8**, 3373
- 6 Stockmayer, W. H. and Fixman, M. *J. Polym. Sci. (C)* 1963, **1**, 137
- 7 Inagaki, H., Suzuki, H. and Kurata, M. *J. Polym. Sci. (C)* 1966, **15**, 409
- 8 Flory, P. J. 'Principles of Polymer Chemistry', Cornell University Press, Ithaca, 1953
- 9 Ptitsyn, O. B. and Eizner, Yu. E. *Zh. Techn. Fiz.* 1958, **29**, 1020
- 10 Pyun, C. W. and Fixman, M. *J. Chem. Phys.* 1965, **42**, 3838
- 11 Berry, G. *J. Chem. Phys.* 1966, **44**, 4450
- 12 Bates, T. W. *PhD Thesis* Leeds University (1965)
- 13 Flory, P. J. *Proc. Nat. Acad. Sci. US* 1964, **51**, 1060
- 14 Flory, P. J. and Jernigan, R. L. *J. Chem. Phys.* 1965, **42**, 1965
- 15 Hoeve, C. A. J. *J. Chem. Phys.* 1960, **32**, 888
- 16 Mark, J. E. *J. Polym. Sci. (B)* 1966, **4**, 825
- 17 Hendrickson, J. B. *J. Am. Chem. Soc.* 1961, **83**, 4537
- 18 Oi, N. and Coetzee, J. F. *J. Am. Chem. Soc.* 1969, **91**, 2478
- 19 Abraham, R. J., Cavalli, L. and Pachler, K. G. R. *Mol. Phys.* 1966, **11**, 471
- 20 Fawcett, A. H. *PhD Thesis* The Queen's University of Belfast (1968); Ivin, K. J. and Navrátil, M. *Prepr. IUPAC Int. Symp. Macromolecules, Boston*, 1971, p 755
- 21 Ivin, K. J., Ende, H. A. and Meyerhoff, G. *Polymer* 1962, **3**, 129; Bates, T. W., Biggins, J. and Ivin, K. J. *Makromol. Chem.* 1965, **87**, 180
- 22 Bates, T. W., Ivin, K. J. and Williams, G. *Trans. Faraday Soc.* 1967, **63**, 1976
- 23 Mark, J. E. and Flory, P. J. *J. Am. Chem. Soc.* 1966, **88**, 3702; Brant, D. A. and Flory, P. J. *J. Am. Chem. Soc.* 1965, **87**, 2788

# Study of molecular packing density in boundary layers of some polymers

Yuri S. Lipatov, E. G. Moysya and G. M. Semenovich

*Institute of Macromolecular Chemistry, Academy of Sciences of the Ukrainian SSR, 252160, Kiev 160, USSR*

*(Received 9 September 1974; revised 11 November 1974)*

Packing density of macromolecules of some amorphous polymers, poly(methyl methacrylate), polystyrene and polydimethylsiloxane, in boundary layers formed at the solid-polymer interface, was studied by a 'molecular probe' technique. It was shown that the boundary layers of the above polymers have a complex structure composed of regions with different densities of molecular packing: a surface region of thickness 2 to 4  $\mu\text{m}$ , and a transient and loosely-packed region of thickness of the order of 30 to 60  $\mu\text{m}$ . It was established that both the structure and the thickness of boundary layers for each of the polymers depends both on polymer chain flexibility, and on cohesion energy density of a polymer.

## INTRODUCTION

Current interest in the phenomena occurring at the solid-polymer phase interface is readily explained by their role in the properties of filled polymers. Experimental data accumulated during recent years leads one to conclude that in the vicinity of the polymer-solid interface a boundary layer is formed, the properties of which markedly differ from those of polymer in bulk<sup>1-4</sup>. Physico-chemical investigations of the layer have shown that the polymer-solid interaction results in the net decrease of segmental mobility of macromolecules near the interface, and may lead in some cases to the shift of glass transition temperature of a polymeric matrix and/or change of molecular packing density in the latter. However, studies of packing density in filled polymers in different laboratories have given seemingly discordant results. For example, experimental data obtained by methods which permit the estimation of the overall effect of a solid-polymer interface on the properties of a filled polymer, suggest<sup>1</sup> that packing efficiency of macromolecules in filled systems is worse than that in pure samples. This was attributed by some authors<sup>1</sup> to the loosening of molecular packing in boundary layers. On the other hand, investigation of properties of very thin polymeric films on various fillers reported by Nesterov and Lipatov<sup>5</sup> indicates that boundary layers have a rather complex structure and that the packing density change with distance from the filler surface is not smooth.

The purpose of the present paper is to study the packing density of macromolecules near the polymer-solid interface as a function of chain flexibility, cohesion energy density (*CED*) of a polymer and energetic properties of a filler surface. We have chosen for this study polystyrene (PS), poly(methyl methacrylate) (PMMA) and polydimethylsiloxane (PDMS). As shown in *Table 1*, the first two polymers have similar values of a flexibility parameter  $\sigma^*$ , while their *CED*'s are different, and the last two (PS and

PDMS) possess approximately equal *CED* values, but markedly different  $\sigma^{3,6}$ . This choice allows us to elucidate the contribution of polymer chain flexibility and its energetic interaction with the substrate to the change of packing density at the solid-polymer interface.

## EXPERIMENTAL

We used in this study the 'molecular probe' (MP) technique<sup>7-10</sup> which is especially suitable for estimation of magnitude of the packing density change in polymeric matrix under various environmental conditions. This information is provided by measurements of the magnitude of the absorption spectral shifts,  $\Delta\nu$ , or luminescence spectra of impurity molecules dissolved in a matrix polymer with respect to the spectra of these molecules in the 'free' state (vapour). Since the magnitude of spectral shifts for 'probe' molecules in non-polar or weakly polar media exhibits quadratic dependence on the density of a medium, the equation for a molecular packing density change in polymer boundary layers with respect to polymer density in the bulk phase<sup>10</sup> is:

$$\frac{\rho_{\text{boundary}}^2}{\rho_{\text{bulk}}^2} = \frac{\Delta\nu_{\text{boundary}}}{\Delta\nu_{\text{bulk}}} \quad (1)$$

where  $\rho_{\text{boundary}}$  and  $\rho_{\text{bulk}}$  are polymer 'apparent' densities in boundary layers and in the bulk,  $\Delta\nu_{\text{boundary}}$  is the difference  $\nu_{\text{vapour}} - \nu_{\text{boundary}}$ , and  $\Delta\nu_{\text{bulk}}$  is the difference  $\nu_{\text{vapour}} - \nu_{\text{bulk}}$ ,  $\nu_{\text{boundary}}$  and  $\nu_{\text{bulk}}$  are band positions for a

*Table 1* Values of cohesion energy density, *CED* (cal/cm<sup>3</sup>) and flexibility parameter,  $\sigma$

Polymer	<i>CED</i> <sup>3</sup>	$\sigma^6$
PMMA	132.0	2.14
PS	72.8	2.22
PDMS	77.0	1.47

\*  $\delta = \langle r^2 \rangle_0 / \langle r^2 \rangle_f$ , where  $\langle r^2 \rangle_0$  and  $\langle r^2 \rangle_f$  are mean-square end-to-end dimensions of an 'unperturbed' macromolecule and of a model freely rotating chain respectively.

pure electron transition or a position of one band of vibrational electronic sequence in spectra of absorption or luminescence of probe molecules, incorporated into the boundary layers or bulk phase respectively, and  $\nu_{\text{vapour}}$  is the position of the same band in the vapour spectrum of the impurity molecules. Having determined experimentally the values  $\nu_{\text{boundary}}$  and  $\nu_{\text{bulk}}$  and knowing  $\nu_{\text{vapour}}$ , we may estimate the deviation of packing density in the boundary layers from that in the bulk phase from equation (1). In this work change of packing density of macromolecules in the boundary layers was estimated from the shift of position of  $(\nu_{00} + 2 \times 1405) \text{ cm}^{-1}$  band of luminescence spectra of anthracene probe molecules which are in a molecularly dispersed state in studied polymers.

Luminescence spectra of anthracene molecules in polymeric matrices were recorded at the liquid nitrogen temperature (77 K) using the spectrometer model DFS-12. Luminescence was excited with a high pressure mercury lamp model DRS-500 equipped with a glass filter  $\lambda_{\text{max}} = 365 \text{ nm}$ . Since both excitement and recording spectra were effected from the substrate side, the latter had to satisfy the following requirements: (i) the substrates had to have different surface energies (see above); (ii) they should be transparent in the u.v. region. These requirements seemed to be met by the fused silica and Teflon polymer. Prior to use the fused silica slides were annealed at  $600^\circ\text{C}$  for 1.5 to 2 hours, while Teflon films were carefully washed with the same solvents which were used for casting of polymer samples. The following polymers with a rather narrow molecular weight distribution were used: atactic PS of high purity (product of Waters Associates Co., USA) with  $\bar{M}_w = 867\,000$  and  $\bar{M}_n = 773\,000$ ; atactic PMMA (product of suspension polymerization supplied by Miss N. Averbakh, Dzerzhinsk) with the 'viscosity-average' molecular weight (chloroform,  $25^\circ\text{C}$ ) 590 000, which was obtained by a step-by-step precipitation fractionation in acetone-water and subsequent solvent evaporation; and commercial sample of PDMS (trademark SKT, supplied by Dr Yu. Godovsky, Moscow) with the viscosity molecular weight 237 000 purified by a double precipitation. It is pertinent to note that sudden quenching of PDMS in liquid nitrogen virtually excludes any possibility of its crystallization, so that it forms a glass below its glass transition temperature<sup>11</sup>. This means that all the data obtained in the present work refer to glassy polymers. Films from the above polymers were cast from 'good' solvents (chloroform, dichloroethane and benzene for PMMA, PS and PDMS respectively) on a substrate. All solvents used were carefully purified, dried and fractionally distilled according to standard methods<sup>12</sup>. To insure the homogeneous distribution of impurity molecules in the solution, an amount of anthracene corresponding to desired concentration in polymer was added to a solvent before a polymer. The polymer concentration in solution was always 0.2 g/100 ml. Polymer films were formed at room temperature on the substrates and then dried in a vacuum oven to a constant weight. The thickness of the polymer films on the substrates remained constant, while the thickness of the layer from which the information was obtained was varied by changing the concentration of impure probe molecules in the range from  $10^{-2}$  to  $10^{-4}$  g/g. This method allowed us to follow the packing density change in the polymer matrix at different distances from the substrate, since all other conditions being equal, the higher the concentration of probe molecules in a matrix, the lower the depth of penetration of exciting radiation into the polymer surface layers. Hence, we obtain information on the den-

sity of an environmental phase of impurity molecules which refers only to those polymer layers which are in the immediate vicinity of a solid surface. On the other hand, when the probe molecules concentration is low, the radiation penetrates to greater depth (Lambert-Beer law), and we obtain information on the density of the medium in the more distant layers, the thickness of which is greater, the lower the concentration of impurity molecules in a polymer. Using eight different anthracene concentrations (see Figure 1) we calculated from a knowledge of the absorptive characteristics of anthracene<sup>13</sup>, the dependence of an 'apparent' polymer layer thickness on impurity concentration. The experimental error (i.e. resolution of an adjacent weak band on the wing of a principal luminescence band) is about 10%, and therefore our calculations were limited to those thicknesses corresponding to a 90% absorption at a given concentration. Noticeable differences between impurity molecules spectra in surface layers and in the bulk or in the loosely packed regions would imply that the former might be superimposed on the latter. This effect, however, should not be taken into account because transition from higher concentrations ( $10^{-2}$  g/g) to the lower ones is accompanied by a rather large decrease of relative intensity of probe molecules in the surface layers, and will not exceed about 10% at a concentration of  $10^{-3}$  (10% on the band wing will be close to the experimental accuracy limit), while at a concentration of  $10^{-4}$  g/g it will drop to only 1% with respect to the overall intensity of anthracene spectra.

## RESULTS AND DISCUSSION

The observed changes in the position of fluorescence spectra of probe molecules at different concentrations of the latter are shown in Figure 1. The ordinate shows the values of the ratio  $\rho_{\text{boundary}}/\rho_{\text{bulk}}$  (in %) calculated from the experimental values of spectral shifts of impurity molecules and the abscissa  $\log C$  from which the thickness of the surface layer was calculated.

It can be seen that increase of packing density of macromolecules in the immediate vicinity of the solid surface is a common feature for all polymers and substrates used. Since this effect is observed both for high energy, as well as low energy solid surfaces, it seems reasonable to propose that the orientation of macromolecules under the influence of the solid is dominating<sup>14</sup>. The corresponding packing density increment for this surface layer with respect to the bulk polymer for the three polymers amounts to 3 to 5%. Comparison of the influence of high energy and low energy substrates on the packing density of macromolecules in the surface layers shows that the difference was most pronounced for PMMA, which has a high CED value ( $132 \text{ cal/cm}^3$ ) and rather stiff chain ( $\sigma = 2.14$ ), somewhat less for PS which has similar chain stiffness but lower CED, whereas for PDMS which possesses the lowest values of  $\sigma$  and CED, the nature of the substrate plays a rather minor role. This comparison alone shows that the mode of molecular packing in the polymer boundary layers depends significantly on values of  $\sigma$  and CED. Moreover, the whole spectrum of changes of packing density (i.e., quantitative differences between packing densities in boundary layers and in the bulk, thickness of the layer where structural rearrangement due to the solid surface effect is still observed, and differences between effects of a high energy and low energy solids, etc.) was also most noticeable for PMMA with the high CED and  $\sigma$ , while it was the least for PDMS with



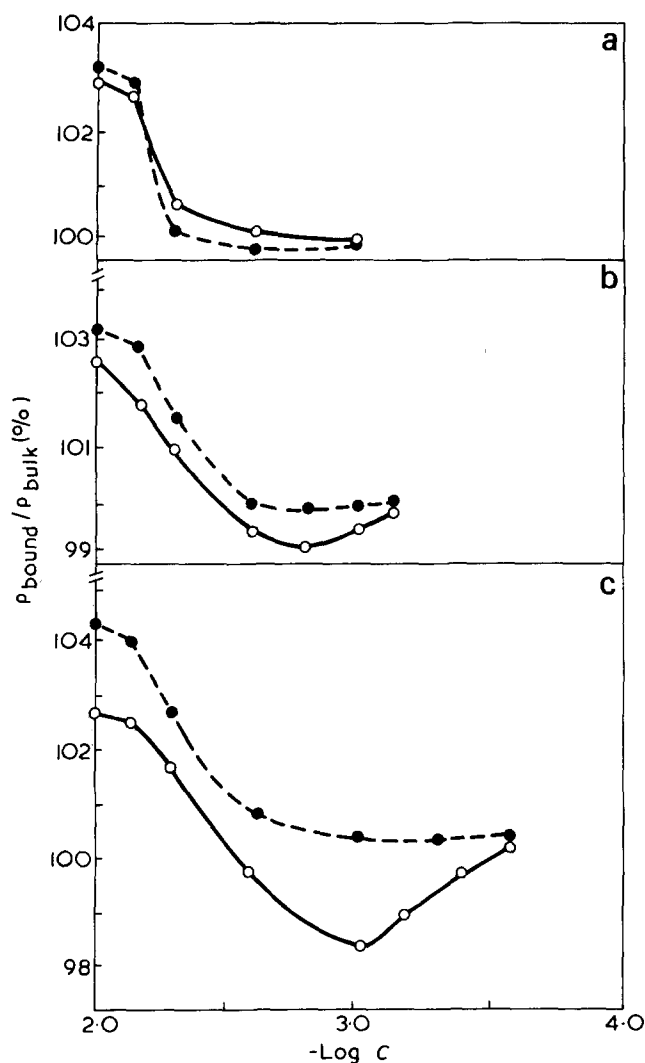


Figure 1 Change of packing density of macromolecules in boundary layers as function of the distance from the polymer—solid interface. (a) PDMS; (b) PS; (c) PMMA; —, boundary layers on fused silica; ---, those on Teflon

minimum values of  $CED$  and  $\sigma$ , PS exhibiting an intermediate effect. Structural rearrangement in the surface layers of films cast on Teflon was limited to formation of a densified surface layer with thicknesses of 2 to 3  $\mu\text{m}$  for PDMS and 3 to 4  $\mu\text{m}$  for PS and PMMA. In the more remote regions for the most flexible polymer (PDMS) the orienting effect of both high energy and low energy substrates virtually disappears and the packing density at distances of more than 3  $\mu\text{m}$  from the solid corresponds to that for a bulk polymer. In the case of PMMA and PS the structure of the layer formed on the high energy substrate (fused silica) is rather complex: here the regions in the immediate vicinity of interface that show an enhanced packing density are followed presumably by regions where packing density is close to that in the bulk ('transient' layers), after which packing of macromolecules becomes looser than in the bulk ('loosely-packed' regions). The thickness

of the boundary layers on the high energy substrate where the change of molecular packing density compared to that of the bulk phase is still observed, was estimated as 30  $\mu\text{m}$  for PS and 60  $\mu\text{m}$  for PMMA.

## CONCLUSIONS

The results indicate that the surface layers have a complex structure. The layer nearest to the solid exhibits enhanced packing density of macromolecules as compared with the bulk, and this can be tentatively attributed to the orienting effect of the solid surface. At larger distances from the solid the orientation induced by a substrate surface greatly weakens, especially in the case of low energy solids and/or polymers with high chain flexibility and low cohesion energy density, the effect being more pronounced the lower the flexibility parameter,  $\sigma$ . For polymers with stiffer chains and stronger interactions with a substrate, however, such structural changes are far more evident. In this case and for films cast on a high energy substrate the 'transient' layer is followed by a 'loosely-packed' region with the packing density lower than that for bulk polymer. This effect is observable in the more remote regions, the higher the  $CED$  of the polymer.

## ACKNOWLEDGEMENTS

We wish to express our gratitude to Miss N. Averbakh and Dr Yu. Godovsky for the gift of PMMA and PDMS samples used in the present study.

## REFERENCES

- 1 Lipatov, Yu. S. 'Physical Chemistry of Filled Polymers', Naukova Dumka, Kiev, 1967 (in Russian)
- 2 Lipatov, Yu. S. and Privalko, V. P. *Vysokomol. Soedin. (B)* 1973, 15, 749
- 3 Lipatov, Yu. S. and Privalko, V. P. *Vysokomol. Soedin. (A)* 1972, 14, 1643
- 4 Kwei, T. K. and Kumins, C. A. *J. Appl. Polym. Sci.* 1964, 8, 1483
- 5 Nesterov, A. E. and Lipatov, Yu. S. *Vysokomol. Soedin. (A)* 1973, 15, 2601
- 6 Kurata, M. and Stockmayer, W. H. *Fortschr. Hochpolym. Forsch.* 1963, 3, 196
- 7 Moysya, E. G. and Egorov, Yu. P. *Zh. Prikl. Spektrosk.* 1964, 1, 363
- 8 Egorov, Yu. P., Moysya, E. G. and Ar'ev, I. A. *Teor. Eksp. Khim.* 1967, 3, 772
- 9 Egorov, Yu. P. and Moysya, E. G. *J. Polym. Sci. (C)* 1967, 16, 2031
- 10 Moysya, E. G. and Egorov, Yu. P. *Teor. Eksp. Khim.* 1967, 3, 131
- 11 Godovsky, Yu. K., Levin, V. Yu., Slonimsky, G. L., Zhdanov, A. A. and Andrianov, K. A. *Vysokomol. Soedin. (A)* 1969, 11, 2444
- 12 'Techniques of Organic Chemistry', (Ed. A. Weissberger), Interscience, New York, 1955, Vol 7
- 13 Brodin, M. S. and Marisova, S. V. *Opt. Spektrosk.* 1965, 19, 235; Anri, V. *Trans. Gos. Optich. Inst.* 1919, 1, 27
- 14 Kwei, T. K. *J. Polym. Sci. (A)* 1965, 3, 3329

# Effect of pressure on the formation of poly(methyl methacrylate) glasses

Colin Price

Department of Chemistry, University of Manchester, Manchester M13 9PL, UK

(Received 8 December 1974)

Poly(methyl methacrylate) (PMMA) glasses were formed by cooling from the fluid state at constant pressures in the range 0.1–295 MN/m<sup>2</sup> and then decompressing at 20°C. The densities of the glasses determined at 30°C and atmospheric pressure were found to increase with increasing cooling pressure; for the highest cooling pressure investigated the percentage densification was 1.43. Heats of solution of the PMMA glasses in toluene were measured at 30°C using a Calvet microcalorimeter. The results showed that for cooling pressures up to 70 MN/m<sup>2</sup> the enthalpy of the glasses remained approximately constant, but increased progressively over the upper part of the range covered. The results for PMMA glasses were compared quantitatively with results obtained earlier for polystyrene glasses. Using hole energies determined by Smith and assuming that rotational isomerism became frozen in at the glass transition, conformational contributions of 0.13 and 0.07 J g<sup>-1</sup> K<sup>-1</sup> were calculated for PMMA and polystyrene respectively.

## INTRODUCTION

Tammann and Jenckel<sup>1</sup> showed that formation of organic glasses by cooling from the fluid state at elevated pressures leads to samples which are more dense (at say 20°C and 0.1 MN/m<sup>2</sup>) than those formed by cooling at atmospheric pressure. Some years later Shishkin<sup>2</sup> carried out a lengthy investigation of the densification process for a range of glass forming substances including poly(methyl methacrylate), polystyrene, phenolphthalein and boron trioxide. From the results it was possible to conclude that densification was a general phenomenon for glass forming substances and that it was not merely an artifact associated with the method of transmitting the pressure. Shishkin's interpretation of the effect was that the substances had been artificially moved down their supercooled fluid curves and therefore were in a state closer to thermodynamic equilibrium than glasses formed by conventional cooling methods.

Renewed attention has been given in recent years to the effect of conditions of formation on the properties of organic glasses and in particular of the effect of pressure<sup>3–7</sup>. A thermodynamic analysis carried out by Gee<sup>6</sup> for temperatures and pressures up to 126°C and 125 MN/m<sup>2</sup> respectively indicated that densification of a polystyrene sample by means of a temperature/pressure cycle had very little influence on the enthalpy of the sample as determined at 20°C and atmospheric pressure. Calorimetric studies<sup>8–10</sup> on polystyrene glasses confirmed this somewhat surprising result and further showed that if higher pressures and temperatures were used in the cycle the enthalpy actually increased with densification.

In the present study an investigation is reported of the effect of densification on the enthalpy of poly(methyl methacrylate) glasses and the results are compared with those obtained earlier for polystyrene.

## EXPERIMENTAL

### *Poly(methyl methacrylate) (PMMA)*

The polymer was prepared by free-radical polymerization and separated into three fractions by liquid–liquid

separation using benzene/iso-octane as the solvent/non-solvent mixture. The investigation was carried out on the middle fraction; the weight-average molecular weight of this fraction determined by light scattering was 180 000, and the  $\bar{M}_w/\bar{M}_n$  from gel permeation chromatography was 1.6. The material was compression moulded into sheets ~3 mm in thickness. Residual water was removed by maintaining the samples at a temperature of 112°C for several days. Until required for study the sheets were stored in a desiccator at room temperature.

### *High-pressure equipment*

A pressurized reservoir fed oil into the low-pressure end of a high compression pump. The pump, which was an air-driven reciprocating pump manufactured by Pressure Products Inc., could generate pressures up to 1000 MN/m<sup>2</sup> and these were transmitted to a pressure vessel containing the sample using a hydrocarbon oil as the hydrostatic fluid. Pressures were measured by means of a calibrated Astra pressure gauge. The dimensions of the internal cylindrical cavity of the pressure vessel were 1.9 cm (diam.) and 15.2 cm (length). Inside the pressure vessel, samples (pieces cut from the sheets) were kept within a stainless-steel container filled with mercury; the mercury transmitted the hydrostatic pressure to the samples but prevented any contact of the samples with the oil. An electrically heated jacket permitted the pressure vessel to be thermostated to ±0.2°C. An outer water jacket facilitated cooling at lower temperatures. Temperatures were measured using thermocouples inserted into the base of the vessel.

### *Densification procedure*

The polymer was heated at a constant pressure to a temperature  $T_x$  above the ordinary glass transition temperature (105°C). The pressure was then built up over a period of 15 min to a value  $P_a$  which was insufficient to bring about glass formation at  $T_x$ . Maintaining the pressure constant the system was then cooled down at ~1 K/min to 20°C. At this stage the applied pressure was released and the polymer was recovered and stored in a desiccator at -5°C. This

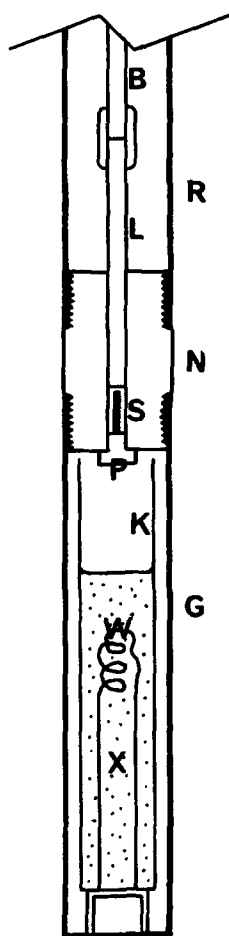


Figure 1 Experimental assembly of the microcalorimeter cell

procedure was repeated for different values of  $P_a$  up to  $295 \text{ MN/m}^2$ . (The constant pressure used in the initial heating part of the cycle was  $\sim P_a/3$ .) The densities of the glasses were determined by a flotation method at  $30^\circ\text{C}$  using the mixture of non-solvents utilized by Kimmel and Uhlmann<sup>11</sup>. The observed percentage densifications were checked dilatometrically for the glasses to be used later in the heat of solution studies. In this procedure mercury was used as the dilatometric fluid, and the change in volume of the sample brought about by annealing at  $115^\circ\text{C}$  overnight was determined at  $30^\circ\text{C}$ .

#### Microcalorimetry

A detailed description of the theory, construction, calibration and operation of the Calvet microcalorimeter may be found elsewhere<sup>12</sup>. Briefly the instrument consisted of an aluminium heat sink containing two cavities into which fitted twin cylindrical cells (referred to as 'laboratory' and 'reference' cells). The twin cells, 1.7 cm (diam.) and 8.5 cm (length), were constructed of stainless steel and were held on Teflon tubes (R) via screw threaded Teflon plugs (N) (see Figure 1). The temperature of the aluminium block was controlled to  $\pm 0.001 \text{ K}$ . In each cavity a thermopile (496 copper/constantan thermocouples) was interposed between cell and metallic block. Either a quarter or three-quarters of the thermocouples in the pile surrounding the 'laboratory' cell could be used to generate the compensating Peltier effect. The remaining thermocouples were connected in opposition to their counterparts surrounding the 'reference' cell, and the net output from these fed to a

recorder assembly (Sefram Verispot galvanometer, projection lantern, and photodyne spot-follower).

During the course of an experiment the recorder deflection  $\Delta$  was measured as a function of time. The thermal power,  $W$ , developed in the 'laboratory' cell (relative to the 'reference' cell) at time  $t$  was given by

$$W = (p/g)\Delta + \tau(p/g)(d\Delta/dt) + Pi(1 - iI^{-1}) \quad (1)$$

where  $(p/g)$ ,  $\tau$ ,  $P$  and  $I$  are calibration constants and  $i$  is the applied Peltier current. Thus the quantity of heat emitted by the cell contents between times  $t_1$  and  $t_2$  was given by:

$$q = (p/g) \int_{t_1}^{t_2} \Delta dt + \tau(p/g) \int_{\Delta_1}^{\Delta_2} d\Delta + \sum_{j=1}^{j=n} Pi_j(1 - i_j I^{-1})(t)_j \quad (2)$$

In the heat of solution measurements, the second term on the righthand side of equation (2) was zero, since experiments were started and ended on the same base line (i.e.  $\Delta_1 = \Delta_2 = 0$ ). The first term was determined from the area under the recorder curve and the third term from the times  $(t)_j$  for which each Peltier current  $i_j$  was applied.

The experimental assembly within the 'laboratory' cell (G) is shown schematically in Figure 1. In a mixing experiment the glass rod (L) was depressed by means of brass push rod (B) attached to a microsyringe head until the Teflon stopper (P) was forced out of the roof of the cell. The sample (S) then dropped into the solvent (X), toluene, contained in the inner glass cell (K). To facilitate mixing the sample was prevented from falling straight to the bottom of the cell by means of a copper wire (W). Forcing out the Teflon stopper inevitably generated a small quantity of heat near the roof of the cell; it was possible to compensate for this small effect by setting up a reference system in which the sample was replaced by a piece of Pyrex glass.

Each experimental run was conducted as follows: the 'laboratory' and 'reference' cells were first loaded and inserted in position by means of the Teflon tubes (R). When the base-line had stabilized, the two push rods were screwed down simultaneously by turning each micrometer screw approximately six turns. During the mixing process the deflection of the recorder was kept as small as possible by means of the Peltier effect; normally, it was possible to compensate for about 90% of the total heat output. The complete mixing experiment usually took about 4 h.

#### RESULTS AND DISCUSSION

In Figure 2 the percentage density increase of the PMMA at 1 atm pressure and  $30^\circ\text{C}$  is plotted against the pressure ( $P_a$ ) applied during the cooling part of the temperature/pressure cycle. The density of a PMMA glass formed by cooling from  $120^\circ\text{C}$  under 1 atm pressure at a rate of 1 K/min was taken as the reference ( $\rho = 1.184_0$ ). As observed previously for polymeric glasses<sup>2,5,9</sup>, the densification produced by a given pressure increment falls off with increasing pressure. For the highest cooling pressure investigated,  $P_a = 295 \text{ MN/m}^2$ , the percentage densification was 1.43. Allowing for the somewhat different molecular weight characteristics of the samples, the percentage densifications obtained in the present study are in fair agreement with those obtained by Shishkin for PMMA<sup>2</sup>.

It has been argued<sup>13,14</sup> that if a single ordering parameter was sufficient to describe the excess thermodynamic pro-

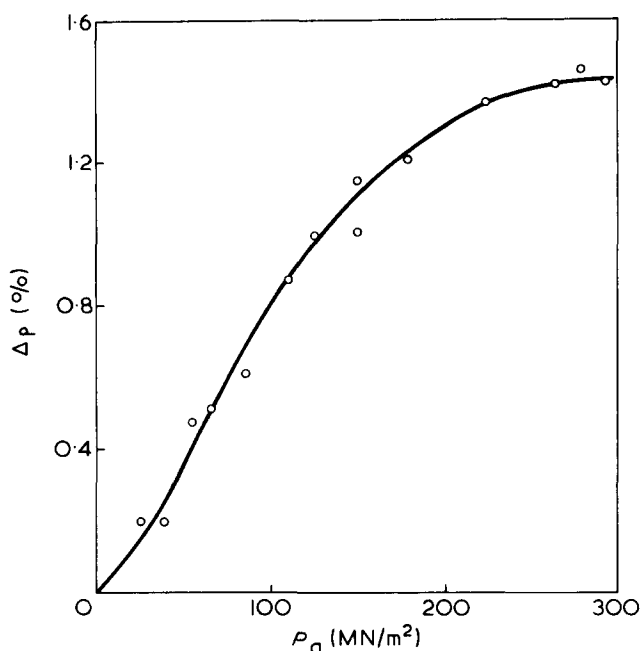


Figure 2 Percentage increase in density of PMMA glasses determined at 30°C and atmospheric pressure as a function of the pressure applied during cooling from the fluid state

properties of the fluid state over those of the glassy state then the following relationships would hold:

$$dT_g/dP = \Delta K/\Delta a \quad (3)$$

$$dT_g/dP = TV\Delta a/\Delta C_p \quad (4)$$

where  $\Delta K$ ,  $\Delta a$  and  $\Delta C_p$  are the discontinuities in the compressibility, the thermal expansion coefficient and the heat capacity at the transition, and  $dT_g/dP$  is the dependence of the glass transition temperature on pressure. Even if this description does not hold, Goldstein<sup>4</sup> has suggested that if the transition occurs at a constant value of the excess volume  $V_e$ , equation (3) should apply, whilst if the transition occurs at a constant value of the excess entropy or the excess enthalpy, equation (4) should apply. From assessments<sup>4,6</sup> of the available data it appears that  $dT_g/dP < \Delta K/\Delta a$ , whilst  $dT_g/dP \approx TV\Delta a/\Delta C_p$ . The densification phenomenon can be accounted for on a thermodynamic basis in terms of the inequality attached to the first of these relationships. Following the line of argument put forward by Beuche<sup>3</sup> let us consider the two processes (a) and (b) shown in Table 1.

The fractional changes in volume which occur during the processes are

$$\Delta V_a/V = a_f[(T_g)_p - (T_g)_0] + K_g P \quad (5)$$

and

$$\Delta V_b/V = K_f P + a_g[(T_g)_p - (T_g)_0] \quad (6)$$

where  $a_f$  and  $a_g$  are the coefficients of expansion and  $K_f$  and  $K_g$  the compressibilities of the polymer in the fluid and glassy states respectively. Hence,

$$(\Delta V_a - \Delta V_b)/V = \Delta a[(T_g)_p - (T_g)_0] - \Delta K P \quad (7)$$

Since it has been shown that  $\Delta a[(T_g)_p - (T_g)_0] < \Delta K P$  the sample produced by process (a) should be denser than that

produced by process (b). It should be noted, however, that the validity of this simple argument rests on the assumption that it is possible to ignore relaxation effects (i.e. it is possible to establish time-independent values of  $a_g$  and  $K_g$  for all the conditions of interest). If further we assume that densification has no influence on the values of  $a_g$  and  $K_g$ , equation (7) will provide us with a rough estimate of the percentage densification expected from the temperature/pressure cycle used in the present study. Setting<sup>6</sup>  $\Delta K = 1.23 \times 10^{-4} \text{ MN}^{-1} \text{ m}^2$ ,  $\Delta a = 2.95 \times 10^{-4} \text{ K}^{-1}$  and  $dT_g/dP = 0.23 \text{ K MN}^{-1} \text{ m}^2$  we obtain  $(\Delta V_a - \Delta V_b)/V = -1.63 \times 10^{-2}$  for glasses formed by cooling at  $P = 295 \text{ MN/m}^2$  which corresponds to a percentage densification of 1.65 (cf 1.43, Figure 2). The discrepancy between the calculated and observed values is not serious in view of the assumptions made; better agreement would be obtained by taking account of the temperature and pressure dependence of  $\Delta a$  and  $\Delta K$ , but this refinement was not felt worthwhile in view of the general uncertainty posed by relaxation effects.

Heats of solutions  $\Delta H_s$  of the PMMA glasses in the solvent, toluene, at  $P = 1 \text{ atm}$  and  $T = 30^\circ \text{C}$  are recorded in Table 2; the final concentration of each solution was  $0.01 \text{ g/cm}^3$ . For the purpose of discussion the dissolution process can be considered to take place in two stages:

glass  $\rightarrow$  hypothetical fluid

hypothetical fluid + solvent  $\rightarrow$  solution

Hence we have  $\Delta H_s = (H_f - H_g) + \Delta H_{sf}$ , where  $H_g$  and  $H_f$  are the enthalpies of the glass and hypothetical fluid respectively and  $\Delta H_{sf}$  is the enthalpy change on dissolution of

Table 1

Process (a)			Process (b)		
State	Pressure	Temperature	State	Pressure	Temperature
fluid	0	$(T_g)_0$	fluid	0	$(T_g)_0$
↓			↓		
fluid	0	$(T_g)_p$	glass	$P$	$(T_g)_0$
↓			↓		
glass	$P$	$(T_g)_p$	glass	$P$	$(T_g)_p$

$(T_g)_0$  and  $(T_g)_p$  are the glass transition temperatures of the polymer at pressures 0 and  $P$  respectively for the chosen experimental time-scale

Table 2 Dependence of the density and enthalpy of poly(methyl methacrylate) glasses on the pressure applied during cooling from the fluid state

Pressure during cooling (MN/m <sup>2</sup> )	Properties at 30°C and atmospheric pressure		
	Density (g/cm <sup>3</sup> )	$-\Delta H_s$ (J/g)	$\Delta H_d$ (J/g)
—	1.184 <sub>0</sub>	31.9	(0)
25	1.186 <sub>4</sub>	31.9	0.0
40	1.186 <sub>4</sub>	32.0	0.1
55	1.189 <sub>7</sub>	31.8	-0.1
65	1.190 <sub>0</sub>	32.1	0.2
110	1.194 <sub>3</sub>	32.6	0.7
150	1.195 <sub>8</sub>	33.1	1.2
180	1.198 <sub>2</sub>	33.8	1.9
225	1.200 <sub>2</sub>	34.3	2.4
280	1.201 <sub>3</sub>	35.2	3.3
295	1.200 <sub>9</sub>	35.7	3.8

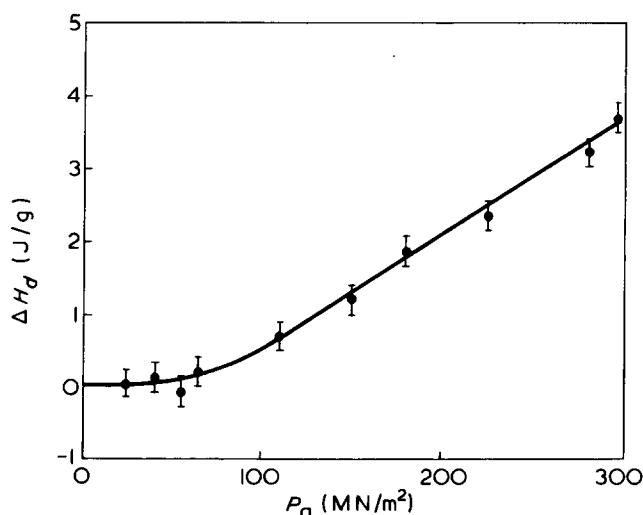


Figure 3 Dependence of the enthalpy of PMMA glasses on the pressure applied during cooling from the fluid state

the hypothetical fluid. The first contribution,  $(H_f - H_g)$ , is large and exothermic due in part to a substantial volume relaxation and is responsible for the large exothermic heat of solution on dissolution of the glass; the second contribution,  $\Delta H_{sf}$ , is much smaller than the first and may be slightly endothermic. The difference in enthalpy between any two glasses is obtained by taking the negative difference of their heats of solution. Relative enthalpies of densified PMMA glasses calculated in this way are given in Table 2; again a PMMA glass cooled from 120°C under 1 atm pressure at a rate of 1 K/min was taken as the reference material.

In Figure 3 the difference in enthalpy between densified and reference glasses ( $\Delta H_d$ ) is plotted against the pressure ( $P_d$ ) at which the densified glass was cooled from the fluid state. Over the lower part of the pressure range (up to 70 MN/m<sup>2</sup>) the enthalpy is seen to be approximately independent of volume. The result is similar to that first observed by Allen *et al.*<sup>8</sup> for polystyrene and later verified by Ichihara *et al.*<sup>10</sup>. With further increase in densification however there is a significant increase in enthalpy. A similar trend was observed by Price *et al.*<sup>9</sup> on studying polystyrene over an extended pressure range. In disagreement with the present results, Kimmel and Uhlmann<sup>11,15</sup> using a d.s.c. method found that the enthalpy of PMMA decreased on densification. Since the percentage densifications were very similar to those obtained in this work, it is difficult to account for the discrepancy. It may be associated in some way with the fact that they used a Bridgeman anvil device in their temperature/pressure cycles, whereas here hydrostatic pressures were used.

The calorimetric results obtained for polystyrene in previous studies and those reported for PMMA in this paper are inconsistent with the suggestion<sup>2</sup> that densified glasses are closer to thermodynamic equilibrium than ordinary glasses, since if a substance was artificially moved down its supercooled-fluid curve its enthalpy would be expected to fall. The results imply that for pressures up to 70 MN/m<sup>2</sup>,  $T_g$  occurs at an approximately constant value of the excess enthalpy, but that on going to higher pressures  $T_g$  occurs at progressively increasing values of this function.

Let us now consider the factors which will govern the relative enthalpies of the glasses. Within the framework of free-volume theories the total volume of a liquid is considered to be divided into a part 'occupied' by the molecular segments and a 'free volume' which is shared communal-

ly and distributed in the form of disconnected holes<sup>16-18</sup>. Each hole is characterized by its molar volume,  $v_h$ , and the molar excess energy,  $e_h$ ; for PMMA and polystyrene,  $e_h/v_h = 400$  and 350 J/cm<sup>3</sup> respectively<sup>19</sup>. In a liquid the holes and phonons associated with the liquid matrix are in thermal equilibrium. A glass may be distinguished from a liquid in that the free volume is independent of temperature, and continual redistribution of free volume no longer occurs. If the densification phenomenon observed in the present studies was associated solely with a reduction of frozen-in free volume, the enthalpy of a densified glass would be lower than that of the reference glass by  $\Delta H_v \approx (e_h/v_h)(\rho_r^{-1} - \rho_d^{-1})$ . Since as shown in Figure 3 the enthalpy does not fall in this way, there must be some compensation factor involved,  $\Delta H_c$ , having a value of  $\Delta H_d + \Delta H_v$ . As suggested previously<sup>6,8</sup> the conformational energy of the chains is a possible source of this compensation factor. Rotational isomerism will be frozen-in at a temperature in the region of  $T_g$ , so that the magnitude of the compensation factor will be a function of the temperature of glass formation. In Figure 4,  $\Delta H_c$  is plotted against  $[(T_g)_p - (T_g)_0]$  for PMMA and polystyrene; the results for polystyrene were determined from data given in ref 9. In calculating the effect of pressure on  $T_g$ ,  $dT_g/dP$  was taken as 0.23 K MN<sup>-1</sup> m<sup>2</sup> for PMMA and 0.31 K MN<sup>-1</sup> m<sup>2</sup> for polystyrene. Using the method of least squares to establish the best linear plots passing through the origin, the conformational contributions of PMMA and polystyrene were calculated to be 0.129 and 0.071 J g<sup>-1</sup> K<sup>-1</sup> respectively.

It is possible, however, that 'internal strain' within the densified glass may be responsible for part of the compensation factor. On removing the pressure at the end of the cycle the volume will increase in a manner which is consistent with the minimizing of the free energy of the system within the limits imposed by the restricted translational motion of the molecules. Depending on the volume change involved, some 'internal strain' such as distortion of main-chain bond angles could be introduced during this process. This would make a positive contribution to the

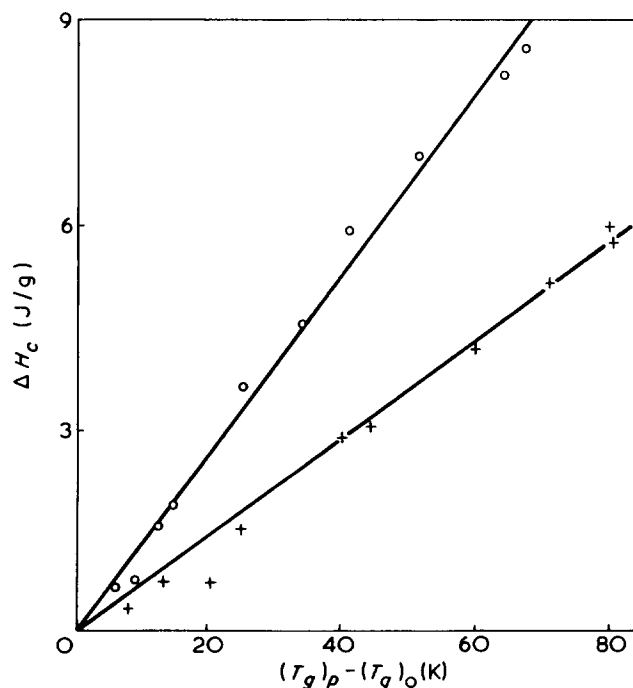


Figure 4 Dependence of the compensation enthalpy  $\Delta H_c$  of PMMA (○) and of polystyrene (+) on  $(T_g)_p - (T_g)_0$

compensation energy and would lead to a lower estimated value for the conformational contribution arising from freezing-in of rotational isomerism.

#### REFERENCES

- 1 Tammann, G. and Jenckel, E. *Z. Anorg-Allgem. Chem.* 1929, **184**, 416
- 2 Shishkin, N. I. *Sov. Phys. (Solid State)* 1960, **2**, 322
- 3 Beuche, F. *J. Chem. Phys.* 1962, **36**, 2940
- 4 Goldstein, M. *J. Chem. Phys.* 1963, **39**, 3369
- 5 Breuer, H. and Rehage, G. *Kolloid-Z. Z. Polym.* 1967, **216**, 159; Rehage, G. and Borchart, W. in 'The Physics of Glassy Polymers', (Ed. by R. N. Haward), Applied Science, London, 1973, Ch 1, pp 54–107
- 6 Gee, G. *Polymer* 1966, **7**, 177
- 7 Nose, T. *Polym. J.* 1971, **4**, 445
- 8 Allen, G., Ayerst, R. C., Cleveland, J. R., Gee, G. and Price, C. *J. Polym. Sci. (C)* 1968, **23**, 127
- 9 Price, C., Williams, R. C. and Ayerst, R. C. in 'Amorphous Materials', (Ed. by R. N. Douglas and B. Ellis), Wiley-Interscience, London, 1972, Ch 12, pp 117–124
- 10 Ichihara, S., Komatsu, A. and Hata, T. *Polym. J.* 1971, **2**, 664
- 11 Kimmel, R. M. and Uhlmann, D. R. *J. Appl. Phys.* 1970, **41**, 2917
- 12 Calvet, E. and Prat, H. 'Recent Progress in Microcalorimetry', (Ed. by H. A. Skinner) Pergamon Press, New York, 1963
- 13 Prigogine, I. and Defay, R. 'Chemical Thermodynamics', (Trans. D. H. Everett), John Wiley, New York, 1962
- 14 Davies, R. O. and Jones, G. O. *Proc. R. Soc. (A)* 1953, **26**, 217
- 15 Kimmel, R. M. and Uhlmann, D. R. *J. Appl. Phys.* 1971, **42**, 4917
- 16 Hirai, N. and Eyring, H. *J. Appl. Phys.* 1958, **29**, 810
- 17 Hirai, N. and Eyring, H. *J. Polym. Sci.* 1959, **37**, 51
- 18 Wunderlich, B. *J. Phys. Chem.* 1960, **64**, 1052
- 19 Smith, P. R. *J. Polym. Sci. (A-2)* 1970, **8**, 1337

# Catalytic action of metallic salts in autoxidation and polymerization: 11. Polymerization of methacrylic acid esters with sodium hexanitrocobaltate in methanol–water

Zenjiro Osawa, Hitoshi Kanazawa, Yuji Kuwako and Yoshitaka Ogiwara

Department of Polymer Chemistry, Faculty of Engineering, Gunma University, Kiryu City, Gunma 376, Japan

(Received 26 March 1973; revised 2 September 1974)

The polymerization of a series of methacrylic acid esters (methyl, ethyl, isopropyl and n-butyl) with sodium hexanitrocobaltate,  $\text{Na}_3[\text{Co}(\text{NO}_2)_6]$  was carried out in a methanol–water mixed solvent. The homogeneity of the polymerization system was dependent on the composition of the mixed solvent and greatly affected the rate of the polymerization. A maximum rate was obtained at approximately equimolar fractions of methanol and water in the polymerization of methyl methacrylate. The effect of bulkiness of ester groups on the polymerizability of each monomer was indistinguishable in the mixed solvent system. Kinetic study of the polymerization of methyl methacrylate in a mixed solvent of about an equimolar fraction of methanol and water gave the following polymerization equation:  $R_p = k [I]^{1/2} [M]^2$ , and an apparent activation energy of 10.6 kcal/mol. The copolymerization of methyl methacrylate and styrene with the initiator suggested that polymerization proceeded via a radical mechanism. The possibility of a certain interaction between initiator, solvent and monomer in the initial stage of the polymerization is discussed on the basis of the kinetic data, properties of oligomers of methyl methacrylate, spectroscopic and other data.

## INTRODUCTION

This paper discusses the polymerization of methacrylic acid esters (methyl, ethyl, isopropyl and n-butyl) with sodium hexanitrocobaltate,  $\text{Na}_3[\text{Co}(\text{NO}_2)_6]$ , in various alcohol–water mixed solvents and the initiation mechanism.

Extensive studies have been made on the vinyl polymerization of methyl methacrylate with metal salts or metal chelates<sup>1–9</sup>, and it has been reported that a few cobalt (III) complexes could initiate the polymerization of vinyl monomers in an aqueous medium<sup>10–14</sup>. In a previous paper<sup>15</sup> of this study we reported that sodium hexanitrocobaltate could initiate the polymerization of methyl methacrylate in mixed solvent of acetone and water. By further study we found that the same initiator could polymerize methyl methacrylate in a methanol–water mixed solvent much faster than in an acetone–water solvent. We have now carried out a kinetic study on the polymerization of methyl methacrylate with  $\text{Na}_3[\text{Co}(\text{NO}_2)_6]$  in about an equimolar fraction of water and methanol and here discuss the possibility of a certain interaction between initiator, solvent and monomer in the initial stage of the polymerization.

## EXPERIMENTAL

### Materials

Sodium hexanitrocobaltate  $\text{Na}_3[\text{Co}(\text{NO}_2)_6]$  was prepared according to a literature method<sup>16</sup>, from reagent grade sodium nitrite and cobalt nitrate  $\text{Co}(\text{NO}_3)_2 \cdot 6\text{H}_2\text{O}$ , and was identified by its infra-red spectra<sup>17</sup>. Purification of monomers and solvents was performed in the usual manner<sup>18</sup>.

### Polymerization

Kinetic studies were carried out in a simple dilatometer and rapid preparative polymerizations in a glass tube under nitrogen. The polymerization products were treated in the usual manner<sup>19</sup>. For the oligomeric materials, the contents of a glass tube were poured into a large amount of water and the precipitates were purified by precipitation from acetone into water. The polymerization conditions are shown in the Figure captions.

### Characterization of polymers and oligomers

Molecular weights of the polymers were measured viscometrically in benzene solution at 25°C with the aid of the intrinsic viscosity molecular weight relationship of Fox *et al.*<sup>20</sup>. Oligomers were characterized by i.r. spectral analysis, elemental analysis and determination of molecular weight by a vapour pressure method. Ultra-violet spectroscopic measurements were made with a Hitachi double beam type spectrometer.

## RESULTS AND DISCUSSION

### Dependence of conversion on solvent composition

The relationships between conversion of methacrylic acid ester monomers and molar fraction of water in alcohol–water mixed solvents are shown in *Figures 1* and *2*. As shown in *Figures 1* and *2*, homogeneity of the polymerization system at the initial stage is greatly affected by mole fractions of water and alcohols, and the conversion of each monomer is extremely dependent on the homogeneity of the system. In general, homogeneous systems give higher conversion than heterogeneous ones. The effect of bulki-

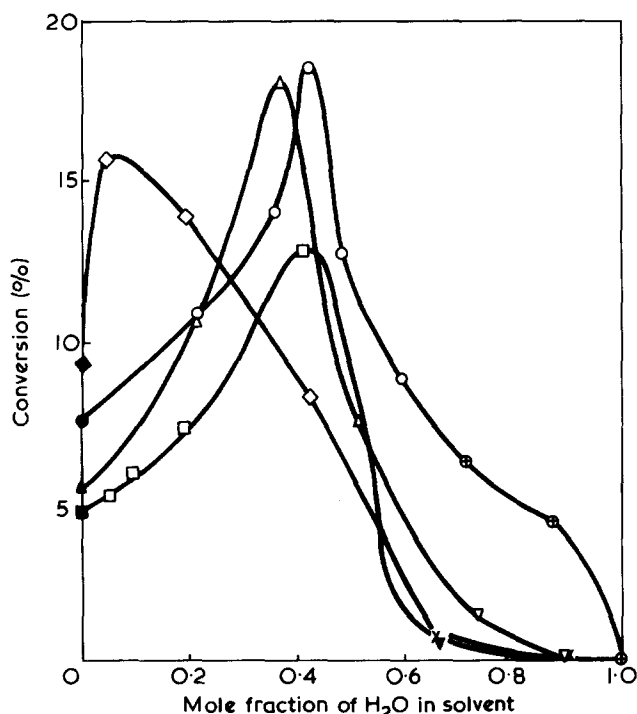


Figure 1 Conversion versus mole fraction of H<sub>2</sub>O in mixed solvent of methanol and water. Polymerization conditions: concentration of Na<sub>3</sub>[Co(NO<sub>2</sub>)<sub>6</sub>] = 8.25 × 10<sup>-4</sup> mol/l; [M] = 2.0 mol/l; time = 6 h; temperature = 50°C

Monomer	Initial state of system		
	Homogeneous	Two layers	Heterogeneous
Methyl methacrylate (MMA)	○	⊕	●
Ethyl methacrylate (EMA)	△	▽	▲
Isopropyl methacrylate (iso-PMA)	□	×	■
n-Butyl methacrylate (n-BMA)	◇	▼	◆

ness of the ester group on the polymerizability of each monomer is, therefore, indistinguishable in these mixed solvent systems. In the case of methyl methacrylate a maximum conversion is observed at about an equimolar fraction of water and methanol. The following kinetic study was, therefore, made in a mixed solvent of 0.49 mole fraction of water.

#### Kinetic study

The dependence of the polymerization rate,  $R_p$ , on the concentration of initiator and monomer was examined at very low conversion and in homogeneous solutions. Usually time-conversion curves were approximately linear for 50 min, and during this time the degree of polymerization was almost constant and no appreciable increase in the degree of polymerization was observed thereafter.

The overall rates of polymerization,  $R_p$ , were calculated from the initial linear time-conversion curves, and it was found that the rate was proportional to the square root of the initiator concentration and to the square of monomer concentration, respectively. The plots of the overall rate of polymerization obtained against the product of the square root of initiator concentration and the square of monomer concentration are clearly linear (see Figure 3). Accordingly, the polymerization rate equation can be expressed as follows:

$$R_p = k [I]^{1/2} [M]^2$$

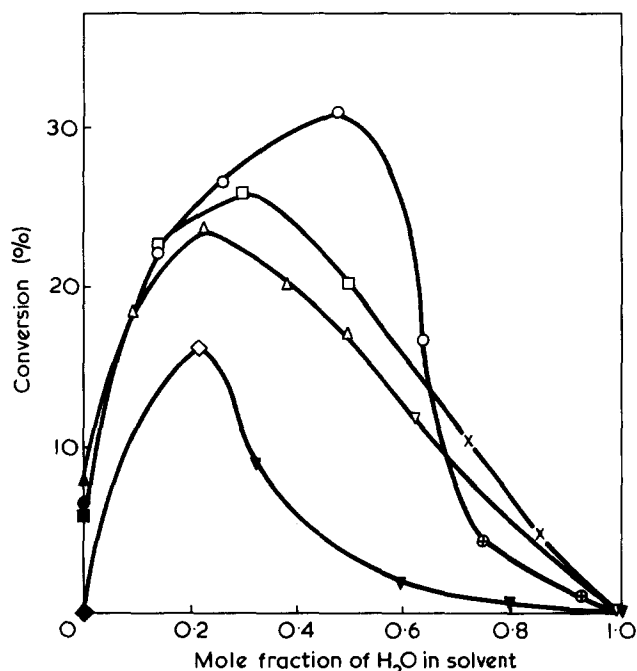


Figure 2 Conversion versus mole fraction of H<sub>2</sub>O in mixed solvent of various alcohols and water. Polymerization conditions: concentration of Na<sub>3</sub>[Co(NO<sub>2</sub>)<sub>6</sub>] = 8.25 × 10<sup>-4</sup> mol/l; [M] = 3.9 mol/l; time = 6 h; temperature = 50°C

Monomer	Solvent	Initial state of system		
		Homogeneous	Two layers	Heterogeneous
MMA	MeOH-H <sub>2</sub> O	○	⊕	●
EMA	EtOH-H <sub>2</sub> O	△	▽	▲
iso-PMA	iso-PrOH	□	×	■
n-BMA	n-BuOH	◇	▼	◆

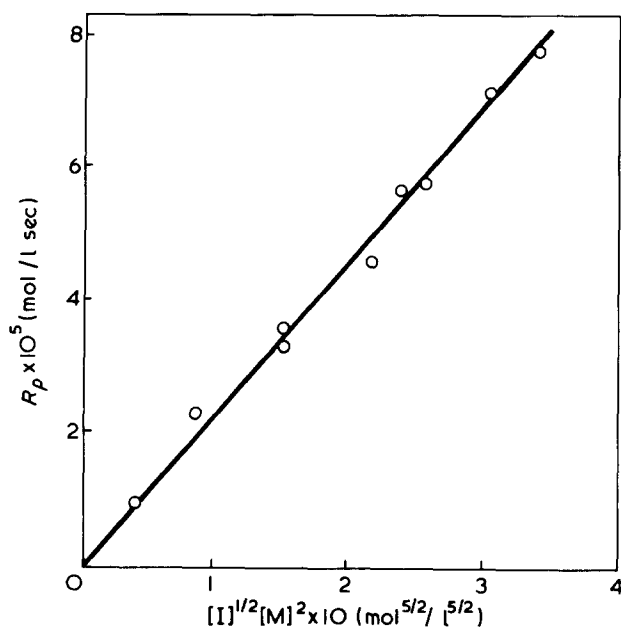


Figure 3 Plot of  $R_p$  against  $[I]^{1/2}[M]^2$ . Polymerization conditions for dependence on initiator concentration: [M] = 3.51 mol/l; [I] = 1.55 × 10<sup>-4</sup> to 7.74 × 10<sup>-4</sup> mol/l; total solvent = 10 ml (3 ml H<sub>2</sub>O and 7 ml MeOH); temperature = 50°C; for dependence on monomer concentration: [I] = 6.19 × 10<sup>-4</sup> mol/l; [M] = 1.17 to 3.51 mol/l; total solvent = 10 ml (3 ml H<sub>2</sub>O and 7 ml MeOH); temperature = 50°C



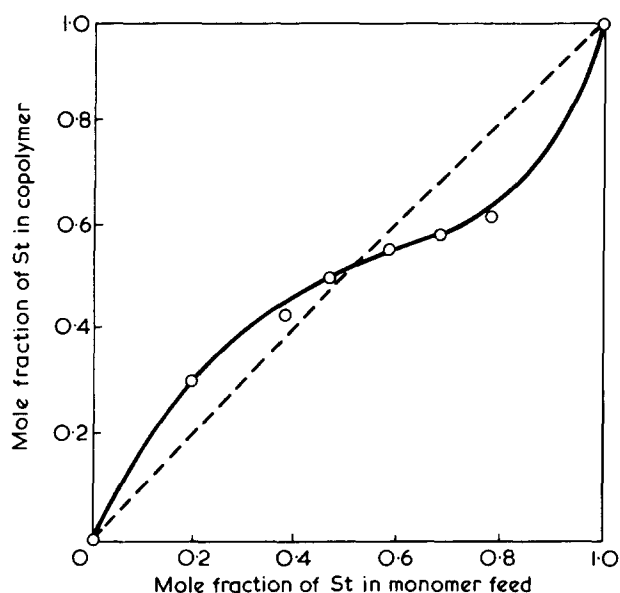


Figure 4 Radical copolymerization curve of methyl methacrylate with styrene. Polymerization conditions:  $[I] = 8.26 \times 10^{-4}$  mol/l; total monomer = 5 ml (MMA and St); solvent = 7 ml (2 ml H<sub>2</sub>O and 5 ml MeOH, corresponding to 0.47 fraction of water); time = 3 h; temperature = 50°C

The dependence of the polymerization rate on temperature was examined between 40° and 60°C. An Arrhenius plot was linear over the temperature range 40 to 60°C and gave an activation energy of 10.6 kcal/mol.

The degree of polymerization ranged from ~1400 to 5800 and decreased with increasing initiator concentration and increased with increasing monomer concentration.

In order to elucidate whether the polymerization proceeded via a radical mechanism, copolymerization of methyl methacrylate and styrene with Na<sub>3</sub>[Co(NO<sub>2</sub>)<sub>6</sub>] was carried out. The copolymerization curve shown in Figure 4 is apparently the same as that obtained by a conventional radical copolymerization. The polymerization of this system was also inhibited by conventional inhibitors such as hydroquinone and diphenylpicrylhydrazyl (DPPH). These results indicate that the polymerization proceeds via a radical mechanism.

Furthermore, we also confirmed that the overall rate of polymerization of methyl methacrylate with a conventional radical initiator, azobisisobutyronitrile (AIBN), in the same methanol–water mixed solvent was proportional to the first power of monomer concentration.

The dependence of the polymerization rate on the square of monomer concentration suggests the participation of monomer in the initiation reaction. In order to examine the initiation mechanism, oligomeric materials were prepared and were characterized by their molecular weight, i.r. spectra, and elemental analyses. The i.r. spectra of the oligomers and the polymers are shown in Figure 5 and clearly show the presence of nitro groups, namely two peaks at 1560 cm<sup>-1</sup> due to C–NO<sub>2</sub> and 1650 cm<sup>-1</sup> due to N–O, whereas those of the polymers indicate the presence of the nitrogen groups only in minor amounts. The nitrogen content of the oligomers was measured and compared with their average molecular weights determined by a vapour pressure method. The results obtained are summarized in Table 1. Since the nitrogen content of the oligomers observed was almost equal to that of the calculated one, the oligomers presumably contain two nitro groups at

both ends of the molecule. If the oligomers contain two nitro groups, possible termination reactions may be recombination of growing oligomer radicals themselves, recombination of chain radicals with primary radicals, and chain transfer of chain radicals to the initiator.

Baysal and Tobolsky<sup>22</sup> suggested a well known kinetic scheme for vinyl polymerization with an initiator, and proposed that the following equation could be used to estimate the chain transfer reaction in solution polymerization:

$$1/\bar{P}_n = C_M + C_I[I]/[M] + C_S[S]/[M] + R_p\delta^2/[M]^2$$

where  $\bar{P}_n$  = the number-average degree of polymerization,  $C_M$ ,  $C_I$ ,  $C_S$  = chain transfer constants for monomer, initiator, and solvent, respectively,  $[I]$ ,  $[M]$ ,  $[S]$  = concentrations of initiator, monomer, and solvent, respectively,  $R_p$  = overall rate of polymerization,  $\delta^2$  = a constant and equal to  $(2k_{td} + k_{tc})/k_p^2$ , and  $k_{td}$ ,  $k_{tc}$ ,  $k_p$  = rate constants of termination by disproportionation, termination by recombination and rate constant of propagation. Recently, Potnis and Deshpande<sup>23,24</sup> presented a comprehensive kinetic study of the polymerization of vinyl acetate using the Baysal and Tobolsky method. The same treatment was, therefore, made in order to examine the possibility of chain transfer reaction to initiator in this polymerization system. The relationship between  $1/\bar{P}_n$  and  $R_p/[M]^2$  is shown in Figure 6. From Figure 6,  $\delta^2$  was estimated to be  $0.57 \times 10^2$ . The relationship between  $(1/\bar{P}_n - R_p\delta^2/[M]^2)$  and  $[I]/[M]$  is shown in Figure 7. The slope of the linear curve shown in Figure 7 is almost zero ( $C_I = 0$ ). Therefore, the results indicate that no chain transfer to initiator is present in the polymerization system.

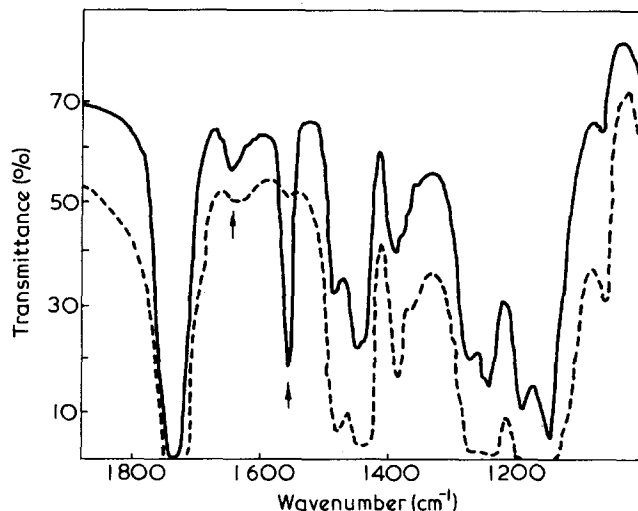


Figure 5 Infra-red spectra of polymers (---) and oligomers (—)

Table 1 Number-average molecular weight and nitrogen content of the oligomers

Expt. No.	$\bar{M}_n$	N content (%)	
		Obs.	Calc.*
1	1590	1.80	1.76
2	1540	1.83	1.82

\* Assumed that one oligomer molecule contains two NO<sub>2</sub> groups. Polymerization conditions:  $[I] = 2.45 \times 10^{-2}$  mol/l;  $[M] = 3.06$  mol/l; solvent = 7 ml (2 ml H<sub>2</sub>O and 5 ml MeOH); time = 30 min; temperature = 47°C (for exp.1), 40°C (for exp.2)

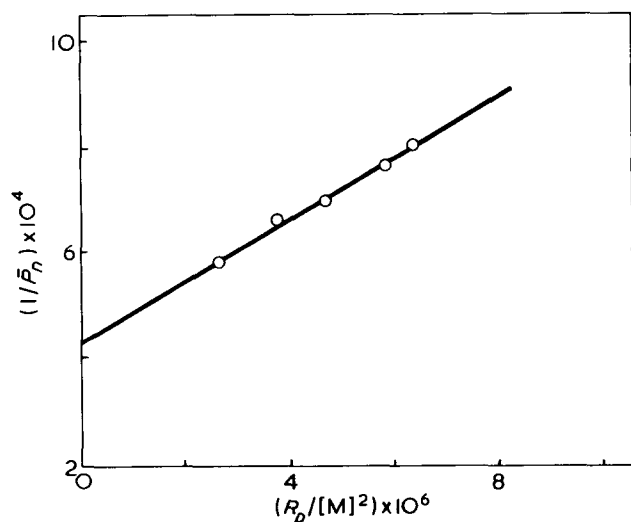


Figure 6 Relationship between  $1/\bar{P}_n$  and  $R_p/[M]^2$ . Polymerization conditions:  $[M] = 3.51$  mol/l;  $[I] = 1.55 \times 10^{-4}$  to  $7.74 \times 10^{-4}$  mol/l;  $[S] = 10.8$  mol/l; MeOH-H<sub>2</sub>O mixed solvent (0.49 molar fraction of water); time = 1 h; temperature = 50°C

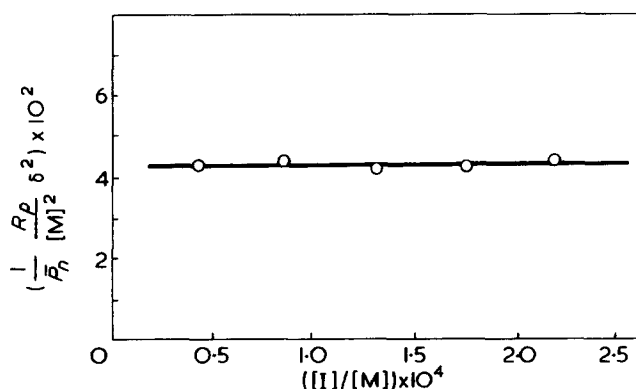


Figure 7 Relationship between  $(1/\bar{P}_n - R_p^2/[M]^2)$  and  $[I]/[M]$ . Polymerization conditions are the same as in Figure 6

The other two possibilities for termination are recombination of oligomer radicals themselves and recombination of oligomer radicals with primary radicals. However, it is well known that termination in methyl methacrylate polymerization is normally predominantly by disproportionation. Thus, the more probable termination to produce oligomers containing two NO<sub>2</sub> groups in one molecule seems to be recombination of chain radicals with primary radicals.

#### Spectrophotometry

The aforementioned dependence of the polymerization rate on the square of monomer concentration implies the participation of monomer in the initiation process. Spectroscopic measurements seem to give some information for the elucidation of the initiation mechanism. An aqueous solution of Na<sub>3</sub>[Co(NO<sub>2</sub>)<sub>6</sub>] shows four absorption peaks in the visible and u.v. regions, namely, 240, 280, 360 and 470 nm. Among them the absorption peak at 360 nm is the clearest and decays with slight blue shift. Based on these facts, the u.v. spectra of the initiator in water and in a methanol-water mixed solvent in the presence and absence of monomer were measured at 20° and 50°C. The decay of the absorption peak at 360 nm is shown in Figure 8. This apparently shows that the decay of the

absorption peak at 360 nm is fairly fast in water and the addition of methanol and monomer enhance further the rate of decay. Furthermore, the rate of decay of the absorption is substantially increased with the rise of temperature and at 50°C the peak at 360 nm becomes almost constant within 10 min. No evidence of the formation of a complex between initiator and monomer was observed by spectrophotometry. However, these results may indicate that the initiator changes to other active species by the partial replacement of ligand with solvent, and that the primary radicals may be generated by the interaction of the active species and monomer. In other words, the results suggest the presence of a certain interaction between initiator, solvent and monomer at the beginning of the polymerization.

To confirm the assumption of the interaction, the effect of standing time of the initiator in the mixed solvent on conversion was examined. After the addition of mixed solvent of methanol-water into a glass tube containing the initiator, the solution was kept at 50°C for various times and then polymerization was started by adding monomer. By the treatment of the initiator with solvent, the rate of polymerization was decreased remarkably. For example, after 1 h standing the rate of polymerization became almost half the rate observed when all components were added together, and after 24 hours standing no polymer was obtained, during 3.5 h polymerization. The kinetic treatment was, of course, made without prior standing of the initiator in solvent, and the rates of polymerization were calculated by the use of the initial linear time-conversion curves. Thus, the active species formed by the interaction of the initiator and solvent or monomer should be sufficiently unchanged to allow one to assume a stationary state in the polymerization system.

The results mentioned above may imply the presence of a certain interaction between initiator, solvent and monomer in the initial stage of the polymerization. However, the polymerization mechanism of the examined system is fairly complex and various elementary reactions may be considered.

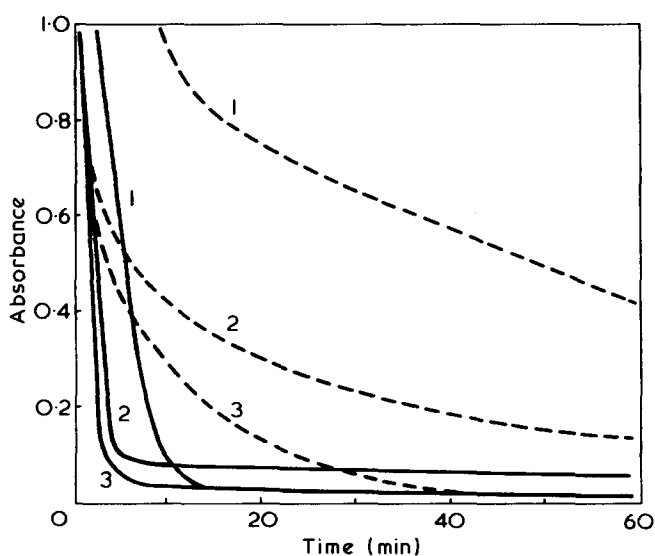


Figure 8 Decay of absorption intensity at 360 nm in various solutions. Concentration of Na<sub>3</sub>[Co(NO<sub>2</sub>)<sub>6</sub>] =  $1.44 \times 10^{-4}$  mol/l; ---, 20°C; —, 50°C. 1, H<sub>2</sub>O; 2, H<sub>2</sub>O-MeOH (0.49 mole fraction of water); 3, H<sub>2</sub>O-MeOH-MMA (0.49 mole fraction of water in solvent,  $[M] = 1.31 \times 10^{-1}$  mol/l)

#### ACKNOWLEDGEMENTS

Thanks are due to Professor C. Schuerch of the State University of New York, College of Environmental Science and Forestry for helpful suggestions and to the Ministry of Education, Japan for giving financial assistance in the form of a Science Research Fellowship to one of the authors (Z.O.).

#### REFERENCES

- 1 Otsu, T. 1970 *A. Rev. Soc. Polym. Sci., Japan* 1971, p 13
- 2 Otsu, T. 1971 *A. Rev. Soc. Polym. Sci., Japan* 1972, p 11
- 3 Imoto, M. 'Radical Polymerization Mechanism. I. Initiation Reaction', Kagaku Dojin, Tokyo, 1969, p 64
- 4 Bamford, C. H., Eastmond, G. C. and Maltman, W. R. *Trans. Faraday Soc.* 1965, 61, 267
- 5 Bamford, C. H. and Denyer, R. *ibid.* 1966, 62, 1567
- 6 Bamford, C. H. and Hargreaves, K. *ibid.* 1967, 63, 392
- 7 Bamford, C. H., Eastmond, G. C. and Rippon, J. A. *Trans. Faraday Soc.* 1963, 59, 2548
- 8 Bond, J. and Hobson, D. B. *J. Polym. Sci. (A)* 1963, 1, 2179, 2185
- 9 Kastning, E. G., Naarman, H., Reis, H. and Berding, C. *Angew. Chem.* 1965, 77, 313
- 10 Biswas, A. M. and Mukherjee, A. R. *Indian J. Chem.* 1965, 3, 412
- 11 *Idem, ibid.* 1966, 4, 160
- 12 Takemura, F., Omori, M. and Tanaka, H. *Nippon Kagaku Zasshi* 1968, 89, 576
- 13 Takemura, F., Matsuyama, R., Mori, K. and Nagai, M. *ibid.* 1971, 92, 1102
- 14 Takemura, F. and Morita, E. *ibid.* 1971, 92, 1107
- 15 Osawa, Z., Sorimach, M., Kanazawa, H. and Ogiwara, Y. *J. Polym. Sci. (A-1)* 1973, 11, 523
- 16 Chemical Society of Japan, 'Textbook of Chemical Experiments, Vol 11: Coordination Chemistry', Maruzen, Tokyo, 1956, p 18
- 17 Nakamoto, K. 'Infrared Spectra of Inorganic and Coordination Compounds', John Wiley, New York, 1970, pp 150, 153, 160, 178
- 18 Society of Polymer Science, Japan, 'Textbook of Polymer Experiments, Vol 9: Monomer Preparation Method', Kyoritsu Shippun, Tokyo, 1959, pp 72, 141
- 19 Otsu, T. and Takemoto, K. 'Experimental Methods of Vinyl Polymerization', Kyoritsu Shippun, Tokyo, 1964, pp 88, 91
- 20 Flory, P. J. 'Principles of Polymer Chemistry', Cornell Univ. Press, Ithaca, 1953, p 312
- 21 Dyer, J. R. 'Application of Absorption Spectroscopy of Organic Compounds', Prentice-Hall, Englewood Cliffs, NJ, 1965
- 22 Tobolsky, A. V. and Baysal, B. *J. Polym. Sci.* 1952, 8, 529
- 23 Potnis, S. F. and Deshpande, A. *Makromol. Chem.* 1969, 125, 45
- 24 *Idem, ibid.* 1972, 153, 139
- 25 Tsuruta, T. 'Reactions of Polymer Synthesis', Nikkan Kogyo, Tokyo, 1962, p 20; Bevington, J. C., Melville, H. W. and Taylor, R. P. *J. Polym. Sci.* 1954, 12, 449

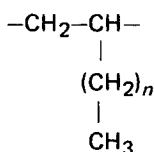
# Low temperature internal friction in some poly( $\alpha$ -olefins)

M. Pineri

Centre d'Etudes Nucléaires de Grenoble, Département de Recherche Fondamentale, BP 85, 38041 Grenoble Cédex, France

(Received 6 December 1974; revised 11 February 1975)

1 Hz internal friction experiments have been carried out using a torsion pendulum. The temperature range was between 4 and 100K. The existence of a very low temperature  $\delta$  peak has been studied in poly( $\alpha$ -olefins)



where  $n = 0-3$ . Polyethylenes have been studied in the same way. Evidence has been given for the existence of a low temperature peak coming from the presence of nitrogen or air. After purification we obtained  $\Delta W/W$  against temperature curves without a  $\delta$  peak for polyethylene and polypropylene samples. Evidence has been given for the existence of such  $\delta$  peaks in polypentene and polyhexene. A possible mechanism involving the rotation of the alkyl group is proposed.

## INTRODUCTION

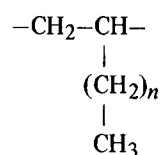
Frequency spectra of chain motions define the dynamical physical properties of polymers. During the last ten years many experiments have been carried out in this field. Dielectric measurements, nuclear magnetic resonance experiments, dynamic mechanical techniques and more recently incoherent inelastic neutron scattering spectroscopy have given much information about molecular motion<sup>1-7</sup>.

This paper considers the  $\delta$  type processes which occur at low temperatures (below 100K) when using 1 Hz dynamic mechanical techniques. Many experiments have been carried out between liquid helium and nitrogen temperatures<sup>8-19</sup>. Yet many questions are still unsolved as far as we are concerned with the interpretation of this  $\delta$  peak. When the temperature is lowered, molecular motions are more and more frozen in. At very low temperatures only very local motions are possible, such as methyl rotation. Many polymers containing pendant methyl groups, PMMA, polypropylene, polybutene, have been studied. Relaxation peaks appeared in some polymers.

It has been proposed that methyl group rotation is the mechanism responsible for the existence of this peak. Yet this explanation is not consistent with experiments performed with polybutene (no  $\delta$  peak) and poly(vinyl chloride) (one peak at 20K). Another inconsistency arises from the position of the peak compared to the value of the barrier of potential ( $\sim 2$  kcal). Quantum mechanical tunnelling as suggested by Eisenberg<sup>11</sup> can explain this last inconsistency.

Another explanation for the very low temperature peaks in semi-crystalline polymers has been advanced by some authors<sup>8-10</sup>. Motions of dislocation jogs and their interactions with specific conformational kink defects would produce  $\delta$  maxima.

Our purpose of the present study is to review the influence of the size of the side group in polymers such as:



where  $n$  is 0-3. In addition we have used polyethylene as a reference. If  $\delta$  peaks arise from methyl rotation we must have such a peak in polyhexene, polypentene, polybutene and polypropylene. The position of this peak must stay at the same temperature. The amplitude of the maximum must change with the relative number of methyl groups.

## EXPERIMENTAL

### Procedure

A 1 Hz torsion pendulum was used for the experiments described in this paper. It consists of an inverted free oscillating apparatus which has been previously described<sup>20</sup>. We plot against temperature the values:

$$\Delta W/W = 1 - \exp\left(-\frac{2}{n} \ln \theta_o/\theta_n\right)$$

and

$$G_T/G_4 = P_4^2/P_T^2$$

where  $\theta_o$  and  $\theta_n$  are the amplitudes of the oscillations  $o$  and  $n$ .  $P_T$  is the period of the decrease at temperature  $T$ .

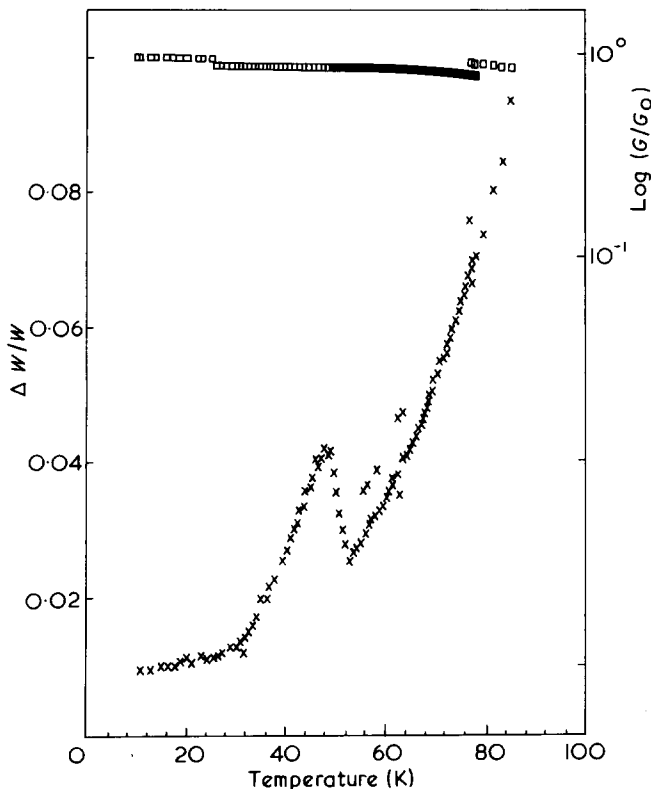


Figure 1 1 Hz  $\Delta W/W$  (x) and  $G/G_4$  (□) against temperature curves for a polyethylene

When the damping is low, as in the case of our experiments, we have:

$$\frac{\Delta W}{W} \approx 2\delta \approx 2\pi Q^{-1}$$

**Materials**

Six different commercial types of polyethylene have been studied. The density varies from 0.9 for the most branched polyethylene to 0.97 for the most linear.

Polypropylene, polybutene, polypentene and polyhexene were synthesized in the laboratory of 'Cinetique chimique macromoleculaire' by Dr Guyot.

The characterization of the different samples which have been studied was carried out in the Laboratoire de Chimie Macromoleculaire de l'Universite Claude Bernard Lyon I. Infra-red spectroscopy, X-ray diffraction experiments, differential enthalpic analysis and density measurements were done on the different polymers.

The polymorphism of polybutene (I, II and III), polypentene (I and II), polypropylene ( $\alpha$ ,  $\beta$  and  $\gamma$ ) and polyhexene has been taken into account.

Using quenching and annealing treatments the influence of crystallinity has been studied in these polymers.

Different catalytic systems were used in order to have polymers of different tacticity and of different molecular weights.

No important difference has been observed when changing these parameters in a polymer in the low temperature range studied. For this reason we will speak of a polymer without considering the different values which define it.

All the samples were prepared by compression moulding into sheets 0.5 mm thick. Differential enthalpic experiments have been performed so as to define the heat of fusion and the onset of melting temperature for each specimen.

**RESULTS**

Figure 1 shows the curve of  $\Delta W/W$  against temperature for a polyethylene. We can see a peak, the maximum of which is located at 50K for 1 Hz experiments. We have obtained such a peak in many experiments studying specimens of polybutene, polypentene, polyhexene, nylon, etc. This peak is characterized by a very quick decrease in the high temperature side. The amplitude of the maximum seemed to change in a hazardous manner.

In the same way we have obtained such a peak in experiments with graphite to define the origin of this peak. When having an entry of air or nitrogen we have observed such a peak while nothing appears with oxygen. For 1 Hz experiments the peak appears at 60K with air and 54K with nitrogen: Figure 2 shows the different curves.

From these last experiments we can conclude that the peak shown in Figure 1 is connected with a presence of nitrogen. We suppose that the formation of a very thin coat of solid nitrogen on the specimen has occurred. Internal friction damping comes from this coat.

Such a peak was no longer observed when we used the following procedure. After the sample had been mounted in the pendulum chamber, the entire system was evacuated to  $10^{-2}$  mmHg overnight. Purified helium gas was introduced to give 15 mmHg pressure. Purification of helium was achieved by adsorbing  $O_2$ ,  $N_2$ ,  $H_2O$  molecules on a synthetic zeolite molecular sieve. The chilling of the molecular sieve to liquid nitrogen temperature was accomplished by plunging the trap in liquid nitrogen. Thus when the  $\delta$  peaks are studied, we must pay particular attention to the purity of the exchange gas and to the quality of the initial vacuum.

Figure 3 shows the curves of  $\Delta W/W$  against temperature for a polyethylene;  $G_T/G_4$  is similarly plotted. It is seen that we have a continuous increase in  $\Delta W/W$  beginning from 4K. This increase corresponds to the  $\gamma$  peak, the maximum of which is located between 123 and 153 K depending on the percentage of  $CH_3$  in the polyethylene. For all the

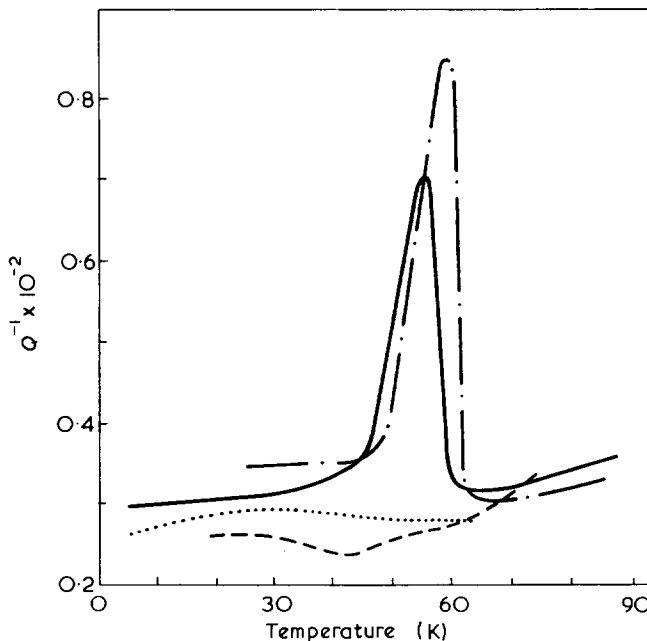


Figure 2 1 Hz  $Q^{-1}$  against temperature curves for nuclear graphite without exchange gas (....) and with oxygen (---), with nitrogen (-.-.) and air (—) as exchange gases

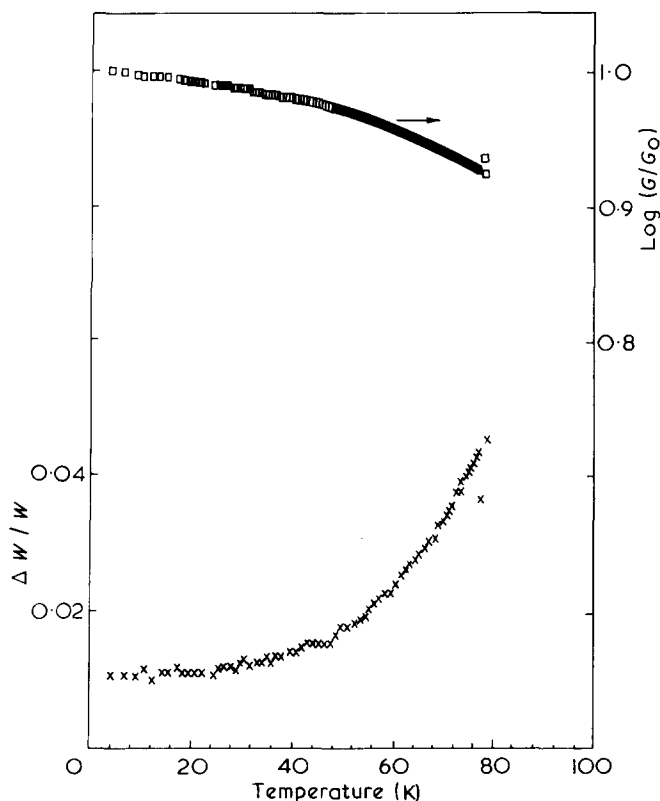


Figure 3 1 Hz  $\Delta W/W$  (x) and  $G/G_4$  (□) against temperature curves for a polyethylene after purification of the exchange gas

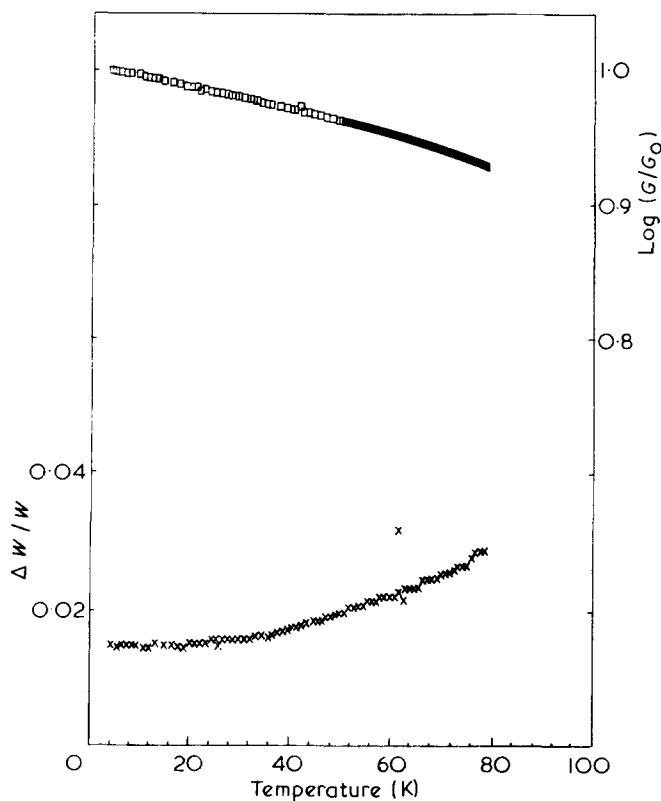


Figure 4 1 Hz  $\Delta W/W$  (x) and  $G/G_4$  (□) against temperature curves for a polypropylene specimen

polyethylene specimens we have studied, no  $\delta$  peak has been seen.

Figure 4 shows the same curves obtained for a polypropylene sample. The increase in  $\Delta W/W$  values is not very important between 4 and 80K. The decrease in the values of  $G_T/G_4$  is uniform in this range of temperatures. Figure 5

shows the curves of  $\Delta W/W$  and  $G_T/G_4$  for the polybutene specimen. No important change in the curves appears when we change the phase (I, II or III) or the crystallinity.

Figure 6 shows the same curves obtained for the poly-pentene specimen. In the same way no change has appeared when we change the phase or crystallinity. The important increase of the  $\Delta W/W$  value between 20 and 80K is con-

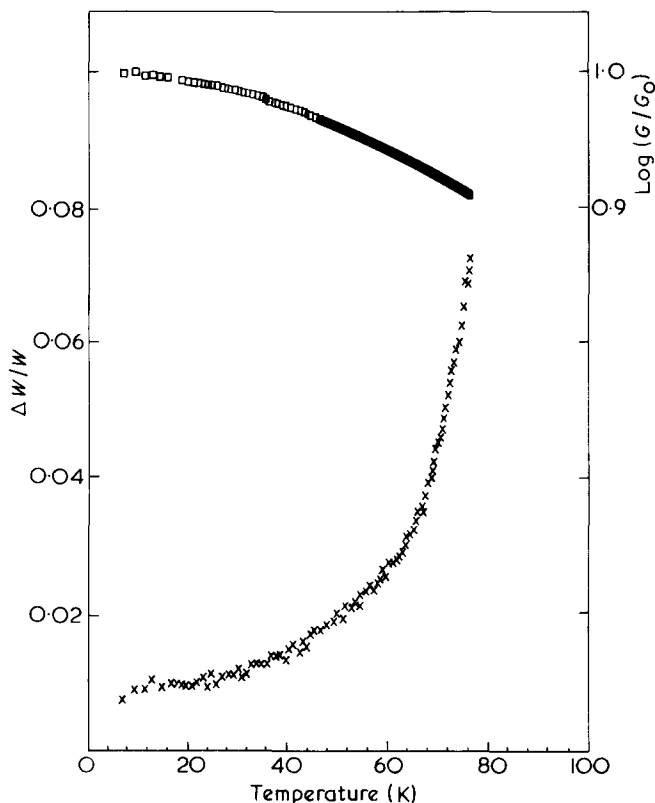


Figure 5 1 Hz  $\Delta W/W$  (x) and  $G/G_4$  (□) against temperature curves for a polybutene specimen

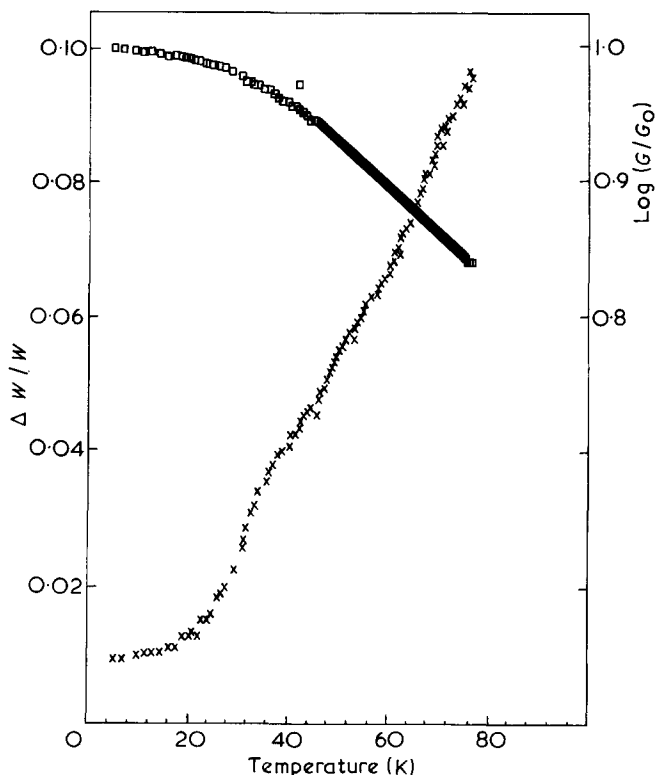


Figure 6 1 Hz  $\Delta W/W$  (x) and  $G/G_4$  (□) against temperature curves for a poly-pentene specimen

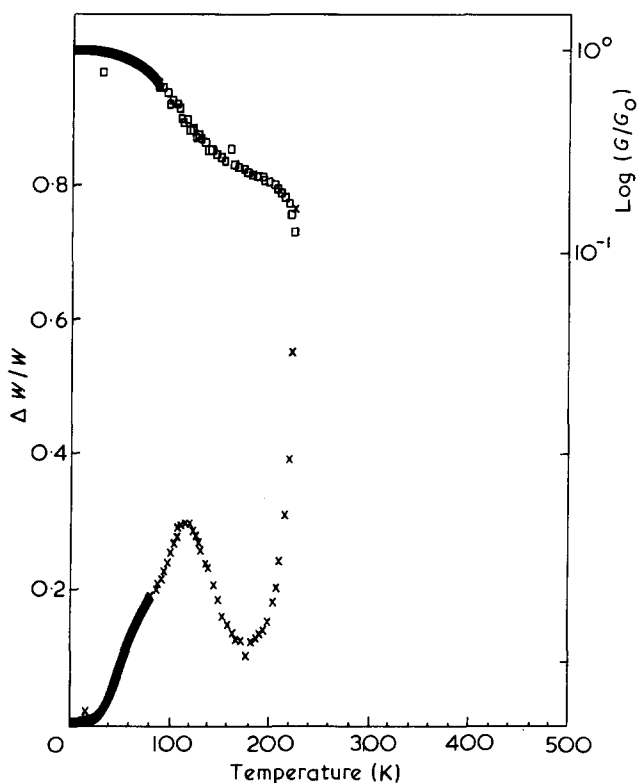


Figure 7 1 Hz  $\Delta W/W$  (X) and  $G/G_4$  ( $\square$ ) against temperature curves for a polyhexane specimen

nected with the  $\gamma$  peak. We have the superposition of a  $\delta$  peak as shown by an inflection point at  $\sim 34$ K.

Figure 7 shows the same curves for polyhexene. The range of temperatures is between 4 and 210K. The  $\gamma$  peak has its maximum at 120K. The large increase in the  $\Delta W/W$  value from 180K is associated with the  $\beta$  peak corresponding to the glass temperature. An important decrease in the modulus is associated with these peaks. Evidence of the existence of a  $\delta$  peak, superimposed to the low temperature side of the  $\gamma$  peak, is given by the change of slope in the  $\Delta W/W$  against temperature curve.

Another kind of experiment has been carried out, similar to that recently made by Papir and Baer<sup>8,9</sup>. We start with a linear polyethylene which as previously seen gives no evidence of a  $\delta$  peak. The specimen is annealed for 2 h at 128°C, being submitted *in situ* to a 660 g/cm<sup>2</sup> tension. After cooling at 4K we obtain the curve shown in Figure 8. A new peak centred at 35K appears. When annealing in the same way but without tension, we do not obtain this peak. With polypropylene we have not obtained a peak when annealing with tension or not.

### DISCUSSION

First, we wish to demonstrate that classical rotation of methyl groups cannot give a maximum in dynamic mechanical experiments.

Let us consider such a chain:



which gives the Newman representation and the potential curve of Figure 9.

If  $n_1$  = the number of  $\text{CRH}_2$  groups with R in position number 1 or 2,  $E_1$  = the energy of  $\text{CRH}_2$  in such a position,

$n_2$  = the number of  $\text{CRH}_2$  groups with R in number 3 position,  $E_2$  = the energy of  $\text{CRH}_2$  in such a position, we have  $n = n_1 + n_2$  (total numbers of  $\text{CRH}_2$ ). Therefore the total energy is:

$$E_0 = n_1 E_1 + n_2 E_2$$

$$n = n_1 + n_2$$

$$\frac{n_1}{n_2} = \exp(V/KT)$$

which gives:

$$E_0 = \frac{n}{1 + \exp(V/KT)} \left[ \exp\left(\frac{V}{KT} E_1 + E_2\right) \right]$$

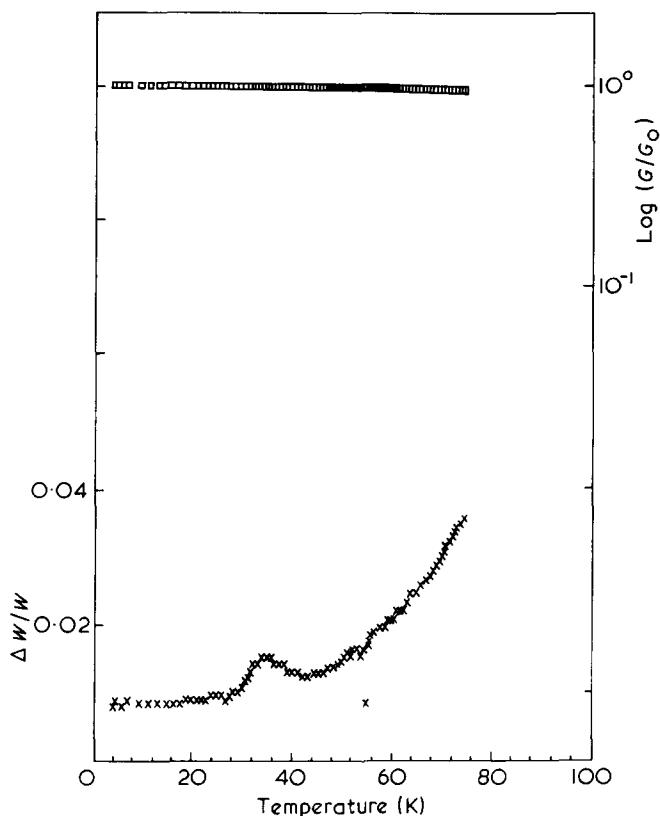


Figure 8 1 Hz  $\Delta W/W$  (X) and  $G/G_4$  ( $\square$ ) against temperature curves for a polyethylene after annealing for 2 h at 128°C. A 660 g/cm<sup>2</sup> tension was maintained during the annealing

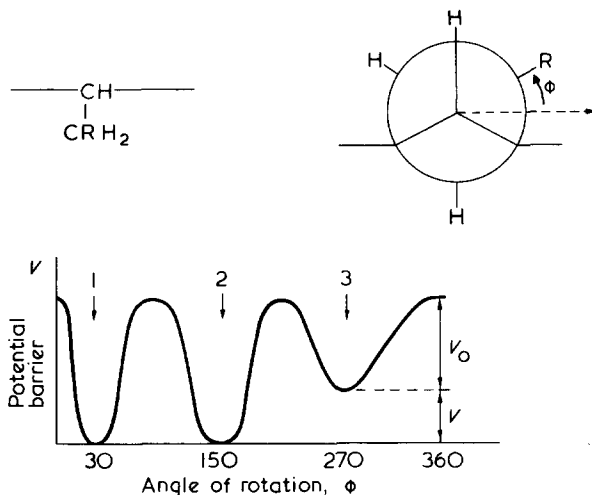


Figure 9 Potential barrier associated to the rotation of alkyl groups

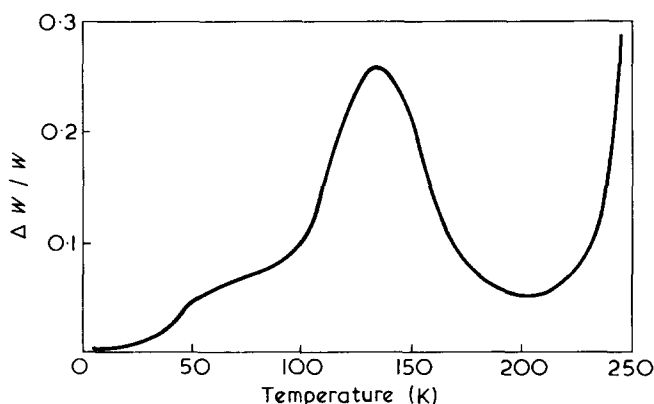


Figure 10 60 Hz  $\Delta W/W$  against temperature curve for a polypentene specimen

If now at a given time  $t$  we have a deformation, we will change the value  $V \rightarrow V'$ . Therefore, we have two consequences:

(1) We will change the energies:  $E_1 \rightarrow E'_1$  and  $E_2 \rightarrow E'_2$ . This change is instantaneous. The energy of the system becomes:

$$E_0 = \frac{n}{1 + \exp V/KT} \left[ \exp \left( \frac{V}{KT} E'_1 + E'_2 \right) \right]$$

(2) We will change the populations. Since this last change is not instantaneous, it will depend on the value of  $V_0$  and  $KT$ . The new energy will be for  $t \rightarrow \infty$ :

$$E'_0 = \frac{n}{1 + \exp V'/KT} \left[ \exp \left( \frac{V'}{KT} E'_1 + E'_2 \right) \right]$$

If the deformation is periodic:

$$V' = V + a \sin \omega t$$

Such a system will give a loss of energy, the maximum of which will be for  $\omega\tau \approx 1$  where  $\omega$  is the frequency of oscillation:

$$\tau = \frac{1}{2K \exp(V_0/KT)}$$

If now  $R = H$  (methyl group rotation), for the deformation there will be an instantaneous change of the  $CH_3$  energy. But there will be no change of this energy by rotation because of the identity of the H groups. No peak in internal friction experiments can appear in that case.

The problem to be discussed now is are there  $\delta$  peaks in polyethylene, polypropylene, polybutene, polypentene, and polyhexene? If such a peak appears, what is the mechanism involved?

From our experimental results we can draw the following conclusions: no  $\delta$  peak appears in polyethylene and polypropylene samples, and there is a  $\delta$  peak superimposed on the low temperature side of the  $\gamma$  peak in polypentene and polyhexene specimens. An internal friction experiment carried out at a frequency of 60 Hz in Figure 10 gives more evidence of the presence of a  $\delta$  peak in a polypentene specimen.

We are unable to draw a conclusion about the presence or absence of such a peak in polybutene.

It seems now impossible to separate the  $\gamma$  and  $\delta$  contributions in the  $\Delta W/W$  curve since we do not know the exact mechanisms which are involved in the relaxation peaks. We can only obtain qualitative information about the existence or non-existence of a  $\delta$  process if we plot  $\Delta W/W$  (Figure 6) or  $G''$  (Figure 11) against temperature. Only experiments at higher frequencies are perhaps able to give such a separation.

What is now the mechanism which is able to give a  $\delta$  peak? Methyl rotation was proposed to explain such a peak. As we have seen classical rotation is unable to give such a peak and there is no evidence of maximum in polypropylene. Inelastic tunnelling as proposed by Eisenberg<sup>11,12</sup> is a possibility to explain a very low temperature peak ( $\sim 6K$ ) in PMMA.

Classical rotation of a  $CRH_2$  group in polybutene, polypentene, and polyhexene is able to take into account the presence of a low temperature peak.

If we suppose an Arrhenius law,  $v = v_\infty \exp(W/KT)$ , for the rotation of the alkyl group we can define the energy activation  $W$  from the position of the maximum. We must take an arbitrary value for  $v_\infty$ . In polypentene and polyhexene the maximum of the  $\delta$  peak is located around 40K. With  $V_\infty = 10^{13}$  we obtain  $W \approx 2$  kcal which is relatively low compared to the values defined for the rotation of small molecules.

Polyhexene is an amorphous polymer, polypentene is a semi-crystalline one. Therefore it is impossible to propose a mechanism involving defects and dislocations in the crystalline phase to explain the  $\delta$  peak.

The aim of this paper is not to discuss the interpretation for the  $\gamma$  peak. However, we can state that the  $\gamma$  peak in polyhexene (amorphous) must be connected to the motions of the backbone involving side groups. In the same

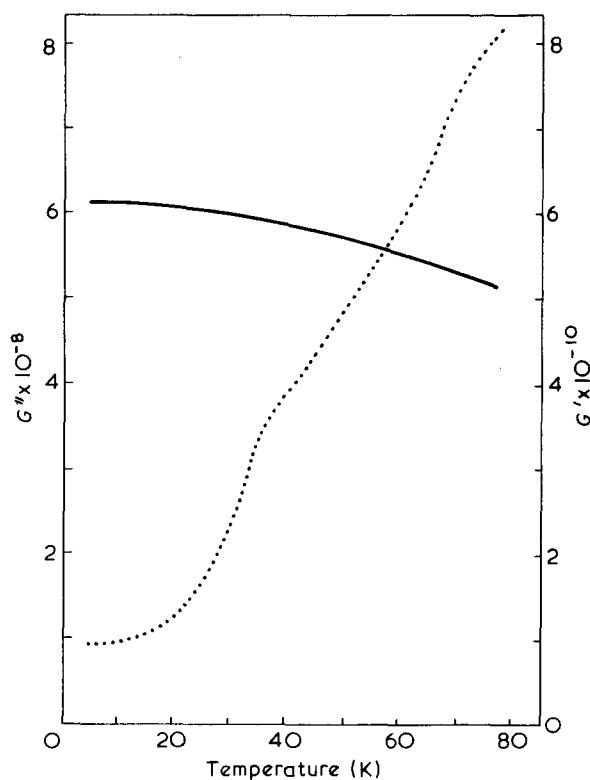


Figure 11 1 Hz  $G'$  (—) and  $G''$  (···) against temperature curves for a polypentene specimen



way an important part of the  $\gamma$  peak in polypropylene and polybutene must correspond to the same mechanism.

## CONCLUSIONS

A low temperature peak associated with nitrogen or air disappears after purification. No evidence of a  $\delta$  peak has been given in polyethylene and polypropylene samples. In polypropylene and polyhexene strong evidence of such a peak has been seen. As for polybutene it is very difficult to draw any conclusions from 1 Hz experiments.

The mechanism involved in this  $\delta$  process must be side group motion. Rotation of ethyl, propyl and butyl side groups are able to give an internal friction peak. Mechanisms involving defects in a crystalline part must be eliminated because of the amorphous character of the polyhexene. However, the activation energy of  $\sim 2$  kcal which is found for the  $\delta$  process seems to be low compared to the energies usually found for this type of motion.

## ACKNOWLEDGEMENTS

This work was supported in part by the CNRS (Action thématique programmée No.1C06). We are grateful to Dr Guyot (Cinetique chimique macromoléculaire in Villeurbanne) for supplying samples and to Dr P. Berticat and Dr May (Université Claude Bernard Lyon I) for characterizing the samples. We are indebted to Drs P. Berticat, Gilchrist, Isnard, May and Odin for very useful

discussions. Thanks are also due to Mr M. Brotte for the mechanical measurements.

## REFERENCES

- 1 McCrum, N. G., Read, B. E. and Williams, G. 'Anelastic and dielectric effects in polymer solids', Wiley, New York, 1967
- 2 Iwayanagi, S. and Sakurai, I. *J. Polym. Sci. (A-1)* 1966, 4, 29
- 3 Olf, H. G. and Peterlin, A. *J. Polym. Sci. (A-2)* 1970, 8, 753
- 4 Hoffman, J. D., Williams, G. and Passaglia, E. *J. Polym. Sci. (C)* 1966, 14, 173
- 5 Sauer, J. A. and Woodward, A. E. *Rev. Mod. Phys.* 1960, 32, 1
- 6 Higgins, J. S., Allen, G. and Brier, P. N. *Polymer* 1972, 13, 157
- 7 Heijboer, J. *Kolloid Z.* 1956, 148, 36
- 8 Papir, Y. S. and Baer, E. *J. Appl. Phys.* 1971, 42, 4669
- 9 Papir, Y. S. and Baer, E. *Mater. Sci. Eng.* 1971, 8, 310
- 10 Armeniades, C. D., Baer, E. and Rieke, J. K. *J. Appl. Polym. Sci.* 1970, 14, 2635
- 11 Eisenberg, A. and Reich, S. *J. Chem. Phys.* 1969, 51, 5706
- 12 Reich, S. and Eisenberg, A. *J. Chem. Phys.* 1970, 53, 2847
- 13 Sauer, J. A. and Saba, R. G. *J. Macromol. Sci. (A)* 1969, 3, 1217
- 14 Frosini, V. and Woodward, A. E. *J. Macromol. Sci. (B)* 1969, 3, 91
- 15 Armeniades, C. D., Kuriyama, I., Roe, J. M. and Baer, E. *J. Macromol. Sci. (B)* 1967, 1, 777
- 16 Takayanagi, M. *IUPAC Microsymp. IV, Prague* 1969
- 17 Takayanagi, M. *Proc. IV Int. Congr. Rheol., Kyoto* 1963
- 18 Grissman, J. M., Sauer, J. A. and Woodward, A. E. *J. Polym. Sci. (A)* 1964, 2, 5075
- 19 Grissman, J. M., Woodward, A. E. and Sauer, J. A. *J. Polym. Sci. (A)* 1965, 3, 2693
- 20 Pineri, M., Bonjour, E., Gerard, P. and Martin-D'Hermont, F. *Plast. Mod. Elastomères* 1972, (10),

# Polymerization of methyl methacrylate by tri-n-butylborane in the presence of amino acid esters\*

Kuniharu Kojima, Susumu Iwabuchi, Yuichi Moriya and Masako Yoshikuni  
Department of Applied Chemistry, Faculty of Engineering, Chiba University, Chiba 280, Japan  
(Received 7 October 1974)

The polymerization of methyl methacrylate by tri-n-butylborane in the presence of amino acid esters was investigated. The binary systems of tri-n-butylborane and amino esters were found to be more effective for initiating the polymerization than tri-n-butylborane alone. Co-catalytic effects of amino acid esters were in the order: tyrosinate > glutamate > aspartate ≧ phenyl alaninate > serinate > glycinate. The rate of polymerization in a mixture of dimethylsulphoxide and toluene was proportional to the square root of the concentration of the initiator system, to the monomer concentration, and to the concentration of dimethylsulphoxide in the solvent. The overall energy of activation was estimated to be 4.6 kcal/mol for the tri-n-butylborane/methyl tyrosinate system. Copolymerization curves gave a typical free-radical character.

## INTRODUCTION

It is known that alkylboranes can initiate the polymerization of vinyl monomers in the presence of oxygen<sup>1,2</sup>. Both organic and metal peroxides show co-catalytic effects on the alkylborane-initiated polymerization<sup>3,4</sup>. Previous investigations of the polymerization and copolymerization of vinyl monomers by tri-n-butylborane<sup>5-8</sup> showed that nitrogen-containing compounds (e.g. pyridine<sup>5</sup> and its derivatives<sup>6</sup>) and alkyl halides (e.g. butyl iodide<sup>7</sup>) exhibit co-catalytic effects. Furthermore, the polymerization of methyl methacrylate by tri-n-butylborane was found to be accelerated in the presence of silk<sup>8</sup>. In order to clarify this, the polymerization of methyl methacrylate by tri-n-butylborane was studied in the present work in the presence of methyl esters of amino acids which contain structural units of silk.

## EXPERIMENTAL

### Materials

The monomers and solvents used were purified by distillation. Tri-n-butylborane (TBB) was prepared from boron trifluoride etherate and n-butyl bromide by a Grignard reaction. TBB was distilled under nitrogen in a dry box and stored in a sealed glass ampoule (b.p. 111–112°C at 25 mmHg)<sup>9</sup>. Methyl esters of amino acids were prepared in accordance with the method of Fischer<sup>10</sup>. The esters so obtained were identified by means of i.r. spectroscopy and m.p. or b.p.

### Polymerization procedure

To a mixture of 10 ml (3.7 mol/l) of methyl methacrylate (MMA) and a given amount of the esters in solvent (dimethylsulphoxide and/or toluene) the TBB was added quickly by means of a microsyringe. The mixture was poured into a 20 ml dilatometer or a tapered glass tube

(capacity about 40 ml) and was immersed in a thermostated bath at 25°C. After a specified time, the mixture was poured into 200 ml of methanol, the precipitate was filtered, washed with methanol, and dried *in vacuo* at 40°C to constant weight.

### Measurements

Intrinsic viscosities of the polymers were determined at 25°C in chloroform with a modified Ubbelohde viscometer and average molecular weights were calculated from<sup>11</sup>:

$$[\eta] = 0.48 \times 10^{-4} \cdot M_n^{0.8} \text{ (dl/g; 25°C).}$$

Dilatometry showed that the rate of polymerization was of pseudo first-order at the initial stage of reaction and the rates of polymerization and the rate constants reported in this paper were calculated as a reaction of first-order.

## RESULTS AND DISCUSSION

### Co-catalytic effects of various amino acid esters

Polymerizations of methyl methacrylate (MMA) by tri-n-butylborane (TBB) were carried out in dimethylsulphoxide (DMSO) and/or toluene in the presence of methyl esters of amino acids. The results (Table I) show that methyl tyrosinate (MeTyr), dimethyl glutamate (DMGlu), and dimethyl aspartate (DMAsp) promoted, while methyl phenylalaninate (MePhe), methyl serinate (MeSer), and methyl glycinate (MeGly) retarded the polymerization. The co-catalytic effects of the esters were in the order: MeTyr > DMGlu > DMAsp ≧ MePhe > MeSer > MeGly.

### Effects of the molar ratios of the esters on the rate of polymerization

In order to investigate the optimum catalytic activity of the TBB/amino acid ester systems, polymerizations were

\* Presented in part at the 28th Annual Meeting of the Chemical Society of Japan, April 1973, Tokyo, Japan.

Table 1 Polymerization of MMA by TBB in the presence of amino acid ester<sup>a</sup>

Amino acid esters NH <sub>2</sub> CH(R)COOCH <sub>3</sub>	(g)	Conversion (%)	Time (min)	$\bar{M}_n \times 10^{-3}$
Methyl tyrosinate MeTyr <sup>b</sup> R = -CH <sub>2</sub> C <sub>6</sub> H <sub>4</sub> OH	0	11.0	60	100
	0.020	16.8		87
	0.039	12.6		130
Dimethyl glutamate DMGlu <sup>c</sup> R = -CH <sub>2</sub> CH <sub>2</sub> COOCH <sub>3</sub>	0	3.0	35	132
	0.030	5.3		82
Dimethyl aspartate DMAsp <sup>c</sup> R = -CH <sub>2</sub> COOCH <sub>3</sub>	0	3.0	35	132
	0.030	5.1		80
Methyl phenylalaninate MePhe <sup>c</sup> R = -CH <sub>2</sub> C <sub>6</sub> H <sub>5</sub>	0	10.3	60	62
	0.035	9.1		76
Methyl serinate MeSer <sup>c</sup> R = -CH <sub>2</sub> OH	0	10.5	60	56
	0.027	8.4		81
Methyl glycinate MeGly <sup>c</sup> R = -H	0	9.9	60	64
	0.018	4.6		164

<sup>a</sup> [MMA] = 3.75 mol/l; [TBB] = 8.0 × 10<sup>-3</sup> mol/l; temperature = 25°C

<sup>b</sup> Solvent = DMSO

<sup>c</sup> Solvent = toluene

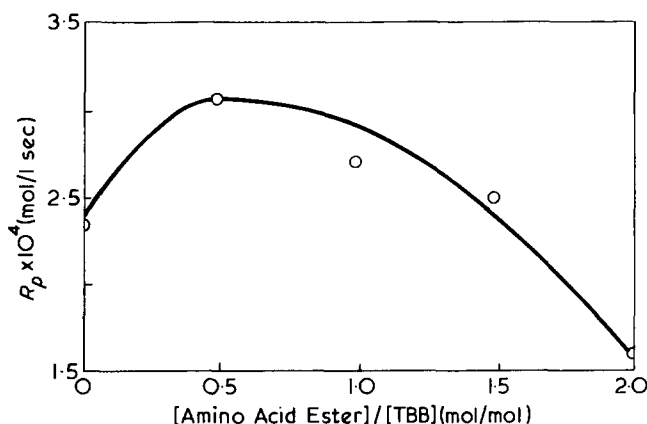


Figure 1 Optimum molar ratios of amino acid ester and TBB. [MMA] = 3.75 mol/l; [TBB] = 8.0 × 10<sup>-3</sup> mol/l; solvent = DMSO; temperature = 25°C

Table 2 Dependence of the rate of polymerization on initiator concentration<sup>a</sup>

Run no.	Initiator concentration × 10 <sup>3</sup> (mol/l)	Rate of polymerization × 10 <sup>4</sup> (mol/l sec)
1	2.4	1.32
2	6.1	2.92
3	8.0	3.86
4	12.0	4.05

<sup>a</sup> Initiator = equimolar mixture of MeTyr and TBB; [MMA] = 3.75 mol/l; solvent = DMSO; temperature = 25°C

performed in DMSO and toluene, at varying concentrations of amino acid ester and constant concentration of TBB. The results plotted in Figure 1 show the rate of polymerization was a maximum near 0.5 for the TBB/MeTyr system.

Effects of initiator concentration

The dependence of the rate of polymerization in initiator concentration was studied at varying initiator concen-

trations and constant molar ratios of [TBB]/[ester] (Table 2). The plots of  $R_p$  against [initiator] was non-linear and the extrapolation of [TBB-MeTyr] to  $R_p = 0$  gave a value of about 1.6 × 10<sup>-3</sup> mol/l. This means that no polymerization could occur at this concentration and lower. When this amount of the initiator system was added to a solution of MMA in DMSO under the same conditions, no polymerization in fact was observed. Therefore, the effective initiator concentration ([I]<sub>eff</sub>) was assumed to be the concentration of the added initiator system ([I]) - the critical initiator concentration ([I]<sub>c</sub> = 1.6 × 10<sup>-3</sup> mol/l). The log of the rate of polymerization ( $R_p$ ) was plotted against the log of the effective initiator concentration ([I]<sub>eff</sub>) (Figure 2). The plot was linear and the rate was found to be proportional to the square root of [I]<sub>eff</sub>.

Effects of initial monomer concentrations

Polymerizations were performed, at initial monomer concentrations from 1.87 to 7.5 ml/l and constant initiator concentration. The plot of the rate of polymerization against the initial monomer concentration was non-linear i.e. the rate was assumed to depend on [DMSO]. The plot of  $R_p/[MMA]$  against [DMSO] (Figure 3) was linear and

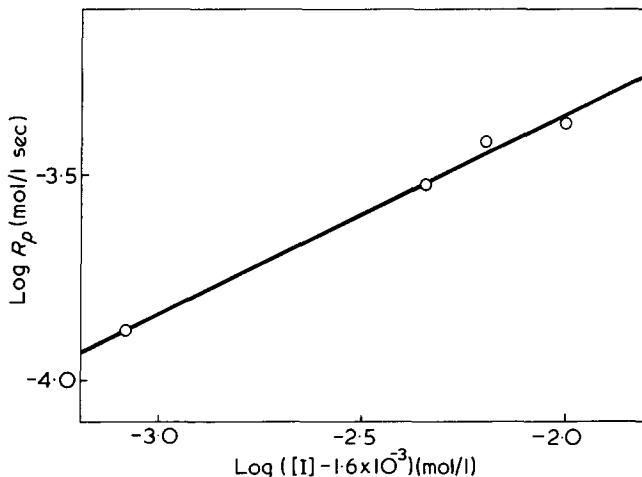


Figure 2 Plots of the rate of polymerization vs. the effective initiator concentration, [I]<sub>eff</sub>. [MMA] = 3.75 mol/l; solvent = DMSO; temperature = 25°C

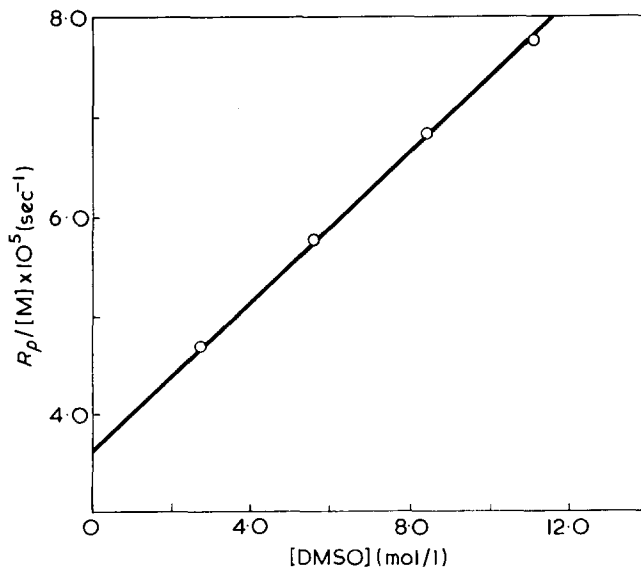


Figure 3 Solvent effects on the rate of polymerization. [TBB] = 8.0 × 10<sup>-3</sup> mol/l; [MeTyr] = 4.0 × 10<sup>-3</sup> mol/l; temperature = 25°C

thus  $R_p/[MMA] \propto [DMSO]$ . In order to keep the solvent effects constant, polymerizations were repeated using a constant amount of DMSO (5 ml), to which MMA and toluene were added to bring the total volume up to 25 ml. As can be seen from Figure 4, the rate of polymerization was found to be proportional to the initial monomer concentration. The above results show that:  $R_p = k \cdot [I]_{eff}^{1/2} \cdot [MMA] \cdot [DMSO]$ .

Temperature dependence of rate constants

The plots of rate constants ( $R_p$ ) against reciprocals of temperatures ( $1/T$ ) gave the overall energy of activation of 4.6 kcal/mol for the TBB–MeTyr system in DMSO (Figure 5). The corresponding activation energy of the polymerization of acrylonitrile by TBB in tetrahydrofuran is 3.8 kcal/mol<sup>12</sup>, that of MMA by the TBB–methyl nicotinate system 4 kcal/mol<sup>6</sup>, and that of vinyl chloride by triethylborane 8.23 kcal/mol<sup>13</sup>.

Reaction mechanism

The polymerization of vinyl monomers by alkylboranes in the presence of oxygen or electron donors is known to proceed via a free-radical mechanism<sup>14–18</sup>. In order to elucidate the reaction mechanism of the polymerization of MMA by the TBB/amino acid ester systems, MMA and styrene were copolymerized by TBB in the presence of MeTyr in DMSO. Figure 6 shows the copolymerization curve; this was found to be of the typical free-radical mechanism<sup>19</sup>. Monomer reactivity ratios of MMA ( $M_1$ ) and styrene ( $M_2$ ) were  $r_1 = 0.42$  and  $r_2 = 0.46$  for the TBB–MeTyr system. The result agrees closely with those for the typical free-radical copolymerization of MMA and styrene within experimental errors ( $r_1 = 0.42$  and  $r_2 = 0.54$ )<sup>20</sup>.

Borsini and Cipolla<sup>21</sup> found that the alkylborane-initiated polymerization of vinyl chloride is accelerated by electron-donating solvents, such as ether and pyridine, and they assumed the formation of the complex of alkylborane and these donors. We previously showed that the electron-donating property of hydrophilic groups, such as amino and hydroxyl groups, plays an important role in the polymerization and copolymerization of vinyl monomers by TBB<sup>5–8,22–26</sup>. Analogously, the amino acid esters seems to act as electron donors.

The following reaction mechanism, similar to that previously suggested for the polymerization of MMA by TBB/

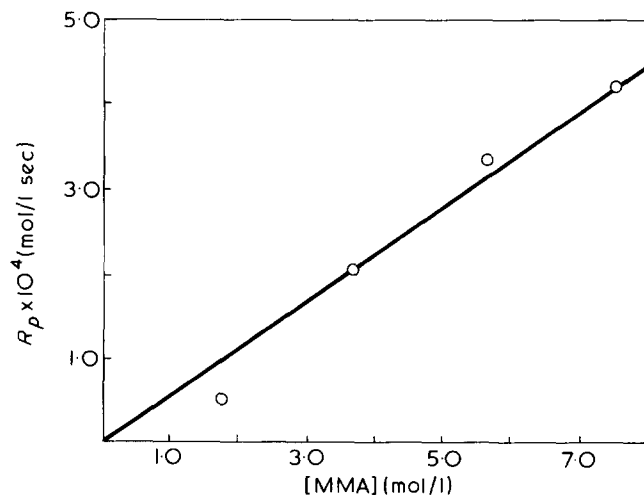


Figure 4 Effects of the initial monomer concentration on the rate of polymerization. [TBB] =  $8.0 \times 10^{-3}$  mol/l; [MeTyr] =  $4.0 \times 10^{-3}$  mol/l; solvent = mixtures of DMSO (5 ml) and toluene

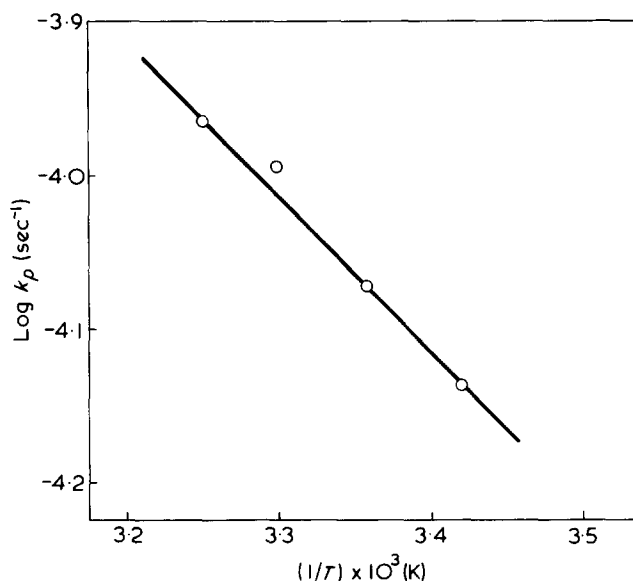


Figure 5 Arrhenius plots for the systems MeTyr/TBB and DMGlu/TBB. [TBB] =  $8.0 \times 10^{-3}$  mol/l; [MeTyr] =  $4.0 \times 10^{-3}$  mol/l; [DMGlu] =  $8.0 \times 10^{-3}$  mol/l; solvent = mixtures of DMSO (5 ml) and toluene

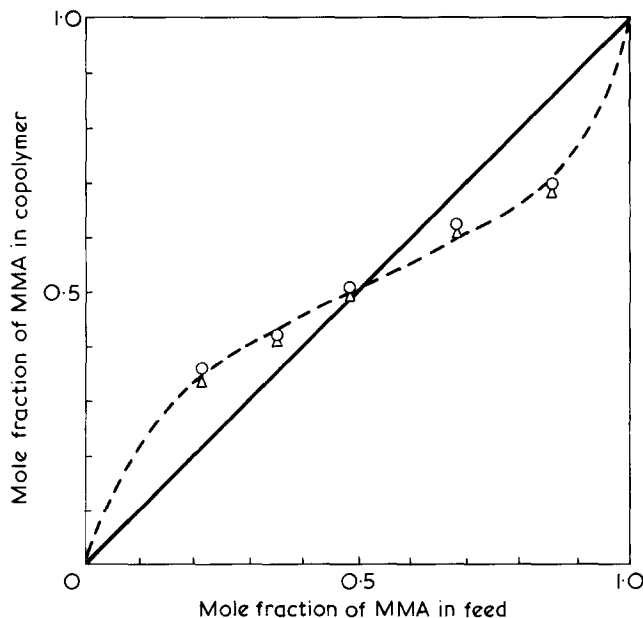
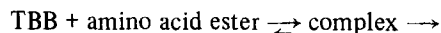


Figure 6 Composition of copolymer as a function of monomer composition for the copolymerization of methyl methacrylate ( $M_1$ ) and styrene ( $M_2$ ) initiated by the system amino acid ester/TBB.  $\circ$ , MeTyr/TBB in DMSO;  $\triangle$ , DMGlu/TBB in toluene. Temperature = 25°C

pyridine system<sup>5</sup> or by the TBB/alkyl halide system<sup>7</sup> is proposed:



free radicals  $\rightarrow$  initiation

Further studies on the polymerization of vinyl monomers in the presence of polymeric model compounds for silk (e.g. synthetic polypeptides) are now in progress.

ACKNOWLEDGEMENT

The authors are grateful to Dr T. Nakahira for helpful discussions.

REFERENCES

- 1 Furukawa, J., Tsuruta, T. and Inoue, S. *J. Polym. Sci.* 1957, **26**, 234
- 2 Kolesnikov, G. S. and Klementova, N. V. *Izv. Akad. Nauk. USSR* 1957, p 652; *Chem. Abstr.* 1957, **51**, 15458
- 3 Furukawa, J. et al. *Kogyo Kagaku Zasshi* 1958, **61**, 728
- 4 Furukawa, J., Tsuruta, T., Iwata, T. and Fukutani, H. *Makromol. Chem.* 1959, **31**, 122
- 5 Kojima, K., Iwata, Y., Nagayama, M. and Iwabuchi, S. *J. Polym. Sci. (B)* 1970, **8**, 541
- 6 Kojima, K., Habu, T., Iwabuchi, S. and Yoshikuni, M. *Nippon Kagaku Kaishi* 1972, p 2165
- 7 Yoshikuni, M., Asami, M., Iwabuchi, S. and Kojima, K. *J. Polym. Sci. (A-1)* 1973, **11**, 3115
- 8 Kojima, K., Suzuki, T., Iwabuchi, S. and Tarumi, N. *Nippon Kagaku Kaishi* 1972, p 1943
- 9 Johnson, J. R., Snyder, H. R. and Van Campen, M. G. *J. Am. Chem. Soc.* 1938, **60**, 115
- 10 Fischer, E. *Chem. Ber.* 1901, **34**, 451
- 11 Bischoff, J. and Desreux, V. *J. Polym. Sci.* 1953, **10**, 437
- 12 Ogata, Y. and Minoura, Y. *Kogyo Kagaku Zasshi* 1963, **66**, 1707
- 13 Furukawa, J., Tsuruta, T., Kawasaki, A. and Shiotani, S. *ibid.* 1958, **61**, 1363
- 14 Furukawa, J., Shiotani, S. and Kawasaki, A. *ibid.* 1959, **62**, 268
- 15 Furukawa, J., Tsuruta, T. and Nakayama, Y. *ibid.* 1960, **63**, 876
- 16 Furukawa, J. et al. *Makromol. Chem.* 1959, **31**, 122
- 17 Zuty, N. L. and Welch, F. J. *J. Polym. Sci.* 1960, **43**, 445
- 18 Welch, F. J. *ibid.* 1962, **61**, 243
- 19 e.g. Billmeyer, Jr. F. W. 'Textbook of Polymer Science', 2nd Edn, Wiley, New York, 1965, p 349
- 20 'Polymer Handbook', (Eds. Brandrup, J. and Immergut, E. H.) Interscience, New York, 1965
- 21 Borsini, G. and Cippola, M. *J. Polym. Sci. (B)* 1964, **2**, 291
- 22 Kojima, K., Iwabuchi, S., Kojima, K. and Tarumi, N. *ibid.* 1971, **9**, 25
- 23 Kojima, K., Iwabuchi, S., Kojima, K. and Tarumi, N. *ibid.* 1971, **9**, 453
- 24 *Idem*, *Bull. Chem. Soc. Japan* 1971, **44**, 1891
- 25 Kojima, K., Iwabuchi, S., Kojima, K., Tarumi, N. and Masuhara, E. *J. Polym. Sci. (A-1)* 1971, **9**, 3213
- 26 Kojima, K., Iwabuchi, S., Murakami, K., Kojima, K. and Ichikawa, F. *J. Appl. Polym. Sci.* 1972, **16**, 1139

# Kinetic study of anionic polymerization of butadiene in a polar solvent

A. Siove and P. Sigwalt

Laboratoire de Chimie Macromoléculaire de l'Université Paris VI, 4 Place Jussieu, 75005 Paris, France

and M. Fontanille

Laboratoire de Recherches sur les Macromolécules de l'Université Paris-Nord, Place du 8 Mai 1945, 93206 Saint-Denis, France

(Received 12 December 1974)

The kinetics of the propagation reaction for the polymerization of butadiene initiated by cumyl potassium in tetrahydrofuran solution at several temperatures have been studied. Kinetic data and electrolytic behaviour indicate that polybutadienyl free ions assume the whole of the propagation reaction. At 0°C, the respective rate constants for ion-pairs and free ions are  $1 \text{ l mol}^{-1} \text{ s}^{-1}$  and  $4.8 \times 10^4 \text{ l mol}^{-1} \text{ s}^{-1}$  respectively. The ionic dissociation constant is  $7.8 \times 10^{-9} \text{ mol/l}$ . The activation energy of the propagation reaction for free ions is 6.5 kcal/mol.

## INTRODUCTION

The kinetics of anionic polymerization of dienes initiated by organo-alkali derivatives in polar solvents such as tetrahydrofuran (THF) are difficult to study owing to the very low stability of active centres propagating the polymerization.

Medvedev and coworkers<sup>1,2</sup> measured overall rate constants for the propagation of butadiene in THF solution, for several alkali cations associated with carbanionic end groups, at temperatures between  $-96^\circ\text{C}$  and  $+10^\circ\text{C}$ . These authors deduced from their experimental data a very small influence of free ions on overall reactivity, especially in the case of species associated to  $\text{Li}^+$  and  $\text{Na}^+$  cations. These conclusions are surprising if compared to results obtained by Bywater and Worsfold<sup>3</sup> who studied the kinetics of isoprene polymerization initiated by *n*-BuLi in THF solution. The measurement of homopolymerization rate constants and the determination of dissociation constants from ion-pairs to free ions showed the preponderance of free ions over ion-pairs in the kinetic scheme. Their relative concentration is low, but their reactivity is much higher than the reactivity of ion-pairs.

THF is an aprotic solvent having a dissociating power high enough to show the influence of free ions. We have chosen  $\text{K}^+$  as counter-ion because its compounds have a stability higher than those of species associated with  $\text{Na}^+$  and  $\text{Li}^+$ .

## EXPERIMENTAL

Purification of solvent, monomer and initiator were carried out in all-sealed high vacuum apparatus as described in previous papers<sup>5</sup>. Polymerizations were carried out in an adiabatic calorimeter similar to the one used by Sigwalt *et al.*<sup>6</sup> for kinetic studies of cationic polymerizations. This sealed apparatus (shown in Figure 1) also permits operation at any temperature lower than room temperature.

Cumyl potassium was used as initiator and was prepared by direct reaction of methyl cumyl ether on a potassium mirror, washed with hexane over sintered glass, dissolved in THF and filtered.

The introduction of the initiator solution into the calorimeter was made from a side storage vessel. A breaking-bulb system was used to introduce the monomer into the initiator solution.

As butadiene has a low boiling point, we verified that under vacuum and between  $-80^\circ$  and  $0^\circ\text{C}$ , more than 95% of the monomer is in the THF solution. At higher temperatures, monomer concentration in the gas phase is not

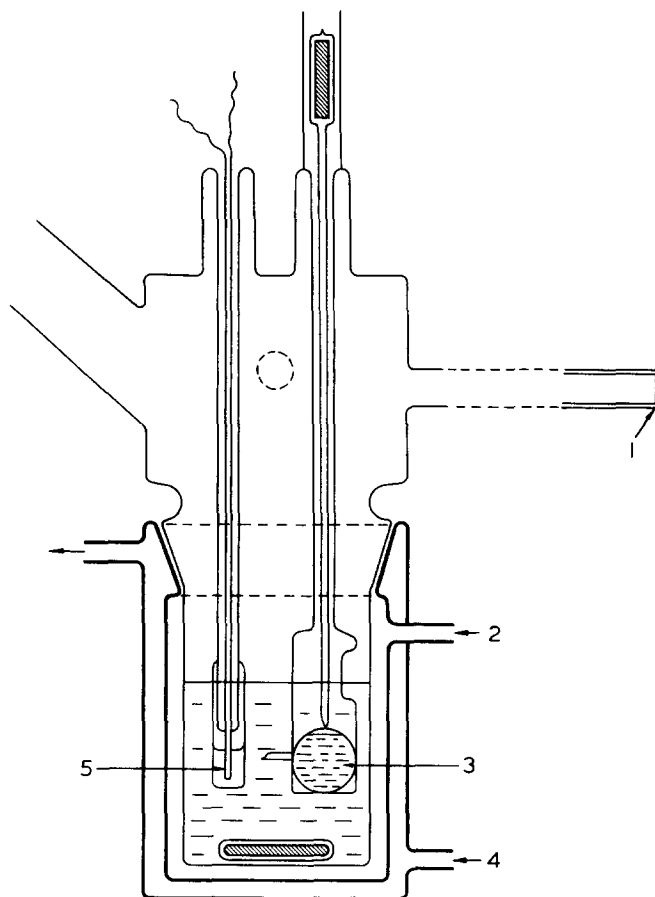


Figure 1 Polymerization apparatus. 1, U.v. cell; 2, vacuum; 3, bulb containing the monomer; 4, thermoregulation; 5, thermistor

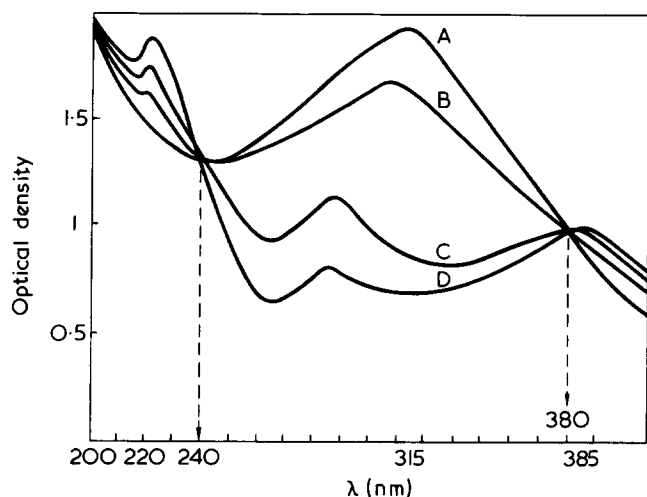


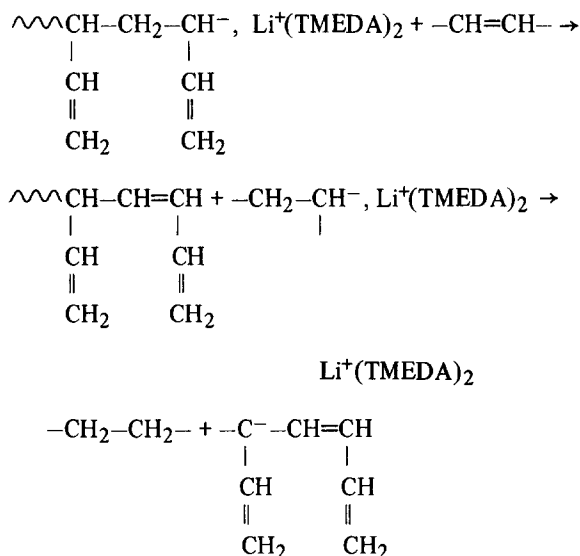
Figure 2 Absorption spectra of polybutadienyl potassium in THF at  $-20^{\circ}\text{C}$  (initiated with a potassium mirror). A, 2 min; B, 1 h; C, 5 h; D, 8 h after initiation

negligible but with this technique, it is not possible to operate at a temperature higher than  $0^{\circ}\text{C}$ .

Initiation is very rapid, and the active centre concentration was assumed equal to initiator concentration (see later). The variation of the concentration of active centres was followed with a u.v. spectrometer in a low-temperature cell as previously described<sup>7</sup>.

### RESULTS AND DISCUSSION

We have shown that the stability of active species is very dependent on their concentration and on temperature. Indeed, as shown in Figure 2, it is possible to follow the transformation from polybutadienyl initial species to 'isomerized' species by using a high concentration ( $2 \times 10^{-2}\text{ M}$ ) of active centres, whereas at a low concentration ( $10^{-4}\text{ M}$ ), the isomerization is fast above  $-20^{\circ}\text{C}$ . In that case, the overall transformation cannot be followed by spectrophotometry. The isomerization corresponds to a disappearance of the initial absorption maximum ( $\lambda_{\text{max}} = 315\text{ nm}$ ) and to the appearance of 3 peaks at 220, 285 and 385 nm. A satisfactory scheme was proposed by Hay and McCabe<sup>8</sup> for analogous conditions:



Moreover, several polymerizations initiated by cumyl potassium have shown that isomerization phenomena are faster when the temperature is increased, the general behaviour remaining similar.

Nevertheless, several observations permit us to conclude that the stability of propagating species is such that their concentration may be considered as constant during the propagation step. The study of spectra realized at room temperature about 2 min after the polymerization was achieved, shows that at least 50% of active species still exist in the system. One can estimate that active centres destroyed during the propagation step is less than 3%.

This estimation was corroborated by the fact that no important modification of electrolytic behaviour (see Figure 3) or of the reaction kinetics (see Figure 4,  $\log(M_0/M) = f(t)$  is a straight line) are observed during the reaction.

### Kinetic measurements

We have verified for each temperature that the order in monomer is equal to unity. Homopolymerizations were

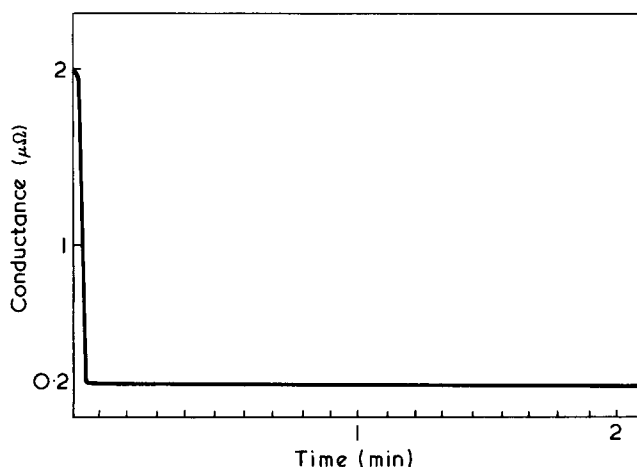


Figure 3 Variation of the conductance during the polymerization of butadiene. The initial value is that of the cumyl potassium solution ( $10^{-4}\text{ M}$ )

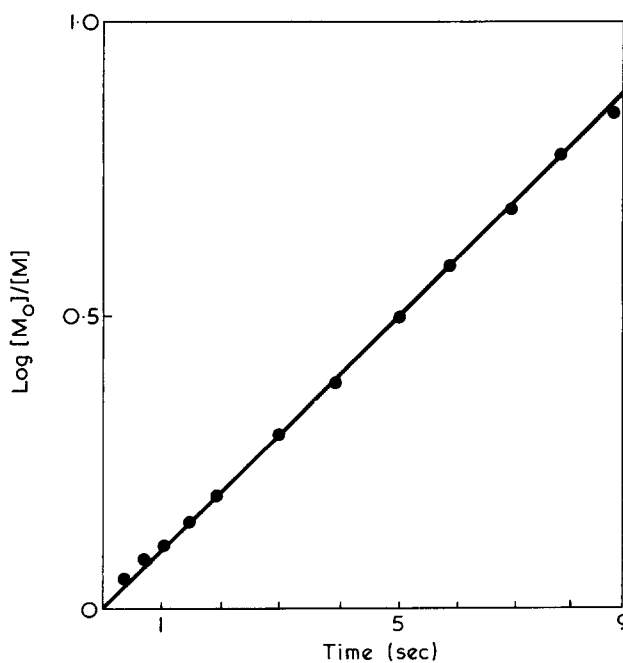


Figure 4 Order in monomer for a polymerization at  $0^{\circ}\text{C}$ .  $[\text{C}^-] = 1.07 \times 10^{-3}\text{ M}$ ;  $k_p = 125\text{ M}^{-1}\text{ s}^{-1}$

Table 1 Overall rate constants measured for several concentrations of active centres and potassium cation at several temperatures

$T$ (°C)	[but <sup>-</sup> , K <sup>+</sup> ] × 10 <sup>4</sup> (M)	[φ <sub>4</sub> B <sup>-</sup> , K <sup>+</sup> ] × 10 <sup>4</sup> (M)	$k_p$ (M <sup>-1</sup> s <sup>-1</sup> )
0	10.7	0	125
	3.02	—	254
	1.77	—	325
	1.11	—	400
	11	22.4	2.3
	10.2	8.9	3.3
	3.1	4.3	3.9
-6	3.05	2.68	5.5
	9.2	0	116
	3.13	—	198
	1.47	—	305
	1.03	—	340
	10	14.6	2
	9.8	6.65	2.9
-13	6.75	5.28	3.3
	3	3.1	4.05
	8.65	0	100
	4	—	132
	1.53	—	216
	1.05	—	276
	11	12.3	1.65
7.2	6.21	2.7	
2.5	2.77	3.5	

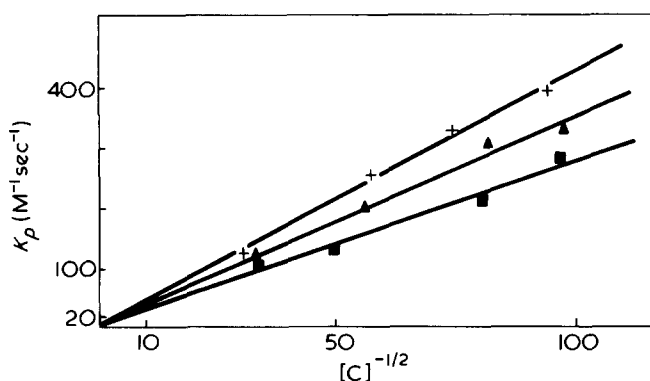
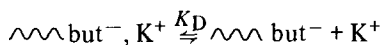


Figure 5 Dependence of overall rate constants on polybutadienyl potassium concentrations. +, 0°; ▲, -6°; ■, -13°C

realized between 0° and -13°C. At temperatures lower than -13°C, polymerization rates are too slow to obtain a satisfactory adiabaticity of the system.

Kinetic results given in Table 1, show an important variation of the overall rate constants with the concentration in active centres. This behaviour can be ascribed to the existence of an equilibrium between two types of active centres with different reactivities. Addition of potassium tetraphenylboride to the solution displaces this equilibrium and this permits us to conclude that as in the case of styrene, electrolytic dissociation of ion-pairs into free ions determines the kinetic behaviour.



The rate of polymerization can be represented by the following kinetic law:

$$V_p = k_p [C] [M]$$

where [M] = monomer concentration, [C] = concentration of active centres,  $k_p$  = overall rate constant, but  $k_p$  varies

with [C]<sup>9</sup>:

$$k_p = k_p(\pm) + k_p(-) \left( \frac{K_D}{[C]} \right)^{1/2}$$

where  $k_p(\pm)$  and  $k_p(-)$  are the absolute rate constants for propagation upon ion-pairs and free ions respectively, and  $K_D$  the ion-pairs dissociation constant.

Extrapolations of  $k_p = f([C]^{-1/2})$  (Figure 5) at several temperatures, show that the dependence of propagation rate constants upon ion-pairs are close to zero.

The dissociation constants  $K_D$  cannot be measured by conductimetry with the experimental conditions used as the transformation of the active centres is fast. It was necessary to use the effect of an electrolyte possessing a common cation (potassium tetraphenylboride) upon the kinetics of the propagation reaction. With added electrolyte the overall rate constant<sup>10</sup> is given by:

$$k_p = k_p(\pm) + k_p(-) \cdot \frac{K_D}{[K^+]}$$

Figure 6 shows that extrapolations of straight lines  $k_p = f([K^+]^{-1})$  correspond to very low values for absolute rate constants for polybutadienyl potassium ion-pairs ( $k_p(\pm) \sim 1 \text{ l mol}^{-1} \text{ s}^{-1}$ ). The exact values are difficult to estimate.

For concentration in active centres higher than 10<sup>-3</sup> M, the heat evolution from the propagation reaction is disturbed by the initiation reaction. Moreover the least squares method shows that in all cases the extrapolations of  $k_p = f([K^+]^{-1})$  give ion-pairs absolute rate constants close to unity. These results are in agreement with those obtained for electrochemically initiated polymerization by Funt and Hornoff<sup>11</sup>, for polybutadienyl sodium ion-pairs at -10°C ( $k_p(\pm) = 1.15 \text{ l mol}^{-1} \text{ s}^{-1}$ ). Table 2 shows that the free

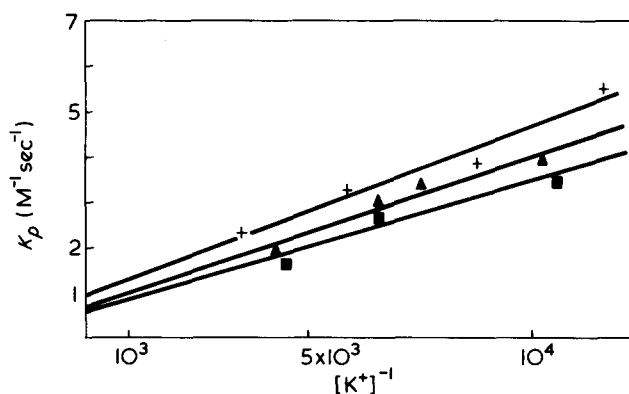

 Figure 6 Dependence of overall rate constants on K<sup>+</sup> cation concentrations. +, 0°; ▲, -6°; ■, -13°C

Table 2 Dissociation constants and absolute rate constants for polybutadienyl potassium in THF

$T$ (°C)	$K_D \times 10^9$ (M)	$k_p(-)$ (M <sup>-1</sup> s <sup>-1</sup> )	$k_p(\pm)$ (M <sup>-1</sup> s <sup>-1</sup> )
0	7.8	48000	<1
-6	9.4	36000	<1
-13	11.0	26000	<1



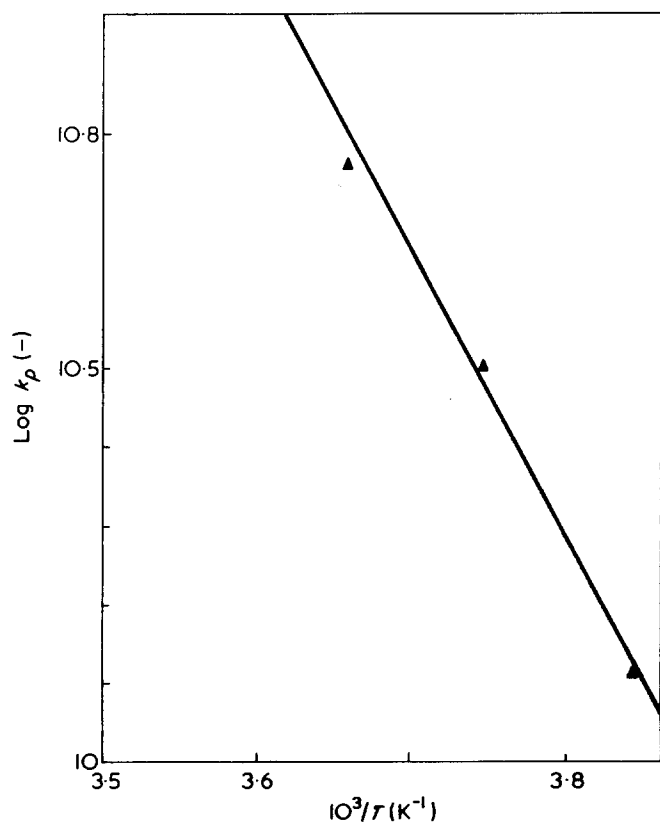


Figure 7 Determination of the activation energy upon free ions

ions assume practically the whole of the propagation process. Their relative concentration is low, but their reactivity is much higher than that of ion-pairs.

The slope of the straight line  $\ln k_p(-) = f(1/T)$  (Figure 7) gives a value for the activation energy for the propagation reaction by free ions:  $E(-) = 6.5$  kcal/mol. This value is near those observed for 2-vinylpyridine ( $E(-) = 6.5$  kcal/mol) and styrene ( $E(-) = 5.9$  kcal/mol) anionic polymerizations in THF. We were not able to measure with sufficient precision the activation energy for the propagation by ion-pairs, because the exact value of the corresponding absolute rate constants are difficult to estimate.

#### REFERENCES

- 1 Arest-Yakubovich, A. A. and Medvedev, S. S. *Dokl. Akad. Nauk SSSR* 1964, 159, 1066
- 2 Arest-Yakubovich, A. A., Gantmakher, A. R. and Medvedev, S. S. *Dokl. Akad. Nauk SSSR* 1966, 167, 1069
- 3 Bywater, S. and Worsfold, D. J. *Can. J. Chem.* 1967, 45, 1821
- 4 Bywater, S., Johnson, A. F. and Worsfold, D. J. *Can. J. Chem.* 1964, 42, 1255
- 5 Fontanille, M. and Sigwalt, P. *Bull. Soc. Chim. Fr.* 1967, p 4083
- 6 Cheradame, H., Vairon, J. P. and Sigwalt, P. *Eur. Polym. J.* 1968, 4, 13
- 7 Gourdenne, A. and Sigwalt, P. *Bull. Soc. Chim. Fr.* 1967, p 2249
- 8 Hay, J. N. and McCabe, J. F. *J. Polym. Sci. (A-1)* 1972, 10, 3451
- 9 Bhattacharyya, D. N., Lee, C. L., Smid, J. and Szwarc, M. *J. Phys. Chem.* 1965, 69, 612
- 10 Hostalka, H. and Schulz, G. V. *Z. Phys. Chem.* 1965, 45, 286
- 11 Funt, B. L. and Hornoff, V. *J. Polym. Sci. (A-1)* 1971, 9, 2429

# Fibrillation in the flow of polyoxymethylene melts

G. V. Vinogradov and B. V. Yarlykov

*Polymer Rheology Laboratory, Institute of Petrochemical Synthesis, USSR Academy of Sciences, Moscow 117912, USSR*

and M. V. Tsebrenko, A. V. Yudin and T. I. Ablazova

*Synthetic Fibres Laboratory, Kiev Technological Institute of Light Industry, Kiev 252011, Ukrainian SSR, USSR*

*(Received 23 October 1974)*

The phenomenon of specific fibrillation from melts of polymer mixtures is considered (using mixtures of polyoxymethylene with copolyamide as an example) when, in contrast to conventional fibre spinning methods, a complex thread consisting of hundreds of thousands of ultrafine fibrils oriented along the extrusion axis is obtained as a result of compressing the melt mixture through a single orifice (or upon extension of one stream of the polymer melt mixture). Here we deal with a radically new process of fibrillation of one of the polymers of the mixture (under the effect of the rheological forces at the capillary inlet) in the matrix of the other, when the number of the filaments in the thread is not determined by the number of the orifices in the die.

After solvent extraction (from the solidified extrudate) of the polymer forming the matrix the other component remains as a bundle of fine fibrils less than  $1\ \mu\text{m}$  in diameter. The microstructure of mixture extrudates depends on the rheological properties of the melt, the mixture composition, the conditions of mixing and extrusion. Capillary viscometry methods have revealed a drastic difference in the viscoelastic properties of melt mixtures as compared with the separate components.

## INTRODUCTION

As a rule, polymers in mixtures are thermodynamically incompatible. However, in spite of the multiphase structure of polymer systems, the polymers considerably affect each other as a result of mixing, and this is manifested in a radical change of their fine and supermolecular structure, thermodynamic and physicochemical properties. Owing to this, mixing of polymers is an efficient method for modifying their properties and obtaining products with pre-assigned new properties<sup>1,2</sup>. Thus, we have demonstrated the possibility of obtaining ultrafine fibrils and thin films by extruding melts of mixtures of thermodynamically incompatible polymers differing in crystallization rate, degree of crystallinity, or melting point, as well as melts of mixtures of crystallizable and amorphous polymers<sup>3</sup>. At present this problem is given some attention, mainly in the patent literature<sup>4</sup>. It should be noted that the production of fine synthetic fibres (of diameter less than  $1\ \mu\text{m}$ ) is extremely important and urgent. Such fibres are used in the production of filters for high-precision purifications (entrapment of particles  $0.01$  to  $0.001\ \mu\text{m}$  in size)<sup>5</sup>, high-quality materials, etc. Conventional methods for spinning (from polymer melts and solutions) can produce fibres of  $10$  to  $15\ \mu\text{m}$  diameter. The spinning of fibres, even of such a small diameter, involves great difficulties and requires intricate equipment.

Of particular importance are the problems of reinforcing polymer products with ultrafine fibrils. It was shown<sup>3,6</sup> that ultrafine synthetic fibrils can be obtained by extruding (or extending) melts of polymer mixtures of various nature: polyoxymethylene-copolyamides; polyoxymethy-

lene-homopolyamides; polyoxymethylene-polystyrene; polyoxymethylene-copolymers of ethylene and vinyl acetate (and other copolymers of ethylene); polyesters-polyamides; polyolefins-copolyamides; polyolefins-polyesters; polyamides-copolymers of ethylene, etc. The most significant results were obtained on mixtures of polyoxymethylene (POM) with copolyamides (CPA).

Since the phenomenon of specific fibrillation under review depends on rheological factors and results from the compression (by any method) of a melt of a polymer mixture through a duct, the present work investigates the viscous properties of melts of POM-CPA mixtures over a wide range of shear stresses, as well as the effect of the flow regimes on the microstructure of extrudates.

## EXPERIMENTAL

The objects under investigation were mixtures of a copolymer of formaldehyde with 2% of 1,3-dioxalane (POM) and a mixed copolyamide (CPA), which is a copolymer of caprolactam (44%), hexamethylene adipate (37%) and hexamethylene sebacate (19%). The characteristics of the polymers were reported earlier<sup>7</sup>.

The content of CPA in the mixtures varied from 0 to 100 wt %. The properties and microstructure of the extrudates of mixtures with a POM/CPA ratio of 60 : 40, 30 : 70, 20 : 80 were thoroughly investigated; they were selected on the basis of the results of Tsebrenko *et al.*<sup>8</sup> according to which these compositions showed the most pronounced change in the thermodynamic and structural properties of the polymers in the mixture as compared with the

Table 1 Capillary dimensions and deformation conditions

	Capillary diam., $D$ (mm)	Capillary length, $L$ (mm)	$L/D$	$\tau \times 10^4$ ( $N/m^2$ )	$\dot{\gamma}$ ( $sec^{-1}$ )
1	0.500	22.8	22.8		
2	0.786	7.9	10.0		
3	0.992	5.0	5.0		
4	1.000	22.5	22.5	0.27	1.2 to
5*	1.056	1.1	1.0	to 32	$5 \times 10^3$
6	1.118	46.6	41.6		
7	1.800	39.3	21.9		
8	3.000	79.7	26.6		

\* Capillary with  $L/D = 1.0$  was used with the aim of assessing the effect of  $L/D$  on the microstructure of mixture extrudates

initial components. For the other mixtures, the viscosity–composition relationships in the shear stress range of  $(0.89–5.76) \times 10^4 N/m^2$  were obtained. The polymers were mixed as described previously<sup>3</sup>. The viscous properties of the melts of the indicated systems were investigated on constant-pressure capillary viscometers at temperatures of 170, 190 and 210°C.

The capillary dimensions and the shear stress ( $\tau$ ) and rate ( $\dot{\gamma}$ ) range are given in Table 1.

The experimental data were treated by the conventional procedure, so that  $\tau$  and  $\dot{\gamma}$  were determined on the capillary wall. The root mean square of the arithmetical mean in determination of viscosity ( $\eta$ ) and ( $\dot{\gamma}$ ) was  $\pm 5\%$  (with 95% confidence).

The formed extrudate structure (obtained under definite conditions) was observed in thin transverse or longitudinal sections with the aid of a polarization microscope. To obtain sections, a piece of extrudate, 1 mm long, was dipped in epoxy resin in a gelatine capsule and held in a thermostat for 48 h until solidified. With the aid of a piezoelectric ultramicrotome UMTP-2, sections of 10–15  $\mu m$  thickness were obtained. The sections were inspected (in polarized light) under a microscope (magnification 57–420x) and photographed. The copolyamide was entirely dark (almost in all cases) in the microscope field of vision, the structural formations of the polyoxymethylene being very prominent against its background. In addition, the fibre bundles obtained after the polyamide was washed from the extrudate and distributed in the immersion liquid were investigated visually under a microscope. The copolyamide was extracted in a Soxhlet apparatus with ethyl alcohol at a temperature of 75°C. The time of removal of CPA depends on the size and the conditions under which the extrudate is obtained. The i.r. spectra of the ultrafine fibres were recorded on a UR-10 spectrometer with the use of NaCl/LiF prisms.

## RESULTS

### Viscous properties

Some authors<sup>9–11</sup> indicate the specific features of the properties of melts of polymer mixtures, which are hard to predict, knowing the viscosity and the elastic properties of the separate components. This also refers to the POM–CPA mixtures investigated in the present work. Having relatively close values of melt viscosities, POM and CPA form, on mixing, systems which differ drastically from the initial polymers as regards the viscous properties of their melts (Figure 1). It can be seen from Figure 1 that the nature of the curve  $\eta = f(\text{composition})$  depends on the

shear stress: at  $\tau < 6.30 \times 10^4 N/m^2$ , the curves lie above the viscosities of POM and CPA. In the shear stress regions above  $6.30 \times 10^4 N/m^2$  the nature of the viscosity–composition relationship changes radically; the curves lie below the viscosities of the POM and CPA melts and they have a minimum in the region of 80% concentration of the copolyamide. Besides, at high shear stresses for melt mixtures, the viscosity anomaly is very pronounced. Thus, if in the range of  $\tau$  from  $1.2 \times 10^4$  to  $3.2 \times 10^5 N/m^2$  the viscosities of the POM and CPA melts decrease about three times, for 60 : 40, 30 : 70, 20 : 80 mixtures POM/CPA, they decrease 17.6 and 38 times, respectively. In this respect the flow behaviour of the mixtures are like certain filled polymers<sup>14,15</sup>. The behaviour of these POM–CPA melt mixtures is probably connected, primarily, with the change of the phase state, shape, size and nature of distribution of the POM regions in the mixture melt, and this (as will be shown below) is supported by the results of the investigation into the microstructure of extrudates of mixtures obtained at high shear stresses.

Proceeding from the temperature dependence of the melt viscosity of the systems investigated we calculated the values of the apparent activation energy of the viscous flow  $E$ , which proved to be 12–15 kcal/mol. This means

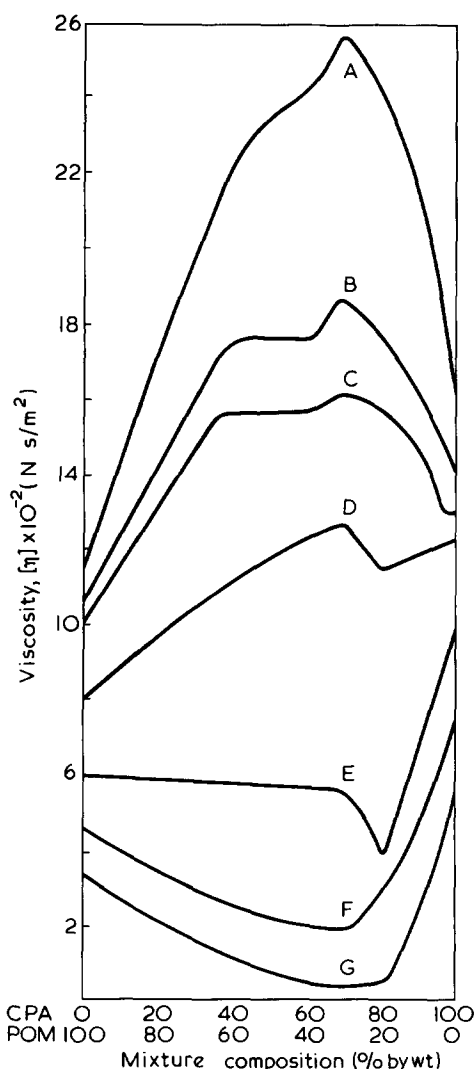


Figure 1 Dependence of viscosity of POM/CPA melt on composition at 190°C. Shear stress: A, 1.27; B, 3.93; C, 5.44; D, 6.30; E, 12.59; F, 19.52; G,  $31.62 \times 10^{-5}$  dyne/cm<sup>2</sup>

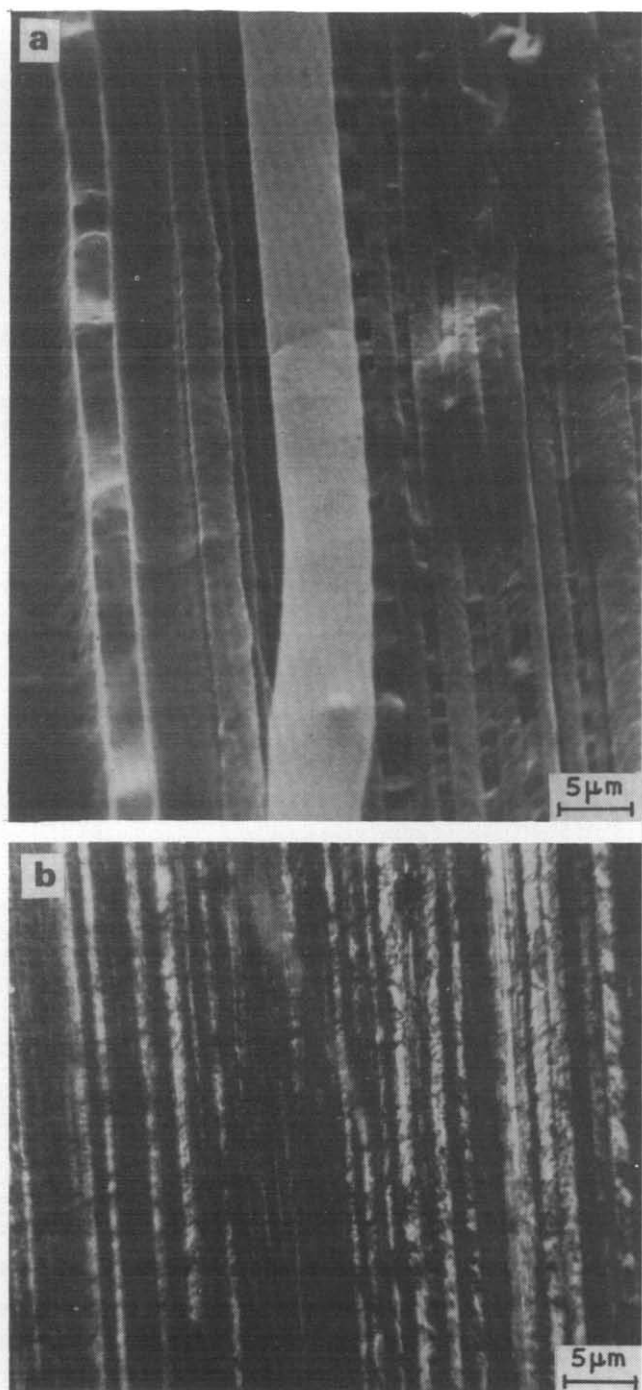


Figure 2 Electron photomicrograph of longitudinal section (a) and photomicrograph of longitudinal section (b) of POM/CPA extrudate

that in the temperature range from 190 to 210°C (when both polymers are in the fluid state) the fluidity of the mixtures is determined by the copolyamide ( $E_{\text{CPA}} = 12\text{--}15$  kcal/mol,  $E_{\text{POM}} = 7\text{--}9$  kcal/mol).

For POM/CPA melts, the pressure losses at the capillary inlet are small – the inlet corrections are equal to one radius at low shear stresses and two or three radii at high  $\tau$ . However, in flowing through a capillary, melt mixtures, unlike the initial polymers, manifest three-to-four-fold swelling of the melt stream after it leaves the capillary (with the exception of specimens obtained at 170°C). With an increase in the degree of dispersity of the initial POM powder the swelling increases. Thus, for instance, if the average diameter of the POM powder particles is 2  $\mu\text{m}$ , the issuing stream of the POM–CPA melt swells to about ten

times the capillary diameter and has a milky-white colour.

The above features of the viscoelastic properties of POM–CPA melts are due, primarily, to the above-described phenomenon of specific fibrillation, and this confirms the results of the investigation into the microstructure of mixture extrudates.

#### Extrudate microstructure

At a temperature of 170°C (i.e. below the melting point  $t_m$  of POM), composition mixtures of 60 : 40, 30 : 70, 20 : 80 POM/CPA are capable of flowing, but no fibres are then formed. The swelling of the stream leaving the capillary is insignificant and therefore difficult to record. After extraction of the CPA from the extrudate, the POM remains in powder form. Ultrafine polyoxymethylene fibres can be obtained only at temperatures above melting point of POM,  $t_m$  (Figure 2). An analysis of sections and washed fibre bundles (freed from CPA) has shown that with an increase in melt temperature the degree of dispersion of the POM in the extrudate increases (in the sense of reduced fibril diameter and increased number of the fibrils), and a more uniform fibril bundle is obtained, both from the point of view of fibril diameter distribution and the presence of balls, short fibrils, and films. The principal cause of this is evidently a reduction in melt viscosity with increasing melt temperature, which facilitates deformation of the POM particles in the direction of flow.

The shear stress strongly affects the microstructure of mixture extrudates. As  $\tau$  increases, the average diameter of the POM fibres decreases (from 3  $\mu\text{m}$ ) at  $\tau = 3.9 \times 10^4$  N/m<sup>2</sup> to values beyond the resolution of optical microscopes at  $\tau > 10^5$  N/m<sup>2</sup>; layer-like arrangement of the POM fibrils is observed, the layers being located closer to the capillary wall. The extrudate centre is impoverished in POM and the fibrils it contains are practically unobservable with an optical microscope (Figure 3). After the CPA is removed from such an extrudate, a set of concentric ultrafine fibrous tubes (films) remains with a small number of fibrils between them.

A similar ‘telescopic’ distribution of one polymer in the melt of the other (with the components being incompatible) was observed by Walczak<sup>14</sup> on polypropylene with an addition of poly(ethylene oxybenzoate) and by White *et al.*<sup>15</sup>, and Han and Yu<sup>9</sup> for polyolefin–polystyrene mixtures. On short capillaries, the concentricity of the extrudate structure is less pronounced (and is practically nil, for  $L/D = 1$ ), probably because the melt remains in the

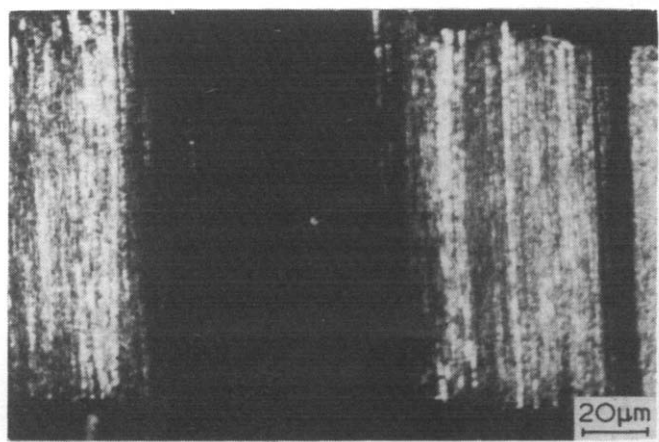


Figure 3 Photomicrograph of longitudinal section of extrudate of POM + 70% CPA mixture obtained at  $\tau = 3.2 \times 10^6$  dyne/cm<sup>2</sup>

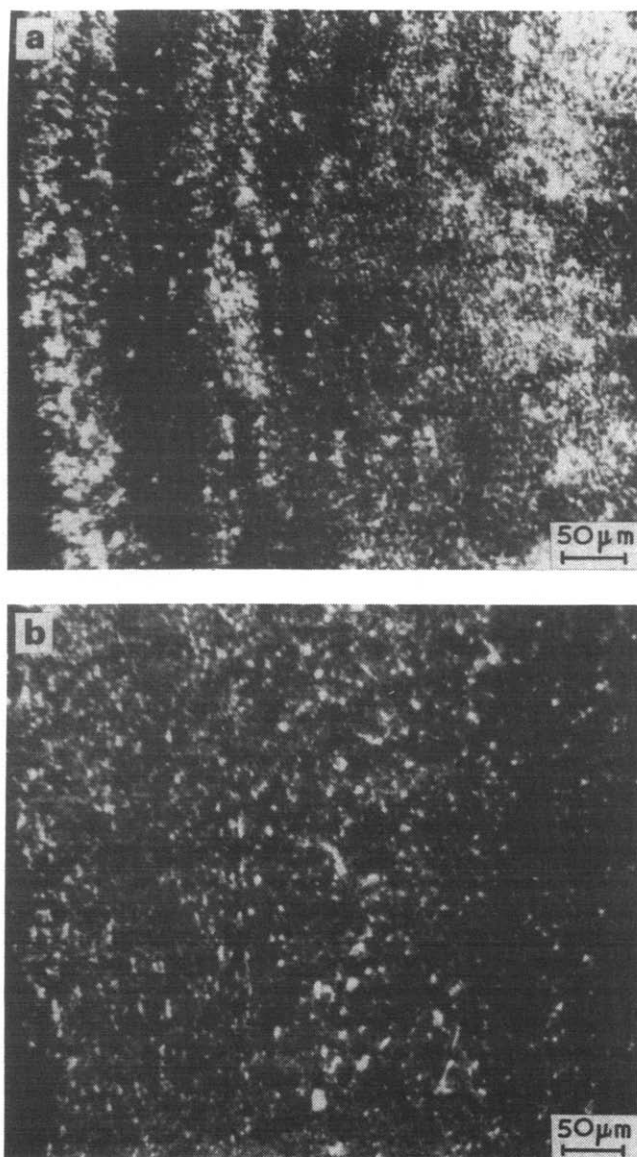


Figure 4 Effect of cooling conditions on microstructure of extrudate of POM + 70% CPA mixture. Temperature of extrudate reception: (a) +20°; (b) -40°C

capillary for only a short time. The shear stresses at which the extrudate has a 'telescopic' structure correspond to the region of sharp viscosity anomaly on the flow curves of the mixture melts. The aggregation of POM into tubular films is probably the main reason for the drastic increase in mixture fluidity.

If mixture extrudates are received, not in an air medium at -20°C, but in a dry ice-acetone mixture (-40°C), it is possible to considerably suppress the swelling of the stream and to fix the structure formed in the flow in the capillary.

An analysis of sections (and washed fibrils) has shown a strong influence of the cooling conditions (and hence of the swelling) of the extrudate on its microstructure, size, and the nature of distribution of the POM fibrils (Figure 4).

It is also possible to considerably restrict the adverse effect of stream swelling on the structure of the formed extrudate by die drawing (i.e. receiving the issuing stream at a constant rate). Here, the average diameter of the POM fibres decreases and the uniformity of the diameter distribution of the fibrils greatly improves (Figure 5); already on 1000% extension of the spinneret draw ratio 90% of all the fibres have a diameter of 1 μm. Extension

also results in a certain additional orientation of the POM fibres formed in the copolyamide matrix. It should be particularly emphasized, however, that fibrils obtained with a free flow of the melt from the capillary (i.e. practically without spinneret extension or with its negative value) prove to be well oriented in the direction of the extrusion axis. All this is clearly confirmed by X-ray analysis and by the infra-red dichroism method (Figure 6): thus, for instance, the dichroic ratio of the bands in the region of 1385 cm<sup>-1</sup> is 1.60.

Experimental data indicate a qualitative difference in the process of fibrillation for 60 : 40, 30 : 70, 20 : 80 POM/CPA mixtures. With decreasing content of the high-crystalline component (POM) the uniformity and homogeneity of the fibrils improves, their diameter decreases and their number increase considerably. This is in good agreement with the data of Bakeyev *et al.*<sup>16</sup>, according to which for most of the mixtures of incompatible polymers a decrease in the content of the higher-crystalline component in mixtures results in a gradual increase in its degree of dispersity and a decrease in scattering of the particle size.

Thus, the microstructure of extrudates depends on the composition of the mixture, the geometric dimensions of the capillary, and the conditions of flow and reception of the melt stream leaving the capillary.

## DISCUSSION

The numerous experimental results obtained by us in investigating the properties of melts and solutions of poly-

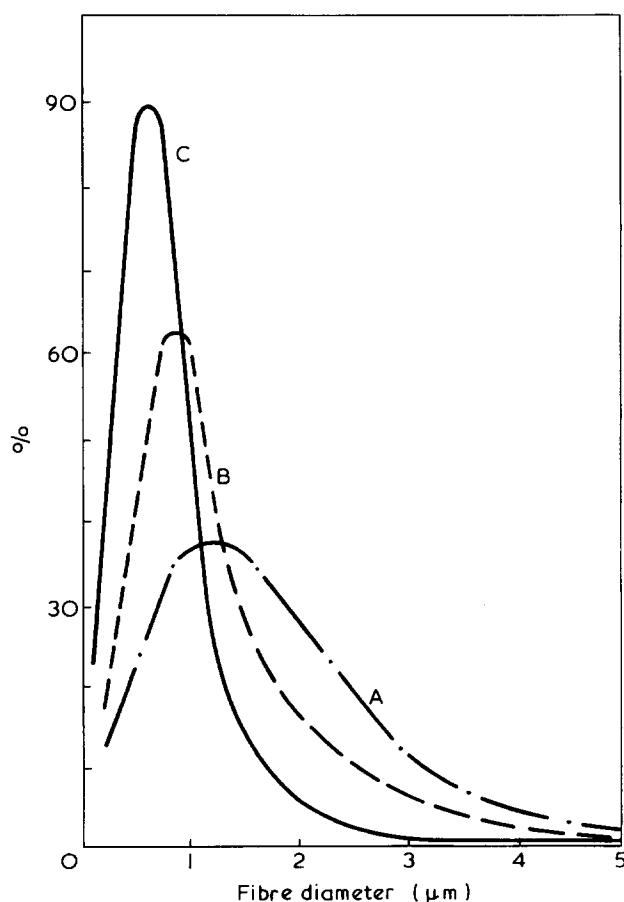


Figure 5 Differential curves of distribution of ultrafine POM fibrils obtained from extrudate of POM + 80% CPA mixture. Die extension: A, 200; B, 500; C, 1000%



Figure 6 I.r. spectra of ultrafine POM fibrils in polarized light parallel (---) and perpendicular (—) to fibre axis

mer mixtures indicate that fibrillation in the systems at hand is achieved, not after the melt leaves the die (i.e. not in the stage of stream solidification), but in the inlet zone of the capillary with a considerable longitudinal rate gradient. This constitutes the specificity of such fibrillation. Thus, when using capillaries with  $L/D \leq 1$  (i.e. actually dies), extrudates with extremely uniform ultrafine POM fibrils (in the absence of spinneret extension) were obtained.

Proceeding from the available experimental data, the mechanism of specific fibrillation can be visualized as follows.

A melt of two polymers, under certain conditions of mixture preparation and melting, is a heterogeneous system in which the dispersion medium is, for instance, copolyamide, and the dispersed phase, polyoxymethylene. The polymer melts under consideration are not homogeneous. It can be assumed that POM (at temperatures relatively close to its melting point) is in a liquid-crystalline state<sup>17</sup> in the melt mixture and therefore differs from the copolyamide in its viscoelastic characteristics. In the inlet zone of the capillary the POM droplets elongate mainly under the effect of extension, with the formation of ultrafine fibrils oriented along the extrusion axis. Here, directed crystallization of POM may occur under the influence of tensile and shear forces. Indeed, it is known from the literature<sup>18</sup> that the extremely high crystallization rate of POM and the absence of the latent period of crystallization are due to the small difference in the structure of the liquid and crystalline phases (the molecules in the melt have the same spiral conformation as in the crystal), and the presence of highly ordered melt regions. Therefore

shear or extension (even of low intensity) may initiate crystallization of POM, as has actually been observed for a number of other polymers<sup>19,20</sup>. Moreover, Mikhailov and Nedkov<sup>21</sup> have shown that on cooling of the melt POM crystallizes (at  $t > 160^\circ\text{C}$ ) with the formation of plastic crystals (this should be considered as a phase transition), and then, on further cooling, the plastic crystals transform to solid ones. Under the effect of shear and extension, directed crystallization of POM may be initiated in the form of such plastic crystals even at the investigated spinning temperatures ( $190^\circ\text{C}$ ), and this must yield fibrils of infinite length, given the appropriate component ratios and flow conditions. It is due to such directed crystallization in the capillary that POM fibrils acquire a considerable orientation (Figure 6) immediately after leaving the capillary.

The presence of ultrafine crystallized POM fibrils in a flowing melt explains the observed peculiarities of the viscous and elastic properties of POM-CPA melts. Indeed, the viscosity of such a highly filled (virtually reinforced) system must be much higher than the viscosity of the initial components, which is actually the case at  $\tau < 6.3 \times 10^4 \text{ N/m}^2$ . The directed flow of streamlets and crystallization of POM in the form of ultrafine fibrils is also associated with enormous swelling of the stream on leaving the capillary. In connection with the above it is necessary to mention the work<sup>22</sup> where increased swelling of the extrudate (by a factor of 2.5) of polyethylene or polystyrene was observed on addition of small fractions of 1% of long flexible fibrils of Teflon to the melt.

No swelling was observed for POM/CPA extrudates obtained at  $170^\circ\text{C}$  (i.e. when a suspension of the POM powder in the CPA melt was present). A change in the phase state of POM must also increase the swelling. Thus, according to the data of Southern *et al.*<sup>23</sup>, the beginning of crystallization of polyethylene when flowing through a capillary coincided with strong swelling of the stream leaving the capillary.

The drastic decrease in mixture melt viscosity is probably due to the change in the nature of distribution of the POM fibrils along the capillary radius; the fibrils are thrust towards the capillary wall with the formation of tubular films, the central part of the flow being enriched in CPA (Figure 3). In the rheological sense the behaviour of the systems investigated is similar to the behaviour of a flow of filled polymers<sup>12,13</sup>.

Direct experimental results indicate that the microstructure obtained in a flow through a capillary undergoes considerable changes in the swelling zone (Figure 4): 'telescopicity' of the distribution of the POM fibres is observed, the latter aggregating into tubular films; the fraction of short fibrils and balls increases. Han and Yu have also shown experimentally<sup>9</sup> that in the course of cooling of extrudates of polyolefin-polystyrene mixtures on leaving the capillary, their structure changes, and this is accompanied by the rupture of the regions of the dispersed phase elongated in the direction of the flow, with the formation of drops.

The phenomenon of specific fibrillation from polymer melt mixtures is of interest not only from the point of view of obtaining a new type of fibrous material and mastering the spinning of a complex thread or yarn through a single orifice, but also from the point of view of the theory of processing of mixtures, and methods of fibrillation of one of the polymers in the mass of the other with the formation of reinforced materials.

REFERENCES

- 1 Natov, M. A. and Dzhagarova, E. Khr. *Vysokomol. Soedin. (A)* 1966, 8, 1835
- 2 Starita, J. M. *Trans. Soc. Rheol.* 1972, 16, 339
- 3 Tsebrenko, M. V., Yudin, A. V., Kuchinka, M. Yu., Vinogradov, G. V. and Zubovich, K. A. *Vysokomol. Soedin. (B)* 1973, 15, 566
- 4 Br. Pat. 1 280 676 (1972); FDR Pat. 1 931 822 (1971)
- 5 Petryanov, I. V. and Kozlov, V. I. 'Voloknistyie filtruyuschiye materialy' FP (Fibrous Filtering Materials), Znaiye, Moscow, 1968
- 6 Yudin, A. V., Tsebrenko, M. V., Kuchinka, M. Yu. and Vinogradov, G. V. *Compl. Sci. Res. Work Ukr. High Coll.* 1974, issue 7, p 3
- 7 Tsebrenko, M. V., Yakob, M., Kuchinka, M. Yu., Yudin, A. V. and Vinogradov, G. V. *Int. J. Polym. Mat.* 1974, 3, 81
- 8 Tsebrenko, M. V., Vinogradov, G. V., Yudin, A. V., Goikhman, A. Sh. and Benzar, A. I. *Vysokomol. Soedin. (A)* 1973, 15, 1719
- 9 Han, C. D. and Yu, T. C. *J. Appl. Polym. Sci.* 1971, 15, 1163
- 10 Han, C. D. and Yu, T. C. *Polym. Eng. Sci.* 1972, 12, 81
- 11 Minoshima, N., Kobayashi, S., Shimura, M. and Kinoshita, Y. *Kobunshi Kagaku* 1971, 28, 953
- 12 Malkin, A. Ya., Epple, G. V. and Grishchuk, A. I. *Kolloid-Z.* 1972, 34, 550
- 13 Vinogradov, G. V., Malkin, A. Ya., Plotnikova, E. P., Sabsay, O. Yu. and Nikolayeva N. B. *Int. J. Polym. Mat.* 1972, 2, 1
- 14 Walczak, Z. K. *J. Appl. Polym. Sci.* 1973, 17, 169
- 15 White, J. L., Ufford, R. C., Dharod, K. R. and Price, R. C. *J. Appl. Polym. Sci.* 1973, 16, 1313
- 16 Bakeyev, N. F., Berestneva, Z. A., Zharikova, Z. F. and Kazhdan, M. V. *Vysokomol. Soedin. (A)* 1973, 15, 2128
- 17 Smit, P. P. A. *Kolloid-Z. Z. Polym.* 1972, 250, 27
- 18 Roshchupkin, V. P., Andreyev, N. S. and Goncharov, T. K. *Vysokomol. Soedin. (A)* 1972, 14, 477
- 19 Cristal, R. G. and Southern, J. H. *J. Polym. Sci. (A-2)* 1971, 9, 1641
- 20 Keller, A. and Machin, M. J. *J. Macromol. Sci. (B)* 1967, 1, 41
- 21 Mihajlov, M. and Nedkov, E. *J. Polym. Sci. (C)* 1972, 38, 33
- 22 Busse, W. F. *J. Polym. Sci. (A-2)* 1967, 5, 1249
- 23 Southern, J. H., Weeks, N., Porter, R. S. and Cristal, R. G. *SPE Techn. Paper* 1971, 17, 232

# Some basic aspects of flame resistance of polymeric materials

D. W. van Krevelen

Akzo Research and Engineering bv, Arnhem, The Netherlands

(Received 27 November 1974; revised 27 January 1975)

For a better insight into flame resistance and flame extinction it is useful to split the combustion process into its constituent elements. It then appears that the thermal decomposition is the first link in a series of reactions and therefore a better understanding of this decomposition is a prerequisite. Further, it is found that the amount of char and the amount of incombustible gases that may be formed in thermal decomposition are very important quantitative measures of flame resistance. For a large number of model substances the char residue upon pyrolysis has been determined. The residue is found to be very clearly related to the chemical structure of the polymer, so much so that the amount of char can be predicted from the structure. Finally, it has been demonstrated that there is a very significant relation between the pyrolysis residue (%) and the (limiting) oxygen index.

## INTRODUCTION

Never before has there been such interest in the problem of the flammability of materials, now that we are faced with the imminent introduction of stringent legislation.

People have always been accustomed to the presence and use of flammable matter in the form of, for instance, building, clothing and auxiliary materials. But the problem at issue has become acute because of the present-day phenomenon of people crowding in confined spaces (sometimes of great height), such as blocks of flats, office buildings, department stores, hospitals and jumbo jets, with all the hazards this implies.

The point to be considered here in particular may, in short, be formulated as follows: is it possible to predict the degree of flammability of a polymeric material on the basis of its chemical structure?

As index of the flame resistance (ignition and flame propagation) we have chosen the (limiting) oxygen index  $OI$  value<sup>1</sup>. This limiting  $OI$  is the minimum fraction of oxygen in an oxygen-nitrogen mixture that is just sufficient to maintain combustion (after ignition) of the material. Table 1 gives the  $OI$  values for a number of polymeric materials. A material must be considered flammable as long as the  $OI$  value  $\leq 0.26$ .

## ESSENTIALS OF FLAMMABILITY AND FLAME RETARDANCE

What happens in broad outline when a material burns is schematically indicated in Figure 1<sup>2</sup>. Fundamentally there are two consecutive chemical processes — decomposition and combustion — connected by ignition and thermal feedback. Primarily the material decomposes (pyrolysis), which requires heat. The decomposition products are combusted, during which heat is generated. This heat is (partly) used to support the decomposition. An ignition mechanism is essential. Of great importance are the heat effects  $Q_1$  and  $Q_2$  as well as the available area,  $A$ , for exchange of heat and matter. To be flame-resistant a material should have a high  $Q_1$  value, a low  $Q_2$  value and

a low  $A$  value.  $Q_2$  will be low if only small amounts of combustible gases develop in the pyrolysis, for instance, because the material chars considerably and mainly splits off carbon dioxide and water. The residue of pyrolysis (or the sum of this residue and the weight of carbon dioxide

Table 1 Oxygen indices of polymers

Polymer	$OI$	Polymer	$OI$
Polyformaldehyde	0.15	Wool	0.25
Poly(ethylene oxide)	0.15	Polycarbonate	0.27
Poly(methyl methacrylate)	0.17	Nomex®	0.285
Polyacrylonitrile	0.18	PPO®	0.29
Polyethylene	0.18	Polysulphone	0.30
Polypropylene	0.18	Phenol-formaldehyde resin	0.35
Polyisoprene	0.185	Neoprene®	0.40
Polybutadiene	0.185	Polybenzimidazole	0.415
Polystyrene	0.185	Poly(vinyl chloride)	0.42
Cellulose	0.19	Poly(vinylidene fluoride)	0.44
Poly(ethylene terephthalate)	0.21	Poly(vinylidene chloride)	0.60
Poly(vinyl alcohol)	0.22	Carbon	0.60
Nylon-6,6	0.23	Polytetrafluoroethylene	0.95
Penton®	0.23		

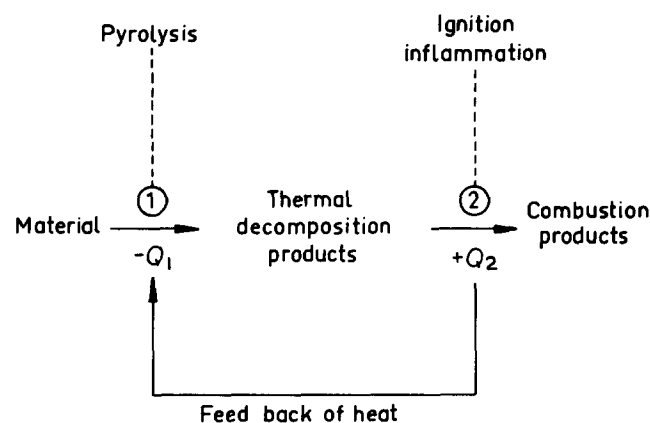


Figure 1 Consecutive reactions during burning



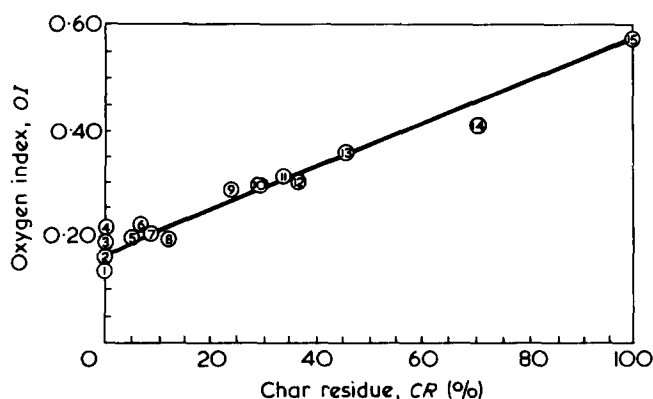


Figure 2 Correlation between OI and CR. 1, Polyformaldehyde; 2, polyethylene, polypropylene; 3, polystyrene, polyisoprene; 4, nylon; 5, cellulose; 6, poly(vinyl alcohol); 7, PETP; 8, polyacrylonitrile; 9, PPO®; 10, polycarbonate; 11, Nomex®; 12, polysulphone; 13, Kynol®; 14, polyimide; 15, carbon

and water formed by pyrolysis) may be used as a measure of the non-flammability.

This is proved by the fact that there is a significant correlation<sup>3</sup> between the char residue (CR) and the oxygen index of polymers, as is shown in Figure 2\*. This linear relationship can be represented by:

$$OI \times 100 = 17.5 + 0.4CR \quad (1)$$

where CR is the char residue in wt % at 850°C. In view of this interesting correlation it seemed useful to make an elaborate investigation into the relation between the residue of pyrolysis and the constitution of polymers.

### ESSENTIALS OF PYROLYTIC DECOMPOSITION

Thermal decomposition of a non-volatile organic material is accompanied with the phenomena illustrated schematically in Figure 3<sup>3</sup>. The pyrolysis generally proceeds in two stages: a primary decomposition in the range 350° to 550°C; in this stage there will often be softening of the material and formation of tar mist. Very often a residue of pyrolysis (semicoke) is obtained; this, however, does not happen in the pyrolysis of fully aliphatic polymers which are free from halogen and -OH groups.

Softening need not occur either, provided that the starting substance is strongly crosslinked or contains reactive dehydrogenating groups (-OH, =OH, halide). Basically the decomposition of the polymeric starting material into tar and gas on the one hand and char on the other is a disproportionation reaction which leads to hydrogen-enriched and hydrogen-poor fragments.

Above 550°C there will often be a second pyrolysis stage; primary char of the first stage will then be carbonized into a final char residue with attendant formation of a gas very rich in hydrogen. This second pyrolysis stage terminates in the range of 800° to 1000°C.

This scheme of pyrolysis as just described, or variants of it, will be recurrently encountered. This mechanism of pyrolysis is considered in the light of pyrolysis experiments with different series of model substances. For the purpose of comparison (some materials are highly heat resistant!) a pyrolysis temperature of 850°C is selected in all cases.

\* This correlation is not valid for halogen-containing polymers. This is a direct consequence of the fact that halogen radicals are combustion inhibitors and therefore influence the interaction between pyrolysis and ignition.

### INVESTIGATION INTO THE PYROLYSIS OF MODEL SUBSTANCES

#### Aliphatic and cyclo-aliphatic polymers

Table 2 summarizes the pyrolysis results for these substances on the basis of our own measurements. In general, aliphatic and cyclo-aliphatic polymers do not give any residue on pyrolysis. This even applies to substances such as polystyrene and poly(vinyl carbazole), although they have an aromatic or heterocyclic side group linked to an aliphatic chain. This absence of a pyrolysis residue is due to the high hydrogen content of these polymers, as a result of which the entire decomposition product can be disproportionated into volatile substances.

There are, however, a number of exceptions, viz. those polymers that contain free -OH groups and those that contain halogen or cyanide groups. The -OH-containing polymers are found to yield a small char residue when they contain the group -CHOH- [cellulose, poly(vinyl alcohol)]. The halogen-containing polymers are a special class. Some of them form a small char residue, others none at all. That these polymers are non-flammable is partly to be attributed to the splitting off of non-combustible gases such as HCl, HF and C<sub>2</sub>F<sub>4</sub>, which seal the surface of the material from the combustion air.

The -CN-containing polymer polyacrylonitrile must be considered an exception in that it readily cyclizes and therefore does give a char residue; but on the other hand, it gives off much flammable gas, so that it is not flame resistant.

#### Polymers of the (-ArCH<sub>2</sub>-)<sub>n</sub> type with variable Ar group

Polymers of this type have been prepared by Wolfs *et al.*<sup>5</sup> and also subjected to pyrolysis experiments. The object then was to unravel the mechanism of pyrolysis from coal to coke by means of model substances. The polymers were prepared by reacting the respective aromatic hydrocarbons with formaldehyde in the form of paraformaldehyde, using nitrobenzene as solvent and anhydrous zinc chloride (dissolved in glacial acetic acid) as condensation catalyst. The reaction temperature was about 110°C, the reaction time about 24 h. The paraformaldehyde used was radioactive, so that from the measured value of the

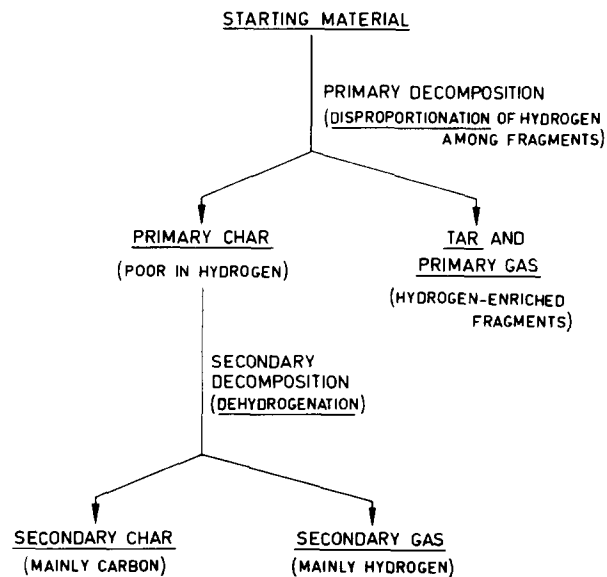
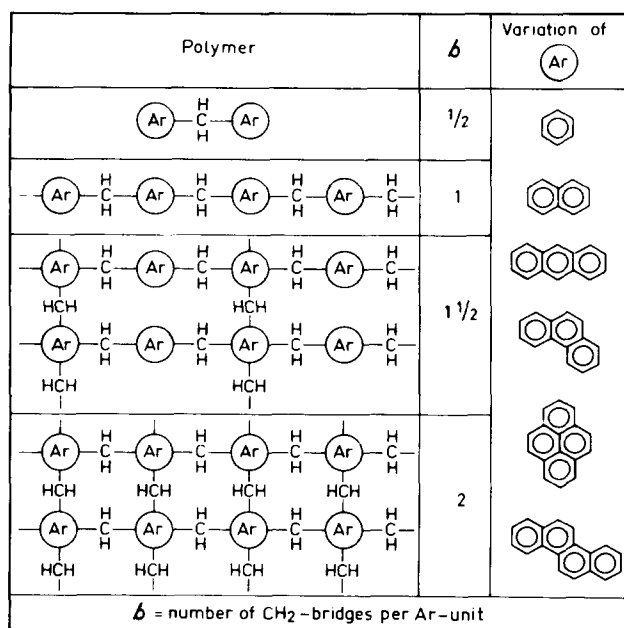
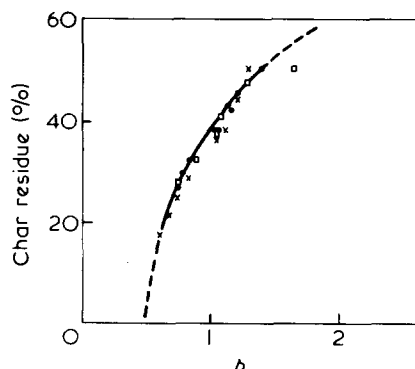


Figure 3 Basic mechanism of pyrolysis

Table 2 Pyrolysis of polymers with aliphatic chains

Polymer	Elemental composition	Residue of pyrolysis (%)	Per structural unit		
			Mol. wt	Residue	C equiv.
Polyethylene	$\text{C}_2\text{H}_4$	0	28	0	0
Polypropene	$\text{C}_3\text{H}_6$	0	42	0	0
Polyisobutene	$\text{C}_4\text{H}_8$	0	56	0	0
Polybutadiene	$\text{C}_4\text{H}_6$	0	54	0	0
Polyisoprene	$\text{C}_5\text{H}_8$	0	68	0	0
Polystyrene	$\text{C}_8\text{H}_8$	0	104	0	0
Poly(vinyl carbazole)	$\text{C}_{14}\text{H}_{11}\text{N}$	(0.3)	193	0	0
Poly(methylene oxide)	$\text{CH}_2\text{O}$	0	30	0	0
Poly(ethylene oxide)	$\text{C}_2\text{H}_4\text{O}$	0	44	0	0
Nylon-6	$\text{C}_6\text{H}_{11}\text{ON}$	0	113	0	0
Qiana®	$\text{C}_{25}\text{H}_{44}\text{O}_2\text{N}_2$	0	404	0	0
Polyacrylonitrile	$\text{C}_3\text{H}_3\text{N}$	12	53	6.3	0.53
Poly(vinyl chloride)	$\text{C}_2\text{H}_3\text{Cl}$	10	62.5	6.3	0.53
Poly(vinylidene chloride)	$\text{C}_2\text{H}_2\text{Cl}_2$	26	97	25	2.1
Polytetrafluoroethylene	$\text{C}_2\text{F}_4$	0	100	0	0
Poly(vinyl alcohol)	$\text{C}_2\text{H}_5\text{O}$	7	44	3.1	0.25
Cellulose	$\text{C}_6\text{H}_{10}\text{O}_5$	5	162	8.1	0.67
Poly(methyl methacrylate)	$\text{C}_5\text{H}_8\text{O}_2$	0	100	0	0


 Figure 4 Polymers of type  $(\text{Ar})(\text{CH}_2)_b$ 

 Figure 5 Char residue as a function of parameter  $b$ . ●, Anthracene; X, phenanthrene; □, pyrene

radiation intensity of the purified polymer the exact number of  $-\text{CH}_2-$  bridges per aromatic unit,  $b$ , could be determined. The parameter  $b$  was varied from about 0.6 to about 1.5.

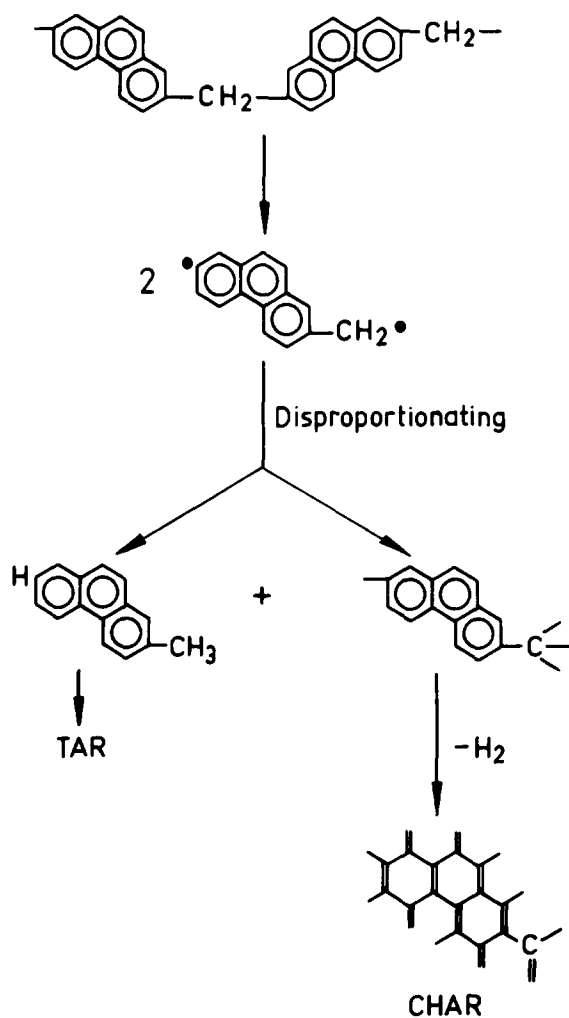
Figure 4 indicates the structure of the polymers and the variation of the aromatic unit (Ar). The thermal behaviour of the polymers was in accordance with expectation. As long as  $b \leq 1$ , the polymers were soluble and fusible. If  $b \leq 0.5$  (dimer), total volatilization becomes possible without giving a char residue, since then the boiling point is sufficiently low ( $<350^\circ\text{C}$ ).

With  $b$  higher than 1, so that crosslinking occurs, softening will take place merely as a result of thermal decomposition, when also a high degree of swelling is observed. This swelling decreases with increasing value of  $b$ ; at  $b > 1.3$  softening and swelling no longer take place. Figure 5 shows the percentages of char residue. By following the decomposition with thermogravimetric and elemental analysis and radiology, it was possible to unravel the mechanism of this pyrolysis. The results of this investigation led to the following conclusions: (1) with the type  $(-\text{ArCH}_2-)_n$  polymer the division between the primary and secondary stages of the pyrolysis is very sharp (selective). Below  $550^\circ\text{C}$  all tar is formed, but hardly any gas; above this temperature there is only gas evolution; (2) the radioactive carbon fraction which is left in the primary residue (semi-coke) at  $500^\circ\text{C}$  is equal to that in the starting material; the carbon in the  $\text{CH}_2$  bridges consequently is not split off selectively; (3) in each structural unit the amount of hydrogen left at  $550^\circ\text{C}$  in the residue is exactly equal to the amount of aromatic hydrogen in the starting material, so that hydrogen splits off selectively; (4) in the secondary pyrolysis all the (originally aromatic) hydrogen is removed, but only little carbon. Quantitative interpretation of the results of these experiments is possible with the aid of the rough and somewhat idealized reaction scheme shown in Figure 6.

Additional experiments have shown that when the Ar group concentration becomes large, i.e. when it contains more than about 25 C atoms, the entire Ar group is left in the residue and only the  $\text{CH}_2$  bridges are cracked.

Table 3 Pyrolysis of  $[-Ar(X)CH_2-]_n$  polymers

Aromatic starting material	X	Elemental composition	Residue of pyrolysis (%)	Per structural unit		
				Mol. wt	Residue	C equiv.
Benzene	—	$C_7H_6$	37	90	33.5	2.8
Phenetole	$-OC_2H_5$	$C_9H_{10}O$	40	134	53.5	4.5
Phenol	$-OH$	$C_7H_6O$	45	106	47.5	4.0
Cresol	$-CH_3, -OH$	$C_8H_8O$	30	120	36	3.0
Naphthalene	—	$C_{11}H_8$	37	140	51.5	4.2
Methylnaphthalene	$-CH_3$	$C_{12}H_{10}$	37	154	57	4.8
Naphthol	$-OH$	$C_{11}H_8O$	60	156	93.5	7.8


 Figure 6 Pyrolysis of  $(ArCH_2)_n$  polymer

#### Polymers of the $[-Ar(X)CH_2-]_n$ type (with variable X)

A second type of polymers prepared by Wolfs *et al.*<sup>5</sup> is that of substituted aromatic units linked by  $CH_2$  bridges. Some results are listed in Table 3. The nature of the functional group X appears to have considerable influence on the results of the pyrolysis. Roughly, 3 types of functional groups may be distinguished. (a)  $X = -CH_3, (-alkyl, -C_6H_5)$ : the division between primary and secondary pyrolysis is less sharp here, and formation of tar is accompanied by the production of gas. In the disproportionation alkyl hydrogen as well as the  $CH_2$  bridge hydrogen are used. (b)  $X = -OCH_3, -O-alkyl$ : in the primary pyrolysis the entire alkoxy group appears to split off, these polymers behaving similarly to those of the series  $(ArCH_2-)_n$ . (c)  $X = -OH, (-Cl, -Br, =O)$ : these groups are capable of

 Table 4 Pyrolysis of  $[-Ar(X)Y-]_n$  polymers

Polymer	Groups		Elemental composition	Residue %	Per structural unit		
	Y	X			MW	Residue	C-equiv
$-C_6H_4-OH$	—	—	$C_8H_4$	65	76	49	4.1
$-C_6H_4-O-$	—	$-OH$	$C_8H_4O$	75	92	69	5.7
$-C_6H_4-CH_2-$	$-CH_2-$	—	$C_7H_6$	37	90	33	2.8
$-CH_2-C_6H_4-CH_2-$	$-CH_2-CH_2-$ (p)	—	$C_8H_8$	30	104	31	2.6
$-CH_2-C_6H_4-CH_2-$	$-CH_2-CH_2-$ (m)	—	$C_8H_8$	10	104	10	1.0
$-C_6H_4-CH_2-$	$-CH_2-$	$-OH$	$C_7H_6O$	45	106	48	4.0
$-C_6H_4-O-$	$-O-$	—	$C_6H_4O$	50	92	46	3.9
$-C_6H_4-O-$	$-O-$	—	$C_6H_4O$	47	92	43	3.7
$-C_6H_4-O-$	$-O-$	$2-CH_3$	$C_8H_8O$	28	120	33.5	2.8
$-C_6H_4-O-$	$-O-$	$-CH(CH_3)_2$	$C_9H_{10}O$	10	134	13	1.1
$-C_6H_4-O-$	$-O-$	$2-C_6H_5$	$C_{18}H_{12}O$	44	244	107	9.0
$-C_6H_4-S-$	$-S-$	—	$C_8H_4S$	41	108	44	3.7
$-C_6H_4-NH-$	$-CO-NH-$ (p)	—	$C_7H_5ON$	43	119	51	4.3
$-NH-C_6H_4-CO-$	$-CO-NH-$ (m)	—	$C_{12}H_{10}O_2N_2$	35	238	83	6.9
$-OC-C_6H_4-COO-$	$-C-O-(CH_2)_2-O-C-$	—	$C_{10}H_8O_4$	8	192	15	1.25
$-C(CH_3)_2-C_6H_4-C(CH_3)_2-$	$-C-(CH_2)_2-O-C-$	—	$C_{18}H_{16}O_2$	24	254	61	5.1
$-O-C(CH_3)_2-C_6H_4-C(CH_3)_2-O-$	$-C-(CH_3)_2-+2O-C-$	—	$C_{27}H_{20}O_2S$	40	442	177	16.7
$-O-S-C_6H_4-S-O-$	$-SO_2-+2O-$	—	$C_{12}H_8O_2S$	34	248	84	7.0

reacting with H atoms and therefore give rise to post condensation (crosslinking). The plastic range in the decomposition is consequently strongly narrowed and swelling will hardly occur. The char residue is higher than in the case of the non-substituted aromatic units.

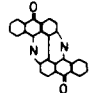
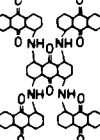
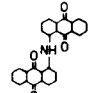
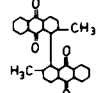
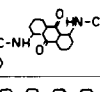
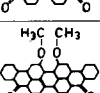
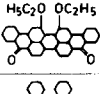
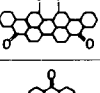
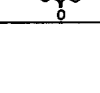
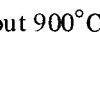
#### Polymers of the $[-Ar(X)Y-]_n$ type (with variable $-Y-$ )

A number of representatives of this type of polymer, where Y is a varying bridge structure, have been prepared and investigated by Wolfs *et al.*<sup>5</sup> Table 4 gives the data of Wolfs as well as results of recent measurements carried out with commercial polymers at the author's laboratory. Both the group X and the bridge structure Y appear to have considerable influence on the amount of char residue. In general,  $CH_2$  bridges reduce the char residue; this residue is also decreased by side groups of the alkyl type but increased by side groups of the OH type.

#### Condensed aromatic model substances containing multi-ring systems

Some years ago Riley and coworkers<sup>6</sup> carried out pyrolysis experiments with dyes built up of highly condensed aromatic systems, derivatives of anthrone and benzanthrone. Although these are not polymeric substances, the volatility upon heating (without decomposition) is nil, so that for our purpose they are particularly useful. Table 5 gives the results of the experiments, from which the following conclusions arise: (a) during pyrolysis alkoxy groups as well as alkyl groups split off entirely; (b) phenyl groups and phenoxy groups also split off entirely; phenyl groups contribute to a very small extent to the formation of char

Table 5 Pyrolysis of condensed aromatic model substances

Substance	Formula	Residue of pyrolysis (%)	Per structural unit		
			MW	Residue	C-equiv
Flavantrone $C_{28}H_{12}O_2N_2$		84	418	350	29
1,1',4',5',8'-Pentanthrimide $C_{70}H_{36}O_{10}N_4$		76	1092	830	69
1,1'-Dianthrimide $C_{28}H_{15}O_4N$		76	429	326	27
2,2'-Dimethyl-1,1'-dianthraquinoyl $C_{30}H_{10}O_4$		63	442	279	23
1,5-Dibenzoyl-aminoanthraquinone $C_{28}H_{18}O_4N_2$		45	446	201	168
Dioxanthrone $C_{34}H_{16}O_2$		82	444	364	30
16,17-Dimethoxy-dibenzanthrone $C_{36}H_{20}O_4$		77	516	396	33
16,17-Diethoxy-dibenzanthrone $C_{38}H_{24}O_4$		77	544	418	35
16,17-Dibenzoxy-dibenzanthrone $C_{46}H_{24}O_4$		62	640	396	33
Ananthrone $C_{22}H_{10}O_2$		77	306	236	19.6

residue; (c) at about 900°C oxygen and nitrogen have largely split off.

Heterocyclic polymers of the [-Het(X)Y-]<sub>n</sub> type

A fair amount of data on these classes of substances is to be found in the literature<sup>7-11</sup>. The available data are listed in Tables 6-8. Further analysis shows that the general rules found for the previously mentioned classes of substances also apply here.

CONCLUSIONS FROM EXPERIMENTS WITH MODEL SUBSTANCES

Careful analysis of all experimental data indicated that during pyrolysis all the functional groups making up a polymer behave very regularly. Each functional group in principle contributes to the residue of pyrolysis in its own characteristic way. Some corrections must be made as a result of the disproportioning mechanism, which is primarily influenced by the non-aromatic hydrogen. This means that the char-forming tendency of a polymer is an additive property which may be calculated from group contributions. The char-forming tendency (CFT) is quantified here as the amount of char per structural unit of the

Table 6 Pyrolysis of heterocyclic polymers

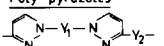
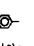

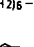

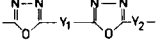
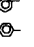
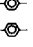
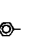
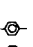
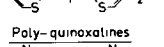
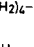

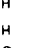
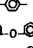
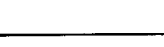
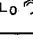
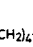
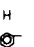

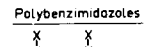
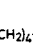

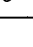
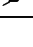
Polymer	Groups		Elemental composition	Residue of pyrolysis (%)	Per structural unit		
	Y1 or X	Y2 or Y			MW	Residue	C-equiv
Poly-pyrazoles 			$C_{18}H_{12}N_4$	59	284	168	14.0
			$C_{18}H_{20}N_4$	42	292	123	10.3
Poly-oxadiazoles 			$C_{16}H_8O_2N_4$	35	288	101	8.5
			$C_{16}H_8O_2N_4$	40	288	115	9.6
Poly-thiazoles 			$C_{18}H_8N_2S_2$	58	316	183	15.3
			$C_{16}H_{12}N_2S_2$	39	296	115	9.6
Poly-quinoxalines 	H		$C_{22}H_{12}N_4$	78	332	259	21.5
	H		$C_{26}H_{16}N_4O$	65	424	275	22.9
			$C_{40}H_{24}N_4O$	70	576	405	33.6
Polybenzimidazoles 	H		$C_{12}H_{12}N_4$	43	212	91	7.6
	H		$C_{14}H_8N_4$	70	232	162	13.6
			$C_{24}H_{16}N_4$	68	360	245	20.4

Table 7 Pyrolysis of heterocyclic polymers (continued)







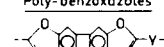

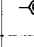
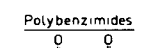

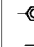
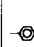

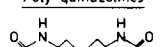

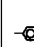


Polymer	Group -Y-	Elemental composition	Residue of pyrolysis (%)	Per structural unit		
				MW	Residue	C-equiv
Poly-benzimidazoles (cont'd) 	$(CH_2)_4$	$C_{18}H_{16}N_4$	46	288	132	11.0
		$C_{16}H_{10}N_4$	67	258	173	14.4
		$C_{20}H_{12}N_4$	75	308	231	19.2
		$C_{24}H_{14}N_4$	73	358	261	21.8
		$C_{24}H_{14}N_4$	40 ?	358	143	11.9
		$C_{24}H_{14}N_4$	67	358	240	20.0
Poly-benzoxazoles 		$C_{20}H_{10}O_2N_2$	74	310	229	19.1
		$C_{26}H_{14}O_3N_2$	63	402	253	21.0
Polybenzimidides 		$C_{16}H_6O_4N_2$	63	290	183	15.2
		$C_{22}H_{10}O_5N_2$	63	382	240	20.0
		$C_{22}H_{10}O_4N_2$	70	366	256	21.3
		$C_{23}H_{12}O_4N_2$	62	380	236	19.7
Poly-quinazolines 		$C_{22}H_{12}O_4N_4$	80	396	316	26.6
		$C_{23}H_{14}O_4N_4$	62	410	254	21.2
		$C_{29}H_{18}O_4N_4$	88	484	425	35.4
		$C_{26}H_{14}O_4N_4$	76	446	339	28.2

Table 8 Pyrolysis of heterocyclic polymers (continued)

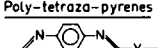
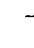

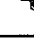
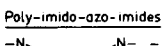
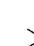
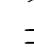
Polymer	Group -Y- or -X-	Elemental composition	Residue of pyrolysis (%)	Per structural unit		
				MW	Residue	C-equiv
Poly-tetraza-pyrenes 		$C_{18}H_8N_4$	77	280	216	17.9
		$C_{18}H_8N_4$	80	280	224	18.6
		$C_{22}H_{10}N_4$	73	330	241	20.0
Poly-imido-azo-imides 		$C_{16}H_6O_2N_4$	63	284	179	14.9
		$C_{20}H_6O_2N_4$	72	332	239	19.9

Table 9 Group contributions to char formation

GROUP	CFT in C-equiv	GROUP	CFT in C-equiv
<b>ALIPHATIC GROUPS</b>		<b>HETEROCYCLIC GROUPS</b>	
—CHOH—	1/3		1
ALL OTHER *)	0		3 1/2
<b>AROMATIC GROUPS</b>			3 1/2
	1		3 1/2
	2		3 1/2
	3		3 1/2
	4		7
	6		7
	6		9
	10		11
	14		10
	1 1/4		12
<b>CORRECTIONS DUE TO DISPROPORTIONING (H-SHIFT):</b>			10
<b>GROUPS DIRECTLY CONNECTED TO AROMATIC NUCLEUS</b>			15
>CH <sub>2</sub> and >CH—CH <sub>2</sub> —	-1		
—CH <sub>3</sub>	-1 1/2		
>C(CH <sub>3</sub> ) <sub>2</sub>	-3		
—CH(CH <sub>3</sub> ) <sub>2</sub>	-4		
*) NO HALOGEN GROUPS INCLUDED			
N.B. SYSTEM IS NOT VALID FOR HALOGEN-CONTAINING POLYMERS			

polymer divided by 12 (the atomic weight of carbon); in other words: the amount of C equivalents in the char per structural unit of the polymer.

Table 9 shows the group contributions to the CFT per structural unit. For all the polymers investigated the char residue was calculated by means of the formula:

$$CR = 1200 \left\{ \sum_i (CFT)_i \right\} / M \quad (2)$$

where  $M$  is the molecular weight per structural unit.

Figure 7 shows the comparison between calculated and experimental values and the result is really satisfactory for a complex process like thermal decomposition. For about 100 polymers investigated the mean deviation is  $\pm 3.5\%$ .

#### RELATION BETWEEN FLAME RESISTANCE AND CHAR RESIDUE

Since the CR value can be calculated with the aid of Table 9, it is interesting to see which (calculated) OI values result from these (calculated) CR values when use is made of the combination of the derived formulae (1) and (2). The

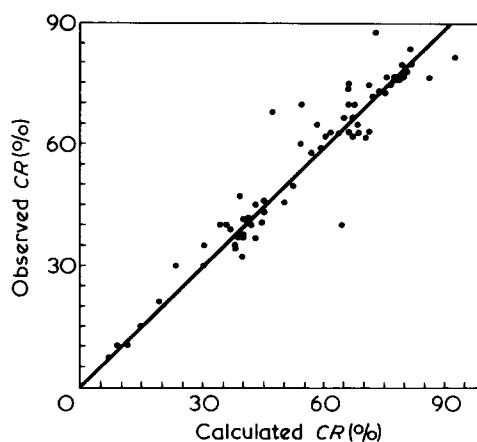


Figure 7 Calculated versus observed CR values

Table 10 Examples of estimated CR and OI values

Polymer	Flame resistance (OI value x 100)				
	Char residue		Predicted using		
	Exp.	Predicted	Exp. CR value	Predicted CR value	Exp.
Polyoxymethylene	0	0	17.5	17.5	15.3
Poly(methyl methacrylate)	0	0	17.5	17.5	17.3
Polyethylene	0	0	17.5	17.5	17.4
Polystyrene	0	0	17.5	17.5	18.3
Cellulose	5	5	19.5	19.5	19.9
Polyester (PETP)	8	8	20.7	20.7	20.6
Polycarbonate	24	24	27.5	27.5	29.4
Nomex®	35	30	31.5	29.5	29.8
PPO®	28	30	28.9	29.5	30.5
Kynol® (phenol-formaldehyde)	45	45	35.5	35.5	35.5
Polybenzimidazole (PBI)	70	67	45.5	43.5	41.5
Carbon	100	100	57.5	57.5	56–64

results are shown in Table 10 (halogen-containing polymers have not been included) and the result is fairly satisfactory.

It may therefore be concluded that, in the absence of factual information, the flame resistance of a polymer can be assessed fairly accurately on the basis of its chemical structure alone.

#### REFERENCES

- 1 Wolfhard, H. G. *et al. Combust. Flame* 1957, 1, 53, 155;
- 2 Fenimore, C. P. and Martin, F. J. *Mod. Plast.* 1966, 44, 141
- 3 van Krevelen, D. W. *Angew. Makromol. Chem.* 1972, 22, 133
- 4 van Krevelen, D. W. *Chimia* 1974, 28, 504
- 5 van Krevelen, D. W. 'Coal', Elsevier, Amsterdam, 1962, Ch 25 and 26
- 6 Wolfs, P. M. J. *Thesis Delft University of Technology* (1959);
- 7 Wolfs, P. M. J., van Krevelen, D. W. and Waterman, H. J. *Brennst.-Chem.* 1959, 40, 155, 189, 215, 241, 314, 342, 371; *Fuel* 1960, 39, 25
- 8 Riley, H. L. *et al. Inst. Fuel Wartime Bull.* 128 1945
- 9 Korshak, V. V. 'The Chemical Structure and Thermal Characteristics of Polymers', (Transl.) Israel Program for Scient. Transl., Jerusalem, 1971
- 10 Lee, H., Stoffey, D. and Neville, K. 'New Linear Polymers', McGraw-Hill, New York, 1967
- 11 'High Temperature Resistant Fibres', (Ed. A. H. Frazer), Interscience, New York, 1967
- 12 Behr, E. 'Hochtemperaturbeständige Kunststoffe', Hanser Verlag, München, 1969
- 13 'High Temperature Resistant Fibres from Organic Polymers', (Ed. J. Preston), Interscience, New York, 1969



mol/l), the polymerization of nitrogen vinyl monomers such as *N*-vinylcarbazole ( $10^{-1}$  mol/l) or *N*-vinylpyrrolidone (1–2 mol/l). The general kinetic and related features of the polymerization of *N*-vinylpyrrolidone by  $\text{POCl}_3$  in methylene chloride include the first order dependence of the rate on  $[\text{POCl}_3]$  and  $[\text{N-vinylpyrrolidone}]$ , its retardation in presence of basic additives and  $\text{H}_2\text{O}$ , and the independence of  $\bar{P}_n$  on both  $[\text{POCl}_3]$  and  $[\text{N-vinylpyrrolidone}]$  which incidentally are similar to those reported for the polymerization of *N*-vinylcarbazole by  $\text{AsCl}_3^5$ , or  $\text{SOCl}_2^{10}$ . However, the molecular weights of these polymers are extremely low ( $\bar{P}_n = 8$ ) which limits the use of this initiator.

#### ACKNOWLEDGEMENTS

The authors thank CSIR, India for a research grant and the Authorities of the Indian Institute of Technology, Kharagpur, for facilities.

## Chitosan gel: a novel polysaccharide gel

Shigehiro Hirano, Sumiyo Kondo and Yasuo Ohe  
Department of Agricultural Biochemistry, Tottori University, Tottori 680, Japan  
(Received 24 February 1975)

Chitosan<sup>1</sup>, (1→4)-2-amino-2-deoxy-β-D-glucopyranan is found in some micro-organisms<sup>2</sup> and is readily prepared from naturally abundant chitin by de-*N*-acetylation with alkali<sup>3</sup>.

In this communication, we wish to report that chitosan, in solution in dilute acetic acid, readily undergoes partial acetylation with acetic anhydride to afford a novel polysaccharide gel.

Chitin was prepared by the conventional procedure from shells of crab, *Chionoecetes opilio*, and its de-*N*-acetylation was carried out with 40%  $\text{NaOH}^4$  in the presence of 1%  $\text{NaBH}_4$  to produce an almost completely de-*N*-acetylated product, chitosan,  $[\alpha]_D^{15} - 3.1^\circ$  (*c* 1.3, 50% formic acid),  $-10.5^\circ$  (*c* 1.3, 10% acetic acid).

Chitosan (500 mg) was dissolved in 25 ml of 10% acetic acid by shaking at room temperature<sup>5</sup>. To the solution was added 12.5 ml of acetic anhydride. The excess acetic anhydride added is important to the gel formation and is considered to be used for the acetylation of both amino and hydroxyl groups present in chitosan as well as for the reaction with water. The mixture was kept at room temperature for about 30 min to afford a rigidly solidified gel to the whole solution in a flask or even in a Visking cellulose tube. The solidified gel was kept at room temperature overnight and then suspended in a large volume (about 2 l) of distilled water, which was changed several times, at room temperature for three days or dialysed against running water. This treatment exchanged free acetic acid present in the gel for water and removed unreacted chitosan as its acetate salt which is soluble in dilute acid. Thus, the chitosan gel free of acetic acid was obtained by filtration in about 31.4 g yield. The gel was colourless, transparent and rigid, and gave no smell of acetic acid and almost no taste. The gel was soluble in formic acid but insoluble in water, 50% formic acid, 10% acetic acid, alcohols and acetone. The gel in a test tube did not melt by heating over a flame and could be sliced with a knife without destruction.

In order to examine its components, the gel was lyophilized or dehydrated in a large volume of acetone, and the product was further dried over  $\text{P}_2\text{O}_5$  *in vacuo* at  $110^\circ\text{C}$

#### REFERENCES

- 1 Biswas, M. and Mishra, P. K. *J. Polym. Sci. (B)* 1973, **11**, 639
- 2 Biswas, M. and Chakravorty, D. *Bull. Chem. Soc., Japan* 1970, **43**, 1904
- 3 Payne, D. S. 'Non Aqueous Solvent Systems', Academic Press, New York, 1965
- 4 Pepper, D. C. *Trans. Faraday Soc.* 1949, **45**, 397
- 5 Biswas, M. and Chakravorty, D. *J. Polym. Sci. (A-1)* 1973, **11**, 7
- 6 Dainton, F. S. and Tomlinson, R. H. *J. Chem. Soc.*, 1953, p 151
- 7 Worsfold, D. J. and Bywater, S. *J. Am. Chem. Soc.* 1957, **79**, 4917
- 8 Zlamal, Z. 'Vinyl Polymerization', Part II, Vol 1, Marcel Dekker, New York, 1969
- 9 Plesch, P. H. 'The Chemistry of Cationic Polymerization', Pergamon, New York, 1963
- 10 Biswas, M. and Kamannarayana, P. *J. Polym. Sci. (A-1)* 1975 (in press)

for 3 h to afford an amorphous product in 470–540 mg yield,  $[\alpha]_D^{15} - 1.4^\circ$  (*c* 0.72, formic acid). Calculated for  $[\text{C}_{10}\text{H}_{14}\text{NO}_5(\text{OH})_{0.6}(\text{OCOCH}_3)_{0.4} \cdot 0.7\text{H}_2\text{O}]_n$ : C, 47.22; H, 6.31; N, 5.09%. Found: C, 47.75; H, 6.65; N, 5.47%. I.r. (KBr), 3250–3450 (OH, NH), 1730 and 1240 (C=O in OAC), 1650 (C=O in NAC),  $1040\text{ cm}^{-1}$  (C–O–C). N.m.r. ( $^2\text{HCOO}^2\text{H}$ )  $\delta$  (ppm, sodium 2,2,3,3-tetradeutero-3-(trimethylsilyl)propionate as an internal standard), 6.00–3.00 (methine and methylene), 2.13 (*N*- and *O*-acetate-methyl). The ratio of (*N*- and *O*-acetate-methyl)/(methine and methylene) = 0.89 was found, and this value corresponds to a degree of substitution = 2.36 per monosaccharide residue. The dried gel was soluble in formic acid and 50% resorcinol but insoluble in other solvents examined. The solubility is similar to that of a peracetylated chitin prepared with acetic anhydride by passing dry  $\text{HCl}^6$ .

On the basis of these data, it is concluded that the novel polysaccharide gel is a chitosan hydrate which is partly acetylated to a degree of substitution = 2.36 per monosaccharide residue. Mechanism of the gel formation is under investigation. However, a molecular aggregation is considered to occur with frameworks that are crosslinked by micelles among chitosan chains. This is similar to the formation of cellulose gels through chemical modification of the polymer<sup>7,8</sup>.

#### ACKNOWLEDGEMENT

Partial financial support was provided by a research grant from the Ministry of Education of Japan.

#### REFERENCES

- 1 Brimacombe, J. S. and Webber, J. M. 'Mucopolysaccharides', Elsevier, Amsterdam, 1964, p 18
- 2 Kreger, D. R. *Biochim. Biophys. Acta* 1954, **13**, 1
- 3 Horton, D. and Lineback, D. R. *Methods Carbohydr. Chem.* 1965, **5**, 403
- 4 Meyer, K. H. and Wehrli, H. *Helv. Chim. Acta* 1937, **20**, 353
- 5 Horton, D. and Just, E. K. *Carbohydr. Res.* 1973, **29**, 173
- 6 Shorruigin, P. P. and Hait, E. *Ber. Dtsch. Chem. Ges.* 1935, **68B**, 971
- 7 Rees, D. A. *Chem. Ind.* 1972, p 630
- 8 Arnott, S., Hukins, D. W. L., Whistler, R. L. and Baker, C. W. *Carbohydr. Res.* 1974, **35**, 259

mol/l), the polymerization of nitrogen vinyl monomers such as *N*-vinylcarbazole ( $10^{-1}$  mol/l) or *N*-vinylpyrrolidone (1–2 mol/l). The general kinetic and related features of the polymerization of *N*-vinylpyrrolidone by  $\text{POCl}_3$  in methylene chloride include the first order dependence of the rate on  $[\text{POCl}_3]$  and  $[\text{N-vinylpyrrolidone}]$ , its retardation in presence of basic additives and  $\text{H}_2\text{O}$ , and the independence of  $\bar{P}_n$  on both  $[\text{POCl}_3]$  and  $[\text{N-vinylpyrrolidone}]$  which incidentally are similar to those reported for the polymerization of *N*-vinylcarbazole by  $\text{AsCl}_3^5$ , or  $\text{SOCl}_2^{10}$ . However, the molecular weights of these polymers are extremely low ( $\bar{P}_n = 8$ ) which limits the use of this initiator.

#### ACKNOWLEDGEMENTS

The authors thank CSIR, India for a research grant and the Authorities of the Indian Institute of Technology, Kharagpur, for facilities.

## Chitosan gel: a novel polysaccharide gel

Shigehiro Hirano, Sumiyo Kondo and Yasuo Ohe  
Department of Agricultural Biochemistry, Tottori University, Tottori 680, Japan  
(Received 24 February 1975)

Chitosan<sup>1</sup>, (1→4)-2-amino-2-deoxy-β-D-glucopyranan is found in some micro-organisms<sup>2</sup> and is readily prepared from naturally abundant chitin by de-*N*-acetylation with alkali<sup>3</sup>.

In this communication, we wish to report that chitosan, in solution in dilute acetic acid, readily undergoes partial acetylation with acetic anhydride to afford a novel polysaccharide gel.

Chitin was prepared by the conventional procedure from shells of crab, *Chionoecetes opilio*, and its de-*N*-acetylation was carried out with 40%  $\text{NaOH}^4$  in the presence of 1%  $\text{NaBH}_4$  to produce an almost completely de-*N*-acetylated product, chitosan,  $[\alpha]_D^{15} - 3.1^\circ$  (*c* 1.3, 50% formic acid),  $-10.5^\circ$  (*c* 1.3, 10% acetic acid).

Chitosan (500 mg) was dissolved in 25 ml of 10% acetic acid by shaking at room temperature<sup>5</sup>. To the solution was added 12.5 ml of acetic anhydride. The excess acetic anhydride added is important to the gel formation and is considered to be used for the acetylation of both amino and hydroxyl groups present in chitosan as well as for the reaction with water. The mixture was kept at room temperature for about 30 min to afford a rigidly solidified gel to the whole solution in a flask or even in a Visking cellulose tube. The solidified gel was kept at room temperature overnight and then suspended in a large volume (about 2 l) of distilled water, which was changed several times, at room temperature for three days or dialysed against running water. This treatment exchanged free acetic acid present in the gel for water and removed unreacted chitosan as its acetate salt which is soluble in dilute acid. Thus, the chitosan gel free of acetic acid was obtained by filtration in about 31.4 g yield. The gel was colourless, transparent and rigid, and gave no smell of acetic acid and almost no taste. The gel was soluble in formic acid but insoluble in water, 50% formic acid, 10% acetic acid, alcohols and acetone. The gel in a test tube did not melt by heating over a flame and could be sliced with a knife without destruction.

In order to examine its components, the gel was lyophilized or dehydrated in a large volume of acetone, and the product was further dried over  $\text{P}_2\text{O}_5$  *in vacuo* at  $110^\circ\text{C}$

#### REFERENCES

- 1 Biswas, M. and Mishra, P. K. *J. Polym. Sci. (B)* 1973, **11**, 639
- 2 Biswas, M. and Chakravorty, D. *Bull. Chem. Soc., Japan* 1970, **43**, 1904
- 3 Payne, D. S. 'Non Aqueous Solvent Systems', Academic Press, New York, 1965
- 4 Pepper, D. C. *Trans. Faraday Soc.* 1949, **45**, 397
- 5 Biswas, M. and Chakravorty, D. *J. Polym. Sci. (A-1)* 1973, **11**, 7
- 6 Dainton, F. S. and Tomlinson, R. H. *J. Chem. Soc.*, 1953, p 151
- 7 Worsfold, D. J. and Bywater, S. *J. Am. Chem. Soc.* 1957, **79**, 4917
- 8 Zlamal, Z. 'Vinyl Polymerization', Part II, Vol 1, Marcel Dekker, New York, 1969
- 9 Plesch, P. H. 'The Chemistry of Cationic Polymerization', Pergamon, New York, 1963
- 10 Biswas, M. and Kamannarayana, P. *J. Polym. Sci. (A-1)* 1975 (in press)

for 3 h to afford an amorphous product in 470–540 mg yield,  $[\alpha]_D^{15} - 1.4^\circ$  (*c* 0.72, formic acid). Calculated for  $[\text{C}_{10}\text{H}_{14}\text{NO}_5(\text{OH})_{0.6}(\text{OCOCH}_3)_{0.4} \cdot 0.7\text{H}_2\text{O}]_n$ : C, 47.22; H, 6.31; N, 5.09%. Found: C, 47.75; H, 6.65; N, 5.47%. I.r. (KBr), 3250–3450 (OH, NH), 1730 and 1240 (C=O in OAC), 1650 (C=O in NAC),  $1040\text{ cm}^{-1}$  (C–O–C). N.m.r. ( $^2\text{HCOO}^2\text{H}$ )  $\delta$  (ppm, sodium 2,2,3,3-tetradeutero-3-(trimethylsilyl)propionate as an internal standard), 6.00–3.00 (methine and methylene), 2.13 (*N*- and *O*-acetate-methyl). The ratio of (*N*- and *O*-acetate-methyl)/(methine and methylene) = 0.89 was found, and this value corresponds to a degree of substitution = 2.36 per monosaccharide residue. The dried gel was soluble in formic acid and 50% resorcinol but insoluble in other solvents examined. The solubility is similar to that of a peracetylated chitin prepared with acetic anhydride by passing dry  $\text{HCl}^6$ .

On the basis of these data, it is concluded that the novel polysaccharide gel is a chitosan hydrate which is partly acetylated to a degree of substitution = 2.36 per monosaccharide residue. Mechanism of the gel formation is under investigation. However, a molecular aggregation is considered to occur with frameworks that are crosslinked by micelles among chitosan chains. This is similar to the formation of cellulose gels through chemical modification of the polymer<sup>7,8</sup>.

#### ACKNOWLEDGEMENT

Partial financial support was provided by a research grant from the Ministry of Education of Japan.

#### REFERENCES

- 1 Brimacombe, J. S. and Webber, J. M. 'Mucopolysaccharides', Elsevier, Amsterdam, 1964, p 18
- 2 Kreger, D. R. *Biochim. Biophys. Acta* 1954, **13**, 1
- 3 Horton, D. and Lineback, D. R. *Methods Carbohydr. Chem.* 1965, **5**, 403
- 4 Meyer, K. H. and Wehrli, H. *Helv. Chim. Acta* 1937, **20**, 353
- 5 Horton, D. and Just, E. K. *Carbohydr. Res.* 1973, **29**, 173
- 6 Shorruigin, P. P. and Hait, E. *Ber. Dtsch. Chem. Ges.* 1935, **68B**, 971
- 7 Rees, D. A. *Chem. Ind.* 1972, p 630
- 8 Arnott, S., Hukins, D. W. L., Whistler, R. L. and Baker, C. W. *Carbohydr. Res.* 1974, **35**, 259



## Inverse isotope effect on the rate of polymerization of deuterated methyl methacrylate

There are relatively few reports on the effect of deuterium substitution on rate of free radical polymerizations. Allyl[1-<sup>2</sup>H<sub>2</sub>] acetate polymerizes 2–3 times faster than allyl acetate owing to a primary kinetic isotope effect on the rate of degradative chain-transfer termination step<sup>1</sup>. Styrene [ $\alpha$ -<sup>2</sup>H] also shows a small inverse isotope effect<sup>2–4</sup>. Conflicting results have been reported for styrene [ $\beta$ -<sup>2</sup>H<sub>2</sub>] where there is either no effect<sup>5,6</sup> or a small inverse isotope effect<sup>2–4</sup>. In the latter case the effect was ascribed to a secondary deuterium isotope effect on the propagation step. We report here the preliminary results of a radiochemical investigation of the polymerization of methyl methacrylate [<sup>2</sup>H<sub>5</sub>] [CD<sub>2</sub> = C(CD<sub>3</sub>)CO<sub>2</sub>CH<sub>3</sub>].

Polymerizations (~10% conversion) were conducted in bulk in evacuated sealed tubes or dilatometers at 60°C using <sup>14</sup>C-azoisobutyronitrile as initiator. The results, obtained as described previously<sup>7</sup>, are recorded in Table 1. The overall rate constant,  $k$ , for polymerization of the deuterated monomer is ~36% greater than that of the undeuterated monomer and the isotope effect  $k_H/k_D = 0.73$ . The increased rates of polymerization are also reflected in the higher molecular weights of the deuterated polymers.

Since  $k = k_p(fk_d/k_t)^{1/2}$ , where  $k_p$ ,  $k_d$  and  $k_t$  are the velocity constants for propagation, initiator decomposition and termination and  $f$  is the initiator efficiency it follows that any one or all of the constants might have been affected by deuterium substitution. By making the reasonable assumption that  $k_d$  was not affected it was shown by

Table 1 Polymerization of methyl methacrylate and methyl methacrylate [<sup>2</sup>H<sub>5</sub>] in bulk at 60°C\*

Exp.	Monomer	$k$		$\bar{M}_n$ x 10 <sup>-5</sup>	$n$
		[I] <sub>0</sub> x 10 <sup>3</sup> (mol/l) <sup>1/2</sup>	(mol <sup>-1/2</sup> sec <sup>-1</sup> )		
1	CH <sub>2</sub> =C(CH <sub>3</sub> )CO <sub>2</sub> CH <sub>3</sub>	6.68	3.16	4.55	1.38
2		11.2	3.00	3.32	1.24
3		17.2	3.00	2.85	1.19
4		17.2	3.13	2.85	1.25
5		22.6	3.05	2.47	1.26
6		24.8	3.10	2.30	1.28
	Mean values		3.07 ± 0.07		1.27 ± 0.06
7	CD <sub>2</sub> =C(CD <sub>3</sub> )CO <sub>2</sub> CH <sub>3</sub>	8.08	4.19	6.63	1.52
8		11.7	4.14	5.53	1.51
9		18.1	4.17	4.44	1.53
10		23.9	4.25	3.82	1.55
11		23.9	4.16	3.82	1.51
12		33.6	4.23	3.18	1.49
	Mean values		4.19 ± 0.04		1.52 ± 0.02

\* [I]<sub>0</sub> = initial initiator concentration;  $k = R_p/[M]_0[I]_0^{1/2}$  where  $R_p$  = rate of polymerization measured gravimetrically and [M]<sub>0</sub> = initial monomer concentration;  $\bar{M}_n$  = number average molecular weight determined osmotically;  $n$  = number of initiator fragments per polymer molecule

radiochemical assay that the rates of initiation,  $R_i$ , and hence values of  $f$ , were identical within the limits of experimental error. Chain transfer to monomer can also be neglected in these systems. Thus, the isotope effect must be associated with either the propagation or the termination reaction.

Secondary inverse isotope effects have been observed when free radicals add to carbon double bonds. Addition of methyl or trifluoromethyl radicals to deuterated olefins gives rise to inverse isotope effects of about 3% per deuterium atom at 65°C<sup>8</sup>. An isotope effect of 0.94–0.90 was observed for the addition of methyl radicals to styrene [ $\alpha, \beta$ -<sup>2</sup>H<sub>3</sub>]<sup>9</sup> and the effect of deuterium substitution on styrene polymerization at 60°C can be accounted for by an inverse effect on the propagation reaction of about 5% per atom of deuterium<sup>2</sup>. However, the value of  $k_H/k_D = 0.73$  reported here seems rather large to be accounted for solely in terms of an inverse secondary effect on the propagation reaction, particularly as only two hydrogens are involved in the change from  $sp^2$  to  $sp^3$  hybridization.

The termination reaction is clearly affected since the value of  $n$ , the number of initiator fragments per polymer molecule is increased from 1.27 to 1.52 by deuteration. These values correspond to 42% and 68% combination of polymer radicals. This may be interpreted as an isotope effect on hydrogen transfer during termination by disproportionation which would explain all the results reported in the Table. The ratio of the velocity constants for termination by disproportionation may then be calculated as  $k_{td,H}/k_{td,D} = 2.93$  which is about right for a hydrogen transfer reaction having a low activation energy. This in turn could be taken as clear evidence that the combination and disproportionation reactions proceed by way of different transition states.

The work with styrene<sup>2</sup> cannot be explained by the above mechanism, however, since polystyrene radicals terminate solely by combination. Thus, it seems possible that in the case of methyl methacrylate both  $k_p$  and  $k_t$  may be affected by deuterium substitution and it will be necessary to examine these constants individually to further delineate the system.

G. Ayrey and D. J. D. Wong

*Isotope Unit, Queen Elizabeth College (University of London),  
Campden Hill, London W8 7AH, UK  
(Received 6 May 1975)*

### References

- Bartlett, P. D. and Tate, F. A. *J. Am. Chem. Soc.* 1953, 75, 91
- Pryor, W. A., Henderson, R., Palsiga, R. A. and Carroll, N. *J. Am. Chem. Soc.* 1966, 88, 1199
- Kirchner, R. *Makromol. Chem.* 1966, 96, 179
- Kopecky, K. R. and Evani, S. *Can. J. Chem.* 1969, 47, 4049
- Hammond, G. S. and Kopecky, K. R. *J. Polym. Sci.* 1962, 60, S54
- Burkalov, I. M., Goldanskii, V. I. and Kuo, M. K. *Dokl. Akad. Nauk SSSR* 1964, 155, 883
- Ayrey, G., Levitt, F. G. and Mazza, R. *J. Polymer* 1965, 6, 157
- Feld, M., Stefani, A. P. and Szwarc, M. *J. Am. Chem. Soc.* 1962, 84, 4451
- Matsulka, M. and Szwarc, M. *J. Am. Chem. Soc.* 1961, 83, 1260

# Book Reviews

## The chemistry of organolithium compounds

B. J. Wakefield

Pergamon Press, Oxford, 1974. 335 pp. £10.20

The author aimed to write an account which is comprehensive, though not exhaustive. The selection of examples from more recent full papers, which give experimental details, rather than from preliminary communications or older work, was also a stated aim. This is perfectly reasonable in view of the available reviews covering the literature into the mid-fifties. The author admits some bias in the selection of examples and perhaps some readers may find too great an emphasis on, for example, the chemistry of perhalogeno-organolithium reagents. On the other hand, the selection of examples within such terms of reference does add a personal touch and a reasonable number of references are to papers published in 1972.

The book is divided into four parts. Two short chapters are devoted to the constitution and the preparation of organolithium compounds. The majority of the book is, in the reviewer's opinion, quite properly devoted to organic and organometallic synthesis. The book is clearly aimed at researchers in industrial and university laboratories and as such delineates the most important preparative and synthetic applications of these versatile reagents.

The book is well produced and is so free from proof-reading errors that a positive effort had to be made to detect any. The majority of the structural formulae are very clear but certain of the *schemes* are less clear and do not use a consistent method of indicating bonds (see for example *scheme* 9.1 on p 124). The book is relatively easy to use but I should have preferred the references to have been present as a footnote on individual pages or alternatively collected at the end of the whole book.

These minor criticisms do not detract from the general usefulness of the book which should find a place in all chemical libraries. It is unfortunate that the price will probably result in the book not finding its way onto many individual bookshelves, particularly since there has been a 20% increase in price since it was originally published less than a year ago.

H. Heaney

## Reviews in macromolecular chemistry, Volume 11

Edited by G. B. Butler, F. O'Driscoll and M. Shen

Marcel Dekker, New York, 1974. 373 pp. \$29.50

At first sight, the prospect of reading six lengthy articles on unconnected topics in polymer science appears a daunting one. It is therefore a pleasure to report that in the event this particular volume proved both interesting and rewarding. The standard of

presentation is uniformly high and the exposition is pitched at a level which requires no more than a reasonable general knowledge of the physics and chemistry of polymers.

The first article in this book by S. Wu provides a comprehensive survey of Interfacial and surface tensions of polymers. It is clear that the present state of the state does not embrace much definitive theory, but this review covers the published work in the area in a very satisfactory fashion. The next topic, Mixing in polymer reactors by E. B. Nauman, is an unfamiliar one to this reviewer. In complete contrast to the previous article, the behaviour is discussed from the outset in terms of basic equations originated by Danckwerts and others. The whole discussion is developed in a systematic manner, always keeping in touch with the theoretical models. This article is followed by a very well written account of modern theories of polymer crystallization by I. C. Sanchez. The review is very much up-to-date in discussing the author's own theories (in collaboration with E. A. Di Marzio), comparing and contrasting these theories with those of Lauritzen and Hoffman, Frank and Tosi, Price and Lauritzen, Di Marzio and Passaglia.

The articles by Nauman and Sanchez rely on formal mathematical exposition and are comparatively short (~35 pages). In complete contrast the next article by G. L. Wilkes forms a comprehensive account of some 110 pages on Rheo-optical methods and their application to polymeric solids. This is an extremely valuable review, with much to stimulate anyone who is interested in structure/property relationships in solid polymers.

A rather shorter article, on the thermal decomposition of poly(vinyl chloride), covers new ground for this reviewer, but Z. Mayer must be congratulated on the clarity of this exposition. He makes out the case for thermal dehydrochlorination of PVC proceeding by non-radical mechanism, discusses the catalytic effect of free hydrogen chloride, and generally shows how ideas have changed dramatically in the subject over recent years. The final article in this volume is an account of the Thermodynamics of copolymerization by H. Sawada. This is a straightforward account of comparatively simple theories.

In conclusion, it can be seen that the articles in this volume range from informal reviews of experimental research to formal expositions of recent theoretical developments. There is something for most polymer scientists, written at a uniformly good standard, so that the book can be warmly recommended for any library where the subject of polymer science is to be included.

I. M. Ward

### Conference Announcement

#### Plastics in Medicine and Surgery

Glasgow, 24–25 September 1975

This conference, organized by the Plastics and Rubber Institute, will be held at the University of Strathclyde, Glasgow on 24 and 25 September 1975. Thirty one contributions will cover aspects including implantable materials, artificial organs and assist devices and design, safety and standards. Further details and registration forms are available from Mr J. N. Ratcliffe, Plastics and Rubber Institute, 11 Hobart Place, London SW1W 0HL, UK.

### Conference Announcement

#### Polymer Rheology and Plastics Processing

Loughborough, 16–19 September 1975

An international conference on polymer rheology and plastics processing, sponsored by the British Society of Rheology and the Plastics and Rubber Institute, will be held at Loughborough University from 16 to 19 September 1975. Over 30 contributions from industrial and academic workers are scheduled, with four sessions on principles and properties, three on plasticization and processing and one on attitudes to research in polymer rheology and plastics processing in industry and universities. The final day will consider shaping flows. Further information and registration forms are available from Miss S. Keeble, Plastics and Rubber Institute, 11 Hobart Place, London SW1W 0HL, UK.

# Texture of elastin gels

R. B. Beevers

Belvoir Research Laboratory, 160 Chatham Road, Eastwood, New South Wales, 2122, Australia

(Received 7 April 1975)

Elastin gels which show a filamentous texture have been observed when an elastin fraction was swollen in buffer solutions between pH 5.85 and 8.16. This fraction, previously completely soluble in aqueous solutions, had been obtained during the hydrolysis of bovine *ligamentum nuchae* and stored for over three years at about 3°C. The diameter of the filaments was about 2 μm and microscopic examination showed that the texture of the gel depended on the protein concentration, pH and the ionic strength of the buffer solution used to cause swelling. Amino acid analysis of this protein fraction showed a slightly higher proportion of lysine and it is considered that the gel is the result of the reformation of a few lysinonorleucine and/or desmosine crosslinkages recreating an insoluble elastin matrix.

## INTRODUCTION

Elastin may be isolated from bovine *ligamentum nuchae* by extraction at neutrality followed by periods of autoclaving in distilled water<sup>1</sup>. The insoluble elastin can then be degraded by reflux with oxalic acid to yield a soluble product ( $M_n = 70\,000$ , Partridge method<sup>2</sup>).

There have been a number of reports of attempts to reconstitute an insoluble form of elastin from this soluble product. For example, Wood<sup>3</sup> obtained elastomeric gels by heating elastin solutions to form a coacervated phase which was then collected and these experiments may readily be repeated. A limited amount of success also has been achieved in the reconstitution of elastin through the addition of synthetic heparinoids to elastin solutions<sup>4</sup>. The gels obtained by these methods have elastic properties but show no structural features even when examined under the electron microscope.

As part of a detailed study of the solution properties of soluble elastin<sup>5</sup>, bovine elastin obtained from a 1.5 year old ox was solubilized by the Partridge method. However, instead of following the usual procedure and pooling the solubilized elastin as it was produced, each of the five stages of reflux were separately treated dialysing the elastin obtained against water and then freeze-drying. These fractions were completely re-soluble in water and have remained so except for the fourth fraction. This fraction was found to contain some insoluble material after about 15 months storage at 3°C although initially completely re-soluble. At the time the insoluble component was discarded without further examination. Two years later, when further solution studies were contemplated, it was found that this elastin fraction had become almost completely insoluble. Microscopic examination of the water-swollen gel revealed a filamentous texture. A report is given here of the result of a more detailed examination of the elastin gel texture.

## GEL TEXTURE

Mixtures of elastin (fourth fraction) were prepared with 0.05 M sodium formate buffer at pH 8.16 and had nominal concentrations in the range 6 to 98 mg dry protein/g. The mixtures were equilibrated at room temperature and then part of the gel was transferred by pipette to an excavated cell in a microscope slide and sealed with a coverslip. Each

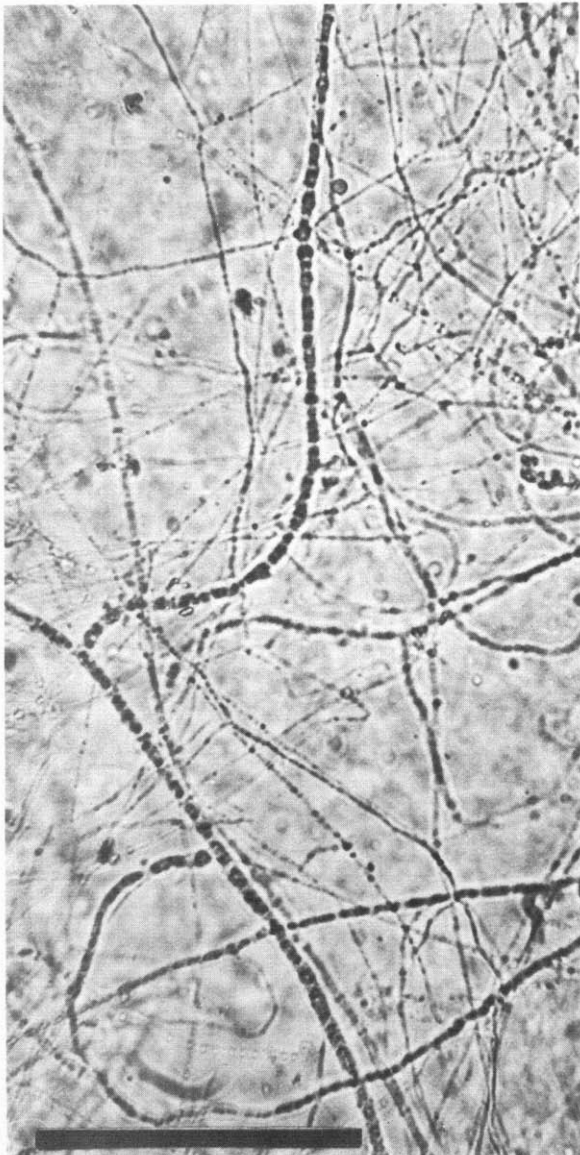
cell usually contained a portion of liquid to maintain equilibrium conditions of swelling. Examination of the gels under a polarizing microscope showed no indication of birefringent structures within the gel.

At the lowest protein concentration the general appearance of the gel was of a coarse grained texture similar to that which may be observed in elastin gels prepared by the method of Wood<sup>3</sup>. In the latter case the gel comprises a conglomerate of spherical coacervate particles which have sedimented to form a layer. At a high protein concentration, as shown in *Figure 1*, the gel comprises an amorphous granular base together with a distinctly filamentous component.

Examination of microphotographs of elastin gels prepared with increasing protein concentration reveals changes in the texture which strongly suggest the development of a filamentous structure, the final stage being shown in *Figure 1*. It was found that when gels were prepared at a lower pH filaments were obtained at a lower protein concentration. An example of the gel filaments prepared at pH 5.85 is shown in *Figure 2*. Further reduction in pH reversed this trend and no filaments could be found at pH 4.50. The boundaries to the development of filaments with respect to pH, protein concentration and temperature still remain to be clarified.

A comparison of the filamentous texture in gels prepared at pH 5.85 and 8.16 reveals a number of differences. For example, it was found that at the lower pH the gel consisted entirely of filaments and no amorphous gel component could be detected. Well developed branched structures were common and a typical example is shown in *Figure 2*. More detailed examination showed that at the lower pH there was an increase in the number of branches per unit length of filament and generally the branches were shorter in length.

Further it was observed that in gels prepared at pH 8.16 more than one type of filament could be detected. The prominent filament shown crossing the field in *Figure 1* was only found in small numbers. Some internal structure could be discerned and appears to be of a random, globular type. Also shown in *Figure 1*, close to this filament, is another distinct type occurring in small numbers and which have a characteristic 'I' cross-spacing at roughly regular intervals along the length of the filament. These two types are roughly 2–3 times the width of those forming the major



**Figure 1** Microphotograph of part of an elastin gel swollen in 0.05 M sodium formate buffer at pH 8.16 and with a protein concentration of 95 mg dry protein/g. The bar indicates 0.1 mm

part of the gel. As far as can be judged the various types of filament exist independently.

A feature of the microphotographs of gels equilibrated at pH 5.85 is the large number of small particles in the surrounding protein solution. These particles often cluster in the region of the filaments as shown at the bottom of *Figure 2*. A possible explanation is that the particles are nuclei from which the filaments grow by accretion. Examination of gel filament at higher magnifications shows there to be some evidence for this view. This may also explain the absence of optical anisotropy in the filaments.

#### DIAMETER OF THE FILAMENTS

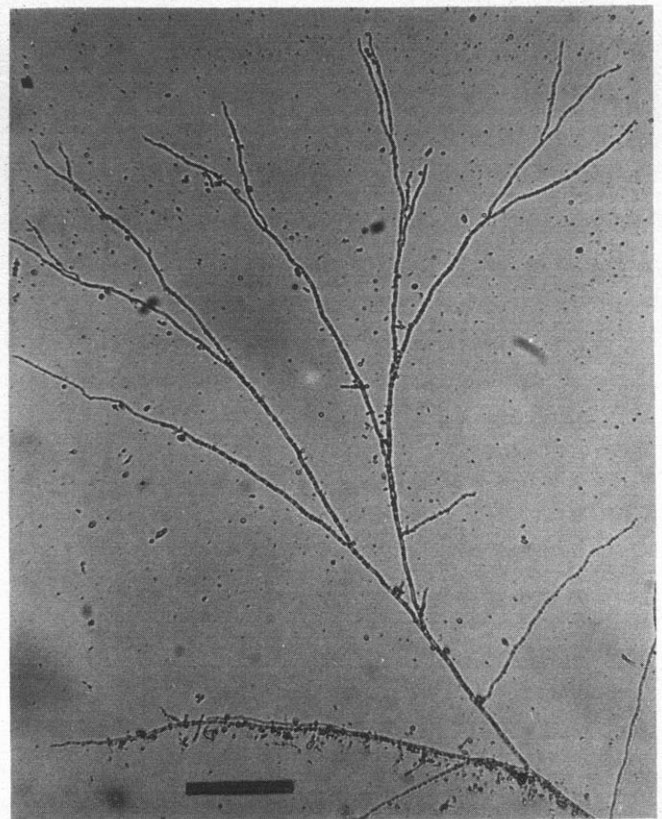
Measurement of filament diameter ( $\Phi$ ) was made with a calibrated micrometer eyepiece assuming the filaments to be of circular cross-section. In each gel a large number of filaments were measured and the mean filament diameter could be determined to  $\pm 0.3 \mu\text{m}$ . At pH 8.16 the distribution diagram of the filament diameters was skewed as a result of the presence of a small number of filaments of different type and significantly larger diameter.

An examination has been made of the effect of change of pH and ionic strength of the buffer solution on filament diameter. Preparatory to this work, part of an elastin solution containing gel was transferred to Visking tubing and dialysed against conductivity water. Fragments of filamentous gel were then transferred by pipette to tubes containing buffer solution of known pH and ionic strength. After equilibration for several days at 20°C small fragments of gel were then transferred to microscope slide cells for measurement of filament diameter with the results shown in *Figure 3b*. Adjustment to the ionic strength was made with KCl. Swelling measurements made on adult bovine *ligamentum nuchae* elastin by Jackson *et al.*<sup>6</sup> are reproduced in *Figure 3a* for comparison where  $w_s$  is the weight of water taken up by 1 g of dry ligament.

The two sets of data show an interesting correlation with a maximum at about pH 8 although the proportionate changes are not the same. Below pH 7, however, the swelling behaviour shows opposite trends. Differences here may be expected since quite severe hydrolysis conditions have been used to obtain the elastin fraction from the original insoluble bovine ligament. The ability to make use of the gel filaments in this manner demonstrates that they have a reasonable degree of coherence and are not simply an aggregation of particles.

#### ORIGIN OF THE GEL

The elastin gel filaments show many of the features exhibited by *in vivo* bovine *ligamentum nuchae* elastin that is, a fibrous texture with branching of the fibres<sup>7</sup> and an unordered molecular structure as detected by X-rays<sup>8</sup>. It has been found that X-ray scattering from wet gel filaments



**Figure 2** Microphotograph showing part of a branched gel filament in an elastin gel swollen in 0.05 M sodium acetate buffer at pH 5.85 and with protein concentration of 40 mg/g. The bar indicates 0.1 mm

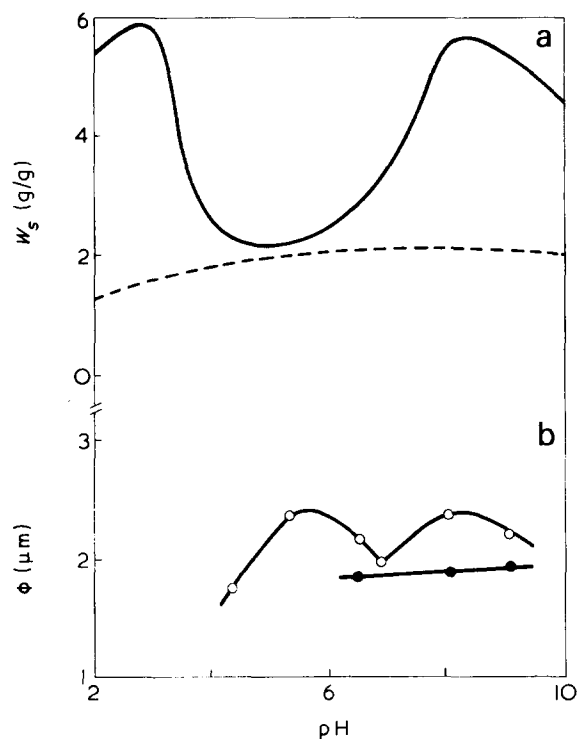


Figure 3 The dependence on pH and ionic strength of: (a) swelling of adult bovine *ligamentum nuchae* elastin determined in non-saline (—) and 2M NaCl (----). Results of Jackson *et al.*<sup>6</sup>; (b) diameter ( $\mu\text{m}$ ) of elastin gel filaments determined at 20°C and at molar ionic strengths of 0.05 (O) and 1.0 (●)

mounted in Lindemann glass specimen tubes is similar to that obtained from water-swollen bovine ligament (results to be reported shortly).

The reason for the development of insolubility in this elastin fraction has not yet been established. Amino acid

analysis has shown that the fractions are all similar in composition with no major differences. There is a small decrease in the amounts of valine and a slight but progressive increase in alanine, phenylalanine and lysinonorleucine with increase in fraction number. It has been found that the fourth fraction has a slightly larger amount of lysine than the other fractions and this permits a possible explanation for the development of insolubility.

It is now well established that there is a decrease in lysine during the development of foetal elastin the lysine residues becoming incorporated into desmosine and/or lysinonorleucine crosslinkages, the elastin becoming an insoluble protein<sup>9</sup>. The slight excess of lysine in this elastin fraction, determined shortly after preparation and whilst still completely water-soluble, would indicate that there may be a formation or reformation of the same type of crosslinkages. Only a few crosslinkages would be necessary to create an insoluble network structure and it may be that the observation of the gel texture is the most sensitive determinant of the presence of these cross-bridges.

#### REFERENCES

- 1 Jackson, D. S. and Cleary, E. G. in 'Methods of Biochemical Analysis', (Ed. D. Glick), Interscience, New York, 1967, Vol 15, p 56
- 2 Partridge, S. M., Davis, H. F. and Adair, G. S. *Biochem. J.* 1955, **61**, 11
- 3 Wood, G. C. *Biochem. J.* 1958, **69**, 539
- 4 Podrazky, V. *Nature* 1967, **215**, 1161
- 5 Beevers, R. B. *Biochim. Biophys. Acta* 1971, **243**, 102
- 6 Jackson, D. S., Cleary, E. G. and Sandberg, L. G. *Biochem. J.* 1965, **96**, 813
- 7 Gross, J. *J. Exp. Med.* 1949, **89**, 699
- 8 Gotte, L., Mammi, M. and Pezzin, G. in 'Symposium on Fibrous Proteins', (Ed. W. G. Crewther), Butterworths, Australia, 1967, p 236
- 9 Cleary, E. G., Sandberg, L. B. and Jackson, D. S. *Biochem. Biophys. Res. Commun.* 1966, **23**, 139

# Thermodynamic properties of concentrated poly( $\gamma$ -benzyl-L-glutamate) solutions

K. Kubo and K. Ogino

Department of Pure and Applied Sciences, College of General Education, University of Tokyo, Tokyo, Japan  
(Received 21 October 1974; revised 7 February 1975)

Solvent activities for the poly( $\gamma$ -benzyl-L-glutamate)–chloroform system were obtained in the concentration range of 20 to 100 vol % polymer at 30°C by isothermal distillation and vapour pressure measurements. The results were combined with osmotic pressure data reported previously and were compared with the existing theories for solutions of rodlike molecules. Coexistence of two phases was not found. The data could be explained by the Flory theory, as modified by Wee and Miller, in a low or intermediate concentration range, and could be explained by the Flory–Leonard model at high concentrations.

## INTRODUCTION

It is known that poly( $\gamma$ -benzyl-L-glutamate) (PBLG) exists in the form of the rodlike,  $\alpha$ -helical conformation in *N,N*-dimethylformamide (DMF) and chloroform. Below a limiting concentration (A-point) the solutions are isotropic, while above another concentration (B-point) they are anisotropic. The coexistence of these isotropic and anisotropic phases is observed in an intermediate concentration range.

Flory<sup>1</sup> proposed a theory of equilibrium properties for solutions of rodlike molecules based on a lattice theory. The important result of this treatment was that the phase separation arises from the contribution of entropy as a consequence of an asymmetric shape of the molecules. The enthalpy term in the free energy of mixing of the polymer and solvent was assumed to be of the van Laar type and to be characterized by a thermodynamic interaction parameter  $\chi$ . A phase diagram for  $\chi$  and composition was obtained for the stiff polymer–solvent system.

Robinson *et al.*<sup>2</sup> found the A- and B-points for PBLG solutions in methylene chloride and dioxane using a polarizing microscope. The dependence of the concentrations of these points on the axial ratio was semi-quantitatively explained by Flory's theory, provided the  $\chi$  is sufficiently small or negative. Nakajima *et al.*<sup>3</sup> obtained the phase diagram from the observation of turbidity for the three component system, PBLG/DMF/poor solvent, in which the increase of the poor solvent content caused an increase in the thermodynamic parameter. Wee and Miller<sup>4</sup> determined the temperature–composition phase diagram for PBLG solutions in DMF from n.m.r. spectroscopy measurements. These phase diagrams were similar to those predicted by Flory's theory. Because the relation between  $\chi$  and the poor solvent content or temperature was unfortunately not given in these experiments, an ambiguity for the propriety of the Flory model for rodlike molecules still remains.

Only limited thermodynamic studies have been made on the application of the Flory model. The results of vapour sorption studies for PBLG and poly( $\beta$ -benzyl-L-aspartate) solutions at high polymer concentrations by Flory and Leonard<sup>5</sup> could not be explained by the Flory model, but could be explained by assuming that mixing of solvent with flexible side chains dominates the thermodynamic

behaviour at high concentrations. Rai and Miller<sup>6</sup> obtained similar results for the PBLG–DMF system at high concentrations. They also showed that the results could be explained by the Wee–Miller theory, in which modification of Flory's lattice theory to allow for side chain flexibility had been made, i.e. the flexible side chains were assumed to be attached to a rigid main-chain backbone.

Osmotic pressure studies were recently reported for PBLG solutions in chloroform and ethylene dichloride in the concentration range of 2 to 15 vol % polymer at 29°C<sup>7</sup>. Because the measured osmotic pressures were a monotonic function of concentration, no phase boundaries were found. The value of  $\chi$  was found to be 0.44–0.47 in the isotropic phase. In view of this large value of  $\chi$ , it was concluded that the system cannot be treated without regarding net attraction between solute molecules.

In this paper determination of solvent activities for the PBLG–chloroform system are reported in the concentration range of 20 to 100 vol % polymer at 30°C. The solvent activities were determined from vapour pressure and isothermal distillation. The results are combined with those obtained by osmotic pressure measurements, and are compared with the existing theories.

## EXPERIMENTAL

### Materials

PBLG ( $M_n = 98\,000$ ) was the same as that used in the previous work, and its axial ratio was 45. Chloroform was dried over  $\text{CaCl}_2$  and then distilled. Triphenylmethane (TPM), used as a reference solute for the isothermal distillation, was purified by recrystallization from ethanol, and was vacuum dried for more than 24 h.

### Vapour pressure

Vapour pressure measurements were performed by two independent sets of apparatus, with different manometers. The basic part of the apparatus is a manometer, a chamber for housing a quartz spring balance, and a tube for storing pure solvent after vacuum-distillation. Direct and indirect vapour pressures were measured by a Bourdon gauge (60–100 vol % polymer) and by a U tube manometer (50–70 vol % polymer). The chamber, in the former, or together

with the tube, in the latter, was immersed in a bath ( $30 \pm 0.02^\circ\text{C}$ ), and the other parts of the system accessible to solvent vapour, including the manometer, were maintained at a slightly higher temperature ( $+0.3^\circ\text{C}$ ) above that of the bath to prevent condensation of solvent. Dried PBLG film, after weighing (40–50 mg), was placed on a quartz pan, suspended from the calibrated spring which was housed in the chamber. Solvent was admitted to the chamber and the manometer from the tube using a high-vacuum Teflon stopcock, and the resulting pressure was measured by the manometer, after evacuation to  $10^{-4}$  mmHg through a vacuum line. The increase in weight owing to sorption of solvent by the polymer was observed from the elongation of the spring. Sorption equilibrium was usually attained within 6 h except at relatively high solvent concentration, where 24 h was generally necessary. The data were taken randomly by increasing or decreasing vapour pressure. The volume fraction was obtained assuming no volume change on mixing. The specific volume of PBLG was taken as  $0.787 \text{ cm}^3/\text{g}^5$ . Prior to the isothermal distillation measurements, the activity coefficient of chloroform was determined using solutions of the standard solute (TPM) by the U tube method.

#### Isothermal distillation

Isothermal distillation was performed in the concentration range of 20 to 50 vol % polymer at  $30^\circ\text{C}$ . The diagram of a glass vacuum desiccator is shown in Figure 1. The PBLG (0.5–1.0 g) was weighed in fibrous form at the beginning of the experiment. Two weighing bottles, A and B were put on a glass plate, and their lids were placed above the bottles. Polymer solution was set in one bottle, and a reference solution of TPM in chloroform was placed in the second bottle. All joints, C, D, and E were sealed with

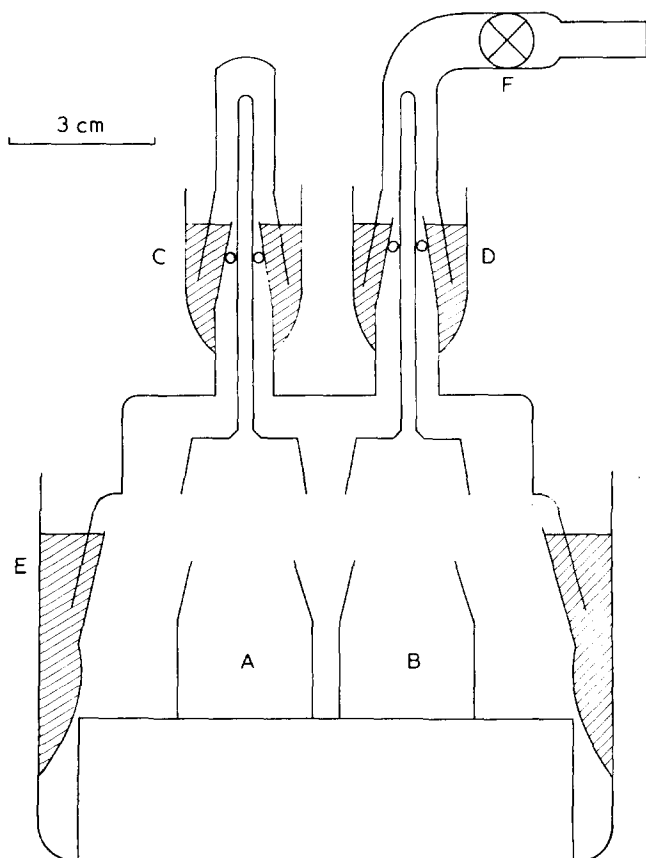


Figure 1 Diagram of apparatus for isothermal distillation

Table 1 Manometric data for PBLG in chloroform at  $30^\circ\text{C}$

Run 1		Run 2	
$v_1$	$a_1$	$v_1$	$a_1$
Direct vapour pressure			
0.110	0.310	0.185	0.472
0.139	0.380	0.285	0.612
0.178	0.450	0.386	0.741
0.198	0.480	0.423	0.796
0.246	0.546		
Indirect vapour pressure			
0.306	0.635	0.376	0.729
0.346	0.687	0.391	0.755
0.461	0.829	0.423	0.802
0.503	0.883	0.438	0.815
0.540	0.920	0.465	0.865

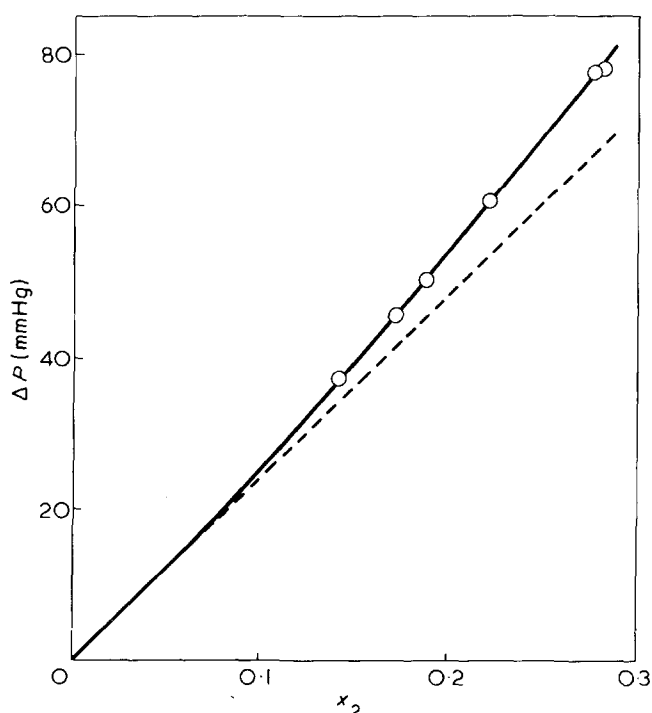


Figure 2 Vapour pressure depression of chloroform vs. mole fraction of TPM at  $30^\circ\text{C}$ . ----, Raoult's law

mercury, and the desiccator was evacuated through a high vacuum Teflon stopcock F. The desiccator was then immersed in a bath at  $30 \pm 0.01^\circ\text{C}$ . To take out the weighing bottles, the stopcock was opened, and the joints, C and D were removed. After the weighing bottles were quickly covered, the desiccator was opened. The volume fraction was obtained by weighing using the same assumption as was made in the vapour pressure measurements.

Isothermal distillation between polymer solutions whose initial concentrations were different by about 20 vol % polymer was performed. These concentrations coincided within the experimental error for the run after seven days. Therefore, we assumed that this was a sufficient condition for attainment of equilibrium for isothermal distillation.

## RESULTS

### Vapour pressure

Results for solvent activities are given in Table 1.

Vapour pressure depression for the reference solution of TPM in chloroform is plotted as a function of solute  $x_2$  in Figure 2. The broken line represents Raoult's law. The

solvent activity coefficient  $\gamma_1 = a_1/x_1$  was calculated from the vapour pressure depression,  $\Delta P$ , by:

$$\gamma_1 = (1 - \Delta P/P_1^0)/(1 - x_2) \quad (1)$$

where  $P_1^0$  is the vapour pressure over the pure solvent,  $a_1$  the solvent activity, and  $x_1$  the mole fraction of the solvent. These values are plotted as  $(\gamma_1 - 1)/x_2^2$  versus  $x_2$  in Figure 3. The expression for the activity coefficient of chloroform in TPM from this plot is:

$$\gamma_1 = 1 - 0.668x_2^2 - 0.273x_2^3 \quad (2)$$

#### Isothermal distillation

Results for isothermal distillation are summarized in Table 2. The second column lists the mole fraction of TPM in chloroform at equilibrium. The solvent activities listed in the third column were calculated using equations (1) and (2).

#### DISCUSSION

The thermodynamic properties of the PBLG-chloroform system over the entire concentration range could be obtained by combining the isothermal distillation and vapour pressure data with osmotic pressure data reported previously<sup>7</sup>. Although it is difficult to choose a function which describes the entire behaviour of the activity for a wide concentration range, we can satisfy this criterion by choosing a function,  $\ln a_1/\ln v_1$ , which was first used by Krigbaum and Geymer<sup>8</sup>. Here,  $a_1$  and  $v_1$  are the activity and the volume fraction of the solvent, respectively. The function  $\ln a_1/\ln v_1$  obtained from three different types of measurements is plotted in Figure 4 against volume fraction of polymer,  $v_2$ . At infinite dilution this function must approach a constant value  $1/X$ , where  $X$  is the ratio of the molar volume of polymer

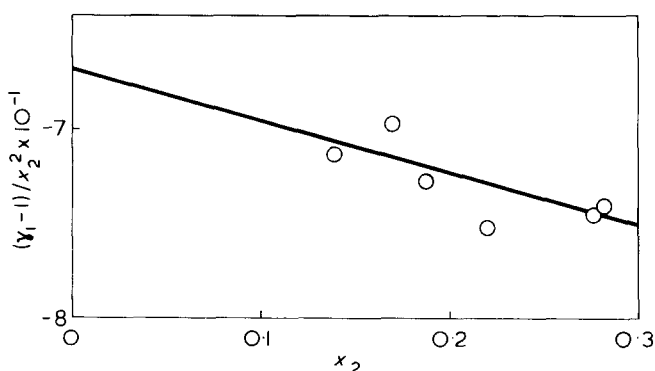


Figure 3 Activity coefficient of chloroform in solution of TPM at 30°C

Table 2 Isothermal distillation data for PBLG in chloroform at 30°C

$v_2$	$x_2 \times 10^2$	$a_1$
0.207 4	0.350	0.996 49
0.239 3	0.619	0.993 72
0.304 7	1.23	0.987 6
0.322 0	1.54	0.984 5
0.395 6	3.08	0.968 6
0.448 3	5.47	0.943 4
0.486 3	8.73	0.907 9
0.552 6	16.97	0.813 2

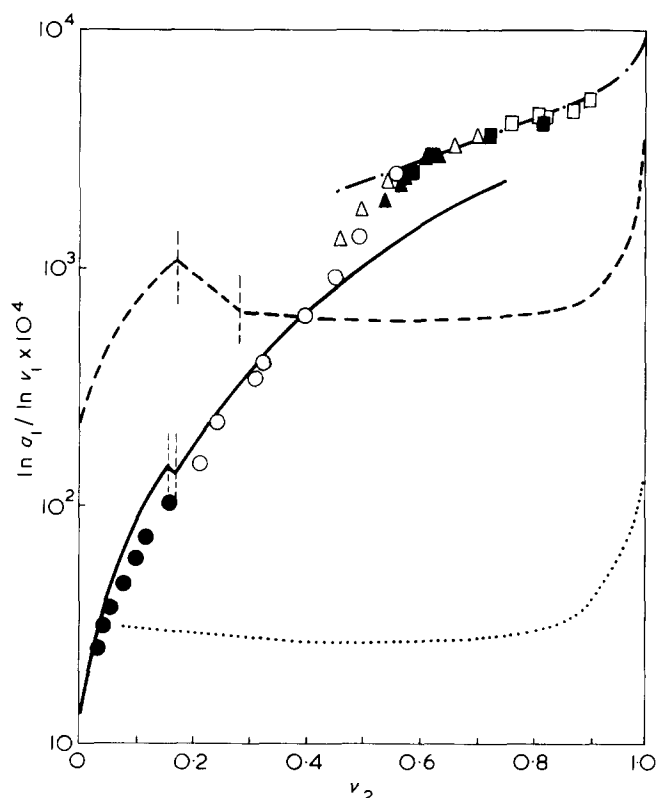


Figure 4 Comparison of activity data for PBLG-chloroform with various theoretical curves: ●, osmotic pressure; ○, isothermal distillation; □ and ■, runs 1 and 2 of direct vapour pressures, respectively; △ and ▲, runs 1 and 2 of indirect vapour pressures, respectively; ---- and ····, Flory's theory with  $\chi = 0$  for  $r = 45$  and 948.8, respectively; - · - ·, Flory-Leonard model with  $\chi_s = -0.2$ ; —, Wee-Miller theory with  $x = 242.6$ ,  $a = 706.2$ , and  $\chi = 0.46$ . Vertical broken lines indicate calculated positions of phase boundaries

to that of solvent. At the other limit of concentration the function must approach unity. Although the osmotic pressure and isothermal distillation data do not overlap perfectly, Figure 4 shows that the two sets of data complement each other. The A-point for the PBLG (axial ratio 85)/chloroform system was found to be  $v_2 \approx 0.065 - 0.070$ <sup>7</sup>, and the B-point should exist at a somewhat higher concentration. If the bisphasic region existed, this function  $\ln a_1/\ln v_1$  must decrease with increasing concentration within this region. The existence of certain phase boundaries is not seen in the Figure.

In Flory's lattice theory of rodlike molecules, the thermodynamic properties are represented as follows. Activity of solvent  $a_1$  and of polymer  $a_2$  for the isotropic phase are:

$$\ln a_1 = \ln(1 - v_2) + \{(r - 1)/r\}v_2 + \chi v_2^2 \quad (3)$$

$$\ln a_2 = \ln(v_2/r) + (r - 1)v_2 - \ln r^2 + \chi r(1 - v_2)^2 \quad (4)$$

and those for the anisotropic phase are:

$$\ln a_1 = \ln(1 - v_2) + \{(y - 1)/r\}v_2 + 2/y + \chi v_2^2 \quad (5)$$

$$\ln a_2 = \ln(v_2/r) + (y - 1)v_2 + 2 - \ln y^2 + \chi r(1 - v_2)^2 \quad (6)$$

where  $v_2$  is the volume fraction of the polymer,  $r$  the axial ratio of the polymer, and  $y$  a disorientation index, determined using the following equation:

$$v_2 = \{r/(r - y)\} \{1 - \exp(-2/y)\} \quad (7)$$



At high concentrations, where  $y = 1$  (i.e. perfect alignment of rodlike molecules prevails at equilibrium) the activity of solvent is given by the expression for a solution with ideal entropy of mixing:

$$\ln a_1 = \ln x_1 + \chi v_2^2 \quad (8)$$

where  $x_1$  is the mole fraction of solvent.

In Figure 4,  $\ln a_1/\ln v_1$  versus  $v_2$  calculated from equations (3)–(8) for  $\chi = 0$  with  $r = 45$  and  $948.8^*$  is plotted.

From the general features of these curves, the discrepancy between the predicted values and experimental data cannot be removed by adjusting the value of  $r$ . The experimental curve may be aligned with a curve obtained by assuming a large value of  $\chi$ , but Flory's theory predicted that the system with a large value of  $\chi$  must be biphasic at extremely low concentration. It must also have a large concentration difference between the two phases in equilibrium, so our results cannot be accounted for by such an assumption.

Flory and Leonard<sup>5</sup> measured vapour pressures for PBLG–pyridine, PBLG–ethylene dichloride, and poly( $\beta$ -benzyl-L-aspartate)/chloroform in the concentration range of 60 to 100 vol % polymer. They found that their data could not be fitted with the results predicted by Flory. To take account of this discrepancy, the mixing of solvent with flexible side chains of polymer was considered and the arrangement of main chains was assumed to be fixed where the volume fraction of solvent was small. Their data were compared with the following expression:

$$\ln a_1 = \ln(1 - v_2') + v_2' + \chi_s (v_2')^2 \quad (9)$$

where  $v_2'$  is the volume fraction of the side chains calculated on the basis of mixing being confined to the side chains,

\* This value given for  $r$  corresponds to the value of  $X$  for this system.

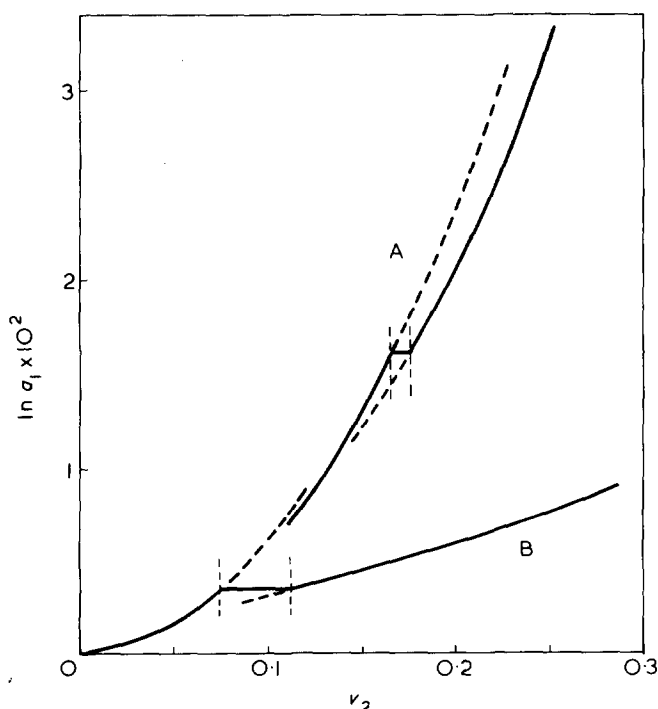


Figure 5 Curves of  $\ln a_1$  vs.  $v_2$  calculated from Wee–Miller theory with  $\chi = 0$ . A,  $x = 110$  and  $a = 110$ ; B,  $x = 110$  and  $a = 0$ . Vertical broken lines indicate positions of phase boundaries

and  $\chi_s$  is the interaction parameter related to the side chain and solvent. The  $v_2'$  is given by:

$$v_2'/(1 - v_2') = (M_s/M_u)\{v_2/(1 - v_2)\} \quad (10)$$

where  $M_s$  and  $M_u$  are the molecular weights of the side chain and of the entire peptide unit. The data of Flory and Leonard were found to fit equation (9) reasonably, below the concentration of 10–15 vol % solvent, if  $\chi_s$  for PBLG–pyridine, PBLG–ethylene dichloride, and poly( $\beta$ -benzyl-L-aspartate)/chloroform were assumed as 0.35, 0.2, and 0, respectively. In Figure 4,  $\ln a_1/\ln v_1$  versus  $v_2$  calculated from equations (9) and (10) with  $\chi_s = -0.2$  is shown. Reasonable agreement is found between the predicted and experimental results above  $v_2 \approx 0.6$ . Rai and Miller<sup>6</sup> reported similar results obtained by vapour pressure measurements for the PBLG–DMF system in the concentration range of 70–100 vol % polymer. The experimental results were explained by equations (9) and (10) with  $\chi_s = 0.6$ . They also showed that these results can be explained by Flory's lattice theory, as modified by Wee and Miller. In this theory, polymer chain was assumed to be composed of rigid main chain and flexible side chains. A partition function for the system, in which the main chains were partly oriented about an axis, was derived on the basis of a lattice model as in the original Flory model. However, we did not adopt the Wee–Miller theory for explaining the present experimental results at high concentrations, because the assumption that arrangement of main chains is affected by dilution would not be reasonable at high concentrations.

We considered that the Wee–Miller theory for polymer molecules composed of rigid main chains and flexible side chains does not apply at high concentrations, but rather at low or intermediate concentrations. This has been briefly mentioned in a report by Rai and Miller<sup>6</sup> and is discussed in some detail below.

Activities of solvent and polymer for the isotropic phase are:

$$\ln a_1 = \ln(1 - v_2) + [(x + a - 1)/(x + a)]v_2 + \chi v_2^2 \quad (11)$$

$$\ln a_2 = \ln [v_2/(x + a)] + (x + a - 1)v_2 - \ln x^2 + \chi(x + a)(1 - v_2)^2 \quad (12)$$

and those of for the anisotropic phase are:

$$\ln a_1 = \ln(1 - v_2) + [(y + a - 1)/(x + a)]v_2 + 2/y + \chi v_2^2 \quad (13)$$

$$\ln a_2 = \ln [v_2/(x + a)] + (y + a - 1)v_2 + 2 - \ln y^2 + 2a/y + \chi(x + a)(1 - v_2)^2 \quad (14)$$

where  $x$  is the axial ratio of the main chain,  $a$  the number of segments of side chains per main chain, and  $y$  the disorientation index. The value of  $y$  is given by the expression:

$$v_2 = \{(x + a)/(x - y)\} \{1 - \exp(-2/y)\} \quad (15)$$

These equations lead back to equations (3)–(7) in the case of  $a = 0$ . Solvent activities for the system with  $x = 110$  and  $\chi = 0$  calculated from equations (11)–(15) are shown in Figure 5 in the cases of  $a = 0$  and 110. The difference

between solvent activities for isotropic and anisotropic phases in the latter case is much smaller than that for the former. The concentrations of the A- and B-points are given as  $v_2 = 0.073$  and  $0.112$  for  $a = 0$ , and  $v_2 = 0.165$  and  $0.174$  for  $a = 110$ .

The segments of main chain and of side chain, and the solvent molecules to be occupied on a lattice site must be primarily limited to the same size on the basis of the lattice model. In order to allow the theory to be applied to actual solutions, we take  $x$  and  $a$  as adjustable parameters. Because the value of the function  $\ln a_1/\ln v_1$  must approach  $1/X$  at infinite dilution, it is reasonable to take the ratios of the molar volume of main chain and of side chains per main chain to the molar volume of solvent as  $x$  and  $a$ . The curve of  $\ln a_1/\ln v_1$  versus  $v_2$  calculated from equations (11)–(15) with  $x = 242.6$ ,  $a = 706.2$ , and  $\chi = 0.46$  is shown in Figure 4. The behaviour of solvent activities fits reasonably for the experimental data below  $v_2 \approx 0.4$ . The concentrations of the A- and B-points given as  $v_2 = 0.153$  and  $0.164$  would be respectively higher than those observed using a polarizing microscope. This is, perhaps, due to the fact that the PBLG–chloroform system is not perfectly within the limitations of applicability of the lattice model in choosing values for  $x$  and  $a$ . The fact that the phase boundaries were not found from the thermodynamic measurements may be because the biphasic region was too narrow and the difference between the activities for the isotropic and anisotropic states was too small to be detected experimentally (see Figures 4 and 5).

The parameter  $\chi$ , characterizing the enthalpy term in equations (11)–(14), is approximately given by the following expression, provided that the interaction between main chain and side chain is omitted:

$$\chi = [x/(x+a)]\chi_m + [a/(x+a)]\chi_s \quad (16)$$

where  $\chi_m$  is the interaction parameter between the main chain and the solvent, and  $\chi_s$  is the parameter related to the side chain. If  $\chi$ ,  $\chi_s$ , and  $x/a$  are respectively taken as  $0.46$ ,  $-0.2$ , and  $0.344$ , the value of  $\chi_m$  is given as  $2.4$  from equation (16). The distinct and very large value of  $\chi_m$  is due to the strength of the net attractive forces, perhaps resulting from the interaction between the large dipole moments of the main chains. We can deduce from these observations that the solubility of PBLG molecules can be attributed to the compatibility between the side chain and the solvent.

#### ACKNOWLEDGEMENT

The authors thank Dr A. Hatano of their Department for helpful discussions. They thank the Ministry of Education in Japan for a Grant-in-Aid.

#### REFERENCES

- 1 Flory, P. J. *Proc. R. Soc. (A)* 1956, 234, 73
- 2 Robinson, C., Ward, J. C. and Beevers, R. B. *Discuss. Faraday Soc.* 1958, 25, 29
- 3 Nakajima, A., Hayashi, T. and Ohmori, M. *Biopolymers* 1968, 6, 973
- 4 Wee, E. L. and Miller, W. G. *J. Phys. Chem.* 1971, 75, 1446
- 5 Flory, P. J. and Leonard, Jr, W. J. *J. Am. Chem. Soc.* 1965, 87, 2102
- 6 Rai, J. H. and Miller, W. G. *Macromolecules* 1972, 5, 45
- 7 Okamoto, A., Kubo, K. and Ogino, K. *Bull. Chem. Soc. Japan* 1974, 47, 1054
- 8 Krigbaum, W. R. and Geymer, D. O. *J. Am. Chem. Soc.* 1959, 81, 1859

# Thermodynamic studies of solid polyethers: 5. Crystalline–amorphous interfacial thermal properties\*

Mitsuru Ikeda†, Hiroshi Suga and Syuzo Seki

Department of Chemistry, Faculty of Science, Osaka University, Toyonaka, Osaka, Japan  
(Received 17 June 1974; revised 10 February 1975)

The influence of the crystalline–amorphous interface on the bulk melting phenomena of poly(ethylene oxide) and poly(octamethylene oxide) was studied. For this purpose, heats of solution of various kinds of specimens prepared by precise heat treatment were measured at various temperatures with an isoperibol calorimeter. The crystallinity and the lamellar thickness were determined by dilatometric and small-angle X-ray scattering methods, respectively. Melting points of each sample were determined using a differential scanning calorimeter. The thermodynamic quantities obtained were correlated by theoretical consideration, so that the effects of crystalline–amorphous interfacial thermal properties on bulk quantities such as heat of fusion were derived.

## INTRODUCTION

The nature of the surfaces of folded-chain crystals of solid high polymers has been the subject of intensive study in recent years. There are two methods of investigation in general. One of them is the kinetic approach. Hoffman and Lauritzen<sup>1</sup> have determined the surface free energy of folded-chain crystals by studying the kinetics of the crystallization of polymers. The other is based on thermodynamic considerations<sup>2,3</sup>. The investigation by Fisher and Hinrichsen<sup>2</sup> is a typical example.

As is well known, a crystalline high polymer is considered as consisting of crystallites embedded in an amorphous region. This model is widely supported by measurements of density<sup>4</sup>, small-angle X-ray scattering<sup>5</sup>, broadline n.m.r.<sup>6</sup> and of etching phenomena<sup>4</sup>. We have adopted this kind of model for the analysis of the surface-excess thermodynamic functions.

The present study aims to elucidate the effect of the nature of interface on the bulk properties such as melting phenomena, etc. Dynamic techniques such as differential scanning calorimetry may be useful for semi-quantitative discussion, but for more precise estimation of the free energy of the interface it is desirable to obtain accurate data under static conditions. In this respect, we have employed another technique to determine heats of fusion, through the determination of heats of solution with a precision solution calorimeter.

\* Parts of this paper were presented at the 20th (1971) and the 21st (1972) Annual Meetings of the Society of Polymer Science, Japan.

† Present address: Research Laboratory, Tokyo, Fuji Photo Film Co. Ltd., Asaka, Saitama, Japan.

Table 1 Viscosity-average molecular weight ( $M_\eta$ ), number-average molecular weight ( $M_n$ ) and the ratio of the weight-average to the number-average molecular weight ( $M_w/M_n$ ) of three PEO samples

Sample	$M_\eta$	$M_n$	$M_w/M_n$
I	$1.29 \times 10^3$	$1.52 \times 10^3$	1.13
II	$7.80 \times 10^3$	$6.84 \times 10^3$	1.11
III	$2.02 \times 10^4$	$1.96 \times 10^4$	1.18

We have determined thermodynamic quantities for characterized samples of poly(ethylene oxide) (PEO) and poly(octamethylene oxide) (POMO), since their crystal and molecular structures have been studied very precisely by Tadokoro *et al.*<sup>7,8</sup>.

## EXPERIMENTAL

### Preparation and characterization of samples

*Poly(ethylene oxide)*. Of three samples employed for the present research, sample I (PEO 1500) and sample II (PEO 6000) were obtained from Wako Junyaku Co. Ltd, sample III (PEO 20 000) being obtained from Union Carbide Co. Ltd.

They were recrystallized by precipitation of chloroform solution (Wako special grade) with petroleum ether (Wako special grade) at ice-bath temperature and then dried under high vacuum ( $10^{-3}$  N/m<sup>2</sup>) for a week at room temperature.

The molecular weight distribution and number-average molecular weight of the samples were determined by use of gel permeation chromatography (g.p.c.). The g.p.c. analysis of sample I was carried out in tetrahydrofuran (THF) solution at 35°C, by means of a Shimadzu GPC packed with crosslinked polystyrene–divinylbenzene gel. Samples II and III were treated in dimethylacetamide solution at 80°C using Bio-Glass 200 (Bio-Rad Lab. Co. Ltd) as the packing. For the determination of  $M_\eta$  values of these samples the viscosities of their benzene solution were measured at 25°C. In this case the following equation<sup>9</sup> was employed:

$$[\eta] = 3.97 \times 10^{-4} M_\eta^{0.686} \quad (1)$$

The results are listed in Table 1.

Four samples of sample III, prepared under different annealing conditions, were used for the measurements of heat of solution, lamellar thickness, and degree of crystallinity. They were crystallized from the melts at the constant temperatures of 28°, 42°, 50° and 55°C, respectively. These samples are called hereafter samples I', II', III' and IV', respectively.

As PEO is very hygroscopic, special care was taken to isolate the sample from open air by handling in a dry-box.

*Poly(octamethylene oxide).* The monomer n-octamethylene glycol was purified by repeated recrystallization from an acetone solution of a commercial sample (Nakarai Chemical Co. Ltd) by precipitation with ethyl ether. Polymerization was then performed in a special reaction tube which was designed by Rhoad and Flory<sup>10</sup>. After a small amount of concentrated sulphuric acid and  $(C_2H_5)OBF_3$  (Nakarai Co. special grade) had been introduced into the tube, it was evacuated and degassed. The mixture was then heated up and polymerized in the temperature region 160°–210°C under a constant stream of dry nitrogen gas. The product was purified by repeated precipitation from benzene solution with methanol and finally dried in vacuum ( $10^{-3}$  N/m<sup>2</sup>) at 30° to 50°C for a week.

The molecular weight distribution and number-average molecular weight of POMO were determined by Yoshida *et al.*<sup>11</sup>. Based on this result the average molecular weight was evaluated to be ~7000. POMO exists in two crystalline forms. Although the chain conformation is planar zig-zag in both forms, their packing in the unit cell differs. In this study, PTHF-type prepared by cooling the molten sample was used<sup>8</sup>. Four kinds of sample with different annealing conditions were prepared for the purpose mentioned above. They were crystallized from the melts at the constant temperatures of 30°, 40°, 50° and 60°C. These samples are called hereafter samples I', II', III' and IV', respectively. All the procedures of handling the samples were carried out in a dry-box as described above.

#### Heat of solution

The heat of solution was measured by making use of an isoperibol-type precision calorimeter, LKB 8700-1. This calorimeter was calibrated by measuring the heat of solution of tris(methyl hydroxy)amino methane in 0.1 N HCl solution and the inaccuracy was found to be 0.01%. The amount of sample used in each measurement was about 500 mg which was dissolved in 100 cm<sup>3</sup> water.

The heats of solution in water for each of samples I, II, and III of PEO were measured at 20°, 25° and 30°C. In every case two kinds of sample, quenched or annealed, were investigated. For the quenching treatment each sample was dried under high vacuum ( $10^{-4}$  N/m<sup>2</sup>) for 30 min at 350 K and then immersed directly into liquid nitrogen. On the other hand, an annealed sample was prepared by a slow cooling (0.4 K/h) down to room temperature. For samples I', II', III' and IV' of PEO, the measurements of the heats of solution in water were carried out at 25°C.

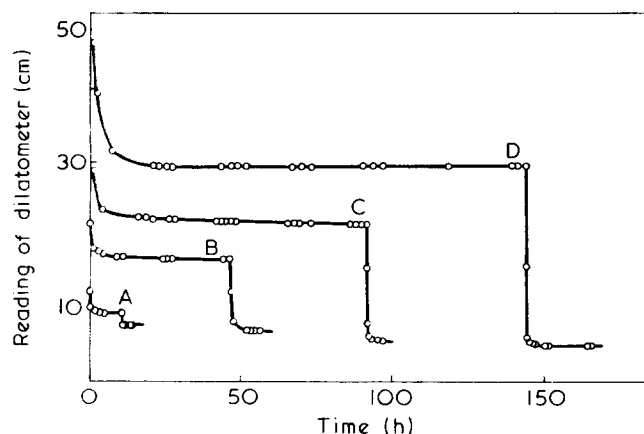


Figure 1 Reading of dilatometer of PEO at different temperatures. A, Sample I'; B, sample II'; C, sample III'; D, sample IV'

The heats of solution of POMO (sample I') in benzene were measured at 25°, 30° and 35°C. The heats of solution in benzene for samples I', II', III' and IV' of POMO were also measured at 35°C.

#### Dilatometry

After complete degassing of the melts (347 K) of each sample the volume changes on crystallization were measured with a dilatometer. An ordinary dilatometer made of glass was used with a cathetometer (to  $\pm 0.01$  mm). The degree of crystallinity of each sample was determined using the method by Skoulios *et al.*<sup>12-14</sup>.

#### Small-angle X-ray scattering

The measurement of small-angle X-ray scattering was carried out by using a Rigaku Denki RU-3HM. Small-angle X-ray diffraction photographs for samples I', II', III' and IV' of PEO were obtained at 25°C. The exposure time was about 24 h for each measurement. For the samples of POMO, the measurements were made at 20°C. These data were analysed by use of a photometer. The lamellar thickness of the samples was determined according to the method of Fisher and Hinrichsen<sup>2</sup>.

#### Melting point determination

The melting points of all the samples were measured by use of a DSC-model 1B (Perkin-Elmer).

## RESULTS AND DISCUSSION

#### Poly(ethylene oxide)

*Determination of the degree of crystallinity.* The degree of crystallinity of sample III was determined using the data of the dilatometric study described in the previous section. The relationship between the reading of dilatometer and the time elapsed immediately after dipping the sample into the water-bath is illustrated in Figure 1. Each curve consists of two parts: the initial drop of the reading corresponding to the process of crystallization from the melt at a definite temperature, and the second drop expressing the thermal contraction which takes place on cooling the sample from the crystallization temperature down to the final temperature, 25°C.

For the determination of the degree of crystallinity, the following relations proposed by Skoulios *et al.*<sup>12-14</sup> were adopted:

$$\tau(t) = [V(t) - V_1(t)] / [V_c(t) - V_1(t)] \quad (2)$$

where  $\tau(t)$  is the degree of crystallinity of the sample at  $t^\circ\text{C}$ ,  $V$  the specific volume of crystalline polymer and  $V_c$  and  $V_l$ , the specific volume of the crystalline as well as the amorphous regions on the assumption that the specific volume of the amorphous region is equal to that in the supercooled liquid state.

In the present case, the degrees of crystallinity were calculated by adopting the following numerical data:  $V_c(25^\circ\text{C}) = 0.8104 \text{ cm}^3/\text{g}$ ,  $V_c(t_c) = 0.8104 + 1.5 \times 10^{-4}(t_c - 25)$ <sup>13</sup>;  $V_l(25^\circ\text{C}) = 0.8860 \text{ cm}^3/\text{g}$  and  $V_l(t_c) = 0.8860 + 7.0 \times 10^{-4}(t_c - 25)$ . The degrees of crystallinity based on these values are given in Table 2.

*Heat of solution.* In Figure 2, the dissolution curve into pure water of sample II at 25°C is shown. It is interesting to note here that the first process is endothermic, which is followed by a subsequent exothermic one. Presumably, the

former corresponds to a swelling effect, while the latter to a dissolving one. In order to analyse this mechanism in more detail, the dissolution curve of the same sample into a saturated aqueous solution of PEO at 25°C was measured. The result is shown in Figure 3. In this case we observe only the first abrupt rise of the temperature. This fact supports the above-mentioned interpretation, since no dissolution should occur in this case. The value of the heat of swelling amounts to 3.36 kJ/mol monomer unit. In the following experiments with PEO, 100 cm<sup>3</sup> water were always used as the solvent. In such experiments the process of swelling and dissolution takes place simultaneously.

The dissolution curves of sample II in chloroform and benzene at 25°C are shown in Figure 4. After the swelling process was over, the exothermic process was observed in chloroform, while in benzene we could not observe any such tendency, and a monotonous approach to equilibrium was observed. The much slower process of dissolution in the cases of benzene and chloroform in comparison with that of water makes it impossible to determine the exact heat of solution from these data. However, we can observe the total effect due to the simultaneous swelling and dissolution processes. As a result, we can point out the important fact that at 25°C there appears to be an exothermic process in polar solvents but not in non-polar solvents.

To investigate the temperature dependence of the heat of solution in water in more detail than the results reported by Nakayama<sup>15</sup> and Lakhanpal *et al.*<sup>16</sup>, we studied the heat of solution at various temperatures (20°, 25° and 30°C) for samples I, II and III, each of which had undergone two kinds of treatment, annealing and quenching. These results are given in Table 3 and Figure 5. The experimental error was estimated to be  $\pm 0.2$ –0.4%. As is shown in Figure 5, the heats of solution for all the samples shift from the exothermic side to the endothermic one with increasing tem-

Table 2 Degree of crystallinity, lamellar thickness and heats of solution of four PEO samples

Sample	$t_c$ (°C)	$\tau(t_c)$	$\tau(25)$	$L$ (nm)	$\Delta H_{sol}^{ob}$ (25°C) (J/mol monomer unit)
I'	28	0.845 3	0.843 9	16.95	-222.1
II'	42	0.841 3	0.857 1	18.05	-119.3
III'	50	0.831 0	0.874 3	25.86	108.2
IV'	55	0.776 0	0.881 0	27.43	248.4

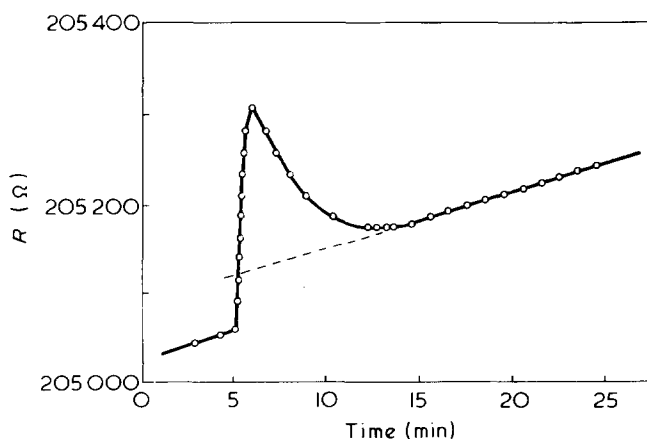


Figure 2 Thermogram of solution process of PEO (sample II) in water at 25°C (0.092 1 mol/dm<sup>3</sup>). Sensitivity at 25°C is 55 (Ω/K) ( $=\Delta R/\Delta T$ )

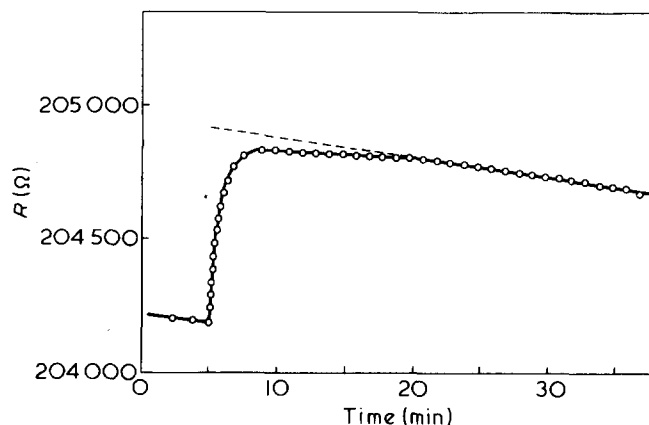


Figure 3 Thermogram of solution process of PEO (sample II) in saturated aqueous solution of PEO at 25°C

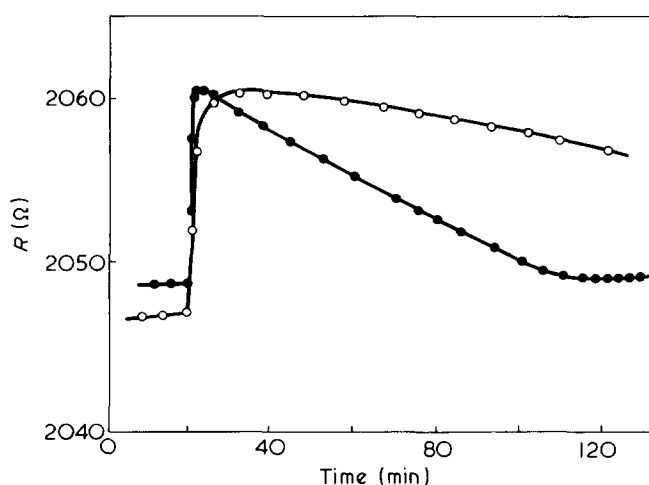


Figure 4 Thermograms of solution processes of PEO (sample II) in chloroform (0.094 3 mol/dm<sup>3</sup>; ●) and into benzene at 25°C (0.091 8 mol/dm<sup>3</sup>; ○)

perature. It is rather difficult to find out the systematic influence of the molecular weight on the heat of solution from these results, because the curves also reflect the influence of the degree of crystallinity on the heat of solution.

In order to illustrate this, we measured the heat of solution into water at 25°C for the samples of sample III with various degrees of crystallinity. These results are listed in Table 2 and illustrated in Figure 6. This curve indicates that the heat of solution of this sample of PEO in water at 25°C becomes zero at a degree of crystallinity of about 86.7%.

**Determination of lamellar thickness of folded-chain crystal.** Small-angle X-ray diffraction patterns were taken for the samples which were recrystallized from the melt at crystallization temperatures of 28°, 42°, 50° and 55°C. To analyse these diffraction patterns, we referred to the collagen crystal<sup>17</sup> as a standard substance. Since the polymer crystal contains the amorphous region, a true lamellar thickness is obtained by taking into account the degree of crystallinity on the basis of Fisher's method<sup>2</sup>. This relates the lamellar thickness,  $L$ , to the crystallinity,  $\tau(t)$ , and the length of long period,  $l$ , obtained by the small-angle X-ray scattering method by:

$$L = \tau(t) \times l \quad (3)$$

The relationship between lamellar thickness and crystallization temperature obtained is illustrated in Figure 7 and

Table 3 Values of the heats of solution of PEO samples measured at different temperatures

$t$ (°C)	$\Delta H_{\text{sol}}^{\text{ob}}$ (J/mol monomer unit)					
	Sample I		Sample II		Sample III	
	Quenched sample	Annealed sample	Quenched sample	Annealed sample	Quenched sample	Annealed sample
20	-403.1	-392.2	-28.03	208.9	-160.0	-143.4
25	-179.6	-150.1	241.0	539.8	59.36	155.2
30	68.31	109.0	—	—	353.4	490.5

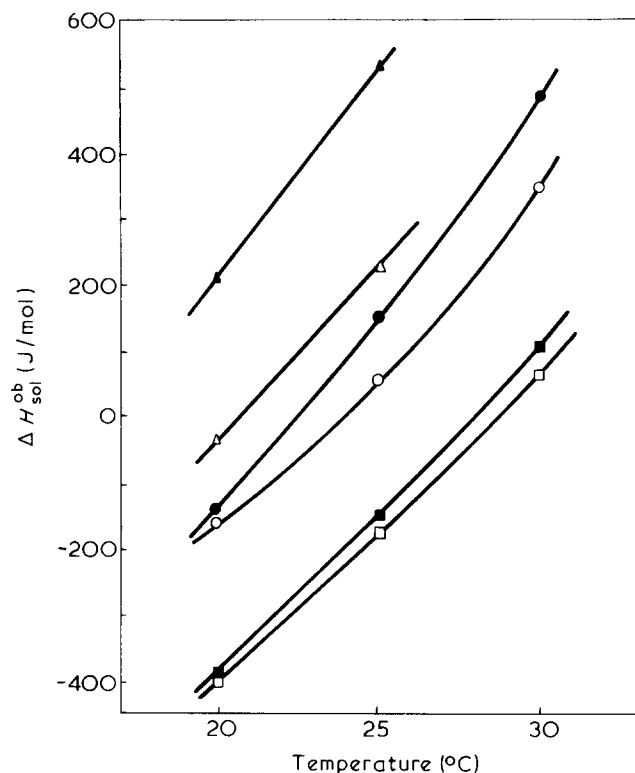

 Figure 5 Temperature dependence of the heats of solution in water for PEO.  $\square$ , Sample I;  $\triangle$ , sample II;  $\circ$ , sample III. Solid symbols, annealed sample; open symbols, quenched sample

Table 2. As is shown from these results, the lamellar thickness increases with the crystallization temperature appreciably around 45°C. This fact indicates that the lamellar thickness is determined mainly during the period of crystal growth. The sharp change mentioned above seems to agree fairly well with the result of Skoulios *et al.*<sup>14</sup> and also is consistent with the theory of Lindenmeyer<sup>18</sup>. After the completion of our study we have noted the new results of Booth *et al.*<sup>19</sup> and Spegt<sup>20</sup>. The former investigated the change of the melting point as well as the interfacial free energies with the variation of molecular weight mainly for low molecular weight specimens, while the latter investigated the effect of variation of molecular weight on the lamellar structure. According to the latter's results it may be concluded that our sample corresponds to his sample H-20000.

*Estimation of the melting point of an assumed ideal crystal.* Melting points of samples I', II', III' and IV' were measured by using a Perkin-Elmer DSC 1B. The curve of melting points vs. reciprocal lamellar thickness is shown in Figure 8, in which we can see a linear relationship. This fact seems to reflect a continuous change in the lamellar thickness of our sample as was mentioned in the previous

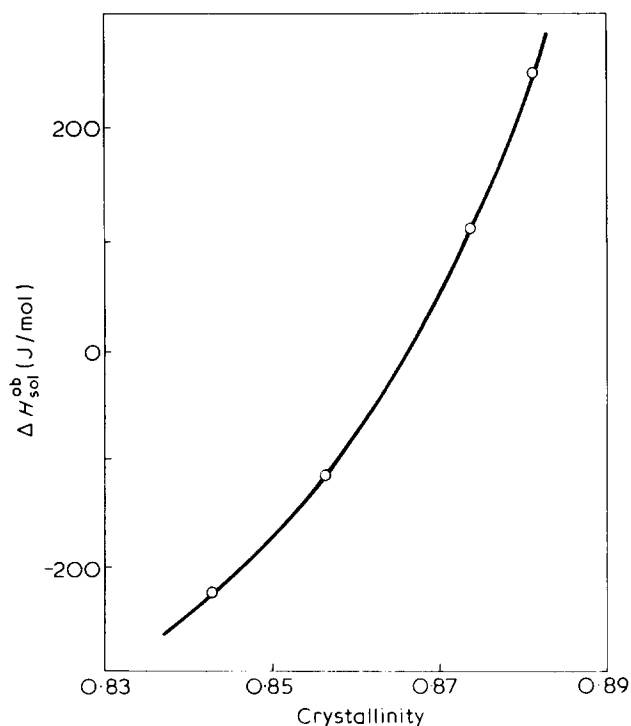


Figure 6 Heat of solution of PEO (samples I', II', III' and IV') in water at 25°C plotted against crystallinity

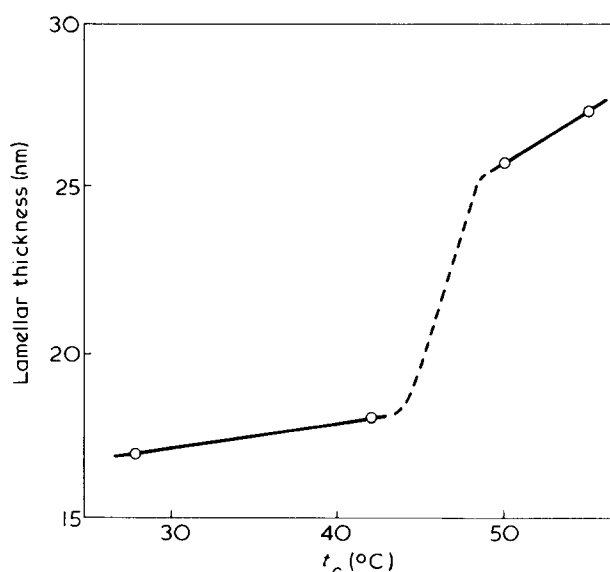


Figure 7 Lamellar thickness (25°C) of PEO plotted against crystallization temperatures for samples I', II', III' and IV'

section. If this assumption is correct, the melting point of an ideal crystal which consists of infinite extended-chain polymer may be estimated by extrapolating to  $L^{-1} = 0$  and found to be 341.8 K.

## Poly(octamethylene oxide)

**Determination of the degree of crystallinity.** The degrees of crystallinity for four samples (samples I', II', III' and IV') of POMO were determined in the same way as in PEO and the results are shown in Figure 9. In this case the final temperature was 30°C. In the calculation of the degree of crystallinity, the density of the crystalline part of POMO was found to be  $d(25^\circ\text{C}) = 1.03 \text{ g/cm}^3$  from the X-ray diffraction data measured by Tadokoro *et al.*<sup>8</sup>. In addition, the following data were employed:  $V_c(25^\circ\text{C}) = 0.9709 \text{ cm}^3/\text{g}$ ,  $V_c(t_c) = 0.9770 \times [1 + 1.48 \times 10^{-3}(t_c - 30)]^{21}$ ,  $V_l(30^\circ\text{C}) = 1.1916 \text{ cm}^3/\text{g}$  and  $V_l(t_c) = 1.1916 \times [1 + 7.53 \times (t_c - 30)]$ . The degree of crystallinity data obtained are listed in Table 4.

**Heat of solution.** Measurements of the heat of solution into benzene for the samples recrystallized from the melts at 30°, 40°, 50° and 60°C, were carried out at 35°C. Below 35°C, the solubility and the rate of dissolution decreases markedly. Here, we can observe heat data as given in Table 4 in which the experimental error was found to be  $\pm 2\%$ . The heats of solution of sample I' were measured at 25°, 30° and 35°C: their values were found to be 19.74, 22.07 and 24.30 kJ/mol monomer unit respectively.

**Determination of lamellar thickness of folded-chain crystal.** The small-angle X-ray diffraction photographs for the samples recrystallized from the melts were taken at crystallization temperatures of 30°, 40°, 50° and 60°C. As in the case of PEO, a change of diffraction patterns was observed. The experimental results of lamellar thickness are given in Table 4.

**Estimation of melting point of an assumed ideal crystal.** The corresponding procedure to the case of PEO (see Figure 8) was carried out and the melting point of an assumed

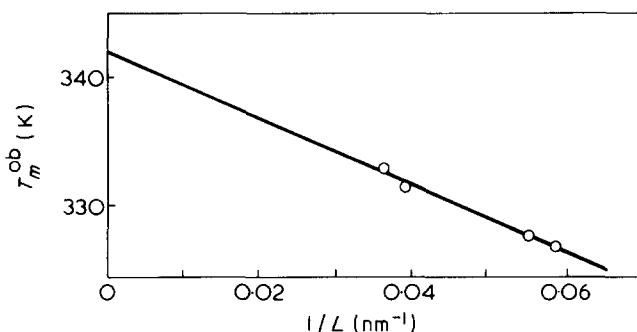


Figure 8 Melting point of PEO (samples I', II', III' and IV') plotted against reciprocal lamellar thickness.  $T_m^\infty = 341.8 \text{ K}$

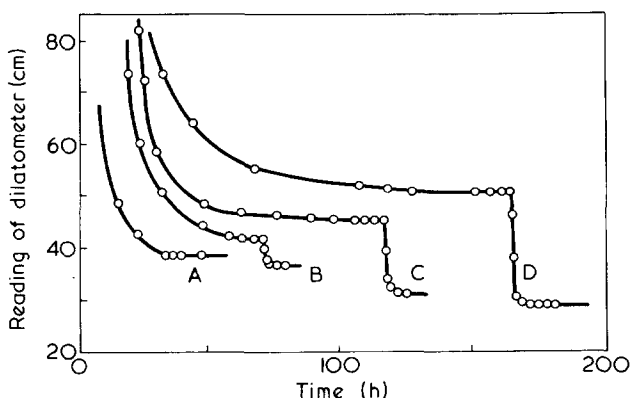


Figure 9 Reading of dilatometer of POMO at different temperatures. A, Sample I; B, sample II; C, sample III; D, sample IV

Table 4 Degrees of crystallinity, lamellar thickness and heats of solution of four POMO samples

Sample	$t_c$ ( $^\circ\text{C}$ )	$\tau(t_c)$	$\tau(30)$	$L$ (nm)	$\Delta H_{\text{sol}}^{\text{ob}}$ (35 $^\circ\text{C}$ ) (J/mol monomer unit)
I'	30	0.681 0	0.681 0	9.66	24.66
II'	40	0.677 2	0.722 3	10.52	25.33
III'	50	0.653 0	0.781 1	11.90	26.78
IV'	60	0.621 9	0.820 5	13.58	29.08

ideal crystal was obtained as 347 K. This result is compatible with that obtained by Yoshida *et al.*<sup>11</sup> (347 K) who determined it by use of an adiabatic calorimeter.

## Interfacial enthalpy and enthalpy of fusion of folded-chain lamellar crystal

As was mentioned in the introduction, the main purpose of the present work is to determine the interfacial enthalpy of the two crystalline polymers, based on the measurement of the heats of solution as well as the crystallinities of the samples.

In this respect, the first step was to derive the relationship between the heat of solution and the interfacial enthalpy. By using the equation suggested by Fisher<sup>2</sup>, the observed molar heat of fusion can be expressed as follows:

$$\Delta H_m^{\text{ob}} = \tau(t) \times \{ \Delta H_m^\infty - (2V_c H^\sigma / L) \} \quad (4)$$

where  $\Delta H_m^{\text{ob}}$  is the observed molar heat of fusion of polymer per monomer unit,  $\Delta H_m^\infty$  is the molar heat of fusion for the ideal crystal which is made up with the perfect crystalline part of infinitely extended-chain,  $H^\sigma$  is the molar interfacial enthalpy of folded-chain crystal,  $V_c$  is the molar volume,  $\tau(t)$  is the degree of crystallinity at  $t^\circ\text{C}$  and  $L$  is the lamellar thickness of folded-chain crystal.

Assuming the additivity of the molar enthalpies of crystalline and amorphous regions, the observed molar heat of solution,  $\Delta H_{\text{sol}}^{\text{ob}}$  at  $t^\circ\text{C}$  is given by:

$$\Delta H_{\text{sol}}^{\text{ob}} = \tau(t) \times \Delta H_{\text{sol}}(\text{cryst}) + \{1 - \tau(t)\} \times \Delta H_{\text{sol}}(\text{amorph}) \quad (5)$$

where  $\Delta H_{\text{sol}}(\text{cryst})$  is the molar heat of solution at  $t^\circ\text{C}$  for the crystalline part and  $\Delta H_{\text{sol}}(\text{amorph})$  is the molar heat of solution at  $t^\circ\text{C}$  for the amorphous region of the partly crystalline polymer. By setting

$$\Delta H_{\text{sol}}(\text{cryst}) = H(\text{sol}) - H(\text{cryst}) \quad (6)$$

$$\Delta H_{\text{sol}}(\text{amorph}) = H(\text{sol}) - H(\text{liq}) \quad (7)$$

and substituting equations (6) and (7) into equation (5), we obtain:

$$\Delta H_{\text{sol}}^{\text{ob}} = \tau(t) \times [H(\text{liq}) - H(\text{cryst})] + \Delta H_{\text{sol}}(\text{amorph}) \quad (8)$$

where  $H(\text{liq})$  and  $H(\text{cryst})$  are the enthalpies at  $t^\circ\text{C}$  of liquid and crystalline regions of high polymer, respectively.

Then, we obtain the following approximate equations from equations (4) and (8):

$$\Delta H_{\text{sol}}^{\text{ob}} = \tau(t) \times [ \Delta H_m^\infty - (2V_c H^\sigma / L) ] + \Delta H_{\text{sol}}(\text{amorph}) \quad (9)$$

Table 5 Various thermodynamic data obtained from our experiments

Sample		$\Delta H_m^\infty$ (kJ/mol monomer unit)	$\Delta S_m^\infty$ (J/K per bond)	$T_m^\infty$ (K)	$H^\sigma \times 10^{-7}$ (J/cm <sup>2</sup> )	$G^\sigma \times 10^{-7}$ (J/cm <sup>2</sup> )	$S^\sigma \times 10^{-7}$ (J/cm <sup>2</sup> )
PEO	our data (25°C)	9.41 ± 1.05	9.11	341.8	104 ± 27	97.7	0.018 4
POMO	our data (30°C)	29.85 ± 1.30	9.70	347.1	80.8 ± 23	73.4	0.021 3

$$\Delta H_{\text{sol}}^{\text{ob}} - \Delta H_{\text{sol}}(\text{amorph}) = \tau(t) \times [\Delta H_m^\infty - (2V_c H^\sigma / L)] \quad (10)$$

From equation (9), we obtain the following equation by taking the difference of the  $\Delta H_{\text{sol}}^{\text{ob}}$  of different samples:

$$[(\Delta H_{\text{sol}}^{\text{ob}})_i - (\Delta H_{\text{sol}}^{\text{ob}})_j] = \Delta H_m^\infty [(\tau(t))_i - (\tau(t))_j] - 2V_c H^\sigma \{[(\tau(t))_i / L_i] - [(\tau(t))_j / L_j]\} \quad (11)$$

where we assume that  $\Delta H_m^\infty$  and  $H^\sigma$  are constant for *i*th and *j*th different samples, since we have employed rather high molecular weight polymers which have average lamellar thicknesses as was described in the preceding section\*. In this way, we can eliminate  $\Delta H_{\text{sol}}(\text{amorph})$  which is not measurable, and we are in a position to evaluate a kind of averaged  $\Delta H_m^\infty$  and  $H^\sigma$  from the  $\Delta H_{\text{sol}}^{\text{ob}}$  data by means of the method of least squares.

Substituting our experimental results into this equation, the interfacial enthalpy and the enthalpy of fusion of PEO and POMO were evaluated. The results obtained correspond to 25°C for PEO and to 30°C for POMO. The enthalpies of fusion obtained are converted to those at  $T_m^\infty$  by use of the  $C_p$  data of Beaumont *et al.*<sup>23</sup>. The final values are shown in Table 5.

Now, we proceed to the discussion of the significance of these values for PEO. If the interfacial term in equation (4) is neglected the  $\Delta H_m^\infty$  of PEO will have an unreasonably large value of  $13.30 \pm 7.37$  kJ/mol monomer unit with large probable error. This result suggests strongly that we should take the interfacial enthalpy into consideration. As far as we are aware the derivation of the enthalpy of fusion of ideal PEO crystals has been carried out either by the measurement of heat capacity<sup>23</sup> or by use of the method of the depression<sup>24</sup> of melting point for samples with different crystallinities. However, the former gives the enthalpy of fusion of folded-chain crystalline polymer with 100% crystallinity, not of the perfectly extended ideal crystal. So, the effect of the interfacial region is not taken into account. The latter method is rather inaccurate owing to the difficulty of accurate determination of the melting point. The value in this study corresponds to that of a perfect extended-chain crystal excluding the effect of interfacial enthalpy.

Skoulios *et al.* reported<sup>13</sup> the interfacial Gibbs energy of  $74 \times 10^{-7}$  J/cm<sup>2</sup> by using an enthalpy of fusion of 8.28 kJ/mol monomer unit estimated by Mandelkern and Flory<sup>25</sup>. In general it seems to be important in the case of a high

polymer that we should adopt a physical property for the definitely characterized specimen. In this respect, the data of Skoulios *et al.* are not so reliable, since the value of  $\Delta H_m^\infty$  adopted for their calculation is taken from a different sample employed by Mandelkern and Flory. In passing it may be added here that after the completion of our study Maron and Filisko<sup>26</sup> reported the enthalpy of fusion for PEO ( $M_n = 6000$ ) as  $242 \pm 1.7$  J/g by the measurement of heat of solution in water.

The enthalpy of fusion and interfacial enthalpy of POMO crystal consisting of infinitely extended-chain were calculated in the same way. The results are also shown in Table 5. Little is known about the enthalpy of fusion of POMO, except for the value of 29.7 kJ/mol monomer unit which was estimated by Yoshida *et al.*<sup>11</sup> from the measurement of heat capacity and which agrees approximately with our result of  $29.85 \pm 1.30$  kJ/mol monomer unit.

This fact indicates that the effect of folding on the enthalpy of fusion and melting point seems to be rather small for the POMO samples employed.

#### Interfacial entropy

The thermodynamic relation suggested by Flory<sup>24</sup> follows:

$$T_m^{\text{ob}} = T_m^\infty [1 - (2G^\sigma V_c / \Delta H_m L)] \quad (12)$$

The combination of this equation with equation (4) and the following thermodynamic relation:

$$S^\sigma = [(H^\sigma - G^\sigma) / T_m^\infty] \quad (13)$$

gives the interfacial entropy  $S^\sigma$ . Here we have used our data on  $H^\sigma$  and  $T_m^\infty$  given above. The results are as follows:  $S^\sigma = 0.184 \times 10^{-7}$  and  $0.021 3 \times 10^{-7}$  J/cm<sup>2</sup>, for PEO and POMO, respectively.

#### Entropy of fusion

The entropy of fusion of the ideal crystal is evaluated by the relation of  $\Delta S_m^\infty = \Delta H_m^\infty / T_m^\infty$  and  $\Delta S_m^\infty = 9.24$  and  $9.84$  J/K per bond for PEO and POMO, respectively.

#### Mixing enthalpies of PEO and POMO

From equation (10),  $\Delta H_{\text{sol}}(\text{amorph})$ , which is equal to the mixing enthalpy of the supercooled liquid of polymer with the solvent, is obtained by using the data of  $\Delta H_m^\infty$ ,  $H^\sigma$  and  $L$  of solid high polymer obtained in the present study. Figure 10 shows the  $\Delta H_{\text{sol}}(\text{amorph})$  vs.  $t_c$  curve for PEO and POMO which were derived by substituting experimental values of the degree of crystallinity and the lamellar thickness into equation (10). We obtained the following data:  $\Delta H_{\text{sol}}(\text{amorph}) = -7.11 \pm 0.42$  and  $5.46 \pm 0.27$  kJ/mol monomer unit for PEO and POMO, respectively.

\* In contrast with our case Afifi-Effat and Hay<sup>21</sup> studied the case of low molecular weight samples and found an apparent variation of  $G^\sigma$  with the lamellar thickness. Booth *et al.*<sup>22</sup> proposed a new formula for the relation between melting point and lamellar thickness for this kind of sample.



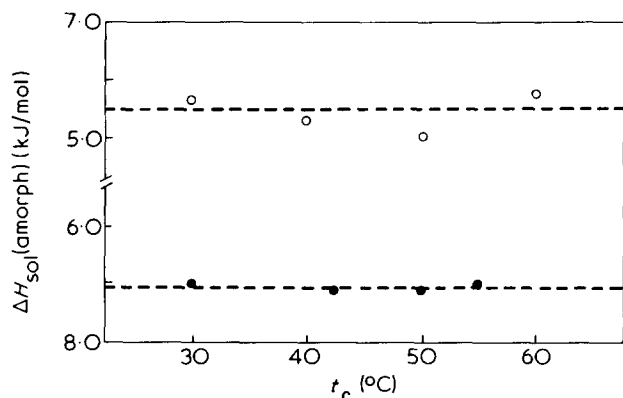


Figure 10 Mixing enthalpies vs. crystallization temperatures. ○, POMO; ●, PEO

## CONCLUSION

In the present study it has been shown that the interfacial enthalpy of PEO makes a significant contribution to the total magnitude of the enthalpy of fusion. The dependencies of the heats of solution of PEO and POMO on temperature and degree of crystallinity were determined. The mixing enthalpies of these materials were also estimated experimentally. It was found to be reasonable that the additivity of the heats of solution of the crystalline and the amorphous regions holds in derivation of the heat of solution of real high polymer solid.

## ACKNOWLEDGEMENTS

The authors would like to express their sincere thanks to Dr Katsuzo Wakabayashi and Dr Tatsuo Ueki, Osaka University, Faculty of Engineering Science, who kindly permitted us to use an X-ray diffraction apparatus for the measurement of the lamellar thickness of the samples. The authors are also grateful to Dr Minoru Ueda of the Kurare Co. Ltd, who kindly performed the characterization of the samples by use of gel permeation chromatography. The

authors are also indebted to Dr Syohei Yoshida for fruitful discussions.

## REFERENCES

- Hoffman, J. D. and Lauritzen, J. I. *Kolloid-Z. Z. Polym.* 1967, **231**, 93
- Fischer, E. W. and Hinrichsen, G. *Kolloid-Z. Z. Polym.* 1966, **213**, 93
- Atkinson, C. M. L. and Richardson, M. J. *Trans. Faraday Soc.* 1969, **65**, 1764
- Peterlin, A. *J. Macromol. Sci.* 1958, **50**, 12
- Tsvankin, D. Ya. *Polym. Sci. USSR* 1964, **6**, 2304
- Law, G. H. and Field, J. A. *Ind. Eng. Chem.* 1958, **50**, 12
- Tadokoro, H. *J. Polym. Sci. (C)* 1966, **15**, 1
- Kobayashi, S., Tadokoro, H. and Chatani, Y. *Makromol. Chem.* 1968, **112**, 225
- Allen, G., Booth, C., Hurst, S. J., Jones, M. N. and Price, C. *Polymer* 1967, **8**, 391
- Rhoad, M. J. and Flory, P. J. *J. Am. Chem. Soc.* 1950, **72**, 2216
- Yoshida, S., Suga, H. and Seki, S. *Polym. J.* 1973, **5**, 33
- Arlie, J. P. and Skoulios, A. E. *Makromol. Chem.* 1966, **99**, 160
- Spegt, P., Terrise, J., Gilg, B. and Skoulios, A. E. *Makromol. Chem.* 1967, **107**, 29
- Arlie, J. P., Spegt, P. and Skoulios, A. E. *Makromol. Chem.* 1967, **104**, 212
- Nakayama, H. *Bull. Chem. Soc. Japan* 1970, **43**, 1683
- Lakhanpal, M. L., Kappor, V., Sharma, R. K. and Sharma, S. C. *Indian J. Chem.* 1966, **4**, 59
- Kratky, O. *J. Polym. Sci.* 1948, **3**, 195
- Lindenmeyer, P. H. *J. Chem. Phys.* 1967, **46**, 1902
- Beach, D. R., Booth, C., Pickles, C. J., Sharpe, R. R. and Waring, J. R. S. *Polymer* 1972, **13**, 246
- Spegt, P. *Makromol. Chem.* 1970, **140**, 167
- Afifi-Effat, A. M. and Hay, J. N. *JCS Faraday Trans. II* 1972, **68**, 656
- Beech, D. R. and Booth, C. *J. Polym. Sci. (B)* 1970, **8**, 731
- Beaumont, R. H., Clegg, B., Gee, G. et al. *Polymer* 1966, **7**, 401
- Flory, P. J. *J. Chem. Phys.* 1949, **17**, 223
- Mandelkern, L. and Flory, P. J. 'Principles of Polymer Chemistry', Cornell University Press, Ithaca, 1953, p 573
- Maron, S. H. and Filisko, F. E. *J. Macromol. Sci. (B)* 1972, **6**, 79

# Thermal degradation of poly(diethyl vinylphosphonate) and its copolymer

Norihiro Inagaki, Kiyoshi Goto and Kakuji Katsuura

Polymer Chemistry Section, Faculty of Engineering, Shizuoka University, Hamamatsu 432, Japan  
(Received 15 January 1975)

Thermal degradation of poly(diethyl vinylphosphonate) and diethyl vinylphosphonate/vinyl alcohol copolymer was investigated using thermogravimetry, infra-red spectroscopy and g.c.—mass spectrometry. For poly(diethyl vinylphosphonate), little chain scission occurred and the high stability may be attributed to P—O—P crosslinkages between phosphonate units. With the diethyl vinylphosphonate/vinyl alcohol copolymer, the presence of hydroxyl groups in the polymer chains inhibited the formation of the P—O—P crosslinkages. The main degradation products from the copolymer were aldehydes having the general formula  $\text{HC(O)(CH=CH)}_n\text{—CH}_3$  and methyl ketones having the formula  $\text{H}_3\text{CC(O)(CH=CH)}_n\text{—CH}_3$  and  $\text{CH}_3\text{C(O)(CH=CH)}_n\text{—CH=CH}_2$ , where  $n = 1, 2, 3$ . The introduction of phosphonate unit into poly(vinyl alcohol) is less effective than that of phosphate unit in enhancement of thermal stability.

## INTRODUCTION

This paper reports an investigation of the effect of phosphonate units incorporated in poly(vinyl alcohol) on its thermal degradation.

The flame-proofing effect of phosphorus-containing polymers is dependent on the constitution of the phosphorus components. For example, Sander and Steininger<sup>1</sup> reported that the flame resistance of polymers of unsaturated phosphonates was higher than that of unsaturated phosphates, and this was ascribed to their different thermal stabilities. However, the flame resistance of polymers containing functional groups cannot be explained solely on the basis of their thermal stabilities. Thermal reactions induced by the interaction of functional groups with phosphorus residues need to be taken into account. For example, a relationship between the flame-proofing effect of cellulose and the induced reactions have been recognized<sup>2</sup>.

In a previous paper<sup>3</sup> on the action of phosphate unit in poly(vinyl alcohol) on thermal degradation, it was shown that the introduction of phosphate units accelerated dehydration and inhibited the scission of polymer chains. This inhibition was due to the formation of conjugated double bonds in the polymer chains by the *cis*- $\beta$ -elimination of the phosphorus ester groups.

Simple phosphonates are well known to be more stable than phosphates<sup>4</sup> and the elimination of phosphonate groups to give olefins rarely occurs<sup>5</sup>. The comparison of the thermal degradation of poly(vinyl alcohol) containing phosphonate units with that of phosphate units is therefore of interest.

## EXPERIMENTAL

### Materials

Diethyl vinylphosphonate was prepared from triethyl phosphite and 1,2-dibromoethane according to the method of Kosolapoff<sup>6</sup>. The product was identified by i.r. and n.m.r. spectroscopy<sup>7-9</sup>. Vinyl acetate was purified by distillation under nitrogen atmosphere before use. Azobisisobutyronitrile (AIBN) was recrystallized from ethanol solution. Other chemicals were analytical grade commercial materials and were used without further purification.

### Polymerization

The homopolymerization was carried out by heating the degassed monomer containing 0.01 mol% AIBN in a sealed glass tube at 70°C for 200 h. The polymer was dissolved in benzene and precipitated with petroleum ether. This process was repeated three times.

The copolymer of vinyl alcohol and vinylphosphonate was prepared by alkaline hydrolysis of vinyl acetate/diethyl vinylphosphonate copolymer, according to the procedure of Tsuda and Yamashita<sup>10</sup>. The monomer reactivity ratio for the copolymerization at 70°C was estimated to be 1.3 and 0.73 for vinyl acetate and diethyl vinylphosphonate, respectively.

### Thermogravimetry

Samples (10 mg) were placed in the quartz pan provided with a Rigaku—Denki thermogravimetric analyser. All analyses were carried out in vacuum ( $10^{-4}$  mmHg) at a programmed rate of 1.5°C/min.

### Analysis of degraded products

Polymers contained in a Pyrex tube connected to a liquid nitrogen trap, were pyrolysed at a prescribed temperature for 1 h in vacuum. The infra-red (i.r.) spectra of the residual products were examined as a KBr disc using a Nihon—Bunko spectrophotometer IRA-1.

The oily products condensed in the trap were analysed by g.c.—mass spectrometry using a Nihon—Denshi GC—Mass spectrometer JMS-07. A separation column (3 mm i.d. x 2 m) containing 25 wt % of poly(ethylene glycol) 4000 coated on C-22(30–60 mesh) was used. The column was heated in a temperature range from room temperature to 150°C.

## RESULTS AND DISCUSSION

### Thermogravimetry (t.g.)

The thermogravimetric curves (Figure 1) showed that the thermal degradation of poly(diethyl vinylphosphonate) proceeded in two stages: (a) in the temperature range from 220° to 250°C, with weight loss of 34.3%. This was followed by a thermally pseudo-stable stage up to 430°C; (b) in



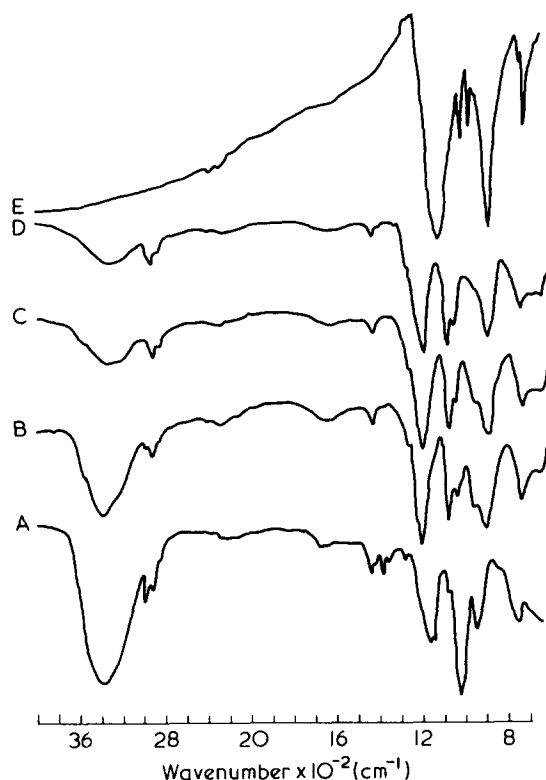
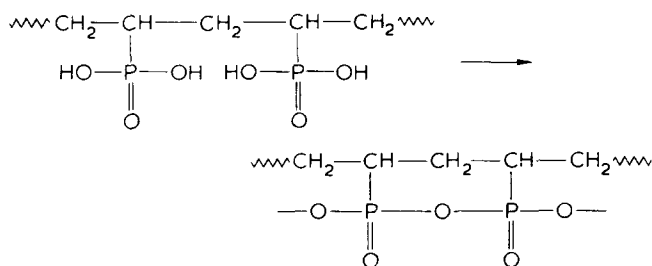


Figure 3 I.r. spectra of copolymer I residue. A, original; B, degraded at 250°C; C, degraded at 300°C; D, degraded at 350°C; E, degraded at 450°C

The suggestions were supported by the pyrolysis-gas chromatographic results which showed that only ethylene was the evolved product in the first stage degradation. In the second stage the absorption band of OH groups disappeared and a new band assigned to be P-O-P groups appeared at 975 and 955  $\text{cm}^{-1}$ . The absorption of the phosphoryl groups shifted to the lower frequency at 1120  $\text{cm}^{-1}$ . Weak absorptions at 1700 (C=O) and 1600  $\text{cm}^{-1}$  (C=C) were observed and the strong absorption of P-C groups (at 720  $\text{cm}^{-1}$ ) remained up to 530°C where the degradation was complete. The above results show that intra- and/or inter-molecular P-O-P crosslinkage is possible.



The elimination via a five-membered ring intermediate<sup>5</sup> occurs infrequently, although this polymer has an available  $\beta$ -hydrogen atom.

The i.r. spectra of copolymers I and III on heating are shown in Figures 3 and 4, respectively. Since the changes of bands attributed to the poly(vinyl alcohol) part of the copolymer were identical with the results<sup>3</sup> reported previously only other spectral changes are discussed here. In the first degradation step all the bands attributed to P-O-C<sub>2</sub>H<sub>5</sub> group disappeared and absorption bands at 1050 and 1720  $\text{cm}^{-1}$  appeared. The former absorption was assigned to the vinyl ester group and the latter to the

carbonyl group. In the second degradation stage a small amount of P-O-P crosslinked structure was formed, especially for copolymer III. A large amount of P-OH group (at 1080  $\text{cm}^{-1}$ ) and C-OH group (at 1430  $\text{cm}^{-1}$ ) remained after the complete degradation. The conjugated double bond group (at 1600  $\text{cm}^{-1}$ ) was less intense in absorption. The comparison between poly(diethyl vinylphosphonate) and the phosphonate copolymers shows that the formation of a P-O-P crosslinking structure is inhibited by the incorporation of a vinyl alcohol unit in polymer chains and that the phosphonate copolymer is more subject to chain scission at a vinyl alcohol unit than the phosphate copolymer.

#### Analysis of oily product

Poly(diethyl vinylphosphonate) on pyrolysis gave only trace amounts of oily products. The main products were ethylene and water, indicating that chain scission rarely occurs.

G.c.-mass spectrometric results presented in Table 2 for the large yield of oily products from copolymer IV, showed the presence of unsaturated carbonyl compounds. No phosphorus compounds were detected. Tsuchiya and Sumi<sup>13</sup> reported that the main products from poly(vinyl

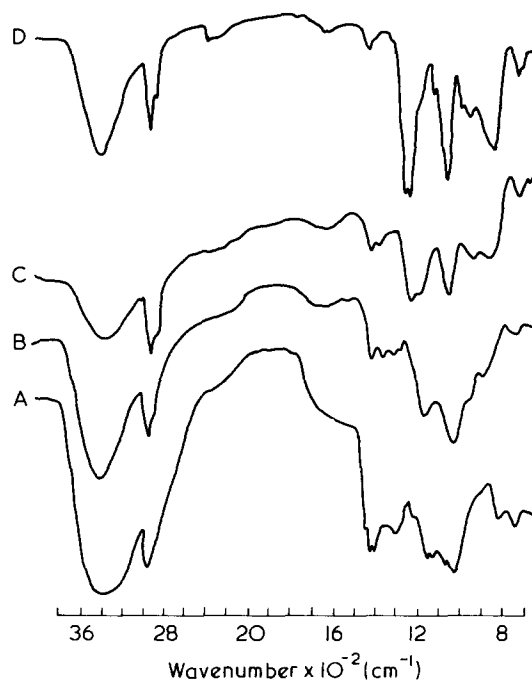


Figure 4 I.r. spectra of copolymer III residue. A, original; B, degraded at 250°C; C, degraded at 320°C; D, degraded at 400°C

Table 2 Oily degradation products (wt%) on heating at 500°C. Copolymer IV, 1 g; Oily products, 154 mg

CH <sub>2</sub> =CHCH=CHC(O)CH <sub>3</sub>	18.0
CH <sub>2</sub> =CHCH <sub>2</sub> C(O)H	14.0
CH <sub>3</sub> C(O)CH <sub>3</sub>	11.5
CH <sub>2</sub> =CHCH <sub>2</sub> C(O)CH <sub>3</sub>	8.5
CH <sub>3</sub> CH=CHCH=CHC(O)CH <sub>3</sub>	6.6
CH <sub>3</sub> C(O)H	6.0
CH <sub>2</sub> =CH(CH=CH) <sub>2</sub> C(O)CH <sub>3</sub>	5.5
CH <sub>2</sub> =CHCH=CHCH <sub>2</sub> C(O)CH <sub>3</sub>	4.7
C <sub>6</sub> H <sub>6</sub>	2.9
CH <sub>2</sub> =CH(CH=CH) <sub>3</sub> C(O)CH <sub>3</sub>	2.3
C <sub>6</sub> H <sub>5</sub> C(O)CH <sub>3</sub>	2.3

alcohol) were aldehydes having the general formula  $\text{HC(O)(CH=CH)}_n\text{-CH}_3$  and methyl ketones having the formula  $\text{H}_3\text{CC(O)(CH=CH)}_n\text{-CH}_3$ , where  $n = 1, 2, 3$ , etc. In addition to these carbonyl compounds, methyl ketones having the formula  $\text{CH}_3\text{C(O)(CH=CH)}_n\text{-CH=CH}_2$ ,  $n = 1, 2, 3$ , were main products from the phosphonate copolymer. The comparison with the phosphate copolymer<sup>3</sup> reported previously shows that the introduction of phosphonate unit in polymer chain is ineffective in inhibition of chain scission.

#### ACKNOWLEDGEMENT

The authors express their thanks to Mr Shoji Ito of Research Institute for Polymer and Textiles for g.c.-mass spectrometric measurements.

#### REFERENCES

- 1 Sander, M. and Steininger, E. 'Reviews in Macromolecular Chemistry', Marcel Dekker, New York, 1967, Vol 2, p 13
- 2 Katsuura, K. and Inagaki, N. *Text. Res. J.* 1975, 45, 103
- 3 Inagaki, N., Tomiha, K. and Katsuura, K. *Polymer* 1974, 15, 335
- 4 Canovan, A. E., Dowden, B. F. and Eaborn, C. E. *J. Chem. Soc.* 1962, p 331
- 5 Baily, W. J., Muir, W. M. and Marktscheffel, F. *J. Org. Chem.* 1962, 27, 4404
- 6 Kosolapoff, G. M. *J. Am. Chem. Soc.* 1948, 70, 1971
- 7 Lancaster, J. E. *Spectrochim. Acta* 1967, 23A, 1449
- 8 Williamson, M. P., Castellano, S. and Griffin, C. E. *J. Chem. Phys.* 1968, 72, 175
- 9 Williamson, M. P. and Griffin, C. E. *J. Chem. Phys.* 1968, 72, 4043
- 10 Tsuda, T. and Yamashita, Y. *Kogyo Kagaku Zasshi* 1962, 65, 811
- 11 Harwood, H. J. and Ritchey, W. M. *J. Polym. Sci. (B)* 1964, 2, 601
- 12 Pike, R. M. and Cohen, R. A. *J. Polym. Sci.* 1960, 44, 531
- 13 Tsuchiya, Y. and Sumi, K. *J. Polym. Sci. (A-1)* 1969, 7, 3151

# Small angle neutron and X-ray scattering by poly(methyl methacrylate) chains

D. Y. Yoon and P. J. Flory

Department of Chemistry, Stanford University, Stanford, California 94305, USA

(Received 20 February 1975)

The intensity of radiation scattering by poly(methyl methacrylate) (PMMA) chains is computed as a function of scattering angle over the range  $0 < \mu = (4\pi/\lambda) \sin(\vartheta/2) < 0.3 \text{ \AA}^{-1}$ , on the basis of a realistic rotational isomeric state model. The scattering functions  $F_x(\mu)$ , corresponding to  $I\mu^2$ , are developed for chains of  $x$  units in terms of the even moments  $\langle r_{ij}^{2p} \rangle$  of the separation distance between pairs of the monomer units  $i$  and  $j$ . Whereas the theoretical scattering function  $F_x(\mu)$  for isotactic PMMA increases monotonically with  $\mu$ , for predominantly syndiotactic PMMA it exhibits a maximum at  $\mu \approx 0.05 \text{ \AA}^{-1}$ . This is in agreement with experimental results on small angle neutron and X-ray scattering by PMMA (in bulk and in solution, respectively). The appearance of the maximum in  $F_x(\mu)$ , heretofore considered anomalous, is shown to be a direct consequence of the preference of racemic diads of PMMA for the *trans*, *trans* conformation and of the inequality of the skeletal bond angles at  $-\text{CH}_2-$  and at the doubly substituted  $\text{C}^\alpha$ .

## INTRODUCTION

Radiation scattering by polymer chains provides a preferred method for investigating their configurations both in solution and in the bulk state. In particular, small angle scattering of neutrons has received special attention recently as a means for direct determination of configurational characteristics of polymer chains in the absence of diluent. A wealth of experimental results<sup>1-5</sup> gathered within the past three years demonstrates beyond question that the radii of gyration of poly(methyl methacrylate) (PMMA), polystyrene and polymethylene, in either the glassy or the amorphous states, conform within close limits to their values in dilute solution in theta solvents. The dependences of the radii of gyration on chain length confirm the adherence to ideal behaviour, without perturbation of the configuration either by interactions with neighbouring chains or by effects of excluded volume<sup>6</sup>. For small magnitudes of the wave vector  $\mu = (4\pi/\lambda) \sin(\vartheta/2) < 0.03 \text{ \AA}^{-1}$ , the scattering function  $P(\mu)$  expressing the ratio of scattered intensity at angle  $\vartheta$  to that at zero angle follows the Debye equation<sup>7</sup>:

$$P(\mu) = (2/v^2)(v - 1 + e^{-v}) \quad (1)$$

where  $v$  is defined according to<sup>8</sup>:

$$v = \mu^2 \langle s^2 \rangle \quad (2)$$

$\langle s^2 \rangle$  being the mean-square radius of gyration.

The Debye equation (1) rests on two assumptions<sup>7</sup>:

(i) that the mean-square distance  $\langle r_{ij}^2 \rangle$  between units  $i$  and  $j$  is proportional to the number  $t = |i - j|$  of units separating these scattering centres; and (ii) that the distribution function  $W(\mathbf{r}_{ij})$  for vector  $\mathbf{r}_{ij}$  is Gaussian (rather, that the Fourier transform of  $W(\mathbf{r}_{ij})$  is Gaussian<sup>7</sup>). These assumptions hold for small values of  $\mu$  where the pairs of units that contribute significantly to  $P(\mu)$  are far apart in sequence along the chain. At larger scattering angles such that  $\mu > \sim 0.03 \text{ \AA}^{-1}$ , the intensity depends increasingly on correlations between units separated by shorter sequences. Conditions (i) and (ii) are not then fulfilled, and departures from the Debye equation may be expected.

The discrepancies that may be encountered upon extending the Debye equation to larger values of the scattering wave vector are demonstrated most strikingly in the results of Kirste and coworkers on the small angle neutron<sup>1,2</sup> and X-ray<sup>9,10</sup> scattering by PMMA. For both syndiotactic and atactic PMMA they observed that  $I\mu^2$ , where  $I$  is the scattered intensity, passes through a maximum at  $\mu \approx 0.1 \text{ \AA}^{-1}$ , instead of increasing monotonically with  $\mu$  as is usually observed for most other polymers<sup>4,5</sup>. These unusual deviations from the Debye equation have been attributed variously to helical sequences, or to ordered regions in the case of the bulk polymers investigated by neutron scattering.

In this communication we show that the abnormalities observed in the scattering functions for PMMA are consistent with the random-coiled configurations peculiar to predominantly syndiotactic PMMA chains. The configurational characteristics of relatively short sequences within long chain molecules of the isotactic, syndiotactic, and atactic PMMA are examined, and their contributions to the scattering functions are evaluated.

## SCATTERING THEORY

The scattering function for a system of independent molecules oriented at random is given with full generality by<sup>7,11</sup>:

$$P(\mu) = (x + 1)^{-2} \sum_{i,j} G_{ij}(\mu) \quad (3)$$

where

$$G_{ij}(\mu) = \langle (\mu \mathbf{r}_{ij})^{-1} \sin(\mu \mathbf{r}_{ij}) \rangle \quad (4)$$

and  $r_{ij}$  is the distance between the groups  $i$  and  $j$ ; the angled brackets denote the statistical mechanical average over all configurations of the chain. The function  $G_{ij}(\mu)$ , which is the Fourier transform of the distribution function  $W(\mathbf{r}_{ij})$ , may be expressed as a series in the even moments of  $r_{ij}$  in the following manner developed by Nagai<sup>12</sup>:

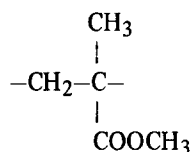
$$G_{ij}(\mu) = \exp(-\mu^2 \langle r_{ij}^2 \rangle / 6) [1 + g_{2;ij}(\mu^2 \langle r_{ij}^2 \rangle / 3) + g_{4;ij}(\mu^2 \langle r_{ij}^2 \rangle / 3)^2 + g_{6;ij}(\mu^2 \langle r_{ij}^2 \rangle / 3)^3 \dots] \quad (5)$$

where

$$\begin{aligned} g_{2;ij} &= 0 \\ g_{4;ij} &= -2^{-3} [1 - 3\langle r_{ij}^4 \rangle / 5\langle r_{ij}^2 \rangle^2] \\ g_{6;ij} &= -2^{-4} [(1 - 3\langle r_{ij}^4 \rangle / 5\langle r_{ij}^2 \rangle^2) - \\ &\quad \frac{1}{3} (1 - 9\langle r_{ij}^6 \rangle / 35\langle r_{ij}^2 \rangle^3)] \\ g_{8;ij} &= -2^{-6} [(1 - 3\langle r_{ij}^4 \rangle / 5\langle r_{ij}^2 \rangle^2) - \\ &\quad \frac{2}{3} (1 - 9\langle r_{ij}^6 \rangle / 35\langle r_{ij}^2 \rangle^3) + \\ &\quad \frac{1}{6} (1 - 3\langle r_{ij}^8 \rangle / 35\langle r_{ij}^2 \rangle^4)] \end{aligned} \quad (6)$$

etc.<sup>13</sup>.

In this paper we identify the scattering group with the repeating unit:



For sufficiently long chains, it is legitimate to replace all moments  $\langle r_{ij}^{2p} \rangle$  for which  $|i - j| = t$  by  $\langle r_t^{2p} \rangle$  without regard for the location of the sequence of  $t$  units within the chain. When 'end effects' may thus be neglected, it is preferable to use the scattering function defined as follows:

$$F_x(\mu) = (x + 1)\mu^2 P(\mu)$$

where  $x$  is the number of units in the chain. With the introduction of equations (3)–(6), this expression simplifies to:

$$F_x(\mu) = \mu^2 + 2\mu^2(x + 1)^{-1} \sum_{t=1}^x (x + 1 - t) \times \exp(-\mu^2 \langle r_t^2 \rangle / 6) [1 + g_{4;t}(\mu^2 \langle r_t^2 \rangle / 3)^2 + g_{6;t}(\mu^2 \langle r_t^2 \rangle / 3)^3 + \dots] \quad (7)$$

#### ROTATIONAL STATES AND STATISTICAL WEIGHTS

A detailed investigation of the conformational energies of PMMA diads has been reported in a recent paper<sup>14</sup>. The C–C bond was assigned the length  $l = 1.53$  Å. The supplements of the skeletal bond angles at the CH<sub>2</sub> group and at the substituted carbon (C<sup>α</sup>) were concluded to be  $\theta' = 58^\circ$  and  $\theta'' = 70^\circ$ , respectively. Well-defined minima were identified at bond rotations  $\phi$  approximating  $0^\circ$  and  $120^\circ$ , the latter being measured in the sense depending on the chirality of the bond, as previously defined<sup>15</sup>. These two

states, *trans*( $t$ ) and *gauche*( $g$ ), are the only ones of significance in PMMA<sup>14</sup>. The energy in the vicinity of the  $g$  state at  $\phi = -120^\circ$  is excessive owing to severe steric interactions involving the planar ester group<sup>14</sup>. Hence, the required statistical weight matrices are of order  $2 \times 2$ . They take the form<sup>14</sup>:

$$U' = \begin{bmatrix} 1 & 1 \\ 1 & 0 \end{bmatrix} \quad (8)$$

$$U_m'' = \begin{bmatrix} 1 & \alpha \\ \alpha & \alpha^2/\beta \end{bmatrix} \quad (9)$$

$$U_r'' = \begin{bmatrix} \beta & \alpha \\ \alpha & \alpha^2/\beta \end{bmatrix} \quad (10)$$

for the pair of bonds flanking C<sup>α</sup>, for the pair of bonds of a meso diad, and for those of a racemic diad, respectively. Rotational states are indexed in the order  $t, g$  on rows and columns of these matrices. Adjustment of the statistical weights calculated from the conformational energies as required to achieve reasonable agreement with experimental measurements of chain dimensions yields<sup>14</sup>:

$$\begin{aligned} \alpha &= 1.6 \exp(-1100/RT) \\ \beta &= 1.4 \exp(600/RT) \end{aligned} \quad (11)$$

#### NUMERICAL CALCULATIONS

The disubstituted carbon atom C<sup>α</sup> was treated as the point scatterer representing the repeating unit in the calculations presented in this communication. (Calculations carried out using more realistic approximations offering refinements for larger values of  $\mu$  will be presented in a paper now in preparation<sup>16</sup>.) Accordingly,  $r_t$  was measured from the C<sup>α</sup> of the first unit to the C<sup>α</sup> of the  $t$ th unit of the sequence. The even moments  $\langle r_t^{2p} \rangle$  with  $p = 1, 2, 3$  and 4 were computed for chains of  $t$  units centred within a longer chain of  $100 + t + 100$  units; i.e., terminal sequences of 100 units were appended at each end of the  $t$ -unit sequence to which  $r_t$  refers. The calculations were carried out using matrix generation methods<sup>7,17</sup>. The range  $t = 2$  to 200 was covered by direct calculation for all of the moments with  $p = 1$  to 4 for the stereoregular isotactic and syndiotactic PMMA chains. The calculations refer to the unperturbed state, usually denoted by a subscript 0, which is here omitted for simplicity.

Values of the ratios  $\langle r_t^4 \rangle / \langle r_t^2 \rangle^2$ ,  $\langle r_t^6 \rangle / \langle r_t^2 \rangle^3$  and  $\langle r_t^8 \rangle / \langle r_t^2 \rangle^4$  required for the evaluation of  $g_{2;t}$ , etc., reflect characteristics of the distribution function  $W(\mathbf{r}_t)$ . They reach limiting values of  $5/3$ ,  $35/9$  and  $35/3$ , respectively, as  $t$  increases indefinitely, these being the values for a Gaussian distribution of the vector  $\mathbf{r}_t$ . These ratios for  $200 < t < \infty$  are readily evaluated with high accuracy by extrapolation from the calculations for  $t \leq 200$ .

Calculations were carried out also for 'atactic' PMMA chains in which the average fraction  $w_m$  of meso diads is 0.20. This composition corresponds approximately to PMMA prepared in the conventional manner using a free radical initiator at elevated temperatures<sup>18</sup>. Chains were generated by Monte Carlo methods, the distribution of meso and racemic diads being Bernoullian. The sequence of  $t$

units was embedded between terminal sequences of 100 'atactic' units each, in the same manner as for the stereoregular chains.

Evaluation of  $\langle r_t^6 \rangle$  and  $\langle r_t^8 \rangle$  by the Monte Carlo methods necessary for generation of atactic chains would require excessive computing time. Accordingly, we have employed the 'equivalent freely jointed' model chain as a basis for estimating their higher moments<sup>†</sup>. For the model chain composed of  $n^*$  freely jointed bonds<sup>7</sup>,

$$\langle r^4 \rangle / \langle r^2 \rangle^2 = \frac{5}{3} - \frac{2}{3n^*} \quad (12)$$

$$\langle r^6 \rangle / \langle r^2 \rangle^3 = \frac{35}{9} - \frac{14}{3n^*} + \frac{16}{9n^{*2}} \quad (13)$$

$$\langle r^8 \rangle / \langle r^2 \rangle^4 = \frac{35}{3} - \frac{28}{n^*} + \frac{404}{15n^{*2}} - \frac{48}{5n^{*3}} \quad (14)$$

From the given value of  $\langle r_t^4 \rangle / \langle r_t^2 \rangle^2$  for the atactic chain of  $t$  monomer units, the number of equivalent freely jointed bonds,  $n^*$ , is obtained from equation (12). Then  $\langle r_t^6 \rangle / \langle r_t^2 \rangle^3$  and  $\langle r_t^8 \rangle / \langle r_t^2 \rangle^4$  are evaluated by inserting  $n^*$  into equations (13) and (14).

The validity of this approximate method was tested by comparing the exact calculations for isotactic and syndiotactic chains with the values of  $\langle r_t^6 \rangle / \langle r_t^2 \rangle^3$  and  $\langle r_t^8 \rangle / \langle r_t^2 \rangle^4$  obtained from equations (12)–(14). Agreement is within 15%. Although the indirect method is subject to some inaccuracy, it nevertheless affords a practicable approximation.

## RESULTS

In Figure 1 the characteristic ratio  $C_n = \langle r_t^2 \rangle / 2t^2$ , where  $n = 2t$  denotes the number of bonds, is plotted against  $1/t$  for isotactic, syndiotactic and atactic PMMA. The passage of  $C_n$  through a maximum at  $t \approx 15$  for the syndiotactic and atactic PMMA is the most striking result of these calculations. It is in marked contrast to the behaviour of  $C_n$  for most other polymers<sup>7</sup> and for isotactic PMMA as well.

<sup>†</sup> The present method resembles superficially the one applied recently to the moments of polymethylene chains<sup>19</sup>. The method of ref 19 differs, however, in taking account of the persistence vector and in the normalization transformation applied to render the distribution spherically symmetric.

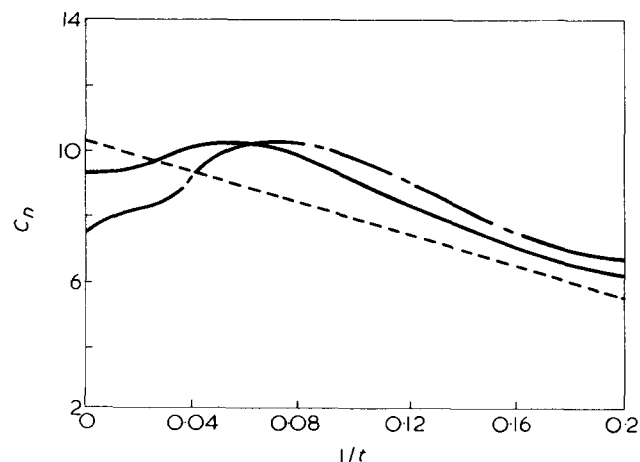


Figure 1 Characteristic ratio,  $C_n = \langle r_t^2 \rangle / 2t^2$ , for PMMA sequences of  $t$  repeating units situated within a very long chain plotted against  $1/t$ . —, a-PMMA; ----, s-PMMA; - · - ·, i-PMMA

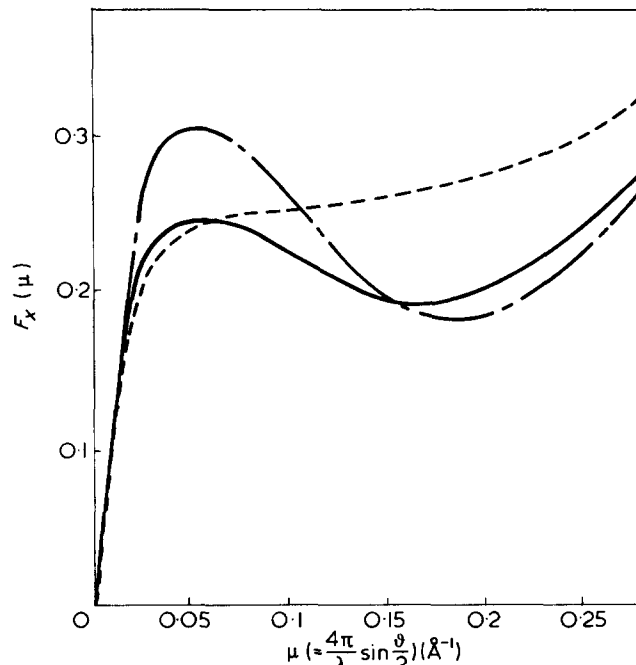


Figure 2 Scattering function,  $F_x(\mu)$  plotted against  $\mu$  for PMMA chains consisting of  $x = 1000$  monomer units. Calculations were carried out according to equation (7) truncated at  $g_8$ . —, a-PMMA; ----, s-PMMA; - · - ·, i-PMMA

This unusual variation of  $C_n$  with chain length arises from the inequality of the two skeletal bond angles in PMMA ( $\theta'' = 70^\circ$ ,  $\theta' = 58^\circ$ ) in conjunction with the predominance of the  $|tt|$  conformation for racemic diads. The energy of  $|tt|$  state for this diad is lower than that of  $|gt|$  by 1700 cal/mol; for the meso diad this difference is 1100 cal/mol. The average length of sequences over which  $|tt|$  states are perpetuated, as calculated according to well established methods<sup>7</sup>, is about nine units for syndiotactic PMMA. For isotactic PMMA it is only about three units.

The scattering functions  $F_x(\mu)$  obtained from equation (7) are presented in Figure 2 over the range  $0 < \mu < 0.3 \text{ \AA}^{-1}$  for PMMA chains of 1000 monomer units. The series expansion of  $F_x(\mu)$  was truncated at  $g_8$ . As stated above, values of  $\langle r_t^2 \rangle$ ,  $\langle r_t^4 \rangle / \langle r_t^2 \rangle^2$ , etc. for  $t > 200$  were obtained by extrapolation. It is to be noted that  $F_x(\mu)$  is equivalent to the quantity  $I\mu^2$  frequently plotted as a function of  $\mu$  in the presentation of experimental results.

The scattering function  $F_x(\mu)$  for isotactic PMMA increases monotonically with  $\mu$ , rapidly at first and then more slowly as  $\mu$  increases further. For syndiotactic and atactic PMMA, however,  $F_x(\mu)$  passes through a maximum at  $\mu \approx 0.05 \text{ \AA}^{-1}$  and a minimum at  $\mu \approx 0.18 \text{ \AA}^{-1}$ . The maximum in  $F_x(\mu)$  is directly related to the maximum observed in the characteristic ratio shown in Figure 1. This connection follows from the fact that the variation of  $\langle r_t^2 \rangle$  with  $t$  is a major factor in determining  $F_x(\mu)$  [see equation (7)].

These features of the variation of  $F_x(\mu)$ , or  $I\mu^2$ , with  $\mu$  and their dependence on the stereochemical configuration of PMMA are in satisfactory qualitative agreement with the experimental results of small angle neutron and X-ray scattering as reported by Kirste *et al.*<sup>1,2,9,10</sup>, as will be apparent from comparison of Figure 3 with Figure 2. However, the agreement is by no means quantitative<sup>†</sup>. Improvement in

<sup>†</sup> Neither acetone nor benzene is a theta solvent for PMMA. Hence, in these solvents, the configurations of the chains are perturbed by excluded volume effects. These effects should be small in the range of main interest here, i.e., for  $\mu > 0.03 \text{ \AA}^{-1}$ , where the principal contributions come from sequences much shorter than the molecular chain length  $x \approx 1000$ .



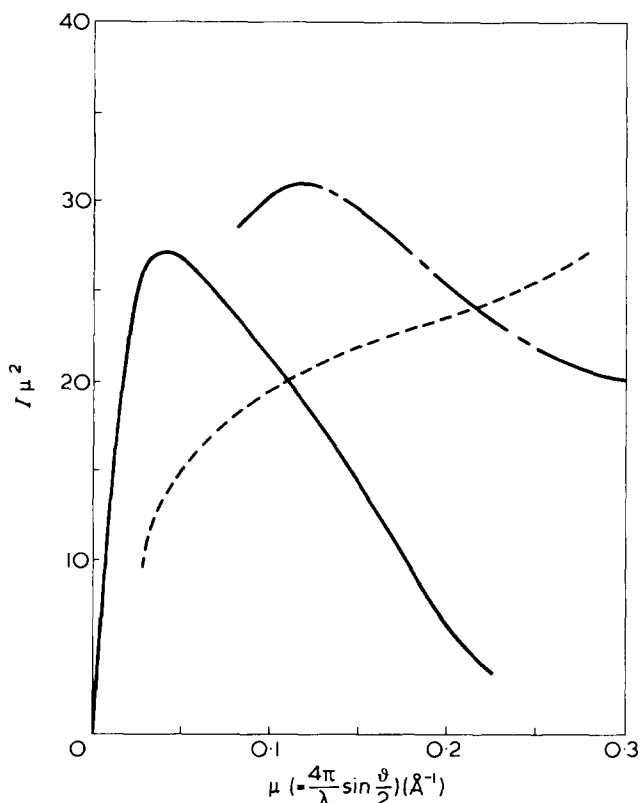


Figure 3 Experimental results on the relative values of  $I\mu^2$  plotted against  $\mu^2$ : —, neutron scattering by a-PMMA in the bulk ( $w_m = 0.2$ ,  $M_w = 250\,000$ ); ---, X-ray scattering by s-PMMA in acetone (independent of  $M_w$  for  $M_w > 10\,000$ ); - · - ·, X-ray scattering by i-PMMA in benzene ( $M_w = 275\,000$ )

this regard appears to require refinement of the present treatment in two respects as follows: (i) the series expansion of  $F_x(\mu)$  in equation (7) is not satisfactorily convergent when truncated at  $g_8$ . Terms of higher order  $g_{10}$ ,  $g_{12}$ , etc. are required for  $\mu > 0.05$ ; (ii) the representation of the monomer unit as a point scatterer located at the  $C^\alpha$  atom is subject to error for larger value of  $\mu$ , i.e., for  $\mu > 0.2$ . This is especially important in small angle neutron scattering by the deuterated polymer in a protonated host. The locus of the scattering is situated at the  $CD_3$  groups;

these groups are separated from the  $C^\alpha$  atom by appreciable distances.

Improvement of the present theoretical calculations through measures designed to overcome those inadequacies are in progress. Results of the newer calculations together with similar computations on other polymers will be published in the near future.

#### ACKNOWLEDGEMENT

This work was supported by the National Science Foundation, Grant No. DMR-74-07655 A01.

#### REFERENCES

- 1 Kirste, R. G., Kruse, W. A. and Schelten, J. *Makromol. Chem.* 1972, **162**, 299
- 2 Kirste, R. G., Kruse, W. A. and Ibel, K. *Polymer* 1975, **16**, 120
- 3 Benoit, H. *et al. Nature (Phys. Sci.)* 1973, **245**, 13
- 4 Ballard, D. G. H., Wignall, G. D. and Schelten, J. *Eur. Polym. J.* 1973, **9**, 965; 1974, **10**, 861
- 5 Fischer, E. W., Wendorff, J. H., Dettenmaier, M., Leiser, G. and Voigt-Martin, I. *Polym. Prepr.* 1974, **15**(2), 8
- 6 Flory, P. J. *J. Chem. Phys.* 1949, **17**, 303
- 7 Flory, P. J. 'Statistical Mechanics of Chain Molecules', Interscience, New York, 1969, pp 340-350
- 8 Flory, P. J. and Jernigan, R. L. *J. Am. Chem. Soc.* 1968, **90**, 3182
- 9 Kirste, R. G. *Makromol. Chem.* 1967, **101**, 91
- 10 Kirste, R. G. and Kratky, O. *Z. Phys. Chem. (NF)* 1962, **31**, 363
- 11 Fujiwara, Y. and Flory, P. J. *Macromolecules* 1970, **3**, 288
- 12 Nagai, K. *J. Chem. Phys.* 1963, **38**, 924
- 13 Ref 7, pp 309-311
- 14 Sundararajan, P. R. and Flory, P. J. *J. Am. Chem. Soc.* 1974, **96**, 5025
- 15 Flory, P. J., Sundararajan, P. R. and DeBolt, L. C. *J. Am. Chem. Soc.* 1974, **96**, 5015
- 16 Yoon, D. Y. and Flory, P. J. in preparation
- 17 Flory, P. J. *Macromolecules* 1974, **7**, 381
- 18 Frisch, H. L., Mallows, C. L., Heatley, F. and Bovey, F. A. *Macromolecules* 1968, **1**, 533
- 19 Yoon, D. Y. and Flory, P. J. *J. Chem. Phys.* 1974, **61**, 5366
- 20 Ref 7, pp 313-314

# Heat capacity of linear high polymers

K. C. Wong, F. C. Chen and C. L. Choy

*Department of Physics, The Chinese University of Hong Kong, Shatin, N.T., Hong Kong*

*(Received 18 November 1974; revised 14 January 1975)*

The molar heat capacity of a 45:55% copolymer of ethylene and tetrafluoroethylene has been measured from 80 to 340 K by the use of an adiabatic calorimeter, to an accuracy of 0.3%. The results are found to be in close agreement with values calculated from the known optical lines of related polymers and the Tarasov model; they are also analysed together with the available data on polyethylene and four other fluoropolymers, showing that the principle of additivity for heat capacities is generally valid to within 2%. The logical relations between these two phenomenological frameworks and their resultant implication on the effective one-dimensional force constant of the carbon backbone are discussed at some length.

## INTRODUCTION

Two fairly successful phenomenological frameworks are at present available for analysing the heat capacities of linear high polymers. The temperature dependence of the heat capacity can be understood in the Tarasov model<sup>1</sup>, which treats the acoustical modes of a polymer like those of a one-dimensional continuum superimposed on a three-dimensional continuum. The relation among different polymers, on the other hand, roughly obeys the principle of additivity proposed by Wunderlich and Jones<sup>2</sup>, who found that the heat capacity of a particular polymer in the temperature range from 60 K up to the glass-transition point is approximately the linear combination of the contributions from its various segments.

It is mainly for the sake of the further verification of these two frameworks that we measured the heat capacity of a 45:55% copolymer of ethylene and tetrafluoroethylene (TFE), in the range 80 to 340 K. The results obtained turned out to be in good agreement with both frameworks: in the temperature range 80–200 K the acoustical contribution predicted by the Tarasov model together with the optical contribution are in close agreement with experimental data, even though above 200 K a definite discrepancy similar to those observed in previous works<sup>3–6</sup> appears between the two. As for the principle of additivity, the straightforward superposition of the observed heat capacities of polyethylene (PE)<sup>7</sup> and polytetrafluoroethylene (PTFE)<sup>8</sup> in 45:55% proportions is also found to fit the data extremely well up to the first-order transition point of PTFE at 270 K. This analysis can be extended to include the recently available data<sup>5</sup> on three other fluoropolymers: poly(vinyl fluoride) (PVF), poly(vinylidene fluoride) (PVF<sub>2</sub>) and polytrifluoroethylene (PVF<sub>3</sub>). Only three distinct 'segments' CH<sub>2</sub>, CHF and CF<sub>2</sub> are involved in the six polymers named, and their values can be easily deduced by least-squares fit to the data. The linear combinations of these 'segmental' heat capacities again agree with all the data throughout the appropriate temperature ranges, bearing out the basic validity of the principle of additivity.

While the general agreement of these two models with our result is gratifying, it also raises a question: what are the logical and physical connections between these two models, if any? We are only able to give partial and tentative answers to this question, mainly because neither model is sufficiently refined and rigorous to allow a meaningful detailed analysis.

## EXPERIMENTAL

The TFE sample used in this experiment was kindly provided by Dr M. Ragazzini of Montecatini Edison, SpA at Milan, and reported to contain 55 mol% of tetrafluoroethylene. This copolymer is known<sup>9–11</sup> to have a high melting temperature (516–545 K), and to be highly alternating between the two monomers, the degree of alternation generally exceeding 90% for the case of equimolar composition such as ours.

The sample stock came in the form of fine powder, 52 g of which were used without further preparation in an adiabatic calorimeter. The measurement of heat capacity at constant pressure,  $C_p$ , was made in the temperature range 80–340 K, to an accuracy of about 0.3%. Since experimental details have already been reported in previous papers<sup>4,5</sup>, they will not be repeated here.

## RESULTS AND DISCUSSIONS

The smoothed data of our measurements on the molar heat capacity  $C_p$  of TFE at constant pressure are given in *Table 1* and shown in *Figure 1*. We define a repeat unit of the copolymer as consisting of two chain atoms, so that the corresponding effective molecular weight is the sum of the atomic weights of two carbon atoms, 45% of two hydrogen atoms and 55% of two fluorine atoms, that is, 67.64.

### *Comparison with the Tarasov model*

The analysis of our results in the framework of the Tarasov model<sup>1</sup> closely parallels several previous works of the same nature<sup>4,5,7</sup>, the notations and basic assumptions of which are adopted below without detailed explanations. Since no spectroscopic data on TFE are available, the optical contributions to the heat capacity at constant volume  $C_v$  is estimated by a linear combination of the optical contributions calculated from the known spectral lines of PE<sup>12</sup> and PTFE<sup>13</sup>, with weight factors 0.45 and 0.55, respectively. For each of these two polymer segments there are seven optical lines, including the stretching mode of the carbon chain, making a total of 14 lines. The acoustical contribution is calculated from the well-known Tarasov function<sup>1</sup>. For convenience in computation, we have used a polynomial (and, for large argument, another closed analytical form) to approximate this function to within 0.05% (Appendix A). As in refs 4, 5 and 7, only four acoustical modes with identical characteristic parameters

$\theta_1$  and  $\theta_3$  are assigned to each repeat unit, because the two stretching modes have already been included in the optical contribution. Furthermore, in our temperature range the Tarasov function is practically independent of the parameter  $\theta_3$ , so it is set arbitrarily at 100 K, about midway between the values for PE (147 K) and PTFE (58 K). It was then found that the optimum value for the variable parameter  $\theta_1$  is 360 K, for which the sum of the optical and the acoustical contributions fit the experimental data to within 2% from 90 to 200 K (Curves I, II and III of Figure 1).

As in previous calculations<sup>4,5,7</sup>, the prediction falls below the data at higher temperatures, and naturally we ascribe the discrepancy to the difference between  $C_p$  and  $C_v$ . While the correction term  $C_p - C_v$  does explain similar discrepancies quite satisfactorily in the cases of PVF and PCTFE<sup>6</sup> and, to a lesser extent, in that of PE<sup>3</sup>, its effect on our data is not so clear. We evaluate  $C_p - C_v$  by the well-known formula  $\beta^2 VT/K$ , where the expansivity  $\beta$ , molar volume  $V$  and isothermal compressibility  $K$  can all be estimated from the available data<sup>14</sup> on the specific volume  $v$  of TFE gathered by static measurements at different temperatures and pressures. Unfortunately, this term overcompensates for the discrepancy and seems to have too small a temperature dependence (Figure 1), which, however, may only be due to the experimental error in  $v$ .

#### The principle of additivity

The principle of additivity<sup>2</sup> can be applied to our data in a particularly simple manner: the linear combination of the

Table 1 Heat capacity of TFE

Temperature (K)	Observed heat capacity (J/mol K)	Calculated heat capacity (1) <sup>a, c</sup> (J/mol K)	Calculated heat capacity (2) <sup>b, c</sup> (J/mol K)
80	25.9	24.7	24.7
90	28.2	27.7*	27.5
100	30.4	30.6	30.0*
110	32.8	33.3	32.6
120	35.1	35.9	35.1
130	37.4	38.2	37.6
140	39.6	40.5	40.0
150	41.9	42.5	42.2
160	44.1	44.5	44.5
170	46.2	46.4	46.8
180	48.3	48.2	49.0
190	50.4	49.9	51.2
200	52.6	51.6*	53.2
210	54.9	53.3	55.3
220	57.0	54.9	57.0
230	59.3	56.5	58.9
240	61.5	58.1	60.7
250	63.8	59.6	63.0
260	66.0	61.2	65.5
270	68.3	62.7	69.2*
280	70.6	64.2	75.5
290	73.0	65.7	76.8
300	75.3	67.2	80.3
310	77.5	68.7	75.1
320	80.1	70.1	75.8
330	82.8	71.6	77.1
340	85.6	73.0	78.3
350	88.9	74.4	80.0

<sup>a</sup> Calculation based on the Tarasov model and spectral lines

<sup>b</sup> Calculated from the combination of the heat capacities of PE<sup>7</sup> and PTFE<sup>8</sup> by proportional factors 0.45 and 0.55, respectively

<sup>c</sup> Calculated values at and between the two \* marks within each column agree with the observed values to within 2%

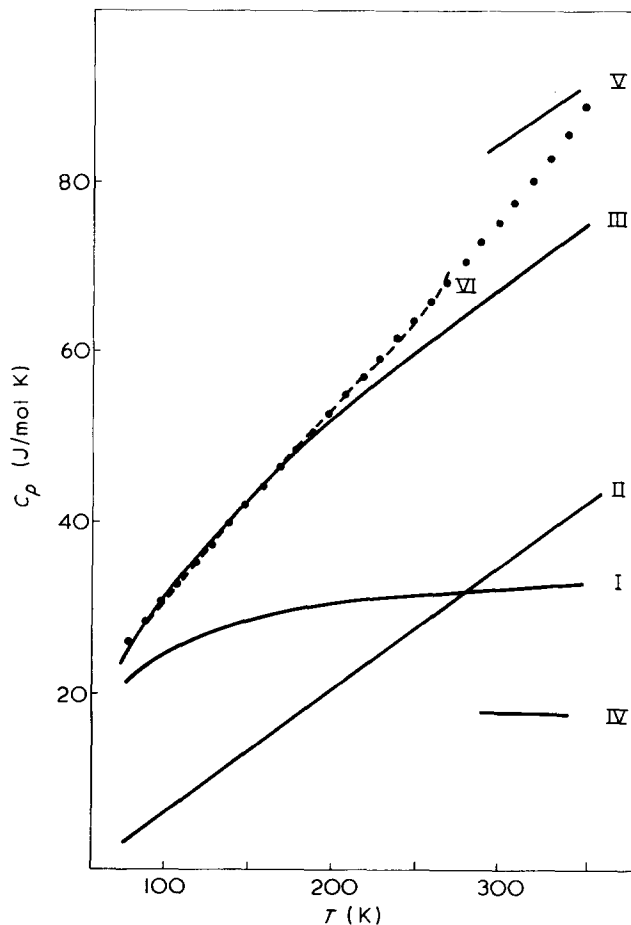


Figure 1 Heat capacity of TFE vs. temperature. I, Calculated acoustical contribution according to the Tarasov model, at  $\theta_1 = 360$  K; II, calculated optical contribution from 14 lines; III, calculated total heat capacity,  $C_v$ ; IV,  $C_p - C_v$  estimated from specific volume data<sup>14</sup>; V, sum of III and IV; VI, calculated from observed PE and PTFE heat capacities, in 45:55 proportions. ●, smoothed measured heat capacities

heat capacity data of PE<sup>7</sup> and PTFE<sup>8</sup> available in the literature with the respective coefficients 0.45 and 0.55 should match the TFE data. As shown by the broken curve in Figure 1, there is indeed close agreement (<2%) between the two up to 270 K, at which point the transition effect of PTFE begins to set in, and additivity is no longer valid. The relatively poor agreement at below 100 K is probably due to experimental uncertainty.

However, we can subject the principle of additivity to a much more stringent test by analysing our results together with the data on PE<sup>7</sup>, PTFE<sup>8</sup>, and the recently available data on the following series of fluoropolymers: PVF, PVF<sub>2</sub>, PVF<sub>3</sub><sup>5</sup> and PCTFE<sup>4</sup>. Only three distinct segments CH<sub>2</sub>, CHF and CF<sub>2</sub> are involved in the first six polymers, and one extra segment CFCI is involved in PCTFE. Additivity amounts to the following seven approximate equations:

$$\text{PE} \approx 2x \quad (1)$$

$$\text{PTFE} \approx 2y \quad (2)$$

$$\text{TFE} \approx 0.9x + 1.1y \quad (3)$$

$$\text{PVF} \approx x + z \quad (4)$$

$$\text{PVF}_2 \approx x + y \quad (5)$$

$$\text{PVF}_3 \approx y + z \quad (6)$$

$$\text{PCTFE} \approx y + w \quad (7)$$

where the left-hand sides refer to the heat capacities of the respective polymers named, and  $x$ ,  $y$ ,  $z$  and  $w$  on the right-hand sides refer to the additive contributions of the  $\text{CH}_2$ ,  $\text{CF}_2$ ,  $\text{CHF}$  and  $\text{CFCI}$  segments, respectively.

The segmental contributions  $x$ ,  $y$  and  $z$  can be determined by least-squares fit to the six heat capacities on the left of equations (1)–(6) at each temperature, and  $w$  is then obtained directly from equation (7) (Table 2). Values of the first six heat capacities predicted from the segmental values so determined are shown in Figure 2, where it is seen that there is very close agreement between calculation and data for PE, TFE, PVF and  $\text{PVF}_3$  up to 350 K and for  $\text{PVF}_2$  and PTFE up to their respective transition points at 220 and 260 K. As a matter of fact, if we disregard points above these two transition points then the fit is better than 2% for all six polymers from 80 to 340 K except for a few points near 80 K, and the average error for all 142 points is less than 1%. The success of such a three-parameter fit to six independently observed quantities is a clear indication of the validity of the principle of additivity, and gives us confidence that the segmental values tabulated in Table 2 should be a reliable basis for predicting heat capacities of other related polymers.

Additivity may in fact be valid above or around the glass-transition point provided the associated jump in  $C_p$  is small or diffused. Such seems to be the case for PE (Figure 2), which probably has a crystallinity-dependent double glass-transition between 190 and 280 K<sup>15–17</sup>, and possibly also for PTFE (Figure 2), which may have a 'lower' glass-transition at 223 K<sup>16</sup>. Similarly contributions to  $C_p$

Table 2 Heat capacities of segments (J/mol K)

Temperature (K)	$\text{CH}_2$	$\text{CF}_2$	$\text{CHF}$	$\text{CFCI}^a$
80	8.2	16.0	11.4	16.6
90	8.9	17.7	12.7	19.0
100	9.6	19.4	14.0	21.2
110	10.3	21.1	15.2	23.5
120	10.9	22.8	16.3	25.4
130	11.6	24.4	17.3	27.3
140	12.3	26.0	18.2	29.1
150	13.0	27.5	19.1	30.7
160	13.7	28.9	20.0	32.3
170	14.4	30.4	20.7	34.0
180	15.1	31.8	21.5	35.5
190	15.7	33.2	22.5	37.0
200	16.4	34.6	23.7	38.4
210	17.2	36.0	24.7	39.8
220	17.7	37.4	26.4	41.0
230 <sup>b</sup>	18.0	38.9	27.2	42.1
240	18.3	40.5	28.8	43.2
250	18.8	42.1	30.4	44.2
260	19.2	44.0	31.9	45.1
270 <sup>c</sup>	19.8	45.6	33.2	46.2
280	20.7	47.0	34.6	47.6
290	21.3	48.6	35.9	48.8
300	22.1	50.1	37.4	50.5
310	22.7	51.8	39.1	50.9
320	23.6	53.2	40.4	53.2
330	25.0	54.1	41.0	55.3
340	26.2	55.3	42.1	58.1

<sup>a</sup> Heat capacities in this column are obtained by subtracting values of the  $\text{CF}_2$  segment from the observed values of PCTFE

<sup>b</sup> Values of segmental heat capacities below 230 K are obtained by least squares fit to the observed values of PE, PTFE, TFE, PVF,  $\text{PVF}_2$  and  $\text{PVF}_3$ . At 230 K and above the observed values of  $\text{PVF}_2$  are not used in the fit

<sup>c</sup> At 270 K and above the values of PTFE are not used in the fit

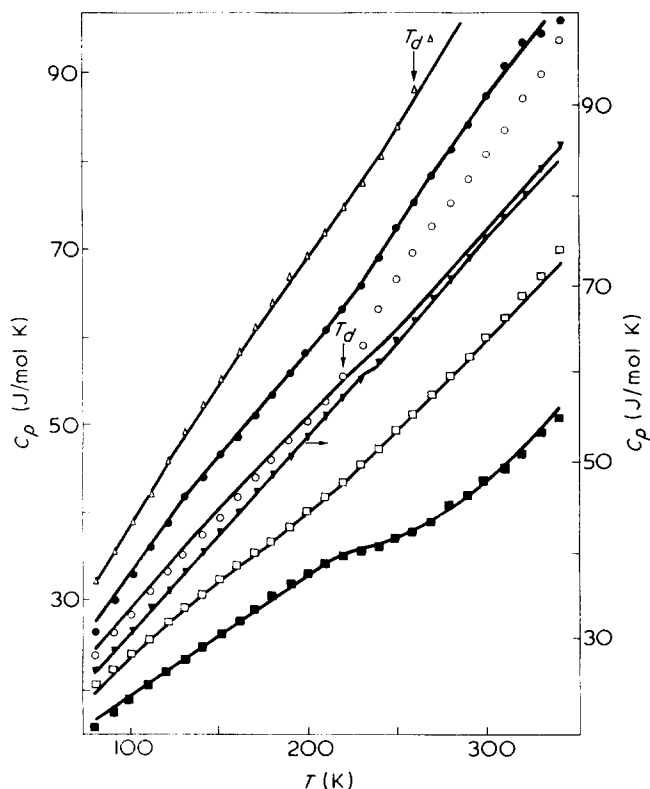


Figure 2 Heat capacities of PE and five fluoropolymers vs. temperature. Solid lines are obtained from appropriate linear combinations of the fitted segmental contributions. Observed data points: ■, PE; □, PVF; ▼, TFE; ○,  $\text{PVF}_2$ ; ●,  $\text{PVF}_3$ ; △, PTFE.  $T_d$ , transition points. The scale for TFE has been shifted

arising from possible subglass transitions at low temperature are usually limited to only a few per cent and, what is more important, are rather featureless as well<sup>17</sup>, so that they are not expected to affect the Tarasov model (except perhaps the numerical value of  $\theta_1$ ) or the principle of additivity in any significant manner.

#### Connection between the Tarasov model and additivity

Since both the Tarasov model and the principle of additivity are in good agreement with data, at least for the series of fluoropolymers being studied, it is natural to ask whether any relation can be established between these two models, or, in other words, whether one model can be derived from the other. We limit our attention to the region in which additivity is expected to be valid, that is from about 60 K up to the transition point of any particular polymer.

The Tarasov model consists of two terms, of which the optical contribution is clearly additive in the sense of equations (1)–(7) on physical grounds. This is precisely the principle one makes use of in estimating the optical contribution where direct spectroscopic data are not available. If the total contribution to  $C_v$  is additive as postulated then clearly the second term, i.e. the acoustical contribution, must also be additive. In a particularly simple case such as TFE this means, for an entire range of temperature  $T$ ,

$$D_1\left(\frac{\theta_C}{T}\right) = \alpha D_1\left(\frac{\theta_A}{T}\right) + \beta D_1\left(\frac{\theta_B}{T}\right) \quad (\alpha + \beta = 1) \quad (8)$$

where  $\theta_A$ ,  $\theta_B$  and  $\theta_C$  refer to the  $\theta_1$ -values of PE, PTFE and TFE, respectively;  $\alpha$  and  $\beta$  refer to the molar fractions of PE and PTFE, respectively; and we have approximated the

Tarasov function by  $D_1(\theta_1/T)$  in the region where additivity is valid, i.e., above 60 K.

Mathematically equation (8) puts a constraint on the permissible form of  $D_1(x)$ ; it can be shown (Appendix B) that, contrary to the known analytic form of  $D_1(x)$ , this equation implies it must have either one of the following forms:

$$r + sx^p$$

or

$$r + s \ln x \quad (9)$$

where  $x = \theta/T$  and  $r$ ,  $s$  and  $p$  are constants. However, this contradiction is not disastrous, since, after all, equation (8) is but an approximate relation correct to, say, 3 or 5%. One can actually approximate the known form of  $D_1(x)$  to within 2% by the simple linear form:

$$D_1(x) \approx 1.06551 - 0.08846x \quad (10)$$

in the interval  $0.5 \leq x \leq 7$ , which already covers all the  $T$  and  $\theta_1$  ranges of interest (Figure 3). It is therefore possible to reconcile  $D_1$  with equation (8) by choosing  $p = 1$  in the first form of equation (9). ( $p = 0.9$  gives an even bet-

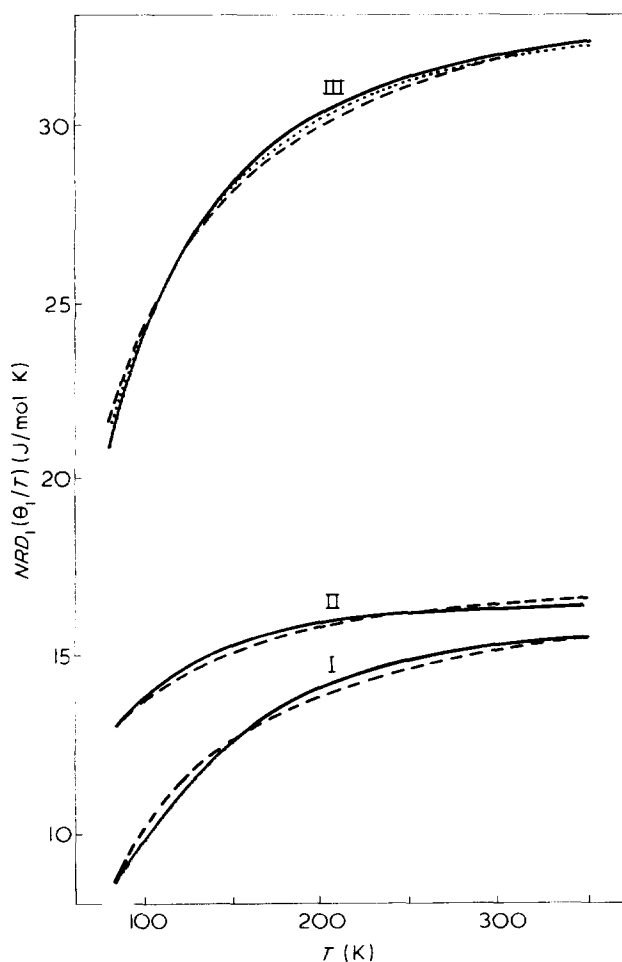


Figure 3  $NRD_1(\theta_1/T)$  vs.  $T$ , showing the approximate additivity of acoustical contributions as given by  $D_1$ . I,  $\theta_1 = 515$  K,  $N = 2$ ; II,  $\theta_1 = 260$  K,  $N = 2$ ; III,  $\theta_1 = 0.45(515 \text{ K}) + 0.55(260 \text{ K}) = 374.75$  K,  $N = 4$ . —, Exact  $D_1$ ; ----, corresponding approximations linear in  $x$ ; ····, sum of I and II (solid lines), with weight factors 0.9 and 1.1, respectively. Note that, by construction, broken line III is an exact sum of dashed lines I and II, with weight factors 0.9 and 1.1, respectively

Table 3 Additivity of  $\theta_1$

Polymer	$\theta_1$ (K)		
	Fitted values <sup>a</sup>	Calculated <sup>b,c</sup> values	Deviation (%)
PE	515	503	-2.4
PVF	430	432	+0.5
PVF <sub>2</sub>	357	377	+5.0
TFE	360	364	+1.0
PVF <sub>3</sub>	308	306	-0.7
PTFE	260	250	-4.0

<sup>a</sup> Obtained by direct fittings of the Tarasov model to the experimental heat capacities. The values for PE and PTFE are obtained by our own fitting of the published data<sup>7,8</sup> and differ slightly from the corresponding published values<sup>7,18</sup>; the rest are taken from refs 4 and 5

<sup>b</sup> A least-squares fit yields the segmental values  $\theta_x = 251.5$  K,  $\theta_y = 125.0$  K and  $\theta_z = 180.5$  K, from which the  $\theta_1$  values in this column are calculated through equations (1)–(6)

<sup>c</sup> From equation (7) and  $\theta_1(\text{PCTFE}) = 235$  K one can also deduce the segmental value  $\theta_w = 110$  K for the CFCI segment

ter fit, but  $p = 1$  is more convenient.)

So in the region where the difference between  $C_p$  and  $C_v$  is negligible<sup>4,5,7</sup> ( $60 \text{ K} < T < 200 \text{ K}$ ) the principle of additivity as applied to  $C_p$  can be understood as a consequence of the separate additivity of the optical and the acoustical contributions, the latter being approximately valid by virtue of the mathematical form of  $D_1(x)$ .

But from 200 K up the difference  $C_p - C_v$  becomes appreciable. Rewriting this term in the form  $(\beta^2\nu/K)MT$ , where  $M$  is the molecular weight and other symbols bear the same meanings as before, we see that it would also be roughly additive if the factor  $\beta^2\nu/K$  is approximately the same for different polymers. Using the specific volume data available in the literature<sup>14</sup>, this factor is estimated to vary by about  $\pm 20\%$  at 300 K for the six polymers we have studied. Since  $C_p - C_v$  accounts for no more than 15–20% of the total heat capacity, the variation in  $\beta^2\nu/K$  would introduce at most 3–4% error in the additivity of  $C_p$ , which thus can again be understood as a consequence of the rough additivity of its individual components. Nevertheless, it is still quite surprising that  $C_p$  is additive to within 2%, whereas the individual components are expected to be additive to within 2–4% only. Whether this is merely due to fortuitous circumstances, or deeper reasons are involved, we cannot say.

#### Connection between $\theta_1$ , the mass, and the force constant

A simple and immediate consequence of equation (10) and the additivity of  $C_p$  is that the one-dimensional Debye temperature  $\theta_1$  should also be additive. In other words, we can replace the heat capacities on the left of equations (1)–(6) by the corresponding experimentally determined  $\theta_1$  values of the respective polymers, carry out a least-squares fit to determine the three 'segmental'  $\theta_1$  values:  $\theta_x$ ,  $\theta_y$ ,  $\theta_z$ , and then calculate a set of predicted  $\theta_1$ . The results are given in Table 3, where we see that the agreement between data and prediction is fair ( $< 5\%$ ), especially in view of the fact that several successive approximations are involved in this prediction and  $D_1(x)$  is not really very sensitive to  $\theta_1$ .

It remains for us to point out that such a linear relation among the various  $\theta_1$  is inconsistent with the general impression<sup>4,5,7</sup> that the effective one-dimensional force constant  $k_1$  of the carbon chain is the same throughout the series of polymers we study. By definition  $k_1$  is propor-

tional to  $M\theta_1^2$ ,  $M$  being the molecular weight of a repeat unit. Since  $M$  is additive the constancy of  $k_1$  would imply that  $1/\theta_1^2$  is also additive, or according to equation (9) that  $D_1$  could be approximated by the form  $r + s/x^2$ . Unfortunately such an approximation involves on the average a 20% error and is clearly much inferior to the linear approximation. It does not seem to us that this inconsistency can be resolved within the phenomenological frameworks we are working in, since a 2–3% approximation is involved in each logical step, and any deduction involving several steps is always expected to have 5–10% uncertainty.

## CONCLUSION

From the foregoing analysis it is clear that the Tarasov model and the principle of additivity are both valid and consistent with each other to within the degree of precision usually expected (about 2%), even though the surprisingly close fit of the predictions of additivity in regions where  $C_p - C_v$  is appreciable certainly needs further clarification. Similarly, it remains to be seen whether the Tarasov model is also generally valid at higher temperatures after the  $C_p - C_v$  correction is made, preferably by using the more accurately determinable ultrasonic data. On the other hand, it may not be meaningful to ask whether the effective one-dimensional force constant  $k_1$  is indeed the same for different polymers, unless a reasonable and unambiguous definition of 'equality' can first be agreed upon. In any case, one should now be able to apply these two frameworks to other polymers and copolymers with increased confidence, and it would be interesting to see, for instance, whether other polymer series with different backbones are equally amenable to this line of investigation.

## ACKNOWLEDGEMENTS

The authors wish to express their gratitude to Dr M. Ragazzini of Montecatini Edison, SpA, Milan, Italy for supplying the sample, and to Dr K. Young of this Department for a reading of the manuscript and supplying the proof given in Appendix B.

## REFERENCES

- 1 Tarasov, V. V. *Zh. Fiz. Khim.* 1950, **24**, 111
- 2 Wunderlich, B. and Jones, L. D. *J. Macromol. Sci. (B)* 1969, **3**, 67
- 3 Bares, V. and Wunderlich, B. *J. Polym. Sci. (A-2)* 1973, **11**, 397
- 4 Lee, W. K., Lau, P. C. and Choy, C. L. *Polymer* 1974, **15**, 487
- 5 Lee, W. K. and Choy, C. L. *J. Polym. Sci.* to be published
- 6 Choy, C. L. to be published
- 7 Wunderlich, B. *J. Chem. Phys.* 1962, **37**, 1203, 1207
- 8 Furukawa, G. T., McCoskey, R. E. and King, G. J. *J. Res. Nat. Bur. Stand.* 1952, **49**, No.4
- 9 Modena, M., Garbuglio, C. and Ragazzini, M. *J. Polym. Sci. (B)* 1972, **10**, 153
- 10 Starkweather, H. W. *J. Polym. Sci. (A-2)* 1973, **11**, 587
- 11 Wilson, F. C. and Starkweather, H. W. *J. Polym. Sci. (A-2)* 1973, **11**, 919
- 12 Tasumi, M., Shimanouchi, T. and Miyazawa, T. *J. Mol. Spectros.* 1962, **9**, 261
- 13 Hannon, M. J., Boerio, F. J. and Koenig, J. L. *J. Chem. Phys.* 1969, **50**, 2829
- 14 Weir, C. E. *J. Res. Nat. Bur. Stand.* 1954, **53**, 245
- 15 Boyer, R. F. *Macromolecules* 1973, **6**, 288
- 16 Boyer, R. F. *J. Macromol. Sci. (B)* 1973, **8**, 503
- 17 O'Reilly, J. M. and Karasz, F. E. *J. Polym. Sci. (C)* 1966, **14**, 49
- 18 Wunderlich, B. *Adv. Polym. Sci.* 1970, **7**, 351

## APPENDIX A

For computational purposes it is much more convenient to approximate the one- and three-dimensional Debye functions  $D_1(x)$  and  $D_3(x)$  by close analytical forms rather than relying on the defining integrals or tabulated values. The following approximations are good to within 0.05% of the published tabulations<sup>7</sup>, and should suffice for most practical purposes.

$$D_n(x) \equiv \frac{n}{x^n} \int_0^x \frac{y^{n+1} e^y}{(e^y - 1)^2} dy \quad n = 1, 2, 3, \dots \quad (\text{A1})$$

$$D_1(x) \simeq \sum_{n=0}^5 a_n x^n \quad 0 \leq x \leq 7$$

$$\simeq [A - (x^2 + 2x + 2)e^{-x}]/x, \quad 7 < x \quad (\text{A2})$$

where  $A = 3.28987$ ,  $a_0 = 0.99980522$ ,  $a_1 = 0.00387191$ ,  $a_2 = -0.03452752$ ,  $a_3 = 0.00394121$ ,  $a_4 = 0.00000410$ ,  $a_5 = -0.00001401$ .

$$D_3(x) \simeq \sum_{n=0}^6 b_n x^n \quad 0 \leq x \leq 6.2$$

$$\simeq 3[B - (x^4 + 4x^3 + 12x^2 + 24x + 24)e^{-x}]/x^3$$

$$6.2 < x \quad (\text{A3})$$

where  $B = 25.97576$ ,  $b_0 = 0.99993481$ ,  $b_1 = 0.00122983$ ,  $b_2 = -0.05209779$ ,  $b_3 = 0.00074816$ ,  $b_4 = 0.00218456$ ,  $b_5 = -0.00032884$ ,  $b_6 = 0.00001496$

## APPENDIX B

Let us define  $\theta_A/T = x$ ,  $\theta_B/\theta_A = \lambda$ ,  $\theta_C/\theta_A = \eta$  and specialize to the case  $\alpha = \beta = 1/2$ . Then equation (10) can be written as

$$f(\eta x) = 1/2[f(x) + f(\lambda x)] \quad (\text{B1})$$

where  $\eta$  is a function of  $\lambda$ , but not  $x$ , and  $D_1$  has been replaced by a general function  $f$ . We now look for the most general  $f$  consistent with this equation.

Let  $e^v = x$ ,  $e^g = \eta$ ,  $e^y = \lambda$  and  $F(v) = f(x) = f(e^v)$ , so that equation (B1) takes on the form

$$F(v + g) = 1/2[F(v) + F(v + y)] \quad (\text{B2})$$

where  $g = g(y)$ . If we make a Taylor's expansion of  $F$  at  $v$  and also of  $g$  at  $y = 0$ , and equate the coefficients of powers of  $y$ , then with the reasonable assumption  $g(0) = 0$  we obtain for the first two powers  $g'(0) = 1/2$  and  $F''(v) = 4g''(0)F'(v)$ . If  $g''(0) \neq 0$  then the latter equation leads to  $F = C_1 \exp(4g''(0)v) + C_2$ , or the form  $f = C_1 x^p + C_2$ . If  $g''(0) = 0$  then one obtains  $F = C_1 v + C_2$  or  $f = C_1 \ln x + C_2$ . Clearly all functions satisfying equation (B1) necessarily belong to one of these two forms. Since it is easy to verify that these functions do indeed satisfy equation (B1), they must be the only solutions of that equation, and the proof is complete. Extension of the proof to other values of  $\alpha$  along the same lines is trivial.

# An anionically prepared flexible adhesive: 1: Synthesis

A. V. Cunliffe, M. B. Huglin\*, P. J. Pearce and D. H. Richards

Explosives Research and Development Establishment, Ministry of Defence, Waltham Abbey, Essex EN9 1BP, UK

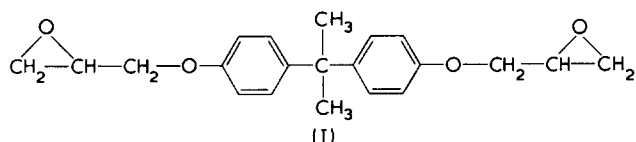
(Received 6 February 1975)

A method is described whereby epoxides based on a diglycidyl ether of bisphenol A (DGEBA) may be flexibilized by reaction with dienes such as butadiene or isoprene (M). The process requires the reaction of a tetrahydrofuran solution of DGEBA and diene with excess alkali metal, and the initial step is that of formation of diene dianion which homopropagates until terminated by DGEBA. The isolated product consists of a mixture of unreacted DGEBA and modified DGEBA. Preliminary tests indicate that this mixture exhibits adhesive properties superior to that of the original epoxide.

## INTRODUCTION

Epoxy resins have a wide and increasing use in industry owing to their unique combination of properties. They and their curing agents are generally liquids which are easily processable and systems may be selected which will effect cures at temperatures ranging from ambient to 200°C. The absence of volatile by-products and low shrinkage during cure results in good moulding characteristics, and the minimization of internal stresses gives the thermoset excellent mechanical properties. Further, the cured resins possess good electrical insulation and outstanding chemical resistance, and they have high adhesive strengths due mainly to the generation of polar hydroxyl groups during cure. It is this last property which is the subject of this series of papers.

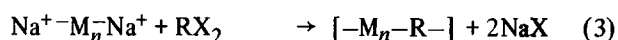
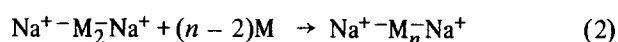
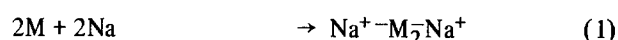
By far the most commonly used epoxy resins are those derived from bisphenol A by reaction with epichlorhydrin. The simplest diepoxide formed in this process is the diglycidyl ether (I):



and the work to be described involves the flexibilization of commercial resins such as Araldite MY 750 or Epikote 828 in which this compound predominates. Although these materials are used as adhesives, they suffer from a lack of flexibility, and hence reduced shear strength and low peel, when cured with conventional 'small molecule' reagents. The epoxide contents of the resins are high and curing leads to a densely crosslinked structure so that this, plus the presence of rigid aromatic groups in the chain, results in severe restriction of segmental motion and thus to low flexibility. Improvements in flexibility can be obtained by incorporating long chain aliphatic compounds into the resin before cure; these may either remain unreacted during cure when they act as plasticizers, or they may be linked

chemically into the system by the cure process when they may be described as flexibilizers.

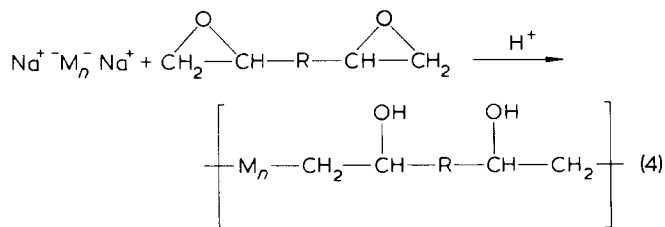
An alternative but hitherto relatively unexplored approach is to devise reactions which will modify the epoxide resin itself such that the product, whilst remaining a diepoxide, will be more flexible, and accordingly will, hopefully, exhibit shear strengths superior to the original material on curing with conventional reagents. It seemed that techniques which we had been developing to synthesize novel anionic condensation copolymers<sup>1,2</sup> could be adapted to prepare such flexibilized adhesives. These methods are modifications of the 'living' polymer systems developed by Szwarc *et al.* in which a suitable monomer (M), such as styrene, butadiene, isoprene etc., is reacted in tetrahydrofuran (THF) with alkali metal in the presence of a linking agent. Alkyl dihalides (RX<sub>2</sub>) constitute a class of linking agents which were extensively examined and shown to react in a manner illustrated by the following reaction sequence:



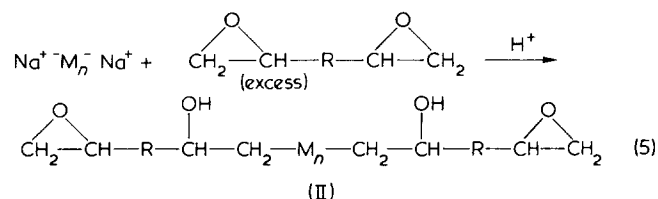
The initial step is a surface reaction with the alkali metal to form a dimer dianion which then diffuses away, reacting with more monomer until the carbanionic ends are terminated by a metathetical reaction with the dihalide to form a copolymer. It has been shown by n.m.r. spectroscopy<sup>2</sup> and by model compound synthesis<sup>3</sup> (using the equivalent monohalide HRX) that when the molar ratio of monomer to dihalide is 2 : 1, a regular copolymer is formed where greater than 90% of the repeat units have  $n = 2$ .

Difunctional epoxides constitute another class of compounds which react with vinyl and diene monomers in an analogous way. Both diepoxides and halo-epoxides have yielded polyalcohols under these conditions<sup>4</sup>. It is well known that the epoxide group is subject to additive nucleophilic attack at the  $\alpha$ -carbon atom<sup>5,6</sup>, and so the generation of oligomeric dianions *in situ* results in the formation of alcoholate groups along the growing polymer chain, viz:

\* Department of Chemistry and Applied Chemistry, University of Salford, Salford, M5 4WT, UK.



Thus, if these reactions were carried out in the presence of an excess amount of diepoxide, modified diepoxides (II) should be produced which possess a central oligomeric unit as shown in equation (5):



Thus, by using diene as monomer, the rubbery central block should result in a significant flexibilization of the resin whilst retaining epoxide groups which would have a reactivity to curing agents very similar to that of the parent material.

This paper describes the synthesis and preliminary evaluation of such a material. Part 2<sup>7</sup> deals with a more detailed study of the effect of reaction variables on the structure of the product, and Part 3<sup>8</sup> describes tests carried out to evaluate the adhesive properties of a selected flexibilized epoxide as compared with those of the unmodified starting material. The whole process is the subject of a patent application<sup>9</sup>.

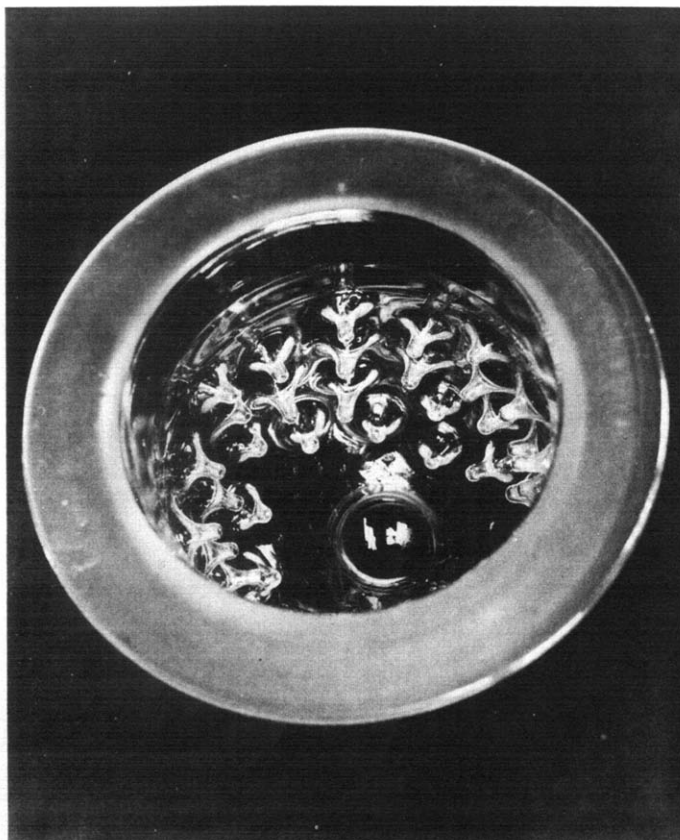


Figure 1 'Spiked' flask used in the synthesis

## EXPERIMENTAL

### Materials

15 mm diameter sodium pellets (BDH Ltd) were washed with low boiling petroleum ether under a blanket of dry nitrogen, extruded into wire or cut into thin slices.

Tetrahydrofuran (THF) was first dried over molecular sieves and then treated, under dry nitrogen, with a solution of sodium naphthalene in THF until a permanent green colour characteristic of the complex remained to indicate complete drying. The solvent was subsequently distilled, stored over fresh sodium wire and used within two days.

The diepoxide was a diglycidyl ether of bisphenol A (DGEBA) supplied as either MY750 (Ciba-Geigy) or Epikote 828 (Shell) and used without further purification. These two materials were found to be of very similar composition and were used indiscriminately.

Butadiene was collected by condensation from a cylinder into a graduated container after passage through molecular sieves. Isoprene was used freshly distilled from powdered calcium hydride.

### Apparatus

Gas-liquid chromatography (g.l.c.) was performed with the aid of a Pye series 104 chromatograph. 7 ft columns were used with Chromosorb 80/100 mesh support coated with 2½% OV17 silicone oil. Separations were effected using a temperature programme in the range 100 to 300°C at 8°C/min.

N.m.r. spectra were recorded on a Jeol PS-100 100 MHz spectrometer using approximately 10% solutions in deuteriochloroform with tetramethylsilane as internal standard. Details of the analytical procedures employed are fully described in Part 2<sup>7</sup>.

Mild steel lap joints, which had been prepared in a manner described in Part 3<sup>8</sup>, were tested with a Monsanto Type E tensometer. Loading was applied at a constant crosshead speed of 0.2 in/min and continued until failure occurred.

### Synthetic method

Conventional laboratory scale glass apparatus was used for the synthesis, with one important exception. Because of the problem of gel formation (see below) which initially appeared on the surface of the sodium metal, thereby causing the reaction rate to decline and eventually to cease, it was necessary to devise methods to overcome this difficulty. Two approaches were considered: first, the reaction flask was filled to about 50% capacity with glass beads of 6 mm diameter before introduction of the reagents. The beads had a 'ball mill' effect when agitated with a powerful stirrer, and caused a constant abrading of the metal surface. Despite the success of this method it had several drawbacks. The relatively large amount of beads required for optimum gel removal resulted in a considerable diminution of the available reaction volume. Furthermore, constant stirring rates were difficult to achieve and the risk of flask breakage was a potential fire hazard.

The second method involved modifying the glass reaction flask by forming a series of indentations projecting inwardly as spikes (Figure 1). When the reactants were stirred, the sodium slices repeatedly collided with the spikes and efficient cleaning of the surface resulted. A comparison of the product obtained from the two methods showed little difference in the epoxide content of the final product (Table 1) and so the 'spiked' flask procedure was adopted as standard for all further preparations.



The reaction was slightly exothermic but was maintained at  $0 \pm 1^\circ\text{C}$  with the aid of a Thermo-watch and Jack-o-matic manufactured by Instruments for Research and Industry.

The reaction between isoprene and DGEBA in equimolar proportions is typical of the procedure; the ratio may be changed over a wide range or butadiene substituted for isoprene without changing appreciably the method outlined here.

A glass, multinecked, spiked, flanged flask of 2 litres capacity was charged with 1000 ml THF containing 280 g (0.8 mol) of DGEBA. It was cooled and maintained at  $0^\circ\text{C}$  whilst purified nitrogen was bubbled through to maintain an inert atmosphere. With constant stirring a two-fold molar excess, 37 g (1.6 mol), of sliced sodium metal was added followed by 54.4 g (0.8 mol) isoprene. The nitrogen flow was then stopped and the vessel was sealed. Following a short induction period, the sodium metal surface became yellow thus indicating that the reaction had started. After about 4 h the reaction mixture had become fairly viscous with signs of gel formation, and the metal surface had reverted to a dull grey. A few millilitres of methanol were then added to disperse the gel and to lower the viscosity, and the excess sodium was removed by coarse filtration to yield a clear orange-brown solution.

Most of the solvent was removed on a rotary film evaporator after which the residue was hydrolysed. Saturated brine was used to effect hydrolysis as this produced a better phase separation than water alone. The organic layer was extracted with ether and again shaken with aliquots of brine until the washings were neutral. Finally, the ether extract was dried over anhydrous magnesium sulphate filtered, and evaporated under vacuum to yield 300 g (87% yield) of product.

The freshly prepared modified resin is opaque, and on standing separates slowly into two layers, the top being very viscous and rubbery. The separation time is a few days at ambient temperature but may be accelerated to a matter of hours by warming to  $50^\circ\text{C}$ . The upper layer may be peeled off by careful manipulation with a spatula, or removed by accurate breaking of the container at the interface. Reblending is best achieved by mixing the two phases at  $40\text{--}50^\circ\text{C}$ .

Numerous procedures are available for the determination of epoxide content<sup>10</sup>. In this work a rapid, highly reproducible method of titration with a very sharp end point was used which has been developed by Jay<sup>11</sup> and by Dijkstra and Dahmen<sup>12</sup>. The epoxide content has been

described using a variety of units; in this series of papers the results are given in equiv./kg.

## RESULTS AND DISCUSSION

The reproducibility of the process was evaluated from the epoxide contents and the yields of materials produced in a series of experiments involving equimolar proportions of isoprene and DGEBA under a variety of conditions. Analyses were carried out immediately after isolating the materials and before any effective separation of the two phases could occur. The results are given in Table 1.

It appears that the reaction is insensitive to the changes effected in the experiments listed; neither the scale of reaction, the type of vessel, nor the form of the sodium metal seems to affect significantly the yield of product or its epoxide content. The former averages out over the thirteen experiments at 85% with a standard deviation of 5.5% whilst the latter averages at 3.74 with a 4.5% standard deviation. Considering the heterogeneous nature of the process, this reproducibility can be considered as good.

### Reaction characteristics and mechanism

The reaction between dienes, excess epoxide and alkali metal may be carried out under a variety of conditions, but the following characteristics are invariably observed: (1) during the reaction the alkali metal assumes a silvery yellow coloration, and at low stirring rates yellow striations are seen to diffuse from the metal into the bulk of the solution where they are eliminated; (2) the rate of reaction is very sensitive to the rate of stirring; (3) as the reaction proceeds, the viscosity of the solution increases until gel is formed and the stirring can only be maintained with difficulty; (4) after the reaction is complete, the alkali metal takes on a matt appearance, and the gel is easily dispersed by adding small quantities of a protonating agent such as methanol; (5) the product isolated is an opaque material which can vary in colour from a pale yellow to a light orange-brown. On standing for a few days this material separates into two layers. The top layer is rubbery, opaque and viscous whereas the bottom is almost clear with a viscosity comparable to that of the original DGEBA.

These observations are important in elucidating the reactions occurring in the system and will be used, with evidence obtained from related experiments, to deduce the mechanistics of the processes involved.

Previous work, which has concerned the reaction of styrene or its derivatives with alkali metal in the presence of alkyl dihalides, has shown that it is the monomer which is adsorbed preferentially on to the alkali metal surface to form the dimer dianion, and that this subsequently desorbs and reacts with alkyl dihalide to form copolymer<sup>3</sup>. This dimer dianion is observed by the red coloration appearing on the metal surface and diffusing into the bulk solution. In a similar way, reactions of butadiene with alkali metal in the presence of dihalides<sup>13</sup>, monohalides<sup>14</sup> or monoepoxides<sup>15</sup> have all been initiated by the diene dimer dianion and all exhibit the yellow-orange coloration characteristic of the diene dicarbanion. Thus the observation that similar coloration occurs in the present system is strong evidence for preferred reaction of diene monomer with the metal to form the initiating diene dianion. Experiments carried out where the monomer was omitted and a THF solution of the epoxide was allowed to stand in contact with sodium metal showed no significant reaction in the time span required for the present synthesis.

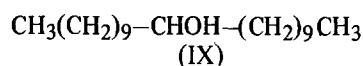
Table 1 Batch reproducibility of product prepared from equimolar quantities of DGEBA and isoprene

Scale (mol)	Apparatus	Sodium form	Yield (%)	Epoxide value
0.40	Flask and glass balls	Slices	—	3.44
0.40	Flask and glass balls	Thin wire	82	3.86
0.40	Flask and glass balls	Thin wire	87	3.64
0.85	Flask and glass balls	Slices	—	3.70
0.40	Flask and glass balls	Thick wire	79	3.47
0.20	'Spiked' flask	Slices	78	3.85
0.80	'Spiked' flask	Slices	83	3.67
0.86	'Spiked' flask	Slices	92	3.92
0.86	'Spiked' flask	Slices	91	3.86
0.86	'Spiked' flask	Slices	87	3.93
0.86	'Spiked' flask	Slices	88	4.03
0.86	'Spiked' flask	Slices	90	3.69
0.86	'Spiked' flask	Slices	89	3.60



of the epoxide. Fortunately the basicity of the alkoxide ion is very much less than that of the carbanion so that the initiation step must be considerably slower. Nevertheless the concentration of alkoxide ion increases as the reaction proceeds so that its effect towards the end of the reaction could become significant.

To see whether homopolymerization of DGEBA by alkoxide ions occurs under these experimental conditions, the following experiment was carried out. A 0.25 M solution of the sodium salt of heneicosanol-11 (IX):



in THF was prepared by titrating a 20% excess of the alcohol with the calculated amount of sodium naphthalene in THF, and sufficient DGEBA was then dissolved in the solution to give a concentration of 1 M. A suitable hydrocarbon was then added as a marker and the solution was stirred under nitrogen for 5 h at 0°C. Samples removed before and after reaction, and subjected to g.l.c. analysis after acidification, showed that none of the heneicosanol-11 had been consumed. As the concentration and conditions of the experiment had been planned to duplicate as far as possible those obtaining in the flexibilization reaction, this result is a strong indication that negligible homopolymerization of DGEBA occurs in this system.

It is a feature of this reaction, and of other systems involving epoxy compounds, that the solution becomes more viscous as reaction proceeds until finally gelling may occur. This phenomenon is not observed when the epoxides are replaced by reagents such as alkyl halides which are capable of metathetical reaction with the carbanions to produce electrically neutral molecules. Thus the gelling must be directly related to the formation of alkoxide-alkali metal ion pairs. This effect has been noticed previously when 'living' polystyrene has been terminated with ethylene oxide<sup>19,20</sup>, and has been ascribed to the formation of ion pair agglomerates which act as pseudo crosslinks and consequently produce a polymeric network which results in a gel. This hypothesis is supported by the observation that only small quantities of a suitable proton donor are required to destroy the gel by hydrolysing the alkoxide ion pairs. It is also significant that when monofunctional 'living' polymers are terminated with ethylene oxide, no gelling occurs but only an increase in viscosity because in this situation no network can result. Thus gelling appears as a direct consequence of the reactions being carried out and, although many additives have been tried in order to

minimize this effect in the present study, no significant improvement has as yet been achieved.

#### Preliminary evaluation

The lap joint shear strengths of the re-blended DGEBA resin modified with an equimolar quantity of isoprene were compared with those obtained with unmodified DGEBA using a number of different curing agents. Details of the experimental techniques and the curing cycles are given in Part 3. Table 2 lists the results obtained using mild steel strips at ambient temperatures; the average shear strength of four replicates are listed together with the maximum value obtained, to give some indication of the spread of results. The results clearly show that the flexibilized material possesses significantly superior shear properties to the unmodified epoxide regardless of the cure system employed.

These preliminary results, therefore, confirm that this technique can produce materials with enhanced adhesive properties. It was therefore decided to study the reaction system and its products in more detail and these investigations are reported in Part 2<sup>7</sup>. When the reaction parameters were thus optimized, the resulting modified material was subjected to the more comprehensive series of physical tests described in Part 3<sup>8</sup>.

[© Crown Copyright. Reproduced with permission of the Controller, HMSO, London]

#### REFERENCES

- Richards, D. H., Scilly, N. F. and Williams, F. J. *Polymer* 1969, 10, 603
- Richards, D. H., Scilly, N. F. and Hutchison, S. M. *Polymer* 1969, 10, 611
- Davis, A., Richards, D. H. and Scilly, N. F. *Makromol. Chem.* 1972, 152, 121
- Gleaves, M. H., Pearce, P. J., Richards, D. H. and Scilly, N. F. *Eur. Polym. J.* 1970, 6, 1469
- Gee, G., Higginson, W. C. E., Levesley, P. and Taylor, K. J. *J. Chem. Soc.* 1959, p 1338
- Gee, G., Higginson, W. C. E., Taylor, K. W. and Trenholme, M. W. *J. Chem. Soc.* 1961, p 4298
- Cunliffe, A. V., Huglin, M. B., Pearce, P. J. and Richards, D. H. *Polymer* 1975, 16, 659
- Cunliffe, A. V., Huglin, M. B., Pearce, P. J. and Richards, D. H. *Polymer*, 1975, 16, 665
- Br. Pat. Appln 52 910/73 (Ministry of Defence)
- Dobinson, B., Hofmann, W. and Stark, B. P. 'The Determination of Epoxide Groups', Pergamon Press, Oxford, 1969
- Jay, R. R. *Analyt. Chem.* 1964, 36, 667
- Dijkstra, R. and Dahmen, E. A. M. F. *Analyt. Chim. Acta* 1964, 31, 38
- Pemberton, M. G., Richards, D. H. and Scilly, N. F. *Eur. Polym. J.* 1970, 6, 1083
- Davis, A., Richards, D. H. and Scilly, N. F. *Eur. Polym. J.* 1970, 6, 1293
- Burgess, F. J., Cunliffe, A. V. and Richards, D. H. *Makromol. Chem.* 1973, 165, 39
- Morton, M., Sanderson, R. D. and Sakata, R. *J. Polym. Sci. (B)* 1969, 7, 821
- Rembaum, A., Ells, F. R., Morrow, R. C. and Tobolsky, A. V. *J. Polym. Sci.* 1962, 61, 155
- Jenkins, A. D. and Ledwith, A. 'Reactivity, Mechanism and Structure', John Wiley, London, 1974, p 367
- Brody, H., Richards, D. H. and Szwarc, M. *Chem. Ind.* 1958, p 1473
- Richards, D. H. and Szwarc, M. *Trans. Faraday Soc.* 1959, 55, 1644

Table 2 Comparison of lap shear strengths (MN/m<sup>2</sup>) of product from reaction with equimolar DGEBA and isoprene, and DGEBA

Curing system	DGEBA		Modified DGEBA	
	Av.	Max.	Av.	Max.
Aliphatic amine	24.5	25.2	34.2	35.8
Aromatic amine	15.6	17.7	24.4	25.9
Polyamide	24.6	26.6	31.3	32.8
Anhydride	19.7	20.6	31.9	33.9
Catalytic	17.5	18.3	19.4	20.7

# An anionically prepared flexible adhesive: 2. Product analysis

A. V. Cunliffe, M. B. Huglin\*, P. J. Pearce and D. H. Richards

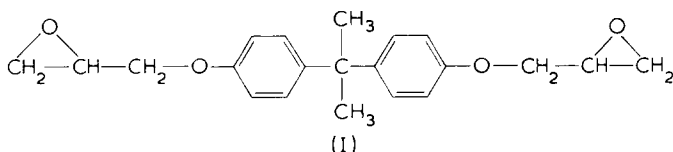
Explosives Research and Development Establishment, Ministry of Defence, Waltham Abbey, Essex EN9 1BP, UK

(Received 6 February 1975)

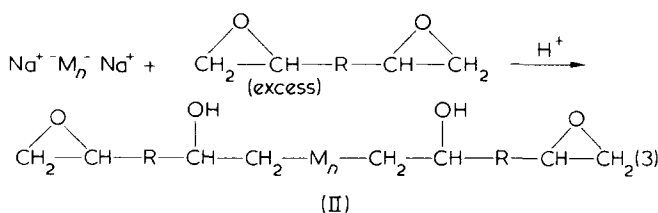
The previously described reaction whereby epoxides based on a diglycidyl ether of bisphenol A (DGEBA) may be flexibilized by reaction with dienes such as butadiene or isoprene (M) is studied in more detail. The process transforms a proportion of the DGEBA into a modified DGEBA structure and the relative amounts of these components in the product have been examined as a function of reagent molar ratios. Similarly the effect of reaction parameters on the degree of polymerization,  $n$ , of the diene moiety has been studied and the behaviour of isoprene compared with that of butadiene. The reaction product separates out into two phases on prolonged standing and the composition of these phases has been estimated. The upper layer has been shown to consist principally of modified material and the lower principally of DGEBA, although fractionation of the modified material occurs between the phases.

## INTRODUCTION

In Part 1<sup>1</sup> it was shown that commercial epoxides based on bisphenol A and comprised principally of molecules of structure (I):



could be flexibilized by reacting tetrahydrofuran (THF) solutions of mixture of the epoxide and of dienes, such as isoprene or butadiene, with excess sodium metal. Flexibilization was established as occurring via reactions represented schematically as follows:



Thus the diene (M) reacts preferentially with the alkali metal to form a diene dianion which diffuses away from the surface and propagates further before reacting with the excess diepoxide present in the system. Under these conditions new diepoxides (II) are formed which contain a central oligomeric unit of diene in the molecule. It was shown that after standing for a few days the isolated material separated into two phases, the upper being opaque and rubbery and the lower having a consistency and appearance approximating to those of the starting material (I).

\* Department of Chemistry and Applied Chemistry, University of Salford, Salford M5 4WT, UK.

The modified epoxide, produced from isoprene at a reactant molar ratio of unity, when rebled and mixed with a variety of curing agents exhibited in all cases significantly improved lap shear strengths on comparison with the original diepoxide (DGEBA).

This paper examines the structure of the product in greater detail and studies the effect of changing the epoxide to diene ratio on the nature of the material produced.

## EXPERIMENTAL

The materials used were prepared and purified in the manner described in Part 1. The synthetic method and product isolation techniques are also given in detail in that publication and will therefore not be repeated here.

Gel permeation chromatography (g.p.c.) was carried out using a Waters Associates model ALC 100 chromatograph with a differential refractometer as detector. Five columns, each 5 ft x 0.375 in diameter were packed with Styrogel of porosity 2000–700 AU, 5000–2000 AU, 2000–700 AU, 700–350 AU and 350–150 AU respectively. An operating pressure of 4.8 MN/m<sup>2</sup> (700 lbf/in<sup>2</sup>) was used to give a flow rate of 0.85 ml/min. <sup>1</sup>H n.m.r. spectra were recorded on a Jeol PS-100 100 MHz spectrometer using approximately 10% solutions in deuteriochloroform with tetramethylsilane as internal standard.

## RESULTS AND DISCUSSION

### N.m.r. spectra

The spectrum of unmodified DGEBA is shown in *Figure 1a*. The characteristic four line pattern at about 3 $\tau$  arises from the two pairs of aromatic protons in each aromatic ring. Also prominent is the sharp singlet at 8.1 $\tau$  due to the methyl peaks. Absorptions due to the –OCH<sub>2</sub>– groups can be found at 6.0 $\tau$  whilst those due to the –CH– and –CH<sub>2</sub>– groups of the epoxide ring occur at 7.0 $\tau$  and 7.8 $\tau$  respectively.

*Figure 1b* represents a typical spectrum obtained from the top layer of the product given by reaction of equimolar quantities of DGEBA and isoprene, and *Figure 1c*

shows the spectrum characteristic of the lower layer of this product. In addition to the peaks described for DGEBA, Figure 1b also possesses a characteristic pattern in the 4.5 $\tau$  to 5.5 $\tau$  region due to the aliphatic resonances of the isoprene units. The relatively complicated pattern arises because there are several types of alkylenic protons in the 1,2-, 1,4- and 3,4-isomeric forms. Similarly, the spectrum shows several broad absorptions in the 8.0 $\tau$  to 9.0 $\tau$  range due to the aliphatic isoprenyl groups. These peaks are also in evidence in the spectrum of the lower layer shown in Figure 1c, but to a much lower extent.

From a quantitative standpoint the most straightforward measurement to be obtained from the n.m.r. spectrum is the ratio of the aromatic peaks to the remainder. Since the aromatic peaks arise only from the DGEBA units, this ratio can be used to calculate the relative amounts of DGEBA to isoprene present in the sample (see Appendix).

Similar spectra are obtained when butadiene is used as monomer. In the alkylenic region characteristic patterns

are obtained due to the  $-\text{CH}=\text{CH}-$  and  $-\text{CH}=\text{CH}_2$  groups which absorb at about 4.7 $\tau$ , and to the  $-\text{CH}=\text{CH}_2$  hydrogens at 5.0 $\tau$ . Broad aliphatic resonances also occur at 8.0 $\tau$  and 8.7 $\tau$  and are due to the  $-\text{CH}_2-\text{CH}=\text{CH}-$  and the  $-\text{CH}_2-\text{CH}-$  hydrogens respectively. The proportion of 1,2-units ( $p$ ) can be calculated from the easily derived relationship  $p = (4 - 2a)/(a + 1)$ , where  $a$  = ratio of aliphatic to alkylenic hydrogens in the butadiene units.

#### Bulk material

Table 1 in Part 1 shows that the epoxide value of the resin, originally at 5.2 equiv./kg had been reduced by reaction with equimolar amounts of isoprene to an average of 3.74 equiv./kg with a standard deviation of 4.5%. If the initial assumption be made that the reaction is quantitative, and that no loss of product due to fractionation factors has occurred during the work-up stage, then the molar ratio of the components in the product mixture,  $r$ , is the same as that of the reactants,  $r_0$ . On this basis, application of equations (A2) and (A3) (see Appendix) to these data enables the mole fraction of adduct formed,  $p_0$ , and the number-average chain length of the diene oligomers,  $n_0$ , to be estimated. Despite the obvious inaccuracy in the assumption of quantitative conversion and isolation, it is instructive to apply these equations to the average value of the epoxide content previously obtained assuming  $r = 1$ . These give a value of  $n_0 = 6.5$ , and the percentage of DGEBA converted to adduct as 30%. Since the standard deviation of the results is 4.5%, this allows ' $n_0$ ' to vary between 5.2 and 8.6, and the percentage conversion to have limits of 23% and 38%. Thus calculations of ' $n_0$ ' and ' $p_0$ ' by this method are very sensitive to the accuracy of the epoxide determination, and so can safely be used only to give semi-quantitative indications of any trends in the process.

Although fractionation at the work-up stage may invalidate the absolute figures given above, the spread in the calculated results is probably still significant since any deviations due to this effect will probably be similar in the circumstances where reproducibility is being examined. However, when the reagent composition is changed this need no longer apply and an independent assessment of the molar ratio in the product is necessary. This is carried out by  $^1\text{H}$  n.m.r. spectroscopy prior to phase separation of the material.

A series of reactions were carried out using isoprene as monomer where the molar ratio of isoprene to DGEBA was varied from 0.5 to 2.5. The products were then isolated and both the molar ratios and the epoxide contents of the bulk materials were evaluated before phase separation

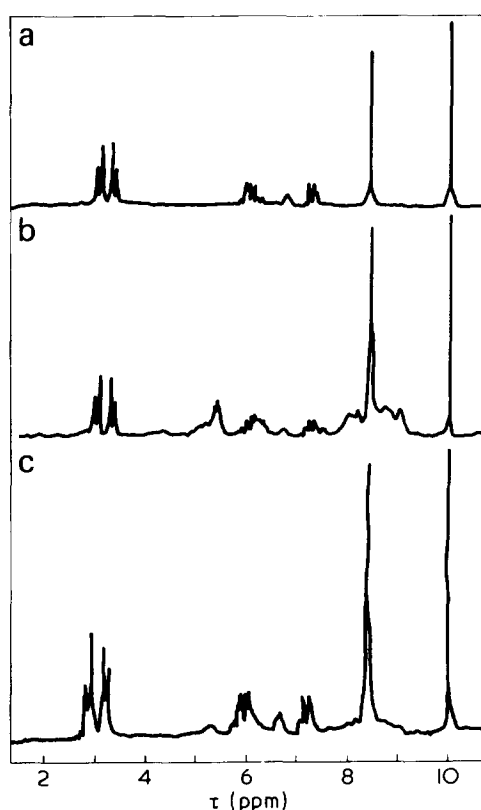


Figure 1 100 MHz  $^1\text{H}$  n.m.r. spectra of: (a) unmodified DGEBA; (b) DGEBA modified with equimolar isoprene — top layer; (c) DGEBA modified with equimolar isoprene — bottom layer

Table 1 Analysis of total product obtained from reaction of DGEBA and diene at various molar ratios of diene to DGEBA

Monomer	Starting molar ratio				Spectroscopic molar ratio			
	$r_0$	$f(E)$	$p_0$	$n_0$	$a$	$r$	$p$	$n$
Isoprene	0.5	0.82	0.106	4.7	2.45	0.58	0.095	5.9
	0.75	0.76	0.140	5.4	2.62	0.82	0.142	5.8
	1.0	0.73	0.140	7.2	2.75	0.90	0.154	6.0
	1.5	0.65	0.179	8.4	3.02	1.48	0.180	5.6
	2.0	0.62	0.160	12.5	3.42	1.67	0.196	8.6
	2.5	0.42	0.332	7.5	3.83	2.10	0.370	5.7
Butadiene	1.0	0.77	0.120	8.3	2.61	0.99	0.122	8.2
	2.0	0.675	0.134	14.9	3.07	1.72	0.160	10.7
	3.0	0.605	0.139	21.6	3.62	2.52	0.178	14.3

occurred. The former values were calculated using equations (A8) and (A9). A similar series of preparations and analyses was also carried out with butadiene as monomer. Equations (A10) and (A9) were employed in the spectroscopic analysis of these materials.

The results from both these series of modified epoxides are given in *Table 1* where, for purposes of comparison, calculations of the percentage modified material and of the average chain length of its diene component were carried out using values of the molar ratio derived from the initial mix ( $r_0$ ) and from the spectroscopic analyses ( $r$ ).

It can be seen that the relative quantity of either diene found in the isolated material is less than that introduced in the reagent mixture, and that this trend becomes more pronounced as the starting ratio increases. Agreement at ratios near unity is relatively close so that use of the initial reagent ratio in the reproducibility calculations mentioned previously should be reasonably sound. However, with butadiene using either method of calculation, the chain length increases with the reagent ratio although its degree does not match that of the reagents. Thus, increase in the diene proportion not only increases the degree of polymerization but also the number of chains initiated. Isoprene is less sensitive to reagent ratio and change is principally reflected in the number of chains formed rather than their length.

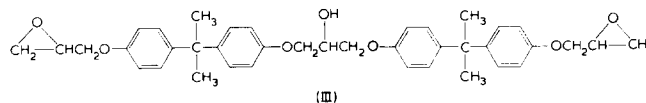
The average chain lengths of the butadiene moieties are significantly greater than those of isoprene under identical conditions. Furthermore, the rate of increase of chain length with reagent ratio is larger for butadiene so that the values for the two monomers diverge as the reagent ratio increases. These observations are consistent with the fact that the rate constant of anionic propagation in THF of butadiene is greater than that of isoprene.

#### Phase separated materials

The opaque bulk material gradually separates into two layers until, after about one week the viscous rubbery top layer may be physically removed.

The separated layers of products from a series of different syntheses were examined by g.p.c. and were subsequent-

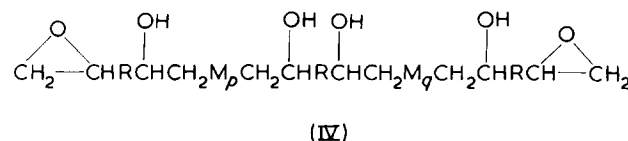
ly analysed for epoxide content, and by n.m.r. spectroscopy. The g.p.c. traces of starting material and of the products from reactions involving equimolar proportions of either diene and DGEBA are shown in *Figure 2*. The DGEBA trace shows a main peak characteristic of material of structure I having a molecular weight of 340, and a minor peak at higher molecular weight which is almost certainly the derivative:



This has a molecular weight of 624 and, as the average molecular weight of the material is given as 384, this would require 15.5% by wt of the commercial DGEBA to consist of III, which is roughly in accord with the relative areas.

The traces of the upper and lower layers both show the presence of DGEBA and the modified material, although their relative abundances are very different. This means that the modified material has a significant solubility in DGEBA and *vice versa* and/or that the separation process is not complete. The transparency and comparatively low viscosity of the bottom layer suggest that solubility is the reason for the presence of modified material in this phase, whereas the opacity and high viscosity of the upper layer indicate that kinetic factors could be important in determining its composition.

The shapes of the traces of the modified material in both layers show that there is a high dispersity of chain lengths of the diene segments, although it is possible that the broadness reflects the formation of appreciable quantities of 'dimers' of structure IV (see Part 1)<sup>1</sup>:

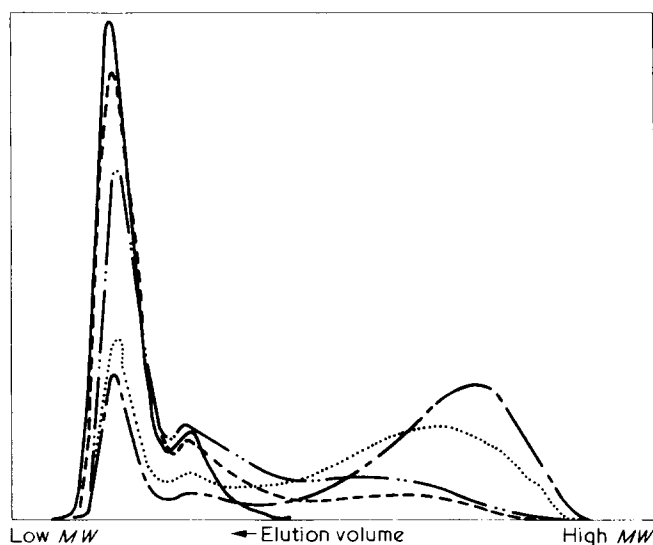


It is interesting and significant to note that the maximum in the trace of the modified material from the upper layer is at a higher molecular weight than that of the lower layer. Thus some fractionation of the modified material has occurred on separation. It is to be expected that those molecules containing the smallest diene oligomers would be most compatible with, and hence most soluble in, DGEBA and this appears to be confirmed.

A point of significance to the spectroscopic analysis described in the Appendix is whether the relative proportions of structures I and III in each phase have changed as a result of fractionation between the layers. Nothing conclusive may be derived from examination of the g.p.c. traces other than that any changes which have occurred are not large. It has therefore been assumed that the relative ratios of structures I and III have been maintained and are as recorded for unmodified DGEBA, although it is realized that this assumption introduces a further uncertainty in the results calculated by this method.

A more quantitative analysis of the g.p.c. traces is difficult because of the variation in the refractive index of the components of the layers with the size of the diene oligomeric units contained therein.

The weights of accurately known volumes of the upper and lower phases were determined for the products of isoprene and DGEBA reactions carried out at various reagent molar ratios. The resultant densities were shown to be



*Figure 2* Gel permeation chromatograms of modified and unmodified DGEBA. —, DGEBA; ---, equimolar butadiene/DGEBA — top layer; - · - ·, equimolar butadiene/DGEBA — bottom layer; · · ·, equimolar isoprene/DGEBA — top layer; - - - -, equimolar isoprene/DGEBA — bottom layer

**Table 2** Analysis of layers formed from products obtained from reaction of DGEBA and diene at various molar ratios of diene to DGEBA. No allowance made for mutual solubility of DGEBA and modified material

Monomer	$r_0$	Top layer				Bottom layer	
		Epoxide content		Volume fraction		Epoxide content	
		Exp.	Calc.	Exp.	Calc.	Exp.	Calc.
Isoprene	0.5	1.52	1.70	0.10	0.30	4.51	5.2
	0.75	1.43	1.75	0.13	0.40	4.27	5.2
	1.0	1.56	1.71	0.21	0.42	4.26	5.2
	1.5	1.51	1.51	0.28	0.54	4.08	5.2
	2.0	1.32	1.49	0.44	0.58	4.47	5.2
	2.5	1.32	1.73	0.50	0.84	3.37	5.2
Butadiene	1.0	1.56	1.65	0.20	0.39	4.35	5.2
	2.0	1.50	1.49	0.33	0.50	4.38	5.2
	3.0	1.50	1.31	0.50	0.58	4.55	5.2

**Table 3** Analysis of layers formed from products obtained by reaction of DGEBA and diene at various molar ratios of diene to DGEBA

Monomer	$r_0$	$a_T$	$a_B$	$v$	$(y+z)$	$n_T$	$n_B$	$v_0^*$	$(x-y)_0^\dagger$
Isoprene	0.5	6.25	2.22	0.10	0.029	10.7	3.7	0.84	0.09
	0.75	6.67	2.33	0.13	0.041	11.5	3.7	0.87	0.13
	1.0	6.67	2.56	0.20	0.070	12.9	7.0	0.71	0.10
	1.5	7.14	2.56	0.31	0.122	14.3	5.9	0.70	0.13
	2.0	7.14	2.44	0.47	0.176	12.3	9.2	0.92	0.07
	2.5	7.14	2.42	0.50	0.248	12.3	1.7	0.94	0.44
Butadiene	1.0			0.14	0.050				
	2.0			0.33	0.100				
	3.0			0.50	0.220				

\*  $v_0 = y/(y+z)$  = mole fraction of modified material in top layer

†  $(x-y)_0 = (x-y)/(1-y-z)$  = mole fraction of modified material in bottom layer

insensitive to this parameter and to average at 0.96 and 1.11 g/ml respectively. These values compare with a density of 1.16 g/ml found for unreacted DGEBA. Although these results are not sufficiently accurate to serve as the basis of a quantitative analysis of phase compositions, the observation that the density of the bottom layer is slightly lower than that of pure DGEBA is explained by the observed solubility of the less dense modified material in this phase.

The volume fraction of top layer obtained in the separated product is very dependent on the molar ratio of starting materials; for example, the measured volume fraction increases from 0.10 to 0.50 as the molar ratio of isoprene to DGEBA rises from 0.5 to 2.5, and the rate of increase is roughly proportional to the change in reagent ratio (Table 2). Thus the epoxide equivalent of the top layer is relatively insensitive to the ratio of reactants and the change is principally reflected in the amount of modified material formed.

If one assumes that the upper and lower layers consist exclusively of modified epoxide and unreacted DGEBA respectively, then the epoxide content and volume fraction of the upper phase will be given by equations (A11) and (A13). This assumption is clearly justified from the foregoing observations but, nevertheless, the discrepancies between those values calculated on this basis and those observed highlight the significance of 'solubility' effect. The results are recorded in Table 2 using the data obtained from the n.m.r. analysis given in Table 1. Inspection of Table 2 leads to the following conclusions: (a) the calculated volume fractions of top layer are significantly larger than those observed, especially at low  $r_0$ ; (b) the epoxide content of the bottom layer is appreciably lower than the value of 5.2 required if it were unreacted DGEBA only; (c) the epoxide content of the top layer is closer to, although

consistently lower than, the calculated value. These observations may be interpreted on the basis of mutual solubility of the two components in the system; particularly that of the modified material in DGEBA. If, however, the solubility of the modified epoxide were independent of molecular weight, the epoxide content of the top layer could not be lower than that calculated as is in fact obtained. This last observation can be explained only on the basis of a preferential solubility of the lower molecular weight component of the modified material in DGEBA, leaving the top layer with a distribution weighted towards the high molecular weight end, and hence with an epoxide number lower than that predicted.

The weight fraction of modified layer may be derived from the observed epoxide numbers by use of equation (A19) and converted into volume fraction via equation (A21). The results of these calculations are given in Table 3 and shown to be in good agreement with those measured (Table 2). Further, the total mole fraction of both modified epoxide and DGEBA molecules in the top layer may be derived from equation (A20) and the results are listed in Table 3. The relative amounts of these two species cannot be determined without recourse to further compositional data. These were obtained for the isoprene modified series by n.m.r. analysis of the separated layers and the use of equation (A8). The degree of polymerization of the isoprene moieties in the top phase,  $n_T$ , and in the bottom phase,  $n_B$ , were derived in this way and are quoted in Table 3. It is clear that some of the values of  $n_T$  and  $n_B$  are inconsistent with those of  $n$  in Table 1 since  $n$  should lie between these two extremes. It is easily shown, however, that the values of  $n_T$  are more accurate than  $n_B$  because  $n_B$  is very sensitive to small changes in  $f(E)_B$  and

$a_B$  since the amount of modified material in the bottom layer is small. Thus, the absolute values of  $n_B$  show a large scatter, although it is evident that  $n_B$  is always significantly less than  $n_T$  indicating that fractionation of the modified epoxide has occurred between the two phases.

These results may in turn be used in equations (A14) and (A15) to calculate the relative proportions of modified material and DGEBA in each phase. The values obtained are given in Table 3 and despite wide variation, indicate that there is about 10 mol % of DGEBA in the top layer and a similar quantity of modified material in the bottom layer.

Lastly, it is necessary to consider the assumptions inherent in the analysis. First, it has had to be assumed that the ratio of compounds I and III, determined for the starting material, has been maintained in the composition of each of the phases. This is clearly an approximation as it has been shown that fractionation occurs on separation and the derivatives of these structures should be similarly affected under these circumstances. Secondly, the presence of dimers of structure IV has not been considered. If  $n$  in the calculations be regarded as the number-average degree of polymerization between DGEBA residues regardless of whether the epoxide groups in those residues have totally or partly reacted, then its values will be unchanged by the presence of structure IV. By the same token, however, this means that the analysis cannot be used to assess the importance of structure IV in the composition of the final products.

[© Crown Copyright. Reproduced with permission of the Controller, HMSO, London]

## REFERENCE

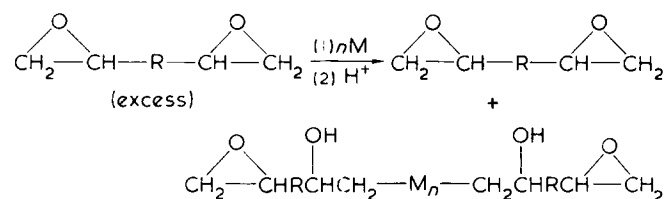
- 1 Cunliffe, A. V., Huglin, M. B., Pearce, P. J. and Richards, D. H. *Polymer* 1975, 16, 654

## APPENDIX

### Overall composition of the reaction product

If the molar ratio,  $r$ , of diene to total DGEBA present in the isolated product, whether as unreacted diepoxide or as ligand, be known then the average chain length of the diene moieties,  $n$ , and the mole fraction of unreacted DGEBA may be calculated from the epoxide content.

Let the overall reaction be represented by the equation:



where  $M$  = diene monomer of molecular weight  $m$ .

If the mole fraction of DGEBA converted into adduct =  $2p_0$  then mole fraction of adduct relative to original DGEBA =  $p_0$  and the total number of moles is reduced to  $1 - p_0$ . Therefore, mole fraction of DGEBA in product =  $(1 - 2p_0)/(1 - p_0)$ , and of adduct =  $p_0/(1 - p_0)$ .

The molecular weight of the commercial DGEBA used = 384, and, ignoring the molecular weight contribution of the  $-\text{OH}$  hydrogens in the product, the molecular weight of the adduct =  $2 \times 384 + mn_0 = 768 + mn_0$  ( $n_0$  = degree of polymerization of diene units assuming complete conversion). This approximation introduces an error well within

that of the determination of the epoxide content, and can therefore be applied where such figures are used. It is not permissible under other circumstances, as will be seen when the n.m.r. spectroscopic results are considered.

The epoxide content of DGEBA is given by  $E_0 = 2000/384$  equiv./kg and the epoxide content of the product is similarly given by:

$$E^1 = \frac{2000(1 - p_0)}{(1 - 2p_0)384 + p_0(768 + mn_0)}$$

Thus:

$$\frac{E^1}{E_0} = f(E) = \frac{1 - p_0}{1 + (m/384)n_0p_0} \quad (\text{A1})$$

If it be assumed that all reactants are retained in the product then we have  $n_0p_0 = r_0$ , where  $r_0$  = molar ratio of isoprene to DGEBA introduced into the reaction so that equation (A1) becomes:

$$f(E) = \frac{1 - p_0}{1 + (m/384)r_0} \quad (\text{A2})$$

or

$$n_0 = \frac{r_0}{1 - [1 + (m/384)r_0]f(E)} \quad (\text{A3})$$

and, for isoprene:

$$n_0 = \frac{r_0}{1 - [1 + 0.177r_0]f(E)} \quad (\text{A4})$$

Without the assumption of quantitative reaction and isolation, the product composition can be estimated by combining the epoxide value with the results of n.m.r. analysis.

Under these circumstances, if the mole fraction of modified epoxide in the product =  $x$ , the epoxide number is given by:

$$E^1 = \frac{2000}{(1 - x)384 + x(768 + mn)}$$

from which

$$f(E) = \frac{1}{1 + [1 + (mn/384)]x} \quad (\text{A5})$$

which, for isoprene, gives:

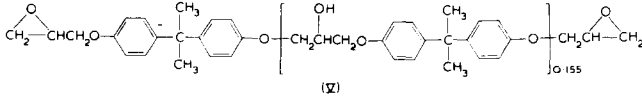
$$f(E) = \frac{1}{1 + (1 + 0.177n)x} \quad (\text{A6})$$

As the n.m.r. analysis gives the ratio of aliphatic to aromatic hydrogens, the composition of the DGEBA and of the modified material must be considered in more detail.

G.p.c. measurements have shown commercial DGEBA to consist of a mixture of structures I and III and calculation from the average molecular weight of 384 gives the mole fraction of III = 0.155. The best model to use to describe the starting material is therefore structure V:



An anionically prepared flexible adhesive (2): A. V. Cunliffe et al.



Thus the aliphatic to aromatic hydrogen ratio of V is given by:

$$\left(\frac{\text{Al}}{\text{Ar}}\right)_{\text{DGEBA}} = \frac{16 + 12 \times 0.155}{8 + 8 \times 0.155} = 1.93$$

If we assume that the relative concentrations of I and III in the isolated product are identical with those in DGEBA, then V may be considered as undergoing the reaction with diene. Thus, including the hydrogens of the OH groups produced by the reaction, the aliphatic to aromatic hydrogen ratio in the isoprene modified product is now given by

$$\left(\frac{\text{Al}}{\text{Ar}}\right)_{\text{Mixture}} = a =$$

$$\frac{[2 \times (17 + 12 \times 0.155) + 8n]x + (16 + 12 \times 0.155)(1 - x)}{2 \times (8 + 8 \times 0.155)x + (8 + 8 \times 0.155)(1 - x)} = \frac{1.93 + (2.15 + 0.866n)x}{1 + x} \quad (\text{A7})$$

Equations (A6) and (A7) may now be combined to evaluate  $n$ :

$$n = \frac{a - 2.15 + 0.22f(E)}{0.866[1 - f(E)] - 0.177(a - 1.93)f(E)} \quad (\text{A8})$$

Knowing  $n$ ,  $x$  may be evaluated from equation (A6), whence an *apparent* conversion fraction  $p$  may be calculated from the relationship  $p = x/(1 + x)$ . Finally, the molar ratio ( $r$ ) of diene to total DGEBA (unreacted or as ligand) can be derived from the equation:

$$np = r \quad (\text{A9})$$

In an identical way an equation analogous to equation (A8) for the butadiene modified system may be derived:

$$n = \frac{a - 2.15 + 0.22f(E)}{0.65[1 - f(E)] - 0.146(a - 1.93)f(E)} \quad (\text{A10})$$

*Analysis of separated layers*

Ignoring again the contribution to the molecular weight of the  $-OH$  hydrogen in the product, the epoxide content of the modified material is given by:

$$E = \frac{2000}{768 + mn} \quad (\text{A11})$$

and it may be readily shown that the weight fraction of the modified epoxide is given by:

$$w_0 = \frac{1}{1 + \frac{1 - x}{x \left(2 + \frac{mn}{384}\right)}} \quad (\text{A12})$$

and that its volume fraction is given by:

$$v_0 = \frac{1}{1 + \frac{D(1 - x)}{dx \left(2 + \frac{mn}{384}\right)}} \quad (\text{A13})$$

where  $D$  = density of modified epoxide, and  $d$  = density of DGEBA.

Assume that the two components are mutually soluble and that fractionation has occurred between the two phases.

If the top phase contains  $y$  and  $z$  mole fractions of modified material and DGEBA respectively, then the bottom phase is composed of  $(x - y)$  and  $(1 - x - z)$  mole fractions of these components. Finally, if  $n_T$  and  $n_B$  are the average degree of polymerization of the diene moieties in the top and bottom phase respectively, and  $E_T$  and  $E_B$  be their epoxide number, then the following relationships may be derived for isoprene:

$$f(E_T) = \frac{E_T}{E_0} = \frac{y + z}{z + (2 + 0.177n_T)y} \quad (\text{A14})$$

$$f(E_B) = \frac{E_B}{E_0} = \frac{1 - (y + z)}{(1 - x - z) + (2 + 0.177n_B)(x - y)} \quad (\text{A15})$$

$$nx = n_T y + n_B(x - y) \quad (\text{A16})$$

and

$$f(E) = wf(E_T) + (1 - w)f(E_B) \quad (\text{A17})$$

where  $w$  = weight fraction of top layer. The weight fraction  $w$  may also be derived from the relationship:

$$w = \frac{(768 + mn_T)y + 384z}{(768 + mn_T)y + 384z + (768 + mn_B)(x - y) + (1 - x - z)384}$$

which, by use of equation (A16) may be simplified to:

$$w = \frac{(2 + 0.177n_T)y + z}{1 + (1 + 0.177n)x}$$

Again, using equations (A6) and (A14) this reduces to:

$$w = (y + z) \frac{f(E)}{f(E_T)} \quad (\text{A18})$$

but from equation (A17):

$$w = \frac{f(E_B) - f(E)}{f(E_B) - f(E_T)} \quad (\text{A19})$$

so that

$$y + z = \frac{f(E_T)[f(E_B) - f(E)]}{f(E)[f(E_B) - f(E_T)]} \quad (\text{A20})$$

Thus the weight fraction  $w$  may be derived via equation (A19) from the epoxide numbers of the phases and may be related to the experimentally determined volume fraction by the equation:

$$v = \frac{1}{1 + [(1 - w)/w](D/d)} \quad (\text{A21})$$

# An anionically prepared flexible adhesive:

## 3. Physical testing

A. V. Cunliffe, M. B. Huglin\*, P. J. Pearce and D. H. Richards

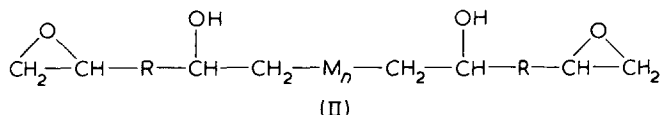
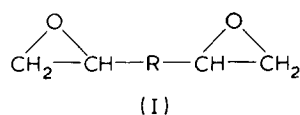
Explosives Research and Development Establishment, Ministry of Defence, Waltham Abbey, Essex  
EN9 1BP, UK

(Received 6 February 1975)

The physical properties of flexibilized epoxides produced by reaction of a diglycidyl ether of bisphenol A with dienes are examined and the reaction conditions necessary to produce materials giving maximum lap shear strengths are determined. It is shown that these optimum conditions occur when equimolar proportions of isoprene and bisphenol A based epoxides are reacted together with excess sodium metal. Tests carried out which involve ageing at elevated temperature, and exposure to adverse environmental conditions show that the improvements in lap shear strengths observed on flexibilization are retained under these adverse conditions.

### INTRODUCTION

Part 1<sup>1</sup> of this series of papers describes a process by which conventional diepoxides based on a diglycidyl ether of bisphenol A (DGEBA) can be flexibilized by reaction with a diene and excess alkali metal. The chemistry of the reaction is fully covered in the paper, but the process may be represented as a transformation of a proportion of the starting material from the structure represented schematically as I to the flexibilized form II, where  $M_n$  represents an oligomeric diene unit of length  $n$ .



The isolated material separates on standing for a few days into two layers. The upper component, which is opaque and rubbery, has been shown to be composed principally of the modified epoxide II, whilst the lower layer consists predominantly of the unreacted starting material I. In Part 2<sup>2</sup> it was established that the volume fraction of the modified layer was directly dependent on the molar ratio of the diene to epoxide in the reaction whilst the diene oligomeric chain length was relatively insensitive to this change; for example, with isoprene as monomer, the average chain length  $n$  only changed from 5.6 to 8.6 over a five-fold increase in isoprene concentration.

Preliminary lap shear strength measurements on the product obtained from an equimolar isoprene-epoxide reagent mixture, reblended and mixed with a variety of curing agents, indicated that in all cases significant improvements in strength were obtained over the similarly mixed unmodified material<sup>1</sup>.

This communication describes experiments carried out to establish whether isoprene or butadiene modified epoxide exhibits the better adhesive properties, and to decide

on the proportion of top to bottom layer which on blending results in the maximum synergism. The material with the optimum adhesive strength having been selected, there follows a discussion of the results of physical tests carried out under a variety of experimental conditions on lap joints bonded together by this adhesive.

### EXPERIMENTAL

The experimental details relating to the purification of reagents and the synthesis and isolation of the flexibilized epoxides have been described in Part 1<sup>1</sup> and will not be repeated here.

#### Test method for adhesive shear strength using lap joints

This method is based on test specification ASTM D1002-64<sup>3</sup> which is universally accepted for lap shear examination.

Test specimens were prepared from metal sheets of 0.064 in gauge, cut into 4 in × 1 in strips. Immediately prior to use they were cleaned and dried carefully by a process which was dependent on the substrate. Two metals were used in this work, aluminium coated aluminium alloy (BS 2L73 specification) and mild steel; in both cases the surface was degreased in trichloroethylene vapour before further treatment.

The aluminium specimens were chemically etched by immersion for 30 min at 60–65°C in an agitated chromic acid solution, washed in tap water followed by distilled water and dried at 60°C. The acid solution was prepared by dissolving 5 parts chromium trioxide and 15 parts by wt concentrated sulphuric acid (s.g. 1.84) in 80 parts water.

A phosphate treatment recommended for etching the mild steel strips failed to give good reproducibility under test, but consistent results were obtained with pressure impact abrasion using alumina of 180–220 mesh, and this latter technique was adopted for mild steel strips throughout.

The cleaned strips were assembled in pairs and the adhesive, prepared by mixing resin and curing agent, was applied to a length across the end of each specimen sufficient to cover a space at least 0.25 in longer than the 0.5 in overlap required. The joints were then assembled, held rigidly under slight pressure and allowed to cure for the recommended period of time. Glue line thickness was controlled

\* Department of Chemistry and Applied Chemistry, University of Salford, Salford M5 4WT, UK.

at 0.004 in by inserting into the joint two or three very short lengths of stainless-steel wire of this diameter during the joint assembly.

Testing was carried out using a Monsanto Type E tensometer adjusted to ensure that the breaking load of the specimen fell between 15 and 85% of full scale capacity. The joint was held by a suitable pair of self-aligning grips allowing the outer inch of each end to be firmly engaged. Loading was applied at a constant crosshead speed of 0.2 in/min and continued until failure occurred.

#### Curing systems and cycles employed

The proportion of curing agent added to the modified epoxides was the subject of experiment (Table 2) whereas the proportion added to the unmodified material (DGEBA) was that recommended by the manufacturers. The cure cycles employed were as described below unless otherwise specified in the text.

1. *Aliphatic primary amine*: triethylenetetramine (Ciba HY951). Cure cycle of 2 hours at 80°C.
2. *Aromatic amine*: 4,4'-diaminodiphenylmethane (Ciba HT972). Cure cycle of 2.5 hours at 100°C.
3. *Polyamide*: (Versamid 140). Cure cycle of 2 hours at 100°C.
4. *Anhydride*: hexahydrophthalic anhydride (Ciba HT907). Cure cycle of 2 hours at 120°C followed by 2 hours at 150°C.
5. *Catalytic*: borontrifluoride-ethylamine (Ciba HT973). Cure cycle of 3 hours at 120°C followed by 3 hours at 150°C.

#### Elevated temperature and environmental testing

In order to assess the performance of the modified resin under a variety of conditions, lap joints were assembled as described and subjected to the four tests given below. Unmodified DGEBA was used throughout as a standard for comparison.

*Ageing at elevated temperatures.* Lap joint specimens were treated at temperatures in the range 150–250°C in thermostatically controlled ovens and periodically sampled. Lap shear measurements were carried out at room temperature and the results were plotted as a function of time.

*Lap shear measurements at elevated temperature.* For this test the tensometer was fitted with a thermostatically controlled oven which totally enclosed the grips and lap joint. The test specimen was heated from ambient to the required temperature at a rate of 6 to 10°C/min and held for 15 min before application of the load.

*Test at 96% r.h. for 1000 h at 43°C.* These conditions, taken from Ministry of Defence specification D.T.D. 5577<sup>4</sup>, were achieved by placing the specimens over a saturated solution of sodium sulphate in a desiccator and storing in a thermostatically controlled oven. Lap shear measurements

were then carried out at room temperature after 1000 h exposure.

*Exposure to de-icing fluid for 1000 h at 43°C.* This test, especially important to the aeronautical industry, is carried out by totally immersing the specimens in a mixture of water and methanol (56:44 parts by wt) in an enclosed cylinder heated in an oven at 43°C. Lap shear measurements were carried out at room temperature after a 1000 h exposure.

## RESULTS AND DISCUSSION

### Product composition

Preliminary tests with the product from the reaction of equimolar quantities of DGEBA (structure I) and isoprene with excess sodium had shown superior adhesive properties to DGEBA with a variety of curing agents. Two points were still to be resolved before a more detailed examination of properties could be launched: (a) whether isoprene or butadiene produces the better adhesive; and (b) which blend of top to bottom layer results in the optimum adhesive properties.

The former problem was investigated by carrying out comparative tests on the lap shear strengths of the products of reactions between equimolar quantities of each diene and DGEBA. Triethylene tetramine (TETA) was chosen as curing agent and blended with both of the modified resins and with DGEBA in stoichiometric proportions based on the determined epoxide content of the materials. The cure cycle employed was 1.5 h at 80°C followed by a postcure of 1 h at 250°C. The results of lap joint tests on these materials are given in Table 1 where the average of four replicates are listed together with the maximum value obtained to give a measure of the dispersity of the results.

These results indicate that flexibilization to this degree gives a significant improvement in lap shear strength in both cases, but that the isoprene modified material gives higher values than the butadiene system. It was therefore decided to concentrate further investigation on isoprene based materials. This choice has the added advantages that: (a) during the synthesis the induction period before onset of reaction is usually very short for isoprene whereas an induction period in excess of 0.5 h has been observed with butadiene; (b) isoprene, being liquid at ambient temperature, is more convenient to purify and manipulate than butadiene; (c) the degree of polymerization of the isoprene moieties in the modified material is less sensitive to changes in the initial molar ratio of the reagents than is butadiene<sup>2</sup>. Thus experiments may be carried out to maximize the amount of upper layer without drastically affecting its composition. This is relevant to the question of determining the layer ratio necessary to optimise the shear strength.

This problem of maximizing the shear strength of the isoprene modified material was approached in the following way. The top layer of an equimolar preparation was removed and re-blended with various amounts of bottom layer and of DGEBA. Six mild steel lap joint specimens were prepared at each composition using triethylene tetramine (TETA) as the curing agent and with the curing cycle described above. The average lap shear strengths are given as a function of percentage top layer in Figure 1. The maximum in both sets of blends occurs at about 20% top layer, although the shear strength at this point is significantly lower if pure DGEBA is used. This last observation

Table 1 Comparison of the shear strengths of isoprene modified and butadiene modified epoxide resin (TETA cured with cycle of 1.5 h at 80°C followed by 1 h at 250°C)

Resin	Lap shear strength (MN/m <sup>2</sup> )	
	Av.	Max.
DGEBA	24.5	25.1
1:1 isoprene-DGEBA	33.9	35.7
1:1 butadiene-DGEBA	30.2	31.6

could be due to the absence of low molecular weight modified epoxide in the pure DGEBA which would increase compatibility between the phases, thus ensuring on cure a maximum transmission of stresses to the rubbery micelles. However, the important observation is that maximum synergism occurs with the system containing 20% top layer. This is close to the proportion obtained in the reaction of equimolar quantities of isoprene and DGEBA and it was decided, therefore, that a further and more comprehensive examination of the adhesive properties of the product of this reaction would be carried out.

*Mild steel substrate*

The physical properties of cured resins are to a large degree determined by the curing agent employed; hence it is clearly of importance to evaluate the properties of the isoprene modified material with a number of cures. Five

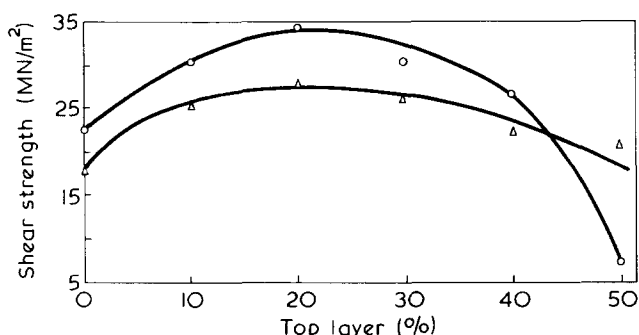


Figure 1 Maximization of shear strength by blending. O, Top layer/bottom layer; Δ, top layer/DGEBA

different curing systems were chosen to represent the wide variety available, namely, aliphatic amine, aromatic amine, polyamide, anhydride and catalytic. These were blended with the modified resin in various proportions to determine which resulted in the optimum shear strengths; DGEBA was used as a control with the hardner ratio recommended by the manufacturers. Eight replicates were tested for each variation and the results are given in Table 2. Particularly marked gains in performance were obtained with the aliphatic amine and anhydride cure systems, with 104% and 73% improvements over DGEBA recorded. It is also of interest to note that even when a flexible polyamide is used further gain in strength can be obtained by using the flexibilized epoxide, the resulting lap shear strengths being the highest recorded with any of the cure systems employed.

Thus, having established that the modified epoxy resin exhibits superior adhesive properties to those of DGEBA under ambient conditions, it is now necessary to consider whether these improvements are retained under a variety of adverse environmental conditions. The first of these to be considered is the effect of ageing at elevated temperature on lap shear strengths.

*Effect of ageing on shear strength*

Tests were carried out at 150°, 200° and 250° C; TETA was used as curing agent at all three temperatures whilst specimens cured with aromatic amine and anhydride were treated in parallel at 250° C. All curing agents were used at concentrations for optimum shear strength as determined in Table 2. Testing was carried out in quadruplicate, and the averaged results were plotted against time as shown in Figures 2 to 6.

Table 2 Determination of curing agent concentration for maximum shear strength with mild steel substrate (optimum curing agent concentration underlined)

Curing system	Resin	Curing agent (pph)	Lap shear strength (MN/m <sup>2</sup> )		Maximum improvement (%)
			Av.	Max.	
Aliphatic amine	Modified	6	14.7	17.5	104
	Modified	8	26.7	28.1	
	Modified	10	21.7	23.3	
	Modified	12	20.8	23.0	
	Unmodified	10	13.1	14.8	
Aromatic amine	Modified	15	19.3	24.1	57
	Modified	22	24.4	25.9	
	Modified	24	23.2	24.9	
	Unmodified	27	15.6	17.7	
Polyamide	Modified	110	18.3	19.5	30
	Modified	100	20.6	21.8	
	Modified	90	24.2	26.3	
	Modified	80	25.1	27.2	
	Modified	70	29.4	30.8	
	Modified	60	29.1	32.1	
	Modified	50	32.1	33.3	
	Modified	40	31.3	32.8	
	Modified	30	27.2	30.5	
	Unmodified	100	24.6	26.5	
Anhydride	Modified	63	14.7	15.8	73
	Modified	51	20.3	21.9	
	Modified	41	27.4	27.8	
	Modified	30	29.3	30.3	
	Modified	20	31.9	32.5	
	Modified	10	30.7	31.5	
Catalytic	Unmodified	100	18.4	20.0	11
	Modified	1	Did not cure		
	Modified	4	19.4	20.7	
	Modified	8	15.6	17.0	
	Unmodified	3	17.5	18.3	

It is seen that a postcure strength increase is frequently observed with one or both of the resins. This is almost certainly caused by the reaction of last traces of curing agent leading to a more complete network structure with consequent increase in strength, as it occurs primarily with the systems cured at low temperature with aliphatic amine. The modified resin may also crosslink further through its unsaturation and, since the postcure effect is generally more marked with the modified resin, both reactions could well occur simultaneously.

More importantly, however, it is clear that at all temperatures and with each of the curing agents used the improvement in shear strength is maintained throughout the useful life span of the resin despite the potential instability present at the aliphatic double bonds. In fact, these double

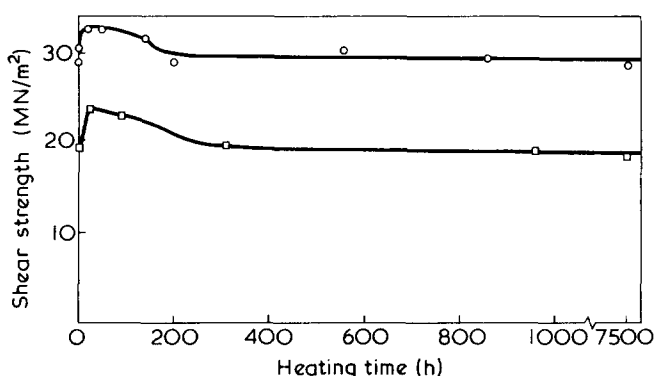


Figure 2 Effect of temperature on shear strength for aliphatic amine cure at 150°C. ○, Modified; □, unmodified

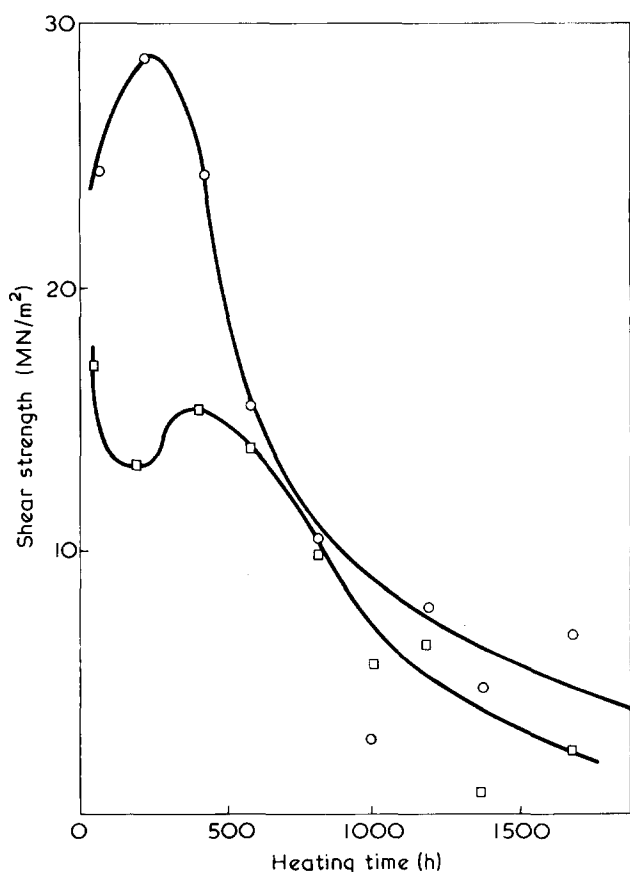


Figure 3 Effect of temperature on shear strength for aliphatic amine cure at 200°C. ○, Modified; □, unmodified

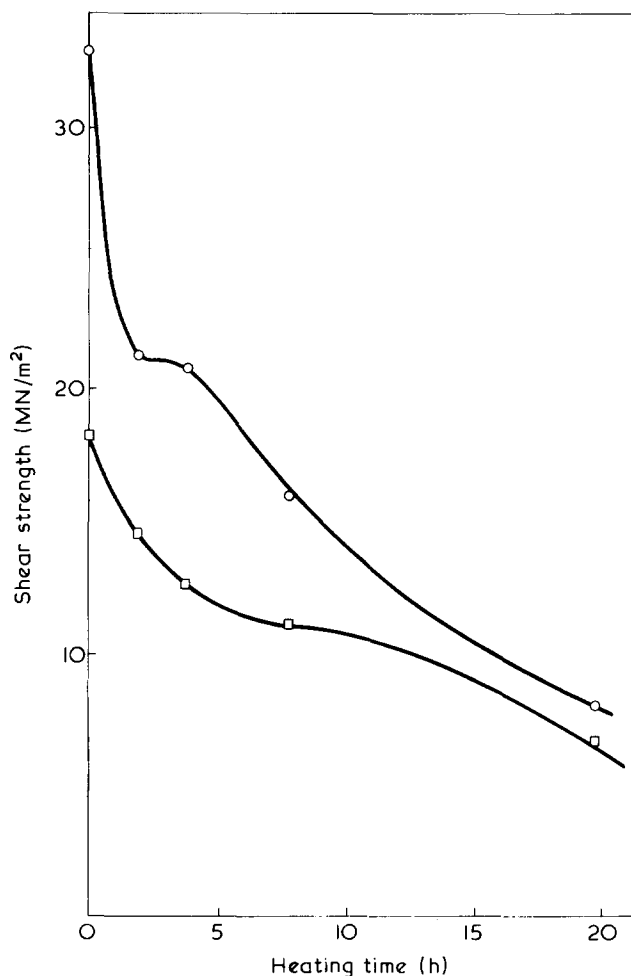


Figure 4 Effect of temperature on shear strength for aliphatic amine cure at 250°C. ○, Modified; □, unmodified

bonds might act as crosslinking sites at high temperatures and thus partly compensate for the thermally induced chain scission.

Finally, the aliphatic amine cured specimens which are unaffected at 150°C over a period of 1500 h have a useful life span of about 800 h at 200°C, but show rapid degradation at 250°C with a total useful life span of only about 13 h. This may be improved by replacing TETA with the more rigid aromatic amine or anhydride hardener. The former gave specimens which still retained a lap shear strength of 10 MN/m<sup>2</sup> after 20 h at 250°C whilst the latter averaged at 14 MN/m<sup>2</sup> after the same exposure period.

#### Environmental testing

One of the more important tests which evaluates the practical applicability of a material, and especially an adhesive, is that which assesses its ability to withstand conditions of high humidity. This is standardized for an adhesive by measuring the fall in shear strength after exposure to a relative humidity of 96% for 1000 h at 43°C. The results of such a test on the modified material and on DGEBA, expressed as the average of eight replicates, are contained in Table 3.

Both aliphatic and aromatic amine cured specimens, and those cured with polyamide gave significant drops in shear strengths averaging at about 17%. This is not unexpected as it is known that the curing process with nitrogen containing hardeners of these types gives bonds which are susceptible to hydrolysis. Hence, although these figures

are within most specifications, it indicates that these curing agents should be used with caution. On the other hand, very little change in strengths was observed when the resins

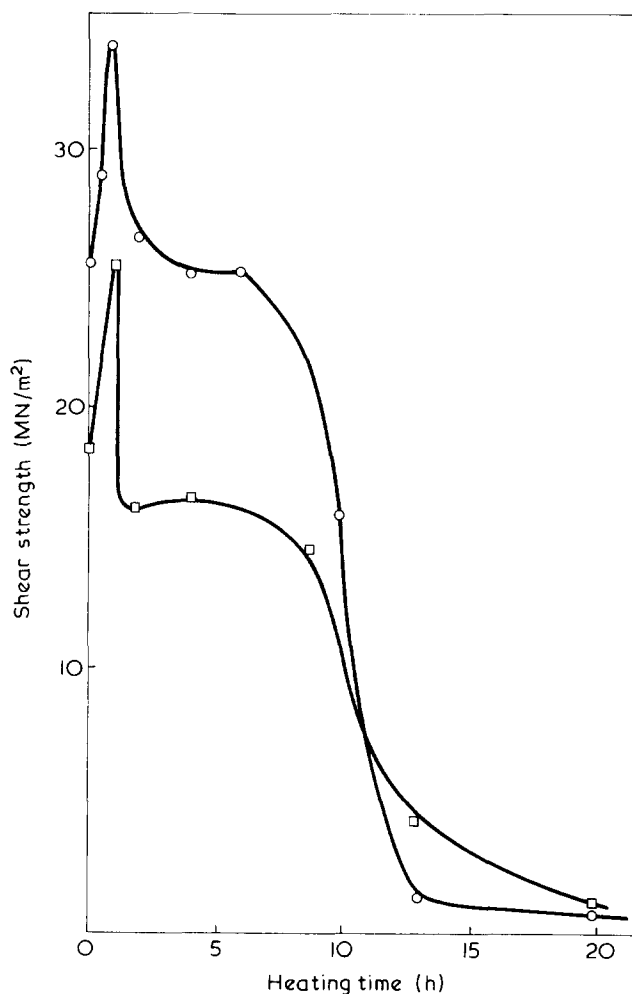


Figure 5 Effect of temperature on shear strength for anhydride cure at 250°C. ○, Modified; □, unmodified

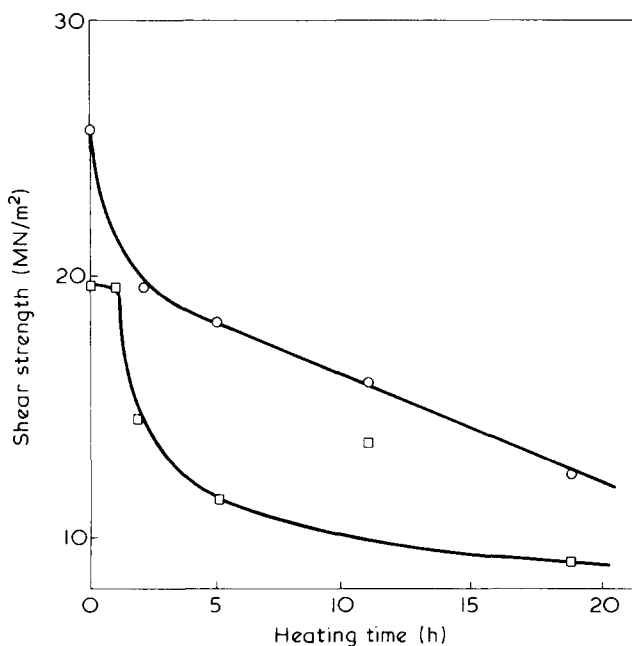


Figure 6 Effect of temperature on shear strength for aromatic amine cure at 250°C. ○, Modified; □, unmodified

Table 3 Effect on lap shear strengths of exposure to 96% r.h. for 1000 h at 43°C

Curing system	Resin	Average lap shear strength (MN/m <sup>2</sup> )		Change (%)
		Unexposed	Exposed	
Aliphatic amine	Unmodified	13.2	11.0	-16.7
	Modified	25.6	21.3	-16.8
Aromatic amine	Unmodified	15.6	12.8	-17.9
	Modified	21.9	16.7	-23.8
Polyamide	Unmodified	21.3	17.5	-17.9
	Modified	28.0	24.6	-12.1
Anhydride	Unmodified	15.9	16.7	+5.0
	Modified	29.4	28.1	-4.4
Catalytic	Unmodified	12.2	10.9	-10.7
	Modified	22.6	22.9	+1.3

Table 4 Comparison of lap shear strengths of isoprene modified and unmodified DGEBA using aluminium substrate

Curing system	Average lap shear strength (MN/m <sup>2</sup> )		Improvement (%)
	Unmodified	Modified	
Aliphatic amine	16.7	24.8	49
Anhydride	19.0	31.8	67

were cured with anhydride or catalytically and it is evident that these would be preferred hardeners for use in circumstances where high humidity is expected.

Lastly, it is again observed that the improvements in shear strengths obtained by flexibilizing DGEBA are retained under the conditions of this test, and that the behaviour patterns of the modified and unmodified DGEBA are roughly parallel.

#### Aluminium coated aluminium alloy substrate

All the tests covered so far were carried out with mild steel testpieces. However, aluminium coated aluminium alloy is widely used in the aerospace industry and, as the shear strengths of adhesives are also critically dependent on the nature of the substrate, it is evident that tests should also be conducted using this material. The remaining tests to be described were therefore carried out using aluminium substrate.

The adhesive shear strengths of modified DGEBA and pure DGEBA were again determined as with mild steel, but only TETA and anhydride were used as hardeners. The results obtained (average of four replicates) are summarized in Table 4. Again, superior strengths were obtained with the modified resin, and similar enhancement was achieved with the anhydride cured material as when mild steel test pieces were used. The percentage improvement with the amine cure was lower than formerly, although this was due principally to a large increase in the shear strength obtained with the pure DGEBA.

#### Lap shear measurements at elevated temperature

The modification of a material by introducing a component which is flexible and hence has a low  $T_g$ , is expected to have a deleterious effect on its strength at elevated temperatures. It is therefore important to assess this effect and so lap joints were prepared with various hardeners and tested at 70°C. The results, which are the average of six replicates, are given in Table 5.

Table 5 Comparison of the lap shear strengths of modified and unmodified DGEBA at ambient and 70°C

Curing system	Resin	Average lap shear strength (MN/m <sup>2</sup> )		Change (%)
		Ambient	70°C	
Aliphatic amine	Unmodified	17.3	17.1	-1.2
	Modified	27.0	14.7	-45.6
Aromatic amine	Unmodified	27.2	28.2	+3.7
	Modified	30.8	21.7	-29.5
Polyamide	Unmodified	27.7	10.0	-63.9
	Modified	26.1	14.4	-44.8
Anhydride	Unmodified	19.0	21.3	+12.1
	Modified	31.8	23.3	-26.7

The results indicate clearly the adverse effect of the aliphatic polymeric moieties on the elevated temperature performance of the cured adhesive. In all cases the modified resin shows a marked drop in shear strength, ranging from 27% for the anhydride to 45% with TETA and polyamide when compared with those recorded at ambient. This contrasts with the much smaller fall in values obtained with pure DGEBA so that the shear strengths of the two materials are more comparable at 70°C than at ambient temperature.

#### Environmental testing

The test at 96% relative humidity for 1000 h at 43°C was repeated using aluminium substrate and anhydride cured modified material. The average value from six replicates showed a 16% loss compared with the shear strength obtained from laboratory stored specimens. This relatively small loss is acceptable for an aeronautical adhesive.

#### Exposure to de-icing fluid for 1000 h at 43°C

Six replicates of anhydride cured modified resin were used and the average loss in shear strength was 15%. Again this is a satisfactory result for an aeronautical adhesive.

[© Crown copyright. Reproduced with permission of the Controller, HMSO, London]

#### REFERENCES

- 1 Cunliffe, A. V., Huglin, M. B., Pearce, P. J. and Richards, D. H. *Polymer* 1975, 16, 654
- 2 Cunliffe, A. V., Huglin, M. B., Pearce, P. J. and Richards, D. H. *Polymer* 1975, 16, 659
- 3 ASTM Standards No.16, American Society for Testing and Materials, Philadelphia, 1964
- 4 Ministry of Defence, Specification D.T.D. 5577, HMSO, London, 1966

# Phosponitrilic chloride: 27. Synthesis and properties of cyclophosphazene polymers

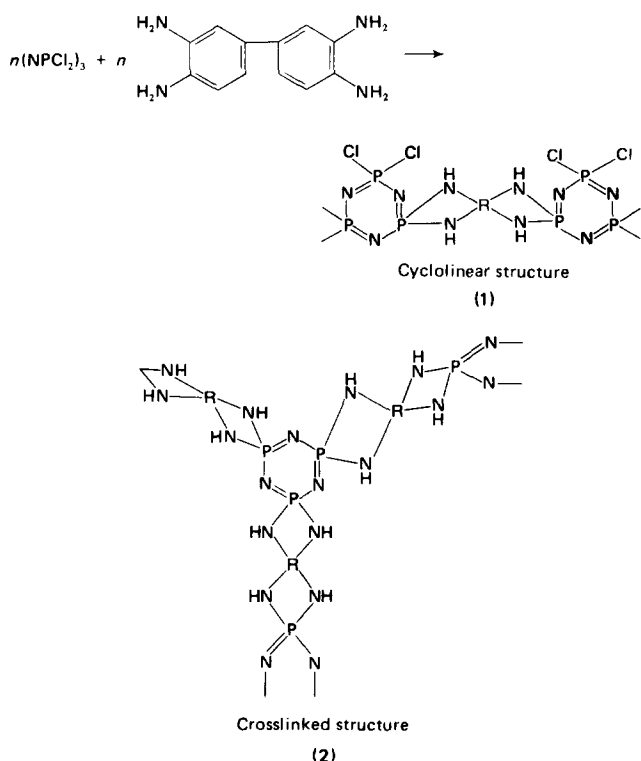
Meisetsu Kajiwara and Hajime Saito

Department of Applied Chemistry, Faculty of Engineering, Nagoya University, Nagoya, Japan  
(Received 9 December 1974)

The products of the reaction between dichlorocyclophosphazene,  $(\text{NPCl}_2)_3$ , and 3,3'-diaminobenzidine,  $(\text{H}_2\text{N})_2\text{C}_6\text{H}_3\text{C}_6\text{H}_3(\text{NH}_2)_2$ , in pyridine were shown to be amorphous, black coloured solids and slightly soluble in polar organic solvents, but insoluble in non-polar organic solvents. Measurement of the degree of swelling showed that the products were not crosslinked structures. The products were decomposed by heating at relatively low temperatures and by dilute acids and alkalis.

## INTRODUCTION

Cycloliner- and cyclomatrix-phosphazene or crosslinked polymers prepared by the polycondensation reaction between dichlorocyclophosphazene and 3,3'-diaminobenzidine were usually rigid, with high melting points, of resinous composition, and had good stability at high temperature. The polycondensation reactions (1) or (2) are assumed to occur if the reaction is carried out in pyridine.



The properties of the products are described in this paper.

## EXPERIMENTAL

Dichlorocyclophosphazene,  $(\text{NPCl}_2)_3$ , was prepared by the modified method of Saito and Kajiwara<sup>1</sup>. The pure trimer (m.p. 112°C) was obtained by repeated fractional crystallization from light petroleum ether.

Dichlorocyclophosphazene ( $10^{-2}$  mol) and 3,3'-diaminobenzidine ( $3 \times 10^{-2}$ ,  $2 \times 10^{-2}$  and  $1 \times 10^{-2}$  mol) in pyridine (200 ml) were heated under reflux for 24 h. The insoluble products removed by filtration were washed with 150 ml of dry chloroform, distilled water and were dried over  $\text{P}_2\text{O}_5$  for 24 h.

## Analytical data

The infra-red spectra were recorded on a Shimadzu Model-450 type spectrometer in the region 4000 to 200  $\text{cm}^{-1}$  using the pressed KBr disc technique.

The thermal analyses were recorded on a Shimadzu Model-20B and the thermal decomposition products formed by heating were determined by a Hitachi RMS-4 mass spectrometer. The properties of the products were measured by the methods described in previous papers<sup>2,3</sup>. The volume fraction ( $VF$ ) and the degree of volume swelling ( $DVS$ ) of the products formed by the polycondensation reaction were calculated by the following equation:

$$VF = \frac{1}{1 + (\rho_2/\rho_1)(W_a/W_b) - \rho_2/\rho_1}$$

where  $W_b$  is weight of the product,  $W_a$  is weight of the product reached at steady state in benzene solution,  $\rho_1$  is specific gravity of benzene and  $\rho_2$  is specific gravity of the product in benzene.

## RESULTS AND DISCUSSION

The properties and yield of the products are summarized in Table 1. All of the products are amorphous, black coloured

Table 1 Yield, molecular weight, volume fraction and degree of swelling of the products obtained by polycondensation reaction between dichlorocyclophosphazene and 3,3'-diaminobenzidine

Mole ratio $(\text{NPCl}_2)_3$ / diamine	Yield (g)	Molecular weight	Volume fraction	Degree of swelling
1:1	9.78	17 500	1.03	0.97
1:2	6.92	5 800	0.96	1.04
1:3	5.32	4 300	0.93	1.07



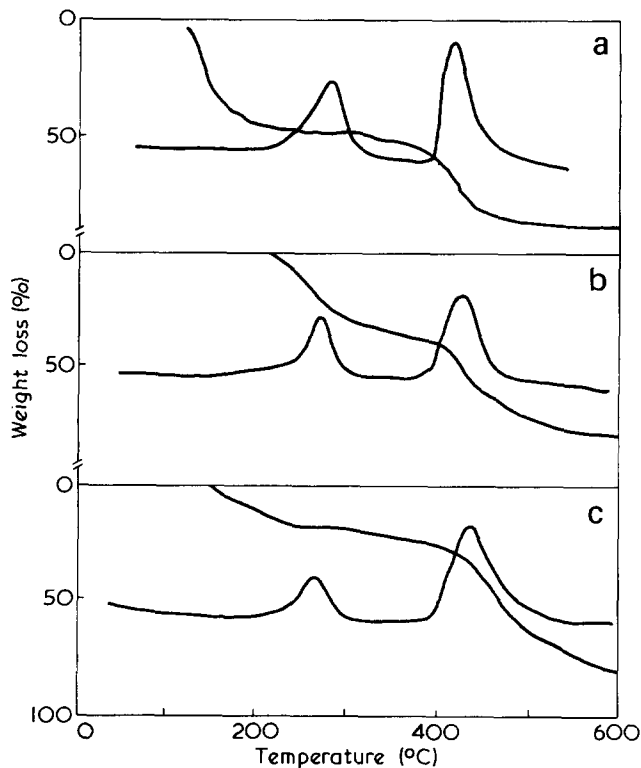


Figure 1 Thermal gravimetric and differential thermal analysis of the products formed by polycondensation reaction between dichlorocyclotriphosphazene and 3,3'-diaminobenzidine in air at heating rate of 5°C/min. (NPCl<sub>2</sub>)<sub>3</sub>/diamine: (a) 1:1; (b) 1:2; (c) 1:3

solids, slightly soluble in polar organic solvents. However, the solubility was adequate for molecular weight measurement using vapour pressure or other methods.

The i.r. spectra of the products showed a characteristic band in the region 1300 to 1100 cm<sup>-1</sup> attributable to the presence of P=N in P<sub>3</sub>N<sub>3</sub> ring. On the other hand, P-NH-R formed by the polycondensation reaction between PCl<sub>2</sub> group and -NH<sub>2</sub> group, appears in the region 1000 to 900 cm<sup>-1</sup><sup>4</sup>.

The low value of the degree of swelling (Table 1) supports the view that polycondensation occurred by reaction (1).

The softening points of the products appear to be over 300°C. Thermal decomposition temperatures as measured by differential thermal analysis and thermogravimetric analysis are shown in Figure 1. For all the products, the exothermic reaction peaks appear at 430°C and 270°C, respectively. Other properties of the products are specific gravity (25°C) 1.56 and water absorption (25°C) 22.0%.

The product is decomposed by 10% aqueous sulphuric acid, 5% and 10% aqueous sodium hydroxide and 5% and 10% aqueous nitric acid.

#### REFERENCES

- 1 Saito, H. and Kajiwara, M. *J. Chem. Soc. Japan (Ind. Chem. Sect.)* 1963, 66, 618
- 2 Kajiwara, M. and Saito, H. *J. Chem. Soc. Japan (Ind. Chem. Sect.)* 1970, 73, 1947
- 3 Kajiwara, M. and Saito, H. *J. Chem. Soc. Japan (Ind. Chem. Sect.)* 1970, 73, 1954
- 4 Pustinger, J. V., Cave, W. T. and Nielsen, M. L. *Spectrochim. Acta* 1959, p 909

# Crystallization of polyamides under elevated pressure:

## 2. Pressure-induced crystallization of nylon-6 (polycapramide) from the melt

S. Gogolewski\* and A. J. Pennings

Laboratory of Polymer Chemistry, State University of Groningen, Groningen, The Netherlands  
(Received 30 December 1974)

A study has been made on the crystallization of nylon-6 from the melt under elevated pressures. Crystallization induced by pressures of up to 8 kbar at temperatures between 270° and 310°C did not lead to a significant increase of the melting temperature for nylon-6 containing 8% caprolactam. However, the melting peak temperature, as determined by differential scanning calorimetry was found to increase from 220° to 250°C for nylon-6 without caprolactam and crystallized under pressures exceeding 5 kbar for 50 h. The heat of melting of the nylon specimen crystallized under these conditions increased from 14 to 37 cal/g. Thermal decomposition of the polymer could be diminished by heating under pressure and extruding the nylon under vacuum prior to the high pressure crystallization experiments. The specific volume diminished gradually during isothermal crystallization and the melting temperature was found to increase with crystallization time. These observations point to a one stage process for the development of extended-chain crystals of nylon-6. The highest melting peak temperature of 256°C was recorded on nylon-6 which was crystallized at 315°C and 8 kbar for a period of 320 h.

### INTRODUCTION

Pressure may have a pronounced effect on the solidification of polymers such as linear polyethylene. Extended chain crystals of polyethylene are formed if the crystallization is induced at an appropriate temperature by pressures exceeding 3 kbar as was shown by Wunderlich and Arakawa<sup>1</sup>. It was found by Rees and Bassett<sup>2</sup> that the molecules may not be fully extended after crystallization under elevated pressure but the fold length or lamellar thickness may increase with time. Additionally, Rees and Bassett provided evidence that extended chain crystals could also be produced by annealing polyethylene folded chain crystals near the melting temperature. Furthermore from differential thermal analysis as well as from dilatometry under pressure Bassett and Turner<sup>3</sup> concluded that above 3 kbar a new high-pressure phase<sup>27</sup> is formed in polyethylene and that the melting and crystallization process under these conditions occur in two stages. The effect of pressure on the crystallization of thin films of natural rubber was studied by Phillips and Andrews<sup>4</sup>. Edwards and Phillips<sup>5</sup> further developed the intensified argon high pressure system by which they were able to determine the increase of the lamellar growth rates with pressure and to observe concurrently the growth of single crystals, spherulites and oblate spheroids at different pressures applied to thin films of *cis*-polyisoprene.

So far little attention has been devoted to the effect of pressure on the crystallization of polyamides. Katayama and Yoneda<sup>6</sup> measured the crystallization kinetics and the increase in melting temperature of nylon-6 with pressure up to 2.5 kbar but they did not report any effect of pressure on the crystallinity, the structure and morphology of nylon-6. In general melt crystallized nylon-6 has a rather

low crystallinity in the order of 35% but a highly crystalline specimen may be prepared by zone-polymerization of  $\epsilon$ -caprolactam as described by Liberti and Wunderlich<sup>7</sup>. The step heights in the fracture surfaces of this sample ranged up to 6700 Å which corresponds roughly to the extended chain length.

The main objective of the present investigation was to explore the possibilities of growing extended chain crystals of nylon-6 by subjecting the melt to elevated pressures. In the case of the high pressure crystallization of nylon-6 one may expect some complication resulting from the thermal degradation which is likely to occur when the polymer is heated to high crystallization temperatures above the ceiling temperature of roughly 250°C. This thermal decomposition, which is affected by catalyst residues and water present in the polymer, may be suppressed to some extent by high pressures if the thermodynamic stability of nylon-6 is similar to that of other polymers for which it was established that the ceiling temperature increased with pressure<sup>8</sup>. That the rate of formation of monomer and possibly oligomers may form a major problem in the high pressure crystallization of nylon-6 is strongly suggested by our finding<sup>9</sup> that application of this technique only led to an increase of crystallinity and melting temperature when previously the free caprolactam was removed from the polymer. This finding is well in line with the observation by Wunderlich<sup>10</sup> that pressure did not have a significant effect on the lamellar thickness of folded chain crystals of polyethylene grown from dilute xylene solutions. In their recent publication Treiber *et al.*<sup>11</sup> reported that about 8% of xylene in polyethylene suffice to inhibit the formation of extended chain crystals under pressure.

The present paper describes in detail the effect of pressure, temperature, time, thermal treatment, and sample purification on the crystallization behaviour of nylon-6. Changes in the solid state of the polymer as a result of vary-

\* Present address: Institute of Polymers, Polish Academy of Sciences, 41-800 Zabrze, Poland.

ing the crystallization conditions were assessed by using differential scanning calorimetry.

## EXPERIMENTAL

### High pressure technique

The crystallization experiments were carried out using a simple piston-cylinder apparatus<sup>12</sup>. The thick-walled cylinder was equipped with a heating mantle of 500 W which was connected to a temperature regulator. This was monitored by a thermocouple inserted in the lower piston. The upper one was connected to a high-pressure ball-bearing so that the piston could be rotated during the crystallization experiments. By this set-up the stick-slip effect of the upper piston could be overcome<sup>13</sup>. The sealing of the cell was achieved by using small triangular shaped Teflon rings in conjunction with small anti-extrusion rings of graphitized bronze. The pressure was generated by a hydraulic press which was fitted with a Bordon gauge, a pressure regulator and a valve by which the pressure could be varied more accurately. Volume changes could be determined by measuring the displacement of the upper piston using a dial indicator that could be read to 0.001 mm. The inside diameter of the cylinder was 14 mm  $\pm$  0.001 and the polymer samples examined were approximately 1 cm in height. We did not employ a liquid as a pressure transmitting medium in these experiments.

The calibration of the Bordon gauge was performed with the aid of a Philips unbonded strain gauge. Pressure losses were assessed by measuring the pressure at which the solid-solid phase transition occurs in ammonium fluoride<sup>14</sup> (analytical reagent containing 5% H<sub>2</sub>O). This I-II transition, accompanied by a volume decrease of 24%, takes place at a pressure of 3606 bars at a temperature of 25°C. The piston displacement *versus* pressure cycles were measured up to 10 kbars and were found to be reproducible if readings of the piston height were taken after some vibration of the piston by quickly opening and closing the release valve. Nevertheless the compression and decompression curves displayed a hysteresis which may in part be due to the internal friction of the medium. In the compression stroke the I-II transition was observed at 3800 bars. The phase change was completed in 6 min. It could be interrupted by a slight variation of the pressure. The II-I transition on decompression occurred at 3440 bars and was finished in 42 min. In general pressure losses for increasing and decreasing pressure in the case of non-hydrostatic systems may not be equal. This casts some doubt on the validity of averaging the two values of the transition pressure<sup>15</sup>. Nevertheless, the difference between the two pressures is relatively small and averaging gives the correct value so that further correction for the applied pressures were omitted. This seems certainly justified in view of the fact that the volume-pressure and volume-temperature curves for the solid and the melt did not exhibit any hysteresis if volume readings were made after moving the piston three times over a small distance and the time interval between successive volume changes was not less than 10 min. This period of time might be needed for dissipation of the heat of compression or decompression and for relaxation of stress and pressure gradients<sup>23</sup>.

### Thermal analysis

For the thermal analysis of the samples a Perkin Elmer differential scanning calorimeter 1B was used which was

calibrated with benzoic acid and indium according to standard procedures. Thermograms were measured at a scan speed of 8°C/min if not stated otherwise.

### Materials

In the course of this study four nylon-6 samples were used which will be referred to as samples A, B, C, and D.

*Sample A* was unfractionated nylon-6 (received from Akzo) obtained by catalytic polymerization of caprolactam. The polymer did not contain titanium dioxide. The viscosity-average molecular weight was  $85 \times 10^3$ . The viscosity measurements were carried out on 98% sulphuric acid solutions at 25°C and the viscosity-average molecular weights were calculated from the Matthes equation<sup>16</sup>. The amount of free caprolactam in the nylon-6 was 8% by wt.

*Sample B* was prepared by dissolving sample A in concentrated formic acid to a 5% solution. Subsequently the polymer was precipitated by pouring the solution into an excess of a 50% by wt mixture of acetone and water. The precipitate was washed with water and methanol and finally with acetone before drying to a constant weight in a vacuum desiccator at room temperature. The polymer, purified by this technique, had a viscosity-average molecular weight of  $90 \times 10^3$  and did not contain caprolactam according to the infra-red analysis. Absorption bands at 11.2 and 11.5  $\mu\text{m}$  ascribed to caprolactam were absent<sup>17</sup>.

*Sample C* was obtained by the following treatment of the original nylon-6. Pellets were first extracted with hot water and acetone to remove the caprolactam. After drying the polymer was extruded under vacuum according to the technique developed by Gogolewski<sup>18</sup>. By this method residual caprolactam is removed effectively. After purification the polymer had a viscosity-average molecular weight of  $95 \times 10^3$ .

*Sample D* was prepared by polycondensation of caprolactam in the presence of water. This fibre-forming quality was free from TiO<sub>2</sub> and caprolactam. It was extracted with water in a Soxhlet, washed with alcohol and acetone and dried in a vacuum desiccator over P<sub>2</sub>O<sub>5</sub> for 24 h (Toyo Rayon Company Ltd). The viscosity-average molecular weight was  $29.8 \times 10^3$  and  $M_w/M_n = 1.48$ <sup>19</sup>.

## RESULTS

### Characterization

The effect of pressure on the crystallization of nylon-6 may be evaluated by using several techniques such as scanning and transmission electron microscopy on fracture surfaces, i.r. reflection spectroscopy, wide and small-angle X-ray diffraction and differential scanning calorimetry (d.s.c.). Although it is recognized that the application of all these methods is needed to gain a better understanding of the phase transition under pressure, in our search for the optimum conditions for producing extended chain crystals of nylon-6 it was found appropriate to rely primarily on the calorimetric technique for characterization of the samples crystallized under high pressures.

Thermograms for various nylon-6 samples crystallized under widely different conditions of pressure and temperature are shown in *Figure 1*. The melting peak temperatures of these endotherms vary from 175° to 250°C and furthermore the heat of fusion is seen to differ considerably. Thermograms were also taken at temperatures in the neighbourhood of the glass transition temperature which may appear at about 50°C if the nylon is conditioned properly<sup>20</sup>.

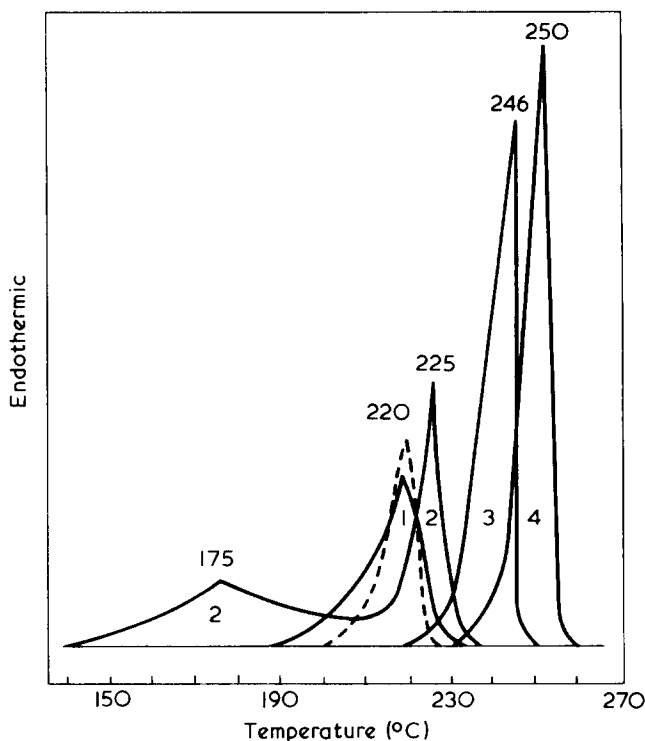


Figure 1 Melting thermograms for various nylon-6 samples. 1, endotherm for the original sample (A); ---, sample without caprolactam, both crystallized at ambient pressure. Crystallized at 295°C and 6.5 kbars for 50 h: 2, original sample (A); 3, sample B free from caprolactam; 4, sample C extruded under vacuum

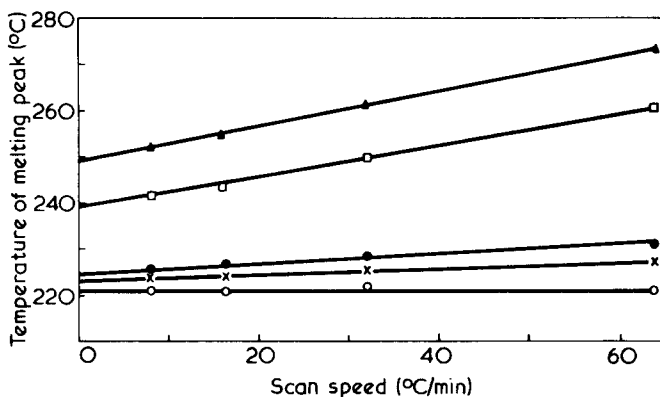


Figure 2 Effect of the scan speed on the melting peak temperature for various nylon-6 samples.  $\circ$ , Original sample (A);  $\times$ , sample B free from caprolactam;  $\bullet$ , sample C extruded under vacuum;  $\square$ , sample B crystallized at 295°C and 6.5 kbars for 50 h;  $\triangle$ , sample C crystallized at 295°C and 6.5 kbars for 50 h

The d.s.c. scans for the nylon-6 crystallized under high pressure did not exhibit any endothermic peak or change in the specific heat between room temperature and the melting range. The high pressure crystallized samples could be distinguished from those crystallized under ambient pressure in a marked difference in superheatability. Figure 2 illustrates the effect of the scan speed on the melting peak temperature. Samples crystallized at atmospheric pressure exhibit only a slight superheating whereas the melting peak temperature for the high pressure crystallized nylon-6 increases from 250°C at a scan speed of 8°C/min to 274°C at a scan speed of 64°C/min.

#### Effect of pressure on the melting temperature

In order to be able to select the appropriate crystallization conditions it was necessary to dispose of information

about the dependence of the melting temperature on pressure. For this reason the specific volume was determined as a function of temperature at various pressures. At first the nylon specimen of 2 g was compressed under a pressure of 10 kbars for 2 h. After adjustment of the pressure to the proper value, the temperature was raised in steps of 5°C. When temperature equilibrium was attained the piston was moved three times in order to reduce the pressure loss by friction and the height of the piston was measured. Each temperature step was carried out in about 25 min. A typical volume-temperature curve for sample B measured at a pressure of 5 kbars is shown in Figure 3. In general such curves did not display an abrupt beginning of the melting process but the end of melting could be determined rather accurately from the sudden change in thermal expansion ( $T_3$ ). Also the beginning of crystallization upon reversing the temperature programme could be detected ( $T_2$ ). It should be noted that the curves for the change in volume on increasing and decreasing the temperature for the polymer melt coincide. This indicates that the pressure losses due to internal stresses and interfacial friction appear to be within experimental error for the applied method. The effectiveness of the crystallization under pressure is indicated by the final volume contraction at the end of the temperature-volume cycle.

The effect of pressure on the final melting temperature ( $T_3$ ) for two melt-crystallized nylon-6 samples is illustrated in Figure 4. The increase in melting temperature with

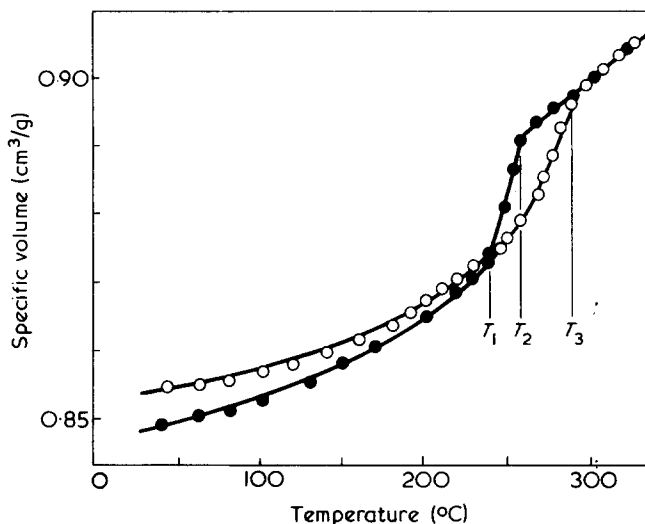


Figure 3 Dependence of the specific volume on temperature for nylon-6 (free from caprolactam) under a pressure of 5 kbars. The end of melting and the beginning and end of crystallization are indicated by  $T_3$ ,  $T_2$ , and  $T_1$  respectively.  $\circ$ , Heating run;  $\bullet$ , cooling run

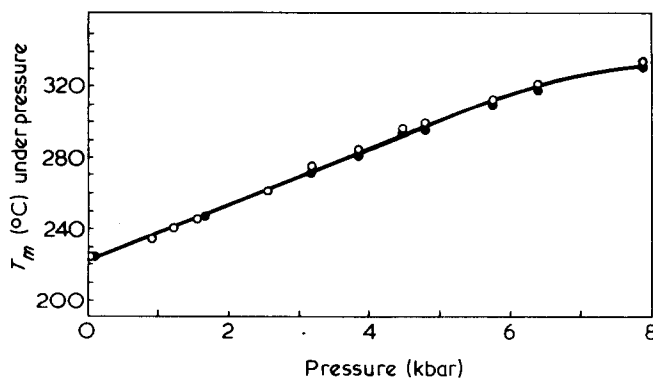


Figure 4 Dependence of the end melting temperature on the applied pressure for nylon-6.  $\circ$ , Sample C ( $\bar{M}_v = 85 \times 10^3$ );  $\bullet$ , sample D ( $\bar{M}_v = 29.8 \times 10^3$ )

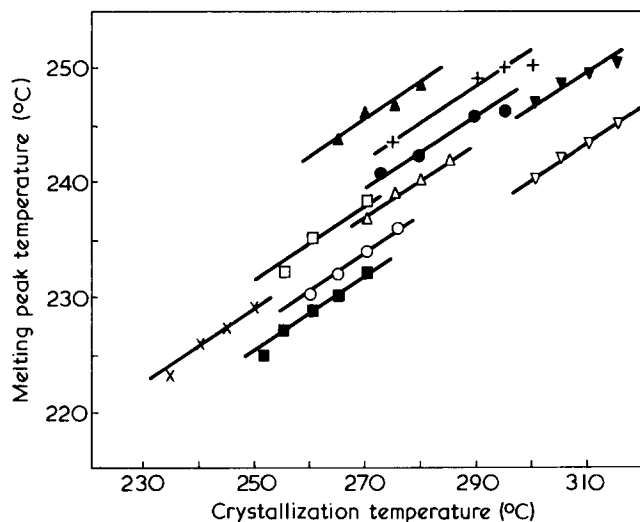


Figure 5 Dependence of the atmospheric melting peak temperature on the crystallization temperature and pressure for various nylon-6 samples. The crystallization time amounted to 50 hours. Sample B:  $\times$ , 3.2;  $\blacksquare$ , 3.9;  $\circ$ , 4.5;  $\triangle$ , 4.9;  $\bullet$ , 6.5;  $\nabla$ , 8 kbars. Sample C:  $\square$ , 4.5;  $\blacktriangle$ , 4.9;  $+$ , 6.5;  $\blacktriangledown$ , 8 kbars

pressure amounts to 16°C/kbar and appears to be the same for the high molecular weight nylon-6 (sample B) ( $M_v = 90 \times 10^3$ ) and the fibre forming quality with  $M_v = 29.8 \times 10^3$  (sample D).

#### Pressure induced crystallization of sample A

The first high pressure crystallization experiments were carried out on the original nylon-6 containing 8% by wt caprolactam. Crystallization was induced by heating the polymer to temperatures in the range of 225°C to 260°C and applying pressures ranging from 0.65 to 4.5 kbars. After 60 h the high pressure dilatometer was cooled down to room temperature and subsequently the pressure was reduced to 1 atmosphere. The d.s.c. thermograms of these samples displayed a melting peak at 225°C and a tail at lower temperatures. These thermograms should be compared with that of the original nylon-6 which only had a melting peak at 220°C (Figure 1).

Attempts were made to improve the crystalline structure of the nylon-6 by heating sample A to temperatures between 270° and 310°C and inducing crystallization by pressures between 4.9 and 8 kbars. Samples crystallized for 60 h under these conditions were found to be rather sticky, smelled of ammonia and the d.s.c. traces showed a melting peak at 215°C and a long low temperature tail originating from crosslinking and from the low molecular weight polymer that was formed by thermal degradation<sup>21</sup>.

#### Pressure induced crystallization of sample B

Thermal stability of the nylon-6 may be improved by removal of the catalyst residues<sup>21</sup> and for this reason the polymer was dissolved in formic acid and recovered by pouring the solution into an excess of acetone water mixture. By this method of purification also the caprolactam is removed and thermal stability may have improved additionally as a result of blocking the amine end-groups by reaction with formic acid. This nylon, referred to as sample B, was first compressed at room temperature by applying 8 kbars for 30 min. After releasing the pressure to 1 bar the sample was heated up to 290°C and crystallization was initiated by applying 6.5 kbars. It should be mentioned that for melting of the nylon at 290°C, a period of 15 min was required to obtain samples that appeared to be homo-

geneous. If heating at this temperature was carried out for a shorter period the core of the specimen remained powder-like. Crystallization under these conditions for 48 h resulted in a marked shift in the melting peak temperature from 220° to 235°C. This increase in melting temperature seems to be caused by the isothermal crystallization at 290°C since a variation in the cooling rate between 10°C/h and 100°C/h did not affect the melting behaviour.

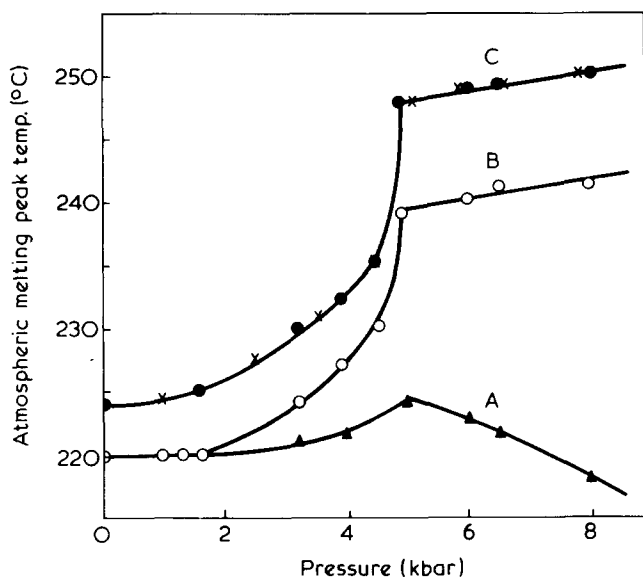
In this exploratory stage of this investigation several treatments of the nylon-6 were tried out for improving the crystalline order during high pressure crystallization. For instance, nylon-6 specimens were annealed in order to bring about complete conversion from the  $\gamma$ - to the more stable  $\alpha$ -crystalline modification<sup>20</sup>. If sample B was aged at 100°C and 8 kbars for 15 h, prior to the high pressure crystallization according to the method described above, a d.s.c. melting peak temperature of 240°C was found. Thus the annealing step resulted in an additional increase of 5°C in melting temperature. Infra-red analysis of this sample revealed that a small amount of caprolactam was formed in the course of this crystallization experiment. Since the removal of caprolactam from nylon-6 had such a pronounced effect on the crystallization under pressure it was considered to be pertinent to avoid all experimental conditions that may favour the formation of monomer and other compounds. Therefore the nylon-6 was heated to the crystallization temperature of 290°C under a pressure of 6.5 kbars. Subsequently the pressure was reduced to 100 bars for 15 min to melt the polymer and crystallization was set in by enhancing the pressure to 6.5 kbars. Applying this alternative method to sample B gave rise to a melting temperature at ambient pressure of 246°C another gain of 6°C due to heating under pressure.

It seems justified to conclude from these experiments that it is of basic importance for the high pressure crystallization of nylon-6 to avoid any thermal depolymerization and degradation. It was found that the thermal decomposition was negligible if the samples were melted for 15 min at temperatures up to 315°C (under pressure).

The next step in this research was to find the optimum crystallization conditions as regards pressure and temperature. At first the crystallization temperature was varied while the other steps of the procedure remained unchanged. As is illustrated in Figure 5 the melting peak temperature measured at atmospheric pressure increased with the crystallization temperature. For a pressure of 6.5 kbars and crystallization temperatures of 273°C and 290°C melting temperatures were found of 240°C and 246°C respectively. Such experiments were also carried out at different pressures. This allows crystallizing the polymer in different temperature ranges under similar degrees of supercooling. At low pressures up to 3.9 kbars an increase in crystallization temperature range of 20°C appears to have only little effect on the crystallization process as judged from the d.s.c. thermograms. The same holds for crystallization temperatures of about 280° and 310°C and pressures of 6.5 and 8 kbars, respectively, although the level of the melting peak temperatures of these nylon-6 crystals is substantially higher than that of samples crystallized at lower pressures.

#### Sample C

Similar experiments were performed on sample C which was obtained by extruding the original nylon-6 under vacuum. Characteristic of this sample was that it did not contain caprolactam and since it was extruded in a glass pipe



**Figure 6** Dependence of the atmospheric melting peak temperature on the applied crystallization pressure for various nylon samples. The crystallization temperature was  $40^{\circ}\text{C}$  below the end melting temperature for all specimens. Crystallization time was 50 h.  $\blacktriangle$ , Sample A containing 8% caprolactam;  $\circ$ , sample B free from caprolactam;  $\bullet$ , sample C free from caprolactam and extruded under vacuum;  $\times$ , sample C with additional ageing at  $100^{\circ}\text{C}$  for 15 h prior to crystallization

with an inside diameter equal to that of the high pressure dilatometer, sample C contained considerably less voids and trapped air at the beginning of the high pressure experiments than samples A and B. Some of the data for sample C are compiled in *Figure 5* which illustrates that by applying the same crystallization procedure the atmospheric melting peak temperature is about  $5^{\circ}\text{C}$  higher than that for sample B crystallized under corresponding conditions.

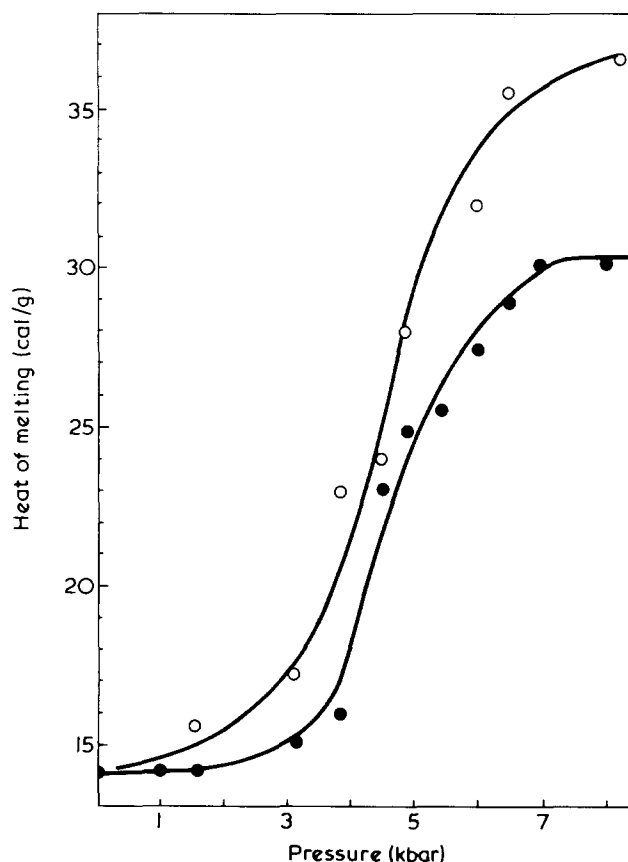
A comparison of the effect of pressure on the melting temperature of the three nylon-6 samples A, B, and C is made in *Figure 6*. All data points in this graph were obtained by crystallizing the samples for 50 h and at the same degree of supercooling of  $40^{\circ}\text{C}$ , viz., the crystallization temperature was  $40^{\circ}\text{C}$  below the end melting temperature of the folded chain crystals under the corresponding pressure. *Figure 6* clearly illustrates that the pressure induced crystallization had little effect on sample A and raised the melting temperature of sample C and B about  $25^{\circ}\text{C}$ . The difference in melting temperature of  $5^{\circ}\text{C}$  between sample C and B was already found for crystallization from the melt at ambient pressure. At 8 kbars the difference amounts to  $8^{\circ}\text{C}$ . A further distinction between these two nylon-6 specimens is that annealing of the extruded sample at  $100^{\circ}\text{C}$  under 8 kbars for 15 h had no measurable effect on the high pressure crystallization. The data points for the annealed and unannealed sample C lie on the same curve demonstrating the reproducibility of the measurements. The most conspicuous observation is that up to 2 kbars there is hardly any effect of pressure noticeable but the most pronounced influence of pressure occurs between 3 and 5 kbars. Especially for sample C a strong increase in melting peak temperatures is observed for crystallization pressures close to 5 kbars. For pressures exceeding 5 kbars there is a decrease in melting temperatures for sample A whereas for samples B and C there is still a slight increase. It was verified whether thermal degradation had occurred during the crystallization at these pressures beyond 5 kbars

but i.r. analysis and viscosity measurement could not detect any change in molecular structure. In conclusion, 5 kbars seems to be the most effective pressure to induce crystallization in nylon-6 for crystallization times of  $\sim 50$  h.

Another thermal quantity that reflects the degree of order of the nylon-6 samples is the heat of fusion. The curve in *Figure 7* represents the dependence of the heat of fusion as measured in d.s.c. on the crystallization pressure, and a comparison is made between sample C and B for the 50 h crystallization experiments. Again sample C has the highest values for the heat of fusion which varies from 15 to 37 cal/g for crystallization under 8 kbars. A marked increase in this heat of melting occurs around 5 kbars.

#### Crystallization time

The preceding sections have been concerned with experiments in which the isothermal crystallization was extended over periods of 48 or 50 h. These crystallization times were rather arbitrary and it was considered pertinent to investigate the influence of time on the solidification process under pressure. *Figure 8* shows that there is a rather strong dependence of the crystallization time on the crystalline state as reflected by the d.s.c. melting peak temperature. The rise in the melting temperature is most pronounced up to a crystallization time of 80 h and appears to depend on pressure and crystallization temperature. There is a trend that at lower pressures the melting temperature continues to increase over a longer period than at higher crystallization pressures. These data suggest again that the crystallization process proceeds more rapidly at the higher temperatures and pressures. For instance at a crystallization temperature of  $295^{\circ}\text{C}$  and a pressure of 6.5 kbar the



**Figure 7** Dependence of the heat of melting on the crystallization pressure. The crystallization time was 50 h and the temperature  $40^{\circ}\text{C}$  below the end melting temperature.  $\circ$ , Sample C;  $\bullet$ , sample B

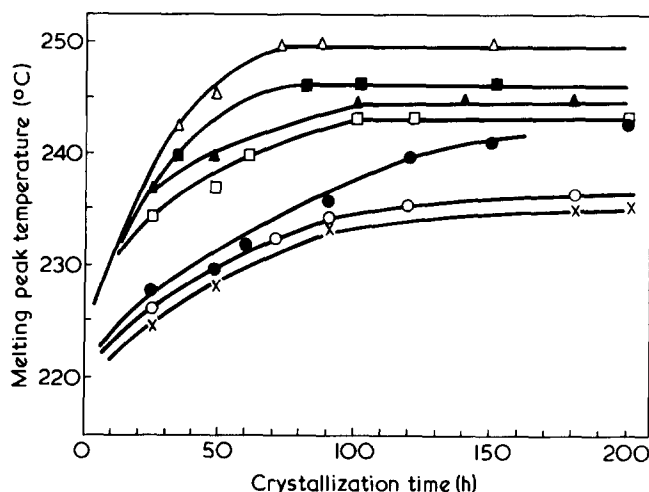


Figure 8 Dependence of the atmospheric melting peak temperature on the crystallization time. Sample B: x, 245°C and 3.2 kbars; o, 260°C and 3.9 kbars; ●, 265°C and 4.5 kbars; □, 270°C and 4.9 kbars; ■, 295°C and 6.5 kbars. Sample C: ▲, 270°C and 4.9 kbars; △, 295°C and 6.5 kbars

maximum melting temperature of 246°C for sample B was reached after 50 h but at 245°C and 3.2 kbars the melting temperature still increased after 200 h. It should be mentioned that although the melting temperature appeared to be constant after a certain period the crystallization process seemed to continue for considerably longer times as disclosed by the piston displacement that was recorded during crystallization (Figure 9). In separate experiments at this temperature of 295°C and 6.5 kbars the crystallization was interrupted at various crystallization times and the nylon-6 samples were analysed by differential scanning calorimetry. These thermograms are inserted in Figure 9 at the corresponding crystallization time. They show a considerable narrowing of the melting peak as the crystallization proceeds and there seems to be no two peak melting processes as might be expected if folded chain crystals would transfer abruptly into extended chain crystals.

The results described above clearly indicate that also the crystallization time is an important variable and extension to longer times may lead to a more perfect crystalline state. The ultimate conditions for pressure induced crystallization were tried out at 315°C and 8 kbars for a period of 320 h. The ultimate melting temperature of sample B, crystallized under these circumstances, turned out to be 246°C which is the same value as was obtained by crystallization under less extreme circumstances. According to the i.r. analysis some caprolactam was formed. However, sample C appeared to be able to withstand these severe conditions better and no decomposition could be detected after such a crystallization experiment. The melting peak temperature of this nylon-6 specimen was 256°C.

## DISCUSSION

The experimental observations described above clearly demonstrate that pressure has a marked effect on the crystallization process of nylon-6 if the polymer has been purified prior to the crystallization experiment. Removal of the free caprolactam either by dissolving the polymer or by the extrusion under vacuum does not lead to the same increase of the melting temperature and the heat of fusion of the high pressure crystallized nylon-6. The difference in crystallization behaviour between the nylons purified by these two methods is to be attributed to a difference in

void content. Compression of the nylon powder, obtained by the precipitation method, even at 10 kbars and 100°C did not yield a material with homogeneous appearance when examined under the microscope. The presence of voids, remaining as a result of internal friction, and possibly of trapped air, apparently enhanced the rate of thermal degradation. The nylon, that was extruded under vacuum, turned out to be more resistant to be exposed for longer times to high temperatures which resulted in a more perfect solid state. It seems to be the amount of the caprolactam rather than for instance a variation in the water content that interferes with the development of a highly crystalline nylon. The effect of the water content has not been investigated systematically but variation in exposure time to the humidity in the laboratory and keeping specimen in a vacuum desiccator over P<sub>2</sub>O<sub>5</sub> did not give rise to any discernable difference in high pressure crystallization behaviour<sup>24</sup>.

The basic question that may be raised is therefore why caprolactam inhibits the chain extension during the high pressure crystallization. This may essentially be the same phenomenon as the suppression of chain extension in polyethylene by the presence of xylene. In the case of polyethylene the formation of extended chain crystals occurs through the intermediate phase as concluded by Bassett *et al.*<sup>25</sup>. For nylon-6 we did not notice any plateau in the volume-temperature curve and the gradual decrease in volume upon isothermal crystallization also did not show any interruption indicative of a two-stage process. The crystallization mechanism of polyethylene may differ substantially from that of nylon in which the breakage and formation of hydrogen bonds plays such a prevailing role. Hydrogen bond formation was also the rate determining step in the formation of folds during annealing of oriented nylon-6. If indeed the lower melting temperatures and heat of fusions need be ascribed to the presence of folds then one may say that the caprolactam molecules stabilize the folds and that thereby the effect of pressure on the crystallization has been diminished. Another difference between polyethylene and nylon-6 is that a pressure of 5 kbars seems to be most effect for the latter while for the former polymer chain extension occurs already at 3 kbars.

Finally, some remark should be made about the melting temperature. The value of 256°C, found for the extruded

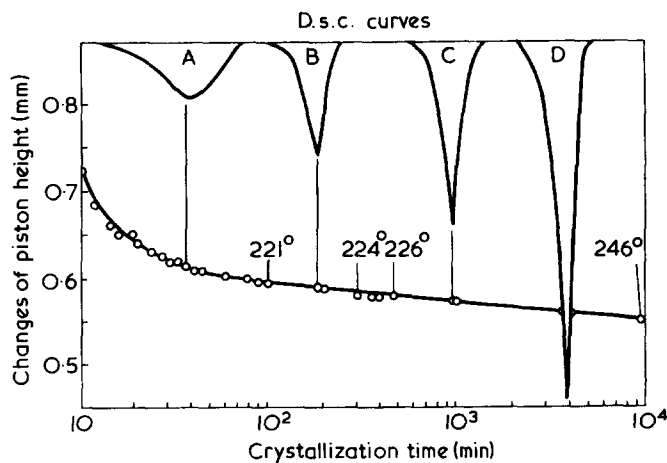


Figure 9 Change of piston height versus the crystallization time for sample B at 295°C and 6.5 kbars as well as thermograms and melting peak temperatures of the nylon-6 at various crystallization times. A,  $T_m = 220^\circ$ ,  $\Delta H_m = 12.3$ ; B,  $T_m = 223^\circ$ ,  $\Delta H_m = 22.1$ ; C,  $T_m = 230^\circ$ ,  $\Delta H_m = 26.7$ ; D,  $T_m = 246^\circ$ ,  $\Delta H_m = 36.5$  cal/g

nylon crystallized at 315°C and 8 kbars, exceeds substantially the melting point of an equilibrium crystal which is reported<sup>7</sup> to be 232°C. On the other hand, Arakawa and Nagastoshi<sup>26</sup> estimated that the melting point of nylon-6 might be at least 270°C or even 306°C. It is our impression that values higher than 256°C may be achievable if extreme measures are taken to remove caprolactam and conditions for improvement of the solid state are adopted that avoid any formation of the monomer.

## REFERENCES

- 1 Wunderlich, B. and Arakawa, T. *J. Polym. Sci. (A)* 1964, **2**, 3697; Geil, P. H., Anderson, F. R., Wunderlich, B. and Arakawa, T. *J. Polym. Sci. (A)* 1964, **2**, 3707
- 2 Rees, D. V. and Bassett, D. C. *Nature* 1968, **219**, 368; *J. Polym. Sci. (A-2)* 1971, **9**, 385
- 3 Bassett, D. C. and Turner, B. *Nature* 1972, **240**, 146
- 4 Phillips, P. J. and Andrews, E. H. *J. Polym. Sci. (B)* 1972, **10**, 321
- 5 Edwards, B. C. and Phillips, P. J. *Polymer* 1974, **15**, 491
- 6 Katayama, Y. and Yoneda, K. *Rev. Com. Lab.* 1972, **20**, 921
- 7 Liberti, F. N. and Wunderlich, B. *J. Polym. Sci. (A-2)* 1968, **6**, 833
- 8 Ivin, K. J. *IUPAC Symp. Macromol. Chem. Montreal 1961* 1962, p 273
- 9 Gogolewski, S. and Pennings, A. J. *Polymer* 1973, **24**, 463
- 10 Wunderlich, B. *J. Polym. Sci. (A)* 1963, **1**, 1245
- 11 Treiber, G., Melillo, L. and Wunderlich, B. *J. Polym. Sci. (B)* 1973, **1**, 435
- 12 Pennings, A. J. and Pijpers, M. F. J. to be published
- 13 Bridgeman, P. W. 'The Physics of High Pressures', Bell, London, 1949
- 14 Kaneda, R., Yamamoto, S. and Nishibata, K. in 'Accurate Characterization of the High-Pressure Environment', (Ed. E. C. Lloyd) NBS, Washington, D.C., 1971, p 257
- 15 Tamayama, M. and Eyring, H. *Rev. Sci. Instrum.* 1967, **38**, 1009
- 16 Matthes, A. *J. Prakt. Chem.* 1943, **162**, 245; *Makromol. Chem.* 1950, **5**, 165
- 17 Haslam, J. and Willis, H. A. 'Identification and analysis of plastics', Iliffe, London, 1965, pp 125-128
- 18 Gogolewski, S. *Polimery* 1971, **16**, 130
- 19 Turska, E. and Gogolewski, S. *Polymer* 1971, **12**, 616
- 20 Northolt, M. G., Tabor, B. J. and van Aartsen, J. J. *Kolloid-Z. Z. Polym.* to be published
- 21 Boer, E., Kohn, R. and Papir, Y. S. *J. Macromol. Sci. (B)* 1972, **6**, 761
- 22 Kroes, G. H. *PhD Thesis Delft* (1963)
- 23 Piermarini, G. J., Block, S. and Barnett, J. D. *J. Appl. Phys.* 1973, **44**, 5377
- 24 Rybnikar, F. *Chem. Prum.* 1961, **11**, 217
- 25 Bassett, D. C. and Turner, B. *Phil. Mag.* 1974, **29**, 285
- 26 Arakawa, T. and Nagatoshi, F. *J. Polym. Sci. (B)* 1970, **8**, 41
- 27 Bassett, D. C., Block, S. and Piermarini, G. J. *J. Appl. Phys.* 1974, **45**, 4146



# Effect of molecular weight on crystallization isotherms of high molecular weight poly(ethylene oxide) fractions

J. Q. G. Maclaine and C. Booth

Department of Chemistry, University of Manchester, Manchester M13 9PL, UK

(Received 8 January 1975)

Dilatometric crystallization isotherms have been determined for a set of poly(ethylene oxide) fractions ranging in molecular weight from  $2 \times 10^4$  to  $1.6 \times 10^6$ . For a given fraction the isotherms obtained for different crystallization temperatures can be superimposed over most of the crystallization. For a given crystallization temperature the degree of crystallinity obtained in the primary stage of the crystallization varies greatly with molecular weight, and superimposition of the isotherms is not possible. Secondary crystallization processes are pronounced when the molecular weight ( $\bar{M}_v$ ) exceeds  $10^5$ .

## INTRODUCTION

In a recent paper<sup>1</sup> we have reported the molecular weight dependence of spherulite growth rate for a set of poly(ethylene oxide) fractions with molecular weights in the range  $10^4$  to  $10^6$  (g/mol). The molecular weight dependence of other features of the crystallization process are of interest. The bulk crystallization rate and the final extent of crystallinity are accessible, in principle at least, via dilatometric determination of the crystallization isotherm<sup>2,3</sup>. Most work, in this area, on poly(ethylene oxide) fractions has been with molecular weights less than  $20\,000^{4-8}$  or with one or two high molecular weight fractions only<sup>6,8,9</sup>. In this paper we present dilatometric data for seven poly(ethylene oxide) fractions covering the molecular weight range ( $\bar{M}_v$ ) 23 000 to 1 600 000.

## EXPERIMENTAL

### Preparation and characterization of fractions

The preparation and characterization of fractions has been described earlier<sup>1</sup>. The fractions used in the dilatometric work are listed in Table 1, together with their intrinsic viscosities (benzene at 25°C), viscosity-average molecular weights<sup>10</sup>, and molecular weight ratios ( $\bar{M}_w/\bar{M}_n$ , g.p.c.). [Shear corrections were not applied to the intrinsic viscosity of fraction N1600000, so the molecular weight of this fraction will be too low by a few per cent.] The prefixes used in denoting the fractions refer to their sources: H to Hoechst Chemicals; R to our own preparation; W to Polyox

Table 1 Characteristics of poly(ethylene oxide) fractions

Fraction	$[\eta]$ in benzene at 25°C (cm <sup>3</sup> /g)	$\bar{M}_v$	$\bar{M}_w/\bar{M}_n$ (g.p.c.)
H23000	37	23 000	1.20
R42000	59	42 000	1.30
W84000	95	84 000	1.21
N130000	125	126 000	1.35
W240000	194	244 000	1.22
W540000	339	538 000	1.53
N1600000	707	1 570 000	1.85

WSR-35 and N to Polyox N-750, both supplied by Union Carbide Ltd.

### Dilatometry

The dilatometers were constructed of glass, being L-shaped with a horizontal tube (4–6 mm i.d., volume 1 to 2 cm<sup>3</sup>) part-filled with polymer and with a vertical capillary (0.5 mm i.d. Veridia tubing). A known weight of polymer (100–200 mg) was moulded in high vacuum, sealed into the dilatometer, outgassed and confined with mercury. In a crystallization experiment the dilatometer was usually placed in boiling water for 10 min and then transferred to a stirred oil bath held (to  $\pm 0.05K$ ) at the required crystallization temperature,  $T_c$ . The temperature of the dilatometer fell almost to  $T_c$  within 0.5 min and reached  $T_c$  within 2 min. The height of mercury in the capillary was followed by means of a cathetometer (to  $\pm 0.004$  cm). The total contraction owing to crystallization was usually in the range 3 to 8 cm. The time of transfer was taken as the starting time for the crystallization, and the height of mercury in the capillary 2 min from transfer was taken as the starting height. Our technique was suitable for determination of crystallization isotherms with half-lives as low as 10 min.

In order to assess the possible loss of polymer during its incorporation into the dilatometer, certain dilatometers were opened after measurements were completed and the polymer was recovered. These experiments show that the weight of polymer is known to within 2%. The largest error in determining the crystallization isotherms is in determining the initial height of the mercury in the capillary. We estimate an overall precision of  $\pm 3\%$  for our estimates of the extent of crystallinity.

## RESULTS AND DISCUSSION

Observations with the polarizing microscope of thin films of these fractions have been reported earlier<sup>1</sup>. Results pertinent to this work are as follows: (i) spherulites were initiated sporadically with time over the initial part of the crystallization; (ii) for given crystallization conditions the spherulite number density,  $\nu$ , varied from fraction to fraction. Fraction W84000 had an abnormally low value of

$\nu$ ; (iii) spherulite radii increased linearly with time up to the point of impingement. Impinged spherulites eventually filled the field of view; (iv) the spherulites had a close-textured appearance which did not differ from fraction to fraction.

We have also used low-angle X-ray scattering (the method has been described earlier<sup>11</sup>) to check that the essential structure of the crystalline state, i.e. a stacked crystalline lamella system, was unchanged across the range of molecular weights studied. Lamella spacings ( $T_c = 55.7^\circ\text{C}$ ) ranged from 23 nm (H23000) to about 30 nm (N1600000).

Volume contractions were usually measured for fractions melted at  $100^\circ\text{C}$  for 10 min. Certain crystallizations were studied after melting at  $80^\circ\text{C}$  for 10 min. The crystallizations were faster under these conditions, in keeping with the higher spherulite number densities observed<sup>1,6</sup> at lower melting temperatures. Otherwise the crystallization isotherms were identical with those obtained normally. The results given below all pertain to melting at  $100^\circ\text{C}$  for 10 min.

**Crystallization isotherms,  $X_v(t)$**

The weight fraction of polymer in the crystalline state at crystallization temperature  $T_c$  and at time  $t$  can be defined by:

$$X_v(t) = \frac{V(t) - V_l^0}{V_c^0 - V_l^0} \quad (1)$$

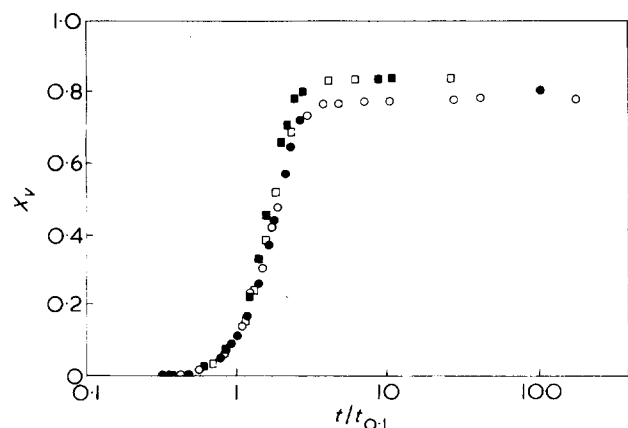


Figure 1 Superimposed crystallization isotherms of poly(ethylene oxide) fraction H23000 for crystallization temperatures of:  $\circ$ ,  $54.7^\circ$ ;  $\bullet$ ,  $55.6^\circ$ ;  $\square$ ,  $57.0^\circ$ ;  $\blacksquare$ ,  $58.1^\circ\text{C}$

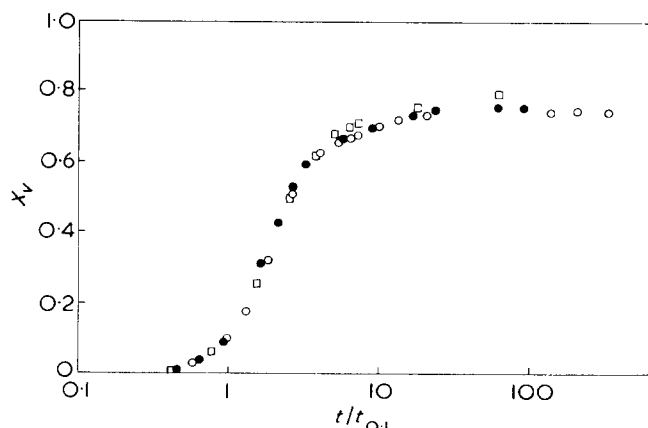


Figure 2 Superimposed crystallization isotherms of poly(ethylene oxide) fraction N130000 for crystallization temperatures of:  $\circ$ ,  $57.0^\circ$ ;  $\bullet$ ,  $58.1^\circ$ ;  $\square$ ,  $59.4^\circ\text{C}$

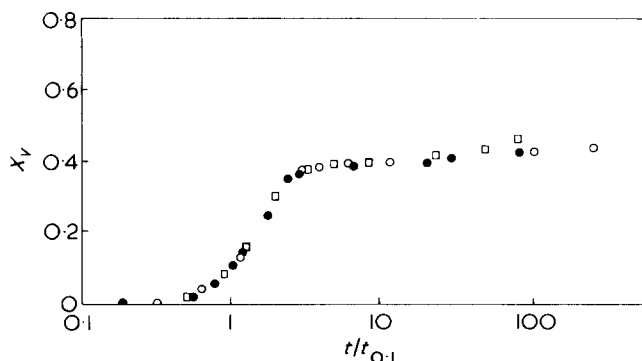


Figure 3 Superimposed crystallization isotherms of poly(ethylene oxide) fraction N1600000 for crystallization temperatures of:  $\circ$ ,  $57.0^\circ$ ;  $\bullet$ ,  $58.1^\circ$ ;  $\square$ ,  $59.4^\circ\text{C}$

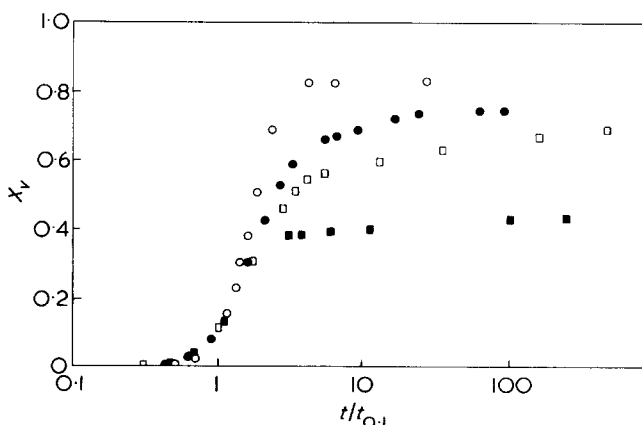


Figure 4 Superimposed crystallization isotherms at crystallization temperature  $57.0^\circ\text{C}$  for poly(ethylene oxide) fractions:  $\circ$ , H23000;  $\bullet$ , N130000;  $\square$ , W540000;  $\blacksquare$ , N1600000

where  $V_l^0$  and  $V_c^0$  represent the specific volumes of liquid and crystalline polymer at temperature  $T_c$ , and  $V(t)$  represents the specific volume of the system at temperature  $T_c$  and time  $t$ . Values for  $V_l^0$  and  $V_c^0$  can be determined, for a given  $T_c$ , from known values of the specific volumes of molten polymer (from pycnometric measurements) and crystalline polymer (via unit cell dimensions from wide-angle X-ray measurements) together with appropriate coefficients of expansion ( $\alpha_l^0, \alpha_c^0$ : from dilatometric measurements). For poly(ethylene oxide) we use the following data:

$$\text{Liquid: } V_l^0(25^\circ\text{C, cm}^3/\text{g}) = 0.891^{12}, \alpha_l^0(\text{cm}^3 \text{ g}^{-1} \text{ K}^{-1}) = 0.00069^{12,13}$$

$$\text{Crystal: } V_c^0(25^\circ\text{C, cm}^3/\text{g}) = 0.813^{14}, \alpha_c^0(\text{cm}^3 \text{ g}^{-1} \text{ K}^{-1}) = 0.00015^{12}$$

Evaluated in this way the crystallization isotherm  $X_v(t)$  represents the absolute degree of crystallinity of the polymer (as assessed by dilatometry).

Crystallization isotherms (semilogarithmic plots of  $X_v$  against  $t$ ) are illustrated in Figures 1 to 5. These isotherms are all superimposed at the point  $X_v(t) = 0.1$ : crystallization times to  $X_v(t) = 0.1$  ( $t_{0.1}$ ) are listed in Table 2. For a given fraction the isotherms obtained for different crystallization temperatures can be superimposed over most of the crystallization. This is illustrated in Figures 1 to 3 for fractions H23000, N130000 and N1600000. Over the range of

fractions we have studied the superimposition of isotherms improves as the molecular weight increases (compare Figures 1 and 3). This is because the degree of crystallinity achieved in the primary stage of crystallization is less influenced by  $T_c$  when the molecular weight of the fraction is high.

For a given crystallization temperature the isotherms  $X_v(t)$  obtained for different fractions cannot be superimposed (Figures 4 and 5) except for the two fractions of lowest molecular weight (Figure 6). It is possible that the nature of the spherulite initiation process varies somewhat within the range of molecular weights we have investigated<sup>6</sup>. Most obviously, however, it is clear that the degree of crystallinity achieved in the primary stage of the crystallization varies markedly with  $\bar{M}_v$ , when  $\bar{M}_v > 50\,000$  (see Table 3). It is also apparent that the isotherms of the higher molecular weight fractions are affected by a slow secondary process.

We know, from observations with the polarizing microscope, that the termination of the space filling process (i.e. the point at which the spherulites completely fill space) is at or about the end of the fast part of the crystallization process (as judged by the crystallization isotherm). For the lower molecular weight fractions (H23000, R42000) this is at or about the end of the crystallization process. For the higher molecular weight fractions ( $\bar{M}_v \geq 84\,000$ )  $X_v$  increases slowly with time long after the space filling process is complete. Such a slow volume contraction is usually<sup>3</sup> called a secondary crystallization process, to distinguish it from the primary (space filling) process. Further observations on the secondary process in the crystallization of our highest molecular weight fraction (N1600000) are reported in the Appendix to this paper.

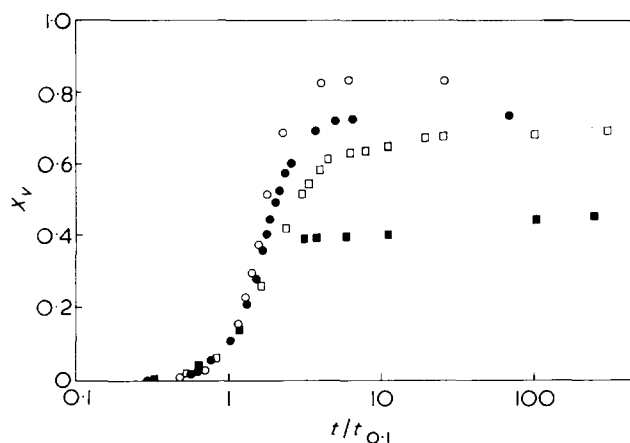


Figure 5 Superimposed crystallization isotherms at crystallization temperature 57.0°C for poly(ethylene oxide) fractions: ○, H23000; ●, W84000; □, W240000; ■, N1600000

Table 2 Crystallization times ( $t_{0.1}$ , min) for poly(ethylene oxide) fractions

Fraction	$T_c$ (°C)				
	54.7	55.6	57.0	58.1	59.4
H23000	7.2	13	44	120	—
R42000	—	—	16	49	270
W84000	16	24	60	—	—
N130000	—	—	7.7	20	77
W240000	—	—	13	23	—
W540000	—	—	8.7	11	—
N1600000	—	—	9.3	16	56

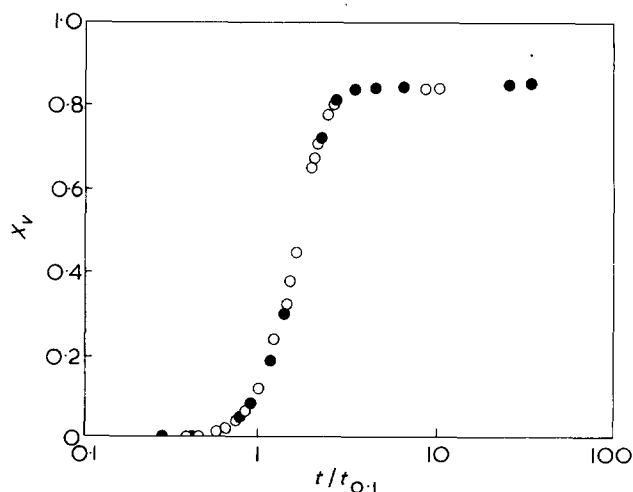


Figure 6 Superimposed crystallization isotherms at crystallization temperature 58.1°C for poly(ethylene oxide) fractions H23000 (○) and R42000 (●)

Table 3  $X(t')$ \* for poly(ethylene oxide) fractions

Fractions	$T_c$ (°C)				
	54.7	55.6	57.0	58.1	59.4
H23000	0.77	0.80	0.83	0.83	—
R42000	—	—	0.86	0.83	0.87
W84000	0.67	—	0.72	—	—
N130000	—	—	0.72	0.74	0.78
W240000	—	—	0.66	0.67	—
W540000	—	—	0.65	0.67	—
N1600000	—	—	0.43	0.43	0.44

\*  $t' = 100t_{0.1}$

In view of the secondary process, and the limited time scale of our experiments, it is not possible to identify the ultimate degree of crystallinity for most of the fractions. Here we compare  $X_v(t)$  evaluated at a comparable stage of each crystallization by taking as the point of comparison a time  $t' = 100t_{0.1}$ . Values of  $X_v(t')$ , obtained by extrapolation or interpolation of the isotherms, are listed in Table 3. Only for fractions H23000 and H42000 do the values of  $X_v(t')$  coincide with the ultimate extents of crystallinity<sup>15</sup>: for the highest fractions the ultimate crystallinity may greatly exceed the values we quote (see Figure 4 and Appendix). For a given fraction  $X_v(t')$  is increased slightly as  $T_c$  is increased. For a given  $T_c$ ,  $X_v(t')$  is decreased markedly as  $\bar{M}_v$  is increased beyond 50 000. The variation of  $X_v(t')$  at 57°C with  $\bar{M}_v$  is illustrated in Figure 7. Other data<sup>12</sup> for a fraction of  $\bar{M}_v \sim 11\,000$  are included in Figure 7. Fractions with  $\bar{M}_v$  in the range 6000–4000, when crystallized at 57°C, form extended chain crystals<sup>11,16</sup> and have low crystallinities (at 57°C) due to fractionation.

#### Crystallization rates

The time ( $t_{0.1}$ ) to attain a degree of crystallinity  $X_v = 0.1$  is a measure of the overall crystallization rate which can be sensibly compared for different fractions because the isotherms  $X_v(t)$  are roughly superimposable before  $t_{0.1}$  (Figures 4 and 5). Reciprocal tenth-lives, taken from Table 2, are plotted against  $\bar{M}_v$  (double logarithmic plot) in Figure 8. Data for fraction W84000 are omitted from this plot in view of the anomalously low spherulite number density observed for this sample. The overall crystallization rate ( $1/t_{0.1}$ ) measured at constant  $T_c$  is increased

as  $\bar{M}_v$  is increased, and perhaps attains a maximum near  $\bar{M}_v = 8 \times 10^5$ . Bearing in mind that the spherulite number density in the fractions is observed<sup>1</sup> to increase as  $\bar{M}_v$  is increased, these results are consistent with the molecular weight dependence of the spherulite growth rates,  $G_s$  presented elsewhere<sup>1</sup>, i.e. a maximum in  $G_s$  versus  $\bar{M}_v$  at or about  $\bar{M}_v = 2 \times 10^5$ .

The temperature dependence of  $t_{0.1}$  leads, via the usual assumptions<sup>1</sup>, to values of end interfacial free energy  $\sigma_e$  for the higher molecular weight fractions ( $\bar{M}_v > 10^5$ ) of 5 to 6 kJ/mol of chains emerging. This is in good agreement with the value of  $\sigma_e$  obtained<sup>1</sup> from the temperature dependence of the spherulite growth rates of the higher molecular weight fractions, i.e.  $\sigma_e \sim 5.5$  kJ/mol. This correspondence between the temperature dependence of spherulite growth rate and of overall crystallization rate (provided that elementary precautions are taken with regard to melting and crystallization procedures) has been noted earlier<sup>17</sup>

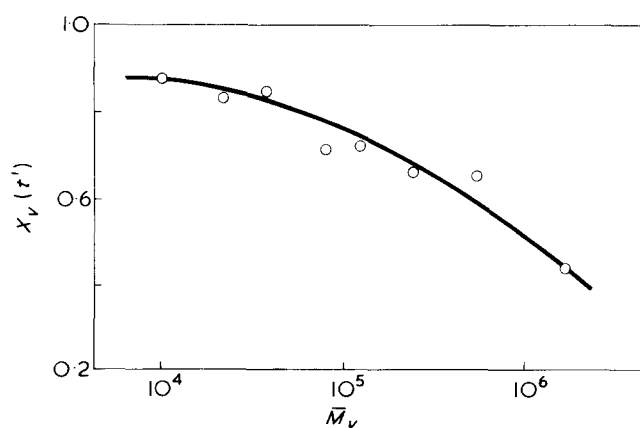


Figure 7 Weight fraction crystallinity at  $t' = 100t_{0.1}$  versus viscosity-average molecular weight for poly(ethylene oxide) fractions crystallized at 57.0°C

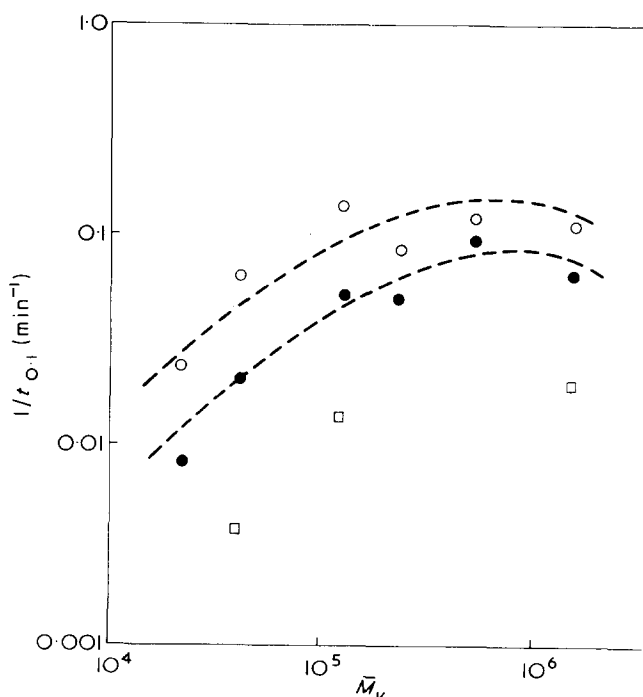


Figure 8 Reciprocal tenth-life of crystallization versus viscosity-average molecular weight for poly(ethylene oxide) fractions crystallized at temperatures of: ○, 57.0°C; ●, 58.1°C; □, 59.4°C

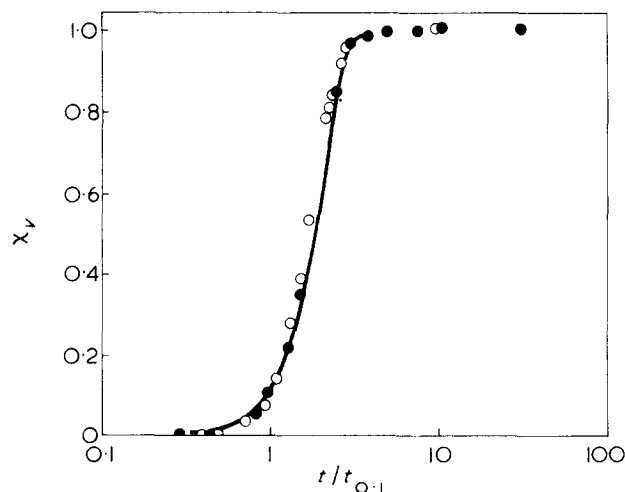


Figure 9 Superimposed crystallization isotherms at crystallization temperature 58.1°C for poly(ethylene oxide) fractions H23000 (○) and R42000 (●). Curve is the Avrami isotherm (equation 4) with  $n = 3$

#### Crystallization isotherms, $\chi_v(t)$

The weight fractions of polymer incorporated into the crystalline (spherulitic) phase at the crystallization temperature and at time  $t$  can be defined by:

$$\chi_v(t) = \frac{V(t) - V_l^0}{V_c(t) - V_l^0} \quad (2)$$

where  $V_c(t)$  represents the specific volume of the crystalline phase at temperature  $T_c$  as it actually exists within the spherulite at time  $t$ . (The other symbols have been defined earlier.) This specific volume,  $V_c(t)$ , cannot be determined except in the simple case that the crystallization is by a single process, occurring at the spherulite boundary, and that the (impinging) spherulites eventually fill space. For this case  $V_c$  is independent of  $t$  and equal to the specific volume of the system when crystallization is complete, and:

$$\chi_v(t) = \frac{V(t) - V(0)}{V(\infty) - V(0)} \quad (3)$$

where the specific volumes relate to zero time [ $V(0) = V_l^0$ ] and infinite time [ $V(\infty) = V_c$ ].

For a given phase morphology and phase initiation process, a simple crystallization process as described above leads to a crystallization isotherm  $\chi_v(t)$  which can be described by an Avrami equation<sup>2,3</sup>:

$$1 - \chi_v(t) = \exp(-zt^n) \quad (4)$$

The phase morphology is spherulitic which, together with the observation that not all spherulites are initiated instantaneously, means that the exponent  $n$  should have a value somewhat greater than 3. The rate constant  $z$  depends upon the spherulite growth rate and the spherulite number density (which is a function of time) and can be related directly to  $t_{0.1}$  only if the crystallization isotherms fit equation (4)<sup>2,3</sup>.

Fractions with molecular weights exceeding 50 000 cannot be analysed in this simple way because of the prominent secondary process. Crystallization isotherms (semilogarithmic plots of  $\chi_v$  against  $t$ ) for fractions H23000 and R42000 are illustrated in Figure 9. The isotherms are superimposed

at the point  $X_v(t) = 0.1$ . The curve drawn through the data is the Avrami isotherm with  $n = 3$ . The best value of  $n$  to fit equation (4) to the data of Figure 9 is about 3.5. In view of the complexity of the crystallization process the agreement between the prediction (from the observations with the microscope) and the experimental result is satisfactory.

#### Comparison with polyethylene

Crystallization isotherms for a set of fractions of linear polyethylene with molecular weights in the range 4000 to 8 000 000 have been reported by Ergoz *et al.*<sup>18</sup>. In most respects our results for poly(ethylene oxide) parallel the results for polyethylene. For example our data can be superimposed to a similar extent; the variation of the extent of crystallinity  $[X_v(t')]$  with molecular weight is similar, as is the range of  $X_v(t')$  observed; and the variation of crystallization rate with molecular weight is also similar. We have considered fitting the crystallization isotherms  $X_v$  with an Avrami equation (as advocated by Ergoz *et al.*) but we do not find integral values of the exponent  $n$ .

#### ACKNOWLEDGEMENTS

We thank Mr D. J. Roy for assistance with the characterization of the polymers. J. Q. G. M. acknowledges receipt of a Science Research Council Studentship.

#### REFERENCES

- 1 Maclaine, J. Q. G. and Booth, C. *Polymer* 1975, **16**, 191
- 2 Mandelkern, L. 'Crystallisation of Polymers', McGraw-Hill, New York, 1964
- 3 Sharples, A. 'Introduction to Polymer Crystallisation', Arnold, London, 1966
- 4 Mandelkern, L., Quinn, F. A. and Flory, P. J. *J. Appl. Phys.* 1954, **25**, 840
- 5 Barnes, W. J., Luetzel, W. G. and Price, F. P. *J. Phys. Chem.* 1961, **65**, 1742
- 6 Hay, J. N., Sabir, M. and Steven, R. L. T. *Polymer* 1969, **10**, 187; Hay, J. N. and Sabir, M. *Polymer* 1969, **10**, 203
- 7 Godovsky, Yu. K., Slonimsky, G. L. and Garbar, N. M. *J. Polym. Sci. (C)* 1972, **38**, 1; *Vysokomol. Soedin. (A)* 1973, **15**, 813; *Polym. Sci. USSR*, 1973, **15**, 914
- 8 Beech, D. R., Booth, C., Dodgson, D. V. and Hillier, I. H. *J. Polym. Sci. (A-2)* 1972, **10**, 1555
- 9 Price, C., Evans, K. A. and Booth, C. *Polymer* 1975, **16**, 196
- 10 Allen, G., Booth, C., Hurst, S. J., Jones, M. N. and Price, C. *Polymer* 1967, **8**, 391
- 11 Beech, D. R., Booth, C., Dodgson, D. V., Sharpe, R. P. and Waring, J. R. S. *Polymer* 1972, **13**, 73
- 12 Arlie, J. P., Spegt, P. and Skoulios, A. E. *Makromol. Chem.* 1966, **104**, 212
- 13 Simon, F. T. and Rutherford, J. M. *J. Appl. Phys.* 1964, **35**, 82
- 14 Price, F. P. and Kilb, R. W. *J. Polym. Sci.* 1962, **57**, 395
- 15 Godovsky, Yu. K., Garbar, N. M. and Slonimsky, G. L. *Vysokomol. Soedin. (A)* 1972, **14**, 1833; *Polym. Sci. USSR* 1972, **14**, 2053
- 16 Kovacs, A. J. and Gonthier, A. *Kolloid-Z.* 1972, **250**, 530
- 17 Beech, D. R., Booth, C., Hillier, I. H. and Pickles, C. J. *Eur. Polym. J.* 1972, **8**, 799
- 18 Ergoz, E., Fatou, J. G. and Mandelkern, L. *Macromolecules* 1972, **5**, 147
- 19 Beech, D. R. and Booth, C. *J. Polym. Sci. (B)* 1970, **8**, 731
- 20 Hoffman, J. D. *SPE Trans.* 1964, **4**, 315

#### APPENDIX

We have investigated the secondary process in the crystallization of fraction N1600000 in some detail. A sample was crystallized at 57.0°C for 100 min (to  $X_v = 0.38$ ), by which time the primary crystallization was complete (see Figure 3). The dilatometer was then transferred to an oil bath usually held at a higher temperature  $T_a$ . After 15 to 30 min the dilatometer was returned briefly to the primary crystallization bath in order to determine whether partial melting had occurred at  $T_a$ ; in the event partial melting only occurred to an appreciable extent at  $T_a = 66.4^\circ\text{C}$  when the value of  $X_v$  dropped by 0.015. The changes in  $X_v$ , from the values 2 min after transfer to the bath at  $T_a$ , are plotted against time in Figure A1. In the range  $55 < T_a < 60^\circ\text{C}$  the secondary process is practically temperature independent. In the range  $60 < T_a < 67^\circ\text{C}$  the secondary process varies with temperature, though not in a systematic way. Melting temperatures for samples held at  $T_a$ , measured as described earlier<sup>11,19</sup>, are listed in Table A1. The increase in  $T_m$  during the secondary process may be taken to indicate that some process of crystal perfecting occurs.

Taken together these data give no indication that the secondary process in the crystallization of this high molecular weight fraction of poly(ethylene oxide) can be reduced to a simple mechanism, be it lamella crystal thickening<sup>20</sup> or volume relaxation<sup>9</sup>.

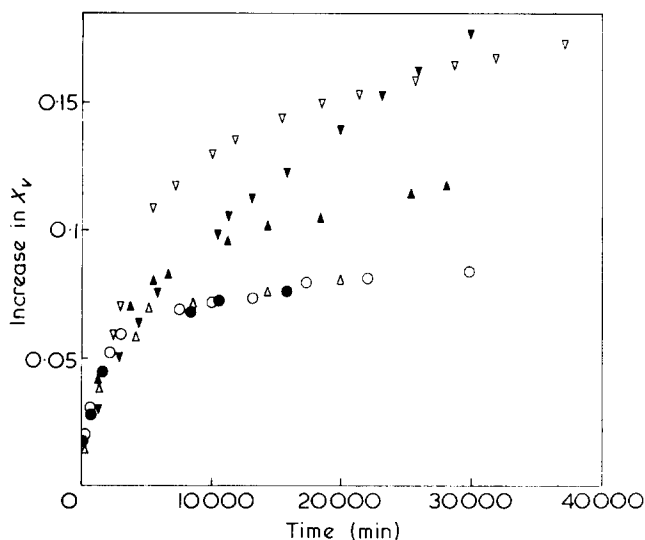


Figure A1 Increase in  $X_v$  versus time for poly(ethylene oxide) fraction N1600000 initially crystallized at 57.0°C for 100 min and held at temperatures ( $^\circ\text{C}$ ) of:  $\circ$ , 55.6;  $\bullet$ , 57.0;  $\triangle$ , 59.4;  $\blacktriangle$ , 61.7;  $\nabla$ , 63.9;  $\blacktriangledown$ , 66.4°C

Table A1 Melting points of poly(ethylene oxide) fraction N1600000

Treatment of sample	$X_v$	$T_m$ ( $^\circ\text{C}$ )
Primary process:		
100 min at 57.0°C	0.38	68.0
Secondary process:		
30 000 min at 59.4°C	0.46	68.5
63.9°C	0.54	68.9
66.4°C	0.55	69.1

# Dynamic transition of grafted polybutadiene in ABS resins

T. Riccò, A. Pavan and F. Danusso

Industrial Chemistry Department, Macromolecular Chemistry and Materials Section, Polytechnic Institute, 20133 Milan, Italy

(Received 31 December 1974)

Dynamic mechanical properties of a series of ABS (acrylonitrile–butadiene–styrene) resins, having a constant rubber basis grafted to different extents, were studied in the temperature range  $-120^{\circ}$  to  $20^{\circ}\text{C}$ . The observed viscoelastic transition of the rubbery phase shows two main effects: the amplitude of the transition and the transition temperature decrease as the degree of grafting increases. The grafted component had been prepared by graft copolymerization of butadiene rubber in emulsion with different comonomers/rubber ratios. Both the dynamic effects observed on ABS are discussed in terms of structure variations induced by the change of the grafting condition.

## INTRODUCTION

Toughening of a normally brittle glassy polymer by incorporation of dispersed particles of rubber is well established. The mechanism of this reinforcement remains to be fully understood, but it is now generally accepted that a two phase structure is necessary and a good adhesion between phases is requisite to the dispersed phase toughening action<sup>1–3</sup>.

Good interfacial adhesion is usually achieved by grafting the glassy polymer to the rubber particles. To what extent and way these have to be grafted in order to obtain the maximum toughening efficiency seems to be still one of the points for clarification.

To this aim we have undertaken experimental work on ABS samples with rubber particles grafted to different degrees and in this paper report some first results of a dynamic mechanical characterization.

Table 1 Comonomers/rubber ratio in the feed and degrees of grafting obtained

Graft sample	$w_{\text{mo}}/w_{\text{r}}$	GD	
		Measured	Calculated*
1	0	—	0
2	0.16 <sub>s</sub>	(0.22)	0.15
3	0.29 <sub>s</sub>	0.23 <sub>s</sub>	—
4	0.37	0.30	0.32
5	0.43	0.27	—
6	0.64	(0.79 <sub>s</sub> )	0.49 <sub>s</sub>
7	0.64 <sub>s</sub>	0.54	—
8	0.80	0.69	—
9	0.97	0.67	—
10	1.00	0.76	0.69
11	1.10 <sub>s</sub>	0.64	—
12	1.22	0.76	—
13	1.50	0.91	0.92
14	1.73	0.92	—
15	1.86	1.13	—
16	2.08	1.14	1.12
17	2.51	1.08	—

\* According to equation (3)

## EXPERIMENTAL

### Materials

A series of grafted rubber latexes was prepared by graft copolymerization of a nearly azeotropic mixture of styrene and acrylonitrile onto a prevalingly *cis*-tactic polybutadiene latex. The grafting process was carried out by adding the glassy resin-forming comonomers to the rubber latex in the presence of a water-soluble free-radical initiator. To obtain samples grafted to different extent, the comonomers: rubber ratio  $w_{\text{mo}}/w_{\text{r}}$  was varied from sample to sample as reported in Table 1, all other conditions having been kept constant. Practically, the reaction was carried out to complete conversion, so that  $w_{\text{mo}}/w_{\text{r}}$  also represents the whole resin/rubber ratio in the graft product.

The samples for the dynamic mechanical examination (i.e. samples 1, 2, 4, 6, 10, 13 and 16) were then brought to the same resin/rubber ratio 2.08 (that of sample 16) by mixing each graft latex with the appropriate amount of a stock latex of nearly azeotropic styrene–acrylonitrile copolymer (SAN resin) and the final ABS samples were recovered from these latexes by coagulation. As the final ABS samples have the same basic rubber content (32.5 wt % polybutadiene), the correlation of the mechanical properties with the degree of grafting may be regarded as of actual meaning\*.

### Determination of degree of grafting

The degree of grafting (GD) defined as the mass ratio of grafted glassy polymer to rubber, will be in general less than  $w_{\text{mo}}/w_{\text{r}}$ , i.e. the total glassy polymer/rubber ratio in the graft product, owing to a limited 'grafting efficiency' of the copolymerization. The degree of grafting of each sample was measured by extracting the ungrafted (or 'free') SAN resin by methyl ethyl ketone, according to a separation technique described elsewhere<sup>4</sup>.

\* The SAN resin added and that formed in the course of the grafting process could be structurally different. However, the reaction conditions used in this work yield molecular weights high enough not to substantially affect the mechanical properties studied here, and monomeric units disposition is likely to be similar to that of the added resin.

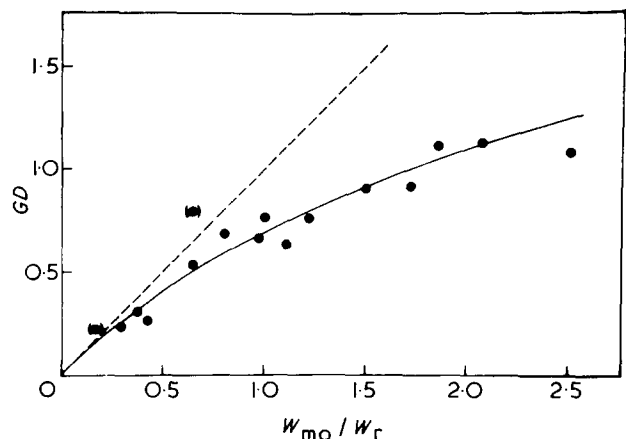


Figure 1 Degree of grafting ( $GD$ ) versus comonomers/rubber ratio in the feed. ---, complete grafting; —, equation (3); ●, experimental

#### Test specimens

The specimens needed for dynamic mechanical measurements are strip bars of about  $2.5 \times 1.0$  cm, 0.10–0.15 cm thick. All specimens were compression moulded at  $180^\circ\text{C}$ , annealed at  $105^\circ\text{C}$  for 2 h and then slowly cooled to room temperature (cooling rate  $0.2^\circ\text{C}/\text{min}$ ).

#### Dynamic mechanical measurements

The measurements were performed by an INUA tester<sup>5</sup>, at different temperatures, from  $-120^\circ\text{C}$  to room temperature. The apparatus used allows measurement, for a given material at a given temperature, of the resonance frequency  $\nu_r$  of transversal vibrations of a slab-shaped sample of known dimensions, and the width of the resonance band as the difference  $\Delta\nu$  between the frequencies at which the amplitude of the vibrations is  $1/\sqrt{2}$  of its maximum value. From these data the real part of the elastic modulus,  $E'$ , and the loss angle tangent,  $\tan \delta$ , can be calculated by the following equations<sup>6</sup>:

$$E' = \rho K_1 \frac{L^4}{d^2} \left[ \nu_r^2 + \frac{(\Delta\nu)^2}{2} \right] \quad (1)$$

$$\tan \delta = \frac{\Delta\nu}{\nu_r} \left[ 1 - 1/2 \left( \frac{\Delta\nu}{\nu_r} \right)^2 \right] \quad (2)$$

where  $\rho$  is the density of the examined material,  $L$  and  $d$  are the specimen length and thickness respectively, and  $K_1$  is a dimensionless constant which is related to the particular observed vibrational mode.

As may be seen from equation (1), the determination of  $E'$  can be strongly affected by small errors in the measurement of the dimensions of the specimen, so that only a qualitative meaning can be attributed to the curves  $E'(T)$  obtained. We shall therefore discuss only  $\tan \delta$  vs. temperature curves. Each specimen was stepwise cooled from room temperature at intervals of 5 to  $7^\circ\text{C}$ , and conditioned at the desired temperature for 10 to 15 min before each measurement. The resonance frequencies of each specimen varied by about 200 Hz when the temperature was lowered from room temperature to  $-120^\circ\text{C}$ .

## RESULTS

Experimental degrees of grafting are listed in Table 1 and plotted in Figure 1 against comonomers/rubber ratio. Also

shown in Figure 1 is the 'ideal' degree of grafting that would have resulted if all of the resin-forming comonomers fed would have been grafted on the pre-formed rubber, equal to  $w_{\text{mo}}/w_r$  (broken line).

According to Rosen<sup>3</sup> an upper limit to the extent of grafting arises from thermodynamical incompatibility between rubber and glassy phase formed in the course of the copolymerization process. Regardless of the chemical nature of the grafting process itself, a simple model has been developed which provides a quantitative estimate of that upper limit as a function of the conversion, and monomer/rubber ratio in the feed. At total conversion, the maximum possible degree of grafting,  $GD_{\text{max}}$ , should be:

$$GD_{\text{max}} = \ln \left( 1 + \frac{w_{\text{mo}}}{w_r} \right) \quad (3)$$

corresponding to the solid line also reported in Figure 1.

The observed agreement can seem striking, considering the very simplifying assumptions on which the Rosen's model is based.

In Figure 2 the experimental values of  $\tan \delta$  are reported as a function of the temperature, for each sample. Each curve shows a peak indicating a dynamic transition of the material or part of it. This transition is to be associated with the glass transition of the microphase of differently grafted polybutadiene embodied by each ABS sample.

The amplitude  $(\tan \delta)_{\text{max}}$  and the location  $T_d$  of each peak maximum are plotted against the degree of grafting in Figure 3. As the degree of grafting increases  $T_d$  shifts to lower temperatures and  $(\tan \delta)_{\text{max}}$  decreases, except for the ungrafted sample 1.

In Table 2 the temperatures  $T_d$  are reported together with the frequencies at which the peak maxima occur. It is noticeable that, although these frequencies are not equal, they do not differ greatly and the relationship between  $T_d$  and  $GD$  should not be substantially inferred by such a variation. Anyway, to remove this doubt we have tentatively reduced the  $T_d$  values to the same mean frequency ( $\nu = 565$  Hz) through the empirical correlations between  $T_d$  and  $\nu$  found by Lewis for various polymers<sup>7</sup>. According to

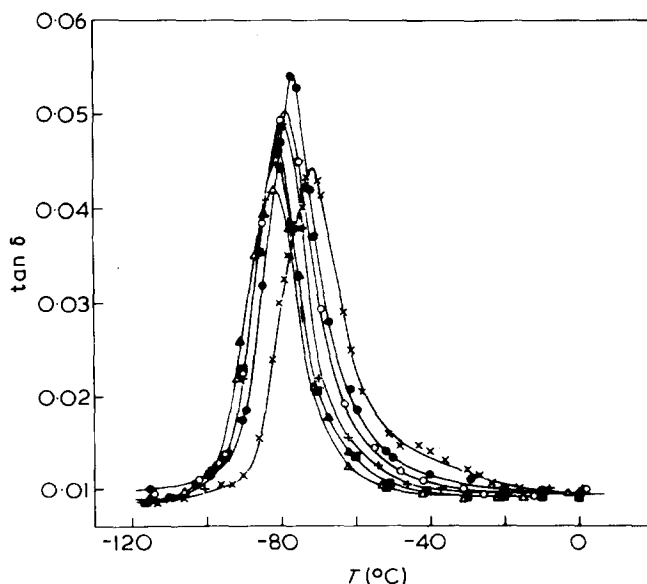


Figure 2 Loss factor  $\tan \delta$  versus temperature  $T$ , for the series of ABS samples examined: x, sample 1; ●, sample 2; ○, sample 4; +, sample 6; ■, sample 10; ▲, sample 13; △, sample 16

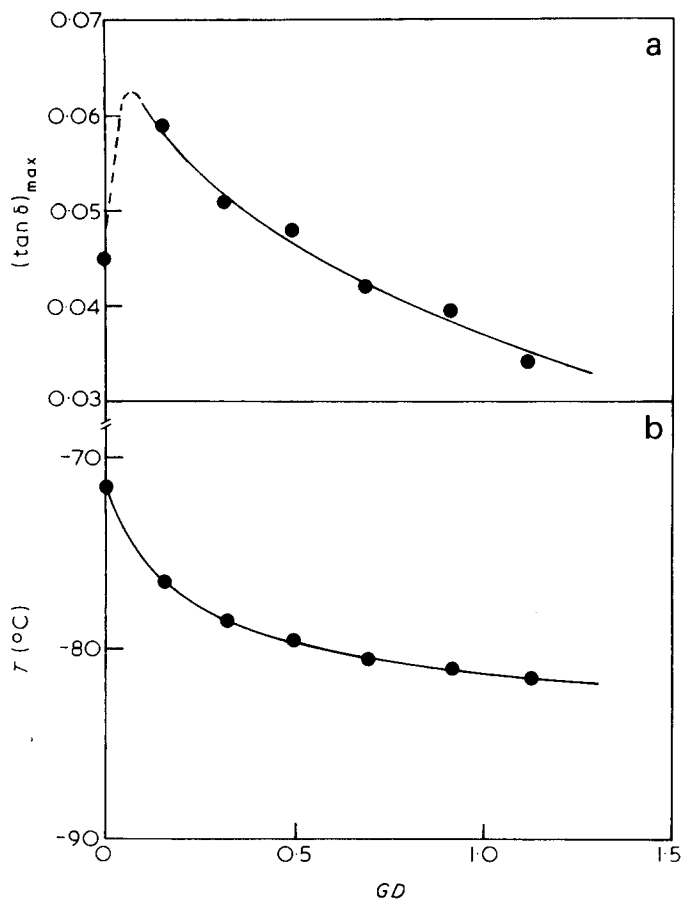


Figure 3 Loss factor maxima  $(\tan \delta)_{\max}$  (a) and dynamic transition temperatures  $T_d$  (b) as functions of degree of grafting (GD)

Lewis, plots of  $\log \nu$  versus  $1/T_d$  for polymeric materials are straight lines passing, with an approximation, through a common point, which is different for two characteristic classes of polymers: (a) with a rigid chain and/or bulky lateral groups (sterically restricted polymers), and (b) with a more flexible chain, without bulky lateral groups (sterically non-restricted polymers). Since we do not possess enough elements to assign the polybutadiene with different degrees of grafting of our samples to either of these classes, we have taken into account both possibilities. From the known coordinates of the common point and our experimental values of  $\nu$  and  $T_d$ , the relationship between  $\log \nu$  and  $1/T_d$  has been determined for each sample. From these relationships we have interpolated the values of  $T_d$  corresponding to the mean frequency of 565 Hz. These values do not differ substantially from the experimental ones (see Table 2).

Lewis also proposed an empirical correlation between the 'static' glass transition temperature,  $T_g$ , and the dynamic transition temperature  $T_d$  at  $\log \nu = -1.5$ :

$$T_d (\log \nu = -1.5) = aT_g + b \quad (4)$$

where  $a$  and  $b$  are two constants different for the two classes of polymers, the sterically restricted and the sterically non-restricted polymers. From this equation we have calculated the values of  $T_g$  for our samples: the results are reported in Table 2 and plotted against the degree of grafting in Figure 4. As may be expected, the glass transition temperatures  $T_g$  are lower than the dynamic transition temperatures,  $T_d$ ; however, the dependence of  $T_g$  on the degree of grafting is quite similar to that of  $T_d$ .

The value  $T_g = -115.8^\circ\text{C}$  obtained for the ungrafted polybutadiene (sample 1) in the hypothesis of sterically non-restricted polymer, compares fairly well with literature values of  $-112^\circ\text{C}^8$  and  $-108^\circ\text{C}^{9-11}$  of free (and pure) *cis*-tactic polybutadiene.

## DISCUSSION

The two main results, i.e. the decrease of  $(\tan \delta)_{\max}$  and of  $T_g$  as the degree of grafting increases, although related to each other, can be discussed separately.

As for the first result, Illers and Jenckel<sup>12</sup> and McCrum<sup>13-16</sup> have found that the amplitude of the dynamic transition of a component of a composite material is directly related to the relative quantity of the component itself. The same result has been obtained by Dickie<sup>17</sup> from a theoretical calculation based on a simple mechanical model of composite material.

The observed decrease of  $(\tan \delta)_{\max}$  may then appear as a reduction of the relative quantity of a rubber 'active' in the dynamic transition. Since the weight fraction of polybutadiene in the examined ABS samples was kept constant, such a reduction may be interpreted as due to a progressive immobilization of the rubber particles at least on their outer shells when they are increasingly grafted.

Table 2 Effect of frequency on transition temperature

ABS sample	Experimental		Calculated			
	$\nu$ (Hz)	$T_d$ ( $^\circ\text{C}$ )	Sterically restricted	$T_d$ ( $\nu = 565$ Hz) ( $^\circ\text{C}$ )	Sterically non-restricted	$T_d$ ( $\nu = 565$ Hz) ( $^\circ\text{C}$ )
1	580	-71.5	-71.5	-123.5	-71.6	-115.8
2	470	-76.5	-75.4	-126.4	-76.1	-120.6
4	675	-78.5	-80.4	-130.3	-79.1	-123.7
6	552	-79.5	-79.5	-129.5	-79.5	-124.1
10	540	-80.5	-81.0	-130.0	-79.2	-124.1
13	520	-81.0	-79.5	-129.5	-80.4	-125.1
16	620	-81.5	-82.3	-131.8	-81.8	-126.5

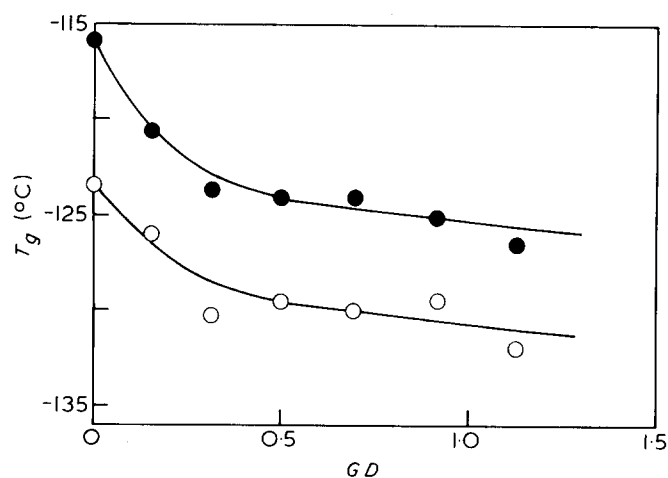


Figure 4 Glass transition temperatures  $T_g$  calculated according to equation (4), as function of degree of grafting (GD): ●, hypothesis of sterically non-restricted polymers; ○, hypothesis of sterically restricted polymers



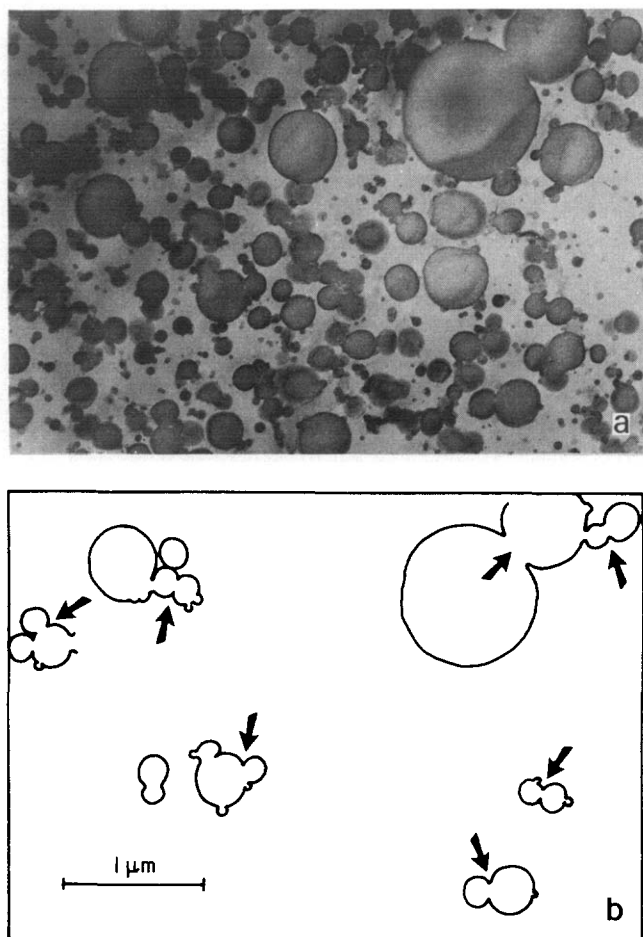


Figure 5 Evidence of coalescence of rubber particles in lightly grafted ABS samples. (a) Phase contrast electron photomicrograph of sample 2 and (b) pattern showing coalescence points

Photomicrographs obtained by electron microscopy\* of sections of the specimens (see, e.g., the pictures taken from samples 2 and 16 shown in Figures 5a and 6a respectively), support this hypothesis. As one may see from Figure 5a, for the scarcely grafted sample, sample 2, the incompatibility of the polybutadiene particles with the matrix induces them to coalesce (see examples indicated in Figure 5b); in the case of sample 16 a sort of barrier seems to prevent them from coalescing (see examples indicated in Figure 6b), which may be evidence of the existence of an outer shell formed by the glassy copolymer grafted on the rubber particles.

The behaviour of sample 1 remains, however, unexplained under the described hypothesis.

From the series of photomicrographs obtained for the different samples, one can observe an increasing amount of glassy polymer subinclusions distributed in the rubber particles as the  $GD$  increases. From the aforesaid considerations it may be inferred that these subinclusions too can immobilize part of the rubber, further reducing  $(\tan \delta)_{\max}$ . On the other hand, they increase the overall volume fraction of the dispersed phase, which is known to raise  $(\tan \delta)_{\max}$ <sup>17-19</sup>

The experimental results must then be interpreted by assuming that the immobilization of the rubber shells at the boundaries with the glassy polymer is the prevailing effect.

As for the second result, i.e. the decrease of the transition temperature  $T_d$ , or  $T_g$ , it can be ascribed to the presence of thermal stresses built up by cooling the samples, as a consequence of the different thermal expansion coefficients of rubber phase and glassy matrix<sup>20-22</sup>. Because of the greater thermal contraction of rubber with respect to glassy matrix, a state of triaxial tension is to be expected in each rubber particle. As a consequence the free volume of rubber increases, and results in a decrease of the glass transition temperature<sup>21,23</sup>.

Of course, such an effect presupposes a sufficient adhesion between the two phases, generally believed to be secured by the usual grafting operation. However, the progressive shift of the transition to lower temperatures observed as the degree of grafting increases can be explained only by assuming that the degree of adhesion varies together with the degree of grafting.

As for other possible factors, the increasing amount of glassy subinclusions in the rubber particles should give an opposite effect, both because it increases the overall fraction of dispersed phase<sup>17</sup> and reduces the level of thermal stresses in rubber<sup>24</sup>. Other minor effects, such as copolymerization effects and crosslinking, would also play a role in the same direction.

We must conclude that the first effect prevails, and a substantial degree of grafting has to be reached for a high degree of adhesion between rubber particles and glassy

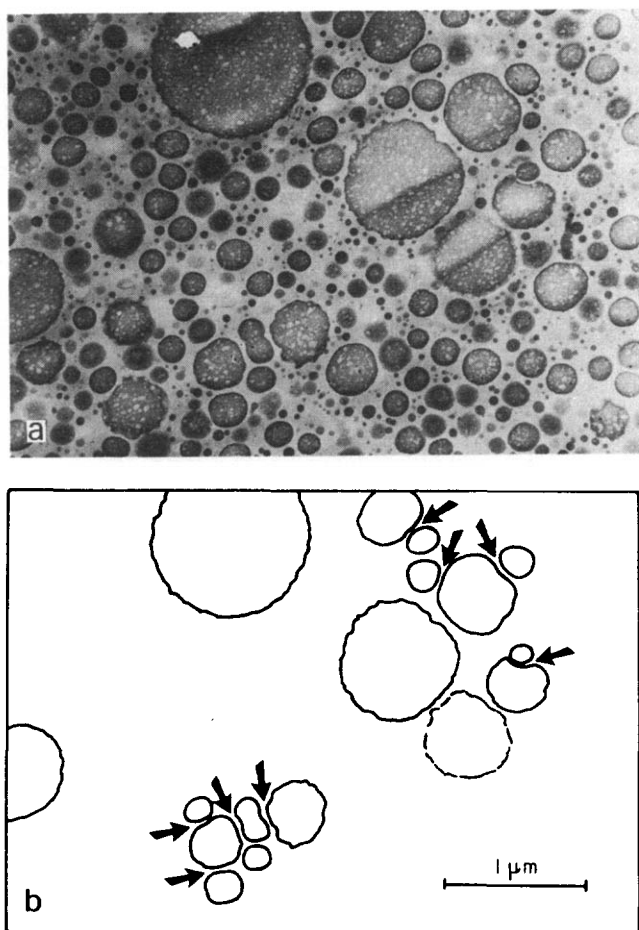


Figure 6 Evidence of hindrance to coalescence of rubber particles in highly grafted ABS samples. (a) Phase contrast electron photomicrograph of sample 16 and (b) pattern showing points of hindrance to coalescence by shells of grafted glassy polymer. Subinclusions of glassy polymer in the rubber particles are also evident in (a)

\* These photomicrographs have been supplied by courtesy of the ANIC SpA, S. Donato Milanese (Italy).

matrix, even if rather low degrees of grafting are usually satisfactory in the production of high impact composite materials.

#### ACKNOWLEDGEMENTS

This work was supported by ANIC SpA, San Donato Milanese (Italy), with partial contribution of Consiglio Nazionale delle Ricerche, Roma (Italy).

#### REFERENCES

- 1 Bevilacqua, E. M. *J. Polym. Sci.* 1957, **24**, 292
- 2 Haward, R. N. and Mann, J. *Proc. R. Soc. (A)* 1964, **282**, 120
- 3 Rosen, S. L. *Polym. Eng. Sci.* 1967, **7**, 115
- 4 Pavan, A. to be published
- 5 Danusso, F., Pegoraro, M. and Szilagy, L. *Mater. Plast. Elastomeri* 1969, No.10
- 6 Szilagy, L., Locati, G. and Pegoraro, M. *Kolloid-Z. Z. Polym.* 1968, **223**, 97
- 7 Lewis, A. F. *J. Polym. Sci. (B)* 1963, **1**, 649
- 8 Sanders, J. F. *PhD Thesis* University of Wisconsin (1968)
- 9 Baccaredda, M. and Butta, E. *Chim. Ind. (Milan)* 1960, **42**, 978
- 10 Dainton, F. S., Evans, D. M., Hoare, F. E. and Melia, T. P. *Polymer* 1962, **3**, 297
- 11 Dannis, M. L. *J. Appl. Polym. Sci.* 1963, **7**, 231
- 12 Illers, K. H. and Jenckel, E. *Kolloid-Z. Z. Polym.* 1958, **160**, 97
- 13 McCrum, N. G. *J. Polym. Sci.* 1958, **27**, 555
- 14 McCrum, N. G. *Am. Soc. Test. Mat. Bull.* 1959, No.242
- 15 McCrum, N. G. *J. Polym. Sci.* 1959, **34**, 355
- 16 McCrum, N. G. *Makromol. Chem.* 1959, **34**, 50
- 17 Dickie, R. A. *J. Appl. Polym. Sci.* 1973, **17**, 45
- 18 Cigna, G. *J. Appl. Polym. Sci.* 1970, **14**, 1781
- 19 Wagner, E. R. and Robeson, L. M. *Rubber Chem. Technol.* 1970, **43**, 1129
- 20 Beck, R. H., Gratch, S., Newman, S. and Rusch, K. *J. Polym. Sci. (B)* 1968, **6**, 707
- 21 Bohn, L. *Angew. Makromol. Chem.* 1971, **20**, 129
- 22 Morbitzer, L., Ott, K. H., Schuster, H. and Krank, D. *Angew. Makromol. Chem.* 1972, **7**, 57
- 23 Newman, S. 'Polymer Technology and Engineering', (Ed. L. Naturman), Marcel Dekker, New York, 1974, Vol 2, p 67
- 24 Pavan, A. and Riccò, T. to be published

## Notes to the Editor

### Synthesis and characterization of styrene–butadiene graft copolymers

D. C. Evans, M. H. George and J. A. Barrie

Department of Chemistry, Imperial College of Science and Technology, London, SW7 2AY, UK

(Received 31 July 1974; revised 23 April 1975)

#### INTRODUCTION

Synthesis of graft copolymers by anionic polymerization techniques have been widely reported. There are two principal methods<sup>1</sup>. In the first of these, living polymer is deactivated by a backbone polymer molecule containing a suitable functional group. In the second, anionic polymerization of the grafted polymer is initiated by a backbone polymer molecule which has been converted into a multifunctional initiator. It is generally considered that the former method gives products that can be more fully characterized<sup>1</sup> and its use in the synthesis of well characterized branched polystyrenes<sup>2</sup> and polystyrene-*g*-polyisoprene copolymers<sup>3</sup> has been reported recently. This report describes attempts to prepare styrene–butadiene graft copolymers of approximately predetermined structure using the second method. This method is of importance since the grafted side chains remain active after polymerization is complete, and so the grafts can be terminated with functional groups. For example, controlled crosslinking of graft copolymers with grafts terminated with a carboxyl group should lead to network polymers of controlled structure.

When polystyrene is metalated by *n*-butyl lithium (*n*-BuLi) in the presence of *N,N,N',N'*-tetramethylethylenediamine (TMEDA), metalation occurs at the *meta* and *para* positions on the aromatic ring<sup>4,5</sup>. The metalated polymer behaves as a multifunctional anionic initiator and addition of butadiene results in graft polymerization of butadiene onto polystyrene. The synthesis of such a copolymer by this technique has been reported earlier<sup>6</sup>, but few details were given.

The graft copolymers were isolated, purified and characterized with respect to molecular weight, composition and chain microstructure. Solution and bulk properties of one copolymer were investigated and the results are presented below and compared to those for similar systems.

#### EXPERIMENTAL AND RESULTS

##### *Synthesis and characterization of graft copolymers*

Polystyrene, prepared anionically and of molecular weight above 110 000, was metalated by *n*-BuLi/TMEDA in cyclohexane at 55°C under dry argon as described previously<sup>4</sup>. At a known time of reaction, the mixture was cooled in ice and butadiene in cyclohexane was added under a pressure of argon. The reaction mixture was stirred continuously and allowed to warm to room temperature during the polymerization of the butadiene. The molecular weight of the polybutadiene grafts was designed to be less than approximately 15 000. The reaction was terminated by degassed methanol. After dilution, the polymer was precipitated into methanol containing a trace of antioxidant (2,6-di-*t*-butyl-*p*-cresol).

Difficulties were encountered in the purification of the graft copolymer, owing to the presence of homopolybutadiene, produced by the polymerization of butadiene initiated by the *n*-BuLi that did not take part in the metalation reaction. Product separation was achieved by fractional precipitation. A 1:1 v/v toluene/*n*-heptane mixture, containing approximately 0.05% w/v antioxidant was used as solvent and methanol as precipitant. The composition of the fractions obtained was followed by gel permeation chromatography (g.p.c.). Full details of these experimental procedures have been given elsewhere<sup>7</sup>.

Yields of graft copolymer were low; the weight of graft copolymer finally obtained was generally only slightly higher than the starting weight of polystyrene. This is probably a result of polystyrene molecules with a small number of branches remaining in solution after the remainder of the graft copolymer had been extracted during fractional precipitation.

The graft copolymers and samples of homopolybutadiene which were isolated from the initial reaction product were characterized as described below.

*Number-average molecular weights* ( $\bar{M}_n$ ) of all samples were determined by membrane or vapour phase osmometry.

*Weight-average molecular weights* ( $\bar{M}_w$ ) of graft copolymers were measured by light scattering from toluene solutions at room temperature and values of  $\bar{M}_w$  were obtained from Zimm plots.

*Ultra-violet spectroscopy* was used to determine overall compositions of graft copolymers by estimation of the polystyrene content<sup>8</sup>.

*Infra-red spectra* of all samples were recorded. Spectra of graft copolymers were equivalent to the sum of those of polystyrene and ungrafted polybutadiene. By comparison with published spectra<sup>9</sup> grafted polybutadiene was shown to have a predominantly 1,2-microstructure.

*Proton n.m.r. spectra* of ungrafted polybutadiene were analysed<sup>10</sup> and corresponded to a microstructure of approximately: 1,2-, 84% and 1,4-, 16%. It has been reported elsewhere<sup>11</sup> that polybutadiene, initiated by *n*-BuLi/TMEDA in hydrocarbon solvent has a high 1,2-content.

##### *Properties of graft copolymers*

Limiting viscosity numbers of the graft copolymers were measured as a function of temperature and of solvent composition in mixed solvent systems. In all solvent mixtures, changes in the limiting viscosity number  $[\eta]$  of the copolymer were virtually the same as those in that of the polystyrene backbone. An example is shown in *Figure 1* in which toluene–cyclohexane solvent mixtures were used.

For a variety of graft copolymers it has been reported<sup>14,15</sup> that  $[\eta]$  increases in mixed solvent systems as the solvent becomes more selective for one of the components of the

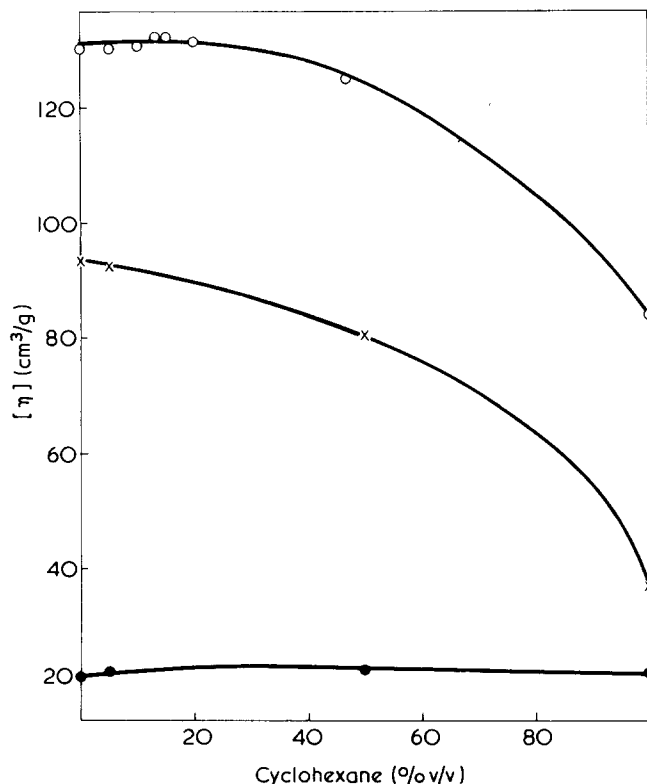


Figure 1 Dependence of limiting viscosity number of styrene-butadiene graft copolymer (O), polystyrene backbone (X) and polybutadiene samples (●) on solvent composition in toluene-cyclohexane solvent mixtures at 25°C

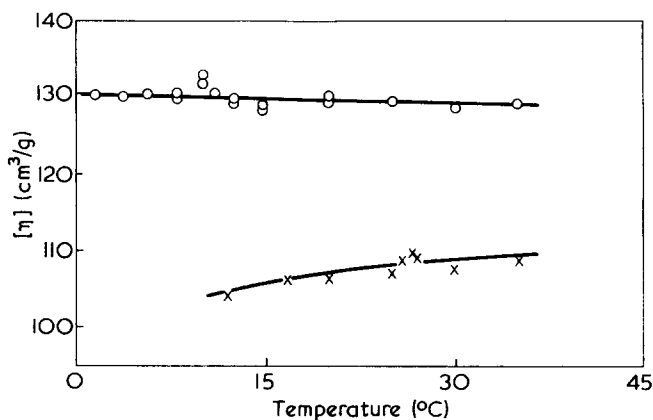


Figure 2 Dependence of limiting viscosity number of styrene-butadiene graft copolymer sample on temperature in toluene (O) and dioxane (X)

graft copolymer. The increase in  $[\eta]$  is maintained until one of the components collapses and 'monomolecular micelles' are produced<sup>16</sup>, resulting in a sharp fall in  $[\eta]$ . This behaviour was not observed with the styrene-butadiene graft copolymers described in this study.

Limiting viscosity numbers of the styrene-butadiene graft polymers in toluene and in dioxane were almost independent of temperature within the temperature range studied (Figure 2), as were those of the homopolymers. These results differ from those reported for other graft copolymers in good solvents for both components<sup>17,18</sup>. In these cases, a transitory increase in  $[\eta]$  of the copolymer was observed, generally at or just below room temperature.

These results suggest that in the sample of styrene-butadiene graft copolymer, repulsive interactions between

unlike polymer chains are weak. Such interactions result from a positive heat of mixing of unlike polymers and are responsible for the phase separation that is generally observed in solutions of two homopolymers<sup>19</sup> and for the microphase separation of block copolymers in the solid state<sup>20</sup>. The weakness of these interactions in the graft copolymers of this study is probably a result of the low molecular weight of the polybutadiene branches since polystyrene and polybutadiene are inherently incompatible as demonstrated by the complete microphase separation obtained with styrene-butadiene block copolymers<sup>20</sup>. Molecular weight results and some related data for one sample of graft copolymer are given in Table 1. Also included are data for the polystyrene, used as the backbone polymer, and for the homopolybutadiene prepared during the grafting reaction. Since  $\bar{M}_w$  for the graft copolymer was determined from measurements in a single solvent, its value will be an apparent one only and will be higher than the true  $\bar{M}_w$ <sup>12</sup>. However, the high value of  $\bar{M}_w/\bar{M}_n$  (2.1) is chiefly a result of oxidative crosslinking during fractionation of the polymer. The use of antioxidant reduced, but did not completely eliminate, crosslinking. In Table 1, the branching frequency is defined as the average number of polybutadiene branches per backbone molecule. It is emphasized that this is an average value since it has been shown<sup>13</sup> that there is a distribution of metalated sites among polystyrene molecules.

The results of differential thermal analysis are given in Table 2; for comparison, the experimentally measured glass transition temperatures ( $T_g$ ) of the sample of homopolybutadiene prepared with the graft copolymer and a literature value for the  $T_g$  of polystyrene<sup>21</sup> are included.

With block and graft copolymers, if microphase separation is not complete, the  $T_g$  of each block moves towards that of a random copolymer of similar overall composition<sup>22</sup>. On this the results in Table 2 indicate that microphase separation of unlike blocks in the graft copolymer is not complete.

That microphase separation does occur, is demonstrated by transmission electron microscopy. Thin films of polymer were prepared from benzene solution directly onto copper grids by flash evaporation of the solvent, and were stained with osmium tetroxide<sup>23</sup>. Micrographs, such as shown in Figure 3, were obtained with a VEM-7 electron microscope operated at 100 kV. In Figure 3, the dark

Table 1 Molecular weight and related data for a styrene-butadiene graft copolymer

	Polystyrene	Homopolybutadiene	Graft copolymer
$\bar{M}_n \times 10^{-4}$	25.6	0.9	37.0
$\bar{M}_w \times 10^{-4}$	27.6	—	79.0
Overall composition (wt % styrene):			
u.v. spectroscopy			69
from $\bar{M}_n$			69
Branching frequency			13

Table 2 Glass transition temperatures of a styrene-butadiene graft copolymer

Polymer	$T_g$ (°C)
Polystyrene-g-polybutadiene	-27,95
Homopolybutadiene	-32
Polystyrene	100

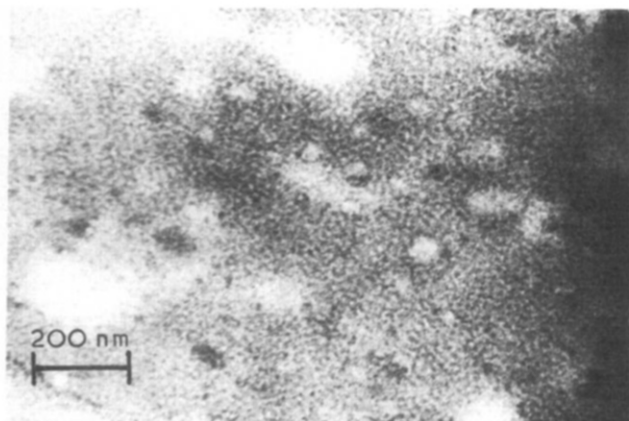


Figure 3 Transmission electron micrograph of styrene-butadiene graft copolymer

regions correspond to those of predominantly osmium tetroxide-stained polybutadiene grafts.

#### ACKNOWLEDGEMENTS

Financial support for this work and a maintenance award (to D.C.E.) were provided by the Science Research Council. G.p.c. measurements were made by Dr J. M. Evans of the Rubber and Plastics Research Association (RAPRA). Proton n.m.r. spectra were recorded by Mr S. J. Roberts of the Chemistry Department, Imperial College, and Mrs Barbara Robinson recorded the electron micrographs in the Chemical Engineering Department.

#### REFERENCES

- 1 Rempp, P. and Franta, E. *Pure Appl. Chem.* 1972, 30, 229
- 2 Pannell, J. *Polymer* 1971, 12, 558
- 3 Price, C. and Woods, D. *Polymer* 1973, 14, 82
- 4 Evans, D. C., George, M. H. and Barrie, J. A. *J. Polym. Sci. (A-1)* 1974, 12, 247
- 5 Evans, D. C., Phillips, L., Barrie, J. A. and George, M. H. *J. Polym. Sci. (B)* 1974, 12, 199
- 6 Sun Oil Co. Br. Pat. 1 121 195 (1968)
- 7 Evans, D. C. *PhD Thesis* University of London (1974)
- 8 Meehan, E. J. *J. Polym. Sci.* 1946, 1, 175
- 9 Haslam, J. and Willis, H. A. 'Identification and Analysis of Plastics', Iliffe Books, London, 1965
- 10 Simak, R. and Fahrback, G. *Angew. Makromol. Chem.* 1970, 12, 73
- 11 Hay, J. N., McCabe, J. F. and Robb, J. C. *JCS Faraday Trans. I* 1972, 68, 1
- 12 Bushuk, W. and Benoit, H. *Can. J. Chem.* 1958, 36, 1616
- 13 Cha, C. Y. *Polym. Prepr.* 1971, 12, 282
- 14 Dondos, A., Rempp, P. and Benoit, H. *J. Polym. Sci. (B)* 1966, 4, 293
- 15 Gosnell, A. B., Woods, D. K., Gervasi, J. A., Williams, J. L. and Stannett, V. *Polymer* 1968, 9, 561
- 16 Gallot, Y., Franta, E., Rempp, P. and Benoit, H. *J. Polym. Sci. (C)* 1964, 4, 473
- 17 Dondos, A. *Makromol. Chem.* 1966, 99, 275
- 18 Dondos, A. *Eur. Polym. J.* 1969, 5, 767
- 19 Dobry, A. and Boyer-Kawenoki, F. *J. Polym. Sci.* 1947, 2, 90
- 20 Dawkins, J. V. in 'Block Copolymers', (Eds D. C. Allport and W. H. Janes), Applied Science, Barking, 1973, 8A
- 21 'Polymer Handbook', (Eds J. Brandrup and E. H. Immergut), Interscience, New York, 1966
- 22 Childers, C. W. and Kraus, G. *Rubber Chem. Technol.* 1967, 40, 1183
- 23 Kato, K. *J. Polym. Sci. (B)* 1966, 4, 35

## Effect of annealing on thermomechanical properties of poly(ethylene oxide)

E. Alfthan and A. de Ruvo

Department of Physics, Swedish Forest Products Research Laboratory, Box 5604, S-114 86, Stockholm, Sweden  
(Received 24 March 1975; revised 23 April 1975)

#### INTRODUCTION

The purpose of this note is to demonstrate how the thermal prehistory of poly(ethylene oxides) influences their dynamic mechanical properties, especially with regard to the second order transition. Samples with different molecular weights have been used in this investigation, which confirmed the results obtained by previous authors on the relationship between first and second order transition and molecular weight.

Many previous papers have dealt with similar studies of poly(ethylene oxides), and the first and second transitions have been determined by means of mechanical spectroscopy<sup>1,2</sup>, dielectric measurements<sup>3</sup>, n.m.r.<sup>4</sup> and e.s.r.<sup>5</sup>. It is noteworthy that the theoretically predicted inverse relationship<sup>6</sup> between the glass transition temperature and molecular weight is not obtained. Instead, the glass transition temperature reaches a maximum at intermediate molecular weights (4000–10 000). This anomalous behaviour has been attributed to the presence of the crystalline phase, which restrains the chain mobility in the amorphous regions. In terms of the concept of free volume, this implies a corresponding reduction in the free volume of the amorphous phase<sup>7</sup>. This may be achieved either by compressional restraints or by the interaction or adhesion

between the crystalline surfaces and the amorphous chain segments.

#### EXPERIMENTAL

The samples used in this investigation were kindly provided by J. Törmala and J. Lindberg and used in their investigation of the relaxations of poly(ethylene oxides) (PEO) at temperatures above  $T_g$ <sup>5</sup>. This investigation employed e.s.r. studies of the rotational relaxation of nitroxyl radicals used as probes or labels in the polymer.

The PEO samples were of commercial origin (Fluka AG and E. Merck AG) and were labelled according to the technique described by Lindberg. All samples had a fairly narrow distribution of molecular weight. The data obtained by Törmala and Lindberg are reproduced in Table 1 together with the transition temperatures measured in this study.

#### Thermal prehistories

In the first series the samples were dried at 105°C in a nitrogen atmosphere for 1 h after which the temperature was lowered at the rate of 40°C/h to 20°C. The sample was conditioned for 1 h before testing. These samples were

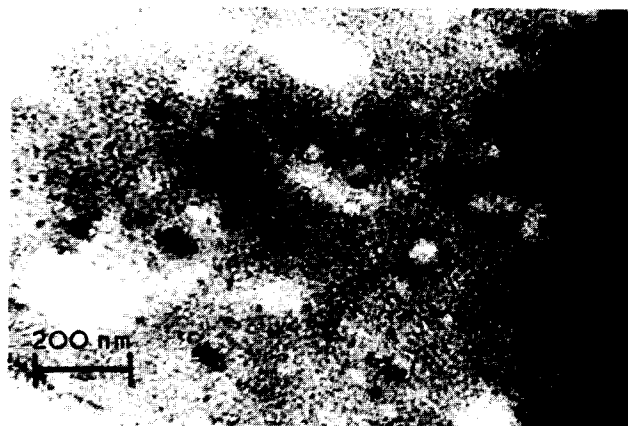


Figure 3 Transmission electron micrograph of styrene-butadiene graft copolymer

regions correspond to those of predominantly osmium tetroxide-stained polybutadiene grafts.

#### ACKNOWLEDGEMENTS

Financial support for this work and a maintenance award (to D.C.E.) were provided by the Science Research Council. G.p.c. measurements were made by Dr J. M. Evans of the Rubber and Plastics Research Association (RAPRA). Proton n.m.r. spectra were recorded by Mr S. J. Roberts of the Chemistry Department, Imperial College, and Mrs Barbara Robinson recorded the electron micrographs in the Chemical Engineering Department.

#### REFERENCES

- 1 Rempp, P. and Franta, E. *Pure Appl. Chem.* 1972, 30, 229
- 2 Pannell, J. *Polymer* 1971, 12, 558
- 3 Price, C. and Woods, D. *Polymer* 1973, 14, 82
- 4 Evans, D. C., George, M. H. and Barrie, J. A. *J. Polym. Sci. (A-1)* 1974, 12, 247
- 5 Evans, D. C., Phillips, L., Barrie, J. A. and George, M. H. *J. Polym. Sci. (B)* 1974, 12, 199
- 6 Sun Oil Co. Br. Pat. 1 121 195 (1968)
- 7 Evans, D. C. *PhD Thesis* University of London (1974)
- 8 Meehan, E. J. *J. Polym. Sci.* 1946, 1, 175
- 9 Haslam, J. and Willis, H. A. 'Identification and Analysis of Plastics', Iliffe Books, London, 1965
- 10 Simak, R. and Fahrback, G. *Angew. Makromol. Chem.* 1970, 12, 73
- 11 Hay, J. N., McCabe, J. F. and Robb, J. C. *JCS Faraday Trans. I* 1972, 68, 1
- 12 Bushuk, W. and Benoit, H. *Can. J. Chem.* 1958, 36, 1616
- 13 Cha, C. Y. *Polym. Prepr.* 1971, 12, 282
- 14 Dondos, A., Rempp, P. and Benoit, H. *J. Polym. Sci. (B)* 1966, 4, 293
- 15 Gosnell, A. B., Woods, D. K., Gervasi, J. A., Williams, J. L. and Stannett, V. *Polymer* 1968, 9, 561
- 16 Gallot, Y., Franta, E., Rempp, P. and Benoit, H. *J. Polym. Sci. (C)* 1964, 4, 473
- 17 Dondos, A. *Makromol. Chem.* 1966, 99, 275
- 18 Dondos, A. *Eur. Polym. J.* 1969, 5, 767
- 19 Dobry, A. and Boyer-Kawenoki, F. *J. Polym. Sci.* 1947, 2, 90
- 20 Dawkins, J. V. in 'Block Copolymers', (Eds D. C. Allport and W. H. Janes), Applied Science, Barking, 1973, 8A
- 21 'Polymer Handbook', (Eds J. Brandrup and E. H. Immergut), Interscience, New York, 1966
- 22 Childers, C. W. and Kraus, G. *Rubber Chem. Technol.* 1967, 40, 1183
- 23 Kato, K. *J. Polym. Sci. (B)* 1966, 4, 35

## Effect of annealing on thermomechanical properties of poly(ethylene oxide)

E. Alfthan and A. de Ruvo

Department of Physics, Swedish Forest Products Research Laboratory, Box 5604, S-114 86, Stockholm, Sweden  
(Received 24 March 1975; revised 23 April 1975)

#### INTRODUCTION

The purpose of this note is to demonstrate how the thermal prehistory of poly(ethylene oxides) influences their dynamic mechanical properties, especially with regard to the second order transition. Samples with different molecular weights have been used in this investigation, which confirmed the results obtained by previous authors on the relationship between first and second order transition and molecular weight.

Many previous papers have dealt with similar studies of poly(ethylene oxides), and the first and second transitions have been determined by means of mechanical spectroscopy<sup>1,2</sup>, dielectric measurements<sup>3</sup>, n.m.r.<sup>4</sup> and e.s.r.<sup>5</sup>. It is noteworthy that the theoretically predicted inverse relationship<sup>6</sup> between the glass transition temperature and molecular weight is not obtained. Instead, the glass transition temperature reaches a maximum at intermediate molecular weights (4000–10 000). This anomalous behaviour has been attributed to the presence of the crystalline phase, which restrains the chain mobility in the amorphous regions. In terms of the concept of free volume, this implies a corresponding reduction in the free volume of the amorphous phase<sup>7</sup>. This may be achieved either by compressional restraints or by the interaction or adhesion

between the crystalline surfaces and the amorphous chain segments.

#### EXPERIMENTAL

The samples used in this investigation were kindly provided by J. Törmala and J. Lindberg and used in their investigation of the relaxations of poly(ethylene oxides) (PEO) at temperatures above  $T_g$ <sup>5</sup>. This investigation employed e.s.r. studies of the rotational relaxation of nitroxyl radicals used as probes or labels in the polymer.

The PEO samples were of commercial origin (Fluka AG and E. Merck AG) and were labelled according to the technique described by Lindberg. All samples had a fairly narrow distribution of molecular weight. The data obtained by Törmala and Lindberg are reproduced in Table 1 together with the transition temperatures measured in this study.

#### Thermal prehistories

In the first series the samples were dried at 105°C in a nitrogen atmosphere for 1 h after which the temperature was lowered at the rate of 40°C/h to 20°C. The sample was conditioned for 1 h before testing. These samples were

used for determining  $T_m$ . In a second series the temperature of the samples was lowered from 105° to -60°C in 30 min (rapid cooling). In the third series the samples were cooled to a temperature of 10°C. After a certain time, the sample was cooled to -60°C in 5 min after which its glass transition temperature and melting temperature were measured. Samples kept for more than three days were considered to be annealed. Finally, the samples were quenched from 105°C to -60°C.

### Thermomechanical testing

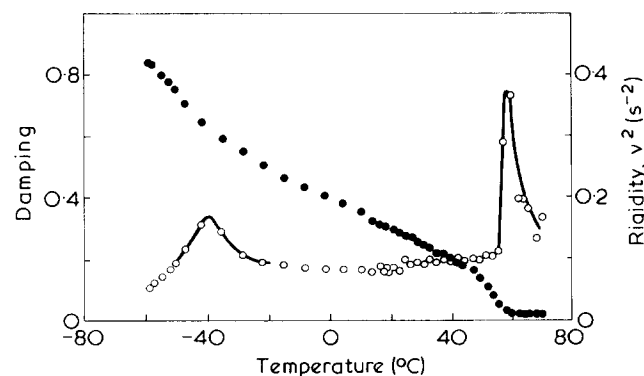
All measurements were performed in a commercial torsional pendulum, TBA (Chemical Instruments Corp.). The basic principle of this instrument has been described previously<sup>8</sup>. All samples were impregnated on a glass braid and the resonance frequency and damping of the composite sample were recorded. All changes in these parameters were assumed to be caused by thermally induced changes in the polymer. The polymers were impregnated on the braid from an aqueous solution of 10% concentration. Total deposition on the braid was 20–40 wt %.

Thermomechanical spectra were recorded at a scanning rate of 1°C/min and the damping and resonance frequency were measured automatically by a computer at every second degree. This ensured that the evaluation of the damping was performed in an objective and reproducible manner, which is especially necessary at high damping numbers.

## RESULTS

It can be seen from *Figure 1* that damping rises sharply to a maximum in the region of melting. The temperature of maximum damping corresponds to the  $T_m$  as measured with d.s.c.<sup>9</sup> Previous work<sup>10</sup> on similar samples using the TBA technique has not shown that damping reaches a maximum at the temperature of melting. This may to some extent be ascribed to the difficulty of evaluating high damping numbers in an objective manner. Furthermore, previous work on homogeneous samples also indicates the existence of a maximum level of damping at the melting temperature<sup>11</sup>.

A linear relationship is obtained between  $1/T_m$  and  $1/M$ . However, the application of the Flory theory to evaluate the heat of fusion is questionable primarily as it can only be applied to polymers having a most probable molecular weight distribution<sup>14</sup>. Previous authors have accordingly noted a significant discrepancy between a calculated heat of fusion and that experimentally determined by means of calorimetry<sup>13</sup>.

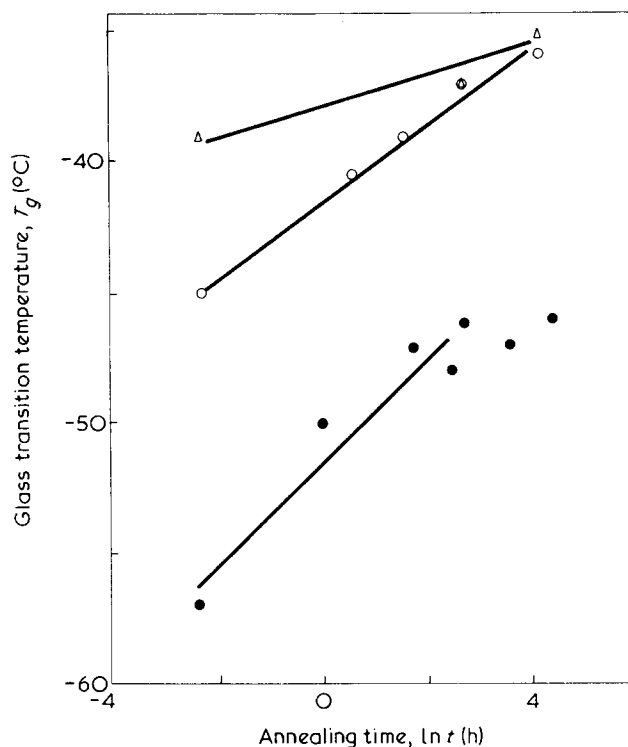


*Figure 1* Thermomechanical spectrum of PEO ( $M = 4000$ ). ○, Damping; ●, rigidity

*Table 1* Molecular characteristics and transition temperatures of PEO samples

$M_n$	$M_w/M_n$	$T_g$ (°C)			$T_m$ (°C)	
		Quench- ed	Rapid cool- ed	Anneal- ed	TBA	D.s.c.*
2050 ± 150	1.28	-45	-39	-36	50.3	48.5
4000 ± 500	1.28	-39	-38	-35	56.7	55.5
6700 ± 700	1.23	-	-38	-	58.7	55.5
9500 ± 500	1.10	-	-39	-	60.4	57.5
15000 ± 2000	1.09	-	-45	-	61.8	60.5
22000	1.08	-57	-47	-46	63.0	62.0

\* D.s.c. values reproduced from the work of Törmala and Lindberg



*Figure 2* Glass transition temperature as a function of annealing time for PEO of various molecular weights,  $M$ : ○, 2000; △, 4000; ●, 22000

From *Table 1* it is evident that  $T_g$  reaches its maximum value at intermediate molecular weights, in accordance with previously reported results<sup>1–5</sup>. In this case the maximum values are somewhat lower than those obtained by Read. It seems likely that these differences are the result of annealing effects. Thus, as can be seen in *Table 1* and *Figure 2*, longer annealing times result in an increase in  $T_g$  values. The dependence of  $T_g$  on the length of the annealing process can presumably be explained by the kinetics of crystallization. It is worth noting that the extent of the change in  $T_g$  depends on the molecular weight. This should mean that each sample will differ in its rate of crystallization. Moreover, the effect of the time of annealing on  $T_g$  is most pronounced at the lowest (2000) and highest (22000) molecular weights. At  $M = 4000$  the change in  $T_g$  for different times of annealing is noticeably lower than is the case with the other samples.

It is significant that a transition from chain-extended to chain-folded structures takes place in the crystallites at the intermediate molecular weight<sup>12–14</sup>. Moreover, the fact that chain-folded structures are formed at a faster rate tends to

### Notes to the Editor

favour their presence when crystallization occurs at low temperatures<sup>14</sup>. Thus the low sensitivity of  $T_g$  to the annealing time at  $M = 4000$  may be attributed to the rapid completion of crystallization and the resultant preferential forming of chain-folded structures.

At the lowest molecular weight, therefore, the pronounced dependence of  $T_g$  on the time of annealing can be ascribed to a slow and therefore incomplete crystallization. This corresponds to the previously mentioned forming of chain-extended structures at low molecular weights.

Finally, the extent to which  $T_g$  changes in response to the length of annealing time is greater at high molecular weights. This is probably caused by the retarding effect of the increased melt viscosity.

### CONCLUSIONS

Wide variations exist in the literature for the  $T_g$  of PEO and for the maximum  $T_g$  obtained at a given molecular weight. These inconsistencies probably stem from the rather complicated crystallization mechanism of the polymer, in which both crystallization temperature and molecular weight govern the rate of crystallization and the preferred type of crystalline structure<sup>12</sup>. Consequently, these parameters and the time of annealing essentially control the resulting crystallinity and morphology, and thus also determine the location of  $T_g$ . It is apparent that both  $T_g$  and crystallinity reach a maximum in the region of mole-

cular weight where the transition from chain-extended to chain-folded structure takes place. Thus it can be expected that the absolute value and the intensity of the maxima will be greatly influenced by the thermal prehistory of the sample. It is this which differs significantly in many previous investigations.

### REFERENCES

- 1 Read, B. E. *Polymer* 1962, 3, 529
- 2 Faucher, J. A. *et al. J. Appl. Phys.* 1966, 37, 3962
- 3 Connor, T. M., Read, B. E. and Williams, G. J. *Appl. Chem.* 1964, 14, 74
- 4 Allen, G., Connor, T. M. and Pursey, H. *Trans. Faraday Soc.* 1963, 59, 1525
- 5 Törmälä, P., Lattilä, H. and Lindberg, J. J. *Polymer* 1973, 14, 481
- 6 Fox, T. G. and Flory, P. J. *J. Appl. Phys.* 1950, 21, 581
- 7 Boyer, R. F. *Rubber Chem. Technol.* 1963, 36, 1303
- 8 Lewis, A. F. and Gillham, J. K. *Polymer* 1966, 7, 331
- 9 Törmälä, P. and Savolainen, A. *Acta Chem. Scand.* 1973, 27, 1430
- 10 Hartmann, B. *Polymer* 1972, 13, 460
- 11 Wetton, R. E. and Allen, G. *Polymer* 1966, 7, 331
- 12 Spegt, P. *Makromol. Chem.* 1970, 140, 167
- 13 Godovskij, J. K., Slononimskij, G. L. and Garbar, N. M. *Sowj. Beitr. Faserforsch. Textiltech.* 1973, p 396; *Vysokomol. Soedin.* 1973, A15, 813
- 14 Beech, D. R., Booth, C., Dodgson, D. V., Sharpe, R. R. and Waring, J. R. S. *Polymer* 1972, 13, 73
- 15 Booth, C., Bruce, J. M. and Buggy, M. *Polymer* 1972, 13, 475



# Letter

## Spectroscopic evidence for ion-pair equilibria involving polyvinylbiphenyl carbanions

### Introduction

The absorption spectra of solutions of the ions of several aromatic hydrocarbons exhibit a sensitivity to temperature, counterion and solvent which provides direct evidence for the existence of tight and loose ion-pairs, in addition to free ions<sup>1</sup>. The simultaneous participation of some, or all, of these species in the propagation of the anionic polymerization of monomers such as styrene was proposed by Szwarc and coworkers on the basis of kinetic evidence<sup>2</sup>. The present report presents preliminary spectroscopic data for the ion-pairs of the polymer anions derived from vinyl biphenyl and isopropenyl biphenyl.

### Experimental

The monomers were purified by recrystallization from ethanol, followed by vacuum sublimation. Polymerization was initiated by butyl lithium or by brief contact with a mirror of sodium metal, using standard high vacuum techniques. The solutions so obtained were stable for several days. Spectroscopic measurements were conducted using quartz cells (0.1 cm pathlength) immersed in ethanol contained in an unsilvered Dewar vessel. The temperature was lowered by the controlled passage of liquid nitrogen through a copper coil submerged in the alcohol.

### Results

At ambient temperatures the visible absorption spectrum of poly(vinylbiphenyl lithium) in 2-methyltetrahydrofuran

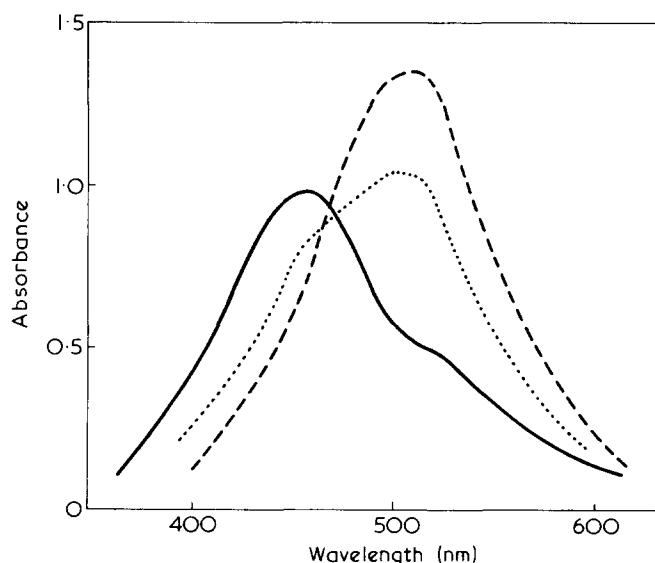


Figure 1 Absorption spectrum of poly(vinylbiphenyl lithium) in 2-methyltetrahydrofuran. —, +25°; ····, -10°; - - -, -45° C

Table 1 Changes in entropy ( $\text{J mol}^{-1} \text{K}^{-1}$ ) and in enthalpy ( $\text{kJ/mol}$ ) for the conversion of tight to loose ion-pairs

Monomer	Cation	Solvent	$-\Delta H^\circ$	$-\Delta S^\circ$
VB	Li	MTHF	27	97
VB	Li	Oxepane	13	46
VB	Na	THF	23	85
IB	Li	MTHF	35	123

VB = 4-vinylbiphenyl; IB = 4-isopropenylbiphenyl; MTHF = 2-methyltetrahydrofuran; oxepane = oxacycloheptane

consisted of a single absorption band whose maximum lay at 452 nm (Figure 1). As expected, the spectra of samples prepared using lithium metal and butyl lithium were identical. When the temperature was lowered, the absorbance decreased and a new band was formed at 512 nm. The spectra recorded at a series of temperatures passed through an isosbestic point at 476 nm and the changes in the spectrum were completely reversible. Such behaviour is in accordance with the conversion of a tight ion-pair ( $\lambda_{\text{max}}$  452 nm) to a loose ion-pair ( $\lambda_{\text{max}}$  512 nm). The absence of electrical conductivity and the independence of the spectra of the concentration of the solution supported this conclusion and eliminated the possibilities of dissociation or aggregation.

Analysis of the absorption spectrum, making the necessary adjustment for overlap, enables the determination of the equilibrium constant  $K = [\text{loose ion pair}] / [\text{tight ion pair}]$ . The van't Hoff plot of  $\ln K$  vs.  $1/T$  was linear and corresponded to  $\Delta H^\circ = -27 \text{ kJ/mol}$  and  $\Delta S^\circ = -97 \text{ J mol}^{-1} \text{K}^{-1}$  for the conversion of tight to loose pairs. Similar spectral sensitivity to temperature was exhibited by several other systems based on vinyl and isopropenyl biphenyl and the results of detailed analysis are summarized in Table 1.

The potassium, rubidium and caesium based polymers were prepared in methyltetrahydrofuran but the extent of the conversion of these to the loose ion-pairs even at the glass temperatures of the solvent was insufficient to permit the determination of the thermodynamic parameters.

These results offer a clear opportunity of testing the correlation of ion-pair equilibria with the kinetics of polymerization. Work on the latter is presently in progress.

R. N. Young

Department of Chemistry,  
University of Sheffield,  
Sheffield S3 7HF, UK  
(Received 19 June 1975)

### References

- 1 Szwarc, M. 'Carbanions, Living Polymers and Electron Transfer Processes'. Interscience, New York, 1968
- 2 Bhattacharyya, D. N., Lee, C. L., Smid, J. and Szwarc, M. *Polymer* 1964, 5, 54

# Book Reviews

## Fire resistant and flame retardant polymers

M. W. Ranney

Noyes Data Corporation, Park Ridge, NJ, 1974,  
395 pp. \$36.00

This book is one of the well known Noyes Chemical Technology Reviews and provides detailed descriptive information on fire resistant and flame retardant polymers based on US patent literature. In all 273 patents are cited (ranging from USP 2 590 211 to USP 3 784 509 dated January 8, 1974). Each patent is summarized in readable technical language, free from legal jargon and phraseology. The claims and essential technical details of manufacture and use are given. The book is organized in a systematic and easy-to-follow manner and deals with: polyurethanes; polyesters, epoxides, silicones; polypropylene and polyethylene; polystyrene and ABS; polyamides, acrylics and other thermoplastics, and finally with patents on general utility additives. The individual chemical approaches are systematically listed in a contents and subject index at the beginning of the book.

The text is easy to read but the size of the print may prompt some of the older readers to feel the need of a magnifying glass. This is particularly true for tables which have been reproduced from patents, some of which have 16 lines to the inch.

It is felt that this book will be invaluable to chemists working in the field, even taking into account that they will probably have access to the original patents.

It is well bound and printed. The author and publishers are to be congratulated in producing it so quickly and including such recent patent literature.

K. A. Scott

## Thermal analysis of polymers

*Advances in Polymer Science, Volume 13*

W. Wrasidlo

Springer Verlag, Berlin, 1974. 99 pp. DM 46

Any experiment in which quantitative account is taken of a temperature change or a heat flow falls within the scheme of thermal analysis. The author, recognizing the breadth of his title, chooses to review two important areas: (a) glass formation and the glassy state; and (b) crystallization, melting and the crystalline state. My feeling is that he has attempted too much, for a proper consideration of either of these subjects might occupy the space available.

The review of the glass transition emphasizes the rationalization of experimental results by use of free volume or kinetic theories.

### Conference Announcement

## VII International Congress on Rheology

Gothenburg, Sweden, 23–27 August 1976

The VIIth International Congress on Rheology will take place at Chalmers University of Technology, Gothenburg, Sweden from 23 to 27 August, 1976. All aspects of rheology will be discussed and contributions that aim at a reduction of the diversity of the theoretical and empirical framework by introducing new unifying concepts will be especially welcome. Prospective contributors should send their title and 300 word summary by 1 October 1975 to the Chairman of the Organizing Committee, Professor Josef Kubát, Department of Polymeric Materials, Chalmers University of Technology, Fack, S-402 20 Gothenburg 5, Sweden, from whom Circular 2 will also be available.

It includes a useful summary of thermal ( $T_g$ ,  $\alpha$ ,  $C_p$ ) and viscometric data for more than 60 polymers and copolymers. This section is concise and informative.

Not so the review of crystallization and melting, which is something of a *pot-pourri* of effects and examples. In this case there is no accepted framework of theory within which to present the experimental observations. Nevertheless an opportunity has been missed to emphasize those experiments and ideas which lead to useful (if oversimplified) models of the crystallization process and the crystalline state.

The editing is noticeably lax: several references are incomplete; several names are misspelt; several entries in the tables are incomprehensible. There is no evidence that the review was rushed into print, since the references terminate in mid-1972.

Altogether, at a cost of more than £8.00, this is a disappointing volume.

C. Booth

## Macromolecular syntheses, Volume 5

*Edited by Emerson L. Wittbecker*

John Wiley, London & New York, 1974. £5.40

To those familiar with this series it suffices to say that the new volume extends the range of reactions documented in its four predecessors. For others the essential information is that the book contains detailed practical instructions for the preparation of twenty-three different polymers by methods which have been carefully checked by independent assessors. In passing, one notes that one of the preparations was checked by a team in the same laboratory as the originators of the procedure, a fact which detracts somewhat from the value of the monitoring process.

Although, as might be expected, emphasis falls on the addition and condensation routes, there are examples of cyclo-addition and ring-opening reactions as well as of polymer transformations by means of chemical reagents and mechanical forces. Some of the polymers are esoteric but any collection which includes as diverse a range of materials as thiocarbonyl fluoride, cyanoethyl cellulose, squaric acid and isotactic polypropylene can scarcely be condemned for lack of variety or originality.

This book will surely be a welcome addition to all polymer chemistry libraries.

A. D. Jenkins

## Publications Received

### Reviews in macromolecular chemistry, Volume 12

*Edited by G. Butler, K. O'Driscoll and M. Shen*  
Marcel Dekker, New York, 1975. 390 pp. \$29.50

### Disposal of plastics

J. A. Shelton  
Fulmer Research Institute, Stoke Poges, 1975. 90 pp. £15.00

### Factors influencing the performance of polyolefin mouldings

A. C. Morris  
Plastics (and Rubber) Institute, London, 1974. 14 pp. £1.20

### Formulations, Part 1

(*Treatise on Coating, Volume 4*)  
*Edited by R. R. Myers and J. S. Long*  
Marcel Dekker, New York, 1975. \$68.00

### Progress of rubber technology, 1975

Volume 38  
Plastics and Rubber Institute, London, 1975. 115 pp. £5.25  
(£1.75 to members)

### Polymer-plastics technology and engineering, Volume 3

*Edited by Louis Naturman*  
Marcel Dekker, New York, 1974. 252 pp. \$29.50

### Polymer handbook

*Edited by J. Brandrup and E. H. Immergut*  
Wiley-Interscience, New York, 1975. 2nd Edn. 1368 pp. £16.50

# Segregation and conformational transitions in triblock copolymers in dilute solution: 3. Viscometric investigations in solvent mixtures

Anastasios Dondos

Laboratory of Physical Chemistry, University of Athens, 144 Athens, Greece

and Paul Rempp and Henri Benoit

Centre de Recherches sur les Macromolécules, CNRS, 6 rue Boussingault, 67083 Strasbourg, France

(Received 12 February 1975; revised 7 April 1975)

Viscometric measurements were carried out on a triblock copolymer PMMA/PS/PMMA at two temperatures in two binary solvent mixtures, in order to establish to what extent segregation between the two kinds of blocks is maintained as the composition of the solvent mixture i.e. its preferential affinity to one of the blocks, changes. From the variation of the limiting viscosity number of the polymer *versus* composition of the solvent mixture, taking into account the corresponding plots for the two homopolymers, it was established: that at relatively low temperature the molecular dimensions of the block copolymer are very close to those calculated neglecting the heterocontact interactions, i.e. assuming segregation, and that at higher temperatures the dimensions observed for the block copolymer are higher than the values calculated by assuming segregation, thus showing that the heterocontacts exert some influence, inducing the chain to expand. A comparison with a PS/PMMA random copolymer of the same composition showed, however, that in the same solvent mixtures the number of heterocontacts was far lower in the case of the block copolymer than in the case of the random copolymer, even at elevated temperatures.

## INTRODUCTION

For more than ten years now, block copolymers of various kinds have been investigated thoroughly, using many different techniques, in dilute solution as well as in bulk.

There are, however, still large discrepancies between the proposed structures of block copolymers in dilute solution. Some authors<sup>1-3</sup> claim that, owing to the strong repulsions between chemically unlike sequences of the same molecule, the block copolymer adopts 'segregated' conformations, i.e. conformations in which the A part and the B part of the molecule are located in different domains of space, involving consequently very few A-B contacts. Other authors<sup>4,5</sup> do not agree with segregation and they claim that the conformations of a block copolymer chain obey Gaussian statistics, with some extra expansion originating from A-B type interactions, as in the case of random copolymers<sup>6</sup>.

In previous investigations along this line<sup>6-8</sup> we have shown that the viscosity of a block copolymer can be calculated from those of the corresponding homopolymers applying some additivity rule<sup>8</sup>, and taking no account of AB interactions. The good fit between the calculated values and the corresponding experimental limiting viscosity numbers is a strong argument in favour of segregation.

In a subsequent step we carried out viscosity and light scattering experiments on BAB triblock copolymers at various temperatures. We were thus able to detect some 'transition' phenomena which can be attributed to a conformational change<sup>8,9</sup>: on raising the temperature above  $T_c$ , the probability of AB heterocontacts increases. These 'transitions' are readily observable for triblock copolymers, as they introduce discontinuities in the variation of  $[\eta]$

and of the second virial coefficient  $A_2$  as a function of temperature. Similar transitions were observed by other authors, especially on polystyrene/polyisoprene/polystyrene triblock copolymers<sup>10</sup>. In the case of two block copolymers, however, no such transition has been observed. If there is segregation it is independent of temperature. In one case only a similar change was observed for a two-block copolymer of styrene and  $\alpha$ -methylstyrene<sup>11</sup>.

In the present communication, the behaviour of triblock copolymers in dilute solution in solvent mixtures is discussed with reference to the problem of segregation of unlike sequences and of possible conformational transitions.

Let us first recall that the morphology of a homopolymer in a binary solvent mixture is influenced by two factors: (i) the segment-segment interaction parameter  $\chi$ ; it does not vary linearly with the solvent composition, since it also depends upon the interactions between solvent 1 and solvent 2<sup>12</sup>; and (ii) preferential solvation<sup>13,14</sup>, which is a consequence of the thermodynamic interactions existing in the system, leads to experimentally detectable differences of the solvent mixture composition within the polymer coils.

In the case of a block copolymer, if segregation is established one can expect each part of the molecule to exhibit on its own preferential solvation and not necessarily by the same constituent of the solvent mixture. Furthermore, the AB heterocontact interaction parameter, usually referred to as  $\chi_{AB}$ , which should exert an influence at higher temperatures, when segregation decreases, can be expected to noticeably depend upon solvent composition.

For the present investigation we used the same BAB triblock copolymer of styrene (A) and methyl methacry-

late (B)<sup>8,9</sup>, and we measured the limiting viscosity number of that copolymer in two solvent mixtures: benzene–chloroform and benzene–tetrahydrofuran, as a function of solvent composition.

It should be recalled that poly(methyl methacrylate) (PMMA) homopolymer exhibits a conformational transition in benzene at around 30°C<sup>15</sup>, whereas no discontinuity is observed in the  $[\eta]$  versus temperature plots in THF or in CHCl<sub>3</sub>. It was shown recently, however, that in both solvent mixtures used here, PMMA exhibits, at a given content of polar solvent (THF or CHCl<sub>3</sub>) a slightly temperature dependent<sup>16</sup> transition of the same type. This transition is thus a characteristic feature of the individual PMMA chain, and this may be helpful in the interpretation of the observed behaviour of the triblock copolymer.

In spite of the complexity of these systems and of the numerous parameters to be considered an investigation of the limiting viscosity number of triblock copolymers in binary solvent mixtures is of great interest, if it is carried out in close comparison with the corresponding homopolymers. An attempt had already been made along the same line<sup>17</sup>, using a two-block copolymer of styrene and methyl methacrylate, in three different solvent mixtures. But in this early work the conformational transition of PMMA in these solvent mixtures had been overseen, and furthermore segregation was totally achieved throughout the systems of solvents investigated.

## EXPERIMENTAL

The triblock copolymer BAB with a centre block of polystyrene (PS) surrounded by two B blocks of poly(methylmethacrylate) was made anionically, according to a well known procedure<sup>8</sup>.  $\alpha$ -Methylstyrene 'tetramer' was used as initiator and THF as solvent. After completion of the styrene polymerization a few drops of diphenylethylene were added to prevent side reactions involving the ester functions of the methyl methacrylate from occurring. Then this latter monomer was added.

Characterization of the obtained polymer involved gel permeation chromatography and light scattering measurements. Satisfactory homogeneity of the sample was attained, and the presence of two-block copolymer, arising from deactivation of one out of two living ends of the precursor polystyrene, was not detectable.

The weight-average molecular weight of the block copolymer amounted to 425 000, and its styrene content was 53% by weight.

The two homopolymers (PS and PMMA) which were used in this investigation were also prepared anionically, and their polydispersities as estimated from the ratios of their weight- and number-average molecular weights were of the order of 1.1 for PS and 1.2 for PMMA. Their molecular weights were:  $M_{PS} = 400\,000$  and  $M_{PMMA} = 435\,000$ .

All the viscosity measurements were carried out using a capillary viscometer of the modified Ubbelohde type, requiring no corrections for flow kinetics or hydrostatic pressure. The temperature control of the thermostat was better than  $\pm 0.1^\circ\text{C}$ .

When working on solvent mixtures, we always dissolved the polymer in a mixture of the solvents of adequate composition. We never adjusted the composition of a polymer solution by addition of a single constituent.

The calculation of the theoretical values of  $[\eta]_{\text{cal}}$  are based upon the following considerations<sup>8</sup>. It is well known

that under the assumption of segregation the limiting viscosity number in a  $\theta$ -solvent (for both parts of the copolymer) is given by:

$$[\eta]_{\theta} = \left\{ x[\eta]_{\theta,A}^{2/3} + (1-x)[\eta]_{\theta,B}^{2/3} \right\}^{3/2} \quad (1)$$

since  $K_{\theta} = xK_{\theta,A} + (1-x)K_{\theta,B}$  where  $x$  is the A content of the block copolymer, and  $K_{\theta}$  is the well known parameter characterizing the unperturbed dimensions, and defined by:  $K_{\theta} = [\eta]_{\theta}/M^{1/2}$ . As we are working here in thermodynamically good solvents we have to evaluate the viscometric expansion coefficient  $\alpha_{\eta}^3$  which, assuming segregation, can be put in the very simple form:

$$\alpha_{\eta}^3 = x\alpha_{\eta A}^3 + (1-x)\alpha_{\eta B}^3$$

and it follows:

$$\alpha_{\eta}^3 = x \left( \frac{[\eta]_{\theta,A} M^{-1/2}}{K_{\theta,A}} \right) + (1-x) \left( \frac{[\eta]_{\theta,B} M^{-1/2}}{K_{\theta,B}} \right) \quad (2)$$

Since  $\alpha_{\eta}$  is molecular weight dependent the calculated value of the expansion was evaluated from data on homopolymers A and B exhibiting the same molecular weight as the whole copolymer (and not as its A part respectively, its B part alone).

It is therefore possible to calculate the limiting viscosity number of the copolymer:

$$[\eta]_{\text{cal}} = \alpha_{\eta}^3 \cdot [\eta]_{\theta} \quad (3)$$

using equations (1) and (2).

## RESULTS AND DISCUSSION

### Measurements in benzene–chloroform mixtures

The excess free enthalpy of mixing of benzene and chloroform has been found to be negative<sup>18</sup>. This means that the interaction energy between unlike molecules is higher than the average energy between pairs of molecules of the same species; for any polymer dissolved in this solvent mixture the variation of  $[\eta]$  with solvent composition should exhibit a negative deviation from linearity<sup>12</sup>. This is what is observed, at any temperature, for polystyrene (Figure 1). In the case of poly(methyl methacrylate) the variation of  $[\eta]$  with solvent composition has two characteristic features: first, the slope is much higher, showing that chloroform is a better solvent for PMMA than benzene; secondly, the conformational transition of PMMA is shown in the curve around 35% of chloroform by a sharp variation. This discontinuity is more pronounced at 55°C than at 25°C (Figure 1).

From these curves it is possible to calculate the anticipated viscosity behaviour of the block copolymer as a function of solvent composition, under the assumption of segregation, using equation (3). These calculated curves are shown in Figures 2 and 3, together with the actual experimental curves.

At 25°C (Figure 2) a temperature at which a very high degree of segregation can be expected<sup>8,9</sup>, no discontinuity is visible on the experimental curve, and for all compositions the measured values of  $[\eta]$  are below the calculated ones, except for pure chloroform and for pure benzene.

At 55°C, (Figure 3) previous results have shown that the heterocontacts are no longer negligible. This can explain

that even for pure benzene and for pure chloroform there is no good agreement between the measured values of  $[\eta]$  and the values calculated under the assumption of segregation. It should be noted that the PMMA transition appears here very distinctly around 40% of chloroform, and that the two parts of the  $[\eta]$  versus composition curve exhibit sharp negative deviations from linearity.

Since, at the lower temperature, we assume no interactions between PS and PMMA, the copolymer should show the transition of PMMA. It is possible that this abnormal behaviour is due to the difference in solubility of both types of blocks: the outside of the molecule will be made mainly of PS hiding the transition of PMMA.

Furthermore, the very marked negative deviations from linearity observed in the  $[\eta]$  vs. composition plot may be due to the fact that incompatibility between the homopolymer sequences in mixtures of these solvents is less than would be expected from the  $\chi_{AB}$  values in the pure solvents.

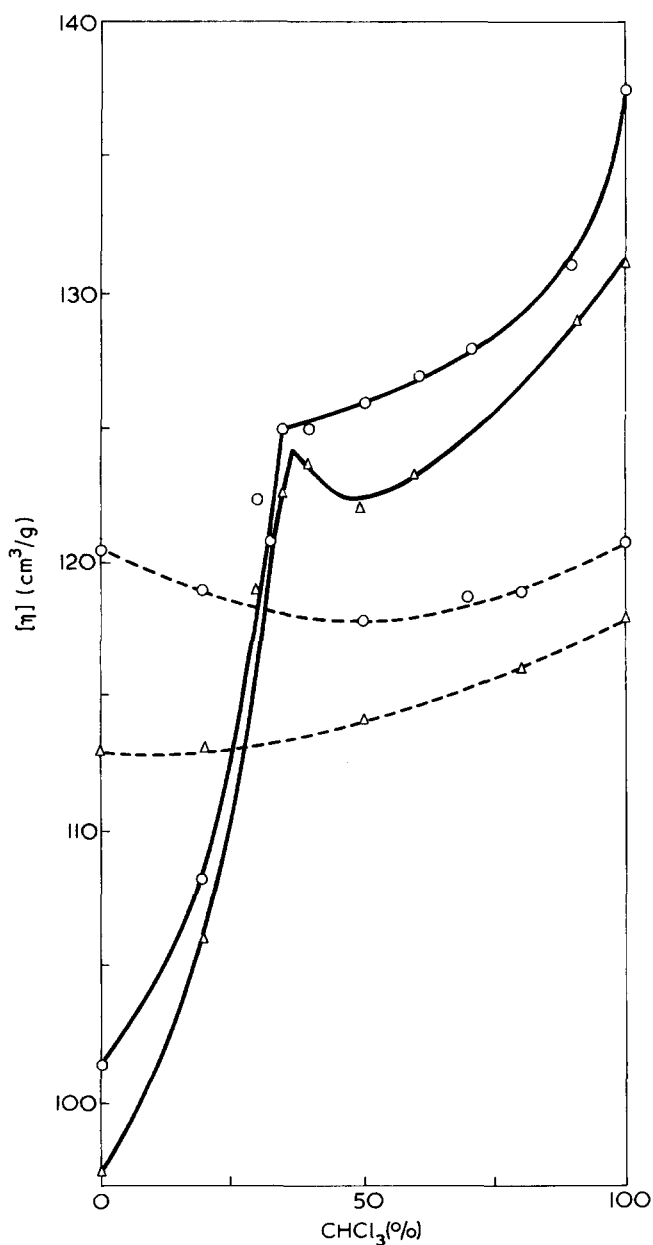


Figure 1 Variation of the limiting viscosity number of polystyrene (----) and of poly(methyl methacrylate) (—) versus the  $\text{CHCl}_3$  content of the benzene-chloroform solvent mixture.  $\circ$ , 25°C;  $\Delta$ , 55°C

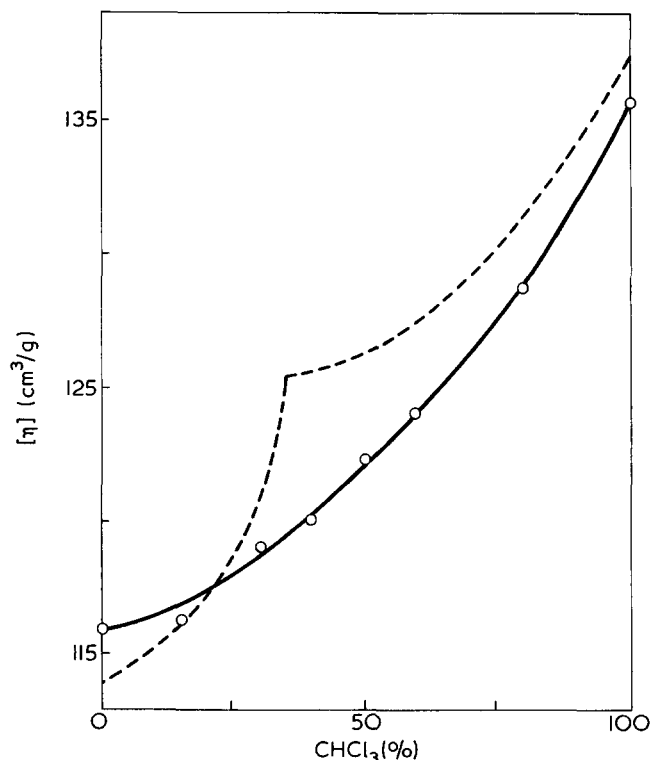


Figure 2 Variation of measured limiting viscosity number of the triblock copolymer (PMMA/PS/PMMA) as a function of  $\text{CHCl}_3$  content of the solvent mixture (benzene-chloroform) at 25°C. ----, Calculated values under the assumption of segregation

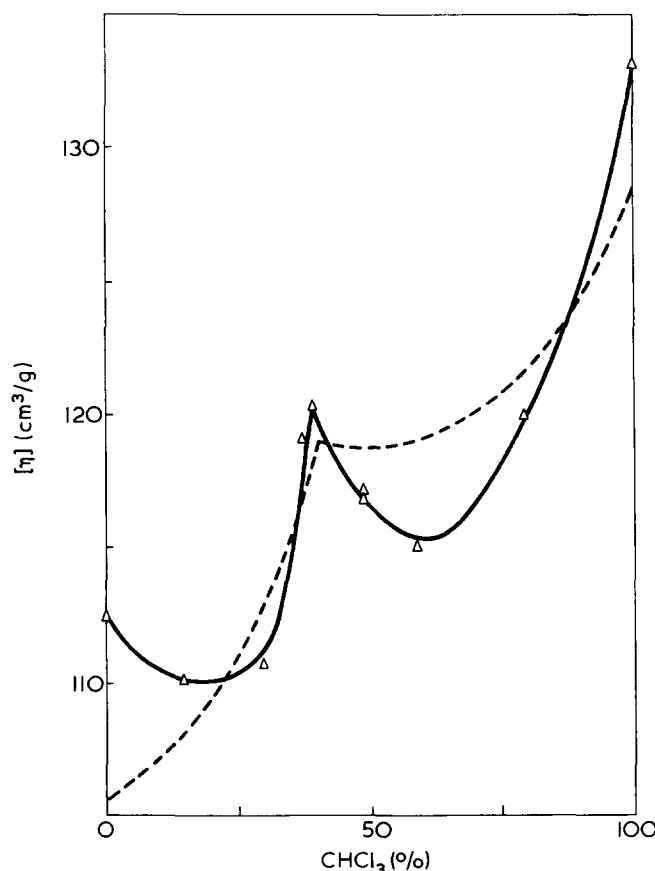


Figure 3 Same as Figure 2, except temperature = 55°C

All these conclusions are very qualitative since it is impossible to write equations for such a four-component system.

## Measurements in benzene-THF mixtures

This solvent mixture is also characterized by a negative deviation from linearity observed in the  $[\eta]$  vs. composition curve for pure polystyrene (Figure 4). For PMMA a discontinuity is observed in the  $[\eta]$  vs. composition plot, and both parts of the curve exhibit upward curvatures (i.e. negative deviations from linearity). As the temperature rises the magnitude of the discontinuity increases, and its position in the composition diagram moves slightly to higher THF contents. An interpretation of this behaviour was proposed recently<sup>16</sup>.

It was also of interest to investigate how the incompatibility of the two homopolymers changes with solvent composition. It is known that the critical demixion concentration  $c_D$  of the two homopolymers in a given solvent is a measure of the  $\chi_{AB}$  interaction parameter. Figure 5 shows a plot of  $c_D$  versus solvent composition; this plot was obtained using equal amounts of a PS sample of molecular weight  $M_w = 700\,000$  and of a PMMA sample of  $M_w = 438\,000$  at room temperature. The plot obtained shows a positive deviation from linearity, which indicates that the two polymers are less incompatible in benzene-THF mixtures than would be expected from the critical demixion concentrations measured (for the same polymers and at the same temperature) in pure benzene and in pure THF.

A further proof of this fact is given by the variation of the limiting viscosity number of a PS/PMMA random copo-

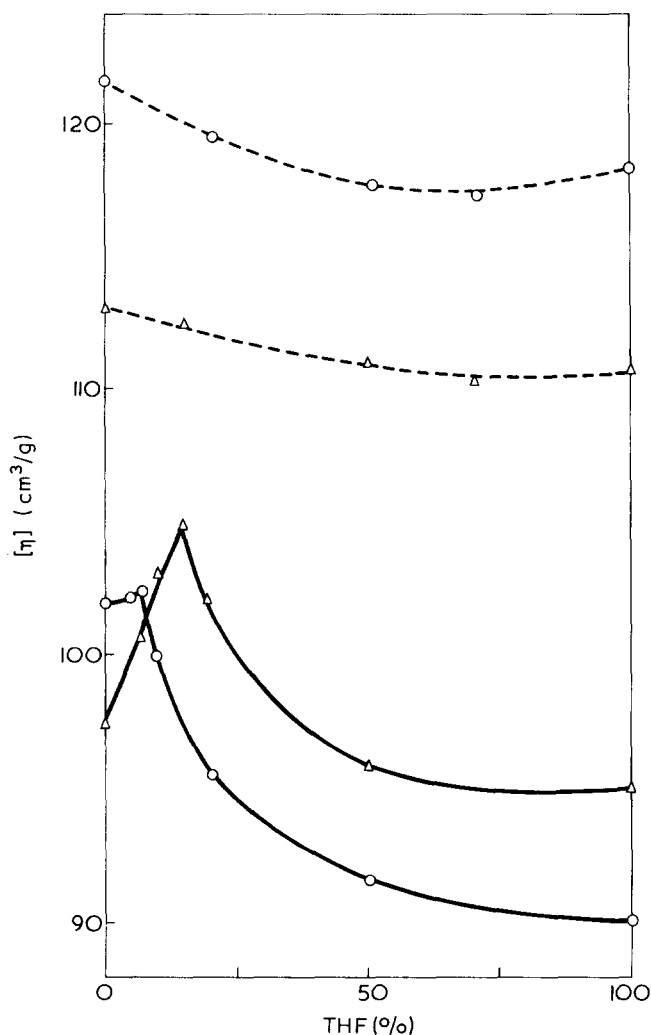


Figure 4 Variation of the limiting viscosity number of polystyrene (---) and of PMMA (—) versus THF content of the solvent mixture (benzene-THF).  $\circ$ , 17°C;  $\triangle$ , 55°C

lymer ( $M_w = 210\,000$ , 52% styrene) over the whole composition range of the solvent mixture. The sharp negative deviation from linearity of this plot (Figure 6) cannot be explained without assuming that  $\chi_{AB}$  is smaller in these mixtures with respect to its values in the two pure solvents. In the same Figure we have plotted the viscosity of the completely segregated block copolymer of the same molecular weight and composition, as a function of the composition of the solvent mixture, using equation (3). This

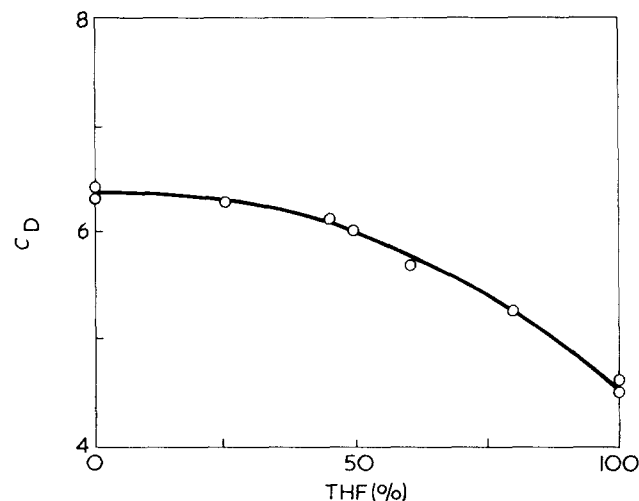


Figure 5 Critical demixion concentration  $c_D$  of a polystyrene ( $M = 700\,000$ )/PMMA ( $M = 435\,000$ ) mixture in benzene-THF mixed solvents versus THF content of the solvent ( $c_D$  is expressed in g PS + PMMA/100 cm<sup>3</sup> of the solvent mixture)

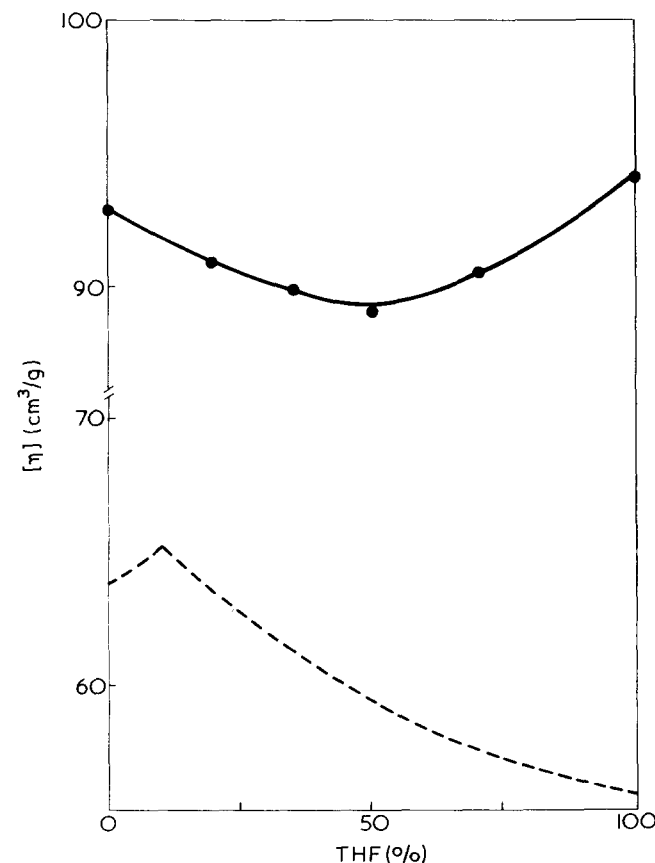


Figure 6 Variation of the limiting viscosity number for a given random copolymer of styrene and MMA as function of the THF content of the benzene-THF solvent mixture. Measurements carried out at 25°C; ---, values calculated neglecting heterocontacts

curve is always below the curve corresponding to the statistical copolymer showing that  $\chi_{AB}$  is positive, increasing when the mixture becomes rich in THF.

Figure 7 shows the experimental viscosities of the triblock copolymer at 17°C as a function of composition of solvent mixture. As in the preceding case, we have calculated a theoretical curve using equation (3).

The agreement is excellent showing that no contribution of the  $\chi_{AB}$  term on the viscosity number can be detected, and thus bringing new arguments in favour of a completely segregated model. In this case, as in the preceding benzene-CHCl<sub>3</sub> mixture at 25°C the transition of PMMA is not detected. The same type of experimental and calculated results have been plotted in Figure 8, in this case at 55°C.

There is now no agreement: the experimental points are higher than the calculated curve. The difference between experimental and calculated curves varies with composition similarly<sup>1</sup> to that observed for statistical copolymers (Figure 6), but to a much lesser extent suggesting that the behaviour of this copolymer is somewhere between the completely segregated and the statistical copolymer.

### CONCLUSION

The present investigation was mainly aimed to study segregation effects in triblock copolymers as a function of solvent composition and at different temperatures.

The samples used were interesting since they contained two PMMA blocks which exhibit a conformational transition in non-polar solvents. This transition is also observed in solvent mixtures, for a given content of polar solvent. The solvent mixtures used were chosen such as to cover a wide range of polarity and to vary the solvation of the individual sequences as much as possible within the composition range of the mixtures.

In both solvent mixtures investigated the behaviour of the triblock copolymer of styrene and MMA is not the same at 15–25°C as at temperatures of the order of 50°C.

In the lower temperature range segregation apparently prevents AB heterocontacts from occurring and the fit is good (especially in benzene-THF mixtures) between the experimental  $[\eta]$  values and those calculated on the basis of segregation. It is interesting to note that under these con-

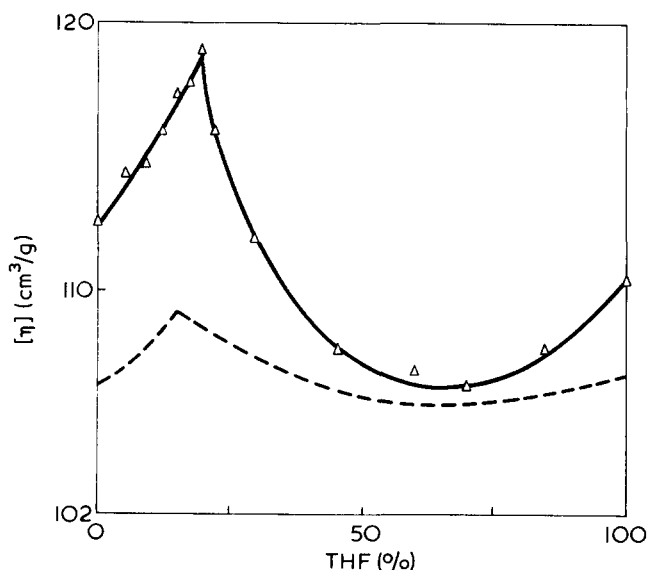


Figure 8 Same as Figure 7 except temperature = 55°C

ditions the conformational transition of the PMMA disappears almost entirely. Whether this is due to the fact that PMMA is hidden by the more soluble PS block or that the contribution of PMMA to viscosity is too small to be detected, is questionable.

At elevated temperature the behaviour of the triblock copolymer in the chosen solvent mixtures cannot be accounted for on the basis of complete segregation.

One can state that it is intermediate between segregated and statistical copolymers. This shows that if segregation does exist there is no abrupt transition between the completely segregated and unsegregated status but that one goes progressively for a segregated to a less segregated conformation, as temperature increases.

Finally, it should be noted that equation (3) which was used to evaluate the dimensions in the segregated conformation does not take into account the fact that we have a triblock copolymer.

### REFERENCES

- 1 Burnett, G. M., Meares, P. and Paton, C. *Trans. Faraday Soc.* 1962, **58**, 737
- 2 Dondos, A., Froelich, D., Rempp, P. and Benoit, H. *J. Chim. Phys.* 1967, **64**, 1012
- 3 Girolamo, M. and Urwin, J. R. *Eur. Polym. J.* 1972, **8**, 299
- 4 Krause, S. *J. Phys. Chem.* 1964, **68**, 1948
- 5 Utiyama, H. et al. *Macromolecules* 1974, **7**, 515
- 6 Dondos, A. and Benoit, H. *Makromol. Chem.* 1968, **118**, 165
- 7 Dondos, A., Rempp, P. and Benoit, H. *Makromol. Chem.* 1969, **130**, 233
- 8 Dondos, A. *Makromol. Chem.* 1971, **147**, 123
- 9 Dondos, A., Rempp, P. and Benoit, H. *Polymer* 1972, **13**, 97
- 10 Girolamo, M. and Urwin, J. R. *Eur. Polym. J.* 1971, **7**, 693
- 11 Dondos, A. *J. Polym. Sci. (B)* 1971, **9**, 871
- 12 Dondos, A. and Patterson, D. *J. Polym. Sci. (A-2)* 1969, **7**, 209
- 13 Dondos, A. and Benoit, H. *Makromol. Chem.* 1970, **133**, 119
- 14 Strazielle, C. and Benoit, H. *J. Chim. Phys.* 1961, **58**, 675, 678
- 15 Dondos, A., Rempp, P. and Benoit, H. *Makromol. Chem.* 1973, **171**, 135
- 16 Dondos, A., Havredaki, V. and Mitsou, A. *Makromol. Chem.* 1975, **176**, 1481
- 17 Dondos, A., Rempp, P. and Benoit, H. *Eur. Polym. J.* 1967, **3**, 657
- 18 Barker, J. A. and Smith, F. *J. Chem. Phys.* 1954, **22**, 375

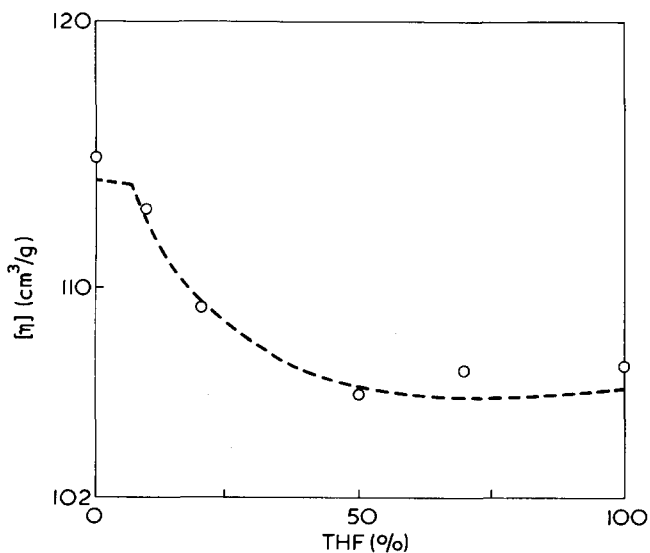


Figure 7 Variation of the measured limiting viscosity number of the triblock copolymer (PMMA/PS/PMMA) as a function of the THF content of the solvent mixture (benzene-THF) at 17°C. ----, Calculated curve

# Crystallization of isotactic polystyrene induced by organic vapours

N. Overbergh, H. Berghmans and G. Smets

Laboratory of Macromolecular and Organic Chemistry, University of Leuven, 3030 Heverlee, Belgium  
(Received 3 January 1975; revised 24 March 1975)

The crystallization of isotactic polystyrene induced by dichloromethane and acetone was studied. From equilibrium absorption data, the critical concentration for crystallization was deduced. The crystallization kinetics were followed and diffusion coefficients were calculated. It was found that the crystallization was diffusion controlled. The increase in the rate of crystallization is explained by the high rate of diffusion and nucleation in the presence of the organic solvents. Evidence for the high nucleation probability was found in morphological observations (SAXS and electron microscope observations). The melting behaviour of the solvent crystallized samples suggests formation of a very unstable crystalline structure which re-organizes rapidly on heating.

## INTRODUCTION

The crystallization of polymers is facilitated by the presence of organic vapours<sup>1-6</sup>. These low molecular weight plasticizers greatly increase the rate of crystallization owing to an increase of nucleation probability and/or a higher rate of chain segment diffusion. Both factors influence the onset of the crystallization as well as the growth of the crystalline phase.

In order to gain some insight into the mechanism of this crystallization, we have studied the crystallization of isotactic polystyrene (IPS) induced by dichloromethane and acetone. The morphology and the melting behaviour of the structures formed were also studied.

## EXPERIMENTAL

### Polymers

The synthesis of isotactic polystyrene (IPS) was reported elsewhere<sup>7</sup>. Atactic polystyrene (APS) was prepared by thermal polymerization in benzene at 125°C<sup>8</sup>.

### Absorption measurements

The apparatus used for the absorption measurements is shown in *Figure 1*. The organic solvent was introduced under high vacuum into flask A which was then attached to the apparatus (B). The polymer sample of about 50 mg was suspended on a calibrated quartz spring with an average extension of 1.8 mm/mg. When the high vacuum in B is obtained, solvent vapour is allowed to flow from A to B by breaking the breakseal which separates the two compartments. The vapour pressure of the solvent was determined by a thermostatic bath (T<sub>1</sub>). The water jacket (T<sub>2</sub>) surrounding the sample determines the crystallization temperature; this corresponds to the temperature of the air chamber around the apparatus. The extension of the quartz spring measures the degree of vapour absorption and is followed with a cathetometer.

For determining the kinetics of absorption, the spring extension is followed as a function of time under different vapour pressures. Equilibrium absorption measurements as a function of the vapour pressure were carried out with one sample, beginning with the lowest vapour pressure. Before

measurement the sample was kept under constant vapour pressure for at least 24 h.

### Density measurements

Densities were measured using a density gradient column, filled with an aqueous solution of potassium chloride, thermostated at 23°C. The densities at the top and the bottom of the column were respectively 1.040 and 1.099. For the calculation of the degree of crystallinity values of 1.057 and 1.125<sup>9</sup> were taken for the densities of the amorphous phase and the crystal lattice respectively.

### Annealing

About 20 mg of the crystallized samples were annealed under vacuum under various conditions of temperature and time.

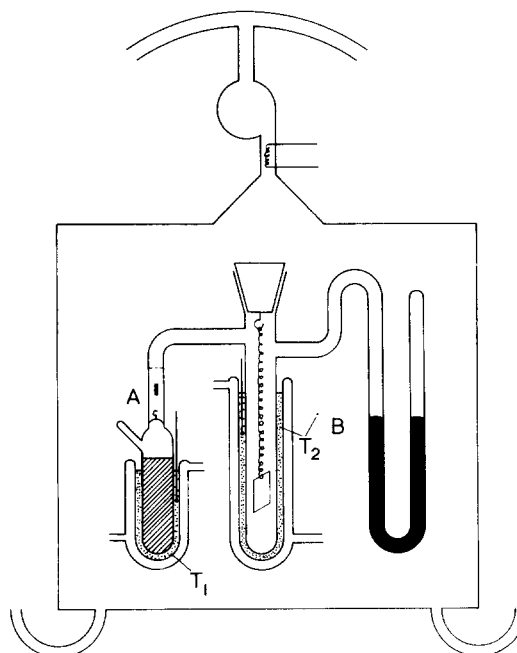


Figure 1 Absorption apparatus



**Calorimetric observations**

Calorimetric measurements were made with a Perkin-Elmer DSC-1B, after drying the samples for two weeks at room temperature followed by 60–70°C for one week.

The glass transition temperature of polymer–solvent mixtures was measured at a heating rate of 32°C/min. In order to prevent evaporation of the solvent, liquid sample pans were used<sup>10</sup>.

**Microscopy**

Optical observations on microtome sections (~5 μm) were carried out with a polarizing microscope (Leitz-Dialux-Pol). The spherulitic morphology was examined on ultramicrotome sections of about 500 Å (LKB Ultratome III) with a Jeol 100U electron microscope.

**X-ray analysis**

Small angle X-ray scattering (SAXS) experiments were performed with a Kratky camera with counting equipment. Monochromatic Cu-radiation was obtained by using a NiKβ filter and detected by a proportional counter and pulse height discrimination. Appropriate slit height collimation corrections were applied using a computer program described by Vonk<sup>11</sup>. Wide angle X-ray diffraction patterns were recorded with a vertical diffractometer in the transmission mode. A Cu-target tube was used and the diffracted radiation was passed through a curved crystal focalizer.

**RESULTS AND DISCUSSION**

**Equilibrium absorptions**

Equilibrium absorption data for polystyrene–dichloromethane and polystyrene–acetone systems are represented in Figure 2, where the degree of absorption is plotted

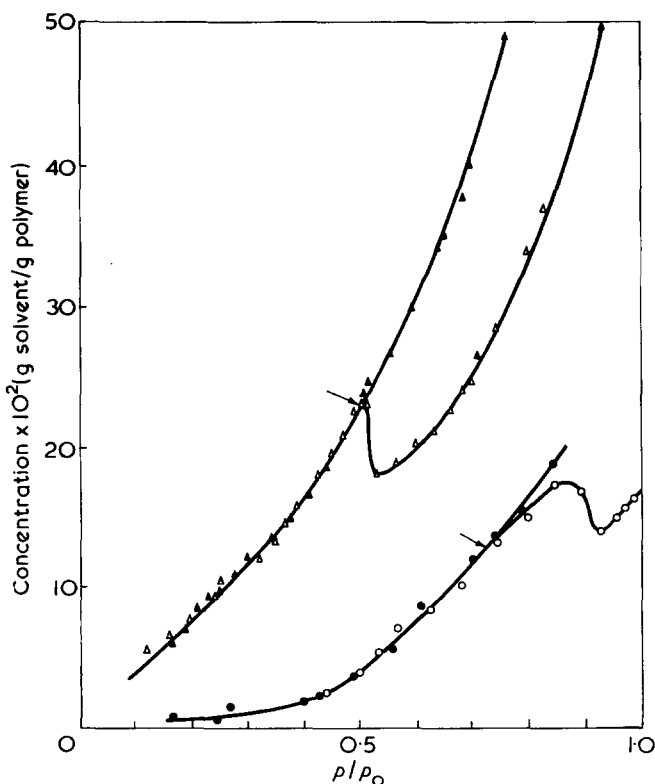


Figure 2 Equilibrium absorption isotherms for IPS (dichloromethane, ▲; acetone, ●) and for APS (dichloromethane, △; acetone, ○)

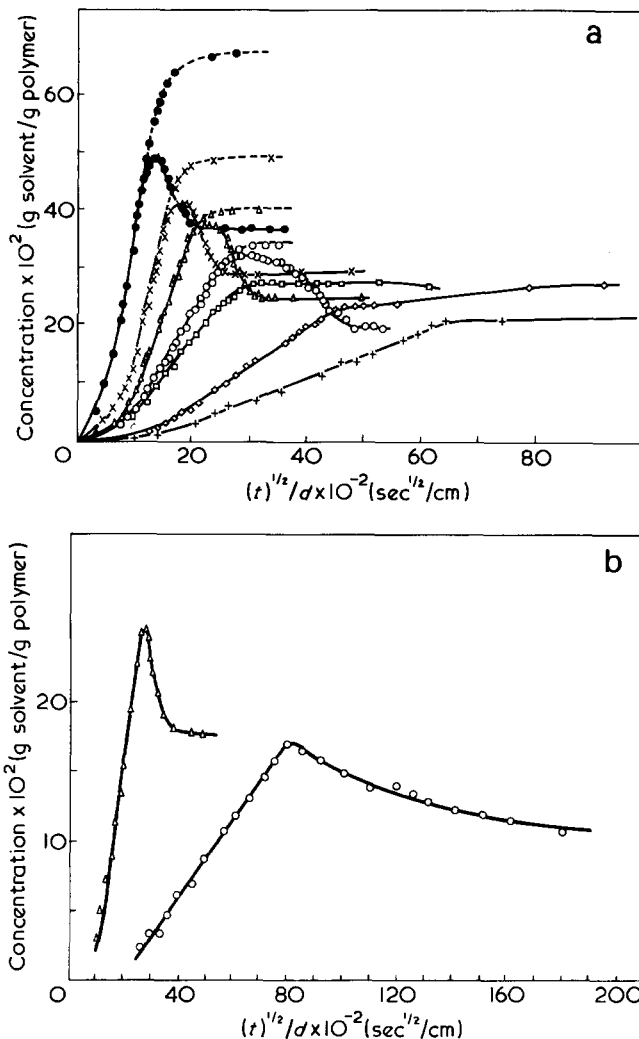


Figure 3 (a) Integral dichloromethane absorption kinetics of IPS (—) and APS (---) at 25°C and different partial vapour pressures (sample thickness 0.25 mm).  $p/p_0$ : ●, 0.85; ×, 0.76; △, 0.69; ○, 0.63; □, 0.61; ◇, 0.575; +, 0.532. (b) Integral acetone absorption kinetics of IPS at 30°C (sample thickness 0.25 mm).  $p/p_0$ : ○, 0.81; △, 0.91

against the reduced vapour pressure  $p/p_0$ ,  $p$  being the actual vapour pressure and  $p_0$  the equilibrium vapour pressure at the temperature of the experiment.

At low degrees of absorption, the curves for IPS and APS coincide. From dichloromethane and acetone contents of 22% and 11% respectively ( $p/p_0$  0.50 and 0.73 respectively) onwards, the equilibrium absorption of IPS falls below that of APS. This is ascribed to the onset of crystallization; indeed, during this process solvent is rejected from the crystallizing region, lowering the overall degree of absorption. Increasing the vapour pressure still further causes a marked difference in the behaviour of both polystyrenes. This is the consequence of a gradual increase of the crystallinity with increasing vapour pressure. At  $p/p_0 = 0.62$  for dichloromethane and 0.92 for acetone, the degrees of crystallinity determined by d.s.c. are respectively 0.23 and 0.27. At higher vapour pressure, the degree of crystallinity remains constant and further solvent absorption occurs parallel to the absorption in APS.

From these data we conclude that the minimum solvent content required for crystallization is 22% for dichloromethane and 11% for acetone. The glass transition temperature at these critical concentrations of both solvents is -5°C (d.s.c.) This is about 30°C below the crystallization temperature.

## Kinetics of absorption and crystallization

The absorption isotherms for dichloromethane and acetone are represented in Figures 3a and 3b. In agreement with Fick's equation<sup>12</sup> the uptake of solvent is plotted against  $(t)^{1/2}/d$  where  $t$  is the absorption time and  $d$  the half thickness of the sample. After a small induction period the curves are linear up to an absorption of 80% and 70% (for dichloromethane and acetone respectively) of the maximum amount that can be absorbed. The curves of APS and IPS are coincident. Above this content a deviation of the IPS curves occurs, owing to a decrease of the absorption rate, followed by an important desorption. This behaviour is ascribed to the onset of crystallization; the samples become opaque.

The rates of absorption and desorption as well as the degree of desorption increase by increasing the reduced vapour pressures. At low  $p/p_0$  values (0.532 and 0.575 for dichloromethane) no desorption occurs, although the samples crystallize ( $x_c$  is respectively 0.12 and 0.18).

From the linear part of the reduced absorption curves of IPS, diffusion coefficients were calculated, using the equation of Fick<sup>12</sup>:

$$M_t/M_\infty = \frac{2}{d} \left[ \frac{\bar{D}t}{\pi} \right]^{1/2} \quad (1)$$

where  $M_t$  is the quantity of solvent absorbed at time  $t$ ,  $M_\infty$  the equilibrium value and  $\bar{D}$  the integral diffusion coefficient. This integral diffusion coefficient is temperature and concentration dependent.

The concentration dependence is given by:

$$\bar{D} = D_{c \rightarrow 0} \exp(kc) \quad (2)$$

where  $D_{c \rightarrow 0}$  is the diffusion coefficient at zero concentration,  $c$  is the concentration and  $k$  a positive parameter characteristic of a polymer system at a given temperature<sup>13</sup>. The numerical results for the absorption of dichloromethane are given in Table 1; the  $D_{c \rightarrow 0}$  values are by given combination of equations (1) and (2).

The kinetics of absorption depend not only on the reduced vapour pressure but also on the temperature and film thickness.

Table 1 Integral diffusion coefficients and diffusion coefficients at zero concentration for different temperatures

Temperature (°C)	$\bar{D} \times 10^7$ (cm <sup>2</sup> /sec)	Concentration (g dichloromethane/g polymer) $\times 100$	$p/p_0^a$	$D_{c \rightarrow 0} \times 10^9$ (cm <sup>2</sup> /sec)
25	0.118	23	0.57	0.85
	0.227	27.3	0.61	
	0.530	31.7	0.63	
	0.954	37.2	0.69	
	1.59	41.5	0.76	
30	2.47	49	0.85	1.4
	0.197	22.3	0.50	
	9.12	37.4	0.69	
35	2.25	43.8	0.76	2.5
	0.504	28.5	0.51	
	0.595	35.5	0.57	
40	2.41	47.5	0.76	4.3
	0.61	27.4	0.47	
	1.0	32.6	0.58	

<sup>a</sup> Reduced vapour pressure:  $p$  = actual vapour pressure;  $p_0$  = equilibrium vapour pressure at the given temperature

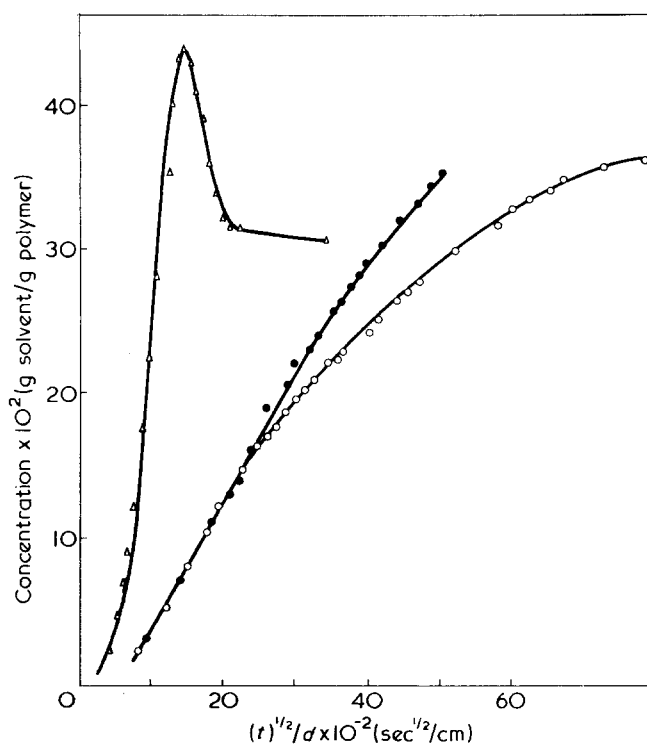


Figure 4 Integral dichloromethane absorption kinetics of IPS at 30°C and different thicknesses (○, 2 mm; △, 0.25 mm) The absorption kinetics of APS are also represented (●, 2 mm)

The critical concentration for crystallization decreases with increasing temperature. In the presence of 23% dichloromethane, IPS crystallizes readily at 40°C, but very slowly at 25°C. At 35°C, 13% of acetone is sufficient while at 25°C no crystallization occurs at that concentration.

The influence of film thickness on the absorption kinetics is illustrated in Figure 4.

With a thin sample (Figure 4, 0.25 mm,) an important desorption is observed, while no desorption occurs with a thicker sample (Figure 4, 2 mm). This is explained by a diffusion controlled crystallization. In the thin sample, the critical concentration is obtained practically over the whole sample before the onset of crystallization. As a consequence, solvent is rejected from the sample during the crystallization as evidenced by this desorption. In thicker samples, a solvent gradient is built up in the sample and the critical concentration for crystallization is attained initially at the surface of the sample. As a consequence crystallization begins at the surface. As the absorption proceeds, a front with this critical concentration moves into the sample followed by a crystalline front. During this crystallization, part of the rejected solvent is absorbed into the centre of the sample. Therefore no desorption is observed while the rate of absorption is strongly reduced. This absorption rate is also lower than in the case of atactic polystyrene of the same thickness (Figure 4).

This diffusion controlled crystallization is illustrated in Figure 5 on microtomed sections of samples of different thickness, made during the initial stages of crystallization; a crystalline border can be observed (crossed polarizers) while the interior of the sample is still amorphous. In Figure 5a, the arrow indicates the centre of the sample. The crystalline phase is composed of small spherulites as revealed by electron microscope observations on ultramicrotomed sections (Figure 6). The spherulites have an average diameter of 6 μm. The arrow indicates the diffusion direction.

Because of this diffusion controlled crystallization, it is impossible to follow the crystallization kinetics in order to derive Avrami parameters<sup>4,14-16</sup>. The crystallinity measured by conventional methods is only an average value. Difficulties also arise from the continuation of the crystallization during the elimination of the solvent under vacuum. Because of the presence of the crystalline layer, evaporation is retarded and it is impossible to bring the sample quickly below the critical concentration for crystallization.

In the presence of organic vapours the rate of crystallization is greatly enhanced. A sample with a thickness of 0.25 mm, crystallized in dichloromethane vapour ( $p/p_0 =$

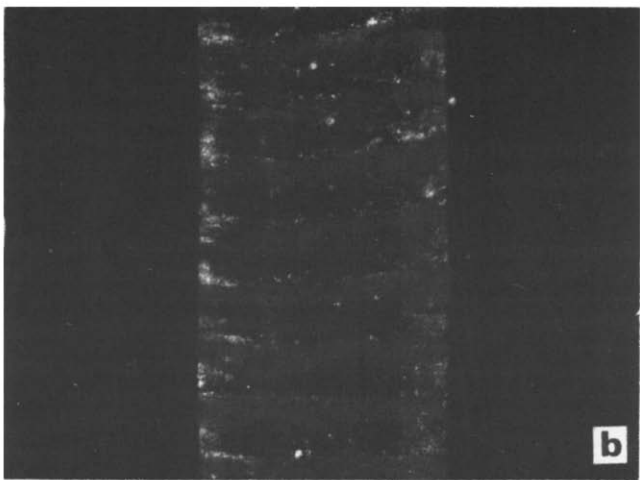
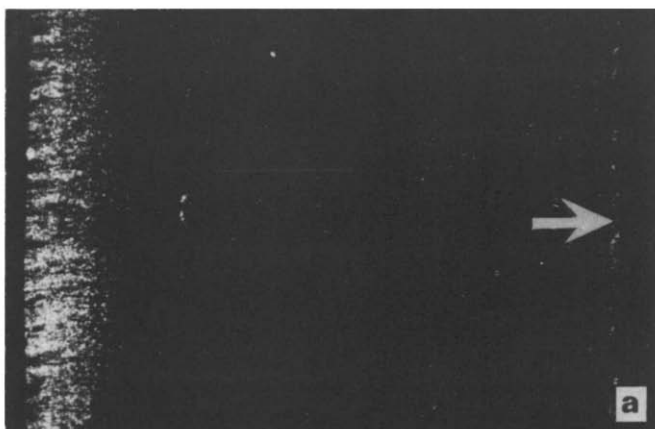


Figure 5 Optical micrographs (crossed polarizers) of a microtomed section of IPS crystallized in dichloromethane vapour. Sample thickness: (a) 2 mm; (b) 0.25 mm at maximum degree of absorption



Figure 6 Electron micrograph of an ultramicrotomed section of IPS crystallized by swelling with dichloromethane vapour

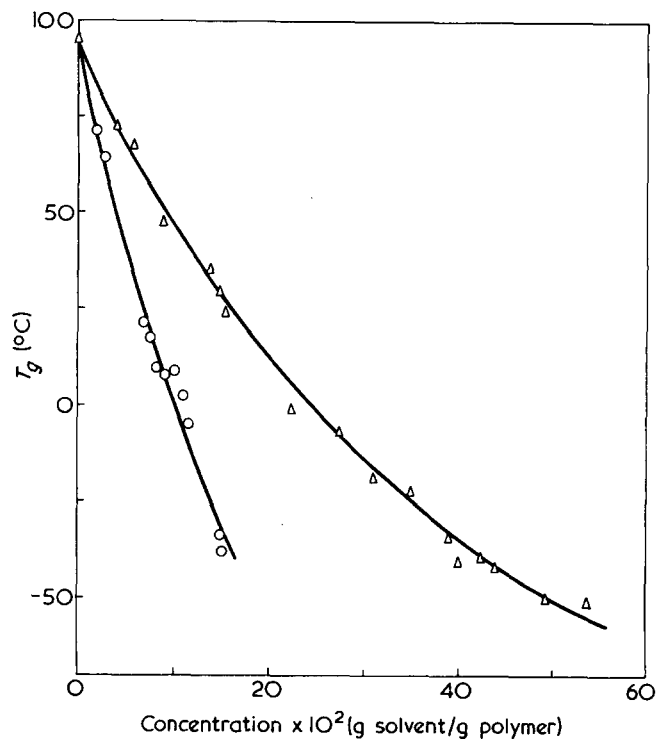


Figure 7 Glass transition temperature ( $T_g$ ) of IPS as a function of dichloromethane ( $\Delta$ ) and acetone ( $\circ$ ) concentration

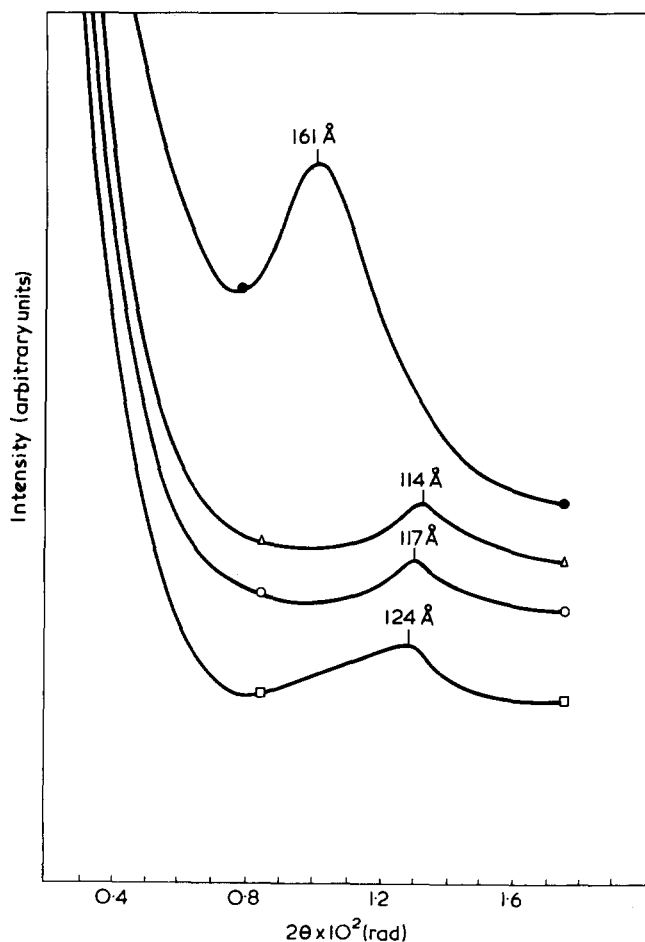


Figure 8 Desmeared SAXS curves of crystallized IPS:  $\circ$ , by swelling with acetone at 25°C;  $\Delta$ , by swelling with dichloromethane at 25°C;  $\square$ , at 135°C in the absence of any organic vapour;  $\bullet$ , in acetone at 25°C followed by annealing at 207°C for 15 h

Table 2 Crystallinity ( $X_v$ ) as a function of annealing time at different annealing temperatures ( $T_a$ ), of a sample crystallized in dichloromethane vapour (amorphous at 220°C)

Annealing time (min)	$T_a$ (°C)						
	150	170	195	200	205	210	215
2	0.25	0.25	0.25	0.25	0.235	0.23	0.10
5	0.26	0.26	0.255	0.26	0.28	0.26	0.13
15	0.265	0.265	0.27	0.29	0.31	0.30	0.25
30	0.265	0.27	0.28	0.30	0.32	0.31	0.30
60	0.27	0.275	0.29	0.31	0.33	0.32	0.32
180	0.27	0.28	0.30	0.31	0.33	0.32	0.33
300	0.28	0.285	0.31	0.32	0.33	0.33	0.33
600	0.29	0.295	0.31	0.33	0.33	0.33	0.33
900	0.295	0.30	0.32	0.33	0.33	0.33	0.33
1440	0.31	0.31	0.32	0.33	0.33	0.33	0.33

0.75 and  $T_c = 25^\circ\text{C}$ ), is completely crystalline in 25 min. The crystallization of a sample without solvent, prepared under the same conditions, takes many hours even at the temperature of maximum crystallization rate. Crystallization kinetics depend upon ability of diffusion and nucleation. They are determined by the difference between the crystallization temperature,  $T_c$ , and the glass transition temperature ( $T_c - T_g$ ) and the equilibrium melting point ( $T_m^0 - T_c = \Delta T$ ) respectively<sup>17,18</sup>. We have taken  $T_m^0 = 240^\circ\text{C}$  and  $T_g = 95^\circ\text{C}$ .

The dependence of  $T_g$  on solvent concentration was investigated and is shown in Figure 7. At high solvent concentrations the onset of crystallization cannot be prevented. This introduces an error of the order of a few degrees in this domain.

A  $T_g$  of  $25^\circ\text{C}$  was obtained with a concentration of 15% by wt for dichloromethane and 7% by wt for acetone. A  $T_g$  of  $23.5^\circ\text{C}$  was found by Jenckel<sup>19</sup> for APS containing 16.8% of dichloromethane.

Owing to the volatility of the solvents, it is impossible to determine experimentally the dependence of  $T_m$  on solvent concentration. As a consequence, the degree of undercooling ( $\Delta T$ ) at different concentrations cannot be calculated.

This degree was estimated from the SAXS measurements. The SAXS maximum of samples crystallized by swelling with a solvent are broad and low in intensity (Figure 8). In the presence of 40% dichloromethane or 24% acetone these maxima appear at greater diffraction angles than for samples crystallized in the absence of any solvent at  $T_c = 135^\circ\text{C}$  ( $\Delta T = 105^\circ\text{C}$ ). The long periods are reported in the Figure. It is known from crystallization theories that  $L$  is related to the reciprocal of the degree of undercooling,  $\Delta T$ . The crystals with the smallest long period are grown at the largest degree of undercooling. Consequently during crystallization in the presence of 40% dichloromethane or 24% acetone,  $\Delta T$  is larger than during the thermal crystallization at  $135^\circ\text{C}$ , i.e.  $\Delta T > 105^\circ\text{C}$ . This also implies that in the presence of a solvent, the nucleation probability is higher. But under these conditions, the diffusion of the chains to the growing crystal surface is also enhanced. In the presence of 40% of dichloromethane,  $T_g = -40^\circ\text{C}$  and at  $25^\circ\text{C}$   $T_c - T_g = 65^\circ\text{C}$ . At  $T_c = 135^\circ\text{C}$  without solvent  $T_c - T_g$  is only  $40^\circ\text{C}$ .

The high crystallization rate in the presence of a solvent can therefore be ascribed to an increased nucleation probability and a lower diffusion activation energy.

Further confirmation of the high degree of undercooling

in the presence of solvent is found in the high nucleation density, reflected in the large number of small spherulites formed (Figure 6). A much smaller number of spherulites is formed in samples, prepared under the same conditions as the samples used in this work and crystallized in absence of solvent at the highest possible degree of undercooling.

Because of the small crystallite thickness (Figure 8) a low melting point is expected for these structures. However, under different rates of heating the solvent crystallized (dried) samples show only one melting endotherm with a final melting point depending only on the heating rate. A melting point dependent on heating rate is an indication for a re-organization of an unstable crystalline structure, which was clearly illustrated for thermally crystallized IPS<sup>7</sup>. The final melting points of solvent crystallized samples are the same as those obtained with thermally crystallized samples which re-organize during heating at the same rate. This demonstrates that the crystallites must be very unstable so they re-organize easily on heating.

Annealing experiments clearly illustrate this fast re-organization (Table 2). During heating above the crystallization temperature, the crystallinity of the samples increases. Above  $200^\circ\text{C}$  partial melting followed by recrystallization is observed. At lower temperatures, no initial drop of the crystallinity can be detected, although the annealing temperature is in the melting region of the originally formed crystallites. This suggests that during the annealing the crystallites re-organize directly to a more stable phase. This is reflected in the SAXS patterns.

After annealing below  $200^\circ\text{C}$  the maxima shift to smaller scattering angles, the width increases and the intensity increases (Figure 8). In the WAXS, a sharpening of the (211) reflections is observed. These changes in the SAXS and WAXS indicate an increase in crystallite thickness and improvement of the perfection of the crystals.

We can conclude that during this very rapid crystallization an unstable crystalline structure is formed, which re-organizes very quickly by heating.

#### ACKNOWLEDGEMENTS

The authors are indebted to the Ministry of Scientific Programmation for a fellowship to one of them (N.O.), as well as for equipment and financial support given to the laboratory.

REFERENCES

- 1 Siegmann, A. and Geil, P. H. *J. Macromol. Sci. (B)* 1970, **4**, 239
- 2 Kambour, R. P., Karasz, F. E. and Daane, J. H. *J. Polym. Sci. (A-2)* 1966, **4**, 327
- 3 Assukelov, M. A., Krasnikova, N. P. and Kargin, V. A. *J. Polym. Sci. USSR* 1972, **14**, 33
- 4 Zachmann, H. G. *Kolloid-Z. Z. Polym.* 1963, **189**, 67
- 5 Mercier, J. P., Groeninckx, G. and Lesne, M. *J. Polym. Sci. (C)* 1967, **16**, 2059
- 6 Horikiri, S. and Kodera, K. *Polym. J.* 1973, **4**, 213
- 7 Overbergh, N., Berghmans, H. and Smets, G. *J. Polym. Sci. (C)* 1972, **38**, 237
- 8 Campbell, T. W. and Sorenson, W. 'Preparative Methods of Polymer Chemistry', *Interscience, New York*, 1968, p 160
- 9 Natta, G. and Corradini, P. *Makromol. Chem.* 1955, **16**, 77
- 10 Kambour, R. P., Romagosa, E. E. and Gruner, C. I. *Macromolecules* 1972, **5**, 335
- 11 Vonk, C. G. *J. Appl. Crystallog.* 1971, **4**, 340
- 12 Crank, J. and Park, G. S. 'Diffusion in Polymers', Academic Press, London, 1968
- 13 Kishimoto, A. and Fujita, A. *J. Polym. Sci.* 1958, **28**, 569
- 14 Sheldon, R. P. *Polymer* 1962, **3**, 27
- 15 Sheldon, R. P. and Blakely, P. R. *Nature* 1962, **195**, 172
- 16 Moore, W. R. and Sheldon, R. P. *Polymer* 1961, **2**, 315
- 17 Hoffman, J. D. and Lauritzen, Jr, J. I. *J. Res. Nat. Bur. Stand.* 1961, **65A**, 297
- 18 Lauritzen, Jr, J. I. and Hoffman, J. D. *J. Res. Nat. Bur. Stand.* 1960, **64A**, 73
- 19 Jenckel, E. and Heusch, R. *Kolloid-Z. Z. Polym.* 1953, **130**, 89

# Determination of unsaturation in ethylene-propylene terpolymers and butyl rubber by time-averaged $^1\text{H}$ n.m.r. measurements

Yasuyuki Tanaka, Hisaya Sato and Yukio Ozeki

*Department of Textiles and Polymer Science, Faculty of Technology, Tokyo University of Agriculture and Technology, Koganei, Tokyo, Japan*

and Masaru Ikeyama and Takefumi Sato

*Tokyo Research Laboratory, Japan Synthetic Rubber Co., Ikuta, Kawasaki, Japan*

*(Received 28 January 1975)*

The time-averaged  $^1\text{H}$  n.m.r. spectra of ethylene-propylene-dicyclopentadiene, ethylene-propylene-ethylidene norbornene and isobutylene-isoprene copolymers were measured. Assignments of the olefinic resonances were carried out by comparing the spectra with those of each homopolymer and starting monomers. The concentration of the olefinic unit in copolymer was determined by measuring the intensity ratio between the olefinic proton signal and the signal of trichloroethylene which was added as an internal standard of intensity measurements. The concentrations of unsaturation in copolymers determined by using the iodine-mercuric acetate method were proportional to those determined by the n.m.r. method. The accuracy and precision of the n.m.r. measurements were shown to be better than 10% for a mixture of polyisobutylene and polyisoprene containing 1.24 mol % of unsaturation as a model compound of isobutylene-isoprene copolymer.

## INTRODUCTION

In the polymerization of isobutylene or copolymerization of ethylene and propylene a small amount of unsaturation is introduced into the chain to facilitate the sulphur vulcanization of the polymers. Several different types of diene monomer are employed in commercially produced rubber, i.e., dicyclopentadiene, ethylidene norbornene, methylidene norbornene, or 1,4-hexadiene for ethylene-propylene terpolymer (EPDM) and isoprene for butyl rubber (IIR). Identification and quantitative analysis of those diolefinic units in copolymers have been technically rather difficult owing to the low concentration of the units and also to the fact that these diene units polymerize to give several types of the isomeric structure.

Chemical and infra-red (i.r.) spectroscopic analyses have been widely used to determine the unsaturation in copolymers. The iodine number methods utilize the addition reaction of halogen using reagents such as iodine monochloride<sup>1</sup>, iodine-mercuric acetate<sup>2</sup> or pyridinium bromide perbromide<sup>3</sup> were investigated in detail. However, this is still somewhat unsatisfactory because of the presence of side reactions and of incomplete addition reaction of these reagents. On the other hand, the infra-red method is of limited application, e.g., the content of isoprene units in butyl rubber cannot be determined by this method owing to the absence of characteristic infra-red bands as well as small absorptivity of the units. Recently, time-averaged  $^1\text{H}$  n.m.r. spectroscopy has been used for the determination of small amounts of copolymer components<sup>4-6</sup> and the isomeric structure of polyisoprene<sup>7,8</sup>. A low signal-to-noise ratio of the spectrum can be improved by the use of this technique. However, direct measurements of the relative intensity of the olefinic proton signals are practically

impossible in EPDM and IIR, because the intensity of these signals is usually very small in comparison with that of the other aliphatic proton signals. Different settings of output signal attenuations in the instrument were used in the spectra of the olefinic signals and aliphatic signals of EPDM<sup>6</sup>, but there still remains uncertainty for calibrating the attenuation differences.

The present investigation was undertaken to develop a new method for determining a small amount of unsaturation in EPDM and IIR by the time-averaged  $^1\text{H}$  n.m.r. measurement. In addition, the accuracy and precision of the analysis were checked in detail. The concentration of unsaturation in commercially produced EPDM and IIR sample was determined by the n.m.r. method. The results were compared with those obtained by the iodine-mercury acetate method<sup>2</sup>.

## EXPERIMENTAL

### *Materials*

The commercially produced ethylene-propylene-dicyclopentadiene (EPDM-D), ethylene-propylene-ethylidene norbornene (EPDM-N), and isobutylene-isoprene (IIR) rubbers were purified by repeated reprecipitations from cyclohexane solution with methanol. The viscosity of the polymer solution was reduced by irradiating the ultrasonic wave at 25 kHz under nitrogen atmosphere.

### *$^1\text{H}$ n.m.r. measurements*

The  $^1\text{H}$  n.m.r. spectra were measured at 24°C in a 5 mm o.d. or 10 mm o.d. sample tube on a JEOL-4H-100 spectrometer. A JNM-SB-2 S/N booster equipped with spectral

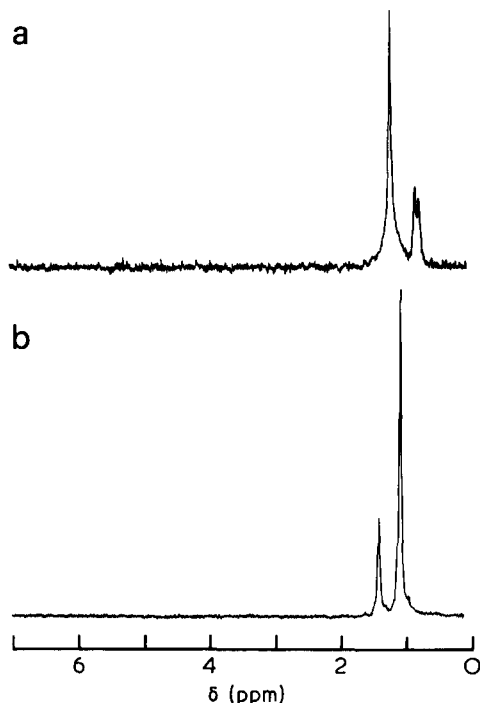


Figure 1 N.m.r. spectra of (a) EPDM and (b) IIR

data points of 1024 bits was used for the time-averaging work. The signal-to-noise ratio of the spectrum was enhanced by the multiple scan average technique. The olefinic proton resonances were time-averaged with a sweep time of 85 sec for 8 to 4 ppm ( $\delta$ ) sweep width. The samples were dissolved in carbon tetrachloride to give a concentration of 20% w/v for the measurement of olefinic proton resonances and 5% for aliphatic proton resonances. Trichloroethylene was used as an internal standard of intensity measurements. The relative intensities between the trichloroethylene signal and the olefinic proton signal were measured by cutting and weighing each peak area of a Xerox copy of the spectrum. The time-averaged spectra were taken with the accumulation of 32 to 128 scans using a 10 mm o.d. sample tube and 64 to 256 scans using a 5 mm o.d. sample tube for the determination of unsaturation in IIR and EPDM, respectively. The settings of a radiofrequency field were decided in such a way that trichloroethylene exhibited a well resolved signal in the time-averaged spectrum.

#### Iodine number method

The degree of unsaturation in the copolymers was determined using the iodine-mercury acetate-trichloroacetic acid method<sup>2</sup> according to the procedure developed by McNall and Eby<sup>9</sup>. A solution of copolymer in carbon tetrachloride was reacted for 30 min with iodine in the presence of mercuric acetate and trichloroacetic acid. Afterwards, the excess iodine was titrated with sodium sulphate.

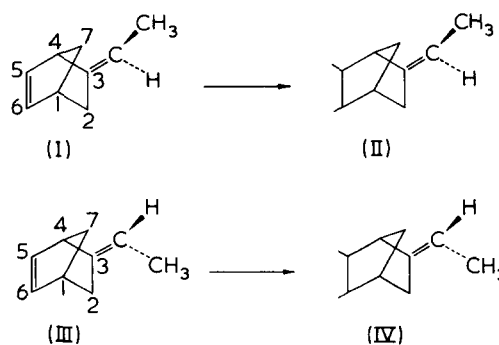
## RESULTS AND DISCUSSION

#### Assignments of the signals

The unsaturation units in EPDM or IIR cannot be detected with the usual n.m.r. measurements, since the signals from the olefinic protons are of such low intensity that they cannot be distinguished from the background noise as shown in Figure 1. On the other hand, the olefinic

resonances of isoprene, dicyclopentadiene and ethylidene norbornene units in the copolymers were clearly observed by means of the time-averaged measurements as shown in Figure 2. The signal at 5.02 ppm in the spectrum of IIR (Figure 2a) is assigned to the methine protons of *cis*-1,4- and/or *trans*-1,4-isoprene units on the basis of the assignments in the spectrum of polyisoprene<sup>10-13</sup>. It is noteworthy that the olefinic resonances due to the isoprene units in 3,4- and 1,2-addition are not detected in the spectrum of IIR. This fact gives support to the early findings obtained in the degradation of IIR by ozone that all of the isoprene units are present in 1,4-addition along the polymer chain<sup>14</sup>.

The olefinic resonances of ethylidene norbornene units in EPDM-N appeared as two doublets centred at 5.20 and 4.95 ppm (Figure 2b). Similar resonance was observed in the spectrum of ethylidene norbornene monomer. In view of the fact that the starting ethylidene norbornene monomer is a mixture of two steric isomers (I and III), the signals at 4.95 and 5.20 ppm are attributed to the substituted methine protons in the configuration of II and IV, respectively<sup>15-17</sup>. No signals from the olefinic 5,6-methine protons were observed in the spectrum.



This indicates that the ethylidene norbornene units are incorporated into the copolymer in a structure polymerized through norbornene double bond. Therefore, the concentration of unsaturation can be determined from the relative intensity of the peak around 5.0-5.2 ppm.

It was found by i.r. analysis that dicyclopentadiene is incorporated in EPDM by addition at 9,10-double bond<sup>18</sup>. The olefinic resonance of the dicyclopentadiene units in EPDM appeared as a doublet centred at 5.48 ppm (Figure 2c), which is assigned to two methine protons of 1,2-position (VI).



The time-averaged spectra of the samples irradiated with ultrasonic wave at 25 kHz were compared with those of the starting copolymer samples. No significant difference was observed between them for IIR and EPDM samples except for the improvement in resolution of the spectra by irradiation. This indicates the usefulness of the ultrasonic treatment to obtain a well resolved spectrum in the time-averaged measurement. Ultrasonic irradiation results in chain scission of polymer<sup>19</sup> and lowering of solution viscosity as well as homogenizing of polymer solution. These effects might bring great advantages for measuring the n.m.r. spectrum of high molecular weight polymer. An improve-

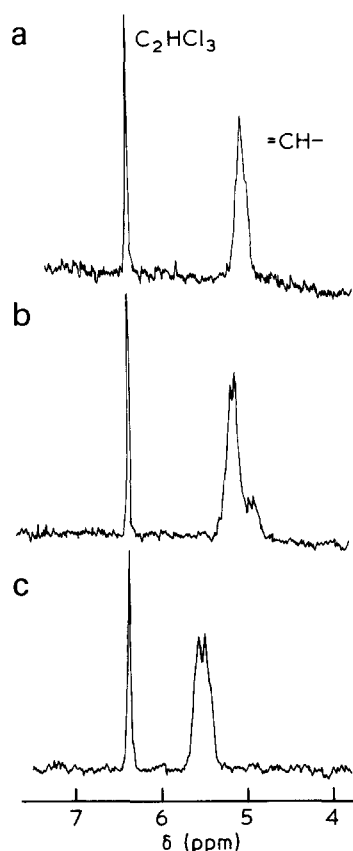


Figure 2 Time-averaged n.m.r. spectra of (a) IIR, (b) EPDM (ethylidene norbornene) and (c) EPDM (dicyclopentadiene) containing  $\text{C}_2\text{HCl}_3$  as an internal standard of intensity measurement. The spectra were obtained with accumulations of 128 scans

ment of resolution by the ultrasonic treatment was observed also in the  $^{13}\text{C}$  n.m.r. measurement of polybutadiene<sup>20</sup>.

#### Quantitative determination of copolymer composition

The signals from olefinic protons in IIR and EPDM are of such low intensity that the direct measurement of the relative intensity against the aliphatic proton signals is practically impossible even if the time-averaging technique is adapted. As a method for measuring intensity ratios, the settings of the output signal attenuation in the n.m.r. instrument were calibrated for each of the olefinic and aliphatic resonances<sup>6</sup>. However, it is very difficult to maintain the same conditions as calibrated beforehand for a long time. In our method an internal standard for intensity measurement was adapted as shown in Figure 2. For this purpose known quantities of trichloroethylene were added into the sample as a solution in carbon tetrachloride.

The concentration of the isoprene, ethylidene norbornene or dicyclopentadiene units (mol/g copolymer) were determined according to the following equations:

$$[\text{IP}] \text{ or } [\text{ENB}] = C \cdot W_s/W_c \cdot I(=\text{CH})/I(\text{C}_2\text{HCl}_3) \quad (1)$$

$$[\text{DCP}] = C \cdot W_s/W_c \cdot I(=\text{CH})/2I(\text{C}_2\text{HCl}_3) \quad (2)$$

where  $C$  is the concentration of  $\text{C}_2\text{HCl}_3$  in  $\text{CCl}_4$  (mol/g),  $W_s$  and  $W_c$  are weights of the  $\text{C}_2\text{HCl}_3$  solution and copolymer incorporated into the n.m.r. tube, respectively, and  $I(\ )$  represents the relative integrated intensity of the signal due to the proton indicated in parenthesis.

The concentration of the isobutylene unit in IIR is determined from the concentration of the isoprene unit:

$$68.11[\text{IP}] + 56.10[\text{IB}] = 1 \quad (3)$$

The concentration of the ethylene and propylene units in EPDM is determined from the intensity ratio between the methyl proton signal around 0.85 ppm and the other aliphatic proton signals centred at 1.3 ppm (Figure 1b) by considering overlap of the signals from termonomer units.

$$\begin{cases} 3[\text{P}]/(3[\text{P}] + 4[\text{E}] + 11[\text{ENB}]) = \\ I(-\text{CH}_3)/I(>\text{CH}_2, >\text{CH}-) \quad (4) \\ 28.05[\text{E}] + 42.08[\text{P}] + 120.19[\text{ENB}] = 1 \end{cases}$$

$$\begin{cases} 3[\text{P}]/(3[\text{P}] + 4[\text{E}] + 10[\text{DCP}]) = \\ I(-\text{CH}_3)/I(>\text{CH}_2, >\text{CH}-) \quad (5) \\ 28.05[\text{E}] + 42.08[\text{P}] + 130.20[\text{DCP}] = 1 \end{cases}$$

In Tables 1 and 2 are shown the compositions of commercially obtained IIR and EPDM samples determined by the n.m.r. measurements together with those determined by the iodine number method using the following equation<sup>9</sup>:

$$\text{Unsaturation (mol/g)} = \frac{\text{Iodine No.}}{126.91F} \times 10^{-2} \quad (6)$$

Here,  $F$  is a stoichiometric factor depending on the reaction condition. The concentration of unsaturation in IIR and

Table 1 Determination of isoprene unit in isobutylene-isoprene copolymer

No.	[Isoprene] $\times 10^4$ (mol/g copolymer)	Composition (mol %)		Iodine number*
		Isoprene	Isobutylene	
1	2.64	1.5	98.5	8.9
2	2.82	1.6	98.4	8.9
3	2.61	1.5	98.5	10.2
4	1.47	0.8	99.2	5.9

$$* \text{Iodine number} = \frac{\text{ml} \times \text{N of Na}_2\text{S}_2\text{O}_3 \times 126.91}{\text{g copolymer} \times 1000} \times 100$$

Table 2 Determination of termonomer unit in ethylene-propylene terpolymer

No.	[Termonomer unit] $\times 10^4$ (mol/g copolymer)	Composition (mol %)			Iodine number	
		Ethylene	Propylene	Termonomer		
1	DCP	4.14	65.4	33.1	1.4	12.0
2	DCP	3.99	64.7	33.9	1.4	11.8
3	DCP	3.34	68.2	30.6	1.1	9.1
4	DCP	1.90	72.0	27.4	0.6	6.3
5	DCP	3.36	75.3	23.6	1.1	9.6
6	ENB	5.94	56.9	41.0	2.1	19.5
7	ENB	0.967	62.6	37.1	0.3	3.5
8	ENB	4.96	75.0	23.4	1.6	15.3
9	ENB	1.93	71.9	27.5	0.6	4.6
10	ENB	3.72	62.1	36.6	1.3	10.8
11	ENB	2.46	60.3	38.9	0.8	7.6
12	ENB	6.85	58.4	39.2	2.4	20.7



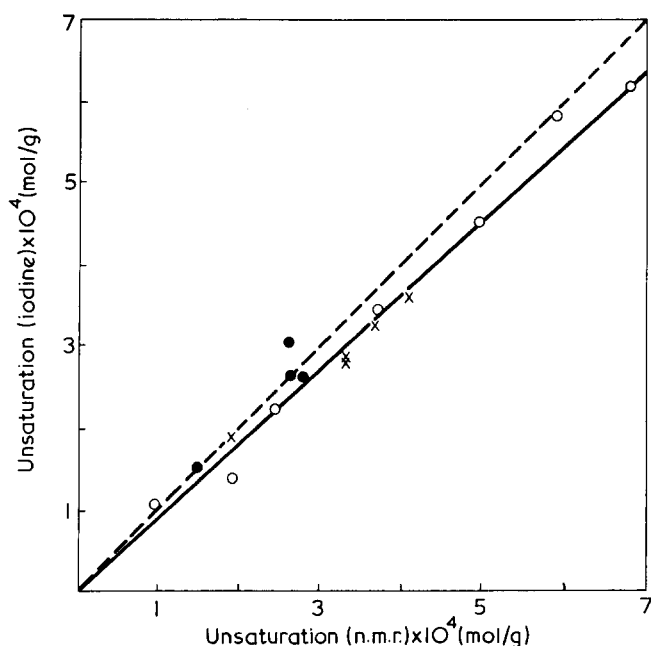


Figure 3 Comparison of the n.m.r. measurements with the iodine number measurements.  $\circ$ , EPDM (ENB);  $\times$ , EPDM (DCP);  $\bullet$ , IIR

EPDM was calculated by the use of an  $F$  value of 2.61 which was decided by McNall and Eby<sup>9</sup> for IIR using the radio-isotope tracer analysis as a standard. The correlation of these two determinations gave a good straight line as shown in Figure 3. The apparent deviation from the expected correspondence, which is illustrated by the broken line in the Figure, may arise from the  $F$  value employed in equation (6). The  $F$  value expected for these ethylidene norbornene and dicyclopentadiene units is assumed to be 2.38 on the basis of the n.m.r. measurements.

#### Accuracy and precision of n.m.r. analysis

The accuracy and precision of intensity measurements, i.e. the deviation from theoretical values and the scatter of the measurements, respectively, were evaluated for a mixture of polyisobutylene and polyisoprene (1.24 mol %) as a model of IIR. The concentration of the isoprene units in the mixture was determined according to the procedure mentioned above using the accumulation of 64 scans. The composition of the mixture was found to be 1.33, 1.13, 1.31, 1.27, and 1.10 mol % (mean value 1.23 mol %). These observed values are in close agreement with the theoretical value of 1.24 mol %. The accuracy and the precision of these five measurements were calculated as percentages as follows:

$$\text{Accuracy} = 100 \cdot (\bar{x} - x_t)/x_t$$

$$\text{Precision} = 100 \cdot t_{\phi}(\alpha)(S/n^{1/2})/\bar{x}$$

where  $\alpha = 0.05$ ,  $n = 5$ ,  $\phi = 4$ . Here,  $x_i$ ,  $x_t$  and  $\bar{x}$  represent the observed, theoretical, and mean values, respectively,  $S$ ,  $n$  and  $t_{\phi}(\alpha)$  denote the root mean square  $\{\sum(x_i - \bar{x})^2/(n - 1)\}^{1/2}$ , number of measurements and critical value of the Student  $t$  distribution for confidence coefficient of 95%, respectively. The accuracy and the precision of these measurements are 0.8 and 10.3%, respectively.

The actual reproducibility of the time-averaged n.m.r. measurements was evaluated with statistical treatments of five measurements using accumulations of 32, 64, 128,

and 256 scans for an EPDM sample (No.12 in Table 2). The results are given in Table 3. The precision of the measurements was calculated to be 4.14%. The result of the analysis was practically independent of the number of scans employed. In the case of commercially obtained IIR and EPDM samples the most satisfactory results were obtained by the accumulation of 32 to 256 scans. The measurement of integrated intensity was almost impossible in the spectrum obtained with the accumulation less than 32 scans, even when a 10 mm o.d. sample tube was used. The scatter of intensity measurements might decrease with increasing the accumulation. However, the overall precision of measurement is affected rather by the stabilization of the n.m.r. instrument, i.e. the stability of magnetic field against slow drift and of the detection phase. In the time-averaged measurement the detection phase is adjusted to a pure absorption mode at the beginning for the aliphatic proton signals. Consequently, a slight change in the phase during the accumulation results in a significant deformation of the time-averaged signals.

The accuracy and precision of the usual n.m.r. measurements were evaluated for squalene as a model compound of ethylene-propylene copolymer. The intensity ratio between the methyl-proton peak (0.85 ppm) and the other aliphatic proton peak (1.2 ppm) was measured for the spectrum of squalene. The mean value of five measurements was 0.633 (theoretical value 0.6316). The accuracy and the precision of the intensity measurement are 0.25 and 1.96%, respectively. This indicates that highly accurate results can be obtained by this n.m.r. method.

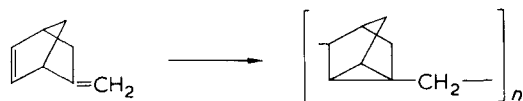
It was reported that the accuracy of the n.m.r. analysis was improved by the use of an internal standard of the intensity measurement<sup>21</sup>. The main advantage of the internal standard method is that it is possible to measure the relative intensity using the peaks of similar intensities. In the case of the time-averaged measurement, it is difficult to decide the optimum value of radiofrequency field because of the uncertainty of knowing whether saturation is occurring in the spectrum. Therefore, the settings of output signal attenuations in the instrument are decided so as to get a well resolved signal of the internal standard. Under these conditions the errors arising from saturation will be less than the amount of saturation itself<sup>21</sup>. Trichloroethylene was chosen as an internal standard in our experiments, because the chemical shift of it is close to that of the olefinic proton signals under examination. It is preferable to use an internal standard having a similar half-width of peak as that of the olefinic proton signal in copolymer.

The radio-isotope labelling method has been employed to determine the unsaturation in IIR or EPDM using copolymer containing  $^{14}\text{C}$ -labelled diolefin monomers. The tracer analysis has been reputed to be the most reliable method and was employed as a standard method for the

Table 3 Reproducibility of the measurement of ethylidene norbornene unit in ethylene-propylene terpolymer

No. of scans	ENB content	
	$\times 10^4$ mol/g copolymer	mol %
32	6.57	2.35
64	6.84	2.45
128	6.90	2.47
256	6.85	2.45
256	7.21	2.59

determination of a stoichiometric factor in the iodine number method<sup>9</sup> or for the determination of extinction coefficients in i.r. methods<sup>18,23</sup>. However, it should be considered that the content of unsaturation in copolymer is not always compatible with that of the  $^{14}\text{C}$ -labelled monomer unit. In the case of methyldene norbornene, it was reported that some of the monomer unit polymerized to give a saturated structure through a transannular reaction by the use of cationic catalysts<sup>24,25</sup>. Occurrence of a similar polymerization process is expected for ethylidene norbornene:



since the aliphatic resonance corresponding to methyl proton is observed in the spectrum of ethylidene norbornene homopolymer prepared with  $\text{VOCl}_3/\text{AlEt}_2\text{Cl}$  catalyst. The loss of some unsaturation has been suggested also in the case of dicyclopentadiene through side reactions such as branching or oxidation in the course of copolymerization<sup>18</sup>. In practice, it is necessary to determine the content of unsaturation in EPDM and IIR in order to evaluate the facility of vulcanization. In this sense the n.m.r. method is well suited for the analysis of unsaturation in copolymer.

The i.r. spectroscopy and refractive index measurements are widely used for the determination of unsaturation in copolymer, which provide facilities for routine analyses of a series of samples in a short time. These analyses are carried out by the use of extinction coefficients or calibration curves determined on the basis of the chemical analysis of unsaturation. Another advantage of the n.m.r. method against the chemical or radio-isotope procedure is that it takes only one or two hours to obtain the time-averaged spectrum. Taking account of these facts, this n.m.r. method is available for determining a calibration curve for physical procedures of unsaturation analysis.

## REFERENCES

- 1 Lee, T. S., Kolthoff, I. M. and Johnson, E. *Analyt. Chem.* 1950, **22**, 995
- 2 Gallo, S. G., Wiese, H. K. and Nelson, J. F. *Ind. Eng. Chem.* 1948, **40**, 1277
- 3 Tunnicliffe, M. E. *J. Appl. Polym. Sci.* 1970, **14**, 827
- 4 Chen, H. Y. and Field, J. E. *J. Polym. Sci. (B)* 1967, **5**, 501
- 5 Sewell, P. R. and Skidmore, D. W. *J. Polym. Sci. (A-1)* 1968, **6**, 2425
- 6 Attenau, A. G., Headley, L. M., Jones, C. O. and Ransaw, H. C. *Analyt. Chem.* 1970, **42**, 1280
- 7 Chen, H. Y. *J. Polym. Sci. (B)* 1966, **4**, 891
- 8 Carman, C. J. and Wilkes, C. E. *Polym. Prepr.* 1969, **10**, 1435
- 9 McNall, L. R. and Eby, L. T. *Analyt. Chem.* 1957, **29**, 951
- 10 Golub, M. A., Fuqua, S. A. and Bhacca, N. S. *J. Am. Chem. Soc.* 1962, **84**, 4981
- 11 Schué, F. and Dole Robbe, J-P. *Bull. Soc. Chim. Fr.* 1963, p 975
- 12 Chen, H. Y. *Analyt. Chem.* 1962, **34**, 1793
- 13 Tanaka, Y., Takeuchi, Y., Kobayashi, M. and Tadokoro, H. *J. Polym. Sci. (A-2)* 1971, **9**, 43
- 14 Rehner, J. Jr. *Ind. Eng. Chem.* 1944, **36**, 46
- 15 Moen, R. V. and Makowski, H. S. *Analyt. Chem.* 1967, **39**, 1860
- 16 Moen, R. V. and Makowski, H. S. *Analyt. Chem.* 1971, **43**, 1629
- 17 Laszlo, P. and Schleyer, P. R. *J. Am. Chem. Soc.* 1964, **86**, 1171
- 18 Cooper, W., Eaves, D. E., Tunnicliffe, M. E. and Vaughan, G. *Eur. Polym. J.* 1965, **1**, 121
- 19 Chandra, S., Row-Chowdhury, P. and Biswas, A. B. *J. Appl. Polym. Sci.* 1966, **10**, 1089
- 20 Tanaka, Y., Sato, H., Ogawa, M., Hatada, K. and Terawaki, Y. *J. Polym. Sci. (B)* 1974, **12**, 369
- 21 Paulsen, P. J. and Cooke, W. D. *Analyt. Chem.* 1964, **36**, 1713
- 22 Tunnicliffe, M. E., Mackillop, D. A. and Hank, R. *Eur. Polym. J.* 1965, **1**, 259
- 23 Tosi, C., Ciampelli, F. and Cameli, N. *J. Appl. Polym. Sci.* 1972, **16**, 801
- 24 Sartori, G., Valvassori, A., Turba, V. and Lachi, M. P. *Chim. Ind. (Milano)* 1963, **45**, 1529
- 25 Kennedy, J. P. and Makowsky, H. S. *J. Macromol. Sci. (A)* 1967, **1**, 345

# Structural effects in the sub-millimetre wave spectrum of isotactic polypropylene

J. Haigh, A. S. M. Ali and G. J. Davies

Post Office Telecommunications Headquarters Research Department, Dollis Hill, London NW2 7DT, UK

(Received 17 February 1975; revised 28 April 1975)

A partial resolution of the polypropylene submillimetre crystal lattice band has been observed at low temperatures. At room temperature, the band profile varies, at constant crystallinity, with the free energy of fusion of the crystallites. Amorphous polypropylene shows no peak, indicating that there is no pseudo-lattice mode.

## INTRODUCTION

Recent developments in telecommunications systems<sup>1</sup> suggest that a material of low dielectric loss at millimetric wavelengths (30–300 GHz, 1–10 cm<sup>-1</sup>) may soon be required. Isotactic polypropylene (IPP) is an attractive candidate for such a material. Chantry and coworkers<sup>2,3</sup>, Goldstein *et al.*<sup>4</sup> and Ayers *et al.*<sup>5</sup> have shown that the dielectric loss spectrum has a weak broad peak near 1000 GHz (33 cm<sup>-1</sup>) which tails into the millimetric region. (The corresponding peak in the absorption spectrum lies near 1500 GHz (50 cm<sup>-1</sup>.) Goldstein *et al.* have shown qualitatively that the sharpness and peak height increase with X-ray crystallinity, and that its frequency shifts upwards by about 250 GHz on lowering the temperature to 100 K. This indicates that a part of the absorption at least is due to crystal lattice modes. They predict that five infra-red active lattice modes should be distinguishable. Alternatively Chantry<sup>2</sup> has pointed out that the absorption profile resembles those found in liquids and attributed to dipolar fluctuations caused by collisions. He has postulated that a collisional fluctuation mechanism in the amorphous regions (a 'pseudo-lattice' mode) may contribute to the peak. Because of the technological importance a detailed analysis of the mechanism is needed. The present work attempts to define the effects of making small changes in crystallization parameters such as might be feasible in component production.

## EXPERIMENTAL

### Sample preparation

Polypropylene powder free of additives and of high tacticity was supplied by ICI Ltd (Plastics Division). They also supplied atactic polypropylene gum. These materials were cast into solid blocks by the vacuum-melt-extraction and casting technique (VMEC), which is described elsewhere<sup>5,6</sup>. Samples of varied crystal growth rate were produced by cooling in vacuum through the temperature band 450–410 K, at various rates. Crystallization was complete at 415 K, so that no  $\beta$ - (hexagonal) crystal modification was formed<sup>7,8</sup>. Practical considerations of the rate of heat removal, the response of the control equipment, and the need to avoid oxidative degradation, limited the cooling rate range.

Because of the very low submillimetre absorption thick samples (>1.0 cm) had to be made, using a falling-tempera-

ture solidification method. To avoid cracks and voids between contracting spherulites it was necessary to cool the polymer melt in such a way as to maintain flat isothermal surfaces in it, and hence a flat solid/melt interface. This was done by imposing a linear temperature gradient from top to bottom of the sample, hotter at the top. Although isothermal crystallization is impossible with this technique, by imposing a linear temperature-time profile all parts of the sample can be given the same thermal history, so that an average crystal growth rate calculated for the whole sample has meaning. Using this method (suggested by Mr K. A. Buckingham, of ICI Plastics Division) void-free cylinders 5 cm in diameter and up to 5 cm thick can be made.

### Sub-millimetre wave spectra

Two Grubb Parsons/NPL cube interferometric spectrometers were modified to cover the spectral ranges 60–930 GHz and 600–12 000 GHz. Collimating optics were incorporated to remove beam convergence effects<sup>9</sup>. Over the range 600–3000 GHz quartz and diamond-windowed Golay detectors were used, the resolution was 120 GHz, and reproducibility between consecutive runs was 1%. Over the range 60–930 GHz a Rollin InSb liquid helium-cooled detector<sup>10</sup> was used with a 4 mm black polyethylene filter; resolution was 60 GHz and reproducibility about 0.2%. The method used to compute the sample absorption spectrum removed errors due to radiation reflected from sample surfaces<sup>11</sup>. The 4 K spectrum was obtained with a liquid helium cooled sample cell. It was not corrected for surface reflection effects, and the sample cell design prevented observations above 60 cm<sup>-1</sup>. Assuming a frequency-independent refractive index of 1.5, the loss tangent spectrum against frequency is

$$\tan(\delta(\nu)) \approx \frac{\alpha(\nu) \cdot c}{3\pi\nu}$$

where  $c$  is the speed of light.

### Density measurements

Density measurements were made using a Davenport density gradient column at 23°C with a resolution of 0.001 g/cm<sup>3</sup>. X-ray diffraction scans were obtained using a Philips PQ 1010 diffractometer with CuK $\alpha$  radiation and pulse height discrimination, working in transmission. Finally,

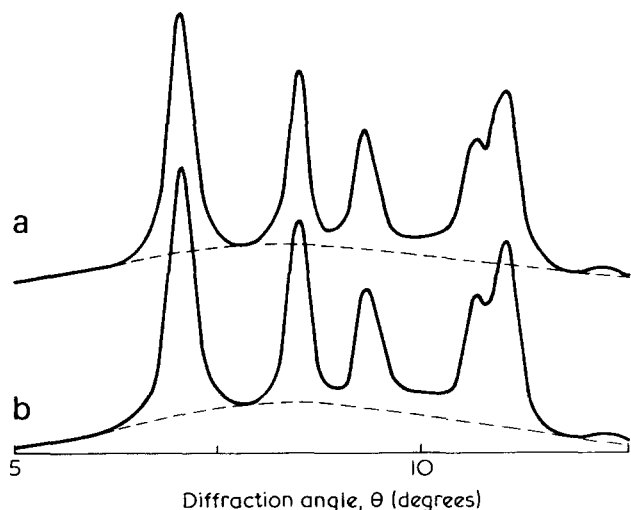


Figure 1 Wide-angle X-ray diffraction patterns of isotactic polypropylene samples cooled from the melt at (a) 50 and (b) 25 K/h

differential scanning calorimetry (d.s.c.) traces of the melting endotherms were obtained with a Perkin-Elmer thermal analysis system, the d.s.c. module being calibrated with indium. Heating rates of 8, 4 and 2 K/min gave the same pattern of results, but those at 4 K/min were most reproducible.

## RESULTS

### Crystal structure of the isotactic samples

The X-ray diffraction patterns (Figure 1) relate to samples cooled at 25 and 50 K/h. Crystalline/amorphous ratios were defined, dividing the scans into areas *A* and *C* corresponding to amorphous scatter and crystalline diffraction, as  $C/(C + \gamma A)$  where  $\gamma$  is a correction factor of 0.94. The values were 62 and 63%. The densities were 0.9094 and 0.9100 g/cm<sup>3</sup>. The d.s.c. endotherms showed a single peak in each case, due to the melting of the crystalline regions. This lay at 430 K (50 K/h cooling), 431 (25 K/h) and 433 K (10 K/h).

### Sub-millimetre wave spectra

Dielectric loss tangent spectra are shown in Figures 2 and 3 on a logarithmic frequency scale. Small voids in the sample used for curve D (Figure 2) distort the spectrum by scattering below 1000 GHz, so this section is omitted.

Reducing the crystal growth rate sharpens the absorption band and shifts it up in frequency (Goldstein *et al.* showed that a similar sharpening, but not the frequency shift, occurred when X-ray crystallinity was increased). The atactic material, which was almost completely amorphous, shows only a trace of a lattice band on top of a large background absorption which is featureless up to at least 6000 GHz (200 cm<sup>-1</sup>).

Figure 3 shows that partial resolution of the lattice mode components in the isotactic material occurs at 4 K, and that the separation of resolvable lattice mode frequencies at this temperature is 300 GHz.

## DISCUSSION

Technologically significant changes in the submillimetre loss spectrum can be brought about by small changes in polymer structure. Their explanation requires hypotheses

relating structure to molecular motions in the 10–3000 GHz range. We would expect, on a simple view, that slowing crystal growth from the melt would (a) increase the crystalline/amorphous ratio, and (b) increase the size of individual crystallites while suppressing disorder-producing features such as surface loop distortion<sup>12</sup>. X-ray crystallinity data show that over the range considered here there is no significant change in the crystalline/amorphous ratio. The small upward shift in melting endotherm temperature confirms that the crystal free energy is lowered<sup>13</sup> as growth rate is reduced: this could be due to increased crystal size, reduced defect concentration or decreased surface fold distortion. The latter factor, as Bank and Krimm showed<sup>14</sup> in polyethylene, would also account for the upward shift in lattice vibration frequency.

The almost featureless continuum observed in the amorphous atactic polymer indicates that we should expect no

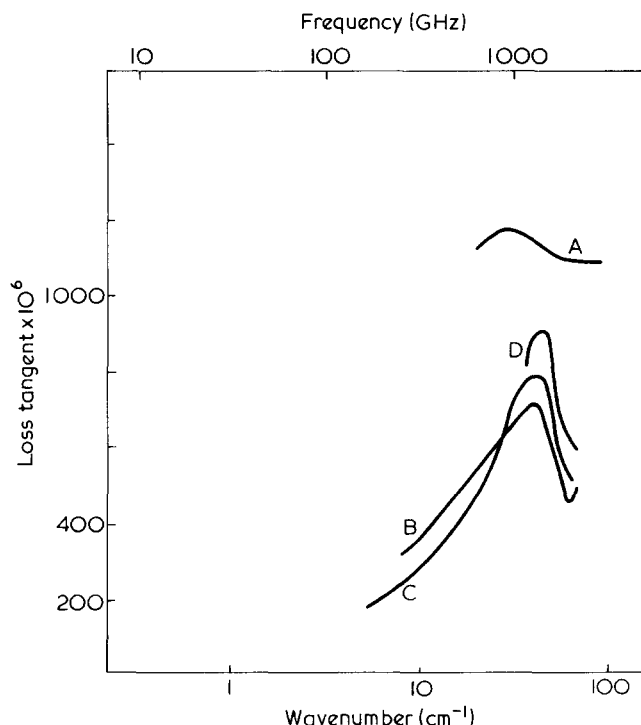


Figure 2 300 K submillimetre wave loss tangent spectra of atactic polypropylene (A) and isotactic polypropylene cooled from the melt at: B, 50; C, 25; D, 10 K/h

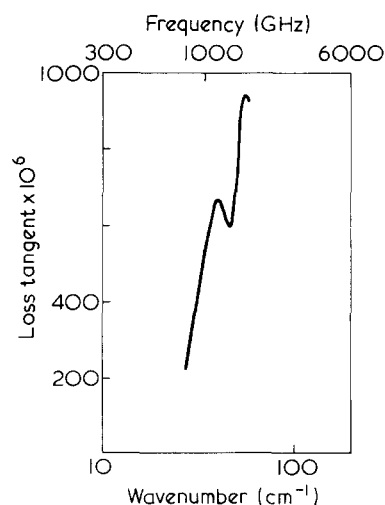


Figure 3 4 K submillimetre wave loss tangent spectrum of isotactic polypropylene sample cooled from the melt at 25 K/h

pseudo-lattice band structure in the amorphous regions of the isotactic polymer. Indeed if the absorptions of the two types of chain, in random conformation, are comparable, then the truly amorphous fraction in the isotactic polymer must be much less than the figure from X-ray data, since the total dielectric loss of the isotactic polymer away from the lattice band centre is much less than 38% of that of the atactic polymer (Figure 2). This is to be expected since the amorphous domains contain chainfolds, cilia etc. which are attached to crystallites and therefore constrained in their motions.

More extensive studies are clearly needed, but it appears that the submillimetre absorption band is a true lattice absorption broadened by imperfections such as surface loop distortion: the amorphous regions appear to contribute only a featureless continuum.

#### ACKNOWLEDGEMENTS

We thank Miss P. Daffurn, ICI Polymer Science Division, Plastics Division, Welwyn, for the X-ray data, and Mr E. Puplett, Queen Mary College, London, for the 4 K spectrum. We also thank Dr H. A. Willis and Dr G. W. Chantry for useful discussions.

Acknowledgement is made to the Director of Research of the Post Office for permission to publish this paper.

#### REFERENCES

- 1 Ravenscroft, I. A. and Jackson, L. A. *Proc. Eur. Microwave Conf., Brussels 1973*
- 2 Chantry, G. W., Fleming, J. W., Pardoe, G. W. F., Reddish, W. and Willis, H. A. *Infrared Phys.* 1971, **11**, 109
- 3 Chantry, G. W., Fleming, J. W., Smith, P. M., Cudby, M. E. A and Willis, H. A. *Chem. Phys. Lett.* 1971, **10**, 473
- 4 Goldstein, M., Seeley, M. E., Willis, H. A. and Zichy, V. J. I. *Polymer* 1973, **14**, 530
- 5 Ayers, S., Davies, G. J., Haigh, J., Marr, D. and Parker, A. E. *Proc. IEE* 1974, **121**, 1447
- 6 Davies, G. J. and Haigh, J. *Infrared Phys.* 1974, **14**, 183
- 7 Turner Jones, A., Aizlewood, J. M. and Beckett, D. R. *Makromol. Chem.* 1964, **75**, 134
- 8 Samuels, R. J. and Yee, R. Y. *J. Polym. Sci. (A-2)* 1972, **10**, 385
- 9 Fleming, J. W. *Infrared Phys.* 1970, **10**, 57
- 10 Clegg, P. E. and Huizinga, J. S. *IERE Conf. Techniques, Reading 1971*
- 11 Chamberlain, J. *Infrared Phys.* 1972, **12**, 145
- 12 Ewers, W. M., Zachmann, H. G. and Peterlin, A. *Kolloid-Z. Z. Polym.* 1972, **250**, 1187
- 13 Hoffman, J. D. and Weeks, J. J. *J. Res. Nat. Bur. Stand.* 1962, **66A**, 13
- 14 Bank, M. I. and Krimm, S. *J. Appl. Phys.* 1968, **39**, 4951

# Stereoregular polymerization of vinyl chloride with the redox system ferrous sulphate/hydrogen peroxide/oxalic acid:

## 2. Process kinetics

L. Slavtcheva and K. Dimov

Higher Institute of Chemical Technology, Sofia 56, Bulgaria

(Received 27 January 1975; revised 2 April 1975)

Kinetics relationships of the polymerization of vinyl chloride with the redox system ferrous sulphate/hydrogen peroxide/oxalic acid in the presence of emulsifier have been determined. The investigations have been made at constant monomer, initiator and emulsifier concentrations in the temperature range  $-30^{\circ}\text{C}$  to  $+15^{\circ}\text{C}$ . The influence of the polymerization temperature on the rate and the activation energy of the process has been clarified. The process is discussed from the point of view of simultaneous polymerization in solution, emulsion and solid phase and the order of the total reaction with respect to monomer concentration has been determined.

### INTRODUCTION

Emulsion polymerization has found wide application in the production of poly(vinyl chloride) (PVC). The theory of Smith and Ewart<sup>1</sup> is the basis of its quantitative kinetic description. However, during the polymerization of vinyl chloride (VC), owing to the insolubility of the polymer in the monomer and to the solubility of VC in water (0.25% by wt at  $0^{\circ}\text{C}$ ), the process deviates from the Smith and Ewart theory and can be best described by the theory of Medvedev and Sheinker<sup>2</sup>.

In the initial stage of emulsion polymerization and before the stationary condition determined by the constant concentration of  $N$  particles, is reached, it is possible that the process takes place in the solution and thus it can be formally described by the relationships of radical homogeneous polymerization.

The increase of conversion during polymerization leads to lowering of the stability of the polymer particles and results in their consolidation and coagulation. However, the process can continue in the solid phase of the polymer by diffusion of the monomer molecules. Therefore, in its last stages the process is similar to a bulk heterogeneous polymerization and can be described by the equation of Bengough and Norrish<sup>3</sup>.

This investigation aims at the elucidation of some problems of the formal kinetics of emulsion polymerization using the redox initiation system ferrous sulphate/hydrogen peroxide/oxalic acid in water-methanol over the temperature range  $-30^{\circ}\text{C}$  to  $+15^{\circ}\text{C}$ .

### EXPERIMENTAL

The polymerization of VC was carried out by a method previously described<sup>4</sup>. The rate was experimentally determined by gas chromatographic analysis. The initial components of the mixture in the reactor are given in Table 1. The operating conditions were constant reagent concentrations, as calculated with respect to the total volume of the reac-

tion medium and different polymerization temperatures,  $T_p$ . The monomer concentration in the reaction medium was determined by use of an inner standard — in our case *n*-pentane added in the reactor before the beginning of the process.

### RESULTS AND DISCUSSION

Emulsion polymerization of VC in water-methanol with the redox system ferrous sulphate/hydrogen peroxide/oxalic acid is a heterogeneous process. The presence of methanol in the reaction medium increases the monomer solubility. The initiation system is soluble in water-methanol and the process can be considered as a homogeneous one; its velocity is formally described by the equation of the homogeneous radical polymerization. The newly formed polymer in the presence of methanol forms a sludge that carries away part of the emulsifier of the system thus reducing its concentration  $[E]$  in the solution and therefore reducing the number of the particles,  $N$ , and thus their contribution to the polymerization.

The polymerization in the micelles obeys the kinetics of the Medvedev-Sheinker theory and the spectral analysis shows the presence of linear polymer<sup>5</sup>. This supports the view that the polymerization takes place on the surface of

Table 1 Initial mixture in the reactor

Substance	Concentration (mol/l)
water	24.5200
methanol	5.5200
<i>n</i> -pentane	0.2330
vinyl chloride	4.4000
ferrous sulphate (hydrated)	0.0040
hydrogen peroxide	0.0377
oxalic acid	0.0029
sodium salt of mepasin sulphonic acid	0.0638

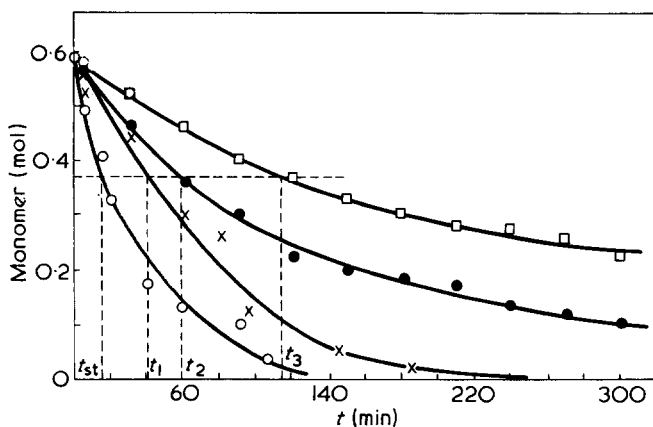


Figure 1 Polymerization of VC with the redox system ferrous sulphate/hydrogen peroxide/oxalic acid in water-methanol and in the presence of emulsifier. □, 15°; ●, 0°; X, -14°; ○, -25° C

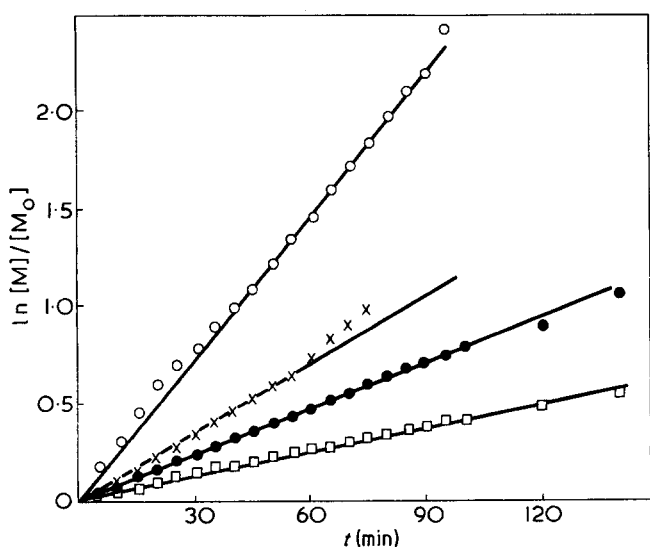


Figure 2 Order of reaction towards the monomer concentration at different polymerization temperatures. □, 15°; ●, 0°; X, -14°; ○, -25° C

the particles. Otherwise, the chain growth would occur within the polymer because of its high concentration and the result would be branch-chained PVC.

The presence of methanol in the reaction medium leads to precipitation of the PVC (or the macroradical) and the polymerization recurs by the monomer diffusion. This process is similar to a bulk polymerization and can be described by the equation of Bengough and Norrish.

The monomer distribution in the reaction medium at any time would be as follows:

- [M] total monomer concentration,
- [m<sub>1</sub>] monomer concentration in the water-methanol phase (dissolved monomer): [m<sub>1</sub>] = α[M],
- [m<sub>2</sub>] monomer concentration in the micelles: [m<sub>2</sub>] = β[M] = γ[m<sub>1</sub>],
- [m<sub>3</sub>] monomer concentration in the solid phase (absorbed monomer): [m<sub>3</sub>] = δ[M] = ε[m<sub>1</sub>],
- [m<sub>4</sub>] monomer concentration in the drops (dispersed monomer): [m<sub>4</sub>] = τ[M].

α, β, γ, δ, ε and τ are constants depending on the polymerization conditions. Since we operated at constant reagent concentrations and only the polymerization temperature, T<sub>p</sub> varied, it was to be expected that these coefficients would depend on T<sub>p</sub>.

The experimentally determined monomer concentration can be considered as the sum total of [m<sub>1</sub>], [m<sub>2</sub>] and [m<sub>4</sub>]. We accept that [m<sub>3</sub>] has a very small value since the monomer diffuses from the solution into the solid phase which is much denser. Since the monomer concentration is determined by quantitative analysis by means of an independent standard, soluble in the monomer, the error made in all analyses will be of the same order and the equation [M] = f(t) will give the kinetic curve of the process (Figure 1).

The order of the total reaction towards the monomer is approximately first order. This can be seen from the integral curves (Figure 2) that show the plot ln [M]/[M<sub>0</sub>] = f(t). The conditions of the polymerization using the redox system in water-methanol in the presence of emulsifier may occur by three separate processes that take place according to different mechanisms:

1. Polymerization in solution – polymer separates from the reaction medium. Its rate of formation can be formally described by the equation of the homogeneous radical polymerization:

$$R_{p1} = k_{p1} [m_1] \left( \frac{R_i}{2k_{01}} \right)^{1/2}$$

where k<sub>p1</sub> is the rate constant for propagation of the chain; R<sub>i</sub> is initiation rate. In our case R<sub>i</sub> = k<sub>r</sub> [H<sub>2</sub>O<sub>2</sub>] [FeSO<sub>4</sub> · 7H<sub>2</sub>O], where k<sub>r</sub> is the initiation rate constant and k<sub>01</sub> is rate constant for termination.

2. Emulsion polymerization that takes place on the surface of the particles and its rate will be determined according to the Medvedev-Sheinker theory:

$$R_{p2} \propto N^{1/5}, [E]^{1/2}, [I]^{1/2}$$

where [I] is the initiator concentration.

3. Polymerization in the solid phase – according to the equation of Bengough and Norrish:

$$R_{p3} = k_{p3} [I]^{1/2} [m_3] \left\{ 1 + \frac{k' [P]^{2/3}}{[m_3]} \right\}$$

where k<sub>p3</sub> is the propagation rate constant; [P] is concentration of the polymer formed; and k' is a constant.

The auto-acceleration, noticed in the course of our investigations, is due to the high degree of the conversion

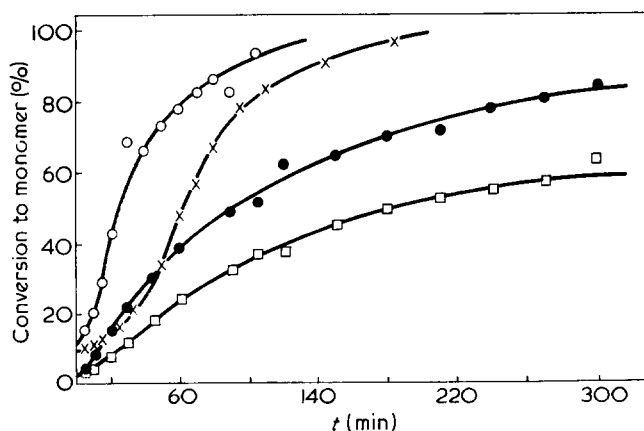


Figure 3 Monomer conversion at different temperatures. □, 15°; ●, 0°; X, -14°; ○, -25° C

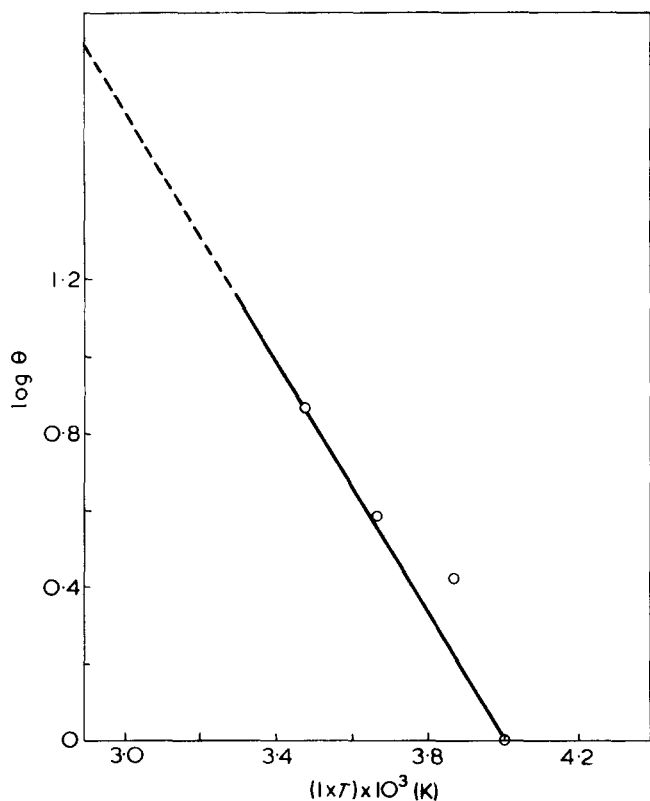


Figure 4 Temperature dependence of the polymerization rate

and to the gel effect (or the so-called Trommsdorff effect) and is favoured by the third process. This can be proved by the S shape of the conversion–time curve (Figure 3).

The overall rate will be a sum total of the rates of the three kinds of polymerization:

$$R_p = R_{p1} + R_{p2} + R_{p3}$$

The value of  $R_p$  depends on the reaction conditions which in our case were constant values of  $[M_0]$ ,  $[I_0]$ ,  $[E_0]$ , constant composition of the medium and continuous agitation. Therefore,  $R_p$  depends only on  $T_p$  and on the degree of conversion. This dependence can be expressed by means of the activation energy  $E_R$  which will be the sum total of the activation energies of the three separate polymerizations:

$$E_R = E_{R1} + E_{R2} + E_{R3}$$

$E_{R1}$  can be considered as the activation energy of the polymerization in solution. With increasing  $T_p$ ,  $[m_1]$  and  $R_i$  increase. This results in an increase of  $R_{p1}$  and a decrease of  $E_{R1}$ .

The experimentally determined  $E_R$  has a negative absolute value  $-7.63$  kcal/mol ( $31.8 \times 10^3$  J/mol).  $E_R$  was calculated from the slope of the line expressing the dependence  $\log \theta = f(1/T)$ . The values of  $\theta$  are calculated by transformation of the curves  $[M] = f(t)$  ( $\theta = t_{st}/t$ , determined under conditions of constant conversion, Figure 4). The value of  $E_R$  is considerably lower than most of the values of the activation energies of polymerization processes, initiated by the thermal decomposition of the initiator ( $\sim 20$  kcal/mol;  $83.6 \times 10^3$  J/mol).

#### REFERENCES

- 1 Smith, W. V. and Ewart, R. W. *J. Chem. Phys.* 1948, 16, 592; Smith, W. V. *J. Am. Chem. Soc.* 1948, 70, 3695
- 2 Sheinker, A. and Medvedev, S. S. *Dokl. Akad. Nauk SSSR* 1954, 97, 111
- 3 Bengough, W. F. and Norrish, R. G. *Proc. R. Soc. (A)* 1950, 218, 149
- 4 Dimov, K. and Slavtcheva, L. *Polymer* 1973, 14, 234
- 5 Slavtcheva, L. and Dimov, K. *Godishnik NIICHP* 1973, 12, 75
- 6 Emanuel, N. M. and Knorre, A. G. 'Kurz Khimicheskoi Kinetiki, Vishshaya Shkola', Moscow, 1962, p 50



# Stiffness of aqueous sodium carboxymethyl cellulose from electric birefringence data

Alan R. Foweraker and Barry R. Jennings

Department of Physics, Brunel University, Uxbridge, Middlesex UB8 3PH, UK

(Received 24 March 1975)

Electric birefringence studies have been made on some five samples of sodium carboxymethyl cellulose of different molecular weights ( $M$ ) in water. The orientational relaxation times were evaluated from the decay rates of pulsed field experiments. These were analysed in terms of theories for rigid rods, weakly bending rods and worm-like chains. At  $M$  less than  $5 \times 10^3$ , the rod model appeared to be representative of the molecular conformation. The optical anisotropy factor ( $g_3 - g_1$ ) and the electrical polarizability anisotropy ( $\alpha_3 - \alpha_1$ ) were also evaluated at each molecular weight and in terms of the rod model. It appears that, the electrical polarizability anisotropy when reduced to unit length is a sensitive parameter which is constant in the rod-like region but deviates rapidly with the onset of flexibility. It is suggested that this parameter may be of value (a) to indicate the molecular weight at which the flexibility is significant, and (b) as an indicator of the relative flexibility of different members of the polysaccharide family.

## INTRODUCTION

The experimental investigation of flexibility in solutions of linear polymers has long been of interest. Apart from the characterization of this property, flexibility has proved something of a *bête noir* in that theories are generally developed for the completely rigid or completely randomly coiled molecule. The intermediate situation has been described often only through comparisons with either extreme model. Whereas hydrodynamic methods such as viscosity and flow birefringence have been used traditionally, recent electro-optic techniques have been shown to lead to useful qualitative data<sup>1-3</sup>.

In this study five differing molecular weight samples of sodium carboxymethyl cellulose (SCMC) were studied in aqueous solution in which they exhibit polyelectrolytic behaviour.

In an effort to study both the molecular properties and the flexibility of SCMC the electric birefringence technique was employed<sup>4,5</sup>.

Measurements were made on each sample as a function of the applied field strength and the data were interpreted in terms of molecular hydrodynamical, optical and electrical parameters.

## THEORY

In a dilute solution, each macromolecule can be considered as isolated and in some random orientation relative to any arbitrary direction. Thus the overall effect of these optically anisotropic molecules is to present a bulk isotropic solution. However, on application of a pulsed electric field, the individual molecules experience an orienting torque owing to the interaction of the applied pulsed field and their inherent or induced electrical dipoles. These torques lead to an ordering of the molecular array and the bulk solution begins to manifest the optical anisotropy of the individual molecules.

The conventional method of measuring the birefringence is thus to measure the light transmitted through a system consisting of polarizer, cell containing the solution under test, and analyser. The field is applied to the solution at an azimuth of  $45^\circ$  to the polarizer transmission axis. In this work, the analyser was not crossed with the polarizer but was offset by a small angle  $\sigma$ . The birefringence accompanying particle orientation was indicated as a change in the transmitted intensity, recorded by means of a photodetector. If  $I^*$  and  $a^*$  are the intensity and the amplitude respectively of the linearly polarized beam incident on the cell, and  $K$  is a constant which accounts for the light loss due to absorption and reflection losses in the optical components, then, with *no* electric field applied to the cell, the transmitted intensity is given by the law of Malus, namely:

$$I_{E=0} = KI^* \sin^2 \sigma \quad (1)$$

Upon application of the field, the solution becomes birefringent. The incident beam can be visualized as two equivalent linear oscillations of equal amplitude, one parallel to and the other perpendicular to the field direction. After leaving the cell, these components would have amplitudes given by the equations:

$$\begin{aligned} a^{\parallel} &= \frac{a^*}{\sqrt{2}} \sin(\omega t - \delta) \\ a^{\perp} &= \frac{a^*}{\sqrt{2}} \sin \omega t \end{aligned} \quad (2)$$

where the superscripts indicate the parallel and perpendicular components. The phase lag  $\delta$ , arising from the birefringence or refractive index difference  $\Delta n$  for these two directions at a wavelength  $\lambda$  and for a cell length  $l$  is given

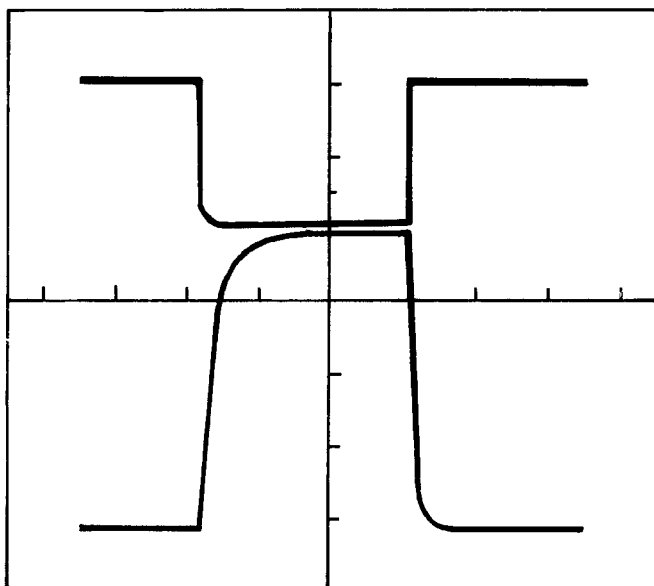


Figure 1 Tracing of a typical transient obtained using a SCMC sample of molecular weight 30 000 at an applied field of  $E = 8.4$  kV/cm and 145  $\mu$ s duration. Time scale is from left to right

by:

$$\delta = \frac{2\pi l \Delta n}{\lambda} \quad (3)$$

The result of these two components passing through the analyser is a beam of intensity:

$$I_E = \frac{KI^*}{2} (1 - \cos 2\sigma \cos \delta) \quad (4)$$

Hence, the relative intensity change of the light beam reaching the photomultiplier on application of the electric field is given by:

$$\frac{\Delta I}{I_{E=0}} = \frac{I_E - I_{E=0}}{I_{E=0}} = \frac{\sin^2(\delta/2) \cos 2\sigma}{\sin^2 \sigma} \quad (5)$$

Hence, one can determine  $\delta$ , and from equation (3),  $\Delta n$ .

For a solution of concentration  $c$  g/ml, and  $\bar{v}$  partial specific volume, Peterlin and Stuart<sup>6</sup> have shown that:

$$\Delta n = \frac{2\pi c \bar{v} (g_3 - g_1)}{n} \Phi \quad (6)$$

where  $n$  is the refractive index and  $(g_3 - g_1)$  the optical anisotropy factor for the solute molecules, which are distributed and oriented as controlled by the orientation function,  $\Phi$ . For rigid particles and low degrees of orientation<sup>4</sup>, as at low field strengths ( $E$ ),

$$\Phi = \frac{1}{15} (\beta^2 + 2\gamma) \quad (7)$$

where  $\beta = \mu_3 E / kT$  and  $\gamma = (\alpha_3 - \alpha_1) E^2 / 2kT$  for molecules with a permanent moment  $\mu$  and polarizability components  $\alpha$ . Subscripts 3 and 1 indicate the major and a minor

(transverse) axis respectively. At high applied fields, such that the condition of full molecular orientation is attained,  $\Phi = 1$ .

Experimentally one applies a square wave pulsed electric field. This induces an optical response which is recorded by the photomultiplier as a transient signal (Figure 1). For easier analysis, we consider this as consisting of three distinct regions:

1. This is an initial rise region which is characterized by a compound interaction of the electrical, optical and geometrical properties of the molecules. It is rather more difficult to handle theoretically than the following.
2. This is a saturation region in time where the electrical orientating forces are equally balanced by the Brownian randomizing factors. In this region, measurements of the induced birefringence ( $\Delta n$ ) as a function of the applied field strength ( $E$ ) are made. The data are then plotted in the form of  $\Delta n$  vs.  $E^2$  which leads to a characteristic plot for the molecules under study (Figure 2). The initial linear slope at low applied field strengths is described by the combination of equations (6) and (7) and leads directly to the electrical properties of the molecules. The saturation value of the plot as  $E$  approaches infinity leads to the optical anisotropy factor ( $g_3 - g_1$ ).
3. The third region is a field free relaxation region which is, to a first approximation, dependent solely on the hydrodynamical properties of the molecules. If the molecular motion be characterized through a molecular rotary relaxation time  $\tau$ , then the latter stage is a first order diffusion process, which for a monodisperse system is described by the equation<sup>5</sup>:

$$(\Delta n)_t = (\Delta n)_0 \exp(-t/\tau) \quad (8)$$

where  $(\Delta n)_t$  is the birefringence at any time  $t$  after the start of the decay and  $(\Delta n)_0$  is the measured birefringence at time  $t = 0$ . Analysis of the transient decays in terms of a log-linear plot of normalized amplitude versus time (Figure 3) gives a value for  $\tau$ , which in turn leads to molecular dimensions on consideration of specific molecular models.

## EXPERIMENTAL

The samples were kindly supplied by Dr I. Robb of Unilever Research Limited, Port Sunlight, Cheshire, the molecular weights of which were obtained from viscosity measurements. Each sample was dissolved in water by

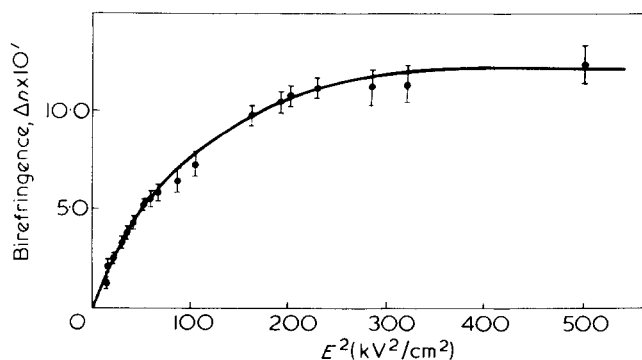


Figure 2 Variation of  $\Delta n$  versus  $E^2$  for a SCMC sample of molecular weight 30 000, concentration  $c = 0.2$  mg/cm<sup>3</sup> at a wavelength of  $\lambda = 546$  nm

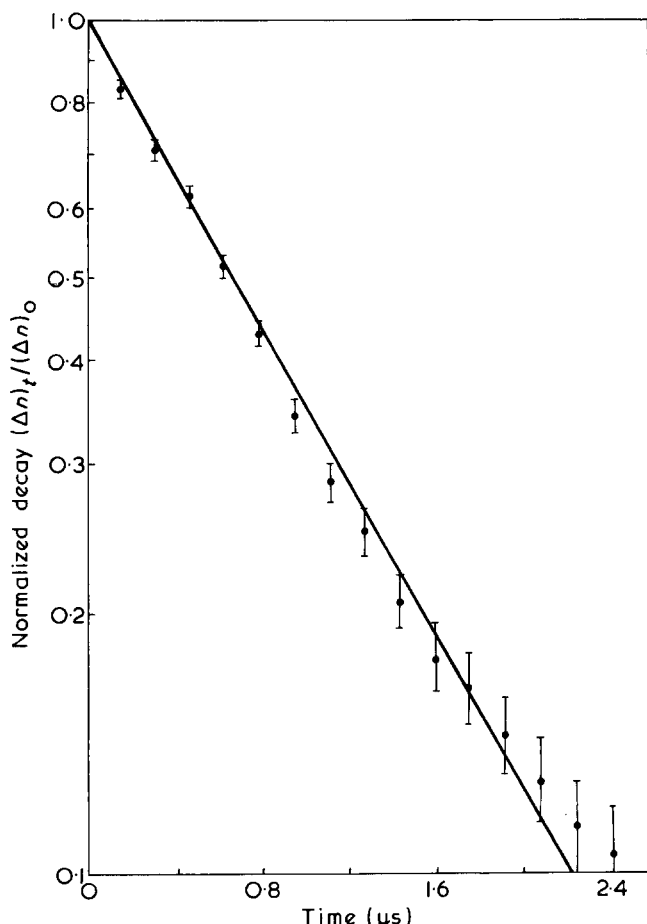


Figure 3 Normalized semi-logarithmic plot for the transient decay of the 30 000 molecular weight sample. The applied field strength was in the order of 5 kV/cm

Table 1 Parameters obtained from the rotary relaxation data

$M$ $\times 10^{-3}$	$\tau$ ( $\mu$ s)	Equivalent rod length		Persistence length	
		$l_r$ (nm)	$L$ (nm)	$q$ WBR (nm)	$q$ WLC (nm)
30	0.94	48.5	85.9	4.57	2.0
35	1.16	52.2	100.2	4.12	1.9
50	1.87	61.7	143.1	3.4	1.75
90	2.09	64.5	257.6	1.27	0.93
250	2.13	64.9	715.5	0.2	0.3

Subscripts  $r$ , WBR, WLC refer to the true equivalent rod, the 'weakly bending rod' and 'worm-like chain' models respectively

continuous stirring to form a stock solution of known concentration. This was subsequently diluted as required with de-ionized water. Measurements were made on all samples at a molecular concentration of  $5 \times 10^{-4}$  g/cm<sup>3</sup> and at a wavelength of 546 nm.

The apparatus used was similar to that described elsewhere<sup>3</sup> for electric dichroism measurements. An additional polarizer was incorporated as the analyser in the detecting system. Measurements were made in the linear birefringence<sup>7</sup> mode in which the analyser was offset by an angle  $\sigma$ . This allowed the sign of the birefringence to be measured and also enabled fluctuations in the lamp output to be monitored. A typical transient response, taken from the oscilloscope, is shown in Figure 1 in which the photomultiplier load resistance was 1 k $\Omega$ . Such a load reduced the detection system time constant to the order of

0.1  $\mu$ s, which was well below that of the molecular relaxation time. Pulses of 40 to 100  $\mu$ s duration and of 0 to 7 kV amplitude were applied to the solutions.

## RESULTS AND DISCUSSION

The relaxation data were analysed by means of normalized semi-logarithmic plots (Figure 3). In each case the initial slope of the decay was measured as being the most characteristic average for the sample<sup>8</sup>. The relaxation times obtained for each sample are shown in Table 1.

Interpretation of the rotary relaxation times in terms of molecular sizes depends upon the assumed molecular model and in this case three such models were considered namely:

(a) the rigid rod model<sup>9</sup> whence

$$\tau = \frac{\pi\eta_0 l_r^3}{18kT[\ln(2p) - 0.8]} \quad (9)$$

(b) the weakly bending rod model<sup>10</sup> whence

$$\tau = \frac{\pi\eta_0 M^3}{6kT\rho^3} \left\{ 3 \ln\left(\frac{M}{2\rho b}\right) - 4.92 + 4\left(\frac{b}{a}\right) + \frac{M}{4\rho q} \left[ 4.5 \ln\left(\frac{M}{2\rho b}\right) - 10.2 + 4\left(\frac{b}{a}\right) \right] \right\}^{-1} \quad (10)$$

and (c) the worm-like chain model<sup>10</sup> whence

$$\tau = \frac{\eta_0 q M^2}{6kT\rho^2} \left[ 0.126\left(\frac{M}{q\rho}\right)^{1/2} + 0.159 \ln\left(\frac{2q}{b}\right) - 0.37 + 0.16\left(\frac{b}{a}\right) \right]^{-1} \quad (11)$$

where  $\eta_0$  is the viscosity of the solvent,  $l_r$  is designated the equivalent rigid rod length,  $p$  is the axial ratio,  $\rho$  is the mass per unit length,  $q$  is the persistence length<sup>11</sup> and the parameters  $a$  and  $b$  are frictional parameters. In this, as in earlier<sup>12</sup> work, they are assumed to be equal to the rod diameter.

The relaxation data were analysed in terms of each of the above models and the results are presented in Table 1 along with the estimated hydrodynamical length  $L$  calculated assuming each monomer unit to be of lengths 0.69 nm. This length was estimated from an unfolded amylose helix<sup>13</sup>. Hence, for a degree of polymerization  $Z$ ,  $L = 0.69Z$  nm. Figure 4 compares the equivalent rigid rod

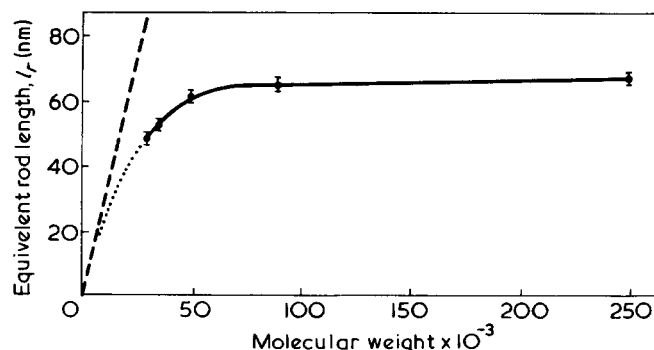


Figure 4 Plot of the equivalent rigid rod length,  $l_r$ , as a function of molecular weight. ---, True extended rod behaviour based on a length of 0.69 nm per monomer unit

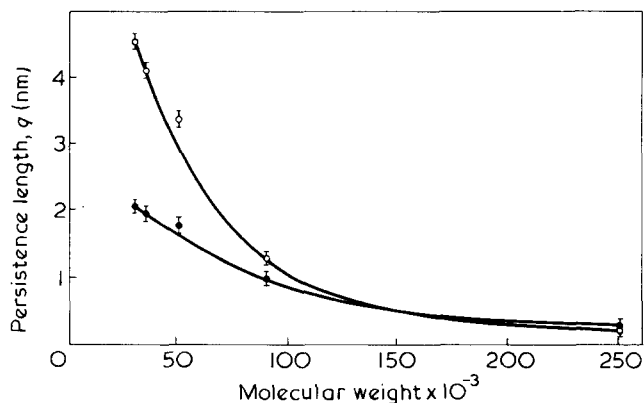


Figure 5 Graph of the measured persistence lengths for the 'weakly bending rod' (WBR) (O) and the 'worm like chain' (WLC) (●) models as functions of molecular weight

Table 2 Optical and electrical anisotropy parameters

$M$ $\times 10^{-3}$	$(g_3 - g_1)$ $\times 10^3$	$(\alpha_3 - \alpha_1)$ $\times 10^{31}$ (Fm <sup>2</sup> )	$[(\alpha_3 - \alpha_1)/l_r]$ $\times 10^{24}$ (Fm)	$[(\alpha_3 - \alpha_1)/L]$ $\times 10^{24}$ (Fm)
30	7.11	2.03	4.18	2.36
35	12.3	2.07	3.97	2.07
50	12.4	2.75	4.45	1.92
90	12.7	3.72	5.77	1.44
250	11.5	4.78	7.37	0.67

data ( $l_r$ ) and the calculated extended length ( $L$ ) as a function of molecular weight. If the molecules were rigid rods these curves would remain coincident and linear with increasing molecular weight. It is seen that there is almost immediate deviation from the rigid rod model at molecular weights exceeding  $5 \times 10^3$ .

Figure 5 shows the persistence lengths  $q$ , evaluated from equations (10) and (11), for both the weakly bending rod and the worm-like chain models plotted as a function of molecular weight. The similarity between the values obtained for either model does not enable us to differentiate between them.

The approach through the use of equations for rigid rod-like molecules does indicate the rigid behaviour of the SCMC molecule at low molecular weights and the degree of departure from this model at  $M > 5 \times 10^3$ . No such sensitivity is offered through the evaluation of  $q$ .

In order to analyse the electrical parameters, one needs to know the relative contributions of the permanent and induced dipoles to the factor  $\Phi$ . In principle, one of two methods could be used. The first is to use pulses or bursts of alternating current in order to obtain a frequency dispersion plot<sup>14</sup>. We had no suitable apparatus at our disposal which could give fields of high enough amplitude and frequency and which could be switched with fast relays. The second method is to apply a reversing pair of d.c. pulses in juxtaposition. We were unable to generate such a pair at the voltages required. Because of the polyelectrolytic nature of this polymer in water, it is realistic to assume that counter-ion polarization processes must play an important role and that induced dipole moments predominate. Should all of the observed birefringence be attributed to permanent dipoles (for a rod molecule applied to the appropriate low molecular weight data), then dipole moments of some  $10^2$  D ( $3.34 \times 10^{-28}$  C m) per monomer unit would be obtained. This is clearly unrealistic by more than an order of magnitude.

A typical plot of the dependence of the observed birefringence on field strength is shown in Figure 2. At high  $E$ , the effect becomes field independent,  $\Phi \rightarrow 1$  and  $(g_3 - g_1)$  can be evaluated (Table 2). The high molecular weight material has the biggest dipole moment in a field  $E$  and is thus more readily saturated. As  $(g_3 - g_1)$  is evaluated from the high field (saturation) data, we accept the high  $M$  average of  $(g_3 - g_1) = 12.2 \times 10^{-3}$  as the most reliable estimation of this parameter.

We are not aware of other determinations of this optical factor for SCMC but note the order of magnitude similarity with the following water-borne macromolecules: 6 to  $9 \times 10^{-3}$  for tobacco mosaic virus<sup>15</sup>, 7 or  $34 \times 10^{-3}$  for DNA, depending on the experimental method used<sup>16</sup> and  $8 \times 10^{-3}$  for sodium polyethylene sulphonate<sup>17</sup>.

From the low field dependence of  $\Delta n$  on  $E^2$ , the electrical anisotropy values listed in Table 2 were obtained. The molecular origin of this anisotropy may be ascribed to a volume effect<sup>6</sup> or a surface polarizability<sup>18</sup> or a combination of the two. Whichever is the case, one would expect the polarizability to be dependent on the molecular length for a rod-like model. This appears to be the case at low molecular weights where the rod behaviour is closely indicated in Figures 4 and 6. By this argument one would expect, for a rigid molecular system, that the parameter  $(\alpha_3 - \alpha_1)$  per unit length would be independent of molecular weight. In Figure 7 the parameters  $(\alpha_3 - \alpha_1)/l_r$  and

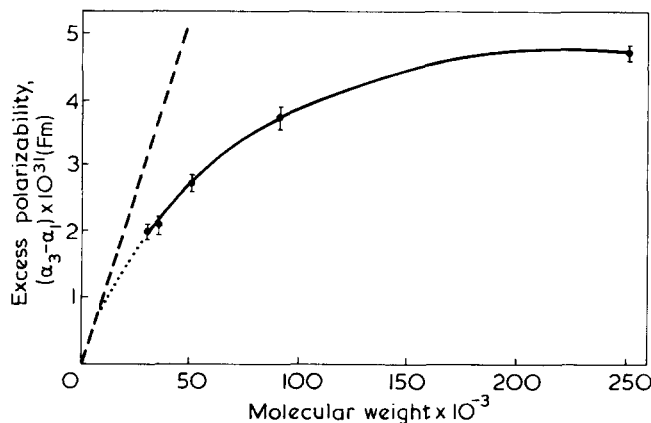


Figure 6 Excess molecular polarizability difference as a function of molecular weight. ---, Semi-theoretically predicted rigid rod-like behaviour based on the excess polarizability per unit length parameter at the low molecular weight limit of Figure 7

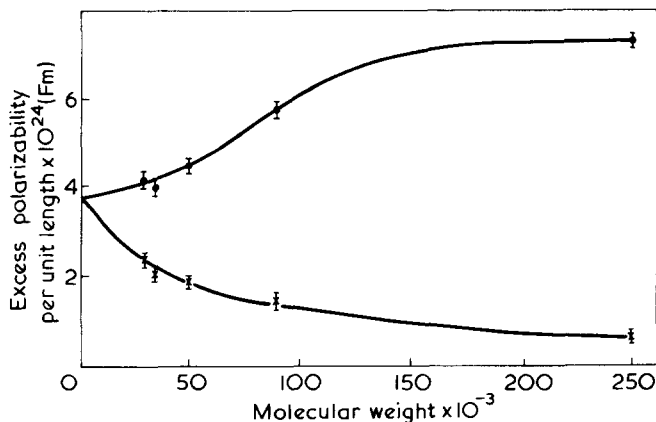


Figure 7 Excess polarizability per unit length as a function of molecular weight using hydrodynamical contour lengths  $L$  (X) and effective rod lengths  $l_r$  (O)

$(\alpha_3 - \alpha_1)/L$  are plotted as a function of  $M$ . The graph exhibits a number of important features. First, the parameters plotted are *not* constant throughout the molecular weight range studied. This indicates that the molecules are not rigid, at least at the higher molecular weights, but do flex. Secondly, as  $M$  is reduced towards zero the molecules indicate increasing conformity to the rigid rod-like behaviour. In the low  $M$  limit, the parameter  $(\alpha_3 - \alpha_1)$  per unit length is constant whether  $l_r$  or  $L$  are used for the equivalent length. This can only indicate that  $l_r$  becomes identical with the length  $L$  at low  $M$ . Thirdly, the intercept suggests the value of  $3.7 (\pm 0.3) \times 10^{-24}$  Fm as the truly characteristic value for the excess polarizability per unit length for the SCMC molecular system. At this low  $M$ , the theory used herein becomes fully appropriate.

Finally, there are two further points which are worthy of comment. (a) We note the similarity between the value of the excess polarizability per unit length obtained here for SCMC and that obtained ( $3.5 \pm 0.2 \times 10^{-24}$  Fm) for amylose<sup>3</sup> in complexed aqueous dispersion even though different electro-optic methods were used in the two studies. It has not escaped our notice that this parameter might be a useful characteristic of the polysaccharide family. (b) Although the persistence length values determined herein for SCMC are similar to those found for amylose, we note differences in the curves of  $(\alpha_3 - \alpha_1)$  per unit length *versus*  $M$  for these two systems. Not only is the degree of polymerization at which the curves of  $(\alpha_3 - \alpha_1)$  per unit length depart from linearity different, (25 for SCMC and 350 for amylose), but also the *rate* of divergence is different. It seems to us that the reduced electrical polarizability anisotropy per unit length is a potentially useful parameter which is very sensitive to the departure from rigid rod behaviour and hence the increasing flexibility, of stiff but flexible polymers as their molecular weight increases. It would appear to be much more indicative of flexibility than  $q$ .

#### ACKNOWLEDGEMENTS

The majority of the apparatus was obtained from a grant originally given by the Science Research Council. The oscilloscope was purchased with funds from ICI Ltd. One of us (A.R.F.) thanks Unilever Research Ltd for a post-doctoral fellowship and for the provision of samples.

#### REFERENCES

- 1 Tsvetkov, V. N., Rjuntsev, E. I., Pogodina, N. V. and Shtennikova, I. N. *Eur. Polym. J.* 1975, 11, 37
- 2 Jennings, B. R. in 'Light Scattering from Polymer Solutions', (Ed. M. Huglin), Academic Press, London, 1972, Ch 13
- 3 Foweraker, A. R. and Jennings, B. R. *Adv. Mol. Relaxation Processes* 1974, 6, 241
- 4 O'Konski, C. T. 'Encyclopedia of Polymer Science and Technology', John Wiley, New York, 1969, Vol 9, p 551
- 5 Fredericq, E. and Houssier, C. 'Electric Dichroism and Electric Birefringence', Clarendon Press, Oxford, 1973
- 6 Peterlin, A. and Stuart, H. A. 'Handbuch und Jahrbuch der Chemischen Physik' 1943, Vol 8, Section 1B
- 7 Badoz, J. *J. Phys. Radium (Paris)* 1956, 7, (Suppl. 11) 143A
- 8 Schweitzer, J. and Jennings, B. R. *Biopolymers* 1973, 12, 2439
- 9 Broersma, S. *J. Chem. Phys.* 1960, 32, 1626
- 10 Hearst, J. E. *J. Chem. Phys.* 1963, 38, 1002
- 11 Kratky, O., and Porod, G. *Rec. Trav. Chim.* 1949, 68, 1106
- 12 Hearst, J. E. and Stockmayer, W. H. *J. Chem. Phys.* 1962, 37, 1425
- 13 Rundle, R. E. *J. Am. Chem. Soc.* 1947, 69, 1769
- 14 Schweitzer, J. and Jennings, B. R. *J. Phys. (D)* 1972, 5, 297
- 15 Stoylov, S. P. *Adv. Colloid. Interface Sci.* 1971, 3, 45
- 16 Weill, G., Hornick, C. and Stoylov, S. P. *J. Chim. Phys.* 1968, 65, 182
- 17 O'Konski, C. T., Yoshioka, K. and Orttung, W. H. *J. Phys. Chem.* 1959, 63, 1558
- 18 O'Konski, C. T. *J. Phys. Chem.* 1960, 64, 605

# Molecular motion in polystyrene–plasticizer systems as studied by dielectric relaxation\*

Philip J. Hains and Graham Williams

Edward Davies Chemical Laboratories, University College of Wales, Aberystwyth SY23 1NE, UK  
(Received 7 February 1975; revised 20 March 1975)

The dielectric relaxation behaviour of mixtures of polystyrene with the glass-forming liquids di-n-butyl phthalate, tri-tolyl phosphate and di-octyl phthalate, has been studied over a wide range of compositions. Three distinct dipole relaxation processes are observed, the  $\alpha$  process being due to the re-orientation of solvent molecules as modified by the polymer molecules in the environment, the  $\alpha''$  process is due to the motion of solvent molecules in cooperation with, and largely determined by, the motion of the polymer molecules, and the  $\alpha'$  process is due to the partial re-orientation of solvent molecules. A comparison is made between the behaviour of these systems and of pure solid dipolar polymers and of supercooled molecular liquids.

## INTRODUCTION

It is now well known that both amorphous solid polymers<sup>1–3</sup> and supercooled non-associated molecular liquids<sup>4–8</sup> exhibit quite similar dielectric relaxation behaviour. The  $\alpha$  process, which is due to large-scale Brownian motions, has a contour in the plot  $\epsilon''$  against  $\log(\text{frequency})$  which is quite similar for many polymers and molecular liquids<sup>4,9</sup>. In addition, the observation of a temperature dependent apparent activation energy in both systems is suggestive of a common mechanism<sup>4,5,9</sup>. The  $\beta$  process, which is thought to be due to local motions of dipole units, gives rather broad loss curves and low apparent activation energies. No simple mechanism can be proposed for the  $\beta$  process<sup>1,3,8</sup>. In view of the apparent similarity between the dielectric behaviour of amorphous solid polymers and supercooled molecular liquids, it seemed desirable to study their mixtures. In order that the dielectric loss processes could be assigned to the motions of only one component, we studied the polar solutes, di-n-butyl phthalate (DBP), tri-tolyl phosphate (TTP) and di-n-octyl phthalate (DOP), in (essentially non-dipolar) atactic polystyrene. DBP and TTP form glasses without the complication of crystallization, with glass transitions near 193 K and 217 K respectively, and with  $T_g$  (polystyrene) being near 363 K, the variation in relaxation frequency with composition was expected to be very large. We note that Davies and Edwards<sup>10</sup> and Davies and Swain<sup>11</sup> studied the low frequency dielectric relaxation of several small molecules in polystyrene, while Thurn and Würstlin<sup>12</sup> and Hartmann<sup>13</sup> studied poly(vinyl chloride)/plasticizer systems.

\* This paper contains 21 illustrations which have been deposited with the British Library Lending Division, Boston Spa, Wetherby, Yorkshire LS23 7BQ, UK as Supplementary Publication No. SUP 90013 (20 pages). Applications for copies of supplementary publications should be made to the British Lending Library, quoting the SUP number and enclosing prepaid coupons or their equivalent in cash. One prepaid coupon is required for every 10 pages or part thereof and the present costs are: UK & Eire, £4 for 20 or 20p each; Europe, £11 for 20 or 55p each; elsewhere, £13 for 20 or 65p each. These costs include postage (by airmail where available).

## EXPERIMENTAL

Di-n-butyl phthalate (BDH) was distilled before use, tri-tolyl phosphate (BDH, Chromatography Grade) and di-n-octyl phthalate (BDH) were used as received. Polystyrene (BDH No.29790,  $M_w$   $2.5 \times 10^5$  g/mol) gave negligible dielectric loss, so was used as received. Dielectric measurements were made using two and three terminal cells together with a General Radio 1620-A Assembly ( $10^2$ – $10^5$  Hz) and a Scheiber Bridge ( $10^{-1}$  to  $10^2$  Hz). Mixtures were prepared by dissolving the components in *trans*-1,2-dichloroethylene followed by vacuum removal of this solvent on a water bath. For high polystyrene concentrations (>80% w/w) the materials were glassy solids at room temperature, and discs were made by compression moulding at temperatures exceeding the softening temperature.

## RESULTS

### *Di-n-butyl phthalate–polystyrene*

Dielectric measurements were made on the following mixtures: 9.6, 20.5, 28.4, 35.4, 41.1, 58.7, 73 and 100% DBP/polystyrene (wt %). The detailed results are deposited with the British Library Lending Division, SUP 90013. *Figures 1–4* show† representative loss data at three frequencies, while these and other data are summarized in *Table 1*. The overall behaviour is as follows. Pure DBP exhibits one process, the  $\alpha$  process, which is due to the large-scale Brownian motions of the molecules. As the polystyrene content is raised, the  $\alpha$  process broadens very considerably and moves to higher temperatures at a given frequency. At approximately 40% polystyrene, the single broad  $\alpha$  process separates into two broad processes; the lower temperature process ( $\alpha'$  process) appears to be a continuation of the  $\alpha$  process; the higher temperature process ( $\alpha''$  process) appears to be associated with the plasticization of polystyrene. These variations are conveniently illustrated in *Figure 5*. We note that the  $\alpha$ ,  $\alpha'$  and  $\alpha''$  processes are

† The Figures in the SUP are numbered *Figures 1–21* and should not be confused with *Figures 1–6* of the present paper.

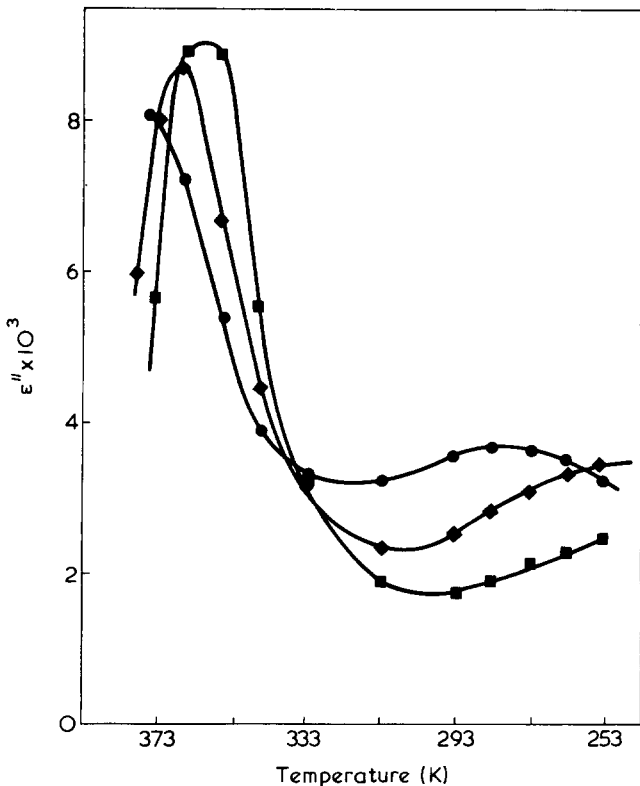


Figure 1  $\epsilon''$  against temperature for 9.63% DBP in polystyrene at 120 Hz (■), 1 kHz (◆) and 10 kHz (●)

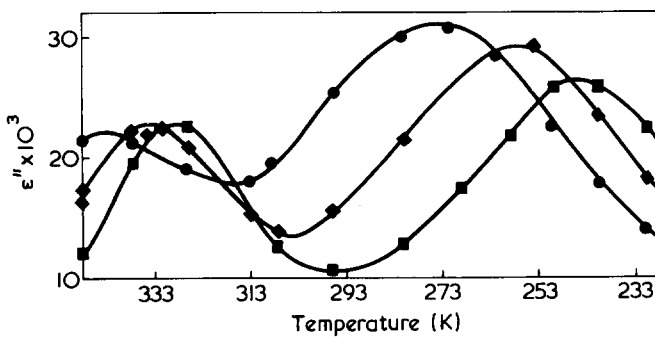


Figure 2  $\epsilon''$  against temperature for 20.5% DBP in polystyrene at 120 Hz (■), 1 kHz (◆) and 10 kHz (●)

all due to the motions of the (dipolar) DBP molecules, but are an indirect measure of the motions of the (non-dipolar) polystyrene. Table 1 shows that the apparent activation energy,  $Q$ , for the  $\alpha'$  process decreases with increasing polystyrene content, whereas  $Q$  for the  $\alpha''$  process remains approximately constant.  $Q(\text{DBP})$  is given as 98 kJ/mol by Shears and Williams<sup>7</sup>.  $Q_{\alpha''} > Q_{\alpha'}$  in all cases, and  $Q_{\alpha''}$  is similar to that commonly found for the glass-transition ( $\alpha$ ) process in amorphous solid polymers and for polystyrene in particular<sup>1</sup>. The half-width of the plot  $\epsilon''$  versus  $\log(\text{frequency})$  for the  $\alpha$  process increases from 1.8 to 3.5 decades on going from 0 → 40% polystyrene; then the  $\alpha'$  process, being a continuation of the  $\alpha$  process, has a half-width ranging from 3.5 decades at 40% polystyrene to 5 decades at 80% polystyrene. It was not possible to obtain a half-width for the  $\alpha''$  process with any degree of certainty, but it is in excess of five decades of frequency. Thus the  $\alpha$  and  $\alpha''$  processes are extremely broad in comparison with the  $\alpha$  process observed in most amorphous solid polymers<sup>1</sup>, and in supercooled liquids<sup>4-9</sup>. The suggestions that there is a common mechanism<sup>4-8</sup> for the  $\alpha$  process in both

systems may well be true, but it appears that other factors are involved in their mixtures, leading to the observed complex behaviour.

Figures 1-4 show that the maximum loss factor  $\epsilon''_m$  for the  $\alpha'$  process exceeds that of the  $\alpha''$  process for the 9.6% DBP system, but the reverse is the case for DBP greater than 14%. Now  $(\epsilon''_{m\alpha'}/\epsilon''_{m\alpha''}) = (\Delta_{\alpha'}\bar{\beta}_{\alpha''})/(\Delta_{\alpha''}\bar{\beta}_{\alpha'})$  where  $\Delta$  and  $\bar{\beta}$  are the dispersion magnitude and the distribution parameter for a given process. We find that  $\bar{\beta}_{\alpha'} \approx \bar{\beta}_{\alpha''}$  for  $C_{\text{DBP}} < 14\%$ , and hence deduce that the relative variation of  $\epsilon''_{m\alpha'}$  and  $\epsilon''_{m\alpha''}$  with increasing DBP concentration corresponds to the relative variations in the dispersion magnitudes. Both  $\Delta_{\alpha'}$  and  $\Delta_{\alpha''}$  increase with increasing DBP, but

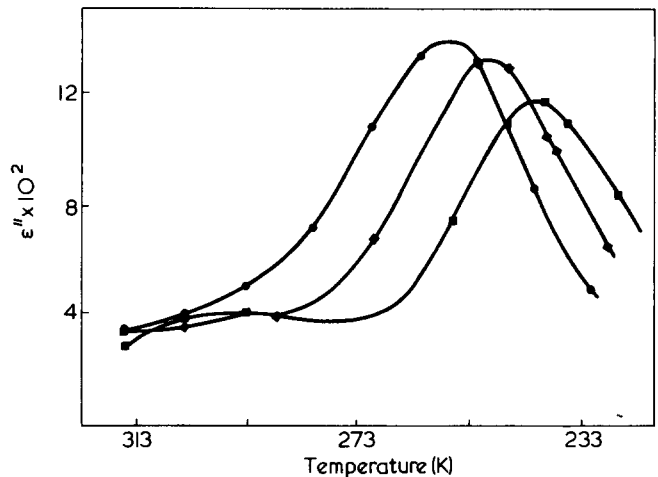


Figure 3  $\epsilon''$  against temperature for 35.5% DBP in polystyrene at 120 Hz (■), 1 kHz (◆) and 10 kHz (●)

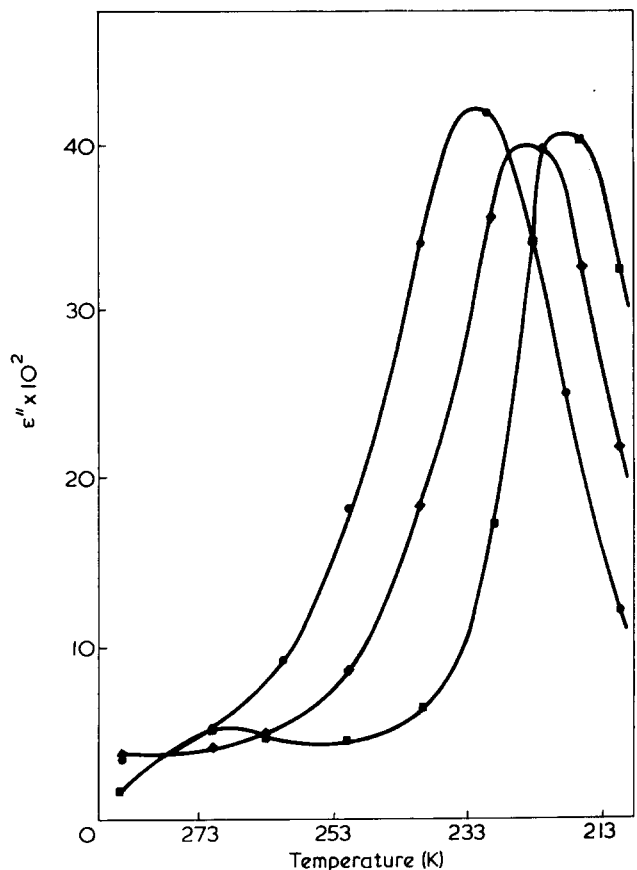


Figure 4  $\epsilon''$  against temperature for 58.1% DBP in polystyrene at 120 Hz (■), 1 kHz (◆) and 10 kHz (●)

Table 1 Relaxation quantities for the  $\alpha$ ,  $\alpha'$  and  $\alpha''$  processes for DBP in polystyrene

Conc. (% w/w)	$T_m$ (K)		$f$ (kHz)	$\epsilon''_m$		$Q$ (kJ/mol)	
	$\alpha''$	$\alpha'$ or $\alpha$		$\alpha'$	$\alpha'$ or $\alpha$	$\alpha''$	$\alpha'$ or $\alpha$
9.6	377.2	280.2	10	—	0.003	303.8	—
	366.2	249.2	1	0.008	0.003		
	359.2	—	0.12	0.009	—		
20.52	342.7	273.7	10	0.022	0.032	284.5	94.5
	334.2	256.7	1	0.023	0.029		
	328.2	244.2	0.12	0.023	0.026		
28.80	314.7	268.2	10	0.033	0.080	303.8	115.9
	311.2	257.2	1	0.033	0.068		
	304.2	242.7	0.12	0.034	0.060		
35.45	—	257.2	10	0.04	0.136	306.3	127.0
	259.7	249.2	1	0.040	0.130		
	290.7	240.2	0.12	0.039	0.115		
41.15	—	249.7	10	—	0.174	—	134.8
	—	240.7	1	0.035	0.172		
	279.2	233.2	0.12	0.04	0.166		
58.07	—	231.7	10	—	0.420	—	134.8
	—	223.2	1	—	0.40		
	268.7	216.7	0.12	0.05	0.408		

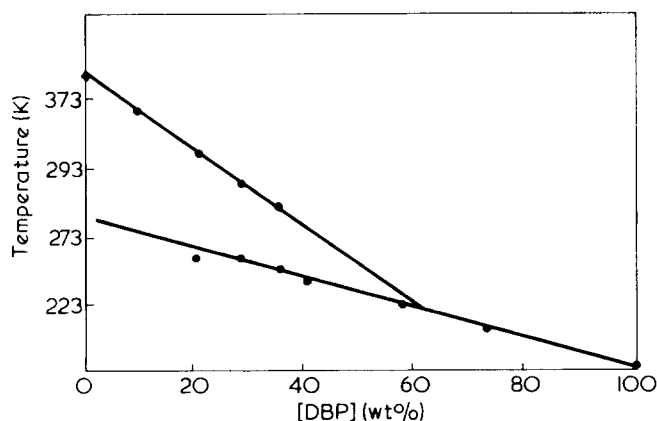


Figure 5 Temperature of maximum loss at 1 kHz as a function of composition for DBP/polystyrene

$\Delta_{\alpha'}$  increases more rapidly than  $\Delta_{\alpha''}$  leading to a reversal in their relative magnitudes for  $C_{\text{DBP}} > 14\%$ .

One explanation for the mechanism of  $\alpha'$  and  $\alpha''$  processes would be that at low DBP concentrations, certain DBP molecules are 'free' to re-orientate, uninfluenced by the polymer matrix, leading to the  $\alpha'$  process, while others are 'bound' in the immediate vicinity of polymer chains. These 'bound' molecules may only move in cooperation with the motions of the polymer chains, leading to the  $\alpha''$  process, which corresponds then to the  $\alpha$  relaxation of the plasticized polymer. This cannot be the complete explanation however, since both the  $\alpha'$  and  $\alpha''$  processes are very broad in the frequency domain, indicating a variety of mechanisms for both processes. Also the location of the  $\alpha'$  process differs from that of the  $\alpha$  process, indicating that the motions are hindered by the presence of polymer chains. A more satisfactory rationalization for the mechanism of  $\alpha$ ,  $\alpha'$  and  $\alpha''$  processes is as follows. For very small DBP concentration, the DBP molecules are isolated from each other in the polymer matrix. These molecules find themselves in a variety of environments, so that some are fairly free to re-orientate their dipole moment in the fixed local potential field of the polymer chains. The re-orientation of these molecules leads to the  $\alpha'$  relaxation

and is partial relaxation of their dipole moments. The unrelaxed moment can only be relaxed by the Brownian motions of the environment<sup>8,14</sup>, i.e. the motions of the polymer chains, leading to a contribution to the  $\alpha''$  relaxation. Some DBP molecules will be completely constrained from local motion ( $\alpha'$  process) by the environment, thus all of their mean square moment will be relaxed only by the Brownian motions of the environment, again making a contribution to the  $\alpha''$  process. The DBP molecules will be distributed over a whole range of local environments, thus leading to the  $\alpha'$  process, being partial relaxation in an environment which does not change its configuration within the timescale of the process, and the  $\alpha''$  process, being the cooperative, large scale, Brownian motions of the polymer matrix and DBP molecules. In terms of this general approach, both  $\alpha'$  and  $\alpha''$  processes are expected to, and do, have broad loss curves in the frequency domain. At low DBP concentration the observation  $\Delta_{\alpha'} < \Delta_{\alpha''}$  indicates that the polymer environment suppresses the local relaxation of DBP molecules. As the DBP concentration is increased there is a corresponding increased probability that DBP molecules are adjacent in the medium, and their cooperation in re-orientational motions leads to an increase in the magnitude of the  $\alpha'$  process at the expense of the magnitude of the  $\alpha''$  process, in accord with experiment since  $\Delta_{\alpha'} > \Delta_{\alpha''}$  for  $C_{\text{DBP}} > 14\%$ . The  $\alpha'$  process, being the partial relaxation of DBP molecules in the polymer environment tends to the character of the  $\alpha$  process as the DBP concentration is further increased, and for  $C_{\text{DBP}} > 60\%$  the polymer chains have only a modifying influence on the DBP motions, leading to the  $\alpha$  process (Figure 5) which contains within it all the available relaxation strength. When the partial relaxation ( $\alpha'$ ) becomes the  $\alpha$  relaxation all of the relaxation strength will be contained in the  $\alpha$  relaxation thus only one process can be observed\*. The  $\alpha$  relaxation, observed in the range 60–100% DBP, becomes faster (see Figure 5) and narrows as the DBP concentration is raised. The half-width of the

\* The  $\alpha''$  curve in Figure 5 cannot cross the  $\alpha$ - $\alpha'$  line to give an observable  $\alpha''$  process at higher DBP concentrations. A similar condition applies to the  $\alpha$ ,  $\beta$ , ( $\alpha\beta$ ) relaxations in solid polymers<sup>15,16</sup>.



plot  $\epsilon''$  versus  $\log$  (frequency) at 73% DBP is near 3 decades of frequency, which should be compared with 1.8 decades for pure DBP. Thus although the polymer chains do not limit the equilibrium orientation distribution of the DBP molecules in this concentration range, the DBP molecules clearly move in a cooperative manner with the polymer chains, and broad loss curves result.

*Tri-tolyl phosphate-polystyrene, di-octyl phthalate-polystyrene and related mixtures*

Dielectric measurements were made on 14.3, 27.9 and 50% TTP/polystyrene (wt %) and 15.5, 34.7 and 50% DOP/polystyrene (wt %). The data are given in SUP 90013. The behaviour of these systems was analogous to that observed for DBP/polystyrene;  $\alpha$ ,  $\alpha'$  and  $\alpha''$  relaxations being observed, and the  $\alpha''$  relaxation being larger in magnitude than the  $\alpha$  relaxation at low solute concentrations, the converse being true at higher solute concentrations. Figure 6 and Table 2 summarize a portion of the results for TTP/polystyrene, and the general behaviour is seen to be quite analogous to that for DBP/polystyrene. For  $C_{TTP} = 14.3\%$  the magnitude of the  $\alpha''$  relaxation exceeds that of the  $\alpha'$  relaxation, while the converse is true for  $C_{TTP} = 27.9\%$ . For  $C_{DOP} = 15.5\%$  the magnitudes of the  $\alpha'$  and  $\alpha''$  processes are comparable, and for  $C_{DOP} = 34.7\%$  the  $\alpha'$  relaxation is dominant. Some measurements were made on the  $\alpha''$  relaxation in the systems anthrone/polystyrene/*o*-terphenyl, anthrone/polystyrene and phthalic anhydride/polystyrene, all at low (<10%) dipolar solute concentration. The process was found to be extremely broad and reflected the cooperative Brownian motions of solute and polymer matrix, i.e. is a measure of the relaxation of plasticized polystyrene.

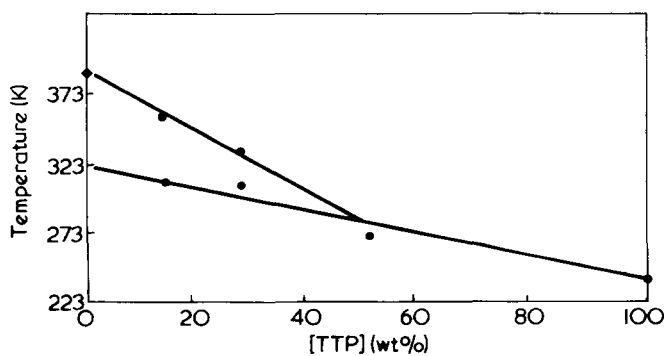


Figure 6 Temperature of maximum loss at 1 kHz as a function of composition for TTP/polystyrene

Table 2 Relaxation quantities for the  $\alpha$ ,  $\alpha'$  and  $\alpha''$  processes for TTP in polystyrene

Conc. (% w/w)	$T_m$ (K)		$f$ (kHz)	$\epsilon''_m$		$Q$ (kJ/mol)	
	$\alpha''$	$\alpha'$ or $\alpha$		$\alpha''$	$\alpha$ or $\alpha'$	$\alpha''$	$\alpha'$ or $\alpha$
14.35	364.7	318.2	10	0.029	—	438.0	—
	358.2	308.2	1	0.030	—		
	353.7	298.2	0.12	0.028	0.016		
27.91	323.0	309.2	10	0.11	0.125	—	202.9
	328.0	304.2	1	0.09	0.105		
	319.7	294.2	0.12	0.08	0.090		
50.81	—	277.2	10	—	0.290	—	202.9
	—	271.2	1	—	0.275		
	—	263.2	0.12	—	0.240		
100	—	241.2	10	—	2.040	—	158.5
	—	234.2	1	—	1.900		

## DISCUSSION

The occurrence of  $\alpha$ ,  $\alpha'$  and  $\alpha''$  relaxations was unexpected, especially since these relaxations arise only from the dipolar solute. Similar studies on dipolar solutes in supercooled non-polar solvents<sup>4-8</sup> give an  $\alpha$  relaxation, and a lower temperature  $\beta$  relaxation. There the  $\alpha$  relaxation corresponds to the cooperative Brownian motions of solute and solvent, and the  $\beta$  relaxation is thought<sup>8</sup> to be due to partial re-orientation of the solute molecules. It is significant in Table 1 that the apparent activation energy for the  $\alpha''$  relaxation is approximately a constant and large, being comparable with the  $\alpha$  relaxation in both solid amorphous polymers and in supercooled molecular liquids. The apparent activation energy for the  $\alpha'$  relaxation decreases with decreasing DBP. It appears that the apparent activation energy for the  $\alpha'$  relaxation is a little high to be regarded as analogous to that for the  $\beta$  relaxation in polymers<sup>1</sup> ( $Q_\beta \approx 40$  kJ/mol) or in supercooled molecular liquids<sup>4,5</sup> ( $Q_\beta \approx 20$  kJ/mol). The  $\alpha'$  relaxation appears to be due to partial re-orientation of solute in a (predominantly) polymer environment, and the  $\alpha''$  and  $\alpha$  relaxations appear to be due to the cooperative Brownian motions of solute and polymer as discussed above.

Obviously one interpretation of the occurrence of  $\alpha'$  and  $\alpha''$  processes would be that our systems were two-phase in nature. All specimens were optically transparent suggesting that if certain compositions were two-phase that this was not at a macroscopic level. We note that Jenckel and Heusch<sup>17</sup> observed only one  $T_g$  in their study of plasticized polystyrene, a study which included the TTP/polystyrene system, again suggesting a one-phase system. Also Wasser and Kurath<sup>22</sup> studied the viscoelastic relaxation of TTP/polystyrene systems over the range 5 to 67% by wt of polystyrene and the observed behaviour is consistent with a one-phase system for this range of composition. The present data show systematic variations with composition, suggestive of a one-phase system at all compositions, and we did not observe discontinuities seen in poly(vinyl chloride)/plasticizer systems by Thurn and Würstlin<sup>12</sup> (their Fig.2) and by Hartmann<sup>13</sup> (his Fig.2). Thus we consider it likely that our systems are essentially one-phase systems at all compositions but we should not ignore the possibility that there may be a tendency towards a separation at the microscopic level for systems containing a small proportion of the plasticizer (TTP or DBP).

Much of the earlier work on polymers containing small molecules relates to poly(vinyl chloride) as the polymer. The simplest such system appears to be that of PVC/di-

phenyl, which in polarity is the reverse of the systems studied here. Fuoss<sup>18</sup> showed that the dielectric  $\alpha$  relaxation moved uniformly to lower temperatures, without any appreciable change in shape as the diphenyl concentration was raised from 0 to 20%. In this case the dielectric measurements correspond to the *direct* observation of the motion of the (dipolar) polymer chains, in contrast with the  $\alpha'$  relaxation of the present work in which the motions of the DBP, TTP or DOP molecules are in cooperation with the motions of the polymer chains, but the correlation is not exact. This would explain our observation that the  $\alpha''$  process is rather broad in comparison with the  $\alpha$  relaxation of a pure amorphous polymer. Other work on PVC systems has involved plasticizing the dipolar polymer with dipolar plasticizers<sup>12,13,19,20</sup>. For example, Würstlin<sup>19</sup> found one dielectric process at each extreme of composition, and two processes at intermediate compositions, being assigned to polymer and plasticizer contributions.

At lower concentrations of plasticizer the loss peak is largely due to the polymer chain motions as modified by the plasticizer molecules. The plasticizer exhibits a separate peak when the polymer molecules are fully solvated<sup>19</sup> (see also ref 1, p 433), and it has been suggested<sup>13</sup> that there will be  $\sim 4$  to 6 repeat units of the chain per 'bound' plasticizer molecule. Later works by Luther and Weisel<sup>20</sup> and by Thurn and Würstlin<sup>12</sup> have suggested that the PVC/plasticizer results are consistent with the superposition of individual processes. The interpretation of multiple loss peaks in two component mixtures in which both components are dipolar is perhaps more difficult than in the present case where the intensity of the multiple loss peaks is due only to the plasticizer molecule.

It is of interest to consider the  $\alpha$ ,  $\alpha'$  and  $\alpha''$  processes in terms of cooperative relaxation as envisaged by Simmons and Macedo<sup>21</sup> for inorganic oxide glasses and by Shears and Williams<sup>7</sup> for organic molecular liquids in their supercooled state. Simmons and Macedo have suggested that cooperative relaxation may be considered in terms of  $\Lambda$ , the 'range' of concentration fluctuations and  $r_0$ , the finite range for interactions which lead to relaxation. For the low frequency relaxation region,  $\Lambda \geq r_0$ , relaxing species are well embedded within the range of fluctuations, and the width of the loss curves is predicted to be broad, being a superposition of individual curves each arising from a different environment. A similar model has been suggested by Shears and Williams<sup>7</sup>, and was introduced to rationalize the unusual variation, with composition, of the width of dielectric loss curves for DBP/*o*-terphenyl mixtures. For the polystyrene/plasticizer systems studied here we suggest the following model for relaxation. The natural Brownian motions of the system, involving the re-orientational and translational motions of chain segments and plasticizer molecules, lead to gross fluctuations (in time)

of the local composition of the medium. The reorientational motions of molecules, giving rise to  $\alpha$ ,  $\alpha'$  and  $\alpha''$  relaxations will occur on a much shorter time scale than that for fluctuations in composition, thus the dipoles reorientate in an environment of apparently fixed composition. The wide range of local environments then leads to very broad  $\alpha$ ,  $\alpha'$  and  $\alpha''$  relaxations. The partial relaxation ( $\alpha'$ ) and total relaxation ( $\alpha''$ ) processes are themselves allowed to occur by local density fluctuations, and are a measure of these fluctuations; similarly for the  $\alpha$  process, except now the local fluctuations succeed in re-orientating the small molecules completely, and no  $\alpha''$  process can be observed in the concentration range where the  $\alpha$  process occurs.

#### ACKNOWLEDGEMENT

We thank the Courtauld Educational Trust Fund for an award to P.J.H.

#### REFERENCES

- 1 McCrum, N. G., Read, B. E. and Williams, G. 'Anelastic and Dielectric Effects in Polymeric Solids', John Wiley, New York, 1967
- 2 McCall, D. W. in 'Molecular Dynamics and Structure of Solids', (Ed. R. S. Carter and J. J. Rush), (*Nat. Bur. Stand. Spec. Publ. 301*) 1969, NBS, Washington, D.C.
- 3 Ishida, Y. *J. Polym. Sci. (A-2)* 1969, 7, 1835
- 4 Johari, G. P. and Smyth, C. P. *J. Chem. Phys.* 1972, 56, 4411
- 5 Johari, G. P. and Goldstein, M. *J. Chem. Phys.* 1970, 53, 2372
- 6 Williams, G. and Hains, P. J. *JCS Faraday Symp.* 1972, 6, 14
- 7 Shears, M. F. and Williams, G. *JCS Faraday Trans. II* 1973, 69, 608
- 8 Williams, G. in 'Dielectric and Related Molecular Processes', Chem. Soc. Specialist Periodical Reports, Vol 2, (Ed. M. Davies), 1975, The Chemical Society, London, Ch 4, p 151
- 9 Williams, G., Cook, M. and Hains, P. J. *JCS Faraday Trans. II* 1972, 68, 1045
- 10 Davies, M. and Edwards, D. A. *Trans. Faraday Soc.* 1967, 63, 2163
- 11 Davies, M. and Swain, J. *Trans. Faraday Soc.* 1971, 67, 1637
- 12 Thurn, H. and Würstlin, F. *Kolloid-Z.* 1957, 156, 21
- 13 Hartmann, A. *Kolloid-Z.* 1956, 148, 30
- 14 Williams, G. and Watts, D. C. *Trans. Faraday Soc.* 1971, 67, 1971
- 15 Williams, G. *Trans. Faraday Soc.* 1966, 62, 2091
- 16 Williams, G. and Watts, D. C. in 'NMR, Basic Principles and Progress: NMR of Polymers', Vol 4, Springer-Verlag, Berlin, 1971, p 271
- 17 Jenckel, E. and Heusch, R. *Kolloid-Z.* 1953, 130, 89
- 18 Fuoss, R. M. *J. Am. Chem. Soc.* 1941, 63, 378
- 19 Würstlin, F. *Kolloid-Z.* 1949, 113, 118
- 20 Luther, H. and Weisel, G. *Kolloid-Z.* 1957, 154, 15
- 21 Simmons, J. H. and Macedo, P. B. *J. Res. Nat. Bur. Stand.* 1971, 75A, 175
- 22 Wasser, R. B. and Kurath, S. F. *J. Colloid Sci.* 1966, 21, 182

# E.p.r. study of radicals produced mechanically in PGMA and their interaction with oxygen

J. Pilař and K. Ulbert

*Institute of Macromolecular Chemistry, Czechoslovak Academy of Sciences, 162 06 Prague 6, Czechoslovakia*

*(Received 11 October 1974; revised 15 May 1975)*

The vibrational grinding of poly(ethyleneglycol methacrylate) (PGMA) *in vacuo* at the liquid nitrogen temperature gives rise to polymer radicals in high concentrations. Changes in the radical concentration as a function of temperature in the presence and absence of oxygen were followed by means of electron paramagnetic resonance. It was found that polymer radicals reacted at very low temperatures with oxygen with simultaneous formation of polymer peroxy radicals and of a non-paramagnetic polymer tetroxide. This polymer tetroxide, which has been proved indirectly, can decompose to yield polymer peroxy radicals and non-paramagnetic products; the observed anomalies on the curve of the thermal decomposition of radicals may be thus elucidated. The relative participation of polymer tetroxide depends on the oxygen concentration, on the temperature of the sample in contact with oxygen and on the concentration of polymer radicals arising by grinding predominantly on the surface of polymer particles.

## INTRODUCTION

The formation of polymer radicals during the mechanical degradation of a polymer by vibrational grinding was first observed by Bresler<sup>1</sup> and Butyagin *et al.*<sup>2</sup>. Later, Butyagin<sup>3,4</sup> studied in detail processes taking place during the grinding of the polymer. Bresler *et al.* investigated, in the temperature range of 40–100°C, the decay of polymer radicals prepared by the vibrational grinding of poly(methyl methacrylate) (PMMA) *in vacuo* at the liquid nitrogen temperature<sup>5</sup>, the interaction of the radicals with oxygen accompanied by the formation of polymer peroxy radicals<sup>6</sup> at temperatures ranging from –20° to –80°C and the decay of polymer peroxy radicals<sup>5</sup> at temperatures from 5 to 37°C. Butyagin *et al.*<sup>7</sup> studied transformations of the polymer peroxy radicals *in vacuo* and in an oxygen atmosphere at temperatures above –30°C. In this paper we report some results obtained in the study of polymer radicals prepared by the vibrational grinding of PGMA and of their transformations due to an interaction with oxygen at lower temperatures, ranging from –150 to –60°C.

## EXPERIMENTAL

### Material

The starting polymer material was poly(ethyleneglycol methacrylate) (PGMA) crosslinked to 40% with ethyleneglycol dimethacrylate prepared<sup>8,9</sup> in the form of porous globules (Spheron 300®). The size of the globules varied from 100 to 200 μm.

### Sample preparation and grinding

400 mg of PGMA globules were evacuated at room temperature for 2–3 h in a glass grinding vessel (Figure 1) at 10<sup>–3</sup> mmHg. After sealing off, the glass grinding vessel containing the polymer and glass beads was fixed in a quickchange chuck of a driving grinding unit. The latter consisted of an adapted vibratory stirrer (100 W) with an

adjustable vibration amplitude at a frequency of 100 Hz. The vibration amplitude was adjusted within a range of 2–4 mm. During the grinding, which proceeded for 15–60

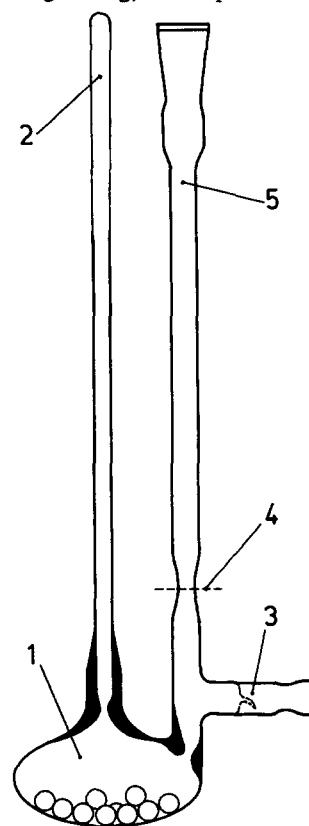


Figure 1 Glass grinding vessel used for evacuation, vibrational grinding and measuring e.p.r. spectra of the polymer: 1, milling part with glass beads; 2, measuring tube; 3, break-type glass valve; 4, final seal; 5, evacuation port

min, the holder and the vessel were immersed in liquid nitrogen. After completion of grinding the holder was quickly disconnected, turned by 180° and fixed to the driving unit by its other end. The ground polymer sticking to the inner walls of the vessel and to the glass beads was (while still in liquid nitrogen) shaken off by short-time vibrations (1–2 min) into a measuring tube with an outer diameter of 5 mm, forming part of the grinding vessel. The measuring tube was filled up to such a level which equals the length of the cavity of the spectrometer to eliminate the 'filling factor' effect. A break-type glass valve was also part of the vessel, allowing oxygen or other gases to be admitted into it. It was found that the radical concentration in the ground polymer strongly depended on the vibration amplitude; the dependence on the time of grinding had the same character as the dependence established by Butyagin<sup>3</sup>.

#### E.p.r. spectra measurements

Electron paramagnetic resonance (e.p.r.) spectra were recorded with a JES-3B JEOLCO Tokyo spectrometer, the measuring cavity of which can be thermostated within a temperature of –150° to +200°C with an accuracy of ±1°C. Mn<sup>2+</sup> in MgO was used as the internal standard. The first derivative and first and second integral of the spectrum were recorded simultaneously. An analogue electronic integrator and a digital electro-optical integrator<sup>10</sup>, respectively, were used for integration.

#### Determination of relative and absolute radical concentrations

When comparing radical concentrations measured in the sample under various conditions (before and after introduction of oxygen, at different temperatures etc.), we expected changes in the quality of the cavity (from change in the amplitude of the signal of the internal standard) and changes in the occupation of the energy levels of the unpaired electron in the magnetic field due to temperature (from the Boltzmann distribution law<sup>11</sup>). All measurements were performed at the same amplitude of the high-frequency magnetic modulation and at the same power input to the measuring cavity of the spectrometer (~1 mW) in virtually identical measuring specimen tubes. The experimental error of determination of relative radical concentrations was estimated to be about 15%. The absolute radical concentrations in the samples were determined by a comparison with a standard sample – benzene solution of diphenylpicrylhydrazyl (DPPH). The radical concentration in this solution was determined from electron spectra in the visible region<sup>12</sup> ( $\lambda_{\text{max}} = 520 \text{ nm}$ ,  $\epsilon = 11\,500 \text{ l mol}^{-1} \text{ cm}^{-1}$ ). For e.p.r. spectra measurements the benzene solution of DPPH was filled into the same measuring tubes and measured at room temperature under otherwise the same conditions as for polymer samples. The absolute concentrations of polymer radicals in the samples measured immediately after grinding at –150°C ( $[R^*]_0^{-150}$ ) varied between 1 and  $3 \times 10^{18} \text{ g}^{-1}$  depending on the conditions of grinding. In those cases when two different radicals appeared in the sample simultaneously, a WANG 600 14 computer was used for computing the first derivatives of simulated superimposed spectra, and for computing the second integrals of both components forming the superimposed spectrum, by twofold numerical integration.

## RESULTS

### Polymer radicals R\*

Szöcs and Ulbert<sup>13</sup> have found that the spectrum of polymer radicals formed in an X-irradiated PGMA coincides with the characteristic spectrum referred to in the literature as the '5 + 4 line' spectrum and most frequently attributed to the radical of type Ia. A spectrum of the same shape was also obtained in the study of PGMA irradiated by a high-frequency discharge in rarefied nitrogen gas. The spectrum of polymer radicals obtained by vibrational grinding of PGMA *in vacuo* at the liquid nitrogen temperature recorded at –150°C (Figure 2b) differs from the former spectrum by the width and ratio of intensities of the individual components of the hyperfine structure (third and seventh lines of the spectrum exhibit a stronger intensity than the central fifth line). An increase in the sample temperature has as a consequence a narrowing of the spectral lines accompanied by gradual transformation of the spectrum into the '5 + 4 line' shape and a decrease in the radical concentration of the sample (Table 1). The spectrum of a sample left for several minutes at room temperature (Figure 2a) has also the form '5 + 4 line'. If the sample temperature is kept constant within a range of –150° to –60°C, the radical concentration changes do not exceed the experimental error. The observed changes in the shape of the spectrum and in the radical concentration with temperature are not reversible.

### Interaction of polymer radicals with oxygen

After the introduction of oxygen at atmospheric pressure and a temperature  $T_r = -150^\circ\text{C}$  a very fast decrease in the radical concentration takes place in the sample, and the observed spectrum (Figure 2c) is a superposition of the spectrum of polymer radicals R\* (Figure 2b) and of that of polymer peroxy radicals ROO\* (Figure 2d). If the sample is left at –150°C for several tens of minutes the further decrease in the concentration of radicals R\* is very small. The concentration of ROO\* remains virtually unchanged. An increase in the sample temperature (by 20°C up to –60°C) leads to a fast decrease in the concentration of R\* to zero, and to an increase in the concentration of ROO\* attaining at –60°C a maximum value which is higher than the total radical concentration measured in the sample immediately after the introduction of oxygen at –150°C ( $[R^*]^{-150} + [\text{ROO}^*]^{-150}$ ). At temperatures –60°C and higher the concentration of ROO\* rapidly decreases with time and temperature. The measured relative radical concentrations are given in the first line of Table 1. Further lines contain the results of experiments in which oxygen was introduced into the sample at higher  $T_r$ , the result of an experiment in which air was introduced into the sample, and also of an experiment in which the sample after grinding was left at room temperature for some 30 min. Changes in the radical concentration with temperature are very fast as mentioned above. All measurements were carried out on samples in an almost stationary state when on the contrary changes in the shape of the spectra and in the radical concentrations are very small and slow. Table 1 summarizes mean values of measurements carried out during a time between 10 and 60 min after the change in temperature or the introduction of oxygen. In order to rule out the possibility that the decrease in the radical concentration in the sample is due to a heating of the sample cooled to –150°C owing to the introduction of uncooled gas (the gas introduced was always at room temperature), we carried out an

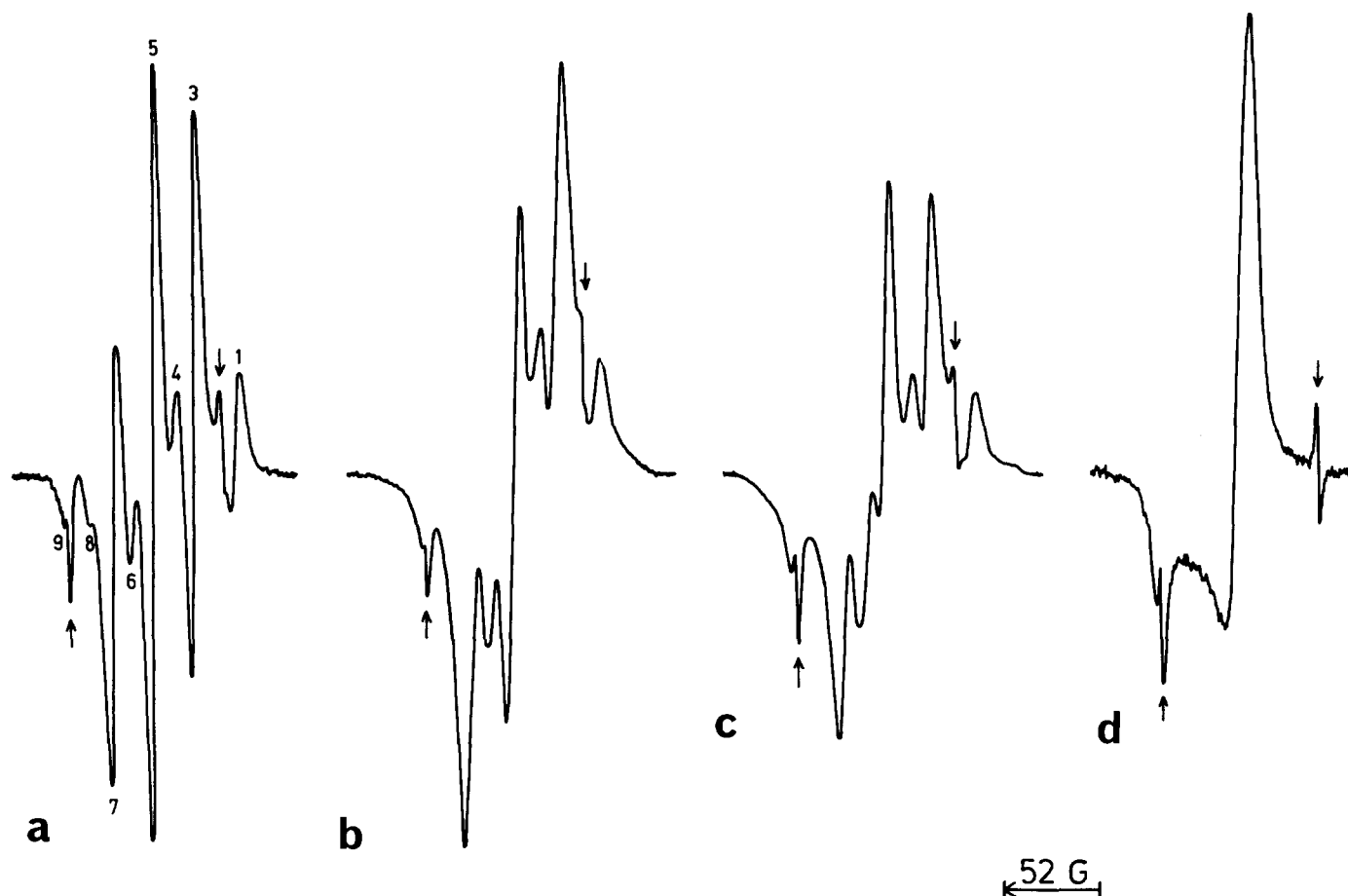


Figure 2 E.p.r. spectra of polymer radicals obtained by vibrational grinding of PGMA *in vacuo* at liquid nitrogen temperature. Arrows denote positions of third and fourth lines of the internal standard  $Mn^{2+}$  in  $MgO$ ; their distance is 86.9 G. (a) spectrum of a sample left after grinding 30 min in vacuum at room temperature measured at  $-150^{\circ}C$ ; (b) spectrum of the sample measured immediately after grinding in vacuum at  $-150^{\circ}C$ ; (c) spectrum measured at  $-150^{\circ}C$  after introduction of oxygen into the sample at the same temperature; (d) spectrum of polymer peroxy radicals measured at  $-60^{\circ}C$

Table 1 Relative radical concentrations in samples at various temperatures<sup>a</sup>

$T_r$ ( $^{\circ}C$ )	$\frac{[R']_{T_r}}{[R']_0^{-150}}$	$\frac{[R']^{-150}}{[R']_0^{T_r}}$	$\frac{[ROO']^{-150}}{[R']_0^{T_r}}$	$\frac{[R']^{-120}}{[R']_0^{T_r}}$	$\frac{[ROO']^{-120}}{[R']_0^{T_r}}$	$\frac{[R']^{-100}}{[R']_0^{T_r}}$	$\frac{[ROO']^{-100}}{[R']_0^{T_r}}$	$\frac{[R']^{-80}}{[R']_0^{T_r}}$	$\frac{[ROO']^{-80}}{[R']_0^{T_r}}$	$\frac{[R']^{-60}}{[R']_0^{T_r}}$	$\frac{[ROO']^{-60}}{[R']_0^{T_r}}$
-150	1.00	0.20	0.05	0.08	0.15	0.06	0.30	0	0.37	0	0.40
-120	0.88			0.12	0.16	0.03	0.30	0	0.39	0	0.40
-100	0.78					0.05	0.41	0	0.47	0	0.47
-80	0.70							0	0.53	0	0.53
-60	0.60									0	0.61
-150 <sup>c</sup>	1.00	0.32	0.17	0.13	0.35	0.05	0.47	0.03	0.51	0	0.50
-150 <sup>d</sup>	0.26	0.70	0.10	0.24	0.32	0.07	0.39	0.04	0.52	0	0.58

<sup>a</sup>  $[R']_0^{-150}$  is concentration of radicals  $R'$  measured in the sample immediately after grinding at  $-150^{\circ}C$ .  $[R']_0^{T_r}$  is concentration of radicals  $R'$  measured in the sample at  $T_r^{\circ}C$  closely before introduction of oxygen.  $[R']^{-150}$  and  $[ROO']^{-150}$  respectively are concentrations of radicals  $R'$  and  $ROO'$  measured in the sample after introduction of oxygen at  $-150^{\circ}C$  ( $-120^{\circ}C$ ,  $-100^{\circ}C$ ,  $-80^{\circ}C$ ,  $-60^{\circ}C$ ). The numbers are mean values determined from several measurements. The experimental error of radical concentration in relative units does not exceed 15%

<sup>b</sup>  $T_r$  is sample temperature at the time of introduction of oxygen

<sup>c</sup> Air introduced into the sample

<sup>d</sup> The sample after grinding left at room temperature about 30 min

experiment in which nitrogen was introduced into the sample. However, both the shape of the spectrum and the radical concentration remained unchanged after nitrogen had been introduced into the sample at  $-150^{\circ}C$ .

## DISCUSSION

The primary process taking place after the introduction of oxygen into the sample is clearly the formation of polymer peroxy radicals:



Ingold and Thomas<sup>14,15</sup> assume that at a low temperature low molecular tertiary peroxy radicals can form non-paramagnetic tetroxide via a fast mutual exothermal reaction:



By using the e.p.r. method, Barlett and Guaraldi<sup>16</sup> have found that with increasing temperature the equilibrium in reaction (2) is shifted towards the peroxy radicals; changes in the concentration of the peroxy radicals are completely reversible within a temperature range of  $-150$  to  $-70^{\circ}C$ .

On consuming some activation energy the low molecular tertiary tetroxides can decompose via possible formation of trioxide and alkoxy radicals as intermediates to give peroxides ROOR, oxygen and further products<sup>14,15</sup>

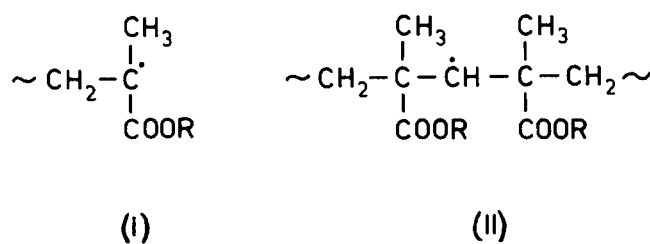
The observed changes in the radical concentrations in polymer samples (*Table 1*) may be elucidated by assuming the possible formation of a polymer tetroxide with similar properties. The introduction of oxygen into the sample at  $T_r = -150^\circ\text{C}$  has as a consequence the transformation of some 75% of polymer radicals  $R^\bullet$  via reactions (1) and (2) into non-paramagnetic polymer tetroxide. With an increase in the sample temperature from  $-150$  to  $-60^\circ\text{C}$  the remaining polymer radicals react with oxygen while giving rise to polymer peroxy radicals and partly also to polymer tetroxide. The latter decomposes to a greater extent directly into stable non-paramagnetic products, and to a lesser extent back into polymer peroxy radicals. At temperatures  $-60^\circ\text{C}$  and higher reactions transforming peroxy radicals directly into final products seem to predominate. In contrast with low molecular peroxy radicals<sup>16</sup> the concentration changes of polymer peroxy radicals with temperature are not completely reversible, which may be due, on the one hand, to their lower mobility, and on the other to a partial decomposition of polymer tetroxide into non-paramagnetic products already at very low temperatures. It may also be deduced from what has been said above that the method applied by Bresler *et al.*<sup>6</sup> in their study of the interaction of polymer radicals prepared by the vibrational grinding of PMMA with oxygen at atmospheric pressure and temperatures ranging from  $-80$  to  $-20^\circ\text{C}$ , which is based only on measurements of the concentrations of forming polymer peroxy radicals, does not adequately describe an important region of behaviour of the mechanically degraded polymer. We believe that the formation and gradual decomposition of polymer tetroxide is also the cause of the so far unexplained increase in the total concentration of polymer radicals and polymer peroxy radicals after heating of samples prepared by the mechanical degradation of polymers by filing as observed by Kawashima *et al.*<sup>17</sup> in their investigation of polypropylene and other polymers.

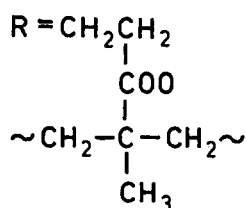
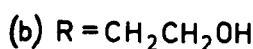
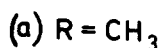
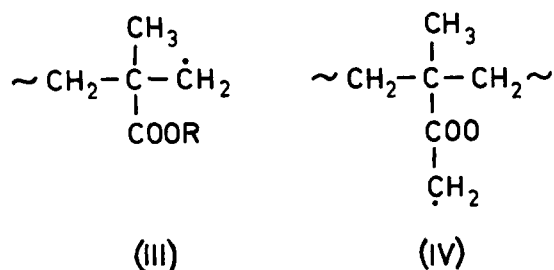
The conditions of formation of polymer tetroxide become worse with increasing temperature  $T_r$  at which oxygen is introduced into the sample. This is due to an increase in temperature at which polymer radicals react with oxygen, and particularly to the decrease in the concentration of polymer radicals on the surface of particles of the ground polymer which during the rise in the sample temperature under vacuum from  $-150^\circ\text{C}$  to  $T_r$  disappear by recombination. At the same time the portion of polymer radicals from  $[R^\bullet]_0^{T_r}$  transformed into non-paramagnetic products by the decomposition of the polymer tetroxide is decreasing, while the relative concentration of polymer peroxy radicals in the sample is rising (*Table 1*). We assumed that the polymer radicals were prevailing localized on the surface of microscopic polymer particles produced by grinding. This is supported by the high rate of their reaction with oxygen even at very low temperatures. The observed recombination of polymer radicals is probably related to a steep decrease in the surface area of the ground polymer observed by Butyagin<sup>4</sup> in his study of PMMA in the temperature region around  $-140^\circ\text{C}$  and attributed by him to the sintering of the polymer.

If air is introduced into the sample instead of oxygen at  $T_r = -150^\circ\text{C}$ , only some 50% of polymer radicals are transformed into the non-paramagnetic tetroxide form, which is evidence that the transformation is a function of the partial

concentration of oxygen. The overall radical concentration remains practically unchanged during heating of the sample: either the remaining polymer radicals are only oxidized to polymer peroxy radicals, or the formation of polymer tetroxide (if any) is in a dynamic equilibrium with its decomposition back to polymer peroxy radicals. The introduction of oxygen at  $T_r = -150^\circ\text{C}$  into the sample left after grinding at room temperature for some 30 min has as a consequence the transformation of only about 20% of the remaining polymer radicals into the non-paramagnetic form. We suppose that on exposure of the sample to room temperature surface radicals predominantly recombine, thus raising the relative participation of radicals existing at various depths below the surface of microscopic polymer particles. These subsurface radicals do not any more react readily with oxygen, and the formation of polymer tetroxide by reactions (1) and (2) accompanied by a decrease in the overall radical concentration proceeds to a great extent also at increasing sample temperature from  $-150^\circ$  to  $-100^\circ\text{C}$ . During the further increase in temperature the decomposition of polymer tetroxide probably prevails, and the concentration of polymer peroxy radicals increases.

In the discussion of the results one cannot avoid an analysis of the shape of the spectrum, and consequently of the structure of polymer radicals formed by the vibrational grinding of PGMA. In particular, one has to analyse the difference in the shapes of the spectra of polymer radicals obtained by X-irradiation<sup>13</sup> and vibrational grinding. The first explanation that comes to mind is that the spectrum in *Figure 2b* is a superposition of the '5 + 4 line' spectrum (*Figure 2a*) attributed to radical Ib and of the spectrum of another radical or several radicals which with increasing temperature of the sample recombine faster than radicals Ib. Butyagin *et al.* in their study of radicals formed by the vibrational grinding of PMMA<sup>18,19</sup> observed similar departures from the shape of the '5 + 4 line' spectrum deepening with the time of vibrational grinding of the polymer to such an extent that after 28 h of grinding the spectrum of polymer radicals was only a broad doublet. They assigned the doublet to radical IIa and found that its decay *in vacuo* at constant temperature in the interval between  $-36^\circ$  and  $-0^\circ\text{C}$  was controlled by second order kinetics<sup>19</sup>. A doublet observed on heating of the X-irradiated PGMA<sup>13</sup> at  $65^\circ\text{C}$  in vacuum for 6 h is assumingly due to the radical IIb the superposition of which on the '5 + 4 line' spectrum is reflected in an increase in the intensities of the fourth and sixth lines of the spectrum. However, some difficulties are met when one is trying to explain the formation of radicals II during the mechanical destruction of polymers. In the vibrational grinding of PMMA, radicals IIIa should be formed simultaneously with radicals Ia as primary radicals owing to the breaking of the polymer chain. In the cross-linked PGMA, radicals IV should perhaps arise in addition to radicals Ib and IIIb owing to breaking of the connecting chains. Radicals III and IV could not be recorded so far,





probably because of their high reactivity. Radicals II may be formed as secondary radicals in the mechanical degradation of the polymer owing to the tearing off of the hydrogen atom of the methylene group in the polymer chain by reactive radicals III or IV rather than as primary radicals by direct breaking of the C–H bond of the methylene group, as has been suggested by Butyagin *et al.*<sup>18</sup>. Besides the fact that the observed shape of the spectrum can be due to the superposition of some of radicals IIb, IIIb, and IV, or of all of them simultaneously on the spectrum of radical Ib, the possibility should also be borne in mind that the observed departures from the shape of the '5 + 4 line' spectrum may be caused by intermolecular interactions alone between radicals Ib at a high concentration of the latter on the surface of the polymer particles. The changes in the shape of the spectrum could also be a result of the formation and decay of radical pairs similarly to irradiated polyethylene<sup>20,21</sup>, but so far no spectra corresponding to the  $\Delta M_s = 2$  transition have been recorded. The results of an attempt to simulate numerically the shape of the spectrum in *Figure 2b* and also the results of measurement of the differential spectrum of a sample kept after grinding at  $-150^\circ\text{C}$  and a sample left at room temperature have only led to a conclusion that the spectrum given in *Figure 2b* can be produced by the superposition of a very broad unresolved singlet on the '5 + 4 line' spectrum. This singlet can be the spectrum of any of radicals IIb, IIIb and IV. Moreover, the superposition of such singlet does not rule out the possibility that both spectra differ only owing to the above mentioned intermolecular interaction of radicals Ib.

If the ground PGMA contains also some of radicals IIb, IIIb, and IV, one may expect that after the introduction of oxygen into the sample the above radicals would react similarly to radicals Ib. It can be expected of course that the properties of the respective polymer tetroxide would be different from those of the tetroxide of radical Ib. In such case the observed fact that with increasing  $T_f$  the relative concentration of polymer peroxy radicals  $[\text{ROO}^*]^{-60}/[\text{R}^*]_0^{T_f}$  increases, but their relative concentration  $[\text{ROO}^*]^{-60}/[\text{R}^*]_0^{150}$  remains practically the same could be explained by the finding that at low temperatures the decomposition of the tetroxide proceeds prevalingly

by a mechanism leading directly to non-paramagnetic products. Owing to the observed shapes of the spectra, radicals IIb, IIIb and IV should recombine faster on heating of the sample than radicals Ib, and their participation in the polymer radical concentration  $[\text{R}^*]_0^{T_f}$  should decrease with increasing  $T_f$ .

It is clear that the suggested mechanism of interaction of polymer radicals with oxygen at low temperatures requires a further experimental investigation. Attempts are needed to obtain more insight into the problem by analysing reaction products using chemical and physicochemical methods, which along with a further examination of the transformations of polymer radicals and shapes of their spectra are the object of a further study.

Experiments have been carried out with the aim of revealing the role played by an antioxidant in the reaction of polymer radicals with oxygen under the described conditions. The first results obtained with samples prepared by grinding the polymer with 1% of added antioxidant show that a pronounced interaction of polymer peroxy radicals with the antioxidant occurs at temperatures  $-60^\circ\text{C}$  and higher.

#### ACKNOWLEDGEMENTS

The authors wish to thank Dr J. Pospíšil for stimulating discussions, Dr J. Čoupek for kindly supplying the polymer material Spheron 300, Dr J. Jokl for writing the program for numerical simulation and integration of the e.p.r. spectra, and Mrs J. Vaňková for technical assistance.

#### REFERENCES

- Bresler, S. E., Zhurkov, S. N., Kazbekov, E. N., Saminskij, E. M. and Tomashevskij, E. E. *Zh. Tekh. Fiz.* 1959, 29, 358
- Butyagin, P. Yu., Berlin, A. A., Kalmanson, A. E. and Bljumenfeld, A. A. *Vysokomol. Soedin.* 1959, 1, 865
- Butyagin, P. Yu. *Vysokomol. Soedin. (A)* 1967, 9, 136
- Butyagin, P. Yu. *Vysokomol. Soedin.* 1963, 5, 1829
- Bresler, S. E., Kazbekov, E. N., Fomitchev, V. N., Szöcs, F. and Smejtek, P. *Fiz. Tverd. Tela* 1963, 5, 675
- Bresler, S. E., Kazbekov, E. N. and Fomitchev, V. N. *Kinet. Katal.* 1965, 6, 820
- Butyagin, P. Yu., Kolbanov, I. V., Dubinskaya, A. M. and Kisluk, M. U. *Vysokomol. Soedin. (A)* 1968, 10, 2265
- Coupek, J., Kriváková, M., and Pokorný, S. *Prepr. IUPAC Int. Symp. Macromolecules, Helsinki 1972*
- Czech. Pat. 148 828
- Czech. Pat. 105 555
- Poole, Ch. P., Jr. 'Electron Spin Resonance', Interscience, New York, 1967
- Henglein, A., Boysen, M. and Schnabel, W. Z. *Phys. Chem. (N.F.)* 1957, 10, 137
- Szöcs, F. and Ulbert, K. *J. Polym. Sci. (B)* 1967, 5, 671
- Ingold, K. U. *Acc. Chem. Res.* 1969, 2, 1
- Thomas, J. R. and Ingold, K. U. *Adv. Chem. Ser.* 1968, 75, 258
- Bartlett, P. D. and Guaraldi, G. *J. Am. Chem. Soc.* 1967, 89, 4799
- Kawashima, T., Shimada, S., Kashiwabara, H. and Sohma, J. *Polym. J.* 1973, 5, 135
- Butyagin, P. Yu., Kolbanov, I. V. and Radtzig, V. A. *Fiz. Tverd. Tela* 1963, 5, 2257
- Butyagin, P. Yu. *Dokl. Akad. Nauk SSSR* 1965, 165, 103
- Fujimura, T., Hayakawa, N. and Tamura, N. *Prepr. IUPAC Conf. Chem. Transform. Polym. Bratislava 1971*
- Iwasaki, M., Ichikawa, T. and Ohmori, T. *J. Chem. Phys.* 1969, 50, 1984, 1991

# A route to anionic hydrophilic films of copolymers of L-leucine, L-aspartic acid and L-aspartic acid esters

W. L. Sederel, A. Bantjes and J. Feijen

Polymer Division, Department of Chemical Technology, Twente University of Technology, Enschede, The Netherlands

(Received 11 November 1974; revised 24 March 1975)

A series of copolymers of L-leucine and  $\beta$ -benzyl-L-aspartate [Leu/Asp(OBz)] covering the range 30–70 mol % of L-leucine, was synthesized by the *N*-carboxyanhydride (NCA) method. The copolymers were characterized by elemental analysis, infra-red spectroscopy and viscometry. For all compositions high molecular weight copolymers were prepared with excellent film-forming properties. Tercopolymers of L-leucine,  $\beta$ -benzyl-L-aspartate and  $\beta$ -methyl-L-aspartate [Leu/Asp(OBz)/Asp(OMe)] were obtained after an ester interchange reaction (conversion 85–95%) with the original copolymer systems. These tercopolymers were characterized by elemental analysis and i.r. spectroscopy. Films of the tercopolymers, cast from organic solvents, could be converted into hydrophilic films by saponification of the methyl ester groups using alkaline water/organic solvent media. The hydrophilic films, which will be further investigated for their use as haemodialysis membranes were characterized by potentiometric titration and i.r. spectroscopy.

## INTRODUCTION

During the last decade, there has been an intensified search for biomaterials. Synthetic polypeptides, well known as model compounds for the elucidation of natural processes, show great potential as biomaterials. These materials have already been studied for the utilization as biodegradable sutures<sup>1</sup>, artificial skin<sup>2,3</sup>, tissue implants<sup>4</sup> or as membranes in haemodialysers<sup>5–8</sup> and blood oxygenators<sup>9</sup>.

In haemodialysis membrane applications, where the materials are exposed to blood, it is necessary to get an understanding of the phenomena, which take place at the blood–material interface. In this respect negatively charged materials are of special interest, since it is thought that negatively charged surfaces repel platelets, erythrocytes and other blood elements, which are also negatively charged. Therefore, we are interested in the synthesis of a series of well characterized, negatively charged, water insoluble films, which can be made from synthetic polypeptides in a reproducible way.

Two approaches can be followed: (a) incorporation of L-glutamic acid or L-aspartic acid in hydrophobic polypeptides, such as poly (L-leucine); (b) crosslinking of polyacids such as poly (L-glutamic acid) or poly (L-aspartic acid). One disadvantage of many chemically crosslinked polymers is that the crosslinking (and sometimes the polymerization) is accomplished at the same time the membrane is being formed. As a result, it is often difficult to obtain reproducible pinhole free membranes. Therefore we decided to follow approach (a).

In principle copolymers of L-leucine and L-aspartic acid [Leu/Asp(OH)] can be made by hydrogen bromide treatment of the corresponding  $\beta$ -benzyl-ester derivatives [Leu/Asp(OBz)] (I). The copolymers of L-leucine and  $\gamma$ -benzyl-L-glutamate [Leu/Glu(OBz)] were treated in this way by Klein *et al.*<sup>6</sup>. The resultant polymers [Leu/Glu(OH)] were generally poorly soluble in common solvents. Membrane formation from mixtures of solvents yielded weak membranes.

On the basis of the results with the glutamic acid series an alternative pathway was chosen to reach our goal. This report describes the synthesis and characterization of hydrophilic films of high molecular weight copolypeptides of L-leucine,  $\beta$ -benzyl-L-aspartate,  $\beta$ -methyl-L-aspartate and L-aspartic acid [Leu/Asp(OBz)/Asp(OMe)/Asp(OH)] (III). The films were obtained: (a) directly from films made of copolymers of L-leucine,  $\beta$ -benzyl-L-aspartate and  $\beta$ -methyl-L-aspartate [Leu/Asp(OBz)/Asp(OMe)] (II) by treatment with alkaline aqueous/organic solvent mixtures; and (b) by dissolving polymers (III) in pyridine and casting films from these solutions. The copolypeptides (II) were obtained from L-leucine and  $\beta$ -benzyl-L-aspartate [Leu/Asp(OBz)] (I) copolymers via an ester interchange reaction.

## EXPERIMENTAL

### Materials

$\beta$ -Benzyl-L-aspartate was synthesized by the method described by Benoiton<sup>10</sup>, (m.p. 220°C). The monomers  $\beta$ -benzyl-L-aspartate-NCA (m.p. 125–126°C) and L-leucine-NCA (m.p. 76°C) were prepared by methods described in the literature<sup>11,12</sup>.

### Typical polymerization procedure for 50:50 Leu/Asp(OBz) (I)

L-Asp(OBz)-NCA (9.96 g, 40 mmol) was dissolved in a mixture of dry dioxane (70 ml) and of dry benzene (130 ml); L-leucine-NCA (6.28 g, 40 mmol) was dissolved in dry benzene (150 ml). The two solutions were filtered and introduced in the polymerization flask. Triethylamine (TEA) was used as an initiator at anhydride: initiator ratios (A/I) of 200 and 500. Polymerization reactions were allowed to proceed for 5 days at room temperature. A part of the clear viscous solution (35 ml) was slowly poured into methanol (500 ml) and the fibrous polymer was isolated and dried *in vacuo* at 50°C.



Elemental analyses (I) (%) Leu <sub>x</sub> /Asp(OBz) <sub>1-x</sub>			
x	Element	Calculated	Found
0.70	C	64.01	63.92
	H	7.82	7.75
	N	9.95	9.83
0.67	C	64.04	63.67
	H	7.66	7.75
	N	9.74	9.68
0.60	C	64.09	63.36
	H	7.34	7.25
	N	9.34	9.19
0.50	C	64.15	63.71
	H	6.92	6.82
	N	8.81	8.60
0.40	C	64.21	63.63
	H	6.54	6.90
	N	8.32	8.57
0.30	C	64.26	64.06
	H	6.20	6.26
	N	7.89	7.74

#### Leu/Asp(OBz)/Asp(OMe) (II)

The polymer solution of (I) (315 ml) was diluted with benzene (300 ml) and the solution was heated to 65°C and treated with methanol (150 ml) containing concentrated sulphuric acid (6 ml) for 60 h.

On cooling the polymer precipitated and the mixture was concentrated by evaporation. The resulting gel was dissolved in tetrahydrofuran (THF) and the solution was poured into water (1.8 l). The polymer was isolated and washed with water until neutral and then dried *in vacuo* at 50°C. The composition of copolymers (II) was determined by elemental analyses.

Elemental analyses (II) (%) Leu <sub>x</sub> /Asp(OBz) <sub>1-x-y</sub> /Asp(OMe) <sub>y</sub>			
	Element	Calculated	Found
x = 0.70	C	58.06	58.19
y = 0.30	H	8.32	8.33
	O	21.74	22.26
x = 0.60	C	57.23	57.63
y = 0.36	H	7.81	7.93
	O	23.52	24.30
x = 0.50	C	55.77	55.20
y = 0.45	H	7.37	7.57
	O	25.64	25.40

#### Leu/Asp(OBz)/Asp(OMe)/Asp(OH) (III)

II (2 g) was dissolved in THF (50 ml) at 45°C. The viscous solution was poured onto a glass plate and films were cast by use of a Dokter's knife. A second glass plate placed over the first one at a distance of about 1–2 cm was used to control the evaporation rate. The films (20 x 35 cm, 20–40 μm thick) were placed in a mixture of acetone (500 ml) and 0.1 N sodium hydroxide (500 ml) for various times (0–4 h). The films were then placed in 0.2 N hydrogen chloride (200 ml). After washing with distilled water the films were dried and stored.

#### Measurements

Viscosity measurements of Leu/Asp(OBz) copolymers were carried out in Ubbelohde type capillary viscometers at 25°C. Elemental analyses were carried out in the section of Chemical Analyses of our Department (Mr W. Potman).

The mol % of ionic groups in the end-products were determined by potentiometric titration in the same division (Dr M. Bos). Infra-red absorption spectra of solid films were measured with a Beckmann IR-33 spectrophotometer in the region 600–4000 cm<sup>-1</sup>.

## RESULTS AND DISCUSSION

Hydrophilic copolymers of L-leucine, L-aspartic acid and L-aspartic acid esters can be obtained by saponification of β-alkyl aspartate residues.

The β-alkyl ester groups can be introduced following two approaches: (a) copolymerization of L-leucine and β-alkyl-L-aspartates; and (b) copolymerization of L-leucine with β-benzyl-L-aspartate, followed by an ester interchange reaction to convert the β-benzyl ester groups into β-alkyl ester groups<sup>13</sup>. Until now poly(β-alkyl-L-aspartates) can only be prepared with low molecular weights, whereas β-benzyl-L-aspartate-NCA can be polymerized with molecular weights over 100 000<sup>13</sup>. Therefore we started with the synthesis of the as yet unknown high molecular weight random copolymers Leu/Asp(OBz) (I). In 1972 the synthesis of the low molecular weight sequential poly[Leu-Leu-Asp(OBz)] was reported<sup>14</sup>.

High molecular weight Leu/Asp(OBz) (I) polymers are prepared by polymerization of the corresponding α-amino acid *N*-carboxyanhydrides (NCAs). Optimum polymerization results are dependent on the choice of solvent(s) and molar ratios of the α-amino acid-NCAs for a particular polymerization reaction.

Polymers (I), containing more than 50 mol % of L-leucine can be polymerized best in benzene/dioxane (4:1 up to 6:1 v/v) mixtures. When the content of L-leucine in I is less than 50 mol %, the use of benzene/dioxane leads to lower yields and the polymerization solution becomes turbid. The polymerization of β-benzyl-L-aspartate-NCA in mixtures of dioxane and chloroform, using triethylamine as an initiator yields irreproducible products<sup>15</sup>. Notwithstanding the partial insolubility of β-benzyl-L-aspartate-NCA in chloroform, better results are obtained by using this solvent<sup>15</sup>. Therefore the 30:70 mixture of NCAs was polymerized in chloroform resulting in a polymer with a comparable composition.

Table 1 Reaction conditions and characterization of Leu/Asp(OBz) (I) copolymers<sup>a</sup>

Molar ratios of Leu-NCA and Asp/(OBz)-NCA	A/I	Polymer composition <sup>b</sup> (mol % Leu)	η <sub>sp</sub> /c (c = 0.2, DCA, 25°C) (dl/g)	[η] <sup>c</sup> 25°C CHCl <sub>3</sub> (dl/g)
70:30	200	68	0.92	1.7 <sup>c</sup>
67:33	200	67	0.96	2.8
60:40	200	57	0.79	—
60:40	500	—	1.23	3.4
50:50	200	47	0.56	1.7
50:50	500	—	1.52	5.3
40:60	200	49	0.56	—
40:60	500	—	0.76	—
30:70	200	26	0.53	1.1

<sup>a</sup> The total NCA concentration is 5% by weight; triethylamine was used as an initiator. All the reactions were performed in benzene/dioxane (4:1 up to 6:1 v/v) mixtures except the 30:70 copolymer where chloroform was used

<sup>b</sup> Based on hydrogen and nitrogen elemental analysis (Figure 2)

<sup>c</sup> In CHCl<sub>3</sub>-DCA (90:10 v/v)

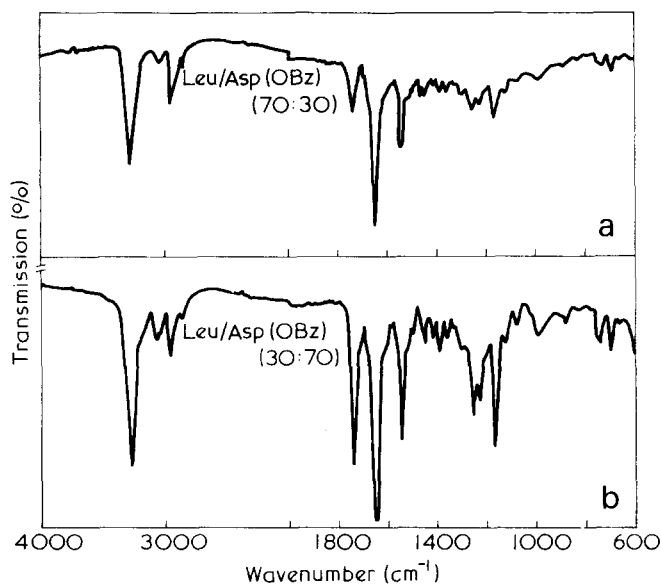


Figure 1 Infra-red spectra of (a) Leu/Asp(OBz) (70:30) and (b) Leu/Asp(OBz) (30:70). Films: 70:30 cast from benzene/dioxane; 30:70 from chloroform

The compositions of polymers (I) based on molar ratios of NCAs used can be verified by elemental analyses (hydrogen and nitrogen). The results are given in Table 1. In general, good agreement was observed.

The polymers described in Table 1 are soluble in chloroform, except Leu/Asp(OBz), (70:30). All the polymers are soluble in dichloroacetic acid. Polymers containing from 50 to 80 mol % L-leucine are soluble in benzene/dioxane (4:1 v/v) mixtures. Non-solvents for all the polymers are alcohols, dimethylformamide (DMF), dimethylsulphoxide, acetonitrile and water.

Viscosity measurements on polymers (I) have been carried out at 25°C in dichloroacetic acid (DCA) solutions ( $\eta_{sp}/c$ ,  $c = 0.2$  g/dl.) as well as in chloroform solutions ( $[\eta]$ ;  $c = 0.05$ – $0.25$  g/dl). It is clear that by using higher NCA–initiator (A/I) ratios the viscosity values are increasing for the same polymer compositions. Preliminary o.r.d. measurements on Leu/Asp(OBz) (50:50) dissolved in DCA indicate that this polymer was not completely in the random coil conformation. Therefore it is not possible to determine the molecular weight of these polymers using the equation of Doty *et al.*<sup>16</sup> for poly ( $\gamma$ -benzyl-L-glutamate). The viscosity values in chloroform indicate a rod-like structure and/or strong association of the polymer chains.

Figure 1 shows the i.r. spectra of films of Leu/Asp(OBz) (70:30 and 30:70). The absorption at  $1745\text{ cm}^{-1}$  reveals the change in the amount of benzyl ester groups in the copolymers. The occurrence of the amide I band at about  $1650\text{ cm}^{-1}$  and the amide II band at  $1548\text{ cm}^{-1}$  in combination with a weak absorption at  $1516\text{ cm}^{-1}$  indicates that in the films the polymer chains are predominantly in the  $\alpha$ -helical conformation.

The copolymers (I) are converted to II using the method of Bradbury *et al.*<sup>13</sup>. Viscous solutions of I ( $\pm 4\%$  w/v in benzene/dioxane) are diluted with one volume of benzene. After the addition of an excess of methanol containing catalytic amounts of sulphuric acid reactions are performed at 65°C for 60 h. The copolymers are isolated and purified by standard methods. Films having thicknesses from 20 to 40  $\mu\text{m}$  can be cast from 1, 1, 2, 2-tetrachloroethane (II, 70 mol % L-leucine) or from THF (II, 60, 50 and 40 mol %

L-leucine). The ester interchange reaction can be followed by i.r. spectroscopy (Figure 2a).

When we compare the spectrum of II (50 mol % L-leucine) (Figure 2a) with the spectra of I (70 and 30 mol % L-leucine) (Figure 1), the peaks at  $3080$ ,  $745$ – $735$  and  $690\text{ cm}^{-1}$  (benzyl absorbance) disappear, whereas the peak at  $1435\text{ cm}^{-1}$  (methyl) becomes stronger. These data in combination with elemental analyses of the methylated products indicate that the ester interchange occurs with 85–95% conversion.

Films of II originally based on 50, 60 and 70 mol % of L-leucine are saponified at room temperature by treatment for up to 4 h in 0.1 N sodium hydroxide/acetone (1:1 v/v) mixtures. Wet films of Leu/Asp(OBz)/Asp(OMe)/Asp(ONa) are strongly swollen and are mechanically weak and difficult to handle. Upon treatment with acetone the films shrink

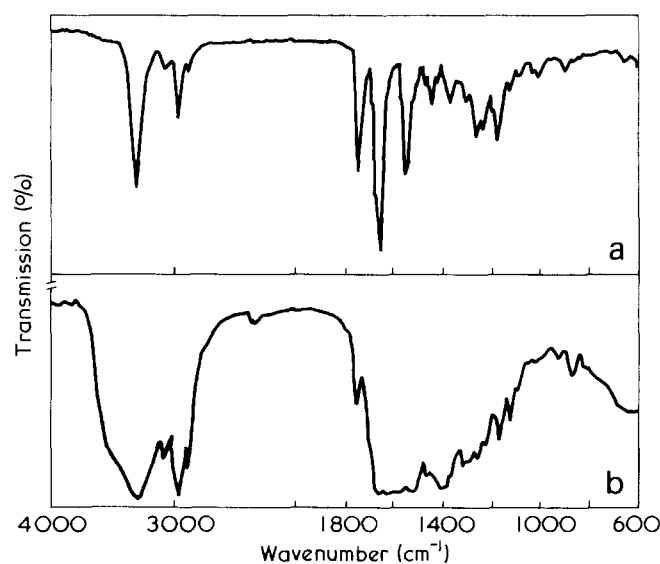


Figure 2 (a) Infra-red spectrum of Leu/Asp(OBz)/Asp(OMe), 50 mol % of L-leucine. Film cast from tetrahydrofuran. (b) Infra-red spectrum of partially hydrolysed Leu/Asp(OBz)/Asp(OMe)/Asp(ONa) with 50 mol % of L-leucine

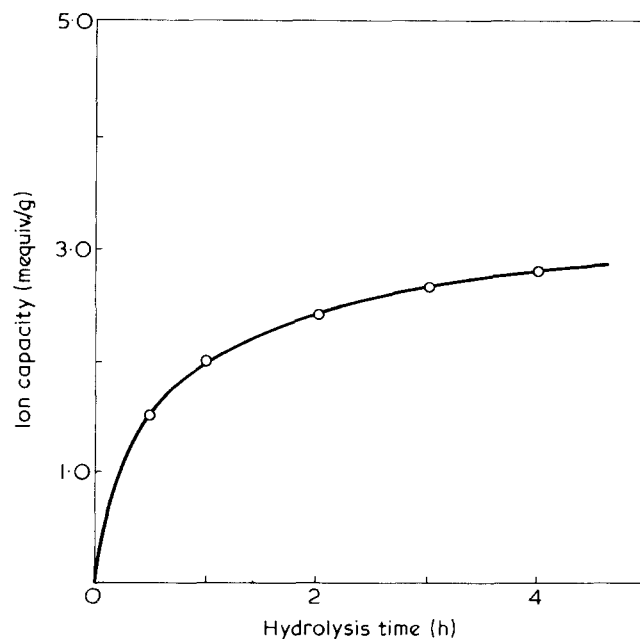


Figure 3 Ion capacity of hydrolysed film of Leu/Asp(OBz)/Asp(OMe) (47:3:50) 50 mol % of L-leucine (40  $\mu\text{m}$  thickness) as a function of hydrolysis time

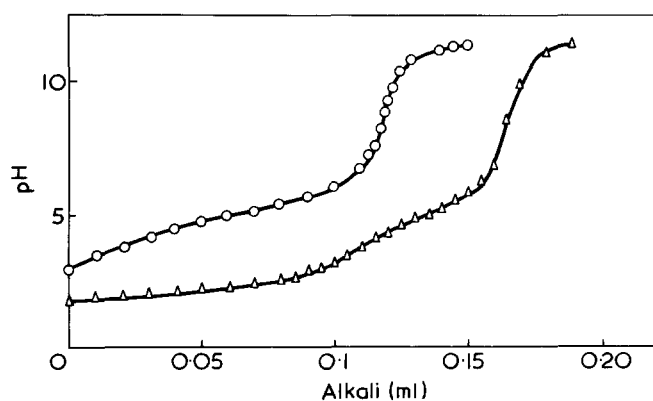


Figure 4 Potentiometric titration curve for Leu/Asp(OBz)/Asp(OMe)/Asp(OH) and Leu/Asp(OBz)/Asp(OMe)/Asp(ONa). ○, 52.10 mg 'Leu/Asp(OH)' in 8 ml 0.1 M NaClO<sub>4</sub> titrated with 1.003 N NaOH; △, 31.52 mg 'Leu/Asp(ONa)' treated with 0.15 ml 1.056 N HClO<sub>4</sub> in 10 ml 0.1 M NaClO<sub>4</sub> and titrated with 1.013 N NaOH

markedly and can be better handled. After the reaction, alkali is removed by using an excess of 0.2 N hydrogen chloride. Wet films of Leu/Asp(OBz)/Asp(OMe)/Asp(OH) are much stronger than wet films of the sodium salt derivatives. Probably because acetone is a non-solvent for Leu/Asp(OBz)/Asp(OMe)/Asp(ONa) saponification levels off after a certain time. For Leu/Asp(OBz)/Asp(OMe) (47:3:50) we found this to occur after 2 h (Figure 3), at 2.7 mequiv./g or 34 mol % of COOH groups. When higher ionic contents are required treatment with 0.1 N sodium hydroxide in acetone for 2 h and then treatment with 0.1 N sodium hydroxide is an appropriate procedure. The copolymers (III) are soluble in pyridine (1.5–2.7 mequiv./g) or tetrahydrofuran. Therefore it is also possible to cast films from these solutions. The composition of these films will be more homogeneous than the films obtained directly after the saponification treatment.

The saponification can be followed by i.r. spectroscopy (Figure 2b). The mol % of ionic groups in the polymer (III) is dependent on saponification times and film thicknesses.

The determination of the amount of ionic groups can be carried out by potentiometric titration in the presence of 0.1 N NaClO<sub>4</sub> by two ways: (a) titration of the acid form with sodium hydroxide; (b) titration of the sodium salt form by adding excess HClO<sub>4</sub> and after equilibrium has been established, titration with sodium hydroxide (Figure 4). A pK<sub>a</sub> value of 5.0 for Leu/Asp(OBz)/Asp(OMe)/Asp(OH) (60% Leu) is found graphically from Figure 4 using method (a). The method of least squares to obtain the best theoretical curve yields a value of pK<sub>a</sub> = 5.18.

## CONCLUSION

A series of well characterized negatively charged films of random copolymers of L-leucine, β-benzyl-L-aspartate, β-methyl-L-aspartate and L-aspartic acid [Leu/Asp(OBz)/Asp(OMe)/Asp(OH)] (III) was obtained after saponification of hydrophobic films of random copolymers of L-leucine, β-benzyl-L-aspartate and β-methyl-L-aspartate [Leu/Asp(OBz)/Asp(OMe)] (II) in alkaline water/organic solvent media. Polymers (II) were obtained after an ester interchange reaction with random copolymers of L-leucine and β-benzyl-L-aspartate, [Leu/Asp(OBz)] (I).

The series of copolymers (I) covering the range 30–70 mol % of L-leucine was synthesized by the *N*-carboxyanhydride (NCA) method.

## ACKNOWLEDGEMENTS

Thanks are due to Mrs H. M. J. Hammink-Siers for typing the manuscript.

The contribution of Mr H. Hof's to part of this work is gratefully acknowledged.

## REFERENCES

- Miyame, T., Mori, S. and Takeda, Y. U.S. Pat. 3 371 069 (27.2.68)
- Spira, M., Fiset, J., Hall, C. W., Hardy, S. N. and Gerow, F. J. *J. Biomed. Mat. Res.* 1969, 3, 213
- Hall, C. W. *et al. Trans. Am. Soc. Artif. Int. Organs* 1970, 16,
- Anderson, J. M., *et al. 5th A. Biomat. Clemson Symp.* 1973
- Klein, E., May, P. D., Smith, J. K. and Leger, N. *Biopolymers* 1971, 10, 647
- Klein, E. and Smith, J. K. *3rd A. Rep. PB 210181 (1970–71)* p 13
- Klein, E., Lindholm, D., Smith, J. K. and May, P. D. *5th A. Contractors Conf. Artif. Kidney Program Nat. Inst. Arthr. Metab. Dis.* 1973
- Klein, E., Lindholm, D., Vieira, J. A., Smith, J. K. and May, P. D. *ibid.* 1973, p 162
- Martin, E. C., May, P. D. and McMahon, W. A. *J. Biomed. Mat. Res.* 1973, 5, 53
- Benoiton, L. *Can. J. Chem.* 1962, 40, 570
- Karlson, R. H., Norland, K. S., Fasman, G. D. and Blout, E. R. *J. Am. Chem. Soc.* 1960, 82, 2268
- Fasman, G. D., Lindblow, C. and Bodenheimer, E. *Biochemistry* 1964, 3, 155
- Bradbury, E. M., Carpenter, B. G. and Goldman, H. *Biopolymers* 1968, 6, 837
- D'Alagni, M., Bemporad, P. and Garofolo, A. *Polymer* 1972, 13, 419
- Bradbury, E. M., *et al. Proc. R. Soc. (A)* 1960, 259, 11d
- Doty, P., Bradbury, J. H. and Holtzer, A. M. *J. Am. Chem. Soc.* 1956, 78, 947

# Structure and molecular relaxation of alternating copolymers of styrene and *N*-substituted maleimides

H. Block, P. W. Lord and S. M. Walker

Department of Inorganic, Physical and Industrial Chemistry, University of Liverpool, PO Box 147, Liverpool L69 3BX, UK

(Received 18 March 1975; revised 30 April 1975)

The dielectric relaxations of twelve differing styrene/*N*-substituted maleimide alternating copolymers are reported. Five processes common to most member copolymers have been observed, and their molecular origins are discussed. Supplementary evidence based on measured X-ray structural factors and differential scanning calorimetry, together with comparative literature data on *N*-substituted polymaleimides and a styrene-maleic anhydride copolymer is presented as further evidence supporting the suggested origins for loss peaks in these structurally related polymers.

## INTRODUCTION

Mechanical, dielectric and nuclear magnetic resonance (n.m.r.) techniques are of increasing importance in the study of molecular motion in polymeric materials in the solid state. However, the assignment of particular molecular re-arrangements to an observed relaxation presents problems whose solution often necessitates the study of a series of polymeric materials with only rather minor structural variations.

One such series of polymers is the homologous group based on *N*-substituted polymaleimides whose relaxation behaviour has formed the basis of a previous report<sup>1</sup>. Another allied macromolecular system is the alternating copolymer of styrene with maleic anhydride<sup>2</sup>. Below we report on the relaxation behaviour of alternating copolymers of twelve *N*-substituted maleimides with styrene. These were readily obtained from a styrene-maleic anhydride copolymer precursor. In their dielectric and n.m.r. relaxation behaviour these materials show five processes ( $\alpha$  to  $\epsilon$ ), two assignable to main chain motions, two to maleimide ring deformations and a further process which is probably a ring deformation but whose assignment is less well substantiated. Thus, the copolymer system presents the same general relaxation behaviour as that of the homopolymers<sup>1</sup> but with significant and informative differences of detail, discussed below. Also presented is evidence based on X-ray investigation as to the structure and morphology of the styrene/*N*-substituted maleimide copolymers, and this evidence is discussed in relation to the molecular motions which occur.

The investigation described below covers a frequency range of  $10^{-5}$  to  $10^6$  Hz over a temperature range from 90 to 500 K.

## EXPERIMENTAL

### Materials

Styrene-maleic anhydride copolymer was prepared by free radical initiation (0.15% azobisisobutyronitrile) of equimolar proportions of monomers in acetone as diluent (~75%). Polymerization was carried out under vacuum

(< $10^{-3}$  mmHg) at 50°C for several hours<sup>3</sup>. The resulting polymer was isolated by precipitation into light petroleum ether and vacuum dried. Alternating *N*-substituted maleimide copolymers were synthesized from the anhydride copolymer by reacting a 6% solution with an excess of the appropriate amine in refluxing glacial acetic acid for 4 h<sup>4</sup>. After complete precipitation into light petroleum ether the copolymers were reprecipitated from chloroform and vacuum dried. All materials showed strong imide absorption bands at  $1690\text{ cm}^{-1}$  and an absence of the  $1850\text{ cm}^{-1}$  anhydride band, present in the precursor copolymer. Elemental analysis and other characterizing data are shown in Table 1.

### Differential scanning calorimetry

Thermograms were obtained using a Perkin-Elmer DSC 1B differential scanning calorimeter operating at a scan rate of  $16^\circ\text{C}/\text{min}$  and using small compressed pellets (~0.5 mm thickness) of polymer. The  $T_g$  values obtained are shown in Table 2.

### X-ray structural studies

X-ray diffraction photographs were obtained from small disc samples (~1 mm thickness) made by pressing the powdered polymer. These were mounted in a flat-plate camera and irradiated with vanadium-filtered  $\text{CrK}\alpha$  radiation (wavelength  $0.22896\text{ nm}$ ) for small angle scattering and nickel-filtered  $\text{CuK}\alpha$  radiation (wavelength  $0.15405\text{ nm}$ ) for large angle scattering. The calculated spacings for the amorphous halos were corrected by Ehrenfest's relation<sup>5</sup> [ $d = 1.25d_{\text{Bragg}}$ ]. Derived spacings are shown in Table 2.

### Molecular weights

For polymers soluble in tetrahydrofuran, weight- and number-average molecular weights were estimated from gel permeation chromatograms performed at the Rubber and Plastics Research Association. Data so obtained are given in Table 1.

### Dielectric studies

Discs of polymer (51 mm in diameter  $\times$  ~1 mm thick) were prepared by pressing powdered material (which had

Table 1 Data characterizing the *N*-substituted maleimide/styrene copolymers

R	Code	$\langle M_n \rangle^*$ $\times 10^5$	$\langle M_w \rangle^*$ $\times 10^5$	Elemental analysis					
				Found (%)			Calculated (%)		
				C	H	N	C	H	N
CH <sub>3</sub>	SMM	3.2	28.6	71.2	6.1	6.1	72.6	6.1	6.5
C <sub>2</sub> H <sub>5</sub>	SEM	2.4	11.1	70.5	6.8	6.2	73.4	6.6	6.1
<i>n</i> -C <sub>5</sub> H <sub>11</sub>	SAM			74.4	7.9	4.9	75.3	7.8	5.2
<i>n</i> -C <sub>7</sub> H <sub>15</sub>	SHM			75.7	8.5	4.5	76.2	8.4	4.7
<i>n</i> -C <sub>9</sub> H <sub>19</sub>	SNM			75.8	8.6	4.1	77.1	8.9	4.3
<i>n</i> -C <sub>12</sub> H <sub>25</sub>	SDDM			76.8	9.3	3.5	78.0	9.5	3.8
<i>n</i> -C <sub>14</sub> H <sub>29</sub>	STDM			77.8	9.7	3.5	78.6	9.8	3.5
<i>n</i> -C <sub>16</sub> H <sub>33</sub>	SHDM			78.9	10.0	3.2	79.0	10.1	3.3
<i>n</i> -C <sub>18</sub> H <sub>37</sub>	SODM			78.6	10.1	3.3	79.5	10.4	3.1
C <sub>6</sub> H <sub>5</sub>	SPM	5.1	49.0	75.1	5.5	4.9	78.0	5.4	5.1
<i>m</i> -C <sub>6</sub> H <sub>4</sub> Cl	SCPM	3.6	7.5	68.0	4.6	4.0	69.2	4.8	4.5
<i>m</i> -C <sub>6</sub> H <sub>4</sub> CH <sub>3</sub>	STM			77.0	5.9	5.3	78.1	6.2	4.8

\* Molecular weight averages were estimated from gel permeation chromatograms using tetrahydrofuran as solvent. Where estimates are not given the copolymers were insoluble in solvents (toluene or tetrahydrofuran) suitable for the available analytical gel permeation chromatography equipment

Table 2 X-ray diffraction spacings, glass-rubber transition temperatures ( $T_g$ ) and activation energies ( $E_a$ ) for the  $\alpha$ -process in styrene/*N*-substituted maleimide copolymers

Sample code <sup>a</sup>	X-ray spacings (nm)		$T_g^c$ (°C)	$E_a$ (mJ/mol)
	$d_1^b$	$d_2$		
SMM	1.65	*	171	2
SEM	1.40 (1.45)	*	144	2
SPRM	(1.46)	—	—	—
SBM	(1.6)	—	—	—
SAM	1.57	0.48	128	0.7
SHM	—	—	104	0.3
SOM	(2.41)	—	—	—
SNM	2.89	*	105	0.3
SDDM	3.76	<0.62	83	0.3
STDM	—	—	60	0.3
SHDM	—	—	53	1
SODM	3.76	0.41	59	0.5
SPM	*	<5.9	146	0.3
SCPM	—	—	167	0.4
STM	—	—	200	—

<sup>a</sup> For code see Table 1. SPRM = *N*-propyl, SBM = *N*-*n*-butyl and SOM = *N*-*n*-octyl derivatives

<sup>b</sup> Cubbon<sup>4</sup> values (corrected by Ehrenfest relation<sup>5</sup>), in parenthesis

<sup>c</sup> From d.s.c. measurement

\* No significant halo for measurement

previously been vacuum dried for  $\geq 24$  h) in a stainless-steel die using an Apex hydraulic press. The press had facility for working at thermostatically controlled elevated temperatures. Discs prepared at ambient temperatures were pressed for  $\sim 1$  h at  $1.6 \times 10^7$  N/m<sup>2</sup> whilst those prepared at 20–30°C above their  $T_g$  were pressed at  $3.2 \times 10^6$  N/m<sup>2</sup> for  $\sim 1/2$  h. Certain sample discs were treated by heating at 30°C above their  $T_g$  for several hours and then quenching in liquid nitrogen to provide a more disordered morphology. For measurements performed in two terminal dielectric cells the discs were provided with tin foil electrodes (25  $\mu$ m thickness) using a thin layer of petroleum jelly (refined by passage down an alumina column at 90°C) as bonding agent.

Capacitance/conductance measurements in the range 105–20  $\times 10^3$  Hz were made with a B221 Wayne–Kerr

transformer ratio-arm bridge energized externally with a TSA 635/2 Venner Electronics wide range oscillator fitted with a RSC TA6 amplifier and matching transformer. Null detection was achieved with a Brookdeal Electronics model 464 high gain tuned amplifier. For the frequency range 10<sup>5</sup>–10<sup>6</sup> Hz a Wayne–Kerr radiofrequency B601 bridge was used with a SR268 combined source–detector unit.

Dielectric relaxation measurements in the range 10<sup>–5</sup>–10<sup>–1</sup> Hz were obtained by the dielectric step-response technique in which the charge/discharge currents of a capacitor are monitored as a function of time. After subtracting the steady state current in the charging mode from the time dependent charge current, charge and discharge current curves were practically identical; their mean values were Fourier transformed. A stable, continuously variable high voltage d.c. source (E. M. Wareham Ltd, Model SO7) acted as charging source (in the range 0–40 V) and a Keithley 602 electrometer (input resistance  $> 10^{14}$   $\Omega$ ) was employed as a picoammeter. Data were automatically logged using a Solartron LM1620 digital voltmeter gated at fixed preset intervals using digital timing circuitry. These data were recorded, either manually or onto paper tape with a Solartron punch drive unit and Addo punch head acting as a decimal-binary converter. The capacitor cell and electrometer were shielded by enclosing them in a ground box and all electrical connections were made with the minimum lengths of low-loss coaxial cable screened to earth. These precautions were essential to obtain a low random noise level of  $\pm 10^{-14}$  A which was uninfluenced by variations in temperature.

Measurements were made using three alternative dielectric cells. A General Radio type 1690A two-terminal micro-meter electrode assembly mounted in a Perspex box through which was passed heated or cooled nitrogen, served for the temperature range –80° to +90°C. Temperature control ( $\pm 0.5^\circ$ C) was achieved by adjustment of gas flow rate which was preheated or cooled (liquid nitrogen). A copper–constantan thermocouple embedded in the lower electrode enabled the continuous monitoring of temperature. In order to achieve a wider temperature range (–196° to +220°C) the cell shown in Figure 1 was constructed. This

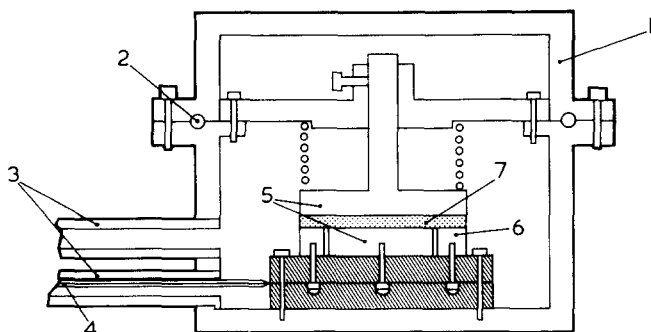


Figure 1 Wide temperature range three terminal capacitance cell. 1, Outer casing; 2, silicone 'O' ring seal; 3, chimneys carrying leads (4); 5, measuring electrodes; 6, guard ring; 7, sample. Hatched sections denote Teflon

was a three terminal cell enclosed in a brass housing sealed by a silicone 'O' ring and the entire assembly had facility for total immersion in a cooling bath, or for the introduction of precooled or heated nitrogen through the 20 cm long chimneys. These also served as inlet ports for the electrode and thermocouple connections. A wide versatility in temperature was achieved with this construction. A similar cell provided with an externally wound heater, but without facility for gas streaming, was used in the step-response measurements, which were all made at temperatures above ambient.

The Fourier transformation of current/time data was processed using the University of Liverpool KDF 9 computer and the procedure suitable for dielectric data, previously described<sup>6</sup>. This method of transforming the charge/decay curves makes no assumptions such as that of the Hamon approximation<sup>7</sup>, as to the nature of current decay functions.

## RESULTS AND DISCUSSION

### X-ray diffraction

The X-ray photographs of all the copolymers studied exhibited only one or two diffuse halos, indicating that they all had an essentially amorphous morphology. An identical lack of crystallinity has been reported for those poly(*N*-substituted maleimides) investigated<sup>8</sup>. Calculated spacings based on the positions of maximum intensity of the halos are shown in Table 2. Of the two observable spacings only the larger one, derived from the more dominant inner halo, is significantly influenced by the nature of the substituent on the maleimide nitrogen. Thus we attribute this spacing to the average interchain separation. Such a view is supported by the variation of this spacing with substituent chain length in the alkyl series [Table 2 which also includes data reported by Cubbon<sup>4</sup> and corrected by the Ehrenfest relation<sup>5</sup> for the amorphous chain environment].

There is a linear increase in spacing with methylene group content from the amyl to the dodecyl members whilst up to and including C<sub>5</sub> the spacing remains approximately constant at ~1.5 nm. Finally, the octadecyl copolymer appears anomalous. The increase in spacing above C<sub>5</sub> is consistent with increasing side chain bulk; the near constancy of the spacing below C<sub>5</sub> we attribute to the dominance of the phenyl group in determining the interchain separation in these cases. The intermolecular spacing for the octadecyl polymer is of similar magnitude to that of the dodecyl polymer and these observations suggests that above C<sub>12</sub> inter-side chain stacking of the methylene

groups may terminate the trend of separation with increasing side chain size, although further studies including more members above C<sub>12</sub> are necessary before such a hypothesis can be confirmed. The magnitude of 1.5 nm for the average chain separation of the lower members (one to five carbon atoms) is consistent with a local 3<sub>1</sub> helical chain conformation (cross-section 1.52 nm) depicted in Figure 2. The pitch of this helix is ~0.45 nm and we believe that the smaller spacing calculated for favourable cases from the position of the weaker halo (Table 2) reflects this regularity. Two polymers, those with dodecyl and phenyl substituents on the nitrogen, appear to have a larger helical pitch than the remainder. The pitch in these cases may indicate a change of dominant conformer to a 4<sub>1</sub> helix (depicted in Figure 2). Such a duality of helix type has been reported to occur in substituted maleimide homopolymers both from X-ray<sup>8</sup> and dielectric studies<sup>1</sup>. In the present study, dielectric observations (next section) lend support to the view that two local structures are also present in the copolymer systems. The estimated cross-section of the 4<sub>1</sub> helix from measurements on space-filling models is 2.17 nm. Either 3<sub>1</sub> or 4<sub>1</sub> helices result from a *trans* addition to the double bonds to give a *three* diisotactic local order.

### Relaxation studies

*α*- and *β*-processes. The least facile of all the dielectric relaxation processes (the *α*-processes) are displayed in Figure 3 in the temperature plane at a fixed frequency of 10<sup>-3</sup> Hz. These loss peaks are all temperature-dependent, and frequency maxima (*f<sub>m</sub>*)-temperature dependencies are shown in Figure 4 in the form of Arrhenius plots. With the heptyl-, nonyl- and dodecyl-maleimide copolymers two linear portions of differing slope were observed. In these cases we believe that the results obtained at the higher frequency and temperatures are influenced by the *β*-process, whose resolution from *α*-process has not been

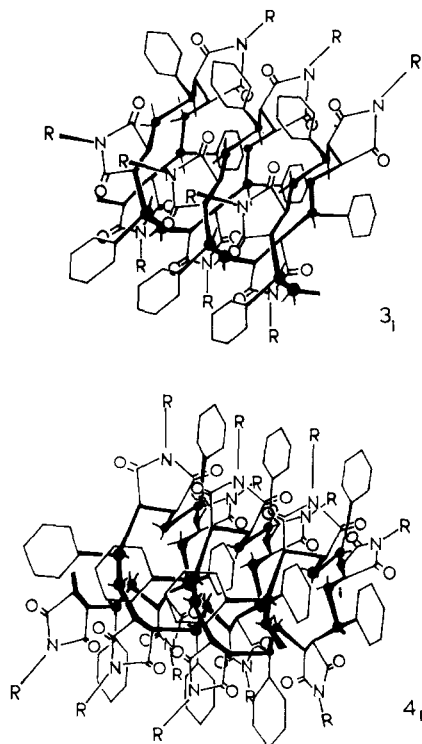


Figure 2 The proposed 3<sub>1</sub> and 4<sub>1</sub> helical forms of styrene/*N*-substituted maleimide copolymers

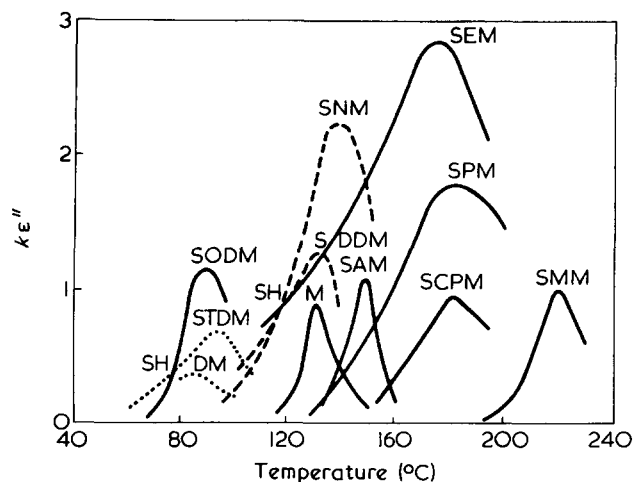


Figure 3 Temperature dependence of dielectric loss at  $10^{-3}$  Hz for the  $\alpha$ -process for styrene/*N*-substituted maleimide copolymers. —,  $k = 1$ ; ---,  $k = 5$ ; ····,  $k = 10$

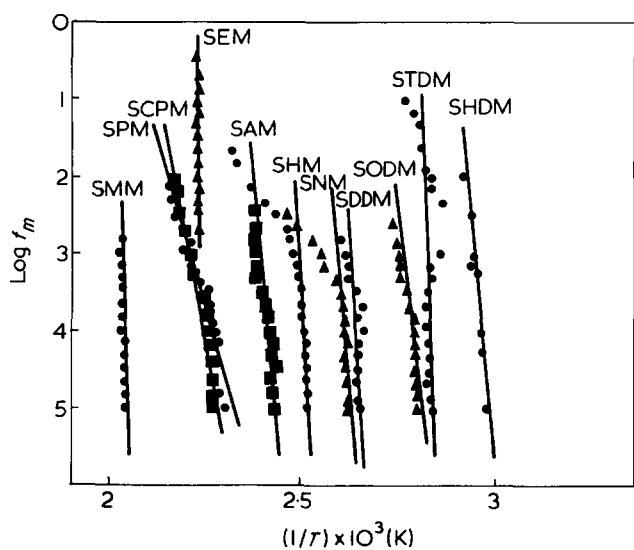


Figure 4 Arrhenius plots for the  $\alpha$ -process in styrene/*N*-substituted maleimide copolymers

adequately achieved in these ranges. For this reason the true  $\alpha$ -process parameters have been taken from the linear low temperature portions of the curves. The  $\alpha$ -process in this region for all polymers investigated tends to extrapolate at very low frequencies towards the  $T_g$  observed on the d.s.c. traces and enumerated in Table 2. Although the slopes of the Arrhenius plots are very steep and therefore subject to substantial errors they do provide estimates for an apparent activation energy (Table 2) which are of considerable magnitude. The position and slope of the temperature dependence of maximum frequency strongly support the presumption that the  $\alpha$ -process in all these copolymers correspond to micro-Brownian motion accompanying the glass-rubber transition. This is so even though the data do not obey the WLF equation<sup>9</sup>, a discrepancy known to occur with other polymer systems<sup>10</sup>. The trends in magnitude of the apparent activation energies as a function of hydrocarbon chain lengths mirrors the interchain separation obtained from X-ray data. Thus, chain separation due to side chains, which commences to have significance at  $C_5$  to  $C_7$ , results in an easier glass-rubber process because of the extra free volume available. Alternatively, self-plasticization commences at about  $C_5$  to  $C_7$ . Increasing the side chain bulk still further has little effect on the

apparent activation energy of the  $\alpha$ -process until  $C_{16}$  is reached whereupon the apparent activation energy again rises. Although the information for these higher alkyl members is restricted, it may be that at and above  $C_{16}$  the glass-rubber transition becomes less free, because of the start of some inter-side chain stacking.

The presence of a phenyl or substituted phenyl ring on the maleimide nitrogen appears to provide enough free volume to make the chain movement equivalent to hydrocarbon chains between  $C_6$  and  $C_{14}$ .

The distribution of relaxation times making up the  $\alpha$ -peaks is generally narrow and results in slightly asymmetric Cole-Cole diagrams. A typical example is shown in Figure 5 which depicts the results for the amyl derivative: the Cole-Cole distribution parameter  $\alpha$  for this system is 0.8 and other members of the series show similar values for  $\alpha$ , as do the maleimide homopolymers<sup>1</sup>. The skewed arc behaviour is attributable to the presence of the  $\beta$ -relaxation close to the  $\alpha$ -peak. This  $\beta$ -relaxation is manifest by a small loss peak or shoulder close to the  $\alpha$ -peak on the low frequency/high temperature side of most of the copolymers studied (the exception being STDM and SHDM). In the main the  $\beta$ -relaxation could not be completely resolved from the large neighbouring  $\alpha$ -process, but its partial resolution in the temperature plane could be optimized by the judicious choice of frequency. Values of  $\epsilon''$ ,  $T$  and optimum frequency for the peak maxima are shown in Table 3 and examples of the peak for SNM and SDDM are depicted in Figure 6.

Because of the difficulties in resolving the  $\beta$ - and  $\alpha$ -peaks, and because of the small magnitude of the former with respect to the latter, quantitative evaluation of the activation energy for the  $\beta$ -processes was not possible. In qualitative terms the activation energies for the  $\beta$ -process in any copolymer were less, sometimes considerably less, than those for the  $\alpha$ -process. Trends in the facility of both processes with side chain length can best be illustrated (Figure 7) by changes in the temperature at relaxation

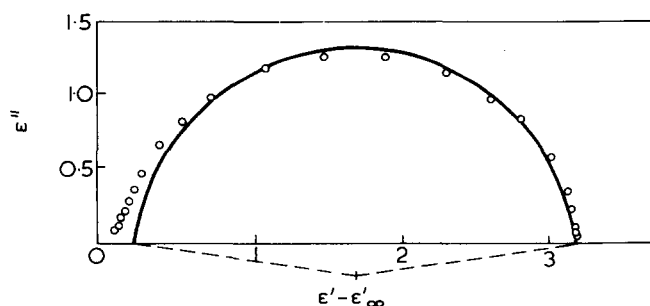


Figure 5 Plot to determine the Cole-Cole distribution parameters for the  $\alpha$ -process in SAM at a temperature of 422K

Table 3  $\beta$  relaxation in styrene/*N*-substituted maleimide copolymers

Polymer	$f$ (Hz)	$\epsilon''_{\max} \times 10^2$	$T_{\max}$ (K)
SMM	$10^{-2}$	1	320
SEM	$10^{-2}$	2	314
SAM	$5 \times 10^{-4}$	14	328
SHM	$5 \times 10^{-2}$	1	346
SNM	$10^{-2}$	5	371
SDDM	$10^{-2}$	5	365
SODM	$10^{-2}$	8	318
SPM	$10^{-2}$	12	333
SCPM	$10^{-2}$	39	302

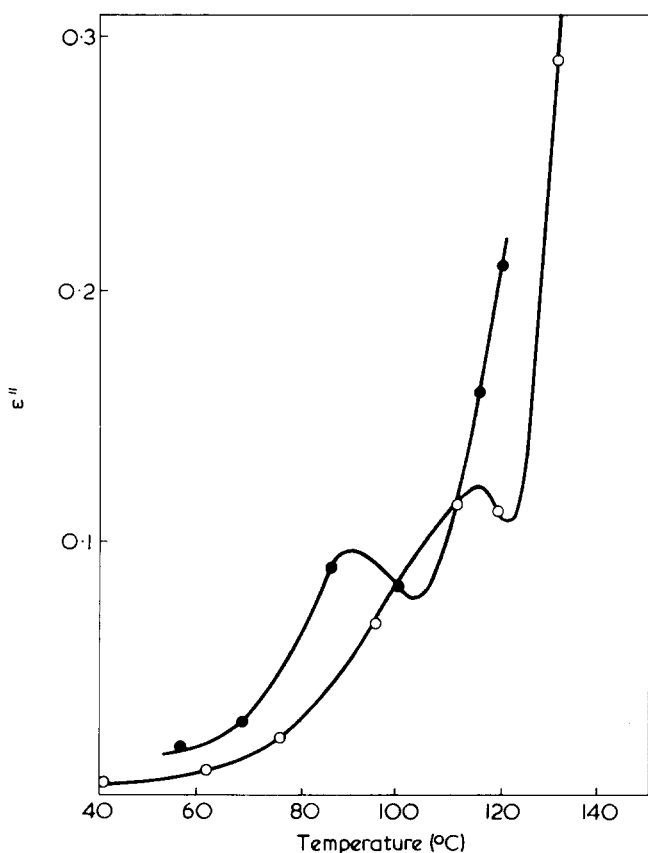


Figure 6  $\beta$ -relaxation appearing as a shoulder on the  $\alpha$ -relaxation in SNM (O) and SDDM (●). Measuring frequency:  $5 \times 10^{-3}$  Hz

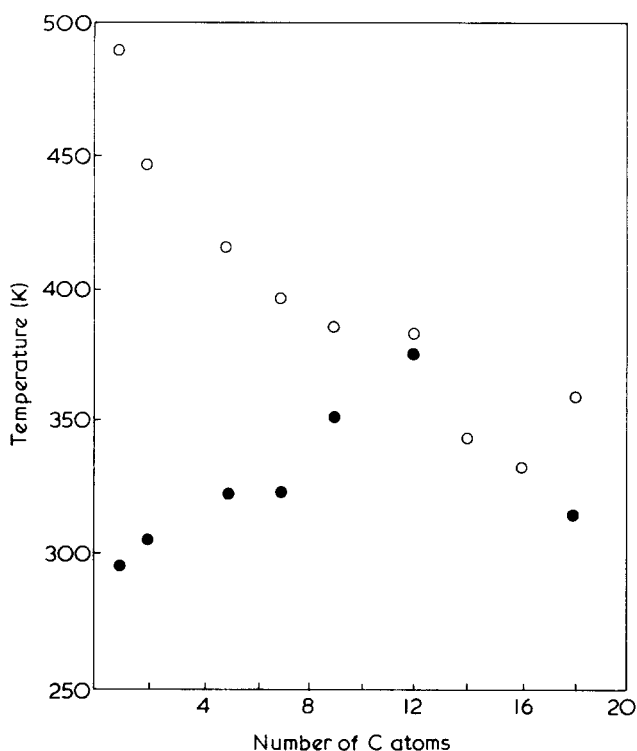


Figure 7 Interdependence of the  $\alpha$ - (O) and  $\beta$ - (●) processes as illustrated by the temperature for loss maximum at  $10^{-3}$  Hz for the series of styrene/*N*-*n*-alkyl substituted maleimide copolymers

maximum measured at a fixed frequency of  $10^{-3}$  Hz. As can be seen, the  $\beta$ -process becomes more difficult with increasing chain length up to  $C_{12}$ , which is the inverse of the behaviour of the  $\alpha$ -process. For ODM this trend has

been reversed. The apparent inverse correlation supports the view that main chain motion is involved in the  $\beta$ -process also, probably as some form of local mode. The behaviour shown in Figure 7 then reflects, that up to  $C_{12}$ , increasing chain length eases the micro-Brownian movement of the  $\alpha$ -process, because of increased free volume, but decreases the ease of localized motion because as the chain length increases, steric factors make side chain rotation about the main chain more difficult. With the SDDM copolymer these trends may have changed because of the possibility of the side-chain/side-chain interaction already referred to.

*$\gamma$ - and  $\delta$ -relaxations.* A selection for the copolymers were studied in the frequency range  $10^2$  to  $10^6$  Hz. In this region relaxations were observed to occur at temperatures below that characteristic for the  $\beta$ -process. In most cases two distinct maxima were observed by a suitable choice of measuring frequency; the SDDM copolymer was an exception in that it was found impossible to satisfactorily resolve its low temperature/high frequency processes. The loss peaks in these regions are designated  $\gamma$  and  $\delta$  and are shown in Figure 8. The intensities of the  $\gamma$  and  $\delta$  loss peaks and their relative magnitudes were markedly affected by the thermal history of the sample. Quenching of the sample from above the  $T_g$  to liquid nitrogen temperature caused a reduction in loss peak magnitudes which was most marked for the high temperature  $\gamma$  peak (Figure 8). Typical activation energies for the  $\gamma$  and  $\delta$  processes are tabulated in Table 4; estimates for the  $\gamma$  process, which exhibits the smaller loss peak are subject to the larger error because of overlap of peaks. It is evident that although both processes have different activation energies, with most copolymers only minor variations in activation energy result from change of substituent. Also, quenching has, with the exception of STM no significant effect on the activation energy. The  $\gamma$  and  $\delta$  processes occurring in STM show anomaly in activation energy from the lower chain length members of the series.

The magnitude of the activation energies for the  $\gamma$  and  $\delta$  processes suggest that a localized dipole relaxation in the

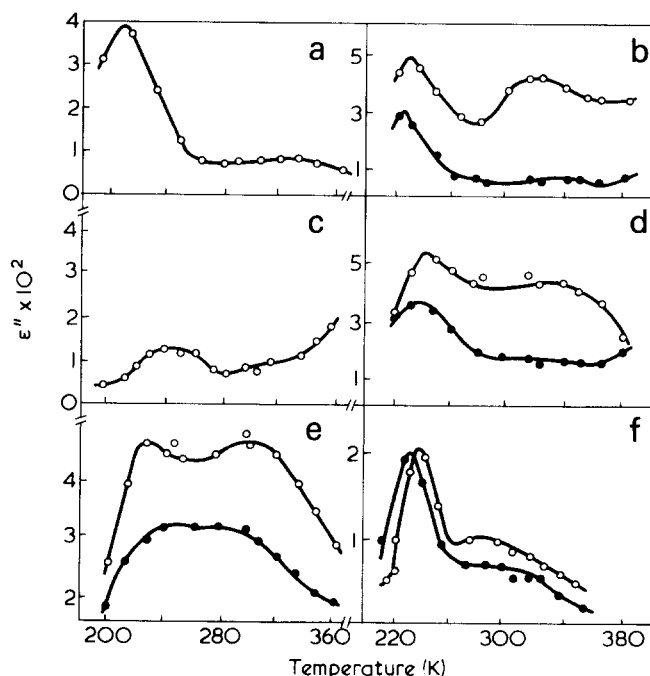


Figure 8  $\gamma$ - and  $\delta$ -processes in some styrene/*N*-substituted maleimide copolymers measured at 1 kHz. ●, Quenched sample data. (a) SMM; (b) SEM; (c) SDDM; (d) SPM; (e) SCPM; (f) STM



Table 4  $\gamma$  and  $\delta$  processes in styrene/*N*-substituted maleimide copolymers

Polymer	$T_{\max}$ (K)	$\epsilon''_{\max}$ $\times 10^2$	$T_{\max(Q)}$ (K)	$\epsilon''_{\max(Q)}$ $\times 10^2$	$E_a$ (kJ/mol)
$\gamma$ -Process:					
SMM	332	0.9	a	a	b
SEM	300	4.3	320	0.7	85
SDDM	b	b	a	a	b
STM	282	1.1	285	0.7	190
SPM	292	4.8	305	1.7	85
SCPM	296	4.6	283	3.3	120
$\delta$ -Process:					
SMM	206	4.2	a	a	50
SEM	211	4.9	205	3.0	45
SDDM	244	1.26	a	a	50
STM	238	2.05	233	2.00	100 (70 <sup>c</sup> )
SPM	223	5.5	220	3.6	45
SCPM	230	4.65	245	3.4	50

Q = quenched samples; a = quenching causes insignificant change; b = parameters not determined because of insufficient resolution; c = activation energy for quenched sample in STM which was the only observed case where  $E_a$  was significantly influenced by thermal treatment

side chain is responsible for the dielectric loss. Very similar relaxations have been observed in the maleimide homopolymers, both dielectrically<sup>1</sup> and by pulsed and broad-line proton n.m.r.<sup>11</sup> The copolymer of styrene and maleic anhydride also exhibits similar dielectric relaxations<sup>2</sup> but in this case the process is not observed in pulsed proton n.m.r.<sup>11</sup> For the maleimide co- and homo-polymers we suggest that inversion of the non-planar succinimide ring is the mode responsible for both the  $\gamma$  and  $\delta$  processes. Support for non-planarity of the succinimide ring is already to hand<sup>12</sup>. With the styrene-maleic anhydride system a similar process implies a non-planar ring system, and is consistent with its appearance in the dielectric experiments (presence of a dipole change) and its absence in the proton n.m.r. experiments (absence of protons in the inverting part of the ring system).

That the loss magnitudes of the  $\gamma$  and  $\delta$  processes are decreased by quenching, suggests that both processes occur in regions of structural order. The X-ray evidence already discussed indicates that any such structure is of limited extent and does not represent the presence of fully crystalline regions. There is also some minimum evidence that more than one structure (3<sub>1</sub> and 4<sub>1</sub> helices) may be present, and similar variants in conformation are known for the maleimide homopolymers<sup>8</sup>. It is possible that the  $\gamma$  and  $\delta$  doublet which occurs in this system, and also in some polymaleimides<sup>1</sup> and the styrene-maleic anhydride copolymer<sup>2</sup>, reflects heterocyclic ring deformations in two such essentially different conformational environments. The lower appearance temperature for  $\gamma$  and  $\delta$  loss peaks in the maleimide-styrene copolymers *vis-à-vis* the homopolymers, when measured at a common frequency, indicates that the deformations are easier in the copolymer systems. This is consistent with the likely increase in

free volume for such a process, when styrene residues separate the heterocyclic rings.

*$\epsilon$ -relaxation.* At low temperatures and high frequencies, SCPM, SDDM and the homopolymer poly(*N*-*n*-amylmaleimide) exhibit a small relaxation peak. Similar relaxations have been observed for poly(*N*-*n*-amylmaleimide) by n.m.r.<sup>11</sup> for SDDM by pulsed n.m.r. studies ( $\epsilon''_{\max} = 1.56 \times 10^{-2}$  at 1 MHz and  $-120^\circ\text{C}$ ). In the dielectric mode adequate resolution from the  $\gamma - \delta$  losses for activation energy determination has only been achieved for the homopolymer, providing an estimate of 15 kJ/mol for this system. The close correspondence of these relaxations in SDDM, SCPM and poly(*N*-*n*-amylmaleimide) suggests that a common molecular origin is responsible for the  $\epsilon$  process. Since the process occurs in the homopolymer, the presence of styrene residues is not causative; the low activation energy essentially precludes a form of main chain motion and the presence of the relaxation in SCPM suggests that relaxation of alkyl side chain is not the mode involved. In view of the assignment of the  $\gamma$  and  $\delta$  relaxations to ring deformation in a defined conformational environment, it is possible that the  $\epsilon$  relaxation has a similar origin but in regions of gross chain disorder where steric hindrances are at a minimum. This would be consistent with the low activation energy observed. The small magnitude of the loss suggests that if ring deformation is involved, then the number of dipoles in such a free, disordered environment is small. A final assignment of  $\epsilon$  relaxations to molecular processes does, however, require further study.

#### ACKNOWLEDGEMENTS

The authors wish to acknowledge the support of the Science Research Council by the provision of a Polymer Centre Research Grant and for a Postgraduate Award to P.W.L.

#### REFERENCES

- Block, H., Groves, R. and Walker, S. M. *Polymer* 1972, **13**, 527
- Block, H., Collinson, M. E. and Walker, S. M. *Polymer* 1973, **14**, 68
- Bawn, C. E. H. and Huglin, M. B. *Polymer* 1962, **3**, 615
- Cubbon, R. C. P. *J. Polym. Sci. (C)* 1967, **16**, 387
- Klug, H. P. and Alexander, L. E. 'X-ray diffraction procedures for polycrystalline and amorphous materials', John Wiley, New York, 1954, p 631
- Block, H., Groves, R., Lord, P. W. and Walker, S. M. *JCS Faraday Trans. II* 1972, **68**, 1890
- Hamon, B. V. *Proc. IEE* 1952, **99**, (iv), 27
- Balta-Callaja, F. J., Ramos, J. G. and Barrales-Rienda, J. M. *Kolloid-Z.* 1972, **250**, 474
- Williams, M. L., Landel, R. F. and Ferry, J. D. *J. Am. Chem. Soc.* 1955, **77**, 3701
- McCrum, N. G., Read, B. E. and Williams, G. 'Anelastic and Dielectric Effects in Polymeric Solids', John Wiley, London, 1967
- Bailey, J., Block, H., Cowden, D. R. and Walker, S. M. *Polymer* 1973, **14**, 45
- Hargreaves, M. K., Pritchard, J. G. and Dare, H. R. *Chem. Rev.* 1970, **70**, 439

# Thermoluminescence and induced phosphorescence in irradiated doped PMMA

D. J. Morantz and C. S. Bilen

London College of Printing, London SE1 6SB, UK

(Received 5 December 1974; revised 20 February 1975)

Thermoluminescence (t.l.) is reported for doped poly(methyl methacrylate) (PMMA), irradiated by X-rays and u.v. light. The results are correlated with those we previously reported for induced phosphorescence in the same system. These luminescence results are accounted for in terms of transient species which have been reported for irradiated PMMA and which were detected by e.s.r. and optical absorption techniques. The transient species responsible for t.l., and induced phosphorescence, appears to be the same, namely a radical derived from PMMA. A brief outline is given of the production of such transients and their subsequent reactions in the post-irradiation period. The energy transfer processes involved are discussed in terms of an energy level diagram.

## INTRODUCTION

Phosphorescence<sup>1,2</sup> of organic substances is well known and has been extensively studied in glassy solutions at low temperatures. Thermoluminescence of irradiated inorganic materials<sup>3-5</sup> above room temperature is also well known as is the thermoluminescence of irradiated organic glasses<sup>6-8</sup> at low (77 K) temperatures. The correlation of these two luminescence effects has, however, been attempted by few authors<sup>9</sup>.

Recently, we have found and reported<sup>10</sup> the existence of strong *room temperature* phosphorescences in certain doped irradiated polymeric glasses. The ability to phosphoresce may be induced in a doped matrix by irradiation using X-rays, u.v. light, or electron bombardment; prolonged heating of the matrix at 200°C will also produce this result. The term 'induced phosphorescence' has been proposed by us for this effect<sup>10</sup>. The induced phosphorescence was found to be associated with species which were created by irradiation of the polymeric glass and which could be destroyed, i.e., 'bleached', by heating the doped matrix above its glass transition. We now report that during such bleaching of the induced phosphorescence, thermoluminescence takes place. This report outlines the features of the thermoluminescence and a model to account for the phenomenon. Previous studies of thermoluminescence in organic materials generally depend on the creation of charged species at *reduced* temperatures. We now find that there is a direct correlation between induced phosphorescence and thermoluminescence in that their kinetics, during and after irradiation, are similar. Indeed, there is strong evidence that the same species are responsible for both of these effects. Our thermoluminescence results provide an indication of the nature of these active species and these would appear to be radical species.

## EXPERIMENTAL

The induced phosphorescence investigations used a laboratory built spectrophotometer with a HBO 200 W mercury lamp as the source of excitation light, focused through a quartz lens and filtered to remove infra-red through 15 cm

of a 3% nickel sulphate solution. The excitation band was selected by means of a Hilger and Watts grating monochromator (M/65/7) in conjunction with an OX7 filter to cut off any stray visible light. The sample box had a locating device for a matching sample holder so that the emission from the same area of the sample was analysed using a high resolution grating monochromator (Hilger and Watts D 330/1 Mark II). The spectrum was plotted by means of a motor drive scan of 25 nm/min. The detection system for the emission was a photomultiplier (EMI 5824 B) connected to a d.c. amplifier and chart recorder.

Sample preparation and irradiation procedures have been described elsewhere<sup>10</sup>.

The thermoluminescence apparatus is shown schematically in *Figures 1a* and *1b*. The doped samples were irradiated in the X-ray apparatus or by an unfiltered HBO 200 W u.v. lamp for 10-60 min. The irradiated samples were inspected under a u.v. inspection lamp (CAMAG Meetlenz Schivanz 220 V/50 Hz) for fluorescence and phosphorescence. The non-irradiated part showed normal fluorescence, whereas the irradiated part showed both fluorescence and phosphorescence. The sample was then placed in the thermoluminescence apparatus sample chamber and its glow curve was recorded.

During some experiments, the irradiated samples were first placed in the emission spectrophotometer, their emission spectra (including fluorescence and phosphorescence bands) were recorded, and then the same samples were examined in the thermoluminescence apparatus to obtain the thermoluminescence curves. This allowed direct comparison of the two effects. A sample which was to be used for a variety of irradiation periods was annealed, after each experiment, in an electric oven at 160°C for 20 min and then kept in the dark for 30 min to cool to room temperature. Otherwise each irradiation experiment was undertaken using a fresh sample.

## RESULTS

A typical emission spectrum for dibenzothiophene (DBT) doped PMMA showing the presence of induced phosphorescence bands, after X-ray irradiation for 1 h is shown in

Figure 2a. The thermoluminescence of a similar sample after X-ray irradiation is shown in Figure 2b. The thermoluminescence peak was found to be at 340 K i.e., approximately at the glass transition temperature of the matrix when the induced species are created by X-ray irradiation. However, in the case of u.v. irradiation of doped polymer samples, the situation is more complex. In the earlier stages of the u.v. irradiation the peak position corresponded, as for X-ray irradiation, to the glass transition temperature. As irradiation with u.v. proceeded, the peak appeared to shift to higher temperatures and new higher temperature peaks appeared. The intensity of the 340 K peak was down by an order of magnitude (see Figure 3a).

Figure 3b shows the emissions of a DBT doped PMMA sample at various stages of u.v. irradiation. The solid curve shows the DBT emission (fluorescence only) of an un-irradiated sample. The curve showing the emission of a sample after optimum u.v. irradiation includes fluorescence as well as phosphorescence bands. The effect of further u.v. irradiation, producing an induced fluorescence peak at 380 nm is shown in the broken curve. For X-ray excitation, the induced phosphorescence peak intensity rises to a maximum with increasing irradiation period as shown in Figure 4 (solid curve); the broken curve in Figure 4 shows the corresponding curve of thermoluminescence peak intensity against X-ray irradiation periods. The u.v. irradiation behaviour follows a different pattern as shown in Figure 5. The thermoluminescence curve of triphenylene (TP) doped PMMA after excessive irradiation is shown in Figure 6a and the corresponding u.v. induced phosphorescence is shown in Figure 6b. The induced fluorescence at 390 nm is much more pronounced for TP (Figure 6b) than for DBT (Figure 3b).

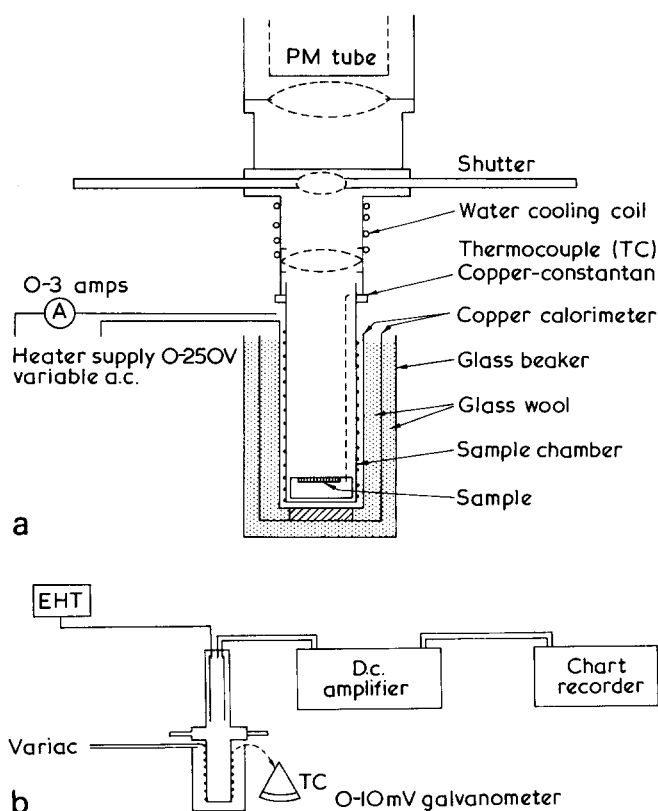


Figure 1 Experimental apparatus for thermoluminescence; (a) sample chamber; (b) schematic diagram of the apparatus. The cold junction of the thermocouple was held at 0°C

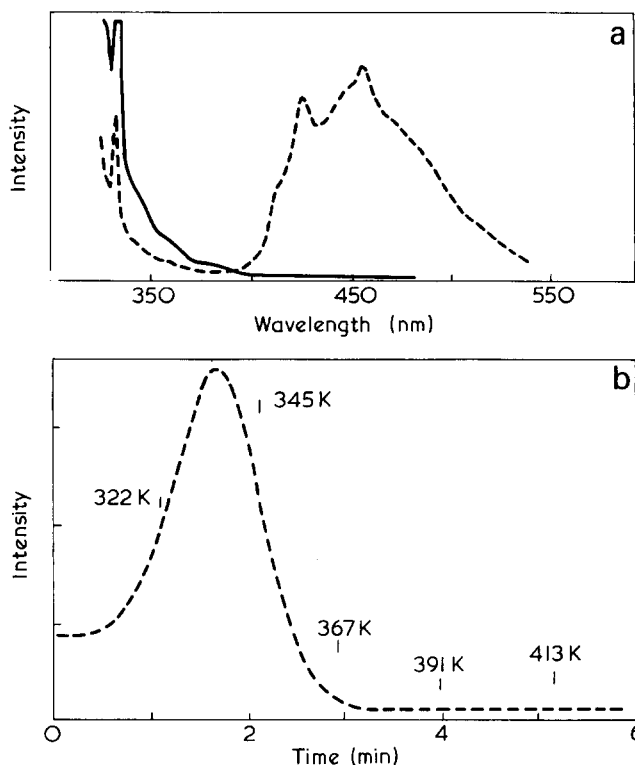


Figure 2 Effect of X-ray irradiation on dibenzothiophene (DBT) doped PMMA; (a) photoluminescence spectra before (—) and after (---) irradiation; (b) thermoluminescence curve showing strong peak at 338 K

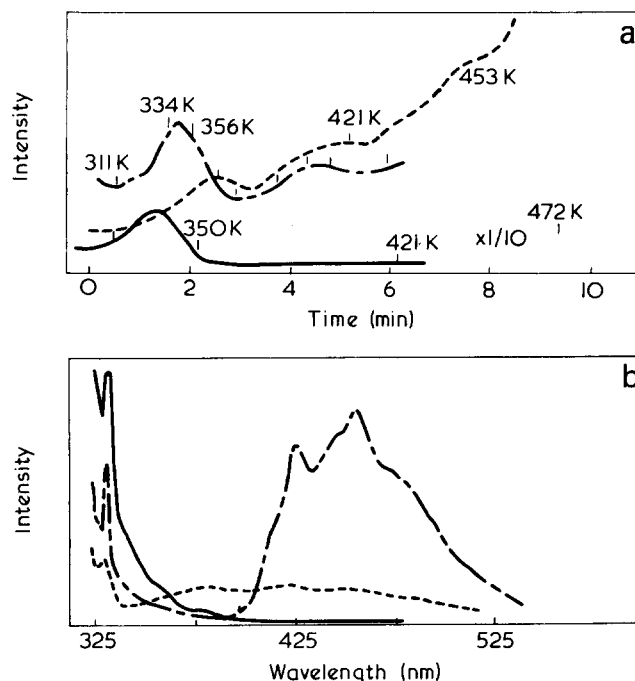


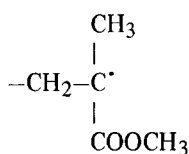
Figure 3 Effect of u.v. irradiation on DBT doped PMMA. (a) Thermoluminescence curves after irradiation of: —, 10; ---, 220; ----, 480 min. (b) Photoluminescence spectra before u.v. irradiation (—), after 10 min (---) and 220 min (----) u.v. irradiation

### DISCUSSION

These thermoluminescence results and our previously reported induced phosphorescence<sup>10</sup> results, as well as the reported e.s.r. and optical studies, may all be explained in terms of common transient species produced by irradiation

in the matrix. Previous studies using e.s.r.<sup>11,12</sup> and t.l. (thermoluminescence)<sup>13</sup> with X-ray and  $\gamma$ -irradiated PMMA samples, demonstrated that a variety of charged as well as uncharged species are present under various experimental conditions. David *et al.*<sup>13</sup> found that most of the charged species produced by  $\gamma$ -irradiation in PMMA samples doped with acridine will recombine to give a t.l. peak at 160 K. However, the absorption spectrum, due to uncharged radicals, continued to exist until the glass transition point (360 K) of the matrix. There was also a correlation between the t.l. decay curve and the decay curve for the disappearance of the radical anion absorption band due to the dopant. After the t.l. and anion decay most of the anions were converted to uncharged radicals.

Recently, Geuskens and David<sup>11</sup> studied the evolution of the e.s.r. spectrum of PMMA after  $\gamma$ -irradiation, between 110 K and 320 K, and suggested that up to six different types of radicals may be found depending on the temperature range. At room temperature, the radical, R, predominated and was of the form:



This was identified by a strong 9 line e.s.r. spectrum.

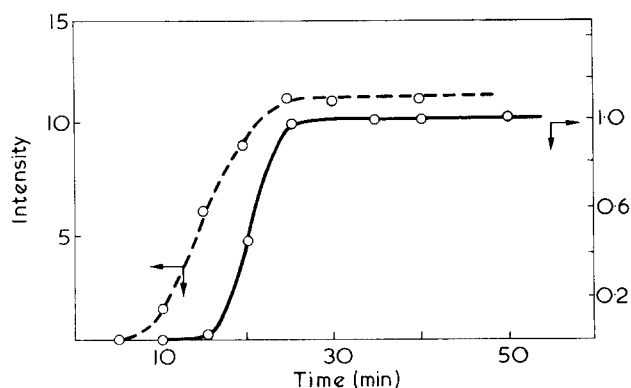


Figure 4 Induced phosphorescence and thermoluminescence (---) rise curves for X-ray irradiated DBT doped PMMA

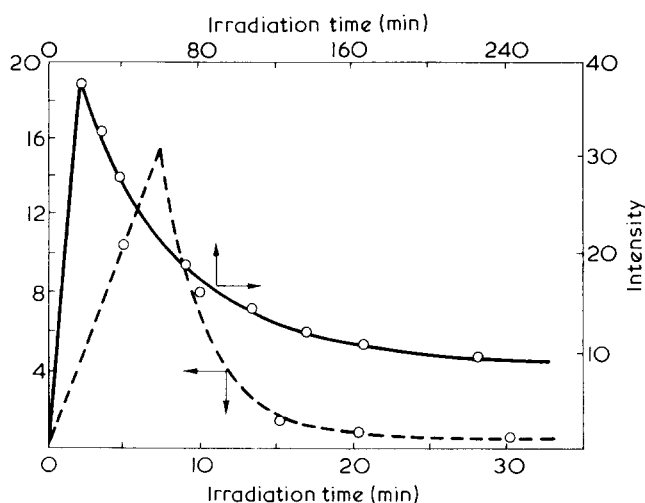


Figure 5 Induced phosphorescence (—) and thermoluminescence (---) rise curves for u.v. irradiated DBT doped PMMA

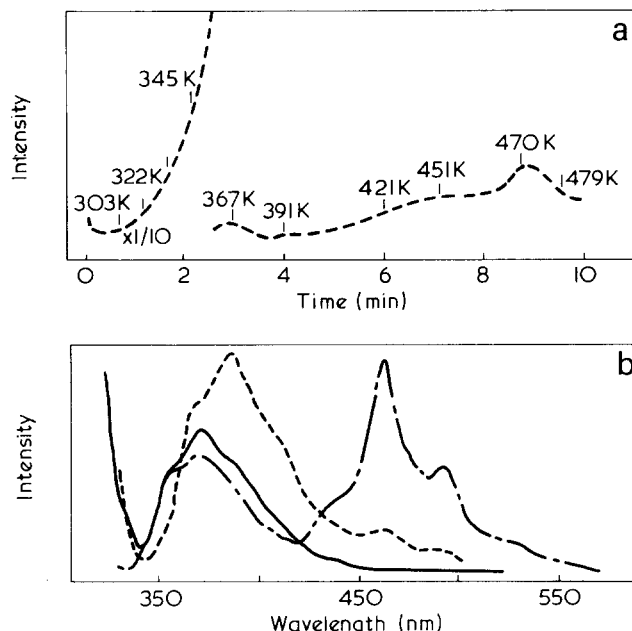


Figure 6 Effect of u.v. irradiation on triphenylene (TP) doped PMMA: (a) thermoluminescence curve after 226 min of u.v. irradiation; (b) photoluminescence spectra at different stages of u.v. irradiation; —, before irradiation; ---, 20 min irradiation; - · - ·, 226 min irradiation

Szocs and Lazar<sup>12</sup> found that at or above room temperature the radical responsible for the nine line spectrum decayed rapidly at 340 K while some other radical species, giving doublet and singlet e.s.r. peaks, persisted and decayed at about 373 K and higher. The nine line spectrum did not appear in irradiated PMMA samples even at room temperature when these were carefully freed from monomer before irradiation. However, doublet and singlet peaks, occurring in such samples, changed very rapidly to a strong nine line signal when monomer vapour was allowed to diffuse into the irradiated sample.

The induced phosphorescence effect in our X-ray irradiated doped PMMA samples also decays rapidly at 340 K and furthermore these samples show a strong t.l. peak at about the same temperature during the glow experiment, suggesting therefore that the species responsible for the induced phosphorescence and t.l. effects may be the same radical, R. Such species have also been observed by e.s.r., for u.v. irradiated PMMA<sup>14</sup>.

We confirm that, during the initial u.v. irradiation periods (up to 20 min) of our doped PMMA samples, such transient species were produced, and we note the similarity of the emission curves of X-ray and u.v. irradiated samples (see Figures 2a and 3b); in both cases the induced phosphorescence peaks appear to be due to the presence of radiation induced radical species. These species are affected by oxygen in a similar manner to that reported for the species observed using e.s.r.<sup>11,12</sup>. The t.l. peaks for X-ray and u.v. irradiated samples (Figures 2a and 3b) are both approximately at the same temperature (340 K). The curve in Figure 4 which describes the increase in the induced phosphorescence during X-ray irradiation shows similar features to the corresponding curve for the t.l. effect. Again the behaviour of the two luminescence effects in the case of u.v. irradiation (Figure 5) shows strikingly similar kinetic behaviour, owing to the presence of the same species. Such species may, moreover, be responsible for the current peak under a thermal gradient observed at 340 K, when

X-ray and  $\gamma$ -irradiated samples were heated<sup>15</sup>. However, during our studies in some cases (where long u.v. irradiations were carried out in air), t.l. peaks were observed at temperatures higher than 340 K. Such peaks are shown in *Figure 3b*, and also in *Figure 6a*. Samples showing these later t.l. peaks did not show much induced phosphorescence but exhibited new induced fluorescence peaks (see *Figure 3a* and *Figure 6a*). In these cases, the species responsible for induced phosphorescence and the t.l. peak at 340 K appear to have undergone further reaction with oxygen (in the presence of u.v. light) so as to give new species responsible for induced fluorescence and high temperature t.l. peaks. It is also seen that with excessive u.v. irradiation not only does the intensity of the 340 K peak decrease, but also the peak maximum appears to shift towards higher temperatures (*Figure 3b*). This indicates that those species (SP 1) which are at shallow trapping depths are more readily converted to the other species (SP 2) responsible for the higher temperature t.l. peaks. Those species, of kind SP 1, at deeper trapping depths, are left behind and are not converted to SP 2. We propose the following scheme for production, and subsequent reactions of these species. During irradiation and the primary reactions, chain scissions of the polymer matrix occur. The species produced may be any one of those suggested by David *et al.*<sup>13</sup>, dependent upon temperature and other experimental conditions. At room temperature where X-ray irradiation is carried out in our samples in the presence of oxygen, uncharged radicals, R, will predominate. These radicals, by virtue of the energy levels they possess, will take part in energy transfer processes resulting in induced phosphorescence<sup>10</sup> until and unless they are consumed by various secondary reactions. The latter reactions comprise radical-radical recombinations and radical reactions with oxygen in the presence or absence of u.v. light. In the case of X-ray irradiation, charged species and radical fragments of both main and side chains are produced. There is also a small probability of the production of monomer radical and dissociation of the dopant molecule. During u.v. irradiation of the system both types of radical fragmentation as well as excitation of the dopant occur. There is little probability of the production of charged species. The other distinction between the effects of these two types of

irradiation is the bulk (for X-ray) and surface (for u.v.) nature of the reactions. In the post-irradiation period the predominant reaction is recombination of the transient radical species (SP 1). In the presence of oxygen and u.v. light combination these transient species may be converted to stable species (SP 2) by secondary reactions. Whenever the products of any of these reactions are formed in their excited states, these undergo normal deactivation processes leading to fluorescence, phosphorescence and non-radiative thermal degradation.

We conclude that the species responsible (SP 1) for the 340 K t.l. peak is radical R and that this radical is also involved in the transfer of energy to the triplet level of the dopant molecule and hence the induced phosphorescence. The energy transfer processes involved, between the energy levels of the species (SP 1), the normal matrix and the dopant molecules are shown schematically in *Figure 7*. The species responsible for the higher temperature t.l. peaks and the induced fluorescence peaks, in the case of excessive u.v. irradiated samples, are thought to be radical peroxides as the products (SP 2) of radical reactions. The energy levels corresponding to species SP 2 are shown in *Figure 7*, which demonstrates, as well, the difference in the nature of SP 1 and SP 2. The latter is emissive and SP 1 is non-emissive. We recall as well that the SP 1 species are transient and are converted, in secondary reactions to stable, SP 2 species. We recall, moreover, that e.s.r. studies<sup>13</sup> show that the signals corresponding to SP 2 were absent when irradiation was carried out in the absence of oxygen. These considerations support the view that SP 2 are oxidized products of SP 1.

#### ACKNOWLEDGEMENT

We acknowledge an ILEA Research Fellowship to one of us (C.S.B.).

#### REFERENCES

- Lewis, G. N. and Kasha, M. *J. Am. Chem. Soc.* 1944, **66**, 2100
- Craig, D. P. and Ross, I. G. *J. Chem. Soc.* 1955, p 1589
- Curie, D. 'Luminescence in Crystals', Methuen, London, 1960, p 147
- Cameron, J. R. and Suntharalingam, N. 'Radiation Dose Measurement', European Nuclear Energy Agency, Paris, 1967, p 71
- Nokolskiy, V. *Sov. Sci. Rev.* 1972, **3**, 77
- Hamil, W. H. 'Radical ions', (Ed. E. T. Kaiser and L. Keven), Interscience, New York, 1968
- Morantz, D. J. and Foster, D. J. *Discuss. Faraday Soc.* 1971, **51**, 123
- Burton, M. and Funabashi, K. in 'Organic Solid State Chemistry', (Ed. G. Adler), Gordon and Breach, New York, 1969
- Boustead, I. and Charlesby, A. *Proc. R. Soc. (A)* 1970, **315**, 271
- Morantz, D. J. and Bilen, C. S. in 'Reactivity of Solids', (Eds J. S. Anderson, M. W. Roberts and F. S. Stone), Chapman & Hall, London, 1972, p 525
- Geuskens, G. and David, C. *Makromol. Chem.* 1973, **165**, 273
- Szocs, F. and Lazar, M. *Eur. Polym. J. (Suppl.)* 1969, p 337
- David, C., Janseen, P. and Geuskens, G. *Int. J. Radiat. Phys. Chem.* 1972, **4**, 51
- Wong, P. K. *Polymer* 1974, **15**, 60
- Murphy, P. H. and Hoecker, F. E. *Radiat. Res.* 1971, **46**, 1

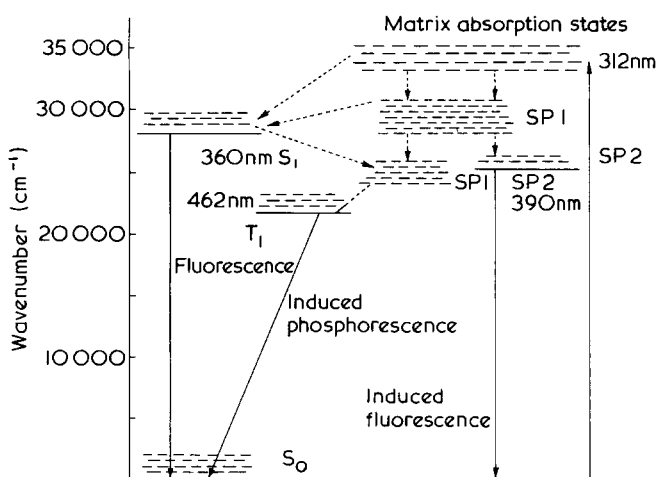


Figure 7 Energy level diagram showing energy transfer processes leading to fluorescence; induced phosphorescence and induced fluorescence of triphenylene doped PMMA

# Kinetics of the thermal oxidation of isotactic poly(1-pentene)\*

S. M. Gabbay, S. S. Stivala and L. Reich

Department of Chemistry and Chemical Engineering, Stevens Institute of Technology, Hoboken, New Jersey 07030, USA

(Received 7 April 1975)

The kinetics of the thermal oxidation of isotactic poly(1-pentene) was studied in the bulk phase. The experimental data were obtained from the quantitative estimation of carbonyl groups formed in the non-volatile oxidation products using infra-red spectroscopy. Reaction temperature varied from 100° to 115° and oxygen concentrations from 10% to 100% by volume. A general kinetic scheme and mathematical expressions previously reported for the thermal autoxidation of polyolefins satisfactorily explained the experimental results. Activation energies of this polymer for various steps in the kinetic scheme were compared with polypropylene and poly(1-butene).

## INTRODUCTION

Among the thermal oxidation studies of polymers, the polyolefins, e.g., polyethylene, polypropylene, and poly(1-butene), have received considerable attention<sup>1,2</sup>. Stivala and Reich have previously presented a general kinetic scheme for the thermal oxidation of polyolefins<sup>1</sup>. Mathematical expressions derived from the scheme were satisfactorily applied to the thermal oxidation of isotactic polypropylene (IPP)<sup>3</sup>, atactic polypropylene (APP)<sup>4-9</sup>, isotactic poly(1-butene) (IPB)<sup>10</sup>, and atactic poly(1-butene) (APB)<sup>11</sup> in the bulk phase under various experimental conditions (temperatures, oxygen concentrations, and metal catalyst concentrations). Bawn and Chaudri<sup>12,13</sup> successfully used this kinetic scheme to both metal catalysed and uncatalysed autoxidation of APP in solution in explaining various kinetic dependencies. The purpose of this paper is to examine the kinetics of the thermal oxidation of isotactic poly(1-pentene) (IPP-1) in the bulk phase using infra-red (i.r.) spectroscopy. The rates of formation of the non-volatile products, at various temperatures and oxygen concentrations, were assessed from the i.r. bands of the carbonyl groups. The volatile products evolved during the thermal oxidation of IPP-1 were identified by thermal and mass chromatography<sup>14</sup>; this method was also used in studying the volatile products evolved from the thermal oxidation of poly(4-methyl-1-pentene)<sup>15</sup>.

## EXPERIMENTAL

### Starting material

The IPP-1 sample used in this study was unstabilized pure polymer obtained through the courtesy of Dr Gianotti from Montedison Company, Italy. Its intrinsic viscosity in tetralin at 135°C was 4.7 g/dl. Upon ignition, the sample gave an ash content of 0.01% by weight. A crystal-

line melting point of 78°C was determined by a Perkin-Elmer Differential Scanning Calorimeter (DSC) using a programmed heating rate of 10°C/min. IPP-1 studied in this work was modification 1.

### Apparatus

A Perkin-Elmer recording spectrophotometer, Model 21, was used. Attached to this instrument was an oxidation cell which was essentially similar to that previously described<sup>4</sup>. The temperature controller, a Fisher Proportional Temperature Control, had a temperature range up to 250°C, with a nominal temperature variation of  $\pm 0.02^\circ\text{C}$ . The cell chamber temperature was measured with an iron-constantan thermocouple connected to a millivolt potentiometer (Leeds and Northrup). The thermometer temperature reading was calibrated against the potentiometer.

### Procedure

Clear and uniform films of approximately 2 to 2.5 mil thickness of modification 2 were prepared when IPP-1 sample was compression moulded in vacuum at 140°C and cooled to room temperature over a 20 min period. These films were converted to modification 1 by refluxing them in absolute ethanol overnight and subsequently dried in a vacuum oven at 50°C for 12 h (thickness not appreciably affected). These films were then placed on sodium chloride discs which were assembled in the oxidation cell mounted onto the infra-red spectrophotometer. By means of i.r. spectra, as shown in *Figure 1*, it was ascertained that no pre-oxidation of the sample occurred, during film preparation or when the sample was heated to the desired reaction temperature under a blanket of nitrogen.

Known mixtures of pure dry oxygen and nitrogen were passed into the oxidation cell at a constant rate of 30 cm<sup>3</sup>/min after the desired reaction temperature was reached. The ratios of oxygen to nitrogen mixtures used were (by volume): 10 : 90, 25 : 75, 50 : 50, 75 : 25, and 100 : 0. Reaction temperatures were 100°, 105°, 110° and 115°C. I.r. spectra of the carbonyl (5.50–6.00  $\mu\text{m}$ )

\* From the thesis submitted by S. M. G. in partial fulfillment of the requirements for the degree of Doctor of Philosophy, Stevens Institute of Technology, 1975.

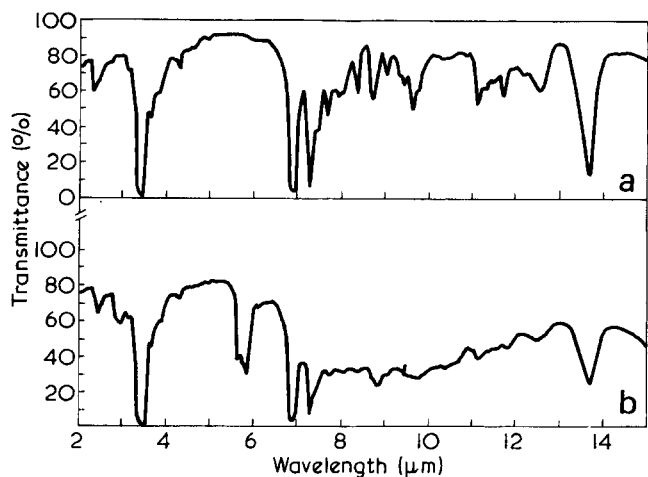


Figure 1 I.r. spectra of IPP-1 (modification 1). (a) Before oxidation; (b) after oxidation at 115°C

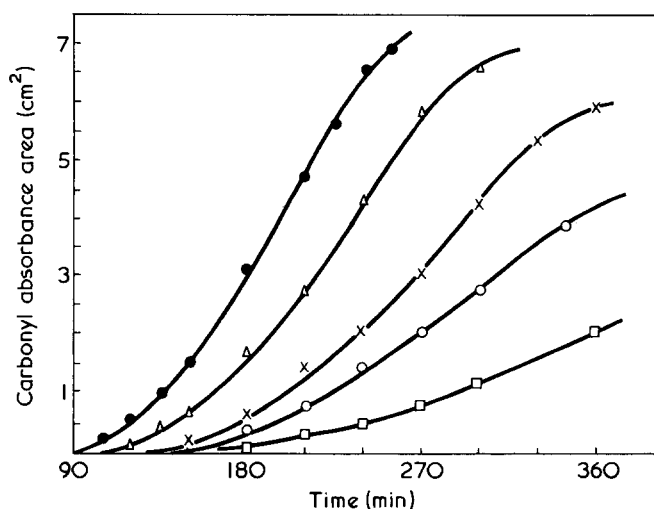


Figure 2 Plots of carbonyl absorbance area versus time for IPP-1 at 100°C under various oxygen concentrations: □, 10; ○, 25; ×, 50; △, 75; ●, 100%

region were recorded at various temperatures and oxygen concentrations, as a function of exposure time. The carbonyl areas for a given film were computed in terms of the total absorbance area ( $\text{cm}^2$ ) of the carbonyl band using a Fortran IV program<sup>16</sup>. This program converts the carbonyl transmittance band to absorbance, and then replots the area computed by the trapezoid method while maintaining the same baseline as previously reported<sup>4</sup>. The computed absorbance area is normalized to unit film thickness from an *a priori* calibration of maximum absorbance at  $7.30 \mu\text{m}$  (due to  $-\text{CH}_2\text{CH}_3$ ) versus known film thicknesses<sup>16</sup>. Thus, the computed carbonyl area of a given film thickness was divided by the value of the maximum absorbance of the corresponding film thickness from the linear calibration curve at a given oxygen concentration and temperature<sup>16</sup>. The weight loss of modification 1 was 1% at 115°C under 100% oxygen for 75 min. Diffusion control was found to be absent for the mil thickness of the films used in this study, pursuant to procedure described earlier<sup>1,4</sup>.

## RESULTS

As in the cases of IPP<sup>3</sup>, APP<sup>4</sup>, IPB<sup>10</sup>, and APB<sup>11</sup>, it was observed that at all oxygen concentrations employed, the reaction rate increased while the induction period decreased with increasing reaction temperature. Further, as the

oxygen concentration was increased, the rate of formation of total carbonyl increased while the induction time decreased, at any one given temperature (Figure 2). Maximum rates of formation of total carbonyl ( $\rho_m$ ) were determined from plots of carbonyl absorbance area versus time (cf. Figure 2) for various temperatures and oxygen concentrations. These values are listed in Table 1. Figure 3 has been constructed from the data in Table 1.

## DISCUSSION

Modification 2 was found to resist oxidation at 65°C in pure oxygen for 4 h. Higher temperatures of oxidation would approach the melting point of this form (78°C), thus rendering thermal oxidative studies in the bulk phase impractical. On the other hand, modification 1, by virtue of its higher melting point (128°C), was more amenable for examining its thermal oxidative properties. At 65°C modification 2 would have required, for less than 100%

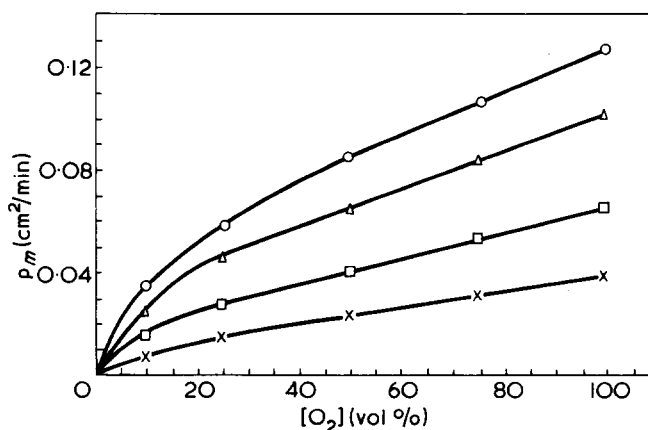


Figure 3 Plots of maximum rate ( $\rho_m$ ) versus  $[\text{O}_2]$  at various temperatures for IPP-1: ×, 100°; □, 105°; △, 110°; ○, 115°C

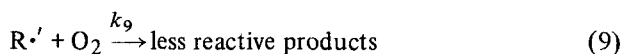
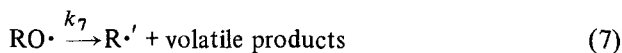
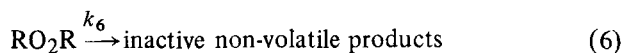
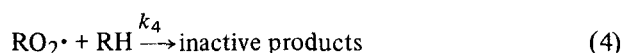
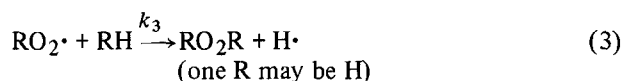
Table 1 Comparison of theoretical and observed maximum rates ( $\rho_m$ ) of total carbonyl at various temperatures and oxygen concentration

Temp. (°C)	$[\text{O}_2]$ (vol. %)	$K_1 \times 10^4$	$K_2$	$K_3$	$\rho_m$ ( $\text{cm}^2/\text{min}$ )	
					Calc.	Obs.
115	100	8.61	46.31	49.88	0.124	0.129
	75				0.103	0.107
	50				0.080	0.085
	25				0.056	0.059
	10				0.037	0.036
110	100	7.42	34.42	38.95	0.099	0.103
	75				0.080	0.085
	50				0.060	0.065
	25				0.040	0.046
	10				0.025	0.025
105	100	5.11	29.65	31.10	0.066	0.067
	75				0.053	0.055
	50				0.040	0.041
	25				0.0270	0.029
	10				0.018	0.016
100	100	3.21	20.92	24.66	0.039	0.040
	75				0.030	0.031
	50				0.022	0.023
	25				0.014	0.015
	10				0.008	0.007

$K_1$ ,  $K_2$ ,  $K_3$  defined in equations (10a), (10b) and (10c)

oxygen, very long exposure time to detect carbonyl formation. (Diffusion rate is low at lower temperatures thus requiring long exposure times at lower oxygen concentrations.)

The kinetic scheme and assumptions presented previously by Stivala *et al.*<sup>3</sup> for the thermal oxidation of polypropylene were used in this study. For convenience, the scheme is reproduced below:



where RH represents the polyolefin. The pertinent expressions which were derived are summarized in equations (10)–(13).

The maximum rate of formation of non-volatile carbonyl products,  $\rho_m$ , at a given temperature and oxygen concentration is expressed as:

$$\rho_m = \frac{K_1 [\text{O}_2]}{1 - K_2/(K_3 + [\text{O}_2])} \quad (10)$$

where

$$K_1 = \frac{Ck_i k_3 k_6 [\text{RH}]}{(k_3 + k_4)(k_5 + k_6)} \quad (10a)$$

and  $C = (1 - e^{-At_m}) \approx \text{constant}$ , since  $At_m$  (where  $t_m$  equals the time to reach maximum reaction rate) is approximately constant under the experimental conditions used over the range of temperatures and oxygen concentrations employed.

$$K_2 = \frac{2k_3 k_5 k_8 [\text{RH}]}{k_9(k_3 + k_4)(k_5 + k_6)} \quad (10b)$$

$$K_3 = \frac{k_8}{k_9} [\text{RH}] \quad (10c)$$

$$K_5 = \frac{(k_3 + k_4)k'K_2}{2k_3K_3} \quad (11)$$

$$A' = 1 - \frac{K_2}{K_3 + [\text{O}_2]} \quad (12)$$

where

$$A' = \frac{A}{k'} = \frac{A}{k_5 + k_6} \quad (12a)$$

and

$$-\ln(\rho_m - \rho)/\rho_m = At \quad (13)$$

when  $\rho \ll \rho_m$ . For relatively high values of  $[\text{O}_2]$ , equation (10) becomes:

$$\rho_m = K_1 K_3 + K_1 [\text{O}_2] \quad (10d)$$

From equation (10d), it can be seen that a plot of  $\rho_m$  versus  $[\text{O}_2]$  should give a linear curve of slope  $K_1$  and intercept  $K_1 K_3$ . By rewriting equation (10) in the form:

$$\{K_3 + [\text{O}_2]\} \{\rho_m - K_1 [\text{O}_2]\} = K_2 \cdot \rho_m \quad (10e)$$

and plotting the left hand side of equation (10e) versus  $\rho_m$ , a linear curve of slope  $K_2$  can be obtained. Hence, values for  $K_1$ ,  $K_2$ , and  $K_3$  may be estimated. Values for these constants are given in *Table 1* for various temperatures (from 100° to 115°C) and oxygen concentrations (from 10 to 100%). From these values, various values of  $\rho_m$  were calculated and found to agree satisfactorily with observed values (cf. *Table 1*). From equation (13) values of  $A$  were determined at various temperatures and oxygen concentrations (*Table 2*). Corresponding values of  $A'$  were calculated from equation (12). The values of  $k'$ , at a given temperature and for various oxygen concentrations, were about constant. Arrhenius plots of  $\log K_3$  and  $\log [K_2/(K_1 K_3)]$  were constructed as shown in *Figure 4*. From the slopes of the linear relationships obtained and from equations (10a) to (10c), the following values were obtained:  $E_8 - E_9 \approx 13$  kcal/mol and  $E_i + E_6 - E_5 \approx 20$  kcal/mol. From equation (11), it can also be seen that if  $k_4/k_3$  is constant over the temperature range used [this was previously indicated to be true<sup>17</sup>], then an Arrhenius plot of  $-\log [k'K_2/K_3]$  should afford a value of  $E_5$ . In

*Table 2* Values of  $A$  and  $k'$  for various temperatures and oxygen concentrations

Temp. (°C)	[O <sub>2</sub> ] (vol. %)	A (min <sup>-1</sup> )	k' (min <sup>-1</sup> )
115	100	0.014	0.020
	75	0.009	0.014
	50	0.006	0.011
110	25	0.003	0.008
	100	0.009	0.012
	75	0.006	0.009
	50	0.005	0.008
105	25	0.003	0.006
	100	0.007	0.009
	75	0.005	0.008
100	50	0.004	0.007
	25	0.003	0.006
	100	0.005	0.006
	75	0.003	0.004
100	50	0.002	0.003
	25	0.001	0.002



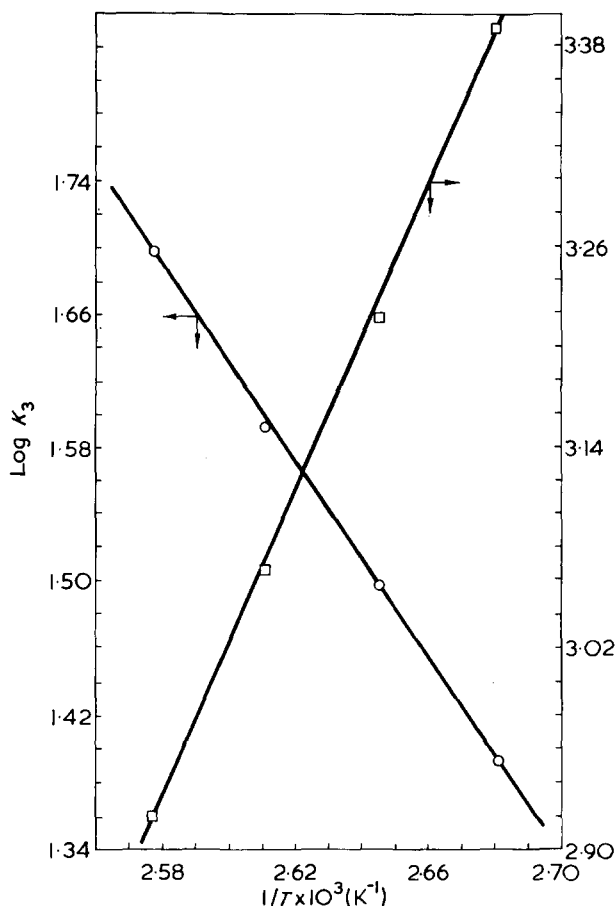


Figure 4 Plots of  $\log K_3$  (○) and  $\log (K_2/K_1K_3)$  (□) versus reciprocal temperature,  $1/T$

Table 3 Comparison of activation energies of IPP-1 at various oxidation stages to other polyolefins

Polyolefins	Activation energies (kcal/mol)			
	$(E_8 - E_9)$	$(E_j + E_6 - E_5)$	$(E_j + E_6)$	$(E_5)$
IPP (3)	6	18	51	33
APP (4)	9	17	48	31
IPB (10)	14	13	38	25
APB (11)	10	14	43	29
IPP-1 (this work)	13	20	46	26

this manner,  $E_5 \approx 26$  kcal/mol (cf. Figure 5). This value was checked by means of a plot of  $-\log \rho_m A/[O_2]$  versus reciprocal temperature [cf. Figure 5 and equations (10), (10a), and (12a)] to yield a value of  $E_i + E_6 \approx 46$  kcal/mol from which a value of  $E_5 \approx 26$  kcal/mol was calculated.

Values of the activation energies for the various stages obtained in this work for IPP-1 are compared with corresponding values for other polyolefins, previously reported from this laboratory in Table 3. From this Table, it appears that various autoxidation process may be occurring less rapidly for IPP-1 than for IPB but more so than in IPP, under similar experimental conditions.

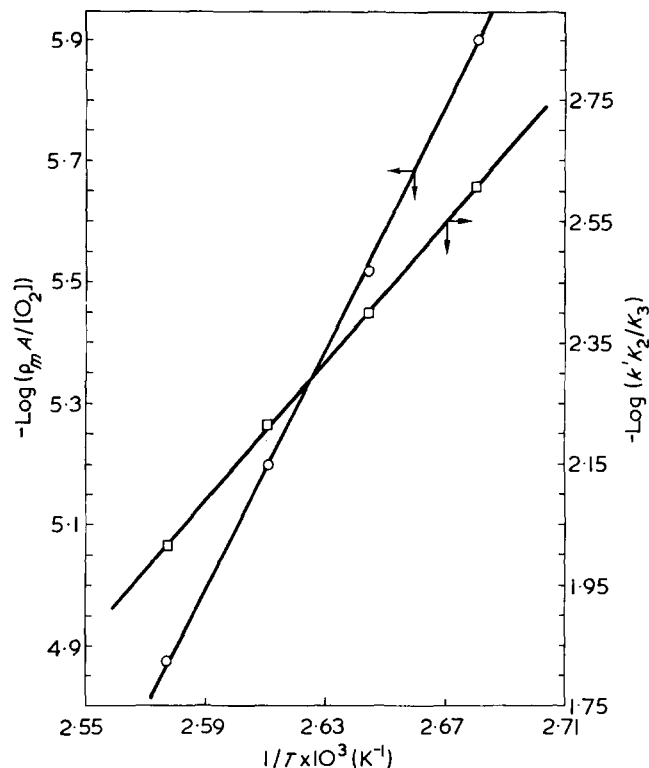


Figure 5 Plots of  $-\log (\rho_m A/[O_2])$  (○) and  $-\log (k'K_2/K_3)$  (□) versus reciprocal temperature,  $1/T$

## REFERENCES

- 1 Reich, L. and Stivala, S. S. 'Autoxidation of Hydrocarbons and Polyolefins', Marcel Dekker, New York, 1969
- 2 Reich, L. and Stivala, S. S. 'Elements of Polymer Degradation', McGraw-Hill, New York, 1971
- 3 Stivala, S. S., Reich, L. and Kelleher, P. G. *Makromol. Chem.* 1963, 59, 28
- 4 Jadrnicek, B. R., Stivala, S. S. and Reich, L. *J. Appl. Polym. Sci.* 1970, 4, 2537
- 5 Stivala, S. S., Jadrnicek, B. R. and Reich, L. *Macromolecules* 1971, 4, 61
- 6 Reich, L., Jadrnicek, B. R. and Stivala, S. S. *J. Polym. Sci. (A-1)* 1971, 9, 231
- 7 Reich, L., Jadrnicek, B. R. and Stivala, S. S. *Polym. Eng. Sci.* 1971, 11, 265
- 8 Stivala, S. S., Jadrnicek, B. R. and Reich, L. *J. Appl. Polym. Sci.* 1971, 15, 2185
- 9 Jadrnicek, B. R., Stivala, S. S. and Reich, L. *Macromolecules* 1972, 5, 20
- 10 Stivala, S. S., Kaplan, E. B. and Reich, L. *J. Appl. Polym. Sci.* 1965, 9, 3557
- 11 Stivala, S. S., Yo, G. and Reich, L. *J. Appl. Polym. Sci.* 1969, 13, 1289
- 12 Bawn, C. E. H. and Chandri, S. A. *Polymer* 1968, 9, 81
- 13 Bawn, C. E. H. and Chandri, S. A. *Polymer* 1968, 9, 123
- 14 Gabbay, S. M., Stivala, S. S. and Reed, P. R. *Analyt. Chim. Acta* in press
- 15 Gabbay, S. M., Stivala, S. S. and Reich, L. *J. Appl. Polym. Sci.* in press
- 16 Gabbay, S. M. *PhD Thesis* Stevens Institute of Technology (1975)
- 17 Reich, L. and Stivala, S. S. *J. Appl. Polym. Sci.* 1969, 13, 17

# Derivation of accurate glass transition temperatures by differential scanning calorimetry

M. J. Richardson and N. G. Savill

*Division of Materials Applications, National Physical Laboratory, Teddington, Middlesex TW11 0LW, UK*

*(Received 3 March 1975)*

Glass transition temperatures,  $T_g$ , cannot be directly determined from differential scanning calorimetry (d.s.c.) curves because of kinetic effects which are especially serious for well annealed samples. Using an anionic polystyrene as an example it is shown how d.s.c. data can be transformed to enthalpy curves which give  $T_g$  with an accuracy of  $\pm 1$  K. As the rate of cooling through the glassy region is lowered  $T_g$  is found to decrease by 2.2 K per decade decrease in cooling rate. Quantitative data are given for the specific heat increment at  $T_g$ .

## INTRODUCTION

The specific heat,  $c_p$ , of a polymer changes abruptly at the glass transition temperature,  $T_g$ , and, since the signal from a differential scanning calorimeter (d.s.c.) is proportional to  $c_p$ , this form of calorimetry has found a ready application in the characterization of  $T_g$ . Unfortunately a d.s.c. is a dynamic instrument and because the glass transition is a strongly rate dependent phenomenon, kinetic effects make the interpretation of experimental d.s.c. curves difficult, if not impossible. Consistent, but arbitrary, treatment allows the definition of a dynamic glass temperature,  $T_{gd}$ , but such a quantity has little value other than for showing differences between samples. In particular, it cannot be related to values obtained by other techniques.

This paper describes how a simple treatment of d.s.c. data gives 'equilibrium' values of  $T_g$ , which are independent of the heating rate. By contrast, the rate of cooling (annealing) through the transition region has a well defined effect on the glass temperature and quantitative data are given for this and also for the specific heat increment at  $T_g$ .

## EXPERIMENTAL

The polymer was an anionic polystyrene of  $M_n = 36\,000$  (Pressure Chemical Co., Batch No.7b). Before any measurements were made, samples were heated in the d.s.c. to about 450 K with the dual purpose of removing any residual low molecular weight impurities and giving a stable sample geometry for subsequent experiments (polystyrene of this molecular weight slowly flows above  $T_g$  and without this pretreatment the calorimeter output may be perturbed). Polymer was transformed to the glassy state by cooling through  $T_g$  at various rates in the calorimeter itself, the only exception being for the slowest rate (2.5 K/day) where the stabilized sample was cooled, in an atmosphere of nitrogen, in an oil bath.

Experiments were carried out with a Perkin-Elmer DSC-2 using alumina as the enthalpy calibrant. Full details have been given earlier<sup>1-3</sup> but we emphasize the important points here. The calorimeter temperature was raised from one

steady value,  $T_1$ , to another,  $T_2$ , where  $T_1 < T_g < T_2$ , in the sequence: (i) empty, (ii) calibrant, (iii) sample. The results of (i) and (ii) gave the area-to-enthalpy conversion factor and reference data for specific heats which, in conjunction with (i) and (iii), led to the total enthalpy change in the polymer  $H_l(T_2) - H_g(T_1)$ , where  $g$  and  $l$  refer to the glassy and liquid states, respectively, as well as specific heats in the interval  $T_1$  to  $T_2$ .

## RESULTS

Results for a variety of thermal treatments are summarized in *Table 1*. The computer programme transformed the d.s.c. output into the overall enthalpy change, column 4, and a table of specific heats at intervals of about a Kelvin, the actual figure depending on the heating rate and the frequency of sampling for the tape output. Specific heat data for the glassy and liquid states were then fitted to separate polynomials in temperature, care being taken to exclude data from the transition region itself. Simple linear relationships were found to adequately represent the  $c_p$ /temperature behaviour of both the glassy and the liquid state in the range  $T_g \pm 70$  K and columns 5-8 show values calculated from these least squares fits at rounded temperatures. They give a good idea of the reproducibility of the experimental data, a figure of  $\pm 1\%$  encompasses all results from 20 separate experiments. *Table 1* cannot reveal rate effects in the transition region itself and these are shown in *Figures 1* and *2*. Specific heat curves should be coincident, at least in the liquidus (the glassy state is discussed below), and the observed deviations in *Figures 1* and *2* reflect the experimental errors discussed above. We should emphasize that our computer procedure<sup>3</sup> is based on the isothermal temperature calibration plus a correction for thermal lag, owing to the finite heating rate, which is derived from the sample curve itself. This correction was 0.7 (5), 1.6 (10) 3.1 (20) and 6.3 K (40 K/min) for the heating rates noted in parentheses and it is clear that the lag varies, as expected, in direct proportion to the heating rate. We therefore believe sample temperatures are properly corrected and features of *Figures*

Table 1 Glass transition temperatures and related properties

Cooling rate (K/min)	Heating rate (K/min)	$T_g$ (K)	J/g		$c_p$ (glass) (J/g/degree)		$c_p$ (liquid) (J/g/degree)		$\Delta c_p$ (J/g/degree)	$\Delta c_p \cdot T_g$ (J/g)
			$H(456.8 \text{ K}) - H(302.0 \text{ K})$	$H(460 \text{ K}) - H(280 \text{ K})$	300 K	350 K	400 K	450 K		
			20	5	371.0	266.2		1.250		
20	10	371.3	268.5		1.252	1.473	1.953	2.102	0.301	111.8
20	20	370.4	267.0		1.239	1.456	1.939	2.109	0.294	108.9
20	40	372.0	265.6		1.233	1.459	1.929	2.093	0.279	103.7
2.5 day <sup>-1</sup>	10	362.7	268.6		1.240	1.453	1.931	2.111	0.289	104.9
0.625	10	367.7	268.9		1.246	1.464	1.948	2.106	0.306	112.5
20	10	371.3	268.5		1.252	1.473	1.953	2.102	0.301	111.8
20	—	372.2		300.7	1.237	1.471	1.945	2.109	0.279	104.0
20	20	371.6		298.6	1.234	1.453	1.930	2.094	0.289	107.5

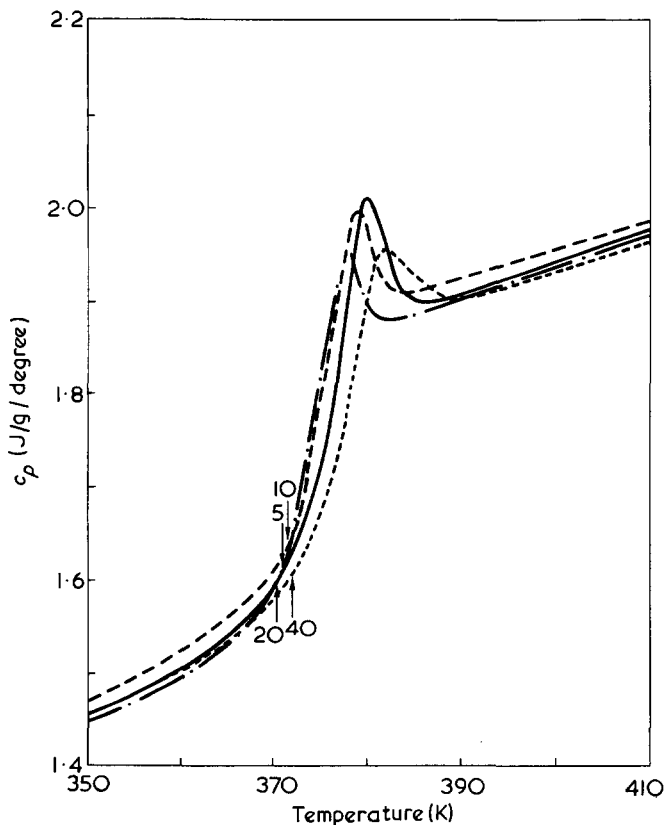


Figure 1 Effect of heating rate on samples cooled at 20 K/min. —, 5; —, 10; —, 20; —, 40 K/min. Arrows show calculated values of  $T_g$  for the heating rates indicated

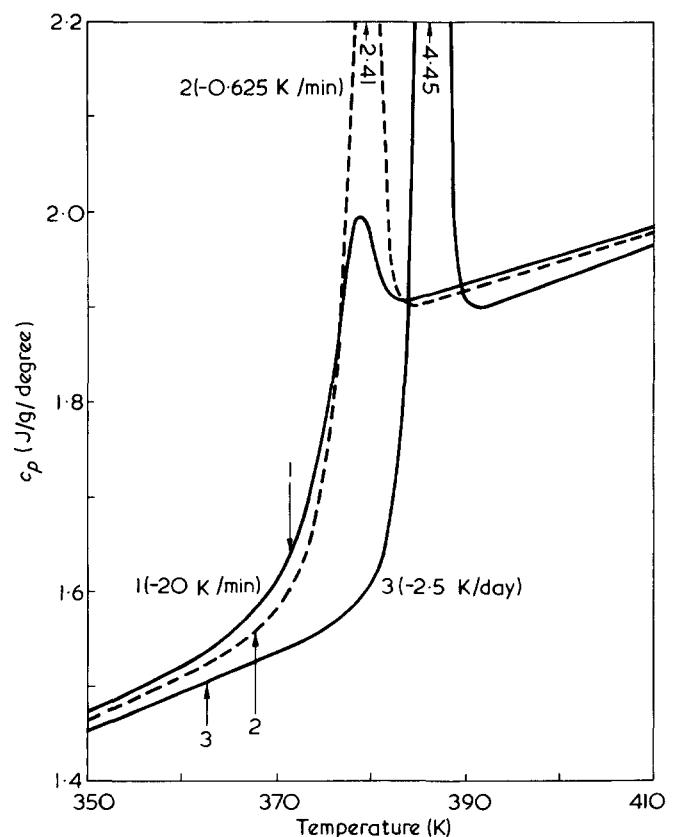


Figure 2 Effect of annealing, at the cooling rates shown, on samples heated at 10 K/min. Arrows show calculated values of  $T_g$

1 and 2 may be ascribed to material, rather than instrumental, effects. An exception is the anomalous peak height for the 40 K/min heating rate (Figure 1). This is low because the true peak was missed owing to the slow sampling rate (one point per 1.3 K) used.

DISCUSSION

Calculation of  $T_g$

$T_g$  is defined by the point of intersection of enthalpy curves for the glassy and liquid states. The glassy state is generally not well defined thermodynamically but under particular circumstances pseudo-equilibrium conditions can be assumed and thermodynamic arguments employed. The specific assumption of this paper is that a given cooling rate yields a reproducible configuration so that the overall enthalpy change  $H_l(T_2) - H_g(T_1)$  is a meaningful thermo-

dynamic quantity.  $T_1$  was always arranged to be some 70 or 80 K below  $T_g$  so that any 'glassy annealing' effects would require a time-scale orders of magnitude larger than that of the experiments.

Schematic enthalpy and specific heat curves for both quenched and well annealed samples are shown in Figure 3. The well known tendency of annealed material to superheat is apparent in Figure 3, and calculation of the dynamic  $T_{gd}$  from the  $c_p$  discontinuity yields a value which is higher than that for quenched materials, the opposite of the true situation.

Our approach has been to construct enthalpy curves for the glass and solid which are linked by the overall enthalpy change but which ignore all details of transition region itself. In effect, enthalpy curves from well defined regions are extrapolated to the glass temperature which is defined by  $H_g(T_g) = H_l(T_g)$ . Integration of the specific heat equations  $c_{pg} = a + bT$  and  $c_{pl} = A + BT$  gives:

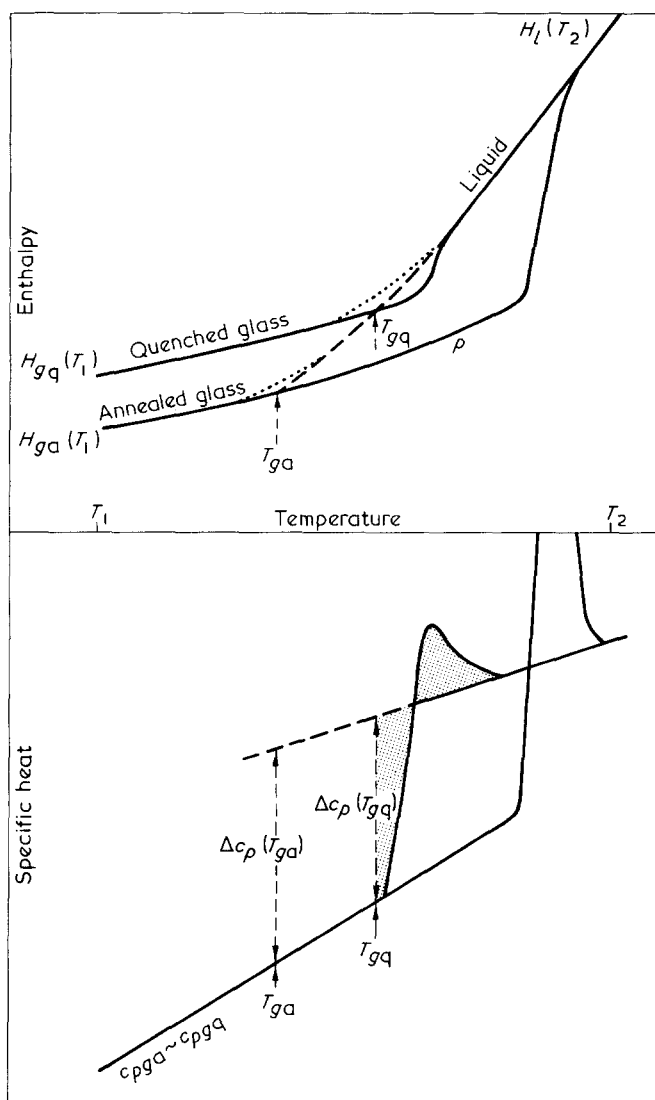


Figure 3 Schematic enthalpy and corresponding specific heat curves. Full lines show typical experimental paths; broken lines, which represent ideal conditions in the absence of rate effects, show how  $T_g$  is defined

$$H_g(T) = aT + \frac{1}{2}cT^2 + P$$

$$H_l(T) = AT + \frac{1}{2}BT^2 + Q$$

and, since  $H_l(T_2) - H_g(T_1)$  is an experimental quantity, the integration constant  $Q - P$  is readily obtained. It is then a trivial matter to solve the quadratic equation for  $T_g$  as defined by the point of intersection of the two enthalpy curves and the glass temperatures shown in Table 1 and Figure 4 have been calculated in this way.

#### Effects of heating rate

Figure 1 shows small but systematic displacement of both the point of maximum slope and the peak position with respect to heating rate,  $R$ . These are to be expected since the superheating effect (Figure 3) is rate dependent but they give the misleading impression that  $T_g$  is also a function of  $R$  whereas it should, if it is to have any thermodynamic significance, be independent of such an experimental parameter. Table 1 shows that this is indeed true when enthalpy curves are used to calculate  $T_g$ . These calculated values have been inserted on Figure 1 and it is clear that there is no simple

construction (such as the point of deviation from the low temperature baseline, or the point of intersection of this baseline with a tangent to the point of maximum slope) whereby the 'dynamic' quantity  $T_{gd}$  can be transformed to the equilibrium or 'enthalpy' value  $T_{gH}$ . In one sense it is fortunate that for this rapidly cooled polymer, which simulates the conditions under which most components are fabricated, there are only a few Kelvins difference between  $T_{gd}$ , however defined, and  $T_{gH}$ . However, the following results obtained on more carefully annealed samples show that the confidence thereby generated in the  $T_g$  values is in fact misplaced.

#### Effects of annealing

Anomalies in the definition of  $T_g$  from  $c_p$  curves alone are clearly illustrated in Figure 2 in which curves 1 and 3 are quantitative examples of, respectively, the schematic quenched and annealed samples of Figure 3. Again,  $T_{gH}$  values have been inserted and the most striking feature is the total lack of structure in curve 3 until more than 10 K above  $T_{gH}$ . It is not the purpose of this paper to comment on the kinetic implications of these results, we restrict ourselves to the 'equilibrium' characteristics of the glassy region. However, it must be emphasized that, since relaxation times around  $T_g$  are of the order of normal experimental time scales, anomalies are not peculiar to d.s.c. but are the general rule. For example, in dilatometry a glass brought to a point on the volume-temperature curve corresponding to  $P$  (Figure 3) shows a steady increase in volume for a time that can extend to many hours.

When  $T_{gH}$  is plotted against  $\log(\text{cooling rate})$  there is an excellent linear correlation (Figure 4), a result which is completely hidden in the specific heat curves and is in fact not easily attainable by any other technique. Transformation of specific heat data as described in this paper shows that  $T_g$  decreases by 2.2 K per decade decrease in cooling rate, a figure which is constant over the molecular weight range  $2 \times 10^3$  to  $2 \times 10^6$ .

Dilatometry<sup>4</sup> gives 363.6 K for the glass temperature of this polymer after cooling at 2.5 K/day, a figure which agrees well with the value shown in Table 1 and which confirms the validity of our procedure.

It is appropriate to mention here that the overall enthalpy change is affected by the annealing treatment in two ways. Not only does  $T_g$  change, as in Figure 4, but also  $c_{pg}$ , which should strictly be written  $c_{pg\alpha}$  where  $\alpha$  represents a particular configuration corresponding to a given thermal treatment, for example, the 'annealed' or 'quenched' samples of Figure 3. Thus:

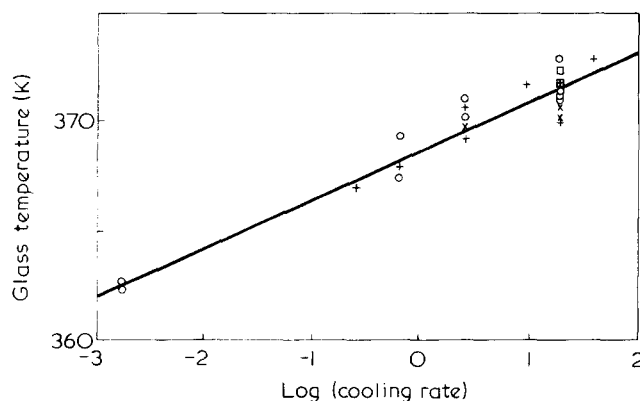


Figure 4 Glass temperatures as a function of the rate of cooling through  $T_g$ . Heating rates: X, 5; O, 10; +, 20; □, 40 K/min

$$H_l(T_2) - H_g(T_1) = \int_{T_1}^{T_{g\alpha}} c_{pg\alpha} dT + \int_{T_{g\alpha}}^{T_2} c_{pl} dT$$

Table 1 clearly shows that  $c_{pg}$  does not change markedly with differing annealing processes but we have preliminary evidence, from very accurate measurements where the bulk of the signal is backed off against a reference material<sup>5</sup>, that  $c_{pg}$  decreases by 0.1–0.2% as the cooling rate is decreased from 20 to 0.625 K/min.

#### Cooling curves

A d.s.c. gives quantitative results on cooling, as well as heating, and Figure 5 shows  $c_p$  curves for a sample cooled at 20 K/min and subsequently reheated at the same rate. Calculated values of  $T_{gH}$  are nearly equal (Table 1), as indeed they should be since the same glass is considered in both cases but although the two curves are remarkably similar, values of  $T_{gd}$ , however derived, are different. A rough correlation between  $T_{gd}$  and  $T_{gH}$  is again found and it is clear that this simply reflects the low degree of 'superheating' in this relatively quenched sample.

It would be wrong to suggest that, lacking rate effects,  $T_g$  is defined by a sharp intersection of two enthalpy curves. Rather, there is curvature indicated by the dotted lines of Figure 3 and by the fact that the cooling curve of Figure 5 enters the transition region some 10 K above  $T_{gH}$ . A wide range of relaxation times is needed to explain experimental observations<sup>6</sup> and the particular temperature chosen has to reflect an average value.

#### Accuracy

At  $T_g$  the specific heat difference between the two states  $\Delta c_p = c_{pl} - c_{pg}$  is about 0.3 J/g/degree (column 9, Table 1) so that an error of  $\pm 0.3$  J/g would, at first sight, imply an error of  $\pm 1$  K in  $T_g$ . Since the overall enthalpy change may be 200–300 J/g this would seem to call for unprecedented

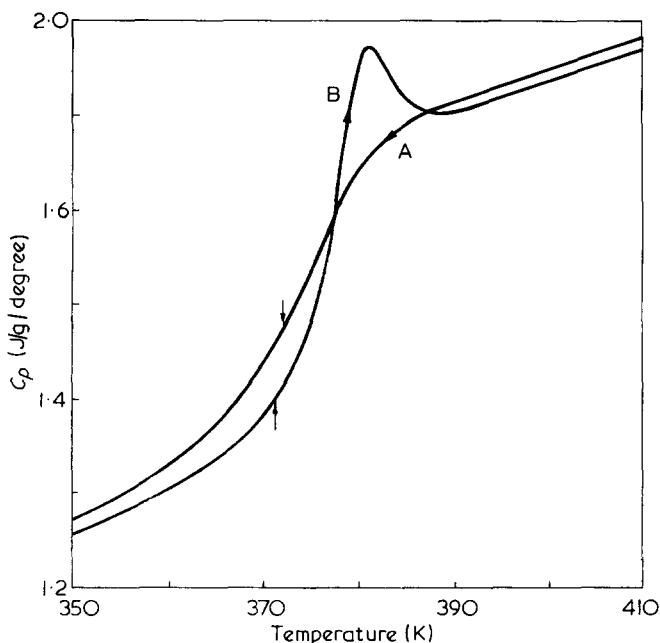


Figure 5 Specific heat curves on cooling (A) and subsequent reheating (B) through  $T_g$ ; all 20 K/min

calorimetric accuracy. Fortunately this is not so since, although we are indeed looking for enthalpy differences of this order, we use results which are internally calibrated in the sense that  $H_l(T_2) - H_g(T_1)$  is related to  $c_{pg}$  and  $c_{pl}$  so that if the last are in error by a certain amount, so is the overall enthalpy change and the net result is a cancellation of errors. For example, in the first four rows of Table 1  $H_l(T_2) - H_g(T_1)$  should be the same; as it is, observed values are well within our anticipated  $\pm 1\%$  accuracy and the highest enthalpy change is simply associated with the highest  $c_p$  values.

Reproducibility of  $T_{gH}$  is excellent. Eleven determinations on different samples cooled at 20 K/min, using a variety of heating rates, gave an average  $T_{gH}$  of 371.7 K with a standard deviation of  $\pm 0.8$  K. The overall accuracy of  $T_{gH}$  is less easy to assess. It has been seen that results are internally consistent with respect to the influence of annealing and, more significantly in the present context, agree to within one Kelvin with a dilatometric value and we feel that this uncertainty,  $\pm 1$  K, is a realistic estimate of the accuracy of the technique.

#### General remarks

Karasz *et al.*<sup>7</sup> have shown that for the very low heating rates of about 0.1 K/min which are used in adiabatic calorimetry,  $T_{gH}$  is essentially the same as  $T_{gd}$ , defined as the point of inflection of the sigmoid  $T_g$  transition. This is clear evidence of the diffuse nature of the glass transition and should suggest that, if an attempt is made to extract  $T_g$  from specific heat curves, the 'onset' temperature should *not* feature in the suggested method. This point was made by Strella and Erhardt<sup>8</sup> who recommend the extrapolation of points of inflection to zero heating rates. However, even if this is a valid procedure, there are ambiguities in the definition of the point of inflection and, of course, it is inconvenient to sacrifice the practical benefits of high heating rates in the d.s.c. A technique based on enthalpy curves has been devised by Guttman and reported by Flynn<sup>9</sup> and this should be used where the full analysis reported here is not possible. However, since the present technique is so simple, and the additional information regarding the glass transition so valuable, we feel that it should always be used when any form of data treatment, and this is increasingly common, is available.

#### Specific heats at $T_g$

There has recently been considerable interest in numerical values of  $\Delta c_p$  at  $T_g$  and various generalizations have been suggested either for  $\Delta c_p$  or the product  $\Delta c_p T_g$ <sup>10,11</sup> Since our technique gives all these quantities we comment briefly on results for this particular polymer. Specific heats at  $T_g$  were extrapolated from the linear equations used to describe the glass and liquid and  $\Delta c_p$  and  $\Delta c_p T_g$  are given in Table 1. There are fairly large uncertainties in  $\Delta c_p$  because there is only a 20% difference between  $c_{pl}$  and  $c_{pg}$ , although, even here, errors partly compensate – only partly since extrapolated values are used. The fluctuations in  $\Delta c_p$  conceal real differences which, if  $c_{pga} \sim c_{pgq}$  (section on annealing above) where a and q refer to different annealing processes, originate in the change of  $T_g$  with annealing. For example, when  $T_g$  decreases by 10 K,  $\Delta c_p$  would be expected to increase by about 3%, a figure which is almost exactly compensated by the drop in  $T_g$ , so that the product

$\Delta c_p T_g$  should be constant. It is encouraging that adiabatic calorimetry<sup>7</sup> gives  $\Delta c_p = 0.296$  J/g/degree and  $\Delta c_p T_g = 107$  J/g. The suggested value of 0.33 J/g/degree<sup>10</sup> is based on an unusually high figure for  $c_{pl}$  which subsequent work has shown to be incorrect<sup>12</sup>.

## CONCLUSIONS

Transformation of d.s.c. data to enthalpy curves gives accurate values of  $T_g$  when the curves for the glass and liquid which lie outside the transition region are extrapolated to meet. The point of intersection is  $T_g$  and this is independent of the d.s.c. heating rate unlike the directly recorded curves. Quantitative data are now readily available for the effects of annealing and the technique should allow the influence of other important parameters such as pressure and drawing, to be studied directly rather than by inference.

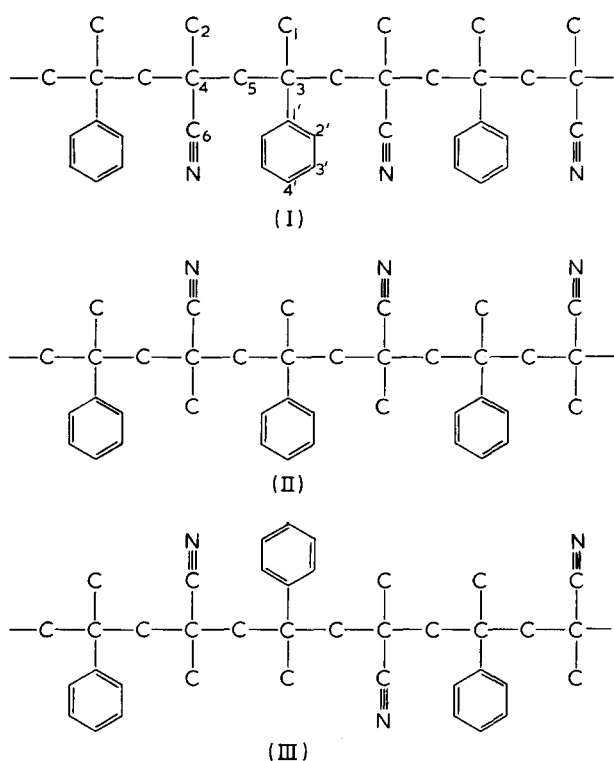
## REFERENCES

- 1 Richardson, M. J. *J. Polym. Sci. (C)* 1972, **38**, 251
- 2 Mills, K. C. and Richardson, M. J. *Thermochim. Acta* 1973, **6**, 427
- 3 Richardson, M. J. and Burrington, P. J. *Thermal Anal.* 1974, **6**, 345
- 4 Richardson, M. J. and Savill, N. G. to be published
- 5 Cassel, B. *Pittsburgh Conf. Analyt. Chem., Cleveland* March 1974
- 6 Roberts, G. E. and White, E. F. T. in 'The Physics of Glassy Polymers', (Ed. R. N. Haward), Applied Science, London, 1973
- 7 Karasz, F. E., Blair, H. E. and O'Reilly, J. M. *J. Phys. Chem.* 1965, **69**, 2657
- 8 Strella, S. and Erhardt, P. F. *J. Appl. Polym. Sci.* 1969, **13**, 1373
- 9 Flynn, J. M. *Thermochim. Acta* 1974, **8**, 69
- 10 Wunderlich, B. and Jones, L. D. *J. Macromol. Sci. (B)* 1969, **3**, 67
- 11 Boyer, R. F. *J. Macromol. Sci. (B)* 1973, **7**, 487
- 12 Bares, V. and Wunderlich, B. *J. Polym. Sci. (Polym. Phys. Edn)* 1973, **11**, 861

# Letters

## On the $^{13}\text{C}$ n.m.r. spectrum of alternating copolymers from $\alpha$ -methylstyrene and methacrylonitrile

N.m.r. spectra of random copolymers from  $\alpha$ -methylstyrene (A) and methacrylonitrile (N) consist of several groups of resonance signals with complicated substructure concerning configurational and compositional sequences of monomeric units. Thus, for understanding the complexity of the spectra it should be reasonable to study the spectra of alternating copolymers first. Alternating copolymers from  $\alpha$ -methylstyrene and methacrylonitrile composed in a head-to-tail arrangement are prepared easily by a method described by Gaylord<sup>1,2</sup>.



Formulae (I), (II) and (III) represent segments of the polymer chain. Each monomeric unit contains an asymmetric carbon atom leading to a ditactic arrangement according to Natta's ditacticity designation<sup>3</sup>. If a polymer is isotactic with respect to the substituents of the monomeric units A and N, two structures are possible: erythro-diisotactic (I) and threo-diisotactic (II). The relative configurational enchainment of A and N in (I) is *m* (meso), whereas the relative enchainment in (II) is *r* (racemic). Hence, the configurational sequence of I and II are  $A_m N_m A_m N_m A$  and  $A_r N_r A_r N_r A$ , respectively. As shown by III a disyndiotactic polymer consists of equal amounts of erythro- and threo-diisotactic placements. The relative configurational enchainment of segment III is  $A_r N_m A_r N_m A$ . However, since  $^{13}\text{C}$  n.m.r. spectroscopy cannot observationally distinguish between a sequence and its reverse form, e.g.  $A_r N_m A$  and  $A_m N_r A$ , the sum of both sequences,  $A_m N_r A + A_r N_m A$ , is marked by  $A_r N_m A^+$  in the following. Numbered carbon atoms in formula I refer to spectra in Figures 1 and 2. For

assignment it is important to compare the spectra of the homopolymers with the spectrum of the alternating copolymer. As shown in Figure 2 the shape of the resonances of carbon  $C_1$ ,  $C_2$ ,  $C_3$ ,  $C_4$  and  $C_5$  of the alternating copolymer appears similar to the shape of the resonances of the two corresponding homopolymers. Especially the resonances of the non-protonated carbon in poly( $\alpha$ -methylstyrene) and methacrylonitrile correspond to the resonance spectrum of the alternating copolymer. Whereas large chemical shifts of a particular carbon nucleus depend on its bonding and chemical environment the substructure of these resonances stems from pronounced sensitivity of the  $^{13}\text{C}$  chemical shift to configuration. Since both homopolymers of A and N, the spectra of which are shown in Figures 1 and 2, are dominantly syndiotactic<sup>4-6</sup>, the alternating copolymer too has to be considered dominantly

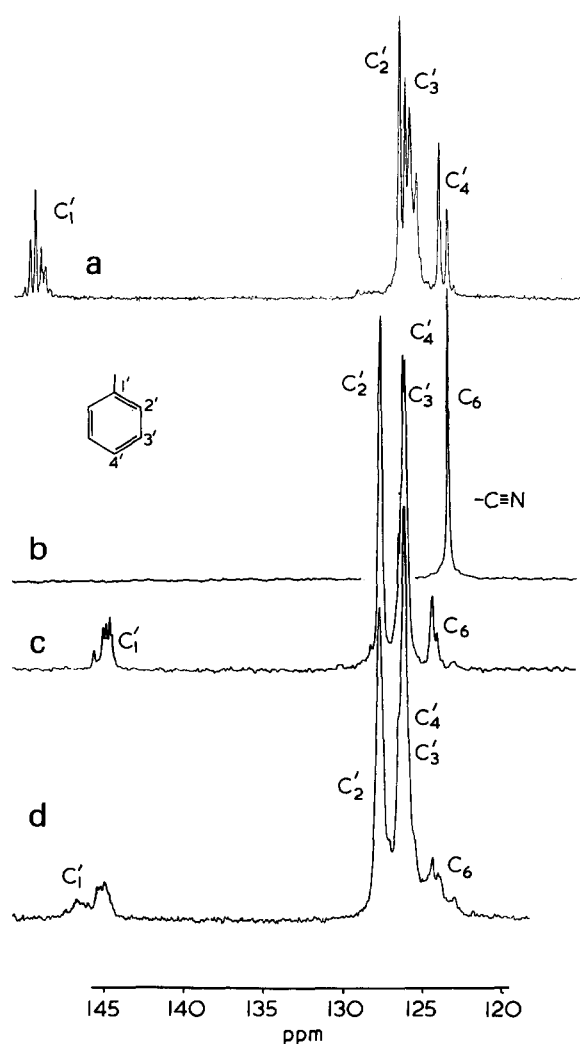


Figure 1  $^{13}\text{C}$  n.m.r. spectra of poly( $\alpha$ -methylstyrene), methacrylonitrile and their copolymers. Resonance region of the aromatic carbons and the nitrile group. Spectra are continued in Figure 2. (a) Poly( $\alpha$ -methylstyrene), for assignment see refs 5 and 6; (b) polymethacrylonitrile, for assignment see ref. 7; (c) alternating copolymer from  $\alpha$ -methylstyrene and methacrylonitrile; (d) random copolymer from  $\alpha$ -methylstyrene and methacrylonitrile; fraction of monomeric unit corresponding to  $\alpha$ -methylstyrene in copolymer,  $m_A = 0.47$

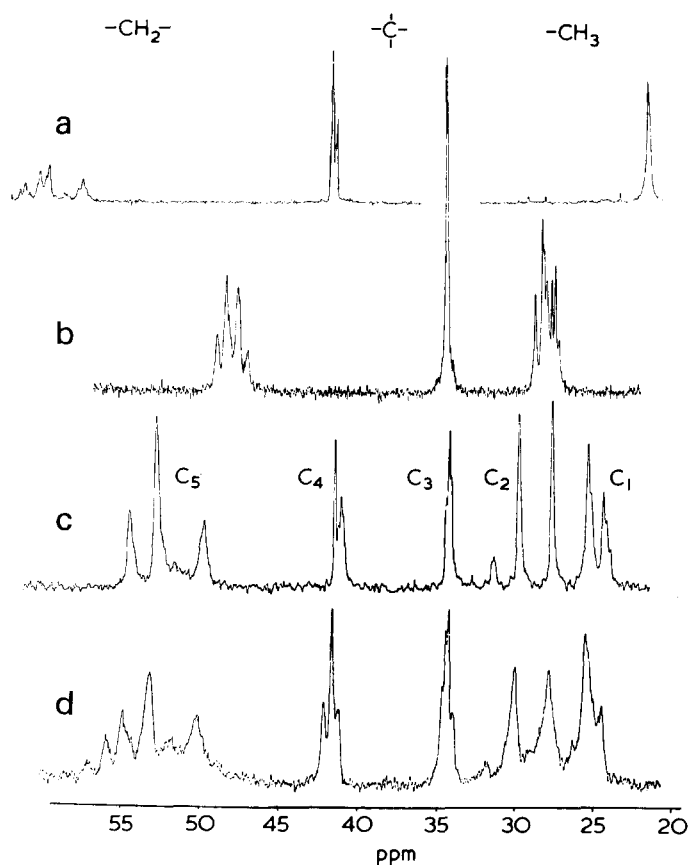


Figure 2  $^{13}\text{C}$  n.m.r. spectra of poly( $\alpha$ -methylstyrene), methacrylonitrile and their copolymers. Spectra continued from Figure 1. Resonance region of the aliphatic carbons. (a) Poly( $\alpha$ -methylstyrene); (b) polymethacrylonitrile; (c) alternating copolymer; (d) random copolymer

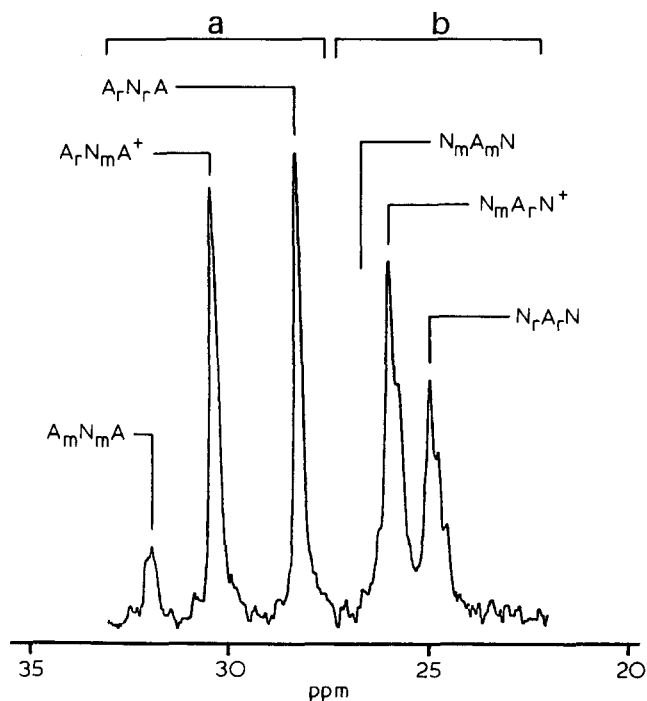


Figure 3  $^{13}\text{C}$  n.m.r. spectrum of an alternating copolymer from  $\alpha$ -methylstyrene and methacrylonitrile. Enlarged spectrum according to Figure 2c. Resonance region of the  $\text{CH}_3$  groups. (a) Monomeric unit corresponding to methacrylonitrile; (b) monomeric unit corresponding to  $\alpha$ -methylstyrene

syndiotactic in contrast to results obtained by  $^1\text{H}$  n.m.r. spectroscopy<sup>1</sup>.

The assignment of the resonance signals of both  $\text{CH}_3$  groups can be performed as shown in Figure 3. The splitting of the resonance signals of the  $\text{CH}_3$  group of the monomeric unit due to N (see Figure 2c, carbon  $\text{C}_2$ ) appears in the same succession as in the homopolymer but with larger chemical shifts as given in Table 1 and without pentad splitting. On the other hand, the triad splitting of the  $\text{CH}_3$  group of the monomeric unit due to A (see Figure 2c, carbon  $\text{C}_1$ ) is smaller but with outlined pentad splitting. It is remarkable that the  $\text{CH}_3$  resonance signal provides information on configuration, since in homopolymer spectra as shown in Figure 1a no splitting has yet been observed.

The enlarged resonance spectrum of the carbon  $\text{C}'_2$ ,  $\text{C}'_3$ ,  $\text{C}'_4$  and  $\text{C}_6$  is shown in Figure 4. Triad assignment in analogy to  $\alpha$ -methylstyrene-acrylonitrile copolymers<sup>7</sup> and peak intensities of the aromatic carbons are given in Table 2. Triad fractions have been determined by curve fitting techniques. Within experimental error observed and calculated values are in good agreement.

The assignment of the resonances of the carbon atoms  $\text{C}_1$ ,  $\text{C}_2$ ,  $\text{C}'_2$ ,  $\text{C}'_3$  and  $\text{C}'_4$ , given in Tables 1 and 2, respectively, rests on the dominantly syndiotactic enchainment of the monomeric units in poly( $\alpha$ -methylstyrene) and polymethacrylonitrile and validity of Bernoullian statistics. The assumption of Bernoullian statistics is valid for the alternating copolymer, too, if  $\rho = 2 \cdot m \cdot r/mr = 1$ . A value of  $\rho = 1.00 \pm 0.1$  has been calculated from triad fractions of the corresponding carbons  $\text{C}_1$ ,  $\text{C}_2$ ,  $\text{C}'_2$ ,  $\text{C}'_3$  and  $\text{C}'_4$ , respectively.

Resonance signals of the aromatic carbon  $\text{C}'_1$  occur in the downfield part of the  $^{13}\text{C}$  n.m.r. spectrum. The expanded resonance region is shown in Figure 5. The well resolved lines are assigned to configurational pentads, since there are more lines than expected for triad splitting. Chemical shift data and line intensities determined by curve fitting are presented in Table 3. Within experimental error observed peak intensities and intensities calculated from Bernoullian statistics are in good agreement.

The alternating copolymer under study is thus of random configuration with dominantly syndiotactic enchainment of the monomeric units. The resonance spectra of carbon  $\text{C}_3$ ,  $\text{C}_4$ ,  $\text{C}_5$  as well as  $\text{C}_6$  will be discussed in a later paper concerning the  $^{13}\text{C}$  n.m.r. spectra of random copolymers from  $\alpha$ -methylstyrene and methacrylonitrile. Attention should be directed to a resonance signal at 123.1 ppm shown in Figure 4. This signal is unambiguously assigned to the triad  $\text{NNA}^+$  or its corresponding pentads. This means that there is slight deviation from exact alternating copolymerization.

Table 1 Triad intensities in  $^{13}\text{C}$  n.m.r. spectrum of an alternating copolymer from  $\alpha$ -methylstyrene and methacrylonitrile. Resonances of the  $\text{CH}_3$  groups according to Figure 2c

Sequence	Carbon	Chemical shift		Intensity	
		ppm	$\Delta\text{Hz}$	Observed	Calculated*
$\text{N}_r\text{A}_r\text{N}$	$\text{C}_1$	21.19 <sup>†</sup>	78	0.43	0.46
$\text{N}_r\text{A}_m\text{N}^+$		22.34 <sup>†</sup>		0.47	0.44
$\text{N}_m\text{A}_m\text{N}$		23.26		0.10	0.12
$\text{A}_r\text{N}_r\text{A}$	$\text{C}_2$	25.07	171	0.47	0.46
$\text{A}_r\text{N}_m\text{A}^+$		27.59		0.44	0.44
$\text{A}_m\text{N}_m\text{A}$		29.61		0.09	0.12

\* Calculated for Bernoullian statistics;  $r = 0.66$ ,  $m = 0.34$

<sup>†</sup> Corresponding to peak maximum



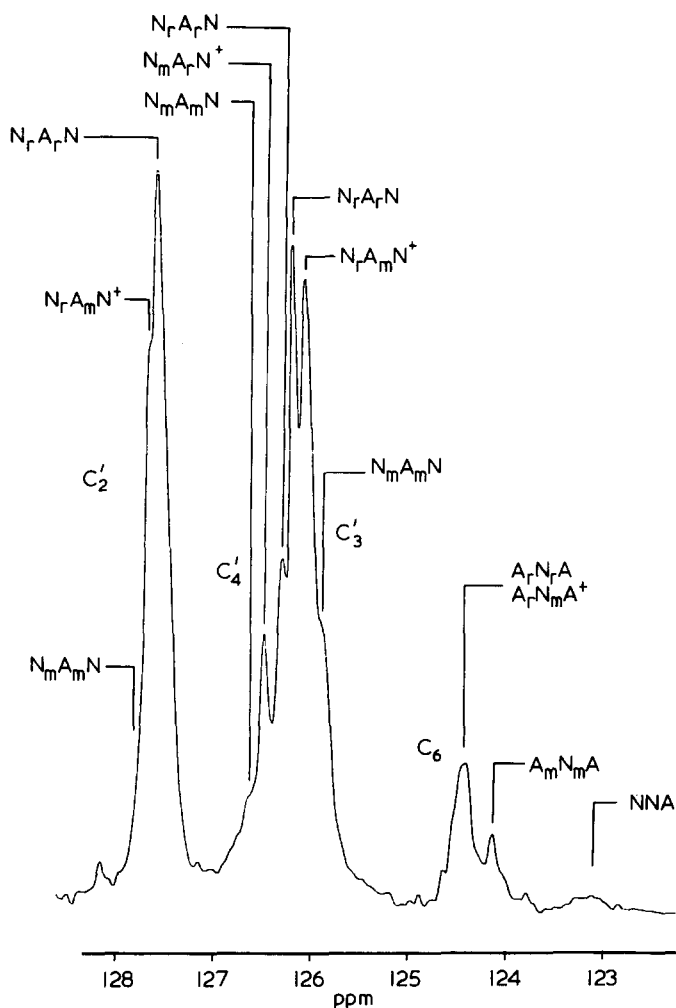


Figure 4 <sup>13</sup>C n.m.r. spectrum of an alternating copolymer from  $\alpha$ -methylstyrene and methacrylonitrile. Enlarged resonance region of aromatic carbons C<sub>2</sub>', C<sub>3</sub>' and C<sub>4</sub>' and nitrilic carbon C<sub>6</sub> according to Figure 1c

Table 2 Triad intensities in the <sup>13</sup>C n.m.r. spectrum of an alternating copolymer from  $\alpha$ -methylstyrene and methacrylonitrile. Resonances of the aromatic carbons C<sub>2</sub>', C<sub>3</sub>' and C<sub>4</sub>' according to Figure 5

Sequence	Carbon C <sub>2</sub> '		Carbon C <sub>3</sub> '		Carbon C <sub>4</sub> '		Inten- sity calc.*
	ppm	Inten- sity	ppm	Inten- sity	ppm	Inten- sity	
N <sub>r</sub> A <sub>r</sub> N	127.66	0.47	126.19	0.41	126.09	0.44	0.44
N <sub>r</sub> A <sub>m</sub> N <sup>†</sup>	127.80 <sup>†</sup>	0.43	126.06	0.44	126.51	0.40	0.45
N <sub>m</sub> A <sub>m</sub> N	127.90 <sup>†</sup>	0.10	125.96	0.15	126.90 <sup>†</sup>	0.16	0.12

\* Calculated for Bernoullian statistics; m = 0.34, r = 0.66  
 † Extrapolated from curve fitting

Experimental

The alternating copolymer was prepared as described by Gaylord *et al.*<sup>1</sup>. The polymerization was started by adding methacrylonitrile to the n-hexane solution of ethyl aluminium sesquichloride at -78°C. After adding  $\alpha$ -methylstyrene at -10°C the polymerization was carried out at this temperature.

The proton decoupled <sup>13</sup>C n.m.r. spectra of the polymer samples were obtained in CDCl<sub>3</sub> at 40°C using a Bruker-Spectrospin HX 270 operating at 67.88 MHz. Spectro-

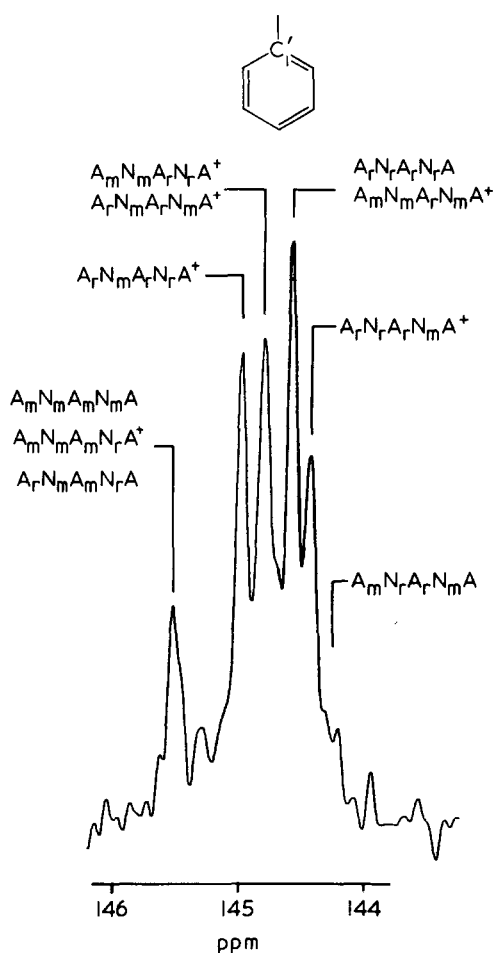


Figure 5 <sup>13</sup>C n.m.r. spectrum of an alternating copolymer from  $\alpha$ -methylstyrene and methacrylonitrile. Enlarged spectrum according to Figure 1c. Resonance region of the aromatic carbon C<sub>1</sub>'

Table 3 Triad and pentad assignment in the <sup>13</sup>C n.m.r. spectrum of an alternating copolymer from  $\alpha$ -methylstyrene and methacrylonitrile. Resonance of the aromatic carbon C<sub>1</sub>'

Sequence		Chemical shift (ppm)	Intensity	
Triad	Pentad		Observed	Calculated*
N <sub>r</sub> A <sub>r</sub> N	A <sub>m</sub> N <sub>r</sub> A <sub>r</sub> N <sub>m</sub> A	144.46	0.05	0.05
	A <sub>r</sub> N <sub>r</sub> A <sub>r</sub> N <sub>m</sub> A <sup>†</sup>	144.57	0.16	0.20
	A <sub>r</sub> N <sub>r</sub> A <sub>r</sub> N <sub>r</sub> A	144.68	0.26 <sup>‡</sup>	0.19
N <sub>r</sub> A <sub>m</sub> N <sup>†</sup>	A <sub>r</sub> N <sub>m</sub> A <sub>r</sub> N <sub>r</sub> A <sup>†</sup>	145.09	0.20	0.20
	A <sub>r</sub> N <sub>m</sub> A <sub>r</sub> N <sub>m</sub> A <sup>†</sup>	144.89	0.23	0.20
	A <sub>m</sub> N <sub>m</sub> A <sub>r</sub> N <sub>r</sub> A <sup>†</sup>	144.68 <sup>†</sup>	0.26 <sup>‡</sup>	0.06
	A <sub>m</sub> N <sub>m</sub> A <sub>r</sub> N <sub>m</sub> A <sup>†</sup>	144.68 <sup>†</sup>	0.26 <sup>‡</sup>	0.06
N <sub>m</sub> A <sub>m</sub> N		145.66	0.11	0.12

\* Calculated for Bernoullian statistics; m = 0.34, r = 0.66  
 † Determined by curve fitting  
 ‡ Due to combined intensity of A<sub>r</sub>N<sub>r</sub>A<sub>r</sub>N<sub>r</sub>A + A<sub>m</sub>N<sub>m</sub>A<sub>r</sub>N<sub>m</sub>A<sup>†</sup>

meter settings were: sweep width, 12 kHz; pulse width, 35  $\mu$ sec; transients, 8 K; data points of spectrum, 8 K. Internal standard was octamethyltetrasiloxane (OMTS) = 0 ppm.

Spectra simulations have been performed by a DuPont 310 curve resolver adjusted to Lorentzian line shape.

### Acknowledgement

The financial support of Arbeitsgemeinschaft Industrieller Forschungsvereinigungen is gratefully acknowledged.

K.-F. Elgert and B. Stützel

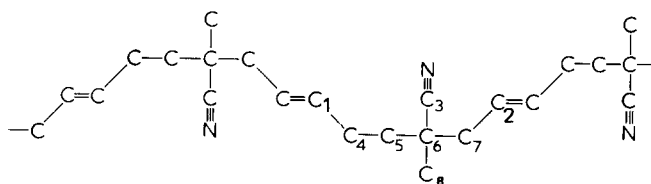
Institut für Makromolekulare Chemie,  
Universität Freiburg,  
D-78 Freiburg i. Br., West Germany  
(Received 11 March 1975)

### References

- Gaylord, N. G. and Patnaik, B. K. *J. Polym. Sci. (A-2)* 1966, **4**, 155
- Patnaik, B. K. and Gaylord, N. G. *J. Macromol. Sci. (A)* 1971, **5**, 843
- Natta, G., Peraldo, M., Farina, M. and Bressan, G. *Makromol. Chem.* 1962, **55**, 139
- Inoue, Y., Nishioka, A. and Chújó, R. *Makromol. Chem.* 1972, **156**, 207
- Elgert, K.-F., Wicke, R., Stützel, B. and Ritter, W. *Polymer* 1975, **16**, 465
- Inoue, Y., Koyama, K., Chújó, R. and Nishioka, A. *Makromol. Chem.* 1974, **175**, 277
- Kuntz, I. and Chamberlain, N. F. *J. Polym. Sci.* 1974, **12**, 1695
- Elgert, K.-F. and Stützel, B. *Makromol. Chem.* in preparation

### On the $^{13}\text{C}$ n.m.r. spectrum of alternating copolymers from butadiene and methacrylonitrile

$^{13}\text{C}$  n.m.r. spectroscopy has been used frequently for studying the structure of polybutadienes. Especially, the resonance spectrum of the carbon double bond<sup>1</sup> is very sensitive to differences in the sequence distribution of monomeric units forming the polymer backbone chain. Thus, an extension of  $^{13}\text{C}$  n.m.r. spectroscopy on copolymers from butadiene should be quite promising. This letter deals with the assignment of the  $^{13}\text{C}$  n.m.r. spectrum of the alternating copolymer as a first attempt to study the complicated spectra of random copolymers from butadiene and methacrylonitrile.



The formula represents a chain segment of the alternating copolymer. Numbered carbons refer to spectra in Figures 2 and 3. This sequence of six monomeric units is designated by T-NT-NT-N. In this abbreviation T stands for *trans*-1,4-butadiene and -N for methacrylonitrile with respect to the relative position of the methylene carbon C<sub>5</sub>. As a consequence, carbon nuclei C<sub>1</sub> and C<sub>2</sub> are expected to have different chemical shifts owing to their different distances to the nitrilic group.

Alternating copolymers from butadiene and methacrylonitrile can be prepared according to the method described by Furukawa<sup>2,3</sup>, originally developed for alternating copolymers from butadiene and acrylonitrile. As expected<sup>4</sup>, methacrylonitrile and butadiene undergo alternating copolymerization by the same catalyst system. The polymerization is assumed to generate a head-

to-tail arrangement of the monomeric units. Crystallinity, observed in the Debye-Scherrer diagram is a proof of predominantly *trans*-1,4-enchainment of butadiene.

Figure 1a represents the proton-decoupled  $^{13}\text{C}$  spectrum of the alternating copolymer. With respect to their different bonding, individual carbon nuclei are identified from the non-decoupled spectrum as shown in Figure 1b. Consequently, C<sub>3</sub>, C<sub>6</sub> and C<sub>8</sub> are assigned to corresponding resonance signals at 122.96, 35.94 and 22.99 ppm, respectively. Exact peak positions and assignment are given in Table 1.

For comparison spectra of homopolymers, alternating and random copolymers are shown in Figures 2 and 3. Resonance signals of both homopolymers cannot be observed in the resonance spectrum of the alternating copolymer. On the other hand, owing to compositional sequences, the spectrum of the random copolymer is of increased complexity as compared to the alternating copolymer. In low molecular weight compounds such as alkanes<sup>5</sup>, alkenes<sup>6</sup> and nitriles<sup>7</sup> the study of substituent effects has given rise to empirical additivity correlations. Additionally, the nitrile triple bond has been found to

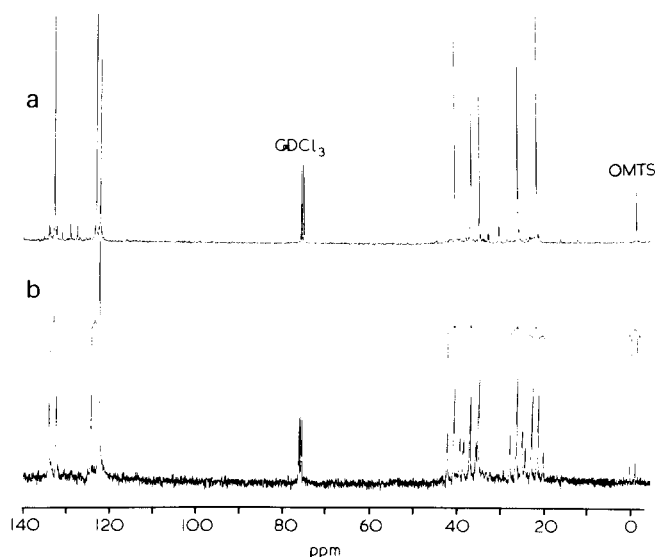


Figure 1  $^{13}\text{C}$  n.m.r. spectra of an alternating copolymer from butadiene and methacrylonitrile. (a) Proton-decoupled spectrum; (b) non-decoupled spectrum

Table 1 Chemical shift data for an alternating copolymer. Monomeric units are *trans*-1,4-butadiene and methacrylonitrile

Signal	Carbon*	Chemical shift	
		Observed	Calculated
1	-C=C-	133.62	131.01 <sup>a</sup>
2	-C=C-	123.90	127.48 <sup>a</sup>
3	-C≡N	122.96	-
4	-CH <sub>2</sub> -	27.32	27.08 <sup>b</sup>
5	-CH <sub>2</sub> -	37.85	38.20 <sup>b</sup>
6	-C-	35.94 <sup>c</sup>	35.16 <sup>b</sup>
7	-CH <sub>2</sub> -	41.55	41.20 <sup>b</sup>
8	-CH <sub>3</sub>	22.99 <sup>c</sup>	23.54 <sup>b</sup>

\* Carbon atoms of chain segment T-NT-NT according to formula

<sup>a</sup> Calculated according to ref. 1, substituting -C≡N by -CH=CH<sub>2</sub>

<sup>b</sup> Calculated according to refs 6 and 7 substituting -C≡N by -CH<sub>2</sub>-CH<sub>3</sub>

<sup>c</sup> Assignment from non-decoupled spectrum in Figure 1b

### Acknowledgement

The financial support of Arbeitsgemeinschaft Industrieller Forschungsvereinigungen is gratefully acknowledged.

K.-F. Elgert and B. Stützel

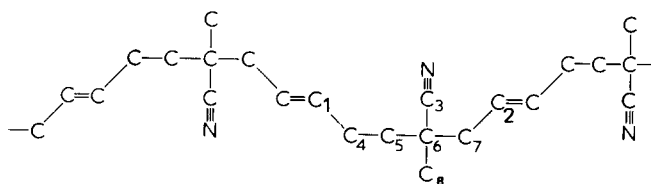
Institut für Makromolekulare Chemie,  
Universität Freiburg,  
D-78 Freiburg i. Br., West Germany  
(Received 11 March 1975)

### References

- Gaylord, N. G. and Patnaik, B. K. *J. Polym. Sci. (A-2)* 1966, **4**, 155
- Patnaik, B. K. and Gaylord, N. G. *J. Macromol. Sci. (A)* 1971, **5**, 843
- Natta, G., Peraldo, M., Farina, M. and Bressan, G. *Makromol. Chem.* 1962, **55**, 139
- Inoue, Y., Nishioka, A. and Chújó, R. *Makromol. Chem.* 1972, **156**, 207
- Elgert, K.-F., Wicke, R., Stützel, B. and Ritter, W. *Polymer* 1975, **16**, 465
- Inoue, Y., Koyama, K., Chújó, R. and Nishioka, A. *Makromol. Chem.* 1974, **175**, 277
- Kuntz, I. and Chamberlain, N. F. *J. Polym. Sci.* 1974, **12**, 1695
- Elgert, K.-F. and Stützel, B. *Makromol. Chem.* in preparation

### On the $^{13}\text{C}$ n.m.r. spectrum of alternating copolymers from butadiene and methacrylonitrile

$^{13}\text{C}$  n.m.r. spectroscopy has been used frequently for studying the structure of polybutadienes. Especially, the resonance spectrum of the carbon double bond<sup>1</sup> is very sensitive to differences in the sequence distribution of monomeric units forming the polymer backbone chain. Thus, an extension of  $^{13}\text{C}$  n.m.r. spectroscopy on copolymers from butadiene should be quite promising. This letter deals with the assignment of the  $^{13}\text{C}$  n.m.r. spectrum of the alternating copolymer as a first attempt to study the complicated spectra of random copolymers from butadiene and methacrylonitrile.



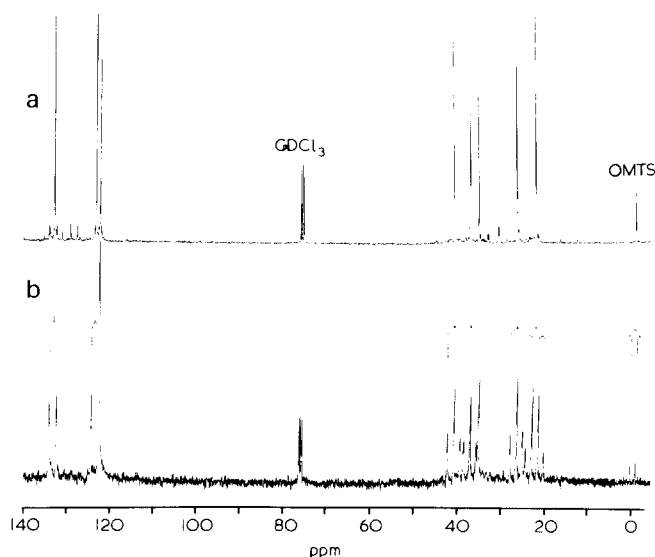
The formula represents a chain segment of the alternating copolymer. Numbered carbons refer to spectra in *Figures 2 and 3*. This sequence of six monomeric units is designated by T-NT-NT-N. In this abbreviation T stands for *trans*-1,4-butadiene and -N for methacrylonitrile with respect to the relative position of the methylene carbon C<sub>5</sub>. As a consequence, carbon nuclei C<sub>1</sub> and C<sub>2</sub> are expected to have different chemical shifts owing to their different distances to the nitrilic group.

Alternating copolymers from butadiene and methacrylonitrile can be prepared according to the method described by Furukawa<sup>2,3</sup>, originally developed for alternating copolymers from butadiene and acrylonitrile. As expected<sup>4</sup>, methacrylonitrile and butadiene undergo alternating copolymerization by the same catalyst system. The polymerization is assumed to generate a head-

to-tail arrangement of the monomeric units. Crystallinity, observed in the Debye-Scherrer diagram is a proof of predominantly *trans*-1,4-enchainment of butadiene.

*Figure 1a* represents the proton-decoupled  $^{13}\text{C}$  spectrum of the alternating copolymer. With respect to their different bonding, individual carbon nuclei are identified from the non-decoupled spectrum as shown in *Figure 1b*. Consequently, C<sub>3</sub>, C<sub>6</sub> and C<sub>8</sub> are assigned to corresponding resonance signals at 122.96, 35.94 and 22.99 ppm, respectively. Exact peak positions and assignment are given in *Table 1*.

For comparison spectra of homopolymers, alternating and random copolymers are shown in *Figures 2 and 3*. Resonance signals of both homopolymers cannot be observed in the resonance spectrum of the alternating copolymer. On the other hand, owing to compositional sequences, the spectrum of the random copolymer is of increased complexity as compared to the alternating copolymer. In low molecular weight compounds such as alkanes<sup>5</sup>, alkenes<sup>6</sup> and nitriles<sup>7</sup> the study of substituent effects has given rise to empirical additivity correlations. Additionally, the nitrile triple bond has been found to



*Figure 1*  $^{13}\text{C}$  n.m.r. spectra of an alternating copolymer from butadiene and methacrylonitrile. (a) Proton-decoupled spectrum; (b) non-decoupled spectrum

*Table 1* Chemical shift data for an alternating copolymer. Monomeric units are *trans*-1,4-butadiene and methacrylonitrile

Signal	Carbon*	Chemical shift	
		Observed	Calculated
1	-C=C-	133.62	131.01 <sup>a</sup>
2	-C=C-	123.90	127.48 <sup>a</sup>
3	-C≡N	122.96	-
4	-CH <sub>2</sub> -	27.32	27.08 <sup>b</sup>
5	-CH <sub>2</sub> -	37.85	38.20 <sup>b</sup>
6	-C-	35.94 <sup>c</sup>	35.16 <sup>b</sup>
7	-CH <sub>2</sub> -	41.55	41.20 <sup>b</sup>
8	-CH <sub>3</sub>	22.99 <sup>c</sup>	23.54 <sup>b</sup>

\* Carbon atoms of chain segment T-NT-NT according to formula

<sup>a</sup> Calculated according to ref. 1, substituting -C≡N by -CH=CH<sub>2</sub>

<sup>b</sup> Calculated according to refs 6 and 7 substituting -C≡N by -CH<sub>2</sub>-CH<sub>3</sub>

<sup>c</sup> Assignment from non-decoupled spectrum in *Figure 1b*

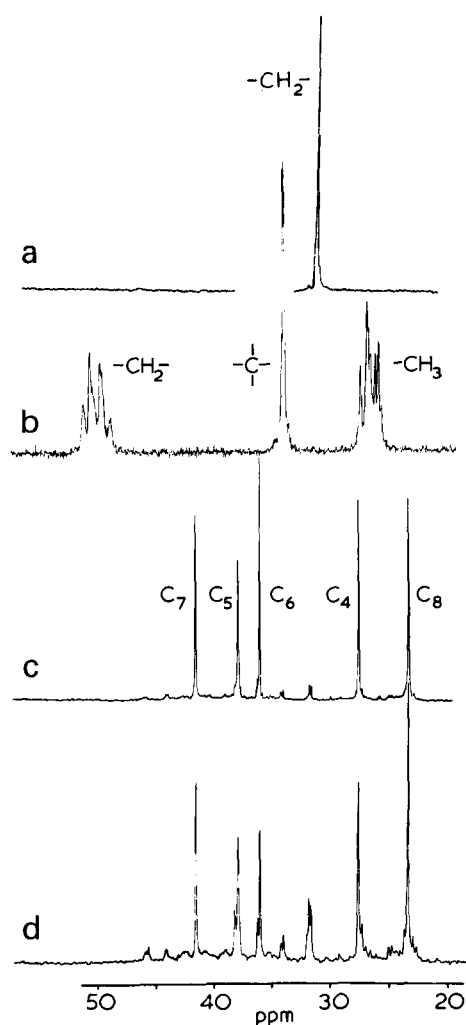


Figure 2  $^{13}\text{C}$  n.m.r. spectra of polybutadiene, polymethacrylonitrile and their copolymers. Resonance region of the aliphatic carbons. Spectra are continued in Figure 3. (a) *trans*-1,4-polybutadiene; (b) polymethacrylonitrile; for assignment see ref. 10; solvent,  $\text{CD}_3\text{NO}_2$ ; (c) alternating copolymer from butadiene and methacrylonitrile; upfield part of spectrum shown in Figure 1a; (d) random copolymer from butadiene and methacrylonitrile; fraction of monomeric unit corresponding to butadiene,  $m_B = 0.47$

exhibit a very much reduced  $\alpha$ - and  $\beta$ -deshielding effect<sup>7</sup>. Thus, the above mentioned additivity correlations should be applicable to some degree to nitrile substituted alkanes as well. In this way chemical shifts for  $\text{C}_4$ ,  $\text{C}_5$  and  $\text{C}_7$ , respectively, have been predicted in analogy to alkanes. Results are given in Table 1. The agreement is good even for  $\text{C}_6$  and  $\text{C}_8$ , which have been assigned independently from the non-decoupled spectrum in Figure 1b. With respect to the increased  $\gamma$ -shielding effect<sup>7</sup> the tendency of chemical shift of the carbon atoms  $\text{C}_1$  and  $\text{C}_2$  of the carbon double bond can be predicted by analogy to alkenes.

Thus, the assignment can be performed as shown in Figures 4 and 5. With respect to a particular carbon atom all signals of high intensity ( $\text{C}_1$  to  $\text{C}_8$ ) are assigned to pentads,  $\text{T-NT-NT}$  and  $-\text{NT-NT-N}$ , respectively. Signals of low intensity in Figures 4 and 5 indicate deviation from exact alternation and, therefore, have to be

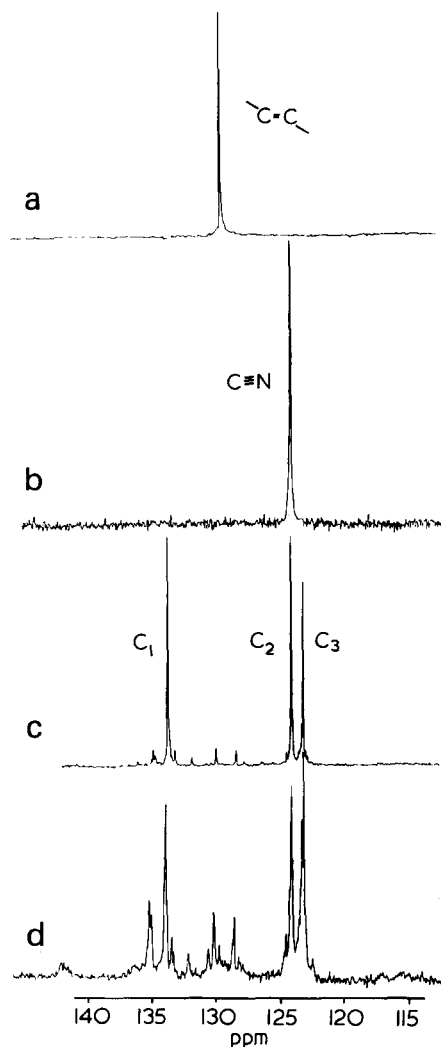
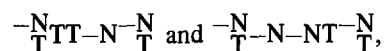


Figure 3  $^{13}\text{C}$  n.m.r. spectra of polybutadiene, polymethacrylonitrile and their copolymers. Resonance region of the carbon double bond and the nitrilic group. Spectra are continued from Figure 2. (a) *trans*-1,4-polybutadiene; (b) polymethacrylonitrile; (c) alternating copolymer; downfield part of spectrum shown in Figure 1a; (d) random copolymer

assigned to  $\text{TT-N}$  and  $-\text{N-NT}$ , respectively. The amount of deviation can be diminished by using only aluminium sesquichloride as catalyst. As a result, intensities of  $\text{TT-N}$ ,  $-\text{N-NT}$ , and hence their corresponding pentads



respectively, tend to zero. Pentad assignment will be discussed in a later paper<sup>8</sup> concerned with random copolymers from butadiene and methacrylonitrile.

#### Experimental

The alternating copolymer under study was prepared as described by Furukawa<sup>2,3</sup>. The copolymerization was carried out at  $0^\circ\text{C}$  in *n*-hexane using ethyl aluminium dichloride and  $\text{VOCl}_3$  as a catalyst. Additionally, an alternating copolymer was prepared using only aluminium sesquichloride as a catalyst. This copolymerization was carried out at  $-10^\circ\text{C}$ . The yield was 10 and 3%, respectively.

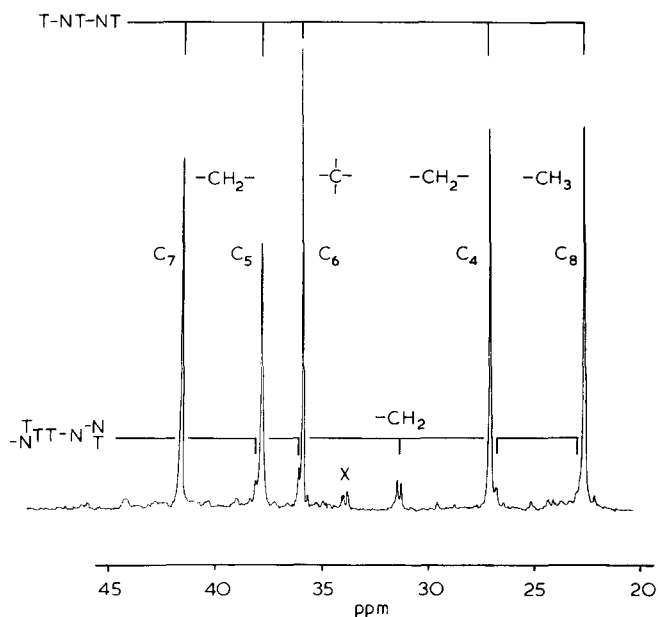


Figure 4  $^{13}\text{C}$  n.m.r. spectrum of an alternating copolymer. Monomeric units correspond to *trans*-1,4-butadiene and methacrylonitrile. Enlarged spectrum according to Figure 2c. Resonances of aliphatic carbons. X = sequence T-N-NT-N, non-protonated carbon

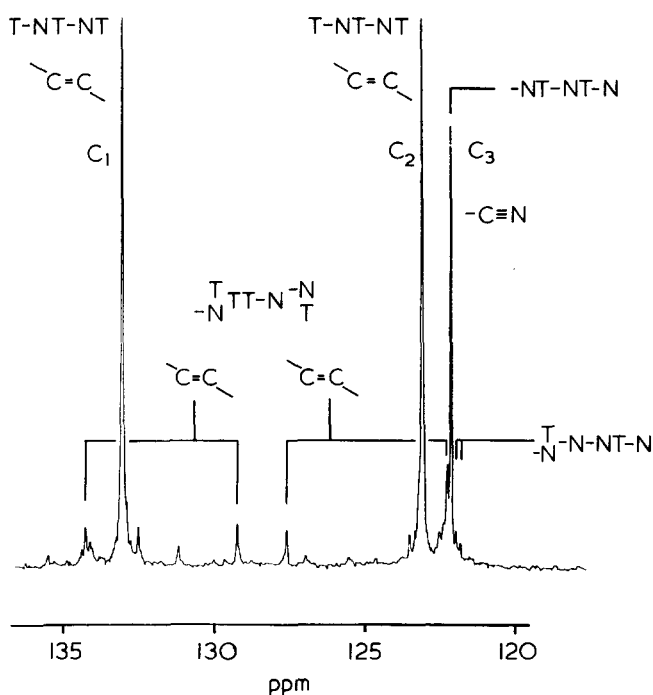


Figure 5  $^{13}\text{C}$  n.m.r. spectrum of an alternating copolymer. Enlarged spectrum according to Figure 3c. Resonances of the carbon double bond and the nitrilic group

$^{13}\text{C}$  n.m.r. spectra of the polymer samples were obtained in  $\text{CDCl}_3$  at  $40^\circ\text{C}$  using a Bruker-Spectrospin HX 270 operating at 67.88 MHz. Unless otherwise indicated, the spectra have been proton-decoupled. The concentration of the polymer solution was 30% (w/v). Spectrometer settings were: sweep width, 12 kHz; pulse width, 35  $\mu\text{sec}$ ; pulse repetitions rate, 0.8 sec; transients, 8 K; data points of spectrum, 8 K. Internal standard was octamethyltetrasiloxane (OMTS) = 0 ppm.

#### Acknowledgements

The financial support of the Arbeitsgemeinschaft Industrieller Forschungsvereinigungen is gratefully acknowledged. The authors thank A. Kuppel for running the Debye-Scherrer diagrams.

K.-F. Elgert and B. Stützel

Institut für Makromolekulare Chemie,  
Universität Freiburg,  
D-78 Freiburg i. Br., West Germany

and Imre Forgó

Ciba - Geigy AG,  
CH-4002 Basel,  
Switzerland  
(Received 1 April 1975)

#### References

- 1 Elgert, K.-F., Quack, G. and Stützel, B. *Polymer* 1975, **16**, 154
- 2 Furukawa, J., Kobayashi, E., Iseda, Y. and Arai, Y. *Polym. J.* 1970, **1**, 442
- 3 Furukawa, J., Iseda, Y., Haga, K. and Kataoka, N. *J. Polym. Sci. (A-1)* 1970, **8**, 1147
- 4 Kobayashi, E., personal communication
- 5 Lindeman, L. P., and Adams, J. Q. *Analyt. Chem.* 1971, **43**, 1245
- 6 Dorman, D. E., Jautelat, M. and Roberts, J. D. *J. Org. Chem.* 1971, **36**, 2757
- 7 Pehk, T. and Lippmaa, E. *Org. Magn. Reson.* 1971, **3**, 679
- 8 Elgert, K.-F. and Stützel, B. *Makromol. Chem.* in preparation
- 9 Pino, P. *Fortschr. Hochpolym. Forsch.* 1966, **4**, 399
- 10 Inoue, Y., Koyama, K., Chujó, R. and Nishioka, A. *Makromol. Chem.* 1974, **175**, 277

#### Detection of tacticity in polypropylenimine by $^{13}\text{C}$ n.m.r.

Linear isotactic polypropylenimine, prepared by Saegusa's method<sup>1</sup> starting from L-alanine and using dimethyl sulphate at  $120^\circ\text{C}$  to polymerize the intermediate L-4-methyloxazoline, was found to have the expected three lines in its  $^{13}\text{C}\{^1\text{H}\}$  n.m.r. spectrum. With  $\text{D}_2\text{O}$  at  $60^\circ\text{C}$  as solvent these occur at 55.11 (CH), 53.75 ( $\text{CH}_2$ ) and 20.08 ppm ( $\text{CH}_3$ ) relative to TSP. The corresponding polymer made from DL-alanine has an almost identical spectrum (Figure 1a) but with the methine peak broadened and shifted very slightly upfield to 54.92 ppm. On adding sufficient concentrated hydrochloric acid to react with all the imine groups, the spectrum shown in Figure 1b is obtained. The methine resonance moves downfield by 0.77 ppm and splits into two equal peaks separated by 0.14 ppm; the methylene resonance moves upfield by 4.11 ppm and splits into three peaks covering a range of 0.37 ppm and in intensity ratio 1:2:1; and the methyl resonance also moves upfield (by 2.83 ppm) and splits into two approximately equal peaks separated by 0.28 ppm. Addition of some of the isotactic polymer to this solution causes the peaks labelled *m* or *mm* to increase in intensity. The polymer made from the racemic monomer

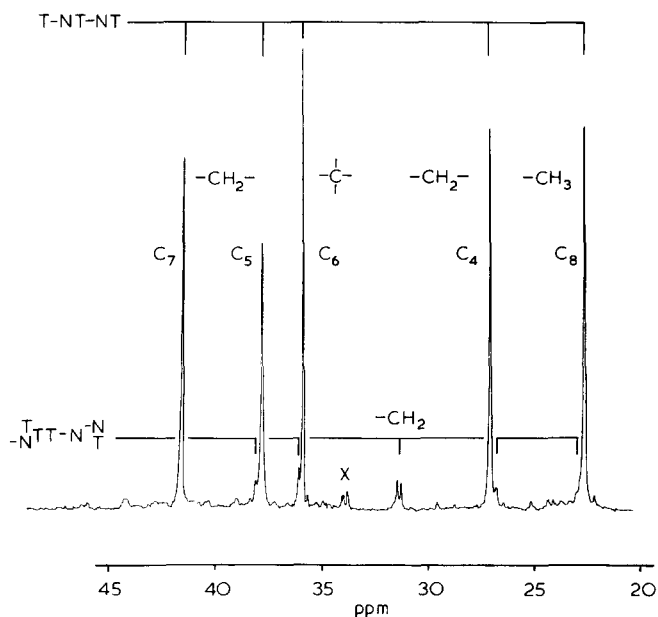


Figure 4  $^{13}\text{C}$  n.m.r. spectrum of an alternating copolymer. Monomeric units correspond to *trans*-1,4-butadiene and methacrylonitrile. Enlarged spectrum according to Figure 2c. Resonances of aliphatic carbons. X = sequence T-N-NT-N, non-protonated carbon

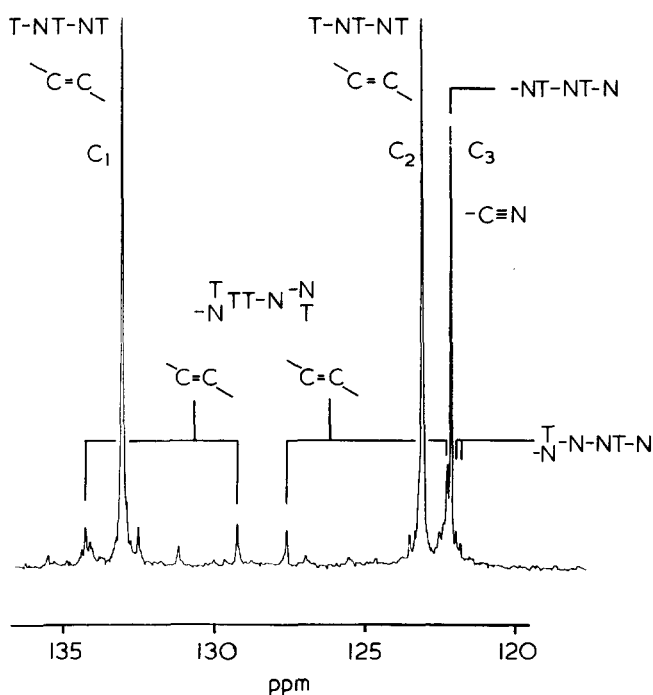


Figure 5  $^{13}\text{C}$  n.m.r. spectrum of an alternating copolymer. Enlarged spectrum according to Figure 3c. Resonances of the carbon double bond and the nitrilic group

$^{13}\text{C}$  n.m.r. spectra of the polymer samples were obtained in  $\text{CDCl}_3$  at  $40^\circ\text{C}$  using a Bruker-Spectrospin HX 270 operating at 67.88 MHz. Unless otherwise indicated, the spectra have been proton-decoupled. The concentration of the polymer solution was 30% (w/v). Spectrometer settings were: sweep width, 12 kHz; pulse width, 35  $\mu\text{sec}$ ; pulse repetitions rate, 0.8 sec; transients, 8 K; data points of spectrum, 8 K. Internal standard was octamethyltetrasiloxane (OMTS) = 0 ppm.

#### Acknowledgements

The financial support of the Arbeitsgemeinschaft Industrieller Forschungsvereinigungen is gratefully acknowledged. The authors thank A. Kuppel for running the Debye-Scherrer diagrams.

K.-F. Elgert and B. Stützel

Institut für Makromolekulare Chemie,  
Universität Freiburg,  
D-78 Freiburg i. Br., West Germany

and Imre Forgó

Ciba - Geigy AG,  
CH-4002 Basel,  
Switzerland  
(Received 1 April 1975)

#### References

- 1 Elgert, K.-F., Quack, G. and Stützel, B. *Polymer* 1975, **16**, 154
- 2 Furukawa, J., Kobayashi, E., Iseda, Y. and Arai, Y. *Polym. J.* 1970, **1**, 442
- 3 Furukawa, J., Iseda, Y., Haga, K. and Kataoka, N. *J. Polym. Sci. (A-1)* 1970, **8**, 1147
- 4 Kobayashi, E., personal communication
- 5 Lindeman, L. P., and Adams, J. Q. *Analyt. Chem.* 1971, **43**, 1245
- 6 Dorman, D. E., Jautelat, M. and Roberts, J. D. *J. Org. Chem.* 1971, **36**, 2757
- 7 Pehk, T. and Lippmaa, E. *Org. Magn. Reson.* 1971, **3**, 679
- 8 Elgert, K.-F. and Stützel, B. *Makromol. Chem.* in preparation
- 9 Pino, P. *Fortschr. Hochpolym. Forsch.* 1966, **4**, 399
- 10 Inoue, Y., Koyama, K., Chújó, R. and Nishioka, A. *Makromol. Chem.* 1974, **175**, 277

#### Detection of tacticity in polypropylenimine by $^{13}\text{C}$ n.m.r.

Linear isotactic polypropylenimine, prepared by Saegusa's method<sup>1</sup> starting from L-alanine and using dimethyl sulphate at  $120^\circ\text{C}$  to polymerize the intermediate L-4-methyloxazoline, was found to have the expected three lines in its  $^{13}\text{C}\{^1\text{H}\}$  n.m.r. spectrum. With  $\text{D}_2\text{O}$  at  $60^\circ\text{C}$  as solvent these occur at 55.11 (CH), 53.75 ( $\text{CH}_2$ ) and 20.08 ppm ( $\text{CH}_3$ ) relative to TSP. The corresponding polymer made from DL-alanine has an almost identical spectrum (Figure 1a) but with the methine peak broadened and shifted very slightly upfield to 54.92 ppm. On adding sufficient concentrated hydrochloric acid to react with all the imine groups, the spectrum shown in Figure 1b is obtained. The methine resonance moves downfield by 0.77 ppm and splits into two equal peaks separated by 0.14 ppm; the methylene resonance moves upfield by 4.11 ppm and splits into three peaks covering a range of 0.37 ppm and in intensity ratio 1:2:1; and the methyl resonance also moves upfield (by 2.83 ppm) and splits into two approximately equal peaks separated by 0.28 ppm. Addition of some of the isotactic polymer to this solution causes the peaks labelled *m* or *mm* to increase in intensity. The polymer made from the racemic monomer

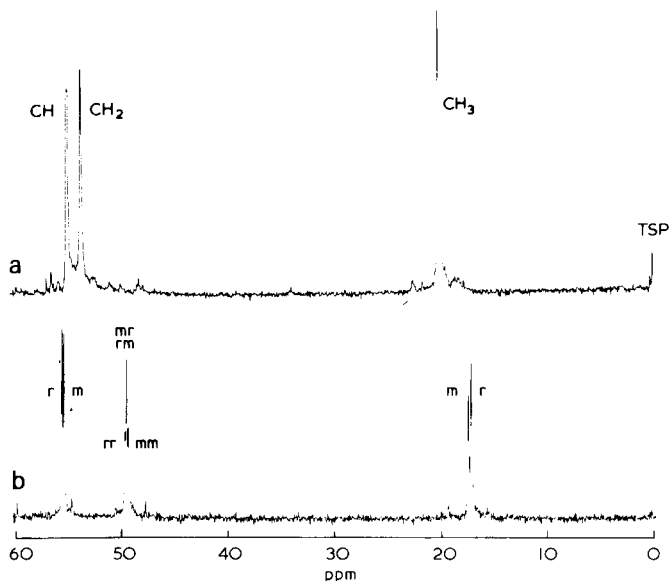
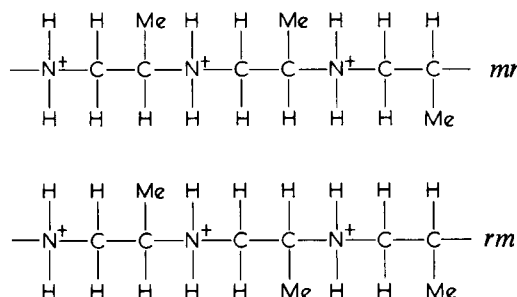


Figure 1  $^{13}\text{C}\{^1\text{H}\}$  n.m.r. spectra (22.63 MHz) of (a) atactic polypropylenimine in  $\text{D}_2\text{O}$  at  $60^\circ\text{C}$ , and (b) with added concentrated hydrochloric acid. 28 000 scans in each case. Sweep width 2000 Hz. Reference signal, TSP (sodium trimethylsilyl-1-propane sulphonate). The assignment for (a) was made by an off-resonance experiment. The line order  $\text{CH} > \text{CH}_2 > \text{CH}_3$  is the same for (b)

is thus atactic, with equal proportions of the four possible triads, which may be labelled *mm* (isotactic), *mr*, *rm* (heterotactic), *rr* (syndiotactic), where *m* denotes that adjacent methyl groups in the Fischer projection structure are written on the same side of the chain, and *r* denotes that they are written on the opposite side of the chain. (The terms meso and racemic are not strictly applicable to such a chain although the letters *m* and *r* can be retained with the above meaning.)

It should be noted that the two heterotactic structures *mr* and *rm* are not identical



One cannot say, without use of model compounds, to which *m* and *r* dyad peaks the centre methine and methyl carbons contribute in each case. A similar situation exists for poly(propylene sulphide)<sup>2</sup>. The line order for the two downfield methylene peaks, *rr*, (*rm*, *mr*), is assumed by analogy with many other polymers. The line order for the CH *r* and *m* shifts is evidently reversed by the addition of HCl.

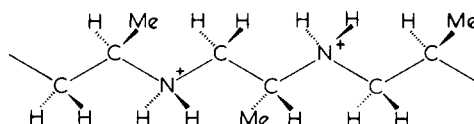
The shifts caused by the addition of acid, known as titration shifts<sup>3</sup>, are to be interpreted in terms of electric field effects and conformational changes. In primary amines the shifts are usually upfield, partly as a result of the greater polarizability of C—H bonds compared with C—C bonds<sup>3</sup>. Each carbon atom in the polymer will be subject to electric field effects from two adjacent  $\text{NH}_2^+$  groups as well as from more distant parts of the chain. The net effect of nearest

Table 1 Titration shifts<sup>3</sup>  $\delta$  (ppm upfield) for  $\text{RNH}_2 \rightarrow \text{RNH}_3^+$  compared with the observed shifts for  $[\text{CH}_2\text{CH}(\text{CH}_3)\text{NH}]_n$

Polymer	Model compound	$\delta$	Sum	Observed
CH	$(\text{CH}_3)_2\text{CHNH}_2$	-2.36	2.46	-0.77
	$\text{CH}_3\text{CH}_2\text{CH}_2\text{NH}_2$	4.82		
CH <sub>2</sub>	$\text{CH}_3\text{CH}_2\text{CH}_2\text{NH}_2$	1.44	5.90	4.11
	$(\text{CH}_3)_2\text{CHNH}_2$	4.46		
CH <sub>3</sub>	$(\text{CH}_3)_2\text{CHNH}_2$	4.46	5.02	2.83
	$\text{CH}_3\text{CH}_2\text{CH}_2\text{NH}_2$	0.56		

neighbours is less than the sum of the individual effects in the primary amines (see Table 1), as might be expected, but the relative order of magnitude of the shifts ( $\text{CH} < \text{CH}_3 < \text{CH}_2$ ) is the same. In the polymer it appears that the shift caused by the  $\beta\text{-NH}_2^+$  group is only about half that in the corresponding primary amine.

A further effect may result from electrostatic repulsion of adjacent  $\text{NH}_2^+$  groups in the polymer, which will lead to a change in the proportion of *gauche* interactions suffered by the different carbon atoms. Thus if we write the isotactic chain in its fully extended form:



we see that the gamma-interactions to left and right of each carbon atom are as follows: methine (*t*; *t*); methylene (*t*, *g*; *t*); methyl (*g*; *g*). Hence stiffening of the chains will cause: (a) an increase in *gauche* interactions for methyl carbons, which may be expected to result in an additional upfield shift; and (b) a decrease in *gauche* interactions for the methine carbons, resulting in an additional downfield shift. The fine structure for each carbon resonance presumably results from subtle variations of this conformational effect with the tacticity.

#### Acknowledgements

We thank Dr I. A. Stenhouse and Mr M. W. Cooper, PCMU Harwell, for the spectra; also the Science Research Council for financial support.

J. G. Hamilton, K. J. Ivin,  
L. C. Kuan-Essig and P. Watt

Department of Chemistry,  
Queen's University of Belfast,  
Belfast BT9 5AG, UK  
(Received 19 May 1975; revised 16 June 1975)

#### References

- 1 Saegusa, T., Kobayashi, S. and Ishiguro, M. *Macromolecules* 1974, 7, 958
- 2 Boileau, S., Cheradame, H., Lapeyre, W., Sousselier, L. and Sigwalt, P. *J. Chim. Phys.* 1973, 70, 879
- 3 Batchelor, J. G., Feeney, J. and Roberts, G. C. K. *J. Magn. Reson.* in press

## Solvent effect on the unperturbed dimensions of poly(aryl isocyanates)

### Introduction

The conformation and the rigidity of poly (*n*-alkyl isocyanate) molecules in solution have been investigated by various physical methods<sup>1-5</sup>. Although there are some significant qualitative differences among the data reported, all these studies are in agreement concerning the high degree of rigidity of these chains. However, the precise origin of this high rigidity is still uncertain.

Considerably less attention has been given to the study of poly (aryl isocyanates); some dynamo-optical and electro-optical data reports by Tsetkov<sup>6</sup> on an unfractionated sample of poly(4-methylphenyl isocyanate) leads us to believe that the conformation of this polymer is quite different from that of the polymers with aliphatic side chains.

In order to shed some light on the problem of the conformation of the polyisocyanates, we are actually carrying out a systematic investigation on the hydrodynamic properties of both types of polymers. The present communication concerns essentially the study of the hydrodynamic properties of poly (4-methoxyphenyl isocyanate) (PMIC) and poly (4-methylphenyl isocyanate) (PTIC) in several solvents. The results clearly show that: (i) the replacement of the aliphatic side chain by an aromatic one induces an important decrease in the rigidity of the main chain; and (ii) the two-parameter theory does not strictly apply to the aromatic polymers i.e., the unperturbed dimensions of the chains strongly depend on the nature of the solvents.

### Experimental

Polymers were synthesized by the method of Shashoua<sup>7</sup> with DMF as solvent and NaCN as catalyst at the initial temperature of  $-58^{\circ}\text{C}$ . They were fractionated by the precipitation technique using  $\text{CH}_2\text{Cl}_2$  as solvent and heptane as non-solvent. The fractions were analysed by gel permeation chromatography. They exhibit a polydispersity of 1.2–1.4.

Viscosity measurements were carried out at  $25^{\circ}\text{C}$  in Desreux–Bischoff suspended level dilution viscometers and as a function of temperature with a new type of sealed capillary viscometer<sup>8</sup>.

Light scattering measurements were performed at  $25^{\circ}\text{C}$  in  $\text{CHCl}_3$  and  $\text{C}_6\text{H}_5\text{Cl}$  with a standard Sofica diffusometer using vertically polarized light ( $\lambda = 5460 \text{ \AA}$ ).

Sedimentation coefficients of some fractions of both polymers were determined in  $\text{C}_6\text{H}_5\text{Cl}$  at  $25^{\circ}\text{C}$  using a Spinco Model E ultra-centrifuge.

### Results

The temperature dependence of limiting viscosity numbers of solutions of PMIC in  $\text{CHCl}_2\text{CHCl}_2$  ( $10\text{--}80^{\circ}\text{C}$ ),  $\text{CHCl}_3$  ( $10\text{--}55^{\circ}\text{C}$ ) and  $\text{C}_6\text{H}_5\text{Cl}$  ( $10\text{--}80^{\circ}\text{C}$ ) does not show any anomaly as is the case for polymers with aliphatic side groups<sup>9</sup>.

The relationships between the intrinsic viscosity and the molecular weight were obtained over a wide range of molecular weight (80 000 to 1 500 000 for PMIC and 150 000 to 1 100 000 for PTIC). The  $K$  and  $a$  values for the Mark–Houwink relations are given in *Table 1* and are quite different from those reported for poly (alkyl isocyanates)<sup>1,2,4</sup>; they are characteristic of flexible polymers.

The Flory constants  $K_{\theta}$  were evaluated by plotting the data at  $25^{\circ}\text{C}$  according to the treatments of Kurata–Stockmayer–Roig, Burchard–Stockmayer–Fixman (BSF), Inagaki–Suzuki–Kurata and Cowie. As an example the BSF plot for PMIC is shown in *Figure 1*; this relation fits satisfactorily our data for each solvent. The four extrapolation methods lead almost to the same  $K_{\theta}$  value for each solvent considered separately, but the values are different from one solvent to another.

The  $K_{\theta}$  values and the corresponding characteristic ratios  $A$  or  $(\langle r_0^2 \rangle / M)^{1/2}$  obtained from the well-known Flory relation are given in *Table 1*. A few characteristic ratios obtained by light scattering and sedimentation, using the Baumann<sup>11</sup> (*Figure 2*) and Cowie–Bywater<sup>12</sup> treatments are also given in this Table. In the calculation of the ratios, the theoretical limiting value of the Flory universal parameter  $\Phi$  was chosen and appropriate heterogeneity corrections were made<sup>10,13</sup>. The characteristic ratios obtained by these different methods are in good agreement with each other and their magnitude is of the expected order for polymers with flexible chain.

### Discussion

In conflict with the two-parameter theory for polymer solutions, the influence of the solvent on the unperturbed dimensions has already been reported several times<sup>10,14</sup>.

Analysing the literature data for polyvinyl chains, Donos and Benoit<sup>15</sup> have recently shown that small variations of  $K_{\theta}$  with the nature of solvent are found for this type of

*Table 1*  $K$  and  $a$  values of the Mark–Houwink relations,  $K_{\theta}$  and characteristic ratios  $A$  for PMIC and PTIC in several solvents at  $25^{\circ}\text{C}$  1,3- $\text{Cl}_2\text{C}_6\text{H}_4$  = *m*-dichlorobenzene;  $\text{C}_6\text{H}_{10}\text{O}$ : cyclohexanone

Polymer	Solvent	$K \times 10^5$ (dl/g)	$a$	Viscosity		$A \times 10^{11}$ (cm/mol <sup>1/2</sup> )	
				$K_{\theta} \times 10^5$ (dl/g)	$A \times 10^{11}$ (cm/mol <sup>1/2</sup> )	Light scattering	Sedimentation
PMIC	$\text{CHCl}_2\text{CHCl}_2$	22.0	0.68	124	765	—	—
	$\text{CHCl}_3$	14.7	0.69	87	675	665	—
	$\text{CH}_2\text{ClCH}_2\text{Cl}$	13.5	0.67	72	640	—	—
	$\text{CH}_2\text{Cl}_2$	11.4	0.69	72	640	—	—
	$\text{C}_6\text{H}_5\text{Cl}$	44.1	0.53	57	595	590	630
PTIC	$\text{CHCl}_3$	12.4	0.73	120	755	765	—
	$\text{C}_6\text{H}_5\text{Cl}$	18.3	0.66	108	730	—	730
	$\text{CH}_2\text{Cl}_2$	10.2	0.72	86	670	—	—
	1,3- $\text{Cl}_2\text{C}_6\text{H}_4$	14.0	0.68	86	670	—	—
	$\text{C}_6\text{H}_{10}\text{O}$	13.4	0.66	70	640	—	—
	THF	9.6	0.69	65	615	—	—



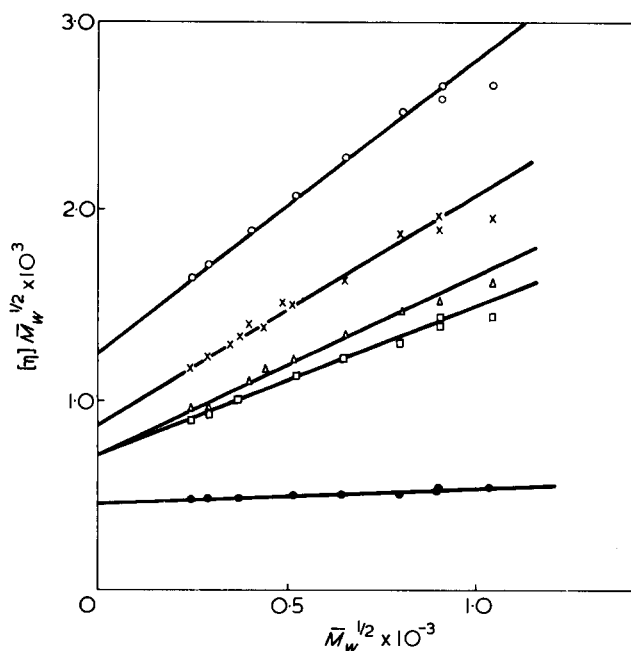


Figure 1 Burchard-Stockmayer-Fixman plot for PMIC in several solvents at 25°C. ○, CHCl<sub>2</sub>CHCl<sub>2</sub>; X, CHCl<sub>3</sub>; △, CH<sub>2</sub>Cl<sub>2</sub>; □, CH<sub>2</sub>ClCH<sub>2</sub>Cl; ●, C<sub>6</sub>H<sub>5</sub>Cl

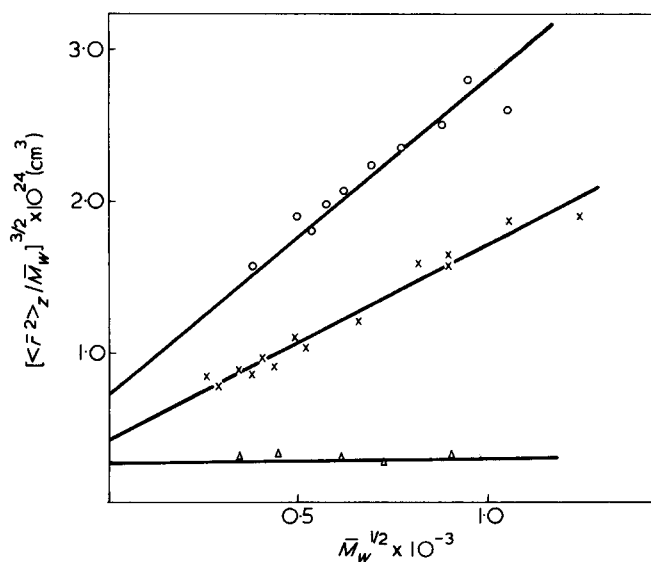


Figure 2 Baumann plot to estimate unperturbed dimensions at 25°C. ○, PTIC in CHCl<sub>3</sub>; X, PMIC in CHCl<sub>3</sub>; △, PMIC in C<sub>6</sub>H<sub>5</sub>Cl.

flexible polymer when polar side groups interact with solvent molecules. In this connection, it is important to point out that the experimental data are not always very precise and their comparison is often rather hazardous, except when they have been obtained under identical conditions (temperature, sample preparation, experimental procedure . . .).

In 1961, Ivin *et al.*<sup>16</sup> in a study of the solution properties of poly (hexene-1-sulphone) expressed the hypothesis that the solvent effect on the unperturbed dimensions might be particularly important in the case of polymers with polar groups in their main chains; important variations of  $K_\theta$  have been reported for such polymers: poly (propylene

sulphide)<sup>17</sup>, poly (ethylene oxide)<sup>18</sup>, polytetrahydrofuran<sup>19</sup> amylose derivatives<sup>20</sup>.

The solvent effect in the case of the poly (aryl isocyanates) is also fairly great since the ratios of the extreme  $K_\theta$  values equal two; from this point of view, the behaviour of these polymers is quite different from that of common flexible polymers such as polymethacrylates.

This influence of the solvent on the  $K_\theta$  values of poly (aryl isocyanates) is very likely due to interactions between the solvent molecules on the one hand, the aromatic side chains and especially the carbonyl groups of the backbone on the other hand. A correlation between the  $K_\theta$  values and some physical properties of solvents is rather difficult to find; several parameters have been considered, such as internal cohesive density, dielectric constant, but without success when solvents of different chemical nature are considered. Yet, the  $K_\theta$  values for PMIC and PTIC dissolved in aliphatic chlorinated solvents increase regularly with the molar volume or the molar refraction of these solvents (Figure 3); the increase in the unperturbed dimensions is probably due to the steric hindrance of the backbone motions resulting from the solvation of the carbonyl groups.

The infra-red spectra bring complementary data; contrary to what is observed in the case of the poly(n-alkyl isocyanates), we have found that the carbonyl absorption band of the poly(aryl isocyanates) can be resolved into several components, the relative intensities of which depend on the particular solvent considered. Moreover, the complexity of this band decreases in solvents where high  $K_\theta$  values are obtained, namely CHCl<sub>3</sub> and CHCl<sub>2</sub>CHCl<sub>2</sub>. Recently, Volchek and Nikitin<sup>21</sup> reported a difference between the i.r. spectra of poly(n-butyl-) and poly(n-methylphenyl isocyanates) in CHCl<sub>3</sub> as in solid state. They attributed the complexity of the carbonyl vibration band in the case of PTIC to the existence of rotational isomers associated with the possibility of rotation about the C-N bond. In this hypothesis, a change in the degree of the main chain flexibility should involve a redistribution of the intensities of the band components. This is supported by our results for PMIC and PTIC in several solvents.

Lastly, from the study of the dielectric properties of PMIC and PTIC solutions<sup>22</sup>, we may discard the hypothesis that the increased rigidity of these polymers in some solvents might be due to short rigid sequences [as in poly(n-alkyl isocyanates)] statistically distributed in a more flexible backbone.

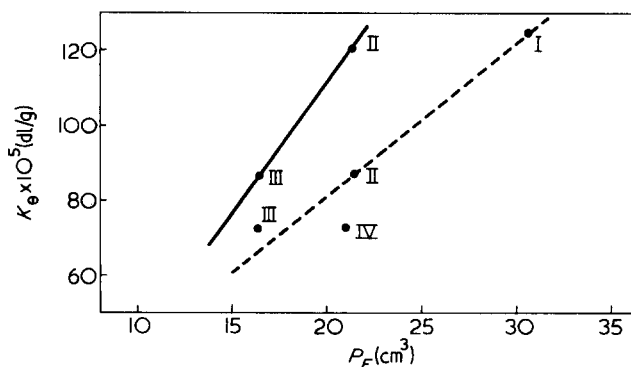


Figure 3  $K_\theta$  dependence on the electronic polarizability of the solvent; —, PTIC; - - -, PMIC; I, CHCl<sub>2</sub>CHCl<sub>2</sub>; II, CHCl<sub>3</sub>; III, CH<sub>2</sub>Cl<sub>2</sub>; IV, CH<sub>2</sub>ClCH<sub>2</sub>Cl

### Conclusion

In conclusion, if the aromatic polyisocyanates may be considered as flexible polymers, their hydrodynamic behaviour is nevertheless quite different, the solvent effect being important; the presence in the main chain of polar groups reacting with the solvent molecules is very probably an important factor of the  $K_\theta$  variations; the series of chlorinated aliphatic solvents still containing one or more hydrogen atoms ( $\text{CCl}_4$  and  $\text{Cl}_2\text{C}=\text{CCl}_2$  are non-solvent) is particularly interesting, the corresponding solutions of the aromatic polyisocyanates being characterized by practically the same exponent  $a$  of the Mark-Houwink relation. These observations raise once more the question of the exact meaning of the  $K_\theta$  values for polymers strongly interacting with the solvent molecules and of the corresponding unperturbed dimensions.

Investigations on low molecular weight samples would probably clarify these problems as well as the determination of the  $K_\theta$  values in pure  $\theta$  solvents.

L. Lecomte and V. Desreux

Laboratoire de Chimie Physique,  
Université de Liège,  
B 4000 Liège, Belgium  
(Received 7 July 1975)

### References

- Burchard, W. *Makromol. Chem.* 1963, **67**, 182
- Schneider, N. S., Furusaki, S. and Lenz, R. W. *J. Polym. Sci. (A)* 1963, **1**, 933
- Bur, A. J. and Roberts, D. E. *J. Chem. Phys.* 1969, **51**, 406
- Berger, M. N. *J. Macromol. Sci. (C)* 1973, **9**, (2), 269
- Tsetkov, V. N. *et al. Eur. Polym. J.* 1975, **11**, 37
- Tsetkov, V. N. *et al. Vysokomol. Soedin. (A)* 1968, **10**, 2132
- Shashoua, V. E., Sweeny, W. and Tietz, R. F. *J. Am. Chem. Soc.* 1960, **82**, 866
- to be published
- Pierre, J. and Desreux, V. *Polymer* 1974, **15**, 685
- Kurata, M. and Stockmayer, W. H. *Adv. Polym. Sci.* 1961, **3**, 196
- Baumann, M. *J. Polym. Sci. (B)* 1965, **3**, 1069
- Cowie, J. M. G. and Bywater, S. *Polymer* 1965, **6**, 197
- Gouinlock, E. V., Flory, P. J. and Scheraga, H. A. *J. Polym. Sci.* 1955, **16**, 383
- Moore, W. R. 'Progress in Polymer Science', Pergamon Press, London, 1967, Vol I
- Dondos, A. and Benoit, H. *Macromolecules* 1971, **4**, 279
- Ivin, K. J., Ende, H. A. and Meyerhoff, G. *Polymer* 1962, **3**, 129
- Nash, D. W. and Pepper, D. C. *Polymer* 1975, **16**, 105
- Beech, D. R. and Booth, C. *J. Polym. Sci. (A-2)* 1969, **7**, 575
- Kurata, M., Utiyama, H. and Kamada, K. *Makromol. Chem.* 1966, **88**, 281
- Bohdanecky, M. *J. Polym. Sci. (B)* 1965, **3**, 201
- Volchek, B. Z. and Nikitin, V. N. *Dokl. Akad. Nauk. SSSR* 1972, **205**, 622
- Lecomte, L. and Marchal, E. to be published

# SCIENCE & PUBLIC POLICY

the international journal of the Science Policy Foundation

current awareness for busy people in

**government · industry · business ·  
education · research**

#### SCIENCE & PUBLIC POLICY

- provides information on national policies for science and technology and their effects
- examines the roles of science and technology in the operations of government (local, national and international), industry and business
- analyses the social and political environments within which science and technology operate
- assesses appropriate methodologies, information systems and organisational forms
- explores various types of public participation and their influence on national and international policies

The journal contains short, pithy news items, concise reports, comment, commissioned reviews, facts in figures, book reviews and extensive bibliographies.

The information is gathered through a worldwide network of national correspondents who are intimately involved in researching and applying science and public policy in their country.

Subscription £25.00 (\$65.00) per year (12 issues) including postage by fastest route. A special annual rate of £10.00 (\$26.00) is available for the individual who certifies that the copies are for his/her personal use and who is the full-time employee of a current full-price establishment subscriber at the same address.

**IPC Business Press Ltd, Oakfield House, Perrymount Road,  
Haywards Heath, Sussex, England**

*Published monthly by IPC Science and Technology Press Ltd:  
publishers of FUTURES, ENERGY POLICY and RESOURCES  
POLICY.*

# Book Reviews

## Adhesive bonding

J. Shields

Oxford University Press, London (for Design Council of BSI and CEI). 1974, 24 pp. £1.00

This book is one of a series intended for 'engineering designers' and is particularly intended to introduce them to the scope and application of adhesive materials and processes.

It certainly gives a very wide and informative review of adhesive types but the balance, considering the intended audience, is surprising. The various adhesives for the manufacture of plywood and their durability are discussed fully. The range of thermosetting adhesives, which are those of major importance for structural engineering, is somewhat limited and the account of their properties does less than justice to their significance. One is particularly struck by the paucity of detail on the various types of adhesive involving epoxides.

The review of the geometry on the various types of adhesive involving epoxide joints, their features, and consequent strengths is very good and clear. It should leave a designer in no doubt about some of the less immediately obvious stress patterns and their consequences.

The bibliography is one of the weaker features. It contains only 20 references up to fourteen years old and omitting direct reference to some of the most useful general monographs although including several rather elementary and superficial tests.

The style and presentation is very satisfactory but because of the amount which is included within small compass it necessarily demands careful reading.

At contemporary prices it is very reasonable value and in spite of its shortcomings represents a useful contribution to the review literature in this area.

K. W. Allen

## Molecular behaviour and the development of polymeric materials

Edited by A. Ledwith and A. M. North

Chapman and Hall, London. 1975. £12.00

This book has been prepared in commemoration of the work of Professor C. E. H. Bawn (an Editor of *Polymer* since its inception in 1960 and formerly of the University of Liverpool), who retired in 1973, and indeed the eminence of the contributors and the effort which has been put into its production is a remarkable tribute to one to whom the world of polymers owes so much.

The opening chapters deal more specifically with the chemistry of polymerization processes, the roles of Ionic intermediates and of Radical intermediates being treated respectively by M. Szwarc and C. M. Bamford, while the subject of Transition metal catalysts for olefin polymerization is examined by D. G. H. Ballard. This leads on to two chapters dealing with elastomers, the first by E. W. Duck, which is concerned primarily with butadiene-based polymers, and the next by W. Cooper, of more general scope. Each of these considers industrial developments in a historical setting and examines the progress made in achieving desirable physical characteristics. The production and properties of polyolefins are systematically examined in a chapter by P. A. Small, the emphasis here being more on the relation between physical properties and morphology, while the class of materials known as polyurethanes, which are in many respects more versatile than other types of polymers, is comprehensively surveyed from both chemical, physical, and industrial standpoints by C. Hepburn and R. J. W. Reynolds in the following chapter.

Further primarily chemical topics included are Chemical reactions on polymeric fibre surfaces (H. N. Friedlander and V. Menikheim) which has important practical applications, particularly in connection with bond formation, and Catalytic applications of synthetic polymers (A. Ledwith and D. C. Sherrington).

Later chapters contain valuable reviews of structure and mor-

phology as well as of associated techniques of investigation. Applications of X-ray diffraction are surveyed broadly by C. W. Bunn, while A. M. North, in a penetrating article, discusses the fundamentals of molecular motion in polymers as revealed by mechanical and dielectric relaxation phenomena. This is followed by a critical discussion of the glassy state, including the controversial question of the physical interpretation of the glass transition, by R. N. Haward. Closely related to this is the chapter on the Microstructure and properties of polymers, as revealed by ingenious experimental techniques, by D. Hull. The concluding chapter by H. Block grapples with the difficult but potentially important question of the reduction of turbulent drag by polymers.

This brief summary of its contents is necessarily inadequate, and fails to do justice to this stimulating work, which is marked throughout by careful selection of material and lively presentation. It is reliable, informative, and a pleasure to read.

L. R. G. Treloar

## The role of additives in plastics

L. Mascia

Arnold, London, 1974. 172 pp. £4.00

A report on a recent meeting of the Polymer Properties Group of the Plastics Institute (*Plastics and Polymers* 1975, 43, 6) reads '... the full effect of making additions of materials such as plasticizers, process aids and fillers to polymers was only partly understood and in only a few cases had it been studied to any depth. Little recent work appeared to have been published'. With this statement in mind the present book was received with considerable interest for it was felt that the author had wisely selected an area which well merited attention. The book is written so as to deal with a wide range of additives in plastics compositions and to this extent he does much to meet this. It is devoted to theory rather than practice, presenting a background of the principles involved.

After a general introduction dealing with types of additives employed in service, compatibility, mixing, hazards, and electrical properties, five chapters deal respectively with: processing aids; plasticizers, fillers and reinforcing materials; additives to modify surface colour, and optical properties; and resistance to ageing. The final chapter relates to the use of blowing agents and fire retardants. Over a third of the book (chapter 3) discusses in some detail the mechanical properties of polymers and their modification by plasticizers and the use of fibrous or particulate additions, considerable attention being given to the rheological and materials engineering principles involved. Elsewhere the treatment is less uniform or detailed; sometimes (e.g. on test methods) it is perhaps barely adequate, although one appreciates the limitations imposed by space in a book of only some 170 pages.

References to relevant literature are given at the end of each chapter and in this respect the reader has guidance to a number of useful publications. Unfortunately the text is not always easy to follow and a serious criticism is the inexcusable number of vagaries or errors in the print. These are far too numerous to detail here but, for example, we read on p 5, 'i.e.  $\Delta FM$  must be negative or  $\Delta FM$  positive'; Table 2.1 omits the butyl groups in the chemical formula for Santowhite, and gives a grouping as 'di-tibutyl'; Table 2.1 (p 25) should read Table 2.3; oxirane is given as 'oxyrane' (p 30); some errors occur in the references for Chapter 3: R. A. Horsely should read R. A. Horsley, F. R. Einrich should be F. R. Eirich and the relevant page number in Gordon's book is 114, not 14. In the index (which is comprehensive and useful) one is surprised to read 'Arrhenius plot' and an incorrect page number given (on p 22 the spelling is Arrhanus). Many of the errors are of a minor nature but serve to undermine confidence in the reliability of other parts of the text.

However, despite these faults the book is a brave attempt to deal with a diverse and often difficult subject in a uniform manner and it can be a useful introduction to some aspects of polymer science and technology which are often regarded as empirical.

R. J. W. Reynolds

# Copolymerization behaviour of $N,N'$ – divinylureas

G. C. Corfield and H. H. Monks

Department of Chemistry and Biology, Sheffield Polytechnic, Sheffield S1 1WB, UK

and L. P. Ellinger

The British Petroleum Company Limited, Research and Development Department, Epsom, Surrey, UK

(Received 14 May 1975; revised 23 June 1975)

Copolymerizations of 1,3-divinylimidazolid-2-one (DVI), 1,3-divinylhexahydropyrimid-2-one (DVHHP) and 1-ethyl-3-vinylimidazolid-2-one (EVI) with ethyl acrylate (EA) have been carried out and reactivity ratios determined. For DVI-EA,  $r_1 = 0.090$ ,  $r_2 = 0.388$ ; DVHHP-EA,  $r_1 = 0.137$ ,  $r_2 = 0.549$ ; EVI-EA,  $r_1 = 0.094$ ,  $r_2 = 0.530$ . The  $Q$  and  $e$  values for these  $N$ -vinylureas have been calculated. 1,3-Diphenyl-1,3-divinylurea inhibits or retards the polymerization of other monomers. The results support the proposal that the  $N,N'$ -divinylureas are highly conjugated molecules.

## INTRODUCTION

The homopolymerization of a number of  $N,N'$ -divinylureas has been reported in earlier papers<sup>1,2</sup>. 1,3-Divinylimidazolid-2-one (DVI) and 1,3-divinylhexahydropyrimid-2-one (DVHHP) gave insoluble crosslinked polymers not cyclopolymers and 1,3-diphenyl-1,3-divinylurea (DPDVU) could not be polymerized under a variety of conditions. These results were attributed to the continuous overlap of  $\pi$  orbitals of the vinyl and carbonyl groups with  $p_z$  orbitals on the nitrogen atoms.

As a means of gaining further information on the nature and reactivity of  $N,N'$ -divinylureas and the radicals produced from them, a number of copolymerization studies have been carried out.

## COPOLYMERIZATION OF $N$ -VINYLUREAS WITH ETHYL ACRYLATE

The copolymer composition equation is used to determine the reactivity ratios and  $Q$  and  $e$  parameters for the copolymerization of DVI, DVHHP and 1-ethyl-3-vinylimidazolid-2-one (EVI) with ethyl acrylate.

Mixtures of the  $N$ -vinylureas and ethyl acrylate in benzene were copolymerized to low conversions using azobisisobutyronitrile as initiator. After precipitation

and purification, the copolymers were analysed for nitrogen content from which the  $N$ -vinylurea residues in the copolymer were calculated. Results are summarized in Table 1.

Beynon<sup>3,4</sup> investigated the copolymerization of difunctional monomers (diallyl phosphonates and diallylureas) with monofunctional comonomers using the normal form of the copolymerization equation (equation 1). He decided that this equation could be used if the two groups in the difunctional monomer were equivalent, whether or not both functional groups are involved in the polymerization. Thus, for the copolymerization of the  $N$ -vinylureas with ethyl acrylate equation (1) (and its derivatives) has been used for the determination of reactivity ratios:

$$\frac{d[M_1]}{d[M_2]} = \frac{[M_1]}{[M_2]} \cdot \frac{r_1[M_1] + [M_2]}{r_2[M_2] + [M_1]} \quad (1)$$

The reactivity ratios were calculated by computer<sup>5</sup> using the method of Fineman and Ross<sup>6</sup> and are given in Table 2.

The  $Q$  and  $e$  values<sup>7</sup> obtained for the  $N$ -vinylureas, using values of  $Q = 0.52$ ,  $e = 0.22$  for ethyl acrylate, are given in Table 3. The values obtained for some other  $N$ -vinyl monomers are included for comparison.

The reactivity ratios  $r_1$  and  $r_2$  for the copolymerization of all the  $N$ -vinyl monomers studied and ethyl acrylate were both less than one. In such cases there is a strong tendency to form alternating copolymers. The values of  $r_2$  are the reactivity ratios for ethyl acrylate relative to the  $N$ -vinyl-

Table 1 Copolymerization of  $N$ -vinylureas with ethyl acrylate

Mole fraction EA in feed	Mole fraction EA in copolymer with DVI	Mole fraction EA in copolymer with DVHHP	Mole fraction EA in copolymer with EVI
0.90	0.763	0.842	0.928
0.80	0.720	0.757	0.748
0.70	0.692	0.714	0.662
0.60	0.637	0.687	0.631
0.50	0.640	0.639	0.608
0.40	0.613	0.632	0.568
0.30	0.595	0.597	0.531
0.20	0.592	0.588	0.512
0.10	0.562	0.456	0.519

Table 2 Reactivity ratios for copolymerization of  $N$ -vinylureas with ethyl acrylate

System	$r_1$	$r_2$
DVI( $M_1$ ), EA( $M_2$ )	0.090	0.388
DVHHP( $M_1$ ), EA( $M_2$ )	0.137	0.549
EVI( $M_1$ ), EA( $M_2$ )	0.094	0.530

Table 3 *Q* and *e* parameters for some *N*-vinyl monomers<sup>a</sup>

Monomer	<i>e</i>	<i>Q</i>
<i>N</i> -vinylurethane	-1.62	0.19
1,3-Divinylimidazolid-2-one <sup>c</sup>	-1.58	0.84
<i>N,N'</i> -Divinylaniline	-1.54	0.19
<i>N</i> -ethyl- <i>N</i> -vinylurea	-1.53	0.13
1-Ethyl-3-vinylimidazolid-2-one <sup>c</sup>	-1.53	0.67
<i>N</i> -vinylphthalimide	-1.53	0.36
<i>N</i> -vinylcarbazole <sup>b</sup>	-1.49	0.28
1,3-Divinylhexahydropyrimid-2-one <sup>c</sup>	-1.40	0.68
<i>S</i> -ethyl- <i>N</i> -methyl- <i>N</i> -vinylmonothiocarbamate	-1.29	0.11
<i>N,N'</i> -ethylene- <i>N'</i> -vinylurea	-1.19	0.18
<i>N</i> -vinylglycidylurethane	-1.15	0.18
<i>N</i> -vinylpyrrolid-2-one	-1.14	0.14
<i>N</i> -methyl- <i>N</i> -vinyl- <i>p</i> -toluenesulphonamide	-1.10	0.082
<i>N</i> -vinyl-2-oxazolidone	-0.80	0.057
<i>N</i> -vinylsuccinimide	-0.34	0.13

<sup>a</sup> Values taken from ref 8 unless otherwise stated

<sup>b</sup> Ref 9

<sup>c</sup> This work

urea molecules. If the reactivity ratios ( $R_2$ ) of ethyl acrylate relative to the *N*-vinyl groups in the *N*-vinylureas are calculated, we obtain:

ethyl acrylate/1,3-divinylimidazolid-2-one ( $R_2 = 2r_2$ ),  
 $R_2 = 0.776$

ethyl acrylate/1,3-divinylhexahydropyrimid-2-one  
( $R_2 = 2r_2$ ),  $R_2 = 1.098$

ethyl acrylate/1-ethyl-3-vinylimidazolid-2-one ( $R_2 = r_2$ ),  
 $R_2 = 0.530$

Thus, the *N*-vinyl groups in 1,3-divinylimidazolid-2-one and 1,3-divinylhexahydropyrimid-2-one are less reactive than the *N*-vinyl group in 1-ethyl-3-vinylimidazolid-2-one. This seems to support the proposal of Crawshaw and Jones<sup>1</sup> that a conjugated (resonance stabilized) structure would explain their inability to cyclopolymerize.

The values in Table 3 show that the *e* values for the new *N*-vinyl compounds are consistent with other *N*-vinyl monomers. Since the *N*-vinyl group will dominate the copolymerization behaviour, and the influence of the various *N*-substituents will be very similar, it is understandable that the parameter, *e*, which denotes the polar properties of the monomers and their radicals, will be similar for this series of compounds.

The *Q* values for the new monomers are much higher than those for the other monomers. However, since the *Q*-*e* scheme is an empirical method of analysis, the parameters of which are susceptible only to a quasi-theoretical interpretation, it would be extending the significance of the scheme to attach fundamental importance to these high results.

#### ATTEMPTED COPOLYMERIZATIONS OF 1,3-DIPHENYL-1,3-DIVINYLUREA

It has already been noted that 1,3-diphenyl-1,3-divinylurea (DPDVU) could not be polymerized by free radical initiators under various conditions, and this was attributed to resonance stabilization of the free radical derived from this monomer<sup>2</sup>.

To characterize the polymerization behaviour of DPDVU further, copolymerizations were attempted with certain comonomers. 50% w/w mixtures of DPDVU with vinyl

acetate, ethyl acrylate, methyl acrylate or acrylic anhydride were heated in the presence of 2–3% of initiator (azobisisobutyronitrile) under conditions under which the comonomer alone was shown to be polymerized to high conversion; from none of these mixtures could any (co)polymer be isolated. When styrene was examined as comonomer its polymerization in benzene solution, initiated by azobisisobutyronitrile, was found to be retarded by DPDVU; the product appears to be a copolymer. The rate of copolymerization declines and the DPDVU content of the copolymer increases as the proportion of DPDVU in the comonomer mixture is increased (Table 4). This retardation by DPDVU was observed also in a dilatometric study of the thermally initiated polymerization of styrene alone and with DPDVU (5%) in benzene solution.

DPDVU (50% w/w) was also found to inhibit the polymerization of DVI or DVHHP using 1–5 mol % di-*t*-butyl peroxide as initiator at 150°C for periods up to 10 h. With 101 mol % initiator (based on DPDVU), during 4.5 h at 150°C glassy polymers were obtained with both comonomers. The infra-red spectra of the latter (after extraction with ethanol) were found to be almost identical to those of poly(1,3-divinylimidazolid-2-one) or poly(1,3-divinylhexahydropyrimid-2-one) respectively.

The results of these copolymerization studies are consistent with the radical derived from DPDVU being rather unreactive; this may be ascribable to resonance stabilization.

## EXPERIMENTAL

### Purification of monomers and solvents for copolymerization

1,3-Divinylimidazolid-2-one and 1,3-divinylhexahydropyrimid-2-one were crystallized twice from light petroleum ether (b.p. 40–60°C) (analytical reagent) dried at reduced pressure and stored at -5°C.

1-Ethyl-3-vinylimidazolid-2-one was distilled through a Nester–Faust spinning band distillation column equipped with an 18 in stainless-steel band and partial take off head, b.p. 110°C at 1.0 mmHg and stored at -5°C. Ethyl acrylate (mid.cut) was redistilled through a 30 cm column packed with glass helices equipped with a partial take off head (reflux ratio 3:1) b.p. 98.8–99.0°C and stored at -5°C.

Benzene (analytical reagent) was redistilled, b.p. 80.5°C.

Azobisisobutyronitrile was crystallized twice from methanol (analytical reagent) dried over phosphorus pentoxide under reduced pressure and stored at -5°C.

Table 4 Attempted copolymerization of 1,3-diphenyl-1,3-divinylurea with styrene<sup>a</sup>

Feed		Copolymer		
DPDVU (%)	Styrene (%)	Conversion <sup>b</sup>	DPDVU <sup>c</sup> in polymer (wt %)	Reduced <sup>d</sup> viscosity
0.0	100.00	22	0.0	0.256
5.0	95.0	20	1.5	0.228
10.0	90.0	18	2.3	0.166
20.0	80.0	16	2.7	0.124
30.0	70.0	14	3.5	0.109

<sup>a</sup> Polymerized at 50% w/w monomer concentration in benzene with 0.5% w/w azobisisobutyronitrile as initiator for 5 h at 70°C

<sup>b</sup> Estimated gravimetrically by precipitation in methanol

<sup>c</sup> Calculated from nitrogen analysis

<sup>d</sup> Determined in toluene

*Copolymerization of 1,3-divinylimidazolid-2-one, 1,3-divinylhexahydropyrimid-2-one or 1-ethyl-3-vinylimidazolid-2-one with ethyl acrylate*

Vinylurea monomer and ethyl acrylate (total weight 2.000 g) were weighed into stoppered bottles and transferred using two aliquots of benzene (5 ml each) to polymer tubes containing azobisisobutyronitrile (0.13 mol %). The contents of each polymer tube were made up to 20.0 g with benzene, purged with dry nitrogen and sealed with a rubber serum cap. The tubes were vigorously agitated and placed in a thermostated water bath at  $60^{\circ} \pm 0.1^{\circ}\text{C}$ . When the reaction was judged to have proceeded to a few per cent conversion the contents of the tube were slowly poured into vigorously stirred light petroleum ether (b.p.  $40\text{--}60^{\circ}\text{C}$ ) (200 ml). The precipitate was collected by filtration, washed repeatedly with light petroleum ether and dried at  $55^{\circ}\text{C}$  and 0.1 mmHg for 6 h. The polymers were ground to a fine powder, washed repeatedly with light petroleum ether and dried at  $55^{\circ}\text{C}$  and 0.1 mmHg for 24 h. The nitrogen content of the copolymer gave the percentage of vinylurea in the copolymer.

#### ACKNOWLEDGEMENTS

This paper results from work carried out at the Department of Chemistry and Biology, Sheffield Polytechnic, to whom

one of us (H.H.M.) is grateful for a research assistantship, and at The British Petroleum Company Ltd, Epsom Division, Research and Development Department, whom we thank for support and facilities.

#### REFERENCES

- 1 Crawshaw A. and Jones, A. G. *J. Macromol. Sci. (A)* 1971, **5**, 51
- 2 Corfield, G. C., Crawshaw, A. and Monks, H. H. *J. Macromol. Sci. (A)* 1975, **9**, in press
- 3 Beynon, K. I. *J. Polym. Sci. (A)* 1963, **1**, 3343
- 4 Beynon, K. I. and Hayward, E. J. *J. Polym. Sci. (A)* 1965, **3**, 1793
- 5 McCaffery, E. M., 'Laboratory Preparation for Macromolecular Chemistry', McGraw-Hill, New York, 1970, p 362
- 6 Fineman, M. and Ross, S. D. *J. Polym. Sci.* 1950, **5**, 259
- 7 Young, L. J. *J. Polym. Sci.* 1961, **54**, 411
- 8 Young, L. J., in 'Polymer Handbook', (Eds J. Brandrup and E. H. Immergut) Interscience, New York, 1966, Ch II, p 341
- 9 Negulescu, I., Feldman, D. and Simionescu, Cr. *Polymer* 1972, **13**, 149

# Light scattering Rayleigh linewidth measurements upon solutions of globular proteins containing high molecular weight impurities

D. B. Sellen

Astbury Department of Biophysics, University of Leeds, Leeds LS2 9JT, UK  
(Received 24 February 1975)

A theory is presented showing that the effect of a very small amount of high molecular weight impurity on a globular protein solution is to decrease the measured diffusion constant and increase the weight average molecular weight in equal proportions. This applies when the diffusion constant is determined by a light scattering Rayleigh linewidth measurement using the autocorrelation method. Experimental verification of this is provided by the results of measurements upon a solution of bovine plasma albumin containing a high molecular weight impurity. The effects of different amounts of impurity were simulated by making measurements at different angles of scatter. The limitations of the theory are discussed.

## INTRODUCTION

Investigation of the spectra of light scattered from macromolecular solutions is now an established technique for the determination of translational diffusion constants<sup>1-7</sup>. The most convenient method of making these measurements is by means of the optical homodyne technique in which the power spectrum of a photoelectric signal is investigated. In recent years it has been found advantageous to do this by obtaining the autocorrelation function by use of a suitable computer<sup>4,5,7</sup>. The present paper discusses the effect which a small amount of high molecular weight impurity or a small number of large aggregates (henceforward called agglomerates), has upon the measured diffusion constant of a globular protein, when the autocorrelation method is used.

## THEORY

As the diffusion constant of a globular molecule of given shape and density is inversely proportional to the cube root of its molecular weight, it might at first appear that the presence of a small number of large agglomerates in a solution of globular protein would have little effect upon the measured diffusion constant. However, it will be shown that, owing to the types of average involved, this is not the case.

Where spectral broadening is due to translational diffusion alone, the autocorrelation function of the photoelectric signal resulting from light scattered from a polydisperse solution of macromolecules is given by<sup>7</sup>:

$$\phi(\tau) = \frac{c^2 \gamma^2}{2} [\sum_n I_n \exp(-K^2 D_n \tau)]^2 \quad (1)$$

$c$  is the overall photosensitivity of the detecting system and

$\gamma$  a coherence factor depending upon the geometry of the optics<sup>6</sup>.  $\tau$  is the autocorrelation delay time,  $I_n$  the scattered intensity from that component having diffusion constant  $D_n$  and:

$$K = \frac{4\pi}{\lambda} \sin \theta/2 \quad (2)$$

where  $\lambda$  is the wavelength in the solution and  $\theta$  is the angle of scatter. If  $\ln \phi(\tau)$  is plotted against  $\tau$  the slope of the graph at  $\tau = 0$  is  $-2K^2 D_z$  where  $D_z$  is the  $Z$ -average diffusion constant<sup>7</sup>. Unless the degree of polydispersity is very high however,  $\phi(\tau)$  will not differ significantly from a single exponential, in which case a logarithmic plot will be a straight line of slope  $-2K^2 D_z$ <sup>7</sup>.

Light scattering measurements therefore yield weight average molecular weights and  $Z$ -average diffusion constants. A mixture of a globular protein and a small number of agglomerates has a weight average molecular weight given by:

$$M_w = M_G(1 + I_A/I_G) \quad (3)$$

where  $C_A/C_G \ll 1$ ,  $M$ ,  $I$  and  $C$  refer to the molecular weight, scattered intensity and concentration, and the subscripts G and A refer to the protein and agglomerates respectively. The  $Z$ -average diffusion constant is given by:

$$D_z = \frac{D_G(1 + D_A I_A/D_G I_G)}{1 + I_A/I_G} \quad (4)$$

$D_G$  here is the diffusion constant of the protein and  $D_A$  the  $Z$ -average diffusion constant of the agglomerates.  $D_A$  will always be less than  $D_G$  and if:

$$D_A I_A/D_G I_G \ll 1 \quad (5)$$

then:

$$D_z = \frac{D_G}{1 + I_A/I_G} \quad (6)$$

Thus the proportionate decrease in diffusion constant due to the presence of a small number of agglomerates is equal to the proportionate increase in weight average molecular weight, i.e.

$$D_z M_w = D_G M_G \quad (7)$$

It must be emphasized that no assumptions have been made here about the nature of the agglomerates or their range of sizes.  $I_A$  refers to their total scattered intensity. The only assumption is that the Z-average diffusion constant of the agglomerates is much less than that of the protein.

### EXPERIMENTAL VERIFICATION

When a solution of bovine plasma albumin is left to stand for some time it acquires a dissymmetry of scatter. This is due to the formation of very high molecular weight aggregates which make a greater contribution at lower angles. From the point of view of the light scattering technique therefore, the protein may be regarded as being in a different state of 'agglomeration' for different angles of scatter, and each angle will have a corresponding weight average molecular weight associated with it. Thus by making conventional light scattering measurements and light scattering Rayleigh linewidth measurements at various angles, it should be possible to verify the above theory.

A stock solution of bovine plasma albumin [fraction  $\bar{V}$  from bovine plasma (Armour Pharmaceutical Co.)] was made up at a concentration of approximately 2% with a 0.1 M aqueous solution of NaCl plus 0.01 M phosphate buffer (pH = 7) as solvent. This was centrifuged at 20 000  $\times g$  for 1 h and then made to pass through a 1.2  $\mu\text{m}$  Millipore filter directly into the light scattering cell. No dissymmetry of scatter was observed and the molecular weight was determined in the usual way using the Aminco (American Instrument Co. Inc., Silver Spring, Maryland, USA) apparatus. The cell was transferred to the light scattering Rayleigh linewidth apparatus and the diffusion constant was determined in the manner previously described<sup>7</sup>. The stock solution was then allowed to stand at room temperature for 2 days and refiltered into the light scattering cell. A rise in scatter of some 16% at  $\theta = 25^\circ$  was observed with light of wavelength 546 nm. It is necessary, however, to find effective molecular weights at various angles for light of wavelength 633 nm (the wavelength of the He-Ne laser). To do this, plots were made of  $KC/R_\theta$  against  $(\sin^2 \theta/2)/\lambda^2$  (where the symbols have their usual meaning) for the wavelengths 546 and 436 nm. The Debye theory<sup>8</sup> predicts that these should form a single plot and this was found to be the case. Effective molecular weights for 633 nm were found by interpolation. The fact that the plots at the two wavelengths could be superimposed to yield a single plot indicated that the dissymmetry of scatter was due to agglomerated material and not to large dust particles. In the latter case  $KC/R_\theta$  would be much lower at 546 than 436 nm for the lower values of  $(\sin^2 \theta/2)/\lambda^2$ . The absence of dust particles is important as they are mostly

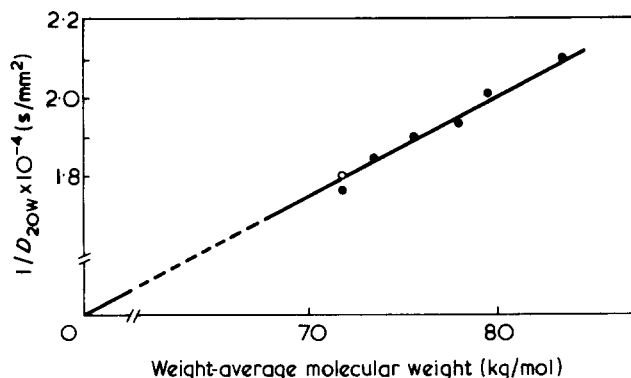


Figure 1 Diffusion constant of bovine plasma albumin containing various amounts of high molecular weight impurity (see text) as a function of weight average molecular weight: O, measurements taken on first making up the solution; ●, after standing at room temperature for 2 days

comparable in size to the illuminated volume from which scattered light is received in the Rayleigh linewidth apparatus,  $\sim(0.1 \text{ mm})^3$ , and lead to spasmodic vertical movements of the recorded autocorrelation function<sup>7</sup>, whereas in the conventional light scattering apparatus they simply increase the overall scatter. Effective diffusion constants were determined for  $\theta = 30^\circ, 35^\circ, 40^\circ, 50^\circ, 70^\circ, 90^\circ$  and a plot made (Figure 1) of  $1/D$  against the molecular weight determined at the same angle. According to equation (7) the data should lie within experimental error on a straight line through the origin and this is seen to be the case. The straight line through the origin which best fits the data has a slope  $1/D_G M_G$  and in this case  $D_G M_G$  is found to be  $4.00 \times 10^{-3} \text{ kg mm}^2 \text{ s}^{-1} \text{ mol}^{-1}$ . In practice the accuracy of this figure is limited by the accuracy of calibration of the conventional light scattering apparatus ( $\sim \pm 5\%$ ).

### DISCUSSION AND CONCLUSION

It must be emphasized that the above results are presented merely in order to illustrate the theory. It is *not* recommended that such a procedure be followed in place of normal clarification procedures such as differential centrifugation which in most cases are sufficient to remove any dissymmetry of scatter. The theory, however, applies in many cases where there is no detectable dissymmetry of scatter and the exact conditions under which it applies will now be discussed. The inequality (5) may be written:

$$\frac{D_A}{D_G} < p \frac{I_G}{I_A} \quad (8)$$

where  $p$  is the precision required expressed as a fraction. In fact this is the *only* condition necessary as the further condition to validate equation (3), i.e.  $C_A/C_G < p$  is automatically fulfilled as equation (8) may be written  $C_A/C_G < p(M_G/M_A)(D_G/D_A)$  where  $M$  indicates weight average molecular weight.  $(M_G/M_A)(D_G/D_A)$  is always less than unity although its actual value depends very much on the polydispersity of the agglomerates ( $M_A$  is a weight average and  $D_A$  a Z-average). If the arbitrary but typical values  $p \sim 0.02$  and  $I_G/I_A \sim 5$  are taken then equation (8) yields  $D_A/D_G < \sim 10$ . The *larger* agglomerates ( $D_A$  is a Z-average) should therefore be typically greater than about 50 nm in diameter for the theory to be applicable (or proportionately smaller if a lower precision is acceptable or



if the agglomerates make a lower contribution to the total scatter). The presence of particles of this size which account for 20% of the scattered intensity would result in a dissymmetry of scatter,  $D_{45/135}$ , of only 1.04. Thus although these large agglomerates may be removed by high speed centrifugation there is no way of knowing when complete clarification has been achieved. In fact it is the presence of very small but variable amounts of material of this sort which is likely to lead to variable weight average molecular weights as determined by light scattering, and it is the purpose of this paper to point out that this will lead to the same proportionate variability in the measured diffusion constants. The latter is far more serious than the former in assessing the size of the protein. If, however, both conventional light scattering measurements and light scattering Rayleigh linewidth measurements are made on the same solutions it might be possible to correct the measured diffusion constant using equation (7) if the molecular weight of the globular protein is known by other means, e.g. osmotic pressure measurements. The procedure would be self-justifying if the appropriate correlation could be obtained between molecular weight and diffusion constant for different attempts at clarification.

So far the only case considered is where the increase in scattered intensity is due to very small amounts of high molecular weight material. This does not mean that low molecular weight aggregates (i.e. dimers, trimers, etc.) cannot be present provided that inequality (8) is satisfied. The maximum proportion of the material (by weight) which may in any circumstance contain anything but the pure monomer is  $p$ . The theory does not apply in cases where the increase in scatter arises from a very much higher proportion of low molecular weight aggregates. However, if

the distribution is such that the low molecular weight aggregates and the high molecular weight agglomerates may be regarded as distinct from each other then the theory may be re-interpreted so that  $D_G$ ,  $M_G$ ,  $I_G$ ,  $C_G$  now refer to the Z-average diffusion constant of the monomer plus low molecular weight aggregates and the corresponding weight average molecular weight, scattered intensity and concentration respectively. If it is possible to find the weight average molecular weight in the absence of the agglomerates,  $M_G$ , possibly by the use of a sedimentation equilibrium method, then equation (7) yields the Z-average diffusion constant of the monomer plus low molecular weight aggregates.

In conclusion it must once again be emphasized that the results of light scattering Rayleigh linewidth measurements are likely to be much more useful if conventional light scattering measurements are made at the same time on identical solutions.

#### REFERENCES

- 1 Pecora, R. *Discuss. Faraday Soc.* 1970, **49**, 222 and references cited therein
- 2 Cummins, H. Z., Knable, N. and Yeh, Y. *Phys. Rev. Lett.* 1964, **12**, 150
- 3 Dubin, S. B., Lunacek, J. H. and Benedek, G. B. *Proc. Nat. Acad. Sci. US* 1967, **67**, 1164
- 4 Foord, R., Jakeman, E., Oliver, C. J., Pike, E. R., Blagrove, R. J., Wood, E. and Peacocke, A. R. *Nature* 1970, **227**, 242
- 5 Ford, N. C., Lee, W. and Karasz, F. E. *J. Chem. Phys.* 1969, **50**, 3098
- 6 Sellen, D. B. *Polymer* 1970, **11**, 374
- 7 Sellen, D. B. *Polymer* 1973, **14**, 359
- 8 Debye, P. *Ann. Phys.* 1915, **46**, 809

# Study of the conformational rigidity of polyelectrolytes by elastic neutron scattering: 1. Carboxymethylcelluloses in the intermediate momentum range

Michel Moan and Claude Wolff

Laboratoire d'Hydrodynamique Moléculaire, Université de Bretagne Occidentale, 29283 Brest Cedex, France

(Received 28 April 1975)

Small angle elastic neutron scattered intensity  $I(q)$  by dilute solutions of a high molecular weight and low charge density carboxymethylcellulose (CMC) in  $D_2O$ , without added-salt has been measured. The variation of  $I(q)$  is proportional to  $q^{-2}$  ( $q$  = momentum transfer) for  $q < q^*$ , and to  $q^{-1}$  for  $q > q^*$ . The dependence on  $q^{-2}$  shows that the distribution of the statistical units is Gaussian whereas the existence of  $q^*$  provides the possibility of calculating the length of such a unit; according to the dependence on  $q^{-1}$ , we conclude that these units are rigid. The length increases with dilution and charge density, which agrees with our previous results obtained by viscosity.

## INTRODUCTION

Many workers<sup>1,2</sup> have shown that the root mean square end-to-end distance of polyelectrolytes in aqueous solutions decreases as the concentration or the ionic strength increases; but to explain such phenomena as the non-Newtonian viscosity, besides the expansion of the polyion, it is necessary to take a certain rigidity into account. The quantitative study of this last parameter is very difficult: we thought that neutron small-angle scattering, previously applied to the study of non-ionic polymers in dilute or concentrated solutions and in the solid state<sup>3,4</sup>, could be very fruitful for conformational studies of polyelectrolytes in dilute solutions, as was recently showed by preliminary measurements<sup>5</sup>.

After a brief theoretical outline, neutron diffraction will be used to study the mechanism of the conformational changes of polyelectrolytes with the concentration, the ionic strength and the charge density along the chain, and compared to viscometric results. The first part of this work deals only with carboxymethylcelluloses (CMC), the second part with poly(methacrylic acid) (PMA).

## SCATTERING THEORY

In elastic neutron scattering on polymer solutions, the dependence of scattered intensity on scattering vector  $q$ , defined by:

$$q = k - k'$$

and

$$q = |q| = \frac{4\pi}{\lambda} \sin \theta/2 \simeq \frac{2\pi\theta}{\lambda} \text{ (for small } \theta \text{)}$$

where  $k'$  and  $k$  are the wave vectors of the incident and scattered beams,  $\theta$  the scattering angle and  $\lambda$  the wavelength of the neutron, can be written in the following form, assuming that the interactions between macromolecules are negligible:

$$I(q) = kN^2S(q) \quad (1)$$

$N$  is the number of independent sub-units in the polymer chain,  $k$  the contrast factor between polymer and solvent and  $S(q)$  a function of intrachain correlation for which several expressions have been proposed according to the statistical configuration of the chains and the range of the  $q$  values. For an ideal Gaussian chain, the Debye approximation<sup>6</sup> is:

$$S(q) = \frac{2}{x^2} [e^{-x} - 1 + x] \quad (2)$$

with  $x = q^2R_g^2$  and  $R_g^2$  the radius of gyration of the chain. When the chain dimensions are such as  $qR_g \ll 1$  (Guinier's approximation<sup>7</sup>) relation (2) gives:

$$S(q) = (1 - q^2R_g^2/3) \quad (3)$$

In the intermediate momentum-transfer range,  $qR_g > 1$ ,  $S(q)$  can be formulated in first approximation as follows:

$$S(q) = \frac{2}{q^2R_g^2} \quad (4)$$

This last result holds for  $q$  smaller than the inverse of the persistence length  $b$  of the chain; for  $qb > 1$ , the scattered intensity should reveal an asymptotic  $q^{-1}$  law<sup>8</sup>. Moreover, different factors such as the concentration<sup>9</sup> or the polydispersity have an effect on the scattering law.

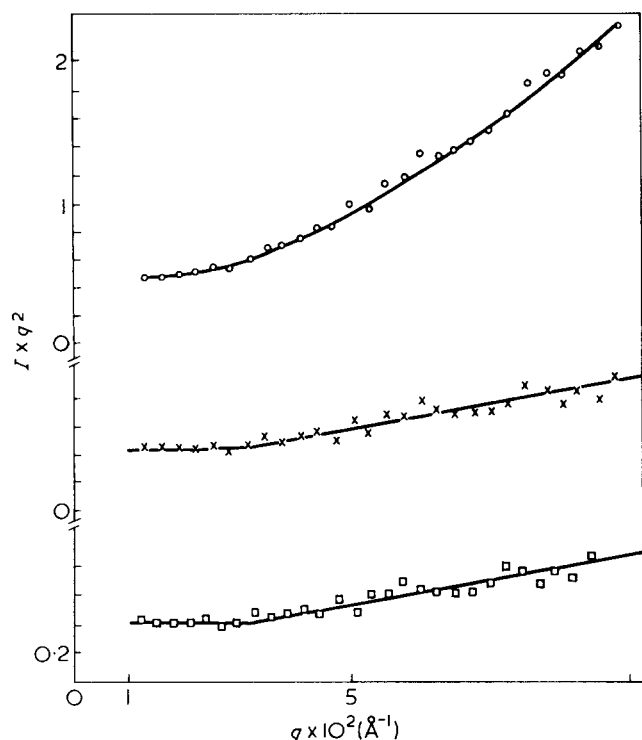


Figure 1 Variation of  $I \times q^2$  with  $q$ , for  $C = 2 \times 10^{-2} \text{ g/cm}^3$ .  $\circ$ , Curve uncorrected for the hydrogen background;  $\times$  and  $\square$ , corrected curves and  $q$  respectively calculated with  $\bar{\lambda} = 7.60 \text{ \AA}$  and  $(\bar{\lambda}^2)^{1/2} = 8.02 \text{ \AA}$ . In all the plots, the scattered intensity is given in arbitrary units

## EXPERIMENTAL

### Neutron diffraction

The experiments were performed on the EL-3 reactor of the Commissariat à l'Énergie Atomique. The instrument<sup>10</sup> used in this work allows a precise angular resolution of the neutron beam while keeping a suitable intensity by a broad wavelength distribution. The characteristics of the wavelength spectrum are the following: mean value of the wavelength distribution,

$$\bar{\lambda} = \int_0^{\infty} \lambda f(\lambda) d\lambda = 7.60 \text{ \AA}$$

wavelength of the maximum of the distribution density,  $\lambda_M = 5.12 \text{ \AA}$ . The distance between the sample and the detector is 2.60 m, and the momentum-transfer  $q$  (calculated with  $\bar{\lambda}$ ) ranges from  $10^{-2}$  to  $10^{-1} \text{ \AA}^{-1}$ . The cell containing the solution has a 15 mm diameter and is 5 mm thick.

Two corrections must be brought to the scattered intensity. For polymer solutions in  $\text{D}_2\text{O}$ , the first correction comes from the very high incoherent scattering cross-section of the hydrogen atoms of the solute molecules; this background, which is independent of the scattering vector, has been measured with a  $\text{D}_2\text{O}$  solution containing the same amount of protons as the polymer solution. In practice, the scattered intensity  $I(\theta)$  recorded for an angle depends on the wavelength distribution and the discussion of the experimental results must be made using the statistical mean of each quantity. For example, in the small

momentum range, using equation (3),  $I(\theta)$  is given by:

$$I(\theta) = \int_0^{\infty} f(\lambda) S(q) d\lambda$$

$$= \int_0^{\infty} f(\lambda) \left[ 1 - \frac{1}{3} \left( \frac{2\pi\theta}{\lambda} \right)^2 R_g^2 \right] d\lambda$$

$$I(\theta) = 1 - \frac{4\pi^2\theta^2}{3} R_g^2 \int_0^{\infty} [f(\lambda)/\lambda^2] d\lambda$$

and the momentum transfer  $q$  will be computed with a wavelength defined by:

$$\langle 1/\lambda^2 \rangle^{-1/2} = \int_0^{\infty} [f(\lambda)/\lambda^2] d\lambda$$

in the same way for a  $q^{-1}$  scattering law, the mean value  $\bar{\lambda}$  will be used.

The respective effects of these two corrections, which have been made systematically, are shown in Figure 1 in a typical plot of the results  $I(q) \times q^2 = f(q)$ ; the abscissa value of the intersection of the two parts of the curve is independent of the average wavelength.

### Viscosity

The viscosity measurements have been performed at  $25 \pm 0.005^\circ\text{C}$ , using a capillary viscometer with automatic measurement of efflux times<sup>11</sup>. For the measurements at fixed shear rate, we used an Ostwald viscometer with a capillary diameter 0.4 mm, giving for water an efflux time of 120 s and a shear rate of  $1400 \text{ s}^{-1}$  at the wall.

### Polyelectrolyte

The carboxymethylcelluloses (CMC) are polyelectrolytes prepared from Linters powder<sup>12</sup>. The mean degree of substitution  $\overline{DS}$ , i.e. the number of carboxymethyl groups by monomeric unit was 0.68; the molecular weight determined by viscosity<sup>13</sup> was  $M_v = 300\,000$ , i.e., a mean degree of polymerization,  $\overline{DP} = 1400$ . The electrical charges of the chain are due to the dissociation of carboxylic groups obtained by the progressive neutralization of the acid form H-CMC (stoichiometric degree of neutralization  $\alpha_s = 0$ ) by sodium hydroxide to the fully neutralized form Na-CMC ( $\alpha_s = 1$ ). To improve the contrast between solute and solvent, the solutions were prepared with  $\text{D}_2\text{O}$  (contrast ratio  $\text{D}_2\text{O}/\text{H}_2\text{O} \approx 2$  for CMC).

The domain of polyelectrolyte concentrations was  $2.57 \times 10^{-2}$  to  $10^{-3} \text{ g/cm}^3$ ; it corresponds, at least for the highest concentrations, to a state in which the chains can overlap. This 'semi-dilute' regime holds for  $C$  higher than a critical concentration defined for Gaussian coils by  $C^* = M/NR_g^3$  ( $M$  = molecular weight and  $N$  = Avogadro number). Using the  $R_g$  values of Table 1, we obtain  $C^* = 10^{-2} \text{ g/cm}^3$  for  $R_g = 368 \text{ \AA}$  and  $C^* = 4.5 \times 10^{-3}$  for  $R_g = 481 \text{ \AA}$ ; this result could mean that the regime is semi-dilute for the highest concentrations and dilute for the lowest.

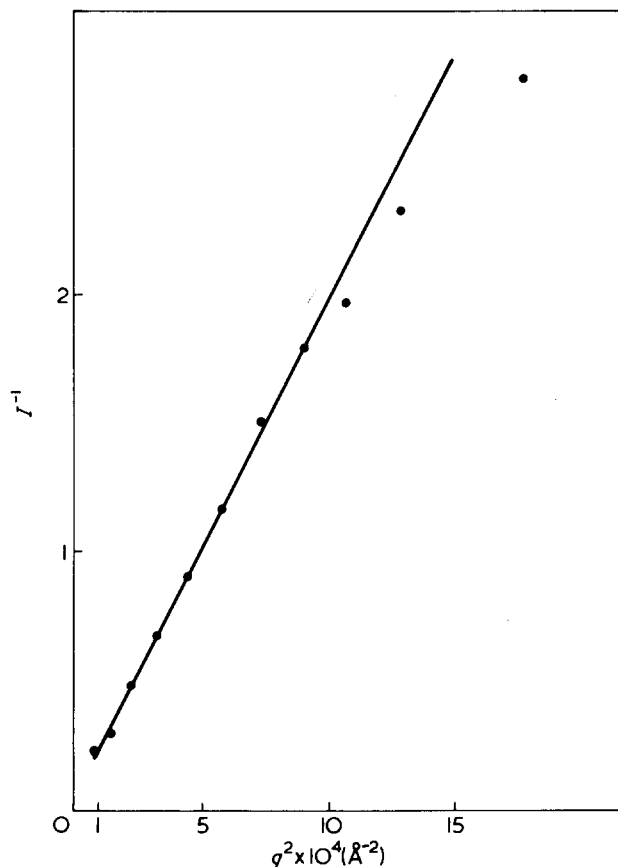


Figure 2 Variation of the inverse of the scattered intensity with  $q^2$ , for  $C = 2.57 \times 10^{-2} \text{ g/cm}^3$

## RESULTS AND DISCUSSION

### Scattering curve of the carboxymethylcelluloses

As a consequence of the high molecular weight, the measurements of neutron scattering have been made in the intermediate momentum transfer range  $q$ , that is for  $qR_g > 1$ , to study the effect of the polyelectrolyte concentration and the charge density on the conformation of the polyion. In practice, the scattering curves have been studied, as shown in Figure 1, plotting  $I(q) \times q^2$  vs.  $q$  since the product  $I(q) \times q^2$  must be constant when the scattering law is described by the Debye approximation.

The plots of Figures 3, 6 and 7, show two different scattering branches on both sides of a critical value  $q^*$  of the scattering vector: for  $q < q^*$ , the horizontal line indicates a  $q^{-2}$  scattering law; this result is confirmed by the plot of  $I^{-1}(q)$  vs.  $q^2$  shown in Figure 2; for  $q > q^*$ , the oblique line corresponds to a  $q^{-1}$  dependence of the scattered intensity.

The  $q^*$  value, which corresponds to the intersection of the two lines of the  $I(q) \times q^2 = f(q)$  plots, can be determined with an accuracy of  $0.2 \times 10^{-2} \text{ \AA}^{-1}$ . On the basis of the persistence length model, Kratky and Porod<sup>14</sup> have shown that the persistence length  $b$  of the chain and the length  $a$  of a statistical unit in the Kuhn model<sup>15</sup>, can be deduced from the transition point of the scattering curve by:

$$a = 2b = 2/q^* \quad (5)$$

As we have observed a  $q^{-2}$  behaviour in our range of concentrations, we can conclude that the chain of the polyion is a Gaussian distribution of rigid segments, whose length is approximately  $a$ . However, this result cannot be generalized to all CMC, because our sample has two particular characteristics which can explain a Gaussian conformation, in spite of our experimental conditions (zero external ionic strength and low enough concentration): the length of the chain which is relatively large and the low charge density, i.e., an average minimum distance of about 8 Å between charges, if all carboxylic groups are ionized.

### Polyelectrolyte concentration dependence of $q^*$

The effect of the concentration on the conformation of the polyion was first studied by successive dilutions of the Na-CMC ( $\alpha_s = 0.6$ ) in pure D<sub>2</sub>O without simple electrolyte added.

The  $I(q) \times q^2 = f(q)$  plots of Figure 3 show very clearly the effect of the concentration on  $q^*$ ;  $q^*$  decreases with the polyelectrolyte concentration. The different  $q^*$  values obtained and the corresponding characteristic lengths  $b$  (equation 5) are summarized in Table 1. This  $q^*$  value permits an approximate determination of the characteristic lengths  $b$  of the chain; the increase of  $b$  when the concentration decreases confirms the results obtained by viscosity, i.e. the rigidity of the polyion increases with dilution, which increases the electrostatic repulsions between the charged sites along the chain. Figure 4 shows a linear variation of  $q^*$  with  $C^{1/2}$ , which is the same as the

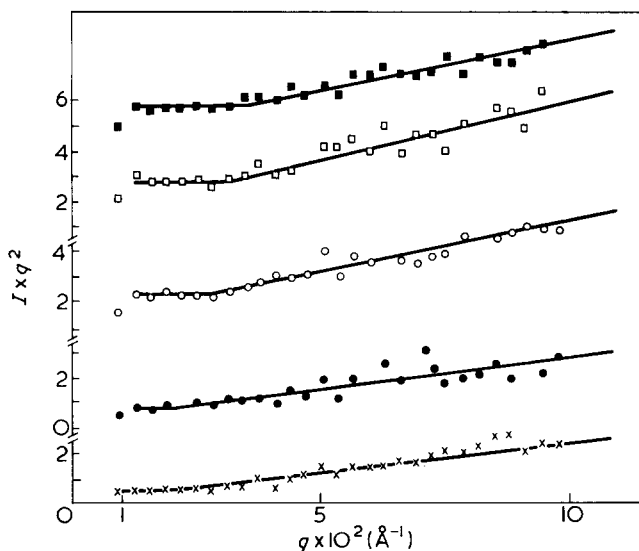


Figure 3 Variation of  $I \times q^2$  with  $q$  for different concentrations: ■,  $2.57 \times 10^{-2}$ ; □,  $10^{-2}$ ; ○,  $8 \times 10^{-3}$ ; ●,  $2.5 \times 10^{-3}$ ; ×,  $10^{-3} \text{ g/cm}^3$

Table 1 Effect of the polyelectrolyte concentration on  $q^*$ ,  $b$  and  $R_g$  values

$C$ ( $\text{g/cm}^3$ )	$q^* \times 10^2$ ( $\text{\AA}^{-1}$ )	$b$ ( $\text{\AA}$ )	$R_g$ ( $\text{\AA}$ )
$2.57 \times 10^{-2}$	3.60	27.7	368
$2 \times 10^{-2}$	3.25	30.7	387
$10^{-2}$	3.15	31.7	394
$8 \times 10^{-3}$	2.75	36.4	421
$2.5 \times 10^{-3}$	2.20	45.5	471
$10^{-3}$	2.05	47.6	481

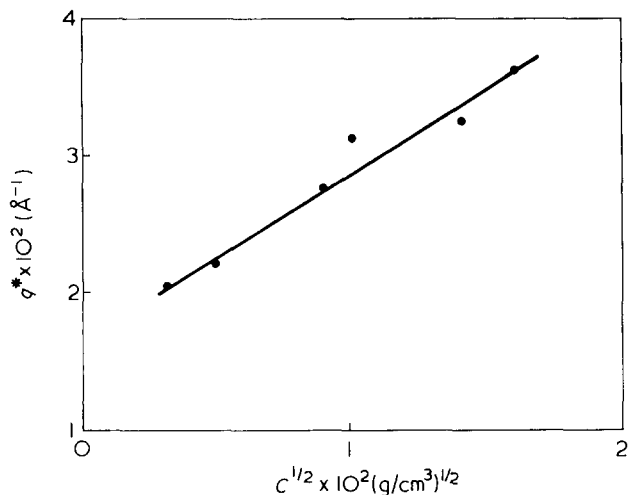


Figure 4 Variation of the critical value  $q^*$  with the square-root of the concentration

variation of the reciprocal of the reduced viscosity of polyelectrolyte solutions according to the Fuoss relation<sup>16</sup>, typical of electrostatic interactions.

The extrapolation of the  $b$  values to zero concentration is  $b = 61 \text{ \AA}$ , but it seems unreasonable to give a particular meaning to this value, because very dilute solutions could not be studied here and the existence, in that range of concentrations, of cooperative phenomena<sup>17</sup> which leads to a variation of the viscosity no longer proportional to  $C^{-1/2}$ .

The distance of effectiveness of these electrostatic interactions can be evaluated by calculating the radius  $\chi^{-1}$  of the ionic atmosphere around fixed charges on the polyion; if we assume that all the charged sites of the chain are not ionized, but only a fraction corresponding to the osmotic coefficient  $\Phi$  ( $\Phi$  is the fraction of free counterions) which has been determined by Rinaudo and Milas<sup>18</sup> for CMC, we obtain  $\chi^{-1}$  by the following relation<sup>19</sup>:

$$\chi^{-1} = \left[ \frac{\nu \cdot \epsilon_0 k T}{n \cdot 4\pi e^2} \right]^{1/2} \quad (6)$$

where  $\nu$  is the volume occupied by a polyion,  $n$  the number of effective charges of the chain,  $e$  the charge of the electron,  $k$  the Boltzmann constant,  $T$  the absolute temperature, and  $\epsilon_0$  the dielectric constant of the medium. Figure 5 shows a linear variation of  $b$  with  $\chi^{-1}$  and this clearly indicates again that the  $b$  values are directly connected to the interactions between charged sites along a chain.

If the polyion is represented by a distribution of quite-rigid segments of length  $a = 2b$  freely joined by the bond between two glucose units (bond angle  $\alpha = \pi - \theta \approx 110^\circ$ ), then the radius of gyration  $R_g$  is given by:

$$R_g^2 = \frac{Na^2}{6} \left[ \frac{1 + \cos \theta}{1 - \cos \theta} \right] \quad (7)$$

where  $N = L/a$ ,  $L$  being the length of the fully extended chain; the calculated values of  $R_g$  are shown in Table 1.

We have demonstrated by viscosity measurements<sup>20</sup> that the conformation of the polyion does not change if the dilutions are made by the procedure of 'isoionic dilution' which keeps the total ionic strength of the polyelectrolyte solution constant. The decrease of ionic strength with dilution is prevented by the addition of a simple

electrolyte, such as NaCl. These 'isoionic dilution' procedures have been used at the departure from the most concentrated polyelectrolyte solution,  $C = 2 \times 10^{-3} \text{ g/cm}^3$ , which corresponds to an ionic strength  $I = 3 \times 10^{-2} \text{ mol/l}$ . The  $I(q) \times q^2$  plots of Figure 6 do not show, contrary to the plots of Figure 3, a variation of  $q^*$  with the polyelectrolyte concentration. Thus, the neutron scattering also confirms in this case the deductions made from the viscosity results. Under the same experimental conditions, the intrinsic viscosity, extrapolated to zero shear-rate is  $[\eta] = 561 \text{ cm}^3/\text{g}$ ; from this result, the radius of gyration can be calculated by the Fox-Flory<sup>21</sup> equation for a statistical coil:

$$R_g^3 = \frac{M[\eta]}{6^{3/2} \cdot \Phi}$$

where  $\Phi = 2.5 \times 10^{23}$ ; the value obtained  $R_g = 357 \text{ \AA}$ , is in unexpected agreement with the value  $R_g = 387 \text{ \AA}$ , deduced from  $q^*$  by equations (5) and (7).

#### Effect of the charge density on $q^*$

As pointed out<sup>20</sup>, viscosity studies show that the expansion of the polyion increases progressively with the charge density along the chain; such a variation of the charge density is obtained by changing  $\alpha_s$  from 0.2 to 1. The

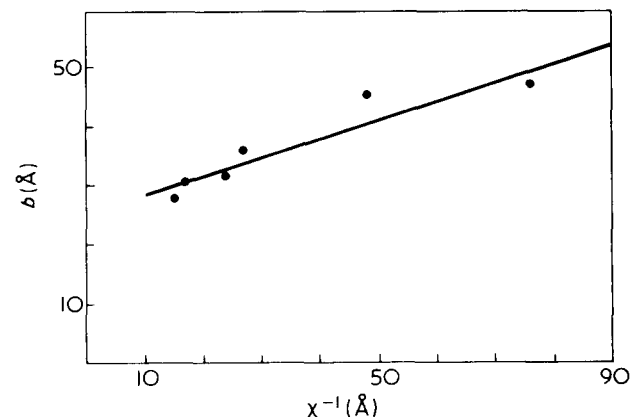


Figure 5 Variation of the  $b$  length with the radius  $\chi^{-1}$  of the ionic atmosphere of the charges

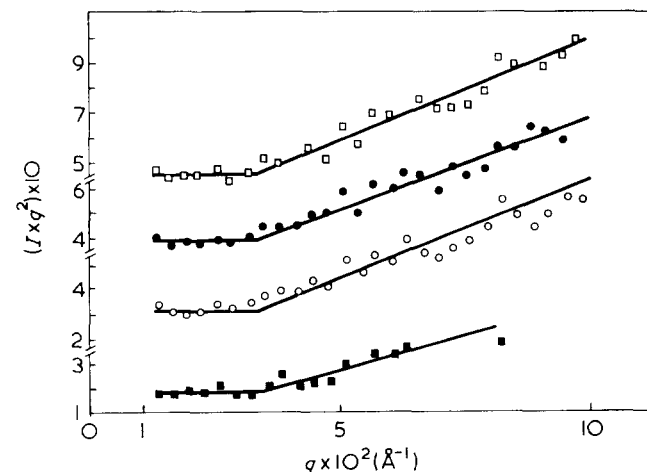


Figure 6 Variation of  $I \times q^2$  with  $q$ , in the case of the 'isoionic' dilution.  $\square$ ,  $C = 2 \times 10^{-2}$ ;  $\bullet$ ,  $1.38 \times 10^{-2}$ ;  $\circ$ ,  $10^{-2}$ ;  $\blacksquare$ ,  $5 \times 10^{-3} \text{ g/cm}^3$

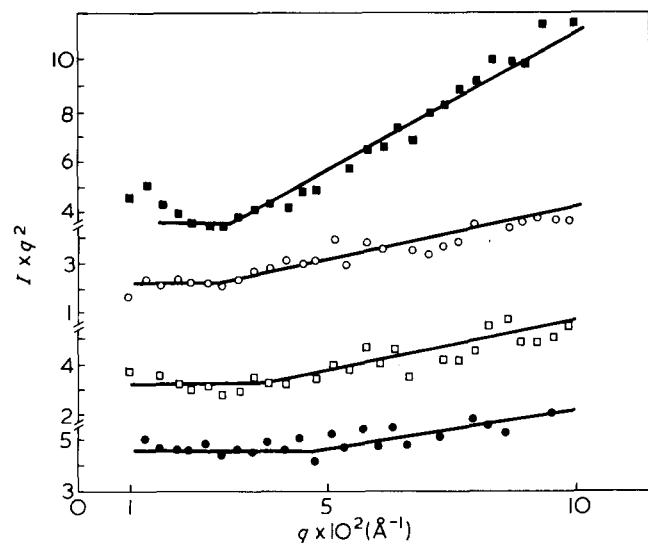


Figure 7 Effect of the charge density on the variation of  $I \times q^2$  with  $q$ . ■,  $\alpha_s = 1$ ; ○,  $\alpha_s = 0.6$ ; □,  $\alpha_s = 0.4$ ; ●,  $\alpha_s = 0.2$

Table 2 Effect of the charge density on  $q^*$ ,  $b$  and  $R_g$  values

$\alpha_s$	$q^* \times 10^2$ ( $\text{\AA}^{-1}$ )	$b$ ( $\text{\AA}$ )	$R_g$ ( $\text{\AA}$ )
0.2	4.9	20.4	316
0.4	3.65	27.4	366
0.6	2.75	36.4	421
1	—	—	—

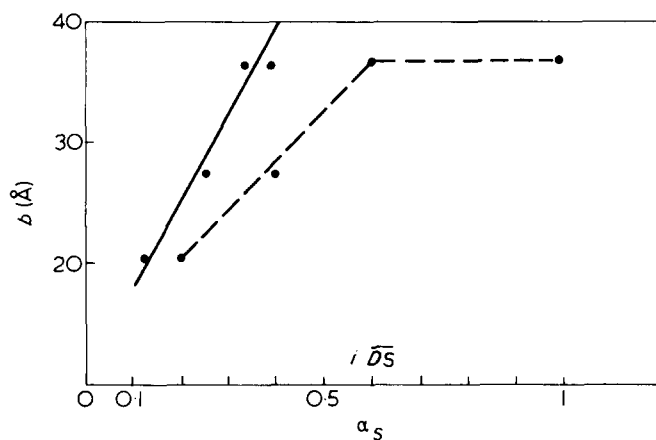


Figure 8 Effect of the charge density on the  $b$  length; --- and —, variation of  $b$  with  $\alpha_s$  and  $i\overline{DS}$ , respectively

$I(q) \times q^2 = f(q)$  plots of Figure 7, for a polyelectrolyte concentration  $C = 8 \times 10^{-3} \text{ g/cm}^3$  show the influence of  $\alpha_s$  on  $q^*$  values, and on the corresponding  $R_g$  values; the data are reported in Table 2. Figure 8 shows that the greatest stretching of the polyion occurs at  $\alpha_s = 0.6$ ; a similar conclusion has been drawn from earlier viscosity measurements<sup>20</sup>. Since all the sites are not ionized, the most interesting parameter is not  $\alpha_s$ , but  $i\overline{DS}$ , the effective charge per monomeric unit; Figure 8 also shows that the variation of  $b$ , which is equivalent to the rigid segment length, is linear with  $i\overline{DS}$ .

## CONCLUSION

The law of the small-angle scattered intensity  $I(q)$  of a high molecular weight and low charge density CMC is different on the two sides of a critical value  $q^*$  of the scattering vector: for  $q < q^*$ , the law is proportional to  $q^{-2}$  and for  $q > q^*$ ,  $I(q) \sim q^{-1}$ .

According to this behaviour, it is concluded that, under our experimental conditions, these CMC macromolecules behave as a Gaussian distribution of rigid segments, whose  $a = 2/q^*$  length increases with dilution and charge density. These results agree fairly well with previous results obtained by viscometric methods; but, because of the sample characteristics (high molecular weight and low charge density) and the impossibility to perform neutron scattering experiments on higher dilute solutions, we have not succeeded, on this sample, in showing that the extension of the polyion may become anisotropic, as suggested by our previous viscosity results.

## ACKNOWLEDGEMENTS

We are grateful to Professor M. Rinaudo, CERMAV Grenoble, for her help in this work, particularly for providing the CMC samples and the know-how of their use. Elastic neutron scattering experiments have been performed at the Centre d'Etudes Nucléaires, Saclay; we are very thankful to Dr Janninck and his group, for his welcome and assistance during the experiments. We also thank Professor H. Benoit for his interest in this work which has been done within the framework of the RCP 194 'Polyelectrolytes' whose Chairman he was.

## REFERENCES

- 1 Tanford, C. 'Physical Chemistry of Macromolecules', Wiley, New York, 1961
- 2 Schneider, N. S. and Doty, P. *J. Phys. Chem.* 1954, **58**, 762
- 3 Cotton, J. P., Farnoux, B. and Janninck, G. *J. Chem. Phys.* 1972, **57**, 290
- 4 Benoit, H. *et al. Nature (Phys. Sci.)* 1973, **245**, 13
- 5 Moan, M., Wolff, C. and Ober, R. *Chem. Phys. Lett.* 1974, **28**, 505
- 6 Debye, P. *Techn. Rep. CR 637* Office of Rubber Reserve, Washington, 1945
- 7 Guinier, A. 'Théorie de la Radiocristallographie', Dunod, Paris, 1964
- 8 Porod, G. *J. Polym. Sci.* 1953, **10**, 157
- 9 Janninck, G., de Gennes, P. G. *J. Chem. Phys.* 1968, **48**, 2360
- 10 Cotton, J. P. *Thesis* Paris (1973)
- 11 Gramain, P. and Libeyre, R. *J. Appl. Polym. Sci.* 1970, **14**, 283
- 12 Rinaudo, M. and Hudry-Clergeon, G. *J. Chem. Phys.* 1967, **63**, 1746
- 13 Moan, M. *Speciality Thesis* Strasbourg (1972)
- 14 Kratky, O. and Porod, G. *Rec. Trav. Chim.* 1949, **68**, 1106
- 15 Kuhn, W. *Kolloid-Z.* 1934, **68**, 2
- 16 Fuoss, R. M. *J. Polym. Sci.* 1948, **3**, 603
- 17 Moan, M. and Wolff, C. *C.R. Acad. Sci. (Paris) (C)* 1972, **274**, 1492
- 18 Rinaudo, M. and Milas, M. *C.R. Acad. Sci. (Paris) (C)* 1971, **269**, 1190
- 19 Oosawa, F. 'Polyelectrolytes', Marcel Dekker, New York, 1971
- 20 Moan, M. and Wolff, C. *Makromol. Chem.* 1974, **175**, 2881
- 21 Flory, P. J. and Fox Jr, T. G. *J. Am. Chem. Soc.* 1951, **73**, 1904

# Study of the conformational rigidity of polyelectrolytes by elastic neutron scattering: 2. Molecular dimensions and conformation of poly(methacrylic acid)

Michel Moan and Claude Wolff

Laboratoire d'Hydrodynamique Moléculaire, Université de Bretagne Occidentale, 29283 Brest Cedex, France

and Raymond Ober

Laboratoire de la Matière condensée, Collège de France, 75231 Paris-Cedex 05, France  
(Received 14 May 1975)

Elastic neutron scattering at small angles allows the radius of gyration of a PMA sample of molecular weight  $M_v \sim 13\,000$  to be measured in highly dilute solution; the variation of this parameter with concentration and charge density to be followed, and the viscometric results to be confirmed. The scattered intensity is proportional to  $q^{-2}$  ( $q$  = momentum transfer) for the highest concentrations studied, which correspond to a Gaussian distribution function of the sub units of the chain, and to  $q^{-1}$  at the lowest concentrations, of which it is concluded that the polyion is then a zig-zag with only a few subunits.

## INTRODUCTION

In Part 1<sup>1</sup>, small angle neutron scattering was used for the study of the conformation of polyelectrolytes, when the values of the scattering vector are such that  $qR_g > 1$  ( $R_g$  = radius of gyration). Under the same experimental conditions ( $10^{-2} < q < 10^{-1} \text{ \AA}^{-1}$ ), the investigation of Guinier's range, where  $qR_g < 1$ , requires a macromolecule whose radius of gyration lies between 10 to 100 Å. For this purpose, we used a sample of poly(methacrylic acid) (PMA) with a very low degree of polymerization ( $DP = 150$ ) and thus a radius of gyration of about 100 Å if we assume that the chain is fully extended.

## EXPERIMENTAL

The experimental conditions of measurement of neutron scattering and viscosity are the same as in Part 1. The molecular weight of the poly(methacrylic acid) (PMA-A)

Table 1 Variation of  $R_g$  with the polyelectrolyte concentration  $C$

$C(\text{g/cm}^3)$	$R_g(\text{Å})$	$C^{*a}(\text{g/cm}^3)$
$3.2 \times 10^{-2}$	33.5	$5.8 \times 10^{-1}$
$2 \times 10^{-2}$	33.3	—
$10^{-2}$	33.7	$5.7 \times 10^{-1}$
$8.2 \times 10^{-3}$	35.4	$4.9 \times 10^{-1}$
$3.2 \times 10^{-3}$	36.7	$4.4 \times 10^{-1}$
$10^{-3}$	43	$2.7 \times 10^{-1}$
$5 \times 10^{-4}$	49	$1.8 \times 10^{-1}$

<sup>a</sup>  $C^* = M/NR_g^3$ ,  $M$  = molecular weight and  $N$  = Avogadro number

Table 2  $R_g$  and  $\eta_{sp}/C$  values determined for various  $\alpha_s$  at a constant concentration  $C = 10^{-2} \text{ g/cm}^3$

$\alpha_s$	$R_g(\text{Å})$	$\eta_{sp}/C(\text{cm}^3/\text{g})$	$C^*(\text{g/cm}^3)$
0.27	33.7	13.9	$5.7 \times 10^{-1}$
0.37		19	
0.48		58	
0.6	74	150	$5.3 \times 10^{-2}$
0.9	83	251	$3.8 \times 10^{-2}$
1	88	248	$3.2 \times 10^{-2}$

determined from the viscometric law of Katchalsky *et al.*<sup>2</sup> was  $M_v = 13\,000$ . The domain of polyelectrolyte concentrations was  $3.2 \times 10^{-2}$  to  $5 \times 10^{-4} \text{ g/cm}^3$ ; it corresponds for all the solutions to a state in which the chains cannot overlap; indeed, the values of the critical concentration  $C^*$  reported in Tables 1 and 2, clearly show that the conditions  $C < C^*$  is always satisfied. As in Part 1, the scattered intensity has been systematically corrected to take into account the broad wavelength distribution and the incoherent scattering of the hydrogen atoms of PMA.

## RESULTS AND DISCUSSION

In the elastic scattering, the study of Guinier's range allows us to obtain directly the radius of gyration of the molecule, without assumptions on its geometrical form. When it was possible, the measurements were carried on beyond this range to obtain information on the conformation of the polyion<sup>1</sup>.

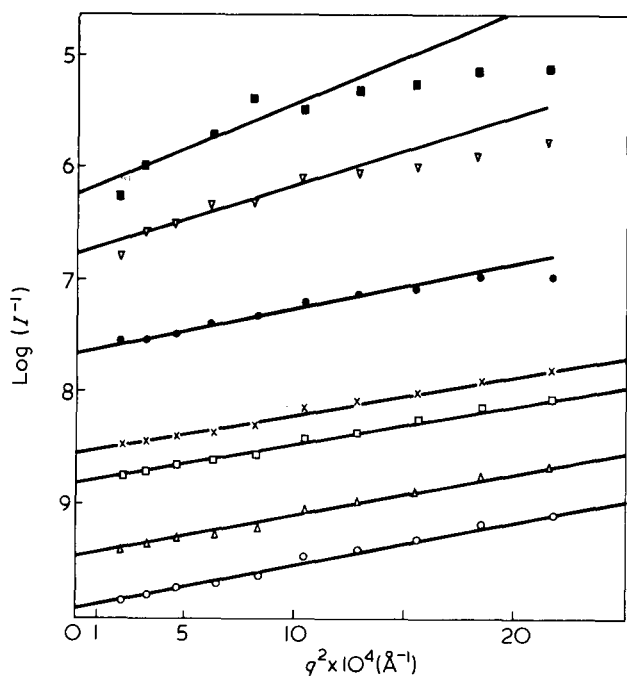


Figure 1 Guinier's plots for solutions of PMA ( $\alpha_s = 0.27$ ) in  $D_2O$ .  $\circ$ ,  $3.2 \times 10^{-2}$ ;  $\triangle$ ,  $2 \times 10^{-2}$ ;  $\square$ ,  $10^{-2}$ ;  $\times$ ,  $8.2 \times 10^{-3}$ ;  $\bullet$ ,  $3.2 \times 10^{-3}$ ;  $\nabla$ ,  $10^{-3}$ ;  $\blacksquare$ ,  $5 \times 10^{-4} \text{ g/cm}^3$

#### Study of the gyration radius

**Effect of the polyelectrolyte concentration.** This study was made on sodium salt (PMA-Na) whose stoichiometric degree of neutralization by sodium hydroxide was  $\alpha_s = 0.27$ ; the solutions were prepared with pure water (respectively  $D_2O$  and  $H_2O$  in neutron scattering and viscosity) without simple electrolyte added.

Qualitatively, the effect of the polyelectrolyte concentration on the dimensions of the polyion can be shown by the increase of reduced viscosity  $\eta_{sp}/C$  ( $\eta_{sp} = (\eta - \eta_0)/\eta_0$ , with  $\eta$ ,  $\eta_0$  absolute viscosities of solution and solvent,  $C$  polyelectrolyte concentration) when the concentration decreases; for this sample in pure water solution without external salt, the 'polyelectrolyte' behaviour clearly appears only at concentrations lower than  $10^{-2} \text{ g/cm}^3$ . This concentration is much lower than the critical concentration  $C^* = 5.7 \times 10^{-1} \text{ g/cm}^3$  calculated for  $R_g = 33.7 \text{ \AA}$ .

In neutron scattering experiments, the intensity scattered by these solutions is sufficient (after the various corrections) to carry on the study down to dilutions of about  $5 \times 10^{-4} \text{ g/cm}^3$ . Figure 1 shows Guinier's plots  $\log(I^{-1}(q)) = f(q^2)$ , for various PMA-Na concentrations; the slope of these straight lines gives the apparent polyion gyration radius, if the interparticle effects are negligible (see relations (2) and (3) of Part 1<sup>1</sup>). The values obtained at various concentrations, are summarized in Table 1 and Figure 2. The radius of gyration remains almost constant at the highest concentrations, then increases from  $C = 8 \times 10^{-3} \text{ g/cm}^3$ ; this result is in agreement with the variation of reduced viscosity. The second part of Figure 2 also shows that, in the concentration range where the sample has a 'polyelectrolyte' behaviour, the radius of gyration has a linear variation with  $C^{-1/2}$ ; this fact is characteristic of the expansion of the polyion as a consequence of the electrostatic repulsions which increase with the dilution.

The  $R_g = 49 \text{ \AA}$  value obtained for the lowest concentration ( $C = 5 \times 10^{-4} \text{ g/cm}^3$ ) is still far from the radius of gyration of the fully stretched polyion (about  $100 \text{ \AA}$ ). It

can be accounted for by the low degree of neutralization  $\alpha_s = 0.27$ . There is less than one electrical charge for three monomeric units, so the electrostatic repulsions are much lower than the forces of hydrogen bonding between the non-ionized carboxylic groups which keep the structure of the polyion compact.

**Effect of the charge density.** As in Part 1<sup>1</sup>, the variation of the charge density along the chain is obtained by progressive neutralization of the acid form PMA-A; the effect of the charge density, which is a function of the stoichiometric degree of neutralization  $\alpha_s$ , was studied at a constant concentration  $C = 10^{-2} \text{ g/cm}^3$  for various  $\alpha_s$ . Several workers<sup>3</sup> have shown that the increase of the reduced viscosity with the increase of  $\alpha_s$  was then very important, except at low charge density, as indicated by the data of Figure 3.

The neutron scattering allows us to obtain directly the variation of the radius of gyration under the same conditions; the  $R_g$  values obtained by this method are shown in Table 2 and the variation of  $R_g$  with  $\alpha_s$  is also given in Figure 3. From this important increase of the polyion dimensions it follows that the condition  $qR_g < 1$  is no longer satisfied except in a more and more restricted range of the  $q$  values, and an accurate determination of  $R_g$  is then more difficult.

The highest value obtained  $R_g = 88 \text{ \AA}$  differs little from the radius of gyration of the fully stretched chain and it suggests that the polyion has then a rod-like conformation.

#### Interactions between polyions

The previous results only consider the apparent radii of gyration, i.e., measured at finite polyelectrolyte concentra-

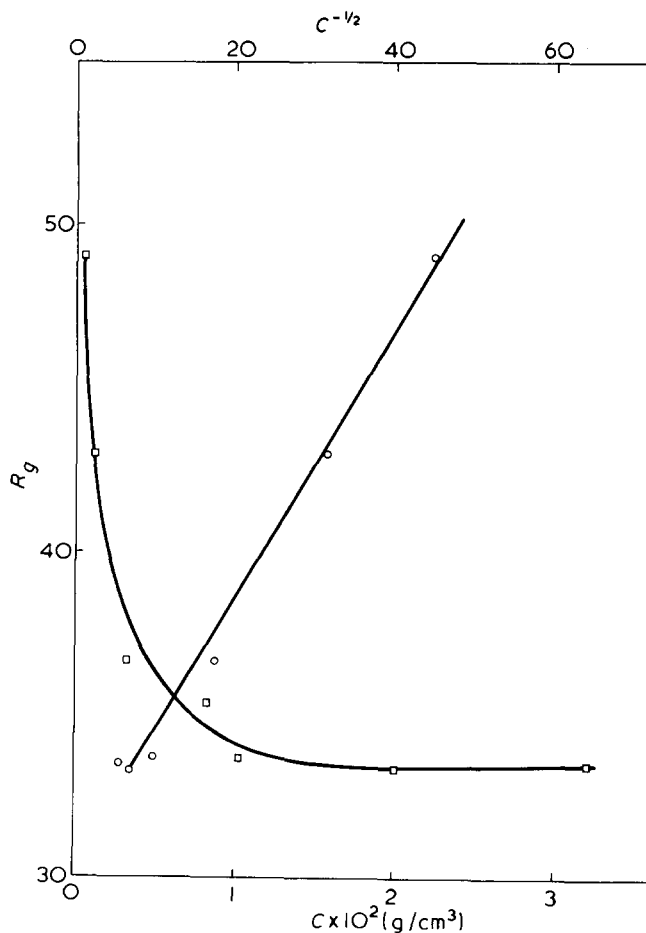


Figure 2 Variation of gyration radius  $R_g$ , respectively with  $C$  and  $C^{-1/2}$



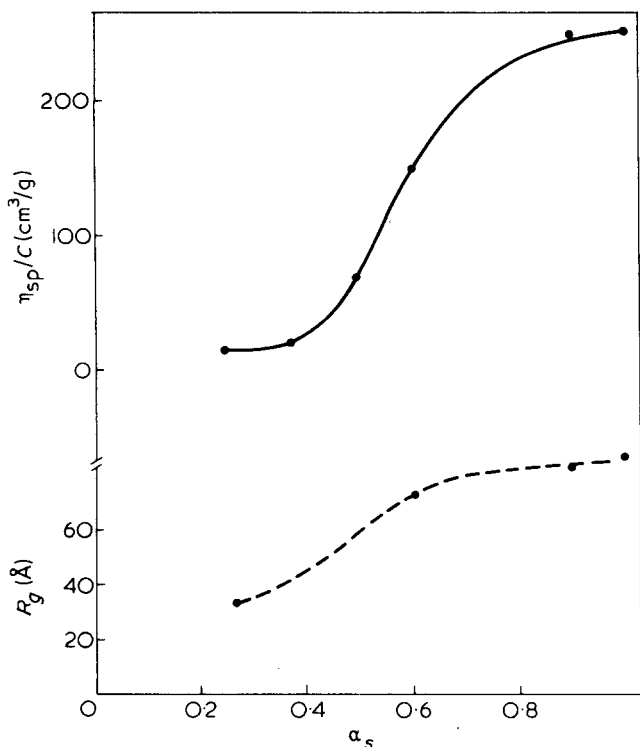


Figure 3 Variation of reduced viscosity  $\eta_{sp}/C$  (—) and gyration radius (---) with the degree of neutralization  $\alpha_s$ , at constant concentration

tion. The Zimm method<sup>4</sup>, used in light scattering, allows us to obtain by extrapolation to both zero concentration and zero angle the radius of gyration at zero concentration and the second virial coefficient  $A_2$ . However, it is unrealistic to use the Zimm method when there are important conformational changes due to intra- and inter-molecular interactions. So, the Zimm plot of Figure 4 was drawn only for the four highest concentrations (at  $\alpha_s = 0.27$ ) when the radius of gyration is almost constant. The relation<sup>4</sup>:

$$\frac{KC}{I(q)} = \frac{1}{M} (1 + q^2 R_g^2/3) + 2A_2C \quad (1)$$

yields  $A_2 = 7 \times 10^{-5} \text{ g}^{-2} \text{ cm}^3$ .

For non-ionic polymers,  $A_2$  is related to the effect of excluded volume arising from the interactions between the solvent and the polymer; thus, the low value  $A_2$  can be explained by the hydrophobic character of methyl groups of PMA.

According to relation (1), the intensity extrapolated to zero angle at each concentration can be written in the form:

$$\frac{KC}{I(0)} = \frac{1}{M} + 2A_2C \quad (2)$$

Figure 5 shows the variation of  $C/I(0)$  with  $C$ , in the whole range of concentrations studies:  $C/I(0)$  decreases sharply at the lowest concentrations and does not follow relation (2). If we only consider the range of concentrations down to  $4 \times 10^{-3} \text{ g/cm}^3$ , an approximate value  $A_2 = 3.5 \times 10^{-3} \text{ g}^{-2} \text{ cm}^3$  can be obtained. It is much higher than the preceding value; this anomalous decrease of  $C/I(0)$  can be explained by the important increase of the polyion interactions, as the concentration is reduced, caus-

ing further expansion of the ionic atmosphere of each polyion<sup>5</sup>.

#### Intermediate momentum-transfer range

When  $qRg > 1$ , the scattering law gives information on the conformation and the rigidity of the polyion<sup>1</sup>. This study has been made on this sample in the whole preceding range of concentrations, but only for a degree of neutralization  $\alpha_s = 0.27$ . Figure 6 shows the variation of the product  $I(q) \times q^2$  with  $q$ , for the most concentrated PMA solution ( $C = 3.2 \times 10^{-2} \text{ g/cm}^3$ ) and the most diluted one ( $C = 5 \times 10^{-4} \text{ g/cm}^3$ ); the plots obtained in these two cases are very different. For  $C = 3.2 \times 10^{-2} \text{ g/cm}^3$  after Guinier's range, the  $I(q) \times q^2$  term is constant and, then the scattered intensity is proportional to  $q^{-2}$ ; this result, which is valid for  $C \geq 3 \times 10^{-3} \text{ g/cm}^3$ , indicates that the polyion has a Gaussian conformation<sup>6</sup>. A careful statistical analysis shows that a law  $I(q) \sim q^{-5/3}$  as predicted theoretically by Des Cloizeaux<sup>8</sup> and De Gennes<sup>9</sup> for Gaussian coil with excluded volume is more probable in this case than the  $I(q) \sim q^{-2}$  law. With respect to Part 1<sup>1</sup>, it can be noted that in the investigated momentum-range, a critical value  $q^*$  is not observed; however, that study which has not been carried on beyond  $q = 10^{-1} \text{ \AA}^{-1}$ , does not allow the existence of such a  $q^*$  value to be denied.

In the case of very dilute solutions  $C \leq 10^{-3}$  the scattered intensity varies as  $q^{-1}$  and not as  $q^{-2}$ ; for example, the data of Figure 7 plotted for  $C = 5 \times 10^{-4} \text{ g/cm}^3$  show this

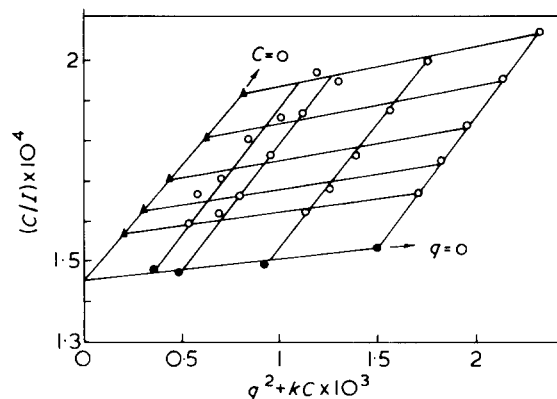


Figure 4 Zimm plot for the four highest concentrations of Figure 1

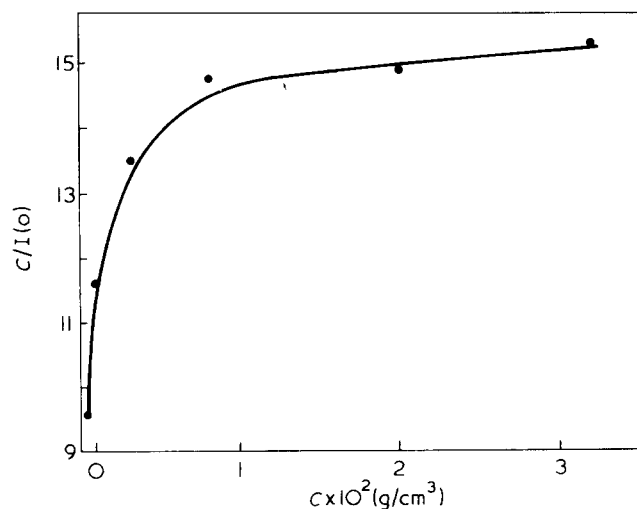


Figure 5 Variation of  $C/I(0)$  with concentration, for the same solutions as in Figure 1

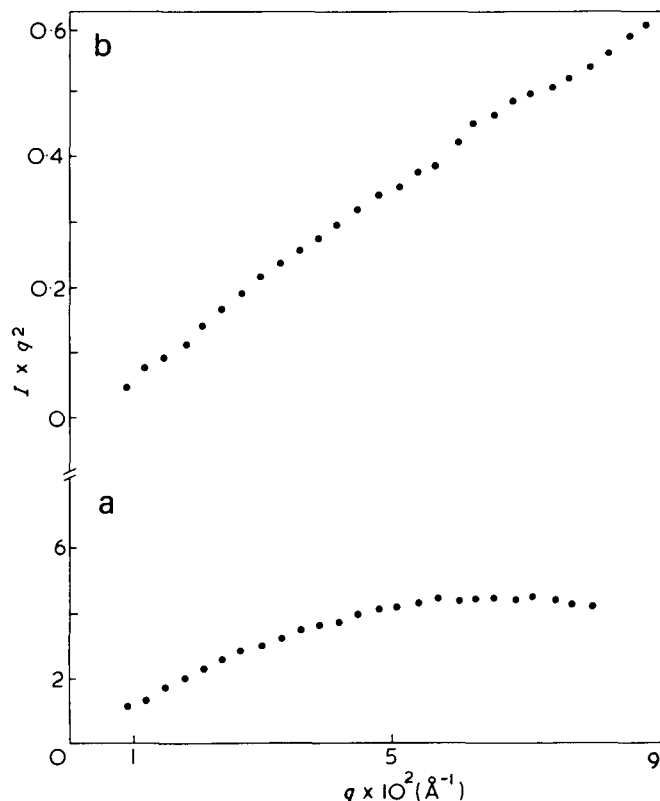


Figure 6 Variation of  $I \times q^2$  with  $q$  for (a)  $C = 3.2 \times 10^{-4}$  and (b)  $C = 5 \times 10^{-4}$  g/cm<sup>3</sup>. The intensity  $I$  is given in arbitrary units

behaviour; from this curve, we can draw two conclusions: (1) the  $q^*$  value, if  $q^*$  exists, is lower than  $q_m = 2.5 \times 10^{-2} \text{\AA}^{-1}$  which corresponds to a rigid segment length higher than  $a_m = 2/q_m = 80 \text{\AA}$ ; (2), although the  $q^{-1}$  behaviour is predicted by the calculation of Porod and Kratky<sup>7</sup> in the case of rod-like particles, we can reasonably suppose that the polyion conformation is closer to a chain of a few rigid segments rather than to a long rod, if we consider the respective values of the gyration radius  $R_g$ , of the fully extended length and of  $a_m$ .

In such a case (low molecular weight polyelectrolyte in a low ionic strength solvent), it is possible to calculate from the values of  $R_g$  and  $a_m$  the few configurations which are possible; this will be discussed later.

#### ACKNOWLEDGEMENTS

We are grateful to Dr Zana (CNRS, Strasbourg) for the

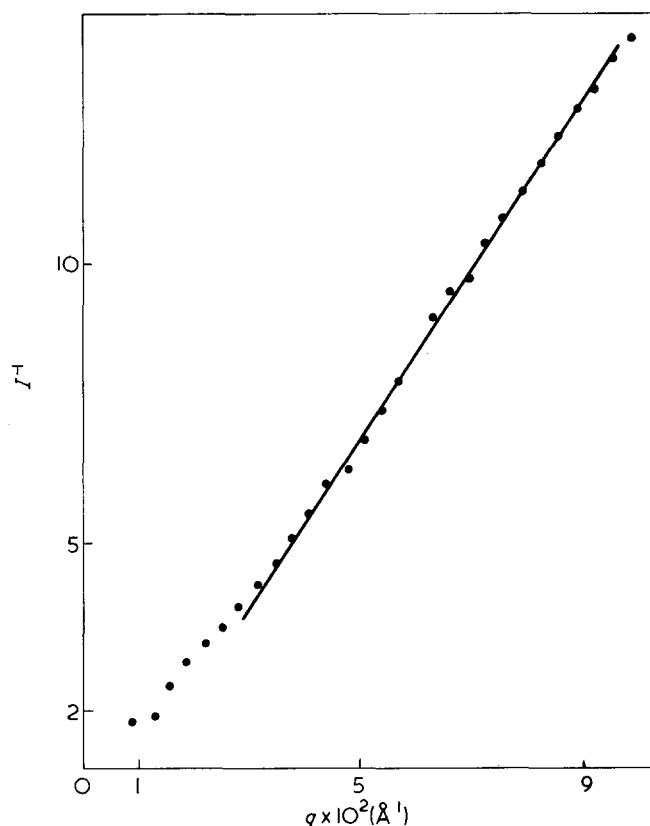


Figure 7 Variation of the inverse scattered intensity with  $q$ , for  $C = 5 \times 10^{-4}$  g/cm<sup>3</sup>

supply of the PMA sample and to the C.E.N. Saclay for allowing us to use the E. L 3 Reactor.

#### REFERENCES

- 1 Moan, M. and Wolff, C. *Polymer* 1975, **16**, 776
- 2 Katchalsky, A., and Eisenberg, H. *J. Polym. Sci.* 1951, **6**, 145
- 3 Noda, I., Tsuge, T. and Nagasawa, M. *J. Phys. Chem.* 1970, **74**, 710
- 4 Zimm, B. H., *J. Chem. Phys.* 1948, **16**, 1093
- 5 Tanford, C. 'Physical chemistry of Macromolecules', John Wiley, New York, 1965
- 6 Debye, P., *Techn. Rep. Cr 637* Office of Rubber Reserve, Washington, 1945
- 7 Kratky, O., Porod, G. and Kahovec, L. *Z. Elektrochem.* 1951, **55**, 53
- 8 Des Cloizeaux, J. *J. Phys. (Paris)* 1970, **31**, 715
- 9 De Gennes, P. G. *Phys. Lett.* 1972, **38A**, 339

# Potentiometric study of poly(L-glutamic acid) in water–dioxane mixtures

Michel Morcellet and Claude Loucheux

Laboratoire de Chimie Macromoléculaire, Université des Sciences et Techniques de Lille, BP 36, 59650 Villeneuve d'Ascq, France

(Received 14 April 1975; revised 29 May 1975)

The potentiometric behaviour of poly(L-glutamic acid) (PLGA) has been studied in several water–dioxane mixtures and 0.2 M NaCl/dioxane mixtures. The intrinsic ionization constant  $pK_0$  was found to increase with dioxane content and decreasing temperature. This variation of  $pK_0$  with dioxane content can be explained by the variation of the dielectric constant,  $\epsilon$  of the solvent. The free energy change  $\Delta F^\circ$  associated with the helix–coil transition for the uncharged conformers has been determined. At 25°C, the absolute value of  $\Delta F^\circ$  increases when decreasing the dielectric constant (i.e. when increasing the dioxane content) but the comparison with the experimental results of other authors show that a change in  $\epsilon$  is not sufficient to explain the variations of  $\Delta F^\circ$  in all solvent mixtures. The temperature dependence of  $\Delta F^\circ$  in different 0.2 M NaCl/dioxane mixtures was determined between 3° and 55°C. The experimental results show that the stabilization of the  $\alpha$  helix by dioxane has an entropic origin as it was already found for a 0.1 M KCl/ethanol/PLGA system. In the absence of salt, a sharp change in the variation of  $\Delta F^\circ$  is observed for the solvent composition at which a solvent induced conformational transition occurs, along with a change in the absolute adsorption of dioxane on the PLGA molecule. The free energy change involved in the adsorption of a molecule of dioxane on a PLGA residue has been evaluated.

## INTRODUCTION

The potentiometric behaviour of poly(L-glutamic acid) (PLGA) has been extensively studied especially in aqueous solutions because the experimental data allows the standard free energy change  $\Delta F^\circ$  for the transition between the uncharged  $\alpha$  helix and the (hypothetical) uncharged random coil to be determined. The effect of the ionic strength<sup>1–3</sup>, of the nature of the counterion<sup>4–7</sup>, and of the temperature<sup>3,8,9</sup> have also been studied.

The addition of an organic solvent to aqueous solutions of PLGA increases the absolute value of  $\Delta F^\circ$  and thus increases the stabilization of the  $\alpha$  helix. Such an effect has been shown for ethanol<sup>10,11</sup> and other aliphatic alcohols<sup>12</sup>. Dioxane is known to have a stabilizing effect on the  $\alpha$  helical conformation of PLGA which is qualitatively similar to that of ethanol (for example the pH of the transition which is 4.9 in 0.2 M NaCl becomes 6.00 in the presence of 33% dioxane<sup>13,14</sup> and 5.8 in the presence of 20% ethanol at 25°C<sup>10</sup>). Nevertheless only few potentiometric measurements have been carried out in water–dioxane mixtures in the presence of salt<sup>3,14</sup>.

The purpose of this work has been to study more completely the potentiometric behaviour of PLGA in water–dioxane mixtures in the presence or in the absence of salt, at different temperatures. Moreover, PLGA is known to undergo, at constant pH, a solvent induced transition which has been shown to be correlated to a sharp increase in the absolute adsorption of the organic solvent on the polymer<sup>13</sup>. Therefore it was interesting to seek a possible further correlation between this preferential adsorption and the value of  $\Delta F^\circ$  when varying the composition of the water–dioxane mixtures.

## EXPERIMENTAL

The PLGA sample (in the acid form) was prepared in the laboratory by debenzoylation of a poly( $\gamma$ -benzyl-L-glutamate) sample according to the method of Idelson and Blout<sup>15</sup>. The intrinsic viscosity, measured under the standard conditions of Wada<sup>1</sup>, i.e. 25°C, pH 7.3 in 0.2 M NaCl, is 29.0 ml/g, corresponding to a weight-average molecular weight  $M_w = 12\,200$ . In some cases measurements were also carried out on another sample ( $M_w = 33\,000$ ). The results obtained for both samples were always self consistent within experimental errors. pH measurements were made with a Radiometer pH M 26 pHmeter with the use of a G 202 C glass electrode in conjunction with a K.101 calomel electrode. The pHmeter was standardized with aqueous buffers (pH 8.00 and 4.45). No corrections were made for the actual hydrogen ion activity in water–dioxane mixtures. Thus apparent pH values were used throughout this paper. The temperature in the titration vessel was maintained at the desired value within  $\pm 0.1^\circ\text{C}$ .

The solutions were prepared by dissolving a weighted amount of PLGA in the solvent of the required composition, containing a slight excess of NaOH.

The titrations were carried out on fresh solutions containing about 40 mg in 20 ml of solution. Appropriate blank titrations of the solvent were also performed.

### Dielectric constant

The dielectric constant of pure water was taken as  $\epsilon_w = 78.3$  at 25°C. For salt solutions the relation  $\epsilon = \epsilon_w + 2\delta c$  was used, where  $c$  is the salt concentration in mol/l and  $\delta$  is a constant depending on the nature of the salt<sup>16</sup>. For

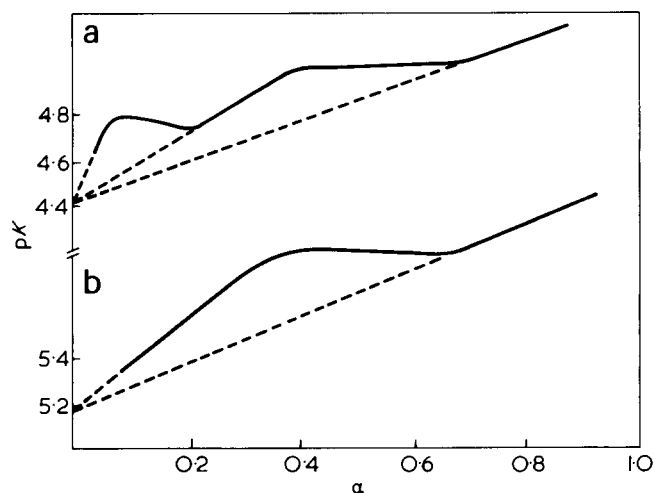


Figure 1 Modified titration curves for PLGA in (a) 0.2 M NaCl and (b) 0.2 M NaCl/dioxane mixture (70:30 v/v) at 25°C

NaCl and KCl,  $\bar{\delta} = -5.51/\text{mol}$  and  $-5.01/\text{mol}$  respectively. Thus  $\epsilon$  is 76.1 for 0.2 M NaCl and 77.3 for 0.1 M KCl. In the case of mixtures with dioxane ( $\epsilon = 2.2$ ) or ethanol ( $\epsilon = 24.3$ ) the dielectric constant was assumed to be linearly dependent on the composition.

## RESULTS AND DISCUSSION

### pH induced transition

**Values of  $pK_0$ .** Some of the modified titration curves where the apparent  $pK$ ,  $pK_{\text{app}} = \text{pH} - \log \alpha/(1 - \alpha)^{17}$  are plotted as a function of the degree of ionization  $\alpha$ , are shown in Figure 1. At 25°C, in the presence of salt (0.2 M NaCl) (Figure 1a) the parts of the curve corresponding to the pure helix ( $\alpha < 0.38$ ) and to the pure coil ( $\alpha > 0.70$ ) are straight lines. A linear extrapolation at  $\alpha = 0$  for the helix and for the coil gives the same value for the intrinsic ionization constant  $pK_0$  of the polyacid. The values of  $pK_0$  obtained as a function of the dioxane content at different temperatures are given in Table 1.

It can be seen that  $pK_0$  increases when increasing the dioxane content and/or decreasing temperature. The value of  $pK_0 = 4.40$  obtained at 25°C in 0.2 M NaCl is in good agreement with those of other authors: 4.45<sup>2</sup>, 4.37<sup>14</sup>. In 0.2 M NaCl/dioxane mixtures the enthalpy of ionization of PLGA can be deduced from the temperature dependence of  $pK_0$ . This value was found to be  $\Delta H = 3100$ , 3000 and 2900 cal/mol for 10, 20 and 30% of dioxane respectively. Thus, an increase of  $\Delta H$  is observed by adding dioxane as in the case of ethanol<sup>10</sup> (the value of  $\Delta H$  is only 550 cal/mol in the absence of any organic solvent<sup>10</sup>).

At 25°C, in the lower pH range, a deviation from a pure helix titration curve is observed below  $\alpha = 0.18$ , which is known as the 'aggregation peak'. The extrapolation of this part of the titration curve leads to a value of  $pK_0$  which is the same as the value obtained when extrapolating either the 'coil part' or the 'helix part' of the titration curve. When adding dioxane, the aggregation disappears and the preceding peak vanishes (see in Figure 1 the curve corresponding to a 30% dioxane mixture). In the absence of salt curvilinear extrapolations<sup>2,14</sup> were used in order to determine the value of  $pK_0$  at  $\alpha = 0$  assuming also that  $pK_0$  must be the same for the helix and for the coil. The values obtained are also given in Table 1. It can be seen that  $pK_0$  increases in the same manner in the presence or in the

absence of salt being, however, slightly smaller in the first case.

The increase in the values of  $pK_0$  when adding dioxane, accounts for the changes observed in the values of pH 1/2, the pH at the midpoint of the helix–coil transition of PLGA. For instance, the helix–coil transition was monitored by circular dichroism in several solvent mixtures. The values of pH 1/2 and  $pK_0$  are collected in Table 2. It can be concluded that pH 1/2 and  $pK_0$  increase simultaneously.

Conio and Patrone<sup>10</sup> have suggested that the variations of  $pK_0$  with the solvent composition should be qualitatively explained by a variation of the dielectric constant  $\epsilon$ , as it is the case for model aliphatic monofunctional carboxylic acids.

In Figure 2 the values of  $pK_0$  measured in different solvent mixtures are plotted as a function of  $\epsilon$ . Some literature data are also given in this Figure along with data relative to acetic acid in water–dioxane mixtures<sup>18</sup>. The small difference of 0.1  $pK$  unit observed between the two curves corresponding to water–dioxane mixtures and 0.2 M NaCl/dioxane mixtures can be assigned to the variation of the ionic strength<sup>3,19</sup>. In all cases the variation of the dielectric constant accounts for the variation of  $pK_0$ , in water–dioxane mixtures and in ethanol–water mixtures where the variations of  $pK_0$  with organic solvent composition are much smaller. This effect can be quantitatively described by the Born's relation<sup>20</sup>:

$$-\log \frac{{}_sK_A}{{}_wK_A} = \frac{e^2}{rkT \ln 10} \left[ \frac{1}{\epsilon} - \frac{1}{\epsilon_w} \right]$$

where  ${}_sK_A$  and  ${}_wK_A$  are the ionization constants in the solvent mixture and in water,  $e$  is the charge of the proton,  $k$  the Boltzmann's constant,  $T$  the absolute temperature,  $\epsilon$

Table 1 Values of  $pK_0$  for 0.2 M NaCl/dioxane and water–dioxane solutions of PLGA at different temperatures

Dioxane (% v/v)	$t$ (°C)	$pK_0$ (0.2 M NaCl)	$pK_0$ (H <sub>2</sub> O)
0	25	4.40	4.45
10	3.5	4.85	—
	11.5	4.63	—
	25	4.68	4.80
20	41	4.53	—
	55	4.46	—
	3.5	5.02	—
	15	4.80	—
	25	4.95	5.05
30	41	4.83	—
	55	4.71	—
	3.5	5.16	—
	11.5	5.25	—
	25	5.18	5.26
40	41	5.11	—
	55	4.98	—
	25	—	5.60
50	25	—	5.75

Table 2 Values of pH 1/2 and  $pK_0$  for different solvent mixtures

Solvent	pH 1/2	$pK_0$
5 M NaCl	4.50	3.67
0.2 M NaCl/H <sub>2</sub> O	4.90	4.41
	5.35	4.45
0.2 M NaCl/dioxane (2:1)	6.00	5.50
	H <sub>2</sub> O/dioxane (2:1)	6.95

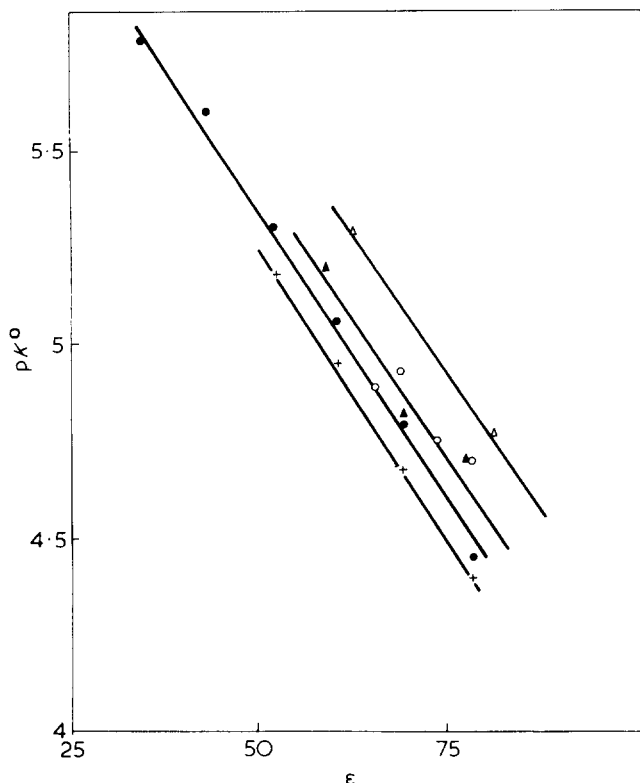


Figure 2 Variation of  $pK_0$  versus the dielectric constant  $\epsilon$  at 25°C: +, PLGA in 0.2 M NaCl/dioxane mixtures; ●, PLGA in water-dioxane mixtures; ○, PLGA in 0.1 M KCl/ethanol mixtures<sup>10</sup>; ▲, PLGA in 0.1 M KCl/ethanol mixtures<sup>11</sup>; △, acetic acid in water-dioxane mixtures<sup>18</sup>

and  $\epsilon_w$  the dielectric constant of the solvent mixture and of water respectively. The use of this equation constant gives for the water-dioxane-PLGA system:

$$-\log \frac{sK_A}{wK_A} = -1.79 + \frac{140}{\epsilon}$$

which can be compared with:

$$-\log \frac{sK_A}{wK_A} = -1.77 + \frac{140}{\epsilon}$$

obtained for the propionic acid in the same solvent mixture<sup>21</sup>.

Thus, the effect of the solvent on the ionization constant of PLGA is quite similar to that observed for the low molecular weight models. This result is not surprising if one considers that the  $pK_0$  values are obtained by an extrapolation at  $\alpha = 0$ , in order to eliminate the effect of the interactions between neighbouring carboxylic groups.

**Values of  $\alpha$  at the midpoint of the transition.** The values  $\alpha_{1/2}$  of  $\alpha$  at the midpoint of the transition are plotted in Figure 3 as a function of the temperature for the different solvent mixtures. It can be seen that  $\alpha_{1/2}$  decreases when increasing the temperature in each solvent mixture. This decrease of  $\alpha_{1/2}$  is accompanied by a decrease of the pH at the midpoint of the transition. This result was easily foreseeable, for it is well known that an increase of the temperature decreases the stability of the  $\alpha$  helix.

**Free energy of the helix-coil transition.** The free energy  $\Delta F^\circ$  of the transition between the uncharged conformers can be determined from the preceding modified titration curves. According to Zimm and Rice<sup>17</sup> the area

$A$  between the actual curve and the extrapolated curves for the helix and the coil is related to the free energy of transition:  $-\Delta F^\circ = A RT \ln 10$ . The experimental values of  $\Delta F^\circ$  have been determined at 25°C for several water-dioxane and 0.2 M NaCl/dioxane mixtures. These data are plotted in Figure 4 as  $\Delta F^\circ$  versus the dioxane content (% v/v) along with data of Conio and Patrone<sup>10</sup> relative to 0.1 M KCl/ethanol mixtures. At 0% dioxane in 0.2 M NaCl,  $\Delta F^\circ = -106$  cal/mol is in very good agreement with the values of other authors<sup>22</sup>. In the absence of salt, the values of  $\Delta F^\circ$  are somewhat less accurate owing to the use of curvilinear extrapolation necessary to obtain the same  $pK_0$  value for helix and coil. In the absence of salt and dioxane, the value of  $\Delta F^\circ$  is  $-175 \pm 10$  cal/mol, in rather good agreement with the value of  $-192$  cal/mol reported by Olander and Holtzer<sup>3</sup> for PLGA in 0.01 M NaCl.

The effect of dioxane is to increase the absolute value of  $\Delta F^\circ$  i.e. to stabilize the  $\alpha$  helix as observed for ethanol<sup>10</sup>. In both cases (i.e. in the presence or in the absence of salt) the variation of  $\Delta F^\circ$  with the solvent composition is linear until about 25% dioxane. In the presence of salt the variation of  $\Delta F^\circ$  with the composition of the solvent is much greater in the case of ethanol. The question arises whether that difference is due or not to a difference in the ionic strength or in the nature of the salt.

In the case of KCl or KSCN, it has been shown that a variation of the ionic strength from 0.1 to 1.2 was of little effect on the value of  $\Delta F^\circ$ <sup>22</sup>. Moreover, the counterions  $K^+$  and  $Na^+$  have the same effect on the variation of  $\Delta F^\circ$ <sup>7</sup>. Thus the change from 0.1 M KCl to 0.2 M NaCl has probably a negligible effect on the variation of  $\Delta F^\circ$ . As confirmation we determined the value of  $\Delta F^\circ$  in a mixture of 0.2 M NaCl/ethanol (81:19 v/v). It was found to be  $-190$  cal/mol, in good agreement with the results of Conio and Patrone<sup>10</sup> for 0.1 M KCl/ethanol mixtures.

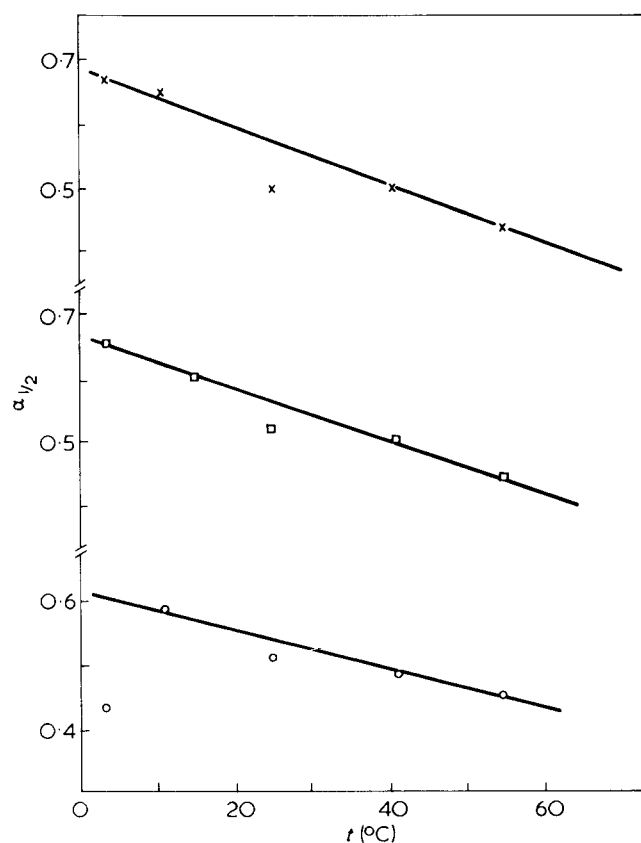


Figure 3 Variation of  $\alpha_{1/2}$  versus the temperature for PLGA in different 0.2 M NaCl/dioxane mixtures: ○, 10%; □, 20%; ×, 30%

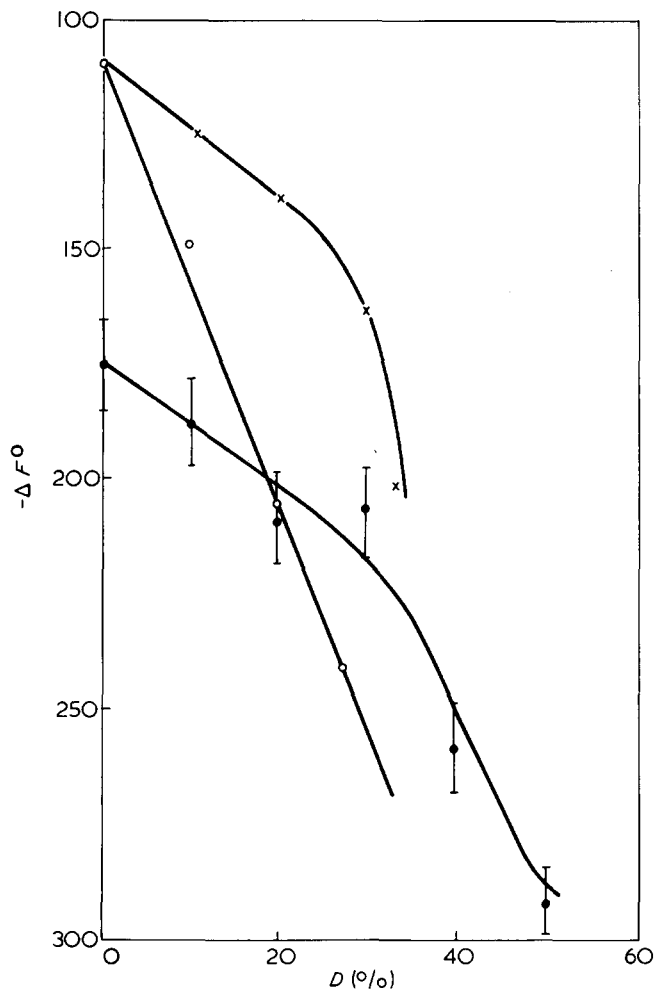


Figure 4 Variation of  $\Delta F^\circ$  at 25°C versus the dioxane content. X, PLGA in 0.2 M NaCl/dioxane mixtures; ●, PLGA in water-dioxane mixtures; ○, PLGA in 0.1 M KCl/ethanol mixtures<sup>10</sup>

In 0.2 M NaCl, the value of  $\Delta F^\circ$  obtained for 33% dioxane is very different from the linear behaviour exhibited for lower dioxane contents. Beyond this solvent composition, further addition of dioxane causes the polymer to precipitate<sup>23</sup>. Pederson *et al.*<sup>24</sup> have determined the free energy involved by the transfer on the peptidic backbone of poly(L-lysine) from pure water to 10% ethanol mixture. They found  $\Delta F^\circ = 41$  cal/mol, a value which is close to the free energy of transfer of a peptidic group from water to 10% ethanol (60 cal/mol)<sup>25</sup> for model low molecular weight amides or amino acids.

In the case of PLGA the transfer from water to 10% ethanol mixture gives  $\Delta F^\circ = 41$  cal/mol<sup>10</sup> while the transfer from water to 10% dioxane gives 16 cal/mol in our experiments. Thus dioxane has a much less stabilizing effect on the PLGA helix than ethanol.

Rather than in terms of organic solvent composition, the experimental results may be treated as a function of the methylene molarity according to Von Hippel and Wong<sup>26</sup>. On this ground, Conio *et al.*<sup>12</sup> found that the increment of the free energy per methylene molarity [ $\Delta(\Delta F^\circ)/\text{mmol}$ ] was constant for PLGA or poly(L-ornithine) in mixtures of water with methanol, ethanol, propanol, and butanol on the entire range of solvent composition. This value is  $\Delta(\Delta F^\circ)/\text{mmol} = -13$  cal/mmol. Such a calculation, applied to the PLGA/water/dioxane system gives an increment of the free energy per methylene molarity equal to  $-3$  cal/mmol. This result supports the

conclusion that dioxane has a much less stabilizing effect than ethanol. In a more recent paper, Dubin<sup>27</sup> proposed an alternative way to account for experimental results in the domain. Using the data of Conio *et al.*<sup>12</sup>, he showed that a plot of  $\Delta F^\circ$  versus the dielectric constant  $\epsilon$  was a unique curve regardless of the nature of the alcohol. This is in good agreement with the fact that  $\Delta F^\circ$  depends only on methylene molarity, at least in water/alcohol mixtures. Nevertheless, Dubin suggests that parameters other than the dielectric constant must have an influence on  $\Delta F^\circ$ . Our experimental results obtained in 0.2 M NaCl/dioxane mixtures support this suggestion. Figure 5 shows that in this case a linear variation of  $\Delta F^\circ$  with  $\epsilon$  is obtained, but the curve is very different from the corresponding curve for alcohols. Thus it seems that the nature of the organic solvent plays an important role in the stabilization of the  $\alpha$  helix.

Further investigation must be carried out in other water/organic solvent systems to cast some light on this problem.

#### Temperature dependence of the free energy of transition

The temperature dependence of  $\Delta F^\circ$  in 0.2 M NaCl/dioxane mixtures was previously studied by Bychkova and Coll<sup>14</sup> for 25% and 33% dioxane mixtures. They found that a common straight line can be drawn through the values corresponding to these two mixtures, giving  $\Delta H^\circ = -1700$  cal/mol and  $\Delta S^\circ = -4.86$  for the enthalpy and the entropy of transition.

Nevertheless, the results of Figure 4 show that, at 25°C, the values of  $\Delta F^\circ$  beyond 25% of dioxane are disturbed by the vicinity of the limit of precipitation. Thus we re-investigated the temperature dependence of  $\Delta F^\circ$  in mixtures with 10, 20 and 30% of dioxane. The results obtained are shown in Figure 6. The corresponding values of  $\Delta H^\circ$  and  $\Delta S^\circ$  are given in Table 3. These results are similar to those previously reported for PLGA in 0.1 M KCl/ethanol mixtures<sup>10</sup> leading to the conclusion that the stabilization of the  $\alpha$  helix by dioxane is essentially an entropic effect. Conio *et al.* have suggested that, in the case of ethanol, the solvation of the peptide amide group in the randomly coiled conformation may be responsible for the observed increase in  $\Delta S^\circ$ . In the case of dioxane, we have shown<sup>13</sup> that a strong preferential adsorption of dioxane occurs on the ionized coil PLGA molecule. This supports the assumption that the solvation of the random coil takes an important part in the changes of  $\Delta S^\circ$ .

#### Solvent-induced transition

In the absence of salt, the solubility limit is reached beyond 50% of dioxane. Between 30 and 50% of dioxane,

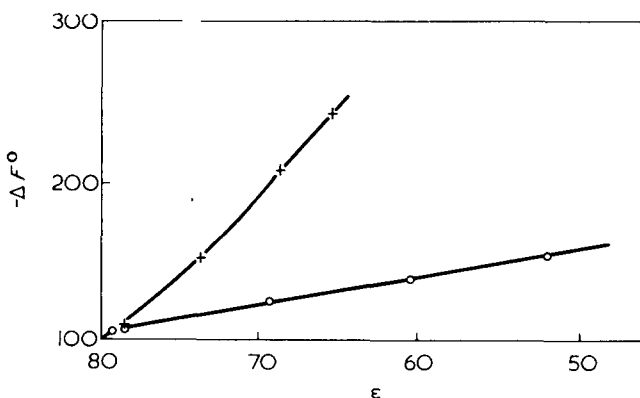


Figure 5 Variation of  $\Delta F^\circ$  at 25°C versus the dielectric constant  $\epsilon$ . ○, PLGA in 0.2 M NaCl/dioxane mixtures; +, data of Conio and Patrone<sup>10</sup> for PLGA in 0.1 M KCl/ethanol mixtures

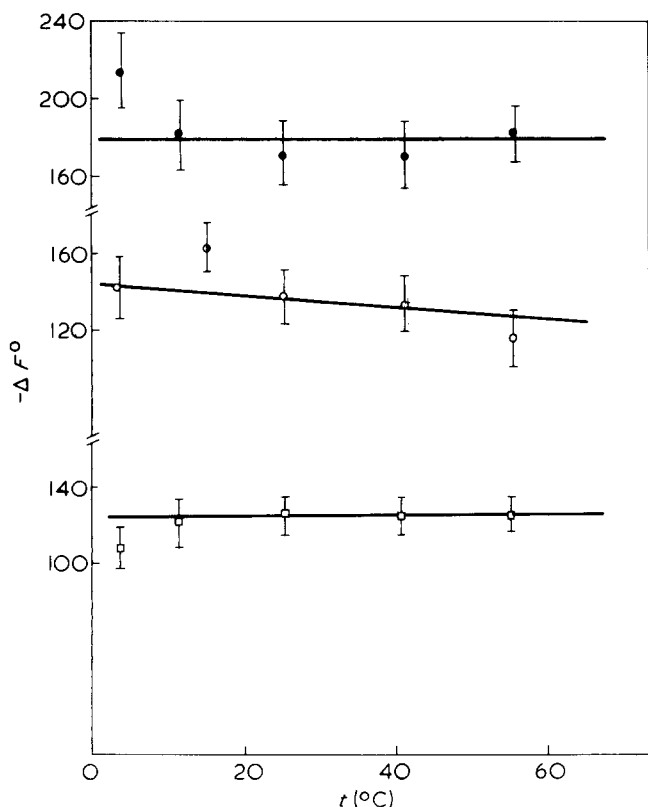


Figure 6 Variation of  $\Delta F^\circ$  versus the temperature for PLGA in different 0.2 M NaCl/dioxane mixtures:  $\square$ , 10%;  $\circ$ , 20%;  $\bullet$ , 30%

Table 3 Thermodynamic parameters for PLGA in 0.2 M NaCl/dioxane mixtures

	Dioxane (% v/v)			
	0% <sup>a</sup>	10%	20%	30%
$\Delta F^\circ$ (25°C)	-107	-124	-137	-164
$\Delta H^\circ$	-1200	-124	-200	-180
$\Delta S^\circ$	-3.3	0	-0.3	0

<sup>a</sup> Data of Ciferri *et al.*<sup>22</sup>

a sharp variation of  $\Delta F^\circ$  is observed (Figure 4). This sharp variation occurs at a solvent composition for which, at constant pH, a solvent induced helix–coil transition takes place. This transition has been monitored by circular dichroism by plotting the ellipticity at 222 nm,  $[\theta]_{222}$  as a function of the solvent composition<sup>13</sup>. Figure 7 shows that the variation of  $\Delta F^\circ$  parallels exactly the transition followed by circular dichroism.

Moreover, light scattering and differential refractometry studies on some proteins<sup>24–27</sup> and on PLGA<sup>13</sup> in solvent mixtures have shown that the preferential and absolute adsorption of the organic solvent on the polymer can be related to the conformational transition induced by the change of the solvent composition. Especially it has been pointed out that the absolute adsorption of organic solvent increases with the helix content.

In Figure 7, is also plotted the variation of the absolute adsorption  $A_3$  of dioxane on PLGA<sup>13</sup>. The change of the absolute adsorption between 30 and 50% of dioxane (i.e. between the beginning and the end of the transition) is about half a molecule of dioxane per residue of PLGA. (There is about half a molecule of dioxane adsorbed at 30% of dioxane and about one molecule at 50% when extrapolating the experimental curve to 100% helicity.) Taking

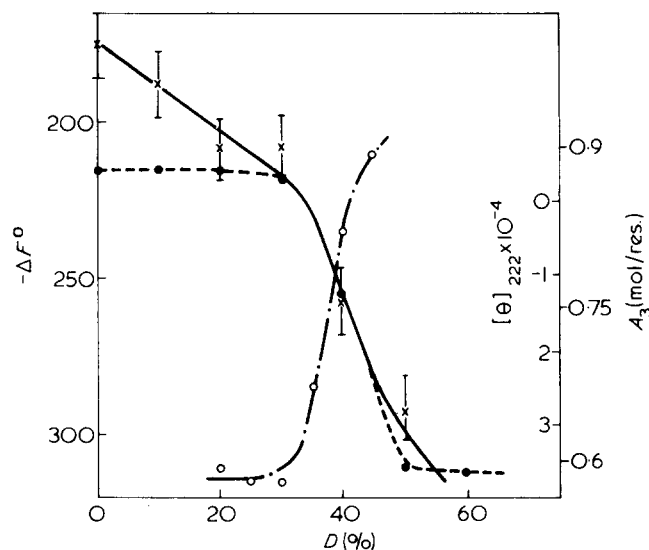


Figure 7 Variation of  $\Delta F^\circ$  (X),  $[\theta]_{222}$  (●) and  $A_3$  (○) versus the dioxane constant for PLGA in different water–dioxane mixtures

into account the value of about 50 cal/mol for the change in  $\Delta F^\circ$ , the free energy change involved by the adsorption of a dioxane molecule on a PLGA residue can be estimated to be 80–100 cal/mol. This value must be considered only as an estimation for two reasons: first the unreliability on the values of  $\Delta F^\circ$  measured in the absence of salt; secondly, the unreliability on the number of dioxane molecule bound to a PLGA residue, partly due to the fact that PLGA begins to precipitate before the transition is completely achieved. Moreover, the observed change in  $\Delta F^\circ$  is the sum of at least two contributions: (i) the change in  $\Delta F^\circ$  due to the adsorption of dioxane on the molecule which has been shown to increase strongly beyond 30% of dioxane; (ii) the change in  $\Delta F^\circ$  involved by the solvent induced transition which is not achieved when the solubility limit is reached. At the present time, the splitting between the different contributions is difficult.

## CONCLUSION

The experimental results show that the variation of the  $pK_0$  of PLGA in solvent mixtures depends on the variation of the dielectric constant  $\epsilon$  as it is in the case for model carboxylic acids. The free energy of the helix coil transition is also dependent on  $\epsilon$  but other parameters are probably involved in the stabilization of the  $\alpha$  helix. In the absence of salt, a sharp variation of  $\Delta F^\circ$  is observed which is related to the solvent induced helix–coil transition and to the absolute adsorption of the organic solvent on the polymer, showing that the free energy of the helix–coil transition is strongly dependent on the state of solvation of the polymer.

## REFERENCES

- 1 Wada, A. *Mol. Phys.* 1960, 3, 409
- 2 Nagasawa, M. and Holtzer, A. *J. Am. Chem. Soc.* 1964, 86, 538
- 3 Olander, D. S. and Holtzer, A. *J. Am. Chem. Soc.* 1968, 90, 4549
- 4 Jacobson, A. L. *Biopolymers* 1963, 1, 269
- 5 Jacobson, A. L. *Biopolymers* 1964, 2, 207
- 6 Barone, G., Crescenzi, V. and Quadrioglio, F. *Biopolymers* 1966, 4, 529
- 7 Conio, G. *et al. Biopolymers* 1974, 13, 1483
- 8 Miller, W. G. and Nylund, R. E. *J. Am. Chem. Soc.* 1965, 87, 3542

- 9 Hermans, Jr J. *J. Phys. Chem.* 1966, **70**, 510
- 10 Conio, G. and Patrone, E. *Biopolymers* 1969, **8**, 57
- 11 Hermans, Jr J. *J. Am. Chem. Soc.* 1966, **88**, 2418
- 12 Conio, G., Patrone, E. and Brighetti, S. *J. Biol. Chem.* 1970, **245**, 3335
- 13 Morcellet, M. and Loucheux, C. *Polymer* 1975, **16**, 401
- 14 Bychkova, V. E., Ptitsyn, O. B. and Barskaya, T. V. *Biopolymers* 1971, **10**, 2161
- 15 Idelson, M. and Blout, E. R. *J. Am. Chem. Soc.* 1958, **80**, 4631
- 16 Hasted, J. B., Ritson, D. M. and Collie, C. H. *J. Chem. Phys.* 1948, **16**, 1
- 17 Zimm, B. H. and Rice, S. A. *Mol. Phys.* 1960, **3**, 391
- 18 Harned, H. S. and Kazanjian, G. L. *J. Am. Chem. Soc.* 1936, **58**, 1912
- 19 Harned, H. S. and Owen, B. 'The Physical Chemistry of Electrolytic Solutions', 3rd Edn, Reinhold, New York, 1963, pp 676, 677
- 20 King, E. J. 'Acid/Base Equilibria: The International Encyclopedia of physical Chemistry and Chemical Physics', Pergamon Press, New York, 1st Edn, 1965, pp 255-258
- 21 Robinson, R. A. and Stokes, R. H. 'Electrolyte solutions', 2nd Edn, Butterworths, London, 1959, Ch 12
- 22 Ciferri, A., Puett, D., Rajagh, L. and Hermans, Jr J. *Biopolymers* 1968, **6**, 1019
- 23 Iizuka, E. and Yang, J. T. *Biochemistry* 1965, **4**, 1249
- 24 Pederson, D., Gabriel, D. and Hermans, Jr J. *Biopolymers* 1971, **10**, 2133
- 25 Cohn, E. J. and Edsall, J. T. 'Proteins, Amino Acids and Peptides', Reinhold, New York, 1943
- 26 von Hippel, P. H. and Wong, K. Y. *J. Biol. Chem.* 1965, **240**, 3909
- 27 Dubin, P. L. *Biopolymers* 1973, **12**, 685
- 28 Inoue, H. and Timasheff, S. N. *J. Am. Chem. Soc.* 1968, **90**, 1890
- 29 Timasheff, S. N. and Inoue, H. *Biochemistry* 1968, **7**, 2501
- 30 Timasheff, S. N. *Acc. Chem. Res.* 1970, **3**, 62
- 31 Inoue, H. and Timasheff, S. N. *Biopolymers* 1972, **11**, 737



# Electro-optical properties of poly( $\epsilon$ -carbobenzoxy-L-lysine) in organic solvents

Masaharu Nishioka, Kazuo Kikuchi and Koshiro Yoshioka

Department of Chemistry, College of General Education, University of Tokyo, Meguroku, Tokyo, Japan  
(Received 17 February 1975; revised 25 March 1975)

The electric birefringence of poly( $\epsilon$ -carbobenzoxy-L-lysine) (PCBL) in various helicogenic organic solvents and solvent mixtures has been measured over a wide range of field strengths by application of rectangular pulses. The apparent permanent dipole moment and the optical anisotropy factor were separately determined from the field strength dependence of the steady-state birefringence. The apparent dipole moment per residue for a PCBL sample with molecular weight close to  $1 \times 10^5$  fell in the range of 4.7 to 5.9 D in spite of the large variation of the solvent dielectric constant. The optical anisotropy factor was appreciably small and changed its sign depending upon the solvent. The intrinsic birefringence of PCBL was found to be negative in sign on the basis of the Peterlin-Stuart theory. This was interpreted in terms of the orientation of the side chains with respect to the helical backbone. The apparent dipole moment per residue for high molecular weight PCBL samples was much smaller, indicating a considerable flexibility of the helix.

## INTRODUCTION

Poly( $\epsilon$ -carbobenzoxy-L-lysine) (PCBL) is a precursor of poly(L-lysine) in the ordinary synthetic procedure. The optical rotatory dispersion and circular dichroism spectra indicate that this un-ionized polypeptide exists in a helical conformation in a variety of organic solvents<sup>1-4</sup>. Helix-coil transitions of PCBL in solution, induced by changing the solvent composition or the temperature, have been investigated by polarimetric, calorimetric and viscometric measurements<sup>4,5-9</sup>. The stability of the helix of PCBL was shown to be weaker than that of poly( $\gamma$ -benzyl-L-glutamate) (PBLG), a closely analogous polypeptide<sup>5</sup>. The transition in PCBL systems was found to be considerably more cooperative, compared with PBLG or poly( $\beta$ -benzyl-L-aspartate)<sup>4,6</sup>.

Light scattering and hydrodynamic studies (including viscosity, diffusion, sedimentation and flow birefringence) on PCBL samples of widely different molecular weights have revealed that the PCBL helix is distinctly more flexible than the PBLG helix<sup>1,2,4,10,11</sup>. This was attributed to the existence of more frequent breaks in the PCBL helix. The nature of the side chain might play an important role in determining both the stability and the flexibility of polypeptide helices<sup>2,10</sup>.

Recently, two dielectric studies on PCBL solutions have been reported. Frolov *et al.*<sup>12</sup> have measured the dielectric dispersion of dilute chloroform solutions of various PCBL samples, determining the specific static dielectric increment and the critical frequency as functions of the molecular weight. From the results the persistence length and the permanent dipole moment per amino acid residue were calculated to be 26 nm and 4 D, respectively. Omura *et al.*<sup>13</sup> have measured the dielectric dispersion of PCBL preparations with relatively low molecular weights (rang-

ing from  $2.3 \times 10^4$  to  $8.7 \times 10^4$ ) in *m*-cresol at various temperatures. As found by Matsuoka *et al.*<sup>4</sup>, PCBL in *m*-cresol undergoes a sharp, thermally induced helix-coil transition of inverse type near the room temperature. From the temperature dependence of the dielectric dispersion and the optical rotation, the square average of the dipole moment and the dielectric relaxation time were obtained as functions of the helical content.

Only one electro-optical study on PCBL has ever been published, as far as we are aware. Tsvetkov *et al.*<sup>14</sup> have measured the electric birefringence of one sample of PCBL in dimethylformamide (DMF) and dichloroacetic acid. The specific Kerr constant of the helical conformation of PCBL in DMF was found to be much smaller than that of PBLG with nearly the same molecular weight in the same solvent.

In the present work we have studied the electro-optical properties of a number of PCBL samples in various helicogenic organic solvents and their mixtures. From the field strength dependence of the electric birefringence the permanent dipole moment and the optical anisotropy factor were separately determined according to the usual procedure. The results indicate that the optical anisotropy factor of PCBL is appreciably smaller than that of PBLG and changes its sign depending upon the solvent.

## EXPERIMENTAL

The PCBL samples were prepared by the polymerization of  $\epsilon$ ,*N*-carbobenzoxy-L-lysine *N*-carboxyanhydride in dioxane using sodium methoxide as an initiator according to the method of Fasman *et al.*<sup>5</sup>. The resulting polymers were precipitated with ethanol, dissolved in chloroform and reprecipitated with *n*-hexane. Finally they were lyophilized from dioxane and stored in a refrigerator at low tempera-

**Table 1** Intrinsic viscosity in DMF and molecular weight data for PCBL samples

Sample	Intrinsic viscosity (dl/g)	Molecular weight $\times 10^{-4}$
I	0.549	9.9
II	0.633	12
III	5.77	62
IV	8.92	88

tures. Measurement of the intrinsic viscosity in DMF at 25°C enabled the molecular weight of these samples to be determined using the relationship obtained by Matsuoka et al.<sup>4</sup>. Intrinsic viscosity and molecular weight data for the PCBL samples used are quoted in Table 1.

The solvents used were dichloroethane, chloroform, tetrabromoethane, dioxane, tetrahydrofuran, DMF, hexamethylphosphoramide (HMPA) and *m*-cresol. Most of these solvents were purified by the standard procedure. The tetrabromoethane was of reagent grade and used without further purification. Mixed solvents were made up on a volume basis.

The electric birefringence measurements were carried out in the apparatus previously described<sup>15-17</sup>. The electric field was applied to the solution in a Kerr cell in the form of single rectangular pulses of up to 6 kV amplitude. The Kerr cell contained two platinum electrodes spaced 0.205 cm apart.

The optical retardation  $\delta$  of the solution due to the electric field was obtained following the procedure described in a previous paper<sup>17</sup>. The electric birefringence,  $\Delta n$ , is related to  $\delta$  by:

$$\Delta n/\lambda = \delta/2\pi l \quad (1)$$

where  $l$  is the path length of light through the birefringent medium and  $\lambda$  is the wavelength of light *in vacuo*. In this experiment,  $l = 0.979$  cm and  $\lambda = 546$  nm. We define the Kerr constant  $B$  by:

$$B = (\delta/2\pi l E^2)_{E \rightarrow 0} = (\Delta n/\lambda E^2)_{E \rightarrow 0} \quad (2)$$

where  $E$  is the applied field strength.

In the case of determining the sign of the electric birefringence of the solution, a Babinet-Soleil compensator was interposed between the Kerr cell and the analyser crossed with the polarizer<sup>18</sup>. Its optic axis was parallel to the electric field. For this optical system the change in light intensity at the photomultiplier produced by the field,  $\Delta I$ , is given by:

$$\Delta I = I_0 \sin(\delta/2) \sin(\delta/2 + \delta_c) \quad (3)$$

where  $I_0$  is the change in light intensity upon rotating the analyser from the crossed to the parallel position in the absence of optical retardation and  $\delta_c$  is the retardation of the compensator. For large  $\delta_c$  and small  $\delta$ , equation (3) is approximated by:

$$\Delta I = I_0(\delta/2) \sin \delta_c \quad (4)$$

Thus the light signal increases if  $\delta$  is positive and decreases if  $\delta$  is negative. This permits us to determine the sign of the birefringence.

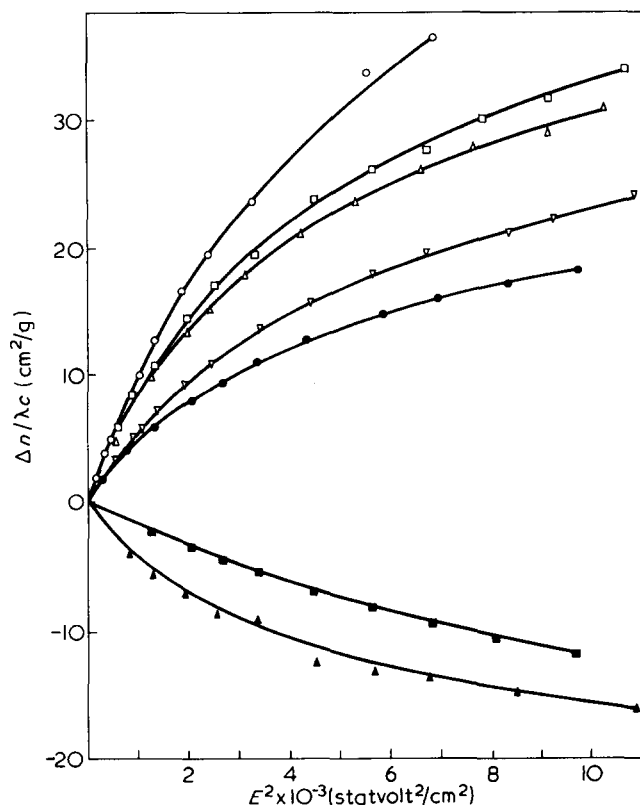
The contribution of the solvent to the birefringence

was subtracted from the experimental values for solutions, whenever it was not negligible. This solvent correction is especially large in the case of DMF, HMPA and *m*-cresol, since these solvents have large Kerr constants. For solutions we employ the specific Kerr constant defined by  $B/c$ , where  $c$  is the polymer concentration in  $\text{g}/\text{cm}^3$ . Strictly speaking, it is defined by  $(B_{\text{solution}} - B_{\text{solvent}})/c$ .

## RESULTS

The steady-state electric birefringence of the PCBL samples in various organic solvents was measured as a function of field strength. Figure 1 shows the  $\Delta n/\lambda c$  versus  $E^2$  plots for sample I in dichloroethane, chloroform, dioxane, tetrahydrofuran, DMF, HMPA and *m*-cresol. All these solvents are helicogenic solvents for PCBL. The measuring temperature was 25°C except for *m*-cresol solution. Measurement of the latter was made at 35°C; PCBL is partly helical in this condition<sup>4</sup>. The concentration dependence of  $\Delta n/\lambda c$  was small in the range of  $0.5 \times 10^{-3}$  to  $3.5 \times 10^{-3} \text{ g}/\text{cm}^3$ . PCBL molecules are to some extent associated in dioxane, as judged from the relaxation time of the rise and decay process of the birefringence. The sign of the birefringence was negative in HMPA and *m*-cresol and positive in other solvents.

The plots in Figure 1 are linear at low fields, i.e., Kerr's law holds. The initial slope gives the specific Kerr constant. However, large deviations from Kerr's law are observed at higher fields. These plots can be fitted to a theoretical equation of the electric birefringence for the



**Figure 1** Plots of  $\Delta n/\lambda c$  versus  $E^2$  for sample I ( $M = 9.9 \times 10^4$ ) in organic solvents:  $\circ$ , DMF ( $c = 1.3 \times 10^{-3} \text{ g}/\text{cm}^3$ );  $\square$ , dichloroethane ( $c = 1.6 \times 10^{-3} \text{ g}/\text{cm}^3$ );  $\triangle$ , tetrahydrofuran ( $c = 2.7 \times 10^{-3} \text{ g}/\text{cm}^3$ );  $\nabla$ , dioxane ( $c = 1.6 \times 10^{-3} \text{ g}/\text{cm}^3$ );  $\bullet$ , chloroform ( $c = 3.2 \times 10^{-3} \text{ g}/\text{cm}^3$ );  $\blacksquare$ , *m*-cresol ( $c = 2.0 \times 10^{-3} \text{ g}/\text{cm}^3$ );  $\blacktriangle$ , HMPA ( $c = 1.5 \times 10^{-3} \text{ g}/\text{cm}^3$ ). The solid curves are calculated by means of equation (5) selecting appropriate values of  $\mu'$  and  $g_1 - g_2$ .

Table 2 Specific Kerr constant, dipole moment, dipole moment per residue and optical anisotropy factor of sample I in organic solvents

Solvent	Temp. (°C)	$B/c \times 10^3$	$\mu'$ (D)	$\mu'/\text{res.}$ (D)	$(g_1 - g_2) \times 10^4$	$n_D$	$\epsilon$
Dichloroethane	25	10.2	2120	5.6	9.4	1.442	10.36
Chloroform	25	5.4	2240	5.9	4.9	1.443	4.81
Dioxane	25	6.4	1880	5.0	7.0	1.420	2.21
Tetrahydrofuran	25	10.0	2060	5.5	8.7	1.405	7.58
DMF	25	11.5	1780	4.7	11	1.428	36.7
HMPA	25	-5.3	1960	5.6	-4.7	1.457	30
<i>m</i> -Cresol	35	-2.0	1100	2.9	-7.0	1.540	11.8

case of pure permanent dipole moment orientation. The electric birefringence of a dilute solution of rigid, axially symmetric macromolecules with a permanent dipole moment along the symmetry axis is given by:

$$\Delta n = \frac{2\pi\bar{v}c}{n} (g_1 - g_2) \left[ 1 - \frac{3(\coth\beta - 1/\beta)}{\beta} \right] \quad (5)$$

with

$$\beta = \mu'E/kT \quad (6)$$

where  $n$  is the refractive index of the solution,  $\bar{v}$  is the partial specific volume of the solute,  $g_1 - g_2$  is the optical anisotropy factor (i.e., the difference between the excess optical polarizability per unit volume of the macromolecule along the symmetry axis and that along the transverse axis),  $\mu'$  is the apparent permanent dipole moment,  $k$  is the Boltzmann constant and  $T$  is the absolute temperature<sup>19</sup>. The solid curves in Figure 1 are the theoretical curves obtained by assigning appropriate values to the two parameters,  $\mu'$  and  $g_1 - g_2$ , in equation (5). The partial specific volume of PCBL is taken as  $0.803 \text{ cm}^3/\text{g}^4$ . The agreement between the calculated and experimental values is fairly good in spite of the polydispersity of the sample. Thus the apparent permanent dipole moment and the optical anisotropy factor can be separately determined. The data for the specific Kerr constant, the apparent dipole moment, the apparent dipole moment per residue and the optical anisotropy factor are summarized in Table 2. In this Table are also included literature values of the refractive index and the dielectric constant of the solvents. The specific Kerr constant is given in  $\text{statvolt}^{-2} \text{ cm}^4 \text{ g}^{-1}$  ( $1 \text{ statvolt}^{-2} \text{ cm}^4 \text{ g}^{-1} = 1.113 \times 10^{-10} \text{ V}^{-2} \text{ m}^4 \text{ kg}^{-1}$ ) and the dipole moment in Debye unit ( $1 \text{ D} = 3.336 \times 10^{-30} \text{ C m}$ ).

As can be seen from Table 2, the apparent dipole moment per residue is of the same order of magnitude as that of PBLG and does not depend very much upon the solvent. The exceptionally small value of  $\mu'$  in *m*-cresol may be ascribed to the incomplete helix in this condition. On the other hand, the optical anisotropy factor is considerably small and changes its sign depending upon the solvent. It is to be noted that the sign of the optical anisotropy factor is negative in HMPA and *m*-cresol which have large refractive indices.

The  $\Delta n/\lambda c$  versus  $E^2$  plots for PCBL samples of different molecular weights in DMF and HMPA are presented in Figures 2 and 3, respectively. The solid curves in these Figures are those calculated according to equation (5). Contrary to expectation, the agreement between the calculated and experimental values is fairly good even for high molecular weight samples (samples III and IV). Thus it is possible to assign pertinent values to  $\mu'$  and  $g_1 - g_2$

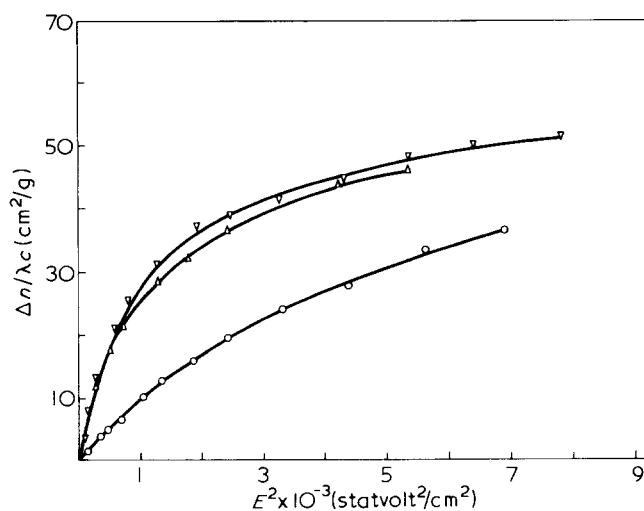


Figure 2 Plots of  $\Delta n/\lambda c$  versus  $E^2$  for samples I (○), III (△) and IV (▽) in DMF at 25°C

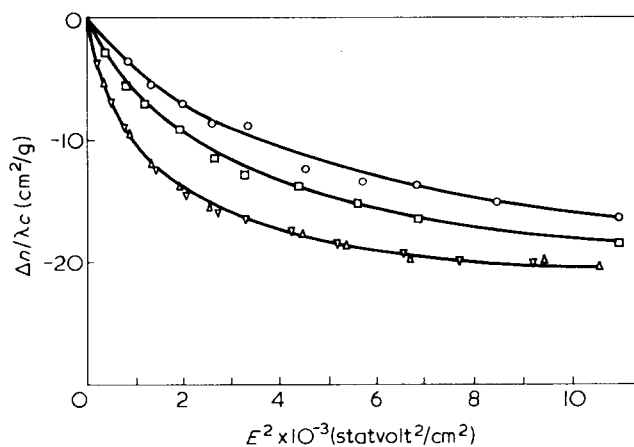


Figure 3 Plots of  $\Delta n/\lambda c$  versus  $E^2$  for samples I (○), II (□), III (△) and IV (▽) in HMPA at 25°C

Table 3 Specific Kerr constant, dipole moment, dipole moment per residue and optical anisotropy factor of PCBL samples in DMF

Sample	Temp. (°C)	$B/c \times 10^3$	$\mu'$ (D)	$\mu'/\text{res.}$ (D)	$(g_1 - g_2) \times 10^4$
I	25	11.5	1780	4.7	11
III	25	48.2	4170	1.8	11
IV	25	53.2	4340	1.3	11

for these samples. However, these values must be regarded as tentative, since the high molecular weight PCBL helices behave as flexible rods<sup>2,10</sup>. The data for  $B/c$ ,  $\mu'$  and  $g_1 - g_2$  of PCBL samples in DMF and HMPA are listed in Tables 3 and 4, respectively. The small values of the apparent dipole

Table 4 Specific Kerr constant, dipole moment, dipole moment per residue and optical anisotropy factor of PCBL samples in HMPA

Sample	Temp. (°C)	$B/c \times 10^3$	$\mu'$ (D)	$\mu'/res.$ (D)	$(g_1 - g_2) \times 10^4$
I	25	-5.3	1960	5.6	-4.7
II	25	-8.4	2660	5.8	-4.7
III	25	-21.0	4400	1.9	-4.3
IV	25	-21.6	4470	1.3	-4.3

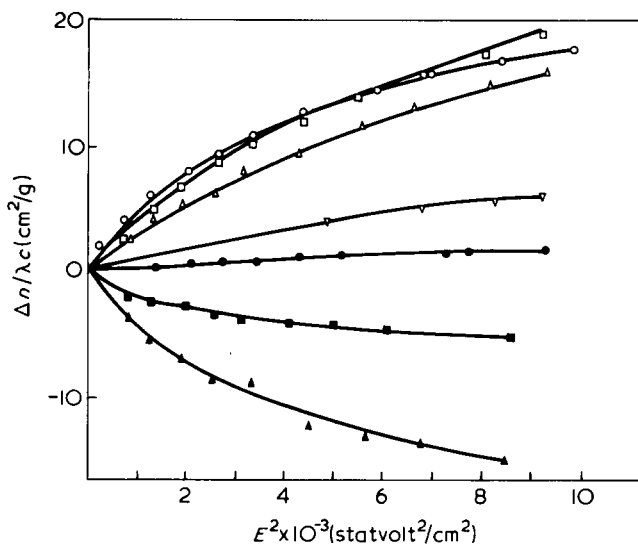


Figure 4 Plots of  $\Delta n/\lambda c$  versus  $E^2$  for sample I in chloroform-HMPA mixtures at 25°C: ○, chloroform; □, 20%; △, 40%; ▽, 60%; ●, 70%; ■, 80%; ▲, 100% HMPA

moment per residue for high molecular weight samples reflect a considerable flexibility of the helix.

Furthermore, the electric birefringence of sample I was studied in mixed organic solvents. Figure 4 shows the field strength dependence of the birefringence in chloroform-HMPA mixtures. The solid curves in this Figure represent the theoretical ones based on equation (5). The specific Kerr constant and the optical anisotropy factor obtained in the same manner as above are plotted against the solvent composition in Figure 5. A reversal in the sign of the specific Kerr constant and the optical anisotropy factor is observed in the vicinity of 70 vol % HMPA. Another example of the sign reversal is encountered in the case of PCBL in chloroform-tetrabromoethane mixtures, as shown in Figure 6. Incidentally we note that PCBL is not soluble in pure tetrabromoethane. We also noticed that the negative sign of the electric birefringence of helical PCBL in *m*-cresol turned positive with the addition of methanol. In Figure 6, the electric birefringence of PCBL in a *m*-cresol-methanol mixture (75:25 by vol) is also presented.

## DISCUSSION

The following discussion is mainly concerned with the electro-optical properties of sample I, since the low molecular weight PCBL helices (with molecular weight below  $1 \times 10^5$ ) show the characteristic behaviour of rigid rods according to the study of Daniel and Katchalski<sup>10</sup>.

As can be seen from Table 2, the apparent dipole moment per residue lies in the range of 4.7 to 5.9 D in spite of the large variation of the dielectric constant of the solvents used. This indicates that the internal field correction factor is rather small for such elongated, thin macromole-

cules. The values quoted are somewhat larger than those for PBLG in the corresponding solvents.

The reversal of the sign of the optical anisotropy factor accompanied by the variation of the solvent can be explained on the basis of the theory of Peterlin and Stuart<sup>20</sup> for rigid ellipsoids of revolution. In their theory the particle is assumed to be a continuous dielectric and immersed in a continuous medium (solvent). The dimensions of the particle are assumed to be small compared to the wavelength of light. Resting on these assumptions, the optical anisotropy factor is given by:

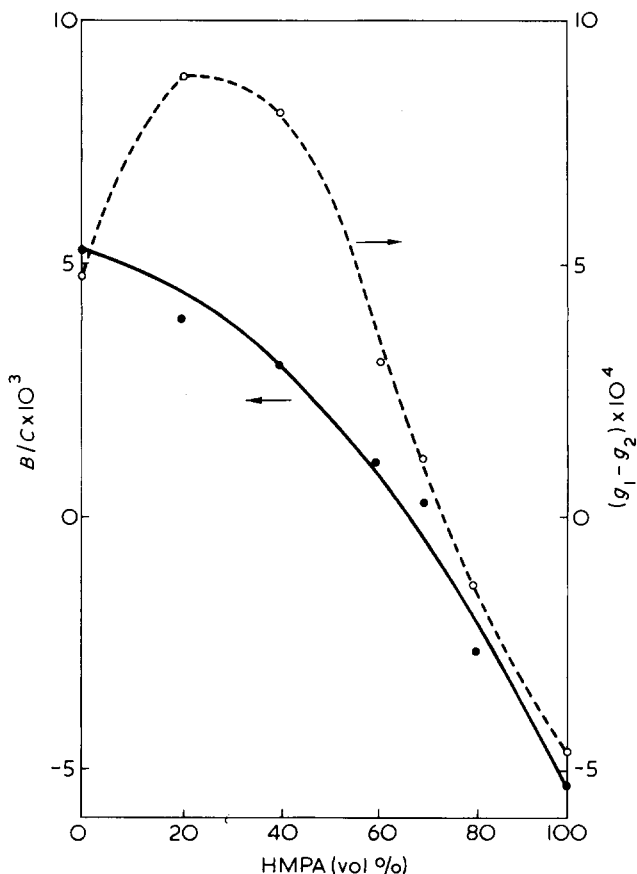


Figure 5 Specific Kerr constant (●) and optical anisotropy factor (○) of sample I plotted against the solvent composition of chloroform-HMPA mixtures

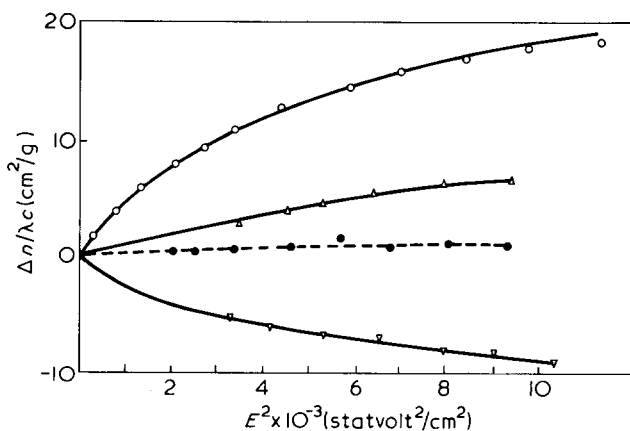


Figure 6 Plots of  $\Delta n/\lambda c$  versus  $E^2$  for sample I in chloroform-tetrabromoethane mixtures at 25°C and in a *m*-cresol-methanol mixture at 35°C: ○, chloroform; △, 16.7% tetrabromoethane; ▽, 50% tetrabromoethane; ●, *m*-cresol-methanol mixture (75:25 by vol)

Table 5 Optical parameters of PCBL in organic solvents

Solvent	$n_0$	$(g_1 - g_2) \times 10^3$	$(g_1 - g_2)_{\text{form}} \times 10^3$	$(g_1 - g_2)_{\text{intrinsic}} \times 10^3$	$(n_1 - n_2) \times 10^2$
HMPA	1.457	-0.47	2.2	-2.7	-1.2
Chloroform	1.443	0.49	2.7	-2.2	-1.0
Dichloroethane	1.442	0.94	2.8	-1.9	-0.8
DMF	1.428	1.1	3.4	-2.3	-1.0
Dioxane	1.420	0.70	3.8	-3.1	-1.4
Tetrahydrofuran	1.405	0.87	4.5	-3.6	-1.6

$$g_1 - g_2 = \frac{1}{4\pi} \frac{(n_1^2 - n_2^2) + e(n_1^2 - n_0^2)(n_2^2 - n_0^2)/n_0^2}{\left[ \frac{n_1^2 + 2n_0^2}{3n_0^2} - \frac{2e}{3} \frac{n_1^2 - n_0^2}{n_0^2} \right] \left[ \frac{n_2^2 + 2n_0^2}{3n_0^2} + \frac{e}{3} \frac{n_2^2 - n_0^2}{n_0^2} \right]} \quad (7)$$

where  $n_1$  and  $n_2$  are the refractive indices of the particle along the symmetry and transverse axes,  $n_0$  is the refractive index of the solvent and  $e$  is a form factor which depends only on the axial ratio.

In the case of a prolate ellipsoid the value of  $e$  approaches its asymptotic value of 0.5 when the axial ratio is very large. Then, equation (7) reduces to:

$$g_1 - g_2 = \frac{2n_0^2(n_1^2 - n_2^2)}{4\pi(\bar{n}^2 + n_0^2)} + \frac{(\bar{n}^2 - n_0^2)^2}{4\pi(\bar{n}^2 + n_0^2)} \quad (8)$$

where  $\bar{n}$  is the mean refractive index of the particle. The first term in the right side of equation (8) arises from the intrinsic anisotropy of the particle itself and the second from the form anisotropy, which depends on the difference in the refractive indices of the particle and the solvent. Let the former be represented by  $(g_1 - g_2)_{\text{intrinsic}}$  and the latter by  $(g_1 - g_2)_{\text{form}}$ . While  $(g_1 - g_2)_{\text{form}}$  is always positive except for the special case of  $n_0 = \bar{n}$ ,  $(g_1 - g_2)_{\text{intrinsic}}$  is positive, zero or negative according as  $n_1 > n_2$ ,  $n_1 = n_2$  or  $n_1 < n_2$ . If  $n_1 > n_2$ ,  $g_1 - g_2$  is positive for all values of the refractive index of the solvent. On the other hand, the sign of  $g_1 - g_2$  can be changed by suitable variation of  $n_0$ , if  $n_1 < n_2$ .

The mean refractive index of the solute particle can be obtained from the specific refractive index increment of the solution,  $dn/dc$ , using the simple equation<sup>21</sup>:

$$dn/dc = \bar{v}(\bar{n} - n_0) \quad (9)$$

For PCBL,  $dn/dc = 0.117 \text{ cm}^3/\text{g}$  (in DMF, at 546 nm)<sup>4</sup>. Thus  $\bar{n} = 1.574$ . Using this value,  $(g_1 - g_2)_{\text{form}}$  was calculated for each PCBL-solvent system. Then,  $(g_1 - g_2)_{\text{intrinsic}}$  was obtained by subtracting  $(g_1 - g_2)_{\text{form}}$  from the experimental value of  $g_1 - g_2$ . Finally, the intrinsic birefringence,  $n_1 - n_2$ , was calculated from  $(g_1 - g_2)_{\text{intrinsic}}$ . These data are quoted in Table 5.

The intrinsic birefringence should be constant in different solvents. However, it varies to some extent with the solvent according to Table 5. This might be due to the experimental inaccuracy and the inadequacy of the Peterlin-Stuart theory. Cassim and Taylor<sup>22</sup> examined the sources of error in the Peterlin-Stuart theory and showed that this theory overestimated the form contribution to the optical anisotropy factor. The error produced will become larger as the refractive index of the solvent departs from that of the solute particle. Subsequently their conclusions were supported by Oriol and Schellman<sup>23</sup>.

Notwithstanding these uncertainties, we can conclude

that the intrinsic birefringence of PCBL is negative in sign. The sign reversal and the small absolute value of the optical anisotropy factor are explained on this basis. On the other hand, the intrinsic birefringence of PBLG has been found to be positive in sign<sup>22</sup>. Correspondingly the optical anisotropy factor of PBLG is fairly large; for example,  $g_1 - g_2 = 4 \times 10^{-3}$  in dichloroethane<sup>19,24</sup>.

Recently, particular attention has been paid to the orientation of the side chains of polypeptide molecules with respect to the helical backbone<sup>25</sup>. Charney *et al.*<sup>26</sup> measured the electric dichroism of PBLG in dichloroethane at 258 nm and inferred that the electronic transition moment lying in the plane of the phenyl group makes an angle of 53.5° with the helix axis. Since the side chain of PCBL [ $-(\text{CH}_2)_4\text{NHCOOCH}_2\text{C}_6\text{H}_5$ ] is longer than that of PBLG [ $-(\text{CH}_2)_2\text{COOCH}_2\text{C}_6\text{H}_5$ ] and contains an amide group with planar character, the former will assume a transverse conformation rather than a longitudinal one<sup>27</sup>. If the terminal phenyl ring is so oriented as to protrude relative to the helical backbone, it will contribute greatly to the optical polarizability along the transverse axis. This will give rise to the negative intrinsic birefringence of PCBL.

Evidently the sign reversal of the optical anisotropy factor of PCBL in chloroform-HMPA mixtures is not due to a conformational change of the helical backbone, since the values of the Moffitt parameter  $b_0$  are nearly the same in chloroform and in HMPA<sup>4</sup>. However, the possibility of the change of side-chain conformations cannot be entirely excluded.

## ACKNOWLEDGEMENTS

This work was supported in part by research grants from the Ministry of Education of Japan. We are indebted to Professor Akio Teramoto of Osaka University for valuable instructions on the preparation of PCBL samples.

## REFERENCES

- 1 Applequist, J. *PhD Thesis* Harvard University (1959)
- 2 Applequist, J. and Doty, P. 'Polyamino Acids, Polypeptides, and Proteins', (Ed. M. A. Stahmann), University of Wisconsin Press, Madison, 1962, p 161
- 3 Parrish, Jr. J. R. and Blout, E. R. *Biopolymers* 1971, **10**, 1491
- 4 Matsuoka, M., Norisuye, T., Teramoto, A. and Fujita, H. *Biopolymers* 1973, **12**, 1515
- 5 Fasman, G. D., Idelson, M. and Blout, E. R. *J. Am. Chem. Soc.* 1961, **83**, 709

- 6 Karasz, F. E., O'Reilly, J. M. and Bair, H. E. *Biopolymers* 1965, 3, 241
- 7 Cortijo, M., Roig, A. and Garcia Blanco, F. *Biopolymers* 1969, 7, 315
- 8 Giacometti, G., Turolla, A. and Boni, R. *Biopolymers* 1970, 9, 979
- 9 Štokrová, Š., Fišer, V. and Bláha, K. *Macromolecules* 1973, 6, 523
- 10 Daniel, E. and Katchalski, E. 'Polyamino Acids, Polypeptides, and Proteins', (Ed. M. A. Stahmann), University of Wisconsin Press, Madison, 1962, p 183
- 11 Spach, G., Freund, L., Daune, M. and Benoit, H. *J. Mol. Biol.* 1963, 7, 468
- 12 Frolov, V. I., Valsov, G. P. and Kalikhevich, V. N. *Vysokomol. Soedin. (A)* 1973, 15, 162
- 13 Omura, I., Matsumoto, T., Teramoto, A. and Fujita, H. *Prepr. 22nd Soc. Polym. Sci. Japan Polym. Symp., Tokyo* 1973, Vol III, p 111; *Macromolecules* 1975, 8, 284
- 14 Tsvetkov, V. N., Shtennikova, I. N., Ryumtsev, E. I. and Pirogova, G. F. *Vysokomol. Soedin. (A)* 1967, 9, 1575
- 15 Ikeda, K., Watanabe, H., Shirai, M. and Yoshioka, K. *Sci. Pap. Coll. Gen. Educ., Univ. Tokyo* 1965, 15, 139
- 16 Yoshioka, K. and Watanabe, H. 'Physical Principles and Techniques of Protein Chemistry, Part A', (Ed. S. J. Leach), Academic Press, New York, 1969, p 335
- 17 Kikuchi, K. and Yoshioka, K. *J. Phys. Chem.* 1973, 77, 2101
- 18 Tsuji, K., Ohe, H. and Watanabe, H. *Polym. J.* 1973, 4, 553
- 19 O'Konski, C. T., Yoshioka, K. and Orrtung, W. H. *J. Phys. Chem.* 1959, 63, 1558
- 20 Peterlin, A. and Stuart, H. A. *Z. Phys.* 1939, 112, 129
- 21 Heller, W. *J. Phys. Chem.* 1965, 69, 1123
- 22 Cassim, J. Y. and Taylor, E. W. *Biophys. J.* 1965, 5, 531
- 23 Oriel, P. J. and Schellman, J. A. *Biopolymers* 1966, 4, 469
- 24 Nishinari, K. and Yoshioka, K. *Kolloid-Z. Z. Polym.* 1970, 240, 831
- 25 Scheraga, H. A. *Chem. Rev.* 1971, 71, 195
- 26 Charney, E., Milstien, J. B. and Yamaoka, K. *J. Am. Chem. Soc.* 1970, 92, 2657
- 27 Yan, J. F., Vanderkooi, G. and Scheraga, H. A. *J. Chem. Phys.* 1968, 49, 2713

# Acoustic studies of chain flexibility in copolymers of *N*-vinylcarbazole

P. N. Shankar Iyer, Alastair M. North, Richard A. Pethrick and Daniel B. Steinhauer

Department of Pure and Applied Chemistry, University of Strathclyde, Glasgow G1 1XL, UK

(Received 30 January 1975; revised 25 February 1975)

Acoustic relaxation studies of a series of copolymers of *N*-vinylcarbazole with methyl acrylate and with styrene have shown that the incorporation of up to 20% of the sterically less hindered comonomer promotes very little flexibility in the stiff poly(*N*-vinylcarbazole) chain.

## INTRODUCTION

Interest in the molecular physics of poly(*N*-vinylcarbazole) has led to studies of segmental rotation by both dielectric relaxation<sup>1,2</sup> and luminescence<sup>3,4</sup> techniques. These have shown that the chain is relatively 'stiff', with a room temperature segmental rotation frequency between 1 MHz (dielectric relaxation) and 3 MHz (fluorescence depolarization) in dilute solution. Furthermore, observations of electronic energy transfer down poly(*N*-vinylcarbazole) chains containing methyl acrylate comonomer units have suggested<sup>4</sup> that the comonomer has surprisingly little effect on the ease of energy migration, and so presumably on the separation of neighbouring carbazole units. Since relatively unhindered comonomers such as methyl acrylate are often added to increase the 'flexibility' of 'stiff' polymer chains, it becomes a matter of interest as to whether such a comonomer exerts its normal 'flexibilizing' action on the very hindered poly(*N*-vinylcarbazole) chain. In this context it is the resistance to segmental motion caused by intramolecular energy barriers that is of interest and not the factors arising from the strong inter-chain interactions of the carbazole groups in solid polymer. For this reason we refer to the speed of segmental rotation of the dissolved (isolated) chain as the 'intrinsic flexibility'.

Consideration of the reactivity ratios for copolymerization of *N*-vinylcarbazole with methyl acrylate<sup>5</sup> and styrene<sup>6</sup> suggests that while the former comonomer exhibits a strong tendency to alternation ( $r_1, r_2 < 1, r_1, r_2 \ll 1$ ) there is a tendency for sequences of more than one styrene unit to occur in the appropriate copolymer ( $r_2 > 1$ ). Consequently an added point of investigation concerns the effect of sequence distribution of any 'flexibilizing' action.

## EXPERIMENTAL

A series of copolymers of *N*-vinylcarbazole with methyl acrylate and with styrene were prepared by conventional

Table 1 Characteristics of copolymers of *N*-vinylcarbazole

Comonomer	$M_w \times 10^{-4}$	Mole ratio carbazole/comonomer
styrene: 1	63	6
2	25	5
3	59	4
methyl acrylate: 4	5.1	13
5	6.4	6
6	3.0	4

free radical polymerization of the mixed monomers at 353 K using di-*t*-butyl peroxide as initiator. The polymer compositions as determined by elemental analysis are recorded in Table 1. Molecular weights were determined by light scattering from dilute solutions in benzene. The refractive index increment in each case was measured in a Brice-Phoenix differential refractometer and ranged from +0.13 to +0.16 for the styrene copolymers and +0.16 to +0.175 for the methyl acrylate series. The determinations had a precision of 10%, but in view of the difficulty of interpretation of light scattering data from copolymers we do not place a significance greater than 30% on the calculated values. They are reported, however, to confirm that the chains studied were sufficiently long to make acoustic effects due to end-groups insignificant.

Acoustic measurements were carried out using pulse and resonator techniques as described previously<sup>7</sup>.

## RESULTS

As an example, the acoustic absorption observed in a 2.5% w/v solution of the copolymer, methyl acrylate 4, in toluene at 318 K, is illustrated in Figure 1. The normal mode contribution<sup>7</sup> to the absorption was calculated from the solution viscosity using the model of Yu and Stockmayer<sup>8</sup> for stiff chains. The remaining absorption was analysed<sup>7</sup> to give the internal relaxation amplitude, frequency and Cole-Cole distribution parameter.

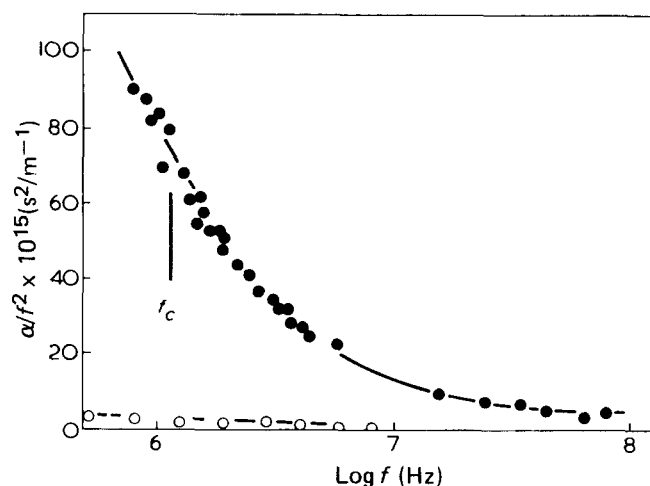


Figure 1 Acoustic absorption in the *N*-vinylcarbazole/methyl acrylate copolymer designated methyl acrylate 4, in toluene at 318 K. ●, Observed absorption; ○, normal mode contribution

Table 2 Relaxation parameters of copolymers

Copolymer	Temp. (K)	Relaxation amplitude $\times 10^{15}$ ( $m^{-1} s^{-2}$ )	Relaxation frequency (MHz)	Cole–Davidson distribution parameter
styrene: 1	308	114	$1.4 \pm 0.6$	0.6
	2	308	$1.4 \pm 0.4$	0.6
		328	$1.3 \pm 0.4$	0.6
	3	308	$1.2 \pm 0.4$	0.6
		328	$1.2 \pm 0.4$	0.6
methyl acrylate: 4	308	124	$1.3 \pm 0.3$	0.7
		328	$1.3 \pm 0.4$	0.7
	5	308	$1.4 \pm 0.6$	0.6
		328	$1.3 \pm 0.7$	0.6
	6	308	$1.4 \pm 0.5$	0.7
		328	$1.6 \pm 0.4$	0.6

Because the complete relaxation extended in frequency below the accessible instrument range, the error in the calculated acoustic parameters is larger (see below) than that reported<sup>7</sup> for polystyrene and similar systems. The absorption curves for the other copolymers are very similar to the example illustrated. When the data are portrayed on the same graph the individual curves cannot be distinguished over most of the frequency range. The derived relaxation data are presented in Table 2.

## DISCUSSION

For all the polymers studied the relaxation frequencies are indistinguishable (within experimental error) from that reported for poly(*N*-vinylcarbazole). The rather surprising conclusion is that incorporation of up to 20% comonomer promotes a negligible increase in the intrinsic rate of segmental motion in the hindered poly(*N*-vinylcarbazole) chain. This is true although the copolymer containing 20% styrene units has an observable probability of containing sequences of two or more styrene units.

The reason for the lack of comonomer effect must lie in the fact that the barriers to segmental rotation have

their origin in long range dipole–dipole interactions between carbazole groups as well as in the strong short range 'steric' effects. Thus the acoustic results confirm the conclusions of the dielectric studies<sup>2</sup> that the rotating unit contains several monomer residues and so is little affected by a 'chemical defect'.

For all of the styrene copolymers and the methyl acrylate copolymer of lowest comonomer content the relaxation amplitudes are the same within 10% spread. There is no consistent trend in the relaxation amplitudes of the two polymers of higher methyl acrylate comonomer content, and it may be that the discrepancy arises in the difficulty of estimating the absorption at frequencies well below the experimental measurements by curve fitting to the upper half of the relaxation. These relaxation amplitudes (though not the relaxation frequencies) are particularly sensitive to errors in the lowest frequency points obtained by the resonator technique.

## ACKNOWLEDGEMENT

The authors acknowledge with pleasure the support of the Science Research Council (P.N.S.I. and D.B.S.).

## REFERENCES

- 1 North, A. M. and Phillips, P. J. *Chem. Commun.* 1968, p 1340
- 2 Dev, S. B., Lockhead, R. Y. and North, A. M. *Discuss. Faraday Soc.* 1970, **49**, 244.
- 3 North, A. M. and Soutar, I. *JCS' Faraday Trans. I* 1972, **68**, 1101
- 4 North, A. M. and Treadaway, M. F. *Eur. Polym. J.* 1973, **9**, 609
- 5 North, A. M. and Whitelock, K. E. *Polymer* 1968, **9**, 590
- 6 Brandrup J. and Immergut, E. H. 'Polymer Handbook', Wiley–Interscience, New York, 1966
- 7 Cochran, M. A., Dunbar, J. H., North, A. M. and Pethrick, R. A. *JCS Faraday Trans. II* 1974, **70**, 215
- 8 Yu, H. and Stockmayer, W. H. *J. Chem. Phys.* 1967, **45**, 1369



# Saturated hydrocarbon prepolymers by ozonolysis\*

R. A. Rhein and J. D. Ingham

*Jet Propulsion Laboratory, California Institute of Technology, Pasadena, Ca 91103, USA*

*(Received 13 March 1975; revised 1 July 1975)*

The preparation and isocyanate cure of hydroxyl-containing, saturated hydrocarbon prepolymers is described, with emphasis on ethylene-propylene copolymers. The preparation consists of ozonolysis and subsequent reduction, with alkylaluminium hydride materials, of precursors derived from commercially available polymers. The methods for obtaining the precursors are: (a) no prior treatment; (b) bromination followed by dehydrobromination, so as to create sites of main-chain unsaturation; or (c) thermal degradation of the parent polymer to a viscous, unsaturated oligomer. Liquid ethylene-propylene (copolymer) prepolymers, approximately difunctional in hydroxyl, were prepared and cured with di-isocyanates; analogous prepolymers of polyisobutylene and amorphous polypropylene were also prepared.

## INTRODUCTION

The objective of this work is the preparation of saturated hydrocarbon prepolymers with terminal hydroxyl groups for use in solid propellant binders.

Relatively low molecular weight polymers containing reactive terminal or pendant functional groups are useful as precursors or components of castable polymer systems, and as additives in formulations of inherently hard or brittle polymers such as epoxy resins, to increase toughness or decrease hardness. The work described in this paper is part of a long-term investigation to prepare and evaluate saturated hydrocarbon prepolymers that are not generally available. Besides allowing increased versatility in formulating castable polymeric systems, such prepolymers are expected to have enhanced thermal and oxidative stability compared with available polybutadiene and polyether prepolymers. Although hydroxyl<sup>1</sup> and carboxyl<sup>2</sup> terminated polyisobutylene can be prepared by ozonolysis and subsequent conversion of ozonolysis and subsequent conversion of ozonized butyl rubber to the desired product, this process is generally limited to isobutylene polymers because other high molecular hydrocarbon polymers containing occasional sites of main-chain unsaturation are not readily obtained.

This paper describes the preparation, and isocyanate curing, of saturated hydrocarbon prepolymers containing hydroxyl functionality of the following types: ethylene-propylene copolymer, amorphous polypropylene, and polyisobutylene; it is an extension of a published<sup>3</sup> preliminary study on the preparation of ethylene-propylene (copolymer) prepolymers. Following the preparation of hydroxy-terminated polyisobutylenes by ozonization of butyl rubber, we attempted the preparation of the ethylene-propylene analogues by bromination followed by dehydrobromination so as to create occasional main-chain unsaturation, followed by ozonolysis and reduction, and obtained hydroxyl-containing ethylene-propylene prepolymers in this manner.

\* This paper presents the results of one phase of research carried out at the Jet Propulsion Laboratory, California Institute of Technology, under Contract number NAS7-100 sponsored by the National Aeronautics and Space Administration.

It was found, also, that hydroxyl prepolymers could be prepared by ozonolysis of a solution of ethylene-propylene copolymer, amorphous polypropylene, or polyisobutylene followed by reduction. A more convenient method of prepolymer preparation was subsequently developed in which ethylene-propylene copolymer or amorphous polypropylene was partly thermally degraded at elevated temperatures and then ozonized and reduced.

## EXPERIMENTAL AND RESULTS

Solution viscosities were measured using a Ubbelohde viscometer held at  $30.00 \pm 0.02^\circ\text{C}$  by a Hallikainen Thermotrol Viscometer Bath. Intrinsic viscosities were estimated from the equation<sup>15</sup>:

$$\eta_{sp}/C = [\eta] + 0.4[\eta]^2 C$$

where  $\eta_{sp}$  is the specific viscosity,  $C$  the concentration (g/dl) and  $[\eta]$  the intrinsic viscosity (dl/g).

Ozone was produced from oxygen by a Welsbach T-816 Ozonator at a concentration of  $0.055 \text{ kg/m}^3$ . The flow rate of oxygen-ozone mixture was generally held at 1.0 l/min.

Di-isobutyl aluminium hydride (DIBAL-H)<sup>4,5</sup>, sodium aluminium diethyl dihydride (OMH-1), and sodium dihydrobis(2-methoxyethoxy)aluminum (Red-Al)<sup>7,8</sup> were found to be effective in reducing the ozonized polymer terminal groups to hydroxyl. The temperatures, reaction times, solvents, and mole ratios of hydride-ozonized terminal group for DIBAL-H were  $100^\circ\text{C}$ , 2 h, heptane, and mole ratio 3.2; for OMH-1,  $25^\circ\text{C}$ , 30 min, benzene, and mole ratio 2.0; for Red-Al,  $80^\circ\text{C}$ , 2 h, benzene, mole ratio 2.42. These reagents replace the more costly  $\text{LiAlH}_4$  suggested in the literature<sup>7</sup>.

Number-average molecular weights were determined by vapour pressure osmometry (v.p.o.) (in benzene at  $30^\circ\text{C}$ ); number- and weight-average molecular weights were determined from gel permeation chromatography, calibrated from the v.p.o. measurements.

We prepared samples of hydroxy-terminated polyisobutylene by ozonolysis and reduction of butyl rubber by

Table 1 Hydroxyl prepolymers prepared by ozonization and reduction

Designation	Initial polymer	Solvent	Ozone admitted (equiv./kg)	Prepolymer product yield (%)	$M_w$	$M_n$	Hydroxyl (equiv./kg)	Hydroxyl (equiv./mol)
PIBLM	Exxon Butyl LM-430 <sup>†</sup>	Heptane	1.5	93	2140	1203	1.483	1.78
PIBH	Exxon Butyl 365 <sup>‡</sup>	Heptane	0.7	80	3630	1963	0.677	1.33
PP4282	Eastman M-5L	CCl <sub>4</sub>	4.5	58	2920	1210	0.99	1.20
PP10041C	Eastman M-5L	CCl <sub>4</sub>	12.0	>50	2060	1055	2.5	2.64
PP10024	PP700B*	CCl <sub>4</sub>	4.0	68	1803	676	1.76	1.19
EPDM 5174C	EPDM-1040*	CCl <sub>4</sub>	6.0	49	2430	1230	1.91	2.35
EPDM 5204A	EPDM-1440*	CCl <sub>4</sub>	6.0	43	2130	1110	2.33	2.56
EPDM 5204B	EPDM-301*	CCl <sub>4</sub>	6.0	54	2550	1330	1.87	2.50
EPDM 5204C	EPDM-2504*	CCl <sub>4</sub>	6.0	59	2170	1193	1.83	2.18

\* See Table 3

<sup>†</sup> 4.2% unsaturation<sup>‡</sup> 2.0% unsaturation

Table 2 Hydroxyl prepolymers prepared from ethylene-propylene copolymer Exxon Vistalon 404

Designation	Treatment	Solvent	Ozone admitted (equiv./kg)	Product yield (%)	$M_w$	$M_n$	Hydroxyl (equiv./kg)	Hydroxyl functionality (equiv./mol)
EPR 6281 A	Br <sub>2</sub> then potassium t-butoxide	Heptane	1.8	>50	8050	2300	0.786	1.81
EPR 2102	N-ethylpiperidine	Heptane	2	>50	11 670	2758	0.698	1.92
EPR 5042A	—	Heptane	10.8	55	4750	1700	1.22	2.08
EPR 5042B	—	Heptane	8.24	72	5620	2152	1.37	2.95
EPR 5122	—	Heptane	7.46	73	5730	1962	1.38	2.71
EPR 6132	—	Heptane	12	>50	8950	1820	1.67	3.04
EPR 10041A	—	CCl <sub>4</sub>	16	>50	1537	870	4.2	3.65
EPR 7233A6	—	CCl <sub>4</sub>	6	>50	3480	1503	1.06	1.6
EPR 10183	—	CCl <sub>4</sub>	9	>50	2330	1122	2.18	2.45
EPR 12123A6	540°C in N <sub>2</sub>	CCl <sub>4</sub>	6	57	2658	1054	1.87	1.97
EPR 12123B6	430°C in N <sub>2</sub>	CCl <sub>4</sub>	6	93	3035	1222	1.79	2.19
EPR 10173CS	540°C in N <sub>2</sub>	CCl <sub>3</sub> F	2	52	3750	1701	0.97	1.65
EPR 12203-2S	540°C then 350°C in N <sub>2</sub>	Freon-113	2	66	2580	1025	1.32	1.35
EPR 12203-4S	540°C then 350°C in N <sub>2</sub>	Freon-113	4	73	2295	857	2.12	1.81
EPR 12203-6S	540°C then 350°C in N <sub>2</sub>	Freon-113	6	66	2003	866	2.30	1.99

the method of Jones and Marvel<sup>1</sup> except that DIBAL-H was used as the reducing agent. The results are presented in Table 1.

This work was extended in an attempt to prepare hydroxy-terminated ethylene-propylene copolymer by ozonolysis of an ethylene-propylene copolymer containing occasional main-chain unsaturation sites, prepared in turn by bromination and dehydrobromination. The parent polymer used was Exxon Vistalon 404, an ethylene-propylene copolymer containing 43% ethylene. This copolymer was first subjected to bromination and dehydrobromination for polymers designated in Table 2 as EPR 6281A and EPR 2102. A 5 wt % solution in carbon tetrachloride was treated with 1.0 mol Br<sub>2</sub>/kg of copolymer; bromination was complete in about 1 hour upon exposure of the solution to sunlight. This brominated polymer was then precipitated in acetone and solvent removed by vacuum evaporation. For dehydrobromination, the polymer, EPR 6281A (Table 2) was treated with potassium t-butoxide in tetrahydrofuran (24 equiv./kg polymer) (from a suggestion by Dr F. P. Baldwin, Exxon Corp.), for 1.75 h, at 66°C; polymer EPR 2102 (Table 2) was treated with N-ethylpiperidine (50 equiv./kg polymer) in decalin, for 1.75 h, at 131°C. The polymers were then dissolved in heptane (5 wt %), ozonized and reduced to yield products with properties given in Table 2.

Polymers EPR 5042A, EPR 5042B, EPR 5122, and EPR

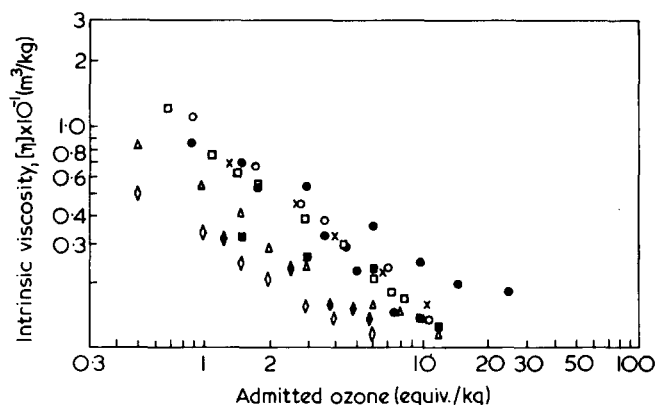


Figure 1 Degradation of saturated hydrocarbons by ozonolysis: intrinsic viscosity versus ozone exposure. ○, EPR 5042A; □, EPR 5042B; ×, EPR 5102; ⊗, EPR 5122; △, EPR 10041A; ◇, 10041B, polyisobutylene in CCl<sub>4</sub>; ●, 10041C, polypropylene in CCl<sub>4</sub>; ■, 10041D, poly(1-butene) in CCl<sub>4</sub>; ◆, 6092, polypropylene in heptane

6132 (Table 2) were prepared by direct ozonolysis of ethylene-propylene copolymer in heptane (5 wt % solution) followed by DIBAL-H reduction (in the same heptane solvent); polymers 10041A, 7233A6, and 10183 (Table 2) were prepared by ozonizing 5 wt% ethylene-propylene copolymer in CCl<sub>4</sub>, followed by solvent stripping, redissolving in heptane, and reduction by DIBAL-H. Figure 1 shows the decrease in intrinsic viscosity with ozonization in heptane and in CCl<sub>4</sub>.

Table 3 Oligomers resulting from thermal degradation of polymers

Degradation		Parent polymer	$M_w$	Unsaturation	Degradation temp. (°C)	Yield of oligomer (%)	$M_w$	$M_w$	Unsaturation/kg	Unsaturation/mol
EPR 350	Exxon Vistalon	404	113 000	0	350	85	17 400	4260	0.38	1.62
EPR 430	Exxon Vistalon	404	113 000	0	430	93	8 290	2690	0.94	2.53
EPR 430—air	Exxon Vistalon	404	113 000	0	430	60	6 400	2720	0.75	2.02
EPR 450	Exxon Vistalon	404	113 000	0	450	83	5640	2350	1.02	2.40
EPR 500	Exxon Vistalon	404	113 000	0	500	88	5990	2570	0.68	1.75
EPR 540	Exxon Vistalon	404	113 000	0	540	60	4 130	2160	0.82	1.77
EPR 600	Exxon Vistalon	404	113 000	0	600	0	—	—	—	—
EPR 540—350A	Exxon Vistalon	404	113 000	0	540 then 350	73	2 000	1030	1.99	2.03
EPR 540—350B	Exxon Vistalon	404	113 000	0	540 then 350	73	2 000	1030	1.99	2.03
EPDM-2504	Exxon Vistalon	2504	120 000	0.33	540	54	1 990	870	1.76	1.53
EPDM-301	Uniroyal Royalene	301	84 000	0.95	540	27	2 280	1420	1.32	1.88
EPDM-1040	Dupont Nordel	1040	119 000	0.48	540	63	2 080	870	1.83	1.59
EPDM-1440	Dupont Nordel	1440	128 000	0.79	540	60	2 400	1040	1.75	1.82
PP 500	Eastman M-5L	—	20 250	0	500	40	4 215	1970	1.08	2.13
PP 600	Eastman M-5L	1440	20 250	0	600	67	6 562	2112	1.03	2.18
PP 700A	Eastman M-5L	1440	20 250	0	700	81	3 117	677	2.95	2.00
PP 700B	Eastman M-5L	1440	20 250	0	700	47	2 192	550	3.2	1.76
PP 800	Eastman M-5L	1440	20 250	0	800	0	—	—	—	—

This study of the ozonolysis of saturated polymers was extended to amorphous polypropylene (Eastman M-5L), polyisobutylene (Exxon Vistanex 80), and poly(1-butene) (Cellomer Associates). Figure 1 shows the decrease in intrinsic viscosity with ozonization for these polymers. The polypropylene samples were ozonized in  $CCl_4$ , the solvent removed, the ozonized product re-dissolved in heptane and reduced with DIBAL-H. The hydroxyl content and molecular weight of the resulting prepolymers are presented in Table 1.

The observation (M. F. Humphrey, personal communication) that ethylene-propylene rubber degraded to a viscous liquid upon heating to elevated temperatures prompted an investigation of thermal degradation as a means of preparing precursors of liquid oligomers. The polymers subjected to thermal degradation were the commercially available EPR and EPDM parent polymers, listed in Table 3. The apparatus used for thermal degradation consists of a Vycor tube, 0.0254 m diameter and 0.5 m long, with 24/40 male joint at each end, suspended vertically, the bottom joint fitting in the cover of a 500 ml resin kettle. A constriction 0.09 m from the bottom of the tube held in place a small, very loose-fitting Pyrex disc. Borosilicate Raschig rings added to the tube filled a space 0.127 m above the disc. The tube was fitted in a tube furnace (Hoskins FH 303A) so that the bottom of the tube furnace (length 0.33 m) lined up with the constriction/disc. A gas inlet tube was attached to the resin kettle cover. At the top of the reaction tube was attached a condenser and a 500 ml flask for collecting the volatile degradation products.

In the experiments, the furnace temperature was controlled to a preset level, and in most cases nitrogen was passed into the resin kettle, hence upwards through the reaction tube, at 100 ml/min. Small pieces of polymer were added periodically from above into the reaction tube. Table 3 gives the results for the various polymers and degradation temperatures. It was observed that during the course of thermal degradation the polymer, initially resting at the top of the Raschig rings, would liquefy and flow downwards between the rings while the countercurrent nitrogen flow swept gaseous and volatile liquid products upwards and out through the condenser.

Although nitrogen was generally selected as the carrier

gas, in the preparation of sample EPR430—air (Table 3) air was used in place of  $N_2$ , resulting in a somewhat lower yield of liquid polymer. We found that at furnace temperatures above about 500°C, the use of air as carrier gas resulted in combustion within the furnace. Two-step processing of EPR was used in the preparation of samples EPR540—350A and —B. The first step, at 540°C occurred in the presence of  $N_2$ , but without countercurrent flow. The rather fluid product from the first step was added dropwise to the apparatus held at 350°C with countercurrent  $N_2$  flow to remove the volatiles. Experiment EPR600, conducted at 600°C, gave no liquid polymer in the resin kettle.

Higher temperatures were required to degrade amorphous polypropylene; the products resulting from temperatures of 500° to 700°C, i.e., samples PP500, —600, —700A, and —700B are shown in Table 3. Only volatile products resulted at a degradation temperature of 800°C. The polypropylene samples were also degraded in the presence of nitrogen, but only sample PP500 was subjected to countercurrent  $N_2$  flow.

The degradation products from EPR, EPDM, and polypropylene were found to contain olefinic unsaturation, identified from the infra-red spectrum by absorption peaks at 6.0–6.1 and then quantitatively determined by the mercuric acetate method, and shown in Table 3.

Several of these precursors were ozonized and then reduced with OMH-1 (benzene solvent, 30 min, ambient temperature) (Tables 1 and 2).

Curing studies on a number of prepolymers prepared in this effort were conducted. Generally, the curing experiments consisted of degassing 0.005–0.01 kg of prepolymer in a vacuum, mixing in the isocyanate — generally tolylene-2,4-diisocyanate (TDI) or the di-isocyanate derivative of dimer acid (General Mills Corp.; isocyanate equivalent wt. 300) (DDI) in the amounts recorded in Tables 4 and 5, and pouring the mixture into an aluminium dish 2½ in. in diameter, pretreated with MS122 fluorocarbon Release Agent (Milles-Stephenson Chemical Co.). If ferric acetylacetonate was used it was dissolved in the isocyanate to give a concentration of  $4.95 \times 10^{-3}$  kg/l (TDI) or  $1.09 \times 10^{-3}$  kg/l (DDI) as isocyanate (i.e., mole ratio FeAA/isocyanate =  $10^{-3}$ ) before adding the isocyanate to the prepolymer. The mixture was heated at 70°C in an oven

Table 4 Curing of hydroxyl polyisobutylene and polypropylene oligomers

Prepolymer	Coreactant (phr)	Curing agent	Mole ratio isocyanate: hydroxyl	Curing time (days)	Hardness Shore A	Gel swelling ratio	Gel fraction
PIBLM	—	TDI/FeAA	1.05	2	a	—	0
PIBLM	—	PAPI <sup>b</sup>	1.0	10	49	3.50	0.875
PIBLM	—	VORITE63 <sup>c</sup>	1.0	10	22	5.17	0.730
PIBLM	DB oil <sup>d</sup> 43.7	TDI	1.05	10	28	3.37	0.886
PIBLM	EPR 6132, 97.0	TDI	1.05	3	47	2.82	0.836
PIBLM	TMP <sup>e</sup> , 1.33 <sup>f</sup>	DDI	1.00	7	49	g, h	—
PIBH	—	TDI/FeAA	1.05	2	i	—	0
PIBH	—	PAPI	1.0	10	24	4.54	0.812
PIBH	—	VORITE 63	1.0	10	5	13.10	0.443
PIBH	DB oil, 56.4	TDI	1.05	10	15	5.99	0.707
PIBH	EPR 6132, 90.5	TDI	1.05	10	37	3.00	0.814
PP4282	—	TDI/FeAA	1.05	3	26	5.03	0.692
PP4282	—	DDI/FeAA	1.20	10	15	4.14	0.749
PP4282	—	PAPI	1.0	10	37	2.59	0.938
PP4282	—	VORITE 63	1.0	10	10	2.16	0.886
PP10024	TMP, 1.88	TDI	1.05	1	5j	—	—

<sup>a</sup> A chain-extended product, soluble in benzene, of  $M_w$  96 000 resulted

<sup>b</sup> Poly(methylene polyphenyl isocyanate), (Upjohn Co.) trifunctional isocyanate equiv. wt 133.7

<sup>c</sup> Trifunctional isocyanate derivative from ricinoleic acid, (Baker Castor Oil Co.) NCO equiv. wt 228

<sup>d</sup> Refined castor oil (triol) (Baker Castor Oil Co.) hydroxyl equiv. wt 342

<sup>e</sup> Trimethylolpropane, hydroxyl equiv. wt 44.7

<sup>f</sup> Processed as a solid propellant, with 75% solids (NH<sub>4</sub>C104 and A1 powder) added

<sup>g</sup> Breaking stress, 35 lbf/in<sup>2</sup>; breaking strain, 98%

<sup>h</sup> Performed by Mr D. Udlock, Jet Propulsion Laboratory

<sup>i</sup> A chain-extended product, soluble in benzene,  $M_w$  96 000

<sup>j</sup> Sample PP10024 cured and analysed by Dr S. Kalfayan, Jet Propulsion Laboratory

Table 5 Curing of hydroxyl ethylene-propylene (copolymer) prepolymers

Prepolymer	Curing agent	Ratio isocyanate: hydroxyl	Curing time (days)	Hardness, Shore A	Gel swelling ratio	Gel fraction
EPR 5042B	TDI	1.05	10	41	2.20	0.914
EPR 5042B	DDI	1.20	10	47	4.55	0.923
EPR 5122	TDI	1.05	10	40	2.16	0.886
EPR 6122	DDI	1.20	10	45	2.59	0.938
EPR 6132	TDI	1.05	3	61	2.08	0.452
EPR 6132	TDI-FeAA	1.05	3	57	2.00	0.358
EPR 6132	DDI	1.05	3	49	2.22	0.911
EPR 6132	DDI	1.05	10	51	2.24	0.917
EPR 6132	DDI	1.20	3	39	2.76	0.868
EPR 6132	DDI	1.20	10	46	2.20	0.914
EPR 6132	DDI-FeAA	1.20	3	30	3.05	0.879
EPR 6132	DDI-FeAA	1.20	10	44	2.56	0.897

for either 3 or 10 days. If the mixture cured, the Shore A hardness was measured, and  $9 \times 10^{-6}$  m diameter samples ( $\sim 2 \times 10^{-4}$  kg) were immersed in 100 ml of toluene for determination of gel fraction and gel swelling. The curing results are shown in Tables 4 and 5.

## DISCUSSION

This effort was initiated by the need for saturated hydrocarbon prepolymers with reactive functional groups for solid propellant binders.

The successful preparation of hydroxy-terminated polyisobutylene by ozonolysis of butyl rubber in solution, followed by reduction with LiAlH<sub>4</sub>, by the method of Jones and Marvel<sup>1</sup> prompted the investigation of other, less expensive and more convenient, reducing agents. We found that commercially available reducing agents capable of reducing the carbonyl (resulting from ozonolytic scission

of main-chain unsaturation) to hydroxyl, besides LiAlH<sub>4</sub>, were di-isobutyl aluminium hydride<sup>4,5</sup> (DIBAL-H), sodium bis(2-methoxyethoxy) aluminium hydride<sup>7,8</sup> (Red-Al), and sodium aluminium diethyl dihydride<sup>6</sup> (OMH-1). Since economics favour DIBAL-H and OMH-1, they were used extensively in this effort for the reduction of ozonized groups of saturated prepolymers.

The successful preparation of hydroxyl-terminated polyisobutylene prompted investigation of the preparation of prepolymers of ethylene-propylene copolymer by the method of bromination, dehydrobromination to produce main-chain unsaturation, and ozonolysis followed by reduction. Bromination was expected to take place at tertiary carbon sites<sup>9</sup>, and bromination of ethylene-propylene copolymer in CCl<sub>4</sub> solution has been reported<sup>10,11</sup>. We found here that bromination of the ethylene-propylene copolymers in CCl<sub>4</sub> solution occurred readily under ordinary laboratory fluorescent lighting in either Pyrex or quartz vessels.

For dehydrobromination, we found potassium *t*-butoxide in tetrahydrofuran and *N*-ethylpiperidine in heptane to be satisfactory, but have used a substantial excess of dehydrobromination agent; further research may show that appreciably less is required.

The process of bromination, dehydrobromination, ozonolysis, and reduction successfully produced viscous, liquid hydroxyl-containing curable prepolymers from ethylene-propylene rubber. We found that a sample of ethylene-propylene copolymer, Exxon Vistalon 404, brominated to the extent of 1.0 equiv. Br<sub>2</sub>/kg polymer, when not subjected to dehydrohalogenation also was degraded by ozonolysis; this observation prompted the investigation of ozonolysis of saturated hydrocarbon polymers as a means of prepolymer preparation.

Although there is substantial literature on the reaction between olefins and ozone and the reactions involved have been clearly defined<sup>12</sup>, there have been relatively few investigations of the effects of ozone on saturated compounds. However, Geiseler and coworkers found that ozone reacts with *n*-octadecane to form carboxyl and carbonyl species, and have investigated the reaction mechanism<sup>13</sup>. Subsequently they examined the degradation of polyolefins by ozone in oxygen<sup>14</sup>. The saturated hydrocarbon polymers investigated included high and low density polyethylene, and polypropylene as suspensions in carbon tetrachloride and polyisobutylene dissolved in carbon tetrachloride. They observed substantial reductions of intrinsic viscosities for these polymer systems, as well as infra-red evidence for the formation of carboxyl and other species containing oxygen.

In this work it has been found that solutions of ethylene-propylene rubber (EPR), amorphous polypropylene and poly(1-butene) can be ozonized to give low molecular weight products that can subsequently be reduced to prepolymers containing hydroxyl groups. The prepolymers can then be reacted with di-isocyanates to obtain crosslinked polyurethane hydrocarbon elastomers.

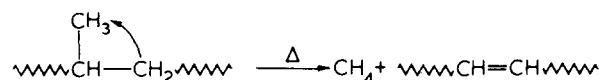
Figure 1 shows the observed relationships of polymer intrinsic viscosities and ozone consumption for the three types of polymers. Since the values for ozone required represent the total amount bubbled into the reaction mixtures, and concentrations were variable, no rigorous conclusions about the kinetics of ozonization are possible. However, the slopes generally appear to be slightly larger for ethylene-propylene rubber than the other polymers. Following ozonization, the products were treated with diisobutylaluminum hydride (DIBAL-H, Texas Alkyls) 25 wt % in heptane and reduced, using the same procedure as for lithium aluminum hydride<sup>1</sup>. Ozonization conditions, approximate intrinsic viscosities, hydroxyl concentration and functionalities are shown in Table 1. Functionality is the number of hydroxyl groups/mol of prepolymer. Since these products often have functionalities exceeding two, some hydroxyl groups must be present along the chains as well as at the ends. Preliminary experiments have shown that crosslinked polymers are obtained when these prepolymers are cured with approximately equivalent amounts of di-isocyanates. Since the cured polymers usually contained about 10% sol or less, it can be concluded that relatively few monofunctional species were formed during ozonolysis and reduction.

Although the reaction times and amounts of ozone required for ozonization of saturated hydrocarbon polymers are greater than for ozonolysis of butyl rubber<sup>1,2</sup> the process described here allows preparation of hydrocarbon

prepolymers of different chemical structure and with high functionality that can be used in the formulation of a variety of castable hydrocarbon polymer systems.

We observed in each experiment that EPR and EPDM underwent thermal degradation to viscous oligomers, suggesting chain scission rather than unzipping, as in the case of polyisobutylene<sup>16</sup>. The molecular weight of the residue, as non-volatile oligomer, decreased with increasing degradation temperature. The EPDM materials were apparently more subject to thermal degradation than was EPR (Table 3) as indicated by lower molecular weight product.

The relatively high unsaturation functionality (~2) of the EPR degraded products is difficult to explain, since chain scission alone would be expected to give monofunctional unsaturated materials<sup>17</sup>, one possible explanation is the reaction:



occurring in addition to chain scission for the EPR products. This reaction is indicated by the fact that ozonolysis results in further reduction in molecular weight. (Ozonolysis of isobutylene-diene copolymer containing main-chain unsaturation results in substantial molecular weight reduction due to olefin cleavage<sup>1</sup>.)

The viscous oligomers that were ozonized to the extent of 6.0 equiv./kg, were substantially over-ozonized since the unsaturation levels in the oligomers were ~2 equiv./kg (Table 2). Consequently, not only were ozone-olefin reactions<sup>12</sup> occurring, but also ozone degradation of saturated EPR was taking place.

After reduction of these ozonized oligomers, essentially complete conversion of all oxygen species to hydroxyl was observed from the infra-red spectra.

The preliminary curing experiments of the hydroxy-terminated polyisobutylene samples prepared from butyl rubber (Table 4) indicate that since crosslinking took place only upon the addition of triols to the polymer that the polyisobutylene samples were mixtures of diol with species less than difunctional in hydroxyl. The polyisobutylene sample PIBLM, prepared from butyl containing 4.2% unsaturation, warrants further investigation. Its molecular weight is lower than that prepared from butyl of only 2% unsaturation, resulting in a lower bulk viscosity [2460 P (Dr S. Kalfayan, Jet Propulsion Laboratory) at 23°C vs. 8000 P at 21°C for an analogous polyisobutylene<sup>2</sup> of  $M_n$  1800].

The ethylene-propylene prepolymer cured readily with TDI and DDI (Table 5); with TDI the cured products were rather hard materials. With DDI the cured products were flexible and had a high gel fraction.

The polypropylene prepolymers also cured with isocyanates, as shown in Table 4, producing rather soft polymer.

## CONCLUSIONS

Ozonolysis of polymers (with or without main-chain unsaturation) in solution, followed by reduction, leads to curable, viscous liquid prepolymers containing hydroxyl groups. Ethylene-propylene copolymers with main-chain

unsaturation are much more readily cleaved by ozonolysis than are fully saturated polymers.

Main-chain unsaturation can be produced in a saturated hydrocarbon by bromination followed by dehydrobromination.

Bromination occurs readily in CCl<sub>4</sub> solution; potassium t-butoxide and *N*-ethylpiperidine have been found to be effective in dehydrobromination.

The thermal degradation at temperatures ranging from 350–550°C of one type of EPR and several types of EPDM, and at temperatures from 500 to 700°C for amorphous polypropylene resulted in viscous liquid oligomers which were mono- to di-functional in unsaturation. The molecular weight of the oligomers is inversely related to the degradation temperature. Ozonolysis followed by reduction of these oligomers produced prepolymers approximately di-functional in hydroxyl.

Reduction of ozonized, degraded polymer to produce hydroxyl groups can be effected with lithium aluminium hydride, di-isobutyl aluminium hydride, sodium bis(2-methoxyethoxy) aluminium hydride, and sodium aluminium diethyl dihydride.

Saturated ethylene-propylene prepolymers with hydroxyl groups can be cured with difunctional isocyanates under a variety of conditions.

## REFERENCES

- 1 Jones, E. B. and Marvel, C. S. *J. Polym. Sci. (A)* 1964, **2**, 5313
- 2 Baldwin, F. P., Burton, G. W., Griesbaum, K. and Hanington, G. *Adv. Chem. Ser.* 1969, **91**, 448
- 3 Rhein, R. A. and Ingham, J. D. *Polym. Prepr.* 1974, **15**, 60
- 4 'Diisobutyl Aluminum Hydride and Triisobutyl Aluminum', Technical Bulletin, Texas Alkyls Inc., 1970
- 5 Bruno, G. 'The Use of Aluminum Alkyls in Organic Syntheses', Report ICD-1008, Ethyl Corp., 1970
- 6 Davenport, T. F. 'Reductions with OHM-1', Ethyl Corp., 1971
- 7 'Red-Al' Technical Bulletin, Adrich Chemical Co., 1970
- 8 Vit, J. *Eastman Org. Chem. Bull.* 1970, **42** (3)
- 9 Gould, E. S. 'Mechanism and Structure in Organic Chemistry', Holt, Rinehart, and Winston, New York, 1959, pp 698–699
- 10 Makowski, H. S. and Seelbach, C. W. U.S. Pat. 3 084 145 (April 2, 1963)
- 11 Dontsov, A. A., Novitskava, S. P. and Dogadnin, B. A. *Rubber Chem. Technol.* 1971, **44**, 721
- 12 Bailey, P. S. *Chem. Rev.* 1958, **58**, 925
- 13 Geiseler, G., Asinger, F. and Wien, H. *Chem. Ber.* 1959, **92**, 958
- 14 Geiseler, G. and Wergin, H. *J. Prakt. Chem.* 1964, **25**, 135
- 15 Flory, P. J. 'Principles of Polymer Chemistry', Cornell University Press, Ithaca, 1967
- 16 Madorsky, S. L. 'Thermal Degradation of Organic Polymers', Interscience, New York, 1964, pp 113, 114
- 17 Simha, R. and Wall, L. A. *J. Polym. Sci.* 1950, **5**, 615

# An infra-red investigation of cardo polymer solutions

B. I. Lirova, A. A. Tager and L. I. Lazareva  
*Ural State University, Sverdlovsk, USSR*

and S. N. Salazkin and Ya. S. Vygodskii  
*Institute of Element-Organic Compounds, Moscow, USSR*  
(Received 2 February 1975)

Intermolecular interaction of certain cardo polyarylates, polyamides, polyimides with solvents such as chloroform, *sym.*-tetrachloroethane, *m*-cresol, has been investigated. Integrated intensities for the carbonyl stretching bands point to the formation of hydrogen bonds with solvent molecules. The lactone carbonyl is most capable of forming such a bond. The formation of hydrogen bond in polyamides is weakened by the polymer interchain interaction. The proportion of the solvated lactone carbonyls decreases when passing to polymers with more rigid chains.

## INTRODUCTION

In recent years soluble cardo polymers<sup>1,2</sup> with increased heat resistance have aroused considerable interest. The solubility of such polymers is dependent on their chemical structure<sup>3</sup>. Because of this, determination of the mechanism of dissolution of these polymers seems to be a topical problem from the scientific and practical viewpoints.

Since the interaction of individual groups of the macromolecule with the molecules of the solvent plays a significant part in dissolution, the need for studying intermolecular interactions in the polymer-solvent system becomes obvious. Infra-red analysis is one of the most direct methods; it was, therefore, of interest to use it for studying solutions of the cardo polymers.

## EXPERIMENTAL

In this study aromatic polyesters (polyarylates), polyamides, and polyimides have been investigated.

The polyarylates were synthesized by high temperature polycondensation of bisphenols (phenolphthalein, phenolfluorene, and phenolanthrone) and dicarboxylic acid dichlorides (sebacic, terephthalic, 4,4'-diphenyl dicarboxylic, and 4,4'-diphenyloxide dicarboxylic acids)<sup>1-3</sup>.

The polyamides were prepared by low temperature solution polycondensation of anilinephthalein, anilinefluorene, anilineanthrone with isophthaloyl and terephthaloyl chlorides<sup>1-3</sup>. The polyimides were prepared by high temperature one-step polycondensation of anilinephthalein and anilinefluorene and pyromellitic, 3,3', 4,4'-diphenyloxide tetracarboxylic, and 3,3',4,4'-diphenyl tetracarboxylic dianhydrides<sup>1-3</sup>. All polymers were dried under vacuum at 100-120°C. Water content (by Karl-Fischer reagent) does not exceed 0.2-0.3%. Model compounds were prepared by known methods; melting points and solvents for crystallization were as follows: phthalide,

71°C (water); 3,3-diphenylphthalide, 117-118°C (ethanol); anthrone, 161-162°C (benzene/petroleum ether); 9,9-diphenylanthrone, 194-195°C (ethanol).

Polymethylenephthalide selected as a model polymer was synthesized by polymerization in dimethylformamide (DMF) in the presence of benzoyl peroxide initiator<sup>1,2</sup>.

Chloroform, *sym.*-tetrachloroethane (TCE) dimethyl sulphoxide (DMSO), and *m*-cresol dissolve the polymers and do not absorb selectively in the investigated region of the spectrum. The water content did not exceed 0.01%.

The i.r. spectra were recorded on a UR-20 double-beam spectrophotometer.

The spectra of films of polymers were taken in the 700-1800 cm<sup>-1</sup> region with a NaCl prism. The polymer solutions (0.035 mol/l) were investigated in the carbonyl absorption region of 1600-1800 cm<sup>-1</sup>. The compensation method was applied to polymer solution investigation, using two similar demountable cells (sample cell and compensation cell), the thickness of which was checked interferometrically before each run.

The films of polyarylates and all polyimides were obtained from solutions in TCE and those of the polyamides from solutions of the polymers in DMF.

The 800 cm<sup>-1</sup> band was used to control the drying of polymer films obtained from DMF. Integrated intensities of the absorption bands were determined by the Ramsay method<sup>4</sup>. In the case of the overlapped bands, the integrated intensity was determined by direct area measurements with correction for wings. Such bands were preliminarily separated graphically.

## SPECTRA OF POLYMER SOLUTIONS

### *Polyarylates*

*Figure 1a* gives the spectra of solutions of polyarylates I-III in TCE. It can be seen (*Table 1*) that there is a band

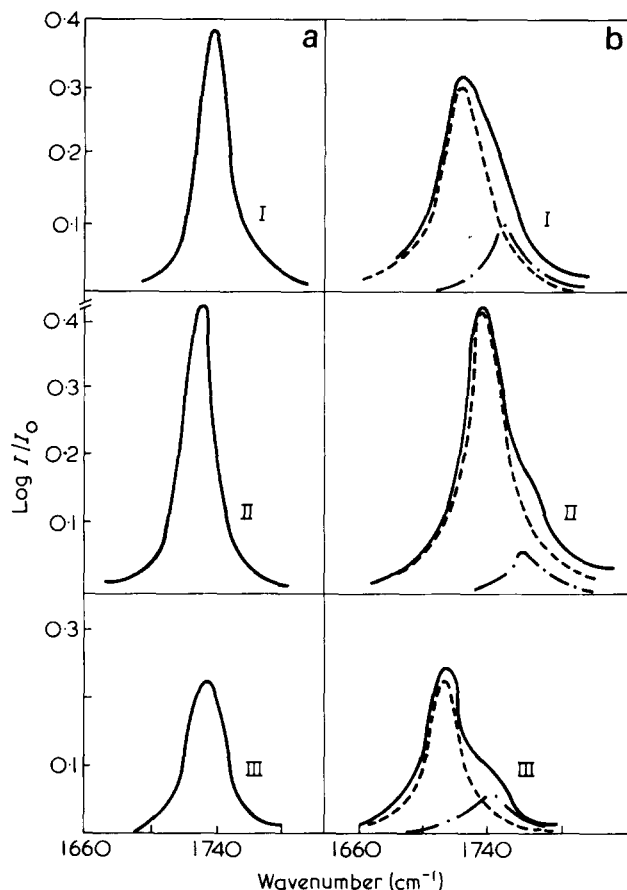


Figure 1 I.r. spectra of 0.035 mol solutions of polyarylates I-III in (a) TCE and (b) *m*-cresol

in the spectrum that is slightly shifted to low frequency as compared to that of the film.

Similar spectra were obtained with solutions of polyarylates II and III in chloroform. The half-band widths of the  $\nu_{C=O}$  band in this solvent is  $25\text{ cm}^{-1}$  as in the spectrum of the film, and the integrated absorption coefficient  $A_{C=O}$  for carbonyl groups is  $3.1 \times 10^4\text{ cm}^{-2}\text{ mol}^{-1}$ .

The integrated absorption coefficients  $A_{C=O}$  of the ester group for solutions of polyesters in TCE are given in Table 1.

The spectrum of the polyarylate V solution in TCE is given in Figure 2a. There is double band with maxima at  $1741$  and  $1766\text{ cm}^{-1}$  which are shifted to the low frequencies as compared to the spectra of films. The spectra of solutions of polyarylate V in chloroform are similar. It is interesting that in both cases, that the carbonyl stretching band of the lactone is shifted most in going from film to solution.

The integral absorption coefficient  $A_{C=O}$  of the lactone in TCE solution (Table 1) was determined from the value calculated for the polymethylenephthalide.

The shift towards low frequencies, when passing from film to solutions in chloroform and TCE, is also observed for polyarylate VI (Figure 2a). But, unlike polyarylate V, both bands in the spectrum of the solution reveal practically the same shift under the influence of solvent.

The integrated coefficient for the carbonyl band of anthrone in TCE solutions calculated after graphical separation from the integrated coefficient of the carbonyl band of the ester bond of polymers I-III is given in Table 1. The shift of the carbonyl bands in solutions of the polyesters in TCE and chloroform towards low frequencies is indicative

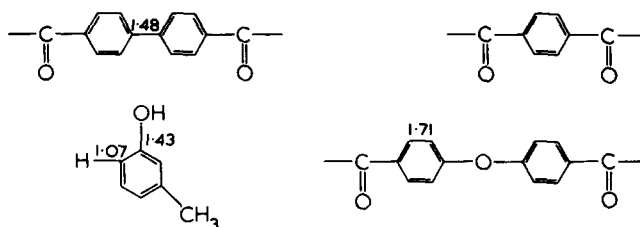
of the formation of hydrogen bonds between the solvent molecules and the carbonyl groups of polymer molecules. This is also confirmed by the increase of the integrated absorption coefficient of the carbonyl band in solutions as compared to its value for carbonyl groups unperturbed by hydrogen bonds.

More substantial changes in spectral parameters of the carbonyl band take place in the spectra of solutions of the polyarylates in *m*-cresol.

Figure 1 shows the spectrum of polyarylate I in *m*-cresol. The complex band with a maximum at  $1723\text{ cm}^{-1}$  is markedly shifted towards low frequencies as compared to its position in the film, and this again points to the formation of a hydrogen bond between the carbonyl groups of the polymer with the OH groups of solvent molecules. The presence of a shoulder in the high frequency region indicates that not all carbonyl groups participate in hydrogen bond formation. H-bond formation is also confirmed by an increased half-band width as well as by an increased integral absorption coefficient for the ester groups.

The integral absorption coefficient of the solvated carbonyl group was calculated after determination of the number of unassociated carbonyl groups from the known coefficient of the unperturbed band in the spectrum of the film (Table 1). The content of the free carbonyl groups in the solution was 0.5.

The same changes in spectral parameters, when passing from film to *m*-cresol solution, occur also for polyarylates II, III (Figure 1b) but the content of unbonded carbonyl groups is less than in the polyarylate I and is equal to 0.2. This can be connected with decreasing steric hindrance in the interaction of the carbonyl with solvent molecules, when passing from polyarylate I to polyarylates II-III. Indeed, the linear dimensions of diphenyl and diphenyl-oxide dicarboxylic acids are more than twice the distance between the carbonyl groups of terephthalic acid (polyarylate I), the dimensions of which are commensurable with those of the solvent.



It is known that molecules containing two adjacent polar groups can have two conformations (rotational isomers):



In the latter case the steric effect will probably be particularly significant.

It should be noted that the possibility of rotational isomerism does not exclude the fact that the splitting of the carbonyl band in *m*-cresol solutions could be associated with the field effect due to proximity of the carbonyl groups<sup>5-7</sup>.

Figure 2b shows the spectrum of the solution of polyarylate V in *m*-cresol. It is seen that the carbonyl of both the lactone and the ester group are shifted to low frequencies. It should be noted that if both carbonyl groups interact with



Table 1 Spectral parameters of the absorption band  $\nu_{C=O}$  of polyarylates

No.	Structural unit of the polymer	Assignment of the band $\nu_{C=O}$	Solutions in									
			Chloroform			sym-tetrachloroethane			m-Cresol			
		Film $\nu_{max}$ ( $cm^{-1}$ )	$\nu_{max}$ ( $cm^{-1}$ )	$\Delta\nu$ ( $cm^{-1}$ )	$\nu_{max}$ ( $cm^{-1}$ )	$\Delta\nu$ ( $cm^{-1}$ )	$\Delta\nu^{1/2}$ ( $cm^{-1}$ )	$A \times 10^{-4}$ ( $l \text{ cm}^{-2} \text{ mol}^{-1}$ )	$\nu_{max}$ ( $cm^{-1}$ )	$\Delta\nu$ ( $cm^{-1}$ )	$\Delta\nu^{1/2}$ ( $cm^{-1}$ )	$A \times 10^{-4}$ ( $l \text{ cm}^{-2} \text{ mol}^{-1}$ )
I		1743	—	—	1740	3	25	3.6	1723	20	32	5.5
II		1739	1738	1	1735	4	25	3.5	1715	24	32	6.0
III		1739	1738	1	1735	4	26	3.5	1715	24	32	5.2
IV		1765	—	—	1758	7	—	—	1743	22	—	—
V		1776 1743	1769 1742	7 1	1766 1741	10 2	26 25	6.8 3.6	1748 1729	28 14	34 32	8.5 5.5
VI		1743 1672	1741 1670	2 2	1740 1669	3 3	25 20	3.6 3.4	1723 1657	20 15	32 25	5.5 5.0
*		1776	—	—	1777†	—	26	5.4	1761	15	36	8.0

\* For comparison  
† In DMSO

the solvent, changes in the position of the ester carbonyl groups was slightly less than in the spectra of solutions of polyarylates I–III in *m*-cresol. Simultaneously with the shift of the band in the polyarylate V spectrum a redistribution of the intensities of two carbonyl bands in favour of the high intensity lactone carbonyl band has occurred.

The integral absorption coefficient of the lactone of polyarylate V was calculated from that of carbonyl absorption of the ester groups associated with *m*-cresol in the solution of polyarylate I. The value of integral coefficient  $A_{C=O}$  of the acetone carbonyl groups of polyarylate V was  $8.5 \times 10^4 \text{ l cm}^{-2} \text{ mol}^{-1}$ , the same as for solutions of polymethylenephthalide and 3,3-diphenylphthalide in *m*-cresol.

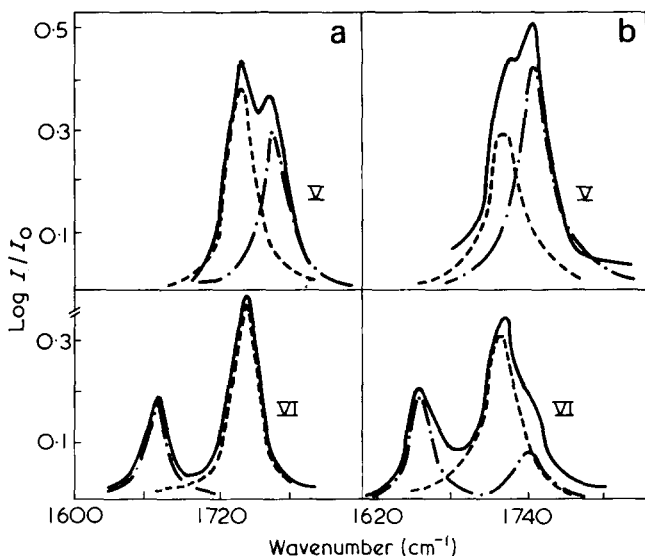
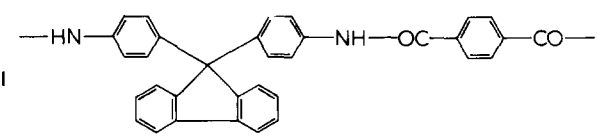
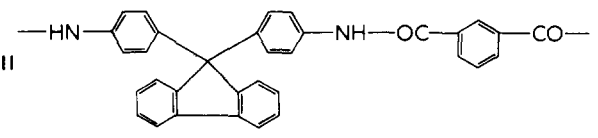
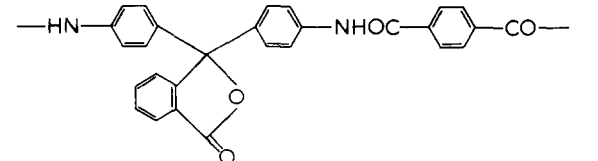
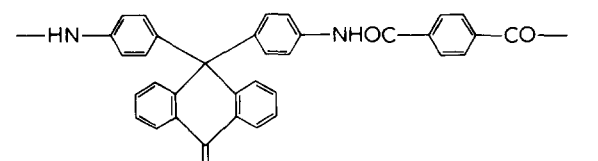


Figure 2 I.r. spectra of 0.035 mol solutions of polyarylates V and VI in (a) TCE and (b) *m*-cresol

Table 2 Position of  $\nu_{C=O}$  in polyamides

No.	Structural units of the polymer	Film $\nu_{max}$ ( $\text{cm}^{-1}$ )	Assignment of C=O	Solution in <i>m</i> -cresol	
				$\nu_{max_1}$ ( $\text{cm}^{-1}$ )	$\Delta\nu$ ( $\text{cm}^{-1}$ )
VII		1668	Amide-I	1660	8
VIII		1668	Amide-I	1662	6
IX		1668	Amide-I	1663	5
		1770	lactone	1746	24
X		1669	Anthrone and Amide-I	1660	9

Hydrogen bonds are formed in solutions of polyarylate VI in *m*-cresol but, unlike sample V, the magnitude of the shift and the integral coefficients  $A_{C=O}$  of the C=O absorption of the anthrone and ester bond are close to each other (Table 1, Figures 1, 2a and 2b).

Thus, the spectrum parameters (the shift of carbonyl band is 20–30  $\text{cm}^{-1}$ ) undergo more significant changes in *m*-cresol solutions as a consequence of the greater proton-donating ability.

An analysis of the spectrum parameters of absorption bands of different carbonyl groups in solutions of polyarylates in TCE and *m*-cresol indicates that all groups participate in H bonding. But the considerable shifts and the high value of  $A_{C=O}$  for the lactone point to the greater ability of this group to form H bonds. This can be explained both by higher basicity of the lactone carbonyl as compared to the carbonyl groups of ester and ketones<sup>8</sup> and by steric factors.

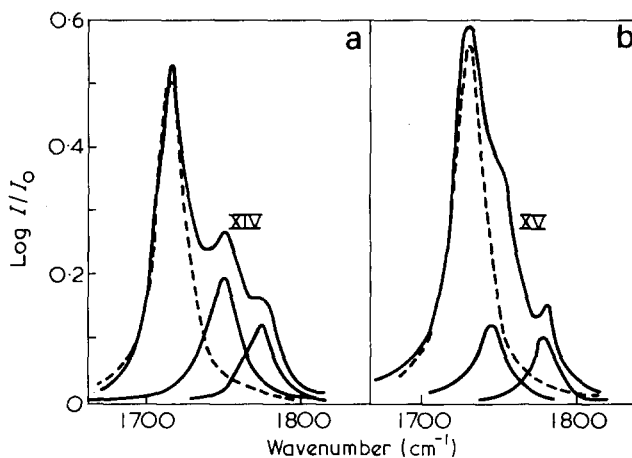
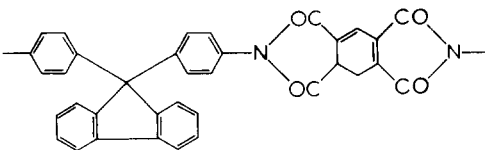
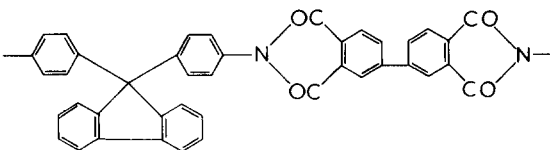
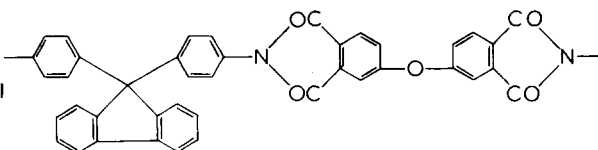
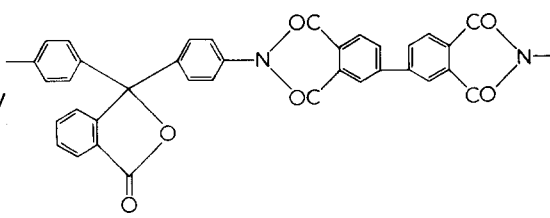
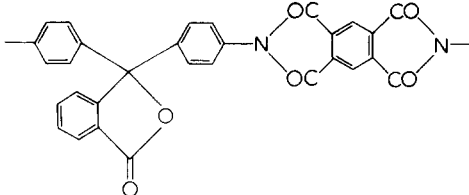


Figure 3 I.r. spectra of 0.035 mol solutions of polyimides (a) XIV and (b) XV in *m*-cresol

Table 3 Position of  $\nu_{C=O}$  in polyimides

No. Structural unit of the polymer	Film $\nu_{\max}^{(1)}$ ( $\text{cm}^{-1}$ )	Assignment of C=O	Solution in <i>m</i> -cresol	
			$\nu_{\max}^{(1)}$ ( $\text{cm}^{-1}$ )	$\Delta\nu$ ( $\text{cm}^{-1}$ )
XI 	1780 1724	imide ( <i>sym</i> ) imide ( <i>asym</i> )		
XII 	1778 1724	imide ( <i>sym</i> ) imide ( <i>asym</i> )	1773 1712	5 12
XIII 	1780 1726	imide ( <i>sym</i> ) imide ( <i>asym</i> )	1775 1711	5 15
XIV 	1778 1724	imide ( <i>sym</i> ) and lactone imide ( <i>asym</i> )	1774 1749 1713	4 27 10
XV 	1781 1732	imide ( <i>sym</i> ) and lactone imide ( <i>asym</i> )	1780 1745 1727	1 31 5

### Polyamides

Table 2 shows the results obtained by investigations of the polyamide films and solutions. The spectra of the solutions of polyamides VII, VIII and X in *m*-cresol reveal one absorption band slightly shifted to low frequencies as compared to the film spectra.

The spectrum of the solution of polyamide IX has two bands shifted to low frequencies, the higher frequency band corresponding to the lactone carbonyl group as in the case of polyarylate V.

However, it is interesting that the magnitude of the shift of the carbonyl band in polyamides is considerably less than that of ester groups in the spectra of solutions of similarly composed polyarylates in the same solvent.

This can probably be explained by the fact that the polyamide carbonyl groups participate in the formation of H bonds  $-\text{NH} \dots \text{O}=\text{C}<$  in the polymer.

### Polyimides

The spectra of the solutions of polyimides XII and XIII in TCE and *m*-cresol contain two absorption bands and the shift to low frequencies compared to the films of these polyimides points to the formation of hydrogen bonds with

the solvents (Table 3). It should be emphasized that the absorption band corresponding to the antisymmetric C=O vibration of the cyclic imide is shifted to a greater extent than that corresponding to the symmetric vibration.

In the spectra of *m*-cresol solutions of the polyimides XIV–XV (Figure 3) there are three bands in the carbonyl absorption region as opposed to two bands in the spectra of their films and TCE solutions. The appearance of a band at  $1750 \text{ cm}^{-1}$  probably characteristic of C=O stretching of the lactone (as in solutions of polyarylate V and polyamide IX) can be explained by the fact that this band in the presence of the solvent shifted to a greater extent than the band which overlaps the former in the film spectrum and this is assigned to the symmetric C=O vibration of the imide. The shift value of the carbonyl band of the lactone is  $30 \text{ cm}^{-1}$ .

The proportion of the lactone carbonyl groups of polyimide participating in the H bond formation with the solvent molecules was calculated from the known  $A_{C=O}$  value for the lactone in *m*-cresol.

The proportion of the bonded carbonyl groups of the lactone in polyimide XV was 0.09 and almost half that of polyimide XIV (0.17). An increased proportion of the lactone carbonyl groups participating in the H bond formation for polyimide XIV as compared to polyimide XV can

apparently be explained by better flexibility of the polymeric chain of polyimide XIV, which facilitates the interaction of the carbonyl groups of the polymer with the molecules of the solvent. It should be noted that the proportion of the solvated lactone carbonyl groups increases still further ( $\sim 0.43$ ) in solutions of polymers with less rigid chains, e.g. polyarylates.

Thus the comparative investigations of solution of regularly changing cardo polyarylates, polyamides, polyimides, and polymethylenephthalide has shown that, besides the polar groups of the polymer backbone, the polar groups of the cardo group, in particular the carbonyl group of the anthrone and especially phthalide rings, make a considerable contribution to intermolecular interaction of the macromolecule with the molecules of the solvent.

## REFERENCES

- 1 Vinogradova, S. V. and Vygodskii, Ya. S. *Usp. Khim.* 1973, **42**, 1225
- 2 Korshak, V. V., Vinogradova, S. V. and Vygodskii, Ya. S. *J. Macromol. Sci.* 1974, **11**, 45
- 3 Korshak, V. V. and Vinogradova, S. V. 'Non-equilibrium Polycondensation', Nauka, Moscow, 1972
- 4 Ramsay, D. A. *J. Am. Chem. Soc.* 1952, **74**, 72
- 5 Bellamy, L. J. 'Advances in the Infra-red Group Frequencies', Methuen, Suffolk, 1968
- 6 West, W. (Ed). 'Chemical Applications of Spectroscopy', Wiley, New York, 1956
- 7 Mikhailov, G. P. and Smolyansky, A. A. *Opt. Spektrosk.* 1963, **15**, 566
- 8 Bellamy, L. J. 'Infra-red Spectra of Complex Molecules', Wiley, New York, 1960

# Transport of water in synthetic *cis*-1,4-polyisoprenes and natural rubber

J. A. Barrie, D. Machin\* and A. Nunn†

Department of Chemistry, Imperial College of Science and Technology, London SW7 2AY, UK

(Received 25 April 1975; revised 11 July 1975)

The sorption, permeation and diffusion of water in two synthetic *cis*-1,4-polyisoprenes and natural rubber and of methanol in natural rubber have been measured in the range 25 to 60°C. At the higher relative pressures the diffusion coefficient in all systems decreases with concentration and activation energies for diffusion increase with concentration. The results are consistent with increased clustering of the sorbed penetrant at higher relative pressures which renders an increasing fraction of the penetrant relatively immobile. The effect of polar impurities on the sorption and diffusion process is discussed to account for differences in behaviour of the various samples at lower relative pressures.

## INTRODUCTION

For a number of water-polymer systems, the diffusion coefficient  $D$  decreases as the total concentration  $C$  of water sorbed is increased<sup>1-4</sup>; the effect is more pronounced with elastomers containing amounts of water-soluble salts such as sodium chloride<sup>2</sup>. It is generally accepted that clustering of the sorbed water through hydrogen-bond formation is responsible and that the molecules in clusters are virtually immobilized relative to the unassociated water, the fraction of which decreases as  $C$  increases.

Of the elastomers, the silicone and polyurethane rubbers have been studied in some detail<sup>2,5-8</sup>. The results of earlier work on the water-natural rubber system indicate that  $D$  should decrease with  $C$  for this elastomer<sup>9,10</sup>. In the present investigation water transport in high purity synthetic *cis*-1,4-polyisoprenes and natural rubber is investigated in some detail. Some measurements have also been made with methanol as it was observed that in the silicone rubber systems  $D$  for this penetrant again decreased with  $C$ <sup>2</sup>. The effect of sodium chloride 'filler' on the transport process is examined briefly in the region of relative pressure,  $p/p_0 < 0.75$ ; the region of higher water activity has been the subject of another investigation<sup>11</sup>.

## EXPERIMENTAL

Rubber samples in the form of thin sheets, 0.5 to 1 mm in thickness were supplied by the Malaysian Rubber Producers Research Association (UK). The samples comprised: a natural rubber in the form of deproteinized pale crepe (NR); two synthetic polyisoprenes, Natsyn 2200 (Goodyear Chemical Co.) and Cariflex IR 305 (Shell Chemicals UK) with a high *cis*-1,4-content, >92%; a Cariflex IR 305 sample containing 0.5 parts of crushed sodium chloride per 100 parts of rubber.

All of the sheets were cured with 3% dicumyl peroxide for 35 min at 140°C, refluxed with acetone for two days under an atmosphere of nitrogen in a darkened Soxhlet

apparatus and stored under vacuum in darkened containers. To investigate the effect of a 'limited' degree of ageing on the solubility of water in natural rubber, a few measurements were made with a sample which had been stored for ~3 years in the dark and under vacuum with occasional exposures to air and light. Sorption isotherms for water were obtained using an electronic microbalance (Sartorius 4102) and for methanol using a calibrated silica spiral as described earlier<sup>2</sup>. Steady-state permeation rates were determined as a function of the pressure on the ingoing face of the membrane by sorbing the outgoing vapour in a dehydrated aluminosilicate suspended from a calibrated silica spiral<sup>12</sup>. Alternatively, the pressure at the outgoing face of the membrane was monitored using an electronic micromanometer (M.K.S. Instruments Inc.) with a receiving volume of not less than 6 litres so as to minimize effects arising from the sorption of water on glass surfaces<sup>13</sup>.

## RESULTS

Typical sorption isotherms are shown in Figures 1-3. The water isotherms for the synthetic polyisoprenes are of the same type as observed with the silicone rubbers and have a

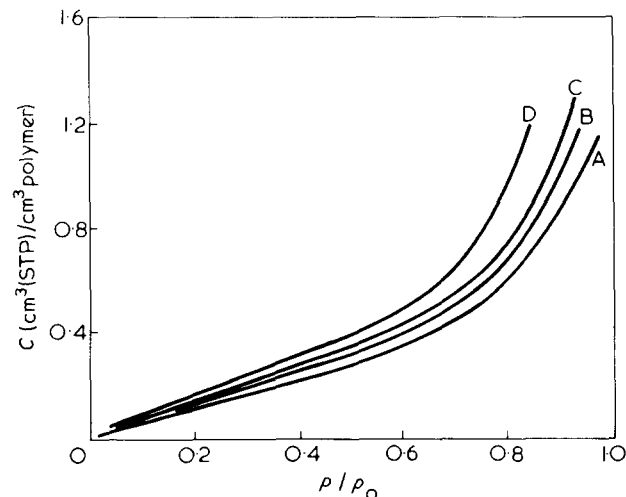


Figure 1 Sorption of water in Cariflex IR305. A, 36.6°; B, 42.2°; C, 50.3°; D, 61.3°C

\* Unilever Research Laboratory, Port Sunlight, Wirral, Cheshire L62 4XN, UK.

† Graphic Systems, London, UK.

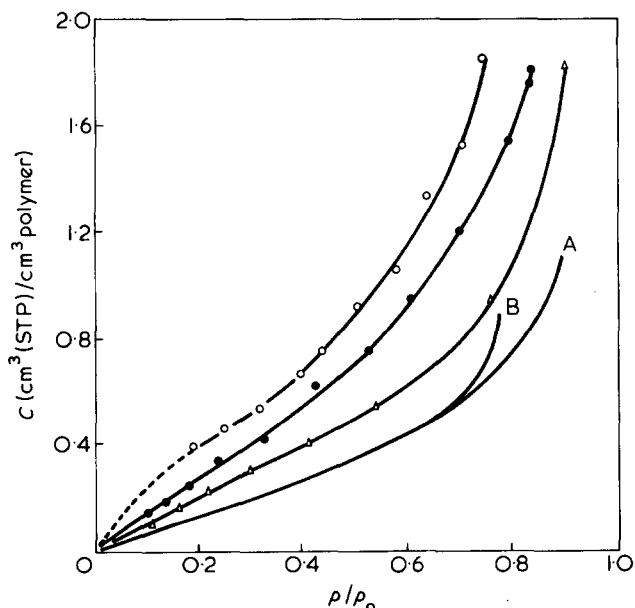


Figure 2 Water sorption at  $\sim 50^\circ\text{C}$ . A, Cariflex IR305; B, Cariflex IR305. +, NaCl;  $\Delta$ , Natsyn 2200;  $\circ$ , 'aged' natural rubber

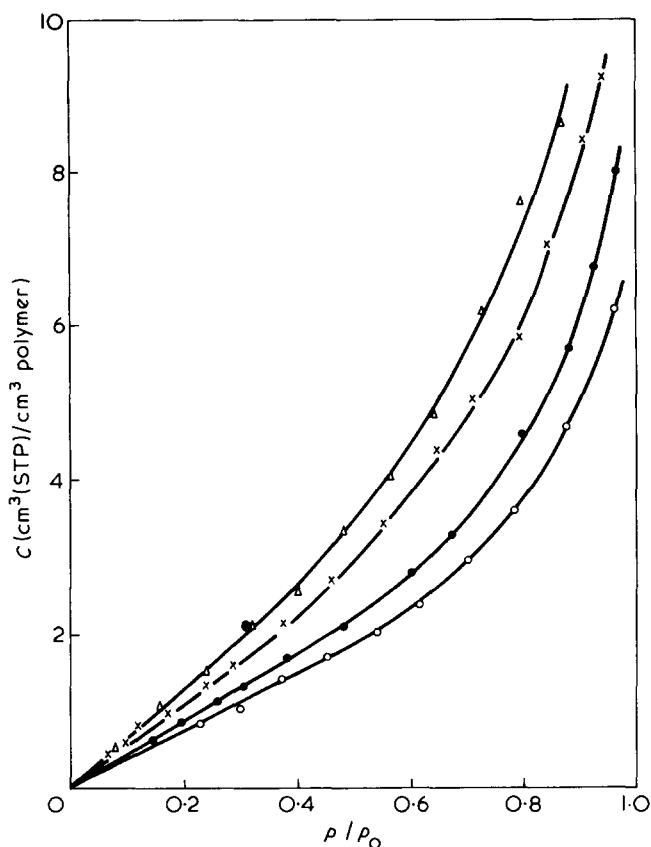


Figure 3 Sorption of methanol in natural rubber.  $\circ$ ,  $26^\circ$ ;  $\bullet$ ,  $35.1^\circ$ ;  $\times$ ,  $50^\circ$ ;  $\Delta$ ,  $60^\circ\text{C}$

linear region at low relative pressures from which values of  $\sigma_{C=O}$ , the Henry's law solubility constant, were obtained and are given in Table 1. For the natural rubber samples, particularly at the lower temperatures, there was an indication of a Langmuir-type sorption at lower relative pressures. This feature of the natural rubber isotherms is more evident for the 'aged' specimen as shown in Figure 2. Since the shape of the isotherm at the lower relative pressures was not established with sufficient accuracy, values of  $\sigma_{C=O}$  are not estimated for the natural rubber samples.

The tendency for penetrant to cluster in the polymer was examined using the clustering functions  $G_{AA}/V_A$  and  $[1 + \phi_A(G_{AA}/V_A)]$  of the Zimm/Lundberg theory where  $G_{AA}$  is a cluster integral for the penetrant and  $V_A$  and  $\phi_A$  are the partial molecular volume and volume fraction of the penetrant, respectively<sup>14,15</sup>. Values of  $G_{AA}/V_A > -1$  and  $< -1$  denote, respectively, clustering and segregation of the penetrant molecules, and the function  $[1 + \phi_A(G_{AA}/V_A)]$  is a measure of the mean cluster size. The clustering functions for the synthetic polyisoprene-water and natural rubber-methanol systems are given as a function of concentration in Table 2. Some heats  $\Delta\bar{H}_A$  and entropies  $\Delta\bar{S}_A$  of dilution were obtained as a function of concentration and are given in Table 3.

Steady-state permeation measurements were made for all samples with the exception of the 'aged' natural rubber and, in all cases, the permeation rate  $J$  varied linearly with the ingoing relative pressure in the range 0 to 0.9. Typical plots of the normalized flux  $Jl$  against relative pressure are shown in Figure 4; for water these are linear but for methanol in natural rubber there is curvature at the higher

Table 1 Solubility coefficients and heats of sorption

System	$T$ ( $^\circ\text{C}$ )	$\sigma_{C=O}$ ( $\text{cm}^3$ (STP)/ $\text{cm}^3$ (cm Hg))	$\Delta\bar{H}_s$ (kJ/mol)
Cariflex IR305/H <sub>2</sub> O	61.3	0.049 (0.054)	
	50.3	0.072 (0.072)	
	42.2	0.100 (0.101)*	-31 (-30.5)
Natsyn 2200/H <sub>2</sub> O	36.6	0.119 (0.152)†	
	49.6	0.105	
Natural rubber/MeOH	44.4	0.129	-38
	32.0	0.238	
	60	0.105	
	50	0.137	
	35.1	0.213	-28
	26	0.278	

Figures in parenthesis refer to Cariflex IR305 with 0.5% NaCl  
\* At  $41.5^\circ\text{C}$ ; † at  $30.5^\circ\text{C}$

Table 2 Clustering functions at  $\sim 50^\circ\text{C}$

System	$p/p_0$	$G_{AA}/V_A$	$1 + \phi_A (G_{AA}/V_A)$
Cariflex IR305/H <sub>2</sub> O	0.3	-1	1
	0.5	640	1.17
	0.7	2150	1.9
Natsyn 2200/H <sub>2</sub> O	0.3	-1	1
	0.5	290	1.07
	0.7	1300	1.88
Natural rubber/MeOH	0.3	-1	1
	0.5	46	1.25
	0.7	100	1.80

Table 3 Heats and entropies of dilution

System	$C$ ( $\text{cm}^3$ (STP)/ $\text{cm}^3$ )	$\Delta\bar{H}_A$ (kJ/mol)	$\Delta\bar{S}_A$ ( $\text{J K}^{-1}$ $\text{mol}^{-1}$ )
Cariflex IR305/H <sub>2</sub> O	0.3	12.1 (4.6)	39 (11)
	0.6	5.9 (3.3)	18 (5.4)
	0.75	5.4	14
Natural rubber/MeOH	1.6	15	56
	4.8	7.9	29
	8.0	4.6	15

Figures in parenthesis refer to Natsyn 2200/H<sub>2</sub>O system

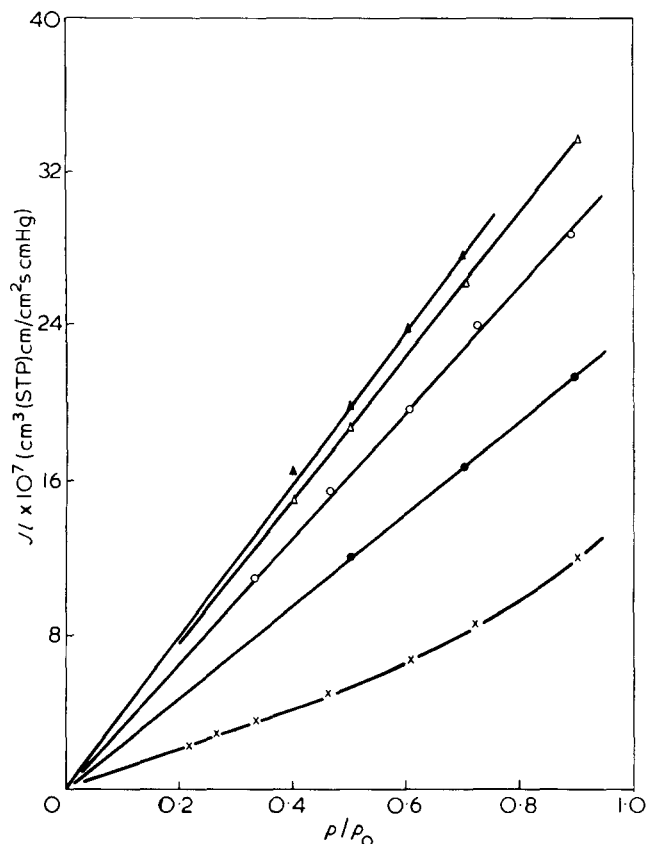


Figure 4 Flux vs.  $p/p_0$  at  $\sim 50^\circ\text{C}$ . X, Natural rubber/MeOH ( $50.3^\circ\text{C}$ ); ●, Natsyn 2200/H<sub>2</sub>O ( $45.2^\circ\text{C}$ ); ○, natural rubber/H<sub>2</sub>O ( $50^\circ\text{C}$ ); △, Cariflex IR305/H<sub>2</sub>O ( $50^\circ\text{C}$ ); ▲, Cariflex IR305 + NaCl/H<sub>2</sub>O ( $50^\circ\text{C}$ ). For methanol the ordinate is  $Jl \times 10^6$

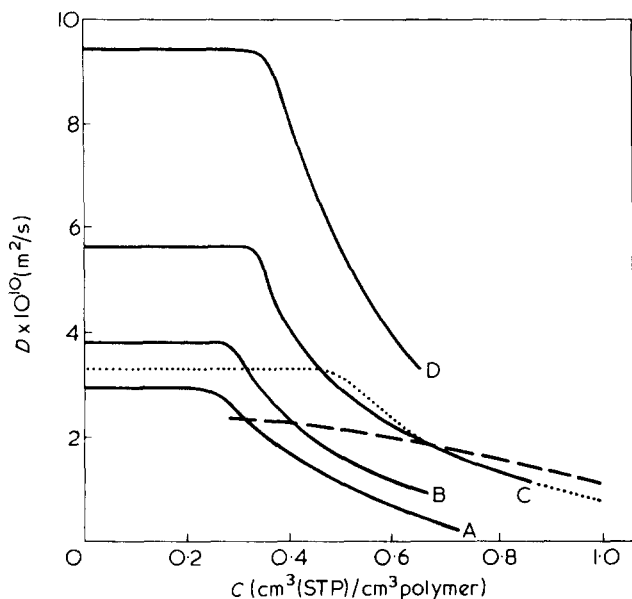


Figure 5 Concentration dependence of  $D$  for water. Cariflex IR305: A,  $36.6^\circ$ ; B,  $42.2^\circ$ ; C,  $50.3^\circ$ ; D,  $61.3^\circ\text{C}$ . ---, natural rubber ( $49.7^\circ\text{C}$ ); ·····, Natsyn 2200 ( $49.7^\circ\text{C}$ )

relative pressures. Steady state diffusion coefficients were obtained from the relation  $D = dJ/dc$  by graphical differentiation of plots of  $Jl$  against the concentration of penetrant in the ingoing face of the membrane. The concentration dependence of  $D$  is illustrated in Figures 5 and 6 and values of  $D_{C=0}$ , the diffusion coefficient in the limit of zero concentration, and of  $\bar{P}_{C=0}$  are given in Table 4. The temperature dependences of  $D$  and of  $\bar{P}$  were described

respectively by the expressions  $D = D_0 \exp(-E_D/RT)$  and  $\bar{P} = \bar{P}_0 \exp(-E_{\bar{P}}/RT)$  and values of  $E_D$  and  $E_{\bar{P}}$  are given as a function of penetrant concentration in Table 5.

## DISCUSSION

The results indicate that the solubility of water in the Cariflex sample is comparable with that in polydimethylsiloxane but for the Natsyn sample it is significantly greater and

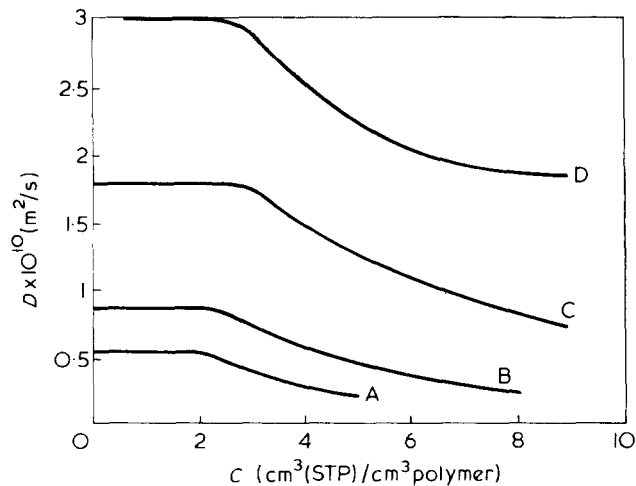


Figure 6 Concentration dependence of  $D$  for methanol. A,  $26^\circ$ ; B,  $35.1^\circ$ ; C,  $50^\circ$ ; D,  $60^\circ\text{C}$

Table 4 Diffusion and permeability coefficients at zero concentration

System	$T$ ( $^\circ\text{C}$ )	$P_{C=0} \times 10^7$ ( $\text{cm}^3$ (STP) $\text{cm} / \text{cm}^2 \text{ s}$ (cmHg))	$D_{C=0} \times 10^{10}$ ( $\text{m}^2/\text{s}$ )
Natural rubber/H <sub>2</sub> O	49.7	3.48	—
	42.5	3.17	—
	39.0	3.02	—
	31.4	2.71	—
Natsyn 2200/H <sub>2</sub> O	49.6	3.49	3.3
	44.4	3.32	2.6
Cariflex IR305/H <sub>2</sub> O	32.0	2.93	1.2
	61.3	4.56 (4.90)	9.3 (9.7)
	50.2	4.02 (4.26)	5.6 (6.0)
	42.2	3.75 (3.76)*	3.8 (3.7)
Natural rubber/MeOH	36.6	3.41 (3.15)†	2.9 (2.1)
	60	3.19	3.0
	50	2.57	1.8
	35.1	1.86	0.87
	26	1.50	0.53

Figures in parenthesis refer to Cariflex IR305 with 0.5% NaCl  
\* At  $41.5^\circ\text{C}$ ; † at  $30.5^\circ\text{C}$

Table 5 Activation energies for diffusion and temperature coefficients of the permeability

System	$C$ ( $\text{cm}^3$ (STP) / $\text{cm}^3$ )	$E_{\bar{P}}$ (kJ/mol)	$E_D$ (kJ/mol)
Cariflex IR305/H <sub>2</sub> O	0	9.2 (8.4)	42 (46)
	0.3	9.2	58
	0.5	9.2	58
	0.6	8.4	— (54)
Natural rubber/MeOH	0	18	42
	5	18	54
	8	18	71

Figures in parenthesis refer to Natsyn 2200/H<sub>2</sub>O

even more so for the natural rubber and 'aged' natural rubber. The results for the synthetic polyisoprenes suggest that impurities of a polar nature are present to a greater extent in the Natsyn sample. The more exothermic heat of sorption  $\Delta\bar{H}_s$  for Natsyn at low coverages and the somewhat greater tendency for water to cluster in the Cariflex sample supports this view. Further support comes from typical ash contents of the two materials, namely 0.35 and 0.05% for the Natsyn and Cariflex samples respectively. The most likely sources of impurities are metallic salts which may not extract readily on refluxing or polar groups arising from partial oxidation of the polymer.

It was previously established for silicone rubbers that the introduction of water-soluble metallic salts, by milling prior to crosslinking, had little effect on water sorption at relative pressures below that of the saturated salt solution<sup>2</sup>. The results of Table 1 and of Figure 2 show that the addition of crushed sodium chloride to the Cariflex rubber has no marked effect on the water sorption at lower relative pressures. It is unlikely therefore that metallic salt impurities can account for the differences between the Natsyn and Cariflex samples and it appears that partial oxidation of the former sample has occurred. It has been established that water sorption in natural rubber increases appreciably on oxidative degradation<sup>16</sup> and it is probable that this factor partly accounts for the higher water sorptions of the natural rubber and 'aged' natural rubber samples. In addition the presence of residual protein groups in natural rubber will also lead to an enhanced water sorption. The effect of impurities on the equilibrium sorption of water by natural rubber has already been reviewed<sup>17</sup>. In general the results of the present investigation are consistent with those of earlier studies.

The clustering functions indicate a strong tendency for water to cluster in all samples at higher relative pressures. The tendency for  $\Delta\bar{H}_A$  and  $\Delta\bar{S}_A$  to decrease with  $C$  is also consistent with clustering of the penetrant molecules. The linear variation of the water flux with relative pressure and the decrease of  $D$  with increasing  $C$  for the synthetic polyisoprenes and natural rubber can be interpreted in terms of a relative immobilization of penetrant molecules in clusters<sup>2</sup>. The  $D-C$  curves for the synthetic polyisoprenes are similar in shape to those for water diffusing in silicone rubber and show an initial region of constant  $D$ . The tendency for  $E_D$  to increase with  $C$  subscribes further to the view that clustering of penetrant occurs. As indicated there was some indication of curvature in the water isotherms for natural rubber at low relative pressures suggesting that the  $D-C$  curve in this region would pass through a maximum. Since the sorption measurements were not of sufficient accuracy to determine precisely the isotherm shape it is not possible to analyse the  $D-C$  dependence accurately in this region. Unfortunately permeation measurements were not made on the 'aged' natural rubber sample, for which the isotherm at low relative pressures shows more marked curvature and one anticipates a stronger maximum in this region for this sample.

Although the Natsyn sorbs more water than the Cariflex sample, the latter has the greater permeability; this reflects the higher  $D$  for the Cariflex and is again consistent with a greater fraction of the penetrant being immobilized in the Natsyn sample by some form of specific-site sorption. Similarly the permeability of natural rubber is comparable to that of Natsyn and since  $\sigma_{C=O}$  will be higher for the natural rubber then one anticipates a considerably smaller  $D_{C=O}$  for this polymer consistent with a higher degree of localized sorption.

Finally, the sorption and permeation results for methanol in natural rubber indicate that a significant degree of clustering with immobilization also occurs with this penetrant. There is no indication of a Langmuir-type sorption at low relative pressures and methanol sorption for natural rubber is in fact somewhat smaller than for silicone rubber. The increase in the permeability at higher relative pressures can be attributed to some degree of plasticization compatible with the relatively high uptake of penetrant in this region.

#### ACKNOWLEDGEMENTS

We thank the Science Research Council for a Research Studentship to A. S. and the Malaysian Rubber Producers Research Association for the preparation of the membranes. This work was carried out with the support of Procurement Executive, Ministry of Defence.

#### REFERENCES

- 1 Barrie, J. A. in 'Diffusion in Polymers', (Ed. J. Crank and G. Park), Academic Press, New York, 1967, Ch 8
- 2 Barrie, J. A. and Machin, D. *J. Macromol. Sci. (B)* 1969, **3**, 645, 673
- 3 Barrie, J. A. and Machin, D. *Trans. Faraday Soc.* 1971, **67**, 244, 2971
- 4 Machin, D. and Rogers, C. E. *CRC Crit. Rev. Macromol. Sci.* 1972
- 5 Schneider, N. S., Dusablon, L. V., Spano, L. A. and Hopfenberg, H. B. *J. Appl. Polym. Sci.* 1968, **12**, 527
- 6 Schneider, N. S., Dusablon, L. V., Snell, E. W. and Rosser, R. A. *J. Macromol. Sci. (B)* 1969, **3**, 623
- 7 Barrie, J. A., Nunn, A. and Sheer, A. *Polym. Sci. Technol.* 1974, **6**, 167
- 8 Illinger, J. L., Schneider, N. S. and Karasz, F. E. *Polym. Sci. Technol.* 1974, **6**, 183
- 9 Taylor, R. L., Herrman, D. B. and Kemp, A. R. *Ind. Eng. Chem.* 1936, **28**, 1255
- 10 Taylor, R. L. and Kemp, A. R. *Ind. Eng. Chem.* 1938, **30**, 409
- 11 Southern, E. *Thesis London University* (1969)
- 12 Barrer, R. M. and Barrie, J. A. *J. Polym. Sci.* 1958, **28**, 377
- 13 Yasuda, H. and Stannett, V. *J. Macromol. Sci. (B)* 1969, **3**, 589
- 14 Zimm, B. H. and Lundberg, J. *J. Phys. Chem.* 1956, **60**, 425
- 15 Lundberg, J. *Pure Appl. Chem.* 1972, **31**, 261
- 16 Tester, D. A. *J. Polym. Sci.* 1946, **19**, 535
- 17 van Amerongen, G. J. *Rubber Chem. Technol.* 1964, **37**, 1065



# Cationic copolymerization of vinyl ethers with styrene derivatives and their model reactions: selectivity of a growing carbocation

Kenji Yamamoto and Toshinobu Higashimura

Department of Polymer Chemistry, Faculty of Engineering, Kyoto University, Kyoto 606, Japan  
(Received 11 March 1975; revised 9 June 1975)

In order to assess the possibility of cross propagation in cationic copolymerization, vinyl ethers were copolymerized with styrene derivatives using  $\text{BF}_3\text{O}(\text{C}_2\text{H}_5)_2$  catalyst in toluene and methylene chloride at  $-78^\circ\text{C}$ , and the monomer reactivity ratios were determined. The experimental results were compared with the relative reactivity of these olefins in the electrophilic addition of diethyl acetal and of  $\text{Ph}_3\text{CSnCl}_5$ . The addition of diethyl acetal could be a model for the reaction of vinyl ether-type propagating species, and that of  $\text{Ph}_3\text{CSnCl}_5$  for styrene-type propagating species. Either in the copolymerizations or in the model reactions a carbocation preferred to react with one having a similar structure to the two olefinic compounds, provided that a steric interruption between the carbocation and the olefins is not significant.

## INTRODUCTION

In most cationic copolymerizations it has been observed that the product of monomer reactivity ratios,  $r_1 \times r_2$ , is close to unity. This indicates that the relative reactivity of a monomer depends only on the kind of the monomer and is independent of the type of growing carbocation<sup>1</sup>. However, in cationic copolymerizations of a pair of monomers having different structures such as vinyl ethers/styrene derivatives<sup>2</sup> or styrene/isobutene<sup>3</sup> pair, both  $r_1$  and  $r_2$  tend to become larger than unity. This means that a propagating carbocation prefers to react with a monomer having a structure more similar to the carbocation. For example, in the copolymerization of vinyl ethers with styrene derivatives, a carbocation produced from a vinyl ether reacts preferentially with a vinyl ether and a carbocation produced from a styrene derivative with a styrene derivative. The present authors define this sort of phenomenon as 'selectivity of carbocation', and use this term throughout this paper. The selectivity leads to a difficulty of cross propagation and a formation of block-like copolymers in cationic copolymerizations.

As propagation in cationic polymerization is an electrophilic addition of a propagating carbocation to an olefinic compound, it is very unlikely that a block copolymer is produced through the cationic copolymerization. This study was undertaken to assess the possibility of cross propagation in the cationic copolymerization of vinyl ethers with styrene derivatives. Moreover, the selectivity was also tested with other electrophilic additions. Ethoxyethyl cation produced from diethyl acetal and triphenylmethyl cation produced from triphenylmethyl pentachlorostannate were chosen as the models for a vinyl ether-type and a styrene-type propagating carbocation, respectively. The addition of acetal to vinyl ethers<sup>4,5</sup> and styrene derivatives<sup>6,7</sup> in the presence of acid and that of triphenylmethyl

cation to vinyl ethers<sup>8</sup> and styrene derivatives<sup>9,10</sup> have been reported. However, no insight into the experimental results from a standpoint of the selectivity has been given.

In the present study, non-vinyl type olefins such as  $\alpha$ -methylstyrene and *cis*-phenyl propenyl ether were also used to investigate the steric effect of  $\alpha$ - or  $\beta$ -methyl group on the selectivity of the monomers.

## EXPERIMENTAL

### Materials

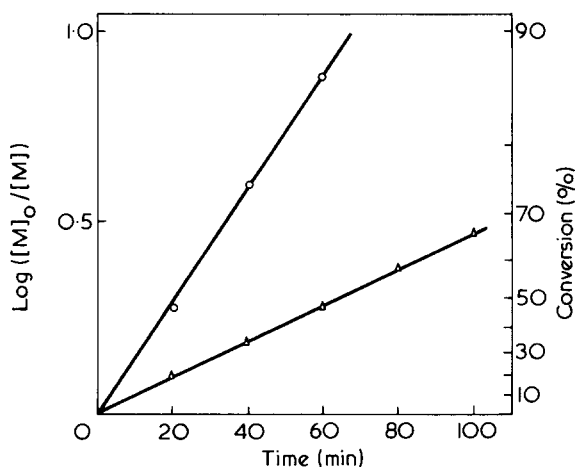
$\alpha$ -Methylstyrene ( $\alpha$ -MS), *p*-methylstyrene (*p*-MS), phenyl vinyl ether (PhVE), and 2-chlorethyl vinyl ether (CEVE) were commercially available. These olefinic compounds were purified by usual methods and distilled from calcium hydride before use. *p*-Methoxystyrene (*p*-MOS) was synthesized from *p*-methoxyacetophenone through reduction and dehydration<sup>11</sup>. The synthesis of *cis*-phenyl propenyl ether (*cis*-PhPE) has been reported previously<sup>12</sup>. The purity of these olefins was more than 99.5% by gas chromatography.

Toluene, methylene chloride and ethylene dichloride were purified by usual methods and distilled from calcium hydride before use.  $\text{BF}_3\text{O}(\text{C}_2\text{H}_5)_2$  was purified by distillation. Tetralin and bromobenzene, which were used as internal standards for gas chromatography, were purified by distillation. Diethyl acetal was distilled twice or more from calcium hydride before use. The purity was more than 99.9% by gas chromatography. Triphenylmethyl pentachlorostannate ( $\text{Ph}_3\text{CSnCl}_5$ ) was synthesized from  $\text{Ph}_3\text{CCl}$  and  $\text{SnCl}_4$  according to the method reported<sup>13</sup> and recrystallized twice from toluene.

**Table 1** Monomer reactivity ratios in the copolymerization of vinyl ethers with styrene derivatives

M <sub>1</sub>	M <sub>2</sub>	Solvent	r <sub>1</sub>	r <sub>2</sub>	r <sub>1</sub> r <sub>2</sub>
PhVE	p-MOS	C <sub>6</sub> H <sub>5</sub> CH <sub>3</sub>	0.27 ± 0.09	12.2 ± 1.3	3.27
		CH <sub>2</sub> Cl <sub>2</sub>	0.15 ± 0.11	11.1 ± 1.1	1.69
PhVE	p-MS	C <sub>6</sub> H <sub>5</sub> CH <sub>3</sub>	8.96 ± 0.72	0.61 ± 0.14	5.48
		CH <sub>2</sub> Cl <sub>2</sub>	1.45 ± 0.03	0.89 ± 0.02	1.29
PhVE	α-MS	C <sub>6</sub> H <sub>5</sub> CH <sub>3</sub>	2.99 ± 0.10	0.60 ± 0.04	1.80
		CH <sub>2</sub> Cl <sub>2</sub>	0.57 ± 0.04	1.98 ± 0.07	1.13
cis-PhPE	α-MS	C <sub>6</sub> H <sub>5</sub> CH <sub>3</sub>	0.75 ± 0.09	2.16 ± 0.16	1.62
		CH <sub>2</sub> Cl <sub>2</sub>	0.22 ± 0.07	5.14 ± 0.32	1.12
cis-PhPE	p-MOS	C <sub>6</sub> H <sub>5</sub> CH <sub>3</sub>	0.52 ± 0.16	13.6 ± 1.3	7.05
		CH <sub>2</sub> Cl <sub>2</sub>	0.68 ± 0.16	12.8 ± 1.1	8.70

[M]<sub>0</sub> = 10% v/v; catalyst = BF<sub>3</sub>O(C<sub>2</sub>H<sub>5</sub>)<sub>2</sub>; temp. = -78°C



**Figure 1** First-order plot of the monomer consumption in the competitive addition of diethyl acetal to PhVE and p-MOS in CH<sub>2</sub>Cl<sub>2</sub> at 0°C: △, PhVE; ○, p-MOS, BF<sub>3</sub>O(C<sub>2</sub>H<sub>5</sub>)<sub>2</sub>, 3.0 mmol/l

### Methods

Copolymerization was carried out in a closed vessel equipped with a stopcock under dry nitrogen. The concentration of inevitable water was in the order of 10<sup>-4</sup> mol/l in all the runs. Details of the copolymerization have been described elsewhere<sup>12</sup>. Copolymer compositions were calculated on the basis of the amounts of unreacted monomers measured by gas chromatography. Monomer reactivity ratios were calculated by the curve-fitting method and the improved Finemann-Ross method<sup>14</sup>.

The relative reactivity of two olefinic compounds in the addition of diethyl acetal was determined by a competitive method. Solvent, 2% v/v of olefins (1% v/v for each olefin), 10% v/v of diethyl acetal and 1% v/v of the internal standard for gas chromatography were introduced by a syringe into the vessel under dry nitrogen and the mixture was kept at 0°C. Tetralin was chosen as an internal standard. Only for the CEVE/p-MOS system was a mixture of tetralin and bomobenzene used. The reaction was started by introducing a catalyst solution to the mixture by a syringe under dry nitrogen. At specified time intervals small portions of the reaction mixture were withdrawn by a syringe, and mixed with ammonia-methanol to stop the reaction. The consumption of the two olefinic compounds was determined by measuring the amount of unreacted compounds by gas chromatography to give the relative reactivity.

The relative reactivity of two olefinic compounds in the addition of Ph<sub>3</sub>CSnCl<sub>5</sub> was determined by following the consumption of Ph<sub>3</sub>CSnCl<sub>5</sub>. The reaction was started by

adding the specific amount of Ph<sub>3</sub>CSnCl<sub>5</sub> solution to an ethylene dichloride solution containing an olefinic compound at 30°C. The rate of the consumption of Ph<sub>3</sub>CSnCl<sub>5</sub> was followed by measuring the optical density at 430 nm due to triphenylmethyl cation with Shimadzu UV-210 double-beam spectrophotometer. Two sets of experiments with different olefins gave the relative reactivity.

## RESULTS

### Copolymerization of vinyl ethers with styrene derivatives

PhVE was copolymerized with p-MOS or p-MS in toluene and methylene chloride at -78°C by BF<sub>3</sub>O(C<sub>2</sub>H<sub>5</sub>)<sub>2</sub> as catalyst. cis-PhPE and α-MS were also used in order to examine the steric effect of α- or β-methyl substituent. The monomer reactivity ratios are summarized in Table 1. White methanol-insoluble copolymers were produced in all the copolymerizations. The formation of a true copolymer of the vinyl ethers and the styrene derivatives was verified by the same method as described in a previous paper<sup>2</sup>.

As Table 1 shows, a polarity of a solvent strongly affected the monomer reactivity ratio in copolymerization of a polar monomer with a non-polar one (PhVE/p-MS, PhVE/α-MS and cis-PhPE/α-MS). The solvent effect on the monomer reactivity ratios could be explained in terms of the selective solvation of a growing carbocation by the polar monomer in the non-polar solvent.

The selectivity of growing carbocation in the copolymerization will be discussed later.

### Diethyl acetal additions to vinyl ethers and styrene derivatives

In order to compare the relative reactivity of vinyl ethers against styrene derivatives towards a vinyl ether-type carbocation, the addition of diethyl acetal to these olefins was investigated in toluene and methylene chloride at 0°C. In this series of experiments, CEVE was also investigated for comparison. Figure 1 shows the first-order plot of the concentrations of PhVE and p-MOS consumed competitively by a carbocation produced from diethyl acetal. This reaction was performed in methylene chloride at 0°C with BF<sub>3</sub>O(C<sub>2</sub>H<sub>5</sub>)<sub>2</sub> as a catalyst. The first-order plot with respect to each olefin was so linear that the reaction of each olefin was not interfered with by the other olefin. The relative reactivity was estimated by comparing the slopes of the straight lines. The relative reactivities of vinyl ethers against styrene derivatives towards an ethoxyethyl cation are listed in Table 2. It shows, with some exceptions,

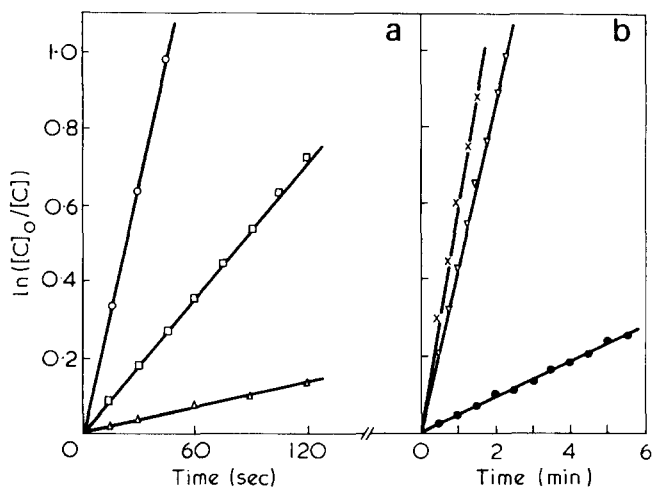
**Table 2** Relative reactivities of vinyl ethers against styrene derivatives in diethyl acetal addition catalysed by BF<sub>3</sub>O(C<sub>2</sub>H<sub>5</sub>)<sub>2</sub> at 0°C

Monomer pair	Relative reactivity of vinyl ethers against styrene derivatives	
	in C <sub>6</sub> H <sub>5</sub> CH <sub>3</sub>	in CH <sub>2</sub> Cl <sub>2</sub>
PhVE/p-MOS	1.43	0.33
CEVE/p-MOS	23.7	1.92
PhVE/p-MS	3.41	9.56
PhVE/α-MS	8.77	1.61
CEVE/α-MS	—	5.36
cis-PhPE/α-MS	6.38	2.20
cis-PhPE/p-MOS	1.62	0.63

that the vinyl ethers are more reactive than the styrene derivatives in the diethyl acetal addition.

### Ph<sub>3</sub>CsSnCl<sub>5</sub> additions to vinyl ethers and styrene derivatives

In order to know the relative reactivity of vinyl ethers against styrene derivatives towards a styrene-type carbo-



**Figure 2** First-order plot for the consumption of Ph<sub>3</sub>CsSnCl<sub>5</sub> in (CH<sub>2</sub>Cl)<sub>2</sub> at 30°C. (a): ○, *p*-MOS ([M]<sub>0</sub> = 0.020 mol/l, [C]<sub>0</sub> = 0.97 × 10<sup>-5</sup> mol/l); □, *p*-MS ([M]<sub>0</sub> = 0.089 mol/l, [C]<sub>0</sub> = 4.26 × 10<sup>-5</sup> mol/l); △, α-MS ([M]<sub>0</sub> = 0.082 mol/l, [C]<sub>0</sub> = 5.23 × 10<sup>-5</sup> mol/l); (b): X, CEVE ([M]<sub>0</sub> = 0.001 mol/l, [C]<sub>0</sub> = 4.26 × 10<sup>-5</sup> mol/l); ▽, PhVE ([M]<sub>0</sub> = 0.042 mol/l, [C]<sub>0</sub> = 1.95 × 10<sup>-5</sup> mol/l); ●, *cis*-PhPE ([M]<sub>0</sub> = 0.077 mol/l, [C]<sub>0</sub> = 5.23 × 10<sup>-5</sup> mol/l);

**Table 3** Rate constant of Ph<sub>3</sub>CsSnCl<sub>5</sub> addition to vinyl ethers and styrene derivatives

Monomer	$k \times 10^2$ (l/mol sec)
<i>p</i> -MOS	102 ± 3.3
<i>p</i> -MS	6.5 ± 0.2
α-MS	1.3 ± 0.05
CEVE	97 ± 1.7
PhVE	18 ± 0.8
<i>cis</i> -PhPE	0.85 ± 0.05

Solvent = (CH<sub>2</sub>Cl)<sub>2</sub>; temp. = 30°C

**Table 4** Comparison between the monomer reactivity ratios in copolymerizations and the relative reactivities in electrophilic addition of vinyl ethers and styrene derivatives

No.	Olefin		Copolymerization <sup>a</sup>		Relative reactivity of M <sub>1</sub> against M <sub>2</sub>		Selectivity	
	M <sub>1</sub>	M <sub>2</sub>	r <sub>1</sub>	1/r <sub>2</sub>	Diethyl acetal addition (c <sub>1</sub> ) <sup>b</sup>	Ph <sub>3</sub> CsSnCl <sub>5</sub> addition (1/c <sub>2</sub> ) <sup>c</sup>	Copolymerization	Addition reactions
A	PhVE	<i>p</i> -MOS	0.15	0.09	0.33	0.18	Yes	Yes
B	CEVE	<i>p</i> -MOS	3.08 <sup>2</sup>	0.22 <sup>2</sup>	1.92	0.96	Yes	Yes
C	PhVE	<i>p</i> -MS	1.45	1.12	9.56	2.84	?	Yes
D	CEVE	<i>p</i> -MS	8.80 <sup>2</sup>	2.50 <sup>2</sup>	—	15.1	Yes	—
E	PhVE	α-MS	0.57	0.51	1.61	14.1	?	No
F	CEVE	α-MS	2.05 <sup>2</sup>	1.47 <sup>2</sup>	5.36	74.9	?	No
G	<i>cis</i> -PhPE	α-MS	0.22	0.19	2.20	0.65	No	Yes
H	<i>cis</i> -PhPE	<i>p</i> -MOS	0.68	0.078	0.63	0.0083	Yes	Yes

<sup>a</sup> Reaction temp. = -78°C; solvent = CH<sub>2</sub>Cl<sub>2</sub>

<sup>b</sup> Reaction temp. = 0°C; solvent = CH<sub>2</sub>Cl<sub>2</sub>

<sup>c</sup> Reaction temp. = 30°C; solvent = (CH<sub>2</sub>Cl)<sub>2</sub>

cation, the addition of Ph<sub>3</sub>CsSnCl<sub>5</sub> to these olefinic compounds was studied. As Ph<sub>3</sub>CsSnCl<sub>5</sub> is not soluble in non-polar solvents such as toluene, all the reactions were carried out in ethylene dichloride at 30°C. Details of the procedure have been described elsewhere<sup>9</sup>. The concentration dependence of the rate was determined by varying the initial concentration of an olefin or Ph<sub>3</sub>CsSnCl<sub>5</sub>. In the present study, the apparent molar extinction coefficient at 430 nm was found to be 1.71 × 10<sup>4</sup> l/mol cm (lit.<sup>9</sup> 1.69 × 10<sup>4</sup> l/mol cm). For all the compounds used in this experiment the following relationship held over the whole range of conversion:

$$-d[C]/dt = k [C] [M] \quad (1)$$

[C] and [M] being the concentration of Ph<sub>3</sub>CsSnCl<sub>5</sub> and an olefin, respectively. Figures 2a and 2b show the typical first-order plot for the consumption of vinyl ethers and styrene derivatives, respectively. Table 3 summarizes the rate constant, *k*, in the Ph<sub>3</sub>CsSnCl<sub>5</sub> addition defined by equation (1). The reactivity of olefinic compound towards the triphenylmethyl cation decreased, as is clear from Table 3, in the following order: *p*-MOS ≥ CEVE > PhVE > *p*-MS > α-MS ≥ *cis*-PhPE. The *k* values for α-MS and *p*-MOS obtained in the present study are comparable with those previously reported under similar conditions<sup>9,15</sup>.

## DISCUSSION

Table 4 summarizes the relative reactivities of vinyl ethers against styrene derivatives towards various carbocations in a polar solvent. The results of the copolymerization of CEVE with *p*-MOS and with *p*-MS<sup>2</sup> are also shown in this Table.

Table 4 shows that a carbocation prefers to attack a monomer which has a structure similar to that of the carbocation, i.e. the selectivity of carbocation is observable in most cases. For example, in the copolymerization of PhVE(M<sub>1</sub>) with *p*-MOS(M<sub>2</sub>), *r*<sub>1</sub> is larger than 1/*r*<sub>2</sub> so that the selective addition of a propagating carbocation is observed. The selective addition is also concluded on the basis of the relative reactivity of PhVE against *p*-MOS in diethyl acetal addition (*c*<sub>1</sub>) and Ph<sub>3</sub>CsSnCl<sub>5</sub> addition (1/*c*<sub>2</sub>). The former, *c*<sub>1</sub>, corresponds to *r*<sub>1</sub> and the latter, 1/*c*<sub>2</sub>, to

$1/r_2$  in the copolymerization of these olefins, and  $c_1$  is larger than  $1/c_2$ . Thus, the selectivity of carbocation does exist either in copolymerization or in addition reaction with the pair PhVE/*p*-MOS.

As the conditions in copolymerization are somewhat different from those in addition reactions, the comparison of these reactions cannot be made on a completely quantitative level. However, there is no trouble from the viewpoint of a qualitative investigation about the selectivity of carbocation.

In the first place, the copolymerization and the addition reaction of vinylic olefins ( $\text{CH}_2=\text{CHR}$ ) will be discussed, where the steric interruption between substituents is not very important (A–D in Table 4). The selective addition occurs with the olefin pair, PhVE/*p*-MOS, as was described above. Similarly, the selective addition is observed for all other olefin pairs, vinyl ether ( $M_1$ )-ring substituted styrene ( $M_2$ ). This conclusion is based on the fact that  $r_1 > 1/r_2$  and  $c_1 > 1/c_2$ . For the olefin pair, PhVE( $M_1$ )/*p*-MS( $M_2$ ), the selectivity in the copolymerization was not high in methylene chloride ( $r_1 \sim 1/r_2$ ), but it was large in toluene ( $r_1 = 8.96$ ,  $1/r_2 = 1.64$ ). However, the selectivity in the electrophilic addition is clearly observable with this olefin pair.

On the other hand, when  $\alpha$ -MS or propenyl ether ( $M_2$ ) is used as a pair for PhVE or CEVE (E ~ H in Table 4), the selectivity was not clearly observed. This could be explained in terms of a steric interruption between a bulky triphenylmethyl cation or propagating carbocation formed from  $M_2$  and an  $\alpha$ - or  $\beta$ -methyl groups in  $M_2$ .

In conclusion, we can safely say that a carbocation adds to a monomer having a similar structure to the carbocation when vinyl ethers and styrene derivatives are involved, pro-

vided that steric interactions between the substituents of the carbocation and the olefin is not significant. However, the reason for the selective addition in these monomer pairs is not clear at present. It is necessary to know the precise nature of the propagating species in these systems (i.e. free ions, ion pairs) in order to know the reason and further study of this problem is in progress.

## REFERENCES

- 1 Landler, Y. *C. R. Acad. Sci.* 1950, **230**, 539; *J. Polym. Sci.* 1952, **8**, 63
- 2 e.g., Masuda, T., Higashimura, T. and Okamura, S. *Polym. J.* 1970, **1**, 19
- 3 e.g., Imanishi, Y., Higashimura, T. and Okamura, S. *J. Polym. Sci. (A)* 1965, **3**, 2455
- 4 Hoaglin, R. I. and Hirsh, D. H. *J. Am. Chem. Soc.* 1949, **71**, 3468
- 5 Okuyama, T. and Fueno, T. *J. Polym. Sci. (A-1)* 1969, **7**, 3045
- 6 Paul, R. and Tchelitcheff, S. *Bull. Soc. Chim. Fr.* 1951, p 425
- 7 Dermer, O. C. and Hawkins, J. J. *J. Am. Chem. Soc.* 1952, **74**, 4595
- 8 Kunitake, T., Matsuguma, Y. and Aso, C. *Polym. J.* 1971, **2**, 345
- 9 Higashimura, T., Fukushima, T. and Okamura, S. *J. Macromol. Sci. (A)* 1967, **1**, 683
- 10 Sambhi, M. S. and Treloar, F. E. *J. Polym. Sci. (B)* 1965, **3**, 445; Sambhi, M. S. *Macromolecules* 1970, **3**, 351
- 11 Nystron, R. F. and Brown, W. G. *J. Am. Chem. Soc.* 1947, **69**, 1197
- 12 Yamamoto, K. and Higashimura, T. *J. Polym. Sci. (Polym. Chem. Edn)* 1974, **12**, 613
- 13 Sharp, D. W. A. and Sheppard, V. J. *Chem. Soc.* 1957, p 674
- 14 Ezrielev, A. I., Brokhina, E. L. and Roskin, E. S. *Vysokomol. Soedin.* 1969, **11**, 1670
- 15 Cotrel, R., Sauvet, G., Vairon, J. P. and Sigwalt, P. *Int. Symp. Cation. Polym. Rouen* 1973, C8

# Reactivity and mechanism in the cationic polymerization of *p*-methoxystyrene initiated by cycloheptatrienyl hexachloroantimonate

A. M. Goka\* and D. C. Sherrington

Department of Pure and Applied Chemistry, University of Strathclyde, Glasgow G1 1XL, UK

(Received 16 December 1974; revised 4 February 1975)

The cationic polymerization of *p*-methoxystyrene initiated by cycloheptatrienyl hexachloroantimonate in dichloromethane solution has been studied in some detail. Reactions proved to be highly exothermic, and rates of monomer consumption were measured using an adiabatic calorimetric technique. Termination was deduced to be insignificant during kinetic lifetimes, and  $\bar{M}_n$  values in the range 10 000–50 000 showed chain breaking to occur by transfer mechanisms. Appropriate analysis of conversion/time curves allowed computation of enthalpies of polymerization and rate coefficients for propagation,  $k_p$  (obs), under various conditions. Data for  $k_p$  (obs) were found to vary with the initial concentrations of initiator and monomer employed, and these dependences are discussed in terms of current theories regarding ion pair/free ion equilibria in non-aqueous solvents. In particular values of  $3.6 \times 10^3 \text{ M}^{-1}\text{s}^{-1}$  and  $4.8 \times 10^3 \text{ M}^{-1}\text{s}^{-1}$  at  $0^\circ$  and  $+10^\circ\text{C}$  respectively for the rate constant for propagation by free poly(*p*-methoxystyryl) cation have been deduced, and a tentative value of  $450 \text{ M}^{-1}\text{s}^{-1}$  at  $0^\circ\text{C}$  has been estimated for the rate constant for propagation by the corresponding hexachloroantimonate ion pairs. These data and the related activation parameters are compared with independent results in the literature. Polymerizations carried out in the presence of excess common ion salt, dimethyl benzyl phenyl ammonium hexachloroantimonate, showed rate depressions far in excess of those predicted by a simple mass law effect, arising possibly as a result of a more dramatic ionic association than simple ion pairing.

## INTRODUCTION

Of all the substituted styrene monomers, *p*-methoxystyrene is one of the most useful since it is readily polymerized with high reactivity by free radical<sup>1</sup>, anionic<sup>2</sup> and cationic<sup>3</sup> means. In principle therefore it should be possible to assess quantitatively the difference in reactivity which arises with these mechanisms.

Molecular iodine has been most widely investigated<sup>3–5</sup> as an initiator of cationic polymerization of *p*-methoxystyrene. Okamura and his coworkers<sup>3</sup> have reported rate constants for the propagation reaction,  $k_p$ , in solvents of varying polarity. The interpretation of these results in terms of current theories of ionic equilibria is difficult, and the overall low order of magnitude of  $k_p$  ( $\sim 10\text{--}0.1 \text{ M}^{-1}\text{s}^{-1}$ ) would seem to indicate that the data may be seriously affected by a kinetic term from the initiation processes. The same system has been investigated by Ise and his group<sup>4</sup>. They were particularly interested in the effect of an applied electric field, and have shown that the overall rate of polymerization increases under such conditions. The increase was attributed to a field-facilitated dissociation of propagating ion pairs into free ions, the latter, it was assumed, being the more reactive. Unfortunately the complexity of the system precluded evaluation of the

various contributing rate constants.

More recently, Sigwalt and his collaborators<sup>6</sup> have studied in detail the kinetics of the polymerization of this monomer initiated by triphenylmethyl hexachloroantimonate. They have also recognized the possibility of contributions from various types of ionic intermediate, though they do not report any quantitative estimation of individual reactivities.

The present work represents a continuation of our studies of absolute reactivity in cationic polymerizations<sup>7–9</sup> and extends those monomers investigated to include *p*-methoxystyrene. Polymerizations were carried out homogeneously in dichloromethane solutions under high vacuum conditions employing preformed cycloheptatrienyl hexachloroantimonate ( $\text{C}_7\text{H}_7^+\text{SbCl}_6^-$ ) as the initiator. Reaction rates were measured by an adiabatic calorimetric technique as before<sup>7</sup>, employing initiator concentrations covering a wider range ( $\sim 10^{-4}$  to  $10^{-6} \text{ M}$ ) than previously for a single monomer. This was possible because of the clean and highly reproducible polymerizations exhibited by this monomer, which was readily converted to 100% polymer with rates measurable by our technique, over this wide range of catalyst concentrations. Rather conveniently data for ion pair dissociation constants ( $K_d$ ) for a variety of organic hexachloroantimonate salts<sup>10</sup> fall within this range, and the results of the present kinetic experiments are discussed later with this in mind.

\* Present address: Department of Chemistry, University of Cape Coast, Cape Coast, Ghana.

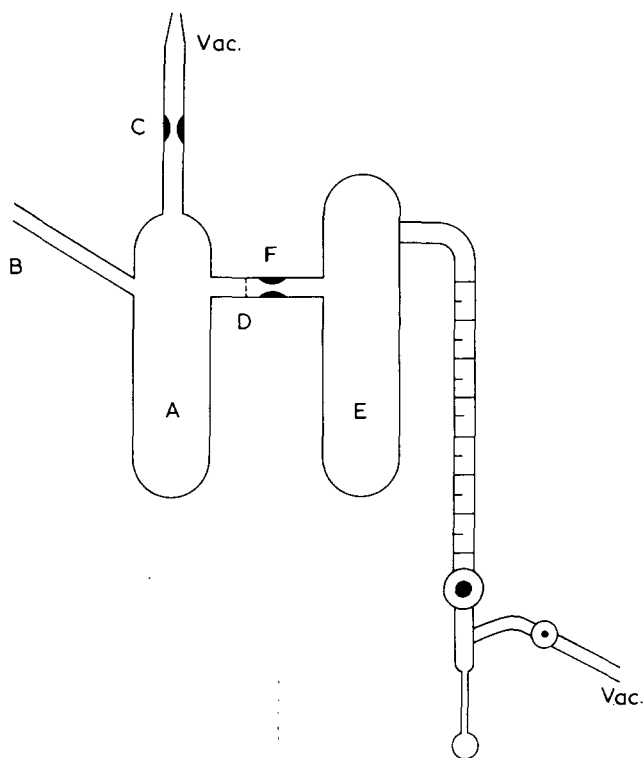


Figure 1 Monomer storage and metering vessel

## EXPERIMENTAL

### Materials

Dichloromethane was dried and purified as previously reported<sup>7</sup>. Its method of storage and metering under vacuum has also been described elsewhere<sup>8</sup>. Cycloheptatrienyl hexachloroantimonate, used for the kinetic experiments, was prepared as before<sup>7</sup>; however, on this occasion the salt was recrystallized from dry dichloromethane, without addition of carbon tetrachloride. It was stored *in vacuo* in the absence of light. Both melting point and micro-analysis were consistent with previous reports. The corresponding tetrafluoroborate salt was used in a 1:1 molar reaction with *p*-methoxystyrene in methanol, in order to characterize the initiation mechanism. It was prepared according to the method reported by Conrow<sup>11</sup> and was recrystallized from acetonitrile before use. Benzyldimethylphenyl ammonium hexachloroantimonate was also prepared, purified and characterized as described previously<sup>12</sup>.

*p*-Methoxystyrene (10 ml) (Koch-Light Laboratories) was diluted with petroleum ether (20 ml, b.p. 30–40°C). The solution was shaken with 1% aqueous sodium hydroxide (3 × 50 ml) to remove the stabilizer, *t*-butyl catechol, and finally with distilled water (4 × 50 ml) until the pH of the washings remained constant. After drying over anhydrous calcium chloride for 2 h the solution was decanted onto freshly crushed calcium hydride, where it was left overnight. The following day the solution was transferred to a fresh sample of calcium hydride, refluxed for 40 min, and then fractionated under vacuum ( $\sim 10^{-3}$  mmHg). After removal of the petroleum ether, a middle fraction of the monomer (b.p.  $\sim 60^\circ\text{C}$  at  $\sim 10^{-3}$  mmHg) was collected, and then pipetted into limb A of a previously prepared storage/metering vessel (Figure 1). Freshly crushed calcium hydride was added via side arm B, which was then sealed in the usual manner. The monomer was then degassed several

times at  $10^{-5}$  mmHg and allowed to stand on the drying agent overnight, well protected from light by a black polyethylene sleeve. After further degassing the next day, the vessel was sealed from the vacuum line at constriction C, and the monomer was filtered from the drying agent by tipping through sinter D (pore size 3). Finally the monomer was chilled in limb E, and the unwanted limb A was sealed off at constriction F. The storage vessel with its vacuum burette arrangement for metering of the monomer was then stored in the dark in a deep freeze.

### Calibration technique

The adiabatic calorimeter used in these experiments was similar to one described before<sup>8</sup>, and employed a resistance thermometer as the temperature sensor. The temperature coefficient of the latter was determined using the freezing points of pure solvents as definitive temperatures. The heat capacity of the calorimeter and its contents (100 ml of solvent) was determined at 0°C by polymerizing isobutyl vinyl ether under the same conditions as those used in the kinetic experiments. The known heat of polymerization of this monomer<sup>7</sup> allowed computation of the required heat capacity. Data at other temperatures were then calculated assuming the same temperature dependence of the heat capacity as previously determined<sup>7</sup>.

### Kinetic technique

The operation of the calorimeter has already been adequately described<sup>7</sup> and the only significant variation in the procedure was the method of introduction of the monomer. Because of the high boiling point of *p*-methoxystyrene, direct quantitative distillation into the calorimeter was found to be impossible. Instead glass phials of monomer were prepared under vacuum in a similar manner to the phials of initiator solution, using the vacuum burette described earlier (Figure 1). For a normal kinetic run a phial of monomer was placed in the upper position in the phial holder, and a catalyst phial in the lower (see diagram p122, ref 7). After sealing the calorimeter and distilling in solvent, the upper phial was crushed first, and the monomer was allowed to mix thoroughly with the solvent. The temperature of the solution was then adjusted to the steady value required using a Dewar of chilled methanol, and then the initiator phial was crushed. The temperature rise was recorded on a Bryans 27 000 chart recorder, and after polymerization the polymer yield was established gravimetrically as in the polymerization of *N*-vinylcarbazole<sup>8</sup>. Molecular weights of polymer samples were determined by gel permeation chromatography using a Waters Anaprep machine fitted with polystyrene gel columns. The latter were calibrated using narrow molecular weight polystyrene standards, and the data generated for the samples therefore refer to equivalent polystyrene molecular weights. In the analysis of chromatograms no attempt was made to correct for dispersion effects and so distributions will tend to appear larger than they really are.

In one experiment involving successive additions of two monomer samples a slightly modified procedure was adopted. The required weight of initiator was weighed directly into the calorimeter base and two monomer phials (each containing 1 ml of monomer and 1 ml of solvent to prevent freezing at 0°C) were placed in the phial holder. Crushing of the first phial initiated polymerization, and

Table 1 Calorimeter calibration data

	Temperature (°C)		
	-25	0	+10
Thermometer resistance (Ω)	20.95	23.10	24.00
Temperature coefficient of resistance (Ω/degree)	0.0861	0.0861	0.0861
Heat capacity (kJ/degree)	273.4	282.6	287.6

Table 2 Polymerization of *p*-methoxystyrene by  $C_7H_7^+SbCl_6^-$  in  $CH_2Cl_2$  at 10°C

$[p\text{-MeOSt}]_0 \times 10^2$ (M)	$[C_7H_7^+SbCl_6^-]_0 \times 10^5$ (M)	$k_p$ (obs) $\times 10^{-3}$ (M <sup>-1</sup> s <sup>-1</sup> )	$\Delta H_p$ (kJ/mol)	$M_n \times 10^{-4}$	$M_w \times 10^{-5}$
7.46	0.261	4.0	78.6	1.66	4.99
7.46	0.522	4.1	78.6	2.82	5.75
7.46	1.04	3.0	74.4	1.74	4.61
7.46	1.33	2.1	70.6	1.47	4.43
7.46	2.66	1.9	75.2	4.86	4.33
7.46	5.31	1.3	74.0	5.53	4.56
7.46	10.7	0.83	75.2	1.66	4.99
7.46	20.1	0.47	79.4	4.52	2.79
7.46	20.1	0.50	81.1	—	—
3.73	5.31	0.50	70.2	3.34	2.52
5.60	5.31	0.98	77.3	3.74	2.84
7.46	5.31	1.3	74.0	5.53	4.56
11.2	5.31	2.2	79.0	4.49	5.52

when this was complete the second phial was crushed and polymerization resumed.

A number of experiments involving a common ion salt were also performed. In these the common ion salt, benzyldimethylphenyl ammonium hexachloroantimonate, was weighed directly into the calorimeter base, and then the normal procedure followed.

#### Measurements of dielectric constants

The dielectric constants of dichloromethane and dichloromethane/*p*-methoxystyrene mixtures were measured at 0° and +10°C using an automatic liquid dielectric bridge (Calvert Designs).

## RESULTS

#### Calibration of the calorimeter

Kinetic experiments were carried out at -25°, 0° and +10°C. The calorimeter calibration parameters required at these temperatures are shown in Table 1.

#### Kinetic data

Without exception the normal kinetic runs produced S-shaped conversion curves similar to those reported in the polymerizations of vinyl ethers<sup>7,9</sup> and some solutions became pale red in colour. Unlike vinyl ether reactions, however, even at very low initiator concentrations (~10<sup>-6</sup> M) a steady polymerization to 100% conversion was obtained. Only when attempts were made to extend the range even further, did termination appear to become significant during kinetic lifetimes. Indeed absence of any appreciable termination was dramatically demonstrated by

addition of a second monomer sample to a completed polymerization, whereupon reaction was resumed and 100% polymer was obtained. Recorder traces were analysed by a technique reported earlier (see appendix to ref 7), based on a simple two stage mechanism involving only initiation and propagation reactions. This analysis produced the data for rate coefficients for propagation,  $k_p$  (obs), shown in Tables 2-4. The calorimetric technique also readily allows the evaluation of corresponding enthalpies of polymerization,  $\Delta H_p$ , and these are also shown in the Tables, together with appropriate molecular weight data.

#### Common ion experiments

The results of experiments involving addition of a common ion salt are shown in Table 5. No attempt was made to analyse the recorder traces obtained, since polymer yields were always less than quantitative during the time of observation.

#### Dielectric constant measurements

The influence of *p*-methoxystyrene on the dielectric constant of dichloromethane in the concentration range used in polymerizations is shown in Table 6. As might be expected a steady fall is observed as the volume fraction of monomer increases.

Table 3 Polymerization of *p*-methoxystyrene by  $C_7H_7^+SbCl_6^-$  in  $CH_2Cl_2$  at 0°C

$[p\text{-MeOSt}]_0 \times 10^2$ (M)	$[C_7H_7^+SbCl_6^-]_0 \times 10^5$ (M)	$k_p$ (obs) $\times 10^{-3}$ (M <sup>-1</sup> s <sup>-1</sup> )	$\Delta H_p$ (kJ/mol)	$M_n \times 10^{-4}$	$M_w \times 10^{-5}$
7.46	0.498	3.0	89.9	0.683	2.21
7.46	1.25	2.3	73.6	1.51	5.25
7.46	1.30	2.7	76.1	—	—
7.46	2.15	1.5	76.5	0.713	6.54
7.46	2.47	1.2	85.7	—	—
7.46	4.98	0.94	76.5	1.25	4.69
7.46	7.47	0.91	86.9	3.23	2.50
7.46	9.96	0.70	82.3	2.56	7.57
7.46	21.6	0.60	86.1	—	—
7.46	21.8	0.49 <sup>a</sup>	88.2	1.41	4.03
7.46	21.8	0.72 <sup>b</sup>	—	—	—
3.73	4.94	0.50	76.1	—	—
5.60	4.94	0.73	72.7	2.55	1.83
7.46	4.98	0.94	76.5	1.25	4.69
11.2	4.94	1.7	75.7	4.21	9.01

<sup>a,b</sup> refer to the experiment in which a second sample of monomer was added to a completed polymerization. <sup>a</sup> was computed from the first conversion envelope and <sup>b</sup> from the second. Since the latter was non-sigmoid  $k_p$  (obs) was calculated directly from the initial slope, and showed a marginal increase within the experimental error

Table 4 Polymerization of *p*-methoxystyrene by  $C_7H_7^+SbCl_6^-$  in  $CH_2Cl_2$  at -25°C

$[p\text{-MeOSt}]_0 \times 10^2$ (M)	$[C_7H_7^+SbCl_6^-]_0 \times 10^5$ (M)	$k_p$ (obs) $\times 10^{-3}$ (M <sup>-1</sup> s <sup>-1</sup> )	$\Delta H_p$ (kJ/mol)	$M_n \times 10^{-4}$	$M_w \times 10^{-5}$
3.73	2.50	0.50	64.3	2.38	8.15
3.73	4.94	0.32	54.3	1.17	3.23
3.73	9.98	0.14	68.1	1.88	5.64
3.73	20.0	0.092	84.0	—	—
3.73	20.0	0.077	83.2	1.71	5.65
3.73	9.98	0.14	68.1	1.88	5.64
7.46	9.98	0.22	84.4	2.27	1.75

**Table 5** Effect of the common ion salt, Me<sub>2</sub>. PhCH<sub>2</sub>. Ph.N<sup>+</sup> SbCl<sub>6</sub><sup>-</sup>, on the polymerization of *p*-methoxystyrene initiated by C<sub>7</sub>H<sub>7</sub><sup>+</sup> SbCl<sub>6</sub><sup>-</sup> in CH<sub>2</sub>Cl<sub>2</sub> at 0°C

[ <i>p</i> -MeOSt] <sub>0</sub> × 10 <sup>2</sup> (M)	[C <sub>7</sub> H <sub>7</sub> <sup>+</sup> SbCl <sub>6</sub> <sup>-</sup> ] <sub>0</sub> × 10 <sup>5</sup> (M)	[Common ion] × 10 <sup>4</sup> (M)	Polymer yield (%)		<i>M<sub>n</sub></i> × 10 <sup>-4</sup>	<i>M<sub>w</sub></i> × 10 <sup>-5</sup>
			A	B		
7.46	2.15	10.2	2.00	18.0	4.29	4.41
7.46	2.15	5.38	36.6	56.8	7.32	4.82
7.46	2.15	2.90	68.0	76.7	8.10	5.05
7.46	2.15	0.98	87.0	92.5	7.13	6.54

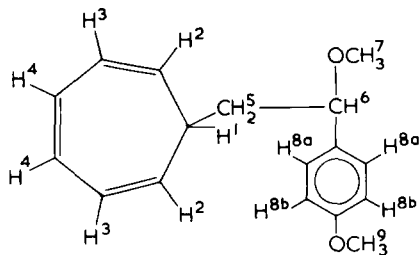
Yield A was calculated from the maximum temperature rise recorded on the trace. Yield B was obtained a short time later, after the reaction was killed with methanol, by gravimetric analysis

#### Reaction of *p*-methoxystyrene with cycloheptatrienyl tetrafluoroborate in methanol

The tetrafluoroborate salt (5.0 g) was dissolved in dry acetonitrile (100 ml) in a three-necked flask, fitted with a dropping funnel containing a solution of *p*-methoxystyrene (4.0 g) in dry methanol (50 ml). This solution was added slowly to the initiator solution over a period of 7 min, with constant stirring at room temperature. The orange red colour that developed after the initial addition grew progressively more intense as the remainder of the solution was added. After allowing the reaction mixture to stand for a further 8 min it was shaken with a 1% aqueous solution of caustic soda (200 ml), the resulting mixture being slightly alkaline. The organic products were then extracted into dichloromethane, and after separation this solution was washed with water and dried over anhydrous calcium chloride. Finally, the solvent was removed on a rotary evaporator, and the product, a yellow oil, dried in a vacuum oven at 30°C (yield 6.5 g).

A high resolution mass spectrum of the impure product showed a parent ion C<sub>17</sub>H<sub>20</sub>O<sub>2</sub><sup>+</sup>, mass = 256.15, and a fragmentation pattern totally consistent with this as the major species. Thin-layer chromatography (t.l.c.) analysis using a silica solid phase and a liquid phase, 90% petroleum ether (b.p.30–40°C): 10% diethyl ether, confirmed the presence of one major product accompanied by five other species in much smaller proportions. Only one of these was developed faster than the major product.

Two grammes of the product were purified by column chromatography using 100 g of silica gel (MFC) and the same solvent mixture as that used in the t.l.c. analysis. The first detectable sample from the column was shown to be unreacted monomer by infra-red analysis. The second and major sample, a pale yellow oil, was shown by high resolution proton n.m.r. spectroscopy to have the following structure:



$\tau$	Protons
2 → 3.3	8a, 8b
~ 3.4	4
~ 3.8	3
~ 4.8	2
~ 5.8	6
~ 6.2	9
~ 6.9	7
~ 7.7–8.4	1, 5

#### DISCUSSION

All polymerizations of *p*-methoxystyrene were complete within 4 min under the conditions described, and invariably produced quantitative yields of polymer. Reactions were highly exothermic and the average values of the heats of polymerization determined are summarized in Table 7.

The S-shaped conversion curves obtained provide strong evidence for a relatively slow initiation process followed by a faster propagation reaction. Significant termination was shown to be absent in the experiment in which successive additions of monomer were made. Molecular weight data for the polymers isolated at the end of polymerizations showed little correlation with initiator concentrations, and indicated that chain breaking occurs as a result of transfer processes. Detailed mechanistic features of the initiation and propagation reactions will be discussed in detail.

#### Initiation

The pale red coloration formed on breaking initiator phials (particularly the ones of higher concentration) persisted during polymerizations, but disappeared on addition of methanol, used to kill reactions. Attempts to record a visible spectrum of this failed. Cycloheptatrienyl cation is known to form coloured charge transfer complexes with various substituted aromatic residues<sup>13</sup>, and the initial coloration may indeed be due to this. However, Olah and his coworkers have recorded the ultra-violet/visible spectra of a number of benzylic cations including a *p*-methoxy-substituted derivative<sup>14</sup>. Although very different conditions were employed to those in the present work, their results are not inconsistent with the view that the pale red colour

**Table 6** Influence of *p*-methoxystyrene on the dielectric constant of dichloromethane

<i>p</i> -MeOSt (vol %)	Temperature (°C)	
	+10	0
0.00	9.467	9.860
0.50	9.454	9.820
1.00	9.440	9.760
1.50	9.420	9.690
2.00	9.400	9.596

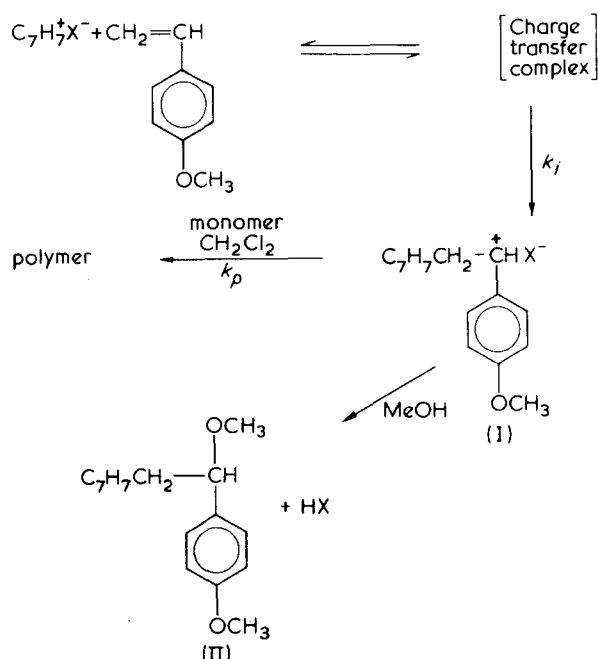
**Table 7** Average enthalpies of polymerization of *p*-methoxystyrene in CH<sub>2</sub>Cl<sub>2</sub>

Temperature (°C)	$\Delta H_p$ (kJ/mol)
+10	76.1
0	80.5
-25	73.0



persisting during our polymerizations may be due to the poly- (*p*-methoxystyryl) cation. On the other hand, as with the colours observed in related polymerizations of vinyl ethers<sup>7,9</sup> and indene<sup>15,16</sup> those remaining after complete reaction may arise as a result of post-polymerization interactions with the polymer backbone.

In a separate experiment in which a catalyst phial was broken into a monomer solution below  $\sim -50^\circ\text{C}$  a stable pale red colour formed\*. No polymer was precipitated on addition of excess methanol, providing the solution was not allowed to warm up before the addition took place. It does seem likely therefore that initiation is preceded by formation of a charge transfer complex, which under favourable conditions collapses to yield a propagating cation. Overwhelming evidence that this collapse involves addition of the cycloheptatrienyl cation to the double bond of the monomer-producing species (I), is provided by the isolation and characterization of derivative (II), from the 1:1 molar reaction in methanol.



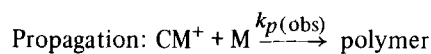
Closely related addition reactions of cycloheptatrienyl cation have been reported previously<sup>17-19</sup>.

In contrast to this mechanism triphenylmethyl cation is known to abstract hydride ion from suitable substrates under many reaction conditions, rather than undergo addition<sup>20,21</sup>. It is generally accepted that this carbocation has a relatively hindered electrophilic centre, with an overall propeller symmetry. Whereas approach of a nucleophile to a planar cycloheptatrienyl cation can take place without steric hindrance, close approach to the central carbon atom of triphenylmethyl cation is difficult, particularly for vinyl monomer molecules. In fact steric hindrance can force reaction to take place preferentially in the *para* position of one of the phenyl groups<sup>21,22</sup>, via one of the resonant structures believed to contribute to the delocalization of this cation. This inherent difference between cycloheptatrienyl and triphenylmethyl cation may well give rise to different initiation mechanisms, with correspondingly different efficiencies. This point will be raised again in the discussion of the propagation data obtained in this study.

\* Concentrations similar to those used in kinetic experiments.

### Propagation

The derived rate coefficients for propagation,  $k_p$  (obs), in Tables 2-4 were obtained assuming a simple two stage mechanism as below



(counterion omitted for simplicity)

The data at  $0^\circ$  and  $10^\circ\text{C}$  are most complete and show  $k_p$  (obs) to be a function of both the initial catalyst,  $[\text{C}]_0$ , and monomer concentrations,  $[\text{M}]_0$ . These dependences are shown graphically in Figures 2 and 3.

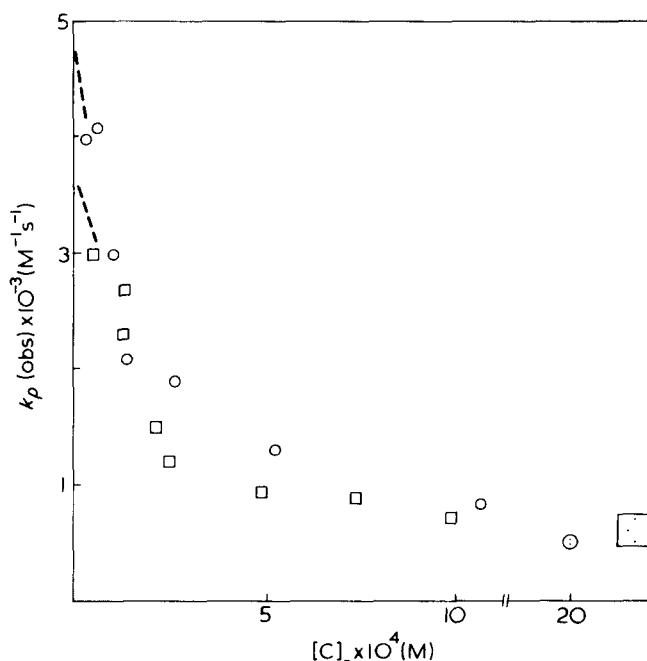


Figure 2 Plot of  $k_p$  (obs) versus  $[\text{C}]_0$ .  $\circ$ ,  $+10^\circ$ ;  $\square$ ,  $0^\circ\text{C}$

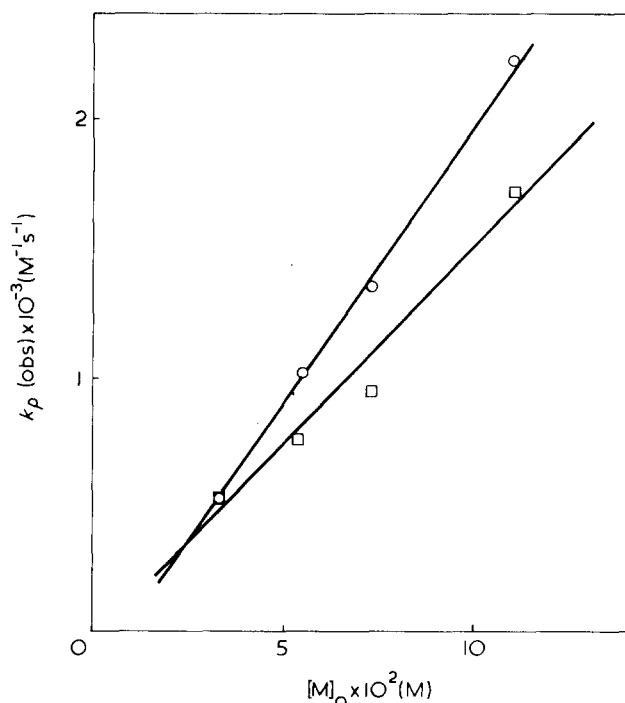


Figure 3 Plot of  $k_p$  (obs) versus  $[\text{M}]_0$ .  $\circ$ ,  $+10^\circ$ ;  $\square$ ,  $0^\circ\text{C}$

Close examination of previous results<sup>9</sup> shows a similar though less well defined variation of  $k_p(\text{obs})$  with  $[C]_0$ . The range of  $[C]_0$  used in the present work was in fact much larger, and therefore more likely to identify such a trend.

#### Variation of $k_p(\text{obs})$ with $[C]_0$

The decrease in  $k_p(\text{obs})$  with  $[C]_0$  can be explained reasonably in three ways: (a) inefficient conversion of initiating cations into propagating active centres; (b) contributions to propagation from free cations in equilibrium with ion pair species; (c) a combination of these effects. The first two possibilities will be examined separately in more detail.

The method of kinetic analysis assumes that during the earlier part of polymerizations (say below ~15% conversion) all cycloheptatrienyl cations are converted to growing active centres, (i.e.  $[C]_0 \rightarrow [P_n^+]_t$ , the concentration of active centres at time  $t$ ), the concentration of which thereafter remains constant, i.e.

$$\frac{-d\ln[M]_t}{dt} = k_p(\text{obs}) [P_n^+]_t$$

Sigwalt and his coworkers<sup>6</sup> have shown that in the case of triphenylmethyl cation as initiator only about 10% of the catalyst is consumed in the initiation process. If such a situation prevailed in the present system then clearly the estimation of  $[P_n^+]_t$  would be in error. Furthermore as  $[C]_0$  is increased it might be argued that the proportion of cations successfully initiating polymer chain growth would fall. Hence the error in the value of  $[P_n^+]_t$  employed in the calculation would rise, and the deviation of  $k_p(\text{obs})$  from a constant value would also increase. In fact inspection shows that  $k_p(\text{obs})$  would be expected to fall in value as  $[C]_0$  rises, precisely the trend observed in practice.

Contrary to this argument, however, are a number of observations. First, cycloheptatrienyl cation is likely to react more efficiently with monomer than triphenylmethyl cation for the reasons already advanced. Also if there is non-quantitative use of initiator then no steady state can be achieved during these polymerizations. Hence in the experiment in which a second addition of monomer was carried out, a continuing generation of active centres would be expected, and should be reflected in the data for  $k_p(\text{obs})$ . However, analysis of the two conversion envelopes occurring within this experiment, yields values of  $k_p(\text{obs})$  which differ only within the known experimental error (see Table 3).

Attempts to settle this question unequivocally by observing directly the consumption of initiator were unfortunately only partly successful. Cycloheptatrienyl cation has a characteristic singlet proton n.m.r. peak at  $\tau = 0.63$ . Using Fourier transform n.m.r. spectroscopy this signal was successfully detected in solutions of concentration as low as  $\sim 10^{-4}$  M in  $\text{CD}_2\text{Cl}_2$  i.e. the upper end of the concentration range employed in the polymerization reactions, and within the region where inefficient use of catalyst is most likely to be detectable. Addition of *p*-methoxystyrene in the same concentration as that used in the polymerizations destroyed the cycloheptatrienyl resonance. However, because of computer limitations, this second spectrum had to be accumulated over a period of ~10 min after the addition

of monomer. Since polymerization is complete within ~3 min under these conditions, the disappearance of cycloheptatrienyl cation (at  $\sim 10^{-4}$  M) cannot be unambiguously attributed to the initiation reaction alone. Excess unused initiator may be consumed for example in post-polymerization processes such as aromatic alkylation. Nevertheless the new ability of Fourier transform proton n.m.r. to detect low concentrations, typical of those of active centres in ionic polymerizations is extremely important, and considerable scope remains for further investigations in this area.

The second and perhaps more attractive explanation for the variation of  $k_p(\text{obs})$  with  $[C]_0$  has proved equally difficult to substantiate. It is generally accepted that where an equilibrium exists between free ions and ion pair species, the latter are generally the less reactive. Thus with the present results, if the kinetic analysis is assumed to be correct, it can be argued that the variations in  $k_p(\text{obs})$  merely reflects the contributions from free ion and ion pair growth according to the general expression:

$$k_p(\text{obs}) = \alpha k_p^+ + (1 - \alpha) k_p^\ddagger$$

where,  $k_p^+$  is the rate constant for propagation by free ions and  $k_p^\ddagger$  that by ion pairs,  $\alpha$  being the fraction of free ions present.

Under conditions when propagating ions are either largely associated ( $\alpha \rightarrow 0$ ) or substantially dissociated ( $\alpha \rightarrow 1$ ) then it can be shown that:

for  $\alpha \rightarrow 0$

$$k_p(\text{obs}) = k_p^\ddagger + K_d^{1/2} k_p^+ [P_n^+]_t^{-1/2} \quad (1)$$

for  $\alpha \rightarrow 1$

$$k_p(\text{obs}) = k_p^+ - k_p^\ddagger K_d^{-1} [P_n^+]_t \quad (2)$$

where  $K_d$  is the ion pair dissociation constant of the growing ion pair. These approximations are most accurate under the condition  $k_p^+ \gg k_p^\ddagger$ , which, by analogy with the results from anionic polymerizations<sup>23</sup>, is the situation often assumed to prevail in cationic systems. The latter very often employ more polar solvents, however, and this assumption may well require modification in the future. If for example the major ion pair species is a solvent separated one, then reactivity may be comparable with the free ion. This appears to be the case in ring opening polymerizations by cationic mechanisms<sup>24,25</sup>.

In spite of this, however, if the present results do simply reflect some ionic equilibria as above, then addition of a suitable common ion salt should be able to disturb this equilibrium, and change  $k_p(\text{obs})$  at least within the range of values obtained experimentally. The results of such experiments are summarized in Table 5. Polymerizations were found to be retarded much more dramatically than would be predicted from a simple common ion effect, and kinetic analysis of the recorder traces was not attempted. The increase in polymer yields detected between stopping the calorimeter (calculated from recorder trace) and killing the reaction (gravimetric analysis) showed that in all cases the polymerization process was continuing, although very slowly. It is possible therefore that the concentrations of added salts were such that agglomerates of propagating cations and counterions much larger than ion pairs are

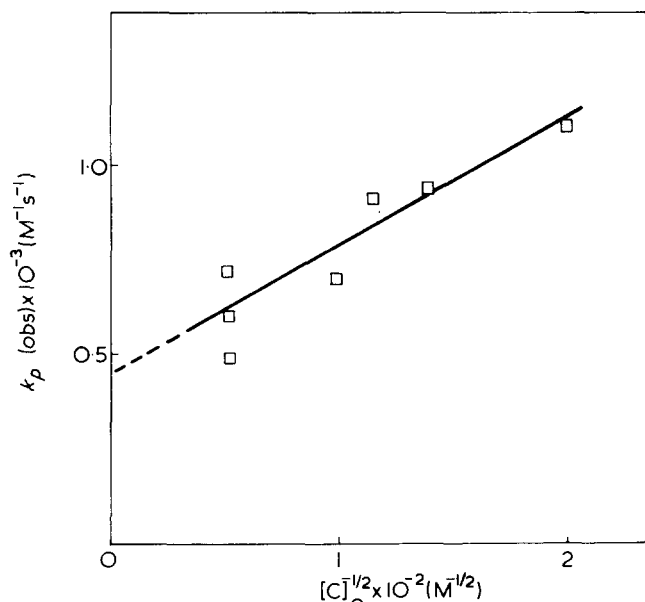


Figure 4 Plot of  $k_p$  (obs) versus  $[C]_0^{-1/2}$  at  $0^\circ\text{C}$

formed, and that these give rise to much slower polymerizations. The detailed nature of solutions of high ionic strength in which one ion possesses a long 'polymeric tail' still requires investigation, and work in this direction has been embarked upon recently.

#### Significance of kinetic data

If it is assumed that  $K_d$  for the propagating species is of the same order of magnitude as that for simple hexachloroantimonate salts under similar conditions (i.e.  $10^{-4}$  to  $10^{-5}\text{M}$ )<sup>10</sup> then the data for  $k_p$  (obs) at the higher concentrations of  $[C]_0$  may be analysed according to equation (1) above. Indeed a plot of  $k_p$  (obs) versus  $[C]_0^{-1/2}$  (i.e.  $[P_n^+]_t^{-1/2}$ ) for data at  $0^\circ\text{C}$  does produce a straight line in this region as shown in Figure 4, allowing a tentative estimation of the rate constant for ion pair propagation,  $k_p^\pm$ , of  $450\text{M}^{-1}\text{s}^{-1}$  at  $0^\circ\text{C}$ . A much poorer fit is obtained at  $+10$  and  $-25^\circ\text{C}$ .

It is rather fortuitous, that irrespective of which explanation for the variation of  $k_p$  (obs) is the correct one, the same prediction can be made concerning the significance of the extrapolated value of  $k_p$  (obs) at the lower extremes of  $[C]_0$ . Under such conditions, i.e.  $[C]_0 < 10^{-6}\text{M}$ , initiation is most likely to be quantitative and therefore the kinetic analysis most likely to be valid. Furthermore in this limit the vast majority of ions will be free (assuming the same magnitude for  $K_d$  as before). The extrapolated value of  $k_p$  (obs) will therefore represent a measure of the reactivity in propagation of free poly(*p*-methoxystyryl) cation i.e.  $k_p^+$ . Even if the second explanation for the variation of  $k_p$  (obs) were the correct one, this also predicts the data to approach  $k_p^+$  linearly as the concentration of active centres is reduced substantially below  $K_d$  (i.e. equation 2). Such an extrapolation yields estimated data for  $k_p^+$  at  $0^\circ\text{C}$  of  $3.6 \times 10^3$  and  $4.8 \times 10^3\text{M}^{-1}\text{s}^{-1}$  respectively. The corresponding Arrhenius activation energy is  $\sim 20\text{kJ/mol}$  and the pre-exponential factor  $\sim 1.3 \times 10^7$ . The latter value is consistent with a free ionic mechanism since it compares favourably with similar data from free radical propagations where entropy factors would be expected to be similar. It is also anticipated that pre-exponential factors for ion pair growth will be some orders of magnitude less than this<sup>26</sup>.

Rather interestingly the rate constant for propagation via ion pairs appears to be only one order of magnitude less

than that for propagation via free ions. Such a result has been reported previously<sup>24,25</sup> and may well indicate that the major ion pair species present in dichloromethane is a loose or solvent separated entity. Such comparable reactivity has already been unambiguously demonstrated in anionic systems<sup>23</sup>.

Sigwalt and his coworkers<sup>6</sup> have reported a value of  $2.8 \times 10^4\text{M}^{-1}\text{s}^{-1}$  for the overall rate constant for propagation in cationic polymerization of *p*-methoxystyrene in dichloromethane at  $10^\circ\text{C}$ . Though these authors made no attempt to place quantitative significance on these data in terms of the possible ionic species present, at least superficially some measure of agreement seems to emerge. Ise and his collaborators<sup>2</sup> have determined a value of  $4 \times 10^4\text{M}^{-1}\text{s}^{-1}$  for the rate constant for propagation by free poly(*p*-methoxystyryl) anion, i.e.  $k_p^-$ , in tetrahydrofuran (dielectric constant  $\sim 7$ ) at  $25^\circ\text{C}$ . The present data would predict a value for  $k_p^+$  at  $25^\circ\text{C}$  in dichloromethane (dielectric constant  $\sim 9$ ) of  $\sim 7 \times 10^3\text{M}^{-1}\text{s}^{-1}$ . Media of increasingly higher solvation power are known to reduce the rates of elementary reactions involving charge dispersal in going from initial to transition states e.g. propagation. Hence taking the dielectric constants as indicative of solvating abilities, values of  $k_p^-$  and  $k_p^+$  would be expected to be very similar in a common solvent. It is usually anticipated that under similar conditions  $k_p^-$  should be less than  $k_p^+$ , since the attack of a nucleophile on a vinyl double bond requires the use of high antibonding orbitals on the monomer, whereas attack of an electrophile can proceed via overlap of the  $\pi$ -electron cloud of the monomer with vacant orbitals (of relatively lower energy) on the electron deficient centre. The latter process should therefore be less activated. This argument, however, neglects to account for the relative stabilities of the nucleophilic and electrophilic species. In the case of *p*-methoxystyrene, the free cationic derivative would be expected to be more stabilized by the *para* substituent than the corresponding free anionic species. It is not unreasonable, therefore, to argue that these opposing factors may well balance each other, making  $k_p^+$  and  $k_p^-$  of comparable numerical size.

The increased stability of the propagating free cation in the polymerization of *p*-methoxystyrene, relative to that in styrene polymerizations, would also explain the increased activation energy ( $\sim 20\text{kJ/mol}$ ) relative to that for propagation by free polystyryl cation<sup>27</sup> ( $\sim 0\text{kJ/mol}$ ).

#### Variation of $k_p$ (obs) with $[M]_0$

The other major observations made from the data in Tables 2–4 and shown graphically in Figure 3 is that  $k_p$  (obs) varies almost linearly with the initial concentration of monomer used in polymerizations. It could be argued therefore that this merely reflects a second order rate dependence on monomer. However, a second order plot over the whole conversion range in a single polymerization showed poor linearity hence excluding this possibility, and showing the relationship to be fortuitous. It seems most likely therefore that the effect has its origins in the differing solvation ability of monomer and solvent. Indeed Table 6 shows clearly that the dielectric constant of a reaction solution falls progressively, as the percentage of monomer added rises through the range of values used in the polymerizations. If it is assumed that the solvation effects of a methoxy phenyl residue are the same in the monomer as in the polymer, then at least in a given polymerization the overall dielectric constant can be taken as fixed.

In any reaction involving a number of different ionic species in equilibrium, the solvent can influence the absolute reactivity of each of the species, and simultaneously disturb the equilibrium between them. In ionic propagation reactions whether the active centre is a free ion or an ion pair, decreasing the solvation ability of the medium increases data for individual rate constants. This may explain the observed increase in  $k_p$  (obs) with increase in  $[M]_0$  (i.e. decrease in dielectric constant). The overall change in the dielectric constant is, however, small and it seems unlikely that such changes in  $k_p$  (obs) could be attributed to the above effect alone. It is more likely that a disturbance of the equilibrium between free ions and ion pairs takes place. Unfortunately little is known about the effects of monomer type molecules on the ion pair dissociation constants of organic salts. Dryvers and Goethals<sup>25</sup> have reported that excess sulphide functions (in the cationic polymerization of cyclic sulphides) do not influence the ion pair dissociation constant of the initiator salt used in their studies. However, Jones and Plesch<sup>28</sup> have observed an increase by a factor of  $\sim 2$  in the dissociation constant of triphenylmethyl hexafluorophosphate in dichloromethane, on addition of traces of diethyl ether, despite the latter being a less polar solvent. These authors interpreted the results in terms of specific solvation of the cation by ether molecules.

In the case of *p*-methoxystyrene both *n*- and  $\pi$ -donor sites are present, and it is possible that specific solvation of active centres may occur, increasing the proportion of free ions as  $[M]_0$  is increased. Since free ions are likely to be more reactive than ion pairs,  $k_p$  (obs), which probably includes contributions from both, would be expected to increase also. In order to enable a deeper understanding of this and related polymerizations, a systematic study of the effect of additives on the dissociation constants of some model salts is being carried out at the present moment.

#### ACKNOWLEDGEMENTS

We wish to thank Professor A. M. North for helpful discussions about the work, Drs T. H. Sadler and A. Boyd of the University of Edinburgh for their invaluable help and with Fourier transform n.m.r. spectra, and Mr J. Carruthers for the determination of polymer molecular weights.

One of us (A.G.M.) is also indebted to the Commonwealth Scholarship Commission for a maintenance award.

#### REFERENCES

- 1 Axford, D. W. E. *Proc. R. Soc.*, 1949, **A197**, 374
- 2 Takaya, K., Hirohara, H., Nakayama, M. and Ise, N. *Trans. Faraday Soc.* 1971, **67**, 119
- 3 Okamura, S., Kanoh, N. and Higashimura, T. *Makromol. Chem.* 1961, **68**, 19
- 4 Sakurada, I., Ise, N. and Ashida, T. *Makromol. Chem.* 1966, **95**, 1
- 5 Janjua, K. M. and Johnson, A. F. *Int. Symp. Cationic Polymerization, Rouen* 1973, C15-1
- 6 Cotrel, R., Sauvet, G., Vairon, J. P. and Sigwalt, P. *ibid.* 1973, C8-1
- 7 Bawn, C. E. H., Fitzsimmons, C., Ledwith, A., Penfold, J., Sherrington, D. C. and Weightman, J. A. *Polymer* 1971, **12**, 119
- 8 Bowyer, P. M., Ledwith, A. and Sherrington, D. C. *Polymer* 1971, **12**, 509
- 9 Ledwith, A., Lockett, E. and Sherrington, D. C. *Polymer* 1975, **16**, 31
- 10 Bowyer, P. M., Ledwith, A. and Sherrington, D. C. *J. Chem. Soc. (B)* 1971, p1511
- 11 Conrow, K. *Org. Synth.* 1963, **43**, 101
- 12 Cowell, G. W., Ledwith, A., White, A. C. and Woods, H. J. *J. Chem. Soc. (B)* 1970, p 227
- 13 Sambhi, M. *PhD Thesis* University of Liverpool (1966)
- 14 Bollinger, J. M., Comisarow, M. B., Curpas, C. A. and Olah, G. A. *J. Am. Chem. Soc.*, 1967, **89**, 5687
- 15 Eckard, A. D., Ledwith, A. and Sherrington, D. C. *Polymer* 1971, **12**, 444
- 16 Prosser, H. J. and Young, R. N. *Eur. Polym. J.* 1972, **8**, 879
- 17 McGeachin, S. G. *Can. J. Chem.* 1969, **47**, 151
- 18 Kursanov, D. N., Vol'pin, M. E. and Akhrem, I. S. *Dokl. Akad. Nauk USSR* 1958, **120**, 531
- 19 Vol'pin, M. E., Akhrem, I. S. and Kursanov, D. N. *Zh. Obshch. Khim.* 1960, **30**, 159
- 20 Dauben, H. J., Honnen, L. R. and Harmon, K. M. *J. Org. Chem.* 1960, **25**, 1442
- 21 Olah, G. A. and Svobada, J. J. *J. Am. Chem. Soc.* 1973, **95**, 3794
- 22 Heck, R., Magee, P. S. and Winstein, S. *Tetrahedron Lett.* 1964, p 2033
- 23 Szwarc, M. 'Carbanions, Living Polymers and Electron Transfer Processes', Interscience, New York, 1968
- 24 Sangster, J. M. and Worsfold, D. J. *Polym. Prepr.* 1972, **13**, 72
- 25 Drijvers, W. and Goethals, E. J. *IUPAC Symp. Macromol. Chem. Boston* 1971, p 663
- 26 Higashimura, T. 'Structure and Mechanism in Vinyl Polymerisation', (Ed. T. Tsuruta and K. F. O'Driscoll), Marcel Dekker, New York, 1969, p 313
- 27 Williams, F., Hayashi, K., Ueno, K., Hayashi, K. and Okamura, S. *Trans. Faraday Soc.* 1967, **63**, 1501
- 28 Jones, F. R. and Plesch, P. H. *Chem. Commun.* 1970, p 1018



Table 1 Molecular weight data of the backbone copolymers

	Sample 3	Sample 6
vinyl acetate in feed (mol %)	60.0	23.4
vinyl acetate in copolymer (mol %)	1.9 <sub>3</sub> <sup>a</sup>	0.38 <sup>b</sup>
% conversion (styrene)	8.9	8.6
$M_n \times 10^{-5}$	1.03	4.2
$M_w \times 10^{-5}$	1.58	6.6 <sub>5</sub>
	Sample 3 fraction c	Sample 6 fraction b
total copolymer (wt %)	31	30
$M_n \times 10^{-5}$	1.43	6.2
$M_w \times 10^{-5}$	1.58	6.9
after hydrolysis: $M_n \times 10^{-5}$	—	6.2
$M_w \times 10^{-5}$	—	7.0
after chlorosilylation: $M_n \times 10^{-5}$	1.33	—
$M_w \times 10^{-5}$	—	6.7
theoretical no. of branch sites per molecule	26.5	22.7

<sup>a</sup> Vinyl acetate content determined by i.r. analysis of the C=O bond at 1730 cm<sup>-1</sup> in chloroform measured against a polystyrene solution and calculated using poly(vinyl acetate) standards

<sup>b</sup> Calculated from the experimental reactivity ratios

The characteristics of two large polymer samples are collected in Table 1. These polymers were fractionally precipitated from a benzene-methanol mixture. A middle fraction of sample 3 was retained. The middle fraction of sample 6 was subjected to one further fractionation. The data of the resulting polymers retained for further modification and, as such the parent backbone polymers, are given in Table 1.

#### Chemical modification of the backbone copolymer

The vinyl acetate groups of the copolymer were hydrolysed with KOH at room temperature. The completeness of the reaction was checked by the absence of C=O absorption in the i.r. spectrum of the polymer. The polymer was precipitated three times from filtered benzene solutions into methanol, freeze-dried from benzene and further dried at 50°C at 10<sup>-5</sup> mmHg for 24 h. All subsequent manipulations were performed using high vacuum techniques. To a 2 to 3% polymer solution in benzene-pyridine (90:10 v/v) was added distilled and degassed Si(CH<sub>3</sub>)<sub>2</sub>Cl<sub>2</sub> in 100-fold excess over hydroxyl groups. The mixture was stirred for 18 h at room temperature. The benzene, pyridine and excess Si(CH<sub>3</sub>)<sub>2</sub>Cl<sub>2</sub> were removed by freeze-drying. The polymer was redissolved in benzene (distilled from n-butyllithium), the solution was filtered and freeze-dried. Finally, a 5 to 10% solution of the polymer in benzene was subdivided into ampoules with break-seals. Molecular weight data of the copolymers after the modification are given in Table 1. A sample of copolymer 3c was treated with n-butyllithium. N.m.r. analysis of the Si(CH<sub>3</sub>)<sub>2</sub>CH<sub>2</sub> protons indicated a 66% yield. When Si(CH<sub>3</sub>)<sub>2</sub>Cl<sub>2</sub> was replaced by Si(CH<sub>3</sub>)<sub>3</sub>Cl an 80% conversion was obtained. In order to obtain comb polymers with the same number of branches from one backbone polymer the chlorosilylation reaction was performed in one batch.

#### Preparation of the comb polymers

The living polystyrene, which was to be used as the branch material, was prepared with s-butyllithium in benzene<sup>15</sup>. A sample was removed for molecular weight characterization. The chlorosilylated polystyrene was slowly added through a filter to a two-fold excess of living

polystyryllithium over a period of 2 to 3 h under vigorous stirring. The reaction mixture was left for 18 h at room temperature. The polystyryllithium concentration changed very little during this time. Excess living polymer was terminated with t-butanol. The polymer was fractionally precipitated. The comb polymer was recovered almost entirely in the first fraction which contained less than 1% of the unreacted branch material as indicated by g.p.c. and ultracentrifugation sedimentation.

#### Measurements of physical properties

Osmotic molecular weights were determined in toluene at 35°C with a Mechrolab 503 osmometer. Molecular weights lower than 10 000 were determined with a Perkin-Hitachi vapour pressure osmometer in toluene at 37°C. Light scattering measurements were performed in cyclohexane at 35°C unless otherwise specified with either a Sofica photogoniometer or with a Fica 50 instrument. Technical details of the measurements and required constants are given in previous reports<sup>10,11</sup>. Ultracentrifugation (u.c.) sedimentations were run on a Beckmann model E instrument at 59 780 rev/min. Cyclohexane at 35°C was the solvent. Gel permeation chromatograms (Waters 301) were obtained in toluene at 35°C. Three foot columns of 3 × 10<sup>6</sup>, 5 × 10<sup>5</sup>, 6.5 × 10<sup>4</sup>, 2.5 × 10<sup>4</sup>, 8.5 × 10<sup>3</sup>, 2.5 × 10<sup>3</sup>, 500 and 100 Å were used. Viscosity measurements were performed in a Cannon-Ubbelohde viscometer, with negligible kinetic energy correction.

## RESULTS AND DISCUSSION

#### Preparation and characterization of comb polystyrenes

A comparison of the properties of comb polymers with theory demands the correct determination of the molecular weight and molecular weight distribution of the samples obtained. The latter has seldom been done previously and is quite difficult in practice. Estimation of the degree of branching depends on the sample polydispersity. In the present case modification of the backbone polymer involves three reactions. The first, hydrolysis of the acetate groups has been shown to go to completion and no change in the molecular weight and molecular weight distribution of the sample could be detected. The second step, dimethylchlorosilylation is a variant of the trimethylsilylation reaction used extensively in analytical derivation. This reaction normally goes to completion in less than 10 min with isopropanol. With the polymeric hydroxyl compound, however, only 70–80% yields are observed as determined by n.m.r. analysis on the butyldimethylsilyl or trimethylsilyl model substitutions. This may be due to the low concentration of the hydrolysable groups which poses analytical problems but the possibility cannot be excluded that some hydroxyl groups are not readily available for derivation<sup>16</sup>. Intra- and inter-molecular crosslinking between a pendant silicon chloride group and a residual hydroxyl group has been minimized by rapidly adding an excess of dichlorodimethylsilane. In any case the data in Table 1 show no evidence for an increased molecular weight of the backbone after the chlorosilylation reaction. The efficiency of the coupling reaction can only be assessed by examining the ratio between the calculated and observed molecular weight of the comb polymers. The experience gained in the synthesis of star polymers suggests it should be quantitative<sup>10–12</sup>.

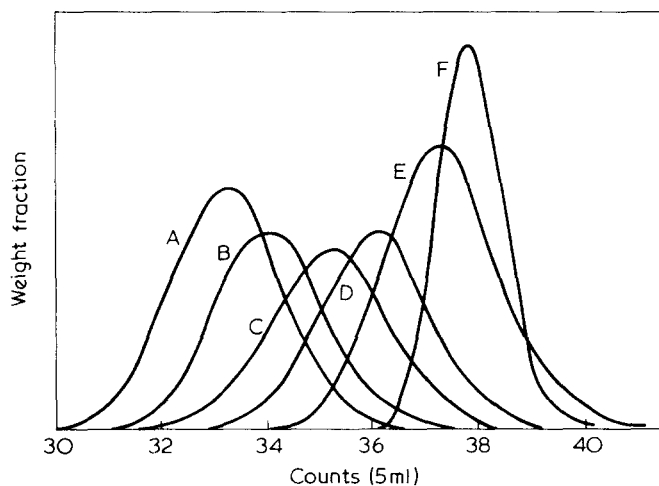


Figure 1 Gel permeation chromatograms of comb polystyrenes: A, C051; B, C031; C, C041A; D, C061; E, bb3c; F, narrow molecular weight distribution polystyrene PS100f2<sup>10</sup>

Examination of the final g.p.c. (Figure 1) and u.c. data shows that the comb polymers have a fairly narrow molecular weight distribution, little wider than the original backbone polymer. It should nevertheless be noted that if different degrees of branching are present in the samples g.p.c. analysis will underestimate the broadness of the molecular weight distribution. The data from number-average and weight-average molecular weight determinations (Table 2) suggest a broader distribution. The  $M_n$  values from stoichiometry (Table 2, column 4) are subject to error in the quantity of starting backbone polymer admitted to react and also relies on quantitative recovery of the comb polymer in the fractionation process. The osmotically determined  $M_n$  values, available for two comb polymers, can be seriously affected by small amounts of branch material. Therefore, from the latter values one derives  $M_w/M_n \leq 1.35$  in poor agreement with g.p.c. results but consistent with a 70–80% yield in the chlorosilylation reaction.

Some broadening of the molecular weight distribution over that of the backbone is expected for the complete coupling of near monodisperse branches to a randomly substituted backbone according to<sup>17</sup>:

$$\left(\frac{M_w}{M_n}\right)_{\text{comb}} = \left(\frac{M_w}{M_n}\right)_{\text{bb}} + \frac{\bar{p}_n y^2 (\bar{x}_n - \bar{p}_n)}{\bar{x}_n (\bar{x}_n + \bar{p}_n y)^2} \quad (1)$$

in which  $\bar{x}_n$  and  $\bar{x}_w$  are number- and weight-average degrees of polymerization of the backbone and  $y$  is the degree of polymerization of the branch. But this broadening is small in the present experiments and would lead to an increase in the  $M_w/M_n$  ratio of less than 0.04 in all cases. A final  $M_w/M_n$  ratio of 1.35 for the combs is therefore not entirely consistent with the  $M_w/M_n$  ratio of 1.11 for the original backbone polymer, or the value of 1.15 derived from the g.p.c. curve of the backbone polymer after correction for axial dispersion.

Because the molecular weight distribution is known with uncertainty and because no  $M_n$  values for the high molecular weight combs are available,  $p$  was determined from:

$$p = \frac{M_{w,\text{comb}} - M_{w,\text{bb}}}{M_{n,\text{br}}} \quad (2)$$

This is essentially equivalent to using  $M_w$ 's throughout as the branch material is not likely to have  $M_w/M_n > 1.1$  and usually much less than that. The error in using  $M_{w,\text{comb}}$  is reduced by simultaneously using  $M_{w,\text{bb}}$ . Equation (2) will, however, overestimate the number of branches.

#### Physical measurements

Light scattering measurements on dilute polymer solutions furnish, beside the weight-average molecular weight, the second virial coefficient,  $A_2$ , and through its temperature dependence  $\theta(A_2)$  the temperature at which  $A_2 = 0$ . The  $\theta(A_2)$  temperature for each comb polymer in cyclohexane is given in Table 3. Decreases of the  $\theta(A_2)$  temperature for branched polymers are now well documented<sup>6,8,11,12,18,19</sup>. In each series of comb polymers with a common backbone the  $\theta$  temperature decreases more from that of linear polystyrene (34.5°C) as the branch length decreases. A comparison of the two series of combs show that the one with the smaller backbone has the largest  $\theta(A_2)$  temperature depression. The  $\theta(A_2)$  temperature decreases observed here are similar to those for comparable comb polystyrenes 1B and 2A of Candau<sup>8</sup>. On the basis of these results polymers A53.2 and A68.4 of Berry<sup>20</sup> would not have a sufficiently high branch density to exhibit a  $\theta(A_2)$  temperature lowering, as was indeed observed.

The decrease in the  $\theta(A_2)$  temperature has been related to increased segment density and hence number of triple contacts in branched polymers<sup>41</sup>. From this hypothesis an expression for  $\theta(A_2)$  was derived:

$$\frac{\theta}{\theta(A_2)} - 1 = \frac{3^{3/2}}{2^4} \frac{C_M}{C_M} \frac{(1/3 - \chi_2)}{\psi} \frac{H(K')}{M^{1/2} g_{\text{exp}}^{3/2}} \quad (3)$$

Table 2 Molecular weight data for the comb polystyrenes

Sample	Backbone	$M_{n,\text{br}} \times 10^{-3}$	$M_{n,\text{comb}}^a \times 10^{-5}$	$M_{n,\text{comb}} \times 10^{-5}$	$M_{w,\text{comb}} \times 10^{-5}$	$p^b$
C061	3c	7.4	2.6	2.8 <sub>6</sub>	3.8 <sub>5</sub>	31
C041A <sup>c</sup>	3c	15.8	4.0	4.1 <sub>8</sub>	5.8 <sub>3</sub>	27
C031	3c	30.1	7.2	—	10.7	30
C051	3c	53.7	12.8	—	16.7	28
C131	6bc	7.0	6.2	—	8.6 <sub>4</sub>	25
C111	6bc	10.7	8.3	—	9.4 <sub>2</sub>	24
C101	6bc	24.0	11.5	—	12.8 <sub>5</sub>	25
C121	6bc	49.1	16.5	—	18.5	24
C141A <sup>c</sup>	6bc	112.1	>28.8	—	36.0	26

a  $M_{n,\text{comb}} = \frac{\text{weight}_{\text{comb}}}{\text{weight}_{\text{bb}}} \times M_{n,\text{bb}}$

b Equation (2)

c Refractionated

Table 3 Physical properties of comb polystyrenes

Sample	$M_w \times 10^{-5}$	$\lambda$	$g_{\text{th}}^a$	$\theta(A_2)$ (°C)	$(S^2)_{\theta(A_2)} \times 10^{-2}$	$g_{\text{exp}}$
C061	3.8 <sub>5</sub>	0.410	0.447	25.5	—	—
C041A	5.8 <sub>3</sub>	0.271	0.326	27.5	—	—
C031	10.7	0.148	0.224	29.6	—	—
C051	16.7	0.0946	0.180	30.8	3.9 <sub>4</sub>	0.281
C131	8.6	0.799	0.803	31.1	5.9 <sub>8</sub>	0.82 <sub>8</sub>
C111	9.4 <sub>2</sub>	0.723	0.741	33.0	6.5	0.821
C101	12.8	0.537	0.563	35.0	8.0	0.74 <sub>4</sub>
C121	18.5	0.373	0.421	34.8	8.8	0.56 <sub>6</sub>
C141A	36.0	0.192	0.271	34.5	12.4	0.41 <sub>0</sub>

a Using  $p = 29$  for combs C031–C061 and  $p = 25$  for combs C101–C141 in equation (4)

b In cyclohexane, linear polystyrene at 34.5°C

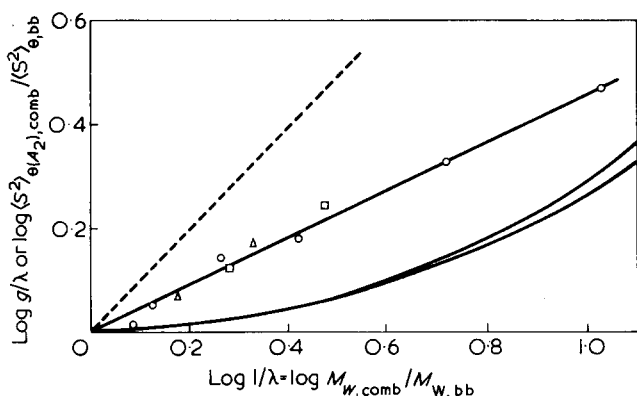


Figure 2 Log-log plot of the ratio of the mean square radius of gyration of a comb to that of its backbone against the ratio of their molecular weights. Experimental points:  $\circ$ , this work;  $\square$ , ref 20;  $\triangle$ , ref 21. — — —, represents linear polystyrene. Curves: equation (5) with  $p = 25$  (upper) and  $p = 29$  (lower)

in which  $C'_M$  and  $C_M$  contain polymer and solvent constants,  $(1/3 - \chi_2)$  is the triple contact term and  $H(K')$  is a function that depends on  $\alpha$ . A plot of  $\alpha^8 - \alpha^6$  versus  $\alpha^3 [1 - (\theta/T)]$  allows the evaluation of  $(1/3 - \chi_2)$  and  $\psi$  for each comb polymer<sup>22</sup>. However, no consistent set of these parameters could be obtained by this analysis, as was also observed previously<sup>21</sup>. Using values of  $(1/3 - \chi_2) = 0.045$  and  $\psi = 0.321$ , obtained for four- and six-branched star polystyrenes<sup>11</sup>, equation (3) predicts  $\theta(A_2)$  temperatures that vary much less with branch length than observed experimentally.

The angular dependence of light scattering after extrapolation to zero concentration gives the radius of gyration of the polymer in solution. Branched polymers have a smaller radius of gyration than linear polymers of the same molecular weight. Random flight statistics allow the calculation of the theoretical ratio,  $g$ , between the radius of gyration of a randomly branched comb and that of its linear homologue<sup>22</sup>:

$$g = \frac{\langle S^2 \rangle_{0, \text{comb}}}{\langle S^2 \rangle_{0, \text{lin}}} = \lambda + \frac{3}{p} (1 - \lambda)^2 + \frac{(1 - \lambda)^3}{p^2} \quad (4)$$

where  $\lambda$  is the fraction of polymer in the backbone. Since  $\lambda \cdot \langle S^2 \rangle_{0, \text{lin}} = \langle S^2 \rangle_{0, \text{bb}}$ , a more useful relation between the radius of gyration of a comb and its backbone can be derived from equation (4)<sup>20</sup>:

$$\frac{\langle S^2 \rangle_{0, \text{comb}}}{\langle S^2 \rangle_{0, \text{bb}}} \approx 1 + \frac{3}{p \cdot \lambda} (1 - \lambda)^2 \quad (5)$$

Any effect of polydispersity on  $\langle S^2 \rangle_{0, \text{comb}}$  is cancelled largely by comparing it with the experimentally measured  $\langle S^2 \rangle_{0, \text{bb}}$ . The initial slope was obtained using the  $P(\theta)$  function for linear polymers as outlined previously<sup>11</sup>. The variable  $\mu = 16\pi^2 (\langle S^2 \rangle / \lambda^2) \sin^2 \theta / 2$  is always smaller than 2, and the  $P(\theta)$  function of combs and linear polymers having the same radius of gyration differ very little<sup>22</sup>. Table 3 lists the calculated (equation 4) and experimentally determined  $g$  values for the comb polymers. The latter are derived with  $\langle S^2 \rangle_{0, \text{lin}} / M_w = 8.4 \times 10^{-12} \text{ cm}^2 \text{ g mol}$  as obtained on the slightly polydisperse backbone polymer 6bc. At  $\theta(A_2)$ , where on the average polymer-polymer and polymer-solvent interactions cancel, all experimental  $g$  values are larger than the theoretical ones (equation 4). The

increase of  $\langle S^2 \rangle_{\theta(A_2), \text{comb}}$  over that of  $\langle S^2 \rangle_{0, \text{bb}}$  on grafting a constant number of progressively larger branches is shown in Figure 2. In contrast to the theoretical prediction, short branches increase the radius of gyration significantly.

Figure 2 also indicates that, to a first approximation and for combs with 20–30 branches:

$$\frac{\langle S^2 \rangle_{\theta(A_2), \text{comb}}}{\langle S^2 \rangle_{0, \text{bb}}} = \left( \frac{1}{\lambda} \right)^{0.46} \quad (6)$$

independent of the molecular weight of the backbone. In the case of linear polymers the exponent is, of course, equal to one. Comb polymers with a near star structure deviate from this line, however<sup>6</sup>.

Intrinsic viscosity measurements on the comb polymers were performed in cyclohexane at  $\theta(A_2)$ , in cyclohexane and in toluene at 35°C. When the intrinsic viscosities of the comb polymers are measured at their individual  $\theta(A_2)$  temperature, where, on the average polymer-polymer and polymer-solvent interactions cancel and the excluded volume becomes zero, the data for the two series of comb polymers fall on a single line and are equal to that of the parent backbone polymer whenever  $M_{w, \text{comb}} / M_{w, \text{bb}} < 4$ . Above this ratio there is a small increase in the intrinsic viscosities which reaches 15% when  $M_{w, \text{comb}} \approx 10 \cdot M_{w, \text{bb}}$  as shown in Figure 3.

The curves obtained for the dependence of the intrinsic viscosity on  $1/\lambda$  in cyclohexane at 35°C are caused by the varying thermodynamic conditions in which the combs exist in that solvent. The larger the  $\theta$ -temperature depression of the comb, the more expanded is the polymer at 35°C and the more the intrinsic viscosity is increased from that at  $\theta(A_2)$ . Clearly, this effect is most pronounced for combs with small branches and/or a high branch density. Similar curves were observed previously, the highly branched combs showing the largest increase in the intrinsic viscosity from that of their backbone<sup>7</sup>.

In toluene at 35°C the thermodynamic conditions of the combs are probably not very different. The intrinsic

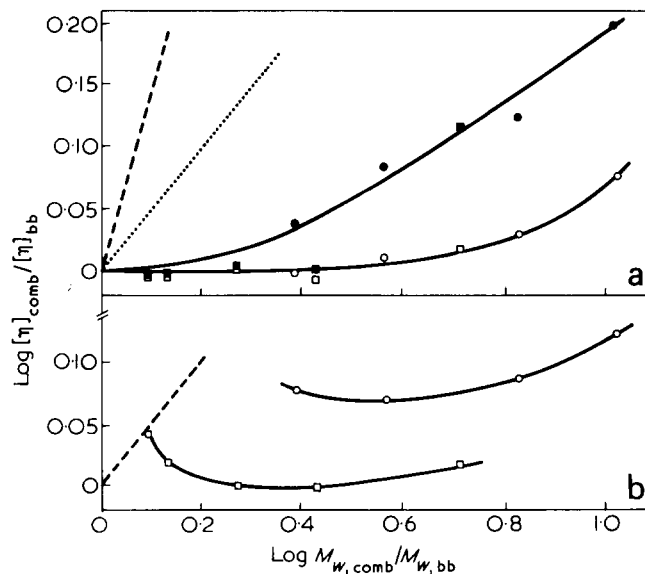


Figure 3 Ratio of the intrinsic viscosity of comb polystyrene to that of its backbone plotted against the ratio of their molecular weights.  $\circ$ , C03–C06;  $\square$ , C10–C14. (a): full symbols, toluene, 35°C; open symbols, cyclohexane at  $\theta(A_2)$ ; — — —, toluene; ···, cyclohexane. (b): cyclohexane, 35°C. — — —, linear polystyrene



Table 4 Intrinsic viscosities of comb polymers

Sample	$M_w \times 10^{-5}$	[ $\eta$ ] (dl/g)			$g'^a$		
		CH 35°C	CH $\theta(A_2)$	Tol. 35°C	$g_{th}^{1/2}$	CH $\theta(A_2)$	Tol. 35°C
bb 3c	1.58		0.278	0.605			
C061	3.8 <sub>5</sub>	0.332	0.276	0.66	0.669	0.536	0.541
C041A	5.8 <sub>3</sub>	0.325	0.284	0.73	0.571	0.448	0.442
C031	10.7	0.338	0.295	0.80	0.473	0.343	0.311
C051	16.7	0.367	0.328	0.94	0.424	0.306	0.265
bb 6bc	6.9		0.61	1.67			
C131	8.6	0.68	0.61	1.70	0.846	0.79	0.77
C111	9.4 <sub>2</sub>	0.645	0.59	1.61	0.861	0.73 <sub>5</sub>	0.69
C101	12.8		0.61	1.69	0.750	0.64	0.58
C121	18.5		0.59	1.64	0.649	0.52	0.43
C141A	36.0	0.6	0.64	2.16	0.521	0.40 <sub>5</sub>	0.35

<sup>a</sup>  $g' = [\eta]_{comb}/[\eta]_{lin}$  with  $[\eta]_{lin} = 8.3 \times 10^{-4} M_w^{0.5}$  in cyclohexane at 35°C and  $[\eta]_{lin} = 1.02 \times 10^{-4} M_w^{0.73}$  in toluene<sup>10</sup>

viscosities show a behaviour similar to that found under  $\theta(A_2)$  conditions. However, the increase of the intrinsic viscosity above that of the backbone as the molecular weight increases occurs at lower molecular weight and is somewhat greater. Nevertheless, the increase is much smaller than observed on increasing the molecular weight in linear polymers.

The results in Table 4 reveal that all intrinsic viscosities at  $\theta(A_2)$  and in toluene are lower than predicted by the Zimm–Kilb relation<sup>23</sup>:

$$g' = \frac{[\eta]_{comb}}{[\eta]_{lin}} = g_{th}^{1/2} \quad (7)$$

A similar although smaller effect was observed in regular star polymers<sup>10–12</sup>. As with the star polymers, the experimental  $g'$  values are lower in the good solvent than under  $\theta$ -conditions. A search for a correlation between  $g'_{exp}$  and  $g_{th}$  of the form:

$$g' = g_{th}^m \quad (8)$$

failed to yield a constant exponent<sup>20</sup>. It is more likely that progress in deciphering the factors determining the intrinsic viscosities of comb polymers will be made by comparison with the intrinsic viscosity of the parent backbone as shown in Figure 3. While the effect of the backbone length was investigated, the effect of the number of branches requires further study; so do the factors influencing the upswing of the intrinsic viscosities and the effect of the polydispersity.

The comb polymers, that have intrinsic viscosities that do not differ from that of the backbone, have nevertheless increased hydrodynamic volumes ( $V_e$ ) through the increase in  $M_w$ .

$$[\eta] \cdot M_w = \text{constant} \times V_e = \phi \langle S^2 \rangle^{3/2} \quad (9)$$

For the comb polymers with  $1/\lambda < 10$   $[\eta]_{\theta(A_2)} \cdot M_w \approx 1/\lambda$ . It follows from equation (6) that  $\langle S^2 \rangle_{\theta(A_2), comb}^2$  varies according to  $(1/\lambda)^{0.69}$ . Therefore:

$$\phi_{\theta(A_2), comb} \approx \phi_{0, lin} \cdot \left( \frac{1}{\lambda} \right)^{\sim 1/3} \quad (10)$$

This approximation seems to hold for combs with 20–30 branches with backbone polymers between  $1.5 \times 10^5$  and  $1.3 \times 10^6$ <sup>20</sup>. When  $1/\lambda > 10$  the comb polymers become

star-like polymers and  $\phi_{\theta, comb}$  will increase faster than indicated by equation (10). There is some evidence that in a good solvent  $\phi_{comb} \approx \phi_{lin}$ <sup>20</sup>. Since the polydispersity of the polymer sample has an important effect on the exact value of  $\phi$ , these variations of  $\phi$  with polymer branching have to be considered exploratory.

## CONCLUSIONS

It is shown that Si–Cl bonds can be introduced into polystyrene and can be used to react with living anionic polymer. The number-average number of branches in the resulting comb polymer is somewhat less than calculated from the original reaction sites in the backbone polymer, probably because of incomplete chlorodimethylsilylation or loss of Si–Cl bonds in the work-up of the polymer. A series of combs with a constant number of branches are obtained. Their exact molecular weight distribution is difficult to determine and leaves some uncertainty as to the exact meaning of the physical properties of the comb polymers. The effect of the unreacted groups in the polymers, especially polar groups, is not known and forms another limitation on the results. These are areas for future improvement.

The  $\theta(A_2)$  temperatures of the combs are lower than for linear polystyrene. At  $\theta(A_2)$  the radii of gyration of the combs are larger than can be calculated from random flight statistics. The intrinsic viscosities at  $\theta(A_2)$  and also in a good solvent are lower than predicted by the Zimm–Kilb relation. The ratio of the radii of gyration of the combs and their backbone varies with the ratio of the molecular weight of the combs and their backbone. Similar variation is found for the intrinsic viscosities of the combs. Both these variations do not seem very sensitive to the exact number of branches between 20–30 branches per chain and are independent of the molecular weight of the backbone polymer between  $1.5 \times 10^5$  and  $1.5 \times 10^6$ .

## ACKNOWLEDGEMENTS

The author wishes to thank Dr S. Bywater for many inspiring discussions, Mr R. Ironside for the i.r. spectra and Mr P. Toporowski for technical assistance.

## REFERENCES

- Altare, Jr T., Wyman, D. P., Allen, V. R. and Meyerson, K. *J. Polym. Sci. (A)* 1965, 3, 4131

*Synthesis and solution properties of comb polystyrenes: J. E. L. Roovers*

- 2 Orofino, T. A. and Wenger, F. *J. Phys. Chem.* 1963, **67**, 566
- 3 Yen, S.-P. S. *Makromol. Chem.* 1965, **81**, 152
- 4 Bryce, W. A. J., McGibbon, G. and Meldrum, I. G. *Polymer* 1970, **11**, 394
- 5 Meunier, J.-Cl. and Van Leemput, R. *Makromol. Chem.* 1971, **142**, 1
- 6 Fujimoto, T., Narukawa, H. and Nagasawa, M. *Macromolecules* 1970, **3**, 57
- 7 Pannell, J. *Polymer* 1971, **12**, 558; 1972, **13**, 2
- 8 Candau, F. and Franta, E. *Makromol. Chem.* 1971, **149**, 41
- 9 Price, C. and Woods, D. *Polymer* 1973, **14**, 82
- 10 Roovers, J. E. L. and Bywater, S. *Macromolecules* 1972, **5**, 384
- 11 Roovers, J. E. L. and Bywater, S. *Macromolecules* 1974, **7**, 443
- 12 Hadjichristidis, N. and Roovers, J. E. L. *J. Polym. Sci. (Polym. Phys. Edn)* 1974, **12**, 2521
- 13 Mayo, F. R., Walling, C., Lewis, F. M. and Hulse, W. F. *J. Am. Chem. Soc.* 1948, **70**, 1523
- 14 Cameron, G. G., Kerr, G. P. and Russell, D. A. *Eur. Polym. J.* 1971, **7**, 1029
- 15 Bywater, S. and Worsfold, D. J. *J. Organomet. Chem.* 1967, **10**, 1
- 16 Ushakov, S. N. and Belogorodskaya, K. V. *Proc. Acad. Sci. USSR (Chem. Sect.)* 1960, **134**, 1159
- 17 Orofino, T. A. *Polymer* 1961, **2**, 295
- 18 Decker, D. *Makromol. Chem.* 1969, **125**, 136
- 19 Zilliox, J.-G. *Makromol. Chem.* 1972, **156**, 121
- 20 Berry, G. C. *J. Polym. Sci. (A-2)* 1971, **9**, 687
- 21 Candau, F., Rempp, P. and Benoit, H. *Macromolecules* 1972, **5**, 627
- 22 Casassa, E. F. and Berry, G. C. *J. Polym. Sci. (A-2)* 1966, **4**, 881
- 23 Zimm, B. H. and Kilb, R. W. *J. Polym. Sci.* 1959, **37**, 19

# Use of organotin compounds in the thermal stabilization of PVC: 6. A radiochemical study of the effect of variations in molecular weight on the reaction between PVC and di(butylthiolato)dibutyltin

F. Alavi-Moghadam, G. Ayrey and R. C. Poller

Department of Chemistry, Queen Elizabeth College, Campden Hill Road, London W8 7AH, UK

(Received 2 May 1975)

Reactions between PVC samples of differing molecular weight and di(butyl<sup>35</sup>S) thiolato)dibutyltin have been examined. There is an inverse relationship between the amount of radioactivity taken up by the polymer and its molecular weight.

## INTRODUCTION

In a previous paper<sup>1</sup> we showed that when a specimen of PVC ( $\bar{M}_n$  28 000) in chlorobenzene was heated with di(butyl<sup>35</sup>S) thiolato)dibutyltin at 180°C *in vacuo* there was only limited uptake of radioactivity during an induction period. This was ascribed to exchange between allylic chlorine atoms in the polymer with <sup>35</sup>S groups. At the end of the induction period incorporation of radioactivity occurred more rapidly due to addition of liberated [<sup>35</sup>S] butane thiol to double bonds in the degrading polymer. In the present paper we report the results obtained when a series of PVC samples of differing molecular weight reacted with the labelled stabilizer.

## EXPERIMENTAL

The suspension polymerized PVC used in this work was a gift from Mr R. Khana of ICI Ltd (Plastics Division). The samples were purified by precipitation from tetrahydrofuran solution using methanol and dried to constant weight in a vacuum oven at 45°C. The molecular weights were determined by gel permeation chromatography and by osmometry. Tetrahydrofuran was allowed to stand over sodium and then refluxed with lithium aluminium hydride. Immediately before use it was fractionally distilled through a 40 cm × 2.6 cm column packed with Fenske helices and the pure material shown to be free from peroxides. Chlorobenzene was similarly fractionally distilled immediately before use. Methanol was Analar grade without further purification.

Details of the preparation of di(butyl<sup>35</sup>S) thiolato)dibutyltin and of the radiochemical assays are given in our previous paper<sup>1</sup>.

### Interaction between PVC and Bu<sub>2</sub>Sn(<sup>35</sup>SBu)<sub>2</sub>

A solution of PVC in chlorobenzene (10–40 cm<sup>3</sup> depending upon concentration) containing 0.200 g of polymer and Bu<sub>2</sub>Sn(<sup>35</sup>SBu)<sub>2</sub> in chlorobenzene (0.20% w/v, 5 cm<sup>3</sup>) was

degassed, sealed at <10<sup>-4</sup> mmHg pressure and heated at 180°C. The polymer was precipitated with methanol, washed and dried. Standard cycles of dissolution in tetrahydrofuran, followed by precipitation with methanol were then carried out (6–8 times) until the radioactivity reached a constant value.

## RESULTS AND DISCUSSION

In our previous study<sup>1</sup> of the reaction between PVC and di(butyl<sup>35</sup>S) thiolato)dibutyltin, reaction periods of up to 8 h were used and there was no indication of any decrease in the rate of uptake of <sup>35</sup>S. The present work arose when this phenomenon was further investigated using PVC of higher molecular weight. The specimen of PVC used was identical with that used earlier except that it had  $\bar{M}_n$  79 800. The amounts of radioactivity incorporated into the polymer are shown in Table 1, from which it can be seen that the uptake of radioactivity continues steadily for 45 h at which point the polymer is highly degraded. When these results are compared with those obtained earlier<sup>1</sup> it is seen that the retained radioactivity after a reaction period of 8 h is 72.4 × 10<sup>3</sup> for PVC with  $\bar{M}_n$  79 800 compared with 364 × 10<sup>3</sup> disintegrations min<sup>-1</sup>g<sup>-1</sup> PVC for polymer having  $\bar{M}_n$  28 000 (the same specimen of labelled stabilizer being used). It seemed possible that the lower molecular weight

Table 1 Retention of radioactivity by PVC ( $\bar{M}_n$  79 800) after interaction with Bu<sub>2</sub>Sn(<sup>35</sup>SBu)<sub>2</sub>

Reaction period (h)	Retained radioactivity × 10 <sup>-3</sup> (disintegrations min <sup>-1</sup> g <sup>-1</sup> PVC)
0	1.6
4	33.1
8	72.4
15	142
25	252
45	533

Table 2 Molecular weights of PVC samples

Sample No.	$\bar{M}_n(A)^*$	$\bar{M}_n(B)^*$
1	28 000	27 500
2	38 000	31 400
3	45 500	39 800
4	55 000	45 000
5	64 000	56 000
6	82 000	79 800

\* Set (A) determined in the ICI (Plastics Division) laboratories by g.p.c.; set (B) determined in this laboratory by osmometry

Table 3 Retention of radioactivity by PVC samples after interaction with  $Bu_2Sn(^{35}SBu)_2$  and decrease in weight of samples after various cycles of dissolution and precipitation

Sample No.	Retained radioactivity $\times 10^{-3}$ * (disintegration $min^{-1}g^{-1}$ PVC)		Weight of PVC sample remaining (g)	
	After 6 cycles	After 8 cycles	After 6 cycles	After 8 cycles
1	114	109	0.0964	0.0638
2	97.8	96.5	0.1013	0.0823
3	69.7 (73.3)	66.7	0.1127	0.0948
4	76.9 (78.7)	71.5	0.1163	0.0956
5	54.8	57.4	0.1183	0.1019
6	36.2	35.0	0.1203	0.1000

\* Figures in parenthesis are repeat experiments

material has a higher concentration of allylic chlorine atoms leading to more rapid degradation and consequently an enhanced rate of addition of  $Bu^{35}SH$  to the formed polyene. It was of interest to examine more closely the relationship between molecular weight and uptake of radioactivity.

The six samples of PVC having molecular weights shown in Table 2 were each treated, in solution, with  $Bu_2Sn(^{35}SBu)_2$ , at  $180^\circ C$  *in vacuo* for 5 h. The polymer samples were then purified, as before, by repeated dissolution in tetrahydrofuran followed by precipitation with methanol until essentially constant values for radioactivity were obtained (at least 6 cycles in each case). The results are shown in Table 3 from which it can be seen that uptake of radioactivity depends inversely on the molecular weight of the

polymer. Although the values for samples 3 and 4 are not in the expected order, repeated experiments showed that the radioactivity values could be reproduced to within 5% or better. The apparent discrepancy is undoubtedly due to the fact that the error in the molecular weight determinations is unlikely to be better than  $\pm 10\%$ . This method of purification underestimates the dependence of uptake of radioactivity on molecular weight since the lower molecular weight components in each sample are preferentially removed. This is clearly seen in columns 4 and 5 of Table 3 where after 6 or 8 cycles of dissolution and precipitation, significantly smaller amounts of the original 0.200 g of sample are left in the case of the lower molecular weight polymers.

Although previous workers have shown that there is an inverse relationship between the rate of dehydrochlorination and the molecular weight of PVC<sup>2-4</sup> this is the first demonstration that the rate of incorporation of X groups from a stabilizer  $R_2SnX_2$  shows a similar relationship. This confirms the view proposed earlier<sup>1</sup> that, after the induction period, the stabilizer  $Bu_2Sn(^{35}SBu)_2$  absorbs hydrogen chloride to give  $Bu_2SnCl_2$  and  $Bu^{35}SH$ , the latter then adds to the double bonds in the degrading polymer. Thus the organotin stabilizer functions not only by prolonging the induction period before the onset of dehydrochlorination but exerts a continuing favourable influence by inhibiting hydrogen chloride catalysis and also by reducing the lengths of the conjugated polyene systems.

#### ACKNOWLEDGEMENTS

We thank the Anglo-Iranian Oil Company for support and ICI (Plastics Division) for samples of characterized PVC.

#### REFERENCES

- 1 Alavi-Moghadam, F., Ayrey, G. and Poller, R. C. *Eur. Polym. J.* in press
- 2 Bengough, W. L. and Sharpe, H. M. *Makromol Chem.* 1963, 66, 31
- 3 Geddes, W. C. *Eur. Polym. J.* 1967, 3, 267
- 4 Bataille, P. and Van, B. T. *J. Polym. Sci. (A-1)* 1972, 10, 1097

# Dielectric and dynamic mechanical relaxation studies of styrene–acrylonitrile copolymers\*

M. Cook and G. Williams

Edward Davies Chemical Laboratories, University College of Wales, Aberystwyth SY23 1NE, UK

and T. Tyssul Jones

Research Department, Monsanto Chemicals Ltd, Corporation Road, Newport, NPT OXF, UK

(Received 27 May 1975)

Dynamic mechanical measurements ( $\sim 1$  Hz) and dielectric measurements ( $10^{-4}$  to  $10^5$  Hz) are presented for styrene–acrylonitrile copolymers containing 25 and 32.5% acrylonitrile. Two dielectric ( $\alpha$ ,  $\beta$ ) and one mechanical ( $\alpha$ ) processes were observed and their mechanisms are discussed. It is shown that the Montrose–Litovitz fluctuation theory and Phillips–Barlow–Lamb defect-diffusion theory give reasonable representations of the dielectric  $\alpha$  relaxation process.

## INTRODUCTION

Styrene–acrylonitrile (S–AN) copolymers are commercial thermoplastic materials whose importance arises from the fact that they are relatively inexpensive and possess an excellent balance of physical and chemical properties. They are strong, rigid and transparent, have excellent dimensional stability and high craze resistance and are relatively easy to fabricate. S–AN copolymers are superior to unmodified polystyrene in their greatly improved resistance to chemical attack and their somewhat greater tensile strength and elongation. In this investigation the dielectric and mechanical relaxation of two S–AN copolymers, containing 25 and 32.5% acrylonitrile, have been studied over a large temperature range. The investigation was carried out for two reasons. First, we wished to see how the magnitude, location and shape of the multiple relaxations varied with acrylonitrile content, and secondly, we wished to obtain information about the relaxation behaviour as a necessary basis for the more complicated, but related, acrylonitrile–butadiene–styrene (ABS) materials.

## EXPERIMENTAL

The dynamic mechanical measurements were made using a torsion pendulum of a design similar to that described by Heijboer *et al.*<sup>1</sup> Using a combination of liquid nitrogen and heating elements, the temperature range 90 to 473 K could be covered. Values of the real ( $G'$ ) and imaginary ( $G''$ ) parts of the complex shear modulus ( $G^*$ ),

\* This paper contains 14 illustrations and 2 tables which have been deposited with the British Library Lending Division, Boston Spa, Wetherby, Yorkshire LS23 7BQ, UK as Supplementary Publication No. SUP 90015 (19 pages). Applications for copies of supplementary publications should be made to the British Lending Library, quoting the SUP number and enclosing prepaid coupons or their equivalent in cash. One prepaid coupon is required for every 10 pages or part thereof and the present costs are: UK and Eire, £4 for 20 or 20p each; Europe, £11 for 20 or 55p each; elsewhere, £13 for 20 or 65p each. These costs include postage (by airmail where available).

the quantity  $G = (G'^2 + G''^2)^{1/2}$ , the logarithmic decrement  $\Delta$ , the loss tangent  $\tan \delta_G$  and the measurement frequency were evaluated at each temperature. The dielectric measurements were made using: (i) a General Radio 1620-A Bridge ( $10^2$  to  $10^5$  Hz); (ii) a Scheiber Bridge ( $10^{-2}$  to  $10^2$  Hz); and (iii) a d.c. transient current method ( $10^{-4}$  to  $10^{-2}$  Hz). The latter technique gave information on the  $\alpha$  relaxation in the time domain which was transformed into the frequency-dependent loss factor  $\epsilon''(f)$  using the Hamon approximation<sup>2,3</sup> together with correction factors given by Williams *et al.*<sup>4,5</sup> for the special case of a Williams–Watts distribution with  $\bar{\beta} = 0.5$  which is appropriate for these copolymers. The two S–AN copolymers (I and II) were suspension polymerized materials with molecular weight near  $6 \times 10^4$  g/mol. S–AN I and S–AN II contained 25 and 32.5% (w/w) acrylonitrile, respectively. Samples were compression moulded at 433 K, and for mechanical measurements rectangular specimens 7 cm  $\times$  0.6 cm  $\times$  ( $4 \times 10^{-2}$  cm) were used, and for electrical measurements disc samples 3.5 cm diameter and 0.1 to 0.3 cm in thickness were used.

## RESULTS

Only representative data are presented in this paper, the full experimental data are given in the SUP. *Figure 1* shows  $G$  and  $\tan \delta_G$  against temperature for S–AN I (i.e. 25% acrylonitrile copolymer). Only one mechanical relaxation region is observed in the range 173 to 403 K, and is associated with the glass transition of the copolymer ( $T_g = 368$  K). *Figure 2* shows the dielectric loss factor  $\epsilon''$  as a function of temperature for S–AN I at a fixed frequency of 1 kHz. Two relaxation regions are observed, the large high temperature process ( $\alpha$  process) correlates in its location with the mechanical process, and is due to the large scale Brownian motions of the dipoles. The lower temperature process ( $\beta$  process) is due to limited

† The Figures in the SUP are numbered *Figures 1–14* and should not be confused with *Figures 1–8* of the present paper.

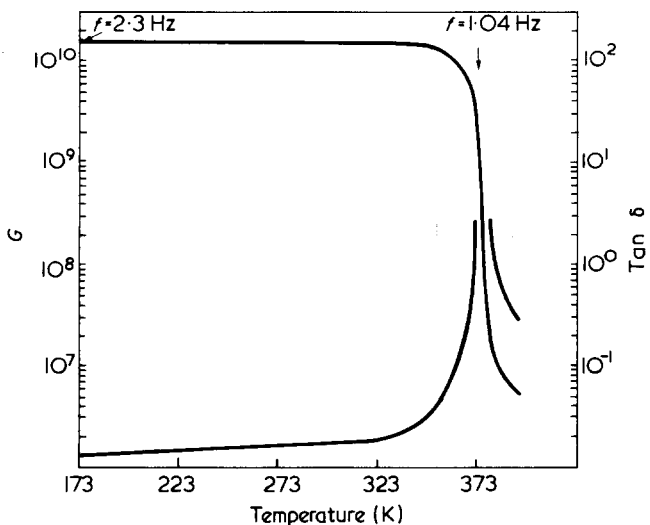


Figure 1  $G$  and  $\tan \delta_G$  against absolute temperature for S-AN I. The frequency of measurement for  $T < 320$  K is 2.3 Hz and falls to 1.04 Hz at the peak of  $\tan \delta_G$

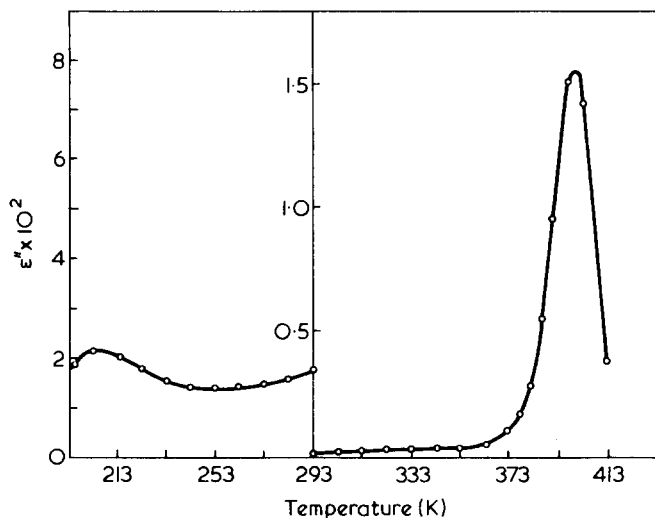


Figure 2  $\epsilon''$  against absolute temperature for S-AN I at 1 kHz

motions of dipoles in the glassy state of the copolymer. Figures 3 and 4 show plots of  $\epsilon'$  and  $\epsilon''$  against  $\log$  (frequency) for the  $\alpha$  and  $\beta$  processes in S-AN I. The results for S-AN II were similar to those shown in Figures 1-4 for S-AN I, and are given in the supplementary publication. Dielectric experiments contain information on: (a) the magnitude of the dipole relaxation processes; (b) their frequency-temperature locations; and (c) the form of the dipole-correlation function as given by the shape of the  $\epsilon''$  vs.  $\log$  (frequency) plots.

**Magnitude**

The values of  $\epsilon_0$  and  $\epsilon_\infty$  ( $\epsilon_0$  and  $\epsilon_\infty$  are the limiting low and high frequency permittivities for a given relaxation process) for the  $\alpha$  process in S-AN I and S-AN II are given in the supplementary publication. The magnitude of the relaxation could be obtained by the difference ( $\epsilon_{0\alpha} - \epsilon_{\infty\alpha}$ ) where these are the experimental permittivities, or more approximately, but conveniently, using the relation<sup>5</sup>:

$$(\epsilon_{0\alpha} - \epsilon_{\infty\alpha}) = K(\bar{\beta}) \epsilon_m'' \Delta \log f \quad (1)$$

where  $\Delta \log f$  is the half width of the loss curve for the  $\alpha$

process,  $\epsilon_m''$  is the maximum loss factor and  $K(\bar{\beta})$  is a function of the distribution parameter  $\bar{\beta}$ . For the curves of Figure 3,  $\bar{\beta} = 0.5$  thus  $K(\bar{\beta}) = 1.66$ . The ratio of the magnitude of the  $\alpha$  relaxation in S-AN II to that in S-AN I was found to be<sup>†</sup>:

$$\frac{(\epsilon_{0\alpha} - \epsilon_{\infty\alpha})_{S-AN II}}{(\epsilon_{0\alpha} - \epsilon_{\infty\alpha})_{S-AN I}} = 1.26 \pm 0.02 \quad (2)$$

Similarly for the  $\beta$  relaxation:

$$\frac{(\epsilon_{0\beta} - \epsilon_{\infty\beta})_{S-AN II}}{(\epsilon_{0\beta} - \epsilon_{\infty\beta})_{S-AN I}} = 1.36 \pm 0.04 \quad (3)$$

† Further details are given in the SUP, Table 1.

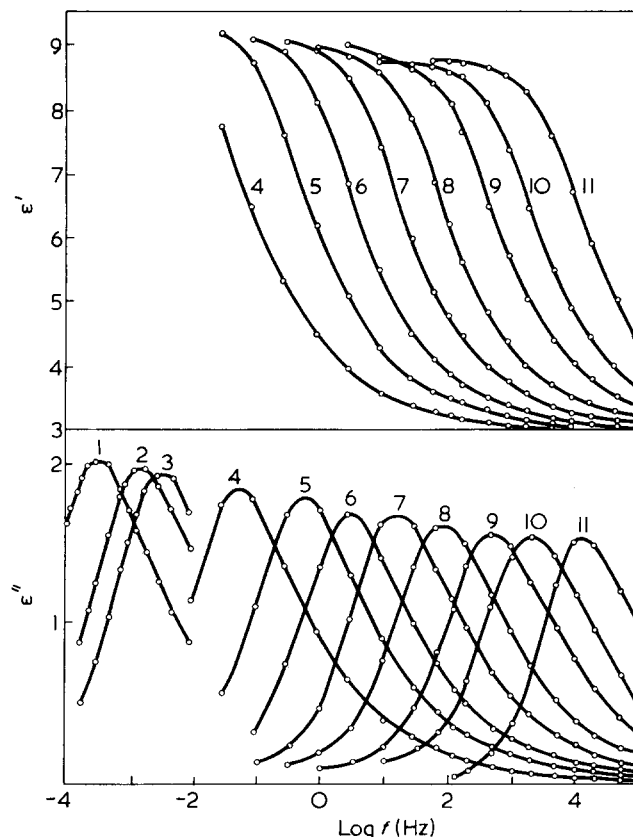


Figure 3  $\epsilon'$  and  $\epsilon''$  against  $\log$  (frequency) for the high temperature process in S-AN I. 1, 367; 2, 368; 3, 369; 4, 373; 5, 377; 6, 381; 7, 385.5; 8, 390; 9, 397; 10, 403; 11, 413 K

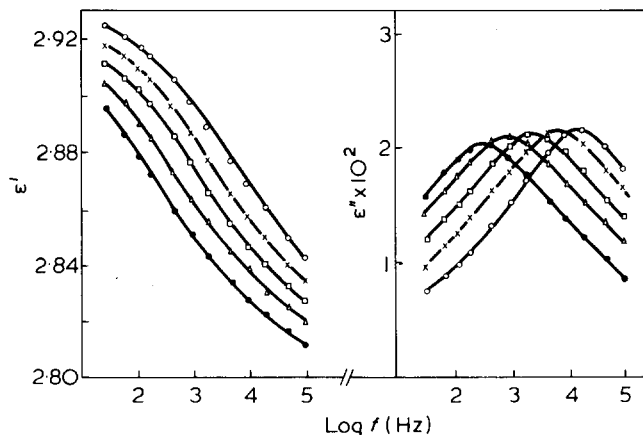


Figure 4  $\epsilon'$  and  $\epsilon''$  against  $\log$  (frequency) for the low temperature process in S-AN I.  $\circ$ , 233;  $\times$ , 223;  $\square$ , 213.5;  $\triangle$ , 203.5;  $\bullet$ , 194.5 K

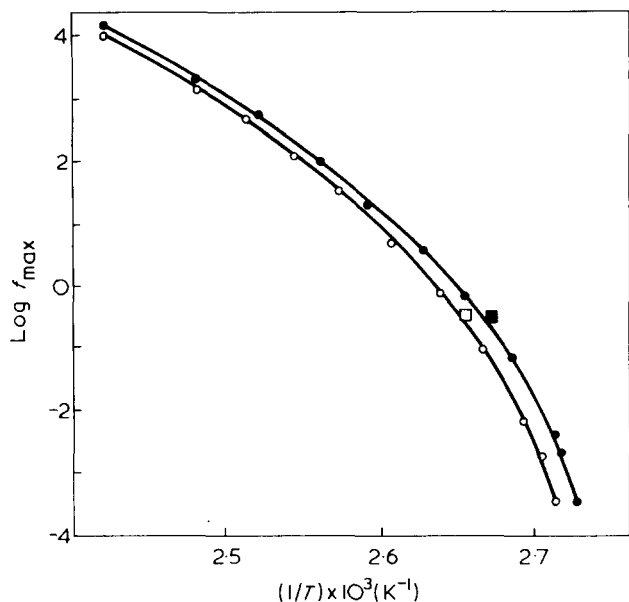


Figure 5 Log  $f_{\max}$  against  $1/T$  for the  $\alpha$  process in S-AN I and S-AN II. ● and ○, dielectric data; ■ and □, mechanical ( $\tan \delta$ ) data for S-AN I and S-AN II, respectively. The dielectric data relate to frequency of maximum  $\epsilon''$  at a given  $T$ ; the mechanical data relate to temperature of maximum  $\tan \delta$  from Figure 1 and Fig. 9 of SUP

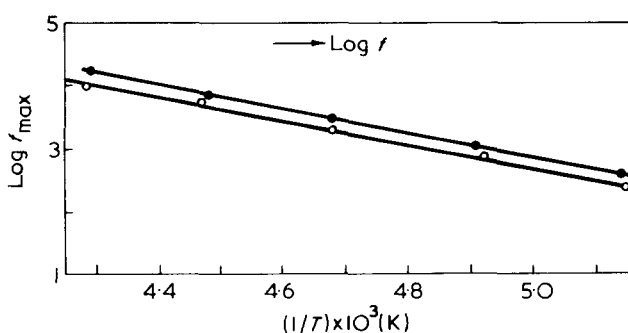


Figure 6 Log  $f_{\max}$  against  $1/T$  for the dielectric  $\beta$  process in S-AN I (●) and S-AN II (○)

These are to be compared with the known ratio of acrylonitrile contents in the two copolymers, being  $32.5/25 = 1.30$ . The good agreement suggests that the dielectric technique provides a convenient method for determining the acrylonitrile content in these copolymers, and also confirms that both the  $\alpha$  and  $\beta$  dielectric relaxations are associated with the motions of acrylonitrile groups in the copolymer.

#### Location

Figures 5 and 6 show the plots of  $\log f_{\max}$  against  $1/T(K)$  for the  $\alpha$  and  $\beta$  relaxations in S-AN I and S-AN II. First, the location of the  $\alpha$  process is quite similar for both polymers and the correlation between the dielectric data and mechanical data for the  $\alpha$  process is good, confirming that the same motional process is being observed by the two techniques, and that the dynamic  $T_g$  is nearly independent of composition for the range studied here. The  $\alpha$  process (Figure 5) shows WLF type behaviour while the  $\beta$  process (Figure 6) exhibits a constant apparent activation energy  $Q$ . Typical values are 300 kJ/mol at 413 K for the  $\alpha$  process in both copolymers, and 39 kJ/mol at 233 K for the  $\beta$  process in both copolymers.

#### Shape

The shape of the plots of  $\epsilon''_{\alpha}$  against  $\log f$  remains approximately constant as temperature is changed from 369 K to 413 K for both copolymers. Figures 7 and 8 show the normalized plots for both the dispersion and absorption in S-AN I and S-AN II. The excellence of the superposition should be noted. The complex dielectric permittivity in normalized form may be related to frequency according to<sup>2,6</sup>:

$$\frac{\epsilon'(\omega) - \epsilon_{\infty}}{\epsilon_0 - \epsilon_{\infty}} = \int_0^{\infty} \frac{\phi(\tau) d\tau}{1 + \omega^2 \tau^2} \quad (4a)$$

$$\frac{\epsilon''(\omega)}{\epsilon_0 - \epsilon_{\infty}} = \int_0^{\infty} \frac{\phi(\tau) \omega \tau d\tau}{1 + \omega^2 \tau^2} \quad (4b)$$

and the curves of Figures 7 and 8 could be fitted by choice of a suitable distribution function. However, such a procedure implies that the relaxation is to be regarded as a weighted sum of single relaxation time functions, which may not be the physical situation<sup>6</sup>. An alternative approach is to deduce the form of the transient step-response function  $\phi_{\alpha}(t)$  from the data of Figures 7 and 8 via the relation<sup>2,5,7</sup>:

$$\left[ \frac{\epsilon_0 - \epsilon'(\omega)}{\epsilon_0 - \epsilon_{\infty}} \right]_{\alpha} = \omega \int_0^{\infty} \phi_{\alpha}(t) \sin \omega t dt \quad (5a)$$

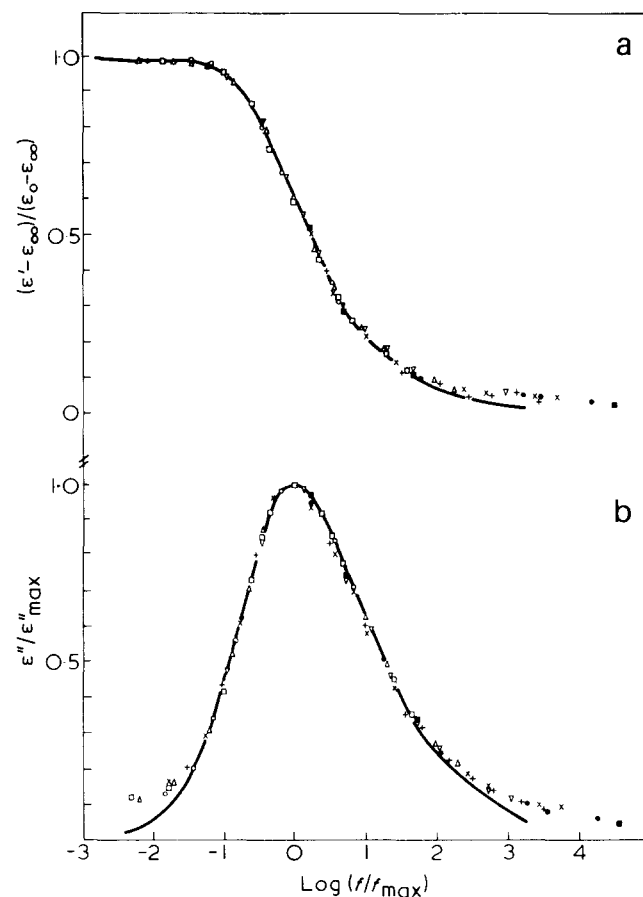


Figure 7 (a)  $(\epsilon' - \epsilon_{\infty})/(\epsilon_0 - \epsilon_{\infty})$  and (b)  $(\epsilon''/\epsilon''_{\max})$  against  $\log f/f_{\max}$  for the  $\alpha$  dielectric relaxation in S-AN I. ■, 373; ●, 377; +, 381; x, 385.5; ▽, 390; △, 397; □, 403; ○, 413 K

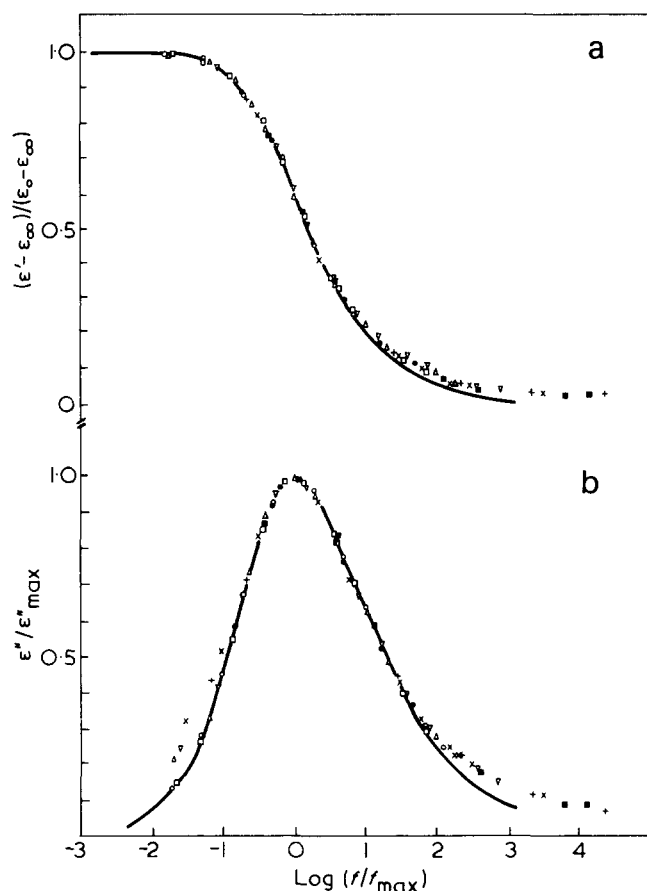


Figure 8 (a)  $(\epsilon' - \epsilon_\infty)/(\epsilon_0 - \epsilon_\infty)$  and (b)  $(\epsilon''/\epsilon''_{\max})$  against  $\log f/f_{\max}$  for the  $\alpha$  dielectric relaxation in S-AN II. ■, 375; ●, 379; +, 383.5; ×, 388.5; ▽, 393; △, 398; □, 403; ○, 413 K

$$\left[ \frac{\epsilon''(\omega)}{\epsilon_0 - \epsilon_\infty} \right]_\alpha = \omega \int_0^\infty \phi_\alpha(t) \cos \omega t dt \quad (5b)$$

$\phi_\alpha(t)$  may be obtained by Fourier inversion of equation (5) or by fitting  $\epsilon'(\omega)$  and  $\epsilon''(\omega)$  to an empirical form of  $\phi_\alpha(t)$ . We have found that the data of Figures 7 and 8 are fairly well represented by the function  $\phi_\alpha(t) = \exp - (t/\tau_0)^\beta$  where  $\beta = 0.5$  and the solid lines in Figures 7 and 8 were calculated using this function. The inadequacy of this representation is only apparent at  $\log(f/f_m) > 2$ , and means, of course, that the short-time behaviour of the empirical function is inconsistent with the experimental data for the  $\alpha$  relaxation, as was found for poly(vinyl acetate) and poly(vinyl octanoate)<sup>5</sup>. Inspection of Figures 5 and 6 shows that the  $\alpha$  relaxation has an appreciable overlap with the higher frequency portion of the  $\beta$  relaxation so the observation in Figures 7 and 8 that the observed loss exceeded the calculated loss may be associated with the  $\beta$  process.

## DISCUSSION

Both S-AN I and S-AN II show only one mechanical relaxation process and in both materials this occurs in the temperature range 343 to 393 K. The sudden fall in modulus and the accompanying maximum in mechanical damping is typical of amorphous polymers when they pass through a range of temperature where a group on the chain or segments of the chain pass from a state of im-

mobility, a frozen-in state, to one of comparative freedom or mobility with respect to the frequency of measurement. In the mobile state groups and chain segments will execute continual Brownian motion. The mechanical  $\alpha$  relaxation is related to motion at the molecular level by a rather complicated time-correlation function<sup>8</sup>. The dielectric  $\alpha$  and  $\beta$  relaxations are related to the time correlation function  $\langle \vec{M}(0) \cdot \vec{M}(t) \rangle$  where  $\vec{M}(t)$  is the macroscopic dipole moment of a suitably chosen assembly of dipoles<sup>6,7</sup>. In the absence of orientational correlations between polymer chains, which would be the case if the polymer molecules do not interpenetrate (see ref 9, pp 549–551), then this time correlation function may be expanded<sup>7</sup> in terms of autocorrelations  $\langle \vec{\mu}_i(0) \cdot \vec{\mu}_i(t) \rangle$  and cross-correlations  $\langle \vec{\mu}_i(0) \cdot \vec{\mu}_j(t) \rangle$  within a given polymer chain. The work of Leffingwell and Beuche<sup>10</sup> indicates that the time dependence of the auto- and cross-correlation functions are quite similar for styrene/*p*-chlorostyrene copolymers, and the fact that the curves of Figures 7 and 8 are essentially identical suggests that here too the auto- and cross-correlation functions have similar time dependencies. Williams *et al.*<sup>11</sup> have emphasized the similarity between the shapes of the  $\alpha$  relaxations in several polymers and copolymers and in certain supercooled liquids as was noted earlier by Johari and Smyth<sup>12,13</sup> and Johari and Goldstein<sup>14,15</sup>, and this has been reviewed recently<sup>16</sup>. Thus the present data for the  $\alpha$  relaxation (Figures 7 and 8) for styrene-acrylonitrile gives direct information on the dipole correlation function  $\langle \vec{\mu}_i(0) \cdot \vec{\mu}_i(t) \rangle$  for a reference dipole in the copolymer chain. Ignoring the internal field factors<sup>6,7</sup> which are involved in relating  $\langle \vec{\mu}_i(0) \cdot \vec{\mu}_i(t) \rangle$  to the complex permittivity, we have  $\langle \vec{\mu}_i(0) \cdot \vec{\mu}_i(t) \rangle \simeq \mu^2 \exp - (t/\tau_0)^{0.50}$ . The question now arises as to how one can interpret such behaviour in terms of a molecular model for the re-orientational process. The observation that the  $\alpha$  relaxation has similar characteristics in a wide range of materials<sup>2,10–16</sup> means that the detailed molecular structure, whilst it determines the magnitude of the relaxation process through  $\langle \mu^2 \rangle$  and the frequency of maximum loss at a given temperature, is not the dominant factor determining the form of dipole correlation function (i.e. the shape of the  $\epsilon''$  vs.  $\log f$  plot). We therefore look for mechanisms which are of quite general applicability to include S-AN and other systems.

One approach is to consider that the dipole in S-AN may only move if it is allowed to do so by the immediate environment. One mechanism would be that via the diffusion of a defect to the reference dipole from the environment. The defect-diffusion model of Glarum<sup>17</sup> as modified by Phillips *et al.*<sup>18</sup> leads to a correlation function:

$$\phi_\alpha(t') = \phi_0(t') [(1 - 2t')\phi_0(t') + 2(t'/\pi)^{1/2}] \quad (6)$$

where  $t' = t/\tau_\alpha$ ,  $\tau_\alpha$  is the defect-diffusion time, and  $\phi_0(t') = \exp(t') \operatorname{erfc}(t')^{1/2}$ . This correlation function, which is deduced for one dimensional diffusion of defects and takes into account nearest and second nearest neighbour defects, is numerically fitted<sup>19</sup> by the empirical decay function with  $\beta = 0.514$ . Then we might say that the gross motions of the acrylonitrile portions of the chain, which give rise to the  $\alpha$  relaxation, occur via the diffusion of 'defects' through the polymer medium. However, the model is one of one dimensional diffusion, and its generalization to the three-dimensional case gives results quite different<sup>20</sup> from equation (6).



DiMarzio and Bishop<sup>21</sup> have generalized the Debye theory for the re-orientation of a sphere to include a viscoelastic medium rather than a viscous medium. Their result differs from the Debye theory in that the relaxation time  $\tau$  is now replaced by  $\tau(\omega) = 3V\eta(\omega)/kT$ , where  $V$  is the volume of the (spherical) molecule and  $\eta(\omega) = G(\omega)/i\omega$ , where  $\eta$  and  $G$  are the viscosity and shear modulus respectively. DiMarzio and Bishop found that  $\tau(\omega)$ , using published  $G(\omega)$  data for several polymers, generated broad asymmetric loss curves similar to the experimental dielectric data for those polymers and, indeed, very similar to the present data (Figures 7 and 8). Whilst one might employ their approach to the S-AN systems, i.e. the characteristic broad shape arises since dipoles turn in a viscoelastic environment, the approach is a macroscopic one involving a sphere turning in a continuum, and its interpretation in molecular terms seems difficult.

There is little doubt that the relaxation behaviour observed here is best thought of in terms of the natural fluctuations in these amorphous systems. The equilibrium theory of fluctuations in volume, temperature, pressure and entropy for a subsystem of a macroscopic body is well established<sup>22</sup> and we have, for example, that the mean square temperature deviation  $\langle \Delta T^2 \rangle$  and mean square volume deviation  $\langle \Delta V^2 \rangle$  for  $N$  particles are given by:

$$\langle \Delta T^2 \rangle = \frac{kT^2}{C_v} \quad (7a)$$

$$\langle \Delta V^2 \rangle = -kT \left( \frac{\partial V}{\partial T} \right)_P \quad (7b)$$

These fluctuations provide a means whereby the segments of the polymer chains relax from a given initial orientation, but equation (7), being time-averaged quantities (i.e. equilibrium quantities) do not give any indication of the rate of the fluctuations or their evolution in time. Montrose and Litovitz<sup>23</sup> have considered structural relaxation in glass-forming molecular liquids using a model for fluctuations in local order which involve the diffusion of holes and a time constant  $\tau'_0$  (for the average time between molecular jumps). Their resultant relaxation function in time yields, on Fourier transformation, Argand diagrams for the frequency-dependent complex compliance which vary from a semi-circular arc (single relaxation time) for  $\sigma^2/(D\tau'_0) \rightarrow \infty$  ( $\sigma$  and  $D$  are a correlation length and the diffusion coefficient for the order respectively<sup>23</sup>), through a Cole-Debye-like function with  $\beta = 0.5$  for  $\sigma^2/(D\tau'_0) = 4$  to a very depressed arc for  $\sigma^2/(D\tau'_0) \rightarrow 0$ . Since  $\sigma^2/D$  characterizes the interval required for diffusion to effect an equilibration of the structure over the range  $\sigma$  then  $\sigma^2/(D\tau'_0)$  is the ratio of this interval to the 'intrinsic' jump time  $\tau'_0$ . Our data\* of Figures 7 and 8 may be fitted approximately by the function of Montrose and Litovitz<sup>23</sup> for  $\sigma^2/(D\tau'_0) \rightarrow 0$ . Physically this corresponds to the situation where the relaxation is determined by the diffusion of the fluctuations. Clearly there are similarities between the result of this model and that for the diffusion of defects given in equation (6) above.

\* Note that these data which are fitted quite accurately by our empirical function  $\beta = 0.50$  may be approximately fitted to the Davidson-Cole function<sup>24,25</sup> with  $\beta = 0.30$ .

Thus the general features of the  $\alpha$  process in the S-AN copolymers and other amorphous polymers may be consistent with a model of fluctuations or of defect-diffusion in which the dipolar chain segments relax not by their own intrinsic relaxation rate in a fixed environment, but as a cooperative motion between the segments and the environment in which the motions of the environment plays a dominant role. This is in accord with the observations of the dielectric  $\alpha$  relaxation in viscous molecular liquids<sup>16</sup>. With regard to the  $\beta$  process in the S-AN copolymers, whilst it arises due to the local motion of the dipolar groups, the large breadth of the process (Figure 4) precludes its interpretation in terms of any simple mechanism.

#### ACKNOWLEDGEMENTS

The authors acknowledge the assistance of personnel in the Research Department of Monsanto Chemicals and we thank the University College of Wales, Aberystwyth, for the award of a Research Assistantship to M.C. This work is published with the permission of Monsanto Chemicals, UK.

#### REFERENCES

- 1 Heijboer, J., Dekking, P. and Staverman, A. J. in 'Proceedings of the Second International Congress on Rheology', (Ed. V. G. W. Harrison), Academic Press, New York, 1954, p 123
- 2 McCrum, N. G., Read, B. E. and Williams, G. 'Anelastic and Dielectric Effects in Polymeric Solids', Wiley, New York and London, 1967, p 214
- 3 Hamon, B. V. *Proc. IEE* 1952, **99**, Part IV, Monogr. 27
- 4 Williams, G. and Watts, D. C. *Trans. Faraday Soc.* 1970, **66**, 80
- 5 Williams, G., Watts, D. C., Dev, S. B. and North, A. M. *Trans. Faraday Soc.* 1971, **67**, 1323
- 6 Williams, G. *Chem. Rev.* 1972, **72**, 55
- 7 Cook, M., Watts, D. C. and Williams, G. *Trans. Faraday Soc.* 1970, **66**, 2503
- 8 Zwanzig, R. A. *Rev. Phys. Chem.* 1965, **16**, 67
- 9 Vollmert, B. 'Polymer Chemistry', Springer-Verlag, Berlin, 1973
- 10 Leffingwell, J. and Bueche, F. J. *Appl. Phys.* 1968, **39**, 5910
- 11 Williams, G., Cook, M. and Hains, P. J. *JCS Faraday Trans. II* 1972, **68**, 1045
- 12 Johari, G. P. and Smyth, C. P. *J. Am. Chem. Soc.* 1969, **91**, 5168
- 13 Johari, G. P. and Smyth, C. P. *J. Chem. Phys.* 1972, **56**, 4411
- 14 Johari, G. P. and Goldstein, M. *J. Phys. Chem.* 1970, **74**, 2034
- 15 Johari, G. P. and Goldstein, M. *J. Chem. Phys.* 1970, **53**, 2372
- 16 Williams, G. in 'Dielectric and Related Molecular Processes', Specialist Periodical Reports of the Chemical Society, (Ed. M. Davies), The Chemical Society, London, 1975, Vol 2
- 17 Glarum, S. H. *J. Chem. Phys.* 1969, **33**, 639
- 18 Phillips, M. C., Barlow, A. J. and Lamb, J. *Proc. R. Soc. (A)* 1972, **329**, 193
- 19 Shears, M. F. and Williams, G. *JCS Faraday Trans. II* 1973, **69**, 1050
- 20 Bordewijk, P. *Chem. Phys. Lett.* in press
- 21 DiMarzio, E. A. and Bishop, M. J. *Chem. Phys.* 1974, **60**, 3802
- 22 Landau, L. D. and Lifshitz, E. M. 'Statistical Physics', Addison-Wesley, Reading, Mass., 1958
- 23 Montrose, C. J. and Litovitz, T. A. *J. Acoust. Soc. Am.* 1970, **47**, 1250
- 24 Davidson, D. W. and Cole, R. H. *J. Chem. Phys.* 1951, **19**, 1484
- 25 Davidson, D. W. *Can. J. Chem.* 1961, **39**, 571

# Migration of PVC plasticizers into alcohols

Emmanuel M. Kampouris, F. Regas, S. Rokotas, S. Polychronakis and M. Pantazoglou  
*Laboratory of Special Chemical Technology, National Technical University of Athens, Athens 147, Greece*

(Received 14 April 1975; revised 4 July 1975)

The use of labelled plasticizers and radioactivity measurements in conjunction with weight loss, can give quantitative information on the amount of migrated plasticizer, and on the amount of the liquid medium that diffuses into the polymer during the migration process. In the case of PVC plasticized with dibutyl phthalate and dioctyl phthalate and immersed in alcohols, the specimens soon become heterogeneous due to loss in compatibility between the polymer and the mixtures of plasticizer—alcohol high in alcohol. These mixtures are formed in the polymer as a result of continuous migration and diffusion processes. The following factors affecting the migration process were examined: nature of alcohol, nature of phthalate plasticizer, amount of plasticizer, molecular weight of polymer, thickness of specimens, presence of epoxy plasticizers, plasticization process, presence of stabilizers, temperature, and time.

## INTRODUCTION

The problem of plasticizer migration is of special interest in the case of polymers modified with considerable amounts of plasticizers. Of the common polymers PVC is the one used in the largest volume as flexible or plasticized PVC. Therefore any study on the plasticization and migration processes may be of practical importance for the PVC industry.

In all applications a plasticized polymer is in contact with some kind of surrounding medium. Under these conditions the plasticizer must stay in place during the useful life of the formed plastic item, otherwise it migrates with the result that (a) the polymer, because of loss of plasticizer, stiffens and becomes less desirable, and (b) the surrounding medium is contaminated by the plasticizer.

Thus there arises the need for a thorough study of factors affecting the migration process, and for a simple and accurate method of measuring amounts of plasticizer which may be present in a given medium.

The possible factors which can affect the migration process can be classified in relation to: (a) the polymer, i.e. nature, molecular weight, crystallinity; (b) the plasticizer, i.e. nature, amount, possible interactions (especially in the case of mixed plasticization systems); (c) the other components usually present in the plasticized polymer, i.e. stabilizers, lubricants, fillers; (d) the plasticization process and conditions, and therefore the homogeneity of the system; (e) the surrounding medium, i.e. nature, compatibility with the plasticizer, effect on polymer; (f) the conditions of the test, i.e. time, temperature, type of contact.

The plasticizer that migrates can be estimated as: the amount leaving the polymer, or the amount entering into the liquid. In the first case the amount can be measured by weight<sup>1</sup> or radioactivity<sup>2</sup> loss. In the second case the amount of plasticizer can be measured by chromatography<sup>3,4</sup>, spectrometry<sup>5</sup>, impulse-polarography<sup>6</sup>, and radioactivity<sup>7,8</sup>.

This paper presents the results, obtained by radiometric and weight loss methods, of a study of the effect of the

following factors upon the migration of phthalate plasticizers from plasticized PVC into alcohols: nature of alcohol, molecular weight of the polymer, nature of plasticizer, amount of plasticizer, presence of epoxy plasticizers, presence of stabilizers, plasticization process, thickness of specimens, temperature, and time.

## EXPERIMENTAL

### *Synthesis of labelled dibutyl phthalate (DBP)*

5 mg of labelled n-butanol (1-<sup>14</sup>C; 0.25 mCi) were diluted with n-butanol (28 ml) and added to a four-necked flask containing powdered phthalic anhydride (49 g). The flask was equipped with stirrer, thermometer, N<sub>2</sub> inlet tube, and a side condenser. The mixture was heated at 100°C for 1 h, then n-butanol (95 ml) and concentrated sulphuric acid (0.4 ml) were added, and the mixture was heated at 130°C for 3 h. During this period a slow stream of N<sub>2</sub> was passed and n-butanol was periodically added to make up for that distilling. After cooling, the reaction product was diluted with ether (500 ml) and the ethereal solution was washed with 10% aqueous sodium carbonate solution, then with water, and finally evaporated to remove ether and unreacted n-butanol. The diester was purified by vacuum distillation (yield 82 g of labelled DBP of radioactivity 4.8 × 10<sup>3</sup> counts/mg/min). Products with lower radioactivities were obtained by dilution with pure unlabelled DBP.

### *Synthesis of labelled dioctyl phthalate (DOP)*

The product was synthesized according to the literature method<sup>8</sup> from labelled phthalic anhydride (7-<sup>14</sup>C) and 2-ethylhexanol.

### *Preparation of specimens*

Suspension polymerized PVC was blended at 80°C with the calculated amounts of plasticizers and stabilizers. No

Table 1 Effect of the nature of alcohol upon the migration (mg) of plasticizers from plasticized PVC

Time (days)	Methanol		Ethanol		n-Propanol		Isopropanol		n-Butanol		Isobutanol		2-Ethylhexanol	
	DBP	DOP	DBP	DOP	DBP	DOP	DBP	DOP	DBP	DOP	DBP	DOP	DBP	DOP
1	152	57	101	163	73	241	51	82	74	260	47	84	26	94
2	255	82	152	209	110	340	87	119	110	399	81	125	37	135
4	344	110	265	274	175	450	147	153	181	518	138	163	54	178
6	399	140	338	319	230	527	189	181	239	588	174	194	69	224
10	452	187	422	396	322	616	256	230	324	663	217	242	78	274
15	484	228	470	464	401	627	308	275	387	705	252	288	115	325
20	506	254	491	516	444	718	349	307	433	736	280	329	133	361
25	521	272	506	551	475	742	376	332	464	754	308	350	147	390
30	528	282	514	575	497	751	392	354	485	762	332	371	161	412

lubricant was used. For stabilization Ba—Cd (1.5 phr) and alkyl aryl phosphite (0.5 phr) type stabilizers were used. The dry blend was then plasticized by hot working for 7 min in the mixing head of a Brabender Plasticorder at 160°C and 30 rev/min. The plasticized mass was then formed by hot rolling to a sheet from which specimens of 20 × 50 mm were cut.

#### Immersion

Each of the specimens was immersed in 250 ml of the liquid medium contained in a 300 ml glass-stoppered Erlenmeyer flask. The following alcohols were used as liquids: methanol, ethanol, 96% ethyl alcohol, n-propanol, isopropanol, n-butanol, isobutanol, and 2-ethylhexanol. All tests were made in duplicate, the flasks were kept at temperatures maintained to ±2°C, and the specimens were selected with weight differences not exceeding 100 mg.

#### Measurement

The radioactivity of the liquid medium, at a given time after immersion, was measured by transferring 0.5 ml of the content of the flasks to a glass measuring vial containing 10 ml of the scintillation solution, shaking to ensure complete solution, and measuring the radioactivity by means of a Packard Tri-Carb 3385 liquid scintillation spectrometer over a period of 10 min. The scintillation solution was made by dissolving 5 g of 2,5-diphenyloxazole (PPO) and 300 mg of 2,2'-p-phenylenebis(4-methyl-5-phenyloxazole)(Dimethyl-POPOP) in one litre of toluene. From each flask, two samples were taken thus each quoted result represents the average of four measurements. Corrections were made for background and quenching.

The radioactivity loss was calculated from radioactivity measurements of the specimens before and after immersion. In both cases about 10 mg of the specimens were dissolved in 1 ml of tetrahydrofuran, 10 ml of the scintillation solution were added, and the radioactivity was measured in the usual way. Efforts were made to obtain representative samples; all measurements were made in fivefold and the average obtained.

## RESULTS AND DISCUSSION

### Effect of the nature of alcohols

This effect was examined at 25°C using *k* 65 PVC plasticized with 50 phr DBP or DOP. The results obtained are given in Tables 1 and 2. As the data in Table 1 indicate, the amount of migrated DBP is high in the case of n-alcohols

Table 2 Effect of the nature of alcohol upon the migration (mg) of DBP and DOP from plasticized PVC: comparison of the results after 30 days of immersion

Alcohol	DBP				DOP			
	I	II	III	IV	I	II	III	IV
Methanol	545	528	289	239	275	282	124	158
Ethanol	538	514	227	287	582	575	317	258
n-Propanol	507	497	192	305	731	751	428	323
Isopropanol	417	392	164	228	372	354	126	228
n-Butanol	493	485	202	283	745	762	420	342
Isobutanol	312	332	145	187	378	371	133	238
2-Ethylhexanol	145	161	57	104	396	412	160	252

I = Migrated plasticizer, by radioactivity loss; II = migrated plasticizer by radioactivity of the alcohol; III = weight loss; IV = difference II - III (diffused alcohol)

and much lower with iso-alcohols. In both cases the greater the molecular weight of the alcohol, the lower is the amount of plasticizer. In the case of DOP the greater migration rates also occur with n-alcohols, but the effect of the molecular weight of is different. Now the greater the molecular weight n- or iso-alcohols, the greater is the amount of migrated plasticizer.

As the data in Table 2 indicate, the radioactivity loss method can give results approximately the same as obtained by measurements of the radioactivity of the liquid medium. Comparison between the results obtained by the weight loss method and that of the radioactivity of the liquid, for both DBP and DOP, indicates that in no case can the weight loss method be used for the measurement of the amount of migrated plasticizer. Correlation of the results of the two methods, supposing no other matter except plasticizer is migrated, can give quantitative information on the amount of the alcohol diffused into the polymer, during the migration process. In no case can the amount of diffused alcohol be related with the molecular weight. The only clear observation is that n-alcohols diffused in greater amounts than iso-alcohols both in the case of DBP and DOP. It also holds true that the lower alcohols diffused faster in PVC plasticized with DBP, while the higher alcohols diffused faster in PVC plasticized with DOP.

In most cases the specimens gradually lose their transparency and become opaque to white, during the migration process. This can be explained by the fact that the plasticizer-alcohol mixture, which plasticizes the polymer, becomes gradually a non-solvent for the polymer and

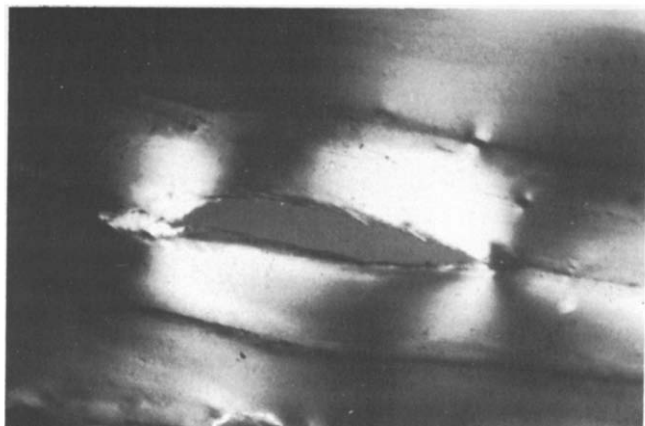


Figure 1 Formation of a long hole, a number of small ones, and lines of differentiation in the mass of PVC plasticized with 50 phr DBP and immersed in ethanol ( $\times 35$ )

Table 3 Effect of the amount of plasticizer upon the migration of DBP from plasticized PVC into ethanol at 30°C

Time (days)	Migrated plasticizer (mg)		
	20 phr	40 phr	60 phr
2	14	108	451
4	19	159	614
6	25	209	688
10	33	301	757
15	40	352	801
20	46	383	827
25	50	415	852
30	56	438	872
40	60	461	899
50	70	482	924
60	76	498	935
70	85	512	943
80	93	523	947
Initial plasticizer content (mg)	464	802	1050
Final plasticizer content (mg)	371	179	103
Final plasticizer content (phr)	16	9	6
Weight loss (mg)	78	180	517
Diffused alcohol (mg)	15	343	430

separates as a second phase in the mass. This is shown in the microphoto of Figure 1.

#### Effect of the nature of phthalate plasticizer

This effect was examined for both DBP and DOP, two common plasticizers with differences in molecular weight, viscosity and volatility. It is often stated, in examining the tendency of plasticizers to migrate, that the greater the molecular weight, the greater the viscosity, or the lower the volatility, the lower is the migration rate<sup>8-10</sup>. The data in Table 1 indicate that there is no firm relationship between molecular weight, viscosity, or volatility of plasticizer and the rate of the migration process. Generally only in the case of contact with methanol does DBP migrate faster than DOP, while the opposite is true in the other cases.

The nature of plasticizer affects the diffusion of alco-

hols exhibiting a selective action. As the data in Table 2 indicate, the lower alcohols diffuse faster in PVC plasticized with DBP, while the higher alcohols do so in PVC plasticized with DOP.

#### Effect of the amount of plasticizer

This effect was examined in the case of *k* 65 PVC plasticized with 20, 40 and 60 phr of DBP. The temperature of the test was 30°C, the duration 80 days, and the liquid medium ethanol. The results obtained are given in Table 3. As the data indicate the amount of plasticizer strongly affects the migration process and the greater the amount of plasticizer, the greater is the amount lost by migration. During the course of the process the migration rate was faster for the specimens plasticized with the greater amounts of plasticizer. The result was a reversal of the order and after a certain time the specimen with the greater amount of plasticizer ends up with the lowest amount. This behaviour can be explained only in cases of high diffusion rates. In the case examined it is evident that the greater the amount of plasticizer, the greater is the amount of diffused ethanol. At the end of the test the specimen plasticized with 20 phr DBP becomes plasticized with about 16 phr of a mixture containing 4% ethanol, the specimen plasticized with 40 phr becomes plasticized with about 26 phr of a mixture containing 65% ethanol, and finally the specimen plasticized with 60 phr DBP becomes plasticized with about 30 phr of a mixture containing 80% ethanol.

#### Effect of the molecular weight of the polymer

For this test four samples of PVC (*k* values 55, 65, 70, and 73 respectively) were plasticized with 50 phr DBP and immersed in ethanol at 30°C for 60 days. The results obtained are given in Table 4. As the data indicate the molecular weight of the polymer affects migration and the greater the molecular weight, the lower is the amount of migrated plasticizer.

#### Effect of the thickness of specimens

In some cases<sup>10,11</sup> short-time tests led to the conclusion that the thickness of specimens has little or no effect on the migration of plasticizers. In this test specimens of *k*

Table 4 Effect of the molecular weight of polymer upon the migration of DBP from plasticized PVC into ethanol at 30°C

Time (days)	Migrated plasticizer (mg)			
	<i>k</i> 55	<i>k</i> 65	<i>k</i> 70	<i>k</i> 73
2	256	203	156	90
4	330	275	205	135
6	377	327	244	170
10	410	370	285	199
15	435	401	324	235
20	450	419	348	260
25	459	425	360	276
30	464	435	370	284
35	469	440	376	298
40	473	445	381	310
45	476	450	385	319
50	480	453	392	326
55	483	457	398	331
60	486	460	405	335

**Table 5** Effect of the thickness of specimens upon the migration of DBP from plasticized PVC into ethanol

Time (days)	Migrated plasticizer (mg)			
	3040 mg	2381 mg	1785 mg	1483 mg
1	317	295	292	287
2	531	442	386	338
4	688	530	463	361
6	738	572	488	377
10	778	599	502	406
15	796	633	515	419
20	814	657	526	435
25	834	675	538	447
30	843	701	547	460
Initial plasticizer content (mg) 1000				
Final plasticizer content (mg) 157				
Final plasticizer content (phr) 7.7				
783				
578				
488				
82				
31				
28				
5.2				
3.5				
3.6				

**Table 6** Effect of epoxy plasticizer upon the migration of DBP and DOP from plasticized PVC into ethanol

Time (days)	Migrated DBP (mg)		Migrated DOP (mg)	
	0 phr	6 phr	0 phr	6 phr
2	186	219	178	223
4	244	269	240	297
6	270	296	282	347
10	302	331	327	402
15	317	360	349	437
20	327	373	360	451
25	333	381	377	460
30	342	384	383	469

65 PVC plasticized with 50 phr DBP were used immersed in ethanol at 30°C. For higher accuracy the weight of 20 × 50 mm specimens was used as an indication of thickness. The results in *Table 5* indicate that the greater the thickness of the specimens, the greater is the amount of migrated plasticizer. At the end of the test the major part of the plasticizer had migrated and the amount remaining was greater for the thicker specimens.

#### Effect of the epoxy plasticizer

In examining the effect of epoxy plasticizers upon the migration of the main (phthalate) plasticizer, specimens were made from *k* 65 PVC plasticized with 50 phr DBP or DOP and 6 phr of epoxy plasticizer (a commercial epoxidized soyabean oil). The specimens were immersed in ethanol for 30 days at 25°C. The results obtained are given in *Table 6*. As the data indicate, the epoxy plasticizer affects migration, promoting that of the main plasticizer. This behaviour seems to be selective; DOP migrates to a greater extent than does DBP.

#### Effect of the plasticization process

This effect was studied for *k* 65 PVC plasticized with 50 phr DBP and immersed in ethanol at 30°C for 60 days. The plasticization process generally used in this work was followed with variations in the time of hot working which

ranged from 2.5 to 15 min. As the data in *Table 7* indicate, differences in the plasticization process (due to variations in plasticization time) affect migration and the greater the working time, the lower is the amount of migrated plasticizer.

#### Effect of stabilization

This effect was examined for *k* 65 PVC plasticized with 60 phr DBP or DOP and immersed in 96% ethanol for 30 days at 25°C. In the case of non-stabilized PVC, plasticized with 60 phr DOP, two series of samples were prepared with different plasticization times, i.e. 7 and 15 min. The results in *Table 8* indicate that stabilization affects strongly the migration process, and the greater amounts are migrating from the stabilized specimens. In the case of unstabilized specimens the effect of the plasticization time is greater than in the case of stabilized ones.

#### Effect of temperature

The effect of temperature was studied in the case of *k* 65 PVC plasticized with 50 phr DBP and immersed in ethanol

**Table 7** Effect of the plasticization process upon the migration of DBP from plasticized DBP ethanol

Time (days)	Migrated plasticizer (mg)			
	2.5 min	5 min	10 min	15 min
2	230	213	208	202
4	327	307	280	262
6	370	352	321	297
10	421	392	368	335
15	445	416	392	380
20	452	430	417	398
30	462	441	425	415
40	467	449	431	424
50	472	459	437	432
60	477	461	442	437
Weight loss (mg) 294				
Ethanol diffused (mg) 183				
290				
171				
273				
169				
265				
172				

**Table 8** Effect of the presence of stabilizers upon the migration of DBP and DOP from plasticized PVC into 96% alcohol

Time (days)	Migrated plasticizer (mg)				
	I	II	III	IV	V
2	222	80	153	79	67
4	283	136	228	123	114
6	333	173	263	164	148
10	379	227	312	207	175
15	424	257	358	246	211
20	451	273	383	276	230
25	469	282	410	303	251
30	483	291	425	328	267

I = Normally stabilized PVC plasticized with 60 phr DBP; II = unstabilized PVC plasticized with 60 phr DBP; III = normally stabilized PVC plasticized with 60 phr DOP, plasticization time 7 min; IV = unstabilized PVC plasticized with 60 phr DOP, plasticization time 7 min; V = unstabilized PVC plasticized with 60 phr DOP, plasticization time 15 min

Table 9 Effect of the temperature upon the migration of DBP from plasticized PVC into ethanol

Time (days)	Migrated plasticizer (mg)		
	10°C	30°C	60°C
2	54	234	442
4	78	334	530
6	100	388	572
10	132	430	599
15	164	457	633
20	199	473	657
30	213	484	701

at temperatures ranging from 10° to 60°C. The results in Table 9 indicate that the temperature affects strongly the migration of plasticizer; any rise in temperature increases drastically the amount of migrated plasticizer. Thus 30 days of immersion at 10°C gave the same amount of migrated plasticizer, as 2 days at 30°C. Schematic presentation of the results leads to the conclusion that the relation temperature/amount of migrated plasticizer is not a linear one.

#### Effect of time

Examining the effect of time, in all the above cases, we can conclude that there is no linear relation between the amount of migrated plasticizer and time, or the square root of time. Contradictory results in the literature may

be explained by the small intervals of time. Generally the greatest migration rates occur in the first stages of the process. They become then lower and tend to minimize. For long enough periods the total amount of plasticizer can migrate, leaving the polymer plasticized, or swelled, by a mixture containing low amounts of plasticizer.

#### ACKNOWLEDGEMENTS

The authors wish to express thanks to Dr G. Akoyunoglou and Mr S. Daousis of the Biology Dept. of N.R.C. Democritos for counting the samples.

#### REFERENCES

- 1 Reed, M. C. and Harding, J. *Ind. Eng. Chem.*, 1949, **41**, 675
- 2 Kampouris, E. and Rokotas, S. unpublished data
- 3 Rost, H. E. *Fette, Seifen, Anstrichm.* 1970, **72**, 552
- 4 Rohleder, K. and Bruchhausen, B. V. *Dsch. Lebensm-Rundsch.* 1972, **68**,
- 5 Gutsalyul, V. G. and Samonova, N. S. *Izv. Akad. Nauk Kaz. SSR, Ser. Khim.* 1962, (2), 95
- 6 Woggon, H. and Koehler, U. *Kunststoffe* 1967, **57**, 583
- 7 Figge, K. and Piater, H. *Dsch. Lebensm-Rundsch.* 1971, **67**, 235
- 8 Kampouris, E. *4th Eur. Conf. Plast. Rubbers, Paris* 1974, Paper 91
- 9 Knappe, W. *Kunststoffe* 1962, **52**, 387
- 10 Quackenbos, H. M. *Ind. Eng. Chem.* 1954, **46**, 1335
- 11 Reed, M. C., Klemm, H. F. and Schultz, E. F. *Ind. Eng. Chem.* 1954, **46**, 1344

# Notes to the Editor

## Effect of temperature and molecular weight on the crystallization of a *cis*-1,4-butadiene/isoprene copolymer

Aurelio De Chirico

Laboratori Ricerche Polimeri, Snamprogetti-Diris, S. Donato Milanese, Milan, Italy  
(Received 19 March 1975, revised 19 May 1975)

### INTRODUCTION

The crystallization rates of polymers depend on their degree of structural regularity, crystallization temperature,  $T_c$ , and according to recent research<sup>1-7</sup> on molecular weight ( $MW$ ) and molecular weight distribution ( $MWD$ ).

There is a substantial dependence of the half-crystallization time,  $t_{1/2}$ , with  $MW$ , as has been found for high density polyethylene<sup>1</sup>, for *cis*-1,4-polyisoprene<sup>5,6</sup>, and *cis*-1,4-polybutadiene<sup>7</sup>.

As a contribution towards a better understanding of the role of  $MW$  on  $t_{1/2}$ , in polymers, the results obtained with a *cis*-1,4-butadiene/isoprene copolymer (7 mol % of isoprene) are now reported.

### EXPERIMENTAL

#### Dilatometry

The sample (~ 1 g) was placed in the cup of a dilatometer and was degassed at  $10^{-2}$  mmHg for about 2 h before the introduction of the mercury. The dilatometer assembly was kept at  $80^\circ\text{C}$  for 1 h and then placed in a cryostat at the predetermined  $T_c$ . During crystallization and fusion, the mercury level in the capillary was followed with a cathetometer. A heating rate of  $0.25^\circ\text{C}/\text{min}$  was maintained throughout the fusion.

#### Polymer sample

A *cis*-1,4-butadiene/isoprene copolymer with 7 mol % isoprene, was prepared using a catalyst based on  $\pi$ -allyl uranium derivatives<sup>8</sup>. The sample had the following characteristics:  $[\eta] = 3.85$  (dl/g) in toluene at  $30^\circ\text{C}$ ;  $\bar{M}_{\text{osm}} = 110\,000$ ; 1,4-trans(%) = 1.1; 1,2-vinyl(%) = 0.8; 1,4-*cis*(%) = 98.1.

#### N.m.r. spectra analysis

The isoprene content was determined from n.m.r. data using  $\text{CCl}_4$  as solvent.

### RESULTS AND DISCUSSION

The crystallization kinetics of the (*cis*-1,4-butadiene/isoprene) copolymer are highly accelerated by lowering

the  $T_c$  in the same way as has been reported for polybutadienes<sup>7</sup> with different 1,4-*cis* content.

The half-time of crystallization, the melting temperature,  $T_m^*$ , and the crystallinity, reported as  $\Delta V_{\text{sp}}$ , as a function of  $T_c$  are plotted in Figure 1. The  $t_{1/2}$  increases exponentially and  $\Delta V_{\text{sp}}$  decreases as  $T_c$  increases (i.e. faster kinetics and a higher degrees of crystallinity at lower  $T_c$  were obtained).

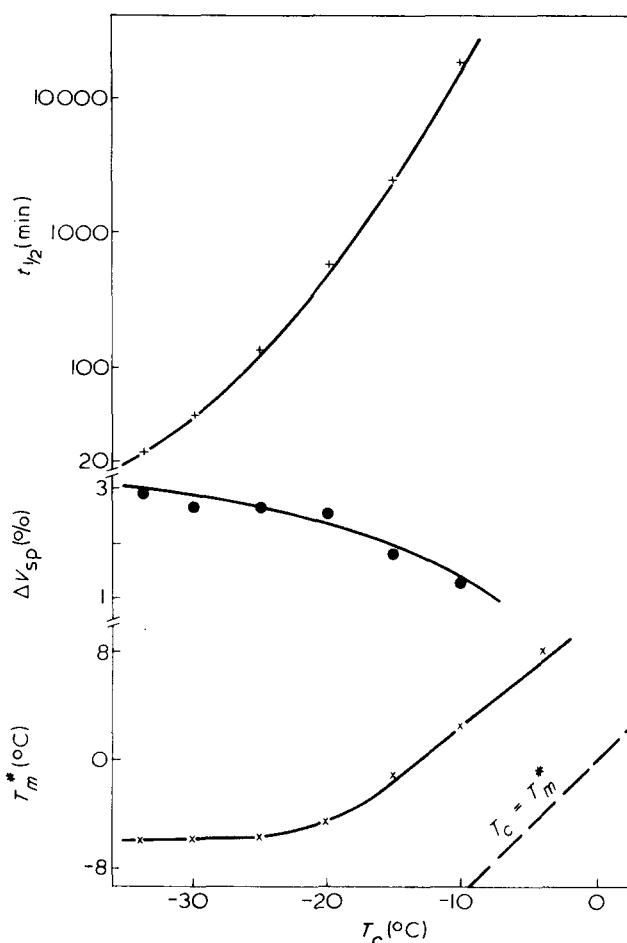


Figure 1 Melting point (X), crystallinity (●) and half crystallization time (+) versus crystallization temperature for the unfractionated *cis*-1,4-butadiene/isoprene copolymer

Table 1 Solution and bulk characteristics of fractions of a *cis*-1,4-butadiene/isoprene copolymer

Fraction	Weight (%)	$[\eta]$ (dl/g)	Isoprene (mol %)	$t_{1/2}$ at $-25^\circ\text{C}$ (min)	$n$	$T_m^*$ ( $^\circ\text{C}$ )
1	6.5	10.38	6	48	(2.2)	-5.4
2	4.95	9.30	6	95	3.6	-8.2
3	7.20	7.18	7.5	250	3.7	-7.8
4	10.23	5.23	7.5	580	2.5	-8.0
5	11.91	3.69	8.9	750	2.7	-8.0
6	11.48	2.78	6.5	1050	2.5	-8.0
7	10.68	2.26	8.6	630	3.0	-8.0
8	11.46	1.80	8.1	680	3.0	-8.0
9	9.62	1.46	7.8	350	3.9	-6.0
10	7.78	1.14	6.9	580	2.6	-5.0
11	8.18	0.66	7.8	180	3.3	-4.8
Whole copolymer		3.85	7.2	130	4.0	-5.8

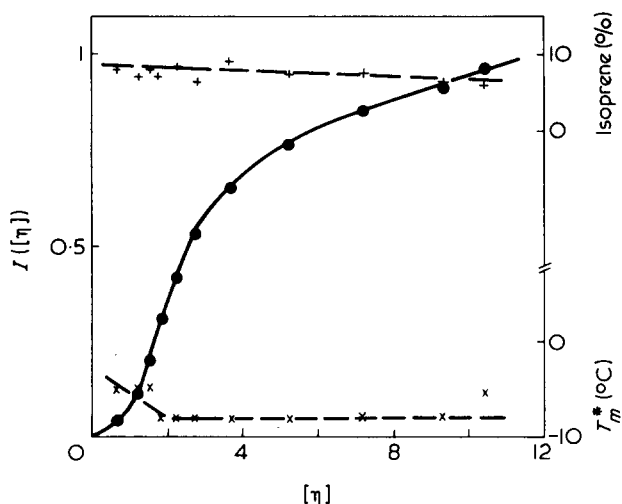


Figure 2 Integral MWD for *cis*-1,4-butadiene/isoprene copolymer (●), isoprene content (+), and melting point of the fractions (X) as a function of intrinsic viscosity

As noted for *cis*-1,4-polybutadiene<sup>7</sup>,  $T_m^*$  cannot be easily extrapolated against  $T_c$  in order to obtain the equilibrium melting temperature,  $T_m^0$ , (Figure 1). The slow rate of the isothermal crystallization kinetics at higher  $T_c$  does not allow other  $T_m^*$  values to be experimentally obtained which approach  $T_m^0$  more closely. This value can be obtained by trial and error by introducing the  $t_{1/2}$  and the corresponding  $T_c$  into the equation recently reported by Giuliani<sup>9</sup>. In this way it has been possible to obtain a  $T_m^0$  of  $22^\circ\text{C}$  for the *cis*-1,4-butadiene/isoprene copolymer used in this paper and a  $T_m^0$  of  $30^\circ\text{C}$  for *cis*-1,4-polybutadiene (99% *cis*-) on the basis of data previously published by us<sup>7</sup>.

In order to elucidate the relationship between bulk isothermal crystallization kinetics and *MW* we have fractionated this copolymer by the fractional precipitation technique. All fractions obtained were characterized by different techniques and the results are collected in Table 1. The isoprene content is essentially constant at around 7 mol %, and there is a large *MWD* (Figure 2).

Half-crystallization times of the fractions, measured at  $-25^\circ\text{C}$ , plotted against their intrinsic viscosities,  $[\eta]$ , show a parabolic shaped curve (Figure 3).

The effect of *MWD* on  $t_{1/2}$  is shown by the position of the point referred to the initial unfractionated sample in

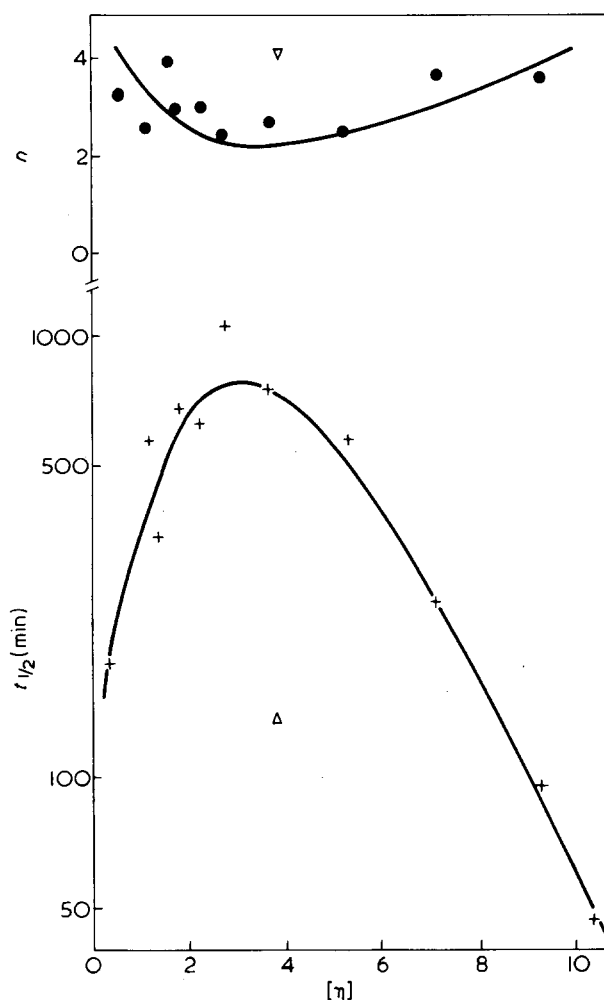


Figure 3 Half-crystallization time (+) at  $-25^\circ\text{C}$ , and Avrami index (●) for fractions and for unfractionated (Δ, ∇) *cis*-1,4-butadiene/isoprene copolymer versus intrinsic viscosity

the same Figure. The polydispersity accelerates  $t_{1/2}$  in some synthetic elastomers<sup>5-7</sup> and in natural rubber<sup>5</sup> at equal viscosity-average molecular weight. It appears that  $t_{1/2}$  of the polydispersed sample is determined by the fractions with highest crystallization rates. The melting temperature is essentially constant except for the last low *MW* fractions (Figure 2).



The Avrami index,  $n$ , shows a broad minimum for the fractions with the highest value of  $t_{1/2}$  (Figure 3). The same dependence of  $n$  with  $MW$  is shown more distinctly by *cis*-1,4-polybutadiene (99% *cis*)<sup>7</sup>. These results and others<sup>2-5,7</sup> previously reported confirm that the dependence of  $t_{1/2}$  on  $MW$  is also affected by a different nucleation mechanism.

#### ACKNOWLEDGEMENT

The author thanks Dr M. Bruzzone for useful discussions.

#### REFERENCES

- 1 Mandelkern, L., Fatou, J. G. and Ohno K. *J. Polym. Sci. (B)* 1968, **6**, 615
- 2 Magill, J. H. *J. Polym. Sci. (B)* 1968, **6**, 853
- 3 Lovering, E. G. *J. Polym. Sci. (A-2)* 1970, **8**, 1831
- 4 Turska, E. and Gogolewski, S. *Polymer* 1971, **12**, 629
- 5 De Chirico, A., Lanzani, P. C., Piro, M. and Bruzzone, M. *Chim. Ind. (Milano)* 1972, **54**, 35
- 6 Marej, A. I., Novikova, G. E., Petrova, G. P. and Tkachenko, G. T. *Int. Symp. Isoprene Rubber, Moscow* November 1972
- 7 De Chirico, A., Lanzani, P. C., Raggi, E. and Bruzzone, M. *Makromol. Chem.* 1974, **175**, 2029
- 8 Lugli, G., Mazzei, A. and Poggio, S. *Makromol. Chem.* 1974, **175**, 2021
- 9 Giuliani, G. P. and Sorta, E. *J. Polym. Sci. (B)* 1974, **12**, 375

# SCIENCE & PUBLIC POLICY

the international journal of the Science Policy Foundation

current awareness for busy people in

**government · industry · business ·  
education · research**

#### SCIENCE & PUBLIC POLICY

- provides information on national policies for science and technology and their effects
- examines the roles of science and technology in the operations of government (local, national and international), industry and business
- analyses the social and political environments within which science and technology operate
- assesses appropriate methodologies, information systems and organisational forms
- explores various types of public participation and their influence on national and international policies

The journal contains short, pithy news items, concise reports, comment, commissioned reviews, facts in figures, book reviews and extensive bibliographies.

The information is gathered through a worldwide network of national correspondents who are intimately involved in researching and applying science and public policy in their country.

Subscription £25.00 (\$65.00) per year (12 issues) including postage by fastest route. A special annual rate of £10.00 (\$26.00) is available for the individual who certifies that the copies are for his/her personal use and who is the full-time employee of a current full-price establishment subscriber at the same address.

**IPC Business Press Ltd, Oakfield House, Perrymount Road,  
Haywards Heath, Sussex, England**

*Published monthly by IPC Science and Technology Press Ltd:  
publishers of FUTURES, ENERGY POLICY and RESOURCES  
POLICY.*

# Temperature dependence of the unperturbed dimensions of poly(*p*-biphenyl methacrylate)

N. Hadjichristidis

Department of Industrial Chemistry, University of Athens, 13A Navarinou Street, Athens 144, Greece  
(Received 9 June 1975; revised 24 June 1975)

## INTRODUCTION

The temperature coefficient of the unperturbed dimensions,  $d\ln\langle r_0^2 \rangle/dT$ , has a fundamental importance in the analysis of chain configuration of macromolecules<sup>1-5</sup>. This coefficient may be positive<sup>6-8</sup>, zero<sup>9,10</sup> or negative<sup>11-13</sup> depending on the polymer and on the solvent<sup>14</sup>. In order to correlate this thermal coefficient with the chemical structure of the side groups of some polymethacrylate esters, we present here the results for poly(*p*-biphenyl methacrylate).

## EXPERIMENTAL

The synthesis of the monomer, the preparation and the fractionation of poly(*p*-biphenyl methacrylate) have been published elsewhere<sup>15</sup>. Five fractions, F1 to F5, were selected for the work reported here. The fractions were analysed by gel permeation chromatography at 25°C in tetrahydrofuran (THF) with a Waters GPC 200 instrument. The polydispersity was 1.3 to 1.4.

Viscosities in benzene at various temperatures, 12.5°C to 60°C, were measured in a new type of sealed capillary viscometer<sup>16</sup> designed to have negligible kinetic energy correction. Solutions were prepared by weight and the concentration was corrected for the change of density with temperature.

Light scattering measurements were carried out at 25°C in benzene with a Sofica apparatus at 5460 Å. Dust free solutions and solvent were obtained by filtration through a flotron membrane. The refractive index increment,  $dn/dc$ , under the same conditions, measured with a differential refractometer was  $0.113 + 0.001 \text{ cm}^3/\text{g}$ .

## RESULTS AND DISCUSSION

The weight-average molecular weight,  $\bar{M}_w$  and the intrinsic viscosities,  $(\eta)$ , in benzene at different temperatures are given in Table 1. The experimental values of the constants for the Mark-Houwink equation:

$$(\eta) = K_a \bar{M}_w^a$$

have been established at different temperatures by plotting

data of  $(\eta)$  against  $\bar{M}_w$  on log-log coordinates. The results are given in Table 2.

By plotting the values of  $a$  vs.  $T$  (Figure 1) and extrapolating at  $a = 0.5$  we obtain the  $\theta$ -temperature of poly(*p*-biphenyl methacrylate) in benzene (11°C).

The value of  $K_\theta$  leading to the unperturbed dimension  $\langle r_0^2 \rangle$ :

$$K_\theta = \Phi (\langle r_0^2 \rangle / M)^{3/2} \quad (1)$$

has been calculated by the well known and simple Stockmayer-Fixman relation<sup>17</sup>:

$$(\eta)M^{-1/2} = K_\theta + 0.51B\Phi M^{1/2}$$

The plots of  $(\eta)\bar{M}_w^{-1/2}$  vs.  $\bar{M}_w^{1/2}$  are linear in the entire molecular weight range.

Variation of  $K_\theta$  with temperature is given in Figure 2. As shown in Figure 2,  $K_\theta$  increases with increasing temperature but more rapidly in the range from 12.5° to 40°C ( $d\ln K_\theta/dT = 3.5 \times 10^{-3}$ ) than in the range from 40° to 60°C ( $d\ln K_\theta/dT = 1.8 \times 10^{-3}$ ).

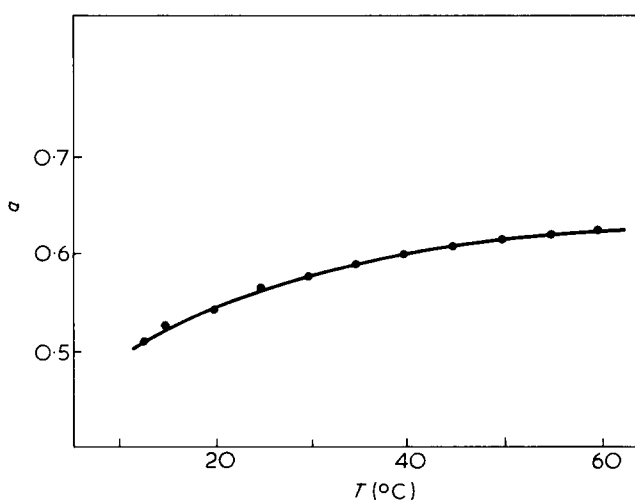


Figure 1 Plot of  $a$  against temperature for poly(*p*-biphenyl methacrylate) in benzene

Table 1 Intrinsic viscosity values (g/dl) of poly(*p*-biphenyl methacrylate) in benzene at different temperatures

Fraction	$\bar{M}_w \times 10^{-6}$	Temperature (°C)										
		12.5°	15°	20°	25°	30°	35°	40°	45°	50°	55°	60°
F1	1.080	0.487	0.515	0.555	0.605	0.650	0.685	0.720	0.750	0.766	0.775	0.795
F2	0.530	0.330	0.350	0.375	0.400	0.425	0.435	0.460	0.470	0.480	0.490	0.500
F3	0.460	0.310	0.330	0.350	0.370	0.390	0.410	0.415	0.430	0.445	0.450	0.465
F4	0.195	0.200	0.205	0.215	0.225	0.235	0.245	0.250	0.255	0.260	0.265	0.270
F5	0.081	0.127	0.130	0.135	0.141	0.145	0.150	0.154	0.156	0.158	0.160	0.163

**Table 2** Constants of the Mark-Houwink relation in benzene at different temperatures

$T$ ( $^{\circ}\text{C}$ )	$K_a \times 10^4$ (dl/g)	$a$
12.5	4.00	0.51
15	3.26	0.53
20	2.85	0.54 <sub>5</sub>
25	2.20	0.57
30	2.06	0.58
35	1.87	0.59
40	1.70	0.60
45	1.54	0.61
50	1.48	0.61 <sub>5</sub>
55	1.41	0.62
60	1.35	0.62 <sub>5</sub>

From equation (1), temperature coefficient of  $\langle r_0^2 \rangle$  is obtained by:

$$d\ln\langle r_0^2 \rangle/dT = (2/3)d\ln K_{\theta}/dT$$

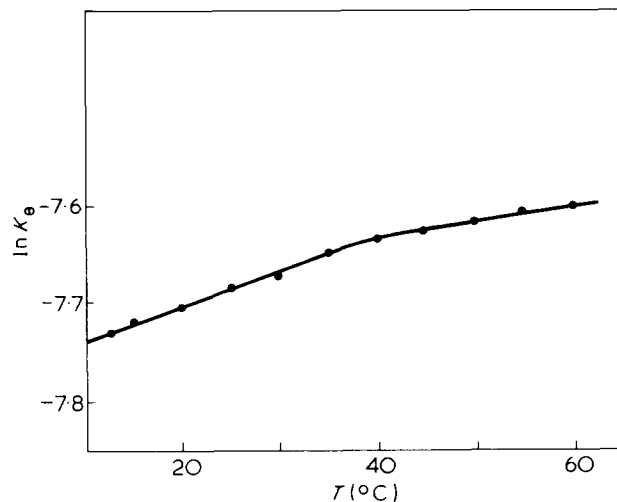
Consequently the value of the thermal coefficient of  $\langle r_0^2 \rangle$  is  $2.3 \times 10^{-3}$  (from  $12.5^{\circ}$  to  $40^{\circ}\text{C}$ ) and  $1.2 \times 10^{-3}$  (from  $40^{\circ}$  to  $60^{\circ}\text{C}$ ). This dependence of  $d\ln\langle r_0^2 \rangle/dT$  from the temperature has been reported elsewhere<sup>18,19</sup>.

#### ACKNOWLEDGEMENT

The author is gratefully indebted to Professor V. Desreux for permission to carry out part of the experimental work in his laboratories at Liège University.

#### REFERENCES

- 1 Ciferri, A., Hoeve, C. A. J. and Flory, P. J. *J. Am. Chem. Soc.* 1961, **83**, 1015
- 2 Flory, P. J., Crescenzi, V. and Mark, J. E. *J. Am. Chem. Soc.* 1964, **86**, 146
- 3 Mark, J. E. and Flory, P. J. *J. Phys. Chem.* 1965, **87**, 1415



**Figure 2** Plot of  $\ln K_{\theta}$  against temperature for poly(*p*-biphenyl methacrylate) in benzene

- 4 Abe, A., Jernigan, R. L. and Flory, P. J. *J. Phys. Chem.* 1966, **88**, 631
- 5 Flory, P. J., Mark, J. E. and Abe, A. *J. Phys. Chem.* 1966, **88**, 639
- 6 Orofino, T. A. and Ciferri, A. *J. Phys. Chem.* 1964, **68**, 3136
- 7 Mark, J. E. and Flory, P. J. *J. Am. Chem. Soc.* 1964, **86**, 138
- 8 Mark, J. E. and Flory, P. J. *J. Am. Chem. Soc.* 1965, **87**, 1423
- 9 Izumi, Y. and Miyake, Y. *Polym. J.* 1973, **4**, 205
- 10 Tani, S., Hamada, F. and Nakazima, A. *Polym. J.* 1973, **5**, 86
- 11 Sitaramaiah, G. and Jacobs, D. *Makromol. Chem.* 1973, **164**, 937
- 12 Moraglio, G., Gianotti, G. and Bonicelli, U. *Eur. Polym. J.* 1973, **9**, 623
- 13 Mark, J. E. and Thomas, G. B. *J. Phys. Chem.* 1966, **70**, 3588
- 14 Abe, M. and Fujita, H. *J. Phys. Chem.* 1965, **69**, 3263
- 15 Alexopoulos, J. B., Hadjichristidis, N. and Vassiliadis, A. *Polymer* 1975, **16**, 386
- 16 Desreux, V. to be published
- 17 Stockmayer, W. and Fixman, M. *J. Polym. Sci. (C)* 1963, **1**, 137
- 18 Noda, I., Mizutani, K., Kato, T., Fuzimoto, T. and Nagasawa, M. *Macromolecules* 1970, **3**, 787
- 19 Utracki, L. A. and Simha, R. *Makromol. Chem.* 1968, **117**, 94

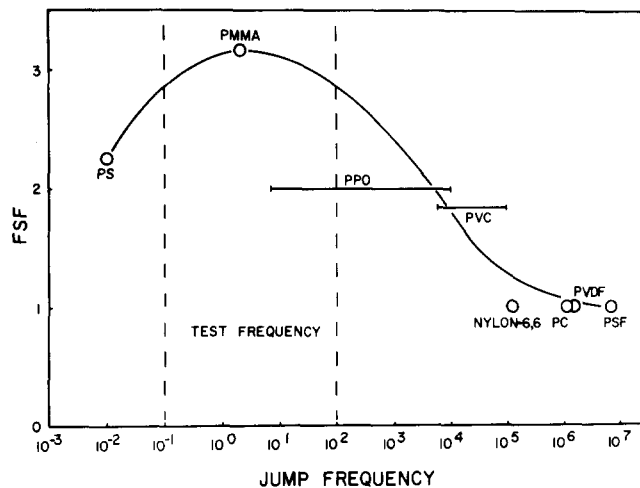
## The $\beta$ transition and frequency sensitivity in fatigue crack propagation of polymers

During the past decade, it has become clear that a number of mechanical phenomena in polymers are closely related to the location (in terms of temperature and frequency) and other characteristics of the  $\beta$  transition. As discussed by Oberst<sup>1</sup>, Heijboer<sup>2,3</sup>, Boyer<sup>4</sup>, and Vincent<sup>5</sup>, impact strength often undergoes a transition in the region of the  $\beta$  relaxation. Retting<sup>6</sup> and Bauwens<sup>7</sup> have shown that the yield stress of PVC is related to the relative position and intensity of the test conditions with respect to the  $\beta$  transition. Broutman and Kobayashi<sup>8</sup> observed that the fracture energy of PMMA was directly related to both the  $\alpha$  (glass) and  $\beta$  (secondary) transitions. Johnson and Radon<sup>9,10</sup>, have also shown that the time to failure in static tests with PMMA and PVC (at the ductile–brittle transition temperature) is approximately equal to the relaxation time of the  $\beta$  process at the same temperature. In this communication we wish to report an apparent correlation between the frequency dependence of fatigue crack propagation (*FCP*) in polymers and the frequency of the  $\beta$  transition at the test temperature concerned.

As part of a continuing study on *FCP*, an examination of the role of frequency, wave-form, and time under load was begun<sup>11</sup>. It was noted that the sensitivity of *FCP* to frequency varied widely from polymer to polymer. Thus, the crack growth rates of polycarbonate (PC) and nylon-6,6 were little affected by changing the frequency from 0.3 Hz to 10 Hz, while 2-fold to 3-fold effects (lower crack growth rates the higher the frequency) were observed for several other polymers such as PMMA and polystyrene(PS).

On examination of the data, it was then found that the behaviour appeared to be correlated with the estimated frequency of motion of the segments concerned with the  $\beta$  process at room temperature ( $\sim 300$  K). Values of this frequency were estimated by extrapolating or interpolating existing data gathered as follows: for PMMA, PC, PS, PVC, poly(vinylidene fluoride) (PVDF), and nylon-6,6 by McCrum *et al.*<sup>12</sup>; for poly(propylene oxide) (PPO) by de Petris *et al.*<sup>13</sup>, Stoelting *et al.*<sup>14</sup> and Eisenberg and Cayrol<sup>15</sup>; and for polysulphone (PSF) by Butta *et al.*<sup>16</sup>. To characterize frequency response, a frequency sensitivity factor (*FSF*) was defined as the multiple by which the *FCP* rate changes per decade change in frequency. Values of *FSF* were determined at low mean stress levels ( $R \leq 0.1$ , where  $R = K_{\min}/K_{\max}$ ,  $K$  being the stress intensity factor) in the range of intermediate crack velocities (around  $10^{-5}$  cm/cycle). *Figure 1* shows the relationship between the *FSF* and the frequency of the  $\beta$  process at the test temperature, and also indicates the range of frequencies used in the fatigue tests.

From the data presented, it certainly seems likely that the greatest sensitivity of *FCP* frequency occurs when the test frequency is close to the frequency of the  $\beta$  process. In all of the insensitive materials, the  $\beta$  frequency is far above the test range, while with the more sensitive materials the  $\beta$  frequency tends to be close to or within the test range. While a precise mechanistic explanation of the behaviour is not yet available, it seems likely that the



*Figure 1* Relationship between *FCP* frequency sensitivity and the room temperature jump frequency for several polymers

behaviour reflects indirectly the tendency of a given polymer to undergo a crazing type of response, at least under the conditions used in these tests<sup>17</sup>. Thus all the polymers exhibiting high values of the *FSF* tend to fail through crazes under the test conditions used, while the other polymers do not. With the more sensitive polymers, a higher frequency may well inhibit the craze-related failure mechanism.

### Acknowledgements

The authors wish to acknowledge discussions with Dr R. F. Boyer, who suggested the examination of  $\beta$  frequencies, and support by the Army Research Office, Durham, Grant Number DAHCO4 74G0010.

J. A. Manson, R. W. Hertzberg,  
S. L. Kim and M. Skibo

*Materials Research Center  
Lehigh University,  
Bethlehem, Pa 18015, USA  
(Received 19 August 1975)*

### References

- 1 Oberst, H. *Kunststoffe* 1963, **53**, 1
- 2 Heijboer, J. *J. Polym. Sci. (C)* 1968, **16**, 3755
- 3 Heijboer, J. *Br. Polym. J.* 1969, **1**, 3
- 4 Boyer, R. F. *Polym. Eng. Sci.* 1968, **8**, 161
- 5 Vincent, P. I. *Polymer*, 1974, **15**, 111
- 6 Retting, W. *Eur. Polym. J.* 1970, **6**, 853
- 7 Bauwens, J. C. *J. Polym. Sci. (C)* 1971, **33**, 123
- 8 Broutman, L. J. and Kobayashi, T. *Int. Conf. Dynamic Crack Propagation, Lehigh University*, 1972
- 9 Johnson, F. A. and Radon, J. C. *Eng. Fract. Mech.* 1972, **4**, 555
- 10 Radon, J. C. *Polym. Eng. Sci.* 1972, **12**, 425
- 11 Hertzberg, R. W., Manson, J. A., and Skibo M., *Polym. Eng. Sci.* 1975, **15**, 252
- 12 McCrum, N. G., Read, B. E. and Williams, G. 'Anelastic and Dielectric Effects in Polymeric Solids', John Wiley, New York, 1967

- 13 De Petris, S., Frosini, V., Butta, E. and Baccarreda, M. *Makromol. Chem.* 1967, **109**, 54  
 14 Stoelting, J., Karasz, F. E. and MacKnight, W. J. *Polym. Eng. Sci.* 1970, **10**, 133  
 15 Eisenberg, A. and Cayrol, B. *J. Polym. Sci. (C)*, 1971, **35**, 129  
 16 Butta, E., de Petris, S. and Pasquini, M. *Ric. Sci.* 1968, **38**, 927  
 17 Kambour, R. P. *J. Macromol. Sci. (Macromol. Rev.)* 1973, **7**, 1  
 18 Rabinowitz, S. and Beardmore, P. *CRC Crit. Rev. Macromol. Sci.* 1972, **1**, 1

### Estimation of the correlation length in polymer melts from nuclear magnetic relaxation dispersion

In this communication we use nuclear magnetic relaxation dispersion measurements for the estimation of the medium length of unidirectional chain orientation in poly(ethylene oxide) melts. This length is considered to be a characteristic size of the short-range order. Thus, a contribution to the discussion of the microstructure in polymer melts can be expected by this kind of investigation.

Molecular motion of molten polymers is anisotropic. We expect a rapid segment re-orientation fluctuation around the chain axis: this type of motion is connected with the diffusion of defects (e.g. kinks and torsions<sup>1</sup>) and will not completely destroy the autocorrelation of the dipolar interaction<sup>2</sup>. Considering for the moment only this anisotropic segment fluctuation process, we can express the unnormalized time autocorrelation function as the sum of a time dependent function  $G_s(\tau)$ , decreasing to zero at infinite times  $\tau$ , and a constant term  $|\bar{R}|^2$ , characterizing the anisotropy of the motion. ( $|\bar{R}|^2$  would be zero for isotropic motions.)

The remaining correlation  $|\bar{R}|^2$  will be finally reduced to zero by any further process which completely destroys the memory to the initial chain orientation at a reference segment. We now define a correlation function  $\bar{R}(0)R^*(\tau)$  concerning this superimposed process. Assuming this type of motion to be slow compared with segment fluctuation, we may write for the total correlation function:

$$G(\tau) \approx G_s(\tau) + \overline{R(0)R^*(\tau)} = G_s(\tau) + |\bar{R}|^2 \tilde{G}_c(\tau) \quad (1)$$

where we have introduced  $\tilde{G}_c(\tau)$  as the normalized autocorrelation function for the second process. [ $G_s(\tau)$  is the time dependent contribution of segment re-orientation to the total correlation function.]

The dominant type of motion responsible for the final disorientation of the reference chain part is expected to be the longitudinal chain diffusion or 'reptation' defined by de Gennes<sup>3</sup>. The reference segment diffuses via defect diffusion on a curvilinear path along the chain's spatial configuration. After a certain diffusion path, the correlation to the initial segment orientation will be lost. Therefore, the time correlation function  $G_c(\tau)$  consists of a configurational and a motional part.

We write:

$$\tilde{G}_c(\tau) = \int_{-\infty}^{\infty} C(X)\eta(X, \tau) dX \quad (2)$$

where  $C(X)$  is the normalized orientation correlation function (with respect to the spatial coordinate dependent function  $R$ ), and  $\eta(X, \tau)$  is the probability that the reference segment diffuses a distance  $X$  during a period  $\tau$ . Thus, the time correlation function  $G_c(\tau)$  is connected with a configurational correlation function.

The simplest, i.e. exponential, correlation function results if the stochastic problem is Poisson like. We therefore assume:

$$C(X) = \exp(-|X|/l) \quad (3)$$

where  $l$  is the orientation correlation length. The solution of the one-dimensional diffusion equation yields:

$$\eta(X, \tau) = \frac{1}{2(\pi D_1 |\tau|)^{1/2}} \exp(-X^2/4D_1 |\tau|) \quad (4)$$

$D_1$  is the one-dimensional (i.e. curvilinear) diffusion coefficient of segments).

We find from equations (2) to (4):

$$\tilde{G}_c(\tau) = \exp(D_1 |\tau|/l^2) \{1 - \text{erf}[(D_1 |\tau|)^{1/2}/l]\} \quad (5)$$

in agreement with the function found by Hunt and Powles<sup>4</sup> for a similar problem.

In the frequency range, slow compared with segment fluctuation rates, we obtain for the intensity function by Fourier transforming equation (1):

$$I(\omega_L) = I_s(\omega) + |\bar{R}|^2 \frac{\tau_l^{1/2}}{\omega_L^{1/2}(1 + 2\omega_L^{1/2}\tau_l + 2\omega_L\tau_l)} \quad (6)$$

with  $\tau_l = l^2/2D_1$ . The constant term  $I_s(\omega)$  arises from segment fluctuation.

For the longitudinal relaxation rate it holds then<sup>5</sup>:

$$\frac{1}{T_1} = |\bar{R}|^2 \left[ k + \frac{\tau_l^{1/2}}{\omega_L^{1/2}(1 + 2\omega_L^{1/2}\tau_l^{1/2} + 2\omega_L\tau_l)} + \frac{4\tau_l^{1/2}}{(2\omega_L)^{1/2}[1 + 2(2\omega_L\tau_l)^{1/2} + 4\omega_L\tau_l]} \right] \quad (7)$$

The constant  $k$  contains the contribution of segment re-orientation in the extreme narrowing condition (divided by  $|\bar{R}|^2$ ). In this equation we have three parameters:  $\tau_l$ ,  $k$  and  $|\bar{R}|^2$ . The latter merely influences the absolute value of the relaxation rate and can therefore easily be fitted to experimental values.

In Figure 1 the experimental  $T_1$ -dispersion of poly(ethylene oxide) melts is plotted in the range  $\omega_L = 5 \times 10^4 \dots 5 \times 10^6$  Hz. The data are taken from ref.6 and were obtained by the aid of a field modulation technique<sup>7</sup>.

Typical orders of magnitude for segment re-orientation rates for this kind of polymers were found to be in the range  $10^{10} \dots 10^{12}$  Hz<sup>8,9</sup>. Thus, even if this re-orientation process is 'broadened' by environmental fluctuations<sup>2</sup>, we may assume the extreme narrowing case for the segmental contribution, and equation (7) can be used for the interpretation of the measurements.

Good agreement between the theoretical and the experimental slope of the dispersion curves was found for  $\tau_l \leq 2.6 \times 10^{-8}$  sec. In order to derive the curvilinear dif-

- 13 De Petris, S., Frosini, V., Butta, E. and Baccarreda, M. *Makromol. Chem.* 1967, **109**, 54  
 14 Stoelting, J., Karasz, F. E. and MacKnight, W. J. *Polym. Eng. Sci.* 1970, **10**, 133  
 15 Eisenberg, A. and Cayrol, B. *J. Polym. Sci. (C)*, 1971, **35**, 129  
 16 Butta, E., de Petris, S. and Pasquini, M. *Ric. Sci.* 1968, **38**, 927  
 17 Kambour, R. P. *J. Macromol. Sci. (Macromol. Rev.)* 1973, **7**, 1  
 18 Rabinowitz, S. and Beardmore, P. *CRC Crit. Rev. Macromol. Sci.* 1972, **1**, 1

### Estimation of the correlation length in polymer melts from nuclear magnetic relaxation dispersion

In this communication we use nuclear magnetic relaxation dispersion measurements for the estimation of the medium length of unidirectional chain orientation in poly(ethylene oxide) melts. This length is considered to be a characteristic size of the short-range order. Thus, a contribution to the discussion of the microstructure in polymer melts can be expected by this kind of investigation.

Molecular motion of molten polymers is anisotropic. We expect a rapid segment re-orientation fluctuation around the chain axis: this type of motion is connected with the diffusion of defects (e.g. kinks and torsions<sup>1</sup>) and will not completely destroy the autocorrelation of the dipolar interaction<sup>2</sup>. Considering for the moment only this anisotropic segment fluctuation process, we can express the unnormalized time autocorrelation function as the sum of a time dependent function  $G_s(\tau)$ , decreasing to zero at infinite times  $\tau$ , and a constant term  $|\bar{R}|^2$ , characterizing the anisotropy of the motion. ( $|\bar{R}|^2$  would be zero for isotropic motions.)

The remaining correlation  $|\bar{R}|^2$  will be finally reduced to zero by any further process which completely destroys the memory to the initial chain orientation at a reference segment. We now define a correlation function  $\bar{R}(0)R^*(\tau)$  concerning this superimposed process. Assuming this type of motion to be slow compared with segment fluctuation, we may write for the total correlation function:

$$G(\tau) \approx G_s(\tau) + \overline{R(0)R^*(\tau)} = G_s(\tau) + |\bar{R}|^2 \tilde{G}_c(\tau) \quad (1)$$

where we have introduced  $\tilde{G}_c(\tau)$  as the normalized autocorrelation function for the second process. [ $G_s(\tau)$  is the time dependent contribution of segment re-orientation to the total correlation function.]

The dominant type of motion responsible for the final disorientation of the reference chain part is expected to be the longitudinal chain diffusion or 'reptation' defined by de Gennes<sup>3</sup>. The reference segment diffuses via defect diffusion on a curvilinear path along the chain's spatial configuration. After a certain diffusion path, the correlation to the initial segment orientation will be lost. Therefore, the time correlation function  $G_c(\tau)$  consists of a configurational and a motional part.

We write:

$$\tilde{G}_c(\tau) = \int_{-\infty}^{\infty} C(X)\eta(X, \tau) dX \quad (2)$$

where  $C(X)$  is the normalized orientation correlation function (with respect to the spatial coordinate dependent function  $R$ ), and  $\eta(X, \tau)$  is the probability that the reference segment diffuses a distance  $X$  during a period  $\tau$ . Thus, the time correlation function  $G_c(\tau)$  is connected with a configurational correlation function.

The simplest, i.e. exponential, correlation function results if the stochastic problem is Poisson like. We therefore assume:

$$C(X) = \exp(-|X|/l) \quad (3)$$

where  $l$  is the orientation correlation length. The solution of the one-dimensional diffusion equation yields:

$$\eta(X, \tau) = \frac{1}{2(\pi D_1 |\tau|)^{1/2}} \exp(-X^2/4D_1 |\tau|) \quad (4)$$

$D_1$  is the one-dimensional (i.e. curvilinear) diffusion coefficient of segments).

We find from equations (2) to (4):

$$\tilde{G}_c(\tau) = \exp(D_1 |\tau|/l^2) \{1 - \text{erf}[(D_1 |\tau|)^{1/2}/l]\} \quad (5)$$

in agreement with the function found by Hunt and Powles<sup>4</sup> for a similar problem.

In the frequency range, slow compared with segment fluctuation rates, we obtain for the intensity function by Fourier transforming equation (1):

$$I(\omega_L) = I_s(\omega) + |\bar{R}|^2 \frac{\tau_l^{1/2}}{\omega_L^{1/2}(1 + 2\omega_L^{1/2}\tau_l + 2\omega_L\tau_l)} \quad (6)$$

with  $\tau_l = l^2/2D_1$ . The constant term  $I_s(\omega)$  arises from segment fluctuation.

For the longitudinal relaxation rate it holds then<sup>5</sup>:

$$\frac{1}{T_1} = |\bar{R}|^2 \left[ k + \frac{\tau_l^{1/2}}{\omega_L^{1/2}(1 + 2\omega_L^{1/2}\tau_l^{1/2} + 2\omega_L\tau_l)} + \frac{4\tau_l^{1/2}}{(2\omega_L)^{1/2}[1 + 2(2\omega_L\tau_l)^{1/2} + 4\omega_L\tau_l]} \right] \quad (7)$$

The constant  $k$  contains the contribution of segment re-orientation in the extreme narrowing condition (divided by  $|\bar{R}|^2$ ). In this equation we have three parameters:  $\tau_l$ ,  $k$  and  $|\bar{R}|^2$ . The latter merely influences the absolute value of the relaxation rate and can therefore easily be fitted to experimental values.

In Figure 1 the experimental  $T_1$ -dispersion of poly(ethylene oxide) melts is plotted in the range  $\omega_L = 5 \times 10^4 \dots 5 \times 10^6$  Hz. The data are taken from ref.6 and were obtained by the aid of a field modulation technique<sup>7</sup>.

Typical orders of magnitude for segment re-orientation rates for this kind of polymers were found to be in the range  $10^{10} \dots 10^{12}$  Hz<sup>8,9</sup>. Thus, even if this re-orientation process is 'broadened' by environmental fluctuations<sup>2</sup>, we may assume the extreme narrowing case for the segmental contribution, and equation (7) can be used for the interpretation of the measurements.

Good agreement between the theoretical and the experimental slope of the dispersion curves was found for  $\tau_l \leq 2.6 \times 10^{-8}$  sec. In order to derive the curvilinear dif-

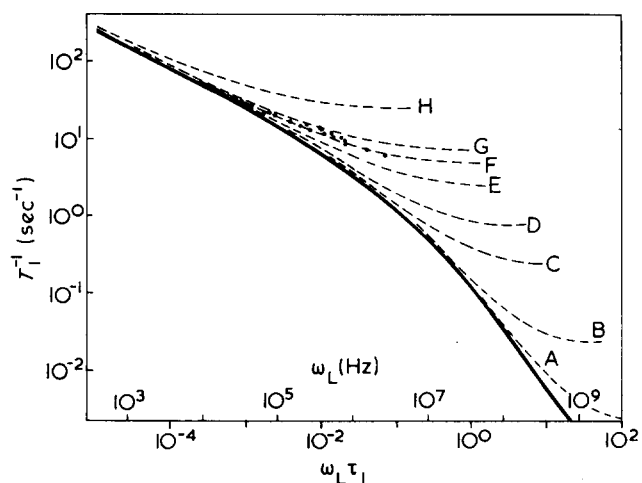


Figure 1 Theoretical curves of the  $T_1^{-1}$  dispersion according to equation (7) for diverse values of  $k$  (constant term of equation 7). The experimental data<sup>6</sup> concern a poly(ethylene oxide) melt at 344K ( $M = 27\,000$ ). They are compatible with the theoretical curves in a certain range of  $k$ , leading to a range  $\tau_1 = 1 \times 10^{-9} \dots 3 \times 10^{-8}$  sec. The  $\omega_L$ -scale and the plotted theoretical curves correspond to  $\tau_1 = 2.6 \times 10^{-8}$  sec and  $|R|^2 = 8.3 \times 10^4$  sec<sup>-2</sup>. —,  $k = 0$ ; A,  $k = 2.7 \times 10^{-8}$ ; B,  $k = 2.7 \times 10^{-7}$ ; C,  $k = 2.7 \times 10^{-6}$ ; D,  $k = 8.1 \times 10^{-6}$ ; E,  $k = 2.7 \times 10^{-5}$ ; F,  $k = 5.4 \times 10^{-5}$ ; G,  $k = 8.1 \times 10^{-5}$ ; H,  $k = 2.7 \times 10^{-4}$  sec

fusion coefficient from the value found from three-dimensional measurements, we have to take into consideration the configuration of the chain. Limiting cases are fully stretched chains and randomly coiled chains.

Estimating the curvilinear diffusion coefficient from field gradient data<sup>10</sup>, we thus find the range:  $2 \times 10^{-8}$  cm<sup>2</sup>/sec  $< D_1 < 2 \times 10^{-6}$  cm<sup>2</sup>/sec. The correlation length  $l$  should therefore be essentially shorter than 30 Å.

The basic assumptions of the suggested interpretation are the dominance of the 'reptation' diffusion process and the validity of the one-dimensional diffusion equation for this process. The complete discussion would exceed the scope of this Letter and will be the subject of a subsequent paper.

R. Kimmich

Sektion Kernresonanzspektroskopie,  
Universität Ulm,  
D-76 Ulm,  
Postfach 4066,  
West Germany  
(Received 21 July 1975; revised 18 August 1975)

## References

- 1 Pechhold, W. *Kolloid-Z. Z. Polym.* 1968, 228, 1
- 2 Kimmich, R. *Colloid Polym. Sci.* 1974, 252, 786
- 3 de Gennes, P. G. *J. Chem. Phys.* 1971, 55, 572
- 4 Hunt, B. I. and Powles, J. G. *Proc. Phys. Soc.* 1966, 88, 513
- 5 Abragam, A. 'The Principles of Nuclear Magnetism', Clarendon Press, Oxford, 1961
- 6 Preissing, G. and Noack, F. *Kolloid-Z. Z. Polym.* 1971, 247, 811
- 7 Kimmich, R. and Noack, F. *Z. Angew. Phys.* 1970, 29, 248
- 8 Liu, K.-J. and Ullman, R. *J. Chem. Phys.* 1968, 48, 1158
- 9 Davies, M., Williams, G. and Loveluck, G. D. *Z. Elektrochem.* 1960, 64, 575
- 10 Tanner, J. E., Liu, K.-J. and Anderson, J. E. *Macromolecules* 1971, 4, 586

## A formula for the $\beta$ -relaxation in polymers

The  $\beta$ -loss peak in polymers is asymmetric in shape in the temperature domain, being steeper on the high temperature side (it can be the opposite in a few cases). In polymers such as poly(vinyl fluoride) (PVF), where it is well resolved from the  $\alpha$  peak, the  $\beta$  peak may be extrapolated on the steeper side to meet the temperature axis at a point, such as  $T_c$ , in Figure 1.  $T_c$  may be taken approximately as the temperature at which the  $\beta$  process would tend to vanish, as the  $\alpha$  process becomes more favoured. 'Cut-off' procedures of this kind are known to yield good approximations to the actual situations and to simplify mathematical treatments, e.g. the Debye treatment of specific heat.

A recently published formula due to Jonscher<sup>1</sup> described dielectric loss in polymers as a function of frequency. No formula as yet exists in the literature, which gives loss as a function of temperature. We report here the loss formula:

$$\tan \delta = A(\omega) \left[ \frac{1}{B(T_c - T)} \right]^2 \operatorname{sech}^2 \left[ \frac{1}{B(T_c - T)} \right] \quad (1)$$

which has been found to agree very well with the dielectric  $\beta$ -relaxation data for a number of amorphous and partly crystalline polymers that have been investigated by the author. In equation (1),  $T_c$  is the  $\beta$  cut-off temperature, as introduced above; and  $T$  is any temperature within the relaxation region at which dielectric loss is being measured.  $B$  is a constant, which was found to be  $1.427 \times 10^{-2}$  K<sup>-1</sup>, for all the polymers investigated.  $A(\omega)$  is a frequency-dependent amplitude. Equation (1) is a peaked function, for which the temperature of maximum loss,  $T_m$ , is related to  $T_c$  via:

$$B|T_c - T_m| = 1.2 \quad (2)$$

$A(\omega)$  is also related to the maximum loss,  $(\tan \delta)_{\max}$ , by:

$$A(\omega) = (\tan \delta)_{\max}/0.44 \quad (3)$$

which is the normalization condition.

To fit experimental data to equation (1), all that has to be done is to match the maximum of equation (1) to that of the experimental curve, using the experimental value of  $T_m$  and the normalization condition (3), and then determining the value of  $T_c$  which gives the best fit. Clearly  $T_c$  is an adjustable parameter.

A typical agreement between equation (1) and experimental data is as shown in Figure 2 for PVF. Other poly-

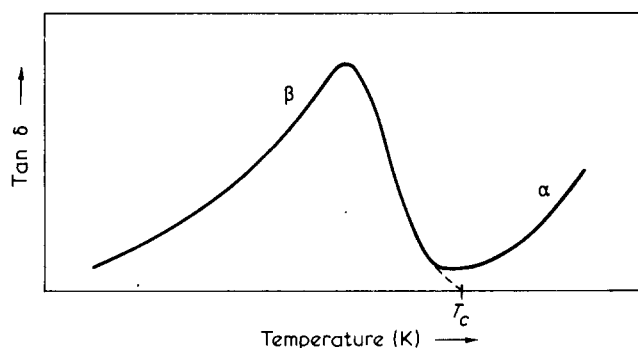


Figure 1 A typical  $\beta$  peak and the high temperature cut-off procedure

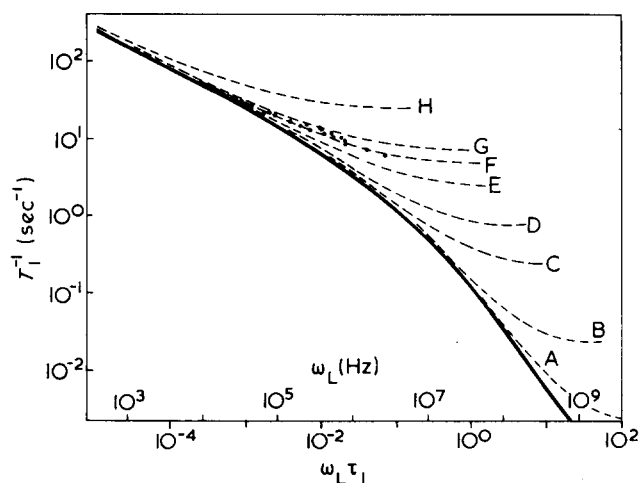


Figure 1 Theoretical curves of the  $T_1^{-1}$  dispersion according to equation (7) for diverse values of  $k$  (constant term of equation 7). The experimental data<sup>6</sup> concern a poly(ethylene oxide) melt at 344K ( $M = 27\ 000$ ). They are compatible with the theoretical curves in a certain range of  $k$ , leading to a range  $\tau_1 = 1 \times 10^{-9} \dots 3 \times 10^{-8}$  sec. The  $\omega_L$ -scale and the plotted theoretical curves correspond to  $\tau_1 = 2.6 \times 10^{-8}$  sec and  $|R|^2 = 8.3 \times 10^4$  sec<sup>-2</sup>. —,  $k = 0$ ; A,  $k = 2.7 \times 10^{-8}$ ; B,  $k = 2.7 \times 10^{-7}$ ; C,  $k = 2.7 \times 10^{-6}$ ; D,  $k = 8.1 \times 10^{-6}$ ; E,  $k = 2.7 \times 10^{-5}$ ; F,  $k = 5.4 \times 10^{-5}$ ; G,  $k = 8.1 \times 10^{-5}$ ; H,  $k = 2.7 \times 10^{-4}$  sec

fusion coefficient from the value found from three-dimensional measurements, we have to take into consideration the configuration of the chain. Limiting cases are fully stretched chains and randomly coiled chains.

Estimating the curvilinear diffusion coefficient from field gradient data<sup>10</sup>, we thus find the range:  $2 \times 10^{-8}$  cm<sup>2</sup>/sec  $< D_1 < 2 \times 10^{-6}$  cm<sup>2</sup>/sec. The correlation length  $l$  should therefore be essentially shorter than 30 Å.

The basic assumptions of the suggested interpretation are the dominance of the 'reptation' diffusion process and the validity of the one-dimensional diffusion equation for this process. The complete discussion would exceed the scope of this Letter and will be the subject of a subsequent paper.

R. Kimmich

Sektion Kernresonanzspektroskopie,  
Universität Ulm,  
D-76 Ulm,  
Postfach 4066,  
West Germany  
(Received 21 July 1975; revised 18 August 1975)

## References

- 1 Pechhold, W. *Kolloid-Z. Z. Polym.* 1968, 228, 1
- 2 Kimmich, R. *Colloid Polym. Sci.* 1974, 252, 786
- 3 de Gennes, P. G. *J. Chem. Phys.* 1971, 55, 572
- 4 Hunt, B. I. and Powles, J. G. *Proc. Phys. Soc.* 1966, 88, 513
- 5 Abragam, A. 'The Principles of Nuclear Magnetism', Clarendon Press, Oxford, 1961
- 6 Preissing, G. and Noack, F. *Kolloid-Z. Z. Polym.* 1971, 247, 811
- 7 Kimmich, R. and Noack, F. *Z. Angew. Phys.* 1970, 29, 248
- 8 Liu, K.-J. and Ullman, R. *J. Chem. Phys.* 1968, 48, 1158
- 9 Davies, M., Williams, G. and Loveluck, G. D. *Z. Elektrochem.* 1960, 64, 575
- 10 Tanner, J. E., Liu, K.-J. and Anderson, J. E. *Macromolecules* 1971, 4, 586

## A formula for the $\beta$ -relaxation in polymers

The  $\beta$ -loss peak in polymers is asymmetric in shape in the temperature domain, being steeper on the high temperature side (it can be the opposite in a few cases). In polymers such as poly(vinyl fluoride) (PVF), where it is well resolved from the  $\alpha$  peak, the  $\beta$  peak may be extrapolated on the steeper side to meet the temperature axis at a point, such as  $T_c$ , in Figure 1.  $T_c$  may be taken approximately as the temperature at which the  $\beta$  process would tend to vanish, as the  $\alpha$  process becomes more favoured. 'Cut-off' procedures of this kind are known to yield good approximations to the actual situations and to simplify mathematical treatments, e.g. the Debye treatment of specific heat.

A recently published formula due to Jonscher<sup>1</sup> described dielectric loss in polymers as a function of frequency. No formula as yet exists in the literature, which gives loss as a function of temperature. We report here the loss formula:

$$\tan \delta = A(\omega) \left[ \frac{1}{B(T_c - T)} \right]^2 \operatorname{sech}^2 \left[ \frac{1}{B(T_c - T)} \right] \quad (1)$$

which has been found to agree very well with the dielectric  $\beta$ -relaxation data for a number of amorphous and partly crystalline polymers that have been investigated by the author. In equation (1),  $T_c$  is the  $\beta$  cut-off temperature, as introduced above; and  $T$  is any temperature within the relaxation region at which dielectric loss is being measured.  $B$  is a constant, which was found to be  $1.427 \times 10^{-2}$  K<sup>-1</sup>, for all the polymers investigated.  $A(\omega)$  is a frequency-dependent amplitude. Equation (1) is a peaked function, for which the temperature of maximum loss,  $T_m$ , is related to  $T_c$  via:

$$B|T_c - T_m| = 1.2 \quad (2)$$

$A(\omega)$  is also related to the maximum loss,  $(\tan \delta)_{\max}$ , by:

$$A(\omega) = (\tan \delta)_{\max} / 0.44 \quad (3)$$

which is the normalization condition.

To fit experimental data to equation (1), all that has to be done is to match the maximum of equation (1) to that of the experimental curve, using the experimental value of  $T_m$  and the normalization condition (3), and then determining the value of  $T_c$  which gives the best fit. Clearly  $T_c$  is an adjustable parameter.

A typical agreement between equation (1) and experimental data is as shown in Figure 2 for PVF. Other poly-

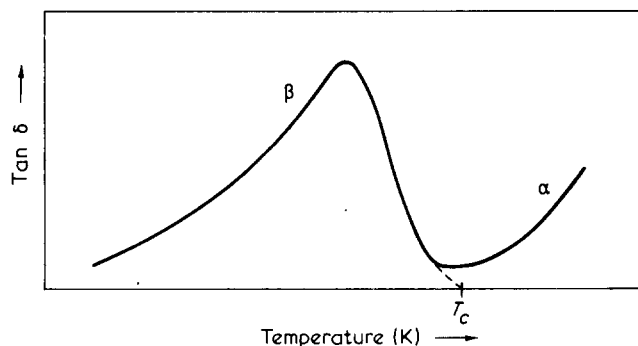


Figure 1 A typical  $\beta$  peak and the high temperature cut-off procedure



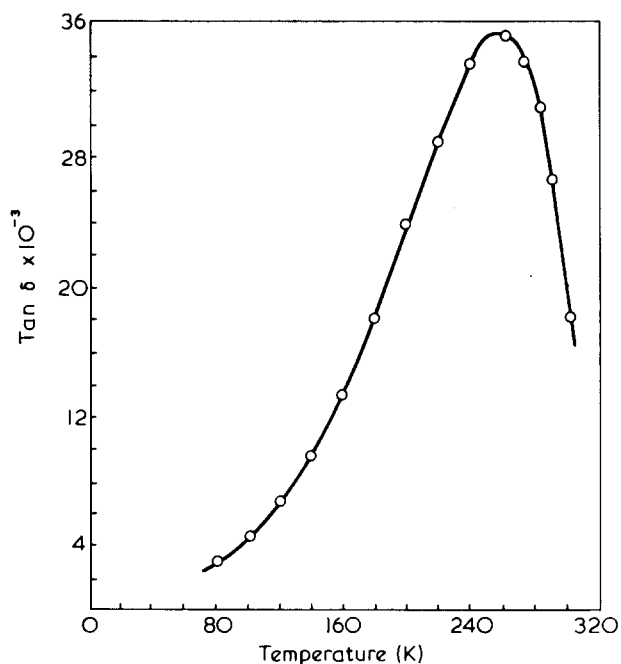


Figure 2 A comparison between equation (1) and experimental data for PVF at 1 kHz

mers which were studied and found to show similar agreement are phenoxy resin; poly(ether sulphone), poly(ethylene terephthalate) and a poly(vinyl chloride)–poly(vinylidene chloride) copolymer, at frequencies from 100 Hz to 100 kHz. Polysulphone showed fairly good agreement above 1 kHz. Equation (1) was applied to the glass–rubber relaxation in poly(vinylidene fluoride), and agreement was fairly good.

#### Acknowledgements

The author wishes to thank Drs D. J. Hourston and R. R. Smith, Department of Chemistry, Lancaster University, and Dr R. A. Pethrick, Department of Chemistry, University of Strathclyde, for helpful discussions on  $\beta$ -relaxations.

G. Makaya

Department of Physics,  
University of Lancaster,  
Lancaster, LA1 4YB, UK  
(Received 21 August 1975)

#### Reference

- 1 Jonscher, A K. *Colloid Polym. Sci.* 1975, 253, 231

## Book Reviews

### Plastics materials

J. A. Brydson

Newnes–Butterworths, London, 1975. 3rd Edn.  
731 pp. £13.75

This book aims at providing an account of the preparation and properties of all the important plastic materials in a single large volume. It is, of course, based on previous editions of the same work though these have been updated, e.g. by adding information on two phase polymers and by including a useful chapter on additives in plastics.

The book consists essentially of two parts, the first part in which the general properties of plastics are outlined and the second, and larger part, where the various plastics materials are described in turn. The latter includes chapters on virtually all the commercially significant plastics in use today.

A book of this type makes very formidable demands on the author concerned, more particularly as it is often difficult to locate authoritative descriptions of the different processes used for manufacturing plastics. Generally the book maintains a satisfactory standard, but inevitably, a reviewer looks at certain parts from the standpoint of his own particular expertise, and such an examination reveals some limitations.

For example the level of low strain modulus in rigid plastics ( $DOE$  in Tuckett's original classification) is now generally explained in terms of intermolecular forces and not due to bond bending, which has been shown by Sakurada and Treloar to lead to much higher modulus figures. Again in the suspension polymerization of styrene, it is not true that 70% of the kettle is taken up by water. Generally more than 50% by volume of monomer is used along with a stabilizer which is often a special calcium phosphate [but not poly(vinyl alcohol)]. This, of course, makes the process more viable compared with the bulk process than would otherwise be the case.

The reviewer understands that the complete elimination of errors of this type in a comprehensive work is not at all easy.

Generally the information given is satisfactory but the reader should be wary of taking the process details given as authoritative. With this reservation the book may be recommended as a useful starting point for the understanding and comparison of different plastic materials.

R. N. Haward

### Selected papers on rheology

Markus Reiner

Elsevier, Amsterdam, 1975. 463 pp. Dfl. 110

Rheology, the study of deformation and flow, is generally accepted to have been born, as a separate science, about fifty years ago. This book is a record of and tribute to one man's contribution during the first fifty years.

Professor Reiner has played a stimulating central role in the development of this subject: his best known work 'Deformation and Flow' is still one of the most readable general texts available. The most appealing aspect of this work is the broad range of materials and concepts which it embraces. From the volumetric creep of concrete to considerations of the rigidity of gases the author is at his best in the description and discussion of phenomena. Professor Reiner is also a pioneer and adept of 'spring and dashpot' imagery – a powerful tool though now largely neglected. The theoretical aspect of the 'Selected Papers' makes a less satisfying pattern and the reader is left with a suspicion that this collection represents a defence of the author's views as well as a statement thereof. It is true that some of Professor Reiner's views are unfashionable today but they need no defence. In a young science where everything flows views are bound to change as new evidence becomes available and in the last fifteen years the abundance of experimental and theoretical work on polymers, an area in which Professor Reiner has done little work himself, has shifted the balance within rheology. Times will change again.

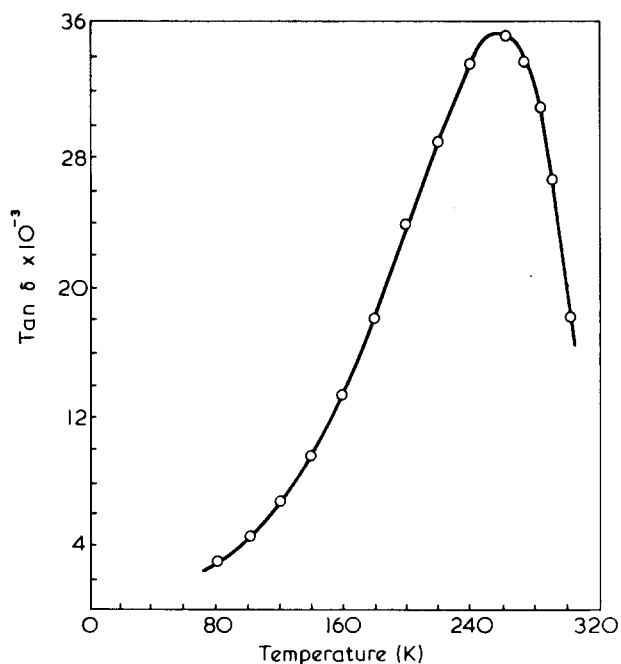


Figure 2 A comparison between equation (1) and experimental data for PVF at 1 kHz

mers which were studied and found to show similar agreement are phenoxy resin; poly(ether sulphone), poly(ethylene terephthalate) and a poly(vinyl chloride)–poly(vinylidene chloride) copolymer, at frequencies from 100 Hz to 100 kHz. Polysulphone showed fairly good agreement above 1 kHz. Equation (1) was applied to the glass–rubber relaxation in poly(vinylidene fluoride), and agreement was fairly good.

#### Acknowledgements

The author wishes to thank Drs D. J. Hourston and R. R. Smith, Department of Chemistry, Lancaster University, and Dr R. A. Pethrick, Department of Chemistry, University of Strathclyde, for helpful discussions on  $\beta$ -relaxations.

G. Makaya

Department of Physics,  
University of Lancaster,  
Lancaster, LA1 4YB, UK  
(Received 21 August 1975)

#### Reference

- 1 Jonscher, A K. *Colloid Polym. Sci.* 1975, 253, 231

## Book Reviews

### Plastics materials

J. A. Brydson

Newnes–Butterworths, London, 1975. 3rd Edn.  
731 pp. £13.75

This book aims at providing an account of the preparation and properties of all the important plastic materials in a single large volume. It is, of course, based on previous editions of the same work though these have been updated, e.g. by adding information on two phase polymers and by including a useful chapter on additives in plastics.

The book consists essentially of two parts, the first part in which the general properties of plastics are outlined and the second, and larger part, where the various plastics materials are described in turn. The latter includes chapters on virtually all the commercially significant plastics in use today.

A book of this type makes very formidable demands on the author concerned, more particularly as it is often difficult to locate authoritative descriptions of the different processes used for manufacturing plastics. Generally the book maintains a satisfactory standard, but inevitably, a reviewer looks at certain parts from the standpoint of his own particular expertise, and such an examination reveals some limitations.

For example the level of low strain modulus in rigid plastics ( $DOE$  in Tuckett's original classification) is now generally explained in terms of intermolecular forces and not due to bond bending, which has been shown by Sakurada and Treloar to lead to much higher modulus figures. Again in the suspension polymerization of styrene, it is not true that 70% of the kettle is taken up by water. Generally more than 50% by volume of monomer is used along with a stabilizer which is often a special calcium phosphate [but not poly(vinyl alcohol)]. This, of course, makes the process more viable compared with the bulk process than would otherwise be the case.

The reviewer understands that the complete elimination of errors of this type in a comprehensive work is not at all easy.

Generally the information given is satisfactory but the reader should be wary of taking the process details given as authoritative. With this reservation the book may be recommended as a useful starting point for the understanding and comparison of different plastic materials.

R. N. Haward

### Selected papers on rheology

Markus Reiner

Elsevier, Amsterdam, 1975. 463 pp. Dfl. 110

Rheology, the study of deformation and flow, is generally accepted to have been born, as a separate science, about fifty years ago. This book is a record of and tribute to one man's contribution during the first fifty years.

Professor Reiner has played a stimulating central role in the development of this subject: his best known work 'Deformation and Flow' is still one of the most readable general texts available. The most appealing aspect of this work is the broad range of materials and concepts which it embraces. From the volumetric creep of concrete to considerations of the rigidity of gases the author is at his best in the description and discussion of phenomena. Professor Reiner is also a pioneer and adept of 'spring and dashpot' imagery – a powerful tool though now largely neglected. The theoretical aspect of the 'Selected Papers' makes a less satisfying pattern and the reader is left with a suspicion that this collection represents a defence of the author's views as well as a statement thereof. It is true that some of Professor Reiner's views are unfashionable today but they need no defence. In a young science where everything flows views are bound to change as new evidence becomes available and in the last fifteen years the abundance of experimental and theoretical work on polymers, an area in which Professor Reiner has done little work himself, has shifted the balance within rheology. Times will change again.

## Book Reviews

For the man interested in the flow of polymers this book is a firm reminder that there are other materials. In indicating the broader horizon this collection of papers will be found both stimulating and challenging.

*F. N. Cogswell*

### **Kinetics and mechanisms of polymerisation reactions**

*P. E. M. Allen and C. R. Patrick*

Ellis Horwood, Chichester, 1974. 596 pp. £18.00

This book carries a main sub-title – Applications of physico-chemical principles – and the authors have really kept to this objective as indicated by the seven chapter headings: Basic physical chemistry of polymerization reactions, diffusion-controlled reactions, Chain reactions in polymerizations, Thermodynamics of polymerization processes, Polyesterification and polyamidation, Reactivity of radicals and ions and the susceptibility of unsaturated and cyclic compounds to their attack, Kinetics of addition polymerization.

Overall the book is extremely well written and well researched. It contains many lists of rate coefficients for the various propagation processes in chain reaction polymerization and will be very useful to active workers in the field. As might be expected, from the research interests of the authors, the chapters on diffusion effects and chain reactions are particularly informative and well presented.

Whilst the objective of integrating reactivity of active intermediates in both polymerization and small molecule processes is to be commended, there must be some reservation as to the method chosen in this particular book. Thus chapter 6 entitled Reactivity of radicals and ions etc. comprises 140 pages of text and really is a somewhat arbitrary compilation of electrophilic, nucleophilic and radical reactions. There are many existing textbooks in physical organic chemistry which provide better discussions of these topics. Similarly the final, and very important, chapter dealing with kinetics of addition polymerization, treats the subject as a whole without any major separation into radical, cationic, anionic etc. processes. Whilst this approach is both novel and readily comprehended by those expert in the field it will be much less valuable to readers drawn from other areas of polymer science or physical organic chemistry.

In summary the book is extremely well presented and is strongly recommended to those concerned with kinetics of polymerization processes. It is remarkably free from typographical errors but, at the price, it is not likely to be acquired for personal use by the general body of polymer scientists.

*A. Ledwith*

### **Immobilized enzymes: preparation and engineering techniques**

*S. J. Gutcho*

Noyes Data Corporation, Park Ridge, NJ, 1974.

198 pp. \$36.00

This book consists almost entirely of a series of abstracts of relevant United States patents. Each abstract contains detailed technical information which will be valuable to researchers wishing to design their own immobilization procedures and enzyme derivatives described because the author often leaves this aspect to emerge solely from the factual abstracts. In general, the author's personal contribution by way of informed discussion and criticism is minimal.

The text includes a forward and list of points expressing the importance of information gathered from the US patent literature. Doubtless most of the arguments presented are valid but the book as a whole leaves one with the feeling that a much more balanced and informative account would have resulted if the author had drawn also on the learned journals for his material. The claim is made that innovations derived from research are frequently first disclosed in the patent literature. However, in many instances, this is not the case. It is recognized that many research workers file

provisional patents immediately prior to publication in the periodical literature. The latter may be in print before a complete patent specification is on file, let alone examined and published. Furthermore, a number of important and far reaching discoveries in immobilized enzyme technology have not been the subject of patent application.

Just over 170 pages of the text are devoted to patents dealing with the synthesis and properties of enzyme conjugates. Much of the experimental information has not been abstracted in such detail elsewhere and, as such, is of value. The reviewer found a number of passages repetitive and, consequently, boring. For example, the basic advantages of immobilized enzymes, including ease of recovery, re-use potential and improved stability to heat denaturation and storage, are restated several times. Too often a given abstract reviews irrelevant or very elementary material such as the state of the art at the date of filing, the general methods available for enzyme immobilization or the relatively few current commercial applications.

A mere 20 pages are devoted specifically to enzyme reactors and detailed applications. It is an inevitable consequence of the method of selecting material that the section on engineering techniques leaves much to be desired. There is a lack of information on enzyme reactors employing magnetic separators and fluidized beds.

Another deficiency is the lack of an alphabetical subject index. The device of presenting a combined table of contents and subject index is inadequate. For example, it is no easy task to find all the references in the text to a particular enzyme. On the other hand, the inclusion of separate company, inventor and patent indexes is useful.

Newcomers to the subject will find it difficult to gain an understanding in depth of such essential problems in enzyme immobilization as matrix and conjugate micro-architecture, compatibility considerations and mechanisms of enzyme stabilization. However, the book will be of value to those with established interests in the field or with extensive knowledge of practical enzymology. It is sturdily bound and would be a useful laboratory handbook.

*R. Epton*

### **Structural polymers – testing methods, Volumes I and II**

*P. M. Ogibalov, N. I. Malinin, V. P. Netroko and B. P. Kishkin* (translated from the Russian)

John Wiley, London & New York, 1974. 600 pp. £22.10

This 600 page work is not, as the title suggests a handbook of standard test methods. It comprises a collection of treatises on a variety of topics related to the physical properties of polymers. Subjects covered include various types of mechanical tests, visco-elastic theory, environmental effects and stress optical behaviour with shorter sections on processing stresses, adhesion and data analysis. With the exception of some useful details of Russian testing instruments the general emphasis is on the theoretical considerations underlying various test methods and hence the book will appeal more to the postgraduate student concerned with theoretical aspects of polymer behaviour than the industrial polymer technologist. As a concise summary, well translated by present standards, of current Russian literature the book is undoubtedly a success and it contains much information which is not otherwise readily available. Composite materials and in particular GRP are treated in particular detail but here, as in other areas, the general usefulness of the text would have been greatly increased by the inclusion of more examples describing the applications of the theories discussed to real situations. A more minor comment also concerns the extensive use of Russian designations for materials, tests and instruments which without further details renders some of the text difficult to follow. For these reasons coupled with the relatively high cost it is doubtful if the book will enjoy a wide readership but it is certainly a useful addition to the reference library and with the exception of the photographic plates the presentation and reproduction is of a high standard.

*G. H. West*

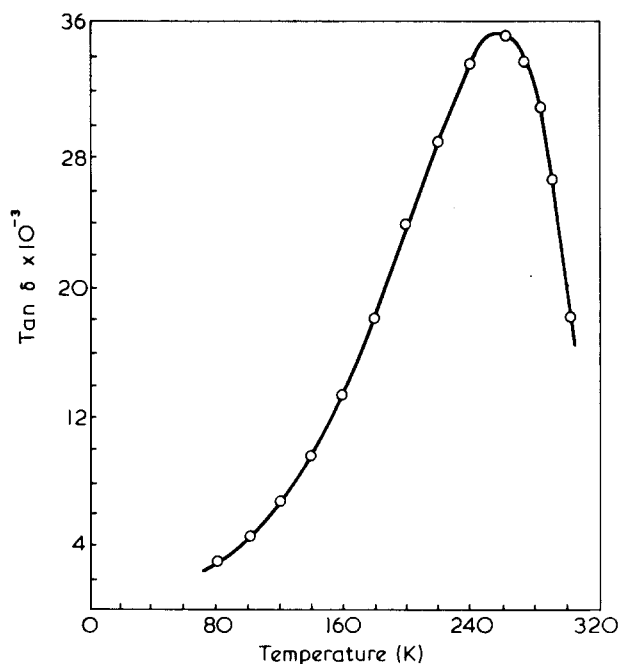


Figure 2 A comparison between equation (1) and experimental data for PVF at 1 kHz

mers which were studied and found to show similar agreement are phenoxy resin; poly(ether sulphone), poly(ethylene terephthalate) and a poly(vinyl chloride)–poly(vinylidene chloride) copolymer, at frequencies from 100 Hz to 100 kHz. Polysulphone showed fairly good agreement above 1 kHz. Equation (1) was applied to the glass–rubber relaxation in poly(vinylidene fluoride), and agreement was fairly good.

#### Acknowledgements

The author wishes to thank Drs D. J. Hourston and R. R. Smith, Department of Chemistry, Lancaster University, and Dr R. A. Pethrick, Department of Chemistry, University of Strathclyde, for helpful discussions on  $\beta$ -relaxations.

G. Makaya

Department of Physics,  
University of Lancaster,  
Lancaster, LA1 4YB, UK  
(Received 21 August 1975)

#### Reference

- 1 Jonscher, A K. *Colloid Polym. Sci.* 1975, 253, 231

## Book Reviews

### Plastics materials

J. A. Brydson

Newnes–Butterworths, London, 1975. 3rd Edn.  
731 pp. £13.75

This book aims at providing an account of the preparation and properties of all the important plastic materials in a single large volume. It is, of course, based on previous editions of the same work though these have been updated, e.g. by adding information on two phase polymers and by including a useful chapter on additives in plastics.

The book consists essentially of two parts, the first part in which the general properties of plastics are outlined and the second, and larger part, where the various plastics materials are described in turn. The latter includes chapters on virtually all the commercially significant plastics in use today.

A book of this type makes very formidable demands on the author concerned, more particularly as it is often difficult to locate authoritative descriptions of the different processes used for manufacturing plastics. Generally the book maintains a satisfactory standard, but inevitably, a reviewer looks at certain parts from the standpoint of his own particular expertise, and such an examination reveals some limitations.

For example the level of low strain modulus in rigid plastics ( $DOE$  in Tuckett's original classification) is now generally explained in terms of intermolecular forces and not due to bond bending, which has been shown by Sakurada and Treloar to lead to much higher modulus figures. Again in the suspension polymerization of styrene, it is not true that 70% of the kettle is taken up by water. Generally more than 50% by volume of monomer is used along with a stabilizer which is often a special calcium phosphate [but not poly(vinyl alcohol)]. This, of course, makes the process more viable compared with the bulk process than would otherwise be the case.

The reviewer understands that the complete elimination of errors of this type in a comprehensive work is not at all easy.

Generally the information given is satisfactory but the reader should be wary of taking the process details given as authoritative. With this reservation the book may be recommended as a useful starting point for the understanding and comparison of different plastic materials.

R. N. Haward

### Selected papers on rheology

Markus Reiner

Elsevier, Amsterdam, 1975. 463 pp. Dfl. 110

Rheology, the study of deformation and flow, is generally accepted to have been born, as a separate science, about fifty years ago. This book is a record of and tribute to one man's contribution during the first fifty years.

Professor Reiner has played a stimulating central role in the development of this subject: his best known work 'Deformation and Flow' is still one of the most readable general texts available. The most appealing aspect of this work is the broad range of materials and concepts which it embraces. From the volumetric creep of concrete to considerations of the rigidity of gases the author is at his best in the description and discussion of phenomena. Professor Reiner is also a pioneer and adept of 'spring and dashpot' imagery – a powerful tool though now largely neglected. The theoretical aspect of the 'Selected Papers' makes a less satisfying pattern and the reader is left with a suspicion that this collection represents a defence of the author's views as well as a statement thereof. It is true that some of Professor Reiner's views are unfashionable today but they need no defence. In a young science where everything flows views are bound to change as new evidence becomes available and in the last fifteen years the abundance of experimental and theoretical work on polymers, an area in which Professor Reiner has done little work himself, has shifted the balance within rheology. Times will change again.

## Book Reviews

For the man interested in the flow of polymers this book is a firm reminder that there are other materials. In indicating the broader horizon this collection of papers will be found both stimulating and challenging.

*F. N. Cogswell*

### **Kinetics and mechanisms of polymerisation reactions**

*P. E. M. Allen and C. R. Patrick*

Ellis Horwood, Chichester, 1974. 596 pp. £18.00

This book carries a main sub-title – Applications of physico-chemical principles – and the authors have really kept to this objective as indicated by the seven chapter headings: Basic physical chemistry of polymerization reactions, diffusion-controlled reactions, Chain reactions in polymerizations, Thermodynamics of polymerization processes, Polyesterification and polyamidation, Reactivity of radicals and ions and the susceptibility of unsaturated and cyclic compounds to their attack, Kinetics of addition polymerization.

Overall the book is extremely well written and well researched. It contains many lists of rate coefficients for the various propagation processes in chain reaction polymerization and will be very useful to active workers in the field. As might be expected, from the research interests of the authors, the chapters on diffusion effects and chain reactions are particularly informative and well presented.

Whilst the objective of integrating reactivity of active intermediates in both polymerization and small molecule processes is to be commended, there must be some reservation as to the method chosen in this particular book. Thus chapter 6 entitled Reactivity of radicals and ions etc. comprises 140 pages of text and really is a somewhat arbitrary compilation of electrophilic, nucleophilic and radical reactions. There are many existing textbooks in physical organic chemistry which provide better discussions of these topics. Similarly the final, and very important, chapter dealing with kinetics of addition polymerization, treats the subject as a whole without any major separation into radical, cationic, anionic etc. processes. Whilst this approach is both novel and readily comprehended by those expert in the field it will be much less valuable to readers drawn from other areas of polymer science or physical organic chemistry.

In summary the book is extremely well presented and is strongly recommended to those concerned with kinetics of polymerization processes. It is remarkably free from typographical errors but, at the price, it is not likely to be acquired for personal use by the general body of polymer scientists.

*A. Ledwith*

### **Immobilized enzymes: preparation and engineering techniques**

*S. J. Gutcho*

Noyes Data Corporation, Park Ridge, NJ, 1974.

198 pp. \$36.00

This book consists almost entirely of a series of abstracts of relevant United States patents. Each abstract contains detailed technical information which will be valuable to researchers wishing to design their own immobilization procedures and enzyme derivatives described because the author often leaves this aspect to emerge solely from the factual abstracts. In general, the author's personal contribution by way of informed discussion and criticism is minimal.

The text includes a forward and list of points expressing the importance of information gathered from the US patent literature. Doubtless most of the arguments presented are valid but the book as a whole leaves one with the feeling that a much more balanced and informative account would have resulted if the author had drawn also on the learned journals for his material. The claim is made that innovations derived from research are frequently first disclosed in the patent literature. However, in many instances, this is not the case. It is recognized that many research workers file

provisional patents immediately prior to publication in the periodical literature. The latter may be in print before a complete patent specification is on file, let alone examined and published. Furthermore, a number of important and far reaching discoveries in immobilized enzyme technology have not been the subject of patent application.

Just over 170 pages of the text are devoted to patents dealing with the synthesis and properties of enzyme conjugates. Much of the experimental information has not been abstracted in such detail elsewhere and, as such, is of value. The reviewer found a number of passages repetitive and, consequently, boring. For example, the basic advantages of immobilized enzymes, including ease of recovery, re-use potential and improved stability to heat denaturation and storage, are restated several times. Too often a given abstract reviews irrelevant or very elementary material such as the state of the art at the date of filing, the general methods available for enzyme immobilization or the relatively few current commercial applications.

A mere 20 pages are devoted specifically to enzyme reactors and detailed applications. It is an inevitable consequence of the method of selecting material that the section on engineering techniques leaves much to be desired. There is a lack of information on enzyme reactors employing magnetic separators and fluidized beds.

Another deficiency is the lack of an alphabetical subject index. The device of presenting a combined table of contents and subject index is inadequate. For example, it is no easy task to find all the references in the text to a particular enzyme. On the other hand, the inclusion of separate company, inventor and patent indexes is useful.

Newcomers to the subject will find it difficult to gain an understanding in depth of such essential problems in enzyme immobilization as matrix and conjugate micro-architecture, compatibility considerations and mechanisms of enzyme stabilization. However, the book will be of value to those with established interests in the field or with extensive knowledge of practical enzymology. It is sturdily bound and would be a useful laboratory handbook.

*R. Epton*

### **Structural polymers – testing methods, Volumes I and II**

*P. M. Ogibalov, N. I. Malinin, V. P. Netroko and B. P. Kishkin* (translated from the Russian)

John Wiley, London & New York, 1974. 600 pp. £22.10

This 600 page work is not, as the title suggests a handbook of standard test methods. It comprises a collection of treatises on a variety of topics related to the physical properties of polymers. Subjects covered include various types of mechanical tests, visco-elastic theory, environmental effects and stress optical behaviour with shorter sections on processing stresses, adhesion and data analysis. With the exception of some useful details of Russian testing instruments the general emphasis is on the theoretical considerations underlying various test methods and hence the book will appeal more to the postgraduate student concerned with theoretical aspects of polymer behaviour than the industrial polymer technologist. As a concise summary, well translated by present standards, of current Russian literature the book is undoubtedly a success and it contains much information which is not otherwise readily available. Composite materials and in particular GRP are treated in particular detail but here, as in other areas, the general usefulness of the text would have been greatly increased by the inclusion of more examples describing the applications of the theories discussed to real situations. A more minor comment also concerns the extensive use of Russian designations for materials, tests and instruments which without further details renders some of the text difficult to follow. For these reasons coupled with the relatively high cost it is doubtful if the book will enjoy a wide readership but it is certainly a useful addition to the reference library and with the exception of the photographic plates the presentation and reproduction is of a high standard.

*G. H. West*

**Developments with thermosetting plastics***Edited by A. Whelan and J. A. Brydson*

Applied Science, London, 1975. 198 pp. £7.00

Thermosetting plastics account for 25–30% of the total plastics consumed in Britain and this timely review contains eleven papers written by practising industrial specialists in the thermosetting plastics field originally presented at a symposium at the National College of Rubber Technology, London. Authoritative accounts are given of materials currently developed or in which there is present industrial interest and most of the contributions are well to the fore in achieving their objectives with special attention to economic trends of up and coming grades, crosslinking reagents and applications to 1972–73.

The first chapter is concerned with trends, prospects, and tonages of materials used followed by five chapters covering separately amino resins, polyesters, Friedel–Crafts resins, furane resins, and polyurethanes. These are followed by another five chapters reviewing a selected number of processing technology aspects specific to powder coating, polyurethane foam processing, fire reinforced plastics, and injection moulding of thermosets.

Emphasis is on practice, only the minimum of theory necessary to understand the text being given and resulting in a lucid easily read text of interest to the general technical reader rather than a specialist in the field. Nevertheless all who are professionally active in this field should find it a considerable convenience to have this state of the art review in a single slim volume.

Editing has been to a good standard and no errors noted though meticulous transcription of all units to apparent SI nomenclature has produced its share of strange bedfellows. A reasonable index is provided; paper, printing quality, and binding is acceptable and the price, while high for a book of moderate length and simple line diagrams, probably necessary when a limited specialist circulation is envisaged. In brief this is a useful addition to topical literature in the thermosetting plastics field.

C. Hepburn

**The mathematics of diffusion***J. Crank*

Clarendon Press, Oxford, 1975. 2nd Edn. 414 pp. £12.50

Since the first edition appeared in 1956 this book has become one of the most important reference texts for those interested in diffusion problems. This is shown by referring to *Science Citation Index* which has listed almost 200 references every year to this book. Relatively few of these citations have been in polymer journals and in view of the increasing importance of polymers in diffusion technology it is particularly interesting that this new edition includes two extra chapters that are of special relevance to the polymer scientist. The first of these deals with the so-called non-Fickian diffusion and gives a very valuable summary of the mathematics of the time dependent diffusion effects that occur in glassy polymers. The second new chapter on heterogeneous media includes a synoptic examination of past mathematical solutions relating to diffusion in layer structures and to the geometrical effects of fillers and crystallites on diffusion. This chapter also includes the author's most recent work in this field.

The other thirteen chapters in this second edition are expanded versions of those in the first edition and include many of the recent mathematical developments of the last 20 years. Chapter 8, however, on numerical methods has been practically completely redone to tie in with the modern use of high speed digital computers. It enables a novice to work out the answers for himself in simple diffusion situations and to understand what is involved in more complicated problems. The clear and unambiguous style of writing of the new edition, like that of the first edition, will make it extremely useful to those who are interested in diffusion but are not mathematical specialists.

The book is nicely produced and is good value at a cost of about 3p per page. Every polymer scientist with an interest in diffusion will find it necessary to have access to this book.

G. S. Park

Announcing a new international journal from IPC Science and Technology Press

APPLIED MATHEMATICAL  MODELLING  
ADVANCES IN NUMERICAL SIMULATION APPLICABLE TO ENVIRONMENTAL,  
SOCIAL & ENGINEERING PROBLEMS

Editor Dr. C. A. Brebbia Southampton University Southampton SO9 5NH, UK  
Associate Editor Professor J. J. Connor Massachusetts Institute of Technology, Cambridge, Mass. 02139, USA

The journal will aim to coordinate the recent rapid advances in mathematical modelling as applied to multidisciplinary problems. Special emphasis will be given to the practical applicability, the reliability of the models, and the adequacy of the mathematical formulae and the numerical techniques used. Associated computer techniques will also fall within the scope of the journal.

APPLIED MATHEMATICAL MODELLING will feature mainly short communications (approx. 3000 equivalent words), which will be published in less than six

months. Longer papers and review papers covering specific fields of application will also appear.

To minimize delays in publication, the Editors will ensure rapid refereeing of all contributions. Manuscripts should be sent in triplicate to the Editor.

The cost of a one year subscription (four issues) to APPLIED MATHEMATICAL MODELLING will be £25.00 (\$65.00) but you can order your first year's copies NOW at the special pre publication offer price of £18.00 (\$46.80) if ordered before 31st March 1976.

To be published quarterly in 1976 commencing with June issue

For full details apply to:

IPC Science and Technology Press Ltd,  
IPC House, 32 High Street,  
Guildford, Surrey, England, GU1 3EW.  
Telephone Guildford (0483) 71661.  
Telex: Scitechpress Gd. 859556

# Heat capacity of copolymers of chlorotrifluoroethylene and vinylidene fluoride

K. C. Wong, F. C. Chen and C. L. Choy

Department of Physics, The Chinese University of Hong Kong, Shatin, N.T., Hong Kong  
(Received 19 May 1975; revised 16 June 1975)

The heat capacities of two copolymers of chlorotrifluoroethylene and vinylidene fluoride, one 30:70 mol % and the other 44:56 mol % in composition, were measured in an adiabatic calorimeter from 80 to 340 K. The glass-transition points  $T_g$  observed at 256 and 269 K for the 30:70 and 44:56 samples, respectively, closely agree with the prediction of the theory of Flory and Fox; the accompanying jump of heat capacities at these points was found to be 2.2 cal/K 'per bead' for both samples, in fair agreement with the 'constant  $\Delta C_p$  rule'. A small peak was observed immediately above  $T_g$ , and interpreted as a time-dependent effect arising from the lack of equilibrium in the region. The data of the heat capacities were analysed in detail in the framework of the Tarasov model and the principle of additivity, and were found to agree well ( $\leq 1-3\%$ ) with theory up to the respective glass-transition points in all cases, thus giving support to the validity of the previously published segmental values of heat capacity and of characteristic temperature  $\theta_1$ .

## INTRODUCTION

In a previous paper<sup>1</sup> we reported measurements of the heat capacity of a copolymer of ethylene and tetrafluoroethylene (TFE), and showed that the results could well be understood in the framework of the Tarasov model<sup>2</sup> and the principle of additivity<sup>3</sup>. We also extracted the heat capacities of the four segments  $\text{CH}_2$ ,  $\text{CF}_2$ , CHF and  $\text{CFCl}$  from an analysis of the available heat capacities of TFE, polyethylene (PE) and four other fluoropolymers, and showed that the characteristic temperature  $\theta_1$  in the Tarasov model roughly obeys additivity, too.

Similar measurements in the temperature range 80 to 340 K have now been completed on two copolymers of chlorotrifluoroethylene and vinylidene fluoride (CTFE/ $\text{VF}_2$ ), one 30:70 mol % and the other 44:56 mol % in composition. The results give further support to the above-mentioned framework, and confirm the validity of the segmental values of the heat capacities and of  $\theta_1$  obtained in the previous work<sup>1</sup>. In addition, we have observed the glass-transition in both copolymers, and discussed the behaviour of the heat capacity around the transition regions.

## EXPERIMENTAL

The two CTFE/ $\text{VF}_2$  samples used in this experiment were obtained from the Minnesota Mining and Manufacturing Company and bear the trade names Kel-F 3700 and Kel-F 5500, respectively. Kel-F 3700 is known to contain 30 mol % of CTFE, but there is some slight uncertainty as to the exact molar composition of Kel-F 5500<sup>4,5</sup>. The data have therefore been analysed on the assumption of various compositions ranging from 44 to 56 mol % content of CTFE, but all were found to yield nearly exactly the same results and features. In the rest of this paper we shall follow Wall and Florin<sup>4,5</sup> and simply take the CTFE content of Kel-F 5500 to be 44 mol %.

The sample stocks in the form of a white rubbery foam were cut into small pieces, and approximately 70 g were used for each measurement of heat capacity at constant pressure  $C_p$  from 80 to 340 K in an adiabatic calorimeter. Details of the measurement have already been reported previously<sup>6</sup> and will not be repeated here.

## RESULTS AND DISCUSSION

The smoothed data on  $C_p$  obtained from 2 to 3 runs on each of the two samples are shown in *Figures 1* and *2*. A repeat unit of the copolymer is defined to consist of two chain atoms, so that the effective molecular weights of the 30:70 and 44:56 mol % samples are 79.7657 and 87.1066, respectively.

### Transitions

The heat capacity curves show a jump and then a change of slope at 256 and 269 K for the 30:70 and 44:56 mol % samples, respectively. These can readily be identified with the glass-transition points  $T_g$  of the copolymers. If we apply the phenomenological theory of Fox and Flory<sup>7</sup> and assume that the inverse of the glass-transition temperatures of the constituent homopolymers ( $T_g = 228$  K for  $\text{PVF}_2$ <sup>8</sup> and = 325 K for  $\text{PCTFE}$ <sup>9</sup>) combine linearly by their respective weight fractions then the two resultant  $T_g$  values for the copolymers come out respectively to be 262 and 277 K, which are within 3% of the above experimental values.

The jump  $\Delta C_p$  in heat capacity at  $T_g$  is 18 J/K mol for both samples, or 2.2 cal/K 'per bead' which is on the low side but still in fair agreement with the 'constant  $\Delta C_p$  rule', i.e.  $\Delta C_p = 2.7 \pm 0.5$  cal/K bead<sup>3</sup>.

We also observe a small peak in the  $C_p$  curve immediately above  $T_g$  (*Figure 3*). The measurement was then scanned three times through the transition region in 0.8–2.5 K steps on the 44:56 mol % sample. Since all the points obtained in

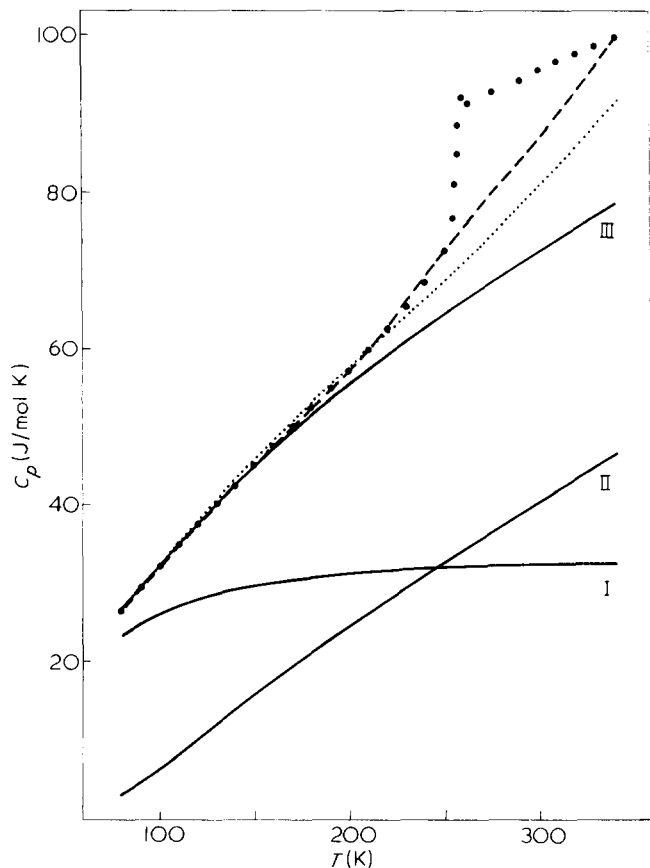


Figure 1 Heat capacity of 30:70 mol % CTFE/VF<sub>2</sub>. I, Acoustical contribution calculated from the Tarasov model; II, optical contribution; III, total heat capacity,  $C_p$ ; ●, observed values of  $C_p$ ; ----, linear combinations of segmental values; ....., linear combinations of experimental values of  $C_p$  for PCTFE and PVF<sub>2</sub>

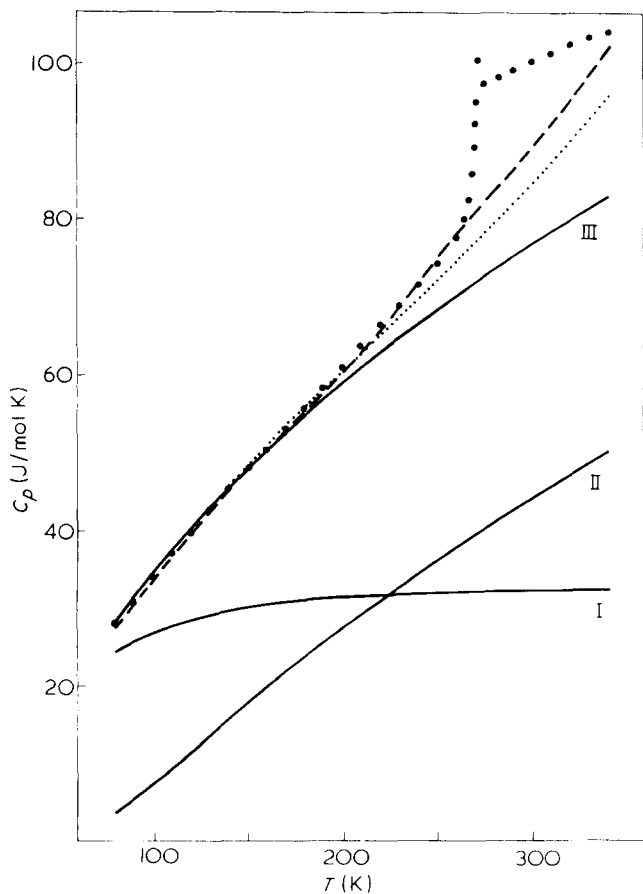


Figure 2 Heat capacity of 44:56 mol % CTFE/VF<sub>2</sub>. The legends are as given in the caption to Figure 1

these latter runs lie consistently on the same smooth curve, the peak seems to be quite genuine. The same phenomenon in many other polymers has been studied systematically by differential thermal analysis<sup>10</sup>, and it is believed to be a time-dependent effect arising from the lack of equilibrium in the glass-transition region through relatively fast heating. In this respect we note that in each run of our experiment the sample was cooled down very slowly through the transition region at a rate of 2–5 K/h and under high vacuum, while the equilibrium time allowed for each measured point at 0.8 to 2.5 K intervals was about 2–5 min, amounting to an effective heating rate of about 0.2–0.5 K/min, considerably lower than the heating rates reported earlier<sup>10</sup>.

#### The Tarasov model

The Tarasov model<sup>2</sup> approximates the acoustical vibrations of a polymer by those of a one-dimensional continuum superimposed on a three-dimensional continuum, with respective cut-off temperatures  $\theta_1$  and  $\theta_3$ ; the optical vibrations are calculated from the spectroscopic data, with the assumption that each mode gives rise to a sharp line. The heat capacity of a polymer is then calculated from the resultant vibrational spectrum. The analysis of the experimental results in this model is practically identical to our previous work<sup>1,6</sup>: the optical contribution to  $C_p$  (heat capacity at constant volume) of the copolymer is obtained by a linear combination of the optical contributions to  $C_p$  of the constituent homopolymers deduced from their respective spectral lines<sup>8,11</sup>, in proportion to their respective molecular fractions; 4 acoustical modes with identical characteristic temperatures  $\theta_1$  and  $\theta_3$  are assigned to each repeat unit;  $\theta_3$  (which does not affect  $C_p$  appreciably in our temperature

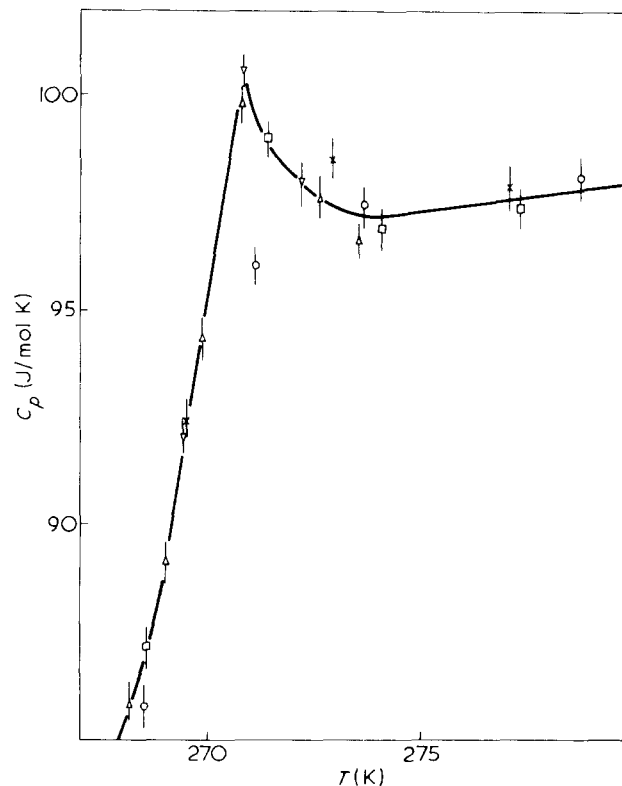


Figure 3 Details of the peak at the glass-transition region of 44:56 mol % CTFE/VF<sub>2</sub>: △, ▽ and □ are experimental points of three separate scans at 0.8 to 2.5 K intervals; × and ○ are points obtained at 4 to 5 K intervals, and hence not reliable in the vicinity of the peak. The solid line is drawn freely through the more reliable experimental points △, ▽ and □



Table 1 Additivity of  $\theta_1$ 

Sample (mol %)	Observed <sup>a</sup> values	$\theta_1$ (K)	
		Calculated values	
		1 <sup>b</sup>	2 <sup>c</sup>
30:70	320	320 (0%)	334 (4%)
44:56	290	303 (5%)	314 (8%)

<sup>a</sup> Obtained by a direct fit of the Tarasov model to experimental data

<sup>b</sup> Calculated from the appropriate linear combination of the observed values for PCTFE and PVF<sub>2</sub>, as given by refs 6 and 10

<sup>c</sup> Calculated from the appropriate linear combination of the segmental values given by ref. 1

range) is set quite arbitrarily to 70 K, midway between the values for PVF<sub>2</sub> and PCTFE, and  $\theta_1$  is adjusted for the best fit to data up to 200 K. The results are  $\theta_1 = 320$  K for the 30:70 mol % CTFE-VF<sub>2</sub> sample and  $\theta_1 = 290$  K for the 44:56 mol % sample. At these values of  $\theta_1$  the Tarasov model gives reasonably good fit to the data (within 3%) from 80 to 200 K (curves I, II, and III of Figures 1 and 2).

As usual, the fit falls considerably below the data above 200 K because of the difference between  $C_p$  and  $C_v$ . Since no data exist for the expansivity and compressibility of the copolymer, it is not possible to make correction for this discrepancy as in previous work<sup>1,8</sup>.

#### Principle of additivity

The principle of additivity<sup>3</sup> can be studied in three slightly different and yet closely related aspects. One can compare  $C_p$  of the copolymer to the appropriate linear combination of  $C_p$  of the constituent homopolymers. With the exception of one point at 80 K, the agreement is excellent ( $\leq 1\%$ ) for both samples up to their respective glass-transition temperatures (Figures 1 and 2). One can also directly 'calculate'  $C_p$  of the copolymer from the segmental heat capacities of CH<sub>2</sub>, CF<sub>2</sub> and CFCl tabulated in our previous work<sup>1</sup>. This affords an opportunity to verify the validity of the CFCl segmental values, which, unlike the other segmental values, were not obtained from least-squares fits to several different experimental values. As shown in the Figures,

the results of the calculation are also in good agreement ( $\leq 3\%$ ) with the data for both samples up to the glass-transition region.

We have previously advanced an argument that the characteristic temperature  $\theta_1$  is approximately additive in the same way as  $C_p$ , and extracted  $\theta_1$  values for the four fluoropolymer segments<sup>1</sup>. It is thus straightforward to make a test of this statement on the two CTFE/VF<sub>2</sub> samples. As seen from Table 1, the agreement is reasonably good ( $\leq 8\%$ ) for both samples, especially in view of the considerable uncertainty usually connected with the determination of  $\theta_1$ .

In summary, it is seen that both the Tarasov model and the principle of additivity in its various aspects can be relied on to give reasonably good (i.e. within 3%) prediction of the heat capacities of copolymers, even though the additivity of  $\theta_1$  generally holds to no better than 10% and should only be used with caution.

#### ACKNOWLEDGEMENTS

The authors wish to acknowledge their gratitude to the 3M Co. for kindly providing the samples and to Dr R. E. Florin of the National Bureau of Standards, USA for a clarification of the composition of the samples.

#### REFERENCES

- 1 Wong, K. C., Chen, F. C. and Choy, C. L. *Polymer* 1975, **16**, 649
- 2 Tarasov, V. V. *Zh. Fiz. Khim.* 1950, **24**, 111
- 3 Wunderlich, B. and Jones, L. D. *J. Macromol. Sci. (A)* 1969, **3**, 67
- 4 Florin, R. E. and Wall, L. A. *J. Res. Nat. Bur. Stand.* 1961, **65A**, 375
- 5 Florin, R. E. personal communications
- 6 Lee, W. K., Lau, P. C. and Choy, C. L. *Polymer* 1974, **15**, 487
- 7 Fox, T. G. and Flory, P. J. *J. Appl. Phys.* 1950, **21**, 581
- 8 Lee, W. K. and Choy, C. L. *J. Polym. Sci. (A-2)* 1975, **13**, 619
- 9 Hoffman, J. D. and Weeks, J. J. *J. Res. Nat. Bur. Stand.* 1958, **60**, 465
- 10 Wolpert, S. M., Weitz, A. and Wunderlich, B. *J. Polym. Sci. (A-2)* 1971, **9**, 1887
- 11 For details of the spectral assignments of PVF<sub>2</sub> and PCTFE, see Lee, W. K. *M. Phil. Thesis* The Chinese University of Hong Kong (1974), and refs. 6 and 8

# Phosphonitrilic chloride: 30. Synthesis of chelating polymers from cyclophosphazene derivatives and studies of their electrical conductivity and thermal properties

M. Kajiwara, M. Hashimoto and H. Saito

Department of Applied Chemistry, Faculty of Engineering, Nagoya University, Nagoya, Japan  
(Received 24 February 1975)

Chelating polymers containing copper, nickel and cobalt have been formed by reaction of the cyclophosphazene derivatives  $P_3N_3(NCSNHC_6H_5)_6$  or  $P_3N_3(NCSNHHC_6H_5)_6$  and the corresponding metal ions. The polymers prepared are amorphous solids and insoluble in most organic solvents.

The electrical conductivity of the products range from  $8.8 \times 10^9$  to  $1.8 \times 10^{14} \Omega\text{-cm}$ . The products are more stable than the corresponding ligand compounds.

## INTRODUCTION

The electrical conductivity of chelating polymers prepared from cyclophosphazene thiocarbamate and metals has been described previously<sup>1</sup>. In this work, some cyclotriphosphazene derivatives are synthesized from hexathiocyclophosphazene,  $N_3P_3(SCN)_6$ , and the electrical conductivity of the chelated products containing copper, nickel and cobalt is described.

## EXPERIMENTAL

Hexachlorocyclophosphazene trimer,  $(NPCl_2)_3$ , was prepared by the modified method of Saito and Kajiwara<sup>2</sup>. The pure trimer (m.p.  $112^\circ\text{C}$ ) was obtained by repeated fractional crystallization from light petroleum ether. Hexathiocyclophosphazene trimer,  $N_3P_3(SCN)_6$  (PTT) and hexaphenylthiouredocyclophosphazene trimer  $N_3P_3(NHCSNHC_6H_5)_6$  [PNP(I)] were prepared by the methods described by Audrith<sup>3,4</sup> and Shvetsov<sup>5</sup>. Hexaphenylthiosemicarbamatecyclophosphazene trimer,  $N_3P_3(NHCSNHHC_6H_5)_6$  (PNPS) (mp.  $165^\circ\text{C}$ ) was prepared from PTT and phenylhydrazine.

Chelated polymers were formed from PNP and copper, nickel or cobalt as follows. 1.04 g (0.001 M) were dissolved in 20 ml of methanol, and 10 ml of pyridine were added. 0.006 M aqueous acetate or nitrate salt solutions of metal ions in 50 ml water and 10 ml pyridine, were added dropwise to the PNP solution with vigorous stirring. The mixture was then warmed for 20 min, the precipitate was filtered, washed with water, ethanol and ether, and then dried over  $P_2O_5$  or under vacuum at 1.5 mmHg for 24 h. The products formed from copper, nickel and cobalt are designated as (II), (III) and (IV).

Chelated polymers were formed from PNPS and copper, nickel or cobalt as follows. 1.13 g (0.001 M) PNPS were dissolved in 20 ml of methanol, and then 5 ml of pyridine were added. 0.006 M aqueous acetate or

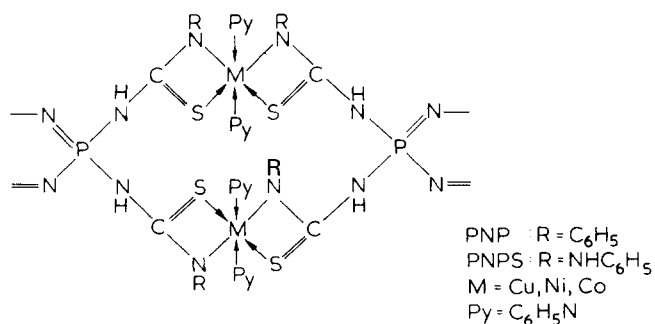
nitrate salt solutions of the metal ions in 60 ml water and 5 ml pyridine, were added dropwise to the PNPS solution with vigorous stirring at room temperature. The reaction mixture was refluxed for 3 h, the precipitate was filtered, and washed or dried as described above. The products are designated as (V), (VI) and (VII).

Infra-red (i.r.) spectra of the products were obtained using the pressed KBr disc technique with a Shimadzu Co. IRG-2 type spectrometer. The variation of resistivity with temperature for the chelated polymers were measured by the method described by Kajiwara<sup>1</sup>.

## RESULTS AND DISCUSSION

### Spectro-analysis of the products

I.r. spectra of the chelated products formed are shown in *Figure 1*. The  $-\text{NH}_2$  frequency of the products II, III, IV, V, VI and VII observed in the region of  $3360 \text{ cm}^{-1}$  is shifted to long wavelengths compared with PNP or PNPS. The  $-\text{NCS}$  frequency of the products II, III, IV, V, VI and VII observed in the region of  $1450 \text{ cm}^{-1}$  is slightly weaker than PNP or PNPS. These observations suggest that metal ions are attached to  $-\text{NH}_2$  or  $-\text{NCS}$  groups. Although the structure of the products have not been elucidated, it is assumed that they have a similar structure to that previously described<sup>1</sup> viz:



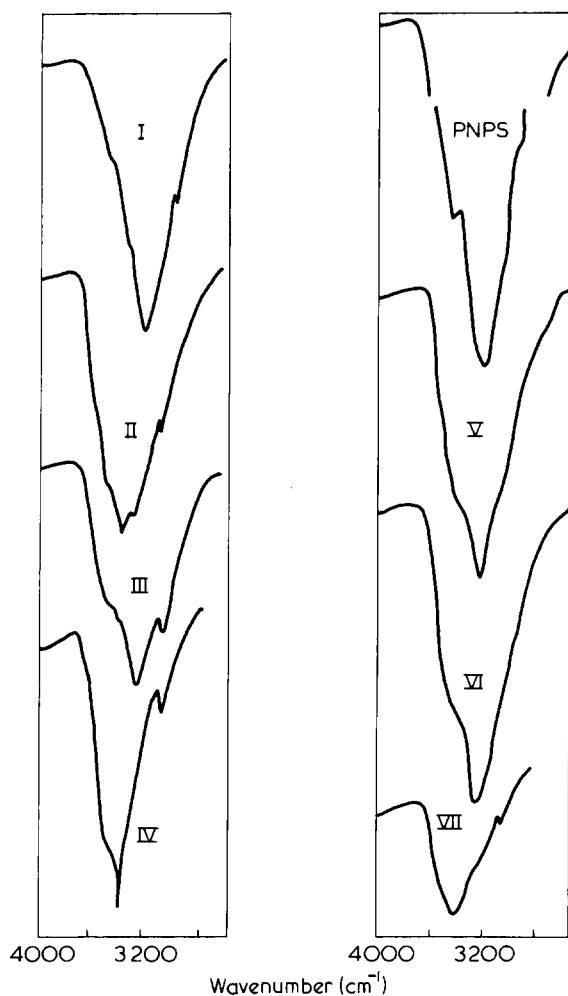


Figure 1 Infra-red absorption of chelating polymers in the region of 4000 to 2800  $\text{cm}^{-1}$ . I, PNP; II, PNP/Co/Py; III, PNP/Ni/Py; IV, PNP/Cu/Py; V, PNPS/Co/Py; VI, PNPS/Ni/Py; VII, PNPS/Cu/Py

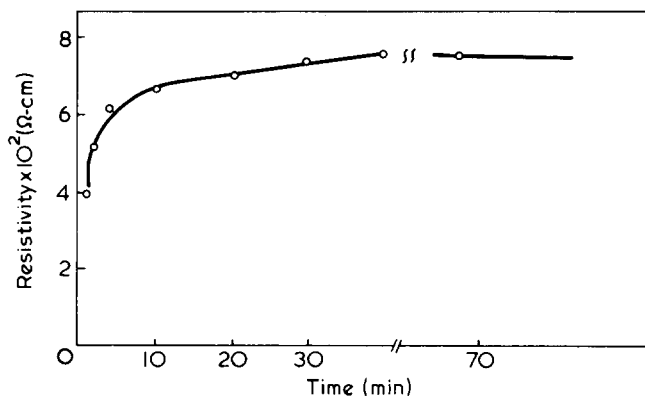


Figure 2 Resistivity vs. time at 25°C for product III

The products are amorphous solids, and insoluble in most organic solvents.

#### Electrical conductivity of the products

The relationship between the resistivity and time is shown in Figure 2. The resistivity of product II attains a constant value only after considerable time and this suggests that the electrical conductivity contributes to an ionic mechanism. Products IV, VI and VII show similar behaviour. On the other hand, products II and V immediately approach the con-

stant value. The variation of resistivity with temperature is shown in Figures 3 and 4, and the energy gaps of the products calculated from the general relation for semi-conductors are summarized in Table 1.

The value of  $\Delta E$  of the products in PNP system and all of the same order, but in PNPS system the value of  $\Delta E$  tend to decrease in the order: V < VII < VI. It can therefore be

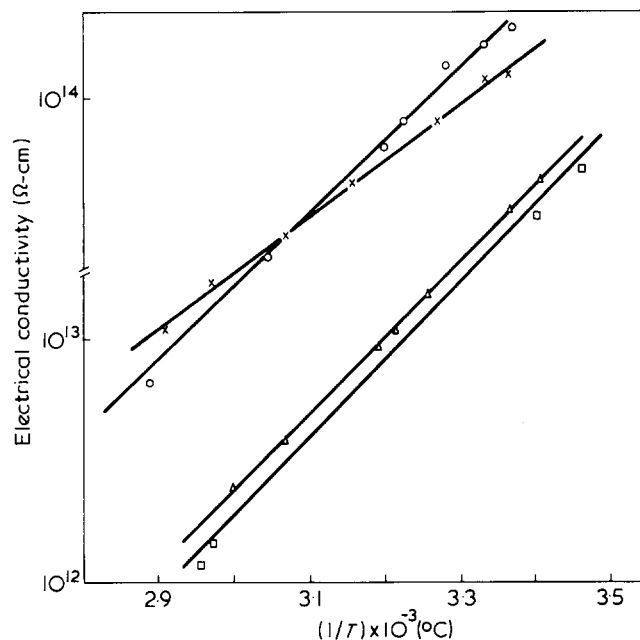


Figure 3 Electrical conductivity of the products formed from PNP and metal salts. X, I; □, II; △, III; ○, IV

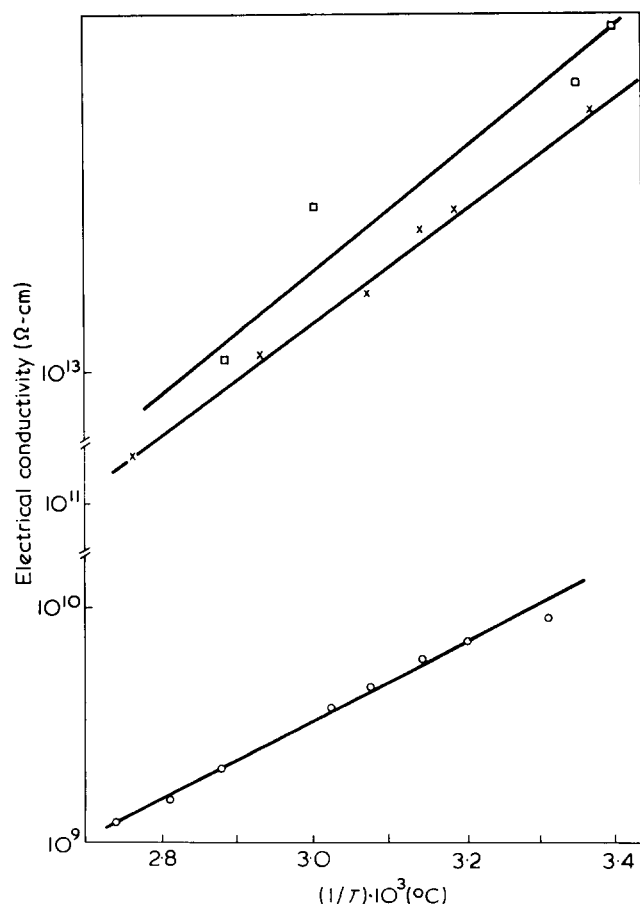
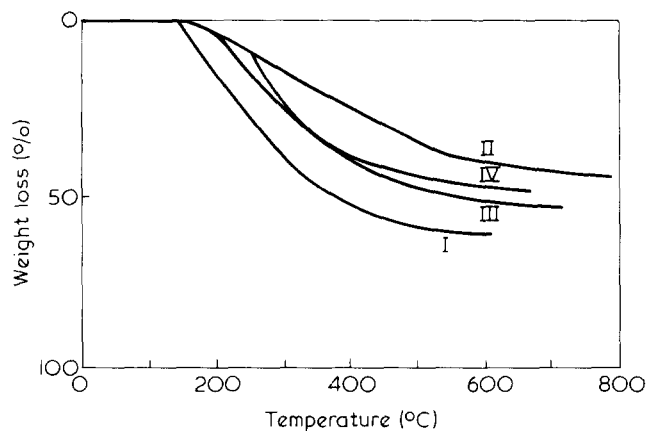


Figure 4 Electrical conductivity of the products formed from PNPS and metal salts. ○, V; □, VI; X, VII

**Table 1** Energy gaps and the value of resistivity of chelated products

Chelated products	$\rho$ (25°C) ( $\Omega$ -cm)	$\Delta E$ (eV)
(I) PNP	$1.2 \times 10^{14}$	0.94
(II) Cu	$2.3 \times 10^{13}$	1.29
(III) Ni	$3.0 \times 10^{13}$	1.27
(IV) Co	$1.8 \times 10^{14}$	1.28
PNPS	—	—
(V) Cu	$8.8 \times 10^9$	0.59
(VI) Ni	$1.4 \times 10^{14}$	0.98
(VII) Co	$2.8 \times 10^{12}$	0.93

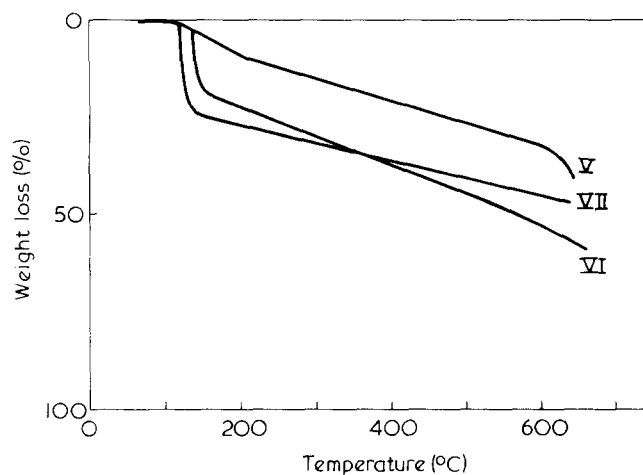


**Figure 5** Thermal decomposition of the products formed from PNP and metal salts in air at 5°C/min

presumed that the lowest value observed with (V) arises from the influence of spin interaction of copper atoms.

#### Thermal stability of the products

The thermal stability of the products investigated using a thermal balance, are shown in *Figures 5* and *6*.



**Figure 6** Thermal decomposition of the products formed from PNPS and metal salts in air at 5°C/min

The thermal decomposition of PNP(I) occurred at 150°C; however, products II, III and IV are more stable than PNP(I) itself. On other hand, PNPS decomposes dramatically owing to the presence of hydrazine groups. It seems that the thermal stability of products V, VI and VII is similar to the products formed from PNP system.

#### REFERENCES

- 1 Kajiwara, M., Hashimoto, M., and Saito, H. *Polymer* 1973, **14**, 488
- 2 Saito, H. and Kajiwara, M. *J. Chem. Soc. Japan (Ind. Chem. Sect.)* 1963, **66**, 618
- 3 Audrith, L. F. *J. Am. Chem. Soc.* 1960, **82**, 528
- 4 Audrith, L. F. *J. Am. Chem. Soc.* 1958, **80**, 5894
- 5 Shvetsov, N. I. *Zh. Obs. Khim.* 1963, **33**, 3936

# Effect of intra-chain double bonds on the crystallization of polyethylene from the melt

L. Amelino and E. Martuscelli

Laboratorio di Ricerche su Tecnologia dei Polimeri e Reologia, CNR, 80072 Arco Felice (Napoli), Italy  
(Received 27 May 1975; revised 30 July 1975)

Crystallization rates, from the melts of linear polyethylene and ethylene-butadiene copolymers, have been measured by differential thermal analysis. The effect of the intra-chain double bonds on the crystallization is discussed. The results are analysed in terms of the Avrami equation. Analysis of the dependence of the rate of crystallization on the undercooling shows that the growth of the spherulites is controlled by a process of surface secondary coherent nucleation. The free energy of formation of a nucleus of critical dimensions depend upon the number of *trans* double bonds in the polymer chain.

## INTRODUCTION

The investigation reported in the present paper was undertaken with the objective of studying the effect of intra-chain *trans* double bonds on the rate of crystallization, from the melt, of samples of ethylene-butadiene copolymers. This work is part of a more general research leading to the knowledge of the properties of polymers with chemical defects or structural irregularities statistically distributed along the chain<sup>1</sup>. The final goal is the improvement of some technological and mechanical properties of polymeric materials by insertion of a known amount of constitutional or configurational irregularities in the macromolecular chain.

## EXPERIMENTAL

### Materials

The polymers used were unfractionated samples of random ethylene-butadiene copolymers (1,4-enchainment) and of high density polyethylene (Vestolen 6013). The polymers were kindly provided by Dr Bruzzoni (ENI-Snam Progetti, Milano, Italy). The copolymers were synthesized using vanadium-based catalysts.

The composition of the samples, determined by i.r. and n.m.r., and some melt rheological properties related to molecular weight values and to their distribution are reported in *Table 1*. The polymers have a rather sharp distribution

*Table 1* Chemical composition and values of the melt flow index (MFI) of samples of ethylene-butadiene (EB) copolymers and of linear polyethylene

Sample	Butadiene composition (mol %)	MFI [2.16(g/10')]	MFI [21.6 (g/10')] MFI [2.16 (g/10')]	Viscosity average molecular weight <sup>a</sup>
Vestolen	0.0	2.0	30	80 000
EB copolymer (1)	0.7	3.0	20	75 000
EB copolymer (2)	1.0	2.6	20	70 000
EB copolymer (3)	1.7	3.0	22	75 000
EB copolymer (4)	2.85	3.0	34	75 000

<sup>a</sup> In decalin at 135°C

of molecular weight; the samples are comparable in both distribution and average molecular weight (see *Table 1*). The presence in the copolymer samples of butadiene units in the *cis* configuration is excluded by i.r. analysis.

### Calorimetry

Crystallization isotherms were obtained using a Perkin-Elmer differential scanning calorimeter DSC-1B. The calorimeter had been previously calibrated with standard low molecular weight substances. The general procedure used for obtaining the crystallization exotherm of the polymer samples was as follows: the polymer was placed in the calorimetric cell and first melted by raising the temperature 10°C above the melting point with a scan rate of 16°C/min. After maintaining the samples at this temperature for about 15 min, to remove any traces of crystallinity, the temperature indicator dial was manually adjusted to the desired crystallization temperature. Zero time of crystallization was taken as the time when the control light came on indicating thermal equilibrium. The crystallization exotherm is registered by running the chart at a suitable rate. A typical curve of crystallization, recorded by using a scanning calorimeter, is shown in *Figure 1*. The weight fraction  $X_t$  of crystallized material at time  $t$  is determined by means of the relation:

$$X_t = \frac{Q_t}{Q_\infty}$$

where  $Q_\infty$ , the total heat generated from the sample at the end of the crystallization, is proportional to the overall area of the exotherm.  $Q_t$ , the heat generated at time  $t$ , is proportional to the shaded area of *Figure 1*. The melting temperature of each sample was determined, after isothermal crystallization, from the maximum of d.s.c. endotherm of fusion.

## RESULTS AND DISCUSSION

Typical crystallization isotherms of samples of linear polyethylene and of ethylene-butadiene copolymers are shown in *Figures 2a* and *2b*. From such plots the half time  $t_{1/2}$  of

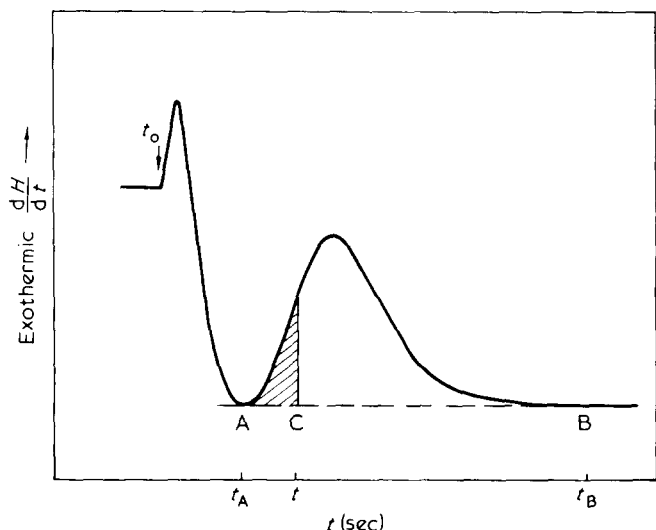


Figure 1 Typical curve of crystallization obtained by use of a differential scanning calorimeter.  $t_0$  is the zero time of crystallization (see text)

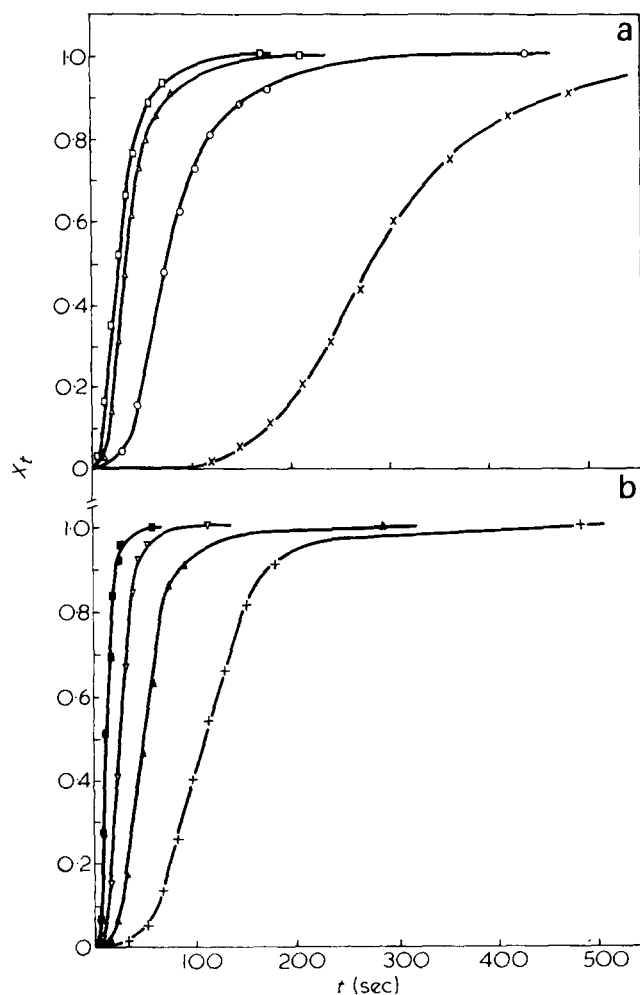


Figure 2 Crystallization isotherm for (a) linear polyethylene and (b) ethylene-butadiene copolymer (4).  $T_c$ : □, 392.5; △, 394; ○, 396; ×, 398; ■, 383.3; ▽, 387.5; ▲, 389.3; +, 391.8 K

the polymers was determined for various crystallization temperatures. The values are reported in Table 2. The crystallization exotherm of the polymers can be analysed by means of the Avrami equation<sup>2</sup>:

$$(1 - X_t) = \exp[-K_n t^n] \quad (1)$$

where  $X_t$  is the weight fraction of crystallizable polymer crystallized at time  $t$ ,  $K_n$  is a kinetic rate constant and  $n$  the Avrami exponent.

In a more useful form equation (1) can be written as:

$$\log[-\log(1 - X_t)] = n \log t + \log \frac{K_n}{2.3} \quad (2)$$

By plotting the quantity  $\log[-\log(1 - X_t)]$  against  $\log t$  it is possible from the slope of the curve, providing that the trend is linear, to determine the values of the Avrami exponent  $n$ .

Plots of  $\log[-\log(1 - X_t)]$  as a function of  $\log t$  are reported in Figure 3 for samples of linear polyethylene and ethylene-butadiene copolymers. In all cases examined a linear trend was observed.

The values of  $n$  determined from the slopes of such curves are reported in Table 2. An average value of 2.6 was calculated.

The rate constant  $K_n$  was calculated from half-life times  $t_{1/2}$  using the following relation:

$$K_n = \frac{\ln 2}{t_{1/2}^n} \quad (3)$$

The melting temperature of the polymers increases with the crystallization temperature with a linear trend according to<sup>3</sup>:

$$T_m = T_m^0 \left( \frac{\gamma - 1}{\gamma} \right) + \frac{T_c}{\gamma} \quad (4)$$

where  $\gamma$  is a parameter that is constant with temperature. The intersection of the  $T_m$  versus  $T_c$  line with the line  $T_c = T_m^0$  yields the value of the equilibrium melting temperature  $T_m^0$ . Examples of the method used for the determination

Table 2 Crystallization temperature,  $T_c$ , half-time,  $t_{1/2}$ , Avrami exponent,  $n$ , and equilibrium melting temperature,  $T_m^0$  for samples of polyethylene and ethylene-butadiene (EB) copolymers isothermally crystallized from the melt

Polymer	$T_c$ (K)	$n$	$t_{1/2}$ (sec)	$T_m^0$ (K)
Vestolen	392.5	2.3	30	412
	394.0	2.3	36	
	396.0	2.5	74	
	398.0	2.7	290	
	400.0	2.7	628	
EB (1)	389.5	2.8	28.5	412
	392.5	2.8	57.5	
	395.5	3.0	25.9	
EB (2)	387.1	2.4	22	412
	389.1	2.4	41.5	
	391.1	2.4	102.5	
	393.1	2.4	211.0	
	395.1	2.3	1000	
EB (3)	387.3	2.4	23.5	412
	389.3	2.5	47	
	391.3	2.5	116	
	393.3	2.5	382	
EB (4)	385.3	2.6	18.5	412
	387.3	2.8	26	
	389.3	2.9	47.5	
	391.3	3.1	108	
	393.3	2.8	346	

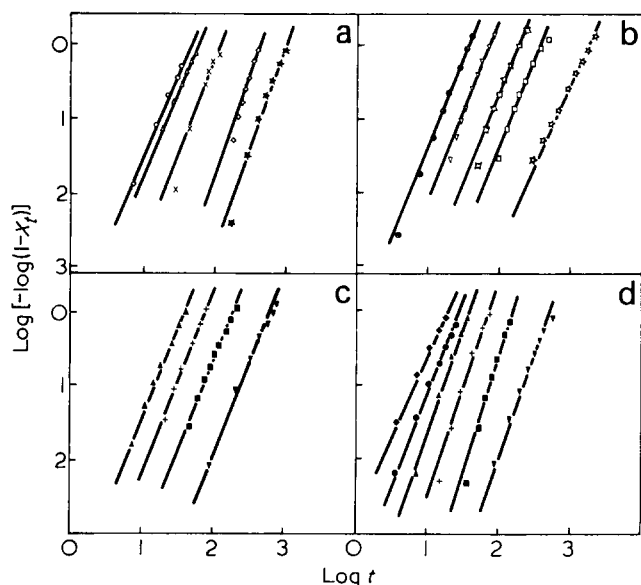


Figure 3 Avrami plots for the crystallization of samples of linear polyethylene (Vestolen 6013) and of ethylene-butadiene copolymers: (a) linear polyethylene; (b) EB copolymer (2); (c) EB copolymer (3); (d) EB copolymer (4). Crystallization temperatures:  $\circ$ , 392.5;  $\triangle$ , 394;  $\times$ , 396;  $\diamond$ , 398;  $\star$ , 400;  $\oplus$ , 387.1;  $\nabla$ , 389.1;  $\boxplus$ , 391.1;  $\square$ , 393.1;  $\star$ , 395.1;  $\blacktriangle$ , 387.3;  $+$ , 389.3;  $\blacksquare$ , 391.3;  $\blacktriangledown$ , 393.3;  $\blacklozenge$ , 383.3;  $\bullet$ , 385.3 K

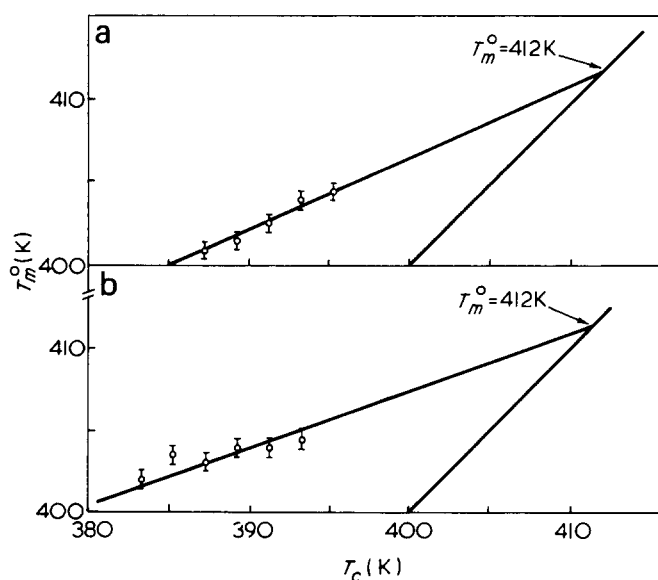


Figure 4 Dependence of the melting temperature  $T_m$  upon the crystallization temperature,  $T_c$ . (a) EB copolymer (3); (b) EB copolymer (4). The value of the equilibrium melting point is also indicated (see text)

of  $T_m^0$  are illustrated in Figures 4a and 4b. No significant influence of the number of intra-chain double bonds on the value of  $T_m^0$  had been observed at least for our range of composition. For linear polyethylene and for ethylene-butadiene copolymers we found, in fact, almost the same value of 412 K for  $T_m^0$ .

The dependence of  $\log(1/t_{1/2})$  on the percentage of butadiene in the polymer chain is shown in Figure 5 for values of the undercooling between 25 and 17°C. The trend of the curves shows that for lower values of the undercooling the rate of crystallization decreases with increasing the number of double bonds in the macromolecule. The extent of this effect becomes negligible at higher values of the undercooling.

It is well known that the crystallization of linear polymers, from the melt, leads to the formation of lamellar spherulites. The linear growth rate  $G$  of the spherulites can be expressed as:

$$G = G_0 \exp \left\{ -\frac{\Delta F^*}{RT_c} \right\} \exp \left\{ -\frac{\Delta \Phi^*}{KT_c} \right\} \quad (5)$$

In this equation  $G_0$  is a parameter usually considered constant,  $\Delta F^*$  represents the activation energy characteristic of transport across the liquid-crystal interface,  $\Delta \Phi^*$  is the work required to form a nucleus of critical size,  $T_c$  is the crystallization temperature and  $K$  is the Boltzmann constant.

When a coherent two-dimensional surface secondary nucleation process controls the radial growth of lamellar spherulites, then the following expression holds for  $\Delta \Phi^*$ <sup>4</sup>:

$$\Delta \Phi^* = \frac{4b_0\sigma \cdot \sigma_e \cdot T_m^0}{\Delta H_F \cdot \Delta T} \quad (6)$$

where  $b_0$  is the thickness of the surface layer,  $\sigma$  and  $\sigma_e$  are interfacial free energies per unit area parallel and perpendicular respectively to the molecular chain direction,  $\Delta H_F$  is the heat of fusion,  $T_m^0$  the equilibrium melting temperature and  $\Delta T = T_m^0 - T_c$  is the undercooling. By using equations (5) and (6) the rate of overall crystallization may be expressed by the equations<sup>4,5</sup>:

$$\frac{1}{3} \log K_n = A_0 - \frac{\Delta F^*}{2.3RT_c} - \frac{4b_0\sigma\sigma_e T_m^0}{2.3K\Delta H_F \cdot T_c \Delta T} \quad (7)$$

or

$$\frac{n}{3} \log (1/t_{1/2}) = A_0 - \frac{\Delta F^*}{2.3RT_c} - \frac{1}{3} \log \ln 2 - \frac{4b_0\sigma\sigma_e T_m^0}{2.3K\Delta H_F \cdot T_c \Delta T} \quad (8)$$

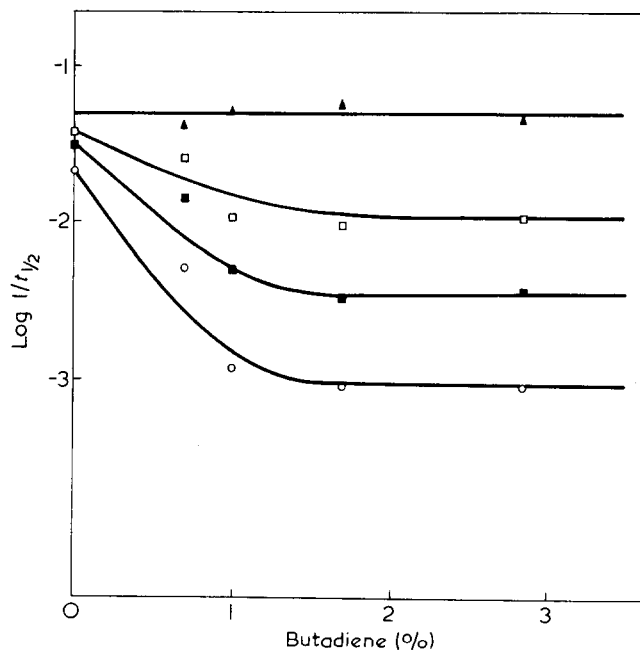


Figure 5 Variation of  $\log(1/t_{1/2})$  with the percentage of butadiene in the chain for samples of polyethylene and ethylene-butadiene copolymers. Undercooling:  $\circ$ , 17;  $\square$ , 19;  $\triangle$ , 21;  $\blacklozenge$ , 25 K

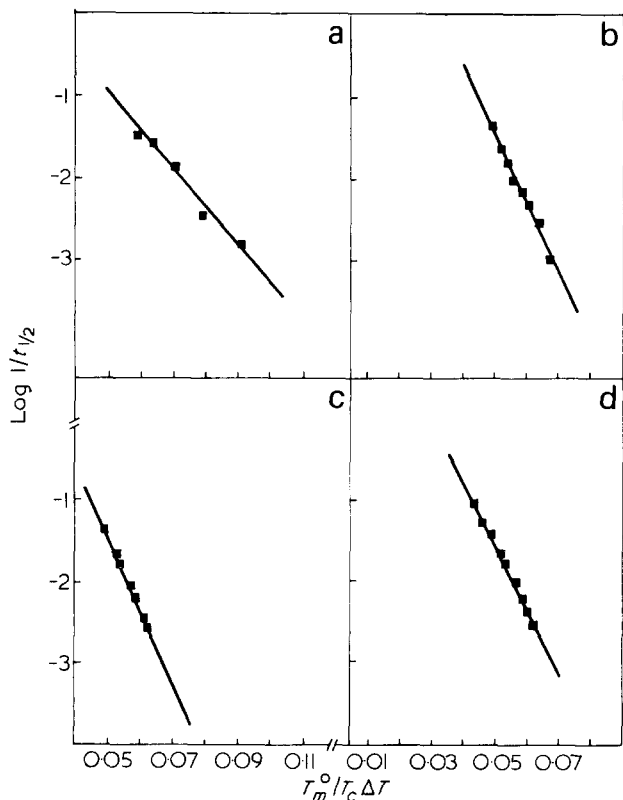


Figure 6 Plots of  $\log(1/t_{1/2})$  against  $T_m^0/T_c \Delta T$  for polyethylene and ethylene-butadiene copolymers isothermally crystallized from the melt. (a) Linear polyethylene; (b) EB copolymer (2); (c) EB copolymer (3); (d) EB copolymer (4)

Table 3 Values of  $4b_0\sigma\sigma_e/K\Delta H_F$  calculated from the slopes of the curves of Figures 6 and 7 and the corresponding average

Polymer	$\frac{4b_0\sigma\sigma_e}{K\Delta H_F}$ (K)		Average
	From slopes of curves of Figure 6	From slopes of curves of Figure 7	
Vestolen	108.0	106.9	107.5
EB (1)	155.0	134.5	144.7
EB (2)	194.0	198.9	196.4
EB (3)	208.0	211.6	209.8
EB (4)	200.0	184	192.0

The variation of the quantity  $\log(1/t_{1/2})$  as a function of  $T_m^0/T_c \Delta T$  in the case of samples of polyethylene and ethylene-butadiene copolymers is reported in Figure 6.

A linear trend is observed indicating that the transport term  $\Delta F^*/2.3RT_c$  in equation (8) almost maintains a constant value when the polymers are isothermally crystallized at a relatively low value of undercooling. From the slopes of the curves of Figure 6 the quantity  $4b_0\sigma\sigma_e/K\Delta H_F$  was calculated. The values are reported in Table 3.

In this calculation, we assumed for the exponent of the Avrami equation  $n$ , an integral value of 3 for all polymers.

The transport term in equations (7) and (8) may be equated to the activation energy for viscous flow which has a temperature dependence, derived from WLF equations<sup>5,6</sup>:

$$\Delta F^* = \Delta F_{WLF} = \frac{C_1 T_c}{C_2 + T_c - T_g} \quad (9)$$

where  $C_1$  and  $C_2$  are constants generally made equal to 4.12 kcal/mol and 51.5 K respectively and  $T_g$  is the glass transition temperature of the polymer.

In Figure 7 the quantity  $1/3 \log K_n + (\Delta F_{WLF}/2.3RT_c)$  is plotted against  $T_m^0/2.3T_c \Delta T$  in the case of polyethylene and ethylene-butadiene copolymers. In all cases the trend is linear. In the calculation of  $\Delta F_{WLF}$ , by means of equation (9), we assumed for the  $T_g$  of the ethylene-butadiene copolymers a value of 148 K, i.e. the glass transition temperature of linear polyethylene<sup>7</sup>. The value of the quantity  $4b_0\sigma\sigma_e/K\Delta H_F$  calculated from the slopes of the curves of Figure 7 agree fairly well with that calculated from the slopes of the curves  $\log(1/t_{1/2})$  against  $T_m^0/T_c \Delta T$  (see Table 3). As shown in Figure 8 the quantity  $4b_0\sigma\sigma_e/K\Delta H_F$  depends upon the number of *trans* double bonds in the chain. In fact, for linear polyethylene we found an average value of 107.5 K while the same quantity assumes in the case of ethylene-butadiene<sup>4</sup> copolymer a value of 192.0 K.

From the data of Table 3 and by using equation (6) the value of the free energy of formation of a nucleus of critical size  $\Delta\Phi^*$  may be calculated for each sample. The variation of  $\Delta\Phi^*$  with the percentage of butadiene is shown in Figure 9. The comparison is made for the same value of  $\Delta T$ . For lower value of the undercooling,  $\Delta\Phi^*$  drastically increases with the amount of double bonds in the chain.

## CONCLUSIONS

Experimental calorimetric crystallization isotherms of linear polyethylene and ethylene-butadiene copolymers

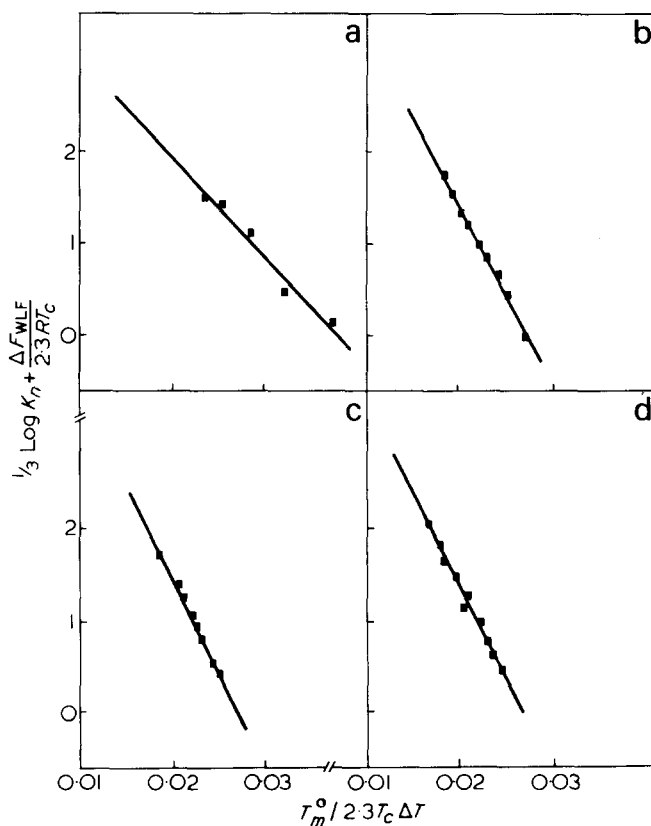


Figure 7 Plots of  $1/3 \log K_n + (\Delta F_{WLF}/2.3RT_c)$  against  $T_m^0/2.3T_c \Delta T$  for polyethylene and ethylene-butadiene copolymers isothermally crystallized from the melt. (a) Linear polyethylene; (b) EB copolymer (2); (c) EB copolymer (3); (d) EB copolymer (4)



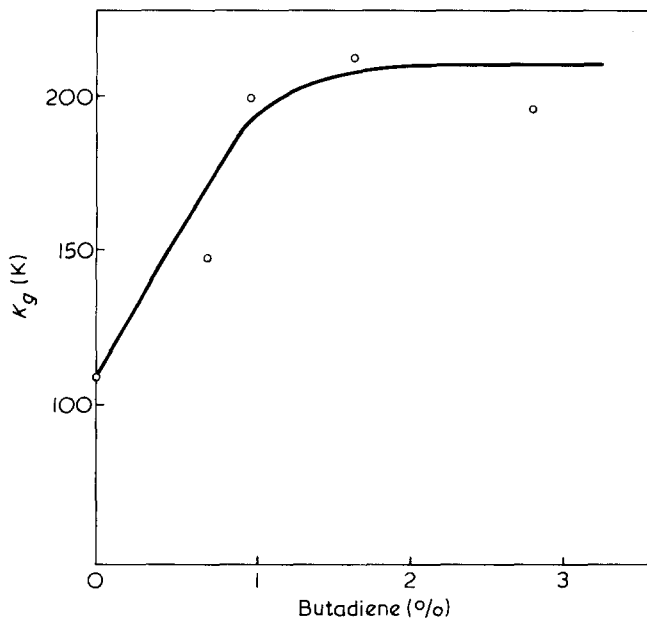


Figure 8 Dependence of the quantity  $K_g = 4b_0\sigma\sigma_e/K\Delta H_F$  upon the percentage of butadiene in the chain for ethylene-butadiene copolymers

fit the Avrami equation for the description of the primary crystallization kinetics. From the analysis of the results, it can be concluded that the random insertion of some *trans* double bonds along the chain of polyethylene decreases the rate of crystallization, from the melt, of the polymer. This effect is more prominent in the vicinity of the melting point.

Analysis of the temperature dependence of crystallization kinetics for linear polyethylene and ethylene-butadiene copolymers, carried out in terms of the kinetic crystallization theory proposed by Hoffman *et al.*<sup>3-5</sup>, agrees with a growth process of spherulites controlled by a surface two-dimensional coherent nucleation. The observed decrease of the rate of crystallization of ethylene-butadiene copolymers, with increasing the percentage of butadiene, is to be ascribed mainly to the fact that *trans* double bonds, when inserted along the chain of polyethylene, cause a rather drastic increase in the value of the free energy of formation  $\Delta\Phi^*$  of a nucleus of critical dimensions. On the contrary, the free energy of activation  $\Delta F^*$ , related to the phenomenon of mass transport at the liquid-crystal interface seems to be almost constant, at least under our crystallization conditions.

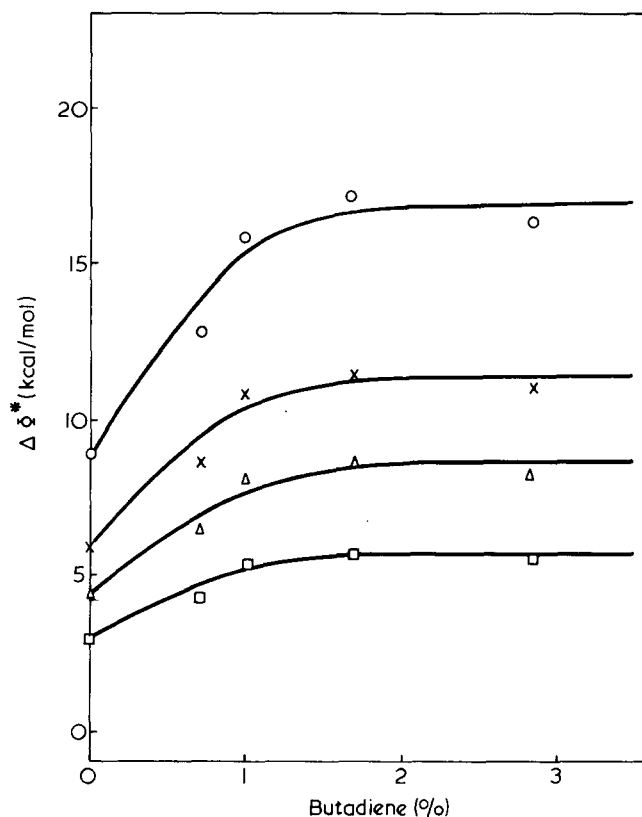


Figure 9 Influence of the composition on the value of the free energy of formation  $\Delta\Phi^*$  (kcal/mol) of a nucleus of critical dimension, at different values of the undercooling  $\Delta T$ , in the case of linear polyethylene and ethylene-butadiene copolymers.  $\circ$ , 10;  $\times$ , 15;  $\triangle$ , 20;  $\square$ , 30 K

## REFERENCES

- 1 Martuscelli, E. and Pracella, M. *Polymer* 1974, 15, 306; Martuscelli, E. *Chim. Ind. (Milan)* 1974, 56, 9; Marchetti, A. and Martuscelli, E. *J. Polym. Sci. (Polym. Phys. Edn)* 1974, 12, 1649; Martuscelli, E. *J. Macromol. Sci. (B)* 1975, 11, 1
- 2 Mandelkern, L. 'Crystallization of Polymers' New York, McGraw-Hill, 1964; Sharples, A. 'Introduction to Polymer Crystallization', Edward Arnold, London, 1966
- 3 Hoffman, J. D. *SPE Trans.* 1964, 4, 315
- 4 Hoffman, J. D. and Weeks, J. J. *J. Chem. Phys.* 1962, 37, 1723
- 5 Godovsky, Ju. K. and Shonimsky, G. L. *J. Polym. Sci. (Polym. Phys. Edn)* 1974, 12, 1053
- 6 Williams, M. L., Landel, R. F. and Ferry, J. D. *J. Am. Chem. Soc.* 1955, 77, 3701
- 7 Brandrup, J. and Immergut, E. H. 'Polymer Handbook', Interscience, New York, 1966

# Dynamic mechanical spectra of poly-(itaconic acid esters) containing phenyl and cyclohexyl rings

J. M. G. Cowie and I. J. McEwen

Department of Chemistry, University of Stirling, Stirling FK9 4LA, UK

and J. Veličković

Faculty of Technology and Metallurgy, Belgrade, Yugoslavia

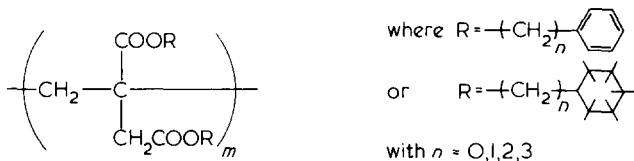
(Received 2 June 1975)

The dynamic mechanical response of a series of poly(itaconic acid esters), in which the ester group,  $-\text{COOR}$ , has  $\text{R} = (\text{CH}_2)_n \phi$  with  $n = 0, 1, 2$  and  $\phi$  is either a phenyl or cyclohexyl ring, was studied over the temperature range 90 to 425K. In each case the glass transition temperature  $T_g$ , of the cyclohexyl derivative is higher than the corresponding phenyl derivative, and  $T_g$  also decreases as  $n$  increases. A  $\beta$ -transition, located in both the phenyl and cyclohexyl series, is attributed to motion of the ester groups. In addition the cyclohexyl polymers exhibit a prominent  $\gamma$ -transition caused by cyclohexyl ring movement and there is also a  $\delta$ -transition in this series which is believed to be a precursor of the  $\gamma$ -transition.

## INTRODUCTION

Polymers based on the esters of itaconic acid have received very little attention in the past. Some work has been reported<sup>1-4</sup> on the solution behaviour of polymers prepared from the dialkyl ester derivatives and their copolymers with styrene, but to date nothing has been published on the mechanical behaviour of either these or related poly(itaconic esters). This area merits study, first because the fundamental monomer, itaconic acid, is not an oil-based product, but is obtained commercially by a fermentation process, and secondly, the esters are similar in structure to the poly(alkyl methacrylates). One can regard poly(itaconic acid di-esters) as poly(alkyl methacrylates) in which one hydrogen of the  $\alpha$ -methyl group is replaced by a second ester group. It is of interest then to explore this area further and to make comparisons with these established polymers.

This is the first in a series of papers in which the physical behaviour of poly(itaconic esters) will be examined. The polymers studied here have the general repeat unit:



Comparison of these two main series also allows one to evaluate the influence of the ring type on the mechanical response.

## EXPERIMENTAL

### Preparation of itaconic acid esters

The synthesis of cycloaliphatic and aromatic esters of itaconic acid was first described by Veličković *et al.*<sup>5</sup>. Dicyclohexyl, dimethyl cyclohexyl, diethyl cyclohexyl,

dibenzyl, diethyl phenyl and dipropyl phenyl itaconate monomers were all prepared by reacting itaconic acid (1 mol) with the appropriate alcohol (3 mol) in toluene, in the presence of sulphuric acid/*p*-toluene sulphonic acid catalyst. The system was refluxed for several hours then the mixture was neutralized with aqueous sodium carbonate. The toluene layer was separated, dried, and filtered, and the toluene was removed by distillation. The monomer was isolated from the residue by vacuum distillation. Diphenyl itaconate was prepared in a different manner. Itaconic acid was dissolved by refluxing a suspension in benzene. A slight stoichiometric excess of phenol was added to the solution and refluxing was continued for 2 h. At this point a slight excess of phosphorus pentoxide was added and the reaction allowed to continue for a further 4 h. The mixture was cooled, washed repeatedly with water and saturated sodium bicarbonate, before separating the organic layer. Benzene was removed from the mixture and the residue was dissolved in diethyl ether. Washing was repeated, followed by drying with sodium sulphate. The ether was removed and the residue dissolved in hot petroleum ether from which the monomer separated on cooling as white crystals (m.p. = 340K).

### Polymerization

The monomers were polymerized in bulk, under vacuum, at temperatures between 333 and 343K; the initiator was  $\alpha, \alpha'$ -azobisisobutyronitrile. Polymerizations, carried out over a period of 24 to 48 h, produced highly viscous or solid products which were dissolved in benzene. The polymer was isolated by precipitation using methanol and purified by repeated dissolution and precipitation. The polymers were characterized and a summary of the data is presented in Table 1.

### Dynamic mechanical measurements

The dynamic thermomechanical response of each sample was measured over the temperature range 90 to 425K and at five frequencies using two techniques.

Table 1 Data characterizing poly(itaconic acid esters) and poly(methyl methacrylate)

Polymer	Code	$[\eta]$ † (cm <sup>3</sup> /g)	$M_v \times 10^{-4}$
poly(dicyclohexyl itaconate)	PDCHI	13.2	6.8
poly(dimethyl cyclohexyl itaconate)	PDMCHI	43.0	50.0
poly(diethyl cyclohexyl itaconate)	PDECHI	40.7	42.0
poly(diphenyl itaconate)	PDFI	26.4	35.0
poly(dibenzyl itaconate)	PDBzI	11.5	13.0
poly(diethyl phenyl itaconate)	PDEFI	23.4	32.0
poly(dipropyl phenyl itaconate)	PDPFI	10.8	10.0
poly(dimethyl itaconate)	PDMI	—	45.1
poly(methyl methacrylate)	PMMA	—	36.0

† Measured in toluene at 298K

**Torsional braid analysis (t.b.a.).** A torsional braid analyzer (t.b.a.), model 100-B1 Chemical Instruments Corporation, was used to obtain thermomechanical spectra at frequencies of less than 1 Hz. Glass braids were impregnated with polymer by immersion in a concentrated solution (10% w/v) of the sample under investigation. The braid was then suspended, under a small load, in a drying cell and the solvent was removed under vacuum. The sample braid was transferred to the measuring chamber of the t.b.a., which was flushed continually by a stream of dry nitrogen, then cooled to liquid nitrogen temperature and equilibrated there for 30 min. The sample chamber and sample were then allowed to warm slowly at a rate of about 1.0 to 1.5 K/min, and the dynamic mechanical response of the sample was recorded at 2 to 4K intervals. The number of oscillations,  $n$ , was counted for each decay pattern between two fixed but arbitrary boundary amplitudes. The characteristic mechanical damping index  $1/n$ , which is related to the logarithmic decrement of the free resonance vibrations, can then be obtained as a function of temperature. Data are plotted as  $-\log n$  against temperature.

**Rheovibron linear viscoelastometer (r.v.).** Measurements of the dynamic mechanical behaviour at frequencies of 3.5, 11.0, 35 and 110 Hz were made using a Rheovibron viscoelastometer model DDV-II-C. The instrument is most useful when the sample is mechanically strong and is sufficiently crystalline to maintain the sample shape as the polymer passes through the glass transition. In order to extend the measurements to the polyitaconates, which form very brittle films and are mechanically weak above their glass transition temperature,  $T_g$ , samples were supported on glass fibre filter paper which was inert over the temperature range of interest.

Strips of GF/C glass fibre filter paper (2.5 cm  $\times$  0.5 cm) were impregnated with polymer solution and allowed to dry. The solvent was removed from the composite as far as possible by further drying under vacuum at room temperature. The instrument measures the damping in the system ( $\tan \delta$ ) directly and spectra were constructed from plots of  $\tan \delta$  against temperature. These were similar in shape to those obtained using the t.b.a. Values of  $\tan \delta$  maxima were also extrapolated to a frequency of 1 Hz, in some cases, for comparison with other data.

#### Differential thermal analysis

Thermograms were obtained using a Du Pont 900-DSO module. Glass transition temperatures were estimated by locating the intersection of the base line with the extrapolated slope of the curve formed during a base line shift.

The instrument was calibrated regularly using gallium and indium as standards.

## RESULTS AND DISCUSSION

Mechanical damping index curves obtained from t.b.a. measurements are shown as a function of temperature in Figure 1 for each cyclohexyl and phenyl pair. Four damping peaks can be located in the spectra of the cyclohexyl derivatives but only two are prominent in the spectra of the phenyl derivatives.

**$\alpha$ -Transitions.** Well defined  $\alpha$ -transitions exist for both series of polymers which are identified as the glass transition. Estimates of the temperatures at which the  $\alpha$ -maxima occur are shown in Table 2 for t.b.a. and for r.v. measurements at 1 Hz, where they can be compared with the values of  $T_g$  obtained from d.s.c. measurements. The  $T_g$  (d.s.c.) values are consistently lower than those obtained from

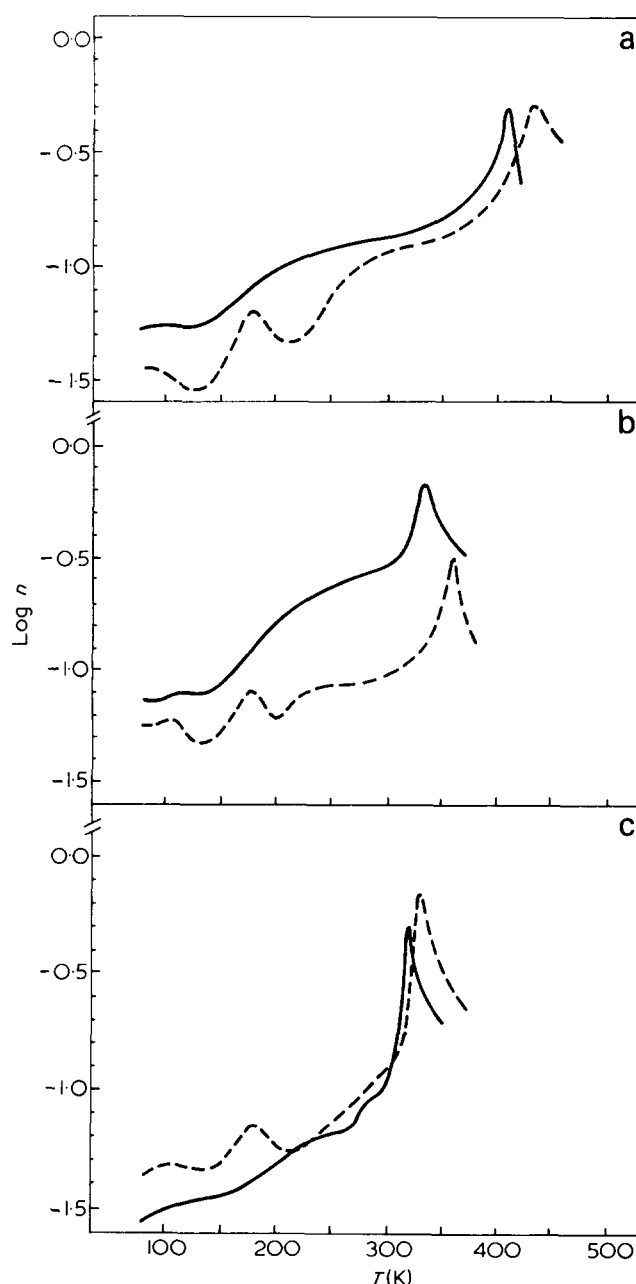


Figure 1 T.b.a. mechanical damping index curves for (a) PDFI (—) and PDCHI (---); (b) PDBzI (—) and PDMCHI (---); (c) PDEFI (—) and PDECHI (---)

Table 2 Glass transition temperatures from d.s.c. and dynamic mechanical measurements

Polymer	$T_g$ (K)			$T_\beta/T_g$
	d.s.c.	t.b.a.	r.v. (1 Hz)	
PDFI	405	414	430	0.58
PDCHI	417	435	446	0.64
PDBzI	328	335	—	0.75
PDMCHI	356	361	379	0.66
PDEFI	308	317	—	—
PDECHI	321	327	322	—
PDPFI	265	—	286	—
PDMI	371	375	395	—
PMMA	396	—	419	—

mechanical measurements although the agreement improves as the ester group lengthens. Heijboer<sup>6</sup> also reported that the damping maxima at 1 Hz ( $\tan \delta$ ), associated with the glass transition or 'softening zone', were often 10 to 30K higher than static  $T_g$  values.

In each case  $T_g$  for the cyclohexyl derivative is higher than the corresponding phenyl derivative, implying that the steric hindrance to rotation in the backbone chain, imposed by the cyclohexyl ring is greater than the phenyl. This was not observed in the analogous poly(phenyl methacrylates) and poly(cyclohexyl methacrylates), both of which exhibited damping curves with  $\alpha$ -transition maxima at 403K<sup>6,7</sup>. Furthermore one can assess the influence of the second ester side chain in poly(itaconic esters) by comparing the  $T_g$  values for poly(methyl methacrylate) (PMMA) and poly(dimethyl itaconate) (PDMI) with the present series using r.v. data extrapolated to 1 Hz. If PDMI is considered to be PMMA with one hydrogen of the  $\alpha$ -methyl group replaced by a  $-\text{COOCH}_3$  group, then it can be seen from the data in Table 2 that this substitution leads to a lowering of  $T_g$  presumably owing to the plasticizing effect of the additional flexible ester group. Replacement of both methyl groups in PDMI by either cyclohexyl or phenyl rings results in a substantial increase in  $T_g$  of between 35 and 50K caused by the increased steric restrictions to rotation arising from the larger molar volume of the rings. Insertion of methylene units to lengthen the ester side chains increases their flexibility and leads to internal plasticization of the polymer. This results in a progressive decrease in  $T_g$  as the side chains lengthen.

$\beta$ -Transition. The  $\beta$ -transition is much more difficult to locate accurately as it appears as a shoulder in the damping curve rather than a pronounced peak. In the PDCHI and PDMCHI samples it occurs in the region of 250K but it is apparently suppressed in the PDECHI polymer. In PDFI and PDBzI the  $\beta$ -shoulder appears in the lower temperature range 200 to 250K and again is less evident in the higher esters PDEFI and PDPFI. The ratio  $T_\beta/T_g$  lies between 0.6 and 0.75 which is similar to that reported for other polymers<sup>8</sup>.

The mechanism underlying the  $\beta$ -damping in poly(alkyl methacrylates) has been discussed at some length by Heijboer<sup>6</sup> who attributes its existence to rotation of the pendant group  $-\text{COOR}$ . Other workers<sup>8</sup> stress that the  $\beta$ -relaxation is a precursor to cooperative chain motion leading to the glass transition and that backbone motion is involved. The two viewpoints are not totally incompatible and we attribute the  $\beta$ -relaxation to rotation of both ester groups which will ultimately aid and reinforce the extensive main chain motion required for the glass transition.

$\gamma$ -Transition. The presence of a damping maximum at about 180K is observed only for the esters containing a cyclohexyl ring. This peak is absent in the phenyl derivatives and leads to the conclusion that the damping is caused exclusively by cyclohexyl ring movement. Heijboer<sup>7,9</sup> detected a comparable transition at 193K for poly(cyclohexyl methacrylate) which was ascribed to a chair-chair transition in the cyclohexyl ring with an apparent activation energy  $\Delta H^\ddagger$  of 48.1 kJ/mol. The frequency dependence of the  $\tan \delta$  maximum for each cyclohexyl derivative examined here is shown in Figure 2. From a least squares analysis of the data  $\Delta H^\ddagger$  can be estimated to be 65.5 kJ/mol for PDCHI, while PDMCHI and PDECHI have slightly lower values of 52.3 and 50.4 kJ/mol respectively. The motion appears to be less impeded when the ring is moved further away from the main chain by the methylene units and in all cases  $\Delta H^\ddagger$  is greater than Heijboer's value for poly(cyclohexyl methacrylate). This may indicate a greater degree of steric hindrance in the itaconic ester polymers. While the transition can be ascribed to cyclohexyl ring motion, we are inclined to favour the idea that it is caused by a chair to skewboat transition. This avoids having the chain, attaching the cyclohexyl ring to the backbone, in an unfavourable axial conformation which it would be forced to adopt for one of the chain positions in Heijboer's mechanism.

$\delta$ -Transition. A small loss peak can be observed in the region of 100K which is more difficult to resolve because it occurs near the lower limit of our attainable temperature range. This  $\delta$ -transition is most obvious in the cyclohexyl derivatives and there is only a very slight suggestion of its presence in PDFI and PDBzI. Molecular motion in this region has been attributed to a variety of mechanisms: methyl group rotation, crankshaft motion, and pendant group re-orientation. Because of the doubt concerning the presence of a  $\delta$ -peak in the phenyl derivatives, it would appear most

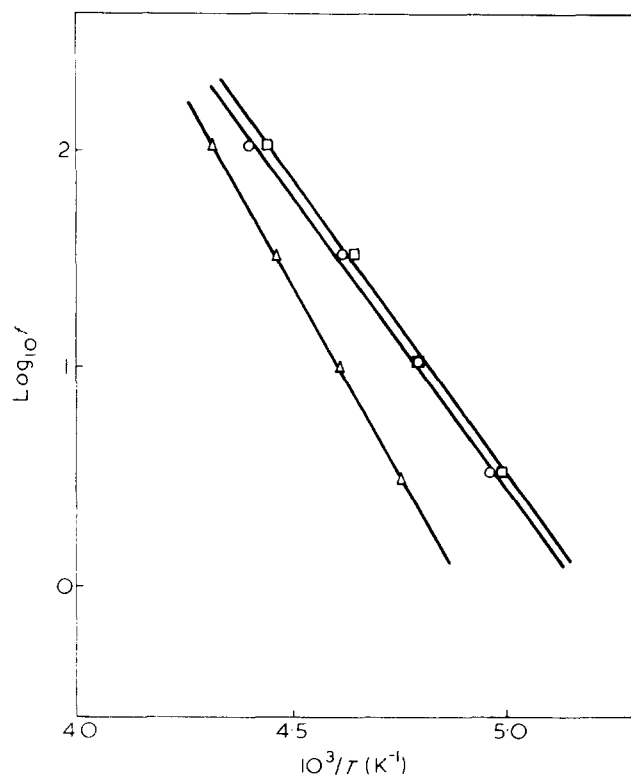


Figure 2 Plots of  $\log_{10}$  (frequency) against reciprocal temperature of the  $\gamma$ -transition  $\tan \delta$  maxima for PDCHI ( $\Delta$ ), PDMCHI ( $\square$ ), and PDECHI ( $\circ$ )

likely that the damping is caused by group motion which is a precursor to the more pronounced movement of the cyclohexyl ring at higher temperatures. This could either be a simple migration of the cyclohexyl ring into a vacant hole or a torsional motion within the ring.

## CONCLUSIONS

The use of glass fibre supports to prepare composites of brittle or mechanically weak polymers for study in the Rheovibron appears to be satisfactory. As with t.b.a., the sample size cannot be defined, consequently the results are not absolute and often yield  $T_g$  values higher than those obtained using static techniques, even after extrapolation to low frequencies. The data can, however, be compared on a relative basis and both glass and subglass transitions are easily located.

The substitution of a ring system in the ester group leads to an increase in  $T_g$  relative to PMMA, and this increase is greater for the cyclohexyl derivatives than for the phenyl derivatives. Observations made on the influence of ring substitution in these samples compared with PMMA, must of course be tempered by the knowledge that the  $T_g$  of PMMA is a function of sample stereostructure. The PMMA sample used here is an atactic sample with ~75% syndiotactic diad placements in the chain; it is assumed that as the polyitaconates were obtained by free radical polymerization the

stereostructure would be roughly the same, namely atactic. Any microstructural differences would only affect conclusions based on the relative magnitudes of  $T_g$ , and should not alter the general trends, detected here, to any marked extent.

## ACKNOWLEDGEMENTS

We wish to thank the Royal Society for a grant-in-aid award to J.M.G.C. for the acquisition of the Rheovibron visco-elastometer.

## REFERENCES

- 1 Tate, B. E. *Adv. Polym. Sci.* 1967, **5**, 214
- 2 Veličković, J., Jovanović, D. and Vukajlović, J. *Makromol. Chem.* 1969, **129**, 203
- 3 Bekturov, Ye. A., Bimendina, L. A. and Bereza, S. V. *Vysokomol. Soedin. (A)* 1970, **12**, 2179
- 4 Veličković, J., Juranicova, V. and Filipović, J. *Angew. Makromol. Chem.* 1972, **24**, 77
- 5 Veličković, J., Muskatirović, M. and Bajic, N. *2nd Yugoslav. Symp. Macromolecules, Zagreb 1971*
- 6 Heijboer, J. *Proc. Int. Conf. Physics Non-Crystalline Solids*, North Holland, Amsterdam, 1965 p 231
- 7 Heijboer, J. *Br. Polym. J.* 1969, **1**, 3
- 8 Hiltner, A., and Baer, E. *Polymer* 1974, **15**, 805
- 9 Heijboer, J. *Kolloid-Z.* 1960, **171**, 7

# Elastic behaviour of ideal polystyrene networks

F. Rietsch and D. Froelich

University of Lille, BP 36, 59650 Villeneuve d'Ascq, France

(Received 23 December 1974; revised 28 May 1975)

Polystyrene gels were prepared by anionic copolymerization of styrene and divinylbenzene in dilute solution (7.5%), the molecular weight between crosslinks ranging from 10 000 to 75 000. A study of the photoelasticity of these networks swollen to equilibrium in benzene and cyclohexane allowed some molecular parameters such as the memory term, the number of elastic chains, the functionality of the crosslinks, and the optical anisotropy of the random links to be calculated. The Mooney–Rivlin representation shows that both in elongation and compression, the  $C_2$  term is nul, the  $C_1$  term becoming identified with the theoretical modulus from the Flory, Wall and Hermans theory.

## INTRODUCTION

Up to now networks have been prepared by radical polymerization in which the chain order of the different monomers results from statistical probability, the parameters being concentrations (initiator and monomer) and ratios of radical reactivity<sup>1,2</sup>. The result is a large distribution of linear sequences between crosslinks and an unknown and varied functionality of the crosslinkage points. Such a method of preparation leads to networks whose structure is not well defined and which, according to certain authors<sup>3,4</sup> can present an inhomogeneous structure.

To ensure a better control of these networks we made use of an anionic polymerization method developed by Rempp and coworkers<sup>5–7</sup>. It is well known that the polymerization of styrene initiated by a bifunctional organometallic initiator, such as naphthalene(sodium salt) or the disodium tetramer of  $\alpha$ -methylstyrene, can by a nucleophile attack of the double bonds, result in a polystyrene with reactive organo-sodium sites at both ends. The dicarbanion obtained in this way is linear and is of low polydispersity. If a difunctional monomer is added, such as divinylbenzene (DVB) which is likely to be initiated by the styryl carbanions, we obtain a three-dimensional network.

This technique offers the following advantages: (1) polystyrene chains are linear and monodisperse; the molecular weights of these chains can be made to vary in large proportions and be measured experimentally before crosslinking; (2) concentration in segments in the gel is equal to the one that already existed in the solution before the DVB was added. Here, the gel point corresponds to multiple linkages between the polymeric chain ends; (3) the total concentration of polymer in its solvent can undergo large variations which makes it possible to avoid syneresis<sup>8</sup>.

On the other hand, those networks very closely related to the ideal model, present the following defects: (1) a certain number of polystyrene chains can become deactivated during preparation. A formation of 'free' chains is observed if deactivation occurs at both chain-ends, whereas pendant chains will appear if deactivation takes place at one chain-end only; (2) physical knots or entanglements can form in the crosslinking process. These can behave like physical crosslinks while the network is being deformed; (3) cyclizations can occur, but this probability is low and experimental results have shown that the phenomenon is

negligible; (4) the functionality of the branching points is not clearly defined.

## THEORETICAL

### *Elasticity and swelling of a three-dimensional Gaussian network*

Over the last few years, the molecular theory of rubber-like elasticity has caused great controversy about two established theories, that of Flory, Wall and Hermans<sup>9–13</sup> on the one hand and of James and Guth<sup>14–17</sup> on the other.

Dusek and Prins<sup>18</sup> have in a recent review, summarized this controversy with emphasis on the variation of free energy in elastic deformation:

$$\Delta F_{\text{network}} = \frac{A\nu_e kT}{2} (\lambda_x^2 + \lambda_y^2 + \lambda_z^2 - 3) - B\nu_e kT \log \lambda_x \lambda_y \lambda_z \quad (1)$$

where  $\nu_e$  stands for the number of elastic chains,  $\lambda_x$ ,  $\lambda_y$ ,  $\lambda_z$ , the deformation ratios projected on three reference axes,  $k$ , the Boltzmann constant, and  $T$ , the Kelvin temperature.

According to Flory, Wall and Hermans  $A = 1$ ,  $B = 2/f$  in which  $f$  represents the functionality of the crosslinks. According to James and Guth  $A = 1/2$  and  $B = 0$ .

When the network is swollen at equilibrium, the chemical potential of the solvent is:

$$\Delta\mu_1 = A\nu_e RT \bar{V}_1 q_0^{-2/3} q_i^{-1/3} - BRT\nu_e \bar{V}_1 q_i^{-1} + RT[\log(1 - q_i^{-1}) + q_i^{-1} + \chi q_i^{-2}] = 0 \quad (2)$$

where  $\bar{V}_1$  = partial molar volume of the diluent

$$q_0^{2/3} = \frac{\langle r_{OS}^2 \rangle}{\langle r_D^2 \rangle} = \frac{\langle r_{OS}^2 \rangle}{\langle r_c^2 \rangle} q_c^{2/3}$$

$q_c^{-1}$  = volume fraction of polymer at crosslinking stage

$q_i$  = swelling ratio of the network

$\chi$  = the Flory–Huggins interaction parameter

Table 1 Network characterization by measurement of molecular weights from linear chains and extractible free chains ratio

	3 003	343	17 102	543	853	743	13 112	2 743	15 112	3 043	5 553
$M_n$	10 450	10 660	11 800	13 100	16 450	19 900	29 300	30 000	40 500	45 600	75 000
$M_w$ (DDL)	10 900	11 900	11 800	15 200	18 600	22 600	29 400	36 200	43 000	47 800	80 000
$M_w$ (g.p.c.)	11 500	12 000	13 000	15 200	17 300	23 000	32 000	35 000	44 000	50 000	85 000
$M_w/M_n$ (g.p.c.)	1.10	1.12	1.10	1.16	1.06	1.15	1.09	1.17	1.10	1.10	1.13
Free chains ratio		0.8%		0.8%	1.4%	1.8%		1.4%		5.8%	4.8%

$\langle r_{OD}^2 \rangle$  and  $\langle r_{OS}^2 \rangle$  = mean square end-to-end distance of network chains in the dry and swollen reference states respectively

$\langle r_D^2 \rangle$  = mean square end-to-end distance of network chains in the dry state

$\langle r_c^2 \rangle$  = mean square end-to-end distance of network chains after crosslinking

$q_0$  = the swelling of the gel in the swollen reference state

It is called the 'memory term' as it is linked to  $q_c^{-1}$ , the volume fraction for the polymer at the crosslinking stage.

When the swollen gel undergoes a unidirectional stress  $\sigma$  (force per unit swollen and strained cross-section) its degree of swelling will change from  $q_i$  to  $q$ . The relation (2) yields:

$$\sigma = Aq_0^{-2/3}q_i^{-1/3}\nu_e^*RT \left[ \Lambda_x^2 - \frac{q}{q_i} \Lambda_x^{-1} \right] \quad (3)$$

where  $\nu_e^*$  = concentration of network chains (per unit dry volume)

$\Lambda_x = L/L_i$  where  $L_i$  = the initial length of the sample swollen at equilibrium and  $L$  = the stressed length of swollen sample

### Stress birefringence

Studies of the photoelastic properties of rubberlike polymers have been interpreted in terms of the Kuhn and Gr $\ddot{u}$  n theory<sup>19</sup> in which the molecule can be described as a chain of randomly jointed optically anisotropic links.

If  $\bar{n}_0$  is the mean refractive index of the network and  $\Delta\alpha_c$  the optical anisotropy of the random link, the optical coefficient is defined as:

$$c = \frac{\Delta n}{\sigma} = \frac{2\pi}{45kT} \frac{(\bar{n}_0^2 + 2)^2}{\bar{n}_0} \Delta\alpha_c \quad (4)$$

where  $\Delta n$  is the stress birefringence.

The knowledge of the optical anisotropy of a monomer unit makes it possible to measure the length of the random link and verify the validity of the Gaussian theory. The optical coefficient is an intrinsic parameter of the polymer, independent of the crosslinking density and the solvent used (except for calculation of  $\bar{n}_0$ ).

## EXPERIMENTAL

### Preparation of samples

All samples were prepared by anionic copolymerization of styrene with divinylbenzene (DVB) according to a method described by Weiss *et al.*<sup>7</sup>

The polymerization initiated by the disodium tetramer of  $\alpha$ -methylstyrene, takes place in inert atmosphere in an equilibrium mixture of toluene and tetrahydrofuran (THF)

at  $-78^\circ\text{C}$ . A mould is fitted under the multi-necked lid of the reactor, so that seven parallelepipedic samples (135 x 42 x 4 mm) and one cylindrical sample (120,  $\phi$  27 mm within the reactor) can be obtained simultaneously.

All these samples were prepared in highly dilute solution (7.5%) with three DVB molecules per living end.

The gel obtained in this way was deactivated by a solution containing 10% THF and tetrahydrofurfuryl alcohol; its alcoholates were removed by successive washings and it was swollen to equilibrium in benzene and cyclohexane.

A sample of the related polystyrene before DVB was added made it possible to measure the molecular weight of the linear chains between crosslinks. Their parameters are given in Table 1.

### Measurements

Elongation was measured by a cathetometer with a precision of  $\pm 1/20$  mm in a rectangular glass cell filled with solvent, the samples being held by means of metallic clamps. To measure the stress a calibrated inductive transducer (Model Q11/100gP Hottinger Balwin) was used. The signal of the transducer was amplified by means of a carrier wave amplifier (Model KWS/35-5 Hottinger Balwin) which gives the force after calibration.

Thickness was measured by a microscope with a precision of  $\pm 5/1000$  mm, and other measurements were taken by means of slide callipers with a precision of  $1/20$  mm.

Taking into account all the experimental errors previously mentioned the elasticity modulus in extension can be calculated to be  $\pm 2.5\%$ .

In compression the samples are pressed in a cylinder by a piston coupled with a transducer (Q11/1kp). The contact surfaces lined with a Teflon film ensure a better sliding on these surfaces under stress. The determination of the initial conditions linked with the parallelism and the surface state of the cross-sections can become inaccurate for weak moduli. Experimental errors of about  $\pm 2.5\%$  can then reach  $\pm 5\%$  in the most unfavourable cases.

We used the arrangement described by Donkersloot and Gouda<sup>3</sup> to measure the optical birefringence  $\Delta n$  when a unidirectional stress  $\sigma$  is exerted on the gel. A galvanometer linked with a photomultiplier gives the phase retardation with a precision of  $\pm 15'$ .

The determination of the optical coefficient  $c = \Delta n/\sigma$  is achieved with a precision of  $\pm 2.5\%$ . All these measurements were made at room temperature.

### Corrections

In equation (3)  $\sigma$  and  $q$  are the stress and the swelling ratio at stress equilibrium. The measurement of  $\sigma$  and  $q$  is usually difficult. In order to avoid this difficulty, we have measured the instantaneous stress  $\sigma_0$ , obtained after deformation.

In this case equation (3) becomes:

$$\sigma_0 = Aq_0^{-2/3}q_i^{-1/3}\nu_e^*RT[\Lambda_x^2 - \Lambda_x^{-1}] \quad (5)$$

This implies the following expression proposed by Dusek and Prins<sup>18</sup>:

$$\frac{q}{q_i} = \Lambda_x^3 + \frac{f}{f_0} (1 - \Lambda_x^3)$$

where  $f$  is the force at equilibrium and  $f_0$  the force measured immediately after deformation.

In order to check the validity of this assumption we have plotted in Figure 1 the value of  $\sigma_0$  versus  $(\Lambda_x^2 - \Lambda_x^{-1})$  and  $\sigma$  versus  $[\Lambda_x^2 - (q/q_i)\Lambda_x^{-1}]$  for two different values of  $\Lambda_x$ , for the gel no. 853 swollen in benzene. The four experimental points are on the same straight line and give the same value of the modulus  $G_{ex}$ . Consequently we have only measured the values of  $\sigma_0$ .

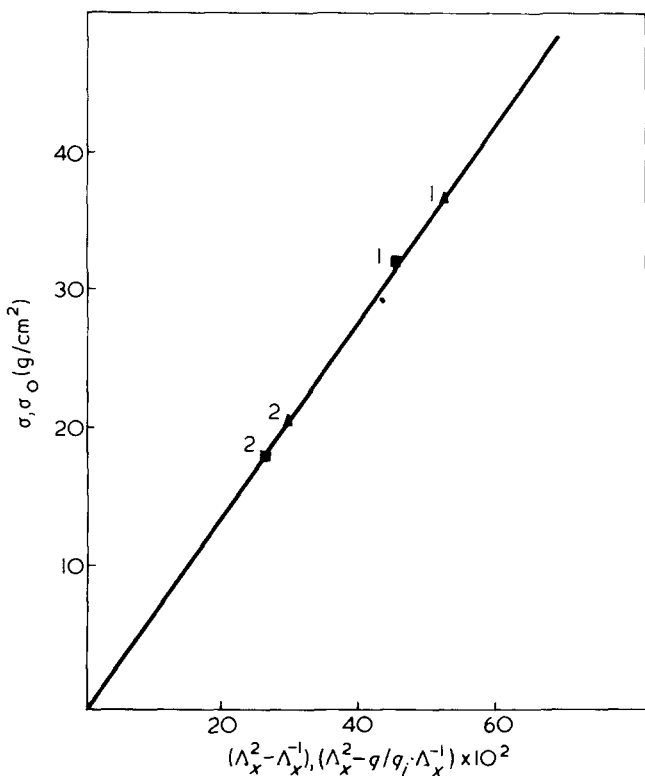


Figure 1 Stress-strain curve for compression measurement in benzene at 18°C for gel no. 853. ▲,  $\sigma_0$  versus  $(\Lambda_x^2 - \Lambda_x^{-1})$ ,  $\sigma_0$  being the stress measured immediately after deformation; ■,  $\sigma$  versus  $(\Lambda_x^2 - q/q_i \Lambda_x^{-1})$ ,  $\sigma$  being the stress at equilibrium

## RESULTS AND DISCUSSION

All the results obtained with gels in equilibrium swelling in cyclohexane and benzene are included in Table 2, the molecular weight of our gels ranged only from 10 000 to 75 000. For lower molecular weights, the crosslinking speed is too high to obtain a satisfactory homogeneous gel. For higher molecular weights, it proved to be impossible to determine the mechanical properties in good solvents, the gels being too weak.

In Figure 2, we have plotted according to equation (5) the values of the stress  $\sigma_0$  (initial stress per strained swollen cross-section) against  $(\Lambda_x^2 - \Lambda_x^{-1})$  for four gels of molecular weights  $\bar{M}_n = 10\,450$ ; 16 450; 19 900; 30 000; swollen in cyclohexane and benzene. The other gels give the same linearity. In all cases we observed a linear variation of  $\sigma_0$

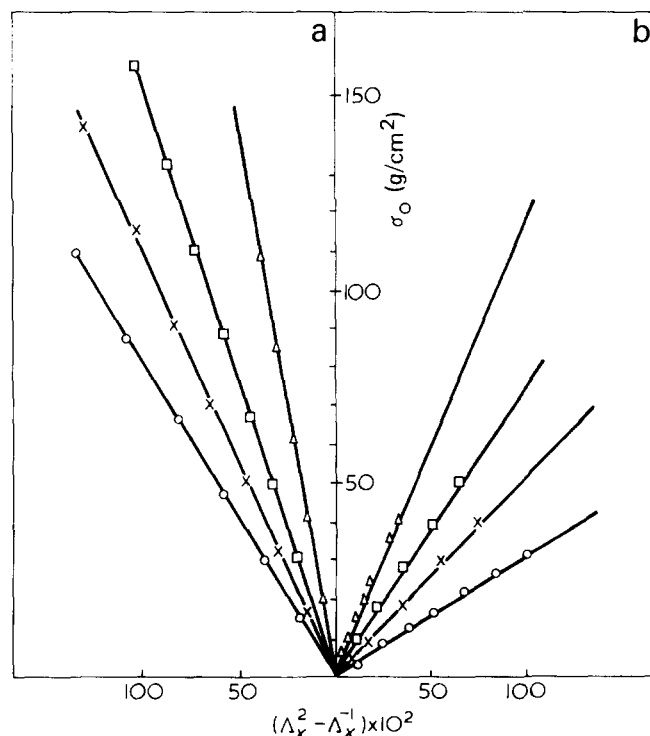


Figure 2 Initial stress-strain curve for four samples swollen in (a) cyclohexane and (b) benzene.  $\bar{M}_n$ : ▲, 10 450; □, 16 450; ×, 19 900; ○, 30 000

Table 2 Mechanical and optical values of samples swollen at equilibrium in benzene and cyclohexane

No.	$\bar{M}_n$	$Q_i$		$G_{ex}$ (benzene) (dynes/cm <sup>2</sup> )		$G_{ex}$ (cyclohexane) (dynes/cm <sup>2</sup> )		$C \times 10^{10}$ (dynes <sup>-1</sup> cm <sup>2</sup> )		$\Delta\alpha_c \times 10^{25}$ (cm <sup>3</sup> )	
		Ben- zene	Cyclo- hexane	Com- pression	Elonga- tion	Com- pression	Elonga- tion	Cyclo- hexane	Ben- zene	Ben- zene	Cyclo- hexane
3033	10450	13.74	3.71	121 000	122 500	194 500	193 000	5.32	4.63	116	130
343	10660	13.31	3.78		125 000	193 000	193 000	5.43	4.50	113	133
17 102	11 800	14.49	3.76		111 700	171 700	171 700		4.67	117	
543	13 100	16.22	3.87	87 200	89 300	153 000	154 600	5.40	4.66	117	132
853	16 450	16.47	4.08	69 000	74 300	130 900	133 500	5.25	4.85	121	129
743	19 900	21.12	4.11	49 670	50 100	105 000	107 700	5.22	4.77	119	128
13 112	29 300	23.52	4.30		33 300		76 300	5.27	4.76	119	129
2 743	30 000	26.64	4.35	30 250	30 900	76 800	77 700	5.25	5.01	125	129
15 112	40 500	29.17	4.40		17 200		45 300	4.70	4.57	115	116
3 043	45 600	53.59	4.51	6 000		24 000	24 500	4.83			118
553	75 000	64.14	4.84				8 700	3.40			83.2



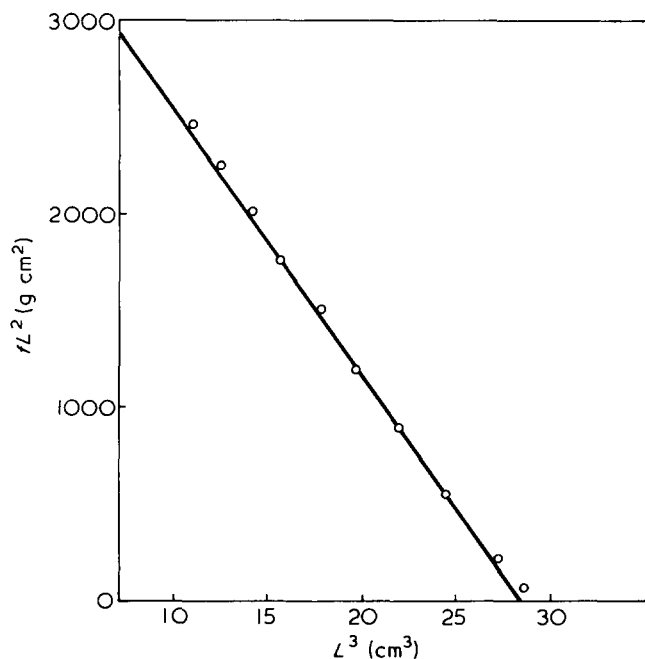


Figure 3 Compression measurement for gel 743 swollen in benzene

against  $(\Lambda_x^2 - \Lambda_x^{-1})$  with an ordinate of zero. The slope allows us to calculate the experimental modulus  $G_{\text{ex}} = \sigma_0 (\Lambda_x^2 - \Lambda_x^{-1})^{-1}$  of our samples whose values are given in Table 2.

In compression, relation (5) can be written:

$$fL^2 = Av_e^* RT V_p q_0^{-2/3} q_i^{2/3} \left[ \frac{L^3}{L_i^2} - L_i \right]$$

where  $L$  and  $L_i$  are the lengths of the deformed and undeformed states;  $f$  = force exerted on the sample; and  $V_p$  = specific volume of the network in the dry state.

In Figure 3, we have plotted  $fL^2$  against  $L^3$  for the gel of molecular weight 19 900 swollen in benzene. We obtained similar curves for all other samples. At low compression ratio a slight deviation from linearity is observed. This is probably due to imperfection in the parallelism of the compressing plates. It can be shown that the slope of the line is  $G_{\text{ex}} S_0 / L_i$ , where  $S_0$  is the cross-section of the samples in the swollen undeformed state. The compression moduli  $G_{\text{exp}}$  for the various gels are given in Table 2.

Relation (5) can also be written in the following way:

$$\sigma_0 = Aq_0^{-2/3} q_i^{-1/3} \left( \frac{\rho}{M_n} - \nu_i \right) RT (\Lambda_x^2 - \Lambda_x^{-1}) \quad (6)$$

in which  $\rho$  is the density of the gels in the dry state and  $\nu_i$  the number of non-elastic network chains.

Therefore we have plotted in Figure 4 the values of  $G_{\text{ex}}/q_i^{-1/3} = Aq_0^{-2/3} [(\rho/M_n) - \nu_i] RT$  against  $1/M_n$  for the various samples, related to the measurements in benzene and cyclohexane. The experimental points obtained are, to within experimental errors, located on a line going through the origin. We are therefore led to conclude that  $\nu_i$  is negligible and that consequently  $\nu_{e1}^* = \rho/M_n$  is a quantity which can be obtained experimentally.

Consequently the behaviour of the gel is ideal, though it may be thought that there is in fact a compensation between eventual pendant chains and the existence of

entanglements. This seems to be all the more probable as in a certain number of our samples and particularly in those whose molecular weights were high, we were able to measure experimentally a certain ratio of extractable chains whose values are shown in Table 1. According to Haeringer<sup>20</sup> those values can be linked with a ratio of pendant chains in the network. The apparently ideal behaviour of the studied samples implies compensation by entanglements.

It can be seen in Figure 4 that the experimental points corresponding to molecular weights higher than 40 000 deviate appreciably from the straight line. This can be accounted for by the ratio of pendant chains becoming too high.

According to relation (6) the slope of the straight lines in Figure 4 allows us to calculate the values of  $Aq_0^{-2/3}$  in benzene and cyclohexane. Those values are equal for both solvents. If we suppose the Flory–Wall–Hermans theory that  $A = 1$ , we can deduce the value of:

$$q_0^{-2/3} = q_c^{-2/3} \frac{\langle r_c^2 \rangle}{\langle r_{OS}^2 \rangle}$$

$q_c^{-2/3}$  being known we can deduce that  $\langle r_c^2 \rangle / \langle r_{OS}^2 \rangle = 0.69$  for both solvents.

It is to be noted that the same memory term value is obtained from modulus measurements in two solvents as different from each other as are benzene and cyclohexane. This then seems to confirm that  $q_0$  is an intrinsic parameter of the gel. Although this value is noticeably different from the one given by Prins<sup>21</sup>, it confirms qualitatively the influence of crosslinking on the dimensions of the chains.

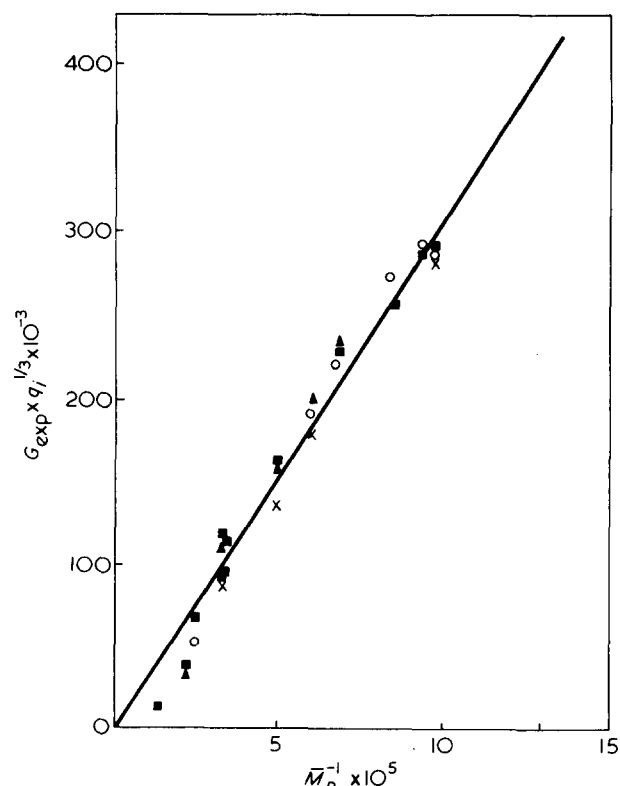

 Figure 4  $G_{\text{exp}} \times q_i^{1/3}$  versus  $M_n^{-1}$  for samples swollen in benzene from compression (X), elongation (O) measurements and in cyclohexane from compression (▲) and elongation (■) measurements

Table 3 Physico-chemical characterization

No.	$\bar{M}_n$	Cyclohexane			$\chi_{cal}$
		$\chi_{Scholte}$	$B$	$f$	
3033	10450	0.613378	0.2884	6.93	0.470
343	10660	0.611052	0.2975	6.72	0.477
17102	11800	0.611707	0.3391	5.89	0.470
543	13100	0.608513	0.3433	5.82	0.479
853	16450	0.602126	0.3701	5.40	0.465
743	19900	0.601316	0.3823	5.23	0.465
13112	29300	0.596492	0.4858	4.12	0.470
2743	30000	0.595303	0.4625	4.32	0.470
15112	40500	0.594145	0.5013	4.00	0.468
3043	45600	0.591702	0.6682	3.00	0.477
553	75000	0.585133	1.6055	1.25	0.479

As could be expected from the Mooney–Rivlin representation:

$$\sigma_0 = (C_1 + C_2\Lambda_x^{-1})(\Lambda_x^2 - \Lambda_x^{-1})$$

the  $C_2$  term is nul in all cases. The  $C_1$  term is then equal to the theoretical modulus defined by the theory of elasticity, in compression as well as elongation. This result could be expected, if we consider the importance of dilution in the crosslinking process and the low polydispersity of the chains<sup>22</sup>.

Using equation (2) in which we introduce the value of  $\Lambda q_0^{-2/3}$  and  $\nu_e^*$  given by the experimental modulus, we obtain a relationship between functionality of the crosslinks  $f$  and the polymer–solvent interaction parameter  $\chi$ , if we suppose that  $B = 2/f$ . It has been shown for linear polystyrene solution in cyclohexane that  $\chi$  is independent of the molecular weight and that for polymer concentration identical to those in our gel, this parameter is the same for a linear and a star polystyrene<sup>6</sup>. In that case we can use the value of  $\chi$  given by the equation of Scholte<sup>23</sup> for our gels:

$$\chi_\phi = 0.2975 + \frac{62}{T} + 0.306\phi + 0.30\phi^2$$

where  $\phi$  = volume fraction of polymer in the solvent.

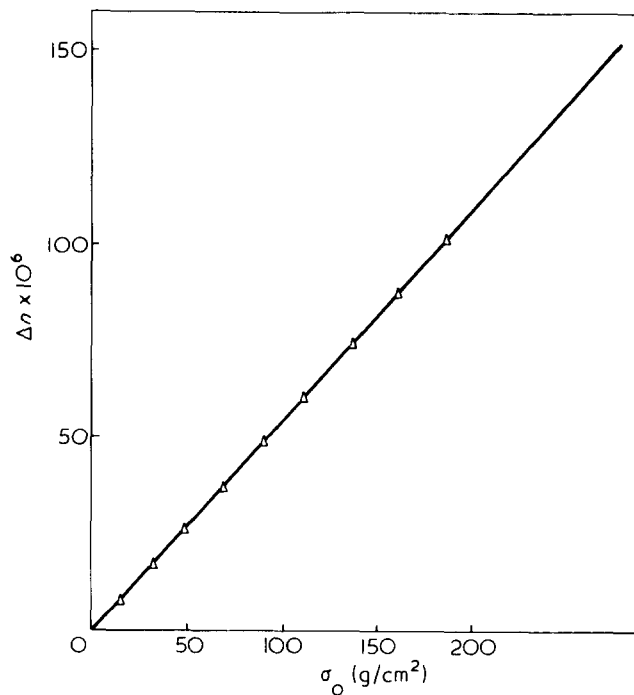
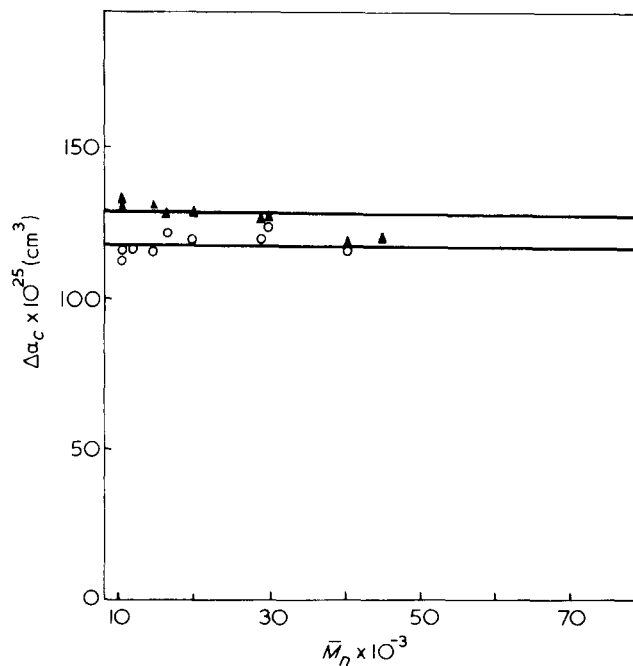
In Table 3 we have given the calculated value of  $\chi$  for each gel and the corresponding value of  $B$  and  $f$  given by equation (2).

The functionality decreases with the molecular weight between crosslinks. This can be due to the kinetics of the crosslinking process which may depend on the viscosity of solute and consequently on the molecular weight, or on the number of pendant chains in the gel which obviously increase with the molecular weight. For the last two gels with the highest molecular weight  $f$  is 3 and 1.25. These values are anomalous because the average values of  $f$  should be higher than 3. This is probably due to the non-ideality of those gels which appears in all the measurements.

In the case of the gels swollen in benzene we cannot apply the same type of calculation, because the value of  $\chi$  is unknown and probably dependent on molecular weight, swelling ratio and molecular structure. Using the value of  $f$  obtained from the measurements in cyclohexane, we have calculated the value of  $\chi$  in benzene, using equation (2). The values are given in Table 3. The parameter  $\chi$  seems to be independent of the molecular weight and in accordance with the value that could be expected.

In Figure 5 for the sample 2743,  $\Delta n$  has been plotted against  $\sigma_0$  and the slope of the straight line is equal to the stress optical coefficient  $c$  as defined in the Kuhn and Gr $\ddot{u}$  n relation<sup>19</sup>. From this value we were able to calculate the anisotropy of the statistical link  $\Delta\alpha_c$  which is plotted against  $\bar{M}_n$  for the different samples swollen in cyclohexane and benzene. The values are given in Table 2 and are in accordance with those given by different authors<sup>24–26</sup>.

From Figure 6 we can conclude that, as was predicted by equation (4),  $\Delta\alpha_c$  is independent of the molecular weight, except for the highest molecular weights where the presence of pendant chains has been shown by other measurements. As has been found by other authors<sup>27–30</sup>, the

Figure 5  $\Delta n$  versus  $\sigma_0$  for the sample 2743Figure 6  $\Delta\alpha_c$  versus  $M_n$  for different samples

values of  $\Delta\alpha_c$  depend on the solvents. Concerning our experiments, it seems most unlikely that the small difference in optical anisotropy between cyclohexane and benzene might account for our results. On the other hand, the anisotropy differences measured in those two solvents can be linked to the important difference in the swelling ratios. In fact it can be supposed that either the chain statistic is modified when another solvent is used<sup>31</sup> or the short-range interactions between chains depend largely on the swelling ratio of the network.

In conclusion it appears that the behaviour of these networks is in good agreement with Gaussian theory. That could be expected knowing the fact that the networks were formed from diluted solutions. The same type of measurement in the dry state is actually in process to verify if the behaviour is still in agreement with Gaussian theory and to check the influence of the short range interaction in the bulk.

#### ACKNOWLEDGEMENTS

The authors acknowledge the helpful discussion of Drs C. Strazielle and M. Hert from CRM Strasbourg and their assistance in molecular weight measurements.

This work was supported by the DGRST under contract 73 711 56.

#### REFERENCES

- 1 Alfrey, T., Bohrer, J. J. and Mark, H. 'High Polymers: 8. Copolymerisation'. Interscience, New York, 1952
- 2 Flory, P. J. 'Principles of Polymer Chemistry', Cornell University Press, Ithaca, 1953

- 3 Donkersloot, M. C., Gouda, J. H., van Aartsen, J. J. and Prins, W. *Recl Trav. Chim. Pays-Bas* 1967, No.4
- 4 Ilavsky, M. and Prins, W. *Macromolecules* 1970, 3, 415
- 5 Rempp, P. *C. R. Acad. Sci.* 1964, 259, 2434
- 6 Worsfold, D. J., Zilliox, J. G. and Rempp, P. *Can. J. Chem.* 1969, 47, 3379
- 7 Weiss, P., Hild, G., Herz, J. and Rempp, P. *Makromol. Chem.* 1970, 135, 249
- 8 Kopecek, J., Jokl, J. and Lim, D. *J. Polym. Sci. (C)* 1968, 16, 3877
- 9 Hermans, J. *J. Polym. Sci.* 1962, 59, 191
- 10 Wall, F. T. and Flory, P. J. *J. Chem. Phys.* 1951, 19, 1435
- 11 Hermans, J. *J. Trans. Faraday Soc.* 1947, 43, 591
- 12 Wall, F. T. *J. Chem. Phys.* 1943, 11, 527
- 13 Flory, P. J. *J. Chem. Phys.* 1950, 18, 108
- 14 James, H. M. and Guth, E. *J. Chem. Phys.* 1953, 21, 1039
- 15 James, H. M. *J. Chem. Phys.* 1947, 15, 651
- 16 Guth, E. *J. Polym. Sci. (C)* 1966, 12, 89
- 17 James, H. M. and Guth, E. *J. Chem. Phys.* 1947, 15, 669
- 18 Dusek, K. and Prins, W. *Adv. Polym. Sci.* 1969, 6, 1
- 19 Kuhn, W. and Grün, F. *Kolloid-Z.* 1942, 101, 248
- 20 Haeringer, A. *Thesis* Strasbourg (1972)
- 21 Froelich, D., Crawford, D., Rozek, T. and Prins, W. *Macromolecules* 1972, 5, 100
- 22 Schwarz, J. *Kolloid-Z. Z. Polym.* 1973, 251, 215
- 23 Scholte, Th. G. *J. Polym. Sci. (A-2)* 1971, 9, 1553
- 24 Grishenko, A. Ye. *et al. Vysokomol. Soedin.* 1963, 5, 1538
- 25 Abe, Y., Tonelli, A. E. and Flory, P. J. *Macromolecules* 1970, 3, 294
- 26 Bazhenov, N. M., Volkenstein, M. V., Gotlib, Yu. Ya. and Rozenstein, D. L. *Zh. Tekh. Fiz.* 1956, 26, 1730
- 27 Ishikawa, T. and Nagai, K. *Polym. J.* 1970, 1, 116
- 28 Gent, A. N. and Kuan, T. H. *J. Polym. Sci. (A-2)* 1971, 9, 51
- 29 Fukuda, M., Wilkes, G. L. and Stein, R. S. *J. Polym. Sci. (A-2)* 1971, 9, 1417
- 30 Gent, A. N. and Kuan, T. H. *J. Polym. Sci. (A-2)* 1971, 9, 927
- 31 Morgan, R. J. and Treloar, L. R. G. *J. Polym. Sci. (A-2)* 1972, 10, 51

# Increase of the melt viscosity of polycapromamide by chromium (III) ions

A. Szafner and J. Karger-Kocsis

Research Institute for the Plastics Industry, Budapest, H-1950, Hungary

(Received 28 April 1975)

The melt viscosity of polycaprolactam can be enhanced by incorporation of chromium (III) ions into the resin. As a possible interpretation of this phenomenon, formation of a mixed complex is suggested by X-ray diffraction, infrared and uv. absorption spectroscopic studies. By comparison with a model compound, it was found that the carbonyl oxygen and the water occurring in the polymer appear to be the coordination centres of chromium (III) ions. The hypothetical composition of the mixed complex is  $[\text{Cr}(\text{CO}_{\text{amide}})_n(\text{H}_2\text{O})_{6-n}]^{3+}$  where  $2 \leq n \leq 6$ .

## INTRODUCTION

The majority of commercial polyamides cannot be used for extrusion of profiles because of their low melt viscosity. The melt viscosity of these polyamides can be increased by introduction of chromium (III) ions<sup>1</sup>. The polymer product is impregnated with an appropriate chromium (III) compound in alcoholic or aqueous medium then dried, extruded and pelletized. The polyamide prepared in this way is capable of extruding as tubes, films, hollow bodies, and other profiles. The chromium (III) compound can also be added to the system before polymerization or polycondensation.

The present paper aims at the interpretation of the effects of chromium (III) compounds.

Changes in the viscosity are shown in *Figure 1* as a function of the amount of chromium (III) compound added. Measurements were carried out using a plastometer at 250°C, a nozzle of 2 mm i.d. and at a load of 500 g. Water content was determined by a vacuum method at 190°C. Thermal stability, resistance to solidification, and water absorption of the polymer product increased while the mechanical properties such as tensile strength and ultimate elongation decreased by about 20% owing to either the change in crystal structure or to the increased proportion of the amorphous phase. In addition, light resistance and

thermal stability of the polymer can be improved by incorporation of chromium (III) compounds<sup>2</sup>. In another process, anionic polymerization of caprolactam in the presence of complex-forming metal cations, led to products of lower degree of crystallinity<sup>3</sup>.

## EXPERIMENTAL AND RESULTS

### X-ray diffraction patterns

X-ray diffractograms were recorded by a Phillips Micro III equipment using Ni-filtered  $\text{CuK}\alpha$  irradiation and operated at 40 kV and 20 mA. It was established that the structure of a polyamide coordinated with chromium was different from that of the original polyamide produced industrially by anionic polymerization at the Borsod Chemical Works *Figure 2*. The X-ray diffraction peaks of the original polyamide at 19.7° and 23.5° were designated according to Roldan<sup>4</sup> as  $\alpha_I$  and  $\alpha_{II}$  respectively.

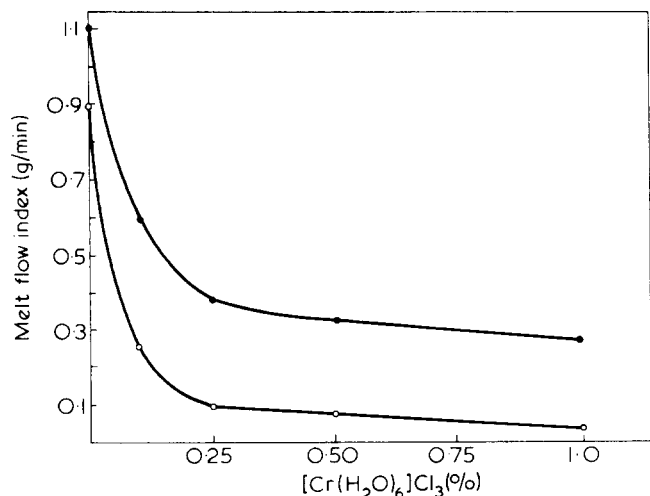
For samples containing chromium compound,  $\alpha_I$  and  $\alpha_{II}$  shifted to 20.3° and 22.8° respectively and a new diffraction band appeared at 21.1° characteristic of a polyamide of  $\gamma$ -structure. The  $\gamma$ -structure is analogous to a polypeptide chain and the molecules are packed more loosely than those of the other crystal forms. This is the reason why polyamide is considered as the model compound for the tanning of collagen after the destruction or weakening of the hydrogen-bonded structure.

Formation of the  $\gamma$ -structure was also observed by infrared spectroscopy through its characteristic band at 975  $\text{cm}^{-1}$ <sup>5</sup>. The chromium-coordinated polyamide has a lower crystalline proportion in comparison to the original one.

### Infrared spectra

Film specimens were investigated by a Zeiss UR-10 spectrophotometer in the range of 400 to 4000  $\text{cm}^{-1}$ . By this method, only the modified crystal structure could be observed. No difference appeared in the carbonyl and amide bands between the original and the chromium-coordinated polyamides owing to the low amount of the chromium (III) ions incorporated. The incorporation of  $10^{-3}$  atomic units to a polyamide unit (having a molecular weight of 113) resulted in changes well below the detection limit of this method. Similar results were obtained in the far infrared range at 0 to 250  $\text{cm}^{-1}$ .

In order to clarify this problem, tricaprolactamo-chromium (III) trichloride  $[\text{Cr}(\text{CLm})_3\text{Cl}_3]$  was prepared by the



*Figure 1* Melt-flow index of chromium-coordinated polycapromamide as a function of the amount of chromium (III) compound added, at different moisture contents.  $\circ$ , 0.03%;  $\bullet$ , 0.10% moisture content

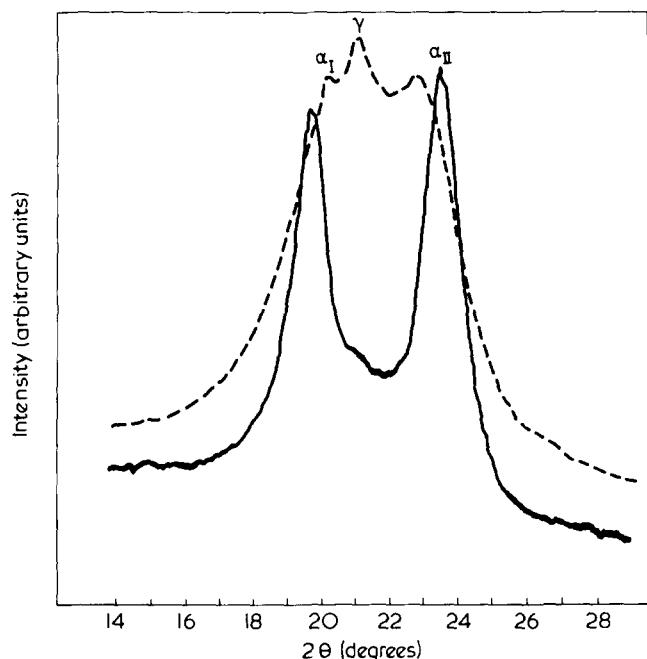


Figure 2 X-ray spectra for the original polyamide (—) and for a chromium-coordinated polyamide (---) containing 0.35% of  $[\text{Cr}(\text{H}_2\text{O})_6]\text{Cl}_3$

standard method and studied as a model compound<sup>6</sup>. Although a hexacoordinated caprolactam-chromium (III) complex could also have been synthesized<sup>7</sup>, an analogous structure to the polyamide-6 might not be expected since, in the practical application, moisture is also present in similar amount to the chromium (III) ion (related to a polyamide unit) and this favours the formation of a mixed complex as it was demonstrated by the absorption spectra (see below).

Caprolactam as a bifunctional compound can coordinate through both lone electron pairs of the oxygen and the nitrogen. If it coordinated through the oxygen, the carbonyl band should shift towards lower frequencies while a coordination through the nitrogen should result in a reverse effect since the amide groups were partly delocalized.

It was established by the KBr pellet technique that the carbonyl oxygen was involved in the complex formation since the CO frequency of caprolactam at  $1662\text{ cm}^{-1}$  shifted to  $1625\text{ cm}^{-1}$  for the model compound. According to Bull *et al.*<sup>8</sup> steric factors also give such a coordination preference.

In addition to the shift of  $\nu_{\text{CO}}$ ,  $\nu_{\text{NH}}$  is changed from  $3305\text{ cm}^{-1}$  of the caprolactam to  $3320\text{ cm}^{-1}$ , due to the coordination, indicating the delocalization in caprolactam. This valence vibration band of the NH group corresponds to the *trans* configuration of the amide group which is sterically more favourable for the coordination.

#### U.v. absorption spectra

U.v. and visible spectra were recorded by a Spektromom 201 spectrophotometer. The  $n-\pi^*$  transition of the caprolactam CO group appears at 210 nm in n-hexane (molar extinction coefficient of  $1380\text{ l mol}^{-1}\text{ cm}^{-1}$ ).

Spectra for the tricapro lactamochromium (III) trichloride and the hexaquo chromium (III) trichloride in ethanol are similar and in dimethylformamide are essentially coincident, showing a bathochromic shift of about 10 nm from those measured in ethanol. This may be attributed to a stronger complex formation rather than to a solvent effect. Since the chromium compound coordinated with caprolactam shows no considerable red shift as compared to that

coordinated with water, the spectra lead to the conclusion that the combined water (bonded strongly or weakly) in the polyamide and the capillary condensed water are involved in the coordination.

In hexacoordinated chromium compounds, three  $d-d$  transitions can be observed within the studied range of wavelength. Two of them at 470 and 650 nm correspond to  $(t_{2g})^3 \rightarrow (t_{2g})^2(e_g^*)^1$  transitions<sup>9</sup>.

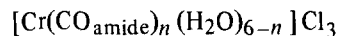
#### DISCUSSION

The infra-red spectra of the model compound shows that the carbonyl of the amide group is involved in the complex formation by the lone electron pair of the oxygen. This kind of coordination is considered for the polyamide as well although in this case, there is no proof of a coordination by the lone electron pair of the nitrogen. A coiled polyfunctional polyamide chain can also contribute to the chelate formation. Incorporation of a chromium compound into the polymer by melting, when the original hydrogen-bonded structure is destroyed, results in a polyamide of lower degree of crystallinity with altered structure ( $\gamma$  form) causing higher hygroscopy of the polymer.

Since chromium (III) ion has a coordination number of six it is unlikely that all of the sites are occupied by the carbonyl oxygens in the amorphous regions. It can be established by the absorption spectra that water is competitive in the coordination with the oxygen of the amide group making the formation of a mixed complex favourable.

A similar mixed coordination of chromium (III) ions was observed with ethylenediaminetetraacetic acid or with various amino acids<sup>10</sup>.

The structure of the hexacoordinated mixed complex is, therefore, supposed as follows:



where  $2 \leq n \leq 6$ .

Since the functional groups of the polymer chains are the ligands of the hypothetical chromium complex, an intermolecular coordination is formed which may explain the changes in the polymer viscosity.

#### ACKNOWLEDGEMENT

The authors are indebted to Professor G. Bodor for the X-ray diffraction measurements.

#### REFERENCES

- Hung. Pat. 165 230 (1972)
- Br. Pat. 649 481 (1948); 689 629 (1950); 718 405 (1952); 862 577 (1959); 1 018 819 (1963); 1 028 530 (1964); 1 030 363 (1964); 1 112 471 (1965); 1 152 905 (1965)
- Fr. Pat. 2 090 428 (1970); FDR Pat. 2 100 943 (1971); US Pat. 3 740 379 (1973)
- Roldan, L. G. *et al.* *J. Polym. Sci. (C)* 1965, 8, 145
- D'Alo, B., Coppola, G. and Palessi, B. *Polymer* 1974, 15, 130
- Rollinson, L. C. and White, R. C. *Inorg. Chem.* 1962, 1, 281
- Madan, S. K. and Denk, H. H. *J. Inorg. Nucl. Chem.* 1965, 27, 1049
- Bull, W. E., Madan, S. K. and Willis, J. E. *Inorg. Chem.* 1963, 2, 303
- Golgotiu, T. and Rosca, I. *Vysokomol. Soedin. (A)* 1973, 15, 2086
- Dobozy, O. *Kolor. Értésítő* 1960, 2, 189

# Polymeric coatings on steel produced by the electroinitiated polymerization of acrylic monomers

G. Mengoli\* and B. M. Tidswell

Postgraduate School of Studies in Polymer Science, University of Bradford, Bradford, West Yorkshire BD7 1DP, UK

(Received 22 November 1974; revised 23 May 1975)

The results of the electropolymerization *in situ* of certain acrylic and methacrylic esters to produce coherent, continuous coatings on steel sheet cathodes using tetra-*n*-butyl ammonium perchlorate as supporting electrolyte in either DMF or DMSO under galvanostatic conditions are described. The effect of monomer concentration, applied current and electrolysis time have been considered. It has been found that the coating formation is favoured when the solubility parameter of the growing polymer is sufficiently different to that of the media. Under these conditions insulating deposits form on the electrode, resulting in strong increases of the electric resistance of the system. The parallel increase of voltage recorded under galvanostatic conditions was used to explain the formation of the films in terms of 'throwing power' and coherence. The best coating results for adhesion and hardness were obtained by copolymerizing *in situ* suitable mixtures of methacrylonitrile and isobutyl methacrylate.

## INTRODUCTION

Electroinitiated polymerization has been the subject of several review articles<sup>1-4</sup>, in many of the examples the cathode behaves as a Lewis acid giving rise to either direct or indirect electron transfer to the monomer resulting generally in the initiation of an ionic process. The electrode is thus entirely concerned with the initiation stage which must therefore be heterogeneous, whilst the propagation reaction takes place homogeneously in the bulk of the solution. Thus the electrode acts as an external source of active species as occurs in photolytic or radiolytic initiation.

For either practical or industrial application electroinitiated polymerization is unlikely to compete with conventional techniques unless the system gives rise to polymers with novel characteristics such as very high molecular weight or controlled programmable molecular weight distributions. However, one aspect of this type of polymerization which may be developed for practical purposes is the polymerization *in situ* of the monomer at the electrode surface when both propagation and initiation occur heterogeneously giving rise to the formation of polymeric coatings which would convert a two stage process, that of polymer preparation followed by a suitable coating technique, into a one stage process.

The patent literature contains examples of successful coating obtained by electropolymerization based on diacetone acrylamide and related monomers<sup>5-7</sup>. Asahara<sup>8-16</sup> has reported the electropolymerization of a wide range of monomers to produce polymeric films on a variety of metal substrates acting as electrodes. This work is exploratory in nature and taking into account the large currents and electrolysis times used may most likely involve the

deposition of a polymeric material produced in the bulk of the solution rather than one produced *in situ* on the metal plate.

Not every monomer capable of undergoing electropolymerization is capable of giving a coating on the electrode. The present work which is restricted to the cathodic polymerization of certain acrylic monomers investigates the conditions that the system should fulfill to be suitable for the production of polymeric coatings as a consequence of the electrode reaction.

## EXPERIMENTAL

### Materials

*N,N'*-dimethylformamide (DMF) and dimethylsulphoxide (DMSO) (BDH Ltd reagent grade) were stored, before use, over granules of either magnesium or calcium oxide; no further purification was attempted.

The monomers, isobutyl methacrylate, methyl methacrylate (Koch Light), *t*-butyl acrylate, *t*-butyl methacrylate and isoamyl methacrylate (Borden Chemical Co.) and methacrylonitrile (Eastman Ltd) were freed of radical scavengers (50–100 ppm) by distillation. However, because of the ionic character of the polymerization similar results were obtained using the commercial materials as received.

*n*-Tetrabutyl ammonium perchlorate, the supporting electrolyte, was prepared by the neutralization of tetrabutyl ammonium hydroxide (Fluka Chemicals) with Analar perchloric acid. The precipitated product was recrystallized from ethanol/water and dried in a vacuum oven at 60°C.

The steel sheet electrodes (0.178 mm thick) were cut from samples of tin free steel supplied by Metal Box Co. Ltd.

Other reagents were used as supplied.

\* Permanent address: Laboratorio di Polarografia ed Elettrochimica Preparativa del CNR, Via Monte Cengio 33, 35100 Padova, Italy.

*Apparatus and procedure*

All the polymerization studies were performed by electrolyzing the monomer–solvent–supporting electrolyte system in a simple two electrode undivided cell. The platinum anode (1 cm<sup>2</sup>) was separated from the steel cathode (11 cm<sup>2</sup>) by a distance of 2 cm.

Experiment showed that in view of the short electrolysis times used, poisoning of the cathode by products discharged at the anode was apparently negligible. Because of the possible practical utilization of *in situ* electropolymerization all electrolyses were performed galvanostatically which combines simplicity of operation with adequate control of initiation rate. The constant current unit used was capable of supplying 1–50 mA in 1 mA steps (Sandmar Electronics Ltd). The voltage across the electrodes was monitored, during the electrolysis, by means of a digital voltmeter. Each polymerization was carried out at room temperature ( $\approx 20^\circ\text{C}$ ) with unstirred solutions.

Prior to electrolysis the sheet steel electrodes were degreased using chloroform and acetone. Immediately following electrolysis the metal electrode was quickly withdrawn from the solution and dried both at room temperature and in an oven at 60–70°C.

The hardness of the polymeric films was metered (relative to a glass standard) using a Pendulum Hardness Rocker to DIN specification 53, 157, equipped with automatic electronic counting (Koenig Pendulum by Sheer Instruments Ltd).

The polymer was recovered from the substrate by dissolution in acetone with subsequent removal of the solvent under vacuum. The molecular weights of the resulting polymer samples were determined using toluene solutions in a Knauer vapour pressure osmometer at 50°C. Thermal analysis of certain samples was carried out using a Perkin-Elmer differential scanning calorimeter DSC 1B.

## RESULTS AND DISCUSSION

*Polymerization mechanism*

The electroinitiated polymerization of the monomers used in this work have not previously been reported. However, there are some reports in the literature of the electroinitiated polymerization of acrylic esters and particularly for the cathodic polymerization of methyl methacrylate in aprotic medium<sup>17,18</sup>. Acrylic and methacrylic esters are capable of cathodic reduction on a mercury electrode in aprotic medium<sup>3,19</sup> with the formation of radical anions and dianions which can easily initiate anionic polymerization. Although no actual mechanistic studies have been carried out it seems more than likely that the reduction of acrylic monomers on a steel electrode which is relatively inert will lead to the same anionic species as produced on mercury. This is substantiated by the following experimental observations.

I. The polymer film formation is not affected by the presence of radical inhibitors.

II. Coating formation is inhibited by small quantities of water or other protic substances.

III. The molecular weight of the polymers is low, which is peculiar to the anionic polymerization of acrylic monomers.

IV. Samples, obtained by electropolymerization *in situ* of isobutyl methacrylate exhibit, by thermal analysis, a  $T_g$  of 284 K which is in good agreement with literature values<sup>20</sup> for poly(isobutyl methacrylate) prepared by anionic initiators.

*Polymerization of isobutyl methacrylate (iBMA) in DMF*

The results referring to the electropolymerization *in situ* of iBMA in DMF are reported in Table 1. Each run was performed using 50 ml of solution containing  $2.35 \times 10^{-2}$

Table 1 Polymerization *in situ* of isobutyl methacrylate in DMF

Run No.	A [Monomer] (mol/l)	B Current (mA)	C Time (sec)	D $\Delta V/V_0 \times 10^2$	E Yield (mg)	F mol/F	G Film hardness
1	3.20	50	30	6	24	0.663	0.19
2	3.20	50	60	6	40	0.555	—
3	3.20	50	90	10	51	0.475	0.16
4	3.20	50	120	8	61	0.425	—
5	3.20	50	180	11	78	0.363	0.25
6	3.20	50	300	7	83	0.232	—
7	3.20	50	600	11	63	0.092	—
8	3.20	25	300	7	24	0.135	—
9	3.20	35	300	9	45	0.180	—
10	3.83	50	30	5	16	0.417	—
11	3.83	50	60	7	38	0.505	—
12	3.83	50	90	13	62	0.540	0.26
13	3.83	50	120	17	61	0.400	—
14	3.83	50	180	19	74	0.320	0.26
15	3.83	50	300	17	62	0.162	—
16	3.83	50	600	16	56	0.073	—
17	3.83	25	300	5	15	0.081	—
18	3.83	35	300	11	47	0.175	—
19	5.10	50	30	9	9	0.225	—
20	5.10	50	90	18	38	0.325	—
21	5.10	50	120	22	35	0.238	0.24
22	5.10	50	180	15	57	0.244	0.24
23	5.10	50	300	15	44	0.114	—
24	5.10	25	300	10	12	0.061	—
25	5.10	35	300	12	37	0.135	—

Table 2 Molecular weight of the products obtained by electropolymerization *in situ* in DMF\* and DMSO

[Monomer] (mol/l)	{Solvent}/ [Monomer]	$\bar{M}_n$
3.20*	2.03	2310
3.83*	1.35	2460
5.10*	0.51	2510
1.28	8.80	1860
1.92 poly(iBMA)	5.12	2160
2.55	3.31	2380
3.20	2.20	3000
3.83	1.47	3320
5.10	0.55	3870
0.61	19.90	1940
0.95	12.60	2730
1.27 poly(t-BMA)	8.85	3300
1.92	5.13	3870
2.54	3.32	4650
1.05	11.40	2000
2.10 poly(t-BA)	4.67	1980
2.80	3.01	1860
3.50	2.01	2010
0.86	13.91	1225
1.72 poly(iAMA)	5.71	1550
2.30	3.67	1790

mol/l of TBAP as background electrolyte and monomer, as shown. The monomer concentrations used are in the range which gave coherent coatings of polymer on the cathode. The first three columns (A, B and C) report the experimental conditions for each run. Column D reports the percentage increase of the potential between the two electrodes [ $\Delta V/V_0 \times 10^2 = 100 \times (V_{\text{final}} - V_{\text{initial}})/V_{\text{initial}}$ ]. Under galvanostatic conditions, the potential increase is due to the increase of resistance of the system as a consequence of the build up of a polymeric film at the cathode surface. Since the polymerization rate is (at least initially) proportional to the number of the active centres, i.e. to the current, the film formation mainly follows the strength of the electric field. When the electric field distribution is modified by the formation of an insulating coating on some part of the cathode, film formation is moved to the points on the electrode when initially the field strength was lower, consequently the greater the increase of resistance of the system with coating the greater will be the homogeneity of the film. As an indication when  $\Delta V/V_0 \times 10^2$  approaches 20, coating occurs on both the back and the front of the electrode. The parameter  $\Delta V/V_0 \times 10^2$  can be taken as an index of the 'throwing power' of the coating system. From the data of Table 1,  $\Delta V/V_0 \times 10^2$  increases with electrolysis time, reaching either a limiting value or rising to a maximum with a subsequent slight decrease. This may be ascribed to the interaction of the conductive solvent with the polymer film which results in some solution or swelling of the film. In systems where  $\Delta V/V_0 \times 10^2$  reaches a maximum for different conditions of monomer concentration and electrolysis time generally correspond to the best experimental conditions for the formation of a coating.

Column E shows the total amount of polymer formed on the cathode during each electrolysis. With increasing electrolysis time this value initially increases quickly but eventually slows to a limiting value; for the longest times a decrease may be observed. For the same electrolysis time the total polymer deposition decreases with increase of the monomer concentration. The first observation may be

explained by the attainment of some steady state condition between rate of polymer formation and rate of polymer solution. The second observation probably results from a decrease of the polymerization rate consequent on the diminution of the dielectric constant of the system for low solvent/monomer ratios, in addition to any increased film solubility at high monomer concentrations.

The current efficiency (column F), the number of polymer moles formed per Faraday probably approaches unity at the very beginning of the process, i.e. each electron transfer initiates a polymer chain, afterwards it decreases rapidly with reaction time. An apparent decrease of efficiency may be due to solution of some of the polymer formed; on the other hand, the polymerization could be diffusion controlled and the decrease of efficiency could be due to a decreased monomer concentration at the electrode surface. The influence of current intensity on polymer yield further confirms the competition existing between electropolymerization *in situ* and interaction of the polymer coating with the solvent. Comparing runs in which the total charge transferred was of the same order (runs 3 and 8, 5 and 9, 13 and 17, 14 and 18, 21 and 24, 22 and 25) one can realise the difference in current intensity. At the lowest currents the polymerization rate is so slow that the time of interaction of solvent with polymer is such that no film is produced.

The last column of Table 1 gives the hardness of certain films. For the same weight of coating, that is the same thickness of the film, the hardness is generally similar for different experimental parameters used. This together with the similarity of molecular weights (Table 2) would imply similar molecular complexity and features in each of the coatings.

#### Polymerization of isobutyl methacrylate in DMSO

The experiments in DMSO were carried out using conditions identical to those using DMF except that in all cases the current was maintained at 50 mA. The results are reported in Table 3. The main differences between DMF and DMSO as solvent lies in the lower compatibility of poly(iBMA) with DMSO which can be appreciated by comparing the solubility parameters; for the polymer  $\delta = 9.2$  with a  $\Delta\delta$  maximum = 1.8<sup>21</sup>, for DMF  $\delta = 12.1$ <sup>22</sup> for DMSO  $\delta = 13.4$ <sup>23</sup>. It is for this reason that in DMSO there is a far greater increase in electrical resistance which is shown in Figure 1, where the parameter  $\Delta V/V_0 \times 10^2$  is considered in terms of different monomer concentrations as a function of electrolysis time. The coatings show a very good 'throwing power' and in most of the coatings the back of the plate is completely and homogeneously coated.

The lower solubility of iBMA in DMSO allows the formation of coherent coatings over a greater range of monomer concentration. Furthermore it is possible to obtain greater amounts of polymer over longer electrolysis periods which means that the current efficiency shows less variation with time. The results show that the best deposition conditions (with respect to rate and current efficiency) are obtained at a volume ratio of about 1:1 solvent:monomer. Both at lower and higher monomer concentration there appears to be a decrease in polymerization rate as a result of diminished monomer activity (at low concentrations) and to diminished dielectric characteristics of the medium (at higher monomer concentration). The data of column E of Table 3 allows comparison of the hardness



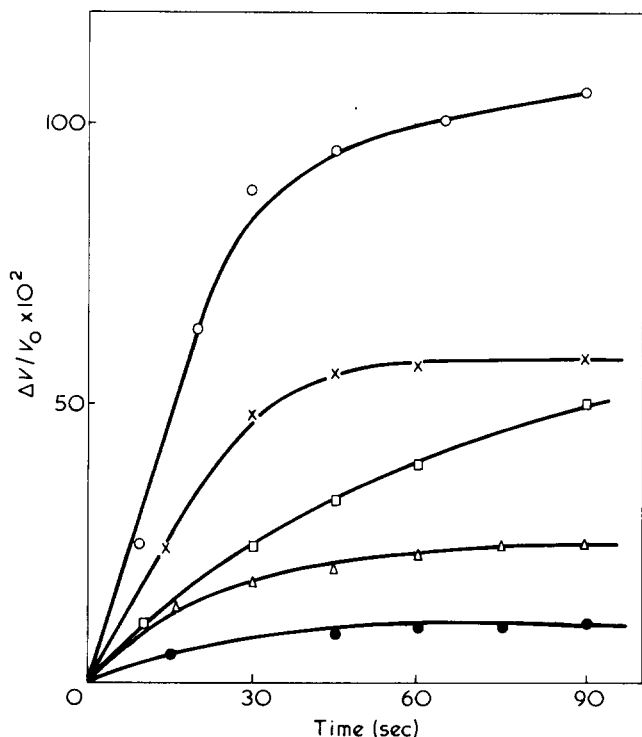


Figure 1 Percentage increase of electrode potential during the electropolymerization *in situ* of isobutyl methacrylate using different monomer concentrations: ○, 5.10; ×, 1.91; □, 3.83; △, 2.55; ●, 3.20 mol/l

Table 3 Polymerization *in situ* of isobutyl methacrylate in DMSO

Run No.	A [Monomer] (mol/l)	B Time (sec)	C Yield (mg)	D mol/F	E Film hardness
26	1.28	30	10	0.347	—
27	1.28	60	19	0.332	—
28	1.28	90	29	0.334	0.19
29	1.28	120	34	0.295	0.19
30	1.28	180	43	0.247	0.15
31	1.28	300	59	0.204	0.15
32	1.91	30	21	0.622	—
33	1.91	60	31	0.465	0.20
34	1.91	90	35	0.352	0.20
35	1.91	120	62	0.462	—
36	1.91	180	66	0.325	0.13
37	1.91	300	96	0.285	0.13
38	2.55	30	21	0.567	—
39	2.55	60	42	0.567	—
40	2.55	90	61	0.555	0.21
41	2.55	120	75	0.510	0.22
42	2.55	180	96	0.430	0.14
43	2.55	300	128	0.348	0.11
44	3.20	30	17	0.375	—
45	3.20	60	42	0.450	0.35
46	3.20	90	73	0.505	0.29
47	3.20	120	80	0.430	—
48	3.20	300	116	0.250	0.26
49	3.83	30	5	0.088	—
50	3.83	60	18	0.193	—
51	3.83	90	40	0.262	0.34
52	3.83	120	68	0.332	0.29
53	3.83	180	75	0.242	—
54	3.83	300	89	0.173	0.210
55	5.10	30	2	0.034	—
56	5.10	60	11	0.092	—
57	5.10	90	28	0.157	0.33
58	5.10	120	37	0.155	0.31
59	5.10	150	30	0.102	0.30
60	5.10	180	30	0.083	0.33
61	5.10	300	37	0.062	0.26

of samples obtained under different conditions. For the same weight of film an increase of hardness generally follows the increase of monomer concentration. This may be explained in terms of a parallel increase of the molecular weights of the samples (Table 2).

#### Polymerization of *t*-butyl methacrylate

The data for the electropolymerization *in situ* of *t*-butyl methacrylate (*t*-BMA) in DMSO are reported in Table 4. The difference between the solubility parameter of this polymer ( $\delta = 8.3$ )<sup>21</sup> and the solvent is greater than with poly(*i*BMA). Figure 2 shows  $\Delta V/V_0 \times 10^2$  as a function of electrolysis time for experiments when only the monomer concentration was varied. The increase of resistance accompanying the coating is greater than that seen in Figure 1 and may be explained by the poor interaction of the insulating film with the conducting solvent. For some monomer:solvent ratios when using the higher current intensities of Figure 2 a value of the difference of potential between the electrodes is soon reached at which the insulating film is broken with a consequent decrease of potential, under these conditions the coating is not homogeneous but is a powdery deposit. As can be seen from the last column of Table 4 coherent polymeric films can be obtained by using lower current intensities. It is interesting to note that the current yield of poly(*t*-BMA) does not generally decrease in applying the same amount of charge by decreasing the current intensities (on the contrary the yield of adherent film formed at low current intensities is greater than that of the powdery deposit obtained at high current intensity).

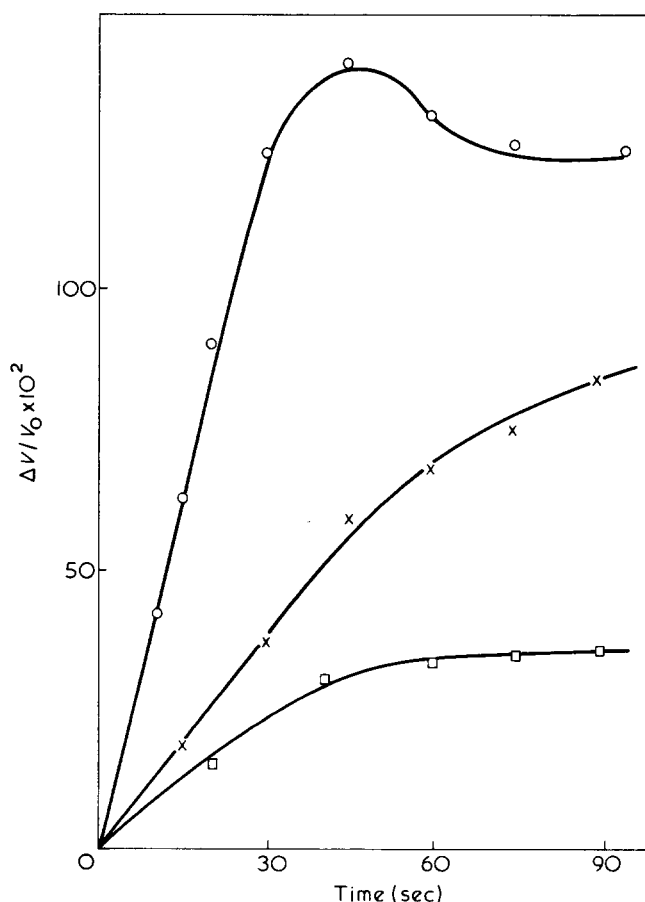


Figure 2 Percentage increase of electrode potential during the electropolymerization *in situ* of *t*-butyl methacrylate for different monomer concentrations: ○, 2.54; ×, 1.92; □, 1.27 mol/l

Table 4 Polymerization *in situ* of t-butyl methacrylate

Run No.	A [Monomer] (mol/l)	B Current (mA)	C Time (sec)	D Yield (mg)	E mol/F	F Film hardness
62	0.63	15	600	23	0.130	0.25
63	0.63	15	720	27	0.124	0.24
64	0.63	15	1080	35	0.107	0.23
65	0.63	15	1800	48	0.088	0.23
66	0.95	50	60	9	0.108	powder
67	0.95	50	90	11	0.090	powder
68	0.95	50	120	20	0.117	powder
69	0.95	50	180	24	0.096	powder
70	0.95	50	300	25	0.061	powder
71	0.95	25	240	24	0.141	0.29
72	0.95	12.5	480	21	0.124	0.29
73	0.95	7	840	36	0.219	0.29
74	0.95	3.5	1680	31	0.136	0.30
75	1.27	20	120	13	0.157	—
76	1.27	20	180	20	0.162	—
77	1.27	20	240	26	0.160	—
78	1.27	20	360	38	0.154	0.33
79	1.27	20	480	51	0.154	0.35
80	1.27	20	780	75	0.140	0.25
81	1.27	20	1200	116	0.142	0.25
82	1.27	40	180	29	0.118	powder
83	1.27	10	720	45	0.184	0.36
84	1.27	5	1440	41	0.166	0.33
85	1.92	50	60	30	0.250	powder
86	1.92	50	90	35	0.195	powder
87	1.92	50	120	50	0.210	powder
88	1.92	50	180	69	0.192	powder
89	1.92	25	120	33	0.274	0.42
90	1.92	12.5	240	36	0.300	0.40
91	1.92	7	600	50	0.300	0.40
92	2.54	50	30	26	0.361	powder
93	2.54	50	60	40	0.280	powder
94	2.54	50	90	45	0.210	powder
95	2.54	50	120	60	0.210	powder
96	2.54	50	180	79	0.182	powder
97	2.54	50	360	129	0.148	powder
98	2.54	25	240	86	0.300	0.35
99	2.54	12.5	480	108	0.374	0.38
100	2.54	7.5	900	106	0.330	0.37
101	2.54	18	1080	151	0.240	0.22

The hardness of the samples (Table 4, column F), generally superior to that obtained for poly(iBMA), may be explained in terms of the higher  $T_g$  of poly(t-BMA) since the molecular weights and probably the molecular complexity are very similar for the two polymers (Table 2).

The hardest films are generally obtained from polymerizations carried out at the lowest currents, an increase of hardness is generally paralleled by an increase in molecular weight (Table 2).

#### Polymerization of t-butyl acrylate with isoamyl methacrylate

For the sake of conciseness the data for t-butyl acrylate (t-BA) and isoamyl methacrylate (iAMA) are not reproduced, only the related molecular weights are given in Table 2.

Both monomers show poor affinity for the solvent and coherent films are obtained; however, because of their low  $T_g$  the poly(t-BA) deposits are very soft and the coatings of poly(iAMA) are mainly viscous oils. The molecular weights are in a similar range to those for the other polymers.

Despite the poor mechanical features the coatings obtained with these monomers are mentioned here for two main reasons: (i) under the same experimental conditions the

isomers with a n-paraffin substituent (n-butyl, n-amyl) are far less suitable for electropolymerization *in situ*; (ii) Both monomers may well be the main component of an electropolymerization *in situ* with monomers capable of improving the features of the coatings.

#### Considerations on the molecular weights of the polymers obtained in situ

The molecular weights reported in Table 2 were obtained from polymer samples obtained by combining the products of several electrolyses similar in concentration and current but differing in reaction time.

In the electroinitiated polymerization of methyl methacrylate<sup>18</sup> and acrylonitrile<sup>2,3,24</sup> in DMF with tetraalkylammonium salts as base electrolyte, it was shown that the molecular weight was largely independent of active centres electrochemically produced, i.e. from the current intensity and electrolysis time. This means that chain propagation and chain limiting reactions have the same kinetic dependence on active centres. On the other hand, Asahara<sup>9</sup> has found some dependence of molecular weights on electrolysis time and current in the polymerization *in situ* of acrylonitrile in the presence of transfer agents. This disagreement may be explained by the heterogeneity of the reaction *in situ*. In addition working in an undivided cell the termination contribution from anodically generated products might well vary with the amount of charge transferred. The molecular weights obtained for different electrolysis times, averaging the contribution from surface or diffusion phenomena, seem however capable of identifying the parameters which control the chain length.

The number-average degree of polymerization  $\bar{X}_n$  of the products can be related to the rate of various stages of polymerization by the Mayo equation:

$$1/\bar{X}_n = R_t/R_p + C_M + C_S [S]/[M]$$

where  $R_p$  and  $R_t$  are the propagation and termination rates respectively and  $C_M$  the transfer constant to monomer and  $C_S$  that to solvent. The data for poly(iBMA) of Table 2 plotted according to the Mayo equation (Figure 3) give a

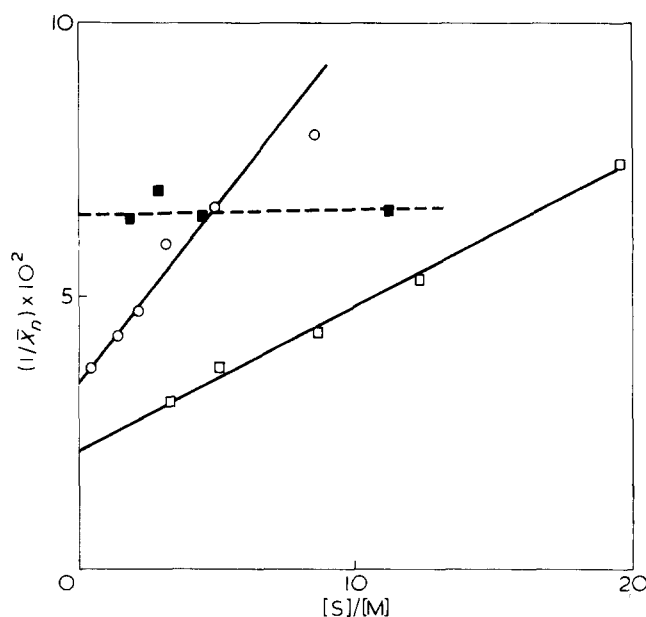


Figure 3 Mayo plot. □, Poly(t-butyl methacrylate); ○, poly(isobutyl methacrylate); ■, poly(t-butyl acrylate)

Table 5 Copolymerization *in situ* of isobutyl methacrylate (A) and methacrylonitrile (B) in DMSO and DMF\*

Run No.	A [Iso-butyl-] (mol/l)	B [Meth-acrylo-] (mol/l)	C Time (sec)	D $\Delta V/V_0 \times 10^2$	E Yield (mg)	F Hardness
156	3.06	0.12	30	6	11	—
157	3.06	0.12	60	14	19	—
158	3.06	0.12	90	22	40	0.36
159	3.06	0.12	120	34	67	0.35
160	3.06	0.12	180	32	69	—
161	3.02	0.18	40	5	13	0.35
162	3.02	0.18	60	13	23	—
163	3.02	0.18	90	21	39	0.28
164	3.02	0.18	120	29	54	0.28
165	3.02	0.18	180	19	55	—
166	2.99	0.24	60	10	24	—
167	2.99	0.24	90	13	32	0.31
168	2.99	0.24	120	20	37	0.32
169	2.99	0.24	180	12	51	0.28
170	2.99	0.24	300	3	43	0.28
171	2.92	0.36	60	2	18	—
172	2.92	0.36	90	6	31	0.37
173	2.92	0.36	120	5	35	0.36
174	2.92	0.36	180	3	43	—
175	2.92	0.36	300	0	42	—
176*	1.25	3.58	15	0.5	16	0.75
177*	1.25	3.58	30	2	26	0.70
178*	1.25	3.58	45	0.5	32	0.63
179*	1.25	3.58	60	0.0	47	—
180*	1.25	3.58	120	0.5	46	0.46
181*	1.25	3.58	180	2	67	0.34
182*	1.25	3.58	300	0.5	61	0.35
183*	0.75	4.52	15	1	28	0.70
184*	0.75	4.52	20	1	30	0.71
185*	0.75	4.52	30	2	40	0.62
186*	0.75	4.52	45	1	51	0.51
187*	0.75	4.52	60	1	68	—
188*	0.75	4.52	90	1	67	0.45

straight line from which  $C_S = 6 \times 10^{-3}$  and  $R_t/R_p + C_M = 3.4 \times 10^{-2}$ . In similar way the Mayo equation applied to the molecular weights obtained for t-BMA (Figure 3) gives the values  $C_S = 2.5 \times 10^{-3}$  and  $R_t/R_p + C_M = 2.25 \times 10^{-2}$ . For poly(t-BA) on the other hand, the molecular weight appears to be quite independent of solvent:monomer ratios (Figure 3) which suggests that the chain limiting process is that of monomer transfer thus differing from methacrylic esters; this monomer does contain an acidic hydrogen atom in the  $\alpha$ -position to the carboxyl group.

#### Copolymerization experiments

The polymer films so far obtained exhibit satisfactory adhesion but generally lack hardness owing to their low  $T_g$ . In order to improve this, copolymerization with a monomer whose homopolymer has a higher  $T_g$  was investigated.

From the previous work iBMA was selected as the common monomer. This was first copolymerized with methyl methacrylate (MMA) ( $T_g = 105^\circ\text{C}$ ) which is useful for hardening polymeric coatings even when present as the minor constituent; in addition it readily undergoes anionic copolymerization with other acrylic and methacrylic esters<sup>25</sup>.

From copolymerization runs carried out in DMSO using conditions identical to those reported earlier it was found that: (1) on increasing the molar ratio [MMA]/[iBMA] from 0.1 to 0.37 both  $\Delta V/V_0 \times 10^2$  and polymer yield decrease; (2) only for systems containing lower amounts

of MMA some slight increase of hardness was observed.

The following explanation seems the most reasonable: iBMA and MMA are likely to have different reactivities. In iBMA the bulky electron releasing substituent would tend to decrease both the electroinitiation and propagation reactions below those to be expected for MMA in the copolymers. However, the solubility parameter of PMMA ( $\delta = 10.2$ ;  $\Delta\delta_{\text{max}} = 2.6$ ) is close to that of the solvent which increase the dissolution of the polymer film. Thus when [MMA] in the feed is low, the coating parameters are affected and the hardness increased. Increasing [MMA] decreases the throwing power and film formation eventually ceases to occur. Unfortunately the usable [MMA] is insufficient to cause a substantial increase in hardness without causing a fall of the other favourable features observed for iBMA homopolymerization *in situ*.

Methacrylonitrile (MAN) the second comonomer to be used is again known to copolymerize readily with acrylic esters<sup>26</sup>. Moreover, PMAN produced anionically does show good hardness characteristics, possibly because of the carbon-nitrogen conjugation present in the structure which also confers increased heat stability. Runs 156–176 (Table 5) were performed in DMSO with [MAN]/[i-BMA] in the range 0.04–0.12. Small amounts of MAN have a pronounced effect on both  $\Delta V/V_0 \times 10^2$  and polymer yield. An explanation similar to that for MMA may be used; however, the higher electronegativity of the nitrile group increases the reactivity of the MAN with respect to both the initiation and propagation processes.

The reaction in DMF is particularly interesting. Mortimer<sup>27</sup> has shown that MAN is particularly suitable for electropolymerization *in situ* in DMF. Despite the fact that DMF is a good solvent for PMAN, coatings of this polymer are resistant to the solvent during the time scale of their formation. The films so formed are of reasonable hardness but with relatively poor adhesion to the substrate.

Using a wide range of comonomer compositions of [MAN]/[t-BMA] leads to some interesting results. When [MAN]/[iBMA]  $\leq 1$  the polymers produced do not give rise to coherent films nor does the solvent swollen film wet the substrate.

On the other hand, when [MAN]/[iBMA]  $> 1$  films are readily produced (Table 5, runs 176–188). Once dried the films are quite hard and exhibit good adhesion properties and in these conditions the coating could have some applied interest; the 'throwing power', on the other hand, is very poor and the system could only be used to coat simple shapes.

#### Compositions of copolymers with MAN

Consideration of the polymer composition as determined by nitrogen analysis leads to some surprising results especially when considered in the light of the higher reactivity which is expected for MAN. Figure 4 shows that for iBMA/MAN in DMF the variation in copolymer composition is almost that of an alternating copolymer for which  $r_1 = r_2 = 1$ . This is interesting in that a product with less than 50 mol% MAN still exhibits the typical coloration of the conjugated carbon-nitrogen bonds shown by pure PMAN. It may be that initial reaction involves the formation of blocks of MAN and that this reaction is faster than the rate of diffusion of MAN to the electrode surface which enables the iBMA (now in relatively greater concentration) to enter into the copolymerization. In addition when the metal plate is withdrawn from the solution after a short electro-

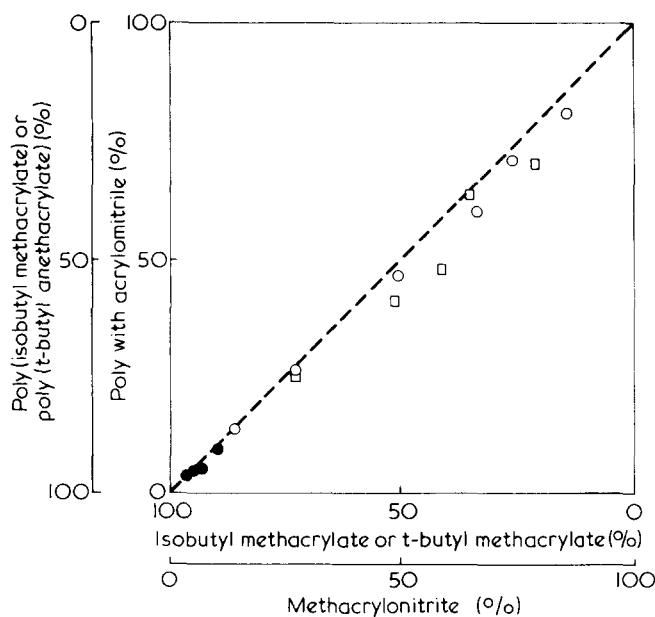


Figure 4 Copolymer composition diagram.  $\square$ , t-butyl methacrylate in DMSO;  $\circ$ , iso-butyl methacrylate in DMF;  $\bullet$ , iso-butyl methacrylate in DMSO. Common comonomer, methacrylonitrile

lysis time, the polymer swollen with the comonomer/solvent mixture will have an average composition very close to that at the onset of reaction. If copolymerization or even homopolymerization proceeds during the drying of the films the resulting products will have a composition similar to that of the comonomer feed.

For longer electrolysis times and lower currents, the different resistance of the products to the solvent at different compositions has to be considered too. This is the case for copolymerization runs carried out in DMSO for the system t-BMA/MAN of which only the data of Figure 4 are reported here.

## CONCLUSIONS

It is clear from the data so far discussed that in order to achieve electrochemical polymerization of acrylic monomers *in situ* (i.e. the formation of polymeric material simultaneous with deposition on the metal substrate) a preliminary condition must be fulfilled; in aprotic media the monomer/solvent couple has to be selected such that the solubility parameter of the polymer is sufficiently different to that of the solvent, or at least the time scale of building up the film should be lower than the time required for the dissolution of the polymer.

The 'throwing power' of the process is related to this condition, once the low conductivity of the insoluble deposition does affect the homogeneity and the morphology of the coating. Although the insolubility of the polymer is a necessary condition it can be a hinderance to obtaining a proper polymeric film; the polymer molecules, because of the poor polymer/solvent interaction will tend to be tightly coiled instead of spreading onto the metal substrate. This effect has to be counterbalanced by other factors: (1) by the existence of some interactions between the growing polymer and the electrode material; (2) by a reduction of the polymer chain length.

An indirect indication of point 1 is that a better coating is formed when the polar monomer contains a bulky secondary or tertiary substituent, n-paraffinic substituents lead to far less satisfactory results. This fact requires further investigation, but it is likely that the adsorption and orientation of monomer molecules on the metal electrode before the polymerization is very important for the subsequent process *in situ* to occur.

Point 2 is banal and requires little further comment. It must be observed that not only the polymer chain but also the average kinetic chain length resulting from each electron transfer need not be very high otherwise the overall polymerization reaction will not be confined to the vicinity of the electrode surface. Thus in the anionic systems examined no careful diminution of impurities and moisture which could possibly act as chain terminating agents was necessary. It is clear that the conditions so far discussed for electropolymerization *in situ* represent a strict limit to this technique either for the range of exploitable monomers or for the physical features of the coatings. In particular the low molecular weights obtained *in situ* do not agree with the general rule that the film forming properties of a surface coating improve as the molecular weight or molecular complexity of the polymer increase.

Copolymerization may overcome these drawbacks. Although some relatively satisfactory results have been obtained with suitable MAN/iBMA mixtures, copolymerization of similar monomer pairs does not generally resolve the problems related to molecular weight and molecular complexity. Addition of a small quantity of a divinyl derivative, which would not affect the 'throwing power' of the systems reported here may be capable of introducing crosslinks either during polymerization or during subsequent drying operations.

## ACKNOWLEDGEMENT

The authors wish to acknowledge a grant in aid from the Italian National Council for Research for one of them (G. M.).

## REFERENCES

- Breitenbach, J. W. and Srna, Ch. *Pure Appl. Chem.* 1962, 4, 245
- Funt, B. L. in 'Macromolecular Reviews', (Ed. A. Peterlin), Interscience, New York, 1967, Vol 1, p 35
- Yamazaki, N., Tanaka, I. and Nakahama, S. *J. Macromol. Sci. (A)* 1968, 2, 1121
- Parravano, G. J. in 'Organic Electrochemistry', (Ed. M. N. Baizer), Marcel Dekker, New York, 1973, p 947
- W. R. Grace and Co. Br. Pat. 1 134 387
- W. R. Grace and Co. Fr. Pat. 1 586 798
- W. R. Grace and Co. Br. Pat. 1 179 543
- Asahara, T., Seno, M. and Tsuchiya, M. *Kinzoku Hyomen Gijutsu* 1968, 19, 511
- Idem, ibid.* 1969, 20, 2
- Idem, ibid.* 1969, 20, 28
- Idem, ibid.* 1969, 20, 64
- Idem, ibid.* 1969, 20, 99
- Idem, ibid.* 1969, 20, 411
- Idem, ibid.* 1969, 20, 414
- Idem, ibid.* 1969, 20, 617
- Idem, ibid.* 1970, 21, 126
- Funt, B. L. and Williams, F. D. *J. Polym. Sci. (A)* 1964, 2, 865

*Polymeric coatings produced in situ by electropolymerization: G. Mengoli and B. M. Tidswell*

- 18 Funt, B. L. and Bhadani, S. N. *J. Polym. Sci. (A)* 1965, **3**, 4191
- 19 Asahara, T., Imoo, M. and Tsuchiya, M. *Kinzoku Hyomen Gijutsu* 1969, **20**, 576
- 20 'Encyclopedia of Polymer Science and Technology', John Wiley, New York, 1964, Vol 1, p 297
- 21 Hughes, L. J. and Britt, G. E. *J. Appl. Polym. Sci.* 1961, **5**, 337
- 22 Walker, E. E. *J. Appl. Chem.* 1952, **2**, 470
- 23 'Encyclopedia of Polymer Science and Technology', John Wiley, New York, 1964, Vol 3, p 841
- 24 Asahara, T., Seno, M. and Tsuchiya, M. *Bull. Chem. Soc. Japan* 1969, **42**, 2416
- 25 Graham, R. K., Panchak, J. R. and Kampf, M. J. *J. Polym. Sci.* 1960, **44**, 411
- 26 'Encyclopedia of Polymer Science and Technology', John Wiley, New York, 1964, Vol 15, p 336
- 27 Mortimer, D. *PhD Thesis* University of Bradford (1975)

# Crystallinity and fusion of ethylene oxide/propylene oxide block copolymers:

## 1. Type PE copolymers

P. C. Ashman and C. Booth

Department of Chemistry, University of Manchester, Manchester M13 9PL, UK

(Received 16 May 1975)

Lamella spacings, specific volumes and melting points have been determined for a series of well characterized poly(propylene oxide)/poly(ethylene oxide) type PE block copolymers with E-block length 40 chain units and P-block lengths 0 to 11 chain units. These properties are interpreted in terms of a stacked lamella model with alternating amorphous and crystalline layers. The crystalline lamella thickness is found to be about 25 E chain units, i.e. the crystals are predominantly of extended-chain type. The specific volume of the polymer in the amorphous lamellae is found to be lower than that of polymer of corresponding composition in the supercooled melt. The melting points are low compared to that of perfectly crystalline poly(ethylene oxide), i.e. 47 to 51°C compared with  $T_m^0 = 76^\circ\text{C}$ . This is due to the positive free energy of formation from the melt of the amorphous layer ( $\sigma_a \sim 3.5$  kJ/mol) and the crystalline/amorphous interface ( $\sigma_o \sim 3$  kJ/mol).

### INTRODUCTION

The crystalline structure and the melting behaviour of low molecular weight poly(ethylene oxide) has been extensively studied. Small-angle X-ray scattering<sup>1-3</sup>, electron<sup>4</sup> and optical<sup>5</sup> microscopy and dilatometry<sup>1,2</sup> have served to show that the crystalline structure is stacked lamellae, i.e. alternating crystalline and amorphous layers, forming a polycrystal. Within the crystalline lamellae the poly(ethylene oxide) chains are folded to an extent which depends upon the molecular weight and the crystallization temperature<sup>1,2,6,7</sup>; samples of molecular weight less than 3000 are essentially unfolded (extended-chain crystals).

The thermodynamic melting point (i.e. the melting point of an infinitely large perfect crystal composed of polymer of infinite molecular length) of poly(ethylene oxide) is near 349 K<sup>8-10</sup>. Melting points of poly(ethylene oxide) fractions range downwards from 343 K, the actual values observed being affected by the average molecular weight<sup>6-11</sup>, the nature of the end group<sup>12-16</sup> and the nature of the chain folding in the crystalline lamellae<sup>6,7,11,14</sup>.

Given that poly(ethylene oxide) is a stacked lamella structure the melting behaviour can be broadly understood in terms of the lamella thicknesses and the free energies of formation (from the melt) of the crystalline and amorphous lamellae. The free energy of formation of the crystalline lamellae can be calculated (using the methods of statistical mechanics<sup>17,18</sup>, known molecular and thermodynamic properties of the polymer, and the lamella thicknesses) and so it is possible to focus attention upon the free energy of formation of the amorphous lamellae and the crystalline/amorphous interface. These two contributions to the free energy of formation from the melt of the polycrystal are usually considered together as the interfacial free energy,  $\sigma_e$ .

For predominantly chain-extended crystals a practicable way of changing  $\sigma_e$  whilst keeping other parameters unchanged is to vary the chemical nature of the chain end-groups<sup>12,13</sup>. If the end-groups are blocks of copolymerized material, such that the block is confined to the amorphous

lamella by the crystallization of the poly(ethylene oxide) block<sup>14,15</sup>, very marked changes in the nature of the amorphous layer are possible.

In order to avoid undue complexity in the interpretation of the thermodynamic properties of a crystallizable block copolymer it is essential that the two polymeric components are compatible in the melt (otherwise the properties of the crystalline copolymer may be determined in part by the two-phase structure of the melt) and that only one component is crystallizable. Accordingly we have chosen to study block copolymers of poly(ethylene oxide) and poly(propylene oxide) rather than the block copolymers favoured by others, i.e. poly(ethylene oxide) with either poly(styrene)<sup>19,20</sup> or poly( $\epsilon$ -caprolactam)<sup>21</sup>. The mixing behaviour of low molecular weight poly(ethylene oxide) and poly(propylene oxide) fractions has been investigated<sup>22,23</sup> and the results give reason to suppose that the poly(ethylene oxide)/poly(propylene oxide) block copolymers we have prepared do not exhibit microphase separation in the melt.

In this paper we report the preparation and properties of diblock copolymers of ethylene oxide and propylene oxide. We denote these PE (where P is a propylene oxide block and E an ethylene oxide block). In subsequent papers we will report on triblock (PEP) and multiblock [P(EP)<sub>n</sub>] copolymers.

### EXPERIMENTAL AND RESULTS

#### Preparation

PE copolymers were prepared by the polymerization of propylene oxide onto  $\alpha$ -methoxy- $\omega$ -hydroxy-poly(ethylene oxide).

Reagents and solvents were purified by the methods described by Perrin *et al.*<sup>24</sup>. Ethylene oxide was refluxed over anhydrous calcium sulphate (2 h) and then distilled through a column of potassium hydroxide pellets. Propylene oxide was refluxed over calcium hydride (4 h) and then distilled. Methanol (50 cm<sup>3</sup>) was reacted with magnesium turnings (2 g), more (200 cm<sup>3</sup>) added and refluxed (3 h), and finally distilled and stored over molecular sieves

Table 1 Characteristics of PE polymers

Sample	$\bar{M}_n$		G.p.c.	$\bar{M}_w/\bar{M}_n$ (g.p.c.)	$w_e^*$ (p.m.r.)	$\bar{M}_n$ (best value)
	V.p.o.	End group analysis				
0-40	1850	1800	1750	1.04	1.00	1750
2-40	—	—	1830	1.05	0.93	1880
3-40	—	—	1920	1.04	0.90	1940
5-40	—	—	2020	1.05	0.85	2030
8-40	—	—	2170	1.04	0.78	2220
11-40	—	—	2270	1.05	0.74	2370

\* Weight fraction of poly(ethylene oxide)

(type 4A). Dioxane (1 dm<sup>3</sup>), water (100 cm<sup>3</sup>) and concentrated hydrochloric acid (14 cm<sup>3</sup>) were mixed and refluxed (12 h) under an atmosphere of nitrogen, the mixture was neutralized with solid potassium hydroxide and refluxed with sodium metal (12 h), and finally distilled and the dioxane was stored over molecular sieves (type 4A). Benzene was dried over and distilled from calcium hydride.

Polymerization was carried out in apparatus similar to that described by Simons and Verbanc<sup>25</sup>. Sodium (2 g) was added to a solution of methanol (46 g) in dioxane (10 cm<sup>3</sup>) under a blanket of dry nitrogen. When reaction was complete (at room temperature) the temperature was raised to 100°C and ethylene oxide (~250 g) was added at a rate sufficient to maintain the temperature. Boiling of the monomer served to agitate the mixture and also blanket the reaction with ethylene oxide vapour; towards the end of the reaction, and whenever the mixture was cooled, dry nitrogen was used for these purposes. After the required amount of ethylene oxide had reacted (i.e. when the ratio of the weight of ethylene oxide reacted to the number of moles of methanol used as initiator indicated an average molecular weight for the poly(ethylene oxide) of  $\bar{M}_n \sim 1750$ ) the system was flushed with dry nitrogen to remove any remaining ethylene oxide. Thereafter propylene oxide was added in increments to prepare the copolymer.

Samples, withdrawn at intervals, were cooled and neutralized with dilute hydrochloric acid. Dioxane, water and unreacted monomer were removed by rotary evaporation followed by evacuation of the melt. Sodium chloride was removed by dissolving the dry polymer in dry benzene and centrifuging the mixture (15 000 × g for 15 min). Finally the polymers were precipitated from the benzene solution by addition of iso-octane (in such a way as to leave the lower molecular weight molecules in solution<sup>26</sup>) and freeze dried (from benzene solution).

#### Notation

We refer to samples by their number-average block lengths (expressed in monomer units) as established by their preparation and subsequent characterization. For example, sample 2-40 denotes a PE block copolymer with a poly(propylene oxide) block length of 2 monomer units and a poly(ethylene oxide) block length of 40 monomer units.

#### Characterization

Average molecular weights were measured by use of a Mechrolab vapour pressure osmometer (benzene at 25°C), by end group analysis (phthaloylation in pyridine)<sup>27-29</sup>, and by gel permeation chromatography (g.p.c.). Condi-

tions for g.p.c. were essentially as described earlier<sup>14</sup>; calibration was by poly(ethylene oxide) and poly(propylene oxide) fractions (which gave practically coincidental results); correction was made for instrumental spreading<sup>14</sup>. The copolymer compositions were determined by proton magnetic resonance spectrometry<sup>14,30</sup>.

The characteristics of the sample are given in Table 1. The measured values of  $\bar{M}_n$  for sample 0-40 are in keeping with the value (1750) calculated from the preparative conditions. The values of  $\bar{M}_n$  finally adopted (last column of Table 1) are calculated from the compositions taking a value of  $\bar{M}_n = 1750$  for sample 0-40; this procedure gives internal consistency and also gives substantial agreement with the g.p.c. results for the copolymers.

#### Dilatometry

Melting points of the samples were determined by dilatometry. The glass dilatometers used have been described elsewhere<sup>31</sup>. A known weight (~0.2 g) of molten polymer was injected into the dilatometer, outgassed (<1 Pa, 4 h), and confined with mercury. Prior to crystallization, the dilatometer was immersed in boiling water (5 min) and then transferred to an oil bath held (to ±0.1 K) at the crystallization temperature. Crystallization was allowed to proceed to completion. The melting point was measured by transferring the dilatometer to a second oil bath held at a temperature 2 K below the expected melting point, and then raising the temperature of the bath at a rate of 6 K/h. The mercury level was observed by means of a cathetometer. The melting point was taken to be the temperature at which the last trace of crystallinity disappeared (as judged by the temperature coefficient of expansion). This melting procedure was chosen so as to avoid<sup>6,8</sup> complications due to overheating and recrystallization.

Melting points, determined for a number of crystallization temperatures ( $T_c$ ), are listed in Table 2. Melting points are seen to be practically independent of  $T_c$ . Multiple melting points<sup>6,7,14,15</sup> were not observed.

#### Picnometry

Specific volumes of the polymers were determined by picnometry. The L-shaped glass picnometers (Figure 1) had a sample chamber (1 cm<sup>3</sup>) joined to a capillary (0.07 cm diameter, 8 cm length) ground to a point at the open end. A dual-bulb apparatus (Figure 1) was used to provide a mercury reservoir during expansion and contraction of the dilatometer contents. Once equilibrium had been achieved the mercury could be syphoned from bulb A to bulb B (Figure 1) leaving the picnometer exactly full to the point of the capillary. The picnometers were calibrated by filling with mercury.

A small amount of molten polymer (~0.4 g) was injected into the weighed picnometer which was then reweighed.

Table 2 Melting points (°C) of PE Polymers

Sample	$T_c$ (°C)		
	33.0	35.2	39.0
0-40	50.6	50.7	50.9
2-40	50.0	50.1	50.2
3-40	49.8	49.8	49.8
5-40	48.6	48.6	48.8
8-40	47.2	47.5	47.7
11-40	47.1	46.9	47.4

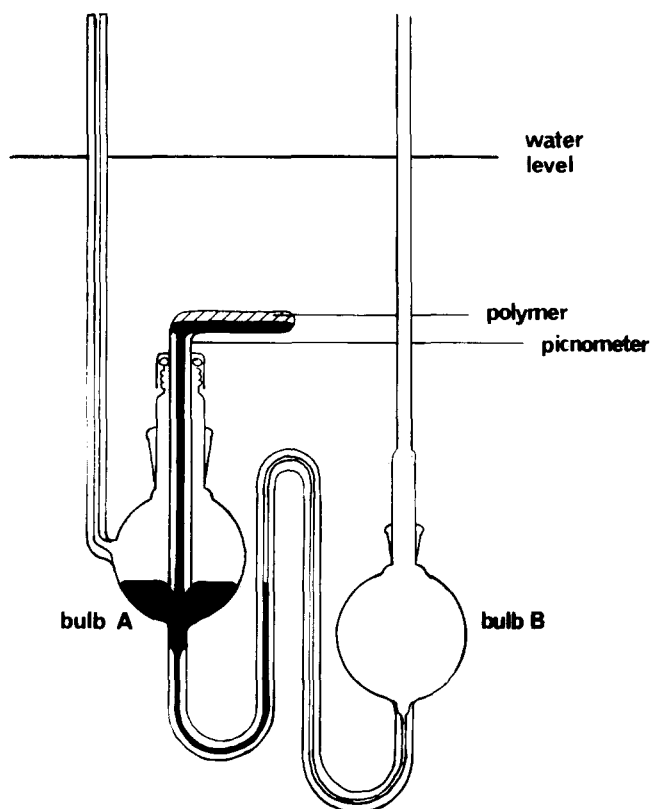


Figure 1 Apparatus used for picnometry

Table 3 Specific volumes (cm<sup>3</sup>/g) of PE polymers

Sample	$T_c$ (°C)	
	25.0	33.0
0-40	0.831	0.832
2-40	0.840	0.840
3-40	0.846	0.846
5-40	0.852	0.853
8-40	0.868	0.871
11-40	0.875	0.876

The polymer was outgassed (<1 Pa, 3 h) and confined with mercury. The picnometer was then attached to the dual-bulb apparatus, immersed in boiling water (5 min), and quickly transferred to a water bath held (to  $\pm 0.1$  K) at the required crystallization temperature. After 3 days, when crystallization was complete, the picnometer was removed and weighed. Specific volumes (calculated with allowance for buoyancy), measured at two crystallization temperatures ( $T_c$ ), are listed in Table 3.

#### X-ray scattering

Lamella spacings were determined by small-angle X-ray scattering. Thin films of polymer (thickness  $\sim 0.1$  cm), supported on Melinex polyester film, were melted at 100°C (5 min) and then transferred to a hot plate held (to  $\pm 0.02$  K) at the required crystallization temperature. Crystallized films were exposed (at room temperature) to CuK $\alpha$  radiation in a Rigaku-Denki slit collimated small-angle camera. The diffraction pattern was recorded photographically. The camera was standardized with powdered sodium stearate.

The diffraction patterns were observed at room temperature for samples crystallized at 33°C. They were similar to those reported<sup>1,6</sup> for low molecular weight poly(ethyl-

ene oxide) homopolymers, i.e. they consisted of several equally spaced maxima of gradually diminishing intensity. Lamella spacings, calculated directly from the photographs by use of Bragg's law (slit smearing affects being unimportant), are listed in Table 4. For purposes of comparison extended chain lengths (nm) are given in Table 4; these are calculated assuming a length of 0.28 nm per chain unit (P or E), in keeping with the repeat distance of 1.95 nm for the 7-2 helix of crystalline poly(ethylene oxide)<sup>32</sup>. The spacings indicate that the polymers form predominantly extended-chain lamellae, as is found<sup>1,6,7</sup> for poly(ethylene oxide) homopolymers of comparable chain length.

#### LAMELLA THICKNESS: SPECIFIC VOLUME OF AMORPHOUS MATERIAL

We interpret the lamella spacings and specific volume in terms of a stacked lamella model as depicted in Figure 2. Initially we focus attention on poly(ethylene oxide) homopolymers.

#### Homopolymers

It is assumed that: (a) the amorphous material in the poly crystal is all contained within the amorphous lamellae which are of uniform thickness  $l_a$ ; (b) the crystalline material is free from defects and is all contained within the crystalline lamellae which are of uniform thickness  $l_c$ ; (c) the interfaces between the alternating amorphous and crystalline lamellae are discrete. Thus the volume fraction of crystalline material,  $\phi_c$ , is simply given by

$$\phi_c = \frac{l_c}{l} \quad (1)$$

where  $l$  is the lamella spacing (measured by X-ray scattering); and the weight fraction of crystalline material,  $w_c$ , is

Table 4 Lamella spacings of PE polymers crystallized at 33°C

Sample	Approximate chain length (nm)	Lamella spacing (nm)
0-40	11.2	11.0
2-40	11.7	11.3
3-40	12.2	11.9
5-40	12.7	12.6
8-40	13.7	13.5
11-40	14.3	14.2

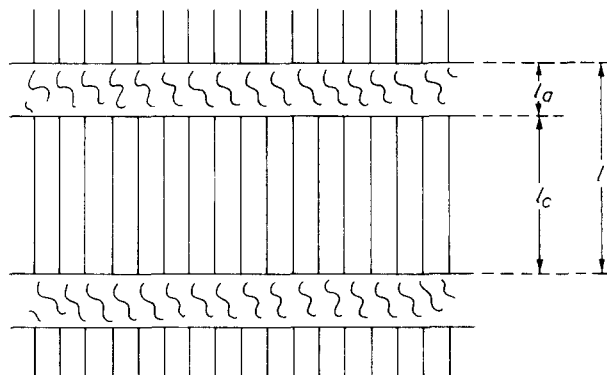


Figure 2 The stacked lamella model of the polycrystal: see text for definition of symbols



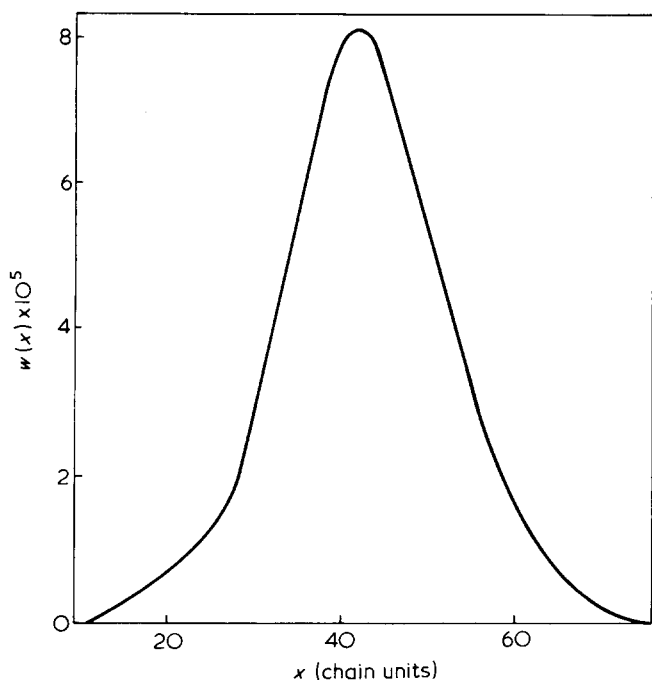


Figure 3 Chain length distribution of sample 0-40:  $l_c = 26$  chain units for  $T_c = 33^\circ\text{C}$

therefore given by:

$$w_c = \frac{l_c \nu}{l \nu_c} \quad (2)$$

where  $\nu$  is the specific volume of the polycrystal (measured by picnometry) and  $\nu_c$  is the specific volume of the crystalline material (calculated from unit cell dimensions).

Equation (2) contains two unknown quantities,  $w_c$  and  $l_c$ . A second relationship between  $w_c$  and  $l_c$  is available if we extend the model further. We assume that: (d) the ends of the molecules are excluded from the crystalline lamellae, and the amorphous material within the polycrystal arises solely from the discrepancy between the length of the polymer ( $x$ ) and the thickness of the crystalline lamellae ( $l_c$ ); (e) the molecules fold to their maximum possible extent (consistent with the crystalline lamella thickness); so that molecules with  $x < l_c$  are rejected from the crystalline lamellae, with  $l_c < x < 2l_c$  pass through the crystalline lamella once, with  $2l_c < x < 3l_c$  pass through the crystalline lamella twice, etc. It may be noted that the assumption of maximum folding implies adjacent re-entry (regular folding) only for those molecules with  $x$  near  $2l_c$ ,  $3l_c$  etc. As these molecules are only a very small fraction of the total in our samples (see Figure 3) the model is not particularly restrictive.

Assumptions (a) to (e) allow us to write:

$$w_c = \sum_{s=1}^{\infty} \int_{sl_c}^{(s+1)l_c} w(x) \left( \frac{sl_c}{x} \right) dx \quad (3)$$

where  $l_c$  is expressed in chain units, i.e.  $l_c/\text{chain units} = (l_c/\text{nm}) (1/0.28)$  since 0.28 nm is the length of a chain unit in crystalline poly(ethylene oxide) at  $25^\circ\text{C}$ <sup>32</sup>, and  $w(x)$  is the weight distribution of chain lengths ( $x$  in chain units) in the sample.

We apply equations (2) and (3) in the following way. The weight distribution of low molecular weight poly(ethylene oxide) samples are narrow (Table 1) and so can be well represented by Schulz-Zimm<sup>33</sup> distributions, i.e. by:

$$w(x) = \frac{b^{(a+1)}}{\Gamma(a+1)} x^a e^{-bx} \quad (4)$$

where  $b = a/\bar{x}_n$  and  $a = 1/(\bar{x}_w/\bar{x}_n - 1)$ , and  $\bar{x}_n$  and  $\bar{x}_w$  are number- and weight-average chain lengths. The two relationships between  $w_c$  and  $l_c$  are plotted in Figure 4 for sample 0-40 for which  $l = 11.0$  nm,  $\nu = 0.832$  cm<sup>3</sup>/g at  $33^\circ\text{C}$ ,  $\nu_c = 0.814$  cm<sup>3</sup>/g at  $33^\circ\text{C}^*$ ,  $\bar{x}_n = 40$  chain units and  $\bar{x}_w/\bar{x}_n = 1.05$ . The intersection of the two curves represents those values ( $l_c = 7.4$  nm,  $w_c = 0.68$ ) which satisfy the two equations. We include in Figure 4 plots of equation (3) for other values of  $\bar{x}_w/\bar{x}_n$ ; it can be seen that the values of  $l_c$  and  $w_c$  obtained are fairly insensitive to this parameter when  $\bar{x}_w/\bar{x}_n \geq 1.05$ .

#### Block copolymers

The above treatment is readily extended to block copolymers with a non-crystallizable block, since all of this material will be in the amorphous lamellae. If  $w_c$  is redefined as the weight fraction of the poly(ethylene oxide) block which is crystalline, and if  $w_e$  is the weight fraction of poly(ethylene oxide) in the copolymer, then the weight fraction of the copolymer which crystallizes is  $w_c w_e$  and equation (2) becomes:

$$w_c = \frac{l_c \nu}{l \nu_c w_e} \quad (5)$$

\* We use  $\nu_c = 0.813$  cm<sup>3</sup>/g at  $25^\circ\text{C}$ <sup>34</sup> and  $\alpha_c = 0.00015$  cm<sup>3</sup>/g K<sup>2</sup>. Note that  $l$  is measured at about  $20^\circ\text{C}$ ; the correction to  $33^\circ\text{C}$  ( $\sim 0.1\%$ ) is negligible compared with experimental error.

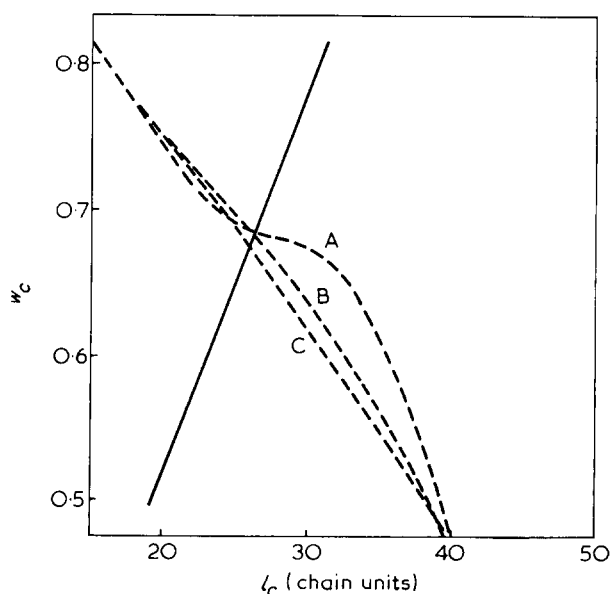


Figure 4 Relationship between  $w_c$  and  $l_c$  for sample 0-40; —, equation (2); ----, equation (3) with  $\bar{x}_w/\bar{x}_n$  equal to 1.05 (A), 1.10 (B) and 1.20 (C)

Table 5 Characteristics of crystalline PE polymers at 33°C

Sample	$l_c$ (nm)	$w_c$	$l_a$ (nm)	$v_a$ (cm <sup>3</sup> /g)	$v_s$ (cm <sup>3</sup> /g)
0-40	7.4	0.68	3.7	0.870	0.897
2-40	7.0	0.69	4.3	0.886	0.917
3-40	7.1	0.69	4.8	0.898	0.927
5-40	7.0	0.69	5.6	0.908	0.937
8-40	6.8	0.69	6.7	0.937	0.952
11-40	6.8	0.69	7.4	0.940	0.957

Equation (3) can be rewritten:

$$w_c = \sum_{s=1}^{\infty} \int_{sl_c}^{(s+1)l_c} w(y) \left( \frac{sl_c}{y} \right) dy \quad (6)$$

where  $w(y)$  is the weight distribution of poly(ethylene oxide) block lengths ( $y$ ).

Solutions of equations (5) and (6) for the PE series of copolymers, using the data of Tables 1, 3 and 4, are given in Table 5. Given  $l_c$  and  $w_c$  we can calculate the thickness of the amorphous lamellae ( $l_a$ ) and the specific volume of the material in the amorphous lamellae ( $v_a$ ) from the equations:

$$l = l_c + l_a \quad (7)$$

$$v = v_c w_c w_e + v_a (1 - w_c w_e) \quad (8)$$

and values of  $l_a$  and  $v_a$  are also given in Table 5.

Crystalline lamella thicknesses ( $l_c$ ) and degrees of crystallinity of the poly(ethylene oxide) block ( $w_c$ ) are practically independent of the copolymer composition. The specific volume of the amorphous material ( $v_a$ ) varies with the copolymer composition mainly because of the changing composition of the amorphous lamellae. The specific volume of a supercooled melt of the same composition as the amorphous lamellae ( $v_s$ ) can be calculated, assuming no volume change on mixing, from the equation:

$$v_s = (w_e w_a v_e + w_p v_p) / (1 - w_c w_e) \quad (9)$$

where  $w_a = 1 - w_c$  is the weight fraction of the poly(ethylene oxide) block which is amorphous,  $w_p = 1 - w_e$  is the weight fraction of poly(propylene oxide) in the copolymer, and  $v_e$  and  $v_p$  are the specific volumes of supercooled liquid poly(ethylene oxide) and poly(propylene oxide) respectively. We use  $v_e = 0.897$  cm<sup>3</sup>/g and  $v_p = 1.007$  cm<sup>3</sup>/g at 33°C\*. Comparison of the specific volume of the amorphous material of the polycrystal ( $v_a$ ) with that of supercooled melt of the same composition ( $v_s$ ) is made in Table 5:  $v_a$  is lower than  $v_s$  by 1 to 3%. This finding is in keeping with studies of crystalline poly(ethylene), which have been reviewed recently<sup>38,39</sup> and which indicate an increased density of the amorphous material in the polycrystal over that of the supercooled melt.

#### END INTERFACIAL FREE ENERGY, $\sigma_e$

Two theories<sup>17,18</sup> may be used to interpret the melting points and lamella thicknesses of low molecular weight

\*  $v_e = 0.891$  cm<sup>3</sup>/g at 25°C<sup>35</sup>;  $\alpha_e = 0.00069$  cm<sup>3</sup>/g K<sup>2,35</sup>.  
 $v_p = 0.997$  cm<sup>3</sup>/g at 20°C<sup>36</sup>;  $\alpha_p = 0.00077$  cm<sup>3</sup>/g K<sup>22,37</sup>.

polymers and block copolymers. These represent extreme cases of independently located chain ends<sup>17</sup> and of chain ends paired at the crystalline lamella surface<sup>18</sup>. A modification<sup>18</sup> of the end-paired model allows for partial melting of the crystalline lamella and the formation of an amorphous layer in which the chain ends are located.

The two models are depicted in Figure 5. In the Flory<sup>17</sup> model of the partly melted system (Figure 5a) the crystalline lamellae are surrounded by melt in which the chain ends are uniformly dispersed. In the modified Flory-Vrij<sup>18</sup> model of the partly melted system (Figure 5b) the alternating crystalline/amorphous lamella structure is the unit which is surrounded by melt. Consequently there is a contribution to the melting point depression in the Flory treatment which arises from dilution of the chain ends in the melt owing to melting of the crystalline phase (Figure 5a), which does not appear in the Flory-Vrij treatment. We have shown earlier<sup>9</sup>, in application of these theories to the melting of low molecular weight poly(ethylene oxide), that the difference between the two models is slight. However, the Flory-Vrij model is consistent with the model we have developed (to account for the lamella spacings and specific volumes of our polymers) in the previous section.

It is convenient to start with a description of the Flory-Vrij theory applied to homopolymers.

#### Homopolymers

The Flory-Vrij theory leads<sup>11</sup> to the following expression for the melting point of a low molecular weight homopolymer in an extended-chain polycrystal:

$$T_m = T_m^0 [1 - 2\sigma_e / \Delta h l_c] / [1 - (RT_m^0 \ln I) / \Delta h l_c] \quad (10)$$

where  $T_m^0$  is the thermodynamic melting point,  $\Delta h$  the thermodynamic enthalpy of fusion, and  $l_c$  the crystalline lamella thickness in chain units. The end interfacial free energy ( $\sigma_e$ ) is the free energy of formation from the melt of the amorphous/crystalline interface and the adjacent amorphous layer. The polymer chains traverse the crystalline lamella  $l$  times each on average. The parameter  $I$  accounts for the

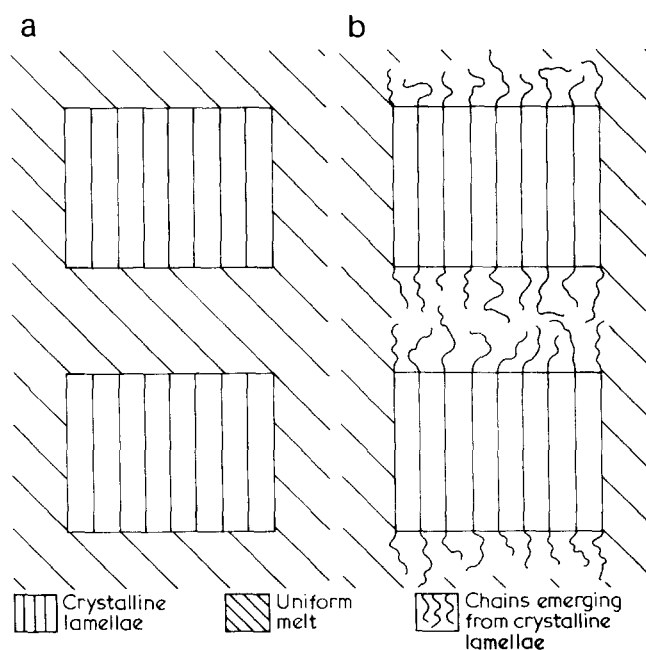


Figure 5 (a) Flory model of the partly melted system, and (b) modified Flory-Vrij model of the partly melted system

Table 6 End interfacial free energies ( $\sigma_e$ ) for PE polymers

Sample	$T_m$ (°C)	$\phi_e^*$	$t$	$\sigma_e$ (kJ/mol)
0-40	50.7	1.00	1.04	6.5
2-40	50.1	0.922	1.10	6.3
3-40	49.8	0.889	1.08	6.4
5-40	48.7	0.834	1.10	6.6
8-40	47.5	0.759	1.14	6.6
11-40	47.1	0.717	1.15	6.7

\* At  $T_m$ :  $l_c$  is negligibly different (<0.1%) from  $l_c$  at 20°C

state of order of the chains in the polycrystal<sup>11,18</sup> and is, effectively, the probability that a sequence of chain units  $sl_c$  long (where  $s$  is a positive integer), folded if  $s > 1$ , does not contain a chain end. For a polydisperse polymer, where each chain folds to its maximum extent (for a given  $l_c$ ),  $I$  has the form<sup>11,18</sup>:

$$I = \sum_{s=1}^{\infty} \int_{sl_c}^{(s+1)l_c} w(x) [(x - sl_c + 1)/x] dx \quad (11)$$

where  $w(x)$  is the weight distribution of chain lengths which, as before, we can represent by a Schulz-Zimm expression<sup>33</sup>. Similarly:

$$t = \sum_{s=1}^{\infty} \left[ \int_{sl_c}^{(s+1)l_c} s \left( \frac{w(x)}{x} \right) dx \right] / \left[ \int_0^{\infty} \left( \frac{w(x)}{x} \right) dx \right] \quad (12)$$

Equations (10) to (12) are consistent with assumptions (a) to (e) of the previous section; however, equations (11) and (12) contain the additional restriction that chain folding must be by adjacent re-entry. The folds are included in the crystalline lamellae.

We apply equations (10) to (12) in the following way. Melting points are calculated for several values of  $\sigma_e$  and compared with the observed melting points to fix  $\sigma_e$ . (Details of this procedure have been given earlier<sup>6</sup>.) For sample 0-40 we have  $T_m^0 = 349$  K<sup>8-10</sup>,  $\Delta h = 8.4$  kJ/(mol of chain units)<sup>40</sup>,  $l_c = 7.3$  nm = 26 chain units,  $\bar{x}_n = 40$  chain units and  $\bar{x}_w/\bar{x}_n = 1.05$ . An observed melting point of 323.9 K (Table 2) leads to a value of  $\sigma_e$  of 6.5 J/(mol of chains emerging) while  $t$ , the folding parameter, is found to be 1.04.

### Block copolymers

For block copolymers equations (10) to (12) must be changed to allow for a changed probability of sequence selection. The molten copolymer chain is considered to be composed of segments of volume equal to that of a molten poly(ethylene oxide) chain unit. The probability that a segment chosen at random is a poly(ethylene oxide) segment is then  $\phi_e$ , the volume fraction of poly(ethylene oxide) in the copolymer melt. This is the probability that the first segment of a chosen sequence is a poly(ethylene oxide) unit\*. The probability that the rest of the sequence does not contain a poly(ethylene oxide) block end is then (for maximum folding)

\* Flory<sup>17</sup> puts this probability equal to the mole fraction of crystallizable polymer units. The use of volume (segment) fraction seems more in keeping with the Flory-Vrij<sup>18</sup> model.

$$I = \sum_{s=1}^{\infty} \int_{sl_c}^{(s+1)l_c} w(y) [(y - sl_c + 1)/y] dy \quad (13)$$

where  $w(y)$  is the weight distribution of poly(ethylene oxide) block lengths ( $y$ ). A similar equation is written for the folding parameter  $t$ . The melting point equation for a block copolymer of type PE is:

$$T_m = T_m^0 [1 - 2\sigma_e/\Delta hl_c] / [1 - (RT_m^0 \ln \phi_e I)/\Delta hl_c] \quad (14)$$

Values of the volume fractions calculated from

$$\phi_e = w_e v_e / (w_e v_e + w_p v_p) \quad (15)$$

are listed in Table 6, together with the values of  $t$  and  $\sigma_e$  obtained by use of these parameters and those listed earlier (note that  $\bar{y}_n = 40$  chain units and  $\bar{y}_w/\bar{y}_n = 1.05$ ). Values of  $t$  are all near to unity, as expected for predominantly extended-chain polycrystals.

The end interfacial free energy  $\sigma_e$  has a formal interpretation which depends upon the model used to describe the system. This is made clear by reference to Figure 5. In the Flory model (Figure 5a)  $\sigma_e$  is the free energy of formation from the melt of the crystal/melt interface. In the Flory-Vrij model (Figure 5b)  $\sigma_e$  is the free energy of formation from the melt of the amorphous/crystalline interface and the adjacent amorphous layer. So it is convenient, for the polycrystalline model, to write  $\sigma_e$  as the sum of three terms:

$$\sigma_e = \sigma_o + \sigma_m + \sigma_a \quad (16)$$

which can be identified as follows:  $\sigma_o$  = the free energy of formation from the melt of the amorphous/crystalline interface;  $\sigma_m$  = the free energy change (enthalpy and non-combinatorial entropy changes) due to the concentration, relative to the melt, of chain ends (blocks or groups) in the amorphous lamellae. (The combinatorial entropy change associated with the formation of the amorphous lamellae is accounted for by the Flory-Vrij theory.);  $\sigma_a$  = the free energy increase due to conformational restriction, relative to the melt, of the chains in the amorphous lamellae, i.e. due to the constraint of the crystal surface. It has been shown elsewhere<sup>14</sup> that the attractive energy of the crystalline lamellae contributes negligibly to  $\sigma_e$ , and we assume (in the absence of any compressive force) that the low specific volume of the polymer in the amorphous layer simply reflects the effects of conformational restriction.

### Estimation of $\sigma_m$

Provided we assume random mixing in the amorphous lamellae and the melt, the non-combinatorial free energy change on mixing per mol of segments can be written:

$$\Delta G_m = RT\chi\phi_e\phi_p \quad (17)$$

where  $\chi$  is the Flory-Huggins parameter for chain segments [segment volume equal to that of poly(ethylene oxide) chain unit] and  $\phi_e$  and  $\phi_p$  are volume fractions. The free energy of mixing on forming the amorphous layer from the melt is:

$$\Delta G_m(\text{layer}) - \Delta G_m(\text{melt})$$

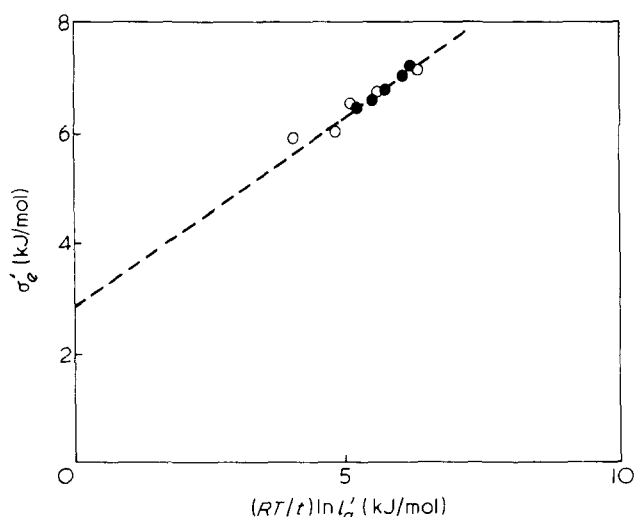


Figure 6 Effect of the length of the emerging chains on the end interfacial free energy: plot of  $\sigma'_e$  against  $(RT/t) \ln l'_a$  in accordance with equations (23) and (25). Broken line (---) has a slope of 2/3. ●, PE block copolymers; ○, poly(ethylene oxide) homopolymers

If we denote volume fractions in the melt by  $\phi_e, \phi_p$  and in the amorphous layer by  $\phi'_e, \phi'_p$  we can write, for the incorporation of 1 mol of segments into the amorphous layer,

$$\Delta g_m = RT\chi \left[ \phi'_e \phi'_p - \frac{\phi_e \phi_p}{\phi_a} \right] \quad (18)$$

where  $\phi_a = l_a/l$ .  $\Delta g_m$  is expressed in J/(mol of chain segments) so that  $l_a$ , the thickness of the amorphous lamellae, is in segments. We have already defined a chain segment as having the volume of a poly(ethylene oxide) chain unit in the melt, so that

$$l_a/\text{segments} = (l_a/nm) \frac{v_c}{0.28v_e} \quad (19)$$

Equilibrium phase composition and cloud point curves have been determined<sup>23</sup> for mixtures of  $\alpha,\omega$ -methoxy-poly(ethylene oxide) ( $\bar{M}_n = 300$  or  $600$ ) and  $\alpha,\omega$ -methoxy-poly(propylene oxide) ( $\bar{M}_n = 1500$  or  $2000$ ). Analysis of these data, in terms of a binary solution with concentration independent  $\chi$ , places  $\chi$  near 0.1. This is in agreement with an earlier<sup>22</sup> estimate of  $\chi$ .

With regard to the contribution of the hydroxy end-group to  $\sigma_m$ , we note that the melting point of  $\alpha,\omega$ -hydroxy-poly(ethylene oxide) of molecular weight  $\bar{M}_n = 2000$  differs little from that of  $\alpha,\omega$ -methoxy-poly(ethylene oxide) of the same molecular weight. [We find<sup>6,41</sup> values of  $53.8^\circ\text{C}$  (hydroxy-) and  $53.5^\circ\text{C}$  (methoxy-).] Accordingly we set  $\chi = 0.1$  and, with sufficient accuracy for our purposes, calculate the values  $\Delta g_m$  listed in Table 7, together with the corresponding values of  $\sigma_m = l_a \Delta g_m$ . The contribution of mixing to  $\sigma_e$  is seen to be fairly small (<10%).

#### Estimation of $\sigma_o$

A simple calculation of the difference in entropy between a free chain and a chain tied at one end to an impenetrable surface can be made for a chain restricted to one dimension (lattice coordination number 2) and with

zero excluded volume<sup>42</sup>. This model leads to:

$$\sigma_a = RT \ln (l'_a)^{1/2} \quad (20)$$

where  $l'_a$  is the length of the tied chain. The form of equation (20) is not greatly dependent on the geometry of the lattice<sup>42</sup>. If allowance is made for excluded volume<sup>43,44</sup> the estimate of  $\sigma_a$  is increased; e.g. the calculation of Bellemans<sup>44</sup> suggests that:

$$\sigma_a = RT \ln (l'_a)^{2/3} \quad (21)$$

For a once-folded polycrystal the corresponding expression is:

$$\sigma_a = (RT/2) \ln (l'_a)^{2/3} \quad (22)$$

since half the chains emerging from the end interface of the crystalline lamellae are assumed to re-enter the crystal via a regular fold. In general we have:

$$\sigma_a = (RT/t) \ln (l'_a)^{2/3} \quad (23)$$

where  $l'_a$  is given by:

$$l'_a = (tl_a/2) + 1 \quad (24)$$

i.e. the average length of the tied chains which emerge into the amorphous lamellae. If we define a quantity  $\sigma'_e$  so that:

$$\sigma'_e = \sigma_e - \sigma_m = \sigma_a + \sigma_o \quad (25)$$

then  $\sigma'_e$  should be independent of the mixing terms and uniform behaviour might be expected for both block copolymers and homopolymers. In Figure 6 we plot  $\sigma'_e$  against  $(RT/t) \ln l'_a$  for the data of Tables 6 and 7 and for results obtained for poly(ethylene oxide) homopolymers (see Appendix). These results are consistent with equation (23) and lead to an estimate of  $\sigma_o$  of about 3 kJ/mol. This value is about 30% of the heat of fusion. It is, therefore, a plausible result; the usual prediction<sup>45</sup> of the lateral interfacial free energy is about 10% of the heat of fusion.

## CONCLUSIONS

We have interpreted the properties of poly(ethylene oxide)/poly(propylene oxide) type PE block copolymers in terms of a simple stacked lamella model with alternating amorphous and crystalline layers. In our systems (E block length = 40, P block length = 0 to 11 chain units) the crystalline lamella thickness is about 7 nm (25 E chain units). The specific volume of the polymer in the amorphous layer, which is predominantly formed of chains

Table 7 Calculation of  $\sigma_m$  for PE polymers

Sample	T	$\phi_a$	$\phi_e$	$\phi'_e$	$-\Delta g_m$ (J/mol)	$l_a$ (segments)	$-\sigma_m$ (kJ/mol)
0-40	50.7	0.332	1.000	1.000	—	11.8	—
2-40	50.1	0.379	0.922	0.787	8.0	13.8	0.1
3-40	49.8	0.404	0.889	0.715	8.7	15.4	0.1
5-40	48.7	0.443	0.834	0.612	16.1	18.0	0.2
8-40	47.5	0.497	0.759	0.493	25.2	21.6	0.3
11-40	47.1	0.524	0.717	0.437	29.9	24.0	0.5

emerging from the end interfaces of the crystalline lamellae, is lower than that of the corresponding polymer in the supercooled melt. The melting temperatures of the stacked lamella structures are low compared with that of perfectly crystalline poly(ethylene oxide): i.e. 47 to 51°C compared with  $T_m^0 = 76^\circ\text{C}$ . This is due to the positive free energy of formation from the melt of the crystal/amorphous interface ( $\sigma_o \sim 3 \text{ kJ/mol}$ ,  $19 \text{ erg/cm}^2$ ) and the amorphous layer ( $\sigma_a \sim 3.5 \text{ kJ/mol}$ ,  $23 \text{ erg/cm}^2$ ). The predominant contribution to the free energy of formation of the amorphous layer from the melt is the reduction in entropy, relative to the melt, of the polymer chain emerging from the crystal surface. This reduction in entropy is quantitatively described by equation (23).

## ACKNOWLEDGEMENTS

We thank Messrs D. J. Roy and D. Rowlinson for assistance with the characterization of the polymers; and Dr D. R. Cooper for helpful discussions. P.C.A. acknowledges receipt of a Science Research Council Studentship.

## REFERENCES

- 1 Arlie, J. P., Spegt, P. A. and Skoulios, A. E. *Makromol. Chem.* 1966, **99**, 160
- 2 Arlie, J. P., Spegt, P. A. and Skoulios, A. E. *Makromol. Chem.* 1967, **104**, 212
- 3 Spegt, P. A. *Makromol. Chem.* 1970, **140**, 167
- 4 Kovacs, A. J.: quoted by Wunderlich, B. *Macromolecular Physics* Vol.1, Academic Press, New York, 1974
- 5 Kovacs, A. J. and Gonthier, A. *Kolloid-Z.* 1972, **250**, 530
- 6 Beech, D. R., Booth, C., Dodgson, D. V., Sharpe, R. R. and Waring, J. R. S. *Polymer* 1972, **13**, 73
- 7 Beech, D. R., Booth, C., Pickles, C. J., Sharpe, R. R. and Waring, J. R. S. *Polymer* 1972, **13**, 246
- 8 Beech, D. R. and Booth, C. J. *Polym. Sci. (B)* 1970, **8**, 731
- 9 Afifi-Effat, A. M. and Hay, J. N. *JCS Faraday Trans. II* 1972, **68**, 656
- 10 Rijke, A. M. and McCoy, S. J. *Polym. Sci. (A 2)* 1972, **10**, 1845
- 11 Ashman, P. C. and Booth, C. *Polymer* 1972, **13**, 459
- 12 Booth, C., Bruce, J. M. and Buggy, M. *Polymer* 1972, **13**, 475
- 13 Ashman, P. C. and Booth, C. *Polymer* 1973, **14**, 300
- 14 Booth, C. and Pickles, C. J. *J. Polym. Sci. (Polym. Phys. Edn)* 1973, **11**, 249
- 15 Booth, C. and Dodgson, D. V. *J. Polym. Sci. (Polym. Phys. Edn)* 1973, **11**, 265
- 16 Galin, J. C., Spegt, P. A., Suzuki, S. and Skoulios, A. E. *Makromol. Chem.* 1974, **175**, 991
- 17 Flory, P. J. *J. Chem. Phys.* 1949, **17**, 273
- 18 Flory, P. J. and Vrij, A. *J. Am. Chem. Soc.* 1963, **85**, 3548
- 19 Skoulios, A. E., Tsouladze, G. and Fanta, E. *J. Polym. Sci. (C)* 1964, **4**, 507
- 20 Short, J. M. and Crystal, R. G. *Appl. Polym. Symp.* 1971, **16**, 137
- 21 Perret, R. and Skoulios, A. E. *Makromol. Chem.* 1972, **162**, 147, 163
- 22 Booth, C. and Pickles, C. J. *J. Polym. Sci. (Polym. Phys. Edn)* 1973, **11**, 595
- 23 Friday, A. *MSc Thesis* University of Manchester (1974)
- 24 Perrin, D. D., Armorego, W. L. F. and Perrin, D. W. 'Purification of Laboratory Chemicals', Pergamon Press, New York, 1966
- 25 Simons, D. M. and Verbanc, J. J. *J. Polym. Sci.* 1960, **44**, 303
- 26 Booth, C. and Price, C. *Polymer* 1966, **7**, 85
- 27 Price, C. C. and St. Pierre, L. E. *J. Am. Chem. Soc.* 1956, **78**, 3432
- 28 Havlik, A. J., Moacanin, J. and Otterness, I. *J. Polym. Sci. (A)* 1963, **1**, 2213
- 29 Blanchard, L. P. and Baijal, M. D. *J. Polym. Sci. (B)* 1966, **4**, 837
- 30 Mathias, A. and Mellor, N. *Analyt. Chem.* 1966, **38**, 472
- 31 Maclaine, J. Q. G. and Booth, C. *Polymer* 1975, **16**, 680
- 32 Brandrup, J. and Immergut, E. H. (Eds.) 'Polymer Handbook', Interscience, New York, 1966, p III-27
- 33 Peebles, L. H. 'Molecular Weight Distribution in Polymers', Interscience, New York, 1971
- 34 Price, F. P. and Kilb, R. W. *J. Polym. Sci.* 1962, **57**, 395
- 35 Simon, F. T. and Rutherford, J. M. *J. Appl. Phys.* 1964, **35**, 83
- 36 Booth, C. and Devoy, C. J. *Polymer* 1971, **12**, 320
- 37 Allen, G., Booth, C., Jones, M. N., Marks, D. J. and Taylor, W. D. *Polymer* 1964, **5**, 547
- 38 Kavesh, J. and Schultz, J. H. *J. Polym. Sci. (A-2)* 1971, **9**, 85
- 39 Mandelkern, L. *J. Polym. Sci. (C)* 1973, **43**, 1
- 40 Devoy, C. J. *PhD Thesis* Manchester University (1966)
- 41 Cooper, D. R., Timson, M. J. and Booth, C. to be published
- 42 DiMarzio, E. A. *J. Chem. Phys.* 1965, **42**, 2101
- 43 McCrackin, F. L. *J. Chem. Phys.* 1967, **47**, 1980
- 44 Bellemans, A. *J. Polym. Sci. (C)* 1972, **39**, 305
- 45 Hoffman, J. D. *SPE Trans.* 1964, **4**, p 315
- 46 Marshall, A. *MSc Thesis* University of Manchester (1973)

## APPENDIX

*Poly(ethylene oxide) homopolymers*

Lamella spacings and specific volumes of several low molecular weight poly(ethylene oxide) homopolymers have been published<sup>1</sup> and the melting points of these polymers are known<sup>6,46</sup>. Published results for samples which form predominantly extended-chain crystals are summarized in *Table A1*. We take  $\bar{x}_w/\bar{x}_n$  to be 1.05 for samples 23 to 45 and 1.10 for sample 68<sup>6,46</sup>.

The characteristics of the polycrystals, calculated from the results of *Table A1* in the manner described heretofore, are listed in *Table A2*. Comparison of these results for homopolymers with those for the PE series of block copolymers (*Tables 5 and 6*) reveals an almost complete correspondence between them. The low value of the folding parameter  $t$  for sample 23 (*Table A2*) reflects the rejection from the crystal of the shorter chains in the distribution: in turn this is consistent with higher value of  $v_a$  found for this sample.

*Table A1* Properties of low molecular weight poly(ethylene oxide)

Sample	$\bar{M}_n$	$T = 25^\circ\text{C}$		
		$l$ (nm)	$v$ (cm <sup>3</sup> /g)	$T_m^0$ (°C)
23	1000	7.1	0.832	39.1
34	1500	9.8	0.826	49.0
45	2000	13.1	0.822	53.8
68	3000	18.5	0.821	59.5

*Table A2* Characteristics of crystalline poly(ethylene oxide) homopolymers

Sample	$w_c$	$T = 25^\circ\text{C}$			$T = T_m$		
		$l_c$ (nm)	$l_a$ (nm)	$v_a^*$ (cm <sup>3</sup> /g)	$l_a$ (segments)	$t$	$\sigma_e$ (kJ/mol)
23	0.68	5.0	2.1	0.87	6.8	0.86	5.9
34	0.68	6.6	3.2	0.85	10.3	0.99	6.0
45	0.68	8.8	4.3	0.84	13.9	0.97	6.6
68	0.68	12.5	6.0	0.84	19.3	1.04	7.0

\* For comparison the specific volume of liquid poly(ethylene oxide) at 25°C is 0.89 cm<sup>3</sup>/g

# Crystallinity and fusion of ethylene oxide/propylene oxide block copolymers:

## 2. Type PEP copolymers

P. C. Ashman, C. Booth, D. R. Cooper and C. Price

Department of Chemistry, University of Manchester, Manchester, M13 9PL, UK

(Received 16 May 1975)

Lamella spacings, specific volumes and melting points have been determined for a series of well characterized poly(ethylene oxide)/poly(propylene oxide) type PEP block copolymers with E-block length 48 chain units and P-block lengths 0 to 7 chain units. These properties are interpreted in terms of a stacked lamella model with alternating amorphous and crystalline layers. Both extended-chain and once-folded-chain crystalline lamellae are found, the former with thickness about 32 E chain units and the latter with thickness about 21 E chain units. Compared with the specific volume of supercooled melt of the same composition the specific volume of the polymer in the amorphous lamellae is lower in the extended-chain polycrystals and higher in the once-folded-chain polycrystals. The melting points of the copolymers are low compared to that of perfectly crystalline poly(ethylene oxide), i.e. 37 to 55°C compared with  $T_m^0 = 76^\circ\text{C}$ . This is due to the large positive free energy of formation from the melt of the crystalline/amorphous end interface ( $\sigma_o$ ) and the amorphous layer ( $\sigma_a$ ). For extended-chain polycrystals we find  $\sigma_o \sim 3$  kJ/mol and  $\sigma_a \sim 3.5$  kJ/mol; for once-folded-chain polycrystals we find  $\sigma_o \sim 6$  kJ/mol and  $\sigma_a \sim 2$  kJ/mol. We also find  $\sigma_{o,x} = 2.5$  kJ/mol for a completely extended-chain end interface and  $\sigma_{o,f} = 10$  kJ/mol for a completely folded-chain end interface.

### INTRODUCTION

In Part 1<sup>1</sup>, we have described the crystallinity and fusion of predominantly extended-chain crystals of type PE poly(ethylene oxide)/poly(propylene oxide) block copolymers, and interpreted the results in terms of a simple stacked lamella model with alternating amorphous and crystalline layers. Previously<sup>2</sup> we have described the melting of predominantly folded-chain crystals of type PEP copolymers. In that work we used E-block lengths of 70 to 100 chain units [E denotes a poly(ethylene oxide) block, P a poly(propylene oxide) block.] Here we report the preparation and properties of type PEP copolymers with an E-block length of 50 chain units and P-block lengths in the range 0–7 chain units. In this series of copolymers we encounter both extended-chain and folded-chain crystals.

### EXPERIMENTAL AND RESULTS

#### Preparation

The method of base catalysed polymerization, using potassium hydroxide as catalyst and ethylene glycol as initiator described in an earlier paper<sup>2</sup> was used in this work without modification.

#### Notation

We refer to samples by their number-average block lengths (expressed in monomer units) as established by their preparation and subsequent characterization. For example, sample 2–48–2 denotes a PEP block copolymer with poly(propylene oxide) block lengths of 2 chain units and a poly(ethylene oxide) block length of 48 chain units.

#### Characterization

Average molecular weights were measured by vapour pressure osmometry (v.p.o.) (Mechrolab, benzene at 25°C), by end group analysis (phthaloylation of hydroxy end-groups<sup>3–5</sup>) and by gel permeation chromatography (g.p.c.). Copolymer compositions were determined by proton magnetic resonance spectroscopy<sup>6</sup> and by hydrogen bromide fusion<sup>6,7</sup>. The application of all these methods to ethylene oxide/propylene oxide block copolymers has been discussed earlier<sup>2</sup>.

The characteristics of the series of copolymers are given in *Table 1*. The observed values of  $\bar{M}_n$  for sample 0–48–0 are in keeping with that (2100) calculated<sup>2</sup> from the preparative conditions. The values of  $\bar{M}_n$  finally adopted (last column of *Table 1*) are calculated from the average composition and the value of  $\bar{M}_n = 2100$  assumed for sample 0–48–0.

#### Dilatometry, picnometry, X-ray scattering

The methods used to determine melting points (dilatometry), specific volumes (picnometry), and lamella spacings (small-angle X-ray scattering) have been described in Part 1<sup>1</sup>. Wide-angle X-ray scattering patterns of the copolymers (Debye–Scherrer camera, CuK $\alpha$  radiation) were identical, except for the amorphous background, to those obtained for poly(ethylene oxide) homopolymers.

The melting point was taken to be that temperature at which detectable crystallinity disappeared: a secondary melting point was defined by the appropriate point of inflection in the dilatometric melting curve (e.g. see Fig. 1 of ref. 9).

Melting points, measured for a variety of crystallization temperatures ( $T_c$ ) are given in *Table 2*. All polymers were

Table 1 Characteristics of the PEP polymers

Sample	$\bar{M}_n$			$\bar{M}_w/\bar{M}_n$ (g.p.c.)	$w_e^*$			$\bar{M}_n$ (best values)
	V.p.o.	End group analysis	G.p.c.		P.m.r.	HBr	Best values	
0-48-0	1900	2100	2000	1.10	1.00	1.00	1.00	2100
1-48-1	2000	—	2000	1.14	0.93	0.96	0.95	2220
2-48-2	2200	—	2200	1.09	0.88	0.90	0.89	2360
5-48-5	2450	—	2300	1.10	0.79	0.79	0.79	2660
6-48-6	2700	—	2500	1.09	0.75	0.75	0.75	2800
7-48-7	3050	—	2600	1.10	0.71	0.74	0.73	2880

\*  $w_e$  = weight fraction of poly(ethylene oxide)

Table 2 Melting of PEP polymers

Sample	$T_c$ (°C)	$T_m$ (°C)		
		Extended chain	Once-folded chain	Twice-folded chain
0-48-0	34.5	54.9	—	—
	37.4	55.0	—	—
	39.8	55.0	—	—
1-48-1	29.1	54.0	—	—
	32.0	53.6	—	—
	37.4	53.7	—	—
2-48-2	32.0	48.3	—	—
	34.5	48.7	—	—
	37.4	48.9	—	—
5-48-5	29.1	—	39.4	—
	30.0	—	39.6	—
	32.0	—	39.4	—
6-48-6	36.0*	—	41.5	—
	20.0	—	38.5	35.4
	25.0	—	38.5	35.6
7-48-7	29.1	—	38.5	37.1
	30.0	—	38.6	37.4
	32.0	—	38.6	37.8
6-48-6	36.0*	—	40.9	—
	29.1	—	37.5	35.2
	30.0	—	37.7	36.0
7-48-7	32.0	—	37.8	37.0
	36.0*	—	39.4	—

\* Low crystallinity

crystallized as completely as possible. At  $T_c = 36^\circ\text{C}$  samples 5-48-5 to 7-48-7 had a low crystallinity and exhibited a high melting point; presumably these effects are due to fractionation during the slow crystallization process at the small undercooling. Two melting points were observed for samples 6-48-6 and 7-48-7 when crystallized at undercoolings exceeding 5 K. (The absence of a melting point is indicated by a rule in Table 2.) The final melting points are practically independent of  $T_c$ , but secondary (lower) melting points increase as  $T_c$  is increased; this behaviour appears to be characteristic of PEP block copolymers<sup>2</sup> and also of partly isotactic poly(propylene oxide)<sup>8</sup>. In Table 2 the melting points are assigned to extended-chain, once-folded-chain, and twice-folded-chain polycrystals on the basis of past experience<sup>2,9,10</sup>, which suggests that the higher melting point is that of the crystal in which the poly(ethylene oxide) chain folds the least number of times, and upon the evidence of the following small-angle X-ray results.

The samples gave small-angle X-ray scattering patterns which resembled those obtained from poly(ethylene oxide) homopolymers<sup>9,11</sup> and copolymers<sup>1,2</sup>, in that the scattering

Table 3 Lamella spacings (nm) of PEP polymers

Sample	Approximate chain length (nm)	$T_c$ (°C)			
		25	29	30	35
0-48-0	13.5	—	—	—	13.5
1-48-1	14.0	—	—	—	14.6
2-48-2	14.6	—	—	—	14.6
5-48-5	16.3	—	10.9	—	—
6-48-6	16.8	10.2	10.9	12.2	—
7-48-7	17.4	—	10.9	—	—

Table 4 Specific volumes (cm<sup>3</sup>/g) of PEP polymers

Sample	$T_c$ (°C)			
	25	29	30	35
0-48-0	0.827	—	0.827	0.829
1-48-1	0.840	—	0.840	0.840
2-48-2	0.848	—	0.855	0.853
5-48-5	0.867	0.871	0.872	—
6-48-6	0.876	0.880	0.881	—
7-48-7	0.883	0.888	0.890	—

comprised several equally spaced lines. However, samples 5-48-5 to 7-48-7 gave very much more intense diffraction maxima than did samples 0-48-0 to 2-48-2. Lamella spacings, calculated directly by means of Bragg's Law, are listed in Table 3. For purposes of comparison extended chain lengths (nm) are given in Table 3: these are calculated assuming a length of 0.28 nm per chain unit (P or E) in keeping with a repeat distance of 1.95 nm for the 7-2 helix of crystalline poly(ethylene oxide)<sup>12</sup>. The spacings are consistent with predominantly extended-chain crystals for samples 0-48-0 to 2-48-2 and predominantly once-folded-chain crystals for samples 5-48-5 to 7-48-7. The temperature dependence of the lamella spacing noted for sample 6-48-6 is curious in view of the constant melting point of the folded-chain crystals (Table 2).

Specific volumes are listed in Table 4.

#### LAMELLA THICKNESS: SPECIFIC VOLUME OF AMORPHOUS MATERIAL

We interpret the lamella spacings and specific volumes of the samples in terms of the stacked-lamella model presented in Part 1<sup>1</sup>, i.e. in terms of the two equations:

$$w_c = \frac{l_c v}{l v_c w_e} \quad (1)$$

Table 5 Characteristics of crystalline PEP polymers

Sample	$l_c$ (nm)	$w_c$	$l_a$ (nm)	$v_a$ (cm <sup>3</sup> /g)	$v_s$ (cm <sup>3</sup> /g)
$T = 35^\circ\text{C}$ :					
0-48-0	8.9	0.68	4.6	0.858	0.898
1-48-1	9.0	0.67	5.6	0.884	0.912
2-48-2	8.5	0.69	6.1	0.912	0.928
$T = 29^\circ\text{C}$ :					
5-48-5	6.2	0.77	4.7	0.959	0.952
6-48-6	5.9	0.78	5.0	0.973	0.961
7-48-7	5.8	0.78	5.1	0.990	0.962

and

$$w_c = \sum_{s=1}^{\infty} \int_{sl_c}^{(s+1)l_c} w(y) \left( \frac{sl_c}{y} \right) dy \quad (2)$$

where  $w_c$  = the weight fraction of the copolymer which is crystalline;  $w_e$  = the weight fraction of poly(ethylene oxide) in the copolymer;  $w(y)$  = the weight distribution of poly(ethylene oxide) block length ( $y$ );  $l$  = the lamella spacing;  $l_c$  = the thickness of the crystalline lamellae;  $v$  = the specific volume of the copolymer;  $v_c$  = the specific volume of perfectly crystalline poly(ethylene oxide).

Equations (1) and (2) can be solved graphically for  $w_c$  and  $l_c$ , as described in Part 1<sup>1</sup>; we assume that  $w(y)$  is well represented by a Schulz-Zimm distribution with parameters evaluated from the molecular weight data in Table 1. Values of  $l_a$ , the thickness of the amorphous lamellae, and  $v_a$ , the specific volume of the polymer in the amorphous lamellae, can then be computed from:

$$l = l_a + l_c \quad (3)$$

and

$$v = v_c w_c w_e + v_a (1 - w_c w_e) \quad (4)$$

Values of  $l_c$ ,  $w_c$ ,  $l_a$  and  $v_a$  are given in Table 5.\* The calculation is straightforward for samples 0-48-0 to 5-48-5 since the information we have (Tables 2 and 3) is consistent with the presence of only one type of crystalline lamella. The model underlying equations (1) and (2) assumes only one type of crystalline lamella in the system. For this reason the calculations for samples 6-48-6 and 7-48-7 are not entirely well founded.

For purposes of comparison with  $v_a$ , the specific volume of the polymer in the amorphous layer, we list in Table 5  $v_s$ , the specific volume of a supercooled melt of the same composition as the amorphous layer, as calculated (assuming no volume change on mixing) from the equation:

$$v_s = (w_e w_a v_e + w_p v_p) / (1 - w_c w_e) \quad (5)$$

where  $w_a = 1 - w_c$  is the weight fraction of amorphous polymer in the polycrystal,  $w_p = 1 - w_e$  is the weight fraction of poly(propylene oxide) in the sample, and  $v_e$  and  $v_p$

are the specific volumes of supercooled liquid poly(ethylene oxide) and poly(propylene oxide) respectively.

The data of Table 5 fall into two groups: (a) samples 0-48-0 to 2-48-2, which form predominantly extended-chain crystals. For these samples  $w_c$  is constant at about 0.68: a value identical, within experimental error, to that found<sup>1</sup> for the PE series of polymers and for poly(ethylene oxide) homopolymers which form extended-chain crystals. Moreover we find that  $v_a$  is lower than  $v_s$  by some 2 to 4% (compared with 1 to 3% found earlier); (b) samples 5-48-5 to 7-48-7, which form predominantly once-folded-chain crystals. For these samples  $w_c$  is constant at about 0.78, and  $v_a$  is higher than  $v_s$  by some 1 to 3%.

This difference between extended-chain and folded-chain crystals is consistent with our model<sup>1</sup>. The increase in  $w_c$  can be attributed to the reduction both in the number of rejected molecules and in the average length of chain ends emerging from the crystalline lamellae. The high value of  $v_a$ , relative to  $v_s$ , observed for the folded-chain polycrystals can be attributed directly to the decrease in the number of chains emerging from the crystal into the amorphous lamellae caused by adjacent re-entry of the crystalline lamellae by the folded chains. The high value of  $v_a$  is consistent with the high intensity of the X-ray scattering maxima which is a characteristic of folded-chain polycrystals (as mentioned earlier), since there is a large density difference between the amorphous and crystalline lamellae.

#### END INTERFACIAL FREE ENERGY, $\sigma_e$

In Part 1<sup>1</sup> we have justified the use of the Flory-Vrij<sup>18</sup> model for the interpretation of the melting points of low molecular weight polymers and block copolymers. Accordingly we write<sup>1,19</sup>:

$$T_m = T_m^0 [1 - 2\sigma_e / \Delta h l_c] / [1 - RT_m^0 \ln \phi_e I / \Delta h t l_c] \quad (6)$$

where  $T_m^0$  is the thermodynamic melting point of poly(ethylene oxide),  $\Delta h$  is the thermodynamic enthalpy of fusion of poly(ethylene oxide),  $\phi_e$  is the volume fraction of poly(ethylene oxide) in the melt, and  $t$  is the average number of times the chains traverse the crystal (i.e.  $t = 1$  for an entirely extended-chain polycrystal,  $t = 2$  for an entirely once-folded-chain polycrystal, etc.). In general  $t$  is given by the equation:

$$t = \sum_{s=1}^{\infty} \left[ \int_{sl_c}^{(s+1)l_c} s \left( \frac{w(y)}{y} \right) dy / \int_0^{\infty} \frac{w(y)}{y} dy \right] \quad (7)$$

Parameter  $I$  is the probability that a sequence of poly(ethylene oxide) units of length  $l_c$  does not contain a block end, and is given by<sup>1</sup>:

$$I = \sum_{s=1}^{\infty} \int_{sl_c}^{(s+1)l_c} w(y) [(y - sl_c + 1)/y] dy \quad (8)$$

In formulating equations (7) and (8) we assume that each chain folds to its maximum possible extent (for a given value of  $l_c$ ) by regular folding, i.e.  $s$  is the number of sequences chosen consecutively from a given molecule, and that folds are included in the crystalline lamellae. In using

\* We use  $v_c = 0.813 \text{ cm}^3/\text{g}$  at  $25^\circ\text{C}$ <sup>13</sup> and  $\alpha_c = 0.00015 \text{ cm}^3/\text{g K}$ <sup>11</sup>  
 $v_e = 0.891 \text{ cm}^3/\text{g}$  at  $25^\circ\text{C}$ <sup>14</sup> and  $\alpha_e = 0.00069 \text{ cm}^3/\text{g K}$ <sup>11,14</sup>  
 $v_p = 0.997 \text{ cm}^3/\text{g}$  at  $20^\circ\text{C}$ <sup>15</sup> and  $\alpha_p = 0.00077 \text{ cm}^3/\text{g K}$ <sup>16,17</sup>



the equations we assume that  $w(y)$  is described by a Schulz-Zimm distribution with parameters evaluated from the molecular weight data in Table 1. The end interfacial free energy,  $\sigma_e$ , is the free energy of formation from the melt of the amorphous/crystalline interface and the adjacent amorphous layer.

In calculating  $\sigma_e$  we have used  $T_m^0 = 349 \text{ K}$ <sup>20-22</sup>,  $\Delta h = 8.4 \text{ kJ}/(\text{mol of chain units})$ <sup>23</sup>,  $\bar{y}_n = 48$  chain units,  $\bar{y}_w/\bar{y}_n = 1.10$ , and the remaining quantities listed in Table 6. The values of  $\sigma_e$ , quoted in Table 6, are in kJ/(mol of chains emerging from the end interface). The values of the folding parameter  $t$ , also listed in Table 6, are consistent with our classification of the crystalline samples into essentially extended-chain and once-folded-chain types.

We have written<sup>1</sup>  $\sigma_e$  as the sum of three terms:

$$\sigma_e = \sigma_o + \sigma_m + \sigma_a \quad (9)$$

which are identified as follows:  $\sigma_o$  = the free energy of formation from the melt of the amorphous/crystalline interface;  $\sigma_m$  = the free energy change (enthalpy and non-combinatorial entropy changes) due to the concentration, relative to the melt, of chain ends (blocks or groups) in the amorphous lamellae;  $\sigma_a$  = the free energy increase due to conformational restrictions, relative to the melt, of the chains in the amorphous lamellae, i.e. primarily due to the constraint of the impenetrable crystal surface.

The estimation of  $\sigma_m$ , assuming random mixing in the melt and the amorphous layer and assuming a concentration independent Flory-Huggins interaction parameter  $\chi = 0.1$ , has been discussed earlier<sup>1</sup>. The calculation is set out in Table 7: the contribution of  $\sigma_m$  to  $\sigma_e$  is seen to be fairly small (<10%). The quantity  $l_a$  in Table 7 is the thickness of the amorphous lamellae at  $T = T_m$  measured in segments, so that:

$$l_a/\text{segments} = (l_a/nm) \frac{v_c}{0.28v_e} \quad (10)$$

We define a quantity  $\sigma'_e$  where

$$\sigma'_e = \sigma_e - \sigma_m = \sigma_o + \sigma_a \quad (11)$$

Table 6 End interfacial free energies ( $\sigma_e$ ) for PEP polymers

Sample	$T_m$ (°C)	$\phi^*$	$l_c^\dagger$ (units)	$t$	$\sigma_e$ (kJ/mol)
0-48-0	54.9	1.000	31.9	1.02	6.3
1-48-1	53.7	0.944	32.2	1.00	6.7
2-48-2	48.7	0.878	30.5	1.08	8.2
5-48-5	39.4	0.770	22.1	1.67	7.9
6-48-6	38.5	0.727	21.1	1.77	8.2
7-48-7	37.5	0.708	20.6	1.83	8.2

\* At  $T_m$  by use of  $v$  and  $\alpha$  values quoted earlier

†  $l_c$  at  $T_m$  is negligibly different from  $l_c$  at 20°C

Table 7 Calculation of  $\sigma_m$  for PEP copolymers

Sample	$T$ (°C)	$\phi_a$	$\phi_e$	$\phi'_e$	$-\Delta g_m$ (J/mol)	$l_a$ (segments)	$-\sigma_m$ (kJ/mol)
0-48-0	54.9	0.340	1.000	1.000	—	14.8	—
1-48-1	53.7	0.384	0.944	0.846	1.8	18.0	0.0
2-48-2	48.7	0.417	0.878	0.692	7.3	19.6	0.1
5-48-5	39.4	0.433	0.770	0.435	33.9	15.3	0.3
6-48-6	38.5	0.459	0.727	0.371	41.3	16.2	0.4
7-48-7	37.5	0.472	0.708	0.342	44.0	16.7	0.5

so that  $\sigma'_e$  should be independent of the mixing terms (if these are properly assessed). We have shown earlier<sup>1</sup> that  $\sigma_a$  depends linearly on the function  $(RT/t) \ln l'_a$ , where  $l'_a$  is the average length of the chains which emerge into the amorphous lamellae given by:

$$l'_a = (tl_a/2) + 1 \quad (12)$$

A plot of  $\sigma'_e$  against  $(RT/t) \ln l'_a$  is illustrated in Figure 1, where we include data for type PE copolymers and homopolymers taken from Part 1<sup>1</sup> together with data for once-folded-chain poly(ethylene oxide) 6000 taken from Appendix I to this paper.

The results for the predominantly extended-chain crystals of the PEP copolymers are in broad agreement with those established in Part 1<sup>1</sup> for PE copolymers and E homopolymers. The high value of  $\sigma'_e$  observed for sample 2-48-2 requires further discussion. There is a clear distinction between PEP and PE block copolymers of high poly(propylene oxide) content in that the PEP copolymers form folded-chain polycrystals, e.g.

PEP 5-48-5	$w_e = 0.79$	$l = 10.9 \text{ nm}$	$t = 1.7$
PE 8-40	$w_e = 0.78$	$l = 13.5 \text{ nm}$	$t = 1.1$

The formation of folded-chain polycrystals must be a consequence of the reduced stability of the extended-chain

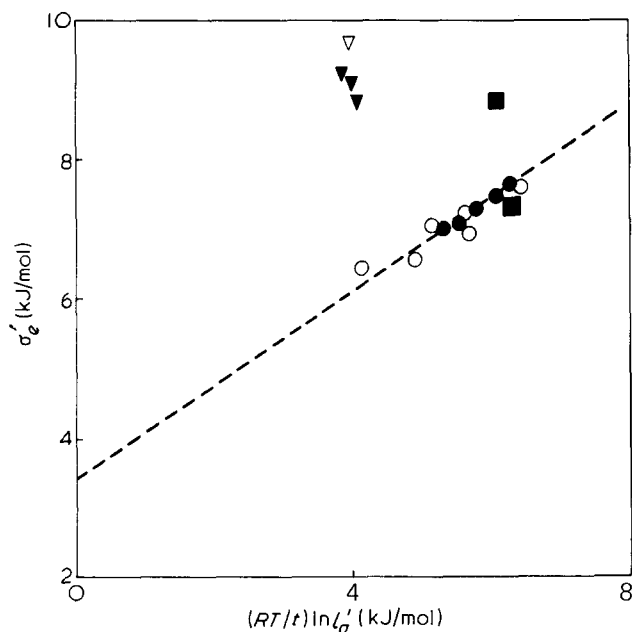


Figure 1 Plot of  $\sigma'_e$  against  $(RT/t) \ln l'_a$ , in accordance with equations (11) and (14). Broken line (---) has slope of 2/3. O and  $\nabla$ , poly(ethylene oxide) homopolymers; ●, PE block copolymers; ■ and  $\nabla$ , PEP block copolymers. The triangles represent data for predominantly once-folded-chain polycrystals; the other symbols represent data for predominantly extended-chain polycrystals

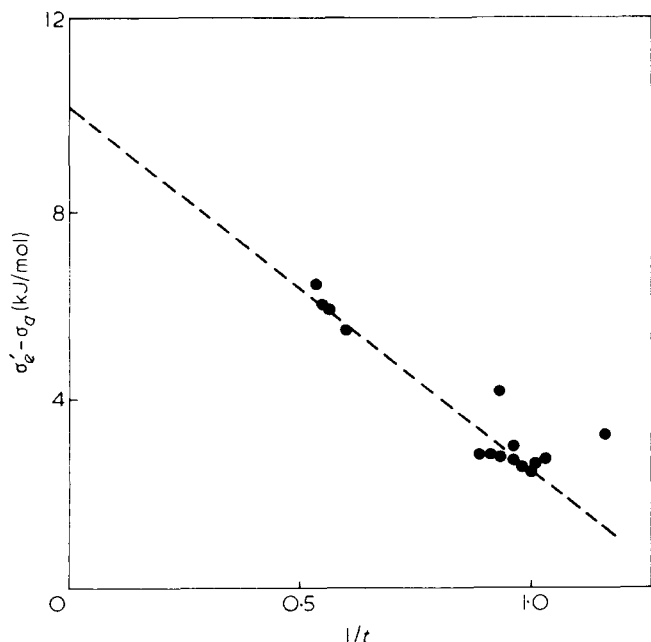


Figure 2 Plot of  $\sigma'_e - \sigma_a$  against  $1/t$ , in accordance with equation (15)

polycrystal: which is consistent with the high value of  $\sigma'_e$  found for sample 2-48-2. The area per chain emerging from the poly(ethylene oxide) end interface can be calculated from lattice dimensions<sup>13</sup> to be  $0.26 \text{ nm}^2$ . The area of cross-section of the poly(propylene oxide) chain is similar to this if it is in the planar zig-zag conformation (we calculate an area of cross-section of  $0.27 \text{ nm}^2$ ) but is higher than  $0.26 \text{ nm}^2$  if the chain adopts a helical conformation (as would be anticipated for isotactic placements: our chains are atactic). In the case of PE copolymers the extension of one end only of the chain leaves a high proportion of terminated poly(ethylene oxide) chains in the amorphous layer. In the case of PEP copolymers the extension of both ends of the poly(ethylene oxide) chains greatly reduces the proportion of chains terminating near to the end interface. Consequently for PEP copolymers forming extended-chain polycrystals there will be a contribution to  $\sigma_e$  (absent or small in PE copolymers) deriving mainly from intramolecular interactions within poly(propylene oxide) sequences constrained to the planar zig-zag form. We have not attempted to quantify this contribution.

The slope of the broken line in Figure 1, which adequately represents the experimental data, is consistent with the theoretical prediction of Bellemans<sup>24</sup> (see Part 1<sup>1</sup> for further discussion of this point). Consequently we would expect a similar dependence of  $\sigma'_e$  on  $l'_a$  for the predominantly once-folded-chain polycrystals, though we have no data to test this prediction. However, with this in mind, it is consistent with our model to write for any type of polycrystal:

$$\sigma'_e = \sigma_{o,x}(1/t) + \sigma_{o,f}(1 - 1/t) + \sigma_a \quad (13)$$

where  $\sigma_{o,x}$  is the free energy of formation from the melt of the completely extended-chain crystal/amorphous interface,  $\sigma_{o,f}$  is corresponding quantity for the completely folded-chain interface,  $1/t$  is the fraction of chains which emerge into the amorphous layer, and  $\sigma_a$  is given by<sup>1</sup>:

$$\sigma_a = (RT/t) \ln (l'_a)^{2/3} \quad (14)$$

as indicated by the broken line of Figure 1. Equation (13)

can be rearranged to the form:

$$\sigma'_e - \sigma_a = \sigma_{o,f} - (\sigma_{o,f} - \sigma_{o,x})(1/t) \quad (15)$$

A plot of  $\sigma'_e - \sigma_a$  against  $1/t$ , for all the samples investigated here and in Part 1, is illustrated in Figure 2. The straight line drawn through the data intercepts  $1/t = 0$  at  $\sigma_{o,f} = 10 \text{ kJ/mol}$  and  $1/t = 1$  at  $\sigma_{o,x} = 2.5 \text{ kJ/mol}$ .

Two crystalline sequences are involved in the formation of one fold, so the above values indicate a free energy of formation within the crystal of a fold of about  $15 \text{ kJ/(mol of folds)}$ . An estimate of the energy of formation within the crystal of a fold, based on conformational changes alone (see Appendix II), is  $13 \text{ kJ/(mol of folds)}$ .

## CONCLUSIONS

We have interpreted the properties of poly(ethylene oxide)/poly(propylene oxide) type PEP block copolymers in terms of the stacked lamella model described in Part 1. Samples with short P-blocks (2 P chain units or less) form predominantly extended-chain polycrystals in which the crystalline lamella thickness is about  $9 \text{ nm}$  (i.e. about 32 E chain units compared with an E-block length of 48 chain units) and in which the specific volume of the polymer in the amorphous layer, which is predominantly formed of chains emerging from the end interfaces of the crystalline lamellae, is lower than that of the corresponding supercooled melt. Samples with long P-blocks (5 P chain units or more) form predominantly once-folded-chain lamellae in which the crystalline lamella thickness is about  $6 \text{ nm}$  (i.e. about 21 E chain units) and in which the specific volume of the polymer in the amorphous layer is higher than that of the corresponding supercooled melt.

The melting temperatures of the polycrystals are low compared with that of perfectly crystalline poly(ethylene oxide): i.e.  $37$  to  $55^\circ\text{C}$  compared with  $T_m^0 = 76^\circ\text{C}$ . This is due to the positive free energy of formation from the melt of the crystal/amorphous interface ( $\sigma_o$ ) and the amorphous layer ( $\sigma_a$ ), the latter being primarily due to the reduction in entropy, relative to the melt, of polymer chains emerging from the crystal surface. The magnitudes of  $\sigma_o$  and  $\sigma_a$  for our systems are typically:

	Extended-chain polycrystal	Once-folded-chain polycrystal
$\sigma_o$	3 kJ/mol (19 erg/cm <sup>2</sup> )	6 kJ/mol (39 erg/cm <sup>2</sup> )
$\sigma_a$	3.5 kJ/mol (23 erg/cm <sup>2</sup> )	2 kJ/mol (13 erg/cm <sup>2</sup> )

A value of  $\sigma_{o,x} = 2.5 \text{ kJ/mol}$  ( $16 \text{ erg/cm}^2$ ) is found for the completely extended-chain end interface and a value of  $\sigma_{o,f} = 10 \text{ kJ/mol}$  ( $65 \text{ erg/cm}^2$ ) for the completely folded-chain end interface.

## ACKNOWLEDGEMENTS

We thank Messrs D. J. Roy and D. Rowlinson for assistance with the characterization of the polymers. P.C.A. acknowledges receipt of a Science Research Council Studentship.

REFERENCES

- 1 Ashman, P. C. and Booth, C. *Polymer* 1975, **16**, 889
- 2 Booth, C. and Pickles, C. J. *J. Polym. Sci. (Polym. Phys. Edn)* 1973, **11**, 249
- 3 Price, C. C. and St. Pierre, L. E. *J. Am. Chem. Soc.* 1956, **78**, 3432
- 4 Havlik, A. J., Moacanin, J. and Otterness, I. *J. Polym. Sci. (A)* 1963, **1**, 2213
- 5 Blanchard, L. P. and Bajjal, M. D. *J. Polym. Sci. (B)* 1966, **4**, 837
- 6 Mathias, A. and Mellor, N. *Analyt. Chem.* 1966, **38**, 472
- 7 Stead, J. B. and Hindley, A. H. *J. Chromatog.* 1969, **42**, 470
- 8 Booth, C., Devoy, C. J., Dodgson, D. V. and Hillier, I. H. *J. Polym. Sci. (A-2)* 1970, **8**, 519
- 9 Beech, D. R., Booth, C., Dodgson, D. V., Sharpe, R. R. and Waring, J. R. S. *Polymer* 1972, **13**, 73
- 10 Beech, D. R., Booth, C., Pickles, C. J., Sharpe, R. R. and Waring, J. R. S. *Polymer* 1972, **13**, 246
- 11 Arlie, J. P., Spegt, P. A. and Skoulios, A. E. *Makromol. Chem.* 1966, **99**, 160; 1967, **104**, 212
- 12 Brandrup, J. and Immergut, E. H. (Eds.) 'Polymer Handbook', Interscience, New York, 1966, p III-27
- 13 Price, F. P. and Kilb, R. W. *J. Polym. Sci.* 1962, **57**, 395
- 14 Simon, F. T. and Rutherford, J. M. *J. Appl. Phys.* 1964, **35**, 82
- 15 Booth, C. and Devoy, C. J. *Polymer* 1971, **12**, 320
- 16 Booth, C. and Pickles, C. J. *J. Polym. Sci. (Polym. Phys. Edn)* 1972, **11**, 595
- 17 Allen, G., Booth, C., Jones, M. N., Marks, D. J. and Taylor, W. D. *Polymer* 1964, **5**, 547
- 18 Flory, P. J. and Vrij, A. *J. Am. Chem. Soc.* 1963, **85**, 3548
- 19 Ashman, P. C. and Booth, C. *Polymer* 1972, **13**, 459
- 20 Beech, D. R. and Booth, C. *J. Polym. Sci. (B)* 1970, **8**, 731
- 21 Afifi-Effat, A. M. and Hay, J. N. *JCS Faraday Trans. II* 1972, **68**, 656
- 22 Rijke, A. M. and McCoy, S. J. *J. Polym. Sci. (A-2)* 1972, **10**, 1845
- 23 Devoy, C. J. *PhD Thesis* Manchester University (1966)
- 24 Bellemans, A. J. *J. Polym. Sci. (C)* 1972, **39**, 305
- 25 Flory, P. J. 'Statistical Mechanics of Chain Molecules', Interscience, New York, 1968

APPENDIX I

*Poly(ethylene oxide) 6000*

Lamella spacings, specific volumes and melting points of poly(ethylene oxide) 6000 have been published<sup>9,11</sup> and are summarized below. This sample forms predominantly once-folded-chain polycrystals at crystallization temperatures below 54°C. We use the data to calculate the characteristics of the polycrystals, in the manner described heretofore. Comparison of these results with those for the PEP copolymers which form predominantly once-folded-chain, i.e. samples 5-48-5 to 7-48-7 (Tables 5 and 6) shows an almost complete correspondence. [We note that the specific volume of supercooled liquid poly(ethylene oxide) at 25°C is 0.89 cm<sup>3</sup>/g so that  $v_a > v_s$  for this once-folded-chain polycrystal as was the case for the others: see Table 5.]

*Experimental data for poly(ethylene oxide) 6000*

$\bar{x}_n = 136$  units;  $\bar{x}_w/\bar{x}_n = 1.1$

$T = 25^\circ\text{C}$ :  $l = 20.6$  nm;  $v = 0.834$  cm<sup>3</sup>/g

$T_m = 60.1^\circ\text{C}$  (once-folded-chain polycrystal)

*Characteristics of crystalline poly(ethylene oxide) 6000*

$T = 25^\circ\text{C}$        $w_c = 0.68$

$l_c = 15.9$  nm;  $l_a = 4.7$  nm

$v_a = 0.91$  cm<sup>3</sup>/g

$T = 60.1^\circ\text{C}$        $l_a = 15.1$  segments

$t = 1.89$

$\sigma_e = 9.1$  kJ/mol

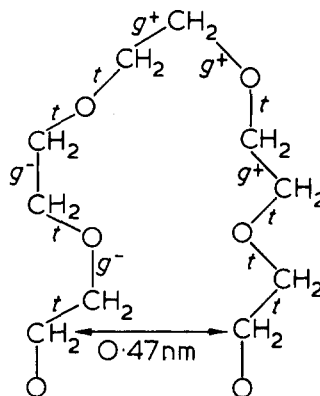


Figure A1 A possible fold conformation in poly(ethylene oxide)

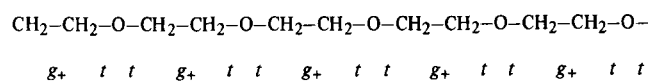
Table A1 Calculation of the energy of fold formation

Conformational change	Energy increase per change (kJ/mol)	Number of changes	Total energy increase (kJ/mol)
CH <sub>2</sub> -CH <sub>2</sub> :g <sub>+</sub> →t	3.8	2	7.6
O-CH <sub>2</sub> :t→g <sub>+</sub>	1.8	2	3.6
CH <sub>2</sub> -CH <sub>2</sub> :g <sub>+</sub> →g <sub>-</sub>	1.5	1	1.5
All changes	-	5	12.7

APPENDIX II

*Calculation of the free energy of fold formation for poly(ethylene oxide)*

Equivalent lattice sites on the end surface of a poly(ethylene oxide) crystal are separated by 0.46 nm<sup>13</sup>. The optimum conformation for adjacent re-entry is that involving the least number of chain units without deformation of bond angles or formation of eclipsed conformations. Such a conformation, involving 5 chain units, is illustrated in Figure A1. The energy of formation of such a fold from crystalline polymer can be calculated from the data of Flory and Mark<sup>25</sup> summarized in Table A1, since the conformational change is from the 7-2 helical form:



to the folded form:



The calculation is set out in Table A1 and the predicted energy of formation of the fold is 12.7 kJ/mol.

# Intrinsically coloured polymers from cellulose carbanilates

Richard Benson, James T. Guthrie and Ransford B. Lartey

Department of Colour Chemistry and Dyeing, University of Leeds, Leeds LS2 9JT, UK  
(Received 20 May 1975; revised 19 June 1975)

The synthesis and characterization of intrinsically coloured polymers from cellulose tricarbonylcarbanilates has been achieved. Data relating to the intermediate stages are given. Spectroscopy, thermal analysis and light fastness tests were used to establish some of the physical properties of the products. Information was obtained regarding the kinetics of nitration of cellulose tricarbonylcarbanilate and the nature of the nitration process has been elucidated. Evidence is presented which indicates that the light fastness characteristics of coloured compounds are not necessarily governed by energy transfer phenomena since the system studied is known to exhibit efficient energy transfer yet the light fastness results are invariably poor. The thermal properties of the products are complex and best dealt with in context.

## INTRODUCTION

The topic of intrinsically coloured polymers has received some attention recently. Various avenues are undergoing investigation and here we report of developments based on the use of cellulose tricarbonylcarbanilate.

Work has been published which deals with the enhanced protection against radiation induced damage which can be afforded cellulose through its conversion to the carbanilate<sup>1</sup>. Similar protection has been observed by a variety of aromatic groups and so the procedures outlined here may be extended to cover these<sup>2-4</sup>. In carbanilation it has been shown that a degree of substitution  $>2.0$  gives almost complete protection to cellulose. Lesser protection is observed at lower levels of substitution. One explanation for the occurrence of poor light fastness properties of dyes and pigments involves the initial absorption of energy which is then transferred to the chromophore, causing its destruction. Thus the incorporation of cellulose tricarbonylcarbanilate into a chromophore system was expected to enhance the light fastness of the chromophore. This is because cellulose carbanilates have a capacity as efficient energy 'sinks'.

Since one important outlet for intrinsically coloured polymers is that of pigmentation it is expedient that this topic be covered in some detail with an attempted classification.

Polymeric pigments can be regarded as largely insoluble polymers which have a chromophoric centre within the structure. Immediately four classes arise which could be further subdivided: (a) polymers, which as a result of secondary reaction become intrinsically coloured. Examples include the thermal or alkali induced degradation of polyacrylonitrile; (b) those polymeric pigments derived from the formation of colour sites within a substrate where hitherto they were absent. The action of reactive dyes on natural polymers can be considered in this category; (c) the products of addition copolymerization reactions in which one of the monomers is coloured. Reports of work along these lines have been published<sup>5,6</sup> and further work is in progress; (d) those intrinsically coloured products of stepwise polymerization reactions. Examples must be legion but perhaps unthought of in this context. Here we can consider the products of reactions of multifunctional coloured compounds. Within this category are the anthraquinones, azo compounds, phthalocyanines etc.

These principles can be extended into related areas such as intrinsically fluorescent polymers, intrinsically biologically active polymers, intrinsically antioxidant polymers, intrinsically flame retardant polymers and intrinsically self-degrading polymers.

In this study we are mainly concerned with the second class of intrinsically coloured polymer. Our interests lie in cellulose tricarbonylcarbanilates, the coloured materials derived therefrom and their physical properties.

## EXPERIMENTAL

### *Cellulose nitrocarbanilates*

Cotton linters were used as the source of cellulose. The preparation of cellulose tricarbonylcarbanilate has been fully described elsewhere<sup>1</sup>. Cellulose tricarbonylcarbanilate (CTC) was partly converted to the *p*-nitro-derivative through direct nitration under both heterogeneous and homogeneous conditions. An alternative route to the nitrocarbanilate from cellulose was by reaction with mixtures of *p*-nitrophenyl isocyanate and phenyl isocyanate.

Cellulose *p*-nitrocarbanilate was subsequently reduced under acid or alkaline conditions (homogeneous and heterogeneous conditions) prior to attempting coupling and exchange reactions involving some standard coupling components and preliminary diazotization. Certain diazotizations were heterogeneous and hence of reduced efficiency.

The details involved in the nitration, reduction, diazotization, coupling and exchange stages are given in *Table 1*.

### *Product characterization*

The intrinsically coloured polymers, together with the various intermediates were characterized through their spectroscopic, thermal and light fastness properties. Light fastness tests were applied only to the intrinsically coloured products.

## RESULTS

Completeness of carbanilation was shown through nitrogen analyses and by the absence of  $\text{-OH}$  absorption frequencies in the infra-red spectrum. The thermal characteristics of

Table 1 Experimental procedures in the preparation of intrinsically coloured polymers

Reaction	Conditions	Reagents
Nitration	heterogeneous/30 min	CTC in CH <sub>3</sub> COOH (glacial):H <sub>3</sub> PO <sub>4</sub> (87%) HNO <sub>3</sub> (70%)
Nitration	homogeneous/various times used in kinetic study	CTC solution in C <sub>6</sub> H <sub>5</sub> NO <sub>2</sub> :HNO <sub>3</sub> (70%) Either H <sub>2</sub> SO <sub>4</sub> (98%) or H <sub>3</sub> PO <sub>4</sub> (87%)
Indirect nitration	homogeneous/48 h	Cellulose; C <sub>6</sub> H <sub>5</sub> NCO: NO <sub>2</sub> -C <sub>6</sub> H <sub>5</sub> -NCO as solution in C <sub>5</sub> H <sub>5</sub> N
Reduction	acidic, 80°C, 8 h	SnCl <sub>2</sub> /HCl
Reduction	alkaline, 100°C, 8 h	Na <sub>2</sub> S.9H <sub>2</sub> O:S in NaOH (5%)
Diazotization	heterogeneous, 3 h, 0°C	HCl(dil):NaNO <sub>3</sub>
Diazotization	homogeneous, 1 h, 0°C	Polymer solution in CH <sub>3</sub> OH:CH <sub>3</sub> COOH (glacial):amyl nitrite
Coupling	10°C, 1 h	β-naphthol in NaOH solution to heterogeneously diazotized CTC
Coupling	10°C, 1 h	(a) β-naphthol in NaOH solution
Coupling	10°C, overnight	(b) pyrazolone in NaOH solution
Coupling	10°C, 1 h	(c) H acid by acid coupling
Coupling	10°C, 1 h	(d) H acid by alkaline coupling
Replacements	Sandmeyer reaction conditions	(a) H <sub>2</sub> O at 75°C (b) CuCl solution at 60°C

CTC are shown in the differential thermogram (Figure 1a) which contains a small endotherm at 125°C, being indicative of incomplete removal of residual solvent, whilst the endotherm at 200°C suggests the beginning of the melting process. This broad endotherm points to the polydisperse character of the sample.

Heterogeneous conditions, normally used in the nitration of cellulose, could not be applied to CTC because of excess charring and the occurrence of degradation. Products from homogeneous nitration of CTC, obtained by reaction in nitrobenzene using phosphoric acid as a catalyst and modifier and nitric acid, were invariably yellow powders. This system was studied in detail to provide information concerning the kinetic features of the nitration reaction. Figure 1b shows the differential thermogram of a typical nitrated sample.

Nitrocarbanilation of cellulose using *p*-nitrophenyl isocyanate alone, in pyridine, proved unsuccessful. Only with mixtures of phenyl isocyanate and *p*-nitrophenyl isocyanate was any nitration observed. One explanation involves the reduced reactivity of *p*-nitrophenyl isocyanate relative to phenyl isocyanate whilst a second cause could result from reduced diffusion of *p*-nitrophenyl isocyanate to the reactive sites of the cellulose. Once substituted with appreciable phenyl isocyanate the resulting carbanilate swells considerably in pyridine, thus facilitating access of *p*-nitrophenyl isocyanate. A thermogram of a typical product of indirect

nitration is shown in Figure 1c. The thermal stability of samples produced by indirect nitration is considerably greater than those achieved from homogeneous direct nitration (Figure 1b). Figure 1b indicates the presence of considerable heterogeneity in the product which could arise from the oxidizing nature of the acidic nitration medium.

For further study of intrinsically coloured polymers, only samples from indirect nitration were considered. However, an investigation of the kinetics of direct homogeneous nitration was considered to be in order as a means of obtaining information of the degradation process.

Reduction of the *p*-nitrocellulose carbanilate was carried out under both acid and alkaline conditions (Table 1). The reductions under acid conditions were heterogeneous with regard to the reducing medium. A thermogram of amino-carbanilated cellulose is shown in Figure 2a. A broad band corresponding to the amino group was found in the infrared spectrum; however, a much reduced absorption corresponding to the nitro group was seen at 850 cm<sup>-1</sup>. Hence reduction is not complete. Decomposition in these samples is seen to be a complex process (Figure 2a). Breakdown occurs at 200°C but there is little evidence of any melting process. The high yields obtained for the reduction and the contradicting evidence of incomplete reduction suggest that the gravimetric process of assessing reaction efficiency is

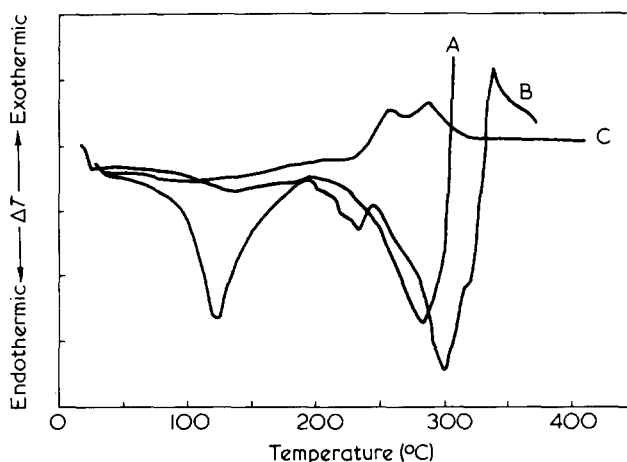


Figure 1 Differential thermograms of (A) cellulose tricarbanilate, (B) cellulose *p*-nitrocarbanilate (homogeneous nitration), (C) cellulose *p*-nitrocarbanilate (indirect homogeneous nitration).  $\Delta T = 0.2^\circ\text{C/in.}$

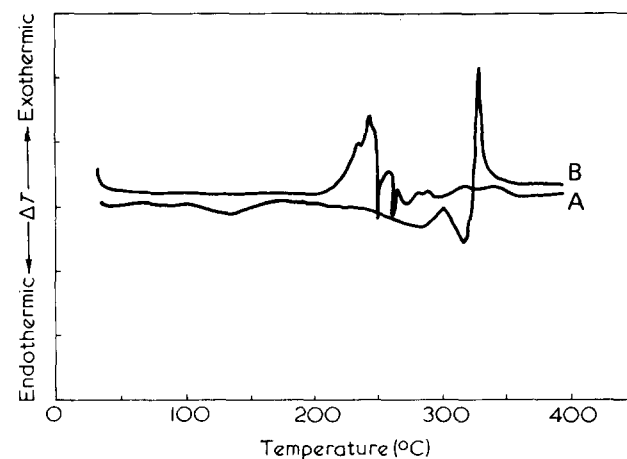


Figure 2 Differential thermograms of (A) *p*-aminocarbanilate produced by reduction under acidic conditions, (B) *p*-aminocarbanilate produced by reduction under alkaline conditions.  $\Delta T = 0.2^\circ\text{C/in.}$

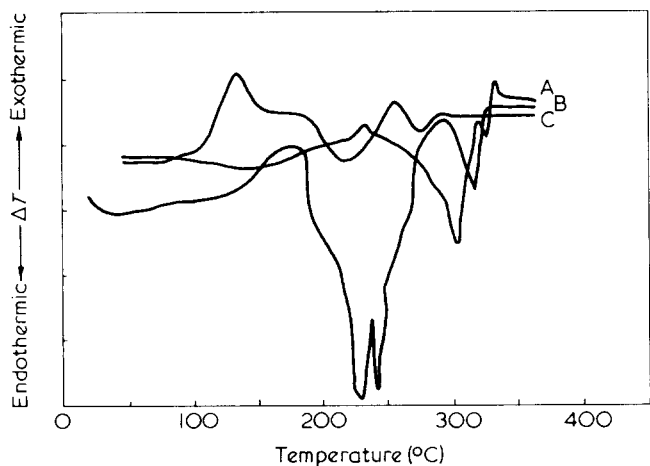


Figure 3 Differential thermograms of the products of coupling the diazo compound to: A,  $\beta$ -naphthol; B, 3-methyl-1-phenyl-5-pyrazolone; C, H acid.  $\Delta T = 0.2^\circ \text{C/in.}$

misleading. Positive confirmation of the presence of low concentrations of tin salts in the *p*-amino carbanilates was obtained subsequently. Stannic salts often adhere strongly to reaction products when they are used and even with thorough washing with warm dilute hydrochloric acid it was not possible to completely remove all the tin salts. Such impurities could well enhance the thermal degradation of the aminocarbanilate and explain the lower decomposition temperature. As a consequence of the degradation process, sealed sample containers used with the DuPont 900 Thermal Analyser were usually split apart at the hermetic seal.

Alkaline reduction was largely ineffective. Although no significant reduction of the nitro groups was achieved, this treatment gave a product of improved thermal stability (Figure 2b) when compared with the product obtained from reduction of the nitro compound under acidic conditions and the nitro compound itself. Decomposition begins at  $315^\circ \text{C}$  compared with  $290^\circ \text{C}$  for the nitro compound.

#### Diazotization reactions

Samples from direct and indirect nitration, subsequently reduced under acidic conditions, underwent heterogeneous diazotization. Diazotizations in solution were carried out only on samples acquired from indirect nitration of cellulose using *p*-nitrophenyl isocyanate and subsequent acid hydrolysis.

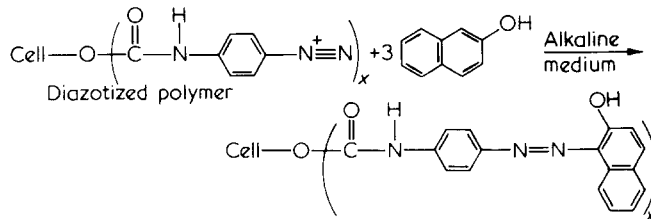
Infra-red analysis showed two new absorption bands from samples prepared above. These are seen at  $2210 \text{ cm}^{-1}$  and  $1580 \text{ cm}^{-1}$  and have been assigned to the absorption of the diazonium group.

The diazo compounds were found to have considerable stability in that re-assessment by i.r. spectroscopy after washing, drying and storing for 48 h still showed the absorptions at  $2210$  and  $1580 \text{ cm}^{-1}$ .

Coupling reactions were carried out on samples produced both by homogeneous and heterogeneous diazotization. The reproducibility of coupling was checked by repeating each process several times. A different coupling component was used for each diazotization process.

For coupling of the product obtained from heterogeneous diazotization,  $\beta$ -naphthol was used as the coupling component. In every instance red coloration occurred as soon as the diazo solution was added to the coupling component. The final products were red materials of varying colour in-

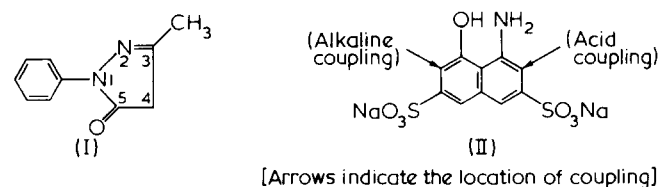
intensities. The coupling process can be represented in simplified form as:



The arrow indicates where coupling occurs.  $x$  is some value between 0 and 3 and will be dependent on the extent of nitration, reduction, diazotization and any degradation of the polymer.

In the i.r. spectrum, absorption bands at  $1550$  and  $1600 \text{ cm}^{-1}$  indicated the presence of azo groups and  $\beta$ -naphthol respectively, though the absorptions were not distinct. The absence of the peak at  $2210 \text{ cm}^{-1}$  showed that coupling had taken place at all the available diazonium group sites.

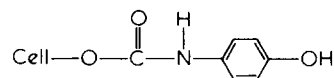
In coupling of those amines diazotized in solution the following coupling components were used, 3-methyl-1-phenyl-5-pyrazolone (I), 4-amino-5-hydroxynaphthalene-2, 7-disulphonic acid (H acid) sodium salt (II) and  $\beta$ -naphthol. The thermograms of the coupled products are given in Figures 3a–3c respectively. The structures of the latter two coupling components are:



A problem met with coupling of the amines diazotized in solution concerns precipitation of the polymer as a consequence of coupling. Thus, the partly coloured polymer precipitated from solution before appreciable coupling could take place. The colour strength of the product intensified gradually on standing. All the i.r. spectra indicate the presence of the azo group by absorption at  $1460\text{--}1570 \text{ cm}^{-1}$ , but interference occurs. The thermograms (Figures 3a–3c) are complex, though the samples decompose at approximately  $300^\circ \text{C}$  as seen in the exotherms.

In the replacement of the diazo group by the hydroxyl group, the yield of product was inversely proportional to the reaction temperature and time of reaction. This is indicative of degradation.

Figure 4a shows complex patterns containing an exotherm at  $\sim 127^\circ \text{C}$ , a gradual endotherm (melting) at  $175^\circ \text{C}$  and delayed decomposition at  $260^\circ \text{C}$ . However, the shift in base line shown in Figure 4a after the initial exotherm shows this to be the major event. Hence the product containing



is thermally less stable than the other products in this series. The i.r. spectrum indicated the stability of the diazo group by the presence of the absorption bands at  $2210$  and  $1575 \text{ cm}^{-1}$ . However, the broad band at  $3000\text{--}3700 \text{ cm}^{-1}$  showed both  $\text{--N--H}$  groups and hydrogen bonded  $\text{--OH}$  groups which could indicate successful replacement.

In the attempted replacement of the diazo group by the chlorine atom, only 84% of the original polymer weight was

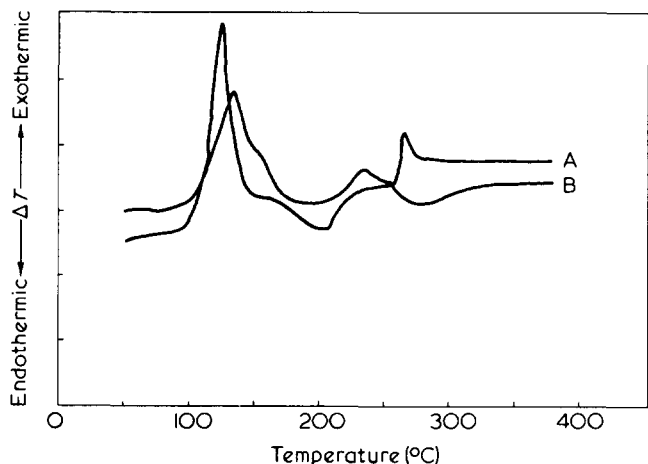


Figure 4 Differential thermograms of the products from attempted replacement of the diazo-group in cellulose *p*-diazocarbanilate by: A, -OH and B, -Cl.  $\Delta T = 0.2^\circ\text{C/in}$

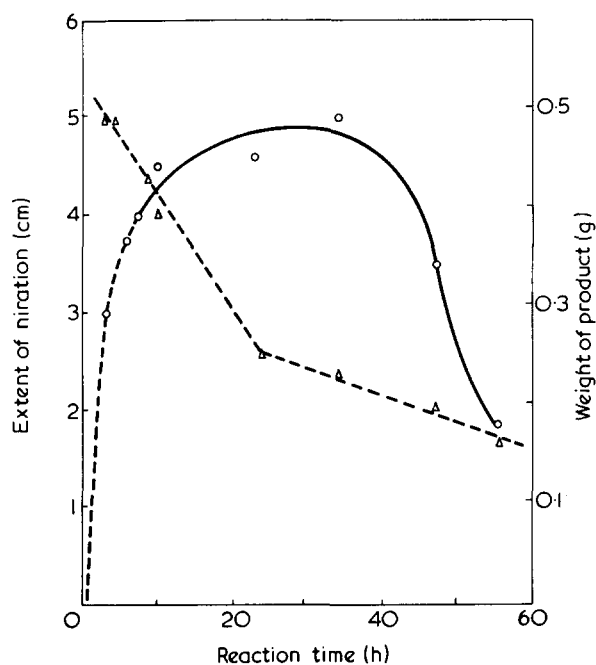


Figure 5 Features of the kinetics of nitration. ○, Variation in the extent of nitration (i.r. spectroscopy) with reaction time; Δ, variation in the weight of product isolated with the reaction time

recovered. Evidence for replacement is by no means conclusive, hence the yield of the chloro derivative is unknown. The i.r. spectrum showed the residual diazo group absorption bands ( $2210$  and  $1570\text{ cm}^{-1}$ ) though a reduction in the extent of -OH hydrogen bonding was observed at  $3000\text{--}3700\text{ cm}^{-1}$ .

The attempted replacement of the diazo groups by chlorine atom results in a product with similar low thermal stability (Figure 4b) to that obtained during replacement by the hydroxy group.

Light fastness<sup>5,6</sup> tests on typical paint 'draw-downs' were made from the various polymeric pigments. These included 'standards' obtained by diazotization of *p*-aminoacetanilide and coupling of the diazo product with each of the previously described coupling components. Comparisons between the 'standards' and the pigments obtained from the diazotized cellulose carbanilates through identical coupling, were made. The light fastness of each class of pigment derived from cellulose nitrocarbanilates was disap-

pointing. In every instance a light fastness of 3 or less was obtained whereas those of the standards were at least 5.

It is known that the medium and nature of the sample affects the light fastness properties of a pigment. No attempt was made to investigate these points. Since, from the applications viewpoint, the results from fading are serious, there arises the topic of the mechanism of the fading phenomenon.

## DISCUSSION

It is unlikely that pigments produced in the manner described have any real value in traditional areas. Points worthy of consideration include the nitration reaction, the thermal decomposition of cellulose nitrocarbanilates and the significance of the poor light fastness properties. Each of these points will be covered in turn.

The system, cellulose tricarbanilate, nitrobenzene as solvent, phosphoric acid as catalyst and modifier, nitric acid as the nitrating species and extended reaction times, was used in an extended study of the nitration process. All the products were obtained as fibrous yellow materials.

Figure 5 correlates the change in nitration with increasing reaction time. It is apparent that higher extents of nitration are achieved at the cost of increased degradation. This is seen in the lower yields recovered from the longer reaction times. Thus low molecular weight (degraded) species are lost in the 'working up' procedures which are designed to recover higher molecular weight, modified polymer. Under the conditions used, a reduction in both the extent of nitration and also the weight of product obtained occurs beyond 35 h of reaction. Again, the indications are that degradation rather than nitration is becoming increasingly significant.

Figures 6 and 7 show the effect of the extent of nitration

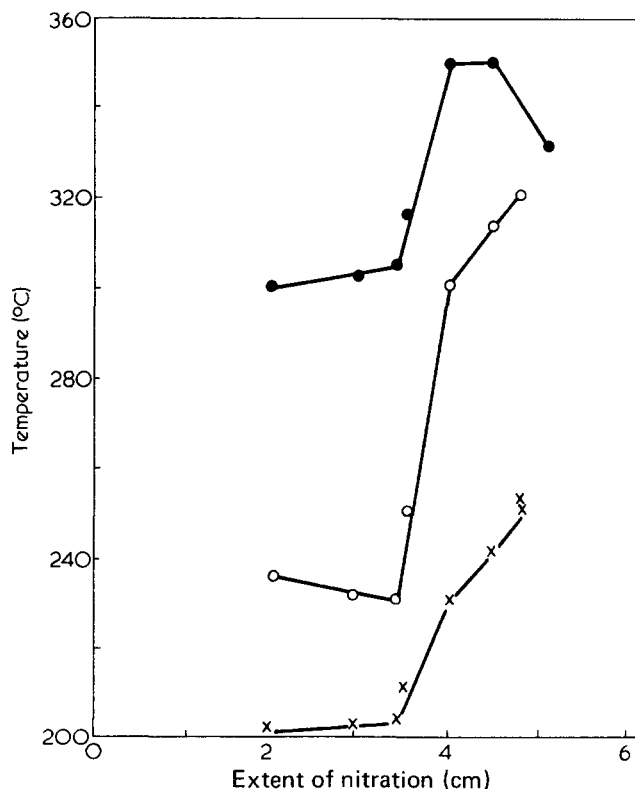


Figure 6 Variation of the temperature of initial melting ( $T_i$ , X), ultimate melting ( $T_m$ , ○) and decomposition ( $T_d$ , ●) with extent of nitration for various samples of cellulose *p*-nitrocarbanilate (homogeneous direct nitration)

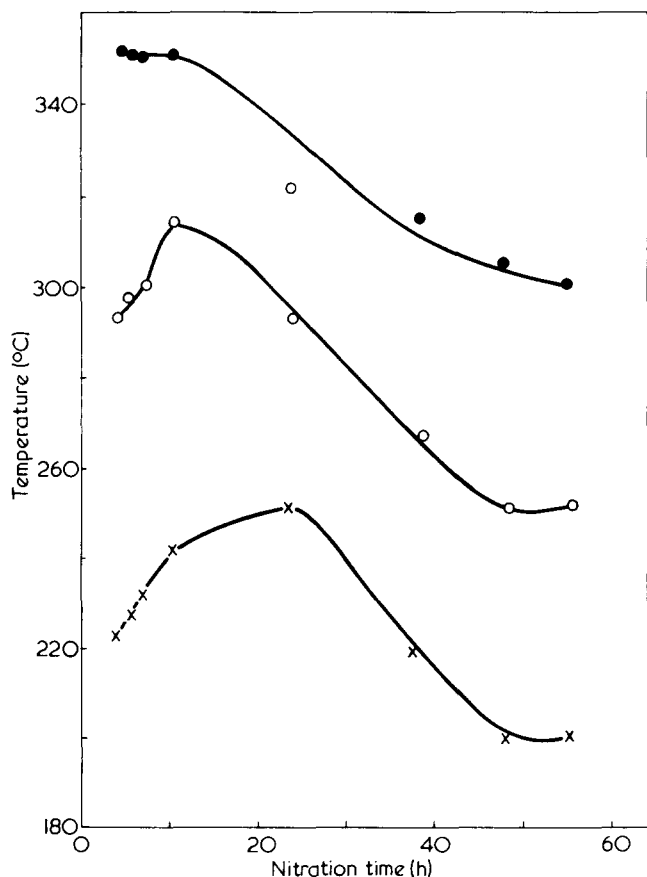


Figure 7 Variation of the temperature of initial melting ( $T_i$ , X), ultimate melting ( $T_m$ , o) and decomposition ( $T_d$ , ●) with nitration time for various samples of cellulose *p*-nitrocarbanilate

and the nitrating time respectively on the thermal properties of cellulose nitrocarbanilates. In these Figures the following terminology applies:  $T_i$ , initial melting temperature (°C);  $T_m$ , ultimate melting temperature (°C);  $T_d$ , ultimate decomposition temperature (°C). The extent of nitration is given in arbitrary units (being the height of the resonance peak obtained from the i.r. spectra). These Figures appear to be somewhat contradictory though on closer examination explanations can be proposed. In Figure 6 the overall trend is one of increasing thermal stability as the extent of nitration increases, although the patterns are not uniform. However, Figure 7 demonstrates that, as the time of nitration increases, the thermal stability of the resulting nitroderivatives passes through a maximum and then decreases. Similar features are shown in each of the measured physical processes, namely  $T_i$ ,  $T_m$  and  $T_d$ . It appears that during the nitration reaction other processes are taking place which eventually result in products with lower thermal stability. Preliminary viscometric data suggest that main-chain cleavage occurs on nitration. Although such cleavage is not instantaneous, it reaches significant proportions within 30 min of commencing nitration. Should any cleavage at the carbanilate linkage have taken place during nitration to produce aromatic nitroamines, then these would have been removed during the 'working up' procedure which was not designed to cope with such a possibility. Hence the yield of product decreases with increasing nitration time (Figure 7). It is noteworthy that the extent of maximum nitration

of the polymer does not coincide with the longest reaction time. Hence the interpretation of an increase in thermal stability with increasing nitration is consistent with observed data. Thus the samples with greatest nitration and thermal stability are those which have been exposed to the nitration medium for intermediate times.

In the nitration of cellulose carbanilate there arises the possibility of nitration in either the *o*- or *p*-position of the phenyl group or in both positions. Using acetanilide as a reference it is found that nitration occurs in the *o*- and *p*-positions. Even with alkyl groups in the position *para* to the amide group only *ortho* substitution is obtained. This indicates that the amide group is reasonably strongly *o*- and *p*-directing. However, with cellulose tricarbnilate, steric hindrance would be expected to reduce the extent of *o*-nitration.

During thermal analysis experiments on nitrated cellulose carbanilates, a green/yellow condensation product was observed on the inside of the Dupont 900 Thermal Analyser bell jar. This was analysed by u.v. spectroscopy and proven to be pure *p*-nitroaniline. This rules out any possibility of *o*-nitration which indicates the role of steric hindrance in the nitration reaction.

The light fastness results are puzzling. Cellulose tricarbnilate is very resistant to damage from exposure to high energy electromagnetic radiation. This protection is thought to involve transfer of incident energy to the phenyl group before its localization and the onset of degradation. It is the stability of the protecting groups' linkage to the cellulosic backbone which is the deciding factor as to whether or not protection occurs and not the nature of that linking group. Since fading concerns modification or destruction of the chromophore and we are again dealing with the absorption of electromagnetic radiation though of much reduced energy, one might have expected that the presence of carbanilate groups would protect the chromophore through energy transfer. Clearly from the poor light fastness results, this expectation is not realized. Certain possibilities arise, namely: (i) light fastness properties and radiation protection operate by different mechanisms. Thus, light fastness is not dependent on energy transfer processes; (ii) the incomplete character of each of the reaction stages could leave residues in the final pigment which are themselves sensitive to exposure to light. Chief among these are unreacted nitro groups which are known to produce oxidizing species. These in turn would have a marked influence on the physical properties of the dye chromophore.

Many questions remain unanswered in this field though work is continuing in the Department which should provide some solutions.

## REFERENCES

- Guthrie, J. T., Huglin, M. B. and Phillips, G. O. *Eur. Polym. J.* 1972, 8, 747
- Moore, J. S. and Phillips, G. O. *Carbohydr. Res.* 1971, 16, 79
- Arthur, Jr. J. C., Stannonis, D. J., Mares, T. and Hinojosa, O. *J. Appl. Polym. Sci.* 1967, 11, 1129
- Singh, S., Hinojosa, O. and Arthur, Jr. J. C. *J. Appl. Polym. Sci.* 1970, 14, 1591
- Batty, N. S. and Guthrie, J. T. *Polymer* 1975, 16, 43
- Batty, N. S. and Guthrie, J. T. *Polymer* 1975, 16, 370



# Some fatigue characteristics of thermoplastics

R. J. Crawford and P. P. Benham

*Department of Mechanical Engineering, The Queen's University of Belfast, Belfast BT9 5AH, UK  
(Received 21 April 1975; revised 25 July 1975)*

Uniaxial and rotating bending fatigue tests were carried out on polypropylene, polycarbonate, poly(methyl methacrylate) (PMMA), poly(tetramethylene terephthalate) (PTMT) and glass filled PTMT to establish the general régimes of thermal softening and fatigue types of failure observed in earlier tests on acetal copolymer. In the uniaxial testing PMMA exhibited both types of behaviour whereas polypropylene and PTMT were particularly prone to the thermal type of failure over a wide range of cyclic frequency and stress and fatigue failure could not be achieved for endurance up to  $10^7$  cycles. However, for PC and filled PTMT only the cracking type of fatigue failure was obtained as there was only a slight temperature rise which stabilized and hence did not lead to thermal softening. It was evident that the two types of failure were related to the magnitude of the loss tangent value for the material.

Under uniaxial loading the effect of a sharp notch in each material was to reduce the thermal effect so that, for example, fatigue failures were produced in polypropylene and PTMT under stresses which would only produce thermal failures in plain material. In general fatigue endurance were reduced owing to the presence of the notch. Rotating bar fatigue tests using the same specimen as in the uniaxial tests exhibited both thermal softening and fatigue type failures, but at higher stress amplitudes and frequencies compared with the uniaxial tests since only the outer surface was subjected to the maximum stress. The results of constant strain rate and creep rupture tests on these materials have also been included for comparison.

## INTRODUCTION

Nowadays thermoplastics are used in a wide variety of load-bearing applications. In many components the applied load is relatively constant in which case creep deformation or static fatigue are the major design criteria. In some components, however, the loading is of a cyclic nature, which may be either in the form of intermittent creep or more rapid and continuous which may lead to dynamic fatigue failure. The high damping and low thermal conductivity of thermoplastics become important factors when the loading is of a fluctuating nature and this, in conjunction with their time and strain dependent properties, means that the dynamic fatigue behaviour of polymers can be quite different from the more familiar concepts in metal fatigue.

The behaviour of polymers under cyclic loading has attracted an increasing amount of attention in recent years. Andrews<sup>1</sup>, Gotham<sup>2</sup> and Plumbridge<sup>3</sup> have all presented good reviews on the subject which describe clearly the extent of the problems involved. Some authors<sup>4,5</sup> have favoured the fracture mechanics approach although the work has been mainly concerned with glassy plastics such as poly(methyl methacrylate). Andrews and Walker<sup>6</sup> have indicated how this type of approach may be used for materials such as polyethylene. A number of authors such as Riddell *et al.*<sup>7</sup>, Tauchert<sup>8</sup>, Oberbach<sup>9</sup> and Constable *et al.*<sup>10</sup> have focused attention on the thermal aspect of fatigue. Few<sup>11</sup>, however, have attempted to present polymer fatigue data in a similar way to those used for metals.

Most of the worthwhile dynamic fatigue literature available on plastics has appeared in the past seven years, but in many cases it has been limited to rather narrow and specific conditions of testing, material etc.

## PREVIOUS FATIGUE STUDIES ON ACETAL COPOLYMER

When the BSI Committee PLC36 was formulating testing procedures for plastics in 1968 there was insufficient information to enable recommendations to be made on dynamic fatigue testing. At that time the authors felt that there was a need for a phenomenological study to establish some of the distinguishing factors that influenced dynamic fatigue of thermoplastics before it was possible to recommend testing procedures. The authors in their previous work<sup>12-14</sup> decided to use initially one engineering thermoplastic, an acetal copolymer, (ICI Kematal M90-04) to study the broad effects of frequency, waveform, mean stress, load or deformation control, notches and mode of testing (uniaxial and bending). Since many components are injection moulded it was decided to design the test specimen to be injection moulded and suitable for a range of tests, e.g. dynamic fatigue in uniaxial tension or bending, creep and creep rupture in tension, and triaxial stress systems. Furthermore by varying the methods of gating into the mould it was possible for the condition of specimens to range from optimum mouldings to those which included defects and undesirable orientation. The geometry of the specimen and the gripping arrangement for all types of fatigue and rupture testing are shown in *Figure 1*.

Perhaps the principal difference between dynamic fatigue in metals and plastics is the effect of cyclic frequency. On the former there is no effect over a wide frequency range so that duration of laboratory testing can be reduced by increasing test frequency. Plastics, on the other hand, have high damping and low thermal conductivity properties which make temperature rise very dependent on frequency

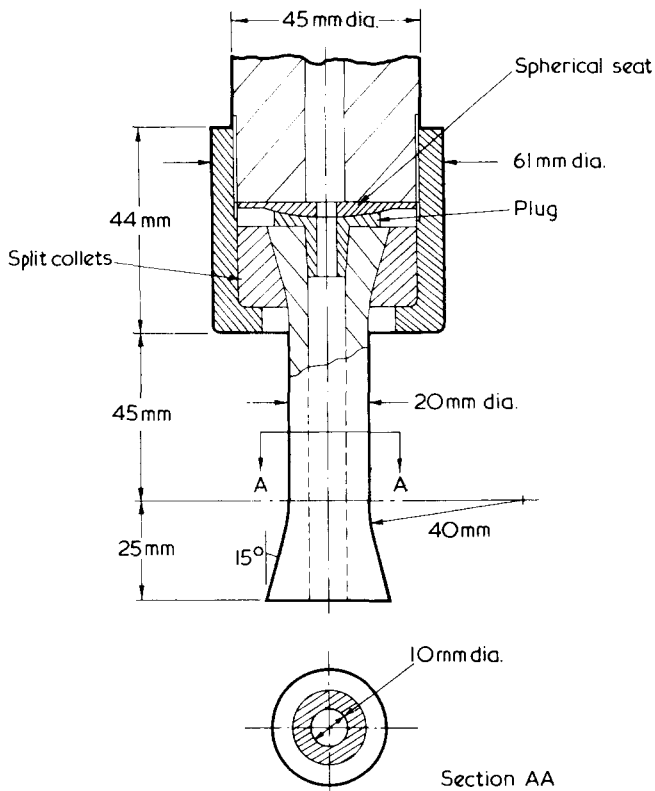


Figure 1 Specimen and grips

and stress level.

Depending on the combination of the latter two parameters the temperature may rise continuously and lead to failure by thermal softening without crack propagation. Alternatively, for certain limits of frequency and cyclic stress the temperature will rise for a period and then achieve a stable value. A conventional form of fatigue crack can then be initiated and propagated to complete failure. The interdependence of stress amplitude, temperature rise and number of cycles is illustrated in Figure 2. There is a complete change in behaviour between stress amplitudes of 21.6 and 22.4 MN/m<sup>2</sup> the former being the highest level of stress amplitude for which crack propagation fatigue can be obtained, while the latter represents the stress for the onset of thermal softening failure. This transition from thermal softening to brittle cracking fatigue is henceforth termed the change-over stress level. It was found to depend on cyclic waveform and frequency, mean stress, and surface area to volume ratio of material.

There is also a distinct difference as between cycling under load control or strain control. A drop in modulus due to temperature rise during load control causes an increase in the energy dissipation, whereas in strain control the drop in modulus causes a decrease in energy dissipation. This means that in the latter case there is a self-stabilizing mechanism with the result that there are no thermal runaway failures under strain control. It is therefore important for designers to consider this aspect of component operation and to select the appropriate fatigue data.

Full details of the thermal softening phenomenon together with an analytical solution for predicting the change-over stress has been given previously<sup>12</sup>.

One of the more important observations in the testing of acetal was the apparent independence of cyclic frequency of the reversed stress-log cycle fatigue cracking relationship and also the limited extent of scatter in results from injec-

tion moulded specimens, as seen in Figure 3. The dependence of thermal softening failure on frequency is also clearly evident in that Figure.

It was found that tensile mean stress reduced the allowable stress amplitude to give a particular endurance. Range/mean stress diagrams have the same form as for metals except that creep rupture is the predominant mechanism at high mean stress values.

Stress concentration, for all materials, is the most common cause of fatigue crack initiation. Apart from the well known effects of sudden change in geometry of components causing stress concentration there are also many possibilities resulting from fabrication processes, e.g. voids, sprue marks, flash lines, welds, contaminating particles, surface finish etc. Many of the foregoing situations have been studied for acetal, which it was hoped would give a general indication of behaviour for other engineering thermoplastics, and the results are detailed in ref. 13. The fatigue performance for injection moulded specimens having a circumferential V-notch (elastic stress concentration factor = 8) carefully machined into the mid-section is shown in Figure 4 together with details of the notch geometry. The fatigue strength reduction due to the notch is not as great as would

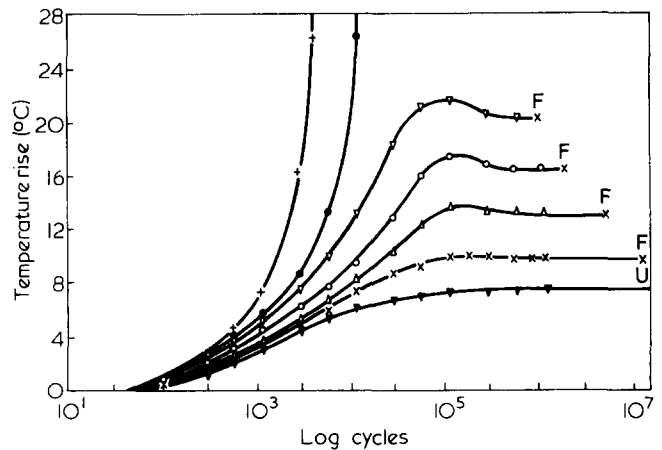


Figure 2 Temperature rise during uniaxial cycling. Frequency = 5.0 Hz (300 cycles/min); load cycle control; sine wave; zero mean stress.  $\blacktriangledown$ , 15.0; X, 16.0;  $\triangle$ , 17.4;  $\circ$ , 19.7;  $\nabla$ , 21.6;  $\bullet$ , 22.4; +, 27.8 MN/m<sup>2</sup>. F = fracture; U = unbroken

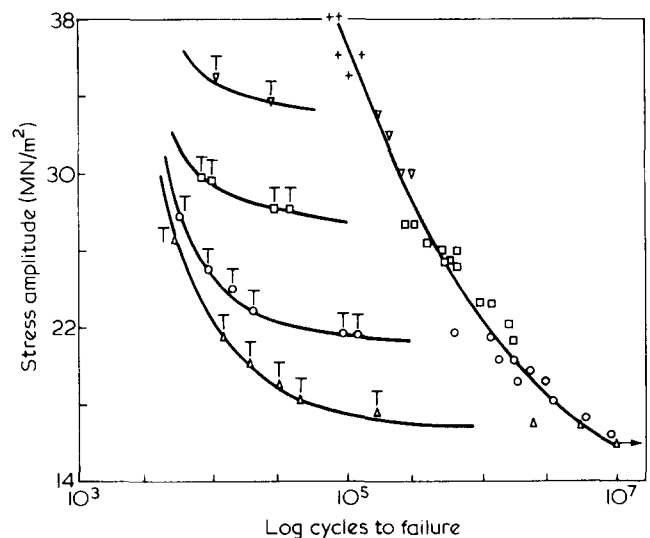


Figure 3 Reversed load cycling fatigue and thermal failures in acetal. +, 0.167;  $\nabla$ , 0.5;  $\square$ , 1.67;  $\circ$ , 5.0;  $\triangle$ , 10.0 Hz. T = thermal failure

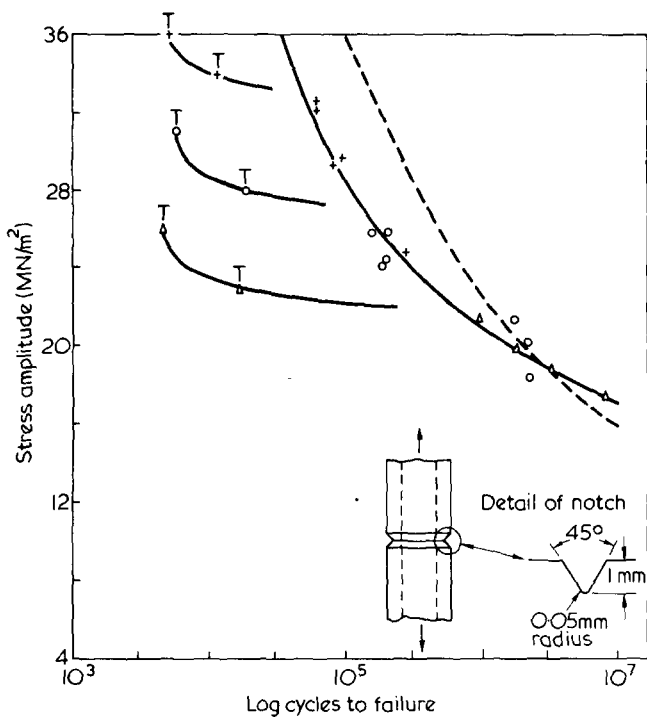


Figure 4 Reversed load cycling and thermal failures for sharp V-notch in acetal. ———, Unnotched single-end gated specimens; T = thermal failure; +, 1.67; o, 5.0; Δ, 10.0 Hz

be expected compared with the so-called plain material, but then in fact the latter is not entirely notch-free because of micro-voids which initiate failure within the wall thickness. Thermal softening failures can occur in the notched specimens, but owing to the localized volume of high stress, higher frequencies can be operated for the same peak stress compared with the unnotched specimens. The effect of other levels and types of stress concentration have been discussed earlier<sup>13</sup>.

All the above work was carried out under uniaxial push-pull stress cycling which, although more satisfactory for instrumented testing, is more costly in equipment for commercial testing. Also many components are subjected to bending deformation rather than simple tension/compression; therefore it was deemed necessary to make some limited study of bending fatigue. Rotating bar fatigue machines for metals were modified to give variable cyclic frequency and to accommodate the same specimen and grips used in the uniaxial fatigue tests. Tests were run at 25 and 50 Hz and the same pattern of thermal softening and fatigue cracking failures as in the uniaxial tests was observed except that since only the outer surface in bending is subjected to the maximum stress, the change-over stress amplitude occurred at much higher values. The basic fatigue curves for plain and V-notched (same as above) material are shown in Figure 5 in which the comparison is made with the corresponding curves obtained from the uniaxial push-pull testing. Apart from the obvious differences in fatigue strength and thermal softening which were exhibited, it became apparent that the tougher skin obtained in the moulding process would have a more beneficial influence in relation to bending fatigue than for uniaxial cycling because the maximum stress in bending only occurs at the outer surface. Another stress concentrator, a transverse hole, and a weld line defect produced by double end gate moulding were also studied and compared with the uniaxial equivalent tests. The details of these results for acetal copolymer may be found in ref. 14.

All types of specimen used in the fatigue programme described above were also tested for tensile creep rupture (static fatigue) of up to 4 weeks duration<sup>13</sup>.

Having produced a fully comprehensive picture of the fatigue behaviour of an acetal copolymer it was decided to study the principal patterns of fatigue behaviour in several other engineering thermoplastics.

### EXPERIMENTAL

The following materials were tested: (i) polypropylene copolymer (PP) (ICI GW701M natural): injection moulded; (ii) poly(tetramethylene terephthalate) (PTMT) (ICI TAP10 unmodified polymer) injection moulded; (iii) poly(tetramethylene terephthalate) (PTMT) (ICI TGA50 glass filled polymer) injection moulded; (iv) poly(methyl methacrylate) (PMMA) (ICI Perspex) machined from 100 mm sheet; (v) polycarbonate (PC) commercially supplied: machined from 40 mm diam. rod.

All the injection moulded specimens, which were manufactured by ICI Plastics Division, were fed from a ring gate at one end of the specimen in an attempt to obtain uniform flow and orientation along the gauge length of the specimen as had been previously achieved with the acetal mouldings. The mould cavity and core bar were highly polished to give good specimen surfaces. The machined specimens were carefully polished to give comparable surface finish to that from moulding.

The specimens were all produced to the dimensions given in Figure 1 and the notch as shown in Figure 4.

The uniaxial fatigue tests were carried out on a ±20 kN servo controlled machine on which the frequency could be varied in the range 0.1–100 Hz. The rotating bending tests were carried out on three fatigue machines which had been modified to take the polymer specimens as used in the uniaxial tests. On one of these machines the frequency could be varied from 2.5 to 25 Hz and on the other two machines the frequency was fixed at 50 Hz. The uniaxial machine and extensometry<sup>13</sup> and the rotating bar machines<sup>14</sup> have been described in greater detail elsewhere. The surface temperature rise of the specimens during cycling was recorded using an infra-red radiation thermometer.

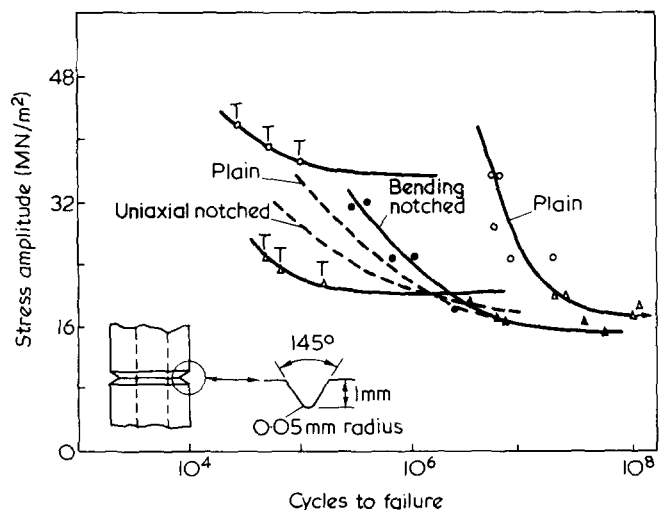


Figure 5 Comparison of uniaxial and rotating bending fatigue for acetal. ———, uniaxial; T = thermal failure (plain). Rotating bending: o, ●, 25; Δ, ▲, 50 Hz

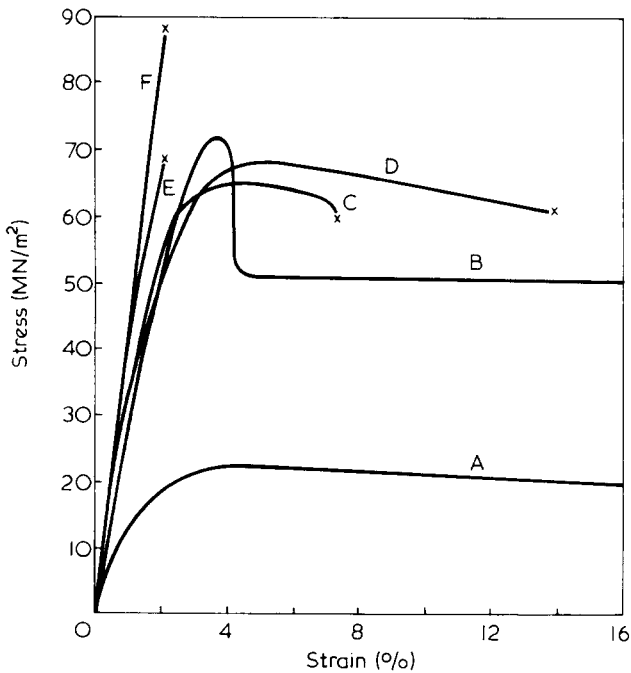


Figure 6 Stress-strain curves at extension rate of 50 mm/min. A, Polypropylene; B, polycarbonate; C, PTMT; D, acetal; E, PMMA; F, glass filled PTMT

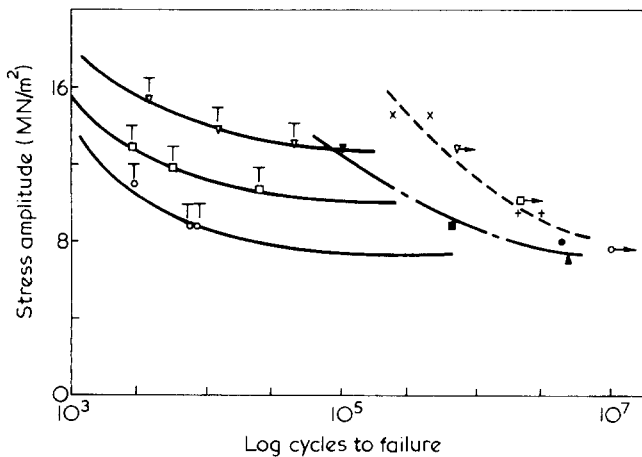


Figure 7 Reversed cycling fatigue and thermal failures in polypropylene. T = thermal failures; → = unbroken, stable temperature. Uniaxial (notched) load cycling: X, 0.5; +, 5.0 Hz. Uniaxial plain (load cycling): ▽, 0.5; □, 1.67; ○, 5.0; △, 10.0 Hz. Uniaxial plain (strain cycling): ▽, 0.5; ■, 1.67; ●, 5.0; ▲, 10.0 Hz

TEST PROGRAMME

Constant strain rate tensile tests

As an initial check on the relative behaviour of each material tensile tests were carried out at a constant extension rate of 50 mm/min on the basic specimen. The stress-strain curves are shown in Figure 6 and generally exhibit the features to be expected.

Fatigue tests

**Polypropylene.** In load-controlled reversed uniaxial loading (Figure 7) this material was very prone to thermal failures owing to its high loss tangent at the testing frequencies, and only at relatively low stress amplitudes did the temperature stabilize. At 5 Hz, for example, the thermal/fatigue failure change-over stress was found to be about 7.5 MN/m<sup>2</sup> and below this the temperature rise did stabilize but no

fatigue failures occurred for endurances up to 10<sup>7</sup> cycles (23 days). At a frequency of 0.5 Hz which allowed stress amplitudes of up to 12.5 MN/m<sup>2</sup> before thermal failures occurred, there were still no fatigue failures up to 7 × 10<sup>5</sup> cycles (16 days). Under these testing conditions therefore only thermal failures were produced in unnotched PP. However, cracking fatigue failure would probably have occurred in those specimens in which the temperature stabilized if the tests could have been continued to longer endurances. Of course, if temperature rise is suppressed by some cooling system then fatigue will occur as found with acetal (Fig. 3<sup>13</sup>). Likewise in a component with large surface area, but small volume, heat transfer would be better and temperature rise would stabilize at lower values and at higher stresses.

A few uniaxial reversed strain cycling controlled tests were conducted since thermal failure does not arise under these conditions. Fatigue failures were obtained in plain specimens as shown in Figure 7.

Circumferentially V-notched specimens (as described earlier) subjected to reversed uniaxial stress cycling at 0.5 and 5 Hz did not exhibit any thermal failure since temperature rise was less. Fatigue failures (using net stress values) are included in Figure 7. A number of problems were experienced in rotating bending tests owing to the pronounced thermal effect, and relatively low modulus, of polypropylene. At 25 Hz thermal failures were produced for stresses above ±8.5 MN/m<sup>2</sup> and for lower stresses no fatigue failures were produced for endurances up to 6 × 10<sup>7</sup> cycles (28 days). At 50 Hz the thermal/fatigue failure change-over stress was 4 MN/m<sup>2</sup> and no fatigue failures could be produced up to 10<sup>8</sup> cycles (23 days).

**Polycarbonate.** Owing to the low loss tangent value (~0.01 at 1 Hz) for this material specimen temperature rise was never very significant and no thermal failures were obtained at any frequencies at stress amplitudes as high as ±30 MN/m<sup>2</sup>. The fatigue data for plain and notched material are illustrated in Figure 8. At the lowest stress ampli-

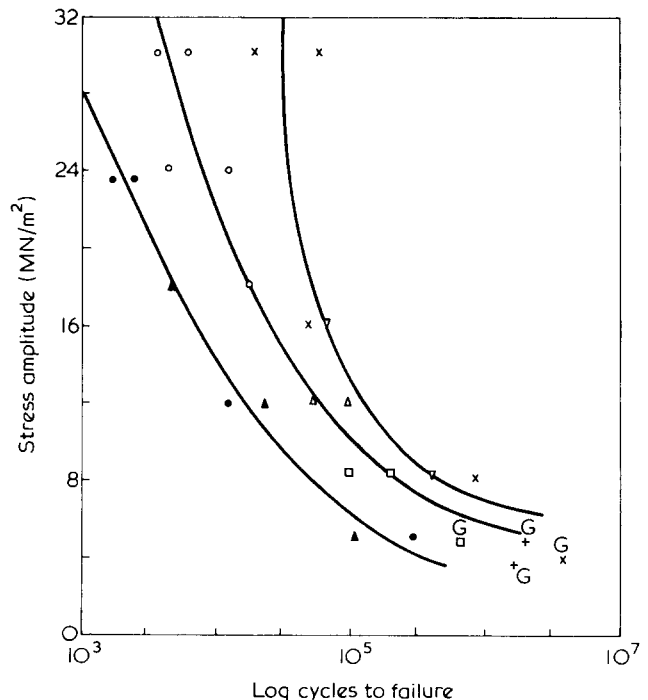


Figure 8 Reversed load cycling fatigue failures in polycarbonate. G = failure in grips. Uniaxial (plain): ○, 5; △, 10; □, 16.7; +, 25 Hz. Rotating bending (plain): X, 25; ▽, 50 Hz. Uniaxial (notched): ●, 5; ▲, 10 Hz

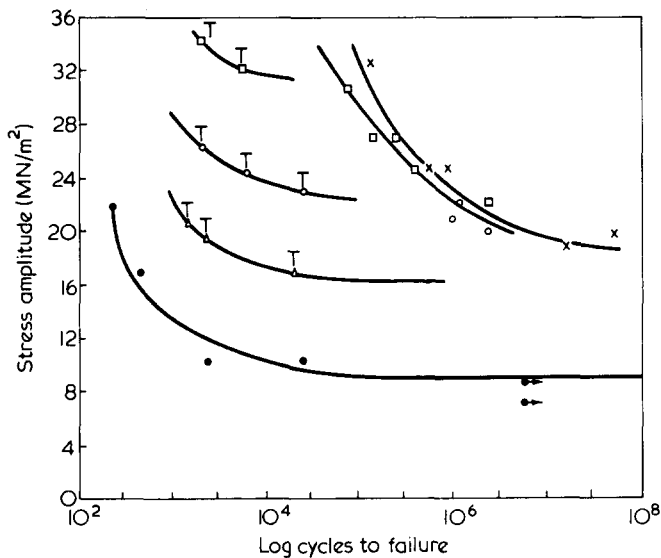


Figure 9 Reversed load cycling fatigue and thermal failures in PMMA. Uniaxial (plain): □, 1.67; ○, 5.0; △, 10.0 Hz. Rotating bending (plain): X, 16.7 Hz. Uniaxial notched (fatigue failures): ●, 5.0 Hz. T = thermal failure

tude of  $\pm 4 \text{ MN/m}^2$  failure occurred for the plain specimens within the grips owing to the stress concentration there. There was no noticeable effect of frequency of testing for either plain or notched results. The ratio of plain to notched fatigue strength does not reflect the high value of stress concentration used and suggests as with the acetal results that the plain material does contain some form of stress raiser in spite of the fact that the carefully machined surfaces were also thoroughly polished.

Under a rotating bending mode of loading PC exhibited a similar general behaviour to that described for uniaxial loading. There was only a small surface temperature rise even for cyclic frequencies of 25 and 50 Hz. The fatigue curve in Figure 8 indicates that there is a slight improvement in endurance over the uniaxial results and that there is no frequency effect. Since there was no tough skin on the PC specimens, as they were machined rather than injection moulded, a much closer agreement is obtained between uniaxial and bending fatigue, the latter being slightly better as generally found in metal fatigue.

**PMMA.** The results of the load controlled fatigue tests on PMMA were in many ways similar to those described for acetal. The loss tangent of  $\sim 0.08$  at 1 Hz is between those for PP and PC and hence both fatigue and thermal failures were observed in the range of cyclic frequencies 1.67–10 Hz as illustrated in Figure 9. However, there is a marked difference in the fatigue behaviour of the two materials when a notch is present, owing to their different levels of fracture toughness. It will be remembered that acetal is not particularly notch sensitive whereas the same geometry of notch in PMMA causes a drastic reduction in endurance. The plain and notched specimen fatigue results for PMMA are compared in Figure 9 and the difference in endurance is always greater than four decades. It was also found that if the surface of the PMMA specimens was not polished after machining there was a considerable reduction in endurance as a result of the surface markings. If the effect of sharp notches on the fatigue behaviour of PC and PMMA is compared it must be concluded that the polishing of the specimens was much more effective for the PMMA.

The rotating bending tests on PMMA again exhibited a similar behaviour to acetal with both thermal and fatigue

failures occurring over the range of frequencies examined (Figure 9). The uniaxial and the rotating bending fatigue strengths agree quite closely in spite of the wide range of test frequencies used.

**PTMT.** The results of the uniaxial reversed load-controlled fatigue tests on unfilled PTMT are shown in Figure 10 and it is seen that only thermal failures were produced. For test conditions at which the temperature rise stabilized no fatigue failures occurred up to  $9 \times 10^6$  cycles at 5 Hz or up to  $2.5 \times 10^6$  cycles at 1.6 Hz. The pronounced thermal behaviour of this material is similar to that described earlier for PP to which it has a comparable loss tangent and the similarity continued when tests were conducted using load controlled cycling on sharply notched specimens. In these tests fatigue failures were produced using frequencies of 1.67 and 5 Hz as shown in Figure 10. Comparing these with the results of tests on plain specimens which produced neither thermal nor fatigue failures it may be concluded that the reduction of endurance, owing to the presence of the notch, is at least in the order of one decade over the range of stresses examined.

In the rotating bending tests thermal failures were again predominant with the thermal/fatigue failure change-over stresses being 21.5 and 28.5  $\text{MN/m}^2$  at frequencies of 50 and 25 Hz, respectively. At both these frequencies several brittle fatigue failures occurred. However, in each case these were at the specimen grips so that no conclusions could be drawn from them and they have not been included in Figure 10.

**Glass filled PTMT.** In the glass filled PTMT the pronounced thermal effect observed in the unfilled material was not present. This can probably be attributed to the greater stiffness of the filled material and the possibility of improved heat transfer owing to the presence of the reinforcement medium in the matrix material. In load controlled cycling fatigue failures occurred for stresses up to  $\pm 40 \text{ MN/m}^2$  at 5 Hz with negligible increase in surface temperature of the specimen. On a stress basis this is twice the value attainable on acetal using the same test conditions.

The results shown in Figure 11 indicate that the material tested was generally weak in fatigue with endurances considerably less than those of the unfilled material. This

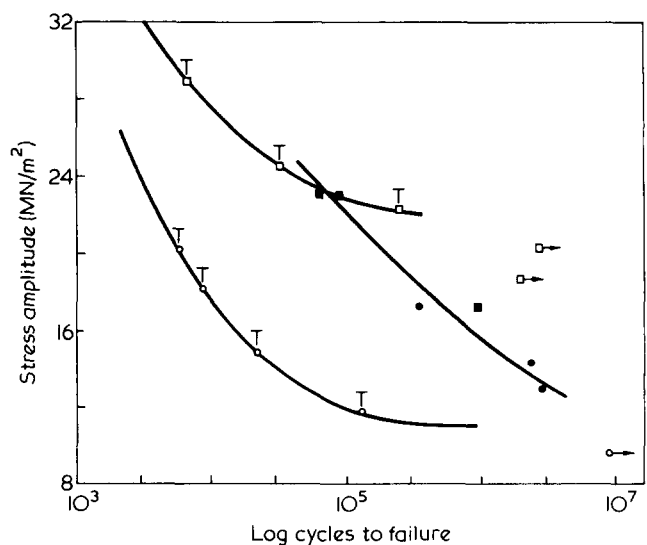


Figure 10 Reversed load cycling fatigue and thermal failures in unfilled PTMT. T = thermal failure; → = unbroken, stable temperature. Uniaxial (plain): □, 1.67; ○, 5.0 Hz. Notched (fatigue failures): ■, 1.67; ●, 5.0 Hz

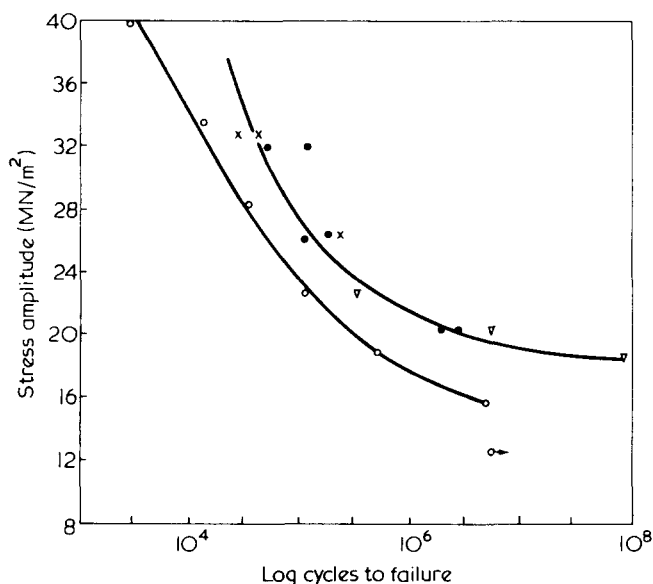


Figure 11 Reversed load cycling fatigue failures in glass filled PTMT. Uniaxial:  $\circ$ , 5 Hz (plain);  $\bullet$ , 5 Hz (notched). Rotating bending (plain):  $\nabla$ , 50;  $\times$ , 25 Hz

type of behaviour is probably to be expected in that the presence of the fibres in the matrix will provide sites for fatigue crack initiation. However, it is also evident that this batch of moulded specimens must have contained additional stress concentrations of considerable magnitude, since the V-notched specimens had longer endurance than the plain material. The presence of incipient flaws in the glass filled material is also evidenced by the fact that in the constant strain rate tests described earlier the fracture stresses obtained were about 30% less than the values quoted by the manufacturers of the material.

In the rotating bending tests there was again no significant temperature rise in the material and only fatigue failures occurred at frequencies of 25 and 50 Hz. The endurance (Figure 11) were slightly better than the uniaxial results and indeed correspond quite closely to the endurance of the notched specimens.

#### Creep rupture tests

A series of tensile creep rupture tests were carried out on each material using exactly the same specimen as for fatigue, and the results are shown in Figure 12. In the tests on acetal it had been found<sup>13</sup> that brittle failure occurred at stresses which caused fracture in less than  $10^3$  sec. At lower stresses and for lives up to  $10^6$  sec it was found that failure was ductile and was preceded by whitening. For endurance in excess of  $10^6$  sec the whitening was barely detectable but a neck formed in the material prior to fracture. In all cases failure initiated from within the wall thickness and was similar to the fractures observed in the constant strain rate tests.

The creep rupture tests on PP produced ductile fractures over the whole range of stress examined. The material whitened and then necked prior to fracture which initiated from within the specimen wall.

The creep rupture endurance in PC were surprisingly large as compared with the relatively short endurance under dynamic loading. In most tests crazing was observed shortly after the load was applied but this did not indicate that failure was imminent. Even in the longest testing time of approximately four weeks the crazes were present throughout the whole life of the specimen. The fracture surfaces

of the PC specimens which failed as a result of creep rupture or fatigue looked very similar under the microscope in that, at the point of crack initiation both had a very smooth area surrounded by finely spaced striations.

Under sustained static loading PMMA was observed to craze at some point during its life and then form a neck at which fracture occurred. Fracture always initiated at the inner or outer surface and had the typical brittle fracture appearance described earlier.

Both filled and unfilled PTMT failed in a brittle manner over the range of stresses examined and as shown in Figure 12 the endurance of the glass filled material are always greater by about two decades. As with the failures in fatigue and constant strain rate tests the fracture surface of the filled PTMT specimens was generally featureless and indeed it was difficult to distinguish one type of failure from the others. The creep rupture fractures in the unfilled material, however, were quite different from those in the other tests.

#### DISCUSSION AND CONCLUSIONS

The behaviour of a thermoplastic under cyclic stress conditions is perhaps even more difficult to interpret and design for than is the case with a metal. First, this can be attributed to the presence in plastics particularly of two distinct failure mechanisms, the thermal softening and the fatigue cracking. The presence of the former is largely related to the loss tangent value for the material at any particular frequency. The larger the  $\tan \delta$  value then the more will thermal softening predominate over fatigue cracking. The present specimen geometry is regarded as quite a good compromise for a representative laboratory specimen to relate to likely proportions of components, injection moulding conditions, usage for various tests, etc. The temperature rise for this specimen can be calculated as a function of stress amplitude, frequency, heat transfer coefficient, surface area, volume, density and phase lag  $\delta^{12}$  and this could similarly be done on an approximate basis for actual components to establish when temperature rise stabilizes and so does not lead to thermal failure. In the present programme it was found that

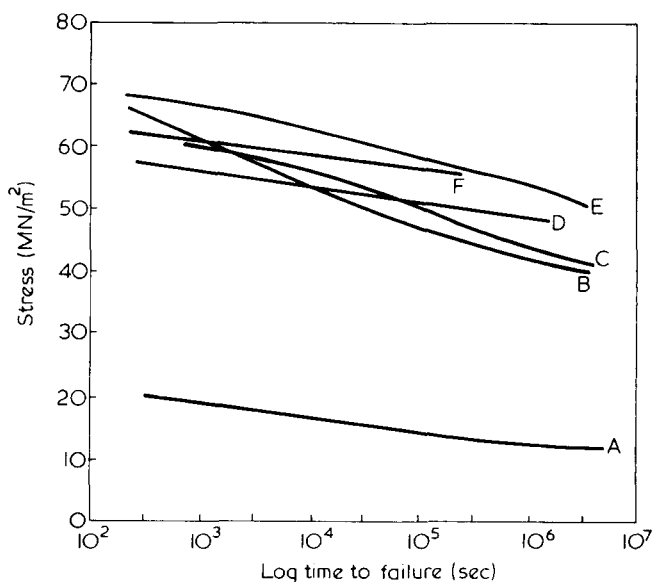


Figure 12 Creep rupture behaviour of several thermoplastics. A, Polypropylene; B, PMMA; C, acetal; D, PTMT; E, polycarbonate; F, glass filled PTMT

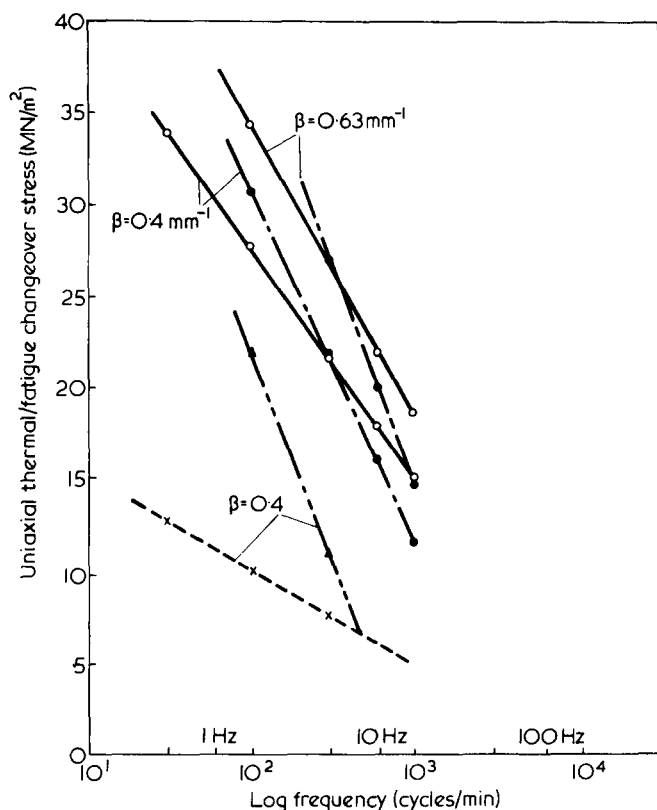


Figure 13 Relationships between stress amplitude and frequency for changeover from thermal softening to fatigue failure.  $\beta$  = surface area/volume ( $\text{mm}^{-1}$ ); load cycle control; sine wave; zero mean stress.  $\circ$ , Acetal;  $\bullet$ , PMMA; X, polypropylene;  $\blacktriangle$ , unfilled PTMT

the changeover stress, cyclic frequency and surface area to volume ratio were related by a single empirical expression of the form:

$$\sigma_c = \left[ \frac{A}{V} \right]^{1/2} \{ C_1 - C_2 \log_{10} f \}$$

where  $\sigma_c$  is the changeover stress amplitude in  $\text{MN}/\text{m}^2$ ,  $f$  is cyclic frequency in Hz, surface area  $A$  and volume  $V$ , are in mm units and  $C_1$  and  $C_2$  are material constants. This equation is illustrated in Figure 13 for four materials and two  $A/V$  ratios. One useful point to note is that the changeover stress value can be pin-pointed quickly and accurately since there is so little scatter with the thermal softening failures.

The dynamic fatigue performance of the six materials is summarized in Table 1 for a reasonably long endurance ( $3 \times 10^6$  cycles) and the constant strain rate maximum tensile strength has been included also for comparison. There is a wide variation in the ratio of fatigue/static strength in which PC is seen to be by far the poorest material and PP the best material in uniaxial dynamic fatigue relative to their static strengths.

The dynamic fatigue strength in bending is in all cases slightly higher than in push-pull, as is generally the case for metals, and of course the thermal softening problem is not as severe in bending owing to the stress gradient through the material. As far as commercial fatigue testing is concerned bending does have the considerable advantage of requiring less complicated and costly apparatus than for uniaxial testing. However, in either type of test, design and

Table 1 Fatigue strength at  $3 \times 10^6$  cycles endurance ( $\pm \text{MN}/\text{m}^2$ )

	Acetal	PP	PC	PMMA	Unfilled PTMT	Filled PTMT
Plain (uniaxial)	18.5*	<10.0	4.5	20.0	<20.0	16.0
Plain (bending)	44.0†	—	6.0	21.0	—	20.0
Notched (uniaxial)	18.5*	9.5	2.0†	8.5	13.0	20.0
Max static strength (from Figure 3)	68	22	72	68	65	88

\* By coincidence the plain and notched curves cross at this endurance

† Extrapolated values

< Actual fatigue failures not reached

condition of specimen is of considerable importance and must always be specified.

The notched fatigue results illustrate the care which is necessary in the selection of plastics to resist cyclic stressing as revealed by the high notch sensitivity of PC and PMMA and in contrast the notch-toughness of acetal.

Two further factors in the present work which are worth mentioning again are the relatively low degree of scatter in the fatigue cracking results and reasonable independence of cyclic frequency.

It is seven years ago since the PLC36 Committee was unable to make recommendations for dynamic fatigue testing of plastics and perhaps with the number and variety of fatigue studies that have been undertaken since then it would now be possible and appropriate for BSI to reconsider the case.

#### ACKNOWLEDGEMENTS

Those specimens which were injection moulded were generously provided by ICI Ltd Plastics Division.

This programme has received financial support from the Science Research Council.

#### REFERENCES

- Andrews, E. H. 'Testing of Polymers', (Ed. W. E. Brown), Wiley, New York, 1968, Vol 4, pp 237-295
- Gotham, K. V. *Plastics and Polymers* 1969, 37; 309
- Plumbridge, W. J. *J. Mater. Sci.* 1972, 7, 939
- Mukherjee, B. and Burns, D. J. *Exp. Mech.* 1971, p 433
- Arad, S., Radon, J. C. and Culver, L. E. *Polym. Eng. Sci.* 1972, 12, 193
- Andrews, E. H. and Walker, B. J. *Proc. R. Soc. (A)* 1971, 325, 57
- Riddell, M. N., Koo, G. P. and O'Toole, J. L. *Polym. Eng. Sci.* 1966, 6, 363
- Tauchert, T. R. *Int. J. Eng. Sci.* 1967, 5, 353
- Oberbach, K. *Kunststoffe* 1969, 59, 37
- Constable, I., Williams, J. G. and Burns, D. J. *J. Mech. Eng. Sci.* 1970, 12, 20
- Johnson, T. A. ASTM STP519, 1973, pp 70-97
- Crawford, R. J. and Benham, P. P. *J. Mater. Sci.* 1974, 9, 18
- Crawford, R. J. and Benham, P. P. *J. Mech. Eng. Sci.* 1974, 16, 178
- Crawford, R. J. and Benham, P. P. *J. Mater. Sci.* 1974, 9, 1297

# Effect of temperature on the impact fracture toughness of polymers

E. Plati and J. G. Williams

Department of Mechanical Engineering, Imperial College, London SW7 2BX, UK

(Received 9 May 1975; revised 17 July 1975)

A method is described by which the true energy release rate at fracture may be determined from a conventional impact test. This method is then used to investigate the effect of temperature on impact strength and the results are described in terms of a yield stress dependent thickness effect. Blunt notch data are also given and plane stress and plane strain energy absorption mechanisms are postulated to account for the observed behaviour.

## INTRODUCTION

Impact testing is of considerable practical importance but suffers from several drawbacks in the test methods currently employed. In the first place, the apparatus used is often not of a good standard resulting in considerable scatter in the data because of poor alignment and friction. Secondly, the test method is designed in such a way that the data are difficult to interpret with any logic. This paper describes an apparatus which overcomes most of these problems so that machine scatter is largely eliminated and an analysis is employed which presents the data in a concise and meaningful form.

The results from conventional impact testing are usually expressed in terms of the specific fracture energy  $w/A$ , where  $w$  is the energy absorbed to break the notched specimen and  $A$  is the cross-sectional area of the fractured ligament. Such an analysis of the data is not satisfactory because the parameter  $w/A$  depends on the specimen geometry and the type of test used. There is only a rough correlation between the Charpy and the Izod impact values for the same material. However, some recent publications<sup>1-4</sup> have shown that if elastic deformations are assumed linear fracture mechanics theory can be extended to impact data and  $G_c$ , the critical strain energy release rate, can be deduced directly from the absorbed energy. The absorbed energy to failure,  $w$ , can be written in the form:

$$w = G_c \cdot BD\phi$$

where  $B$  and  $D$  are the thickness and depth of the specimen respectively and  $\phi$  is a calibration factor which is a function of crack length and may be calculated or measured experimentally.  $w$  is determined for several crack lengths and  $G_c$  determined from the linear plot of  $w$  versus  $\phi$ . Plati and Williams<sup>4</sup> have determined calibration factors for both the Charpy and Izod tests and  $G_c$  for a range of polymers at 20°C in both tests.  $G_c$  was shown to be independent of specimen geometry and identical for both test methods. For highly ductile materials a modification of the method was necessary to obtain values which are comparable with those for the more brittle materials<sup>2,4</sup>.

The work is extended here by measuring  $G_c$  for both sharp and blunt notches over a range of temperatures for several polymers using a temperature control cabinet fitted to the impact machine. The results are analysed in terms

of the concept of a plane stress and a plane strain  $G_c$  and changes in  $G_c$  with both temperature and specimen thickness are described in terms of yield stress changes.

## APPARATUS

The impact testing machine used is shown in *Figure 1* and is of the conventional pendulum type. The machine was made by the Mechanical Engineering Department, Imperial College, from a design supplied by The British Petroleum Co. Ltd. A set of pendulums of various weights are used to give high precision in energy measurements over a wide

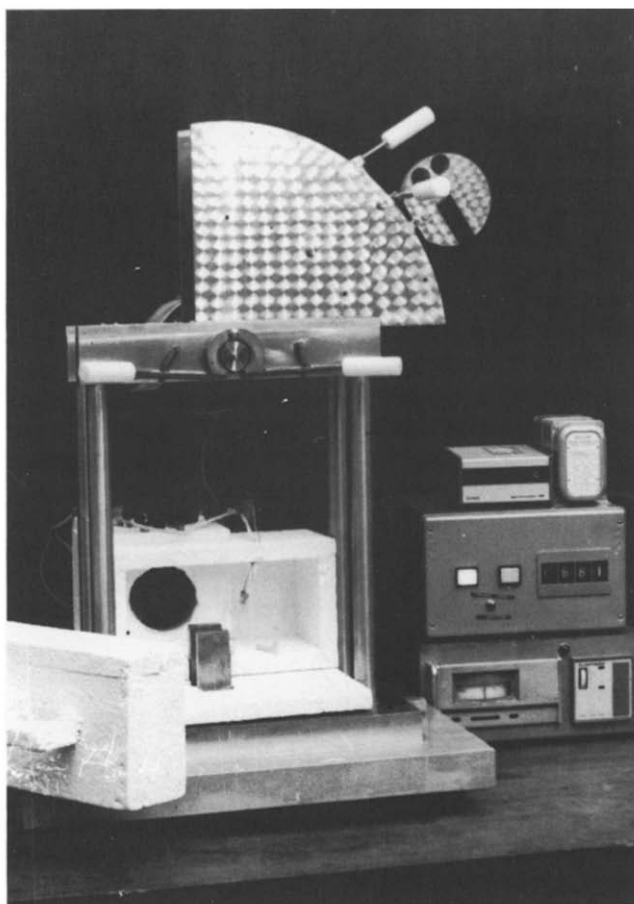


Figure 1 Impact machine with temperature box



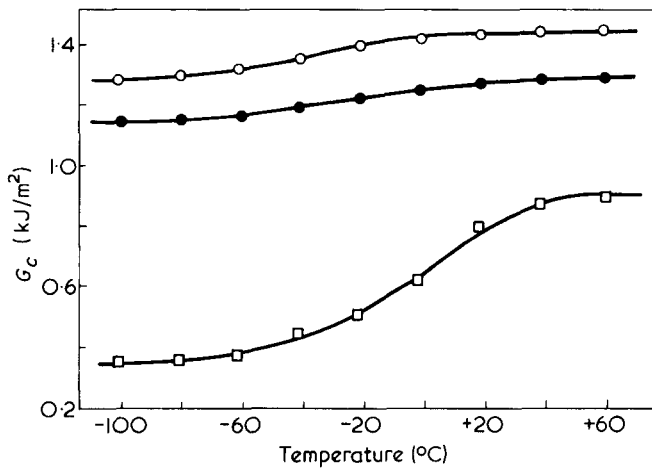


Figure 2 Low impact strength materials. ○, PVC; ●, PMMA; □, GPPS

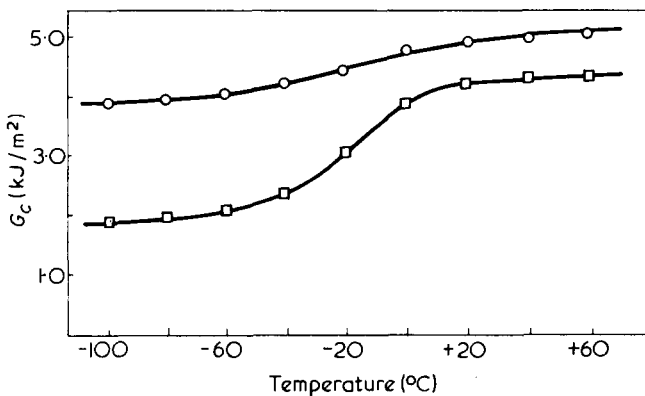


Figure 3 Medium impact strength materials. ○, Polycarbonate; □, nylon-6,6 (dry)

range of values and the usual precautions were taken to ensure that the centre of percussion is at the impact point. Different pendulums were designed such that Charpy, Izod and tensile impact tests could be performed.

Special care was taken in the bearing design to ensure a minimum of friction and play since these factors were found to be of particular importance in achieving consistency<sup>1</sup>. The angular measurements are made using a photo-electric device and a transparent disc marked at 9' of arc intervals. The angles are indicated as a number on a digital counter. Windage and friction losses were determined from free swing experiments so that each reading on the counter could be given an energy value for each pendulum and initial pendulum angle. Tables of values were produced for all counter readings. Speed variations from the four original settings available are rather small and all the data given here are at 3 m/s.

The various temperatures were achieved using a split insulated box surrounding the specimen (see Figure 1). When the required temperature is reached the front part of the box is withdrawn to allow the pendulum to swing down and strike the specimen. A small fan is used to circulate air through the box from a closed loop containing a heater coil. Low temperatures are obtained by blowing liquid nitrogen into the loop. A thermocouple embedded in a dummy specimen located close to the real one controls the nitrogen flow and the heater via a 'Eurotherm' control unit. The range  $-100^{\circ}$  to  $+60^{\circ}\text{C}$  was used and a control of  $\pm 1^{\circ}\text{C}$  was achieved. The box is opened for a very short

period ( $< 1$  s) in order to break the specimen and no appreciable temperature change was observed.

## RESULTS

The  $G_c$  values for 6 mm thick specimens notched with a very sharp ( $< 50 \mu\text{m}$ ) cutter are shown in Figures 2, 3 and 4 for the temperature range  $-100^{\circ}$  to  $+60^{\circ}\text{C}$ . Each point is obtained from the slope of a  $w$  versus  $\phi$  graph and contains the results from 15–20 specimens of various notch lengths as shown for polycarbonate in Figure 5. They are grouped as low, medium and high impact strengths and in the low group ( $\approx 1 \text{ kJ/m}^2$ ) we have unmodified polystyrene and PMMA as expected. The PVC is also unmodified and behaves as a glassy amorphous polymer but PVC would be expected to be in a higher group when impact modifiers or fillers are added. Figure 3 ( $\approx 4 \text{ kJ/m}^2$ ) includes polycarbonate and dry nylon-6,6 which are classified here as medium strength materials. Figure 4 gives the high impact strength materials ( $\approx 20 \text{ kJ/m}^2$ ) and very large changes

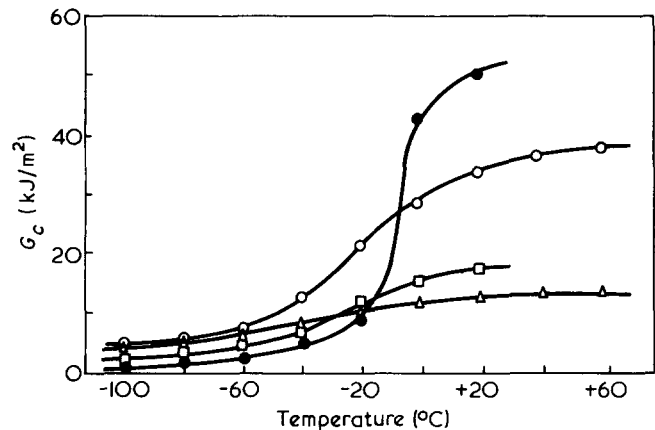


Figure 4 High impact strength materials. ○, Polyethylene (low density); △, polyethylene (medium density); □, HIPS; ●, ABS

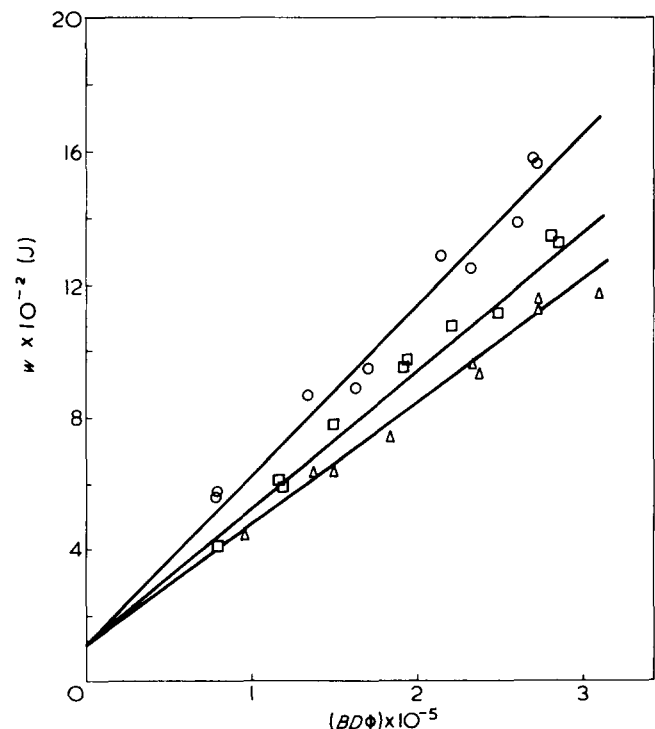


Figure 5 Sharp notch data for polycarbonate at three temperatures: ○,  $+20^{\circ}$ ; □,  $-40^{\circ}$ ; △,  $-100^{\circ}\text{C}$

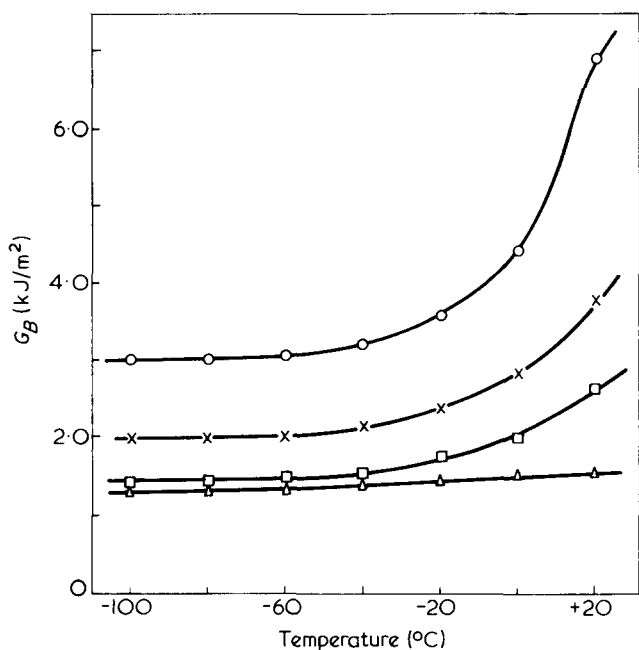


Figure 6 Blunt notch data for PVC.  $\Delta$ , Sharp notches;  $\square$ ,  $\rho = 0.25$  mm;  $\times$ ,  $\rho = 0.5$  mm;  $\circ$ ,  $\rho = 1.0$  mm

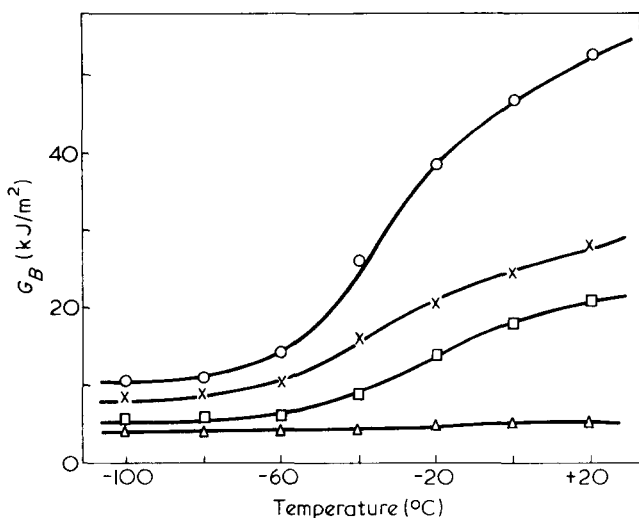


Figure 7 Blunt notch data for polycarbonate.  $\Delta$ , Sharp notches;  $\square$ ,  $\rho = 0.25$  mm;  $\times$ ,  $\rho = 0.5$  mm;  $\circ$ ,  $\rho = 1.0$  mm

with temperature are apparent. Changes of the order of ten are observed here while in the low and medium category they are two or less. There is a noticeable similarity in the curves in that all are sigmoidal in form between constant high and low temperature values within the temperature range covered. It should be noted that all the points are for brittle failures except for some of the high impact strength materials at the higher temperatures. In these cases, ductile failure occurs and the  $G_c$  is calculated from  $2w/A$ <sup>4</sup>.

A series of tests were also performed on specimens with blunt notches of tip radii 0.25, 0.5 and 1 mm. The  $G_c$  determination was as in the sharp notch case and a blunt notch  $G_c$  value, termed  $G_B$ , was obtained. These are shown in Figures 6, 7 and 8 for PVC, polycarbonate and PMMA, respectively. PVC and polycarbonate show the expected elevation of the curves and they remain similar in form. For PMMA, however, a peak appears at  $-60^\circ\text{C}$  which increases with the blunter notches and is totally absent in the sharp notch data. There is no significant

evidence of peaks in the other materials for any notch radius.

### THEORETICAL ANALYSIS

It is postulated here that a polymer exhibits different fracture strengths depending on the stress system imposed. The lowest value is when the material is heavily constrained, as in the centre of a notched specimen, and this is termed  $G_{c1}$ . The highest value is with no constraint as near the surface of the specimen and this is the plane stress value  $G_{c2}$ .

This concept has been used for metals<sup>5</sup> and has been extended to polymers<sup>6,7</sup> but in the form of fracture toughness  $K_c$ . Following the same line of argument, however, similar relationships may be derived for  $G_c$ . The extent of the plane stress region is assumed to be the plastic zone size  $r_{p2}$  which is given by<sup>6</sup>:

$$r_{p2} = \frac{1}{2\pi} \cdot \frac{K_{c2}^2}{\sigma_y^2}$$

and since  $K_{c2}^2 = EG_{c2}$  where  $E$  is the modulus and  $\sigma_y$  the yield stress, we have:

$$r_{p2} = \frac{E}{2\pi} \cdot \frac{G_{c2}}{\sigma_y^2} \quad (1)$$

The specimen may therefore be considered as a sandwich of a plane strain region between two plane stress regions of thickness  $r_{p2}$ . Since energy is measured in this test an average  $G_c$  will be determined (and not  $K_c$  as in ref.6) such that:

$$G_c B = G_{c1}(B - 2r_{p2}) + G_{c2}2r_{p2}$$

i.e.

$$G_c = G_{c1} + \frac{2r_{p2}}{B} (G_{c2} - G_{c1})$$

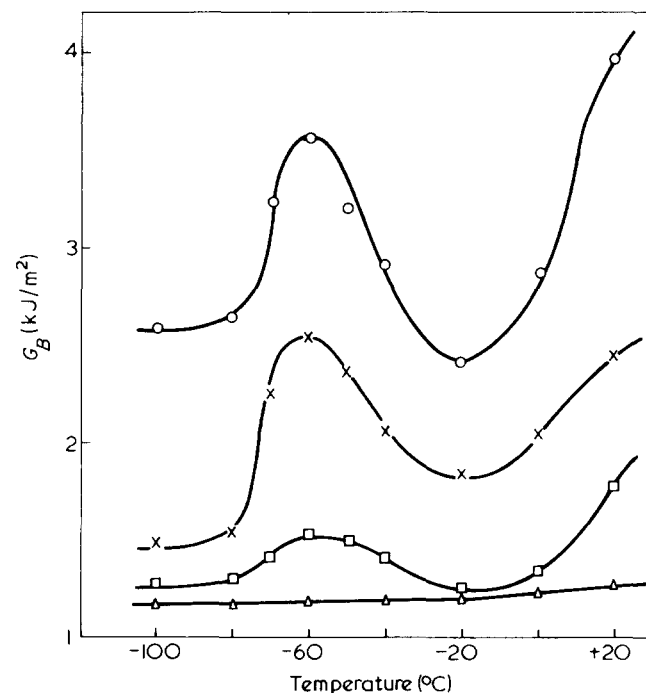


Figure 8 Blunt notch data for PMMA.  $\Delta$ , Sharp notches;  $\square$ ,  $\rho = 0.25$  mm;  $\times$ ,  $\rho = 0.5$  mm;  $\circ$ ,  $\rho = 1.0$  mm

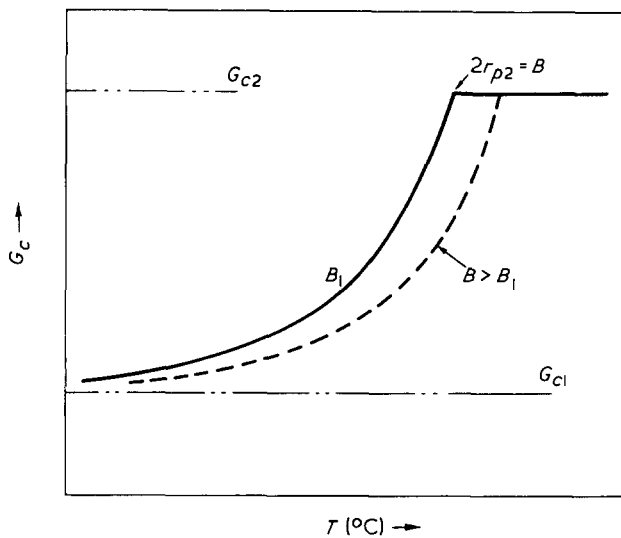


Figure 9 Schematic form of toughness changes with temperature as given by equation (2)

where  $B$  is the specimen thickness. Substituting for  $r_{p2}$  we have:

$$G_c = G_{c1} + \frac{EG_{c2}}{\pi\sigma_y^2 B} (G_{c2} - G_{c1}) \quad (2)$$

Since impact fractures are at quite high speeds they would be expected to be adiabatic and therefore  $G_{c1}$  and  $G_{c2}$  would not be expected to depend on temperature. Similarly,  $E$ , which relates  $K_c$  and  $G_c$  would also be expected to be insensitive to temperature.  $\sigma_y$ , on the other hand, refers to the plastic deformation away from the actual fracture and should be influenced by temperature changes. It would be difficult to determine the  $\sigma_y$  appropriate to impact but the form of the temperature dependence would be expected to be similar to slower rate data. If  $1/\sigma_y^2$  as determined in ordinary slow rate tests at various temperatures is plotted as a function of  $G_c$ , equation (2) would indicate a straight line extrapolating to  $G_{c1}$ . This value should be a reasonably accurate estimate since it is not derived from the particular  $\sigma_y$  values used. It is also clear that when  $2r_{p2} = B$ ,  $G_c = G_{c2}$ . Since  $\sigma_y$  increases with decreasing temperature the form of curve expected would be  $G_c$  remaining at  $G_{c2}$  with decreasing temperature until  $2r_{p2} < B$  when dependence on  $\sigma_y$  comes into force and  $G_c$  tends to  $G_{c1}$ . Since the  $\sigma_y$  dependence on temperature is similar (i.e. approximately linear) for most polymers an explanation is provided for the similar form of curves noted previously. Figure 9 shows the form of equation (2) schematically and also indicated the effect of a thickness change. The deformation properties are contained in the term  $\sigma_y^2/E$  and this may be written as the plane stress elastic work to yielding:

$$w_{p2} = \frac{1}{2} \cdot \frac{\sigma_y^2}{E} \quad (3)$$

It was suggested<sup>4</sup> that blunt notch data could be analysed by assuming that the same plane strain plastic zone of radius  $r_{p1}$  had to form at the tip of the blunt notch at fracture as in the sharp notch. For the condition that the notch tip radius  $\rho$  is much greater than this plastic zone then the

relation:

$$G_B = G_c \left(1 + \frac{\rho}{2r_{p1}}\right)^3 / \left(1 + \frac{\rho}{r_{p1}}\right)^2$$

becomes:

$$G_B = \frac{G_c}{2} + \frac{2}{\pi} w_{p1} \cdot \rho \quad (4)$$

where

$$w_{p1} = \frac{\pi}{16} \frac{G_c}{r_{p1}}$$

and is the elastic energy to yield under the plane strain conditions at the notch tip. Assuming that there is no lateral deformation in the constrained region the ratio of  $w_{p1}$  and  $w_{p2}$  may be expressed in terms of the Poisson's ratio  $\nu$  so that:

$$\frac{w_{p1}}{w_{p2}} = \left(\frac{1-\nu}{1-2\nu}\right)^2 \quad (5)$$

As expected, as  $\nu \rightarrow 1/2$ ,  $w_{p1} \rightarrow \infty$  since complete constraint has been imposed on an incompressible material. However, for most polymers  $\nu$  is around 0.4 giving  $w_{p1}/w_{p2} = 9$  so that  $w_{p1}$  will be expected to be much larger than  $w_{p2}$ .

## DISCUSSION OF RESULTS

Figure 10 shows data for PMMA and PVC plotted as  $G_c$  versus  $1/\sigma_y^2$  and the expected linear relationship is apparent giving the values of  $G_{c1}$  and  $G_{c2}$ . Figure 11 shows data for two thicknesses of polycarbonate and Figure 12 for three thicknesses of polyethylene. The form of the data is in reasonable agreement with equation (2) and when the slopes are plotted against  $1/B$  in Figure 13 good straight lines result. It would seem that equation (2) is a good description of the data given here. Table 1 gives the values of  $G_{c1}$  and  $G_{c2}$  for the materials tested. The effect of specimen thickness reported by Wolstenholme *et al.*<sup>9</sup> is also in accord with equation (2) in indicating a decrease in energy per unit area with increasing thickness. The reported proportionality of fracture load and yield stress<sup>9</sup> is also consistent with equation (4).

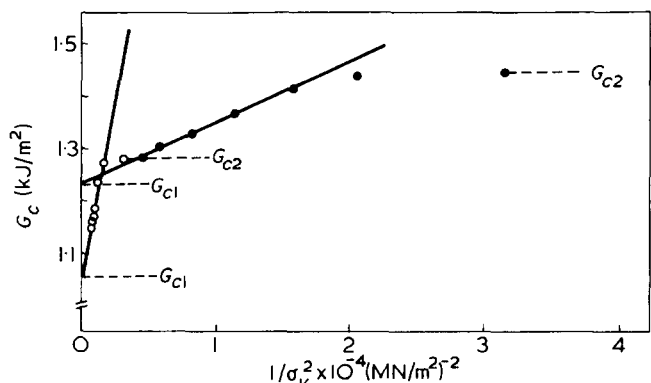


Figure 10 Variation of impact toughness with yield stress. ●, PVC; ○, PMMA

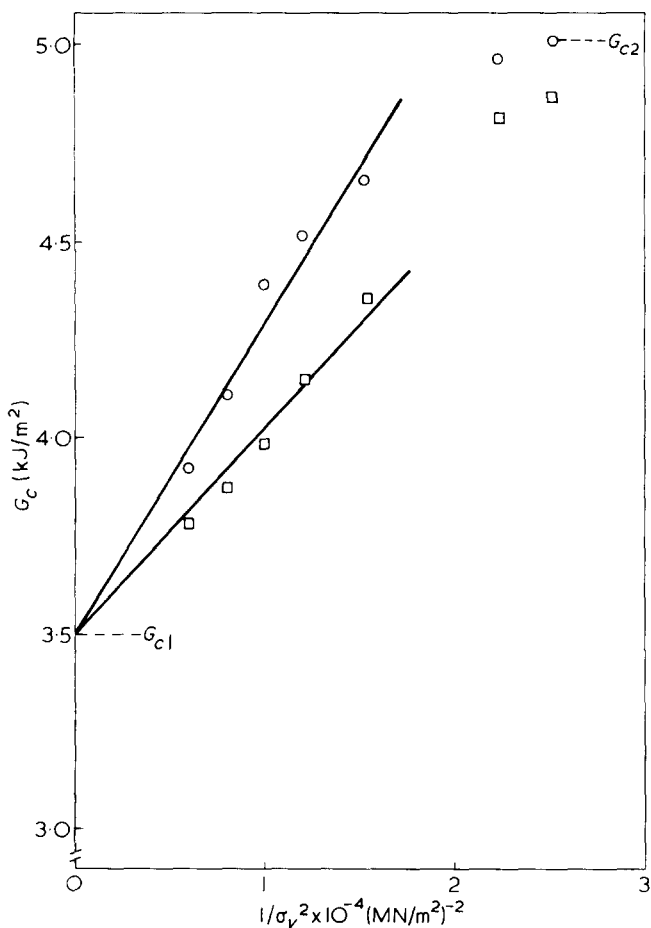


Figure 11 Variation of impact toughness with yield stress for polycarbonate for two specimen thicknesses:  $\circ$ ,  $B = 3$  mm;  $\square$ ,  $B = 6$  mm

Since  $G_{c1}$  is found by extrapolation and  $G_{c2}$  is known it is possible to deduce the parameter  $w_{p2}$  from equation (2). The  $E$  here is an adiabatic value and constant while  $\sigma_y$  is not so that  $w_{p2}$  will be proportional to  $\sigma_y^2$ . Figure 14 shows  $w_{p2}$  as a function of temperature and shows a rapid increase with decreasing temperature consistent with this relationship.

The blunt notch data were plotted in accordance with equation (4) so that  $w_{p1}$  was obtained and this is shown for the three materials in Figure 14.  $w_{p1}$  is much greater than  $w_{p2}$  as expected and corresponds to  $\nu$  values of around 0.45.  $w_{p1}$  also decreases with temperature decrease and there is evidence of peaks in all three materials. Peaks in impact data have been widely reported<sup>10-12</sup> and Vincent<sup>8</sup> has observed that they are more usually found with blunt notches. Their correlation with  $\tan \delta$  peaks has been widely discussed but seems to be somewhat variable. The pronounced peak at  $-60^\circ\text{C}$  here for PMMA and the lesser one for PVC at  $-20^\circ\text{C}$  could be equated with the  $\beta$  process<sup>13,14</sup>. The more modest peak for polycarbonate does not seem to correspond to any  $\tan \delta$  peak which agrees with the findings of Heijboer<sup>10</sup>.

## CONCLUSIONS

The basic hypothesis that impact strength is strongly influenced by the constraint imposed by the specimen geometry seems to provide a good description of the sharp notch data. The concept of  $G_{c1}$  and  $G_{c2}$  coupled with yield stress changes gives an accurate picture of variations with temperature and specimen thickness. The fact that the yield

stress away from the actual fracture zone does show changes with temperature while  $G_{c1}$  and  $G_{c2}$  do not is the basis for the observed variations with temperature. Blunt notch data in effect magnify the plane strain yielding process at the notch root and although the plane stress energy  $w_{p2}$  shows the dependence on temperature typical of slow rate data the plane strain values,  $w_{p1}$ , show peaks.

The strong dependence on volume change is believed to be important here since it seems that it is the changes in

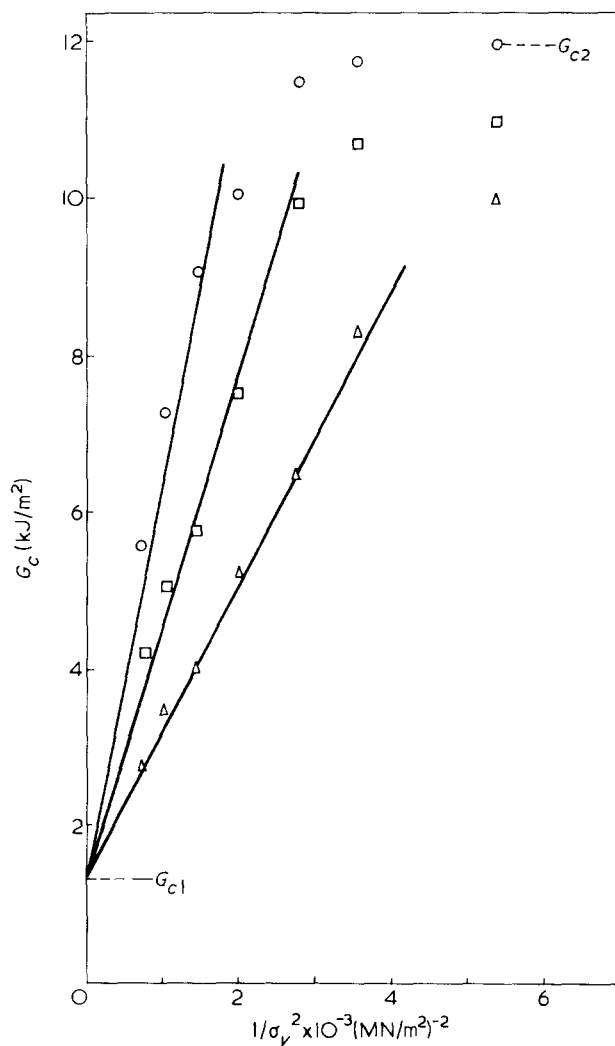


Figure 12 Variation of impact toughness with yield stress for medium density polyethylene for three specimen thicknesses:  $\circ$ ,  $B = 3$  mm;  $\square$ ,  $B = 6$  mm;  $\triangle$ ,  $B = 11$  mm

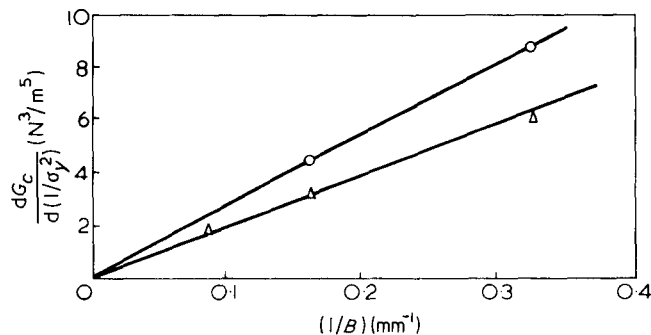


Figure 13 Variation of slope of  $G_c$  versus  $1/\sigma_y^2$  lines with specimen thickness.  $\circ$ , Polycarbonate;  $\triangle$ , polyethylene (medium density)

Table 1

Material	$G_{c1}$ (kJ/m <sup>2</sup> )	$G_{c2}$ (kJ/m <sup>2</sup> )
PMMA	1.06	1.28
Polystyrene	0.35	0.90*
PVC	1.23	1.44
Polycarbonate <sup>a</sup>	3.5	5.02
Nylon-6,6 (dry)	0.25	4.15
Polyethylene (medium density) <sup>b</sup>	1.3	11.90
Polyethylene (low density) <sup>c</sup>	5.0	35.00*
HIPS	1.0	15.00

\* Estimated values — no reliable yield stress data available

<sup>a</sup> Bayer Makrolon extruded sheet. Specimens cut in the extrusion direction

<sup>b</sup> Density = 0.955;  $MI = 0.2$

<sup>c</sup> Density = 0.945;  $MI = 6.0$

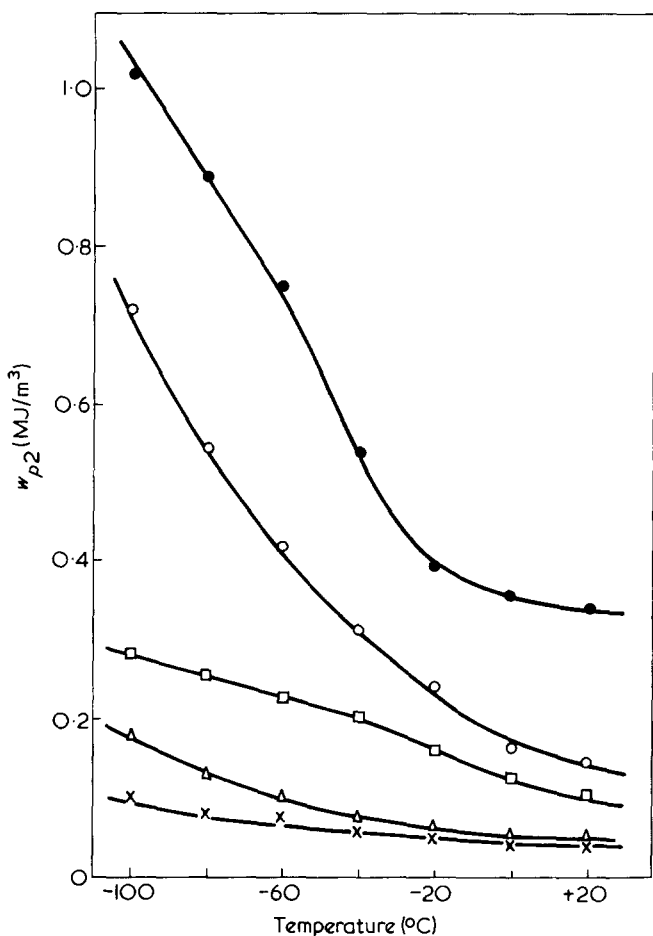


Figure 14 Variation of plane stress yielding energy with temperature. ●, Polyethylene (medium density); ○, polycarbonate; □, nylon-6,6 (dry); △, PVC; ×, PMMA

$\nu$  which dominate over those in  $\sigma_y$ . Data of  $\nu$  are scarce but it seems likely that there would be some correlation between  $\tan \delta$  peaks and volume changes. However, the origins of the effect may be in other factors such as absorbed fluids which are apparent in  $\tan \delta$  and have a strong influence on volume changes. A  $-60^\circ\text{C}$  peak in PMMA, for example, is sometimes ascribed to water. This sensitivity to volumetric effects in the fracture behaviour of polymers

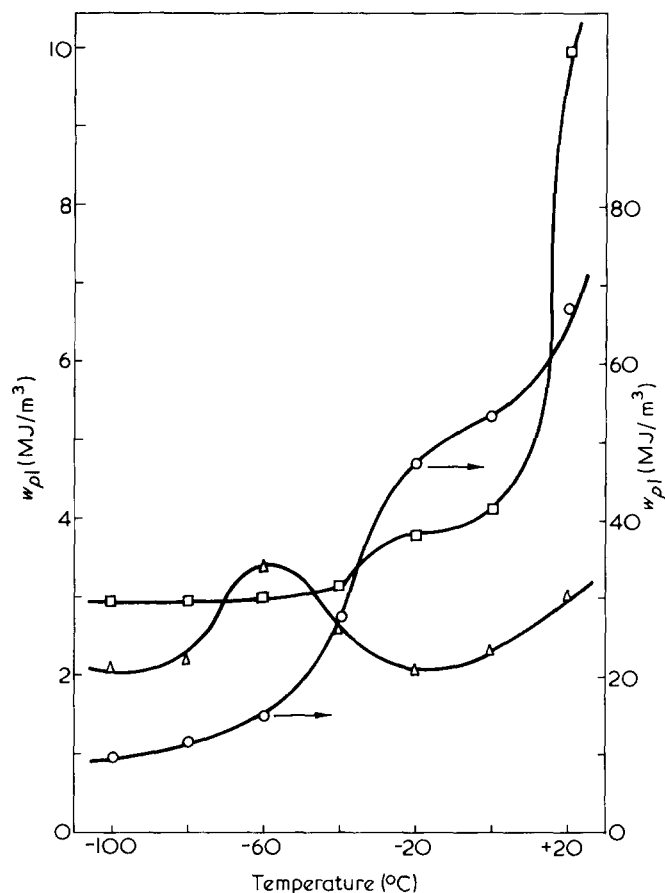


Figure 15 Variation of plane strain yielding energy with temperature. △, PMMA; □, PVC; ○, polycarbonate

is likely to be of importance in an understanding of the fundamental processes involved.

#### ACKNOWLEDGEMENT

The authors wish to thank British Petroleum Chemicals International Ltd for their generous financial support of this work.

#### REFERENCES

- 1 Marshall, G. P., Williams, J. G. and Turner, C. E. *J. Mater. Sci.* 1973, 8, 949
- 2 Brown, H. R. *J. Mater. Sci.* 1973, 8, 941
- 3 Fraser, R. A. W. and Ward, I. M. *J. Mater. Sci.* 1974, 9, 1624
- 4 Plati, E. and Williams, J. G. *Polym. Eng. Sci.* 1975, 15, 470
- 5 Bluhm, J. I. *Proc. ASTM* 1961, 61, 1324
- 6 Parvin, M. and Williams, J. G. *Int. J. Fracture* in press
- 7 Parvin, M. and Williams, J. G. *J. Mater. Sci.* in press
- 8 Vincent, P. I. *Polymer* 1974, 15, 111
- 9 Wolstenholme, W. E., Pregun, S. E. and Stark, C. F. *J. Appl. Polym. Sci.* 1964, 8, 119
- 10 Heijboer, J. J. *Polym. Sci. (C)* 1968, 16, 3755
- 11 Wada, Y. and Kasohara, T. *J. Appl. Polym. Sci.* 1967, 11, 1661
- 12 Turley, S. G. *Appl. Polym. Symp.* 1968, 7, 237
- 13 Johnson, F. A. and Radon, J. C. *Eng. Fracture Mech.* 1972, 4, 552
- 14 Boyer, R. F. *Polym. Eng. Sci.* 1968, 8, 161

# Crazing and the creep behaviour of PMMA in methanol

G. W. Weidmann\* and J. G. Williams

Department of Mechanical Engineering, Imperial College, London SW7 2BX, UK

(Received 9 June 1975; revised 17 July 1975)

A considerable increase in strain was observed when crazes formed during tensile creep tests on poly-(methyl methacrylate) (PMMA) specimens immersed in methanol. A model of craze growth from surface flaws is proposed which is based on craze growth kinetics, and which shows good correlation with the measured time and stress dependent behaviour.

## INTRODUCTION

The phenomenon of crazing is well known and occurs in many glassy thermoplastics. It has been extensively studied since crazes, which although crack-like in appearance are still load-bearing, were first distinguished from cracks<sup>1-3</sup>. Work on the structure of crazes, chiefly by Kambour<sup>4,5</sup> has led to the now generally accepted view that these consist of regions of lower density than the bulk polymer and in which the molecular chains are grouped in aligned bundles separated by voids.

The growth of crazes is dependent both on stress and on environment and many polymers which undergo only slow bulk absorption of organic liquids are very prone to crazing when stressed in the presence of these liquids. This appears to be due to a stress-enhanced preferential absorption of the liquid at the tips of pre-existing surface flaws, leading to local plasticization and subsequent craze growth<sup>6,7</sup>. Studies of the growth of crazes from induced flaws have established growth laws as functions of flaw size and stress level<sup>7,8</sup>. The application of these laws to craze growth in unnotched specimens has enabled estimates to be made of the numbers and sizes of pre-existing flaws<sup>8</sup>.

Although there have been previous investigations into the effect of liquids on the tensile creep behaviour of polymeric materials<sup>9</sup> and, more recently, an explanation proposed for the observed accelerated creep rates in terms of the kinetics of bulk diffusion of the liquid into the specimen<sup>10</sup>, there has been very little reported on the possible role played by crazing in the process. Menges and Schmidt<sup>11</sup> have postulated that a critical strain is required for the onset of crazing which is the same for air as for craze-promoting liquids, the differences in tensile creep behaviour then arising from the different times at which the critical strain was achieved. However, they did not examine the subsequent effect of crazing on the tensile creep strain.

In this work the most intensively investigated polymer-liquid system in craze growth studies, namely PMMA in methanol, is examined under conventional, uniaxial tensile creep test conditions<sup>12</sup>. A comparison with results obtained under similar conditions in air, where no crazing is found, shows that the creep strain in methanol increases much more rapidly with time after crazes are formed and grow. This increasing difference in strain with time between the two environments is considered in terms of craze growth kinetics.

\* Present address: Institut für Festkörpermechanik, 78 Freiburg/Br., Rosastrasse 9, West Germany.

## EXPERIMENTAL

The creep tests were performed on ICI-type uniaxial tensile creep testing machines<sup>12</sup> with specimens 5.5 mm wide and 100 mm parallel section (80 mm gauge length) prepared from 1/8 in. ( $\approx 3$  mm) thick, cast PMMA sheet (ICI Perspex). Strains were determined using modified Lamb's optical extensometers<sup>12</sup> and, for the tests in methanol, the whole specimen-extensometer assembly was immersed in the liquid contained in a glazed tank which was bolted to the machine. In order to calculate the strain from an observed deflection of a light spot on a curved scale, it was necessary to correct for refraction at the methanol-air 'interface' (ignoring refractive effects due to the thickness of glass, which were negligible). The geometry of the situation is illustrated in *Figure 1* and, using the same notation, the true reading for a rotation  $\gamma$  of the light beam would be  $\delta_R$  whilst, due to refraction it appears as  $\delta_A$ . Putting:

$$\theta = \delta_A/R$$

$\gamma$  may be obtained by iteration from

$$R \sin \theta = A \tan \gamma + \frac{\mu \sin \gamma (R \cos \theta - A)}{(1 - \mu^2 \sin^2 \gamma)^{1/2}}$$

and as  $\delta_R = R\gamma$  strains may be calculated from the change in  $\delta_R$  during a test.

Two kinds of specimen surface preparation were used. In some cases the routed edges were left untreated, whilst in others these edges were polished with a very fine emery cloth. Such polishing had a marked effect on creep behaviour, with fewer visible crazes being obtained and smaller strains. Tests were conducted over a range of stress levels for both kinds of surface finish and typical creep curves

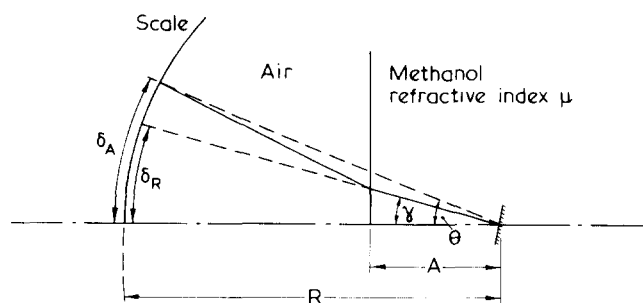


Figure 1 Extensometer scale geometry

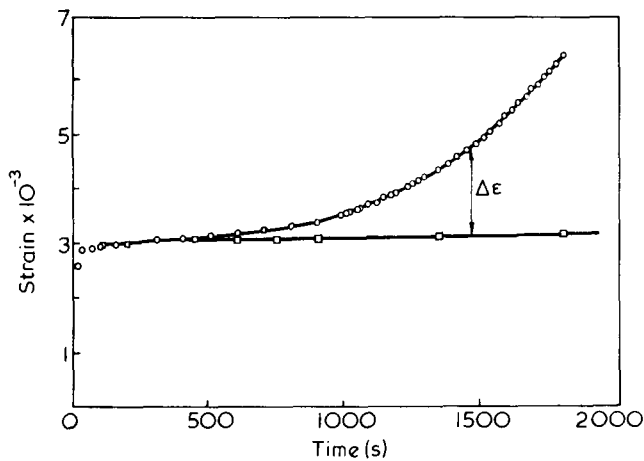


Figure 2 Creep results at  $\sigma = 9 \text{ MN/m}^2$  with 12 observed crazes.  $\square$ , in air;  $\circ$ , in methanol

for methanol and air are shown in Figure 2 at a stress of  $9 \text{ MN/m}^2$ . The difference between the two curves at various times gives the increased strain due to the effect of the methanol,  $\Delta\epsilon$ .

Additional tensile tests were undertaken in order to establish the maximum flaw sizes,  $\hat{a}$ , in the specimens. Three each of the polished and unpolished specimens were strained to failure in air with an Instron testing machine. Taking the stress intensity factor  $K = 2\sigma\hat{a}^{1/2}$  (see later) and the critical  $K$  value as  $1.6 \text{ MN/m}^{3/2}$ <sup>13</sup>, the flaw sizes may be deduced from  $1.6 = 2\sigma_b\hat{a}^{1/2}$  where  $\sigma_b$  is the stress at failure. Both sets of specimens gave an average value of  $\hat{a} = 36 \text{ }\mu\text{m}$ , indicating that the polishing did nothing to remove these large flaws.

This estimate of  $\hat{a}$  does not take into account the possibility of slow growth of the flaw during straining<sup>13</sup>. However, an additional estimate of  $\hat{a}$  can be obtained from the creep test data. Preliminary trials showed that no appreciable effect on the strain and no visible crazes were produced at stresses below about  $5 \text{ MN/m}^2$  and for times less than about 5000 s (at longer times bulk absorption of the methanol became sufficient to accelerate the creep rate). From previous work, the minimum value of  $K$  for initiation of craze growth in methanol is  $K_m = 0.05 \text{ MN/m}^{3/2}$ <sup>7</sup>. Taking this value and using  $\sigma = 5 \text{ MN/m}^2$  gives a value of  $\hat{a} = 25 \text{ }\mu\text{m}$ , assuming that such initiation first takes place at the largest flaws. In view of the possibility of slow growth in the fracture tests and of the observed initiation of both the cracks and the crazes from the machined edges, it is a reasonable supposition that both started at the same large flaws, whose size is approximately  $25 \text{ }\mu\text{m}$ .

Crazes would not grow from the cast surface until the stress had reached  $16 \text{ MN/m}^2$ . Using the same expression for  $K$  and the same value for  $K_m$  as previously with this value of stress implies a maximum flaw size of the cast surface of  $2.5 \text{ }\mu\text{m}$ . However, since there were very large numbers of these crazes, it will be taken that this value represents the mean flaw size for this surface.

### CRAZING CREEP IN POLYMERS

In earlier work<sup>7</sup> it was established that, depending on the value of  $K$ , two different modes of craze growth in the presence of liquids could occur. At stresses corresponding to values of  $K$  below about  $0.25 \text{ MN/m}^{3/2}$  as was the case in the experiments considered in this paper, craze growth is proportional to the square root of time and the craze

length  $x$  after a time  $t$  under load is given by:

$$x^2 = (K^2 - K_m^2)\beta t \quad (1)^*$$

where  $K_m$  is the minimum value of the stress intensity factor  $K$  below which no craze growth occurs, and  $\beta$ , which is a function of the properties of both the polymer and the liquid, is a constant for any polymer-liquid combination. In the case of PMMA-methanol,  $\beta = 2.5 \times 10^{-8} \text{ m}^5 \text{ MN}^{-2} \text{ s}^{-1}$ <sup>6,7</sup>.

If the surface flaws from which the crazes initiate can be considered as semi-elliptical flaws of depth  $a$  and width  $2b$ , as illustrated in Figure 3, with  $b \gg a$ , then:

$$K^2 = 4\sigma^2 a \quad (2)$$

From equations (1) and (2):

$$a = \frac{1}{4\sigma^2} \left\{ \frac{x^2}{\beta t} + K_m^2 \right\} \quad (3)$$

As a mechanism for the contribution,  $\Delta\epsilon$ , of the crazes to the creep strain it is postulated that, first, an initial craze nucleated from a surface flaw adds an increment  $u_0$  to the deflection of the specimen when it has grown a distance  $x_0$  and secondly, that the subsequent extension of the craze in the direction of the tensile stress can be modelled by the parallel growth of additional, unit crazes from the original flaw each adding a unit increment  $u_0$  to the deflection. Thus, after  $n$  crazes per unit length of the specimen have grown to a length of  $x_0$  or greater, the additional strain in the specimen is:

$$\Delta\epsilon = u_0 n \quad (4)$$

Although the first postulate might appear somewhat arbitrary it tends to be supported by the observed initiation of crazes during the creep tests at much earlier times than those at which differences in strain between the tests in methanol and those in air could be detected. The divergence between the two creep curves (Figure 2) only took place after the crazes had grown to, typically, a length of the order of 1 mm.

The distribution of sizes of the flaws on the surface of a specimen may be expressed by a cumulative exponential distribution of the form<sup>14</sup>:

$$N = N_0 \exp - (a/\bar{a}) \quad (5)$$

where  $N_0$  is the total number of flaws per unit area,  $\bar{a}$  is

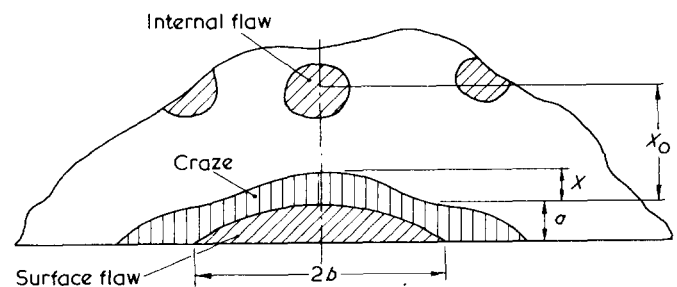


Figure 3 Craze growth from a surface flaw

\* This is a slightly modified form to that given earlier<sup>7</sup>.

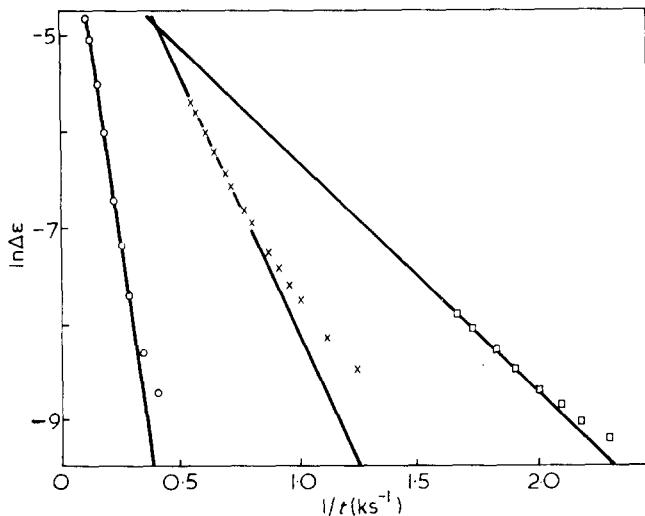


Figure 4  $\ln \Delta \epsilon$  as a function of  $1/t$  at three stress levels: ○, 5.5; ×, 9.0; □, 12.0 MN/m<sup>2</sup>

the modal flaw size, and  $N$  is the number of flaws whose depth is  $a$  or greater.

If  $n$  is proportional to  $N$  then the additional strain  $\Delta \epsilon$  after  $n$  crazes have grown to a length of  $x_0$  or greater, from equations (3)–(5) is given by:

$$\ln \Delta \epsilon = \ln \Delta \epsilon_0 - \frac{K_m^2}{\bar{K}^2} - \frac{x_0^2}{\bar{K}^2 \beta t} \quad (6)$$

where  $\bar{K}^2 = 4\sigma^2 \bar{a}$ .

Equation (6) predicts a linear relationship between  $\ln \Delta \epsilon$  and  $t^{-1}$  for a given pair of creep tests on PMMA in methanol and air at a constant stress  $\sigma$ , and that the slopes of the lines from different sets of creep tests should show a stress dependence of the form:

$$\frac{d(\ln \Delta \epsilon)}{d(1/t)} = - \frac{x_0^2}{4\beta \bar{a}} \cdot \frac{1}{\sigma^2} \quad (7)$$

The intercept,  $\ln \Delta \epsilon_i$ , of a  $\ln \Delta \epsilon$  versus  $t^{-1}$  plot, when  $t \rightarrow \infty$ , should be given by:

$$\ln \Delta \epsilon_i = \ln \Delta \epsilon_0 - \frac{K_m^2}{\bar{K}^2} \quad (8)$$

where  $\Delta \epsilon_0 = u_0 n_0$ , the limiting strain when all the crazes are longer than  $x_0$ , and  $n_0$  is proportional to  $N_0$ .

## RESULTS

Polished and unpolished specimens were tested in both air and in methanol at stress levels ranging from 5.5 to 12 MN/m<sup>2</sup>. The results of each pair of tests at a given stress level were plotted in the form of  $\ln \Delta \epsilon$  versus  $t^{-1}$ . Three typical sets of such data are shown in Figure 4, for which it can be seen that linear relationships are obtained for significant ranges of the points. The divergence from linearity which is apparent at short times represents an approximately constant deflection per observed craze of about 1 μm independent of stress level. This might reflect the short term response of the largest flaws immediately after stressing in methanol, since it seems unlikely that any systematic error could have produced an effect of this sort.

Figure 5 shows the slopes of the linear regions of the  $\ln \Delta \epsilon$  versus  $t^{-1}$  plots as a function of  $\sigma^{-2}$ . The relationship is linear as required by equation (7). However, unlike the theoretical prediction, the line in Figure 5 does not pass through the origin. The accelerated craze growth found at higher stresses in previous work<sup>5</sup> would provide an explanation of this since such behaviour would tend to displace the experimental points upwards at the lower values of  $\sigma^{-2}$ .

From the slope of the line in Figure 5 ( $-6.1 \times 10^5$  MN s m<sup>-4</sup>) and equation (7),  $x_0$  may be calculated. There is, however, an uncertainty in the value of  $\bar{a}$ , the mean flaw size of the machined surface. Upper and lower limits to its value can be provided by the maximum flaw size deduced from the fracture tests, 25 μm, and the estimated mean flaw size on the cast surface, 2.5 μm. This gives  $0.4 \text{ mm} < x_0 < 1.2 \text{ mm}$  which is in agreement with the observed extent of craze growth prior to a detectable contribution to the strain from the crazes.

In order to compare the intercept results from the different tests it is necessary to take into account the effect of different flaw size distributions on the specimens (or, more precisely, different values of  $N_0$ , the total number of flaws). However,  $N_0$  was not known. If instead the number of observed crazes  $N'$  is taken as an indicator of  $N_0$  then, as can be seen from Table 1 which summarizes the experimental results, if there is any systematic variation of the intercept values with stress then it is in the opposite sense to that required by equation (8). This could be explained if the relationship between  $n_0$  and  $N_0$  was a stress-dependent one rather than the simple proportionality assumed earlier.

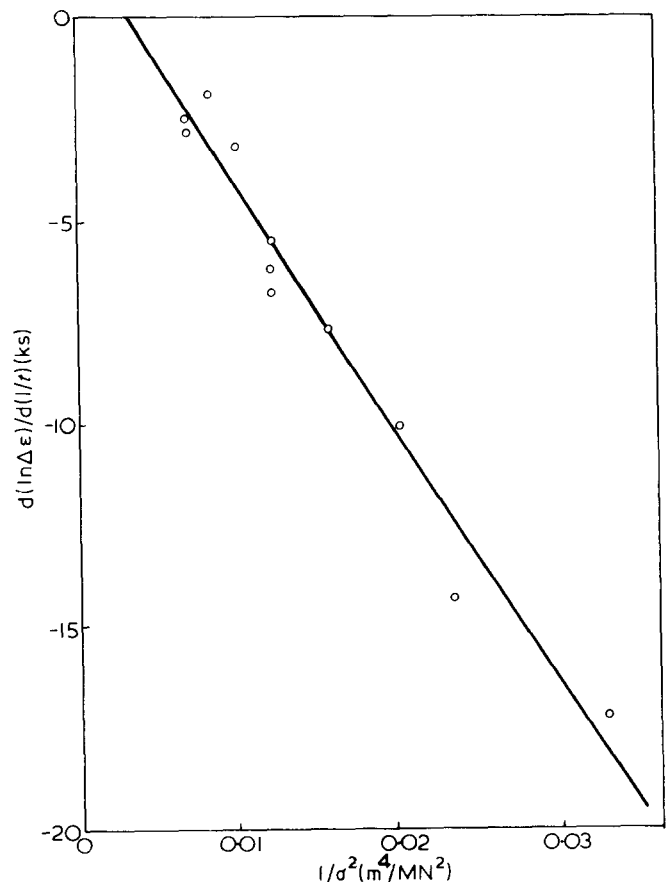


Figure 5 Slopes of  $\ln \Delta \epsilon$  versus  $1/t$  as a function of  $1/\sigma^2$



Table 1

$\sigma$ (MN/m <sup>2</sup> )	$N'$	$\frac{d \ln \Delta \epsilon}{d(t^{-1})}$ (ks)	$\ln \Delta \epsilon_j$	$\ln \frac{\Delta \epsilon_j}{N'}$
5.5 P	4	-17.11	-2.90	-4.29
6.5 P	3	-14.34	-3.22	-4.32
7	29	-10.04	-1.60	-4.97
8 P	2	-7.63	-4.23	-4.93
9 P	4	-6.63	-3.51	-4.90
9	12	-5.46	-2.70	-5.19
9	29	-6.09	-1.90	-5.27
10	103	-3.08	-1.61	-6.25
11	38	-1.81	-2.80	-6.44
12 P	4	-2.41	-3.90	-5.29
12 P	7	-2.77	-3.88	-5.82

P = Polished edges

### CONCLUSIONS

The postulated model of craze thickening through the growth of a number of additional unit crazes from the original flaws, each contributing an increment to the thickness, and the theoretical expressions based on this model, are successful in their ability to describe not only the rate with which the increased strain due to crazing varies with time, but also the rate with which it varies with stress. The correlation of the model with the magnitudes of the observed strains, and their dependence on stress, is not so successful, requiring as it does a more detailed knowledge of the total numbers of flaws on the specimen surfaces.

The initiation data both from craze growth and fracture tests provide reasonable evidence for a maximum flaw size of 25  $\mu\text{m}$ . The mean flaw size has not been so well established, but the values of the parameter  $x_0$  based on upper and lower estimates of the mean flaw size are consistent with the observed extent of craze growth prior to a detect-

able increase in craze strain. The parameter  $x_0$  might then be taken to represent the average spacing between a surface flaw and an internal flaw sufficiently severe to activate an increase of strain in a craze.

### ACKNOWLEDGEMENTS

The authors wish to thank Mr L. H. Coutts and Mr K. H. Jones for their assistance with the experimental work and the Science Research Council for their financial support.

### REFERENCES

- 1 Sauer, J. A., Marin, J. and Hsiao, C. C. *J. Appl. Phys.* 1949, **20**, 507
- 2 Lebedev, G. A. and Kuvshinskii, E. V. *Soviet Phys. Solid St.* 1962, **3**, 1947
- 3 Spurr, O. K. and Niegisch, W. D. *J. Appl. Polym. Sci.* 1962, **6**, 585
- 4 Kambour, R. P. *Polymer* 1964, **5**, 143
- 5 LeGrand, D. G., Kambour, R. P. and Haaef, W. R. *J. Polym. Sci. (A-2)* 1972, **10**, 1565
- 6 Marshall, G. P., Culver, L. E. and Williams, J. G. *Proc. R. Soc. (A)* 1970, **319**, 165
- 7 Marshall, G. P. and Williams, J. G. in 'Deformation and Fracture of High Polymers', (Eds H. H. Kausch, J. A. Hassell and R. I. Jaffee), Plenum Press, New York, 1974, p 557
- 8 Marshall, G. P., Graham, I. D., Zichy, E. L. and Williams, J. G. *Pure Appl. Chem.* 1974, **39**, (1-2), 275
- 9 Bergen, R. L. *SPE J.* 1968, **24**, 77
- 10 McCammond, D. and Ward, C. A. *Polym. Eng Sci.* 1974, **14**, 831
- 11 Menges, G. and Schmidt, H. *Plastics and Polymers* 1970, **38**, 13
- 12 Thomas, D. A. and Turner, S. in 'Testing of Polymers', (Ed. W. E. Brown), Wiley, New York, Vol 4, 1969, p 73
- 13 Marshall, G. P. and Williams, J. G. *J. Mater. Sci.* 1973, **8**, 138
- 14 Freudenthal, A. M. in 'Fracture, An Advanced Treatise', (Ed. H. Liebowitz), Academic Press, London and New York, Vol 2, 1968

# Influence of high injection pressures on the internal stress level in injection moulded specimens

Josef Kubát and Mikael Rigdahl

Division of Polymeric Materials, Chalmers University of Technology, S-402 20 Gothenburg, Sweden  
(Received 17 March 1975; revised 7 July 1975)

Internal stresses in high and low density polyethylene specimens, injection moulded at pressures ranging from 100 MPa to 450 MPa have been measured by a stress relaxation method. The internal stress parameter ( $\sigma_i$ ), which is an average value of the internal stress distribution in the samples, changes from a negative value (compressive stresses) at normal injection pressures to a small positive value (frozen-in tensile stresses) at the highest pressures used. The yield stress increases in approximately the same way with the pressure, while the mould shrinkage in the flow direction decreases. It is suggested that the decrease in the absolute value of the internal stress parameter originates from an increase of the melting temperature with pressure, resulting in a more homogeneous solidification.

## INTRODUCTION

The magnitude and distribution of internal stresses in injection moulded plastics objects is the result of a complicated interplay of a large number of factors, among which the injection pressure seems to occupy an important place.

The influence of the injection pressure on internal stresses in injection moulded samples does not seem to have attracted much interest. On the whole, the variation of the pressure within the range normally used appears to have little effect on the properties of the mouldings, such as yield strength, shrinkage etc.<sup>1</sup>, although some properties, e.g. impact strength, exhibit a somewhat more pronounced dependence on the pressure<sup>1</sup>. In addition there is the well known difficulty of separating the effect of internal stresses and anisotropy. Normally, the properties of the moulding will be determined by a combination of both. In order to measure the influence of the injection pressure Kantz<sup>1</sup> determined the volume proportion of oriented material as dependent on the pressure. Jensen and Whisson<sup>2</sup> determined the degree of orientation and presented the results in terms of a so-called orientation stress. Measured in the flow direction, this quantity decreased only to a minor extent as the pressure was raised. The materials studied were polystyrene, polypropylene, polysulphone and ABS. Similar results were reported by Fett<sup>3</sup> using a hardness method for measuring the combined action of internal stresses and anisotropy. The injection pressures used in these investigations were, however, only moderate.

When the polymer melt solidifies in the mould, internal stresses are frozen-in as a consequence of differences in the solidification rate between the surface parts and the interior of the object. This results normally in compressive stresses at the surface and tensile stresses in the interior. Such effects are well known; they have been analysed both experimentally<sup>3-6</sup> and theoretically<sup>6,7</sup>.

This paper gives an account of an experimental study of the influence of injection pressure on the overall internal stress level ( $\sigma_i$ ) in LDPE and HDPE samples having the shape of small tensile test specimens.

The range of injection pressures extended to 450 MPa, i.e. far above the normally used interval ending at 150–

200 MPa. Increasing the pressure brought about a decrease in the overall  $\sigma_i$  level for both LDPE and HDPE. The yield stress and the mould shrinkage of the samples were also measured. As expected, an increase in the absolute value of  $\sigma_i$  produced larger shrinkage. Also the yield stress showed a tendency to increase with  $\sigma_i$ . The method used to measure the  $\sigma_i$  values was the stress relaxation method described earlier<sup>8,9</sup>.

## EXPERIMENTAL

### Injection moulding

The injection moulding of the samples at varying injection pressures was performed using a modified machine of conventional type (Engel 500/250 AS). This machine was equipped with a special screw (Figure 1). The main feature of this screw was a plunger (diameter 30 mm) at its end, the molten polymer flowing through a central bore in the plunger. Back flow of the melt during injection into the mould was prevented by a non-return valve. In this way injection pressures varying between 100 MPa and 450 MPa could be attained. The holding pressure was identical to the injection pressure. The dimensions of the injection moulded samples are shown in Figure 2.

### Materials used and processing conditions

The experiments were carried out with LDPE and HDPE samples. The characteristics of these materials were as follows: LDPE (BASF, Lupolen 1800 M), density 0.916–

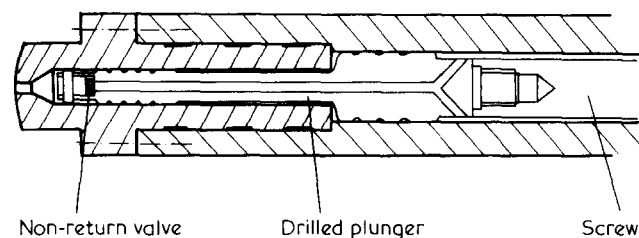


Figure 1 Cylinder and the screw of the modified injection moulding machine

Table 1 Moulding conditions

	HDPE	LDPE
Melt temperature (°C)	200–240	180–200
Mould temperature (°C)	30	30
Injection time (s)	1	1
Holding time (s)	15	14
Cooling time (s)	35	30

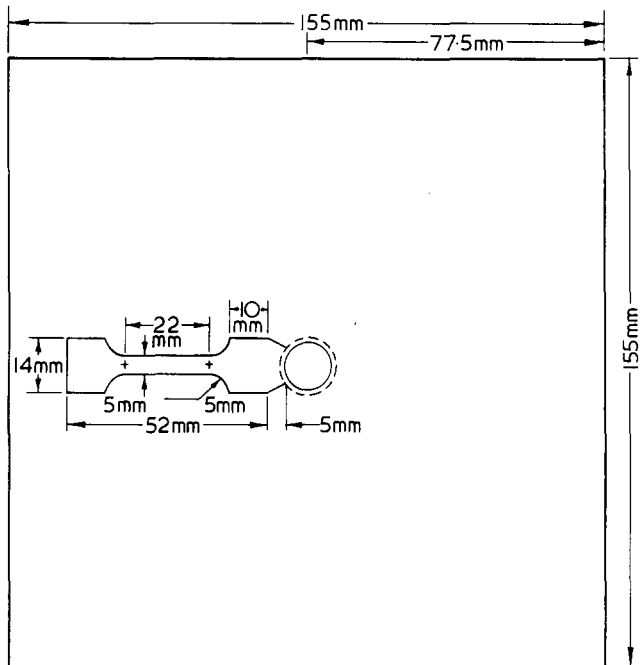


Figure 2 Dimensions of the mould. The thickness of the tensile test specimen is 1.5 mm. + denotes mark from the hardness tester

0.918 g/cm<sup>3</sup>, melt index 6–8 g/10 min (MFI 190/2 I6); HDPE (Hoechst, Hostalen GC 7260), density 0.960 g/cm<sup>3</sup>, melt index 7 g/10 min (MFI as above). The moulding conditions are given in Table 1.

**Measurement of stress relaxation and stress-strain behaviour. Mould shrinkage**

The stress relaxation measurements were performed in the usual way by deforming the sample, keeping the deformation constant and measuring the stress decay. The tensile testing machine used was of a conventional type (L & W Alwetron, TCS 250). The deformation rate was  $\dot{\epsilon} = 10^{-2} \text{ s}^{-1}$ . Every sample was used for a single experiment only.

The measured relaxation curves recorded were transformed into stress-log (time) diagrams and the maximum (inflection) slope of the rectilinear portion of the curves obtained, i.e.

$$F = \left( - \frac{d\sigma}{d \log t} \right)_{\max}$$

was plotted against the initial stress  $\sigma_0$  of the relaxation experiment. The plots were then used for determining the internal stress level  $\sigma_i$  from  $\sigma_0 = \sigma_i$  at  $F = 0$ .

Besides the relaxation measurements, the stress-strain curves of the samples were also recorded. In this case, the deformation rate was  $\dot{\epsilon} = 1.6 \times 10^{-2} \text{ s}^{-1}$ .

The mould shrinkage was determined by measuring with a microscope the distance between two fiducial marks made

in the mould by a Rockwell hardness tester, and the change of this distance when measuring the replicas of these marks on the moulding.

The stress-strain and relaxation experiments were carried out at  $22 \pm 0.5^\circ\text{C}$ .

**RESULTS**

*Internal stresses*

As already mentioned the internal stress data were obtained from an analysis of stress relaxation curves of the various samples. An illustration of the effect of injection pressure on the relaxation kinetics is shown in Figure 3. The two curves, typical of the behaviour under study, relate to HDPE moulded at a pressure of 100 and 400 MPa; the magnitude of their initial stresses was about the same. As can be seen, the relaxation rate is greater for the sample moulded at the higher pressure.

The internal stress analysis using data from a series of relaxation curves measured at varying initial stress  $\sigma_0$  has been carried out in Figure 4 for HDPE samples moulded at

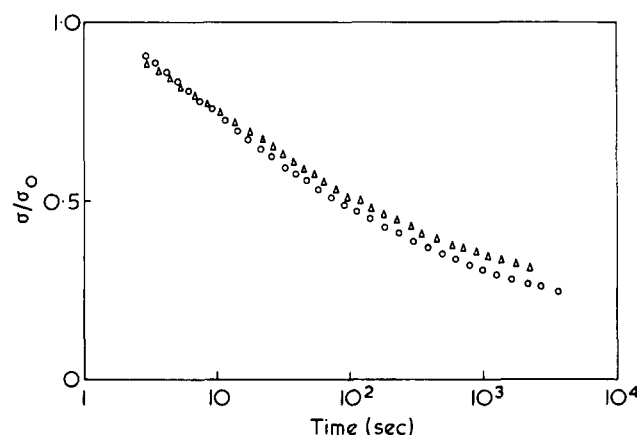


Figure 3 Stress relaxation curves for HDPE, injection moulded at 100 (Δ) and 400 MPa (○). The initial stresses ( $\sigma_0$ ) were 9.7 MPa and 9.9 MPa, respectively

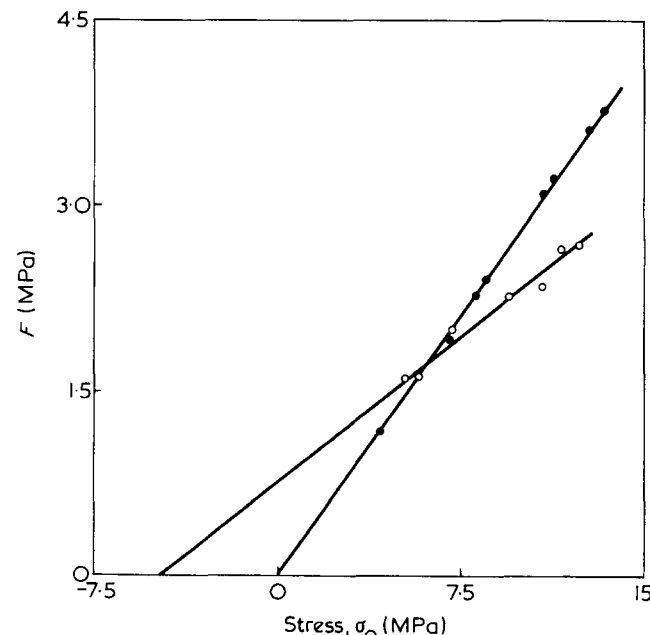


Figure 4 Determination of the internal stress parameter in HDPE using  $F(\sigma_0)$  plots. ○, 100; ●, 400 MPa

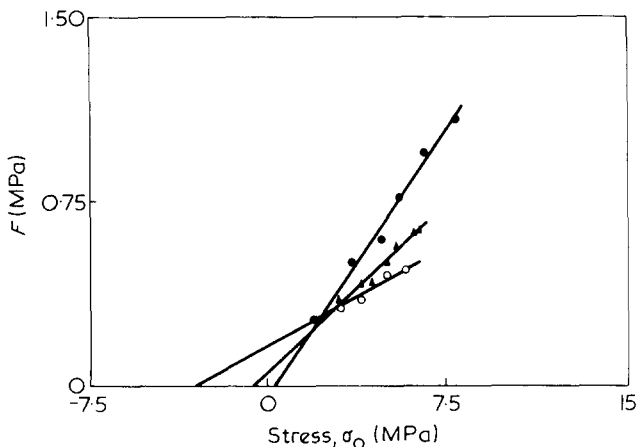


Figure 5 Determination of the internal stress parameter in LDPE using  $F(\sigma_0)$  plots.  $\circ$ , 100;  $\blacktriangle$ , 200;  $\bullet$ , 400 MPa

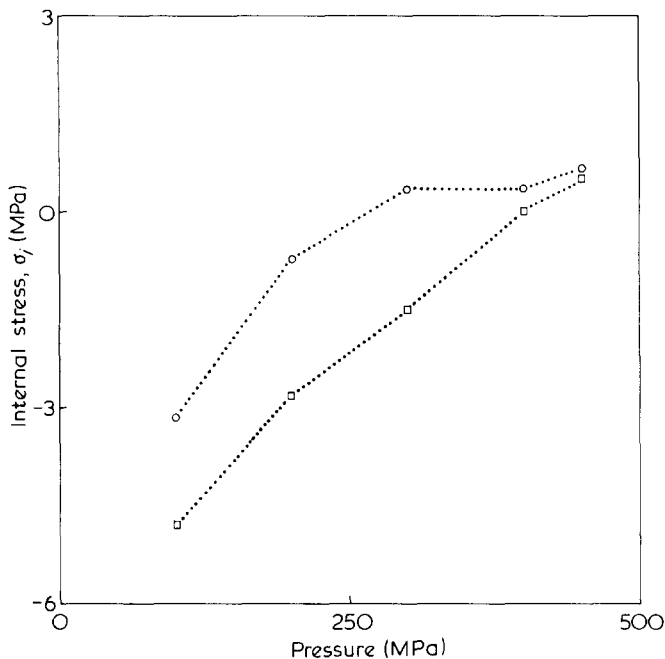


Figure 6 Internal stress parameter as a function of pressure for HDPE ( $\square$ ) and LDPE ( $\circ$ )

100 and 400 MPa. The value of the intercept between the maximum slope  $F$  of the  $\sigma(\log t)$  curves when plotted against the initial stress  $\sigma_0$ , and the axis  $F = 0$  is, as pointed out above, a measure of the internal stress level,  $\sigma_i$ . It can be seen from Figure 4 that the absolute value of  $\sigma_i$  decreases markedly by increasing the injection pressure from 100 to 400 MPa. At the same time, the slope of the  $F(\sigma_0)$  line increases. LDPE samples behave similarly (Figure 5).

The relationship between the internal stress parameter  $\sigma_i$  and the injection pressure is shown in Figure 6 for the two kinds of PE. The  $\sigma_i$  value changes from comparatively large negative values to rather small positive ones. For HDPE, the  $\sigma_i$  value at 100 MPa is larger (negative) than that for LDPE. It should be noted that by a suitable choice of the injection pressure the  $\sigma_i$  value can be reduced to zero.

#### The yield value

The yield value and its variation with the injection pressure or  $\sigma_i$  is another interesting aspect of the experiments reported here. For HDPE, the yield value can be defined without difficulty by relating the maximum stress to the

initial cross-section area of the sample. Such a simple definition cannot, on the other hand, be applied to a material such as LDPE, which does not exhibit a pronounced yielding behaviour. In such a case, one can rely on for instance the ASTM method D 638, according to which the yield point is defined as the stress at which the initial ('elastic') part of the stress-strain curves starts to depart from a straight line, again related to the initial cross-section.

Figure 7 shows the internal stress  $\sigma_i$  plotted against the yield stress value. It can be clearly seen that these two quantities are interrelated. At least for not too high injection pressures, the yield stress increases with the  $\sigma_i$  value.

#### Mould shrinkage

The extent of shrinkage was determined by measuring the distance between two marks along the flow direction in the mould and the corresponding distance between the replicas of these marks left on the moulded samples. The shrinkage value  $\epsilon_s$  was calculated from:

$$-\epsilon_s = \frac{a_s - a_m}{a_m}$$

where  $a_m$  and  $a_s$  denote the distance between the points in the mould and on the sample, respectively.

Figure 8 shows the relationship between internal stress and the mould shrinkage. It follows from this diagram that the lower the absolute value of  $\sigma_i$ , the lower is also the shrinkage. On the other hand, a simple proportionality does not seem to exist.

#### DISCUSSION

When discussing the results obtained, one should keep in mind the complexity of the various factors influencing the residual stress distribution in an injection moulded specimen. In the first place, such stresses are not homogeneous. Normally, their distribution forms a pattern, the characteristics of which depend on processing and material parameters<sup>4,8</sup>. For specimens of the type used here, one usually finds relatively high compressive internal stresses in the surface layers and weak tensile stresses in the interior<sup>7</sup>.

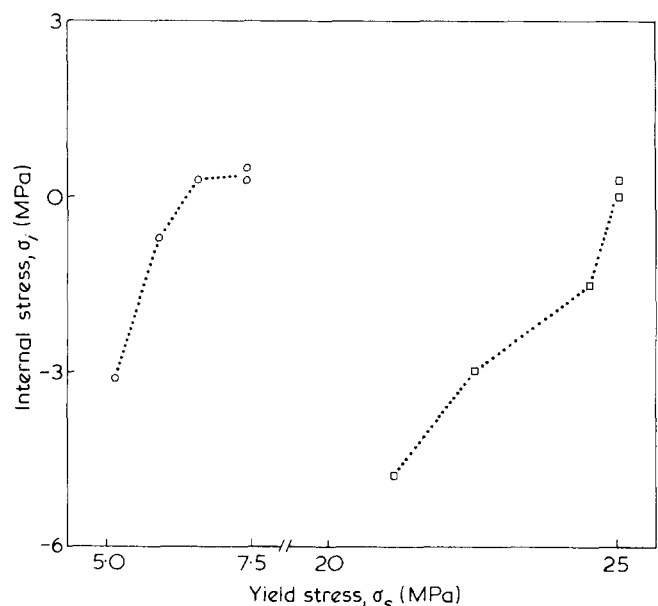


Figure 7 Internal stress parameter vs. yield stress for HDPE ( $\square$ ) and LDPE ( $\circ$ )

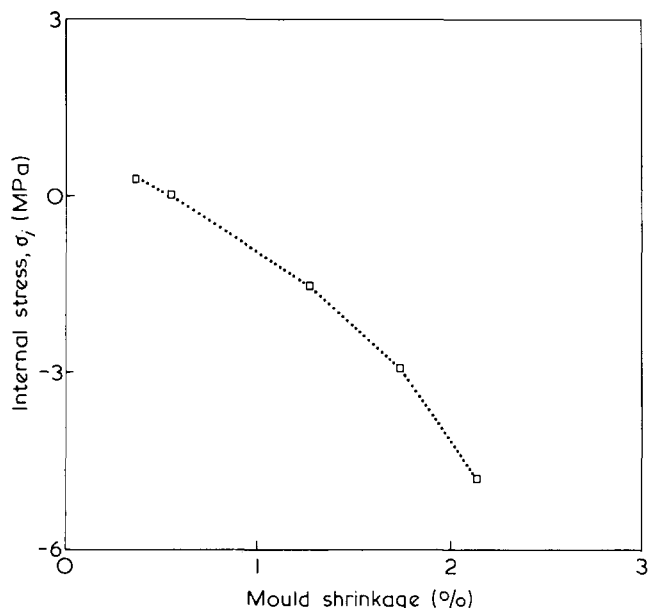


Figure 8 Correlation between internal stress parameter and mould shrinkage for HDPE

The  $\sigma_i$  values presented above are thus to be considered as averages over the various layers having different internal stress levels and also different relaxation behaviour due to the variation of anisotropy over the cross-section<sup>1,10</sup>. As the average  $\sigma_i$  level is evaluated from certain parameters of stress relaxation curves, it is to be assumed that also these parameters in their turn are averages. The course of the stress relaxation is thus the result of a superposition of relaxation processes in the different layers of the specimen having different  $\sigma_i$  values and different relaxation behaviour<sup>10</sup>.

Despite the complications mentioned, the analysis of the relaxation curves and the overall  $\sigma_i$  values obtained from them, point at some interesting results when the general influence of the injection pressure on the properties of the specimen is considered. The first result to be noted is that the residual compressive stress obtained in normal injection moulding practice is reduced by increasing the pressure. At the highest pressures used this compressive stress is reversed into a weak tensile one. It thus appears possible to reduce the average  $\sigma_i$  value to zero by an appropriate rise in the injection pressure (Figures 4 and 5).

The mechanism behind the appearance of an internal stress distribution in an injection moulded specimen has been discussed previously<sup>6,7</sup>. Here, it may suffice to say, that these stresses are due to a temperature gradient during cooling. The outer layers solidify in the initial stage of the cooling process. Owing to differences in specific volume between melt and solid, compressive stresses are frozen into the solidified surface layers when the interior of the specimen becomes solid. For balance reasons, weak tensile stresses prevail in the interior. With regard to the effect of pressure on this process the following may be said. It is known that the melting point of a polymer is relatively sensitive to pressure, an increase of about 20°C/100 MPa having been found for polyethylene<sup>11,12</sup>. Increasing the pressure on the melt in the mould is thus equivalent to an overall increase of the melting point of the polymer. In principle, when the mould has been filled and the peak pressure reached, the whole cavity content can be brought to solidify simultaneously. In normal moulding, the solidification (crystallization) takes place when the temperature in different parts of the mould passes a critical value ( $T_m$ ). The important thing

to note is that this critical temperature is reached in different parts of the specimen at different times. Contrary to this, when using high pressures the crystallization can take place simultaneously in the whole of the specimen. It is thus possible to ascribe to the injection pressure the role of a crystallization regulator, a role not taken advantage of hitherto in the production of stress-free mouldings.

Looking at Figure 6 one may see that the injection pressure corresponding to zero level of  $\sigma_i$  is approximately the pressure by which the melting points of HDPE and LDPE are raised to a temperature<sup>11,12</sup> equal to that of the melt leaving the cylinder.

Another effect which probably contributes to the reduction of the  $\sigma_i$  level on increasing the pressure is a decrease in the thermal shrinkage occurring in the vicinity of  $T_m$ <sup>7,11</sup>.

As could be expected, the average  $\sigma_i$  value correlates well with mould shrinkage. Again, it should be kept in mind that we deal with averages which preclude an exact analysis of these findings. The same is true of the relationship between  $\sigma_i$  and the yield stress. Nevertheless, the results have a clear technical significance, as the samples used have been prepared according to normal practice. For a closer study of the phenomena involved it is, however, necessary to resolve the different components contributing to the average  $\sigma_i$  level and also to compare such results with experiments performed on samples containing a homogeneous internal stress. In a forthcoming paper we will report on a simple mathematical model relating to a distribution of internal stresses in specimens of simple shape with a varying degree of anisotropy over their cross-section<sup>10</sup>. It will be shown that this model will handle the effects of an internal stress distribution on the parameters of stress relaxation curves, which are used in determining the  $\sigma_i$  values. In the first place this applies to the variation of the  $F(\sigma_0)$  relationship and to the value of the  $F(\sigma_0)$  intercept with the  $\sigma_0$  axis (i.e. the  $\sigma_i$  value). For instance, it will be shown that the results of the present paper can be simply handled by assuming a 3-layer model with compressive and tensile internal stresses.

The influence of injection pressure on the  $\sigma_i$  level has been illustrated here using LDPE and HDPE as examples. For other crystalline polymers the melting temperature is shifted in a similar way, e.g. for polypropylene  $T_m$  increases from about 175°C at atmospheric pressure to about 245°C at a pressure of 220 MPa<sup>13</sup> and for polyamide-6 and polyoxymethylene a change in melting temperature of 38° and 44° C per 100 MPa, respectively, in the pressure range 0–200 MPa has been reported<sup>14,15</sup>. The role played by the increase in the melting temperature with pressure is, on the other hand, not restricted to crystalline polymers. It is known, that the corresponding critical temperature for amorphous polymers, i.e. the glass transition temperature, also rises when the pressure is increased, e.g. for polystyrene, PVC and PMMA a shift of  $T_g$  of 32°, 16° and 29° C per 100 MPa, respectively, has been determined<sup>16</sup>. As this increase per 100 MPa is of the same order of magnitude as that in  $T_m$  for crystalline polymers, the effect of increasing injection pressure in reducing the overall internal stress level appears to be a rather general one.

As the main purpose of this paper was a first demonstration of a possible practical significance of increasing the injection pressure, we have not analysed a number of factors which may influence the results. For instance, the concept of melting and crystallization, and their dependence on super-cooling has been treated in qualitative terms only. With regard to the distinction between true internal stresses and anisotropy, the relaxation method used for the mea-

surements of the overall  $\sigma_i$  level does not clearly distinguish between the two contributions. On the other hand, the method is known to produce data consistent with normal practical experience<sup>8,10</sup>. It may also be pointed out that, in the present experiments, the injection rate was kept constant, independent of the final pressure attained. For this reason, the contribution of the anisotropy should be about the same at the different pressure levels.

Rather naturally, a number of problems remain to be solved. Of particular interest would be measurement of the  $\sigma_i$  level in different directions of the sample as well as careful following of the pressure and temperature variation in the mould. It is intended to describe such studies in a forthcoming publication.

It may be pointed out that the present work is a part of an investigation of the properties of specimens injection moulded at high pressures. The experiments cover a pressure range up to 500 MPa under conditions of normal injection moulding practice. The results of this investigation will be published elsewhere.

#### ACKNOWLEDGEMENTS

The authors would like to thank Mrs Ulla Johansson and Mr Krister Djurner for skilful experimental assistance.

Thanks are also due to Engel KG, Schwertberg, Austria, for providing the special screw and cylinder for the injection moulding machine. The project was supported financially by the Swedish Board for Technical Development and AB Volvo.

#### REFERENCES

- 1 Kantz, M. R. *Int. J. Polym. Mat.* 1974, **3**, 245
- 2 Jensen, M. and Whisson, R. R. *Polymer* 1973, **14**, 193
- 3 Fett, T. *Plastverarbeiter* 1973, **24**, 665
- 4 Menges, G. and Wübken, G. 'IKV Kunststofftechnisches Kolloquium', 1972, p 21
- 5 Alpsten, G. 'Residual stresses in hot-rolled steel shapes', *Diss. R. Inst. Technol., Stockholm* 1967
- 6 Knappe, W. *Kunststoffe* 1961, **51**, 562
- 7 Rigdahl, M. *Int. J. Polym. Mat.* 1975, in press
- 8 Kubát, J. and Rigdahl, M. *Int. J. Polym. Mat.* 1975, **3**, 287
- 9 Kubát, J., Petermann, J. and Rigdahl, M. *Mat. Sci. Eng.* 1975, **19**, 185
- 10 Kubát, J. and Rigdahl, M. *Mat. Sci. Eng.* 1975, in press
- 11 Matsouka, S. *J. Polym. Sci.* 1962, **57**, 581
- 12 Osugi, J. and Hara, K. *Rev. Phys. Chem. Japan* 1966, **36**, 28
- 13 Baer, E. and Kardos, J. L. *J. Polym. Sci. (A)* 1965, **3**, 2827
- 14 Katayama, Y. and Yoneda, K. *Rev. Elect. Commun. Laboratories* 1972, **20**, 921
- 15 Starkweather, H. K. *J. Phys. Chem.* 1960, **64**, 410
- 16 Billingham, P. R. and Tabor, D. *Polymer* 1971, **12**, 101

## Crystallization of isotactic poly(methyl methacrylate) from the melt

A. de Boer, G. O. R. Alberda van Ekenstein and G. Challa

*Department of Polymer Chemistry, State University of Groningen, Groningen, The Netherlands*

*(Received 19 May 1975; revised 20 June 1975)*

### INTRODUCTION

In 1958 Fox *et al.*<sup>1</sup> reported the possibility of crystallizing isotactic poly(methyl methacrylate) (i-PMMA). Stroupe and Hughes<sup>2</sup> determined the unit cell of crystalline i-PMMA: a pseudo orthorhombic cell with the lattice distances  $a = 21.08$ ,  $b = 12.17$  and  $c = 10.55$  Å. Coiro *et al.*<sup>3</sup> concluded from X-ray fibre diagrams that i-PMMA crystallizes in a ( $5_1$ ) helix conformation. Tadokoro *et al.*<sup>4</sup> refined this picture by X-ray diffraction and far infra-red measurements and suggested that the ester side groups of i-PMMA in the ( $5_1$ ) helix conformation are rotated somewhat inwards. Also Tanaka *et al.*<sup>5</sup> and Klement and Geil<sup>6</sup> investigated crystalline i-PMMA. In all cases the crystalline i-PMMA was obtained by means of borderline solvents or by annealing stretched thin films. In this note we present some results on the growth rate, shape and melting temperature of crystals of i-PMMA crystallized from the melt.

### EXPERIMENTAL

The sample of i-PMMA was prepared according to a known procedure<sup>7</sup>. Some data of the polymer (sample no. 109) are: isotactic/heterotactic/syndiotactic triads 94:5:1,  $\bar{M}_v = 213 \times 10^3$ ,  $T_g = 40^\circ\text{C}$ . The tacticity was measured on 5 wt% *o*-dichlorobenzene solutions at  $150^\circ\text{C}$  by 60 MHz n.m.r. spectroscopy with a Varian A 60 instrument.  $[\eta]$  was measured in chloroform at  $25^\circ\text{C}$ . For the calculation of  $\bar{M}_v$ , the relation<sup>8</sup>  $[\eta] = 4.8 \times 10^{-5} \bar{M}_v^{0.8}$  was used. The glass transition temperature was measured with a differential scanning calorimeter (Perkin-Elmer DSC IB) at a heating rate of  $8^\circ\text{C}/\text{min}$ .

Films with a thickness of about  $10 \mu\text{m}$  were obtained by evaporation of a 3 wt % chloroform solution of i-PMMA on a glass slide. To remove all solvent, the films were dried afterwards at  $50^\circ\text{C}$  *in vacuo* for 30 min. For crystallization temperatures ( $T_c$ ) below  $110^\circ\text{C}$  the films were first heated at  $180^\circ\text{C}$  for 5 min and then cooled down to  $T_c$ . This was done because otherwise there exist too many nuclei for detecting separate crystals. Temperature control of the crystallization oven was within  $0.2^\circ\text{C}$ . A Zeiss polarization microscope with phase-contrast condenser and objective was used for light microscopic measurements on crystals grown in the films.

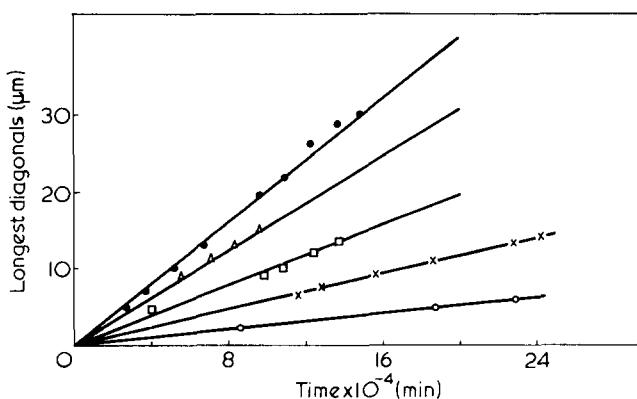
Because of the very low growth rate ( $G$ ) of i-PMMA crystals phase-contrast photographs were taken over several

days. After enlarging the photographs it was possible to measure the diagonal of the crystals with an accuracy of about  $0.6 \mu\text{m}$ . The magnifications were calibrated with a micrometer. Melting temperatures,  $T_m$ , were determined both with d.s.c. and a hot-stage light microscope. We used a hot stage plate (Mettler FP 5) with a heating rate of  $0.2^\circ\text{C}/\text{min}$ .

### RESULTS AND DISCUSSION

In *Figure 1* the average values of the longest diagonals of the crystals are plotted against the crystallization time for various  $T_c$ . From these lines the average growth rates  $G$  were calculated and plotted against crystallization temperature in *Figure 2*. This Figure shows that i-PMMA has a maximum value  $G_{\text{max}}$  of about  $1 \times 10^{-3} \mu\text{m}/\text{min}$  at about  $120^\circ\text{C}$ . For isotactic polystyrene (i-PS) maximum values of about  $300 \times 10^{-3} \mu\text{m}/\text{min}$  were reported<sup>9</sup>. In the literature<sup>10</sup> i-PS is considered a slowly crystallizing polymer. Comparing the maximum values of  $G$  it is clear that i-PMMA should be called a very slowly crystallizing polymer. However, it should be kept in mind that the given maximum value for i-PMMA is not a general one. It will be influenced by molecular weight and tacticity of the sample.

*Figure 3* shows some typical photographs of crystals of



*Figure 1* Longest diagonal ( $\mu\text{m}$ ) of crystals of i-PMMA against crystallization time (min) for various  $T_c$ :  $\circ$ ,  $90^\circ$ ;  $\times$ ,  $100^\circ$ ;  $\triangle$ ,  $110^\circ$ ;  $\bullet$ ,  $120^\circ$ ;  $\square$ ,  $130^\circ\text{C}$

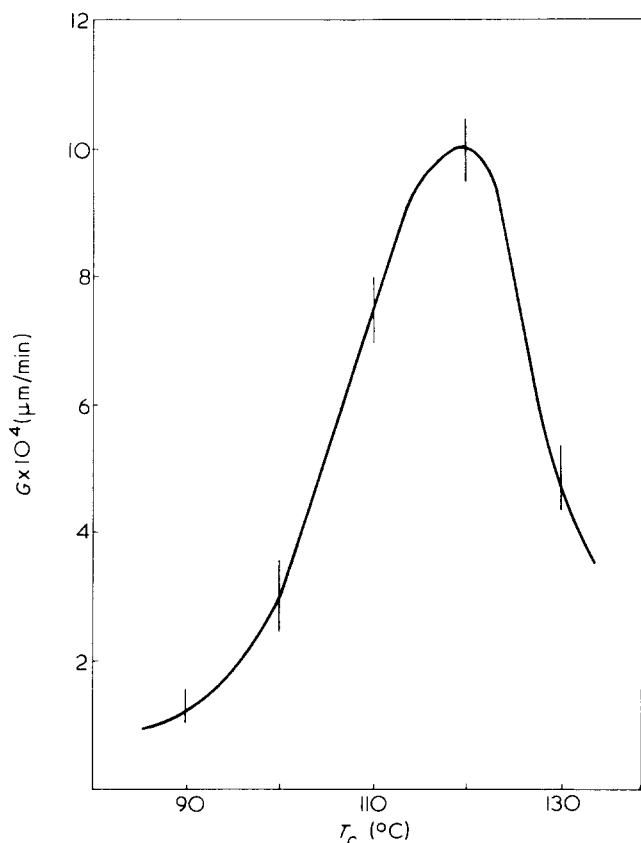


Figure 2 Average growth rate  $G$  ( $\mu\text{m}/\text{min}$ ) of i-PMMA crystals against crystallization temperature  $T_c$

i-PMMA taken at different stages of growth at  $120^\circ\text{C}$ . Initially only hexagonal structures were observed, which showed only little birefringence (Figures 3a and 3d), while in later stages skeletation to starlike structures occurred and finally the crystals became rounded.

Hexagonal structures have also been reported for polyoxymethylene<sup>11</sup>, isotactic polypropylene<sup>11</sup> and isotactic polystyrene<sup>12</sup>. Besides the above mentioned hexagonal structures spherical structures were also observed, especially at lower  $T_c$ , e.g.  $90$  and  $100^\circ\text{C}$ . The spherical crystals had about the same value of  $G$  as the hexagons. In accordance with the literature<sup>11,13</sup> these spherical structures showed more birefringence than the hexagonal structures. At  $130^\circ\text{C}$  no spherical structures could be observed at all.

The above results are in agreement with those of Keith<sup>13</sup> for i-PS. However, we observed hexagons of i-PMMA at crystallization temperatures  $100$ – $120^\circ\text{C}$  below the melting temperature, whereas Keith could detect hexagons of i-PS only at  $30$ – $40^\circ\text{C}$  below the melting temperature. Moreover, the hexagons of i-PMMA could become much larger than those of i-PS, e.g.  $65 \mu\text{m}$  in Figure 3a versus  $5 \text{ nm}$  reported for pure i-PS.

According to Keith<sup>14</sup>  $\delta$  can be considered as a characteristic length for the growing crystal. ( $\delta = D/G$ ;  $D$  = diffusion coefficient for 'impurity' in the unsolidified medium;  $G$  = growth rate of the crystal face). At crystal sizes smaller than  $\delta$ , impurities can easily diffuse out of the way of oncoming growth fronts. In this stage single crystals grow from the melt, producing hexagons which are multilayers of single crystals, also called hedrites.

In the literature no melt viscosity data were available for i-PMMA to calculate  $D$  and it seems troublesome to use the

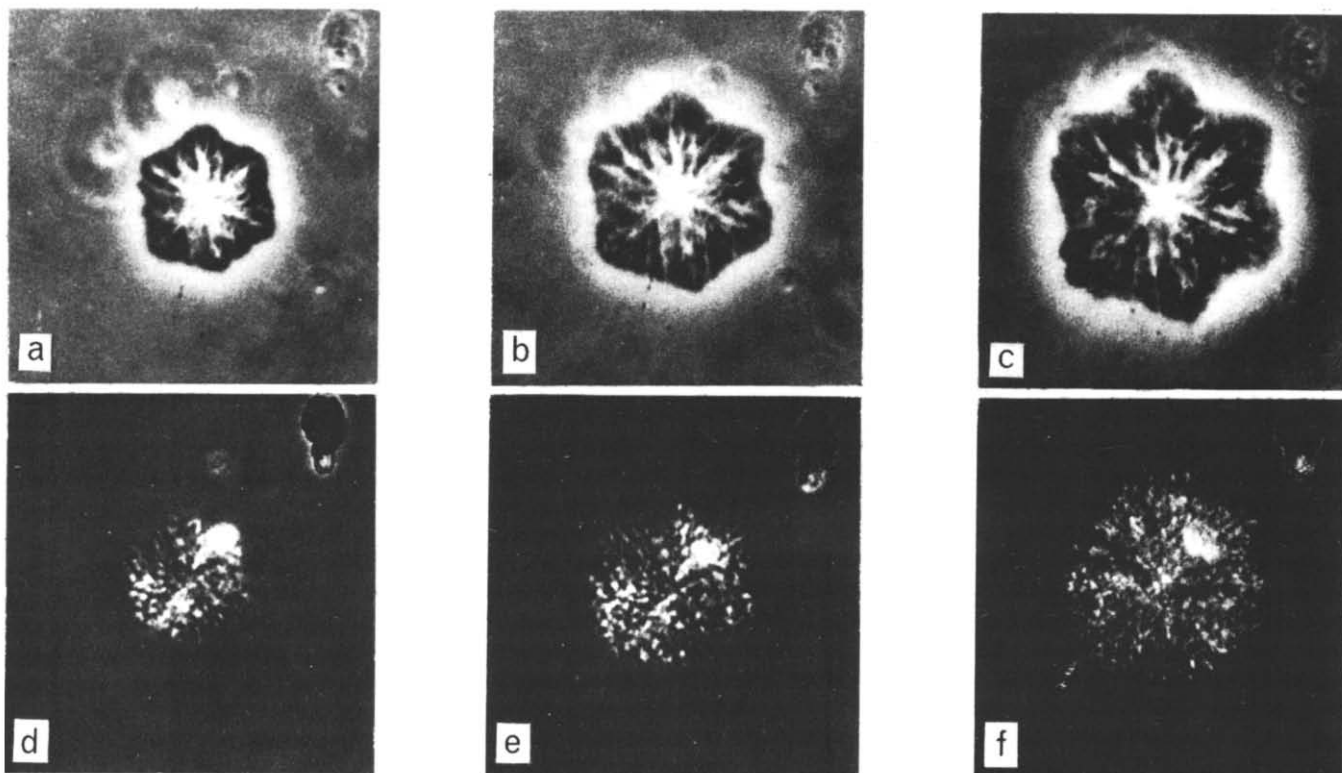


Figure 3 Various stages of crystal growth of i-PMMA at  $120^\circ\text{C}$ . (a), (b) and (c) are phase-contrast photographs. (d), (e) and (f) are bright field photographs between crossed Nicols. Crystallization times: (a) 10 days; (b) 14 days; (c) 18 days; (d) 10 days; (e) 14 days; (f) 18 days (magnification  $640\times$ )



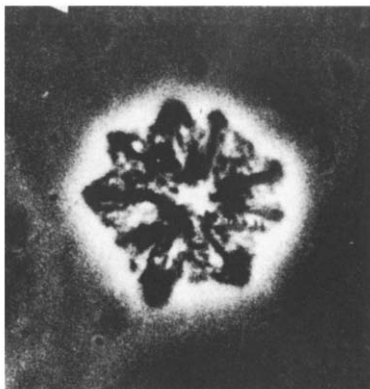


Figure 4 Phase contrast photograph of i-PMMA crystallized at 130°C during 25 days (magnification 640×)

available data of atactic PMMA. For  $\delta = 65 \mu\text{m}$ , the limiting value of the diagonal (Figure 3a) and a  $G$  value of  $1 \times 10^{-3} \mu\text{m}/\text{sec}$  (Figure 2) we calculate a  $D$  value of about  $10^{-9} \text{cm}^2/\text{sec}$ , which is a quite reasonable value. So, it may be assumed that the differences in supercooling and sizes of hexagons for i-PMMA and i-PS are predominantly caused by the much lower growth rate of i-PMMA compared with i-PS.

Figure 4 shows a photograph of a sample crystallized at 130°C. At this temperature  $\delta$  has a larger value than at 120°C because  $D$  increases and  $G$  decreases with temperature (Figure 2). So, we expected to observe still larger hexagons, but even in very early stages no purely hexagonal structures could be observed, only structures with strong skeletation. Maybe, more faceted growth takes place at 130°C.

Finally, Figure 5 shows the  $T_m - T_c$  diagram of i-PMMA. Melting temperatures  $T_m$  were recorded with a d.s.c. at various heating rates. To correct for super heating (maximum effects of 8 and 20°C for crystals grown at 90 and 130°C, respectively),  $T_m$  values were extrapolated to zero scan speed.  $T_m$  values were also estimated on the hot stage light microscope (Figure 5). The middle of the melting range (4–8°C) of the crystals was chosen as  $T_m$ . The difference with d.s.c. values can be explained by the fact that especially for samples crystallized at 90°C and 100°C the beginning of the melting process is not exactly detected as a result of which too high  $T_m$  values are found. Since it is very time consuming to crystallize i-PMMA at temperatures above 130°C, the line in the  $T_m - T_c$  diagram had to be extrapolated over a large distance. This means that the extrapolated melting temperature  $T_m^0$  can only be found approximately. Figure 5 shows that  $T_m^0$  of i-PMMA is about 220°C.

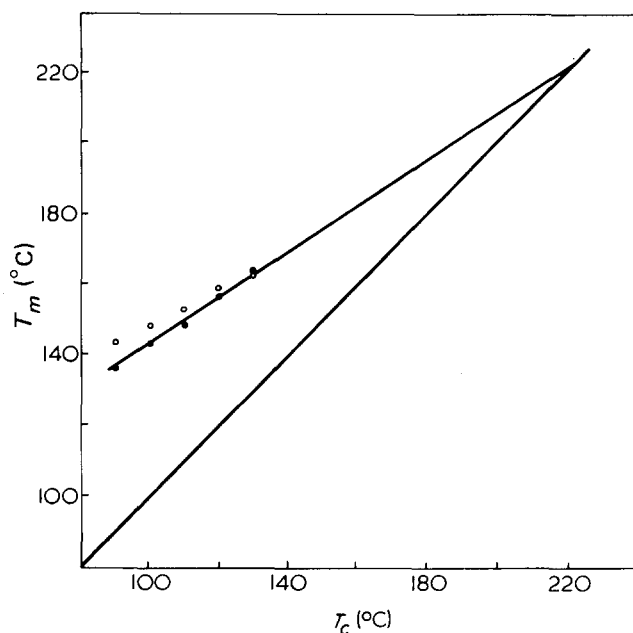


Figure 5 Melting temperatures  $T_m$  of i-PMMA as a function of crystallization temperature  $T_c$ . ●, Recorded by d.s.c. extrapolated values with zero scan speed; ○, estimated by light microscopy with a heating rate of 0.2°C/min

#### REFERENCES

- 1 Fox, T. G., Garret, B. S., Goode, W. E., Gratch, S., Kincaid, J. F., Spell, A. and Stroupe, J. D. *J. Am. Chem. Soc.* 1958, **80**, 1768
- 2 Stroupe, J. D. and Hughes, R. E. *J. Am. Chem. Soc.* 1958, **80**, 2314
- 3 Coiro, V. M., De Santis, P., Liquori, A. M. and Mazzarella, L. *J. Polym. Sci. (C)* 1969, **16**, 4591
- 4 Tadokoro, H., Chatani, Y., Kusanagi, H. and Yokoyama, M. *Macromolecules* 1970, **3**, 441
- 5 Tanaka, A. and Ishida, Y. *J. Polym. Sci. (Polym. Phys. Edn)* 1974, **12**, 335
- 6 Klement, J. J. and Geil, P. H. *J. Macromol. Sci. (B)* 1972, **6**, 31
- 7 Goode, W. E., Owens, F. H., Fellmann, R. P., Snijder, W. H. and Moore, J. H. *J. Polym. Sci.* 1960, **46**, 317
- 8 Bischof, J. and Desreux, V. *Bull. Soc. Chim. Belg.* 1952, **61**, 10
- 9 Lemstra, P. J., Postma, J. and Challa, G. *Polymer* 1974, **15**, 757
- 10 Boon, J. *Thesis*, Delft (1966)
- 11 Geil, P. H. 'Polymer Single Crystals', Interscience, New York, 1963, section III/2
- 12 Danusso, F. and Sabbioni, F. *Rend. Inst. Lomb. Sci. Lett. (A)* 1958, **92**, 435
- 13 Keith, H. D. *J. Polym. Sci. (A)* 1964, **2**, 4339
- 14 Keith, H. D. and Padden, Jr., F. J. *J. Appl. Phys.* 1963, **34**, 2409

# Upper and lower theta temperatures for solutions of *cis*- and *trans*-1,4-polybutadiene

J. M. G. Cowie and I. J. McEwen

Department of Chemistry, University of Stirling, Stirling FK9 4LA, UK  
(Received 21 July 1975)

Variations in polymer dilute solution behaviour due to microstructural differences are now well documented<sup>1</sup>. When polymer tacticity is the variable the differences are most clear in pseudo-ideal solvents and become less apparent as the solvent quality improves. In the 1,4-polydienes, where *cis*-*trans* isomerism is the important feature, structurally dissimilar polymers can be readily distinguished in good solvents in which the polymer coil is highly expanded. Thus the Mark-Houwink equations derived for *cis*- and *trans*-1,4-polybutadiene dissolved in toluene are quite distinct<sup>2</sup>. While some work has been reported on the behaviour of pseudo-ideal solutions of *cis*-1,4-polybutadiene<sup>3,4</sup> we are unaware of any comparable studies for the *trans*-polymer. Vanzo<sup>5</sup> has reported lower critical solution temperatures (*LCST*) for two fractions of a polybutadiene sample in hexane, but the polymer had a mixed structure.

Commercial samples of *cis*- and *trans*-1,4-polybutadiene were used in this work. Infra-red analysis<sup>6</sup> showed that the structures were respectively, 93% *cis*, 4% *trans*, 3% 1,2-addition, and 94% *trans*, 6% 1,2-addition. The samples were fractionated from cyclohexane solutions using isopropyl alcohol as precipitant. The fractions were separated, dried and then stored under vacuum until required for measurement. Viscosity-average molecular weights,  $M_v$ , were calculated from established Mark-Houwink equations by measuring the limiting viscosity number  $[\eta]$  in toluene at 303K for predominantly *cis* samples<sup>3a</sup>, and in cyclohexane at 313K for the *trans* fractions<sup>7</sup>. The results are shown in Table 1.

Cloud point curves for all fractions were determined in three solvents, ethyl propyl ketone, diethyl ketone and propylene oxide. These were established, in both the upper and lower critical regions, by preparing several solutions of each fraction in the concentration range 0.5 to 12% w/v, sealing these in capillary tubes and observing the liquid-liquid phase separation temperatures using methods described elsewhere<sup>8</sup>. As the samples were not monodisperse,

Table 1 Limiting viscosity numbers and molecular weights for *cis*- and *trans*-1,4-polybutadiene fractions

Samples	$[\eta]$ (cm <sup>3</sup> /g)	$M_v \times 10^5$
<i>cis</i> -1,4-polybutadiene:		
1, 1(A)	520	6.92
1, 1(B)	386	4.57
1, 2	256	2.60
2, 2	175	1.53
2, 3	135	1.08
<i>trans</i> -1,4-polybutadiene:		
3	177	1.93
4	110	1.37
5(a)	95	1.00
5(b)	53	0.47

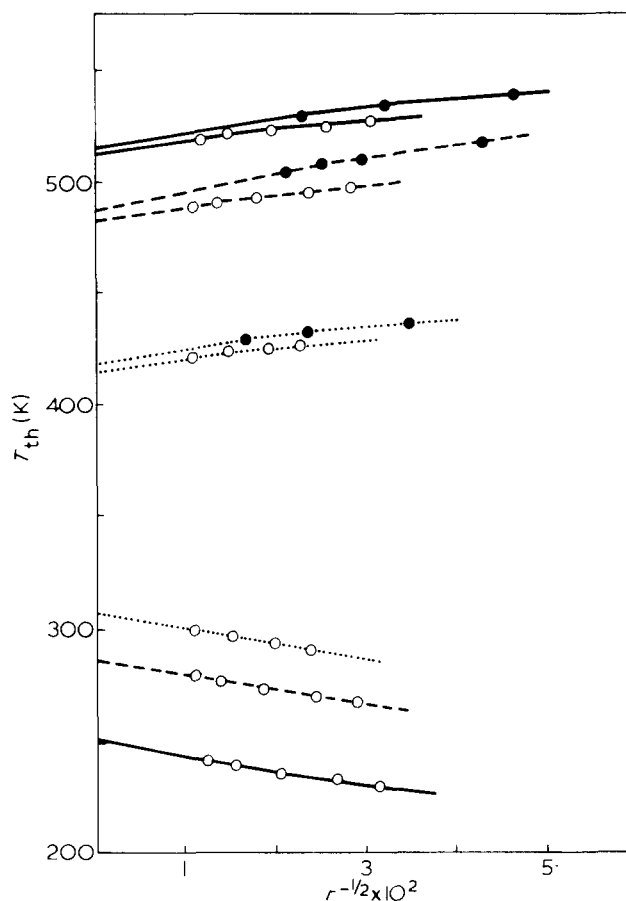


Figure 1 Plots of  $T_{th}$  against  $r^{-1/2}$  for *cis*-polybutadiene (○) and *trans*-polybutadiene (●) in the solvents ethylpropylketone (—), diethyl ketone (---) and propylene oxide (····).  $r$  is the ratio of the molar volumes of polymer and solvent at 298 K

the maxima and minima of the cloudpoint curves represented threshold temperatures,  $T_{th}$ , rather than true critical points, but the difference is probably small in every case because of the flatness of the experimental curves.

In Figure 1,  $T_{th}$  has been plotted against  $r^{-1/2}$ , where  $r$  is the ratio of the molar volume of the polymer to that of the solvent. The data have been extrapolated to  $M = \infty$  in both the upper and lower critical solution regions to obtain  $\theta_U$  and  $\theta_L$  respectively. It can be seen from the summary in Table 2, that the solvent quality varies quite considerably from a miscibility range  $\Delta\theta$  of 109K in propylene oxide to  $\Delta\theta = 259$ K in ethyl propyl ketone. Also shown is the ratio  $(\theta_L/T_c)$ , estimated for each polymer-solvent pair, where  $T_c$  is the critical temperature of the solvent. The values are similar to those reported for other systems. A value of  $\theta_U = 283.5$ K for *cis*-polybutadiene in diethyl ketone has been reported by Abe and Fujita<sup>4</sup> in reasonable agreement

Table 2 Upper and lower theta temperatures for *cis*- and *trans*-1, 4-polybutadienes

Solvent	Polybutadiene	$\theta_U(K)$	$\theta_L(K)$	$(\theta_L/T_c)$
Ethyl propyl ketone	<i>cis</i>	251	510	0.884
	<i>trans</i>	—	513	0.889
Diethyl ketone	<i>cis</i>	287	481	0.847
	<i>trans</i>	—	486	0.856
Propylene oxide	<i>cis</i>	308	414	0.836
	<i>trans</i>	—	419	0.842

with our value, considering that there are slight differences in structure between the samples.

While the *cis* and *trans* forms of the polymer can be distinguished in the lower critical region, the differences in  $\theta_L$  are really quite small. In all cases,  $\theta_L$  for the *trans* form was slightly higher than that for the *cis*. This is consistent with the simple explanation which attributes the existence of the *LCST* to differences in free volume between the rapidly expanding solvent and the more slowly expanding polymer, as the critical temperature of the solvent is approached. The expansion coefficients of 1, 4-polybutadienes appear to be almost independent of the *cis-trans* content<sup>9</sup>, although the results do indicate that the expansion factor for the *trans* form is marginally higher than the *cis*. Thus one would expect both forms to exhibit very similar *LCST*'s, but with the *trans* form having the higher value.

Unfortunately a similar comparison of  $\theta_U$  values could not be made because the *trans*-1, 4-polybutadiene consistently crystallized from all three solvents before liquid—

liquid phase separation could occur. The temperature at which the liquid—crystal phase separation took place was in the range 290–295K and was independent of the sample chain length. For this reason measurement of the *LCST* would be a more general means of distinguishing between the *cis* and *trans* forms of 1, 4-polybutadiene, but because of the small differences observed this would not provide a particularly reliable method of analysis. Consequently, in contrast to polymers with different tactic forms, *cis-trans* isomerism is most easily detected when polymers are dissolved in good solvents.

#### ACKNOWLEDGEMENTS

The authors wish to thank SRC for supporting this work.

#### REFERENCES

- 1 Cowie, J. M. G. in 'Light Scattering from Polymer Solutions', (Ed. M. Huglin), Academic Press, London, 1972, Ch 14
- 2 Takeda, M., and Endo, R. *Rep. Progr. Polym. Phys. Japan* 1963, 6, 37
- 3 (a) Danusso, F., Moraglio, G. and Gianotti, G. *J. Polym. Sci.* 1961, 51, 475; (b) Moraglio, G. *Eur. Polym. J.* 1965, 1, 103
- 4 Abe, M. and Fujita, H. *J. Phys. Chem.* 1965, 69, 3263
- 5 Vanzo, E. *J. Polym. Sci. (B)* 1967, 5, 325
- 6 Binder, J. L. *Appl. Spectros.* 1969, 23, 17
- 7 Kurata, M., Utiyama, H., Kajitani, K., Koyama, T. and Fujita, H. *12th Polym. Symp., Nagoya* 1963
- 8 Cowie, J. M. G. and McEwen, I. J. *Macromolecules* 1974, 7, 291
- 9 Pedemonte, E. and Bianchi, U. *J. Polym. Sci. (B)* 1964, 2, 1025

## Effects of oxygen on vinyl polymerization systems: limitations of conventional dilatometry

A. Garton\* and M. H. George

Department of Chemistry, Imperial College of Science and Technology, London SW7 2AY, UK.

(Received 10 July 1975)

#### INTRODUCTION

Small scale dilatometry is a widely applied technique for following the course of polymerization reactions<sup>1</sup> and many simple, and more complicated types of dilatometer have been described previously<sup>2,3</sup>

Some of the discrepancies associated with the interpretation of dilatometric results may involve the improper use of monomer and polymer densities or the heating effects occurring within dilatometers<sup>4</sup>. However, although the need for adequate stirring of dilatometer contents has been stressed when studying emulsion polymerizations<sup>5</sup>, little attention has been paid to the effect of inadequate reactant mixing in other polymerization systems. We have found in our laboratories that adequate mixing of dilatometer contents was crucial when examining the effect of the gaseous additive, oxygen, at low concentrations, on several free radical vinyl polymerizations.

\* Present address: Applied Chemistry Division, National Research Council, Ottawa, Ontario K1A 0R6, Canada.

#### EXPERIMENTAL AND RESULTS

For example, the effect of oxygen on the liquid-phase polymerization of vinyl chloride at 55°C in the presence of an added initiator, bis(4-*t*-butylcyclohexyl) peroxydicarbonate (Perkadox 16) has been studied<sup>6</sup>. Initial experiments were conducted in a conventional manner similar to that reported in several earlier studies. Thick walled dilatometers were used, each with a bulb volume of about 2.5 cm<sup>3</sup> attached to 2 mm precision-bore capillary. Known amounts of oxygen were added to the previously purified and degassed monomer/initiator mixtures inside each dilatometer bulb. After freezing in liquid nitrogen, the dilatometers were sealed off under vacuum. The dilatometer contents were shaken vigorously at 0°C prior to clamping vertically in a thermostated bath at 55°C. The relationship between the initial oxygen content (0–600 ppm w/w) and the resulting induction period,  $\tau$ , recorded as the time taken for polymer to precipitate from solution, was studied. If ideal solution behaviour of oxygen in vinyl chloride is assumed, at least 98%

Table 2 Upper and lower theta temperatures for *cis*- and *trans*-1, 4-polybutadienes

Solvent	Polybutadiene	$\theta_U(K)$	$\theta_L(K)$	$(\theta_L/T_c)$
Ethyl propyl ketone	<i>cis</i>	251	510	0.884
	<i>trans</i>	—	513	0.889
Diethyl ketone	<i>cis</i>	287	481	0.847
	<i>trans</i>	—	486	0.856
Propylene oxide	<i>cis</i>	308	414	0.836
	<i>trans</i>	—	419	0.842

with our value, considering that there are slight differences in structure between the samples.

While the *cis* and *trans* forms of the polymer can be distinguished in the lower critical region, the differences in  $\theta_L$  are really quite small. In all cases,  $\theta_L$  for the *trans* form was slightly higher than that for the *cis*. This is consistent with the simple explanation which attributes the existence of the *LCST* to differences in free volume between the rapidly expanding solvent and the more slowly expanding polymer, as the critical temperature of the solvent is approached. The expansion coefficients of 1, 4-polybutadienes appear to be almost independent of the *cis-trans* content<sup>9</sup>, although the results do indicate that the expansion factor for the *trans* form is marginally higher than the *cis*. Thus one would expect both forms to exhibit very similar *LCST*'s, but with the *trans* form having the higher value.

Unfortunately a similar comparison of  $\theta_U$  values could not be made because the *trans*-1, 4-polybutadiene consistently crystallized from all three solvents before liquid—

liquid phase separation could occur. The temperature at which the liquid—crystal phase separation took place was in the range 290–295K and was independent of the sample chain length. For this reason measurement of the *LCST* would be a more general means of distinguishing between the *cis* and *trans* forms of 1, 4-polybutadiene, but because of the small differences observed this would not provide a particularly reliable method of analysis. Consequently, in contrast to polymers with different tactic forms, *cis-trans* isomerism is most easily detected when polymers are dissolved in good solvents.

#### ACKNOWLEDGEMENTS

The authors wish to thank SRC for supporting this work.

#### REFERENCES

- 1 Cowie, J. M. G. in 'Light Scattering from Polymer Solutions', (Ed. M. Huglin), Academic Press, London, 1972, Ch 14
- 2 Takeda, M., and Endo, R. *Rep. Progr. Polym. Phys. Japan* 1963, 6, 37
- 3 (a) Danusso, F., Moraglio, G. and Gianotti, G. *J. Polym. Sci.* 1961, 51, 475; (b) Moraglio, G. *Eur. Polym. J.* 1965, 1, 103
- 4 Abe, M. and Fujita, H. *J. Phys. Chem.* 1965, 69, 3263
- 5 Vanzo, E. *J. Polym. Sci. (B)* 1967, 5, 325
- 6 Binder, J. L. *Appl. Spectros.* 1969, 23, 17
- 7 Kurata, M., Utiyama, H., Kajitani, K., Koyama, T. and Fujita, H. *12th Polym. Symp., Nagoya* 1963
- 8 Cowie, J. M. G. and McEwen, I. J. *Macromolecules* 1974, 7, 291
- 9 Pedemonte, E. and Bianchi, U. *J. Polym. Sci. (B)* 1964, 2, 1025

## Effects of oxygen on vinyl polymerization systems: limitations of conventional dilatometry

A. Garton\* and M. H. George

Department of Chemistry, Imperial College of Science and Technology, London SW7 2AY, UK.

(Received 10 July 1975)

#### INTRODUCTION

Small scale dilatometry is a widely applied technique for following the course of polymerization reactions<sup>1</sup> and many simple, and more complicated types of dilatometer have been described previously<sup>2,3</sup>

Some of the discrepancies associated with the interpretation of dilatometric results may involve the improper use of monomer and polymer densities or the heating effects occurring within dilatometers<sup>4</sup>. However, although the need for adequate stirring of dilatometer contents has been stressed when studying emulsion polymerizations<sup>5</sup>, little attention has been paid to the effect of inadequate reactant mixing in other polymerization systems. We have found in our laboratories that adequate mixing of dilatometer contents was crucial when examining the effect of the gaseous additive, oxygen, at low concentrations, on several free radical vinyl polymerizations.

\* Present address: Applied Chemistry Division, National Research Council, Ottawa, Ontario K1A 0R6, Canada.

#### EXPERIMENTAL AND RESULTS

For example, the effect of oxygen on the liquid-phase polymerization of vinyl chloride at 55°C in the presence of an added initiator, bis(4-*t*-butylcyclohexyl) peroxydicarbonate (Perkadox 16) has been studied<sup>6</sup>. Initial experiments were conducted in a conventional manner similar to that reported in several earlier studies. Thick walled dilatometers were used, each with a bulb volume of about 2.5 cm<sup>3</sup> attached to 2 mm precision-bore capillary. Known amounts of oxygen were added to the previously purified and degassed monomer/initiator mixtures inside each dilatometer bulb. After freezing in liquid nitrogen, the dilatometers were sealed off under vacuum. The dilatometer contents were shaken vigorously at 0°C prior to clamping vertically in a thermostated bath at 55°C. The relationship between the initial oxygen content (0–600 ppm w/w) and the resulting induction period,  $\tau$ , recorded as the time taken for polymer to precipitate from solution, was studied. If ideal solution behaviour of oxygen in vinyl chloride is assumed, at least 98%

by wt of the gas should be dissolved in the liquid monomer at 55°C under typical conditions. Any positive interactions between vinyl chloride and oxygen would increase the solubility of the gas.

Nevertheless, irreproducible measurements of induction periods were obtained by this simple 'static' dilatometric method. It was considered that the irreproducibility was largely caused by the existence of an oxygen rich phase within the dilatometer capillary. The restricted rate of diffusion of oxygen from the capillary would therefore result in polymerization occurring within the bulb before the oxygen had been completely consumed. Conventional stirring of the contents of dilatometer bulbs would be of little use in these circumstances.

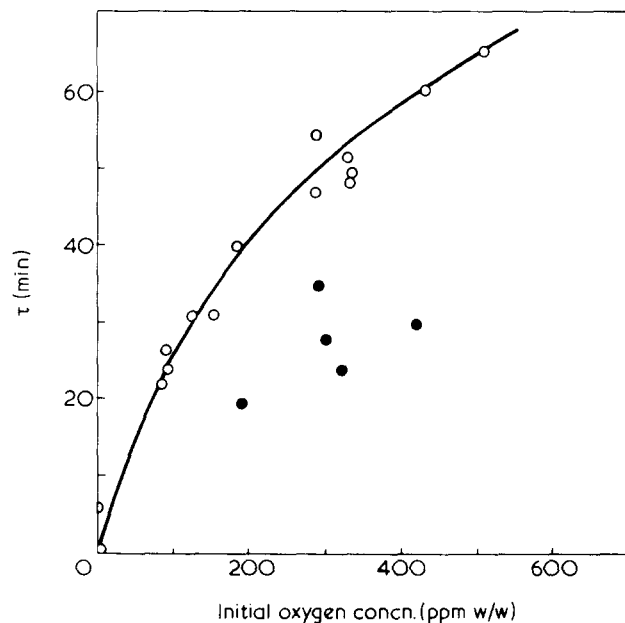
The filled, sealed-off dilatometers were inverted, therefore, in subsequent experiments to allow the gas phase to enter the bulb and then rotated slowly in the thermostated bath. Typically, the dilatometers were rotated about an axis 45° to the vertical at a speed of about 30 rev/min. The oscillation of the gas phase within the bulb coupled with the movement of the liquid reactants within the dilatometer ensured efficient mixing. This tumbling was periodically stopped to allow drainage and refilling of the capillary stem. When polymer precipitation was observed, the dilatometer was returned to its conventional vertical position. The induction period,  $\tau$ , was recorded and the subsequent rate of polymerization was observed, if necessary after cooling to allow drainage of the contents remaining in the capillary stem.

Using this method of 'tumbled dilatometry', the induction period measurements were reproducible, and at constant initiator concentration were proportional to the square root of the initial oxygen concentration. Some typical induction period results obtained by conventional and tumbled dilatometry are shown in *Figure 1*. The extent of peroxide formation during the induction period was also increased by tumbling the dilatometers which again indicated the incomplete oxygen consumption in conventional dilatometry. Further details of experimental procedure are reported elsewhere<sup>6,7</sup>

Further studies have been made of the effects of oxygen on the polymerization of bulk acrylonitrile initiated by 2,2'-azobisisobutyronitrile (AIBN) at 50°C, and of acrylamide dissolved in ethanol initiated by AIBN at 80°C. In general, induction periods measured by conventional (static) dilatometry were irreproducible and less than those recorded by tumbled dilatometry.

## CONCLUSIONS

The method of tumbled dilatometry reported here is applicable to systems in which the onset of polymerization is associated with polymer precipitation. The technique enables reproducible measurements of induction periods to be made due to the presence of added oxygen. The results serve to emphasize the importance of efficient mixing of dilatometer contents involving gaseous additives. Vigorous shaking of reactants at temperatures below that at which



*Figure 1* Induction periods,  $\tau$ , for the polymerization of vinyl chloride at 55°C, as a function of initial oxygen concentration (ppm w/w). Perkadox 16 concentration = 0.05 g/dm<sup>3</sup>. ○, Tumbled dilatometry; ●, conventional dilatometry

polymerization is finally studied may prove to be insufficient because of inhomogeneities produced when the reactants inside a dilatometer bulb expand into the capillary stem.

## ACKNOWLEDGEMENTS

The above technique was involved in a project undertaken as part of a Cooperative Award in Pure Science (CAPS) scheme, financed jointly in this case, by the Science Research Council and BP Chemicals International Ltd. Financial support for one of the authors (A. G.) from these two bodies is gratefully acknowledged.

## REFERENCES

- Collins, E. A., Barès, J., and Billmeyer, Jr. F. W. 'Experiments in Polymer Science', 1973, Wiley, New York, Ch 5
- Rubens, L. C. and Skochdopole, R. E. in 'Encyclopedia of Polymer Science and Technology', (Eds H. F. Mark, N. G. Gaylord and N. M. Bikales), Interscience, New York, 1966, Vol 5, pp 83-98
- Bauer, N. and Lewin, S. Z. in 'Techniques of Chemistry', (Eds A. Weissberger and B. W. Rossiter) 1972, Vol 1, Part IV, Interscience New York, Ch 2
- Allen, P. E. M. and Patrick, C. A. in 'Kinetics and Mechanisms of Polymerization Reactions', Horwood, Chichester, 1974, Ch 3
- Paoletti, K. P. and Billmeyer, Jr. F. W. *J. Polym. Sci. (A) (A-2)* 1964, 2, 2049
- Garton, A. and George, M. H. *J. Polym. Sci. (Polym. Chem. Edn)* 1973, 11, 2153
- Garton, A. and George, M. H. *J. Polym. Sci. (Polym. Chem. Edn)* 1974, 12, 2779

## Anomalous melt elasticity of isotactic ethylene-propylene block copolymers

In comparing the processing properties of polypropylene homopolymers with those of certain ethylene-propylene 'end-block' copolymers containing up to 25 wt % of ethylene at constant melt flow index (MFI)<sup>1</sup>, one obvious difference is that the copolymers have lower swelling ratios than the homopolymers. Within a given manufacturer's series, swelling ratio decreases with increasing ethylene content. Examples are given in *Table 1*.

At least part of the ethylene in the 'end-block' copolymers considered here, is present as a high molecular weight tail of polyethylene or polyethylene-rich molecules<sup>2</sup>. The apparently reduced elastic response (i.e. lower swelling ratio) is contrary to expectation and common experience in homopolymers with wide molecular weight distribution. However, we have also observed that at stress levels much lower than those used to measure swelling ratio, the copolymers do appear to become more elastic.

The following series of experiments clearly demonstrates the difference between the two types of polymers. Samples were stabilized with 1% Topanol OC and the tests were performed at 210°C under a nitrogen blanket in all cases. All measurements compared the same two polymers: a standard homopolymer and a copolymer containing 15 wt % ethylene.

### Dynamic elasto-viscosity

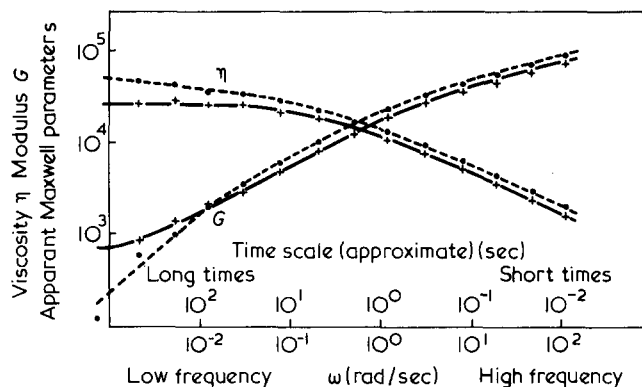
In dynamic measurements an alternating strain of low amplitude is imposed in an oscillation which is sinusoidal with respect to time. For this experiment we used the Contraves balance rheometer interpreting the results in terms of the apparent Maxwell parameters as recommended by Benbow<sup>3</sup>. The inverse of the angular frequency may be interpreted as a time scale.

The Maxwell model comprises an elastic spring of modulus  $G$ , in series with a dashpot of viscosity,  $\eta$ . The ratio viscosity/modulus can be interpreted as the natural time of the material; if the time of deformation is less than the

*Table 1* Swelling ratio versus ethylene content for homopolymers and end-block copolymers

Source	Ethylene content (wt %)	MFI (190°C/10 kg)	Swelling ratio*
Manufacturer A	0	35	2.02
	0	11	2.19
	7	20	1.80
	15	10	1.57
	25	38	1.39
Manufacturer B	0	17	1.98
	14	15	1.58
Manufacturer C	0	19	1.85
	22	9	1.46

\* Diameter of extrudate/die diameter measured at 230°C and a shear stress of  $9 \times 10^4$  N/m<sup>2</sup>, using a 1 mm dia. x 0.25 in long die having a 30° entry angle



*Figure 1* Dynamic elasto-viscosity at 210°C, strain amplitude 0.37. —, Homopolymer; ----, copolymer

natural time of the material then the majority of the deformation will occur in the elastic element. It follows that the combination of higher viscosity with lower modulus allows the qualitative interpretation of greater melt elasticity.

The apparent Maxwell parameters over the angular frequency range  $10^{-3}$  to  $10^2$  sec<sup>-1</sup> (time scale  $10^3$  to  $10^{-2}$  sec) are shown in *Figure 1*.

At time scales of less than 10 sec the modulus of the copolymer is slightly higher than that of the homopolymer but at a time scale of about 10 to 100 sec the two polymers have similar moduli. They then diverge rapidly so that at a time scale of 1000 sec the modulus of the copolymer is only one quarter that of the homopolymer sample; this, combined with the higher viscosity of the copolymer sample, implies a longer natural time (an apparently more elastic response) for that material at these long time scales.

### Steady state flow

Cone and plate rheometry is used to study the steady state flow at stress levels in the range  $10^2$ – $10^4$  N/m<sup>2</sup>; the experiments are again interpreted in terms of the apparent Maxwell parameters as described by Benbow<sup>3</sup>. Capillary rheometry, including studies of converging flow, is used to investigate the rheology at high stress<sup>4</sup>. The steady state flow measurements (*Figure 2*) show two distinct regions for the copolymer sample. At stress levels above  $10^3$  N/m<sup>2</sup> the melt viscosity and elastic modulus follow a similar pattern to that of the homopolymer response; below  $10^3$  N/m<sup>2</sup> there is a separate region of high viscosity and low modulus. Thus in both dynamic and steady state measurements we observe a change in rheological behaviour in going from high to low stress (or rapid to slow deformations).

The transition from highly elastic response to less elastic response is clearly seen in *Figure 3* which depicts the strain recovery after steady state simple shear. The recovery of the homopolymer sample increases approximately in proportion to the applied stress and reaches saturation within about 50 sec. At recovery times of about 10 sec the copolymer recovers a similar amount of strain to the homopolymer but then continues to recover even after 500 sec.

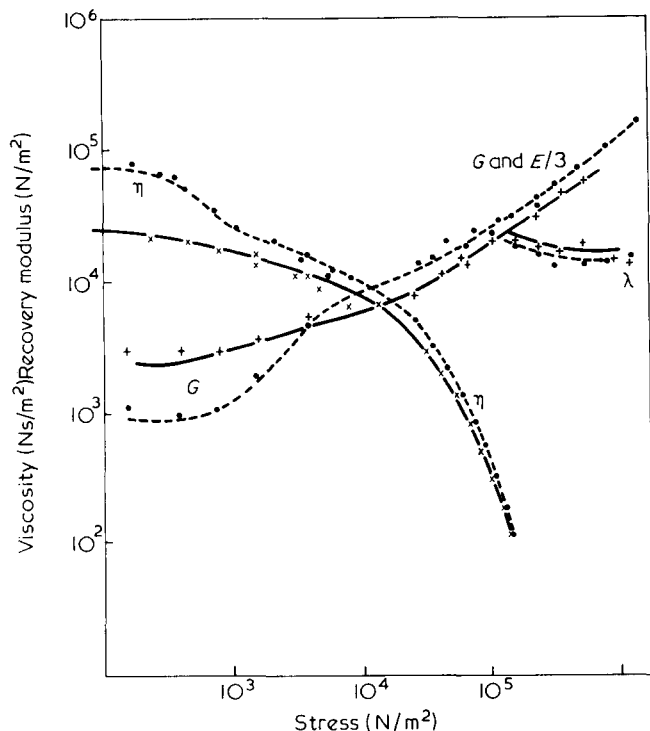


Figure 2 Rheology of polypropylene at 210°C by constant shear rate cone and plate and by capillary extrusion rheometry. Material properties evaluated according to ref 3 for cone and plate measurements and ref 4 for extrusion rheometry.  $\eta$ , viscosity under simple shear;  $\lambda$ , viscosity under extension;  $G$ , modulus under simple shear;  $E$ , modulus under extension. —, Homopolymer; ----, copolymer

	MFI (190°C/10 kg)		MFI (230°C/2 kg)		Swell ratio at 100 sec <sup>-1</sup>	
	MFR	Swell ratio	MFR	Swell ratio	$B_1$	$B_0$
Copolymer	11.5	1.51	1.0	1.20	1.5	2.3
Homopolymer	13.0	1.87	1.3	1.36	2.0	3.1

At higher stress levels this long time scale behaviour does not occur and the recovery curve reverts to a shape which is similar to that of the homopolymers albeit of lesser magnitude.

Discussion

Qualitatively similar viscosity results have been described by Arnold and Meier<sup>5</sup> for styrene-butadiene-styrene block copolymers and by Lee<sup>6</sup> for polypropylene with a dispersed elastomeric phase. Those authors, who did not report any detailed observations of the elastic response, attribute the differences in rheological behaviour to phase separation effects.

Our results form a picture of a highly entangled high molecular weight polymer (polyethylene) dissolved in a different polymer (polypropylene) of lower molecular weight such that at stress levels above 10<sup>3</sup> N/m<sup>2</sup> the high

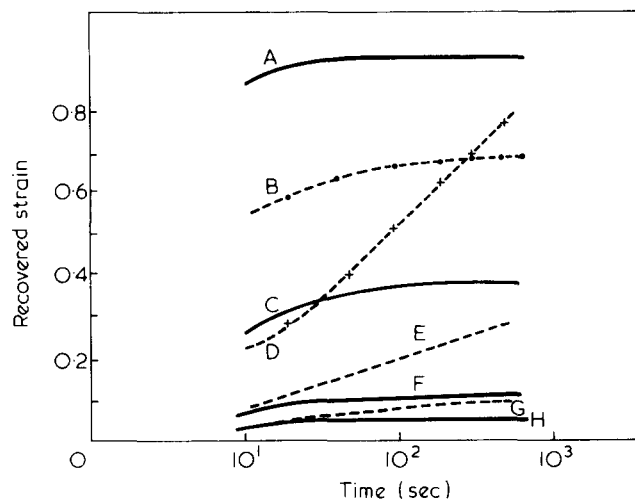


Figure 3 Strain recovery following 100 sec creep under constant shear stress. —, Homopolymer; ----, copolymer. Creep stress for 100 sec: A, B, 7.4 x 10<sup>3</sup>; C, D, 1.5 x 10<sup>3</sup>; E, F, 3.7 x 10<sup>2</sup>; G, H, 1.5 x 10<sup>2</sup> N/m<sup>2</sup>

molecular weight material becomes completely disentangled. After disentanglement the high molecular weight polyethylene chains appear to act solely as a filler, inhibiting the matrix from developing its full melt elasticity. In this respect the high molecular weight polyethylene 'tail' is behaving differently from what would be expected of a comparable high molecular weight polyethylene 'tail' in polyethylene as evidenced by a common experience with wide molecular weight distributions, where the tail enhances the elasticity at all stress levels.

There are several possible mechanisms for a disentanglement process. The two polymers may be sufficiently incompatible in the melt to favour separation on the molecular scale. They are certainly incompatible in the solid state and crystallize in different forms. Other alternatives are the physical separation of 'thin' from 'thick' or 'smooth' from 'barbed wire' structure molecules: in both of these cases separation of unlike molecules might occur in a shear gradient.

Extension of this hypothesis as a basis for achieving easily processable 'alloys' may be feasible if a sufficiently large number of different molecular types can be made available.

F. N. Cogswell and D. E. Hanson

ICI Plastics Division,  
Bessemer Road, PO Box 6,  
Welwyn Garden City, Herts AL7 1HD, UK  
(Received 15 August 1975)

References

- 1 ASTM D1238T
- 2 Heggs, T. G. 'Block Copolymers' (Ed. D. C. Allport and W. H. Janes), Applied Science Publishers, London, 1973, pp 496-502, 513-514
- 3 Benbow, J. J. *Lab. Pract.* 1973, 12, (6), 6
- 4 Cogswell, F. N. *Polym. Eng. Sci.* 1972, 12, 64
- 5 Arnold, K. R. and Meier, D. J. *J. Appl. Polym. Sci.* 1970, 14, 427
- 6 Lee, T-S. *Proc. Vth Int. Congr. Rheology* 1968, 4, 421

### Anomalous behaviour of benzoyl peroxide as an initiator of polymerization

Benzoyl peroxide initiates the polymerization of *N*-vinylcarbazole (VCZ) at 60°C but the process does not have the kinetic characteristics of a radical polymerization<sup>1,2</sup>. The polymer from a polymerization initiated by the peroxide has a molecular weight much lower than that of a polymer from a polymerization performed under similar conditions and proceeding at the same rate but initiated by azobisisobutyronitrile. The average numbers of initiator fragments per polymer molecule are quite different for polymers made using the azonitrile and the peroxide suggesting that the two polymerizations have quite different mechanisms<sup>3</sup>. Further, for the polymers prepared using the peroxide, there is an exceptionally high proportion of benzoyloxy groups among the incorporated initiator fragments. It has been concluded that benzoyl peroxide with VCZ promotes a polymerization most of which is essentially cationic in nature but a small part of which has the characteristics of a radical reaction<sup>2</sup>.

VCZ is very susceptible to cationic polymerization and engages readily in electron-transfer processes; correspondingly, its behaviour in free radical systems is such that it has been assigned a large and negative value ( $-1.34$ ) for  $e^4$ . It seemed desirable, in view of the unusual behaviour of this monomer with benzoyl peroxide, to examine carefully polymerizations involving the peroxide with other monomers known to be active in cationic polymerization and having large and negative values of  $e$ . There is no evidence of abnormalities in the case of styrene ( $e = -0.8$ ) and so

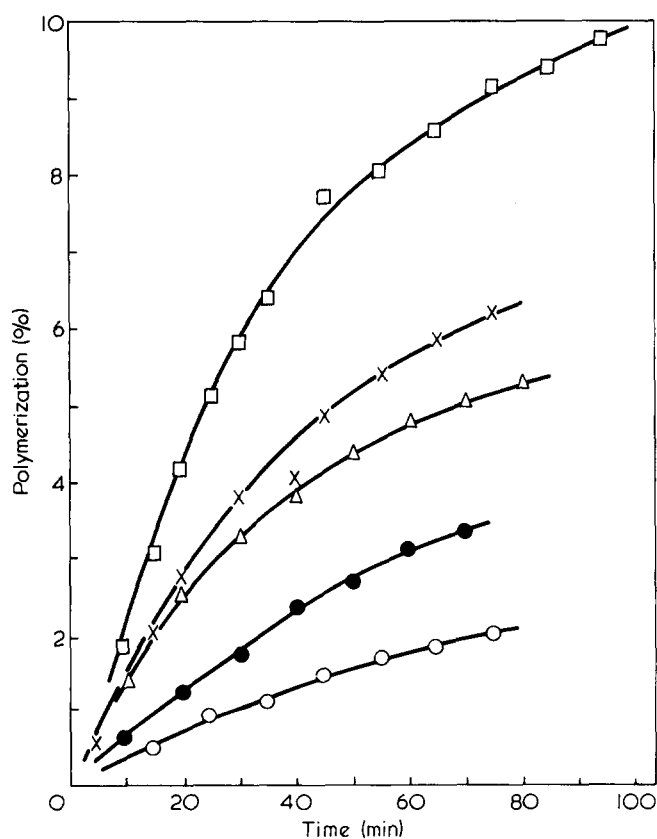


Figure 1 Conversion/time plots for polymerization at 60°C of *N*-vinylpyrrolidone in benzene. Concentration of monomer = 2.81 mol/dm<sup>3</sup>. Concentrations of benzoyl peroxide: ○,  $0.41 \times 10^{-2}$ ; ●,  $1.24 \times 10^{-2}$ ; △,  $2.07 \times 10^{-2}$ ; ×,  $3.02 \times 10^{-2}$ ; □,  $6.16 \times 10^{-2}$  mol/dm<sup>3</sup>

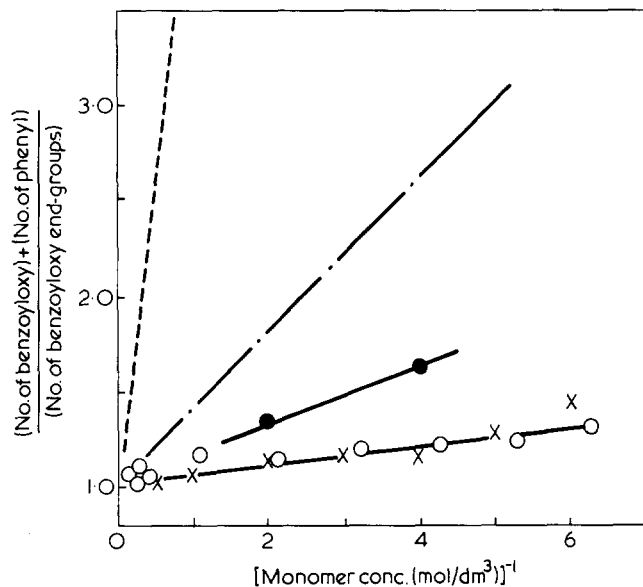


Figure 2 Variation in the relative numbers of benzoyloxy and phenyl end-groups in polymers with the concentration of monomer prevailing during polymerization at 60°C. — — —, Methyl methacrylate; - · - ·, styrene. ●, *N*-vinylcarbazole (polymers believed to have been formed in genuine radical polymerizations<sup>2</sup>); ×, *N*-vinylcarbazole; ○, *N*-vinylpyrrolidone

attention was paid to monomers with more negative values of  $e$ , including *N*-vinylpyrrolidone (NVP) and *p*-methoxystyrene (MOS) for which values of  $-1.14$  and  $-1.11$  respectively have been quoted<sup>4,5</sup>.

The polymerization at 60°C of NVP in benzene with azobisisobutyronitrile shows no abnormalities. Polymerizations at 60°C with benzoyl peroxide do not have steady rates (see Figure 1); even at low conversions and after quite short reaction times, the rates fall off markedly as would be so if the peroxide were consumed much more rapidly than expected by comparison with systems containing monomers such as styrene and methyl methacrylate. The polymers resemble those produced from VCZ under similar conditions in that the proportion of benzoyloxy end-groups is unexpectedly high (see Figure 2). It has been reported<sup>6</sup> that benzoyl peroxide fails to initiate the polymerization of NVP; evidently, this report is wrong but a suggestion that the peroxide is destroyed in a rapid redox reaction with the monomer is essentially correct.

Kinetic abnormalities are not immediately apparent in the polymerization at 60°C of MOS in benzene with benzoyl peroxide but rates seem rather high by comparison with those of polymerizations initiated by azobisisobutyronitrile. The molecular weights of polymers prepared using the peroxide are very much lower than expected by consideration of those of polymers produced with the azonitrile. There is almost as high a proportion of benzoyloxy end-groups as in the cases of VCZ and NVP. The slope of the line in Figure 2 for VCZ and NVP is 20.5 dm<sup>3</sup>/mol; the slope of the corresponding line for MOS is 15.8 dm<sup>3</sup>/mol.

It is clear that unusual behaviour of benzoyl peroxide as an initiator of polymerization is not confined to VCZ as monomer. Further studies, some with substituted benzoyl peroxides, are in progress.

#### Acknowledgement

The work described in this note was performed while



C. J. D. held a studentship awarded by the Science Research Council.

J. C. Bevington and C. J. Dyball

Department of Chemistry,  
University of Lancaster,  
Lancaster LA1 1YA, UK  
(Received 25 September 1975)

#### References

- 1 Jones, R. G., Catterall, E., Bilson, R. T. and Booth, R. G., *Chem. Commun.* 1972, p 22
- 2 Bevington, J. C. and Dyball, C. J., *J. Polym. Sci. (A)* in press
- 3 Bevington, J. C. and Dyball, C. J., *JCS Faraday Trans. I* in press
- 4 Young, L. J., *J. Polym. Sci.* 1961, 54, 411
- 5 Brandup, J. and Immergut, E. H., 'Polymer Handbook', Interscience, New York, 1965
- 6 Solomon, O. F., Corciovei, M. and Boghina, C., *J. Appl. Polym. Sci.* 1968, 12, 1843

## Book Review

### Antioxidants, syntheses and applications

J. C. Johnson

Noyes Data Corporation, Park Ridge, NJ. 1975.  
\$36.00

This book reviews the US patent literature since 1972 on the subject of antioxidants. It provides detailed technical data, taken directly from patents, on the synthesis and evaluation of antioxidants in a wide range of substrates which include polymers, lubricating oils and foodstuffs. By eliminating the legal jargon, the essential technical information has been abstracted from the patents which have been selected from the patent literature apparently on a quite random basis.

The book contains a vast amount of information which will be of value to the practicing antioxidant technologist and the subject index lists the contents both in terms of classes of antioxidant (e.g. phenols, amines, sulphur compounds, etc.) and in terms of the substrates in which they are used (e.g. petroleum products, lubricating oils, elastomers, polyolefins, etc.).

A major deficiency of the book is that it is almost impossible to use it as a reference work as was clearly intended due to the absence of a useful subject index. There is a 'Product stabilisation index' which is little more than an elaboration of the list of substrates in the contents. There is a patent number index which is of value only if the relevant patent number is known. There is a Company index and an Inventor index which are of value if the owners or inventors of the patents are relevant starting data.

Perhaps the most important limitation of this book is its uncritical approach to the patent literature. A forward to the book states its philosophy as follows:

*'The US patent literature is the largest and most comprehensive collection of technical information in the world. There is more practical, commercial, timely process information assembled here than is available from any other source. The technical information obtained from a patent is extremely reliable and comprehensive...'*

This is a point of view which is not shared by many users of the patent literature. Unlike the periodical journal literature with which the patent literature is compared favourably by the author, there is no obligation on the part of the inventors to unequivocally establish the nature of the products reported or the reproducibility of the processes described. Claims as to the usefulness of classes of products are frequently exaggerated to provide adequate legal protection of the invention and the emergence of practically useful

#### Conference Announcement

### The Outlook for Polymer Science

UMIST, Manchester, 24 and 25 March 1976

The Sixth Biennial Manchester Polymer Symposium will be held at UMIST on 24 and 25 March 1976 and will mark the retirement of Professor Geoffrey Gee CBE, FRS as Sir Samuel Hall Professor of Chemistry in the University of Manchester. The programme will consist of a number of papers by distinguished workers from the USA and UK who will assess the present stage in the development of various topics and speculate on their future progress under the symposium title, The Outlook for Polymer Science. Applications for further details and a registration form should be made to The Registrar, University of Manchester Institute of Science and Technology (UMIST), PO Box 88, Manchester M60 1QD, UK.

#### Conference Announcement

### Polymeric Delivery Systems

Midland, Michigan, 23–27 August 1976

An international symposium on polymeric delivery systems will be held at the Midland Macromolecular Institute on 23–27 August 1976. It will consist of both invited and contributed papers. The invited papers will offer critical reviews of: formation, and structure of synthetic membranes, films and microcapsules, by H. Hopfenberg; slow release of macromolecules from synthetic membranes, by J. Folkman; synthetic polymeric drugs, by H. Ringsdorf; carriers for bioactive materials, by A. Trouet; pharmaceutical considerations in the design of devices for prolonged drug delivery, by T. Roseman; release of effectors from polymers and microcapsules, by G. Banker; status of delivery systems for drugs and food additives as viewed by FDA, by C. Kumkumian. Contributed papers are solicited. Further details may be obtained from Symposium Secretary, Midland Macromolecular Institute, 1910 West St Andrews Drive, Midland, Michigan 48640, USA

products from the plethora of patents in the antioxidant field is the very rare exception rather than the rule. The author of this book makes no attempt to distinguish between the small number of patents which have been exploited commercially and the remainder which have not.

This book will be of interest to the industrial chemist who is primarily interested in synthesizing new antioxidants and testing them empirically. It will be of little value to the mechanist who is concerned with the design of new antioxidants on the basis of modern theories of antioxidant action.

G. Scott

C. J. D. held a studentship awarded by the Science Research Council.

J. C. Bevington and C. J. Dyball

Department of Chemistry,  
University of Lancaster,  
Lancaster LA1 1YA, UK  
(Received 25 September 1975)

#### References

- 1 Jones, R. G., Catterall, E., Bilson, R. T. and Booth, R. G., *Chem. Commun.* 1972, p 22
- 2 Bevington, J. C. and Dyball, C. J., *J. Polym. Sci. (A)* in press
- 3 Bevington, J. C. and Dyball, C. J., *JCS Faraday Trans. I* in press
- 4 Young, L. J., *J. Polym. Sci.* 1961, 54, 411
- 5 Brandup, J. and Immergut, E. H., 'Polymer Handbook', Interscience, New York, 1965
- 6 Solomon, O. F., Corciovei, M. and Boghina, C., *J. Appl. Polym. Sci.* 1968, 12, 1843

## Book Review

### Antioxidants, syntheses and applications

J. C. Johnson

Noyes Data Corporation, Park Ridge, NJ. 1975.  
\$36.00

This book reviews the US patent literature since 1972 on the subject of antioxidants. It provides detailed technical data, taken directly from patents, on the synthesis and evaluation of antioxidants in a wide range of substrates which include polymers, lubricating oils and foodstuffs. By eliminating the legal jargon, the essential technical information has been abstracted from the patents which have been selected from the patent literature apparently on a quite random basis.

The book contains a vast amount of information which will be of value to the practicing antioxidant technologist and the subject index lists the contents both in terms of classes of antioxidant (e.g. phenols, amines, sulphur compounds, etc.) and in terms of the substrates in which they are used (e.g. petroleum products, lubricating oils, elastomers, polyolefins, etc.).

A major deficiency of the book is that it is almost impossible to use it as a reference work as was clearly intended due to the absence of a useful subject index. There is a 'Product stabilisation index' which is little more than an elaboration of the list of substrates in the contents. There is a patent number index which is of value only if the relevant patent number is known. There is a Company index and an Inventor index which are of value if the owners or inventors of the patents are relevant starting data.

Perhaps the most important limitation of this book is its uncritical approach to the patent literature. A forward to the book states its philosophy as follows:

*'The US patent literature is the largest and most comprehensive collection of technical information in the world. There is more practical, commercial, timely process information assembled here than is available from any other source. The technical information obtained from a patent is extremely reliable and comprehensive...'*

This is a point of view which is not shared by many users of the patent literature. Unlike the periodical journal literature with which the patent literature is compared favourably by the author, there is no obligation on the part of the inventors to unequivocally establish the nature of the products reported or the reproducibility of the processes described. Claims as to the usefulness of classes of products are frequently exaggerated to provide adequate legal protection of the invention and the emergence of practically useful

#### Conference Announcement

### The Outlook for Polymer Science

UMIST, Manchester, 24 and 25 March 1976

The Sixth Biennial Manchester Polymer Symposium will be held at UMIST on 24 and 25 March 1976 and will mark the retirement of Professor Geoffrey Gee CBE, FRS as Sir Samuel Hall Professor of Chemistry in the University of Manchester. The programme will consist of a number of papers by distinguished workers from the USA and UK who will assess the present stage in the development of various topics and speculate on their future progress under the symposium title, The Outlook for Polymer Science. Applications for further details and a registration form should be made to The Registrar, University of Manchester Institute of Science and Technology (UMIST), PO Box 88, Manchester M60 1QD, UK.

#### Conference Announcement

### Polymeric Delivery Systems

Midland, Michigan, 23–27 August 1976

An international symposium on polymeric delivery systems will be held at the Midland Macromolecular Institute on 23–27 August 1976. It will consist of both invited and contributed papers. The invited papers will offer critical reviews of: formation, and structure of synthetic membranes, films and microcapsules, by H. Hopfenberg; slow release of macromolecules from synthetic membranes, by J. Folkman; synthetic polymeric drugs, by H. Ringsdorf; carriers for bioactive materials, by A. Trouet; pharmaceutical considerations in the design of devices for prolonged drug delivery, by T. Roseman; release of effectors from polymers and microcapsules, by G. Banker; status of delivery systems for drugs and food additives as viewed by FDA, by C. Kumkumian. Contributed papers are solicited. Further details may be obtained from Symposium Secretary, Midland Macromolecular Institute, 1910 West St Andrews Drive, Midland, Michigan 48640, USA

products from the plethora of patents in the antioxidant field is the very rare exception rather than the rule. The author of this book makes no attempt to distinguish between the small number of patents which have been exploited commercially and the remainder which have not.

This book will be of interest to the industrial chemist who is primarily interested in synthesizing new antioxidants and testing them empirically. It will be of little value to the mechanist who is concerned with the design of new antioxidants on the basis of modern theories of antioxidant action.

G. Scott

# Classified Contents

- ABS resins, dynamic transition of grafted polybutadiene, 685
- Acrylonitrile, polymers from, polymerized in the presence of vinylsulphone dyes, 370
- Acrylonitrile, polymerization of, in the presence of vinylsulphone dyes, 43
- Adhesive, anionically prepared flexible: 1. Synthesis, 654. 2. Product analysis, 659. 3. Physical testing, 665
- Aggregation, evidence for, in solutions of poly(ethylene oxide), 306
- Alkali metal adducts of triphenylamine and triphenylphosphine, vinyl polymerization initiated with, 281
- Alternating copolymers, the  $^{13}\text{C}$  n.m.r. spectrum from butadiene and methacrylonitrile, 761
- Alternating copolymers from  $\alpha$ -methylstyrene and methacrylonitrile, the  $^{13}\text{C}$  n.m.r. spectrum, 758
- Alternating copolymers, structure and molecular relaxation of styrene and *N*-substituted maleimides, 739
- Anionic, kinetic study of polymerization of butadiene in a polar solvent, 605
- Anisotropy,  $^{19}\text{F}$  chemical shift, in aligned PTFE fibres, 161
- Annealing, effect on the thermomechanical properties of poly(ethylene oxide), 692
- Benzoyl peroxide as initiator of polymerization, anomalous behaviour, 938
- Biomedical applications of polymeric materials and their interactions with blood components: a critical review of current developments, 409
- Birefringence data, electric, stiffness of aqueous sodium carboxymethyl cellulose from, 720
- Birefringence, flow, studies of polymer conformation: cellulose tricarbanilate in two characteristic solvents, 359
- Bisphenol A, 2,2-bis(4-hydroxyphenyl)propane and 1,4-bis(hydroxymethyl)decafluoro-bicyclo (2.2.1) heptane, synthesis and characterization of some copolycarbonates, 433
- Bisphenol A polycarbonate, observations of craze structure, 549
- Bisphenol A, preparation and properties of some graft copolymers of the poly(2-chlorocyanurate) ester, 38
- Block copolymers, ethylene oxide/propylene oxide, crystallinity and fusion: 1. Type PE copolymers, 889. 2. Type PEP copolymers, 897
- Block copolymers, isotactic ethylene-propylene, anomalous melt elasticity, 936
- Butadiene, kinetic study of anionic polymerization in a polar solvent, 605
- Butadiene, the  $^{13}\text{C}$  n.m.r. spectrum of alternating copolymers from methacrylonitrile, 761
- Butadiene-styrene, n.m.r. studies of copolymers, 338
- $\beta$ -Carotene, persistent polarization in a carotenoid polymer, 5
- Cationic polymerization, absolute reactivity of methyl and other alkyl vinyl ethers, 31
- Cationic polymerization, phosphoryl chloride as an initiator of vinyl monomers, 621
- Cationic polymerization, solvent effect on styrene with  $\alpha$  or  $\beta$ -methylstyrenes, 97
- Cavity field for axially symmetric dielectrics, 477
- Cellulose, aqueous sodium carboxymethyl, stiffness from electric birefringence data, 720
- Cellulose carbanilates, intrinsically coloured polymers from, 903
- Cellulose tricarbanilate in two characteristic solvents: flow birefringence studies of polymer conformation, 359
- Cellulose trinitrate, light scattering Rayleigh linewidth measurements on some solutions, 169
- Chain molecules, an improved model for studying the concentration dependence of the configurational behaviour, 310
- Chitosan gel: a novel polysaccharide gel, 622
- Circular dichroism study of poly(L-tyrosine), poly(L-glutamic acid) and of random and sequential copolymers of L-glutamic acid and L-tyrosine in trimethylphosphate, 16
- Cloud point curves for poly(vinyl methyl ether) and monodisperse polystyrene mixtures, 285
- Coatings, polymeric, on steel produced by the electroinitiated polymerization of acrylic monomers, 881
- Cohesive energy, relationships between  $T_g$ : 1. Dependence of  $T_g$  on the composition of copolymers, 173. 2. Prediction of  $T_g$  of homopolymers, 177
- Conformation of poly(ethylene oxide) in the solid state, melt and solution measured by Raman scattering, 505
- Conformation of polymers, determination, in the amorphous solid state and in concentrated solution by neutron diffraction, 120
- Conformational properties of poly(alkene sulphone)s in solution: 1. Relation between the dielectric properties in solution and the structure of the repeat unit, 569. 2. A rotational isomeric state study of the poly(cyclohexene sulphone) chain, 573
- Conformational studies of *N*-acetyl-*N*-methyl-L-alanine dimethylamide- $d_6$  by n.m.r. spectroscopy, 345
- Conformational study of the sequential (Try-Glu) $_n$  copolymer in aqueous solution, 9
- Conformational transitions, segregation in triblock copolymers in dilute solution: 3. Viscometric investigations in solvent mixtures, 698
- Copolymer, *cis*-1,4-butadiene/isoprene, effect of temperature and molecular weight on the crystallization, 845
- Copolymer, sequential (Try-Glu) $_n$ , conformational study in aqueous solution, 9
- Copolymer, vinyl chloride/vinyl acetate, thermal decomposition, 269
- Copolymers, a route to anionic hydrophilic films of L-leucine, L-aspartic acid and L-aspartic acid esters, 735
- Copolymers, alternating, the  $^{13}\text{C}$  n.m.r. spectrum from butadiene and methacrylonitrile, 761
- Copolymers, alternating, the  $^{13}\text{C}$  n.m.r. spectrum from  $\alpha$ -methylstyrene and methacrylonitrile, 758
- Copolymers, block, of ethylene oxide and isoprene cast from solutions, domain structure and crystalline morphology of AB and ABA type, 249
- Copolymers, butadiene-styrene, n.m.r. studies, 338
- Copolymers of chlorotrifluoroethylene and vinylidene fluoride, heat capacity, 858
- Copolymers, graft, preparation and properties of the poly(2-chlorocyanurate) ester of bisphenol A, 38
- Copolymers, monomeric unit distribution and optical activity: random copolymers of acrylic acid and *N*-(*s*-butyl)-*N*-methyl acrylamide antipodes, 115
- Copolymers, ethylene-vinyl acetate, dielectric behaviour of, 308
- Copolymers of *N*-vinylcarbazole, acoustic studies of chain flexibility in, 797
- Copolymers, POM, synthesis and properties of completely crystalline, 497
- Copolymers, random and sequential, of L-glutamic acid and L-tyrosine in trimethylphosphate, 16
- Copolymers, styrene-acrylonitrile,

- dielectric and dynamic mechanical relaxation studies, 835
- Copolymers, triblock, segregation and conformational transitions in dilute solution: 3. Viscometric investigations in solvent mixtures, 698
- Copolymers, three-block, morphologies and stress-strain properties of samples prepared under various experimental conditions, 531
- Copolymerization behaviour of *N,N'*-divinylureas, 770
- Copolymerization, cationic, of vinyl ethers with styrene derivatives and their model reactions: selectivity of a growing carbocation, 815
- Copolymerization, radical, some kinetic aspects: influence of the reaction medium on the reactivity ratios, 429
- Copolymerization reactivities of alkyl vinyl ketones, structure and radical reactivities of vinyl monomers, 468
- Copolymerization systems styrene/*p*-ethoxystyrene and methyl methacrylate/*p*-ethoxystyrene, reactivity ratios for, 278
- Craze structure, observations of bisphenol A polycarbonate, 549
- Crazing and the creep behaviour of PMMA in methanol, 921
- Crystallinity and fusion of ethylene oxide/propylene oxide block copolymers: 1. Type PE copolymers, 889. 2. Type PEP copolymers, 897
- Crystallinity, measurement of polyamide-6 by d.s.c., 546
- Crystallization of a *cis*-1,4-butadiene/isoprene copolymer, effect of temperature and molecular weight, 845
- Crystallization, effect of molecular weight on isotherms of high molecular weight poly(ethylene oxide), 680
- Crystallization of isotactic poly(methyl methacrylate) from the melt, 930
- Crystallization of isotactic polystyrene induced by organic vapours, 703
- Crystallization of polyamides under elevated pressure: 2. Pressure-induced crystallization of nylon-6 (polycapramide) from the melt, 673
- Crystallization of polyethylene from the melt, effect of intra-chain double bonds, 864
- Crystallization of poly(ethylene oxide) fractions: simultaneous dilatometry and calorimetry, 196
- Decomposition, thermal, effect of dielectric relaxation process of poly(vinyl chloride), 265
- Decomposition, thermal, of polystyrene, 81
- Decomposition, thermal, of a vinyl chloride/vinyl acetate copolymer, 269
- Deformation, heat of, thermomechanical studies on *cis*-polybutadiene, 261
- Deformation mechanisms in polytetrafluoroethylene, 450
- Design of large hot melt extruders, 298
- Dielectric behaviour of ethylene-vinyl acetate copolymers, 308
- Dielectric and dynamic mechanical relaxation studies of styrene-acrylonitrile copolymers, 835
- Dielectric properties of oligomers: 4. Dielectric properties of vinyl acetate and methyl methacrylate oligomers, 101
- Dielectric relaxation, molecular motion in polystyrene-plasticizer systems as studied by, 725
- Dielectric relaxation process of poly(vinyl chloride), effect of thermal decomposition, 265
- Differential scanning calorimetry, derivation of accurate glass transition temperatures, 753
- Elastic behaviour of ideal polystyrene networks, 873
- Elastin gels, texture of, 626
- Elastomers, mechanical response, not too far from equilibrium, 77
- Electrical conductivity of PMMA at linearly increasing temperatures, 166
- Electrical conduction, the role of macromolecules in certain biomedical problems, 25
- Electron microscopy, optimum conditions of radiation-sensitive polymer crystals, 157
- Electro-optical properties of poly( $\epsilon$ -carboboxy-L-lysine) in organic solvents, 791
- Engineering, polymer - *Editorial*, 394
- E.p.r. study of radicals produced mechanically in PGMA and their interaction with oxygen, 730
- E.s.r. study of  $\gamma$ -irradiated isotactic and atactic polypropylene, 510
- Ethylene-propylene, determination of unsaturation in terpolymers and butyl rubber by time-averaged  $^1\text{H}$  n.m.r. measurements, 709
- Extruders, large hot melt, design of, 298
- Extruders, single screw, melting of thermoplastics in, 49
- Fatigue characteristics of several thermoplastics, 908
- Fatigue crack propagation of polymers, the  $\beta$  transition and frequency sensitivity, 850
- Fatigue, effect of temperature and frequency in polymers, 539
- Fibrillation in the flow of polyoxymethylene melts, 609
- Flame resistance, some basic aspects of polymeric materials, 615
- Fluoropolymers, ultrasonic studies of three, 481
- Fracture roughness of polymers, effect of temperature on the impact, 915
- Friction, low temperature internal, in some poly( $\alpha$ -olefins), 595
- Gel permeation chromatography: universal calibration for rigid rod and random coil polymers, 554
- Glass transition of polystyrene, effects of molecular weight and chain ends, 291
- Glass transition temperatures by differential scanning calorimetry, 753
- Graft copolymers, synthesis and characterization of styrene-butadiene, 690
- Graft polymerization to cellulose, developments in radiation-induced: a review, 134
- Grafted polymers from poly(4-vinylpyridinium) salts, 94
- Heat capacity of copolymers of chlorotrifluoroethylene and vinylidene fluoride, 858
- Heat capacity of linear high polymers, 649
- Helix-coil transition of poly( $\epsilon$ -carboboxy-L-lysine) in *m*-cresol, 396
- Infra-red investigation of cardo polymer solutions, 805
- Infra-red study, far, of conformational disorder in PTFE, 74
- Injection moulded specimens, influence of high injection pressures on the internal stress level, 925
- Internal stress level in injection moulded specimens, influence of high injection pressures, 925
- Immobilization of  $\beta$ -D-glucosidase, crosslinked poly[acrylyl *N,N*-bis-(2,2-dimethoxyethyl)amine] and crosslinked poly[acryloylmorpholine/acryloyl *N,N*-bis(2,2-dimethoxyethyl)amine] gel networks and their application to, 314
- $\gamma$ -Irradiation, study of structural change in linear polyethylene by elongation in view of behaviour of free radicals induced, 229
- Ising model, theory of, 335
- Kinetics of water vapour sorption in cellulose, some effects of formaldehyde crosslinking, 2
- Light scattering in an electric field: variations of the  $H_H(\theta)$  component around  $\theta = 90^\circ$ , 329
- Light scattering Rayleigh linewidth measurements on some dextran solution, 561

## Classified Contents

- Light scattering Rayleigh linewidth measurements on some solutions of cellulose trinitrate, 169
- Mechanical and dielectric relaxations in polytrifluoroethylene, 501
- Mechanical response of elastomers not too far from equilibrium, 77
- Melt elasticity, anomalous, of isotactic ethylene-propylene block copolymers, 936
- Melting of thermoplastics in single screw extruders, 49
- Melt viscosity of polycaproyamide, increase by chromium (III) ions, 879
- Methacrylic acid esters, polymerization of sodium hexanitrocobaltate in methanol-water: 11. Catalytic action of metallic salts in autoxidation and polymerization, 590
- Methyl methacrylate, deuterated, inverse isotope effect on the rate of polymerization, 623
- Methyl methacrylate, polymerization of tri-*n*-butylborane in the presence of amino acid esters, 601
- $\alpha$ -Methylstyrene and methacrylonitrile, the  $^{13}\text{C}$  n.m.r. spectrum of alternating copolymers, 758
- Migration of PVC plasticizers into alcohols, 840
- Molecular motions, a broadline n.m.r. study in some multicomponent crosslinked polymers, 377
- Molecular motion in polyisobutylene and poly(propylene oxide) studied by  $^{13}\text{C}$  nuclear magnetic relaxation, 493
- Molecular motion in polystyrene-plasticizer systems as studied by dielectric relaxation, 725
- Molecular packing density in boundary layers of some polymers, 582
- Molecular relaxation, structure of alternating copolymers of styrene and *N*-substituted maleimides, 739
- Molecular weight and chain ends on glass transition of polystyrene, effects of, 291
- Molecular weight, effect on crystallization isotherms of high molecular weight poly(ethylene oxide), 680
- Molecular weight, effect of, on the morphology and drawing behaviour of melt crystallized linear polyethylene, 239
- Molecular weight, effect of, on spherulite growth rates of high molecular weight poly(ethylene oxide) fractions, 191
- Morphology, crystalline, domain structure of AB and ABA type block copolymers of ethylene oxide and isoprene cast from solutions, 249
- Morphology, effect of molecular weight and drawing behaviour of melt crystallized linear polyethylene, 239
- Network properties: 2. A broadline n.m.r. study of molecular motions in some multicomponent crosslinked polymers, 377
- Network structure, study of relationship of g.p.c. gels and molecular size of permeable substance, 321
- Networks, stretched, effect of a non-uniform distribution of crosslinks on the analysis of Raman polarization data, 227
- Neutron diffraction, determination of the conformation of polymers in the amorphous solid state and in concentrated solution, 120
- Neutron scattering, elastic, study of the conformational rigidity of polyelectrolytes: 1. Carboxymethyl-celluloses in the intermediate momentum range, 776. 2. Molecular dimensions and conformation of poly(methacrylic acid), 781
- Neutron, small angle, and X-ray scattering by poly(methyl methacrylate) chains, 645
- Non-linear viscoelastic properties of polymer melts and concentrated solutions, a phenomenological description of, 418
- N.m.r., a broadline study of molecular motions in some multicomponent crosslinked polymers, 377
- N.m.r., broadline, studies of ultra-high modulus polyethylenes, 57
- N.m.r.,  $^{13}\text{C}$ ., detection of tacticity in polypropylenimine, 763
- N.m.r.,  $^{13}\text{C}$ ., spectra at 67.88 and at 90.51 MHz, 465. of poly( $\alpha$ -methylstyrene), 465
- N.m.r.,  $^{13}\text{C}$ ., the spectrum of alternating copolymers from  $\alpha$ -methylstyrene and methacrylonitrile, 758
- N.m.r.,  $^{13}\text{C}$  the spectrum of alternating copolymers from butadiene and methacrylonitrile, 761
- N.m.r. spectroscopy, conformational studies of *N*-acetyl-*N*-methyl-L-alanine dimethylamide-*d*<sub>6</sub>, 345
- N.m.r. spectrum,  $^{13}\text{C}$ ., of polybutadiene with *cis*-1,4-*trans*-1,4- and 1,2-units, 154
- N.m.r. studies of butadiene-styrene copolymers, 338
- N.m.r., time-averaged  $^1\text{H}$ ., determination of unsaturation in ethylene-propylene terpolymers and butyl rubber by measurements, 709
- Nuclear magnetic relaxation dispersion, estimation of the correlation length in polymer melts, 851
- Nuclear magnetic relaxation in linear and branched polyethylene, 125
- Nuclear magnetic relaxation,  $^{13}\text{C}$ ., molecular motion in polyisobutylene and poly(propylene oxide), 493
- Nylon-6 (polycapramide), pressure-induced crystallization from the melt, 673
- Oxygen, effects on the vinyl polymerization systems: limitations of conventional dilatometry, 934
- Ozonolysis, saturated hydrocarbon prepolymers by, 799
- Peptide, sequence, polymers: 3. Synthesis and conformational study in solution of poly(L-leucyl-L-leucyl-*N*-carbobenzyloxy-L-lysine), 234
- Phosphonitrilic chloride: 23. Substitution reaction of phosphonitrilic chloride trimer with sodium hydroxymethylphenolate and polymerization of substitution products, 21. 27. Synthesis and properties of cyclophosphazene polymers, 671. 30. Synthesis of chelating polymers from cyclophosphazene derivatives and studies of their electrical properties and thermal conductivity, 861
- Plasticizers, migration of PVC into alcohols, 840
- Polarization, persistent, in a carotenoid polymer,  $\beta$ -carotene, 5
- Poly(acrylic acid), low molecular weight atactic, solution properties and its sodium salt, 68
- Poly[acrylyl *N,N*-bis(2,2-dimethoxyethyl) amine], crosslinked, and crosslinked poly[acryloylmorpholine/acryloyl *N,N*-bis(2,2-dimethoxyethyl)amine] gel networks and their application to the immobilization of  $\beta$ -D-glucosidase, 314
- Poly(alkene sulphone)s, conformational properties in solution: 1. Relation between the dielectric properties in solution and the structure of the repeat unit, 569. 2. A rotational isomeric state study of the poly-(cyclohexene sulphone) chain, 573
- Polyamides, crystallization, under elevated pressure: 2. Pressure-induced crystallization of nylon-6 (polycapramide) from the melt, 673
- Polyamide-6, measurement of crystallinity by d.s.c., 546
- Poly(aryl isocyanates), solvent effect on the unperturbed dimensions, 765
- Poly( $\gamma$ -benzyl-L-glutamate), growth of lamellar crystals, 69
- Poly( $\gamma$ -benzyl-L-glutamate), thermodynamic properties of concentrated solutions, 629
- Poly(*p*-biphenyl methacrylate), properties of, in dilute solution, 386
- Poly(*p*-biphenyl methacrylate), temperature dependence of the unperturbed dimensions of, 848
- 1,4-Polybutadiene, chlorination, 66
- Polybutadiene, grafted, dynamic transition in ABS resins, 685
- Polybutadiene, structure of: 4.  $^{13}\text{C}$  n.m.r. spectrum of polybutadiene with *cis*-1,4-, *trans*-1,4- and 1,2-units, 154

- cis*-Polybutadiene, thermomechanical heat of deformation studies, 261
- cis*- and *trans*-1,4-Polybutadiene, upper and lower theta temperatures for solutions of, 933
- Poly(butylene terephthalate) multiple melting, 462
- Polycaproyamide, increase of the melt viscosity by chromium (III) ions, 879
- Poly( $\epsilon$ -carbobenzyloxy-L-lysine), helix-coil transition in *m*-cresol, 396
- Poly( $\epsilon$ -carboboxy-L-lysine) in organic solvents, electro-optical properties, 791
- Poly(diethyl vinylphosphonate), thermal degradation of its copolymer, 641
- Polyesteramides, transitions of a series of regularly alternating linear, 565
- Polyethers, solid, thermodynamic studies: 5. Crystalline-amorphous interfacial thermal properties, 634
- Polyethylene, effect of intra-chain double bonds on the crystallization from the melt, 864
- Polyethylene, linear and branched, nuclear magnetic relaxation in, 125
- Polyethylene, linear, study of structural change by elongation in view of behaviour of free radicals induced by  $\gamma$ -irradiation, 229
- Polyethylene, melt crystallized linear, effect of molecular weight on the morphology and drawing behaviour, 239
- Polyethylenes, ultra-high modulus, broadline n.m.r. studies, 57
- Polyethylenes, ultra-high modulus linear: effect of initial crystallization conditions, 469
- Poly(ethylene oxide), conformation in the solid state, melt and solution measured by Raman scattering, 505
- Poly(ethylene oxide), effect of annealing on the thermomechanical properties, 692
- Poly(ethylene oxide), effect of molecular weight on crystallization isotherms of high molecular weight, 680
- Poly(ethylene oxide), evidence for aggregation in solutions, 306
- Poly(ethylene oxide) fractions, crystallization: simultaneous dilatometry and calorimetry, 196
- Poly(ethylene oxide) fractions, effect of molecular weight on spherulite growth rates of high molecular weight, 191
- Poly(ethylene terephthalate), studies on the formation: 3. Catalytic activity of metal compounds in transesterification of dimethyl terephthalate with ethylene glycol, 185
- Poly(L-glutamic acid), potentiometric study in water-dioxane mixtures, 785
- Poly(L-glutamic acid) preferential and absolute adsorption in water-dioxane mixtures, 401
- PGMA, e.p.r. study of radicals produced mechanically and their interaction with oxygen, 730
- Poly(isobutene oxide), studies on: 3. Elastic hard fibre of poly(isobutene oxide), 425
- Polyisobutylene and poly(propylene oxide), molecular motion studied by  $^{13}\text{C}$  nuclear magnetic relaxation, 493
- cis*-1,4-Polyisoprenes, synthetic, and natural rubber, transport of water in, 811
- cis*-1,4-Polyisoprene-*b*-poly(methyl methacrylate) copolymer, synthesis and characterization, 151
- Poly(itaconic acid esters), containing phenyl and cyclohexyl rings, dynamic mechanical spectra, 869
- Poly(L-leucyl-L-leucyl-L-aspartic acid) and poly(L-leucyl-L-leucyl-L-lysine), solvent effects on the optical behaviour of, 382
- Polymerization, anionic, kinetic study of butadiene in a polar solvent, 605
- Polymerization, anomalous behaviour of benzoyl peroxide as initiator, 938
- Polymerization, cationic, absolute reactivity of methyl and other alkyl vinyl ethers, 31
- Polymerization, cationic, of *p*-methoxystyrene initiated by cycloheptatrienyl hexachloroantimonate, 819
- Polymerization, cationic, phosphoryl chloride as an initiator of vinyl monomers, 621
- Polymerization, cationic, solvent effect on styrene with  $\alpha$  or  $\beta$ -methylstyrenes, 97
- Polymerization, electroinitiated, of acrylic monomers, polymeric coatings on steel produced by, 881
- Polymerization, free cationic, kinetic studies of ethyl vinyl ether and isobutyl vinyl ether initiated by triphenylmethyl hexachloroantimonate, 527
- Polymerization, graft, kinetics of styrene on *cis*-1, 4-polybutadiene, 520
- Polymerization, inverse isotope effect on the rate of deuterated methyl methacrylate, 623
- Polymerization of acrylonitrile in the presence of vinylsulphone dyes, 43
- Polymerization of methyl methacrylate by tri-*n*-butylborane in the presence of amino acid esters, 601
- Polymerization, stereoregular of vinyl chloride with the redox system ferrous sulphate/hydrogen peroxide/oxalic acid. 2. Process kinetics, 717
- Polymerization of THF, a new catalytic system, 548
- Polymerization, vinyl, initiated with alkali metal adducts of triphenylamine and triphenylphosphine, 281
- Polymerization, vinyl chloride, effect of oligo-amine (or polyamine) by alkyl aluminium compounds, 406
- Polymerization, Ziegler-Natta, active centre determination in donor-modified, 384
- Polymethacrylate, dilatometric study of monovalent counter-ion association [Comments on Letter by J. Kimiyama, Y. Takeda, M. Ando and T. Iijima (*Polymer* 1974, 15, 468-470)], 228
- PMMA, crazing and the creep behaviour in methanol, 921
- PMMA, electrical conductivity at linearly increasing temperatures, 166
- PMMA, irradiated doped, thermoluminescence and induced phosphorescence, 745
- Poly(methyl methacrylate), association of stereoregular: 2. Formation of stereocomplex in bulk, 515
- Poly(methyl methacrylate), atactic and isotactic, sorption of water vapour by, 441
- Poly(methyl methacrylate), effect of pressure on the formation of glasses, 585
- Poly(methyl methacrylate) influence of tacticity on the compatibility with poly(vinyl chloride), 201
- Poly(methyl methacrylate), isotactic, crystallization from the melt, 930
- Poly(methyl methacrylate), small angle neutron and X-ray scattering by chains, 645
- Poly( $\alpha$ -methylstyrene) solutions, phase equilibria in quasi-binary, 244
- Poly( $\alpha$ -methylstyrene), structure of: 3.  $^{13}\text{C}$  n.m.r. spectra at 67.88 and at 90.51 MHz, 465
- Poly( $\alpha$ -olefins), low temperature internal friction, 595
- Poly(oxybenzhydrylidene-1,4-phenylenemethylene), 545
- Polyoxyethylene, amorphous, stress-strain isotherms and thermoelastic properties of crosslinked in compression, 326
- Polyoxymethylene, fibrillation in the flow of melts, 609
- Poly(1-pentene), isotactic, kinetics of the thermal oxidation, 749
- Poly(*p*-phenylene diacrylic acid diethyl ester), depolymerization behaviour, 218
- Poly(propylene glycols), viscoelastic properties, 110
- Polypropylene, isotactic and atactic, e.s.r. study of  $\gamma$ -irradiated, 510
- Polypropylene, isotactic, structural effects in the sub-millimetre wave spectrum, 714
- Poly(propylene sulphide), solution properties, 105
- Polypropyleneimine, detection of tacticity by  $^{13}\text{C}$  n.m.r., 763
- Polystyrene, effects of molecular weight and chain ends on glass transition, 291
- Polystyrene, ideal networks, elastic behaviour, 873
- Polystyrene, isotactic, crystallization induced by organic vapours, 703

## Classified Contents

- Polystyrene—plasticizer, molecular motion in systems as studied by dielectric relaxation, 725
- Polystyrene, thermal decomposition, 81
- Polystyrenes, comb, synthesis and solution properties, 827
- PTFE fibres, aligned,  $^{19}\text{F}$  chemical shift anisotropy, 161
- PTFE, far infra-red study of conformation disorder in, 74
- Polytetrafluoroethylene, deformation mechanisms in, 450
- Polytrifluoroethylene, mechanical and dielectric relaxations, 501
- Polyvinylbiphenyl carbanions, spectroscopic evidence for ion-pair equilibria involving, 695
- PVC, use of organotin compounds in the thermal stabilization: 6. A radiochemical study of the effect of variations in molecular weight on the reaction between PVC and di(butylthiolato)dibutyltin, 833
- Poly(vinyl chloride), effect of thermal decomposition on dielectric relaxation process, 265
- Poly(vinyl chloride), suspension, particle structure and fusion, 470
- Poly(vinyl methyl ether) and monodisperse polystyrene mixtures, cloud point curves for, 285
- Poly(4-vinylpyridinium) salts, grafted polymers, 94
- Proteins, globular, containing high molecular weight impurities, light scattering Rayleigh linewidth measurements, 773
- Radiation-induced graft polymerization to cellulose, a review, 134
- Radical reactivities, and structure, of vinyl monomers: copolymerization reactivities of alkyl vinyl ketones, 468
- Random and sequential copolymers of L-glutamic acid and L-tyrosine in trimethylphosphate, 16
- Reactivity ratios for the copolymerization systems styrene/*p*-ethoxystyrene and methyl methacrylate/*p*-ethoxystyrene, 278
- Refractive index, specific, increments of certain polysaccharide systems, 474
- Relative reactivities of vinyl monomers, evaluation of, towards *t*-butoxy radical by means of spin trapping technique, 389
- $\beta$ -Relaxation in polymers, a formula for, 852
- Rubber elasticity, the energetic contribution in the range of small uniaxial compression and moderate elongation, 209
- Solvent effect on the unperturbed dimensions of poly(aryl isocyanates), 765
- Solvent motion, a study of, in acetone—PMMA solutions using  $^{13}\text{C}$  and  $^1\text{H}$  spin-lattice relaxation measurements, 489
- Spin-lattice relaxation measurements,  $^{13}\text{C}$  and  $^1\text{H}$ , a study of solvent motion in acetone—PMMA solutions, 489
- Stabilization, thermal, of PVC, use of organotin compounds: 6. A radiochemical study of the effect of variations in molecular weight on the reaction between PVC and di(butylthiolato)dibutyltin, 833
- Star polymers from styrene and divinylbenzene, 180
- Stress—strain isotherms and thermoelastic properties of crosslinked amorphous polyoxyethylene in compression, 326
- Stress—strain properties, morphologies of samples prepared under various experimental conditions, 531
- Styrene—acrylonitrile copolymers, dielectric and dynamic mechanical relaxation studies, 835
- Styrene—butadiene, synthesis and characterization of graft copolymers, 690
- Styrene derivatives and their model reactions, cationic copolymerization of vinyl ethers with: selectivity of a growing carbocation, 819
- Styrene, solvent effect on cationic polymerization with  $\alpha$  or  $\beta$ -methylstyrenes, 97
- Styrene, structure and molecular relaxation of alternating copolymers and *N*-substituted maleimides, 739
- Tacticity, influence of poly(methyl methacrylate) on the compatibility with poly(vinyl chloride), 201
- Temperature dependence of the unperturbed dimensions of poly(*p*-biphenyl methacrylate), 848
- Temperature, effect of, on the impact fracture toughness of polymers, 915
- Thermal degradation of poly(diethyl vinylphosphonate) and its copolymer, 641
- Thermal oxidation, kinetics of isotactic poly(1-pentene), 749
- Thermodynamic properties of concentrated poly( $\gamma$ -benzyl-L-glutamate) solutions, 629
- Thermodynamic studies of solid polyethers: 5. Crystalline—amorphous interfacial thermal properties, 634
- Thermoluminescence and induced phosphorescence in irradiated doped PMMA, 745
- Thermoplastics, fatigue characteristics, 908
- Thermoplastics mouldings, voiding in glass fibre reinforced, 459
- Transport of water in synthetic *cis*-1,4-polyisoprenes and natural rubber, 811
- Ultra-high modulus linear polyethylenes, preparation of: effect of initial crystallization conditions, 469
- Ultrasonic studies of three fluoropolymers, 481
- Upper critical solution temperatures in the polystyrene—cyclohexane system, pressure dependence, 445
- Vinyl chloride, effect of oligo-amine (or polyamine) on the polymerization by alkyl aluminium compounds, 406
- Vinyl chloride polymers, heat treated, solvent sorption of, 387
- Vinyl chloride, stereoregular polymerization with the redox system ferrous sulphate/hydrogen peroxide/oxalic acid: 2. Process kinetics, 717
- Vinyl monomers, evaluation of relative reactivities of, towards *t*-butoxy radical by means of spin trapping technique, 389
- Vinyl monomers, phosphoryl chloride as an initiator for the cationic polymerization of, 621
- Vinyl monomers, structure and radical reactivities of alkyl vinyl ketones, 468
- Vinyl polymerization systems, effects of oxygen: limitations of conventional dilatometry, 934
- Vinylsulphone dyes, polymers from acrylonitrile polymerized in the presence of, 370
- Viscoelastic properties of poly(propylene glycols), 110
- Viscoelasticity, dynamic, of entangled polymers, 223
- Viscosity of Newtonian suspensions, 305
- Voiding in glass fibre reinforced thermoplastics mouldings, 459
- Vulcanizates, SBR sulphur, influence of cure system concentration on crosslink structure, 205
- Ziegler—Natta polymerization, active centre determination in donor-modified, 384

# Author Index

- Ablazova, T. I.: *see* Vinogradov, G. V., Yarlykov, B. V., Tsebrenko, M. V., Yudin, A. V. and Ablazova, T. I.
- Adam, G. A., Parsons, I. W. and Haward, R. N.: Synthesis and characterization of some copolycarbonates of 2,2-bis(4-hydroxyphenyl)propane (bisphenol A) and 1,4-bis(hydroxymethyl)decafluoro-bicyclo(2.2.1)heptane, 433
- Adamec, V. and Mateová, E.: Electrical conductivity of PMMA at linearly increasing temperatures, 166
- Akimoto, Akira: Effect of oligo-amine (or polyamine) on the vinyl chloride polymerization by alkyl aluminium compounds, 406
- Alavi-Moghadam, F., Ayrey, G. and Poller, R. C.: Use of organotin compounds in the thermal stabilization of PVC: 6. A radiochemical study of the effect of variations in molecular weight on the reaction between PVC and di(butylthiolato)-dibutyltin, 833
- Alexopoulos, J. B., Hadjichristidis, N. and Vassiliadis, A.: Properties of poly(*p*-biphenyl methacrylate) in dilute solution, 386
- Alfonso, Giovanni C.: *see* Pedemonte, Enrico; Dondero, Giovanni C. and de Candia, Francesco
- Alfthan, E. and de Ruvo, A.: Effect of annealing on the thermomechanical properties of poly(ethylene oxide), 692
- Ali, A. S. M.: *see* Haigh, J., Ali, A. S. M. and Davies, G. J.
- Allen, G.: *see* de Boos, A. G. and Allen, G.
- Allen, G.: *see* Price, C., Allen, G. and Yoshimura, N.
- Allen, Geoffrey: *see* Wolf, F. P. and Allen, Geoffrey
- Amelino, L. and Martuscelli, E.: Effect of intra-chain double bonds on the crystallization of polyethylene from the melt, 864
- Aoyama, T.: *see* Ikada, E., Sugimura, T., Aoyama, T. and Watanabe, T.
- Ashman, P. C. and Booth, C.: Crystallinity and fusion of ethylene oxide/propylene oxide block copolymers: 1. Type PE copolymers, 889
- Ashman, P. C., Booth, C., Cooper, D. R. and Price, C.: Crystallinity and fusion of ethylene oxide/propylene oxide block copolymers: 2. Type PEP copolymers, 897
- Ayrey, G.: *see* Alavi-Moghadam, F., Ayrey, G. and Poller, R. C.
- Ayrey, G. and Wong, D. J. D.: Inverse isotope effect on the rate of polymerization of deuterated methyl methacrylate, 623
- Bain, D. R.: *see* Margerison, D., Bain, D. R., Lindley, K., Morgan, N. W. and Taylor, Lindsay
- Baird, Martin, E. and Houston, Eve: Dielectric behaviour of ethylene-vinyl acetate copolymers, 308
- Bamford, C. H., Eastmond, G. C. and Whittle, D.: Network properties: 2. A broadline n.m.r. study of molecular motions in some multi-component crosslinked polymers, 377
- Bantjes, A.: *see* Sederel, W. L., Bantjes, A. and Feijen, J.
- Barlow, A. John and Erginsav, Aynur: Viscoelastic properties of poly(propylene glycols), 110
- Barrie, J. A.: *see* Evans, D. C., Barrie, J. A. and George, M. H.
- Barrie, J. A.: *see* Evans, D. C., George, M. H. and Barrie, J. A.
- Barrie, J. A., Machin, D. and Nunn, A.: Transport of water in synthetic *cis*-1,4-polyisoprenes and natural rubber, 811
- Batty, N. S. and Guthrie, J. T.: Polymerization of acrylonitrile in the presence of vinylsulphone dyes, 43. Polymers from acrylonitrile polymerized in the presence of vinylsulphone dyes, 370
- Beevers, R. B.: Texture of elastin gels, 626
- Benham, P. P.: *see* Crawford, R. J. and Benham, P. P.
- Benoit, Henri: *see* Dondos, Anastasios; Rempp, Paul; and Benoit, Henri
- Benson, Richard, Guthrie, J. T. and Lartey, Ransford B.: Intrinsically coloured polymers from cellulose carbanilates, 903
- Berghmans, H.: *see* Overbergh, N., Berghmans, H. and Smets, G.
- Bevington, J. C. and Dyball, C. J.: Anomalous behaviour of benzoyl peroxide as an initiator of polymerization, 938
- Bevington, J. C. and Ratti, L.: Chlorination of 1,4-polybutadiene, 66
- Bilen, C. S.: *see* Morantz, D. J. and Bilen, C. S.
- Biswas, Mukul and Mishra, Prashant K.: Phosphoryl chloride as an initiator for the cationic polymerization of vinyl monomers, 621
- Blanchard, Louis-P.: *see* Malhotra, Shadi L., Hesse, Jean and Blanchard, Louis-P.
- Block, H., Lord, P. W. and Walker, S. M.: Structure and molecular relaxation of alternating copolymers of styrene and *N*-substituted maleimides, 739
- Blow, C. M. and Loo, C. T.: Influence of cure system concentration on crosslink structure in SBR sulphur vulcanizates, 205
- Boicelli, A.: *see* Segre, A. L., Delfini, M., Conti, F. and Boicelli, A.
- Bonta, Giorgio; Gallo, Bianca, M.; and Russo, Saverio: Some kinetic aspects of radical copolymerization: influence of the reaction medium on the reactivity ratios, 429
- Booth, C.: *see* Ashman, P. C. and Booth, C.
- Booth, C.: *see* Ashman, P. C., Booth, C., Cooper, D. R. and Price, C.
- Booth, C.: *see* Maclaine, J. Q. G. and Booth, C.
- Booth, C.: *see* Price, C., Evans, K. A. and Booth, C.
- Borri, C., Sorta, E. and Zotteri, L.: Transitions of a series of regularly alternating linear polyesteramides, 565
- Braud, Christian and Vert, Michel: Monomeric unit distribution and optical activity of copolymers: random copolymers of acrylic acid and *N*-(*s*-butyl)-*N*-methyl acrylamide antipodes, 115
- Braun, D. and Platzek, U.: Poly(oxybenzhydrylidene-1,4-phenylene-methylene), 545
- Bravin, L. and D'Alagni, M.: Sequence peptide polymers: 3. Synthesis and conformational study in solution of poly(L-leucyl-L-leucyl-*e*-*N*-carbobenzyloxy-L-lysine), 234
- Brereton, M. G.: A phenomenological description of the non-linear viscoelastic properties of polymer melts and concentrated solutions, 418
- Bruck, Stephen D.: Biomedical applications of polymeric materials and their interactions with blood components: a critical review of current developments, 409. The role of electrical conduction of macromolecules in certain biomedical problems, 25
- Burchard, Walther: *see* Eschwey, Helmut and Burchard, Walther
- Burfield, D. R.: Active centre determination in donor-modified Ziegler-Natta polymerization, 384
- Burgin, Dennis: *see* Rudin, Alfred and Burgin, Dennis
- Capaccio, G., Chapman, T. J. and Ward, I. M.: Preparation of ultra-high modulus linear polyethylenes: effect of initial crystallization conditions, 469
- Capaccio, G. and Ward, I. M.: Effect of molecular weight on the morphology and drawing behaviour of melt crystallized linear polyethylene, 239



- Caze, Claude: *see* Ghesquiere, Denis; Caze, Claude; and Loucheux, Claude
- Challa, G.: *see* de Boer, A., van Ekenstein, G. O. R. Alberda and Challa, G.
- Challa, G.: *see* Feitsma, E. L., de Boer, A. and Challa, G.
- Challa, G.: *see* Schurer, J. W., de Boer, A. and Challa, G.
- Chantry, G. W.: *see* Willis, H. A., Cudby, M. E. A., Chantry, G. W., Nicol, Elisabeth A. and Fleming, J. W.
- Chapman, T. J.: *see* Capaccio, G., Chapman, T. J. and Ward, I. M.
- Chartoff, Richard P.: Particle structure and fusion of suspension poly(vinyl chloride), 470
- Chen, F. C.: *see* Kwan, S. F., Chen, F. C. and Choy, C. L.
- Chen, F. C.: *see* Wong, K. C., Chen, F. C. and Choy, C. L.
- Choy, C. L.: *see* Kwan, S. F., Chen, F. C. and Choy, C. L.
- Choy, C. L.: *see* Wong, K. C., Chen, F. C. and Choy, C. L.
- Choy, C. L., Tse, Y. K., Tsui, S. M. and Hsu, B. S.: Mechanical and dielectric relaxations in polytrifluoroethylene, 501
- Chung, Y. J., Rooney, J. M., Squire, D. R. and Stannett, V.: Kinetic studies of the free cationic polymerization of ethyl vinyl ether and isobutyl vinyl ether initiated by triphenylmethyl hexachloroantimonate, 527
- Clark, A. T. and Lal, M.: An improved model for studying the concentration dependence of the configurational behaviour of chain molecules, 310
- Cogswell, F. N. and Hanson, D. E.: Anomalous melt elasticity of isotactic ethylene-propylene block copolymers, 936
- Cook, M., Williams, G. and Jones, T. Tyssul: Dielectric and dynamic mechanical relaxation studies of styrene-acrylonitrile copolymers, 835
- Conti, F.: *see* Segre, A. L., Delfini, M., Conti, F. and Boicelli, A.
- Cooper, D. R.: *see* Ashman, P. C., Booth, C., Cooper, D. R. and Price, C.
- Coppola, G., Filippini, R. and Pallesi, B.: Measurement of crystallinity of polyamide-6 by d.s.c., 546
- Corfield, G. C., Monks, H. H. and Ellinger, L. P.: Copolymerization behaviour of *N,N'*-divinylureas, 770
- Cowie, J. M. G. and McEwen, I. J.: Phase equilibria in quasi-binary poly( $\alpha$ -methylstyrene) solutions, 244
- Cowie, J. M. G. and McEwen, I. J.: Upper and lower theta temperatures for solutions of *cis* and *trans* 1,4-polybutadiene, 933
- Cowie, J. M. G., McEwen, I. J. and Velicković, J.: Dynamic mechanical spectra of poly(itaconic acid esters) containing phenyl and cyclohexyl rings, 869
- Crawford, R. J. and Benham, P. P.: A comparison of the fatigue characteristics of several thermoplastics, 908
- Cudby, M. E. A.: *see* Willis, H. A., Cudby, M. E. A., Chantry, G. W., Nicol, Elisabeth A. and Fleming, J. W.
- Culver, L. E.: *see* Radon, J. C. and Culver, L. E.
- Cuniberti, Carla: Evidence for aggregation in solutions of poly(ethylene oxide), 306
- Cunliffe, A. V., Huglin, M. B., Pearce, P. J. and Richards, D. H.: An anionically prepared flexible adhesive: 1. Synthesis, 654. 2. Product analysis, 659. 3. Physical testing, 665
- D'Alagni, M.: *see* Bravin, L. and D'Alagni, M.
- D'Alagni, M. and Giglio, E.: Solvent effects on the optical behaviour of poly(L-leucyl-L-seucyl-L-aspartic acid) and poly(L-leucyl-L-leucyl-L-lysine), 382
- Danusso, F.: *see* Riccò, T., Pavan, A. and Danusso, F.
- Darlington, M. W. and Smith, G. R.: Voiding in glass fibre reinforced thermoplastics mouldings, 459
- Daryanani, R.: *see* Noordermeer, J. W. M., Daryanani, R. and Janeschitz-Kriegl, H.
- Davies, G. J.: *see* Haigh, J., Ali, A. S. M. and Davies, G. J.
- Dawkins, J. V. and Hemming, Malcolm: Gel permeation chromatography: universal calibration for rigid rod and random coil polymers, 554
- de Boer, A.: *see* Feitsma, E. L., de Boer, A. and Challa, G.
- de Boer, A., van Ekenstein, G. O. R. Alberda and Challa, G.: Crystallization of isotactic poly(methyl methacrylate) from the melt, 930
- de Boer, A.: *see* Schurer, J. W., de Boer, A. and Challa, G.
- de Boos, A. G. and Allen, G.: Preparation and properties of some graft copolymers of the poly(2-chlorocyanurate) ester of bisphenol A, 38
- de Candia, Francesco: *see* Pedemonte, Enrico; Dondero, Giovanni; Alfonso, Giovanni C.; and de Candia, Francesco
- De Chirico, Aurelio: Effect of temperature and molecular weight on the crystallization of a *cis*-1,4-butadiene/isoprene copolymer, 845
- Delfini, M.: *see* Segre, A. L., Delfini, M., Conti, F. and Boicelli, A.
- de Ruvo, A.: *see* Alftan, E. and de Ruvo, A.
- Desreux, V.: *see* Lecomte, L. and Desreux, V.
- Dimov, K.: *see* Slavtcheva, L. and Dimov, K.
- Dondero, Giovanni: *see* Pedemonte, Enrico; Dondero, Giovanni C.; and de Candia, Francesco
- Dondos, Anastasios; Rempp, Paul; and Benoit, Henri: Segregation and conformational transitions in triblock copolymers in dilute solution: 3. Viscometric investigations in solvent mixtures, 698
- Dröscher, M., Lieser, G., Reimann, H. and Wegner, G.: Synthesis and properties of completely crystalline POM copolymers, 497
- Durtal, Graham: Observations of craze structure in bisphenol A polycarbonate, 549
- Dyball, C. J.: *see* Bevington, J. C. and Dyball, C. J.
- Eastmond, G. C.: *see* Bamford, C. H., Eastmond, G. C. and Whittle, D.
- Edmondson, I. R. and Fenner, R. T.: Melting of thermoplastics in single screw extruders, 49
- van Ekenstein, G. O. R. Alberda: *see* de Boer, A., van Ekenstein, G. O. R. Alberda and Challa, G.
- Elgert, K.-F. and Stützel, B.: On the  $^{13}\text{C}$  n.m.r. spectrum of alternating copolymers from  $\alpha$ -methylstyrene and methacrylonitrile, 758
- Elgert, K.-F., Stützel, B. and Forgó, Impre: On the  $^{13}\text{C}$  n.m.r. spectrum of alternating copolymers from butadiene and methacrylonitrile, 761
- Elgert, K. F., Wicke, R., Stützel, B. and Ritter, W.: On the structure of poly( $\alpha$ -methylstyrene): 3.  $^{13}\text{C}$  n.m.r. spectra at 67.88 and 90.51 MHz, 465
- Elgert, Karl-Friedrich; Quack, Günther and Stützel, Bernhard: On the structure of polybutadiene: 4.  $^{13}\text{C}$  n.m.r. spectrum of polybutadiene with *cis*-1,4-, *trans*-1,4- and 1,2-units, 154
- Ellinger, L. P.: *see* Corfield, G. C., Monks, H. H. and Ellinger, L. P.
- Emi, Shingo: *see* Hayashi, Toshio; Emi, Shingo; and Nakajima, Akio
- Epton, R., Hibbert, Barbara L. and Marr, G.: Crosslinked poly[acryloyl *N,N*-bis(2,2-dimethoxyethyl) amine] and crosslinked poly[acryloylmorpholine/acryloyl *N,N*-bis(2,2-dimethoxyethyl) amine] gel networks and their application to the immobilization of  $\beta$ -D-glucosidase, 314
- Erginsav, Aynur: *see* Barlow, A. John and Erginsav, Aynur
- Eschwey, Helmut and Burchard, Walther: Star polymers from styrene and divinylbenzene, 180
- Evans, D. C., Barrie, J. A. and George, M. H.: Synthesis and characterization of a *cis*-1,4-polyisoprene-*b*-poly(methyl methacrylate) copolymer, 151

- Evans, D. C., George, M. H. and Barrie, J. A.: Synthesis and characterization of styrene-butadiene graft copolymers, 690
- Evans, K. A.: *see* Price, C., Evans, K. A. and Booth, C.
- Fawcett, A. H. and Ivin, K. J.: Conformational properties of poly(alkene sulphone)s in solution: 1. Relation between the dielectric properties in solution and the structure of the repeat unit, 569. 2. A rotational isomeric state study of the poly(cyclohexene sulphone) chain, 573
- Fedors, R. F.: Viscosity of Newtonian suspensions, 305
- Fedors, R. F. and Landel, R. F.: Mechanical response of elastomers not too far from equilibrium, 77
- Feijen, J.: *see* Sederel, W. L., Bantjes, A. and Feijen, J.
- Feitsma, E. L., de Boer, A. and Challa, G.: Association of stereoregular poly(methyl methacrylate): 2. Formation of stereocomplex in bulk, 515
- Fenner, R. T.: *see* Edmondson, I. R. and Fenner, R. T.
- Fenner, R. T.: The design of large hot melt extruders, 298
- Filippini, R.: *see* Coppola, G., Filippini, R. and Palesi, B.
- Fleming, J. W.: *see* Willis, H. A., Cudby, M. E. A., Chantry, G. W., Nicol, Elisabeth A. and Fleming, J. W.
- Flory, P. J.: *see* Yoon, D. Y. and Flory, P. J.
- Fontanille, M.: *see* Siove, A. Sigwalt, P. and Fontanille, M.
- Forgó, Impre: *see* Elgert, K.-F., Stützel, B. and Forgó, Impre
- Foweraker, Alan R. and Jennings, Barry R.: Stiffness of aqueous sodium carboxymethyl cellulose from electric birefringence data, 720
- Froelich, D.: *see* Rietsch, F. and Froelich, D.
- Gabbay, S. M., Stivala, S. S. and Reich, L.: Kinetics of the thermal oxidation of isotactic poly(1-pentene), 749
- Garton, A. and George, M. H.: Effects of oxygen on vinyl polymerization systems: limitations of conventional dilatometry, 934
- Gallo, Bianca M.: *see* Bontà, Giorgio; Gallo, Bianca M. and Russo, Saverio
- Garroway, A. N., Stalker, D. C. and Mansfield, P.:  $^{19}\text{F}$  chemical shift anisotropy in aligned PTFE fibres, 161
- George, M. H.: *see* Evans, D. C., Barrie, J. A. and George, M. H.
- George, M. H.: *see* Evans, D. C., George, M. H. and Barrie, J. A.
- George, M. H.: *see* Garton, A. and George, M. H.
- Georgescu, L.: On the theory of the Ising model of the macromolecular solution, 355
- Ghesquiere, Denis; Caze, Claude; and Loucheux, Claude: Grafted polymers from poly(4-vinylpyridinium) salts, 94
- Giglio, E.: *see* D'Alagni, M. and Giglio, E.
- Gilbert, Marianne: *see* Gray, A. and Gilbert, Marianne
- Goel, Malti: *see* Pillai, P. K. C. and Goel, Malti
- Gogolewski, S. and Pennings, A. J.: Crystallization of polyamides under elevated pressure: 2. Pressure-induced crystallization of nylon-6 (polycapramide) from the melt, 673
- Goka, A. M. and Sherrington, D. C.: Reactivity and mechanism in the cationic polymerization of *p*-methoxystyrene initiated by cycloheptatrienyl hexachloroantimonate, 819
- Goto, Kiyoshi: *see* Inagaki, Norihiro; Goto, Kiyoshi; and Kustuura, Kakuji
- Gray, A. and Gilbert, Marianne: Solvent sorption of heat treated vinyl chloride polymers, 387
- Greenwood, C. T. and Hourston, D. J.: Specific refractive index increments of certain polysaccharide systems, 474
- Guthrie, J. T.: Developments in radiation-induced graft polymerization to cellulose, 134
- Guthrie, J. T.: *see* Batty, N. S. and Guthrie, J. T.
- Guthrie, James T.: *see* Benson, Richard, Guthrie, James T. and Lartey, Ransford B.
- Hadjichristidis, N.: Temperature dependence of the unperturbed dimensions of poly(*p*-biphenyl methacrylate), 848
- Hadjichristidis, N.: *see* Alexopoulos, J. B., Hadjichristidis, N. and Vassiliadis, A.
- Haga, Y.: *see* Kusumoto, N., Haga, Y. and Motozato, Y.
- Haigh, J., Ali, A. S. M. and Davies, G. J.: Structural effects in the sub-millimetre wave spectrum of isotactic polypropylene, 714
- Hains, Philip J. and Williams, Graham: Molecular motion in polystyrene-plasticizer systems as studied by dielectric relaxation, 725
- Hama, Yoshimasa: *see* Ooi, Toshitami; Shiotsubo, Masami; Hama, Yoshimasa; and Shinohara, Kenjichi
- Hamilton, J. G., Ivin, K. J., Kuan-Essig, L. C. and Watt, P.: Detection of tacticity in polypropylenimine by  $^{13}\text{C}$  n.m.r., 763
- Hanson, D. E.: *see* Cogswell, F. N. and Hanson, D. E.
- Harris, P. A.: *see* Price, C., Harris, P. A., Holton, T. J. and Stubbersfield, R. B.
- Hasegawa, Masaki: *see* Nakanishi, Fusai; Hasegawa, Masaki; and Tasai, Takeshi
- Hashimoto, M.: *see* Kajiwara, M., Hashimoto, M. and Saito, H.
- Hashimoto, Takeji: *see* Hirata, Eiji; Ijitsu, Toshikazu; Soen, Toshiichi; Hashimoto, Takeji and Kawai, Hiromichi
- Haward, R. N.: *see* Adam, G. A., Parsons, I. W. and Haward, R. N.
- Hayashi, Toshio; Emi, Shingo; and Nakajima, Akio: Helix-coil transition of poly( $\epsilon$ -carbobenzyloxy-L-lysine) in *m*-cresol, 396
- Heatley, Frank: Molecular motion in polyisobutylene and poly(propylene oxide) studies by  $^{13}\text{C}$  nuclear magnetic relaxation, 493
- Heatley, Frank and Scrivens, J. H.: A study of solvent motion in acetone-PMMA solutions using  $^{13}\text{C}$  and  $^1\text{H}$  spin-lattice relaxation measurements, 489
- Hemming, Malcolm: *see* Dawkins, J. V. and Hemming, Malcolm
- Hertzberg, R. W.: *see* Manson, J. A., Hertzberg, R. W., Kim, S. L. and Skibo, M.
- Hesse, Jean: *see* Malhotra, Shadi L., Hesse, Jean and Blanchard, Louis-P.
- Hibbert, Barbara L.: *see* Epton, R., Hibbert, Barbara L. and Marr, G.
- Higashimura, Toshinobu: *see* Imanishi, Yukio; Kugimiya, Kazuya; and Higashimura, Toshinobu
- Higashimura, Toshinobu: *see* Yamamoto Kenji and Higashimura, Toshinobu
- Hirano, Shigehiro; Kondo, Sumiyo; and Ohe, Yasuo: Chitosan gel: a novel polysaccharide gel, 622
- Hirata, Eiji; Ijitsu, Toshikazu; Soen, Toshiichi; Hashimoto, Takeji; and Kawai, Hiromichi: Domain structure and crystalline morphology of AB and ABA type block copolymers of ethylene oxide and isoprene cast from solutions, 249
- Hirayama, C.: *see* Motozato, Y., Kusumoto, N., Hirayama, C., Murakami, R. and Isozaki, H.
- Hobbs, S. Y. and Pratt, C. F.: Multiple melting in poly(butylene terephthalate), 462
- Holton, T. J.: *see* Price, C., Harris, P. A., Holton, T. J. and Stubbersfield, R. B.
- Hourston, D. J.: *see* Greenwood, C. T. and Hourston, D. J.
- Houston, Eve: *see* Baird, Martin and Houston, Eve
- Hsu, B. S.: *see* Choy, C. L., Tse, Y. K., Tsui, S. M. and Hsu, B. S.
- Huglin, M. B.: *see* Cunliffe, A. V., Huglin, M. B., Pearce, P. J. and Richards, D. H.

## Author Index

- Ibel, K.: *see* Kirste, R. G., Kruse, W. A. and Ibel, K.
- Ida, Hiroaki: *see* Tomita, Kosuke and Ida, Hiroaki
- Ijitsu, Toshikazu: *see* Hirata, Eiji; Ijitsu, Toshikazu; Soen, Toshiichi; Hashimoto, Takeji; and Kawai, Hiromichi
- Ikada, E., Sugimura, T., Aoyama, T. and Watanabe, T.: Dielectric properties of oligomers: 4. Dielectric properties of vinyl acetate and methyl methacrylate oligomers, 101
- Ikeda, Mitsuru; Suga, Hiroshi; and Seki, Syuzo: Thermodynamic studies of solid polyethers: 5. Crystalline-amorphous interfacial thermal properties, 634
- Ikeyama, Masaru: *see* Tanaka, Yasuyuki; Sato, Hisaya; Ozeki, Yukio; Ikeyama, Masaru; and Sato, Takefumi
- Imanishi, Yukio; Kugimiya, Kazuya; and Higashimura, Toshinobu: Conformational studies of *N*-acetyl-*N*-methyl-L-alanine dimethylamide-*d*<sub>6</sub> by n.m.r. spectroscopy, 345. Conformational studies of poly(*N*-methyl-L-alanine) by n.m.r. spectroscopy, 350
- Inagaki, Norhihiro; Goto, Kiyoshi; and Kastuura, Kakuji: Thermal degradation of poly(diethyl vinylphosphonate) and its copolymer, 641
- Ingham, J. D.: *see* Rhein, R. A. and Ingham, J. D.
- Isozaki, H.: *see* Motozato, Y., Kusumoto, N., Hirayama, C., Murakami, R. and Isozaki, H.
- Ivin, K. J.: *see* Fawcett, A. H. and Ivin, K. J.
- Ivin, K. J.: *see* Hamilton, J. G., Ivin, K. J., Kuan-Essig, L. C. and Watt, P.
- Iwabuchi, Susumu: *see* Kojima, Kuniharu; Iwabuchi, Susumu; Moriya, Yuichi; and Yoshikuni, Masako
- Iyer, P. N. Shankar; North, Alastair M.; Pethrick, Richard A.; and Steinhauer, Daniel: Acoustic studies of chain flexibility in copolymers of *N*-vinylcarbazole, 797
- Janeschitz-Kriegl, H.: *see* Noordermeer, J. W. M., Daryanani, R. and Janeschitz-Kriegl, H.
- Jennings, Barry R.: *see* Foweraker, Alan R. and Jennings, Barry R.
- Jones, T. Tyssul: *see* Cook, M., Williams, G. and Jones, T. Tyssul
- Kajiwara, M. and Saito, H.: Phosphonitrilic chloride: 23. Substitution reaction of phosphonitrilic chloride trimer with sodium hydroxymethylphenolate and polymerization of substitution products, 21.
27. Synthesis and properties of cyclophosphazene polymers, 671
- Kajiwara, M., Hashimoto, M. and Saito, H.: Phosphonitrilic chloride: 30. Synthesis of chelating polymers from cyclophosphazene derivatives and studies of their electrical conductivity and thermal properties, 861
- Kampouris, Emmanuel M., Regas, F., Rokotas, S., Polychronakis, S. and Pantazoglou, M.: Migration of PVC plasticizers into alcohols, 840
- Kanazawa, Hitoshi: *see* Osawa, Zenjiro; Kanazawa, Hitoshi; Kuwako, Yuji; and Ogiwara, Yoshitaka
- Kaneko, M.: *see* Saeki, S., Kuwahara, N., Nakata, M. and Kaneko, M.
- Karger-Kocsis, J.: *see* Szafner, A. and Karger-Kocsis, J.
- Kastuura, Kakuji: *see* Inagaki, Norihiro; Goto, Kiyoshi; and Kastuura, Kakuji
- Kawai, Hiromichi: *see* Hirata, Eiji; Ijitsu, Toshikazu; Soen, Toshiichi; Hashimoto, Takeji; and Kawai, Hiromichi
- Kihira, Yasuhara; Matsusaka, Kijuo; and Murakami, Ichiro: Effect of thermal decomposition on dielectric relaxation process of poly(vinyl chloride), 265
- Kikuchi, Kazuo: *see* Nishioka, Masaharu; Kikuchi, Kazuo; and Yoshioka, Koshiro
- Kim, S. L.: *see* Manson, J. A., Hertzberg, R. W., Kim, S. L. and Skibo, M.
- Kimmich, R.: Estimation of the correlation length in polymer melts from nuclear magnetic relaxation dispersion, 851
- Kirste, R. G., Kruse, W. A. and Ibel, K.: Determination of the conformation of polymers in the amorphous solid state and in concentrated solution by neutron diffraction, 120
- Kojima, Kuniharu; Iwabuchi, Susumu; Moriya, Yuichi; and Yoshikuni, Masako: Polymerization of methyl methacrylate by tri-*n*-butylborane in the presence of amino acid esters, 601
- Kondo, Sumiyo: *see* Hirano, Shigehiro; Kondo, Sumiyo; and Ohe, Yasuo
- Kruse, W. A.: *see* Kirste, R. G., Kruse, W. A. and Ibel, K.
- Kuan-Essig, L. C.: *see* Hamilton, J. G., Ivin, K. J., Kuan-Essig, L. C. and Watt, P.
- Kubát, Josef and Rigdahl, Mikael: Influence of high injection pressures on the internal stress level in injection moulded specimens, 925
- Kubo, K. and Ogino, K.: Thermodynamic properties of concentrated poly( $\gamma$ -benzyl-L-glutamate) solutions, 629
- Kugimiya, Kazuya: *see* Imanishi, Yukio; Kugimiya, Kazuya; and Higashimura, Toshinobu
- Kusumoto, N., Haga, Y. and Motozato, Y.: Study of structural change in linear polyethylene by elongation in view of behaviour of free radicals induced by  $\gamma$ -irradiation, 229
- Kusumoto, N.: *see* Motozato, Y., Hirayama, C., Murakami, R. and Isozaki, H.
- Kuwahara, N.: *see* Saeki, S., Kuwahara, N., Nakata, M. and Kaneko, M.
- Kuwako, Yuji: *see* Osawa, Zenjiro; Kanazawa, Hitoshi; Kuwako, Yuji; and Ogiwara, Yoshitaka
- Kwan, S. F., Chen, F. C. and Choy, C. L.: Ultrasonic studies of three fluoropolymers, 481
- Kwei, K. T.: *see* Nishi, T. and Kwei, K. T.
- Labag, J. J.: *see* Marin, G., Labag, J. J. and Monge, Ph.
- Lal, M.: *see* Clark, A. T. and Lal, M.
- Landel, R. F.: *see* Fedors, R. F. and Landel, R. F.
- Lartey, Ransford, B.: *see* Benson, Richard, Guthrie, J. T. and Lartey, Ransford, B.
- Lau, K. H. and Young, K.: Cavity field for axially symmetric dielectrics, 477
- Lazereva, L. I.: *see* Lirova, B. I., Tager, A. A., Lazereva, L. I., Salazkin, S. N. and Vygodskii, Ya. S.
- Lecomte, L. and Desreux, V.: Solvent effect on the unperturbed dimensions of poly(aryl isocyanates), 765
- Ledwith, A., Lockett, E. and Sherrington, D. C.: Absolute reactivity in the cationic polymerization of methyl and other alkyl vinyl ethers, 31
- Lieser, G.: *see* Dröscher, M., Lieser, G., Reimann, H. and Wegner, G.
- Lindley, K.: *see* Margerison, D., Bain, D. R., Lindley, K., Morgan, N. R. and Taylor, Lindsay
- Lipatov, Yuri S., Moysya, E. G. and Semenovich, G. M.: Study of molecular packing density in boundary layers of some polymers, 582
- Lirova, B. I., Tager, A. A., Lazereva, L. I., Salazkin, S. N. and Vygodskii, Ya. S.: An infra-red investigation of cardo polymer solutions, 805
- Lockett, E.: *see* Ledwith, A., Lockett, E. and Sherrington, D. C.
- Loo, C. T.: *see* Blow, C. M. and Loo, C. T.
- Lord, P. W.: *see* Block, H., Lord, P. W. and Walker, S. M.
- Loucheux, Claude: *see* Ghesquiere, Dens; Caze, Claude and Loucheux, Claude
- Loucheux, Claude: *see* Morcellet, Michel and Loucheux, Claude
- McBrierty, Vincent J. and McDonald, Ian R.: Nuclear magnetic relaxation in linear and branched polyethylene, 125

- McDonald, Ian R.: *see* McBrierty, Vincent J. and McDonald, Ian R.
- McEwen, I. J.: *see* Cowie, J. M. G. and McEwen, I. J.
- McEwen, I. J.: *see* Cowie, J. M. G., McEwen, I. J. and Veličković, J.
- Machin, D.: *see* Barrie, J. A., Machin, D. and Nunn, A.
- Maclaine, J. Q. G. and Booth, C.: Effect of molecular weight on crystallization isotherms of high molecular weight poly(ethylene oxide), 680. Effect of molecular weight on spherulite growth rates of high molecular weight poly(ethylene oxide) fractions, 191
- Makaya, G.: A formula for the  $\beta$ -relaxation in polymers, 852
- Malhotra, Shadi L., Hesse, Jean and Blanchard, Louis-P.: Thermal decomposition of polystyrene, 81
- Malhotra, Shadi L., Hesse, Jean and Blanchard, Louis-P.: Thermal decomposition of a vinyl chloride/vinyl acetate copolymer, 269
- Manaresi, P., Passalacqua, V. and Pilati, F.: Kinetics of graft polymerization of styrene on *cis*-1,4-polybutadiene, 520
- Mansfield, P.: *see* Garroway, A. N., Stalker, D. C. and Mansfield, P.
- Manson, J. A., Hertzberg, R. W., Kim, S. L. and Skibo, M.: The  $\beta$  transition and frequency sensitivity in fatigue crack propagation of polymers, 850
- Manuel, A. J.: *see* Smith, J. B., Manuel, A. J. and Ward, I. M.
- Marcinčin, K. and Romanov, A.: Relationships between  $T_g$  and cohesive energy: 1. Dependence of  $T_g$  on the composition of copolymers, 173. 2. Prediction of  $T_g$  of homopolymers, 177
- Margerison, D., Bain, D. R., Lindley, K., Morgan, N. R. and Taylor, Lindsay: Reactivity ratios for the copolymerization systems styrene/*p*-ethoxystyrene and methyl methacrylate/*p*-ethoxystyrene, 278
- Marin, G., Labaig, J. J. and Monge, Ph.: Dynamic viscoelasticity of entangled polymers, 223
- Mark, J. E.: *see* Yu, C. U. and Mark, J. E.
- Marr, G.: *see* Epton, R., Hibbert, Barbara, L. and Marr, G.
- Martuscelli, E.: *see* Amelino, L. and Martuscelli, E.
- Mateová, E.: *see* Adamec, V. and Mateová, E.
- Matsusaka, Kijuo: *see* Kihira, Yasuhara; Matsusaka, Kijuo; and Murakami, Ichiro
- Maxfield, J. and Shepherd, I. W.: Effect of a non-uniform distribution of crosslinks on the analysis of Raman polarization data in stretched networks, 227
- Maxfield, J. and Shepherd, I. W.: Conformation of poly(ethylene oxide) in the solid state, melt and solution measured by Raman scattering, 505
- Mazeron, P.: *see* Ravey, J. C. and Mazeron, P.
- Mengoli, G. and Tidswell, B. M.: Polymeric coatings on steel produced by the electroinitiated polymerization of acrylic monomers, 881
- Minoura, Yuji: *see* Yamaguchi, Koichi; Yoshida, Takero; and Minoura, Yuji
- Mishra, Prashant, K.: *see* Biswas, Mukul and Mishra, Prashant K.
- Miyagi, Z. and Tanaka, K.: Sorption of water vapour by atactic and isotactic poly(methyl methacrylate), 441
- Moan, Michel and Wolff, Claude: Study of the conformational rigidity of polyelectrolytes by elastic neutron scattering: 1. Carboxymethylcelluloses in the intermediate momentum range, 776
- Moan, Michel; Wolff, Claude and Ober, Raymond: Study of the conformational rigidity of polyelectrolytes by elastic neutron scattering: 2. Molecular dimensions and conformation of poly(methacrylic acid), 781
- Moisya, E. G.: *see* Lipatov, Yuri, S., Moisya, E. G. and Semonovich, G. M.
- Monge, Ph.: *see* Marin, G., Labaig, J. J. and Monge, Ph.
- Monks, H. H.: *see* Corfield, G. C., Monks, H. H. and Ellinger, L. P.
- Morantz, D. J. and Bilen, C. S.: Thermoluminescence and induced phosphorescence in irradiated doped PMMA, 745
- Morcellet, Michel and Loucheux, Claude: Potentiometric study of poly(L-glutamic acid) in water-dioxane mixtures, 785. Preferential and absolute adsorption on poly(L-glutamic acid) in water-dioxane mixtures, 401
- Morgan, N. R.: *see* Margerison, D., Bain, D. R., Lindley, K., Morgan, N. R. and Taylor, Lindsay
- Moriya, Yuichi: *see* Kojima, Kuniharu; Iwabuchi, Susumu, Moriya, Yuichi; and Yoshikuni, Masako
- Motozato, Y., Kusumoto, N., Hirayama, C., Murakami, R. and Isozaki, H.: Study of relationship between network structure of g.p.c. gels and molecular size of permeable substance, 321
- Motozato, Y.: *see* Kusumoto, N., Haga, Y. and Motozato, Y.
- Murakami, Ichiro: *see* Kihira, Yasuhara; Matsusaka, Kijuo; and Murakami, Ichiro
- Murakami, R.: *see* Motozato, Y., Kusumoto, N., Hirayama, C., Murakami, R. and Isozaki, H.
- Nakajima, Akio: *see* Hayashi, Toshio; Emi, Shingo; and Nakajima, Akio
- Nakanishi, Fusae; Hasegawa, Masaki; and Tasai, Takeshi: Depolymerization behaviour of poly(*p*-phenylene diacrylic acid diethyl ester), 218
- Nakata, M.: *see* Saeki, S., Kuwahara, N., Nakata, M. and Kaneko, M.
- Nash, D. W. and Pepper, D. C.: Solution properties of poly(propylene sulphide), 105
- News, A. C.: Some effects of formaldehyde crosslinking on the kinetics of water vapour sorption in cellulose, 2
- Nicol, Elisabeth A.: *see* Willis, H. A., Cudby, M. E. A., Chantry, G. W., Nicol, Elisabeth A. and Fleming, J. W.
- Nishi, T. and Kwei, K. T.: Cloud point curves for poly(vinyl methyl ether) and monodisperse polystyrene mixtures, 285
- Nishioka, Masaharu; Kikuchi, Kazuo; and Yoshioka, Koshiro: Electro-optical properties of poly( $\epsilon$ -carboxy-L-lysine) in organic solvents, 791
- Noordemeer, J. W. M., Daryanani, R. and Janeschitz-Kriegl, H.: Flow birefringence studies of polymer conformation: cellulose tricarbanilate in two characteristic solvents, 359
- North, Alastair M.: *see* Iyer, P. N., Shankar, North, Alastair M.; Pethrick, Richard A.; and Steinhauer, Daniel
- Nunn, A.: *see* Barrie, J. A., Machin, D. and Nunn, A.
- Ober, Raymond: *see* Moan, Michel; Wolff, Claude and Ober, Raymond
- Ogino, K.: *see* Kubo, K. and Ogino, K.
- Ogiwara, Yoshitaka: *see* Osawa, Zenjiro; Kanazawa, Hitoshi; Kuwako, Juji; and Ogiwara, Yoshitaka
- Ohe, Yasuo: *see* Hirano, Shigehiro; Kondo, Sumiyo; and Ohe, Yasuo
- Ooi, Toshitami; Shiotsubo, Masami; Hama, Yoshimasa; and Shinohara Kenichi: E.s.r. study of  $\gamma$ -irradiated isotactic and atactic polypropylene, 510
- Osawa, Zenjiro; Kanazawa, Hitoshi; Kuwako, Yuji; and Ogiwara, Yoshitaka: Catalytic action of metallic salts in autoxidation and polymerization: 11. Polymerization of methacrylic acid esters with sodium hexanitrocobaltate in methanol-water, 590
- Otsu, Takayuki and Tanaka, Hitoshi: Structure and radical reactivities of vinyl monomers: copolymerization reactivities of alkyl vinyl ketones, 468
- Otsu, Takayuki: *see* Sato, Tsuneyuki and Otsu, Takayuki
- Overbergh, N., Berghmans, H. and Smets, G.: Crystallization of isotactic polystyrene induced by organic vapours, 703

Author Index

- Oya, S.: *see* Yamzaki, T., Oya, S., Tsukane, N., Tanaka, K., Toba, H. and Yamagishi, K.
- Ozeki, Yukio: *see* Tanaka, Yasuyuki; Sato, Hisaya; Ozeki, Yukio; Ikeyama, Masaru; and Sato, Takefumi
- Pallesi, B.: *see* Coppola, G., Filippini, R. and Pallesi, B.
- Pantazoglou, M.: *see* Kampouris, Emmanuel M., Regas, F., Rokotas, S., Polychronakis, S. and Pantazoglou, M.
- Parsons, I. W.: *see* Adam, G. A., Parsons, I. W. and Haward, R. N.
- Passalacqua, V.: *see* Manaresi, P., Passalacqua, V. and Pilati, F.
- Pavan, S.: *see* Ricco, T., Pavan, A. and Danusso, F.
- Pearce, P. J.: *see* Cunliffe, A. V., Huglin, M. B., Pearce, P. J. and Richards, D. H.
- Pedemonte, Enrico; Dondero, Giovanni; Alfonso, Giovanni C. and de Candia, Francesco: Three-block copolymers: morphologies and stress-strain properties of samples prepared under various experimental conditions, 531
- Pennings, A. J.: *see* Gogolewski, S. and Pennings, A. J.
- Pepper, D. C.: *see* Nash, D. W. and Pepper, D. C.
- Pethrick, Richard A.: *see* Iyer, P. N., Shankar, North, Alastair M., Pethrick, Richard A., and Steinhauer, Daniel
- Pilař, J. and Ulbert, K.: E.p.r. study of radicals produced mechanically in PGMA and their interaction with oxygen, 730
- Pilati, F.: *see* Manaresi, P., Passalacqua, V. and Pilati, F.
- Pillai, P. K. C. and Goel, Malti: Persistent polarization in a carotenoid polymer,  $\beta$ -carotene, 5
- Pineri, M.: Low temperature internal friction in some poly( $\alpha$ -olefins), 595
- Plati, E. and Williams, J. G.: Effect of temperature on the impact fracture toughness of polymers, 915
- Platzek, U.: *see* Braun, D. and Platzek, U.
- Poller, R. C.: *see* Alavi-Moghadam, F., Ayrey, G. and Poller, R. C.
- Polychronakis, S.: *see* Kampouris, Emmanuel M., Regas, F., Rokotas, S., Polychronakis, S. and Pantazoglou, M.
- Pratt, C. F.: *see* Hobbs, S. Y. and Pratt, C. F.
- Price, C.: *see* Ashman, P. C., Booth, C., Cooper, D. R. and Price, C.
- Price, Colin: Effect of pressure on the formation of poly(methyl methacrylate) glasses, 585
- Price, C., Allen, G. and Yoshimura, N.: Thermomechanical heat of deformation studies on *cis*-polybutadiene, 261
- Price, C., Evans, K. A. and Booth, C.: Crystallization of poly(ethylene oxide) fractions: simultaneous dilatometry and calorimetry, 196
- Price, C., Harris, P. A., Holton, T. J. and Stubbersfield, R. B.: Growth of lamellar crystals of poly( $\gamma$ -benzyl-L-glutamate), 69
- Quack, Günther: *see* Elgert, Karl-Friedrich; Quack, Günther and Stützel, Bernhard
- Radon, J. C. and Culver, L. E.: Effect of temperature and frequency in fatigue of polymers, 539
- Ratti, L.: *see* Bevington, J. C. and Ratti, L.
- Ravey, J. C. and Mazon, P.: Light scattering in an electric field: variations of the  $H_H(\theta)$  component around  $\theta = 90^\circ$ , 329
- Regas, F.: *see* Kampouris, Emmanuel M., Regas, F., Rokotas, S., Polychronakis, S. and Pantazoglou, M.
- Reich, L.: *see* Gabbay, S. M., Stivala, S. S. and Reich, L.
- Reimann, H.: *see* Dröscher, M., Lieser, G., Reimann, H. and Wegner, G.
- Rempp, Paul: *see* Dondos, Anastasios; Rempp, Paul; and Benoit, Henri
- Rhein, R. A. and Ingham, J. D.: Saturated hydrocarbon prepolymers by ozonolysis, 799
- Riccò, T., Pavan, A. and Danusso, F.: Dynamic transition of grafted polybutadiene in ABS resins, 685
- Richards, D. H.: *see* Cunliffe, A. V., Huglin, M. B., Pearce, P. J. and Richards, D. H.
- Richardson, M. J. and Savill, N. G.: Derivation of accurate glass transition temperatures by differential scanning calorimetry, 753
- Rietsch, F. and Froelich, D.: Elastic behaviour of ideal polystyrene networks, 873
- Rigdahl, Mikael: *see* Kubát, Josef and Rigdahl, Mikael
- Ritter, W.: *see* Elgert, K. F., Wicke, R., Stützel, B. and Ritter, W.
- Rokotas, S.: *see* Kampouris, Emmanuel M., Regas, F., Rokotas, S., Polychronakis, S. and Pantazoglou, M.
- Romanov, A.: *see* Marcinčin, K. and Romanov, A.
- Rooney, J. M.: *see* Chung, Y. J., Rooney, J. M., Squire, D. R. and Stannett, V.
- Roovers, J. E. L.: Synthesis and solution properties of comb polystyrenes, 827
- Rudin, Alfred and Burgin, Dennis: Effects of molecular weight and chain ends on glass transition of polystyrene, 291
- Russo, Saverio: *see* Bontà, Giorgio; Gallo, Bianca M. and Russo, Saverio
- Saeki, S., Kuwahara, N., Nakata, M. and Kaneko, M.: Pressure dependence of upper critical solution temperatures in the polystyrene-cyclohexane system, 445
- Saito, Hajime: *see* Kajiwara, Meisetsu and Saito, Hajime
- Saito, H.: *see* Kajiwara, M., Hashimoto, M. and Saito, H.
- Salazkin, S. N.: *see* Lirova, B. I., Tager, A. A., Lazareva, L. I., Salazkin, S. N. and Vygodskii, Ya. S.
- Sato, Hisaya: *see* Tanaka, Yasuyuki; Sato, Hisaya; Ozeki, Yukio; Ikeyama, Masaru; and Sato, Takefumi
- Sato, Takefumi: *see* Tanaka, Yasuyuki; Sato, Hisaya; Ozeki, Yukio; Ikeyama, Masaru; and Sato, Takefumi
- Sato, Tsuneyuki and Otsu, Takayuki: Evaluation of relative reactivities of vinyl monomers towards t-butoxy radical by means of spin trapping technique, 389
- Savill, N. G.: *see* Richardson, M. J. and Savill, N. G.
- Schurer, J. W., de Boer, A. and Challa, G.: Influence of tacticity of poly(methyl methacrylate) on the compatibility with poly(vinyl chloride), 201
- Scrivens, J. H.: *see* Heatley, Frank and Scrivens, J. H.
- Sederel, W. L., Bantjes, A. and Feijen, J.: A route to anionic hydrophilic films of copolymers of L-leucine, L-aspartic acid and L-aspartic acid esters, 735
- Segre, A. L., Delfini, M., Conti, F. and Boicelli, A.: N.m.r. studies of butadiene-styrene copolymers, 338
- Seki, Syuzo: *see* Ikeda, Mutsuru; Suga, Hiroshi; and Seki, Syuzo
- Sellen, D. B.: Light scattering Rayleigh linewidth measurements on some dextran solutions, 561. Light scattering Rayleigh linewidth measurements on some solutions of cellulose trinitrate, 169. Light scattering Rayleigh linewidth measurements upon solutions of globular proteins containing high molecular weight impurities, 773
- Semenovich, G. M.: *see* Lipatov, Yuri, S., Moysya, E. G. and Semenovich, G. M.
- Shepherd, I. W.: *see* Maxfield, J. and Shepherd, I. W.
- Sherrington, D. C.: *see* Goka, A. M. and Sherrington, D. C.
- Sherrington, D. C.: *see* Ledwith, A., Lockett, E. and Sherrington, D. C.
- Shinohara, Kenichi: *see* Ooi, Toshitami; Shiotsubo, Masami; Hama, Yoshimasa; and Shinohara, Kenichi
- Shiotsubo, Masami: *see* Ooi, Toshitami; Shiotsubo, Masami; Hama, Yoshimasa; and Shinohara, Kenichi
- Siesler, H. W. and Tittle, B.: A new catalytic system for the polymerization of THF, 548

- Sigwalt, P.: *see* Siove, A., Sigwalt, P. and Fontanille, M.
- Siove, A., Sigwalt, P. and Fontanille, M.: Kinetic study of anionic polymerization of butadiene in a polar solvent, 605
- Skibo, M.: *see* Manson, J. A., Hertzberg, R. W., Kim, S. L. and Skibo, M.
- Slavtcheva, L. and Dimov, K.: Stereoregular polymerization of vinyl chloride with the redox system ferrous sulphate/hydrogen peroxide/oxalic acid: 2. Process kinetics, 717
- Smets, G.: *see* Overbergh, N., Berghmans, H. and Smets, G.
- Smith, G. R.: *see* Darlington, M. W. and Smith, G. R.
- Smith, J. B., Manuel, A. J. and Ward, I. M.: Broadline n.m.r. studies of ultra-high modulus polyethylenes, 57
- Soen, Toshiichi: *see* Hirata, Eiji; Ijitsu, Toshikazu; Soen, Toshiichi; Hashimoto, Takeji; and Kawai, Hiromichi
- Sorta, E.: *see* Borri, C., Sorta, E. and Zotteri, L.
- Spach, Gerard: *see* Trudelle, Yves and Spach, Gerard
- Squire, D. R.: *see* Chung, Y. J., Rooney, J. M., Squire, D. R. and Stannett, V.
- Stalker, D. C.: *see* Garroway, A. N., Stalker, D. C. and Mansfield, P.
- Stannett, V.: *see* Chung, Y. J., Rooney, J. M., Squire, D. R. and Stannett, V.
- Steinhauer, Daniel: *see* Iyer, P. N., Shankar, North, Alastair M., Pethrick, Richard A.; and Steinhauer, Daniel
- Stivala, S. S.: *see* Gabbay, S. M., Stivala, S. S. and Reich, L.
- Stubbersfield, R. B.: *see* Price, C., Harris, P. A., Holton, T. J. and Stubbersfield, R. B.
- Stützel, B.: *see* Elgert, K.-F. and Stützel, B.
- Stützel, B.: *see* Elgert, K.-F., Stützel, B. and Forgo, Impre
- Stützel, Bernhard: *see* Elgert, Karl-Friedrich; Quack, Günther; and Stützel, Bernhard
- Stützel, B.: *see* Elgert, K. F., Wicke, R., Stützel, B. and Ritter, W.
- Suga, Miroshi: *see* Ikeda, Mitsuru; Sugui, Hiroshi; and Seki, Syuzo
- Sugimura, T.: *see* Ikada, E., Sugimura, T., Aoyama, T. and Watanabe, T.
- Szafner, A. and Karger-Kocsis, J.: Increase of the melt viscosity of polycapraamide by chromium(III) ions, 879
- Tager, A. A.: *see* Lirova, B. I., Tager, A. A., Lazareva, L. I., Salazkin, S. N. and Vygodskii, Ya. S.
- Tanaka, Hitoshi: *see* Otsu, Takayuki and Tanaka, Hitoshi
- Tanaka, K.: *see* Miyagi, Z. and Tanaka K.
- Tanaka, K.: *see* Yamazaki, T., Oya, S., Tsukane, N., Tanaka, K., Toba, H. and Yamagishi, K.
- Tanaka, Yasuyuki; Sato, Hisaya; Ozeki, Yukio, Ikeyama, Masaru; and Sato, Takefumi: Determination of unsaturation in ethylene-propylene terpolymers and butyl rubber by time-averaged  $^1\text{H}$  n.m.r. measurements, 709
- Tasai, Takeshi: *see* Nakanishi, Fusai; Hasegawa, Masaki and Tsai, Takeshi
- Taylor, Lindsay: *see* Margerison, D., Bain, D. R., Lindley, K., Morgan, N. R. and Taylor, Lindsay
- Tidswell, B. M.: *see* Mengoli, G. and Tidswell, B. M.
- Tittle, B.: *see* Siesler, H. W. and Tittle, B.
- Toba, H.: *see* Yamazaki, T., Oya, S., Tsukane, N., Tanaka, K., Toba, H. and Yamagishi, K.
- Tomita, Kosuke and Ida, Hiroaki: Studies on the formation of poly(ethylene terephthalate): 3. Catalytic activity of metal compounds in transesterification of dimethyl terephthalate with ethylene glycol, 185
- Tondre, Christian and Zana, Raoul: Comments on Letter: 'Dilatometric study of monovalent counterion association with polymethacrylate' (J. Komiyama, Y. Takeda, M. Ando and T. Iijima, *Polymer* 1974, 15, 468-470), 228
- Trudelle, Yves: Conformational study of the sequential (Try-Glu)<sub>n</sub> copolymer in aqueous solution, 9
- Trudelle, Yves and Spach, Gerard: Circular dichroism study of poly(L-tyrosine), poly(L-glutamic acid) and of random and sequential copolymers of L-glutamic acid and L-tyrosine in trimethylphosphate, 16
- Tse, Y. K.: *see* Choy, C. L., Tse, Y. K., Tsui, S. M. and Hsu, B. S.
- Tsebrenko, M. V.: *see* Vinogradov, G. V., Yarlykov, B. V., Tsebrenko, M. V., Yudin, A. V. and Ablazova, T. I.
- Tsui, S. M.: *see* Choy, C. L., Tse, Y. K., Tsui, S. M. and Hsu, B. S.
- Tsukane, N.: *see* Yamazaki, T., Oya, S., Tsukane, N., Tanaka, K., Toba, H. and Yamagishi, K.
- Ulbert, K.: *see* Pilař, J. and Ulbert, K.
- van Krevelen, D. W.: Some basic aspects of flame resistance of polymeric materials, 615
- Vassiliadis, A.: *see* Alexopoulos, J. B., Hadjichristidis, N. and Vassiliadis, A.
- Veličković, J.: *see* Cowie, J. M. G., McEwen, I. J. and Veličković, J.
- Vert, Michel: *see* Braud, Christian and Vert, Michel
- Vinogradov, G. V., Yarlykov, B. V., Tsebrenko, M. V., Yudin, A. V. and Ablazova, T. I.: Fibrillation in the flow of polyoxymethylene melts, 609
- Vygodskii, Ya. S.: *see* Lirova, B. I., Tager, A. A., Lazareva, L. I., Salazkin, S. N. and Vygodskii, Ya. S.
- Walker, S. M.: *see* Block, H., Lord, P. W. and Walker, S. M.
- Ward, I. M.: *see* Capaccio, G. and Ward, I. M.
- Ward, I. M.: *see* Capaccio, G., Chapman, T. J. and Ward, I. M.
- Ward, I. M.: *see* Smith, J. B., Manuel, A. J. and Ward, I. M.
- Watanabe, T.: *see* Ikada, E., Sugimura, T., Aoyama, T. and Watanabe, T.
- Watt, P.: *see* Hamilton, J. G., Ivin, K. J., Kuan-Essig, L. C. and Watt, P.
- Wegner, G.: *see* Dröscher, M., Lieser, G., Reimann, H. and Wegner, G.
- Weidmann, G. W. and Williams, J. G.: Crazing and the creep behaviour of PMMA in methanol, 921
- Welch, G. J.: Solution properties of low molecular weight atactic poly(acrylic acid) and its sodium salt, 68
- White, J. R.: Optimum conditions for electron microscopy of radiation sensitive polymer crystals, 157
- Whittle, D.: *see* Bamford, C. H., Eastmond, G. C. and Whittle, D.
- Wicke, R.: *see* Elgert, K. F., Wicke, R., Stützel, B. and Ritter, W.
- Williams, G.: *see* Cook, M., Williams, G. and Jones, T. Tyssul
- Williams, Graham: *see* Hains, Philip J. and Williams, Graham
- Williams, J. G.: *see* Plati, E. and Williams, J. G.
- Williams, J. G.: *see* Weidmann, G. W. and Williams, J. G.
- Willis, H. A., Cudby, M. E. A., Chantry, G. W., Nicol, Elisabeth A. and Fleming, J. W.: A far infra-red study of conformational disorder in PTFE, 74
- Wolf, F. P. and Allen, Geoffrey: The energetic contribution to rubber elasticity in the range of small uniaxial compression and moderate elongation, 209
- Wolff, Claude: *see* Moan, Michel and Wolff, Claude
- Wolff, Claude: *see* Moan, Michel; Wolff, Claude; and Ober, Raymond
- Wong, D. J. D.: *see* Ayrey, G. and Wong, D. J. D.
- Wong, K. C., Chen, F. C. and Choy, C. L.: Heat capacity of linear high polymers, 649
- Wong, K. C., Chen, F. C. and Choy, C. L.: Heat capacity of copolymers

## Author Index

- of chlorotrifluoroethylene and vinylidene fluoride, 858
- Yamagishi, K.: *see* Yamazaki, T., Oya, S., Tsukane, N., Tanaka, K., Toba, H. and Yamagishi, K.
- Yamaguchi, Koichi; Yoshida, Takero; and Minoura, Yuji: Vinyl polymerization initiated with alkali metal adducts of triphenylamine and triphenylphosphine, 281
- Yamamoto, Kenji and Higashimura, Toshinobu: Solvent effect on cationic polymerization of styrene with  $\alpha$ - or  $\beta$ -methylstyrenes, 97
- Yamamoto, Kenji and Higashimura, Toshinobu: Cationic copolymerization of vinyl ethers with styrene derivatives and their model reactions: selectivity of a growing carbocation, 815
- Yamazaki, T., Oya, S., Tsukane, N., Tanaka, K., Toba, H. and Yamagishi, K.: Studies on poly(isobutene oxide): 3. Elastic hard fibre of poly(isobutene oxide), 425
- Yarlykov, B. V.: *see* Vinogradov, G. V., Yarlykov, B. V., Tsebrenko, M. V., Yudin, A. V. and Ablazova, T. I.,
- Yoon, D. Y. and Flory, P. J.: Small angle neutron and X-ray scattering by poly(methyl methacrylate) chains, 645
- Yoshida, Takero: *see* Yamaguchi, Koichi; Yoshida, Takero; and Minoura, Yuji
- Yoshikuni, Masako: *see* Kojima, Kuniharu; Iwabuchi, Susumu; Moriya Yuichi; and Yoshikuni, Masako
- Yoshimura, N.: *see* Price, C., Allen, G. and Yoshimura, N.
- Yoshioka, Koshiro: *see* Nishioka, Masaharu; Kikuchi, Kazuo and Yoshioka, Koshiro
- Young, K.: *see* Lau, K. H. and Young, K.
- Young, Robert J.: Deformation mechanisms in polytetrafluoroethylene, 450
- Young, R. N.: Spectroscopic evidence for ion-pair equilibria involving polyvinylbiphenyl carbanions, 695
- Yu, C. U., Mark, J. E.: Stress-strain isotherms and thermoelastic properties of crosslinked amorphous polyoxyethylene in compression, 326
- Yudin, A. V.: *see* Vinogradov, G. V., Yarlykov, B. V., Tsebrenko, M. V., Yudin, A. V. and Alazova, T. I.
- Zana, Raoul: *see* Tondre, Christian and Zana, Raoul
- Zotteri, L.: *see* Borri, C., Sorta, E. and Zotteri, L.

# SCIENCE & PUBLIC POLICY

the international journal of the Science Policy Foundation

current awareness for busy people in

**government · industry · business ·  
education · research**

## SCIENCE & PUBLIC POLICY

- provides information on national policies for science and technology and their effects
- examines the roles of science and technology in the operations of government (local, national and international), industry and business
- analyses the social and political environments within which science and technology operate
- assesses appropriate methodologies, information systems and organisational forms
- explores various types of public participation and their influence on national and international policies

The journal contains short, pithy news items, concise reports, comment, commissioned reviews, facts in figures, book reviews and extensive bibliographies.

The information is gathered through a worldwide network of national correspondents who are intimately involved in researching and applying science and public policy in their country.

Subscription £25.00 (\$65.00) per year (12 issues) including postage by fastest route. A special annual rate of £10.00 (\$26.00) is available for the individual who certifies that the copies are for his/her personal use and who is the full-time employee of a current full-price establishment subscriber at the same address.

**IPC Business Press Ltd, Oakfield House, Perrymount Road,  
Haywards Heath, Sussex, England**

*Published monthly by IPC Science and Technology Press Ltd:  
publishers of FUTURES, ENERGY POLICY and RESOURCES  
POLICY.*

## UK EDITORS

C. H. Bamford **PhD, ScD, FRS**  
Campbell Brown Professor of Industrial  
Chemistry, University of Liverpool,  
PO Box 147, Liverpool L69 3BX

C. E. H. Bawn CBE, FRS  
Professor  
Springfields, Stoodleigh, Tiverton, Devon

E. M. **Bradbury PhD**  
Head of Biophysics Section,  
Portsmouth Polytechnic,  
Portsmouth PO1 2QG

Geoffrey Gee CBE, FRS  
Sir Samuel Hall Professor of Chemistry,  
University of Manchester,  
Manchester M 13 9PL

R. J. W. Reynolds **PhD, FPI**  
Institute of Polymer Technology,  
Loughborough University of Technology,  
Loughborough LE 11 3TU

I. M. Ward **DPhil, FPI**  
Professor of Physics,  
University of Leeds, Leeds LS2 9JT

J. G. Williams **DSc(Eng), PhD, CEng**  
Reader in Polymer Engineering,  
Department of Mechanical Engineering,  
Imperial College of Science and Technology,  
London SW7 2BX

Annual subscription including postage  
**£36; USA \$90.00** (surface mail)  
Airmail USA \$110; Japan ¥50  
Rates for other countries available on request

Subscription enquiries and orders: IPC Business Press Ltd,  
Oakfield House, Perrymount Road, Haywards Heath,  
Sussex, England

Published monthly by IPC Science and Technology  
Press Ltd, IPC House, 32 High Street,  
Guildford, Surrey, **GU13EW**, England  
Telephone: Guildford **(0483) 71661**  
Telegrams and Telex: Scitechpress Gd. 859556

Reprints (minimum quantity usually 100) of papers  
may be ordered from the publishers. Write to the  
Reprints Dept, IPC Science and Technology Press  
Ltd. at the above address  
**ISSN 00323861**

American Representatives: IPC (America) Ltd,  
205 East 42nd Street, New York, NY 10017, USA

© IPC Business Press Ltd, 1975

## OVERSEAS EDITORS

H. C. Benoit **PhD**  
Professor, University of Strasbourg  
Director, Centre de Recherches  
sur les Macromolécules,  
6, Rue **Boussingault**,  
67 Strasbourg, France

S. **Bywater PhD**  
Head, Polymer Section,  
National Research Council,  
Ottawa KIA **OR9**, Canada

F. Danusso **PhD**  
Professor of Macromolecular Chemistry,  
Istituto Chimica Industriale del Politecnico,  
Piazza Leonardo da Vinci 32,  
20133 Milano, Italy

Hirotao Kambe **DSc**  
Professor; Polymer Research Division,  
Institute of Space and Aeronautical Science,  
University of Tokyo, Tokyo, Japan

Maurice Morton **PhD**  
Director, Institute of Polymer Science,  
University of Akron,  
Akron, Ohio 44325, USA

M. Szwarc **PhD, FRS**  
Director, Polymer Research Center,  
State University of New York,  
College of Environmental Science and  
Forestry, Syracuse, NY 13210, USA

## MANAGING EDITOR

J. A. G. Thomas **PhD**

## ASSISTANT EDITOR

C. J. Rawlins **BSc**